Organized by
The North American Geosynthetics Society
(NAGS)
The Industrial Fabrics Association International
(IFAI)
under the auspices of
The International Geotextile Society
(IGS)

March 30-April 1, 1993

Vancouver Trade &
Convention Centre

Waterfront Centre Hotel

Vancouver,
British Columbia,
Canada

GEO'93

CONFERENCE PROCEEDINGS

VOLUME 1

SPONSORED BY

Geosynthetics '93
Conference Proceedings

Volume 1

Opening Session
Roads and Pavements
Walls, Slopes, Embankments and Foundations
Geotextile Filtration Design and Testing

This volume consists of papers presented at the
Geosynthetics '93 Conference held
March 30 - April 1, 1993 in Vancouver, BC, Canada

Sponsored By:

North American Geosynthetics Society
Industrial Fabrics Association International
under the auspices of the International Geotextile Society

Geosynthetics '93 Organizing Committee

Barry R. Christopher, Co-Chairman
Robert Denis, Co-Chairman
Joseph A. Dieltz, Secretary General
Richard J. Bathurst, Technical Committee Chairman
Robert G. Carroll
Jonathan Fannin
Mark L. Marienfeld
Frank Taylor
John F. Beech, Advisor

Publisher

Industrial Fabrics Association International
345 Cedar Street, Suite 800, St. Paul, MN 55101, USA
612-222-2508, fax 612-222-8215

Notice and Disclaimer

Forward

The 120 papers and invited lecture contained in these volumes represent the Proceedings of Geosynthetics '93 held in Vancouver, British Columbia, Canada, March 30 - April 1, 1993. The conference was co-sponsored by the North American Geosynthetics Society and Industrial Fabrics Association International and held under the auspices of the International Geotextile Society.

The papers in these volumes began with 307 abstracts that were received by the Organizing Committee of Geosynthetics '93 in answer to an international call for papers issued in 1991. A Technical Committee comprising seven knowledgeable persons employed with universities, manufacturers, distributors, consultants, testing laboratories and government agencies reviewed all abstracts. Based on this initial selection process, 179 authors were invited to submit full papers. Each paper was carefully reviewed by at least two qualified referees and the result of this peer-review is the collection of valuable papers gathered here. These 120 papers were presented in 24 technical sessions and a poster session at Geosynthetics '93 and represent the largest number of papers ever presented at a North American Conference devoted to geosynthetics.

A great number of individuals gave their valuable time to review papers and to offer constructive advice to the authors. The efforts of the Technical Committee of Geosynthetics '93 and the session leaders who organized the paper reviews are also gratefully acknowledged. Without their help, Geosynthetics '93 and these Proceedings would not have been possible. In addition, acknowledgements would be incomplete without thanking Mr. Joseph A. Dieltz, Timothy J. Arens and the IFAI staff who smoothly executed the formidable logistics required to organize Geosynthetics '93 and to produce these Proceedings.

This collection of technical papers is not only a valuable record of the state-of-the-art for geosynthetics in North America and worldwide, but also a testament to the co-operative spirit of the geosynthetics community in Canada and the United States.

Richard J. Bathurst
Chairman, Technical Committee
Geosynthetics '93

Table of Contents

Volume 1

Opening Session

Roads and Pavements

Walls, Slopes, Embankments and Foundations

Geotextile Filtration Design and Testing

Volume 2

Geosynthetics Testing

Durability and Long-Term Performance of Geosynthetics

Technical Advances, Innovations, Challenges

Volume 3

Waste Containment Case Histories

Landfill Design, Performance and CQA

OPENING SESSION

GEOSYNTHETICS '93 CONFERENCE
VANCOUVER, BRITISH COLUMBIA

OPENING ADDRESS TO GEOSYNTHETICS '93

Geosynthetics in North America: A Rigorous Attempt to Make a Short Story Long

J.E. Fluet, Jr.
Florida Atlantic University, USA

ABSTRACT

When Bob Denis asked me to give this opening address, I was of course pleased and honored, but I must say that I thought it a bit strange when he asked that I speak of my "personal experiences in the geosynthetics industry" and that I "keep it light". Personal and light? I am an engineer, Bob - how about rigorous and scholarly? Perhaps I misunderstood. Perhaps he was suggesting that I am *personally* only *lightly* experienced in geosynthetics, or that he believed it was high time I shed some *light* on some of my *personal* experiences. I realize I am a little confused, but the last time I felt this way was when I met a fellow who said "I'm from the IRS and I'm here to help". In any case, we settled on the following: my recollections and musings of the geosynthetics industry these past 20 years, occasionally based on rigorous research and scholarly reflections.

INTRODUCTION

Remarkably, it really has been 20 years since I was first exposed to the world of geosynthetics. I guess I must have been destined to work in this field, because the 1973 notion of the North American geosynthetics industry was ephemeral at best. Perhaps it existed in the dreams of a few energetic souls whose vision proved to be as prophetic as it was tenacious. I wish I could say I was one of those visionaries who foresaw the wonderful technological leaps that were to come, but the truth is I was just an engineer focused on a difficult problem - it was several years before my vision broadened enough to see beyond the problem at hand.

I was faced with a problem that had plagued several generations of coastal engineers. Most of us had been taught to design coastal revetments that looked roughly like the schematic shown in Figure 1a. (The drawings in Figure 1 must be considered artifacts, since they were drawn years ago without the aid of a single computer.) Naturally, the details varied from project to project, but the concept was always the same. Large stones,

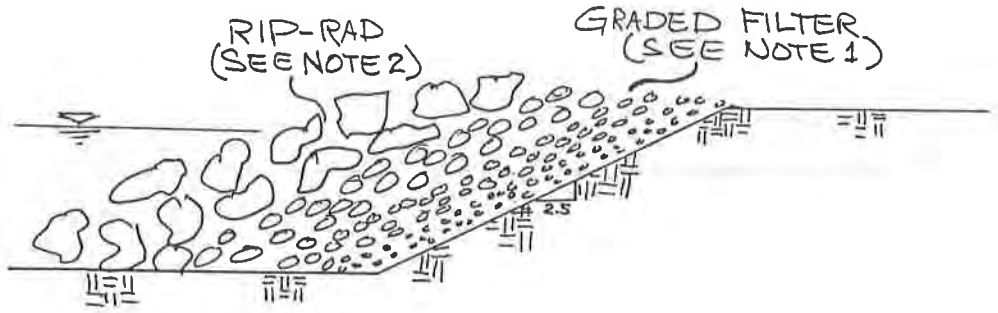

a. The Conventional Design

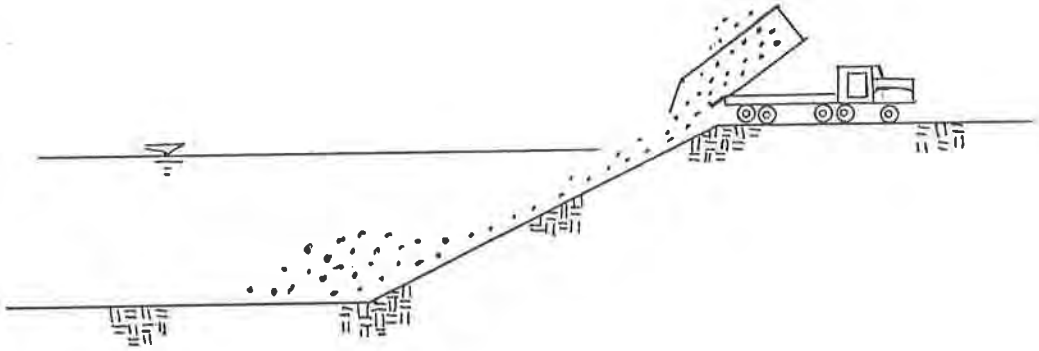

b. The Problem

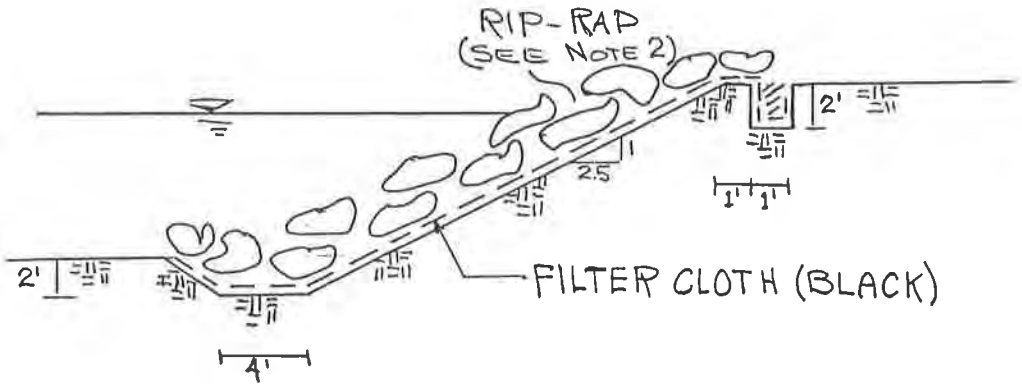

c. The Geotextile Solution

Figure 1: Geotextiles in Early Erosion Control Applications

called rip-rap, were placed on the bank in order to control erosion. This is a great solution except that the soil in the bank escaped through the spaces between the large stones - sort of like trying to screen your porch with chicken wire - a much finer mesh is required. The textbook solution to this problem was to design a "graded granular filter" between the bank soil and the rip-rap, as shown in Figure 1a. Graded granular filters are of course a long established and highly effective solution to such problems, the notion being that each layer in the filter comprises particles which are designed to contain the smaller particles behind them. As is often the case in coastal applications, this elegant solution is much easier to design than to build. As illustrated in Figure 1b, it is nearly impossible to construct this multi-layered structure under water, because, as the truck dumps the filter stones, they of course tend to roll down the bank into a pile at the bottom, rather than arrange themselves nicely parallel to the bank slope as shown in Figure 1a. Fortunately, salvation was at hand, though I must admit its form was somewhat surprising.

One day a jovial fellow named Bob Barrett walked into my office and informed me that he was the purveyor of a wondrous new product that would solve my erosion control filter blues, guarantee me untold fame and riches, and cure the common cold. In fact, his claim proved to be approximately 1/3 correct, and, from my somewhat limited perspective as a frustrated erosion control engineer, it was precisely the third that I most wanted. Bob was touting the wonders of a product known at that time as "Filter-X", and, notwithstanding any excessive claims, Filter-X did indeed solve my erosion control problem. My first geosynthetic design, Figure 1c, was thus born.

A few years later, having successfully constructed a number of such structures, I decided to share the delights of Filter-X with my colleagues, so I made a short presentation at the annual meeting of my local civil engineering society. It happened that a regional representative of the state Department of Transportation (DOT) was in attendance, and, a short time later, DOT offered me the fabulous sum of seven hundred dollars to study and report on the benefits of "filter fabrics". With the stroke of a pen, the DOT had catapulted me into that elite community known as "experts". I soon concluded that the rarified air surrounding experts must be rich with information (probably the excess which falls out of the other experts' minds), because, after breathing that air, I often seemed to know as much as many of the other experts. I was blessed with learning relatively early in my career that there is no better venue for learning than the company of knowledgeable and competent professionals.

THE EARLY DAYS

Then one day in 1978, I met the real geosynthetic experts. I attended one day of an American Society for Testing and Materials (ASTM) meeting in New York. Among others, I heard a presentation by a newly arrived frenchman named J-P Giroud, the man who was to become my technical mentor, my business partner, and, best of all, my friend. By then, I had been hired by Terrafix, a geotextile and erosion control products manufacturing company, which had designated me their representative to the ASTM subcommittee on geotextiles. Some of you may recall that, in those days, we were considered a sub-unit of the textile industry, so we met with ASTM Committee D-13 on Textiles. Well, the next D-

13 meeting was in Philadelphia in the Spring of 1979. (I should mention that a large fraction of D-13 were folks from the garment industry who were apparently competing in a lifelong quest to find the worst hotel in North America.) When I arrived at the conference hotel, I discovered that my room had been sold (no doubt to a more exalted expert), but Ernie Crowe, my counterpart from Terrafix Canada, generously offered to share his room with me, since it had two beds. When Ernie and I arrived at our room, we discovered an engineering/economic marvel - the hotel had somehow stuffed two beds and a dresser into a broom closet, and convinced us to pay a small ransom for the privilege of climbing into the broom closet with the two beds and the dresser. Well, we lost a little sleep, but those of us who survived those trials with D-13 and the garment industry seem to have sustained little permanent damage, because there have been no noticeable repercussions.

Oh, yes, there was one repercussion. That early work by D-13 opened the door for geosynthetics in North America, laid a foundation for an industry that would approach $1,000,000,000 by 1993, and nurtured a technology that would profoundly affect virtually every civil engineering discipline. In fact, as suggested by J-P Giroud at the Fourth International Conference on Geotextiles, the marriage of polymer science and civil engineering has indeed created a new discipline. Whether, as Dr. Giroud suggested, we call it the geopolymer discipline, or refer to it as geosynthetics, geomaterials, geoproducts, or some other term, this new discipline is here to stay[1].

MARKET GROWTH

The development of geosynthetics proceeded on many fronts, all of them working surprisingly well together. Why surprising? Consider that each front comprised people with different backgrounds and personalities, working toward different goals, trying to solve different problems, based on different assumptions, and supported by different funding sources. Upon reflection, the only thing they had in common was geosynthetics - a common solution to uncommon problems.

As early as the 1950's, geotextiles were being used as filters in erosion control applications (you can see how current I was, since I "discovered" this miracle in 1973), and US Army Corps of Engineers (COE) research in geotextile filters had resulted in a COE standard by the mid 1970's. Meanwhile, the 1950's also saw the US Bureau of Reclamation begin to study and specify geomembranes as pond and canal liners.[2] By the mid-1970's, geomembrane pond and canal liners were commonplace, and geotextiles were being specified in several types of drainage applications in addition to erosion control.

---

[1] Several years ago, we appropriately recognized Bob Barrett as the father of the geosynthetics industry. Now, it is long past time for us to recognize Dr. J-P Giroud as the father of the geosynthetics discipline!

[2] It should be noted that the "geo-terms" I have been using so freely in describing the early years were not actually coined until much later. The terms "geotextile" and "geomembrane" were coined by Dr. Giroud in 1977, and I first used the term "geosynthetics" in a document I prepared for ASTM in 1983.

The Marketeers. The credit for providing the initial energy for the development of geosynthetics surely belongs to those early marketeers like Bob Barrett. Armed with no more than a dream and a conviction (frightfully poor choices of weapons when marching to do battle with civil engineers), they intrepidly sallied forth to the tune of "all I know is that it works - try it and you'll see - you can figure out why later". One can imagine how popular this tune was with civil engineers. Nevertheless, the marketeers persisted and eventually acquired a small but impressive portfolio of successful case histories. And, to their great credit, these marketeers, many of whom were weaned in the garment industry, adapted well to their new environment. They learned that engineers insisted on quantifiable design methods based on rational analysis and objective data. So, the marketeers supported technical conferences, hired technical personnel to support their sales staff, developed technical design documents to support their marketing brochures, and, in these and many other ways, redirected their marketing approaches. Today's marketeer is typically a highly qualified professional, often with advanced degrees - I am reminded of Chip Fuller, who holds an engineering degree and a graduate degree in business. Furthermore, we find that many of the technical leaders of our discipline have been, or are, employed by geosynthetic manufacturers. It is no coincidence that this conference, as well as every other major geosynthetics conference ever held in North America, is sponsored by the Industrial Fabrics Association, International (IFAI), a manufacturing and marketing trade association. Furthermore, the geosynthetic conferences sponsored by the IFAI are widely recognized for their technical emphasis and the quality of their proceedings - a far cry from the "convention" atmosphere one might expect.

The Technical Front. On the technical front, we owe great tribute to a small but intrepid group of scientists and engineers. These dedicated pioneers, employed in every facet of technical endeavor - consulting, academia, laboratories, institutes, government and manufacturing - have faithfully and professionally corresponded, convened, and conferred at every opportunity in their common quest to advance the discipline. Their tireless efforts have produced rational design methods for virtually every geosynthetic application, a large and growing body of research data upon which to base future developments, well documented engineering case histories to verify design methods and assumptions, and a vast library of technical books, theses and dissertations, papers, articles and reports (Bob Koerner and J-P Giroud alone have published more than enough to make the average Ph.D. candidate gasp). I think it is especially appropriate, since we are convening here in Canada, to recognize the great technical contributions made by our Canadian colleagues - any perusal of a catalog of geosynthetic publications will reveal an apparently disproportionate number of Canadian authors. (Dr. Kerry Rowe informs me that the number of Canadian publications is only disproportionate when compared to the population of Canada, an arbitrary basis. He is confident, for example, that the number is very consistent with the demands placed on the typical Canadian graduate student.)

Publications. No discussion of the growth of our industry would be complete without mentioning two publications which have provided excellent forums for geosynthetic articles and papers. Geotechnical Fabrics Report (GFR) has become the definitive source of information regarding the progress of the industry. GFR provides its readers with technical articles, case histories, interviews, reviews of conferences, and even an annual Specifier's

Guide. Additionally, it provides manufacturers, consultants and others an advertising medium which reaches a broad cross-section of readers. Geotextiles and Geomembranes (G&G), on the other hand, is a strictly technical publication, in which all papers are critically reviewed, and no advertising is allowed. As such, G&G provides a forum for research results, analytical developments, and similar detailed information, thus serving as an unparalleled resource for the design engineer or geosynthetic researcher.

Market Performance. The geosynthetics market has grown steadily since the early 1980's. Figure 2 was prepared by combining data from a paper I presented at Northeastern University in 1985 with current data provided by IFAI.

	1981	1982	1991	1992
Geotextiles $m^2 \times 10^6$	98	106	298	320
Geomembranes $m^2 \times 10^6$	12	13	55	60

Figure 2. Geosynthetics Market Growth

Comparing the growth from 81-82 to 91-92, most of us would be extremely happy if our personal investments had grown at the same rate.

COMMITTEE WORK

All of these accomplishments beg the question of a venue where the technical gurus and marketeers can meet. The answer of course, lies in conferences and committee work. Since those early struggles at ASTM D-13, the number of available committees and conferences have grown dramatically. To name only the largest North American organizations which have active geosynthetics committees, one may now participate in: NAGS, IFAI, ASTM, CGS, GRI, TRB, ASCE, AREA, NSWMA, and GRCDA. Any of you who are not familiar with any of these acronyms are encouraged to contact me for an explanation and an exhortation to participate. To give credit where it is due, a few of the above organizations deserve special mention: IFAI, ASTM, NAGS, and GRI.

IFAI. It was at a meeting of geotextile manufacturers in the spring of 1980 that a young IFAI conference organizer named Steve Warner (now the President of IFAI) announced the formation of an important new Division of IFAI which would no doubt direct the future of our industry. Not being one to pass an opportunity to participate in anything important, I attended that meeting on behalf of Terrafix, my employer, only to discover that the level of suspicion in that room full of competitors soon approached critical mass. Seeking to accomplish his task and get clear of the fireball as quickly as possible, Steve said his piece and asked for nominations for someone to chair this unstable mass. Apparently I must have dosed off, because as I left the meeting Steve informed me that I had been elected

Chairman. It has now been more than 10 years since I left my position with Terrafix and thus resigned that chair, but I am pleased to say that the Geotextile and Geomembrane Divisions of IFAI function as model examples of competitors working together toward common goals, and both divisions have continued to be actively involved in every step of the evolution of our industry.

ASTM. I have already discussed some of our early days at ASTM - suffice it to say that, in 1980, when we received an invitation to meet with ASTM D-18 on Soil and Rock, we were quick to bid farewell to the garment industry, although , for several years our subcommittee actually served under both D-13 and D-18. Finally, our moment in the ASTM sun had arrived. In 1984, we became ASTM Committee D-35 on Geotextiles and Related Products, and our first official act was to draft the geomembrane group away from D-18. Geosynthetics had arrived at ASTM. Some of my fondest memories surround those long and intense days followed by congenial evenings at ASTM meetings. It seemed to take forever to actually produce standards, but it certainly was not for lack of effort. By ASTM policy, no standard could be approved until every objection was either removed, or, found by consensus to be non-germane. This policy is of course at the core of the quality of ASTM standards, and it works remarkably efficiently for established committees; but, as a newly formed group with highly transient membership, it was the bane of our existence. Every time we approached consensus on a standard, someone new would join our group, and all the old arguments would start anew - to give you just a taste, it took us three years of very hard work to agree whether to name one standard "Apparent Opening Size" or "Equivalent Opening Size". It seems improbable that such a group was ever able to accomplish anything, yet D-35 now stands as one of the most productive and prolific groups in ASTM. This amazing transformation was no accident, I assure you. It was the result of persistent effort by a few undauntable individuals: in particular, Bob Carroll, Barry Christopher, and Dave Suits (listed alphabetically) have been there from the early days, and were instrumental in producing virtually every ASTM geosynthetic standard, and, between them, have held virtually every leadership position in D-35 and the preceding committees.

NAGS. Meanwhile, the International Geotextile Society (IGS) had been founded in Paris, in 1983, and we North Americans were anxious to form ourselves into the first IGS Chapter. Appropriately, it was at our first meeting as D-35 that a core group met to create the American Society on Geosynthetics. The next year, at Geo-'85 in Cincinnati, we officially formed. We then almost immediately changed the name to the North American Geosynthetics Society, or "NAGS" to prove that we were brave as well as international, and, although we were not quick enough to be the first, we did become the second chapter of the IGS. I cannot imagine what prompts technical people who are already overworked and desperately over-committed to take on the additional burden of creating an international society, but we unhesitatingly jumped in, and, if I squint my eyes a little as I look back, I believe we had a good time.

GRI. Finally, we are all indebted to Dr. Bob Koerner, founder and leader of the Geosynthetics Research Institute (GRI). GRI has provided the industry with a forum where competitors can set aside their differences, and industry, government, academia and consultants can join in broad based research efforts which transcend product lines or

applications. I should also comment that, in his spare time, Bob is the author of more geosynthetic books, papers, and articles, and instructor of more geosynthetic short courses, than anyone would have dreamed possible, not to mention being one of the finest gentlemen I have ever known.

CONFERENCES

So, here we are at Geo '93, following in the proud footsteps of Geo '85 in Cincinnati, Geo '87 in New Orleans, Geo '89 in San Diego, and Geo '91 in Atlanta. And these, of course, are in addition to the Second International Conference on Geotextiles, Las Vegas 1982, the International Conference on Geomembranes, Denver 1984, several ASCE and ASTM symposia, an ISSMFE special session, and countless short courses on geosynthetics. I'd say that the geosynthetics discipline has arrived!

I cannot leave the subject of conferences without sharing some of the adventures associated with organizing conferences. Although I have been involved in the organization of several other geosynthetic conferences, the Second International Conference on Geotextiles (ICG II) will always have a special place in my heart. ICG II thrust North America to the forefront of the geosynthetics world, and was the benchmark of the strong growth phase of our industry. The proceedings were replete with well documented successful case histories and newly developed analytical design methods. It became clear that we had a new discipline on our hands - a discipline in technical support of an industry whose great potential was finally becoming apparent. It was no coincidence that the IGS was spawned at ICG II. The attendance at that first meeting to discuss the potential for an international society overflowed the room, and the response was overwhelmingly positive.

ICG II was an undeniable great success, but the five days in Las Vegas, however heady, pale in my mind in comparison to the preceding two years. I remember naively thinking that two years seemed awfully far in advance to start organizing, but I soon discovered that three or four years would have been great. Under the driving leadership of J-P Giroud, whom the other eight members of the Organizing Committee came to know as "Attila the Chairman", we devoted more and more of every passing week (as I recall, our respective employers were less than thrilled at this part) to Organizing Committee work. For example, one day I received four memos from other committee members reminding me of things I had promised at our last meeting, three weeks prior. Two of these were from Attila, and one was labeled "THIRD NOTICE" - - three notices in three weeks? When I called Ara Arman that day, he commented "J-P has missed his calling: he should work for a collection agency!" However trying, those were great times. For two years, we were the epicenter of the geosynthetics world, because all news, events, developments, etc. flowed through us. We were committed to organize a conference that was rigorously technical, comprehensive, and truly international, all in an atmosphere that would provide manufacturers with ample opportunity to promote their wares, and, so we did.

APPLICATIONS

By the 1970's, geosynthetics had become established in filtration, drainage, and pond

and canal liner applications, but the 1980's were surely the decade of geosynthetics (I recently heard someone on television refer to the 1980's as the "Reagan-Bush" era - we must be ever vigilant to question the accuracy of network news delivered by anyone so ill-informed of major civil engineering trends). During the 1980's, geotextiles were standardized in railroad track applications, paved and unpaved roadway applications, and a wide variety of drainage applications. The 1980's also brought us geogrids, geonets, geocomposites, and new types of geotextiles and geomembranes, all of which opened the doors to many new applications - new applications for all types of geosynthetics which were to create major new markets as well as extend the bounds of traditional civil engineering design. The applications which had the greatest impact on the spectacular growth of the industry in the 1980's included:

- asphalt overlay - oh how delicious that moment when I first saw a geotextile featured in a national television ad;
- soil reinforcement - vertical walls and steep slopes made more economical and often safer through geosynthetic soil reinforcement technology; and,
- embankments on soft soils - roads and dikes constructed on soils too soft to walk on, an incredible technology developed by a visionary and courageous engineer, the late Dr. Al Haliburton.
- geosynthetic liner systems - utilizing geomembranes, geotextiles, geonets and sometimes geogrids for waste disposal, mining, industrial, and other applications, a now widely accepted technology pioneered by Dr. J-P Giroud.

Many of the great strides of the 1980's would surely have been more limited had it not been for the tireless efforts of Jerry DiMaggio at the U.S. Federal Highway Administration (FHWA) and Bob Landreth at the U.S. Environmental Protection Agency (EPA), two exemplary models of inspiring leadership in governmental agencies.

Beyond a doubt, the most significant impact of the 1980's was the development and subsequent broad acceptance of geosynthetic liner systems. I was fortunate enough to have been a member of the team which worked with the EPA to develop this concept, and I have been actively involved as a designer, researcher, instructor, permitter, lecturer, witness, and general promoter of the technology ever since. And what a pleasure it has been. I am so grateful to have been involved in a technology that has provided me with ever more interesting challenges, projects with wide scope and impact, a vehicle for personal and corporate growth, and an opportunity to protect the environment - a rare pleasure and a true gift.

CONSULTING

In my 20 years associated with geosynthetics, I have had the pleasure of working as a consultant for, or in conjunction with, many of the best consulting engineering firms in the world. Today, there are many excellent consulting companies with geosynthetic capabilities, but it was not always so - which brings me, of course, to GeoServices.

The 1980's were indeed awesome years for geosynthetics, and they were equally

awesome for two engineers with a dream of founding a consulting company which would specialize in geosynthetics - the first it the world to do so (and hopefully not go broke in the process). To give you an idea of how well funded J-P and I were when we started GeoServices, Inc. Consulting Engineers, (now GeoSyntec Consultants), I still have a plastic cup which was passed around an ASTM meeting with a sign that said "Help Joe Fluet pay his ASTM dues". I still have the foreign currency that was collected in the cup, but I gratefully spent the American money. J-P and I went more than a year without drawing a paycheck, and our "office" was shared with a number of small multi-legged creatures who commuted to the convenience store next door. Nevertheless, we somehow managed to convince some great people to come and work with us - for example, the first year we hired Dr. Jay Beech, who is now the President of NAGS, and Bob Denis who introduced me today. The years went by like a blur, but I savor every memory.

Like most parents, I enjoy talking about my children, even though they are now grown adults and have lives of their own. I have been blessed with my son, Joe, now an Army officer and pilot, my daughter, Jennifer, now headed for Law School, and GeoSyntec, now a large company which has joined the ranks of other international geotechnical/environmental consulting firms. I am inordinately proud of all three:Joe, Jennifer, and GeoSyntec.

CLOSURE

I wish to close by thanking all of you for the many joys I have reaped from my association with geosynthetics. At the opening of Geo '87, I commented that "my association with geosynthetics has provided me with a challenging career, interesting work, a growing list of friends and colleagues, a chance to visit far-away places (perhaps a little more often than I might choose), a decent livelihood, and, it even gives me something to do with my spare time." Well, I am now medically retired from GeoSyntec, and my current status, which I choose to call "semi-retired teacher and consultant", has allowed me some time to reflect on those remarks I made six years ago. Let me assure you that the sentiments I expressed in 1987 ring more truly for me now than ever. I might have worked a few hours less and I could have done without that heart attack, but I would certainly do it again, and with even more gusto. It's a great career, ladies and gentlemen, this industry is still young and expanding, and the secret is to get involved in NAGS, ASTM and as many other committees as you can squeeze in. Join now, and rest assured that your voice will be heard and the echo will resound for years to come!

ACKNOWLEDGEMENTS

I am indebted to many friends and colleagues who helped me prepare for this paper by searching their memories and files to fill in the numerous gaps in my own recollections. It is good, occasionally, to reflect on past times - to pause for a chat with old acquaintances.

ROADS AND PAVEMENTS

GEOSYNTHETICS '93
CONFERENCE
VANCOUVER, BRITISH COLUMBIA

Comparative Laboratory Investigations on Polymer Asphalt Inlays

P.A.J.C. Kunst
Netherlands Pavement Consultants BV, Netherlands

R. Kirschner
Huesker Synthetic GmbH & Co., Germany

ABSTRACT

Three-point-bending-tests on reinforced and unreinforced asphalt specimens were performed investigating the effectiveness of seven different geogrids and nonwovens to retard reflective cracks. Crack propagation was described by means of fracture mechanics and design curves were plotted for reinforced and unreinforced asphalt overlays.

INTRODUCTION

Cracks in asphalt pavements and their durable elimination present a technical and economic problem, in whose solution the use of polymer asphalt inlays as reinforcements has gained considerably in importance. Efforts are made to approximate the effectiveness of the nonwovens and geogrids generally used under real conditions on test roadways. An objective assessment of the reinforcing effect of the different asphalt inlays on the basis of such test roadway results, however, is very difficult if not impossible, since the individual sections of the test roadways are generally subject to different boundary conditions.

An objective comparison of the reinforcing effect of these asphalt inlays is possible in laboratory tests, however, if these simulate conditions similar to those occurring in practice. In the summer of 1991, Huesker Synthetic commissioned the Netherlands Pavement Consultants (NPC, 1991) to carry out such investigations. This paper reports on the results of these investigations.

MATERIALS INVESTIGATED AND MANUFACTURE OF THE TEST SPECIMEN

Five geogrids and two nonwovens were chosen for the comparative laboratory investigation. The most significant characteristics of these materials are summarised in Table 1.

Table 1 Characteristics of the asphalt inlays

Specimen No.	Construction	Raw material	Strength long./lateral (kN/m)	Quantity of binder (kg/m2)
91	geogrid, woven	PET	50/50	0.4
92	geogrid, woven	PET	50/50	0.4
93	geogrid, woven	PET	40/40	0.4
94	geogrid, woven	glass	35/56	0.4
95	geogrid, extruded	PP	14/18	1.3*
96	nonwoven, mech.	PP filament	8.5	1.6
97	nonwoven, mech.	PP staple	8.5	1.6
98	no inlay	--	--	0.3

* with 10 kg/m2 of chippings 8/11

A total of eight two-layer asphalt specimens were manufactured in the laboratory of the NPC: Seven specimens with asphalt inlays and one unreinforced specimen as a reference test specimen. An asphalt concrete 0/16, type B for traffic class 3 with bitumen 80/100 and mineral aggregates corresponding to the Dutch Guidelines was used as asphalt mix.

An asphalt layer of 3 cm thickness was first built up in a special formwork measuring 60 x 60 x 8 cm. A bitumen emulsion U 70 K, type Eshalite, was then applied to this layer as adhesive together with an asphalt inlay. The quantities of binder are also shown in Table 1.

The second asphalt layer was applied on the following day with a thickness of 5 cm. Each asphalt layer was compacted with the same degree of compaction using a hand compactor and then with a hand drawn steel roller. The unreinforced asphalt specimen was produced in the same manner.

After a curing time of one month the specimens were then sawn perpendicularly to the direction of compaction into four beam-like test specimens. Each test specimen measured 60 x 14 x 8 cm.

PERFORMANCE OF THE TESTS AND RESULTS

The tests were conducted as semi-static three-point bending tests on a computer-controlled multi-purpose testing machine, type FTS Seidner 102/300 HV. The static system of the three-point bending tests is illustrated in Figure 1.

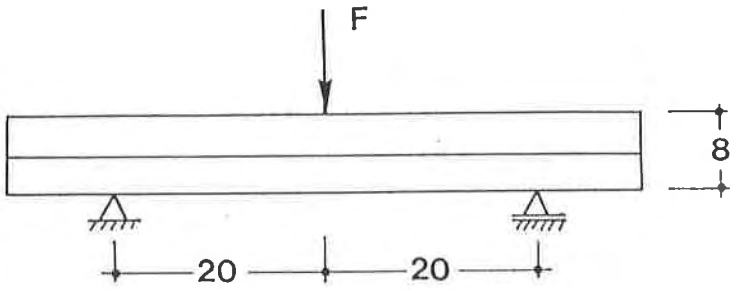

Figure 1 Static system

The load was applied with a hydraulic piston at a deformation rate of 0.85 mm/s. Load and deformation were recorded graphically. The test was conducted at a room temperature of 15° C.

Figure 2 shows schematically the results of two tests in the form of load/deformation curves. The reinforced test specimen No. 91 exhibits a noticeably different behaviour than the unreinforced test specimen No. 98. The maximum load, and in particular the necessary energy applied until failure of the test specimen which can be determined using the integral from the load/deformation curve, is higher for the reinforced test specimen.

The test results for the various asphalt inlays and for the unreinforced test specimen are listed in Table 2 as the mean values from four individual tests. The deformation shown is the deformation at maximum force.

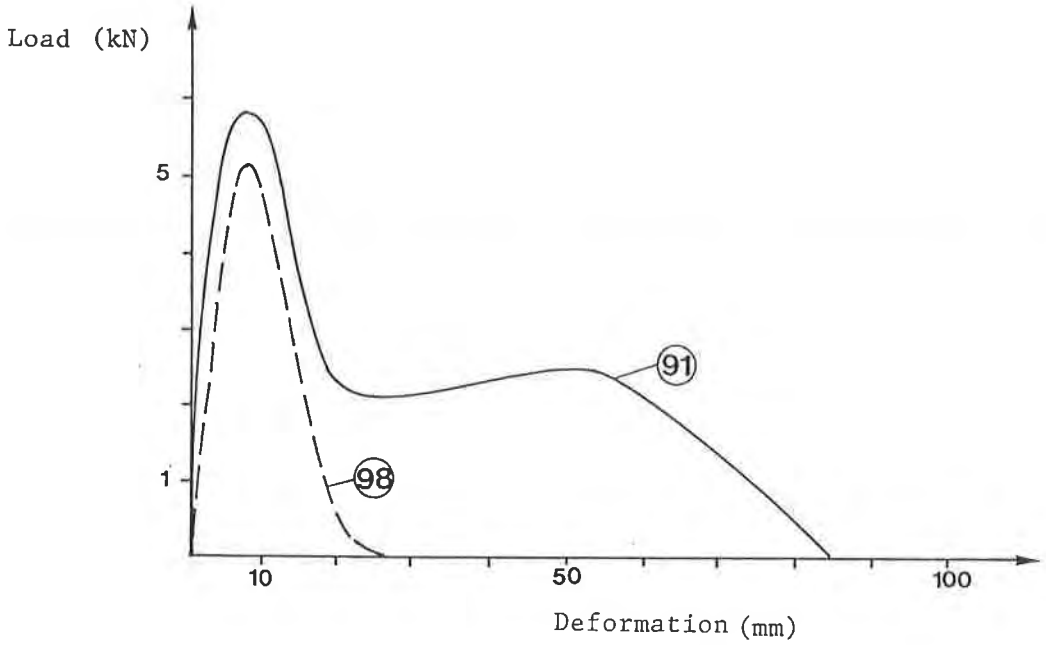

Figure 2 Load/deformation curves

All test specimens, with the exception of No. 94, failed under the bending load as a result of cracking in the middle of the beam. For No. 95 the failure occurred in the form of a shearing of the test specimen in the "interlocking layer" of chippings. All the other grids broke under the tensile load. The nonwovens were appreciably elongated at only a low tensile force but remained intact.

Table 2 Results of the three-point bending tests

Specimen No.	Max. force (N)	Deformation (mm)	Energy required (Nm)	Max. stress (N/mm2)
91	5825	7.15	172	3.49
92	5399	6.19	183	3.37
93	5774	6.82	192	3.52
94	4579	7.52	61	2.97
95	3154	9.95	61	1.97
96	4335	10.62	136	2.94
97	4044	11.39	117	2.76
98	5131	7.35	51	3.23

EVALUATION

In fracture mechanics, the propagation of a crack is described using the differential equation according to Paris (Molenaar 1983):

$$dc/dN = A * K^n \qquad (1)$$

where:
dc/dN - increase in crack length per load cycle
K - stress intensity factor
A,n - material constants

Parameter A is dependent on the stress at failure σ and the energy W required for the propagation of the crack:

$$A = f\left(\frac{1}{\sigma^2} * \frac{1}{W}\right) \qquad (2)$$

Using the results from Table 2 and this function relationship it is possible to calculate the ratios for the stresses at failure of the reinforced and unreinforced test specimens, for the energy required until failure and for the A values. These ratios are listed in Table 3.

The ratio of the A values allows conclusions to be drawn as to the reinforcing effect of the asphalt inlay. The smaller the ratio of the A values, the more effective the reinforcement compared with the unreinforced test specimen. On this basis it is possible to make an objective assessment of the different asphalt inlays with regard to their reinforcing effect. The resulting ranking of the asphalt inlays are shown in Table 3.

Table 3 Ratios for σ, W and A

Specimen No.	$\frac{\sigma}{\sigma_{98}}$	$\frac{W}{W_{98}}$	$\frac{A}{A_{98}}$	Ranking
91	1.08	3.41	0.25	2
92	1.01	3.62	0.27	3
93	1.09	3.80	0.22	1
94	0.86	1.21	1.12	7
95	0.61	1.25	2.15	8
96	0.91	2.69	0.45	4
97	0.85	2.32	0.60	5
98	1	1	1	6

DESIGN CURVES FOR ASPHALT OVERLAYS

The service life of an asphalt overlay or the number of load cycles until a crack in the existing asphalt layer breaks through the asphalt overlay can be calculated from the Paris equation if the material constants A and n and the stress intensity factor K are known. A and n can be determined using the tests described above. The factor K was calculated by the NPC for a variety of boundary conditions using a finite element program, whereby the state of stress in the immediate vicinity of the crack was simulated by a "crack element".

Using the assumptions listed in Figure 3 it is possible to draw up design curves for the various asphalt inlays, and thus to determine the service life of the asphalt overlay at given boundary conditions.

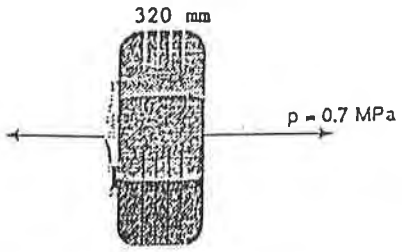

Overlay		E0 = 5000 MPa h0 = 50, 60, 100 mm
Existing asphalt layers	crack	E1 = 7000 MPa h1 = 100, 200, 300 mm
Unbound base courses		E2 = 300 MPa h2 = 300 mm
Subgrade		E3 = 150 MPa

Figure 3 Calculation assumptions

Figures 4 and 5 show examples of design curves for a geogrid (No. 93) and for a nonwoven (No. 96). With an existing asphalt layer of 200 mm thickness and an overlay of 50 mm, the following figures are obtained for the number of load cycles until a crack breaks through the overlay:

Geogrid No. 93	$10^{7.4}$
Nonwoven No. 96	$10^{7.1}$
Without reinforcement No. 98	$10^{6.8}$

Ratios of approx. 4 : 2 : 1 can thus be calculated for the service life of the asphalt overlay for reinforcements with geogrid, nonwoven and without reinforcement.

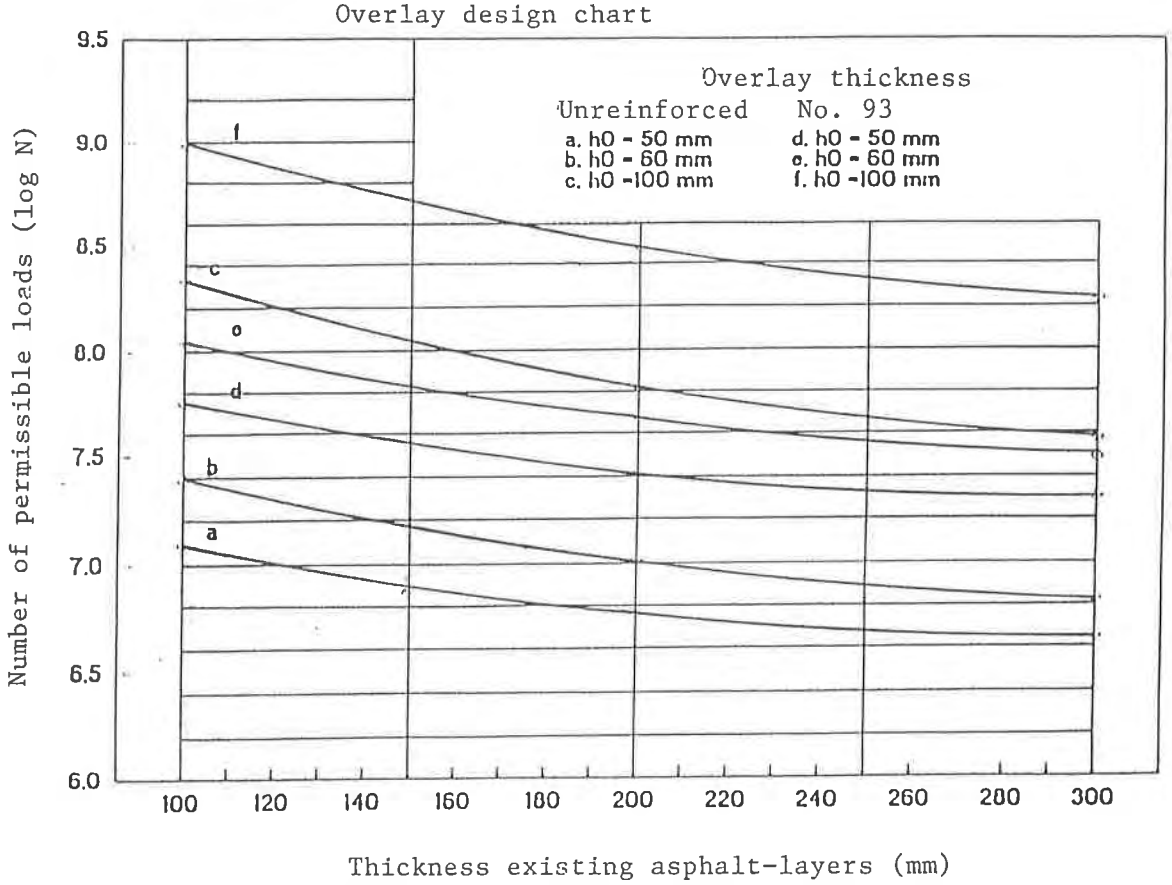

Figure 4 Design curves for a flexible PET geogrid

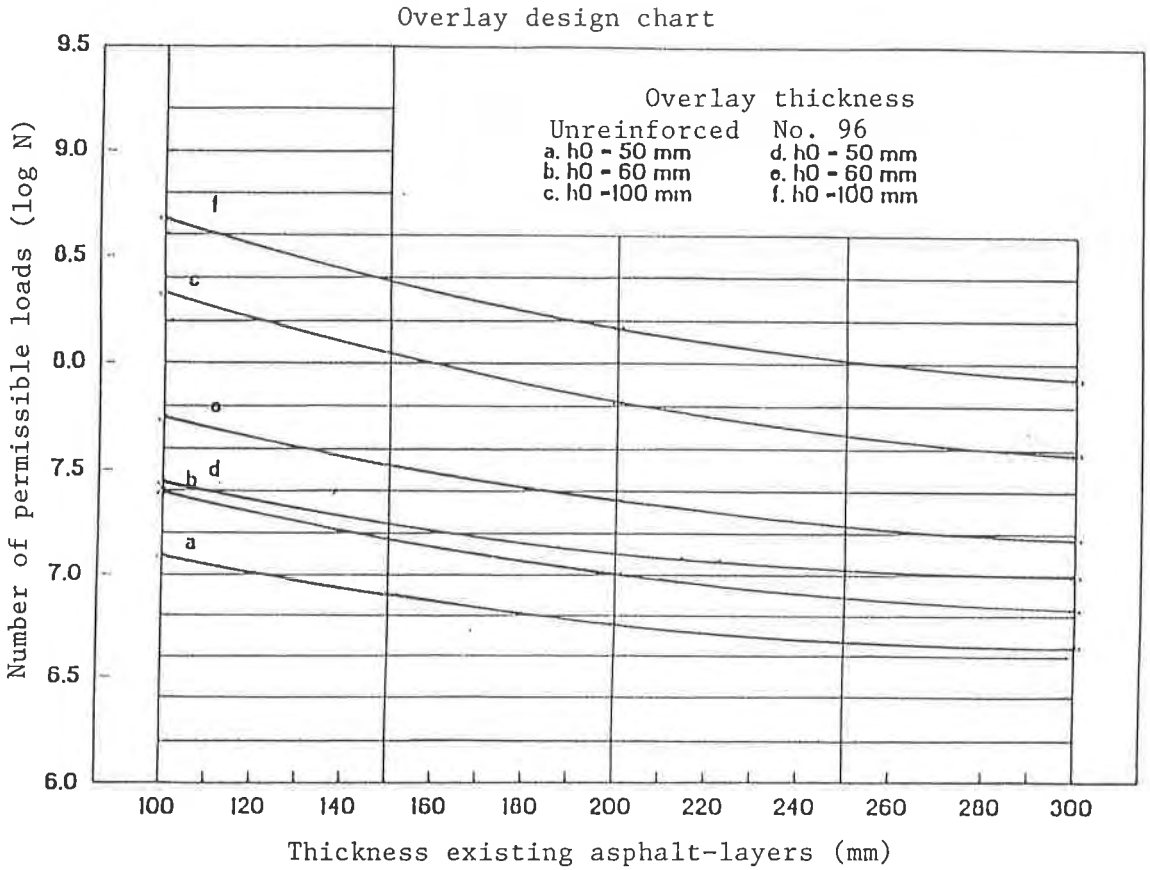

Figure 5 Design curves for a nonwoven of PP continuous filaments

CONCLUSIONS

The laboratory investigation of the reinforcing effect of asphalt inlays produced widely differing results. Flexible geogrids of polyester exhibit a good reinforcing effect. The use of rigid polypropylene geogrids and geogrids of glass, on the other hand, lead to a reduction in the service life of the asphalt overlay.

Asphalt inlays made from nonwovens increase the service life slightly. Compared with flexible geogrids, however, we cannot speak of any notable reinforcing effect. The results of these laboratory tests are confirmed by a Final Research Report of the California Department of Transportation (1990) which, after more than 10 years of observations on 28 test sections of road, comes to a similar assessment of nonwovens.

The results presented here are based on semi-static three-point bending tests. It is planned for the future that these results should be confirmed by further investigations under dynamic loads.

REFERENCES

Netherlands Pavement Consultants (1990) "Results of three-point bending tests on HaTelit-reinforced asphalt concrete beams", Project No. 91431, Hoevelaken, Netherlands, Unpublished.

Molenaar, A.A.A. (1983) "Structural performance and design of flexible pavements and asphalt concrete overlays", Dissertation at the TU Delft, Netherlands.

California Department of Transportation (1990) "Evaluation of paving fabric test installations in California - Final Report" Report No. FHWA/CA/TL-90/02, Sacramento.

Stiffnesses of Geosynthetic-Built Unpaved Road Structures: Experimental Programme, Analysis and Results

R.A. Douglas
University of New Brunswick, Canada

ABSTRACT

The problems of soft subgrades, extremely heavy design axle loads, very low traffic volumes, and very low cost tolerances associated with resource access roads have led designers to adopt access road structure designs using geosynthetics. While design methods which take rut depth as the key criteria exist, it is actually the road *stiffness* that has a large impact on *vehicle* operating costs. Therefore, a long term project to examine geosynthetic-built access road stiffness was embarked upon.

The results of two series of model tests, reported in detail elsewhere, are summarized, together with the results of a third series which has not been reported before. All the data from this eight year test programme are then collected, and an analysis made. All data indicate that a stiffness ratio (road stiffness divided by subgrade stiffness) can be defined, leading to a single design chart that presents all data. The form of this design chart will provide the basis for succeeding numerical analyses and a production design method.

THE DESIGN PROBLEM: GEOSYNTHETIC-BUILT UNPAVED ROADS

Various resources-based industries are heavily dependent on their access roads. In Canadian forestry, for example, 34000 km of access road is built annually, over five times the length of paved, public highway built each year. Annually, approximately $0.7 billion is spent constructing these forest access roads, about 8% of the amount spent on pavement construction, structures and maintenance of public roads (Douglas, 1992: pubic road statistics do not give road construction as a separate item).

Resource access roads are built in a different design environment (Douglas, 1988): the design axle loads can be far heavier than provincial regulations allow on public roads, traffic volumes are far smaller, costs must be kept very low if the operations the roads serve are to remain profitable, and the terrain crossed by the roads can in places be very hostile.

Increasingly, geosynthetics are being used to overcome these problems but unfortunately relatively little R&D is yet available to design engineers.

A further problem is that it appears that a very simple tenet has been forgotten by roads researchers interested in the problem: *roads are built for vehicles* (Douglas and Valsangkar, 1992). The design vehicles for resource hauls are becoming larger and heavier. The performance of these vehicles is greatly affected by the structural behaviour of the roads on which they run:

- one of the largest components of the operating costs of a heavy haul vehicle is fuel consumption,
- one of the largest components of the fuel consumption can be attributed to the requirement to overcome rolling resistance, and
- rolling resistance is heavily influenced by road stiffness

For this reason it was decided some eight years ago to mount a study of how road structural stiffness was influenced by geosynthetic details, dovetailing with parallel heavy vehicle performance research (Douglas et al, 1990).

BACKGROUND

To date, studies of geosynthetic-built access road behaviour have focused on aspects of structural *capacity* rather than *stiffness*. The early work was concerned with bearing capacity (e.g. Milligan and Love, 1984; DeGaridel and Javor, 1986; DeGaridel and Morel, 1986; Resl and Werner, 1986; Hausmann, 1987). Other work was concerned with how geosynthetic inclusions in the road structure influence the development of ruts (e.g. Giroud et al., 1984; Degaridel and Javor, 1986; Delmas et al., 1986; Khay et al., 1986; Hausmann, 1987; Holtz and Sivakugan, 1987). A number of design methods have been put forward, where the basis of the method is the relationship between rut depth, traffic, and geosynthetic characteristics (e.g. Gourc and Riondy, 1984; DeGaridel and Javor, 1986; Delmas et al., 1986; Yasuhara et al., 1986). Some methods are implemented through charts and tables (e.g. Giroud and Noiray, 1981; Giroud et al., 1984; Hausmann, 1987; Holtz and Sivakugan, 1987; Jewell, 1990).

All of this work, however, is directed at setting geosynthetic-built road designs with respect to their capacities, that is, on the basis of some ultimate failure criterion. However, given that it is the *stiffness* that affects vehicle performance (and also noting that ruts are obliterated by periodic routine maintenance operations), it appeared more justifiable to work toward a design method based on the road stiffness, that is, the working load behaviour of the roads (Douglas and Valsangkar, 1992).

Model studies were designed to examine various aspects of the problem from the stiffness point of view. The studies commenced with tests in a 2.5 m square steel test bin (Douglas et al., 1985; Douglas, 1987 and 1990; Douglas and Kelly, 1987) and continued with tests in a 3 × 4 m test pit, a 1.2 × 0.3 m test box, and then returned to the 3 × 4 m test pit (Douglas, 1991; Douglas and Valsangkar, 1991).

All of the model testing was done at scales of about 1:10 and 1:3. Various single layer model aggregate pavement structures were produced with all road structures consisting of an aggregate layer placed on a sheet of geosynthetic, which in turn rested on the subgrade. All

models were built on milled, reconstituted, horticultural, sphagnum peat as the subgrade, chosen because it is similar in behaviour to some of the natural subgrade materials that present such difficulties in practice, because it provides a very compressible subgrade with a behaviour very close to that of a theoretical Winkler foundation, and because it is a material that permits the creation of very consistent subgrades from one test to the next in very large volumes, quickly, and relatively easily.

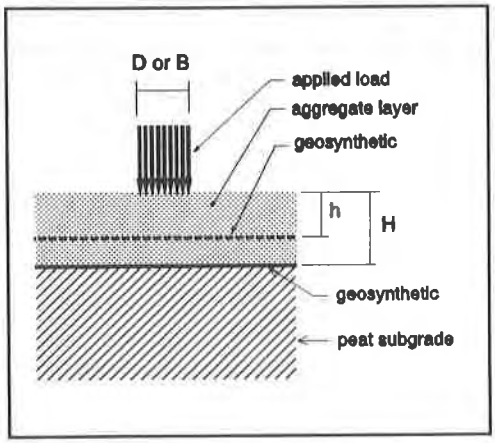

Figure 1. Defining sketch.

Throughout the long term test programme, a consistent set of variables was used. These are shown in the defining sketch, Figure 1. They reduce to a number of dimensionless ratios:

- *H/B* or *H/D*, the aggregate thickness ratio
- *h/H* or *h/B*, position ratio for a second layer of geosynthetic

Other dimensionless ratios will be defined as needed in the discussion, later.

This paper will concentrate on repeated load (Yoder and Witczak, 1975) stiffness tests. In these, the repeated load was applied to a plate or beam resting on the surface of the road structure, at a frequency of about 0.5 Hz, and the road stiffness measured. Stiffness was defined as the slope of the average pressure - average vertical displacement plot loop.

MODEL TESTS: PHASE I, PIT TESTS

In the first phase of the repeated load test programme, tests were carried out in the 3 × 4 m concrete test pit, 2 m deep, equipped with a gravel underdrain in hydraulic connection with a valved sump pump (Douglas and Valsangkar, 1992). Following the preparation of the test subgrades in the pit, model road structures were built and subjected to repeated loading.

The test programme was arranged according to Table 1. Combinations of compaction/no compaction, aggregate type and provision of the geogrid sheet at mid-depth or not were chosen so that the full

Table 1. Phase I Model Construction Details (after Douglas and Valsangkar, 1992)

Designation	*H/D*	Base material	Geotextile at interface	Geogrid at mid-depth
PA1, PA2, PA4	0.0	--	no	no
RA3	0.5	loose pit run gravel	yes	no
RA4, RA5	0.5	compacted crushed rock	yes	yes

range of road structure stiffness, from very poor to very good, would result.

A servo-controlled hydraulic loading system was used to apply repeated loads, at a frequency of 0.5 Hz, to a 300 mm diameter circular plate resting on the model road surface. The loading was thus axisymmetrical, although the geotextile and geogrid themselves were obviously not. The loading system's hydraulic ram reacted against a stiff steel frame over the test pit, repeating the load sinusoidally between peak and trough loads of 4.5 and 0.1 kN respectively (2.0 and 0.1 kN for peat subgrades alone). The vertical load - average vertical displacement response was recorded intermittently using a pen plotter (Figure 2), producing load-displacement loops at number of load repetitions $N = \{1\text{-}10, 30, 100, 300, \ldots \approx 30000\}$.

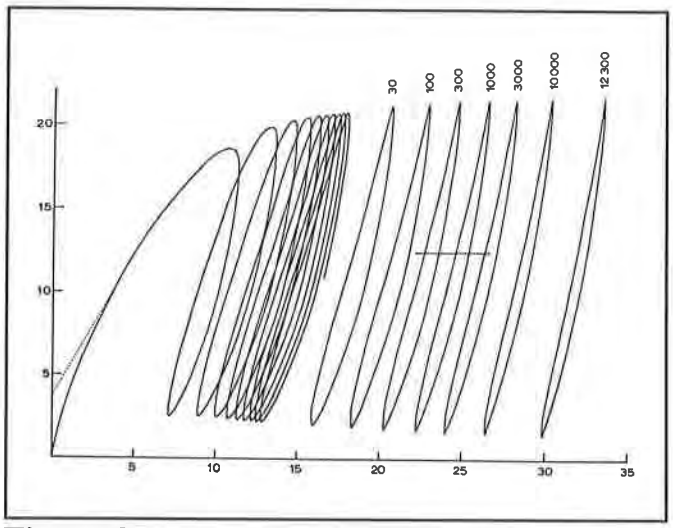

Figure 2. Load-displacement trace. (Douglas and Valsangkar, 1992)

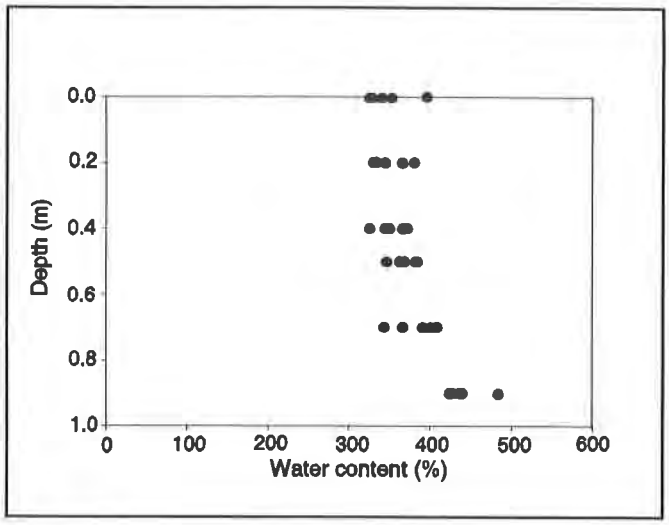

Figure 3. Phase I peat subgrade water contents. (Douglas and Valsangkar, 1992)

Subgrade Preparation. Artificial peat subgrades were prepared in the test pit using previously established techniques (Jarrett, 1984; Douglas et al, 1985; Douglas and Kelly, 1986; Douglas, 1987), whereby the peat was wet-up to a porridge consistency and mixed using a 25 mm diameter pipe equipped with a hinged, 150 mm diameter plate on its end, slowly pushed and pulled vertically through the peat. After mixing, the peat was drained overnight through the fabric filtered gravel underdrain.

Remarkably consistent subgrades were produced. The water contents of samples retrieved with a Hiller sampler are shown in profile in Figure 3. Laboratory CBR tests performed on samples of the same peat, tested at the same drained water content as the model subgrades, yielded a CBR $\ll 1$. In eight loss-on-ignition tests, carried out at 440°C for 5 hours (Landva et al, 1982), the peat had a mean ash content of 26%, with a standard deviation of 4.7%.

Geosynthetics Used. All road sections were built by placing the aggregate on a sheet of non-woven geotextile placed on the peat surface. In some cases (Table 1), a geogrid sheet was placed at mid-depth in the aggregate layer. Geosynthetic characteristics are given in Table 2.

Aggregates. It was desirable in these pilot tests to obtain road structural stiffnesses at the extremes of the practical range. Uncompacted pit run gravel was chosen to represent the poor end of the spectrum, while crushed greywacke compacted by a vibratory plate tamper was chosen to represent the very competent end. Grain size distributions are shown in Figure 4, and additional aggregate characteristics are shown in Table 3. Given the uniformity of the pit run material, Proctor compaction tests could not be successfully carried out. A dry-rodded unit weight test was substituted, carried out according to Canadian standard CSA CAN3 A23.2-10A.

Table 2. Phase I Geosynthetic Characteristics (after Douglas and Valsangkar, 1992)

Geosynthetic	Mass/unit area (g/m^2)	Tensile modulus[a] (kN/m)	Tensile strength[a] (kN/m)	Elongation at failure[a] (%)
Nonwoven geotextile (test results: ASTM D4595)	150	22.0/21.2	4.86/5.26	163/147
Geogrid (manuf. literature - Tensar 1987)	400	NA	15.0/15.0	NA

[a] machine/cross machine-direction

MODEL TESTS: PHASE II, SMALL BOX TESTS

The second phase of tests was performed in a small steel box, 1.2 × 0.3 × 0.6 m (width × depth × height), equipped with a Plexiglas™ front and back. Repeated loading between 0 and 220 N was applied at a frequency of 0.4 Hz by a pneumatic system to single aggregate layer road sections built on subgrades prepared using the same type of peat as in Phase I. Vertical load - average vertical displacement data was recorded digitally through an analogue-to-digital board on a microcomputer.

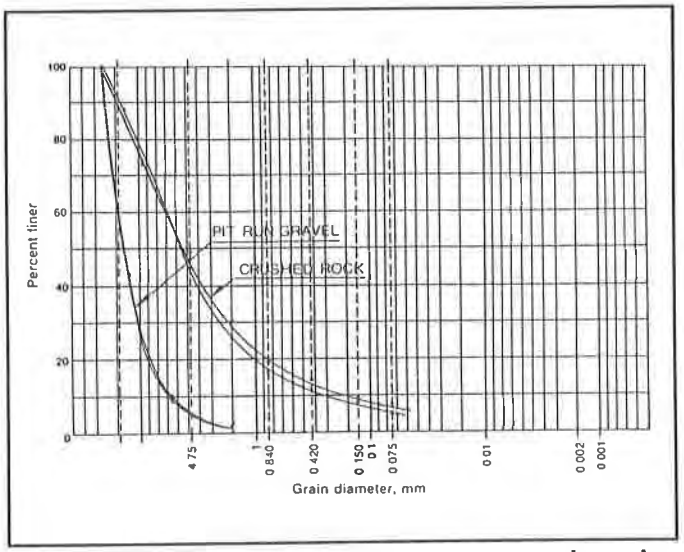

Figure 4. Phase I aggregate grain size distributions. (Douglas and Valsangkar, 1992)

Plane strain loading conditions existed for this batch of tests, as the surface loads were applied to the road sections by a 300 mm long beam of width B = 75 mm.

Table 3. Phase I Aggregate Characteristics (after Douglas and Valsangkar, 1992)

	Pit run gravel	Crushed rock
insitu water content (%)	0.0	2.0
insitu dry unit weight (kN/m^3)	15.2	18.5
standard Proctor maximum dry unit weight (kN/m^3) (ASTM D698[a])	--	20.7
optimum water content (%) (ASTM D698[a])	--	7.0
dry rodded unit weight (kN/m^3) (CSA CAN3 A23.2-10A[b])	17.2	--

[a] except that full range of grain sizes used
[b] except that vibration was used

Subgrade Preparation. Peat subgrades were prepared essentially in the same manner as for Phase I. The peat was wet-up and mixed in the test box with a jetting technique, this time pumping water into the peat through a capped 12 mm diameter copper tube with a pair of 3 mm diameter holes drilled on its diameter, at its end. Following mixing, the peat was drained overnight through a gravel drain in the box's bottom.

The as-drained water content of the peat rose somewhat through the sequence of tests, as shown in Figure 5.

Geosynthetics Used. A woven polyester slit film geotextile with the characteristics shown in Table 4 was used in all tests in Phase II. All model road sections were built with a sheet of the geotextile at the aggregate/subgrade interface. In addition, a number of the road sections were built with a secondary sheet of the same geotextile at a depth *h* below the ground surface.

Aggregate. In order to respect the roughly 10:1 geometric scale in the tests, sand was chosen for the aggregate layer rather than crushed rock. The range in grain size distributions is shown in Figure 6, and other sand characteristics are given in Table 5.

To achieve uniform insitu sand properties from one test to the next, a pluviation technique was used: dry sand was poured through the 12 mm diameter tip of a funnel held a constant height 100 mm above the sand layer surface. Insitu unit weight was determined by placing water content cups on the geotextile, and filling them with sand at the same time the rest of the sand layer was being built up. Following the load test, the water

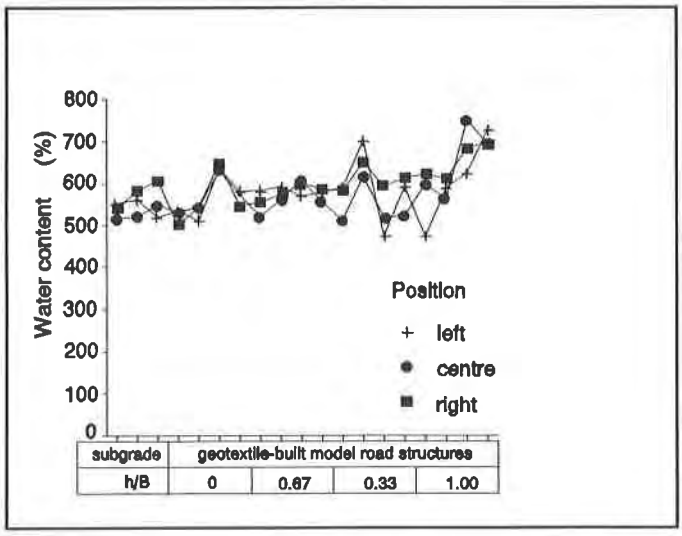

Figure 5. Phase II peat subgrade water contents. (Douglas, 1991)

content cups were retrieved and weighed. The mean insitu dry unit weight over all tests was 15.8 kN/m^3, with a standard deviation of 0.3 kN/m^3. The resultant relative density was 35%.

MODEL TESTS: PHASE III, PIT TESTS

Work returned to the concrete test pit for Phase III. Cycled load tests were carried out on model roads built of the crushed greywacke and the woven geotextile, using the servo-controlled hydraulic loading system. Vertical load - displacement behaviour of the 0.3 mm diameter steel plate acting on the model road structure was logged digitally, for repeated loading carried out at 0.5 Hz between peak and trough loads of 4.5 and 0.1 kN respectively.

Table 4. Phase II/III Geotextile Characteristics (after Douglas, 1991)

Property	Value
(i) Manufacturer's literature: ("typical values", Terrafix, 1991) (to CGSB standards as of Feb 1991)	
grab tensile strength (N)	525
tear (N)	308
elongation at break (%)	20
(ii) Measured in this test programme: ASTM 4595-86	
wide width strip tensile strength (kN/m) machine direction	15.0
wide width strip tensile strength (kN/m) cross-machine direction	13.5

Subgrade Preparation. The same type of peat was used in the third batch of tests, wetted and mixed this time using the water jetting technique. The vane shear strength profile is shown in Figure 7.

Geosynthetics Used. The woven geotextile described earlier (Table 4) was used in this batch of tests. All road structures were built with a sheet of the woven geotextile at the peat/aggregate interface. A number of the model road structures had an additional geotextile sheet at a depth h below the ground surface.

Aggregate. The crushed greywacke described earlier (Table 3, Figure 4) was used in this batch of tests. All model road structures were compacted, using a pedestrian vibratory plate compactor. Insitu dry unit weights averaged 18.6 kN/m^3, with a standard deviation of 1.9 kN/m^3.

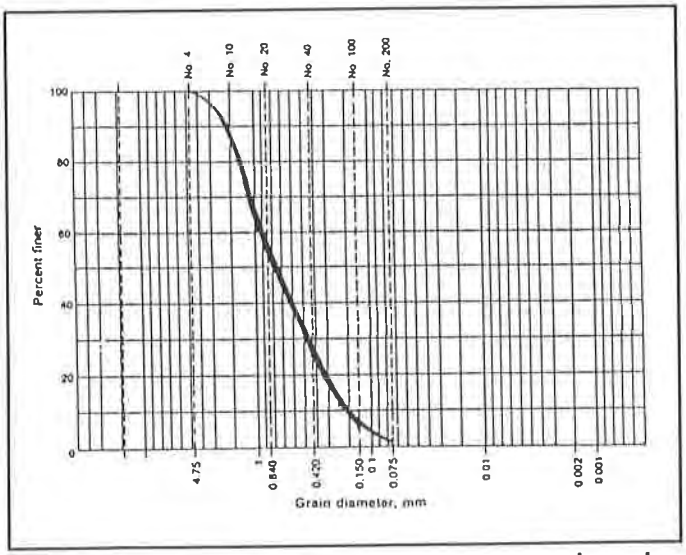

Figure 6. Phase II aggregate grain size distributions. (Douglas, 1991)

TEST RESULTS

Phase I: Test Pit. The recorded load-displacement information was used to produce

plots of vertical stiffness against the logarithm of the number of load repetitions (Figure 8). As shown by the figure, the curves for the peat subgrades were remarkably consistent. In this pilot study, the two compacted crushed rock model road replicates, provided with a geogrid at mid-depth (designated RA4 and RA5) were relatively close. The curve for the single test carried out on the uncompacted pit run road section, built without a geogrid (RA3) fell roughly midway between the peat curves and the crushed rock model road curves.

In general, the curves exhibited a small "jump" at the start, for $1 \leq N \leq 3$, and then settled down. This is attributed to the difficulty of assigning a stiffness to the early load-displacement loops, which were quite wide for the first few repetitions. With $N > 3$, the loops became much tighter, and an average stiffness, defined as the slope of a line through the peak and trough points on the load-displacement loop, was easily determined.

Table 5. Phase II Aggregate Characteristics (after Douglas, 1991)

Property	Value
Grain size distribution:	
percent finer than 0.075 mm	3
coefficient of uniformity, C_u	4.1
coefficient of curvature, C_c	1.2
classification (USCS/AASHTO)	SP/A-1-b(0)
Maximum dry unit weight (kN/m^3)	17.3
Minimum dry unit weight (kN/m^3)	15.0

Phase II: Small Box. The stiffness-log$N$ curves for the small box peat subgrade tests are shown in Figure 9. One set of model road curves, for the case where $h/H = 0$ (i.e. just one layer of fabric used) is shown in Figure 10. Again, the behaviour of the individual peat subgrades was very consistent and again, the model roads exhibit a roughly linear stiffness-log$N$ behaviour, with higher slopes for greater H/B.

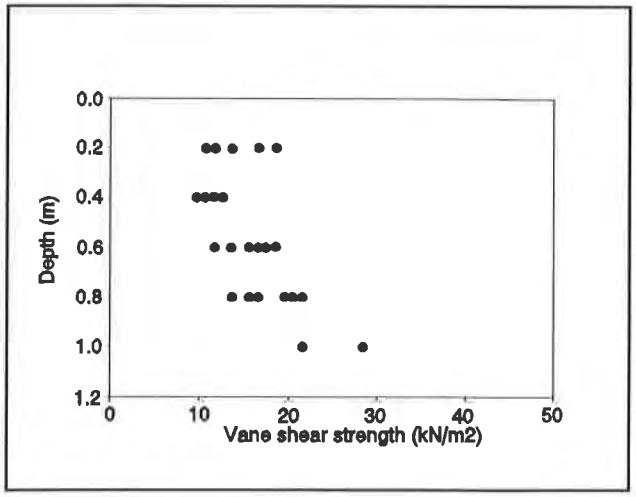

Figure 7. Phase III peat subgrade vane shear strength.

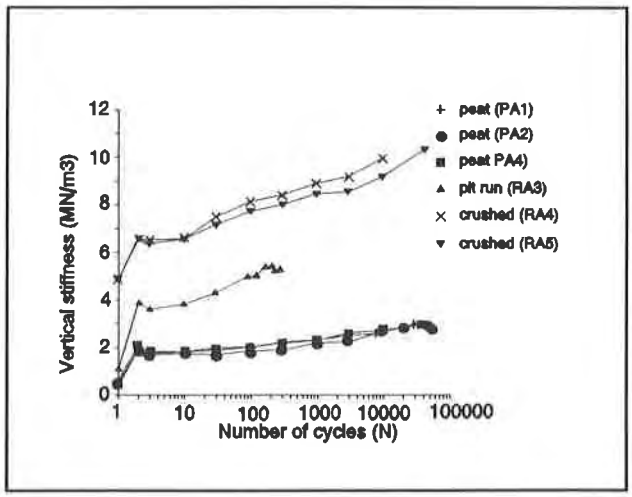

Figure 8. Phase I vertical stiffness against log$N$. (Douglas and Valsangkar, 1992)

Phase III: Test Pit. The stiffness-log$N$ plots for the peat in Phase III are given in Figure 11. The curves were again very consistent, and are roughly linear. Stiffness curves for all model roads tested in this phase are shown in Figure 12. Again, they were somewhat erratic for $N < 10$, but became more regular once $N \geq 10$. The *average* of the peat subgrade curves has been transferred to the figure, and the model road results are identified by a "construction parameter" $C^* = [(H/D)^2 + (h/D)^2]^{0.5}$. Agreement was good for the two replicates each where $C^* = 0.50$ and 0.75, but poorer for the two replicates where $C^* = 0.60$.

Stiffness Ratio. Following the reasoning in Douglas and Valsangkar (1992), stiffness ratios were plotted. Given that the stiffness - log$N$ behaviour was essentially linear both for the model roads and the peat subgrades (see Figure 12), it seemed reasonable to define a stiffness ratio:

$$K^* = k_r/k_p \qquad \ldots (1)$$

where:

K^*	=	stiffness ratio	[unitless]
k_r	=	stiffness of model road section	[MN/m^3]
k_p	=	stiffness of peat subgrade, at corresponding N	[MN/m^3]

The calculated stiffness ratios for the data in Figure 12 for $10 \leq N \leq 10000$ are shown in Figure 13. For all but $C^* = 0.90$, the curves are essentially flat while for $C^* = 0.90$ over same range of N, the stiffness ratio K^* varies $\pm 15\%$ from its mean value.

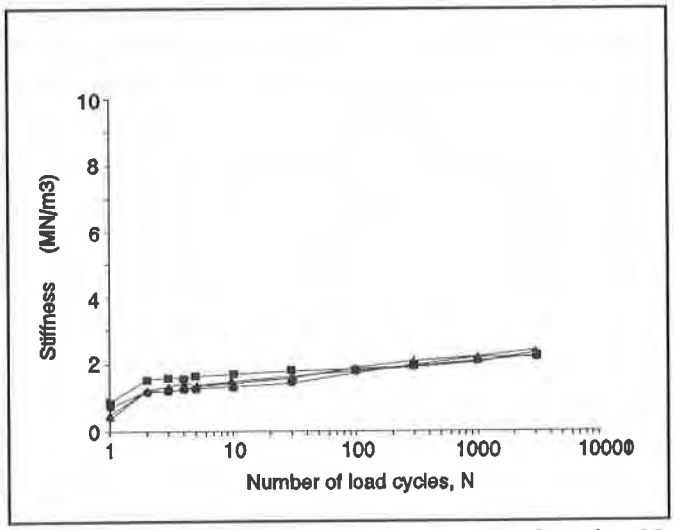

Figure 9. Phase II peat stiffness against log$N$. (Douglas, 1991)

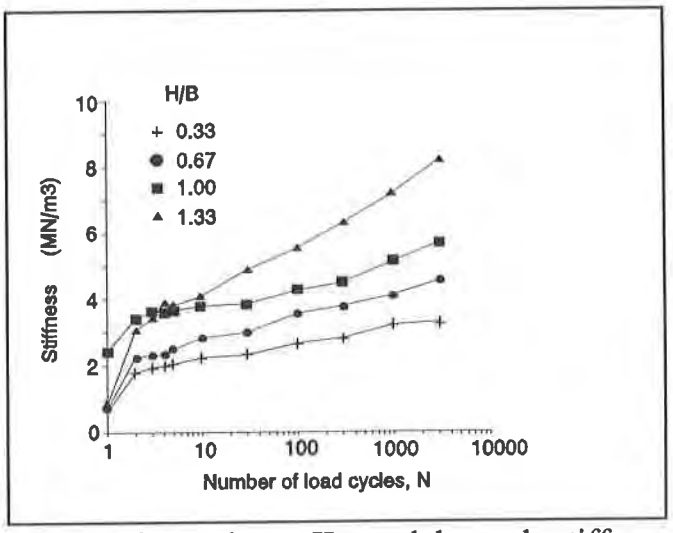

Figure 10. Phase II model road stiffness against log$N$, $h/B = 0$. (Douglas, 1991)

Average Stiffness Ratios, All Tests. Average stiffness ratios K^*_{av} were calculated for the test data from all three phases of the study, and plotted against $C^* = [(H/B)^2 + (h/B)^2]^{0.5}$ or $[(H/B)^2 + (h/B)^2]^{0.5}$, as appropriate for the axisymmetrical pit tests or the plane strain small box tests, Figure 14. Approximately linear K^*_{av} - C^* plots result.

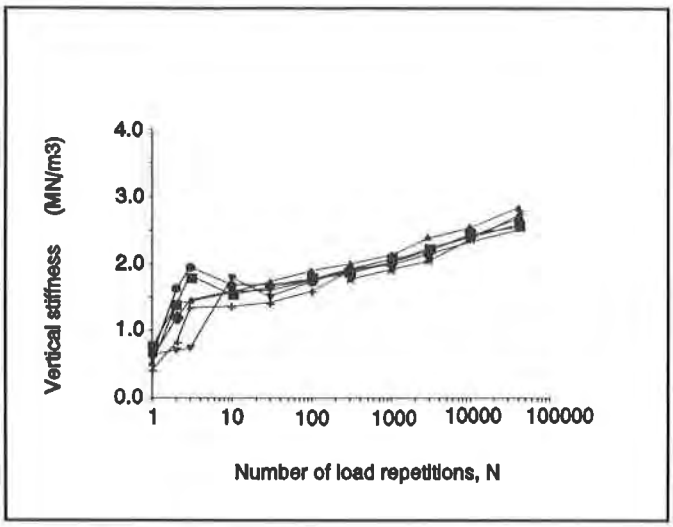

Figure 11. Phase III peat stiffness against log$N$.

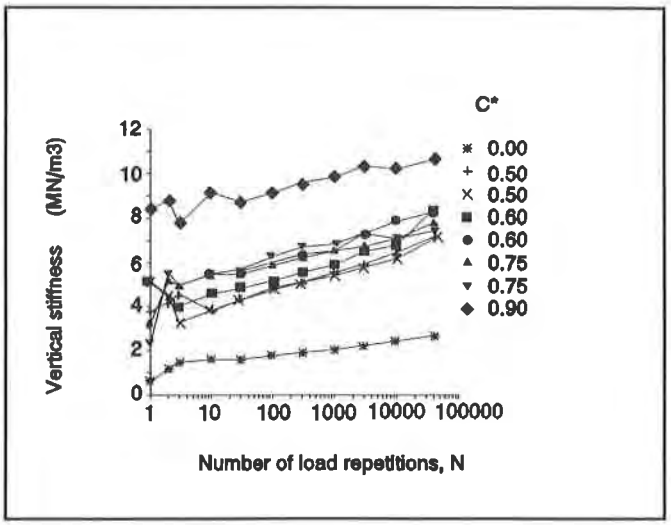

Figure 12. Phase III model road stiffness against log$N$, for various C^*.

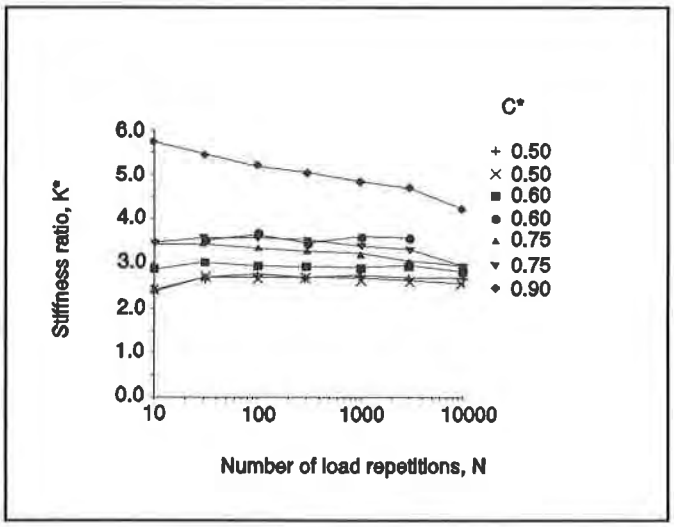

Figure 13. Phase III stiffness ratio against log$N$. for various C^*.

ANALYSIS OF TEST RESULTS

Qualitatively, the results shown in Figure 14 make sense. Average road structure stiffness is seen to increase as construction parameter C^* increased for $C^* \leq 2$. The single point for the well-built road structure in Phase I, which had a compacted, crushed rock aggregate layer provided with a geogrid at mid-depth, lying on the geotextile at the aggregate-peat interface, was considerably higher than the corresponding uncompacted pit-run road structure built without the geogrid layer. In comparison, points for the crushed rock structures in Phase III, compacted but built without a geogrid sheet, lie between the two points for Phase I.

All the data for Phases I and III, where axisymmetrical loading conditions prevailed, are above those for Phase II, where plane strain conditions existed. Insufficient data exists to allow a determination as to whether this was because of the different loading conditions (axisymmetrical or plane strain), or because of the comparatively low relative density achieved by the sand placement method in Phase II.

The average stiffness ratio K^*_{av} degenerates to 1 for $C^* = 0$, since $C^* = 0$ implies that both H and h are 0. All K^*_{av} - C^* curves should therefore pass through the point $(C^*, K^*_{av}) = (0, 1)$. As a first approximation, the curves are assumed to be linear, for $C^* \leq 2$. The slope of these lines can be interpreted as a reflection of the following:

- stiffness (shear modulus) of the aggregate layer used (and thus indirectly the type of material and its treatment, eg. compacted or not, stabilized, cemented, etc.)
- the modulus or moduli of the geosynthetic(s) used
- plane strain or axisymmetrical loading conditions

The *geometry* of the road structure, that is, its aggregate layer thickness and depth to any secondary geosynthetic, is accounted for by the construction parameter, C^*.

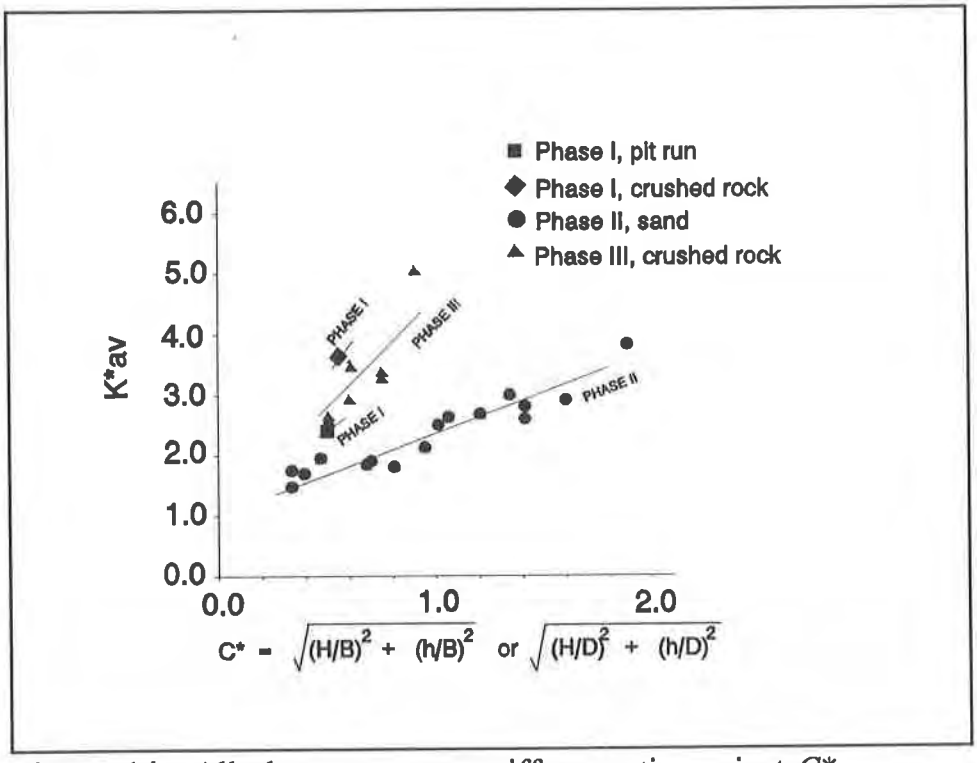

Figure 14. All phases, average stiffness ratio against C^*.

Basis for a Design Method. Designs for single-aggregate-layer, geosynthetic-built access roads could thus be made on the basis of appropriate K^*_{av} - C^* plots. The effect on road behaviour of varying the thickness of the aggregate layer and whether or not a second geosynthetic sheet was included in the structure would be accounted for by C^*. The effects of compacted or uncompacted aggregate, and the quality of aggregate selected, as well as the moduli of the geosynthetic(s) selected, would be accounted for by the slope of the plot.

In practice, to adopt the *stiffness* approach to design of geosynthetic-built access roads on peat subgrades, some predetermined minimum road structure repeated-load stiffness k_r would be set on the basis of *vehicle* considerations. A representative value of subgrade repeated-load stiffness k_p would either be estimated or measured with field plate loading tests. With these two stiffnesses in hand, a minimum tolerable value of $K^*_{av} = k_r/k_p$ would then be calculated. Appropriate K^*_{av} - C^* charts could then be examined, to determine the most economic design, that design being a combination of the aggregate type, aggregate treatment, aggregate layer thickness, and geosynthetic choice. Finally, the design would be checked for adequate bearing capacity, using one of the currently existing methods.

Further Work. The model testing programme, carried out over eight years in soil test boxes and test pits ranging in volume from 0.2 m^3 to 24 m^3 has resulted in the production of Figure 14, where it was demonstrated that a linear K^*_{av} - C^* relationship exists for $C^* \leq 2$. Next, "appropriate K^*_{av} - C^* plots" need to be produced if a viable design method is to be derived. Such charts *could* be produced through continued extensive model and field testing.

However, it will be more efficient if numerical models, properly verified against these model tests and other lab and field data that might be available, can be produced. Work is under way on the development of a three-parameter numerical model. Finite element models will also be examined. Should the numerical models be able to reproduce the relationships found experimentally and shown in Figure 14, then parametric studies, checked against limited laboratory and field tests, can be run to generate the design charts.

CONCLUSIONS

The significance of resource access roads, despite their apparent low standard, has been demonstrated. The design environment for these roads, the combination of design axle load, traffic volume, and economic ceiling, is very different from that for conventional public roads. One solution to the problems presented to designers needing access across soft peat subgrades has been the provision of geosynthetic-built access roads.

To date, little R&D is available to designers of these single-layer geosynthetic-built roads. A handful of design methods exist, where all of the methods are based on bearing capacity or rut depth development.

It has been proposed that rather than rut depth, the key design criteria should be road *stiffness*, since stiffness has a very large effect on the operating cost of vehicles using the roads. A programme of physical model testing to investigate various aspects of geosynthetic-built road stiffness was embarked upon.

The tests have shown that an average stiffness ratio K^*_{av} can be defined for the model road structures, and that K^*_{av} is linear with a parameter C^* describing the construction details of the model road, for $C^* \leq 2$. The slope of the plot of K^*_{av} against C^* reflects the effects of aggregate type and treatment, and geosynthetic characteristics.

Numerical models of the road behaviour are now under development. Once fully verified, they will be used to carry out parametric studies to develop K^*_{av} - C^* charts to facilitate the stiffness approach to the design of geosynthetic-built roads on peat subgrades.

ACKNOWLEDGEMENTS

The funding of three successive three-year Operating Grants provided by the Natural Sciences and Engineering Research Council (NSERC) is gratefully acknowledged. Thanks go as well to the numerous graduate students and undergraduate research assistants who participated enthusiastically in the project's component phases.

REFERENCES

DeGaridel, R. and Javor, E. 1986. Mechanical reinforcement of low-volume roads by geotextiles. Proceedings of the 3rd International Conference on Geotextiles, Vienna. pp. 1021-6.

DeGaridel, R. and Morel, G. 1986. New soil strengthening techniques by tensile elements for low-volume roads. Proceedings of the 3rd International Conference on Geotextiles, Vienna. pp. 1027-32.

Delmas, Ph., Matichard, Y., Gourc, J.-P. and Riondy, G. 1986. Unsurfaced roads reinforced by geotextiles - a seven years experiment. Proceedings of the 3rd International Conference on Geotextiles, Vienna. pp. 1015-20.

Douglas, R.A. 1992. Canadian forest roads and trucks: a technical survey of the country's shadow transportation system. Compendium of Papers, Joint Annual Conference of the Institute of Transportation Engineers, District 1, NE USA and District 7, Canada. May 19, 1992, Ottawa. Session 6A, Paper 1.

Douglas, R.A. 1991. Parametric study of the stiffnesses of unbound, geosynthetic-built roads on compressible subgrades. Proceedings of the 44th Annual Canadian Geotechnical Conference, Calgary, September, 1991. Canadian Geotechnical Society. pp. 80-1 to 80-7.

Douglas, R.A. 1990. Anchorage and modulus in geotextile-reinforced unpaved roads. Geotextiles and Geomembranes 9(3):261-268.

Douglas, R.A. 1988. Forest roads R and D, why it often fails us. UNB Forestry Focus 13(4). Fredericton: Faculty of Forestry, University of New Brunswick. Fall, 1988. 4 pp.

Douglas, R.A. 1987. Modelling geotextile behaviour in thin access road fills over peat subgrades. Proceedings of the 40th Canadian Geotechnical Conference, Regina, Oct. 19-23. Canadian Geotechnical Society. pp. 111-120.

Douglas, R.A., Bessey, B.B. and Small, R.P. 1985. Geotextiles in forest road construction. Proceedings of the Second Canadian Symposium on Geotextiles and Geomembranes, 38th Canadian Geotechnical Conference, Edmonton, Sept. 25-27, 1985. pp. 89-96.

Douglas, R.A., Feng, Z.W. and McCormack, R. 1990. Practical application of truck performance prediction models to forest transportation problems. Presented at the American Society of Agricultural Engineers (ASAE) Winter Meeting, Chicago, December, 1990. Paper No. 907544.

Douglas, R.A. and Kelly, M.A. 1987. Geotextile reinforced logging roads: effect of anchorage. Geotextiles and Geomembranes 4(2):93-106.

Douglas, R.A. and Valsangkar, A.J. 1992. Unpaved geotextile built roads: stiffness rather than rut depth as the key design criterion. Geotextiles and Geomembranes 11(1):45-60.

Giroud, J.-P., Ah-Line, C. and Bonaparte, R. 1984. Design of unpaved roads and trafficked areas with geogrids. Proceedings of the Symposium on Polymer Grid Reinforcement in Civil Engineering. Science and Engineering Research Council, Swindon, and Netlon Ltd., Blackburn. Paper 4.1.

Giroud, J.-P. and Noiray, L. 1981. Geotextile-reinforced unpaved road design. Journal of the Geotechnical Division, ASCE 107(GT9):1233-54.

Gourc, J.-P. and Riondy, G. 1984. Modélisation du comportement à la fatigue des chausées provisoires renforcées par des géotextiles. Proceedings of the Second Canadian Symposium on Geotextiles and Geomembranes, 38th Canadian Geotechnical Conference, Edmonton, Sept. 25-27, 1985. Canadian Geotechnical Society, Edmonton. pp. 97-104.

Hausmann, M.R.. 1987. Geotextiles for unpaved roads - a review of design procedures. Geotextiles and Geomembranes 5(3):201-33.

Holtz, R.D. and Sivakugan, N. 1987. Design charts for roads with geotextiles. Geotextiles and Geomembranes 5(3):191-9.

Jarrett, P.M. 1984. Evaluation of geogrids for construction of roadways over muskeg. Proceedings of the Symposium on Polymer Grid Reinforcement in Civil Engineering. Science and Engineering Research Council, Swindon, and Netlon Ltd., Blackburn. Paper 4.5.

Jewell, R.A. 1990. Strength and deformation in reinforced soil design. Paper presented at the 4th International Conference on Geotextiles, Geomembranes, and Related Products, May, 1990, The Hague, The Netherlands.

Khay, M., Morel, G. and Perrier, H. 1986. Use of geotextiles in construction of low cost highways: an experiment. Proceedings of the 3rd International Conference on Geotextiles, Vienna. pp. 957-61.
Landva, A.O, Korpijaakko, E.O. and Pheeney, P.E. 1982. Geotechnical classification of peats and organic soils *in* Testing of peats and organic soils. ASTM Special Technical Publication 820, P.M. Jarrett, ed. Philadelphia: American Society for Testing and Materials (ASTM). p. 40.
Milligan, G.W.E. and Love, J.P. 1984. Model testing of geogrids under an aggregate layer on soft ground. Proceedings of the Symposium on Polymer Grid Reinforcement in Civil Engineering. Science and Engineering Research Council, Swindon, and Netlon Ltd., Blackburn. Paper 4.2.
Resl, S. and Werner, G. 1986. The influence of nonwoven needle punched geotextiles on the ultimate bearing capacity of the subgrade. Proceedings of the 3rd International Conference on Geotextiles, Vienna. pp. 1009-13.
Yasuhara, K., Hirao, K., Miura, N., Yamanouchi, T. and Ryokai, K. 1986. The use of geotextile against settlement of soft clay under cyclic loading. Proceedings of the 3rd International Conference on Geotextiles, Vienna. pp. 193-8.
Yoder, E.J. and Witczak, M.W. 1975. Principles of pavement design. Toronto: John Wiley and Sons, Inc. p. 246.

Evaluation of Geotextiles as Separators in a Full-Scale Road Test

W.-S. Tsai
University of Washington, USA

B.M. Savage
University of Washington, USA

R.D. Holtz
University of Washington, USA

B.R. Christopher
Polyfelt Inc., USA

T.M. Allen
Washington State Department of Transportation, USA

ABSTRACT

To compare the ability of five different geotextiles to stabilize a soft subgrade during construction, a full scale field test was conducted on Washington state highway SR 507. Performance was compared under two different initial subbase lift thicknesses to evaluate constructibility and installation survivability. Instrumentation was installed to measure vertical strains throughout the cross section, deformations in geotextiles, and changes of water content and temperature. Rut depths were also measured in traffic tests.

The results indicated that the presence of a geotextile resulted in more uniform rut depths. The geotextiles did not however appear to reduce rut depths in test sections where the subgrades had a modest shear strength. All geotextiles had strains in the cross lane direction of less than 8%, except in one failed section. Observations indicated that subgrade drainage during construction was enhanced by the thicker needle-punched nonwoven geotextiles while some types of geotextiles tended to retard pore water dissipation.

INTRODUCTION

Although geotextiles have been widely used as separators in temporary roadways for many years, information on their long term performance in permanent roads is still quite limited. Therefore, an opportunity to investigate geotextile performance arose during the summer of 1991 in connection with the reconstruction of a state highway in Washington. A full scale field test was conducted (1) to compare the ability of different types and weights of geotextiles to stabilize a soft subgrade during construction and (2) to investigate their respective influence on the long-term performance of the pavement system. Five different geotextiles were selected. Their performance was compared under two different initial lift thicknesses (150 and 300 mm) of subbase to evaluate initial lift requirements, constructibility and installation survivability.

SITE DESCRIPTION

The test site was located approximately 32 km south of Olympia on SR 507 in Bucoda, Washington. Both lanes were included in the study.

The area chosen for the test site had a long history of poor performance and was scheduled for major maintenance when the experiment was arranged. The roadway section already contained significant ruts and alligator cracking. The subgrade consisted primarily of clayey soils, with some organic materials found in the northbound lane. The water table was high, especially in the spring, when it was within 0.3–0.6 m of the road surface. The natural water contents were higher than the plastic limits. All soils collected in the subgrades had more than 80% passing the No. 200 sieve; thus the subgrade was suitable for investigating possible soil migration.

FIELD TEST AND INSTRUMENTATION

To accomplish the research objectives, a test site 46 m long and 7 m wide was divided into six sections. One of the six sections was a control section containing no geotextile, while the other five sections each contained a different type of geotextile separator. The geotextiles installed are listed in Table 1 and their respective locations indicated in Figure 1. The geotextiles were selected based on the types of geotextiles conventionally used in stabilization applications, their estimated ability to survive construction, the diversity of filtration characteristics and the potential for lateral drainage. The length of each section was 7.6 m. Instrumentation included soil strain gages for measuring vertical strains throughout the cross section, a grid of rivet points (100 mm by 100 mm on centers) on the geotextile surfaces to measure geotextile deformations in the wheel path, and moisture/temperature sensors for monitoring soil moisture and temperature changes. Schematic diagrams showing the instrumentation locations are given in Figures 1 and 2.

Table 1: Geotextiles installed.

Symbol	Type	Mass/Area (g/m^2)	Survivability Rating based on AASHTO	Manufacture
Soil	no geotextile - control	–	–	–
HB	nonwoven, heat-bonded polypropylene	135	MS	Reemay
NP4	nonwoven, needle-punched polypropylene	135	LS–MS	Polyfelt
NP6	nonwoven, needle-punched polypropylene	202	MS–HS	Polyfelt
NP8	nonwoven, needle-punched polypropylene	270	HS	Polyfelt
SF	woven, slit film polypropylene	250	MS–HS	Exxon

Note:
LS – Low Survivability
MS – Moderate Survivability
HS – High Survivability

Physical Properties of Subgrade Soils. Except for a few silts of high plasticity, all soils collected in the subgrade were classified as clays of high plasticity. There was a large variation in properties of the soils at the site. For example, the initial natural water content was found to be in the range of 20 – 47 %. All soils had more than 80 % passing the No. 200 sieve. The ranges of Atterberg limits were 30 – 77 % for liquid limits, 19 – 35 % for plastic limits and 11 – 42 % for plasticity indices. Table 2 shows the representative subgrade characteristics over the length of the test section in each lane.

Table 2: Representative Characteristics of The Subgrade.

Geotextile	Soil Type	Water Content			Atterberg Limits		
		Initial	Excav 1	Excav 2	LL	PL	PI
Southbound Lane							
HB	CL	20	NA[1]	28	30	19	11
NP4	CL	31	NA[1]	NA[2]	48	27	21
SF	CL	26	NA[1]	NA[2]	34	22	12
Soil	CH	46	NA[1]	46	77	35	42
NP8	CH	38	NA[1]	42	63	28	35
NP6	CH	45	NA[1]	51	74	34	40
Northbound Lane							
HB	CL	27	30	NA[1]	34	23	11
NP4	CL	30	31	NA[1]	44	23	21
NP6	CH	35	23	NA[1]	61	31	30
Soil	CH	37	NA[2]	44	57	28	29
NP8	MH	40	42	43	57	35	22
SF	CH	47	45	50	69	30	39

Note:
1. This set of excavations was not conducted.
2. Data was lost.

Shear Strength of Subgrade. A hand vane tester and a pocket penetrometer were used to measure the in situ shear strengths of the subgrade. The measured shear strengths ranged from 31 to 127 kPa in the northbound lane and from 18 to 98 kPa in the southbound lane using a hand vane tester. The measured shear strengths were found to vary from 48 to 192 kPa in the southbound lane and from 60 to 215 kPa in the northbound lane using a pocket penetrometer. Figures 5 and 6 show the measured subgrade shear strengths using a hand vane tester.

Ground Response. In this study, three traffic tests were conducted using a loaded dump truck. One traffic test was implemented in the southbound lane and two other traffic tests were performed in the northbound lane.

Test Procedure. After removing the top layer of existing fill (0.6 m in the southbound lane and 0.45 m in the northbound lane) to reach the soft clay layer, nuclear density tests were performed on the natural subgrade. Concurrently, in situ shear strength was measured in three locations (within each lane). The locations were: close to the roadway center line and near the middle and outside of each lane, respectively, at approximately every 4.6 m along the length of the lane. Measurements were made using a pocket penetrometer and a hand vane tester. Soil samples were taken for moisture content, grain size distribution and Atterberg limits determinations. As indicated in Figure 3, moisture/temperature sensors were installed at depths of 25 mm and 200 mm below the subgrade surface in each section. A Bison strain coil was placed horizontally at a depth of 200 mm below the subgrade surface in the sections containing: SF, NP8, and the control, in the southbound lane. All instrumentation was placed under the outside wheel path and in the middle of the length of each individual section. The holes dug for the placement of the instrumentation were backfilled with clay and compacted with small hand-operated compactors.

The geotextiles were placed in such a way that the grid points ("pop" rivets) on the geotextiles were located under the outside wheel paths. After the geotextile sections were placed and overlapped 300 mm with adjacent geotextile sections, the rivet spacings were measured. Next Bison coils were attached by duct tape to geotextiles SF and NP8 and a third coil placed at the top of the subgrade in the control section (Figure 3).

A first lift of base course (thickness 300 mm) in the southbound lane and a first lift (thickness 150 mm) in the northbound lane were placed over the entire length of the test section and compacted with a steel wheeled roller. The lift thicknesses were selected based on the minimum lift thickness recommendations for construction on soft subgrade by WSDOT (300 mm) and the minimum lift thickness with geotextile estimated to be required to limit rutting to less than 50 mm during construction as recommended by Steward, et. al. (1977). WSDOT personnel tested the surface of the lift for density and field moisture content using a nuclear densiometer. After the first lift of base course was compacted, samples were taken for moisture content and grain size distribution determinations.

A traffic test was performed (referred to as Traffic 1) on the base course surface using a loaded dump truck weighing 350 kN, having rear tandem axle with dual tires, passing over the entire 46 m experimental zone. A total of 10 passes were made to simulate typical construction traffic. Following passes 1, 2, 5 and 10, readings of the Bison gages and moisture/temperature sensors were taken and rut depths measured. Ground response observations were recorded for each of the intermediate passes. Two rut-depth measurements (one at the north side and one at the south side) were made in both wheel paths in each test section except for the control (soil only) sections. In the control section, only one rut depth measurement was made at the center in both wheel paths as this was the location of the largest rut depth.

After the traffic test, a small test pit was excavated (referred to as Excav 1) down to the geotextile, or to the top of the subgrade in the control section. Grid patterns were measured and visual observations of the geotextiles and subgrade conditions were recorded. Geotextile samples, 0.9 m by 0.9 m, were removed for laboratory testing to determine the extent of physical damage and mechanical property change to the geotextiles. Soil samples were taken from the subgrade.

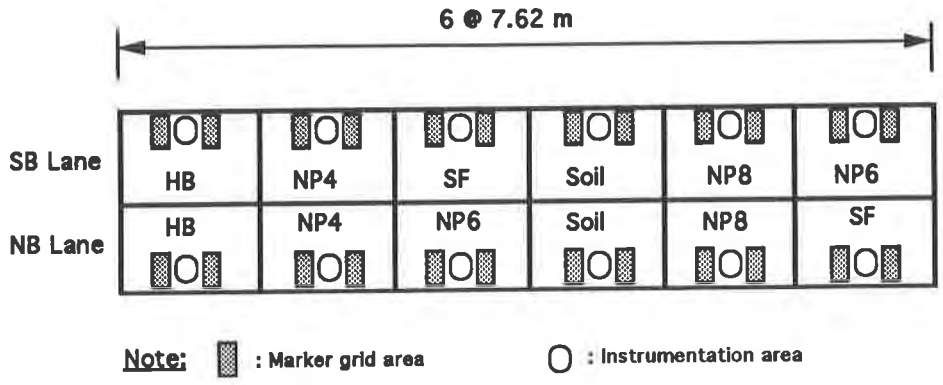

Figure 1: Locations of Geotextile and Instrumentation.

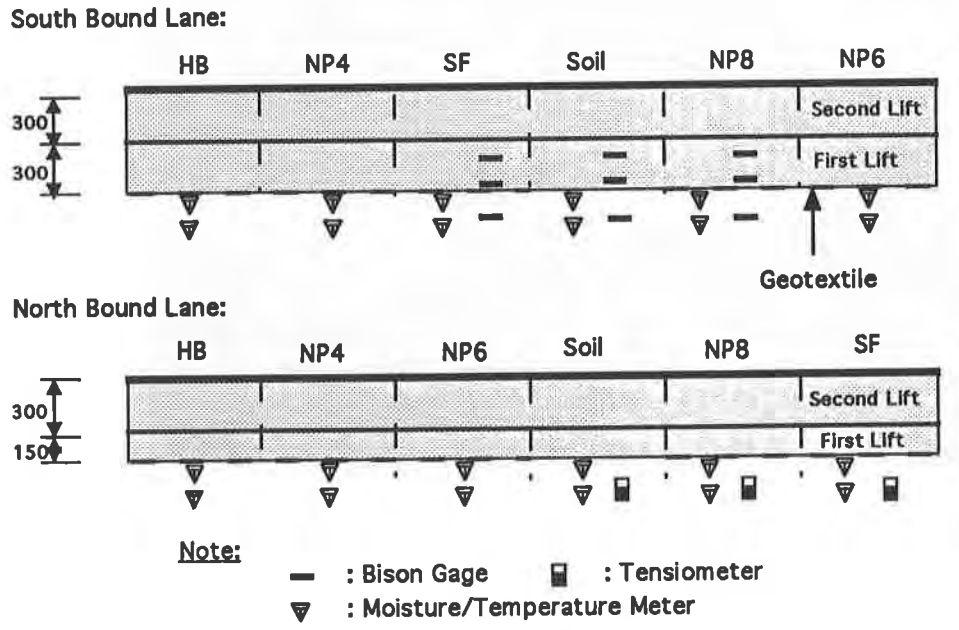

Figure 2: Cross Section Showing Instrumentation Placement (dimensions in mm).

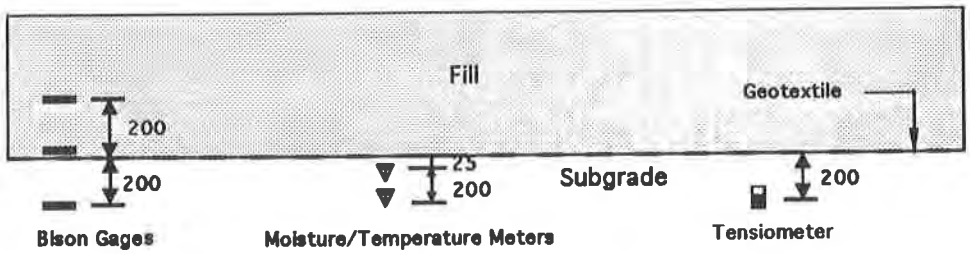

Figure 3: Vertical spacing of instruments (dimensions in mm).

Geotextile patches were placed over the sample removal areas before the excavations were backfilled and compacted.

The second lift of base course was placed and compacted. A traffic test was also performed (referred to as Traffic 2). The second set of test pits was excavated (referred to as Excav 2) to the fabric depth and observations were recorded. The same procedures were followed for the second lift and associated activities as was completed for the first lift. Figure 4 shows a general view of the second excavation in the southbound lane.

Due to time constraints, Excav 1 and Traffic 2 were not performed in the southbound lane.

Figure 4: General View of Field Test during Excav 2 in Southbound Lane.

Falling Weight Deflectometer Tests. To examine the improvement in the stiffness of pavement due to the inclusion of geotextiles, WSDOT personnel performed FWD tests, 37 days before, and 49 days and 173 days subsequent to the placement of the geotextiles in the southbound lane. On each test date, one FWD test was conducted on each section.

RESULTS AND DISCUSSIONS

Only a portion of the study results are presented and discussed herein. Additional study findings will be reported in separate publications as additional data is obtained and analyzed.

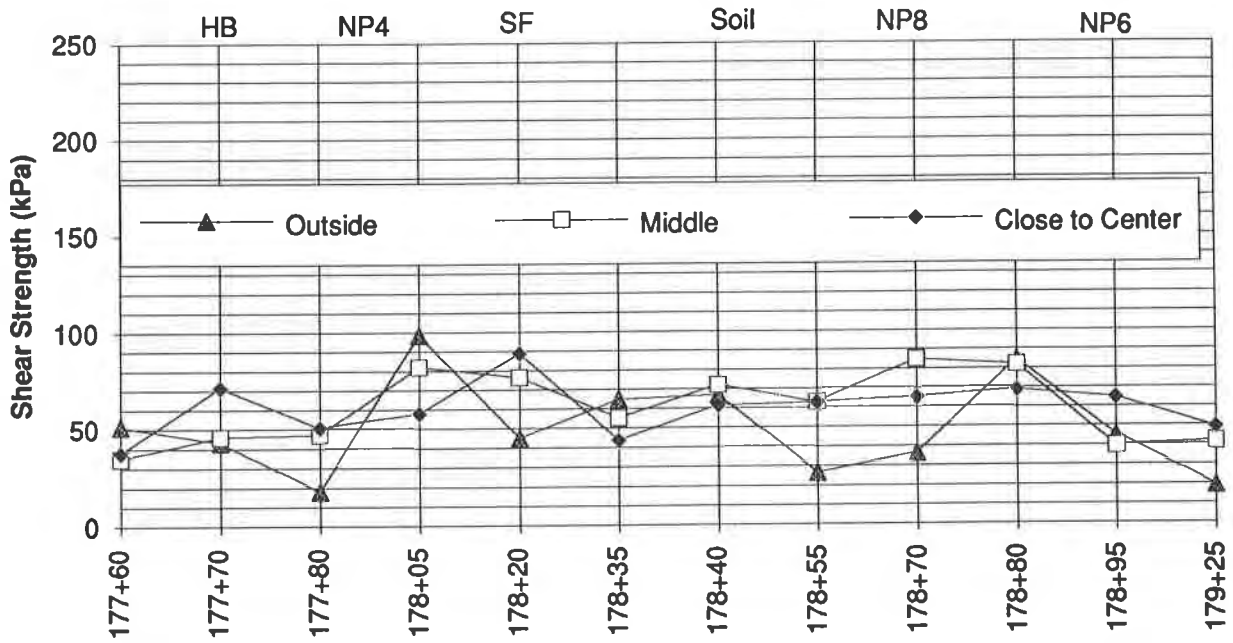

Figure 5: Shear Strength of Subgrade in the Southbound Lane using Hand Vane Tester.

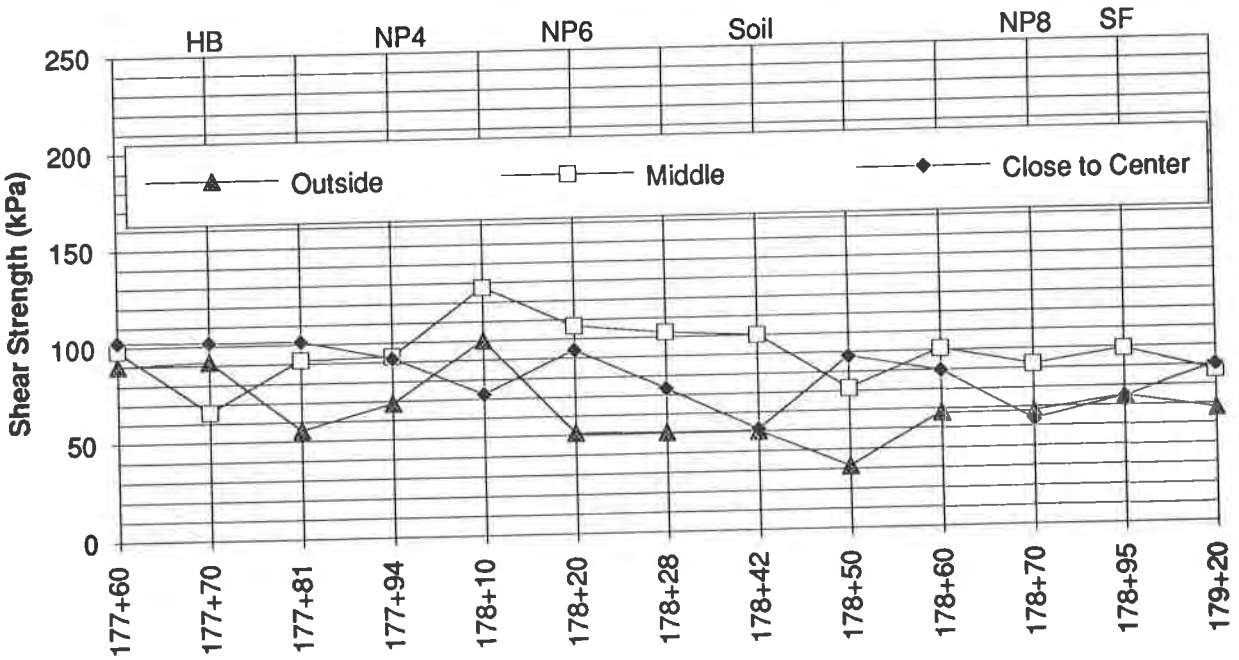

Figure 6: Shear Strength of Subgrade in the Northbound Lane using Hand Vane Tester.

- First Southbound Traffic Test (300 mm base course)

  The performance of the NP4 section was better than the HB section in that the NP4 section had more elastic response and a lower magnitude of elastic deflection than the HB section. As anticipated, based upon the FHWA design method (Christopher and Holtz, 1989), for this lift thickness and the number of passes no plastic deformation occurred during any of the passes. Section NP8 appeared to have the best overall performance.

- First Northbound Traffic Test (150 mm base course)

  The NP4 section became a full mud wave at pass 7 and appeared to have the worst performance than any other section in this lane. Due to the closeness of the wheel path to the fill edge, lateral movement of aggregate was noted as the truck passed over the section having SF and resulted in significant rutting in the first four passes. In contrast with the other sections, the control (soil only) section and NP8 had better overall performance. At this time, there is no obvious explanation why the control section had better performance.

- Second Northbound Traffic Test (450 mm base course)

  In this test, all sections had better performance than in the first traffic test in the same lane. Section HB and Section NP4 had very similar behavior and had the worst performance; after pass 5 both sections began undulating and waving. NP8 and the control section had the best overall performance. Again, there is no obvious reason why the control section performed better.

Rut Depth. All of the measured rut depths in Traffic 1 southbound (300 mm base course) shown in Figure 7 were less than 40 mm. Figure 7 also illustrates that the control section had largest rut depth, which was also less uniform than those in the sections having geotextiles.

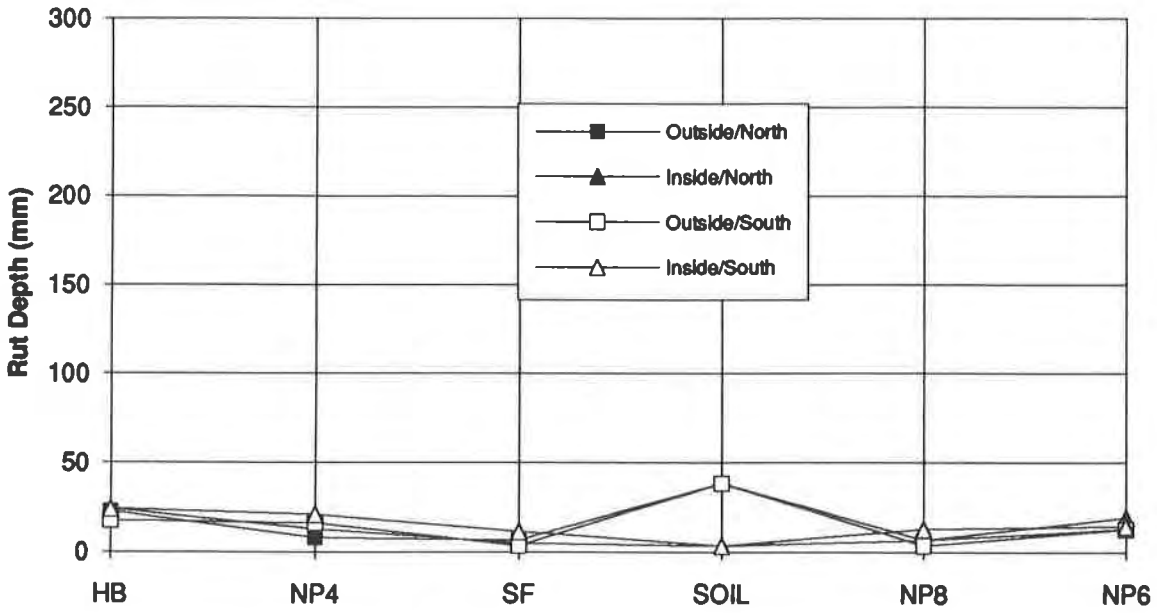

Figure 7: Rut Depth after the Tenth Pass in Traffic 1 in the Southbound Lane.

Figure 8 shows the measured rut depths in each section of the northbound lane in Traffic 1 (150 mm base course). The measured rut depths were relatively low, in the range of 19 to 87 mm, with the exception of NP4. Rut depths in the northbound lane were greater than those in the southbound lane, despite the fact that the sections in the northbound lane had higher average shear strengths. This difference is attributed to the thinner base course in the northbound lane, which was 150 mm less in thickness. Section NP4 had the greatest rut depth (264 mm) in the outside wheel path. This section was found to have failed after the first traffic test (Traffic 1). The thicknesses of the base layer in sections HB and NP4 were found to be less than in any other four sections. The large rut depths observed in Section SF may not reflect its true performance, since these rut depths may have been influenced by the lateral movement of the base course aggregates in the outer wheel path, which was observed during trafficking. Overall, NP8 resulted in the smallest rut depth for this traffic test.

Figure 9 indicates that the rut depths in Traffic 2, northbound, (450 mm thick base course) were very small (less than 25 mm), except in Sections HB and NP4, which had larger rut depths, up to 64 mm. The subgrade of both these sections contained organic materials.

Figures 7 through 9 indicate that geotextiles did not reduce rut depths in comparison with the control sections, probably due to the higher strengths of the involved subgrades; thus the reinforcing effect due to the presence of geotextiles was likely negligible. Hence, the contribution of the geotextile to the reduction of rut depth is very limited if the subgrade has a modest shear strength. In this case, geotextiles are expected to act as separators and drainage media only.

Strains in Subgrade and in Base. Figure 10 shows the induced final strains after traffic tests and the incremental strains during the traffic tests in the subgrade and in first lift in Sections SF and NP8 and the control (soil only) section. The strains in the base were very small; therefore the contribution of the geotextiles with respect to strain reduction could not be evaluated for the first lifts of the base layer. A majority of the strains in the subgrade were measured during placement and compaction of the first lift with much lower strains measured during the traffic tests. The control (soil only) section had the highest final strains, 11% in subgrade and 1% in the base. During the traffic tests, a strain increment of 1.1% was observed in the subgrade. The final measured strains in the section having NP8 were 10% in subgrade and -1% in base. The negative strain in the base may be due to the horizontal movement or a slight rotation of the Bison coils. A strain increment of 2.2% was observed in NP8 during the traffic tests (Figure 10). It should be noted that rut depths were not measured at the exact locations of the Bison coils.

SF had the lowest final strains in the subgrade (1%) and in the base (1%). Thus, the reduction of strain in the subgrade of Section SF was greater than in Section NP8. This may be due to the relatively low modulus of NP8. The low strains in the SF section may have been the result of a combination of high modulus and/or poor drainage observed in that section. Since the subgrade had a lack of uniformity in water content and in shear strength, the differences in the induced strains cannot be directly attributed to the presence of different geotextiles.

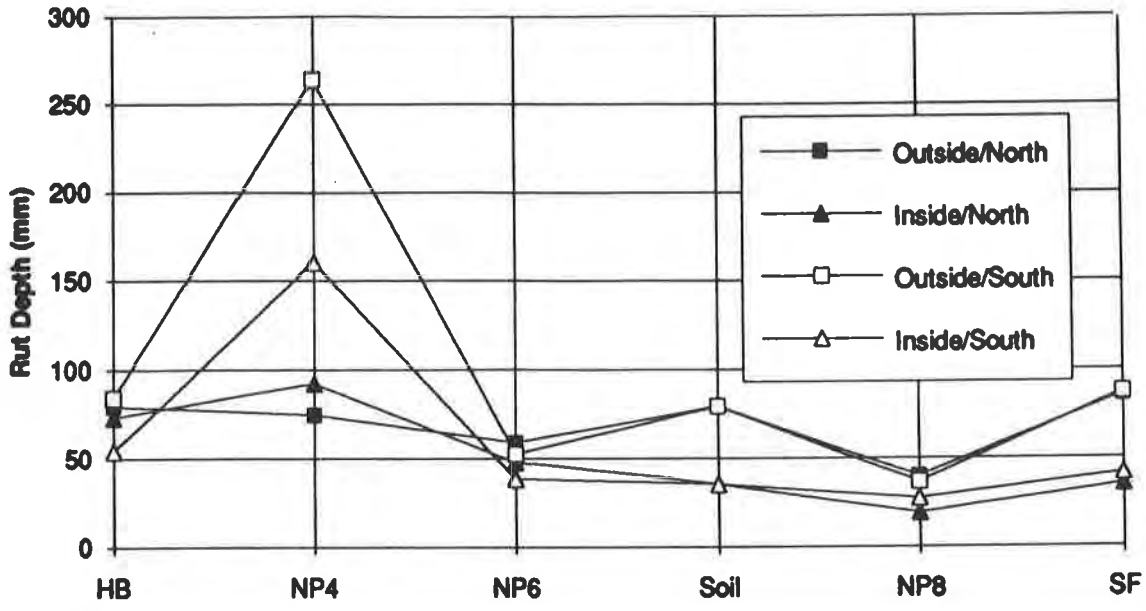

Figure 8: Rut Depth after the Tenth Pass in Traffic 1 in the Northbound Lane.

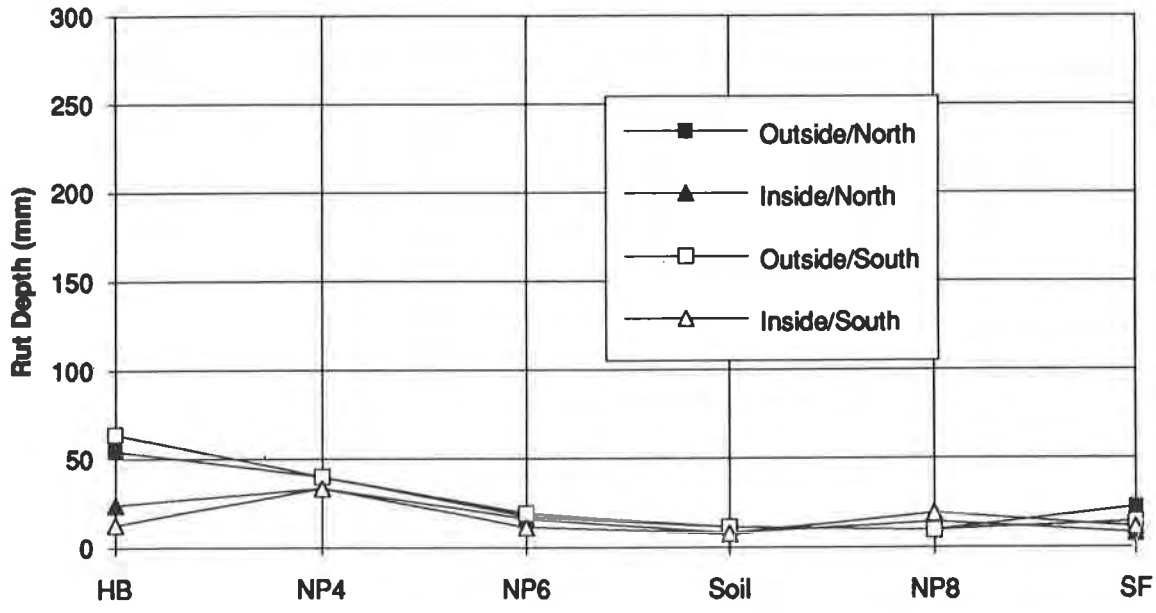

Figure 9: Rut Depth after the Tenth Pass in Traffic 2 in the Northbound Lane.

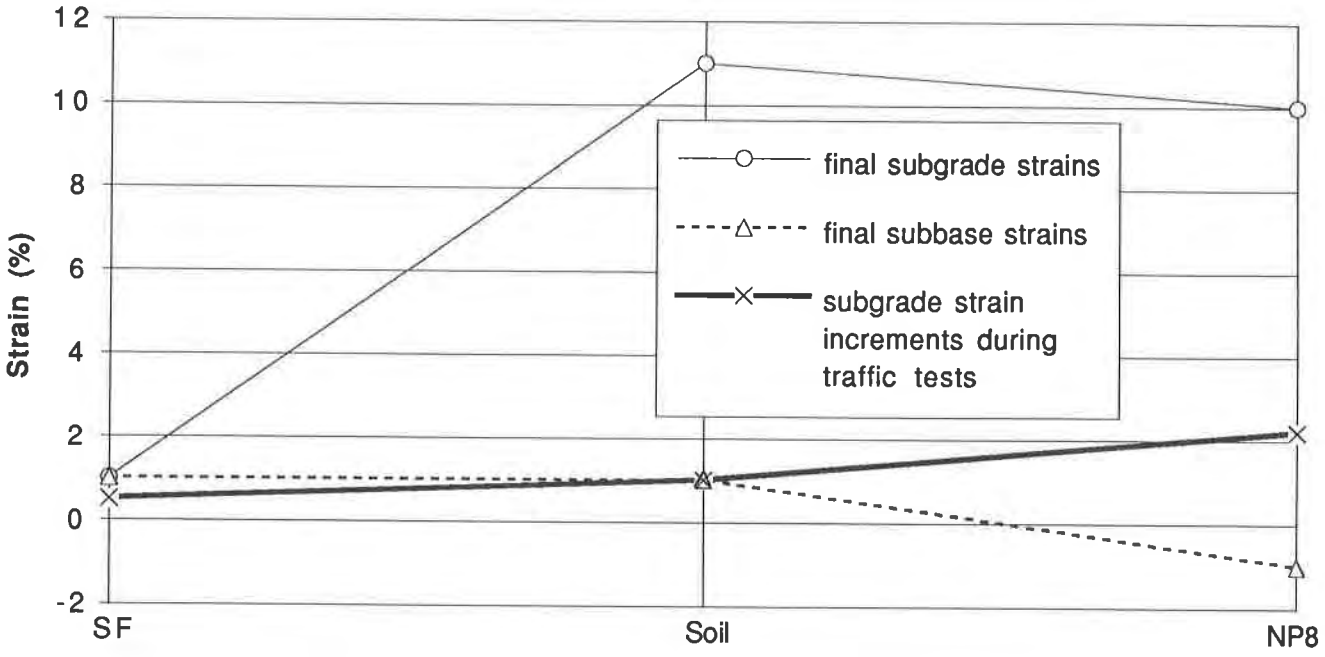

Figure 10: Strains in Subgrade and Base in the Southbound Lane.

Strains in Geotextiles. Figures 11 and 12 summarize the measured strains found in the geotextile surfaces when excavated. The results show that the induced strains in the cross lane direction in SF and NP8 relatively low, about 2% for SF and 4% for NP8. No geotextiles had strains greater than 8% except NP4 in the northbound lane, which had a strain of 136%. The strains in the geotextiles agree well with the measured rut depths; i.e. larger rut depths cause larger strains in the geotextiles.

Visual Observations after Excavations. In the second excavation (southbound lane), all geotextiles performed well. A high ground water table was observed in the test pits during this set of excavations. The designed thickness of fill was 600 mm but the measured thicknesses were not uniform in each section varying as much as 150 mm. SF was not flat and had some ripples (about 50 to 80 mm high) parallel to the lane direction. HB was not in tension and the subgrade was moist and pliable, which is consistent with saturated soft clay conditions. Water ponding under HB existed. NP6 was in tension and wet. NP8 appeared to have less strain. The soil under NP8 was relatively dry compared with the other sections even though the original natural moisture content of the soil was higher in this section indicating a possible influence from lateral drainage potential.

In the control (soil only) section, mixing of subgrade soil and aggregate occurred to a thickness of about 130 mm. However, the intermixture was not observed in the sections containing geotextiles.

In the first northbound lane excavation, SF was in tension but not stretched tightly. Under SF, the subgrade surface was saturated and ponding appeared to be developing. Similarly, NP8 experienced some tension, but was not tight. The soil below NP8 appeared to be relatively dry.

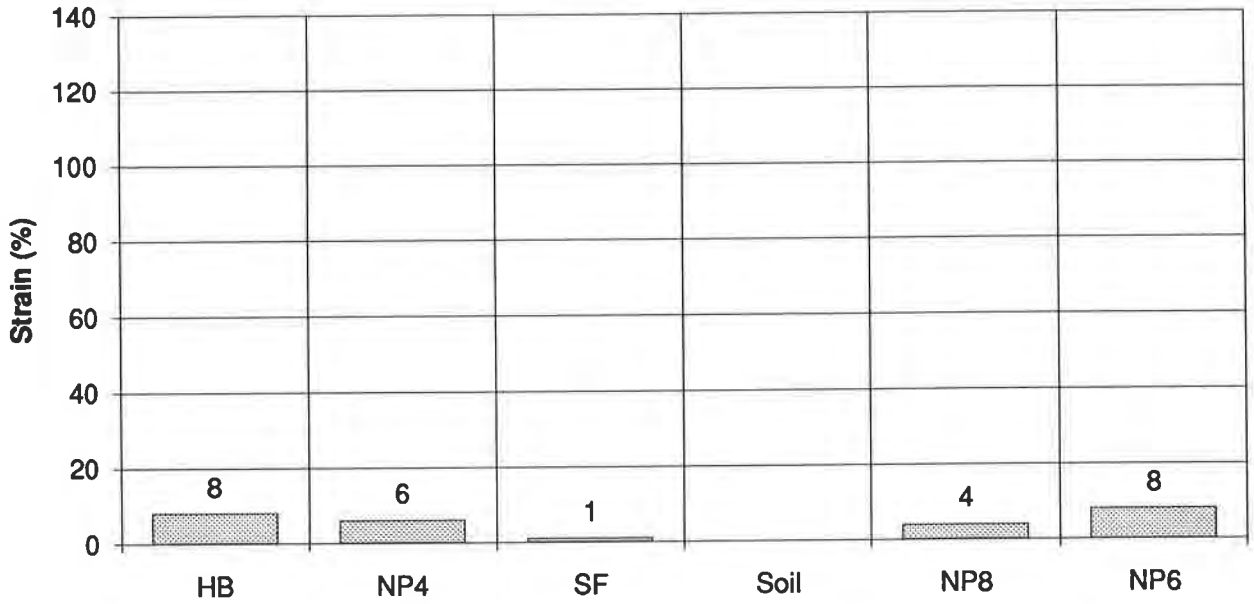

Figure 11: Strains in Geotextiles at Excav 2 in the Southbound Lane.

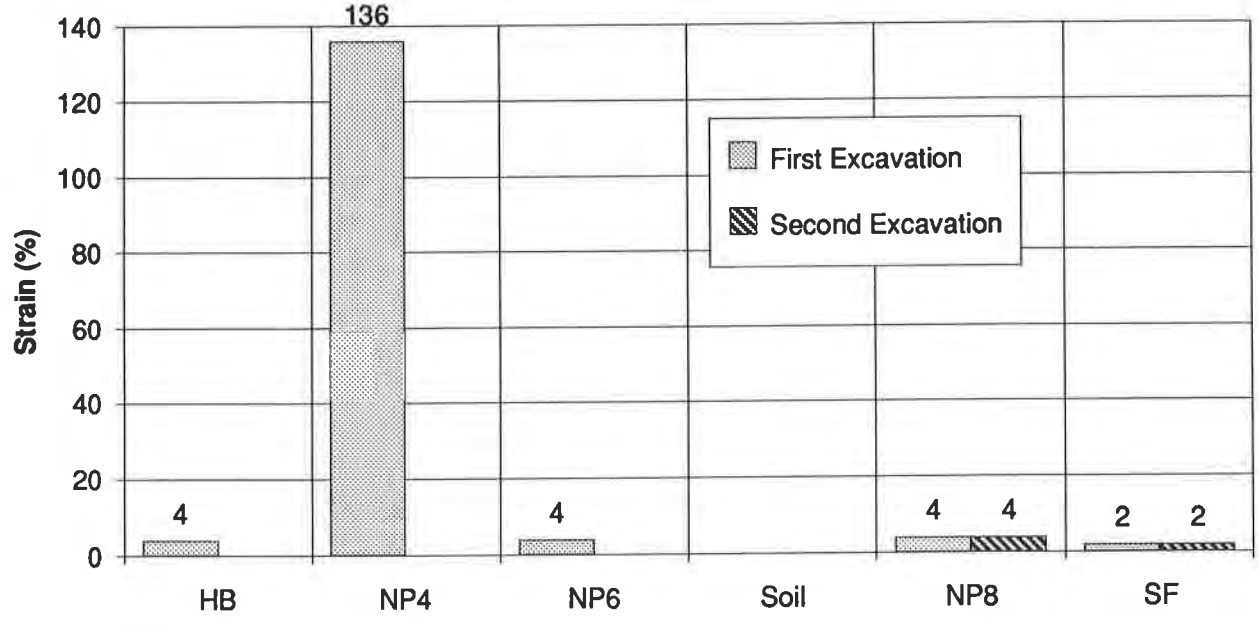

Figure 12: Strains in Geotextiles at Excav 1 and Excav 2 in the Northbound Lane.

NP4 was the only geotextile which did not survive construction. Several holes, which were punched by stones, were found in NP4. This was not surprising considering the subgrade condition, the minimal lift thickness, the amount of rutting observed and the relatively low survivability characteristics of the geotextile. Clay below NP4 appeared wet and slippery. HB was loose as it spanned over discontinuities. A mixture of aggregate and subgrade clay was observed in the control (soil only) section.

In the second excavation (northbound lane), the thickness of fill was less than the design thickness of 460 mm (330 mm for SF and 360 mm for NP8). Soil below NP8 was relatively dry and NP8 appeared tight. Some soil migration was found on the top of the SF, and the surface of the subgrade soil beneath was wet and slightly ponded.

SUMMARY AND CONCLUSIONS

This full scale road test was performed to evaluate the ability of different types of geotextiles to stabilize a soft subgrade for a highway construction. Based on the results of the study, a number of conclusions were drawn:

- The use of a geotextile was in all cases found to eliminate base/subgrade intermixing, if the geotextile survives the installation and placement operations.
- The presence of a geotextile can result in more uniform rut depths, if the geotextile survives the installation and placement operations.
- Rut depth cannot be reduced by geotextiles, if the subgrade has a modest shear strength.
- Compared with the other geotextiles used in this study, NP8 had the best overall performance based on visual observations and rut depths.
- Strains in the subgrade soil appear to be reduced by the SF geotextile; however some pumping of the subgrade may have influenced these results.
- The observations indicate that during construction the needle-punched nonwoven geotextiles allowed unrestricted drainage of the subgrade while the other types tended to retard drainage. The heavier weight needle-punched nonwoven geotextile appeared to enhance drainage.

This paper presents only the initial results of a planned long term monitoring plan. Although the initial results primarily indicate an improvement, the actual benefits of using geotextiles as separators in pavement systems can only be determined after long term monitoring and evaluation.

ACKNOWLEDGEMENTS

Financial support for the instrumentation and field test observations was provided by the Washington State DOT and Polyfelt, Inc. All geotextiles were supplied by Polyfelt, Inc. A special thanks to Mark Wayne for his diligent participation in the program.

REFERENCES

Christopher, B., and Holtz, R. D. (1989) Geotextile Design and Guidelines, National Highway Institute, U.S. Federal Highway Administration, Washington D.C., Report FHWA-HI-90-001.

Steward, J.E., Williamson, R., and Mohney, J., (1977) Guidelines for Use of Fabrics in Construction and Maintenance of Low Volume Roads, U.S. Forest Service, Portland, OR..

A Study of the Cost-Effectiveness of Using Separation Geotextiles in Permanent Road Structures

C.J. Sprague
Sprague & Sprague Consulting Engineers, USA

G.A. Cicoff
Greenville County (South Carolina) Public Services Dept., USA

ABSTRACT

Greenville County, South Carolina, constructs permanent paved surfaces on approximately 20 miles of existing gravel roads each year. The County Engineer sought to protect his new low-cost pavement from premature degradation and more frequent maintenance by including an appropriate geotextile as a separator between the subgrade and the pavement structure.

Three pavement cross-sections and three different types of geotextiles were evaluated in an 8100-foot long trial section. The geotextile strength and hydraulic properties necessary to survive construction and provide long-term filtration and separation between the subgrade and the base aggregate were evaluated based on testing of exhumed geotextile samples and visual pavement condition surveys from a trial installation.

Like-weight geotextiles exhibited the same degree of construction survivability, in terms of retained strength under like conditions. These low-cost, light-weight geotextiles provide subgrade/base interface stability which will generally increase the life of a pavement section without increasing life-cycle costs.

INTRODUCTION

A trial installation was made on an 8000+ foot low volume county road. The purpose of the trial was to determine necessary separation geotextile material properties and to assess the relative performance of different pavement cross-sections with and without separation geotextiles.

In order to assess the ability of the geotextile to survive construction, numerous samples were exhumed from beneath the stone base before the surface course was constructed. Testing indicated that, under comparable conditions, like-weight woven and nonwoven geotextiles exhibit virtually the same degree of construction survivability in terms of percent strength retained. Additionally, the grade on which the installation was made has a significant influence on geotextile survivability.

The long-term performance of the installation was determined through periodic inspections of the road surface. The road surface condition was characterized and ratings were entered into the County's Pavement Management System (PMS) for various segments of the road. The PMS then dictates the timing of the maintenance of the various road segments. This allows for the assessment of the ability to extend maintenance schedules when geotextiles are used with low cost pavement structures. The cost savings associated with extending maintenance schedules can then be compared to the nominal additional cost of including a geotextile.

INSTALLATION LAYOUT

Stockton Road, in southern Greenville County, South Carolina, was selected for this trial installation because it had been surfaced with aggregate twice in the preceding 18 months and was once again in need of additional surfacing. This was a clear indication that the road subgrade was unstable when saturated and could benefit from the installation of a stabilization geotextile.

The full length of the road, approximately 8100 feet, was surfaced with pavement sections as shown in Figure 1 and detailed in Table 1. The following cross-sections were used on approximately one-third of the road each:

- 1" triple treatment surface course over 3" compacted stone base.
- 1-1/2" asphaltic concrete surface course over 3" compacted stone base.
- 2-1/2" full depth asphaltic concrete binder course.

Approximately 500 feet each of three different geotextiles, 4 and 6 oz/sy needle-punched nonwoven geotextile and a 4 oz/sy slit film woven geotextile, were installed between the subgrade and each pavement section. The remaining footage of the road was to act as a control for the long-term evaluation of each pavement section.

A heavier nonwoven geotextile (6 oz/sy) was used in areas involving steep grades and poor drainage while the 4 oz/sy geotextiles were used in areas of more uniform conditions to facilitate more accurate performance comparisons of the like-weight materials.

Typical properties of the separation geotextiles used are shown in Table 2.

Prior to the placement of the geotextiles or pavement systems, the road subgrade was fine graded, surface saturated by water truck, and baseline cone penetration measurements were made.

SITE DATA COLLECTION AND EVALUATION

To facilitate meaningful evaluation of long-term road performance, the following information was obtained during the trial installation:

- Road centerline survey, including staking of stations at 50-foot intervals.
- Centerline plan and profile of roadway, including stations, fabric location and I.D., and pavement location and I.D.
- Saturated soil strength, as measured using the Cone Penetrometer Index.

TABLE 1. STOCKTON ROAD PAVEMENT INSTALLATION

Station	to	Station	Stabilization Geotextile	Pavement Section
0+00		5+00	A	2 1/2" Full Depth Asphalt
5+00		10+00	B	2 1/2" Full Depth Asphalt
10+00		20+00	None	2 1/2" Full Depth Asphalt
20+00		25+00	C	2 1/2" Full Depth Asphalt
25+00		30+00	None	1 1/2" Asphalt over 3" Stone Base
30+00		35+25	A	1 1/2" Asphalt over 3" Stone Base
35+25		40+25	B	1 1/2" Asphalt over 3" Stone Base
40+00		45+50	None	1 1/2" Asphalt over 3" Stone Base
45+50		50+00	C	1 1/2" Asphalt over 3" Stone Base
50+00		55+00	C	Triple Treatment over 3" Stone Base
55+00		61+00	None	Triple Treatment over 3" Stone Base
61+00		66+00	B	Triple Treatment over 3" Stone Base
66+00		71+00	A	Triple Treatment over 3" Stone Base
71+00		81+00	None	Triple Treatment over 3" Stone Base

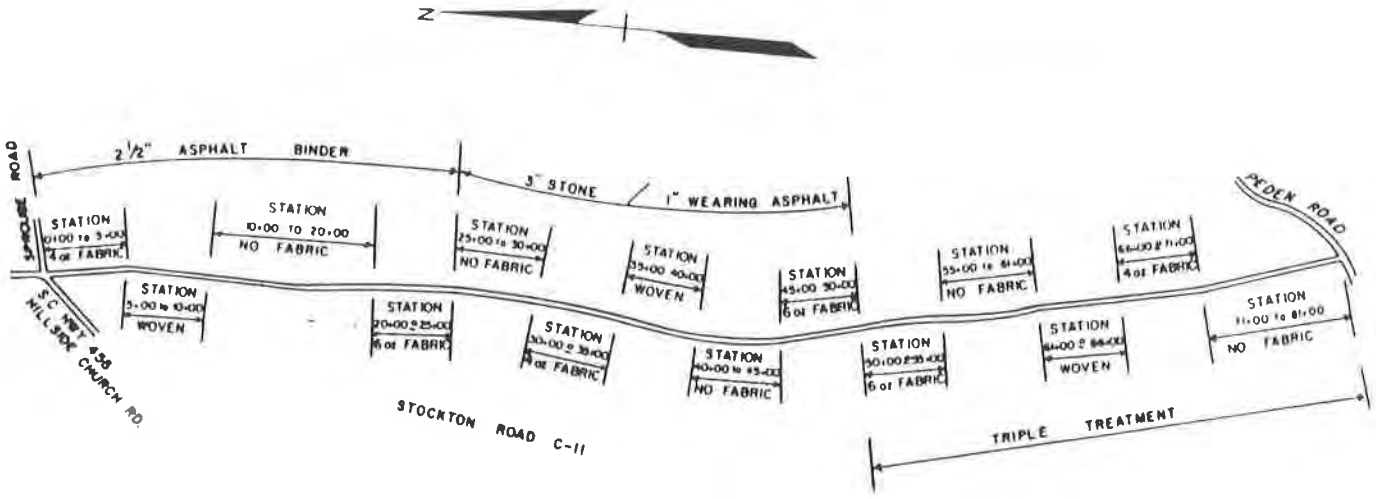

Figure 1
STOCKTON ROAD
EXPERIMENTAL PAVING PLAN
MAY 11, 1987

TABLE 2. TYPICAL PROPERTIES OF SEPARATION GEOTEXTILES

Construction	ASTM Method	A PET Continuous Filament Needlepunched Nonwoven	B PP Silt Film Woven	C PET Continuous Filament Needlepunched Nonwoven
Weight, oz/sy	D3776	4.2	4.0	6.0
Grab Strength, lbs	D4632	135/110	200/200	205/175
Grab Elongation, %	D4632	70/85	20/18	75/85
Puncture, lbs	D3787	60	80	90
Trapezoid Tear, lbs	D4533	60/50	65/65	80/75
Mullen burst, psi	D3786	210	385	315
Water Flow Rage, gpm/sf	D4491	140	5	130
A.O.S., sieve size	D4751	70-100	40	70-100

TABLE 3. ROAD BASE AGGREGATE GRAIN SIZE ANALYSIS

50+00 to 81+00		25+00 to 50+00	
Sieve #	Percent Passing	Sieve #	Percent Passing
1 1/2	100	1 1/2	100
1	92.5	1	96.9
3/4	79.9	3/4	90.0
1/2	69.7	1/2	76.8
3/8	63.1	3/8	69.2
4	52.7	4	56.7
8	45.7	8	47.8
16	37.9	16	39.0
30	30.0	30	30.5
50	19.5	50	19.6
100	10.7	100	10.7
200	5.7	200	5.5
PAN	--	PAN	--

Note: Readings were generally in the 150-180 range (c = 12 to 15 psi) at depths of 1" - 2".

GEOTEXTILE INSTALLATION AND ROAD BASE CONSTRUCTION

With the road and edge drains fine graded for proper cross-slope and drainage, installation of the geotextile began. Construction of very thin lifts of base material with a substantial coarse fraction (see Table 3 for base aggregate grain size analysis) were expected to produce a "worst case" condition on the geotextiles. Lifts of 1-1/2" thickness were used in the triple treatment segment while a single 3" lift was used in the asphalt surfaced segment.

Trucks dumping base aggregate were allowed to run and dump directly on the fabric. This was considered a "practical" acceptance of the typical methods of constructing these low-volume roads as well as providing a "worst case" evaluation.

A motor grader spread the aggregate to the desired depths and an 8-ton steel-wheeled roller provided the compaction of the base material.

Geotextile sampling for construction damage in section one and two was done after the completion of the aggregate base, but before the construction of the surface course.

The third pavement segment consisted of full-depth asphalt binder to a compacted thickness of 2 1/2". No geotextile sampling was done in this segment, but some field observations were made.

The only unsatisfactory observations made during the construction of the full-depth segment involved placement of the 2 1/2" of hot asphalt on the woven slit film geotextile. Circular-arc shaped cracks appeared in the pavement as the paver progressed up a very modest (< 1%) grade and once again when paving a somewhat steeper grade. This is believed to be a result of slippage of the pavement at the geotextile/pavement interface.

EXHUMING GEOTEXTILE SAMPLES

It was assumed that the most severe construction loadings occur during set-up of the base aggregate and that construction of the ensuing surface course would impose less significant stresses on the geotextiles.

Samples were exhumed by shoveling aggregate off areas every 50 feet and cutting out geotextile samples. Patches were then "tucked in" to repair the sampled area.

All samples were marked with the station number corresponding to the sampling location and a note was made if aggregate thickness above the fabric varied significantly from the desired 3 inches.

LABORATORY TESTING AND RESULTS

Ninety-nine field samples were exhumed--twenty-two of each geotextile in segment one and eleven of each geotextile in segment two. Most field samples had puncture damage to a minor extent. To avoid extreme results, both Mullen burst and puncture tests were set up to intentionally exclude obvious puncture holes. Five

Mullen burst and five puncture tests were run on each sample and the results were averaged.

The results, as could be expected, were widely scattered, but when averaged for each sample and for each location (when two samples were exhumed from the same location) the results appeared quite consistent.

As shown in Table 4, the 4 oz/sy fabrics used in the low survivability conditions performed similarly in terms of percent strength retained.

Table 5 gives interesting insight into the need for a more durable geotextile when more demanding survivability conditions are experienced. The six ounce per square yard needlepunched nonwoven geotextile experienced approximately 20% and 40% strength loss in the two pavement segments built using aggregate base. This data points out the importance of considering road grade and drainage when assessing survivability conditions and would indicate that this geotextile may not have been durable enough for the given moderate survivability conditions.

CONSTRUCTION SURVIVABILITY OBSERVATIONS AND RECOMMENDATIONS

Using retained strength as a guide, the following observations are made concerning the construction survivability of geotextiles in low-cost, low-volume pavement structures:

- Like-weight woven slit film and nonwoven needlepunched geotextiles exhibit the same degree of construction survivability, in terms of retained strength, under the like conditions tested here.

- The required level of survivability must include an assessment of lift thickness of base aggregate and roadway grade, as well as saturated subgrade strength and construction vehicle loading.

- 4 oz/sy geotextiles of all types are too light-weight to resist localized puncturing when thin base course lifts are used.

Table 6 summarizes survivability conditions and suggested appropriate geotextile mass per unit area (Cicoff and Sprague, 1991).

MONITORING PAVEMENT PERFORMANCE

In order to characterize the relative long-term performance of the various pavement sections, it was necessary to periodically inspect the road surface to track degradation. An independent visual inspection program was initiated. The program included quantitative assessments of the pavement surface by trained technicians performed on a periodic basis.

The quantitative assessments were entered into a computerized pavement management system which could then project the long-term performance of each pavement segment.

A comparative evaluation was made only of the road sections using like-weight geotextiles (i.e., 4 oz/yd^2) and the control sections since these sections had comparable grades and drainage.

TABLE 4. GEOTEXTILE STRENGTH RETAINED
LOW SURVIVABILITY CONDITIONS*

		4 oz/sy Continuous Filament Needlepunched		4 oz/sy Slit Film	
		NONWOVEN		WOVEN	
		Mullen Burst %	Puncture %	Mullen Burst %	Puncture %
Triple treatment	over 3" Base	80	80	77	100
1 1/2" Asphalt Surface	over 3" Base	100+	100+	93	100+

*Heavy construction equipment operating on firm, dry, well draining subgrade. Road grades are flat to slight.

TABLE 5. GEOTEXTILE STRENGTH RETAINED
MODERATE SURVIVABILITY CONDITIONS**

		6 oz/sy Continuous Filament Needlepunched Nonwoven	
		Mullen Burst %	Puncture %
Triple treatment	over 3" Base	57	73
1 1/2" Asphalt Surface	over 3" Base	77	79

**Heavy construction equipment operating on poorly drained subgrade. Road grades are moderate to steep.

TABLE 6. GEOTEXTILE SPECIFICATIONS FOR CONSTRUCTION
SURVIVABILITY IN LOW COST, LOW-VOLUME ROADS *, ***
(after Cicoff and Sprague, 1991)

Survivability Level	Subgrade Conditions	Base Course Thickness **	Geotextile Mass/Unit Area
Low	Dry, firm, flat	> 6" compacted	4 oz/sy
Moderate	Water sensitive, flat	> 3-4" compacted	6 oz/sy
High	Water sensitive, grade > 2%	> 3-4" compacted	8 oz/sy

* These recommendations incorporate the allowance for construction vehicles to run directly on the fabric during aggregate base construction.

** For base course lifts less than 3", required survivability should be increased one level (i.e. low to moderate).

*** These recommendations expect minor puncture damage to the geotextile. The resulting greater sensitivity to pumping is not considered critical in low volume installations. Required survivability should be increased for higher volume roads to protect against puncture damage to the geotextile.

PAVEMENT CONDITION EVALUATION

Greenville County utilizes the American Public Works Association's Micro Paver Software for Pavement Management. This program was developed by the U. S. Army Corps of Engineers-Civil Engineering Research Laboratories. The basic data entered on the various pavement sections rely on surface distresses. Their quantity and severity establish the overall quality of a pavement. The pavement condition index, or PCI, is established on a ranking scale from 0 to 100. The various qualitative descriptions and the relationship to the PCI numbers are shown on Table 7. Additionally, the various types of distresses identified in the pavement evaluation for a PCI determination are noted at the bottom of Table 6. Each of the 19 distresses associated with asphalt pavements relates to a deduct value from the top rank value of 100. Pavement condition information is entered into and weighting, deduction and projecting calculations are expeditiously handled through the computer software program.

For our purposes, it is assumed that a pavement can be allowed to deteriorate to a PCI of 50 before resurfacing or other rehabilitative work would be required. Pavements exposed to traffic loads and volumes significantly greater than those experienced by the low volume roads being addressed here, should be maintained at some greater level. The action level is established by local preference.

The PCI rankings of the pavement excluded distresses that are not related to the overall structural performance of the pavement. For purposes of this report, sample units without areas damaged by construction, utility work, and other localized distresses were intentionally selected. Sample units within each test section contained approximately 2600 square feet. The sample units selected were typical of the pavement within each section.

The results of PCI evaluations on various segments on Stockton Road are shown on Table 8.

PROJECTING RATE OF DETERIORATION

Micro Paver utilizes a fourth degree equation to simulate the PCI deterioration curve. The pavement performance curve characteristic of Greenville County roads was generated using PCI data on all 1372-miles of roadway within the County's inventory. (Reference Figure 2). A unique, Greenville County-based, deterioration rate curve was selected which best fit the limited PCI data through the first 4-2/3 years. This selected deterioration rate curve is then used to project the expected pavement life (to PCI = 50) for each pavement section. (Reference Figures 3-6). Subsequent evaluations of the roadway may demonstrate variances from the form of the general deterioration curves.

TRAFFIC VOLUMES

Prior to the installation of the pavements, Stockton Road served five (5) homes. The estimated Average Daily Traffic (ADT) was less than fifty (50) vehicles per day. Lacking traffic count data, the general allowance of 10 vehicles per day, per household, was initially used. The current actual traffic counts indicate usage at station 0+00 to be 300 vehicles per day with 5 % truck traffic. At the terminus of the project (Station 81+00), the traffic count is 300 vehicles per day with 5 % truck traffic. The road currently serves a total of seventeen (17) residences. It is interesting to note the drastic impact the paving of this

roadway appears to have had on the development of the area. This rural area is well removed from any area showing development trends.

FULL-DEPTH ASPHALT

Figure 3 shows the projected lives of the various pavement sections utilizing 2 1/2" of full depth asphalt. In terms of pavement life for the 2-1/2 thickness of asphaltic binder, the performance of the 4 ounce non-woven fabric increased pavement life 1.1 years. The slit film material itself, as well as the problems associated with placing asphalt on its relatively slick surface, clearly proved to be a detriment to a full depth asphalt pavement.

ASPHALT OVER BASE COURSE

The predicted PCI values for the 1.5 inch asphaltic wearing course over the 3-inch stone base contained far less deviation than the other types of pavements and are shown in Figure 4. The 4 ounce woven and non-woven fabrics performed equally, increasing projected life by less than 1 year.

TRIPLE TREATMENT OVER BASE COURSE

Figure 5 shows the projected lives of pavement sections using triple treatment over base course. Where triple-treatment was provided over the 3-inch stone base, pavement life was only estimated at 6.0 years. This is the lowest anticipated life of any of the designs used. The four ounce slit-film fabric appeared to out-perform the nonwoven material. It should be noted that the triple treatment produces a relatively rough, coarse surface texture which is somewhat difficult to evaluate.

COMPARING PAVEMENT TYPES

Despite the effort to provide a pavement that would have a projected life of 15 years, all sections performed below expectations by showing a rather rapid decrease in quality during the first two (2) years. Figure 6 was developed to show the relative performance of the three (3) basic pavement designs under the control conditions. The best overall performance was achieved by using a 3" stone base, with a 1-1/2" thick asphalt surfacing overlay. The full depth asphalt binder material, which was expected to have equal performance characteristics, showed approximately seven (7) years of projected pavement life. The porosity of the binder material may have had an impact on the rapid initial deterioration. Had the asphalt binder material performed better as an initial paving surface, it would have been a more desirable structural base for future overlays.

Although triple-treatment provides an all weather surface and protects the subgrade from moisture related failures, overall it performs very poorly as a structural material. Being the most flexible of the three (3) designs, the rutting currently observed will likely continue and develop significant problems.

CONSTRUCTION COSTS

Table 9 details the costs of constructing the pavements utilized in this test. Comparable direct and contracted prices for similar installations are currently being experienced. All hot-laid asphalt materials, as well as the fabric and base under these materials, were placed in conjunction with the County's annual resurfacing program by a private contractor. The costs associated with

TABLE 7. PAVING CONDITION & PCI RANK

Pavement Condition	PCI RANK
Excellent	100
Very Good	85
Good	70
Fair	55
Poor	40
Very Poor	25
Failed	10
	0

ASPHALT PAVEMENTS DISTRESS TYPES

1. Alligator Cracking
2. Bleeding
3. Block Cracking
*4. Bumps and Sags
5. Corrugation
6. Depression
*7. Edge Cracking
*8. Jt. Reflection Cracking
*9. Lane/Shoulder Drop Off
*10. Long & Trans Cracking
11. Patching & Util. Cut Patching
12. Polished Aggregate
*13. Potholes
14. Railroad Crossing
15. Rutting
16. Shoving
17. Slippage Cracking
18. Swell
19. Weathering & Raveling

* All Distresses are Measured in Square Feet Except Distresses 4, 7, 8, 9, and 10 which are Measured in Linear Feet; Distress 13 is Measured in Number of Potholes.

TABLE 8. PAVEMENT PERFORMANCE

BASED ON PAVEMENT MANAGEMENT SYSTEM--APWA--MICROPAVER

PAVEMENT CONDITION INDEX (P.C.I.) AND PROJECTED PAVEMENT LIFE

	2 1/2" Full Depth Asphalt				1 1/2" Asphalt over 3" Stone Base				Triple Treatment Over 3" Stone Base				
	4 oz/sy NW	4 oz/sy SF	Control	6 oz/sy NW	Control	4 oz/sy NW	4 oz/sy SF	Control	6 oz/sy NW	6 oz/sy NW	Control	4 oz/sy SF	4 oz/sy NW	Control
Date of Inspection	0+00 to 5+00	5+00 to 10+00	10+00 to 20+00	20+00 to 25+00	25+00 to 30+00	30+00 to 35+25	35+25 to 40+25	40+25 to 45+50	45+50 to 50+00	50+00 to 55+00	55+00 to 61+00	61+00 to 66+00	66+00 to 71+00	71+00 to 81+00
PCI July 1987	100	100	100	100	100	100	100	100	100	100	100	100	100	100
PCI March 1992	76	17	65	N/A	76	78	81	77	N/A	N/A	58	61	53	57
Projected Pavement Life (Yr)	8.2	2.5	7.1	N/A	8.2	8.6	9.0	8.2	N/A	N/A	6.0	6.5	5.2	6.0
Distress Types	Alligator Edge Cracking	Block Cracking, Edge Cracking	Block Cracking, L & T* Cracking, Edge Cracking	Alligator Edge, L & T Cracking	Block Edge & L & T Cracking	Edge Cracking, Alligator and L&T Cracking	Block Cracking, Edge Cracking, L & T Cracking	Block Cracking, Edge Cracking, L & T Cracking	Edge Cracking, L & T Cracking	Edge Cracking, Rutting, Raveling	Bumps, Edge Cracking, Rutting, Raveling	Bumps, Edge Cracking	Rutting, Raveling	Bumps, Rutting, Raveling

* L & T indicates longitudinal and transverse cracking.

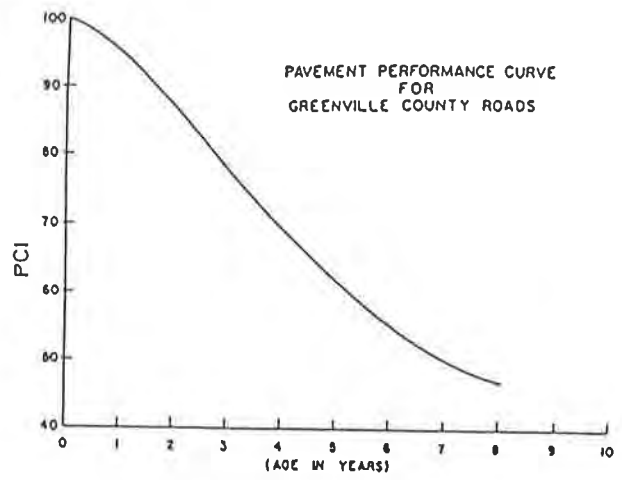

FIGURE 2

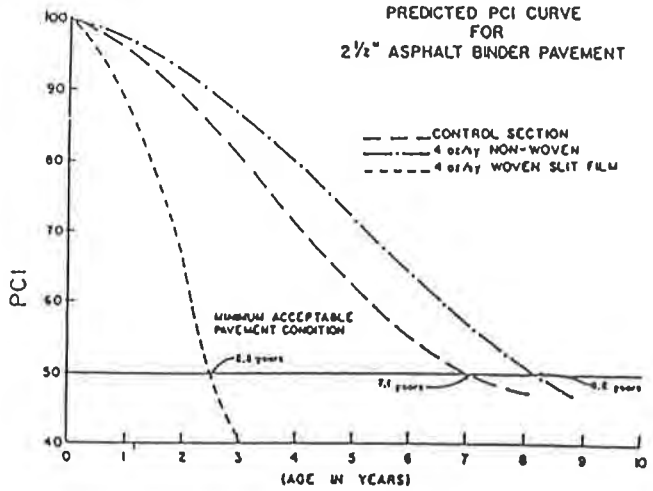

FIGURE 3

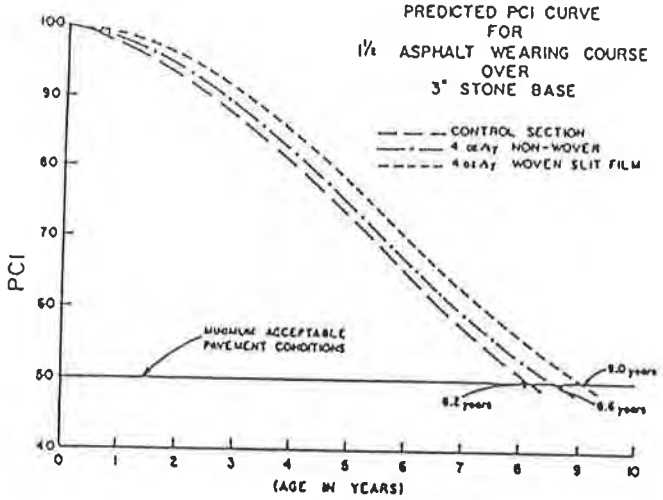

FIGURE 4

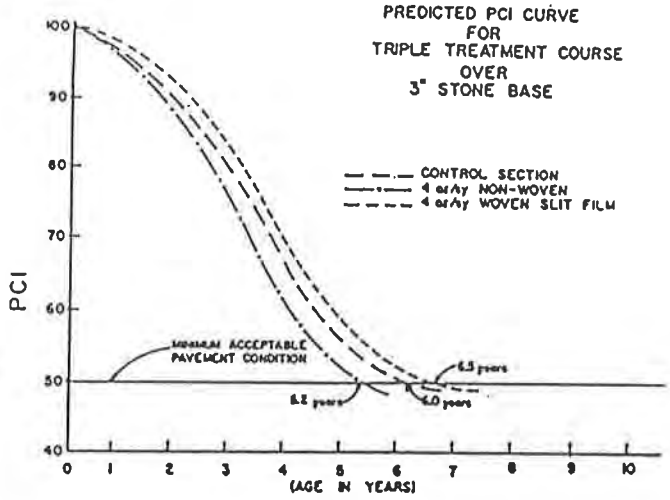

FIGURE 5

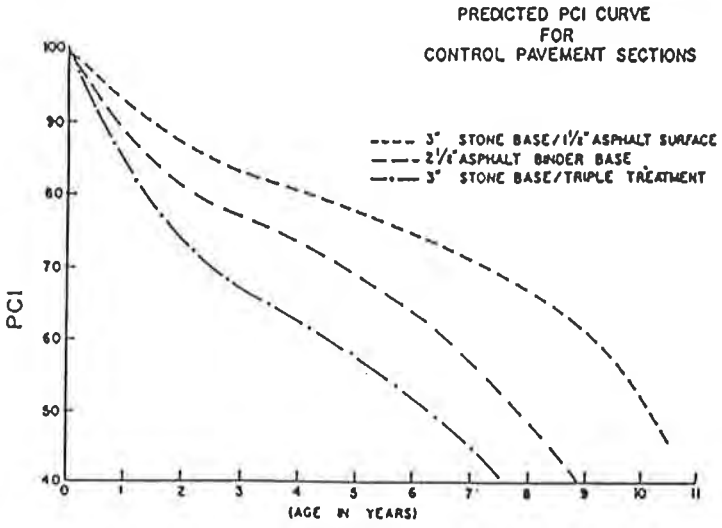

FIGURE 6

TABLE 9. STOCKTON ROAD, GREENVILLE COUNTY, SC, ROAD SURFACING COST DATDATA

I. 2-1/2 FULL DEPTH BINDER (by contractor)

	FABRIC	FABRIC MATERIAL	ASPHALT(1.3" actual)	SQUARE YARD
	$	$	$	$
w/ 4 oz/sy NW	.06	.40	3.50	3.96
w/ 6 oz/sy NW	.06	.55	3.50	4.11
w/ 4 oz/sy WSF	.06	.40	3.50	3.96
None	-	-	3.50	3.50

II. 1-1/2 ASPHALT SURFACE OVER 3" BASE (by contractor)

	FABRIC	FABRIC MATERIAL	BASE	ASPHALT(1.3" actual)	SQUARE YARD
	$	$	$	$	$
w/ 4 oz/sy NW	.06	.40	2.29	1.78	4.53
w/ 6 oz/sy NW	.06	.55	2.29	1.78	4.68
w/ 4 oz/sy WSF	.06	.40	2.29	1.78	4.53
None	-	-	2.29	1.78	4.07

III. TRIPLE TREATMENT OVER 3" BASE

	FABRIC		BASE			TRIPLE TREATMENT			TOTAL
	LABOR	MATERIAL	LABOR	MATERIAL	EQUIPMENT	MATERIAL	LABOR	EQUIPMENT	SQUARE YARD
	$	$	$	$	$	$	$	$	
w/ 4 oz/sy NW	.06	.40	.23	1.94	.49	------1.80------		.85	5.77
w/ 6 oz/sy NW	.06	.55	.23	1.94	.49	------1.80------		.85	5.92
w/ 4 oz/sy WSF	.06	.40	.23	1.94	.49	------1.80------		.85	5.77
None	-	-	.23	1.94	.49	------1.80------		.85	5.31

TABLE 10. STOCKTON ROAD, GREENVILLE COUNTY, SOUTH CAROLINA
ROAD SURFACING COSTS DATA WITH PROJECTED PAVEMENT LIFE-CYCLE COSTS

I. 2-1/2 FULL DEPTH BINDER (by contractor)

	INITIAL COSTS $/SY	PAVING LIFE (YEARS)	EQUIVALENT UNIFORM ANNUAL COST $/SY
4 oz/sy Non-woven	3.96	8.2	0.4618
Woven/Slit Film	3.96	2.5	0.9706
Control/No Fabric	3.50	7.1	0.4615

II. 1-1/2 ASPHALT SURFACE OVER 3" BASE (by contractor)

4 oz/sy Non-woven	4.53	8.6	0.4944
Woven/Slit Film	4.53	9.0	0.4854
Control/No Fabric	4.07	8.2	0.4701

III. TRIPLE TREATMENT OVER 3" BASE

4 oz/sy Non-woven	5.77	5.2	0.7252
Woven/Slit Film	5.77	6.5	0.6553
Control/No Fabric	5.31	6.0	0.6439

construction of the triple treatment section reflect county labor, equipment and materials.

EQUIVALENT UNIFORM ANNUAL COSTS

To account for varying pavement lives when comparing pavement alternatives an annual cost comparison technique was chosen. The Equivalent Uniform Annual Costs (EUAC) were calculated for each pavement test section using pavement lives projected by the selected deterioration curves. The assumptions include an interest rate of 7.5% and a restoration cost of $1.78/sy to provide an asphaltic overlay once the PCI had deteriorated to 50. EUAC equations are described in Engineering Economic Analysis by Donald G. Newman, Engineering Press, 1977 Edition, Page 104.

Table 10 summarizes the Equivalent Uniform Annual Costs for the various pavements installed for this project. The 2-1/2-inch full depth binder control pavement demonstrated equivalent annual costs equal to the pavement section where 4 ounce non-woven fabric was used. The 4 ounce woven slit film materials were not suitable for use under full depth pavement.

For the pavement section constructed of 1-1/2-inch asphaltic wearing surface over a 3-inch stone base, the annual costs for installations utilizing fabric run only slightly higher. This seems to indicate that, even in the relatively short-term, the presence of fabric at the interface may pay for itself by even modestly enhancing overall pavement performance. After long term performance can be monitored, it will be seen if the presence of a fabric substantially increases pavement life by providing protection of the subgrade through its separation characteristics.

The performance of triple-treatment over the 3-inch stone base demonstrated a near equal equivalent annual cost benefit when utilizing 4 oz/sy woven fabrics and no fabric at all. The section with the 4 oz/sy non-woven produced a somewhat higher EUAC.

CONCLUSION

Geotextiles provide subgrade/base interface stability which will generally increase the life of a pavement section. Little is known about low volume pavement design utilizing geotextiles. Principles of reduction in aggregate base depths to offset costs of paving fabrics are not applicable to thin designs.

In most cases, life cycle costs for pavement with fabric were equal to or only slightly greater than the costs associated with the control sections which did not utilize fabrics. Local conditions still warrant the evaluation of life cycle costs associated with any project since the construction costs will vary with the locality. Yet, in general it appears that the additional costs associated with including a fabric do not significantly increase the life-cycle costs of the road.

Low volume pavement designs are very susceptible to accelerated deterioration. Where average daily traffic is less than 500 vehicles per day, the pavement life is significantly impacted by any increases in truck traffic. The presence of fabrics may reduce the susceptibility to rapid deterioration.

Fabrics may or may not enhance initial pavement performance, but as subsequent overlays are placed, fabrics should continue to protect base courses from fouling and therefore may enhance future pavement performance.

In conclusion, the short-term results of utilizing fabric in low volume pavement designs is promising but inconclusive. It is expected that future evaluations will provide insight into the relationships between fabric weights, construction survivability and pavement performance. Many questions remain regarding long-term performance of these test sections. Most notably, will fabrics prevent accelerated deterioration as cracking patterns allow water to pass through the pavement and base material to the detriment of the subgrade.

REFERENCES

Sprague, C.J. and George A. Cicoff, "A Study of Permanent Road Stabilization: Low Cost Pavement Structures and Lightweight Geotextiles, "Proceedings of Geosynthetics `89 Conference, IFAI, 1989, pp. 316-323.

Sprague, C. J. and George A. Cicoff, "Permanent Road Stabilization: Construction Survivability of Lightweight Geotextiles," Geotechnical Fabrics Report, IFAI, July/August, 1989.

Cicoff, G. A., and C. J. Sprague, "Permanent Road Stabilization: Low-Cost Pavement Structures and Lightweight Geotextiles," Proceedings of the Fifth International Conference on Low-Volume Roads, TRR No. 291, Transportation Research Board, 1991, pp 294-310.

A Field Evaluation of Geosynthetic-Reinforced Haul Roads Over Soft Foundation Soils

D.N. Austin
Tenax Corp., USA

D.M. Coleman
Ware Lind Furlow Engineers, USA

ABSTRACT

Although geosynthetics have been used for several decades as effective tools to reinforce soft foundation soils, very few well documented procedures exist to assist the engineer in achieving the most economical designs for temporary access or haul roads. While much laboratory research has been conducted on the use of geogrids and geotextiles to improve roadway performance, only a few full-scale field studies have been completed on the performance improvements geosynthetics offer in temporary roads, haul roads and other relatively low-volume roads constructed over soft soils.

This paper presents the results of a full-scale field study conducted to evaluate the effectiveness of various geosynthetics as the primary reinforcement in aggregate layers placed over very soft subgrades. A test road containing several test sections was constructed on soft, expansive clays. Each test section contained a different geosynthetic, with three unreinforced sections to function as controls. The granular subbase of the test road was constructed of crushed limestone and was between 150 mm and 260 mm thick. A nominal aggregate depth of 200 mm was selected with the anticipation of severe wheel rutting. By promoting "failure" of the test section, a relationship between field observations, loading patterns and current design information/available technical literature could be made. Results from the field evaluation allowed the authors to develop data on the performance of geogrid-reinforced aggregate layers over soft subgrades and to compare the results to accepted design theories.

INTRODUCTION

Haul roads, temporary access roads and other low-volume roads generally demand an economical and efficient design. These aggregate surfaced temporary roads are generally characterized by relatively infrequent, or short-duration traffic and are often constructed over poor (very soft) soil conditions.

The concept of geosynthetic reinforcement of soft soils has existed for several years. In theory, the addition of a stiff horizontal tensile element to the top of a weak foundation soil resists lateral tensile strains in the subbase layer and prevents lateral spreading of the aggregate from beneath the load. Furthermore, geosynthetic reinforcement prevents the aggregate base material from punching into the soft foundation soils. Because base "punching" or localized shear failure is prevented, this results in an improvement of the load distribution capability of the aggregate base layer. Therefore, the stresses induced on a subgrade soil underlying a geosynthetic-reinforced granular layer will be less than the stresses acting on a subgrade soil underlying an unreinforced layer.

Although laboratory testing of geosynthetic-reinforced granular layers over soft soils has demonstrated the effectiveness of the concept, very few full-scale field tests have been conducted to verify existing concepts and laboratory data. Since beneficial effects of geosynthetic reinforcement are greatest when the construction is over soft, cohesive soils having a California Bearing Ratio (CBR) below 2 percent, this study attempts to evaluate the field performance of several different types of geosynthetics placed below a temporary haul road constructed on very soft (a CBR of about 1 percent) clay soils.

GEOTECHNICAL INVESTIGATION

The test road was located near Greenville, Mississippi in a large culvert storage facility owned and operated by Caldwell Culverts, Inc. Originally, the area where the test road was constructed consisted of grass and underbrush. The soil had not been disturbed due to the soft nature of the surface. Approximately 300 mm of humus layer was removed from a 10 meter by 100 meter strip located at the test site. This humus layer was removed using a small dozer with low ground contact pressures to cause a minimal amount of disturbance to the underlying soils. This excavation exposed a stiff gray clay that was consistent over the entire excavated area.

A preliminary soils investigation was conducted in August 1991. This preliminary investigation consisted of five soil borings in the vicinity of the proposed test road. The results of this soils investigation revealed a subgrade with the properties shown in Table 1.

Table 1. Results of Preliminary Soils Investigation (August 16, 1991)

Property of Subgrade	Range of Values
Bearing Ratio (CBR)	3% to 6%
Natural Water Content	27% to 40%
Liquid Limit	73% to 85%
Plastic Limit	23% to 33%
Plasticity Index	48 to 55
Undrained Shear Strength	48 kN/m^2 to 268 kN/m^2
In-Place Dry Density	1220 kg/m^3 to 1270 kg/m^3
Classification (USCS)	CH

These initial soil strengths were too high for the desired field evaluation conditions. The excavated test site was flooded with water and allowed to remain exposed to the environment for nearly eight months in order to soften the soil. In the Spring of 1992, the flooded test area was drained by excavating a small ditch around the test pad and a final soils investigation was performed.

This final soils investigation included field bearing ratio tests, undisturbed sampling of the near-surface soils, and dynamic cone penetrometer (DCP) testing in selected locations. Field bearing ratio tests were used to determine the in-situ strength of the subgrade while the undisturbed Shelby tube samples were used to determine the undrained shear strength, natural moisture content and dry unit weight. A summary of the preconstruction soils investigation results is presented in Table 2.

Table 2. Results of Preconstruction Soils Investigation (April 9, 1992)

Test Number*	Station (meters)	Measured Field CBR (percent)	Moisture Content (percent)	Dry Density (kg/m^3)	Undrained Shear Strength (kN/m^2)	CBR from DCP+ (percent)
T-1	0	-	41.9	1270	31.8	0.9
CBR-4	6.1	0.6	-	-	-	0.9
T-2	12.2	-	43.2	1220	32.1**	0.7
CBR-5	18.3	0.4	-	-	-	0.7
T-3	24.4	-	40.7	1250	24.7	0.8
CBR-6	30.5	0.7	-	-	-	0.6
T-4	36.6	-	39.2	1275	33.5**	0.7
CBR-7	42.7	1.1	-	-	-	0.8
T-5	48.8	-	40.1	1240	16.1	0.7
CBR-8	54.9	0.6	-	-	-	0.9

Notes:
* "T" denotes 75 mm Shelby tube undisturbed sample; "CBR" denotes field bearing ratio test.
** Results from unconsolidated-undrained triaxial test. Other results from unconfined compression tests.
+ Estimated from DCP Index (DCPI) using WES correlation for top 300 mm of subgrade.

The dynamic cone penetrometer (DCP) device used in this study was a dual-mass DCP consisting of a 16-mm diameter steel rod with steel cone attached to one end that is driven into the soil by means of a sliding dual-mass hammer. The penetration cone had an angle of 60 degrees and a base diameter of 20 mm. The diameter of the cone base was 4 mm larger than that of the rod to insure that the resistance to penetration is exerted on the cone and not the rod. The DCP is driven into the soil by dropping either an 8 kg or 4.6 kg sliding hammer from a height of 575 mm. For the low-strength soils encountered in this study, the 8-kg hammer was converted to 4.6 kg by removing a hexagonal set screw and removing the outer steel sleeve. Using the lighter weight hammer, the cone penetration caused by one blow of the 4.6-kg hammer is approximately one-half of that caused by one blow of the 8-kg hammer [1].

The depth of cone penetration was measured at selected drop intervals and the soil shear strength reported in terms of the DCP Index (DCPI). The DCPI is based on the average penetration depth resulting from one blow of the 8-kg hammer. For the 4.6-kg hammer used in this study, the average penetration for each hammer blow must be multiplied by two in order to obtain the corrected DCPI value. Individual DCPI values were determined for each test depth which were used to develop a soil strength versus depth profile for the test location. (It should be noted that in high plasticity clay soils such as those encountered in this study, adhesion of the clay to the rod begins to effect the penetration resistance obtained at depths greater than about 300 mm to 400 mm. For this reason, the DCP Index values obtained in only the top 300 mm were used for correlation with CBR.)

Correlation of the DCPI with CBR is necessary since CBR is the soil strength value generally used for designing and evaluating aggregate-surfaced roads. A data base of field CBR verses DCP Index values has been collected from many sites and for many different soil types by the US Army Corps of Engineers Waterways Experiment Station (WES). Using this data, WES has developed a correlation between CBR and DCPI [1]. This relationship is shown in Equation 1 below:

$$\log CBR = 2.46 - 1.12 (\log DCPI) \quad (1)$$

Where:
CBR = the measured field CBR value; and
DCPI = dynamic cone penetrometer index value.

GEOSYNTHETIC MATERIALS

Six different geosynthetic materials were chosen for the evaluation. These materials included polypropylene geogrids, woven geotextiles and nonwoven geotextiles. These samples were sent to a laboratory and tested in accordance with ASTM D4595 to obtain their wide width tensile strengths. The geosynthetic materials utilized and their respective tensile properties are summarized below in Table 3.

Table 3. Description of Geosynthetic Materials

Station (meters)	Geosynthetic (Product Type)	Wide Width Tensile Strength* (kN/m)		Description (Process)
		MD	CMD	
3.05	Geogrid 1	15.5	20.9	Extruded
9.15	Geogrid 2	17.6	32.9	Sheet-Punched
21.35	Geotextile 1	39.3	44.5	Woven
33.55	Geogrid 4	26.5	26.2	Extruded Triplanar
45.75	Geogrid 1 & Geotextile 2	15.5 50.6 N**	20.9 50.6 N**	Extruded Nonwoven
51.85	Geogrid 3	14.2	15.9	Extruded Triplanar

Notes:
* "MD" indicates machine (or roll) direction; "CMD" indicates cross-machine (or perpendicular to the roll) direction.
** Indicates Grab Tensile Strength (ASTM D4632) reported in absence of actual wide width test values.

CONSTRUCTION OF TEST ROAD

Each geosynthetic was deployed on the evaluated subgrade, carefully overlapping adjacent sections in the direction of anticipated fill placement. A well-graded crushed limestone (classified as GW according to Unified Soil Classification System) was chosen as the aggregate subbase for its strength, availability and acceptance in temporary access and haul road construction. The aggregate subbase, locally referred to as "610 Stone", had the grain size characteristics shown in Figure 1. It had a Standard Proctor maximum dry density of 2210 kg/m^3 at an optimum moisture content of 7.1 percent when tested in accordance with ASTM D698, Method D. Figure 2 presents a plan along the constructed test road showing the location of the test and control sections.

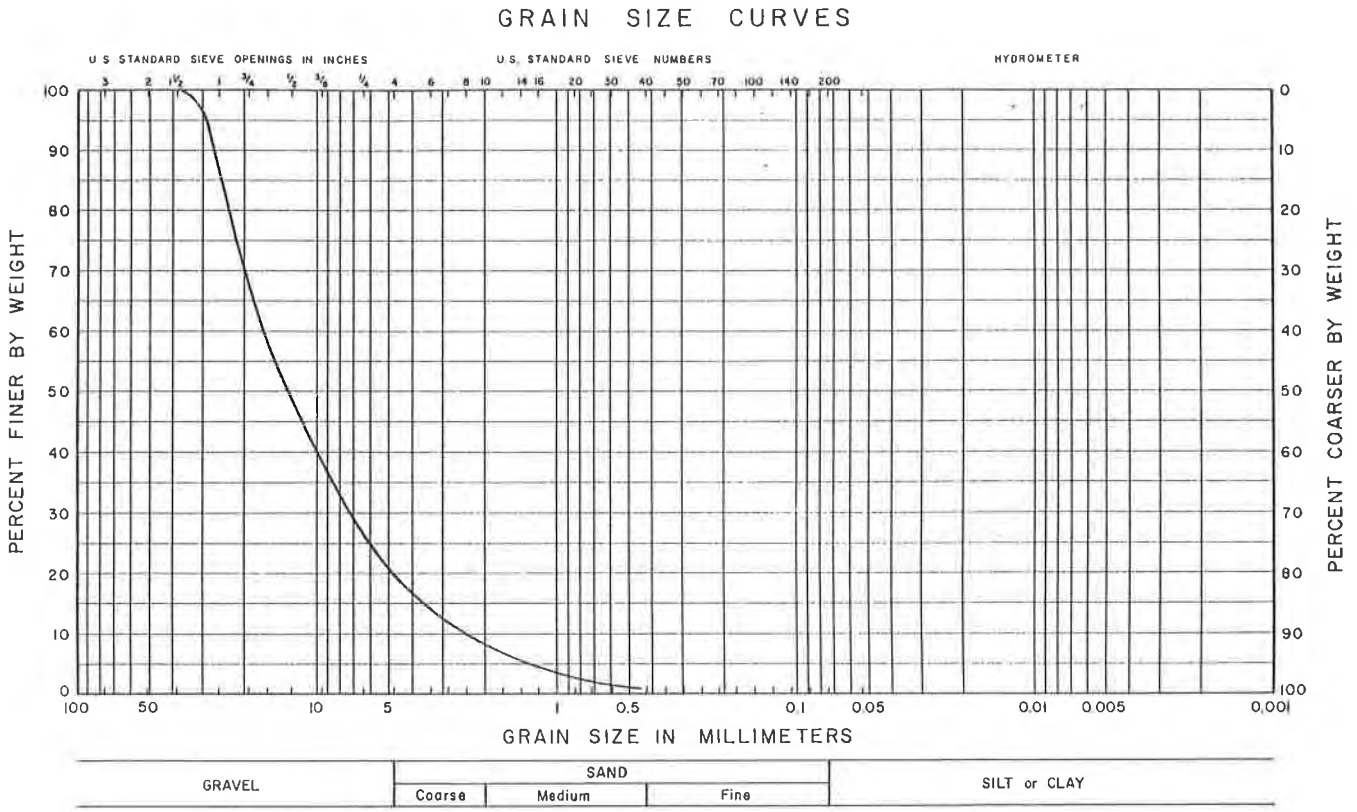

Crushed limestone "610 Stone"

Figure 1. Grain Size Distribution Curve for Aggregate Subbase

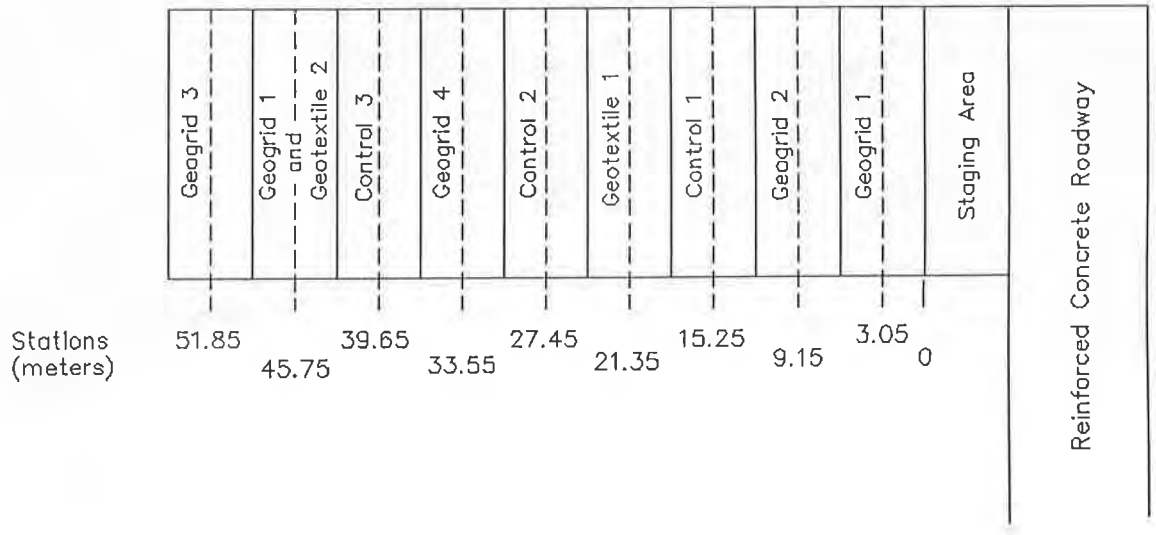

Figure 2. Plan of Test Road

Due to the soft subgrade soils underlying the test road, an attempt was made to minimize construction traffic over the test sections, thereby minimizing the disturbance to the subgrade. A staging area of the aggregate subbase was constructed between Station 0 and the concrete access road to the test site. Dump trucks hauling the aggregate subbase were backed onto the staging area and dumped near Station 0. The aggregate subbase was then spread over the test road using a Caterpillar D4 dozer to an initial depth of about 350 mm to 500 mm. No effort was made to compact the aggregate subbase with equipment other than the small dozer. After the aggregate subbase was walked-in with several passes of the dozer, the dozer was used to cut the thickness to about 200 mm and the surface was back-bladed to provide some leveling of the test section.

Each test section was approximately 6 meters wide by 6 meters long. All geosynthetics were overlapped approximately 1 meter. Since the transition areas contained two different reinforcement products, a data collection station was established at the midpoint of each test section.

After the construction of the test section was complete, additional field testing was performed using the dynamic cone penetrometer to provide an estimate of the CBR and the actual thickness of the aggregate subbase. In addition, a nuclear moisture-density gauge was used to determine the in-place dry density and natural moisture content of the aggregate subbase. This data is presented in Table 4 and is representative of the conditions that existed at the start of the traffic tests. Therefore, this information will serve as the data to be used in the final analysis. Figure 3 presents a profile of subbase and subgrade strengths as determined from this post-construction soils investigation. Photograph 1 presents an overall view of the completed test road, prior to the application of the test road.

Photograph 1. Completed Test Road

Table 4. Results of Post-Construction Soils Investigation (April 13, 1992)

Station (meters)	Subgrade CBR from DCP+ (percent)	Aggregate Subbase Thickness (mm)	CBR from DCP+ (percent)	Coefficient of Variability*** (percent)	Dry Density (kg/m^3)	Moisture Content (percent)
0	0.9	205	20	38.4	2110	2.9
3.05	0.8	265	14	34.8	2130	4.1
6.1	0.9	220	12	7.2	2020	3.9
9.15	0.9	225	15	13.3	2020	4.0
12.2	0.7	190	21	37.8	2060	3.0
15.25	0.6	225	14	68.6	1960	3.2
18.3	0.7	210	18	41.6	2000	3.7
21.35	0.5	250	16	51.4	2070	2.4
24.4	0.8	225	11	57.0	2130	3.0
27.45	1.0	210	8	45.4	2110	7.8
30.5	0.6	180	19	21.5	2100	2.6
33.55	0.6	175	20	39.3	2080	2.8
36.6	0.7	215	18	37.1	1960	3.2
39.65	0.9	200	18	50.6	2020	3.2
42.7	1.0	215	14	43.5	1990	3.8
45.75	0.9	215	13	39.3	1950	3.5
48.8	0.7	225	10	26.2	1930	2.6
51.85	1.0	260	15	41.1	2050	2.8
54.9	0.9	280	12	40.7	2070	3.2

Notes:

\+ Estimated from DCP Index (DCPI) values using WES correlation [1].

*** Coefficient of variation ([Std. Dev./Mean] X 100) of estimated CBR through depth of base course. Provides indication of variability in compaction: the lower the C.V., the less variation in the base strength (i.e. the more uniform the compaction).

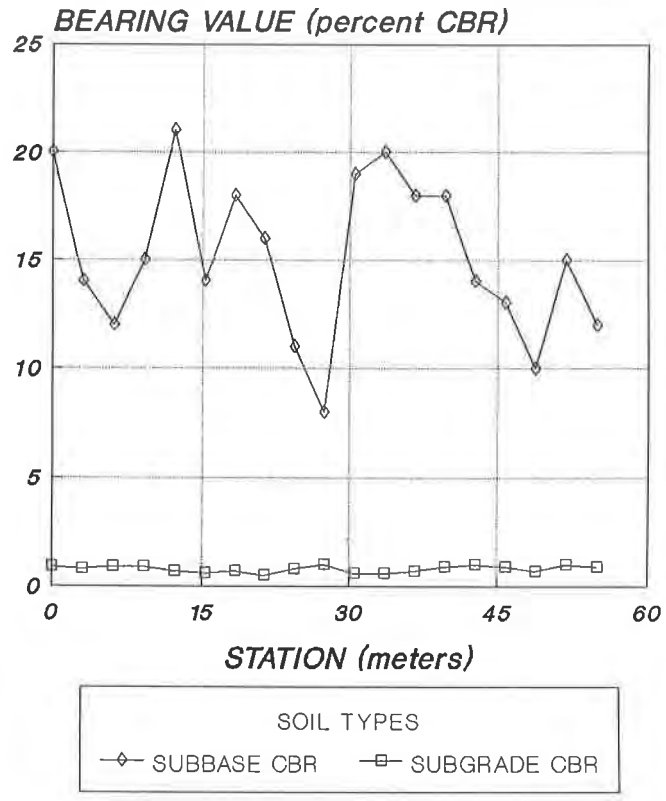

Figure 3. Profile of Soil Strengths in Test Road

FIELD TEST PROGRAM

The test vehicle used in this study was a two axle dump truck with the rear axle loaded to approximately 80 kN using corrugated flat steel. The wheel/axle configuration and other pertinent data for the truck is shown in Figure 4. The tires were inflated to 550 kPa and the axle load was checked at the beginning and end of each day at a truck scale located at the plant. Photograph 2 presents an overall view of the loaded truck.

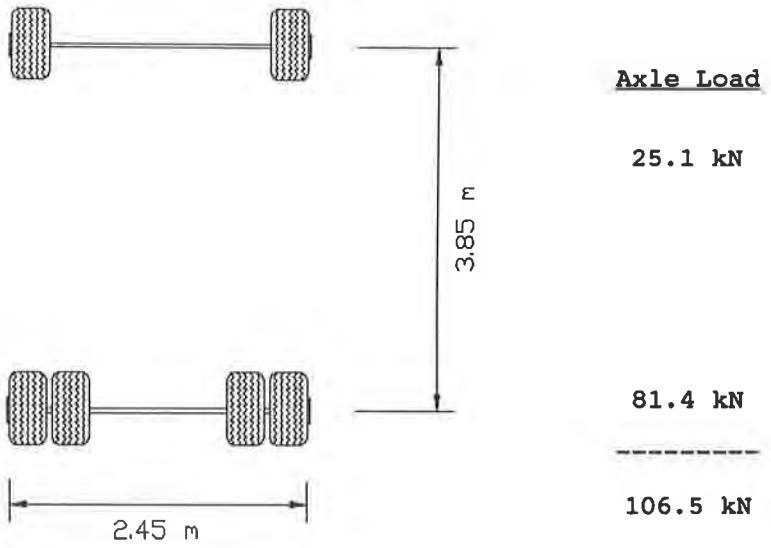

Figure 4. Test Vehicle Configuration

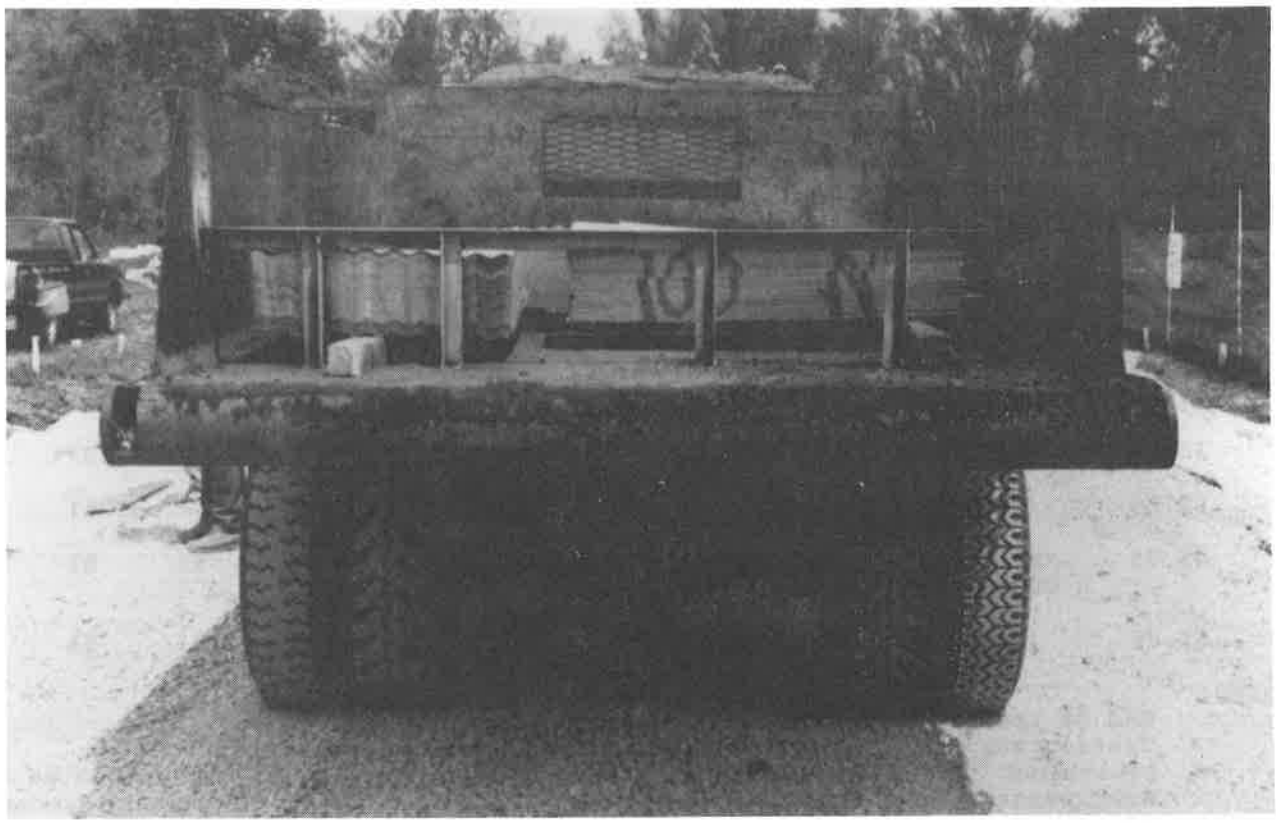

Photograph 2. Loaded Test Vehicle

An initial cross section at each data collection station was obtained at the zero pass level. At selected pass intervals, or at the failure of any test section, the cross-section at each data collection station was measured. Observations made during traffic operations and rutting characteristics were also recorded. The test road was trafficked with the test vehicle until a 75 mm rut occurred or traffic over the section was no longer possible. This rut depth was considered to be failure and the observations made during the testing were documented.

PERFORMANCE OF TEST SECTIONS

All failed sections exhibited similar characteristics of severe rutting with adjacent upheaval. Contamination of the granular subbase by the soft subgrade clay was evident in those sections not containing a geotextile separator. The degree of this contamination varied in each section. However, the rutting, upheaval and contamination observed in all test sections were consistent with shear deformation and failure of the subgrade.

Table 5 presents a summary of the test results showing the number of observed passes to failure. The number of observed passes were converted to equivalent standard axle load (ESAL) passes using a conversion of 1.13 ESAL passes per 1.0 actual passes [2].

Table 5. Summary of Test Results

Station (meters)	Geosynthetic (Product Type)	Observed Passes To Failure			ESAL Passes To Failure++		
		50 mm	75 mm	End*	50mm	75mm	End*
3.05	Geogrid 1	53	63	75	60	71	85
9.15	Geogrid 2	31	43	51	35	49	58
15.25	Control 1	16	20	20	18	23	23
21.35	Geotextile 1	52	59	60	59	67	68
27.45	Control 2	4	12	19	5	14	21
33.55	Geogrid 4	-	-	29**	-	-	33**
39.65	Control 3	2	6	10	2	7	11
45.75	Geogrid 1 & Geotextile 2	30	45	45	34	51	51
51.85	Geogrid 3	21	45	45	24	51	51

Notes:
* End of traffic in that section.
** Traffic stopped at 40 mm rut depth due to failure at transitions.
++ Equivalent Single Axle Load (80 kN Single Axle Dual Wheel) calculated as 1.13 ESAL passes per 1.0 pass of test vehicle using Corps of Engineers Procedure [2].

Results of the cross-sections obtained at selected pass levels were used to develop a plot of rut depth versus number of ESAL passes for each of the test sections. This data is presented in Figures 5 and 6. Figure 5 presents rut depth versus ESAL pass data for Geogrid 1, Geogrid 2, and Geotextile 1. Figure 6 presents rut depth versus ESAL pass data for Geogrid 3, Geogrid 4, and Geogrid 1/Geotextile 2 combination. Additionally, the average rut depth determined from the cross section data was plotted along the length of the test road to produce a profile that indicates the relative magnitude of the rut depths within each test section. This profile is presented in Figure 7.

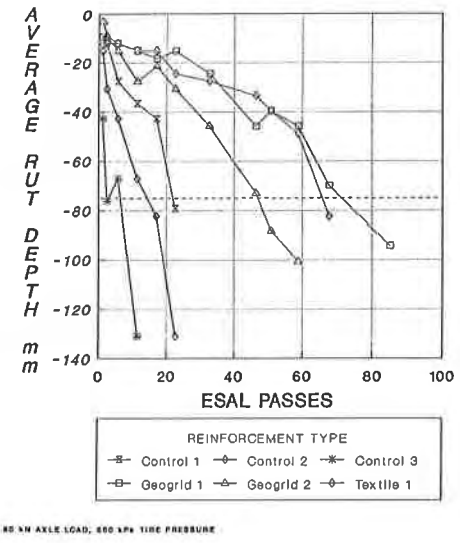

Figure 5. Average Rut Depths

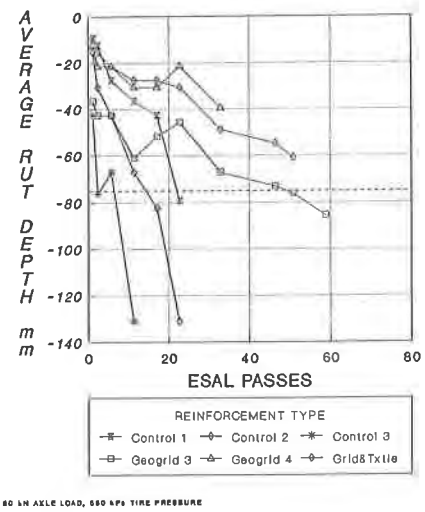

Figure 6. Average Rut Depths

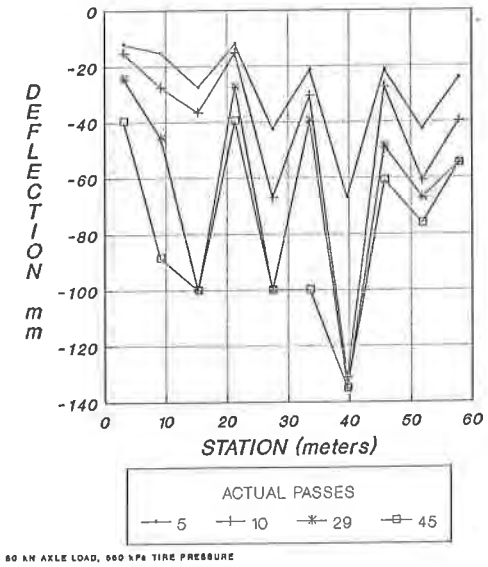

Figure 7. Deflection Profile

Upon completion of the test traffic, excavations were made in the traffic lanes and immediately adjacent the traffic lanes for a post-traffic soils investigation. Excavation of the geogrid sections revealed that individual stones from the aggregate subbase had penetrated and interlocked with the apertures of the geogrid. The aggregate subbase layer was contaminated with the cohesive subgrade soil for thicknesses that ranged from about 35 mm to about 190 mm above the original subgrade elevation. Excavation of the geotextile sections indicated no contamination of the aggregate subbase. The geotextiles did perform their function as separators and there was no evidence of actual tensile failure. However, it was evident that the geotextiles were in tension.

Table 6 presents the results of this post-traffic soils investigation that evaluated the in-place subgrade properties and estimated the amount of aggregate subbase contamination and intrusion into the subgrade.

Table 6. Results of Post-Traffic Soils Investigation*

Station (meters)	Subgrade CBR from DCP+ (percent)	Reference Elevation, feet				Final Aggregate Thickness** (mm)	Contaminated Aggregate Thickness (mm)	Contamination (percent)
		Top of Aggregate	Begin Contamination	Geosynthetic	Top of Clean Subgrade			
3.05	0.8	99.40	98.65	98.6	98.54	260	35	12.8
9.15	0.9	99.45	98.90	98.8	98.75	220	45	21.2
15.25	0.6	99.38	98.62	-	98.40	300	65	21.8[1]
21.35	0.5	99.42	-	98.61	98.60	250	0	0[2]
27.45	1.0	99.34	-	-	98.08	380	190	49.0[1]
33.55	0.6	99.40	98.80	98.52	98.45	290	105	36.8
39.65	0.9	99.23	98.86	-	98.35	270	155	57.7[1]
45.75	0.9	99.34	-	98.64	98.62	220	0	0[3]
51.85	1.0	99.44	98.85	98.78	98.66	240	60	24.2

Notes:

* Data taken from excavation approximately 0.5 m out of traffic lane.

** Final thickness may have been affected by traffic.

\+ Estimated from DCP Index (DCPI) values using WES correlation [2].

1 Control section.

2 Woven geotextile reinforcement.

3 Geogrid reinforcement over nonwoven geotextile separator.

ANALYSIS OF RESULTS

After reducing the data gathered from the field evaluation, several possible relationships were analyzed to determine the relevance and appropriateness of the results. Figures 5, 6, and 7 clearly show the improvements in the performance of the test road when geosynthetics are used to reinforce aggregate subbase placed over soft subgrade soils. However, by themselves, these figures can not quantify the amount of improved performance attributable to the geosynthetics. Improved performance was quantified by normalizing the ESAL passes to failure for a given test section by the ESAL passes to failure of the corresponding control section.

The improved performance of the reinforced sections of the test road was calculated at rut depths of 50 mm and 75 mm. This improved performance is defined as the number of actual passes over the reinforced section to cause the specified rut depth divided by the number of passes over the corresponding control section required to develop the same rut depth. For the purpose of this paper, this term has been defined as the "performance factor". Table 7 presents the performance factors for each reinforced section along the test road at rut depths of 50 mm and 75 mm.

Table 7. Performance Factors from Test Road

Geosynthetic (Product Type)	Control Section	Performance Factor* 50 mm Rut Depth	Performance Factor* 75 mm Rut Depth
Geogrid 1	Control 1	3.3	3.2
Geogrid 2	Control 1	1.9	2.2
Geotextile 1	Control 1	3.2	3.0
Geogrid 4	Control 3	1.3**	-
Geogrid 1 & Geotextile 2	Control 2	4.6	4.4+
Geogrid 3	Control 1	1.4	2.2

Notes:

* Performance Factor = $\frac{\text{Passes over reinforced section}}{\text{Passes over control section}}$

** Calculated at 40 mm rut depth

\+ Calculated at 60 mm rut depth

The data in Table 7 clearly demonstrates that sections containing geosynthetic reinforcement resulted in those sections carrying between 1.9 times and 4.6 times the number of test passes as the unreinforced sections for a 50 mm rut depth. Furthermore, these sections were able to withstand between 2.2 times and 4.4 times the number of passes for a 75 mm rut depth. A similar trend of the improved performance of the geosynthetic-reinforced sections over the unreinforced (control) sections is also seen in the deflection profile shown in Figure 7.

These performance factors were also used to establish possible relationships with the initial field evaluation parameters, the known soil properties, and the physical properties of the geosynthetic reinforcement used in the test road. The tensile characteristics of the various geosynthetics used in this study were determined from laboratory tests and are presented in Table 3. The wide width tensile strength was plotted against the performance factors and the results are shown in Figure 8. As seen from this figure, while there appears to be a trend toward increased performance with increased geosynthetic strength, the data is insufficient to support any such conclusion. This indicates that this measure of performance is somewhat independent of the geosynthetic tensile properties and the specific manufacturing process.

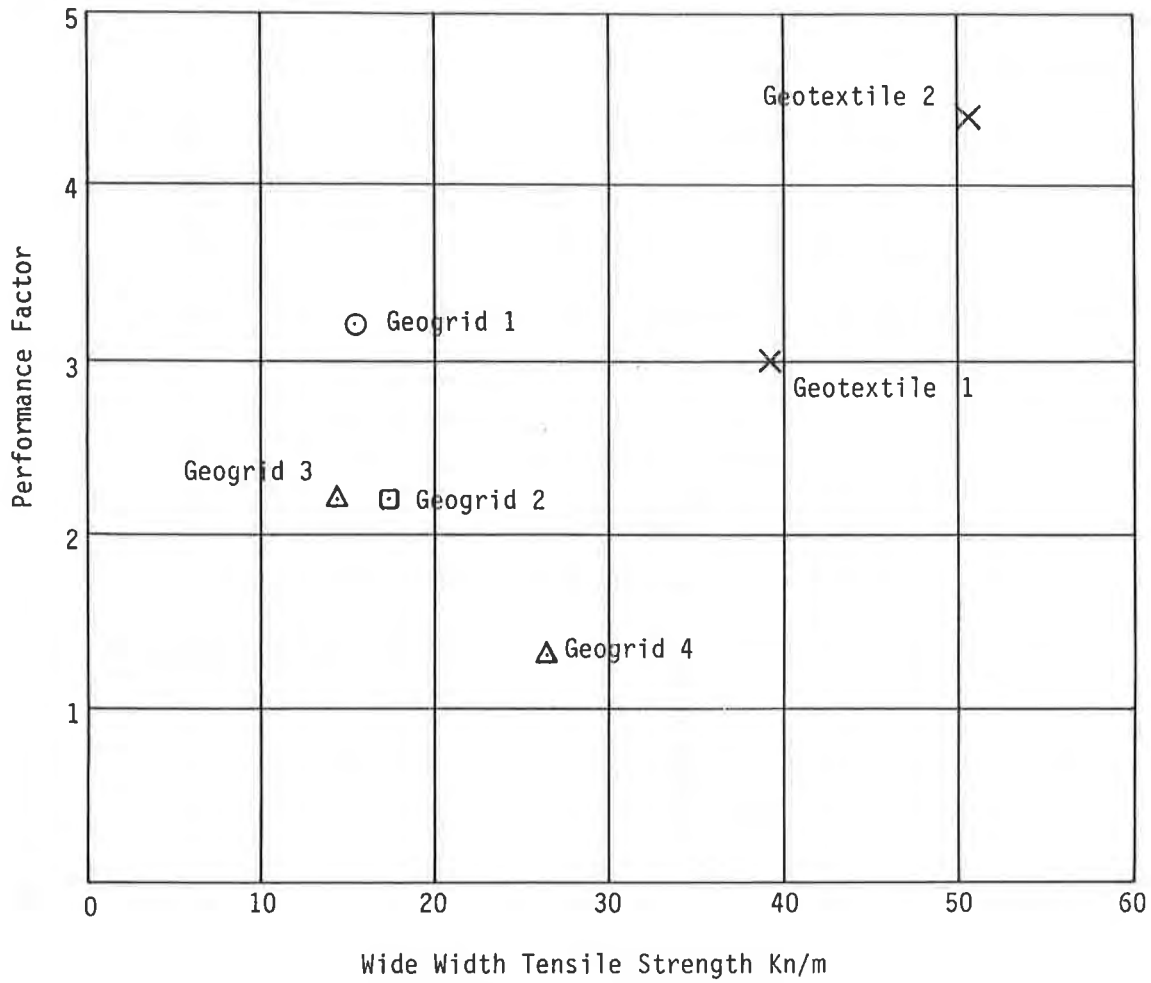

Figure 8. Possible Correlation with Wide Width Tensile Strength

HAUL ROAD DESIGN

The results of this field evaluation of a geosynthetic-reinforced test road built over soft soils were compared to analytical work and theoretical design procedures proposed by Giroud, Ah-Line and Bonaparte [3]. The purpose was to determine the consistency of these results with theoretical design procedures for unreinforced and geogrid-reinforced, aggregate-surfaced roads built over soft soils. The results of this comparison are presented in Figure 9. It appears that the results of this field study correlate fairly well with this previously published theoretical design procedure.

The theoretical aggregate subbase thickness requirements for 80 kN ESAL passes operating on unreinforced aggregate subbase was calculated using the Giroud, et al procedure [3] and plotted as dashed lines in Figure 9. This is presented specifically for a subgrade with a CBR of 0.6 and 1 percent, respectively. The solid line is representative of the theoretical thickness requirements for an unreinforced subbase over a subgrade having an average cohesion value of 27.6 kN/m^2, which was actually the average cohesion of the subgrade at the time of this field test.

The results of the three control, or unreinforced, sections were plotted in Figure 9. The number of passes required to reach a 75 mm rut depth for the initial subbase thicknesses are shown as points on the graph. These data points demonstrate reasonable agreement with the theoretical aggregate subbase thicknesses for an unreinforced subbase that is shown as dashed lines. Therefore, our results indicate that this theoretical procedure can be used with reasonable results to calculate the required thickness of an unreinforced aggregate subbase over soft subgrade soils [3].

The theoretical thickness for a geosynthetic-reinforced aggregate subbase over soft subgrades with a CBR of 0.6 and 1 percent, respectively, was also plotted in Figure 9. These plots were made utilizing reduction factors given for a geogrid similar to those being tested in this study [3]. The theoretical thickness requirements for a geogrid-reinforced aggregate subbase for various pass levels was calculated over a subgrade having an average cohesion value of 27.6 kN/m^2, which was in fact the average cohesion of the subgrade at the time of this field test. This is shown in Figure 9 as a solid line.

The results of the six geosynthetic-reinforced sections were also plotted in Figure 9 as the number of passes required to cause 75 mm of rut depth as a function of the actual initial subbase thickness in the test section. In this case, there is not a definitive agreement between the actual and the theoretical thickness. The thickness of geosynthetic-reinforced aggregate subbase calculated using the theoretical procedures is less than the actual thickness installed in this study to reach the same number of passes prior to failure of the test section.

It is our opinion that this inconsistency is due to the differences in subbase strength between the theoretical assumptions and the actual CBR achieved during construction. The theoretical design equations developed by Giroud, Ah-Line and Bonaparte are based on the assumption that the aggregate subbase will have a CBR of 80 or greater [3]. In this study, the aggregate subbase was placed over the soft subgrade in relatively loose lifts with only light compaction applied by a small dozer while walking-in the aggregate subbase. Based on data obtained from the dynamic cone penetrometer, the subbase strength in the test sections ranged from a CBR of 8 to 20 percent. These CBR values are significantly less than the aggregate subbase strength assumed in the development of the design procedure. The lower compacted subbase strength achieved in these field test sections would require an increased aggregate thickness in order to provide the number of passes predicted by the theoretical procedure [3].

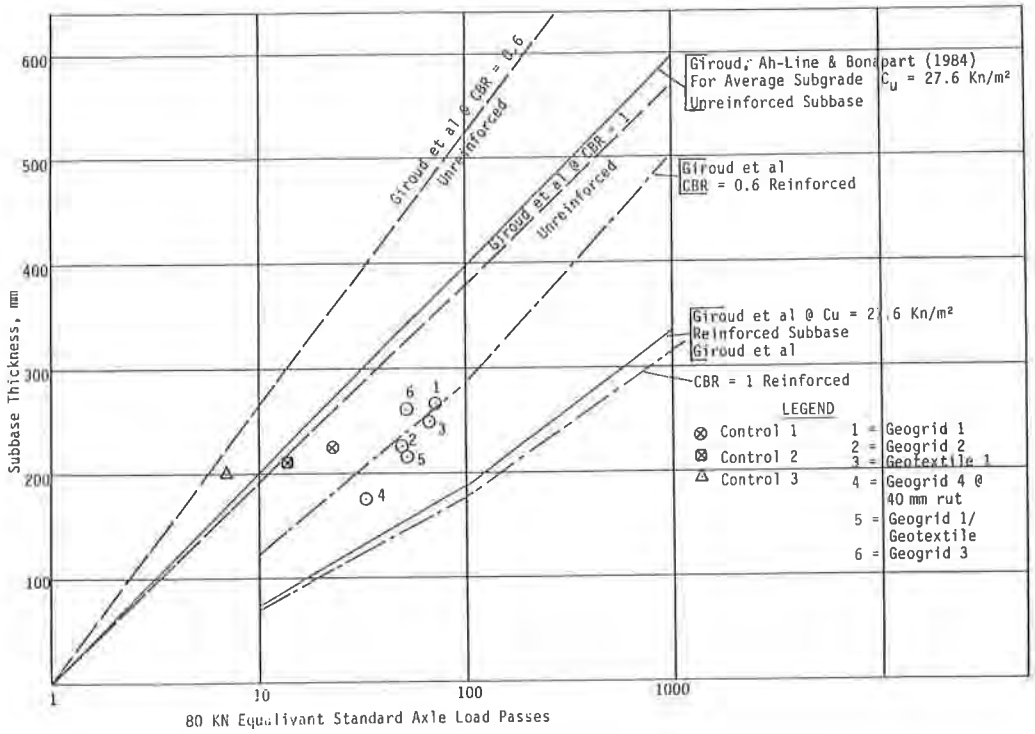

Figure 9. Haul Road Design Comparison
Giroud, Ah-Line and Bonaparte [3]

CONCLUSIONS

Conclusions developed from this full-scale field evaluation of geosynthetic reinforced haul roads are as follows:

1. Geosynthetics are an effective way of reinforcing and stabilizing an aggregate-surfaced haul road constructed on soft cohesive soils having a CBR of less than 1 percent.

2. The performance factors calculated with the test data from this field evaluation indicate that 2 to 3 times the number of ESAL passes were carried by the reinforced sections than the similar unreinforced (control) sections.

3. Limited data from this field evaluation indicates that the performance of polypropylene geogrid-reinforced haul roads constructed on soft soils seems to be independent of the tensile strength and the process used to manufacture the products.

4. The use of a nonwoven geotextile separator together with a polypropylene geogrid reinforcement at the aggregate/subgrade interface resulted in increased performance of haul road when evaluated with calculated performance factors.

5. The number of axle load passes actually achieved for a given thickness of a geosynthetic-reinforced aggregate subbase over soft subgrade soils is less than the expected number of passes calculated based on the design procedure developed by Giroud, Ah-Line and Bonaparte [3]. It is believed that this difference is due to the fact that higher in-place aggregate strengths are assumed in the theoretical design procedure than those actually achieved during the construction of haul roads.

REFERENCES

[1]. Webster, S.L., Grau, R.H., and Williams, T.P. (1992) "Description and Application of Dual Mass Dynamic Cone Penetrometer, Instruction Report GL-92-3, Department of the Army, Waterways Experiment Station, Vicksburg, MS.

[2]. Department of the Army, Waterways Experiment Station (1961), "Revised Method of Thickness Design for Flexible Highway Pavements at Military Installations", Technical Report No. 3-582, Vicksburg, MS.

[3]. Giroud, J.P., Ah-Line, C., and Bonaparte, R. (1984) "Design of Unpaved Roads and Trafficked Areas with Geogrids", Symposium on Polymer Grid Reinforcement in Civil Engineering, London, Paper No. 4.1.

ABE Airport Sinkhole and Subgrade Remediation, Allentown, Pa.

P.E. Gauffreau
NTH Consultants Ltd., USA

C.E. Reynolds
The Reinforced Earth Co., USA

ABSTRACT

Sinkholes and soft subgrade soils have contributed to progressive failure of the taxiway pavements at Allentown-Bethlehem-Easton (ABE) International Airport. A comprehensive subsurface investigation defined the existing conditions and the extent of severe subgrade damage. A cost-effective subgrade stabilization system featuring structural geosynthetics was chosen from among several alternatives. The layered design, which includes geotextiles, compacted soil, and geogrids, serves two purposes: support of the pavement section over a weak foundation and support of an aircraft load over a sinkhole void. Generic testing methods for the geosynthetics were specified to permit competitive bidding among qualified manufacturers. Construction experiences also provided lessons for future geosynthetic designs.

INTRODUCTION

ABE Airport. Allentown-Bethlehem-Easton (ABE) International Airport is located in Hanover Township, Lehigh County, Pennsylvania. Originally a municipal airfield, ABE Airport has grown rapidly into a moderately sized commercial facility serving the Lehigh Valley and the surrounding region. Six major passenger airlines and two major shipping companies currently operate out of the airport while several corporations, a commuter airline, and numerous general aviation aircraft have hangar facilities there.

Future expansion plans for the airport include doubling the size of the passenger terminal, extending the length of the main runway to 10,000 feet, and building a new parallel 6,000-foot runway. The first step of this program, however, was to improve the airfield's existing infrastructure, particularly the deteriorating taxiway pavements. A significant contributor to this problem were the sinkholes which had plagued the airport for years.

Sinkhole Formation. Sinkholes are common phenomena in the limestone regions of southeastern Pennsylvania. Limestone is a carbonate rock which is prone to aggressive solutioning. Water leaching through the soil causes the carbonate bedrock to weather (solution) along planes of weakness (fractures, joints, etc.) which results in the formation of voids or cavities within the rock mass and at the rock surface. As these voids grow, the unsupported soil washes or collapses into them, creating voids at the

soil overburden-rock interface and resulting in the soil overburden arching over the voids. As the soil arches relax, the soil matrix loosens. If this condition persists, the arches collapse into the void and the process is repeated as the cavity propagates to the ground surface as a sinkhole. (See Photo 1).

Photo 1. Typical Sinkhole in Taxiway Subgrade Soil

Such solutioning activity results in a loss-of-support condition for the pavement subgrade soil which threatens the load-carrying capacity of the soil. The potential for loss-of-support conditions at the soil overburden-rock interface and/or sinkhole formation is directly related to the depth of the seamy, cavernous limestone from the ground surface. Shallow limestone with less soil overburden cover is exposed to greater volumes of infiltrating surface water and, as a result, is typically degraded to a higher degree (with more seams and cavities) than the deeper limestone. Furthermore, there is less overburden soil in such cases to arch over a growing void. Therefore, a higher potential for sinkhole development is present when limestone is shallow.

Investigation. Several techniques were employed to located and isolate the zones of weakened subgrade soil, advanced solutioning activity, and sinkhole formation beneath the existing taxiways. The first technique was non-destructive deflection testing (NDT) of the asphalt pavement. NDT is used to estimate the modulus of elasticity (resilient modulus) of the various pavement layers, including the subgrade soils, and was successful in identifying pavement areas with a weakened subgrade.

The second technique involved television inspection of the stormwater lines beneath and adjacent to the taxiways. The videotape records clearly showed sags in the pipelines as well as miscellaneous structural damage which indicated a loss of support from the underlying soils. The locations of these loss-of-support conditions generally coincided with the locations of the weakened subgrade identified by the NDT.

Once the suspect areas had been delineated, a test boring program was performed to define the subsurface conditions. The test borings encountered a typical limestone weathering profile consisting of residual silty clay over intact rock. Advanced solutioning activity was identified when the residual soil became more soft and moist with depth. Some test borings encountered particularly soft soil and even some voids immediately beneath the taxiway pavement which posed significant danger to the aircraft.

DESIGN OF SUBGRADE STABILIZATION

Stabilization Options. Once the zones of weakened subgrade soil and high sinkhole potential had been delineated, a method of stabilization was required. Such a stabilization method would have to restore adequate support of the pavement which would have normally been provided by stable residual soil. Furthermore, the method would have to provide reasonable security against future sinkhole collapses. Three methods were considered and judged on the basis of risk mitigation versus construction costs and durations.

The first method would have consisted of the excavation and replacement of the weakened subgrade soils, including the plugging or repair of limestone seams or cavities. This method was rejected because the tremendous volume of soil to be excavated and the extreme variability in the depth to intact limestone would have resulted in prohibitive construction expenses.

The second method would have involved several stages of grouting to plug subsurface seams and cavities and to recompact loosened subgrade soils. This method was also rejected because of the relative uncertainty associated with grouting under such conditions as well as the potential for excessive costs.

The third method would involve the construction of a subgrade system that would support the pavement over the weakened residual soils, including potential sinkhole voids of a finite size. The subgrade could be modeled as both an "embankment" on a weak foundation and an "embankment" underlain by voids. Such a reconstructed system would consist of geosynthetics placed horizontally within the embankment (subgrade) soils to provide tensile strength. Despite the significant disturbance to the airport facilities, it was believed that this method was relatively simple to construct and, as a result, economical. Furthermore, since the geosynthetics were designed to undergo some strain prior to failure, the system is believed to be capable of providing a visual "early warning" mechanism if sinkholes develop in the future beneath the pavement in the areas of subgrade remediation.

Design Theory. The selected subgrade stabilization method, consisting of alternating horizontal layers of geosynthetics and compacted soil, would perform two tasks. First, it would provide tensile reinforcement of the subgrade (embankment) soils over the weakened (foundation) soils. Second, it would support the subgrade (embankment) soils over the potential sinkhole voids. Both may be accomplished using design theories developed for the transportation industry and which have been applied extensively in the landfill industry.

Reinforced Embankments Over Weak Foundations. The primary design concern with an embankment on weak foundation soils is localized vertical shearing or slip surface failure under the applied load. Horizontal tensile reinforcement, as provided by geosynthetics, decreases the average shear stress and shear strain magnitudes and the extent of the plastic zone in the foundation (Bonaparte and Christopher, 1987). The

reinforcement stiffens the embankment so that it behaves as a semi-rigid mass. However, since the reinforcement does nothing to increase the strength of the foundation soil, the foundation soil must have adequate strength to support the entire reinforced embankment. Therefore, the reinforcement simply reduces the critical failure mechanism to one of bearing capacity under the transmitted uniform load.

The design objective is to determine the required tensile strength per unit width, T, for the geosynthetic reinforcement to support an embankment of height, H. Simplified design charts based on limit equilibrium analyses have been developed for embankments built on saturated clay foundations. The chart presented in Figure 1 provides a conservative estimate of T to obtain a state of limit equilibrium (FS=1). Larger factors of safety may be applied by using factored soil strengths. These charts were developed on the basis of (a) moment equilibrium along the critical circular arc through the foundation and the Coulomb wedge through the embankment, and (b) horizontal force equilibrium along a critical mulipart wedge (Milligan and Busbridge, 1983). The latter equilibrium condition was found to control for ratios of foundation depth (depth to an intact surface), D, to embankment height, H, of less than about 0.5.

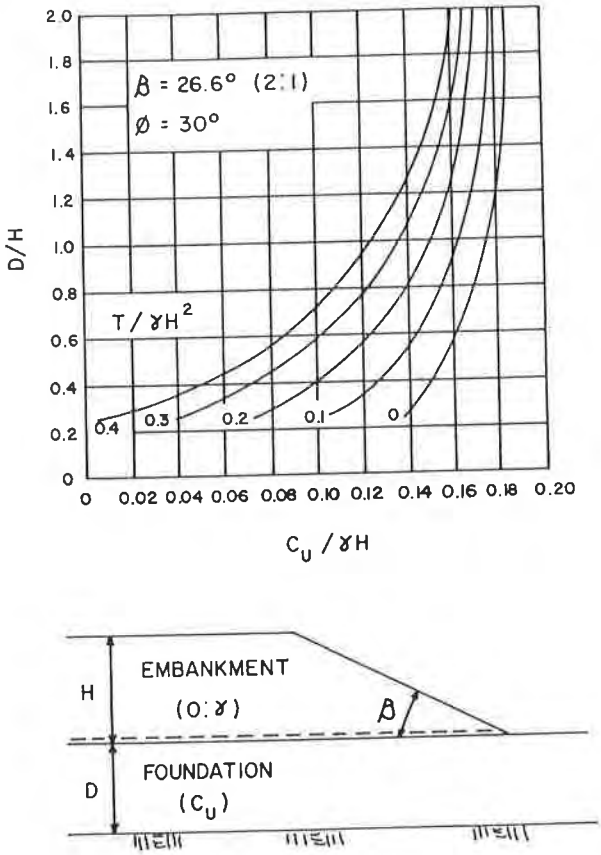

Figure 1. Stability chart for the design of embankments on weak foundations (after Milligan and Busbridge, 1983).

Reinforced Embankments Over Sinkhole Voids. Excavating, repairing, and backfilling known sinkhole voids and known areas of advanced solutioning does not eliminate the potential for future sinkholes. It is prudent to expect and to prepare for such occurrences. A geosynthetic layer placed at the base of the embankment soils may be designed to provide support over a potential void of a finite diameter. After a void

has developed, the geosynthetic will deflect into the opening under the weight of the embankment soil and the applied load. The deflection mobilizes two support mechanisms: bending of the embankment soil and stretching of the geosynthetic (Giroud et al, 1990).

The bending of the embankment soil generates arching in the soil, which transfers a portion of the applied load away from the void area (see Figure 2). As a result, the vertical stress, σ_v, over the void area is smaller than the average vertical stress, $\gamma H+q$. The stretching of the geosynthetic mobilizes a portion of the geosynthetic's strength. Consequently, the geosynthetic acts as a "tensioned membrane" and is able to support a load applied normal to its surface.

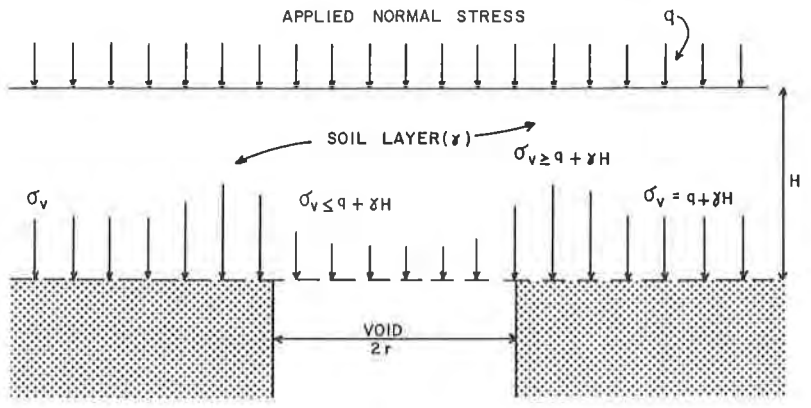

Figure 2. Effect of soil arching on load distribution (after Giroud et al, 1990)

These two mechanisms are considered separately for conservative design purposes, resulting in a two-step approach. First, the behavior of the embankment soil is analyzed using classical arching theory, which yields the vertical pressure, P, being applied to the geosynthetic over the void. For a circular void and an embankment soil with an angle of internal friction, ø, greater than 20°, P may be approximated by

$$P = 2\gamma r\ (1-e^{-0.5H/r}) + qe^{-0.5H/r} \qquad (1)$$

where γ, r and H are defined in Figure 2 (Giroud et al, 1990).

Second, the required horizontal geosynthetic tension per unit width, T, may be determined using tensioned membrane theory. For a circular void, the average value of T may be approximated by

$$T = P\ r\ \Omega \qquad (2)$$

where Ω is a dimensionless factor related to strain in the geosynthetic as shown in Figure 3 (Giroud et al, 1990). Equation (2) is only valid for a geosynthetic with uniform tensile properties in the two principal directions.

Equations (1) and (2) are combined in the design chart presented in Figure 4. A typical design problem may have any one of the four variables: geosynthetic tension per unit width (T), embankment soil height (H), void size (r), or vertical pressure (P). If three variables are known or assumed, Figure 4 may be used to solve for the fourth. Otherwise, if two or more variables are unknown, several combinations of assumed values may be evaluated to determine the most economical design.

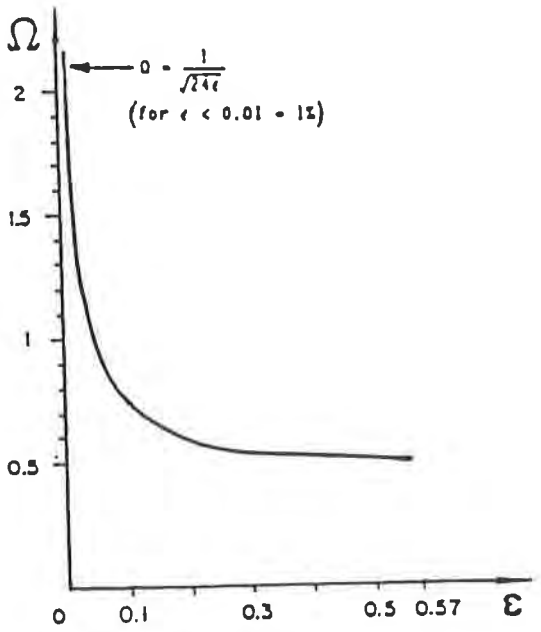

Figure 3. Dimensionless factor Ω (after Giroud et al, 1990).

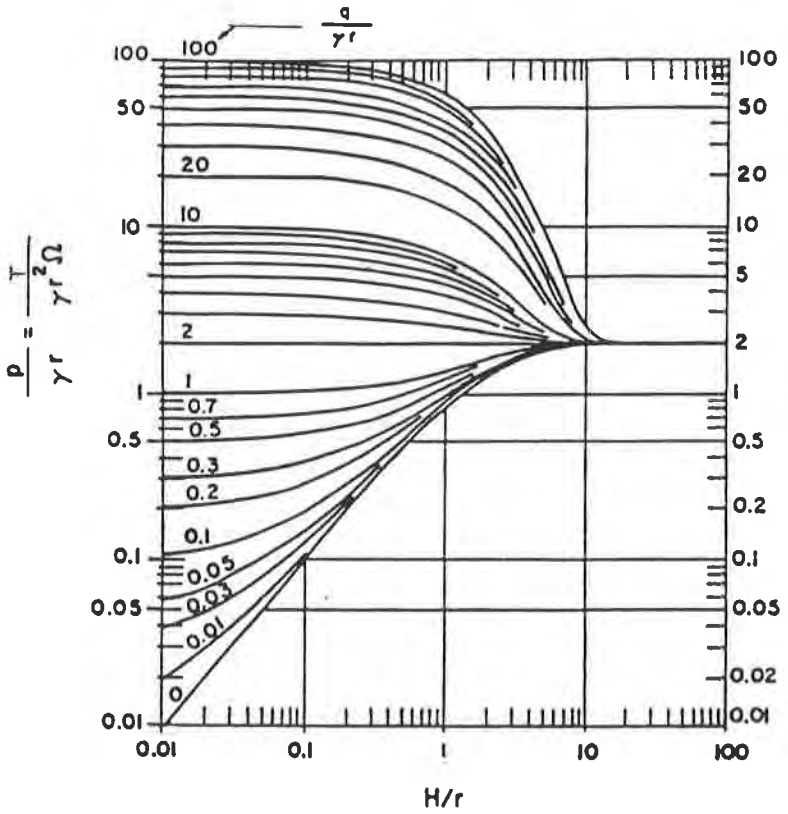

Figure 4. Design chart relating pressure on and tension in the geosynthetic over a void (after Giroud et al, 1990).

Design Assumptions. Since little information regarding similar applications were available to the authors at the time, several assumptions were made prior to beginning the design of the subgrade stabilization. First, since the subgrade stabilization would serve two purposes (support of an embankment over a weak foundation and support of an embankment over a sinkhole void), the designs would be performed separately. Furthermore, the authors believed that two geosynthetic components should be designed to avoid overstressing a single geosynthetic layer performing a dual role. Second, the geosynthetic layers should be separated by a soil layer to encourage independent action. Third, the upper geosynthetic layer should be separated from the pavement section by a similar soil layer to insulate the pavement from the horizontal stresses that may develop in the geosynthetic. These soil layers, consisting of compacted clayey backfill, would comprise the embankment supporting the pavement loads. Fourth, the geosynthetic layer designed for support over a void would be placed at the base of the embankment directly on the weakened subgrade soil.

The asphalt pavement and subgrade cross-section for ABE Airport is shown in Figure 5. Since the geotechnical investigation had determined the allowable bearing capacity of the weakened subgrade soil to be about 71.8 kPa (1,500 psf) (CBR=3.5), the pavement section was designed to transmit a vertical load of less magnitude to the subgrade. Therefore, the applied vertical load, q, at the subgrade elevation, including both the weight of the pavement section [q_{pvmt} = 19.15 kPa (400 psf)] and the maximum transmitted compressive stress from the landing gear of the design aircraft (Boeing 727) at rest [q'_o = 47.88 kPa (1,000 psf)], was about 67.03 kPa (1,400 psf).

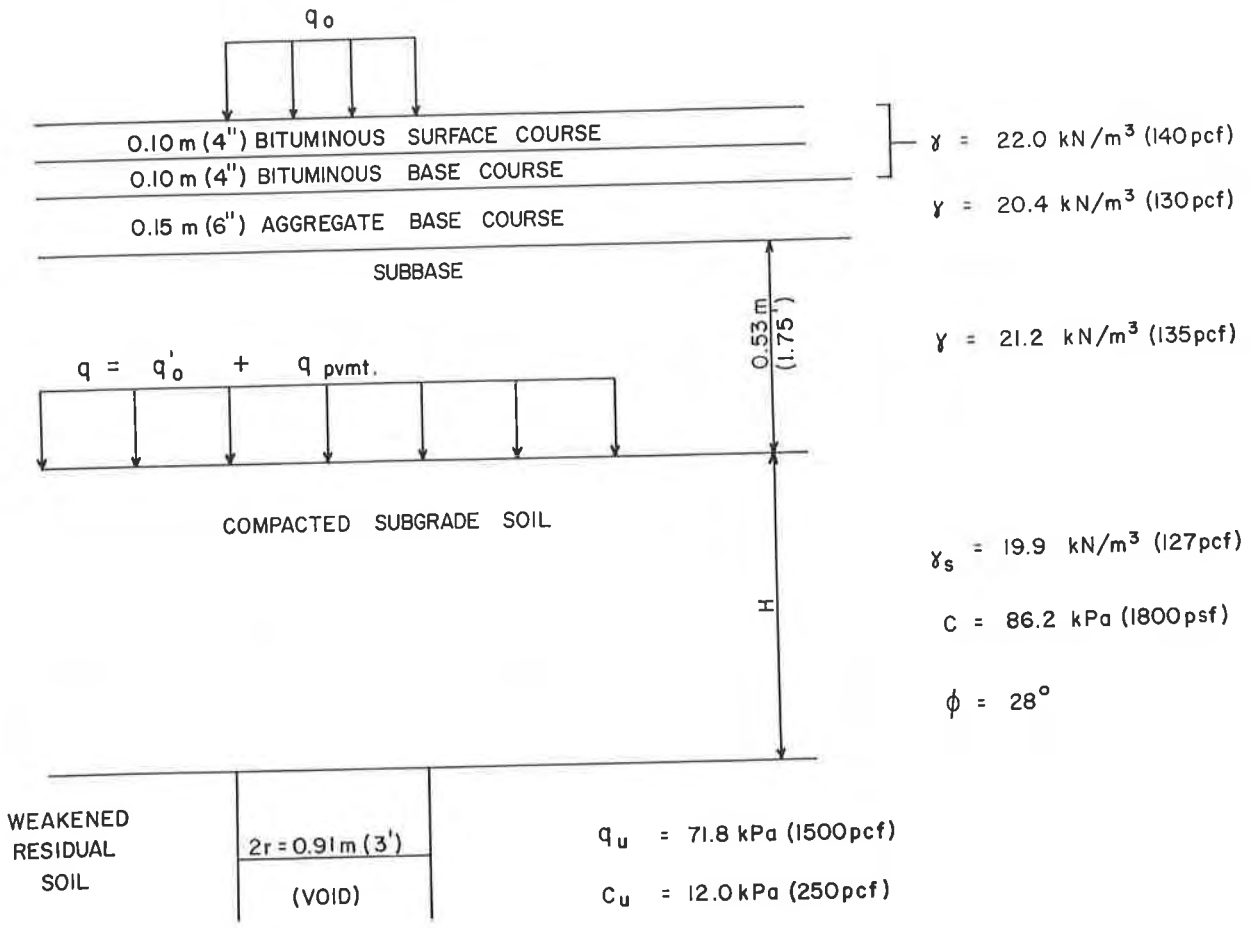

Figure 5. Pavement and subgrade cross-section, ABE International Airport.

Design of the Embankment Over a Weak Foundation. The height of the embankment, H, was assumed to be 0.46 m (1.5 feet) [two 0.23 m (9-inch) soil layers]. The applied vertical load, q, was transformed into an equivalent embankment soil height, resulting in a total theoretical height, H, of 3.81 m (12.5 feet). Using the data shown in Figure 5 and assuming the depth of intact rock, D, to be about 3.05 m (10 feet), the required geosynthetic tensile strength per unit width, T_{design}, was determined from Figure 1 to be about 2,976 kg/m [2,000 lb/ft]. Then, partial factors of safety for installation damage, durability, and creep deformation (GRI GG4, 1991) were applied to establish the required ultimate tensile strength, T, which was product dependent.

Geosynthetics undergo significant strain prior to ultimate failure. A normal stress-strain curve for a given material indicates that progressively increasing load levels will result in progressively increasing strains. Therefore, the required ultimate unit tensile strength must be specified with a corresponding allowable strain. Since no data relating geosynthetic strain to vertical deformation of the embankment was available to the authors at the time, a horizontal strain of 5 percent in the upper geosynthetic layer was assumed to be allowable prior to the potential for damage to the asphalt pavement.

Design of the Embankment Over a Sinkhole Void. The applied vertical pressure, P, on the lower geosynthetic layer at the base of the embankment was conservatively assumed to be 67.03 kPa (1,400 psf). A typical sinkhole void diameter (2r) of 0.92 m (3 feet) was also assumed. The embankment height, H, had previously been established at 0.46 m (1.5 feet). A strain of 10 percent in the geosynthetic was assumed to result in a vertical deflection into the void which, when transmitted through the embankment soils and the pavement section, would be noticeable at the pavement surface but would not result in damage to the asphalt pavement. Figure 3 was then used to determine that $\Omega = 0.73$. The data was entered into Figure 4, resulting in a required geosynthetic tensile strength per unit width, T_{design}, of about 1,637 kg/m (1,100 lb/ft). Applying similar factors of safety as for the embankment over weak foundation design, the required ultimate unit tensile strength, T, was determined.

GEOSYNTHETIC SELECTION AND SPECIFICATION

Upper Geosynthetic Layer. The upper geosynthetic layer was designed to support the pavement structure and embankment soil over the weakened subgrade (foundation) soil. The required design tensile strength was determined to be 2,976 kg/m (2,000 lb/ft) at a strain of 5 percent. The geosynthetic products which achieve this strength at such a relatively low strain are typically limited to uniaxial geogrids. Uniaxial geogrids are high-strength polymer grids which exhibit tensile strength primarily in the machine (principal) direction. The geometry of the geogrids also permits contact and, as a result, continuity between the soil layers.

The required ultimate unit tensile strength at a given strain must be specified in terms of a test method. Two test methods are generally accepted for geogrids: "Tensile Properties of Geotextiles by the Wide-Width Strip" (ASTM D 4595) and "Tension Creep Testing of Stiff or Flexible Geogrids" (Geosynthetic Research Institute Test Method GG3A & GG3B). ASTM D 4595 is a constant strain rate test performed over a relatively brief period of time which is representative of an elastic response to loading and unloading cycles. GG3 is a constant load test performed over 10,000 hours which is representative of a plastic response (creep) to a sustained load. For the ABE Airport case, the specification was based on ASTM D 4595 to model short-term transient and repetitive aircraft loadings as well as GG3 creep data to account for long-term effects.

Lower Geosynthetic Layer. The lower geosynthetic layer was designed to support the pavement structure and embankment soil over a circular sinkhole void. The required design tensile strength was determined to be 1,100 lb/ft at a strain of 10 percent. Since the void would be circular, a biaxial geosynthetic was required. A biaxial material is capable of providing strength in its two principal (machine and cross) directions. High-strength woven geotextiles are a primary type of geosynthetic product which provides the biaxial strength required. Also, a geotextile would limit any erosion of the embankment soils into the void. Using reasoning similar to that for the geogrids, the wide-width tensile test (ASTM D 4595) was used to specify the geotextile tensile strength.

Since the geotextiles are biaxial, the seams between adjacent panels must be sewn to transmit the loads. It is not possible, however, to maintain 100 percent of the geotextile's tensile strength across a sewn seam. Manufacturer's techniques and performances vary, but 70 percent is reasonable to expect. The engineer must determine, therefore, the minimum acceptable percentage of the design strength which the seam should transmit. The manufacturer will use this figure and the performance data for the chosen sewing technique to determine the required tensile strength of the geotextile panels. For example, 90 percent of the ultimate tensile strength was specified for the sewn seams for this project. If the manufacturer's sewing technique can only transmit 70 percent of the panel strength, the manufacturer must provide geotextile panels with a minimum tensile strength which is 128.6 percent (0.9/0.7) of the specified ultimate tensile strength. All sewn seams should be tested in accordance with ASTM D 4884. Another way which has become widely used, and which geotextile manufacturers recommend, is for a designer to specify a seam strength. From this the manufacturer can chose the sewing method and fabric to meet this seam strength.

Final Cross-Section. The final design cross-section for the subgrade stabilization is presented in Figure 6.

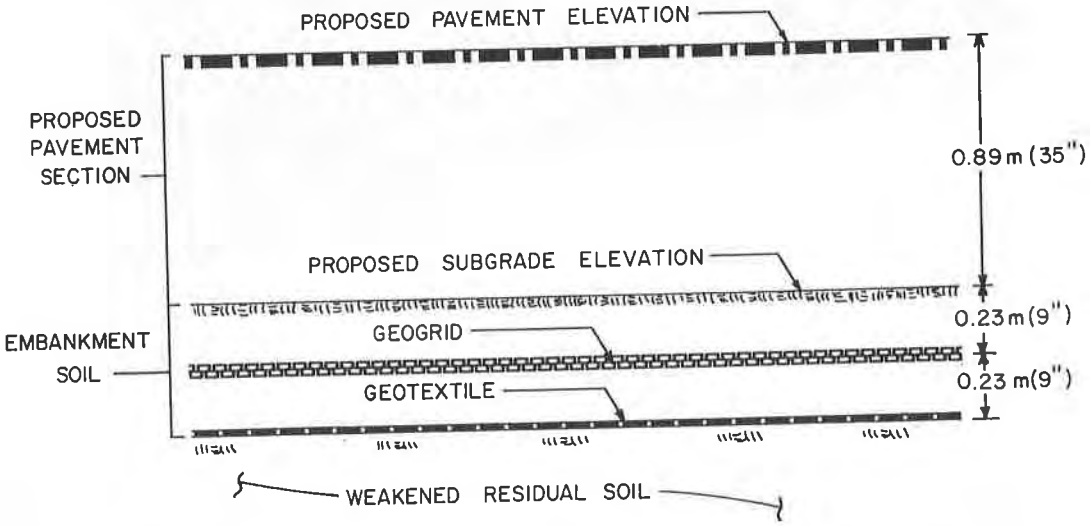

Figure 6. Subgrade stabilization cross-section, ABE International Airport.

CONSTRUCTION EXPERIENCES

One of the attractive aspects of this subgrade stabilization option was the relative ease of construction. However, the inexperience of the earthwork contractor with geosynthetics and a loosely written installation specification contributed to some difficulties and delays which could have been avoided. All of these experiences related to the installation of the geotextile.

The generic specifications permitted the contractor to obtain competitive prices for the geosynthetic products. They also did not prevent the contractor from having the geotextile panels pre-sewn at the manufacturer's plant prior to shipment. The geotextile sheets, some as large of 200 feet by 120 feet, were folded at the plant and shipped in large sacks. Unfortunately, the extremely heavy sacks were shipped in closed trailers with no lift hooks and no markings regarding the size of the enclosed sheet. These problems combined with only rudimentary unfolding instructions, resulted in a trial and error process for the contractor to position the sheets. (See Photo 2) Since the geosynthetic manufacturers have a significant stake in this industry, the authors suggest that they offer more direct assistance and support to contractors during the installation operations.

Photo 2. Pre-Sewn Geotextile Sheet In-Place.

The large and heavy geotextile sheets were too unwieldy to maneuver properly. As a result, the slack in the sheets was never completely eliminated. Also, while the sheets were being backfilled, a wave of slack preceded the advancing pile of soil. Eventually, the soil overran the wave and a fold was formed in the geotextile. Ideally, therefore, the geotextile panels should not be pre-sewn. Adjacent panels should be unrolled in their proper position and sewn together in the field. Then, after the outside panel has been backfilled, the next panel can be stretched to remove the slack. This sequence should be repeated across the subgrade to ensure a taught geotextile layer.

Another problem involved the joining of adjacent, pre-sewn geotextile sheets. The giant sheets were still required to provide bi-axial tensile strength across the entire subgrade, so they had to be field-sewn together. A portable machine was used by the manufacturer's technician to sew a double-stitched butterfly seam perpendicular to the pre-sewn panel seams. (See Photo 3) The cold and wet weather made this task extremely slow and frustrating. Also, since the adjacent geotextile sheets had already been backfilled, the slack along the perpendicular seam could not be removed. The authors believe, therefore, that such perpendicular seams should be minimized if not eliminated whenever possible. If they are still necessary, at least one of the geotextile sheets should not be backfilled so that the slack at the seam may be pulled taught. Finally, a more substantial sewing device is required for such purposes.

Photo 3. Attempting to Sew Perpendicular Seam Between Geotextile Sheets.

An additional difficulty relating to construction damage was also encountered. The geotextile, in one instance, was placed directly on the pavement subgrade over several rounded, slightly protruding limestone knobs. The first 8-inch lift of pavement subbase material, consisting of a dense-graded crushed aggregate, was placed directly on the geotextile and compacted with heavy-duty, vibratory rollers. This operation severely damaged the geotextile over the rock knobs. The manufacturer's recommended solution was to place geotextile patches on top of the first subbase lift over each damaged area. Each patch was extended far enough (about 3 feet) in each direction beyond the area to develop a tensile bond with the underlying geotextile sheet (see Figure 7). This simple remedy helped keep the project on schedule.

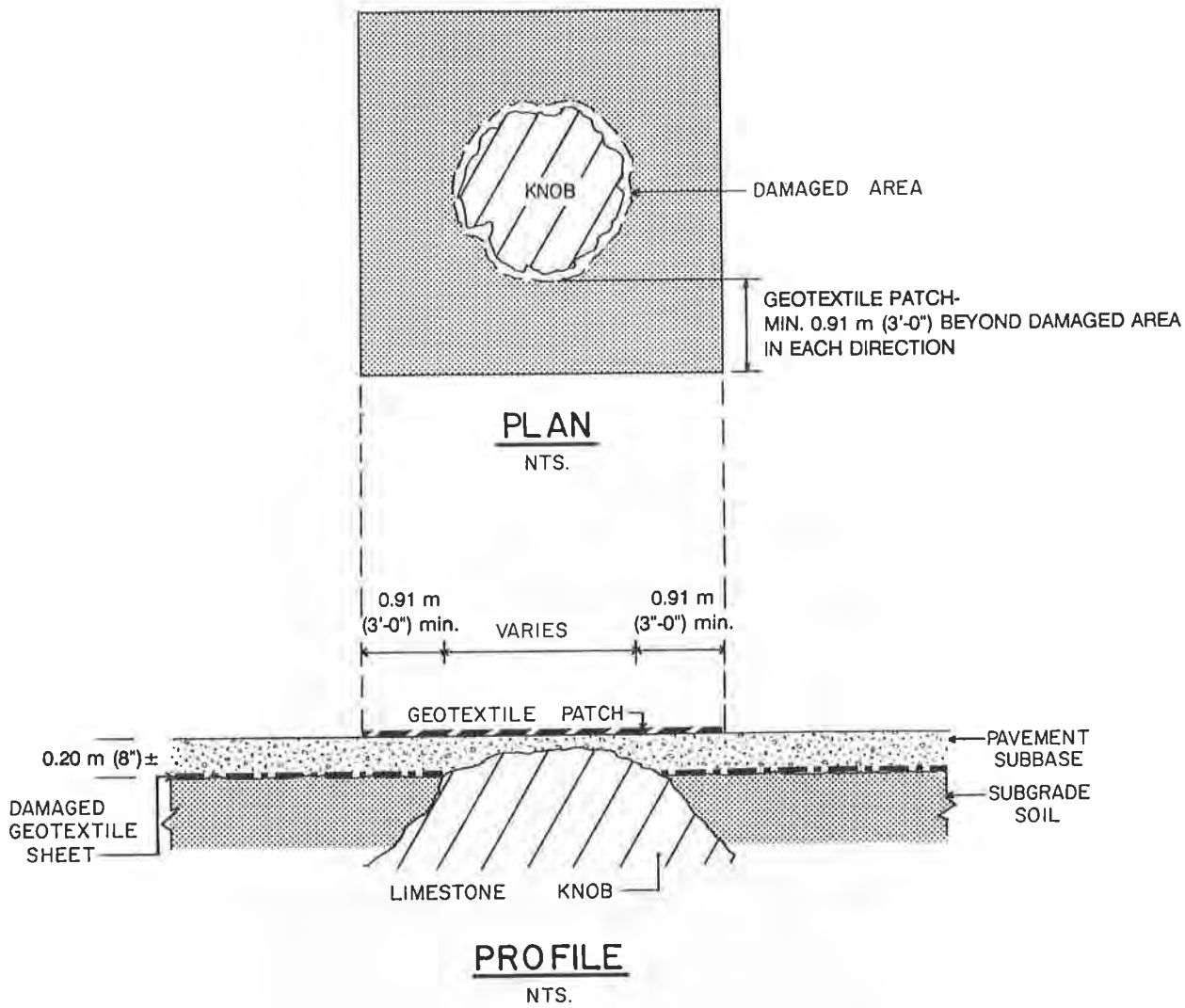

Figure 7. Repair detail for damaged geotextile.

Contrary to these difficulties with the geotextile, the geogrid installation went smoothly. (See photo 4) The geogrids were delivered in individual rolled panels which could be easily maneuvered. The light and flexible characteristics of the geogrid are attributed to its polyester fibers. Adjacent panels were joined by plastic ties placed at 10-foot intervals since the biaxial strength component was not required. To preserve the uniaxial strength, however, consecutive geogrid panels were joined at their ends using a smooth galvanized rod connector.

Photo 4. Installing and Backfilling Geogrids.

CONCLUSIONS

The persistent sinkhole problem at ABE Airport presented a unique engineering challenge. A cost-effective solution which would provide a reasonable measure of security against a catastrophic collapse of the taxiway pavement was required. Such a solution would have to be confined to a relatively small area, be constructed quickly and simply, and require little or no maintenance.

Three unrelated investigative techniques were combined successfully to isolate the zones of advanced solutioning and sinkhole formation. Two distinct design theories were used to develop an innovative subgrade stabilization system. This system, consisting of alternating layers of compacted soil and geosynthetics, did not require excessive excavation, construction time, or disturbance to the airport facilities. Furthermore, it should provide an early-warning mechanism which would permit repairs to be made to a sinkhole prior to the collapse of the pavement.

The unique properties of such structural geosynthetics as geogrids and high-strength woven geotextiles made this design possible. The structural geosynthetic industry is still relatively young with new product developments and applications being made regularly. The geosynthetic manufacturers have taken a lead role in the industry as they attempt to educate the design engineering community. However, since the industry is not evenly regulated, the engineer must be wary of misleading product data or proprietary design methods. Manufacturers' literature should be compared to understand the differences between and the purposes of their products. Most importantly, the engineer must be familiar with the meaning and purpose behind the testing methods being developed by such unbiased agencies as ASTM and the Geosynthetic Research Institute (GRI). Proper specification of these test methods will permit competitive bidding among the manufacturers and verification of the product being supplied.

Installation of these structural geosynthetics is a relatively simple procedure that can be accomplished by most contractors. The engineer should provide installation specifications, however, which address aspects such as material handling, field seaming, and slack. Geosynthetic manufacturers should also provide installation support and guidance along with their products. This type of teamwork is the best form of promotion for the geosynthetic industry.

REFERENCES

Bonaparte, R., and Christopher, B.R. (1987) "Design and construction of reinforced embankments over weak foundations", Transportation Research Record 1153, Transportation Research Board, Washington, DC, January, pp. 26-39.

Gauffreau, P.E., Souto, F., and Russell, T.W. (1991) "Geotechnical and pavement evaluations, ABE International Airport", NTH Consultants, Ltd. Report to the LPA Group, Inc., Tampa, FL.

Giroud, J.P., Bonaparte, R., Beech, J.F., and Gross, B.A. (1990) "Design of soil layer-geosynthetic systems overlying voids", Geotextiles and Geomembranes, Vol. 9, No. 1, pp. 11-20.

GRI GG4 (1991) "Standard practice for determination of the long-term design strength of stiff geogrids", Geosynthetic Research Institute, Drexel University, Philadelphia, PA.

Milligan, V. and Busbridge, J.R. (1983) "Guidelines for the use of Tensar geogrids in reinforcement of fills over weak foundations", Golder Associates Report to the Tensar Corporation, Mississauga, Ontario.

Pavement Test Section to Determine the Effect of Geotextile on Frost Heave

K.S. Henry
U.S. Army Cold Regions Research and Engineering Laboratory, USA

B.R. Christopher
Polyfelt Inc., USA

ABSTRACT

A pavement test section was constructed on U.S. Rte. 3 in Pittsburg, New Hampshire, an area known to be extremely susceptible to frost damage. The test section was subdivided into 10 smaller sections. A 400-g/m^2 (12-oz/yd^2), needle-punched, polypropylene geotextile, with an AOS of 0.105 to 0.15 mm, was installed at the subgrade surface in two test sections at a depth of 0.66 m (26 in.), in one section at 0.96 m (38 in.) and in two sections at 1.27 m (50 in.). Five control areas were included—four on the ends and one in the center of the test section. Subsurface instrumentation included thermocouples and soil moisture sensors. Frost heave was measured by level survey. Results of the first freezing season show that the geotextile reduced frost heave, but not as much as in laboratory tests used to select the optimal product.

INTRODUCTION

Objectives. Laboratory tests have shown that certain geotextiles reduce frost heave when placed horizontally above the water table in soil samples that are frozen vertically from the top down (Henry, 1990 and 1991). In September 1991, a pavement test section was constructed on U.S. Rte. 3 in Pittsburg, New Hampshire, by the U. S. Army Cold Regions Research and Engineering Laboratory, Polyfelt, Inc., and the State of New Hampshire to test the effectiveness of a geotextile in reducing frost heave. There are two objectives of the ongoing research described in this paper. One is to determine whether a geotextile observed to reduce frost heave in a specific soil in a laboratory test actually does so in a field installation. The second is to study the effect of depth of geotextile placement in reducing frost heave. This paper briefly describes the design and construction of the test section, and summarizes and discusses experimental data collected during the 1991–92 freezing season.

Site Location and Description. The test area is located in the town of Pittsburg, Coös County, in northern New Hampshire. Figure 1 shows the general location of the test area. It is 30.5 m (100 ft) long, and 6.7 m (22 ft) wide, extending from State of New Hampshire survey station 224+50 to 225+50, on a relatively flat section of the road; the First Connecticut Lake is approximately 31 m (100 ft) east of the pavement edge. The research project was incorporated into the reconstruction of an 8.4-km (5.2-mile) section of U.S. Rte 3. The reconstruction was needed because of the poor

Figure 1. General location map for geotextile test section.

condition of the pavement, which was probably caused by heavy loading, poor drainage and frost-susceptible soils (Jaworski Geotech, Inc., 1988). The U. S. Department of Agriculture Soil Conservation Service (in preparation) reports that this soil has severe limitations for building sites because of wetness and frost susceptibility.

PREVIOUS WORK ON USE OF GEOTEXTILES TO REDUCE FROST HEAVE

The earliest published investigation regarding the potential use of geotextiles to reduce frost damage in roads was Hoover et al. (1981). Laboratory investigation showed that one horizontal layer of geotextile reduced frost heave slightly and two layers reduced frost heave significantly in frost-susceptible silty clay. The authors suggested that "the lower heaving observed with the fabric-layered specimens may have resulted from a partial cut-off by the fabric of capillary water to the remainder of the specimen" (Hoover et al., 1981).

In another laboratory investigation, Allen et al. (1983) observed that hydrophobic (e.g., polypropylene) geotextiles placed in soil above the water supply in open system freezing tests (i.e., water freely available at the base) reduced frost heave, while a hydrophyllic geotextile increased heave. The "hydrophobicity" of the geotextiles was noted through casual observation of the behavior of the fabric in the presence of water. The capillary equation shows the influence of both pore size and wetting angle on the capillary rise of water in a cylinder (Holtz and Kovacs, 1981):

$$h_c = \frac{2\,T_s \cos\alpha}{R\gamma}$$

where h_c = height of capillary rise in the tube
T_s = surface tension of liquid

R = radius of tube
γ = unit weight of the liquid
α = contact angle between the liquid and the tube.

Thus, both pore size and wetting properties (i.e., degree of hydrophobicity) are expected to influence the capillary rise of water in soils.

In addition to capillary rise, unsaturated flow of soil water is induced by other means. In frost-susceptible soils, water flow to the freezing front is caused by a gradient in chemical potential, which is related to temperature and pressure changes (Gold, 1985). In a recent laboratory investigation, Henry (1991) concluded that geotextiles limit frost heave in soil when placed above the water table and below the depth of freezing by limiting unsaturated water flow to the zone of freezing.

PRELIMINARY INVESTIGATION

Field Investigation. The test location selected had sustained some of the worst damage owing to frost action and/or poor drainage conditions over the entire length of road to be rehabilitated. This site also had no complicating geometries such as culverts, was relatively flat, and would not require fill during reconstruction. Thus, the subgrade would consist of in-situ, frost-susceptible soil.

The field investigation indicated that the subgrade consists of silty, clayey sands of medium stiffness and low sensitivity. Unconfined compressive strengths of the subgrade material ranged from 70 kPa (10 psi) to 202 kPa (29 psi). Representative grain size curves are shown in Figure 2.

During the preliminary investigation, a perched water table at a depth of 0.45 to 0.61 m (1.5 to 2.0 ft) was observed in two of the drilled holes on the west side of the test section. Seasonal streams on the slope adjacent to the west side of the road were also noted. Furthermore, the west lane of the road was significantly more damaged than the east lane at the time of the site visits.

Frost Susceptibility of Soils. Frost groups of the subgrade and base course soils were determined using the U.S. Army Corps of Engineers (USACE) Frost Design Soil Classification System. The subgrade soil belongs to the F3 category, indicating potentially high frost susceptibility, and requiring a maximum base course and pavement thickness in road design (Berg and Johnson, 1983). The base course gravel belongs to either the F1 group, frost-susceptible gravelly soils, expected to show higher bearing capacity during thaw than other frost-susceptible soils, or to the possibly frost-susceptible group—requiring a laboratory test to determine frost category.

Laboratory Investigation. A laboratory investigation was conducted to select a geotextile for use in the test section and to further quantify the frost susceptibility of the subgrade soil.

Two tests were conducted using the standard CRREL frost heave test (Chamberlain and Carbee, 1981). They are shown in Figure 3. Based on the results of these tests, the 400-g/m^2 (12-oz/yd^2) geotextile with an AOS of 0.105 to 0.15 mm was selected for installation in the test section, since it reduced heave rate by an average of 2.5 mm/day, or 63%. Dry cleaning the geotextile to remove surfactants that may influence wetting properties had no influence on its performance.

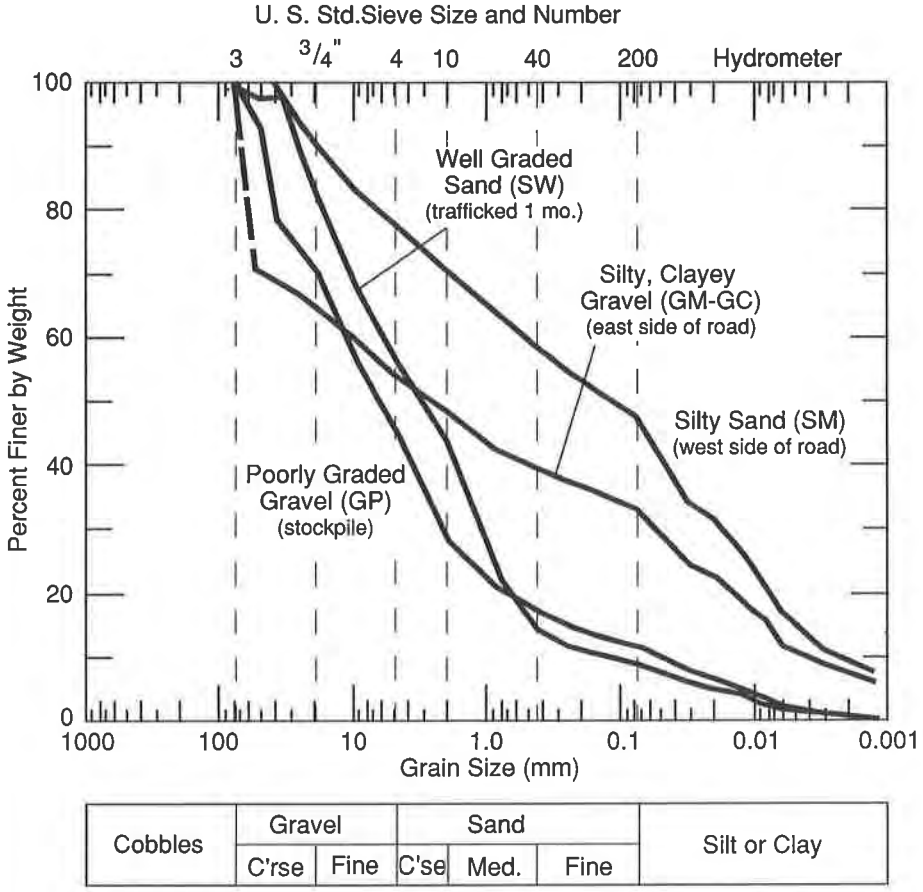

Figure 2. Grain size distribution curbves from Pittsburg, New Hampshire, test section subgrade and base course soils.

The results of the tests are listed in Table 1. Two of three soil reference samples tested resulted in a "high" frost-susceptibility rating of the subgrade, while one soil sample resulted in a medium frost-susceptibility rating.

The AOS of the most effective geotextile, although slightly smaller than the AOS of the other geotextile, is about 200 times larger than the "effective pore diameter" of the soil. The effective pore diameter (0.20 D_{10}) is about 0.0006 mm. This soil parameter is used to estimate the height of capillary rise in soil (Holtz and Kovacs, 1981). It is likely that the greater thickness of the better performing geotextile was a significant factor in the observed difference.

TEST SECTION DESCRIPTION

Test Section Design. The test section consists of 10 smaller test sections, each containing either no geotextile, or a geotextile at a depth of 0.66, 0.97, or 1.27 m below the asphalt surface. Figure 4 is a typical design cross section of the rehabilitation project and Figure 5 is an as-built plan of the test section, showing geotextile and instrumentation locations. It was designed to be able to account for

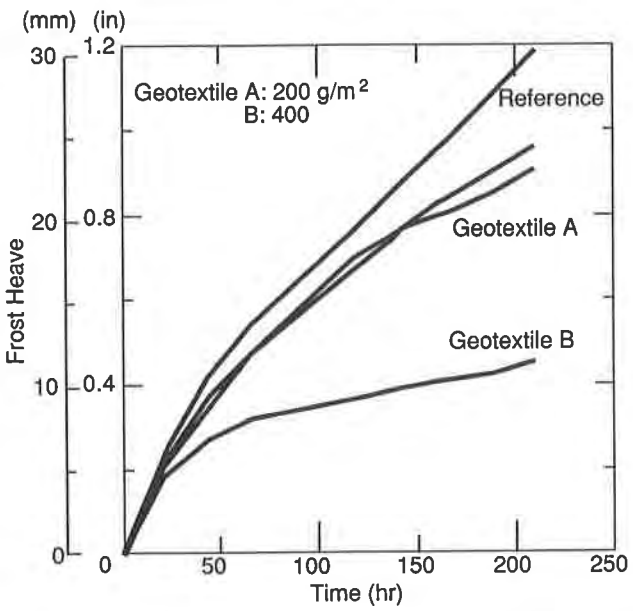

a. Test 1 of geotextiles in subgrade soil.
Geotextile A: AOS = 0.15–0.21 mm
B: AOS = 0.105–0.15 mm

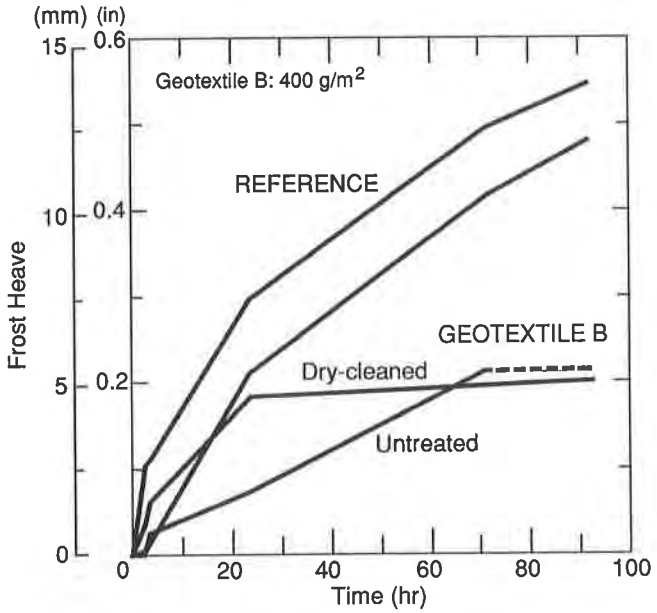

b. Test 2 of dry-cleaned and untreated geotextiles in subgrade soil.

Figure 3. Results of laboratory frost heave tests using a constant freeze rate of approximately 12.5 mm/day.

Table 1. Frost-susceptibility determination of Pittsburg, New Hampshire, geotextile test section soils and soils containing a geotextile layer.

Test series and procedure	Sample	Geotextile treatment	Frost heave rate (mm/day) first cycle	Frost susceptibility
PITTS 1	1	——	4.5	High
	2	——	4.2	High
	3	400 g/m²	2.0	Low-Medium
	4	D.C.* 400 g/m²	1.5	Low
PITTS 2	1	——	3.3	Medium
	2	400 g/m²	1.0	Very Low-Low
	3	200 g/m²	3.8	Medium
	4	200 g/m²	3.8	Medium

* D.C. = dry cleaned.
Average heave rates: no geotextile = 4.0, 400 g/m² = 1.5.

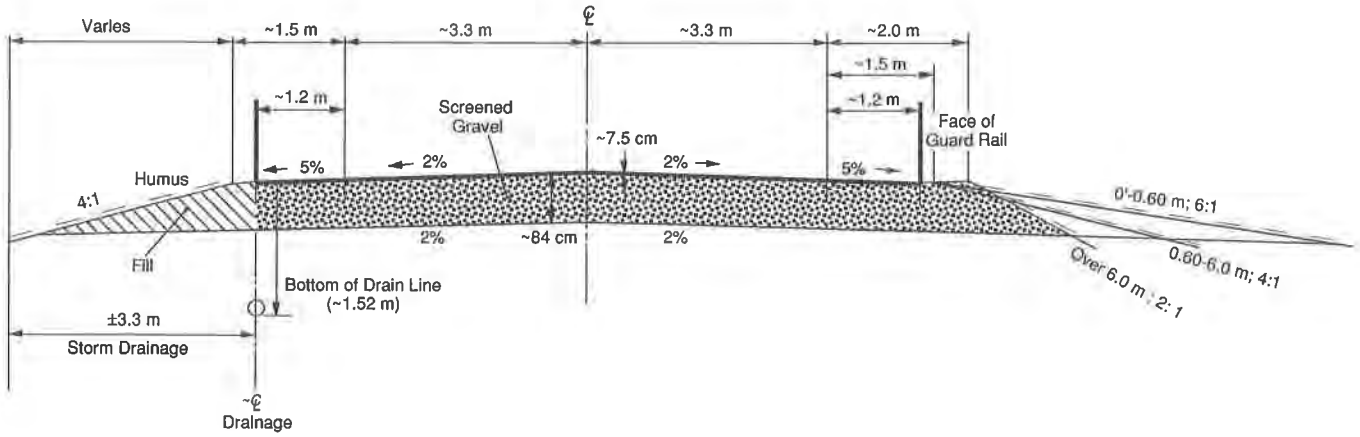

Figure 4. Typical pavement design section for U.S. Rte. 3, Pittsburg, New Hampshire, rehabilitation.

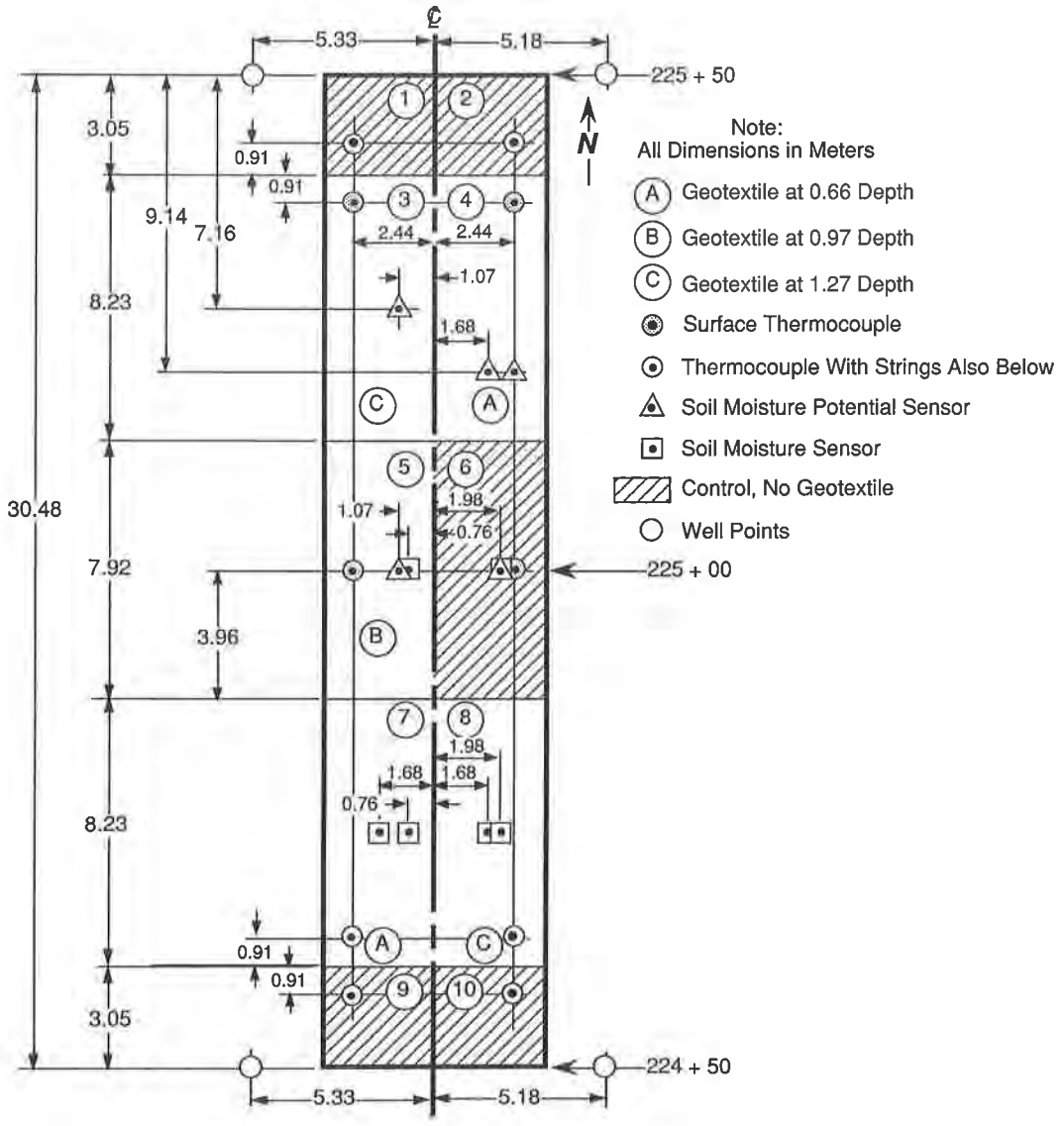

Figure 5. As built plan view of Pittsburg, New Hampshire, geotextile test section.

the effects of location on frost heave so that the response to geotextile presence at the 0.66-m and 1.27-m depths would be clear.

Instrumentation. Change in elevation was the primary variable measured and analyzed since it directly measures frost heave. Other variables determined to be useful in the analysis of the test section behavior were temperature and soil moisture content. Thus, the instrumentation included thermocouple strings and soil moisture sensing devices. Four well points were included in the design at the corners of the test area to monitor water table.

Two types of soil moisture sensing devices were selected. Both types were connected to data logging systems, and recordings were automatic. Neither type of sensor gives reliable information when the soil is frozen, however, and can only be used when the soil is above 0°C.

TEST SECTION CONSTRUCTION

General Construction Procedure. A typical cross section of an individual test section is shown in Figure 6. During construction, all soil layers were removed to a depth of 1.22 m (4 ft) below the base course surface. The entire test area was excavated to this depth to produce uniform treatment of the subgrade. Once the level 1.22 m (4 ft) below base course was reached, a roller compactor made one pass over the subgrade and construction of the test section began, using the subgrade material that had just been removed. Instrumentation located below this depth was then installed. In the

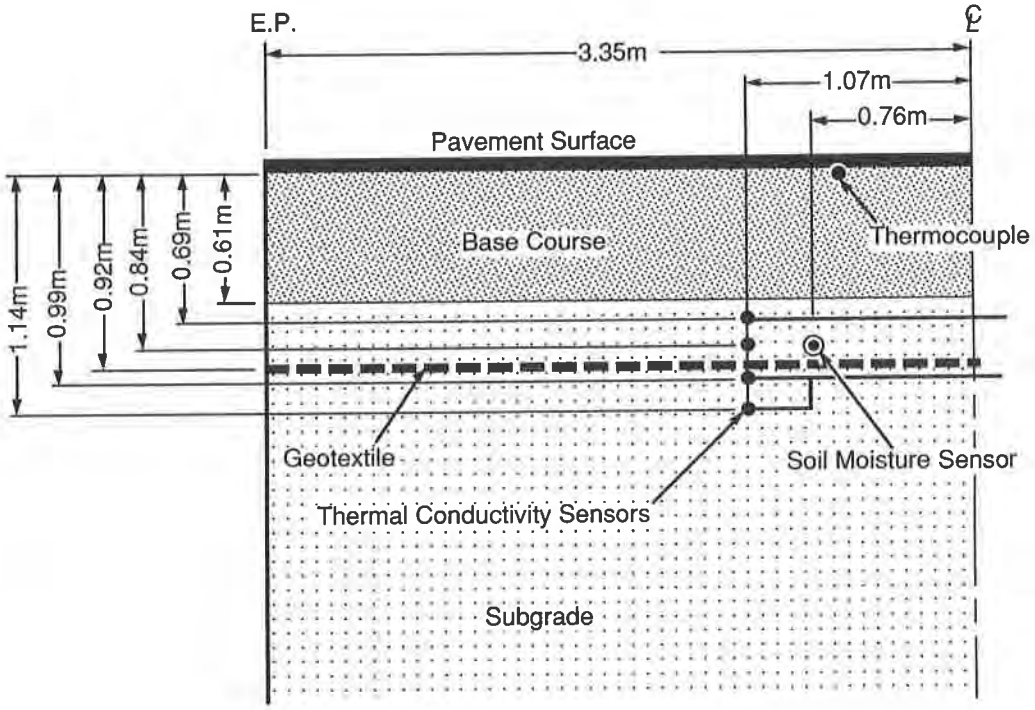

Figure 6. Cross-section view of test section 5 from Pittsburg, New Hampshire, geotextile test section.

appropriate two test sections, the deepest geotextile was placed on this surface. Then in all sections, the first 0.305-m (12-in.) lift was placed and compacted. Instrumentation was installed in the first lift, the geotextile was placed in the appropriate test section on top of this lift, and the second 0.305-m (12-in.) subgrade lift was placed over the entire test section. This process was repeated for the next elevation and the shallowest geotextile layer. The base course material was placed above that level.

Geotextile and Instrumentation Installation. The subgrade at each lift level was shaped so that it sloped toward the right shoulder to avoid potential ponding problems during the life of the pavement. The north and south edges of the geotextile were supported by stakes such that these ends stood vertically for approximately 0.3 m (1 ft). (The geotextile edges on the east and west were laid on the surface with no edges.) This allowed the ends to be wrapped, so each test section was isolated from the adjacent ones. Soil was end-dumped next to the geotextile, then carefully pushed onto it. Once there was a 0.15-m (6-in.) layer of soil on the geotextile, soil was dumped directly onto it.

Prior to construction, all instrumentation leads were placed into appropriately sized conduits for protection during and after construction. Instrumentation below the base course was installed by using a hand auger.Thermocouples were placed on the gravel layer just prior to asphalt placement. They were located so that the reading would indicate temperature at the base of the asphalt layer.

After paving, a grid was set into the test section by driving 6.4-cm (2.5-in.) decking nails into the pavement at a spacing of 1.52 m (5 ft). Three benchmarks were used to provide good control and to evaluate relative benchmark movement during the winter.

SUMMARY OF DATA COLLECTED DURING 1991–92 FREEZE–THAW SEASON

Temperature Data. The reference temperature data from the thermal conductivity sensors show that the freezing season lasted from 27 November 1991 to 26 March 1992. Temperatures as a function of time at various depths for test section 1 are shown in Figure 7. The other test sections show similar variations of temperature with time.

Level Surveys. Twelve level surveys were done to measure frost heave between 17 December 1991 and 1 May 1992. Average frost heave for each test section on each date is contained in Table 2. A statistical technique was used to estimate whether the frost heave of various sections was greater than the frost heave of others. The technique, described in Natrella (1963), tests whether the average of a product A is greater than the average of a product B, when both variances are unknown. The significance level chosen was 0.05; i.e., there is a 5% risk that the hypothesis will be incorrect even when it is accepted.

The center control section, TS 6, consistently heaved significantly less than all other test sections throughout the winter; this was most likely caused by a drainage situation inadvertently created in this area, which will be discussed later. The heave of all other test sections varied in a similar manner and was consistent, with expectations based on site conditions and theory. For these reasons, TS 6 was excluded from being used as a control section, and was evaluated as a "treated" section. The end sections (1, 2, 9 and 10) were used as controls.

Soil Moisture Data. Soil moisture data recorded automatically from the thermal conductivity sensors

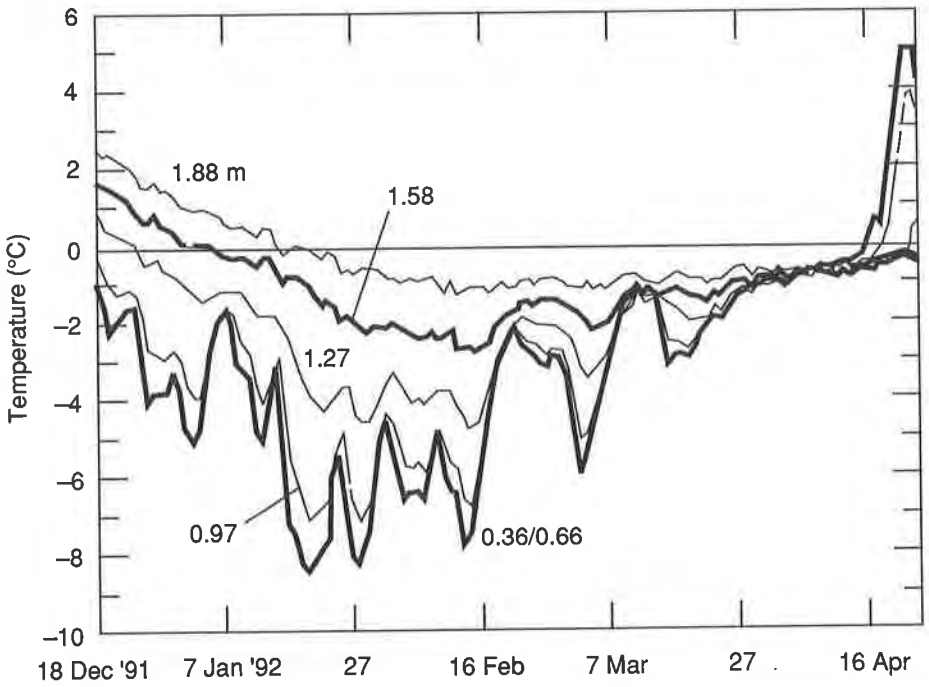

Figure 7. Variation of temperature with time for thermocouples at various depths in test section 1 of the Pittsburg, New Hampshire, geotextile test section.

Table 2. Average frost heave (mm) for Pittsburg, New Hampshire, test sections for 1991–92 freezing season.

	Test section									
Date	1	2	3	4	5	6	7	8	9	10
17 Dec 91	6.8	13.0	11.0	11.0	11.9	7.6	10.4	11.9	10.7	18.3
3 Jan 92	24.4	26.7	21.6	22.3	20.1	18.0	20.1	22.0	20.6	25.9
27 Jan 92	41.2	44.2	34.1	36.6	35.1	32.0	38.1	36.9	40.4	47.2
10 Feb 92	51.1	51.8	42.4	42.7	42.4	37.5	46.0	41.5	47.2	50.3
18 Feb 92	65.5	64.0	57.3	55.2	57.3	46.3	60.4	49.7	63.3	57.2
24 Feb 92	70.9	69.3	59.1	57.6	61.3	49.4	64.3	53.6	67.1	57.9
28 Feb 92	75.4	70.9	65.8	61.0	65.2	53.6	68.3	57.6	71.6	64.8
11 Mar 92	78.5	73.2	69.5	61.6	69.2	53.0	72.2	55.8	74.7	56.4
17 Mar 92	88.4	82.3	79.6	72.5	80.8	63.1	83.2	63.1	84.6	64.8
24 Apr 92	70.9	64.0	64.0	53.6	67.4	45.2	71.6	43.6	71.6	48.8
19 May 92	2.3	9.9	7.6	5.8	8.2	6.7	8.8	8.8	8.4	9.9
8 Jun 92	0.8	8.4	2.7	0.6	2.7	1.2	2.4	2.4	2.3	9.1

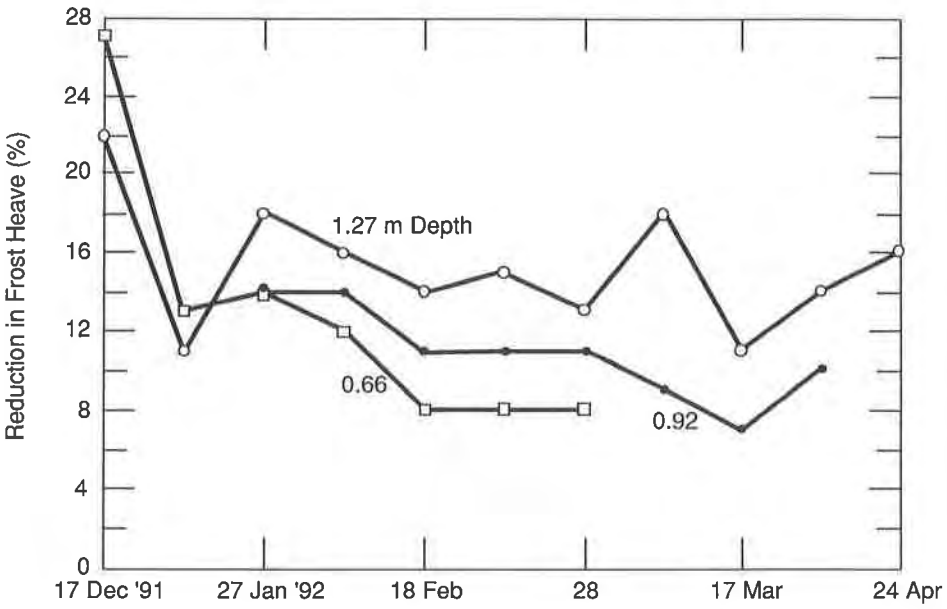

Figure 8. Percent reduction of frost heave due to geotextile presence.

Table 3. Depths of frost penetration, average frost penetration rate and average rate of frost heave for survey dates.

Date	TS no.	Frost penetration (m/in.)	Average rate of frost penetration (mm/day)	Frost heave (mm)	Average rate of frost heave (mm/day)
18 Dec 1991	1	1.031/41		16.8	
	2	0.884/35		13.0	
	8	0.582/20		11.9	
	9	0.813/32		10.7	
	10	0.658/26		18.3	
3 Jan 1992	1	1.534/60	31.4	24.4	0.48
	2	1.252/49	23.0	26.7	0.86
	8	0.968/38	24.1	21.9	0.63
	9	1.336/53	32.7	20.6	0.62
	10	1.107/44	28.1	25.9	0.61
27 Jan 1992	1	frozen		41.1	0.70
	2	1.880/74	26.2	44.2	0.73
	8	1.646/65	28.3	36.9	0.63
	9	frozen		40.4	0.83
	10	1.539/61	18.0	47.2	0.89

were very difficult to interpret for a number of reasons, and are not included in this paper. Eighteen sensors were installed, and only eight gave reasonable values for at least part of the winter. Furthermore, values recorded from some sensors are unstable after dates in which a neighboring sensor began to give erroneous information. The electrical resistance sensors utilized in this project were not calibrated at the time of writing this report, and this information is not yet available.

DISCUSSION

Experimental results show that the geotextiles reduced frost heave. The test sections containing the geotextiles heaved less than the end control sections. Frost heave was evaluated two ways—percentage reduction in frost heave and the total difference in elevation.

Figure 8 shows percentage reduction in frost heave due to geotextile presence on the survey dates for which there was a statistical difference in heave. The geotextiles at 0.66 and 1.27 m show a maximum influence on frost heave early in the season, when freezing temperatures have yet to significantly penetrate the level at which they are placed (see Table 3 for frost penetration). On the first survey date, the shallowest geotextile (0.66 m) exerts the most influence with a 27% reduction in frost heave. After 27 January 1992, the test sections containing geotextile at 1.27 m had the greatest reduction in heave, followed by test sections with geotextile placed at 0.96 and 0.66 m, respectively.

Figure 9 is a graph of the difference in frost heave between the control sections and the geotextile sections (0.66- and 1.27-m geotextile sections). It shows that early in the season, the heave of the

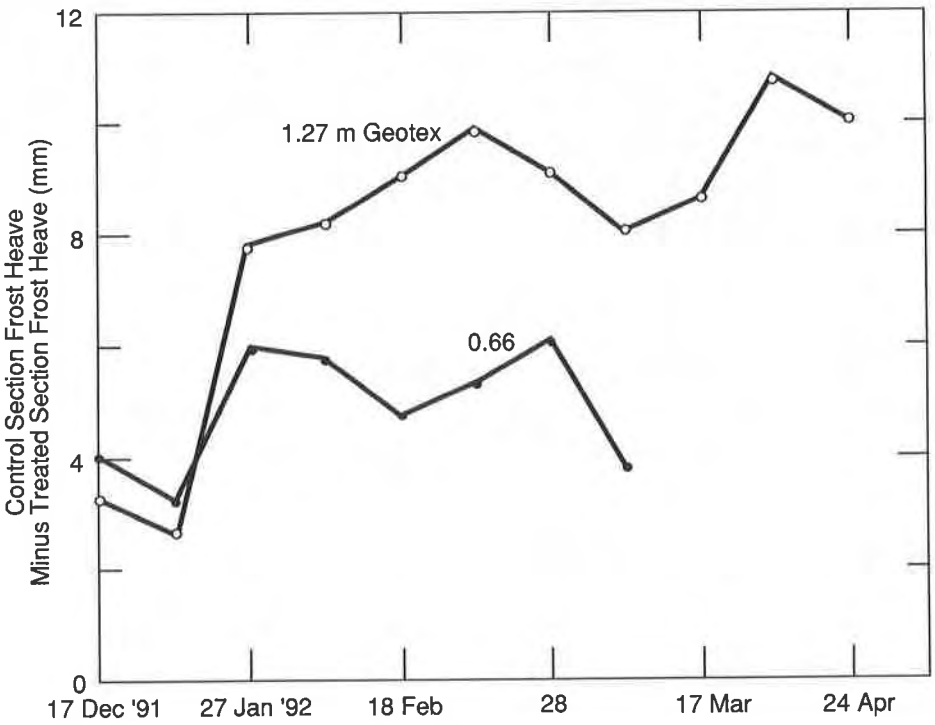

Figure 9. Difference in frost heave between control sections and geotextile treated sections.

test sections containing geotextiles was similar, and then they began to separate at approximately 27 January 1992. The maximum total difference in heave for the sections containing the 0.66-m geotextile occurred on 28 February 1992, with a difference of 6.1 mm (0.24 in.) or a 9% reduction in frost heave. The maximum total difference for the deeper geotextile occurred on 3 April 1992, with a difference of 11.0 mm (0.4 in.) or a 14% reduction.

On the first survey date (17 December 1991), freezing temperatures had just begun to penetrate the 0.66-m depth, the depth of the first geotextile layer (see Table 3). On 3 January, frost was near the 1.27-m level, and on 27 January, it had penetrated well beyond the 1.27-m depth.

The total difference in frost heave due to the presence of the 0.66-m geotextile increased from 3 January, the time at which freezing temperatures were at this level, to 27 January (Figure 9). Likewise, the difference in heave due to the 1.27-m geotextile continued to increase from the date at which frost penetrated that level, 27 January, until 24 February. Thus, the geotextiles reduced frost heave long after freezing temperatures had penetrated them. Figure 8 indicates that they did so; however, this happened by increasingly smaller percentages until there was no statistical difference in elevation.

These results suggest that a "properly designed" geotextile could reduce frost heave for a significant portion of the freezing season, even after frost has penetrated the level at which it is placed. Furthermore, they indicate that frost heave occurred in a large portion of the soil above the "freezing front." This gives good reason to try a "layering" of geotextiles to optimize frost heave reduction.

The center control section, test section 6, heaved significantly less than the two control sections on the east side of the road, as well as less than the sections containing geotextiles that lie on either side of it. This result is most likely explained by the fact that all of the test section instrumentation exited the base and subgrade layers under this section, creating a well-drained area. The wire leads were housed in conduit, and some were laid in an improvised trench of geotextile during construction so that they would be easy to find and splice at later dates. Water was draining from this "trench" shortly after the construction season, and was noted to be draining on 24 April 1992, the first site visit date when snow was absent from the site.

Table 3 shows that the frost penetration rate in the field from 19 December 1991 through 27 January 1992 ranged from 1 1/2 to 2 1/2 times that of the 12.5-mm/day frost penetration rate in the laboratory. The frost heave rates were much lower, however, ranging from 0.12 to 0.23 times those produced in the laboratory. A plot of field data of frost heave vs. frost penetration rate was made, and least squares fit of a line through the data shows the trend that frost heave rate increased as frost penetration rate decreased. Extrapolating this line, the laboratory 12.5-mm frost penetration rate would correlate with a frost heave rate of about 1.3 mm/day. This is about 1/4 that of what was observed in the laboratory, and suggests that field conditions result in significantly less frost heave than that in the laboratory. Furthermore, the geotextiles reduced frost heave by smaller amounts in the field than in the laboratory. From 17 December 1991 through 3 January 1992, the geotextiles at 0.66- and 1.27-m depths reduce the rate of frost heave by 5%; and from 3 January through 27 January 1992, they reduced the rate of heave by 15 and 27%, respectively. However, geotextile presence reduced the rate of frost heave in the laboratory by an average of 60%.

It is worthwhile to consider differences between laboratory and field conditions. The overburden pressure that frost heave must overcome in the field increases as the frost penetration increases. In contrast, the laboratory is set up to include a surcharge of 3.5 kPa to simulate a 15-cm pavement and base overburden at the beginning of the test, and this increases by only 15 cm of soil when the sample is completely frozen. Another condition that is different is the presence of confining pressures around the heaving soil in the field as compared to a frost heave mold that was designed to counteract the effects of side friction to allow free heaving. Water flow in the field during freezing is not restricted to move vertically, and may move horizontally. Soil adjacent to that under the road is probably not frozen as deep as that under the road due to the insulating effect of the snow. This unfrozen soil could act as a source or sink of water during freezing and thawing.

CONCLUSIONS

Based on the research described in this paper as well as past work, the following conclusions are made:

1. Certain geotextiles continue to show promise in reducing frost heave in soils when placed above the water table. Test sections containing geotextiles heaved less than control sections without geotextiles on Rte 3, in Pittsburg, New Hampshire, during the 1991/92 freezing season.

2. Geotextiles in this study continued to reduce frost heave for a considerable time after freezing temperatures penetrated them, although the percentage of reduction decreased after frost penetration. Thus, they may be effective when placed above the greatest depth of frost penetration.

3. Laboratory conditions under which this function of geotextiles have been tested differ significantly from the field conditions during the 1991/92 freezing season. In the laboratory, rate of frost heave and effectiveness of the geotextile is greater.

4. A control section that heaved less than all other test sections probably did so because of drainage unintentionally created where instrumentation exited the pavement section beneath it. For the first freezing season of this test section, providing good drainage was the most effective way to reduce frost heave.

Based on the conclusions made and various observations described above, the following recommendations are made:

1. Future study of this function of geotextiles to reduce frost heave should include a means of correlating laboratory results to results expected in the field.

2. Field studies of geotextiles to reduce frost heave should include the use of more than one layer of geotextile to reduce frost heave.

3. Caution should be exercised when designing future test sections to avoid or control a situation that would result in a condition which, in itself, would reduce frost heave.

The results of this study represent only the initial monitoring phase for this test section. The actual significance and benefits of using geotextiles to reduce frost heave as related to the long-term pavement performance can only be assessed after completion of the long-term monitoring program. However, the initial results are encouraging and indicate an improved condition that should translate into a longer design life for the roadway section.

REFERENCES

Allen, T., J.R. Bell and T.S. Vinson (1983) "Properties of geotextiles in cold regions applications." Transportation Research Report 83-6, Transportation Research Institute. Oregon State University, Corvallis, 275 p.

Berg, R.M. and T. Johnson (1983) "Revised procedure for pavement design under seasonal frost conditions." CRREL Special Report 83-27, U.S. Army Cold Regions Research and Engineering Laboratory, Hanover, NH, 129 p.

Chamberlain, E. and D. Carbee (1981) "The CRREL frost heave test, USA" Frost I Jord. NR22, November, pp. 55-63.

Gold, L.W. (1985) "The ice factor in frozen ground." Chapter 5 in Field and Theory: Lectures in Geocryology, Church, M. and O. Slaymaker, eds., University of British Columbia Press, Vancouver.

Henry, K.S. (1990) "Geotextiles as capillary barriers." Geotechnical Fabrics Report, March/April pp. 30-36.

Henry, K.S. (1991) "Effect of geotextiles on water migration in freezing soils and the influence of freezing on performance." In Proceedings, Geosynthetics "91, Atlanta, GA, p.469-484.

Henry, K.S., S. Taylor and J.E. Ingersoll (1990) "Effects of freezing on the microstructure of geotextiles." In Geosynthetics: Microstructure and Performance, I.D. Peggs, editor, ASTM STP 1076, pp. 147-164.

Holtz, R.D. and W.D. Kovacs (1981) "An introduction to geotechnical engineering." Prentice-Hall, Inc., Englewood Cliffs, NJ 733p.

Hoover, J.M., J.M. Pitt, L.D. Handfelt and R.L. Stanley (1981) "Performance of soil-aggregate-fabric systems in frost-susceptible roads, Linn County, Iowa." Transportation Research Record, No. 827, pp. 6-14.

Jaworski Geotech, Inc. (1988) "Preliminary geotechnical investigation, U.S.Route 3, Pittsburg, New Hampshire." Project No. J87171, January 20, 1988, 217 Rockingham Road, Londonderry, NH 03053.

Natrella, M.G. (1963) "Experimental statistics." United States Department of Commerce, National Bureau of Standards, Handbook 91, U.S. Government Printing Office, Washington, DC.

United States Department of Agriculture, Soil Conservation Service (in preparation) "Nontechnical soils description report for description category - 1SO 2AB 2IN 2PR 6UR: Survey Area- Coos County Area, New Hampshire." USDA-SCS, Lancaster, NH 03584-9612.

Using Geogrids to Limit Longitudinal Cracking of Roads in Interior Alaska

T.C. Kinney
Shannon & Wilson Inc., USA

ABSTRACT

Many roads in Interior Alaska experience lateral spreading resulting in longitudinal cracking of the surface. The lateral spreading is generally caused by thawing permafrost but can be caused by other factors. The rate of spreading can exceed 25 mm per month and many roads require extensive patching several times per year to keep them passable. Several field and laboratory tests have been performed to verify the validity of using geogrids to reinforce laterally spreading roads. This report presents a summary of the design methodology developed and the experimental verification. The results of the study demonstrate that commercially available geogrids can be used cost effectively to reduce maintenance costs in areas where longitudinal cracking is a serious problem. This design methodology is currently being used on roads in Interior Alaska and has been considered for roads over slide areas in other parts of the country. The results appear to be excellent.

INTRODUCTION

Longitudinal cracking of roads in Interior Alaska is a serious problem. Measurements on Farmers Loop Road near Fairbanks indicate that the rate of lateral spreading can exceed 25 mm per month in the spring, summer and fall and extensive patching was necessary several times per year to keep the road passable (Kinney 1992a). Although this is an extreme situation, many roads in Interior Alaska have lateral spreading rates on the order of 25 mm per year or more and require patching at least once a year to keep them safe for the driving public (Kinney 1991). Photograph 1 shows the longitudinal cracking on Farmers Loop Road.

Lateral spreading can be caused by a number of factors including thawing permafrost, creep in the subgrade, and slope instability. Although the mechanism is different for each, the result is the same in that the subgrade spreads laterally leaving cracks in the embankment, base and surfacing material.

One method that is being considered to alleviate this problem is to reinforce the upper portion of the roadbed with a geogrid to keep it from spreading along with the materials below. This report presents a summary of the design methodology developed and the test results used to verify its validity.

Photograph 1 - Longitudinal Cracking on Farmers Loop Road

BACKGROUND

In the spring of 1987 a technique for using geogrids to limit longitudinal cracking was suggested by the author to the Alaskan Department of Transportation and Public Facilities for the reconstruction of the southern 30 miles of the Tok cutoff in Interior Alaska. It was necessary to prove the technology before it could be specified hence a large scale field test was constructed in the summer of 1987 to demonstrate that the technology was viable and economically advantageous. A short section of road was constructed with one lane placed on a series of wooden platforms. The platforms were pulled away from the centerline of the road to simulate the subgrade cracking. A crack up to one meter wide was created and a fully loaded dump truck was used to traffic the road with one wheel path directly over the cracked subgrade. Photograph 2 shows a cross section of the test section after trafficking. The time from inception to the finish of the test was on the order of three weeks. The viability of the technology was established and the road was designed and constructed using the technology (Kinney and Savage 1989).

The test was valuable but very limited in scope. In the spring of 1988 a test section on Farmers Loop Road near the University of Alaska Fairbanks was chosen for a full scale test. The road had been experiencing longitudinal cracking at the rate of about 25 mm per month and was badly cracked and patched as shown in Photograph 1. The upper 1.4 m of the road was excavated for a distance of about 50 m and reconstructed. The test consisted of a control section at each end that was minimally disturbed with two geogrid reinforced test sections and one unreinforced control section in the reconstructed area The test showed that the geogrid dramatically limits the longitudinal cracking, improves serviceability, and reduces the maintenance intervals (Kinney 1992a). Photograph 3 shows the area after three years. The photograph shows one test section with control sections on each end. The control sections have been patched several times to make the road serviceable. The entire section was repaved once to smooth out the patched sections.

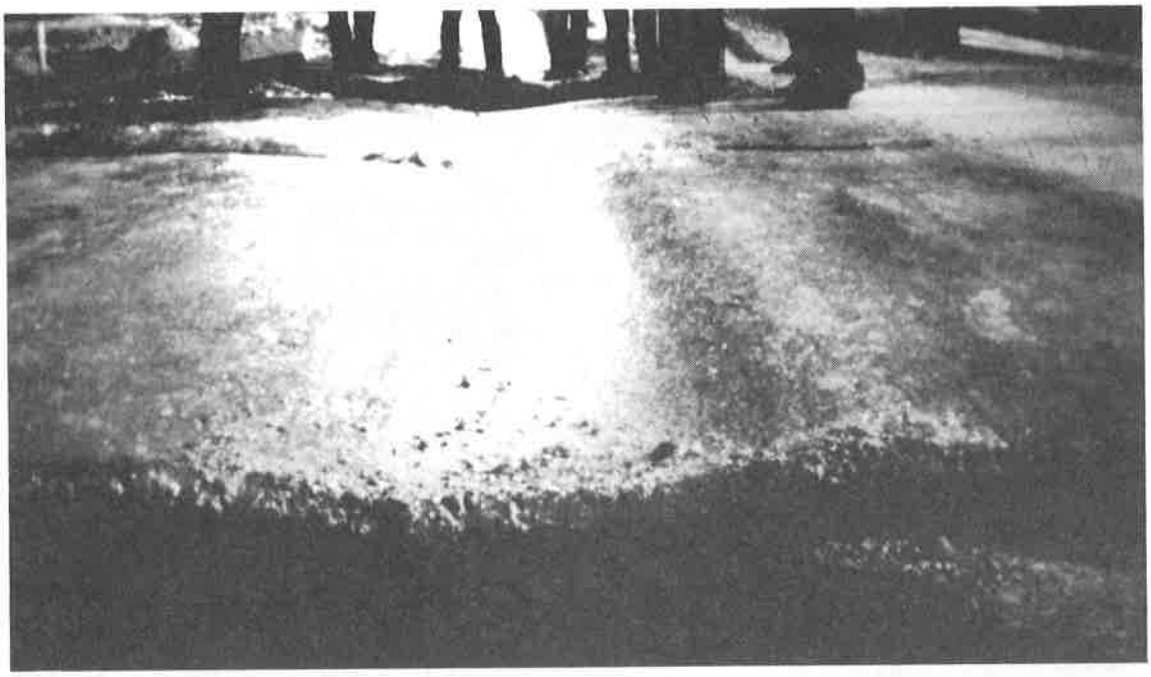

Photograph 2 - Cross Section Through the 1987 Field Test

Photograph 3 - Test Section on Farmers Loop After Three Years

A second large scale field test was constructed during the fall of 1989 to test different geogrids in different configurations. This test resembled the 1987 test but with significantly more sophistication in the data collection and over twice as many different conditions being tested. This test series demonstrated

clearly that some geogrids perform better than others and that the design methodology was valid. Photograph 4 shows the test sections after trafficking.

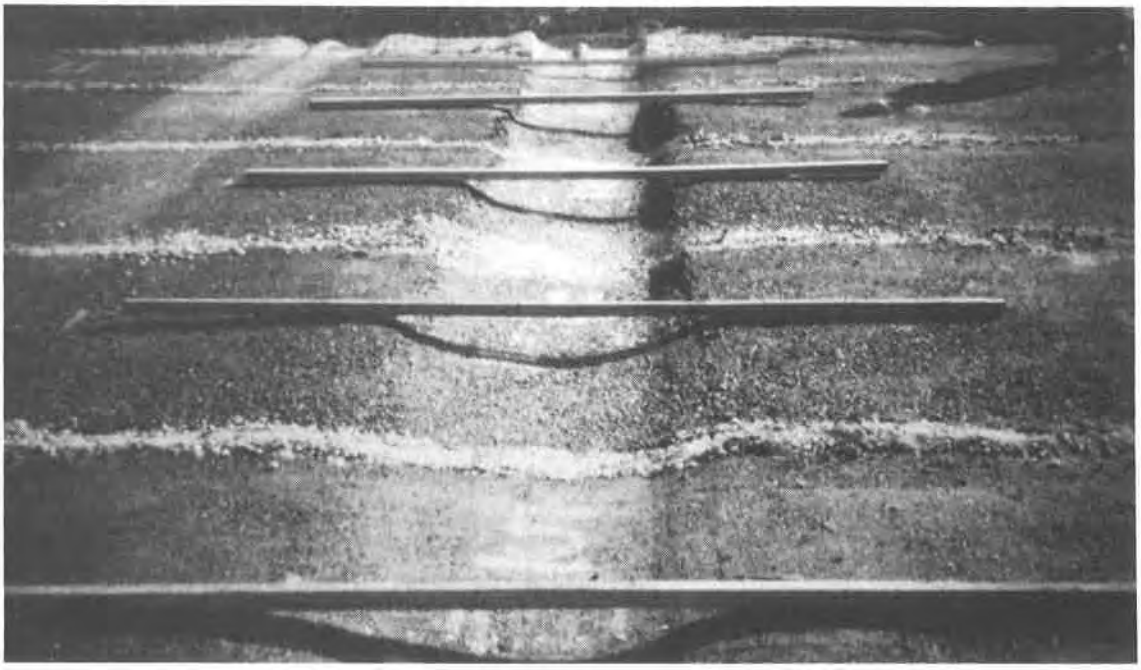

Photograph 4 - 1989 Field Test Sections After Trafficking

Two large scale laboratory test series were constructed in the fall of 1988 to further define the design constraints (Savage 1990 and Neogi 1991). These tests were constructed in a box that was 7.3 m long, 1.2 m deep and 0.6 m wide which was made to represent a thin slice out of a two lane road. One half of the bottom of the box was pulled away from the centerline to simulate the crack development in the subgrade. The results were interesting but not particularly applicable since the material placed over the geogrid was not the same as used in real roads and there were significant edge effects.

Additional laboratory work has been done in the summer of 1990 at the U.S. Army Cold Regions Research and Engineering Laboratory to further refine some of the design parameters.

This report presents the design technique developed as a result of all of these activities.

THEORETICAL DISCUSSION

An embankment will go through two independent stress-strain conditions during development of longitudinal cracks. The first takes place when the subgrade is being stretched and cracking occurs; the second takes place when the traffic load is applied over the stretched embankment. In roads, these two mechanisms take place simultaneously, whereas in the test situations the subgrade was stretched and then the loading was applied. The two mechanisms are discussed separately below because that is the way the tests were performed and therefore that is the way the tests have verified the validity of the theory.

Performance During Subgrade Stretching. The field tests were designed to represent a short section of road. One side of the road was constructed on a silt

subgrade while the other side was constructed on wooden platforms as shown in Figure 1 and Photograph 5. The wooden platforms were pulled out from under the road simulating the condition where one-half of the subgrade was sliding out away from the centerline as shown in Photograph 6. This represents a condition which is common in Alaska over permafrost terrain and exists throughout the world in slide areas.

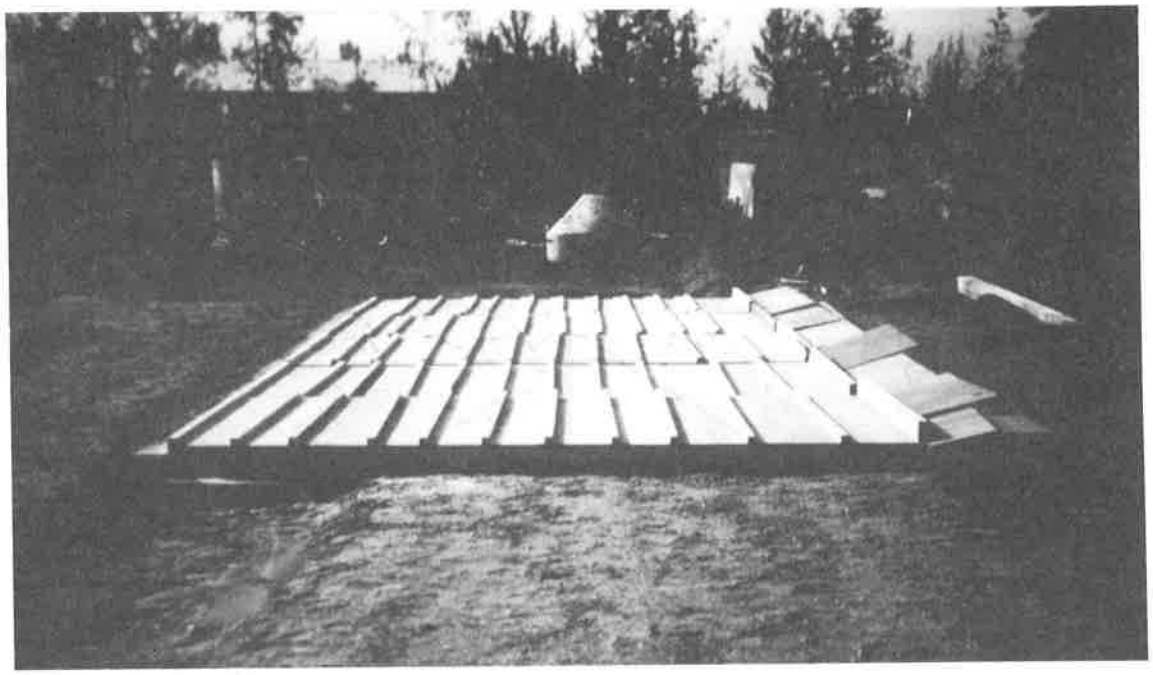

Photograph 5 - Wooden Platforms Under One Side of the 1989 Field Tests

The 1989 test consisted of five test sections each 2.5 m long. The subgrade was compacted and the platforms were constructed to an elevation of 300 mm or 450 mm below final grade. Fifty mm of sand and gravel were compacted over the width of the road and a geogrid was placed over the compacted sand and gravel. A standard paved road section consisting of base, subbase, and asphalt was constructed over the geogrid. One test section had two layers of geogrid at depths of 150 mm and 300 mm, respectively. The road was positioned off-center so that 3.4 m of the road surface was over the platforms and 4.0 m of the road surface was over the silt subgrade as shown on Figure 1. This was done so that the end of the geogrid under the outside edge of the pavement over the silt subgrade would not move when the wooden platforms were pulled out creating the void.

The mechanism creating the stresses and strains during stretching in the test is straightforward. When the platforms are pulled out, resistance to lateral spreading of the road is developed through the geogrid to the other side of the road. The platforms were moved far enough to get complete slippage between the soil on the platform and the geogrid immediately above. The geogrid was shorter over the platforms than it was over the other side, hence the end of the geogrid farthest from the platform never moved. The conditions that existed are discussed below starting with the simplest system and progressing with more complexity until each of the conditions encountered in the test are discussed. Please note that the following discussions consider a two dimensional system. In the analyses of the tests the end effects on the test sections were considered.

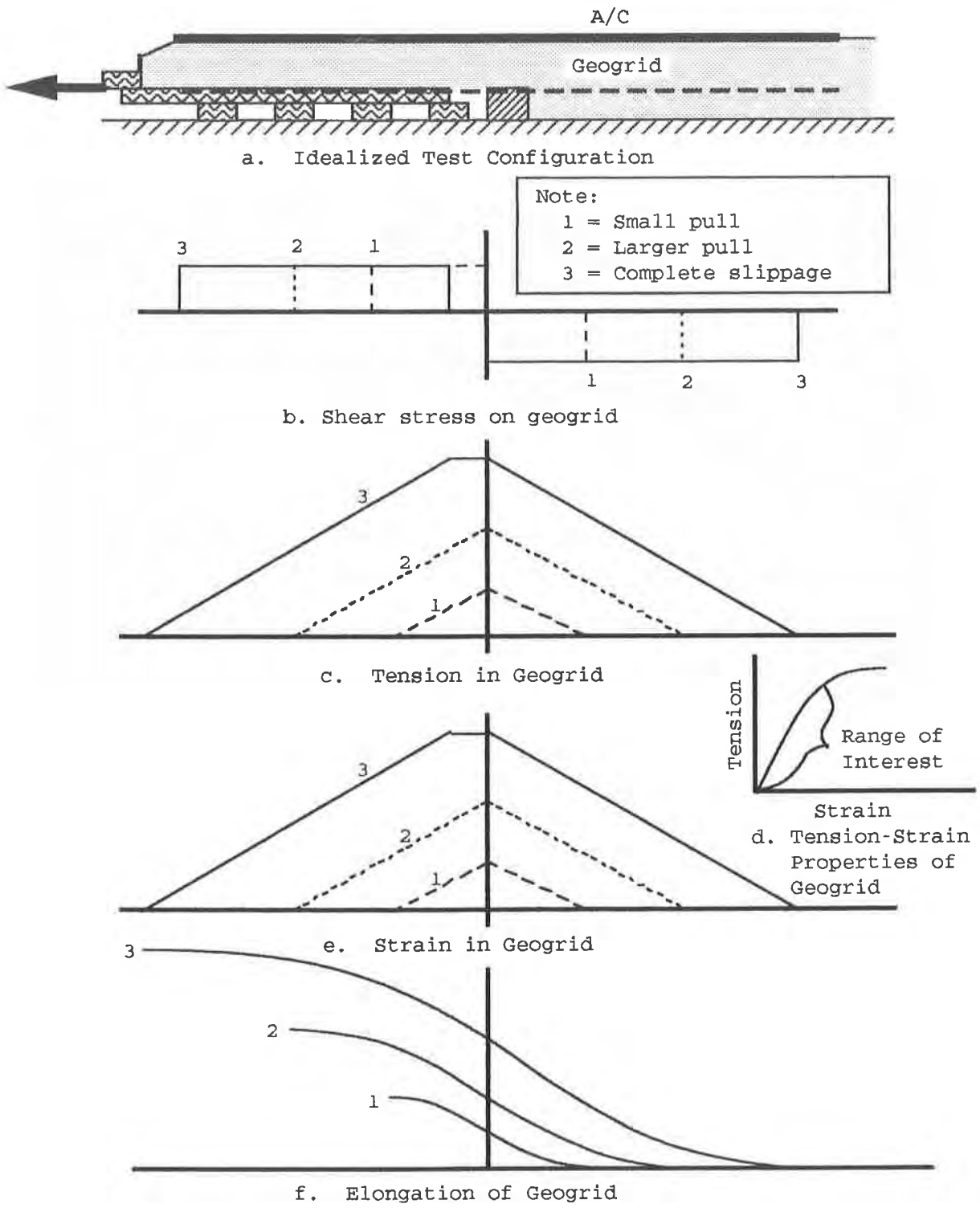

Figure 1. Tension, Strain and Elongation in the Geogrid
Single Layer of Geogrid without Restraint above Geogrid

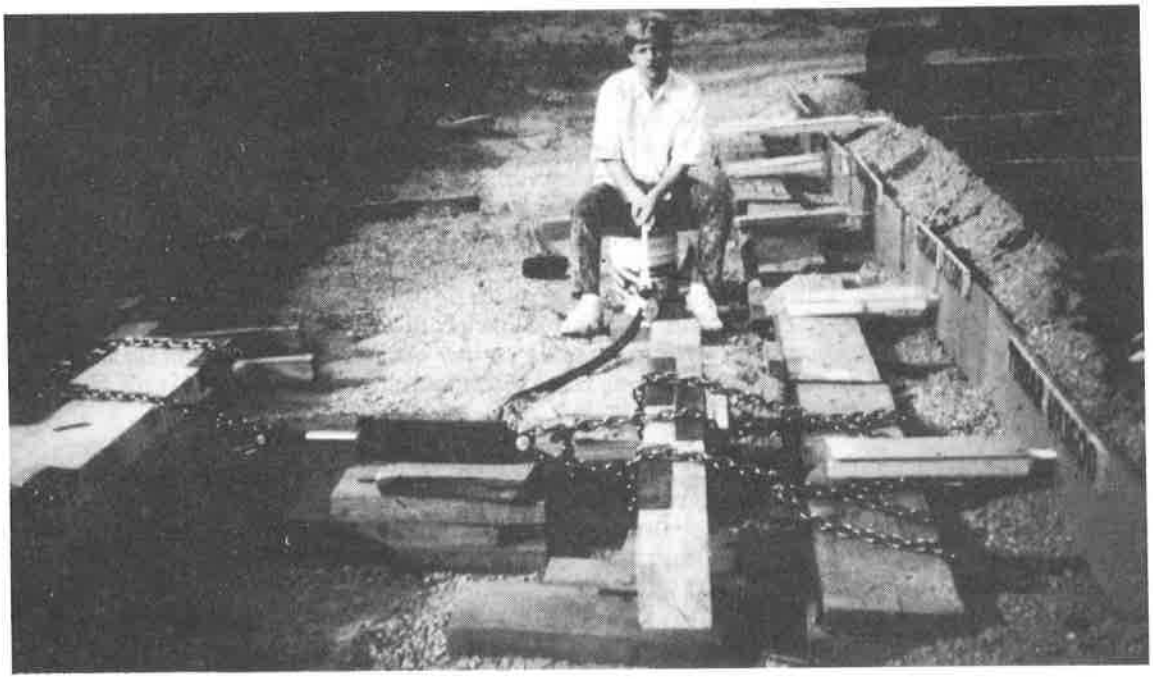

Photograph 6 - Wooden Platforms Being Pulled Out From Under the Road in the 1989 Large Scale Field Tests

Single Layer of Geogrid without Restraint above Geogrid. There are several limiting conditions that exist in this scenario. If there is no tension member above the geogrid, then there can be no tension in the materials above the geogrid and therefore no shear stress can be created on top of the geogrid. There isn't any way to get the resistance needed above the geogrid for shear stresses to develop. Given that all of the shear stress on the geogrid will come from below, the maximum shear stress that can be developed is the shear strength at the boundary between the geogrid and the soil. Since the geogrid openings were large in relation to the particle size and the soil was compacted over the geogrid, it would be reasonable to assume that the shear strength at the boundary would approximate the strength of the soil. If more detailed information were available, it could be used. With the shear stress known, the tension, strain and elongation of the geogrid can be determined mechanistically with the help of Figure 1.

It is easiest to back into the analysis by plotting a generic set of graphs based on expected trends, calculating the coordinates that are known directly and then calculating the coordinates of other points from the known points on that and other graphs. Assume a shear stress distribution on the geogrid as shown on Figure 1b. It is convenient to assume that there is full shear stress developed over a given distance from the edge of the void and no shear stress elsewhere, however there is no requirement in the procedure to do this. The assumption of full shear stress and no shear stress is quite good in situations where a low modulus geosynthetic is used and a small amount of relative displacement between the geogrid and the soil below will create full shear stress. Even though these tests were performed with a high modulus material and something on the order of 3 mm of relative displacement was probably required to develop full shear stress in this test, the assumption still leads to reasonable results and the error introduced by assuming an abrupt change from full to no shear stress is small. This assumption could be completely eliminated in a second iteration if the mechanical properties of the system were known in sufficient detail to warrant the added sophistication.

The tension in the geogrid, Figure 1c, is calculated from the stress on the geogrid by integrating the shear stress over the area of the geogrid starting with no tension at the end of the zone where shear stress is present nearest the edge of the road. Knowing the tension in the geogrid, the strain in the geogrid, shown on Figure 1e, is calculated from the tension-strain relationship for the geogrid shown on Figure 1d. It is convenient, and frequently reasonably accurate, to use a linear relationship for the tension versus strain but there is no requirement for that in the procedure. Once the strain in the geogrid is known it is a simple procedure to determine the elongation of the geogrid as shown on Figure 1f. Simply integrate the strain over the length starting at the point in the geogrid on the stationary side of the road where there is no strain. The maximum elongation in the geogrid is the amount that the platform was moved up to the point where complete slippage had occurred.

This procedure can be redone for other shear stress diagrams, Figure 1b. It is then straightforward to draw relationships between the behavior of the geogrid and the amount the platform is moved. Once the platform has been moved far enough to create full shear stress on the entire length of geogrid over the platform the analysis is essentially over. Further movement of the platform only changes the conditions in that there is no shear stress over the void and the length of the geogrid over the platform gets shorter as the void gets wider.

Note that, without any ability to carry tension, the materials over the geogrid must expand and move with the geogrid. The expansion should loosen the material and cause some thinning of the fill.

Effect of Asphalt. Adding asphalt to the surface has two effects. First it acts as tensile reinforcement and second it may show the results of the stretching more than the soil.

Asphalt is a viscous material and as such will relax if put into tension. The resistance of asphalt to tension is a very complicated function of stress, strain, time and temperature. In general, the tensile strength of asphalt is several hundred kPa which would result in a maximum tension of several thousand Newtons per meter. The actual tension is limited by the shearing resistance along the bottom of the asphalt and therefore the maximum actual tension will be on the order of several hundred Newtons per meter. Therefore, the asphalt should slide along the soil surface and not break. The asphalt will break if the tensile strength is low which can result if the asphalt is cracked by other phenomenon such as fatigue, temperature or vertical deformation. The amount of relaxation of asphalt is more, and hence the tension is less if the asphalt is new, strain rates are slow, temperatures are warm and/or there is increased traffic during straining.

If the asphalt has a high tension modulus in relation to the geogrid and the soil has a high shear modulus, then virtually all of the shear stress on the bottom of the asphalt will be transmitted to the top of the geogrid. This shear stress could be added directly to the maximum shear stress that will develop on the bottom of the geogrid as discussed before. The shear modulus of the compacted crushed rock base course used in these tests is expected to be large enough to behave rigidly for purposes of these calculations. Cured asphalt at low temperatures would have a very high modulus in relation to the geogrid. This test was done within a few days of placing the asphalt and its modulus may have been very low resulting in virtually no additional tensile stress, and subsequently virtually no added shear stress was transmitted to the geogrid.

Multiple Layers of Geogrid. The following guidelines are used to create the shear stress, tension, and elongation diagrams for a two layer system.

a. The lower layer of geogrid is elongated because the platform is moved outward.
b. The shear stress on the bottom of the bottom geogrid above the platform is the same as it was without an upper geogrid layer.
c. The upper layer of geogrid will be stretched because the lower layer of geogrid is stretched.
d. All parts of the bottom geogrid that move, move toward the edge of the road on the side with the platform.
e. All of the shear stresses on the bottom of the upper geogrid would be in the direction of the movement of the lower geogrid if the upper geogrid were anchored.
f. Since the upper geogrid is not anchored it must slip at the end farthest from the platform.
g. Since the maximum shear stress possible on the upper geogrid is the same across its entire length, the shear stress must be opposite on the two ends and change direction at the center.
h. The shear stress on the bottom of the bottom geogrid will be greater than the shear stress on the bottom of the top geogrid because the overburden pressure is more at the plane of the bottom geogrid.
i. The center of the upper geogrid will not change relative location with the lower geogrid. This assumption is not necessarily accurate but the results will be reasonable.
j. The shear stress on the top of the bottom geogrid and the bottom of the top geogrid will be equal and opposite.

With these guidelines one may estimate the shear stress, tension and elongation diagrams shown in Figure 2.

Performance During Trafficking. After the crack formation and before trafficking, the stresses and strains discussed above have developed. The wheel load is then carried over the void by a combination of bridging within the soil and tension in the geogrid.

From a purely elastic standpoint the wheel loads will be distributed outward with depth. The effects of this on the plane of the geogrid can be estimated with reasonable accuracy in a homogeneous soil mass. In a soil mass where there is a soft zone under the load, the analyses are severely complicated. Several design techniques are available, however none of them approximate the situation presented in this series of tests. However, elastic theories, field and laboratory tests, and numerical solutions, all show that the loads are distributed more rapidly if the surface layer is stiffer than the underlying layers. The larger the difference, the wider the distribution.

In the geogrid reinforced sections the geogrid helps spread out the load through a combination of shear stresses on the soil outside the void, upward pressure on the soil above the void and downward pressure on the soils at the edges of the void. In addition, the granular materials over the void are confined and hence stiffened by the interaction with the geogrid. The stiffening of the granular soils allow them to spread the load out more. There have been attempts to quantify some aspects of the load carrying capability of the geogrid (Kinney 1979, Kinney 1986, Kinney and Connor 1987, Kinney 1988, Kinney and Conner 1990, Kinney 1992a and Kinney 1992b) but to date it is not possible to quantify the entire performance.

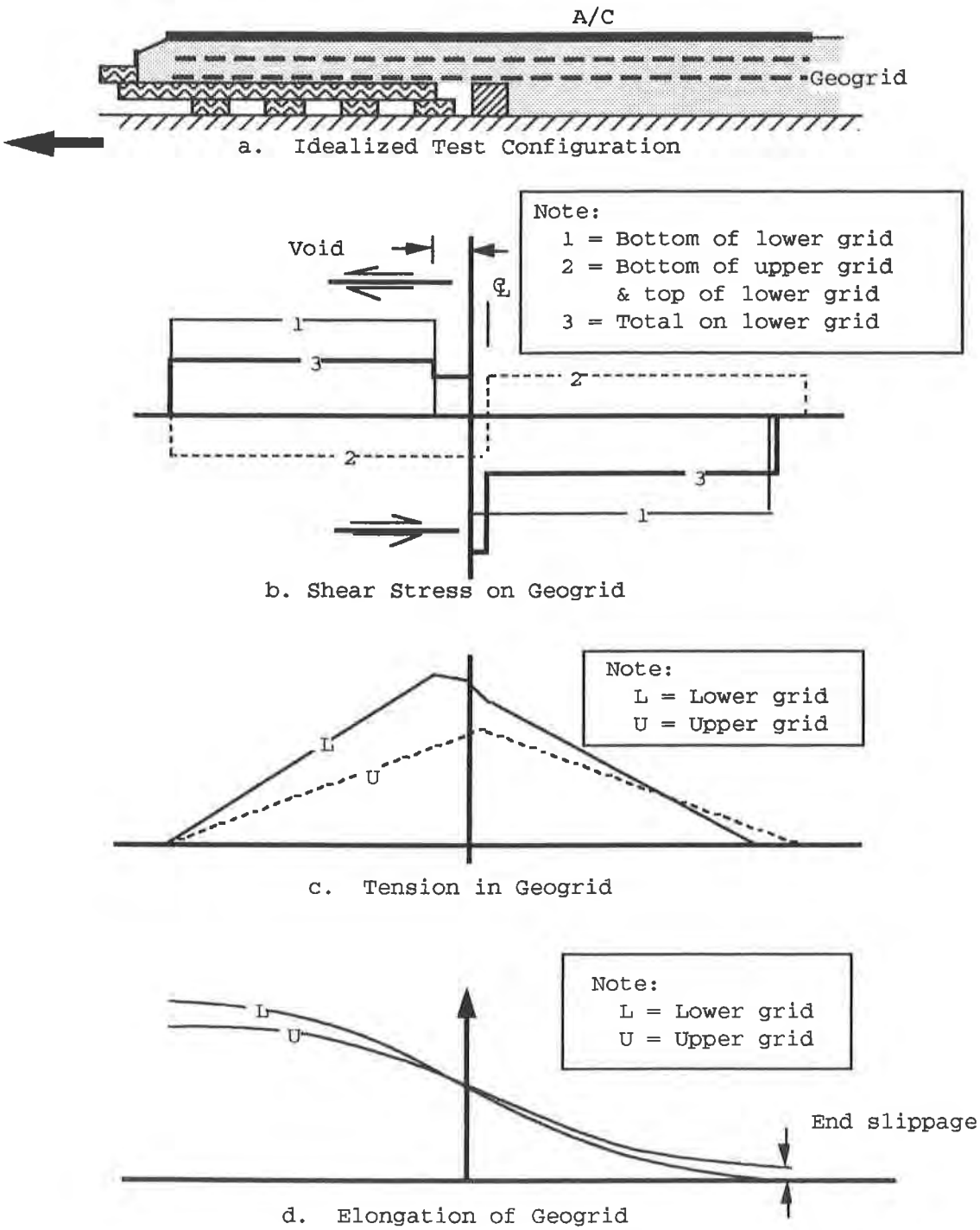

Figure 2. Tension, Strain and Elongation in the Geogrid
Two Layers of Geogrid without Asphalt

FIELD VERIFICATION

Several field and laboratory tests have been performed to verify the theory presented above. The field test on Farmers Loop Road near the University of Alaska Fairbanks (Kinney 1992a) is of particular interest because it is an actual road and it graphically shows the benefits of using the technology. Photograph 1 shows a crack that had opened up in the road within two weeks after patching in the summer prior to construction of the test sections. Measurements over several months indicated that the road was spreading laterally at the rate of at least 25 mm per month throughout the spring, summer and fall.

The road was excavated 1.4 m through asphalt patching and rebuilt using three control sections and two geogrid reinforced test sections. Little, if any, cracking was noted the first year even though the road spread laterally several cm. It is speculated that this was due to the complete reconstruction of the road which allowed the embankment materials to withstand significant lateral spreading by loosening. The asphalt was new and could creep under traffic loading as the embankment spread. The control sections showed considerable cracking and vertical deformation in the second and third years and had to be heavily patched each year. The geogrid reinforced sections showed hairline cracking and no vertical deformation. While patching the control sections at the end of the third year the entire section was overlain because the patched control sections were now higher than the reinforced sections.

Early in the following summer the control sections had several centimeters of cracking and several centimeters of vertical deformation. The geogrid reinforced sections showed up to 25 mm of cracking at the surface but no vertical deformation. Photograph 3 shows the road section with the heavily cracked control sections and the lightly cracked reinforced sections. Photographs 7 and 8 show close-ups of the control and reinforced section cracks. Remember that the control sections had to be patched twice while the reinforced sections had not shown any cracking up to this point.

CONCLUSIONS

Theory and tests have demonstrated that geogrids can be used effectively to limit longitudinal cracking of roads in Interior Alaska. A theory has been developed and proven which will allow design of the section. The technology has been used on roads in Alaska and is expected to be used more in the future. This same technology has been considered in landslide areas in other parts of the country.

ACKNOWLEDGMENTS

The author gratefully acknowledges the following funding agencies: The Tensar Corporation, The Signode Corporation and The State of Alaska Department of Transportation and Public Services(AK DOT&PF). In-kind services in terms of personnel and equipment were donated by: Shannon and Wilson, Inc., H&H Contractors, and AK DOT&PF. Bonny Savage and Jon Bolles received M.S. Degrees on various phases of the project and in doing so devoted many extra hours to the projects. The personal assistance from Bob McHattie and Billy Connor with the AK DOT&PF is especially appreciated.

Photograph 7 - Cracks in the Center Control Section

Photograph 8 - Cracks in Reinforced Section

REFERENCES

Kinney, T.C. (1992b). "Using Tensar geogrid to limit longitudinal cracking in Interior Alaskan roads - a field test." Research report to the Tensar Corporation, Morrow, GA.

Kinney, T.C. (1992a). "The use of geogrids to limit longitudinal cracking on Farmers Loop Road in Fairbanks Alaska." Research report to State of Alaska Department of Transportation and Public Facilities, Fairbanks, AK.

Kinney, T.C. (1991). "Rate of lateral spreading of Interior Alaskan roads." Research report to State of Alaska Department of Transportation and Public Facilities, Fairbanks, AK.

Kinney, T.C. (1988). "Tensile reinforcement of road embankments on polygonal ground using geosynthetics." Report FHWA-AK-RD-87-27 for the Alaska Department of Transportation and Public Facilities, Fairbanks, AK.

Kinney, T.C. (1986). "Reinforced roads bridging voids." Proceedings, Fourth International Conference on Cold Regions Engineering, Anchorage, AK, W.L. Ryan, ed., American Society of Civil Engineers, New York, NY, pp. 320-329.

Kinney, T.C., (1979). "Fabric induced changes in high deformation soil-fabric aggregate systems." Thesis submitted in partial fulfillment of the degree of Doctor of Philosophy at the University of Illinois, Urbana-Champaign IL.

Kinney, T.C, and Abbott R.D, (1984). "Geotextiles used to reinforce roads over voids." Third International Conference on Cold Regions Engineering, Edmonton, Alberta, Canada, D.W. Smith ed., Canadian Society of Civil Engineering, Montreal, Quebec, V.1, pp. 493-505.

Kinney, T.C. Connor, B. (1990). "Geosynthetic reinforcement of paved road embankments on polygonal ground." Journal of Cold Regions Engineering, American Society of Civil Engineers, New York, NY, V4. No. 2.

Kinney, T.C. and Connor, B. (1987). "Geosynthetics supporting embankments over voids." Journal of Cold Regions Engineering, American Society of Civil Engineers, New York, NY, V4, pp. 158-170.

Kinney, T.C. and Savage, B.M. (1989). "Geosynthetics to control lateral spreading of pavements in Alaska - preliminary results." Geosynthetics '89, San Diego, CA, Industrial Fabrics Association International, St. Paul, MN, V.2, pp. 6-13.

Neogi, D. (1991). "An analysis technique using geogrids for limiting lateral spreading of road surfaces and bridging voids." Thesis presented in partial fulfillment of the degree of Master of Science in Civil Engineering at the University of Alaska Fairbanks, Fairbanks, AK.

Savage, B.M. (1990). "Laboratory tests on the use of geogrids to limit longitudinal cracking." Project presented in partial fulfillment of the degree of Master of Science in Civil Engineering at the University of Alaska Fairbanks, Fairbanks, AK.

WALLS, SLOPES, EMBANKMENTS AND FOUNDATIONS

GEOSYNTHETICS '93
CONFERENCE
VANCOUVER, BRITISH COLUMBIA

Instrumentation and Performance of a Tilt-Up Panel Wall

M.A. Knight
University of New Brunswick, Canada

A.J. Valsangkar
University of New Brunswick, Canada

ABSTRACT

A 6.1 m high tilt-up panel wall with geogrid reinforcement was constructed in Fredericton, New Brunswick, Canada, in 1990. The wall was instrumented to monitor: rib strains in geogrids; axial force in temporary prop used during construction; temperature variations in the ground; and lateral earth pressures on the wall panel. The wall movements were monitored by precision survey technique developed at the University of New Brunswick.

This paper describes the details of the instrumentation, and results of the field monitoring. The unique features of this study are: i) use of precision survey to monitor wall movements; ii) behaviour of temporary props during construction; iii) effect of temperature on strain gage readings and iv) effect of construction procedures such as pretensioning of geogrid on strains in geogrids.

INTRODUCTION

In North America, the first reported case of using geosynthethics as a soil reinforcement was in 1974, when a 2.7 m high wall was constructed in the Siskiyou National forest in Oregon (Yako and Christopher, 1988). It was estimated by 1987 that in the order of 200 polymeric reinforced walls and slopes had been constructed (Yako & Christopher, 1988). Out of these projects, 13 retaining walls and slopes were instrumented.

The design of these retaining structures is based on the results of many laboratory and model tests along with conventional design theories. Since there are few instrumented sections that can support the design hypothesis, engineers and researchers are still not confident with the mechanism of interaction between the reinforcement and soil structure. The research reported in this paper was therefore undertaken to study the behaviour of a specific prototype precast waffled concrete panel tilt-up retaining wall known as Waffle-Crete^{R}.

LITERATURE REVIEW

Of the thirteen case studies reported by Yako and Christopher in 1988, only four were geogrid reinforced retaining walls. Since 1987, an additional four instrumented retaining wall projects have been reported in the literature. An extension of Yako and Christopher's 1988 summary of instrumented geogrid walls is given in Table 1.

Ref	Project Name	Location	Year Constr	Structure	Height (m)	Facing	Instrumantation Details
Kutura et.al. 1990	Prototype polymer grid wall	Japan	1988	Full scale test wall	6.0	Precast con-crete panels	Strain gages, Settlement board, Observation points
Jones et. al 1990	Dewbury Ring Road	Yorkshire England	1988	Trial reinforc-ed retaining wall	6.0	Precast con-crete ties	Inductance coils strain gages, Reference points
Simac et. al 1990	Algonquin Full Scale Test Wall	Algonquin Illinois USA	1989	Full scale test wall	6.1	Dry stacked soil filled incre-mentals	Extensometers, Stain gages, Inclinometers Total pressure cells
Bathurst 1991	Highbury Avenue Wall	London, Ontario Canada	1989	Vertical retaining wall	1.25 to 7.1	Full height rein-forced precast panels	Strain gages, Inclinometers, Thermocouples

Table 1. Reported Case Studies of Instrumented Geogrid Retaining Walls

Yako and Christopher, 1988 concluded that it is very difficult, if not impossible, to develop definitive conclusions from the projects surveyed due to significant variations in the instrumented structures, type of backfill, type of reinforcement, facing, instrumentation and construction sequence. This statement is still valid with additional data from instrumented walls.

PROJECT DESCRIPTION

The Site The Carriage Place project site is located north of the Trans Canada Highway on the Hanwell Road in the southwestern part of Fredericton, New Brunswick, Canada. Prior to the wall construction, the site sloped gently to the northeast and at a slightly steeper grade to the southeast towards a gully. The site is bound by an automotive dealership to the northwest and a strip mall to the southeast. The project consisted of building a 5824.8 square metre strip mall along the southeast part of the property (Figure 1). Due to the site's sloping nature and property limitations, a retaining wall was determined to be an economical means for site development.

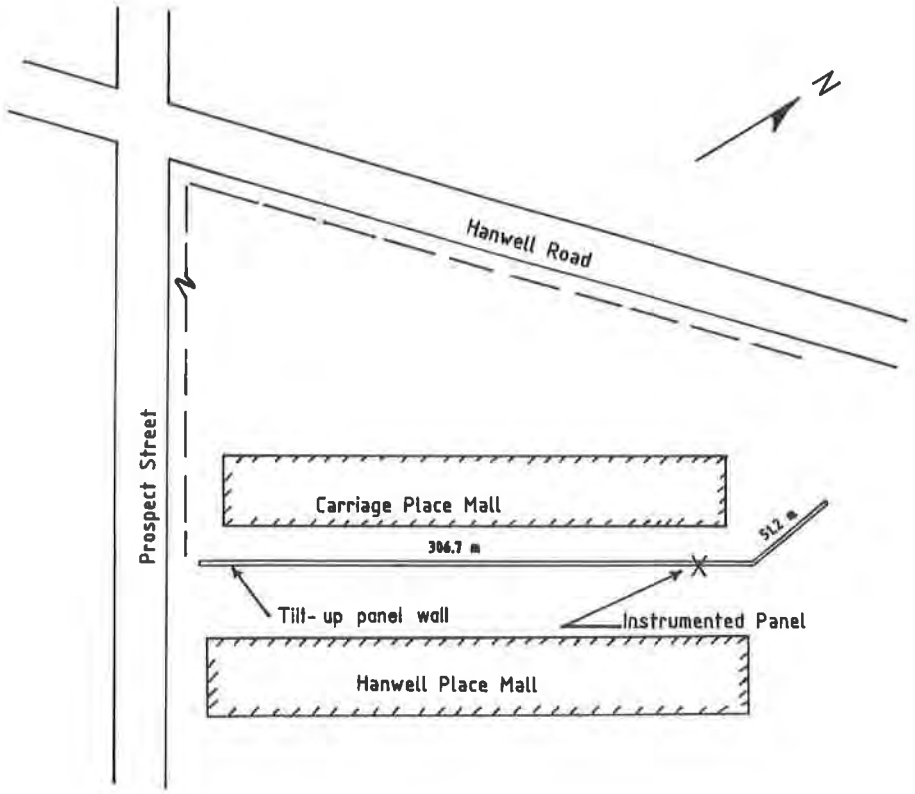

Figure 1. Plan View of Wall

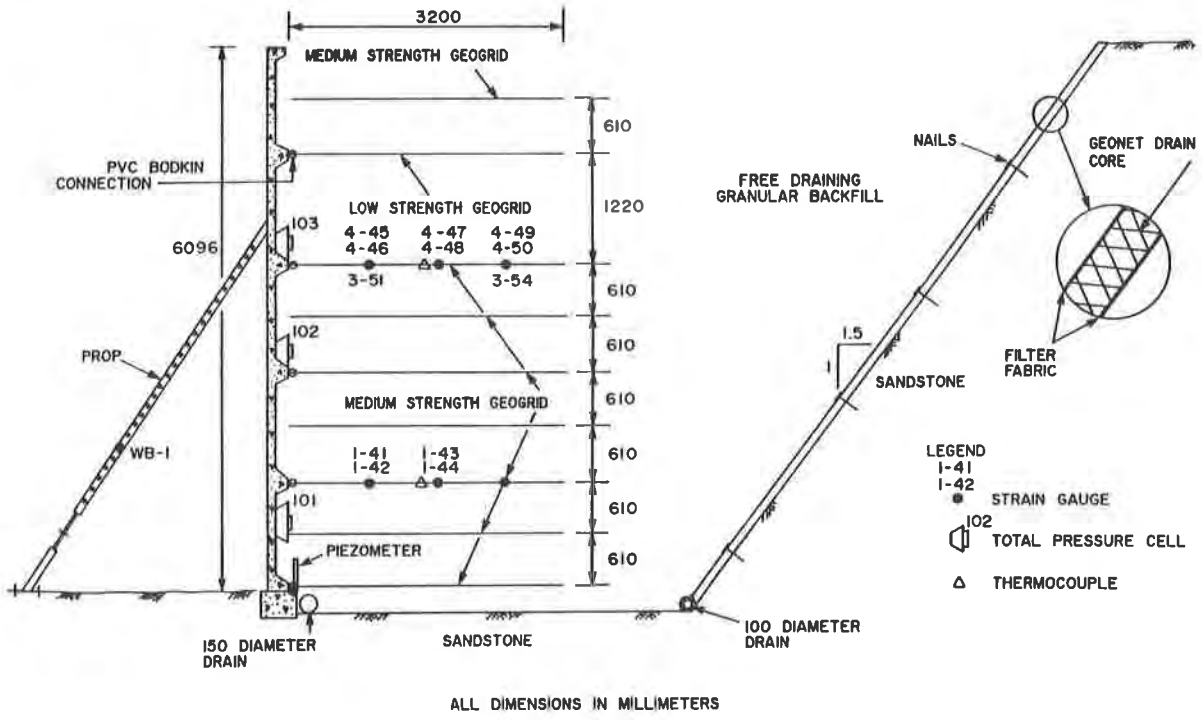

Figure 2. Cross Section of Instrumented Wall Panel

The soils at the site consisted of compact to dense silty sand and gravels generally less than 1.0 m thick, overlying medium to coarse grained horizontally bedded sandstone. The surficial soils are inferred to be glacial tills.

Design of the Wall

The wall, 389.5 metres in length, consisted of individual precast waffled concrete tile-up panels and geogrid soil reinforcement, patented under the Tensa-Crete™ soil structure system. The wall design was carried out by Gordon Wilson and Associates Inc.. The precast facing panels were 2.6 metres wide and varied in height from 2.65 to 6.97 metres. The facing panels were erected by Maritime Precast Ltd., on a 406 mm unreinforced concrete strip footing and fixed to the footing by 12.5 mm diameter and 254 mm long galvanized pins placed in the footing during concrete placement.

Primary geogrid soil reinforcement was mechanically attached to the panel at a vertical spacing of 1.22 meters. At each placement elevation, two adjacent 1.0 meter widths of geogrid reinforcement were placed with principal strength direction perpendicular to the wall face, providing 77 percent coverage of the 2.6 m panel width. Additional unattached geogrid reinforcement was placed between attached geogrid layers to increase internal stability. Based upon design calculations, a total of 8 medium strength (120 yr design strength of 16 kN/m) HDPE geogrids (Tensar SR-2), and one low strength (120 yr. design strength of 8 kN/m) HDPE geogrid (Tensar SR-1) were required as shown in Fig. 2. The method of analysis given in Tensar Technical note (1986) was utilized to determine reinforcement layout.

Adjacent panels were connected via 16 mm diameter friction fit steel pins in precast holes every 1219 mm vertically. The retained backfill material consisted of 76.2 mm minus pit run sand and gravel with approximately 12% passing the 75 μm sieve, which was assigned an internal angle of friction, ϕ, of 35 degrees.

Drainage was provided as per the details shown in Fig. 2.

Wall Construction. The construction of the wall was carried out during the periods of November to December 1989 and April to June 1990. The construction began in early November at the southeast end of the wall. By mid December 1990, the wall construction was halted due to winter conditions. Construction resumed in April 1990, and was completed by the end of June 1990.

The sequence of construction was:

1) Excavation of sandstone rock and overburden soils was carried out with a back slope of 1.5 horizontal to 1.0 vertical extending 4.5 metres behind the wall footing (Figure 2).

2) In situ soils were compacted prior to the placement of a cast in place concrete strip footing, 406 mm wide by 205 mm deep.

3) Subsequent to step 2, installation of inclined drainage blanket and footing drains was completed.

4) Precast full height tilt-up facing panels were erected on the strip footing between galvanized pins. Panels were propped and battered 2% towards the backfill.

5) Sand and gravel backfill was placed and compacted to the level of the first reinforcement layer.

6) Two adjacent 3.4 metre long by 1.0 metre wide geogrid strips were attached to short geogrid tabs embedded within the horizontal ribs of the panel.

7) Each geogrid layer connected to the wall was pretensioned using an adjustable fork rake consisting of two pipes. Tension was applied by extending the rake against the precast panel. Approximately 300 mm of backfill was placed on the tensioned geogrid and then the rake was removed.

8) The backfill was compacted to 90 percent of Modified Proctor maximum dry density (ASTM D1557). Backfilling and compaction continued in approximately 300 mm lifts. Layers of reinforcement not connected to the wall were installed halfway (610 mm) between connected layers. These layers were not pretensioned.

9) Operations 6 to 8 were then repeated until backfilling was completed to 2/3 of the wall height. At this stage individual panels were aligned by shortening the prop length using the screw control located at the bottom of the prop.

10) Operations 6 to 10 were repeated until backfilling was completed to the design grade.

11) The wall panels were aligned using the prop screw adjustment. The prop was removed after the final adjustment.

INSTRUMENTATION

One 6096 mm high precast panel was instrumented during the construction (Figure 1). The objective of the instrumentation program was to monitor the wall performance during and following construction. This program was directed towards monitoring wall movements, geogrid reinforcement strains, wall prop loads during backfilling and lateral earth pressures on the back of the panel.

Instrumentation consisted of: survey targets in the area of the instrumented panel; strain gages attached to the temporary metallic prop and the mid-rib geogrid locations of two different geogrid layers; total stress cells placed along the back face of the wall; one piezometer; and two thermocouples at the location where the reinforcement was instrumented. The details of the instrumentation are also shown in Figure 2.

Geogrid Reinforcement and Thermocouples. Strain gages EA 13 125BT-120, manufactured by Micro-Measurements with an approximate strain limit of 5 percent were chosen to monitor strains in the attached geogrid reinforcement. Geogrid reinforcement layers at depths of 2440 mm, and 4880 mm below the wall surface were instrumented. Both geogrid reinforcement layers were instrumented with 12 strain gages at six locations. The strain gages were attached at mid-rib locations on the top and bottom surfaces of the geogrid reinforcement. All strain gaging was applied in the laboratory with the reinforcement supported on a wooden frame. All strain gages were tested prior to transferring to the construction site. This testing revealed that only 12 of the 24 strain gages remained operational; four on the lower level and eight on the upper level. The locations at which strain gages remain operational are shown in Figure 2. To protect gages and wires from mechanical damage during compaction, a foam packing and 4.75 mm screen sand was hand placed over all gages. All wires were encased in a flexible 12.5 mm diameter PVC conduit that was loosely connected to the reinforcement with plastic ties.

One copper-constant thermocouple was placed in the centre of each instrumented geogrid layer. Thermocouples were used to monitor ground temperatures.

The Wall Prop Instrumentation To monitor forces in the temporary metallic prop during backfilling, four Micro-Measurement EA-13-125BT-120 strain gages were installed around the circumference of the prop at 90 degree intervals. The four gages were connected to form a full wheatstone bridge circuit. The prop was calibrated in the laboratory prior to field installation.

Survey Targets A precision survey was carried out by the University of New Brunswick's Surveying Engineering department. In this survey, a total of twenty two survey targets were installed: eight on the face of the wall panel, two on the concrete footing below the panel, five on the temporary metallic prop, five on the front of the Hanwell Place strip mall opposite the wall and two nails in the asphalt near the bottom bracket of the prop. Using electronic theodolites simultaneously connected to an Apple MacIntosh computer, three dimensional cartesian coordinates of all target points were determined, and used to detect relative movement.

Total Stress Cells and Piezometer In order to measure lateral earth pressure against the panel, three pneumatic cells (101 to 103) were installed behind the precast panel. The cells used were model EPC-9P manufactured by Petur. These cells were placed within the panel waffle in line with the back edge of the panel wall. The total pressure cells 101, 102 and 103 were installed at depths of 2200 mm, 3400 mm, and 5500 mm below the top of the wall.

One Petur P106-1 Canvaspack piezometer was installed with its tip elevation at the top of the footing grade.

RESULTS OF FIELD MONITORING

A 14 month monitoring program began on May 15, 1990 when no backfill was in place, and continued until August 14, 1991. The purpose of this program was to obtain data during and after construction on the installed instrumentation. The construction was considered to be completed on May 25, 1990 when the temporary metallic wall prop was removed and backfill was within 400 mm from the top of the wall.

After each instrument was installed, initial readings were recorded. During the construction period, instruments were monitored on hourly basis. Following the construction period, field monitoring continued daily until June 8, 1990. From June to August 1990, the field monitoring frequency was reduced from 15 to 6 reading per month. For the months of September and October 1990, 2 and 3 sets of readings were obtained respectively. From November 1990 to August 1991 field readings were obtained monthly except for the month of December.

Reinforcement Strains The strain gages were monitored using a Vishay/Ellis Digital Strain Indicator (DSI). Based on a laboratory calibration program all field readings were converted to percent strain. Over the monitoring period ground temperature variation between -5° to 25° C were recorded (Figure 3). In order to determine the effect of temperature changes on strain gage response, five strain gages were attached to geogrid and they were placed in an environmental chamber where the temperature could be controlled over a range of -20° to 33° C. The results of laboratory testing are presented in Figure 4.

Figures 5 and 6 show the data on percent rib strains corrected for temperature. During the construction of the wall, the strains in the ribs in both reinforcement layers were less than 0.5 percent and all gages in each reinforcement layer followed similar trends (Figures 5a and 6a). Over the monitoring period, rib strains in all gages except for 4-48 were observed to be less than 1.0 percent. (Figure 5b and 6b).

Bathurst (1991) reported that gage strain should be converted to gross strain in order to account for the variation in the modulus of elasticity in the reinforcement. Even if this correction is applied, the estimated gross strains in geogrid reinforcement are below 1.5 percent.

During the installation of the lower instrumented reinforcement, one strain gage adjacent to the wall panel was monitored during tensioning of the geogrid. This monitoring revealed that all induced tension was lost upon removal of the tensioning rake.

Temporary Metallic Prop The variation of axial load in the prop during the construction period is shown in Figure 7. This figure indicates that the axial load in the prop was generally constant and less than 50 kN except when the prop screw adjustment was used to change the panel alignment. A precision survey was performed on the survey targets mounted on the prop on May 15, and 17, 1990. This survey data indicate that the prop had bowed in a direction parallel to the wall as backfilling against the panel continued (Figure 8).

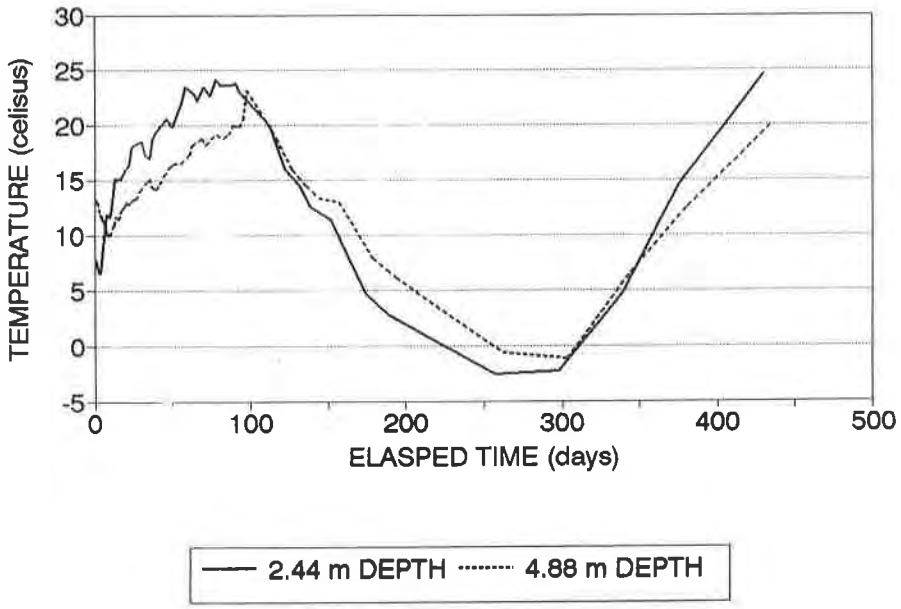

Figure 3. Temperature Variation at Center of Geogrid Layers

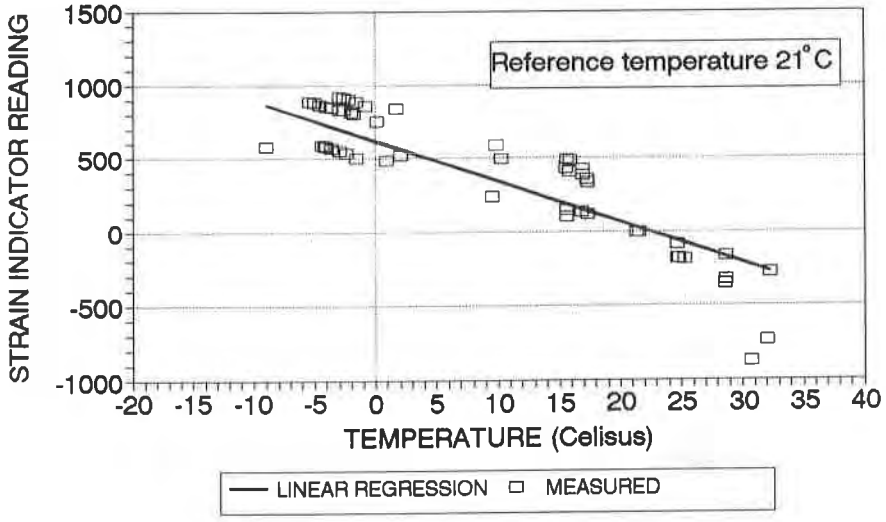

Figure 4. Temperature Calibration for Strain Gages

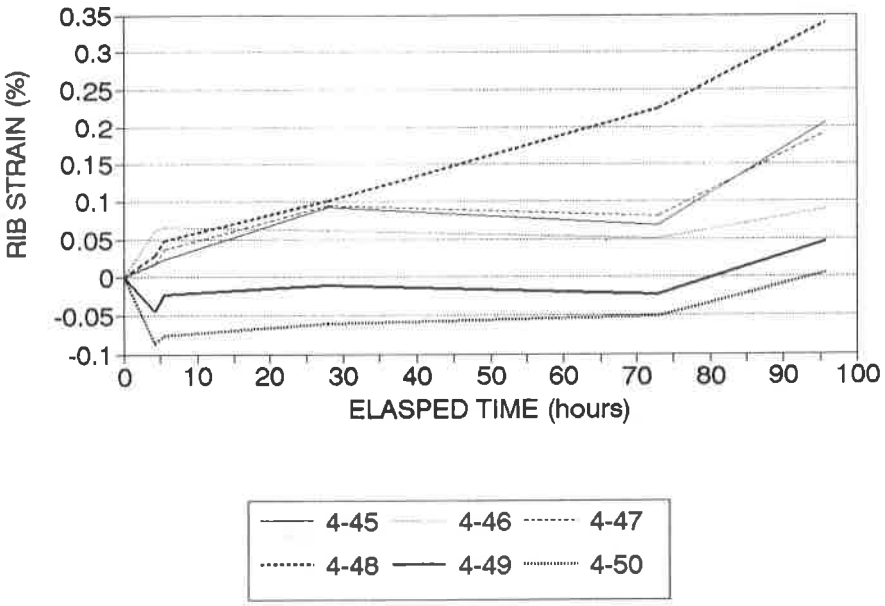

(a) Strains During Construction

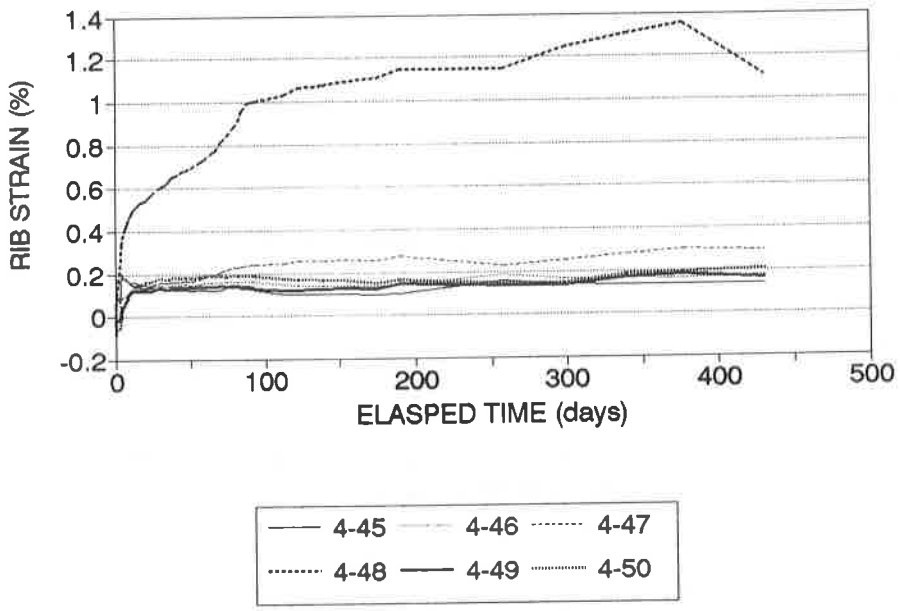

(b) Strains During and After Construction

Figure 5. Geogrid Strains at 2.44 metre Depth

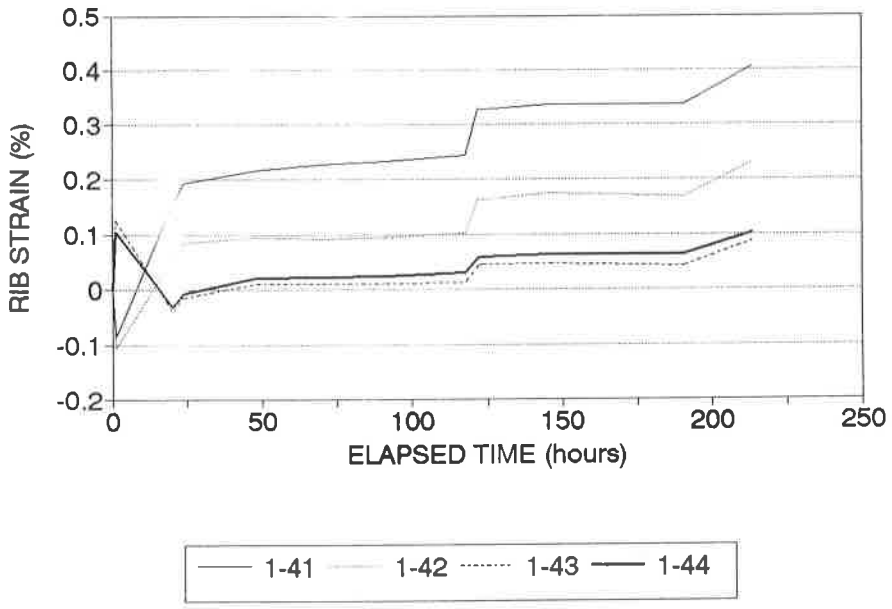

(a) Strains During Construction

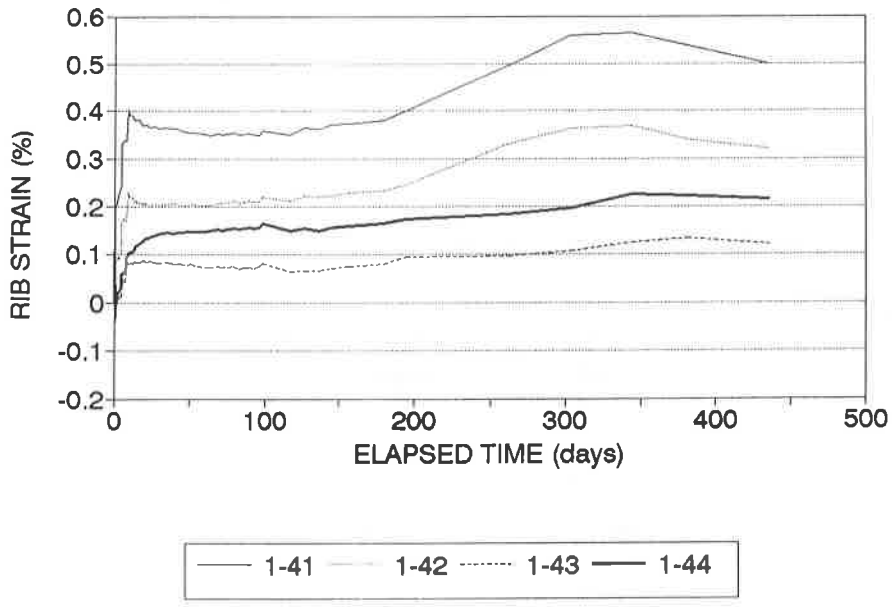

(b) Strains During and After Construction

Figure 6. Geogrid Strains at 4.88 metre Depth

Wall Panel Movements Four precision surveys were carried out on the survey targets placed on the face of the instrumented panel during the monitoring period; two during construction (May 15, and 17, 1990) and two following the construction period (August 10, 1990 and September 2, 1991). The wall panel movements are presented in Figure 9. This data indicate that the wall, which was initially constructed with a 2 percent slope towards the backfill, following construction was near vertical. Definitive conclusions on the total wall deflection during and following the construction period are impossible as the first two surveys were carried with the wall prop in place. During the removal of the prop on May 25, 1990, the prop was used to adjust the panel alignment prior to its removal. The amount of this movement was not measured. Assuming this movement to be minimal the total wall deflection at the top of the wall during construction is in the order of 100 mm. Between the August 10, 1990 and September 2, 1991 survey, a 14 mm defection at the top of wall was measured.

Lateral Wall Pressures Lateral wall pressure variations over the monitoring period are shown in Figure 10. Based on this data, the following observations can be made: during the construction period, the lateral wall pressure was well below the predicted Rankine values and relatively constant with depth; during the winter and spring season following the wall construction, the lateral wall pressure increased to values equal to or greater than the predicted values obtained by the Rankine, Meyerhoff or Trapezoidal pressure distribution theories at the mid-height of the wall. However, pressures remained very low at the base of the wall throughout the monitoring period.

CONCLUSIONS

Based on this study the following conclusions can be drawn:

1) Strains in the ribs of the geogrid reinforcement during and following construction are less than 1.0 percent. This finding is in agreement with other reported case studies.

2) No tension remains in the reinforcement after pretensioning with special designed rakes. The only beneficial effect of pretensioning appears to be straightening of geogrid in the field.

3) Lateral wall pressures appear to be initially very low during and following the construction period. However the pressures appear to increase considerably after the first winter freeze and, thaw and vary with temperature throughout the year.

4) Precision survey method is an acceptable method of measuring small wall movements. Placing the panels at 2 percent slope towards the backfill appears to be a good construction practice as the post construction movements are rather small in relation to the vertical face.

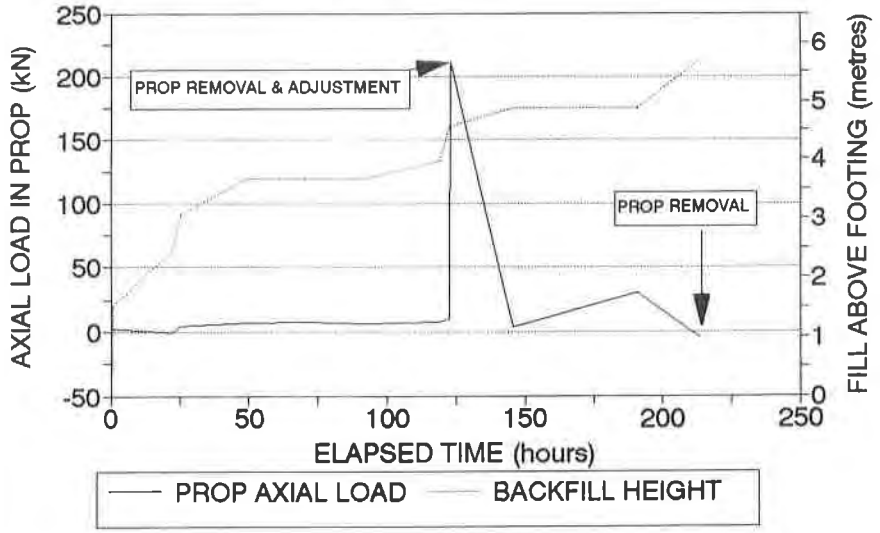

Figure 7. Prop Axial Load

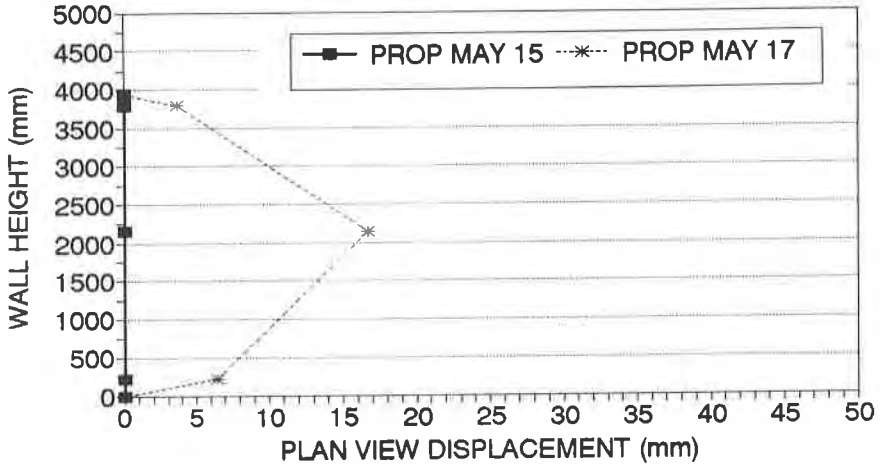

Figure 8. Prop Displacement Parallel to Wall

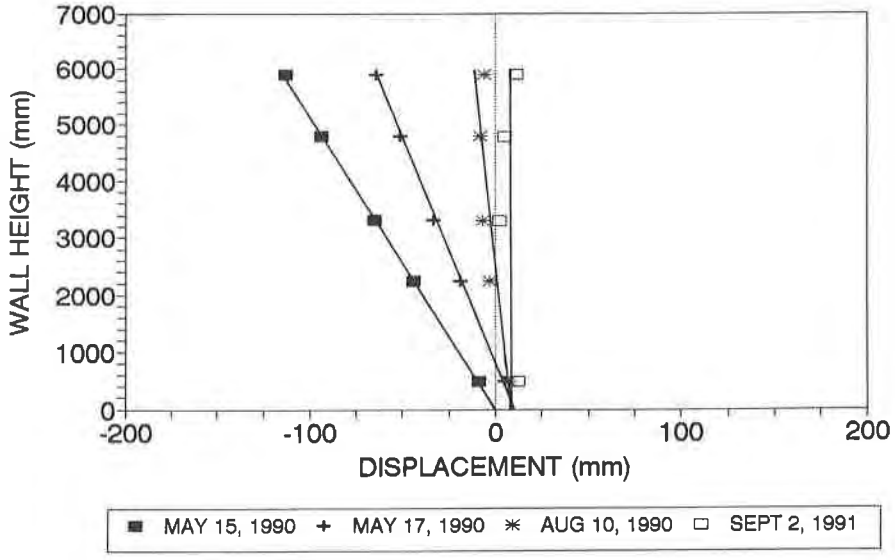

Figure 9. Wall Panel Movements in Time

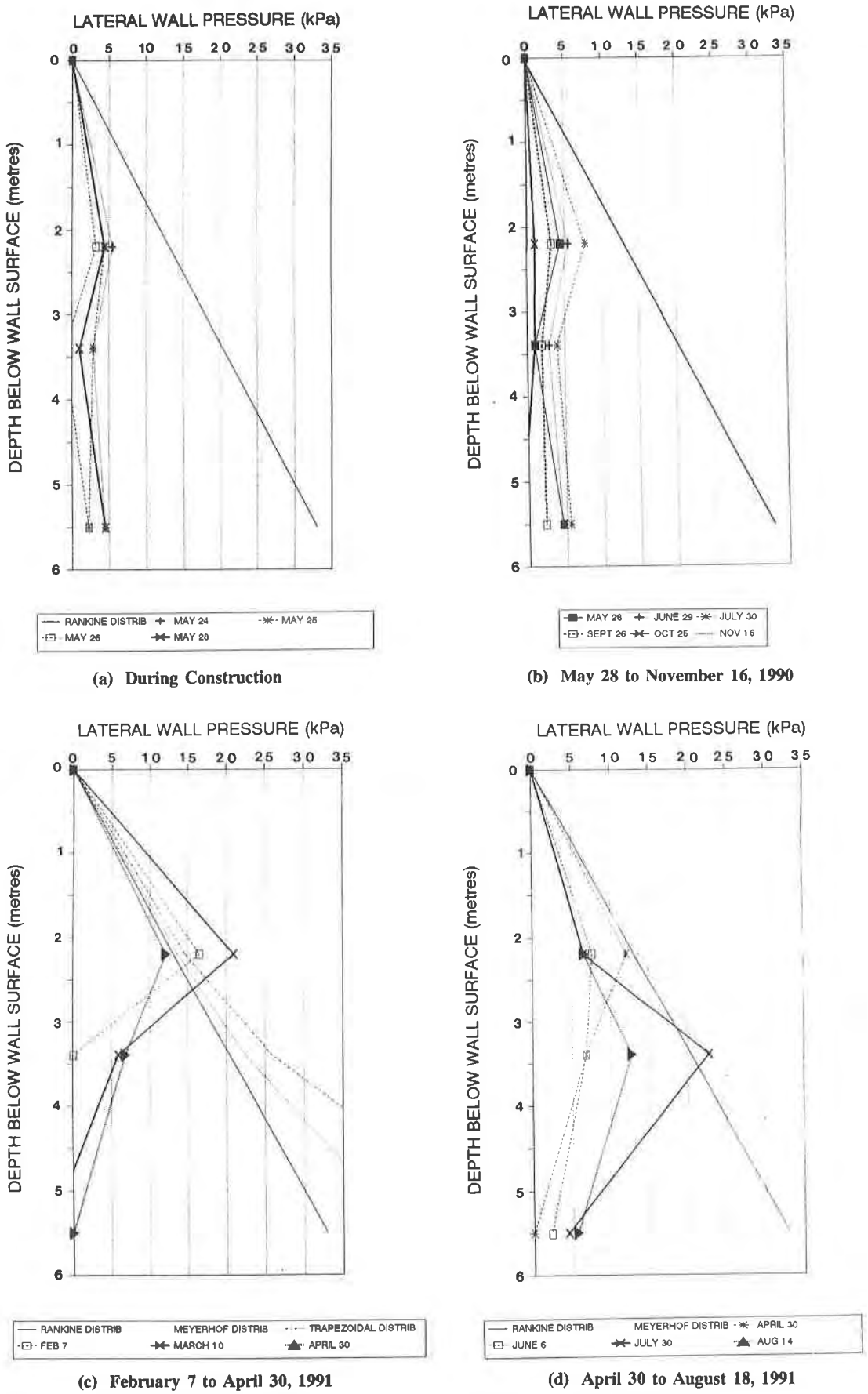

(a) During Construction

(b) May 28 to November 16, 1990

(c) February 7 to April 30, 1991

(d) April 30 to August 18, 1991

Figure 10. Lateral Wall Pressure Variation in Time

ACKNOWLEDGEMENTS

The authors would like to thank owners Ancaster Holdings Ltd., and Contractors Maritime Precast Ltd. for granting the permission to instrument the structure and publishing the results. Input from Dr. R.A. Douglas during the initial stages of this work is highly appreciated. Revisions and comments of Mr. M.R. Simac on the original manuscript are gratefully acknowledged.

REFERENCES

BATHURST, R.J. 1991. "Case Study of a Monitored Panel Wall", International Symposium on Geosynthethic-reinforced Soil Retaining Walls, Denver, Colorado.

BATHURST, R.J. and SIMAC, M.R. 1991. "Review of Three Instrumented Geogrid Reinforced Soil Retaining Walls", 6th Annual Symposium Geosynethetics:Design and Performance, Vancouver B.C., pp. 15.

KUTARA, K. et al. 1990. "Experimental study on Prototype Polymer Grid Reinforced Retaining Wall". Proc. of the Fourth International Conference on Geotextiles, Vol 1, pp 73-78.

JONES, C.J.F.P., CRIPWELL, J.B. and BUSH, D.I. 1990. "Reinforced Earth Trial Structure for Dewsbury Ring Road", Proc. Instn. Civ. Engrs., Part 1, pp 321-345.

SIMAC, M.R., CHRISTOPHER, B.R. and BONCZKIEWICZ, C. 1990. "Instrumented Performance of a 6 m Geogrid Wall", Proc. of the Fourth International Conference on Geotextiles, Geomembranes and Related Products, Vol 1, pp 53-59.

Tensar Technical Note TTN:RW1 1986. "Guidelines for the Design of Tensar Geogrid Reinforced Soil Retaining Walls". The Tensar Corporation, Morrow, GA, USA.

YAKO, M.A. and CHRISTOPHER, B.R. 1988. "Polymerically Reinforced Retaining Walls and Slopes in North America", The Application of Polymeric Reinforcement in Soil Retaining Structures, NATO Advanced Study Institutes Series, Vol.1, pp 239-283.

Shotcrete-Faced Retaining Walls: Application in Flood-Control Channels— Blackland Gully, Kingwood, Texas

J.L. King
Tensar Earth Technologies Inc., USA

W.J. Harper
Southwestern Laboratories Inc., USA

E.D. Carlson
Turner, Collie & Braden Inc., USA

ABSTRACT

Constructibility and economics influenced the design and specification of a unique bridge abutment wing wall system in a high-flow flood control channel at Blackland Gully in Kingwood, Texas. Difficult soil conditions, erosion impact posed by extreme stormwater flows, aesthetic concerns in a high-income subdivision, and the unique connection system for shotcrete-to-wire-basket-wall-face combined to produce an innovative solution and groundbreaking construction techniques. The completed structures illustrate the successful application of geosynthetics (including geogrids, geotextiles and drainage composite) in concert with conventional construction materials (like the wire baskets and shotcrete used in this project) to produce an optimum civil construction solution to extraordinary design constraints.

To support development of a new residential tract, access roads via two bridges over Blackland Gully were required. Channel width and high flows precluded a conventional culvert. To accommodate the high flows and the developer's desire for a 'seamless' abutment wall, clear span bridges with a unique shotcrete-faced, geosynthetically reinforced abutment wall system were utilized.

This paper describes the project parameters, solution development process and successful construction of a shotcrete-faced mechanically stabilized earth wall system in a high-flow channel.

INTRODUCTION, PROJECT CONSTRAINTS AND PROJECT DEVELOPMENT SEQUENCE

In early 1991, Friendswood Development Company, the residential property development unit of Exxon Company, U.S.A., announced plans to develop Section 6 of their holdings in Kingwood, Texas for a new high-income residential community. Expected home prices in the section, which lies between two previously developed sections of the Kingspoint Village area, begin at $250,000. Unfortunately, this section straddled Blackland Gully which is the main drainage channel for a .9833 square kilometers (243 acres) (net) stormwater basin in an area well-known for its high rainfall. Traffic access across this channel would be required at two locations: Hidden Lakes Drive and High Valley Drive.

Kingwood, Texas lies within Harris County. Since Blackland Gully is classified as a stormwater flood control channel in the county, the development plan was required to meet the strict requirements of the Harris County Flood Control District (HCFCD) if it was to be approved. These rules not only concern flow rates and volumes but dictate that slopes cannot exceed a 3H:1V angle. HCFCD also mandates a nine meter (thirty foot) maintenance area from top-of-slope to right-of-way boundary. To compound the developer's problem, Blackland Gully is classified as a wetland area by the U.S. Army Corps of Engineers and the Texas Water Commission which precluded any fill being placed in the channel to modify the slope angle. As a final constraint, Friendswood's development program for planned residential communities like Kingwood incorporates extensive aesthetic and quality-of-life restrictions in their development plans. The thrust of their promotion for Kingwood is "The Livable Forest" and the project's architects, SLA Architects of Houston, Texas were charged with making the Blackland Gully channel a 'greenbelt' with a park-like appeal.

The project's consulting civil engineers, Turner, Collie and Braden of Houston, Texas, undertook an extensive study of the area from a land-use feasibility viewpoint. Soil investigations were contracted to Southwestern Laboratories of Houston while hydraulic studies of the basin and channel were completed in-house. A closed storm sewer system was first considered; however, it became immediately apparent that flows encountered would far exceed the economic viability of hard piping and an improved open channel system for Blackland Gully would be required. Further study revealed that the bridges spanning this channel at the two locations would require either very long spans or unacceptable 'choke points' for water flow. A brief review of typical constructed costs for bridge spans revealed that the long span alternative was economically infeasible. Instead, various options for carrying acceptable water flow under shorter spans were investigated. The first option considered was a box culvert structure, but the 100 year storm volume of 20.6 cubic meters per second (726 cubic feet per second) at a velocity of 1.22 meters per second (4 feet per second) proved this alternative uneconomical. The second short-span alternative investigated was a clear-span bridge over a slightly deepened open-flow channel. Standard available spans of 18.6 meters (61 feet) at Hidden Lakes Drive and 32 meters (105 feet) at High Valley Drive were evaluated for acceptable channel hydraulics and found to meet 100 year stormflow requirements. Unfortunately, these spans reduced the available space at the channel banks which then failed the HCFCD's 3H:1V maximum slope angle.

A short-span, pile-supported bridge section at both crossings with abutment walls angling back to intersect the natural 3H:1V topography appeared to be the best alternative. Eight walls would be required (two at each end of each bridge) with varying heights and lengths. Additionally, the storm sewer system for the roadways being constructed would require outfall in large culverts at locations in three of the walls. Total wall surface area for the eight walls was approximately 465 square meters (5,000 square feet) with the tallest being 4.9 meters (16 feet) at the bridge abutment. To blend with the available topography, four of the walls required construction of internal concave angles of up to 30 degrees.

The architects decided that a 'seamless' facing for the walls was the only acceptable aesthetic facing to complement the 'greenbelt' landscape plan for the channel's recreational utilization. Concern was also expressed that walls with joints would pose a potential problem in the high flow situation of a 100 year storm event. This left cast-in-place concrete walls as the only remaining option. Initial pricing for this option was investigated by the engineer and estimates of $753 (USD) per square meter ($70 per square foot) of wall face were received from local contractors. This was deemed too high a price by the developer and further investigations were mandated. A reinvestigation with contractors confirmed the estimate citing the small wall area and difficult site conditions.

The engineer's previous investigation of MSE-type walls revealed a potential alternative solution which would perhaps meet the owner's and architect's needs at a lower cost: Could the MSE concept of a reinforced earth mass be coupled with a cheaper concrete facing system like shotcrete and still satisfy the wall integrity and 'seamless' construction constraints?

Table 1 shows types of gravity and MSE walls with their relative advantages and disadvantages (in relation to the above parameters) considered by the engineer:

Type Wall	Stability	Economics	Service	'Seamless' Appearance
Gabion	Yes	Yes	Yes	Very Poor
Cast-in-place	Yes	No	Yes	Excellent
Tilt-up Panel	Yes	No	Yes	Marginal
Steel Sheet Pile	Yes	Yes	Yes	Very Poor
Timber-Faced	Yes	Yes	No	Very Poor
MSE Panel	Yes	Yes	Yes	Marginal
Modular Block	Yes	Yes	Yes	Marginal
Shotcrete MSE	Yes	Yes	Yes	Excellent

Table 1: Summary Chart of Wall Alternative Acceptability

Working with manufacturer's representatives of all the elements of a MSE/shotcrete system, the engineers assessed the feasibility, developed a hybrid design methodology, determined a construction procedure and developed specifications. The project was bid according to line-and-grade performance and supply specifications of the civil consultant with contractors to provide final design documents after project award. Competition between extensible geosynthetic reinforcement and inextensible metal reinforcement as well as several shotcrete installers was provided in specified alternatives. A contract was awarded and the project constructed in early 1992 at a 40% cost savings to the original cast-in-place concrete alternative.

This paper describes the project parameters, alternative analysis, design and construction methodology adopted and presents details of the construction technique employed to combine the construction of a geosynthetically reinforced MSE wall system with a seamless, high-strength shotcrete wall facing.

SITE DESCRIPTION (See Figure 1)

Kingwood, Texas is a planned residential community first developed in the early 1960's. It is located approximately 40 kilometers (twenty-five miles) north and slightly east of Houston, Texas in far north Harris County. Current population is approximately 41,000. Developed in sections by Friendswood Development Company, Kingwood has distinct neighborhood developments which range in home value from $100,000 to well over $1 million with townhome/condominium/apartment developments and retail service areas interspersed. The area is heavily forested with native pines and the development methodology has supported maintaining the forested 'rural-urban' theme.

Watersheds in the area are controlled by the Harris County Flood Control District (HCFCD) and consist of a series of streams, gullies and small rivers. The preponderance of the drainage for Kingwood is into the Lake Houston watershed. This large lake is owned by the City of Houston and comprises one of the city's major sources of fresh water. Lake Houston borders this area of Kingwood on the southeast side and lies within 600 meters (2,000 feet) of the project site.

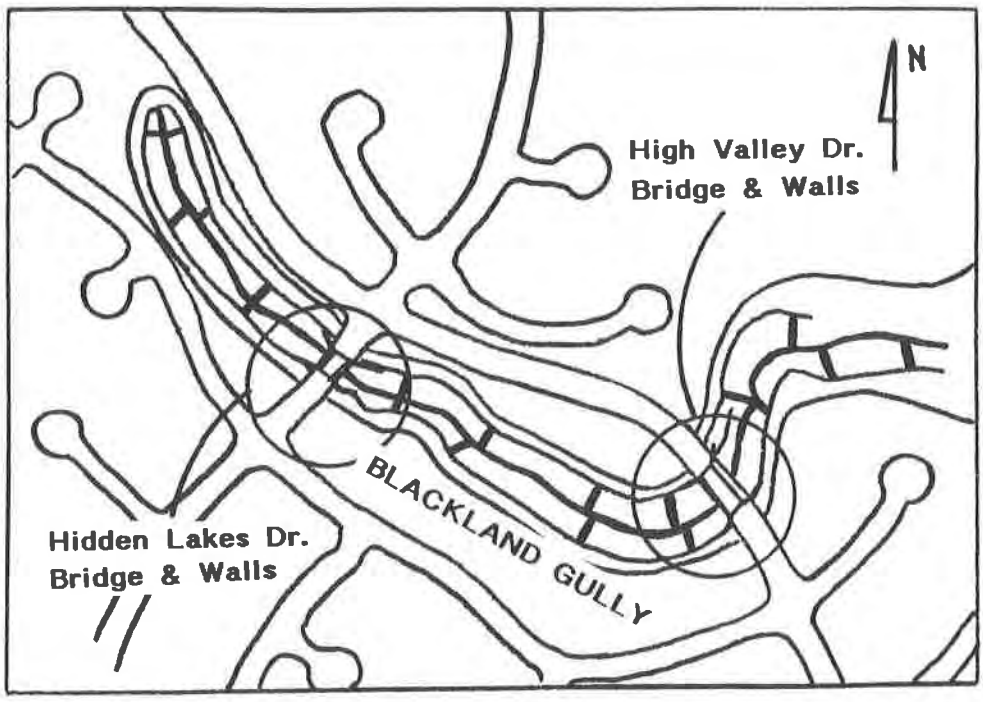

Figure 1: Site Plan View - Blackland Gully Channel Crossings

Soils in the Kingwood area are generally characterized as deltaic deposits on the Beaumont Clay Formation which is comprised of clay, silt and sand. The deltaic deposits largely represent fluvial, bay and interdistributary environment. Soils were deposited during a period of glacial ice retreat and the return of high sea level like that of the present day. Surface fill is classified as firm silty clay varying from 1 to 2 meters (3 to 7 feet) in thickness and overlying a denser layer of sand and silts. Clay layers can be found throughout the area at various depths. Soil borings were completed throughout the development site with one boring at each crossing site which was found to be adequate information for design. Shear strengths generally ranged from 9.6 KN/square meter to 16.8 KN/square meter (200-350 psf). Liquid limits of the plastic clays range from 30 to 80 percent and plasticity indices range from 10 to 50 percent. Overall, the terrain is relatively level except where cut by drainage structures like the gully and its tributaries. Average annual precipitation in the area is approximately 134.6 centimeters (53 inches) with frequent events exceeding 10.2 centimeters (4 inches) in a 24-hour period during the spring season or when Atlantic hurricanes sweep through the area between June and September.

Blackland Gully runs southeast for approximately 488 meters (1,600 feet) through Section 6 of Kingspoint Village before turning east towards Lake Houston. The area of Section 6's development all lies within the upper reach of the gully. It outfalls another 488 meters (1,600 feet) downstream into the East Fork of the San Jacinto River at the river's confluence with Lake Houston. Hydraulic analysis of the basin and flood plain for a 100 year storm indicates that the gully bank in the section being developed is a minimum of 1.22 meters (4 feet) above flood elevation and 3.66 meters (12 feet) above normal flow line of the channel. This elevation above the flood plain is acceptable for development by HCFCD standards. The flow volume and velocity in the channel in the 100 year storm event is 20.6 cubic meters per second (726 cfs) at 1.22 meters per second (4 fps) and governs the development and specific channel design in the project.

The existing gully channel depth averaged 3.66-4.27 meters (12-14 feet) with slopes as steep as 1/2H:1V. Vegetation in the high flow sections of the existing channel was sparse as a result of stormwater erosion while the upper slopes and banks were grassy with light forestation. In various locations, heavy stands of pine were present in the proposed right-of-way which would require clearing and grubbing in the project. The entire right-of-way would require landscaping to flood control district standards as well as the 'greenbelt' requirements of the developer. Right-of-way available to the channel varied from 36.6 to 76.2 meters (120 feet to 250 feet); however, the proposed road crossings are in narrower reaches of 41 meters (135 feet) at the Hidden Lakes Drive crossing and 53.3 meters (175 feet) at the High Valley Drive crossing. Classification by the U.S. Army Corps of Engineers and the Texas Water Commission as a 'wetland area' precluded any fill being placed in the channel as a means of meeting the HCFCD 3H:1V maximum slope angle or maintenance area requirements.

The natural drainage basin served by Blackland Gully encompasses .81 square kilometers (200 acres) south of Kingwood Drive on the east side of Kingwood. An additional .097 square kilometers (24 acres) of drainage from an existing development was previously diverted to Blackland Gully and would be accounted for in the channel design. Channel design must also account for sheet flow in a 100 year storm event which exceeds the capacity of the existing storm sewer system on Kingwood Drive to the north of the basin which would naturally flow down High Valley Drive adding to Blackland Gully's design capacity requirements. Total net drainage area for stormwater design purposes using the HEC-2 hydraulic model was .9833 square kilometers (243 acres). The 100 year storm event volume of 20.6 cubic meters per second (726 cubic feet per second) at a velocity of 1.22 meters per second (4 feet per second) represent the design criteria in the area for this channel section by HCFCD standards. Together, these factors greatly impacted the project's design and alternative selection.

SOLUTION DEVELOPMENT

From their exposure to MSE-type wall systems during the initial investigation, project engineers from the design firm understood the mechanics of mechanically stabilized earth structures but were unaware of any existing system which could combine this type of wall stability with a 'seamless' facing (like cast-in-place concrete) as

desired by the developer. In a project meeting to discuss the options, the possibility of adding a seamless, jointless shotcrete facing to a reinforced soil mass was raised and the following parameters for further investigation of this possible hybrid solution were developed:

1. Strength of the shotcrete facing would have to be similar to cast concrete over the project's 50 year design life.

2. Shotcrete would have to be capable of vertical application with a smooth, seamless finish and close tolerances to design thickness.

3. An effective interface system for the MSE structure would have to be developed to ensure an effective 'grab' or 'bond' with the shotcrete.

4. The reinforcement elements of the MSE structure must be compatible with the shotcrete materials for a 50 year design life.

5. Design of the system must ensure that the interface of the stiff shotcrete facing with the 'flexible' MSE structure does not lead to extensive cracking of the shotcrete facing.

6. The manning coefficient of the shotcrete facing must be similar to that of cast concrete to minimize head losses at the structures.

7. An adequate drainage system must be provided to ensure that water is not allowed to build up behind the wall during rapid draw-down occurrences which could cause wall failure.

8. Wall design must include adequate precautions against scouring effects of high flows at the base and ends of all walls in the project.

9. Concave internal angles would be required in four of the eight walls and drainage culverts through the face of three of the walls must be constructible and effective.

10. Total constructed cost of the proposed system must be attractive to the developer over the cast-in-place wall alternative.

11. Stringent standards for MSE wall design must be developed and applied to the design of the MSE structure.

12. Standards and details for construction, inspection and testing of all elements of the proposed system must be developed without significant departure from existing methodologies and ASTM standards.

Investigation by the project engineer into this hybrid solution began immediately and the expertise of the American Concrete Institute, extensible and inextensible reinforcement manufacturers and shotcrete contractors was enlisted to study the project parameters and solution requirements noted above. Field trips to existing MSE structures and shotcrete operations in the area were undertaken. Sample designs for a variety of wall heights and soil conditions were solicited from reinforcement manufacturers and a literature search completed to gauge the durability of the interface between the shotcrete and the reinforcing elements was completed. Officials at the Texas Department of Transportation (TxDOT) were queried to determine acceptable design parameters and factors of safety for design of MSE structures.

RESULTS OF INVESTIGATION INTO POTENTIAL SOLUTION ELEMENTS

Shotcrete Facing Investigation. Detailed investigation by the project engineer into the viability of the shotcrete facing of an MSE wall structure was accomplished by querying the experts at the American Concrete Institute, meeting with manufacturer's representatives and licensed installers and determining expected material performance characteristics by geotechnical testing laboratory review of similar shotcrete projects.

In general, shotcrete is applied by 'gunning' a mixture of Type II Portland Cement and 6.35 mm (1/4 inch) screened Torpedo Sand (USCS = SW) directly onto a prepared clean surface. These elements are mixed on site from a specially chambered truck in a mixing 'gun' at a ratio of 4.5-sand-to-1-cement. This mixture is pumped through a hose system (powered by a 21.2 cubic meters/min. [750 cfm] air compressor) to the application nozzle where it is further mixed with water from a separate hose. Pressure at the 50.8 mm (2 inch) nozzle exit is 552-621 kPa (80-90 psi).

The nozzle angle to the application surface is controlled manually by the operator. For best results, it should be close to 90 degrees to the application surface and should never exceed 15 degrees from the perpendicular axis to the surface to prevent splatter and slagging of the wet mix. The nozzle should be maintained at a distance from the surface of 1.2-1.5 meters (4-5 feet) which effectively translates the higher nozzle pressure to a non-splattering pressure at the point of application. The operator moves the nozzle over the application surface in an even, slow pattern thus 'coating' the surface with the mix until the desired thickness is attained. Often, wire mesh or steel reinforcing elements are emplaced 50.8 mm (2 inches) above the surface thus becoming a reinforcing element within the shotcrete mass. A skilled operator can apply 3.8-4.6 cubic meters (5-6 cubic yards) of shotcrete per hour in this manner which at 101.6 mm thickness (4 inches) is approximately 42 square meters (450 square feet) of surface area per hour. The labor crew required for normal shotcrete operations is six with the nozzle operator and mixing operator having the greatest impact on quality of the finished product.

Immediately after application, the shotcrete is 'finished' using a trim blade to ensure smoothness of the final surface. Trimming results in a finish similar to cast concrete. Initial drying takes only about 1½ hours while full curing requires 28 days.

Results of the engineer's investigation into shotcrete properties and methods resulted in the following key specification elements:

1. Properly applied shotcrete should be a minimum of four inches thick and attain a 28-day compressive strength of 4,000 psi.

2. Either dry or wet mix shotcrete could be used to apply a smooth, 'seamless' vertical wall over a wire mesh or steel reinforcing bar facing and achieve compressive strength equal to cast concrete. Trimming of the shotcrete would be required to achieve a smooth finish.

3. Weep holes would be required in the wall design to preclude hydrostatic pressure behind the wall during rapid draw-down situations.

4. Shotcrete application must be tied into culvert drainage structures through three of the walls and the concave internal angles in four of the wall plans detailed in the shotcrete application specification.

5. Existing ASTM and American Concrete Institute standards for shotcrete application, inspection and testing would be applicable to the project.

6. While a literature search revealed no documentation of closely-similar applications of shotcrete faced MSE walls, related research into shotcrete properties and MSE structures indicated that they could be acceptably combined in this unique application if properly specified and executed.

7. The Manning coefficient of finished shotcrete is 0.012 (identical to cast concrete) resulting in acceptable head losses at the structures in the channel flow analysis to meet the HCFCD 100 year storm flow requirements.

MSE Wall Investigation. The concept of MSE wall design was well-known to the project engineers and accepted by the design community and the developer. However, the interface of this accepted stabilized earth structure with a 'stiff' shotcrete facing was unknown and therefore required study before approval in the project.

First, Texas Department of Transportation (TxDOT) factors of safety and design parameters for MSE walls from TxDOT project specifications in the Houston District were adopted by the developer and engineer as follows:

Internal Stability		
Geogrid Long-Term Design Strength	F.S.	= 1.5
Geogrid Pull Out	F.S.	= 1.5
Geogrid/Soil Interaction Coefficient	C_i	= 0.9
Percent Geogrid Coverage	P_c	= 100%
External Stability		
Base Sliding	F.S.	= 1.5
Overtuning	F.S.	= 2.0
Bearing	F.S.	= 2.0
External Loading		
Uniform Surcharge	4.8 kN/M^2 (100 psf)	
Design Bearing Pressure	144.0 kN/M^2 (3000 psf)	
Seismic Factors	None	

External and internal hydrostatic loading during a dry condition were assumed insignificant in the design after review of the soil boring data. External hydrostatic forces during a rain event required mitigation using a prefabricated drainage composite supplying minimum conductivity of 50 cm/second (5 gpm per foot width). Conductivity requirements were assumed at 5 kpa (1000 psf) resulting from the planned fill overburden. Internal hydrostatic forces during a rain event were more complex incorporating a rapid drawdown situation with up to 2.44 m (8 feet) of internal hydrostatic head. This hydrostatic situation was accounted for in the design by imposing this phreatic level into the structure during analysis. Potential back pressure created by a high water level in the channel creating an external hydrostatic load on the wall was investigated and determined to be insignificant to the design as the passive resistance of the reinforced soil mass and retained earth zone was sufficient to resist excessive stress imposed on the facing in the event of high water, until the level reached equilibrium. The final design incorporated a series of weep holes near the base of the wall just above final channel grade and free draining backfill materials to rapidly mitigate internal hydrostatic pressure during drawdown.

Manufacturer's representatives for both extensible and inextensible reinforcement were asked to provide conceptual designs for several typical wall heights in the project using a variety of reinforced fill types and the above design parameters to assess economic impact of fill requirements, excavation quantities and project construction. Proposals concerning drainage behind the wall were also requested. The impact of this investigation will be discussed in the **RATIONALE FOR GEOSYNTHETICS USE AND SELECTION** section below.

In this high-flow channel, the impact of scouring below and at the exposed end of the walls was a serious design consideration of the engineer. During the investigation of the MSE wall alternative, the base of the wall was determined to be a potential scouring problem unless it was buried significantly into the channel slope below the wall. Fortunately, the channel is fairly flat at all wall locations. Final design in the project called for burial of the wall footing one meter (3 feet) below channel grade at each location. Additionally, cement stabilized sand was specified for the first three feet of fill behind the MSE wall face to provide additional protection in case of erosion scouring at the base. Scouring at the walls' abutment with the natural channel slope was accounted for in the design by specifying vegetative erosion control materials and landscaping at the interface with the above-mentioned one meter (3 feet) of cement stabilized sand directly behind the wall. The effect of this design is a 'vertical burial' of the end of all walls under landscaped soil to a depth of one meter (3 feet).

Shotcrete-to-MSE Wall Investigation. In this unique hybrid design investigation, the effectiveness, design, constructibility and durability of the interface between the shotcrete facing and the MSE wall structure was a primary concern of the designer.

Since no experience with a similar hybrid system was available, reliance on engineering study and judgement was paramount to acceptance.

Research at the American Concrete Institute indicated extensive experience with shotcrete application over exposed wire mesh and steel reinforcing bars; however, no system to connect such a facing to the reinforcing elements of the MSE soil mass had been specifically developed or tested. It was determined that any wire mesh system proposed must be galvanized to preclude corrosion of the steel mesh in contact with the shotcrete. Similarly, metallic reinforcing strips (if selected) would require galvanizing in the soil mass to prevent corrosion.

Geosynthetics in shotcrete deserved separate study by the engineer. Several published papers regarding the non-corrodibility of organic plastics in concrete were reviewed; however, the only available research on shotcrete interface with plastics was from a series of British Army investigations into shotcrete reinforced bunkers subjected to shelling and bullet fire. While this research was intended to study the improvement of the shotcrete's integrity under ballistic impact when reinforced with plastic elements, it contained conclusory evidence that corrosion or deterioration of the plastics in contact with the shotcrete was not a problem. In fact, these studies convinced the engineer that another of their concerns -- that of potential cracking of the shotcrete after application and curing -- would be significantly reduced by the presence of geosynthetics in the shotcrete as a 'reinforcing' element.

The final interface concern investigated by the engineer was the design of the facing of the MSE structure to afford sufficient 'bond' and 'grab' of the shotcrete during application. A visit to a construction site in the area where a wire-basket faced temporary highway wall was being constructed provided a low cost solution: The MSE wall could be faced with galvanized wire baskets backed by 12 mm X 12 mm (1/2 inch by 1/2 inch) galvanized wire screen with a layer of wrapped geogrid and a geofabric separator inside the basket. As incorporated in the eventual design and project, this MSE facing system provided an outstanding surface for shotcrete application with positive interlock of the MSE structural reinforcement to the gunned shotcrete.

RATIONALE FOR GEOSYNTHETICS USE AND DESIGN

Geogrid reinforcement properties considered critical by the project engineer included strength, chemical compatibility with the soils and shotcrete facing proposed, constructibility, and economics over gravity walls. Geotechnical design parameters and a proven design methodology for geosynthetically-reinforced MSE structures incorporating geogrid properties were considered and specified in the project's special provisions as adopted from TxDOT standards.

Geogrid, geosynthetic drainage materials and geosynthetic fabrics were selected for use in this project and approved by the developer for several key reasons:

1. Chemical compatibility with the shotcrete, cement stabilized sand backfill and native clay backfill materials whose alkalinity would cause rapid deterioration of steel strip reinforcement.

2. Proven long-term durability and tensile strength to provide wall stability throughout the life of the project.

3. Proven long-term creep deformation resistance under sustained load.

4. Adequate transmissivity, durability and chemical resistivity of drainage composites behind the reinforced MSE soil mass to preclude hydrostatic pressure on the wall during rapid draw-down occurrences.

5. High tensile modulus of geogrids to provide strain compatibility with reinforced backfill of two different types.

6. Interaction coefficient with both types of reinforced soils to meet the minimum requirement adopted from TxDOT for the project.

7. Ease of construction for reinforcing elements around culvert structures passing through the reinforced soil mass.

8. Lower cost of geogrids compared to galvanized metallic strip reinforcement.

9. Adequate separation characteristics of geofabrics wrapped at the face of the MSE structure to preclude migration of fines through the wall face until completion of the shotcrete application.

10. Embedment depths which minimized excavation requirements.

11. Confidence in the ability of geogrids wrapped at the face of the MSE structure to provide an adequate 'bond' and 'grab' surface for the application of shotcrete.

GEOSYNTHETICALLY REINFORCED MSE WALL DESIGN

In general, the internal and external stability of the proposed walls was analyzed by engineers at Tensar Corporation who completed final design work under AASHTO Interim Guidelines and AASHTO-AGC-ARTBA Task Force 27 guidelines on computer. Internal stability was analyzed using the tie-back wedge method of analysis along Rankine failure surfaces while four modes of external failure were separately analyzed.

The analysis of external failure modes included sliding (checked against driving lateral thrust force of the retained soil zone), overturning (checked against overturning forces exerted by the retained soil zone), bearing (checked to adequately support the loads imposed by the retaining wall structure against foundation shear failure and excessive settlement) and global stability (checked using limit equilibrium slope stability analysis of the entire MSE structure).

Internal and external stability design and analysis incorporated soils analysis to establish effective strength and moist unit weight parameters of the foundation soils, reinforced backfill and retained backfill zone soils. Soils information from the geotechnical engineering report of borings at both gully crossing locations was used independently for design of the walls at the specific location. Additionally, the engineers specification of one meter (3 feet) of cement stabilized sand behind the wall face to prevent any undermining of the wall by the scouring effect of channel flow was incorporated into the analysis as a separate backfill zone. Equilibrium analysis of forces was then used to determine the strength of reinforcement required and factors of safety for reinforcement strength (1.5), pullout (1.5), durability (1.0), construction damage (1.3), and design uncertainties (1.5) were applied. As a result, long-term allowable design strengths for reinforcing elements were established and a proposed optimal design solution utilizing minimum reinforcing element spacing of 457 mm (18 inches) to match the dimensions of the wire basket facing structure was analyzed by computer using the TENSWAL01 computer program developed by Tensar Corporation using the tie-back wedge method.

Figure 2 is a typical cross-section of the walls as finally designed:

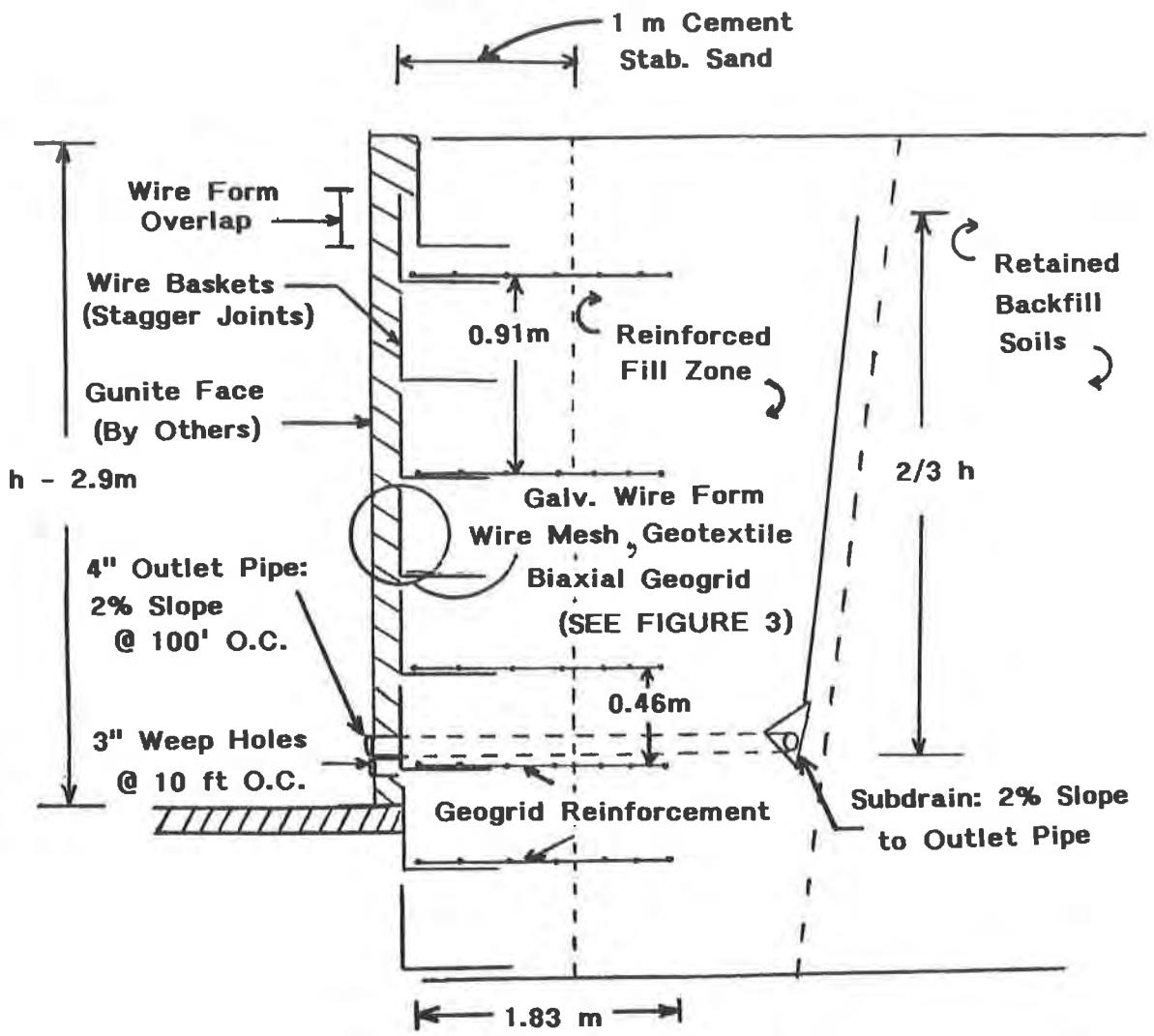

Figure 2: Cross-Section of Wall 3 at Blackland Gully

Geofabric and Geosynthetic Drainage Medium design was relatively simple. Since the only purpose of the geofabric at the facing was to temporarily prevent fines from migrating through the wire basket and biaxial geogrid wrap at the face until completion of the shotcrete application, there was no design consideration taken into account for strength since the wire baskets and geogrid were providing retaining strength. Consequently, a lightweight nonwoven geotextile fabric of 135 gram/sm (4 oz/sy) was acceptable for the designer's purpose. Similarly, the drainage medium requirement behind the reinforced fill zone was a simple prefabricated drainage composite drain application without excessive overburden pressure or transmissivity requirements. The engineer specified standard lightweight drainage composites consisting of a low transmissivity drainage net bonded between two layers of lightweight geotextile. The separator fabrics prevent clogging of the drainage net with fines while groundwater is allowed to pass through and flow to subdrains emplaced at the bottom rear of the reinforced soil zone (See Figure 2). Specified conductivity was 50 cm/sec. (5 gpm per foot width).

DESIGN OF SPECIAL WALL FACING

As a hybrid wall system with many unique design constraints, the detailed design of the facing for the MSE wall structure was critical to the success of the project. It was imperative that a system be developed which afforded maximum 'grab' and 'bond'

for the shotcrete as well as provide a measure of reinforcement within the shotcrete mass.

From the research at the American Concrete Institute, galvanized wire baskets would accomplish both of these tasks; however, these baskets would not protrude from the MSE structure after its construction and compaction to provide a dimensional surface for the shotcrete. The solution developed was to install a 12 mm by 12 mm (1/2 inch by 1/2 inch) galvanized wire mesh between the wire basket and the other elements of the MSE wall and hang an additional wire form structure from the front of each basket. Thus, a dimensional structure was formed which would readily accept the shotcrete and provide a measure of reinforcement within the shotcrete mass to prevent any cracking (See Figure 3).

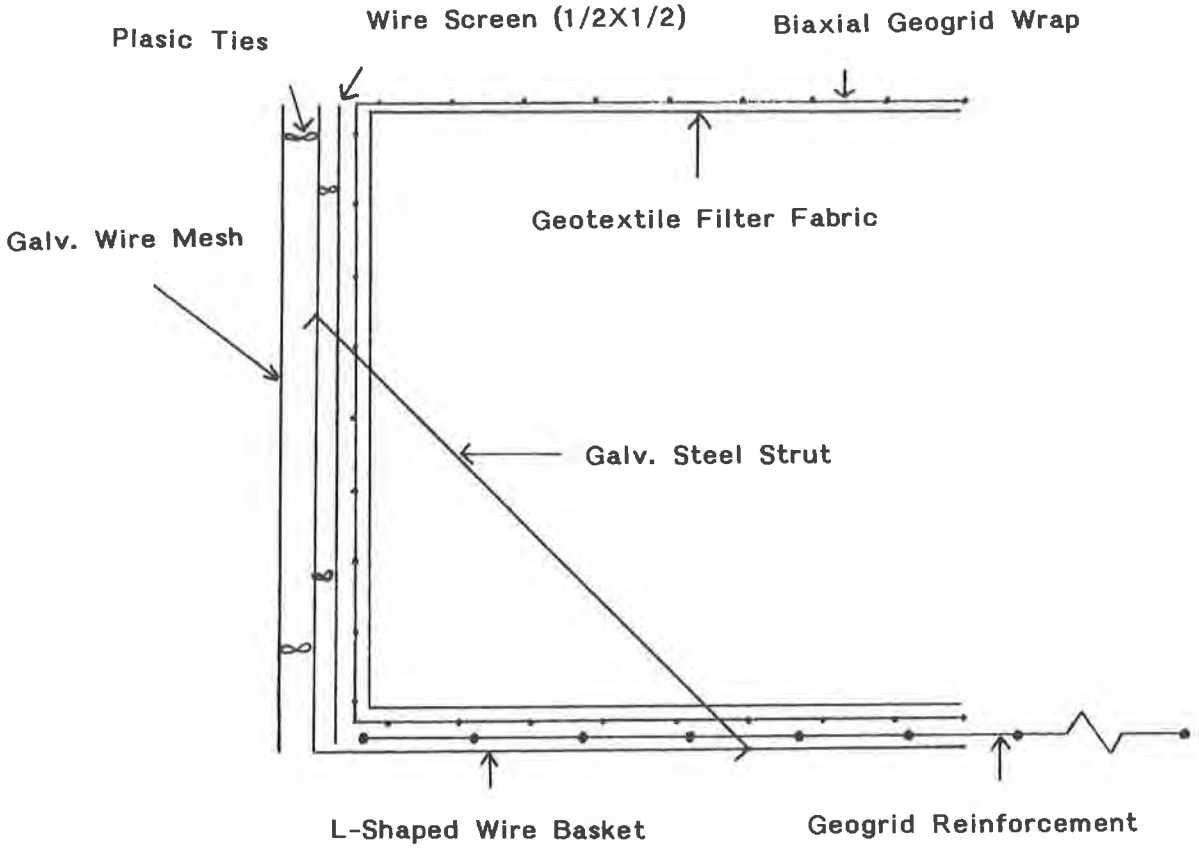

Figure 3: Detail of MSE Structure Facing Prior to Shotcrete Application

CONSTRUCTION SEQUENCE AND DISCUSSION OF TECHNIQUES DEVELOPED

Construction sequencing for the project followed MSE wall construction methods recommended by the geogrid supplier and the project specifications developed by the engineer. The wall sites were first excavated as required and the wall foundations compacted as detailed by the engineer. Wall foundations were compacted to 95% Standard Proctor and the site prepared for wall installation.

The first 457 mm by 457 mm (18 inch by 18 inch) L-shaped, galvanized wire basket was laid on the prepared foundation and plumbed to final wall location. Additional baskets were installed to develop the run of the wall and cut and angled where necessary to form wall angles and terminus point. Where culvert structures intersected the wall, wire baskets were again cut to fit neatly with the culvert outfall. In practice, this first layer of baskets was lightly staked to the ground surface to preclude any movement during backfill operations and subsequent construction.

Next, a primary reinforcing layer of geogrid (cut to specified embedment depth) was laid behind the wire basket's front face overlapping the baskets 457 mm (18 inch) bottom leg. A 457 mm (18 inch) strip of 12 mm by 12 mm galvanized wire mesh (called wire cloth in the industry) was then placed behind the vertical leg of the basket and fastened to it with plastic ties. Similarly, a 457 mm (18 inch) wire basket leg was tied onto the front of the basket face to serve as a 'grab,' 'bond' and reinforcing element for the shotcrete (See Photo 1).

Photo 1: MSE Wire Basket Faced Wall During Construction

A 1.22 meter (4 foot, 6 inch) 'wrap' of biaxial geogrid was placed over the 457 mm (18 inches) bottom leg, up the 457 mm (18 inches) facing leg and laid over the face until completion of backfilling and compaction for this layer of baskets. A similar length of 135 gram/sm (4 ounce/sy) geotextile filter fabric was placed in the same manner to prevent migration of fines during ensuing construction. Galvanized steel struts with hook ends were then emplaced between the two legs of the wire baskets by simply punching them through the geotextile, through apertures in the geogrid wrap and snapping them over transverse bars of the baskets. A minimum of two struts per three meter (10 foot) basket were installed with care taken to ensure that even short sections of cut-to-fit basket locations received two struts. The first wall constructed revealed a problem with off-spec struts which varied considerably in length and affected the final vertical alignment of the wall. No reconstruction was required, however, as the contractor elected to achieve final alignment with a slight increase in shotcrete thickness at the top of this one wall. Struts were henceforth checked for length prior to installation.

Backfilling commenced in six inch lifts with cement stabilized sand comprising the first meter (3 feet) behind the basket face and native soils completing the reinforced zone. Each six inch lift was compacted using a hand operated vibratory compactor and tested by the developer's representative on site. This method worked well even near the basket face with no apparent impact on alignment due to movement of the basket. In practice, the contractor elected to use cement stabilized sand throughout the reinforced zone due to the relatively short embedment lengths of the reinforcing elements and the difficulty of filling the zone with dissimilar types of fill in a simultaneous lift. Consequently, compaction was easily achieved.

When the first basket elevation had been completed, the geogrid and geotextile wraps were laid over the final lift and the next row of baskets installed taking care to stagger the lateral joints of the three meter (10 foot) baskets in succeeding layers.

After the second layer of baskets were completed the subdrains were laid at the back of the reinforced zone location. Prefabricated geosynthetic drainage composite was connected to the subdrains and laid over the rear of the construction site while wall erection proceeded.

Near the bottom of the third basket layer, 76 mm (3 inch) diameter PVC pipes about 152 mm (6 inches) long were placed perpendicular to the basket face on three meter (10 foot) centers and extended at least 102 mm (4 inches) beyond the basket face to serve as weep holes for the completed structure. Their final elevation was approximately 100 mm (4 inches) above final channel grade after burial of the lower basket sections. In practice, these weep drain pipes were stuck into the wire basket immediately prior to shotcrete application since they did not interface with the fill in the MSE structure at all. Upon completion of the shotcrete application, these weep drains are solidly embedded in the wall and allowed the inspector to view the wire cloth, geogrid and geotextile wrap behind the wall for signs of any damage.

The above construction sequence continued until the wall neared its final elevation when a single layer of basket was overlapped with a second basket layer inset as shown in Figure 3. Safety railing posts were set 457 mm (18 inches) into the cement stabilized sand backfill near the basket face as specified and the railings were completed after final shotcrete application. Table 2 summarizes the eight walls in the project.

Wall	Total Length	Maximum Height	Minimum Height	Maximum # Grid Layers	Maximum Grid Length (1.85m min)	Design Tensile Load (kN/M) (lb/ft)
1	26.9m (88.4 ft.)	3.36m (11.04 ft.)	.9m (3 ft.)	4	1.86m (6.1 ft.)	17.78 (1219)
2	22.8m (75 ft.)	2.91m (9.54 ft.)	.9m (3 ft.)	4	1.83m (6 ft.)	15.31 (1049)
3	8.53m (28 ft.)	2.9m (9.5 ft.)	.9m (3 ft.)	4	1.83m (6 ft.)	15.22 (1043)
4	23.16m (76 ft.)	3.72m (12.2 ft.)	.9m (3 ft.)	4	2.05m (6.71 ft.)	23.18 (1589)
5	9.75m (32 ft.)	4.72m (15.5 ft.)	.9m (3 ft.)	5	2.6m (8.53 ft.)	23.25 (1593)
6	31.5m (103.3 ft.)	4.72m (15.5 ft.)	.9m (3ft.)	5	2.6m (8.53 ft.)	23.25 (1593)
7	20.54m (67.4 ft.)	3.96m (13 ft.)	.9m (3 ft.)	5	2.18m (7.15 ft.)	22.6 (1552)
8	8.23m (27 ft.)	3.0m (9.8 ft.)	.9m (3 ft.)	4	1.83m (6 ft.)	15.87 (1088)

Table 2: MSE Retaining Wall Summary - Blackland Gully

All eight walls were constructed in this manner prior to shotcrete application. After an initial 'learning curve' on the first two walls, the six man crew found that they could easily construct a wall of approximately 60 square meters (625 square feet)

of facing (not including burial depth) in a standard workday. Despite construction during Houston's winter rainy season, the walls were completed on schedule without difficulty.

Once all walls were completed, the shotcrete subcontractor applied the shotcrete as detailed in the above Shotcrete Facing Investigation section with a single crew in 1 1/2 days. On-site inspectors representing the engineer verified application parameters and specified thickness attainment for all walls (See Photo 2). Subsequent testing and inspection verified performance of the shotcrete to ASTM standards. The ease of application and trimming operations resulted in effective interface of the shotcrete at bridge abutments, culverts and finishing details like a 'curb' structure at the top of the walls. The inspector on site observed that the shotcrete reached past the wire basket, wire cloth and geogrid wrap to the geofabric ensuring adequate 'grab' and 'bond.' This effectively locked the MSE structure to the shotcrete facing in the completed project.

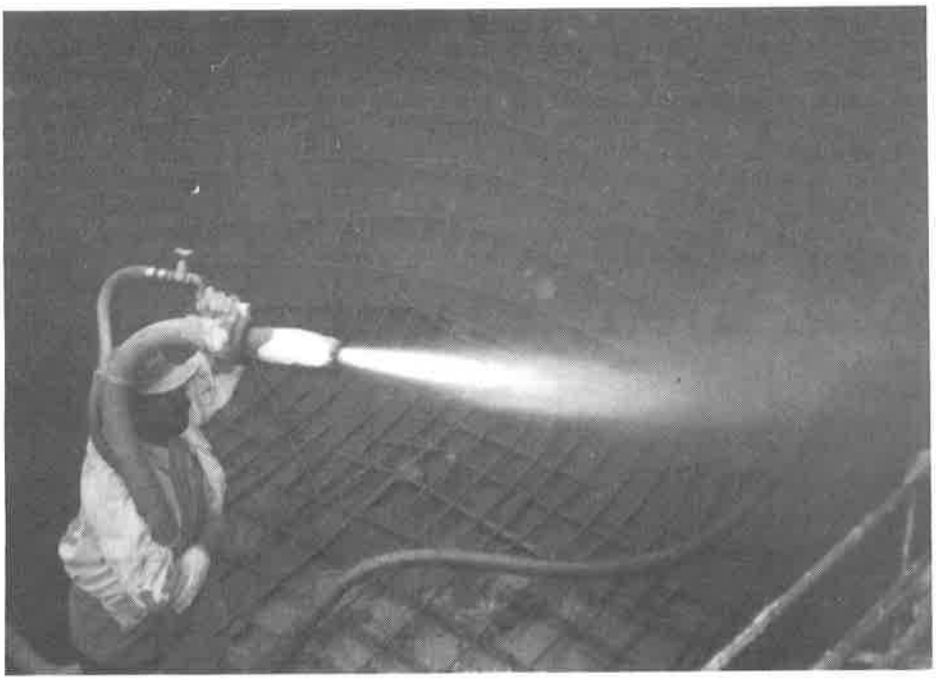

Photo 2: Shotcrete Application Operation

RESULTS AND CONCLUSIONS (See Photo 3 of Completed Walls)

From the experience of the development, design and construction of a unique geosynthetically-reinforced, wire basket faced, shotcrete finished MSE wall in a high-flow flood control channel with many unusual design parameters and constraints, the following conclusions can be drawn:

- Combining elements of standard construction techniques with the advantages of geosynthetic materials offers engineers and designers opportunities for unique solutions at lower costs than other available alternatives.

- Shotcrete facing of MSE structures is an effective lower cost finish for wall applications demanding the appearance of cast-in-place concrete.

- While a factor in project economics, specific backfill type specified is less an overriding economic factor in difficult locations for relatively small walls than often considered; in fact, construction efficiencies with better materials often outweigh the increased costs in final project economics.

- The effects of scouring in high-flow channels can be effectively mitigated by innovative design with MSE walls.

- The expertise of material suppliers and industry agencies can be effectively called upon by designers facing challenging situations to help develop innovative solutions.

- Aesthetic concerns of developers can be met in unique ways by innovative application of the principles of MSE wall design with virtually all desired facing systems and appearances.

- While considerable planning should go into the final detailing of innovative construction techniques, solutions can be found to virtually any potentiality and field construction can proceed with effective completion 'as specified.'

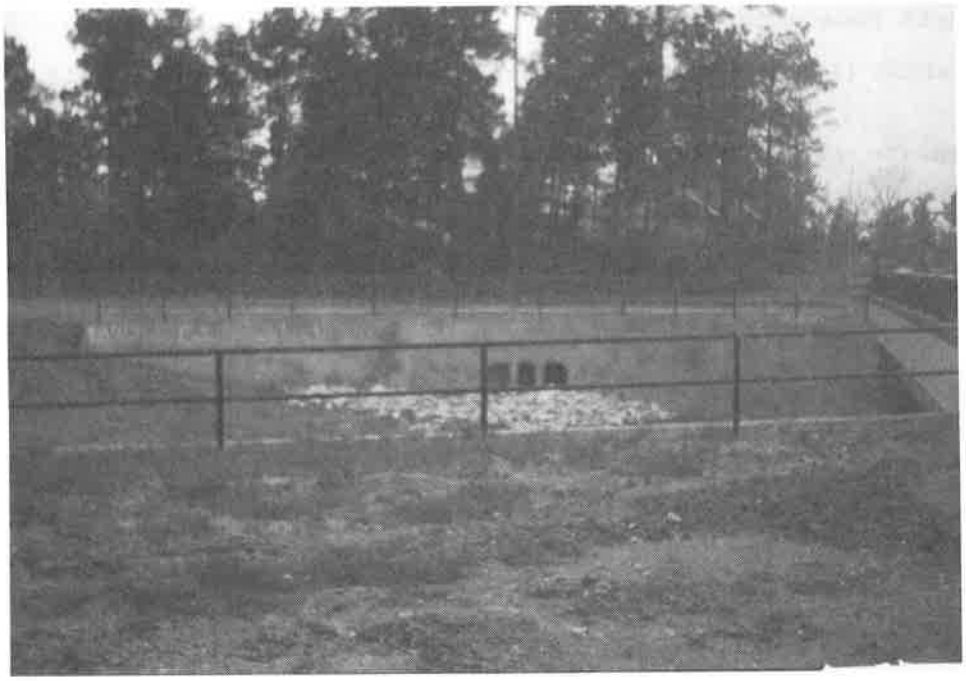

Photo 3: Completed Walls at Blackland Gully Flood Control Channel in Kingwood, Texas

ACKNOWLEDGEMENTS

This paper is presented with the gracious permission of Friendswood Development Company, Harris County Municipal Utility District Number 350, Excalibur Construction Company, Inc. and the City of Kingwood. The authors wish to thank all of their colleagues at Turner, Collie & Braden who participated in the design and construction of this project and all who assisted in preparation and review of this paper. Special thanks are expressed to the experts at the American Concrete Institute and Builder's Gunite for their assistance in both the project's development and the preparation of this paper.

REFERENCES

University of Sheffield, Dept. of Civil Engineering, Dr. R. N. Swamy, et al., "The Behavior of Tensar Reinforced Cement Composites Under Static Loads," 1984.

Federal Highway Administration (August 1986), S. R. Kramer and A. D. Smith, "Geocomposite Drains, Vol. 1, Engineering Assessment and Preliminary Guidelines."

Turner, Collie & Braden, Inc. (1991), Special Specification 4590-080-#1, Item No. A3051-MECHANICALLY STABILIZED EARTH RETAINING WALLS (Kingspoint Village, Section 6, Development Project-Blackland Gully).

Turner, Collie & Braden, Inc. (1991), Special Specification 4590-080-#1, Item No. B1011-SHOTCRETE (Kingspoint Village, Section 6 Development Project-Blackland Gully). American Concrete Institute (1991), ACI506R-90 "Guide to Shotcrete."

AASHTO "Standard Specifications for Highway Bridges, Section 5 - Retaining Walls," 15th Edition, 1991.

AASHTO-AGC-ARTBA Joint Committee (Task Force 27), "Design Guidelines for use of Extensible Reinforcements (Geosynthetic) for Mechanically Stabilized Earth Walls in Permanent Applications," (1990).

TxDOT District 12 (Houston) (1988), "Design and Construction Standards for Mechanically Stabilized Earth Retaining Walls."

Tensar Corporation (1991), "TENSWAL Computer Program for Reinforced Soil Retaining Wall Design."

Tensar Corporation (1992), "GENESIS Highway Retaining Wall System Design Manual and Overview."

The Design and Construction of Geogrid-Reinforced Retaining Walls at the South Carolina Port Authority's Wando Terminal

S. Kemp
South Carolina State Ports Authority, USA

J.S. Martin
Mirafi, USA

A.T. Stadler
S&ME Inc., USA

ABSTRACT

This paper details the design and construction considerations involved in developing an innovative use for geogrids and other geosynthetics at the South Carolina State Port Authority's Wando Terminal. The Wando Terminal is located just north of Charleston, South Carolina on the Wando River. The major application of geosynthetics was the use of geogrid reinforcement to reinforce the soil mass behind a 15.5 feet high and 1,775 feet long modular block retaining wall. Geogrid reinforced wing walls were also used along outfall structures. Interesting design aspects of this project include the treatment of live loads from container storage trucks and equipment and Zone 2 seismic loading. Extensive soil investigation was performed to determine the suitability of the underlying base material to support the retaining wall and to provide construction guidelines to minimize differential settlement. Other aspects of the paper deal with the facing unit/geogrid connection testing which was performed to ensure that the connection strength of the facing unit/geogrid connection was greater than the minimum long term allowable design strength used to design each geogrid layer.

INTRODUCTION

Project Description: In the spring of 1991, the South Carolina State Ports Authority developed a design for the completion of the Wando Terminal - State Pier 41 located north of Charleston, South Carolina on the Wando River. A major part of this terminal completion project was the development of new container yards to service a future wharf addition. The Wando Terminal is located directly adjacent to sensitive wetlands, thus careful consideration had to be given during the design of the new wharf to storm water detention and release, as a significant amount of storm water flow will be generated by the paved surface of the new container yard. The challenge presented to the South Carolina State Ports Authority was to design and build a large storm water detention structure that would require the excavation of over 380,000 cubic yards of earth work, the construction of earthen berms, the installation of geotextile wrapped underdrains and the construction of over 1,800 linear feet of geogrid reinforced modular block retaining wall.

Scope of Project. The storm water detention pond designed by the South Carolina State Ports Authority was an "L" shaped structure with one edge of the "L" forming the southern boundary of the pond and the container storage area. The geogrid reinforced soil wall was constructed along this boundary. The purpose of building a retaining wall along this boundary line was to maximize the amount of space available for containerized storage. Once the decision was made to develop a retaining wall design, a comparison of various retaining wall systems was made by the Ports Authority. Three options were analyzed: 1. A sheet pile retaining wall system. 2. A poured in place concrete wall. 3. A geogrid reinforced modular block retaining wall system. After a careful analysis was performed, it was found that the geogrid reinforced modular block alternative was easily the most cost effective option providing the State with a savings of over $385,000 versus the other retaining wall systems. The savings obtained from the geogrid reinforced option was equivalent to 63% of the modular block wall's total installed cost.

Design Considerations and Project Specifications. The nature of the project and its location presented some interesting design challenges for the South Carolina State Ports Authority. Because the Wando Terminal is located in a seismic zone it was necessary to require that the final contractor designed retaining wall accommodate Zone 2 seismic loadings. The fact that the wall will be supporting a container traffic facility necessitated the use of a 1,000 psf live load design surcharge along the south wall. A 250 psf design surcharge was assumed at the outfall structure wing walls. The maximum allowable soil bearing pressure allowed by the specifications was 2,500 psf, and 1.5 factors of safety against sliding and global stability and 2.0 factors of safety against overturning and bearing capacity were required for the geogrid reinforced soil wall design.

Because of the special loading and drainage considerations, careful attention was given to the specification of wall unit fill, drainage fill and select backfill behind the retaining wall structures. The wall unit fill and drainage fill were required to be compacted gravel or crushed rock conforming to the number six designation of coarse aggregate as defined by ASTM C-33. It was required that twelve inches of drainage fill extend directly behind the modular wall units (see Figure 1). The select backfill placed in the reinforced soil and retained backfill zones was specified to be cohesionless soil containing no more than 15% fines. The complete gradation table as specified by the SCSPA is listed below.

U. S. Standard Sieve Size	Percent Passing and Dry Weight
3/8 inch	100
No. 4	90 - 100
No. 20	60 - 100
No. 40	40 - 90
No. 100	20 - 40
No. 200	0 - 15

For design considerations, the Ports Authority specified the use of a select backfill with an internal friction angle of 35° and a unit weight of 120 pounds per cubic foot.

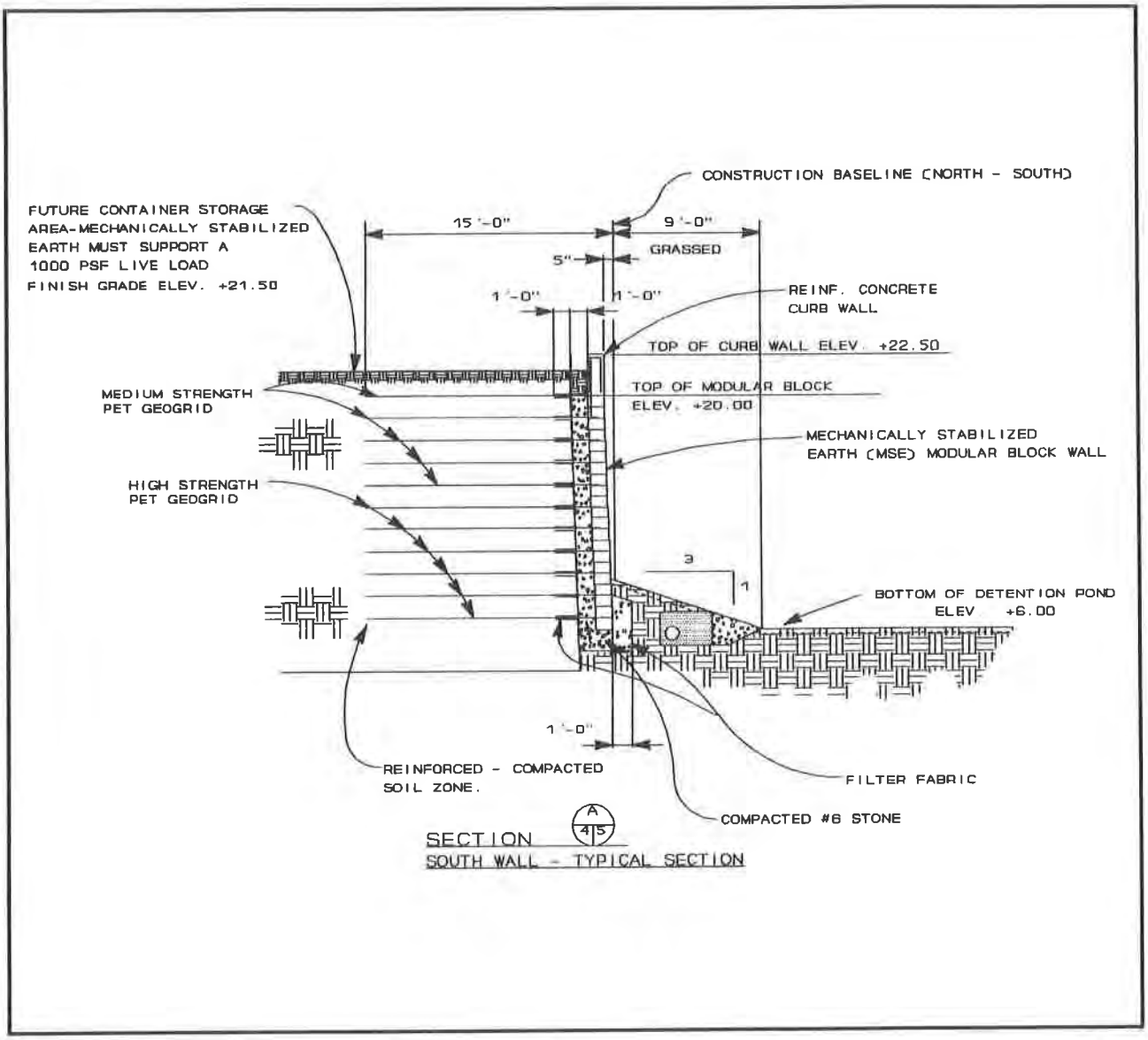

FIGURE 1

Site Exploration and Development of Engineering Soil Parameters. In order to establish the soil strength of the foundation soil directly underneath the retaining wall for global stability analysis purposes, nine soil test borings were performed at regular intervals along the north-south construction baseline. All field testing was performed by engineers from S&ME, Inc. of Mt. Pleasant, South Carolina (formerly Westinghouse Environmental and Geotechnical Services, Inc.). The soil test borings were advanced to depths ranging from 45 to 55 feet using truck mounted drilling equipment. The rotary wash drilling method was used. Split-spoon sampling and standard penetration

testing was performed under the supervision of a geotechnical engineer. Typically, sampling and testing was performed at five foot intervals in the top twenty feet and bottom ten feet of each boring. In between, 2 1/2 foot intervals were typically used. Nine "undisturbed" Shelby tube samples were also obtained at select locations determined by the geotechnical engineers.

Laboratory tests were performed on selected split-spoon and undisturbed samples gathered during the field exploration. The purpose of the laboratory test program was to obtain soil parameters used in material classification and engineering property evaluation. The material classification tests that were performed included Atterberg limits test, grain size analyses, natural moisture tests, and specific gravity tests. The engineering property tests included consolidation, unconfined compression, unconsolidated - undrained triaxial, and consolidated - undrained triaxial tests. In the general location of the retaining wall, a superficial layer of fill was found to be present across the site. The depth of the fill, a sandy clay sand, ranged from 12 to 23 feet below the ground surface (elevation 22.6 mean low water). The bottom of the detention pond and the base of the modular retaining wall system were designed to be at elevation 6.00 mlw. Below the fill, the boring yielded a mixed layer of clay/silty sand, shell hash and clay. The thickness of this layer ranged from 5 to 17 feet and the bottom elevation ranged from approximately 3 to -3 mlw. Below the mixed layer, a layer of highly plastic clay was encountered. The thickness of this layer ranged from 7 to 13 feet and the bottom elevation ranged from roughly -7 to -11 mlw. The materials that generated the greatest concern from an engineering standpoint were the highly plastic clays. Two samples of the highly plastic clay layer were tested to determine the consolidation properties. Samples were taken from boring B-1 and B-6 (see Figure 2). The results indicated that the highly plastic clay possessed relatively high compressibility (average compression index of 0.90 and initial void ratio of 1.76) and had a relatively high preconsolidation pressure of approximately 2.5 ksf.

The laboratory strength tests were performed on undisturbed samples of the highly plastic clay layer. Unconfined compression tests on a sample from boring B-6 yielded an undrained shear strength of 840 psf. Two consolidated - undrained triaxial tests with pore pressure measurements (samples from Boring B-2 and B-7) yielded effective cohesions of 275 and 720 psf and effective internal friction angles of 29° - 14° respectively.

Connection Strength Testing. Prior to developing the completed geogrid reinforced design using the select backfill parameters established by the SCSPA and the foundation soil parameters determined by subsurface exploration, connection strength testing was required to ensure that the geogrid met the connection strength provisions of the specification. The products chosen by the contractor to use in the geogrid reinforced modular wall were three knitted low, medium and high strength polyester geogrids, Miragrid 5T, Miragrid 7T, and Miragrid 10T. The modular block retaining wall unit chosen by the contractor was Amastone, a triangular shaped, 8 inch high block (see Figure 3). The connection strength of the flexible PET geogrids and modular block system was tested at Geosyntec Consultants geomechanics and environmental laboratory in Norcross, Georgia. The test procedure used to conduct the connection strength test was the Geosynthetics Research Institute's GS8 test method for mechanical connection testing.

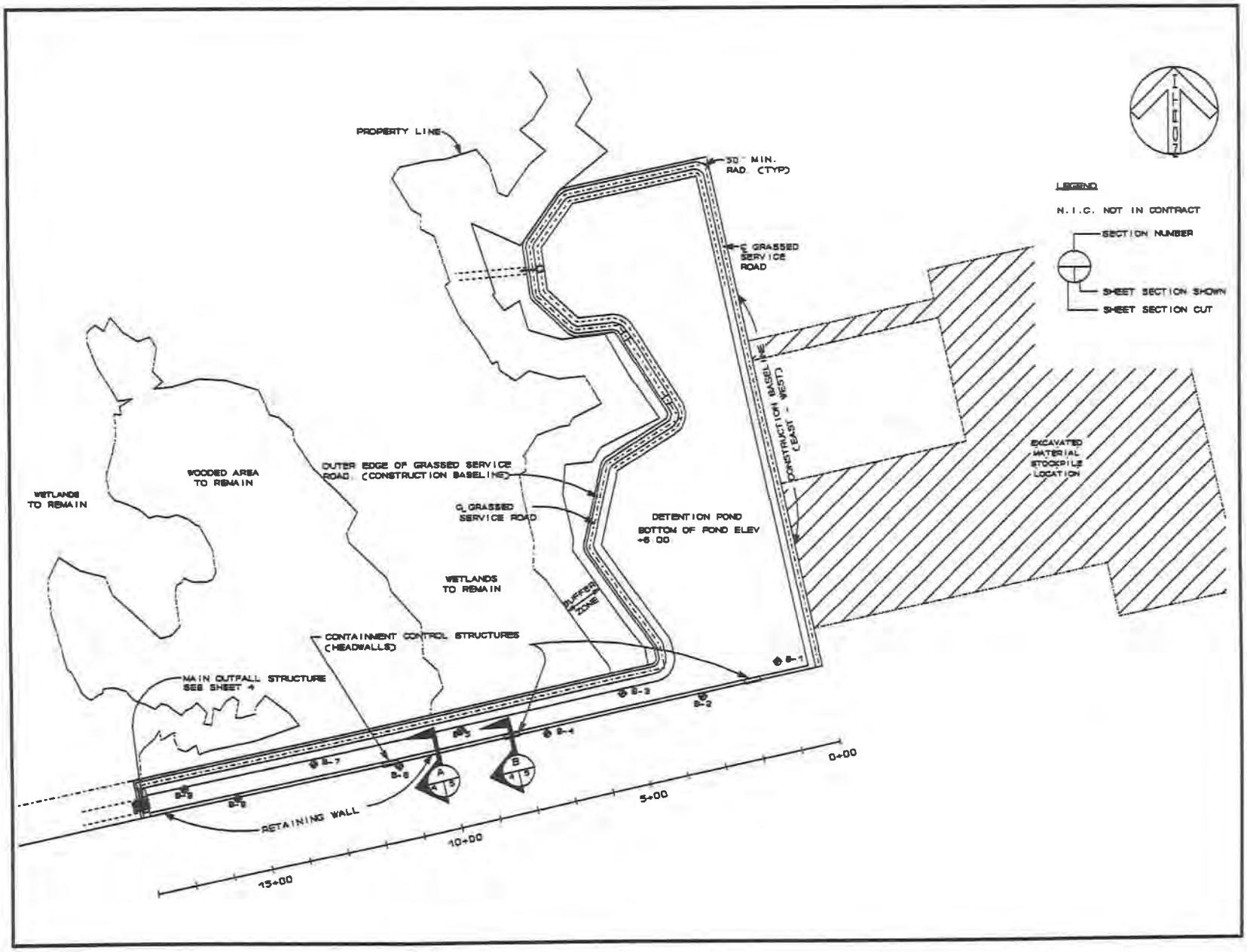
NORTH
PROPERTY LINE
50' MIN. RAD. (TYP)
℄ GRASSED SERVICE ROAD
LEGEND
N.I.C. NOT IN CONTRACT
SECTION NUMBER
SHEET SECTION SHOWN
SHEET SECTION CUT
CONSTRUCTION BASELINE (EAST - WEST)
EXCAVATED MATERIAL STOCKPILE LOCATION
WOODED AREA TO REMAIN
WETLANDS TO REMAIN
OUTER EDGE OF GRASSED SERVICE ROAD (CONSTRUCTION BASELINE)
℄ GRASSED SERVICE ROAD
DETENTION POND BOTTOM OF POND ELEV +6.00
WETLANDS TO REMAIN
BUFFER ZONE
CONTAINMENT CONTROL STRUCTURES (HEADWALLS)
MAIN OUTFALL STRUCTURE SEE SHEET 4
B-1
B-2
B-3
B-4
B-5
B-6
B-7
B-8
B-9
A
4 5
B
4 5
RETAINING WALL
0+00
5+00
10+00
15+00

FIGURE 2

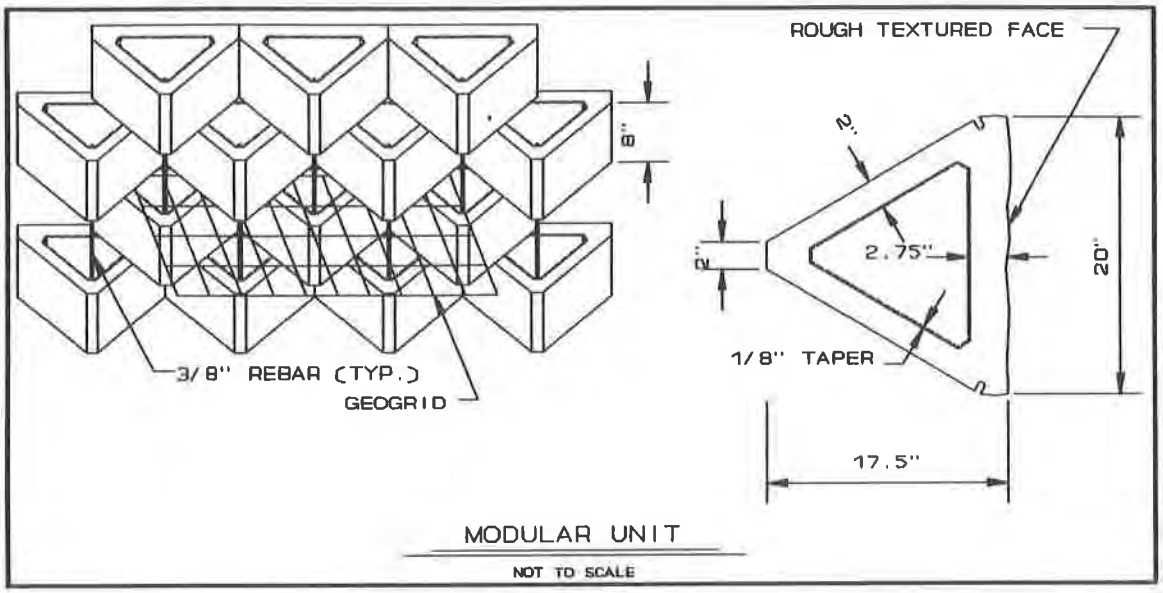

FIGURE 3

Figure 4 provides the results of the connection strength testing. The purpose of the connection strength requirement was to ensure that the blocks did not pull away from the geogrid once the grid was loaded to its design loading. The laboratory tests showed that each flexible polyester geogrid provided an excellent frictional connection between the rock filled modular block and the geogrid interface. This high development of frictional resistance between the aggregate filled voids and the geogrid resulted in excellent connection results in excess of the long term design strengths used to design each geogrid layer.

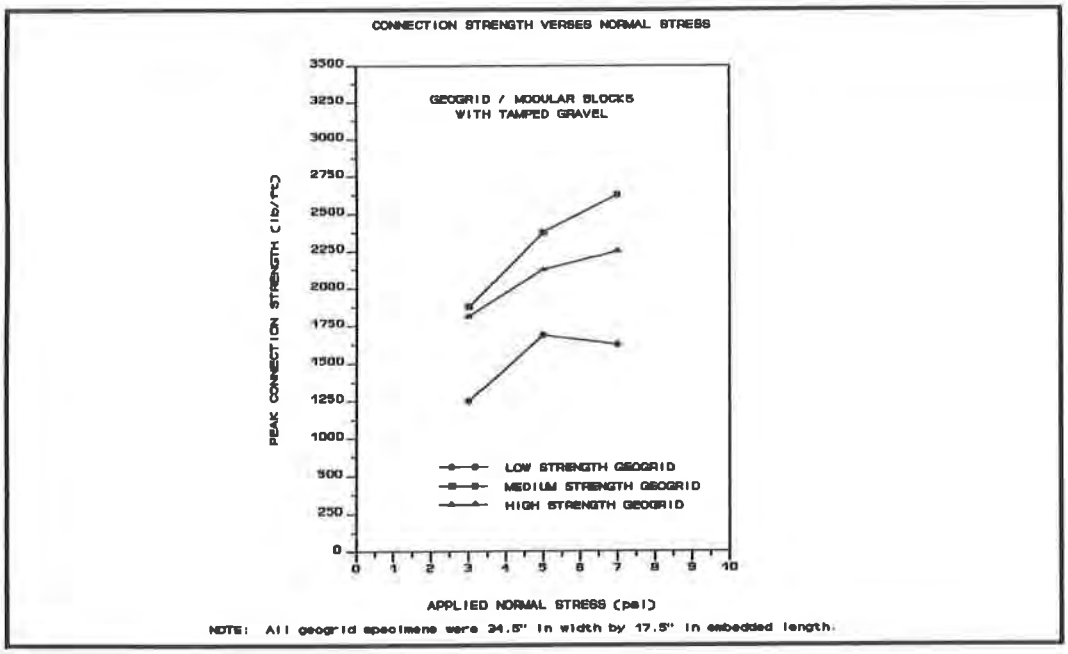

FIGURE 4

Retaining Wall Design Development. Once the soil parameters were established and the connection strength testing was verified, the stability of the reinforced earth modular walls were assessed using two commercially available computer programs, MGWALL (Bathurst) and STABL6 (Humphrey, Holtz). The geogrid design strengths used in the programs were calculated based on GRI-GG4 guidelines. The design strengths of the selected geogrids are shown in Table 1. MGWALL was used to perform the internal and external stability calculations. Specific failure modes addressed included pullout, tensile over-stress, sliding, overturning, and bearing capacity.

TABLE 1

GEOGRID DESIGN STRENGTHS

	Ultimate Strength (lbs/ft)	Long Term Allowable Design Strength (lbs/ft) (See note below)
High Strength PET Geogrid	6,400	1,850
Medium Strength PET Geogrid	3,600	1,050
Low Strength PET Geogrid	2,600	750

Note: Long Term Allowable Design Strength calculated per GRI-GG4 guidelines with an additional Factor of Safety of 1.5 included for design uncertainties.

Assistance in developing the specific wall analysis criteria was also provided by the use of "Design Methodology for Miragrid Reinforced Soil Retaining Walls" (Simac). STABL6 was used to perform the global stability analysis. Both seismic and nonseismic loading conditions were considered. For seismic loading conditions a horizontal acceleration of 0.15 g was assumed. In all cases, the design factors of safety of the reinforced sections shown in Figures 1 and 5 far exceeded the minimum factors of safety indicated in the project specifications with global stability controlling the geogrid reinforced design. Rapid drawdown was not a design consideration because the water level's operational height was not expected to be excessive.

The modular block retaining walls constructed on the project consisted of the main retaining wall located along the southern boundary of the pond and two wing walls constructed on either side of the main outfall structure at the western end of the detention structure. The primary reinforced earth retaining wall located along the southern boundary was designed to be 15.5 feet high and 1,775 feet long. The two wing walls were designed to be 7 feet high and 20 feet long. The wall along the southern boundary was continuous with the exception of three intersections with containment control structures, each containing a minimum 48 inch diameter concrete pipe used to discharge storm water from the future container storage area into the detention pond.

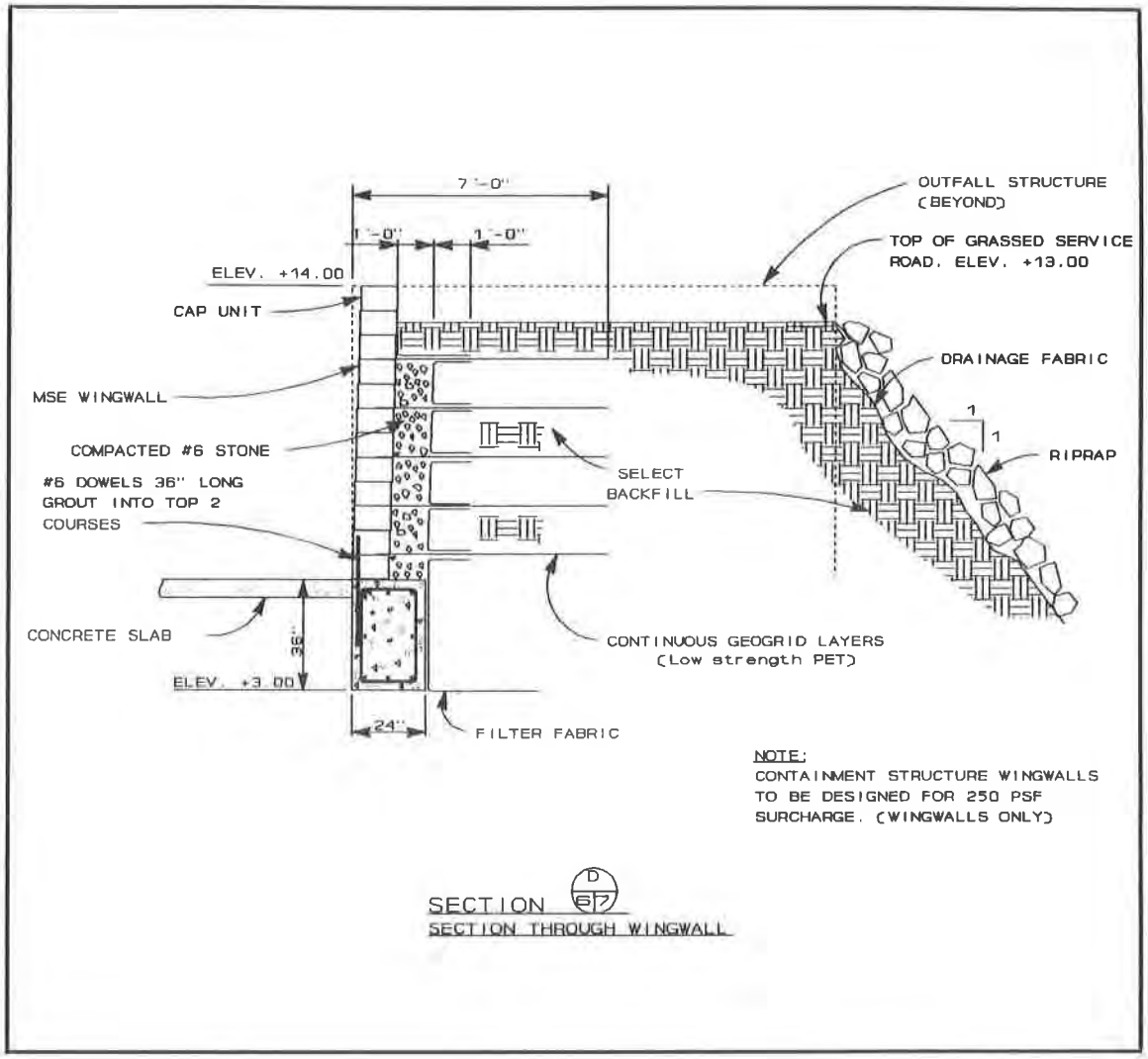

FIGURE 5

At the point of intersection between the containment structure headwall and the modular block retaining wall, the retaining wall blocks were epoxy bonded to the reinforced concrete headwall and dowels were inserted from the modular blocks into the concrete headwall to provide a mechanical attachment.

Two wing walls were designed adjacent to the main outfall structure at the west end of the storm water detention pond (see Figure 6). The wing walls supported a grassed service road which allowed access to the main outfall structure. The loading requirements for the grassed service road was less than that for the container storage area (250 psf versus 1,000 psf) thus, the geogrid strength requirements were not as rigorous. A low strength PET geogrid, was selected for use in the wing wall retaining wall structures. A 10 feet high, 1 to 1 slope was constructed on the wing walls' western side.

FIGURE 6. The Main Outfall Structure and the Geogrid Reinforced Wing Walls

Drainage and Erosion Control Considerations. Geotextile wrapped underdrains were used extensively around the detention pond area to collect drainage and direct it toward the main outfall structure and the underdrain outfall structure located in the northern end of the detention pond. In addition, nonwoven geotextiles were used to wrap the compacted number 6 stone placed directly behind the modular block units and at the base of the modular block retaining wall. This geotextile was used as a means of separating the select backfill from the number 6 stone. Other uses of geosynthetics on the project site included the placement of woven monofilament erosion control geosynthetics underneath rip-rap along emergency spillways and on the wetland side of the earthen containment berms. Sedimentation control fence was also used extensively on the project to prevent the washing of fine construction site sediment into the wetlands.

Construction. The construction of the geogrid reinforced modular block retaining walls began in the Spring of 1992. The first procedure the contractor initiated was to remove the existing fill and excavate to the lines and grades shown on the contract drawings. Once the line and grade was established, a leveling pad was constructed by placing the number 6 stone and compacting to 95% Standard Proctor density. Due to concerns about differential settlement, it was required that a maximum wall height of 5 blocks of wall be constructed over the entire length of the southern retaining wall boundary before additional block placement could take place. This procedure prevented the contractor from building the full height of the wall as he moved from one end of the project to the other. The purpose of this construction sequence was to ensure that equal loading took place across the wall so that differential settlement possibilities could be minimized.

The construction procedure went as follows. Once the leveling pad was established, the first row of blocks were laid and granular unit fill was placed within and behind the blocks. Select backfill was then placed and compacted in the backfill zone. This procedure was repeated until a geogrid layer was required to be placed as per the design drawings. The geogrid was placed by installing the grid in the roll direction, perpendicular to the wall face at the length specified on the design drawings (see Figure 7). Special care was taken to ensure that the geogrid was placed up to the front face of the retaining wall unit to ensure maximum connection between the geogrid and the retaining wall block. Once the flexible polyester geogrid was installed along a given length of wall the next course of blocks were installed directly on top of the geogrid. Unit fill was then placed and compacted within the modular block units, the geogrid was pulled tight and tension was applied while the backfill was placed (see Figure 8 and 9). After 5 blocks of wall height was built along the entire length of the southern boundary, additional block placement was allowed for the entire wall (see Figures 10 and 11). Construction of the wall was completed in the Summer of 1992.

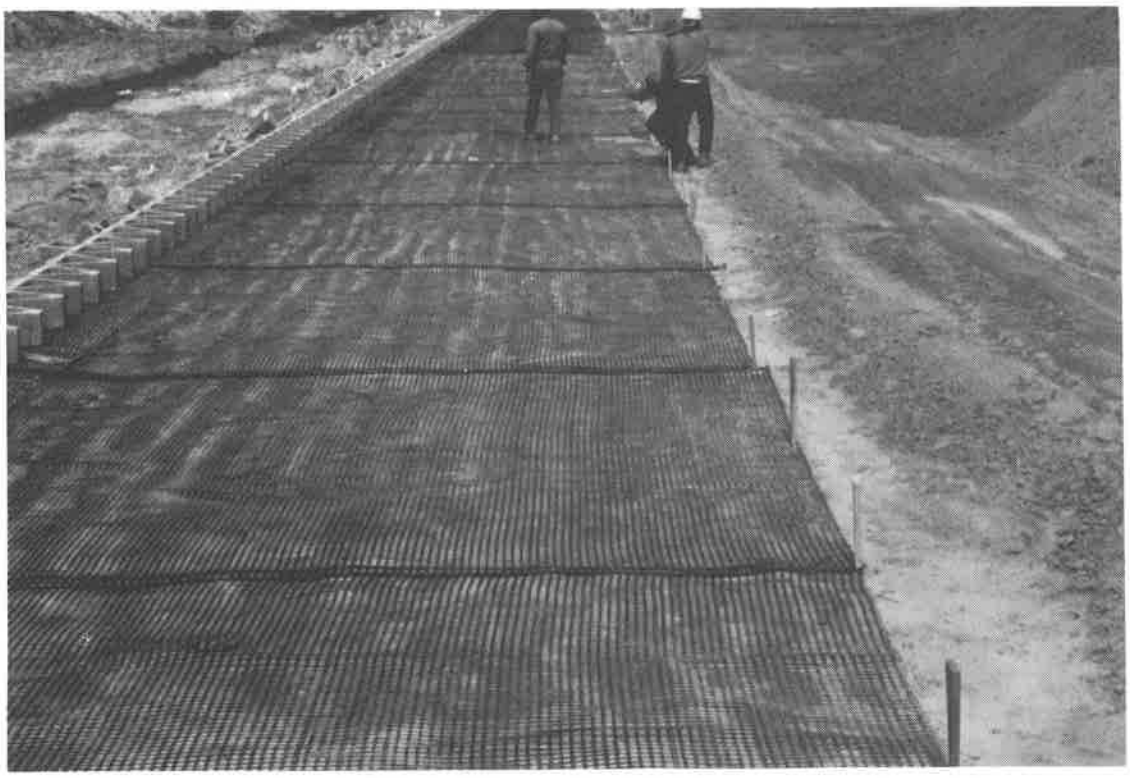

FIGURE 7. The Geogrid was Installed in 15 Feet Embedment Lengths.

FIGURE 8. Number Six Stone was Used as Drainage Fill in and Around the Modular Block Units

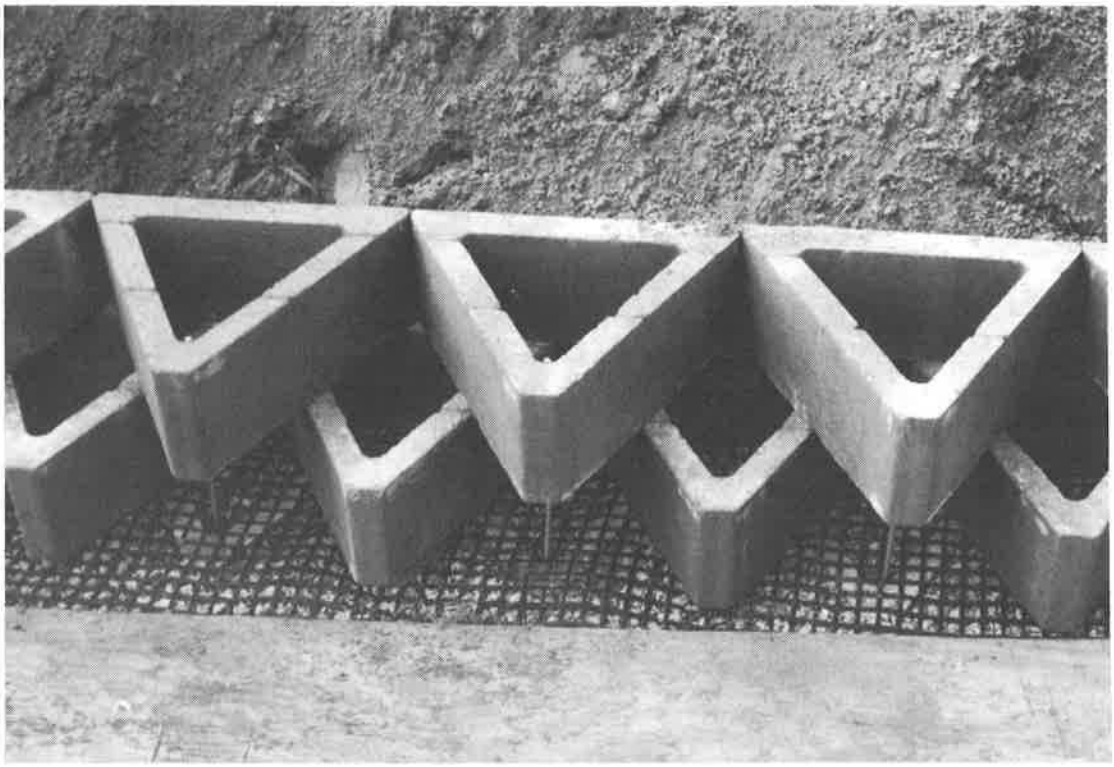

FIGURE 9. Block and Geogrid Placement Configuration

FIGURE 10. The 1,775 Feet Long Modular Block Wall Section Shown Under Construction Along the Project's Southern Boundary

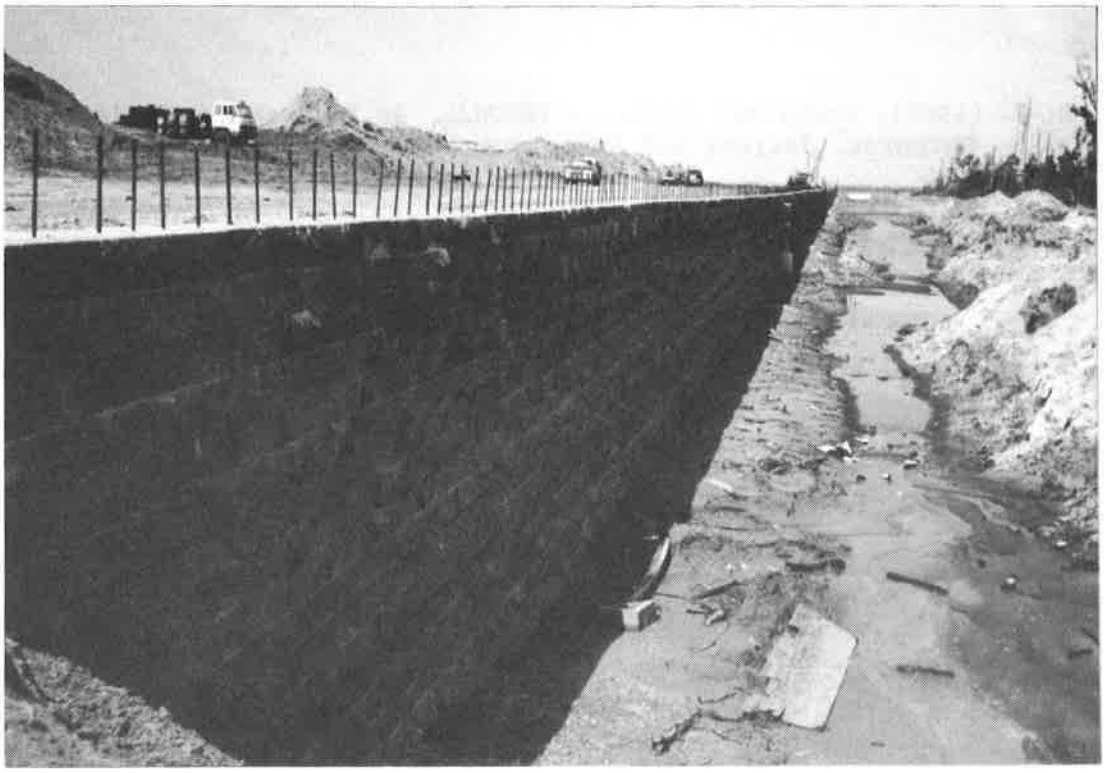

FIGURE 11. The 15.5' High South Wall Nearing Completion

CONCLUSIONS

The significance of this project lies in the use of geogrid reinforcement soil walls to withstand high live loads and seismic loading conditions in areas characterized by typically poor soil load bearing and settlement conditions. The choice of the modular block retaining wall option saved the owner considerable expense. In addition, the use of geogrid reinforcement helped minimize the effects of differential settlement while assuring long term resistance to lateral earth pressures and seismic loadings. It was shown from this project that geogrid reinforced modular walls can provide a significant savings in docking facility acquisition costs by allowing the maximum return from the land available to the owner. Lastly, the project showed once again the ease of installation of modular block retaining walls and lightweight, flexible geogrid reinforcement. The product's ease of installation minimized construction costs, and allowed the project to move quickly, smoothly and on schedule.

ACKNOWLEDGEMENTS

Special acknowledgement must be given to the South Carolina State Ports Authority for implementing the cost effective use of geosynthetics at the Wando Terminal expansion. Further appreciation is also extended to the general contractor, Banks Construction Company of Charleston Heights, South Carolina, for their excellent work and cooperation during the project.

REFERENCES

Bathurst, R. J. (1989), Technical notes for MGWALL: An Interactive Design Program for Miragrid Walls, Bathurst, Jarrett and Associates, Inc.

Humphrey, D. N. and Holtz, R. D. (1986), "STABL6 with Reinforcing Layer Option - User's Manual". Joint Highway Research Project; Engineering Experiment Station, Purdue University, West Lafayette, Indiana.

Simac, M. R. (1990), "Design Methodology for Miragrid Reinforced Soil Retaining Walls", Mirafi Inc, Charlotte, North Carolina.

From a Contractor's Viewpoint: Construction Technicalities of a Tiered Modular Block Wall—The Fiesta, Texas Case

O.A. Moreno
O.A. Moreno and Associates, USA

J.L. King
Tensar Earth Technologies Inc., USA

R.A. MacDonald
Keystone Retaining Wall Systems Inc., USA

ABSTRACT

When the Texas Department of Transportation (TxDOT) began widening Interstate 10 near the new 'Fiesta Texas' theme park in San Antonio, Texas, developers approached highway officials about sharing construction costs. A dramatic entrance was needed to showcase the park which would meet the needs of the department for structural integrity. A system of highway retaining walls including aesthetic pre-cast concrete modules, geosynthetic reinforcement and synthetic drainage materials was chosen for the 5,029 square meter (54,153 square feet), nineteen wall project for its versatility, integrity and aesthetic appeal.

Site conditions, topography, traffic patterns, unique architectural features, construction sequencing, landscaping considerations, and accessibility combined to create special problems for the construction contractor in the field. An understanding by design professionals, owners and general contractors of these difficulties based on actual project experience is helpful in specifying similar projects in other locations.

This paper describes in detail the specialized considerations of wall system design and construction using geosynthetics and modular concrete units as experienced in a major highway wall system project.

INTRODUCTION

In early 1991, developers of a major new theme park in San Antonio, Texas approached the Texas Transportation Institute (TTI), an arm of the Texas Department of Transportation (TxDOT), with an unusual request for a shared-cost project. They needed a special wall system at the access point along Interstate 10 interchange which would service the 'Fiesta Texas' park in a dramatic fashion and highlight the park's musical theme in appearance. The park was being developed as a cultural and musical event specialty amusement center by the owners of Opryland U.S.A. Given the TxDOT's structural integrity requirements for highway retaining wall systems and funding constraints, the architects at TTI proposed a mechanically stabilized earth wall system using geosynthetic reinforcement and modular concrete units. TxDOT investigated the feasibility of the system from a design and economic standpoint. The GENESIS Highway Retaining Wall System was approved for use at a substantial cost savings to other systems considered and TTI began completion of line-and-grade performance and supply specifications.

Since the developer's needs were primarily aesthetic, TTI architects and the developer's consultants (Ralph Bender and Associates) first assessed the site's existing topography, required grade separations, highway right-of-way and project layout to determine a potential wall scheme. The manufacturer of the concrete modular units was asked to present facing options and assess construction feasibility of the

scheme. Together, they developed a system of nineteen walls totalling over 5,029 square meters (54,153 square feet) which ranged in height from 1.0 to 3.14 meters (three to ten feet) and capitalized on the versatility of the system's modularity. Various locations in the project utilized sweeping curves, tiered configurations, step-up elevation changes, planned batters, landscape terraces, and three unique spirals which would resemble musical notes to carry the park's theme to the walls along the interstate highway's interchange. A landscape plan was developed to support the architectural concept and blend the walls to the topography, natural vegetation of the area and the park's musical theme.

TxDOT's Bridge Division structural engineers were called upon in February 1991 to specify the mechanically stabilized earth aspects of the wall system. Following a soils investigation, materials were specified in TxDOT Project Specification IR10-4 (258) 588, and the wall was included in the I-10 widening project let in March 1991 with the successful contractor to provide detailed, stamped design. A contract was let to H. B. Zachry Construction Company and the wall construction was subcontracted to O. A. Moreno & Associates of Houston, Texas, with detailed wall design provided by the Tensar Corporation. Actual construction of the walls began in May 1991 under a "fast-track" sequence and was completed in October 1991.

This paper describes the engineering and architectural aspects of the wall system's specification in this showcase project. Moreover, it presents detailed construction aspects of the project from the installer's viewpoint so that design and construction professionals may gain from the experience and apply the lessons learned to future applications.

SITE DESCRIPTION

The 'Fiesta Texas' theme park is located on the northwest side of San Antonio, Texas in an abandoned rock quarry where little development has occurred. San Antonio, Texas (and specifically the location of the project site) is characterized by low rolling terrain with sparse, yet hardy vegetation which can survive the arid climate. Trees are present only in areas where natural drainage helps support their growth. In fact, landscaping plans throughout the area require meticulous attention to watering systems and vegetation selection. Annual precipitation in the area is 72 centimeters (28 inches). Consequently, the sandy top soil maintains a nearly zero soil moisture content year round. These terrain and vegetation features played a large role in the project's development as the architects strived to specify compatible aesthetics into the construction. Frost and seismic conditions do not exist in San Antonio and are not considered in design.

The site lies in the Pecan Gap Chalk geologic formation. Surface soils are largely weathered limestone blended with clay, sand and silt particles. The subgrade is highly competent with low, shrink/swell potential and consists largely of limestone seams, stiff-hard clay and gravelly clay. This provided an excellent foundation for construction of the project. The soils conditions in the area are extremely favorable to civil construction and consist of very high strength materials with a high limestone content. Subgrade conditions and bearing capacity exceeding 288 kN/square meter (6,000 psi) were not a concern in any area of construction. Select limestone backfill was readily available at a relatively low cost. Actual field conditions encountered during construction verified the above.

The 'Fiesta Texas' site is located on a north-south run along approximately two kilometers (1.25 miles) of Interstate 10 which is the major interstate highway between Florida and California. An existing overpass at the interchange had been constructed in the 1930's primarily to service a rail spur into the rock quarry with little regard for aesthetics. This interchange required extensive modification to service the vehicular entrance to the park and upgrade the aesthetic appearance leading to the entry booths and parking area. Access roads run parallel to the interstate highway on both sides with one-way traffic patterns. The site is flattest on the south end and steepest on the north end where the interstate begins a sweeping curve before resuming its western path to the ranch country of West Texas. (See Figure 1)

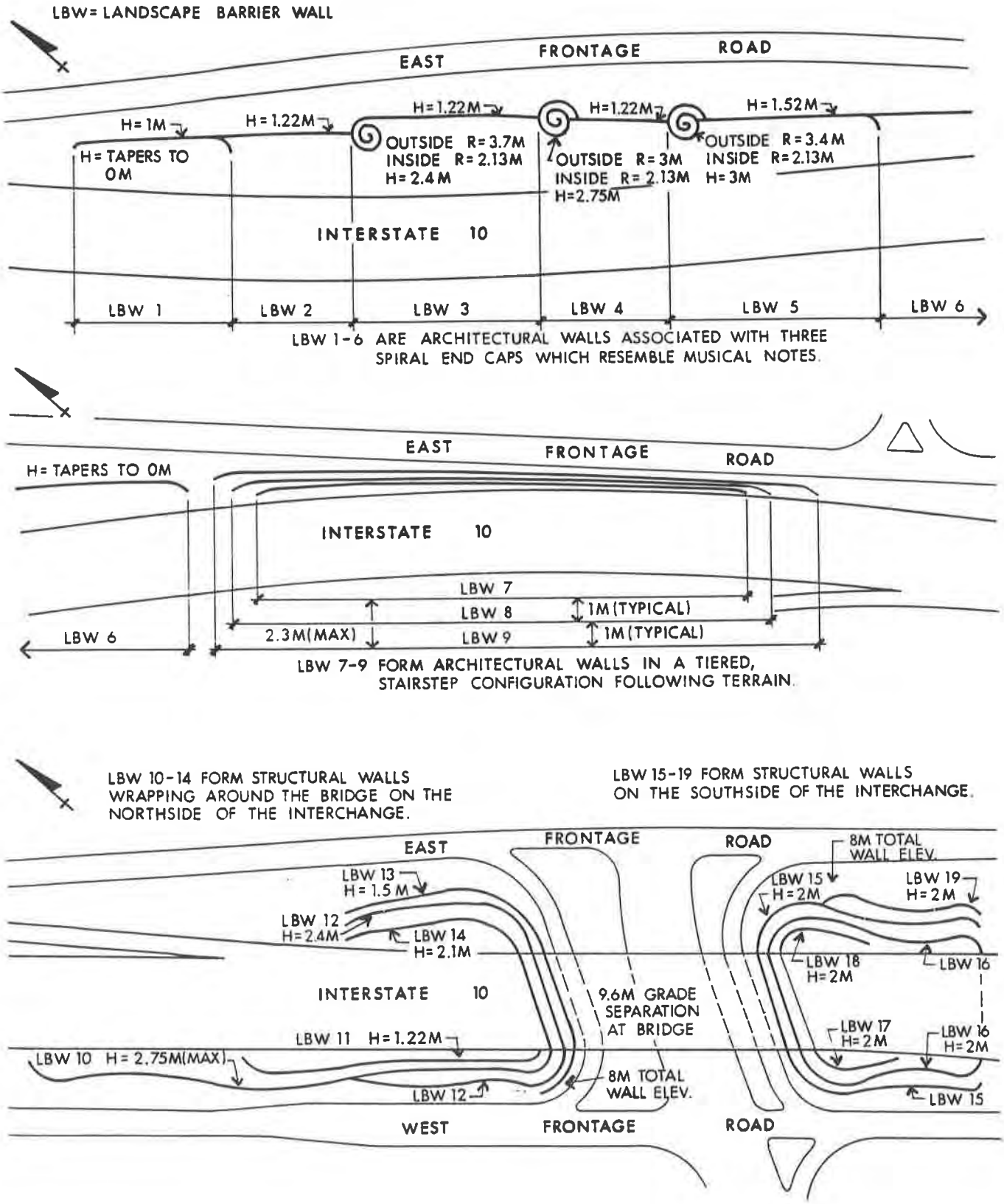

FIGURE 1: Site Plan View Showing Wall Layout - 'Fiesta Texas' Interchange

PROJECT DESCRIPTION PARAMETERS AND CONSTRAINTS

The construction of the walls at the 'Fiesta Texas' interchange comprised part of a $12.4 million (U.S.) upgrade project of a portion of Interstate 10 servicing the new park. Another project to the south of the 'Fiesta Texas' project site totalling $14.9 million (U.S.) was also undertaken by TxDOT in the same time frame to further enhance access through the area. The only impact of this other project was in construction sequencing and traffic diversion to ensure continued trafficability of the interstate highway.

The main objectives of the architects and TxDOT for design and construction of the wall system at the site were as follows:

- The walls must be capable of meeting stringent TxDOT standards for integrity, longevity and stability.
- The walls must provide a significant aesthetic quality in keeping with the developer's and architect's needs as a grand entryway to the park.
- The walls must be constructible within the project's stringent schedule, right-of-way and existing topography without significant disruption of traffic flow.
- The walls must be versatile to handle the unique curves and features envisioned by the architect.
- The walls must be compatible with the architect's planned landscaping and watering system.
- The walls must be cost-effective.

TxDOT Design Parameters in the project specifications called for the following minimum factors of safety for the walls:

Internal Stability		
Overall Geogrid Strength (LTDS with Partial Factors of Safety)	-	F.S. = 1.5
F.S. - Const. Damage = 1.3		
F.S. - Durability = 1.0		
F.S. - Junction Strength = 1.0		
F.S. - Joint Strength = 1.0		
Geogrid Pullout at Connection	-	F.S. = 1.5
Geogrid/Soil Interaction Coefficient	-	C_i = 0.9
Percent Geogrid Coverage (within each layer)	-	P_c = 100%
External Stability		
Base Sliding	-	F.S. = 1.5
Overturning	-	F.S. = 2.0
Global Stability	-	F.S. = 2.0
External Loading		
Uniform Surcharge	-	4.8 kN/m^2 (100. psf)
Foundation Bearing Pressure	-	144.0 kN/m^2 (3000. psf)
Hydrostatic	-	None
Seismic	-	None

DESIGN ALTERNATIVES

While cast-in-place and tilt-up wall systems were originally considered for the project, the architectural detail required by the developer indicated that these

options were cost-prohibitive due to the extensive forming and facing work which would be required to achieve the unique curved and spiraled features and natural stone surface.

A mechanically stabilized earth (MSE) structure was then investigated including panel walls with metallic reinforcement and modular concrete units using geosynthetic reinforcement. The site topography dictated that many of the nineteen walls in the system would be relatively low with extensive tight-radius curves. Large panels could not readily be configured to construct the lower portions of the walls or form the curves envisioned by the architect and developer.

Several types of modular concrete units were investigated seeking a system which could easily form the architectural aspects of the walls and meet the TxDOT's needs for wall integrity, stability and longevity. After reviewing several types of concrete modular units from various manufacturers, the architect selected KeyStone modular concrete units with a curved, natural stone face and presented this recommendation to TxDOT. TxDOT's review of the proposed system was viewed favorably due to the mass of the block, the positive pin connection system and the structural geogrid's compatibility with the available backfill materials. Cost comparisons with other types of walls also favored this system, and it was specified in the project plans for bidding. An ancillary cost benefit was the elimination of a heavy lifting crane for panel unit installation as the 30 kilogram (100 pound) modular units could be handled by hand and on pallets with small 1361 kilogram (3000 pound) lift equipment.

The bidding phase of the project required contractor-supplied designs for review by TxDOT. Each wall over 1.22 meters (four feet) in height was designed per the project specifications to include geosynthetic reinforcement. Figure 2 shows a typical cross-section of these reinforced walls. Additionally, block layouts for the three spirals, leveling pad details for both vertical and '4-inch-in-1-foot' reverse-battered walls were completed as well as associated drainage and separation details using geosynthetics.

RATIONALE FOR GEOSYNTHETIC SELECTION AND USE

Geogrid reinforcement characteristics considered critical by TxDOT during the specification phase included compatibility with the aesthetic concrete modular units selected by the architect, chemical compatibility with the available limestone fill materials, total constructed costs of the MSE walls in the project (both materials and construction economics), constructibility within the project schedule and site restrictions, and adaptability to the architectural curves and features specified by the architects. The values for the geotechnical design parameters including design of geosynthetically reinforced MSE walls were specified by TxDOT in Project Specification IR 10-4 (288) 588. AASHTO Standard Bridge Design Parameters with specified factors of safety were incorporated in TxDOT's project specification.

Geogrid reinforcement was selected for this project and approved by TxDOT for several key reasons:

1. Compatibility and constructibility with selected modular concrete units.
2. Proven long-term durability to maintain reinforcement design characteristics for the life of the project.
3. Proven long-term allowable design strength.
4. Proven long-term creep deformation resistance under sustained load.
5. High tensile modulus to provide strain compatibility with backfill being reinforced.
6. Interaction coefficient with the reinforced soils adequate to meet the TxDOT's 0.9 minimum requirement.
7. Embedment depths which minimized excavation (and fill) behind the proposed walls.

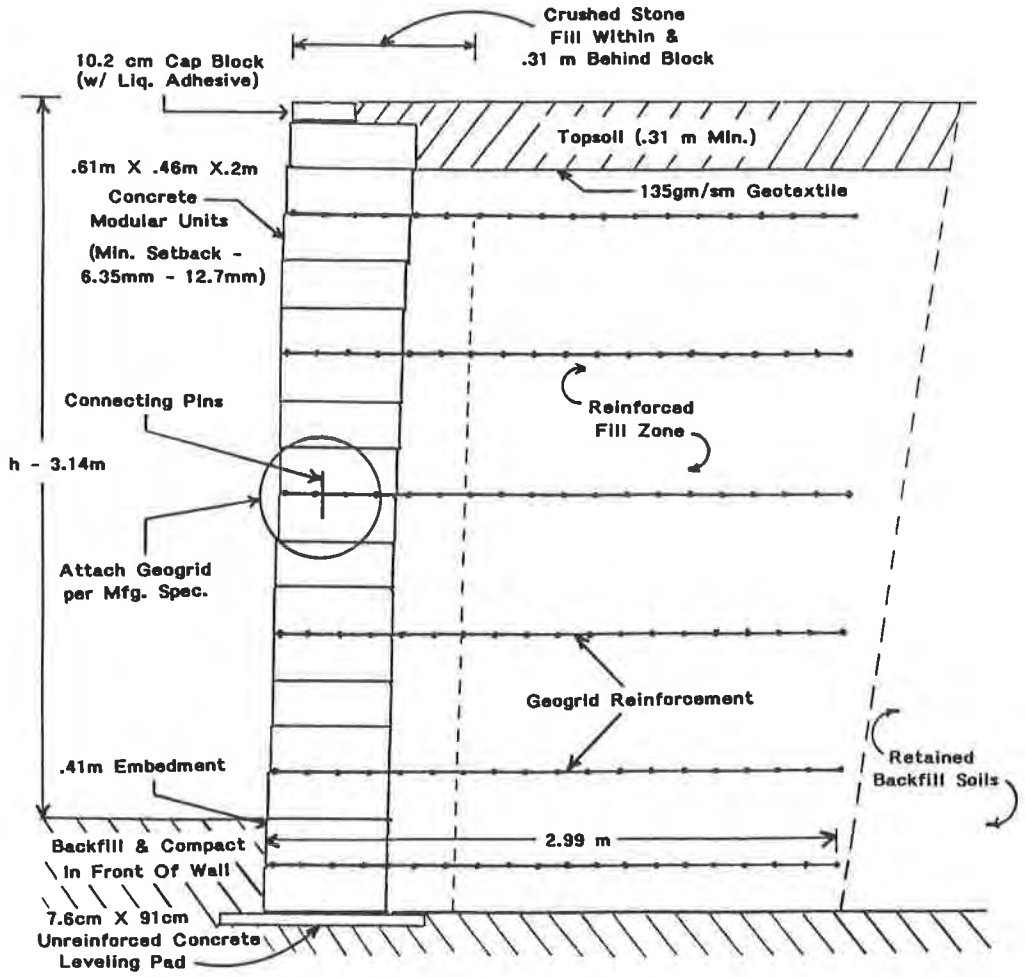

Figure 2: Cross-Section of
Geosynthetically-Reinforced Wall LBW10 (2.75m) at 'Fiesta Texas'

Due to the relatively low heights of the walls and the strength of materials in the retained soils, reinforced fill and subgrade, strength requirements of reinforcing geosynthetics were relatively low. Maximum long-term geogrid design strength of relatively low strength biaxial geogrid (6.13 kN/square meter) met the structural requirements with placement designed to optimize the structure's constructibility and stability. (See Figure 2). The Design methodology employed was Tensar Corporation's TENSWAL 3.0 "Tenswal Computer Program for Reinforced Soil Retaining Wall Design" to analyze all failure modes and optimize reinforcement economics. Global stability of the tiered walls was analyzed separately as a slope using Tensar Corporation's TENSL012 Computer Program. Due to the complexity of the walls, embedment lengths were standardized to 2 meter (6.5 feet) and 2.99 meter (9.8 feet) which met the minimum designed embedment throughout the project. Materials were supplied in only these two dimensions which eliminated the installing contractor's difficulty in properly placing the geogrid per the design.

A field change discussed later removed concrete drainage ditches and drainage composite from the project by capitalizing on the drainage characteristics of the limestone fill. Instead, a 135 gram/square meter (4 oz./square yard) nonwoven geotextile fabric was added as a separator between the topsoil layer and the granular fill. It was chosen for its economics and separation characteristics.

Wall	Total Length (m)	Maximum Height (m)	Minimum Height (m)	Maximum # Grid Layers	Maximum[1] Geogrid Length (m)
1	73	1.0	0.6	1	2.0
2	56	1.22	1.22	1	2.0
3	137	2.1	1.22	3	2.0
4	103	2.1	0.41	4	2.0
5	142	2.1	0.2	3	2.0
6	121	1.31	0.2	1	2.0
7	217	1.31	0.2	2	2.0
8	237	1.31	0.2	2	2.0
9	267	1.52	0.2	2	2.0
10	236	3.14	0.2	6	2.99
11	129	1.22	0.2	1	2.0
12	235	2.96	0.2	6	2.99
13	167	1.5	0.2	2	2.0
14	82	2.53	0.2	4	2.0
15	248	1.74	0.2	2	2.0
16	230	2.7	0.2	4	2.99
17	41	2.7	0.2	4	2.0
18	46	2.74	0.2	6	2.99
19	73	1.0	0.2	1	2.0

Table 1: MSE Retaining Wall Summary - 'Fiesta Texas'

Note 1: Geogrid was cut to standard lengths which exceeded calculated embedment depth for ease of installation by the contractor.

Note 2: The Geogrid long-term design strength used in design was 6.13 kN/square meter (420 pounds/foot). In no case did the calculated load in the geogrid exceed LTDS.

CONSTRUCTION

Construction of the walls was begun in late May of 1991 under a sequential plan which supported the general contractor's project and traffic flow plans. In general, a wall site area was excavated by the general contractor, watering system piping installed, wall footing trenches dug, and footings poured. The site was then turned

over to the wall construction contractor for completion of all walls at that individual location while the next location was being excavated and prepared. In practice, the footing trenches were dug only slightly in advance of wall construction after the construction contractor was on-site and proper layout was established.

Taller tiered walls requiring structural geogrid reinforcement were constructed beginning with the bottom wall. Upper tiers were constructed from the top side after each succeeding tier was completed. In several locations, construction of upper tiers could not be easily accessed from the top and truck ramps were constructed over lower tiers using native soils to haul fill for ensuing tiers.

Lower tiered walls not requiring structural geogrid reinforcement were constructed with the upper tier first and succeeding tiers stepped down the topography. With no reinforced zone the upper tiers could easily be constructed first and succeeding tiers built in front.

The unique spiral structures and curved sections of the walls were constructed using the manufacturer's recommended construction techniques as modified to meet project needs (see discussion in CONSTRUCTION CONSIDERATIONS below).

Each wall in the project was inspected by TxDOT representatives on site during construction and approved upon completion before moving to the next wall for construction. Upon approval of a field change to eliminate concrete drainage swales at the top of all walls, a nonwoven geotextile fabric was required to be placed over the structural backfill as a separator to preclude migration of fines. Topsoil was then hauled in by the general contractor for eventual landscaping.

While the project's initial design called for a concrete drainage ditch behind each wall and a geosynthetic drainage composite at the back of the reinforced zone for all walls taller than 1.22 meters (four feet), a field change was issued to delete both of these items when the drainage properties of the limestone backfill were assessed on-site by TxDOT and contractor personnel and found to have sufficient natural drainage for the expected rainfall and landscape watering. This resulted in an overall cost savings on the project.

A sixty-day demobilization by the wall construction subcontractor was required in the middle of the project to accommodate the general contractor's traffic flow sequencing. A portion of the site was not completed on schedule and traffic could not be rerouted to new lanes which would free the location for wall construction. The subsequent remobilization and completion of wall construction did not hinder project completion deadlines.

CONSTRUCTION CONSIDERATIONS/LESSONS LEARNED

During field erection of the retaining walls, several construction difficulties were encountered which are of educational value to designers, specifiers and constructors of modular block walls. These are presented below in a functional topic format with discussion of each problem encountered and recommendations for dealing with each. The authors recommend that these construction considerations be fully considered during project design, bidding, planning and construction. Each topic should be thoroughly discussed and agreements made by all parties to the project during the pre-construction meeting.

Soils. Due to the relatively high strength of in-situ soils in all zones of the project site, no field construction problems were encountered as a result of actual soil conditions. In fact, the readily-available limestone backfill material was assessed by contractor and TxDOT personnel to have outstanding drainage characteristics. Its availability from the quarry site at low cost and chemical compatibility with the synthetic reinforcement even with high alkalynity offered a field change opportunity beneficial to all parties: The limestone could be used in the entire reinforced zone rather than native soils thus eliminating the need for the concrete drainage swale behind each wall and a vertical drainage system at the back of the reinforced zone. The result was an easier project to construct with more than adequate drainage capacity at a lower cost.

Footings. Layout and construction of the wall footings proved to be a difficulty in the project.

1. Since several of the walls were designed with a batter and others were designed with a '4-inch-in-1-foot' reverse batter emplaced in the poured levelling pad, it was difficult to establish the exact location of the footing. In areas where the wall meets fixed structures like bridge abutments or traffic barriers, this alignment became especially critical. A technique was developed in the field to first survey the top of the wall to be constructed and then plumb to the footing location offset to the designed batter and angle. This technique required close coordination of the wall subcontractor with the general contractor's excavation crew and required a change to project sequencing. The leveling pad excavation and pouring crew worked only slightly ahead of the wall construction crew on sections with battered and angled walls. Thus, the wall construction crew was on-site to properly survey the proper footing location.

2. Watering System conduit which was required to pass under the footing at several locations posed several difficulties. After conduit installation and backfilling, the soil was compacted to 95% Standard Proctor density before pouring of the footing. However, even with this technique, settling of the area above the conduit occurred which eventually cracked the footing and caused a slight anomaly in the wall's alignment. After the problem was discovered, further locations with watering system conduit under the footing were backfilled with cement stabilized sand and compacted to 95% or greater Standard Proctor density. No settling in these locations was encountered. In one location a watering system conduit burst during construction and caused a washout below the leveling pad requiring a rework of the leveling pad before wall construction. The cause of the conduit failure could not be determined so no corrective action to prevent other possible failures was instituted.

3. While the manufacturer's recommended construction technique stated that leveling pads can consist solely of compacted native soils for construction of these relatively low walls, field construction experience at this site showed that straighter, truer walls could be more easily constructed on a properly poured and leveled concrete pad with minimum thickness of 10-12 cm (3 1/2 to 4 inches) of unreinforced concrete. This concrete leveling pad actually reduces the constructed cost of the walls by speeding construction and easing the leveling process. In highway applications, these factors are especially important to the acceptability and aesthetics of the finished walls. Even after compaction of the native soils, it is time consuming to properly level the first course of blocks. Movement by compaction equipment or heavy foot traffic near a laid block can potentially unlevel the block. Concrete leveling pads which are properly poured and leveled eliminate the problem. To aid construction and preclude any future alignment problems due to settling of the first course of concrete units, it is recommended that concrete leveling pads be specified and used for virtually all walls of this type constructed if foundation soils are relatively incompressible, not subject to frost conditions or susceptible to shrink/swell cycles.

4. Curves designed into walls require that the leveling pad be poured to the proper radius. It is important to survey the center point of the curve's arc, establish the top of wall location and plumb the final footing location accounting for batter and reverse tilt before excavating and pouring the leveling pad on the curve's parallel arc. In general, with this project's specified setback and reverse tilt, a curve radius of 3 meters (10 feet) is not a problem for walls constructed using these modules; however, tight curves of 1-2 meters (3-6 feet) radius require special consideration to properly construct. In some cases, field modification of the blocks may be necessary for tight curves as discussed below.

5. Step-up elevation changes in the walls are accounted for in the leveling pad. Since the blocks are 20.3 cm (eight inches) in height and 45.72 cm (eighteen inches) in width, the leveling pad excavation is stepped up in eight-inch increments at the nearest multiple of an eighteen-inch block width to avoid having to cut blocks at the step change. This project's design called for footing changes in 20.3 cm (eight inch) increments. This worked well in locations where elevation steps were widely separated; however, in locations where steeper elevation changes were required, it was found to be easier to make double elevation changes to the leveling pad of 40.6 cm (sixteen inches). This greatly reduced the forming work required for the leveling pad

excavation and pouring thus speeding overall construction. The poured footing made these elevation changes very exact which would not be possible with a compacted native soil footing. Designers should take advantage of opportunities for multiple step changes wherever the topography at the wall's base allows.

Laying the First Course of Concrete Units. Once the concrete footing was installed, the laying of the first course of blocks was straightforward.

1. Blocks are placed side-by-side on the footing. Work from one end of the wall to the other to preclude block fitting in the middle. One should never work from both ends towards the middle to preclude laborious block cutting and fitting requirements. It is also important to lay the blocks on the curves first as their alignment is more critical and less forgiving. Where step-up footings are employed, it is important to work from the lowest elevation to the highest to ensure blocks are set at a 30.48 cm (12 inch) distance between pins in adjacent blocks. This is absolutely critical on curves as tolerances for fitting blocks of ensuing courses are more stringent. These modular units have small manufacturing tolerances for size, pin holes, etc., which can make alignment difficult. Proper placing and sequential construction employing the above rules can help avoid time consuming block fitting and rework.

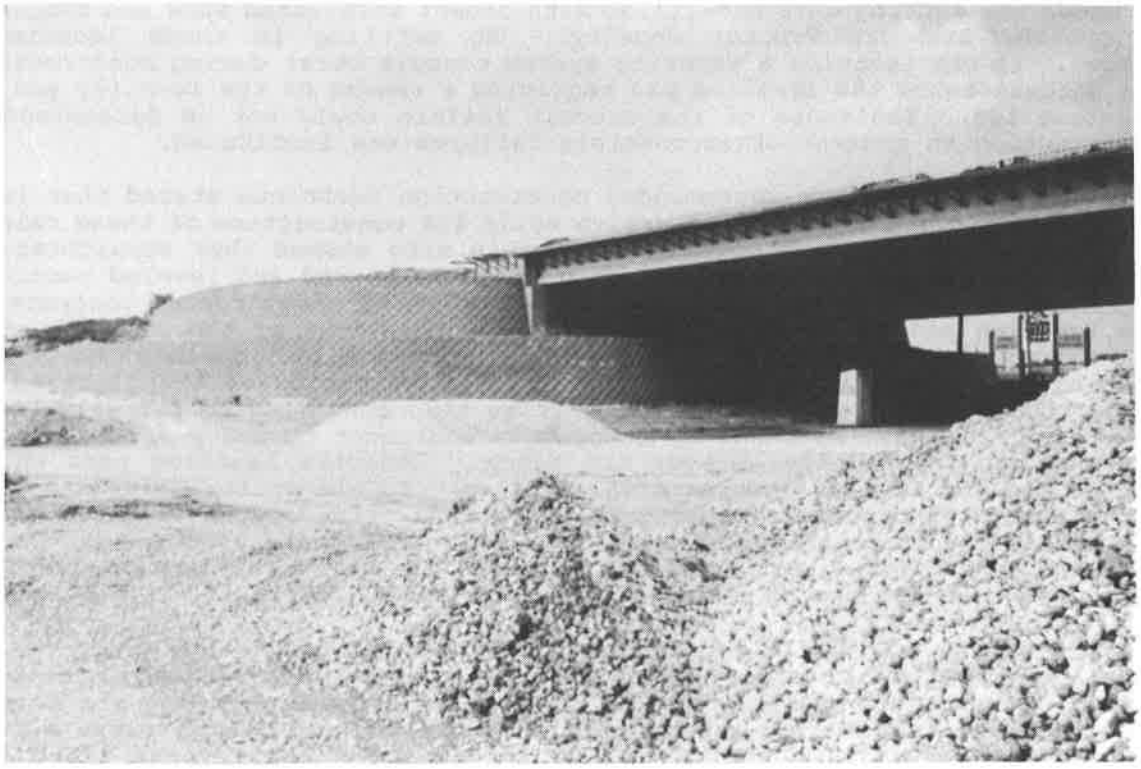

Photograph Taken Near the End of Construction at 'Fiesta Texas'

2. Level must be checked and a string line set over the pins from one end of the wall to the other. This is important because of the difficulty of reading small hand levels placed on individual blocks. By string-leveling the entire wall length, accurate leveling and placement was assured on the project resulting in a near perfect block and wall alignment. High strength fiberglass pins supplied by the block manufacturer were installed manually in the pin holes on the top of each block. A hand hammer was used to gently tap the pins into well-seated position. Immediately after setting each block, place the pins before filling any area with fill to avoid getting fill into the block's pin holes. This lesson is quickly learned by crews who must remove the blocks and turn them over to remove debris before continuing.

3. Clean 6.35 mm to 9.53 mm (1/4-to-3/8) inch washed gravel is poured into the unit voids and one foot behind the units. A single 20.3 cm (eight inch) lift of limestone backfill is then poured to the specified depth and mechanically 'compacted' using a hand-operated plate vibrator with 22.3 kilonewtons (5000 pounds) of compaction force.

Placing the Geogrid and Backfilling. After thoroughly sweeping the top of the unit course with a hand broom to remove any debris which may affect alignment of ensuing courses, the geogrid is placed at specified intervals in the walls by rolling out behind the block and cutting to prescribed embedment depth. The sweeping is important as even small debris has a noticeable impact on alignment of blocks and pins for ensuing courses.

1. Pre-cutting of the reinforcement was not required in this particular project due to the standardized embedment depths of 2.0 m (6.5 feet) and 2.99 m (9.8 feet) specified in the final design. The proper grid was simply placed over the pins in the blocks, pulled by hand to remove slack and the next course of block placed over the grid and pins. The geogrid was found to be easier to work with during sunny portions of the day as it was easier to straighten from the rolled configuration. The grid was easily cut with tin snips or large scissors. Care was taken not to overlay grid in a layered fashion on the pins to avoid impacting wall alignment and leveling.

2. With the clean limestone backfill used on this project, staking of the grid at the back of the reinforced zone was not possible though inspectors initially insisted upon enforcing this provision of the specification. Instead, care was taken to backfill over the grid from the front of the wall back across the grid to the back of the reinforced zone to ensure that no slack was left in the geogrid.

3. Following the manufacturer's recommendations, only rubber-tired equipment was used on top of geogrid and gentle turning and braking techniques were employed. It was found that a four-wheeled drive articulated vehicle with a 1361 kilogram (3000 pound) lift capacity worked best. Its capacity was more than adequate to move pallets of block as necessary. Vehicles with 'skid' type steering caused the geogrid to bunch and wave. In no case were construction vehicles allowed within three feet of the block face to preclude movement of individual block's positioning in the wall. This provision of the specifications must be rigorously enforced or misalignment and reconstruction will result.

4. Soil filling behind the reinforced zone should proceed in parallel with backfill lifts and geogrid installation. This procedure keeps the backfill in place at the back of the zone and reduces waste of backfill which would seek its angle of repose at the back. Since the general contractor was in control of the soil backfilling operation, daily coordination was required to schedule the parallel lifts of reinforced backfill and retained soil.

Construction Sequencing. The complexity of the system of nineteen walls with various tiers, terraces and curves required meticulous planning of the construction sequence.

1. Tiered walls were generally constructed from highest to lowest due to site constraints. This was especially the case in the relatively low walls where it was easy to work in front of completed upper tiers and haul the backfill for lower tiers. Experience soon taught the crew to plan the access route for construction and backfilling equipment for each tier before deciding on the tier construction sequence.

2. Taller tiered walls with easy access from above were more easily constructed with the lower tier first and succeeding tiers in sequence up the slope. In these cases it was found that a wall separation of 3.6 meters (12 feet) was best because it allowed easier access of construction and backfill hauling equipment between walls.

3. In two instances, access from the top on taller walls was not possible requiring construction of a dirt access ramp over the lower tier wall(s) for hauling of backfill and construction equipment access. This was fairly easily accomplished and effective. It is important to construct such a ramp to an elevation at least one foot over the top of the lower tier to keep equipment tires from direct contact with the block and avoid putting stresses on the individual blocks at the top of the wall and staining the block

with tire marks. After completion of upper tiers, these access ramps were easily removed with a small backhoe and hand shovels and the blocks were washed with clean low pressure water.

4. A special problem existed under the interchange bridge where walls were constructed. Overhead bridge beams restricted access for bringing in backfill. The solution was a small backhoe used to lift the backfill into place over the wall. Fortunately, the required reach was not extensive as there were only two tiers of wall affected.

Curves. The batter designed into the walls caused significant difficulties in construction of curves.

1. Inside curves with a reverse batter are naturally narrower at the top than at the bottom. In addition to the surveyed footing considerations mentioned above, the blocks on the lower courses must be placed somewhat further apart. This does not affect pin spacing of adjacent blocks as the angle of curvature allowed maintaining of the 305 mm (12 inch) pin-to-pin spacing. This procedure allowed the succeeding block courses to be laid closer together as the batter required. Failure to properly space the lower block courses will cause extensive cutting of blocks to fit at the narrower top of the wall.

2. In placing succeeding courses of block on curves, it is important to pull the blocks all the way forward on the pins. Again, this helped allow for closer lateral spacing on succeeding block courses. Failure to place the blocks in the far forward position increases the batter and makes the top blocks fit even tighter often requiring special cutting to properly fit.

3. Geogrid placement on inside curves was relatively easy following the manufacturer's overlap recommendations. Overlapping geogrids were separated by approximately three inches of stone to ensure achievement of the specified soil-grid interaction coefficient. No construction difficulties were encountered in this once crews and supervisors were properly educated in the technique.

4. Tight curves often required cutting blocks to fit or breaking off the block tail. Fortunately, the modular units used on this project were easily modified in the field. A hand hammer tapped on the built-in score marks on the side of the block's tail effectively removed the tail. Very few blocks were damaged in this fitting process. For special cutting and fitting of blocks, a gas-powered, hand-held cut-off saw was used. Two types of blades were tested. A dry carbon blade (costing $12-$15) was found to cut only three blocks before dulling to ineffectiveness. A $750 diamond-tipped blade cut over 500 blocks in about one minute per block. It is important for everyone to understand that this modification of the blocks does not impact the structural strength of either the individual blocks or the wall itself or needless arguments with inspectors can ensue.

Spirals. The three unique spirals specified by the architect were not difficult to construct.

1. By modifying the blocks as above, a final radius of 2.13 meters (seven feet) was easily achieved.

2. The spirals were finished off by interconnecting the block back into the preceding curve. While difficult to picture or explain, a few minutes laying blocks into the spiral shape on the ground before construction begins easily resolved the crew's questions.

3. In constructing spirals, it is extremely important to account for the batter in setting the footing and placing the block as previously discussed.

4. Due to the self-containment configuration of the spirals, geosynthetic reinforcement was not required within the spiral but was installed in the backfill behind the entire wall containing the spiral.

Capping. Standard cap units were installed along the top of all nineteen walls in the system. Capping per the manufacturer's recommendation is a relatively simple operation.

1. No special preparation of the surface is required. Simply clean the surface by sweeping away any debris. Debris remaining on the block surface results in a poor seal of the cap unit to the top block.

2. An adhesive product (in this case Liquid Nail) was applied to each block in four spots about the size of a quarter and the cap block set in place over the pins. It is important that the adhesive spots be no closer than two inches to the block face to preclude any adhesive squeezing out over the face which is unsightly and difficult to remove. One tube of adhesive was enough for about ten blocks along the face.

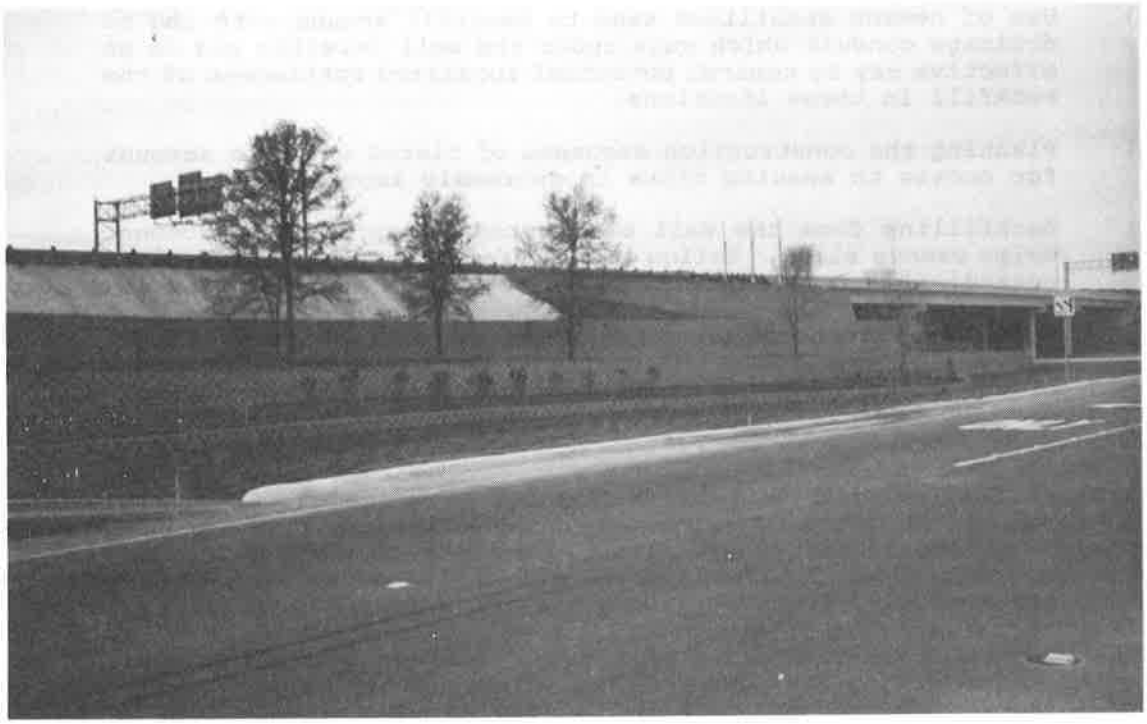

Photograph of a Portion of the Completed Wall Project at 'Fiesta Texas'

CONCLUSIONS

From the experience in design and construction of this large segmental Highway Retaining Wall System at 'Fiesta Texas,' the following conclusions can be drawn:

- The incorporation of synthetic polymer geogrids and modular concrete units into the project reduced the constructed cost of the nineteen walls in the system compared to several other alternatives considered.

- The modularity of the system coupled with its integrity and stability combined to meet the aesthetic architectural needs of the developer and the structural needs of the TxDOT to specified factors of safety.

- The 'showcase' appeal of the constructed wall system exceeded the highest expectations of the architects and developer by effectively tying the park's theme to the landscaped walls of the entrance...all at a lower cost than other options.

- Construction procedures were not complicated but field construction experience with the multiplicity of wall configurations involved can provide an instructional base for designers and constructors of similar wall systems.

Most of the difficulties encountered can be effectively foreseen and accounted for by all parties during the project's design, planning and pre-construction phase. Key lessons learned include:

1) Concrete leveling pads were better than compacted foundation soils for alignment, leveling and construction speed on the competent limestone base at this project site.

2) Leveling pads must be properly placed to account for wall angle and batter to maintain top of wall positioning.

3) Convex curves should be laid first with wider spacing of blocks on lower courses.

4) Use of cement stabilized sand to backfill around watering or drainage conduit which runs under the wall leveling pad is an effective way to control potential localized settlement of the backfill in these locations.

5) Planning the construction sequence of tiered walls to account for access to ensuing tiers is extremely important.

6) Backfilling from the wall back across geogrid reinforcement helps remove slack. Follow the manufacturer's recommendations regarding equipment operation in the fill zone and on geogrid.

7) Think the construction portion of the project through when designing, specifying and bidding. Then discuss all aspects of the construction at a detailed pre-construction meeting.

ACKNOWLEDGEMENTS

This paper is presented with the permission of Mr. Mark McClelland, Supervising Bridge Engineer of the Texas Department of Transportation, H. B. Zachry Construction Company, and 'Fiesta Texas' theme park. The authors wish to thank all of their colleagues who participated in the design and construction of this project and all persons who assisted in preparation and review of this paper.

REFERENCES

1. TxDOT, District 15 (San Antonio) (1990) "Special Specification IR 10-4 (258) 588, I-10, Fiesta, Texas Interchange Improvements."

2. AASHTO "Standard Specifications for Highway Bridges, Section 5, Retaining Walls, 14th Edition, 1989.

3. AAHSTO-AGC-ARTBA Joint Committee (Task Force 27), "Design Guidelines for use of Extensible Reinforcements (Geosynthetic) for Mechanically Stabilized Earth Walls in Permanent Applications," (1990).

4. Tensar Corporation (1991), "TENSWAL Computer Program for Reinforced Soil Retaining Wall Design."

5. Tensar Corporation (1991), "TENSLO12 Computer Program for Slope Stability Analysis Incorporating TENSAR Geogrid Reinforcement."

6. Tensar Corporation (1992), "GENESIS Highway Retaining Wall System Design Manual and Overview.

A New Forming Method and Facing System for Geotextile Walls

M.H. Wayne
Polyfelt Inc., USA

R. Barrows
U.S. Federal Highway Administration, USA

ABSTRACT

Geotextile walls have seen many innovations in material properties since first conceptualized and put into practice by the U.S. Forest Service in the late 1970's.[ref. 1] It is however interesting to note that geotextile walls are for the most part constructed in the same fashion today as they were over 10 years ago.

Most will agree that they have great utility. But many are reluctant to use them today. The authors site three main reasons, all of which are related to the methods used to form and finish the wall face. First, even for temporary use most find geotextile wall faces to be unattractive. They have received the name burritto walls because unless great care and effort is taken the wall lifts tend to sag at the face looking like several burrittos stacked one atop of another. The second reason is a time and constructability issue. The original construction practice of supporting the forms on the lift below has a tendency to amplify error. It can also consume a considerable amount of time if form straps have to be extracted from each lift with construction equipment. Lastly, concerns over construction strain compatibility between geotextile and rigid facing systems have slowed their overall acceptance.

This paper presents an alternative geotextile wall forming and facing method that has been developed and implemented in the construction of a 3 meter high experimental wall. The wall was instrumented with extensometers for monitoring geotextile strain. The paper will also contain construction details and post construction results.

INTRODUCTION

Since the main limitations associated with the construction of a geotextile wall include the appearance of the completed wall, and construction strain compatibility, it was decided that a new forming method and facing system could be evaluated through construction of a test wall. The design of the geotextile wall followed procedures as outlined in reference 2. As such, a 270 gram per square meter nonwoven, needle punched, continuous filament geotextile was used to construct a 3 meter high vertical wall. Soil used for the construction of this test wall consisted of a red silty clayey sand with a liquid limit of 22, plasticity index of 6, and maximum dry unit weight of 19.3 kN/m^3 (123 pounds per cubic foot), when tested in accordance with the American Society of Testing and Materials (ASTM) D-698 [ref. 3], and was native to the project location.

The focus of this paper is geared toward the forming method used to construct this test wall and the attachment of a permanent facing system which is independent of the geotextile wall. This forming and facing system, which should be referred to

as the "Polyfelt Lite Wall System", allows the geotextile to deform during construction and results in a relatively smooth surface vertical wall. After construction of the geotextile wall a facade is then attached to the geotextile wall and is connected using cable supports that were used to construct the wall. This results in an economical and aesthetically pleasing wall.

METHOD OF CONSTRUCTION

To permit construction of the test wall the area was prepared by using a walk behind sheep's foot roller. A trench was then excavated in the location where the wall face was to be constructed. Gravel was then used to construct a leveling pad as depicted in Figure 1.

A wall forming board was constructed such that it was capable of sliding parallel with the wall face and was guided by the vertical supports. Each of the vertical supports was pinned in place by driving rebar into the ground at the appropriate location. Batter boards are then installed as supports for the form board and vertical supports to which they are attached. Although this worked for the experimental wall the author's recommend that these pins be permanently placed within a concrete pad which can be used as both a leveling pad for the geotextile wall and later used as the support pad for the facade. This stage of construction is depicted in Figure 2.

The first two lifts were then constructed using the wrap-around technique which is described in various paper's and design manual's (ref. 1,2,4,5), and is depicted in Figure 2. Care was taken at the form board-geotextile interface. Within the first meter the soil was heavily compacted slightly wet of optimum. For the soil at this site the field density was an average of 17.6 kN/m^3 (112 pounds per cubic foot).

After completion of the second lift the wall form is jacked vertically and pinned in place at the appropriate elevation permitting construction of the next two lifts. A cable connector pin is then driven into the soil approximately two meters behind the wall face and in line with the vertical support. An all thread bar with hook is attached to this connector and a cable is attached at the face. This cable is the attached to the vertical support. The batters are kept in place during this phase of construction which is shown in Figure 4.

The third and fourth lifts were then constructed in a manner similar to the first two. At this point extensometers were placed at locations that were 0.61 m (24"), 1.22 m (48"), 1.83 m (72"), and 2.44 m (96") in from the face of the wall. Prior to moving the form board the plastic coated cable is tightened to a 1" per vertical 1' to release pressure off of the batter boards and provide a batter to the wall face to allow for construction induced deformation. The batter boards were then pivoted and became part of the vertical support for subsequent construction. This sequence is illustrated in Figure 5. Additional lifts were constructed in a similar manner. As a further check, another set of extensometers, similar to the first, were placed between the fifth and sixth lifts.

The wall was complete after the tenth lift above which a 0.61 m (24") surcharge was added and sloped to permit adequate water run off. The forms and batter boards were removed, but the vertical supports remained for attachment of the permanent facade. A cross-section of the completed wall is depicted in Figure 6, and an actual photo of the completed wall is found in Figure 7. Connections used to

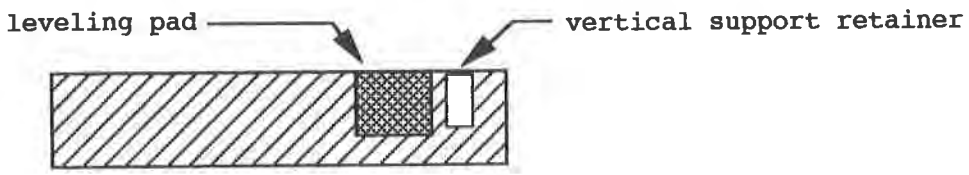

Figure 1 Placement of Leveling Pad

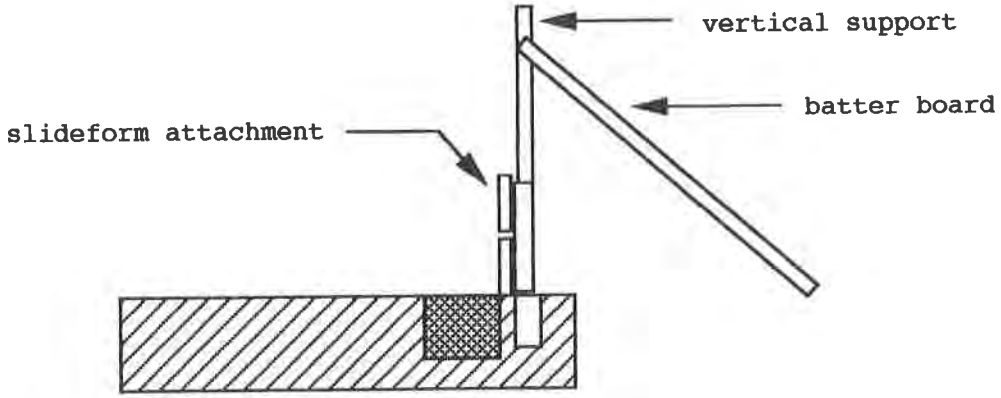

Figure 2 Form Board and Supports Installed

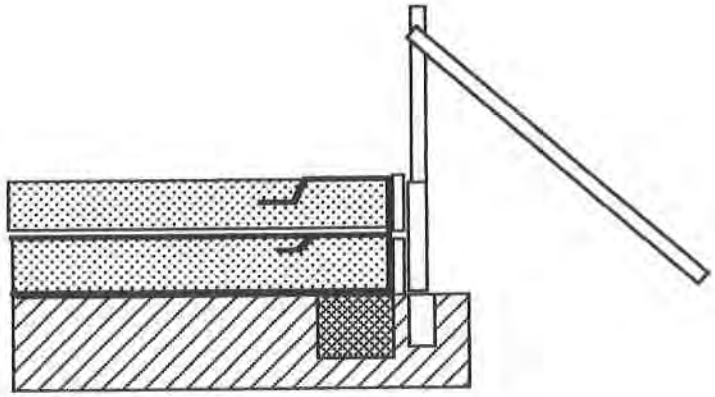

Figure 3 First Two Lifts Constructed

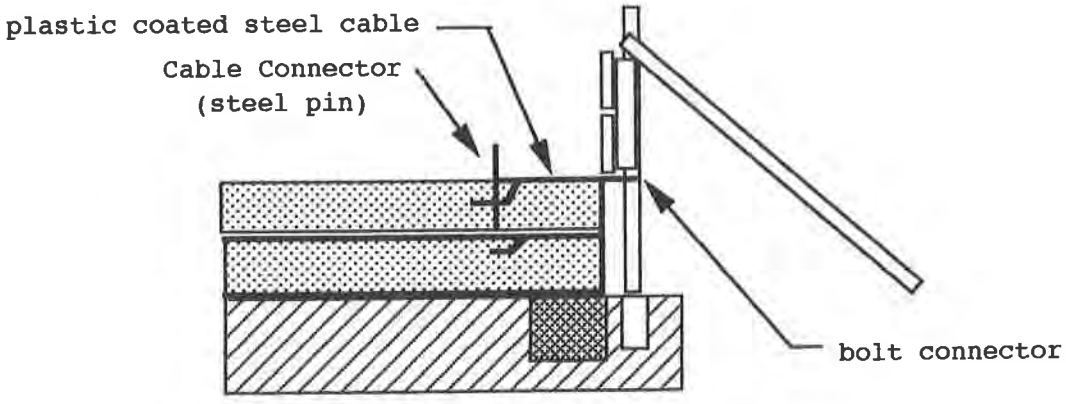

Figure 4 Place Cable Connector & Attach
Cable to Vertical Form Support

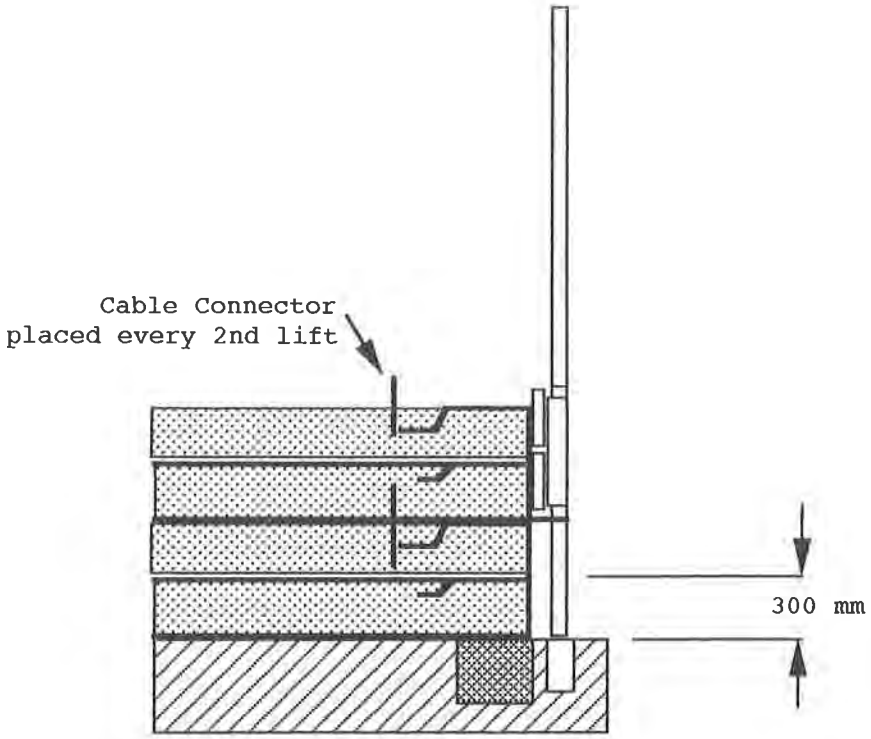

Figure 5 Wall Form Slid Vertical, Batter is Pivoted Vertical, Cable Attached to Vertical Support, Continue Construction

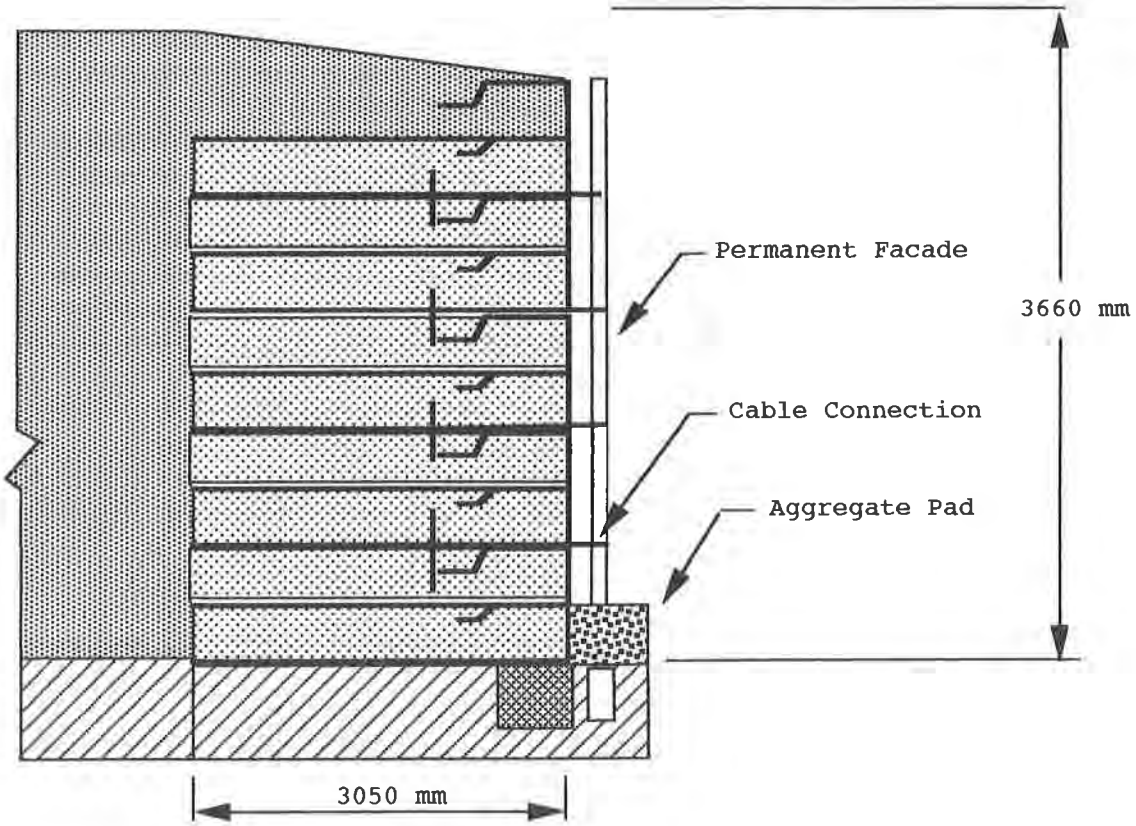

Figure 6 After Completion of Wall, Cable Supports Are Used To Support Permanent Facade.

construct the wall along with additional anchors are then used to attach a facing system as shown in Figure 8. An aggregate pad was placed beneath the facing system to promote drainage, also depicted in Figure 8.

After fourteen months of monitoring this wall, movement of the extensometers was too small to be visually observed. It appears that the movement, which occurred during construction, went undetected by the monitoring systems installed throughout the wall. The 1" horizontal per 1' vertical batter resulted in a 90° wall. This was confirmed by measuring the distance between an existing facility which is located parallel to the geotextile wall. The distance between these two structures, measured over a fourteen month period, has not changed since construction.

Figure 7 Completed Geotextile Wall

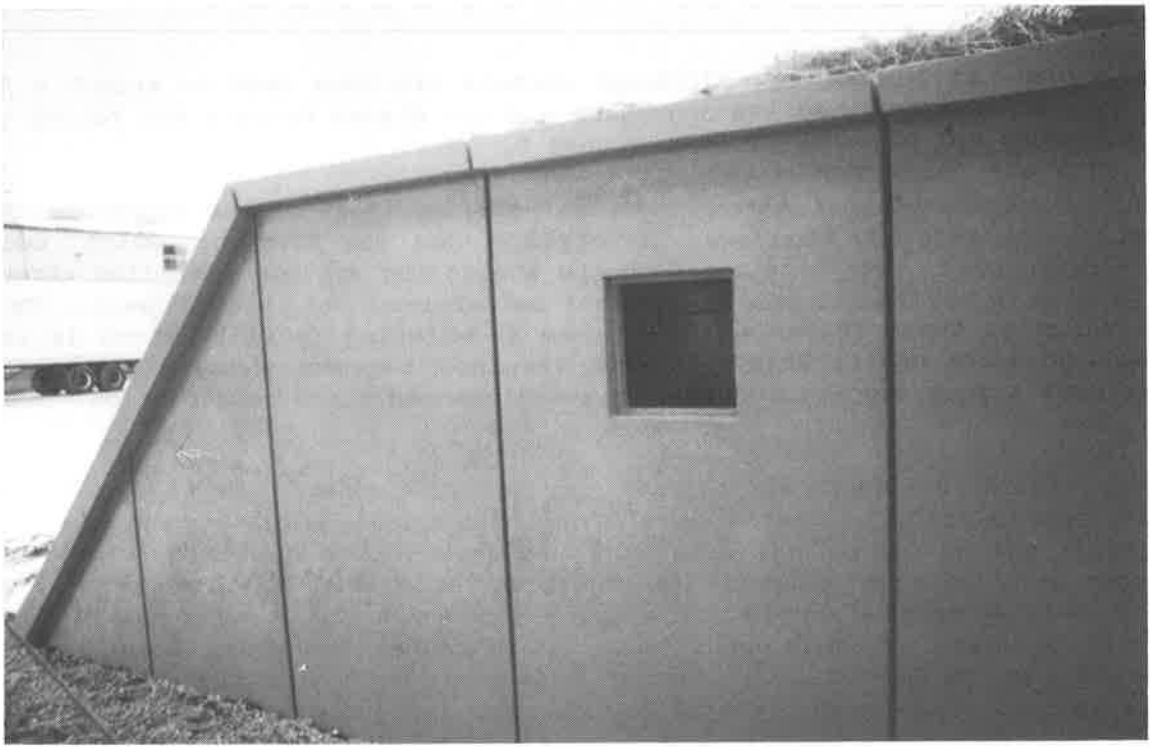

Figure 8 - Completed Polyfelt Lite Wall System

CONCLUSIONS

Construction of an actual test wall confirms the fact that the combination of a spunbonded polypropylene nonwoven geotextile and permanent facade result in a unique and aesthetically pleasing wall system, and at the same time serve as a cost effective means of utilizing existing soils, rather than using clean granular backfill, for construction. After constructing this wall system the author feels the following conclusions apply to this system:

1. The geotextile forming system was successful

2. The new forming system aids in controlling deformation of the geotextile at the face where deformation commonly occurs during construction.

3. The new forming system provides a means for attaching a permanent rigid facade.

Further, the author believes that future efforts should be geared toward the evaluation of the long term benefit afforded by the inclusion of a nonwoven geotextile. Based on excavation of the outer edge of the wall system after 16 months in service field observation indicated the soil to be in a well drained state. It appears that when cohesive soils are used to construct these systems the nonwoven geotextile prevents the buildup of excess pore water pressure through its inherent ability to convey this water within the plane of the geotextile, through transmissivity, and to subsequently exit. This ultimately promotes stability of the wall system.

ACKNOWLEDGEMENTS

The author would like to thank Polyfelt, Inc. for the financial support needed to construct this unique wall. It is hoped that this paper will foster the design of these wall systems.

REFERENCES

1. Steward, J.E., Williamson, R., and Mohney, J., (1977) "Earth Reinforcement," Chapter 5 in *Guidelines for Use of Fabrics in Construction and Maintenance of Low Volume Roads*, U.S. Forest Service, Portland, OR.

2. Polyfelt Inc. (1987), Polyfelt Design and Practice Manual, Evergreen, AL, 146 pp.

3. American Society for Testing and Materials (1991), ASTM Standards on Geosynthetics, Second Edition, Philadelphia, PA, 104 pp.

4. Christopher, B.R. and Holtz, R.D., (1986) "Geotextile Engineering Manual," Report No. FHWA-TS-861203, Federal Highway Administration, Washington, D.C.

5. Bell, J.R., Stilling, A.N. and Vandre, B. (1975) "Fabric Retained Earth Walls," Proceedings, 13th Annual Geology and Soils Engineering Symposium, Moscow, ID.

Effects of Foundations on the Performance of Geosynthetic-Reinforced Soil Walls

N.N.S. Chou
Colorado Department of Transportation, USA

J.T.H. Wu
University of Colorado at Denver, USA

ABSTRACT

Geosynthetic-Reinforced Soil (GRS) walls are inherently flexible; therefore, they may be capable of withstanding large foundation settlements or differential settlement. However, the effects of foundation settlement on the performance of GRS walls have not been fully elucidated. In fact, none of the existing design methods can account for the effects of foundation settlement.

This study was undertaken to investigate the effects of foundation stiffness/strength on the performance of GRS walls. The finite element method of analysis was employed for the study. The analyses were conducted by using a computer program, DACSAR, which was judged to be the best among four finite element programs examined.

The analysis indicated that the foundation soil had a very significant effect on the wall performance. The walls investigated in this study showed maximum lateral wall displacements of 0.45%, 0.67%, 0.75% and 3.0% of the wall height, under a service load of 5 psi, for a rigid foundation, a stiff clay foundation, a medium dense sand foundation, and a soft clay foundation, respectively. The foundation stiffness was also found to affect the mode of deformation. The wall constructed on the rigid foundation rotated about its toe. The wall on the soft clay foundation rotated about the top of the wall, due to the significant movement of its foundation.

INTRODUCTION

Geosynthetic-Reinforced Soil (GRS) walls have demonstrated numerous characteristics that make them more preferable to conventional concrete retaining walls. Among these characteristics is their capability to withstand large foundation settlements or differential settlement due to greater flexibility. In the Glenwood Canyon geotextile test wall (Bell, et al., 1983), for instance, only hairline cracks were detected, although more than two feet of foundation settlement had occurred. This superior feature makes GRS walls well suited for construction over soft foundations, especially when combining with a staged construction technique.

The effects of foundation settlement on the performance of GRS walls have not been fully elucidated. In fact, none of the existing design methods address these effects. All the design methods simply assume that the wall is to be constructed over a rigid foundation.

The objective of this study was to investigate the effects of foundation stiffness/strength on the wall performance. A finite element analysis, using the program DACSAR, was employed in this study. The program features a visco-plastic soil model which can account for the time-dependent deformation of foundations.

THE ANALYTICAL MODEL

A comparative study on finite element analysis of GRS walls was conducted for the purpose of selecting the best analytical tool for this study. Four computer programs were investigated, including SSCOMP (Seed, 1983), CRISP (Britto & Gunn, 1987), CON2D-86 (Schaefer & Duncan, 1987) and DACSAR (Iizuka & Ohta, 1987). The computer program, DACSAR (Deformation Analysis Considering Stress Anisotropy and Reorientation), developed at Kyoto University and Kanazawa University in Japan (Ohta and Iizuka, 1986; Iizuka and Ohta, 1987) was chosen for this study because:

- It is very well organized and appears to be "bug" free.
- It has all the element types needed for simulating the behavior of GRS walls. Namely, the program has bar (truss) element, beam element, and quadrilateral plane strain element.
- It contains both the viscid and inviscid versions of the Sekiguchi-Ohta soil model, which considers the effects of anisotropic consolidation, dilatancy, creep, shearing rate, and stress relaxation.

To analyze the performance of GRS walls, the following modifications were made to DACSAR:

- The Duncan-Chang soil model was implemented to simulate the behavior of backfill.
- A nonlinear, stress-dependent hyperbolic model for the bar element was incorporated to simulate the load-deformation behavior of the reinforcement.

The analytical model has been validated by comparing its results with a closed-form solution; with laboratory "element tests" of soil, reinforcement and facing; with another validated finite element computer program SSCOMP; and with measurements from two full-scale Denver test walls (Chou, 1992). The analytical results agreed well with those of the element tests. Similar analytical results for a GRS wall were obtained from SSCOMP and DACSAR. A class-A prediction on the Denver test walls, using DACSAR, was satisfactory for the cohesive backfill wall under service loads. Analyses, performed after the full-scale tests, showed that the behavior of both test walls can be properly simulated by the numerical model (Chou, 1992).

MATERIAL MODELS

Soil Models

The soil models available in the original DACSAR were a linear elastic model and the Sekiguchi-Ohta (1977) model. The modified Duncan-Chang model was implemented in DACSAR to better simulate the behavior of compacted clay and sand.

The Sekiguchi-Ohta (1977) model was used for simulation of normally consolidated or slightly overconsolidated clayey foundation. The model is an elasto-viscoplastic model which is capable of simulating the anisotropic behavior of clay, including complicated responses to rotation of principal stress directions. This model will reduce to the original Cam-clay model (Roscoe, Schofield and Thurairajah, 1963) under the condition of isotropic initial stress state. Therefore, the Sekiguchi-Ohta model may be considered an extended anisotropic Cam-clay model, or a generalized Cam-clay model, with the original Cam-clay being a special case under isotropic conditions. Detailed derivation of the soil model has been given by Sekiguchi & Ohta (1977), Ohta & Sekiguchi (1979) and Iizuka & Ohta (1987).

Since the Sekiguchi and Ohta model is cast in the framework of classical elastoplasticity via critical state soil mechanics, it is really only well-suited for normally consolidated clay. It should be noted that for most foundation, the clay could be either lightly- to heavily overconsolidated, the analytical result obtained from the Sekiguchi-Ohta and other Cam-clay type model should be viewed as approximation only.

Soil Model Parameters

Detailed descriptions of the determination of the Duncan-Chang and the Sekiguchi-Ohta model have been given by Duncan et. al. (1980) and Iizuka & Ohta (1987), respectively. A brief summary of parameter determination of the Sekiguchi-Ohta model is presented herein.

The soil parameters needed in the inviscid part of the Sekiguchi and Ohta model are λ, κ, e_o, and D. Parameters λ and K are the compression index and the swelling index, respectively, e_o is void ratio at the preconsolidated state, and D is the coefficient of dilatancy defined by Shibata (1963). For simplicity, the irreversibly ratio Λ and the critical state parameter M are chosen as the soil parameters in DACSAR rather than the parameters λ, κ, e_o. They are related by:

$$M = \frac{\lambda - \kappa}{D(1+e_o)} \tag{1}$$

and

$$\Lambda = 1 - \frac{\kappa}{\lambda} \tag{2}$$

The coefficient of secondary compression α and the initial volumetric strain rate $\dot{\nu}_0$ are needed in modelling the viscid characteristics of the material. The initial volumetric strain rate can be determined by $\dot{\nu}_0 = \frac{\alpha}{t_c}$, where t_c is the time required for the completion of the primary consolidation.

Geosynthetic Model

The geosynthetic reinforcement was simulated by a series of bar (truss) elements since geosynthetics, in general, exhibit only axial (tensile) resistance. For most geosynthetics, the tensile stiffness can be described by the following equation:

$$E = E_i \left(1 - \frac{T}{T_{ult}} \right)^2 \quad (3)$$

where T = tensile force per unit width, E_i = initial tensile stiffness, and T_{ult} = ultimate tensile force per unit width. The values of E_i and T_{ult} can be obtained by the transformed linear relationship:

$$\frac{\varepsilon}{T} = \frac{1}{E_i} + \frac{\varepsilon}{T_{ult}} \quad (4)$$

Facing

The behavior of wall facing can be simulated in DACSAR by a series of beam elements with bending and axial resistance. Various facings have been used for GRS wall construction, and their characteristics are described as follows:

- Geosynthetic wrapped-around: negligible bending resistance.
- Timber/forming system: moderate local and global bending resistance;
- Articulated precast panels (modular blocks): high local resistance, but little global bending resistance;
- Continuous concrete facing: high local and global bending resistance.

PERFORMANCE OF GRS WALLS ON DIFFERENT FOUNDATIONS

To study the effects of foundation settlement on the performance of GRS walls, finite element analyses were conducted. The following conditions were assumed in these analyses:

Geometry

- Wall height = 12 ft
- Reinforcement spacing = 1 ft
- Reinforcement length (uniform) = 9 ft
- Vertical, timber/plywood facing
- Horizontal crest
- Flexible foundation with a thickness of 14 ft
- Rectangular wall shape

Materials

- Reinforced backfill: a silty sand and gravel (GP) compacted to 95% of Standard Proctor, with the modified Duncan-Chang model parameters shown in Table 1.
- Unreinforced backfill: same as the reinforced backfill
- Reinforcement: a geosynthetic with hyperbolic model parameters: $E_i = 500$ lb/in. and $T_{ult} = 35$ lb/in.
- Soil-reinforcement interface: no slippage at the soil-geosynthetic interface up to a service load of 5 psi surcharge.
- Facing: continuous timber/plywood facing with EI = 21,000 lb/in^2 /in and A = 4.6 in^2 /in.
- Soil-facing interface: no slippage at the soil-facing interface up to a service load of 5 psi surcharge.

Loading

- A uniform surcharge of 5 psi was applied to the top surface of the wall, except that no surcharge was applied within 1.5 ft of facing. The surcharge represents a combination of dead and live loads of a highway embankment.

The finite element mesh used for the analysis of the control wall is shown in Figure 1. A total of 228 nodes, which define 200 soil elements, 66 bar elements (for the reinforcement) and 12 beam elements (for the wall facing), were employed in the mesh. Based on the authors' experience with DACSAR program, this mesh is considered an adequate representation of the wall system.

The foundation soil was treated as an assembly of "pre-existing" soil elements. The erection of the wall was simulated in twelve construction lifts of soil placement, each one foot thick. Compaction effect was simulated by assigning a high K_o value in the compacted backfill.

It was assumed for this study that the construction took 12 days (one foot high per day) and that another 18 days elapsed before the surcharge was applied. Since the foundation soil for the control wall was assumed to be relatively pervious, the influences due to consolidation are insignificant.

Effect of Foundation

To study the effect of foundation on wall performance, the following subsurface conditions were analyzed:

(1) A medium-stiff sandy clay (SC) with a relatively high permeability (say, k = 1×10^{-6} cm/sec) and a low PI (say, 10), referred to as "medium stiff clay" foundation. The water table is at 3 ft below the existing ground level. This type of soil represents the most commonly encountered overburden soil in Colorado. The Sekiguchi-Ohta model was adopted for simulation of this foundation soil; creep was not considered in the analyses. The Sekiguchi-Ohta model parameters for the foundation soil are listed in Table 2. Above the water table, i.e., the upper 3 ft of the unsaturated foundation soil, development of negative porewater pressures was assumed in the analyses.

Table 1: The Duncan-Chang Soil Parameters for Backfill of the Control Wall

C(psi)	ϕ(deg)	$\Delta\phi$	K_b	m	K_{ur}	K_o	k	n	R_f
0.5	35	7	175	0.2	600	2.5	600	.6	.7

Table 2: The Sekiguchi-Ohta Model Parameters for Foundation of the Control Wall

D	Λ	M	$\acute{o}$	$k/\gamma\varpi$	$\sigma_v^{\cdot}$(psi)	K_o	K_i	α	$\dot{v}_o$	e_o
.023	.86	1.4	.3	$\frac{1.0\ in^4}{day\text{-}\#}$	14	0.9	1.0	0	N/A	0.7

Table 3: The Sekiguchi-Ohta Model Parameters for Soft Clay Foundation

D	Λ	M	$\acute{o}$	k/rw	$\sigma\grave{u}$	K_o	K_i	α	$\dot{v}_o$	e_o
.023	.86	1.4	.3	$\frac{0.01\ in\ 4}{day\text{-}\#}$	14 psi	0.9	1.0	.00124	.0000124	0.7

Table 4: The Duncan-Chang Soil Parameters for the Loose to Medium Dense Sand Foundation

C(psi)	ϕ(deg)	$\Delta\phi$(deg)	K_b	M	K_{ur}	K_o	K	n	R_f
2.0	30	0	110	.2	220	.5	120	.45	.7

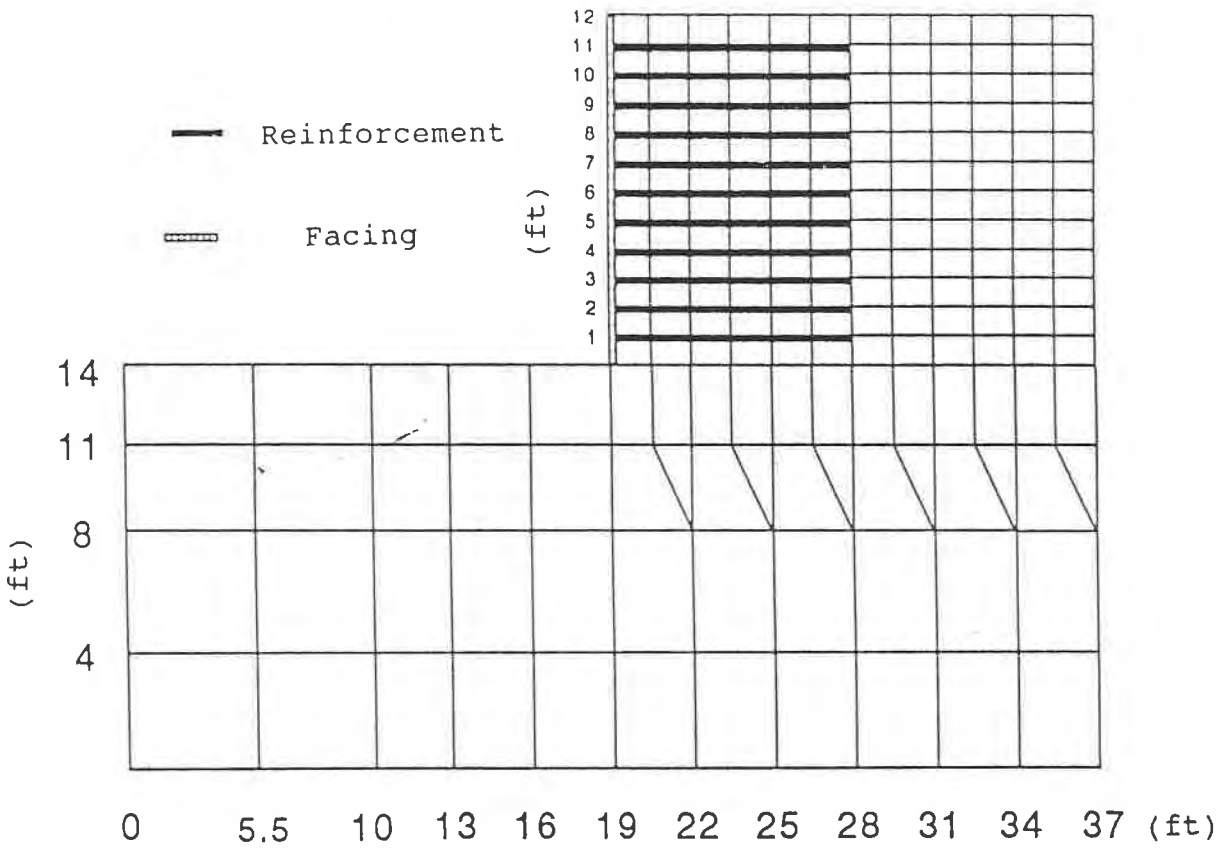

Figure 1: Finite Element Mesh for the Control Wall

(2) A soft-to-medium stiff clay with a relatively low permeability (say, k = $1x10^{-8}$ cm/sec) and a high PI (say, 30) , referred to as "soft clay" foundation. The Sekiguchi-Ohta model parameters for this material are shown in Table 3. Creep was considered in these analyses.

(3) A loose-to-medium dense sand, referred to as "loose sand" foundation. Neither consolidation nor creep was taken into account. The Duncan-Chang model was employed, and the parameters used are listed in Table 4.

(4) A rigid foundation; very hard, such as bedrock or very dense granular material.

Except for the rigid foundation, the foundation depth was assumed to be 14 feet. Wu & Lin (1991) have indicated that the wall movement is not sensitive to the foundation depth varying from 6 to 14 feet for a 12-ft high wall.

Figure 2 shows the lateral wall displacements for the above four foundations, after 10 years consolidation time. As expected, the rigid foundation exhibits the least wall movement, and the wall rotates about the toe of the wall. Lateral wall movement for the medium stiff clay and loose sand foundations are somewhat alike, although different soil models were used. The wall with the soft clay foundation rotates about the top of the wall, due to the significant movement of the foundation. The maximum wall displacements for the rigid foundation and the soft clay foundation were 0.7% of wall height and 3.0% of wall height, respectively. This large difference clearly indicates the importance of including foundation soil in the analysis, especially when soft foundations are present.

The distribution of tensile strains in the reinforcement at three different heights, as shown in Figure 3, indicates that, with the soft clay foundation, the tensile strains induced in the reinforcement are much larger near the bottom of the wall, as reflected by the large wall movement. The wall with a rigid foundation exhibits the lowest tensile strain, and the walls with medium dense sand and stiff clay exhibit about equal tensile strains. The patterns of the strain distribution are very similar for all four foundations.

A preliminary design procedure, based on an allowable lateral wall deformation and limited tensile strain in reinforcement, was proposed (Chou, 1992). The proposed design method accounts for the effects of foundation deformation and facing rigidity and permits judicious use of cohesive backfill.

Staged Construction

GRS walls can be constructed on almost all types of foundation soils except soft clay (i.e., cohesionless than 500 psf). If a soft clay foundation is present and external stability appears to be a problem, the following remedial measures may be considered (Hausmann, 1990): (a) staged (or slow) construction with or without surcharge of the wall, (b) sub-excavation of the existing soft soil and replacement with compacted backfill, (c) lime or lime/fly ash treatment, (d) stone columns, (e) wick drains with or without surcharge, and (f) compaction grouting.

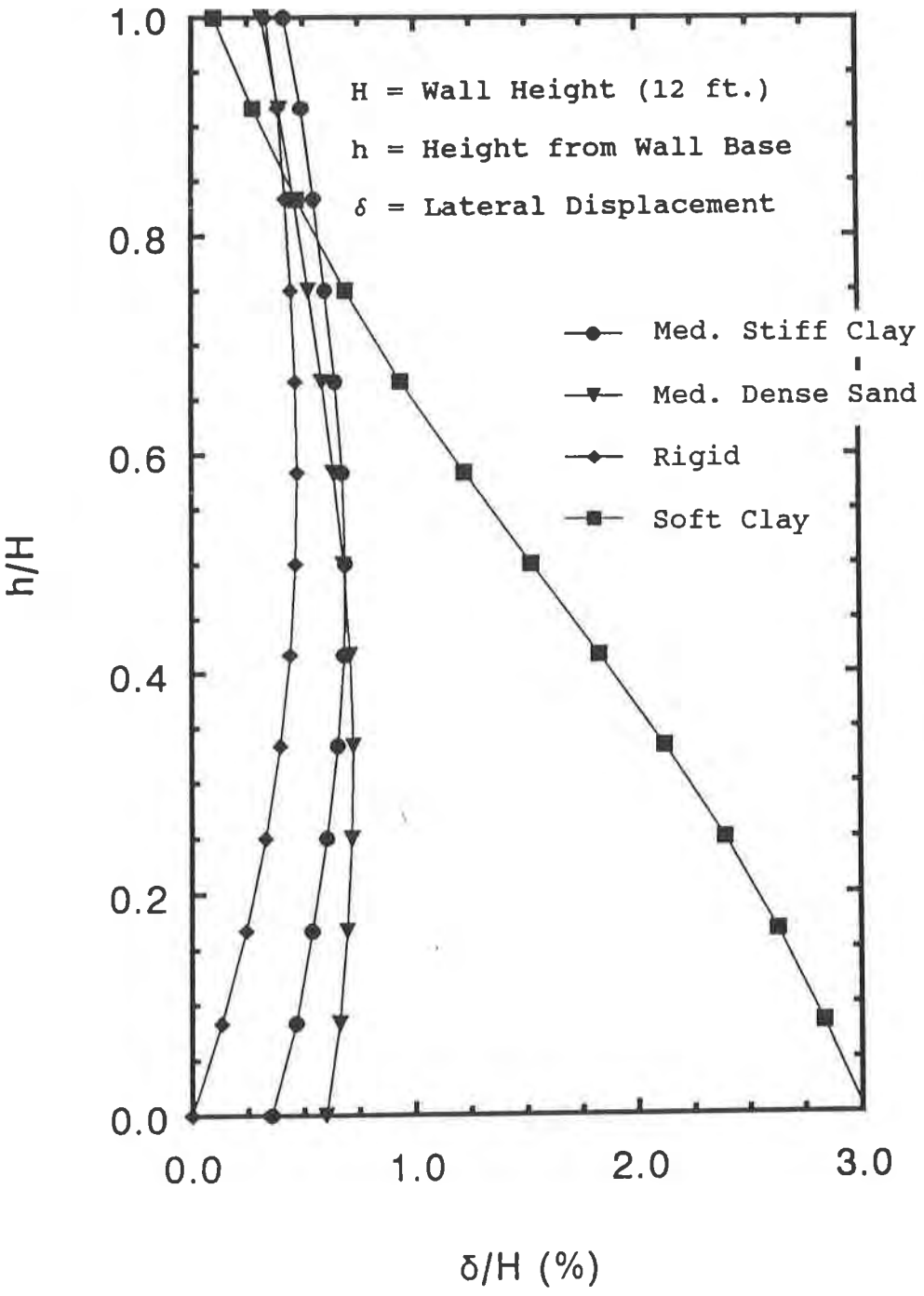

Figure 2: Effect of Foundation on Lateral Wall Displacement

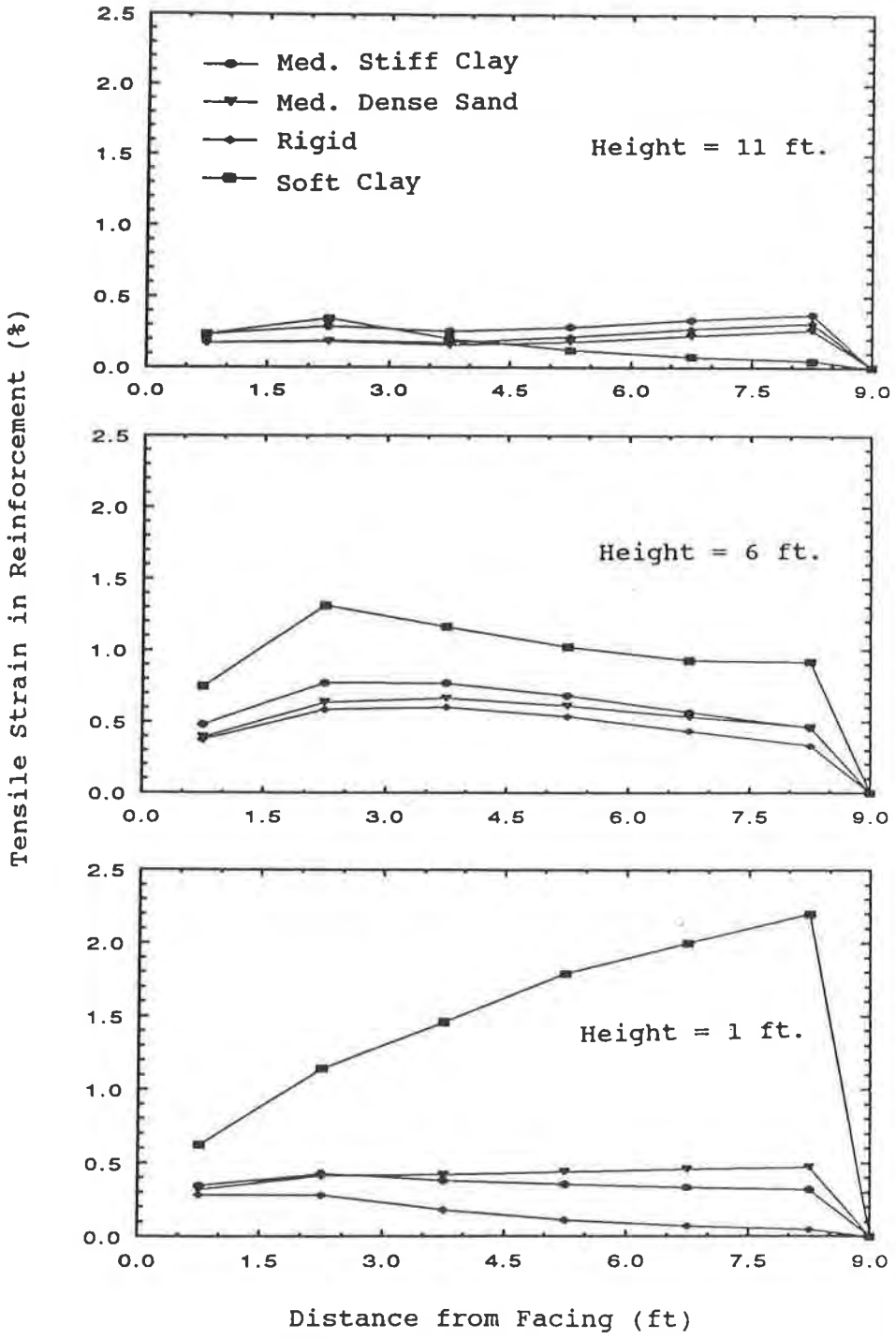

Figure 3: Effect of Foundation Stiffness on Reinforcement Tensile Strains

If time is not a major concern, staged construction, perhaps with surcharge to accelerate consolidation, is often the most cost-effective solution. The external stability of a wall constructed over a soft foundation can be increased significantly (Chou and Su, 1990).

During construction of the wall, the undrained shear strength (S_u) increased due to consolidation. The gain of undrained shear strength, dS_u, was calculated by the following equation (Chou, et. al. 1980):

$$dS_u = m * I * d\sigma_c * U\% \quad (5)$$

where m = Slope of S_u vs σ_c curve
I = Influence factor of loading based on elasticity theory
$d\sigma_c$ = Increase in mean value of consolidation pressure; and
U (%) = Percentage of consolidation.

Equation (5) has been verified by DACSAR if the soil is assumed to be linearly elastic. Since the shear strength is increased due to staged construction, the wall deformation and tensile strain in the reinforcement also can be reduced effectively by staged construction. For a large wall construction project, a "slow construction" technique (i.e., limit the construction speed to an allowable rate) also may be used.

CONCLUDING REMARKS

The analyses indicated that the foundation soil has a very significant effect on the wall performance. The walls investigated in this study resulted in maximum lateral wall displacements of 0.45%, 0.67%, 0.75% and 3.0% of the wall height, under a service load of 5 psi surcharge, for a rigid foundation, a stiff clay foundation, a loose sand foundation, and a soft clay foundation, respectively. The foundation stiffness also affects the mode of deformation. The wall constructed on the rigid foundation rotates about its toe. The wall with the soft clay rotates about the top of the wall, due to the significant movement of its foundation. The wall with a rigid foundation exhibits the lowest tensile strain, and the walls with the medium dense sand and stiff clay foundations exhibit about equal tensile strains in the reinforcement. For a GRS wall situated on the soft foundation, staged construction can be very effective to increase the stability, and reduce the lateral deformation of the wall.

The results presented in this paper are part of a recently completed research study on the performance of geosynthetic-reinforced soil walls (Chou, 1992). The research effort has lead to the development of a preliminary design method. The design concept is based on an allowable lateral wall deformation and limited tensile strain in reinforcement. The proposed design method accounts for the effects of foundation deformation and facing rigidity and permits judicious use of cohesive backfill.

ACKNOWLEDGEMENT

The Colorado Department of Transportation sponsored this research study. The authors gratefully acknowledge Professor Ching S. Chang at the University of Massachusetts for his assistance in the implementation of Duncan-Chang model.

REFERENCES

Akai, K. and Tamura, T. (1976), "An Application of Nonlinear Stress-Strain Relations to Multi-Dimensional Consolidation Problem," Annuals, Disaster Prevention Research Institute, Kyoto University, No. 19, B-2, pp. 15-29 (in Japanese).

ASTM D-4595-86, (1987), "Standard Test Method for Tensile Properties of Geotextiles by the Wide-Width Strip Method," Annual Book of ASTM Standards, Vol. 04.08, pp. 1041-1055.

Bell, J.R., Barrett, R.K, and Ruckman, A.C. (1983), "Geotextile Earth Reinforced Retaining Wall Test, Glenwood Canyon, Colorado," Presented at the Annual Meeting, Transportation Research Board, Washington, D.C.

Britto, A.M., Gunn, M.J., (1987), "Critical State Soil Mechanics Via Finite Elements," Ellis Horwood Limited, Great Britain.

Chou, N.N.S., Chou, K.T., Lee, C.C. and Tsai, K.W. (1980), "Preloading by Water Testing Eliminated Sand Drains for a 65,000 Ton Raw Water Tank in Taiwan," Proceedings of the 6th Southeast Asian Conference on Soil Engineering.

Chou, N.N.S., Su, C.K. (1990), "External Stability of a Reinforced Earth Wall Constructed Over Soft Clay," Proceedings, Conference on Design and Performance of Earth Retaining Structures, ASCE, June 18-21, Ithaca, N.Y.

Chou, N.N.S (1992), "Performance of Geosynthetic Walls," A Dissertation Submitted to the University of Colorado, in partial fulfillment of the requirements for the degree of Doctor of Philosophy, Dept. of Civil, Environmental and Architectural Engineering

Drucker, D.C., Gibson, R.E. and Henkel, D.J. (1957), "Soil Mechanics and Work Hardening Theories of Plasticity," Transportation ASCE, Vol. 122, pp. 338-346.

Duncan, J.M., Byrne, P., Wong, K.S. and Mabry, P. (1980), "Strength, Stress-Strain and Bulk Modulus Parameters for Finite Element Analyses of Stresses and Movements in Soil Masses," Report No. VCB/GT/80-01, Department of Civil Engineering, University of California at Berkeley, August, p. 77.

El-Fermaoui, A. and Nowatzki, E. (1982), "Effect of Confining Pressure on Performance of Geotextiles in Soil," Proceedings of the Second International Conference on Geotextiles, Las Vegas, pp. 799-804.

Hausmann, M.R. (1990), "Engineering Principles of Ground Modification," McGraw-Hill Publishing Company.

Iizuka, A. and Ohta, H. (1987), "A Determination Procedure of Input Parameters in Elasto-Viscoplastic Finite Element Analysis," Soils & Foundation, Vol. 27, No. 3, pp. 71-87.

Ling, H.I. and Tatsuoka, F. (1992), "Nonlinear Analysis of Reinforced Soil Structures by Modified CANDE (M-CANDE)," International Symposium of Geosynthetic-Reinforced Soil Retaining Walls, August 5-9, Denver.

Ling, H.I., Wu, J.T.H., and Tatsuoka, F. (1992), "Short-Term Strength and Deformation Characteristics of Geotextiles Under Typical Operational Conditions, Geotextiles and Geomembranes, Vol. 10, No. 2.

McGown, A., Andrawes, K.Z., and Kabir, M.H. (1982), "Load-Extension Testing of Geotextiles Confined in Soil," Proceedings of the Second International Conference on Geotextiles, Las Vegas, pp. 793-798.

Ohta, H. and Sekiguchi, H. (1979), "Constitutive Equations Considering Anisotropy and Stress Reorientation in Clay," Third International Conference on Numerical Methods in Geomechanics, April 2-6, Aachen.

Ohta, H. and Iizuka, A. (1986), Manual of DACSAR FEM Program, Kanazawa University.

Schaefer, V.R. and Duncan, J.M. (1987), "Analysis of Reinforced Embankments and Foundations Overlying Soft Soil," VPI and State University, Blacksburg, VA.

Seed, H.B. and Duncan, J.M. (1983), "Soil-Structure Interaction Effects of Compaction-Induced Stresses and Deflection," Dept. of Civil Engineering, University of California, Berkeley.

Sekiguchi, H. and Ohta, H. (1977), "Induced Anisotropy and Time Dependency in Clays," 9th International Conference on Soil Mechanics & Foundation Engineering, Tokyo.

Siel, B.D., Wu, J.T.H., and Chou, N.N.S. (1987), "In-Soil Stress-Strain Behavior of Geotextile,", Proceedings, Geosynthetics '87 Conference, Feb 24-25, New Orleans. LA.

Wu, J.T.H and Lin, J.C. (1991), "Analysis and Design of Geotextile-Reinforced Earth Walls, Vol. 3, Parametric Study and Preliminary Design Method," Final Report to Colorado Department of Highways, Department of Civil Engineering, University of Colorado at Denver, March

Wu, J.T.H. (1991), "Measuring Inherent Load-Extension Properties of Geotextiles for Design of Reinforced Structures," Geotechnical Testing Journal, June, Vol. 14, No. 2, pp. 157-165.

Finite Element Analysis of Geosynthetics-Reinforced Soil Walls

S.K. Ho
University of Western Ontario, Canada

R.K. Rowe
University of Western Ontario, Canada

ABSTRACT

The beneficial effect of incorporating geosynthetics as reinforcements in soil retaining structures has been demonstrated by numerous successful applications. However, there are apparent inconsistencies between some of the design assumptions and the observations from field measurements. The finite element method provides complementary means of performing a detailed study. In this paper, the results from a finite element study of a hypothetical geosynthetic reinforced soil wall are presented. Qualitative comparisons between analytical results and field observations may provide insight concerning some of the field observations which have not been fully discussed in the literature. In addition, this information is considered to be useful as a basis for a parametric study of geosynthetic reinforced soil walls.

INTRODUCTION

Despite the fact that a great many geosynthetic reinforced soil walls have been safely constructed and are performing well to date, the interactions between the different components comprising these systems are still not well understood. Most design or analytical methods are either empirical in nature or based on limit equilibrium analysis calculations which do not consider deformations or interactions between the components of the wall system. As a consequence their applications are sometimes limited. Some times, these methods consistently do not make good predictions of field performance, although most approaches are consistently conservative.

Another problem is the apparent inconsistencies evident in the interpretation of the data obtained from instrumented cases. For example, in a trial wall studied by Andrawes et al. (1990) the measured horizontal soil pressure acting at the wall face showed deviation

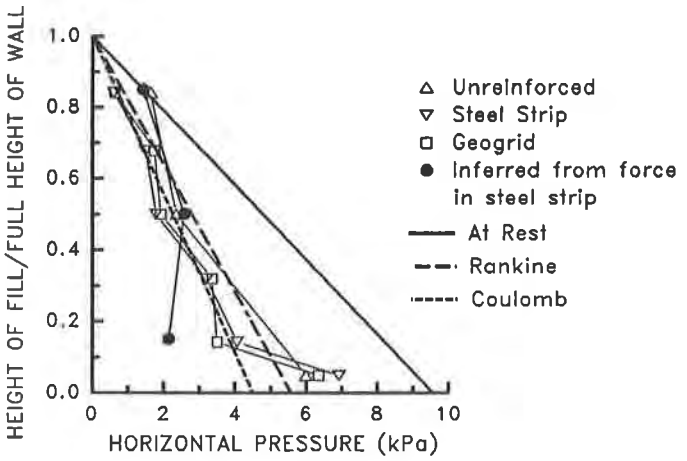

Figure 1 Horizontal Pressure Distribution at Wall Face
(Modified from Andrawes et al., 1990)

from the equivalent horizontal soil stress calculated from the force in the reinforcement (inferred by strain measurement) adjacent to the wall face (Figure 1).

As another example, in some design or analytical methods it is usually assumed that the vertical soil pressure within or at the base of the reinforced soil mass follows one of the three types of distributions shown in Figure 2a (i.e. uniform, trapezoidal or Meyerhof).

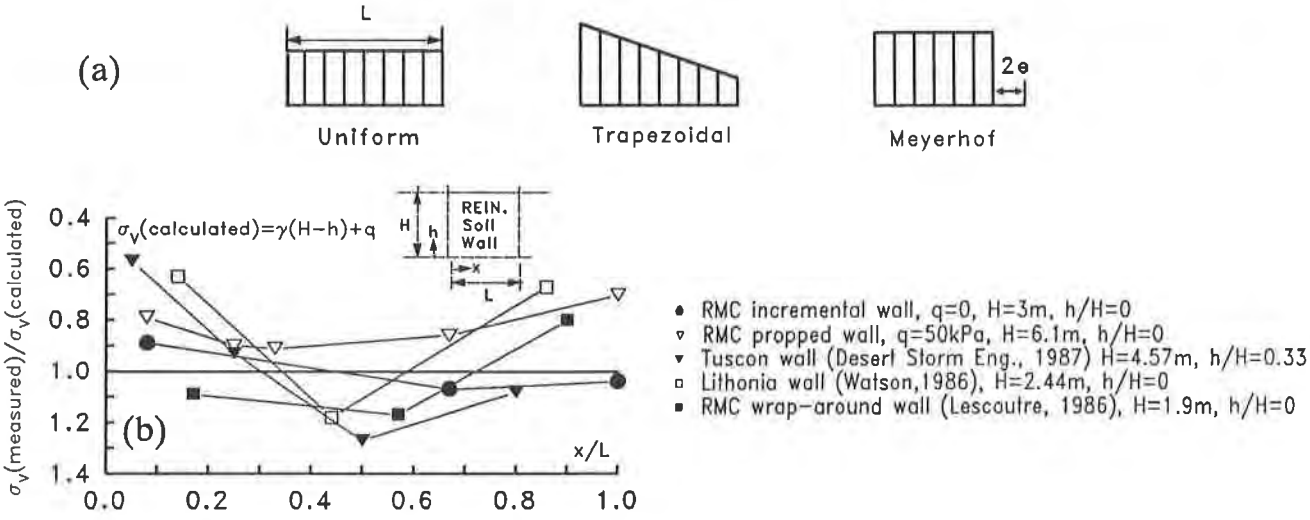

Figure 2 Comparison between a) Design Assumptions and b) Field Observations in Vertical Stress Distribution (Modified from Wawrychuk, 1987)

However, field observations demonstrated that none of these distributions are able to reflect the actual distribution as indicated in Figure 2b. These characteristics cannot be fully appreciated unless sufficient information is available.

"Numerical experiments" or simulations provide a means of gaining insight into the effects of various design assumptions on these walls. Finite elements techniques have been used by some researchers to analyze walls constructed with geosynthetic reinforcement (e.g. International Symposium on Geosynthetic-Reinforced Soil Retaining Walls, Denver, Colorado, 1991). The present paper presents some initial results which form part of a general numerical study of the behaviour of geosynthetic reinforced soil walls. The research program is aimed at providing a parametric study and therefore analyses were performed on a hypothetical reinforced soil wall rather than individual case histories. Results presented herein are for a simple case which considered self-weight of the wall only with no surcharge, these results served to provide a fundamental understanding of reinforced soil wall systems and baseline information for later parametric studies. Qualitative comparison with field observations are made, the findings and implications from the numerical analysis are discussed.

WALL GEOMETRY

This study examines a hypothetical reinforced soil wall with a height (H) of 6 m constructed with cohesionless fill and reinforced with 6 layers of sheet-like geosynthetic reinforcement. The length (L) of each layer was 4.25 m with a typical L/H ratio of 0.71 (Figure 3). The wall was assumed to have a level surface and a continuous full panel concrete facing; and was constructed on a rigid foundation. The facing was allowed to rotate about its toe and provision was made for slippage between the facing/foundation and the fill/foundation interfaces.

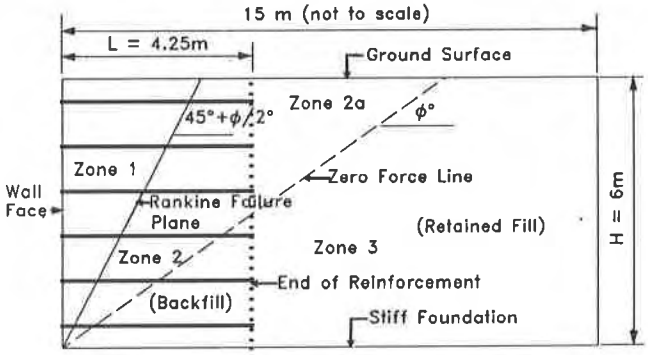

Figure 3 Wall Geometry

NUMERICAL MODELLING

A plane strain finite element analysis was performed on the hypothetical wall using the finite element program AFENA (Carter, 1985) which was modified by the authors to allow modelling of the reinforced soil wall considered herein (this technique has been used with success in the study of a number of case histories, Ho, 1992). The finite element mesh consisted of basically 4237 nodes and 2483 elements. The primary reasons in adopting a fine mesh are to minimize the effect of mesh dependency on the numerical modelling, and to

enable the use of the same mesh (again to minimize the effect of mesh dependency) in cases involving a change in the geometry of the problem (e.g. an increase in the number of layers of reinforcement or an increase in the reinforcement length, etc.).

Soil Element. The backfill and retained fill were modelled using eight-noded isoparametric elements. The fill was assumed to be an elastic-perfectly plastic cohesionless material with a Mohr-Coulomb's failure criterion (i.e. with a friction angle $\phi = 35°$) and a unit weight $\gamma = 20$ kN/m^3. The fill was assumed to have a non-associated flow rule with a dilatancy angle $\psi = 6°$. To capture the nonlinear stress dependent increase in fill stiffness, Janbu's equation was used to update Young's modulus, E, of the fill during the analysis (i.e. $E/P_a = K(\sigma_3/P_a)^n$), where $K = 460$ and $n = 0.5$ are empirical parameters, P_a is the atmospheric pressure and σ_3 is the effective minor principal stress. Poisson's ratio was taken to be $\nu = 0.3$.

Reinforcement And Wall Facing Elements. The reinforcement was modelled using linear elastic bar elements with negligible compressive strength. A reinforcement stiffness J = 2000 kN/m was adopted for the reinforcement. The yield strength α_f was assumed to be 200 kN/m. The continuous full panel facing was assumed to be 140mm thick and was also modelled using eight-noded isoparametric elements with E = 24,000 MPa and $\nu = 0.15$.

Interface (Joint) Element. The interfaces (i.e. interfaces between reinforcement/fill, fill/foundation, fill/facing, facing/foundation) consisted of a pair of dual nodes occupying the same position with independent shear and axial stiffness. Compatible displacement between the pair of dual nodes is ensured by specifying high stiffness until a Mohr-Coulomb's failure criterion is reached. Once the interface shear strength is exceeded, the compatibility conditions are replaced by a failure criterion and a dilatancy equation. In the present study the friction angle for the reinforcement/fill, foundation/fill and facing/foundation interfaces were taken to be 35° (the effect of varying these parameters will be investigated in future parametric studies), the facing/fill interface to be 20°, and the dilatancy angle to be zero at all interfaces.

Temporary Support and Numerical Construction Simulation. In the present study, the wall face was assumed to be fully supported in the horizontal direction during wall construction. The temporary support was modelled by a contact element. The wall was constructed in twenty four layers. Upon completion of construction, the internal forces in the temporary support were released in a number of steps until the deformation at the top of the wall converged to a constant value and the force increment in the reinforcement was negligible in subsequent iterations.

RESULTS OF ANALYSIS

To facilitate later presentation and discussion of results, the wall is divided into three different zones of distinct behaviour as shown in Figure 3. This procedure is similar to that proposed by Jewel (1985) and subsequently used by Bonaparte and Schmertmann (1987).

Zone 1 corresponds to the active zone bounded by the theoretical Rankine's failure plane and the wall face. Zone 2 is referred to the transition zone between the theoretical Rankine's failure plane and the zero force line. The zero force line is the theoretical line beyond which no force is required in the reinforcement for equilibrium, which in this case, corresponds to the theoretical stable slope given by the friction angle of the fill. In addition, there is a sub-zone in Zone 2 (Zone 2a) where curtailment of reinforcement does not extend beyond the zero force line. The area below the zero force line identifies Zone 3.

Stress Distribution in Soil. The average vertical soil stress distributions at each level of reinforcement and at the base of the wall are shown in Figure 4 and Figure 5 respectively.

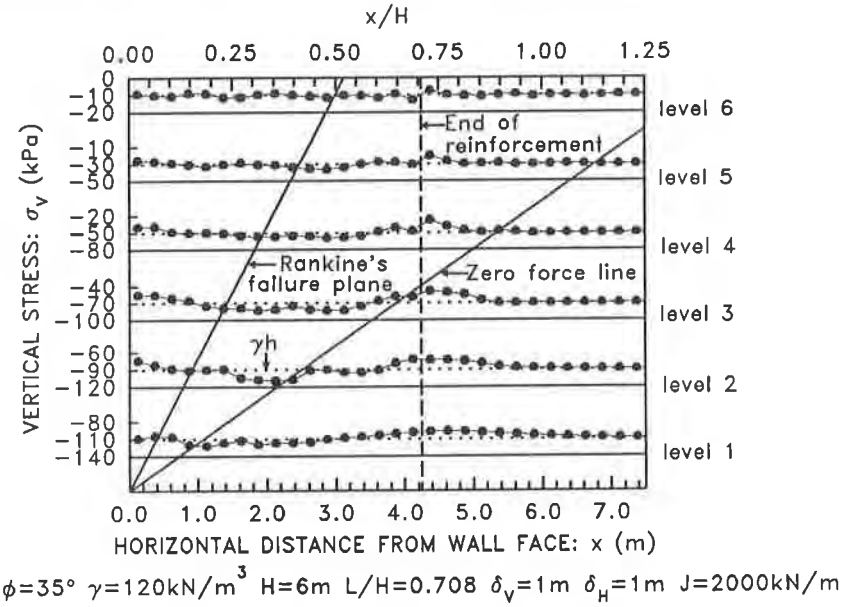

Figure 4 Vertical Stress Distribution within Reinforced Soil Mass

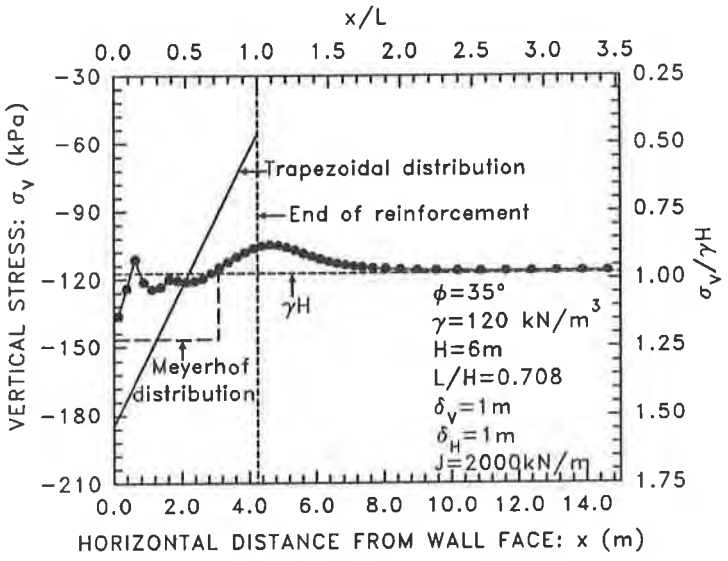

Figure 5 Vertical Stress Distribution at Base of Wall

It can be seen that the pattern of change in vertical soil stress distribution at each level is similar. Close to the fill/facing interface the vertical soil stress is less than the theoretical value (i.e. $\sigma_v = \gamma h$) due to partial transfer of vertical stress from the fill to the facing through fill/facing friction. An exception is in the vicinity of the toe where the rigid foundation prevents significant relative settlement between the fill and the facing. Away from the facing the vertical soil stress increases gradually in the active zone and reaches a maximum exceeding the theoretical value within the transition zone. At each reinforcement level the vertical soil stress reaches a minimum close to the end of the reinforcement with a magnitude less than the theoretical value. A similar trend is observed at the base of the wall (see Figure 5) except again in the vicinity of the toe where the restriction in deformation due to the rigid foundation results in large stress concentration. This pattern of variation in vertical soil stress is comparable to field observations as shown in Figure 2b. It is also clear from Figure 5 that current practice in using either a trapezoidal distribution or a Meyerhof distribution for vertical stress distribution is not applicable. The assumption of a simple uniform distribution appears to be more reasonable in the present case.

Figure 6 shows the average horizontal soil stress distribution at each reinforcement level. It can be seen that the variation of horizontal soil stress mirrors the pattern observed in vertical soil stress variation (see Figure 4).

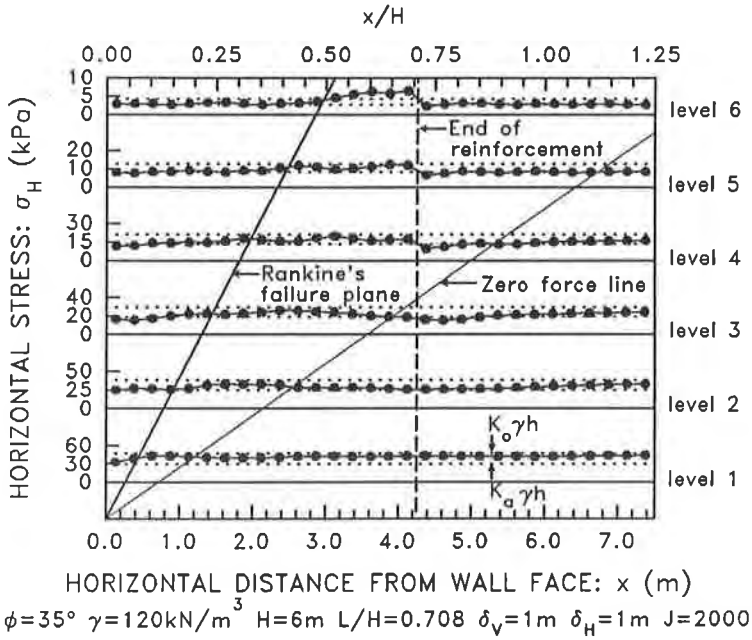

Figure 6 Horizontal Stress Distribution within Reinforced Soil Mass

At the face the magnitude of the horizontal soil stress is very close to that given by the theoretical Rankine active condition, K_a (based on a vertical stress γh at this location). Further back away from the facing, the horizontal soil stress increases and reaches a maximum in the transition zone with magnitude close to or even exceeding the theoretical

at rest condition K_o (i.e. K_o = 1-sinϕ) at the upmost level. Similar to the vertical soil stress variation, the horizontal soil stress reaches a minimum at the end of the reinforcement.

The similarity in the pattern of change in both the vertical and horizontal soil stress distributions indicates that the increase (decrease) in horizontal soil stress is a consequence of an increase (decrease) in vertical soil stress. This is true for a soil element in a state of plastic equilibrium with no rotation in the principal soil stress direction. In order to satisfy the failure criterion an increase (decrease) in vertical soil stress has to be accompanied by an increase (decrease) in horizontal soil stress such that the ratio of horizontal soil stress to vertical soil stress remains constant and equals K_a. However, it is noted that in the vicinity of reinforcement curtailment at the upper levels, there is a large increase (relative to K_a) in horizontal soil stress while the vertical soil stress is close to or even shows a slight decrease from the theoretical value. This suggests that in these local areas the soil elements are not in a plastic state or there are substantial rotations in principal soil stress direction, or both.

Figure 7 shows the state of stress in the reinforced soil mass along each level of reinforcement. Both the horizontal to vertical soil stress ratio (σ_H/σ_V) and the principal soil stress ratio (σ_3/σ_1) from the finite element analysis are plotted for discussion purposes. It should be noted that at a stress point involving rotation of principal soil stress direction, plasticity can only be defined in terms of the principal soil stress ratio, which in this case is numerically equal to the active pressure coefficient K_a.

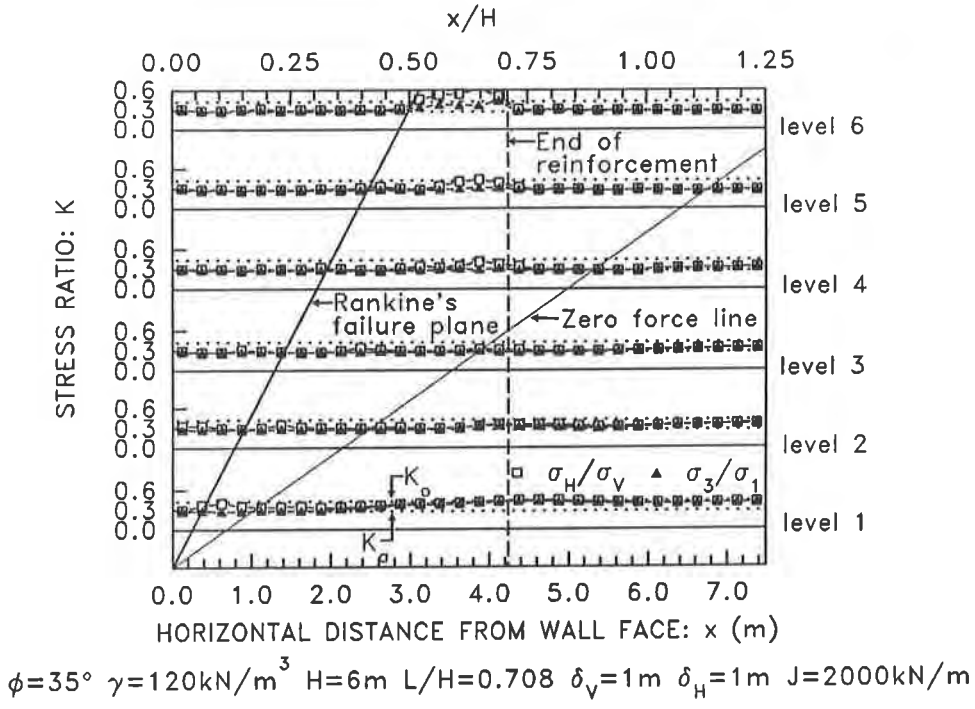

Figure 7 State of Stress within Reinforced Soil Mass

The figure clearly identifies two distinct active earth pressure zones (Zone 1 and the unreinforced portion in the transition zone - Zone 2a). This finding appears to justify the proposal made by Jewel (1987). In particular, the assumption of a rigid foundation does not appear to prevent the soil elements in the vicinity of the toe from developing into an active state. Another significant observation is that while the ratio of horizontal to vertical soil stress may indicate a value greater than K_a, it does not necessary mean that the soil element is not in a plastic state. The only valid indication of plasticity is the principal soil stress ratio. This demonstrates that in field monitoring, merely comparing the measured or inferred horizontal soil stress with the theoretical value will not generally provide a good indication of the state of stress within the soil. Field data (Simac et al., 1990), although limited, support the above finding.

Stress Distribution at Wall Face and at End of Reinforced Fill. The distributions of horizontal soil pressure along the height of the facing are shown in Figure 8. Also shown in the figure are three stress states corresponding to: a) Rankine's active condition K_a, b) at rest condition K_o (i.e. K_o = 1-sinϕ), and c) Coulomb's failure wedge (δ=20°).

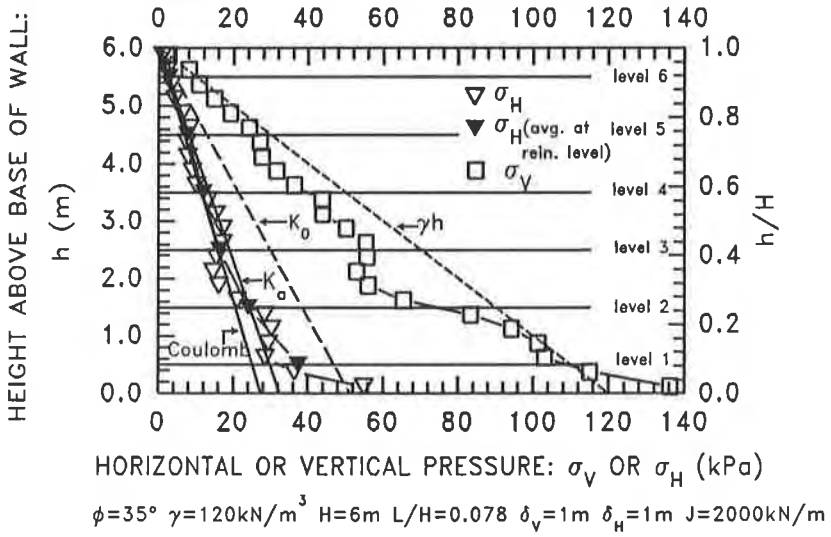

Figure 8 Horizontal and Vertical Pressure at Wall Face

Except at the lower part of the facing where influence of the rigid foundation is significant, the horizontal soil stress is less than the at rest condition. This is reasonable considering the extensible nature of the reinforcement. A more interesting observation is that the horizontal soil stress is even less than that given by the theoretical Rankine active condition and that it oscillates about the pressure line given by Coulomb's failure wedge. The study reveals that this pattern of oscillation (evident in Figure 8) is a result of local variation in vertical soil stress. Both the variations in vertical and horizontal soil stress along the facing follow a similar pattern. It is noted that a similar trend is evident from the experiment data observed by Andrawes et al. (1990) as shown in Figure 1. One might be tempted to attribute the oscillation in Figure 1 to scatter of experimental data, however this

study suggests there is a theoretical basis for the observed oscillation. It should be noted that similar observation is seen at the back of the reinforced soil mass.

Strain Distribution. The force or stress in the reinforcement is directly related to the mobilized reinforcement strain. This, in turn, is closely associated with the strain in the adjacent soil (i.e. the compatibility between soil strain and reinforcement strain). Figure 9 compares the reinforcement strain and the average horizontal soil strain at each reinforcement level (the reinforcement force is also shown at a different scale). It can be seen that compatibility of strain between the fill and the reinforcement is preserved except in the vicinity of the end of reinforcement where curtailment does not extend beyond the zero force line. Curtailment of reinforcement before the zero force line results in a significant increase in horizontal soil strain within the "unreinforced" retained fill, but the magnitude diminishes towards the zero force line. This indicates that the effect of the reinforcement is to suppress the development of horizontal soil strain in an otherwise unreinforced soil mass.

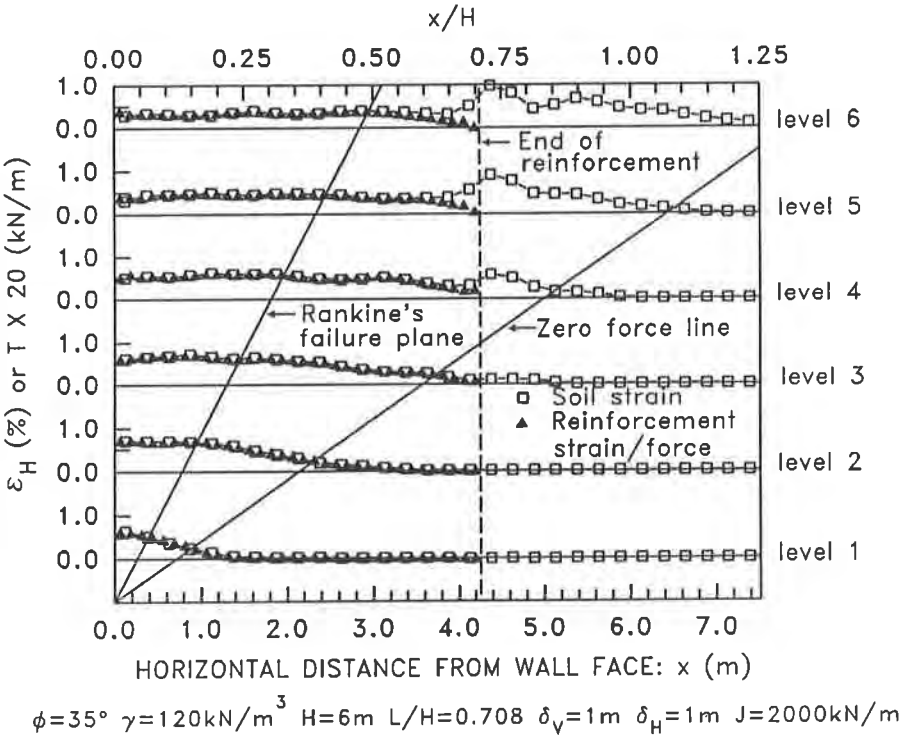

Figure 9 Distribution of Strain/Force along Reinforcement

Force in Reinforcement. As shown in Figure 9, the force at each reinforcement level within the active zone increases gradually from the facing and reaches a maximum (though not distinct in this case) at some locations away from the facing. However, in this particular case the locus of maximum tensile force does not appear to be in the form of a log-spiral; rather, the distribution of tensile force along the reinforcement within the active zone seems to become more uniform towards the top of the wall and the locus of maximum tensile force

appears to conform more to the Rankine failure plane. It should be noted that according to the analytical finding by Leschinsky and Perry (1987) the critical log-spiral failure surface degenerates to Rankine's failure plane for a wall with a vertical face (i.e. 90° slope) constructed of granular soil and horizontal reinforcement as assumed in the present case. However, there are situations (e.g. Christopher et al., 1990) in which the observed locus of maximum tensile force appears to more nearly correspond to a log-spiral. Further investigation is required in this aspect of the problem.

Figure 10 shows the variation of maximum tensile force with depth for the case studied. Similar to most field observations, at upper levels the magnitude of the maximum tensile force exceed that given by Rankine's active condition or even the at rest condition; while at lower levels, the magnitude of the maximum tensile force is significant less.

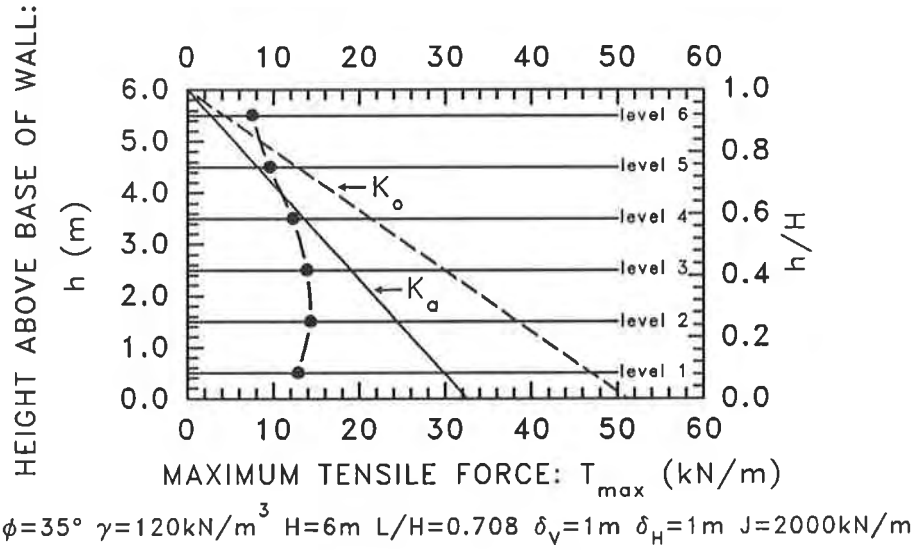

Figure 10 Variation of Maximum Reinforcement Force with Height of Wall

In field observations the relatively large reinforcement force at the top of the wall is usually attributed to compaction effect. However, this analysis, which does not include compaction, suggests that the large reinforcement force close to the top of the wall (i.e. compared to K_a or K_o condition) can arise due to interaction between the soil, the reinforcement and the facing even in the absence of significant compaction. Moreover, the maximum tensile force in the reinforcement does not appear to increase with depth as the horizontal stress in the soil does, suggesting that there is interaction between the foundation and the layers of reinforcement.

Figure 11 indicates an important feature revealed by the present study. At each reinforcement level the tensile force in the reinforcement is compared with the equivalent horizontal soil force from the corresponding contributing soil elements, and the Rankine active and at rest conditions. Within the active zone, the equivalent soil force conforms

closely to the Rankine active condition, while the force in the reinforcement shows significant variation from both the equivalent horizontal soil force and the Rankine active condition. This suggests that the horizontal soil stress is not entirely supported by the reinforcement. In fact, it is found that a significant portion of horizontal soil force (almost 25% in this case) is carried by the toe. If it was assumed that the failure wedge could be approximated by Rankine's failure plane, it could be shown that equilibrium can only be satisfied if the toe reactions are also considered. This indicates that a rigid foundation (as assumed in this study) has a significant effect in the development of tensile force in the reinforcement, especially close to the base of the wall. Similar observations have been reported by Bathurst et al. (1989). However, the extent of the effect of foundation conditions on the force development in the reinforcement requires further investigation.

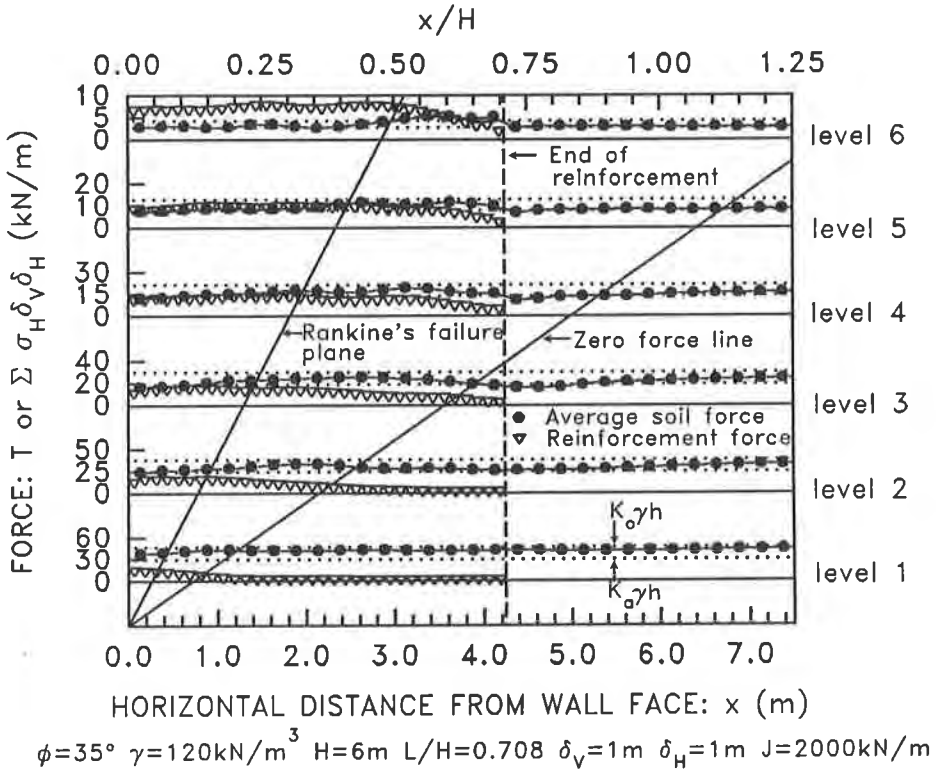

Figure 11 Comparison of Reinforcement Force with Equivalent Horizontal Soil Force

The foregoing results provide some insight to the apparent inconsistency found in the field measurements discussed earlier concerning the limitation in comparing the measured and the equivalent horizontal soil stress inferred from the reinforcement force. The analytical results show that the force in the reinforcement is directly related to the strain developed in the reinforcement and the reinforcement stiffness; and is significantly affected by the stiffness of the foundation. While for a soil element under active condition, the state of stress is independent of both the soil strain and the foundation stiffness. The implication of this finding is that it is generally not valid to assume the tensile force in the reinforcement equal to the equivalent soil force under an assumed stress state. Correct assessment of force

in the reinforcement requires consideration of interaction between the components of the entire reinforced soil system (i.e. soil, reinforcement, facing and foundation).

Horizontal Deformation

Figure 12 shows the horizontal deformation profiles at the wall face and at the end of the reinforced fill. It is evident that the horizontal deformation at the wall face arises from both the internal deformation of the reinforced fill and the deformation of the "unreinforced" retained fill. In agreement with the distribution of horizontal soil strain shown in Figure 9, only limited horizontal displacement exists between the end of reinforcement and the zero force line at levels where the reinforcement extends beyond the zero force line due to the presence of the reinforcement. Field observations reported by Simac et al. (1990), and Christopher et al. (1990) appear to support these findings.

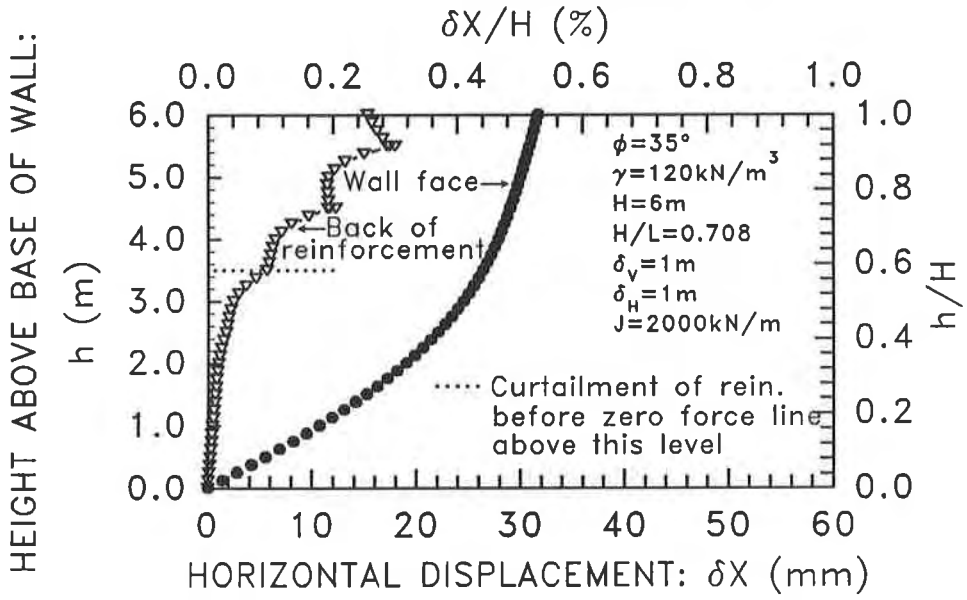

Figure 12 Horizontal Deformation at Wall Face and Back of Reinforced Soil Mass

As a consequence the horizontal deformation at the back of the reinforced fill is limited at levels where the reinforcement extends beyond the zero force line. This is clearly indicated in Figure 12. However, at levels where the reinforcement curtails before the zero force line, substantial horizontal deformation occurs between the end of the reinforcement and the zero force line due to the presence of large amount of soil strain in the "unreinforced" retained fill. For this particular case the magnitude of lateral deformation within the unreinforced fill is significant, e.g., at the top of the wall it accounts for almost half the total magnitude of the horizontal deformation at the wall face.

The implications from these findings are twofold. Firstly, even if the assumption of strain compatibility is satisfied and the force in the reinforcement is correctly predicted,

calculation of horizontal deformation at the wall face merely considering the strain in the reinforcement is unreliable and the horizontal deformation at the wall face would be underestimated. Secondly, the present study assumes a rigid foundation (where horizontal movement at the bottom of the facing is insignificant if shear failure does not occur between the bottom of the wall face and the foundation), this implies that there is sufficient embedment of facing in the foundation and the foundation is non-yielding. However, additional horizontal deformation at the bottom of the facing is anticipated if these conditions are not applicable.

CONCLUSIONS

A finite element method suitable for the analysis of geosynthetic reinforced soil walls has been described. Results have been presented with respect to the state of stress in the fill, the state of strain in both the fill and the reinforcement, the force in the reinforcement and the horizontal deformation. The results demonstrate that the role of reinforcement in reinforced soil walls is to suppress the horizontal soil strain within an otherwise unreinforced soil mass. However, because of the nature of the extensibility of the geosynthetic reinforcement considered herein, the stiffness of the reinforcement is not large enough to prevent the soil elements from developing into a plastic state. Hence, it is anticipated that an active state of stress within the reinforced soil mass would be expected for soil walls utilizing reinforcement with stiffness of similar order to that considered in the present study.

It is shown that caution is required when interpreting the state of stress in a reinforced soil mass based on field measurements. While direct comparison of the measured horizontal soil stress with that derived from the theoretical active condition may indicate some deviations due to variation in vertical stress and rotation of principal stress direction, it does not necessary imply that the soil is not in an active state. The only valid indicator of plasticity is the principal stress ratio. More importantly, inferred horizontal soil stress from force measurement in reinforcement is in general not equivalent to the actual horizontal soil stress. Under active conditions, the force in the reinforcement is no longer controlled by the state of stress in the soil. Results also indicate that there is some variation in the vertical stress distribution; however, for practical purposes the assumption of a uniform distribution appears to be satisfactory (i.e. for wall under self-weight only). Furthermore, the results indicate that calculation of horizontal deformation at the wall face merely considering the strain in the reinforcement without taking into account the soil strain in the unreinforced retained fill will err on the unsafe side.

ACKNOWLEDGEMENTS

The work presented in this paper is funded by the Natural Science and Engineering Research Council of Canada under grant A1007. The authors gratefully acknowledge the value of discussion with Dr. Ian D. Moore of the University of Western Ontario.

REFERENCES

Andrawes, K.Z., Loke, K.H. and Yeo, K.C. (1990) "Application of boundary yielding concept to full scale reinforced and unreinforced soil walls", Performance of Reinforced Soil Structures, British Geotechnical Society, Glasgow, pp. 79-83.

Bathurst, R.J., Benjamin, D.J. and Jarrett, P.M. (1989) " An instrumented reinforced soil wall", Proceedings of the Twelfth International Conference on Soil Mechanics and Foundation Engineering, Rio De Janeiro, Vol. 2, pp. 1223-1226.

Bonaparte, R., Schmertmann, G.R. (1987) "Role of reinforcement extensibility in reinforced soil wall design", The Application of Polymeric Reinforcement in Soil Retaining Structures, Proceedings of NATO Advanced Research Workshop, Kingston, Klumer Academic Publishers, The Netherlands, pp. 409-461.

Carter, J.P. (1985) "AFENA - A General Finite Element Algorithm - User's Manual", School of Civil and Mining Engineering, University of Sydney, N.S.W. 2006, Australia.

Christopher, B.R., Holtz, R.D. and Allen, T.M. (1990) "Instrumentation for a 12.6 m high geotextile-reinforced wall", Performance of Reinforced Soil Structures, British Geotechnical Society, Glasgow, pp. 73-78.

Ho, S.K. (1992) " A numerical investigation into the behaviour of geosynthetic reinforced soil walls", PhD. Thesis (in preparation), Faculty of Engineering Science, University of Western Ontario, London, Canada.

Jewel, R.A. (1985) "Limit equilibrium analysis of reinforced soil walls", Proceedings of the 11th ICSMFE, San Francisco, Vol.3, pp. 1705-1708.

Jewel, R.A. (1987) "Reinforced soil wall analysis and behaviour", The Application of Polymeric Reinforcement in Soil Retaining Structures, Proceedings of NATO Advance Research Workshop, Kingston. Kluwer Academic Publishers, The Netherlands, pp. 365-408.

Leschinsky, D and Perry, E.B. (1987) "A design procedure for geotextile-reinforced walls", Geotechnical Fabrics Report, 5(4), pp. 21-27.

Simac, M.R., Christopher, B.R., and Bonczkiewicz, C. (1990) "Instrumented field performance of a 6 m geogrid soil wall", Proceedings of the 4th Int. Conf. on Geotextiles, Geomembranes and Related Products, A. A. Balkema Publishers, The Netherlands, Vol.1 pp. 53-59.

Wawrychuk, W.F. (1987) "Two geogrid reinforced soil retaining walls", M.Eng. Thesis, Department of Civil Engineering, Royal Military College of Canada, Kingston, Canada.

Partial Material Factors for Polymer Wall Reinforcement

T.S. Ingold
Consulting Engineer, United Kingdom

ABSTRACT

The current trend in defining margins of safety is moving away from the lumped factor of safety approach towards the use of partial factors. However, since the margins of safety associated with lumped factors of safety have been modified with time and experience to render optimum values consistent with safety and economy they are not to be dismissed without impunity. With this in mind this paper introduces a system of partial material factors which might be applied to new reinforcing materials, particularly polymeric reinforcement, to attain acceptable margins of safety. As demonstrated, the partial factor approach is more flexible than the use of lumped factors in as much as partial material factors may be modified as experience accrues with any particular polymeric reinforcement.

INTRODUCTION

Historically the design of engineering structures has been based on the tacit assumptions that design loads are synonymous with applied loads and that material strengths are definitive. To allow for any inadequacies in these assumptions a lumped factor of safety is applied, either as a factor which reduces the rupture strength of the material to an allowable value, or as a ratio of the rupture strength of the material to the design load. With periodic adjustments to the lumped factors of safety, often instigated by unexpected failures, the approach has generally worked well. However, such an approach is limited in as much as it does not separately address the components of material production or behaviour and how these individually affect margins of safety. Additionally lumped factors of safety, developed from long experience with one type of material, can not generally be applied directly to different materials which are new and unproven. The ideal alternative would be a limit state method which effectively considers the probability of variations in material strengths and design loads and with a view to giving a consistent probability against failure irrespective of the reinforcing material used. Unfortunately the variability of the factors controlling soil or fill strengths is so wide as to defy meaningful definition.

A more realistic approach involves the use of partial factors which may be applied discretely to crucial aspects of design loads or material strengths. Whilst a prime objective is to maintain an overall margin of safety consistent with that established by experience with lumped factors of safety, an equally important objective is to permit prescribed modifications to partial factors as experience of any new material accrues with time. In the particular case of reinforced soil walls the industry standard for margins of safety has been established by experience with steel reinforcing strip. This stems from the fact that some 15,000 walls have been constructed over three decades and thereby the failure rate is well defined. If it is accepted that the margin of safety accruing to these walls is satisfactory then it follows that walls reinforced with other materials should be no less safe.

There are many aspects of partial factor design which are beyond the scope of this paper, however, the potential of the approach is illustrated by considering partial factors applied to mitigate against long term tensile rupture of the soil reinforcement. A partial factor approach has been included in the draft code of practice BS8006:1991 Code of practice for strengthened/reinforced soils and other fills, BSI (1991), which has recently been issued for public comment by the British Standards Institution. Although the draft code specifies a minimum value of the partial material factor to be applied to plain steel reinforcement no corresponding value is enumerated for polymeric wall reinforcement. Suggested values are presented below and calibrated against established values of partial factors of safety.

DEFINITION OF PARTIAL FACTORS

Geotechnical engineering, including the design of reinforced soil, is one of the last disciplines using lumped factors of safety. Lumped factors of safety have been applied to geotechnical problems in a variety of inconsistent and often irrational formats. However, in the context of external stability of earth retaining structures the lumped factor of safety, F, has been consistently defined as the ratio of ultimate resisting force, R, to disturbing force, D, eg $F=R/D$. With the advent of reinforced soil certain aspects of internal wall stability involved the introduction of the material properties of the soil reinforcement. In particular knowledge of the ultimate tensile resistance, R, of steel reinforcing strip was needed to determine its adequacy to resist the disturbing force, D, induced by lateral earth pressure. Many early design guides used an allowable stress approach in which stability with respect to tensile rupture of the reinforcement were deemed to be satisfied if $D \leq (R/F)$. One complication was that the ultimate resistance of the reinforcement is time dependent eg ultimate resistance decreases with increasing time as the cross-sectional area of the reinforcement is reduced by corrosion. This did not prove problematical since there was a wealth of existing knowledge on corrosion protection, such as galvanizing, and corrosion rates of steel which permitted allowances to be made for strip thickness to be sacrificed to corrosion. Introduction of polymeric materials added complication since tensile strength is both time and temperature dependent. Additionally different polymers have different inherent strengths and weaknesses. Over and above this, polymeric reinforcement is not produced in the form of a simple strip but takes many forms including composite strips, geotextiles and geogrids. Not surprisingly it was found that the tensile strength of different polymeric products was affected to differing degrees by different environments. For example the tensile strength of one product might be substantially impaired by construction induced damage whilst being totally unaffected by the chemistry of the fill in which it is buried. Conversely another product, under identical conditions, might suffer very slight damage during the construction process but go on to be badly degraded by chemical attack.

To rationalise these effects the geotextiles industry at large adopted the use of partial factors of safety, λ, with one partial factor of safety addressing a particular aspect of potential failure. This approach unravels the lumped factor of safety, F, into a series of partial factors of safety such that $F = \lambda_1 \times \lambda_2 \times \lambda_3 \times ..... \times \lambda_n$. Draft BS8006 uses a partial load factor, f_f, and partial material factor, f_m, to achieve a margin of safety against failure. All the factors take a value of unity, or greater, with the load factor applied to increase the raw calculated load, D, whilst the material factor is applied to decrease the perceived ability of the reinforcement, R, to resist the load. An adequate margin of safety against failure is deemed to operate when the identity $f_f D \leq (R/f_m)$ is satisfied. It should be noted that the material factor, f_m, is applied to the extrapolated long term tensile strength of the reinforcement at the required design life of the structure. The material factor is broken down into number of components, f_{mn}, and sub-components, f_{mnn}, as indicated in Table 1.

Table 1 Partial material factors proposed in draft BS8006

Principal Factor	Component Factor	Intended Purpose
f_{m1}	f_{m11}	Manufacture - to cover the possible reductions in the capacity of the material as a whole compared with the characteristic value deduced from the control test specimens and possible inaccuracies in the assessment of the resistance of a structural element resulting from modelling errors.
	f_{m12}	Extrapolation of test data - to take account of the confidence of the long term capacity assessment. This factor may vary with the required service life of the structure.
f_{m2}	f_{m21}	Susceptibility to damage - to take account of damage during construction. This factor may be derived from site damage tests referred to in the draft code.
	f_{m22}	Environment - to take account of different rates of the degradation due to environmental conditions.

ASSESSMENT OF TENSILE RUPTURE STRENGTH

To avoid reaching the ultimate limit state of collapse induced by tensile failure of polymeric reinforcement it is necessary to estimate the tensile rupture strength of the reinforcement at the projected end of the design life of the structure. The long term tensile creep rupture strength will be a function of many variables including:

- Polymer type and additives.
- Production method and form of reinforcement.
- Mechanical damage caused during construction.
- Environmental attack.
- Operational temperatures.

For a given temperature, the variation of tensile creep rupture strength with time can be assessed by loading samples of the reinforcement at different load intensities so that the times to failure fall inside a predetermined range of time at an appropriate test temperature. In general the load at which tensile rupture will occur, at a given temperature, will decrease with time. If rupture load is plotted against time to a log-log scale, then except for very short times to failure there may be a linear relationship between tensile rupture load and time. At some stage there may be a change in the mechanism controlling tensile failure leading to a transition point or *knee* in the plot of tensile rupture load against time, Figure 1.

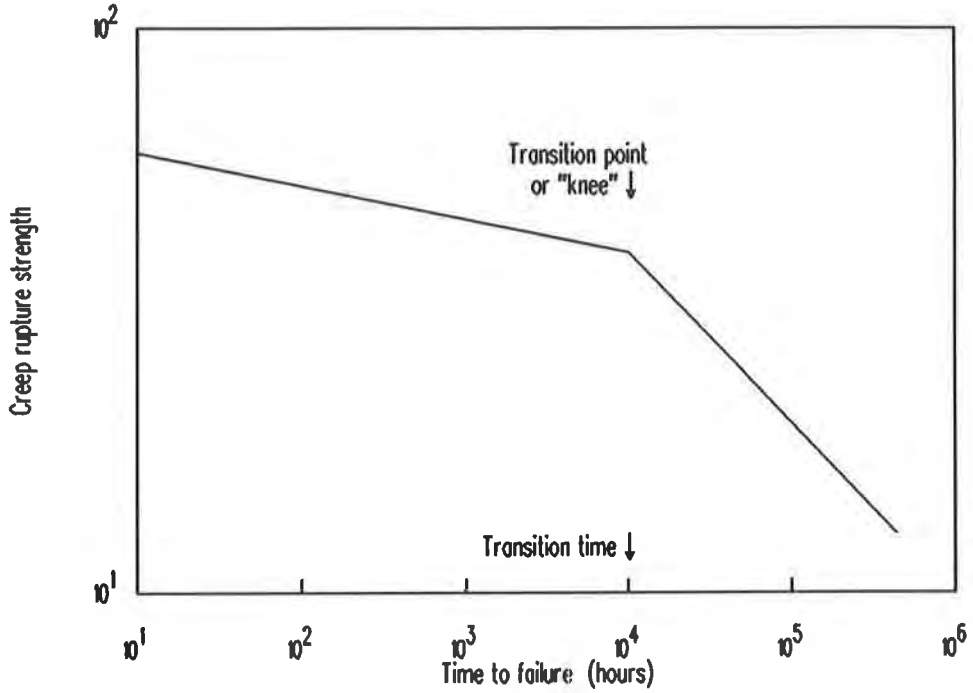

Figure 1 Transition point in tensile creep rupture test

The time at which this transition occurs is important since if the maximum test duration is not long enough the transition may not be detected. Should the transition time be less than the required design life of the structure, then any simple linear extrapolation of the test data could overestimate the rupture load at the end of the design life and so lead to premature collapse of the structure. The time at which a transition may occur will be affected by several factors. For example use of a lower molecular weight polymer to produce a given product will reduce transition time. Similarly an increase of temperature will hasten any transition. More significantly, construction induced damage may invoke a transition in failure mechanism. Finally, any transition will be affected by polymer type and the nature of the environment in which it is required to operate. No creep rupture test duration has been specified in the draft code, however British Gas use 10^4 hours and BS6906 Methods of test for geotextiles specifies a test duration up to 10^4 hours for creep strain tests used to assess serviceability requirements. It is therefore suggested that tensile creep rupture tests for polymeric reinforcement should have a duration of at least 10^4 hours. The need for this becomes evident from Table 2 which reproduces draft BS8006 recommendations for service life. As can be seen for all but temporary and short term short structures Table 2 implies extrapolation of nominally 1 year duration test data by time factors between 10 and 120.

Table 2 Recommendations for service life proposed in draft BS8006

Category	Typical Service Life	Example
Temporary works	1 to 2 years	Contractors site structures
Short term	5 to 10 years	Contractors site structures Basal reinforcement
Industrial	10 to 50 years	Structures at mines
Long term	60 years	Marine structures
Long term	70 years	Retaining walls and embankments
Long term	120 years	Retaining walls, highway structures and bridge abutments

Where the maximum duration of tensile creep rupture tests is less than the required service life the creep rupture strength at the design life has to be estimated by extrapolation. To assist in the detection of any knee or transition, creep rupture tests may be carried out at elevated temperatures. This is the basis of the technique prescribed by British Gas to determine the 50 year rupture strength of certain plastic gas pipes. Tests are run at temperatures of 20°C and 80°C with times to failure falling between 10^1 hours and 10^4 hours, (Greig, 1976). Test data at the design temperature of 20°C indicate a log-log linear relationship, Figure 2.

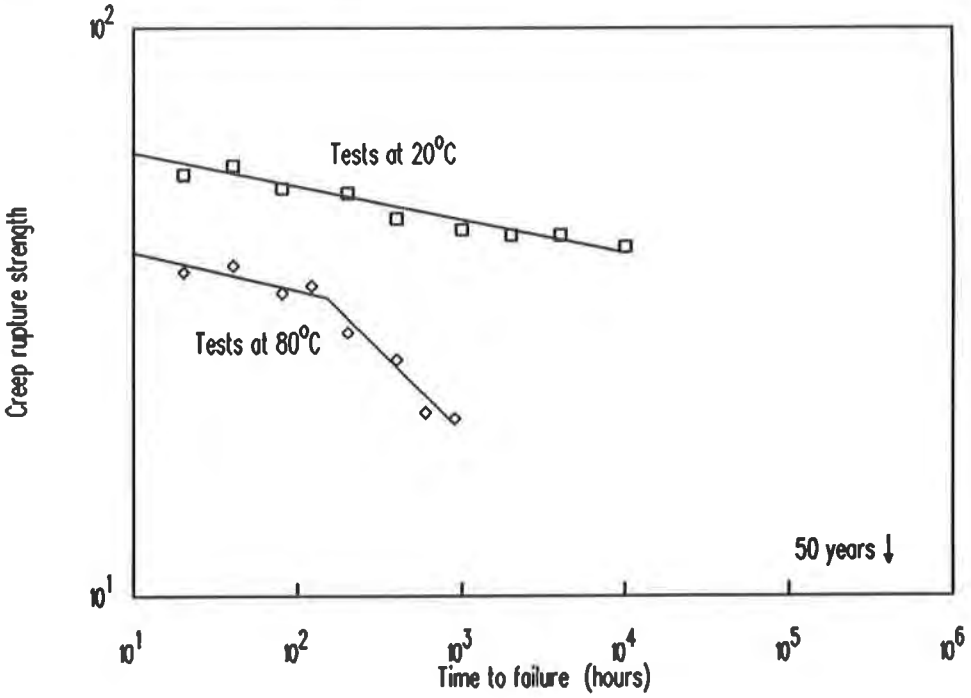

Figure 2 Tensile creep rupture test data at 20°C and 80°C

The perils of extrapolating the 20 °C test data to 50 years are reflected by the knee in the 80 °C test data which defines a transition in failure mechanism. By combining the test data at 20 °C and 80 °C it is possible to calculate the time, beyond the maximum test duration of 10^4 hours, at which any knee might develop. As shown in Figure 3 these combined data are extrapolated to define a tensile rupture load at the end of the required 50 year design life. This involves extrapolation over 1.64 log-cycles of time from 10^4 hours (1.14 years) to 50 years. Since this is in excess of the maximum extrapolation of one log-cycle of time prescribed in BS4618:1970, a factor of safety of 4 is applied to the extrapolated strength to give the 50 year design strength (Greig, 1981). Similar techniques may be applied to determine the long term tensile strength of soil reinforcement.

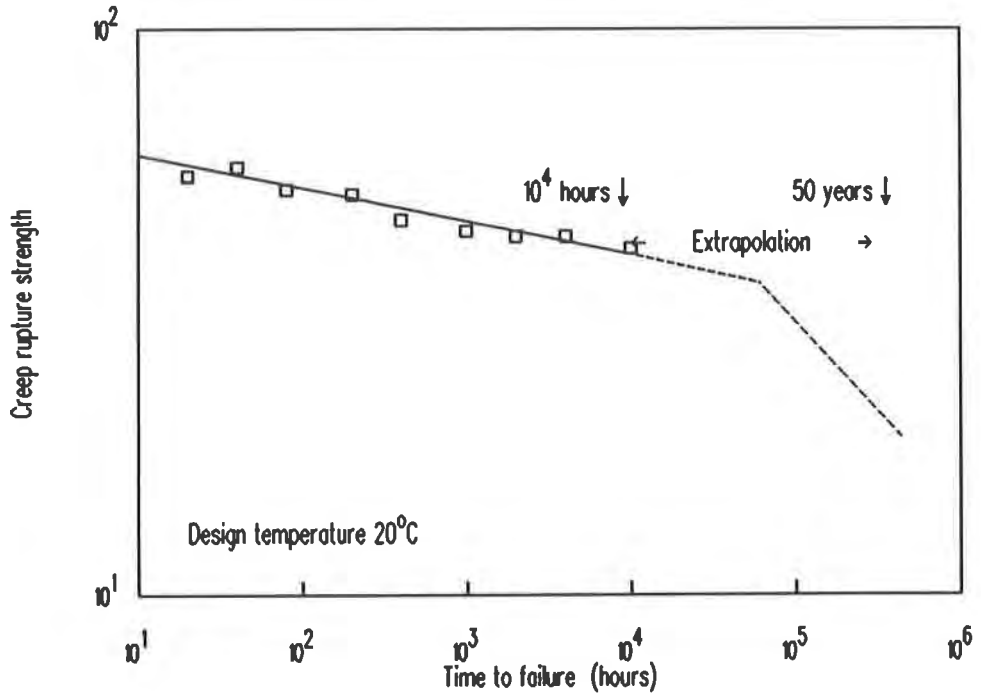

Figure 3 Extrapolation of test data

A clear distinction must be drawn between undamaged control samples tested in a benign medium and operational samples which will be damaged during construction and subject to environmental attack. For a product subject to strict quality control there should be little variation in the extrapolated, undamaged, long term characteristic strength from batch to batch, but, the degree of mechanical damage and aggressiveness of the fill will vary from fill to fill as might the operational temperature. Generally, time restrictions make it impractical to carry out creep rupture tests on samples subject to site specific damage and environment. However, it is practical to carry out tensile creep rupture tests on operational samples, for predetermined categories of fills and environments, to determine how mechanical damage and environment may reduce long term rupture strength. This would allow the determination of various product specific partial factors to be applied to the characteristic control strength to reduce it according to the nature of the particular category of fill to be employed. Laboratory tests on operational samples, which have been pre-damaged, should be carried out in an aggressive environment since the combined effects of environment and damage may be synergistic. Degree of mechanical damage may be assessed using short term tensile testing but this may not reflect long term strength impairment.

The performance of thermo-plastic polymers will be affected by temperature. For this reason the laboratory test temperature should equal or exceed the maximum operational temperature in the reinforced soil structure. In the United Kingdom the mean soil temperature is about 10°C, however, measurement of operational temperatures in a reinforced soil wall shows the seasonal variation is approximately ±10°C (Murray and Farrar, 1988). The upper operational temperature defined by this range is compatible with standard laboratory test temperatures which are usually 20°C or 23°C, however, higher laboratory test temperatures might need to be considered to account for variations of diurnal temperatures in the close vicinity of preformed facing units. As an aside consideration should be given to any spontaneous heating in fill containing industrial waste. For example West and O'Reilly (1986) comment on heating in unburnt colliery shale fill and relate reductions in strengths of plastic reinforcing elements of 30% for a temperature increase of 10°C above a 20°C ambient temperature. A further consideration is the outbreak of fire and the ramifications of this possibility.

VALUES OF PARTIAL MATERIALS FACTORS

There are two routes via which realistic values of partial materials factors can be assessed. The first is to define a lower bound for f_m as being equal to the minimum value of 1.52 which is applied to the characteristic tensile rupture strength of 5 mm thick steel determined from samples having the minimum manufactured cross-sectional area. The logic of this is that the margin of safety pertaining to the characteristic tensile creep rupture strength of polymeric reinforcement should demonstrably not be less than that for steel reinforcement. Allied to this it is useful to compare minimum values of f_m converted from previous studies using a partial load factor, f_f, of 1.5 as prescribed by the draft code for application to lateral earth pressures. Such a comparison is given in Table 3 and shows how partial material factors are considered to vary with degree of extrapolation ranging from 1 log-cycle, which is a factor of 10 in real time, to 2 log-cycles, which is a factor of 100 in real time. Consistently the partial factors suggested by Ingold, (1988) are higher than those derived from Greenwood and Jewell, (1989) but at 1.64 log-cycles of extrapolation, as used by British Gas to determine a 50 years rupture strength, the suggested factor is less than that cited by Greig, (1981) for gas pipe. In all cases the value of f_m at 1 log-cycle extrapolation falls below the prescribed minimum value of 1.52 for steel.

Table 3 Comparison of minimum values of f_m from previous studies

Extrapolation (No. log-cycles)	Greenwood & Jewell (1989)	Ingold (1988)	Greig (1981)
1.00	1.2	1.2	-
1.50	1.5	1.7	-
1.64	1.6	1.9	2.7
2.00	1.8	2.3	-

Minimum values for the components of f_m may be assessed from partial factors of safety published in a wider range of studies. Before doing so it is necessary to establish a relationship between partial material factors and partial factors of safety. Starting with a simple parity between lumped factor of safety and partial material and load factors it follows that for the same margin of safety $F = f_f \times f_m$. The lumped factor of safety F can be resolved into four component partial factors of safety, to reflect the four components cited in Table 1, such that $F = \lambda_{11} \times \lambda_{12} \times \lambda_{22} \times \lambda_{21}$. The product of these four components equates directly to $f_f \times (f_{m11} \times f_{m12} \times f_{m22} \times f_{m21})$. If the load factor, f_f, is taken to apply uniformly to each of n component of the partial material factor then it follows that the parity between these and n corresponding partial factors of safety is defined by the expression $f_{mn} = \lambda_n \times f_f^{-1/n}$. For the particular case of $f_f = 1.5$ and four components of f_m this leads to $f_{mn} \approx 0.9 \times \lambda_n$. Taking the minimum value of f_{m11} to be 1.05, as defined in the draft code, and minimum values of f_{m12}, f_{m22}, and f_{m21} derived from previously defined values of λ_{12}, λ_{22} and λ_{21}, (Ingold, 1988) the nominal minimum values of f_{mn} in Table 4 are obtained.

Table 4 Suggested minimum partial polymeric material factors

Component Partial Materials Factor	Suggested Minimum Factor Value	Comments
f_{m11}	1.05	To cover manufacturing variability
f_{m12}	$\log(t_d/t_t)$	t_d is reinforcement design life t_t is maximum creep test duration
f_{m22}	1.08	Minimum site damage factor
f_{m21}	1.08	Minimum environmental factor
Notes: i) Minimum value of $f_m = 1.52$ ii) Creep rupture test duration and design life in years.		

The effects of construction induced mechanical damage should be assessed using long term tensile creep rupture tests such as those employed to assess the long term tensile rupture strength of intact and undamaged control samples. Short term constant rate of strain tests have indicated reduction factors in the range 1.1 to 1.6 for HDPE grid, (Mitchell and Villet, 1987), and similarly 1.1 to 1.4 for polyester fabric depending on the maximum particle size of the fill, (Voskamp and Risseeuw, 1987). More recently Troost and Ploeg, (1990) quote values, for the same type of geotextile covered with a crushed basalt fill, in the range 1.33 to 2.17, whilst Billing et al (1990) report decreases in tensile strength consistent with reduction factors in the range 1.08 to 1.56. Treating these values as partial factors of safety the corresponding values of f_{m22} would be in the range 1.00 to 1.95. The environmental partial material factor relates to the long term effect of the fill environment on tensile rupture strength. Both chemical and bacteriological attack should be considered and their effects quantified by tensile creep rupture tests in an appropriate aggressive environment at the operational temperature or higher temperatures as appropriate. Environmental

attack will be polymer and therefore product specific. For polyester geotextiles Voskamp and Risseeuw (1987) quote reduction factors for chemical attack up to 1.12 whilst Wrigley (1987) reports no loss of strength in HDPE geogrid tested in a chemically aggressive environment. Overall these observations relate to f_{m21} values in the range 1.00 to 1.01.

All this might infer that the suggested minimum values of $f_{m22} = f_{m21} = 1.08$ are somewhat high. Two counter arguments to this possible inference are synergism and timescale. Where tensile load is applied simultaneously with mechanical damage and aggressive environment the effects of these three agents acting in concert may be synergistic and therefore give rise to a strength reduction which is greater than the sum of the strength reductions caused by the individual agents acting in isolation. Such synergism is not accounted for in the various investigations cited above. Finally there is the question of time scale. Tests to assess the effects of mechanical damage are either very short term constant rate of strain tensile tests or, in some instances, short term creep tests. In both cases a large extrapolation is assumed when arguing that the results of short term damage assessment tests accurately predict the long term effects of damage. More pragmatically it can be demonstrated that the suggested minimum values of f_m given in Table 4 produce a balanced approach to design of polymeric soil reinforcement. Table 5 suggests minimum values of f_m , derived from Table 4, for a range of service lives, as they relate to characteristic tensile creep strength derived from tests with durations of 10^4 hours (1.14 years), 5×10^4 hours (5.71 years) and 10^5 hours (11.42 years). For the 10^4 hours test duration the value of f_m rises above 1.52 for a service life of 20 years or more. For the classified 50 years service life f_m rises to 2.01 and in effect this recognises the uncertainty of extrapolating test data by a time factor of 44 from 1.14 years to 50 years. As a corollary to this the partial material factor for extrapolation by a time factor of 105 from 1.14 years to 120 years warrants a higher f_m of 2.48. For longer creep rupture test durations of 5×10^4 hours (5.71 years) and 10^5 hours (11.42 years) the respective 120 years partial material factors drop to 1.62 and 1.52 and as such reflect the increased confidence in extrapolations where time factors are reduced to 21 and 10 respectively.

Table 5 Illustrative minimum suggested values of f_m

Service Life (Years)	Maximum Tensile Creep Rupture Test Duration (hours)		
	1×10^4	5×10^4	1×10^5
1	1.52	1.52	1.52
10	1.52	1.52	1.52
50	2.01	1.52	1.52
60	2.11	1.52	1.52
70	2.19	1.52	1.52
120	2.48	1.62	1.52

CONCLUSIONS

Draft BS8006 introduces a design approach for reinforced soil in terms of partial load factors and partial material factors. For steel the draft code recommends that a minimum partial material factor, f_m, of 1.45 to be applied to the minimum tensile rupture strength determined from samples with minimum manufactured cross-sectional dimensions and a minimum thickness of 5 mm. Since minimum strengths are used the draft code recommends a value of f_{m111}, a component of f_{m11}, equal to 1.00. Tensile creep rupture strengths for polymeric reinforcing materials are usually couched in terms of characteristic strength rather than minimum strength and therefore the prescribed minimum value of f_{m111} increases to 1.05 which in turn leads to a minimum value of f_m equal to 1.52. To maintain parity with the minimum margin of safety implied by the draft code for steel soil reinforcement it is suggested that the partial material factor, f_m, should not be less than 1.52 when applied to the characteristic strength of polymeric reinforcement with minimum manufactured cross-sectional dimensions. Depending on the standards of material and production quality control employed, appropriate values of f_{m11} may rise above the suggested minimum value of 1.05. The suggested values of f_{m22} and f_{m21} are minimum values. Higher values may apply and these should be determined by field trials and laboratory testing. In general maximum values of f_{m22} and f_{m21} may be predetermined for predefined categories of fill, compaction plant, construction methods and service environments. Appropriate values of these factors will be product specific and will depend upon method of testing, nature of the fill, the construction technique and the service environment. All these variables must be taken into account in assessing values of these partial material factors to be used in design.

Partial material factors intended to mitigate the probability of tensile creep rupture of the soil reinforcement should be applied to the characteristic tensile creep rupture strength of the reinforcement deemed to operate at the end of the service life of the structure. For long term design this value will involve extrapolation of tensile creep rupture test data by time factors up to 105 which exceeds the maximum value of 10 prescribed in BS4618:1970. Consequently where extrapolation exceeds time factors of 10 then time dependent values of $f_{m12} > 1$ should be applied. Tensile creep rupture testing should be carried out at a test temperature at least equal to the maximum operational temperature in the structure which in the United Kingdom is nominally 20°C. In addition to testing at the maximum operational temperature tensile creep rupture tests should be carried out at elevated temperatures with a view to assessing any ductile-brittle transition which may occur during the service life of the structure at its operating temperatures.

This paper does not address the effects of the load factor, f_f, on overall margins of safety since this assumes the same value for both metallic and polymeric reinforcement. However, draft BS8006 does recognise the differences in the axial tensile stiffness of these reinforcements where, in the upper reaches of a wall, non-extensible reinforcement is designed to withstand k_o lateral earth pressure and extensible reinforcement is designed for k_a pressure. Typically the k_o pressure is at least 50% greater than the k_a pressure. For the deadweight of a wall the prescribed value of f_f is 1.5. When combined with the minimum suggested value of f_m of 1.52 this leads to an equivalent minimum lumped factor of safety of 2.28 on long term rupture strength at the end of the required service life. In the US and UK the currently applied factor of safety for steel, at the end of the design life, allowing for corrosion loss, is 2.8. For some polymerics, allowing for construction induced damage, this falls as low as 1.6. Hence a need for rationalisation of margins of safety.

REFERENCES

Billing, J.W., Greenwood, J.H. & Small G.D., (1990) "Chemical and mechanical durability of geotextiles", Proc. IV Int. Conf. on Geotextiles, Geomembranes, Vol. 2. A.A. Balkema, Rotterdam.

BS4618, (1970) "Recommendations for the presentation of plastics design data : Subsection 1.1.1 Creep in uniaxial tension or compression", British Standards Institution, London.

BS4618, (1972) "Recommendations for the presentation of plastics design data: Part 4. Environmental and chemical effects - Section 4.1. Chemical resistance to liquids", British Standards Institution, London.

BS6906, (1991) "Methods of test for geotextiles : Part 5 Determination of creep", British Standards Institution, London.

BS8006, (1991) "Code of practice for strengthened/reinforced soils and other fills", (Draft for public comment), British Standards Institution, London.

Greenwood, J.H. & Jewell, R.A., (1989) "Strength and safety: The use of mechanical property data", Reinforced Embankments Theory and Practice, Thomas Telford, London.

Greig, J.M., (1976) "Fracture and its prevention in plastic gas distribution systems", Gas Engineering and Management, Vol.16, No.2.

Greig, J.M., (1981) "Specification and testing of polyethylene gas distribution systems for a minimum 50 year operational life", Plastics and Polymer Processing and Applications, Vol.1, No.1.

Ingold, T.S., (1988) "Long term performance requirements for polymeric soil reinforcement in the United Kingdom", Theory and Practice of Earth Reinforcement, Balkema, Rotterdam.

Mitchell, J.K. & Villet, W.C.B., (1987) "Reinforcement of earth slopes and embankments", National Co-operative Highway Research Program Report 290, TRB, Washington, D.C.

Murray, R.T., & Farrar, D.M., (1988) "Temperature distributions in reinforced soil retaining walls" Int Jrnl of Geotextiles and Geomembranes, Vol.6.

Troost, G.H. & Ploeg N.A., (1990) "Influence of weaving structure and coating on the degree of mechanical damage of reinforcing mats and woven geogrids caused by different fills during installation", Proc. IV Int. Conf. on Geotextiles, Geomembranes, Vol. 2. Balkema, Rotterdam.

Voskamp, W., & Risseeuw, P., (1987) "Method to establish the maximum allowable load under working conditions of polyester reinforcing fabrics", Proc. Symp. on Very Soft Soil Stabilisation Using High Strength Geosynthetics, Geosynthetic Research Institute, Philadelphia.

West, G. & O'Reilly, M.P., (1986) "An evaluation of unburnt colliery shale as fill for reinforced earth structures", TRRL Research Report 97, Transport Research Laboratory, Crowthorne UK.

Wrigley, N.E., (1987) "Durability and long term performance of Tensar polymer grids for soil reinforcement", Materials Science and Technology, Vol.3.

Geogrid Reinforcement for Surficial Stability of Slopes

D.L. Thielen
GeoEngineers Inc., USA

J.G. Collin
Tensar Earth Technologies Inc., USA

ABSTRACT

Erosion, surficial creep and localized shear failures can create costly maintenance problems for otherwise stable slopes. These surficial instabilities occur in both cut and fill slopes over a wide range of slope face angles. In recent years, geogrid reinforcement has been used to stabilize slopes against surficial instability. An analytical method is presented for evaluating surficial stability of slopes reinforced with geogrids. Existing methods and computer programs are available for evaluating longer "primary" reinforcement. This paper presents a method to determine the length and spacing of shorter "surficial" reinforcement. The method assumes an infinite slope with seepage parallel to the slope face. Geogrid tension failure, and pullout from within and behind the slide mass are considered in the analysis. Surficial reinforcement can be used for: 1) repair of shallow landslides, 2) secondary reinforcement of steep reinforced slopes, 3) stabilizing the face of flatter (e.g., 2H:IV) slopes; and 4) resisting shallow downslope creep.

INTRODUCTION

Surficial failures, forming shallow slip surfaces parallel to the slope face (Figure 1), of both natural and fill slopes have been a problem for land owners and developers on the west coast of the United States for decades. A photograph of a typical surficial slope failure is shown in Figure 2.

In-depth discussions of surficial slope failure mechanisms have been presented by Terzaghi and Peck (1967), and Campbell (1975). These failures are usually initiated by water infiltrating the near surface soils. The source of this water may be rainfall, broken utilities, landscape watering, or failure to intercept upslope drainage. This infiltration can be accelerated by seasonal desiccation and cracking of the soil mantle. When infiltration exceeds the transmissivity of the soil, a perched water table with seepage parallel to the slope face can develop.

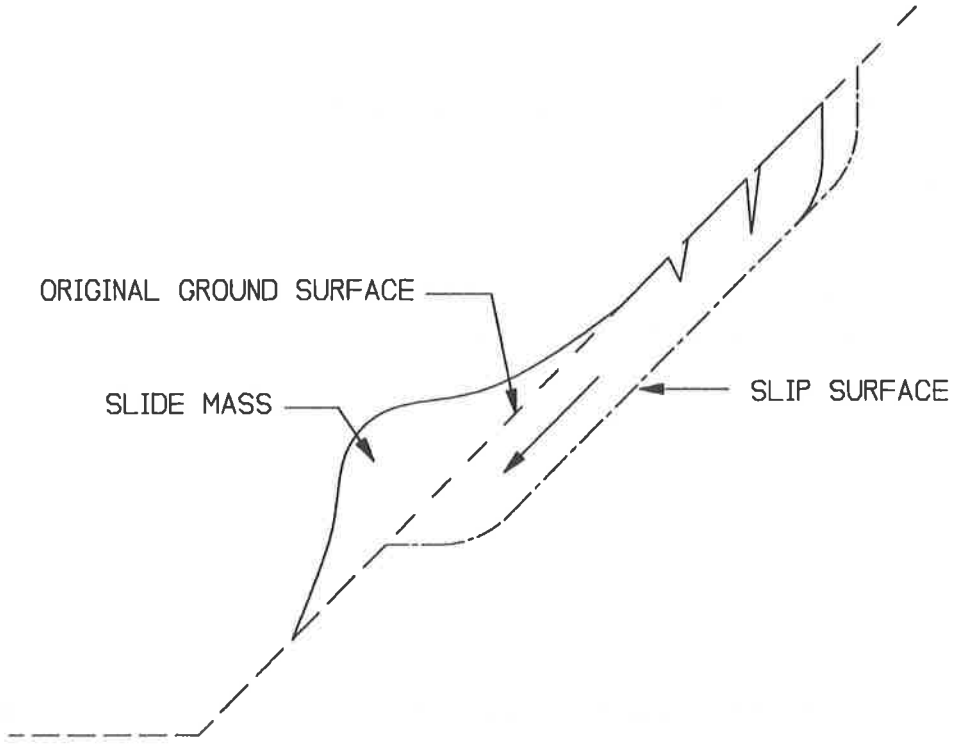

Figure 1. TYPICAL SURFICIAL SLOPE FAILURE

Figure 2. SURFICIAL SLOPE FAILURE

Where a surficial failure has occurred, or has been identified as a potential problem by a low factor of safety, conventional mitigation includes: 1) flattening the slope angle, 2) restricting the slope height, 3) placing a zone of soil-cement treated or lime treated soil at the slope face, or 4) specifying higher strength fill soils. However, another alternative is available: reinforcing the near surface soils with layers of geogrid.

ANALYTICAL MODEL

The inclusion of geogrid reinforcement provides an additional resisting force (anchorage) to the slide mass. Previously published information describes the mechanisms of geogrid reinforcement and overall slope stability with respect to "primary" geogrids (Christopher et al. 1990 and Mitchell and Villet, 1987). This paper presents a method of quantifying the surficial stability of slopes reinforced with geogrids.

Unreinforced Slope The terms which define the geometry and soil properties of a typical infinite slope stability problem are illustrated in Figure 3.

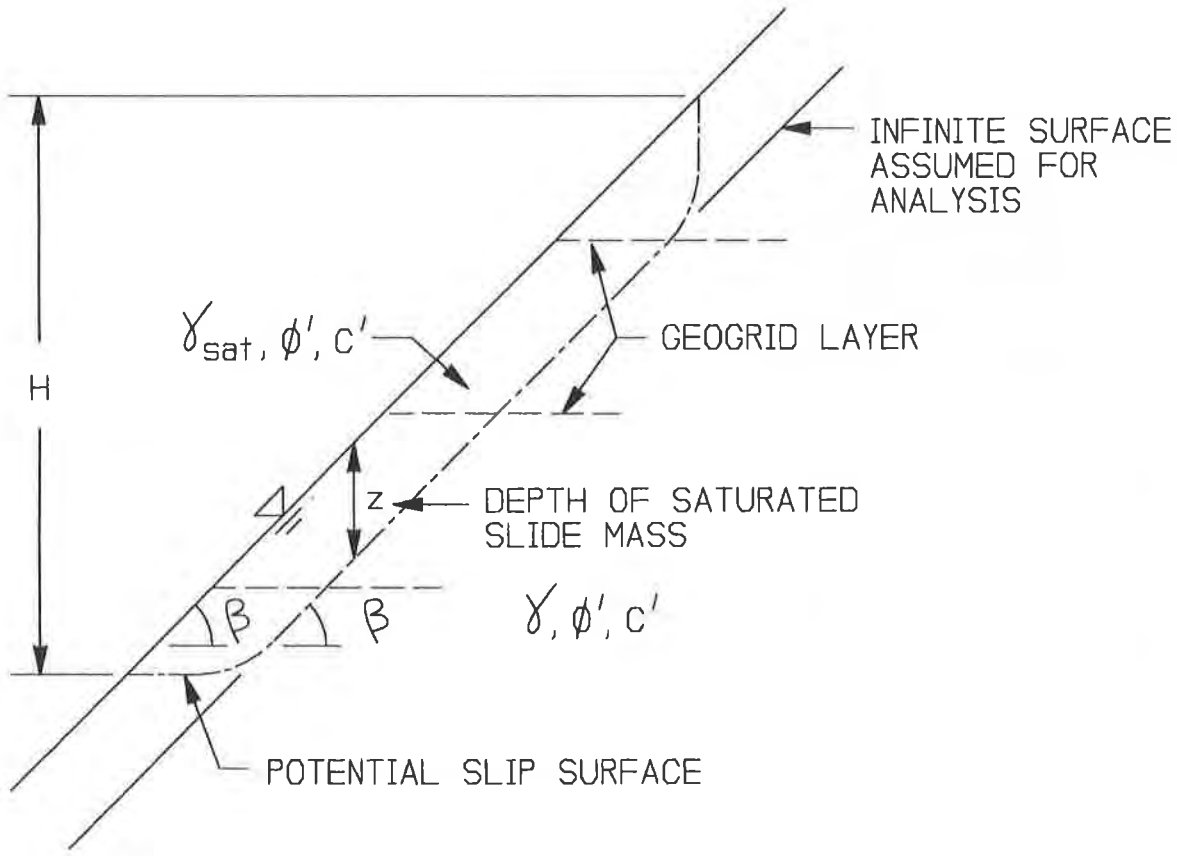

Figure 3. DEFINITION OF TERMS

Analysis of the geometry shown in Figure 3 is based on the following assumptions:

- o The potential slide plane is infinite and parallel to the slope face.
- o A plane strain limit equilibrium condition is assumed.
- o Soil strengths can be described by the Mohr failure envelope. Soil strength is defined by long-term effective stress parameters ϕ', c'.
- o The slide mass is saturated.
- o The depth of the sliding mass, z, is equal to the depth of soil saturation.
- o Seepage occurs parallel to the slope face (i.e. flow lines are parallel to the ground surface).

For the geometry shown in Figure 3, as well as the assumptions listed above, the factor of safety against surficial instability for unreinforced slopes can be calculated from the formula developed by Skempton and Delory (1957) and written in the following form by Campbell (1975):

$$F.S. = \frac{c' + (\gamma_s - \gamma_w) z \cos^2\beta \tan\phi'}{\gamma_s z \sin\beta \cos\beta} \qquad \text{(Eq. 1)}$$

where:

F.S. = Factor of safety
c' = Effective soil cohesion intercept
ϕ' = Effective soil friction angle
γ_s = Soil unit weight, saturated
γ_w = Unit weight of water
z = Depth to failure plane
β = Slope angle

Equation 1 can also be rewritten for an unreinforced slope of finite height "H" as shown below:

$$F.S. = \frac{c'H + (\gamma_S - \gamma_w) H z \cos^2\beta \tan\phi'}{\gamma_S H z \cos\beta \sin\beta} \qquad \text{(Eq. 2)}$$

where:

H = Slope height

Reinforced Slope The addition of geogrids provides anchorage to the potential slide zone as illustrated in Figure 4. This can be modelled using an additional resisting force, F_g. The resulting equation, which describes the factor of safety of a reinforced slope, is given in Equation 3.

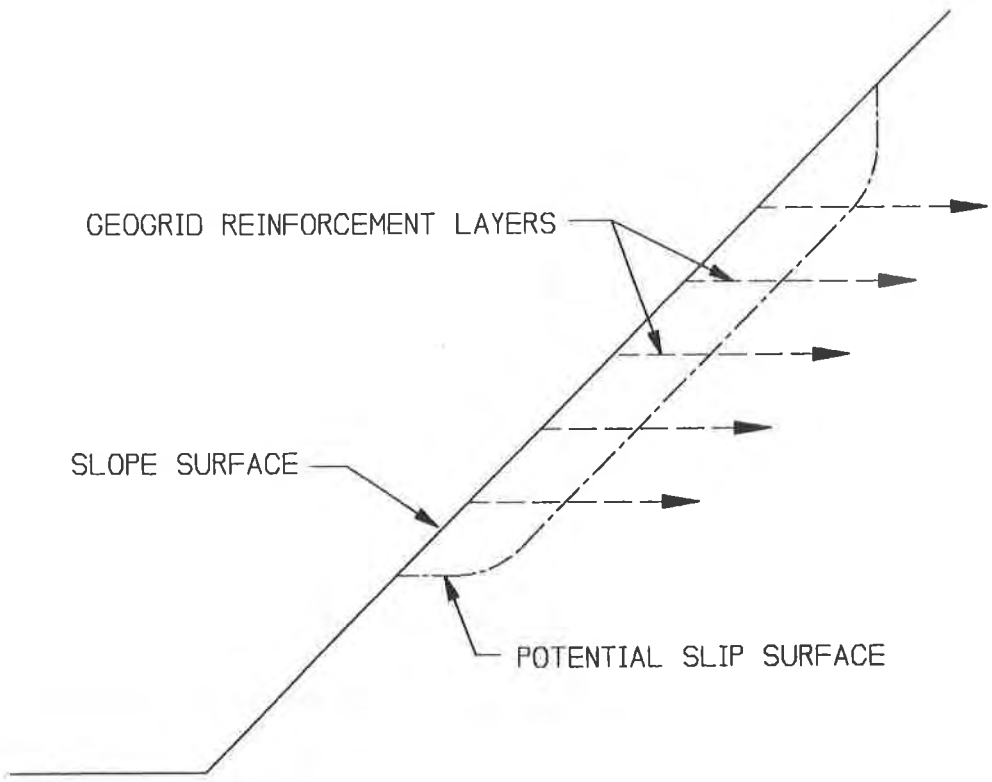

Figure 4. REINFORCEMENT OF A SLOPE FOR SURFICIAL STABILITY

$$FS = \frac{c'H + (\gamma_s - \gamma_w)Hz\cos^2\beta\tan\phi' + F_g\cos\beta}{\gamma_s Hz\cos\beta\sin\beta} \qquad \text{(Eq. 3)}$$

where:

F_g = Summation of geogrid resisting force over slope height H

Grid strength is computed with only the tangential force component. The normal component (which will increase the effective stress across the slip surface) and rotation of the grid (which will increase the tangential component) are ignored. The available geogrid resisting force at each grid layer is limited by 1) the long-term allowable (i.e., limit state), strength of the geogrid, T_a, 2) the allowable long-term pullout resistance of the geogrid in the slide mass, P_{os}, and 3) the allowable long-term pullout resistance of the geogrid behind the slide mass, P_{oa}. These are illustrated in Figure 5.

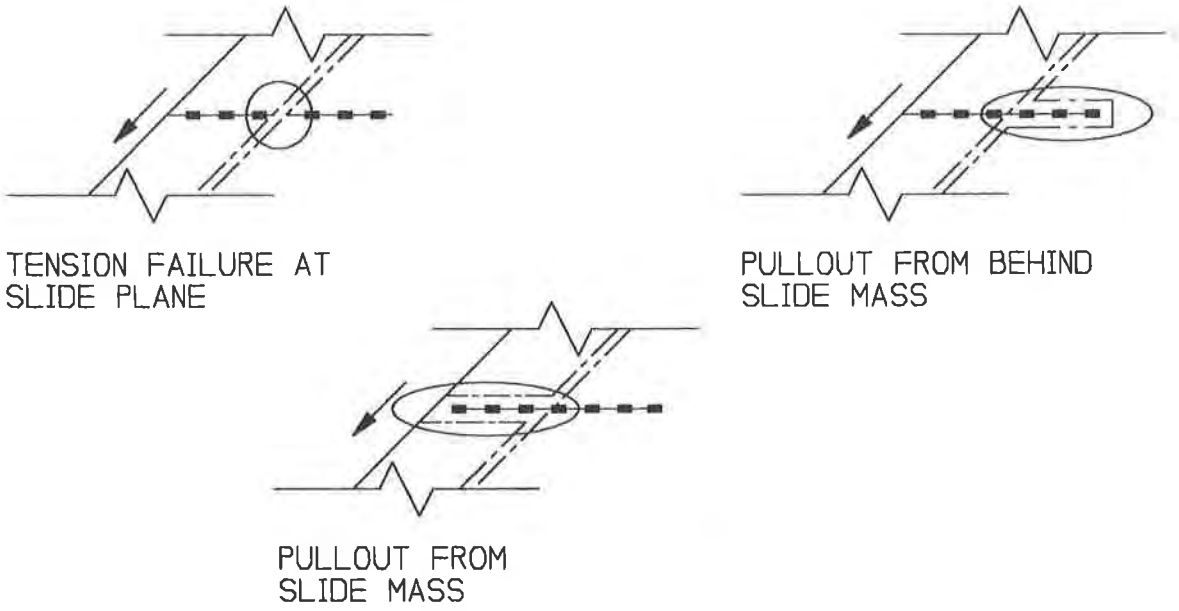

Figure 5. POTENTIAL MODES OF GEOGRID TENSION AND PULLOUT FAILURES

Long-Term Allowable Strength The long-term allowable strength of the geogrid, T_a, is based on the stress-strain behavior of the geogrid structure and is influenced by: 1) construction induced damage; 2) sustained-load deformation (creep); and 3) chemical and biological polymer degradation. The literature contains several resources describing the calculation of long-term allowable strengths of geogrids. (Bonaparte and Berg, 1987, and GRI GG4 Standard Practice, 1991). The current state of the practice is to compute T_a from a partial factor of safety equation that accounts for the above factors (see Equation 16).

It is noted that T_a for reinforced slope applications differs from T_d, which is the design strength used for geosynthetically reinforced soil walls. T_d is determined by dividing the allowable tensile strength by an overall factor of safety (F.S.) as shown in Equation 4.

$$T_d = \frac{T_a}{F.S.} \qquad \text{(Eq. 4)}$$

where:

T_d = Design strength

However, for reinforced slopes the state-of-practice is to use the allowable tensile strength (T_a) and compute the overall factor of safety, F.S., against instability.

Pullout The pullout capacity of the geogrid is a function of the embedment length, the geogrid-soil interaction, and the effective normal stress on the geogrid. Several approaches and design equations have been developed and are currently being used to estimate the pullout resistance by considering frictional resistance, passive resistance or a combination of both. A normalized approach is recommended, as presented by Christopher et al. (1990) and Berg (1991). The ultimate pullout resistance, P_o, of the reinforcement per unit width of the reinforcement is given by:

$$P_o = F^* \cdot \alpha \cdot \sigma_n' \cdot L_E \cdot C \qquad \text{(Eq. 5A)}$$

where:

- L_E = The embedment or adherence length in the resisting zone behind the failure surface
- C = The reinforcement effective unit perimeter; e.g., C = 2 for geogrids
- F^* = The pullout resistance (or friction-bearing-interaction) factor
- α = A scale correction factor
- σ'_n = The effective normal stress at the soil-reinforcement interface

The pullout resistance factor, F^*, can be derived from theoretical or empirical relationships developed for each soil-reinforcement interaction mechanism. For any reinforcement, F^* can be determined using the following general equation:

$$F^* = \text{Passive Resistance} + \text{Frictional Resistance} \qquad \text{(Eq. 5B)}$$

or:

$$F^* = F_q \cdot \alpha_\beta + K \cdot \mu^* \cdot \alpha_f \qquad \text{(Eq. 5C)}$$

where:

- F_q = The embedment (or surcharge) bearing capacity factor
- α_β = A structural geometric factor for passive resistance
- K = A ratio of the actual normal stress to the effective vertical stress; it is influenced by the geometry of the reinforcement
- μ^* = An apparent friction coefficient for the specific reinforcement
- α_f = A structural geometric factor for frictional resistance

Values for these factors can be obtained from Christopher et al. (1990).

Pullout capacity of a geogrid may be determined from laboratory pullout tests. It is imperative, however, that the pullout test conditions are similar to the field conditions. Short embedment lengths (e.g., less than about 1 meter) and low normal pressures (e.g., less than about 60 kN/m^2) are typically encountered for surficial reinforcement applications and should be modelled in laboratory tests. Geogrid and soil materials used in testing should be representative of those used in construction. If these conditions are met, the ultimate pullout resistance may be determined with the following empirical formula:

$$P_o = 2L_E C_i(\sigma_n' \tan\phi' + c') \qquad \text{(Eq. 5D)}$$

where:

C_i = Coefficient of interaction between geogrid and soil

The geogrid-soil interaction coefficient,C_i, is determined from pullout testing (GRI Test Method GG5, 1991). These tests are generally conducted as outlined below: 1) the geogrid is embedded horizontally in soil under a specified confining pressure, 2) the geogrid is pulled horizontally until it comes out of the soil or deforms excessively, and 3) the pullout force is recorded. The geogrid-soil interaction coefficient is the ratio of the recorded pullout force to the available soil shear strength along the plane of the geogrid. It is similar to a friction factor or adhesion value used for design of soil anchors.

To quantify the pullout resistance of a geogrid layer, the effective normal pressure distribution must be defined along the full length of the geogrid (pullout can occur both in front of and behind the potential slip plane). The theoretical normal pressure distribution along the geogrid is shown in Figure 6.

Effective normal stress at points A, B and C are described by Equations 6, 7 and 8, respectively.

At point A:

$$\sigma_n' = z(\gamma_s - \gamma_w \cos^2\beta) \qquad \text{(Eq. 6)}$$

At point B:

$$\sigma_n' = z\gamma_s \qquad \text{(Eq. 7)}$$

At point C:

$$\sigma_n' = z\gamma_s + \gamma_m L_A \tan\beta \quad \textit{(Theoretical)} \qquad \text{(Eq. 8)}$$

where:

γ_m = Moist soil unit weight

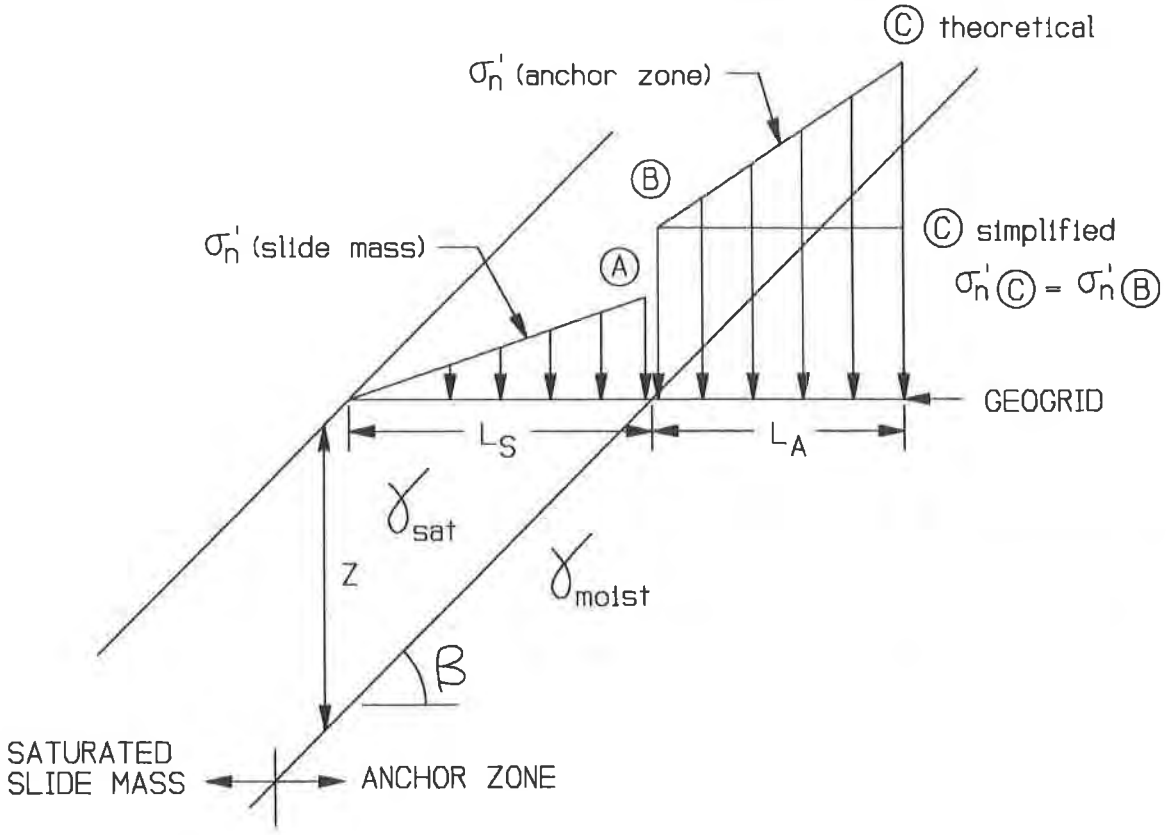

Figure 6. VERTICAL EFFECTIVE STRESS DISTRIBUTION ALONG GEOGRID

However, to simplify the solution, σ'_n in the anchor zone is conservatively assumed to be uniform instead of a function of L_A. Therefore:
At point C:

$$\sigma'_n = z\gamma_s \qquad \text{(For uniform distribution in the anchor zone)} \qquad \text{(Eq. 9)}$$

The average effective normal stress, $\overline{\sigma'_n}$, over the geogrid embedment length in the slide zone and in the anchor zone is computed from equations 6 and 9.

For the slide zone:

$$\overline{\sigma'_{nS}} = \frac{z(\gamma_s - \gamma_w \cos^2\beta)}{2} \qquad \text{(Eq. 10)}$$

For the anchor zone:

$$\overline{\sigma'_{nA}} = z\gamma_s \qquad \text{(For uniform distribution in the anchor zone)} \qquad \text{(Eq. 11)}$$

The available pullout resistance versus embedment length for both the slide zone and anchor zone may be described by combining Equations 10 and 11 with Equation 5.

For the slide zone:

$$P_{OS} = F^* \alpha L_s C \frac{z(\gamma_s - \gamma_w \cos^2\beta)}{2} \quad \text{(Eq.12)}$$

For the anchor zone:

$$P_{OA} = F^* \alpha L_A C z\gamma_s \quad \text{(Eq.13)}$$

From inspection of the equations, pullout in the slide mass will require a longer embedment length than the anchor zone because the effective normal pressure is less in the slide zone. Pullout resistance in the anchor zone can also be increased by lengthening the geogrid behind the slide plane (L_A) to add resistance, whereas the geogrid length within the failure mass (L_S) is fixed by the assumed depth of sliding and slope angle.

Based on the preceding theoretical treatment and equations, the following procedure is proposed to analyze surficial stability:

STEP 1 Compute the total geogrid resistance, F_g, required to achieve an overall safety factor for the slope height H. Rearranging Eq. 3 results in:

$$F_g = \frac{FS\gamma_s Hz\cos\beta\sin\beta - c'H - (\gamma_s - \gamma_w)Hz\cos^2\beta\tan\phi'}{\cos\beta} \quad \text{(Eq.14)}$$

where:

FS = Overall factor of safety against sliding

STEP 2 Compute available geogrid pullout resistance per geogrid as controlled by pullout in the slide mass, P_{OS}. Rearranging Eq. 12 and adding a factor of safety for pullout (FS_{PO}) results in:

$$P_{OS} = \frac{F^*\alpha z^2(\gamma_s - \gamma_w \cos^2\beta)}{FS_{PO}\tan\beta} \quad \text{(Eq. 15)}$$

where the following values were used in Eq. 12.

C = 2 (for geogrids)

$$L_S = \frac{z}{\tan\beta}$$

STEP 3 Compute long-term allowable strength of geogrid, T_a, from partial factor of safety equation. The equation after that presented in the Interim Guidelines for Design, Specification, & Contracting of Geogrid Mechanically Stabilized Earth Slopes on Firm Foundations (Berg, 1991) is as follows:

$$T_a = \frac{T_{ult}}{FS_{ID} \cdot FS_{CR} \cdot FS_{CD} \cdot FS_{BD} \cdot FS_{JNT}} \qquad \text{(Eq. 16)}$$

where:

T_{ult} = Ultimate strength
FS_{ID} = Partial factor of safety for installation damage
FS_{CR} = Partial factor of safety for creep deformation
FS_{CD} = Partial factor of safety for chemical degradation
FS_{BD} = Partial factor of safety for biological degradation
FS_{JNT} = Partial factor of safety for joints (seams and connections)

Values for the above safety factors should be based on laboratory and field testing. Where testing values are not available, default values such as provided in the Interim Guidelines for Design, Specification, & Contracting of Geogrid Mechanically Stabilized Earth Slopes on Firm Foundations (Berg, 1991) can be used.

STEP 4 Compute the required total number of geogrid layers, N. The number of geogrid layers will be controlled by the allowable geogrid tension. This tension will be the lessor of the allowable strength, T_a, or the geogrid pullout resistance in the slide mass, P_{OS}.

$$N = \frac{F_s}{t_g} \qquad \text{(Eq. 17)}$$

where:

t_g = Lesser of T_a or P_{OS}

STEP 5 Compute L_A, the required geogrid length behind the slide plane, by rearranging Eq. 13 and adding a factor of safety against pullout behind the slide plane.

$$L_A = \frac{t_g \, FS_{PO}}{2 \, F^* \, \alpha \, z \, \gamma_s} \qquad \text{(Eq. 18)}$$

where:

$$P_{OA} = t_g \cdot FS_{PO}$$

STEP 6 Finalize spacing and length of geogrids.

$$S = \frac{H}{N} \qquad \text{(Eq. 19)}$$

$$L_G = L_S + L_A = \frac{z}{\tan\beta} + L_A \qquad \text{(Eq. 20)}$$

where:

S = Vertical geogrid spacing at the slope face
N = Total number of geogrids over slope height H
L_G = Total length of geogrid layer

DESIGN AND CONSTRUCTION CONSIDERATIONS

A comprehensive design will result in a surficial reinforcement application that is safe, economical, and can utilize conventional construction methods. The preceding analysis and solution is intended to present a simplified model of a complex subject. The assumed depth of saturation as well as the effective stress parameters of the soils are very important to the final design. For Southern California, the typical depth to saturation assumed for surficial stability analyses is 1.2 meters (4 feet) as specified in the "Minimum Standards for Slope Stability Analysis" (1978). A discussion of the selection of strength parameters for surficial stability (low normal pressures at the slope face) is discussed by Day and Axten (1989, 1990).

In addition to stability issues, surface erosion should be considered. Surface erosion is the degradation of the slope face by external forces such as flowing water, blowing winds, and trafficking or boring by animals. These conditions can be exacerbated by seasonal wetting and drying cycles that may loosen the outer several centimeters of surface soils. Current practice for reinforced slopes is the same as for unreinforced; that is, to vegetate the slope with indigenous plant species that will resist erosion and maintain a relatively constant soil moisture.

Although internal stability and erosion should be treated separately during design, they can affect one another. Slope face erosion can accelerate surface water intrusion, resulting in a saturated condition. A saturated condition at the slope face results in reduced surficial stability. Conversely, geogrids placed in the outer several feet of the slope for surficial stability can enhance resistance to erosion by increasing compaction effectiveness (Christopher et.al 1990) and preventing the formation of surface rills.

Geogrids should meet the following selection criteria: 1) be capable of developing the required long-term allowable tensile strength; 2) have a long-term geogrid-soil coefficient of interaction of 80% or greater to develop pullout resistance over a reasonable length; 3) have favorable long-term durability in order to meet the design assumptions over the life of the slopes; and 4) be resistant to construction induced damage.

Surficial slope reinforcement can be installed using simple modifications to conventional construction methods. The reinforcement layers are placed into engineered fill lifts as the construction proceeds. Photographs of surficial reinforcement installations are presented in Figures 7 and 8. A completed slope having layers of both primary and surficial reinforcement is shown in Figure 9.

CONCLUSIONS

1. The factor of safety of reinforced slopes subjected to downslope translational sliding (i.e., where an infinite slope analysis is appropriate) can be evaluated by the method presented in this paper.

2. Surficial reinforcement with geogrids can be used for: i) repair of shallow landslides, ii) secondary reinforcement of steep reinforced slopes, iii) stabilizing the face of flatter (e.g., 2H:1V) slopes, and iv) resisting shallow downslope creep.

3. The surface of slopes stabilized with geogrid reinforcement, in lieu of stabilization with soil-cement or lime modified soils, may be revegetated.

4. Surficial geogrid reinforcement can be added to new and existing slopes with conventional equipment and easily modified construction methods.

ACKNOWLEDGEMENTS

The authors would like to thank Ryan R. Berg and Connie Adams for their assistance in preparing this paper.

Figure 7. SURFICIAL GEOGRID REINFORCEMENT PLACED AT A SLOPE FACE

Figure 8. PLACEMENT AND COMPACTION OF FILL OVER SURFICIAL GEOGRIDS

Figure 9. CONSTRUCTED SLOPE SHOWING LAYERS OF PRIMARY AND SURFICIAL REINFORCEMENT

REFERENCES

1. Terzaghi, K. and Peck, R.B., "Soil Mechanics in Engineering Practice", Second Edition, John Wiley & Sons, New York, 1967.

2. Campbell, "Soil Slips, Debris Flows and Rainstorms in the Santa Monica Mountains, Southern California", U.S. Geologic Survey Professional Paper 851, 1975.

3. Christopher, B.R., Gill, S.A., Giroud, J.P., Juran, I., Mitchell, J.K., Schlosser, F. and Dunnicliff, J., "Design and Construction Guidelines for Reinforced Soil Structures - Volume I," and Summary of Research - Volume II," Report No. FHWA-RD-89-043, Federal Highway Administration, U.S. Department of Transportation, 1990.

4. Mitchell, J.K. and Villet, W.C.B., "Reinforcement of Earth Slopes and Embankments", National Cooperative Highway Research Program Report No. 290, Transportation Research Board, Washington, DC, 1987.

5. Bonaparte, R. and Berg, R.R., "Long-Term Allowable Tensile Load for Geosynthetic Reinforcement, "Proceedings of Geosynthetic '87", New Orleans, 1987.

6. GRI GG4 Standard Practice, Geosynthetic Research Institute, Drexel University, Philadelphia, PA., 1991.

7. GRI Test Method GG5, Geosynthetic Research Institute, Drexel University, Philadelphia, PA., 1991.

8. "Minimum Standards for Slope Stability Analyses", County of Los Angeles, Los Angeles, CA, 1978.

9. Day, R.W. and Axten, G.W., "Surficial Stability of Compacted Clay Slopes", Journal of Geotechnical Engineering, ASCE, Vol 115, No. 4, April, 1989.

10. Day, R.W. and Axten, G.W., "Softening of Fill Slopes due to Moisture Infiltration", Journal of Geotechnical Engineering, ASCE, Vol 116, No. 9, April, 1990.

11. Berg, R.R., "Interim Guidelines for Design, Specification, & Contracting of Geogrid Mechanically Stabilized Earth Slopes on Firm Foundations", U.S. Dept. of Trans., FHWA., International Fabrics Association International, 1991.

Geogrid Reinforcement for Massive Shear Key Applications

D. Chandra
Leighton and Associates, USA

G.C. Lay
Leighton and Associates, USA

D.L. Thielen
GeoEngineers Inc., USA

ABSTRACT

A case history is presented for geogrid reinforcement of slopes above several massive shear keys constructed for an extensive hillside development located in Southern California. The shear keys were excavated below the base of the hillside to prevent sliding failures along adverse bedding planes. The largest shear key was over 24 meters (80 feet) deep and was constructed below a 549-meter (1,800-foot) long, 24-meter (80-foot) high, 1H:1V (horizontal:vertical), geogrid reinforced slope. The shear keys were designed using Spencer's method of slices, and design of the slopes was accomplished by a slope stability computer program that incorporated geogrid reinforcement. Surficial stability and erosion resistance of the finished slope faces were also evaluated. Critical sections where compressible foundation soils were left in-place due to the constraint from the property line, were analyzed by a finite element method to evaluate the deformation response. In that particular area, a slope inclinometer and five settlement plates were installed to monitor the soil movements at the base of the hillside. The slopes above the shear keys incorporated relatively long primary reinforcement throughout the height of the slopes to increase stability against general circular failures. Short, secondary reinforcement was incorporated at the slope face to increase surficial stability and aid in compaction of the slope face. The design approach, construction considerations, and benefits of geogrid reinforced slopes are presented in this paper.

INTRODUCTION

The natural angle of repose of an unreinforced soil slope typically ranges from 20 to 35 degrees, depending on the types and shear strength of the soils. In Southern California, the governing agencies normally require fill slopes to be built at a gradient of 2H:1V or flatter. The Los Angeles Building Code which is mostly adapted from the Uniform Building Code states that "no fill shall be made which creates an exposed surface steeper than two horizontal to one vertical." However, the use of geogrids for fill slope reinforcement has made it possible to construct a globally and surficially stable slope steeper than what the code calls for. The oversteepened slopes were used in tandem with shear keys to buttress against potential sliding failures on adverse bedding planes. 1H:1V fill slopes were constructed directly over the shear keys to provide higher shear resistance in the keys. In addition, due to the high price of land in Southern California, the monetary value of additional usable land resulting from the steeper slope significantly exceeds the material and construction cost of a geogrid reinforced slope.

PROJECT AND SITE DESCRIPTION

A number of geogrid reinforced slopes were constructed as a portion of a 100-ha

(250-acre) hillside development in the City of Camarillo, Ventura County, California. Prior to grading, the elevations of the study area ranged from 30 meters (100 feet) at the western side to a maximum elevation of 120 meters (393 feet) at the central ridge top, with a maximum topographic relief of approximately 88 meters (290 feet). Over 10.4 million m^3 (13 million cubic yards) of earthwork grading involving significant amounts of cut and fill were required to achieve the final grades. The grading included infilling of most of the north-south trending canyons, some of which were over 30 meters (100 feet) deep. The proposed development will consist of the construction of 159 residential lots, two condominium sites and an 18-hole golf course with the associated clubhouse and maintenance facilities. For the preliminary investigation, over 150 exploratory borings and numerous trenches were excavated on the subject site. The field exploration indicated the presence of adverse bedding planes, and complex landslide and faulting systems. These unfavorable geology features required the construction of massive shear keys below the 1H:1V geogrid reinforced slopes. An aerial view of the project site during construction is shown in Figure 1, and the location of the geogrid reinforced slopes is presented in Figure 2.

In addition, the northwestern area of the subject site (Slope A, Figure 2) was found to be partially underlain by compressible alluvium. Since the alluvium extended beyond the property line, a complete removal of the alluvium and replacement with compacted fill was not feasible. As such, the shear key in this area was constructed against compressible alluvium. A finite element analysis was performed to determine the impact from deformation of the alluvium on the stability of the slope. The maximum tolerable movement at the toe of the slope was determined from the analysis. An inclinometer and five settlement monuments were installed at the toe of the slope to monitor vertical and horizontal ground movements during construction. A typical cross section showing the geogrid reinforced slope and the underlying shear key is shown in Figure 3. This cross-section depicts the northwestern area where Slope A is located (see Figure 2). The inclinometer and two of the settlement monuments were located in the vicinity of this cross-section.

Figure 1 - Aerial View of Project Site During Construction

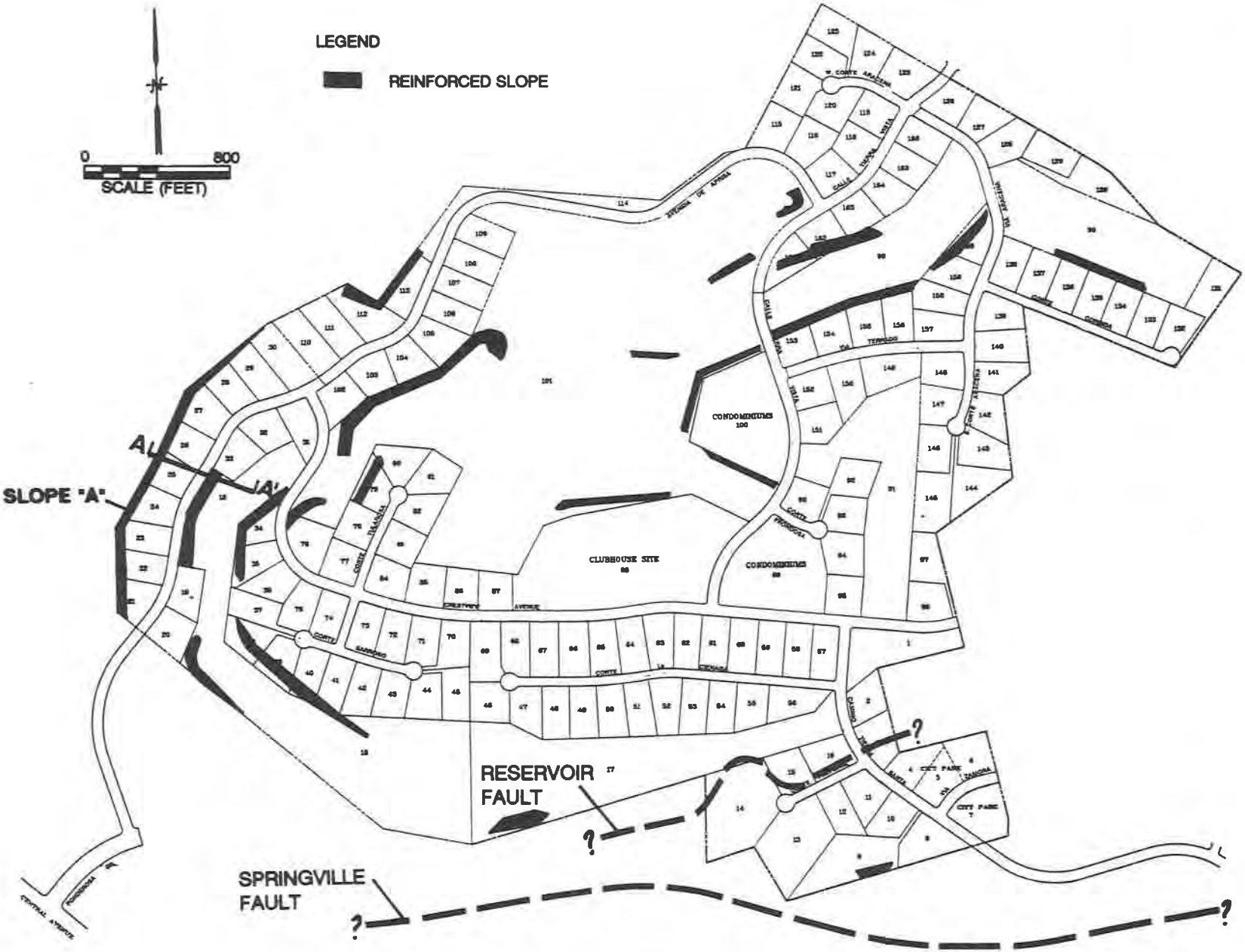

Figure 2 - Location of Geogrid Reinforced Slopes

GEOLOGIC CONDITIONS

Earth Units. Most of the site was covered by a thin colluvial top soil layer, generally less than one meter (three feet) in thickness. Alluvial soils as thick as 12 meters (40 feet) exist at lower elevations around the perimeter of the site and in canyon bottoms. The alluvium mainly consisted of silty fine sand with minor quantities of sandy clay and sandy silt. Saugus Formation bedrock underlaid the surficial deposits. This formation consisted of Plio-Pleistocene-age shallow marine to younger overlying non-marine interbedded sandstones, siltstones, and claystones. Some of the claystones were ruptured, highly plastic, and possessed numerous shiny parting surfaces and slickensides. Shear keys on the study area were designed to prevent potential slope failures along these clay layers.

Landslides. Numerous landslides exist on the subject site, and a relatively large area involving a complex of six translational landslides was identified at the western side. Smaller landslides which might had resulted from erosional undercutting of adversely oriented bedding planes were encountered in the northern and south-central portion of the site. The slide boundaries were clearly marked by rupture surfaces that exhibited slickensides. The landslide material was derived from alluvium and weathered Saugus Formation bedrock. At greater depth, the landslide material was observed to be internally intact bedrock that had moved as a translational block along bedding planes. This material was termed the ancient landslide.

Faulting. Two major faults bisect the southern portion of the site in the east-west direction. The Reservoir fault is located adjacent and approximately parallel to the southern boundary of the site. Based on field exploration, this fault appears to have become inactive during the late Pleistocene. On the contrary, the Springville fault, located south of the Reservoir fault, is potentially active from the evidence of substantial displacement of the "modern" soil resulting from the fault movement. The approximate location of the faults is shown in Figure 2. The presence of the faults had profound effects on the size of the shear keys along the southern boundary of the site since the soil strength along the fault was significantly lower than the intact bedrock.

SOIL STRENGTH PARAMETERS

Direct shear and triaxial tests were conducted on both undisturbed and remolded soil samples to determine the shear strength parameters for design. The parameters for along the bedding clay were obtained from multi-cycle residual direct shear tests. The samples were sheared forward and backward with a normal load of 450 kPa (9,000 psf) and at a rate of 0.0025 centimeters (0.001 inch) per minute until no further decrease in shear strength was observed with continued shearing. After the equilibrium state was reached, the shear value for that normal load was recorded. The normal loads were then reduced gradually without shearing the sample and the shear values were recorded for different normal loads. This method was found to yield conservative residual strength parameters as compared to the conventional method where soil samples were sheared repeatedly under different normal loads.

With the general availability of computer programs that provide fast yet sophisticated means for slope stability analysis, the selection of soil strength parameters has generally become the major task of a project. A summary of all residual test results performed on the claystone is plotted in Figure 4. A lower-bound value of ϕ = 9 degrees and cohesion of 2.5 kPa (50 psf) were selected for the slope stability analysis. The selected parameters for other materials are also summarized in Table 1. These parameters were based on the lower bound of the test results.

For the finite element analysis, the undrained shear strength from the triaxial tests was used because the short-term condition was considered to be more critical. The stability of the compacted fill slope would be favorable in the long term as the pore water pressure induced by the construction dissipated. Moreover, the alluvium was not susceptible to collapse which was a favorable long-term condition.

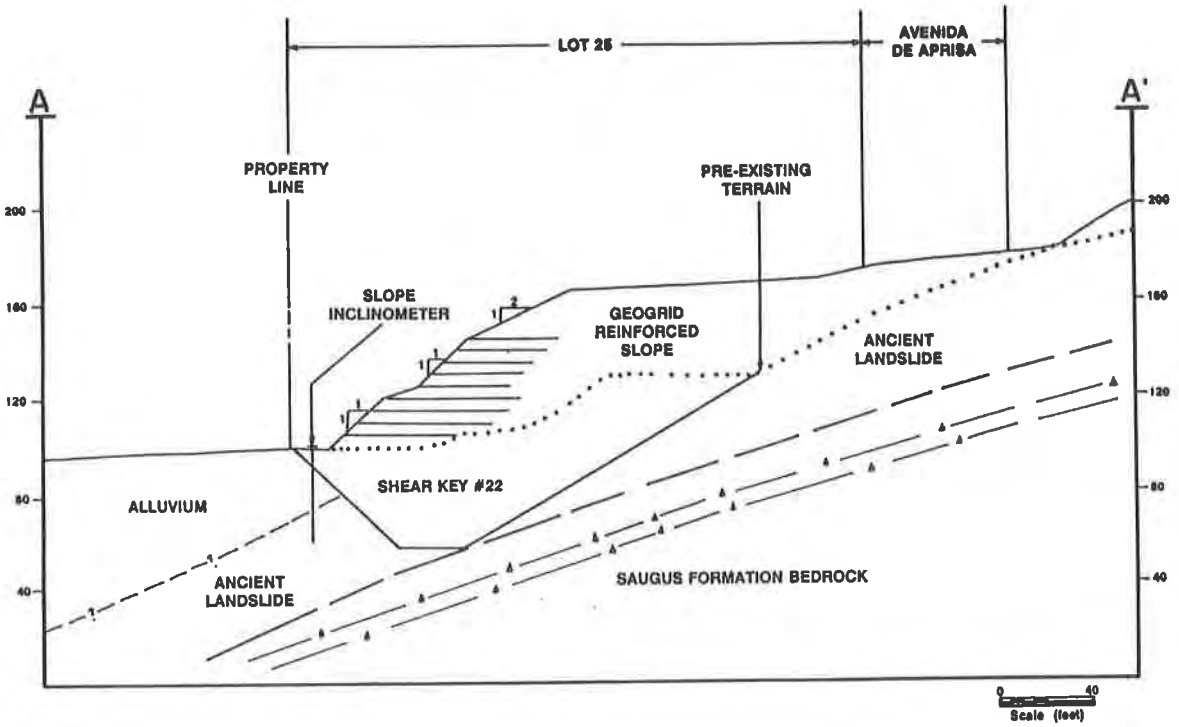

Figure 3 - Cross-Section A-A'

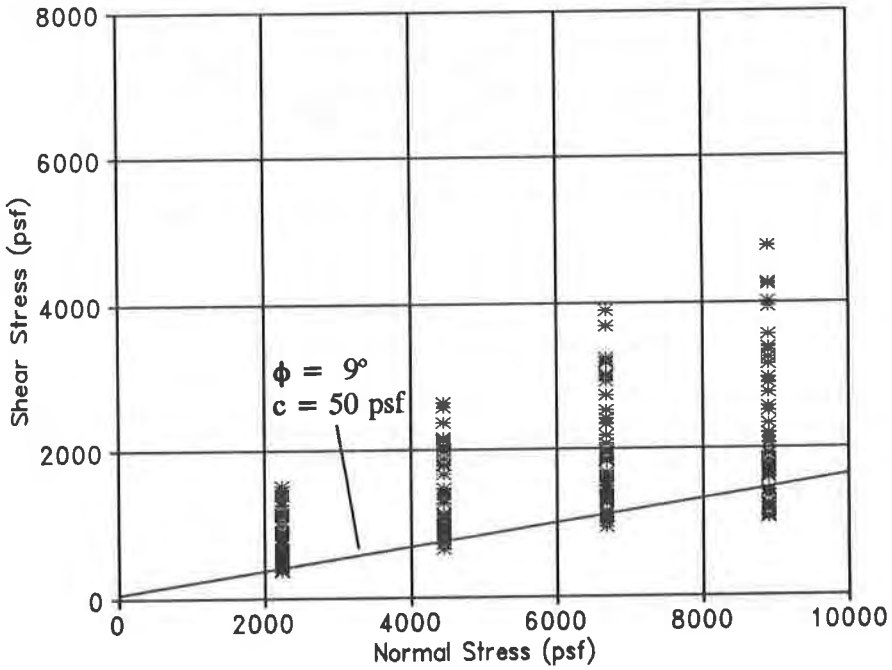

Figure 4 - Summary Plot of Residual Test Results
(Note: 50 psf = 2.5 kPa)

Table 1 - Summary of Soil Strength Parameters

Material Description	Shear Strength Parameters				Unit Weight (pcf)
	Drained		Undrained		
	c (psf)	Phi (deg.)	c (psf)	Phi (deg.)	
Alluvium	0	32.5	3000	0.0	116
Compacted fill	130	30.0	800	15.0	123
Bedrock:					
Across bedding	600	27.5	-	-	116
Along bedding	50	9.0	-	-	116
Along fault	30	19.5	-	-	116

Note: 1 psf = 0.05 kPa; 1 pcf = 0.16 kN/m3

COMPUTER PROGRAMS

The computer programs TENSLO1 and PCSTABL5M were used for design of the reinforced slopes and shear keys, respectively. In addition, the finite element computer program FEADAM84 was utilized for analysis of the deformation characteristics of the reinforced slopes. The capabilities of these computer programs are briefly summarized below.

TENSLO1. This computer program, developed by The Tensar Earth Technology, Inc., considers circular failure surfaces and uses the Modified Bishop method. An additional rotation-resisting moment resulting from the geogrid tensile force is included in the calculation to account for the effect of the geogrid reinforcement. The number, lengths and elevations of the geogrid reinforcement layers required to increase the internal and global stability to acceptable levels are evaluated using an iterative procedure. The most critical failure surface is located using an automatic search routine.

PCSTABL5M. This computer program for two dimensional slope stability analysis was developed at Purdue University (Carpenter, 1986). It includes three different limit equilibrium methods, namely Modified Bishop method, Simplified Janbu, and Spencer's method of slices. It has the random surface generation routines that can be used to search for the most critical potential failure surfaces. It is also capable of modeling the anisotropic soil strength parameters.

FEADAM84. This is a plane strain, two-dimensional, finite element computer program (Duncan et al., 1984). It is capable of modeling the incremental fill construction using non-linear and stress history dependent stress-strain relations. As part of the input of the computer program, the stress-strain relations are approximated by a hyperbolic model (Duncan et al., 1980)

APPROACH OF ANALYSIS

The lengths and numbers of layer of the geogrids were first determined using TENSLO1 for the 1H:1V reinforced slopes. In areas where the shear keys were affected by left-in-place, compressible alluvium, a finite element analysis using FEADAM84 was performed to evaluate the performance of the reinforced slopes from the possible deformation of the alluvium.

The design of the shear key was first accomplished by searching the location of the critical cutoff of the potential failure wedge along the slip surface. Once this was determined, PCSTABL5M was used to generate a search to find the critical breakout at the toe of the hypothetical slip surface. All searches were performed using the Simplified Janbu method. The more elaborate and time-consuming Spencer's method was then used to analyze the critical failure surface determined from the search. Additional analyses were also performed to determine the trend of safety factors for similar potential failure surfaces above and below the critical slip surface. A subroutine has been developed to expedite the search procedures (Chandra and Jiang, 1993). Typical plots of Slope A from TENSLO1 and PCSTABL5M output are presented in

Figures 5 and 6 , respectively.

For the finite element analysis, the stress-strain curves for the alluvium and compacted fill from the triaxial test results were approximated using the hyperbolic model. The finite element mesh used for this study is presented in Figure 7. A higher shear strength was used in the area affected by the presence of the geogrids to account for the effect of the geogrid reinforcement. It was found that a twenty percent increase in shear strength in that particular area was necessary to achieve a safety factor of 1.5 for an identical slope with reinforcement. A detail of the finite element analysis was presented elsewhere (Chandra and Lay, 1992).

GEOGRID SELECTION

In selecting geogrid for geotechnical application, durability is one of the most important elements to be considered. Factors related to durability include the ability to sustain the effects of creep under long-term loading, and resistance to deterioration. Another important property of geogrid is the ability to achieve its working strength at a low strain level. The working strength should develop at a strain level compatible with soils such that no significant movements will be encountered. In addition, the ability of the geogrid to effectively interlock with surrounding soils should be considered since it largely determines the required length of embedment. Generally, the different characteristics of geogrids are readily available from extensive testing performed by geogrid manufacturers. In the design calculation for reinforced slopes, the selection of geogrids eventually depends on the required tensile strength to achieve the required factor of safety. For this project, uniaxial geogrids with allowable working tensile strengths ranging from 454 to 1,317 kilograms (1,000 to 2,900 pounds) per linear foot were selected. The embedment lengths for the geogrids ranged from 1.8 to 25.5 meters (6 to 85 feet). Biaxial geogrids with a typical embedment length of 1.5 meters (4.5 feet) were installed at 0.3-meter (one-foot) intervals for surficial stability and erosion control. For further protection of the slope face, an erosion control mat which retains soil particles and promotes vegetative growth was placed on the slope face.

RESULTS OF FINITE ELEMENT ANALYSIS

The results of the finite element analysis indicated that deformation movement at the toe of Slope A due to the construction of the fill slope would be primarily horizontal. The vertical movement was found to be negligible. The horizontal movement computed at the toe of the slope is plotted as a function of fill elevation in Figure 8. The slope was capable of tolerating this movement as determined from the stress level of each soil element which was calculated to be less than 90 percent. Stress level is the ratio of the stress in the elements to the failure stress. It provides an indication of how close the soil is to shear failure. A stress level over 90 percent indicates the presence of plastic zone, and a stress level greater than 95 percent indicates shear failure. From the analysis, the elements near the toe of the slope were found to have a stress level close to 90 percent. Therefore, the lateral deformation curve from the finite element analysis in Figure 8 was established as the maximum tolerable movement. The top of the slope would have a finish grade elevation of 50 meters (165 feet). From the curve in Figure 8, theoretically, the slope would perform satisfactorily if the movement at the base of the slope was less than 6.4 centimeters (2.5 inches).

CONSTRUCTION CONSIDERATIONS

The main benefit of geogrid reinforced slopes from construction standpoint is that conventional construction methods and equipment can be used, and no additional skilled labor is needed. However, the geogrids must placed at correct elevation and orientation. Proper drainage should be installed to prevent saturation of the reinforced soil from ground water infiltration or surface runoff. Water will significantly reduce soil strength and decrease the factor of safety of the slope. Uniaxial geogrids, like those used for primary slope reinforcement in this project, do not require overlapping. Overlapping of this type of geogrids may produce geogrid on geogrid contact which will create an interlocking capacity that is not uniform to that produced by geogrid and the surrounding soil.

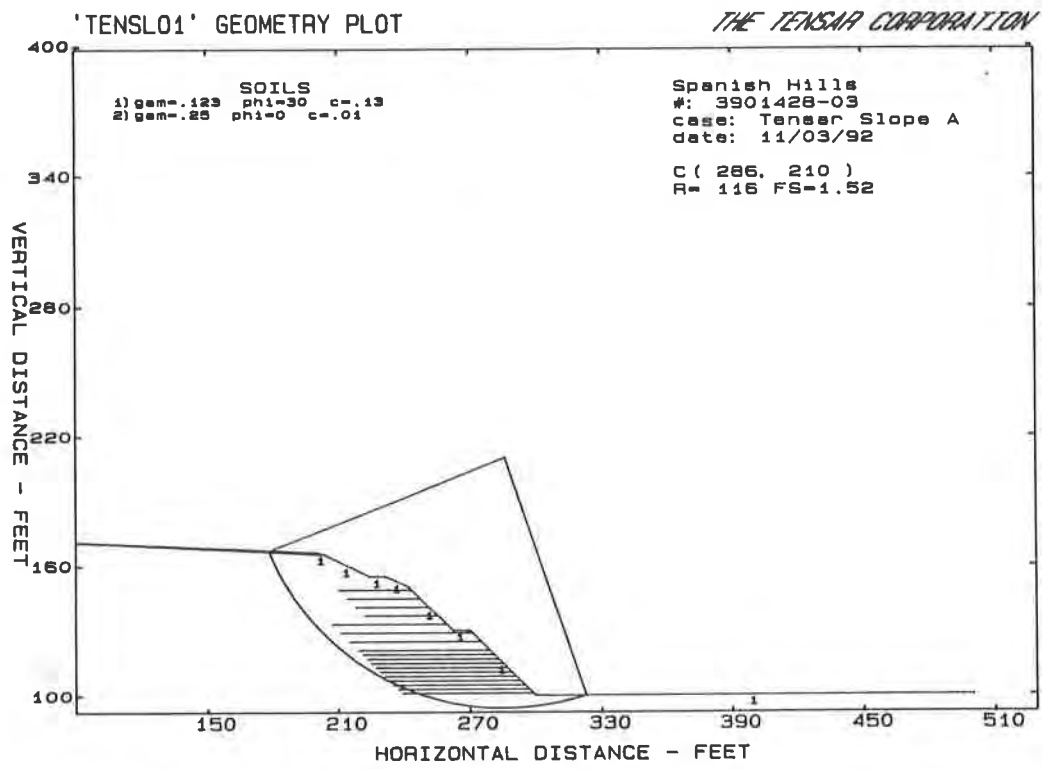

Figure 5 - Typical Output From TENSLO1 for Slope A

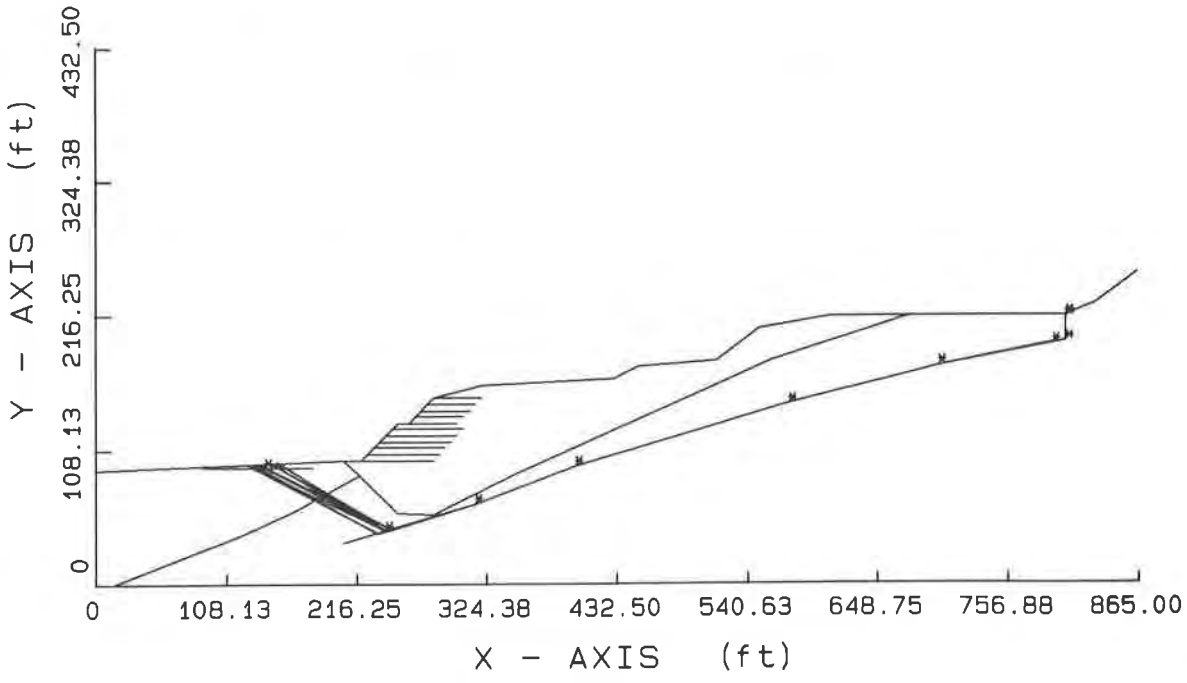

Figure 6 - Typical Output From PCSTABL5M for Slope A

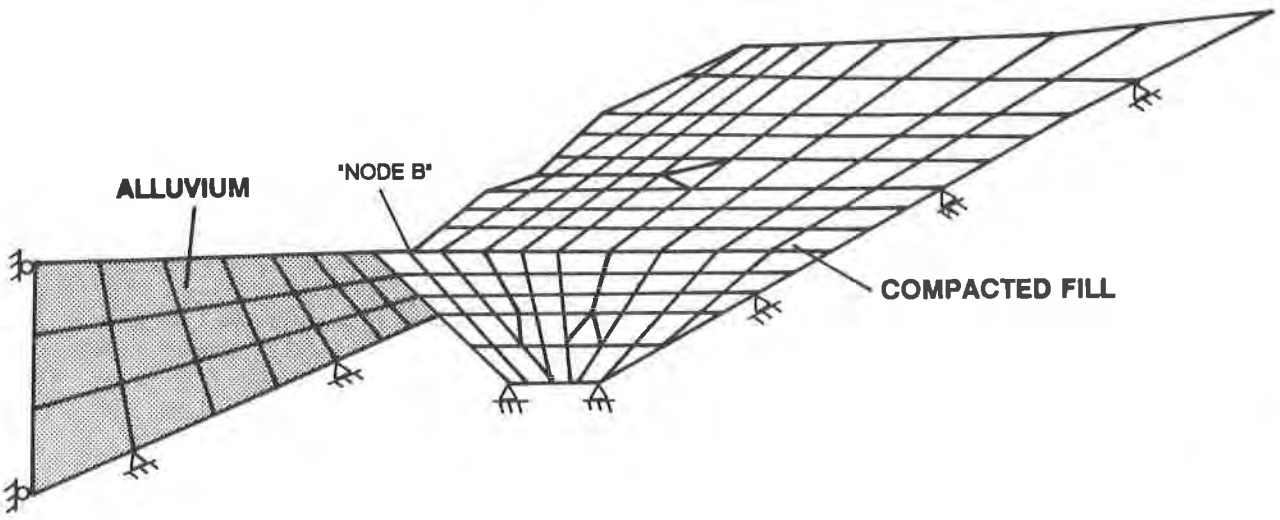

Figure 7 - Finite Element Mesh

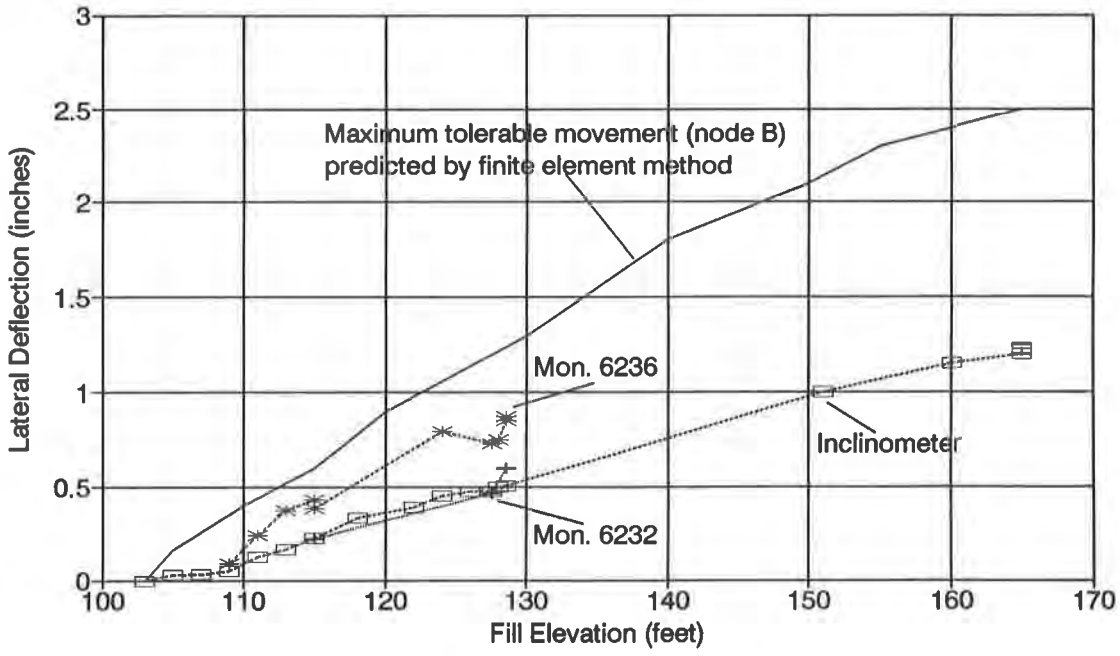

Figure 8 - Lateral Deformation at Toe of Slope A
(Note: 1 feet = 0.3 meter; 1 inch = 2.54 cm)

Prior to construction, one inclinometer and five settlement monuments were installed at the toe of Slope A. Readings were taken periodically during construction to ensure that horizontal movement at the toe of the slope was within the tolerable limit. The construction would be stopped immediately if the readings exceeded the lateral deflection predicted by the finite element analysis. Settlement Monuments 6232 and 6236 were located in the vicinity of Cross-Section A-A'. The readings from these two monuments along with those from the inclinometer are plotted in Figure 8. Later, the two monuments were disturbed, and subsequent readings were not plotted. At the end of construction, the lateral deformation at the toe of the slope as recorded by the inclinometer was significantly less than the calculated maximum tolerable movement.

BENEFITS OF GEOGRIDS

The use of geogrids had steepened the slopes which increased usable property at the top of the slope. Comparing to a 2H:1V slope with no reinforcement, a 1H:1V geogrid reinforced slope with a height of 24 meters (80 feet), for instance, resulted in an additional usable land of 12 meters (40 feet) at the top of the slope. The additional land had tremendous financial value in Southern California.

In addition, the steeper slopes provided increased overburden pressures at the base of the hill. In designing the shear keys to stabilize the hill, these additional overburden pressures increased the resisting force at the base of the hill which permitted shallower and narrower shear key.

CONCLUDING REMARKS

The use of geogrid reinforcement enabled the construction of globally and surficially stable slopes steeper than the maximum 2H:1V gradient required by the governing agency. The benefits included lower construction costs for the shear keys as well as increased usable property at the top of the slopes due to steeper final grades. The deformation response of the reinforced slopes resulting from the possible deformation of the left-in-place, compressible alluvium in the northwestern area of the project site, was evaluated using a finite element analysis. Movements at the toe of the slopes were monitored periodically during and after construction, and the slopes were found to perform satisfactorily.

ACKNOWLEDGEMENT

The authors are grateful for the support from Leighton and Associates, Inc., during the preparation of this paper.

REFERENCES

Carpenter, J.R. (1986), STABL5/PC STABL5 User Manual, Joint Highway Research Project, JHRP-86/14, School of Civil Engineering, Indiana Department of Highways, 47 pp, October 1986.

Chandra, D., and Jiang, C. (1993), Application of Spencer's Method in PCSTABL5M for Wedge Failure Type of Slope Stability Analysis, Abstract Submitted to the Fifth International Conference in Computing in Civil and Building Engineering, Anaheim, California, June 7-9, 1993.

Chandra, D., and Lay, G. (1992), Performance of A Geogrid Reinforced Slope on Compressible Foundation, Proceedings, 28th Symposium on Engineering Geology and Geotechnical Engineering, Boise, Idaho, April 1-3, 1992.

Duncan, J.M., Byrne, P., Wong, K.S., and Mabry, P. (1980), Strength, Stress-Strain and Bulk Modulus Parameters for Finite Element Analyses of Stresses and Movements in Soil Masses, Report No. UCB/GT/80-01, College of Engineering, Office of Research Services, University of California, Berkeley, 70 pp, August, 1980.

Duncan, J.M., Seed, R.B., Wong, K.S., and Ozawa, Y. (1984), FEADAM84: A Computer Program for Finite Element Analysis of Dams, Report No. SU/GT/84-03, Department of Civil Engineering, Stanford University, 78 pp, November, 1984.

Design and Construction of a 13.7 Meter (45 Foot) High, 1:1 Geogrid-Reinforced Slope in Highly Cemented Loess Soils

E. Templeton
Burns, Cooley, Dennis Inc., USA

D.L. Powell
Contech Construction Products Inc., USA

ABSTRACT

In Natchez Mississippi, erosion from a stream was undermining the toe of a 13.72 m (45 ft) high loess slope. When this degradation began to threaten residences at the top, officials evaluated several options for remediation. A 1 vertical (V) to 1 horizontal (H) geogrid reinforced slope was selected for its cost effectiveness, ease of construction and aesthetic appeal.

Design and construction of the slope presented several unique problems. Because of the highly cemented nature of the existing loess deposit, a combination of the tie-back wedge method and the modified Bishop method for slope stability analysis had to be incorporated. An economical solution was developed that incorporated geogrid reinforcement for the entire height of the slope along with a system of rip-rap filled wire forms for protection of that portion of the slope that would be exposed to water flow . Both design and construction had to address the curvilinear geometry of the slope and the proximity of the residences to the crest of the slope.

This paper presents a case history of the design, construction and performance to date of the geogrid reinforced slope.

INTRODUCTION

In late 1989, the Natchez Housing Authority of Natchez Mississippi initiated studies for the Maryland Heights Public Housing Project. A stream at the edge of the property had been, over a period of several years, undermining the toe of a 13.7 meter (45 ft) high loess slope. As this undermining progressed, the highly cemented nature of the loessial soils had resulted in a near vertical bluff. The regression of the bluff was beginning to threaten existing residences at the top.

Jordan, Kaiser & Sessions, a Natchez Mississippi engineering firm, was retained by the housing authority to develop plans for the remediation. Alternates that they studied included; realignment of the channel to allow reconstruction of a flattened slope using conventional means, enclosing the stream and reconstructing a flattened slope over the top of the enclosure, relocation of the residences at the top of the bluff, and reconstruction of a steepened slope by reinforcing the in situ soils with geogrid reinforcement.

The steepened, geogrid reinforced slope was chosen primarily for its low cost. Realignment of the existing channel would require purchasing additional property and it presented problems with state regulatory agencies. Enclosing the channel and reconstructing a flattened slope proved to be cost prohibitive. While at first glance, relocating the residents would appear to be the most cost effective alternative, requirements for relocating residents of public housing resulted in an estimated cost that was almost twice the cost of slope reconstruction. In the end, a geogrid reinforced slope allowed the housing authority to maintain the residences, avoid altering the existing channel alignment and reconstruct a stable steepened slope using site available soils.

DESIGN

General. The design of the slope was based upon the maximum slope height of 13.7m (45 ft) considering a 1V to 1H slope. The reinforcement layout determined for this critical section was conservatively extended throughout transitional slopes steeper than 1V to 2.5H. Analyses indicated that slopes flatter than 1V to 2.5H would not require reinforcement. The minimum factor of safety for slope stability was taken to be 1.5. This factor of safety was considered appropriate due to the proximity of residences to the crest of the slope.

Design of the reinforced slope was accomplished in the following steps:
- Develop the design parameters for the undisturbed and recompacted site soils.
- Evaluate the existing conditions to verify the accuracy of the selected in situ soil parameters.
- Establish the reinforced soil zone geometry by considering the physical constraints of the project.
- Establish the vertical spacing of the reinforcement using a Tie-back Wedge Analysis in junction with the reinforcement properties.
- Analyze the reinforced soil mass using the modified Bishops method for limit equilibrium slope stability analysis.
- Develop surficial stability and erosion protection details.

Soil Parameters Utilized. No site specific soils data was available for the development of the soil parameters utilized in the analysis and design. The design parameters were selected based upon the area geology and local experience with loessial soils. These parameters were then verified through an analysis of the existing conditions.

The project site consisted of a meandering creek channel at the toe of a near vertical bluff. The site is located within the Loess Hills physiographic region immediately adjacent to the eastern edge of the Mississippi River alluvial valley. The soils comprising the bluff generally consist of a thick deposit of loess, underlain at depth by a complex fluvial deposit of the Natchez formation. Recent alluvial and colluvial deposits exist within the creek channel and along the opposing creek bank.

Loess is generally a stable material which provides a safe foundation for properly designed structures. Undisturbed loess has the unusual characteristic of standing in high vertical cuts. This property is primarily attributable to cementation of the soil grains. The effectiveness of the cementation is reduced when the soil becomes wet. Loess typically has a high shear strength and low compressibility when the moisture content is low. However, increases in the moisture content are generally accompanied by dramatic increases in compressibility and a loss of shear strength.

Since loess is composed predominantly of non-plastic, silt size particles, it has a low resistance to erosion resulting in susceptibilities to failure which must be considered if an adequate design is to be achieved.

An extensive investigation of bluff failures along the Mississippi river at Natchez Mississippi was completed by the U.S. Army Corps of Engineers, Vicksburg District, in 1985[1]. This study included detailed mapping of the geologic formations comprising the bluff and the results of consolidated-undrained triaxial tests performed on samples of the loessial silts. These test results indicate a fairly uniform strength for the samples tested with average values of friction angle (Φ) and cohesion (C) of 26 degrees and 28.72 kN/m^2 (600 lb/ft^2), respectively. These values were selected for use in the analysis of existing conditions at the site.

The cementation, which results in an apparent cohesion in undisturbed loess, is lost upon excavation and recompaction. The drained strength of the remolded sample is generally characterized by a friction angle varying from 26 to 33 degrees with no cohesion. Therefore, reasonable yet conservative values of Φ = 26 degrees and C = 0 were assigned to the compacted loess within the reinforced zone of the slope. The moist unit weight of both the in situ and compacted soils was estimated to be 18062 kg/m^3 (115 lb/ft^3).

Loess is seldom saturated unless a perched water table develops. Surface water which infiltrates the soil is able to drain through open pores without causing complete saturation. Improvements to the surface drainage were included in the plans. It is expected that these improvements will prevent any significant percolation of surface water into the in situ soil or the compacted reinforced fill. Therefore, it was assumed in the analysis that no significant water pressures would develop in the slope.

Analyses of Existing Conditions. Analyses were performed for existing slopes to evaluate the accuracy of the assumed shear strength parameters of the in situ loess. Available site mapping indicated that a 2.5V to 1H slope approximately 13.72m (45 ft) in height represented the average condition within the critical reach. An analysis of this geometry using the assumed shear strength parameters of Φ = 26 degrees with C = 28.72 kN/m^2 (600 lb/ft^2) yielded a factor of safety of 1.2. This factor of safety was felt to be consistent with the observed performance of the in situ soils. Therefore, these shear strengths were considered appropriate for use in the design of the reinforced soil mass.

Site Geometry. Physical constraints at the site influenced the selection of the reinforcement lengths. The channel alignment and therefore, slope toe alignment had been established by hydraulic considerations and property constraints. A minimum offset of 4.6m (15 ft) between the residences along the top of the bluff and the crest of the excavated slope was required. These restrictions combined with a maximum acceptable excavation slope of 3 V on 2 H limited reinforcement lengths to 12.2m (40 ft) at the base and 7.6m (25 ft) at the crest.

Reinforcement Properties. The design considered primary and intermediate reinforcement to provide adequate factors of safety for global and surficial stability, respectively. The primary reinforcement had an allowable long-term design strength of 40.9 kN/m (2800 lb/ft) along the principal axis. Since the proposed slope geometry was represented by the plain strain condition,

reinforcement strength along the secondary axis was not a consideration for stability. The long-term design strength accounted for the effects of installation damage, chemical and biological degradation, junction strength and creep. The intermediate reinforcement was a light-weight biaxial geogrid with high junction efficiency extending 1.4m (4.5 ft) into the slope face.

The coefficient of interaction is the ratio of the shear strength developed at the soil-reinforcement interface to the peak soil shear strength. This ratio is used to estimate pullout resistance of the reinforcement for stability calculations. Based upon the manufacturer's recommendations, a value of 0.8 was selected for the analysis.

Method of Analysis. The required vertical spacings of the reinforcement to provide internal stability were determined by the tie-back wedge method of analysis. With this method, it is assumed that the ultimate shear strength of the soil is mobilized and the lateral earth pressures are resisted by the reinforcement tensile force. The assumed failure plane is defined by the Rankine failure surface forming an angle of $45 + \Phi/2$ from the horizontal.

Due to the high undisturbed strength of the in situ loess and, consequently, the ability of loess to stand in high vertical cut sections, it was not considered appropriate to evaluate required geogrid embedment lengths by the usual method. To do so would yield unconservatively short embedment lengths indicating that a thin veneer of reinforced fill would insure global stability. Therefore, minimum lengths of reinforcement at the slope base and crest were based upon the physical constraints described previously. The specifications also required that each layer of primary reinforcement extend from the slope face to the in situ loess.

Limit equilibrium slope stability analyses were performed to evaluate the existing conditions (discussed previously), verify the internal stability of the reinforced fill and evaluate the global stability of the final design. These analyses were performed using the TENSLO1[2] computer program developed by the Tensar Corporation. This program calculates factors of safety for circular failure surfaces using an extended version of the modified Bishop method. The locations of the critical slip surfaces are determined by multiple computer runs using automatic search routines available in the program. The program incorporates the effects of horizontal reinforcement, as a function of the embedment length and the long-term design strength of the reinforcing material, in calculating the factor of safety for each trial circle. The coefficient of interaction is used to compute the available pullout resistance based upon the embedment length of the reinforcement in front of and behind the trial failure surface. The design pullout resistances are determined by applying a pullout factor of safety to these values. The reinforcement tensile strength used in the calculations is the minimum of the pullout resistances calculated or the long-term design strength of the reinforcement.

DESIGN RESULTS

Tie-Back Wedge Analysis. The tie-back wedge method of analysis was utilized to establish the maximum allowable vertical spacings of the primary reinforcement. The Rankine lateral earth pressures were estimated using a factor of safety of 1.5 and an assumed shear strength of $\Phi = 26$ degrees for the recompacted loess. Limiting the tensile stress in the primary reinforcement to 40.9 kN/m (2,800 lbs/ft) resulted in vertical reinforcement spacings ranging from 0.3m (1 ft) at the

base of the slope to 1.24m (4 ft) near the slope crest. The resulting cross section is shown in Figure 1.

Analysis of the Reinforced Slope. Limit equilibrium analyses were performed to verify internal stability and to evaluate global stability. Internal stability was considered to consist of potential failure surfaces confined to the reinforced compacted fill. Failure surfaces located partially or entirely within the in situ soils were classified as global. Multiple computer runs using automatic search routines available in the computer program identified the critical failure surface. The critical failure surface passes through the lower portion of the reinforced mass and up through the in situ loess. The computed factor of safety for this global type failure was approximately 1.5. Computed factors of safety for internal failure surfaces were somewhat higher.

Surficial Stability. While surficial stability was not directly analyzed, the specifications required continuous layers of intermediate reinforcement extending 1.4m (4.5 ft) into the slope face and at 0.3m (1 ft) vertical intervals along the slope face. The intermediate reinforcement was considered a necessity in preventing surficial failure of the essentially non-plastic fill. Inclusion of the intermediate reinforcement at relatively close spacing also improves compaction of the fill materials near the slope face. The intermediate material specified was a light-weight biaxial geogrid with high junction efficiency.

DESIGN DETAILS

Armored Slope Details. The primary cause of the degradation of the existing slope was erosion of the stream bank at the slope toe. The design process, therefore, had to incorporate a protective facing on that portion of the slope where exposure to the water flow in the stream was a concern. The combination of the proposed 1H to 1V slope and the forces generated by the water flow required a facing with a positive connection to the slope. The final detail (Figure 2) incorporated a wire form which was wrapped on the inside with the primary reinforcement. This was filled with an 0.46m (18") thick layer of 0.15m (6") nominal diameter stone and was backed with a nonwoven geotextile to separate the soil fill from the stone facing. The secondary geogrid wrap was supplied in 1.3m (4.26 ft) widths and embedded 1.19m (3.9 ft) on the top and bottom of the wrap, thus providing a positive facing connection. The wire form was manufactured from 10cm (4") X 10cm (4") welded wire fabric. The form was bent to provide the required 1H to 1V face slope and assisted in controlling pillowing of the geogrid wrap as well as getting the lower portion of the slope aligned on the required layback.

Surface Runoff Diversion System. The low plasticity of the loessial silts makes them highly susceptible to erosion from surface runoff. This was evident from the high number of rills and gullies in the existing bluff face. To prevent surface flows from adversely effecting the reinforced slope, concrete lined diversion ditches were incorporated at the slope crest. The collected water was transported down the slope face in an enclosed pipe. Embedment of the pipe in the slope face either during or after construction of the slope would have been a difficult task at best. The pipes were therefore run along the surface of the slope and anchored at intervals with a foundation and strap.

Erosion Mat. While the design did provide for diversion of the surface runoff, the erodible nature

of the loess soils called for protection of the slope face in those areas above the 4.6m (15 ft) high armored protection system. In these areas a three dimensional turf reinforcing mat (TRM) was used. The selected mat consisted of three layers of polyethylene netting that are melt bonded at regular intervals in a manner that creates a three dimensional structure.

Project details called for the mat to be keyed into the slope face on 1.22m (4 ft) vertical intervals with a minimum embedment of 91cm (3 ft) into the slope. The specifications also called for the slope face to be seeded prior to placing the TRM.

CONSTRUCTION

Construction Schedule and Techniques. Construction of the project was started in January, 1991. Weather delayed the start of excavation until March, 1991. The initial phase of construction required the excavation of the existing bluff to provide for the depth of reinforcement embedment and to reach competent, intact loess soils. During this process a berm and channel were constructed to divert the existing stream flow away from the construction area. The excavated material was stockpiled for later use in the reinforced fill zone.

After excavation of the project area was completed, construction of the reinforced fill was started. Construction of the lower portion of the slope required significant coordination of the reinforcing components. Primary reinforcing elements extended from the back of the excavated zone to the face of the soil fill zone (Photo 1). In addition, the geogrid wrap used to contain the stone inside of the wire form, and the geotextile wrap at the back face of the stone, had to be placed prior to placing the soil fill. The soil was placed in 20cm (8 in) loose lifts and compacted to 100% of standard Proctor density in accordance with the project specifications. After the soil fill had progressed 50cm (1.5 ft) vertically, the geotextile was wrapped around the soil face. The stone fill was placed inside the wire form and the geogrid wrap was laid back into the soil fill completing the positive connection of the stone facing to reinforced soil zone. This process was repeated until the fill placement had achieved the required 4.6m (15 ft) vertical height for the stone facing.

Construction of the slope above the stone facing progressed significantly quicker. The primary reinforcement was placed perpendicular to the slope face at the intervals designated by the project plans. The intermediate reinforcement was placed in between the primary reinforcing on 0.3m (1 ft) verticals intervals. The selected material was a biaxial geogrid having its strongest axis in the cross-machine direction. It was provided in 3m (9.8 ft) wide rolls that were cut in half and then rolled out parallel to the slope face. This provided 1.5m (4.9 ft) of embedment.

The turf reinforcing mat was also installed as the slope construction progressed. The mat was cut to the appropriate length embedded 91cm (3 ft) into the slope face and allowed to hang down over the slope below. When the fill had achieved the required elevation, the slope face was seeded, and the mat was wrapped around and embedded into the fill.

Upon completion of the reinforced slope, the drainage improvements at the slope crest were constructed and a protective safety fence was placed at the top of the slope. Construction of the project was substantially completed in November 1991 (Photo 2).

Difficulties Encountered During Construction. The slope was constructed in a curvilinear geometry (Figure 3) involving a significant reverse curve as well as a channel bottom drop of over 0.9m (3 ft) vertically. The slope of the channel required a field determination of the appropriate stepping for the lowest geogrid layers and wire form facing. The severe curvilinear geometry required fanning of the geogrid reinforcement. Because of the radius of curvature and the length of the reinforcement, those layers in the inside curve required an overlap at the tail of the geogrid. Based upon the geogrid manufacturers recommendations, project specifications called for the placement of 10cm (3 in) of soil fill between the overlapping layers. Additionally, the tight horizontal radius of curvature made proper alignment of the 3.1m (10 ft) long wire forms difficult.

Recompacted loessial silts are extremely sensitive to moisture content. This made the specified densities difficult to achieve during the construction process. Weather conditions were either too wet, resulting in an unworkable soil, or too dry, requiring careful control of the additional water. Weather delays, scarification and recompaction were common practice to achieve the specified density.

After completion of the project in November 1991, the lower Mississippi Valley experienced several significant rainfall events. The slope, having been constructed and seeded in late summer and fall, had not had the opportunity to develop any significant vegetative growth. As a result, a portion of the slope experienced some minor surficial slides. The saturated soil slid beneath the TRM, pulling some portions loose from the anchor trenches. The failed areas were covered with a protective plastic sheeting until repairs could be initiated in May 1992.

CONCLUSIONS

Design of the geosynthetic reinforcement was accomplished through the use of conventional methods of slope stability analysis. The single most important factor was an understanding of the unique characteristics of the loessial soils. This was accomplished through the use of locally available studies such as the U.S.A.C.E. investigation and the extensive local experience of the project designers. Care had to be taken to interpret the testing results. Use of the in situ loess strengths alone would have resulted in a potentially unstable design while use of the remolded soil strength would have resulted in an overly conservative and thus expensive design.

Construction of the slope along the curvilinear geometry was difficult to control. The only solution to this would be to provide for a more linear channel alignment; however, the channel geometry was a function of the stream hydraulics and other physical constraints and, therefore, was unavoidable.

The surficial slides that occurred after the completion of the project can be attributed to two factors. First, the vegetative growth did not have adequate time to establish itself. Use of sod in conjunction with the TRM had originally been considered. In light of the delayed construction schedule, this may have made a significant difference. Second, the project details called for keying the TRM into the slope face on 1.2m (4 ft) vertical intervals. There is some evidence that the mat was keyed in at much wider spacings. The performance of a TRM is dependent upon its ability to maintain intimate contact with the soil and its ability to restrain the surface soils. The

increased key interval allowed the shallow surficial sloughing to build up force. This caused the mat to pull away from the slope face and become ineffective in preventing further sliding or in assisting with seed germination. Installing check slots at 1.2m (4 ft) intervals would have controlled the slides more effectively.

Final project costs are around $620,000. These costs were as little as one half of the costs estimated for the other repair alternates. In addition, reconstruction of the slope with reinforcement maintained the existing channel alignment and provided the desired slope stability. While the project has been complete only a short period of time, performance has been as expected.

ACKNOWLEDGMENTS

The authors would like to acknowledge Mr. Phillip Chaffin and Mr. Jim Marlowe of Jordan, Kaiser and Sessions, Natchez Mississippi for their assistance.

References

(1) U.S. Army Corps of Engineers, Vicksburg District, (1985) "The Natchez Bluff Study".

(2) Tensar Corporation (1991), "TENSLO1 Computer Program for Slope Stability Analysis Incorporating TENSAR Geogrid Reinforcement."

Photograph 1. Placement of Primary Geogrid

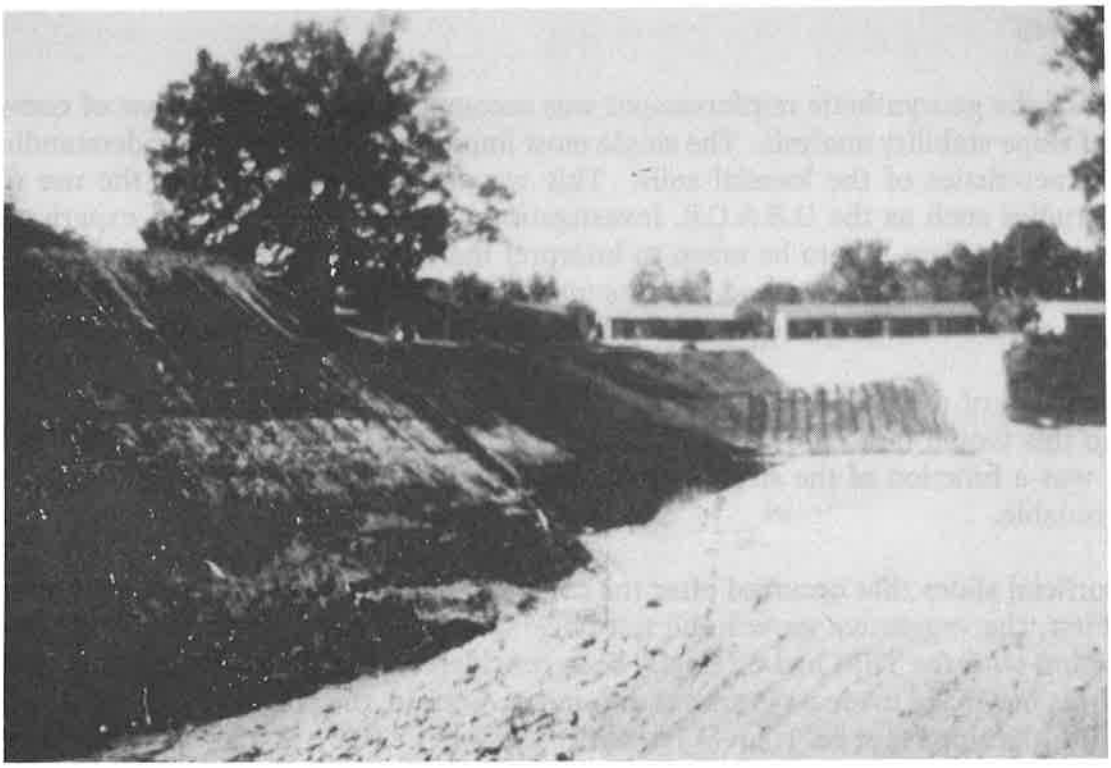

Photograph 2. Finished Slope

Difficulties Encountered During Construction. The slope was constructed in a curvilinear geometry (Figure 3) involving a significant reverse curve as well as a channel bottom drop of over 0.9m (3 ft) vertically. The slope of the channel required a field determination of the appropriate stepping for the lowest geogrid layers and wire form facing. The severe curvilinear geometry required fanning of the geogrid reinforcement. Because of the radius of curvature and the length of the reinforcement, those layers in the inside curve required an overlap at the tail of the geogrid. Based upon the geogrid manufacturers recommendations, project specifications called for the placement of 10cm (3 in) of soil fill between the overlapping layers. Additionally, the tight horizontal radius of curvature made proper alignment of the 3.1m (10 ft) long wire forms difficult.

Recompacted loessial silts are extremely sensitive to moisture content. This made the specified densities difficult to achieve during the construction process. Weather conditions were either too wet, resulting in an unworkable soil, or too dry, requiring careful control of the additional water. Weather delays, scarification and recompaction were common practice to achieve the specified density.

After completion of the project in November 1991, the lower Mississippi Valley experienced several significant rainfall events. The slope, having been constructed and seeded in late summer and fall, had not had the opportunity to develop any significant vegetative growth. As a result, a portion of the slope experienced some minor surficial slides. The saturated soil slid beneath the TRM, pulling some portions loose from the anchor trenches. The failed areas were covered with a protective plastic sheeting until repairs could be initiated in May 1992.

CONCLUSIONS

Design of the geosynthetic reinforcement was accomplished through the use of conventional methods of slope stability analysis. The single most important factor was an understanding of the unique characteristics of the loessial soils. This was accomplished through the use of locally available studies such as the U.S.A.C.E. investigation and the extensive local experience of the project designers. Care had to be taken to interpret the testing results. Use of the in situ loess strengths alone would have resulted in a potentially unstable design while use of the remolded soil strength would have resulted in an overly conservative and thus expensive design.

Construction of the slope along the curvilinear geometry was difficult to control. The only solution to this would be to provide for a more linear channel alignment; however, the channel geometry was a function of the stream hydraulics and other physical constraints and, therefore, was unavoidable.

The surficial slides that occurred after the completion of the project can be attributed to two factors. First, the vegetative growth did not have adequate time to establish itself. Use of sod in conjunction with the TRM had originally been considered. In light of the delayed construction schedule, this may have made a significant difference. Second, the project details called for keying the TRM into the slope face on 1.2m (4 ft) vertical intervals. There is some evidence that the mat was keyed in at much wider spacings. The performance of a TRM is dependent upon its ability to maintain intimate contact with the soil and its ability to restrain the surface soils. The

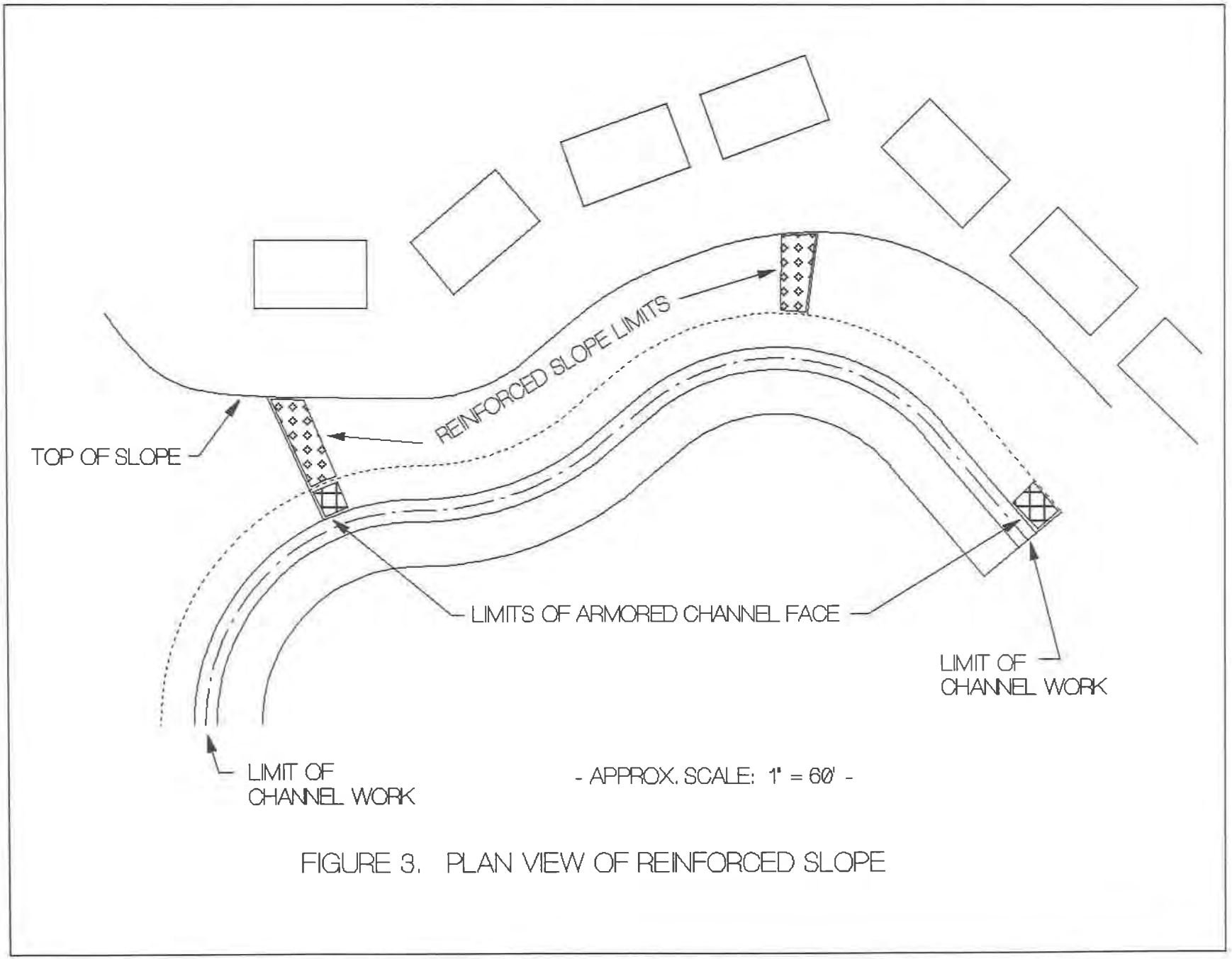

FIGURE 3. PLAN VIEW OF REINFORCED SLOPE

increased key interval allowed the shallow surficial sloughing to build up force. This caused the mat to pull away from the slope face and become ineffective in preventing further sliding or in assisting with seed germination. Installing check slots at 1.2m (4 ft) intervals would have controlled the slides more effectively.

Final project costs are around $620,000. These costs were as little as one half of the costs estimated for the other repair alternates. In addition, reconstruction of the slope with reinforcement maintained the existing channel alignment and provided the desired slope stability. While the project has been complete only a short period of time, performance has been as expected.

ACKNOWLEDGMENTS

The authors would like to acknowledge Mr. Phillip Chaffin and Mr. Jim Marlowe of Jordan, Kaiser and Sessions, Natchez Mississippi for their assistance.

References

(1) U.S. Army Corps of Engineers, Vicksburg District, (1985) "The Natchez Bluff Study".

(2) Tensar Corporation (1991), "TENSLO1 Computer Program for Slope Stability Analysis Incorporating TENSAR Geogrid Reinforcement."

Landform Contour Grading—Natural-Looking Slopes from Geosynthetics

M.T. Peak
Sukut Construction Inc., USA

D.L. Thielen
GeoEngineers Inc., USA

ABSTRACT

Geogrid reinforcement is being used by the hillside development industry to construct natural appearing, undulating landforms. These landforms have included steepened slope sections greater than 30 meters high with surface grades of up to 45 degrees. Additionally, all hillside developments require some degree of corrective grading to mitigate severe engineering and geotechnical constraints such as steep topography and ancient landslides. Conventional solutions, including flatter slopes, soil cement, lime treatment, and battered retaining systems can be uneconomical and aesthetically unacceptable. The landform contour grading concept, its use in land planning, and its design and construction is described. A case history of landform contour grading which included over 13,000,000 m^3 of earthwork is presented describing a hillside development project that is the largest slope reinforcement application in the world. Over 430,000 m^2 of geogrid reinforcement materials were used to increase global and surficial factors of safety while at the same time improving the project's economic viability and environmental acceptance.

INTRODUCTION

Large hillside land developments, such as those which have been occurring in Southern California for the past 30 years or more, are unique. These developments require an enormous amount of earthwork construction (grading) to produce enough useable land for an economically viable project. It is not uncommon to have 30,000 m^3 of grading per housing unit in high end residential developments. The large grading quantities are necessary because the land planner and grading engineer must comply with a variety of city and county grading ordinances and public works standards, which were formulated over the years to protect the public safety and welfare. These codes usually specify a maximum slope gradient of 2H:1V (horizontal:vertical) together with definitive specifications for street grades, widths, vertical curves and radii.

In order to design a development having enough useable land that is not taken up by very high 2H:1V (or flatter) slopes and ample street geometries, the land planner and engineer must literally mass grade most of the site. In addition, almost all hillside land parcels contain many geotechnical constraints that require extensive mitigation. These constraints include high ground water tables, liquefiable soils, compressible soils, creep zones, terrace deposits, organic stratum and expansive soils, adverse (dip slope) bedding planes, folds and flexure-slip surfaces, faults and tectonic shear zones, open joints and fractures, clay and gypsum seams, as well as ancient and historic landslides. Conventional solutions for these problems also create large volumes of grading (corrective grading) in the form of deep removals, overexcavation and recompaction, shear keys and buttress fills. Massive retaining systems, shear pins, compaction grouting, soil cement, lime treatment and other traditional geotechnical engineering solutions are sometimes employed along with the massive earthwork requirements to provide the corrective solutions.

In recent years, hillside projects requiring extensive grading have been severely criticized on environmental and aesthetic grounds. The standard 2H:1V maximum terraced slope mandated by building codes is criticized for having an artificial, regimented and unnatural appearance. Several cities have responded to these concerns by passing ordinances that restrict the heights and lengths of slopes, the depth of cuts and fills, the allowable densities per acre and other measures that further limit or prevent hillside land development.

In an effort to deal with the geotechnical, environmental, political and aesthetic constraints of large hillside developments, a new technology has emerged. The technology combines geogrid reinforcement with state-of-the-art land planning and grading design. This new technology is known as Landform Contour Grading. Landform Contour Grading was introduced to the hillside development industry by Sukut Construction, Inc. in 1987 on a 35 meters high 1H:1V reinforced buttress in San Diego (Chu & Poormand, 1989).

Although other types of geosynthetics, such as geonets and geotextiles are also being used in hillside developments as cost effective alternatives to conventional engineering and construction techniques, this paper will focus on Landform Contour Grading using geogrid reinforcement.

LANDFORM CONTOUR GRADING

Landform Contour Grading is the construction of natural looking slopes that have topographic contours and vegetation similar in appearance to the original and surrounding, ungraded terrain. To achieve this objective, slopes and contours are designed and constructed with variable horizontal and vertical angles. To simulate natural slopes, while at the same time creating enough useable land to produce an economically viable project, the land planner must have the ability to incorporate steepened sections within the designed, variable slope. To ensure both global and surficial slope stability in most soils, tensile reinforcement must be included in the design and construction of any portion of the variable slope that is steeper than approximately 2H:1V. Geogrids have proven to be the most practical and cost effective method of introducing

additional tensile strength to earth materials as will be specifically demonstrated in the case study section of this paper.

Revegetation of the finished, landform contour graded slopes with native and introduced drought tolerant plant materials is mandatory in order to achieve the desired natural appearance. Figure 1 depicts a typical Landform Contour Grading design using 2H:1V angles at the toe and top of a variable slope that includes a 1H:1V reinforced section in the middle. Figure 1 also includes an appropriate natural revegetation specification for landform contour graded slopes. Figure 2 shows a revegetated 21 meters high landform contour graded slope. The upper 9 meters is a geogrid reinforced section.

Landform Contour Grading mitigates environmental and aesthetic concerns by reducing the visual and physical impacts that result from conventional grading design and construction methods. Figure 3 illustrates an actual and typical hillside design situation where a steep walled canyon will be filled to construct a road. The conventional 2H:1V slope with surface drains every 9 meters produces severe physical and visual impacts because of the much larger slope when compared to the landform contour graded slope. Conversely, the landform contour grading design significantly reduces the amount of natural ground and vegetation that is physically impacted by grading. Furthermore, reducing the area to be graded also produces substantial cost savings by reducing the amount of clearing and grubbing, alluvium and colluvium removals, canyon subdrains, embankment, surface drains and landscaping.

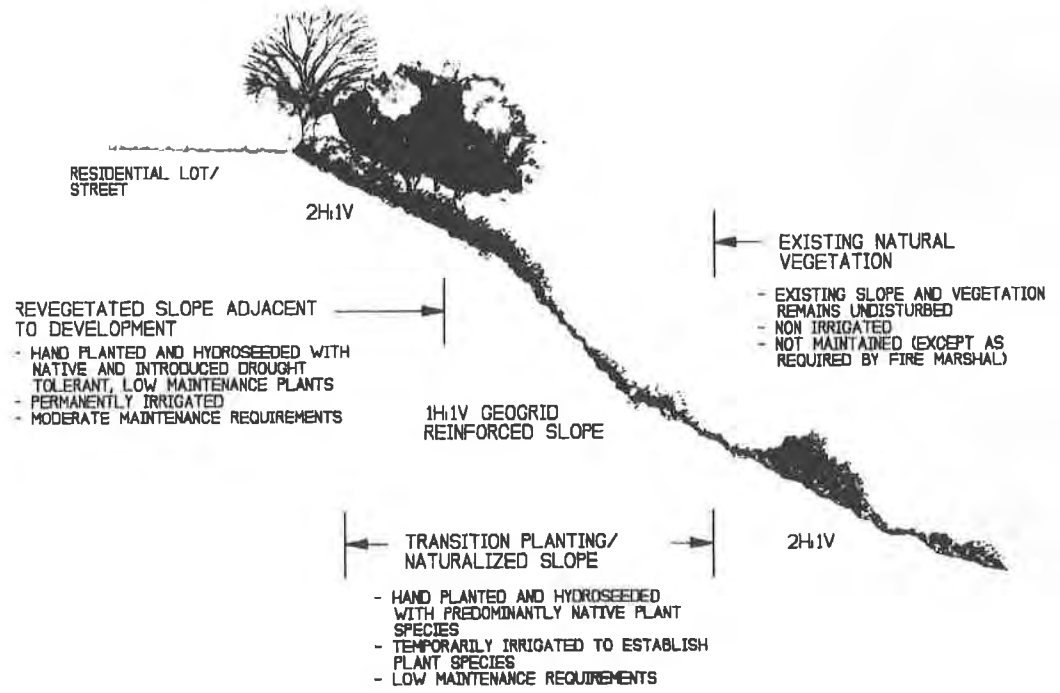

Figure 1. LANDFORM CONTOUR GRADING, SHOWING REINFORCED SLOPE SECTION AND REVEGETATION AT THE EDGE OF A DEVELOPMENT

Figure 2. REVEGETATED 21 METER HIGH LANDFORM CONTOUR GRADED SLOPE HAVING A 1H:1V REINFORCED SECTION IN THE UPPER 9 METERS.

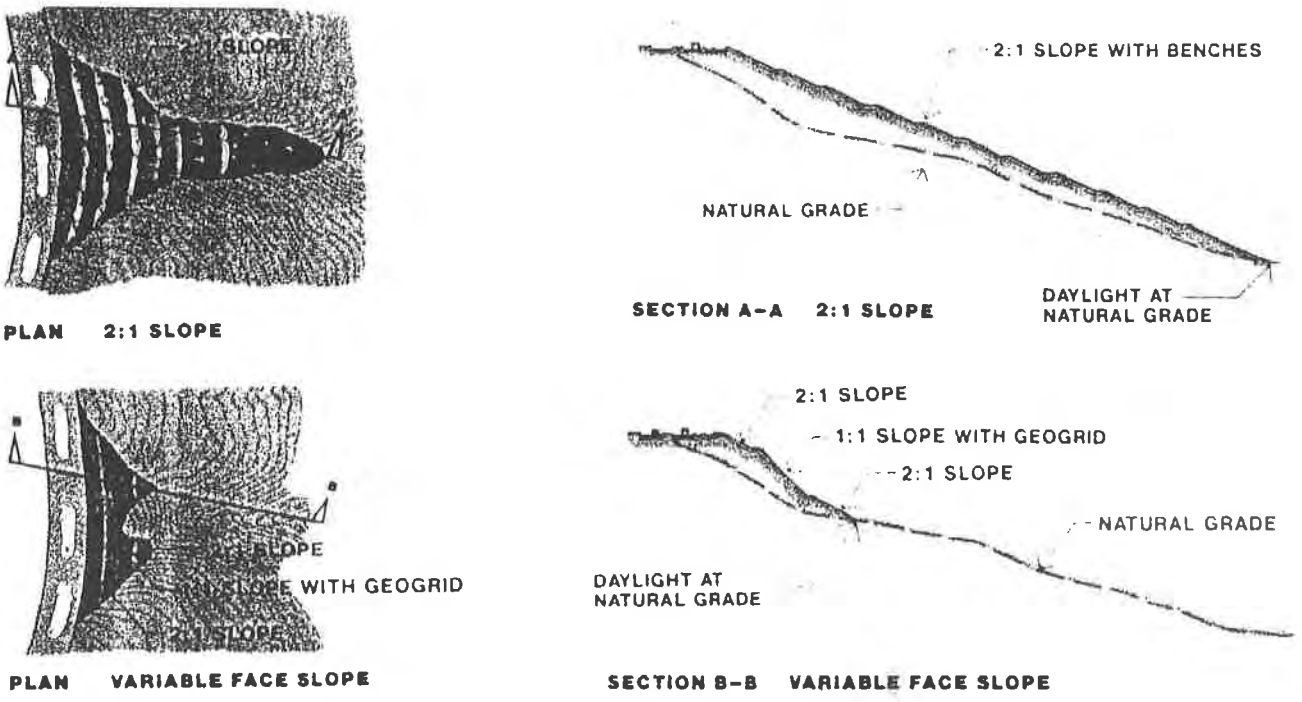

Figure 3. LANDFORM GRADING USED TO REDUCE THE SIZE OF A CANYON FILL

The cost of purchasing and installing the geogrid reinforcement materials is usually minor when compared to the direct, measurable construction cost savings. Indirect benefits can also result from Landform Contour Grading such as the production of more useable land. The natural appearance of Landform Contour Grading also tends to increase both the land values and marketability of a development. Another important indirect benefit of Landform Contour Grading is that more reliable slope performance is possible. Properly selected geogrids provide long-term durability of slopes even if the slopes are neglected and abused. For example, high density polyethylene (HDPE) geogrids are relatively immune to chemical and biological degradation and are indigestible to burrowing rodents. Geogrid reinforced slopes can be designed to resist erosion even if they are saturated from overwatering, as frequently happens.

DESIGN OF LANDFORM CONTOUR GRADED SLOPES

The design process for landform contour graded slopes has only a few differences from that used for conventional fill slopes. The primary difference is the treatment of the geogrid reinforced section. The overall process begins with a geotechnical investigation which identifies maximum safe angles and heights for unreinforced fill slopes. In addition, preliminary reinforcement layouts are identified for steeper slopes (typically up to 1H:1V). Based on the results of the geotechnical investigation, the land planner and civil engineer incorporate multiple slope gradients and slope contouring into the master plan for the development. The reinforced and compound slope sections are analyzed for specific geogrid requirements. The slope reinforcement layout, details and specifications become part of the construction documents.

In areas requiring reinforcement, the goal of a comprehensive design is to determine the type, length, and spacing of geogrids to achieve a safe slope. A safe slope is quantified by the factor of safety against sliding along some critical slip surface. Depending on the final slope conditions, slopes may require only surficial reinforcement or both surficial and global reinforcement.

A significant amount of information has been published which describes the analysis of slopes reinforced with geogrids, the mechanisms of geogrid reinforcement, and the field and laboratory base used to develop design methods (Christopher et al. 1990 and Mitchell and Villet, 1987). Consequently, the following discussion is an overview of the design process.

The required design parameters for reinforced slope sections are: 1) the slope geometry, 2) the soil strength properties of the fill and in-place soils, 3) the tensile and soil interaction properties of the geogrid, and 4) the performance criteria of the slope. The performance criteria are usually defined by acceptable safety factors and long-term durability of the geogrids. Current state-of-the-practice designs utilize soil properties and reinforcement properties developed by extensive laboratory testing. A discussion of important properties for geogrids is presented in the Case Study section.

Analyses of safety factors (slope stability) are generally accomplished by computer. Sound geotechnical engineering practice is utilized to select the type of analyses required for each application. Failures of slopes can occur by several mechanisms: 1) rotational slides generally modelled as cylindrical surfaces and analyzed by a "Simplified Bishop" type equation, 2) wedge failures and general failure surfaces modelled by one or more linear surfaces and analyzed by a "Janbu" type method, and 3) long translational slides modelled as infinite slopes. These analyses generally result in a computed factor of safety, which is the ratio of the forces (or moments) resisting failure and those forces (or moments) tending to cause shear failure along the assumed slip surface.

Many slope stability computer programs have incorporated geogrid reinforcement. The geogrid reinforcement is considered to be an additional resisting force where it crosses the slip surface. The design tensile capacity is the lesser of the allowable tensile strength of the geogrid and pullout resistance of the geogrid where it is embedded behind the failure surface.

Slope sections requiring reinforcement should be analyzed for both surficial and global stability. Surficial stability is usually modelled as a long, downslope translational slip plane of some finite depth, usually less than 1.3 meters. The soil above the slip surface is assumed to be saturated, and an adequate spacing and length of surficial or secondary geogrids is specified to resist failure. A method of analyzing surficial stability of reinforced slopes in presented by Thielen and Collin (1993).

In addition to stability issues, surface erosion should be considered. Surface erosion is the degradation of the slope face by external forces such as flowing water, blowing winds, and trafficking or boring by animals. These conditions can be exacerbated by seasonal wetting and drying cycles that may loosen the outer several centimeters of surface soils. Current practice for reinforced slopes is the same as for unreinforced; that is, to vegetate the slope with indigenous plant species that will resist erosion and maintain consistent soil moisture.

Although internal stability and erosion should be treated separately during design, they can affect one another. Slope face erosion can accelerate surface water intrusion, resulting in a saturated condition. A saturated condition at the slope face results in reduced surficial stability. Conversely, geogrids placed in the outer several meters of the slope for surficial stability can enhance erosion control by preventing the formation of surface rills.

Surficial reinforcement of the slope face of otherwise stable fills is finding increased acceptance on large hillside grading projects. Surficial reinforcement of fill slopes with geogrids is being used by some prudent Southern California hillside land developers to reduce their exposure to the long-term liabilities associated with slope failures. Some geotechnical consultants and engineering contractors, as part of their risk management program, are encouraging their clients to surficially reinforce all of their fill slopes.

CASE STUDY - SPANISH HILLS GOLF AND COUNTRY CLUB

The Spanish Hills Golf and Country Club project is located in the City of Camarillo, County of Ventura, California. It is situated on 1,546,000 m^2 of hillside terrain and includes an 18 hole championship golf course, a 3,534 m^2 club house, 151 estate lots and 2 condominium sites. The grading improvements were started in November of 1990 and were completed in November of 1992.

The project presented a tremendous grading challenge due to an 80 meters high hillside dissected by 11 steep canyons. Adding to that challenge were fault zones and associated tectonic features that traversed the site as well as a bedrock structure that contained out-of slope bedding planes with weak seams. The original grading plan for this project utilized very high conventional 2H:1V perimeter slopes with horizontal terrace drains every 9 meters vertically. In addition, most of the perimeter slopes would have required large shear keys of up to 25 meters deep and over 65 meters wide. Crib-type retaining walls were proposed at numerous locations within these slopes in order to yield enough useable land for an economically viable project.

This original plan was rejected because of political, economic, aesthetic and geotechnical considerations. The City and adjacent land owners would have objected to the unnatural appearance of high, conventional slopes and walls. Furthermore, the regimented appearance of these slopes would have created a marketing and public relations problem for the project. Lastly, the geotechnical consultant discovered that the slopes with the crib walls did not produce acceptable factors of safety.

Conventional engineering solutions to these problems such as flatter slopes, larger walls, and soil-cement or lime-treated buttresses were not feasible. Flatter slopes would have eliminated 32 estate lots or required the purchase of a tremendous amount of off-site acreage. Larger walls would have been unsightly and uneconomical. Soil-cement or lime-treatment was not only uneconomical but would have made it difficult to landscape the slopes.

Landform Contour Grading proved to be the only viable solution. A total of 29 reinforced slopes were contoured both horizontally and vertically. A maximum slope gradient of 1H:1V was used. The highest compound slope, having variable gradients of between 5H:1V and 1H:1V was 41 meters high. The highest 1H:1V slope section was 20 meters high and 550 meters in length. All slope sections steeper than 2H:1V utilized primary reinforcement layers of HDPE geogrids. Intermediate reinforcement consisted of layers of polypropylene geogrids. All of the walls were eliminated by the reinforced slopes.

Landform Contour Grading dramatically reduced the environmental and visual impacts of the perimeter slopes. Also, many of the project's interior slopes, including those surrounding the golf course, utilized steep reinforced slope sections to produce aesthetically pleasing final grades.

The ability to produce steep slopes also provided an economic solution to the adverse bedding plane problems. By placing the 1H:1V sections near the toes of the fills that buttressed against the bedding planes, the sizes of the shear keys were reduced dramatically. This is due to the higher shear resistance in the shear keys that was obtained by increasing the height of the fills over the shear keys. The largest shear key on the project averaged 15 meters deep and 45 meters wide. It was estimated that Landform Contour Grading saved over 3,000,000 m^3 of shear key construction.

Design of the Reinforced Sections and Selection of Geogrids

A typical analysis cross section through a reinforced project slope is shown in Figure 4. The section shows the slope geometry, the geogrid elevations and lengths, the soil properties, and information about the design slip surface. Two types of analyses were conducted to determine the type, spacing, and length of geogrids required for the slopes: circular global stability analysis and surficial stability analysis. These analyses were conducted following the guidelines discussed in the previous section on design. In addition, finite element analyses were conducted to evaluate the deformation of the largest reinforced slope (Chandra and Lay, 1992 and Bray et.al., 1992).

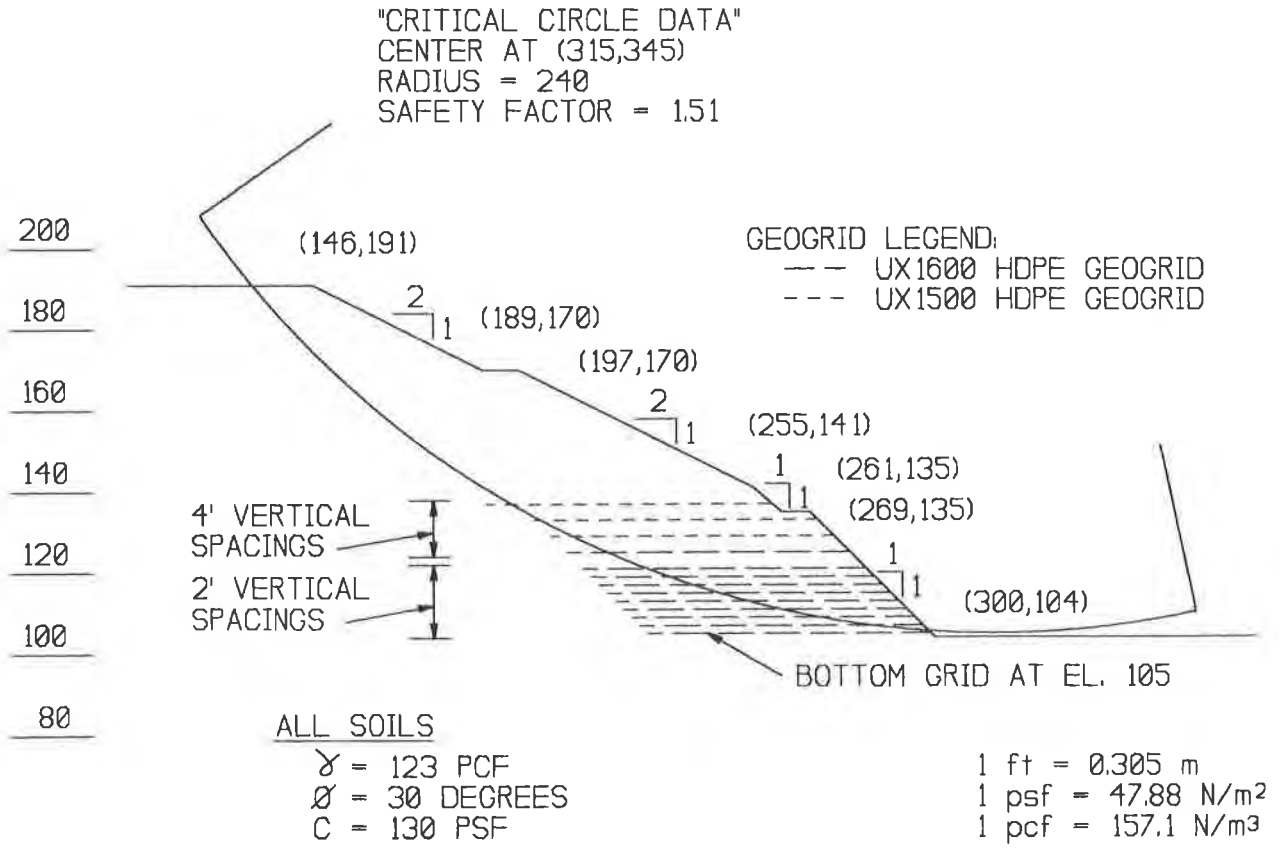

Figure 4. TYPICAL COMPUTER MODEL CROSS SECTION FOR A CONTOUR GRADED SLOPE AT SPANISH HILLS

Geogrids were required to meet the following selection criteria: 1) they had to be capable of developing the required long-term allowable design tensile strength, 2) they had to have high soil interaction to develop pullout resistance over a reasonable length, 3) they had to have long-term durability in order to meet the design assumptions over the life of the slopes, 4) they had to resist construction induced damage, and 5) they had to be suitable for the large scale, high production earthwork operations that were employed on this project.

The specifications for the geogrids were based on testing standards established by both ASTM and the Geosynthetic Research Institute (Koerner and Wilson-Fahmy, 1991). These standards included evaluation of tensile strength, long-term creep, soil interaction, chemical and biological degradation, construction induced damage, and susceptibility to ultraviolet light.

The requirement that the geogrids be suitable for large-scale earthwork projects was very important. The geogrids had to be capable of storage in staging areas for sustained periods of time without losing strength. Furthermore, the geogrids had to be capable of withstanding traffic by large rubber tired construction equipment operating directly on the geogrid. The geogrids had to be stiff enough to retain their shape when compacted in fills and not conform to local irregularities in the fill surface. Based on the selection criteria, HDPE primary geogrids and polypropylene secondary geogrids were used. A typical as-built section of a constructed slope is shown in Figure 5.

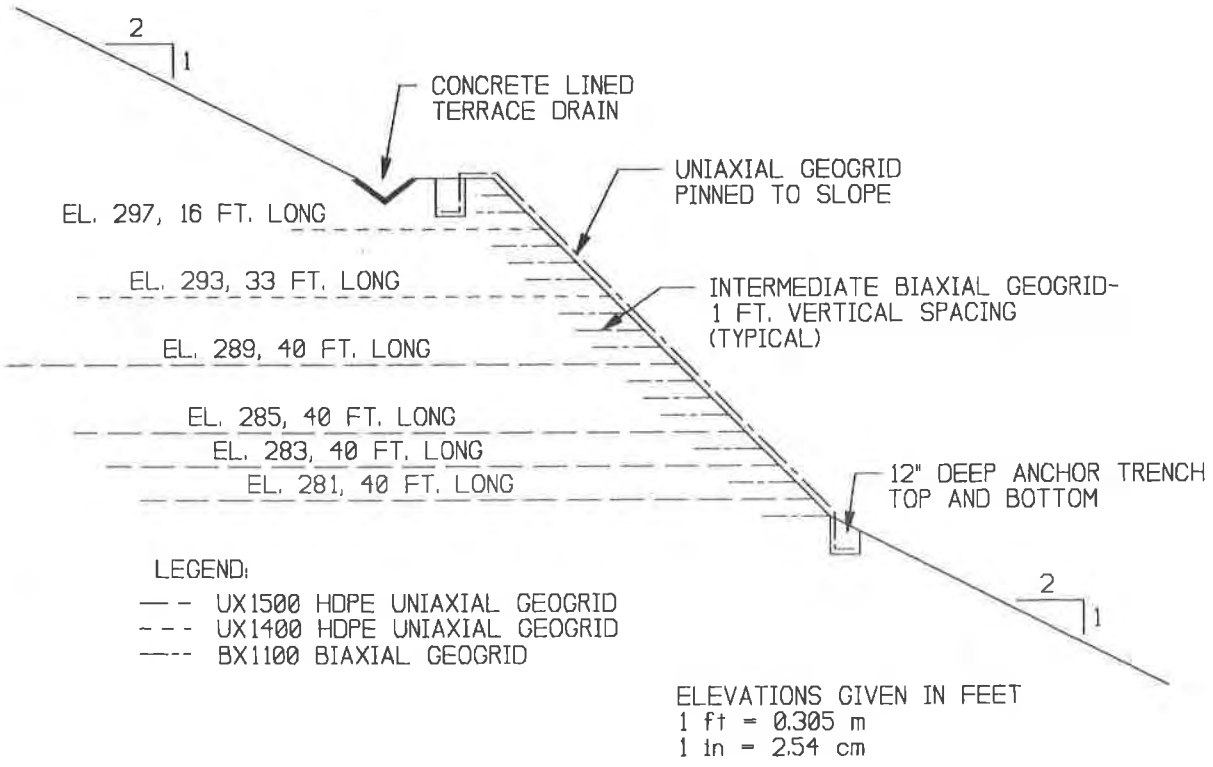

Figure 5. CONSTRUCTION DETAIL OF CONTOUR GRADED SLOPE FOR SPANISH HILLS

Construction of the Landform Contour Graded Slopes

The most complicated and critical component of constructing the landform contour graded slopes and shear keys on this project was not the handling or placement of the geogrid materials, it was the earthwork logistics planning and design. To control potential catastrophic failures in the very high and steep temporary construction slopes associated with corrective grading, the earthwork operations had to be carefully phased. To control earthwork construction costs and to maintain production when placing the geogrids, the construction equipment had to be temporarily assigned to other sectors of the job. If reinforced fill areas were not available, sections of the unreinforced fills were constructed adjacent to the reinforcement materials placement zone in order to keep the equipment working. In severely restricted areas, temporary waiting periods were sometimes unavoidable and had to be factored into the earthwork costs and logistics design.

The specific construction methods for using HDPE geogrids to construct landform contour graded slopes at the Spanish Hills project were as follows:

1) After the geogrids had been delivered to the job site storage area by the manufacturer, they were unrolled and pre-cut to specified lengths. The lengths and placement of a specific grade of geogrid was controlled by a geogrid schedule ("cut sheet") developed by the contractor from the approved reinforcement plans.

2) After the geogrids had been pre-cut, they were re-rolled, marked and stacked in order for delivery to the work area. Two laborers were required for pre-cutting.

3) The geogrids were delivered to the work area on a flat bed truck and rolled out in the predetermined order onto the prepared, tested and approved subgrade. This operation usually required 2 or 3 laborers.

4) Fill materials were dumped at the work area by 30 m^3 wheel tractor-scrapers (scrapers). The scrapers were not allowed to turn or exceed 16 kilometers per hour while traveling directly on the geogrids. This is illustrated in Figure 6. Whenever possible, the fill materials were pre-watered and mixed in the excavation area before delivery to the reinforcement work zone.

5) Each lift of fill was spread in 15 to 20 centimeter thick lifts, mixed and compacted by wheel tractors (rubber-tired dozers), motor graders, track-type tractors (dozers) and scrapers to a minimum of 90% of the maximum density as determined in accordance with ASTM D1557 (Modified Proctor). Compaction tests were required for every 382 m^3. Tracked-type equipment was not allowed to operate without a minimum of 0.3 meters of soil cover on the geogrids. Figure 7 shows geogrids in place and fill being spread over them.

Figure 6. SCRAPER DUMPING FILL SOIL ONTO GEOGRIDS

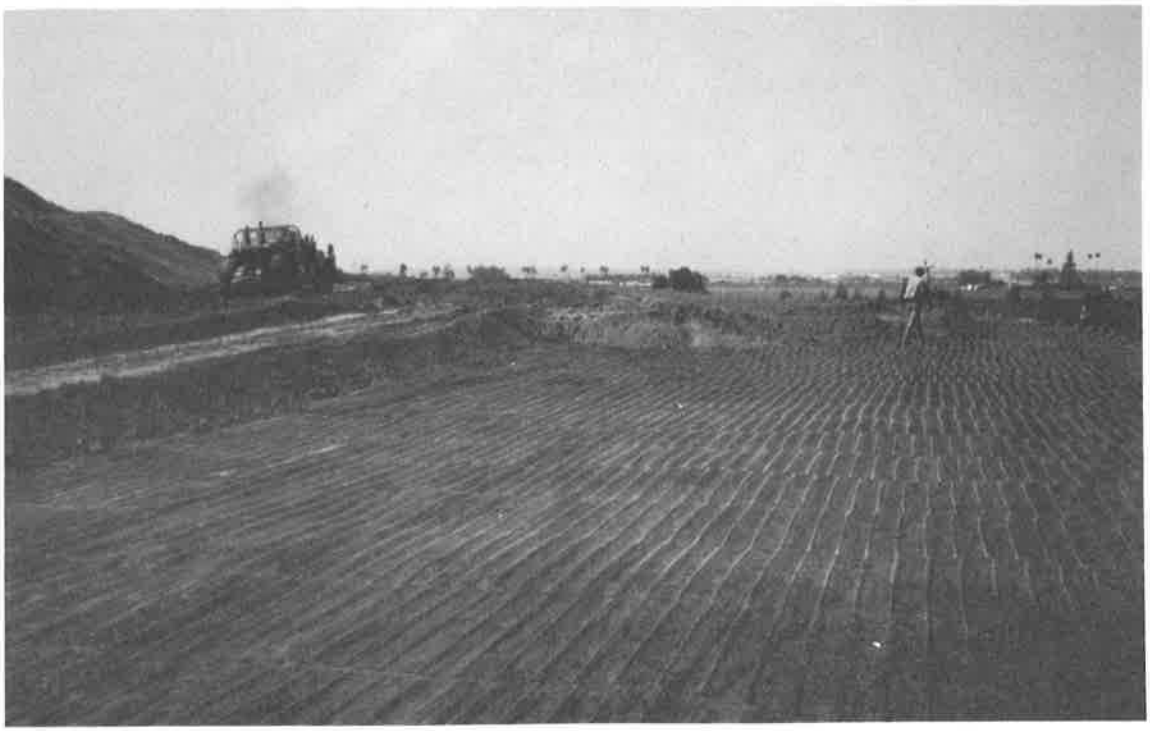

Figure 7. FILL SOIL SPREAD ONTO GEOGRIDS

6) Vertical elevations were checked every 0.6 meters in vertical height to insure that the geogrids were being placed in accordance with the plans and specifications. Also, frequent grade checking and staking were required to control the variable horizontal and vertical angles of the landform contour graded slopes.

7) At the request of the City, a lightweight geogrid was placed directly on the face of the reinforced slope sections. This geogrid was pinned to the slopes with landscape staples or attached to the reinforcement geogrids using hogrings.

Figure 8 shows a completed landform contour graded slope, just prior to revegetation.

Figure 8. COMPLETED LANDFORM GRADED SLOPE PRIOR TO REVEGETATION

The corrective grading quantities on the project totaled 7,952,000 m^3 including the removal and recompaction of 1,835,000 m^3 of alluvium, colluvium and other compressible materials, 1,147,000 m^3 of landslide removals, 1,912,000 m^3 of overexcavation to prevent differential settlement and 3,058,000 m^3 of shear key and buttress fill construction. The general excavation quantity was 5,200,000 m^3. The combined grading quantities were 13,152,000 m^3. In addition, over 40,000 m^2 of nonwoven geotextiles were installed for subdrains in the canyon fills, shear keys and buttress fills. In excess of 314,000 m^2 of primary HDPE uniaxial geogrids and over 117,000 m^2 of secondary polypropylene biaxial geogrids were used in the reinforcement of shear keys, buttress fills and the steep portions of the landform contour graded slopes.

Sukut Construction, Inc. was the earthwork design consultant, grading contractor and general engineering construction manager. Midstate Engineering was the project Civil Engineer. The project geotechnical consultant was Leighton and Associates, Inc. Design of the reinforced slope sections was by Tensar Earth Technologies, Inc. and David Evans & Associates.

CONCLUSIONS

1. Landform Contour Grading that incorporates geogrid reinforcement to produce a variety of surface gradients can be utilized to construct natural-looking slopes. The variation of vertical as well as horizontal grades in a development can produce an attractive alternative to the traditional uniform slope and terrace construction.

2. Landform Contour Grading, incorporating steep slopes can mitigate the environmental and visual impacts of hillside developments. This is most easily illustrated by a traditional canyon fill that can be steepened to significantly reduce the amount of natural canyon that is impacted by the fill.

3. Landform Contour Grading that utilizes steep slopes can result in the benefit of more useable land. The additional land can be used for development or open space.

4. Landform contour graded slopes reinforced with geogrids can be a practical and cost effective solution to engineering and geotechnical problems on hillside land development projects. Geogrids are being used to replace soil-cement and lime reinforcement materials for shear keys, buttress fills and steep slopes. These geogrid reinforced slopes can be revegetated. Steep reinforced slopes can be utilized to provide additional weight over slope shear keys.

5. Landform Contour Grading projects that incorporate geogrid reinforcement can be constructed with conventional equipment and easily modified construction methods.

ACKNOWLEDGEMENTS

The authors gratefully acknowledge the cooperation of Spanish Hills Development Company and the editorial assistance of Linda Adams, Mike Crawford, Margaret Herley, Jerry Pabbruwee, Mary Ann Schulte, Myron Sukut, and Steve Sukut, all with Sukut Construction, Inc.

REFERENCES

1. Christopher, B.R., Gill, S.A., Giroud, J.P., Juran, I., Mitchell, J.K., Schlosser, F. and Dunnicliff, J., "Design and Construction Guidelines for Reinforced Soil Structures - Volume I," and Summary of Research - Volume II," Report No. FHWA-RD-89-043, Federal Highway Administration, U.S. Department of Transportation, 1990.

2. Mitchell, J.K. and Villet, W.C.B., "Reinforcement of Earth Slopes and Embankments", National Cooperative Highway Research Program Report No. 290, Transportation Research Board, Washington, DC, 1987.

3. Chu, D. and Poormand, I., "Reinforcement of an Earthen Buttress with a Polymer Geogrid", Proceedings of Geosynthetics '89 Conference, San Diego, Vol. 1, February 1989, p.p. 243-254.

4. Thielen, D.L. and Collin, J.G., "Geogrid Reinforcement for Surficial Stability of Slopes", Geosynthetics '93 Conference, Vancouver, British Columbia, March 1993.

5. Bray, J.D., Boulanger, R.W., Chew, S.H., and Seed, R.B.,"Finite Element Analysis in Geotechnical Engineering", Proceedings of the Eigth National Conference on Computing in Civil Engineering, ASCE, Dallas, Texas, February 1992.

6. Chandra, D., and Lay, G., "Performance of a Geogrid Reinforced Slope on Compressible Foundation", Proceedings of the 28th Symposium on Engineering Geology and Geotechnical Engineering, Boise, Idaho, April, 1992.

7. Koerner, R.M. and Wilson-Fahmy, R.F., "Application of Geogrids - Volume 1", Report No. FHWA-PA-91-003+90-17, Federal Highway Administration, U.S. Department of Transportation, Pennsylvania Department of Transportation, 1991.

New Construction Techniques Utilized for the Facing of Very Steep Geogrid Reinforced Soil Slopes

C.W. Thompson IV
Contech Construction Products Inc., USA

J.S. Bailey II
Tensar Earth Technologies Inc., USA

ABSTRACT

Construction of geosynthetic reinforced slopes steeper than 1.0 horizontal to 1.0 vertical (1H:1V) has previously been a difficult task as most soil cannot be compacted to hold an angle steeper than 45 degrees. By using a geotextile wrapped face and wooden form work a very steep slope can be built. This method is tedious and the resulting slope face has an unnatural stepped appearance sometimes not aesthetically compatible with natural looking landscaping.

An economical and aesthetically pleasing alternative to a stepped geotextile wrapped slope facing is a slope face built using prefabricated welded steel wire fabric forms and polymer geogrid to retain a natural rock or vegetated face.

This paper will discuss the design and construction of the facing of two 0.5H:1V geosynthetic reinforced slopes built in 1991. W4.0 gage black steel welded wire fabric was formed into light-weight two sided forms used to compact against in the same way wood forms are used in traditional geosynthetic wrapped walls. Wire struts placed on 30 to 60 centimeter (1.0 to 2.0 foot) centers were used to hold the forms to the specific slope angle required for these two projects. Geogrids stabilized against ultra-violet light degradation were wrapped inside of the forms to retain a stone facing in one project. In the other project a lightweight geotextile was wrapped inside of the geogrid to temporarily retain the soil at the slope face until grass vegetation was established.

INTRODUCTION

Conventional grade separation structures have typically been poured concrete cantilever retaining walls with stable unreinforced soil slopes above the walls. Many of these structures could be economically replaced with steep geosynthetic reinforced soil slopes. Constructing permanent facing systems for steep geosynthetic reinforced slopes can be difficult. Synthetic erosion mats or blankets have been used successfully to stabilize reinforced steep slope faces with angles of repose up to 1H:1V (45 degrees from horizontal). For slopes steeper than 1H:1V special considerations usually need to be made in order to insure proper compaction and prevent sloughing or erosion at the slope face. This paper will discuss two projects where 0.5H:1.0V slopes (63.4 degrees from horizontal) were

successfully constructed using a geogrid wrapped face with pre-fabricated welded wire forms to aid in maintaining proper alignment during compaction.

PITTSBURGH, PENNSYLVANIA LANDSLIDE REPAIR - VEGETATED FACING

Project Scope. In 1988 the top half of an existing 1.25H:1.0V slope approximately 9.1 m (30 ft.) high and 46 m (150 ft.) long failed leaving a homeowner with virtually no usable back yard (Figure 1). After consideration of repair options ranging from constructing a poured-in-place concrete retaining wall to "do nothing", a two tier geogrid reinforced 0.5H:1V vegetated slope was chosen by the owner and engineer because of aesthetics and cost. The two tier profile (Figure 2) would allow for the creation of an intermediate plateau while avoiding disturbing an existing sewer line. The project was designed by GeoMechanics, Inc. of Elizabeth, Pennsylvania.

Project Design. The project was designed using Bishop's method of slope stability analysis modified to incorporate reinforcement within the soil structure. The design factor of safety for global stability achieved in this analysis was 1.5. The designer specified 15 layers of HDPE structural geogrids placed every 62 cm (2 ft.) vertically as the slope was constructed in compacted soil lifts. The structural geogrids specified had a creep limited strength of 30 kN/m (2000 lb/ft). The maximum geogrid embedment length into the soil slope was 6.2 m (20.5 ft.).

The facing detail used in this design called for the HDPE geogrids to be wrapped around the face of the slope fill to prevent soil sloughing and erosion. The HDPE geogrid was specified for the structural face wrap due to its excellent chemical durability and weathering resistance. The HDPE geogrid contained approximately 2.5% carbon black to aid in resistance to ultra-violet light degradation until vegetation could be established to shade the geogrid. A light weight non-woven geotextile was placed immediately behind the geogrid wrap to temporarily retain soil fines until vegetation (placed by hydro-seeding) took hold.

Slope Facing Construction Sequence. Construction of the geogrid wrapped slope face was aided by the use of welded wire forms as shown in Figure 3. Unlike the welded wire fabric used in the Hilfiker and other systems as permanent facing and reinforcement, the welded wire forms were used here only as a construction tool and have no long-term structural value. The forms were prefabricated at a 0.5H:1V slope angle.

The slope face was constructed in the following sequence:

1. Reinforcing geogrid is extended out approximately 1.5 m (5 ft.) from slope face. This geogrid "flap" will later be wrapped around a form to confine soil fill (Figure 4).
2. A welded wire form is placed on top of reinforcing geogrid at the slope face.
3. Needle punched non-woven geotextile wrap is placed inside of the welded wire form.
4. Support strut clips are punctured through the geotextile on 30 to 60 cm (1.0 to 2.0 ft) centers and attached to welded wire form to hold slope angle during construction.
5. Soil is compacted in specified 20 cm (8 in.) lifts to top of baskets. Hand operated compaction equipment is to be used within 1m (3 ft.) of slope face.
6. Geogrid "flap" from geogrid mentioned in step 1 is wrapped around wire form.
7. Repeat with next layer of grid at step 1.

Figure 1. Pittsburgh Slope Failure Prior to Repair

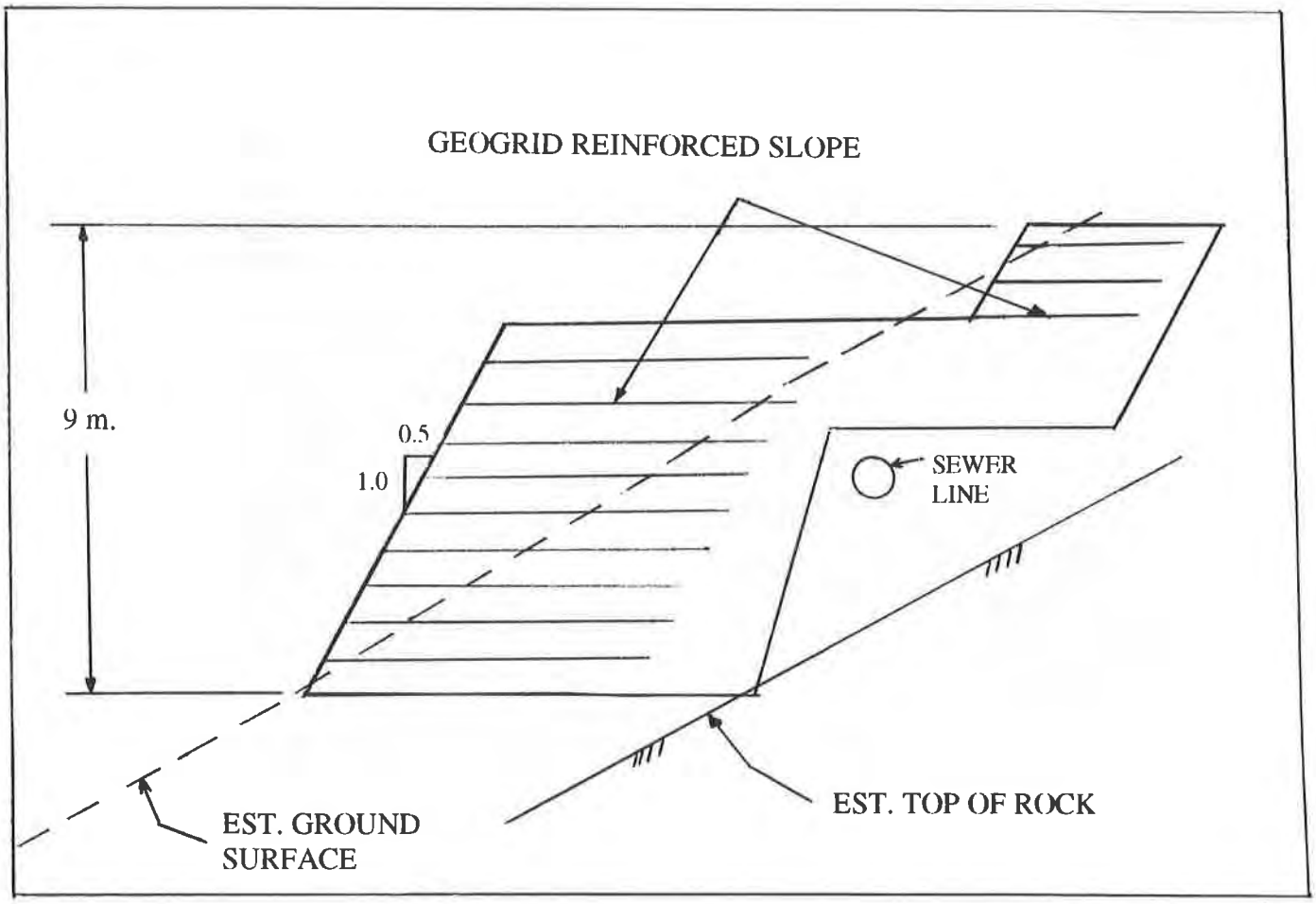

Figure 2. Geogrid Reinforced Slope Cross Section

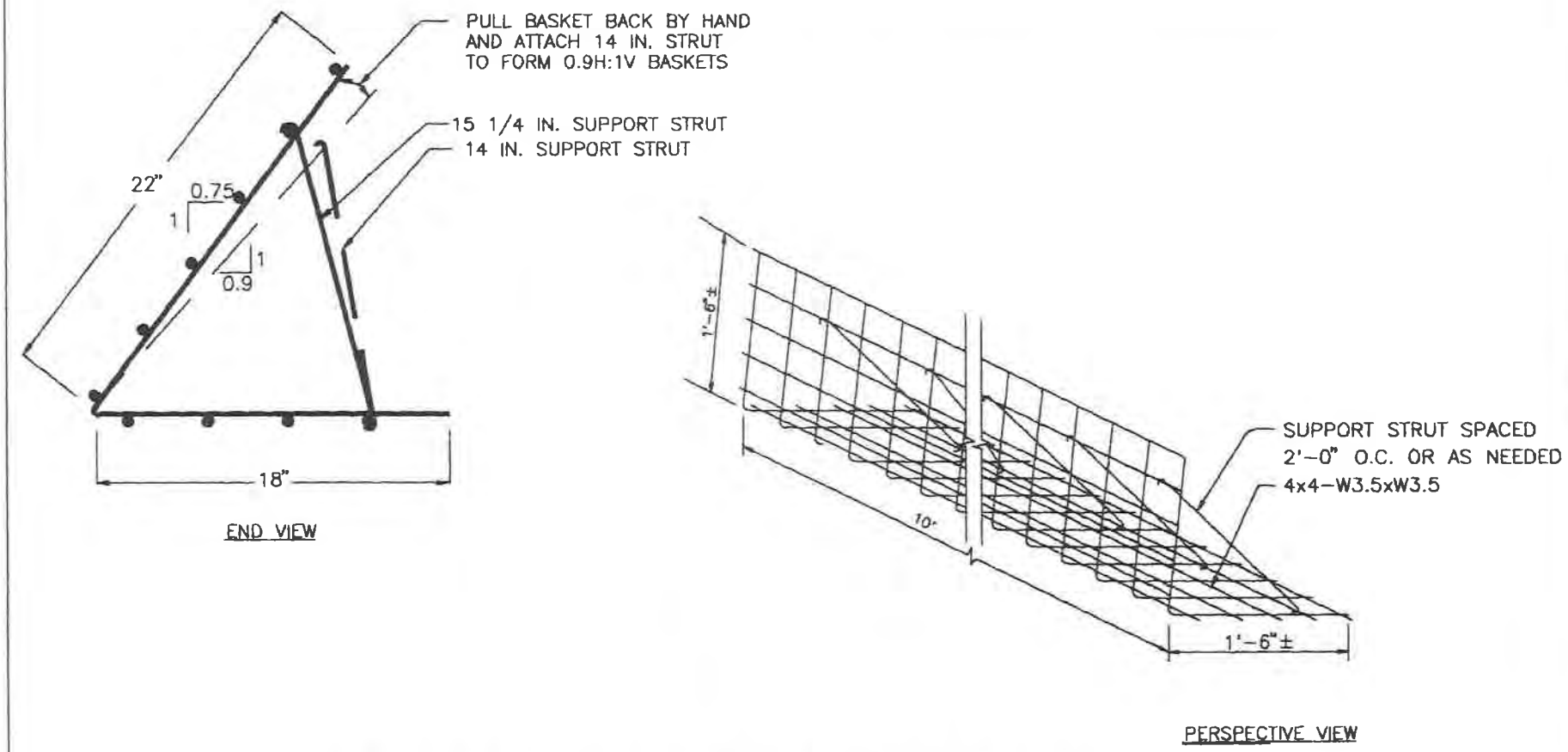

FIGURE 3. WELDED WIRE FORM DETAIL

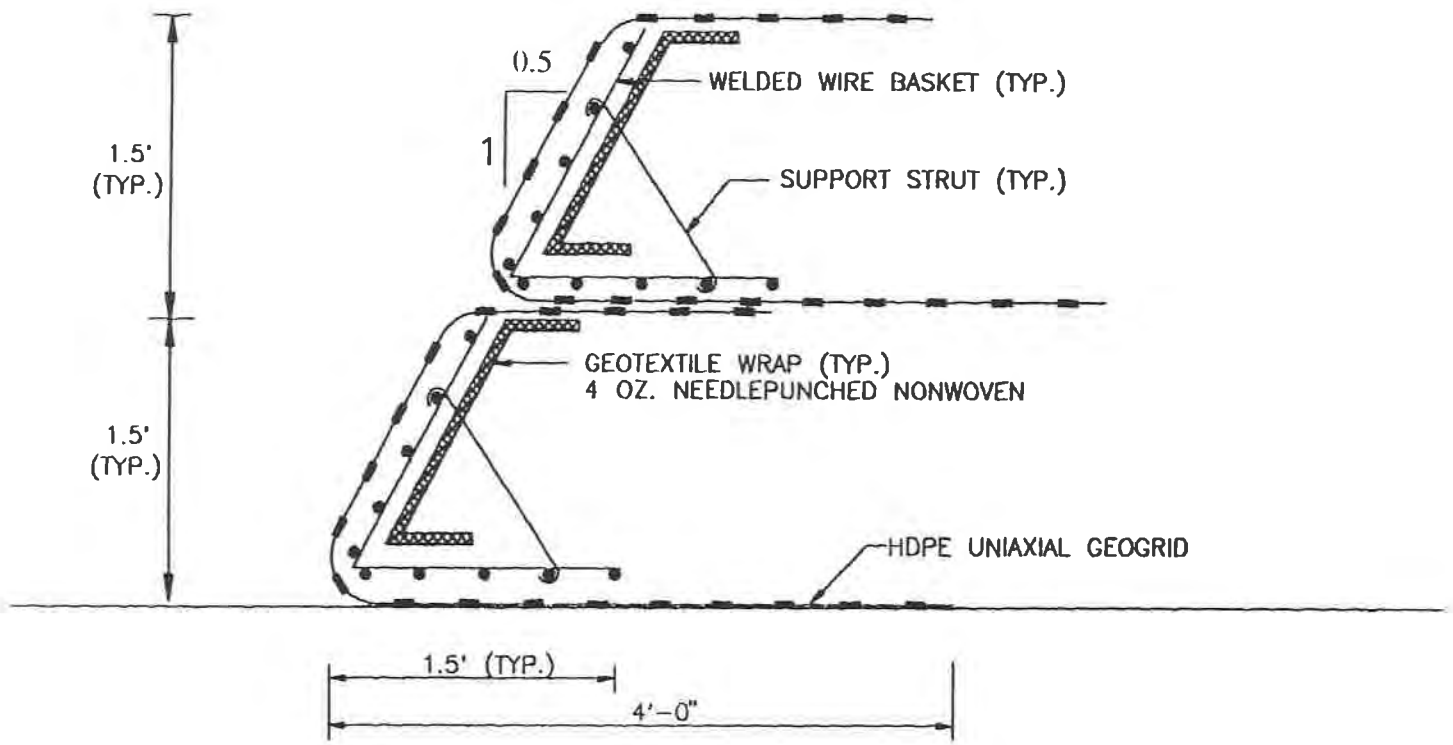

FIGURE 4. VEGETATED 0.5H:1.0V STEEP SLOPE DETAIL

Conclusion. The final constructed slope (Figures 5,6,7) allowed for an estimated 50% savings versus a poured-in-place concrete wall. Vegetation was established within one year of construction (Figures 8,9,10).

MIDDLETOWN, NEW YORK FILL SLOPE - STONE FACE

Project Scope. Site plans for this project were developed by Wehren Associates and called for several retaining walls and reinforced fill slopes to be constructed to allow for parking areas for a large shopping mall. The project was bid with reinforcement design for walls and slopes to be provided by the contractor. Contech Construction Products supplied the geogrid reinforcement and design by Tensar Earth Technologies, Inc. The project involved geogrid reinforced vertical walls and geogrid reinforced steep slopes. A portion of the reinforced slopes required a very steep 0.5H:1V slope angle and abutted New York State Route 84. This slope was to be approximately 6 m (20 ft.) high and 61 m (200 ft.) long.

Project Design. The owner desired a natural looking rock face for the 0.5H:1V slope. The factor of safety for global stability required on this project was 1.3. A modified Bishop's slope stability analysis yielded a requirement of 14 HDPE geogrids approximately 4.5 m (15 ft.) to reinforce the soil fill slope. The HDPE geogrids specified had a creep limited strength of 21 kN/m (1400 lb/ft). These primary reinforcement geogrids were placed at vertical intervals corresponding to one half the height of a welded wire form (22.5 cm or 9 in). Polypropelene (PP) geogrids with apertures measuring 2.5 cm (1 in) x 3.3 cm (1.3in) were used to confine and wrap the rock face. The PP geogrids were manufactured with 2% carbon black to stabilize the polymer against ultra-violet light degradation. This PP geogrid was selected for the wrap of the rock face due to low cost, small aperture size, and the fact that this material is manufactured in large rolls which could be more efficiently installed than smaller primary HDPE reinforcing geogrids. A non-woven geotextile was used as a filter between the backfill soil and the veneer of rock at the slope face (Figure 11).

Slope Facing Construction Sequence. Construction of the geogrid wrapped slope face was aided by the use of welded wire forms as shown in Figure 11.

The slope was constructed in the following sequence:

1. Place first lift of welded wire forms on prepared foundation.
2. Place PP geogrid inside of wire form leaving a 1.32m (4.05ft.) flap over face temporarily. Roll out geogrid parallel to wall face.
3. Place primary HDPE geogrid rolled out perpendicular to wall face at lifts shown on drawings.
4. Attache support strut clips to welded wire form to hold slope angle during construction.
5. Place 4 cm (1.5 in.) + stone into forms a minimum of 30 cm (1 ft.) behind slope face.
6. Place nonwoven geotextile behind stone.
7. Place backfill adjacent to stone and compact. Use light weight hand operated equipment within 1 m (3 ft.) of wall face.
8. Wrap geotextile and geogrid around compacted lift and place next layer of welded wire forms.
9. return to Step 2.

Figure 5. Completed Geogrid Wrapped Slope Prior to Vegetation

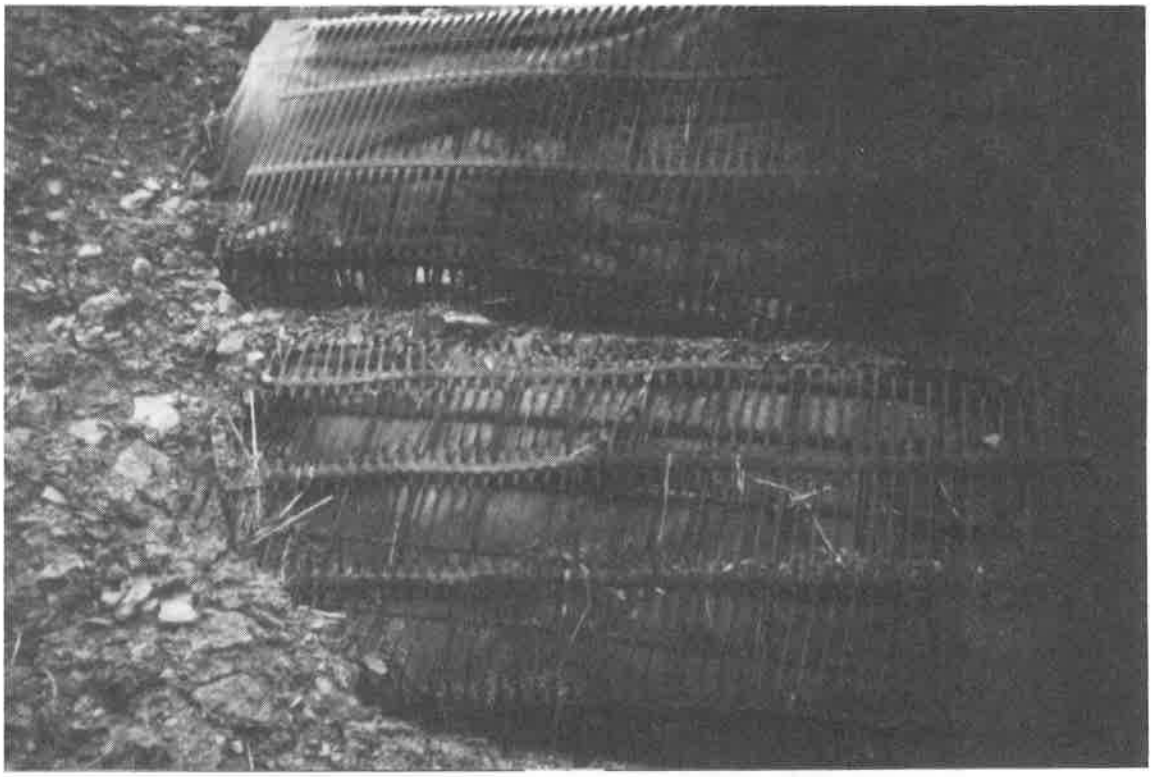

Figure 6. Geogrid Wrapped Slope Face Close Up

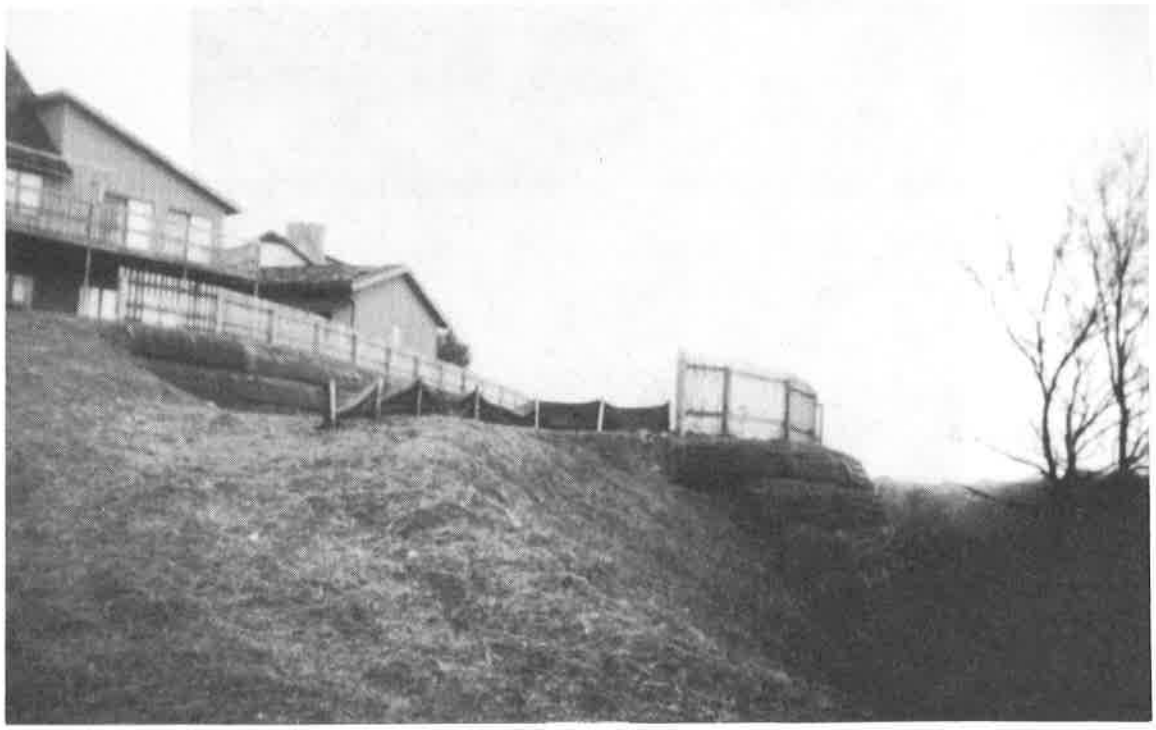

Figure 7. Geogrid Wrapped Slope Prior to Vegetation

Figure 8. Vegetated Slope Face

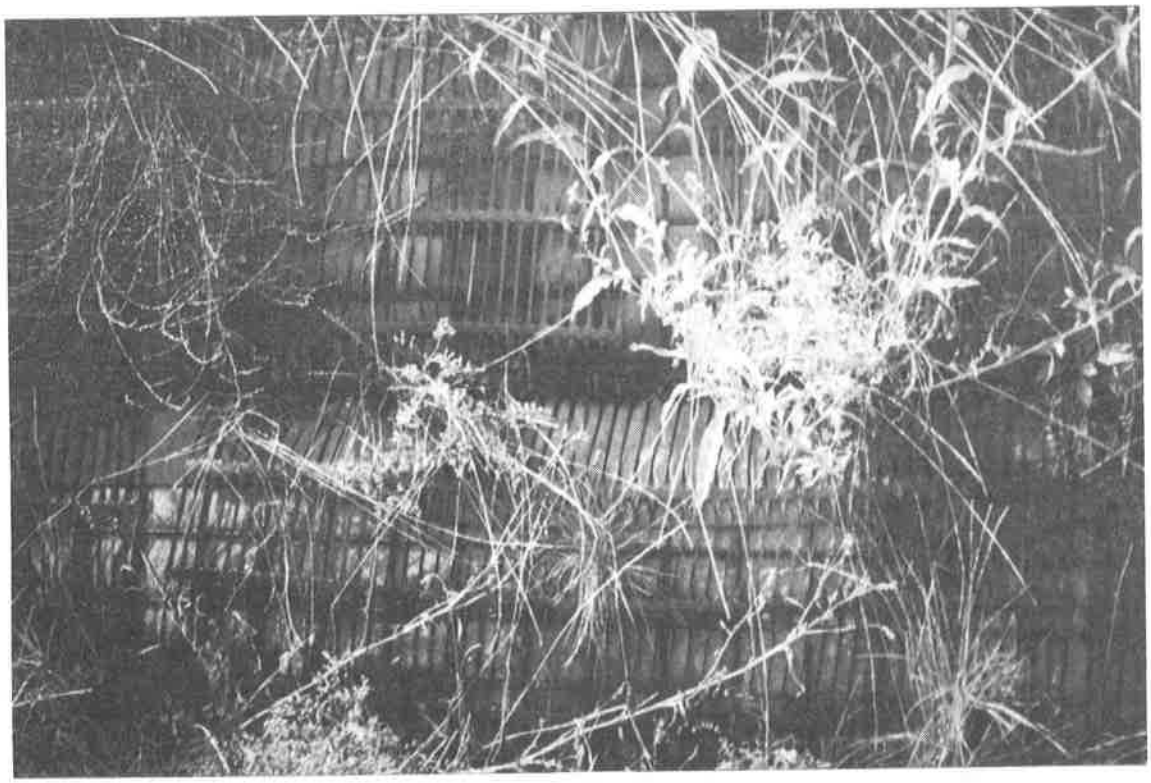

Figure 9. Initial Vegetation of Slope Face

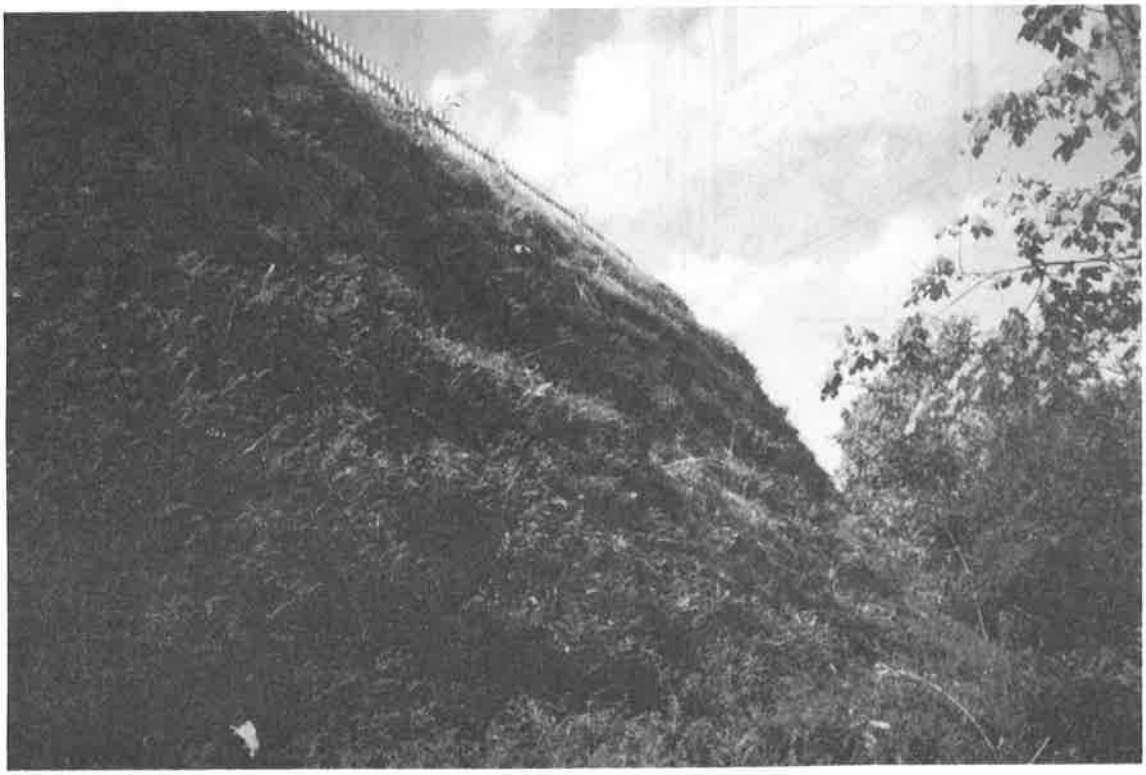

Figure 10. Vegetated Slope Face Eight Months After Construction

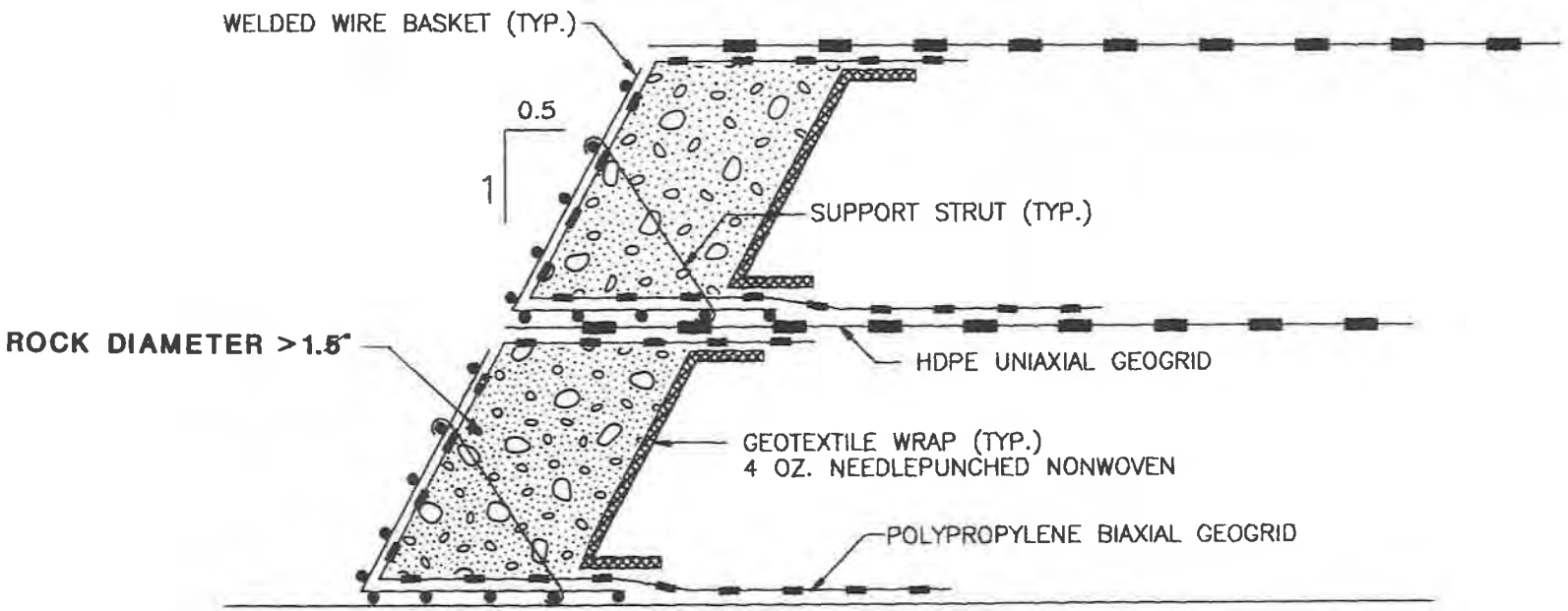

FIGURE 11. ROCK FACE 0.5H:1.0V STEEP SLOPE DETAIL

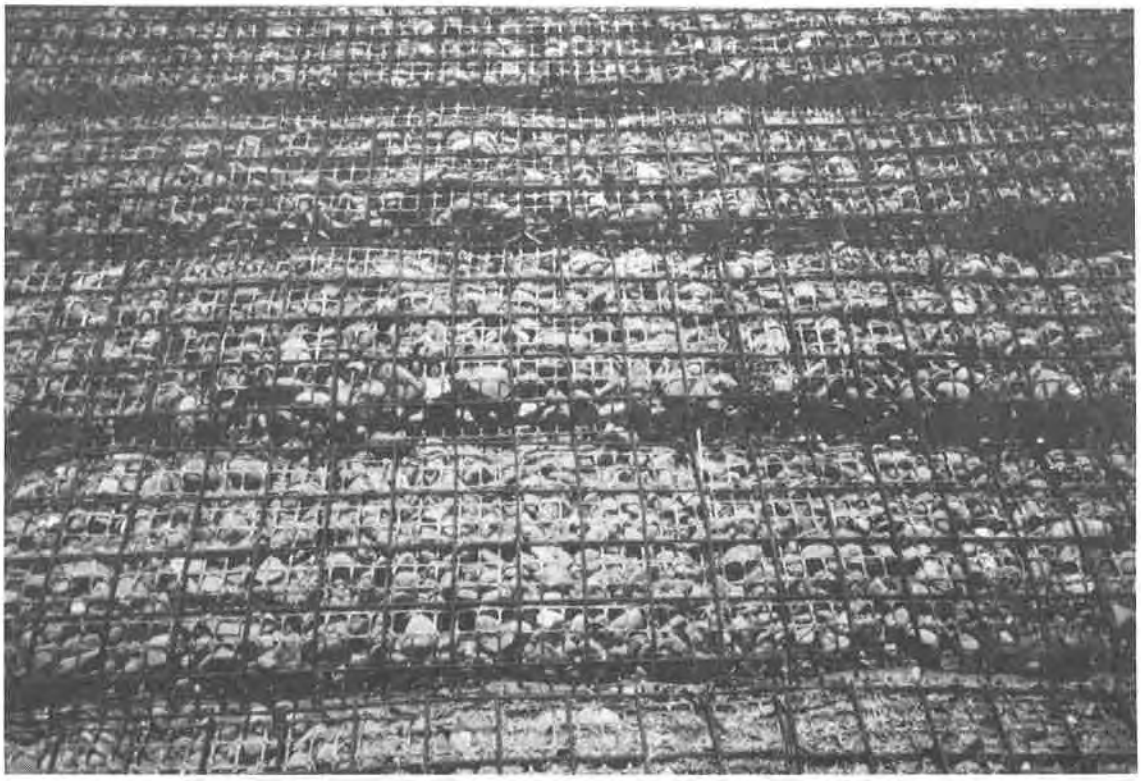

Figure 12. Geogrid Wrapped Rock Slope Face Close Up

Figure 13. Completed Geogrid Wrapped Rock Faced Slope

Figure 14. O.5H:1.0V Rock Face Slope Wrapped With Biaxial Geogrid

Conclusion. The final constructed slope has an attractive appearance similar to gabions and is an economical option to conventional grade separation structures (Figures 12,13,14). The PP geogrid face wrap proved to be more workable for constructing a face wrap then did the HDPE geogrid used in the Pittsburgh project described above.

CONCLUSION

Both vegetated face and stone faced geogrid slope wrapping techniques are economical and constructible steep slope facing methods. The utilization of pre-fabricated welded wire forms greatly aids in efficiently constructing a very steep slope by easing compaction efforts and holding the required slope angle. Both projects were designed for 100+ year design lives. Only time can determine the long-term durability of each facing system in the two projects described.

ACKNOWLEDGEMENTS

The authors wish to thank Randy Frilloux, of Contech Construction Products, Inc and Ronald Johnson of Tensar Earth Technologies for their assistance in construction sequencing determination for geogrid wrapped facing of reinforced soil structures. The authors also wish to thank Ron Sistrunk and Jeff Rodencal of Tensar and Bill Luther and Patrick O'Rourke of Contech for their assistance in providing photographs and details.

Hubrey Road: A Geosynthetic Reinforced Embankment Constructed on a Soft Organic Deposit

B.L.J. Mylleville
Golder Associates Ltd., Canada

R.K. Rowe
University of Western Ontario, Canada

ABSTRACT

A section of a full-scale reinforced embankment constructed on a soft compressible organic deposit was instrumented. Using information obtained from a program of field monitoring together with engineering properties of the soils obtained from laboratory tests, stage I construction was back-analyzed using the finite element method. The results of the analyses are shown to be in very good agreement with the observed performance of the instrumented section. In addition, comments are made regarding the performance of this instrumented section in relation to earlier published recommendations.

INTRODUCTION

This paper briefly summarizes a study which was undertaken to examine the behavior of a geogrid reinforced embankment constructed on a soft, compressible organic deposit. Factors discussed include the geotechnical investigation, the instrumentation, and the monitoring program. In addition, the back-analysis of the embankment will be described and the calculated and observed behavior at the instrumented cross-section will be compared.

The site of the embankment is located just south of the intersection of Hubrey Road and Wilton Grove Road in the Town of Westminster, County of Middlesex (which is located just outside the City of London in Ontario, Canada). As part of the general Hubrey Road Reconstruction project, an embankment fill was constructed to traverse a very wet swampy area, providing a direct link between Hubrey Road to the south of the site and Highway 126 to the north.

SITE CONDITIONS

The Hubrey Road embankment site is located in the physiographic area of southwestern Ontario referred to as the Ingersoll Till Moraine (Chapman & Putnam, 1984). During the retreat of the last glacial ice sheet, large blocks of ice were deposited on the surface of the tills and overlying alluvial outwash to form the moraine as it presently exists. These large ice blocks subsequently melted to form isolated waterfilled depressions. The lack of any continuous deep drainage of these waterfilled depressions resulted in the deposition of considerable depths of peat and organic silts.

In the winter of 1989, the site was cleared and tree stumps and brush were close cut. In August of 1989, three boreholes (U1, U2 and U3) were drilled at the location of the proposed instrumented section as shown on Figure 1 to supplement previous investigations. Samples for classification and laboratory testing were obtained using 70 mm diameter thin-walled, open Shelby tubes and 150 mm diameter thin-walled, piston Shelby tubes.

In general, the soil stratigraphy at the instrumented section consisted of 1.8 to 1.9 m of soft to firm black fibrous peat, underlain by 2.2 to 2.4 m of very soft, tan colored organic silt with numerous shells, which is in turn underlain by 0.4 to 0.6 m of soft fine organic silt with no noticeable shells and an almost jelly-like texture. Fine to medium sands and firm sandy silts with some clay were encountered below the organic silt. At the time of the investigation, the water table was located approximately 0.44 to 0.48 m below the existing ground surface.

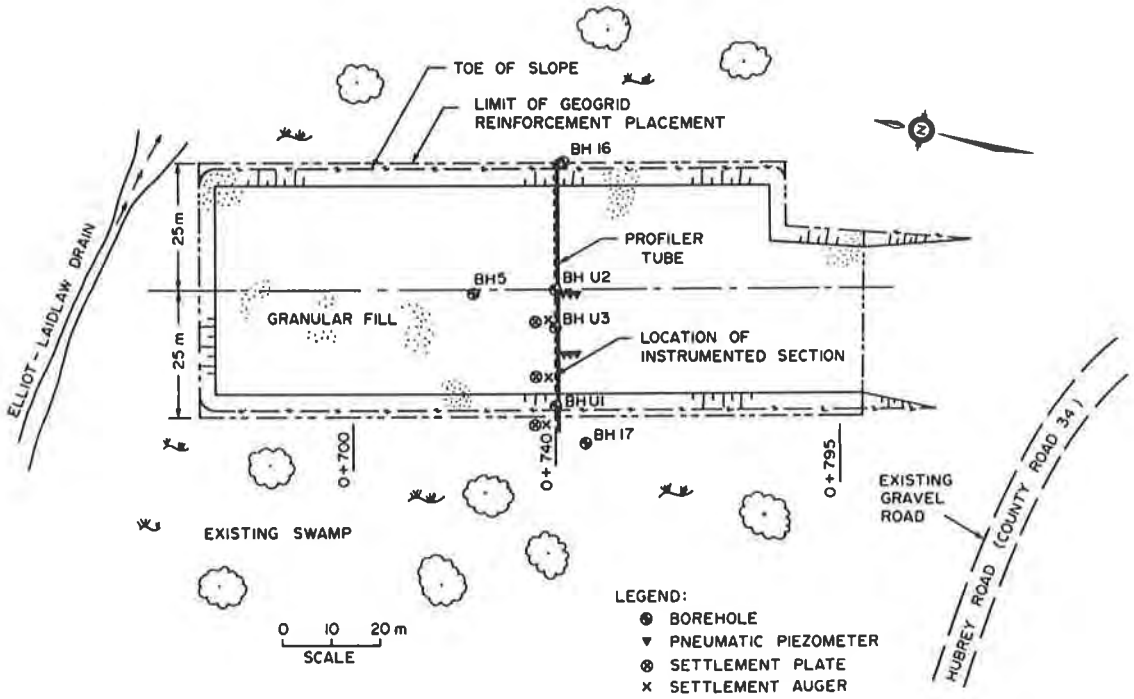

Figure 1. Plan Location of Instrumented Section (Chainage 0+740)

The black fibrous peat had a water content which ranged between 250 and 700%. The organic content of the peat was found to lie in the range between 76 to 90% (as determined by ASTM Standard D2974). The very soft organic silt which underlies the peat had a lower water content, typically ranging from 250 to 480%. Compared to the peat, the organic silt had a significantly lower organic content, typically ranging from 13 to 34%. The organic silt consisted of approximately 60% silt size particulate with the remaining 40% being made up of fine to medium sand, some shells and organic matter.

EMBANKMENT CONSTRUCTION

Several options are available to facilitate embankment construction on very soft compressible foundation soils such as peats and organic silts. One option would be to completely subexcavate the poor foundation soils and replace them with suitable granular fill. Complete subexcavation and back-filling was considered to be impractical in this case because of the quantity of peat and organic silt which would have to be removed. Another option would consider construction directly on top of the poor foundation using lightweight fill (e.g. wood chips and sawdust). Lightweight fill was not locally available. As a result, it was decided to construct the embankment directly on top of the poor foundation soil, using a geosynthetic reinforcement to aid in constructibility, as well as, help maintain embankment stability.

Since the deposit is very soft and a large quantity of fill is required to build the section of roadway to match the existing grades at either end of the site, it was decided to place the fill in stages over a period of time. Constructing the embankment in stages allows time for generated excess pore pressures to dissipate and the soft underlying foundation soil to gain strength as it is compressed under the weight of the fill prior to adding subsequent stages. In addition to using stage construction, reinforcement was placed directly on top of the close-cropped surface of the soft organic deposit prior to adding fill. The reinforcement selected by the design consultants was an extruded polypropylene biaxial grid reinforcement with a tensile strength of 19 kN/m and secant modulus (0-2%) of 450 kN/m as determined by CAN/CGSB 148.1 Method 7.1.

Stage I construction, which is being considered in this paper, consisted of placing 1.5 m of granular fill on top of the geogrid reinforcement. The reinforcement was rolled out in advance of fill placement, overlapped by 1 m and wired together to avoid excessive movement during fill placement. The direction of fill advance was from south to north.

INSTRUMENTED SECTION

In order to monitor the behavior of the embankment fill during and after stage I construction, instrumentation was installed at a section located at chainage 0+740 (see also Figure 1). The arrangement of the instrumentation installed at the section is shown on Figure 2.

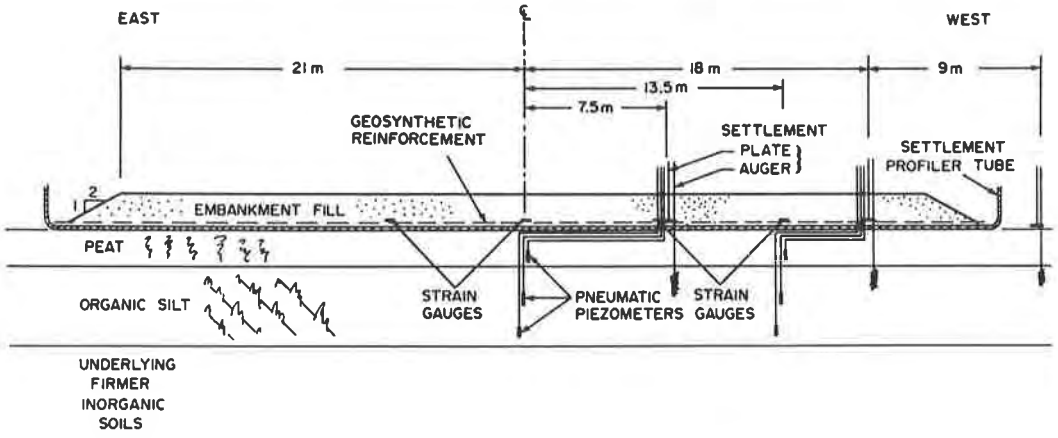

Figure 2. Arrangement of Instrumentation at Section 0+740

A horizontal profiling system (or profiler tube) was installed in order to obtain a continuous settlement profile across the entire instrumented section. Settlement plates and augers were also used to measure vertical movements at several points along the section as shown on Figure 2. The combination of settlement plates and augers was used to obtain readings of total settlement and to provide an estimate of the relative proportions of the total settlement which occurred in the peat and organic silt. Pneumatic piezometers were installed at the time of the geotechnical investigation in order to monitor the development of excess pore pressure during construction (and subsequent dissipation) in both the peat and organic silt. Strain gauges were attached to individual ribs of the geogrid as a means of determining the magnitude of strains which were developed in the geogrid reinforcement transverse to the road alignment.

RESULTS OF FIELD MONITORING

The observed settlement profiles at the initial end of construction (September 12, 1989) and at the end of stage I construction (August 21, 1990), just prior to stage II construction are shown on Figure 3. At the initial end of construction, the maximum settlement was 0.49 m and the average settlement across the section was 0.28 m. Due to variability of the deposit, more settlement occurred on the west half of the section (see Figure 3). The maximum settlement at the end of stage I construction (i.e. August, 1990) was 1.5 m and the average settlement across the section was 1.1 m, again with more settlement occurring in the west half of the section. Given the variability of the organic deposit and the fact that the settlement plates were not located directly on top of the profiler tube, the settlement measured using the profiler tube is considered to be in very good agreement with values obtained using settlement plates (see Figure 3).

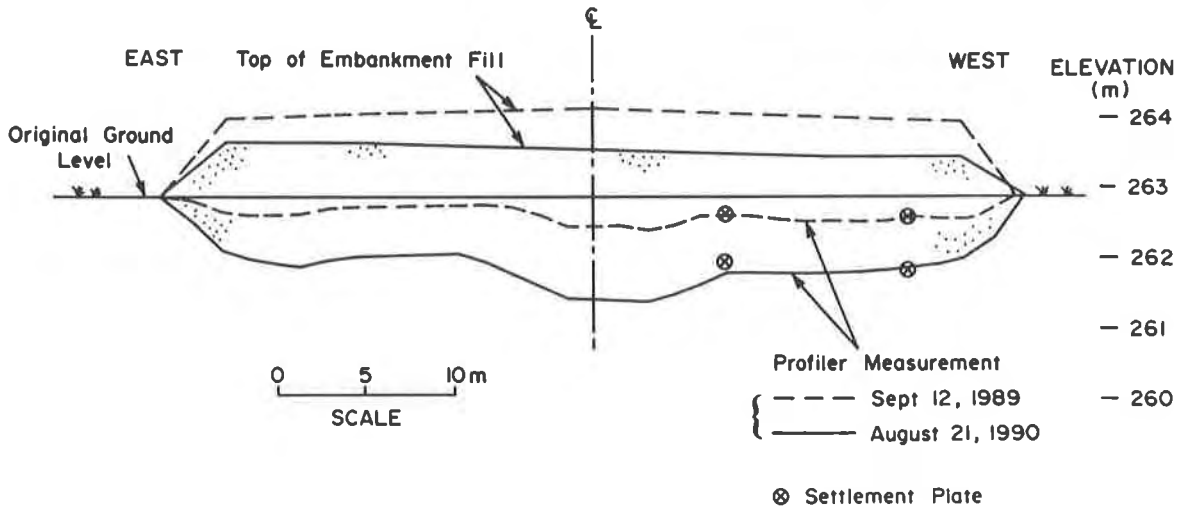

Figure 3. Settlement Profiles at the Instrumented Section

The dip in the settlement profiles shown on Figure 3 is considered to be partly the result of considerable concentration of construction traffic to the central region of the section and partly due to the additional fill thickness in that region. The contractor did add some fill to relevel the surface after the end of the initial construction and hence the average fill thickness across the section at the initial end of construction was 1.46 m as compared to 1.76 m at the end of stage I construction.

Figure 4 shows a plot of excess pore pressure versus time for the three pneumatic piezometers located at the centreline, for a sixty day period starting the day before construction. The actual depths at which each piezometer was installed beneath the ground surface are shown on Figure 4. As one would expect, the excess pore pressures increase rapidly when the fill is placed over the section and then gradually decrease as the excess pore pressures dissipate. What is interesting to note is that the increase in the peat is in the order of 12 kPa whereas in the underlying organic silt, the increase is much higher, 24 to 26 kPa. Assuming an average fill thickness of 1.55 m over the west half of the section (allowing for submergence of some fill material below the watertable) and a fill unit weight of 22 kN/m^3 as measured in the field, the applied load is estimated to be about 31 kPa. The magnitude of these peak excess pore pressure increases, compared to the magnitude of the estimate of applied load, suggests that at the end of construction, although not truly undrained, the organic silt is tending to behave in an undrained manner. On the other hand, the peat response cannot be categorized as truly drained or undrained. This observation was taken into account in performing short term (end of construction) analyses described later in this paper.

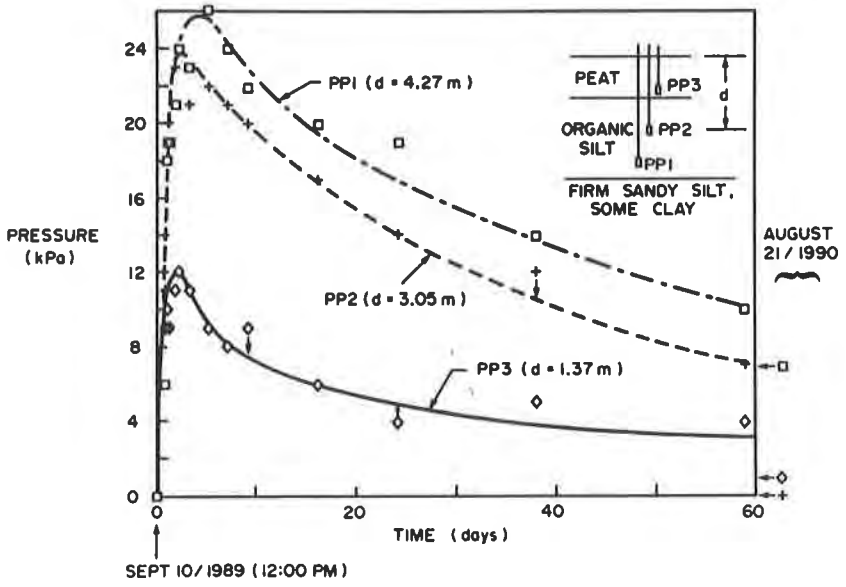

Figure 4. Excess Pore Pressure Observations at the Centreline

Figure 5 shows a plot of strains measured at various locations in the geogrid for the first sixty (60) days of stage I, starting early in the morning on the day fill was advanced over the instrumented section. Also superimposed on the plot are those readings of strain measured at the end of stage I construction (21 August 1990). The strains reached a peak value of strain for each gauge, then decreased slowly with time. This decrease in strain with time is probably due to some relaxation which occurs as the underlying soft organic deposit compresses and subsequently gains strength under the weight of the fill and is similar to that reported by Rowe et al. (1984a,b). The peak strain was generally reached within the first

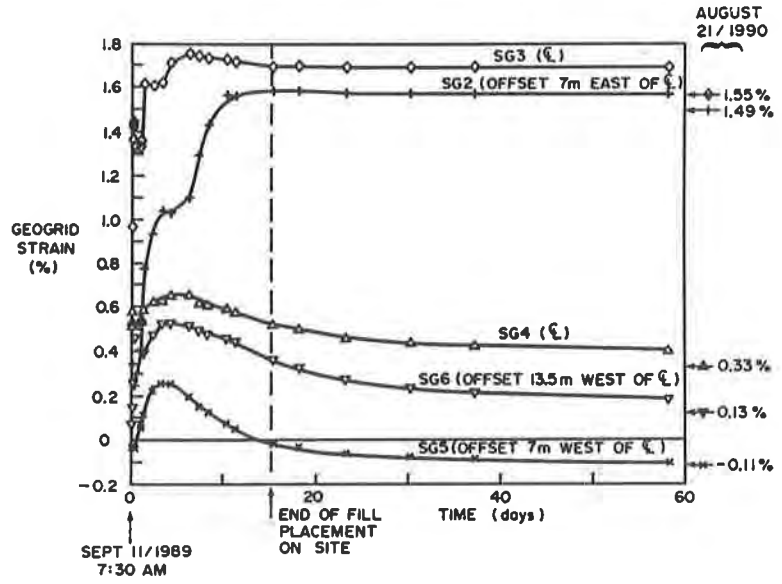

Figure 5. Geogrid strains Measured in the Field

10 days after placement of fill over the section. The peak values of strain measured in the geogrid ranged between 0.25% and 1.75%. The considerable difference in the strains measured for the various gauges is in large part due to the highly variable nature of the organic deposit.

NUMERICAL ANALYSIS

For embankments constructed on soft compressible soils such as peat and organic silts, it is important to take into account the effects of large deformations. This includes considering the decrease in compressibility of the soil as the void ratio decreases and the change in the pore pressure head as points in the soil change their position relative to the water table. The results presented in this paper were obtained using the authors' large deformation adaptation of the program AFENA originally developed by Carter (1985). The modified program takes into account large strain rotational effects and considers the generation of excess pore pressure. The large strain modifications in the program are based on the complete theory for finite consolidation of an elastoplastic soil proposed by Carter et al. (1979). Instead of analyzing the full development and dissipation of excess pore pressures using Biot theory, separate analyses were performed for the limiting cases of the initial end of construction and a long time after construction (end of stage I construction). Because of space restrictions only the initial end of construction will be considered in this paper.

Based on the excess pore pressure observations in the field, the initial end of construction (short term) case was analyzed treating the lower organic silt layer as being undrained and allowing for partial dissipation of excess pore pressures in the overlying peat layer. Due to their porous nature, peats typically experience some dissipation of pore pressures during construction. In principle, it should be possible to calculate the pore pressure at any time during the construction sequence using appropriate large strain consolidation theory. However, at present there is insufficient understanding of peat to allow such an analysis to be meaningfully performed. For example, the large changes in permeability, including changes in the ratio of horizontal to vertical permeability, both with position and loading history, have not been satisfactorily quantified even for a limited range of cases. As a result, the excess pore pressures immediately after construction (end of construction) were calculated using the following equation,

$$\Delta u = \bar{B}\Delta\sigma_1 \tag{1}$$

where Δu is the excess pore pressure at a point; $\Delta\sigma_1$ is the increase in total major principal stress at that point; and $\bar{B}$ is an empirical pore pressure parameter. This parameter, $\bar{B}$, was assumed to vary with depth in the peat and was given by

$$\bar{B} = (u/u_{max})^{*}\bar{B}_{max} \tag{2}$$

where the variation (u/u_{max}) was determined using the "end of construction" curve shown on Figure 6. It should be noted that a limiting isochrone, as shown on Figure 6 (Rowe & Soderman, 1985), was adopted because of the scarcity of available data. This isochrone is likely to provide a conservative estimate of the excess pore pressure distribution.

Based on observations of excess pore pressure in the peat at the instrumented section, the average value of $\bar{B}_{max}$ was calculated to be 0.36. This calculation assumes a fill thickness of 1.55 m and a fill unit weight of 22 kN/m^3. It is worth noting that this magnitude of $\bar{B}_{max}$ is very similar to that reported by Rowe et al. (1984a) for a reinforced embankment at Bloomington Road in Aurora, Ontario. The method described above was successfully used by Rowe et al. (1984b) to analyze the Bloomington Road case history, which consisted of a geotextile reinforced embankment constructed on a deep deposit of highly compressible peat.

A finite element mesh with 2701 degrees of freedom was used to perform the analyses. The results of the borehole investigation were used to define the soft foundation soil profile. The actual fill thickness measured in the field was used in the analyses. To obtain a reinforcement modulus value (J) to be used in the analysis, a sample of geogrid was removed from the roll at the instrumented section and a wide strip test (CAN/CGSB-148.1 Method 7.1) was performed in the machine (roll) direction. The value used in the analysis was J = 450 kN/m, which is representative of the secant modulus in the range 0-2% strain. Details regarding the program of laboratory testing used to determine the engineering properties of the various soils and geogrid reinforcement adopted in the analyses are discussed in detail by Mylleville and Rowe (1991).

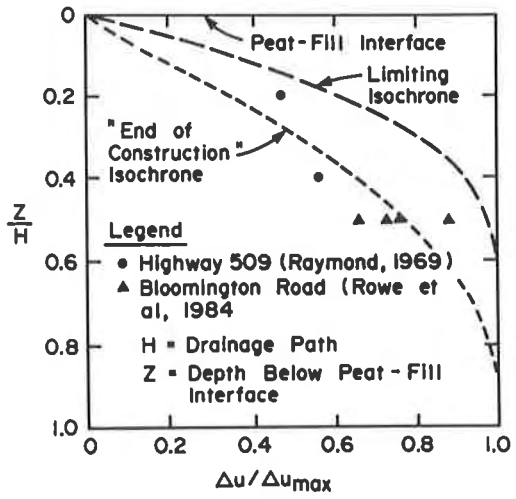

Figure 6. Variation in Excess Pore Pressure With Depth (Rowe & Soderman, 1985)

Initial End of Construction Settlements

Two separate analyses were performed considering the two values of drained Young's modulus obtained from consolidation tests on the peat, namely E′ = 230 kPa and E′ = 130 kPa. Figure 7 compares the observed and calculated settlements of the west half of the section using a value of drained Young's modulus E′ = 230 kPa for the peat. The calculated total settlement of the embankment is in very good agreement with the observed settlement, except near the centreline. The slightly greater observed (compared to calculated) settlement at the centreline is considered to be partially due to the concentration of construction traffic in that area (which was not accounted for in the analysis) and partially due to uncertainty regarding the drained modulus of the peat. It is noted that the calculated vertical movement of the peat/organic silt interface is in excellent agreement with the observed movement of the settlement augers. This suggests that the undrained modulus E_u = 130 kPa adopted in the analysis (based on triaxial test results) is a reasonable value to estimate the end of construction (short term) behavior of the organic silt.

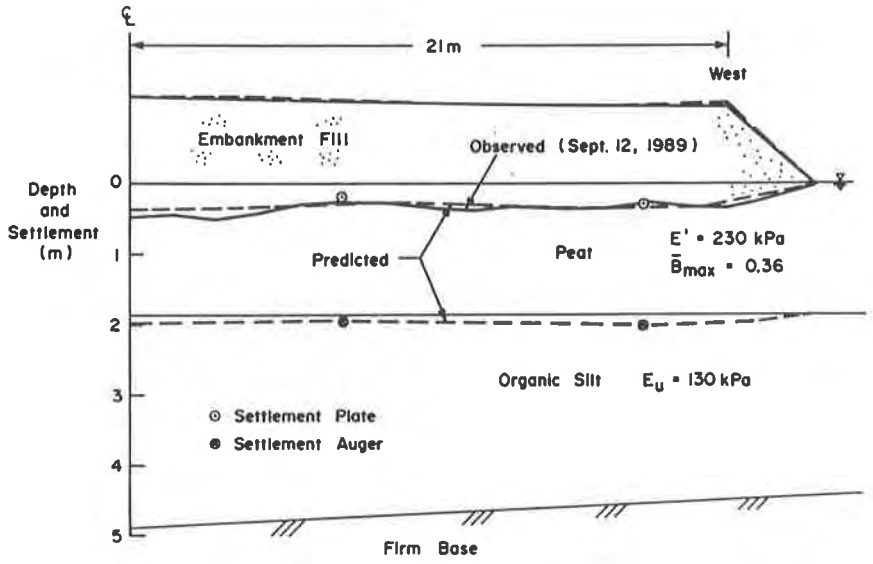

Figure 7. Observed and Predicted Settlements of the West Half of the Section at the Initial End of Construction (Peat, E′ = 230 kPa)

The effect of using a lower drained Young's modulus E′ = 130 kPa on predicted settlements can be seen on Figure 8. The settlements are slightly overpredicted for most of the embankment except near the centreline, where the agreement is excellent, however this is considered to be partially fortuitous since it is anticipated that some of the settlement is due to additional loading from construction traffic. From the foregoing, it would appear that the drained Young's modulus E′ of the peat does lie between 130 and 230 kPa, as

suggested by the laboratory data, and is probably closer to the lower end of this range.

Reinforcement Strains

Figure 9 shows the distribution of calculated strain in the geogrid with position from the centreline (for the west half of the section). Two curves are shown from analyses performed assuming an undrained shear strength profile (based on field vane tests) for the organic silt of c_{uo} = 4 kPa and ρ_c = 2 kPa/m (where c_{uo} is the surface undrained shear strength and ρ_c is the rate of increase in shear strength with depth), with one curve for each of the two drained Young's moduli considered to bracket the modulus of the peat, namely E′ = 130 kPa and E′ = 230 kPa. Also superimposed on the plot are the strains measured for strain gauges SG2 to SG6 at the initial end of construction. In terms of the calculated strain in the reinforcement, the Young's modulus of the peat had very little effect on the magnitude of the strains for the values of modulus considered. This is not surprising since this wide embankment is settling in more or less a one-dimensional manner with very little lateral movement. This also accounts for the relatively low magnitude of calculated strains; in this case less than 1.75%. The maximum calculated strain is developed near the edge of the embankment because displacement conditions change from one-dimensional beneath the embankment to two-dimensional (vertical and horizontal movement) near the edge. The actual measured strain values superimposed on Figure 9 show the same trend as the theoretical values if one considers gauges SG4, SG5 and SG6.

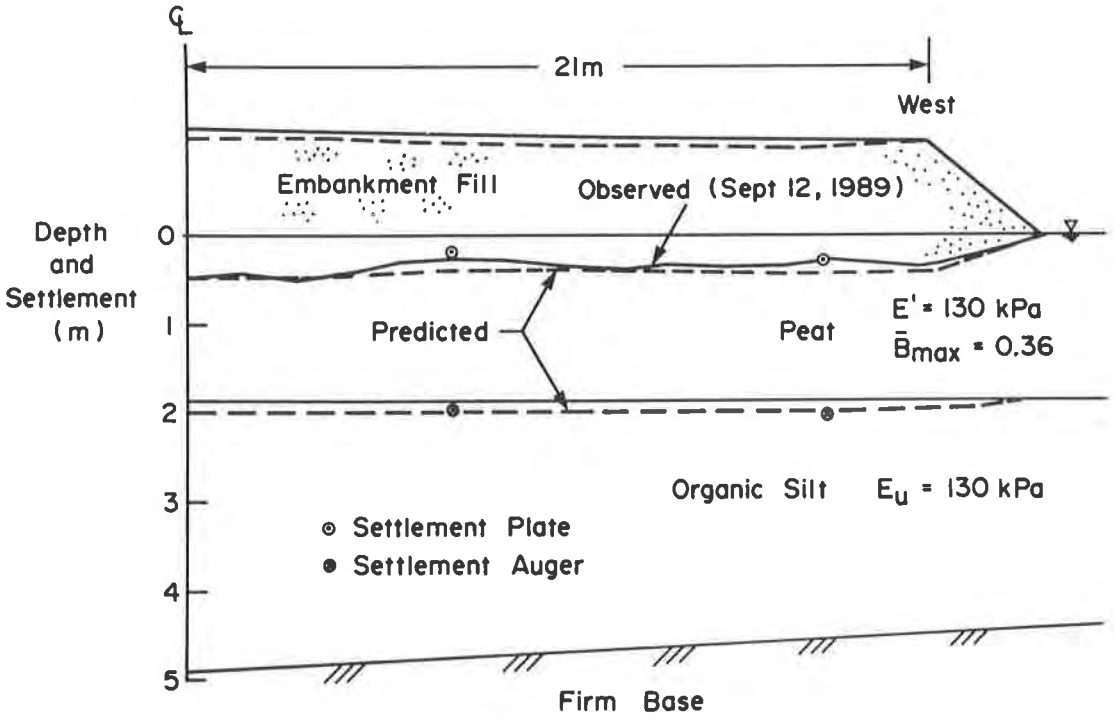

Figure 8. Observed and Predicted Settlements of the West Half of the Section at the Initial End of Construction (Peat, E′ = 130 kPa)

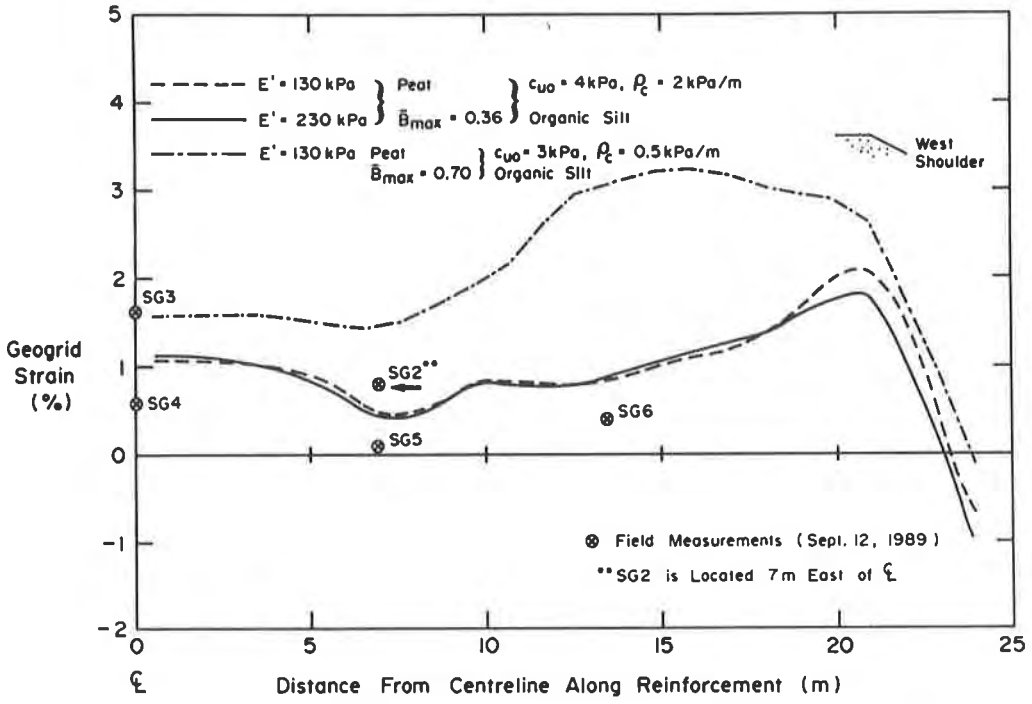

Figure 9. Calculated and Measured Geogrid Strains at the Initial End of Construction

As can be seen from Figure 9, the calculated and measured strains in the geogrid are low at the instrumented section. Although the geogrid was not being loaded to its capacity at the section under investigation, it is considered to have contributed to embankment stability during construction by carrying some of the tensile stresses developed in the peat. The geogrid is considered to have been more beneficial at other softer areas at the site. This is best illustrated by examining the third curve shown on Figure 9 which was obtained from an analysis assuming lower strength parameters for the organic silt (which might approach those at a softer section) namely, c_{uo} = 3 kPa and ρ_c = 0.5 kPa/m, together with a value of $\bar{B}_{max}$ = 0.70 for the peat (simulating a faster construction rate). Clearly, the geogrid develops considerably more strain (as can be seen on Figure 9) and hence should contribute more significantly to embankment stability.

COMPARISON OF BEHAVIOR WITH PUBLISHED RECOMMENDATIONS

In general, it is not practical to construct embankments at a rate so slow that no excess pore pressures develop in the underlying soft organic soil. Rowe and Soderman (1985) discuss the importance of considering the magnitude of excess pore pressures generated during the construction of embankments on peat. They recommended that the construction rate be controlled such that $\bar{B}_{max}$ (which is the ratio of maximum excess pore pressure to applied load; in this case near the bottom of the peat) is less than or equal to

0.34. Serious problems may occur if the embankment is constructed at a rate such that $\bar{B}_{max}$ is substantially greater than 0.34. For the instrumented section (chainage 0+740) at Hubrey Road, $\bar{B}_{max}$ values of 0.34 (at the centreline) and 0.38 (offset 13.5 m west of centreline) were calculated for the two pneumatic piezometers located near the bottom of the peat layer. These values are of the same order as the maximum recommended by Rowe and Soderman (1985). There was no evidence of problems in the vicinity of the section during construction.

During construction of the second half of the embankment fill in the north half of the site (in May of 1990) problems did occur. A second instrumented section was installed at chainage 0+600 in the north half of the Hubrey Road site. During construction, a large rotational failure occurred in a matter of 10 minutes, encompassing at least half of the 42 m crest width embankment. The dish shaped failure passed directly through the instrumented section in the direction of fill advance (from south to north). Based on the pore pressure readings taken just prior to the failure and estimates of applied load due to the fill, $\bar{B}_{max}$ was calculated to be in the order of 0.70 in the peat. The fact that a large rotational failure occurred is not surprising since the $\bar{B}_{max}$ measured at the time of the failure was at least twice the maximum value of 0.34 recommended by Rowe and Soderman (1985) for the level of reinforcement used. Subsequently, the contractor slowed the construction rate and fill advance continued using a much smaller bulldozer.

Just prior to the actual rotational failure, measured strains in the geogrid reinforcement were in the order of 2 to 3%, which is consistent with the calculated values shown on Figure 9 for an assumed, $\bar{B}_{max}$ = 0.70 in the peat.

SUMMARY AND CONCLUSIONS

The geotechnical investigation, instrumentation and field performance (stage I) of an instrumented section of a geogrid reinforced embankment constructed on a very soft compressible deposit of peat and organic silt has been described.

At the end of construction at the section, the amount of fill added varied between 1.30 m and 1.70 m, averaging 1.46 m across the entire section. Maximum settlements of 0.49 m were measured in the vicinity of the centreline at the initial end of construction. The peat behavior was neither truly drained nor undrained, whereas the organic silt tended to behave in an undrained manner (based on an examination of the pore pressure response). Values of $\bar{B}_{max}$ equal to 0.34 and 0.38 were measured in the peat indicating that the rate of construction was generally in accordance with the recommendations of Rowe and Soderman (1985). Maximum measured reinforcement strains ranged between 0.25% and 1.75%, illustrating the highly variable nature of the deposit.

Large deformation finite element analyses have been successfully used to back-analyze stage I construction of the Hubrey Road embankment fill. Analyses were performed for the initial end of construction (short term) where the initial end of construction situation was

analyzed allowing partial dissipation of pore pressure in the peat while treating the organic silt as an undrained material. Parameters for the finite element model were obtained from laboratory tests and data from an extensive program of field investigation and monitoring.

Calculated initial end of construction (short term) settlements were in very good agreement with the actual settlements measured in the field. Distributions of calculated strain developed in the reinforcement were presented for the initial end of construction (short term). The strains measured in the field straddled the theoretical curves, however the trend shown by the measured values is in good agreement with theory. In general, the strains developed in the geogrid were low during stage I construction at the section under consideration (chainage 0+740). This is not surprising since this wide embankment of low height is settling in a manner which may be characterized as largely one-dimensional.

The embankment performed well during stage I construction with no signs of stability problems at the primary instrumented section (chainage 0+740). From a practical standpoint, the use of the geogrid reinforcement was considered to be most beneficial during the placement of fill at the instrumented section. During construction, tension developed in the natural root mat at the surface of the peat, in advance of fill placement, as was evident from the formation of tension cracks. Some of these tensile stresses which developed were carried by the geogrid reinforcement and thus helped to maintain embankment stability during construction by preventing breaking through the stronger root mat and into the much softer underlying peat and organic silt.

Although not utilized to its full capacity at the instrumented section described, the presence of the geogrid was considered to be even more beneficial in helping to maintain embankment stability during construction at other softer areas encountered on the site. This was illustrated by examining results from analyses which demonstrated how the geogrid develops more strain and hence should contribute more to embankment stability for softer areas on the site (assuming a lower strength in the organic silt and faster construction rate). A failure did occur at a second instrumented section, apparently as a result of an excessive rate of construction which resulted in the development of excess pore pressures in the peat approximately twice the maximum recommended by Rowe and Soderman (1985).

ACKNOWLEDGEMENTS

The research in this paper was funded by The North American Geosynthetics Society's Awards of Excellence Program and by NSERC Grant A1007 awarded to Dr. R.K. Rowe. Many thanks are due to a number of people for their contributions to this project: to Dr. K.L. Soderman, and Messrs. G. Lusk, W. Logan and S. Hinchberger at The University of Western Ontario; to Messrs. P.R. Bedell and B. Wilson of Golder Associates Ltd.; to Messrs. B. Huston and G. Knights of M.M. Dillon Ltd.; and to Mr. Don Husson and the County of Middlesex for permission to publish the Hubrey Road case history.

REFERENCES

Carter, J.P., Booker, J.R. and Small, J.C. (1979). The analysis of finite elastoplastic consolidation. International Journal of Numerical and Analytical Methods in Geomechanics, Vol. 3, No. 2, pp. 107-130.

Carter, J.P. (1985). AFENA - A general finite element algorithm - User's Manual, School of Civil and Mining Engineering, University of Sydney, N.S.W. 2006, Australia.

Chapman, L.J. and Putnam, D.F. (1984). The physiography of southern Ontario. 3rd Ed., Ontario Geological Survey, Special Volume 2, Ministry of Natural Resources, Ontario.

Mylleville, B.L.J. and Rowe, R.K. (1991). Hubrey Road: A reinforced embankment case history. Geotechnical Research Centre Report No. GEOT-10-91, The University of Western Ontario, 77p.

Rowe, R.K. and Soderman, K.L. (1985). Geotextile reinforcement of embankments on peat. International Journal of Geotextiles and Geomembranes, Vol. 2, No. 4, pp. 277-298.

Rowe, R.K., MacLean, M.D. and Barsvary, A.K. (1984a). The observed behaviour of a geotextile-reinforced embankment constructed on peat. Canadian Geotechnical Journal, Vol. 21, No. 2, pp. 289-304.

Rowe, R.K., MacLean, M.D. and Soderman, K.L. (1984b). Analysis of a geotextile-reinforced embankment constructed on peat. Canadian Geotechnical Journal, Vol. 21, No. 3, pp. 563-576.

Montana Department of Transportation's Introduction to Geogrid Use for Steepened Embankment Design

T.L. Yarger
Montana Department of Transportation, USA

R.S. Barnes
Montana Department of Transportation, USA

ABSTRACT

This paper gives a brief history of the introduction and use of geogrid for steepened reinforced embankment design on state highways in Montana. Two case histories are presented along with a brief description of an upcoming reinforced embankment bridge approach fill project. One project is a small change order in a highway overlay-widening project which required widening of the roadway over some large diameter pipes in north central Montana. The more detailed case history project is two, 18.3m (60 ft) high, 1:1 and steeper geogrid reinforced embankments around the shore of Dickey Lake in northwestern Montana.

Uniaxial and biaxial geogrid was used to reinforce glacial till fill embankment materials on the Dickey Lake project. Unique features or considerations were; use of prefabricated wire forms on slopes steeper than 1:1, overall slope erosion protection features and the experimental nature of the project which includes slope indicator monitoring and surface surveying of the completed embankments.

INTRODUCTION

The concept of geogrid use for steepened embankment design was first introduced to the Montana Department of Transportation at a Northwest Geotechnical Workshop presentation by the Tensar Corporation in 1984. Since that time the Geotechnical Section has considered the possible use of geogrid reinforced steepened slopes as an alternative to retaining walls, shot rock fills or other design features used to save room or facilitate a highway design.

THE GILDFORD - EAST PROJECT

In April, 1988, an overlay project ready for construction was in need of a retaining or similar type structure for roadway widening. The need for the structure was unaccounted for in design because several large diameter culverts in one area had been omitted in the project survey. These culverts either needed to be lengthened in order to accommodate the additional roadway width or a retaining structure needed to be built on top of them. The Geotechnical Section of the Department recommended the use of a 1:1 steepened slope using geogrid reinforcement. This alternative geometry fit the conditions for roadway widening without having to lengthen the pipes. It was

felt that constructing the grid reinforced steepened slopes should be fairly easy. This feeling prevailed despite a lack of prior experience in the Department as well as the contractor who was to build the overlay. Considering the alternative of having a change order which would require another contractor build a retaining wall or lengthen the pipes, the geogrid was the most logical and economic choice. The most important characteristics of the project are listed below:

1. Typical design (figure 1) called for cohesionless material, 100% passing the 152.4mm (6 in) sieve and no more that 15% passing the #200 sieve. The outer 0.6m± (2 ft) of embankment was to be constructed of a more topsoil-like blend of silt/sand/clay to promote plant growth for erosion protection.
2. Construction issues included:
   a. In one area, grid protruded more extensively on the edge of the fill than is normally acceptable. According to the project manager, this could have been prevented by making sure that the entire lift and grid is established on a good foundation. Loose material apparently had filled a washout missed during the excavation.
   b. Placement of the "topsoil" in the outer edge of the embankment proved difficult. The soil was placed on the pit run gravels and pushed out over the edge causing loss of material down the slope.
   c. Initially it was decided erosion protection was not needed on the slope. It was found, however, that aggregate was being lost through the grid because of water erosion. Because seeding could not take place during construction, a fabric erosion mat was provided to allow for seeding at a later date.

The final cost of widening the roadway using this method was about $40,000. This represents a substantial savings over the $100,000+ estimated for extending the culverts. In his final remarks the Project Manager offered this in his report: "In conclusion, I would like to recommend that this method of construction be used, any time widening needs to be done on large fills, where the cost of extending culverts or the cost of embankment would be prohibitive. I would also recommend that fill material be the closest available A-4 or better, instead of using pit run aggregate. Also, any time the proposed slope is a 1:1 or steeper, embankment protection should be required."

THE DICKEY LAKE PROJECT

Concept Development. Reconstruction of a portion of U.S. 93 around the shore of Dickey Lake, in northwestern Montana (figure 2), required the use of retaining walls or other roadway space saving structures to maintain grade and alignment. Global stability analysis for the two embankment areas requiring retaining structures indicated factors of safety less than 1.5. A minimum factor of safety of 1.5 is normally recommended by Montana Department of Transportation (MDT) standards as well as the Federal Highway Administration (FHWA).

Global stability analysis of a typical section (figure 3) incorporating a Reinforced Earth-Type wall, with reinforcement strips, indicated higher factors of safety. This pointed the way towards possible use of a geogrid reinforced embankment to achieve the required minimum factor of safety of 1.5.

Site Conditions and Geologic Setting. The project site is located in Montana, U.S.A. on U.S. Highway 93 along the northeast shore of Dickey Lake approximately 40 kilometers (25 miles) south of the Canadian border. The roadway follows the Rocky Mountain

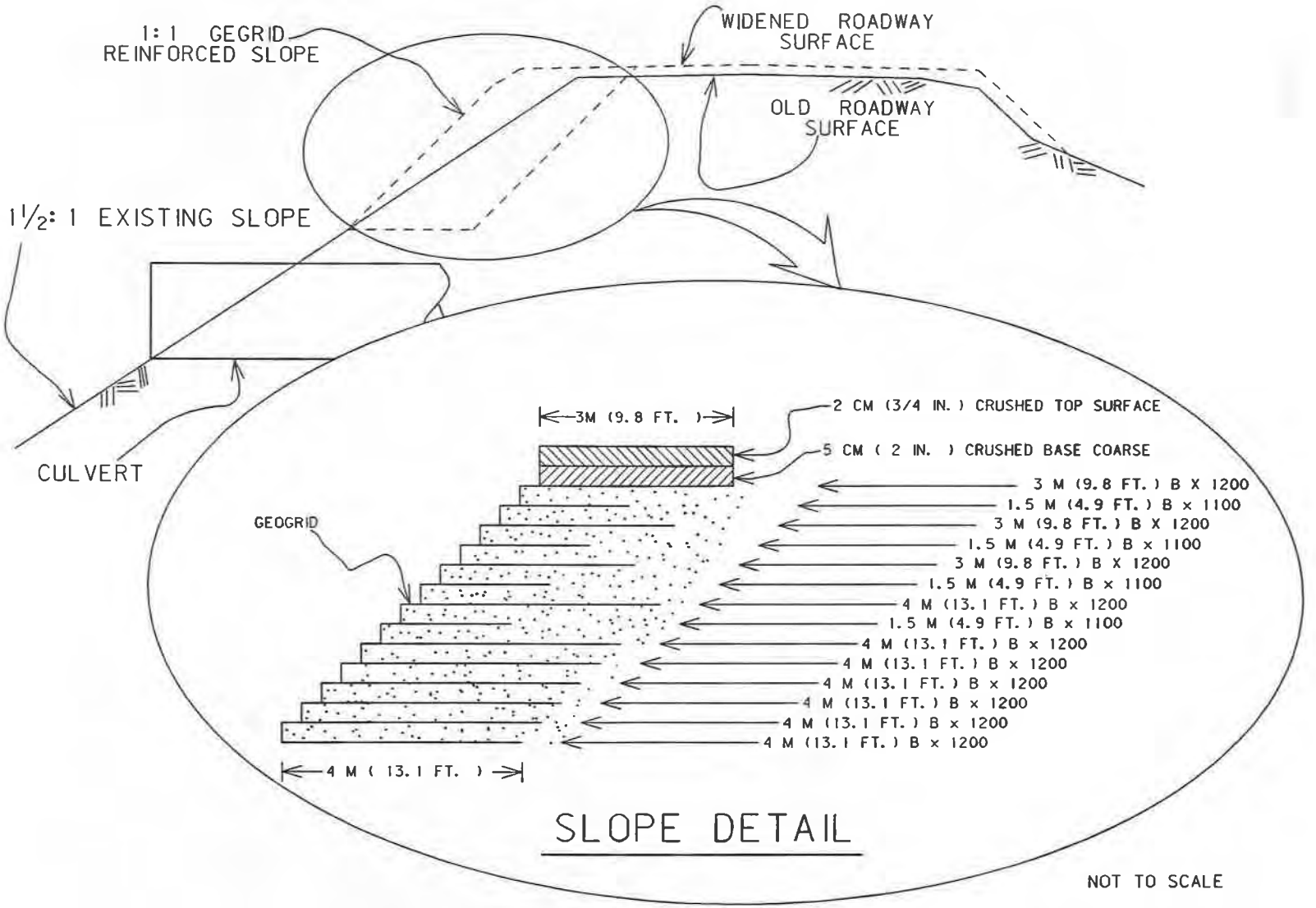

FIGURE 1. DESIGN SKETCH OF GEOGRID REINFORCED SLOPE USED TO WIDEN EXISTING ROADWAY OVER CULVERTS, (GILDFORD - EAST PROJECT).

FIGURE NO. 2 - OBLIQUE VIEW OF THE DICKEY LAKE PROJECT LOOKING NORTHWEST

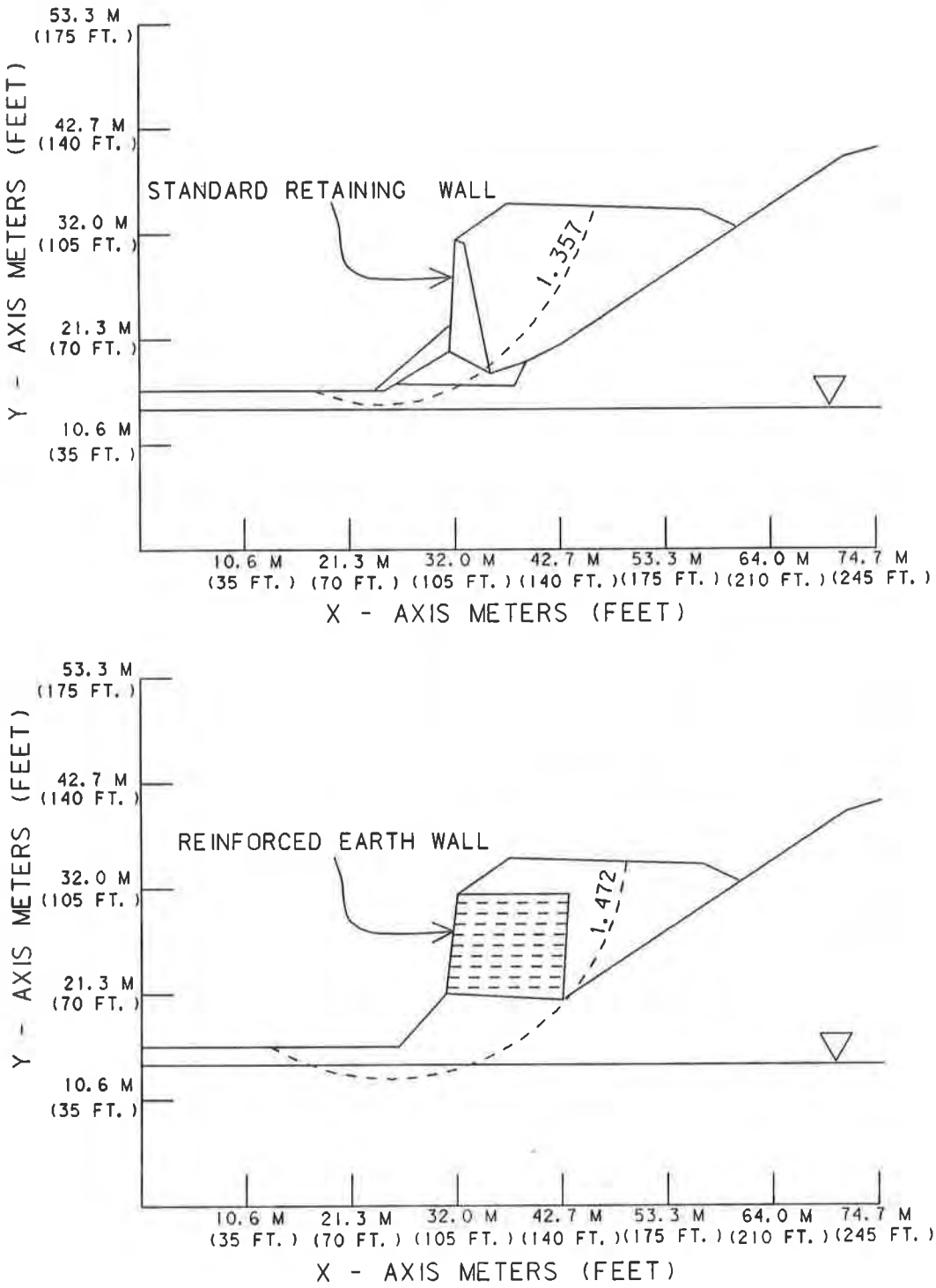

FIGURE NO. 3. - TYPICAL GLOBAL STABILITY ANALYSIS INDICATING THE NEED FOR DEEPER SEATED REINFORCEMENT FOR HIGHER FACTORS OF SAFETY

Trench, a crustal block let down along faults (figure 4). This trench (valley floor) is covered with glacial debris soils left behind when glacial ice melted about 10,000 years ago. The area is fairly heavily forested. Precipitation averages 50 centimeters (19.7 inches) per year. Average annual temperature is 6 degrees celsius (43 degrees fahrenheit).

The glacial till fill borrow and foundation soils on the project area consist of primarily gravel, sand and silt type soils. Classification and shear strength properties of these soils for the areas of proposed steepened embankments are characterized as follows:

a. Foundation soils - Generally medium to very dense silty sands, gravels and gravelly sandy silts.
b. Borrow for critical height fills and reinforced embankment construction - Soils from borrow and cut areas were heterogeneous but dominated by sand and gravel fractions. Minimum friction angle for design was established at 34 degrees. Cohesion was set at 0 n/m^2 (0 psf).

Groundwater is active in this area and its presence was confirmed when many seeps and springs were encountered during construction excavation. The water levels vary seasonally. Many of the aquifers are in perched or channelized configurations because of the nature of the till materials.

Primary Design Activity for the Reinforced Embankments. Following the decision to utilize a reinforced embankment for the Dickey Lake project, preliminary or conceptual design assistance was solicited from a number of manufacturers, including a metal grid/retaining wall supplier. This was done for fairness, and also because of the Department's general lack of design capability and knowledge regarding reinforced embankments. Based on the responses received, design geometry was chosen, and specifications were developed for a geogrid reinforced embankment.

Consideration was given to designing the embankment "in-house", but due to the Department's aforementioned limited experience, it was decided that prospective suppliers would be required to design the embankment. Plans and specifications for a geogrid reinforced embankment(s) were developed, with the plans indicating the desired finished geometry(slope angle, height, etc.). The specifications provided prospective suppliers with soil parameters, design life, required safety factor, and surcharge. The specifications also explained submittal requirements, review procedure, construction requirements, and basis of payment. Minimum acceptable geogrid properties, long term design strength and junction strength/efficiency, were also specified. A minimum design experience level was also specified.

It is perhaps an understatement to say that the above specifications (in particular the minimum geogrid properties and the design experience level) sparked something of a controversy. Prior to this project, the Department had not experienced the continuing debates about creep testing, junction strength, durability, polymer type, etc. It is beyond the scope of this paper or the ability of the Montana Department of Transportation, to discuss these debates in depth. However, for the purpose of the Dickey Lake project, the specifications were developed and upheld based on the following:

1. The Department's need for an experienced embankment designer/supplier.
2. The desire to have a well documented long-term strength.
3. Recommendations of FHWA.

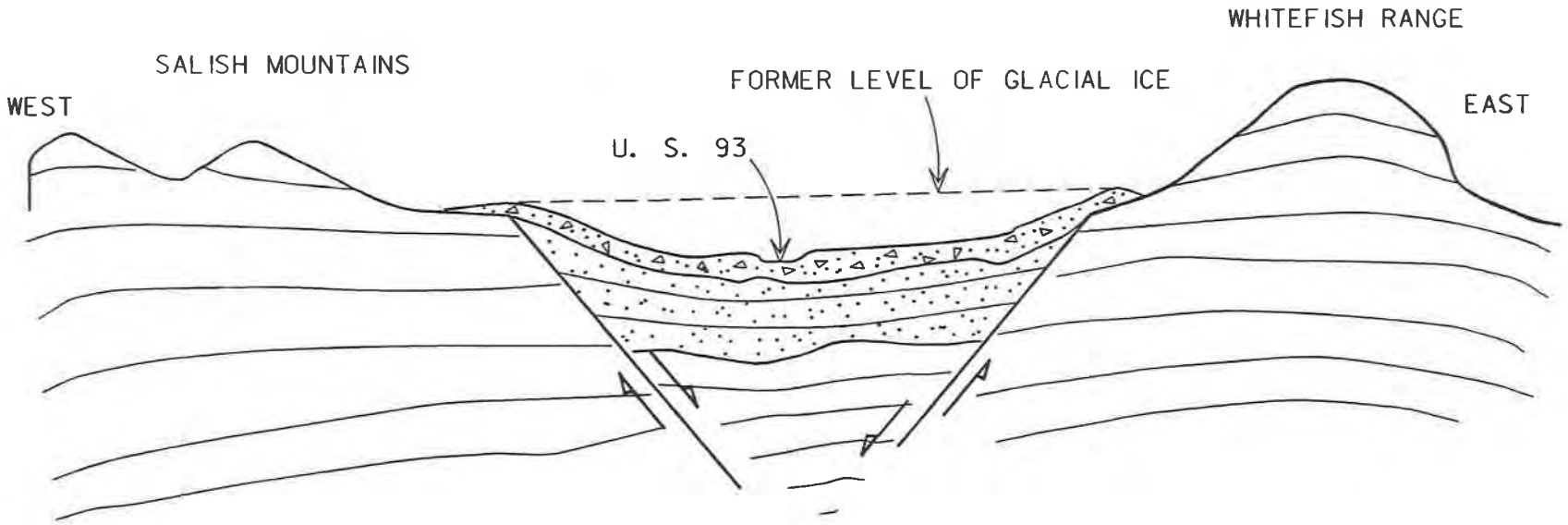

FIGURE NO. 4 - TYPICAL CROSS SECTION OF THE ROCKY MOUNTAIN TRENCH IN NORTHWESTERN MONTANA

It should be noted that the Department utilized the services of an outside consultant, recognized as a geosynthetics expert, in evaluating submittals by prospective geogrid suppliers.

The successful geogrid supplier prepared a submittal in accordance with the plans and specifications. This submittal included a resume of design experience, exhaustive product data verifying long term design strength, and complete construction drawings. Stability analysis of the geogrid reinforced embankment was accomplished using the supplier's software, which is reportedly a simplified Bishop's analysis that accounts for geogrid reinforcement. The resulting design called for primary reinforcing grids 4.6 to 18.3 meters (15 to 60 feet) long and spaced .6 to 1.2 meters (2 to 4 feet) vertically throughout the reinforced embankment (figure 5). In addition, intermediate reinforcement, consisting of lighter, biaxially oriented geogrid, was provided in typical lengths of 1.5 meters (5 feet), and vertical spacing of 0.3 meter (1 foot), at the face of reinforced slopes 1:1 or flatter. Special face treatment for slopes steeper than 1:1 is discussed below.

The design also incorporated subsurface drainage (figure 5). This drainage was judged to be particularly important due to the aforementioned springs or seeps present along the backslope of the embankment. The design incorporated prefabricated drainage composite panels placed along the backslope, draining into a french drain at the toe of the backslope. Laterals to "daylight" the french drain to the embankment face were provided 30.5 meters (100 feet) on centers.

Erosion control material and design was excluded from the geogrid supplier's responsibilities. An organic erosion blanket was specified and utilized to aid establishment of vegetation on the embankment face. For slopes 1:1 or flatter this material was simply rolled down the slope face (figure 6) and staked, following construction.

For embankment faces steeper than 1:1 (maximum 0.84:1 slope) a special detail to control ravelling of material at the face (prior to establishment of vegetation) was provided by the geogrid supplier (figure 7). This consisted of an L-shaped welded wire form, braced by diagonal struts, with a wrap of biaxial grid behind the wire. Initial plans called for the erosion blanket to be placed inside the geogrid wrap.

Construction. Earthwork was accomplished during construction of the reinforced embankment using conventional equipment and methods (figure 8). Scrapers were used to haul and place most of the embankment fill and a patrol grader was used for "delicate" placement of fill around the slope face. Operators of both the scrapers and blade were able to drive directly on the geogrid when necessary, provided that care was taken to avoid sharp turns, high speeds, or other actions that might have shifted or disturbed the geogrid. Compaction was accomplished with conventional equipment.

At several locations, preconstruction grades were as much as a meter different from those shown in the plans. These areas required quick redesigns or checks by the geogrid supplier's design team. These changes were accomplished with minimal delay or extra cost.

Installation of the drainage composite, french drain and laterals required a little more than a week at the beginning of embankment construction. This involved placement of more than 457 linear meters (1500 linear feet) of plastic pipe, all of which had to be trenched in.

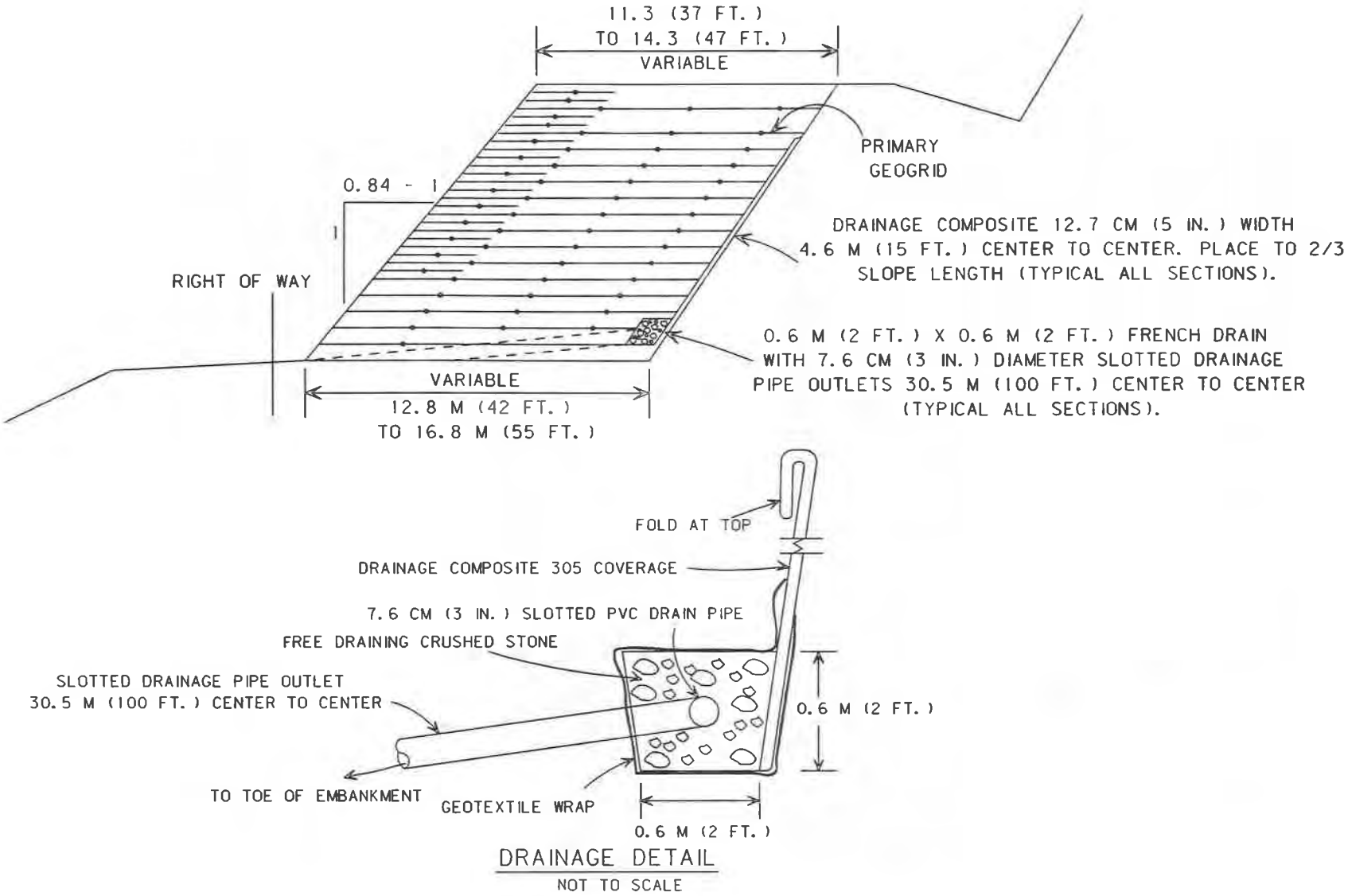

FIGURE NO. 5 - A TYPICAL GEOGRID DESIGN SECTION WITH DRAINAGE DETAIL FOR DICKEY LAKE PROJECT

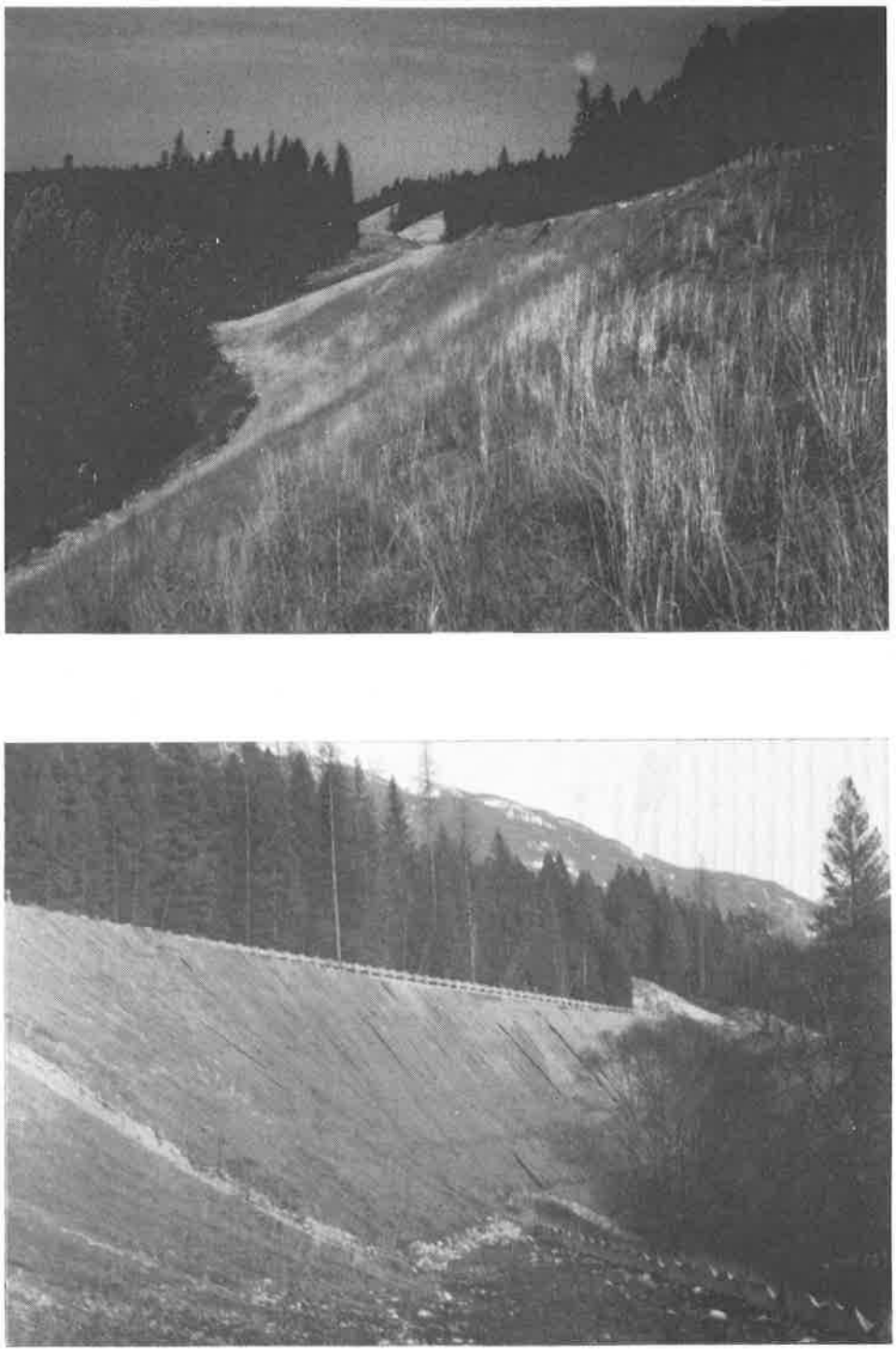

FIGURE NO. 6 - COMPLETED 1:1 GEOGRID REINFORCED EMBANKMENT WITH EROSION CONTROL FABRIC FACING - DICKEY LAKE PROJECT

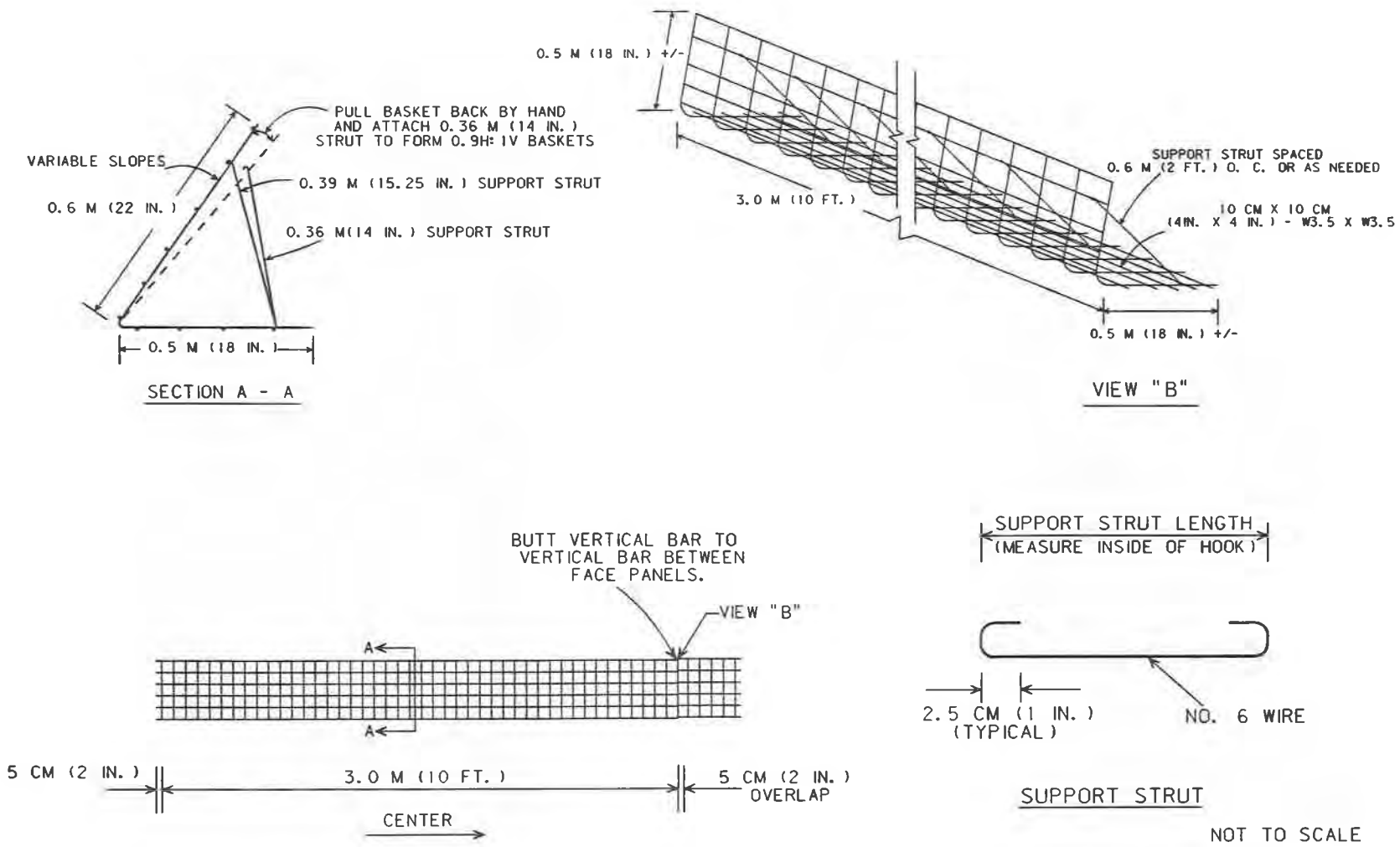

FIGURE NO. 7 - WELDED WIRE BASKET DETAIL

FIGURE NO. 8 - GEOGRID REINFORCED EMBANKMENT UNDER CONSTRUCTION AT DICKEY LAKE

FIGURE NO. 9 - GEOGRID REINFORCED EMBANKMENT UNDER CONSTRUCTION AT BN RAILROAD OVERPASS - BOZEMAN, MONTANA

Laydown of the geogrid and wire baskets (where used) was accomplished during embankment construction using a crew of 3 to 5 laborers. Generally, this crew could stay well ahead of the fill and compaction process.

Several problems were experienced in regard to erosion control during and following embankment construction. As discussed previously, a wire form/wrap detail was utilized to control ravelling of soil down the slope face during or following construction for all slopes steeper than 1:1. The 1:1 "breakpoint" for ravelling control was selected by the geogrid supplier, based on their experience, which was primarily in other locations. However, at the Dickey Lake site, a significant amount of ravelling occurred during and following construction of embankments flatter than 1:1 (perhaps as flat as 1.5:1). The amount of ravelling that occurred in these areas was not enough to require remedial action, but it did cause some concern on the part of the Department's Project Manager. The general consensus among on-site personnel was that it would have been better to extend wire form/wrap coverage out to slopes steeper than 1.5:1, for this site. This can probably be primarily attributed to the granular, non-cohesive nature of the fill used at this site, which would tend to make ravelling more severe.

Where utilized, the wire form/wrap detail proved quite effective in controlling ravelling and assuring a completed slope face in close geometric conformance with the design. Even though it added some cost to the project, it was judged to be well worth it. Due to the gravel quantity present in the import fill, it was possible to eliminate the erosion blanket inside the geogrid wrap, simplifying construction greatly.

An attempt was made to correct these minor erosion control deficiencies in the design of the Bozeman overpass, which is also discussed in this paper. Clearly a more universally effective means of controlling erosion on the face of reinforced embankments needs to be developed. It is believed that in most cases, the facing needs to be "dense" enough to retain soil and yet porous enough to allow seeding to take place.

Monitoring and Present Site Concerns. As part of the experimental portion of this project it is to be evaluated periodically by visual inspection and monitoring. Surface surveys and slope inclinometer installations were established in the reinforced embankment areas.

To date, no major problems have been observed in the embankments, although several minor problems have come up. Erosion control fabric, which is used to aid in seed protection and germination, was placed by rolling the material downslope and stretching it in tension over and above the slope soon after construction. Consequently, grass would not grow well in areas where the fabric did not come in contact with the slope. A simple solution to this would have been to roll the fabric out in several sections rather than one continuous piece.

Sometime between February 19, 1992 and March 2, 1992 cracks appeared in the pavement parallel to the roadway alignment. They appeared around station 20919+50± in the reinforced embankment for this area. A nearby slope inclinometer showed some apparent movement which was difficult to interpret. No discernable movement has occurred in the slope inclinometer since this time. Periodic readings are being taken for cumulative movement. The surface level surveys do not indicate movement in either embankment. The cracks have grown somewhat longer with time, however they have been cracked sealed by maintenance and do not appear to be or indicate a major problem.

The cracking occurred in the embankment section most typified by the plan-cross section at station 20920 + 00.64. Test borings were drilled on May 11, 1992, approximately 3m (9.8 ft) either side of the crack which would represent natural ground versus constructed embankment. Moisture contents were normal or dry of optimum and no indication of a free groundwater table, perched, trapped or otherwise was indicated in the borings.

Movement appears to be caused by some differential strain adjustment reflecting the differences in the overall apparent strength of materials between natural ground or unreinforced backfill and the geogrid reinforced embankment section. This particular embankment section is shorter in height than the majority of the rest of the fill and is situated on sands and gravels which the Project Manager indicated formed some of the densest foundation materials on the project.

THE NEW BOZEMAN RAILROAD OVERPASS PROJECT

Geogrid Reinforced Approach Fills for a Railroad Overpass. Construction of a new railroad overpass with geogrid reinforced approach fills is currently underway near Bozeman, Montana (figures 9 & 10). While it is necessary to maintain traffic on the old structure during construction, use of the reinforced embankments will allow for eventual removal of portions of the old structure without elaborate steps to remove old piers and substructure elements in the embankment areas. It is felt that much time, effort and money was saved on the project for this reason and by the avoidance of possible costly and difficult shoring and utility removal next to the railroad lines.

The design for erosion control features was based on the lessons learned on the Dickey Lake project. The same wire form/wraps are being used on this project as were used at Dickey Lake. The only difference between the two projects is that the wraps are being used on all slopes steeper than 1.5:1 instead of only on slopes steeper than 1:1, which is where they were used at Dickey Lake.

THE FUTURE OF GEOGRID USE IN MONTANA

The future of geogrid use in Montana can be described as nothing but bright. As contractors become more familiar with geogrid use, it will also quickly find its way into the private sector. Use of geogrid for subgrade stability is also being introduced to Montana fairly rapidly.

Difficulties in the use of geogrid in Montana have typically been centered around the design phase and reflect just plain ignorance or lack of knowledge in the makeup of the different types of grid available and what many consider most important, its long term strength.

Another difficulty we have encountered is finishing off the reinforced slope face. Typically, erosion control geotextile, sodding, planting, or other type of slope facing is included in the design but the workability of these alternates is not well thought out. This may be the result of a fine line between recognizing this as a more complicated engineered structure then a standard unreinforced earth embankment. Although reinforced embankments such as this one tend to look fairly natural, sometimes more attention needs to be spent on finishing the embankment face because of its more fragile nature. The slope face treatment is part of the whole system and must be considered in design as such. The treatment must become the responsibility of the embankment designer in order to insure the integrity of the entire system.

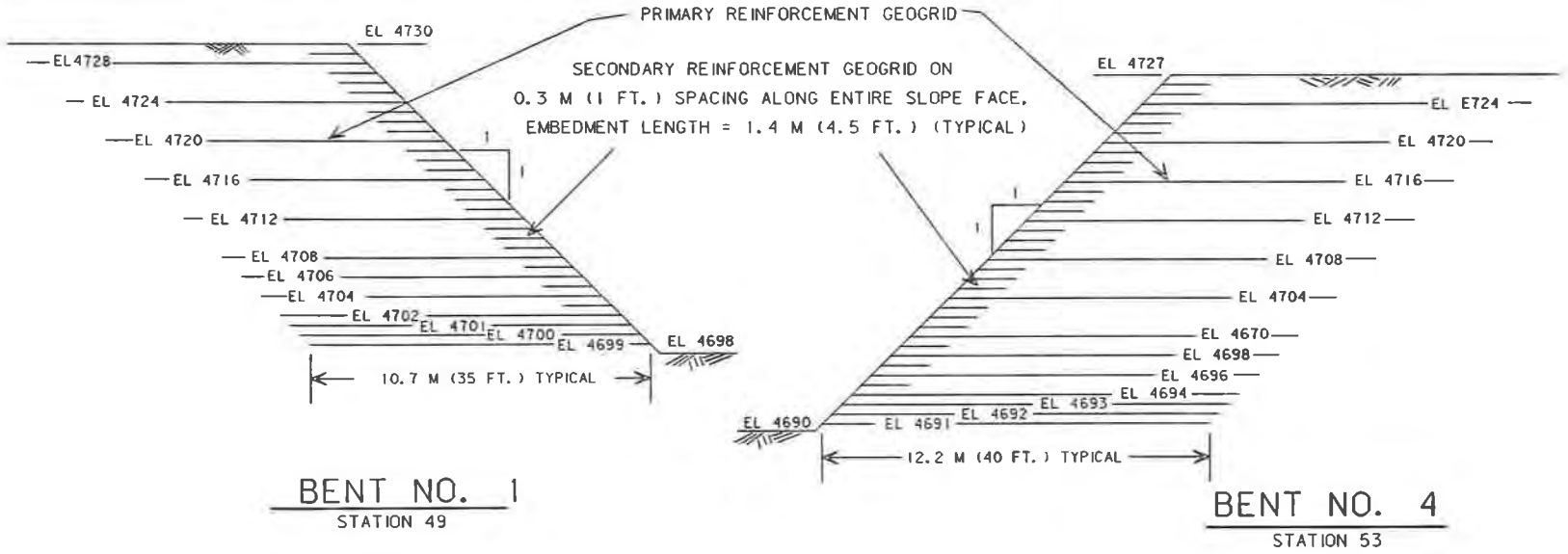

FIGURE NO. 10 - GEOGRID DESIGN TYPICALS FOR BN RAILROAD APPROACH EMBANKMENTS BOZEMAN, MONTANA

ACKNOWLEDGMENTS

The authors wish to express their appreciation to the Montana Department of Transportation (MDT), particularly the Dickey Lake Project Manager, who is now retired, Mr. Eugene Piedalue. Thanks also go to all of the private sector geosynthetic product and engineering people who helped make the Dickey Lake project a truly educational experience for all involved. Also to Matt Strizich, MDT for organizing the authors thoughts.

Specifications for the Dickey Lake project were developed by advice from many different sources. Example specifications were obtained from a Maryland Highway project. California Department of Transportation personnel assisted in supplying us with some example specifications. The Federal Highway Administration also assisted and the list goes on from there.

Example construction drawings from the Dickey Lake project can be found in appendix D of the FHWA's Interim Guidelines for Design, Specification, and Contracting of Geogrid Mechanically Stabilized Earth Slopes on Firm Foundations.

TLY:Q:MT:15.si

Roadway Embankment Construction Over Peat Using Nonwoven Geotextile Reinforcement

P. McCullough
ESA Inc., USA

D. Carter
Polyfelt Inc., USA

ABSTRACT

A paved access road was constructed in the Kitsap Peninsula region of Washington in the fall of 1991. The roadway needed to pass between two existing ponds which necessitated construction over a peat deposit contained between them, a feature common to this part of Washington. The peat extended to a depth of five meters and had an average undrained shear strength on the order of 6KN/m2 based on field and laboratory testing. The initial design analysis indicated that a high strength/high modulus geotextile or geogrid would be required to support the three meter high embankment during construction. Long term subgrade strengths did however appear to be capable of supporting the embankment. After a review of the design analysis, an alternative using staged construction and a heavy weight, needle-punched non-woven geotextile was proposed to provide construction stability and promote drainage of the subgrade. Using this design approach, the embankment was successfully constructed in October of 1991. The geotextile was prefabricated and delivered to the job site in two large panels which facilitated the speed of construction and added to the cost savings. Instrumentation to evaluate settlement and pore pressure response was used to control the rate of construction and allow for long term performance monitoring.

This case study will review the design, construction and performance of the embankment. Subsurface information and design methodology will be reviewed along with the construction sequence and special procedures. The results of the construction monitoring and long term performance will be reviewed and the actual cost of construction versus design alternatives will be discussed.

INTRODUCTION

The building of roads over unstable subgrades produces a variety of problems with a wide range of solutions. This paper presents a case study which will discuss the construction of an embankment over a soft subgrade using a non-woven geotextile. The other design alternatives and reasons for the final design selection will also be reviewed.

SITE DESCRIPTION

The site for this embankment was in Central Washington state on the Kitsap Peninsula. A roadway was to be constructed through a wetland area and would pass between two small ponds (See Figure 1). These ponds were formed by peat mining operations. A soil causeway separated the two ponds and the alignment of the roadway design was required to straddle the causeway as it passed between the ponds. This roadway, which would become 67th Street N.W., would eventually become an arterial route for Pierce County.

VICINITY MAP - FIGURE 1

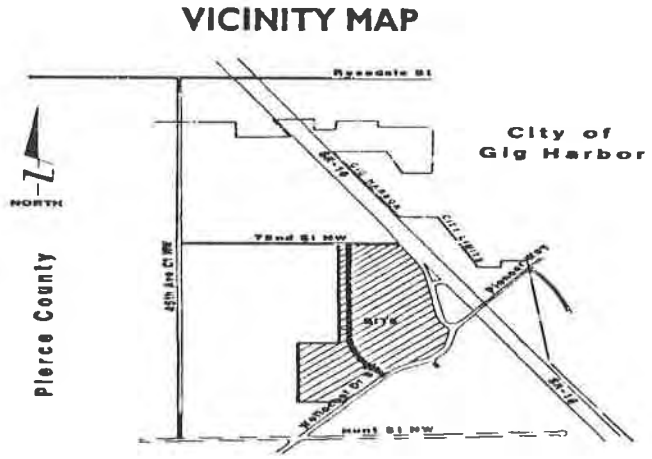

SITE ENVIRONMENT

A Wetland Mitigation Plan was prepared by Pac-Tech Engineering and was submitted to the Pierce County wetland coordinator. The plan included an intention to create a new area of wetland 1.5 times the wetland loss or approximately 2800 m2 to compensate for the loss of wetlands in the fill area. The Pierce County wetland coordinator expressed strong concerns about the placement of any

fill in the wetland which might introduce pollutants into the water.

Another concern was for the travel of small animals from one pond to another. A pathway for small animals has been provided by an arched culvert inserted in the roadway fill. The culvert also allows for storm water flow from one pond to the other.

SOIL ANALYSIS

The surficial soils at the site are shown in Figure 2, Site Soils Map. It was determined from the site soil borings that fibrous peat extended from approximately 1.5m at the northern and southern ends and up to 6m in the center section of the roadway alignment. Absence of significant organic decomposition indicated the peat deposit was relatively recent. Based on field and laboratory testing a shear strength of 6KN/m2 was estimated for the peat. Loose to medium dense silty gravelly sand was encountered beneath the peat and increased in density with depth. In one boring, very soft to soft silty clay was observed between the peat and the sand. The water level in the area of the peat was near the ground surface.

SITE SOILS MAP - FIGURE 2

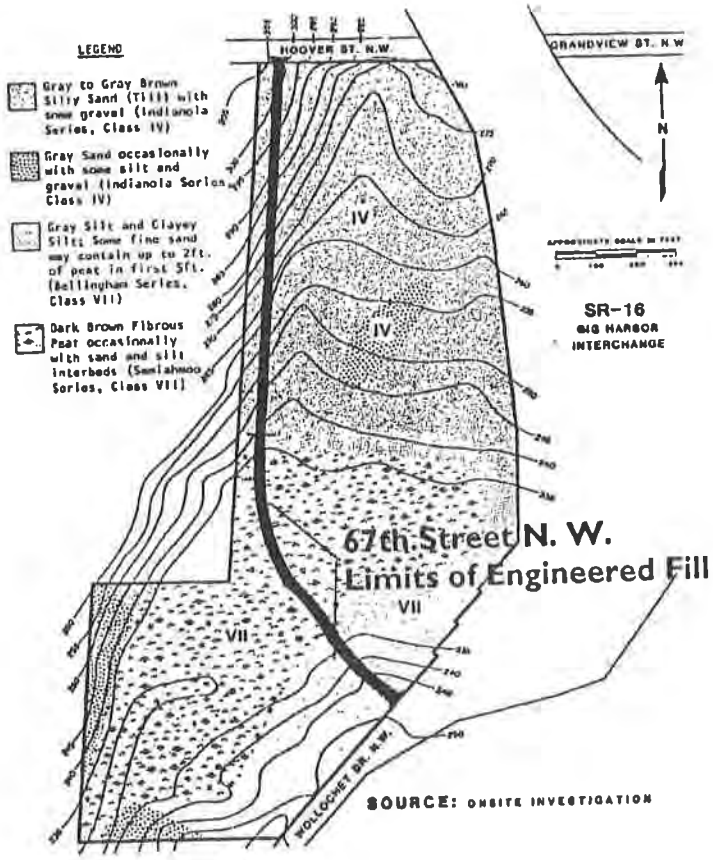

DESIGN ALTERNATIVES

In the original design of 67th Street N.W., the roadway was classified as a collector arterial. It was given this classification in anticipation that the roadway would become part of the Pierce County arterial street system. The road design was based on Pierce County road standards.

Alternative 1, Bridge/Fill Alternative

This alternative consisted of building a bridge over the soft subgrade using steel pipe pilings. This approach would cost over $400,000 and was twice the cost of the chosen design. See Figure 5.

Alternative 2, Aggregate Fill

The initial analysis for feasibility of an aggregate fill for crossing the peat soils was not promising. However, after extensive boring and discussions with the soils consultant, it was decided that an aggregate fill was feasible if geotextiles and proper construction sequencing techniques were used.

The design procedure for all the fill alternatives was similar and began with the modeling of the primary consolidation of the peat soils under load using a computer following the methods reviewed by Christopher and Wagner (1988). First, the peat soils were checked for bearing capacity. Second, slope stability was analyzed using the PC-Slope computer program. The modified Bishop Method of slices for slope analysis was utilized. Geotextile reinforcing requirements were analyzed during this stage and the analysis was checked using a design manual published by Polyfelt (1987). Finally, a sliding analysis was performed to check stability in the sliding mode. The three potential failure modes of the fill are presented in Figure 3.

In all of the fill options, it was necessary to use a synthetic reinforcement placed directly on top of the peat soils to prevent local failures in the subgrade during construction. Local failures can create severe problems and ultimate failure of foundation soils. In addition, the geosynthetic would provide for a more uniform fill placement and limit differential settlement. Several geotextile and geogrid options were investigated. A design and construction approach was selected. It was determined from the engineer's analysis that a geogrid soil reinforcing material would only be required if the owner wished to construct the fill in one continuous construction stage or if peat soils were encountered that would not allow direct access by construction equipment. Neither of these conditions existed on this project. If construction started after the rainy season, the use of geogrid for construction access may have been required. A heavy weight non-woven geotextile was selected based on the strength required

to survive construction, the strength required to increase support for the initial stage, and a high permeability (greater than 0.1 cm/sec) to allow for a rapid drainage and consolidation of the peat. The material selected was an 200g/m2 continuous filament polypropylene needle punched non-woven. The geotextile had a wide width strength of 15.6KN/m and a permeability of 0.4cm/sec which exceeded design requirements. This geotextile also exceeded the survivability requirements as recommended by AASHTO. The use of this non-woven geotextile resulted in a cost saving of $20,000 versus the use of the higher strength geogrid alternative.

FAILURE MODES - FIGURE 3

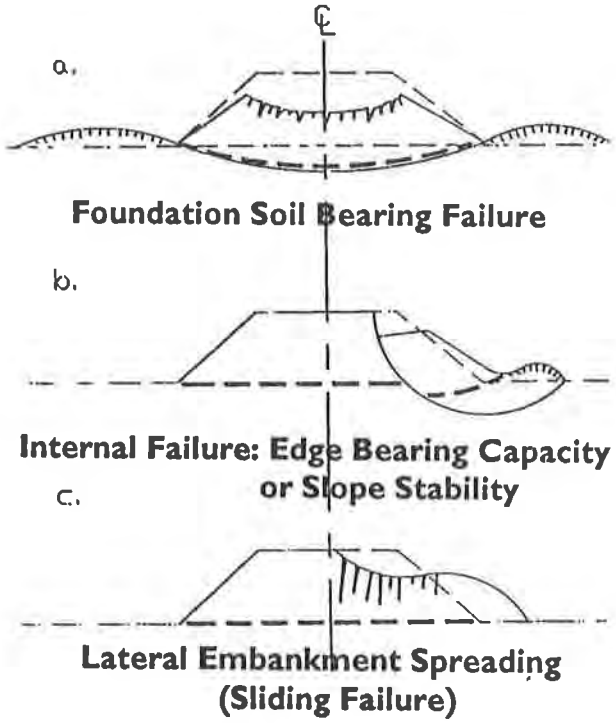

All the fill options were designed for the roadway using a primary consolidation rate of 40%. This rate is less than the average primary consolidation rate taken from the two laboratory tests, but experience has shown from similar projects that the actual consolidation in fibrous peat soils are seldom as high as the lab tests predict.

To determine fill heights and volumes, a spread sheet was constructed. An equation was written in which the primary consolidation equaled .40 times the log of the fill weight. The solution was reiterative until the assumed PC equaled the calculated PC. This technique was used to calculate the total fill height for all the fill alternatives by changing the weight of the fill and recalculations.

A sensitivity analysis was conducted to compare the fill volume and the consolidation ratio for 40%, 47.5% and 55% of the Primary Consolidation. The results are shown in Table 1 and indicate that an additional 2,300 cubic meters of fill material would be required to construct the fill if the consolidation ratio were 55%. If the material were compacted to 100% Proctor unit weight of 22.1KN/m3, and the consolidation ratio were 55%, the fill volume would increase 2,850 cubic meters over the assumed design conditions.

TABLE 1

19.6KN/m3 Fill			
Consolidation Ratio	40%	48%	55%
Fill Volume (cubic meters)	7,023	8,112	9,340
Primary Consolidation in meters	2.38	3.00	3.63
22.1KN/m3 Fill			
Consolidation Ratio	40%	48%	55%
Fill Volume (cubic meters)	7,368	8,548	9,340
Primary Consolidation in meters	2.54	3.19	3.85

In view of the uncertainties of the rate of primary consolidation that will occur in the field during construction, it was recommended that the owner take two precautions during construction.

1) Extend the geotextile five feet beyond the toe of the fill in the event that the fill had to be constructed higher than was currently planned and

2) Retain the soils consultant to closely monitor the fill during construction.

To estimate the secondary settlement of the fill, an additional calculation was made. The soils consultant furnished a copy of secondary settlement rates for similar fibrous peat soils from another project that the firm had worked on. These curves allowed the engineer to estimate the secondary settlement in the next ten years to be 40% of the primary consolidation.

The last column on Figure 4 indicates the minimum road grade to accommodate for the secondary settlement and still maintain a roadway elevation that is one foot above the 100 year flood. It was a delicate balancing operation to design the final construction profile of the proposed roadway for each fill material alternative so that the alternatives could be properly compared.

AGGREGATE FILL ALTERNATIVE - FIGURE 4

Station	Depth of Peat	Calculated Primary Consolidation	Measured Settlement	Minimum Road Grade
13+50	11	3.26	1.37	233.70
13+90	20	7.18	1.84	235.27
15+00	20	7.81	1.70	235.52
16+00	15	4.21	.64	234.08

Conversion: 1 LF = 0.305m

The aggregate fill alternative was designed using the above methodology. The estimated cost of the aggregate fill alternative was $165,478. See Figure 5.

LIGHT WEIGHT FILL ALTERNATIVES

As stated earlier, a major consideration of constructing a roadway over peat soils is the ability of the peat soils to carry the weight of fill and the amount of primary and secondary settlement of the peat soils. In many instances, it is advantageous to construct the fill out of light weight fill to reduce the weight of the fill on the peat, thereby reducing the total settlement. With this strategy in mind, a search for a light weight fill material that was both structurally sound and available locally commenced. Two alternatives emerged; a wood fiber fill material and a bottom ash fill material.

Alternative 3, Wood Fiber Fill

A wood fiber fill was given serious consideration after lengthy discussions with Al Kilian, Tony Allen, and Leroy Wilson of the Washington State Department of Transportation (WSDOT). WSDOT has over 40 wood fiber fills in operation in similar applications and has been extremely pleased with their performance. This design was rejected for the following reasons:

1) This alternative would result in leachate production by the fill. Leachate is high in oxygen demand, has a low pH, and a foul odor. The Washington State Department of Ecology has

been requesting that WSDOT wrap wood waste fills in impervious membrane. A 0.75mm PVC liner was designed into the system for this purpose. This required a leachate collection and a gas release system to be part of the design.

2) Wood fiber fills are subject to secondary settlement in the form of creep. Creep may continue to occur for a number of years and can amount to as high as 10% of the fill height.

3) The cost of this design was less than the cost of the aggregate fill design, but the permitting process for the use of this alternative would be too lengthy to justify the cost savings.

Alternative 4, Bottom Ash Fill

Bottom ash material consists of the "clinkers" from the bottom of coal burning furnaces at the power generating plant at Centrailia, Washington. This material has the consistency of volcanic pumice and weights about 13.3KN/m3 saturated and compacted in place and about 7.1KN/m3 dry. The material has excellent structural properties and makes good roadway fill. Based on discussions with testing agencies, it was concluded that this material was well below the EPA requirements for hazardous waste.

The design of the bottom ash fill proceeded similar to the design of the wood fiber fill with the weight of the fill material being changed to 13.3KN/m3 in the calculations.

The cost of the bottom ash fill was estimated to be $184,785. Transport of the bottom ash made the cost higher than other alternatives.

ENGINEERED FILL COST ESTIMATES - FIGURE 5

BRIDGE/FILL ALTERNATIVE	$414,634
AGGREGATE FILL	$165,478
WOOD FIBER FILL	$146,345
BOTTOM ASH FILL	$184,785

CONSTRUCTION

Construction began in September, 1991. The following construction steps were printed in the plans:

1) Clear roadway base area from STA. 12+50 to STA. 18+00 of all trees and brush. Cut the trees and brush down smooth to the ground. Leave the root mat in the ground.

2) Place the eight oz. (200g/m2) non-woven, needle punched geotextile on the roadway base and field sew the seams.

3) Place 12 inches (0.3m) of free draining gravel base material over the fabric to provide drainage for the underlying peat as it compresses and to provide a cover for the geotextile.

4) Place a two foot (0.6m) depth of the roadway fill on the outer third of each side of the fill form STA. 12+50 to STA. 18+00. Allow the initial fill to complete the primary settlement.

5) Place the remainder of the fill in one foot (0.3m) compacted lifts. Dead roll the material. Do not use a vibratory compactor.

6) A soils engineer from Rittenhouse-Zeman and Associates must be present to monitor the fill operation and to monitor the fill settlement.

7) The fill should be allowed to set through the Winter months and brought up to grade in the Spring. The pavement section should not be placed until authorization is obtained from the soils engineer. The cross section of the roadway embankment is shown in Figure 6.

ROAD EMBANKMENT CROSS SECTION - FIGURE 6

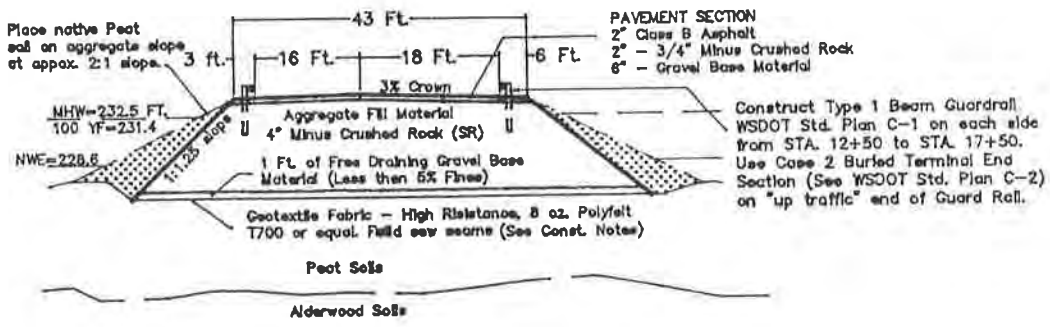

The site was cleared and the root mass was left in place. The 200g/m2 polypropylene, non-woven, needle punched geotextile was sewn together into two large panels by Seattle Tarp and delivered to the job site. The panels were spread out with seams running parallel to the roadway. Any wrinkles in the fabric were pulled out and a 0.3 meter thick drainage layer of free draining material was placed on the geotextile. This layer was followed by a 0.6 meter layer of fill initially placed on the outer third of the embankment.

The primary fill was left in place over the Winter and construction resumed in the Spring after primary settlement had taken place. The remainder of the fill was placed in 0.3 meter lifts and compacted. The paving section will be placed after primary settlement is complete. Settlement was measured through the Winter of 1991-92. The settlement closely followed the design settlement. Settlement readings at four points are shown in Figure 7.

ROADWAY SETTLEMENTS - FIGURE 7

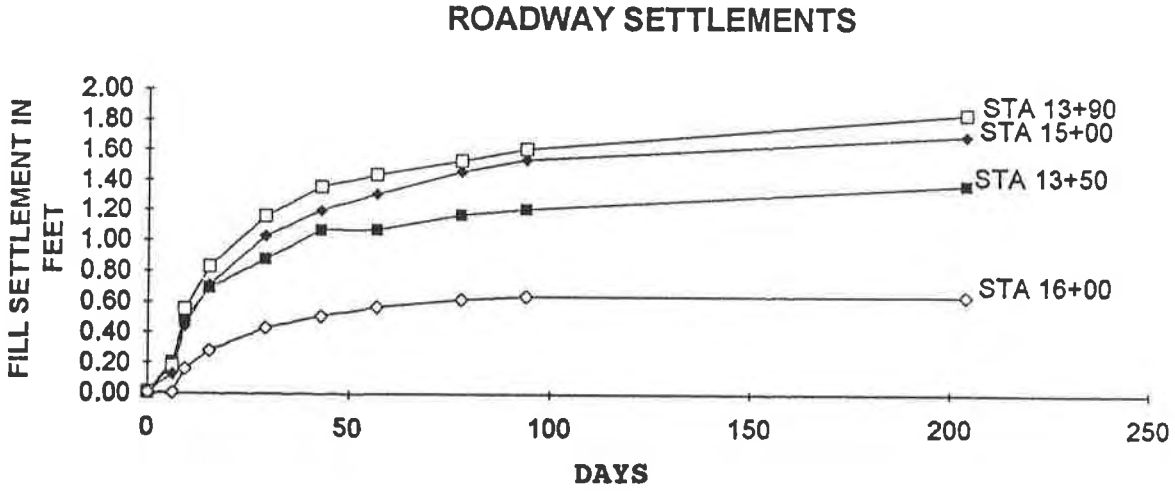

CONCLUSIONS

The redesign of 67th Street N.W. has produced a high quality roadway which meets the needs of the client and Pierce County. Using a geotextile in this application allowed for a design that met the environmental and economic needs of the client and provided a factor of safety which was acceptable to Pierce County.

ACKNOWLEDGEMENTS

The authors would like to thank the contractor for his assistance given us on this project. Jim Talman of Talmo, Inc. was very helpful in documenting and providing information to us. We would also like to thank RZA-AGRA for providing data for this paper. Al Kilian, Tony Allen, and Leroy Wilson of the Washington Department of Transportation were very helpful in sharing their knowledge with us.

REFERENCES

AASHTO M288-90 Standard Specifications for Geotextiles. (1990)

ASTM D4595 Test Method (1991), Annual Book of ASTM Standards, Section 4, Volume 04.08

Christopher, B.R. and Wagner, A.B. (1988) A Geotextile Reinforced Embankment for a Four Lane Divided Highway, Proceedings from 2nd International Conference on Case Histories in Geotechnical Engineering, St. Louis, MO., June, 1988.

Polyfelt, Inc. (1987) Design and Practice Manual, Polyfelt, Inc., Atlanta, GA.

Geogrid and Geotextile Reinforced Foundation for Major Refinery Processing Unit

G. Wharton
Star Enterprise, USA

W.J. Harper
Southwestern Laboratories, USA

C.M. Witt
Contech Construction Products, USA

ABSTRACT

This paper presents a case history of a project where multiple layers of geogrids and geotextiles were utilized to reinforce a granular fill section to create a large load distribution mat. This reinforced section served as foundation support for a major refinery processing unit. The existing soil consisted of a deep strata of primarily organic silt with relatively low shear strength.

The conventional solutions to this situation are described and consist of either excavating the poor soil to a depth of 6 metres (20 feet) and replacing with a competent soil or developing the required support with deep piles spaced very close together.

The layout and construction sequence of the geosynthetic alternate is presented along with discussions on how this load distribution mat was used to spread the surface loads over a series of piles.

Utilization of this concept allowed an increase in the spacing of the piles (decrease in number of piles required) by over 40%, thus saving considerable construction time and dollars.

Design methods for the geogrid/geotextile reinforced mat and modified load distribution effects are presented. Considerations relative to performance of the various options are discussed and general comparative cost data are provided.

SCOPE OF PROJECT

Star Enterprise undertook a new addition to the Residuum Processing facilities in late 1991 at their Port Arthur, Texas oil refinery. The new construction included two new refining process units built partially over the footprint of older defunct units. The new Sulphur Block Unit (SBU) and Hydrotreater Unit (HTU) are comprised of several major vessels and many smaller pieces of equipment: drums, exchangers, pumps and compressors. The major vessels are supported by deep piling groups; the smaller equipment by shallow individual piles. Concrete paving extends to the limits of the SBU and HTU and is supported at grade by the underlying soil. This paving is referred to as unit paving. The unit paving serves many purposes including providing support for

all non-pile supported piping and instrumentation, maintenance and operational access and water containment within the units. The new units are constructed on rectangular sites measuring roughly 91 metres (300 feet) by 107 metres (350 feet). The difficulty of the project comes from the poor support characteristics of the soils upon which the units are to be built. The upper soil strata is very weak and highly compressible to a depth of 6.1 metres (20 feet) and the underlying soil strata is comprised of moderate strength clay and silt to a depth of 6.1 metres (20 feet). Most structures and equipment of these sites are very sensitive to differential foundation movements. Differential settlement between the major vessels and the supporting network of piping can cause significant operational malfunctions.

The scope of the project was to create foundation support for the new processing units. The first step was to excavate 1.5 metres (5 feet) across the SBU site and 3.0 metres (10 feet) across the HTU site to remove the contaminated soils. This excavation would be replaced with imported fill material in order to raise the overall site elevation by 0.6 metres (2.0 feet). This would resort in a final elevation of 1.2 metres (4.0 feet) Mean Low Tide. The project engineer was, Bechtel Inc. Their goal was to design a system that would provide sufficient support while significantly limiting differential settlement. Brown & Root Construction was awarded the contract to construct the SBU and HTU sites.

SITE DESCRIPTION

The Star Enterprise plant is located in Port Arthur, Texas. The plant is located on the Beaumont Clay Formation which is comprised of clay, silt and sand. These soils largely represent fluvial, bay and interdistributary deltaic environment. They were deposited in a period of glacial ice retreat and the return of high sea level. Soil conditions at the SBU and HTU sites can be generalized as 4.5 to 6.1 metres (15 to 20 feet) of soft to very soft, highly plastic and sandy clay. The shear strengths generally ranged from 9.6 kN/m^2 to 16.8 kN/m^2 (200 to 350 psf). Liquid limits for these soils range from 30 to 80 percent and plasticity indices range from 10 to 50 percent. The natural moisture content for the soils ranged from 21 to 97 percent. This upper strata was underlaid by 3.0 to 6.1 metres (10 to 20 feet) of firm silty clay. It's shear strength values were 33.6 kN/m^2 to 62.4 kN/m^2 (700 to 1300 psf) followed by a 9.1 to 15.2 meter (30 to 50 foot) strata of stiff clay. Overall, the site is relatively level with surface elevations that vary from +0.6 to +1.2 meter (+2 to +4 feet). Construction at these sites is complicated by poor drainage and an average annual precipitation of 1346 mm (53 inches). Ground water elevations varied throughout the site with a worse case of +0.3 meter (+1.0 foot) and an average elevation of -4.8 meter (-16.0 feet). After 24 hours the water level in the open boreholes was at depths of .6 to 1.8 metres (2 to 6 feet).

PROJECT CONSTRAINTS/SOLUTION REQUIREMENTS

There were many conditions that needed to be met in order for a given solution to be accepted by all parties. Star Enterprise's conditions, the facility owner, were paramount. The problem was complicated by the fact that these new units were to be constructed within an existing and operating facility.

The main objectives for design and construction of the foundation support system were as

follows:

1. Limit long term differential settlement to 13 mm (1/2 inch)
2. Provide access to underground utilities internal to the sites
3. Complete construction in a timely fashion
4. Limit interference with existing facilities
5. Allow pile driving for major equipment to proceed with minimum hindrance
6. Raise the final elevation above existing grade by up to 0.6 metres (2 feet) to allow for drainage

CONVENTIONAL TECHNIQUES

In the early 80's a unit was built over these same soft soils with poor results. It was not uncommon to experience as much as 304 mm (12 inches) of differential settlement over a 25 year period. Therefore, Star Enterprise's main requirement was to limit long term differential settlement to 13 mm (1/2 inch) over a 25 year period.

This tight restraint led the geotechnical engineer, Southwestern Laboratories, to several costly and time consuming geotechnical recommendations.

The following is a discussion on each of the alternatives considered:

1. The first alternative was to excavate to a depth of 6 metres (20 feet) and replace the highly compressible soils with structural fill. The structural fill would be composed of clean sandy clay with a Plasticity Index between 10 and 20. This solution posed several problems. The sites were close to existing pipe racks which would have to be supported with temporary shoring. The excavation would need to be dewatered, which could become a major problem for a 6.1 metres (20 foot) deep excavation in an area with an elevation of +0.6 to +1.2 metres (+2 to +4 feet) Mean Low Tide . Brown and Root Construction became concerned when they considered that this operation could take as long as six months on a project with an already demanding schedule. Besides the excessive cost and construction time required, it was difficult to determine whether or not the settlement criterion could be met. Therefore, Southwestern Laboratories searched for another alternative.

2. The second major alternative considered was to transfer the pavement loads and the additional 0.6 metres (2 feet) of overburden, to a depth below the compressible clays to the stable soils by means of a deep foundation system such as driven piles. The design called for supporting the entire unit paving directly on 18.3 meter (60 foot) long timber piles, spaced as closely as 1.2 metres (4 feet) on center. There was no doubt the settlement criterion could be met but this option posed a few new problems. Running through the site was a series of buried electrical duct banks and underground piping that had to be installed and accessed. A great deal of coordination would have to be done so as to allow the utilities to be installed during the pile driving operation. This would cause the pile driving to be done in phases, which would be costly and slow. Once the utilities were surrounded by piling, they would be difficult to access in the future.

3. The third alternative, which is typical in tank foundation construction, was to pre-load the area with soil for accelerated consolidation. This solution may have yielded satisfactory results with some secondary treatment. However, the project did not have the luxury of sufficient time necessary for this technique.

4. The fourth alternative considered was to decrease the compressibility of the clays by deep lime/fly ash injection. A testing program was undertaken to determine the effects of this treatment. The test program failed to provide sufficient evidence of the level of required performance.

5. Several combinations of the above alternative solutions were considered, including partial excavation with piles. These attempts were abandoned either because they were too costly or time consuming.

In review of the proposed options to date, it was determined that none of the solutions yielded the results desired. During a meeting to discuss any remaining options, Gary Wharton, Offsites Project Manager of Star Enterprise, proposed a concept that stemmed from his experience in building tank foundations over deep soft soil strata. Mr. Wharton's proposed solution ultimately became the optimum solution as it met nearly all of the project requirements.

SOLUTION DETAILS

The main concept of the solution was to construct a granular load distribution mat which would be supported by a series of piles. The vertical influence of each pile would be enhanced or spread upward through the granular fill section, to support the surface loads. The primary support is offered by the series of piles that extend from the base of the load distribution mat to the underlying stronger soils. The primary function of the load distribution mat is to provide a mechanism to transfer the surface loads to the piling, while allowing for access to underground utilities. The thickness of this load distribution mat could be varied to allow for placement of the underground utilities, thus satisfying project requirement #2. This load distribution mat was reinforced with layers of geogrid to provide increased beam strength for bridging between the piles as well as increased shear strength at the pile tops to prevent the piles from punching through the crushed concrete. Layers of geotextile were placed above and below the granular fill section to prevent contamination from the adjacent fine grained soil zones. Figure 1 details the typical cross-section at the SBU site. Following is a description of this typical cross-section at the SBU site starting from the base and moving towards the top of the fill section. A discussion on material selection is presented in a subsequent section entitled Rationale for Geogrid and Geotextile Selection and Use.

- At elevation -0.9 meter (-3.0 feet), a layer of woven geotextile was placed separating the crushed concrete from the underlying fine grained soil.

- A layer of biaxial geogrid was placed directly on top of the geotextile to provide tensile reinforcement and lateral confinement of the crushed concrete, so that a construction platform could be constructed.

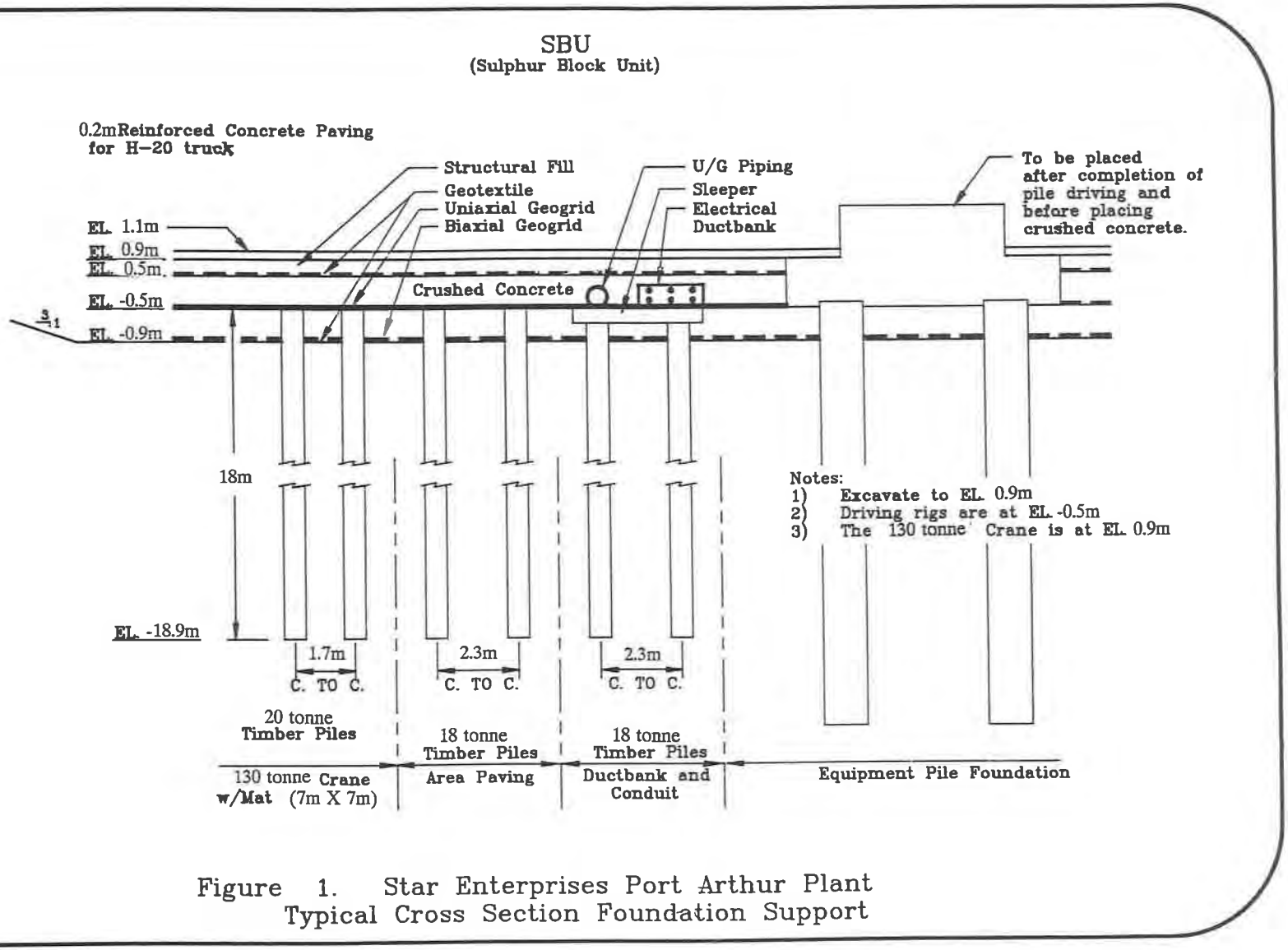

Figure 1. Star Enterprises Port Arthur Plant
Typical Cross Section Foundation Support

- An 0.5 meter (18 inches) thickness of crushed concrete was placed directly on the biaxial geogrid to provide adequate support for construction equipment.

- 18 meter (60 foot) long, 18 tonne (20 ton) capacity timber piles were driven through the above section, flush with the crushed concrete in a 2.3 m x 2.3 m (7'6" x 7'6") grid pattern.

- A layer of uniaxial geogrid, with a wide width tensile strength of 43.8 kN/m (250 lb/in) at 5% strain was placed directly on top of the driven piles to reinforce the crushed concrete section and provide additional shear strength at the pile tops.

- A 0.9 meter (36 inch) thickness of crushed concrete was placed directly on the uniaxial geogrid. The crushed concrete was placed in 0.2 meter (8 inch) lifts and compacted to 98% Standard Proctor Density. This provided a total reinforced thickness, including the initial 0.5 metres (18 inches) of crushed concrete, of 1.4 metres (54 inches). This reinforced thickness of crushed concrete was utilized as a load distribution mat to withstand the loads from a 136 tonne (150 ton) crane.

- A layer of non-woven geotextile was placed to separate the crushed limestone from the above fine grained structural fill.

- A 0.5 meter (18 inch) thickness of structural fill (low plasticity sandy clay) was placed on top of the geotextile to provide the required thickness necessary to fill the remaining thickness left from soil remediation. The structural fill was placed in 0.15 meter (6 inch) lifts and compacted to 98% Standard Proctor Density. This impervious layer also provides protection against runoff.

- A 0.2 meter (8 inch) thick reinforced concrete paving provided the final surface of the unit paving.

This pile supported geosynthetic reinforced load distribution mat proved to be a very cost effective. The initial 0.46 meter (18 inch) thickness of crushed concrete reinforced with geogrid created a stable platform for the pile driving rig to operate.

The initial 0.3 meter (12 inch) thick geosynthetic reinforced crushed concrete layer worked so well that loaded dump trucks were able to transport material over sections of the site that would not initially support the weight of bulldozers.

The pile driving operation proceeded at a fast and uninterrupted pace, because of the lack of interference with underground utility crews. The lack of additional excavation requirements allowed Brown and Root Construction to proceed without major dewatering or temporary shoring requirements.

Bechtel Inc. was satisfied that the differential settlement criterion could be met with this solution due to the fact that unit paving was essentially supported by the grid of piles.

The reinforced load distribution mat sufficiently transferred the pavement loads to the piling. Bechtel Inc. performed two separate design calculations to determine the adequacy of the reinforced pile supported mat to support the unit paving and anticipated loads. The findings of this analysis are presented in the subsequent section entitled Analysis and Design. The unit paving will be closely monitored to determine long term effects of this solution.

CONSTRUCTION SEQUENCE

The depth of the initial excavation was a function of the depth required for removal of contaminated soils and the space required to place the underground utilities. These depths were set by the project group as 1.4 metres (4.5 feet) for the SBU and 3.0 metres (10 feet) for the HTU. The original design called for a layer of woven geotextile to be rolled out over the completed excavation followed by 0.3 metres (12 inches) of crushed concrete. This was intended to serve as a working platform upon which to drive the loaded dump trucks. The biaxial geogrid was intended to be placed at this level prior to receiving an additional 0.15 metres (6 inches) of crushed concrete to create a final platform for the pile driving rig. At the SBU and the HTU, the subgrade was so soft that the woven geotextile with 0.3 meter (12 inches) of crushed concrete could not provide adequate support for the loaded trucks. It was decided that the biaxial geogrid should be moved down in the section and placed directly beneath the crushed concrete to provide additional reinforcement and lateral confinement.

This combination allowed the loaded trucks to haul material over a 0.3 meter (12 inch) section of crushed concrete. Upon placement of the remaining 0.15 metres (6 inches) of crushed concrete the site was ready for the pile driving operation. The pile driving rig was advanced onto the crushed concrete using crane mats for additional support. The timber piles were then driven through the crushed concrete, biaxial geogrid and geotextile section until flush to the surface. There was concern that driving the piles through the geogrid and geotextile would cause significant damage to these materials by vertically deforming them. It was because of these concerns that the geogrid and geotextile were sheared prior to pile driving by driving a flat sharp plate into the location of each pile. The piles were driven through this section with no difficulty or deformation. Pile driving also took place at this elevation for the equipment supports.

When all the piles were driven, concrete pile caps were poured for equipment supports. The uniaxial geogrid was then rolled out over the surface with a 0.15 meter (6 inch) overlap at adjacent rolls. The uniaxial geogrid was hand tensioned and tied together with plastic ties. The 0.9 meter (36 inch) thickness of crushed concrete was placed at this elevation and on top of the geogrid in 0.2 meter (8 inch) lifts. The upper layer of non-woven geotextile was then placed followed by the required thickness of structural fill. The 0.2 meter (8 inch) thick reinforced concrete unit paving was then poured on top of this section for the final surface.

A step-by-step construction sequence is detailed in Figure 2.

RATIONALE FOR GEOGRID AND GEOTEXTILE SELECTION AND USE

The specific geogrids and geotextiles used in this project were selected because they

DETAILED DESCRIPTION OF CONSTRUCTION SEQUENCE
SULPHUR BLOCK UNIT
SBU SITE

- Excavate to El - 0.9 metres (3 feet) over entire area, using a 3:1 slope. Slope surface (approx 1% slope) to outer perimeter drainage trenches.
- Cut drainage ditches around perimeter of site, fill with large stone (highly porous), and wrap with geotextile.
- Haul excavated material away from site.
- Spread geotextile fabric over surface, followed by a layer of Biaxial geogrid.
- Backfill with crushed concrete to a thickness of 0.5 metres (1.5 feet).
- Surface is now ready for pile driver to drive wood piles to support load distribution mat, which in turn will support the support the unit paving.
- Crane driver will spread crane mats over surface, now at El - 0.5 metres (1.5 feet), and begin driving unit paving piles. Piles to be 18 meter (60 foot) long untreated timber piles. Pile driver will drive piles until top of pile is flush with surface (no cut-off of the piles is required). This will permit pile driver good access over entire area.
- This surface will also be used to drive piles for equipment supports (wood, and step-taper), if very large mats are used to distribute the step-taper pile driver's weight.
- Pour concrete pile caps and pedestals for equipment supports, permit to cure and strip forms.
- Place layer of uniaxial geogrid over tops of unit paving piles.
- Place and compact a 0.9 meter (3 foot) deep layer of crushed concrete. This layer would extend from a depth of El - 0.5 metres (1.5 feet) up to El + 0.5 metres (1.5 feet).
- Spread geotextile over entire area, making cut-outs for existing pile caps.
- Backfill and compact with structural fill (probably a CL clay with plasticity index 10-20) to El 0.9 metres (3 feet) (bottom of 0.2 meter (8 inch) slab on grade).
- Pour reinforced concrete unit paving.

Figure 2 Construction Sequence

possessed the required physical properties as determined necessary during the design phase.

The woven geotextile placed at the base of the first lift of crushed concrete provided a separation function. A woven geotextile was chosen over a non-woven geotextile because of its ability to survive the heavy wheel loads of the construction equipment and the high abrasiveness of the crushed concrete. Initially it was thought that the woven geotextile might provide enough tensile strength to allow placement of the initial lifts of crushed concrete, thus allowing the biaxial geogrid to be placed in the center of the initial crushed concrete thickness. Due to the extremely soft soil the biaxial geogrid was moved to the base of the crushed concrete and the woven geotextile performed mainly the function of separation. Key characteristics included the following:

1. Adequate puncture resistance, > 711 N (160 lbs), per ASTM D4833
2. Adequate filtration characteristics, AOS > 50mm, per ASTM D4751-87
3. Adequate grab tensile strength, > 1.3 kN (300 lbs), per ASTM D4632-86

The biaxial geogrid placed at the base of the first lift of crushed concrete provided a tensile reinforcement and lateral confinement function. A biaxial geogrid was chosen because its open grid structure allowed a high degree of interlock with the crushed concrete and its high tensile modulus allowed the addition of the required tensile reinforcement necessary to construct a stiff working platform. The biaxial geogrid was used mainly as a construction expedient to allow placement of the initial lifts of crushed concrete as well as providing sufficient strength to allow access for the construction equipment. Key characteristics included the following:

1. Adequate tensile strength at low strain, tensile modulus @ 2% strain> 262 kN/m (1,500 lb/in), per GRI (Geosynthetic Research Institute) GG1-87.
2. Adequate positive interlock capability, open area > 60%
3. Ability to laterally confine and therefore strengthen granular base material, junction strength > 90%, flexural rigidity > 700,000 mg-cm, per ASTM D1388-64

The uniaxial geogrid placed at the top of the piles beneath the 0.9 meter (36 inch) crushed concrete thicknesses acted as a tensile element to add beam strength to the crushed concrete. A uniaxial geogrid was chosen because of its ability to provide a high degree of tensile reinforcement of the overlying crushed concrete, while possessing high shear strength to resist shear at the pile tops. The uniaxial geogrid chosen is composed of high density polyethylene which has shown excellent chemical compatibility with the materials present at the processing unit. This feature combined with the proven resistance of this material to construction damage made it a good choice for the reinforcement element of the crushed concrete. Key characteristics included the following:

1. High tensile strength at low strain, tensile strength at 5% strain > 43.8 kN/m (250 lb/in), tensile modulus @ 2% strain> 1,750 kN/m (10,000 lb/in), per GRI GG1-87
2. Proven long term resistance to creep deformation under sustained load, design life in excess of 100 years
3. Ability to interlock with surrounding crushed concrete, coefficient of interaction > 0.8, per GRI GG5
4. Adequate durability to maintain reinforcement design characteristics for life of project, chemical and biological compatibility within site material and petrochemical petroleum distillates

The primary function of the non-woven geotextile placed beneath the structural fill was to

separate the fines from the crushed concrete. Therefore, the key characteristics included the following:

1. Adequate puncture resistance, > 222 N (50 lbs), per ASTM D4833
2. Adequate filtration characteristics, AOS > 70mm, per ASTM D4751-87

ANALYSIS AND DESIGN

The basic concept is to reinforce the crushed concrete with geogrid to create a composite structure. This composite geogrid reinforced crushed concrete mat improves the vertical influence of each pile, upward from the pile tops. If geogrid was not used to reinforce the overlying crushed concrete, the degree of load spread through this material would be lessened. This concept of improved verticale pile influence is illustrated in figure 3.

The upward influence of each pile can be approximated as an inverted pyramid or cone. If the influence lines of a pile extending upward intersects those of an adjacent pile (to a high enough degree), this horizontal pile spacing will allow adequate support to be provided, given adequate bearing support of the piles themselves.

Two methods of analysis were employed by Bechtel Inc. to determine the adequacy of the load distribution mat to transfer the anticipated load from the unit paving to the piles.

Primary Method of Analysis

The primary method analyzes the geogrid in the load distribution mat as a tension membrane. This method of analysis is utilized in designing geogrid reinforcement for landfill lining support systems. The design theory is as follows:

When a depression forms below a layer of geogrid reinforcement supporting a landfill lining or cover system, the reinforcement deflects into the depression. The deflection has two effects: arching of the fill materials overlying the reinforcement and tensioning of the geogrid reinforcement.

The arching of the fill materials generates arching inside of the fill materials, which transfers part of the applied load away from the depression. As a result, the vertical stress acting on the reinforcement over the depression is smaller than the vertical stress due to the weight of the overlying fill materials and an applied surcharge, q.

The tensioning of the reinforcement mobilizes a portion of the reinforcement's tensile strength, T. Consequently, the reinforcement acts as a tensioned membrane and can carry a load applied normal to its surface.

The design method utilized combines the arching of the fill materials (arching theory) with the tensioning of the reinforcement (tensioned membrane theory). As a consequence, the reinforcement will only feel a portion of the applied load.

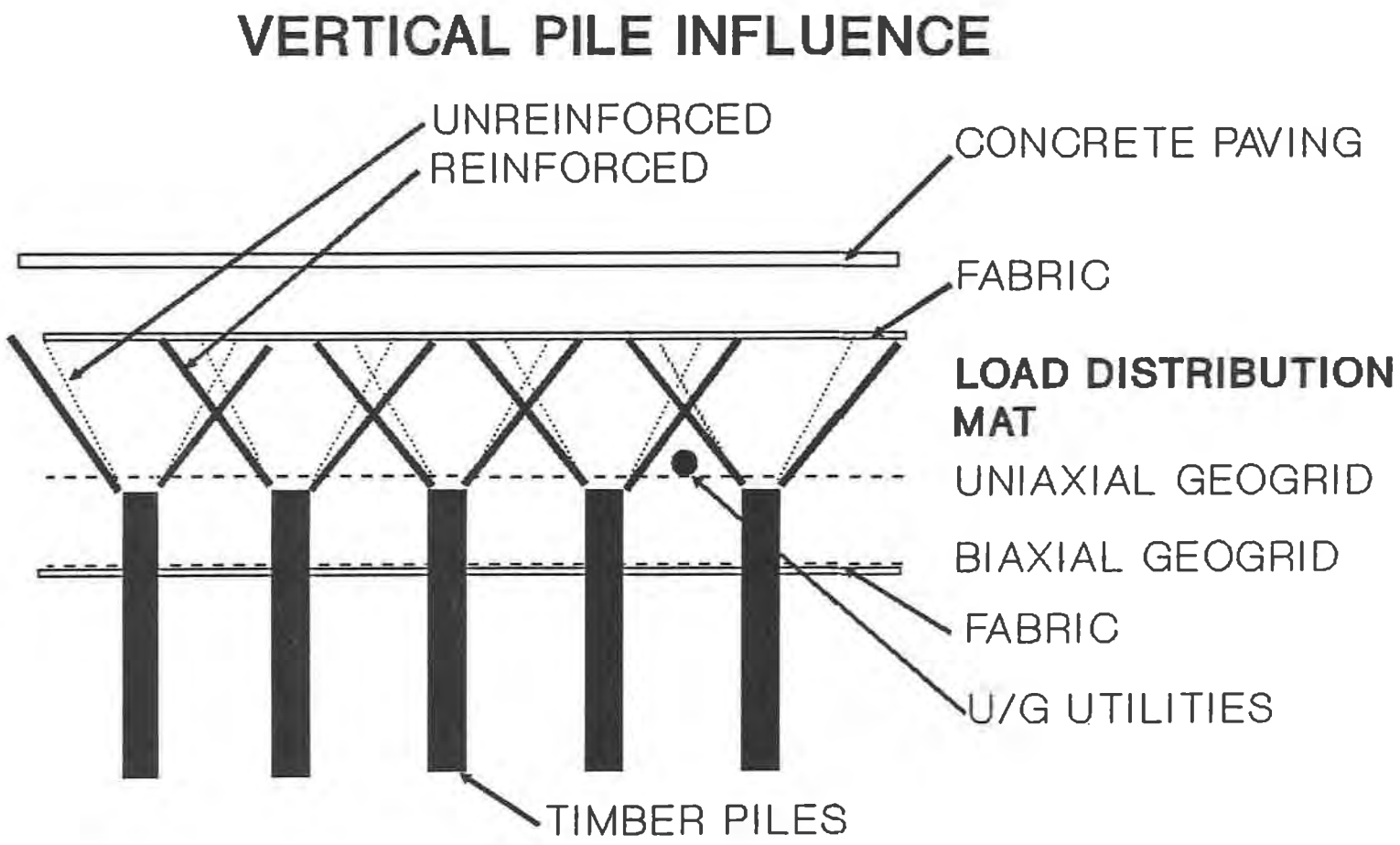

Figure 3. Basic Concept of Vertical Pile Influence Through Load Distribution Mat

Although arching of fill material is generally not fully developed until the fill thickness above the depression is several times greater than the depression radius, the high degree of angularity coupled with geogrid reinforcement suggests that a degree of arching is present.

The design methodology utilized is similar to that used to determine the geogrid reinforcement required to bridge over a depression in a landfill. However, by replacing the depression with the span between piles, the analogy becomes clear. If the maximum diagonal distance between piles is chosen as the depression diameter a tensile force required to support the overlying soils and live load can be calculated. It was determined that a single layer of uniaxial geogrid with a working strength of 43.8 kN/m (250 lb/in) would provide adequate tensile reinforcement.

Secondary Method of Analysis

The second method of analysis was generated by Bechtel's structural department, wherein the reinforced crushed concrete was analyzed as a column supported slab. A compressive strength, f'_c of 553 kN/m² (80 psi) was assumed for the reinforced crushed concrete. The analysis checked punching shear and beam shear along with an analysis of the maximum load per pile versus the allowable load rating for each pile. This analysis concurred with the tension membrane analysis, that a single layer of uniaxial geogrid placed at the base of a 0.9 meter (36 inch) thickness of crushed concrete would provide sufficient beam strength.

The pile spacing of 2.3 metres (7'6") center-to-center, as generated by the design, provides an allowable increase in pile spacing from that of the original geotechnical recommendation of 1.2 metres (4 feet) center-to-center for the HTU. Utilization of the load distribution mat allowed for increased pile spacing in excess of 40 %. This correlated to significant savings in construction time and dollars at the HTU site as approximately 1500 piles were eliminated. If the cost of a driven pile is $300.00, the savings were in excess of $450,000.00.

CONCLUSION

Many of the difficulties associated with constructing a process unit over a deep soft soil strata were overcome by the use of the load distribution mat supported by piles. The foundation portion of this project was constructed during the rainy season which would have caused many delays for the conventional solutions. The project has recently been completed and the processing units were activated 3 months ahead of schedule. The project manager states that the early project completion was due in large part to the speed at which the foundation support was developed, allowing above grade construction to proceed ahead of schedule.

It is expected that the settlement criterion will be met with this solution. Visual inspection had shown no settlement one month after completion of the project. Settlement of the process units will be monitored by the project manager over a 25 year period. Since the project has been completed for only 3 months, there is no other performance data available at this time. The settlement measurements will be charted over time and the performance of the system will be studied.

From the experience in design and construction of the geosynthetic reinforced granular load

distribution mat for Star Enterprise the following conclusions can be drawn:

- Granular load distribution mats reinforced with geosynthetics can offer good support characteristics and limit differential settlements when constructing over deep strata of soft soil.

- Due to the increased load spreading capabilities or beam strength of the geosynthetic reinforced crushed concrete, the horizontal spacing of the supporting piles can be increased by up to 40%.

- Compared to the conventional techniques currently being used to provide foundation support in deep soil strata, the load distribution mat supported by piles offers considerable savings in construction time and dollars.

- The combination of biaxial geogrid and geotextile placed beneath a granular layer can allow construction access and create a working platform over very soft soils, where construction might otherwise be very difficult.

ACKNOWLEDGEMENTS

This paper is presented with permission of Mr. Lee Townsend, Area Manager for Star Enterprise, Port Arthur Plant. The authors would like to express their appreciation to their colleagues who were involved in the design and construction of this unique problem solution.

REFERENCES

(1) Tensar Corporation, (1989), Tensar Geogrid Reinforcement of Landfill Soil Veneer Covers, Tensar Technical note TTN:WM2.

(2) Bonaparte, R. and Berg, R. R., "The Use of Polyer Geosynthetics to Support Roadways over Sinkhole Prone Areas", Proceedings, Second Multidisciplinary Conference on Sinkholes and the Environmental Impacts of Karsts. Orlando, FL, Feb 1987, pp. 437-445.

(3) Giroud, J. P., Bonaparte, R., Beech, J. F., and Gross, B. A., "Load-Carrying Capacity of a Soil Layer Supported by a Geosynthetic", Proceedings of International Geotechnical Symposium on Theory and Practice of Earth Reinforcement, Fukuoka, Japan, Oct 1988, pp. 185-190.

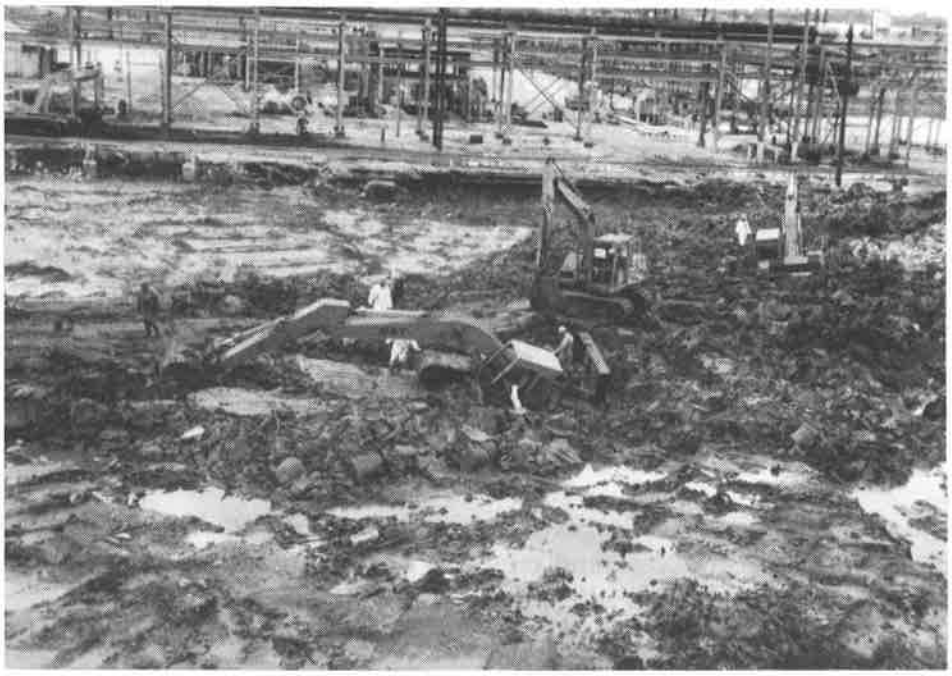

PHOTO 1: Hydrotreater Unit site during initial excavation. Photo shows excavation equipment that had sunk into the soft soils and was being extracted by a third piece of equipment.

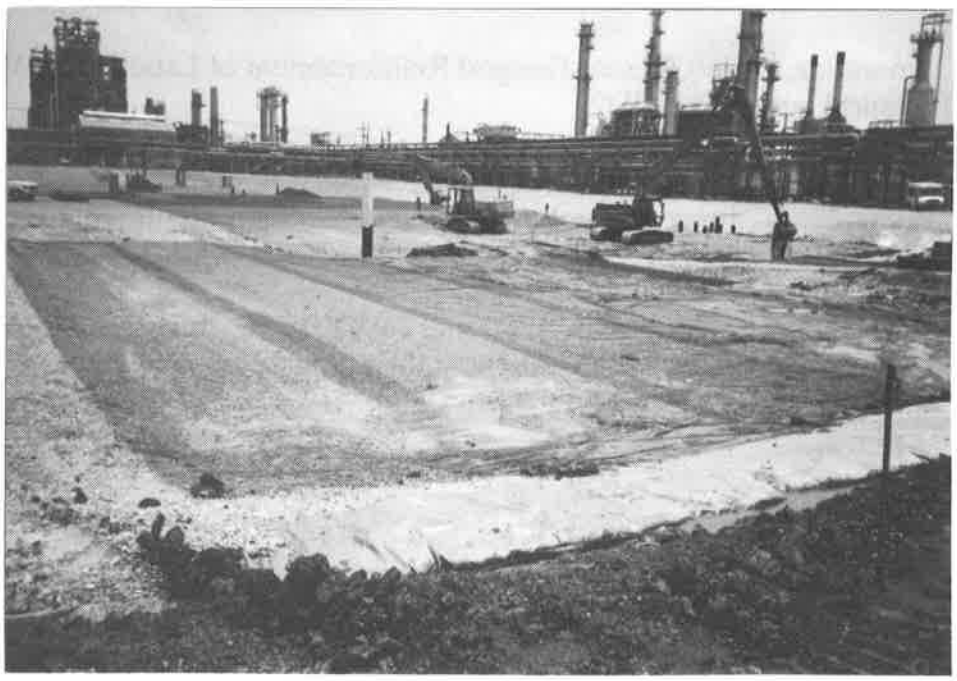

PHOTO 2: Initial lift of crushed concrete being placed on top of geotextile and biaxial geogrid at HTU site.

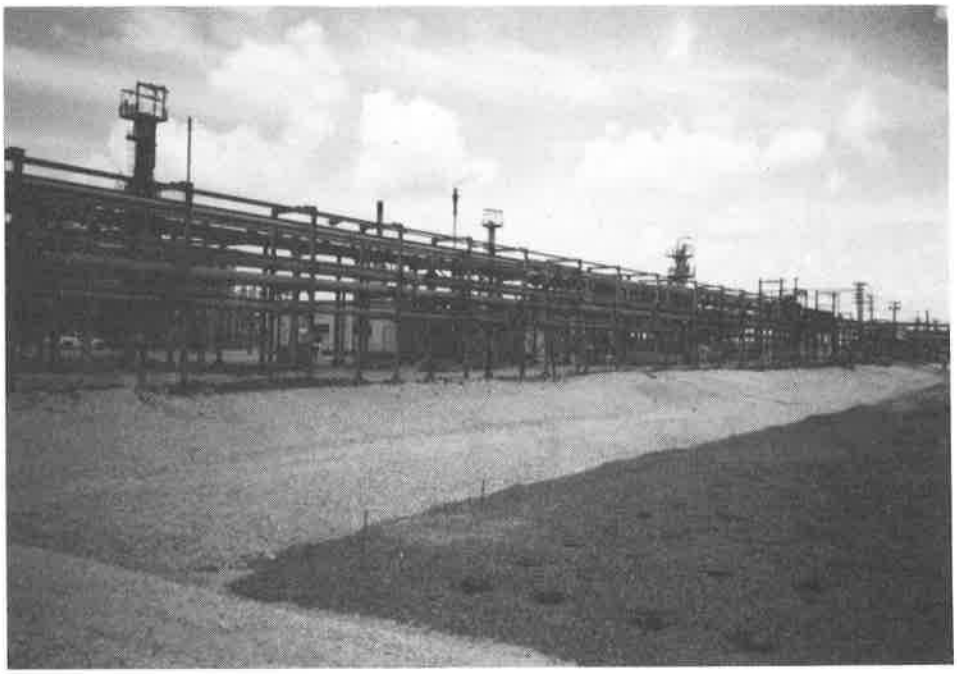

PHOTO 3: Hydrotreater Unit after piles have been driven through the initial 0.46 meter (18 inch) lift of crushed concrete, just prior to uniaxial geogrid placement. Pile tops can be seen in foreground.

PHOTO 4: Sulphur Block Unit Site with geosynthetic reinforced crushed concrete load distribution mat in place. Ready for concrete unit paving.

Geogrid Reinforcement Provides Additional Safety Beneath Buildings in Karst Terrain

A.W. Cadden
Schnabel Engineering Associates Inc. USA

J.S. Bailey II
Tensar Earth Technologies Inc., USA

ABSTRACT

Development in karstic geologic regions poses many potential foundation engineering problems and risks. Typical construction in this geology involves removal of the overburden to reveal potential solution features, grouting the surface of the rock, then backfilling to the design grades, or constructing a concrete mat to span the building area. Alternatively, deep foundations attempting to bear on solid rock are used. Site development with these foundation schemes often proves to be very expensive and is typically riddled with construction cost overruns. Geogrid reinforced mats of dense-graded crushed stone have been utilized, by the authors, on several low rise commercial/industrial projects in order to dissipate the foundation stresses above the soft residual soils. The inclusion of high density polyethylene geogrid at the base of the stone mat provides an additional margin of safety should sinkholes develop beneath the structure following construction. The design and construction of low rise commercial/industrial facilities often require accommodation of loading dock walls and main utility routes within the building limits. The flexibility of placing fill and geosynthetics allows these structures to be handled easily. Experience with this system has also been found to be well suited for preloading of the building area to further limit post construction settlement from floor slab loading over soft overburden soils. This method has proven to be an efficient and cost effective construction technique which is not as adversely affected as traditional foundation schemes are by subsurface uncertainties, such as variable depths of soft overburden soils and the questionable quality of the underlying rock.

INTRODUCTION

The karstic geologies encountered throughout the central and western portions of the mid Atlantic region generally consist of overburden soils which are highly variable in consistency and often become softer near the rock surfaces due to on-going chemical weathering and subsurface erosion. These soils are, therefore, not conducive to shallow foundation support.

Deep foundations consisting of drilled shafts or driven piles are often recommended to limit inherent risks associated with structures over karst geologies. The authors' experience has been that the construction cost overruns typically associated with installation of these foundations are a result of the very same geologic reasons they were selected. The rock surface is highly variable, containing pinnacles, floating boulders and troughs. Driven foundations encountering these features result in highly variable driving lengths and an uncertain final bearing material. Drilled shafts have been used to reduce these uncertainties. In a drilled shaft the bearing material can be inspected directly. However, these foundations still encounter the rock surface at variable depths, requiring costly rock excavation by machine or hand. In addition, probes in the base of these foundations often reveal voids beneath the surface of the rock, requiring further rock removal.

The propagation of solution features is often accelerated by changes in surface or subsurface conditions from construction vibrations, redirection of surface runoff or the creation of impoundments, changes in the overburden depth, and variations in hydrostatic levels and flow volumes. These factors often result in development of sinkholes during construction. Factors such as leaking underground utilities or uncontrolled stormwater runoff around the structures can also lead to problems following completion of construction. The risk of problems following construction can be greatly reduced by considering these factors in the final design to minimize future variations.

Low rise commercial/industrial facilities are typically supported by shallow foundations where suitable soils are present within the zone of stress influence beneath the foundations. In karst geologies these soils are generally not suitable for direct support of shallow foundations. As discussed by DeStephen (1992) construction in karst regions requires not only detailed engineering but also education of the client to the risks of future problems associated with the potential for sinkhole development. The authors have designed several projects of this type incorporating a geogrid-reinforced crushed stone mat to distribute foundation stresses over the soft soils and provide an added measure of safety beneath the structure if a sinkhole should occur in the future, thus limiting the client's risk exposure.

SUBSURFACE EXPLORATION AND TYPICAL SITE GEOLOGY

Subsurface exploration to establish the individual site characteristics is considered essential for any project. Good engineering practice requires test borings to be used to give a general indication of the site conditions. However, due to the variability of karstic sites, excessive exploration programs will not provide any clearer understanding of the subsurface conditions. The benefit from the additional costs of a tight boring spacing is generally not justified.

The Cambrian and Ordovician age limestones and dolomites throughout central and eastern Pennsylvania typify karstic geologies. These formations are highly variable and known to be susceptible to solution features. Figure 1 shows a cross section of conditions which could be interpolated from several borings at a site underlain by a carbonate formation. Conditions similar to this have been observed by the authors in the field, once the overburden has been removed from a site, and are not uncommon. The results of these subsurface features projected

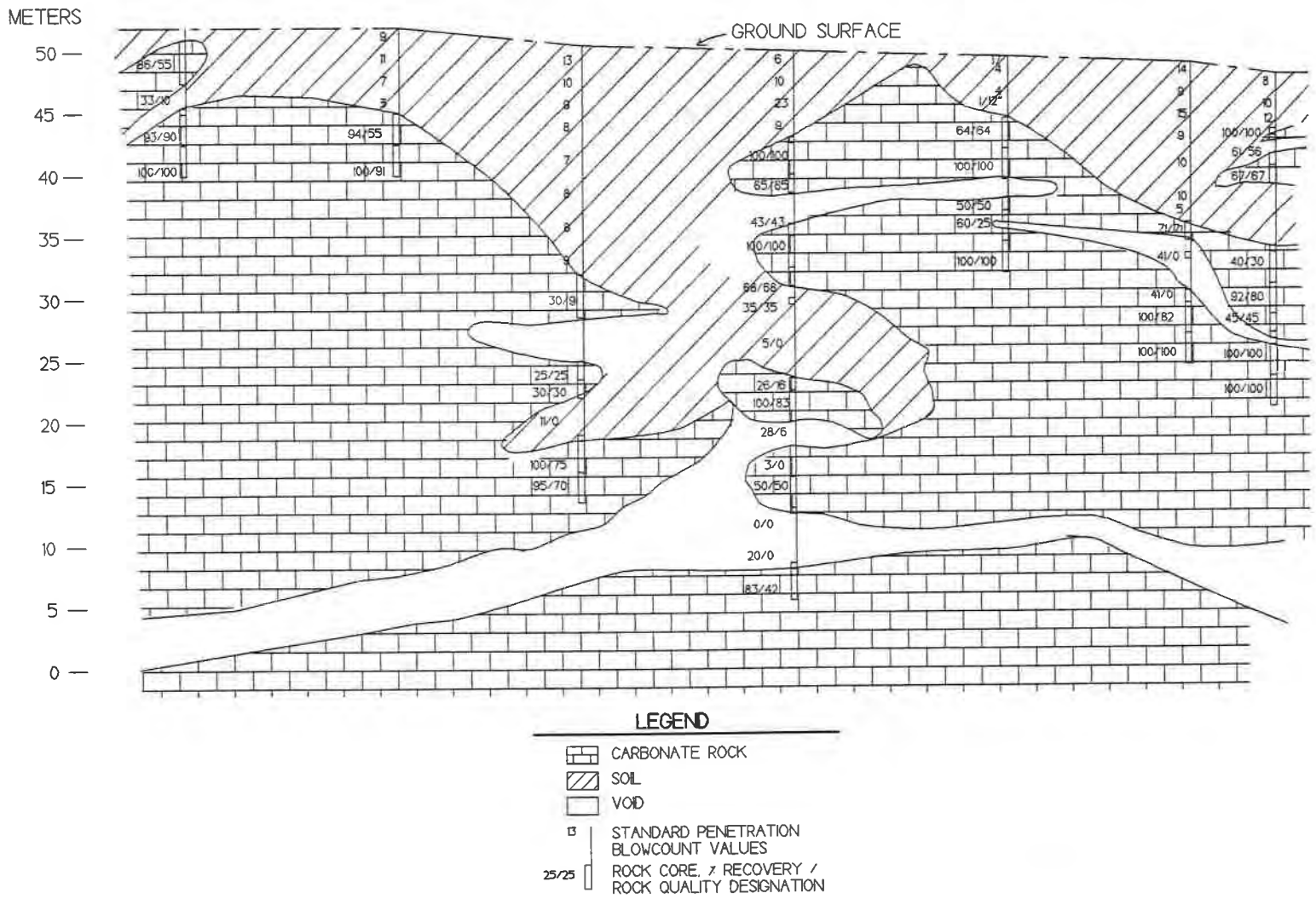

Figure 1. Typical Subsurface Profile

The overburden soils are generally fine grain material varying from medium stiff to very soft consistency. Zones of very soft, unconsolidated material are often encountered near the rock surface where solutioning of the bedrock is continuing and erosion of the overburden soils occurs into the voids or fractures in the rock. The depth of the overburden is also highly variable, often ranging from less than 2 to more than 15 meters at any one site.

Laboratory Tests. Physical soil laboratory test data on overburden soils accumulated through our experience indicates that these soils are generally silt (ML) and lean clay (CL) with variable amounts of sand and gravel size particles. These soils generally contain about 60 to 80 percent material finer by weight than the 75μm sieve. The measured Atterberg Limits generally vary from non-plastic to having liquid limits and plasticity indices of about 40 and 15, respectively. Natural moisture contents of 20 to 30 percent and dry densities of about 1300 kg/m^3 are typical. Additionally, consolidation tests performed on material typical of soils obtained from enhanced weathered zones often indicate that these soils behave as if they were normally to underconsolidated, with a compression ratio on the order of about CR = 0.15.

TYPICAL FOUNDATION EVALUATIONS

In the design of foundations for projects in karstic geologic areas, consideration is given to various foundation alternatives, including: deep foundations, shallow spread footings, and reinforced concrete mats. Limited or total excavation and replacement of the overburden soils and treatment of the rock surface are also often considered as a part of shallow foundation alternatives.

As discussed previously, great difficulty and costs are typically associated with driven pile and drilled shaft foundations in this geology. To further compensate for these risks, many designers and highway departments have resorted to designing redundancies into pile foundations which adds to their cost. For example, the Pennsylvania Department of Transportation has recommended that driven foundation systems be used only if the design considers that 35 percent of the driven members will lose their capacity. This requires additional piles to be driven and the pile caps to be designed so that they are not adversely affected by the loss of pile support in random locations; all of which results in additional costs. Difficulties and large costs in drilled shaft construction include: additional rock excavation, bulging of the shaft during concrete placement, or the necessity to provide permanent steel casing through very soft strata or voidaceous rock.

Concrete mat foundations have been used to support structures and provide a spanning capability if solution features occur beneath the building. Due to the required structural details, the initial costs associated with these foundations are typically high. The variability in the subsurface conditions may also require ground improvement or surcharging to reduce differential settlements to acceptable limits.

Lime or cement treating of soil to create a stiffer mat to distribute loads has also been attempted over soft soils. However, this solution is not considered viable where there is a potential for loss of support since the

structural capacity of the system would not be sufficient to span a solution cavity opening and protect the structure.

Shallow foundations have often been used following complete or partial removal of the overburden soil, treating the rock surface and replacing the area with compacted structural fill. The general variation in the rock surface across a site could require removing overburden soil to depths of up to six meters or more based on the typical stress influence of a soil supported foundation for a low rise commercial/industrial structure with loads of about 1300 kN. However, where the surface of rock is greater than the planned excavation depth, providing long term protection to the foundations and floor can require further excavation to remove soft soils or utilization of ground improvement techniques. Substantial difficulties and expense occur in performing excavations to such depths, especially where existing facilities are nearby.

Other techniques such as deep dynamic compaction, slurry and compaction grouting, or vibro replacement/compaction are being used to induce densification of the overburden soils, thus reducing the risk of future problems following construction, and improving the soils for foundation support. Although generally less costly than deep foundations, these techniques are also often hindered by adjacent facilities.

The risks, uncertainties and potential costs of deep and shallow foundations as well as ground improvement techniques have given cause to explore alternative solutions for lightweight structures which are a large portion of the construction projects throughout karstic regions in Pennsylvania.

GEOSYNTHETIC REINFORCED FOUNDATION ALTERNATIVE

The authors sought a solution which would limit the risk of future damage resulting from the development of solution features following construction. Reducing the costs and difficulties associated with ground improvement or very large excavations was also desired. Reinforced fill has been used extensively to increase bearing capacity and bridge soft subgrade problems. The authors saw this as a means to limit both the depth of undercut as well as direct foundation costs such as footing size. In addition, the use of geosynthetics was explored as a means for reducing the risk of major foundation distortion if a sinkhole occurred. This would reduce costs and overall construction difficulties.

The solution alternatives were evaluated based on constructability, cost and degree of risk of future damage to the structure and its contents while in service. Each of these factors was considered to directly effect a project and the acceptability of the solution to an owner.

Since a reinforced soil mat could not be analyzed as a rigid structure, it was evaluated based on its ability to limit the risk of a catastrophic occurrence. The design for spanning voids with geosynthetics is based on the principle that the reinforcement has no ability to carry moments. Therefore, the reinforcement must deflect into the void to develop the tensile resistance to support the vertical loads applied. The variables in the design are the size of the void, the loads above the void, the maximum allowable deflection (i.e. strain) of the reinforcement and cost. The performance properties of geosynthetics indicate a predictable time related increase in strain under

sustained loading. Therefore, permanent or temporary support can be designed for the structure. The addition of more geosynthetic can reduce the long term strain under a sustained load; however, the associated costs of more material to achieve this increase dramatically.

Once a ground loss occurs, continued solutioning and collapse will take place, resulting in an enlarging of the void over time. The designer must take this into account when a permanent support system is evaluated.

The authors chose to design systems which give an indication of the presence of changing subsurface conditions so that remedial measures can be taken to stabilize and repair them, thus stopping further propagation of the void. By designing a temporary support mechanism which allows limited deflection, the distress to the structural elements can be controlled to within tolerable limits and repairs made before further damage occurs. The geosynthetic material acts as an added safety component in the system, a "safety net", designed only to be utilized when and if a cavity occurs and then just long enough for repairs to be made to restore the soil support to the structure.

Development of the design for a geosynthetic reinforced soil mat foundation requires a combined solution of limiting the stress influence of the new structure on the natural overburden as well as providing sufficient composite strength to temporarily span a developing solution feature. Several geosynthetic reinforced mats are in service for confidential clients of the authors. These are providing a cost effective solution adapted to the specific requirements of the sites.

FOUNDATION DESIGN EXAMPLE

The final design of a geosynthetic reinforced soil mat for support of a structure involves many site and structure specific parameters. In order to describe this process, an example of a typical manufacturing facility is presented which is based on a composite of the authors' experiences.

This facility will be located in a karstic geologic region with rock depths which vary from 1 to 15 meters within an 85 by 85 meter plan area. The overburden soils consist of fine grain soil with Standard Penetration Blowcount values of 1 to more than 30. The low blowcount values are typically present at depths of more than 10 meters. Rock core samples indicate variable quality and the presence of voids greater than one meter thick within the rock mass. The facility will have floor loads of about 25 kPa and maximum column loads of about 1300 kN.

Evaluation of Stress Influence. The stress influence resulting from the foundations and floors of this project is considered too great for support by the natural soils without inducing excessive settlement. In order to control this settlement, limited excavation and replacement of the overburden soil with compacted structural fill is required to the depth where the foundation stress is sufficiently dissipated so that the natural soils can support the increased load. Controlling the magnitude of settlement to an acceptable range is a critical factor in the overall cost of this foundation system. Dense-graded crushed stone fill is used in the design to allow a relatively high foundation bearing

pressure, thus minimizing the size of the foundation elements, depth of stress influence and, therefore, the depth of the excavation.

For this facility, an allowable bearing pressure of 300 kPa is recommended for the foundation design. A bearing pressure of up to about 400 to 500 kPa can be permitted for transient loads but is not considered reasonable for the sustained loads. Foundations are, therefore, sized to have lateral dimensions on the order of 1.5 to 2.0 meters. The necessary thickness of the replacement fill is then evaluated and set to limit the increased stress on the natural soils due to the new foundations to less than about 20 percent of the design bearing pressure. This will result in post construction settlement of less than about 25 mm in this case. A minimum of 2.5 meters of crushed stone fill is therefore necessary beneath the foundations.

The increase in stress due to the application of the uniform floor load, however, can not be dissipated by a stone mat since this behaves more like an area load for the limited depth considered. Therefore, surcharge loading equal to at least 150 percent of the design floor load is recommended to induce this settlement before foundations are constructed. Once the settlement due to this load has essentially ceased, the surcharge can be removed and construction of the foundation commenced.

Determination of Design Void Size and Propagation. Estimation of the potential size of the void likely to occur within the underlying rock and induce a solution feature at the ground surface is a prime site specific requirement. Cavities encountered in the test borings provide some guidance in this endeavor. This, coupled with the expected size of the foundation elements, leads to the selection of a critical void size of 2.0 m in diameter for this example.

Based on a review of available literature on the propagation of sinkholes, the authors have found that two possible shapes are likely to result from a cavity collapse. The first is discussed by Scarborough et al (1989) who presented empirical information related to similar geology in Tennessee which allowed estimation of the vertical surface displacement based on profile functions. The calculated surface deformation of an inverse cone-shaped feature, resulting from a two meter diameter void at a depth of six meters below the ground surface, would be about 40 mm based on Scarborough's discussion.

The second possible void propagation is described by Chen and Beck (1989). Their findings indicate the possibility that development of the void would be cylindrical and would propagate in this manner to the ground surface in stratified overburden containing cohesive layers which is typical in this geology. A collapse of this type is described to occur very quickly in laboratory tests once the underlying support deteriorated.

Since the calculated deformation from the inverse cone development is relatively minor, the remaining soils within the feature are believed to continue to provide some limited support of the overlying loads. Thus the more conservative design approach is the concept of developing a cylindrical-shaped, infinite, solution cavity with no remaining soil within the limits of the feature to resist the overlying foundation stresses. The worst case would be if such a void is occurring directly beneath a fully loaded column foundation. In this case the resulting surface feature would encompass an entire foundation element.

This scenario is considered appropriate and thus utilized throughout the remainder of the design.

Safety Net Design. The method of combining arching theory of fill soil over a geosynthetic with tension membrane theory of geosynthetic reinforcement has been applied to landfill lining systems, roadways and building foundations for the past several years. This design methodology was discussed by the Tensar Corporation (1989) and is based on published information by Giroud (1981 and 1982), Bonapart and Berg (1987), and Giroud, et al (1988).

Utilizing the above discussion of the critical factors, i.e. vertical stress, maximum allowable vertical deflection and design void parameters, a required geosynthetic tensile strength of 26 kN/m is calculated for the footing encompassed by a circular void. The design methodology reqires this strength to be developed by geosynthetics oriented orthogonally.

Geosynthetic Material Selection Criteria. For the purpose of this example, the authors chose to use the following criteria. First, the above design strength is based on limiting the strain in the geosynthetic to a maximum of five percent after one year of sustained loading. This is sufficiently conservative since once the deflection of the structure is noticed, complete repairs are expected to be completed in a much shorter period of time. Second, the geosynthetic is to be sufficiently inert to the effects of high pH (alkaline) solutions which can be formed by calcareous materials and groundwater in order to maintain its integrity for the entire design life of the structure. The geosynthetic as a "safety net" will not experience substantial use until a sinkhole occurs, which could be any time during the useful life of the structure. Thus, the material could remain in a potentially alkaline environment for a long time before it is needed. Third, the reinforcement must have documented testing for installation damage with compacted crushed stone fill. The potential for damage to the geosynthetic from placement and compaction of angular crushed stone would reduce the total structural capacity of the material. These requirements guard against strength reductions would not become apparent until a failure occurred. Use of the material in a similar application is also desired.

Based on these criteria, two layers of Tensar UX 1600 polyethylene geogrids could be specified to be placed with their principal axes at 90 degrees to each other, extending past the building edges to a minimum distance of 1.5 m on each side of the facility. In actual projects the authors have completed, this has been the geosynthetic used. Figure 2 shows a design cross section of a geogrid reinforced mat.

Data which was provided by the Tensar Corporation to support this choice is the result of testing performed in accordance with Geosynthetic Research Institute Standards for Long Term Design Strength of Stiff Grids (GRI-GG4, 1990). An installation list of foundation reinforcement projects for roads, buildings and landfills was also provided.

It should be noted that alternative materials were submitted by contractors on actual projects. A submission for a polypropylene fabric was not accepted since the manufacturer did not have testing information available to confirm the sustained load (creep) and installation damage criteria requirements desired. Another submission for a polyester geogrid was not considered acceptable due to

the lack of EPA 90/90 testing and information published by a number of sources, including Elias (1980) and Montalvo (1989), indicating accelerated hydrolysis of polyester fibers in alkaline environments. Also, neither alternative manufacturer was able to provide an installation list of similar projects.

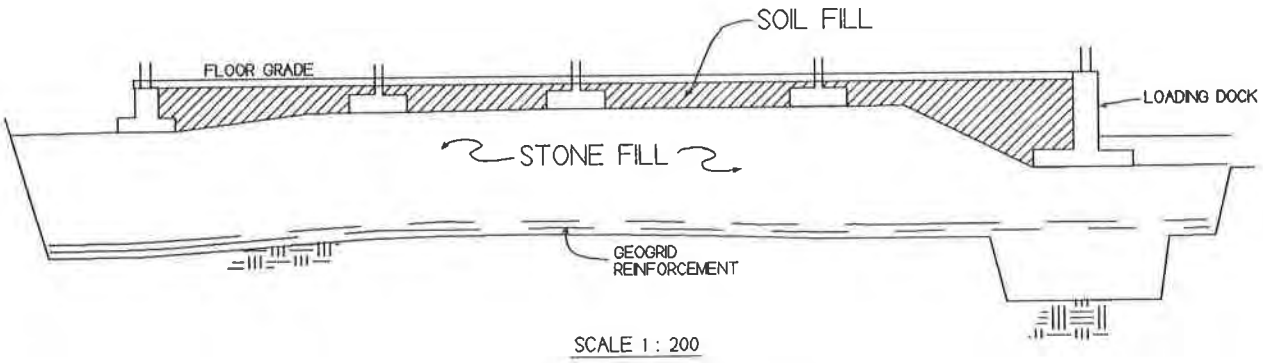

Figure 2. Geogrid Reinforced Mat System Cross Section

CONCLUSIONS

This foundation scheme has been presented to the owners and design teams of several projects. The system limits the settlement of structures, both total and differential, in areas which are highly variable and typically not well suited for foundation loads supported by shallow foundations. In addition, the solution limits the cost of mass excavation and replacement with compacted fill, the initial costs of a concrete mat foundation, and the uncertainties and overrun costs associated with deep foundations. Eliminating the extent of the excavation or potential construction difficulties has also helped maintain tight construction schedules.

Since it is known that the risk of developing solution features is greatest during construction and that measures can be taken in the design to limit the causal factors such as surface water collection or seepage near the structure after construction, the owners are able to optimize the selection of design options tailored to the adverse geologic conditions. The geosynthetic reinforcing provides a measure of protection to the owner against risks to occupants and property when the facility is complete.

Should a sinkhole occur beneath the structure following construction, the reinforcing "safety net" is in place to help support the structure until remedial action can be taken. This would likely involve compaction grouting to fill the void which has occurred and repairing and realigning the structural elements affected.

Construction in karstic regions requires owners to acknowledge the potential and risk of loss in the event of a sinkhole forming under the structure. The previous response has been to expend large amounts of capital to guard against such failures using traditional construction techniques. The use of a geosynthetic reinforced soil mat gives the designer and the owner the opportunity to balance an estimated cost savings of potentially millions of dollars against the limited risk and costs associated with future repairs.

ACKNOWLEDGEMENTS

The authors would like to thank their peers at Schnabel Engineering Associates and Tensar Earth Technologies for their support and assistance throughout the projects which included the geogrid reinforced mats and the development of this paper.

REFERENCES

Allen, Tony M. (1991) "Determination of Long-Term Tensile Strength of Geosynthetics: A State-of-the-Art Review." Proceedings, Geosynthetics '91, Atlanta, Georgia: Industrial Fabrics Association International, pp. 351-371.

Bonapart, R. and Berg, R.R., (1987) "The Use of Polymer Geosynthetics to Support Roadways over Sinkhole Prone Areas", Proceedings, Second Multidisciplinary Conference on Sinkholes and Environmental Impacts of Karsts, pp. 437-445.

Bright, Donald G., (1990) Polymeric Behavior of Geosynthetic Materials: Structural Synthetic Geogrids for Waste Facility Applications, The Tensar Corporation, pp. 5-10.

Chen, J. and Beck, B.F., (1989) "Qualitative Modeling of the Cover-Collapse Process", 3rd Multidisciplinary Conference on Sinkholes Proceedings, pp. 89-94.

DeStephen, R.A. and Wargo, R.H., (1992) "Foundation Design in Karst Terrain", Bulletin of the Association of Engineering Geologists, Volume XXIX, Number 2, pp. 165-173.

Elias, V. (1990) "Durability/Corrosion of Reinforced Soil Structures", Federal Highway Administration RD-89-186.

GRI Standard Practice GG4A, (1990) "Determination of the Long-Term Design Strength of Stiff Geogrids", Geosynthetic Research Institute, Drexel University, Philadelphia, Pennsylvania, pp. 1-12.

Giroud, J.P., (1982) "Design of Geotextiles Associated with Geomembranes", Proceedings of the International Conference on Geotextiles, Volume 4, Las Vegas, p. 130.

Giroud, J.P., (1981) "Designing with Geotextiles", Materiaux et Constructions, Volume 14, No. 82, pp. 257-272.

Giroud, J.P., Bonapart, R., Beech, J.F., and Gross, B.A., (1988) "Load-Carrying Capacity of a Soil Layer Supported by Geosynthetic", Proceedings of International Geotechnical Symposium on Theory and Practice of Earth Reinforcing, pp. 185-190.

Montalvo, J.R., (1989) "Evaluation of the Degradation of Geotextiles", Proceedings of Geosynthetic '89 Conference, pp. 501-511.

Pennsylvania Department of Transportation, Design Manual, (1991) Part 4, Volume 1, Part B, Section 3, p. B.4-9.

Geogrids Strengthen Foundation for Mechanically Stabilized Earth Retaining Wall—A Case History

H.R. Ramos
Law Engineering Inc., USA

G.T. McDaniel
Law Engineering Inc., USA

S.A. Maher
The Reinforced Earth Co., USA

ABSTRACT

Geogrids were used to strengthen the otherwise unstable foundation of a mechanically stabilized earth wall structure constructed on an uncontrolled backfilled borrow pit adjacent to the sloping shoreline of a lake. Four foundation stabilization alternatives were considered: (i) preloading with wick drains; (ii) dynamic compaction; (iii) stone columns and wick drains; and (iv) geogrid reinforcement with wick drains. An analysis indicated that the geogrid/wick drain option was the most economical. Information on the site and surface conditions along with the design and analysis of the structure is summarized and discussed.

INTRODUCTION

The project is located on privately owned property near the Miami International Airport, immediately south of State Road 836 in Miami, Florida (See Figure 1). An existing City Street was required to be extended through the project. This street extension required the construction of a bridge over existing railroad tracks. Earth retaining walls were required for the approach embankments due to the limited right-of-way. The approach fill embankments were 30.5 m (100 ft) wide and ranged from 1.5 to 10 m (6 to 32 ft) high. Mechanically stabilized earth (MSE) walls had been selected based on economy and acceptability to the local governmental agencies. The flexibility and adaptability of MSE walls increased the range of feasible foundation improvement options.

Several man-made lakes are located within the project. In the past, these man-made lakes served as borrow pits for limerock aggregate. In these lakes, limestone and the underlying sands were removed to depths of 9 to 12 m (30 to 40 feet). The water-filled borrow pits were later used as disposal areas for silt sized particles removed during the limerock washing and crushing process. The area was finally reclaimed by backfilling over the previously unconsolidated deposited silt layer, to approximately 1.5 m (5 ft) above the lake water level. This recent fill material generally consists of sand with limerock and possibly construction debris. Due to lack of land availability, the developers were forced to build the roadway extension near the shoreline of Lake Mahar. The east bridge approach MSE fill embankment was located on the reclaimed area, see Figure 2.

GEOTECHNICAL EXPLORATION

Law Engineering Inc. performed the geotechnical exploration and provided geotechnical recommendations for foundation design and site preparation. Ten standard penetration test borings and five exploratory auger borings were drilled along the east approach embankment. The borings revealed a generalized subsurface profile consisting

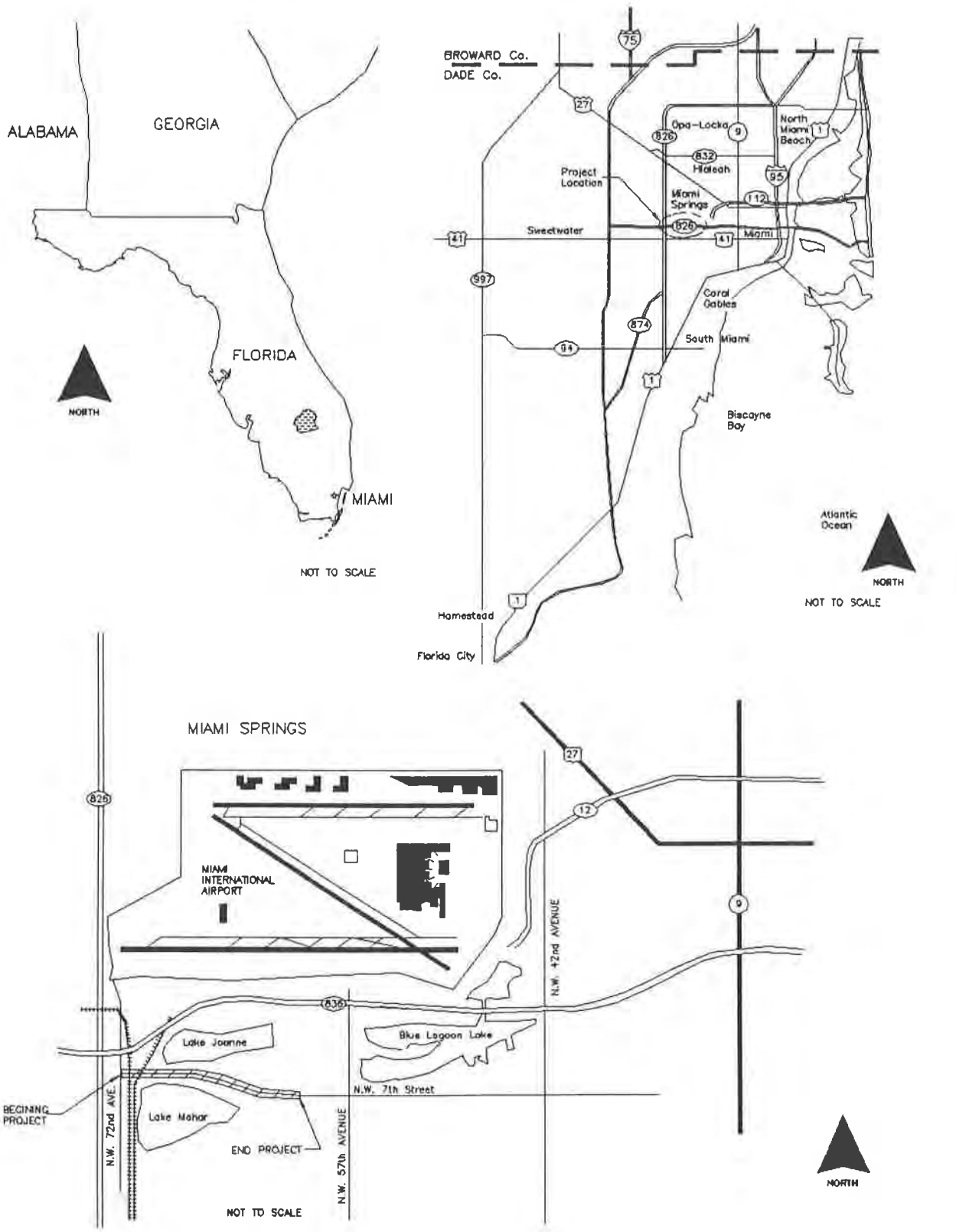

Figure 1. Project Location

of very loose to dense sand and limerock backfill overlying a very soft silt layer encountered below the existing surface at depths ranging from approximately 4.9 to 6.7 m (16 to 22 ft). The silt layer ranged in thickness from approximately 0.9 to 3 m (3 to 10 ft) and consisted of a very soft to soft calcareous silt having Standard Penetration Test (SPT) blow counts ranging from 1 to 2 blows per 0.3 m (1 ft) where encountered. Below the silt layer, sand with limestone layers was encountered to a depth of 15 m (50 ft) which was the maximum depth explored.

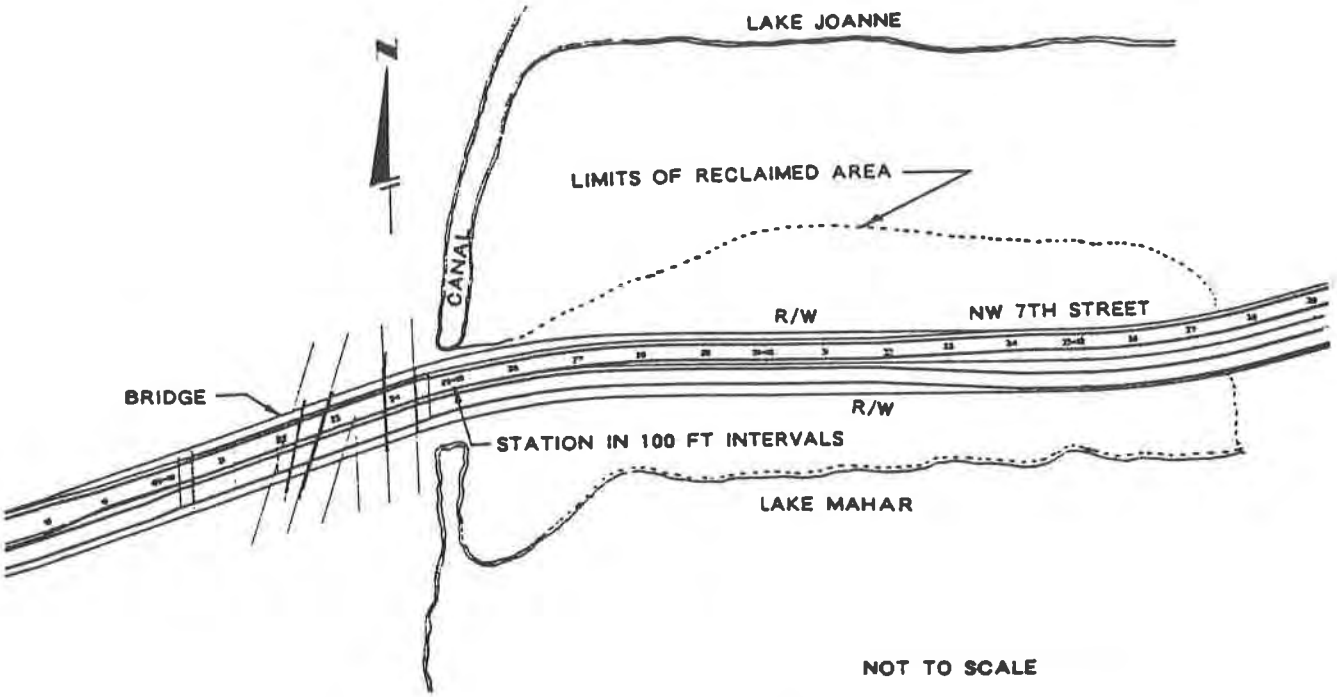

Figure 2. Site Plan

Silt Layer - In-situ and Laboratory Testing - A total of five in-situ vane shear tests were performed to measure the shear strength of the irregular soft silt layer encountered along the MSE approach portion of the roadway extension. The tests were performed using a four-bladed vane 9.2 cm (3.6 inches) in diameter. In addition, several undisturbed soil samples of this material, retrieved with a 7.5 cm (3.0 inches) thin wall tube, were selected for laboratory testing which included natural moisture content tests, percent passing 0.075 mm sieve (No. 200 sieve) and Atterberg limits. Table 1 summarizes the properties of the silt layer.

Table 1. Properties of Silt Layer

TESTS	RESULTS
Natural Moisture, w %	39 to 49
Percent Fines, % 0.075 mm sieve	89 to 100
Liquid Limit, LL %	31 to 40
Plastic Limit, PL %	25 to 30
Plasticity Index, PI %	6 to 10
Undrained Shear Strength, kPa (lb/ft^2)	17.9 to 22.4 - (373 to 467)
Remolded Shear Strength, Kpa (lb/ft^2)	4.5 to 6.7 - (93 to 140)

MSE RETAINING WALL STABILITY ANALYSIS USING UNIMPROVED EXISTING SOILS

Evaluation of the external stability of the MSE retaining wall foundation involved several potential modes of wall instability as well as settlement potential. These evaluation includes:

- Overall stability analysis
- bearing capacity of the unimproved soils
- total and differential settlements along the MSE wall

The external stability of the retaining walls against rotational movement was evaluated using the unimproved existing soil properties presented in Table 2 and the computer slope stability program STABGM (Duncan and Wong, 1984).

The bearing capacity of the subsurface soils was evaluated using conventional soil mechanics theory for the various wall heights and widths of MSE with respect to the soils at various locations. The calculated factors of safety against bearing capacity failure were as low as 1.1 for a wall height of 7 m (23 ft) where underlain by a silt layer of about 3.2 m (10.5 ft) thickness. The area of low bearing capacity generally occurred between Stations 27+00 to 32+00 where the silt layer was thickest. The minimum allowable factor of safety against bearing capacity failure for MSE walls has been established by the local Department of Transportation as 2.0.

Table 2. East Bridge Approach - Design Parameters for Unimproved Soils

Soil Type	Depth Below Ground Surface, m (ft)	Unit Weight kN/m^3 (lbs/ft^3)	Cohesion, c kPa (lb/ft^2)	Angle of Internal Friction ø (Degrees)
I	Embankment	17.3 (110)	0	32
II	Embankment	19.7 (125)	0	34
III	Embankment	19.7 (125)	480 (10,000)	45
IV	0-0.9 (0.0 - 3.0)	18.1 (115)	0	30
IV	0.9-2.4 (3.0-8.0)	18.7 (119)	0	30
IV	2.4-4.0 (8.0-13.0)	17.3 (110)	0	29
IV	4.0-4.9 (13.0-16.0)	17.3 (110)	0	29
V	4.9-8.1 (16.0-26.5)	17.3 (110)	19.2 (400)	0
VI	8.1-11.4 (26.5-37.5)	18.2 (116)	0	33

NOTE:

I: compacted sand; II: compacted limerock
III: mechanically stabilized earth; IV: sand with limerock
V: silt VI: sand with limestone fragments

In the same areas of greatest silt layer thickness where the bearing capacity was indicated to be marginal, the slope stability analysis also indicated that the factors of safety against slope instability ranged from 1.1 to 1.3. Typically, the minimum allowable factor of safety against slope instability ranges from 1.25 to 1.5 for roadway embankment design. The external stability of the proposed MSE wall was considered inadequate without foundation improvement.

FOUNDATION STABILIZATION ALTERNATIVES

In order to construct the mechanically stabilized embankment, the foundation soils had to be improved or strengthened and the following alternatives were analyzed:

Pre-loading with wick drains - Installation of wick drains followed by site surcharge would require a long period of time (6 months or more). Staged construction would also be required in order to control a bearing capacity failure. This alternative would not significantly improve the near surface loose sand and rock fills above the silt layer. Due to project time constraints and since positive improvement of the very soft silt layer and other loose soil layers would be difficult to evaluate, this option was not considered further.

Dynamic compaction - This method would significantly improve the upper soil and rock fill but was not considered able to improve the silt layer sufficiently to increase the factor of safety against bearing capacity failure or rotational instability, or to reduce the settlements. This option was also not considered to be technically feasible.

Stone columns and wick drains - This system was considered feasible for foundation stabilization. The evaluation indicated that 0.9 m diameter (36 inches) stone columns placed on a triangular grid spacing of 2 to 2.2 m (6.5 to 7.0 ft) beneath the reinforced portion of the MSE wall should significantly improve the factor of safety against bearing capacity failure and rotational instability and reduce settlements. Stone columns would densify the sand and limerock fill layers. The shear strength of the silt layer would be reduced due to remolding during the stone column installation. However, the stone would provide the additional shear strength.

Wick drain installation was recommended in the unreinforced portion of the embankment to reduce the settlement potential for the interior of the retained fill. A surcharge fill above the final embankment grade was considered to consolidate and compress the silt layer. The additional fill height was estimated a 20 percent of the retained fill. This construction alternative presented several disadvantages:

- high construction and inspection cost
- Local contractors not familiar with this alternative
- Uncertainty with construction schedule

Due to the above disadvantages, this option was not selected.

Geogrid Reinforcement and Wick Drains - This foundation stabilization option, considered late in the design, resulted in the most economical design. The analysis included the use of a high tensile strength geogrid which in combination with the unimproved soils would provide the required strength to furnish the minimum factors of safety needed by the project specifications. In addition, the geogrid reinforcement would help reduce the differential settlements. This construction alternative was selected based on significant cost savings of the geogrid installation and the reduction in construction schedule. A detailed analysis and evaluation of this construction alternative, as well as a summary of the construction monitoring is presented below.

Consolidation of the silt layer under the fill loading would increase the soil strength. Wick drains were recommended in high fill areas and in the areas underlain by thick silt layers to speed consolidation. Staged construction was required to prevent prematurely overstressing the silt layer.

ANALYSIS OF GEOGRID REINFORCEMENT FOR FOUNDATION OF MSE RETAINING WALL

The Reinforced Earth MSE system was selected and the internal stability of the walls was calculated based on the Task Force 27 Guidelines (AASHTO, 1990).

The geogrid soil reinforcement system analysis involved the selection of the type of geogrid reinforcement to be used, followed by the external and internal stability of the wall system. The Reinforced Earth Company was retained for the selection of

geogrid to be used beneath the wall and the analysis and design of the internal stability of the steel-reinforced wall system. Geogrid reinforcements were provided as foundation reinforcement over the entire area of poor soils and were extended beyond for the purpose of providing minimum factors of safety against rotational instability, bearing capacity failure and reducing potential differential settlements due to variability of soil conditions.

Geogrid Selection - The geogrid selection was based on the tensile strength, tensile modulus at low strain, the ability to withstand creep under the application of the design loads, and economy. High tenacity Matrex woven polyester geogrids offered high design strengths at relatively low costs and helped to reduce the number of layers required which helped minimize excavation and dewatering. Since the loading and reinforcing requirements varied with the soil conditions along the embankment, it was most economical to use more than one type of geogrid. Therefore, three types of geogrid were selected.

Table 3 summarizes the types of geogrids selected and their ultimate tensile strengths. Testing for ultimate tensile strength of the geogrid was performed in accordance with ASTM D-4595.

Table 3. Ultimate Tensile Strength for Geogrids Selected

Geogrid Type	Ultimate Tensile Strength, Kn/m (lb/ft)
Geogrid I	86.0 (5,900)
Geogrid II	181.0 (12,400)
Geogrid III	371.0 (25,400)

Figure 3 shows the limits of reinforced earth backfill. The embankment has a width of 30.5 m (100 ft). The geogrid reinforcement extends 0.9 m (3 ft) outside the front face of the retaining wall to provide an increase of the bearing capacity. Figure 3 also presents a layout of the geogrid coverage. Geogrid I covers from Station 25+90 to 27+00 and from Station 31+00 to Station 32+50, where the wall height is low or the silt layer is relatively thin, minimal reinforcing is required. Geogrid III is used from Station 27+00 to Station 31+00, where the wall is relatively high and the silt layer is thick, a greater soil improvement is required. Geogrid II is placed over Geogrid III and covers from Station 27+00 to Station 28+50 where the greatest thickness of silt occurred.

Determination of Short and Long Term Geogrid Design Strength - For flexible geogrids, standards have been presented (GRI, 1991), to identify and quantify reduction factors for conditions such as construction damage, biological degradation, creep deformation, junction strength, joints and chemical degradation. Partial factors of safety for junction strength and joints for the geogrid products used were both 1.0. Table 4 summarizes the reduction factors for short and long term applications in accordance with GRI Test Method GG4 (GRI, 1991).

Table 4. Reduction Factors for Short and Long Term Applications

Reduction Factor	Short Term Application	Long Term Application
Durability, F_D	1.10	1.50
Construction Damage, F_{CD}	1.20	1.25
Creep, F_C		
Geogrid III	1.82	1.82
Geogrid I, II	1.67	1.67

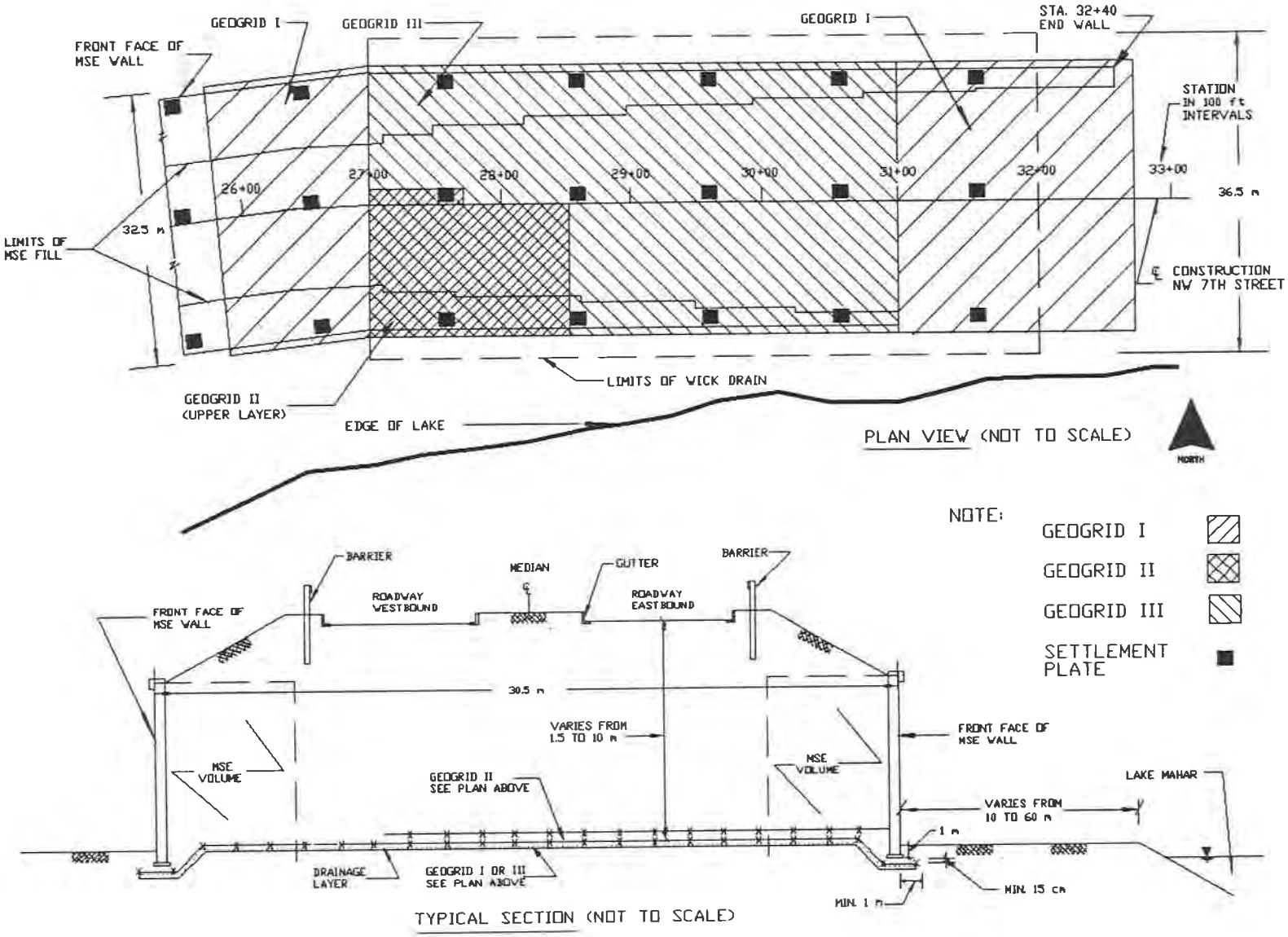

Figure 3. Plain view and typical section of MSE wall

The durability factor is the product of the biological and the chemical reduction factors.

The Derivation of the allowable tensile strength for the geogrid is performed using Equation 1:

$$T_{ALLOW} = T_{ULT} \frac{1}{F_D \times F_{CD} \times F_C} \quad (1)$$

where,

T_{ALLOW} = allowable tensile strength, in kN/m, (lb/ft)
T_{ULT} = ultimate tensile strength, in kN/m, (lb/ft)

Table 5 shows the allowable tensile strength for short and long term applications using Equation 1 and the reduction factors presented in Table 4.

Table 5. Summary of Allowable Tensile Strengths

Geogrid Type	Short Term kN/m (lb/ft)		Long Term kN/m (lb/ft)	
Geogrid I	39.0	(2700)	28.0	(1900)
Geogrid II	82.0	(5600)	58.0	(4000)
Geogrid III	155.0	(10600)	109.0	(7500)

Slope Stability Analysis - Two computer programs were utilized to locate the most critical potential circular failure surfaces: STABL6 and STABGM. Unlike previous programs in the series, STABL6 (FHWA, 1986) can consider soil reinforcement inclusions. The program uses Simplified Bishop's Analysis and analyzes up to 900 trial circles within the limits specified to be searched. STABGM (Duncan and Wong, 1984) computes the slope stability of various circular failures surfaces through a retaining wall embankment which includes geogrid reinforcement using the ordinary method of slices and the Bishop's Modified Method. The inclusion of geogrid reinforcement layers in the embankment provides an improvement in the factor of safety due to the increase of the resisting moment. When a geogrid reinforcement layer is intercepted by a particular slice, a force is calculated and applied as a known resisting force to the base of the slice. This resisting force is added to other resisting forces due to the friction and/or cohesion of the soil.

Figure 4 shows a design cross-section and soil parameters used in the analysis. The design considers a traffic surcharge of 12 Kpa (250 lb/ft^2). Table 6 summarizes the computer results.

Table 6. Summary of Slope Stability Analysis Results

Station	H m	H ft	D m	D ft	Geogrid Type	Factor of Safety Short Term	Long Term
27 + 00	6.9	22.5	21.3	70.0	II+III	1.35	1.45
28 + 00	5.8	19.0	18.3	60.0	II+III	1.35	1.45
29 + 00	4.3	14.0	15.2	50.0	III	1.35	1.50
30 + 00	2.4	8.0	5.8	19.0	III	1.35	1.40
31 + 00	1.8	6.0	9.1	30.0	I	1.40	1.50

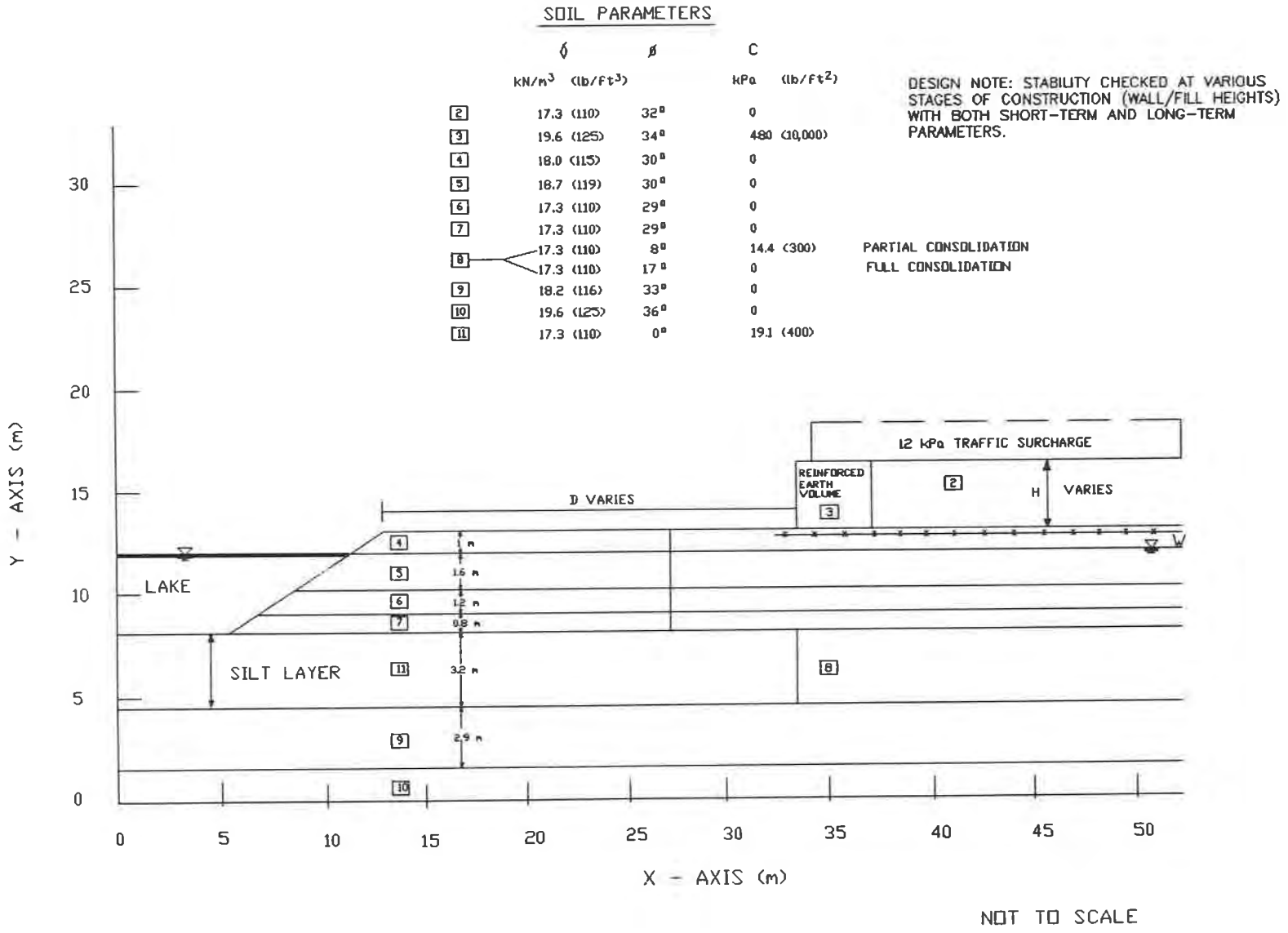

Figure 4. Design section and soil parameters

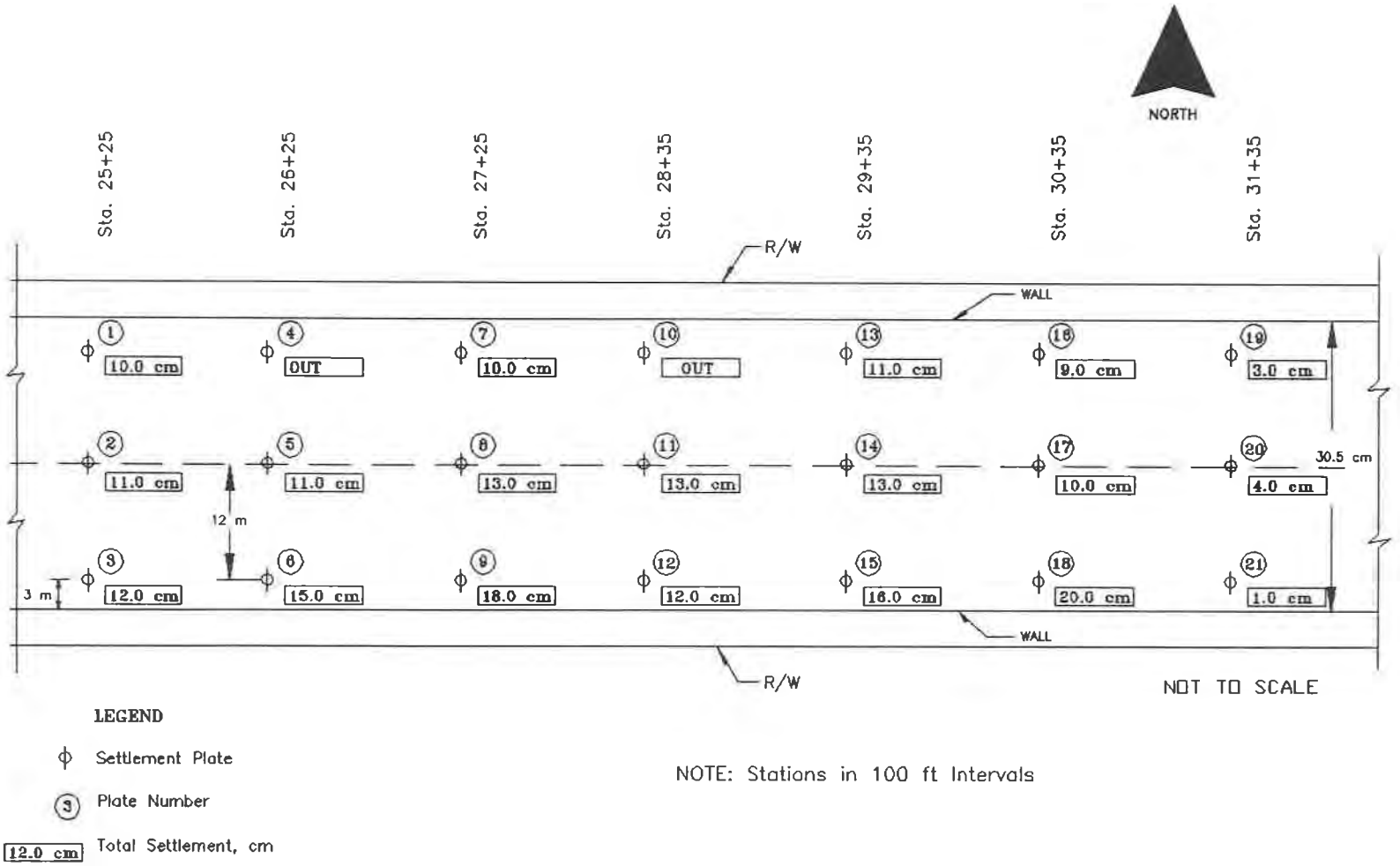

Figure 5. Settlement plate locations and summary of total settlements

Wick Drain Installation - Approximately 24,400 linear meters (80,000 ft) of wick drains were installed within the critical area of the embankment to speed consolidation of the silt layer. As shown in Figure 3, the wick drains covered a width of 36.5 m (120 ft), from Station 27+00 to Station 32+00. The wick drains were installed to an average depth of 9.1 m (30 ft) keeping a spacing of 1.5 m (5 ft) using a square pattern. Due to the gravelly nature of the soils overlying the very soft silt layer, predrilling was needed. After loosening the upper 5 m (16 ft) soil layer, the wick drains were installed using conventional methods.

To prevent prematurely overstressing the silt layer before it had time to consolidate and gain strength, staged embankment construction was planned. After wick drain installation, the embankment was recommended to be initially constructed to approximately 1/2 of its planned height. Settlement monitoring of the fill embankment would indicate when the remainder of the embankment could be constructed.

Settlement Monitoring - Twenty-one settlement plates were installed within the embankment section with wick drains to monitor the settlements caused by the embankment construction. This monitoring helped to determine when the staged embankment construction was ready for more fill placement. The settlement monitoring started on July 17, 1991 and continued until February 14, 1992. A maximum of 20 cm (7.9 inches) of settlement occurred in the area of greatest silt thickness (See Figure 5).

CONSTRUCTION CONSIDERATIONS

Special steps were taken at the base level of the MSE wall at the interface with existing soils and foundation improvements (See Figure 3). The existing soils on the surface were determined to be suitable as select fill for the MSE volume. While typical MSE wall erection procedures involve excavating the wall site to the level of the bottom of the wall facing; however at this site, the existing soils were allowed to remain up to the level of the lowest layer of reinforcement in the MSE volume. A shallow, narrow trench was excavated for the leveling pad and facing panels. A drainage layer of coarse, open-graded crushed limerock was placed over the entire width of the embankment in the area of the wick drains and leveling pad trenches. The first geogrid layer was installed and covered with another layer of drainage rock and the leveling pad construction was started. Once wick drains, geogrid mattress and drainage blanket were in place, MSE wall construction could begin immediately.

The lower level MSE wall steel-reinforcements were sloped gradually upward and away from the wall facing until an elevation was achieved which provided clearance above the geogrid-reinforced mattress and drainage layer.

The geogrid option offered the advantage of direct control of construction procedures to the prime contractor, Redland Construction Company of Homestead, Florida. While the stone column option would require the services of a specialty contractor, the prime contractor was instead able to complete the geogrid installation along with other earthwork operations quickly and without special equipment. The geogrid was provided in 1.0 m (40 inches) wide pieces precut to length which lay flat under their own weight. No field cutting, staking or splicing was required. The project bridge subcontractor, Anzac Contractors of Miami, performed MSE wall construction in conjunction with Redland who provided fill and earthworks for the wall.

Cost Evaluation - Geogrids were the preferred option shown in all construction bids. While the geogrid cost was about US $100,000, including installation; and the geogrid option required about US $20,000 more in wick drains than the stone column option, the stone column installation was priced at US $300,000. Therefore, this option provided about US $180,000 in savings when one also considers the lower cost of inspecting the installation of geogrids when compared to stone columns. The completed wall is shown in Figure 6.

CONCLUSIONS

The external stability of the proposed mechanically stabilized earth wall was considered inadequate without foundation improvement. The critical mode was considered to be a rotational failure on a circle passing behind and beneath the steel

soil reinforcements of the wall system, following the weak silt layer and extending to the sloped face of the lake bottom. The stability was considered to be least during the construction of the wall and embankment due to the time required for the relief of excess pore pressure and consolidation of the silt layer.

A controlled rate of construction, wick drains and geogrid reinforcement of the soils immediately beneath the proposed wall and embankment were determined to be the most cost-efficient option for improving the stability to help prevent any such failure. Pore pressures and settlements were monitored during construction to determine the allowable rate of fill placement and wick drains were used to accelerate the consolidation and strength gain of the silt layer. The use of high-strength geogrids helped to reduce the number of layers of foundation reinforcement required for safety, thereby helping to reduce costs for excavation and dewatering required for geogrid installation. In general, the combined use of mechanically stabilized earth walls and geogrid foundation reinforcement appears to offer a safe and cost-effective alternative to rigidly supported bridges or retaining walls for these conditions.

Figure 6. Wall completed

ACKNOWLEDGEMENTS

The authors would like to express their appreciation to the design engineers on this project Messrs. Eugene Bechamps and Jack Battillo of E.N. Bechamps and Associates. Additionally, the authors thank Ms. Christine Knierim for typing the manuscript and Mr. Manual Escalada for drafting these figures.

REFERENCES

AASHTO. 1990. Task Force 27 report, insitu soil improvement techniques. AASHTO/AGO/ARTBA Joint Committee. Washington, D.C.: American Association of State Highway and Transportation Officials (AASHTO).

Duncan, J.M. and Wong, K.S. 1984. STABGM, a computer program for slope stability analysis with slip circular surfaces and geogrid reinforcement, computer users' manual. Blacksburg, Virginia: Department of Civil Engineering, Virginia Polytechnical Institute and State University.

FHWA. 1986. STABL 6 with reinforcing layer option, users' manual. FHWA/IN/JHRP 86/18. Washington, D.C. : Federal Highway Administration.

GRI. 1991. GRI Standard Practice GG4b, determination of long term design strength of flexible geogrids. Philadelphia: Geosynthetics Research Institute (GRI), Drexel University.

Use of Geosynthetics to Mitigate Earthquake Fault Rupture Propagation Through Compacted Fill

J.D. Bray
Purdue University, USA

A. Ashmawy
Purdue University, USA

G. Mukhopadhyay
Leighton & Associates, USA

E.M. Gath
Leighton & Associates, USA

ABSTRACT

A development project includes structures located in a zone containing minor subsidiary faults on the hanging wall of a potentially active thrust fault. Minor amounts of displacement on these subsidiary faults are possible. Previous studies suggest that differential movement across bedrock faults dissipates as the shear rupture plane rises through overlying fills. The cost of extensive excavation and fill operations, however, may be prohibitive. Hence, the use of fill-reinforcement materials within smaller thicknesses of compacted fill was explored. In this paper, the project and site geology are described, the significant hazards associated with earthquake fault rupture are identified, and the finite element analyses are discussed. The numerical results indicate that the geosynthetic reinforcement is effective in spreading the differential movement across a wider zone. Differential settlement and tensile strains at the depth of the shallow foundations were reduced sufficiently to feasibly construct buildings with acceptable levels of risk at this site.

INTRODUCTION

A mixed use development project is under construction at a 250-acre site located on an anticlinal structure known as the Las Posas Hills in Camarillo, California. The Las Posas anticline is the surface expression of folding and thrusting along the Springville fault zone, a reverse fault system that is located immediately south of the project site. Geologic investigations discovered several extensional normal faults (axial faults) at the Las Posas anticline site. A number of these faults where old soil horizons were present were judged to be inactive. Many of these faults, however, do not have any overlying preserved soil units. In addition, the formational boundaries of the soil profiles are irregular, preventing the measurement of possible fault movements with a resolution level better than 2 to 5 cm. Hence, fault displacements on the order of 2 to 5 cm cannot be precluded for these axial faults. Therefore, the feasibility of attenuating (absorbing) minor fault displacements beneath the future structures at this site was explored.

Previous studies (Asquith and Leighton 1973; Bray et al. 1990) suggest that the differential movement of the underlying bedrock fault dissipates as the shear rupture plane propagates through the overlying compacted fill materials. If the depth of fill is sufficiently large and the underlying fault displacement is relatively small, the

differential displacement of the underlying fault can be "locally absorbed" within the overlying fill. At this site, however, the costs associated with the extensive excavation and fill operations required to mitigate the hazardous effects at the ground surface could prove to be prohibitive. Hence, the use of fill-reinforcement materials was explored to optimize the depth of overexcavation and fill placement.

THE PROPOSED DEVELOPMENT AND PROJECT SITE DESCRIPTIONS

Proposed Development. The project involves balanced cut and fill grading to produce a series of acre-size residential lots, several multi-acre lots for commercial and high density residential use, an 18-hole golf course, and access roads. A schematic diagram of the proposed development and the faults is shown in Figure 1. Approximately twelve million cubic meters of cut and fill will be required to achieve the finish grade. The final graded site will be a series of natural, cut, fill and composite lots, terraced up from the perimeter lowlands to the centrally positioned ridge top. Terraced levels of the site will be separated by slopes of varying heights.

Maximum topographic relief at the site is roughly 90 m, with elevations ranging from 30 m at the property's west side to a maximum elevation of 120 m at the central ridge top. Natural slope gradients are between 4:1 and 2.5:1 (horz. to vert.) and appear to be controlled (to a degree) by the underlying geologic structure. No surface water was noted on the site. Ground water was encountered at a depth of about 12 m in several borings located along the property's perimeter.

Geology of the Las Posas Anticline. The Las Posas anticline and Springville thrust fault system is one of the several east-west trending fold and fault systems that have formed as a result of northeast compression and crustal shortening of the transverse ranges in southern California (Yerkes and Lee 1979). The Las Posas Hills are underlain by fine-grained siltstone, sandstone and several associated paleosols assigned to the Saugus formation. This formation is estimated to be 200 to 600 thousand years old (Rockwell et al. 1985). At the crest of the anticline, these fine-grained deposits are locally overlain by a coarser grained, gravelly alluvial deposit that is estimated to be about 120 thousand years old, and a finer grained colluvial soil with a minimum development age of approximately 15 thousand years (Leighton and Associates 1991). The gravelly sediments at the crest of the anticline were deposited as stream channel deposits by a precursor stream to the modern Santa Clara river at about the same time, or just prior to the hills starting to be uplifted. This suggests that folding and growth of the anticline began no more than 120 thousand years ago. Initially, the anticline grew primarily as a result of folding, with minor compression along a buried (or "blind") thrust fault that developed into the modern Springville fault. The Springville fault is estimated to have broken through to the surface as recently as 15 to 30 thousand years ago. Since then, the hills are growing primarily by thrusting along the Springville fault. Once the blind thrust fault became a surface fault, folding and deformation of the Las Posas anticline was replaced by passive uplift.

Two types of secondary faulting have been observed at the crest of the anticline; namely, east-west trending normal bending moment faults (axial) and north-south trending tear faults (Gath and Whitney 1992). The axial faults formed by extension of the sediments during the time period when the anticline was growing primarily as a result of folding (see Figure 1). Episodic displacements on the axial faults could have also occurred with a movement pattern typical of a normal fault during the seismic events on the blind Springville fault. Formation of the tear faults is associated with the Springville fault having broken through to the surface at different times along the different portions of the anticline. Thus, while some sections of the hill were being

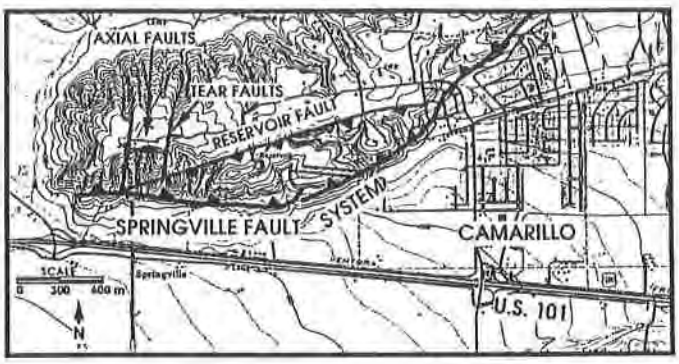

(a) General fault system west of Camarillo, California

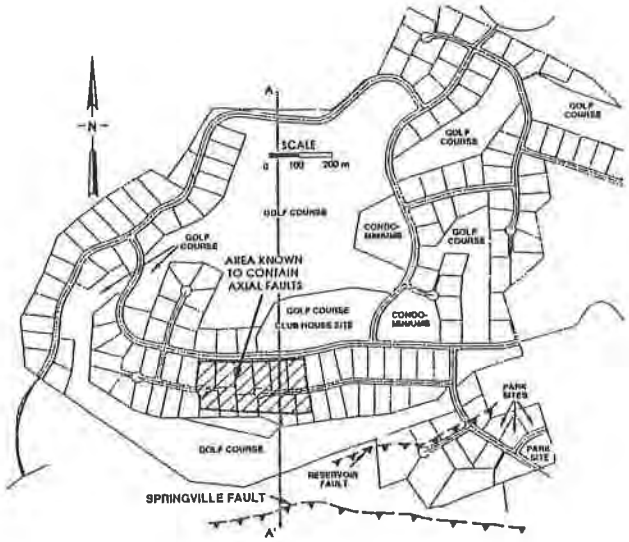

(b) Plan view of the proposed development showing the fault locations

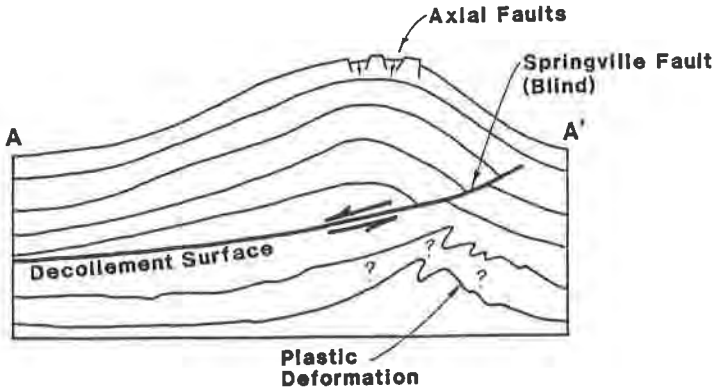

(c) Generalized cross section A-A′ showing the axial faults formed when the Springville fault was a blind structure

Figure 1. Schematic diagram of the proposed development showing the relationship between the Springville thrust fault and the axial faults at the crest of the Las Posas anticline

uplifted primarily by folding, other sections were growing primarily by faulting. Tear faults formed at the margins between these two types of anticlinal growth. Since the Springville fault surfaced, the axial and tear faults have presumably been deactivated, or have been reactivated only coseismically with the movement on the Springville fault. The axial and tear faults themselves are not believed to be seismologically active.

Magnitude and Probability of Axial Fault Displacement. Preliminary results, based on radiocarbon dating of charcoal samples collected in a trench where the Springville fault was exposed, suggest that an event on the Springville fault occurred as recently as 1,000 years ago. A similar magnitude event (based on a similar amount of displacement) occurred about 3,000 to 5,000 years earlier, suggesting that the Springville fault has a recurrence interval of about 3,000 to 5,000 years. The axial and tear faults extend into, and offset the gravelly deposits that are estimated to be 120,000 years old, but they do not appear to affect the 15,000 year-old soils. Because the soil horizons have irregular and gradual lower boundaries, individual displacements on these faults of about 5 cm or less cannot be precluded. The recurrence interval of 3,000 years for the Springville fault suggests that about five earthquakes have occurred on this system in the last 15,000 years. One could interpret that the fault displacements, if any, on the axial and tear faults have occurred during these events, to produce a maximum total displacement of 5 cm.

The probability of occurrence of earthquakes is often assumed to follow a Poisson process and can be estimated using the exponential distribution:

$$P\ (\text{Occurrence}/T,N) = 1-e^{-N/T} = 1-(1-1/T)^{N} \qquad (1)$$

where:
T = the return period in years;
N = the design life in years.

The term 1/T is the annual risk for the occurrence of the design earthquake. Equation (1) can also be used to estimate the displacement if the annual risk for observing the displacement at the site is known. The probability of occurrence of 1, 2.5, and 5 cm displacement on the axial faults at the site were estimated based on these assumptions: (1) Each of the five past significant earthquake event caused the same amount of displacement. Hence, each future earthquake will cause 1 cm of displacement with no uncertainty involved; (2) Only two past earthquakes caused the 5 cm displacement. Hence, the chance of observing 2.5 cm displacement due to a future earthquake is about 2 out of 5; and (3) Only one past earthquake caused the 5 cm displacement. Hence, the chance of observing 5 cm displacement due to a future earthquake is about 1 out of 5. The probability of occurrence of these magnitudes of fault displacement in a 100-year period at the site based on 3,000-year return period for a seismic event on the Springville fault are shown in Table 1.

HAZARDS ASSOCIATED WITH EARTHQUAKE FAULT RUPTURE PROPAGATION THROUGH COMPACTED FILL

Earthquake Fault Rupture. A number of geologists have found that the principal factors controlling the general characteristics of surface faulting are: (a) the type of fault movement (reverse, normal, or strike-slip), (b) the inclination of the fault plane, (c) the amount of displacement on the fault, (d) the depth and geometry of the earth materials overlying the bedrock fault, and (e) the nature of the overlying earth materials (e.g. Bonilla 1988). Two examples which illustrate characteristics of fault rupture propagation through overlying soils are shown in Figures 2 and 3. Typically, reverse faults tend to gradually decrease in dip near the ground surface. Normal

Table 1. Probability of occurrence of axial fault displacement in a 100 year period[a]

Case	Fault Displacement (cm)	Annual Risk (%)	Probability of Occurrence
1	1.0	1/3000	3.3
2	2.5	1/3000 * 2/5	1.3
3	5.0	1/3000 * 1/5	0.7

[a] Based on 3,000 year return period for the Springville fault

faults tend to refract at the soil-bedrock contact and increase in dip as they approach the ground surface. This refraction and variation of the dip of the normal fault plane may produce gravity grabens. Strike-slip faults tend to follow the almost vertical orientation of the underlying bedrock fault, although the rupture zone may spread or "flower" near the ground surface. Relative motion is primarily concentrated within a relatively narrow zone above the bedrock fault. Once failure occurs, differential movement is usually localized to thin, distinct failure planes. Ductile materials, however, may accommodate significant fault movement by warping without actually developing distinct shear surfaces.

Geologic field studies at the project site suggest that the bedrock faults are principally either normal faults dipping between 45 and 60 degrees or nearly vertical strike-slip faults. Most of these fault features are exposed or will be exposed during grading operations. Hence, overexcavation will be required to construct compacted fill over the bedrock faults to mitigate the surficial hazards associated with base rock fault displacements. The depth of overexcavation should be minimized, however, to control costs and to reduce the potentially deleterious effects of the other more routine design considerations (e.g. shrink/swell/collapse under static service loads). The results of previous investigations (Bray et al. 1990) suggest that dip-slip fault movements (especially normal faults which induce extensional strains within the overlying soil) pose a greater hazard than strike-slip fault movements. Hence, two-dimensional (2-D) finite element (FE) analyses of dip-slip base rock axial fault displacements will be investigated. For the purpose of this study, movement on a normal fault plane dipping at 60 degrees has been considered as the baseline case.

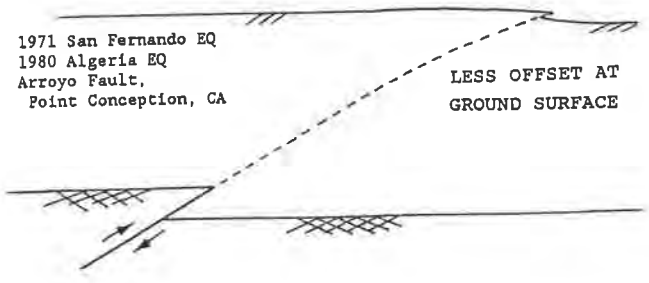

Figure 2. Path of "shallow" reverse fault rupture through "stiff" soils

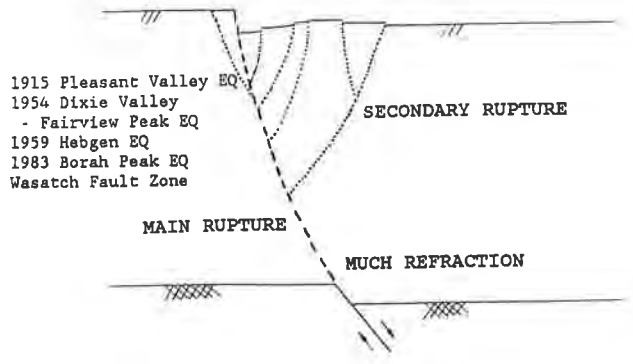

Figure 3. Path of "shallow" normal fault rupture through "stiff" soils

Hazards. The principal surficial hazards of base rock fault displacements are:

(A) propagation of the distinct shear rupture plane to the ground surface,
(B) differential settlement or angular distortion of the ground surface,
(C) compressive or tensile horizontal strains at the ground surface, and
(D) development of surficial tension cracks.

Of course, the earthquake event that produces the relative movement on these subsidiary fault features will also produce strong shaking. This study focuses on the response of the compacted fill to base rock fault displacements and has not considered the potential for building damage due to earthquake strong shaking.

Performance Criteria. Based on an evaluation of the seismicity of the Springville fault and the probable range of displacements on the axial faults, the project's grading specifications were developed based on the 2.5 cm axial fault displacement. The probability of occurrence of the 2.5 cm axial fault displacement was estimated to be 1.3 percent (see Table 1). Conceptually, this risk level is more stringent than the seismic risk level stipulated by the 1991 California Building Code for the design of essential facilities such as hospitals. This degree of conservatism, however, was considered warranted because of the recent discovery of the Springville fault, the uncertainty in the profession's understanding of earthquake fault rupture, and the perceived sensitivity of the potential homeowners to this problem.

Regarding the principal hazards of base rock fault displacements described previously, the project's performance criteria at the 2.5 cm magnitude of fault offset follows. Propagation of the rupture plane to the ground surface was considered unacceptable (Hazard A). The angular distortion over a reasonable length (3 m) should be less than 1/400 (Hazard B). Since post-tensioned foundation slabs were being recommended, this conforms to standard practice in southern California. Based on accepted mining subsidence practices and appropriate foundation design provisions, horizontal tensile strains in the soil were to remain less than 0.3 percent (Hazard C) and tensile stresses at the ground surface were not to exceed 1 kPa (Hazard D).

FINITE ELEMENT ANALYSIS OF EARTHQUAKE FAULT RUPTURE PROPAGATION

Finite Element Procedures. Previous numerical studies of fault rupture propagation through earth materials suggest that the FE method can be applied to this class of problems provided an incremental nonlinear stress-strain soil behavior model is employed (Bray et al. 1990). The plane strain FE computer program SSCOMPPC (Boulanger et al. 1991), which employs a hybrid incremental load solution technique with the Duncan et al. (1980) hyperbolic soil behavior model, was utilized in this study to model the nonlinear stress-dependent stress-strain and volumetric strain behavior exhibited by typical compacted soils. The principal advantages of this particular numerical approach are its relative simplicity and its ability to adequately model the soil's failure strain. The well-validated FE program SSCOMPPC also allows discrete modelling of the soil, the reinforcement, and the soil-reinforcement interface.

Development of Model Parameters. A series of triaxial compression tests were performed on three bulk samples believed to be representative of the fill materials to be used on the project site (USCS soil classifications: SM-SC, ML and SW-SM). Anisotropically consolidated undrained triaxial compression tests (CAU) were performed on all three fill materials at 90% or 95% relative compaction (RC) and at optimum, optimum +3% and optimum +5% moisture contents (MC) with respect to the ASTM 1557 maximum dry density and optimum moisture content. The test specimens were consolidated to stress states

Table 2. Hyperbolic soil model parameters employed to represent baseline soil

Case	Clayey Silty Sand Soil (SM-SC)	ϵ_f (%)	c (kPa)	ϕ (deg)	K	n	R_f	γ (Mg/m^3)
A	MC = Opt+5% & RC = 90%	3-6	36	33	800	1.0	0.95	2.07
B	MC = Opt+3% & RC = 95%	2-3	29	40	600	0.8	0.7	2.15
C	MC = Opt & RC = 90%	4-8	48	28	900	1.0	0.98	1.94
$\Delta\phi = 0$; $K_{ur} = 1.5$ K; $K_b = 1.5$ K and m = n so that $\upsilon_i \approx 0.4$								

representative of field conditions (K_o=0.6), and the strain rate during undrained shear was deliberately high (125%/hr) to simulate at least qualitatively the high strain rates imposed by an earthquake base rock fault displacement.

The stress-strain behavior of the three fill materials at similar RC and relative MC did not differ appreciably. Since the clayey silty sand materials (SM-SC) was judged to be a mix of the predominant materials on site, it constitutes the baseline soil. In addition to the CAU tests, isotropically consolidated drained tests (CID) and undrained tests (CIU) were performed on the baseline soil at slower strain rates to evaluate the volume change behavior and pore pressure response of the soil during loading. These tests also investigated possible strength loss upon saturation of the compacted fill materials. The CID and CIU tests indicated that the material exhibited contractive behavior during shear at the densities and confining pressures representative of field conditions. Based on these test results and previous experience with similar partially saturated compacted fill materials, the initial magnitude of Poisson's ratio (υ) was assumed to be within the range of 0.35 to 0.45. As undrained shear progresses, Poisson's ratio will tend to increase.

Duncan et al. (1980) hyperbolic soil model parameters were developed for each test series, and the model parameters for the baseline soil (SM-SC) are presented in Table 2. The hyperbolic model representation of the stress-strain behavior of the Case A compacted fill test series is shown in Fig. 4. Due in part because of the high strain rates imposed during shear, these model parameters display fairly stiff stress-strain behavior (i.e. high modulus numbers, K) with respect to model parameters typically used in design (Duncan et al. 1980). Multiple analyses were performed to note the sensitivity of the results to variations in the soil model parameters developed to represent the soil's nonlinear stress-dependent behavior.

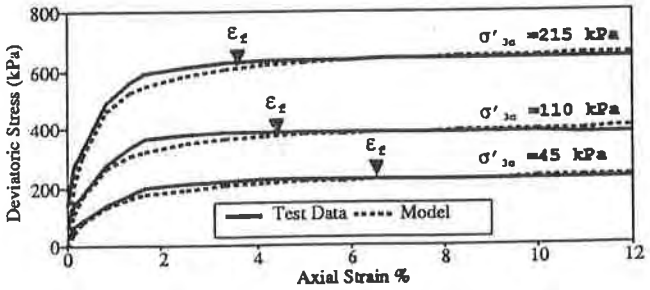

Figure 4. Hyperbolic model's representation of the baseline material (SM-SC) compacted at MC = opt+5% and RC = 90% (Case A)

Table 3. Results of FE analyses of unreinforced compacted fill

Description	Fill Ht. (m)	Base Fault Offset (cm)	HAZARD A Ht. of Shear Zone above bedrock (m)	HAZARD B Angular Distortion over 3m zone (δ/L)	HAZARD C Max. Tensile Strain at Surface (%)	HAZARD D Max. Tensile Stress at Surface (kPa)
SM-SC (Case A) RC=90%, MC=+5%	4.5	2.5	<1.0	1/180	0.6	2.9
		5.0	<1.5	1/85	1.0	7.2
	6.0	2.5	<1.0	1/220	0.4	1.2
		5.0	<1.5	1/100	1.0	4.8
	9.0	2.5	<1.0	1/300	0.25	0.5
		5.0	<1.5	1/130	0.5	2.4
	12.0	2.5	<1.0	1/400	0.2	None
		5.0	<1.5	1/175	0.4	1.2
SM-SC (Case A) over 2m of CL	6.0	2.5	<0.3	1/250	0.3	1.1
		5.0	<0.5	1/115	0.5	2.4
SM-SC (Case B) RC=95%, MC=+3%	6.0	2.5	<1.0	1/230	0.4	3.1
		5.0	<2.5	1/110	1.0	4.8
SM-SC (Case C) RC=90%, MC=+0%	6.0	2.5	<1.0	1/220	0.6	3.6
		5.0	<1.5	1/100	1.0	9.6
ML RC=90%, MC=+5%	6.0	2.5	<1.0	1/220	0.3	12.0
		5.0	<2.0	1/100	0.75	24.0
SW-SM RC=90%, MC=+5%	6.0	2.5	<1.5	1/200	0.4	14.0
		5.0	<4.5	1/100	1.0	17.0

PERFORMANCE OF UNREINFORCED FILL

Representative results of the FE analysis of the unreinforced compacted fill are summarized in Table 3. The deformed FE mesh shown in Figure 5 illustrates the deformation pattern that developed in a 6 m high compacted fill overlying a 60° normal fault displacement of 2.5 cm. The development of the shear rupture plane within the compacted fill for this condition is shown in Figure 6. For this case, the differential movement across the distinct bedrock fault plane is locally "absorbed" within the overlying compacted fill (Hazard A). The distinct bedrock fault offset is spread out over a wider zone of general shear at the ground surface. Because of the compacted fill soil's relatively stiff stress-strain response, however, the majority of differential movement (≈75%) occurs within a fairly narrow zone (≈3 m) along the projection of the base rock fault. The angular distortion across this 3 m wide zone is on the order of 1/220 for the 2.5 cm base rock fault offset (Hazard B). This magnitude of angular distortion can produce structural damage in some of the building's components, however, collapse is unlikely. The fill height must be increased to 12 m to reduce the angular distortion across a 3 m wide zone to roughly 1/400. The maximum

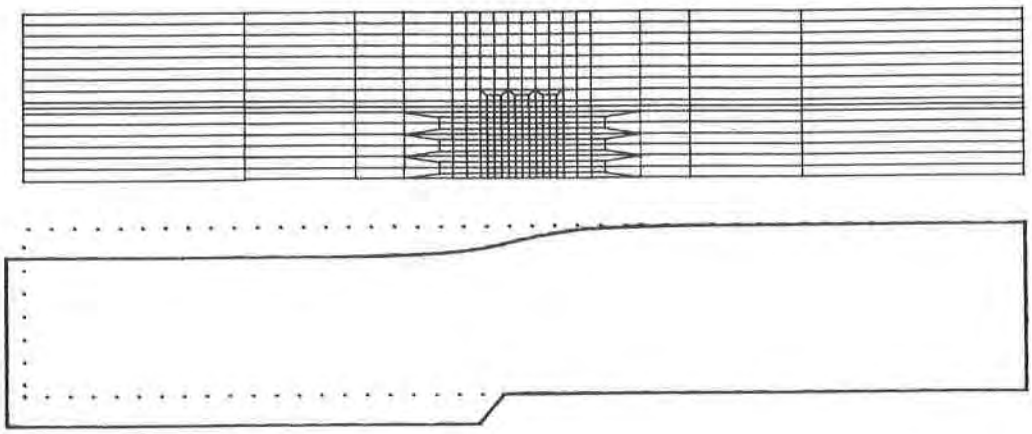

Figure 5. FE mesh and deformed mesh outline for 6m high compacted fill (SM-SC, Case A) and 2.5 cm base fault offset (displacements magnified by 50)

tensile strain for the 6 m high unreinforced fill is 0.4% although the average horizontal tensile strains across a reasonable length (3 m) is less than 0.2% (Hazard C). It is unlikely that (and in fact the foundation can be modified so that) the full horizontal strain developed in the soil below the foundation is not transferred to the structural foundation. Finally, zones at the ground surface where the minor principal stress is negative are not extensive for this case (Hazard D).

As shown in Table 3, the FE results suggest that as the fill height increases or the design base rock fault displacement decreases, the hazards associated with earthquake fault rupture reduce. For a given fill height and magnitude of fault offset, the earthquake fault rupture hazards are reduced as the ductility of the compacted fill increases. For example, the placement of a 2 m thick "ductile" low-plasticity clayey material (CL) directly above the bedrock fault significantly improves the performance of the fill with respect to earthquake fault rupture. The FE results also suggest that the baseline soil (SM-SC) should be compacted wet of optimum and at the lower range of acceptable dry densities. Kneading compaction should be specified to further increase the ductility of the compacted fill.

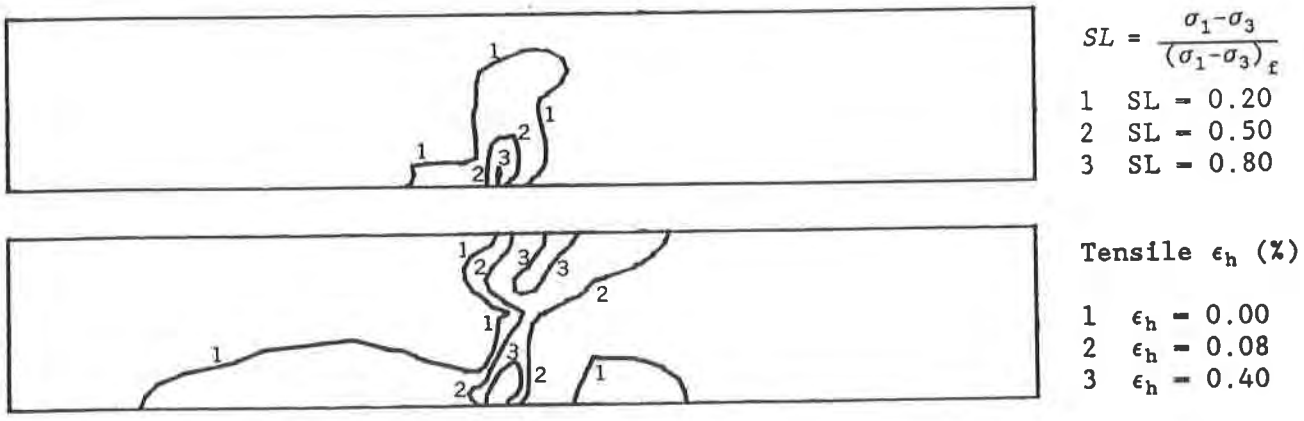

Figure 6. Stress level (SL) contours and horizontal strains for 6 m high compacted fill (SM-SC, Case A) and 2.5 cm base fault offset

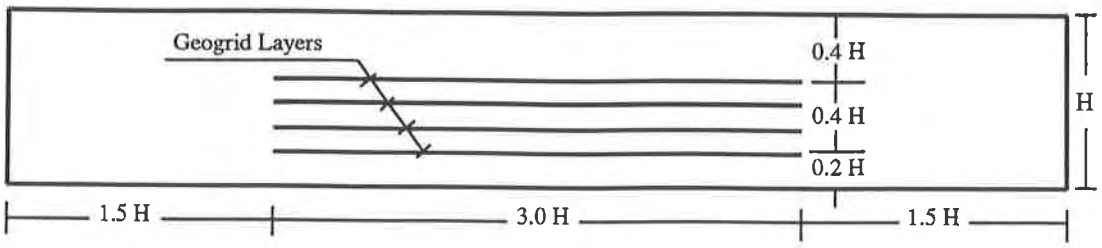

Figure 7. Location of reinforcement layers in compacted fill

Given the project's performance criteria for the 2.5 cm bedrock fault offset, the unreinforced fill height would have to be 12 m high. This fill height requires extensive overexcavating and is considered prohibitive in terms of cost and time.

PERFORMANCE OF REINFORCED FILL

The FE mesh was modified as shown in Figure 7 to include up to four layers of reinforcement. The FE program SSCOMPPC modelled the reinforcement as linear elastic bar elements that sustained only tensile forces and the soil-reinforcement interface as a nonlinear stress-dependent zero thickness element that controlled the relative displacement of adjacent soil and structural element nodal points (Clough and Duncan 1969). Tensar UX1500 (EA = 2920 kN/m, Ultimate Strength = 86kN/m) was selected as the baseline reinforcing material because it was being used at the project site to reinforce compacted fill slopes. Insufficient data were available to quantitatively account for strain rate effects. The hyperbolic model parameters selected to model the soil-geogrid interface were based on the manufacturer's recommended interaction coefficient of 0.9 (i.e. c = 18 kPa, ϕ = 30°, K_{ss} = 27130, R_f = 0.95, n = 1.0). The magnitudes of the geogrid and soil-geogrid interface model parameters are in close agreement with those used in previous studies of reinforced soil (e.g. Collin 1986).

Representative results of the FE analysis of the reinforced compacted fill are summarized in Table 4. Examining the case where two geogrids are placed within a 6 m high compacted fill composed of the baseline soil and subjected to a 2.5 cm base rock fault displacement, the differential movement across the distinct bedrock fault plane is locally "absorbed" within the overlying compacted fill (Hazard A). The angular distortion over a 3 m wide zone along the projection of the bedrock fault plane is roughly 1/400 (Hazard B). The maximum tensile strain at the surface is 0.25% (Hazard C) and the tensile stresses at the surface are minimal (Hazard D). In all cases, the maximum tensile force developed in the geogrid remain less than its established ultimate tensile capacity (FS≈2 for the 5 cm bedrock fault offset).

Given the project's performance criteria for the 2.5 cm bedrock fault offset, the reinforced fill height would have to be 6 m high. This fill height requires minimal overexcavation and is acceptable in terms of cost and time. The additional cost of the two Tensar UX1500 geogrids in-place is only about $15 per square meter in the areas containing identified subsidiary bedrock faults.

As Table 4 indicates, a number of analyses were performed under different conditions to investigate the sensitivity of the results to variations in the input parameters. Limiting angular distortion was the governing performance criteria for this project. Hence, figures which depict the deformed shape of the surface of the compacted fill overlying a 60° normal fault displacement of 2.5 cm will be examined.

As shown in Figure 8, the geogrid reinforcement is effective in spreading the

Table 4. Results of FE analyses of reinforced compacted fill

Description[a]	Base Fault Offset (cm)	HAZARD A Ht. of Shear Zone above bedrock (m)	HAZARD B Angular Distortion over 3m zone (δ/L)	HAZARD C Max. Tensile Strain at Surface (%)	HAZARD D Max. Tensile Stress at Surface (kPa)	Max. Geogrid Force (kN/m)
SM-SC (Case A) without reinf.	2.5	<1.0	1/220	0.4	1.2	--
	5.0	<1.5	1/100	1.0	4.8	--
SM-SC (Case A) with 2 geogrids	2.5	<1.0	1/400	0.25	0.2	22
	5.0	<1.5	1/200	0.5	2.4	44
2 geogrids 4.5m high fill	2.5	<1.0	1/310	0.3	1.3	25
	5.0	<1.5	1/170	0.6	3.6	48
2 geogrids 9.0m high fill	2.5	<1.0	1/670	0.15	None	17
	5.0	<2.0	1/280	0.3	0.7	35
2 geogrids interaction reduced 50%	2.5	<1.0	1/400	0.25	0.5	21
	5.0	<1.5	1/200	0.5	2.4	41
2 geogrids, geogrid EA reduced 90%	2.5	<1.0	1/450	0.25	0.5	3
	5.0	<1.5	1/240	0.5	2.9	6
4 geogrids	2.5	<1.0	1/425	0.2	0.3	27
	5.0	<1.5	1/200	0.4	1.9	42

[a] Results are for 6m high fill (SM-SC, Case A) except where noted.

differential movement, across the distinct bedrock fault across a wider zone of general shear in the fill. Hence, the angular distortion across a reasonable width (3 m) is greatly reduced with the use of the geosynthetic reinforcement. In these plane strain analyses, the FE model enforces uniform displacements at the left and right boundaries of the mesh as one would expect if the underlying bedrock in this area displaced uniformly. The reinforced compacted fill increases the width of the transition zone at the ground surface. Finally, the performance of the compacted fill reinforced with four layers of geogrid instead of two layers is only slightly better, and the improved performance is judged to be inconsequential.

As shown in Figure 9, increasing the reinforced fill height spreads the bedrock fault displacement across a wider zone of general shear in the fill. The results, however, appear to be insensitive to reductions in the soil-geogrid interaction coefficient and the geogrid's stiffness. The stiffness of the reinforcement appears to be less important because it is relatively stiff compared to the soil. Although the magnitudes of angular distortion calculated by the FE analyses are fairly insensitive to the soil-geogrid interaction coefficient within the range of movements examined in this study, the FE results indicate a large number of failed soil-structure interface elements at the 5 cm magnitude of bedrock fault offset for the case with a 50% reduction in the soil-geogrid interaction coefficient. For this case, the reinforcement is beginning to lose its effectiveness at this level of movement. Hence,

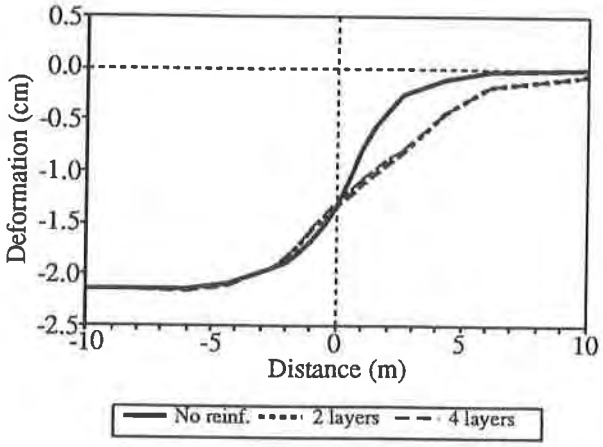

Figure 8. Effect of reinforcement to reduce differential movements at surface of 6 m high fill

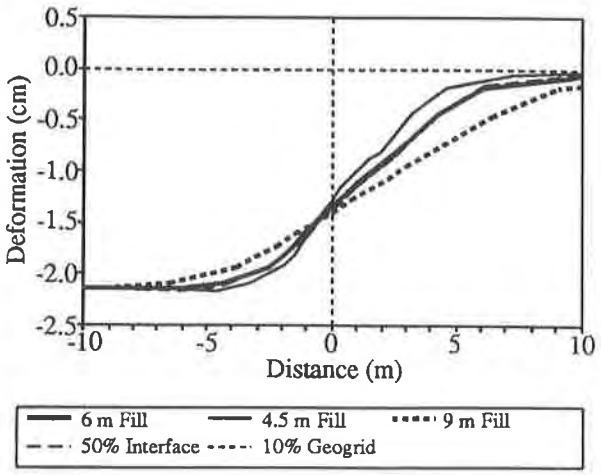

Figure 9. Effect of variations in the reinforced fill height, geogrid properties and interface properties

soil-reinforcement with the higher soil-geogrid interaction coefficients should be used. Finally, the soil-reinforcement must possess adequate tensile capacity with a reasonable safety factor, and the FE results suggest that at least two layers of reinforcement are necessary within the compacted fill.

DISCUSSION OF RESULTS

The FE results suggest that there are principally three construction techniques effective in mitigating the potential hazards associated with earthquake base rock fault rupture propagation through compacted fill. The hazards can be reduced by: (1) increasing the ductility of the compacted fill, (2) increasing the height of the compacted fill, and (3) installing soil-reinforcement within the compacted fill.

On this project, large volumes of fill material were required, and hence it was impractical to not use on-site materials as fill. Laboratory test results indicated that the fill material was fairly stiff, but that ductility could be increased by placing the fill material wet of optimum at lower dry densities with kneading compaction. The performance of the compacted fill could be further enhanced by increasing its thickness. The FE results indicated that the unreinforced compacted fill would have to be 12 m high to meet the project's performance criteria for the 2.5 cm bedrock fault offset. This fill height required extensive overexcavating and was considered prohibitive in terms of additional cost and time.

The soil-reinforcement proved effective in spreading the differential movement across the bedrock fault across a wider zone of shear in the fill, thereby reducing the angular distortion (Hazard B), horizontal tensile strains (Hazard C), and the tensile stresses (Hazard D) at the ground surface. The height of the shear rupture zone in the compacted fill overlying the displaced bedrock fault (Hazard A) was insensitive to the use of soil-reinforcement, but this hazard did not govern the design.

The improved performance of the reinforced compacted fill is shown in Figure 10. In this figure, the angular distortion across a 3 m wide zone at the ground surface and the maximum tensile strain at the ground surface are plotted against the fill height for both the unreinforced and reinforced compacted fill subjected to 2.5 cm and 5.0 cm

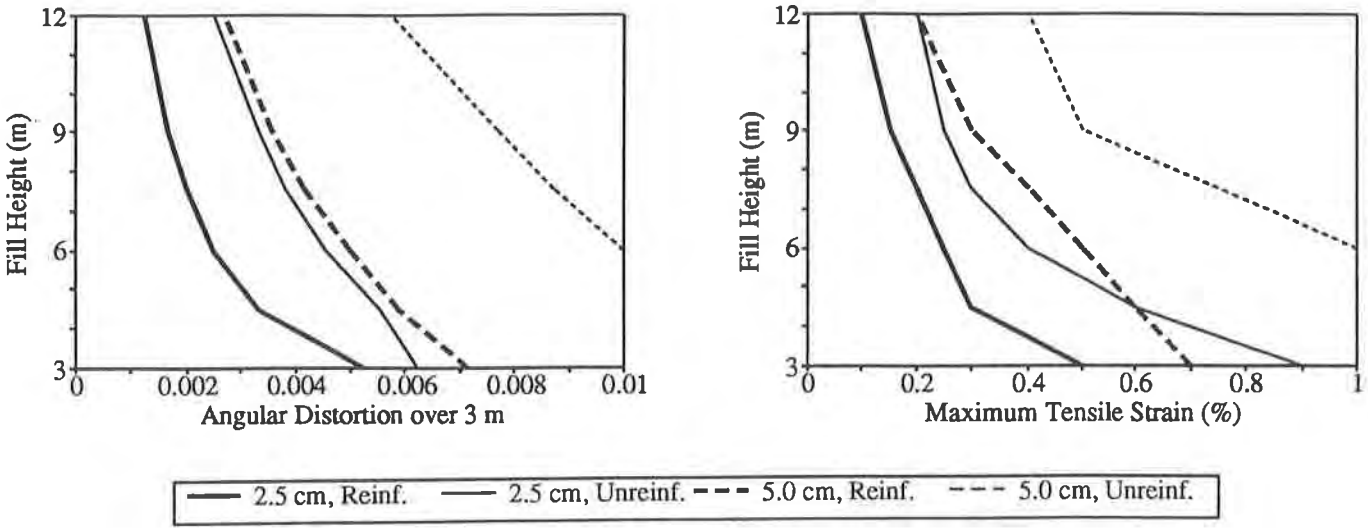

Figure 10. Comparison of unreinforced and reinforced compacted fill for baseline case (SM-SC, MC=opt+5%, RC=90%) for 2.5 cm and 5.0 cm fault offsets

base rock fault offsets. The FE results indicate that the angular distortion (Hazard B) and the maximum tensile strain (Hazard C) are roughly inversely proportional to the fill height. In addition, these potential hazards are significantly reduced by including fill-reinforcement materials within the compacted fill. Specifically, to satisfy the project's performance criteria, a 6 m high compacted fill reinforced with 2 layers of geogrid within the bottom half of the fill is required in lieu of a 12 m high unreinforced compacted fill.

The findings of this FE study agree generally with the results of published laboratory tests which indicated that geosynthetic reinforcement is effective in spreading differential movement in a direct shear apparatus across a wider zone of shear (Shewbridge and Sitar 1989). Moreover, the proposed analytical techniques are applicable to a variety of geotechnical problems where the response of a reinforced soil mass to imposed boundary deformations must be evaluated. Two examples of great practical significance are mitigating hazards due to mining subsidence and due to the subsidence of landfill liner and cover systems. Additional research is required, however, to generalize these findings by evaluating the performance of various compacted fill materials reinforced with a variety of geosynthetic materials and configurations.

CONCLUSIONS

Small amounts of displacement on minor subsidiary faults could produce structural damage in the buildings' shallow foundations at a development project in southern California. The results of this study as well as that of previous studies suggest, however, that differential movement across distinct bedrock faults dissipates as the shear rupture plane rises through overlying fills. At this site, the cost of extensive excavation and fill operations required to mitigate the hazards associated with earthquake fault rupture propagation in this manner proved to be prohibitive. Hence, the use of fill-reinforcement materials within reduced thicknesses of compacted fill was explored. The FE results indicate that the soil-reinforcement is effective in spreading the displacement of the bedrock fault across a wider zone in the reinforced

compacted fill. This spreading of the localized base rock fault displacement over a wider zone would minimize the differential settlement and tensile strains at the depth of the buildings' shallow foundations making it feasible to construct buildings with an acceptable level of risk at this site.

ACKNOWLEDGEMENTS

Leighton and Associates, Inc. served as the project geotechnical engineers. Mid-State Engineers was the design civil engineers. Sukut Construction, Inc. was the constructor. The owner was the Spanish Hills Development Company. Financial support was partially provided by the National Science Foundation under grant No. BCS-9157083.

REFERENCES

Asquith, D.O., and Leighton, F.B. (1973) "Earth Rupture and Structural Damage by San Fernando Earthquake in North Sylmar Housing Development," In San Fernando, California Earthquake of February 9, 1971, U.S. Depart. of Commerce, Washington D.C., pp. 207-212.

Bonilla, M. G. (1988) "Minimum Earthquake Magnitude Associates with Coseismic Surface Faulting," Bull. Association of Engineering Geologists, Vol. XXV, No. 1, pp. 17-29.

Boulanger, R. W., Bray, J. D., Chew, S. H., Seed, R. B., Duncan, J. M., and Mitchell, J. K. (1991) "SSCOMPPC: A Finite Element Analyses Program for Geotechnical Analysis of Soil-Structure Interaction, Earth Dams, and Compaction Effects," Univ. of California, Berkeley Geotech. Engr. Report, UCB/GT/90-02, April.

Bray, J. D., Seed, R. B., and Seed, H. B. (1990) "The Effects of Tectonic Movements on Stresses and Deformations in Earth Embankments," Earthquake Engineering Research Center, Report No. UCB/EERC-90/13, July.

Clough, G. W., and Duncan, J. M. (1969) "Finite Element Analyses of Port Allen and Old River Locks," Univ. of California, Berkeley Geot. Engr. Report, TE-69-3, Sept.

Collin, J. G. (1986) "Earth Wall Design" Ph.D. thesis, Univ. of Calif., Berk., 440 pp.

Duncan, J. M., Byrne, P., Wong, K. S., and Mabry, P. (1980) "Strength, Stress-Strain and Bulk Modulus Parameters for Finite Element Analyses of Stresses and Movements in Soil Masses," Univ. of California, Berkeley Geot. Engr. Report, UCB/GT/80-01, Aug.

Gath, E.M., and Whitney, R.A. (1992) "Faulting and Tectonic Model of the Las Posas Anticline, Western Transverse Ranges, and Implications for Seismic Risk in the Ventura Basin Region, California", Amer. Assoc. of Petrl. Geol. Bull., Vol. 76, No. 3, pp. 419.

Leighton and Associates, Inc. (1991) "Axial Fault Study, Spanish Hills, Tract 4227, Phase II, City of Camarillo, California," Report to the Spanish Hills Development Company, dated June 13, 1991, Project No. 3901427-04.

Rockwell, T.K., Keller, E.A., and Dembroff, G.R. (1985) "Quaternary Rate of Folding of the Ventura Avenue Anticline, Western Transverse Ranges, Southern California," Geological Society of America Bull., Vol. 100, pp. 850-858.

Shewbridge, S.E., and Sitar, N. (1989) "Deformation Characteristics of Reinforced Sand in Direct Shear," J. of Geotechnical Engineering, ASCE, Vol. 115, No. 8, pp. 1134-1147.

Yerkes, R.F., and Lee, W.H.K. (1979) "Late Quaternary Deformation in the Western Transverse Ranges, California," U.S. Geological Survey Circular 799-B, pp. 27-37.

Centrifuge Model Tests on the Consolidation Behavior of Soft Clay With Fabri-Packed Sand Drain

M. Kitazume
Port and Harbour Research Institute, Japan

M. Terashi
Nikken Sekkei Nakase Geotechnical Institute, Japan

N. Aihara
Hokkaido Government, Japan

ABSTRACT

A man-made island for Haneda Offshore Development Project is being reclaimed from the sea by dredged soft sea bottom sediment. Since the thick clay layer of the island has an extremely high water content, a fabri-packed sand drain that is a sand drain wrapped by an envelope made of geotextile, will be used for soil improvement. Centrifuge model tests were performed to investigate its effect on the consolidation of the ground. The study shows that the fabri-packed sand drain functions well as a drain even in such a soft soil. It is also revealed that the stress concentration of the fill pressure to the sand pile remains small if an appropriate geotextile is selected.

INTRODUCTION

Many airport construction projects including the construction of Kansai, Tokyo/Haneda and Tokyo/Narita International Airports, are in progress in Japan to cope with the recent rapid increase of air transport demands. In Tokyo/Haneda Project, a new island is being constructed by sea reclamation adjacent to the currently used Haneda Airport in the Tokyo Bay area. This project, Haneda Offshore Development Project, includes construction of three new runways and terminal buildings to expand airport capacity. Since the thick clay layer at the project site is too weak to support structures without treatment, it must be improved in advance to ensure stability and to minimize the effects of differential settlement. Vertical drains have been widely used for soft clay grounds to accelerate consolidation. Because the construction site has an extremely high water content exceeding 150% (being metaphorically called "Haneda Mayonnaise Layer") sand piles for the ordinary vertical drain method can not stand by themselves and may fail to function as a drainage path. To cope with the problem, fabri-packed sand drains, which are sand drains wrapped by an envelope made of geotextile, are planned. The geotextile is expected to stabilize the sand pile but might cause a concentration of the fill pressure to the sand pile if it has an excessively high tensile rigidity.

A series of centrifuge model tests was performed to investigate the effect of the geotextile on the stability of the sand pile and on the consolidation behavior of the improved ground. In the tests, the model ground corresponding to a typical prototype condition was prepared at a scale ratio of 1/25 and allowed to consolidate under enhanced self-weight at an acceleration of 25g. The effects of the geotextile on stability and the stress concentration were investigated by changing the tensile rigidity of the geotextile.

OUTLINE OF THE PROJECT AND THE CONSTRUCTION SITE

The Haneda Offshore Development Project has been progressing since 1984 to expand air and ground transportation in the currently used Haneda International Airport and to reduce aircraft noise to the nearby areas. In the project three new runways and terminal buildings will be constructed on the man-made island of 468 ha (about 1156 acre). The project has three phases, as shown in Fig. 1: the first phase was completed in 1988 where a new runway was built: in phase 2 new terminal buildings are being constructed and will be completed in 1993: and in phase 3 the construction of two new runways will be completed in 1996 to increase runway capacity and reduce jet noise problems.

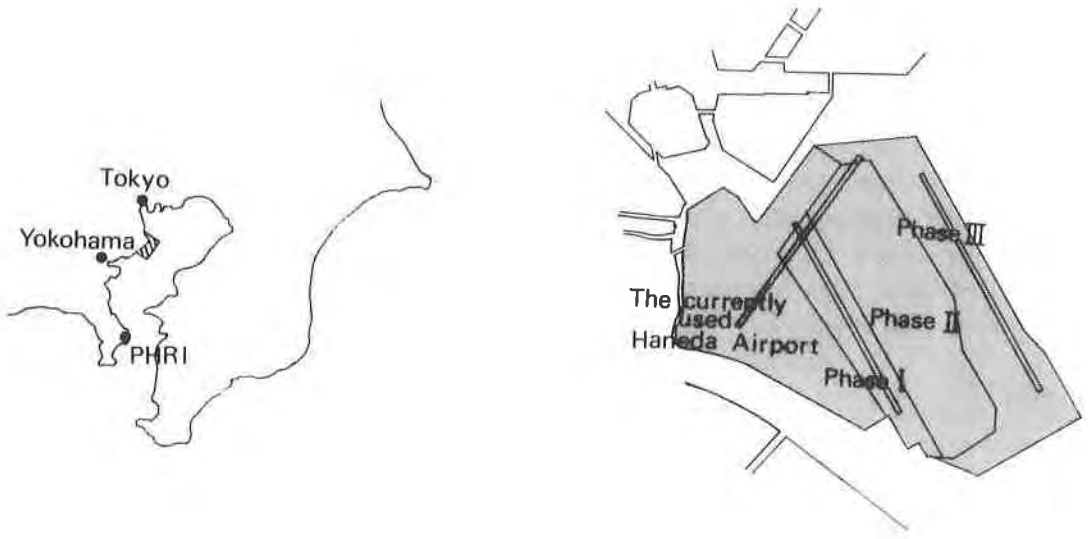

Fig. 1 Outline of the Haneda Offshore Development Project

The reclamation and dredging history of the construction site for some decades is summarized in Fig. 2. A thick sandy layer, As_1 layer, had been accumulated in a loose condition until 1965. But in the latter 1960's this soil was dredged for the reclamation work along the Tokyo Bay shoreline. Since 1971, the site was filled again with sludge from Tokyo Port. The sludge layer, Ac_1, was in turn covered by surplus soil, Bs, from construction sites in Tokyo urban area. Cement stabilization was performed at the surface of the sludge to ensure trafficability during filling with the surplus soil. As the cement-treated soil of about 3.5 m in thickness has a low permeability and covers almost all the Ac1 layer, the Ac_1 layer is practically kept in an undrained condition and, therefore, has an extremely high water content. At the site of phase 3, the objective site in this study, even water contents

exceeding 170 % are still found locally. Therefore the fabri-packed sand drain shown in Fig. 3 will be installed throughout the Ac_1 and at upper half of the Ac_2 layer to accelerate the consolidation. The drain, having a diameter of 50 cm, is planned to be installed at the regular pattern of 2.5 m pitch. Details of the Project were reported by Katayama (1991).

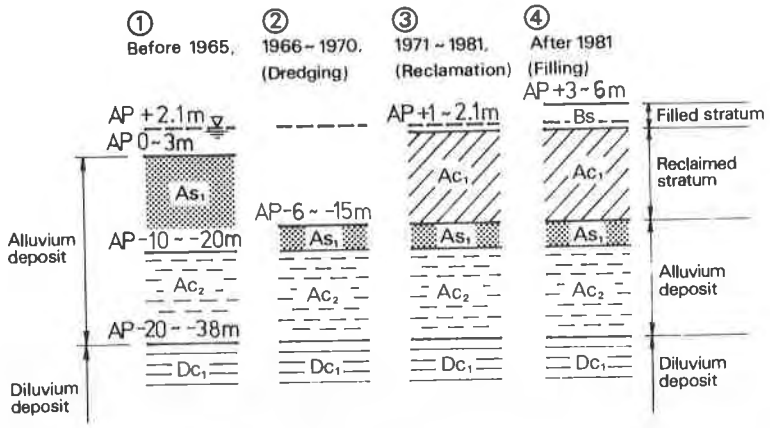

Fig. 2 Reclamation and Dredging History of the Site

Fig. 3 Fabri-Packed Sand Drain

CENTRIFUGE APPARATUS

To predict the prototype behavior correctly from the observation of model behavior, similarity condition must be established for the model and the prototype. The basic concept of centrifuge modeling is that a model with linear dimensions scaled down by a factor of 1/N will, when subjected to a centrifugal acceleration N times greater than that due to gravity, experience the same magnitude and distribution of self-weight stresses as those of prototype.

Figure 4 shows the PHRI (Port and Harbour Research Institute) Geotechnical Centrifuge, which has two swinging platforms at both ends of the arm. The main part of the centrifuge is housed in the underground reinforced concrete pit for safe operation. The drive unit for the centrifuge is mounted on the upper floor of the pit. The centrifuge generates steady acceleration up to 115 g, which means 115 times as large as earth's gravity, at the surface of the platform whose radius during flight is 3.8m. Maximum payload including specimen box, model ground and loading devices is 2.7 tons. Electric signals obtained by various transducers embedded in the model are transmitted through slip rings on the top of the main shaft. The signals are measured by a strain meter in the operation room and automatically recorded by a micro-computer. Monitoring and photographic systems are also available to observe the behavior of the model ground in flight. Major specifications of the Centrifuge are listed in Table 1 and the details of the PHRI Centrifuge and surrounding equipments were reported elsewhere by Terashi (1985).

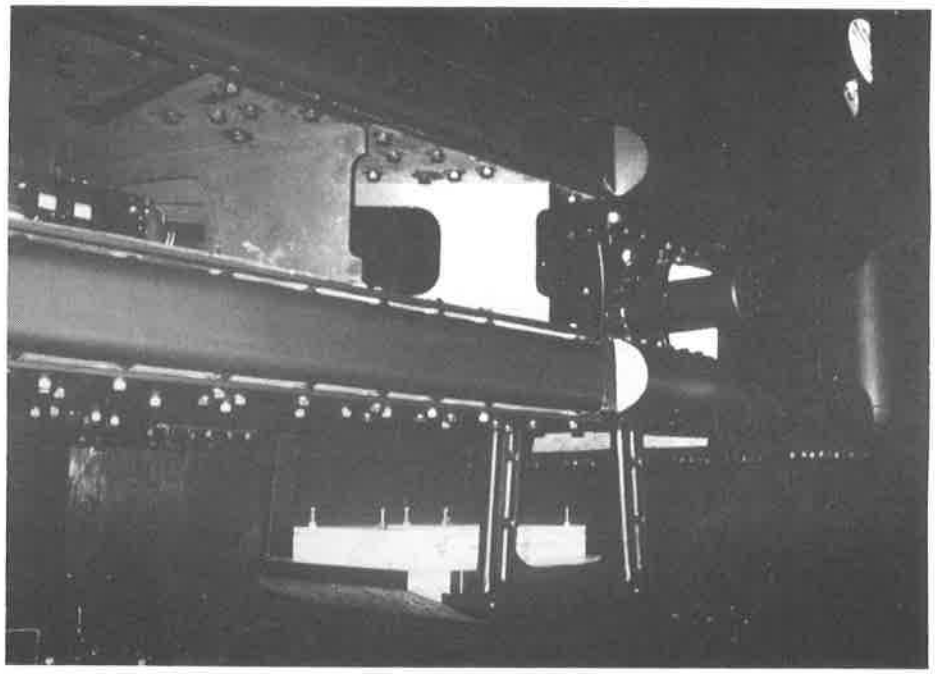

Fig. 4 Photograph of PHRI Geotechnical Centrifuge

Table 1 Major Specifications of PHRI Geotechnical Centrifuge

Maximum acceleration (g)	115
Diameter of rotating arm (mm)	9,650
Maximum effective radius (mm)	3,800
Maximum number of rotation (rpm)	165
Space of swinging platform (mm)	1,600 square
Maximum payload (kg)	2,710
Maximum capacity (g-tons)	300
Main motor (kW)	400
Electric slip ring (poles)	80
Rotary transformer (kVA)	5.2
Total weight of the centrifuge (tf)	87

PREPARATION OF MODEL GROUND

Model fabri-packed sand drains are required to have the identical property throughout the test series to enable the direct comparison of the effect of tensile rigidity. A perspex cylinder of 2 cm in diameter and 20 cm in height was filled with fully saturated Toyoura sand, which has been widely used in Japan for geotechnical study and whose properties are well determined. As shown in Fig. 5, the sand was densified by vibration to the relative density, Dr of 60 %. A set of the sand piles was covered by a thick perspex box so that the sand was gradually frozen from their bottoms in the refrigerator. The frozen sand pile thus densified was extracted from the cylinder by means of an electrical jack, as shown in Fig. 6. An envelope made of non-woven fabric was prepared by gluing the ends of strip together. The fabri-packed sand drain was prepared by installing the frozen sand pile into the envelope and kept frozen not to be disturbed until the installation into the clay ground. The fabric to be used in the prototype is a net made of polyethylene. A model fabric, geometrically scaled to the same material properties as the prototype,

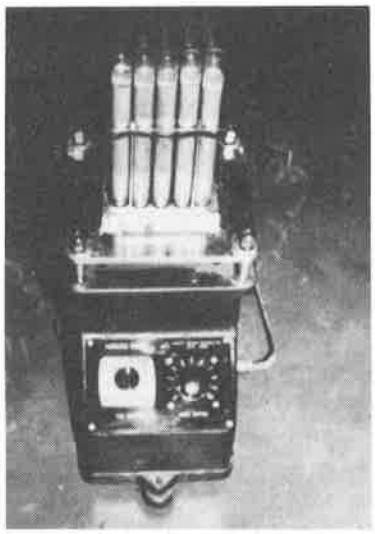

Fig. 5 The Vibrator for Densifying the Sand Pile

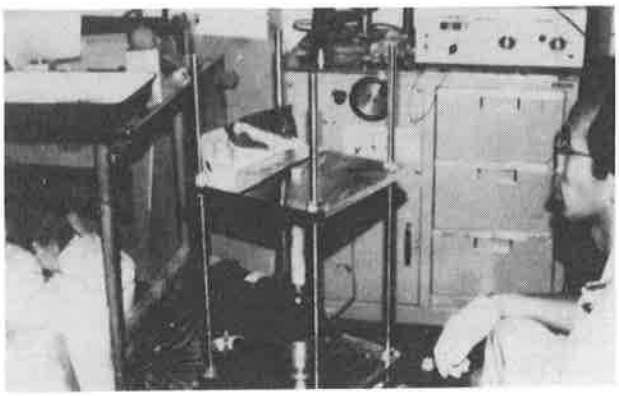

Fig. 6 Extraction of Frozen Sand Pile

should be used in the centrifuge test. However it is not normally possible to find such a material. In the current application, the most important function of the geotextile is reinforcement of the sand pile. Therefor, it was decided to use non-woven fabric having the tensile rigidity and strength that satisfy the similarity requirements for the centrifuge modeling.

Although many fabri-packed sand drains are constructed at a regular interval in the prototype, in the model test only one drain surrounded by a soft clay deposit was simulated for ease of model preparation, as shown in Fig. 7. The model ground was prepared in a perspex cylinder of 10.9 cm in diameter and 64 cm in height. Diameter of the sand pile was scaled down to 2 cm so that the ratio of sand diameter and a maximum drainage path is 5.45 and almost corresponds to the prototype condition of 5.65.

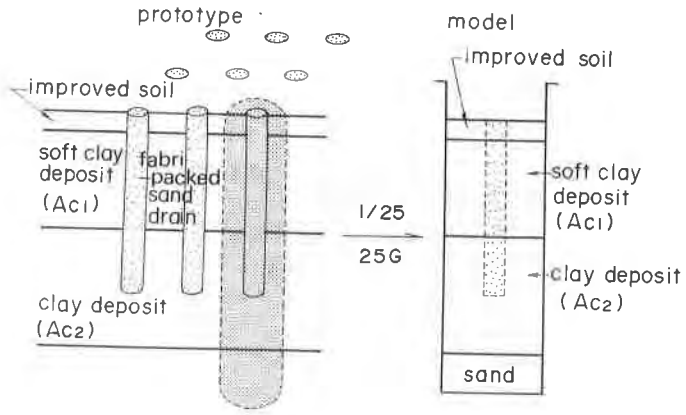

Fig. 7 Modeling of Prototype in Centrifuge

The setup of the model ground was schematically shown in Fig. 8. The inside of the cylinder was well lubricated with silicone grease and silicone oil to reduce friction to a minimum. Toyoura sand was poured first into the cylinder to prepare the sand layer. The sand was saturated by an upward percolation of water introduced

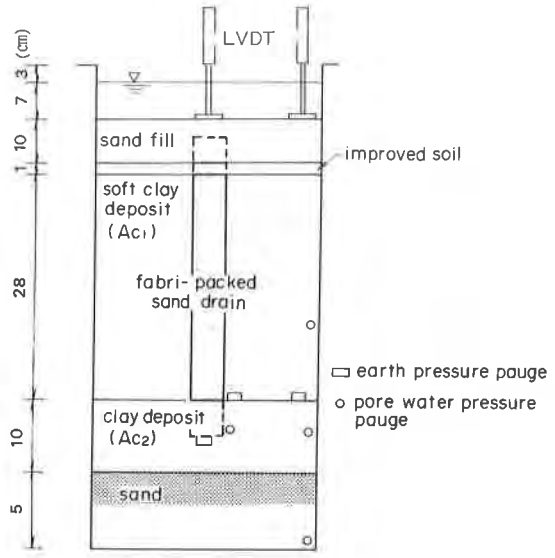

Fig. 8 Setup of Centrifuge Model Ground

through a drainage hole at the base of the cylinder. The clay slurry was then poured on the sand and was gradually compressed one dimensionally to a vertical effective stress of 30 kN/m^2. The Kawasaki clay was used as a clay material because its physical and mechanical properties had been well determined, as shown in Table 2.

Table 2 Major Properties of Kawasaki Clay

G_s	W_L	W_P	I_P	C_u/P	C_v (cm^2/min)	C_c	C_s
2.688	83.4 %	38.6 %	44.8	0.300	0.03	0.59	0.11

As it was considered that the thickness of the clay deposit, Ac_2 has little effect on the consolidation behavior of Ac_1 layer improved by the fabri-packed sand drain, thickness of the Ac_2 was set 10 cm because of the limited length of the cylinder. The thickness corresponds to 2.5 m in the prototype scale. A small hole of 2 cm in diameter and 5 cm in depth was carefully excavated using a small machinery drill at the center of the clay surface. The fabri-packed sand drain in the frozen condition was installed in the hole. Saturated clay slurry mixed at a water content of 150% was carefully poured in the cylinder as shown in Fig. 9. The frozen pile will melt before the test starts. A perspex doughnut plate, whose inner and outer diameters were 2 cm and 10 cm respectively, was placed at the surface of Ac_1 to simulate the stiff and impermeable cement-treated soil. Toyoura sand and lead shot were then poured as fill materials, which were weighted so that the fill pressure at 25 g became 90 kN/m^2. Two LVDTs were mounted on the top of the cylinder to measure the settlements of the sand pile and the clay surface. Earth pressure and pore water pressure transducers were also installed in the model ground to monitor the consolidation process in the centrifuge test.

Fig. 9 Modeling of Ac1 Deposit

CENTRIFUGE TEST

The model ground thus prepared was brought to an acceleration field of 25 g and allowed to consolidate by its enhanced self-weight. During the consolidation, the settlements at the fill surface and pore water pressures within the model ground were monitored. After reaching 90% consolidation, the centrifuge was stopped to end the test. The model ground was pushed out from the cylinder. The deformation of the sand pile was observed after removing the clay deposit. Water contents were also measured at several points to obtain the distribution within the ground.

Seven model tests, including a case without a fabric reinforcement, were carried out changing the tensile rigidity of the geotextiles. The properties of the geotextiles used in the tests were listed in Table 3 in the prototype scale. The test conditions varied so widely that they should include the prototype condition. The tensile rigidity listed in the Table was a tensile force of 5 cm wide specimen at the tensile strain of 1%. The terms horizontal and vertical, in the table mean the tangential and longitudinal directions of the sand pile respectively. Unfortunately the non-woven fabric used in the test had tensile properties different in the fiber direction. The tensile rigidity and the strength in the two directions could not be controlled independently.

Table 3 Test Cases and Properties of the Geotextile

	prototype	1	1'	2	3	4	5	6
material	Polyethylene	non-woven cloth						
tensile rigidity (N/5cm/%)								
horizontal	18	15	15	88	140	140	160	—
vertical	46	160	160	175	50	50	15	—
strength (N/5cm/%)								
horizontal	516	443	443	403	2930	2930	2170	—
vertical	1020	2170	2170	270	1390	1390	443	—
average vertical strain at max. earth pressure (%)		36.1	36.1	33.9	29.2	32.5	31.1	29.3

TEST RESULTS

Preliminary tests were carried out first to obtain the critical water content of the clay at which a sand drain can stand by itself without the geotextile. A thin stainless tube of 2 cm in diameter was filled with a saturated Toyoura sand and stood in the cylinder. After clay slurry was poured into the box, the tube was pulled out from the clay slurry to simulate the construction process in situ. The model ground was immediately brought up to 25 g field to simulate the prototype stress condition. A series of the tests were performed changing the water content of the clay from 160 % to 230 %. The tests showed that a sand pile without geotextile could not stand by itself in the soft clay with the water content exceeding about 170 %. It could be concluded that the fabri-packed sand drain was necessary to improve the construction site where water content exceeded 170 % at many locations.

Figure 10 shows time settlement curves observed in case 1 during the consolidation. The two curves obtained at the top of the sand pile and at the clay surface completely coincide during the consolidation, which shows no differential settlement took place even in the composite ground consisted of the soft clay and the relatively stiff sand pile. This phenomenon was also observed in all cases including a case with no reinforcement by geotextile.

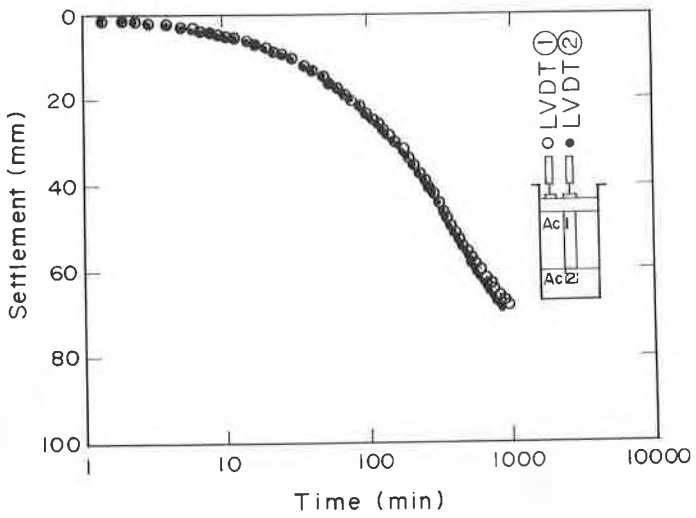

Fig. 10 Time Settlement Curves in Case 1

In case 1', five models having the same ground conditions as in case 1 were tested to observe in detail the development of deformation of the sand piles. All models were mounted on a swing at the same time and brought to the acceleration field of 25 g. At prescribed time intervals the centrifuge was stopped and one of the models was dismounted from the centrifuge. Then the centrifuge was spun again to allow the others to consolidate further. This process was repeated five times until the 90 % consolidation reached. The time settlement curves in this test for five models are shown in Fig. 11. The horizontal axis shows the elapsed time measured after the centrifuge last reached 25 g for each model. Figure 11 also shows the time settlement curve in case 1 by the broken line. The settlement data at the time when each model was dismounted are almost on the broken line and the results show these models could represent the progress of the case 1.

Figure 12 shows the development of the sand pile deformation. Numbers in the figure correspond to the elapsed times for each model already shown in Fig. 11. The sand pile started to expand in diameter to follow the vertical consolidation settlement as long as the settlement remained relatively small. But when a large settlement took place, the pile had a tendency to deform like a snake to absorb the large vertical compression. Measured elapsed times for completion of the consolidation for all case were compared with that calculated by Barron's equation. The measured values were in good agreement with the calculated values(Kitazume et al., 1992). This ensures that such a heavily deformed sand pile could still function as a drainage path, even in a non-packed case.

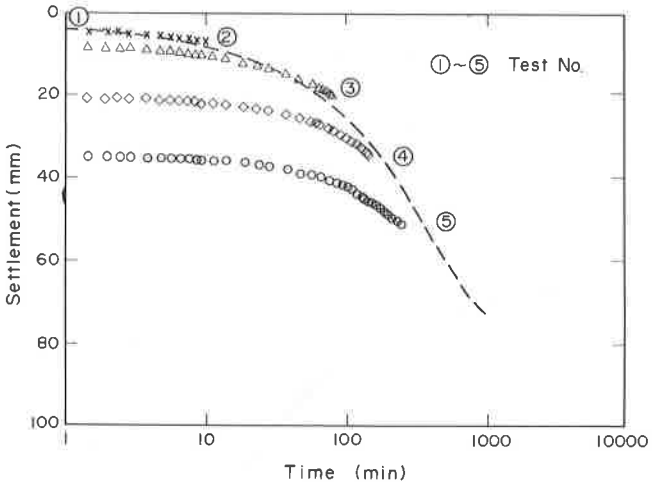

Fig. 11 Time Settlement Curves in Case 1'

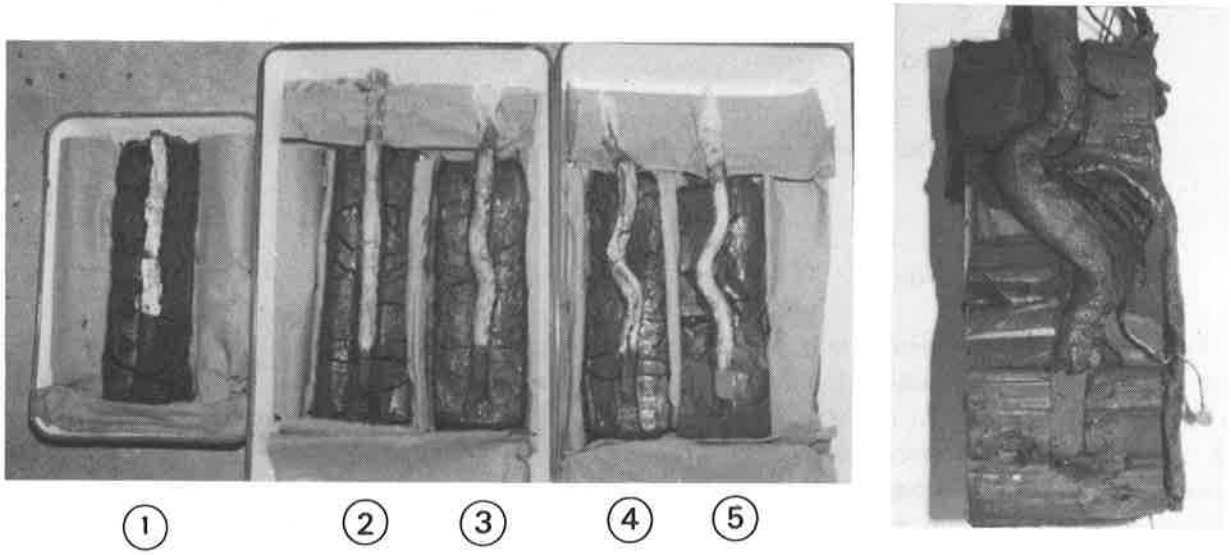

Fig. 12 Progress of the Sand Pile Deformation

Earth pressures measured at the surface of Ac_2 layer are shown in Fig. 13. Pressure measured by the gauge No. 7 that was located at the flush bottom of the sand pile increases to the maximum value with a progress of consolidation. After the pressure reaches to the maximum value, the pressure decreases rapidly. These show the fill pressure gradually concentrates at first to the pile, but redistributes later. As the pile deforms like a snake as shown in Fig. 12, the compressive rigidity of the pile tends to decrease and which seems to cause the redistribution of the fill pressure. The mean vertical strain of the sand pile at the maximum earth pressure is determined by the ratio of the settlement against the initial height of the pile and is listed in Table 1. As shown in the Table, the mean vertical strain at the maximum earth pressure is around 32 % regardless of the tensile rigidity of the geotextile. The redistribution of the fill pressure or the bending of the sand pile seems to start at the similar vertical strain level.

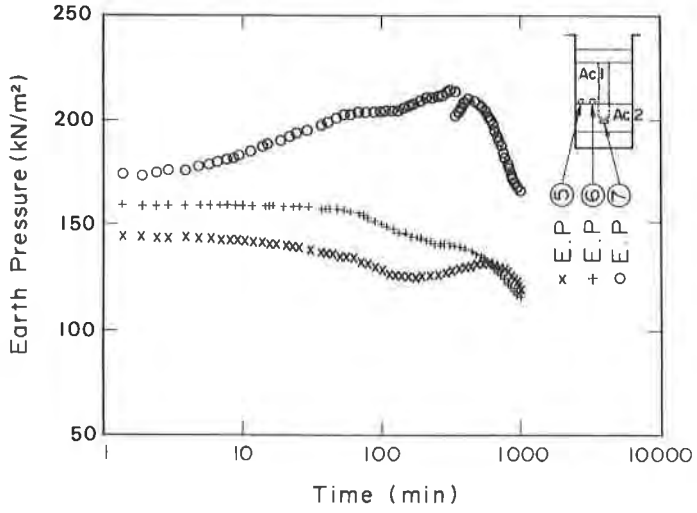

Fig. 13 Time Earth Pressure Curves in Case 1

Three earth pressure gauges were installed beneath the sand pile and at the bottom of Ac_1 deposit, as shown in Fig. 13. While the earth pressure gauge No. 7 was installed 5 cm deeper than the other gauges, the measured pressure was corrected by subtracting the corresponding total earth pressure to enable the direct comparison with those measured by other gauges. Figure 14 shows the change of the earth pressure distributions along radial direction at the bottom of the Ac_1 deposit for the case No. 1. As might be expected from Fig. 13, the pressure distribution changed during the consolidation. The consolidation pressure was also estimated by the water content change and plotted on the same figure by solid circles. Average value of the pressure acting on the sand pile and that on the clay were obtained and shown in the figure by a broken line and a chained line respectively. The stress concentration ratio, n was defined as a ratio of the average effective vertical stress on the sand against that on the clay, and is about 2.0 in the case 1. The same processes were repeated for all test cases.

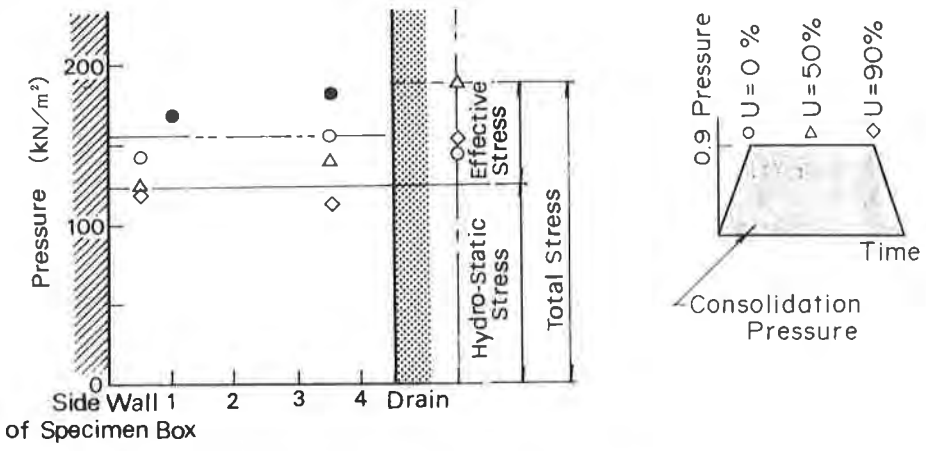

Fig. 14 Pressure Distribution in the Ground

Figure 15 shows the stress concentration ratio against the tensile rigidity of the geotextile in the tangential direction. The ratio, n for the non-packed case is also calculated and plotted by a cross on the vertical axis. It should be noted that the stress concentration of about 1.5 took place even in the non-packed case. Although these values scattered, the ratio increased almost linearly with the tensile rigidity of the geotextiles.

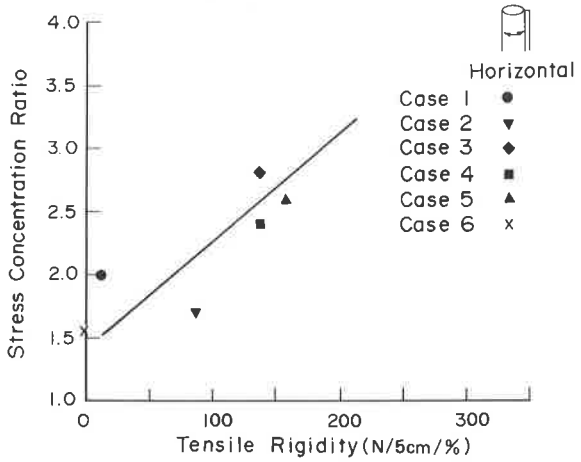

Fig. 15 Relationship Between Stress Concentration Ratio and Tensile Rigidity

The influence of the stress concentration on the consolidation settlement can be evaluated by the following equation, whose validity has been confirmed for the improved ground by sand compaction piles (Aboshi, et al. 1991).

$$\beta = 1 / (A_s * n + (1 - As)) \qquad (1)$$

where:

β = ratio of the settlement of an improved ground against that of un-improved ground,

n = stress concentration ratio,

A_s = replacement area ratio

At the phase 3 site of Haneda, A_s is expected to be around 0.03. The value of β for the prototype is calculated to be 98 % by substituting n of 1.6 into the equation that corresponds to the tensile rigidity of a geotextile to be used in practice. As the replacement ratio of the sand piles is relatively small, the decrease of the settlement due to the stress concentration could remain within 5% as long as the tensile rigidity dose not exceed about 200N/5cm/%.

EVALUATION OF GEOTEXTILE REINFORCEMENT BY SIMPLE ANALYSIS

In this section, a simple calculation is performed to evaluate the relationship between the stress concentration and the tensile rigidity of geotextiles. In the calculation, the Ac_1 deposit with a fabri-packed sand drain is considered to be

composed of two materials; a hollow cylindrical material representing the soft clay and a composite column representing the fabri-packed sand drain as shown in Fig. 16. Assuming these materials are linear elastic materials having Young's modulus and Poisson's ratio, vertical, radial and circumferential stresses in the materials are easily obtained independently by the solution found in textbooks on mechanics. Young's modulus and Poisson's ratio of the fabri-packed drain can be evaluated from each property with the consideration of the effect of hoop tension given by the geotextile.

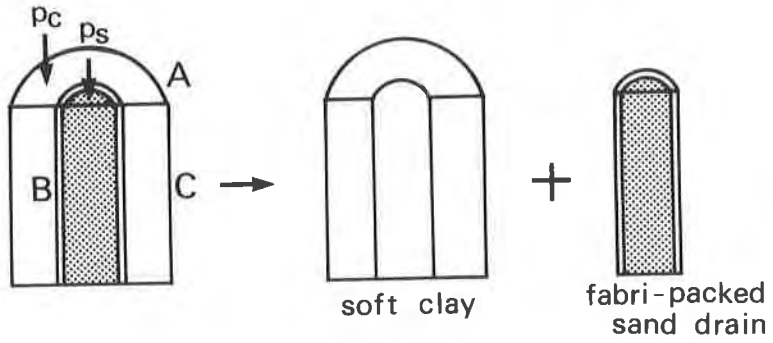

Fig. 16 Break Down of the Ac_1 to Two Elastic Materials

To solve the problem, boundary conditions to be satisfied at three interfaces are listed as follows;

1) Vertical displacements of the sand pile and the clay should be identical at surface A.
2) At the interface B, the interface between the clay and the sand pile, radial stress should be in equilibrium and the same amount of radial displacements should take place.
3) No radial displacement took place at the interface C, which is the outer surface of the clay cylinder.

The stress concentration ratio is evaluated as a ratio of the vertical stresses acting at the sand pile, P_s and the clay, P_c. The Young's modulus of the clay is determined from the coefficient of volume compressibility, m_v, obtained by oedometer test. The modulus of the sand is determined by the compressive rigidity based on the stress-strain curve obtained by triaxial compression tests. The Poisson's ratios of the sand and the clay were assumed to be 0.33, which corresponds to drained condition.

The calculated stress concentration ratio is shown by a range in Fig. 17 against the tensile rigidity of the geotextile. The calculated ratio increases linearly with increasing tensile rigidity. The figure also shows the measured values and a fairly good agreement with the calculation is found. It should be concluded that the simple elastic calculation is able to evaluate the effect of the tensile rigidity on the stress concentration if the Young's modulus of the sand pile is determined appropriately.

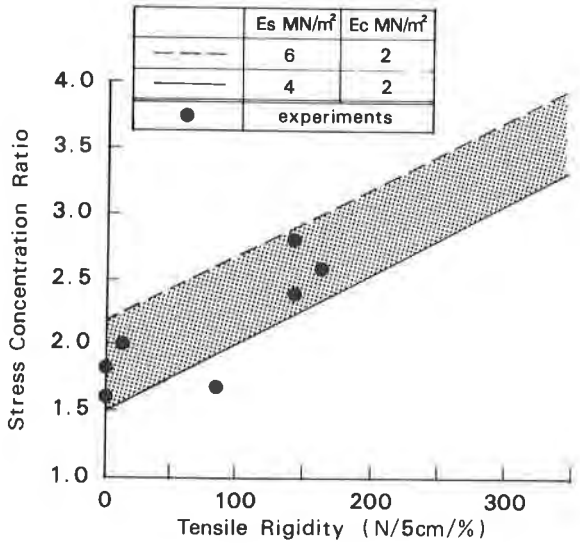

Fig. 17 Relationship Between Stress Concentration ratio and Tensile Rigidity

CONCLUSIONS

A series of centrifuge model tests were performed to investigate the effect of the geotextile on the clay consolidation behavior and to determine the stress concentrations at the fabri-packed drain. The study showed the centrifuge model test was very useful to study the consolidation behavior of the composite ground. The study revealed that the geotextile functioned well to stabilize the sand pile in the extremely soft clay ground. The stress concentrations resulting from the tensile rigidity of the geotextiles evaluated were smaller than anticipated and might not cause undesirable settlement.

As the applicability of the fabri-packed sand drain was confirmed by the centrifuge model study, the method is now being employed in the Haneda Project. The effectiveness of this method, as well as the stability performance, have been confirmed on site. The consolidation behavior will be evaluated soon by the field measurements and will be published elsewhere.

REFERENCE

Aboshi, H., Mizuno, Y. and Kuwabara, M. (1991) "Present state of sand compaction pile in Japan", Deep Foundation Improvements: Design, Construction, and Testing, ASTM STP 1089, ASTM, pp. 32-46.

Katayama, T. (1991) "meeting the Challenge to the Very Soft Ground - The Tokyo International Airport Offshore Expansion Project", GEOCOAST '91.

Kitazume, M., Aihara, N. and Terashi, M. (1992) "Consolidation Behavior of the Soft Ground with Fabri-Packed Sand Drain", The 27th Japan National Conference on Soil Mechanics and Foundation Engineering, JSSMFE, Vol.2, pp.2189-2192 (in Japanese).

Terashi, M., (1985) "Development of PHRI Geotechnical centrifuge and Its Application", Report of the Port and Harbour Research Institute, Vol.24, No.3, pp.73-122.

Improvement of the Bearing Capacity of Footings by a Single Layer of Reinforcement

S. Abdel-Baki
Queen's University, Canada

G.P. Raymond
Queen's University, Canada

P. Johnson
Queen's University, Canada

ABSTRACT

One of the most inspiring aspects of soil reinforcement is structure rehabilitation. For structures such as gantry cranes, railroads and paved roads, rehabilitation has been made easy using a single layer of reinforcement within the ballast or the granular subbase. Such structures are subjected to eccentric and inclined loads in addition to vertical loads. This paper investigates the effect of a single strong reinforcement layer, placed within granular soil, on the bearing capacity of footings subjected to eccentric, inclined and concentric loads.

INTRODUCTION

Soil reinforcement is a method of soil improvement that has gained attention in the past two decades. Soil reinforcement has been used to improve the properties of soils behind retaining walls, inside embankments, and below roads. Recently, it has been used for structure rehabilitation. When the granular layers of paved roads, railroads and gantry cranes are rehabilitated, the cost of undercutting increases significantly as the undercut depth increases. One method of decreasing the undercutting depth is to use a single strong reinforcement layer. This technique is investigated herein through the use of model testing.

THE TESTING MODEL

The objective of the tests was to investigate the effect of the reinforcement on the improvement of the bearing capacity of footings on granular soil. A footing width was selected to negate the effect of the base interference on the bearing capacity and to simulate field dimensions at the same time.

To simulate the dimensions in the field, a 200 mm wide footing was placed on a uniform soil having an average particle diameter of 3 mm. This is comparable to the 2000 mm length of a railroad tie on a ballast with an average diameter of 20 mm.

A review of the literature has proven that the ratio of the soil depth below the footing to the footing width, (H/B), after which no

effect from the base would be felt, changes relative to the footing width. Suklje and Vidmar (1973) used a footing 288 mm wide and concluded that H/B was about 0.33. Pfefifle and Das (1979) using a 51 mm wide footing found this value to be 2 and El-Hakim (1983) using a 75 mm wide footing found it to be 1.5. The variation of the value of H/B with the footing width, B, according to the above mentioned researchers, is shown in Fig. 1.

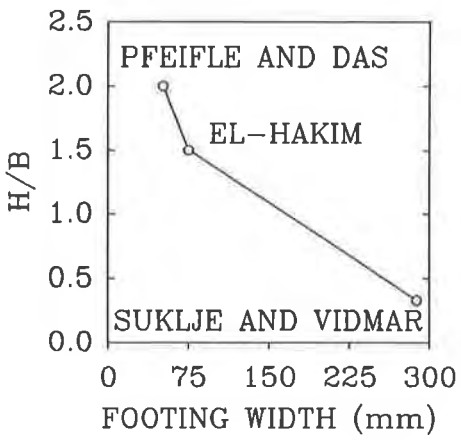

Fig. 1. The minimum value of H/B to give no base effect as determined by different researchers.

A series of tests was thus performed on footings of four different widths , 75 mm, 115 mm, 150 mm, and 200 mm, on the same soil to find the appropriate footing width. The results of these tests are shown in Fig. 2. For the 200 mm wide footing, there was no change in the bearing capacity as the ratio H/B exceeded 1. The 200 mm wide footing was selected for usage in the testing program. It was used by placing it on 200 mm layer of rounded particles overlying the stiff base.

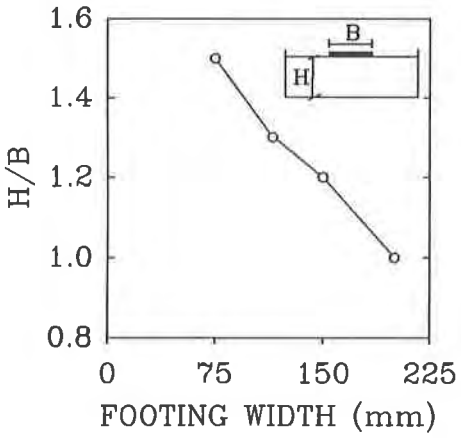

Fig. 2. The minimum value of H/B determined in this study.

THE TESTING EQUIPMENT

The layout of the testing equipment is shown in Fig. 3. The soil used was rounded particles known as denstone particles made by Norton Chemical Processing Co.. The particles had a specific gravity of 2.4 and their maximum and minimum compaction densities were 1.553 and 1.366 gm/cm^3 respectively. The placement density was 1.534 gm/cm^3 giving a relative density of 90%. The angle of friction, ϕ,of these particles from triaxial tests, was 34°.

The reinforcement used for the majority of the tests was a steel mesh manufactured from welded galvanized wire with an aperture size of 19.0 mm X 19.0 mm. Primary tests were performed, however, using a micro mesh with a thickness of 0.3 mm. For all the tests, other than those performed to find the effect of the reinforcement length, the reinforcement was cut to a length and width 25.4 mm less than the length and the width of the tank. The 25.4 mm clearance was more than adequate to prevent any friction between the reinforcement and the tank walls.

The tank used was 900 mm long, 200 mm wide, and 330 mm deep. The sides of the tank were made of Herculite transparent glass with a very small coefficient of friction.

All loading tests used 19 mm thick aluminum model footings extending over the whole width of the tank. This simulates the plane-strain loading condition. Four sets of thrust bearings were seated in

a plate on top of a semi-cylindrical rod in the case of eccentric loading and a triangular prism in the case of inclined loading. The semi-cylindrical rod insured that the load would act vertically even after the footing has settled and tilted. To insure that the load maintained its inclination, in the case of inclined loading, the frame, on which the loading piston was mounted, was inclined to the selected inclination.

A load cell was used to monitor the load and the cell response was recorded by a data acquisition system. Dial gauges, having a travel of 25 mm and sensitivity of 0.0025 mm, were placed near each corner of the footing to monitor the displacement or the heave at that corner. For the case of inclined loading, two more dial gauges were used to measure the horizontal displacement of the footing.

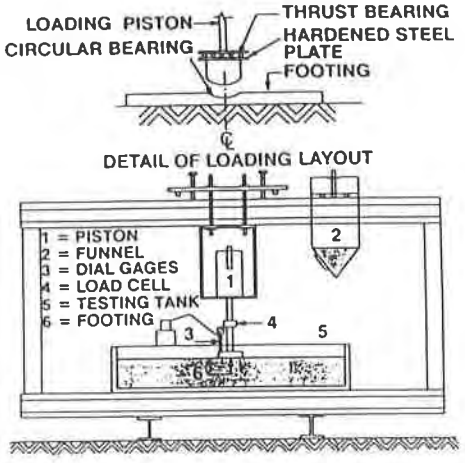

Fig. 3. Layout of the testing equipment.

THEORETICAL AND EXPERIMENTAL RESULTS ON UNREINFORCED SOIL

The second series of tests was performed on unreinforced soil. The values of the bearing capacity obtained from the tests were compared to Meyerhof's theory (1953) for eccentric and inclined loads on cohesionless soil.

According to Meyerhof (1953), the maximum vertical component of the load carried by a footing per unit length for the case of eccentric and inclined loads is shown in equations (1) and (2) respectively.

$$Q_f = \frac{1}{2} \gamma \, (B-2e)^2 \, N_\gamma \qquad (1)$$

$$Q_f = \frac{1}{2} \gamma \, B^2 \, N_\gamma \, i_\gamma \qquad (2)$$

where:

$$i_\gamma = (1 - \frac{i}{\phi})^2 \qquad (3)$$

γ = the unit weight of the soil;
B = the footing width;
e = the load eccentricity;
i = the load inclination;
N_γ = bearing capacity coefficient depending on the angle of friction of the soil, ϕ.

Meyerhof states that the plane-strain angle of friction should be the one to be used in these equations. According to Cornforth (1964), ϕ_{ps} is about 10% greater than ϕ_{tr}. Thus, ϕ_{ps} was calculated to be 38°. The value of N_γ was then calculated, according to Vesic (1973), to be 78. This value was found to be closer to the value obtained from experimental results than other researchers' values. Thus, Vesic's N_γ was used in equations (1) and (2) to predict the maximum load that would be carried by the footing.

The first footing was loaded vertically at 7 different eccentricities, 12.5, 25, 37.5, 50, 62.5, 75, 87.5mm. The footing was in full contact with the soil until failure for eccentricities up to 37.5mm (this compares to the edge of the middle third being at 33.3mm). For larger eccentricities, the unloaded side of the footing lifted above the soil before failure occurred.

The second footing was loaded centrally at 5 different inclinations, 5°, 7.5°, 10°, 15°, 20°. For load inclinations up to 15°, the footing failed and tilted showing a one sided shear failure. For the 20° load inclination, the footing slipped and failure occurred more by sliding rather than shear failure. This fails to verify Meyerhof's concept (1953) that sliding does not occur until the angle of load inclination, i, is equal to the angle of internal friction of cohesionless soil, ϕ. Meyerhof's concept is based on the assumption that the angle of friction between the footing base and the soil, δ, is equal to ϕ. Here δ was closer to the widely used assumption of about (2/3 ϕ) rather than ϕ which may well explain the difference. For this case (2/3 ϕ) = 22.6° which is quite close to the 20° found from these experimental tests.

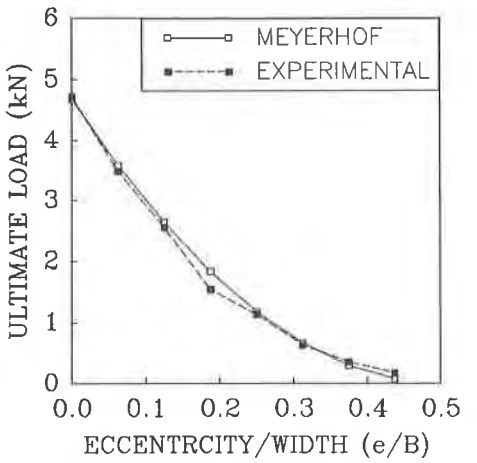

Fig. 4. Comparison between the experimental results and Meyerhof's theory for eccentric loadings.

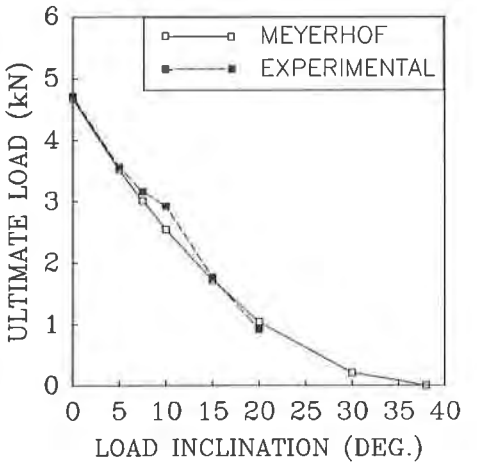

Fig. 5. Comparison between the experimental results and Meyerhof's theory for inclined loadings.

The predicted eccentric and inclined failure values, using Meyerhof's theory (1953), are compared to the experimental values in Figs. 4 and 5. It can be seen that the theoretical values, for surface footings on unreinforced soil subjected to eccentric and inclined loads, are in good agreement with the experimental values.

FOOTINGS ON REINFORCED SOIL

The third series of tests was performed on reinforced soil.

Eccentric and inclined loads were applied to the 200 mm wide footings. The loads were applied at the same eccentricities and inclinations as the unreinforced case. The reinforcement was placed at six different depths. The ratios of the depths of the reinforcement to the footing width, Dr/B, ranged from 0.0625 to 0.5. In no case did the reinforcement fail. This is similar to the prototype since in most cases the reinforcement is selected for survivability and is not expected to fail on loading.

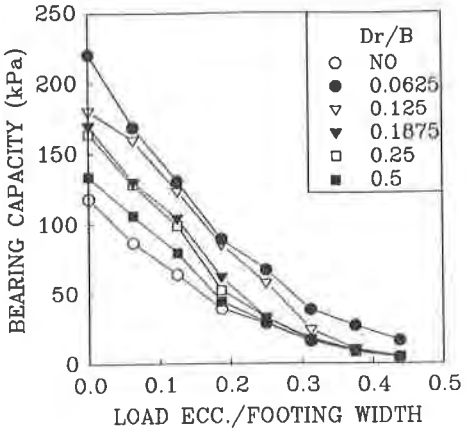

Fig. 6. The bearing capacity of the used footing when loaded at different eccentricities.

Failure for concentric loading cases occurred by general shear failure in a manner similar to the unreinforced case. The results of all the tests are shown in Figs. 6 and 7. It can be seen that the bearing capacity increased when the reinforcement was placed at shallow depths. As the depth of the reinforcement increased, the bearing capacity decreased. For concentric loads, there was no improvement from the reinforcement when it was placed at depths greater than 0.4 times of the footing width. Shallower depths were required for the reinforcement to have any effect on the eccentric and inclined loading.

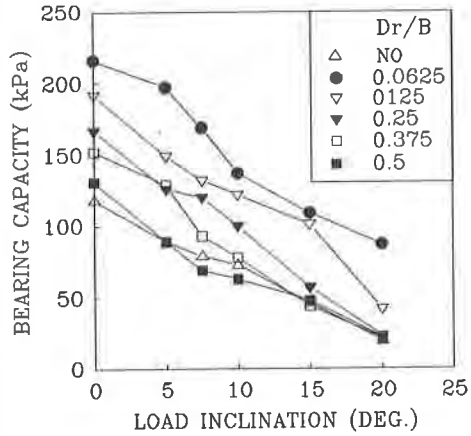

Fig. 7. The bearing capacity of the used footing when loaded at different inclinations.

It is concluded from the analysis of the test results that; for the reinforcement to have any effect on the bearing capacity, it must be placed within the confinement wedge below the footing. The wedge is shallower for the case of eccentric loads. In this case, the wedge is assumed to have a depth related to a footing width of (B-2e) rather than B. The wedge is also shallower in the case of inclined loads (Meyerhof, 1953).

In order to appreciate the effect of the reinforcement position, the Bearing Capacity Ratio, $q_{reinforced}/q_{unreinforced}$, is plotted for different depths of the reinforcement in Figs. 8, and 9 for eccentric and inclined loadings respectively. It can be seen that the increase in bearing capacity is much higher when the reinforcement is placed at shallower depths. For shallower reinforcement depths, the Bearing Capacity Ratio increased as the load eccentricity or inclination increased.

THE EFFECT OF THE LENGTH AND CONTINUITY OF THE REINFORCEMENT

Many values are reported in the literature for the critical reinforcement length (the length, centred about the footing centre, after which any increase in length will be insignificant for the bearing

capacity). The ratios of the recommended length of the reinforcement to the footing width ranged from 1.25 (Guido et al., 1986) to 7 (Fragaszy and Lawyon, 1984). This could be due to the different types of the reinforcements used and the different soils on which the tests were done. A series of tests were conducted to find the effect of the length of the reinforcement and its continuity below the footing on the bearing capacity.

Tests were first done with reinforcements of different lengths, the shortest equalled the footing width. The reinforcements were placed at different depths within the soil. The results of these tests are shown in Fig. 10. It can be seen that, in agreement with Guido et al. (1986), increasing the length of the reinforcement greater than 1.25 the footing's width, had little effect on the bearing capacity. This verifies the assumption, mentioned earlier, that the reinforcement mainly increases the bearing capacity when placed within the confinement wedge.

Another series of tests was performed to investigate the effect of the reinforcement continuity on the bearing capacity. Reinforcement was placed at a depth of 12.5 mm. The reinforcement was cut and a gap below the footing was introduced. The width of the gap was varied from 50 mm to 200 mm. The effect of the gap is shown in Fig. 11. It can be seen that as the gap width increased, the **B**earing **C**apacity **R**atio decreased. This ratio decreased to nearly 1 (i.e., no effect for the reinforcement) as the gap width increased to the footing width. This also verifies the earlier observation that the reinforcement has to be placed within the confinement wedge to have any considerable effect on the bearing capacity.

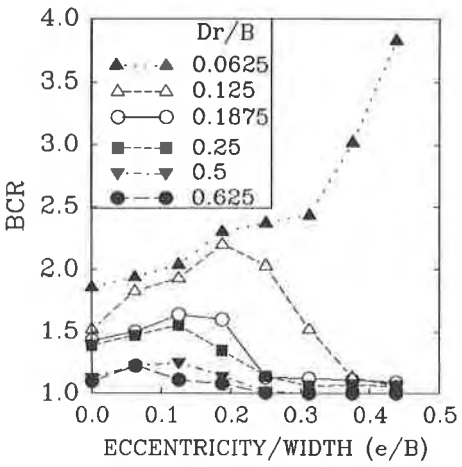

Fig. 8. The BCR for different eccentricities of the load and reinforcement depths.

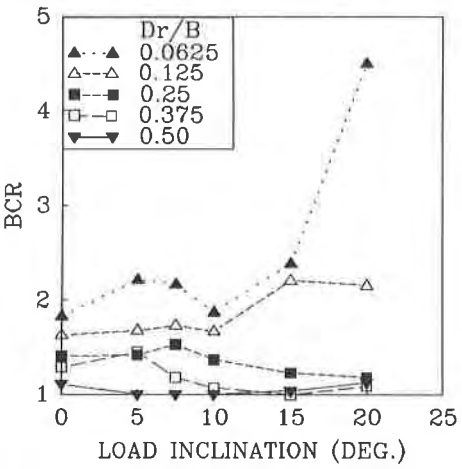

Fig. 9. The BCR for different load inclinations and different reinforcement depths.

DESIGN PROCEDURE

To be able to use the reinforcement for soil improvement below earth slabs, a somewhat simple method of design should be available. Presented herein is a simple design method for footings on reinforced earth subjected to eccentric, inclined or concentric loads using a single strong layer of reinforcement of sufficient strength that it would not fail. The footing is assumed to have a new width that acts at the top of the reinforcement. The new footing width, B1, is determined

according to Fig. 12 as:

$$B1 = B + 2 \tan\theta \, Dr \qquad (4)$$

where θ could be determined as:

$$\theta = \left(\frac{\phi}{\pi/4} - 2\, Dr/B\right) \frac{2\pi}{3} \qquad (5)$$

and $0° \leq \theta \leq 85°$

where:

Dr	=	depth of the reinforcement;
B	=	original footing width;
B1	=	assumed footing width;
ϕ	=	angle of internal friction of the soil;

The bearing capacity can thus be calculated according to Meyerhof with the same notations used in equation (1) as:

$$q = \frac{1}{2} \gamma \, (B1) \, N_\gamma \qquad (6)$$

Eccentric Loading If the loads are applied to surface footings at an eccentricity, e, where, e is less than B/6, then the eccentricity, e1, on the equivalent footing to account for the reinforcement, is calculated as:

$$e1/B1 = \left(\frac{(B1-B)}{B} + 1\right) e/B \qquad (7)$$

The bearing capacity is thus calculated according to Meyerhof with the same notations used in equation (1) as:

$$q = \frac{1}{2} \gamma \, B' \, N_\gamma \qquad (8)$$

where B' = (B1 - 2 e1)

The comparison between the experimental results and the results calculated using the above design procedure is shown in Fig. 13.

Inclined Loading For the case of inclined loads applied to surface

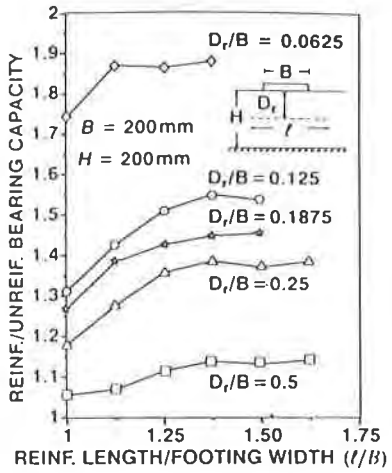

Fig. 10. The effect of the reinforcement length on the bearing capacity.

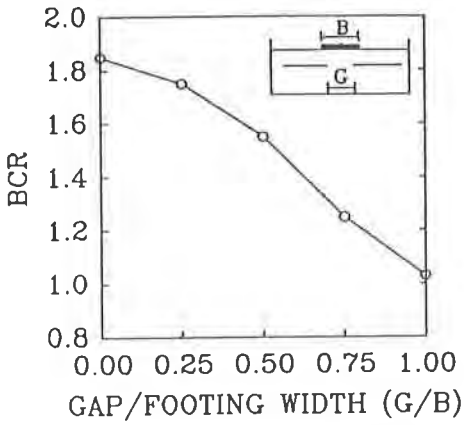

Fig. 11. The effect of having a gap in the reinforcement under the footing on the bearing capacity.

footings, the loads are assumed to be transmitted to the equivalent footing, to account for the reinforcement, with inclination and eccentricity as shown in Fig. 14. The eccentricity, e1, would be calculated using the same notations used in the previous equations as:

$$e1 = Dr \tan i \qquad (9)$$

The bearing capacity is thus calculated as:

$$q = \frac{1}{2} \gamma B' N_\gamma i_\gamma \qquad (10)$$

where i_γ is calculated from equation (3). The experimental values of the bearing capacity, for different load inclinations and reinforcement depths, are compared to the values calculated using the above mentioned design procedure. This comparison is shown in Fig. 15.

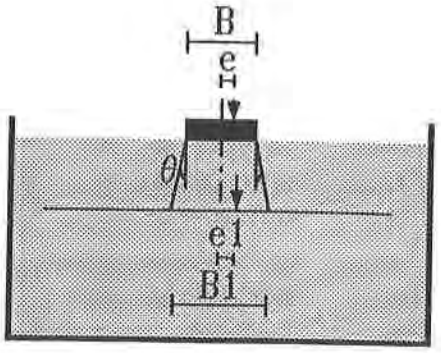

Fig. 12. The equivalent footing width used in the design procedure.

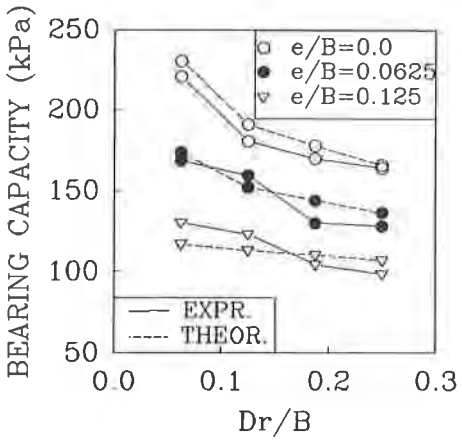

Fig. 13. Comparison between the design procedure and the experimental values.

Tension Force in the Reinforcement The tension force in the reinforcement is assumed to carry the difference in the horizontal load between the unreinforced and the reinforced cases. The tension force in the reinforcement per unit length of the footing would thus be

$$T = K_a (Qr - Qu) \qquad (11)$$

where:

K_a = $(1-\sin \phi)/(1+\sin \phi)$;
Qr = the reinforced load capacity;
Qu = the unreinforced load capacity.

For a more conservative design, K_o can be used instead of K_a where K_o is assumed to be $(1-\sin \phi)$.

There is a limiting load, however, to the reinforcement which could be calculated from the pull-out resistance according to Jewell (1984) or in a very simple form it could be calculated as

$$T_{pull} = Qr \tan \delta \qquad (12)$$

where:

T_{pull} = geogrid pull-out resistance;

δ = the angle of friction between the soil and the reinforcement, assumed to be about 2/3 ϕ.

CONCLUSIONS

Presented are the results of an extensive experimental program for footings on soils reinforced by a single strong layer of reinforcement. Investigated are concentric, eccentric, and inclined loadings. The results of the experimental tests proved that the reinforcement had a considerable effect on the bearing capacity of the footings. The percentage increase in bearing capacity increased as the load eccentricity and inclination increased. The reinforced bearing capacity was in some cases about three times the unreinforced case.

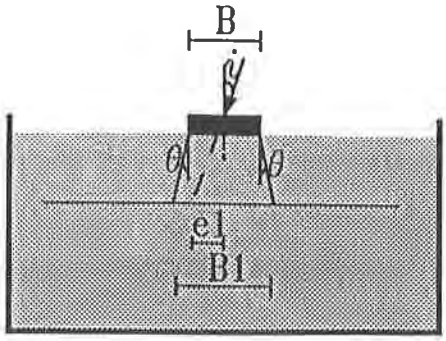

Fig. 14. The loads transmitted to the equivalent design footing.

The effect of the length of the reinforcement beyond the footing width was also investigated. The experimental results indicated that there is no significant effect on increasing the bearing capacity if the reinforcement length is extended over a length of 1.25 the width of the footing.

The effect of the reinforcement continuity below the footing was also investigated. The experimental results proved that the existence of a gap in the reinforcement below the footing decrease the bearing capacity. The increased bearing capacity from the reinforcement decreased as the gap in the reinforcement increased and reached zero when the gap width was equal to the footing width.

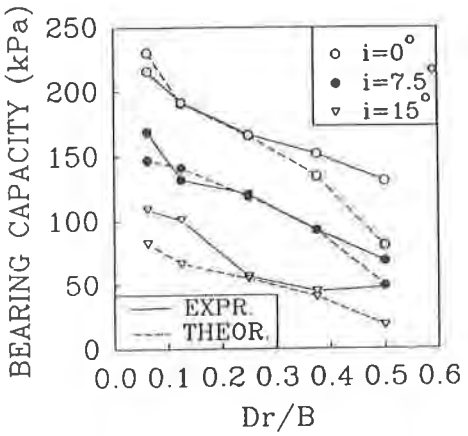

Fig. 15. Comparison between the design procedure and the experimental values for inclined loads.

A simple design procedure was also introduced for the design of footings on reinforced soil. The procedure is valid for concentric, eccentric and inclined loads.

Practical significance The work reported proved that a single strong reinforcement layer has a significant effect on the bearing capacity of footings. Reinforcement using a single strong layer can be used effectively for structure rehabilitation. It is effective under railways, paved and unpaved roads and gantry cranes. The simple design procedure presented represents a simple method of estimating the bearing capacity of reinforced earth slabs and footings on granular soils subjected to concentric, eccentric and inclined loadings.

ACKNOWLEDGEMENTS

Financial support was provided by the National Scientific and Engineering Research Council (NSERC) in the form of grant awarded to Professor G.P. Raymond. This support is gratefully acknowledged. The experimental tests and theoretical analysis were done at the labs of Queen's University at Kingston.

REFERENCES

Cornforth, D.H. (1964), "Some Experiments on the Influence of Strain Conditions on the Strength of Sands", Geotechnique, 14, 143-167.

El-Hakim, A. (1983), "Repeated Loading Of Footing On Sand Layer Overlying Bases of Different Compressibility", Ph.D. Thesis, Dept. of Civil Eng., Queen's University, Kingston, Ontario.

Fragaszy, R.J., and Lawton, A.M. (1984), "Bearing Capacity of Reinforced Sand Subgrades", Journal of the Geotechnical Division, ASCE, Vol 110, GT10, pp. 1500-1507.

Guido, V.A., Chang, D.K., and Sweeney, M.A. (1986), "Comparison Of Geogrids and Geotextiles Reinforced Earth Slabs", Canadian Geotechnical Journal, Vol 23, pp.435-440.

Jewell, R.A. (1984), "Interaction Between Soil and Geogrids", Proceedings of the Symposium on Polymer Grid Reinforcement, London, pp. 18-29.

Meyerhof, G.G. (1953) "The Bearing Capacity of Foundations under Eccentric and Inclined Loads", III ICSMFE Proceedings, Vol 1, pp. 440-445.

Pfeifle, T.W., and Das, B.M. (1979), "Model Tests For Bearing Capacity In Sands", Journal of the Geotechnical Division, ASCE, Vol 105, GT9, pp. 1112-1116.

Suklje, L., and Vidmar (1973), "Critical Loads Depending On Layer Thickness", VIII ICSMFE Proceedings, Vol 1, pp. 253.

Vesic, A.S. (1973), "Analysis of Ultimate Loads of Shallow Foundations", Journal of the Soil Mechanics and the Foundations Division, ASCE, Vol 99, SM1, pp. 45-73.

Simulating Failures of Geosynthetics-Reinforced Earth Structures Under Saturated Conditions

K.M. Chua
University of New Mexico, USA

W. Aspar
University of New Mexico, USA

A. De La Rocha
University of New Mexico, USA

ABSTRACT

Failures of geosynthetics reinforced earth structures are rare. However, if that happens, it is usually related to infiltration of water into the earth structure. This paper discusses the results of an investigation into the effects of high water on the behavior of reinforced earth structures. Laboratory pullout tests were performed with a geogrid in a sand and a clay, in both the dry and the saturated condition. A finite element code called GEOT2D was then used with inputs from laboratory pullout tests to simulate the construction of the reinforced earth structure and the subsequent saturating of it. Backfill soils used include a cohesionless and a cohesive soil. The mechanisms observed at each stage of the simulation are discussed.

INTRODUCTION

Earth structures reinforced with geosynthetics have been known to perform well under conditions which are anticipated in the design. However, unpleasant though it may be, there is an unexpressed concern among users that the performance of the reinforced earth embankment may be drastically affected if the embankment becomes saturated as a result of unexpected water infiltration or a failed drainage system.

This study investigates the effects of high water on the behavior of reinforced earth structures by:

(1) performing laboratory pullout tests with a geogrid in a sand and a clay, in both the dry and the saturated condition;
(2) designing a retaining wall following the state-of-the-practice with the sand and with clay as the backfill; and
(3) simulate these earth structures using a finite element code and observing their behavior at each stage of construction up to where the water table reaches the top at the back of the wall.

The objectives of this study are to determine the change in pullout strength of a material in both sand and clay when flooding takes place, observe the progression of the failure mechanism of earth structures when flooding takes place, and to determine how earth structures may respond to flooding when designed following conventional practice which assumes drainage. Hand-calculations as well as the finite element method [F.E.M.] are employed to this end.

LABORATORY PULLOUT TESTS

Pullout Resistance and Earth Reinforcing Elements

Earth reinforcement is a technique to stabilize soil structure by introducing reinforcing elements which can retain tension into soil mass. The reinforcing elements include metallic (mainly steel or aluminum) and geosynthetic material types. Geosynthetics are usually made of polyester, polypropylene or polyethylene and are available in the form of geogrids or geotextiles. There are two common methods of obtaining soil-reinforcement interface characteristics and they are the direct shear box and the pullout box. The latter is usually larger and has the advantage of being applicable to both geogrids and geotextiles.

Pullout Box Test

The internal dimensions of the steel pullout box at the University of New Mexico are 75 cm (30") long, 70 cm (28") wide and 60 cm (24") deep. Three 20-ton capacity hydraulic jacks are used, one for applying the vertical pressure and the others for the pullout. Strain-gage type load cells are used to measure the pullout force. The vertical load is transmitted to the soil by an assemblage of thick wooden blocks. The reinforcement is pulled at slow and constant rate after the pressure is applied. The pullout displacement of the reinforcement at the front face is measured using linear variable differential transducers. To date, more than 180 tests have been performed with various types of soil-reinforcements including geotextiles and geogrids. A detailed description of the pullout box and typical test results can be found in Yuan and Chua (1990; 1991). Figure 1 shows the setup of the pullout box used.

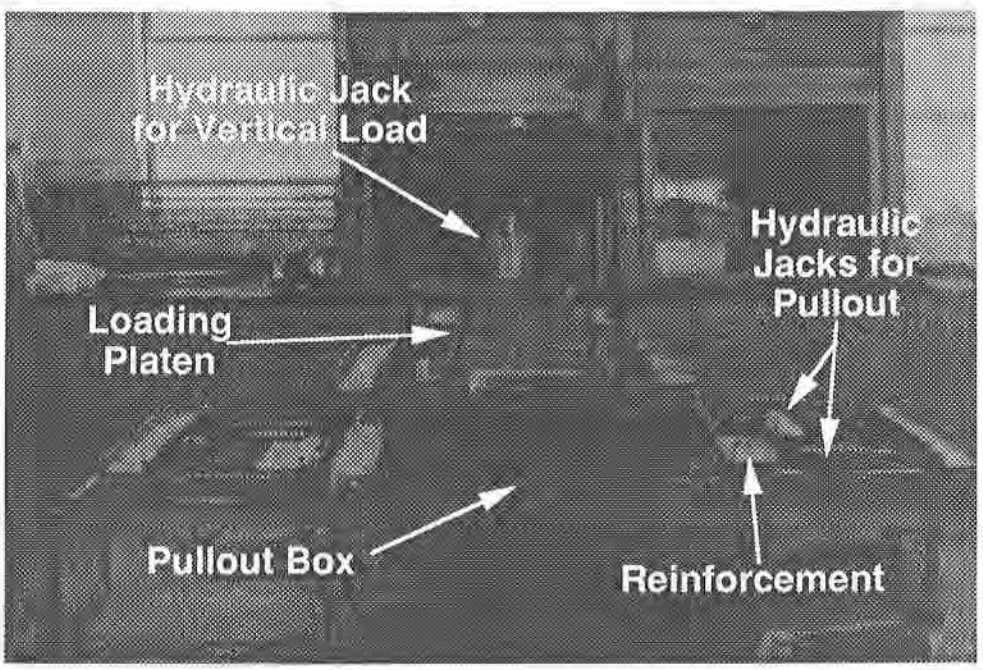

Figure 1. Pullout Box Setup at the University of New Mexico

Obtaining Interface Characteristics

The parameters for the interface materials to be used in the numerical simulation are obtained from the pull-out stress versus displacement curves. The procedure followed to obtain them is to model these results with a hyperbolic curve

$$\tau = \frac{u_r}{a + b\,u_r} \qquad (1)$$

where
τ is the interface shear stress,
u_r is the relative displacement between the soil and the reinforcement at any point along the length of the reinforcement, and
a and b are the hyperbolic model parameters.

The interface shear stiffness (which is the slope of these curves) is defined as

$$\frac{\partial \tau}{\partial u_r} = ks = \frac{a}{(a + b\,u_r)^2} \qquad (2)$$

It was shown by Yuan and Chua (1990) that the interface parameters a and b depend on the normal stress applied as follow

$$a = \alpha\ \sigma_n{}^{\beta}$$

$$b = \gamma\ \sigma_n{}^{\delta} \qquad (3)$$

These stress-independent interface parameters (α, β, γ and δ) are found in the following manner:

1. Obtain the pullout-displacement relationship at the front face of a pullout box,
2. use finite element to simulate the pullout test, and
3. adjust stress independent model parameters until the force-displacement curve at the front face is matched.

Instead of using the finite element method, the analytical approach proposed in Yuan and Chua (1992) can be used.

PULLOUT TEST RESULTS

Two different soil-fabric displacement-dependent interface characteristics were considered and they are, (a) the natural moisture content condition, and (b) the saturated condition. The soil-fabric interactive relationships were obtained from pullout tests. In the second test simulating high water, the box was flooded from the bottom upwards. The water was allowed to flow over the top of the box. Stiff rubber strips were placed at the slits where the reinforcements are slipped into the box to restrict the flow of water. In the saturate case, the clay was placed very wet and then allowed to soak for a period of time. Both tests were performed at a slow pullout rate in order to maintain a quasi-

static condition. The soils were placed in the box in 10 cm (4") lifts and compacted using tampers to the desired density.

Pullout Tests in Sand

The sand used is a fine to medium, well-graded sand (SW) with a coefficient of uniformity of 5.56, according to the Unified Soil Classification System. For the pullout tests, the sand was rained from a height of 35 cm (14") in order to obtain a unit weight of about 15.6 kN/m^3 (105.4 pcf) and a relative density of about 70%. The reinforcement used is a rigid HDPE geogrid. A vertical pressure of 161 kPa (3360 psf) was applied in both tests. Figure 2 shows the results obtained in the tests in sand. The pull-out resistance due to wetting is about 0.57 times that of the dry condition. The interface parameters α, β, γ and δ for the unsaturated condition are 0.003, -0.7, 0.00267 and -1.0, respectively. These values were calculated from results of earlier tests (Chua, 1991) in which the normal pressure were varied. In the wet condition, γ is increased to 0.0045 to reflect the weakening of the interface.

Pullout Tests in Clay

Figure 3 shows the results for the clay tests in which a normal pressure of 28.7 kPa (600 psf) was applied. The clay is obtained from Tierra Amarilla, New Mexico. There are two curves for the unsaturated condition representing a compaction level of 100 % and an 88 % of Standard Proctor. If the unsaturated curve at 88 % Proctor is compared to the saturated curve it is observed that the reduction in pull-out resistance is not as large as the one observed in the tests in sand. The average ratio between saturated and unsaturated pull-out resistance is about 0.81 (considering just the first four inches of displacement). It should be pointed out that the optimum moisture content for this clay is 20.4 % which may explain the small reduction in resistance. The interface parameters α, β, γ and δ for the clay at the optimum moisture content are 0.0004, 0.005, 0.002 and -0.105, respectively. These values calculated from results of earlier tests (Chua, 1991) in which the normal pressure were varied. In the flooded condition, γ is increased to 0.003 to reflect the weakening of the interface.

EXAMPLE PROBLEMS

Designs Based on State-of-the-Practice

Two 20-ft high retaining walls were designed following the procedure described in Koerner (1986). The rigid geogrid tested in the pullout box was used. A sand and a clay backfill was considered. The walls are externally stable, that is for overturning, sliding failure along the base, bearing capacity failure of the base, and settlement. For internal stability checks, the factor of safety against breaking in tension for each of the grid layers is defined as

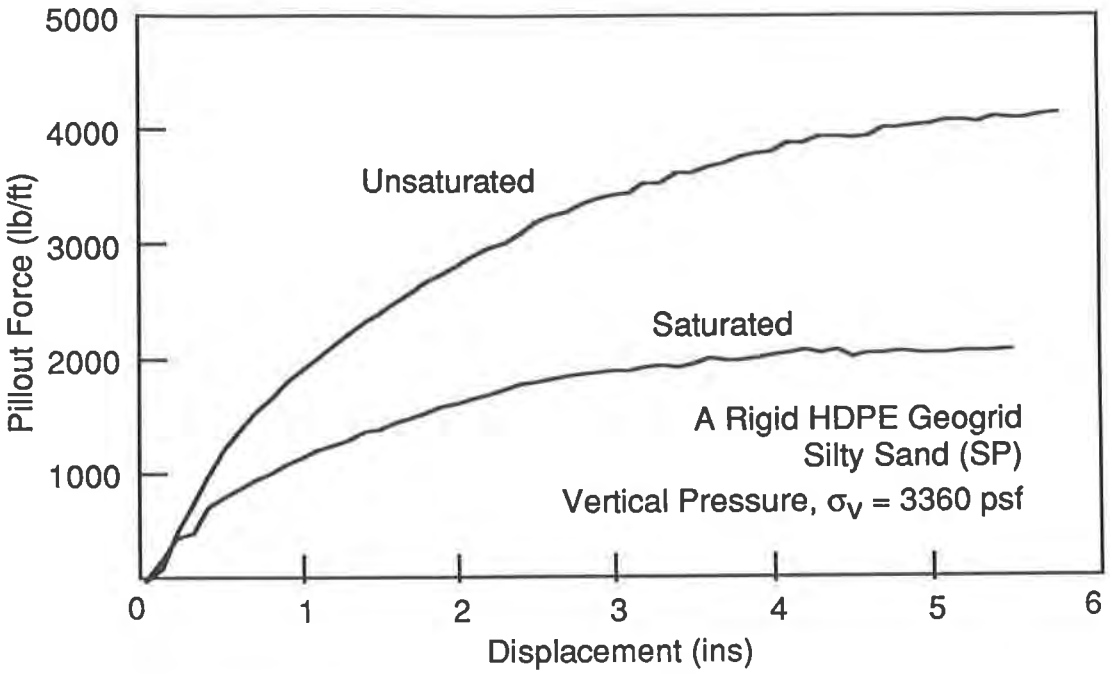

Figure 2. Pullout Force versus Displacement of a Geogrid in Dry and in Saturated Sand

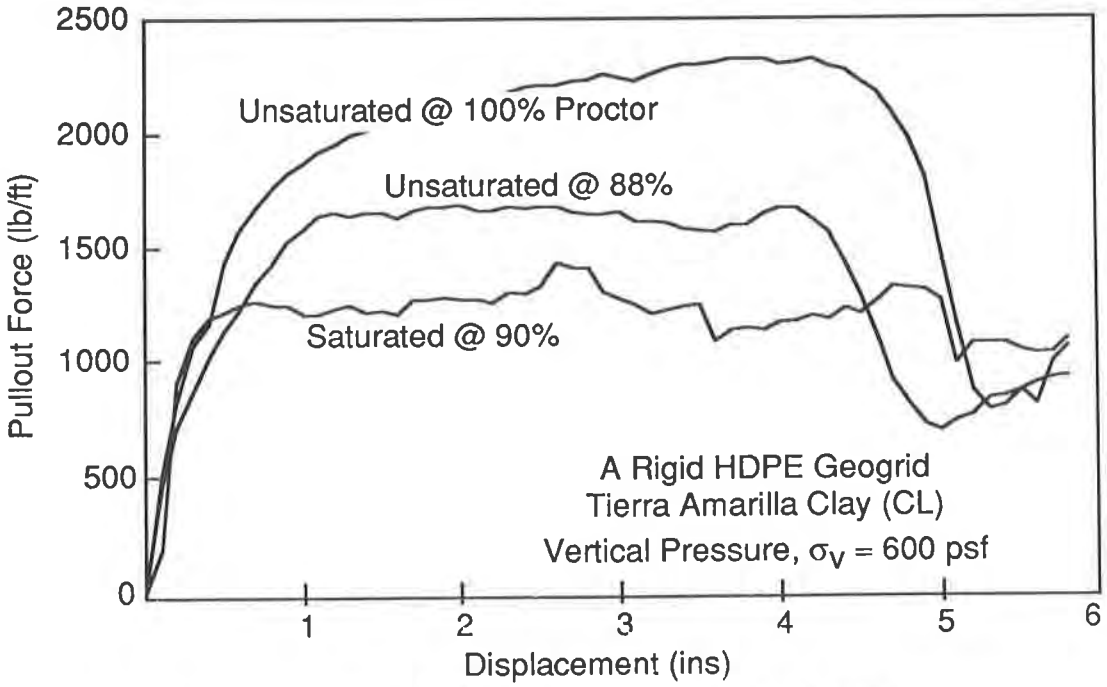

Figure 3. Pullout Force versus Displacement of a Geogrid in Unsaturated and in Saturated Clay

$$F.S._{breaking} = \frac{T_a}{\sigma_h \, S_v} \qquad (4)$$

where T_a is the tensile failure of the grid, σ_h is the lateral earth pressure,
S_v is the vertical separation of the grids,
The lateral earth pressure can be calculated from
$\sigma_h = K_A \, \gamma z$,
K_A is the coefficient of active earth pressure,
γ is the unit weight of the soil, and
z is the depth to the grid.

The factor of safety against pull-out from the soil mass for each of the grid layers is given by

$$F.S._{pullout} = \frac{2 \tau \, L_e}{\sigma_h \, S_v} \qquad (5)$$

where τ, σ_h and S_v are as earlier defined, and
L_e is the length of embedment behind the active or anchorage zone.
Both factors of safety were kept between 1.3 to 1.5. The grids used are all 12 ft long. Table 1 shows the properties for the sand and the clay used in the designs. Other parameters used in the finite element analysis are also given.

The interface properties used in the hand-calculation uses adhesion, c_a and coefficient of friction (tan δ) instead of the hyperbolic relationship presented earlier. These values are also shown in Table 1.

Table 1. Soil Properties Used in Finite Element Analyses

Soil	Unit Weight γ kN/m^3 (pcf)	Friction Angle ϕ (deg)	Cohesion c kPa (psf)	K	n	R_f	Poisson's Ratio	c_a* kPa (psf)	tan δ*
Sand									
Drained	16.6(105.4)	45	0	350	0.5	0.7	0.35	0	1.15
Saturated	18.5(118)	45	0					0	0.66
Clay									
Drained	17.7(112.8)	30	12.0(250)	100	0.45	0.7	0.45	28.7(600)	0
Saturated	19.0(121.1)	25	6.9(144)					23.3(486)	0

* for use in hand-calculations only

FINITE ELEMENT MODELING

The finite element analyses were performed using GEOT2D (GEOTechnical engineering 2-Dimensional analysis code). GEOT2D is an updated Lagrangrian code which allows large deformations in the soil-fabric

system and was initially developed at the University of New Mexico for analyzing reinforced earth structures. The soil-fabric interface is modeled using isoparametric continuum elements, two-node membrane elements and four-node nonlinear interface elements.

The soil is modeled using continuum elements which are described by a hyperbolic stress-strain relationship (Duncan et al., 1980) with the Mohr-Coulomb equation as the failure criterion. The tangent modulus, E_t, is as follows.

$$E_t = k\, P_a \left(\frac{\sigma_3}{P_a}\right)^n \left[1 - \frac{R_f\,(1-\sin\phi)\,(\sigma_1-\sigma_3)}{2c\cos\phi + 2\sigma_3\sin\phi}\right]^n \qquad (6)$$

where
K and n are the modulus number and the exponent, respectively,
R_f, the failure ratio,
P_a, the atmospheric pressure,
c and ϕ are the cohesion and the friction angle, respectively; and
σ_1 and σ_3 are the major and minor principal stresses, respectively.

The stress-strain relationship for rigid HDPE geogrid measured in the laboratory can be described by the following equation

$$k_a = \frac{0.00023}{(0.00023 + 0.0024\,\varepsilon)^2} \qquad (7)$$

where
k_a is the axial stiffness of the reinforcement, and
ε is the strain.

The soil-reinforcement interface properties are according to that described in the earlier section on pullout. The front-face of the earth retaining structure is modeled using beam elements (with stiffness of concrete) hinged to the different reinforcement layers. Interface elements are also used between the beam elements and soil elements.

RESULTS OF FINITE ELEMENT MODELING

Deformed Mesh and Stress Distribution

Figures 4 and 5 show the deformed mesh of the simulation for a sand backfill wall and a clay backfill wall, respectively. The meshes in the left column of both figures, show the sequence in which the walls are built. The meshes in the right column of the figures show steps in which the water table is slowly raised to the top of the backfill behind the walls.

Figures 6 and 7 show the movement of the walls during construction up to the point where the water table is raised to the top of the backfill. It can be seen that at the end of construction, the "sand" wall moved about 1.25 cm (0.5") while the clay wall moved about 3.75 cm (1.5"). Both wall moved about 13 cm (5") when flooding occurs. It is interesting to note that the"sand" wall tends to rotate about the toe

while the "clay" wall slide away from the soil mass.

The magnitude and direction of the major and minor principal stresses for the construction steps through the flooding steps are shown by arrows, with inward pointing arrows showing compression.

Tension in Reinforcements

Figures 8 and 9 show variation of tensile forces in the reinforcements for the construction steps through the flooding steps.

Sand.-- It can be seen from Figure 8(b) that the maximum tension in the reinforcement layer no. 1 occurs at some distance away from the wall and when flooding occurs, maximum tension line moves towards the wall. It can be seen from Figure 8(a) that the reinforcements at top and at the bottom of the wall are more highly stressed.

Clay.-- The observations are comparable with that of a "sand" wall as can be seen from Figure 9. Reinforcement layer no. 1 is more highly stressed than the top layer as the water table is raised in the backfill behind the wall. Again, it can be seen that the soil-reinforcement shear stress nearer the wall is increased with the rising water table.

CONCLUSIONS AND RECOMMENDATIONS

Conclusions

Hand-calculation When Considering Flooding Condition.-- The initial factors of safety of the grids against pullout were kept between 1.3 to 1.5. When flooding in taken into consideration in the hand-calculation, the resulting factors of safety becomes that shown in Table 2. It can be seen that some factors of safety fall below the critical value of 1.0, especially against breaking of the grid. Because the grids were long, the factors of safety against pull-out are adequate for most of the grids except for the higher ones. The low factors of safety against pull-out in the clay material suggest that the length of the grids was too short to resist forces from flooding.

Table 2. Hand-Calculated F.S.for Flooding Behind Wall

Layer No.	Sand Backfill		Clay Backfill	
	$F.S._{breaking}$	$F.S._{pull\text{-}out}$	$F.S._{breaking}$	$F.S._{pull\text{-}out}$
1 Bottom	0.70	0.74	1.02	0
2	0.42	1.35	0.87	0
3	0.36	2.43	0.71	1.03
4	0.93	8.16	0.77	2.26
5			0.76	2.96
6			0.68	3.29
7 Top			1.22	7.11

These simplified hand-calculations show the importance of considering the eventual saturation of the reinforced soil-structure. Without extra provision these structures will fail.

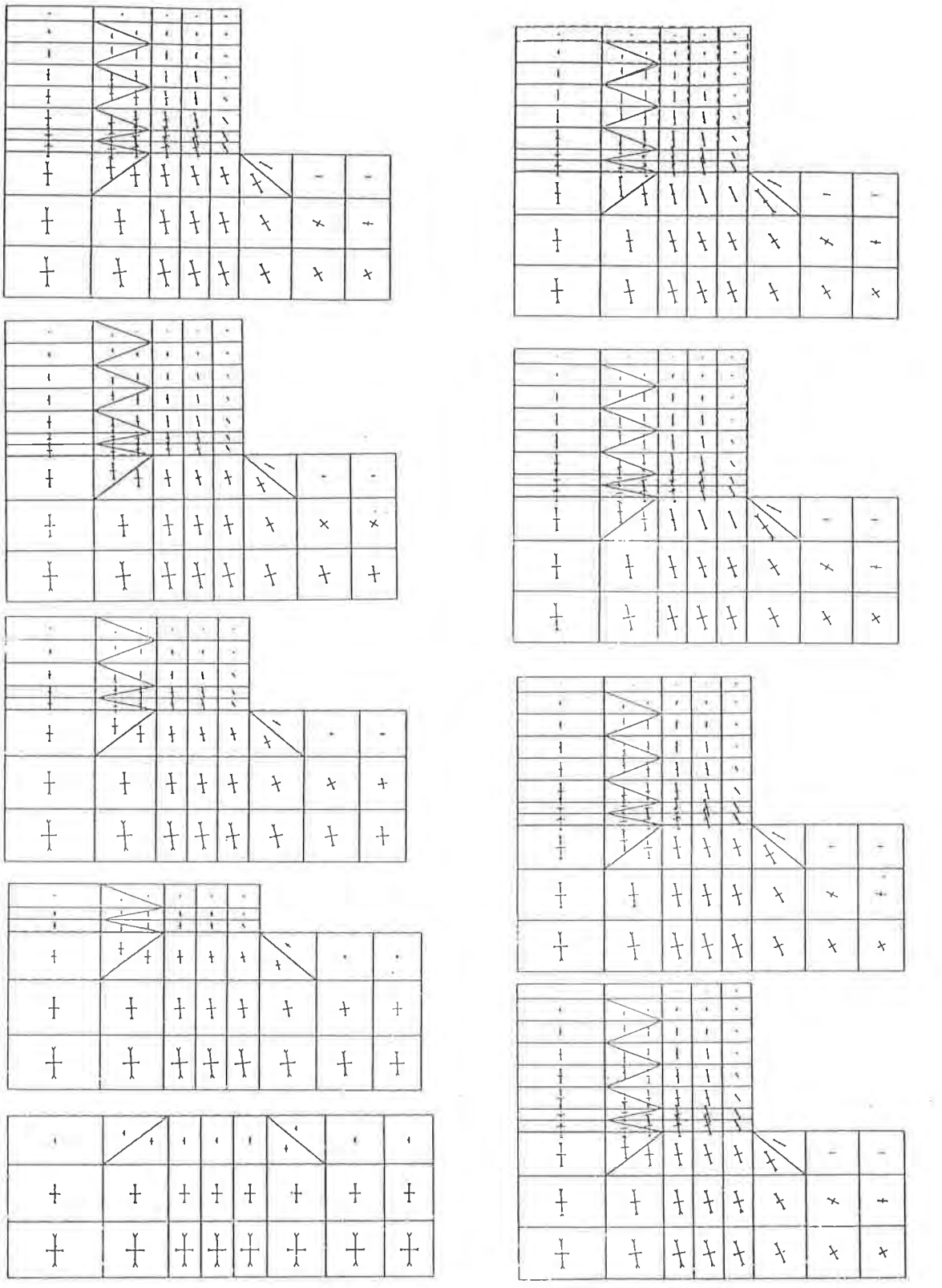

construction sequence

flooding sequence upwards direction

Figure 4. F.E.M. Simulations of Construction and Flooding of Geogrid Reinforced Wall with a Sand Backfill

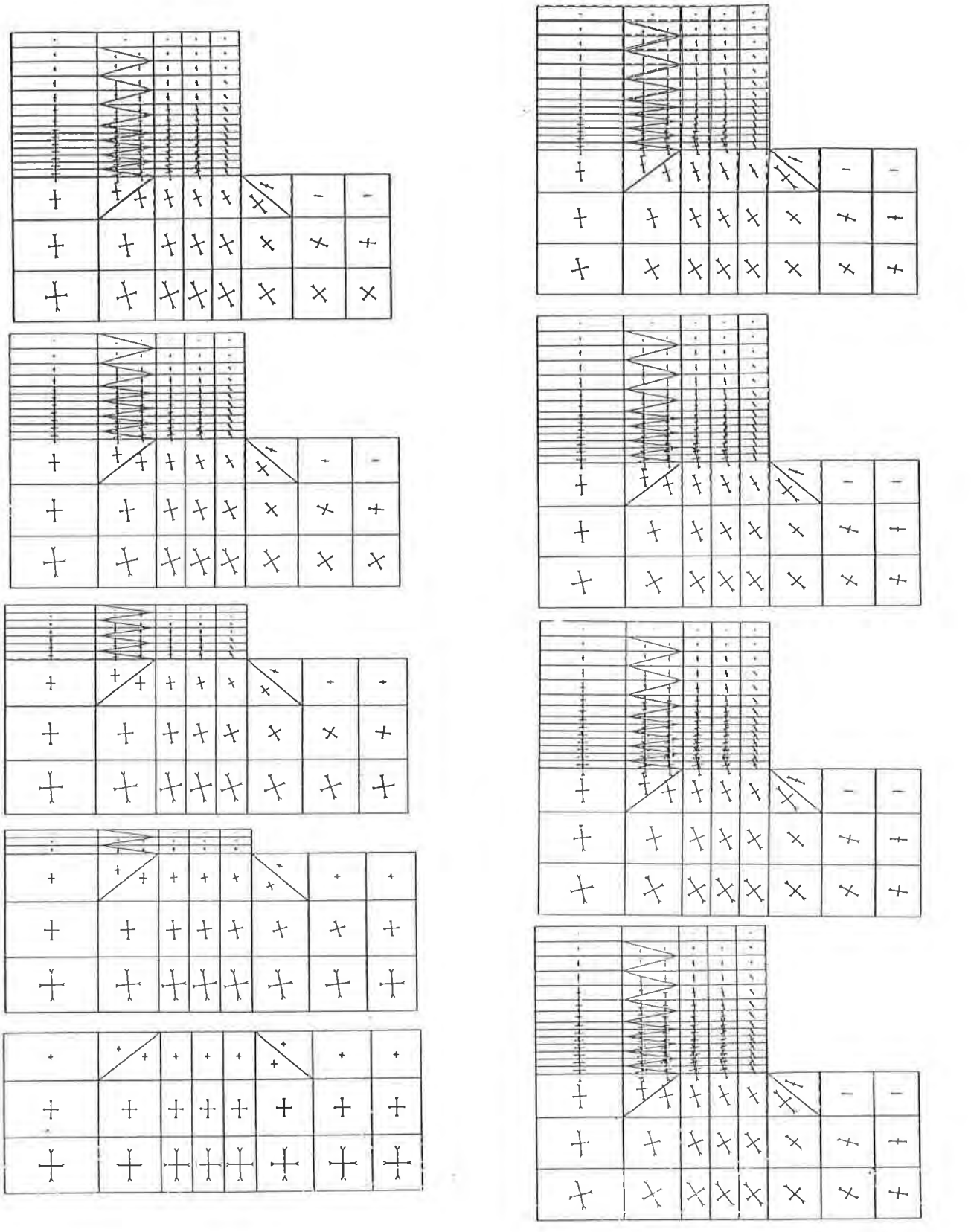

Figure 5. F.E.M. Simulations of Construction and Flooding of Geogrid Reinforced Wall with a Clay Backfill

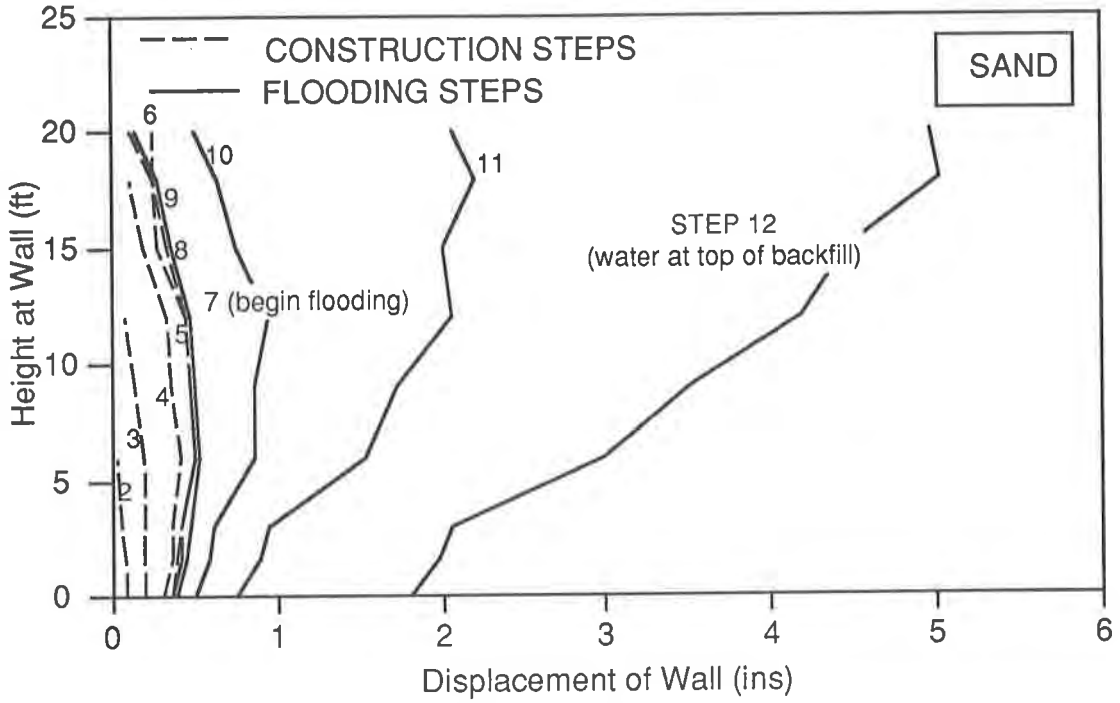

Figure 6. Movement of Wall with a Sand Backfill

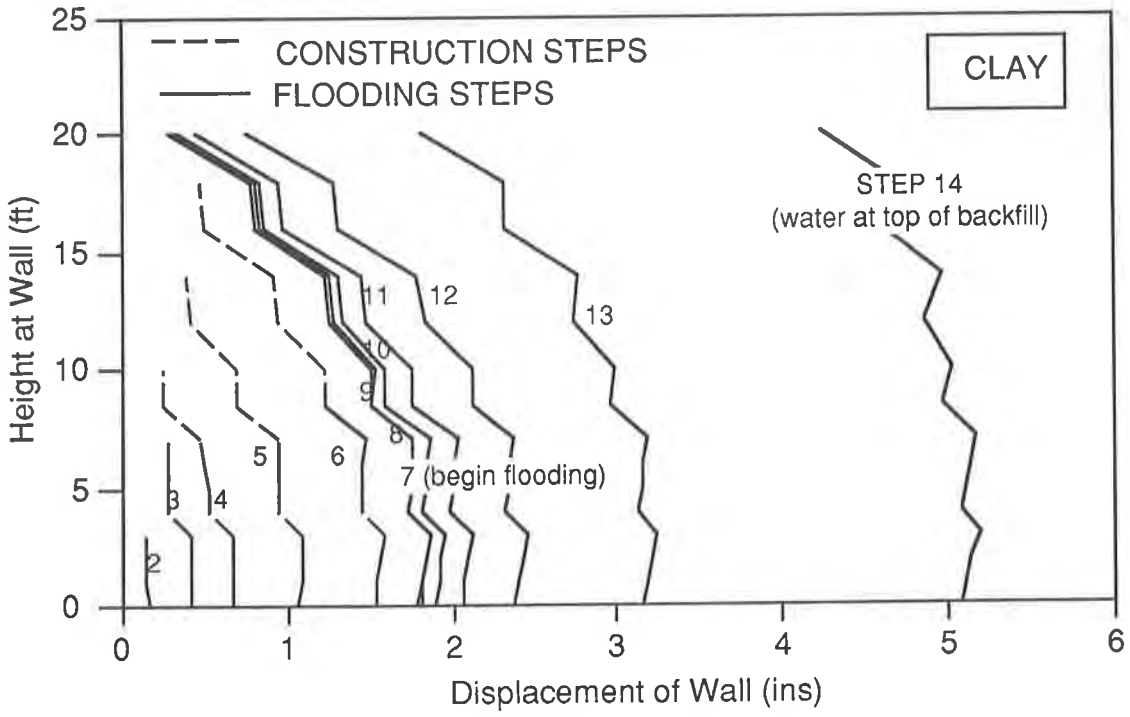

Figure 7. Movement of Wall with a Clay Backfill

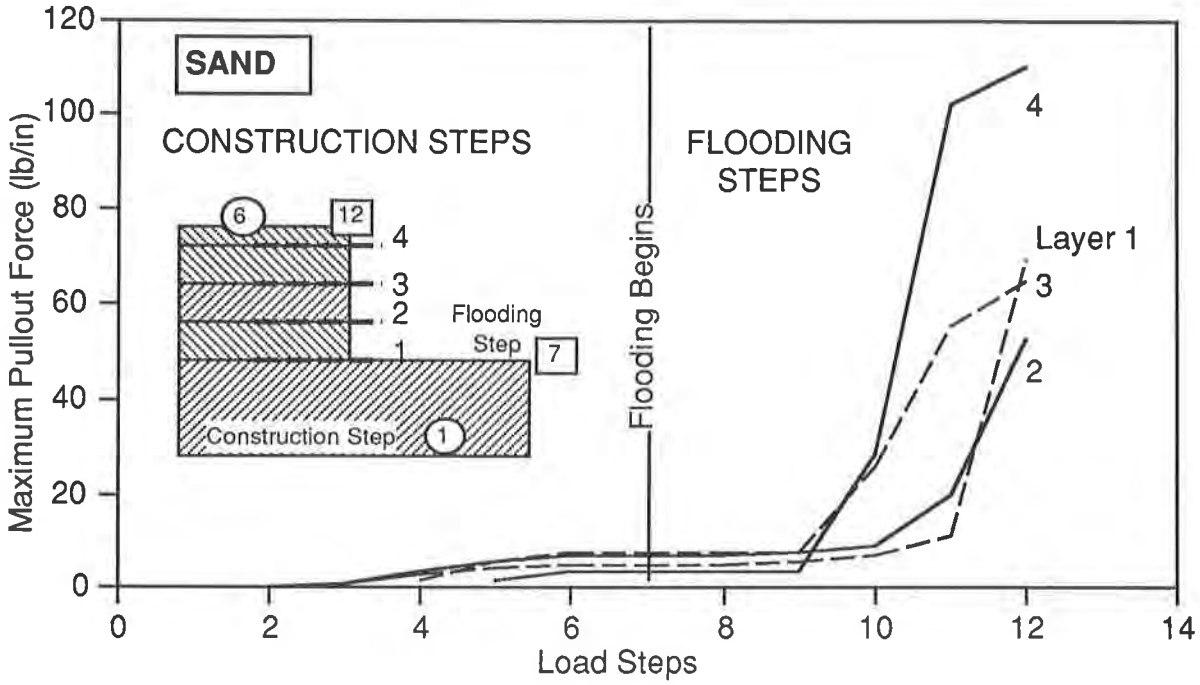

(a) Maximum Tension in Reinforcement Layers for Different Load Steps

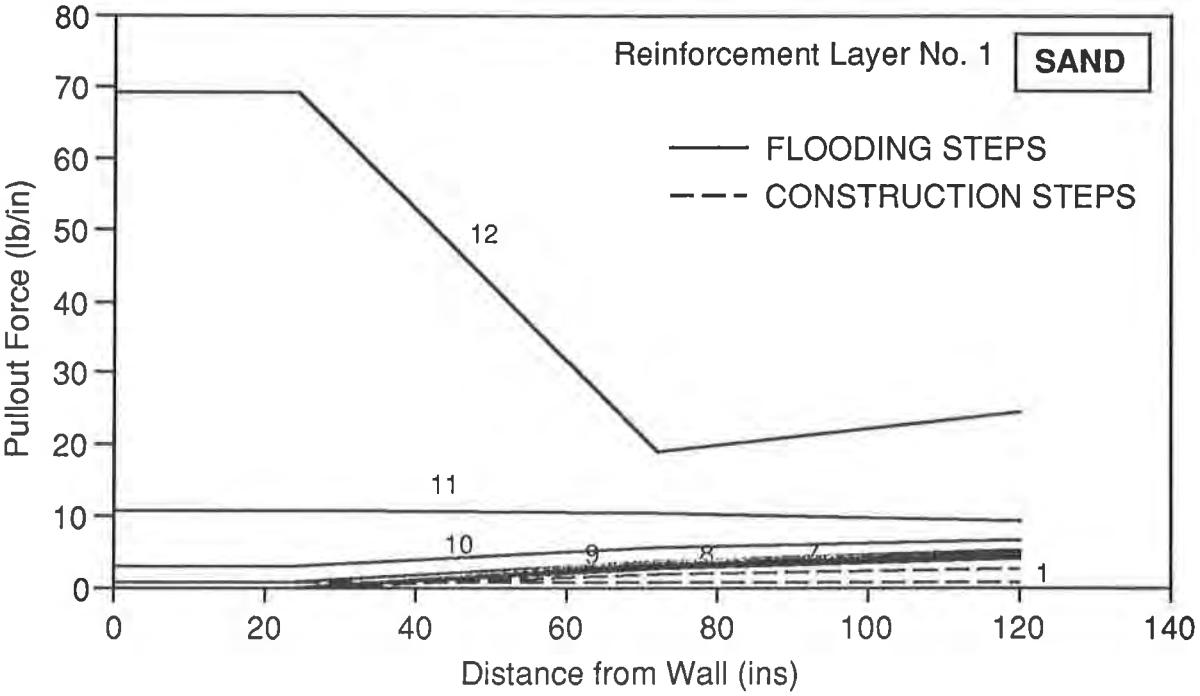

(b) Variation of Tensile Force in Reinforcement Layer No.1 for Different Load Steps

Figure 8. F.E.M. Predictions of Tension in Reinforcements in a Sand Backfill

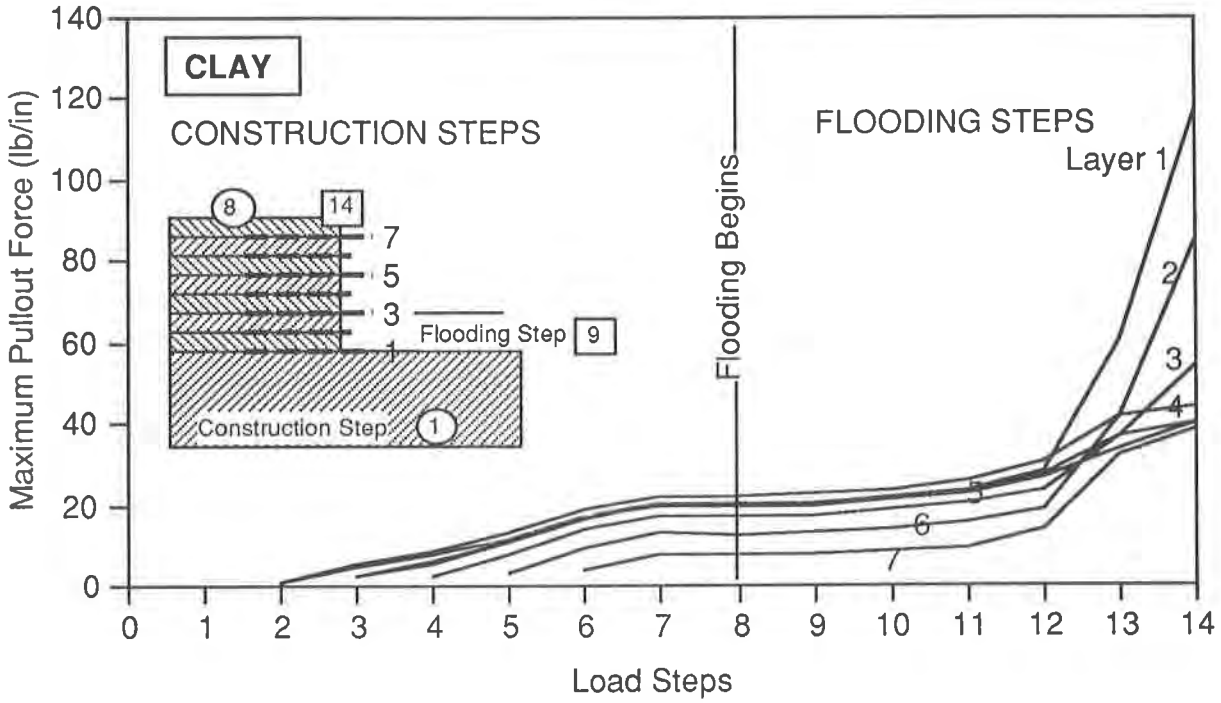

(a) Maximum Tension in Reinforcement Layers for Different Load Steps

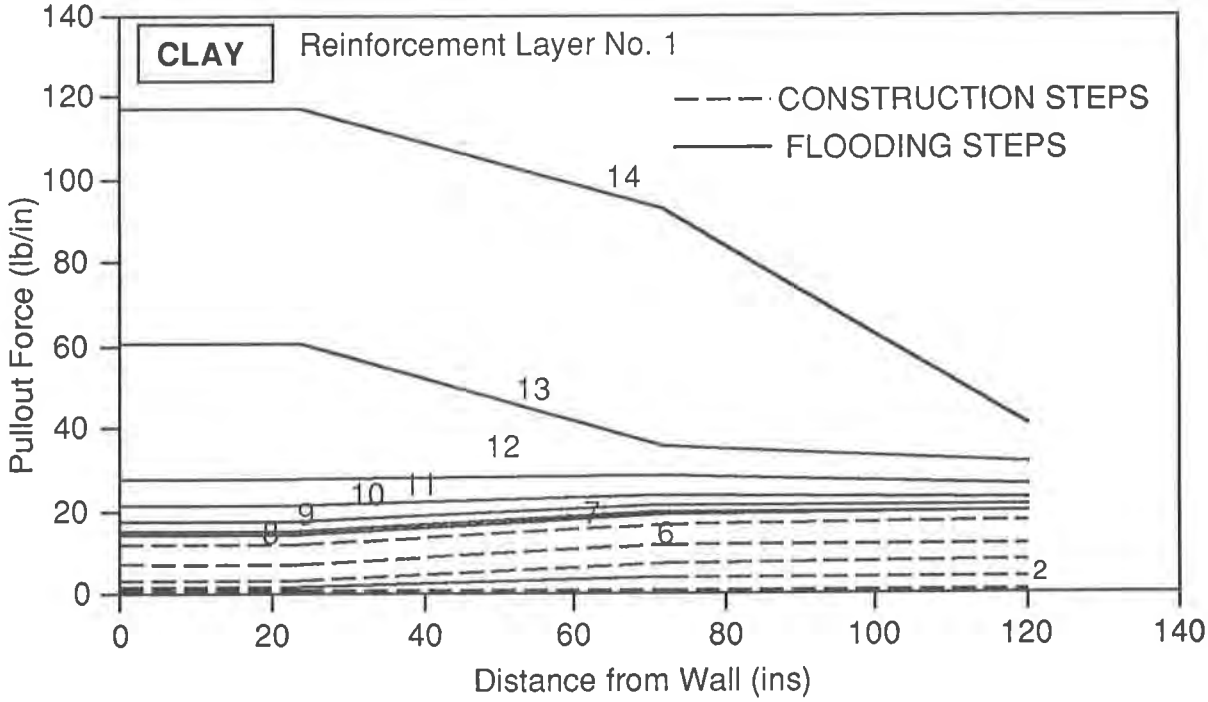

(b) Variation of Tensile Force in Reinforcement Layer No.1 for Different Load Steps

Figure 9. F.E.M. Predictions of Tension in Reinforcements in a Clay Backfill

Numerical Simulations of Flooding.-- From Figures 6 and 7, it can be seen that the wall constructed of sand fill tends to rotate about the toe when flooding occurs. The wall constructed of clay fill tends to slide when flooding takes place.

It can be seen from Figures 8 and 9 that the tensile force in reinforcement can increase substantially for 6 to 10 times more than the end-of-construction tension in the example problems considered here.

Failure Mechanisms.-- Hand-calculation suggests breaking of reinforcements as the primary failure mechanism. However, the finite element analyses suggest that pullout is the primary failure mechanism. The finite element prediction is probably the more accurate one in that the shear stresses are allowed to vary along the entire length of the reinforcements according to the normal stress levels. In the hand-calculation, the entire anchorage length is assumed to be experiencing a uniform shear stress which results in concentrating the tensile force at a point at some pre-determined slip (or shear) plane in the soil mass.

Recommendations

In areas where flooding is likely or where the adequacy of the drainage system is in question, it is suggested that hydrostatic forces be taken into consideration. The pullout resistance of a geosynthetics obtained in a relatively dry sand should be reduced by about 50% and that obtained in a relatively dry clay by about 25% to reflect the effects of saturation. The decrease in pullout resistance is probably caused by changes in the physical properties of the soil and the roughness of the reinforcement as a result of wetting than the reduction of the effective stress. However, in clay, the latter may be more substantial.

The finite element approach may be the more accurate method in that discrete behavior of interfaces and nonlinear response can be more easily incorporate in the simulation. The numerical approach should be considered for analyzing structures involving complex loading sequences.

REFERENCES

Chua, K.M. (1991). "A Database of Reinforcements Pullout Tests Performed at the University of New Mexico". A report submitted to the New Mexico State Highway and Transportation Department.

Chua, K.M. and Scaife, R.P. (1992). "Use of Geofabrics as Tie-Downs for Submerged Large-Diameter Buried Pipes". Geotechnical Fabrics Report, Industrial Fabrics Association International, August.

Duncan, J.M.; Byrne, P.; Wong, K.S.; and Mabry, P. "Strength, Stress-strain and Bulk Modulus Parameters for Finite Element Analysis of Stresses and Movements in Soil Masses." Report No. UCB/GT/80-01, University of California, Berkeley, August.

Koerner, R.M. (1986). "Designing with Geosynthetics." Prentice-Hall, Englewood Cliffs.

Yuan, Z. and Chua, K.M. (1991). "A Numerical Evaluation of the Pullout Box Method of Studying Soil-Reinforcement Interactions". In Transportation Research Record 1278, TRB, National Research Council, Washington, D.C., 1991, pp.116-124.

Yuan, Z. and Chua, K.M. (1992). "An Analytical Model for Pullout of Soil Reinforcement". Presented at the Transportation Research Board, 70th Annual Meeting, Washington, D.C., January 1991.

The Efficiency of Geogrid Connections and the Effects of Temperature

C.J.F.P. Jones
University of Newcastle upon Tyne, United Kingdom

C.D. Lomax
M.R.M., United Kingdom

J. Paul
Netlon Ltd., United Kingdom

ABSTRACT

Geogrids are an accepted form of reinforcement for soils used in vertical retaining structures, embankments and foundations. In some constructions geogrid material can be laid without the need of joints, but in many structures the ability to connect separate lengths of reinforcement and to form connections with facings is an essential requirement. The nature and form of the jointing method can have a significant influence on the joint efficiency and the effective strength of the geogrid material. In addition, temperature influences the performance of polymeric materials and may in turn influence the effectiveness of jointing techniques.

This paper considers the effectiveness of different jointing techniques and materials when used with an established geogrid reinforcing material formed from high density polyethylene and considers the effects of elevated temperatures on selected joints. Comparisons are made to the strength and efficiency of geogrid joints at low temperatures.

INTRODUCTION

Geogrids are established reinforcing materials for soils used in reinforced walls, embankments, slopes and foundations. In some applications geogrid material can be laid without the need of joints, but in many structures the ability to connect separate lengths of reinforcement is required for technical purposes and also to increase the ease and efficiency of the construction process.

Geogrid reinforcements are manufactured by a range of methods including extruding, weaving and knitting, but connection techniques are limited principally to the use of stiff bodkins or sewing with braid, figure 1. The methods used in connecting geotextile reinforcements invariably use sewn joints which provide joint efficiencies ranging from 30 to 95 per cent of the strength of the parent material depending upon the nature and form of the joint adopted, BS 8006 (1991).

As with geotextile reinforcement, the nature and form of the jointing method used with geogrids can have a significant influence on the joint efficiency and the effective strength of the geogrid material. In addition, temperature influences the

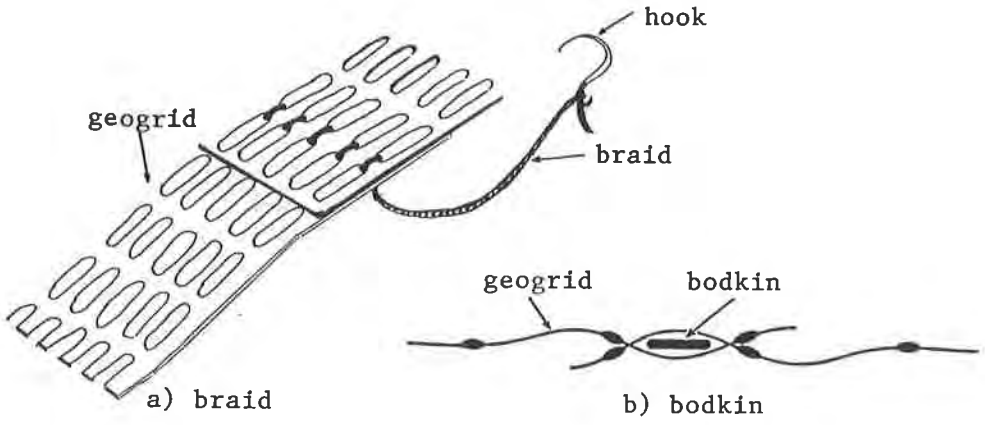

Figure 1. Connection methods for geogrids

performance of polymeric materials and may in turn influence the efficiency and effectiveness of jointing techniques. This paper considers the effectiveness of different jointing techniques and materials on an established and widely used geogrid reinforcing material formed from high density polyethylene (HDPE) and also considers the effects of elevated temperatures on selected joints. A brief comparison is made to the influence of very low temperatures on joint efficiency and strength.

Geogrid reinforcement and joints tested. The longest established geogrid used in reinforced soil is high density polyethylene grid formed using the Tensar process. The development and application of this material has been widely described, SERC (1984). The material selected for this range of tests was standard product Tensar SR80 (batch numbers 8373D 113 and 9253D 002). The form of the material and the basic properties are shown in figure 2.

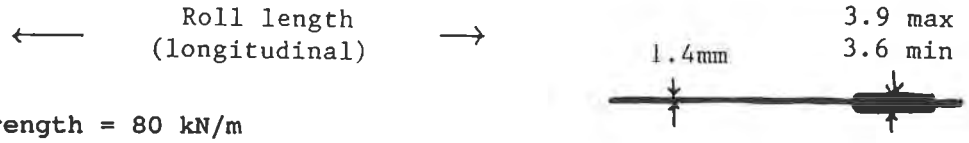

Quality Control Strength = 80 kN/m
Characteristic Long Term Strength = 32.5 kN/m at 10°C
= 30.5 kN/m at 20°C

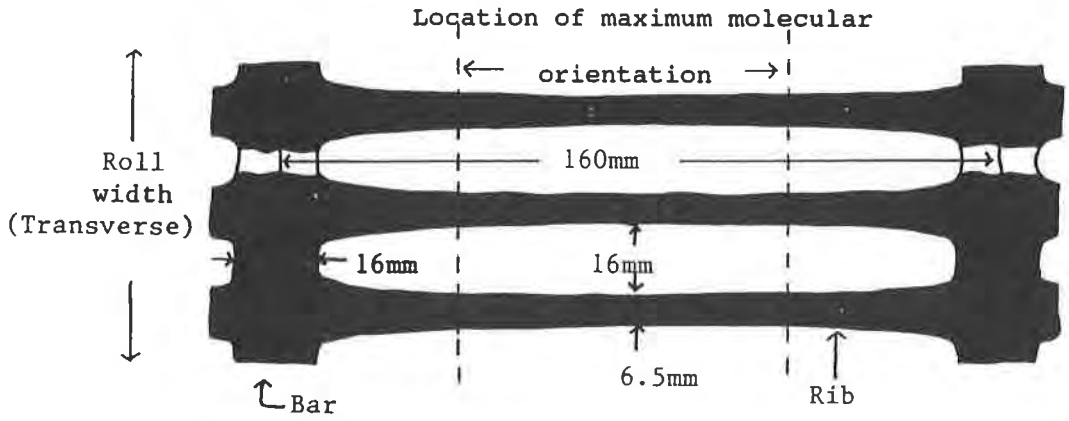

Figure 2 Typical dimensions of 'Tensar' SR80 grid

The joints tested were formed from bodkins made from mild steel, stainless steel, high density polyethylene (HDPE) and polyvinylchloride (PVC), together with polypropylene braid and cast geogrid-concrete connections, Table 1. In the case of the bodkin connections two types of joints were compared with intact material, figure 3. Figure 3 also shows the nature of the geogrid-concrete connection. The dimensions of the test specimens are detailed in Table 2.

Table 1. Connection Materials.

No.	Cross-Sectional Dimensions	Material
1.	19 mm diameter rod	Mild Steel
2.	12 mm diameter rod	Mild Steel
3.	19 mm diameter rod	Stainless Steel
4.	12 mm diameter rod	Stainless Steel
5.	4 x 12 mm	HDPE
6.	3 x 18 mm	HDPE
7.	16 mm diameter rod	HDPE
8.	16 mm tube (5 mm I.D.)	HDPE
9.	25 mm diameter rod	HDPE
10.	9 mm diameter rod	HDPE
11.	6 x 40 mm	HDPE
12.	Bar from SR80	HDPE
13.	4 x 18 mm	PVC
14.	Braid	Polypropylene

Table 2. Dimensions of geogrid specimens for different shaped joints.

Joint Shape	Dimensions
No Connection	5 bars x 5 ribs
No Connection	5 bars x 4 ribs
Normal Joint	(3 bars x 5 ribs) + (3 bars x 5 ribs)
Normal Joint	(3 bars x 5 ribs) + (3 bars x 4 ribs)
Looped Joint	(4 bars x 5 ribs) + (3 bars x 4 ribs)
Looped Joint	(4 bars x 4 ribs) + (3 bars x 5 ribs)

Range of Temperature Tests. Most of the research on geogrids has concentrated on temperate climates, such as that of the United Kingdom which has a mean air temperature of 11°C and an average soil temperature of 10°C, figure 4. Higher temperatures than these occur in tropical and sub-tropical climates and are recorded on facings as a result of solar radiation.

An example of elevated soil temperatures is found in Hong Kong which is situated in the humid tropical zone with a sub-tropical summer climate. The mean air temperature in Hong Kong is 24.7°C (15.6°C in winter and 28.6°C in summer) and the mean soil temperature is 24.7°C (21.4°C in winter and 28.0°C in summer), figure

5, Rudloff (1981). In more extreme climates higher temperatures are possible. Data from a geogrid reinforced soil wall in Tucson, Arizona, shows elevated temperatures occuring at the facing and a relatively high thermal gradient occuring through the

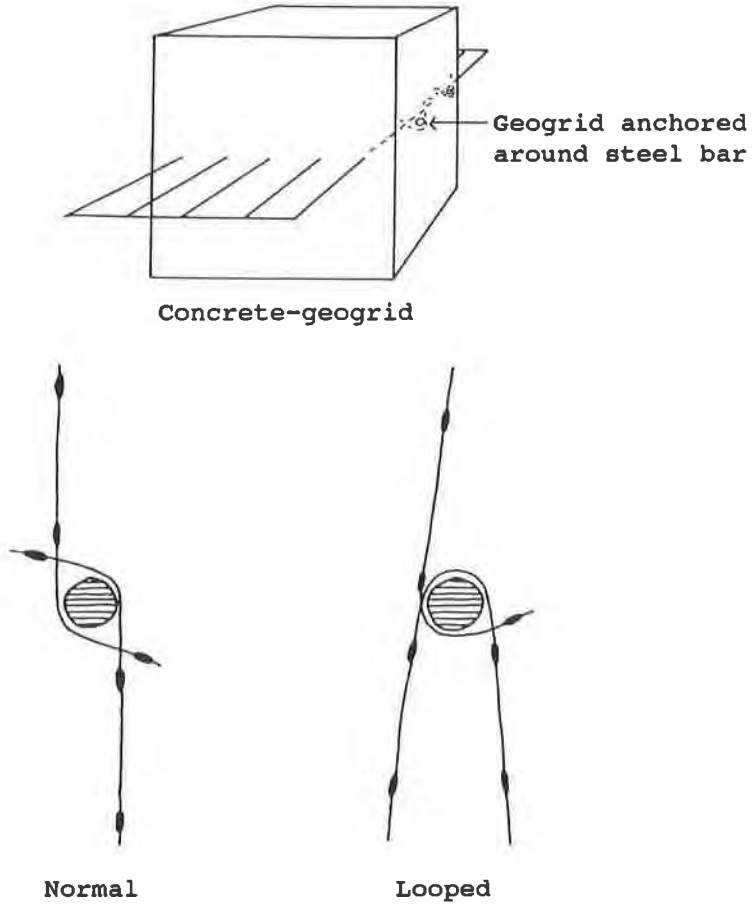

Figure 3 Different joint types

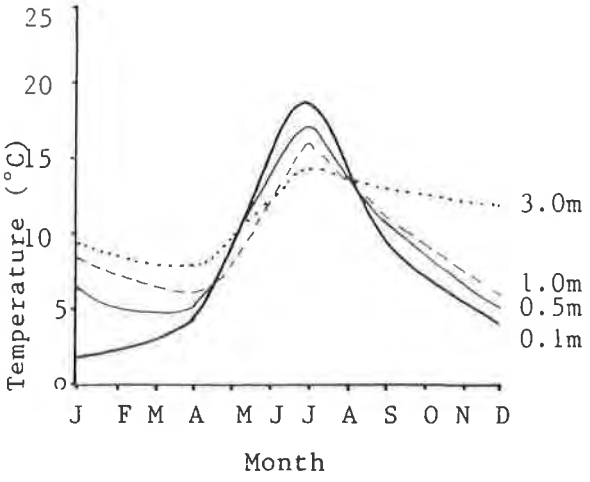

Figure 4. Mean monthly in-soil temperatures at different depths in Britain (After Murray and Farrar, 1988)

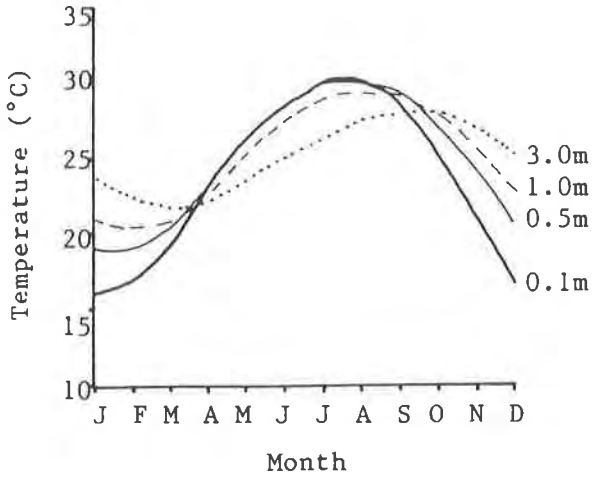

Figure 5. Mean monthly temperatures at different depths in Hong Kong (based on data from Royal Hong Kong Observatory)

structure, figure 6. In winter the hottest part of the structure is <20°C and occurs remote from the facing but in an area close to the maximum line of tension in the reinforcement. In summer the temperature of the facing can exceed 45°C and there is a high thermal gradient behind the facing in the zone where reinforcement joints might occur. Although surface temperatures can be very high, in soil temperatures do not generally exceed 40°C. The soil temperature in Arizona reaches a maximum close to the top of the structure near to the surface and the temperature distribution is similar to the Hong Kong condition.

In order to reflect site conditions the range of temperatures selected for the elevated temperature tests ranged from 20°C to 40°C. The complimentary tests reflecting arctic conditions ranged from -60°C to 0°C, Jones and Mortensen (1992).

Test Procedure and Testing Programme. The tensile tests were performed in accordance with the guidelines of BS6906:Part 1:(1987) using an Avery Dennison 1000kN Universal Testing Machine which was adapted to produce a closed system inside which it was possible to control the temperature and relative humidity, figure 7. The temperature within the test cell was raised by the injection of hot air, provided by a thermostatically controlled electrical fan heater. The hot air entered at the bottom of the test cell and was permitted to exhaust at the top of the cell. An essential part of the test cell was a baffle, positioned in front of the entrance duct to prevent direct heating of the geogrid under test.

The geogrid samples to be tested were positioned, unstressed, in the apparatus until conditions within the cell and geogrid had reached a steady state. This generally required one hour for the first test of the day and 30 - 40 minutes before subsequent tests. Once steady temperature and humidity conditions had been established, the geogrid was preloaded with a load not exceeding 3kN/m, to remove slack from the joints and clamps and to establish initial gauge lengths, figure 6. During testing, load was applied to the sample to produce a controlled average rate of strain of 2 per cent per minute. Readings of the applied load and the associated

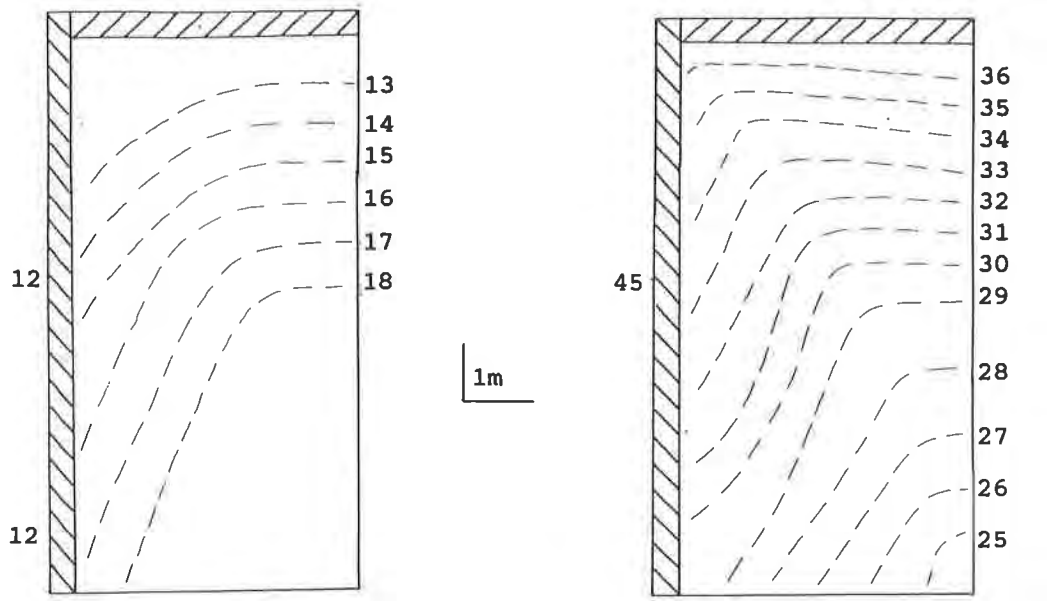

A Winter soil temperature

B Summer soil temperature

	J	F	M	A	M	J	J	A	S	O	N	D
Max	24	27	31	36	40	44	45	43	41	37	31	26
Mean	10	12	16	20	25	30	33	32	29	22	15	11
Min	-1	1	3	6	11	16	20	21	17	8	2	0

C Air temperatures

Figure 6. Temperature conditions in desert environment. A and B show in-soil temperatures (°C) for a reinforced soil wall near Tucson, Arizona (After Berg et al, 1986)
C gives air temperatures (°C) for Phoenix, Arizona (After Rudloff, 1981)

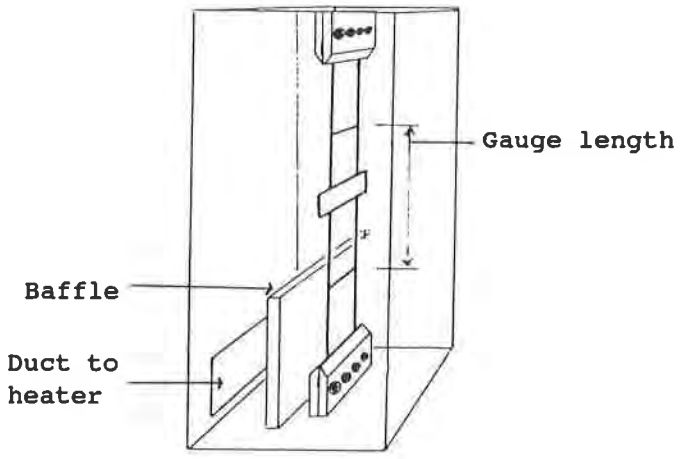

Figure 7. Testing apparatus

strain were taken at 30 second intervals and the tests continued until failure. Strain readings were made to an accuracy of ±1 per cent of the gauge length.

A number of difficulties were experienced in undertaking the tests at elevated temperatures. The first concerned the relative humidity. Various methods of introducing moisture into the system failed to raise the humidity by more than 5 per cent. The result was that humidity varied depending upon the temperature, by 55 per cent at 20°C, 35 per cent at 30°C and 25 per cent at 40°C. The variation in humidity is not considered significant. BS6906 (1987) states that the requirement for a specified relative humidity may be relaxed if it can be shown that the material is not sensitive to humidity. McGown et al (1984) have indicated that the influence of humidity on the properties of high density polyethylene (HDPE) is negligible. This claim is supported by Wrigley (1987) who demonstrated that the microstructure of HDPE has a very low permeability to aqueous solution. In addition the tests were of short duration.

The second difficulty concerned the rate of strain to which the geogrid was subjected during the tests. In some initial tests the geogrid specimens being connected were both of the same width (5 ribs). During loading the overlap of one rib to one side resulted in the connection being loaded slightly eccentrically, producing differential strain across the sample. The eccentric loading was overcome by having one geogrid sample one rib thinner than the other (i.e. one side of the joint had 4 ribs connected to 5 ribs on the other side). This resulted in each half of the test sample being subjected to a different load. The strain rate was constant within each half of the joint and averaged 2 per cent per minute.

The reason for the variation in strain rate is directly associated with the number of ribs loaded. In the test the specimens within 4 ribs strains more quickly as the loading rate is increased. The result is that the 4 rib section is stiffer. The rate of strain of the test specimens is important as this is a parameter which directly determines strain behaviour. In order to eliminate the difference in strain rate from two sides of the test specimens, each side of the test specimen was considered as a separate test and only compared with matching specimens. By adopting this procedure, each test provided two sets of results.

The full range of joint shapes and bodkins detailed in Table 2 were tested at 20±2°C to evaluate the effectiveness and determine the most efficient joints. Following this initial test sequence the more efficient joint types were tested through a parametric sequence of temperatures, at 20±2°C, 30±2°C and 40±2°C to examine the effect of temperature on the connection. In addition the concrete-geogrid connection was tested at 20±2°C to confirm the previous findings concerning the strength of this form of connection, McGown (1985), Berg et al (1987). Details of the initial test results are shown in Table 3 and the results at elevated temperatures on selected connections are shown in Table 4. Also shown on Table 4 are results for tests at -30°C.

Discussion. The results of the tests conducted at 20°C indicate that the best connection system is provided by the specially formed semi-rectangular HDPE bodkin. The efficiency of this joint is better than the 95 per cent figure identified in BS 8006 (1991). The use of bodkins of circular section can reduce the efficiency of the connection by up to 30 per cent and the use of braid results in significant reductions in joint efficiency. The results of geogrid-concrete connection tests confirm previous findings that this is a good connection system with an efficiency of 95 per cent.

Table 3. Results showing effect of joint shape and construction at 20±2°C, 50±5% relative humidity and approximately 2% strain per minute.

Joint construction and composition	Breaking Load (kN/m)	JLCE* (%)	Strain at Breaking Load (%)	10% Secant# Modulus, J_{sec} (kN/m)
No connection	69.1	100	16.5	557
6 x 40 mm HDPE 5 ribs looped	65.6	94.9	24.8	415
6 x 40 mm HDPE 4 ribs looped	58.5	84.7	27.3	371
6 x 40 mm HDPE normal joint	68.1	98.6	28.7	392
PVC normal joint	58.5	84.7	14.5	428
12 mm mild steel normal joint	48.0	69.5	13.2	385
19 mm mild steel normal joint	54.3	78.6	20.5	359
25 mm HDPE normal joint	61.7	89.3	26.1	349
16 mm HDPE normal joint	50.5	73.1	17.2	397
9 mm HDPE normal joint	50.8	73.5	13.8	437
16 mm tube HDPE normal joint	51.5	74.5	16.6	392
Polypropylene Braid	43.6	63.1	19.1	234
Geogrid-concrete	65.8	95.2	28.6	520

* Joint Load Carrying Efficiency (JLCE) defined as the ratio of the average breaking strength of the joint to the average breaking strength of the parent material at 20#C

10% Secant Modulus (J_{sec}) defined as the ratio of the change in load per unit width to 10% strain

Table 4. Results showing effect of temperature on performance of joint, at 20, 30 and 40±2°C, and a rate of strain of approximately 2% per minute.

		No connection	6 x 40mm HDPE 5 ribs looped	6 x 40mm HDPE 4 ribs looped	6 x 40mm HDPE normal joint	12mm mild steel normal joint
Breaking Load (kN/m)	20°C	69.1	65.6	58.5	68.1	46.1
	30°C	62.5	54.7	52.5	63.7	48.3
	40°C	57.5	50.0	49.8	56.3	49.4
	(-30°C)	(115.0)	-	(80.5)	(110.0)	-
JLCE* (%)	20°C	100	94.9	84.7	98.6	66.7
	30°C	100	87.5	84.0	101.9	77.3
	40°C	100	87.0	86.6	97.9	86.1
	(-30°C)	(100)	-	(70.0)	(95.7)	-
Strain at breaking load (%)	20°C	16.5	24.8	27.3	28.7	13.2
	30°C	24.0	37.2	33.3	21.5	20.9
	40°C	33.1	36.7	30.4	35.5	26.6
	(-30°C)	(6.0)	-	(6.4)	(8.8)	-
10% Secant* modulus (J_{sec}) (kN/m)	20°C	557	415	371	392	382
	30°C	513	370	334	330	317
	40°C	450	265	321	338	269
	(-30°C)	-	-	-	-	-

* At -30°C the 10% Secant modulus cannot be measured as failure occurs at <10 per cent strain.

The results of the tests at elevated temperatures suggest that the 6 x 40 mm HDPE normal joint is the most efficient at all temperatures and exceeds the 95 per cent efficienty level identified in BS 8006 (1991). The use of a circular steel bodkin is the least efficient connection system. Increasing the temperature of the geogrid reduces the stiffness of the material and the ultimate breaking load but the results remained within the range already established for HDPE material at elevated temperatures up to 45°C, Bush (1990).

At the lowest temperature of -30°C the geogrid material stiffens and the ultimate strength of the grid increases. The strength of the connections also increased over the 20°C, 30°C and 40°C results. Significantly the efficiency of the 6 x 40 mm bodkin connection remains above the 95 per cent level at the increased strength.

The reason for the superior behaviour of the 6 x 40 mm HDPE bodkin is explained by the geometry of the geogrid and the orientation of the molecules in the parent material. In the geogrid SR80 the maximum draw (orientation) in the ribs occurs at two locations approximately 30 mm from the centreline of the transverse ribs, figure 2. The rectangular bodkin is compatible with this internal geometry whereas the use of circular bodkins results in stress concentration which results in premature breakage.

CONCLUSIONS

Selection of the correct method of jointing geogrid reinforcement is important if the full strength of the parent material is retained in the area of the joint. The use of an inappropriate connection system or material can reduce the effective strength of the geogrid material by over 30 per cent. In addition, the efficiency of different joints is influenced by temperature.

The specialist jointing methods for HDPE geogrids (SR80 Tensar) using shaped bodkins formed from HDPE material produces jointing efficiencies in excess of 95 per cent when used in the temperature range -30°C to +40°C. These temperatures cover the in soil temperatures experienced in most parts of the world including the arctic and the tropics.

ACKNOWLEDGEMENTS

The assistance of Cato Mortensen and Lindsay Moore in conducting the subzero temperature tests is gratefully acknowledged. Mrs. Sandra Dodd produced the text.

REFERENCES

Berg, R.R., Bonaparte, R., Anderson, R.P. and Chonery, V.E., (1986) "Design, Construction and Performance of Two Geogrid Reinforced Soil Retaining Walls", Proc. 3rd Int. Conf. on Geotextiles, Vienna.

Berg, La Rochelle, Bonaparte and Tanguay, (1987) "Sea Wall Reinforced with Tensar SR2" In: The Application of Polymeric Reinforcements in Soil Retaining Structures, Eds. Jarrett & McGown, NATO AS1, Vol. 147.

British Standards Institution, (1987) "British Standard Methods of Test for Geotextiles" BS6906 Part 1. Determination of the Tensile Properties using a Wide Width Strip.

British Standards Institution, (1991) "Code of Practice for Strengthened/Reinforced Soils and Other Fills", BS8006, p.1-232. (Draft for Public Comment.)

Bush, D.I., (1990) "Variation of Long Term Design Strength of Geosynthetics in Temperatures up to 40#C", Proc. 4th Int. Conf. on Geotextiles, Geomembranes and Related Products, pp.673-676, The Hague.

Jones, C.J.F.P. and Mortensen, C. (1992) "The Effect of Lowered Temperatures on HDPE Geogrid Connections", Research Report, Geotechnical Group, University of Newcastle upon Tyne.

McGown, A., (1985) "The Efficiency of the Concrete-Geogrid Connection for Tensar SR", Report, University of Strathclyde.

McGown, A., Andrawes, K.Z., Yeo, K.C. and Dubois, D., (1984) "The Load-Strain-Time behaviour of Tensar Geogrids", Proc. Conf. on Polymer Grid Reinforcement, pp.11-17.

Murray, R.T. and Farrar, D.M., (1988) "Temperature Distribution in Reinforced Soil Retaining Walls", Int. J. Geotextiles and Geomembranes, Vol.VII, pp.33-50.

Murray, R.T., McGown, A., Andrawes, K.Z. and Swan, D., (1986) "Testing Joints and Geotextiles and Geogrids", III Int. Conf. Geotextiles, Vienna, International Geotextile Society, pp.731-736.

Netlon Limited (1989) "The Long-Term Performance of 'Tensar' Geogrids".

Rudloff, W., (1981) "World Climates", Books of the Journal Naturwissenschaftliche Rundschau.

Science Engineering Research Council (1984) "Polymer Grid Reinforcement", Proc. Conf. sponsored by SERC and Netlon Ltd., p.1-249, Thomas Telford, London.

Wrigley, N.E., (1987) "Durability and Long-term Performance of Tensar Polymer Grids for Soil Reinforcement", Materials Science and Technology, pp.161-170.

Failure Criteria for Homogenized Reinforced Soils and Application in Limit Analysis of Slopes

R.L. Michalowski
Johns Hopkins University, USA

A. Zhao
Johns Hopkins University, USA

ABSTRACT

The paper presents application of two methods for estimating failure heights of slopes vertically loaded on the top surface. The first method is based on homogenization of the reinforced soil and solving a set of hyperbolic-type differential equations (the slip-line method) to arrive at the stress field within the soil mass. The second method is that of the kinematic approach of limit analysis, where the upper bound to the failure height is found. A sample of results from both methods is presented. The conditions under which the slip-line technique leads to the lower bound on the failure height are given. For prudent design the slip-line method is recommended.

INTRODUCTION

Analyses of stability of reinforced soil structures are usually performed by extending the existing methods for unreinforced structures to include reinforcement. Reinforced slopes are often analyzed using slice methods, with an additional component resisting failure due to reinforcement. Coulomb and Rankine methods are utilized to arrive at the lateral pressure to be transmitted to the reinforcement. These methods have their origin in engineering intuition and are approximate, as only the global equilibrium equations are required to be satisfied. These methods make no use of deformation characteristics of soil and reinforcement, and, therefore, some of the assumptions as to the mode of failure may be inadmissible. For instance, rigid rotation of a block of soil over a cylindrical failure surface is admissible only for frictionless soils (such as clay), although it is often used as a potential failure mechanism for dilatant materials also (in Bishop's method of slope stability analysis, for instance).

Two more rigorous methods are presented in this paper. The first one is based on

homogenization of reinforced soil and the use of the slip-line technique. The second method is based on the kinematical approach of limit analysis. The purpose of this paper is to indicate the potential of the two methods rather than to produce design charts for a wide range of parameters.

The idea of homogenization and describing the strength of the reinforced soil in terms of the limit stress for an "equivalent continuum" originates from analyses of composite materials. Homogenization (the "unit cell" approach) was used by Romstad *et al.* (1976) to represent the stress-strain relation for reinforced soil, and, more recently, it was used by de Buhan *et al.* (1989) to represent the yield criterion of reinforced soil. The homogenization technique used by de Buhan *et al.* is a particular case of a volumetric averaging method used in the theory of mixtures, with the volume fraction of one constituent (reinforcement) being negligible. This is a purely static approach where no requirement of consistent deformation is placed on the constituents. A different approach to homogenization is presented in this paper. Homogenization of failure properties of the components of reinforced soil will be achieved through the use of an energy balance equation applied to a representative element of the reinforced soil under incipient failure. For the simple case of perfectly plastic constituents in the composite presented here, both the static and kinematic approaches lead to identical macroscopic failure criteria.

The second technique proposed here for analysis of reinforced soil structures is a straightforward application of the kinematical approach of limit analysis. This approach yields the upper bound to limit loads. Selecting a reasonable failure mechanism with variable geometrical parameters allows one to obtain limit loads very close to the true ones. This approach can be used for both densely and sparsely reinforced soils, while the homogenization technique is applicable only to densely reinforced composites. A densely reinforced soil mass is one where the spacing of reinforcement is small relative to the size of the structure. For example, a fifteen-foot tall retaining wall with geotextile spacing up to 18'' can be considered a densely reinforced soil, while an embankment on a soft soil with one or two layers of reinforcement in the fill is a sparsely reinforced soil mass.

The kinematics-based homogenization technique is presented in the following section. The slip-line method for anisotropic material is then used to solve for limit loads on a slope. Next, the solution using the kinematical approach of limit analysis is shown. Finally, the results from the two methods are discussed.

HOMOGENIZATION TECHNIQUE AND FAILURE CRITERIA FOR REINFORCED SOIL

Based on an averaging technique used in mixtures, the stress state in a composite can be represented as a volumetric average of stresses in the constituents

$$\bar{\sigma}_{ij} = \eta^r \sigma^r_{ij} + \eta^m \sigma^m_{ij} \qquad (1)$$

where σ_{ij}^r and σ_{ij}^m are the average stress tensors in the reinforcement and the matrix material,

respectively, and η^r and η^m are the respective volume fractions. It is proposed here, that, rather than using eq. (1), the kinematic approach be used.

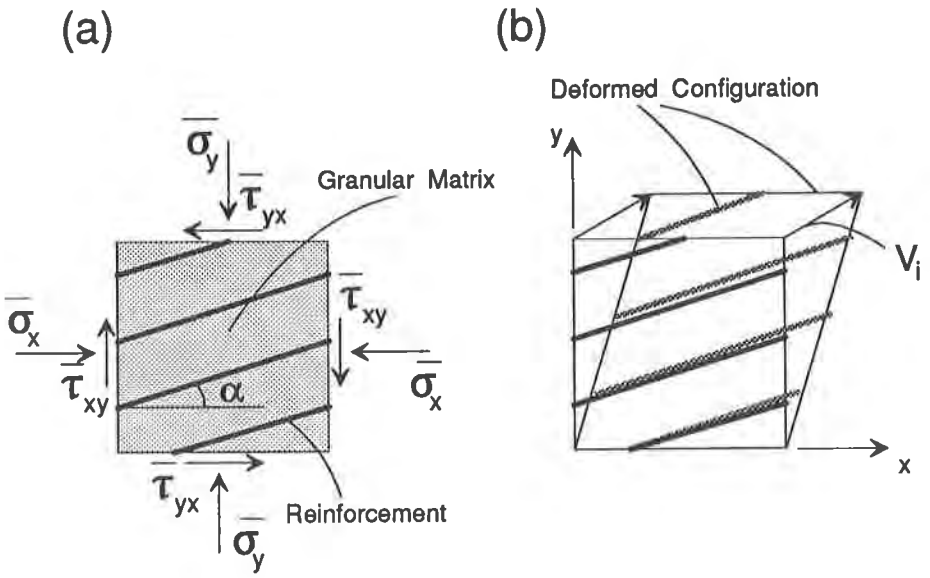

Figure 1. (a) Reinforced soil element; (b) deformation of the composite element (no slip).

The deformation pattern of a reinforced soil element is shown in Fig. 1(b). The deformation of the reinforcement is assumed to be compatible with that of the matrix (no slip). By requiring that the energy balance be satisfied in the incipient flow process of the element in Fig. 1(b), one can calculate one unknown stress component in the stress state representing the limit state associated with the assumed deformation mode. Thus, assuming two out of three stress components (Fig. 1(a)) known, one can calculate the third one. The macroscopic[1] stress ($\bar{\sigma}_{ij}$) necessary to initiate the deformation process represents the limit stress state of the composite. Under plain strain conditions the deformation of the composite element is described as

$$V_i = a_{ij} x_j, \qquad i, j = 1, 2 \tag{2}$$

where V_i is the velocity vector, x_j is the Cartesian co-ordinate system, and a_{ij} is a matrix of coefficients (variables). Constraints on coefficients a_{ij} are imposed by defining a specific dilatancy rate and requiring that the rate of work dissipation during the deformation process always be non-negative. Assuming that two out of three macroscopic stress components are known boundary conditions on the element in Fig. 1(a), the third one is calculated by equating the work performed by the load external to the element to the internal work (dissipation).

[1]The term *macroscopic* here relates to the stress in the composite (anisotropic continuum), and the term *microscopic* pertains to the stresses in the constituents.

Out of all admissible solutions associated with different deformation patterns expressed by different matrices a_{ij}, the one which requires minimum effort is taken as a point on the yield surface in the stress space. If both the granular matrix and the reinforcement obey flow rules associated with their convex yield functions, such approach leads to a strict upper bound to the macroscopic failure criterion. It was found that the upper bound so calculated was identical to the result of the static homogenization, which, for the particular case considered (matrix obeying the Mohr-Coulomb yield condition and the associative flow rule), led to the lower bound for the limit stress. It should be noted that, for a more realistic strain-softening model of the granular material, or reinforcement slip failure with a descending shear stress, the kinematical approach does not lead to a strict upper bound to a macroscopic yield criterion (neither does the static approach lead to the lower bound), but it is still a realistic homogenization technique.

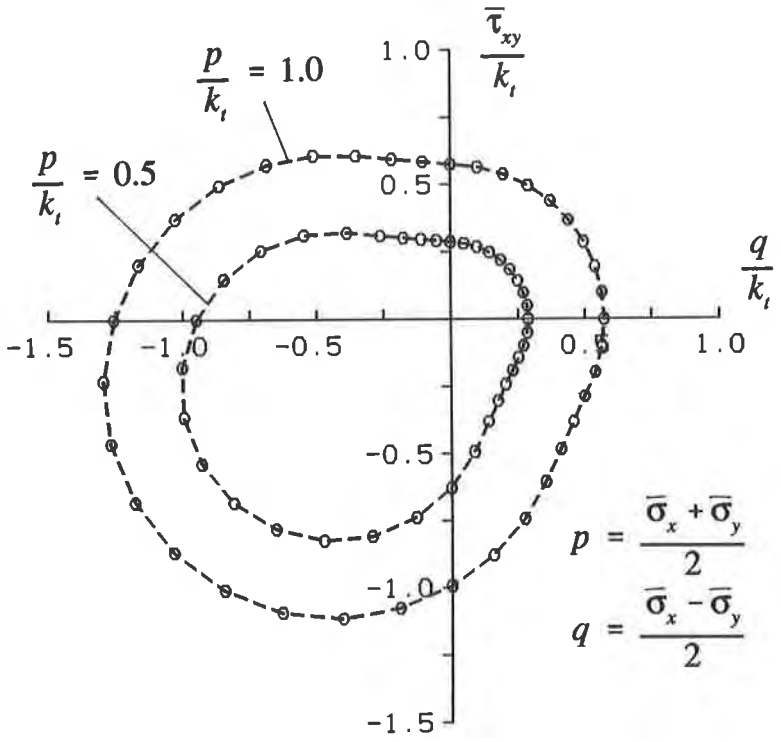

Figure 2. Cross-sections of the macroscopic yield condition of homogenized reinforced soil ($\alpha = 15°$, $\varphi = 35°$).

As the macroscopic yield condition for the homogenized reinforced soil is anisotropic, a p, q, τ_{xy} stress-space was selected to represent the yield surface ($p = (\bar{\sigma}_x + \bar{\sigma}_y)/2$, $q = (\bar{\sigma}_x - \bar{\sigma}_y)/2$). Fig. 2 shows two cross-sections of the macroscopic failure criterion (for two constant hydrostatic stresses p) of a composite for which a representative element is shown in Fig. 1(a). As the normality rule was assumed for the matrix deformation, the only dissipative term in the energy balance equation is that due to work dissipation in the reinforcement

$$\dot{D} = \int_{\vartheta} \langle \dot{\varepsilon}_l \rangle k_t \, d\vartheta \tag{3}$$

where $\langle \dot{\varepsilon}_l \rangle$ is the strain rate in the direction of the reinforcement (zero when compression), ϑ is the volume of the deforming region, and k_t is the tensile strength of reinforcement per unit area of cross-section of the composite.

SLIP LINE SOLUTION TO A REINFORCED SLOPE PROBLEM

The macroscopic yield condition for reinforced soil under plane strain conditions can be represented as

$$f(\bar{\sigma}_x, \bar{\sigma}_y, \bar{\tau}_{xy}) = R - F(p, \psi) = 0 \tag{4}$$

where

$$R = \frac{1}{2}[(\bar{\sigma}_x - \bar{\sigma}_y)^2 + 4\bar{\tau}_{xy}^2]^{\frac{1}{2}}, \quad p = \frac{1}{2}(\bar{\sigma}_x + \bar{\sigma}_y), \quad \tan 2\psi = 2\bar{\tau}_{xy}/(\bar{\sigma}_x - \bar{\sigma}_y)$$

When function F becomes independent of ψ, eq. (4) represents an isotropic yield criterion. Based on numerical calculations, function $f(\bar{\sigma}_x, \bar{\sigma}_y, \tau_{xy}) = 0$ was found (as in Fig. 2), and the following analytical expression was used to describe it

$$f(\bar{\sigma}_x, \bar{\sigma}_y, \bar{\tau}_{xy}) = \left(\frac{a+C}{A}\right)^2 + \left(\frac{b}{B}\right)^2 + Dab^2 - 1 = 0 \tag{5}$$

where A, B, C, and D are correlation coefficients dependent on p and internal friction angle of the matrix material, φ, and

$$a = \frac{q}{k_t}\cos 2\alpha + \frac{\bar{\tau}_{xy}}{k_t}\sin 2\alpha, \quad b = -\frac{q}{k_t}\sin 2\alpha + \frac{\bar{\tau}_{xy}}{k_t}\cos 2\alpha, \quad q = \frac{\bar{\sigma}_x - \bar{\sigma}_y}{2}$$

The correlation of this function to the numerically derived yield condition is very good for large hydrostatic stresses involved in the slope problem.

Equation (4) and the set of differential equilibrium equations lead to a set of two hyperbolic-type partial differential equations which can be solved using the method of characteristics (slip-line method). Equations of characteristics and the relations along characteristics given by Booker and Davis (1972) were adopted in calculations. These equations are considerably different from those of Sokolovskii (1965) for isotropic materials.

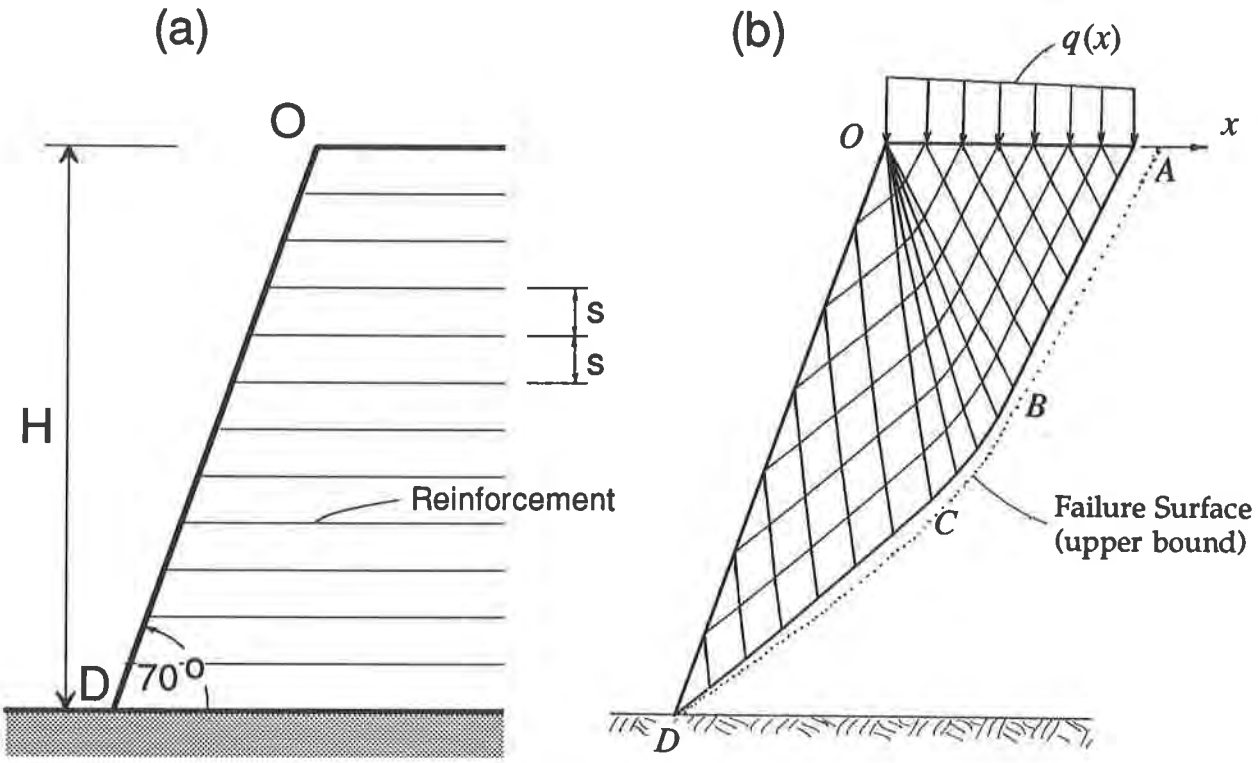

Figure 3. (a) Schematic of a reinforced slope; (b) stress characteristics (slip-line) field.

The limit load on the slope shown in Fig. 3(a) was calculated using the method of characteristics as mentioned above. The slope is built out of granular material with internal friction angle $\varphi = 35°$, and the inclination angle of the slope is $\beta = 70°$. The slope is strengthened with horizontal layers of reinforcement, *e.g.*, geogrid (no flexural or shear strength). The reinforcement is evenly spaced in the vertical direction (s being the spacing), so that the failure criterion derived by the homogenization technique is uniform throughout the slope. Reinforcement is characterized here by its strength per unit area of the soil: $k_t = T/s$ (T being the tensile strength of a single layer of reinforcement per unit length of the slope). The value of k_t enters the reinforced soil failure criterion expressed in eq. (5).

The field of the stress characteristics for the selected example is shown in Fig. 3(b). The solution starts from boundary OD where zero tractions are prescribed. The Cauchy boundary value problem is then solved in region OCD. The load on the top surface is assumed vertical, thus the jump in directions of principal stresses at point O can be found easily (20°). The characteristic problem with a singular point at O is solved next, and, finally, the mixed boundary value problem in triangle OBA allows one to determine the limit tractions $q(x)$ on boundary OA. Note that the limit pressure $q(x)$ on boundary OA decreases from O to A. Numerical results in terms of dimensionless stability factor $\gamma H/k_t$ (γ - unit weight of the reinforced soil) are presented in the last section.

The method of characteristics was used earlier by Sawicki and Lesniewska (1989) to solve for limit loads on reinforced slopes. The solution presented here, however, is quite different. The reinforced soil is described here as an anisotropic continuum, without introducing the mobilization factor for the reinforcement into the equations describing the stress field.

UPPER BOUND SOLUTION

The upper bound technique is based on the use of the upper bound theorem of limit analysis. If the material is perfectly plastic, if its strength is described by a convex yield condition, and if deformation is governed by the normality rule, then the upper bound to the true limit load can be obtained from the balance of external work and internal dissipation during a kinematically admissible incipient failure. There are two possible ways of using this approach in reinforced soils. One is similar to the traditional use of the kinematic approach where the true structure is replaced by a one-phase continuum after the reinforced soil is homogenized. In the second one, the energy dissipation is calculated separately for soil and reinforcement in a failure process where a compatible deformation of soil and reinforcement takes place. The second approach will be used here, and it will be shown that for a slope failing according to a translational mechanism this approach is very efficient.

It is again assumed that the reinforcement is flexible, so that only its tensile strength contributes to work dissipation during failure. The upper bound theorem states that in any kinematically admissible failure mechanism the rate of work done by tractions and the material weight is less or equal to the energy dissipation. Thus, equating the rate of external work to internal dissipation allows one to calculate the upper bound to the true limit load if the velocity along the loaded boundary is uniform. The collapse mechanism considered here (Fig. 4(a)) consists of rigid motion blocks separated by velocity discontinuities. The reinforcement fails in the tensile mode. The slope problem is not well-posed in the sense that the length of boundary OA (Fig. 4(a)) is not defined *a priori*, but follows from the selected collapse mechanism. Therefore, the unknown limit load is taken here as the uniformly distributed load $\bar{q}$ on the top surface of the slope, and not as the total load. Boundary OA is assumed to move with vertical velocity component V_0 (boundary condition), and all the velocities in the mechanism are shown in the hodograph (Fig. 4(b)). The soil again is assumed to be purely frictional, with internal friction angle $\varphi = 35°$. The reinforcement is placed densely in the slope with regular spacing, and is characterized here by the strength per unit area perpendicular to reinforcement, k_t. The energy dissipation rate in one layer of the reinforcement across one velocity discontinuity is

$$\dot{D} = \int_0^{t/\sin\alpha} \dot{\varepsilon}_x T \, dx = T \, [V] \cos(\alpha - \varphi) \tag{7}$$

where [V] is the magnitude of a velocity jump vector (Fig. 4(c)), and T is the tensile strength of the reinforcement (the rate of energy dissipation is independent of thickness t of the rupture

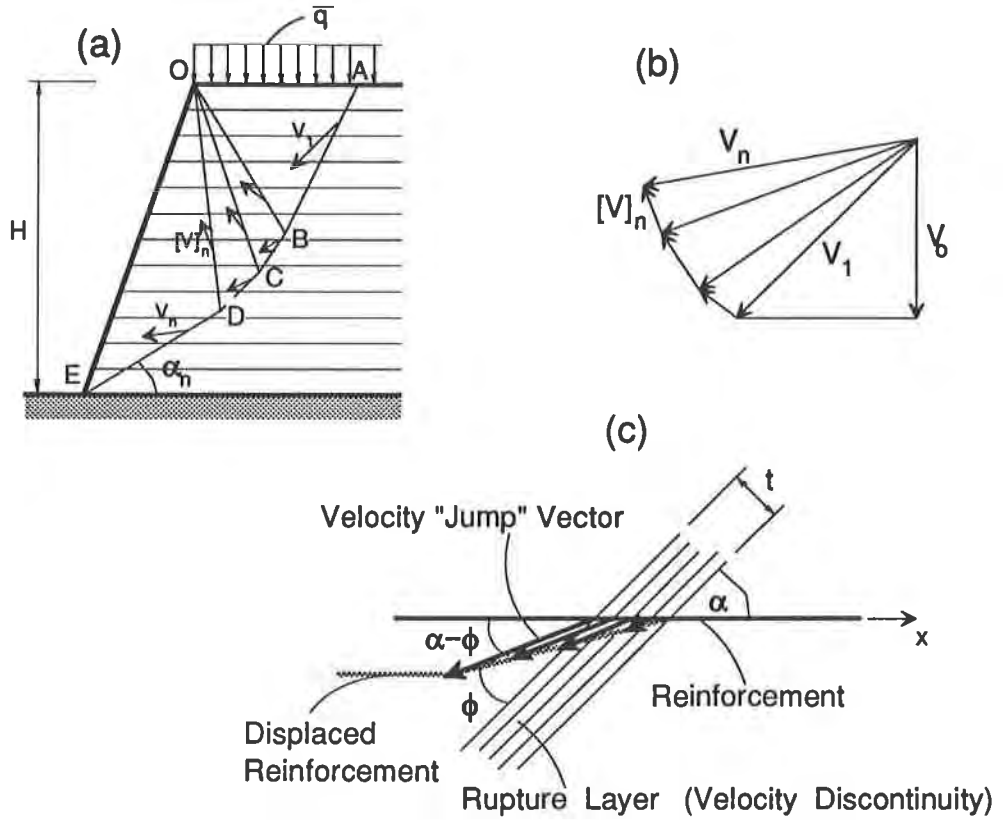

Figure 4. (a) Failure mechanism; (b) hodograph; (c) deformation of reinforcement at rupture layer.

layer). Note that some of the reinforcement layers cross only one velocity discontinuity (ED), while other layers cross more than one discontinuity. A close examination of eq. (6) and the hodograph in Fig. 4(b) leads to the conclusion that the rate of energy dissipation in each reinforcement layer is the same, independent of the number of discontinuities it intersects. The rate of dissipation of energy due to failure of reinforcement in the entire slope can then be found as

$$\dot{D} = H k_t V_n \cos(\alpha_n - \varphi) \tag{8}$$

where H is the height of the slope, V_n is the magnitude of velocity of block ODE, and angle α_n is shown in Fig. 4(a). By equating the rate of work done by the unknown load $\bar{q}$ on boundary OA and the weight of the material to the rate of the energy dissipation in all reinforcement layers, one obtains load $\bar{q}$ related to the assumed failure mechanism. Further, taking all independent angles in the mechanism as variables, one can obtain a minimum limit pressure $\bar{q}$ associated with translational mechanisms of the class shown in Fig. 4(a). The larger the number of blocks in the mechanism, the lower the least upper bound to limit pressure $\bar{q}$. However, for a steep slope as in Fig. 4(a), increasing the number of blocks beyond 4 results in less than 1% difference. Computational results are presented in the next section.

In the kinematical approach of limit analysis the forces in reinforcement must be related to the reinforcement deformation through the flow rule associated with the reinforcement yield condition. As all reinforcement layers undergo extension in the considered mechanism, the forces in reinforcement layers must be equal to their respective tensile strengths (assumed here independent of the confining stress). The contribution of the reinforcement to the stability of the structure (in the kinematical approach) is through the rate of energy dissipated by reinforcement. In the simple translational mechanism of failure in Fig. 4(a), all reinforcement layers contribute equally to the stability of the slope. The sum of the energy dissipation of the upper layer of reinforcement across discontinuities AB, OB, OC, and OD is equal to the dissipation of the lowest reinforcement layer across discontinuity ED. In other admissible mechanisms, *e.g.*, those involving rotation, the dissipation varies in different reinforcing layers.

RESULTS AND FINAL REMARKS

Calculations were performed to find the limit load on the slope using both methods presented. As the objective of the paper is to present the methods and their potential, the calculations were performed only to illustrate the type of results one may expect from the analysis. Calculations were performed for a slope with an inclination angle of 70° and for granular soil with an internal friction angle of 35°, and for different strengths of reinforcement k_t. The slip line method leads to a particular distribution of the failure load on boundary OA (Fig. 3(b)). Therefore, to be able to compare the results from the slip-line method and those from limit analysis, the average limit pressure $\bar{q}$ on boundary OA was calculated from the slip line solution. The results are shown in Fig. 5. The diagram represents dimensionless failure height $\gamma H/k_t$ (where H is the height of the slope and γ is the unit weight of the soil) as a function of limit pressure $\bar{q}/k_t$. Thus, the critical height of a loaded slope can be obtained from the diagram in Fig. 5 if the load on the slope is known, the reinforcement is specified, and the unit weight of the soil is given. It was assumed in the slip-line method that the value of k_t was constant (uniform distribution of the reinforcement), and the upper bound based on the simple mechanism considered is sensitive only to the total reinforcement amount. Pull-out failure was not considered, and the length of reinforcement here is assumed to be large enough so that tensile failure occurs.

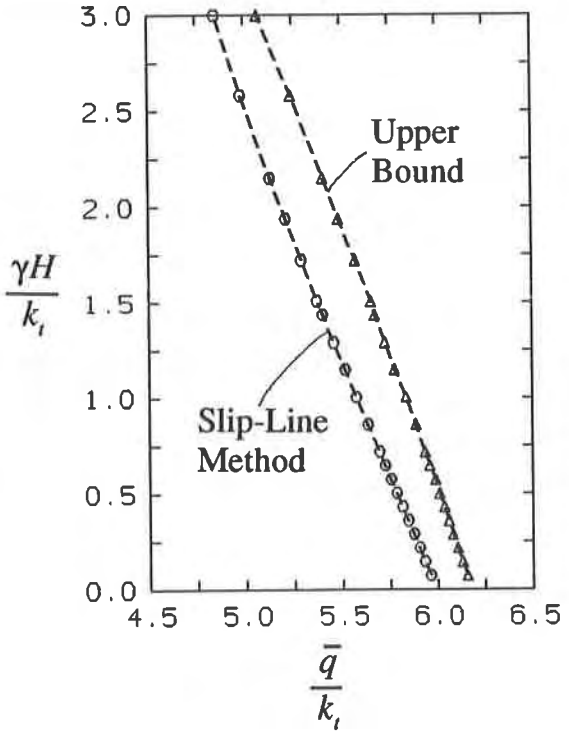

Figure 5. Failure height of a slope as a function of load (slope inclination angle 70°, internal friction angle of soil 35°).

Only the toe failure of the reinforced slope was considered. Fig. 5 suggests that holding $\bar{q}/k_t$ = const., the limit height would increase with an increase in k_t. For large k_t (and large $\bar{q}$), however, failure through the unreinforced soil below the toe will occur. Such a mechanism also should be considered in design, though it was not considered here.

As expected, the slip-line method yields a lower critical height of a reinforced slope than the kinematical approach of limit analysis does. The latter is the upper bound to the true failure height (for a given load). If it is assumed that the soil below the horizontal line passing through point D in Fig. 3(b) is rigid, the interface between this base and the slope is perfectly rough, and external load $\bar{q}$ extends uniformly beyond point A, it is possible to find an admissible extension of the stress field beyond line ABCD. For such case the slip-line solution to the average load on boundary OA is the lower bound to the true collapse load. Consequently, the resulting critical height is also the lower bound.

The difference between the lower and upper bounds to the critical height is significant, which leads to the conclusion that a translational failure mechanism of a slope may not be the best choice in the kinematical approach. This is in accord with findings of Chen (1975), who found the rotational mechanism to be optimal for unreinforced slopes without external tractions.

The slip-line solution becomes somewhat unreasonable for relatively high slopes, where failure occurs at low average pressure $\bar{q}$. The actual distribution of q in such case changes sign along OA. The load along OA is the result of calculations, and cannot be specified *a priori* along with the zero traction condition along boundary OD (overconstrained problem). The slip-line method is then expected to be of some use only for heavily loaded slopes.

Acknowledgement

The research presented in this paper was supported by the National Science Foundation under grant number MSS-9107778.

REFERENCES

Booker, J.R. and Davis, E.H. (1972). A general treatment of plastic anisotropy under conditions of plane strain. *J. Mech. Phys. Solids*, 20, 239-250.

de Buhan, P., Mangiavacchi, R., Nova, R., Pellegrini, G. and Salençon, J. (1989). Yield design of reinforced earth walls by homogenization method. *Géotechnique*, 39, 189-201.

de Buhan, P. and Siad, L. (1989). Influence of a soil-strip interface failure condition on the yield-strength of reinforced earth. *Computers and Geotechnics*, 7, 3-18.

Chen, W.F. (1975). *Limit Analysis and Soil Plasticity*. Elsevier.

Romstad, K.M., Hermann, L.R. and Shen, C.K. (1976). Integrated study of reinforced earth - I: Theoretical formulation. *ASCE J. Geot. Eng. Div.*, 102, 457-471.

Sawicki, A. and Lesniewska, D. (1989). Limit analysis of cohesive slopes reinforced with geotextiles. *Computers and Geotechnics*, 7, 53-66.

Sokolovskii, V.V. (1965). *Statics of Granular Media*. Pergamon Press, New York.

GEOTEXTILE FILTRATION DESIGN AND TESTING

GEOSYNTHETICS '93 CONFERENCE
VANCOUVER, BRITISH COLUMBIA

Geotextile Filter Design Using Flow Nets

S.M. Luettich
GeoSyntec Consultants, USA

J.E. Fluet Jr.
Florida Atlantic University, USA

ABSTRACT

Clogging is a critical design issue for most applications of geotextile filters. The mechanisms that may lead to clogging (particle movement, biological growth, etc.) have been conceptually well defined, but engineering design methods that address flow impedance by the filter zone have not been well developed. This paper presents a four-step engineering methodology for evaluating the potential for drainage system failure due to filter clogging. The methodology utilizes the theory of transformed flow nets and the results of laboratory testing to evaluate the factor of safety against drainage failure due to filter clogging. To demonstrate the methodology, two design examples are presented: (i) a chimney drain in an earth dam; and (ii) a channel sideslope protective revetment system.

INTRODUCTION

Geotextile filter design methodologies typically include criteria for soil retention, and geotextile permeability and porosity. The soil retention criterion is well understood and procedures for ensuring adequate soil retention (i.e., procedures to guard against piping) have, for most applications, proven to be successful (Giroud et al., 1988). This is not the case, however, with the criteria that are intended to ensure adequate permeability of the filter, as evidenced by many drainage failures which have occurred due to filter clogging. Although clogging is often feared by designers, manufacturers and users of geotextile filters, the problem has only been addressed conceptually, and has not yet been *quantified and integrated* into filter design methodologies. The purpose of this paper is to present and demonstrate an engineering method for providing a quantitative definition and evaluation of geotextile filter clogging with respect to the requirements of the drainage application.

The filter design method presented in this paper involves the following four steps:

- **Step 1: determine the filter system drainage requirements;**
- **Step 2: determine the minimum allowable hydraulic conductivity of the filter zone that will satisfy the filter system drainage requirements;**

- **Step 3: conduct laboratory testing to measure the anticipated hydraulic conductivity of the filter zone; and**

- **Step 4: evaluate the factor of safety against filter clogging.**

The authors acknowledge that not every application of geotextile filters warrants the level of design and testing activities set forth in this paper. It is of course incumbent on the designer to assess the level of design required for any project and to compare the cost of the design services against the cost and risk of a failure.

This paper is divided into three sections:

- the first section, *Background Information*, introduces the theory used to incorporate the filter design method into the overall drainage design process;

- the second section, *Design Methodology*, presents a step-by-step procedure for evaluating the factor of safety against drainage failure due to filter clogging; a chimney-drain design example for an earth dam is presented throughout this section to demonstrate the procedure; and

- the third section, *Additional Design Example*, provides a design example for a channel sideslope protective revetment system which further illustrates the design methodology.

BACKGROUND INFORMATION

In order to understand the methods used to incorporate the filter zone into the overall drainage design process, one must first understand the use of *flow nets*. A flow net is an analytical tool that graphically depicts the macroscopic paths (termed *flow lines*) along which water flows through a soil mass, and the contours of equal total head (termed *equipotential lines*) in the flow regime. These two families of lines intersect at right angles to form a pattern of approximately square figures known as a *flow net* (Cedergren, 1977). An example of a flow net for an earth dam with an internal (chimney) drain is shown in Figure 1.

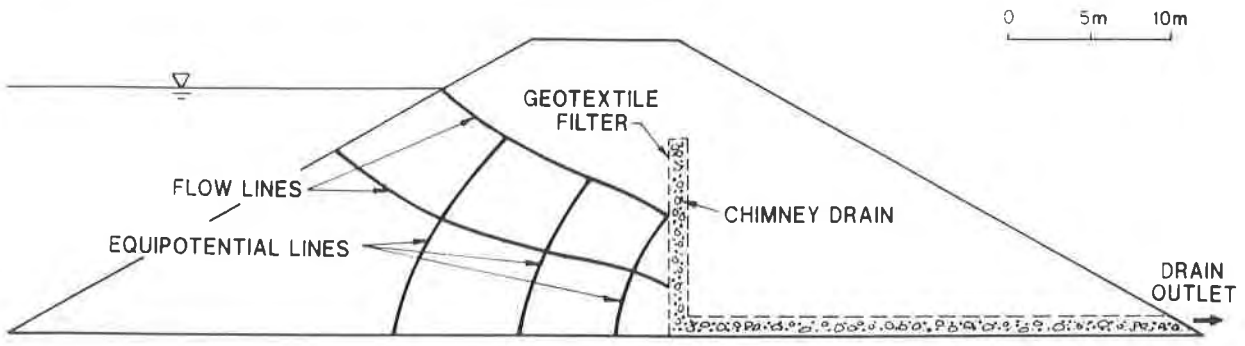

Figure 1. Flow Net for Dam with Chimney Drain

A modification of flow nets, known as the *method of transformed flow nets*, provides a means to evaluate flow through soil layers having different hydraulic conductivities. This technique allows the designer to transform the thickness of soil layers to account for the different hydraulic conductivities. Transformed flow nets can be used to evaluate filter clogging since a clogged filter is merely the development of a thin zone (termed the *filter zone*) which has significantly lower hydraulic conductivity than the adjacent soil.

The supporting concepts for transformed flow nets stem from a mathematical manipulation of Darcy's equation. Consider the soil permeameter, shown in Figure 2(a), that transmits water through a cross sectional area, A, with a total head difference (i.e., head loss), ΔH_a. A soil sample, of length t_a and hydraulic conductivity k_a, is placed in the permeameter and water flow is initiated. According to Darcy's equation, the flow rate through the soil will be:

$$Q_a = k_a \frac{\Delta H_a}{t_a} A \qquad (1)$$

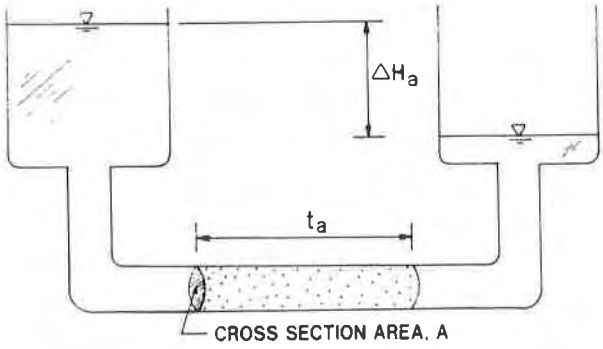

Figure 2(a). Soil Permeameter

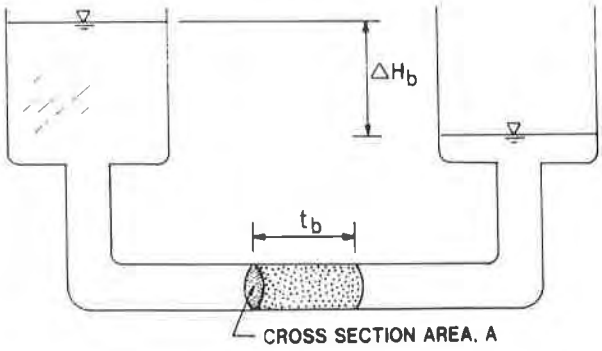

Figure 2(b). Soil Permeameter

Now consider the same permeameter (Figure 2(b)) with the same cross sectional area, A, and head loss, $\Delta H_b = \Delta H_a$, but with a soil sample that is only half the length of the first specimen ($t_b = t_a/2$) and the hydraulic conductivity of which is half that of the first soil ($k_b = k_a/2$). According to Darcy's Equation, the flow rate through the soil will be:

$$Q_b = k_b \frac{\Delta H_b}{t_b} A = \frac{k_a}{2} \frac{\Delta H_a}{t_a/2} A = k_a \frac{\Delta H_a}{t_a} A = Q_a \qquad (2)$$

Hence, the flow rate through these two soils is equal (i.e., $Q_a = Q_b$). Also, the fact that the head loss across the two specimens is equal (i.e., $\Delta H_a = \Delta H_b$) demonstrates conceptually that, for a given cross section, a thin layer of lower-permeability soil can result in the same head loss as a thick layer of higher-permeability soil. This concept is applicable to filter design because a clogged filter (i.e., a thin filter zone having a significantly lower hydraulic conductivity than the adjacent soil) can be graphically transformed such that it is represented by a thicker zone which has the same hydraulic conductivity as the adjacent soil. The transformed filter zone and flow net can be used to determine if the drainage system will fail due to filter clogging. This concept is further described and illustrated in the next section.

DESIGN METHODOLOGY

The four steps of the design methodology, previously presented in the Introduction Section of this paper, are described in detail below, and a design example is used to demonstrate the application of each step. The design example involves a chimney drain in an earth dam. A cross-section of the dam was presented in Figure 1. The dam is 18 m in height, with a base width of 73 m and a crest width of 9 m. The dam is constructed of a homogeneous clayey silt that has a compacted hydraulic conductivity of approximately 5×10^{-6} cm/s. The normal operating water surface elevation is approximately 3 m below the crest elevation of the dam. The chimney drain is included in the design to intercept water seeping through the dam, thereby preventing erosion of the downstream face caused by seepage. For the purpose of this example, it is assumed that the drainage material has been adequately designed such that build-up of hydrostatic pressure does not occur inside the chimney drain.

Step 1: Determine the Filter System Drainage Requirement.

The filter system drainage requirement for a given application is determined by considering the consequences of a drainage system failure due to filter clogging. For the chimney-drain design example, the purpose of the drain is to intercept seeping water prior to the water reaching the downstream face of the dam. Continuous development of a low-permeability filter zone would result in a gradual increase in the elevation of the phreatic surface until it eventually exceeds the top elevation of the chimney drain, thereby allowing water seepage to flow over the chimney drain and ultimately cause erosion of the downstream face of the dam. A conceptual cross section depicting these conditions is shown in Figure 3. Inspection of Figure 3 reveals that "failure" of the drain is defined as the condition when filter clogging (i.e., development of a low-permeability filter zone) results in an elevated phreatic surface that reaches the top elevation of the chimney drain.

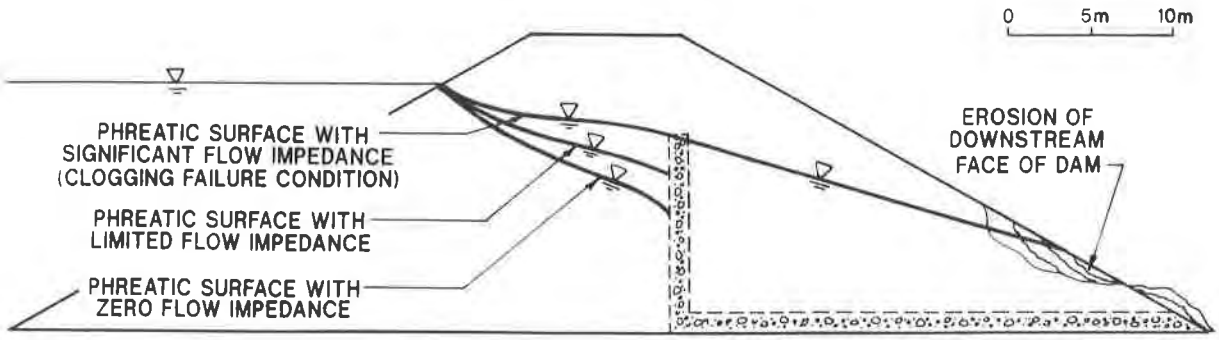

Figure 3. Development of Clogged Filter Drainage Conditions

Step 2: Determine the minimum allowable hydraulic conductivity of the filter zone by using the method of transformed flow nets described below.

- **Step 2.1: Draw a flow net that represents the failure condition** of the drainage system due to filter clogging. This is shown for the chimney-drain design example in Figure 4.

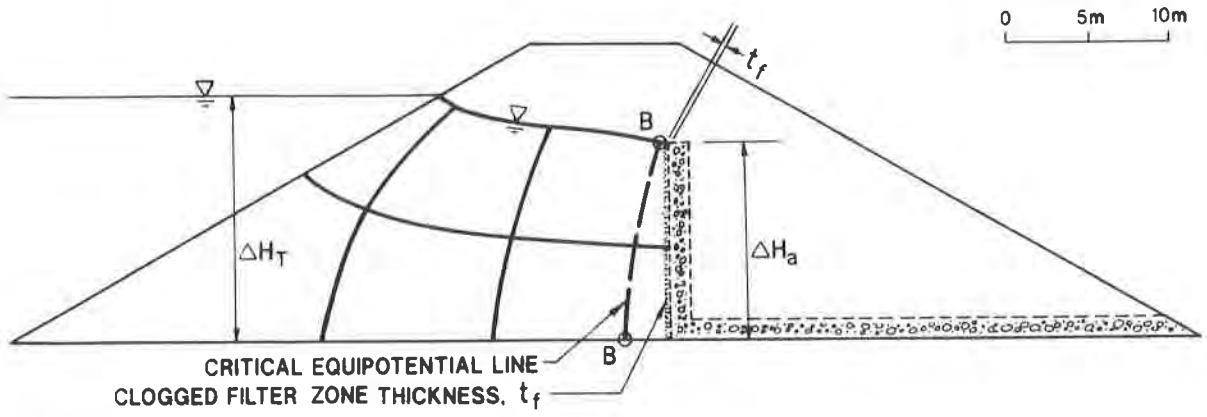

Figure 4. Flow Net for Failure (Clogged Filter) Drainage Condition.

- **Step 2.2: Identify the Critical Equipotential Line** on the failure-condition flow net, which represents the maximum total head condition that would intersect the filter zone if the filter were fully clogged. For the chimney-drain design example, this is the equipotential line which intersects the failed-condition phreatic surface at the top of the chimney drain. The critical equipotential line is depicted in Figure 4 by the heavy broken line B-B.

- **Step 2.3: Draw a flow net that represents the zero-impedance flow condition.** This represents the condition where the hydraulic conductivity of the filter zone, k_{sg}, is equal to the hydraulic conductivity of the soil, k_s, (i.e., zero flow impedance is caused by the filter). This flow net is shown for the chimney-drain design example in Figure 5.

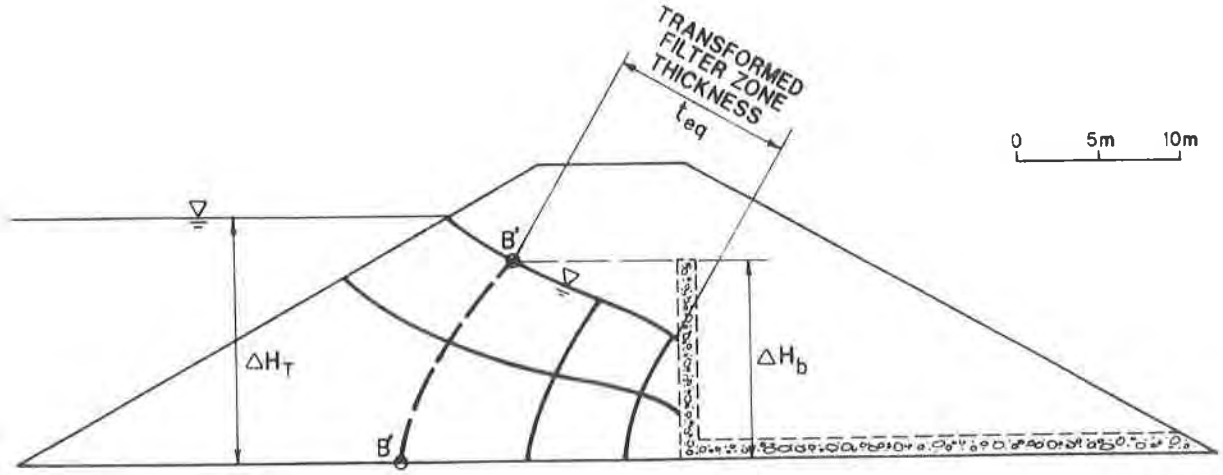

Figure 5. Flow Net for Zero-Impedance Drainage Condition

- **Step 2.4: Identify the Transformed Critical Equipotential Line** on the zero-impedance flow net. The transformed critical equipotential line represents (i.e., is equivalent to) the same hydraulic head condition as the critical equipotential line for the failed condition. The transformed critical equipotential line therefore intersects the zero-impedance phreatic surface at the same elevation as the top of the chimney drain, as depicted in Figure 5 by the heavy broken line B'-B'. The distance from line B'-B' to the drain represents the transformed thickness of the clogged filter zone (i.e., the transformed filter thickness).

- **Step 2.5: Measure the Transformed Filter Thickness, t_{eq}.** This distance represents the transformed thickness of the filter zone which, if it had the same hydraulic conductivity as the soil ($k_{sg} = k_s$), would result in the same head loss as the clogged filter zone having thickness t_f and hydraulic conductivity $k_{sg} << k_s$. For the chimney-drain example, the distance t_{eq} is measured as shown in Figure 5 along the zero-impedance phreatic surface from the drain to the transformed critical equipotential line B'-B', and is found to be 10.7 m.

- **Step 2.6: Determine the minimum allowable hydraulic conductivity of the filter zone, $k_{sg\ min}$.** As previously stated, and as shown in Figures 4 and 5, the head loss, ΔH_a, across the clogged filter zone (of thickness t_f and hydraulic conductivity $k_{sg\ min}$) is equal to the head loss, ΔH_b, across the transformed filter zone (of thickness t_{eq} and hydraulic conductivity k_s). Also, since the cross-sectional area, A, is equal for both layers (t_f and t_{eq}), and the total head loss, ΔH_T, from the upstream water-surface elevation to the chimney drain is equal, the flow rates across the clogged filter zone and the transformed filter zone are equal (i.e., $Q_a = Q_b$). Therefore, in accordance with Equation 2, the equation for determining the minimum allowable hydraulic conductivity of the filter zone can be derived as follows:

$$\Delta H_a = \Delta H_b \tag{3A}$$

$$\frac{Q_a\ t_f}{k_{sg\ min}\ A} = \frac{Q_b\ t_{eq}}{k_s\ A} \tag{3B}$$

$$\frac{t_f}{k_{sg\ min}} = \frac{t_{eq}}{k_s} \tag{3C}$$

Rearranging Equation 3C yields:

$$k_{sg\ min} = \frac{k_s}{t_{eq} / t_f} \tag{4}$$

where: $k_{sg\ min}$ is the minimum allowable hydraulic conductivity of the filter zone;
k_s is the hydraulic conductivity of the soil;
t_f is the thickness of the clogged filter zone and is usually taken to be 5 cm; and
t_{eq} is the transformed filter thickness.

For the chimney-drain design example, $k_{sg\ min}$ is found to be:

$$k_{sg\ min} = \frac{5 \times 10^{-6}\ cm/s}{1070\ cm/5\ cm} = 2.3 \times 10^{-8}\ cm/s$$

The actual thickness of clogged filters (i.e., the thickness of disturbed soil, or of the filter cake) has been the topic of much research and debate. The actual thickness of a clogged filter may vary considerably, and because of its transitional structure, is often not visibly discernable in the soil next to the geotextile. Therefore, the actual thickness is nearly impossible to measure.

To avoid this problem, the thickness of the clogged filter zone, t_f, used in Equation 4, does not represent the actual thickness of the clogged filter or the filter cake. Instead, t_f is the thickness of the filter zone, which is defined as the zone measured 5 cm from the geotextile. The reasons that 5 cm is used are as follows:

- the methodology presented in this paper does not require that the actual hydraulic conductivity of the clogged filter be determined, but rather that the hydraulic conductivity of the composite soil/geotextile filter zone, k_{sg}, be used in the analysis;

- 5 cm is larger than the actual thickness of most clogged filters or filter cakes, and therefore encompasses the zone in which most soil particle rearrangement occurs; and

- 5 cm is the thickness (length) of the laboratory test specimen that is used to measure the composite hydraulic conductivity of the filter zone, k_{sg}, as will be filter described in the next section.

Step 3: Conduct Laboratory Testing.

After determining the minimum allowable hydraulic conductivity of the filter zone, laboratory performance testing should be conducted to evaluate candidate geotextiles by measuring the anticipated hydraulic conductivity of the filter zone, k_{sg}. The testing should be performed using soil from the actual project site and using a candidate geotextile filter that is selected based on conventional geotextile filter selection criteria (Giroud, 1988; Luettich et al., 1991).

Several laboratory test methods have been developed to evaluate the index characteristics and performance of geotextile filters. Whereas most of these test methods are adequate to determine index properties, the laboratory test method that provides the best representation of field performance is the Hydraulic Conductivity Ratio (HCR) test [Luettich and Williams, 1989; Williams and Abouzakhm, 1989; Williams and Luettich, 1990]. The HCR test is currently submitted for approval by the American Society for Testing and Materials (ASTM) under draft designation D35.03.91.01.

The HCR test is performed in a conventional triaxial flexible-wall permeameter. A soil specimen of thickness t_f (usually 5 cm) is placed in the permeameter adjacent to the geotextile filter. Water is permeated through the composite soil/geotextile filter test specimen using the hydraulic gradient and confining conditions expected in the design application. A schematic diagram of the HCR test permeameter and its application to the dam chimney drain design example is shown in Figure 6. The flow rate through the specimen is measured over an extended time period and the hydraulic conductivity of the composite specimen, k_{sg}, is calculated at regular intervals using conventional permeability equations derived from Darcy's equation.

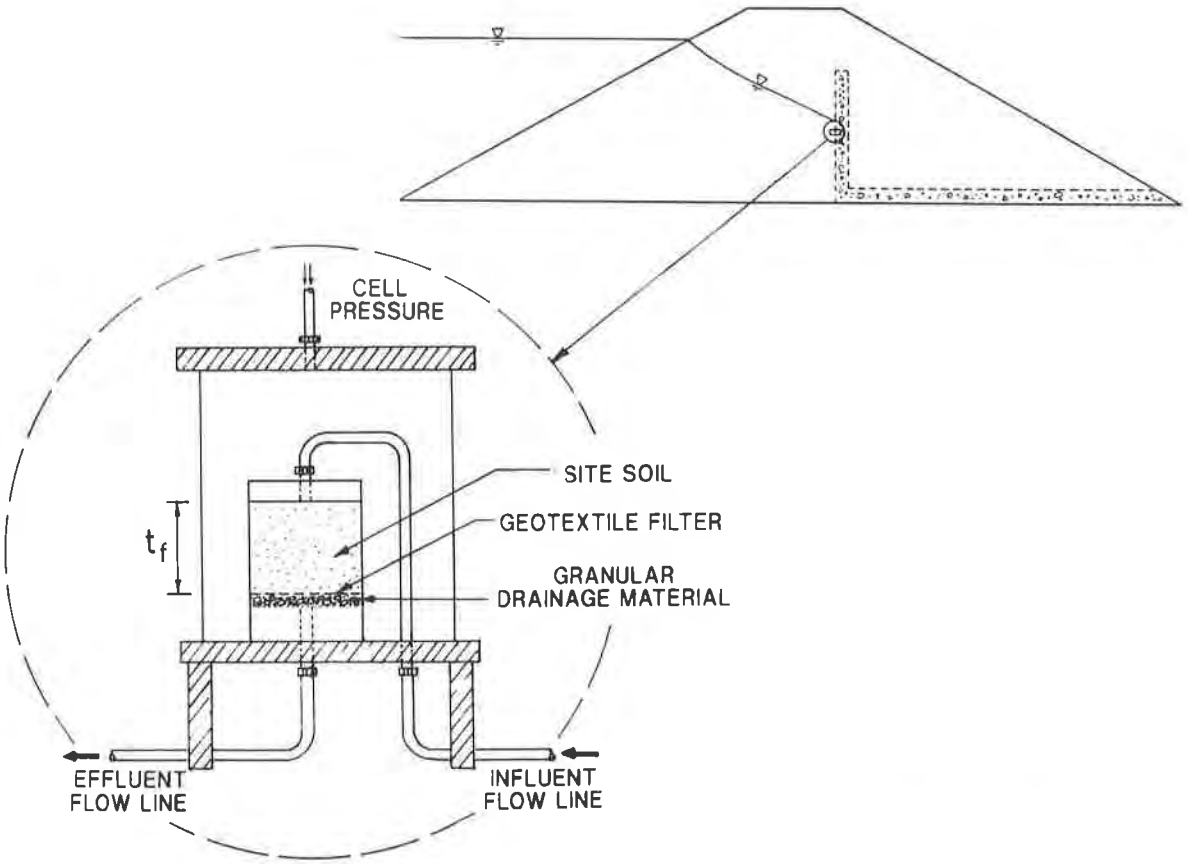

Figure 6. HCR Test Permeameter

The hydraulic conductivity values are plotted as a function of elapsed time. The test is conducted until either:

- the hydraulic conductivity reaches a stabilized value; or
- the hydraulic conductivity falls below the minimum allowable hydraulic conductivity required by the design (i.e., if k_{sg} is less than $k_{sg\ min}$).

Further details of HCR testing can be found in the referenced literature.

Results of a typical HCR test, conducted with conditions and materials applicable to the chimney-drain design example, are presented in Figure 7. The resulting stabilized hydraulic conductivity of the filter zone, k_{sg}, is 1 x 10^{-6} cm/s.

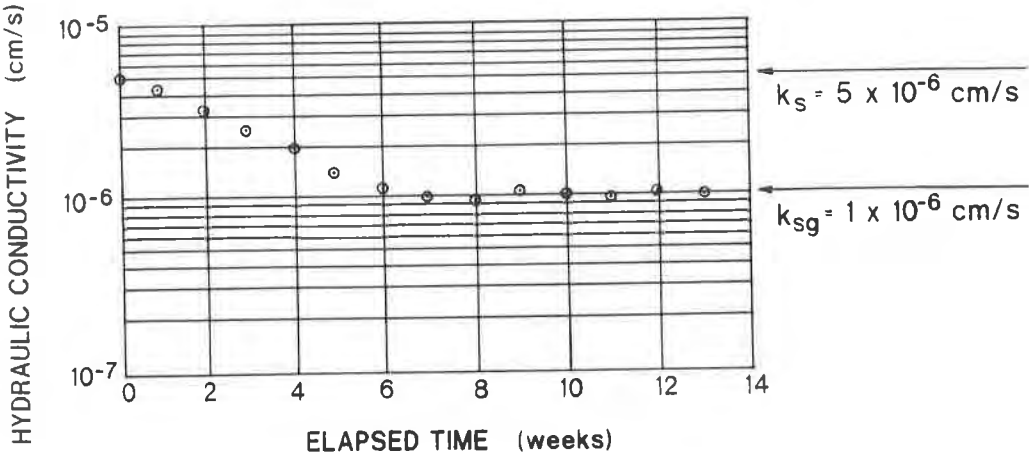

Figure 7. Results of HCR Test for Dam Chimney Drain Design Example

Step 4: Evaluate the Factor of Safety Against Filter Clogging.

The final step in the filter design method is to evaluate the factor of safety, F_s, against drainage failure due to filter clogging. This is accomplished by dividing the anticipated hydraulic conductivity of the filter zone, k_{sg}, measured in the HCR test, by the minimum allowable hydraulic conductivity of the filter zone, $k_{sg\ min}$.

$$F_s = \frac{k_{sg}}{k_{sgmin}} \tag{5}$$

The design engineer must then judge whether, based on the critical nature of the project, the factor of safety against filter clogging is sufficient for the given application.

For the chimney-drain design example, the factor of safety against drainage failure due to filter clogging is:

$$F_s = \frac{1 \times 10^{-6} cm/s}{2.3 \times 10^{-8}\ cm/s} = 43.5$$

For this application, the factor of safety of 43.5 was judged to be suitable by the design engineer. Accordingly, the geotextile used in the HCR test is acceptable as a filter for the project.

ADDITIONAL DESIGN EXAMPLE

To further demonstrate the filter design method, a second design example is presented. This example involves a protective erosion-control revetment system for a dewatering channel located adjacent to a leach field at a waste-water treatment facility. A cross section of the channel is shown in Figure 8.

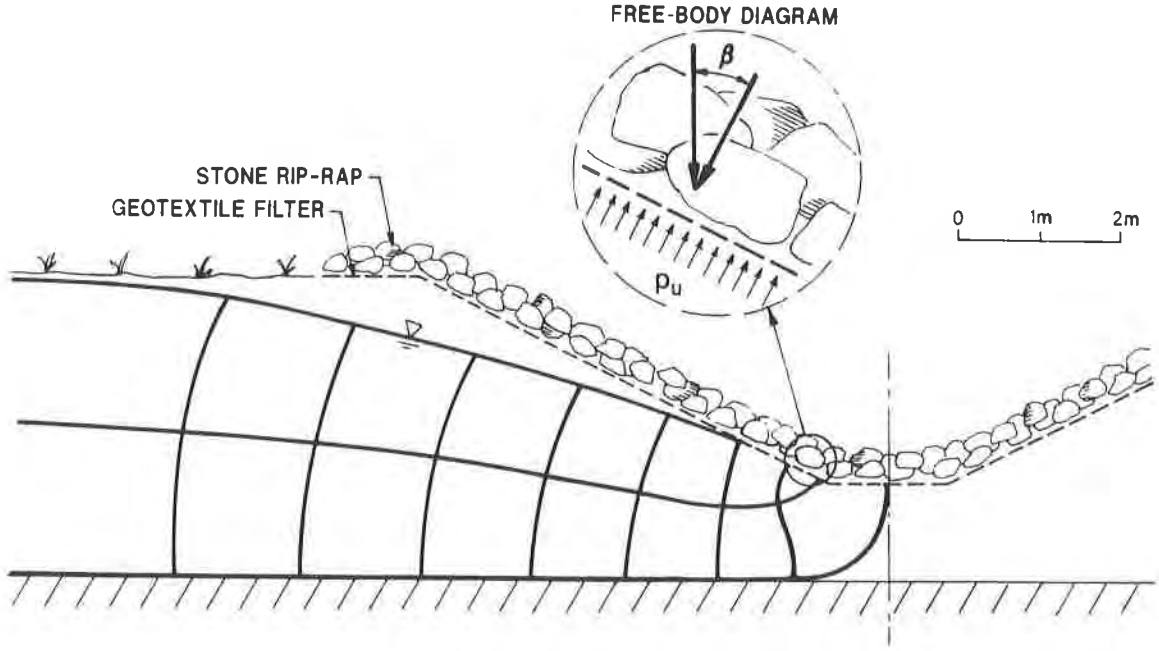

Figure 8. Cross-Section and Flow Net for Channel Revetment System.

The channel is 2.5 m deep and 1.5 m wide at the bottom. The sides of the channel are cut into the existing ground at a slope of 2H:1V (inclined at 26.5 degrees from horizontal). The hydraulic conductivity of the in-situ sandy embankment soil is 1×10^{-2} cm/s.

The proposed revetment system consists of a geotextile filter overlain by stone rip-rap. The stones are approximately 25 cm in average diameter and each weigh approximately 0.3 kN. The stones are placed such that the rip-rap layer ranges from 1 to 2 stones thick and the average pressure exerted on the base of the channel (i.e. on a horizontal surface) is approximately 6.5 kN/m^2. For the purpose of this example, it is assumed that the contact area of the stones with the geotextile does not significantly reduce flow by reducing the overall percentage of open area.

Step 1: Determine the Filter System Drainage Requirements.

The purpose of the revetment system is to prevent erosion of the sandy embankment soil as water seeps from the soil into the channel. Hence, the requirement of the filter system is to allow water from the leach field to drain into the channel without displacing (i.e., causing uplift of) the revetment.

The force that resists uplift is a function of the dead weight of the rip-rap stones and the angle of inclination of the channel side slope. A free-body diagram of a section of the revetment

system, located at the point of greatest uplift where the side slope intersects the base of the channel, is shown in Figure 8. The uplift pressure, p_u, that will cause uplift failure of the revetment system, is calculated using the free-body diagram, as follows:

$$P_u = \sigma \cos\beta \qquad (6)$$

where: p_u is the uplift pressure that will cause uplift failure of the revetment system;
σ is the pressure exerted by the rip-rap layer on a horizontal surface; and
β is the side slope inclination.

For this design example, the maximum allowable uplift pressure is found to be:

$$P_u = 6.5\ kN/m^2 \times \cos 26.5^\circ = 5.8\ kN/m^2$$

The height of hydrostatic head, h_u, that is equivalent to p_u is found by dividing p_u by the unit weight of water:

$$h_u = \frac{5.8\ kN/m^2}{9.81\ kN/m^3} = 0.59\ m$$

Hence, the *quantitative requirement* of the filter system is to allow water to seep into the channel without causing more than 0.59 m of equivalent hydrostatic pressure (head) to build up underneath the revetment system.

Step 2: Determine the minimum allowable hydraulic conductivity of the filter zone by using the method of transformed flow nets.

- **Step 2.1: Draw Failure-Condition Flow Net.** For this design example, the flow net representing the failure condition is shown in Figure 9.

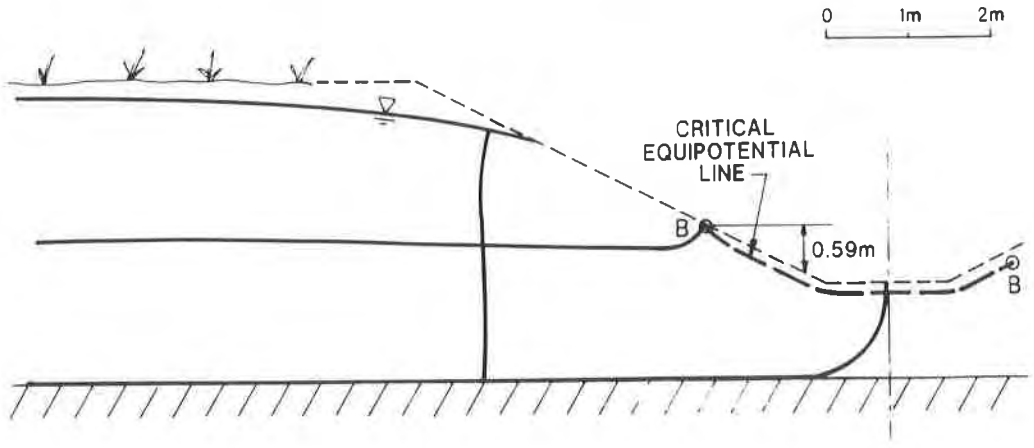

Figure 9. Flow Net for Failed (Clogged Filter) Drainage Condition

- **Step 2.2: Identify the Critical Equipotential Line**, which represents the maximum hydraulic head condition that would intersect the filter zone at the point of uplift, if the filter were clogged. The critical equipotential line is depicted in Figure 9 as the heavy broke line B-B.

- **Step 2.3: Draw Zero-Impedance Flow Net** assuming that the filter zone has the same hydraulic conductivity as the adjacent soil. This is shown in Figure 10.

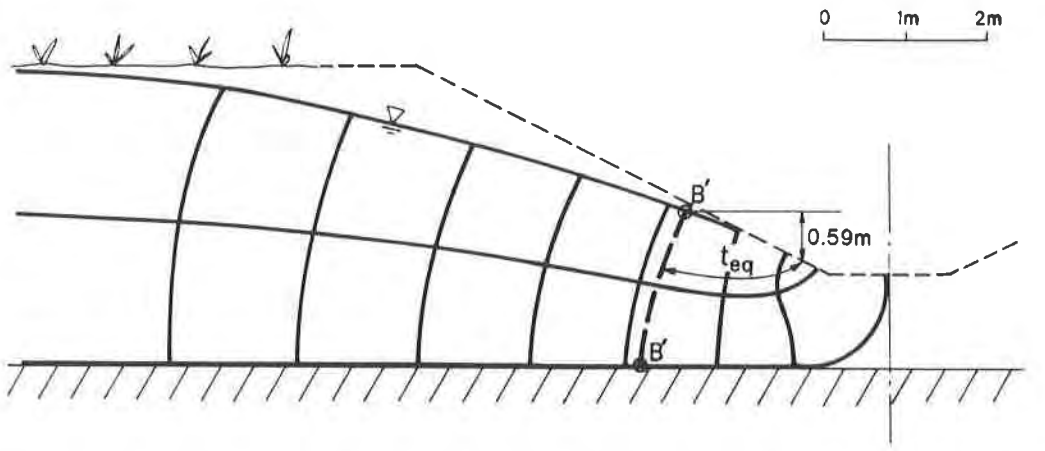

Figure 10. Flow Net for Zero Impedance Drainage Condition

- **Step 2.4: Identify the Transformed Critical Equipotential Line** on the zero-impedance flow net. This is depicted in Figure 10 by the heavy broken line B'-B'. The distance from line B'-B' to the point of uplift is the transformed thickness of the clogged filter zone (i.e., the transformed filter thickness).

- **Step 2.5: Measure the Transformed Filter Thickness, t_{eq}**. For this example, the distance t_{eq} is measured as shown in Figure 10 along a flow line from the point of uplift to the critical equipotential line, and is found to be 2.2 m. The reason that t_{eq} is measured along a flow line instead of the phreatic surface is because, unlike the chimney-drain design example, failure of the revetment system is defined in terms of hydrostatic pressure instead of the actual location of the phreatic surface. In the chimney-drain design example, the flow line along which t_{eq} was measured coincided with the phreatic surface.

- **Step 2.6: Determine $k_{sg\ min}$**
  The minimum allowable hydraulic conductivity of the filter zone, $k_{sg\ min}$, is determined using Equation 4:

$$k_{sg\ min} = \frac{1 \times 10^{-2}\ cm/s}{(\ 220\ cm/5\ cm\ )} = 2.3 \times 10^{-4}\ cm/s$$

Step 3: Conduct Laboratory Testing.

A candidate geotextile filter was selected and HCR testing was performed. The resulting stabilized hydraulic conductivity was determined from the HCR test to be 6 x 10^{-4} cm/s.

Step 4: Evaluate the Factor of Safety Against Filter Clogging.

The factor of safety against failure due to filter clogging is evaluated using Equation 5:

$$F_s = \frac{6 \times 10^{-4} \ cm/s}{2.3 \times 10^{-4} \ cm/s} = 2.6$$

For this application, the factor of safety of 2.6 was judged by the design engineer to be inadequate (i.e., too low) and the geotextile was rejected for this project. A different geotextile was selected and Steps 3 and 4 were repeated. The subsequent HCR test resulted in a stabilized hydraulic conductivity of the filter zone of 2 x 10^{-3} cm/s. The factor of safety against drainage failure due to filter clogging with the second geotextile was calculated using Equation 5:

$$F_s = \frac{2 \times 10^{-3} \ cm/s}{2.3 \times 10^{-4} \ cm/s} = 9.0$$

For this application a factor of safety of 9.0 was judged to be suitable by the design engineer. Accordingly, the geotextile used in the second HCR test is acceptable as a filter for the project.

CONCLUSIONS

To fully understand clogging of geotextile filters, the engineer must understand the entire drainage design process and the requirements of the drainage system for the given application. This paper has demonstrated the following:

- the "failure condition" of the drainage system can be quantitatively defined;
- the minimum allowable conductivity of the filter zone can be determined using the method of transformed flow nets;
- the predicted hydraulic conductivity of the filter zone can be evaluated using HCR laboratory testing; and
- the factor of safety against drainage failure due to filter clogging can be evaluated for the given application.

By following this methodology, the engineer can logically and quantifiably evaluate the potential for failure of a drainage system due to filter clogging. Accordingly, modifications to the drainage design and to the geotextile selection can be made, if necessary, prior to experiencing a drainage failure due to clogging of the geotextile filter.

REFERENCES

Cedergren, H.R., (1977) "*Seepage, Drainage, and Flow Nets*", John Wiley & Sons, New York, NY, 534 p.

Giroud, J.P., (1988) "Review of Geotextile Filter Criteria", *Proceedings of First Indian Geotextiles Conference on Reinforced Soil and Geotextiles*, Bombay, India, pp. 1-6.

Giroud, J.P., Fluet, J.E., Jr., and Gross, B.A., (1988) "*Geosynthetic Design Examples: An Addendum to the FHWA Geotextile Engineering Workshop*", 144 p.

Luettich, S.M., Giroud, J.P., and Bachus, R.C., (1991) "Geotextile Filter Design Guide", *Proceedings of 5th Annual GRI Seminar on Geosynthetics in Filtration, Drainage and Erosion Control*, Philadelphia, PA, pp. 18-33.

Luettich, S.M. and Williams, N.D., (1989) "Design of Vertical Drains Using the Hydraulic Conductivity Ratio Analysis", *Proceedings of Geosynthetics "89 Conference*, San Diego, CA, Vol. 1, pp. 95-103.

Williams, N.D., and Abouzakhm, A.M., (1989) "Evaluation of Geotextiles/Soil Filtration Characteristics Using the Hydraulic Conductivity Ratio Analysis", *Geotextiles and Geomembranes*, Elsevier, England, Vol. 8, pp. 1-26.

Williams, N.D., and Luettich, S.M., (1990) "Laboratory Measurement of Geotextile Filtration Characteristics", *Proceedings of 4th International Conference on Geotextiles, Geomembranes and Related Products*, The Hague, Netherlands, Vol. 1, pp. 273-278.

Geotextile Filter Criteria for Gap-Graded Silty Sands

J.E. Fluet Jr.
Florida Atlantic University, USA

S.M. Luettich
GeoSyntec Consultants, USA

ABSTRACT

Conventional filter criteria may be inadequate when the soil to be filtered is a gap-graded silty sand with less than 20% silt. Such soils are typical of regions such as coastal zones along the southeastern and gulf shores of the United States. Since the structures in such locales are often expensive, the consequences of filter failures can be significant. When conventional geotextile retention criteria are applied, the designer faces a quandary since the associated particle size distribution curve exhibits two slopes - one for the sand portion and one for the silt portion. Most designers choose to ignore this quandary and simply apply the conventional criteria using an average particle size distribution curve. Unfortunately, conventional criteria often lead to selection of a geotextile which retains the silt, and this approach is often non-conservative. This paper proposes design criteria which complement conventional soil retention criteria and are applicable to gap-graded silty sands with less than 20% silt.

CONVENTIONAL GEOTEXTILE FILTER CRITERIA

The conventional approach to geotextile filter design may be summarized as follows:

- Retention criterion - Conventional design methodologies are used to select a geotextile whose Apparent Opening Size (AOS), O_{95}, is sufficiently small to retain the soil to be filtered. Retention criteria are related to some characteristic particle size of the soil to be filtered, e.g., according to Giroud [1982], for soils with $C'_u > 3$,

$$O_{95_{gtx}} \leq \frac{13.5}{C'_U} d_{50_{soil}} \qquad (1)$$

where: O_{95gtx} is the AOS of the geotextile,
d_{50soil} is the particle size whereby 50% by weight of the soil is larger and 50% by weight is smaller, and
C'_U is the linear coefficient of uniformity of the soil.

The retention criteria thus ensures that the soil particles will not pass (pipe) through the geotextile.

- Permeability criterion - Some conventional criteria are very simple, such as the following proposed by Christopher & Holtz [1984],

$$K_{gtx} > 10 K_{soil} \qquad (2)$$

where: K_{gtx} is the geotextile index hydraulic conductivity, and
K_{soil} is the soil hydraulic conductivity,

Some are much more complex, such as the 4-step methodology described by Luettich and Fluet [1993]. Giroud [1988] provided a sound analytical demonstration of a permeability criterion. Permeability criteria either relate the geotextile index hydraulic conductivity to the soil hydraulic conductivity, as shown above, or, for more critical applications, utilize a performance test such as the Hydraulic Conductivity Ratio (HCR) [Williams & Abouzakham,1989]. The choice of criterion is left to engineering judgement based on the consequences of filter failure; but, in all cases, the goal is to ensure that the filter zone (the filter plus the adjacent "filter cake" formed by migrating fine soil particles) allows the fluids in the retained soil to flow through the filter.

- Porosity/Percent-Open-Area (POA) criterion - Porosity criteria apply to non-woven geotextiles and percent-open-area criteria apply to woven geotextiles. Porosity criteria compare the geotextile porosity to that of a comparable sand filter. In fact, virtually all commercially available non-woven geotextiles vastly exceed such porosity criteria. POA criteria simply specify a minimal percent-open-area which, in the judgement of the designer, will ensure an adequate frequency of holes. In both cases, the goal is to ensure enough holes in the geotextile to preclude failure should a few of the holes become randomly clogged. Porosity/POA are the least understood of the filter criteria.

Of the three criteria, retention has been the most discussed and quantitative criteria have been available for the longest time. Although permeability criteria are less well understood by designers, quantitative design criteria have been developed in recent years, and quantitative design methodologies are now available. Porosity/POA criteria are the least understood by design professionals, although ongoing research in this area is continuously increasing the available data.

Essentially, the existing geotextile filter design approach is: (i) to apply retention criteria to ensure the geotextile openings are small enough to retain the soil, and (ii) to apply permeability and porosity/POA criteria to ensure that the openings are large and frequent enough to allow the fluids in the retained soil to flow through the geotextile. One set of criteria tends to make the openings as small as possible, and the other makes the openings as large as possible. Such seemingly contradictory criteria are not unusual in civil engineering applications, e.g., structural engineers design glass thick enough to be strong yet thin enough so as not to distort the view; and they design steel with enough ductility to be flexible and enough brittleness to be strong.

For most geotextile filter applications, established retention criteria may be combined with newly developed permeability criteria to design safe, long lasting filters. Currently, experience seems to dictate that the porosity/POA of many commercially available geotextiles is apparently adequate.

The previous paragraph notwithstanding, established retention criteria are unfortunately not applicable to all soils. In particular, they are often not applicable to gap-graded silty sands with less than 20% silt. Although such silty sands comprise only a small percentage of soils, they nonetheless have a significant impact on filter design because they are most often found in coastal zones such as the southeastern and gulf shores of the United States. Although the areas involved are relatively small, they comprise some of the most desirable and expensive real-estate in the world. Consequently, construction projects are very expensive and filter failures can have enormous economic consequences.

DESCRIPTION OF THE PROBLEM

A typical particle-size distribution (PSD) curve for the soils in question is shown in Figure 1.

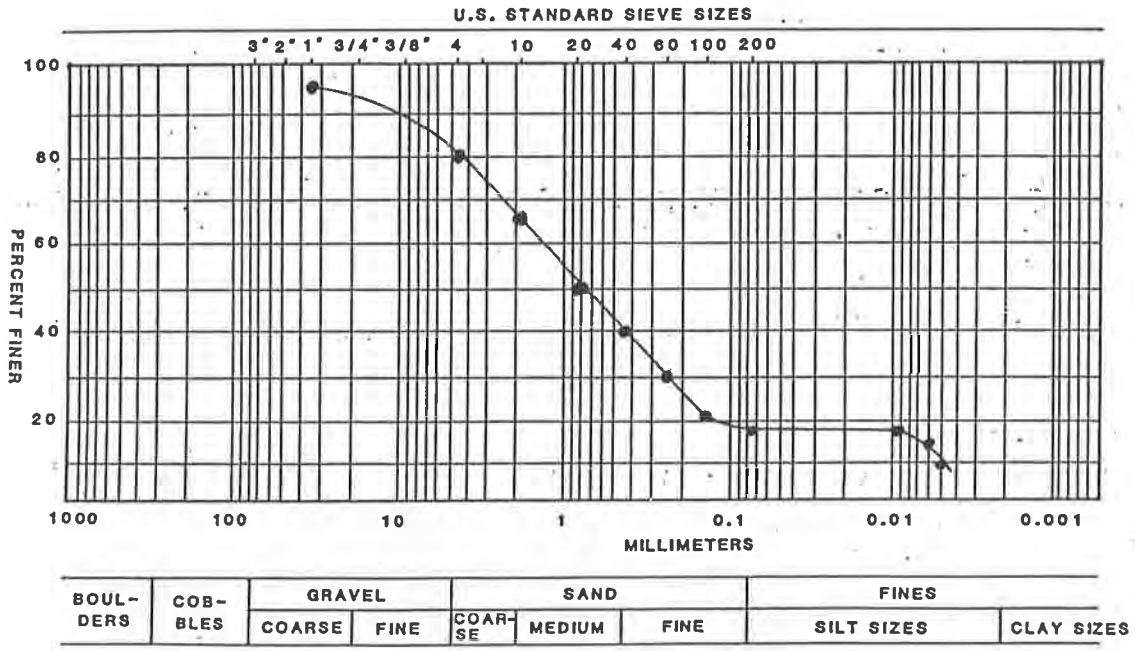

Figure 1. Typical Particle Size Distribution Curve for Flat-Graded Silty Sand

Several aspects of this silty sand PSD curve are particularly noteworthy. First, the soil contains less than 20% silt by weight. Secondly, the largest silt particles are approximately one order of magnitude smaller than the smallest sand particles. Note also that the soil is truly gap-graded, i.e., there are no particle sizes between the largest silt and the smallest sand. The curve thus has a characteristic flat region. To prevent confusion with other silty sands, the soils in question here will hereafter be referred to as "flat-graded" silty sands, the characteristics of which are summarized in Table 1.

Table 1: Characteristics of Flat-graded silty sands

- Contain less than 20% silt by weight.
- Smallest sand particles are at least 10 times larger than the largest silt particles.
- There are no particle sizes between the smallest sand and the largest silt.

A comparison of the interstitial pore space available between the sand particles of flat-graded silty sands to the volume occupied by the silt particles demonstrates that the silt particles can be entirely accommodated in the interstitial spaces between the sand particles. Furthermore, the silt particles are free to move between the sand grains, and, because of the small mass and cohesionless nature of the silt particles, they are easily moved by even small hydraulic gradients. Since the silt particles are "loose" in the sand matrix, they do not contribute to the bearing capacity or structural integrity of the sand, i.e., removal of the silt causes no settlement of the soil matrix even though the silt comprises up to 20% of the soil by weight.

When the conventional retention criteria are applied to such soils, the designer faces a quandary. The PSD curve exhibits two slopes, one for the sand and one for the silt. Most designers simply apply conventional criteria to the overall PSD curve which often leads to selection of a geotextile which retains the silt. This solution is usually perceived by the designers to be conservative. Unfortunately, this solution may result in the development of a low permeability filter-zone (i.e., clogging/blinding), thereby causing failure of the system. Examples of erosion control systems which have failed due to improper geotextile design/selection are shown in photos 1-4.

Photo 1: Example of Erosion Control Structural Problem Caused by Failure of Geotextile Underlying Rip Rap

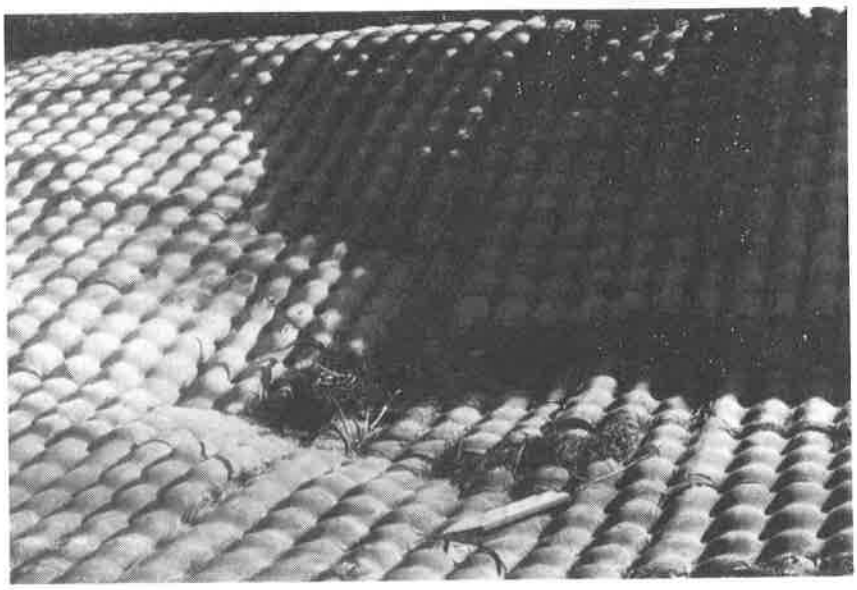

Photo 2: Example of Erosion Control Structural Problem Caused by Failure of Geotextile Underlying Fabric-Formed Concrete

Photo 3: Example of Erosion Control Structural Problem Caused by Failure of Geotextile Underlying Concrete Erosion Control Block

Photo 4: Example of Erosion Control Structural Problem Caused by Failure of Geotextile Underlying Interlocking Concrete Erosion Control Blocks

Each of the erosion control structures shown in Photos 1-4 comprises an armor layer (rip-rap, concrete blocks, fabric-formed concrete) underlain by a geotextile filter. In all cases, the failure shown was caused by failure of the underlying geotextile, not the armor layer. A common failure scenario may be conceptually described as follows:

- a geotextile filter is selected which retains the silt-sized particles;
- the silt particles move freely in the sand matrix (sometimes for distances of several meters) and, upon reaching the geotextile, are trapped in the filter zone (geotextile plus filter cake);
- due to silt accumulation, the permeability of this filter zone progressively decreases to a permeability that is significantly lower than that of the retained sand;
- as a result, water flowing through the retained sand can no longer flow freely through the filter zone; and,
- eventually, the force of the hydrostatic pressure on the geotextile exceeds the retaining force of the armor layer overlying the geotextile and lifts the geotextile and the armor layer, thus allowing shifting of the underlying soils.

Simply stated, the silt is able to move freely through the sand, but is trapped by the geotextile filter, resulting in a filter zone of decreasing permeability.

PROPOSED CONCEPTUAL SOLUTION

It is important to note that with all filter designs, it is incumbent on the designer to determine whether piping or clogging is the greater design problem and to conduct the design accordingly. In those cases where clogging is a major problem and piping is little threat, such as the cases addressed in this paper, the proposed method may be applicable. If, on the other hand, the silt which pipes through the geotextile can lead to downstream problems, the method may not be applicable [Fluet, 1983].

The proposed solution to this problem is to select a geotextile filter which has relatively uniformly sized holes which are small enough to retain the sand but large enough to release the silt. The reader may be justifiably concerned that losing 20% by weight of the soil would lead to: (i) unacceptable levels of settlement in the retained soil or (ii) clogging of the downstream portions of the drainage system; and, the prudent designer may require an analysis (possibly including confirming laboratory tests) to be conducted to ensure that excess settlement is not a problem. However, experience indicates that flat-graded silty sands rarely pose settlement problems. For example, the techniques proposed herein have been used to design the filters for numerous seawalls, and, in each case, the weepholes (protected by the geotextile filter) flow with dirty (silty) water for a period ranging from a few hours to a few days, after which only clean water flows. The "dirty flow" period, of course, is evidence that significant quantities of silt are escaping. Yet, on several of these projects, settlement plates on the retained soil showed only small settlements which were consistent with the normal predicted levels of settlement of the sand alone; i.e., the large fraction (up to 20% by weight) of the soil which passed through the filters and out of the weepholes had no effect on the overall settlement of the soil. The soil which was lost, therefore, was the mobile, interstitial silt which did not contribute to the structural strength of the primary (sand) matrix.

It should be noted here that the soils in question are very specific flat-graded silty sands which exhibit PSD curves similar to the curve in figure 1. These silty sands should not be confused with the more common silty sands which exhibit a "concave-up" PSD curve with a coefficient of curvature of 2 or more as shown in Figure 2 and discussed in detail by Luettich et. al. [1991]. In particular, in flat-graded silty sands, the sands do not act as a filter for (and thus do not prevent the mobility of) silt particles; whereas, in the case of concave-up silty sands, there may be sufficient particle sizes intervening between the silt and the sand to cause the sand and intervening particles to act as a filter for, and thus stabilize, the silt. As a consequence, the designer should always apply granular filter criteria to the silty sands in question to determine whether the silt particles are stable or mobile.

Furthermore, in such "concave-up" silty sands, the silts may contribute to the structural strength of the soil, especially when these are sufficient intervening particle sizes. Accordingly, the design methodology proposed herein may or may not be applicable and the designer should carefully analyze the specific conditions to determine applicability.

The key, therefore, to a design methodology for flat-graded silty sands is to select a filter whose holes are sufficiently small to retain the sand and sufficiently large to allow the silt to escape. The first criterion is, of course, the subject of conventional filter retention criteria except that, in this case, the criterion must be applied only to the sand portion of the PSD curve, i.e., the silt fraction must not be considered.

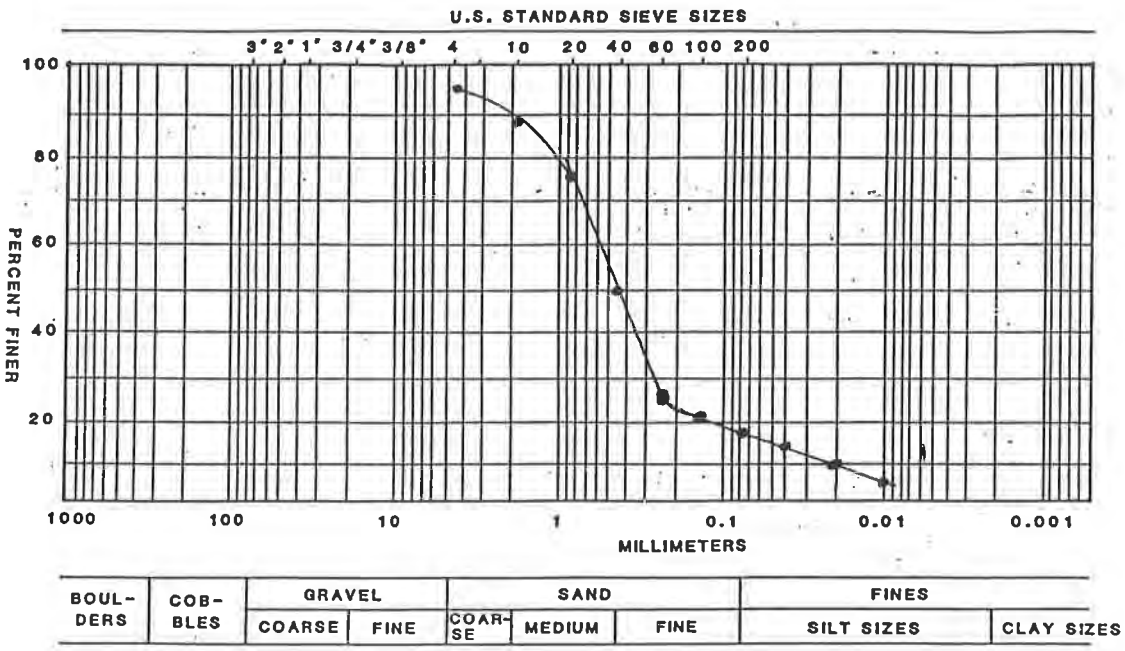

Figure 2. Example of Concave-up PSD Curve

The second criterion, selecting holes large enough to allow the silt to escape may be developed as follows. First, as shown in Figure 3, the AOS of a monofilament woven geotextile is determined by the particle size which is barely retained by the geotextile strands, i.e, the next smaller particle will pass through the strands.

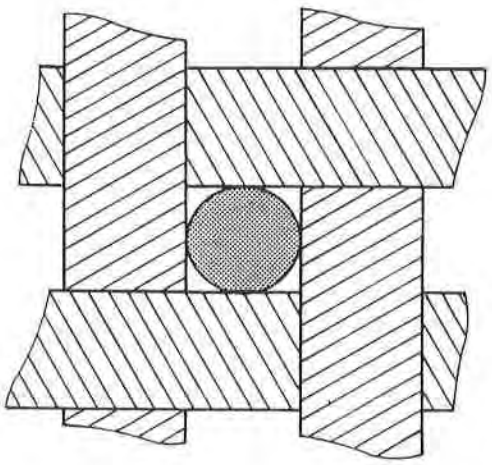

Figure 3. Schematic of Particle Passing Through Woven Geotextile Matrix During AOS Test - AOS is Size of Smallest Particle which will NOT Pass Through Matrix

The preceding discussion would lead one to believe, therefore, that one need only specify that the opening size of the geotextile be larger than the largest silt particles. AOS, however, is determined using rounded particles which are shaken to promote passage. In fact, real silt particles are usually angular, and, in the field, bridging occurs between particles so that a geotextile will often retain soils whose grain size is several times smaller than the opening size of the geotextile. The issue, then, is to determine the minimum AOS which will ensure that silt particles will escape, recognizing that this minimum AOS will be several times larger than the largest silt particles. A detailed analytical development of the minimum AOS is beyond the scope of this paper and is the topic of an ongoing effort. Nonetheless, there is ample experience and empirical evidence available to propose a working method to determine the minimum AOS. Based on years of experience, theoretical discussions, and the results of proprietary laboratory tests, the authors propose the following criterion for the minimum allowable AOS.

$$O_{95} > 10 d_{100_{silt}} \qquad 3$$

In addition to specifying an O_{95} which is large enough to allow the silt to escape, two other criteria are necessary for the silt to escape:

- the geotextile must have relatively uniformly sized openings, and
- there must be a high enough frequency of openings to ensure that approaching silt particles will have an avenue of escape, regardless of where they approach the geotextile.

The first of these additional criteria, uniformly sized openings, is adequately met by many commercially available calendered monofilament woven geotextiles. Based on experience and the results of proprietary laboratory tests, the second additional criterion is satisfied by geotextiles with a POA greater than 15%.

The authors,therefore, propose the following modification to conventional retention criteria, recognizing that the proposed modifications are only applicable to flat-graded silty sands and drainage applications that are not jeopardized by substantial amounts of silt passing through the filter. (Designers should, of course, also design permeability criteria as appropriate.)

Step 1: Conduct a conventional retention design excluding the silt. This will result in a criterion which will specify the largest O_{95} which is allowable to retain the fraction of the soil which is larger than the silt,i.e. a maximum O_{95} .

Step 2: Specify the following minimum O_{95}:

$$O_{95} \geq 10 d_{100_{silt}} \qquad 4$$

Step 3: Specify a geotextile with relatively uniformly sized holes, such as a calendered monofilament woven.

Step 4: In order to ensure a high frequency of holes, specify

$$POA \geq 15\% \qquad (5)$$

It is important to note that steps 1-4 are only applicable to:

- flat-graded silty sands as defined in Table 1
- applications which are not jeopardized by substantial amounts of silt passing through the filter, and
- applications which are subject only to one-way flow (those applications which are subject to two-way dynamic flow require more stringent conventional criteria to prevent piping of some of the smaller sand particles).

It should also be noted that, although a specific type of woven geotextile is most applicable in the specific applications described in this paper, there are many other applications where nonwovens or other types of wovens may be more appropriate.

DESIGN EXAMPLE

Problem: Conduct a geotextile filter retention design for a protective revetment system to be constructed over the soil whose PSD is shown in Figure 1. In this case, the designer has determined that piping of the silt will cause no upgradient or downstream problems.

Step 1: Determine maximum O_{95}

The curve resulting from recasting the PSD for the sand only is shown in Figure 4.

Then, by Giroud,

$$O_{95} \leq 13.5 \frac{d_{50}}{C_u'}$$

$$C_u' = \sqrt{\frac{d_{100}'}{d_0'}} = \sqrt{\frac{18}{.14}} = 11.3$$

$$O_{95} \leq \frac{13.5(1.4)}{11.3} = 1.7mm$$

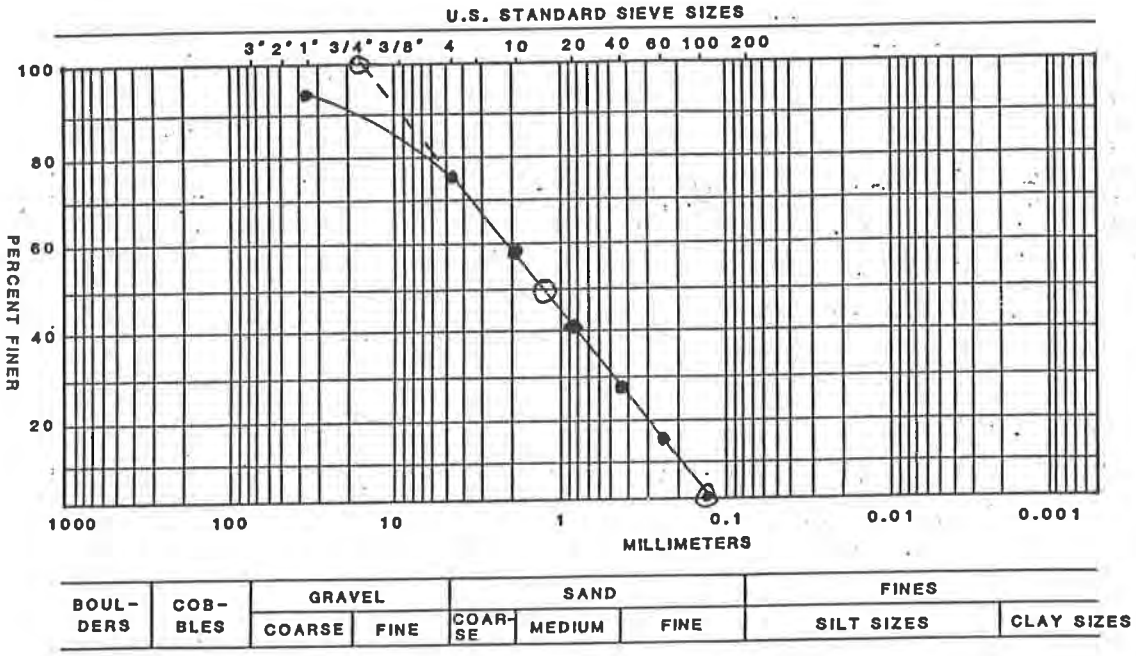

Figure 4. PSD for Sand Fraction Only

Step 2: Determine Minimum O_{95}

$$O_{95} \geq 10 d_{100_{silt}} \geq 10(.01)$$

$$O_{95} \geq 0.1mm$$

Step 3: Specify a calendered monofilament woven geotextile, and

Step 4: Specify a minimum POA

$$POA \geq 15\%$$

In summary, one would specify a calendered monofilament woven geotextile with

$$0.1mm \leq O_{95} \leq 1.7mm$$

and

$$POA \geq 15\%$$

For a much more comprehensive geotextile filter design example, the reader is referred to Giroud, et. al. [1988].

ACKNOWLEDGEMENTS

The authors wish to thank Dr. J.P. Giroud for his thorough review of the paper and Ms. V. B. Fluet for her assistance in preparing the manuscript.

REFERENCES

Giroud, J.P., "Filter Criteria for Geotextiles", Proceedings of Second International Conference on Geotextiles, Las Vegas, Nevada, U.S.A., 1982, pp. 103-108.

Christopher, B.R. and Holtz, R.D., "Geotextile Engineering Manual", FHWA-DTFH61-80-C-00094, 1984.

Luettich, S.M. and Fluet, J.E., Jr., "Geotextile Design Using Flow Nets", Proceedings of Geosynthetics '93, Vancouver, B.C., U.S.A., April 1993.

Giroud, J.P., "Review of Geotextile Filter Criteria", Proceedings of the First Indian Geotextiles Conference, Bombay, December 1988, pp 1-6.

Fluet, J.E., Jr., "Geotextiles Types, Applications and Generalized Design Criteria", ASCE, 1983 Annual Meeting, Cape Coral, FL, Sep 29, 1983.

Luettich, S.M., Giroud, J.P., and Bachus, R.C., (1991) "Geotextile Filter Design Guide", Proceedings of 5th Annual GRI Seminar on Geosynthetics in Filtration Drainage and Erosion Control, Philadelphia, Pa., pp. 18-33.

Williams, N.D., and Abouzakham, A.M., (1989) "Evaluation of Geotextiles/Soil Filtration Characteristics Using the Hydraulic Conductivity Ratio Analysis", Geotextiles and Geomembranes, Elsevier, England, Vol. 8, pp. 1-26.

Giroud, J.P., Fluet, J.E., Jr., and Gross B.A., Geosynthetic Design Examples: An Addendum to the FHWA Geotextile Engineering Workshop, April 1988, 144 p.

* * *

Filtration Performance of Geotextiles With Fine-Grained Soils

U. Siva
Syracuse University, USA

S.K. Bhatia
Syracuse University, USA

ABSTRACT

Geotextiles are more frequently being used as protective filters in embankment and hydraulic fill tailings dams. Poorly established criteria limit their use with fine-grained materials. Performance tests such as the long-term flow (LTF), gradient ratio (GR), and hydraulic conductivity ratio (HCR), are usually needed to evaluate the performance of the selected geotextile with the *in situ* soil. These tests do not reflect the true flow characteristics of low permeability soil-geotextile systems. In this study, the filtration behavior of eleven non-woven geotextiles (from four manufacturers) with six silts was studied using LTF tests. All of the silt-geotextile systems performed satisfactorily under the LTF test conditions. A rapid retention test (RRT) was developed to represent severe hydraulic conditions. In contrast to the LTF tests, as much as 60 to 80 % of the silts passed through the geotextiles under the RRT. Also, the reduction of the geotextile's permeability due to particulate clogging was found to be a factor by no more than 15 of the virgin geotextile.

INTRODUCTION

Geotextiles are used as protective filters or separators in a wide range of applications. In some cases, they have completely replaced the traditional granular filter. An example of this is sub-surface drains where the fabrics are wrapped around perforated pipes to retain and drain the sub-surface soil in place of granular materials (Rollin *et al.*, 1990). Lately, they are increasingly being used in conjunction with fine-grained soils. Typical applications involve filtering fine sands in hydraulic fill tailings dams and small earth dams (Mlynarek *et al.*, 1990), separating rock-fill shells from the silty cores in coffer dams (Lafleur *et al.*, 1991), protecting the railway ballast and rigid pavement sub-base from silty sub-grades, separating clayey silt layers used as a lining material in earth dams (Bertacchi, *et al.*, 1985), and separating a clay liner from the leachate collection layer in landfills.

The selection of a geotextile is a two-step short-listing process.

The first step to comply with filtration criteria; the second step is to meet specific performance test results. The filtration criteria, namely retention and permeability, are mutually compromising. These criteria are well established for coarse soils (Giroud, 1982; Mlynarek et al., 1990; and others). They, however, are not well defined for fine grained and gap-graded soils. For such soils the design is based on a combination of empirical methods, experience-based intuition, and an extension of the criteria established for coarse soils.

In the second step, a performance test is conducted to evaluate the long-term behavior of the geotextile in the field. Tests currently used include the long-term flow (LTF), gradient ratio (GR), hydraulic conductivity ratio (HCR), and lately, the fine fraction filtration (FFF or F^3) test. The last test can be considered as a performance test when an intimate contact is not present between the geotextile and the protected soil (Sasone et al., 1991). All of these tests generally involve placing the field soil atop the fabric in some condition (dry, optimum moisture, slurry) and applying a hydraulic head of some multiple of the expected field value. These performance tests are described below.

In the LTF test, the amount of soil piped and the permeant flow through the system are measured. For the GR test, the pore pressure at various heights of the soil column directly above the geotextile as well as the flow and soil passing are measured. The GR value is computed as the ratio of the hydraulic gradient between the fabric and an inch of soil directly above it to the hydraulic gradient of the entire system (Oberoi, 1992). In the HCR test, a flexible wall permeameter is used to monitor the flow through the soil-geotextile system. In this test, either undisturbed or laboratory-formed soil samples can be used, and a higher degree of saturation can be ensured. In addition, consolidation under typical field stresses can be achieved on the system. The HCR is defined as the ratio of the permeability of the soil to that of the soil-geotextile system (Williams et al., 1989). In the F^3 test, the finer fraction of the soil is mixed into a slurry and introduced in increments into a column containing the fabric under a constant head. To make the slurry, the D_{15} fraction is usually used; however for silty and clayey soils, the entire soil is used (Sasone et al., 1991). The flow through the system is monitored over time. The resulting decrease in flow over time in any of these performance tests is a result of three components. They are geotextile compression under the applied stress, soil sample consolidation or settling, and clogging of the geotextile.

Clogging. Clogging can be particulate, chemical, or biological in nature. The compression component of the geotextile is immediate while the consolidation and particulate clogging components occur within 24 hr of the application of the hydraulic head. Particulate clogging is a short-term phenomenon while chemical and biological clogging are long-term phenomena. Each of these is discussed below.

The normal permeability (or permittivity) of non-woven needle-punched (NP) geotextiles can decrease by an order of magnitude with the application of normal stress (Cancelli *et al.*, 1987). The

transmissivity of NP fabrics, which is related to the normal permeability, can also be reduced by a maximum of an order of magnitude at stresses up to 93 kPa (Koerner *et al.*, 1982).

The soil compression component depends on the sample preparation technique. This component can contribute a significant proportion of the total decrease if flow was initiated on a dry loose sample.

Particulate clogging is a result of soil particles being trapped in the pores of the geotextile. Such clogging depends on, among other factors, the size distribution and shape of the soil particles and the pore structure and opening size distribution of the geotextile. For particulate clogging to occur, there must be some initial movement of the soil particles through the geotextile.

Chemical clogging occurs because various compounds present in the permeant precipitate. For example, leachates from landfills contain a wide range of chemical compounds that can come out of solution. Saline water in coastal structures and high alkalinity ground water can lead to deposition to a chemical layer (sodium, calcium, or magnesium) in the fabric (Sasone *et al.*, 1991).

Biological clogging is the result of bacterial growth on and in the geotextile. It can significantly reduce the flow capacity of the fabric (Koerner *et al.*, 1990; Rios *et al.*, 1989). Such clogging is particularly important in landfills where ample nutrients and moderate temperature can promote bacterial growth.

Fine-grained soil-geotextile permeability. With silts and clays, the geotextile permeability must decrease by two to three orders of magnitude before any significant change in the system (or effective) permeability is observed. Figure 1 shows the theoretically effective permeability of two filters (soil and geotextile) in series. The effective permeability (K_{eff}) is computed using the equation below (Craig, 1987).

$$K_{eff} = \frac{t_g + t_s}{\frac{t_g}{k_g} + \frac{t_s}{k_s}} \qquad \text{.....(1)}$$

The variables t and k in this equation refer to the thickness and permeability respectively, of the geotextile (g) and soil (s). In figure 1, geotextile and soil thicknesses were assumed to be 0.45 cm and 3.5 cm, respectively; the soil permeability ranged from 2×10^{-6} to 2×10^{-1} cm/s.

The figure shows that for soils with permeability (k_s) less than 10^{-3} cm/s, the system or effective permeability is mainly influenced by the permeability of the soil. This implies that during performance tests with silts (and clays), the system permeability will only change after

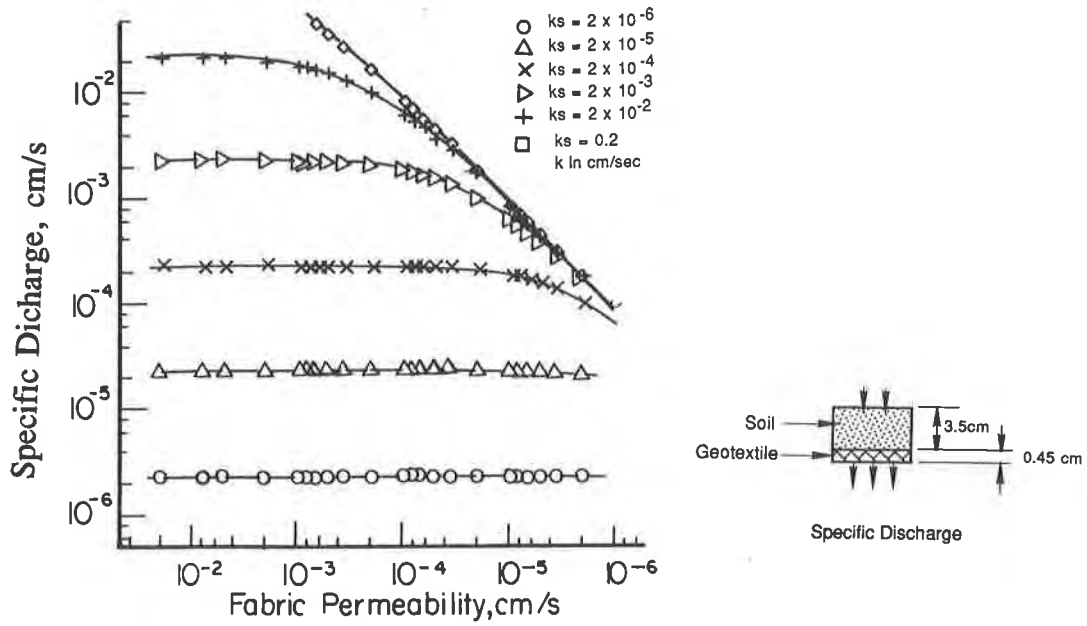

Figure 1: Specific discharge vs. fabric permeability for different soil permeabilities.

a one- to three-order decrease in the geotextile's permeability (K_g); that is, the flow is controlled by the permeability of the soil (Wade *et al.*, 1983).

In the gradient ratio (GR) test, where the hydraulic head at different heights of a soil column above the geotextile is monitored, the GR value can increase only if the permeability of either the fabric or the soil layer directly above the geotextile, or a combination of both, is less than that of the rest of the soil column. This again means that for silts and clays, a two- to three- order decrease in geotextile permeability is required before any excess pore pressure can develop and hence increase the GR value. Oberoi (1992) noticed this phenomena in gradient ratio tests using various gradations of manufactured silts with non-woven (NW) geotextiles; the GR value hardly exceeded 1.4.

Due to the vast difference in the hydraulic properties of fine-grained soils and geotextiles, the performance tests discussed above can only be used to provide qualitative data for silts and clays. As discussed in Wade *et al.* (1983), the LTF test, for example, reflects the behavior of the soil rather than the soil-geotextile conditions. For low permeability soils, these performance tests only provide a means to evaluate the retention capacity of the geotextile with the site-soil under the test conditions; it permits the designer to narrow the choice of geotextiles. If this is the case, a performance test that is easier to perform and does not require long-term monitoring for particulate

clogging is both essential and rewarding, especially with the increasing use of geotextiles with fine grained soils in earth dams, waste containment applications, and agricultural drains.

RESEARCH OBJECTIVES

In this research, a test called the Rapid Retention Test (RRT) was developed to evaluate the retention capacity of geotextiles under severe hydraulic conditions. In this test, the soil was mixed into a slurry at 200% moisture content and poured atop the geotextile. The slurry was continuously stirred to keep the soil particles in suspension and to create turbulence. In addition, the downstream part of the geotextile was kept dry rather than saturated. This condition promoted more soil particle movement through the fabric.

Particulate clogging is the reduction in the fabric permeability due to soil particles being trapped inside the geotextile structure. Such clogging is more applicable or prominent in needle-punched fabrics than thin heat-bonded fabrics. More of this type of clogging can be expected if the size of soil particles are approximately equal to the geotextile pore openings and if the particles are free to move (as in the slurry condition). Hence, the test developed promotes a higher level of particulate clogging. The flow capacities of the fabrics both before and after the RRT were determined using a constant head (3.5 cm) flow test. The ratio of the flow capacity of the virgin fabric to that of the clogged fabric is called the degree of clogging (DC):

$$DC=\frac{Q_{virgin}}{Q_{Clogged}} \qquad (2)$$

In addition LTF tests were performed, and their performance were compared to that under the RRT for similar soil-geotextile combinations.

<u>Significance and use of RRT</u>. The RRT represents the worst-case scenario and can, in general, be applied to all filtration or drainage uses. Specifically, it simulates the following field conditions:

- When the geotextile, for example in an edge drain, is not in good contact with the surrounding soil, the fines from the soil wash and reach the fabric in the form of slurry. This type of gap has been associated with many failures (Giroud, 1982).
- In hydraulically-filled structures, such as tailings dams, the particles are poured in slurry suspension from heights directly on the geotextile (Abadjiev *et al.*, 1990).
- High hydraulic gradients (up to 1000) can develop from concentrated leaks caused by localized cracks in earth dam cores. The cracks can result from differential settlement, construction deficiencies, or hydraulic fracturing; they can also occur at interfaces in a zoned earth dam (Sherard *et al.*, 1984)
- When reversing or non-steady flow conditions exist in the field,

such as in coastal erosion control structures and under highway pavements, the formation of the natural filter cake is impeded (Lafleur *et al.*, 1990). Here the fines move through the fabric in opposing directions numerous times during the life of the structure.

TEST MATERIALS

Geotextiles. Geotextiles from four manufacturers were used in this study. Their relevant properties that influence filtration performance are given in Table 1-a. The opening size of the geotextiles are represented by the apparent opening size (AOS) and filtration opening size (FOS). All geotextiles were non-woven but made with different filament (or fiber) types and bonding processes. Their thicknesses varied from 0.028 to 0.432 cm (or 11 to 170 mils); their masses ranged from 64 to 548 g/m^2 (or 1.9 to 16.2 oz/yd^2).

Table 1-a: Properties of Geotextiles

Geotextile No.	AOS + (mm)	FOS ++ (mm)	Mass (g/m^2)	Thickness (mm)	Flow Capacity* (cm^3/min)	Coeff. of Perm K* (cm/s)	K+ (cm/s)
A1	0.09	0.16	151.9	1.17	909	0.12	0.35
A2	0.038	0.085	202.5	1.22	891	0.13	0.053
A3	0.038	0.064	303.8	1.65	838	0.16	--
B1	0.21	0.193	118.1	1.52	927	0.17	0.31
B2	0.21	0.103	253.2	2.79	906	0.30	0.46
B3	0.125	0.08	455.7	4.32	857	0.43	0.48
C1	0.25	0.15	202.5	2.03	924	0.22	0.4
C2	0.15	0.09	405.1	3.30	897	0.35	0.4
C3	0.1	0.095	546.8	4.06	880	0.42	0.35
D1	0.52	0.2	64.1	0.27	893	0.028	0.07
D2	0.08	0.045	202.5	0.67	468	0.037	0.02

NOTES:
+ From manufacturers' literature.
++ From Powell, J. (1992)
* Measured on geotextile sample with a flow area of 37.93 cm^2 under a constant head difference of 3.75 cm.

Soils. Six different soils were tested. Soils 1 through 5 were natural low-plasticity silts; soil 6 was a commercially manufactured silt made from crushed silica. The particle size distribution and other

properties of the soils are summarized in Table 1-b. The gradation of soils 1 to 5 were obtained using hydrometer analysis; that of soil 6 was obtained by a combination of wet-sieving and hydrometer analyses. The 10% finer size of some the soils required to compute the uniformity coefficient (C_u) and coefficient of curvature (C_c) were beyond the range of the hydrometer method. Therefore, modified ratios, denoted as C_u' and C_c', based on D_{20} rather than D_{10} were computed.

Table 1-b: Properties of Soils

soil No.	LL (%)	PI (%)	soil particle sizes, mm				C_u' (*)	C_c' (+)
			D90	D60	D20	D15		
1	23.8	6.2	0.045	0.015	0.0015		10	0.71
2	NP	NP	0.056	0.031	0.005	0.001	6.2	1.65
3	1.5	4.3	0.041	0.024	0.001		24	4.17
4	28.1	1.2	0.04	0.02	0.0085	0.005	2.4	0.85
5	25.7	8.8	0.035	0.009	0.001		9	0.36
6			0.15	0.05	0.0055	0.0037	9.1	0.44

* $C_u' = D_{60}/D_{20}$
\+ $C_c' = (D_{30})^2/(D_{60}*D_{20})$

Permeant for Long-Term Flow Test. The flow medium for the filtration tests was tap water de-aired to a dissolved oxygen content (DOC) of about 5.5 ppm (under a minimum vacuum of 25 inch Hg). The de-aerator was connected to storage tanks from which water was supplied to the various permeameters. The tanks were not sealed but were open to the atmosphere. Hence, the DOC of the water increased with time. However, the DOC of the water after 24 hr was about 6 ppm, the maximum suggested in related ASTM standards (D 4491, D 5101). For that reason, the stored water was used within 24 hr and replenished with water from a second tank.

APPARATUS

Long-Term Filtration (LTF) Test. The apparatus, shown in figure 2A, was designed such that the soil-fabric system was always saturated. The geotextile, with a flow area diameter of 7 cm, was attached to the bottom of the inner rigid cylinder. Silicone grease was applied to the lower sides of the inner cylinder to minimize local flows between the soil sample and the rigid wall. The outer jacket was filled with the permeant to apply the desired hydraulic head. With this setup, hydraulic heads of up to 35 cm could be applied. The soil sample had a height of 3.5 cm resulting in an applied hydraulic gradient of 10. Any soil that passed through the fabric was retained in the silt-trap. This amount was subsequently determined.

Rapid Retention Test (RRT). The setup of the LTF test without the outer jacket was used in the RRT. In addition, a stirrer with a blade diameter of 2 cm was used to prevent the soil particles from settling on the geotextile. The setup is shown in figure 2B.

The flow capacity of the tested geotextiles was determined using a constant head flow apparatus. The maximum flow capacity of the apparatus itself, i.e. without any geotextile sample, was previously determined to ensure that the apparatus did not compromise or constrict the flow under the test head of 3.5 cm.

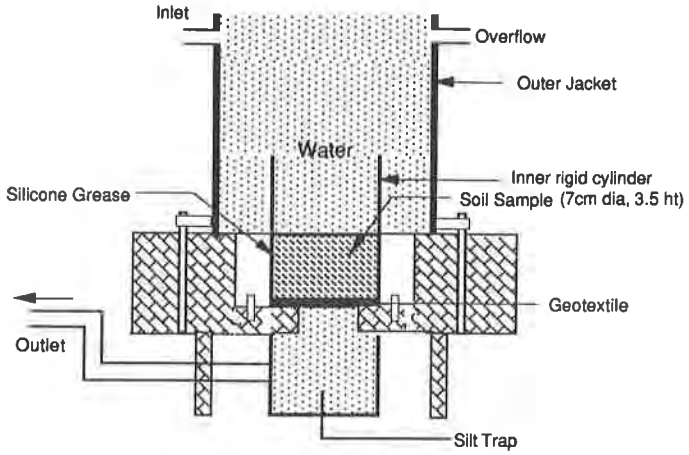

Figure 2A

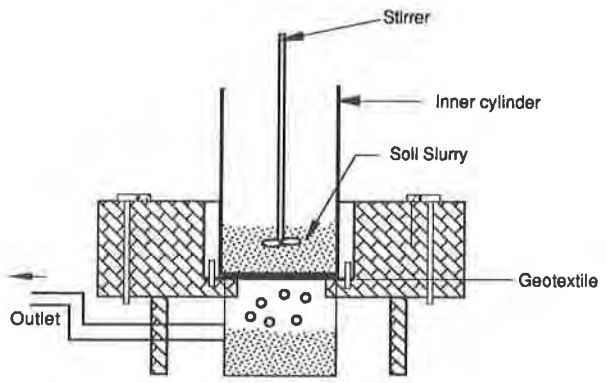

Figure 2B

Figure 2: Schematic diagram of test set-ups for LFT (A) and RRT (B).

TEST PROCEDURE

Long Term Filtration (LTF) Test. For the LTF test, the geotextile was saturated by slowly back-filling the apparatus through the drainage outlet of the silt-trap with the permeant. It was left immersed under a permeant depth of 10 cm by shutting the drainage outlet for a minimum of 1 hr. A small diameter flexible tube was used to siphon air bubbles trapped in the fabric as needed. This was particularly necessary for thick needle-punched fabrics. The soil was mixed separately with just sufficient permeant to form a smooth paste and left to stand for at least 1 hr. (The reason for using this sample preparation method is explained in the discussion section of the paper.) The required soil-permeant ratios (by weight) to get this consistency for the six soils is shown in Table 2.

Table 2: Required Moisture Contents for Slurry-Paste Consistency

SOIL NO.	1	2	3	4	5	6
W_{reg} (%)	38.5	39	45	43	45	30.5

After draining the water from the inner cylinder, the soil paste was poured atop the wet geotextile. Water was filled in the outer jacket carefully to minimize sample disturbance. Observations were made of the clouding of the silt-trap, and flow measurements were taken over time. A minimum interval of 15 min was used to determine the discharge. The

test was continued until the flow was relatively stable, generally between 5 and 20 hr.

Before dismantling the test, a 3 mm diameter hole was punched through the soil sample. This method has been adopted by various researchers (Wade et al., 1983; Sherard et al., 1989) to classify filter performance further; that is, to check if progressive piping or erosion of the hole would occur. The 3 mm hole simulated an open crack in the soil sample. The flow rate was measured until it stabilized.

Rapid Retention Test. For the RRT, the fabric was saturated in a manner similar to that of the LTF test. The soil was mixed separately into a slurry at a water content of between 200 and 250%; about 100 g of air-dried soil was used to make the slurry. Any lumps, especially common with cohesive soils, were broken. The water in the silt-trap was emptied just before the slurry was poured in three increments atop the wet fabric. The soil particles were kept in suspension by a continuously stirring propeller. This was carried out until either all the particles were washed through or until the flow rate was drastically reduced.

The geotextiles' flow capacities both before and after the RRT were determined at a constant head of 3.5 cm. Saturation of the fabrics was ensured by storing them in a moist room and slow back-filling in the constant head permeability apparatus.

RESULTS

Effect of soil sample preparation technique in LTF tests. A series of LTF tests were performed on the various geotextiles and soils using different sample preparation techniques. These included the dry, dry-saturated, slurry-paste, and slurry suspension techniques. In the slurry-paste method, the soil was mixed with just sufficient water to form a smooth-paste. (See Table 2 for required moisture contents.) In the slurry-suspension method, the soil was mixed to a water content of about 200%. In these two methods, flow measurements were taken as soon as the sample was poured and the hydraulic head was applied. In the dry-saturated method, the air-dry soil was placed atop the fabric and was back-saturated overnight before the test was begun. In the dry method, the air-dry sample was again placed atop the fabric, and the test was started by applying the head with no saturation. Figure 3 shows the specific discharge (or flow rate per unit area) over time for geotextile C2 and soil 1 using the different soil sample preparation methods.

Figure 3 shows that the reduction in the specific discharge is highest when flow is initiated on a dry sample and is least for slurry-paste samples. As discussed earlier, the effective flow of a silt-geotextile system is controlled primarily by the permeability of the soil. In the dry method, the soil sample was initially in a very loose condition compared to, for example, the slurry-paste method. Hence, the

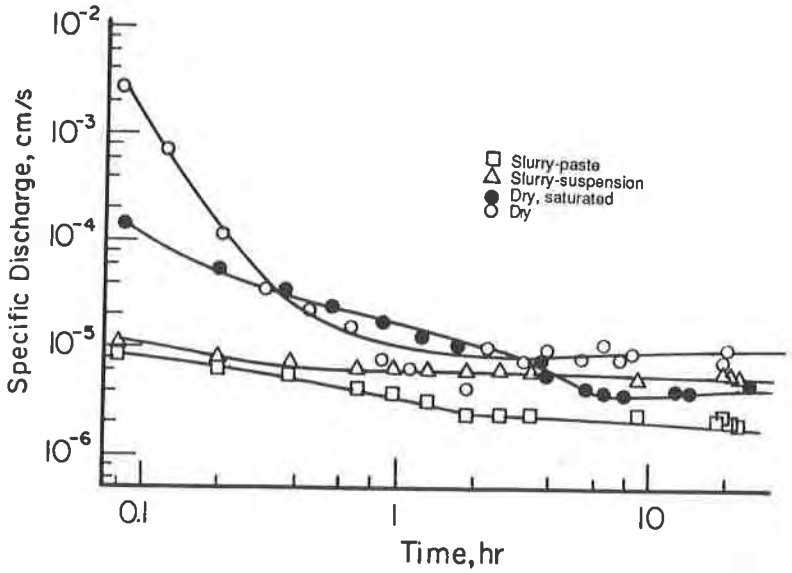

Figure 3: Effects of soil sample preparation techniques

reduction in the flow curve of silt-geotextile systems is due to soil compression and does not necessarily mean particulate clogging of the fabric. At the same time, large air bubbles were observed being displaced from the soil sample (phenomena called boiling) initially. The amount of soil passing through was highest using this method. The passage of soil particles, however, stopped after a few hours from the start of the test. The slurry-suspension method gave the next higher amount of soil piped, followed by the dry-saturated method. No measurable amount of fines passed in the slurry-paste method.

The variation in the amount of piped soil observed is because the particles of dry soil are freer to move than particles of wet soil such as in the slurry paste consistency. This was shown by the difference between the amount of soil passing through the fabric: 1767 g/m^2 for the dry method and 134 g/m^2 for the dry-saturated method. After after some initial soil particle movement and if the geotextile is compatible with the soil, a filter cake will form; otherwise, the piping will continue. In the slurry-suspension method, the slurry is segregated as the coarser soil particles settle on the geotextile before the fines. The coarse particles lead to bridging and are able to retain more of the fines. This is evidenced by the amount of soil piped when using this method: 633 g/m^2.

The slurry-paste method was used in the remainder of the LTF tests because it formed more homogeneous samples (Bhatia *et al*. 1990). It, therefore, displayed better reproducibility and had the least reduction in flow due to sample compression.

Long Term Flow Test. Figures 4A and 4B show typical data for four soils (2, 4, 5 and 6) with two different geotextiles (A1 and B2). An insignificant amount of soil passed through the geotextile in each of these tests. The specific discharge through systems involving soils 2, 4, and 5 was constant with time. This does not necessarily imply that the permeability of the geotextiles was constant. Figures 5A and 5B

show the final specific discharges for soils 2 and 4 with all the geotextiles. These show that the final flow or permeability is not influenced by the type of geotextile but rather by the soil.

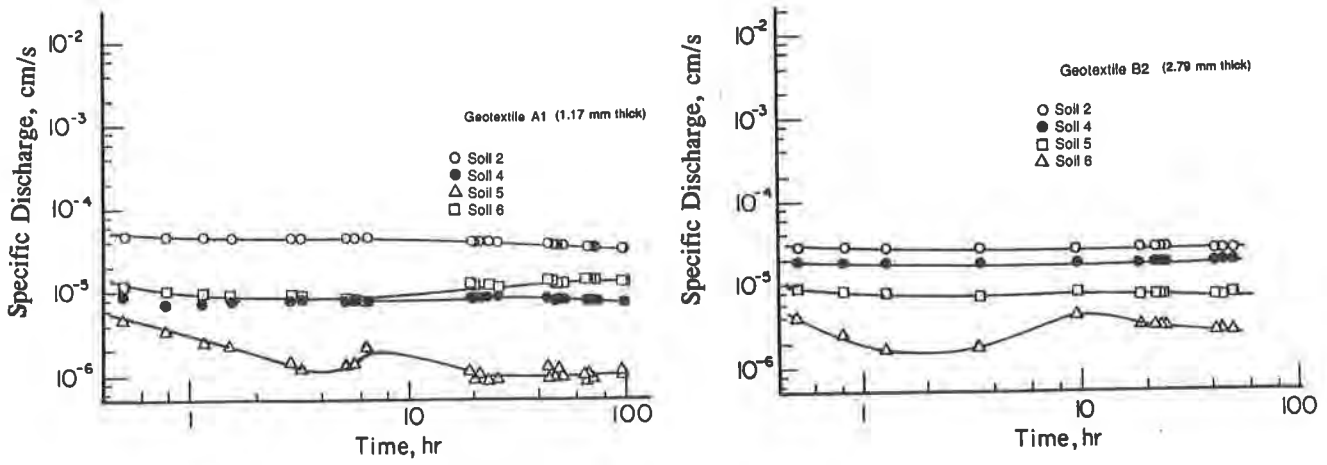

Figure 4: Specific discharge vs Time for geotextiles A1 and B2 in LTF test.

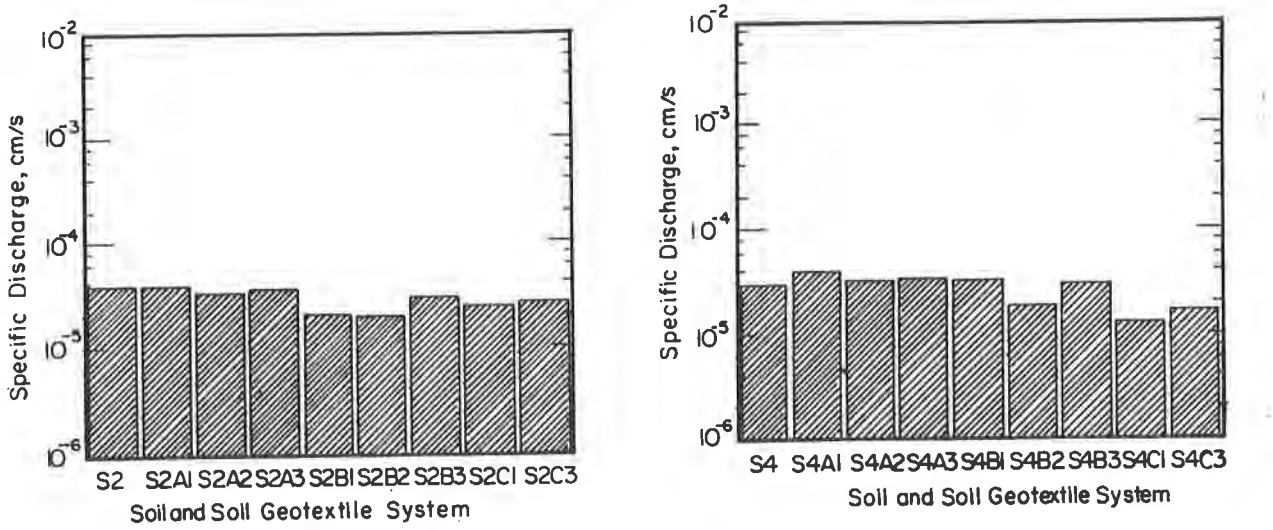

Figure 5: Final specific discharge of Soil 2 and 4 with the different Geotextiles in LTF test.

As can be seen from Figure 1, the geotextile permeability must reduce by two orders of magnitude before any change is detected on the overall system permeability measured in the LTF test. Hence, the soil governs the final permeability of silt-geotextile systems. Soil 5, which is the

most cohesive of the soils tested, showed an initial decrease followed by an increase before stabilizing. The initial reduction was probably due to consolidation or settlement of the soil sample. This behavior was not observed in the other three silty soils because they had settled faster, before flow measurements were started. Flow measurements were usually started after 20 min of sample had poured into the LTF apparatus. The ensuing increase in flow was usually a prelude to a piping failure; piping failure is defined as when a significant amount of the soil passes through the geotextile. Lafleur et al. (1991) set a margin between stable and unstable systems as being when the soil passing through is 2500 g/m^2. In all geotextile and soil systems tested (66 systems) in this study, the amount of fines passing never exceeded 2500 g/m^3; therefore, stable systems were established in all cases.

When a 3 mm hole was punched through the soil sample, some soil passed through the fabric, and the flow increased in all the systems. However, the holes did not continue to erode and, in a short time, the bases of the holes were sealed. Also, the flow stabilized within a few hours of the hole's creation. Thus, it can be concluded that the LTF test flow curve was governed by the soil; the influence of the geotextile was not reflected on the system behavior; and, in all the tested systems, a stable filter was established.

Rapid Retention Test. The amount of soil passing through all of the geotextiles was found to be at least 50% of the original weight in the RRT. In some cases, the soil passing was as much as 90%. Figure 6 shows the plots of the degrees of clogging (defined as $DC=Q_{virgin}/Q_{clogged}$) versus the FOS/D_{85} for the different geotextile types. This figure shows that at some value of the geotextile opening/particle size ratio, more particles were trapped in the geotextile and thereby reduced the final flow capacity of the geotextiles.

The four geotextile types showed similar retention behavior. However, there appeared to be differences in the degree of clogging. When the ratio FOS/D_{85} was less than 1, much tighter fabric relative to the soil, less soil passed through and, hence, fewer particles could become trapped in the geotextile. This led to less reduction in the flow capacity of the fabric. When the same ratio was greater than 2 to 4 (very open fabric relative to soil), most of the soil passed through and did not get trapped inside the geotextile.

The difference in the degree of clogging of the four fabric types was due to the micro-structure of the fabrics. This is shown by the micro-graphs of similar geotextiles used in long-term flow tests in Bhatia *et al.* (1990) and Bhatia *et al.* (1991). The micrographs showed that needle-punched (NP) fabrics, such as types A, B, and C, contain large voids inside them. However, there are differences in the micro-structures of the three NP fabrics. Type A is made from short fibers and has a tight pore structure. Types B and C are made of continuous

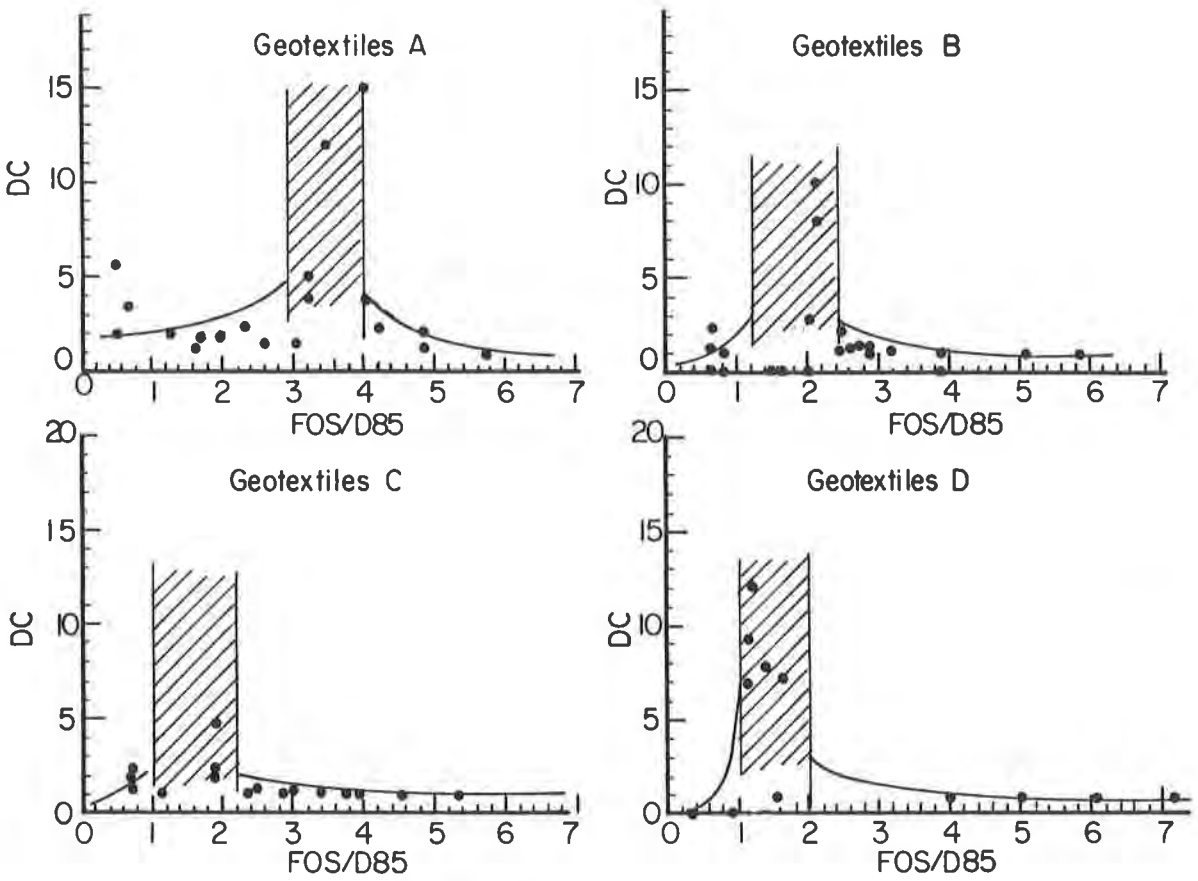

Figure 6: Degree Clogging vs. FOS/D_{85} for Various Geotextiles in Rapid Retention Test.

filaments, and their pore structure has more voids. The trapped soil particles in the NP fabrics do not entirely fill these spaces. The flow rate reduction seemed to occur especially at FOS/D_{85} values between 2.5 and 4.0 for type A, between 1.5 and 2.5 for type B, and between 1 and 2.5 for type C geotextiles. On the other hand, type D geotextile is heat bonded (HB) and is thin with fewer openings. Its flow capacity, therefore, could be reduced by blocking (soil particles lying atop these openings). The reduction in the flow rate appeared to be predominant at FOS/D_{85} values between 1.0 and 2.0 for HB fabrics.

DISCUSSION

The selection of a geotextile for use with any type of soil is based on two compromising criteria: permeability and retention. The permeability criterion requires the fabric to have a long-term permeability, higher than that of the protected soil by some composite factor. This factor should account for geotextile compression (for example, in deep drainage systems), particulate clogging, and chemical and biological clogging. For the geotextiles tested in this study, the flow rate (hence the permeability) due to particulate clogging was reduced by a maximum factor of 15; that is an order of magnitude. This is typical of what has been observed from field data by other

researchers. Mlynarek *et al.* (1990) found this reduction factor not to exceed two for non-woven (NW) geotextiles after 8 years of installation in small earth dams; Saathoff *et al.* (1988) determined the reduction in the permeability of NW geotextiles to range from 2 to 70 after several years of installation in coastal structures; Lafleur *et al.* (1990) found that this factor did not exceed 12 from dynamic consolidation tests between NW geotextile and fine grained soils.

Supplemented by the data from this study, the following conclusions can be made. There will always (inevitably) be a small amount of soil particles trapped within the geotextile structure. This occurs as a result of the soil particles being approximately the same size as the geotextile openings. The reduction in the geotextile's permeability as a result of this phenomena - particulate clogging - is not of serious concern, as the permeability of the fabrics are at least two orders of magnitude higher than that of fine grained soils.

The retention criterion is to ensure that the opening sizes of the fabric are not so large such that a significant portion of the retained soil can pass through the geotextile. On initial hydraulic interaction, a nominal amount of fines can be expected to pass through the geotextile; they would be the soil particles that are smaller than the geotextile's openings. However, this should cease with the formation of a filter cake if the geotextile is compatible with the soil under the test conditions. The prevailing field conditions include the initial soil moisture (for example dry, optimum moisture, or slurry form), soil condition (dense or compacted), hydraulic conditions (reversing or uni-directional, and the highest hydraulic gradient that can occur). In this study, in the long-term flow test results, the maximum amount of soil passing (or piping) through any of the geotextiles tested was within the limits set by Lafleur et al. (1991) of 2500 g/m^2, or equivalent of 9.5 g (or 4.7 %). When the test conditions are made more rigorous, however, as in the RRT, as much as 60 to 80% of the soil washed through the fabrics. Hence, any performance test must reflect the field conditions as closely as possible.

The performance test selected must be able to monitor the whole filtration process. This is especially important when testing silts and clays. The final flow or permeability of the soil geotextile system in the LTF test is governed by the soil as the effect of the large geotextile permeability is governed by the low soil permeability.

CONCLUSION

Any performance test conducted to evaluate the filtration performance of the selected geotextiles with the *in situ* soil must reflect the prevalent field conditions. This research has highlight the importance of the soil sample preparation technique used in the long term flow (LTF) test. This study has also shown that under the LTF test conditions, the selected soils can be retained by the eleven geotextiles that were tested. When the hydraulic conditions are made more rigorous, however, as in the rapid retention test (RRT) developed, at least 60% of the soil passes through the geotextiles. This is an unacceptable

percentage of soil passing. Thus, any performance must reflect the conditions acting in the *in situ* soil. Also, if other forms of clogging are expected because of the field conditions, for example in landfills, typical leachates should be used to conduct performance tests.

In addition, the tests must also predict the soil-geotextile interaction. This is particularly of issue with low permeability soils, such as silts and clays, where the permeability of the geotextile is not easily reflected on the resulting flow curve.

The rapid retention test determined the retention capacity and the extent of clogging of the various geotextiles with the six silts that were examined. The test represented severe field conditions. This test is simple and fast to perform. The following specific conclusions can be drawn:

- For retention under severe conditions, the FOS/D_{85} of the system should as low as possible. Any retention criteria followed in design should reflect the *in situ* hydraulic conditions.
- The maximum reduction in the fabric permeability due to particulate clogging was a factor of 15.
- The rapid retention test developed can be used as a quick test to estimate the soil retention capacity of a geotextile in worst hydraulic conditions.
- If other performance tests, for example the LTF or GR or HCR tests, are conducted on silts, they should be complemented by determining the degree of clogging of the geotextiles.

ACKNOWLEDGMENTS

Research support from the National Science Foundation is gratefully acknowledged. We also wish to thank Mr. Bob Bellandi of O'Brien & Gere Engineers for proofreading the text, and Ms. Jennifer Powell for determining the FOS value of the geotextiles.

REFERENCES

Abadjiev, C.B., and Kaltchev, I.S., (1990) "Investigation of geotextiles as filter in hydraulic fill tailings dams", 4th International Conference on Geotextiles, Geomembranes and Related Products, The Hague, Netherlands, pp. 307-310.

Bertacchi, P., and Cazzuffi, D., (1985) "Geotextile filters for embankment dams", Water Power & Dam Construction, Vol. 37, pp. 11-18.

Bhatia, S.K., Mlynarek, J., Rollin, A.L., and Lafleur, J., (1991) "Effect of pore structure of non-woven geotextiles on their clogging behavior", Geosynthetics '91 Proceedings, Atlanta, USA, pp. 629-642.

Bhatia, S.K., Qureshi, S., and Kogler, R.M., (1990) "Long-Term clogging

behavior of non-woven geotextiles with silty and gap-graded sands", Geosynthetic Testing for Waste Containment Applications, ASTM STP 1081, Edited by Koerner, R.M., ASTM, Philadelphia, pp. 285-298.

Cancelli, A., and Cazzuffi, D., (1987) "Permittivity of geotextiles in presence of water and pollutant fluids", Geosynthetic '87 Proceedings, New Orleans, USA, pp. 471-481.

Craig, R.F., (1987) "Soil Mechanics", 4th Edition, Van Nostrand Reinhold (UK) Co. Ltd., Berkshire, United Kingdom, pp. 36.

Giroud, J.P., (1982) "Filter criteria for geotextiles", Proc. 2nd International Conference on Geotextiles, Las Vegas, USA, pp. 36-38; 103-108.

Kellner, L., and Matei, S., (1991) "Criteria for geotextile filters in clayey soils", Geotextiles and Geomembranes, Vol. 10, pp. 79-88.

Koerner, R.M., and Koerner, M.K., (1990) "Biological activity and potential remediation involving geotextiles landfill leachate filters", Geosynthetic Testing for Waste Containment Applications, ASTM STP 1081, Edited by R.M. Koerner, ASTM, Philadelphia, pp. 313-334.

Koerner, R.M., and Sankey, J.E., (1982) "Transmissivity of geotextiles and geotextile/soil systems", Proc. 2nd International Conference on Geotextiles, Las Vegas, USA, pp. 173-176.

Lafleur, J., and Jacques, P.J., (1991) "Use of geotextiles in the James Bay Hydroelectric Project", Geotextiles and Geomembranes, Vol. 10, pp. 35-52.

Lafleur, J., and Mlynarek, J., (1991) "Filtration of broadly graded cohesionless soils", A.S.C.E. Journal of Geotechnical Engineering, Vol , pp. .

Lafleur, J., Mlynarek, J., and Rollin, A.L., (1990) "Clogging of geotextiles under pumping loads", 4th International Conference on Geotextiles, Geomembranes and Related Products, The Hague, Netherlands, pp. 189-192.

Mlynarek, J., Lafleur,J., and Lewandowski, J.B., (1990) "Field study on long term geotextile filter performance", 4th International Conference on Geotextiles, Geomembranes and Related Products, The Hague, Netherlands, pp. 259-262.

Oberoi, V., (1992) "Filtration studies of geotextile-silt systems using the gradient radio test", Masters degree thesis, Syracuse University, Syracuse, NY.

Powell, J. (1992), "Opening sizes of geotextiles", Masters degree thesis (in preparation) Syracuse University, Syracuse, NY.

Rios, N. and Gealt, M.A., (1989) "Biological growth in landfill leachate collection systems", Durability and Aging of Geosynthetics, Edited by

R.M. Koerner, Elseivier Applied Science Publishers, pp. 244-259.

Rollin, A.L., Mlynarek, J., and Bolduc, G., (1990) "Study of significance of physical and hydraulic properties of geotextiles used as envelopes in subsurface drainage systems", 4th International Conference on Geotextiles, Geomembranes and Related Products, The Hague, Netherlands, pp ???

Sasone, L.J. and Koerner, R.M., (1991) "Fine fraction filtration test to assess geotextile filter performance", Proc. 5th GRI Seminar on Geosynthetics in Filtration, Drainage and Erosion Control, pp. 34-56.

Saathoff, F., (1988) "Examinations of long-term filtering behaviour of geotextiles", Durability of Geotextiles, RILEM, pp. 86-114.

Sherard, J.L., Dunnigan, L.P., and Talbot, J.R., (1984) "Filters for silts and clays", Journal of Geotechnical Engineering, Vol. 110, No. 6, pp. 701-718.

Sherard, J.L., and Dunnigan, L.P., (1989) "Critical filters for impervious soils", Journal of Geotechnical Engineering, Vol. 115, No. 7, pp. 927-947.

Wade, G.T., Klaiber, F.W., and Lohnes, R.A., (1983) "Permeability tests of selected filter fabrics for use with a loess-derived alluvium", TRR 916, Engineering Fabrics in Transportation Construction, Washington, DC, pp. 40-46.

Williams, N.D., and Abouzakhm, M.A., (1989) "Evaluation of geotextile/soil filtration characteristics using the hydraulic conductivity ratio analysis", Geotextiles and Geomembranes, Vol. 8, pp. 1-26.

Correlation Between Long-Term Flow Testing and Current Geotextile Filtration Design Practice

M.H. Wayne
Polyfelt Inc., USA

R.M. Koerner
Geosynthetic Research Institute, Drexel University, USA

ABSTRACT

The use of geotextiles as filters in subsurface drainage applications represents a significant cost savings over traditional granular graded systems. As a result, many geotextiles are chosen on the basis of cost and availability rather than current design methodology.

While geotextiles often serve as adequate filters for inadequately designed subsurface drainage systems which are installed in well graded cohesionless and medium to highly plastic clayey soils, they must be properly designed when placed in gap graded soils containing silt and dispersive clays. For these conditions current design principles stipulate that the designer check the suitability of a given geotextile by conducting a performance based test in addition to use of information from index based tests. Since many designers do not have the time nor the resources to conduct these tests, they often rely solely on the results of index tests. In many cases, this situation has often resulted in the installation of a geotextile which should not have been chosen for the intended application.

This paper presents the results of long term flow testing conducted on four different geotextiles (a heat bonded nonwoven, two different needle-punched nonwovens, and a woven monofilament) and three unique overlying soil conditions. A test apparatus was developed to permit easy evaluation of flow rates at hydraulic gradients of 0.5, 1.0 and 1.5 for a period of up to 5,000 hours. A series of control samples were included in the study to establish baseline flow rates, and both clear and turbid water were used as permeants. At the completion of testing, soil which passed through the soil/geotextile systems was collected and a grain size analysis was performed to determine the retention performance of geotextiles used in the study. In addition, index tests were performed on the geotextiles.

Results of this work are reviewed in conjunction with current design principles along with possible correlation between performance testing, index testing and current design principles.

INTRODUCTION

Since there are numerous papers which have been written on the topic of filtration, the history and subsequent development of these criteria will not be elaborated upon in this paper. Those interested in learning more about these topics should review the works of Koerner (1990) and Christopher and

Holtz (1985), papers written by Christopher and Fischer (1990) and Fischer, Christopher, and Holtz (1990), and a detailed dissertation by Hwu (1990). This literature provides a detailed background on the development of design criteria for the use of geotextiles as filters. After a review of this literature it appears as though there are five fundamental criteria that must be properly evaluated during the design of these systems. These criteria are as follows:

1. Soil Retention - prevent the migration of excessive soil particles through the soil-geotextile system.
2. Permeability - pore water must be able to freely pass through the soil-geotextile system.
3. Blinding and clogging resistance - pore water must pass both immediately after installation and throughout the life of the soil-geotextile system.
4. Construction survivability - the geotextile must survive the installation process without having holes or undue loss of strength.

Although items 1, 2, and 4 are continually elaborated upon in the literature , item 3 is controlled by the internal soil stability. Ultimately, fine grained soils must be evaluated for their ability to migrate toward the soil-geotextile interface. When the geotextile is designed to retain these fine particles it will act as a true filter and the soil-geotextile permeability will reduce to that of the fine grained soil alone. It is unfortunate that although there are numerous papers which discuss the potential problems associated with the use of geotextiles as filters for soils where internal soil stability may result in blinding or clogging, Giroud (1982), many designers are unwilling to have performance testing conducted on candidate geotextiles. This may be due mainly to a greater reliance on the use of easily attainable equations for the design of systems which incorporate man made materials, such as steel and concrete. This often leads to a situation in which a design is based on readily available retention, permeability, and clogging resistance criteria. Many users of these equations fail to recognize the fact that these equations rely on the accuracy of the results obtained through the use of index tests, namely apparent opening size (AOS) , ASTM D 4751-87, and permittivity testing , ASTM D 4491-89 for water permeability requirements . This promotes an unwillingness among designers to conduct performance based tests to serve as the final prequalifier for candidate geotextiles which have been found to satisfy the design requirements. Because of this situation, there is not a sufficient database from which a more thorough analysis can be developed for the case of geotextile usage in varying soil strata which may contain problematic soils, as is often the case for large projects (e.g. geotextiles used in highway edge drains.). Although geotextiles have been successfully used in such applications, there are many instances where geotextiles were found to be inadequate after construction. Sometimes the problem was verified through the use of supplemental performance tests which could have been used to prequalify candidate geotextiles. Currently, there are several performance tests which can be included as part of the prequalification process and include; 1) long term flow test, 2) gradient ratio test, 3) hydraulic conductivity ratio (HCR), 4) dynamic filtration test, and 5) fine fraction filtration test

Before considering which of these tests, or combination of tests, should be

performed, the designer needs to consider the flow regime and soil conditions within which the geotextile is to be placed. With regard to flow regime, one needs to choose either steady-state fully saturated, or dynamic (reversing flow) state fully saturated flow. And although this study focuses on the steady- state fully saturated flow condition, the dynamic filtration test can be used for the latter case . Those interested in dynamic filtration should refer to the paper written by Narejo and Koerner (1991). With regard to soil conditions, gap graded cohesionless soils containing silts and dispersive clays have been found to result in either blinding or clogging when a tight geotextile is used as a filter, and piping when the geotextile is too open. Therefore, a gap graded soil was manufactured for this study to evaluate the usefulness of the long term flow test. Although the gradient ratio test, ASTM D 5101-90, and/or HCR test, as presented by Luettich and Williams (1989), could be used to evaluate the clogging potential of soil-geotextile systems, the author's feel that the long term flow test, proposed by Koerner and Ko (1982), and further defined in the Geosynthetic Research Institute standard GRI-GT1(1987), is the preferred true indicator of long term system performance. For a short term determination of clogging potential investigators at the Geosynthetic Research Institute, see Sansone and Koerner (1991), are currently evaluating the usefulness of the fine fraction filtration test which is based on the work of Hoover (1982) and Legge (1990). At this point in time there is not a sufficient database of information to prove whether this test can predict the long term clogging resistance of a given soil-geotextile system.

Because many believe that extensive time is needed to conduct long term flow testing, some designers believe that this form of testing is only of use in research. It is hoped that this paper will lead to a change in attitude. In contrast to the other performance tests, the main thrust of this test is to determine whether or not the soil-geotextile system will reach equilibrium, and given that it does reach equilibrium one can then determine the equilibrium flow rate. This value can then be used in the final design. If the system does not come to equilibrium, then one of two situations will occur. Either the flow will increase with time, indicating soil piping and inadequate retention, or the flow will continue to decrease with time, indicating either blinding (finer soil particles through mass migration are retained in a layer which forms immediately upstream of the geotextile) or clogging (fine particles get trapped within the geotextile structure). In fact, the current gradient ratio test standard as published by the American Society for Testing and Materials (ASTM), and designated D 5101-90, can be modified to meet the objectives of the long term flow test by requiring the reporting of flow rate versus time to establish the fact that equilibrium flow has been achieved at the end of testing.

This paper presents the results of long term flow testing conducted on four different geotextiles (a heat bonded nonwoven, a polypropylene based needle-punched nonwoven, a polyester based needle-punched nonwoven and a woven monofilament) and four unique overlying soil conditions. A test apparatus was developed to permit easy evaluation of flow rates at hydraulic gradients of 0.5, 1.0 and 1.5 for a period of up to 5,000 hours. A series of control samples were included in the study to establish baseline flow rates, and both clear and turbid water were used as permeants. At the completion of testing, soil which passed through the soil/geotextile systems was collected and a grain size analysis was performed to determine the retention performance of

geotextiles used in the study. In addition, index tests were performed on geotextiles. Results of this work are reviewed in conjunction with current design principles along with possible correlation between performance testing, index testing and current design principles.

GEOTEXTILES USED IN THIS STUDY

To insure that testing was representative, four geotextiles were chosen on the basis that they were representative of the various manufacturing processes by which these materials are currently produced and marketed for the function of filtration .The four geotextiles selected for the long term filtration testing included; monofilament woven, light weight continuous filament needle punched nonwoven, continuous filament heat bonded nonwoven, and a continuous filament heavy weight needle punched nonwoven. The polymer composition of the former three geotextiles consisted of polypropylene and the remaining geotextile consisted of polyester. For convenience each of the four geotextiles was assigned an appropriate designation which is presented in Table 1. The Index properties associated with each of the four geotextiles are found in Table 2. These include physical properties, and hydraulic index properties. The physical properties of mass per unit area and thickness were determined using ASTM D 3776, and ASTM D 1777 respectively. The hydraulic index properties of permittivity, apparent opening size, both AOS and O_{95} are reported, and the average circular-capillary-equivalent pore diameter , designated as O_{50}, were determined using ASTM D4491, ASTM D 4751, and F 902-84 respectively. Although a majority of these tests are well recognized in geosynthetic engineering, the latter of the hydraulic index tests, namely the determination of O_{50} , will be unfamiliar to most. The development of this test method is based on the work performed by Johnston (1983) and further supported through testing performed by Johnston (1985). For geotextiles the equation used to determine this value is as follows:

$$O_{50} = \sqrt{\frac{32 Q \eta z T}{\Delta P \varepsilon A}} \qquad (1)$$

where:

ΔP = pressure drop across the geotextile, N/m^2
z = geotextile thickness, m
η = viscosity of the fluid, N s/ m^2 (a value of 10^{-3} was used for water)
ε = the porosity of the geotextile, which can be calculated through use of equation (2) or via liquid flooding measurement,

$$\varepsilon = 1 - \left[\frac{\text{mass per unit area}}{\text{polymer density x geotextile thickness}} \right] \qquad (2)$$

Where the polymer density is equal to the unit weight of water times the specific gravity of the polymer. For polypropylene a specific gravity of 0.90, and for polyester a value of 1.38 were used in calculating the polymer densities for geotextiles used in this study.

T = the tortuosity factor, a value greater than or equal to 1.0, so that zT equals the average length of a pore defined by fluid flow. Johnston (1983) has found, through the use of probability calculations, that for the case of solvent-cast membranes, or media composed of a random array of fibers or particles that T is equal to $1/\varepsilon$. For woven media, in which the pores are defined by the spaces between the individual fibers, the value of T lies between 1.0 and $1/\varepsilon$, depending on the medium.

Estimated values used for each geotextile are found in Table 3. The authors feel that this determination may ultimately contribute to future design of filter systems in which this value is required. In fact, Fischer , Christopher, and Holtz (1990) have included this value as part of their retention and clogging criteria. As such, its usefulness in evaluating the retention and clogging resistance of the soil-geotextile systems used in this study is explored in the design correlation section of this paper.

Table 1. Designation Assignment

Geotextile	Designation
7 oz/yd^2 heavy weight needle punched nonwoven polyester	NW-NP-PET-H
4 oz/yd^2 heat bonded nonwoven polypropylene	NW-HB-PP
5.7 oz/yd^2 woven monofilament polypropylene	W-MF-PP
4.5 oz/yd^2 light weight needle punched nonwoven polypropylene	NW-NP-PP-L

Table 2. Geotextile Property Values

Geotextile Designation	mass per unit area g/m^2 (oz/yd^2)	Thickness mm (mil)	Permittivity sec^{-1}	AOS O_{95} (mm) (U.S. std. sieve)	O_{50} (mm)
NW-NP-PET-H	249 (7.4)	2.7 (105)	1.8	0.125 (120)	0.0281
NW-HB-PP	128 (3.8)	0.76 (30)	2.5	0.090 (170)	0.0322
W-MF-PP	193 (5.7)	0.36 (14)	.64	0.212 (70)	0.0545
NW-NP-PP-L	158 (4.7)	1.7(68)	2.9	0.125 (120)	0.0291

Table 3 - Values used to determine O_{50}

Geotextile Designation	Q (m^3/sec)	Thickness mm (mil)	ε	T
NW-NP-PET-H	7.6 x 10^{-5}	2.7 (105)	.932	$1/\varepsilon$
NW-HB-PP	1.11x10^{-4}	.76 (30)	.812	$1/\varepsilon$
W-MF-PP	3.0 x10^{-5}	.36 (14)	.403	1.75
NW-NP-PP-L	1.02 x 10^{-4}	1.7(68)	.898	$1/\varepsilon$

SOILS USED IN THIS STUDY

As was stated in the introduction, to illustrate the benefit of using the long term flow test to determine soil-geotextile system performance two gap graded soils were manufactured for this study. These included a 5% silt - 95% ottawa sand, and a 25% silt - 75% ottawa sand mixture. In addition, soil-geotextile systems were constructed with silt and ottawa sand alone. The appropriate grain size values are found in Table 4.

Table 4. Soil Test Values

Soil Type	d_{85} (mm)	d_{60}(mm)	d_{50} (mm)	C_u	d_{15} (mm)	d_{10}(mm)
5% - 95% silty sand	1.0	0.69	0.62	1.7	0.45	0.40
25%- 75% silty sand	1.0	0.54	0.46	24.5	0.04	0.02
Ottawa Sand	1.0	0.80	0.75	1.3	0.65	0.62
Silt	0.05	0.04	0.03	3.2	0.02	0.01

Experimental Setup

This portion of laboratory testing involved evaluation of the fully saturated flow behavior exhibited by four different geotextiles, and geotextile/soil systems as evaluated for periods up to 5000 hours. Permeants chosen for this work included both clear water and turbid water, consisting of 3 grams of silt per liter of water, that had been deaired prior to use. The laboratory test setup used for the clear permeant study is depicted in Figure 1. The test setup used for the turbid water permeant study is similar to Figure 1, with the inclusion of a special turbid water storage tank in place of the clear water storage tank shown. A mechanical stirrer was included within the turbid water tank to keep the fines in suspension throughout testing.

Twenty of the thirty two columns were devoted to clear water flow , while the remaining columns were utilized to establish the influence of turbid water flow on the filtration response. Table 5 lists the cross sections associated with each of the columns tested with clear deaired water. Table 6 lists the cross sections associated with each of the columns through which turbid water served as the permeant. The test columns found in Tables 5 and 6 which are listed as "geotextile alone" were included in the study for two reasons. Firstly, inclusion of this information serves to establish the baseline flow through the geotextiles under the influence of both clear and turbid water. Secondly, this information was used throughout the study to adjust water additives to alleviate possible biological growth problems.

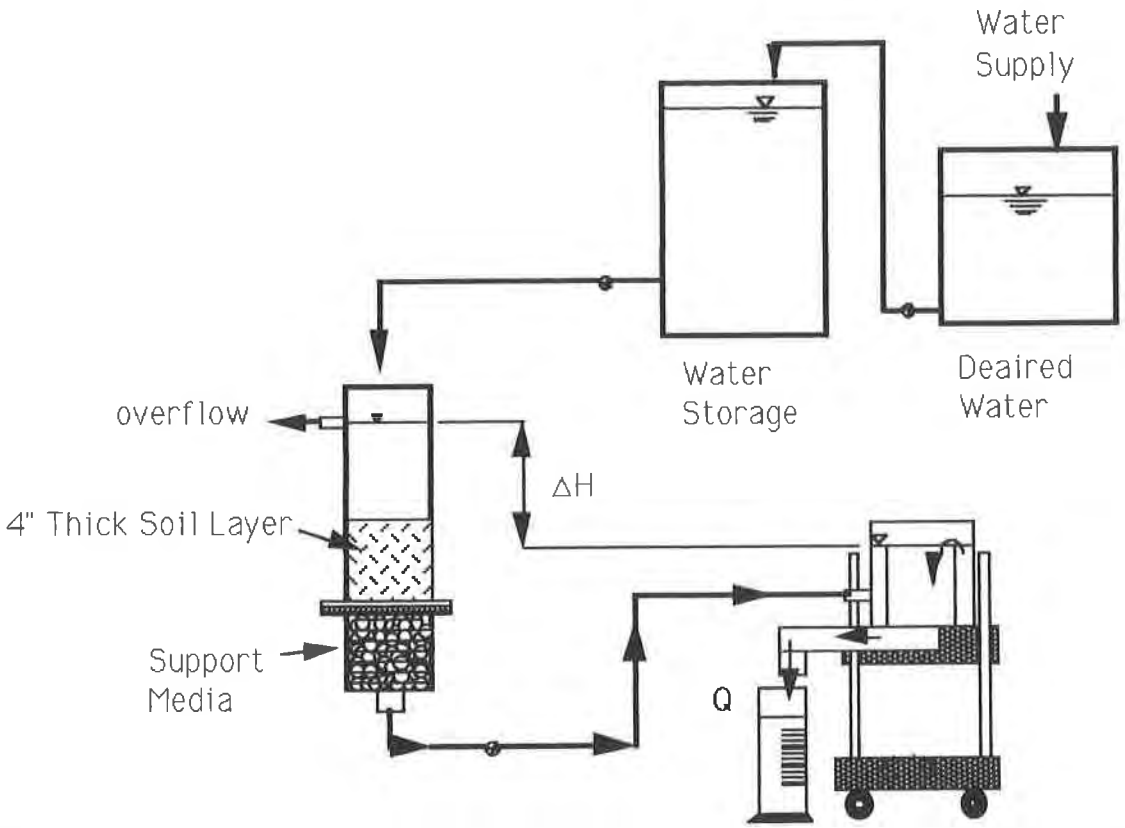

Figure 1 - LTF Clear Water Setup

Table 5 - Details of LTF Tests Conducted with Clear Water Permeant

Designation	Column No.	Test Conditions
NW-NP-PET-H	1	GT/100% Ottawa Sand
	2	GT Alone
	3	GT/Mixture (75-sand/25-silt)
	4	GT/100% Silt
	19	GT/Mixture (95-sand/5-silt)
NW-HB-PP	5	GT/100% Ottawa Sand
	6	GT Alone
	7	GT/Mixture (75-sand/25-silt)
	8	GT/100% Silt
	23	GT/Mixture (95-sand/5-silt)
W-MF-PP	9	GT/100% Ottawa Sand
	10	GT Alone
	11	GT/Mixture (75-sand/25-silt)
	12	GT/100% Silt
	27	GT/Mixture (95-sand/5-silt)
NW-NP-PP-L	13	GT/100% Ottawa Sand
	14	GT Alone
	15	GT/Mixture (75-sand/25-silt)
	16	GT/100% Silt
	31	GT/Mixture (95-sand/5-silt)

Table 6. Details of LTF Tests Conducted with Turbid Water

Designation	Column No.	Test Conditions
NW-NP-PET-H	17	GT/100% Ottawa Sand
	18	GT Alone
	20	GT/Mixture (95-sand/5-silt)
NW-HB-PP	21	GT/100% Ottawa Sand
	22	GT Alone
	24	GT/Mixture (95-sand/5-silt)
W-MF-PP	25	GT/100% Ottawa Sand
	26	GT Alone
	28	GT/Mixture (95-sand/5-silt)
NW-NP-PP-L	29	GT/100% Ottawa Sand
	30	GT Alone
	32	GT/Mixture (95-sand/5-silt)

LONG TERM FLOW DATA

Up to 5000 hours of testing has been conducted using the test setup depicted in Figure 1, and with the overlying conditions listed in Tables 5 and 6. Although the hydraulic gradient was evaluated from 0.5 to 1.5, for the analysis presented in this paper, all of the data was evaluated for a hydraulic gradient of 1. Figures 2 and 3 illustrate the flow rate versus time for clear water and turbid water soil-geotextile systems respectively, involving use of a NW-NP-PET-H geotextile filter. Figures 4 and 5 illustrate the flow rate versus time for clear water and turbid water soil-geotextile systems respectively, involving use of a NW-HB-PP geotextile filter. Figures 6 and 7 illustrate the flow rate versus time for clear water and turbid water soil-geotextile systems respectively, involving use of a W-MF-PP geotextile filter. Figures 8 and 9 illustrate the flow rate versus time for clear water and turbid water soil-geotextile systems respectively, involving use of a NW-NP-PP-L geotextile filter. For the turbid water permeant columns only the sand and 5/95 silty sand are shown since flow rates were too low to show on the same scale for the 25/75 silty sand and the 100% silt.

ANALYSIS OF LONG TERM FLOW DATA

Summary for Clear Water Flow. With the exception of the 5% silt - 95% ottawa sand mixture, all soil-geotextile systems in which clear water was used as the permeant resulted in stable filter systems. For the former case, involving the 5% silt - 95% ottawa sand mixture, based on the curves of flow versus time, (Figures 2, 4, 6, and 8) the silt passed through each soil-geotextile system until an equilibrium flow rate was achieved. In fact, when the soil which passed through each of the soil-geotextile systems was examined through the use of a Microtrac® particle size analyzer, the results of this work are illustrated in Figure 10, with the exception of the NW-HB-PP geotextile all of the other geotextiles allowed the silt, which migrated to the soil-geotextile interface, to freely pass. This appears to prevent blinding and/or subsequent clogging of these systems. For these systems the flow versus time data, Figures 4, 6, 8, appears to be consistent throughout the test program. For the NW-HB-PP, it is evident from the flow data shown in Figure 4, and the analysis on the soil which passed through the system shown in Figure 10, that some of the finer particles were not able to pass through the system. This resulted in the fluctuation of flow versus time which is the result of staged

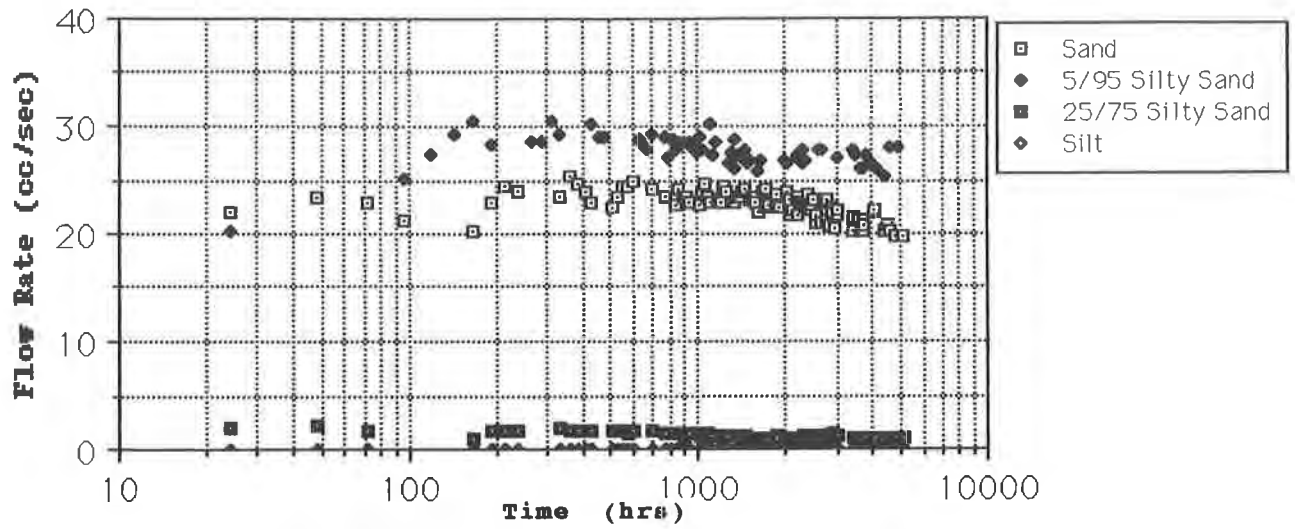

Figure 2 LTF Response of NW-NP-PET-H to Clear Water

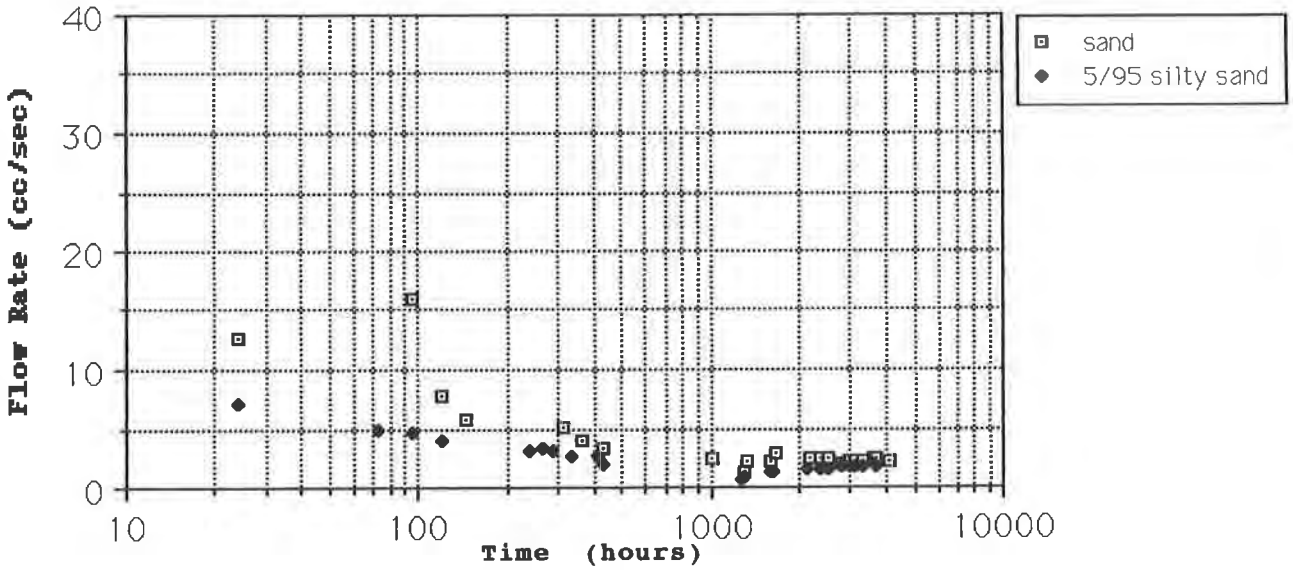

Figure 3 LTF Response of NW-NP-PET-H /Soil to Turbid Water

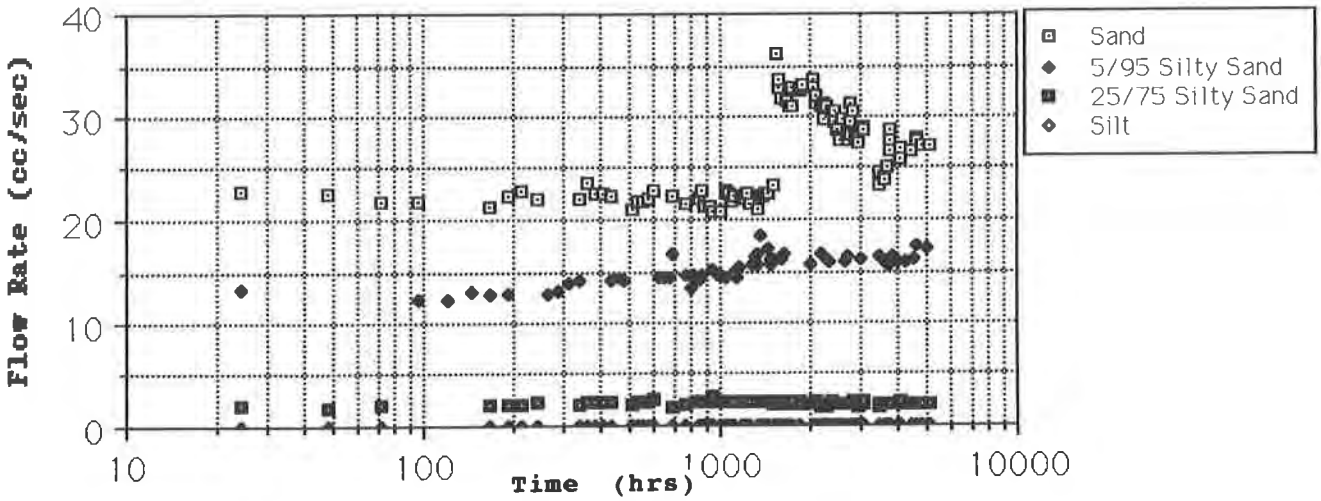

Figure 4 LTF Response of NW-HB-PP to Clear Water

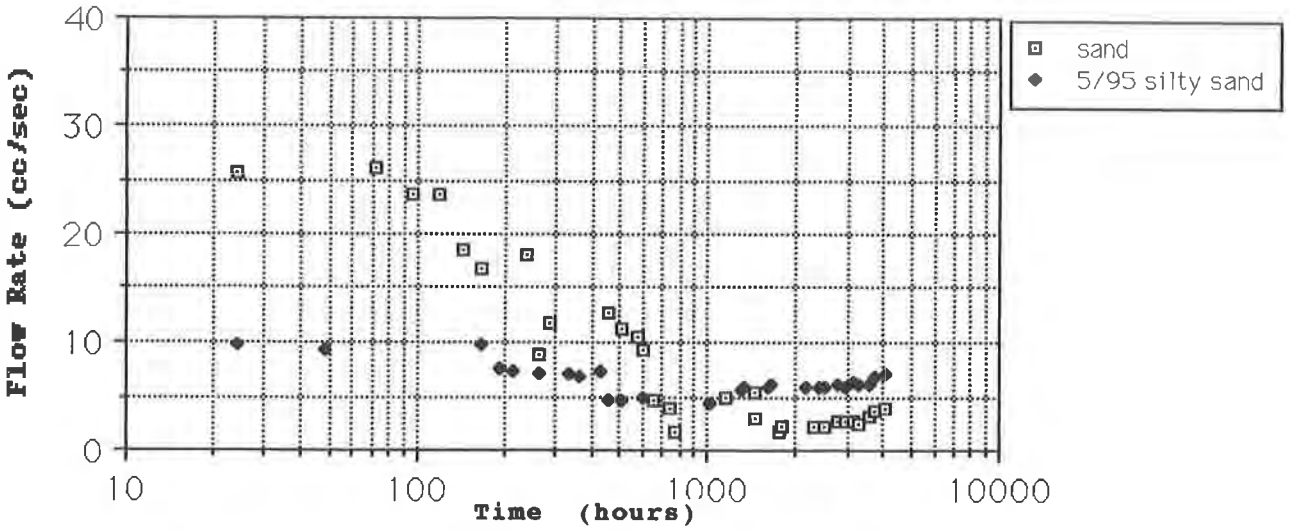

Figure 5 LTF Response of NW-HB-PP / Soil to Turbid Water

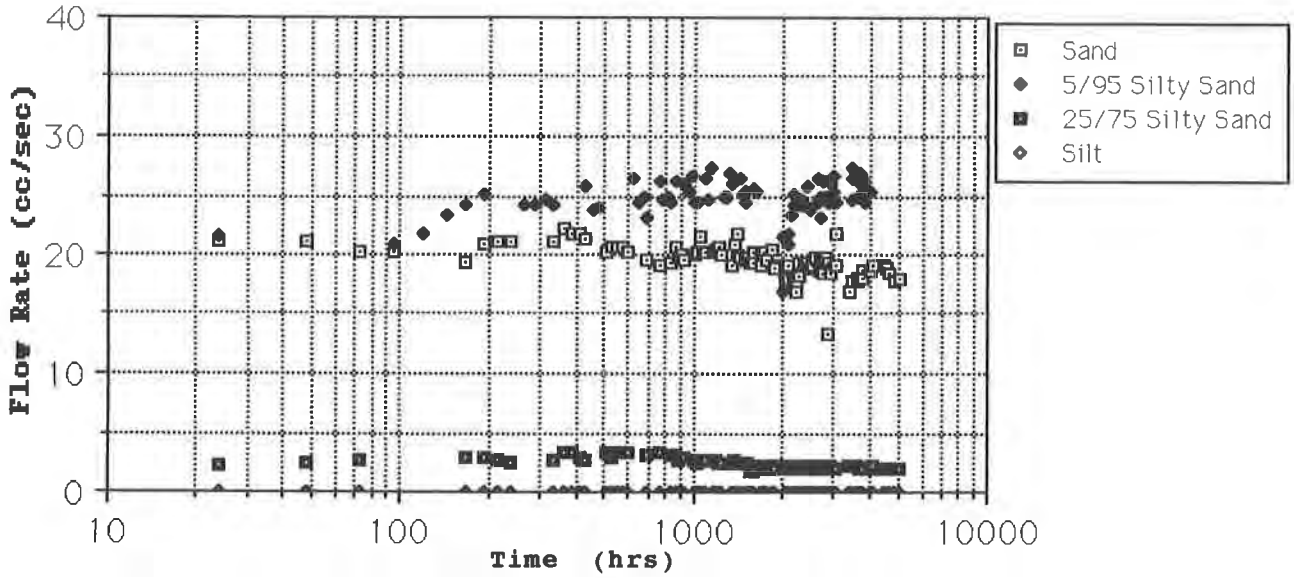

Figure 6 LTF Response of W-MF-PP to Clear Water

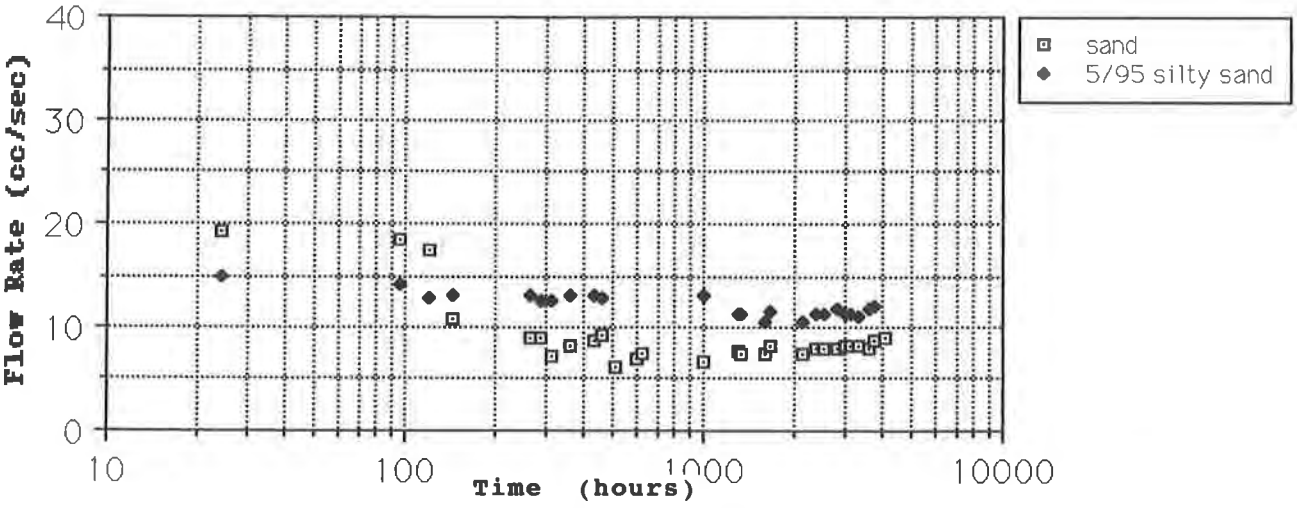

Figure 7 LTF Response of W-MF-PP / Soil to Turbid Water

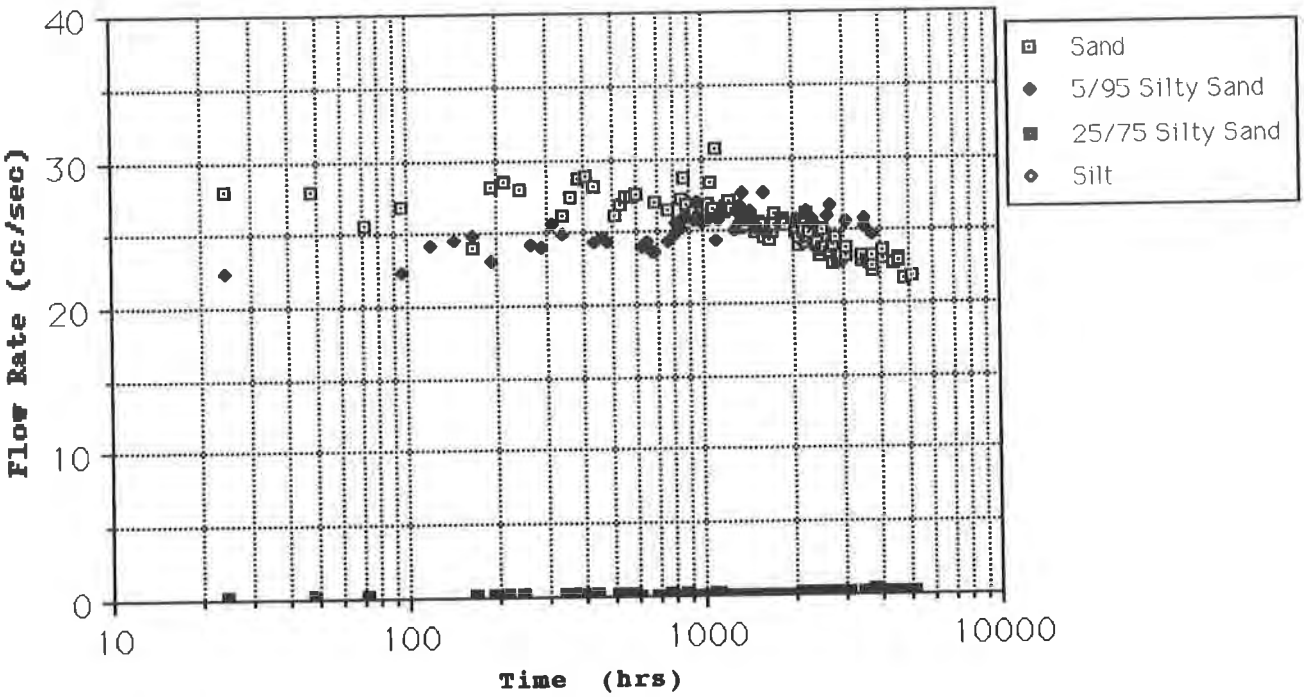

Figure 8 LTF Response of NW-NP-PP-L to Clear Water

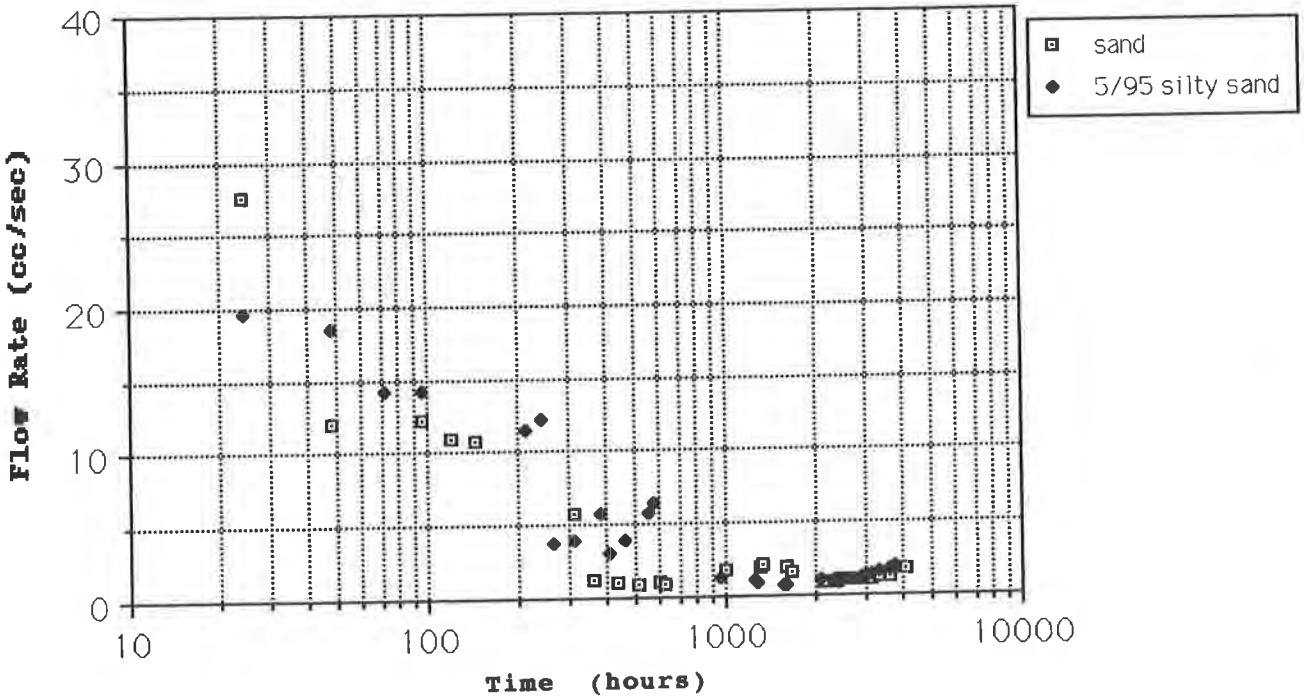

Figure 9 LTF Response of NW-NP-PP-L / Soil to Turbid Water

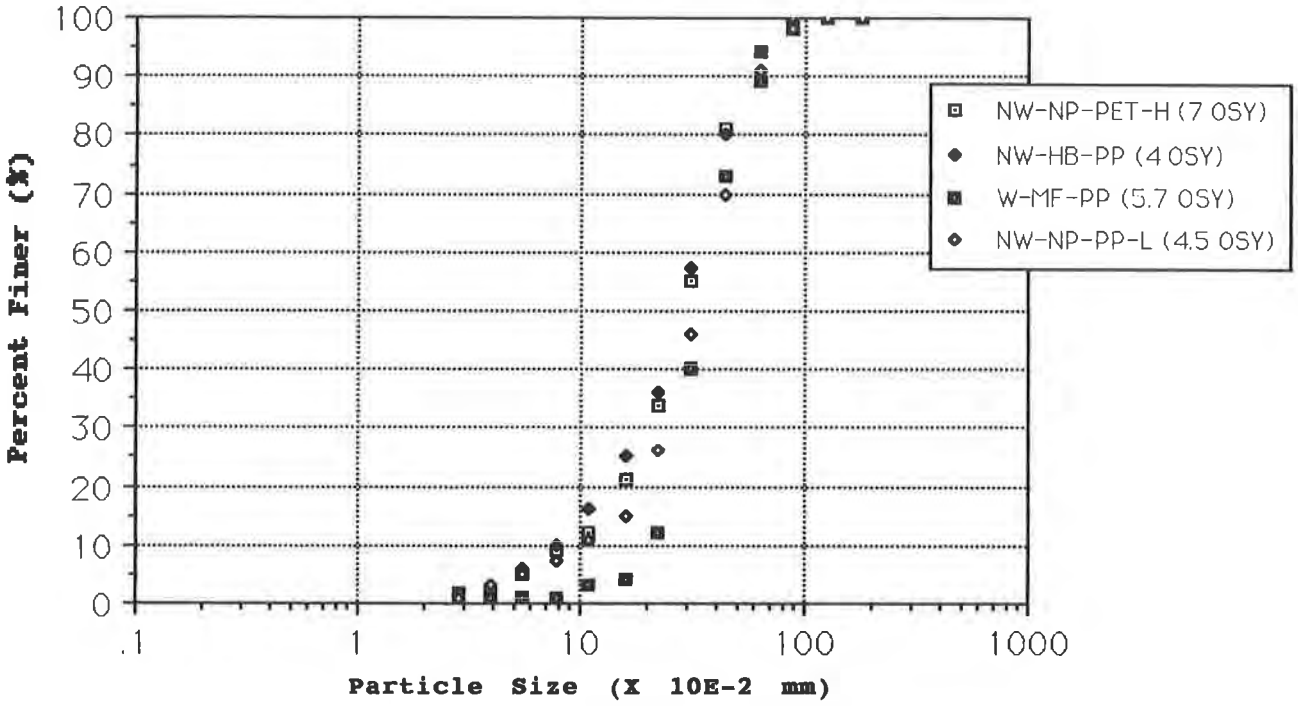

Figure 10 Soil Passing Clear LTF Test Setup (95%-Sand / 5%-Silt Soil)

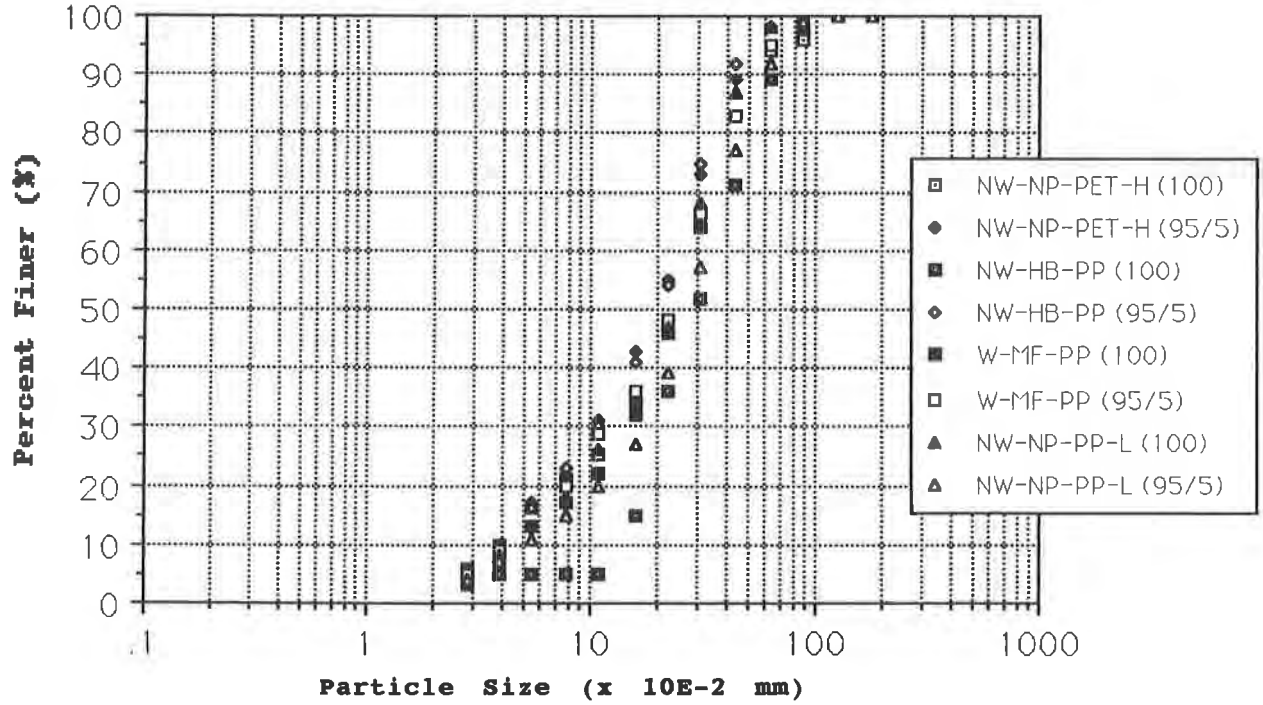

Figure 11 Soil Passing Turbid LTF test Setups

blinding resulting from retention of particles smaller than 0.04 mm. Since daily tests involved changes in gradient from 0.5 to 1.5, it is believed that the higher gradient permitted the passage of fines which incrementally made their way to the soil-geotextile interface. The terminal hydraulic conductivity values, along with values associated with the ratio of geotextile-to-soil permeability (Kg/Ks) are given in Table 8 . This information will be evaluated in the design correlation section of this paper.

Summary for Turbid Water Flow. Results for the cases in which turbid water (at an amount of 3 grams per liter of the silt) was added to the clear water in a mixing tank and used as a permeant are depicted in Figures 3, 5, 7, and 9. Soil which passed through the soil-geotextile systems is depicted in Figure 11. Review of this information clearly indicates the importance of permitting the passage of finer particles which ultimately promotes long term flow. For each of the geotextiles evaluated the transition time, defined as the time at which the change in slope of the flow versus time curve is achieved [GRI (1987)], for passage occurs at approximately 1000 hours. At this point the fine particles which encounter the soil-geotextile interface begin to pass through as indicated by the change in slope at this point. From the summary grain size distribution curve developed through the use of a Microtrac® particle size analyzer, and depicted in Figure 11, it is evident that the silt is able to make its way through all geotextiles to a varying degree. For this segment of the study the NW-HB-PP geotextile appears to have retained more of the finer particles than the other geotextiles and supports the clear water flow segment of this study.

For those columns in which each of the four geotextiles was tested without an upstream soil, all geotextiles retained the silt particles and led to the blinding of all geotextiles. As a result the flow was reduced to the values found in Table 9. These values correlate with those determined for flow through the silt-geotextile systems previously examined.

DESIGN CORRELATIONS

To make use of the information developed during this study, three criteria will be evaluated with current design equations and parameters developed for the soils and geotextiles used in this study. These criteria include: 1) Retention, 2) Permeability, and 3) clogging resistance.

With regard to retention criteria, the ratios of O_{95}/D_{85} , O_{95}/D_{15}, O_{50}/D_{85} , O_{50}/D_{50} , O_{50}/D_{15} , appear in almost all retention criteria established to date. Since the O_{95} (when reported in terms of a standard U.S. sieve size it is referred to as AOS) value is commonly reported, and a method has been described to permit the determination of the O_{50} value, it is believed that this information can be useful in determining the suitability of a given criteria for the soils used in this study.

Based on the ratios shown in Table 7, it appears that Carroll's (1983) criteria in which the ratio of O_{95}/D_{85} must be less than or equal to 3 indicates that only the silt-(W-MF-PP) system will fail to adequately retain the silt. It is evident from testing that this was not the case. Despite this short coming it appears that this criteria is of use. In addition, the Fischer, Christopher, and Holtz (1990) retention criteria, based on pore size

distribution, namely O_{50}/D_{85} should be less than or equal to 0.8, appears to work well for the cohesionless soils used in this study and those soils containing less than 50% minus #200 material. For the case of silt alone, the filter criteria based on D_{15} works well for all geotextiles. For this situation O_{50}/D_{15} must be less than or equal to values between 1.8-7.0 based on the coefficient of uniformity. Given the fact that these criteria have proved satisfactory for all of the soil-geotextile systems evaluated in this study, it is expected that future designs based on these pore size distribution criteria, and the O_{50} determination as described in this paper will confirm their utility.

Table 7. Retention Criteria Values

Geotextile Designation	O_{95}/D_{85}	O_{95}/D_{15}	O_{50}/D_{85}	O_{50}/D_{50}	O_{50}/D_{15}
Silty Sand 5/95 Cu = 1.7					
NW-NP-PET-H	.125	.28	.028	.045	.06
NW-HB-PP	.090	.20	.032	.52	.07
W-MF-PP	.212	.47	.054	.088	.12
NW-NP-PP-L	.125	.28	.029	.047	.06
Silty Sand 25/75 Cu = 24.5					
NW-NP-PET-H	.125	3.1	.028	.061	0.70
NW-HB-PP	.090	2.25	.032	.070	0.80
W-MF-PP	.212	5.3	.054	.118	1.36
NW-NP-PP-L	.125	3.1	.029	.063	0.73
Silt Cu = 3.2					
NW-NP-PET-H	2.5	6.25	.56	.94	1.4
NW-HB-PP	1.8	4.5	.64	1.1	1.6
W-MF-PP	4.2	10.6	1.1	1.82	2.7
NW-NP-PP-L	2.5	6.25	.58	.97	1.5
Ottawa Sand Cu = 1.3					
NW-NP-PET-H	.125	.20	.028	.04	0.04
NW-HB-PP	.090	.14	.032	.04	0.05
W-MF-PP	.212	.33	.054	.1	.1
NW-NP-PP-L	.125	.20	.029	.04	0.04

For the evaluation of permeability, investigators such as Giroud (1982), Carroll (1983), Christopher and Holtz (1985), to name a few, have found that Kg should be greater than or equal to Ks for steady state flow in which the geotextile is to serve in a noncritical application. For critical applications and when geotextiles are placed in severe soil or hydraulic conditions, the investigators have recommended that Kg be greater than or equal to 10Ks. Based on the results of this study, as depicted in Table 8, it appears that due to a reduction in flow over time of all geotextiles, possibly due to contaminants within the permeant, the greatest influence is felt by the

woven monofilament and heat bonded geotextiles. Therefore, it is recommended that for these materials the designer should consider applying the latter criteria. In lieu of this the designer may wish to follow the criteria established by Luettich, Giroud and Bachus (1990) in which this value is determined on the basis of a given application. Based on the hydraulic gradient of the application, these values vary from 1 for a pavement edge drains to 10 for shoreline protection.

With regard to clogging resistance it appears that the 1985 version of the Christopher and Holtz equation is the most useful. This relationship is based on grouting theory which stipulates that for soils containing fines in a non-continuous matrix having a Cu greater than or equal to 3, the ratio of O_{95}/D_{15} should be greater than 2-3. From this study it appears that all of the geotextiles satisfy this criteria. For soils in which Cu is less than 3 it is advisable that the designer check to see if the porosity of the candidate nonwovens is greater than 30%, a value based on graded granular filter porosity, and that woven geotextiles have a POA greater than or equal to 4%. For this study the W-MF-PP geotextile did have a POA of approximately 4%, and all nonwovens had porosity values greater than 30% after compression.

In conclusion, results from this study indicate that both the O_{95} and O_{50} index values along with results obtained from long term flow testing can be of use in determining the suitability of a given candidate geotextile. The author's firmly believe that the only true way to establish the validity of current design criteria is through supplemental testing. These tests ultimately will serve to confirm the validity of existing criteria and aid others through the development of an accurate database.

Table 8 - Permeability of LTF Testing Conducted with Clear Water Permeant

Geotextile	Condition	Column No.	K (cm/sec)	Kg/Ks
NW-NP-PET-H	GT/100% Ottawa Sand	1	0.074	3.0
	GT Alone	2	0.22	
	GT/Mixture (75-sand/25-silt)	3	.0043	51
	GT/100% Silt	4	.0001	2200
	GT/Mixture (95-sand/5-silt)	19	.09	2.4
NW-HB-PP	GT/100% Ottawa Sand	5	.096	0.64
	GT Alone	6	.061	
	GT/Mixture (75-sand/25-silt)	7	.0076	8
	GT/100% Silt	8	.0001	610
	GT/Mixture (95-sand/5-silt)	23	.056	1.1
W-MF-PP	GT/100% Ottawa Sand	9	.073	0.13
	GT Alone	10	.0092	
	GT/Mixture (75-sand/25-silt)	11	.0070	1.3
	GT/100% Silt	12	.0001	92
	GT/Mixture (95-sand/5-silt)	27	.085	0.11
NW-NP-PP-L	GT/100% Ottawa Sand	13	.080	2.25
	GT Alone	14	.18	
	GT/Mixture (75-sand/25-silt)	15	.0004	450
	GT/100% Silt	16	.0001	1800
	GT/Mixture (95-sand/5-silt)	31	.09	2.0

Table 9. Permeability of LTF Tests Conducted with Turbid Water

Geotextile	Condition	Column No.	K (cm/sec)
NW-NP-PET-H	GT/100% Ottawa Sand	17	0.01
	GT Alone	18	0.0009
	GT/Mixture (95-sand/5-silt)	20	.007
NW-HB-PP	GT/100% Ottawa Sand	21	.002
	GT Alone	22	.0001
	GT/Mixture (95-sand/5-silt)	24	.02
W-MF-PP	GT/100% Ottawa Sand	25	.02
	GT Alone	26	.0003
	GT/Mixture (95-sand/5-silt)	28	.04
NW-NP-PP-L	GT/100% Ottawa Sand	29	.003
	GT Alone	30	.0007
	GT/Mixture (95-sand/5-silt)	32	.09

Acknowledgements

This paper was submitted by the primary author for partial fulfillment of requirements for the degree of doctorate in geosynthetic engineering.This study was funded under a National Cooperative Highway Research Project #15-13 and is directed toward the topic of "Long-Term Performance of Geosynthetics in Drainage Applications." The author's would like to thank both the agency and the project officer, Mr. Daniel W. Dearasaugh, Jr., for contributing to the field of geosynthetic engineering.

References

American Society for Testing and Materials (1991), Annual Book of ASTM Standards, Section 4, Volume 04.08.

American Society for Testing and Materials (1990), Annual Book of ASTM Standards, Volume 11.01.

Carroll, R.G. (1983), " Geotextile Filter Criteria," Transportation Research Record, 916, pp.46-53.

Cedergren, H.R. (1989), Seepage, Drainage, and Flow Nets, Third Edition, John Wiley and Sons, 465 p.

Christopher, B.R. and Holtz, R.D. (1985), Geotextile Engineering Manual, U.S. Federal Highway Administration, Report No. FHWA-TS-86/203, 1044 p.

Christopher, B.R. and Holtz, R.D. (1985), Geotextile Construction and Design Guidelines, Prepared for the U.S. Federal Highway Administration, Washington D.C., HI-89-050.

Christopher, B.R. and Fischer, G.R. (1991), "Geotextile Filtration Principles, Practices and Problems," Proceedings of the 5th GRI Seminar on the Topic of Geosynthetics in Filtration, Drainage and Erosion Control, December, Geosynthetic Research Institute, Drexel University, pp. 1-17.

Fischer, G.R., Christopher, B.R. and Holtz, R.D. (1990), " Filter Criteria Based on Pore Size Distribution," Proceedings of the Fourth International

Conference on Geotextiles, Geomembranes, and Related Products, Vol. 1, The Hague, pp. 289-2948.

Geosynthetic Research Institute (1987), " Clogging Potential via Long Term Flow Rate," GRI, Drexel University, Philadelphia, PA.

Giroud, J.P. (1982) " Filter Criteria for Geotextiles," Second International Conference on Geotextiles, vol. 1, Las Vegas, Nevada, pp. 103-108.

Hoover, T.P. (1982), " Laboratory Testing of Geotextile Filter Fabrics," Second International Conference on Geotextiles, vol. 3, Las Vegas, Nevada, pp. 839-844.

Hwu, Bao-Lin (1990), " Design, Evaluation and Behavior of Geosynthetic Drainage Systems," Ph.D. Dissertation, Drexel University, Philadelphia, PA.

Johnston, P.R. (1985), " Fluid Filter Media: Measuring the Average Pore Size and the Pore-Size Distribution, and Correlation with Results of Filtration Tests ," ASTM Journal of Testing and Evaluation, Vol. 13, No. 4, July, pp. 308-315.

Johnston, P.R. (1983), " The Most Probable Pore-Size Distribution in Fluid Filter Media," ASTM Journal of Testing and Evaluation, vol. II, No. 2, March, pp. 117-125.

Koerner, R.M. and Ko, F.K. (1982), " Laboratory Studies on Long-Term Drainage Capabilities of Geotextiles," Second International Conference on Geotextiles, vol. 1, Las Vegas, Nevada, pp. 91-96.

Koerner, R.M. (1990), Designing with Geosynthetics, 2nd Edition, Prentice Hall, Englewood Cliffs, NJ.

Legge, K.R. (1990) " A New Approach to Geotextile Selection," Proceedings of the Fourth International Conference on Geotextiles, Geomembranes, and Related Products, Vol. 1, The Hague, pp. 269-272.

Luettich, S.M., Giroud, J.P. and Bachus, R.C. (1991), " Geotextile Filter Design Guide", Proceedings of the 5th GRI Seminar on the Topic of Geosynthetics in Filtration, Drainage and Erosion Control, December, Geosynthetic Research Institute, Drexel University, pp. 18-33.

Luettich, S.M., and Williams, N.D. (1989), " Design of Vertical Drains Using the Hydraulic Conductivity Ratio Analysis," Proceedings of Geosynthetics '89, San Diego, pp. 95-103.

Narejo, D.B. and Koerner, R.M. (1991) " Technical Note: A Dynamic Filtration Test for Geotextile Filters," Proceedings of the 5th GRI Seminar on the Topic of Geosynthetics in Filtration, Drainage and Erosion Control, December, Geosynthetic Research Institute, Drexel University, pp. 57-62.

Sansone, L.J. and Koerner, R.M. (1991) " Fine Fraction Filtration Test to Assess Geotextile Filter Performance," Proceedings of the 5th GRI Seminar on the Topic of Geosynthetics in Filtration, Drainage and Erosion Control, December, Geosynthetic Research Institute, Drexel University, pp. 34-56.

Determination of Pore Size Distribution Through Filtration Test and Probabilistic Theory

M.H.A. Sória
University of São Paulo, Brazil

E. Viviani
University of São Paulo, Brazil

ABSTRACT

Results of a laboratory investigation carried out to obtain pore size distribution of nonwoven geotextiles, supported by a probabilistic filtration theory, are presented. Hydraulic filtration tests using water-particles suspensions were conducted. Geotextile filters were composed by one, two or three layers, under compressive stresses of 2 kPa and 30 kPa. Sand and glass beads are used as base material for filtration tests. Mercury intrusion porosimetry tests were done with compressed geotextile specimens, and results compared. Experiments have shown that void size curves computed from theoretical equations using the results of filtration tests show acceptable agreement with mercury porosimetry curves.

INTRODUCTION

One of the factors governing the effectiveness of a geotextile filter to protect a base material is the pore size distribution, which determines its capacity to retain soil particles. The choice of geotextiles for application as filter in drainage systems depends on the opening size or more precisely, on the geometry and distribution of voids. In principle, there are two ways for determining the pore size distribution of geotextiles: measuring and counting voids or; making indirect measurement of particles passing through the filter or retained. The first method has almost insurmountable difficulties: geotextiles are almost all voids and such voids don't have clearly defined geometric forms; voids are formed by fibers crossing at various directions. Even optical and image analyzer methods can only measure the actual distance between fibers of nonwoven geotextile and evaluate void's volume "but it lacks interest in simulating filtration behavior" (Rollin, 1986). The second method opens a large spectrum of possibilities. One of them is to run sieve analysis using the geotextile as sieve and determining the "apparent opening size" of the textile. This is the simplest measure that can be done but the parameter reflects only the approximate largest opening dimension available. The hydraulic filtration test offers some advantages: the phenomenon involved is close to the work conditions in real world applications and the variables observed in the laboratory are consonant with behavior in field.

One of the most successful instruments for indirect determination of void size distribution is the probabilistic approach. In 1965 a filtration theory based on probabilistic hypothesis was offered (Silveira, 1965). In a recent paper Silveira (1992), retakes the problem and proposes an experimental procedure for determining the void size curve from hydraulic filtration testes, supported by the theory. A laboratory research on granular filters according to this proposal has already been related (Sória et al, 1992).

This work relates results of an experiment carried out to evaluate the potentiality of the method described, as applied for geotextiles. Basically, two indirect methods for obtaining void size curves are related: hydraulic filtration testes supported by probabilistic filtration theory and mercury intrusion porosimetry tests. The theoretical fundaments for determining void curves from hydraulic filtration results are explained and discussed. The resulting curves are compared with mercury porosimetry results and criticized.

THEORETICAL BASIS

The fundaments of the probability approach here employed has been described elsewhere (Silveira, 1965) and the theory is well known as tool for research on granular filters. The connection between theoretical basis and experimental procedure here described was proposed by Silveira (1992). Following, the basic equations are discussed.

Given a filter and a base material, a particle of an assigned diameter d', will travel the distance S within the filter before being stopped and retained, after a number n of confrontations. The equations describing this process are as follows (Silveira, 1992):

$$n = \frac{\log (1 - P')}{\log P} \qquad (1)$$

$$S = n \cdot s \qquad (2)$$

$$S = \frac{\log (1 - P') \cdot s}{\log P} \qquad (3)$$

where:
P' = confidence level;
P = fraction (or percentage) of voids equal or greater than a given diameter d';
n = number of confrontations;
s = average distance traveled by a particle for one confrontation and;
S = total distance traveled by a particle within the filter.

"Confrontation" may be defined as the event of one particle encountering one void and "testing" that void: if the particle is smaller than the void, it will pass; if not, it will be retained. The average distance covered between one and another confrontation is s. The number of confrontations for covering the total distance S is n. The confidence level P', represents the probability of a given particle to cover the distance S across the filter and consequently also represents the fraction (or percentage) of all particles having diameter d' or smaller, that will penetrate the distance S in the filter. With this hypothesis, a simple and straightforward experimentation program is proposed (Silveira, 1992): to run hydraulic filtration tests with filters of various thicknesses. Assuming filter thickness equal to S, the grain size distributions of the material passing through the filter allow to compute the void size distribution of the filter, from equation 3.

EXPERIMENT

Hydraulic filtration test. The permeameter, shown in Figure 1, is mounted using a CBR (California Bearing Ratio) cylinder as support. The perforated base of the original mold was drilled as to have a perforated area around 60% of the total. One upper plate having the same perforation pattern was provided. Two vertical rods screwed in the upper plate, support the lever bar designed for applying compressive stress over the specimen. The geotextile specimen was placed between sheets of sieve number 30 (aperture 0.595 mm) and mounted between the perforated plates.

General test procedure may be described as follows:

a) A geotextile specimen is placed in the permeameter. One specimen may be composed by one, two or three disks of geotextile;
b) The upper perforated plate is mounted over the specimen and a normal compressive stress is applied. Tests were made for two values of compressive stress: 2 kPa (upper plate and rods) and 30 kPa (plate, rods and lever beam);
c) Water is delivered to the permeameter and, at the same time, the suspension of granular material is introduced into the flow. Hydraulic head is maintained around 15 cm during the test;
d) When about 10 liters has passed through the permeameter the intake is closed and the remaining fluid flows;
e) All material - water plus solids - passing through the filter is collected;
f) The solid portion is separated by sedimentation, filtration and oven drying;
g) Grain size distribution of the collected material is determined by sieve analysis.

It must be emphasized that the granular material used in tests was separated in six grain size fractions in order to have six suspensions, with different grain sizes. The fractions was defined by six intervals of sieves: # 70 to 100; 100 to 140; 140 to 200; 200 to 270; 270 to 400 and smaller than 400. Each specimen was tested for only one suspension. One geotextile thickness was tested in six runs: one for each water-particle suspension, and consequently, using six specimens. This procedure was necessary because in preliminary tests most of granular material stayed at the filter surface blocking the passage of finer material.

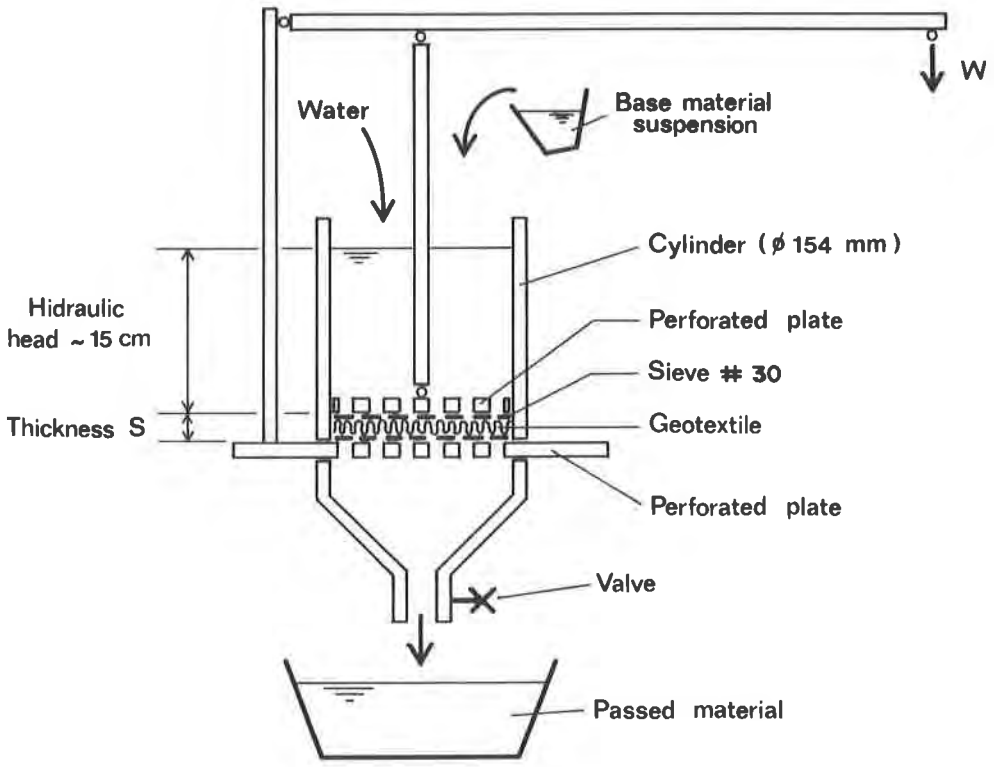

Figure 1 Sketch of test apparatus

Thickness and compressive stress. Since mercury intrusion porosimetry was done with specimen compressed at various thicknesses, it was necessary to obtain curves of thickness versus compressive stress. Geotextiles tested are referred by their nominal thickness given by the manufacturer. Tests have shown that nominal thickness corresponds to that obtained for a compression of about 80 kPa (11.6 psi). A consolidation test machine was used for determining the curves. Results are shown in Figure 2 for one and three layers. Relations between thickness, voids and stresses are in Figure 3.

Mercury intrusion porosimetry. For granular filters, void size distribution curves may be computed from grain size curve and theory; but for geotextiles it is impossible to do this because there is no grain size distribution, since there are no grains. For this reason, in order to have a basis for comparisons, mercury porosimetry tests were done with geotextile specimens. Specimens, measuring 1.0 cm x 1.5 cm, were tested in natural state (uncompressed) and compressed. Compression was acquired placing specimen between two small perforated plates, accomplished with two screws turned to reach a given thickness, consonant to the established compressive stress. Thickness was measured with a caliper and then the assemblage was placed into the mercury porosimeter.

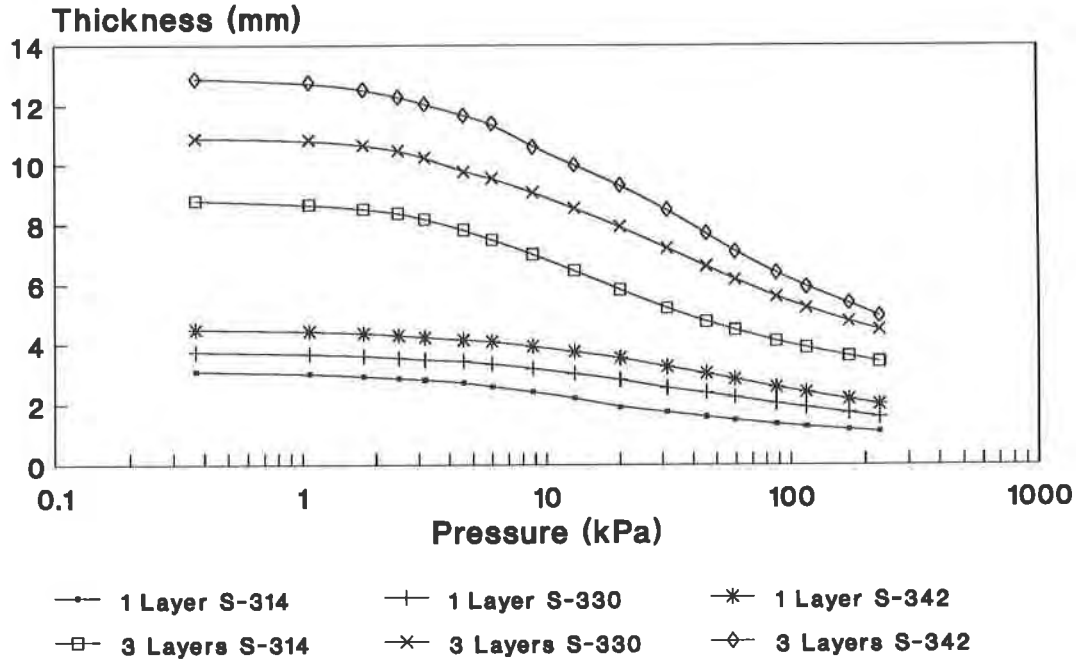

Figure 2 Thickness versus compressive stress

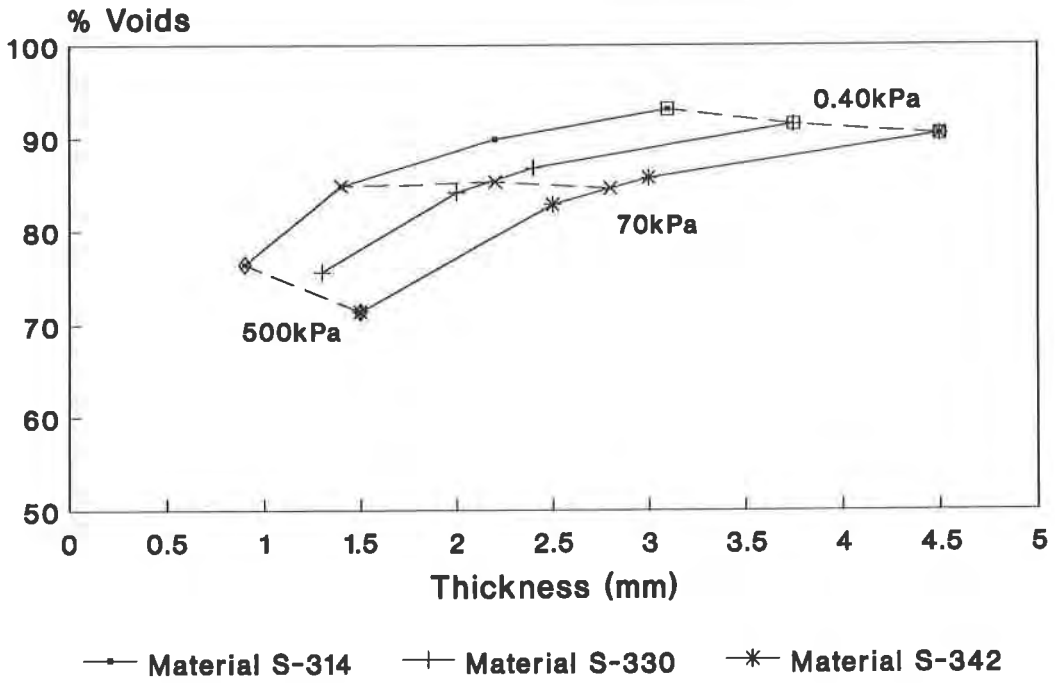

Figure 3 Thickness versus voids

Apparent opening size (AOS). The AOS was determined following the standard method (ASTM, 1987). A mechanical sieve shaker was used and tests were made in a conditioned atmosphere for testing geotextiles. The figures showing void size results contain also AOS points.

MATERIALS

Geotextiles. Materials tested were produced by the same manufacturer at the same industrial plant, at three nominal thicknesses: 1.5 mm, 2.0 mm and 2.8 mm. The product is made of polypropylene (95%) and polyacrylic (5%) fibers, and is a needle punched nonwoven textile. Data given by the manufacturer and obtained by direct measurement are in Table 1. The diameters of fibers are between 0.014 mm and 0.048 mm, with a weighted mean of 0.037 mm.

Table 1. Characteristics of geotextiles

Designation	Nominal thickness mm	Thickness at 80 kPa mm	Mass per unity area kg/m^2 (*)	Mass per unity volume kg/m^3 (*)
S-314	1.5	1.5	0.194	0.129
S-330	2.0	2.0	0.289	0.145
S-342	2.8	2.7	0.391	0.140

(*) measured at 80 kPa

Granular materials. For hydraulic filtration tests two granular materials - referred as "base material" - were used: glass beads and natural sand. Grain size curves of base material are presented in conjunction with results of hydraulic filtration tests. Other characteristics are shown in Table 2.

Table 2. Characteristics of granular material

Material	Specific mass g/cm^3	Sphericity	Roundness
sand and silt	2.52	0.8	0.6
glass beads	2.45	1.0	1.0

RESULTS AND COMPUTATIONS

Mercury intrusion. The test gives results ranging from 0.1 mm to 0.0001 mm. Since the goal was to compare results with hydraulic filtration test, and the granular materials utilized for these tests were coarser than 0.02 mm, the results of mercury intrusion were recalculated taking out the finest part of the curve. Resulting curves have 100% of voids greater than 0.02 mm.

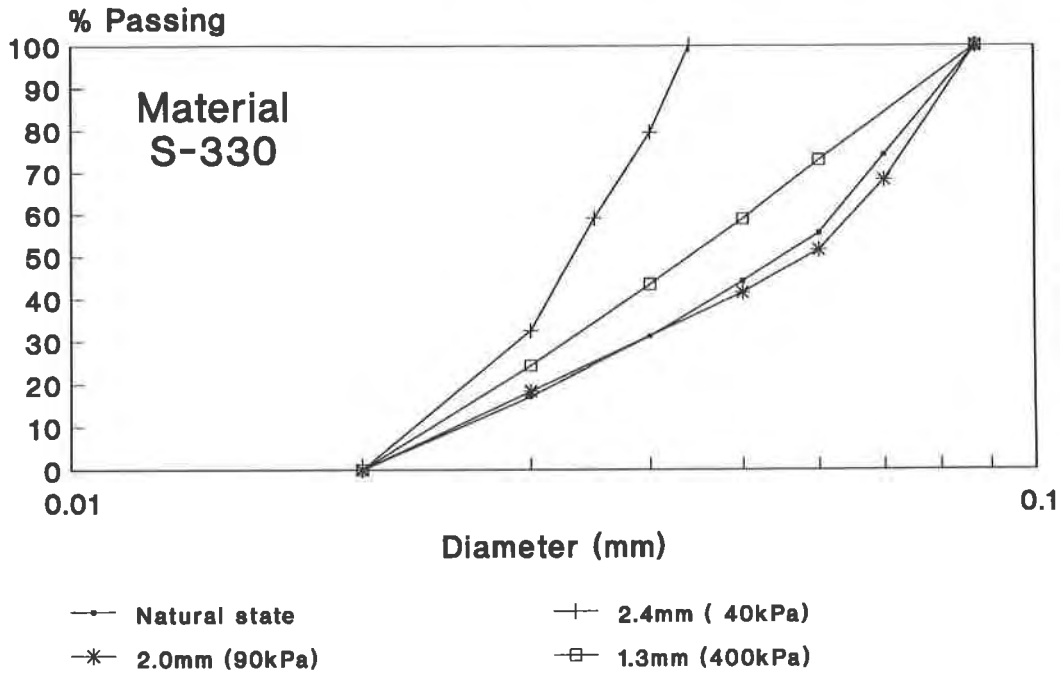

Figure 4 Void curves by mercury intrusion porosimetry

The general aspect of one set of curves (Figure 4) reveals some inconsistencies, contradicting the first expectation. It seams natural that void size curves move to the left as the compressive stress increases, that is, voids would become smaller as thickness decreases with compressive stress; but the results show curves interlaced. The same behavior was found at the original curves, before recalculation. Results for other geotextiles tested are similar.

One of the causes for this behavior, certainly, is that tests use one specimen for each thickness, that is, each point in the graph was obtained with a different specimen. This is aggravated by the fact that specimens are too small (1.5 cm^2) in the face of geotextile heterogeneity. To overcome this problem it would be necessary to test the same specimen at different thickness (compressive stress) in order to have the real variation of void sizes with compression. A method for recuperating the specimen tested is needed. All the mercury contained must be removed before the next test. A suggested procedure is to evaporate the mercury at controlled conditions, but this was not tried. Other point to be discussed about mercury intrusion is concerning to the inherent hypothesis necessary for testing. Computation assumes sphericity of voids; volumes of mercury introduced within the sample are measured and diameters calculated assuming spherical mercury particles. Void with form different than spherical, may be computed as more than one void, overestimating the number of smaller ones. Nonwoven geotextile, having fibers crossing at various directions, with pores or voids poorly defined, can hardly be considered similar to a material containing spherical voids. The effect of this dissimilarity could be minimized herein because the void size curve was recalculated as reported. This fact was not investigated for more detail.

Hydraulic filtration tests. Example of computations is shown in Figure 5. Figures 6 and 7 show sets of grain size curves of material passing through the filter, resulted from batches of hydraulic filtration tests. One point of the void size curve is determined by a pair of values: d' and P, diameter and percentage, respectively. These values may be obtained from one grain size curve and equation 3.

The equation needs three parameters: S, P' and s, respectively, total distance traveled by a particle smaller than d' within the filter, confidence level and average distance traveled by a particle between two confrontations. The points of void size curve are determined as follows:

a) Plot grain size curve of material passing through the filter, for each thickness;

b) Assign a value to S, equal to filter thickness and assign a value to P' near 100%. Values taken are between 95 and 99%. At Figures 5 to 10, P' is equal to 0.98 (98%);

c) With P' assumed , project a line intercepting the grain size curve and then downward to find d'. Note that d' is a function of the pair S and P'. The physical meaning of this is: P' percent of the particles passing through the filter of thickness S are smaller than d'.

d) Assuming a value for s (distance for one confrontation), compute P (percentage) from eq. 3;

e) Enter P and intercept the vertical line representing d' and find the point (d'; P);

f) Repeating the operations for each value of filter thickness S, other points are determined.

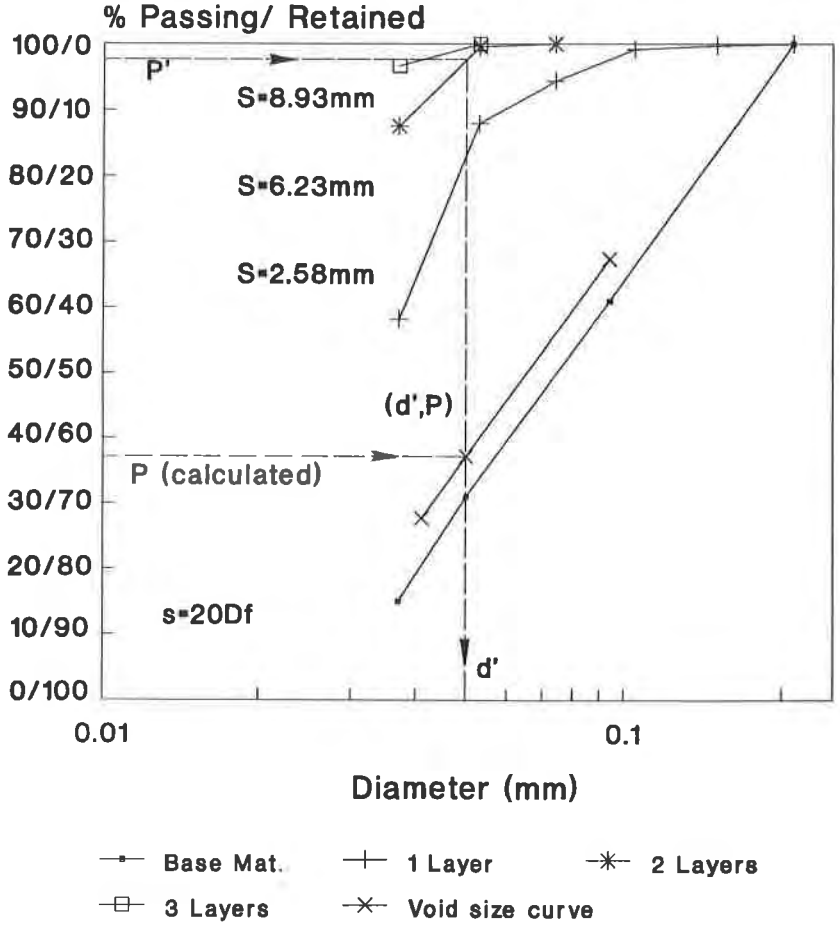

example: with

S = 6.23 mm (filter thickness)
and P' = 0.98 = 98 %

find d' = 0.05 mm ;

assuming:

s = 20 Df = 20 * 0.037 mm
=0.74 mm

compute P from equation 3 :

$$P = 10^{\left[\frac{s \log(1-P')}{S}\right]}$$

$$P = 10^{\left[\frac{0.74 \log(1-0.98)}{6.23}\right]}$$

P = 0.63 (63 % retained)
curve point : (0.05 mm ; 63%)

Figure 5 Determination of void size curve

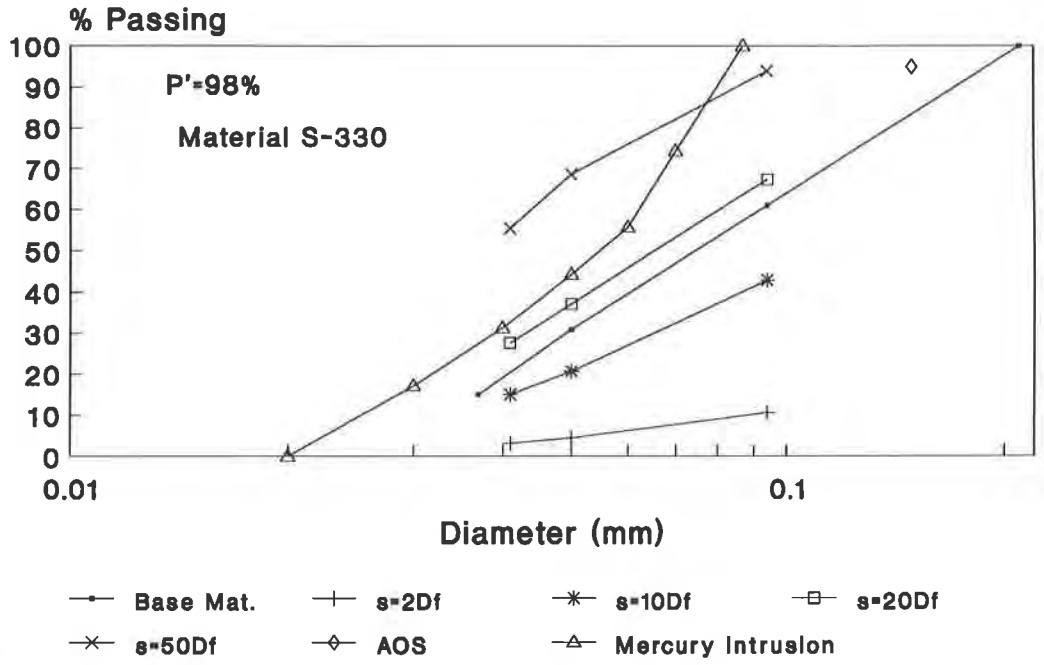

Figure 8 Void size curves for different values of s

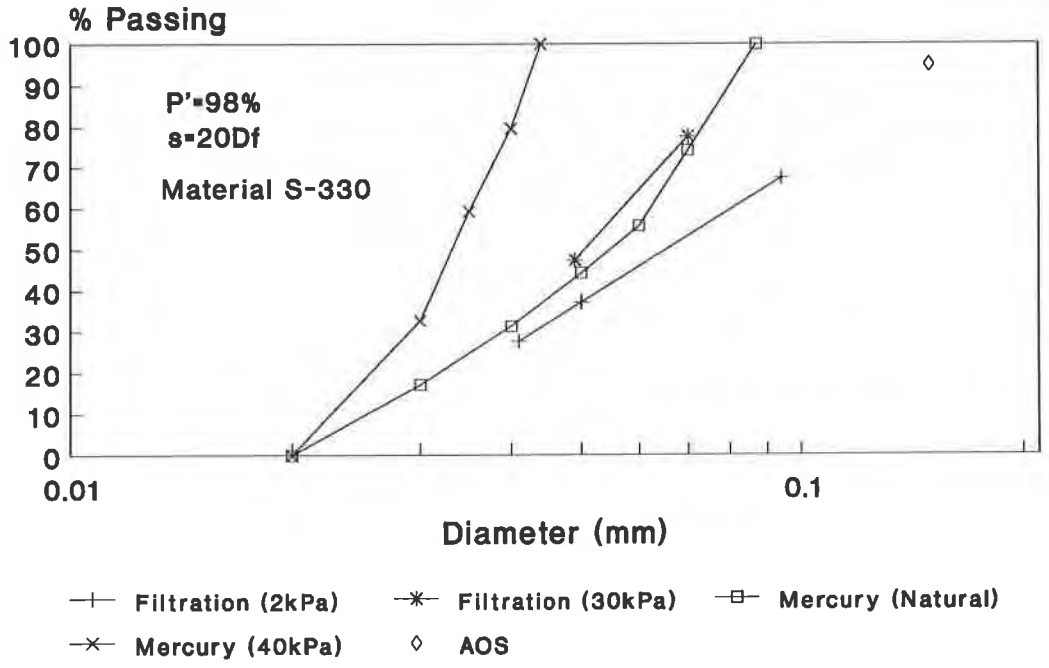

Figure 9 Void size curves for different values of stress

One question about the parameters must be retaken: the value to be assigned to s. The theory assumes an average distance traveled by a particle from one confrontation to another. In the search for a void larger than itself, the particle runs from one void to the next, covering a distance. To measure directly this length seems almost impossible. Silveira (1992) has suggested values for s as function of filter diameter Df. Following this suggestion, computations were done for three values of s :

$$s = 2\ Df = 0.074\ mm;\ s = 20\ Df = 0.74\ mm;\ \text{and}\ s = 50\ Df = 1.85\ mm \quad (4)$$

where Df = fibers diameter = 0.037 mm.

Figures 8 to 11 show the results obtained.

CONCLUSIONS

Concerning to hydraulic filtration tests and computation of void size curves by the theory, some conclusions may be drawn:

- Grain size curves of material passing show consistent results: for greater thicknesses, fines is the material passing. This reveals an expected (but not known in detail) behavior: nonwoven geotextiles tested act more likely as granular filter than as sieve. A laboratory sieve selects material by one dimension, the sieve aperture; in a granular filter, the selection may be better described as a process in which the thickness is a mandatory parameter (Sória et al, 1992).
- For values of s around 20 Df, void size curves obtained by filtration tests supported by the theory are near the curves resulted from mercury intrusion porosimetry.
- Curves obtained with sand and glass beads (Figure 10), have different inclinations. This may probably be due to differences in the surface of particles: glass beads are sensibly more polished than the sand used. This assertion is only speculative, since the point was not investigated.
- The influence of P' in the position of the curves obtained are not significant. It seems that all points, for different P', belong to the same curve;
- Tests for two compressive stresses (2 kPa and 30 kPa) show a shift to the left as compression increases: for larger compression, smaller voids.

CONCLUDING REMARKS

The main purpose of this investigation was to make an evaluation of the approach proposed as instrument for research on geotextiles. As a general conclusion, experiment has shown promising results. The program has some limitations that may be overcome in further research. Tests must be done at different hydraulic conditions, for a larger range of compressive stress and with finer granular material.

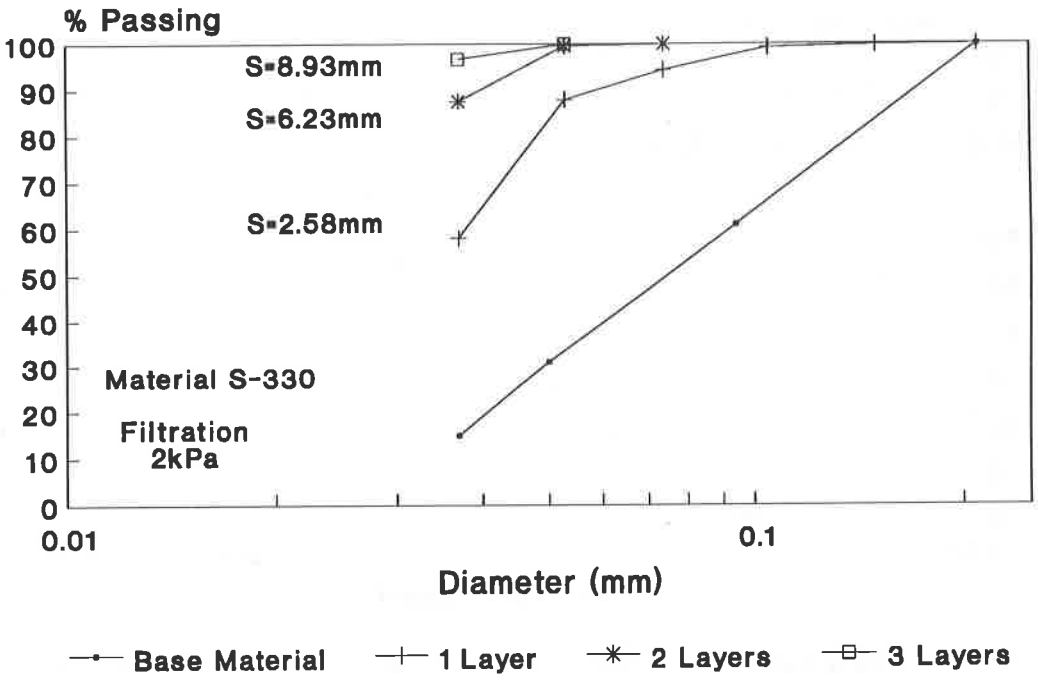

Figure 6 Grain size curves of material passing through filter: stress 2 kPa

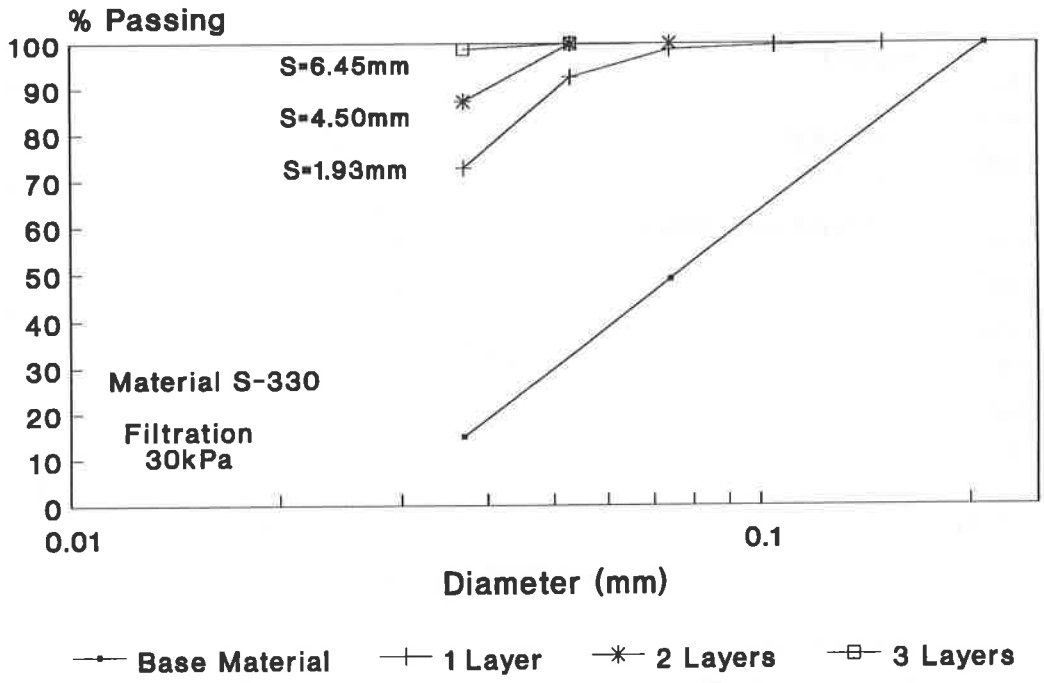

Figure 7 Grain size curves of material passing through filter: stress 30 kPa

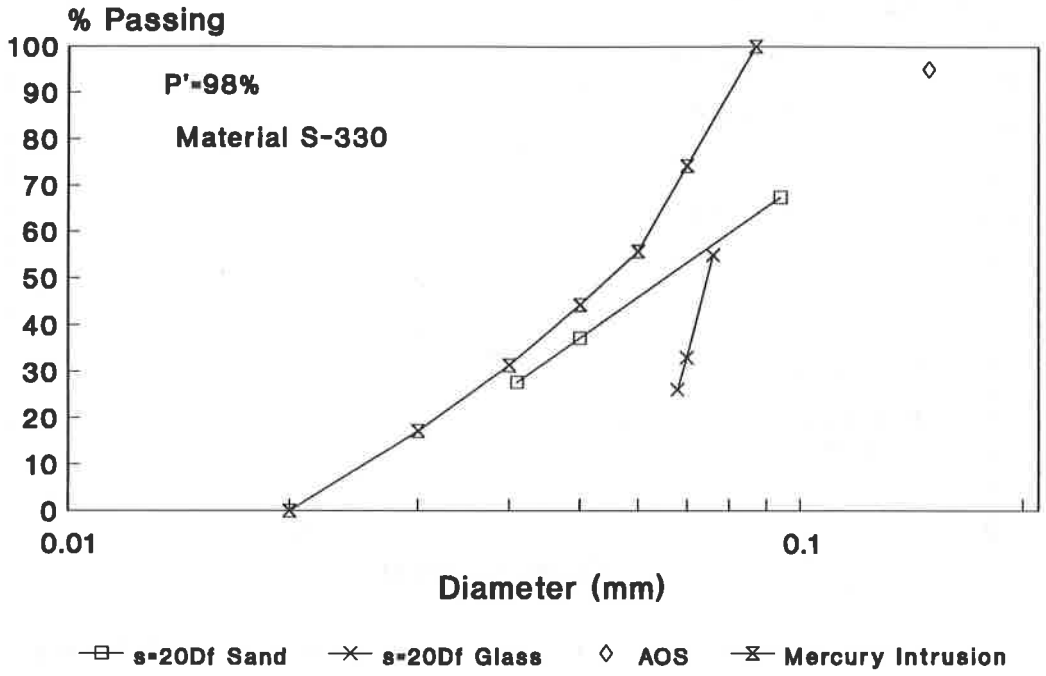

Figure 10 Void size curves for different materials

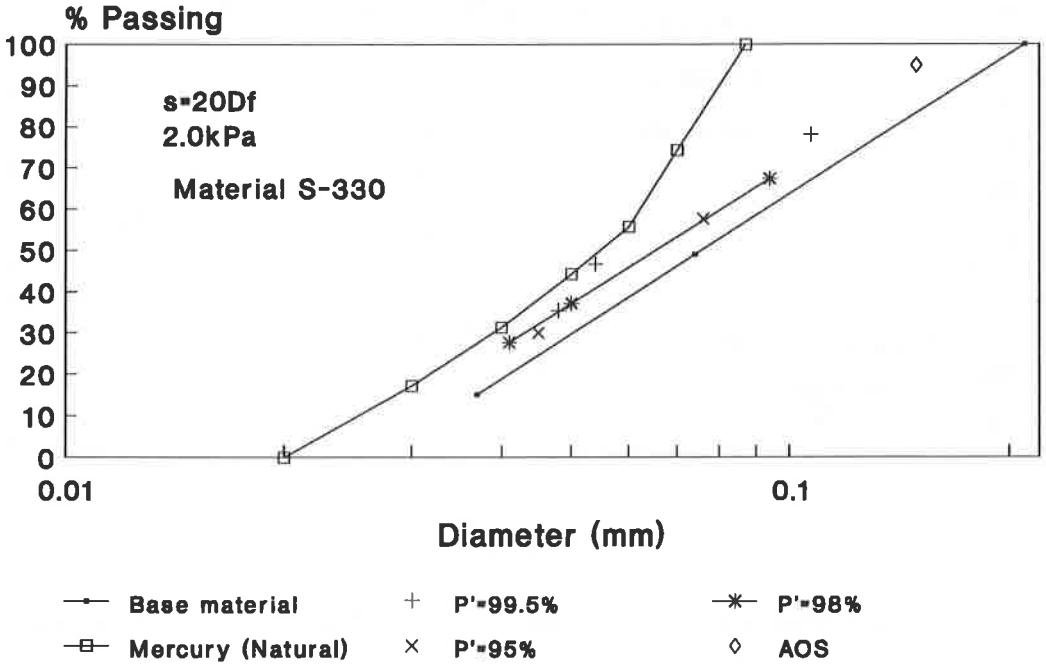

Figure 11 Void size curves for different values of P'

ACKNOWLEDGMENTS

The research herein reported is part of M.S. dissertation to be presented by the second author. Geotextile material and glass beads were kindly provided by the geotextile manufacturer, Tapetes São Carlos Ltda. Mercury intrusion tests were conducted as a kindness of the Materials Department at Federal University of São Carlos. All this support is gratefully acknowledged. The research was done at the Department of Transportation, School of Engineering of São Carlos, University of São Paulo. The authors wish to express their appreciation to Eng. R. Aramaki for the assistance and to Professor Araken Silveira for the incentive and helpful discussions.

REFERENCES

American Society for Testing and Materials, ASTM (1987) "Standard Test Method for Determining Apparent Opening Size of a Geotextile D 4751-87" Annual Book of ASTM Standards , Vol. 04.8, pp. 900-903.

Kenney,T.C. et al (1985) "Controlling constriction size of granular filters" Canadian Geotechnical Journal , Vol. 22, pp. 32-43.

Rollin, A. L. , (1986) "Filtration Opening Size of Geotextiles", ASTM Standardization News , Vol. 14, n. 5, pp. 50-52.

Silveira, A., (1965) "On analysis of the problem of washing through filters in protective filters. Proc. 6th ICSMFE , Vol. 2, pp. 551-555. Montreal.

Silveira, A. , (1992) "A method for determining the void size distribution curve for filter materials", International Conference on Filters and Filtration Phenomena In Geotechnical Engineering. Karlsruhe.

Sória, M. H. A. et al (1992) "Experimental determination of void size curves "International Conference on Filters and Filtration Phenomena In Geotechnical Engineering. Karlsruhe.

Know More.

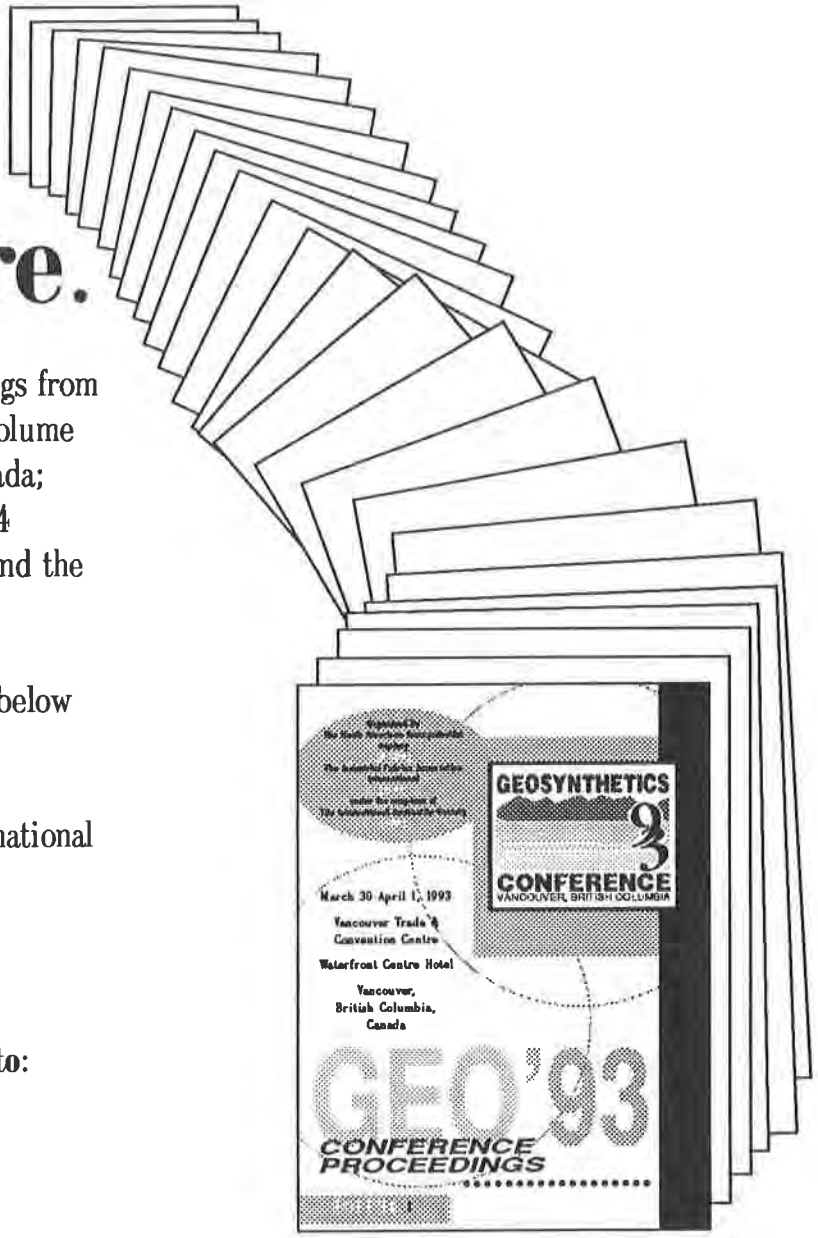

Order extra copies of the proceedings from Geosynthetics '93. Just $85 per 3-volume set, plus postage ($6 U.S.; $19 Canada; $58 South America and Europe; $34 Central America; $70 Asia, Africa and the Middle East).

To order, simply complete the form below and return with payment to:

Industrial Fabrics Association International
345 Cedar St., Suite 800
St. Paul, MN 55101
USA

For faster service, fax your order to:
612/222-8215

GEO'93

Please send _____ copies of Geosynthetics '93 Conference Proceedings @ $85 per set, plus postage

☐ Check enclosed ☐ Please bill my ☐ Visa ☐ Master Card Expiration date _____

Credit Card # _____

SIGNATURE (X) _____

Subtotal _____
Postage _____
TOTAL _____

NAME _____

COMPANY _____

ADDRESS _____

CITY _____ STATE/PROVINCE _____ ZIP/POSTAL CODE _____

COUNTRY _____

PHONE _____ FAX _____

Return to: Industrial Fabrics Association International
345 Cedar St., Suite 800, St. Paul, MN 55101 USA
612/222-2508 • fax 612/222-8215

Geosynthetics '93

Conference Proceedings

Volume 1

Opening Session
Roads and Pavements
Walls, Slopes, Embankments and Foundations
Geotextile Filtration Design and Testing

Volume 2

Geosynthetics Testing
Durability and Long-Term Performance of Geosynthetics
Technical Advances, Innovations, Challenges

Volume 3

Waste Containment Case Histories
Landfill Design, Performance and CQA

Organized by
The North American Geosynthetics Society
(NAGS)
The Industrial Fabrics Association International
(IFAI)
under the auspices of
The International Geotextile Society
(IGS)

GEOSYNTHETICS '93
CONFERENCE
VANCOUVER, BRITISH COLUMBIA

March 30-April 1, 1993

Vancouver Trade & Convention Centre

Waterfront Centre Hotel

Vancouver,
British Columbia,
Canada

GEO'93

CONFERENCE PROCEEDINGS

VOLUME 2

SPONSORED BY

Laboratory Evaluation of a Nonwoven Geotextile for Reinforcing On-Site Soil

H.I. Ling
University of Tokyo, Japan

F. Tatsuoka
University of Tokyo, Japan

ABSTRACT

This paper describes a laboratory testing program which evaluated a nonwoven geotextile for reinforcing a near-saturated silty clay. The operational conditions of a soil-geosynthetic composite in a propped wall, in particular the in-situ stresses and the drainage conditions, were simulated using an automated plane strain device. The test results showed a greater reinforcement effect, in terms of strength and stiffness, for the anisotropically consolidated specimens when compared to the isotropically consolidated specimens, and in both cases, the reinforcement effect has been greater in the drained test when compared to the corresponding undrained test. This investigation indicated the possibility of using low-quality soil as backfill in the reinforced retaining wall with the aid of a permeable nonwoven geotextile.

INTRODUCTION

More than a decade has elapsed since reinforced soil was developed for civil engineering construction. Recently, there is a trend that engineers are trying to put it into permanent use (e.g., Tatsuoka and Leshchinsky, 1993) while on the other hand trying to minimize its construction cost. The conventional reinforced soil structure which uses metallic strips may not be cost effective as it strictly precludes the utilization of low quality backfills. Therefore, the possibility of using on-site soil, which may be cohesive and near-saturated, as backfill of the reinforced soil structure warrants to be studied.

One of the earliest means for studying the mechanism of soil reinforcement has been the triaxial compression test, in which a cylindrical sand-geosynthetic composite was sheared after having been consolidated isotropically (e.g., Yang, 1972). It was reported that the failure strength obtained in the reinforced specimen was greater than that of the unreinforced specimen under otherwise identical conditions. This testing method was also used to study the mechanism of reinforcement in clay-geosynthetic composite under drained and undrained conditions (e.g., Ingold and Miller, 1982; 1983; Yamauchi, 1986; Fabian, 1988). Figure 1a shows the typical result when a spun-bonded nonwoven geotextile was used to reinforce clay, in which no reinforcement effect was realized at undrained condition. The drained test result will be elaborated subsequently.

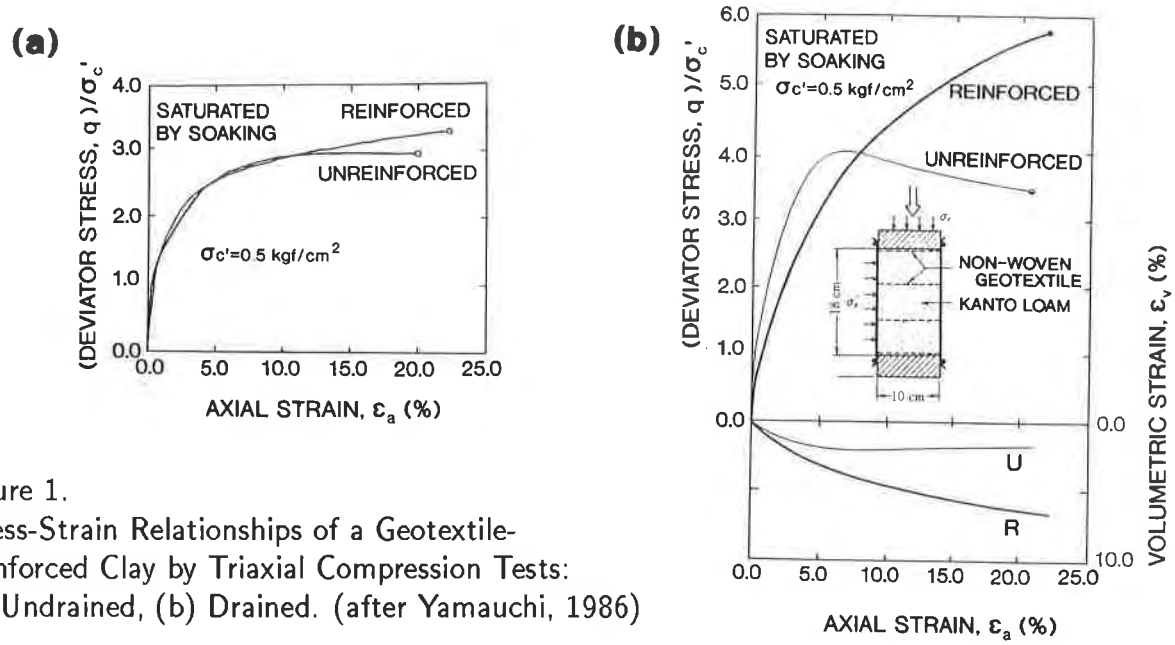

Figure 1.
Stress-Strain Relationships of a Geotextile-Reinforced Clay by Triaxial Compression Tests: (a) Undrained, (b) Drained. (after Yamauchi, 1986)

In contradiction to the results obtained by the laboratory triaxial compression tests, particularly those using an isotropically consolidated undrained specimen, the full-scale prototype model tests (Tatsuoka and Yamauchi, 1986; Murata et al., 1991) constructed with the similar type of nonwoven geotextile and cohesive soil performed satisfactorily. The geosynthetic having a drainage function increased the density of soil, and therefore the failure strength, as can be realized in a drained test (Figure 1b), which may be considered as a result of enhancement in confining stress. However, this does not serve to explain wholly the contradiction in performance between the field and laboratory tests because the stiffness obtained at working strain levels in the reinforced specimen has been less than that in the unreinforced specimen (Figure 1b).

Besides the partially saturated condition in the field, the authors realized that contradiction between the performance of field and laboratory triaxial tests, as described above, could have been mainly because the operational conditions were not simulated correctly from the following view points:

1. The prevailing field condition is plane strain whereas the conventional triaxial test can simulate only an axisymmetric stress condition in which the magnitude of the minor and intermediate principal stresses being equal. It is known that the behavior of soil in plane strain is different from that in triaxial compression. There were studies in the literature reporting the behavior of reinforced soil performed using the plane strain apparatus (McGown et al., 1978; Tatsuoka and Yamauchi, 1986; Whittle et al., 1992), but limited to the isotropically consolidated specimen of sand.

2. The soil in the field is at an anisotropically consolidated state whereas isotropic consolidation has been assumed in the previous studies, which might have significant effects on the soil and geosynthetic from the following arguments:

   (a) The soil behaves differently after having been consolidated isotropically or anisotropically, and a rigorous analysis would require its properties to be determined based on

the anisotropically consolidated specimen (e.g., Ladd, 1991).

(b) When subjected to the incremental construction sequence, a geosynthetic embedded in a vertical wall is always in an 'active state' in which a considerable amount of tensile strain has been mobilized. Even for a propped wall, the strain in it should be close to zero-lateral strain condition. However, when consolidated isotropically, the geosynthetic is compressed in its axial direction, and therefore, does not function as tensile reinforcement until a relatively large shear strain has occurred in the soil upon further loading.

The above mentioned factors undoubtedly rendered a different performance of the simulated soil-geosynthetic composite in the isotropically consolidated triaxial compression test, in terms of strength and stiffness, when compared to that actually existing in the field. In this study, an apparatus has been developed, with an automated stress path control system, which enabled a better understanding of the performance of reinforced soil mass under operational conditions (that is, anisotropically consolidated plane strain compression). The behavior of reinforced clay under both undrained and drained conditions, which is hitherto poorly understood when compared to that of the reinforced cohesionless soil, was studied. The testing program and preliminary results are presented and subsequently discussed.

AUTOMATED PLANE STRAIN TESTING SYSTEM

A rectangular prism specimen of soil or soil-geotextile composite with dimensions 12 x 9.7 x 6.2 (cm) was used (Figure 2a). It was constrained from any lateral strain in the direction of intermediate principal stress (σ_2) using two confining plates. Note that for this apparatus, the length in the minor principal stress direction (σ_3) was designed to be greater than that of σ_2. Four load cells were used to measure precisely the axial load (σ_1), σ_2, and the side friction which may exist between the specimen and the confining plates. However, it was found that very small side friction, at most 5 percent of the peak axial load, existed in this apparatus when the friction elimination technique using the silicon grease layer (Tatsuoka et al., 1984) was used. The friction at the top and bottom ends of the specimen was successfully eliminated using a similar technique.

The effective confining stress was measured using two high-capacity differential pressure transducers (DPT, denoted by 8 and 9 in Figure 2b) located at the top and bottom of the specimen. The cell pressure was also measured with a high capacity DPT (7) for the purpose of stress path control. Meanwhile, a low-capacity DPT (6) and a LVDT were used to measure the volume change and axial displacement, respectively, in the specimen. Besides, the photogrammetric method was used to observe its deformation in σ_2-plane through one of the confining plates which was made of plexiglass. The possible lack of confinement between the specimen and the confining plates in σ_2-direction at the initial stage of shearing, as a result of volumetric contraction during isotropic consolidation, has been successfully overcome by attaching two pieces of metallic wedge to the confining plate. At the end of consolidation, a string connecting them to the external of the triaxial cell was pulled along the length of the wedge to drive the confining plates inward in σ_2-direction.

A feedback stress path control system was incorporated with this apparatus using a pair of analog-to-digital (A/D) and D/A converters, and an electro-pneumatic (E/P) transducer. A computer program, which was coded in Fortran and Assembly languages, was developed to ensure

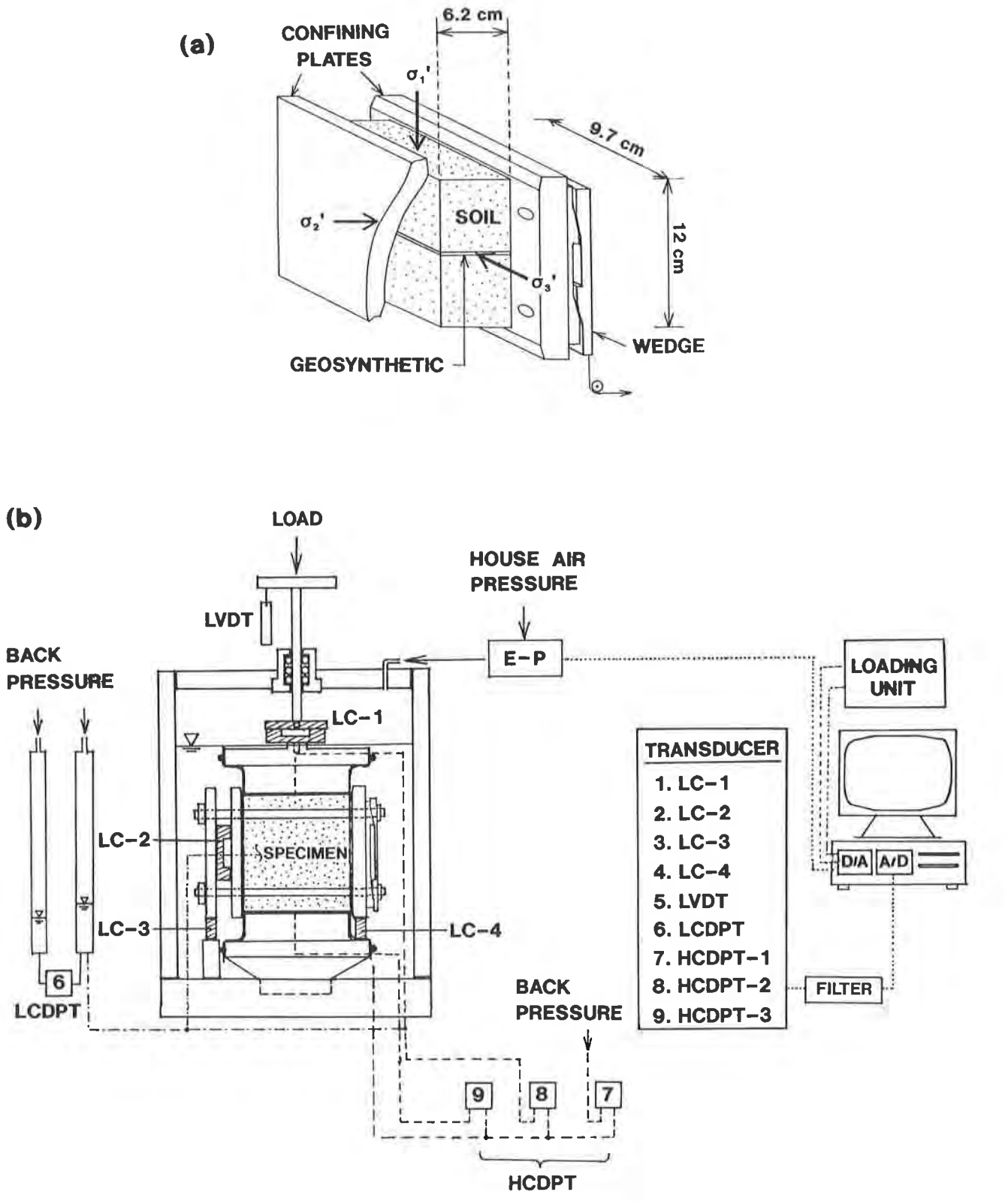

Figure 2. (a) Configuration of Specimen, (b) Automated Plane Strain System. (not to scale)

the efficiency of control. Based on the measured effective axial stress, it calculated the required air pressure, which was supplied to the E/P transducer in the form of direct current through the D/A converter, for controlling the specified stress paths. The stress ratio, which is defined as the ratio of the minor principal stress to the major principal stress ($K = \sigma_3'/\sigma_1'$), was used to control the stress path during anisotropic consolidation. In addition to transmitting voltage to the E/P transducer, the D/A converter also controlled the axial loading unit in this study. Note that the isotropic consolidation was also achieved by means of this system.

Additional details related to this automated plane strain system are found in Ling (1992).

TESTING PROGRAM

A series of plane strain compression tests were performed on both unreinforced and reinforced specimens under undrained (U) and drained (D) conditions, which are of major concern in the short and long-term stability analysis, after having been consolidated isotropically (I) or anisotropically (K). Table 1 summarizes the details of this testing program.

Table 1. Testing Program

Test	Final Consolidation Stress (kgf/cm^2)	Initial Dry Density γ_d (g/cm^3)	Initial Water Content w_i (%)	Initial Void Ratio e_o
1. CIU	$\sigma_1' = \sigma_3'$ = 0.50	0.668	105.23	3.07
2. CIU(R)		0.636	109.08	3.29
3. CID		0.645	117.64	3.46
4. CID(R)		0.724	94.69	2.91
5. CKU	$\sigma_1' = 1.67$ $\sigma_3' = 0.50$	0.772	88.30	2.68
6. CKU(R)		0.686	91.51	3.02
7. CKD		0.750	90.65	2.89
8. CKD(R)		0.729	92.17	2.82

(R) indicates reinforced specimen.

The soil specimen was prepared wet of the optimum water content by compaction in a mold simulating a compaction energy of 5.95 kgf·cm/cm^3 (ASTM Standard D 1557-78). The soil was first compacted into three layers to the mid-height, and the geosynthetic layer was placed. Then, compaction of the soil was continued until it reached the required height. The top end of the specimen was trimmed, installed to the device, and saturated using the dry mounting method (ASTM Standard D 4767-88) under a back pressure of 1.0 kgf/cm^2 (98 kPa). This method has ensured a high degree of saturation in which the measured Skempton's B-value was between 0.96 - 0.99.

The specimen was initially consolidated isotropically to a low confining stress (point A in Figure 3a), and then either isotropically or anisotropically following the specified stress path. After having attained the specified effective confining stress (point C in Figure 3a), the consolidation was allowed for a further 8 hours before shearing was initiated. A swelling-reconsolidation loop was also allowed during consolidation. This paper reports the tests conducted at an effective

confining stress, σ_3', of 0.5 kgf/cm^2 (49 kPa). The rate of consolidation and shearing were both selected as 0.01 percent per minute for the drained and undrained tests, and each test typically took four days to be completed.

PROPERTIES OF SOIL AND GEOTEXTILE

A silty clay, called Kanto Loam, which is widely available near the Metropolitan Tokyo area, was selected for this study. Its index properties are summarized in Table 2. This soil has been used for constructing the test embankments (Tatsuoka and Yamauchi, 1986; Murata et al., 1991), and is being considered a potential candidate for the actual construction of highway and railway embankment with a geotextile having a drainage function.

Table 2. Index Properties of Kanto Loam

Natural water content:	96.7 %
Specific gravity:	2.77
Mean grain diameter, D_{50}:	0.0126 mm
Sand fraction:	13 %
Silt fraction:	57 %
Clay fraction:	30 %

A spun-bonded needle-punched nonwoven geotextile, which has been used in the previously mentioned laboratory triaxial tests and for constructing the test embankments, was used. Its hydraulic and mechanical properties have been thoroughly studied (Ling et al., 1990, 1991, 1992, 1993). The in-plane hydraulic conductivity and axial load-strain relationships of this nonwoven geotextile are highly dependent on the confining stress. Under stress confinement, it is known that the hydraulic conductivity reduces whereas the stiffness and strength increases.

RESULTS AND DISCUSSIONS

The test results for the reinforced and unreinforced specimens at an effective confining stress of 0.5 kgf/cm^2 (49 kPa) are presented in Figures 3 to 10. Note that for the anisotropically consolidated specimens, the effective axial stresses (σ_1') at the end of consolidation was 1.667 kgf/cm^2 (163.37 kPa), since K ($=\sigma_3'/\sigma_1'$) equals 0.3.

Axial Strain of Geotextile at the End of Consolidation. Figure 3b shows the relationships between the axial and lateral strains (ε_1 and ε_3) of the reinforced specimens during isotropic and anisotropic consolidations. The lateral strain, ε_3, was determined indirectly based on the measured axial strain, ε_1, and volumetric strain, ε_v, in the specimen (since $\varepsilon_v = \varepsilon_1 + \varepsilon_3$). At the initial stage of anisotropic consolidation before the desired K value was attained (from point A to point B in Figure 3), the axial load was increased without any increase in the cell pressure, which allowed the lateral tensile strain to be mobilized to a small extent. The lateral strain at the end of anisotropic consolidation (point C in Figure 3) was close to that of the zero-lateral strain condition, and therefore, simulated the condition in a propped wall. On the other hand, it is seen that at the end of isotropic consolidation, the geotextile has been compressed laterally to a greater extent in σ_3-direction when compared to that of the anisotropically consolidated specimen. A kink in the curves was due to the unloading/reloading cycle intentionally applied.

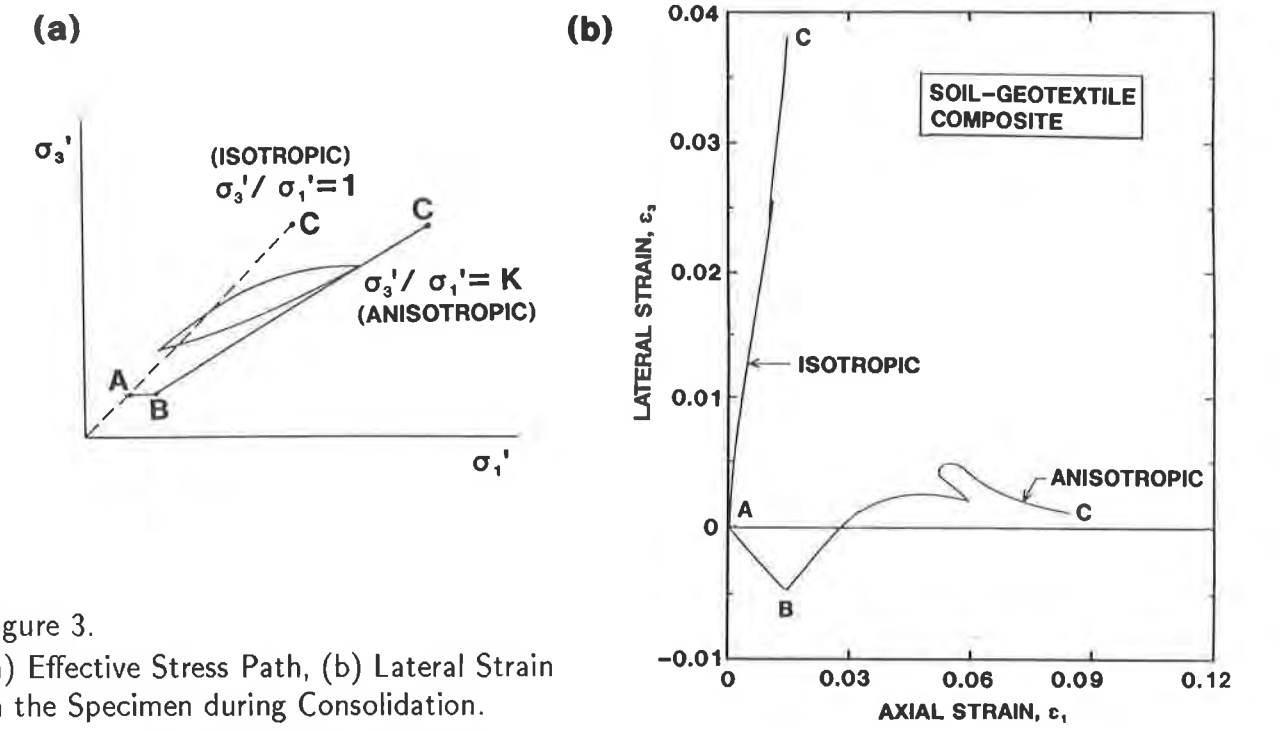

Figure 3.
(a) Effective Stress Path, (b) Lateral Strain in the Specimen during Consolidation.

Stress-Strain Relationships of Reinforced and Unreinforced Specimens. The deviatoric stress-axial strain ($Q - \varepsilon_1$) relationships are shown in Figures 4 and 5 for the undrained and drained tests, respectively, for which $Q = \sigma_1' - \sigma_3'$. The effective stress path for the tests, expressed as ($P' = (\sigma_1' + \sigma_3')/2$, $Q/2 = (\sigma_1' - \sigma_3')/2$), are shown in Figures 6 and 7 for the undrained and drained tests. The effective stress paths are linear for the drained tests, whereas in the undrained tests, they deviated from linearity because of the build-up of positive excess pore water pressure.

Due to anisotropic consolidation, which could have led to a change in the soil fabric structure, the initial portion of Q versus ε_1 curve exhibited a high stiffness. Despite slight variation in the soil index properties as indicated in Table 1, the test produced very consistent results. In the unreinforced undrained tests, the peak stress was attained before 10 percent axial strain level, and after which it remained quite constant. However, the unreinforced drained tests and the reinforced specimens (both drained and undrained) showed a strain hardening behavior without any distinct peak load until the test has been terminated.

From the results, it is seen that at large strain levels, the deviatoric stress is always greater in the reinforced specimens when compared to that of the unreinforced specimens. The low deviatoric stress at small strain levels in the undrained reinforced specimens (isotropically consolidated) when compared to that of the reinforced specimen (Figure 4a) could have been due partly to (i) the lower initial density of soil, and (ii) the compressibility of geotextile in the thickness direction. It has also been due to the positive excess pore water pressure, which was greater in the reinforced specimens when compared to the unreinforced specimens (Figure 8).

Figure 9 shows the volumetric strain versus axial strain relationships of the drained tests, in

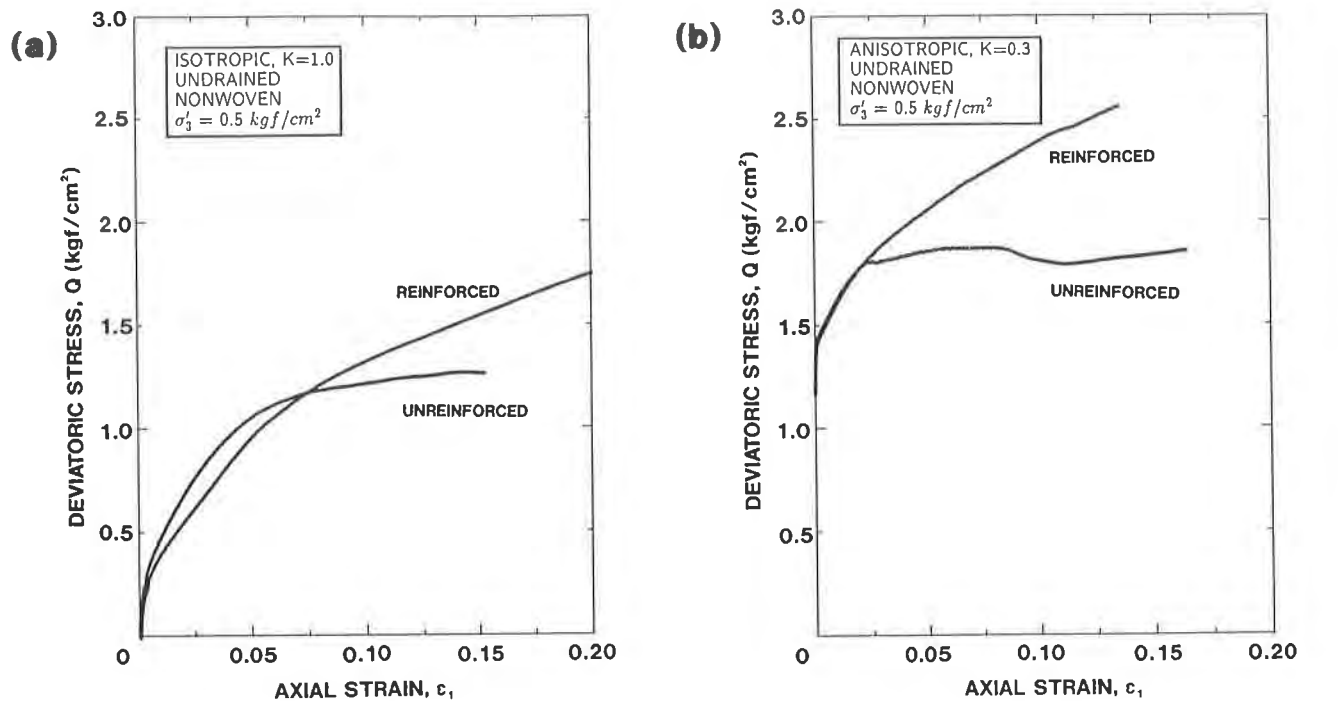

Figure 4. Deviatoric Stress Versus Axial Strain in Undrained Tests: (a) Isotropic, (b) Anisotropic.

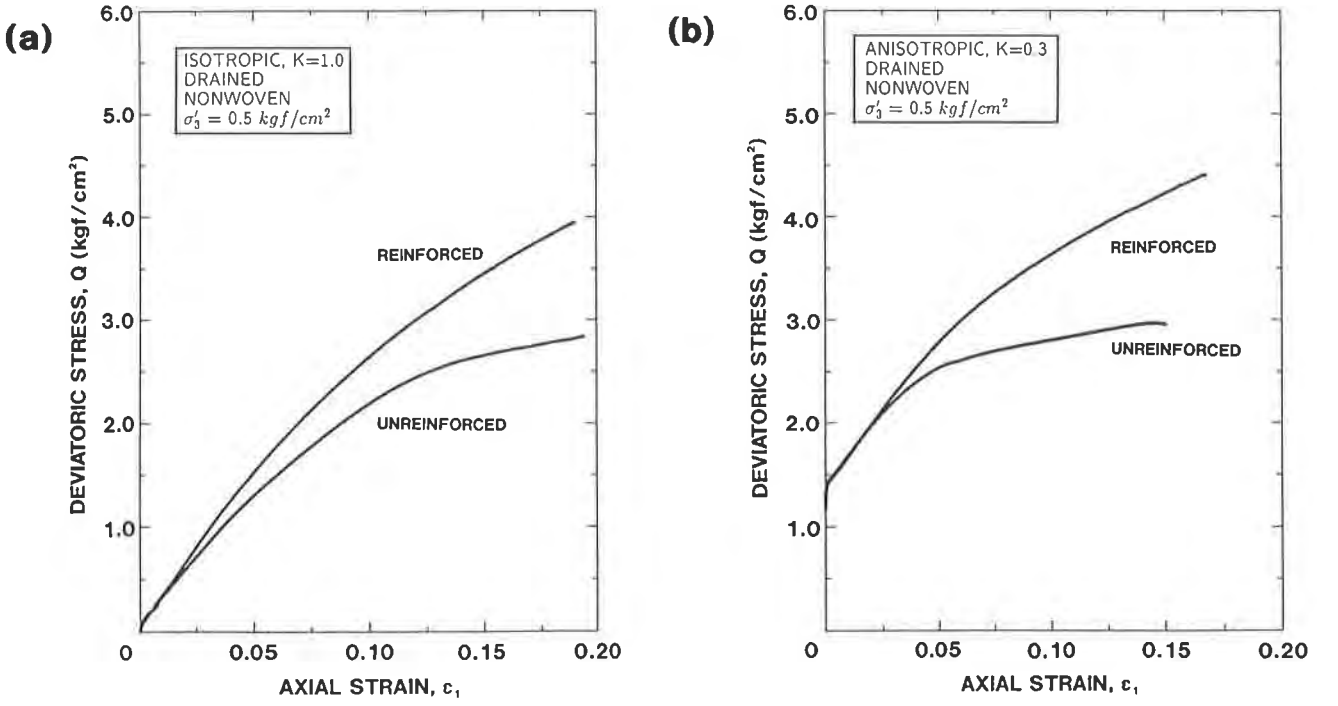

Figure 5. Deviatoric Stress Versus Axial Strain in Drained Tests: (a) Isotropic, (b) Anisotropic.

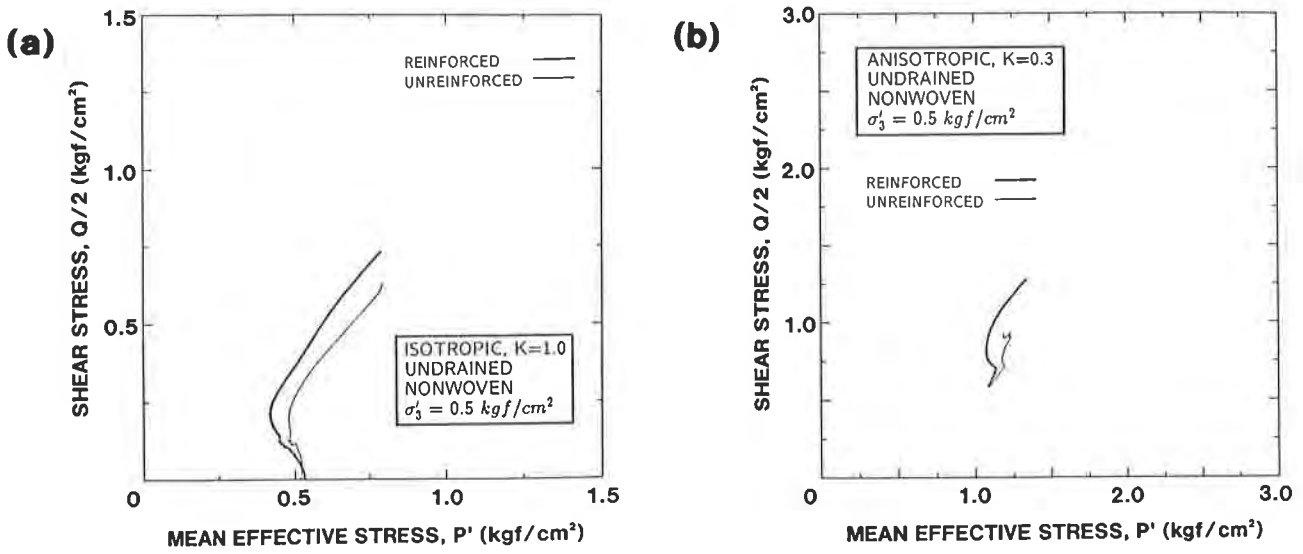

Figure 6. Effective Stress Path in Undrained Tests: (a) Isotropic, (b) Anisotropic.

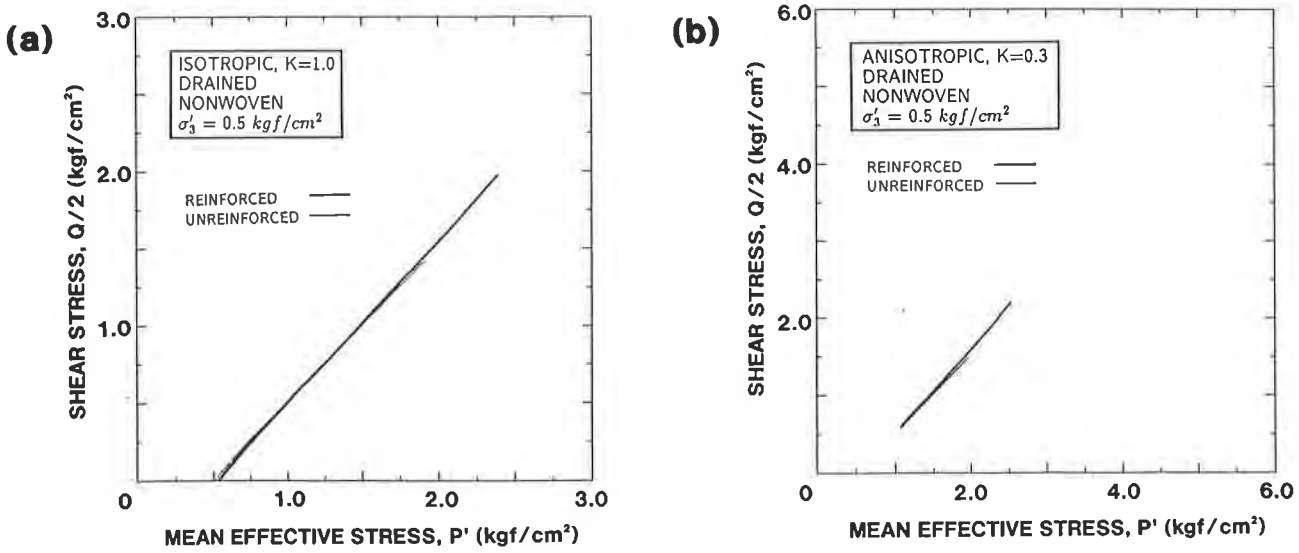

Figure 7. Effective Stress Path in Drained Tests: (a) Isotropic, (b) Anisotropic.

which a greater volumetric strain has been noticed for the reinforced specimens when compared to the unreinforced specimens at the same axial strain level. Upon further investigation, it was found that the larger volumetric strain in the reinforced specimens has been due to the larger deviatoric stress applied, and this tendency was larger in the anisotropically consolidated specimens when compared to the isotropically consolidated specimens.

There are two contradictory aspects of the mechanism of reinforcement; the development of positive excess pore water pressure induced a negative effect whereas the mobilization of tensile strain in the geosynthetic gave rise to a positive effect, both of which affected the performance

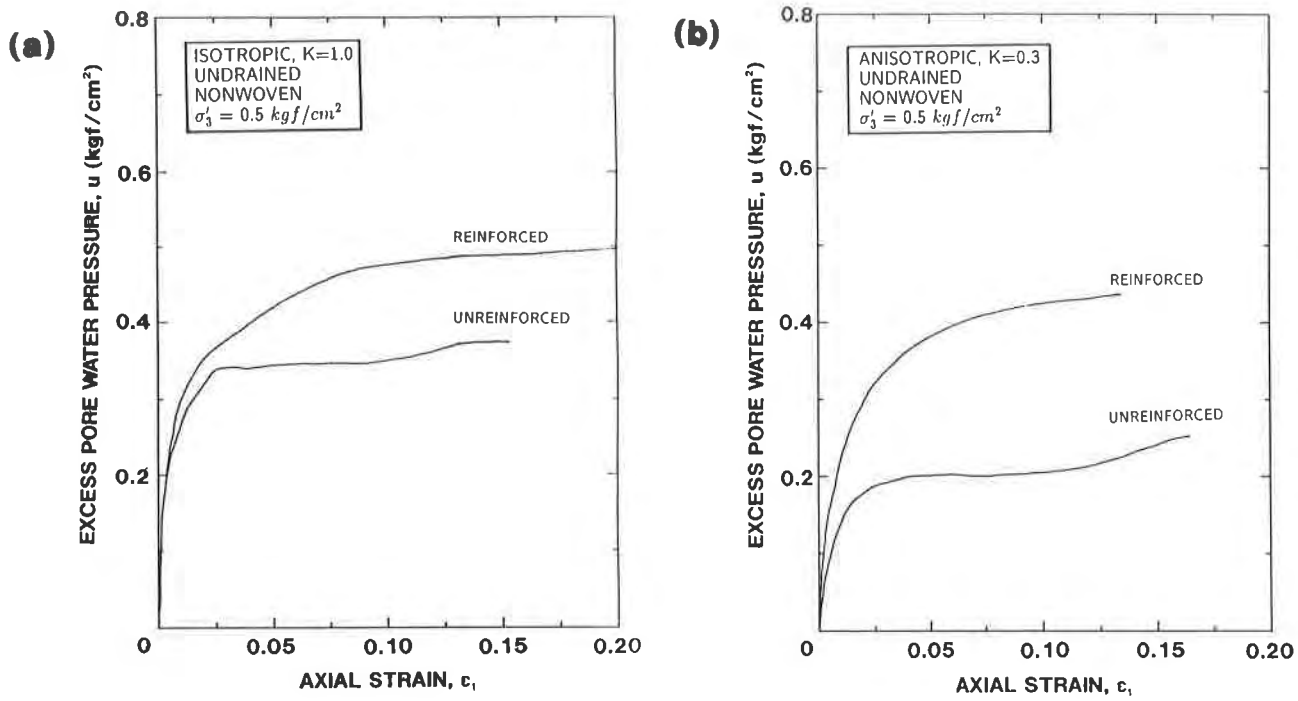

Figure 8. Excess Pore Water Pressure in Undrained Tests: (a) Isotropic, (b) Anisotropic.

of reinforced specimens at undrained condition. During the initial stage of undrained shearing, the negative effect might have suppressed the positive effect, which resulted in a lower deviatoric stress in the reinforced specimen when compared to the corresponding unreinforced specimen, and vice versa at the later stage of the test. The mobilized stress of reinforced specimen exceeded that of unreinforced specimen at about 7.5 and 2.5 percent axial strain, respectively, in the isotropically and anisotropically consolidated tests. However, in the absence of negative effect, the drained tests rendered a larger deviatoric stress in the reinforced specimen when compared to the corresponding unreinforced specimen, and therefore, a greater reinforcement effect has been obtained when compared to the undrained tests.

To the authors' observation, the shear bands which developed in the unreinforced undrained tests did not appear in the reinforced undrained tests. The inclusion of a layer of geotextile has prevented the development of shear band through it and the entire specimen. It seems that this mechanism contributed largely to the increase in strength in the reinforced undrained specimens at large strain levels.

Strength and Stiffness of Reinforced Specimens. Table 3 summarizes the strength at failure and the secant shear modulus at 5 percent axial strain level for the tests. The failure strength is determined as the peak deviatoric stress for the tests which exhibited strain softening behavior or the deviatoric stress at 15 percent strain level for those exhibiting strain hardening behavior. The strength ratio (defined as the failure strength of reinforced specimen to that of unreinforced specimen) and the stiffness ratio (defined as the secant shear modulus at 5 percent strain level of reinforced specimen to that of unreinforced specimen) for the tests are also summarized. In both the undrained and drained tests, the reinforcement effect was greater in the anisotropically consolidated specimens when compared to those consolidated isotropically. Moreover, different from

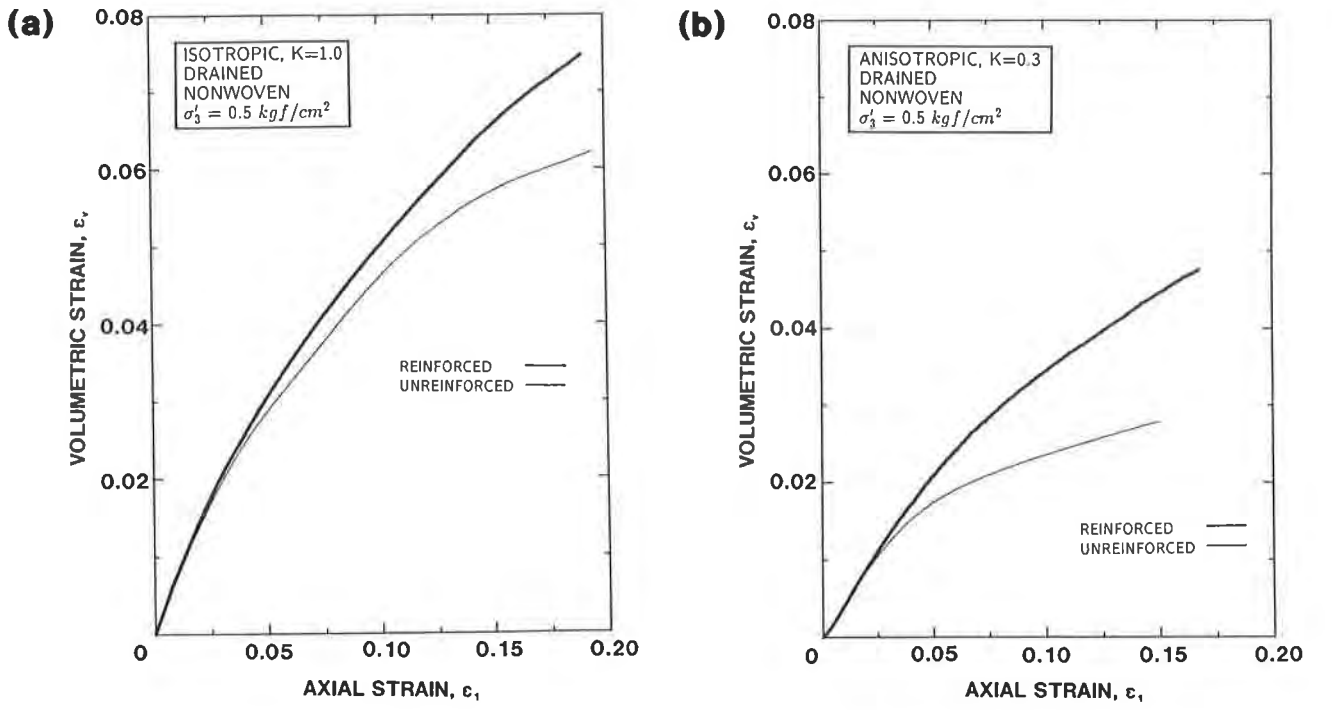

Figure 9. Volumetric versus Axial Strains in Drained Tests: (a) Isotropic, (b) Anisotropic.

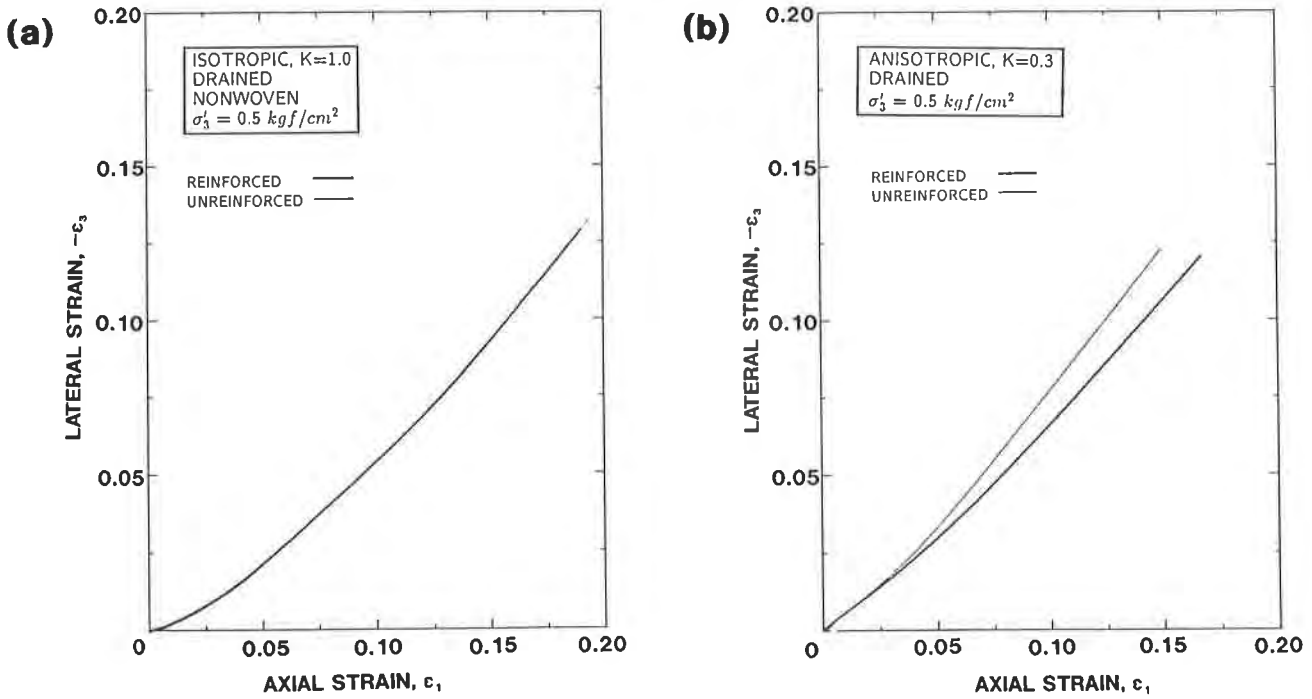

Figure 10. Lateral versus Axial Strains in Drained Tests: (a) Isotropic, (b) Anisotropic.

what has been noticed in the conventional triaxial compression tests on isotropically consolidated specimen as reported in the literature (e.g., Figure 1b) the stiffness ratio has been greater than unity for the anisotropically consolidated specimens.

Table 3. Failure Strength and Secant Shear Modulus of Reinforced and Unreinforced Specimens

Test	Failure Strength Q_f (kgf/cm^2)	Shear Modulus at 5% axial strain G_{sec} (kgf/cm^2)	Strength Ratio	Stiffness Ratio
1. CIU	1.263	10.474		
2. CIU(R)	1.548	8.667	1.23	0.83
3. CID	2.653	18.228		
4. CID(R)	3.451	21.914	1.30	1.20
5. CKU	1.835	6.896		
6. CKU(R)	2.568	8.771	1.40	1.27
7. CKD	2.961	16.397		
8. CKD(R)	4.230	20.206	1.43	1.23

The greater strength and stiffness ratios of the anisotropically consolidated specimens when compared to the isotropically consolidated specimens can be explained with reference to its effects on the properties of geotextile, as follow:

1. At the end of anisotropic consolidation, the axial strain in the geotextile was ready to be activated whereas that of the isotropically consolidated specimen remained to be compressed (Figure 3b). Upon shearing, the tensile strain was mobilized rather rapidly in the anisotropically consolidated specimen which restrained its lateral deformation (Figure 10b), whereas in the isotropically consolidated specimen, it was delayed until shearing occurred to a larger extent that lateral restraining effect was insignificant (Figure 10a).

2. The stiffness and strength of this nonwoven geotextile are highly dependent on the pressure level. At an identical effective confining stress, the effective axial stress acting on the anisotropically consolidated specimen is much larger than that acting on the isotropically consolidated specimen, and therefore, rendered a larger stiffness for the nonwoven geotextile (Ling et al., 1991; 1992) which in turn affected the performance of reinforced soil mass.

CONCLUSIONS

From the results obtained in this study, it is suggested that low quality on-site soil can be improved with the use of a permeable nonwoven geotextile for retaining wall construction. It is shown that the mechanism of reinforcement can be studied in the laboratory by simulating correctly the operational conditions using anisotropic consolidation. The build-up of excess pore water pressure, which could be attributed to the compressibility of both the soil and the nonwoven geotextile, affected to a large extent the stress-strain response of reinforced soil mass at undrained conditions that only a slight reinforcement effect can be realized. However, in the drained tests, the geotextile ensured a positive reinforcement effect due to mobilization of tensile strain in it.

A proper evaluation of the stiffness of reinforced soil mass can be realized only in anisotropically consolidated test. It would be too conservative to study the performance of soil-geosynthetic composite using undrained test in case a geosynthetic with adequate hydraulic conductivity is used.

Additional test results based on different types of geosynthetic and different values of initial stress ratio (K) are highlighted in Ling (1992).

ACKNOWLEDGEMENTS

The first author would like to express gratitude to the Japanese Government for sponsoring his graduate study at the University of Tokyo. Cooperation from the members of the Geotechnical Laboratory, particularly Mr. T. Sato, and the machine shop of Institute of Industrial Science, University of Tokyo, are highly appreciated.

REFERENCES

Fabian, K. (1988). "Clay Geotextile Interaction in Triaxial Tests", Chapter 5 in Clay-Geotextile Interaction Laboratory And Model Tests, Ph.D. Thesis , University of Queensland, Australia.

Ingold, T.S. and Miller, K.S. (1982). "The Behavior of Geotextile Reinforced Clay Subjected to Undrained Loading", Proceedings of Second International Conference on Geotextiles, Las Vegas, pp. 593-597.

Ingold, T.S. and Miller, K.S. (1983). "Drained Axisymmetric Loading of Reinforced Clay." Journal of Geotechnical Engineering, ASCE, Vol. 109, No. 7, pp. 883-898.

Ladd, C.C. (1991). "Stability Evaluation during Staged Construction", Journal of Geotechnical Engineering, ASCE, Vol. 117, No.4, pp. 540-615.

Ling, H.I., Tatsuoka, F., and Wu, J.T.H. (1990). "Measuring In-Plane Hydraulic Conductivity of Geotextiles", Geosynthetic Testing for Waste Containment Application, STP 1081, R.M. Koerner, Editor, ASTM, Philadelphia, pp. 257-272.

Ling, H.I., Wu, J.T.H., and Tatsuoka, F. (1991). "Effectiveness of In-Membrane Test in Simulating Strength and Deformation Characteristics of Nonwoven Geotextiles Under Operational Conditions", Proceedings of Geosynthetics '91 Conference, Atlanta, pp. 601-614.

Ling, H.I., Wu, J.T.H., and Tatsuoka, F. (1992). "Short-Term Strength and Deformation Characteristics of Geotextiles under Typical Operational Conditions," Geotextiles and Geomembranes, Vol. 11, No. 2, pp. 185-219.

Ling, H.I. (1992). Performance of Geosynthetic-Reinforced Cohesive Soil Mass at Plane Strain Compression, Doctoral Thesis, University of Tokyo, December.

Ling, H.I., Tatsuoka, F., and Wu, J.T.H. (1993): "Hydraulic Conductivities of Geotextiles under Operational Conditions", Geotextiles and Geomembranes, Vol. 12, No.4. (to appear)

McGown, A., Andrawes, K.Z., and Al-Hasani, M.M. (1978). "Effect of Inclusion Properties on the Behavior of Sand", Geotechnique, Vol. 28, No. 3, pp. 327-346.

Murata, O., Tateyama, M., and Tatsuoka, F (1991). "A Reinforcing Method for Earth Retaining Walls Using Short Reinforcing Members and a Continuous Rigid Facing", Proceedings of Geotechnical Engineering Congress 1991, Geotechnical Special Publication No. 27, ASCE, pp. 935-946.

Tatsuoka, F., Molenkamp, F., Torii, T. and Hino, T. (1984). " Behavior of Lubrication Layers of Platens in Element Tests", Soils and Foundations, Vol. 24, No. 1, pp. 113-128.

Tatsuoka, F. and Yamauchi, H. (1986). "A Reinforcing Method for Steep Clay Slopes with a Nonwoven Geotextile", Geotextiles and Geomembranes, Vol. 4, pp. 241-268.

Tatsuoka, F. and Leshchinsky, D. (1993). Editors, Proceedings of International Symposium on Recent Case Histories of Permanent Geosynthetic-Reinforced Soil Retaining Walls, Balkema. (under press)

Whittle, A.J., Germaine, J.T., Larson, D.G., and Abramento, M. (1992). "Measurement and interpretation of reinforcement stresses in the APSR cell", Proceedings of International Symposium on Earth Reinforcement Practice, Fukuoka, pp. 179-184.

Yamauchi, H. (1986). A Reinforcing Method for Steep Clay Slopes Using a Non-Woven Geotextile, Doctoral Thesis, University of Tokyo. (in Japanese)

Yang, Z. (1972). Strength and Deformation Characteristics of Reinforced Sands, Ph.D. Thesis, University of California at Los Angeles.

Comparison of Geotextiles—The Correlation Between Test Methods and Practical Performance

J.R. Montalvo
Polyfelt Inc., USA

W. Sickler
Polyfelt Inc., USA

ABSTRACT

"Geotextile xy or equal" is widely used in specifications. What does this mean to the construction contractor? As a basis of comparing different products, values obtained from standard test methods and manufacturing literature are commonly used. Comparison based on some single test methods might be misleading due to the wide range of completely different product types, i.e. wovens, needlepunched or heatbonded nonwovens, continuous or staple fibers, etc. In addition, slight modifications of standard test procedures can lead to significant changes in test results for the different geotextile types. Furthermore, only a limited amount of correlation has been developed between standard test methods and practical applications of geotextiles.

An analysis of current standard test methods with regard to practical relevance is needed. Large scale field studies by others, which consisted of exhuming many different types of geotextiles, are used in an attemp to compare geotextile's field performance. Specifically, published studies such as: GRI Assessment of Installation Damage of Geotextiles, Swiss Association of Geotextile Experts (SVG), and previous geotextile's conference papers as well as in house field studies, are used to better correlate the equivalency of different types of geotextiles. Stress-strain characteristics of fabrics are used to better correlate the equivalency of different types of geotextiles. The short and long-term behavior of a fabric is analyzed showing significant differences in the results compared with short-term tests and their stress-strain properties.

INTRODUCTION

The geotextile market has increased dramatically in recent years as a result of new uses and awareness by the designing engineers. Geotextiles in all forms can trace their origin back to the textile industry rather than to civil engineering which in part explains the early adoption of textile test methods, largely based on woven products. However, the increasing uses of nonwoven geotextiles to provide high performance separation, filtration, and stabilization functions in civil engineering applications demand a fresh look at the validity of current specification assessment criteria and test methods.

Test results obtained using standard testing methods for geotextiles according to ASTM, ISO, DIN, NFG or any other well known standard organization, are just an indication of that property value under the test condition and in most cases do not approximate the actual situation at a site. Slight modifications of standard test procedures can lead to significant changes in test results for the different geotextile types. Complete reliance on laboratory test results might lead to misrepresentation of the simulated situation and consequently to the erroneous selection of the required geotextiles.

The selection of a geotextile and establishment of user specification for a particular field application is often difficult for the potential geotextile user due to a general lack of knowledge relative to the impact of the laboratory test condition such as: clamping length, sample size, test speed, etc., on the geotextile properties and performance.

GEOTEXTILE PROPERTY

The benefit offered by a geotextile to the fabric-soil system for its service life depends to a large extent on the inherent properties of the geotextile used. There are distinct differences in the mechanical behavior of geotextiles since there is a distinct difference in the mechanical structure of them.

Specific properties of significance relative to the optimum use of geotextiles are numerous, although the exact contribution of each is largely unknown. Bell, et al. [1] have listed and discussed in detail a large number of geotextile properties of apparent significance in the broad sense of geotechnical applications which include the following: strength, elongation, modulus, creep, fatigue, tear and puncture resistance, abrasion resistance, permeability, filtration, clogging, biological stability, chemical resistance, and ultraviolet light stability. This list of geotextile properties is great, and in a qualitative sense, all may appear significant. However, the minimum, maximum or optimum level of each property and the combined or interactive effect of these properties are yet to be fully understood and quantified. Test methods to evaluate specific properties have not yet been universally accepted. Currently laboratory tests provide the basis for the selection of the appropriate geotextile type. But, the results obtained from today's methods are only suitable for comparing two geotextiles within certain limitations as they do not take into account specific stresses and site demands.

TENSILE STRENGTH TEST

Numerous tests have been developed for determining the stress-strain characteristics of geotextiles. The most widely used tests are the grab tensile (ASTM D 4632) and wide width strip tensile (ASTM D4595). Both of these tests provide a mean to determine the modulus and strength of the fabric. However, because of the difference in boundary conditions between laboratory and field, neither test provides properties representative of field conditions. When a geotextile is placed in the fabric-soil system, the geotextile may behave in a substantially different manner because of the presence of soil. McGown, et al. [2] reported that the modulus of fabrics in soil situation may be 2-3 times the value in isolation. Complicating the situation even more is the fact that most fabrics are anisotropic; i.e. they have properties which depend upon orientation.

The laboratory clamping conditions for the tensile tests have a great influence in the final result [3,4,5]. In the standard geotextile tensile test method, ASTM D4595, a sample is fixed with a gauge length of 100 or 200 mm and tensioned until rupture occurs. However, this procedure seems to be unsuitable to simulate the actual tensile mechanism inside the soil-geotextile system because of two reasons:

1. The geotextiles are tested without soil confinement. The interlocking effect between soil and geotextile reduce the fiber slippage and therefore higher strength and lower elongation are yielded in the field as compared to standard laboratory tensile test.

2. The geotextiles are "confined" by the soil particles in contact with the fibers in a soil confining condition. The sample's gauge length of 100 or 200 mm is much too high to simulate the actual stress-strain mechanism of the soil-geotextile system.

In order to evaluate the influence of the testing gauge length (confined or unconfined test), a series of tests with woven and nonwoven geotextiles has been carried out, with gauge length of 200 mm and 3 mm [6]. Table 1 shows clearly a great difference in the stress-strain behavior between the large (200 mm) and short (3 mm) gauge distances as well as the difference between wovens and nonwovens. The decrease in the gauge distance produced an increase in the tensile strength. The tensile

strength of the wovens showed an increase of approximately 30%. The nonwoven strength experienced an increase of 65% for the heavy weight, and up to 125% for the light weight geotextile. These test results clearly present the great difference on the behavior of a nonwoven geotextile when tested confined or unconfined.

Table 1. Tensile Strength of Geotextiles with 200 mm and 3 mm Gauge Distance [6]

Geotextile Type	Weight (g/m2)	Tensile Strength (DIN 53857) lo = 200 mm (N/5 cm)	lo = 3 mm (N/5 cm)	Percent Increase
PP Continuous Filament NW	60	137	307	+ 124 %
	90	254	573	+ 126 %
Needlepunched	400	1030	1696	+ 65 %
PP Slit Film Woven	130	973	1300	+ 34 %
	380	3158	4066	+ 29 %
	540	3437	4490	+ 31 %

McGown et al. [7] have shown the effect of confining pressure on the tensile stress-strain characteristics of geotextiles by comparing results obtained from both unconfined and confined "wide width strip" tests. The results of this study suggest that the properties determined from an unconfined wide width strip test are conservative, and that for woven geotextiles there was no significant difference between the properties determined from a confined or unconfined test. In view of these findings, together with consideration of the cost and practical difficulties associated with performing confined tests, it appears to be generally accepted that the unconfined wide width strip test is the most suitable available test for determining the stress-strain properties of geotextiles.

BURST STRENGTH

Geotextile manufacturers have traditionally used the Mullen Burst Method (ASTM D 3786) to identify the burst characteristics of their products. This method was adopted by the textile industry as a standard quality control test. However, after several years of evaluating the results, the procedure has not been found to correlate with field performance. A test specimen 125 mm (5 in.) in diameter is clamped without tension between two steel clamp surfaces a minimum of 75 mm (3 in.) in diameter containing a coaxial aperture of 31 mm (1.22 in.) in diameter. It is known that the test has a significant boundary influence due to the small specimen size evaluated, which leads to erroneous, misleading results. For example, the test imparts a significant bias to results obtained for staple filament products (typically made from short 2 to 3 inch long filaments). The test essentially evaluates the filaments rather than the fabric structure.

For stabilization applications, the burst strength requirements will depend on the applied pressures and aggregate size. Minimum burst strengths for a range of particle sizes can be estimated using Figure 1 [8]. For example, for aggregates less than two inches, the burst strength requirement would be on the order of 50 to 100 psi for lightweight construction equipment, such as bulldozers, and 100 to 200 psi for heavyweight equipment, such as loaded dump trucks.

In order to accurately evaluate the burst characteristics of a geotextile, the size of the specimen must be adequate to evaluate the total structure of the material, as the fabric structure controls its stress-strain response. There is a distinct difference in the mechanical structure and behavior of geotextiles with varied filament types, bonding methods, and manufacturing processes. Recently, a new Large Diameter Multiaxial Burst procedure has been standardized by the Geosynthetic Research Institute (GM4-89) and the Canadian Geotechnical Society (CGSB148.1-6). This procedure should be considered for evaluating geotextile performance when burst resistance is an important design characteristic. Figure 2 shows comparative results using both the Mullen Burst and the Large Diameter Multiaxial Burst procedures performed on three geotextiles with equivalent mass per unit area (340 g/m2). Even though published values (1992 GFR Geotextile Products) for Mullen Burst on staple filament products appear to be higher, in house laboratory actual test data indicates otherwise. The large diameter procedure

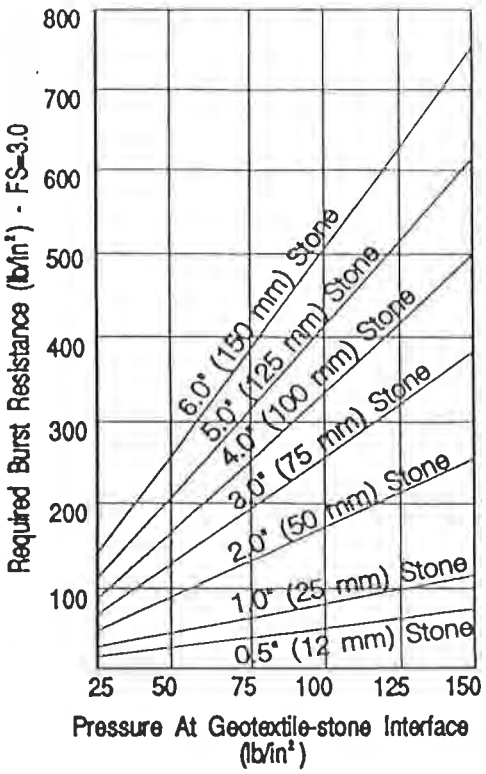

Figure 1. Burst Strength Requirements As a Function of the Applied Pressures and Aggregate Size [8].

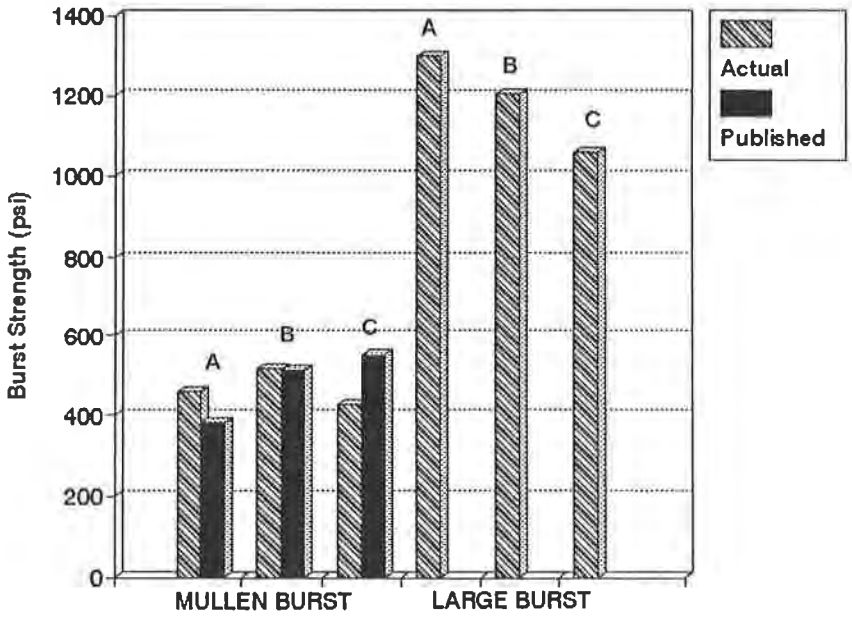

A: NW-PP(Cont.) B: NW-PET(Cont.) C: NW-PP(Staple)

Figure 2. Comparative Results Using Both Mullen Burst and Large Diameter Multiaxial Burst Test Procedures, Approximately 340 g/m2 Geotextiles.

also allows for the evaluation of the biaxial stress-strain characteristics of geotextiles, Figure 3. The results of the large diameter burst indicate a higher burst strength for the continuous filament geotextiles.

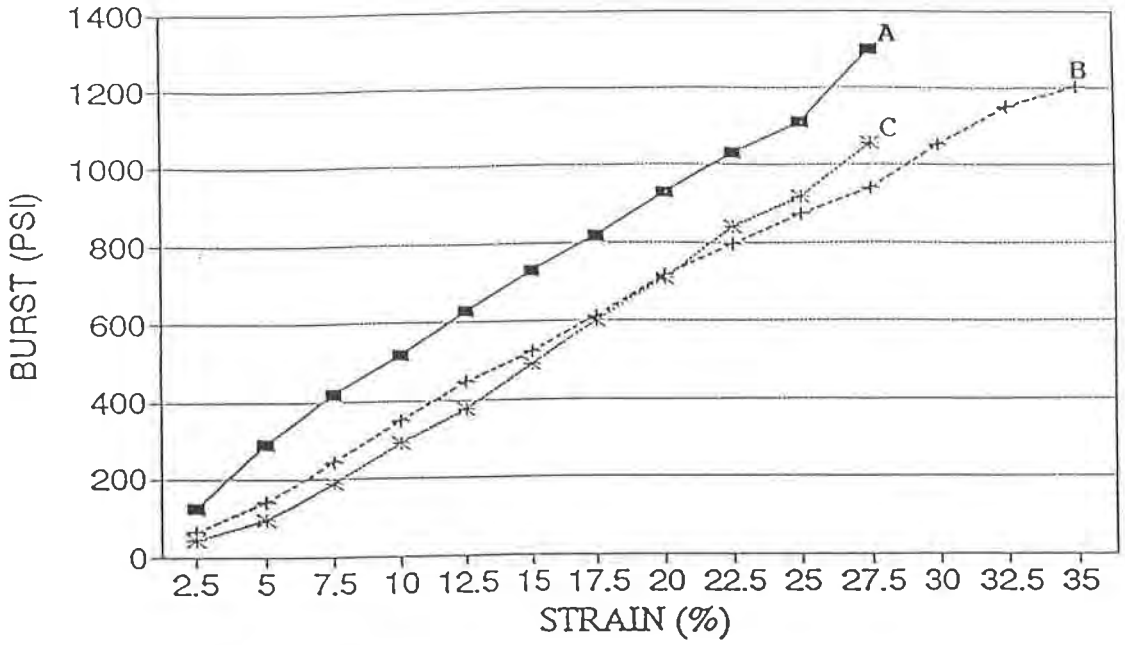

A: NW-PP(Cont.) B: NW-PET(Cont.) C: NW-PP(Staple)

Figure 3. Comparative Evaluation of The Biaxial Stress-Strain Characteristics of Three Typical 340 g/m2 Nonwoven Geotextiles Using The Large Burst Test Method.

INSTALLATION AND PUNCTURE CRITERIA

The greatest mechanical strain on geotextiles occurs during installation through contact with sharp edged fill material. In the following, two important criteria will be drawn upon to evaluate the quality of a geotextile: the puncture resistance and tear resistance tests. Furthermore, various practical experiences and application recommendations will be analyzed.

Puncture Resistance. There are two commonly used standard puncture resistance tests. The standard puncture resistance test according to ASTM D4833 using a 5/16" steel rod does not properly simulate actual field conditions of a sharp object or sharp rock penetrating the structure of the fabric, Figure 4. The test shows the absorption of force when the geotextile absorbs a concentrated load. The standard puncture resistance test (CBR Puncture Test) according to DIN 54307 using a flat piston end, Figure 5, only approximates the actual situation through its simulation. Here a geotextile specimen is clamped in an annular clamp and a piston is impressed upon its surface until penetration is achieved. Clearly this test is atypical of practical application since the flat piston, according to DIN 54307, does not adequately simulate sharp-edged aggregates which is the most important source of stress to a geotextile. This test better evaluates the puncture resistance of the fabric because of the large sample size, so the structure of the geotextile is the one being tested.

Both of these puncture tests evaluate the puncture resistance of the fabric without consideration of the soil, so the results can be used only indirectly. To approximate field conditions, i.e. sharp edged angular stones, the flat piston (DIN 54307, CBR Puncture) was replaced with a pyramidal piston point, 50 mm in diameter, Figure 6 [9]. Table 2 presents pyramid puncture resistance results as compared to the flat CBR piston test. Three different types of fabrics were evaluated, a nonwoven

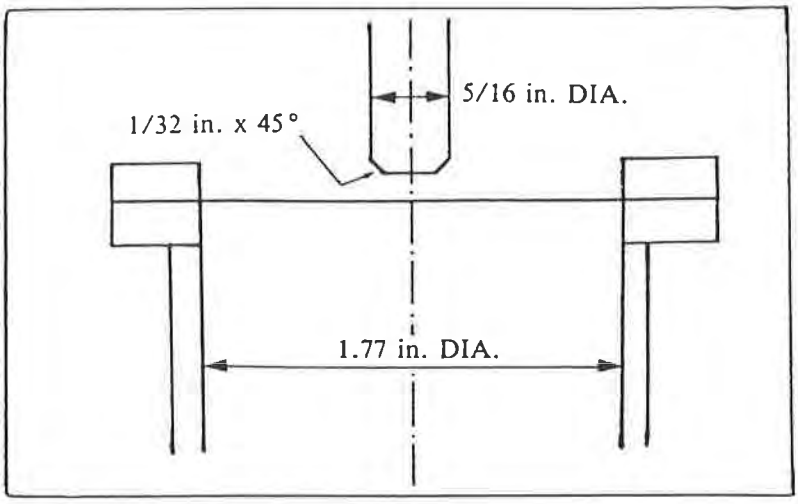

Figure 4. Conceptual Drawing of the Puncture Resistance Test (ASTM D 4833).

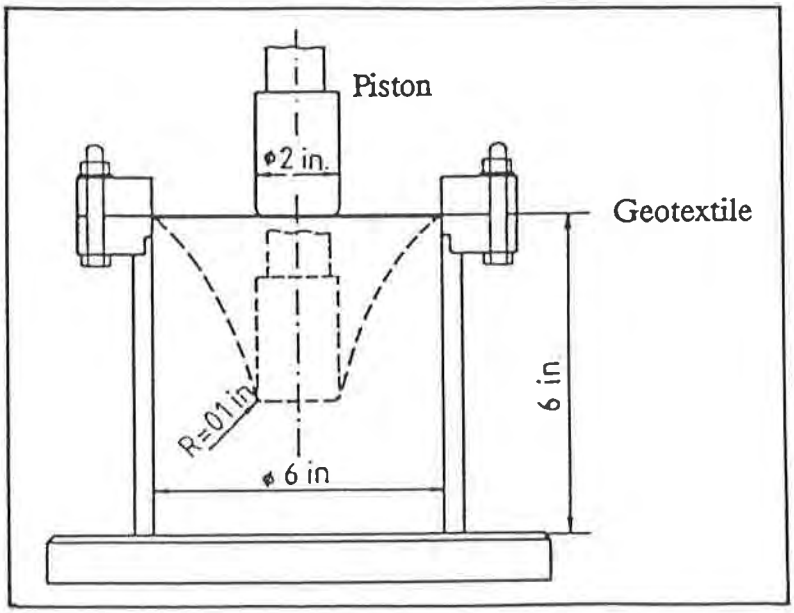

Figure 5. Conceptual Drawing of the CBR Puncture Test (DIN 54307).

continuous filament needlepunched polypropylene, a woven slit film, and a nonwoven continuous filament heatbonded polypropylene. Also, three different weights were evaluated (110, 140, and 200 g/m2).

Table 2. Pyramid Puncture Resistance Test Results As Compared to Flat Piston.

Geotextile Type	Weight (g/m2)	CBR Puncture (DIN 54307) Standard (N)	Pyramid (N)	Reduction (%)
NW Needlepunched	110	1138	569	50
NW Needlepunched	140	1449	724	50
NW Needlepunched	200	2100	1040	50
NW Heatbonded	100	889	267	70
NW Heatbonded	136	1289	387	70
NW Heatbonded	190	1778	533	70
Woven Slit Film	119	2907	436	85
Woven Slit Film	136	3191	480	85

Significantly the tests reveal a clear drop in strength for all the geotextiles, although there is also a clear difference between types, Table 2. It is shown that the puncture resistance of the needlepunched continuous filament nonwoven falls by approximately 50% and yielded much better results than the other geotextiles. The puncture resistance of the heatbonded continuous filament nonwoven falls by 70% and the woven slit film results fall by 85%.

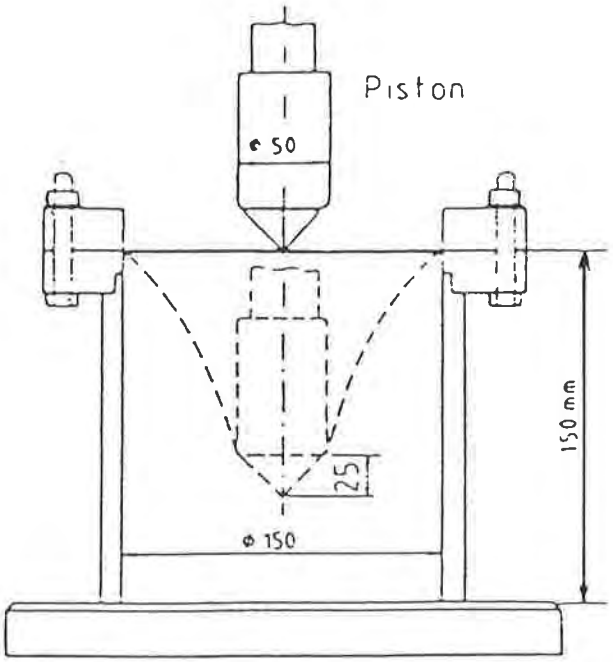

Figure 6. Conceptual Drawing of the Modified CBR Pyramid Puncture [9].

Tear Resistance. If the geotextile is damaged, it is of importance that the material does not continue to tear, thus decreasing the filtering and draining characteristics. In practical applications, the tear propagation strength can influence the geotextile in many different ways. With the trapezoidal tear test (ASTM D4533), an attempt is made to tear a test sample where an incision was made. The side with the incision in the geotextile is clamped down tighly; the other side is attached very loosely between the clamps. The result from this test indicates the tendency of the fabric to continue tearing once torn.

The overall geotextile resistance to damage depends on the combined action of strength (r) and elongation at break (ε_r). The geotextile resistance to damage is achieved either by high strength (Figure 7a), or by high elongation (Figure 7b). This relationship can be expressed by multiplying the tensile strength by the elongation as recommended by the Swiss Association of Geotextile Experts (SVG), which can be expressed as follows [10]:

$$A = r \times \varepsilon_r \qquad (1)$$

where:

A = rupture resistance;
r = rupture strength;
ε_r = rupture elongation.

It can be seen that to overcome critical stress situations during construction stage and in service, two possibilities exist: 1) geotextiles with low elongation can compensate the elongation requirements by accordingly higher strength, and 2) geotextiles with low strength can compensate the strength requirements by higher elongation. Table 3 presents comparison data of the rupture resistance of three types of geotextiles, i.e. needlepunched continuous filament nonwoven, woven slit film, and nonwoven continuous filament heatbonded. For the same mass per unit area, the nonwoven needlepunched continuous filament fabric has the highest rupture resistance.

Table 3. Geotextile Rupture Resistance.

Geotextile Type	Weight	Tensile Strength/Elongation ASTM D 4595		Rupture Resistance
	(g/m2)	(KN/m)	(%)	(A = r x r)
NW Needlepunched	92	5.6	40	224
NW Needlepunched	140	8.9	50	445
NW Needlepunched	200	12.8	50	640
NW Needlepunched	237	14.9	50	745
NW Heatbonded	100	5.1	20	102
NW Heatbonded	136	8.0	30	240
NW Heatbonded	203	12.1	30	363
NW Heatbonded	240	15.0	30	450
Woven Slit Film	92	7.0	20	140
Woven Slit Film	132	21.3	17	362
Woven Slit Film	203	29.9	17	508
Woven Slit Film	240	32.9	20	658

PRACTICAL EXPERIENCE

Installation Damage of Geotextiles. In an attempt to provide design guidance to compensate for possible installation damage to geotextiles, an extended field project was undertaken by the Geosynthetic Research Institute (GRI) "Assessment of Installation Damage of Geotextiles" [11]. The goal of the project was the exhuming of as many geotextiles as possible and measuring their retained strength properties for comparison with the original values of the same materials, as well as counting the holes which occurred. The materials were exhumed directly after installation and compaction of the fill aggregate.

Forty eight (48) geotextiles were exhumed and tested. Among the geotextiles, the most important types were slit film wovens (25) and needlepunched nonwovens (15). The sites were divided into different survivability categories as to the stress level. The survivability degrees are defined in the FHWA "Geotextile Design Manual" [12]. The results for the needlepunched nonwovens and slit film wovens are summarized in Tables 4 and 5. In detail, the results clearly show that the needlepunched nonwovens outperformed the slit film woven fabrics with less holes per square yards and higher percent strength retention for all the survivability degrees.

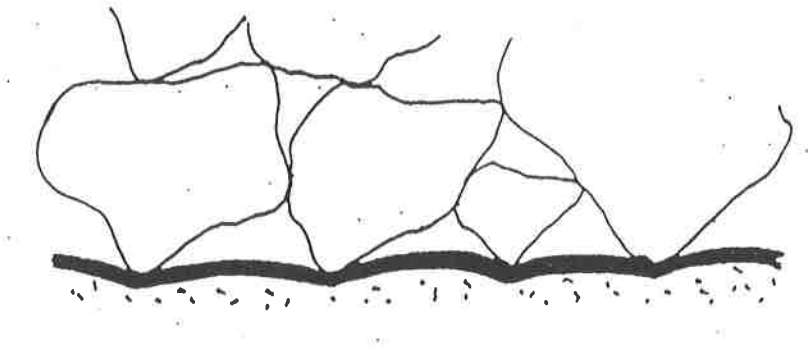

a) Absorption of Puncture Stress due to High Strength.

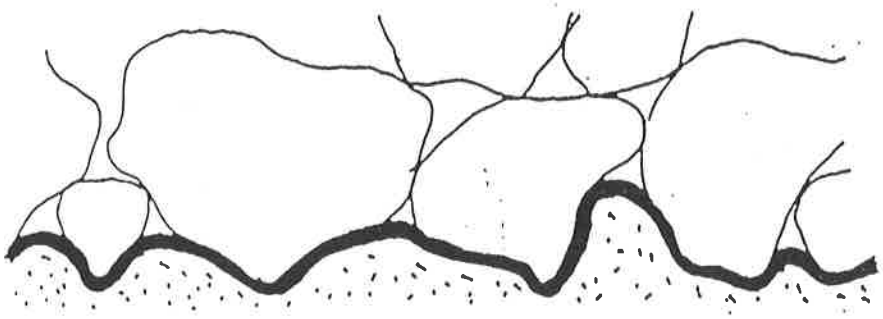

b) Absorption of Puncture Stress due to High Elongation.

Figure 7. Geotextile Resistance to Damage Criterion According to SVG [10].

Table 4. Assessment of Installation Damage on Needlepunched Nonwoven Geotextiles [11].

SURV.	OZ/YD2	HOLES	STR. RET.
N.R./V.H.	5.8	8	71
HIGH	4.5	45	35
	20.0	0	95
	5.3	0	76
MODERATE	4.5	0	92
	5.0	0	96
	5.0	0	87
	5.0	2	80
	5.3	0	80
	10.0	0	96
	5.0	2	77
	15.0	0	91
LOW	5.8	0	95
	5.0	1	92
	6.4	0	92

Table 5. Assessment of Installation Damage on Slit Film Woven Geotextiles [11]

SURV.	OZ/YD2	HOLES	STR. RET.
N.R./V.H.	6.1	6	59
	4.5	36	34
HIGH	4.5	22	63
	4.0	19	65
	4.4	57	50
	3.4	24	46
	5.0	9	63
	4.4	68	31
	4.4	65	51
	4.4	63	39
	3.4	100	13
	3.8	21	66
	4.5	8	54
MODERATE	4.0	0	84
	4.0	0	67
	4.4	11	79
	4.5	0	84
	4.4	14	84
	3.3	21	51
LOW	6.1	0	90
	4.4	12	75
	6.2	0	98
	3.3	12	86
	4.0	5	92
	4.4	0	80

Large Abrasion Test Correlation. To correlate laboratory short-term abrasion tests with long-term field experience, a series of laboratory abrasion tests (7.5 min and 30 min) were carried out using the same ballast materials as were used on the Bruchsal-Bretten separation test section by the Germany Railways Authorities [13]. A conceptual drawing of the laboratory test apparatus is presented in Figure 8.

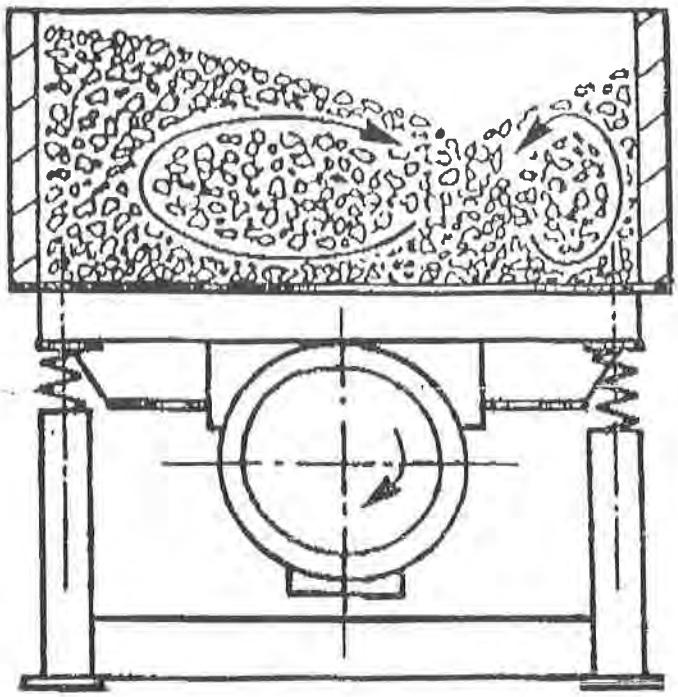

Figure 8. Conceptual Drawing of the Abrasion Laboratory Apparatus [13].

Figure 9 presents the residual strength of the geotextiles tested, a needlepunched continuous filament and a heatbonded nonwovens. The results provide interesting comment on the long-term behavior of nonwoven material.

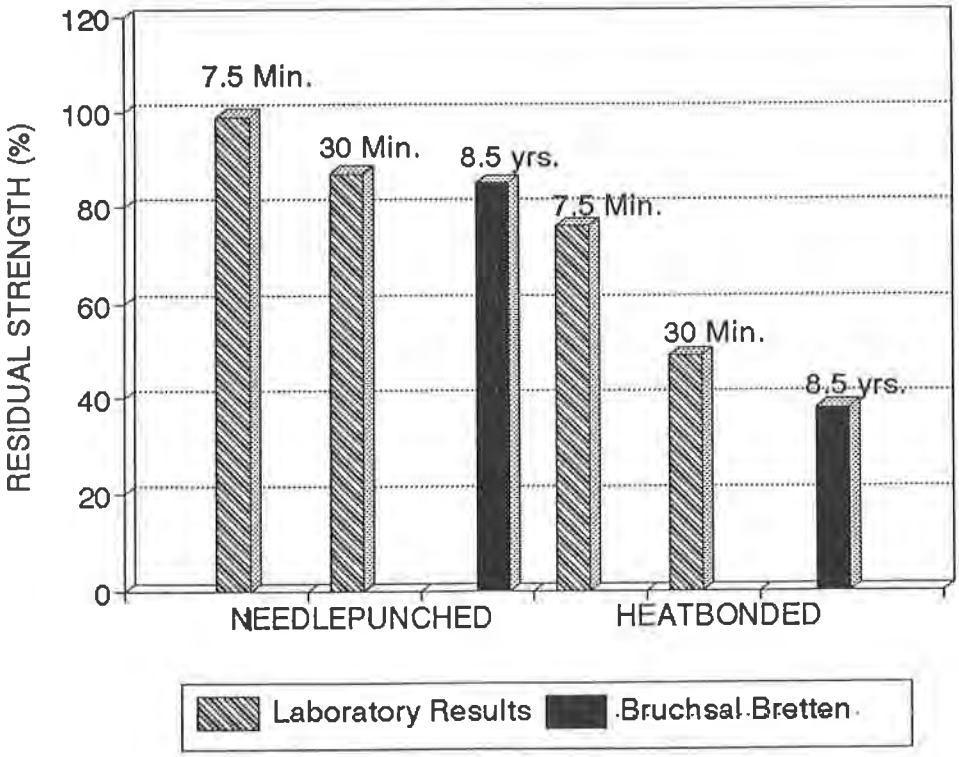

Figure 9. Large Scale Correlation Between the Bruchsal-Bretten and the Laboratory Abrasion Results [13].

These results show that after 30 minutes accelerated abrasion testing gives a very good correlation to the 8.5 years field evaluation of the geotextiles. Also, the needlepunched geotextile retained a strength of 87%, while the heatbonded offered only 47%.

CONCLUSION

Currently laboratory tests provide the basis for the selection of the appropriate geotextile type. However, the results obtained from today's methods are only suitable for comparing two geotextiles within certain limitations, as they often do not take into account specific stresses and site demands. The specifier should look more closely at the published data on geotextile performance.

When a geotextile is placed in a soil system, the fabric may behave in a substantially different manner because of the presence of soil. It was reported that the modulus of fabrics in soil situations may be 2-3 times the value in isolation. Results of studies [2,5,6] suggest that the properties determined from an unconfined wide width strip tensile test are conservative, and that for woven geotextiles there was no significant difference between the properties determined from a soil confined condition or unconfined. There is a clear distinct difference in the stress-strain behavior between the large and short clamping distances as well as differences between wovens, needlepunched, and heatbonded geotextiles. In the case of tensile test the smaller the clamping distance the higher the strength simulating a soil-confining condition. The large diameter burst procedure, larger clamping distance, should be considered for evaluating the geotextile performance when burst resistance is an important design characteristic. The large diameter procedure allows for the evaluation of the structure of the fabric and the biaxial stress-strain characteristics of the geotextile.

The overall geotextile resistance to damage depends on the combined action of strength and elongation at break. The geotextile resistance to damage is achieved either by high strength or by high elongation.

REFERENCES

1. Bell, J. R., et al., "Test Methods and Use Criteria for Filter Fabrics:, Report FHWA-RD-80-021, Federal Highway Administration, U.S. Department of Transportation, 1980.

2. McGown, A., Andrawes, K. Z., And Wilson-Fahmy, R. F., and Brady, K. C., "A New Method of Determining the Load Extension Properties of Geotechnical Fabrics", TRRL Supplementary Report 704, 1981.

3. Fock, G., and McGown, A., "The Creep Behavior of a Needlepunched Polypropylene Geotextile, 9th Southeast Asian Geotechnical conference, Bangkok, pp8-101 to 8-112.

4. Fabian, K., and Fourie, A. "Clay Geotextile Interaction in In-soil Tensile Tests", International Symposium on Theory and Practice of Earth Reinforcement, Kyushu, pp 81-86.

5. Rowe, R. K., and Ho, S. K., "Determination of Geotextile Stress-Strain Characteristics Using a Wide Strip Test", Third International Conference on Geotextiles, Vienna, Austria 1986. pp. 885-890.

6. Resl, S., "Soil-Reinforcing Mechanisms of Nonwoven Geotextiles", 4th International Conference on Geotextiles Geomembranes and Related Products, Den Hoedt 1990.

7. McGown, A., Andrawes, K. Z., and Kakir, M. H., "Load Extension Testing of Geotextiles Confined in Soil", 2nd International conference on Geotextiles", Vol. 3, pp. 745-750.

8. Koerner, R. M., "Designing with Geosynthetics", Prentice Hall, Englewood Cliffs,

New Jersey, 1990.

9. Werner, G., "Design Criteria For The Separation Function of Geotextiles on The Basis of Mechanical Test Procedures", Third International Conference on Geotextiles, Vienna, Austria 1986, pp. 979-983.

10. "Das Geotextil-Handbuch" (Manuel des Géotextiles), édité par l'Association Suisse des Professionnels du Géotextile (SVG), 1986.

11. Koerner, R. M., and Koerner, G. R., "A Quantification and Assessment of Installation Damage To Geotextiles", GRI Report #2, Geosynthetic Research Institute, Drexel University, Philadelphia, PA, 1988.

12. Christopher, B., Holtz, R., and DiMaggio, J. A. "Geotextile Engineering Manual", U.S. DOT, FHWA Contract No. DTFH 61-80-C-00094, Feb., 1984.

13. Martinek, K., "Anwendung von Geotextilien bei der Deutschen Bundesbahn - Erfahrungen und Anforderungen", 23. Int. Chemiefasertagung, Dornbirn, 1984.

A Comparison of Three Commonly Specified Axisymetric Stress Tests for Geosynthetics

R.K. Frobel
R.K. Frobel & Associates, USA

J.R. Montalvo
Polyfelt Inc., USA

ABSTRACT

In response to a growing need for better and more meaningful test methods that are devoted to geosynthetics and their installation performance stress, national and international standardization organizations such as American Society of Testing Materials (ASTM), International Standard Organization (ISO), Geosynthetic Research Institute (GRI), etc. have been instrumental in developing test procedures. Several such test procedures are currently being used to determine the axisymmetric or out-of-plane response to stress as would occur in a burst situation or larger area settlement/subsidence. Three such test methods and size of specimen area for each are as follows:

ASTM D 3786	3.1 cm diameter (7.5 cm^2 stress area)
GRI GS1-86	15.0 cm. diameter (176.6 cm^2 stress area)
GRI GM4	50.0 cm. min. diameter (1962.5 cm^2 stress area)

All three are very different in physical test dimensions, speed of testing, and cost, however all three attempt to measure axisymmetric properties of a geosynthetic, either for index or performance test purposes. This paper describes the three test methods and their advantages and disadvantages. Results of comparison testing of four nonwoven needlepunched geotextiles will be presented and analyzed based on type and mass of geotextile. The load or stress vs. strain characteristics of the selected geotextiles is presented based on this testing. Comparisons of the statistical results of the testing, in particular the standard deviation and coefficient of variation for the CBR and Hydraulic Burst (GRI GS1 and ASTM D 3786) are made in an effort to show the importance of choosing a test method that accurately reflects a products response to axisymmetric loading.

INTRODUCTION

Many geosynthetic products are particularly sensitive to small area index type tests which do not accurately reflect the products true response to axisymmetric stress. One type of product that is particularly sensitive primarily due to manufacturing method is the nonwoven needlepunched geotextile. Three test methods are currently in use in the determination of a products response to burst or axisymmetric stress and many times comparisons are made of this response to similar geosynthetic products without regard to test method, product type or significance in design or application. The suitability of these three test methods in determining comparable axisymmetric values is the subject of this paper.

DESCRIPTION OF TEST METHODS

Hydraulic Bursting Strength. This ASTM standard method (ASTM D 3786) covers the determination of the resistance of fabrics to bursting using a motor driven Hydraulic Diaphragm Burst Tester as shown in Figures 1. A test specimen 125 mm (5 in) in diameter is clamped without tension between two steel clamp surfaces, a minimum of 75 mm (3 in) in diameter, containing coaxial apertures 31 mm (1.22 in) in diameter. The surface of the clamps have concentric grooves for the purpose of restraining the specimen during a test. A synthetic rubber diaphragm is located in the bottom clamp

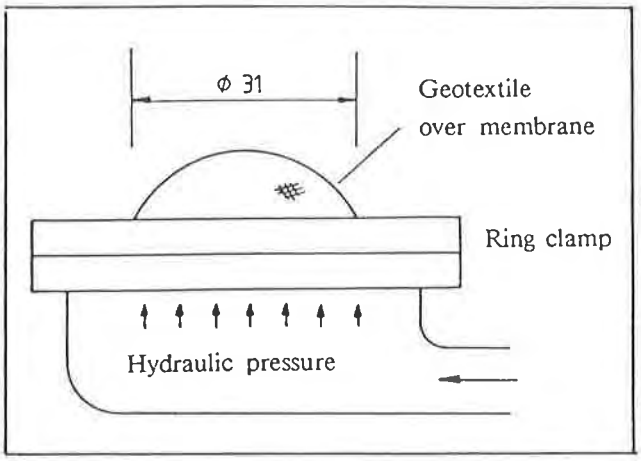

Figure 1 Burst Test Apparatus to ASTM D 3786

assembly for the purpose of transmitting increasing hydrostatic fluid pressure at a rate of 95 + 5 ml/min against the clamped specimen. The fluid is displaced by a piston in the pressure chamber of the apparatus. In general, a geotextile specimen is clamped in position over the expandable rubber diaphragm. The diaphragm is expanded by fluid pressure at a very rapid rate to the point of specimen rupture. The difference between the total pressure required to rupture the specimen and the pressure required to inflate the diaphragm is reported as the bursting strength.

There is no known correlation of this method with other test methods for geosynthetics and precision and accuracy testing for the standard has only been accomplished on knitted spun and filament yarns. There is a known high coefficient of variation for many geosynthetic products, especially nonwoven geotextiles.

CBR Puncture Strength. This GRI (GRI-GS1) Standard is also a standard method in several other countries such as in Germany (DIN 54307) and has been in use since 1977. It is commonly used to characterize both geomembranes and geotextiles as an index test of puncture strength. A test specimen 250 mm (9.8 in) is clamped without tension between two circular plates attached to a California Bearing Ratio (CBR) mold and secured in a tensile/compression test machine (See Figure 2). A force is exerted against the center of the specimen by a steel CBR plunger 50 mm (2 in) in diameter with

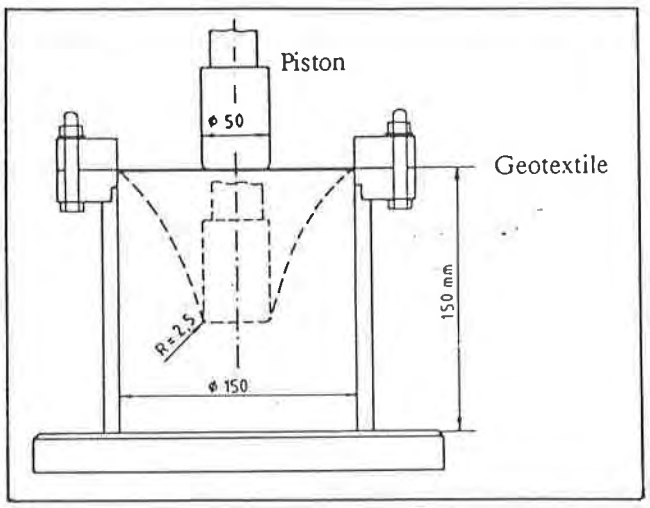

Figure 2 CBR Puncture Resistance Test According to GRI-GS1

a flat end and 45 degree chamfered edges. The opening in the plates is 150 mm (6 in) in diameter. The maximum force required to rupture the specimen with the plunger driven at a speed of 50 mm/min (2 in/min) is recorded along with maximum extension or elongation. In geotextile testing, there is a direct relationship between the CBR puncture strength and the wide width tensile strength of the fabric. This is due to the fact that the fabric between the inner edge of the ring clamps and the outer edge of the plunger piston is in a state of axisymmetric tension (Koerner, 1986). Correlation of CBR puncture strength with strip tensile strength of geotextiles has been made (Cazzuffi, 1986). His research claimed very good comparison between wide width strip tensile and CBR for isotropic nonwoven geotextiles in which the tensile strength of the geotextile can be calculated by the following equation.

$$Tf = 2\pi Fp \quad (1)$$

Where:
Tf = Tensile Force Per Unit Width at Failure in KN/m (lb/in)
Fp = CBR rupture force in KN (lb)

Moritz and Murray (1982) made similar observations using nonwoven geotextiles and concluded that the more isotropic a geotextile, the better the correlation, especially with wider width specimens (greater than 200 mm (8 in).

Multiaxial or Three Dimensional Tensile Test. This test method was originally developed to provide the tensile stress vs. elongation behavior of geomembranes tested in an axisymmetric or out-of-plane loading such as would occur in large area settlement. A standard developed for this purpose is the GRI-GM4 and vessels have been designed for both downward and upward burst/deflection measurements. For this testing, an aluminum frame was used to accommodate 700 mm (27.5 in) diameter specimens and burst pressures to 1.4 mPa (200 psi). The basic frame is similar to that recommended by the German working group AK14 and also recommended as an alternate system in the current ASTM draft method. Figure 3 is a conceptual drawing of the multiaxial load frame used in this testing. The top ring has a 500 mm (20 in) inside diameter with smooth radius edge, O-ring seals and bolt holes. The bottom plate on which the specimen is placed contains inlet/outlet ports for air or water, as well as pressure monitoring. The top of the frame is used for the central deflection measurement via optical or LVDT. Figure 4 illustrates the test device with a nonwoven geotextile under stress. A 0.2 mm (0.008 in.) thick latex rubber diaphragm was used to provide pressurization under the geotextile. This type of diaphragm exhibits very high elongation with negligible contribution to geotextile stress. A coating of talc powder on the diaphragm provides very low surface friction between the geotextile and the latex.

Test Methodology. The following basic procedure was used to test all geotextile specimens in the multiaxial frame:

- Place rubber diaphragm on base plate
- Place geotextile specimen
- Align top ring with base plate
- Install and diametrically torque bolts
- Set vertical deflection measurement to 0
- Back pressure specimen to 1380 Pa (0.2 psi) for 20 min.
- Start testing at pressure increments of 6.89 kPa/min (1 psi/min)
- Incrementally raise pressure/record deflection until failure of the specimen.
- Record fail pressure, pressure increments, deflection increments and observations.

The following stress and strain calculations were used to develop the stress-strain curves for each geotextile type and are based on current GRI and draft ASTM procedures. For $d < D/2$:

$$R = (D^2 + 4d^2)/8d \quad (2)$$

$$\Theta = 2 \tan^{-1}[4(D)d]/(D^2-4d^2) \quad \text{(radians)} \quad (3)$$

$$L = R \times \Theta \quad (4)$$

$$\text{Strain } (\varepsilon) = (L - D)/D \times 100 \quad \text{(percent)} \tag{5}$$

$$\text{Stress } (\sigma) = (P \times D)/[4t \sin(\theta/2)] \tag{6}$$

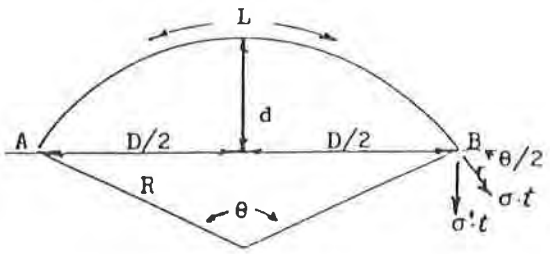

Where:

R = sphere radius
L = length of segment A - B
D = specimen diameter
d = vertical deflection
P = internal Pressure
t = specimen thickness
ε = strain (%)
σ = stress kPa

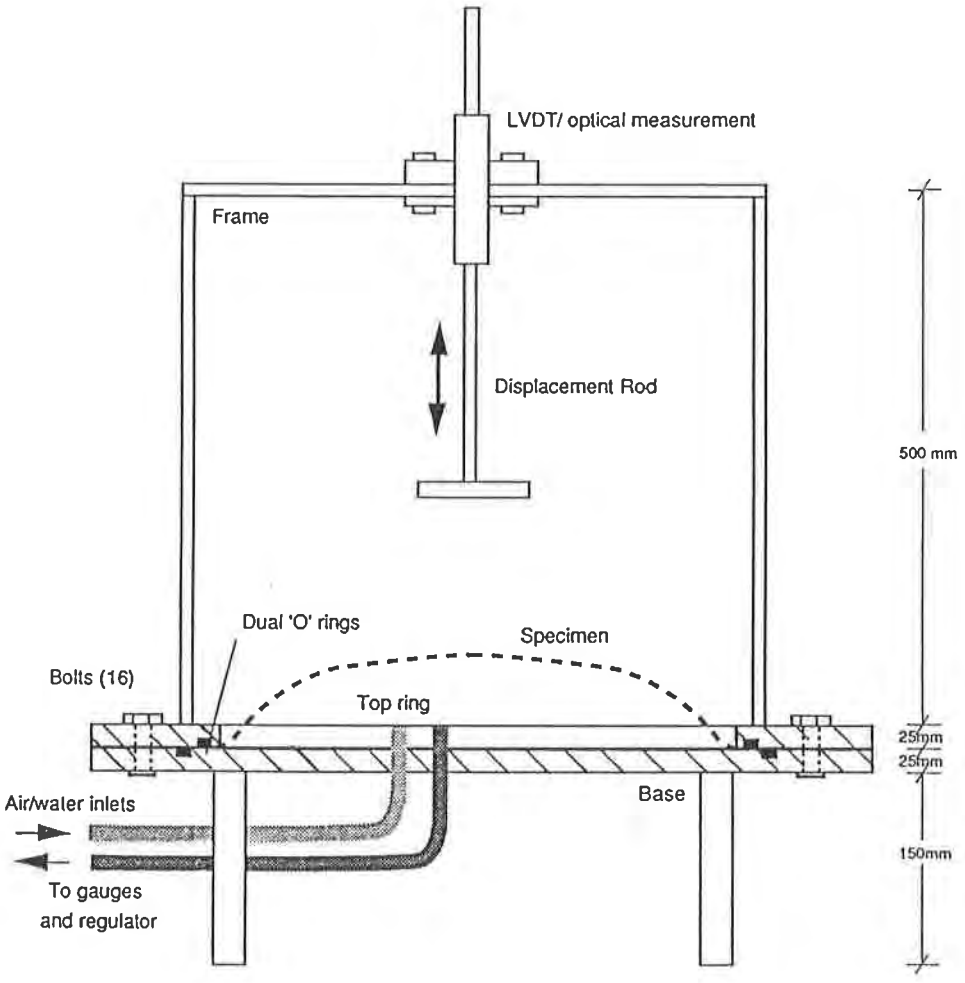

Figure 3 Conceptual Drawing of Multiaxial Load Frame

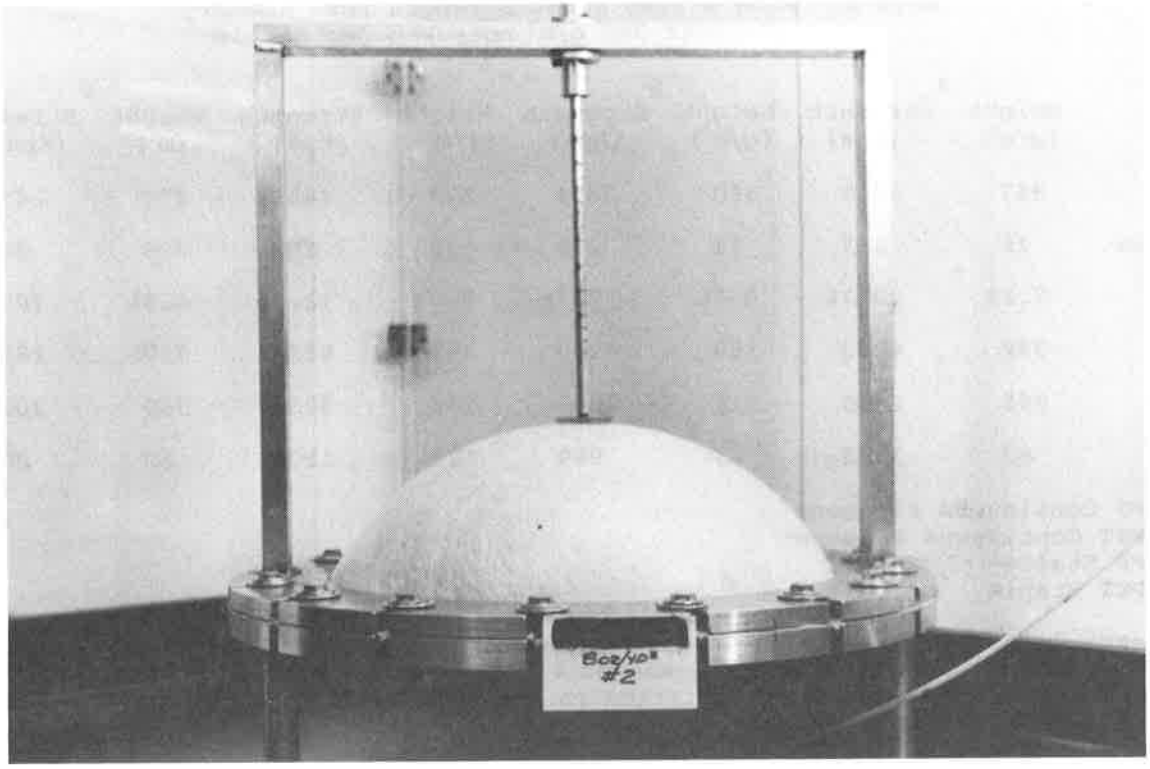

Figure 4 Photo Illustrating the Multiaxial Upward Burst Device With a Nonweven Geotextile under Test.

SELECTION OF GEOTEXTILES

For purposes of comparison, only one type of geosynthetic was chosen for testing: a mechanically bonded (needlepunched) nonwoven geotextile, both staple fiber and continuous filament. One of the primary reasons a mechanically bonded nonwoven was chosen was due to the fact that nonwovens are predominantly used in separation and support/protection functions which contribute to the axisymmetric stress condition.

Four of the most predominant types of needlepunched nonwoven geotextiles were used for comparative testing at a nominal weight of 340 gm/m^2 (10 oz/yd^2). In addition, comparison testing was carried out on a polypropylene, nonwoven needlepunched continuous fiber geotextile at weights of 270 g/m^2 (8 oz/yd^2), 340 g/m^2 (10 oz/yd^2) and 407 g/m^2 (12 oz/yd^2). The types of geotextiles used in this testing were as follows:

Polypropylene	Continuous fiber needlepunched
Polypropylene	Staple fiber needlepunched
Polyester	Continuous fiber needlepunched
Polyester	Staple fiber needlepunched

TEST RESULTS

Summary of Hydraulic Bursting Strength. A minimum of eighteen (18) test specimens were tested for each of the geotextile types. Table 1 presents a statistical summary of the hydraulic burst strength test results on four typical 340 g/m^2 (10 oz/yd^2) fabrics. In general, all geotextile types differed greatly in their response to the hydraulic bursting test. All fabrics were tested according to ASTM D 3786 standard test procedure (also called the Mullen Burst Test).

Table 1. ASTM D 3786 Burst Strength Test Summary
(Typical 340 g/m^2 nonwoven geotextile

	A		B		C		D	
	Weight (g/m^2)	Strength (Kpa)	Weight (g/m^2)	Strength (Kpa)	Weight (g/m^2)	Strength (Kpa)	Weight (g/m^2)	Strength (Kpa)
Mean	347	3345	350	3614	329	4485	375	2455
Std. Dev.	25	457	11	278	32	552	16	259
C.V.	7.2%	13.7%	3.1%	7.7%	9.7%	12.3%	4.3%	10.6%
Max.	388	4283	369	4200	397	5531	410	2834
Min.	295	2490	326	3241	273	3731	350	2034
Range	93	1793	43	959	124	1800	60	800

A: NW_PP Continuous Filament
B: NW_PET Continuous Filament
C: NW_PP Staple
D: NW_PET Staple

Geotextile Type A, a nonwoven needlepunched continuous filament fabric weighing an average of 347 g/m^2 (10.2 oz/yd^2), showed a mean hydraulic burst strength of 3345 Kpa (485 psi) with a coefficient of variation in strength equal to 13.7% and a statistical range of 1793 Kpa (260 psi).

Geotextile Type B, a nonwoven needlepunched continuous filament polyester fiber weighing an average of 350 g/m^2 (10.3 oz/yd^2), showed a mean hydraulic burst strength of 3614 Kpa (524 psi) with a coefficient of variability equal to 7.7% and a statistical range of 959 Kpa (139 psi). This fabric presented the lowest coefficient of variability.

Geotextile Type C, a nonwoven needlepunched polypropylene staple fiber with an average of 329 g/m^2 (9.7 oz/yd^2), showed the highest mean hydraulic bursting strength of 4485 Kpa (651 psi). However, this fabric presented a very high coefficient of variability, 12.3% and the highest range statistical value of 1800 Kpa (261 psi).

Geotextile Type D, a nonwoven needlepunched staple polyester fiber weighing an average of 375 g/m^2 (11 oz/yd^2), showed a hydraulic burst strength of 2455 Kpa (356 psi) with a coefficient of variability of 10.6% and a statistical range of 800 Kpa (116 psi). This fabric presented the lowest average hydraulic burst strength even though the mass per unit area was heavier than all products tested.

Summary of CBR Puncture Resistance. A minimum of ten test specimens were tested for each geotextile. Table 2 presents a statistical summary of the CBR puncture test results and Figures 5 and 6 illustrate the load deflection curves obtained during testing. Referring to Table 2, it can be seen that the coefficient of variability is substantially lower in all cases as compared to the Mullen Burst results in Table 1.

Summary of Multiaxial Test Results. A minimum of three test specimens were tested for each of the geotextile types. Although the geotextiles differed in polymer and fiber length as well as needling density, all were typical 340 g/m^2 (10 oz/yd^2) fabrics. In general, all fabric types differed greatly in their response to multi-axial loading. Figure 7 illustrates the comparative stress-strain response curves generated by this testing for each of the types of geotextiles. All data points for the curves were derived according to the previously described methods of calculation.

Curve A illustrates the stress-strain curve for a nonwoven, needlepunched continuous fiber polypropylene weighing an average of 368.4 g/m^2 (10.8 oz/yd^2). This fabric type exhibited the best overall response for the nominal 340 g/m^2 (10 oz/yd^2) geotextiles. It maintained excellent tensile properties while allowing even strain to maximum 30.7% and 6083 Kpa (882 psi). This product consistently ruptured in the

Table 2. CBR Puncture Resistance Test Summary
(Typical 340 g/m^2 nonwoven geotextiles)

	A Weight (g/m^2)	A Strength (N)	B Weight (g/m^2)	B Strength (N)	C Weight (g/m^2)	C Strength (N)	D Weight (g/m^2)	D Strength (N)
Mean	347	3839	350	3942	329	4348	375	2953
Std. Dev.	25	341	11	201	32	361	16	256
C.V.	7.2%	8.9%	3.1%	5.1%	9.7%	8.3%	4.3%	8.7%
Max.	388	4268	369	4115	397	4907	410	3439
Min.	295	3404	326	3651	273	3944	350	2768
Range	93	864	43	464	124	963	60	671

A: NW_PP Continuous Filament
B: NW_PET Continuous Filament
C: NW_PP Staple
D: NW_PET Staple

machine direction and exhibited consistent test results from specimen to specimen. Stress data comparisons made at 20% strain showed a standard deviation of 5 and a coefficient of variability 0.7%.

Curve B shows the stress-strain curve for a nonwoven, needlepunched, continuous fiber polyester weighing an average 357.7 g/m^2 (10.5 oz/yd^2). The initial modulus and overall response was similar to the continuous fiber polypropylene but lower in stress-strain values. Maximum strain was 37% at 5448 Kpa (790 psi). This product consistently ruptured non directionally with no obvious weaker principal direction. Standard deviation for this product was 7 with a very low coefficient of variability of 0.2%.

Curve C represents the stress- strain curve for a nonwoven, needlepunched stable fiber polypropylene geotextile weighing an average of 312.8 g/m^2 (9.2 oz/yd^2). Although the initial modulus is lower than the continuous fiber products, the stress-strain curve quickly increased to a maximum strain of 37% and 5069 Kpa (735 psi). Mode of failure was in the machine direction. Standard deviation for this product was 9 with a coefficient of variability of 2.3%.

Curve D represents the stress-strain curve for a nonwoven, needlepunched staple fiber polyester geotextile weighing an average 378 g/m^2 (11.2 oz/yd^2). Considering the comparatively higher mass, the stress-strain curve is considerably lower with a low initial modulus but higher extension to failure of 53%. This product showed a standard deviation of 5.7 and a coefficient of variability of 2.1%.

Although the large diameter multiaxial test is more performance related in that it can be used to model anticipated field performance, it is important to note that a relatively large area of specimen is used in the testing and thus the effect of product variability on test results is greatly reduced. The pressure and corresponding deflection measurements taken at one minute intervals are very consistent from one specimen to the next and thus the number of replicate tests can be reduced. This is not the case for the smaller index type tests which rely on small specimen size and thus result in a high coefficient of variability. This is especially true of nonwoven geotextiles which exhibit variable mass across the roll width as well as anisotropic properties. Large diameter axisymmetric tests such as the multiaxial reflect a products true field performance under loading and the test method greatly reduces the influence of manufactured product variability and anisotrophy.

Figure 8 represents multiaxial stress-strain curves as a comparison on between two commonly specified weights of the same product. As the mass of the geotextile is increased and needling density is changed, the modulus of the product increases and the

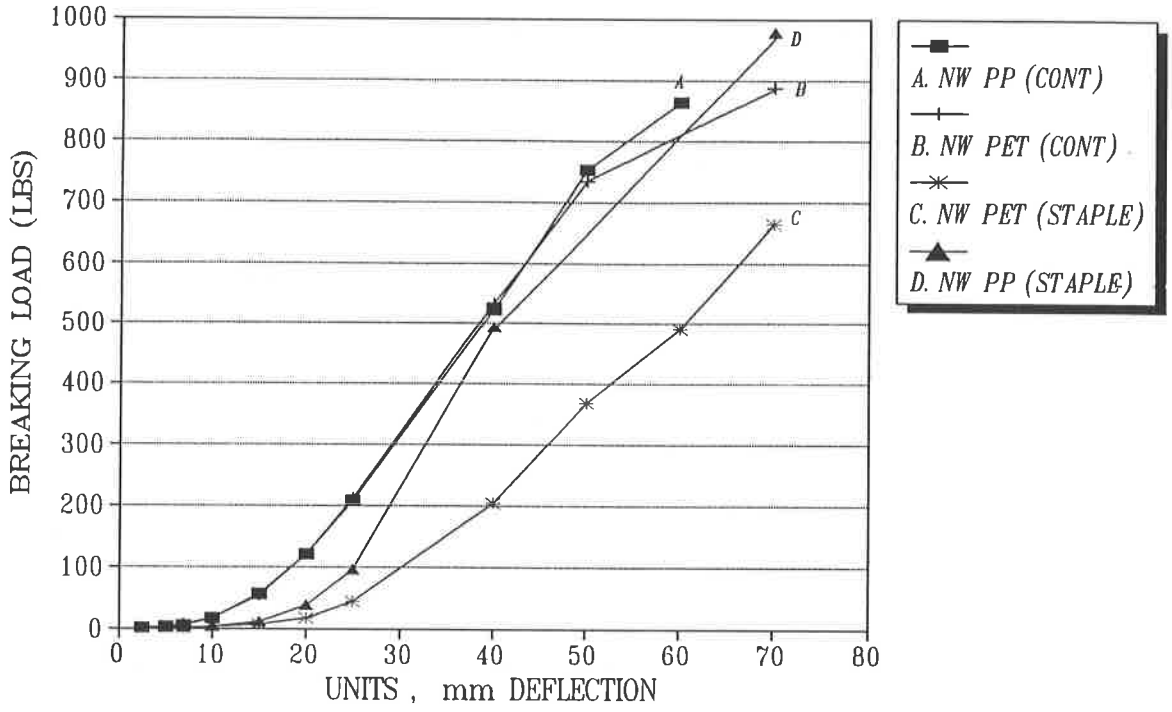

Figure 5 CBR Puncture Resistance Resulting Load-Deflection Curves for Four Typical 340 g/m^2 Nonwoven Needlepunched Geotextiles.

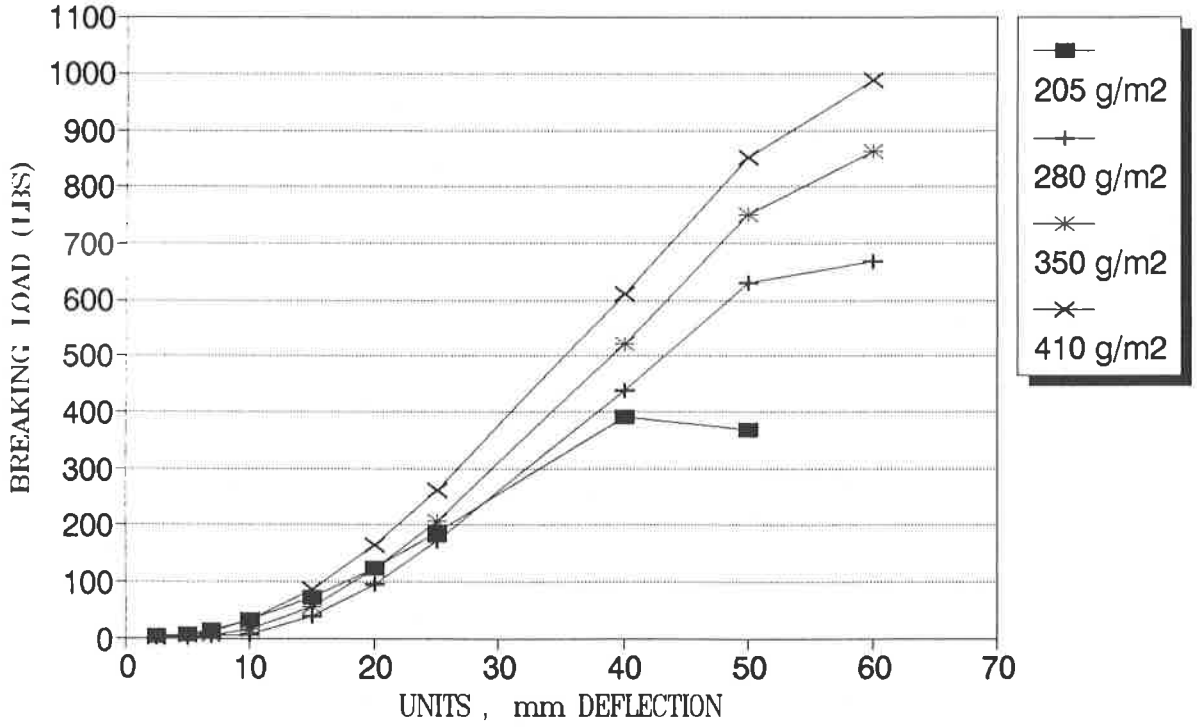

Figure 6 CBR Puncture Resistance Resulting Curves for Four Nonwoven Needlepunched Continuous Filament Polypropylene Geotextiles.

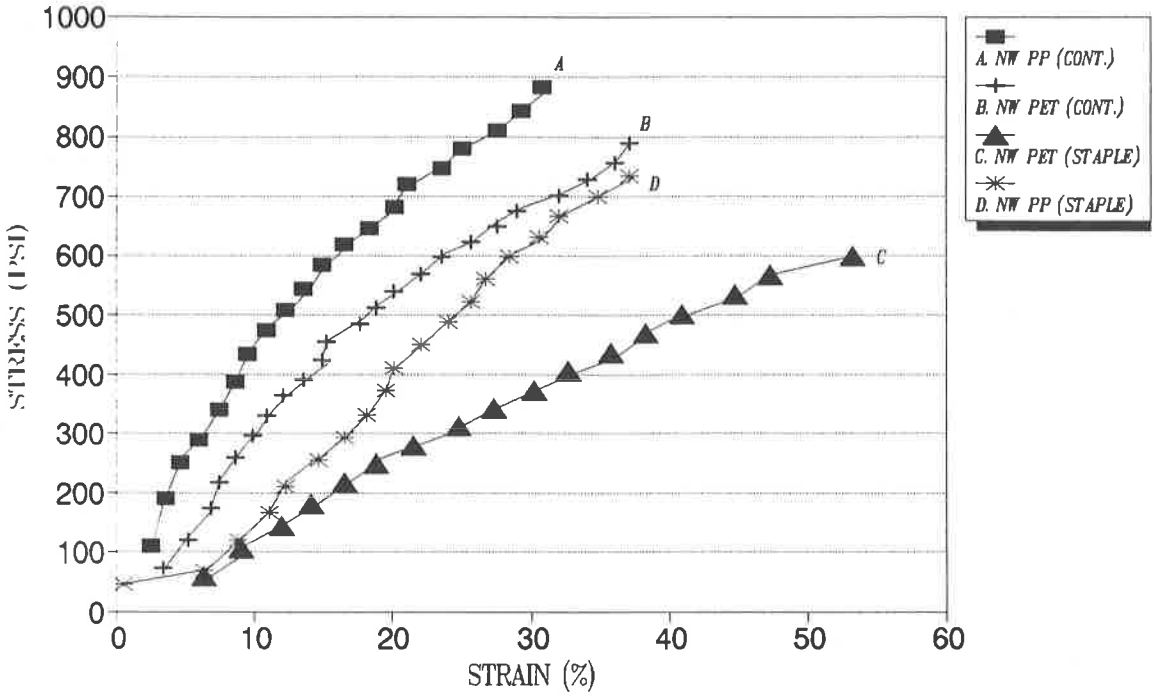

Figure 7 Large Diameter Multiaxial Resulting Stress-Strain Curves for Four Typical 340 g/m² Nonwoven Needlepunched Geotextiles.

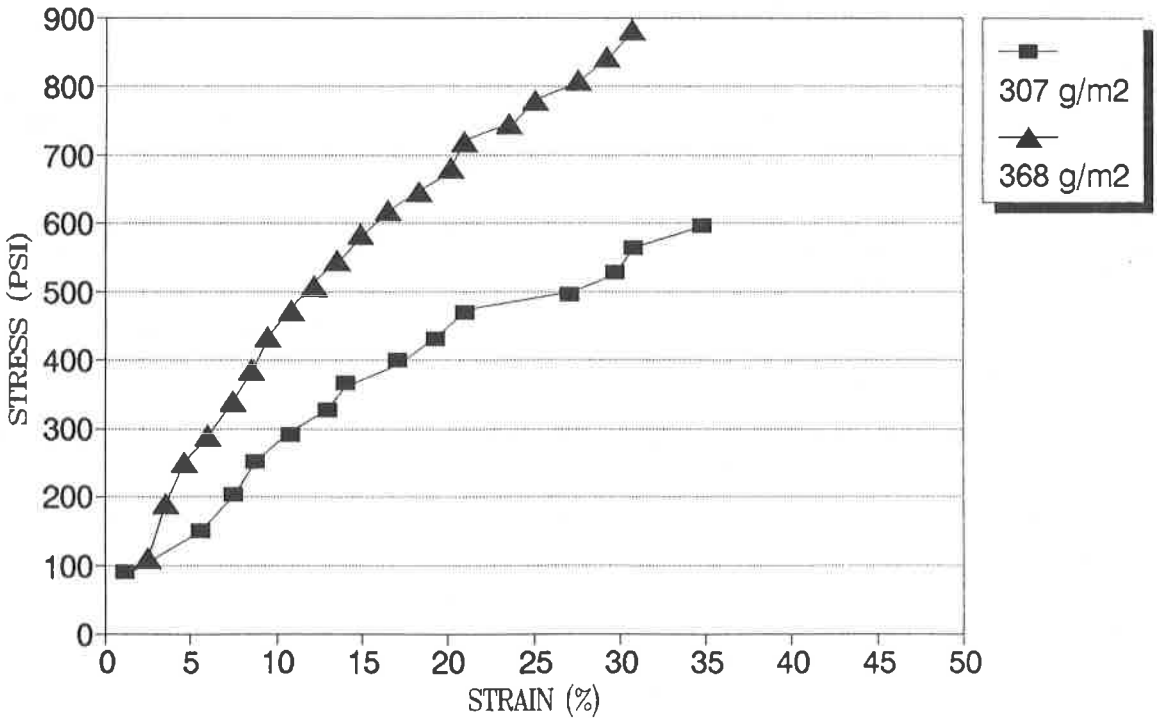

Figure 8 Large Diameter Multiaxial Resulting Stress-Strain Curves for Two Nonwoven Polypropylene Continuous Filament Geotextiles.

ultimate breaking stress is substantially increased but without a significant decrease in elongation.

SUMMARY

Comparison testing was carried out on four type of nonwoven geotextiles using three commonly specified axisymmetric tests in an effort to illustrate the differences in test results when using a smaller index type test vs. larger area tests. It is evident from statistical test results (refer to Table 1) carried out on the four types of nonwoven, needlepunched geotextiles that the coefficient of variation (CV) is very high when the small axisymmetric test (ASTM D 3786) is used to compare products. The CV for this test (usually between 10 and 14 percent) reflects the inappropriateness of using such a small test area on a type of product that historically has a relatively high variability in the mass per unit area and thickness across the roll width.

When the test area is increased to the 176 cm^2 (27.3 in^2) CBR specimen size, the relative coefficient of variation for all products was much closer with the exception of product B, a continuous filament needlepunched PET which exhibited a 5.1% CV. Although the CV's were generally in the range of 8.5%, this is still a much lower variability and more in line with the product's variability in mass and thickness. The CBR test can also be used to compare the strain characteristics of a given product under axisymmetric stress.

The large scale multiaxial test is designed to simulate out of plane loading as would occur during subgrade settlement and as such is performance test which utilizes a large surface area of specimen, 1962.5 cm^2 (290 in^2). It was found that when comparing all replicates at one particular strain (in this case 20%), the coefficient of variation was drastically reduced to between 0.7% and 2.3% for all products. Obviously, the larger the surface area chosen for axisymmetric tests on anisotropic materials, the lower the coefficient of variability in test results and the more meaningful the comparisons. Although the large scale multiaxial test cannot be used for all comparisons due to current scarcely of equipment and high cost, it is recommended that the CBR test be considered for any comparative axisymmetric load-strain comparisons especially on nonwoven needlepunched geotextiles.

REFERENCES

Werner, G., G. Puhringer and R. Frobel (1990) "Multiaxial Stress Rupture and Puncture Resistance of Geotextiles", Proceedings 4th International Conference on Geotextiles, Geomembranes and Related Products, Vol 2, pp 765-770.

Moritz, K. and H. Murray (1982), "Comparisons Between Different Tensile Tests and the Plunger Puncture Test (CBR Test)" Proceedings Second International Conference on Geotextiles, Vol 2, pp. 757-761.

American Society for Testing and Materials (1988), Test Method for Hydraulic Bursting Strength of Knitted Goods and Nonwoven Fabrics - Diaphragm Bursting Strength Test Method, ASTM D 3786, ASTM, Philadelphia, PA.

Geosynthetic Research Institute (1991) CBR Puncture Strength, GRI Test Method GS1-86, GRI, Drexel University, Philadelphia, PA

Koerner, R.M. (1990) Designing with Geosynthetics, Prentice Hall, Englewood Cliffs, New Jersey

Cazzuffi, D., S. Vanesia, M. Rimald, and A. Zocca (1986) "The Mechanical Properties of Geotextiles : Italian Standard and Inter-laboratory Test Comparison", Proceedings Third International Conference on Geotextiles, Vienna, Vol 3, pp. 695-670.

Relationship Between Wide-Width Strip Tensile and Modified Strip Tensile Tests When Testing Nonwoven Geotextiles

M.H. Wayne
Polyfelt Inc., USA

J.R. Montalvo
Polyfelt Inc., USA

M. Boatwright
Polyfelt Inc., USA

ABSTRACT

Current design practice has increasingly included the use of results of the American Society for Testing and Materials' (ASTM) wide-width strip tensile test, designated D 4595, as part of designs in which the geotextile is expected to serve as reinforcement. Examples include the use of geotextiles for reinforced embankments over soft subgrades, reinforced slopes and reinforced retaining walls. Unfortunately, use of the wide-width strip tensile test as a quality control test method by manufacturers' is greatly limited due to the slow testing rate of approximately 10 mm per minute (0.4 inches per minute). Because of their use in reinforcement applications, an increasing number of specifications have been framed around the performance of wide-width strip tensile testing for both quality control, as supplied by manufacturers' or their agents, and as part of conformance testing, as conducted by the owners' representative (e.g. third party inspector). In response to these current design specifications a study was conducted to explore the correlation between this test and the modified strip tensile test which has been standardized in Europe, namely Germany, and is designated as DIN 53857/2. This test method involves a specimen size of 100 mm by 300 mm (4 inches by 12 inches), which is folded toward the centerline of the longer axis to produce a 50 mm by 300 mm (2 inch by 12 inch) sample. The sample is then clamped within a constant rate of extension tensile tester with a 200 mm (8 inch) gauge length and deformed at a rate of 200 mm per minute (8 inches per minute).

The study examines the load-elongation characteristics of both tests as performed on various weight continuous filament and staple fiber needle-punched, nonwoven, polypropylene and polyester based geotextiles. Results of this work indicate the usefulness of this test as an accurate indicator of the ultimate strength of the geotextile as derived from the wide-width strip tensile test. In addition, the authors' examine the differences in modulus and material toughness as determined by each test. It is expected that the use of the modified strip tensile test as a complement to the wide-width strip tensile test will prove to be both cost effective and serve as a quick test which can be used to establish product conformance to design specifications.

INTRODUCTION

Current design practice has increasingly included the use of results of the ASTM wide-width strip tensile test, designated D 4595, as part of designs and specifications where the geotextile is expected to serve as reinforcement. In many cases the manufacturer of a given geotextile is expected to certify that the product meets or exceeds a given minimum average roll value, and provide quality control data as supporting documentation. In general, most manufacturers' conduct grab tensile tests, ASTM designation D 4632, as part of process control testing and one wide-width strip tensile test series per lot as part of the quality control evaluation of a given product. This is done for two reasons. Traditionally the grab tensile test results are required for applications other than reinforcement, and secondly, time constraints involved with process control testing essentially prohibit the use of the wide-width strip tensile test as part of process control testing. Because of this many manufacturers' must conduct additional wide-width strip tensile testing to demonstrate product conformance with project specifications. The authors' of this paper believe that the modified strip tensile test can be used as a quality control test in lieu of grab testing as long as one test series of wide-width strip tensile tests are conducted to substantiate the relationship. As such, this study examines the load-elongation characteristics of both tests as performed on three different geotextile products. These include a continuous filament needle-punched, nonwoven, polypropylene (NW-PP-CONT), a continuous filament needle-punched, nonwoven, polyester (NW-PET-CONT),and a staple fiber needle-punched, nonwoven, polypropylene (NW-PP-STAPLE) based geotextiles. For each of these products, four different mass per unit area products are evaluated for ultimate load and elongation. Actual load-elongation curves for one mass per unit area of each product are then used to compare modulus and toughness results obtained by the wide-width strip tensile and modified strip tensile methods.

TESTING PROGRAM

For each mass per unit area, six specimens were prepared for both wide-width strip tensile and modified strip tensile testing.

Wide-Width Strip Method. As reported in the ASTM Standards on Geosynthetics (1991) this test involves preparation of a 200 mm by 200 mm (8 inch by 8 inch) specimen which is to be tested in a constant rate of extension tensile testing apparatus. The clamping system must be at least 200 mm (8 inches) wide and capable of clamping the specimen while maintaining a 100 mm (4 inch) gauge length at initiation of the test. Testing is initiated at a rate 10.16 mm per minute (0.4 inches per minute) during which the sample load and elongation information is recorded up to the point of product failure. The tensile strength per unit width, in kN/m, is then determined as the observed breaking force, in kN, divided by the specimen width, in m. The actual set-up used for this work is depicted in Figure 1.

Modified Strip Tensile Test. As reported in the Polyfelt Design and Practice Manual (1987), this test method, designated as DIN 53857/2, involves preparation of a 100 mm by 300 mm (4 inches by 12 inches) specimen, which is folded toward the centerline of the longer axis to produce a 50 mm by 300 mm (2 inch by 12 inch) specimen. The specimen is then clamped within a constant rate of extension tensile tester with a 200 mm (8 inch) gauge length and deformed at a rate of 200 mm per minute (8 inches per minute). During testing the sample load and elongation information is recorded

up to the point of product failure. The tensile strength per unit width, in kN/m, is then determined as the observed breaking force, in kN, divided by the specimen width, in m. The actual set-up used for this work is depicted in Figure 2.

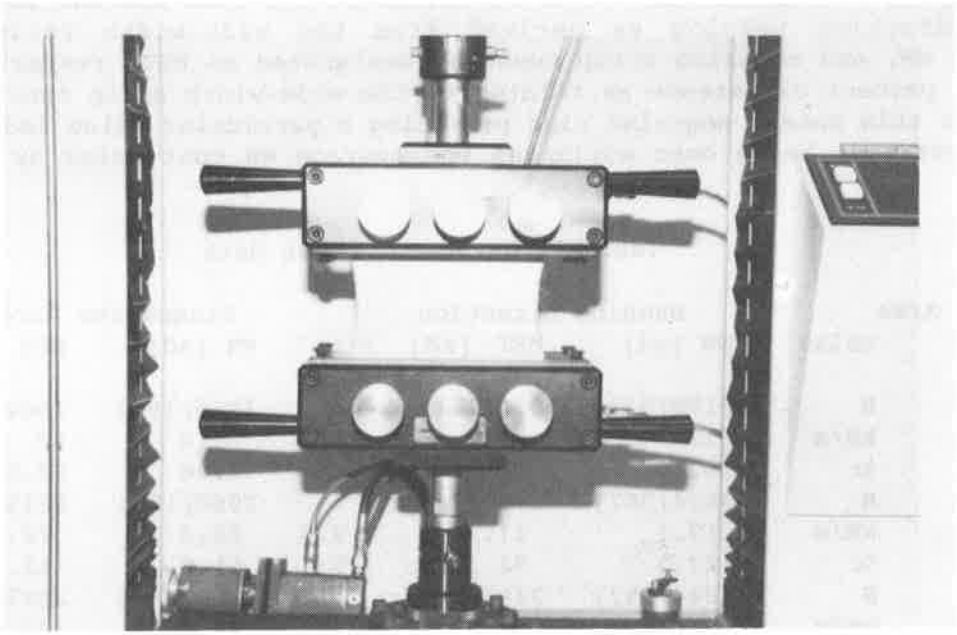

Figure 1 Wide-Width Strip Tensile Test

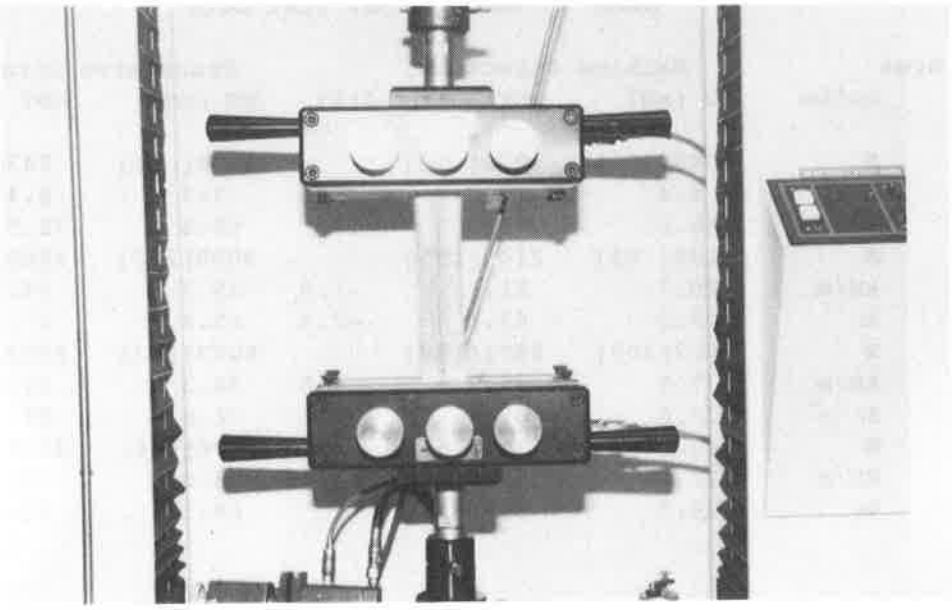

Figure 2 Modified Strip Tensile Test

TESTING RESULTS

Ultimate Load and Elongation. The testing summary for this study is found in Tables 1 for NW-PP-CONT, Table 2 for NW-PET-CONT, and Table 3 for NW-PP-STAPLE products. Within each Table information pertaining to average ultimate load, based on testing six specimens, and the associated standard deviation for both machine direction and transverse direction testing as derived from the wide-width strip tensile, designated as WW, and modified strip tensile, designated as MST, respectively. In addition, the percent difference as related to the wide-width strip tensile test is recorded. For this data a negative sign preceding a particular value indicates that the average MST test value over estimates the average WW test value by the amount indicated.

Table 1. NW-PP-CONT Test Data

Mass per Unit Area		Machine Direction			Transverse Direction		
gms/m^2	units	WW [sd]	MST [sd]	Δ(%)	WW [sd]	MST [sd]	Δ(%)
140	N	2199[833]	970[171]		1916[101]	1002[119]	
	kN/m	11	9.7	11.8	9.6	10	-4.2
	%ε	102.3	86	16	47.6	42.8	10.0
270	N	3824[387]	1727[249]		4060[150]	2215[148]	
	kN/m	19.1	17.3	9.4	20.3	22.2	-9.3
	%ε	123.3	92.3	25	51.8	52.1	-0.6
410	N	4344[357]	2493[284]		4550[115]	2393[139]	
	kN/m	21.7	24.9	-14.7	22.8	23.9	4.8
	%ε	124.1	116.7	6	90.6	68.4	24.5
540	N	5504[1815]	3075[792]		5301[319]	2535[289]	
	kN/m	27.5	30.8	12	26.5	25.4	4.2
	%ε	110	91	17	136.5	101	26

Table 2. NW-PET-CONT Test Data

Mass per Unit Area		Machine Direction			Transverse Direction		
gms/m^2	units	WW [sd]	MST [sd]	Δ(%)	WW [sd]	MST [sd]	Δ(%)
136	N	1888[45]	1034[43]		1544[86]	843[39]	
	kN/m	9.4	10.3	-9.6	7.7	8.4	-9.0
	%ε	58.6	64.3	-10	65.6	72.5	-10.5
240	N	4139[95]	2109[155]		3098[207]	1484[83]	
	kN/m	20.7	21.1	-1.9	15.5	14.8	4.5
	%ε	59.2	63.5	-7.3	65.4	67.2	-2.8
440	N	7502[309]	3571[188]		6067[243]	2982[201]	
	kN/m	37.5	35.7	4.8	30.3	29.8	1.6
	%ε	70.6	69.6	1.4	71.4	67.8	5
540	N	8422[632]	4503[266]		7600[446]	3825[214]	
	kN/m	42.1	45.0	-7	38.0	38.2	-.5
	%ε	69.7	69	1	68.3	65.8	3.7

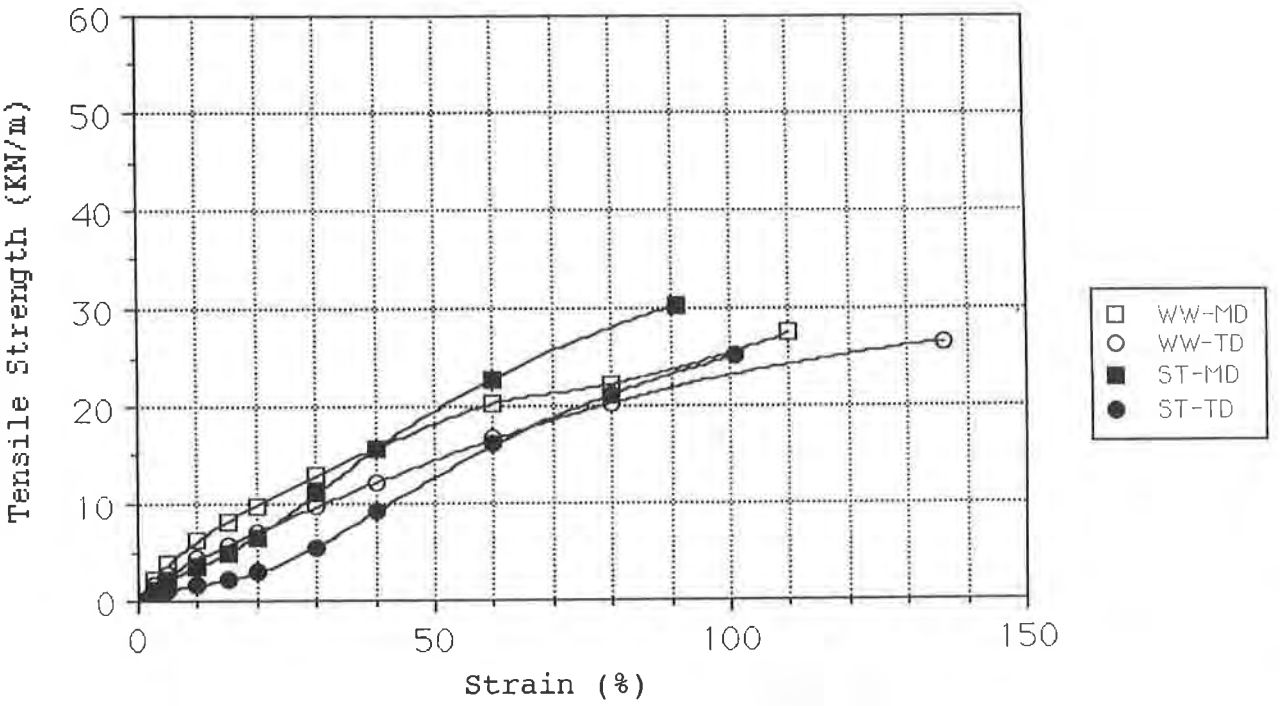

Figure 3 NW-PP-CONT (540 gm/m^2)

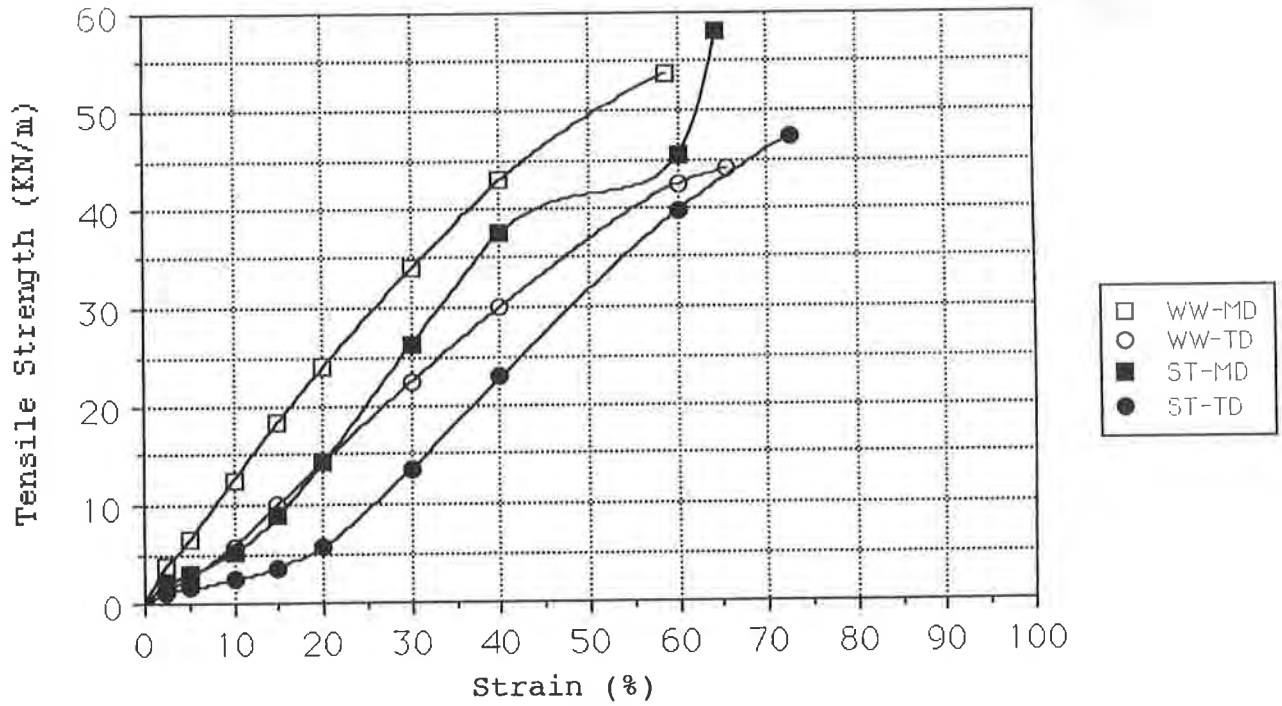

Figure 4 NW-PET-CONT (540 gm/m^2)

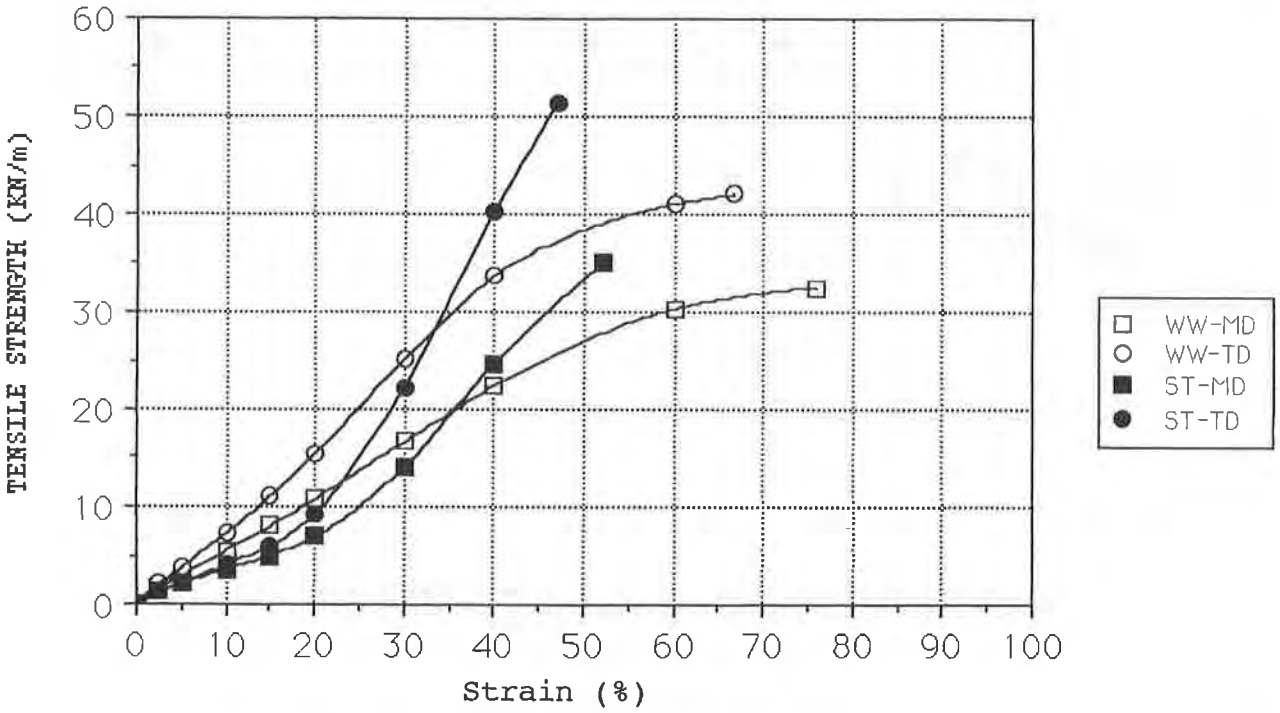

Figure 5 NW-PP-STAPLE (540 gm/m^2)

Table 3. NW-PP-STAPLE Test Data

Mass per Unit Area gms/m^2	units	Machine Direction WW [sd]	MST [sd]	Δ(%)	Transverse Direction WW [sd]	MST [sd]	Δ(%)
150	N	1389[182]	699[81]		2723[392]	1289[139]	
	kN/m	6.9	7.0	1.4	13.6	12.9	5.1
	%ε	49.5	50.4	-2	46.4	43.0	7.3
270	N	2783[210]	1328[82]		5857[480]	2725[176]	
	kN/m	13.9	13.3	4.3	29.3	27.2	7.2
	%ε	53.3	55.6	-4	55	43.7	20.6
410	N	4620[282]	2330[223]		5923[1441]	2986[407]	
	kN/m	23.1	23.3	.9	29.6	29.9	1.0
	%ε	48.5	41.7	14.0	50.3	38.9	22.7
540	N	6530[263]	3560[441]		8400[1343]	5212[451]	
	kN/m	32.6	35.6	9.2	42	52.1	24
	%ε	75.9	52.2	31.2	66.7	47.1	29.4

Load-Elongation Curves. To evaluate the relationship between modulus and toughness associated with the wide-width strip tensile and modified strip tensile tests, curves depicting load per unit width versus percent strain were developed. Figure 3 represents the machine direction and transverse direction responses for the 540 gm/m^2 NW-PP-CONT geotextile. Similar curves were developed for the 540 gm/m^2 NW-PET-CONT, Figure 4, and the 540 gm/m^2 NW-PP-STAPLE, Figure 5. Machine direction and transverse direction offset geotextile tensile modulus values and breaking toughness values for these three products is found in Table 4 and Table 5, respectively.

Table 4. Offset Modulus and Toughness:Machine Direction

Product Designation	Offset Modulus (kN/m)			Breaking Toughness (kJ/m^2)		
	WW	MST	Δ(%)	WW	MST	Δ(%)
NW-PP-CONT	27.7	46.2	67	19	15.2	20
NW-PET-CONT	90	114	27	18.4	17.4	5.4
NW-PP-STAPLE	57.4	107	86	14.8	7.2	51.4

Table 5. Offset Modulus and Toughness:Transverse Direction

Product Designation	Offset Modulus (kN/m)			Breaking Toughness (kJ/m^2)		
	WW	MST	Δ(%)	WW	MST	Δ(%)
NW-PP-CONT	24.7	36.2	47	22.6	12.6	44
NW-PET-CONT	76	93	22	15.6	15.1	3.2
NW-PP-STAPLE	87	181.6	109	16.8	8.6	48.8

SUMMARY

Ultimate Load and Elongation. From the data found in Tables 1,2, and 3 the author's believe that the modified strip tensile test can be used as an indicator of ultimate load, from which the ultimate load per unit width could be derived. It appears that for those tests in which the standard deviation, denoted as sd in the Tables, was the smallest for the results of both tests, the accuracy between the two test methods was within the 10% range. In addition, almost all of the materials tested indicated that the standard deviation associated with the modified strip tensile test is less than that found for the wide-width strip tensile test. It is expected that a greater number of tests conducted in a similar manner would reveal an enhanced correlation. A similar observation can be made for the percent elongation at failure. In evaluating the elongation at failure it appears that the NW-PP-CONT and NW-PET-CONT geotextiles produce results within a reasonable tolerance. Also, it was observed that these materials had values for elongation at failure within approximately 15% for the former and 5% for the latter. And although the NW-PP-STAPLE exhibited elongation at failure within approximately 7% the correlation between the two methods could be better defined through additional testing.

Offset Modulus and Breaking Toughness. The offset modulus and breaking toughness was determined for three products with the same mass per unit area, that being 540 gm/m^2. From the data found in Tables 4 and 5, it appears that the relationship between tests for offset modulus and breaking toughness are less defined. It appears that a larger data base of information will be required to confirm or dispute the correlation between these two tests with regard to offset modulus and breaking toughness.

CONCLUSIONS

The testing conducted for this study has indicated that there is a rather good correlation between ultimate load per unit width as determined from the wide-width and modified strip tensile tests. Based on the information derived from this test program it has been shown that the modified strip tensile test is useful in predicting the wide width tensile strength within ± 15%. It is believed that a larger sampling size will ultimately lead to a better correlation. Also, the correlation of elongation, offset modulus, and toughness for both of these tests was

evaluated. For all of these values, it appears that an increased sampling unit will lead to a possible correlation.

Results of this test program indicate that the modified strip tensile test could serve as a useful indicator of wide-width strip tensile strength. It is believed that future studies are needed to further establish the usefulness of the modified strip tensile test. It is hoped that this study will serve as a starting point for those interested in pursuing this form of testing.

REFERENCES

American Society for Testing and Materials (1991), ASTM Standards on Geosynthetics, Second Edition, Philadelphia, PA, 104 pp.

Polyfelt Inc. (1987), Polyfelt Design and Practice Manual, Evergreen, AL, 146 pp.

Comparison of Pull-Out Performance of Geogrids and Geotextiles

M.J. Cowell
The Reinforced Earth Co., USA

C.J. Sprague
Sprague & Sprague Consulting Engineers, USA

ABSTRACT

A study was performed to compare the interaction coefficients for three woven polyester geogrids with those of three woven geotextiles of similar strengths, when tested in a uniform fine sand. Pullout tests were also performed on the geogrids with the cross ribs completely removed to determine the influence of interlock and junction strength on the pullout performance of the geogrid.

The results of the testing showed that the geotextile and the geogrid have similar pullout performance in terms of their interaction coefficient and ultimate pullout capacity, however the geotextile exhibited a lower in-soil modulus as measured using the load-displacement data.

The results of the pullout tests performed on the geogrids without cross ribs showed that their total pullout resistance and interaction coefficients are slightly less than those for the full geogrid structure; however, their stress-displacement characteristics are virtually the same.

It was also found that inaccuracies in the coefficient of interaction value can be caused due to the relatively large strains that occur within samples during the pullout test. Recommendations are made for calculating C_i values using test data only from tests in which samples pullout, and not from tests in which samples break. Application of the test results to the design of reinforced soil slopes and walls are also discussed.

INTRODUCTION

One of the primary input parameters required in the design of soil structures reinforced with geosynthetics is the coefficient of frictional interaction (C_i) of the geosynthetic with soil. In recent years geogrids have been selected for use as reinforcements in part due to the excellent bond that is created between the soil and the geogrid.

The purpose of this paper is to review a pullout testing program that was performed on three geogrids and three geotextiles. The program was designed to investigate the differences in the pullout performance for geogrids with and without junctions and for geogrids and geotextiles with similar stress-strain characteristics when tested in a uniform fine sand. The objectives of the study were to:

1. Characterize the pullout performance of geogrids and geotextiles of similar ultimate tensile strengths;
2. Compare the pullout performance of geotextiles with those of geogrids;
3. Determine the influence of junction strength on the pullout performance of a geogrid; and
4. Make recommendations on how the results should be used for design.

Three design parameters that are calculated from the results of pullout testing of geosynthetic reinforcements were compared. These parameters are:

- C_i - The coefficient of frictional interaction (C_i) is the ratio of the shear strength that can be developed between the reinforcement and the soil, to the shear strength of the soil alone. This value is used to calculate the bond length of the reinforcement required beyond a critical failure plane.

- PO_{ult} - The ultimate pullout capacity (PO_{ult}) of the reinforcement is the highest load resisted by the reinforcement embedded in the soil regardless of the total displacement. This value is needed to determine if the allowable design strength of a reinforcement can be mobilized for a given bond length.

- $PO_{0.75\ inch}$ - The pullout capacity of the reinforcement at a limiting strain or displacement is used in the design of retaining walls with rigid concrete facings. In this case, it is the pullout capacity associated with a movement of less than 0.75 inches (19 mm) for the leading edge of the sample in the pullout box. (AASHTO 91).

Testing for these parameters for inextensible reinforcements (ie. steel strips) is straight forward since the tension applied to the reinforcement is readily transferred throughout the length of the reinforcement at very low strains. This is not the case for extensible reinforcements such as geogrids and geotextiles, which exhibit relatively large strains within the reinforcements during a pullout test. These large strains, which vary over the length of the sample, can affect the interpretation of the test results. Therefore the stress-strain characteristics of the geosynthetic being tested can have a significant affect on pullout performance and can provide considerable insight into how to interpret pullout test data. In addition, for geogrids, structure and stiffness of the product (Wilson-Fahmy (1990), Berg (1990), Juran (1988), Palmeira (1990)) and for geotextiles, the weave (Swann (1987)), have been investigated and found to have varying

degrees of influence on the frictional interaction that can be developed.

TESTING PROGRAM

The program consisted of running pullout tests on intact geogrids, geogrids from which the cross ribs were completely removed, and woven geotextiles. The three geogrids and three geotextiles were selected to have ultimate strengths of approximately 6000, 12,000 and 24,000 pounds per foot. The ultimate strength, ultimate strain and strength at 5% strain of the geogrids and geotextiles were very similar. In addition all materials were made from high tenacity polyester and manufactured by the same company. Therefore the primary differences between the materials were their structure and as would be found out later, their strength at 2% strain.

Test Equipment and Procedure. The pullout box used was 2 feet (0.61 m) wide by 5 feet (1.52 m) long. A minimum of 6 inches (152 mm) of sand was placed above and below the sample. An air bladder was used to apply the normal stresses directly to the soil. Friction at the face of the box was minimized through the use of a lubricated tapered metal sleeve.

The testing was conducted in accordance with the ASTM draft standard test method for "Determining Geosynthetic Pullout Resistance". Tests were performed at normal stresses of approximately 500, 1000, 2000 and 4000 psf (24, 48, 96, and 192 kN/m^2) on samples approximately 15 inches (381 mm) wide and 45 inches (1143 mm) long. The sand used in the test was placed at approximately 95% of standard Proctor (ASTM D 698) dry density and within approximately 2% of optimum moisture content. Test specimens were instrumented with four "telltales" spaced equally along the length of the sample to measure the variation of displacement within the sample during the test. This was done in order to be able to estimate the load distribution throughout the sample and estimate the actual area of sample that was being mobilized by a given load. Tests were performed at a constant displacement rate of 0.04 inches (1 mm) per minute and run until a constant load was recorded or failure occurred within the test specimen.

MATERIAL PROPERTIES

Soil. The soil used for the pullout testing program consisted of a non-plastic uniform fine sand with a trace of silt (SP) sampled from a Florida Department of Transportation borrow area. The soil is typical of the fill used for embankment fills and for backfill for MSE walls in Florida. The gradation of the soil is summarized below.

Sieve Size	% Passing
No. 20	100
No. 40	96
No. 60	79
No. 100	27
No. 200	2

Coefficient of Uniformity, C_u	2.2
Coefficient of Curvature, C_c	1.23
d_{10}	0.1 mm

The maximum dry density and optimum moisture content of the soil, as measured by ASTM D-698, Method A, was 102.6 pcf (1.64 g/cm^3) and 11.5% respectively.

The shear strength of the soil as measured by direct shear (12 inch (305 mm) by 12 inch box) showed it had peak values of phi = 30 degrees and an apparent cohesion of c'= 10 psf (0.5 kN/m^2), and residual values of phi = 29 degrees and c'= 0 psf.

Geogrids and Geotextiles. The geogrids used in the testing program were manufactured using high tenacity polyester yarns. They were woven using a straight warp weave into a geogrid configuration and then coated with PVC. The geotextiles were also manufactured from similar high tenacity polyester yarns and were woven using a plain weave for samples N 66000 and N 72600 and a twill weave for the N 73400 material. The mechanical properties of each of the materials are provided below:

Material	Structure	Tensile Test Results as per ASTM D4595 (lbs/ft)					
		Ultimate Strength	Strain	@ 2% Strain	% Tult	@ 5% Strain	% Tult
MX 60	Geogrid	5920	11.5%	1590	27%	2474	42%
N 66000	Geotextile	5040	12.2%	720	14%	1716	34%
MX 120	Geogrid	12420	10.4%	2880	23%	5820	47%
N 72600	Geotextile	13008	9.5%	1800	14%	5316	41%
MX 240	Geogrid	25380	12.0%	5640	22%	10020	40%
N 73400	Geotextile	22824	11.2%	3375	15%	9084	40%

TEST RESULTS

Geogrids versus Geotextiles. The results of the pullout testing performed on the geogrids and geotextiles are summarized on Tables 1 and 2. The results showed the following:

- The ultimate pullout capacity, PO_{ult}, of the geotextiles and the geogrids were typically within 15% of each other as shown on Table 1. This variation can be attributed to the slight differences in ultimate strength of the products which ranged up to 15%.

Table 1. Comparison of Ultimate Pullout Capacity of Geogrids to Geotextiles

Material	Pullout Capacity (lbs/ft)			Ultimate Tensile Strength (lbs/ft)
	Normal Stress (PSF)			
	500	1000	2000	
MX 60 N 66000 DIFF %	2483 2693 -210 -8.5%	4772 4258[1] +514 +10.8		5920 5040 +880 +14.9%
MX 120 N 72600 DIFF %	2566 2548 +14 +0.5%	4438 4740 -302 -6.8%	9192 8270 +922 +10%	12420 13008 -588 -4.7%
MX 240 N 73400 DIFF %	3193 2453 +740 +23%	5094 4474 +620 +12.2%	9880 8708 +1172 +11.9%	25380 22824 +2556 +10%

[1]Sample Failed before Pullout

- The coefficient of interaction, C_i, of the geotextile was slightly lower (10% or less) than that for the geogrid as shown on Table 2. For design purposes the lowest value for the geotextile was 0.93, which is high relative to a value of 1.0 for the soil alone.

Table 2. Comparison of C_i of Geogrids and Geotextiles

Material	C_i		
	Normal Stress (PSF)		
	500	1000	2000
MX 60 N 66000 DIFF %	1.09 1.19 -9%	1.05	
MX 120 N 72600 DIFF %	1.15 1.13 +2%	0.99 1.05 -6%	1.03 0.93 +10%
MX 240 N 73400 DIFF %	1.36 1.10 +19%	1.08 1.00 +8%	1.05 0.98 +7%

- The pullout capacity at a 0.75 inch (19 mm) movement, $PO^{0.75\ inch}$, however, was dramatically different for the two materials. This

can be seen on Tables 3, 4 and 5 and on Figure 1 which compares the results for the MX 240 geogrid with the N 73400 geotextile. The allowable design load (T_{AL}) for each material is provided as a reference point on each of these Tables. The results show that all three geogrids reached T_{AL} at 0.75 inches (19 mm) of movement even with junctions removed. However, the corresponding geotextiles could only mobilize 50 to 67% of their T_{AL}. A closer look at the data, on Tables 3, 4, and 5, reveals that the geotextiles were able to achieve their T_{AL} in pullout at the next higher normal stress at which they were tested. Therefore the use of the geotextile in limiting strain applications is controlled by the strength that can be developed at a given normal stress, and not by its ultimate pullout capacity. For designs requiring that strains be limited, such as retaining walls, both bond and pullout at low strains must be checked.

Table 3. Comparison of the Pullout Performance of Geogrids with and without Junctions and Geotextiles at their Allowable Design Load at a 500 psf Normal Stress

Material	Allowable Design Load	PO_{ult}	$PO_{0.75\ inch}$	C_i
MX 60	1890	2483	2000	1.09
MX 60 w/o Junctions	1890	2310	2000	0.99
N 66000	1890	2693	900	1.19
N 66000 @ 1000 psf Normal Stress	1890	4258[1]	1900	0.94[1]

[1] Sample failed prior to pullout

Table 4. Comparison of the Pullout Performance of Geogrids with and without Junctions and Geotextiles at their Allowable Design Load at a 1000 psf Normal Stress

Material	Allowable Design Load	PO_{ult}	$PO_{0.75\ inch}$	C_i
MX 120	3970	4438	4438	0.99
MX 120 w/o Junctions	3970	4140	4000	0.94
N 72600	3970	4740	3000	1.05
N 72600 @ 2000 psf Normal Stress	3970	8270	4000	0.93

Table 5. Comparison of the Pullout Performance of Geogrids with and without Junctions and Geotextiles at their Allowable Design Load at a 2000 psf Normal Stress

Material	Allowable Design Load	PO_{ult}	$PO_{0.75\ inch}$	C_i
MX 240	7400	9880	7400	1.05
MX 240 w/o Junctions	7400	9991	7800	1.12
N 73400	7400	8708	4300	0.98
N 73400[1] @ 4000 psf Normal Stress	7400	---	8700	---

[1] Sample failed before pullout

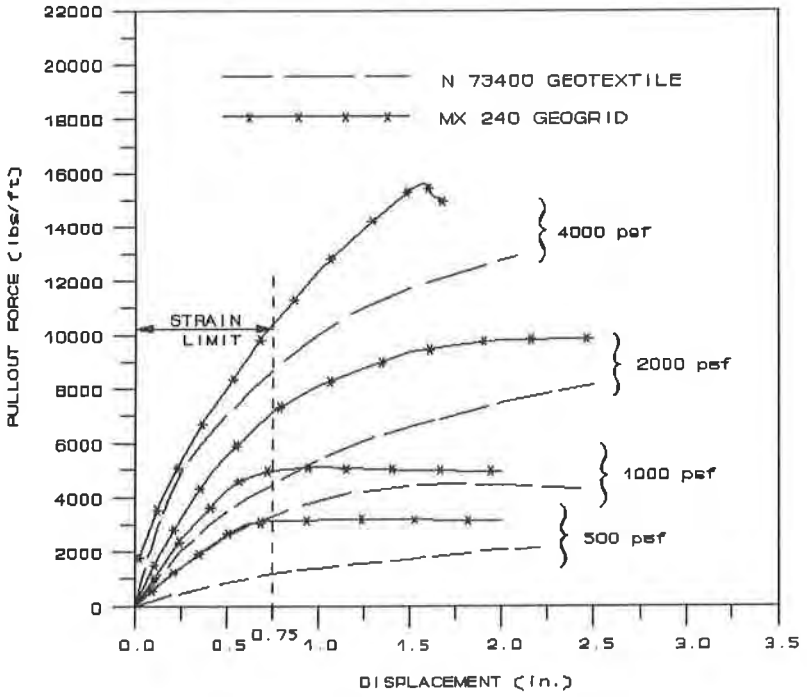

Figure 1 - Pullout Force versus Displacement Curves for MX 240 and N 73400

Comparison of Geogrids With and Without Cross Ribs Removed. Pullout testing of geogrids with and without junctions were performed to determine the influence of junction strength on pullout capacity and interaction coefficients. The cross ribs of the geogrids were completely removed resulting in a structure comprised only of independent longitudinal ribs. Tables 6 and 7 summarize the results of this test series. The conclusions from this testing are as follows:

Table 6. Comparison of Ultimate Pullout, PO_{ult}, for Geogrids with and without Junctions

Material	Ultimate Pullout Capacity PO_{ult}			Allowable Design Load
	Normal Stress (PSF)			
	500	1000	2000	
MX 60	2483	4772	6128[1]	1890
MX 60 w/o Junctions	2310	3768	5774	1890
Difference (%)	-7%	-21%	-6%	
MX 120	2566	4438	9192	3970
MX 120 w/o Junctions	2491	4140	7134	3970
Difference (%)	-3%	-7%	-22%	
MX 240	3193	5094	9880	7400
MX 240 w/o Junctions	2999	5072	9991	7400
Difference (%)	-6%	0%	+1%	

[1] Sample failed before pullout

Table 7. Comparison of C_i of Geogrids with and without Junctions

Material	Coefficient of Interaction, C_i		
	Normal Stress (PSF)		
	500	1000	2000
MX 60	1.09		
MX 60 w/o Junctions	0.99		
Difference (%)	-9%		
MX 120	1.15	0.99	
MX 120 w/o Junctions	1.13	0.94	
Difference (%)	-2%	-5%	
MX 240	1.36	1.08	1.05
MX 240 w/o Junctions	1.34	1.14	1.12
Difference (%)	-1%	+14%	+7%

- The ultimate pullout capacity, PO_{ult}, of the geogrids without junctions (Table 6), was typically within 10% of that for the full geogrid structure. Values ranged from 1% stronger to 22% weaker, with the weaker values being associated with a pullout capacity well above the materials allowable design strength. At the allowable design loads for the MX 60, MX 120 and MX 240 geogrids the differences varied from 0 to 7%.

- The coefficient of interaction, C_i, of the geogrids without junctions as shown on Table 7, was within 10% of that for the full geogrid structure with the lowest value being 0.94. Values ranged from 9% less to 14% greater, with the MX 240 material having higher values without cross ribs. These differences could be attributable to the greater open area of the grid without cross ribs. It is more likely, however, that it is due to the inherent variability between pullout test results since the MX 240 product had higher C_i values without junctions.

- The pullout capacity at 0.75 inches of displacement, $PO_{0.75\ inch}$ (Tables 3, 4 and 5) of the geogrids without junctions indicate that at stress levels close to the materials long term allowable design load, the pullout capacity is virtually the same as that for the full geogrid structure. This is illustrated on Figure 2 in which the load displacement plots for MX 240 with and without junctions are identical for normal stresses of 2000 psf (96 kN/m^2) and below. For stresses above this range the allowable design load is obtained at displacements of less than 0.75 inches (19 mm).

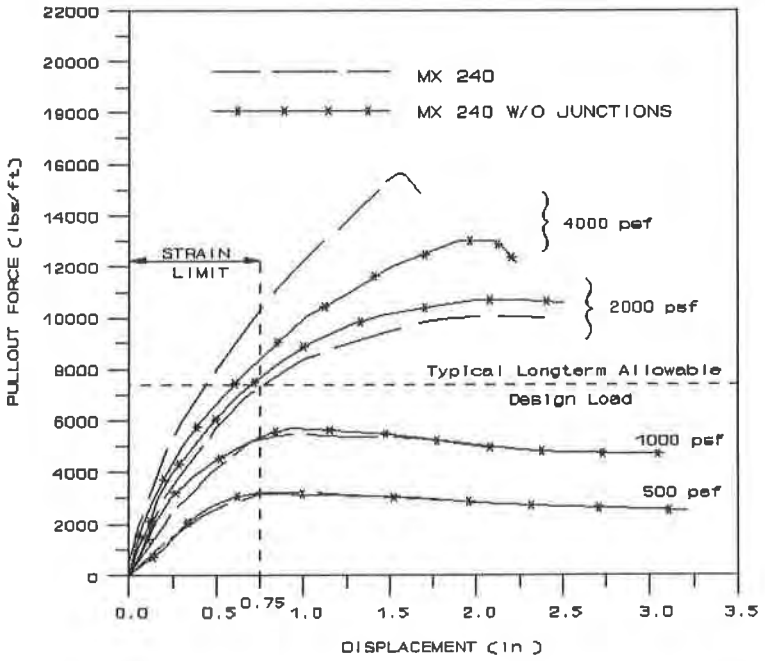

Figure 2 - Pullout Force versus Displacement Curves for MX 240 Geogrids with and without Junctions

APPLICATION OF PULLOUT TEST RESULTS TO DESIGN

In the design of a reinforced soil structure (see Figure 3) there are two problems that need to be solved related to the use of pullout test data. They are:

1. The bond length (L) required beyond a given failure plane that is needed to mobilize the allowable design strength of the reinforcement.

2. The maximum pullout force ($PO_{0.75\ inch}$) that can be used to limit the strains within a structure must be determined for designs where limiting strains are critical to the structure's long term performance.

Design of Reinforced Soil Slopes. For the design of reinforced soil slopes (Figure 3A) the C_i value from pullout testing is used to calculate the bond length behind a critical failure surface using Equation 1 below.

$$L = \frac{PO_{ult} \text{ or } PO_{0.75\ inches}}{2 \times C_i \times \text{Normal Stress} \times \tan \text{phi}} \quad (1)$$

where:

L = Bond Length Beyond a Failure Plane
Tan phi = The tangent of the effective friction angle of the soil

The ultimate pullout load is taken to be less than or equal to the allowable longterm design load and from this the bond length required is calculated. A factor of safety, typically on the order of 1.5, is applied to this length (FHWA, 1991). In slope applications, strains are controlled by using a 10% creep limit strain in the selection of the allowable design load. Likewise embankment slopes can tolerate more movement than a precast concrete wall face, which is why $PO_{0.75\ inch}$ is not typically used for slopes. The critical failure mechanism for a reinforced embankment is global instability and therefore selection of the C_i values used to calculate bond length is the controlling factor. Therefore, the C_i values used in the equation should be those associated with stress levels at or below the allowable design load and those for stress levels or sample lengths at which the shear stress within the samples tend to be more uniform. This is discussed below in more detail.

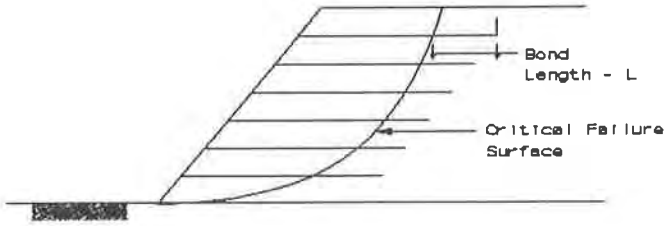

A. Design Controlled by Bond Length

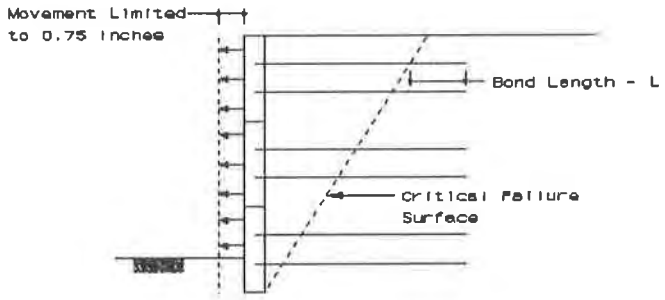

B. Design Controlled by Limiting Strain

Figure 3 - Use of Pullout Data in Slope and Wall Applications

Relationship Between Pullout Load Distribution and C_i. The estimated pullout load within geogrids can vary significantly along the length of the geogrid being tested. This is shown on Figure 4. As the pullout load increases above the allowable design load, the load distribution along the length of the sample becomes less uniform. This is due in part to the unequal strains that are occurring along the length of the reinforcement. In calculating C_i from equation 1, the assumption is made that the pullout force (PO_{ult}) is equally distributed over the length (L) of the reinforcement. Therefore, as this assumption becomes less accurate so will the calculation of C_i. As shown on Figure 4, for C_i data associated with pullout loads well above the allowable design load of a material are not always accurate. This is because these specimens are especially subject to uneven stress distribution. In addition use of this data is not especially meaningful since the reinforcements will not experience these loading conditions.

Therefore to accurately calculate C_i, test data should be used from pullout tests in which pullout of the entire sample has occurred and for pullout load levels closer to the allowable design load of the reinforcement. Uneven stress distribution and reporting of C_i for load levels well above the allowable design load is likely the reason for the large variations in data reported for other geogrids (Berg, 1990).

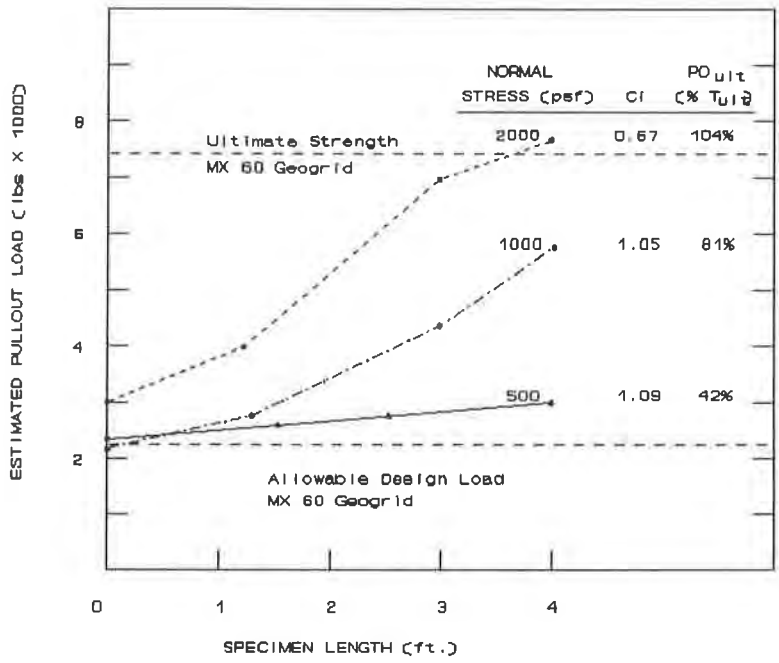

Figure 4 - Estimated Pullout Load Distribution along length of MX 60 Geogrid

Design of Reinforced Soil Walls. For the design of reinforced soil walls with concrete facing panels (Figure 3B) limiting strain of the wall face is critical to performance. Therefore, both the C_i and the $PO_{0.75\ inch}$ for the geosynthetic must be checked to see how they may affect the design. Table 5 illustrates the available pullout capacity at 0.75 inches of displacement for the MX 240 and N 73400 materials at a given normal stress. For the MX 240 geogrid at a normal stress of 2000 psf (96 kN/m^2), the $PO_{0.75\ inch}$ is equal to or greater than the allowable design load. Therefore, bond length will control the design since the allowable design load can be achieved in pullout with less than a 0.75 inch (19 mm) movement. For the N 73400 geotextile, however, the allowable design load is almost two times greater than the pullout resistance that can be obtained at 0.75 inches (19 mm) of movement. Therefore, the allowable design load needs to be lowered to the pullout value at 0.75 inches (19 mm) of movement. This will lower the load carrying capacity available for this material and will require a greater density of reinforcements be used. Therefore, for the design of walls using geosynthetics it is important to check if the allowable design load can be mobilized within a limiting strain in order to assure that wall face movements remain within tolerable limits.

CONCLUSIONS

The results from this testing program can be summarized as follows:

- Geogrids and Geotextiles manufactured from similar fibers, and having similar ultimate strengths and strengths at 5% strain

have similar ultimate pullout capacities and coefficients of interaction.

- The pullout capacity at 0.75 inches (19 mm) of displacement for the geotextiles tested was significantly lower (50 to 67%) than that obtained for geogrids of similar strengths.

- Removal of the cross ribs from the geogrids tested reduced the coefficient of interaction and ultimate pullout capacity of the geogrids by less than 10% and had no effect on the in-soil modulus. It can be concluded that for these types of geogrids that junction strength and the contribution from bearing resistance on the transverse ribs, does not have a significant affect on pullout performance.

- C_i values obtained from pullout tests performed at stress levels above the allowable design strength of the geosynthetic or from specimens that did not pullout can be inaccurate due to the significant variability in load distribution throughout the specimen. C_i values should be calculated only from test results in which the sample pulled out of the soil and for pullout loads close to the allowable design strength of the material being tested.

- Both the C_i and pullout capacity at a given displacement should be investigated for wall designs utilizing concrete facings to see if bond or pullout capacity will control the allowable design strength used for a given material.

ACKNOWLEDGEMENTS

We would like to thank The Reinforced Earth Company and The Nicolon Corporation for funding this project, Mr. Robb Swann and Mr. Zehong Yuan of Geosyntec for their advice and review of the test data, and Ms. Debbie Reynolds for compiling and editing the paper.

REFERENCES

AASHTO 1991 Interim Specifications, "Standard Specification for Highway Bridges", Fourteenth Edition, 1989 as amended by The Interim Specification - Bridges - 1990 and 1991, 295 pp.

Berg, R.G., (1990) "Investigation Into Geogrid Pullout Mechanisms", Proceedings of the International Reinforced Soil Conference, Performance of Reinforced Soil Structures, University of Strathclyde, Glasgow, Scotland, September 10-12, 1990.

Bonczkiewicz, C., Christopher, B, and Simac M., (1991) "Load Distribution in Geogrids with Low Junction Efficiency", Geosynthetics '91, Vol. 2, pp. 643-652.

FHWA (1991), "Interim Guidelines for Design, Specification and Contracting of Geogrid Mechanically Stabilized Earth Slopes on Firm Foundations", 60pp.

Juran, I., and Chen, C.L., (1988) "Soil-Geotextile Pull-out Interaction Properties: Testing and Interpretation", Proceedings of TRB 67th Annual Meeting, January 11-14, 1988, Paper No. 870159, 38 pp.

Palmeira, E.M., and Milligan, G.W.E., (1990) "Large Scale Pull-Out Test on Geotextiles and Geogrids, 4th International Conference on Geotextiles Geomembranes and Related Products, Vol. 2, pp. 743-746.

Swan, R.H., (1987) "The Influence of Fabric Geometry on Soil/Geotextile Shear Strength", Geotextiles and Geomembranes, 6 (1987), pp. 81-87.

Wilson-Fahmy, R.F., and Koerner, R.M., (1990) "Theoretical Analysis of Geogrid Pullout Behavior", Geosynthetic Research Institute, Drexel University, Pennsylvania.

An Interpretation of the Pull-Out Test

D.H. Chan
The University of Alberta, Canada

C.T. Yi
The University of Alberta, Canada

J.D. Scott
The University of Alberta, Canada

ABSTRACT

The pull-out test is a common test in determining the strength and deformation parameters between reinforcement and soil in the design of reinforced earth structures. It is often assumed in the interpretation of the results from the test that the mobilization of shear strength along the reinforcement is uniform. The calculation of the strength parameters is believed to be less affected by this assumption for a strain hardening material than for a strain softening material. However difficulties arise when the pullout test is used in obtaining the deformation behaviour of the soil-reinforcement interface for use in a deformation analysis. The progressive shearing at the soil-reinforcement interface during the pull-out test often leads to incorrect calculations of the shear-displacement response between the reinforcement and the soil.

To investigate the effect of progressive shearing on the calculation of the shear stiffness of the soil-reinforcement interface, the finite element method was used to simulate the pull-out test. The reinforcement, soil and interface behaviour were modelled using linear and non-linear constitutive models. Shear stiffnesses were calculated using conventional methods. It was found that there are considerable discrepancies between the calculated shear stiffnesses and the correct stiffnesses which were used in a finite element analysis. The amount of error depends on the relative stiffness between reinforcement and soil and the size of the specimen being analyzed. The finite element results were also compared with the observed response from laboratory experiments. A revised interpretation of the pull-out test results is discussed.

INTRODUCTION

Design of reinforced soil using geosynthetics currently adopts a limit equilibrium approach. In this approach the stability of the structure is evaluated at a limiting state of incipient failure satisfying force equilibrium but not strain compatibility. A satisfactory design emerges from the analysis by ensuring an adequate factor of safety for the structure. Although this current procedure is a logical extension of the well established method of designing and analyzing unreinforced soil, there is one basic difference between the reinforced and unreinforced structures; namely the unreinforced soil mass usually consists of one material while the reinforced soil mass has at least two materials. The calculation of one

factor of safety for the reinforced soil assumes the same degree of mobilization of shearing resistance for the soil and the soil-reinforcement interface, which obviously is not true for most serviceability conditions except at the state of incipient failure. The use of partial factors of safety is an attempt to account for such discrepancies in mobilized resistance. However it is well recognized that the calculation of mobilized resistance should account for strain compatibility. The importance of strain compatibility in a reinforced soil analysis has been discussed by Beech (1987). Procedures have been proposed to incorporate strain compatibility in conventional methods of design, Rowe and Mylleville (1989). Proper account of strain compatibility, however, can only be made using a deformation analysis. The finite element method is well suited for this purpose.

Numerous studies have been carried out using the finite element method in analyzing reinforced soils, Schaefer and Duncan (1988). In most finite element analyses, the soil is modelled using conventional solid elements. The reinforcement is generally modelled using flexible beam elements incapable of providing bending or compressive resistance. The connection of the reinforcement and the soil can be modelled in two ways. The first approach assumes that the reinforcement is firmly bonded to the soil allowing no slip until the shear stress between the two materials reaches a critical value. This critical value is often determined using the Mohr-Coulomb failure criterion modified to account for the reduced resistance at the interface. Once slip occurs at the interface, a limiting shear stress is assumed. This approach required no special treatment at the interface between the soil and reinforcement.

The second approach is to model the soil and reinforcement interface using an interface element such as that proposed by Goodman et al (1968) or Carol and Alonso (1988). Movement, or partial slip, is allowed between the soil and the reinforcement. This relative movement is controlled by a shear stiffness, k_s, until the shear stress is sufficiently high to cause slippage. The shear stiffness is often defined as:

$$k_s = \frac{\Delta\tau}{\Delta\delta} \qquad (1)$$

where $\Delta\tau$ is the change in shear stress and $\Delta\delta$ is the corresponding change in relative displacement between the soil and reinforcement.

Normal deformation is governed by a normal stiffness, k_n, which is usually uncoupled with shear deformation. The mobilization of resistance is a complicated process. The pull-out resistance of the geogrid reinforcement is basically mobilized by three interaction mechanisms: soil friction on plane surfaces of the reinforcement, soil passive resistance on the transverse elements and particle interlocking in the apertures in the reinforcement. The mechanisms by which the reinforcement resistance develops depend on the size of the apertures, stiffness, geometry, roughness of the surface of the reinforcement, and the grain size of the soil. For small soil-reinforcement displacements there is initially a mobilization of the friction along the longitudinal elements of the reinforcement. The soil passive resistance on the transverse elements is mobilized under larger displacements and is influenced by the stiffness, structure, and geometry of the reinforcement as shown by Schlosser and Delage (1987). Irsyam and Hryciw(1991) show experimentally that shear surfaces develop around the ribs of the reinforcement during the shearing process. The soil passive resistance on the transverse elements plays an important role on the total pullout resistance. It is a function of the soil cohesion, friction angle, and bearing capacity factor (N_q) in the Terzaghi bearing-capacity

equation. The expression for N_q depends on the assumed failure mechanism such as the punching failure mode suggested by Jewell et al.(1984). The particle interlocking resistance is often neglected because the particles of the soil are significantly smaller than the fibre or grid spacing and the grains cannot effectively interlock within the geosynthetics apertures (Sarsby, 1985).

The shear stiffness expressed in equation (1) depends on the soil and type of reinforcement and it is often determined experimentally for use in finite element analysis. The direct shear test and the pull-out test are commonly used to determine the interaction properties between the soil and reinforcement. In particular the pull-out test simulates the anchorage condition of the reinforcement and provides an estimation of the pull-out resistance for design. It is also used to provide an estimate of the shear deformation between the reinforcement and soil, Katagiri et al (1990). In calculating the shear stiffness using equation (1), it is necessary to calculate the shear stress acting on the reinforcing material. In calculating the shear stress, it is assumed that the mobilization of shear stress is uniform along the reinforcement and the change in shear stress is given by:

$$\Delta\tau = \frac{\Delta P}{2A} \tag{2}$$

where ΔP is the measured change in axial force and A is the one sided surface area of the reinforcement.

Therefore equation (1) becomes:

$$k_s = \frac{\Delta P}{2A\,\Delta\delta} \tag{3}$$

The change in displacement in equation (3) is often taken as the displacement measured on the reinforcement at the pull-out slot.

In the present finite element model, the interface between the geogrid and the soil is modelled using an interface element treating the geogrid as a sheet like material with no apertures. Thus the shear stiffness calculated from equations (1) and (3) includes effects due to both interfacial friction and passive resistance.

It is recognized that the mobilization of shear stress is non-uniform along the reinforcement. At failure, that is the fully slipping condition, the mobilization of shear strength is approximately uniform if the interface does not possess a strain weakening characteristic. This behaviour may be true for some soils used in reinforced soil structures which are not dense. For dense soils, the strain weakening behaviour can result in non-uniform mobilization of shear strength.

It is possible to account for the non-linear characteristic of k_s with respect to displacement as well as normal stress, for example see Katagiri et al (1990), but the assumption of uniform shear stress can result in a serious error in obtaining k_s. The mobilization of shear stress is highly non-uniform along the reinforcement during the loading process. Although the shear stress can be estimated using the load transfer approach proposed by Coyle and Reese (1966), the corresponding relative displacement cannot be determined easily.

In this paper, the implication of assuming an uniform shear stress in calculating the shear stiffness from the results of a pull-out test is examined in detail. The progressive development of stress and strain in the reinforcement and its interface are calculated using the finite element method. The approach taken here is to calculate the shear stiffness using equation (3) from numerical simulation of the pull-out experiment. This calculated stiffness is called the apparent shear stiffness. Since the actual stiffness used in the finite element analysis is known, which will be referred to as the true shear stiffness, the discrepancy between the apparent and true stiffnesses can be evaluated. The true stiffness is an equivalent stiffness for use in finite element calculations which combines the effect due to friction and passive resistance. Various factors affecting the shear stiffness are identified.

One can appreciate the advantage of the numerical approach. Since the true shear stiffness between the soil and the reinforcement cannot be determined easily by experiment, it is difficult to examine the effect of progressive deformation on the pull-out test results from laboratory measurements even with extensive measurements of strains and displacements along the reinforcement. The numerical method provides a convenient way of assessing the effect of progressive deformation on the pull-out test results.

FINITE ELEMENT MODELLING OF THE PULL-OUT TEST

The pull-out test was simulated using the finite element method. An interface element was used which was capable of sustaining tensile stress but not bending or compressive stress. A description of the formulation of the joint element can be found in Chalaturnyk (1988).

A two dimensional plane strain idealization of the pull-out specimen is shown in Figure 1. A total of 170 elements, including 17 reinforcing and 34 interface elements, with 636 nodes was used in the simulation. The reinforcing elements are three node elements capable of sustaining only tensile stress. The interface was modelled by 6 node elements. Eight node isoparametric elements were used to simulate the soil.

The reinforcement was extended from one end of the box to the other end. This was the actual experimental set-up carried out at the University of Alberta (Costalonga, 1988). The advantage of this arrangement is that the area of contact between the reinforcement and soil remained constant throughout the experiment. Also the displacement of the reinforcement at the opposite end from the pull-out slot could be monitored to determine the load at which movement occurred.

The reinforcement was modelled using a non-linear force-strain relationship. The tensile force in the reinforcement can be expressed as:

$$F=D_i(\varepsilon_a-\frac{\varepsilon_a^2}{2\varepsilon_f}) \qquad (4)$$

where F, D_i, ε_a and ε_f are the tensile force, initial load modulus, axial strain and axial strain at failure respectively.

Equation (4) is based on a parabolic relationship between stress and strain developed in the reinforcement. This is found to be a good approximation for a polymeric geogrid within

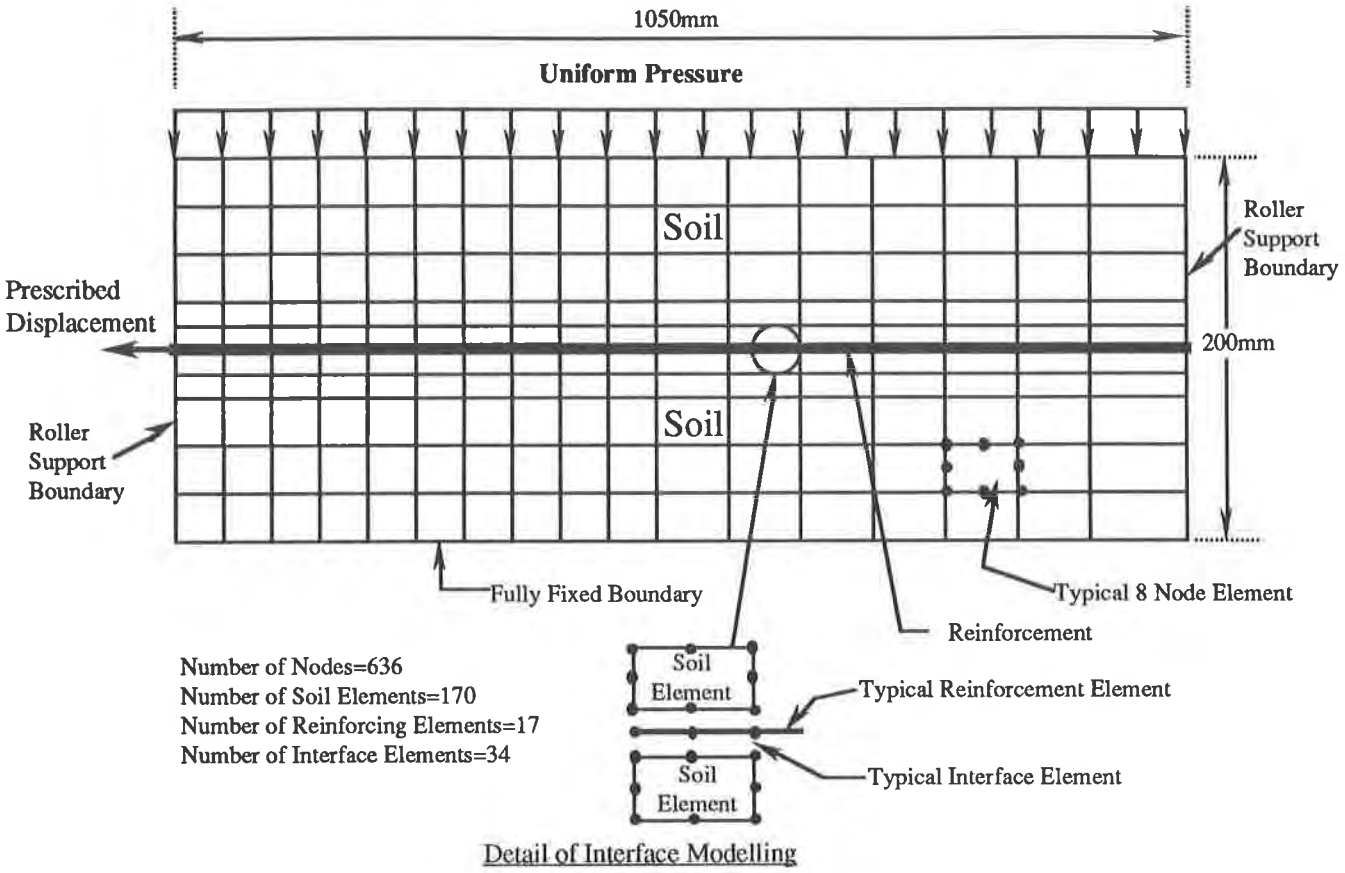

Figure 1. Finite Element Idealization of Soil and Reinforcement for the Pullout Test

the range of strains of interest in this study (Chalaturnyk, 1988). The reinforcement was Tensar SR2 geogrid. The force-strain relationship used in the modelling is shown in Figure 2.

The shear behaviour of the interface between the soil and the reinforcement was modelled using an elastic-plastic model. The shear modulus remained constant until a failure condition was reached along the interface. The failure condition is defined by the Mohr-Coulomb relationship :

$$\tau_f = c_a + \tan\delta \qquad (5)$$

where c_a and δ are the adhesion and frictional resistance between the soil and the reinforcement and;

σ_n and τ_f are the normal and shear stress on the reinforcement respectively.

In the finite element analysis, the shear stress at each integration point was checked with the failure criterion. If failure was reached, a constant shear stress was applied and maintained at the integration point throughout the remainder of the analysis.

A linear elastic model was used to model the behaviour of the soil. Since it was expected that the amount of straining in the soil would be small, smaller than the strain in the interface

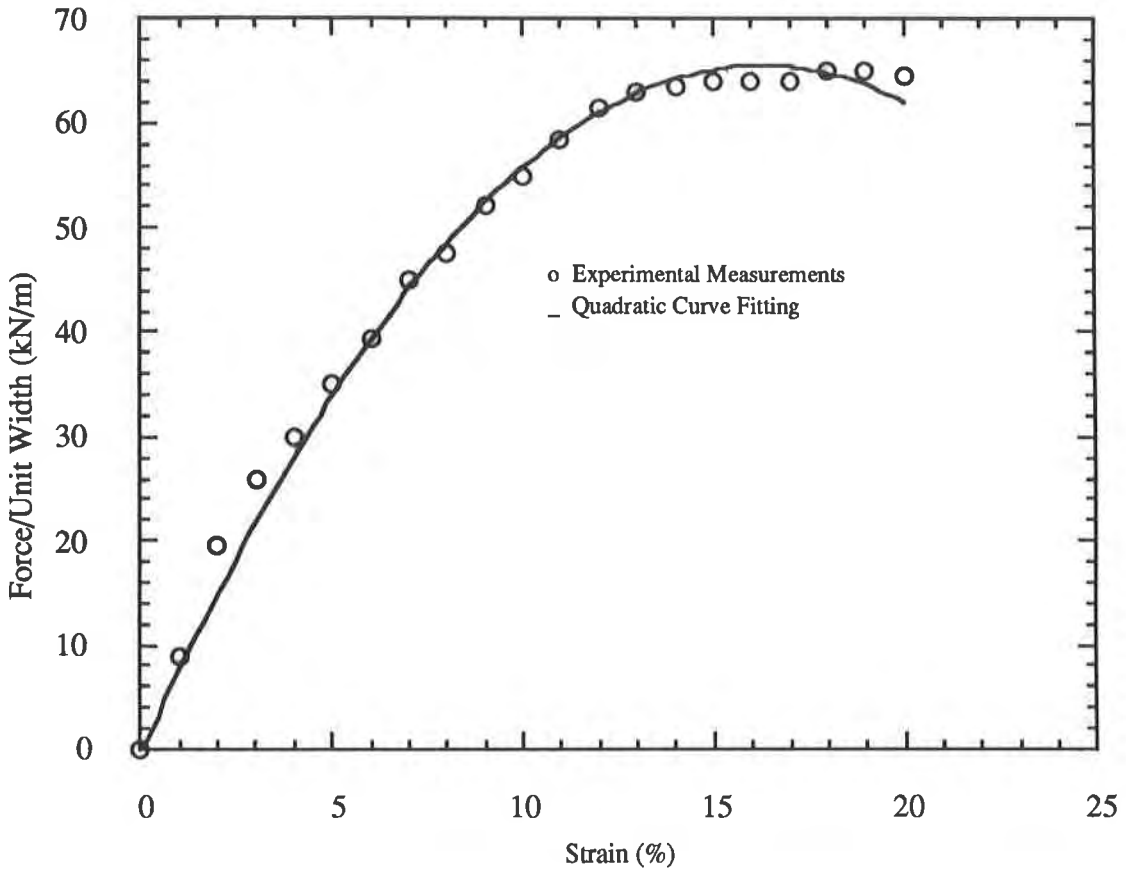

Figure 2. Load-strain Response of Tensar SR-2 used in the Simulation (strain rate, 2%/min.)

and reinforcement, the initial tangent modulus, based on triaxial testing of the soil, was used to calculated the elastic parameters for the model. A summary of the material parameters used in the analysis is given in Table 1. The shear stiffness for the interface was calculated based on a pull-out test conducted by Costalonga (1988). The normal stiffness, K_n, was assigned a very high value to prevent incompatibility in the normal direction.

In simulating the pull-out experiment, a vertical uniform pressure of 51 kPa and the weight of the soil were applied prior to imposing force on the reinforcement located at the mid-height of the apparatus. The pull-out forces acting on the reinforcement during the test were calculated from the prescribed displacements specified on the reinforcement at the pull-out slot. The reinforcement was extended through the back of the apparatus which gave a constantly embedded length during the entire shearing process.

RESULTS OF THE FINITE ELEMENT ANALYSIS

The force-displacement response calculated from the finite element analysis is shown in Figure 3. It is seen that the finite element model underestimated the force required for a certain displacement. It is reminded that the shear stiffness was calculated based on the observed load-displacement response from the pull-out test. It is clear that the assumption of uniform mobilized shear stress along the reinforcement in calculating the shear stiffness underestimated the actual shear stiffness. Katagiri et al. (1990) also simulated the pull-out test

Table 1. Summary of Material Properties Used in the Finite Element Analysis

Material	Properties	Value
SILTY CLAY	Unit Weights (kN/m^3)	18.86
	Initial Elastic Modulus (kPa)	3600
	Poisson's Ratio	0.36
	Cohesion (kPa), c	29
	Internal Friction Angle (°), ϕ	20
GEOGRID	Tensile Strength (kN/m)	78.8
	Initial Load Modulus (kN/m), k_{ri}	800.0
	Failure Strain (%), ε_f	16.4
INTERFACE	Normal Stiffness (kN/m3), k_n	10^{17}
	Shear Stiffness (kN/m3), k_s	1240
	Adhesion (kPa), c_a	2 *
	Friction Angle (°), δ	14 *

* Adhesion and friction angle for the interface are based on the assumption that the geogrid is replaced by an equivalent sheet with no apertures which exhibits the same behaviour.

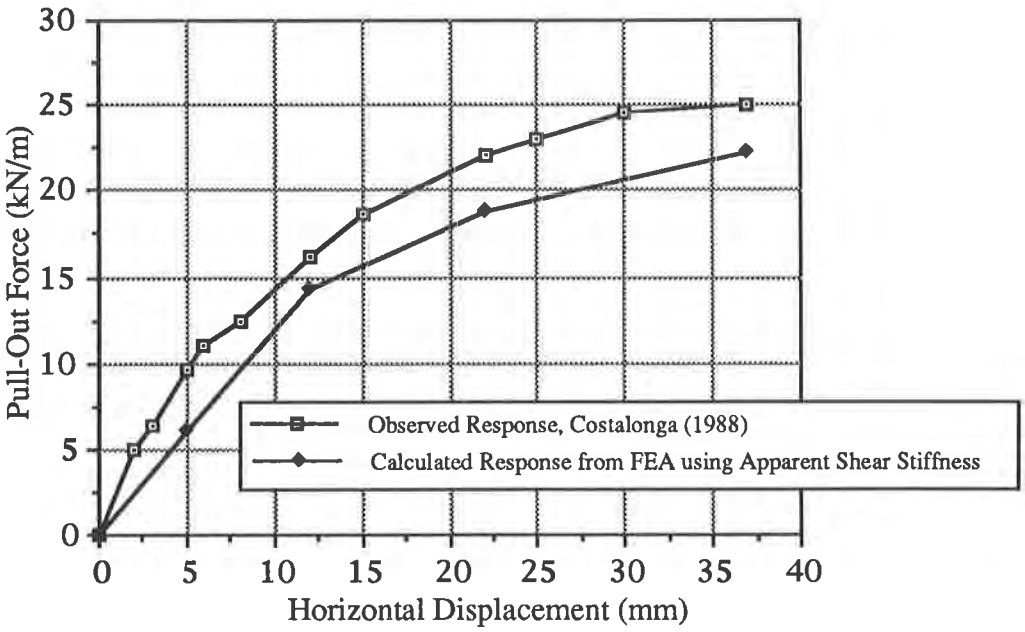

Figure 3. Calculated and Observed Force-Displacement Response of Reinforcement

and the calculated response was softer than the experimental observations.

The mobilized shear stress along the reinforcement is shown in Figure 4. As a result of the progressive shearing along the interface between the soil and reinforcement, the mobilized shear stress is highly non-uniform and decreases along the reinforcement. It does, however, remain relatively constant over the portion of the reinforcement where slip has occurred.

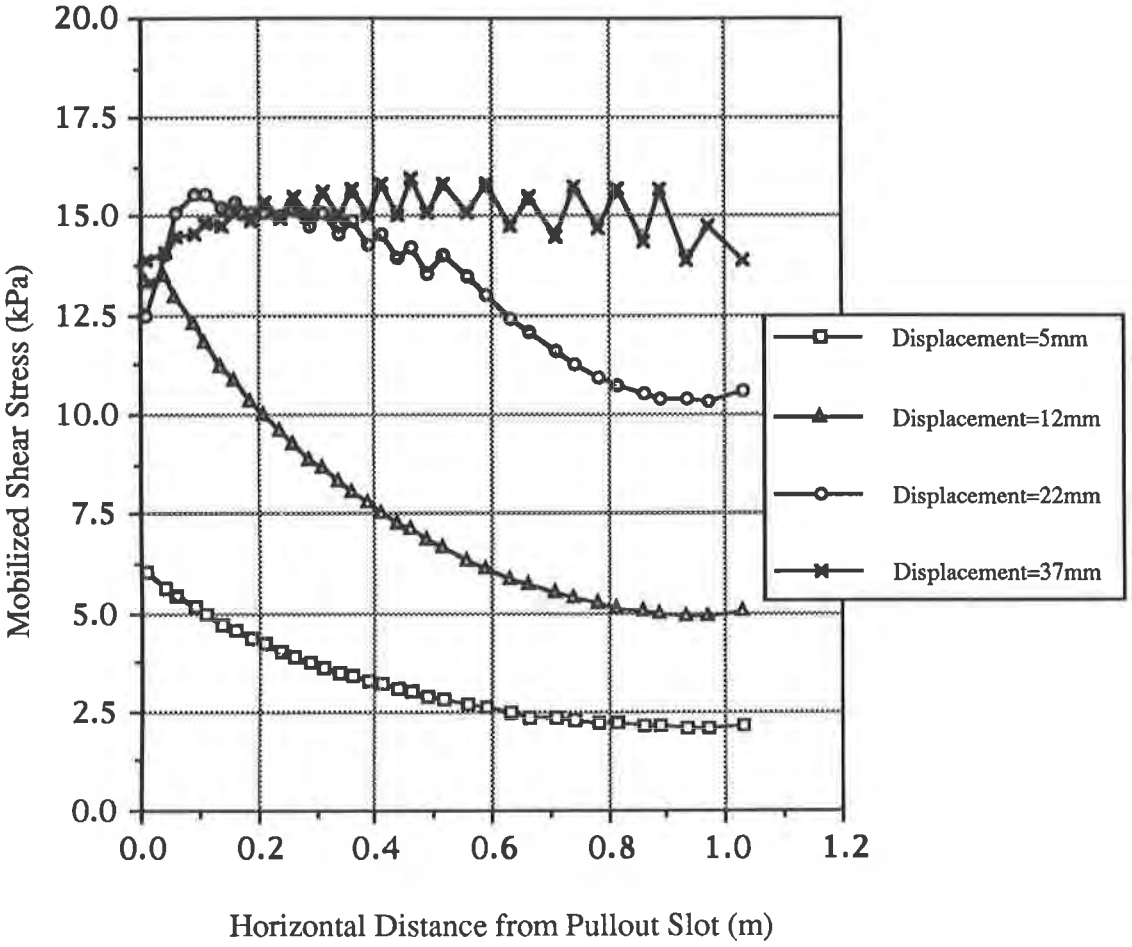

Figure 4. Mobilized Shear Stress Along the Reinforcement

In order to calculate the "true" stiffness for use in a finite element analysis, it is necessary to perform a series of simulations of the pull-out test and determine the apparent stiffness, using Equation 3, from the finite element results. A relationship between the apparent stiffness and the true stiffness then can be determined.

It is realized that the stiffness of the reinforcement influences the load transfer mechanism. The degree of progressive deformation will depend on the relative stiffness between the reinforcement and the interface. It is therefore appropriate to introduce a quantity called the true stiffness ratio, r. The true stiffness ratio is defined as the ratio of the true stiffness of the

interface, k_{st}, over the initial stiffness of the reinforcement, k_{ri};

$$r = \frac{k_{st}}{k_{ri}} \quad . \tag{6}$$

For very stiff reinforcement, such as metallic strips, the value of r is relatively small and the mobilized shear stress and displacements along the reinforcement are uniform. Very soft reinforcement, such as a non-woven geotextile, develops non-uniform shear stress and displacements along the reinforcement. The value of r will be relatively high for this material. It is expected that higher values of r will result in larger errors when calculating the shear stiffness from pull-out test results. A series of numerical simulations of the pull-out test was carried out for different values of the stiffness ratio. In each analysis, a shear stiffness, K_{st}, was specified for the soil interface between the solids and reinforcement. The apparent stiffness, K_{sa}, was calculated from the load-displacement response. The result of the analysis is shown in Figure 5. As r increases, i.e. the stiffness of the reinforcement decreases, progressive shearing becomes more significant and the discrepancy between the apparent shear stiffness and true shear stiffness increases.

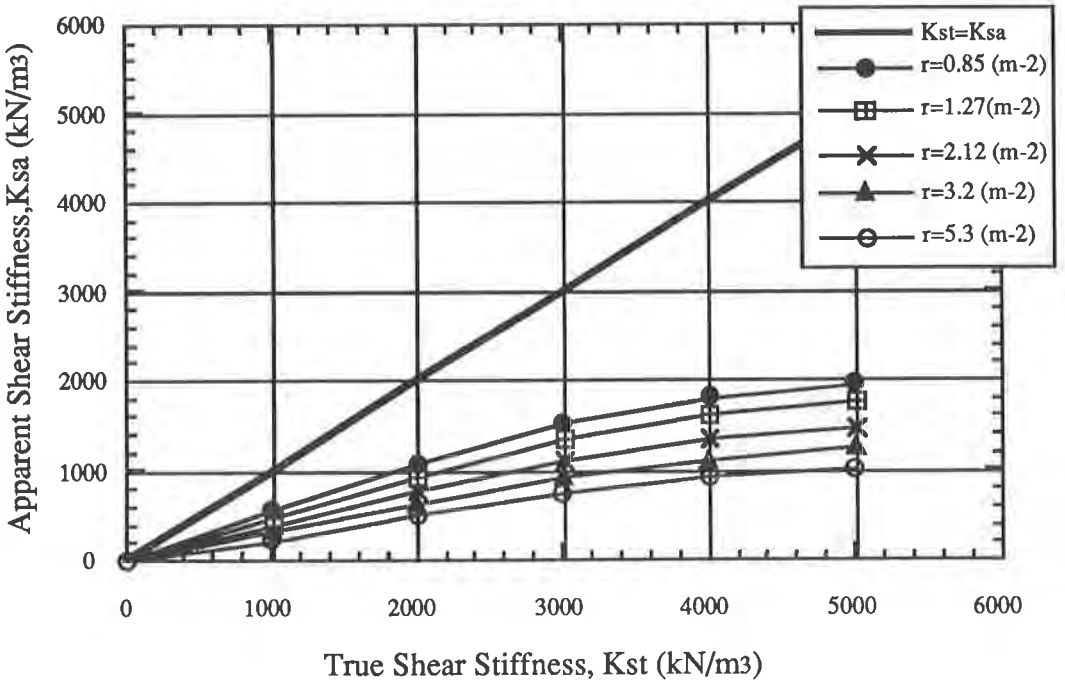

Figure 5. Relationship between the Apparent and Shear Stiffnesses

Based on an apparent shear stiffness of 1.24×10^3 kN/m^3, a true shear stiffness value was found to be 2.0×10^4 kN/m^3 for use in the finite element analysis. Figure 6 shows the observed and calculated load-displacement response using both the apparent and true stiffnesses. It is seen that the corrected stiffness provides better agreement between calculated and observed values. The mobilized shear stress along the reinforcement at different stages of the test is shown in Figure 7. Since the true stiffness is higher than the apparent stiffness, the mobilized shear stress using the true stiffness is higher than that calculated using the apparent

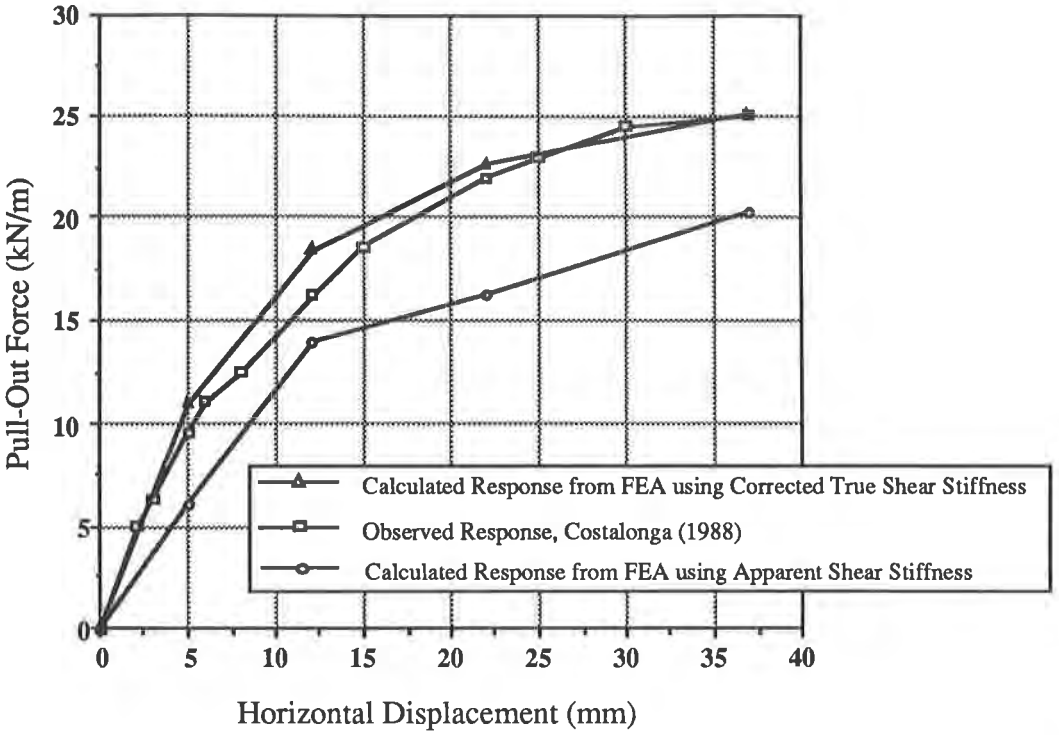

Figure 6. Calculated and Observed Force-Displacement Response of the Reinforcement in the Pullout Test

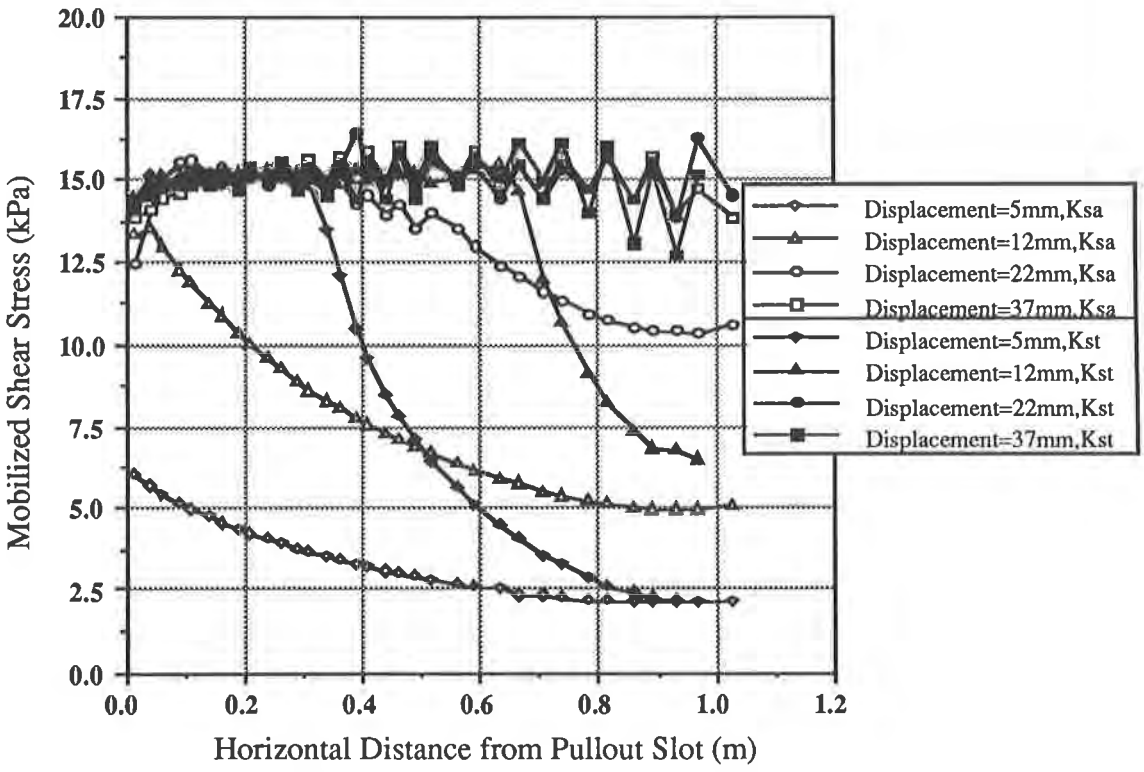

Figure 7. Mobilized Shear Stresses Along the Reinforcement

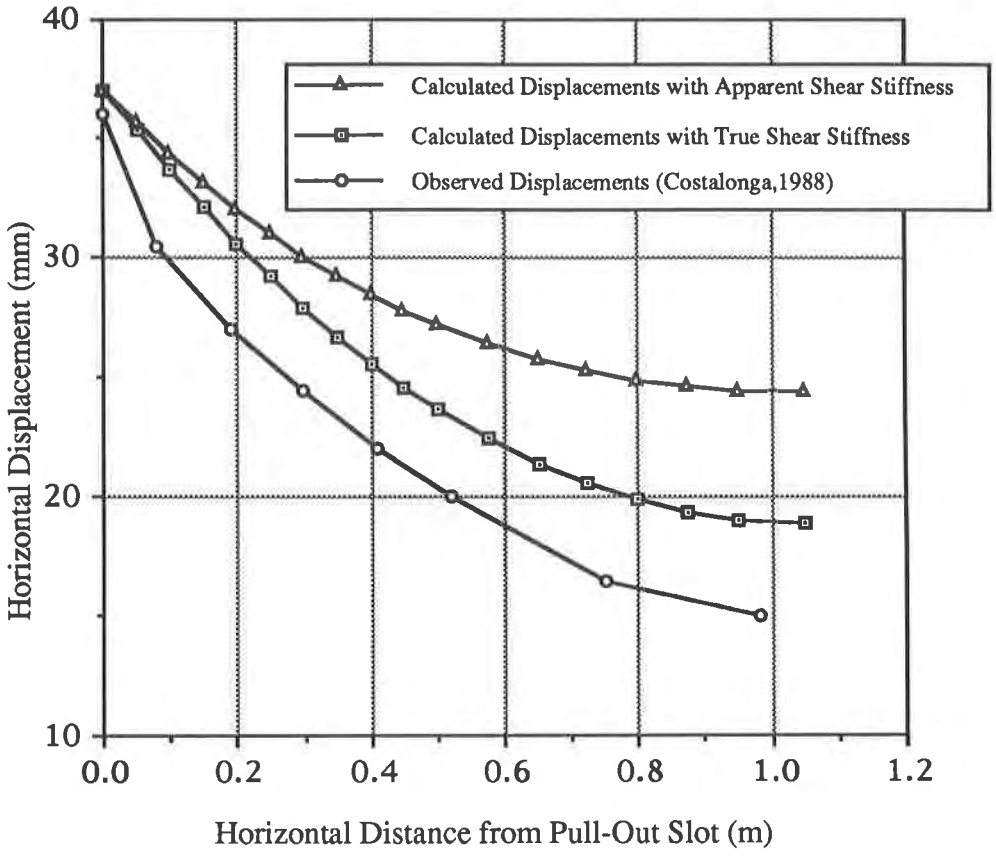

Figure 8. Comparison of Horizontal Displacement Along Reinforcement

stiffness for a given displacement of the reinforcement. The mobilized shear stress is the same for both cases when slipping occurs.

The calculated displacement along the reinforcement is also compared with the experimental results at a displacement of 37 mm when the total length of the geogrid was slipping. The results shown in Figure 8 indicate that the finite element solution slightlyoverestimated the displacement along the reinforcement. It is interesting to note that the difference between the calculated and observed displacements remains relatively constant along the entire length of the reinforcement.

CONCLUSION

The pull-out test was simulated numerically using the finite element method. It was found that the mobilization of shear stress along a reinforcement is highly non-uniform during the initial stage of the test. If the force-displacement response of the pull-out test was used to obtain a shear stiffness for modelling the interface between the soil and reinforcement, the assumption of uniform stress distribution can result in considerable error between the apparent shear stiffness and the true shear stiffness values. This discrepancy depends on the relative stiffness between the interface and the reinforcement. It was illustrated that stiffer reinforcement results in a less degree of progressive shearing and therefore results in less discrepancy between the true and apparent stiffness values. The true stiffness can be

estimated from the results of the pull-out test by using an appropriate stiffness correction. The calculated force-displacement response using a true stiffness value gives better agreement with the experimental observations.

ACKNOWLEDGMENT

The authors wish to thank SNC Inc. and Tensar Earth Technologies Inc. for donating an Award from the North American Geosynthetics Society in support of this research.

REFERENCES

Beech, J.F., (1987) "Importance of Stress-Strain Relationship in Reinforced Soil System Designs", Geosynthetics '87 Conference Proceedings, Vol 1, pp.133-144.

Carol, A.G. and Alonso, E.E., (1988) "An Interface Element Formulation for the Analysis of Soil-Reinforcement Interaction", Computer and Geotechnics, Vol 7, pp 131-151.

Chalaturnyk, R. (1988) "The Behaviour of a Reinforced Soil Slope", M.Sc. Thesis, The University of Alberta, Edmonton Alberta, Canada, 320p.

Costalonga, M.A.R., (1988) "Geogrid Pull-Out Test in Clay", M.Sc. Thesis, The University of Alberta, Edmonton Alberta, Canada, 211 p.

Coyle, H.M. and Reese, L.C. (1966) "Load Transfer for Axially Loaded Piles in Clay", Journal of Soil Mechanics and Foundation Engineering Division, Vol 92, No. SM 2, pp 1-26.

Goodman, R.E., Taylor, R.L. and Brekke T.L., (1968) "A Model for the Mechanics of Jointed Rock", Journal of Soil Mechanics and Foundation Engineering Division, Vol 94, No. SM 3, pp 637-659.

Irsyam, M. and Hryciw, R. D. (1991) "Friction and Passive Resistance in Soil Reinforced by Plane Ribbed Inclusions, Geotechnique, Vol 41, No. 4, pp 485-498.

Jewell, R.A., Milligan, G.W.E., Sarsby, R.W. ,and Dubois, D. (1984) "Interaction Between Soil and Geogrids ", Proceeding from the Symposium on Polymer Grid Reinforcement in Civil Engineering, London, England, pp 18-30.

Katagiri, T., Haneda, H., Moriyama, M., Tsuruoka, T., Toriumi, S., Takaoka, K., Yahaba, T., (1990) "Steep Reinforced Embankment using Geogrid - Laboratory Pull-out Test of Geogrid and its Finite Element Analysis, 4th International Conference on Geotextiles, Geomembranes and Related Products Proceedings, Vol. 1, pp 45-51.

Rowe, R.K. and Mylleville, B.L.J., (1989) "Consideration of Strain in the Design of Reinforced Embankments", Geosynthetics '89 Conference, San Diego, pp 124-35.

Sarsby, R.W., (1985) "The Influence of Aperture Size/Particle Size on the Efficiency of Grid Reinforcement", Proceedings of 2nd Canadian Symposium on Geotextiles and Geomembranes, Edmonton, Alberta, pp 7-12.

Schaefer,V.R. and Duncan, J.M., (1988) "Finite Element Analysis of the St. Alban Test Embankments", ASCE, Geotechnical Special Publication No. 18, pp 158-177.

Schlosser, F. and Delage, P.,(1987) "Reinforced Soil Retaining Structures and Polymeric Materials", The Application of Polymeric Reinforcement in Soil Retaining Structures, NATO ASI Series: Applied Sciences-Vol.147, pp 3-65.

Study on Geotextile Behaviors of Tensile Strength and Pull-Out Capacity Under Confined Condition

D.T.-T. Chang
Chung Yuah University, Taiwan, R.O.C.

W.-T. Wey
Moh and Associates Inc., Taiwan, R.O.C.

T.-C. Chen
Chung Yuah University, Tawiwan, R.O.C.

ABSTRACT

In this research project, 240 x 220 x 50mm soil confining box was adopted to conduct wide-width tensile tests and pullout tests. And the unconfined wide-width tensile tests were also used for comparison purpose. Four types of woven geotextiles were used to evaluate the tensile properties. Also four types of soils, C-190, C-109 ottawa sands, one sandy soil, and the fly ash treated mudstone, were used for confining material. Three confining pressures, 0.5 kg/cm^2, 1.0 kg/cm^2, and 2.0 kg/cm^2 were applied during each testing. According to the results, the developed relationship of elongation behavior can be defined into two portions. For the initial stage, the developed relationship is believed to be controlled by inter-frictional effects. The following stage, until failure reached, the development of increased stress is found to meet the unconfined tensile behavior quite well. To the finer soil, the initial friction-effects period is shorter than that from coarser soil. This also influenced the lower failure strength. For evaluating the frictional resistance from the results of tensile tests, the capacity was analyzed and found to be lower than that from pullout test.

INTRODUCTION

In the application of geotextile reinforcement , the frictional properties and overburden surcharge have been considered as the important factors in the design concept. From the extensive studies, it was indicated that with the soil confinement, geotextiles exhibit different tensile behaviors to that of the unconfining condition. To study the changes of tensile properties causing by the confinement effect, four types of soils with the various confinement effect, pressures are used in this study. Four woven geotextiles were to be selected in the testing program. Not only the tensile behaviors, but also the pullout frictional properties are evaluated. To understand the influncing factors involved, the varied water contents of soils were also evaluated in the study.

TESTING PROGRAM AND METHOD

The following items were to be studied through the laboratory testing program,

1. To review the wide-width tensile behaviors, with and without soil confinement.
2. To evaluate the effect of water contents of soil to the tensile behaviors.
3. To discuss the confined tensile strength to the pull-out resistance.

Based on the major works described as above, the related testing program was set up.

Selected geotextiles and soils. The study evaluated four woven geotextiles and four types of soils. Geotextile samples are denoted by A,B,C, and D, which included the material used (sample A) in the in-situ test wall by Chang et al.(1991). Typical properties performed from ASTM standards(1991) are listed in Table 1.

Table 1 Typical properties of selected geotextiles

Samples	Thickness (mm)	Unit weight (g/cm^3)	AOS (sieve No.)
A	1.92	0.0486	50-60
B	1.10	0.0236	40-50
C	1.65	0.0302	35-40
D	1.80	0.0355	40-45

Of the selected soil samples, two are ASTM C-190 (S-1) and C-109 (S-2) ottawa sands; the other two are sandy soil (S-3) and fly ash treated weathered mudstone (S-4) which were used to construct the test wall by Chang et al.(1991). Pertinent soil characteristics are summarized in Table 2.

Table 2 Related soil properties from direct shear tests

Soil types	Density (g/cm^3)	Water content (%)	Internal frictional Angle (ϕ)	Cohesion (kg/cm^2)
S-1	1.88	< 1	42.0	0
S-2	1.91	< 1	38.5	0
S-3	1.90	< 1	37.5	0.05
$S-3_s$	1.99	12	27.5	0.20
S-4	2.11	18	29.5	0.15

***$S-3_s$: S-3 siol Under saturated condition

Tensile test with soil confinement. Since the wide-width tensile test has been standardized (ASTM 1990) and widely used in design (Christopher and Holtz 1986), the specimen size used in the test was the same, 20cm x 10cm (WxL). For confining purpose, some devices have been developed for the specified studies. Typical examples given by McGown et al.(1982), Christopher and Holtz

(1986), and Kokkalis and Papacharisis (1989) are provided for reference (see Fig.1). Although the device given by Christopher and Holtz is easily assembled for testing, it was concerned that the elongated specimen no longer stay in confined state. For the device from McGown et al., an obvious disadvantage is its limited availability. Reviewing the apparatus from Kokkalis and Papacharisis, some problems during loading were not quite known, such as, soil confinement may be influenced by the metal block. However, the shear box and the similar design concept from McGown et al. were engaged in designing the apparatus. For confining purpose, shear box was 24cm x 22cm x 5.0 cm to ensure the spacing was enough for specimen and the thin clamp aluminum plate. The plate used to hold specimen and transfer load to the outside clamp, was well performed and suggested in the studies by Wu (1990) and Yu (1990).

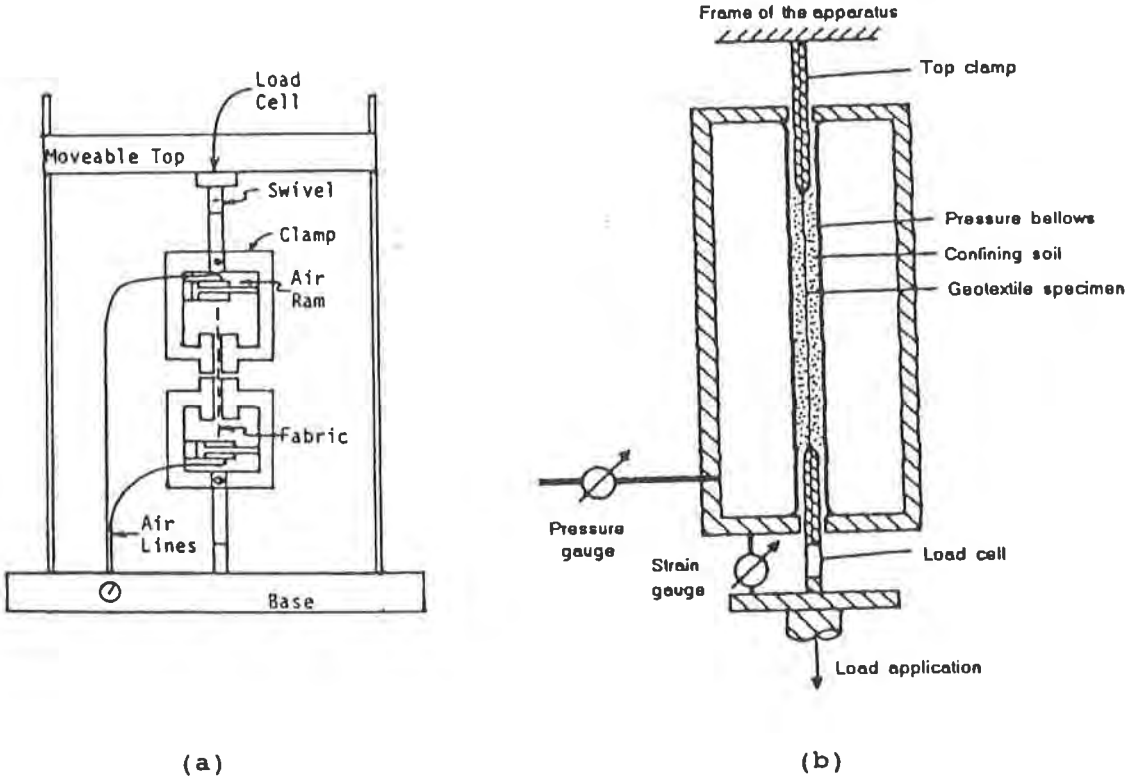

Fig.1 Examples of confined tensile devices
(a) Christopher and Holtz (1982)
(b) McGown and al.(1986)
(c) Kokkalis and Papacharisis(1989)

The details pertaining to the shear box, specimen and clamps are shown in Fig.2 Each specimen was glued with 15.0cm long plate on both sides and clamped from outside of box. For outside clamps, one was connected to a load cell, the other was attached to the fixed arm. For pullout tests, one side of the specimen was free of plate and clamp. During both test, a 10% per min. strain rate was controlled for obtaining the compatible results with the unconfined wide-width tensile strength. And the elongation was measured by a pair of LVDTs from the same clamp with load cell connected. The confining pressures applied by the normal loading plate were set at 0.5kg/cm^2, 1.0kg/cm^2, and 2.0kg/cm^2. Soils used in shear box were placed at the densities given in Table 2. For comparison purpose, the unconfined wide-width tensile tests were also performed on the same equipment without soil confinement. In this paper, only the tensile properties of geotextiles in the machine direction were evaluated.

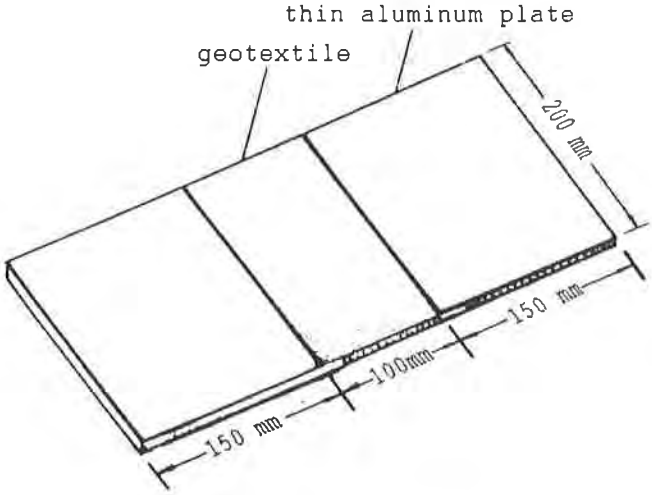

(a) Tensile test specimen

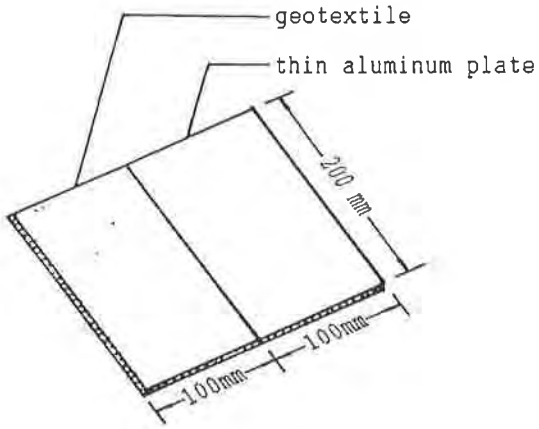

(b) Pullout test specimen

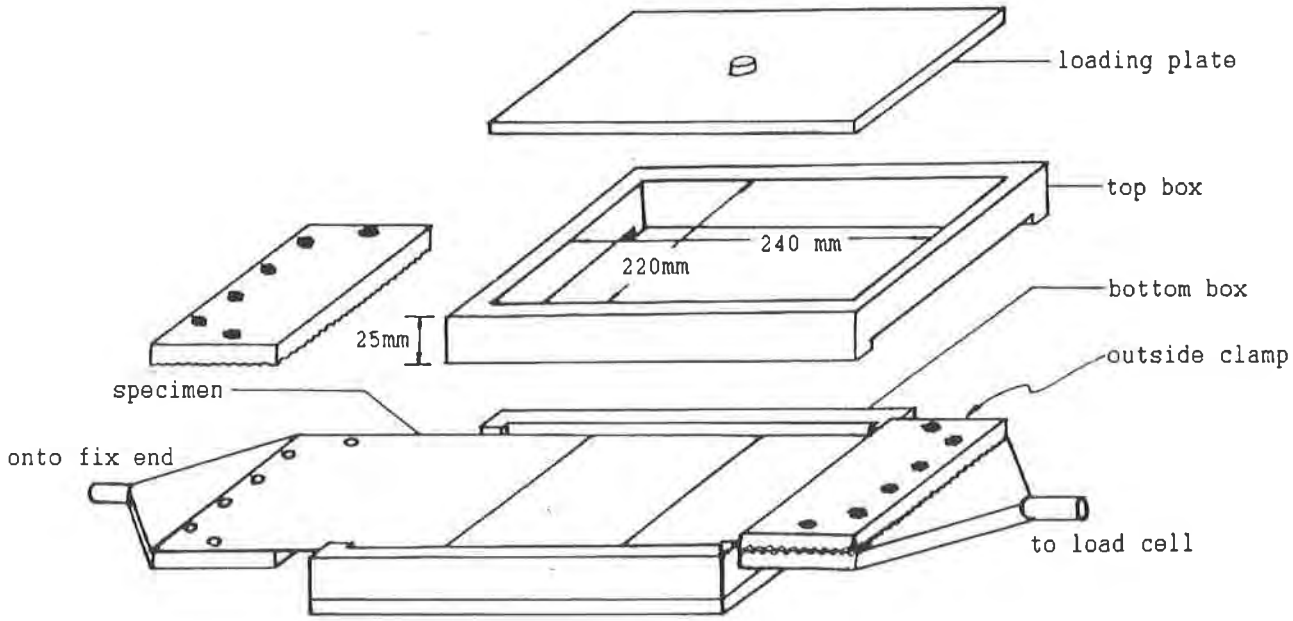

(c) Details of confining box

Fig.2 Schematic drawing of prepared specimens and confining box

Pullout test for aluminum plate. During tensile testing and pullout testing, the aluminum plate may develop friction with soil and results in error. Therefore, it is necessary to measure the resistance for the plate only by pullout test, and to calibrate the test results. The resistance can be obtained by the following equation.

$$F_{al}=2 \times W \times (L-d) \times \sigma_n \times \mu_f \quad (1)$$

where:

F_{al}= resistance of aluminum with soil
W = width of plate which equals to the specimen width(20cm)
L = plate length in the soil, in this testing condition, 6.3cm was set
d = displacement
σ_n= confining pressure
μ_f= coefficient of friction

The test results are presented in Fig.3. Based on this linear calibration relationship, the net tensile stress for a given displacement at the front end of the specimen can be obtained.

ANALYSIS METHOD

Before evaluating the test results, the consideration for analyzing method is necessary to approach herein. First of all, some assumptions were made as follows.

1. For woven geotextiles in the soil, none or little necking occurrence can be neglected. This, leads the linealy increase in contact area with an increase in elongation.
2. The tightened clamp and glued plate are well controlled, thus, no relative movement occurs between specimen and clamped zone.
3. The elongation across the specimen width is uniformly transfer to the clamp. Thus, the way arranged to measure elongation by a pair of LVDTs is appropriate.

Based on the above assumptions, the applied tensile force (T_c) can be defined by three components: F_{al} (frictional resistance between plate and soil), T_w (unconfined tensile strength of specimen), and F_c (friction between soil and specimen). Thus, F_c can be expressed as follows:

$$F_c= T_c - T_w - F_{al} \quad (2)$$

In the expression, F_{al} can be determined from Fig.3 and Eq.1, and T_w is represented by the result of unconfined wide-width tensile test. For F_c, having strickly reviewed, it is believed resulting from the surface friction of specimen gains, within small movement of specimen. During large elongation, is concerned from interlock resistance between soil particles and openings of geotextile. From this analysis, it can be concluded that F_c, somehow, is resulted by soil shearing resistance properties. The

similar conclusion has been made by Christopher and Berg(1990), in defining the pullout resistance of geotextile as given below:

$$F_p = 2 \times A_o \times \mu \times (\sigma_n \times \tan\phi + c) \quad (3)$$

and

$$\mu = F_p / (2A_o \times (\sigma_n \times \tan\phi + c)) \quad (4)$$

where:

F_p = pullout resistace (force) at peak;
A_o = initial contact area of geotextile specimen with soil;
μ = coefficient of interaction between soil and geotextile;
σ_n = normal stress or confining pressure;
ϕ, c= internal friction angle and cohesion of confined soil.

By means of their findings and with the proper modification, F_c can be defined as below:

$$F_c = 2 \times A_c \times \upsilon \times (\sigma_n \times \tan\phi + c) \quad (5)$$

and

$$\upsilon = F_c / (2A_c \times (\sigma_n \times \tan\phi + c)) \quad (6)$$

where:

A_c = corrected area of specimen;
υ = coefficient of interation between soil and specimen for tensile test;
F_c, σ_n, ϕ and c = as given in Eq.2 and Eq.3.

In the expression, modification is made to the area of specimen (A_c) to account for the changes of area during tensile testing. Therefore, A_c can be defined by:

$$A_c = A_o (1 + \epsilon) \quad (7)$$

where:

ϵ = elongation strain of specimen during confined wide-width tensile testing.

Having estabilished the equations 5,6 and 7, the results, therefore, could be evaluated.

RESULT ANALYSIS AND DISCUSSION

To evaluate the stress-strain behaviors from testing results, it is necessary to present all stress-strain curves herein, as shown in Fig.4 to Fig.7. In these results, F_{al} has been already subtracted from the original result data.

Stress-strain behaviors. Observing the shapes of all curves, obviously found that for confined properties, the path of stress development can be divided into two parts. During initial displacement stage, friction developed was more significant than an increase of tensile stress for geotextile, and could be defined as the "friction developing period". In this period, strain ranged

from approxmate 2% to 5%. Beyond this period, friction may remain constant(or somehow drop a little) and tensile behavior plays a most important rule. In addition, the slope of the stress-strain curve within this part, on the whole, is similar to that of the unconfined curve. In comparison the effects from the differences of soil types, coarser sand (S-1) with higher friction angle resulted in a higher strength than that of (S-2). This phenomenon also occure for other soils. For water content effect, because it directly influenced to the internal friction angle, thus, resulted in similar findings.

Moreover, due to the additional component of frictional resistance in the initial period, the tensile moduli increased significantly , but no obvious regularity was observed.

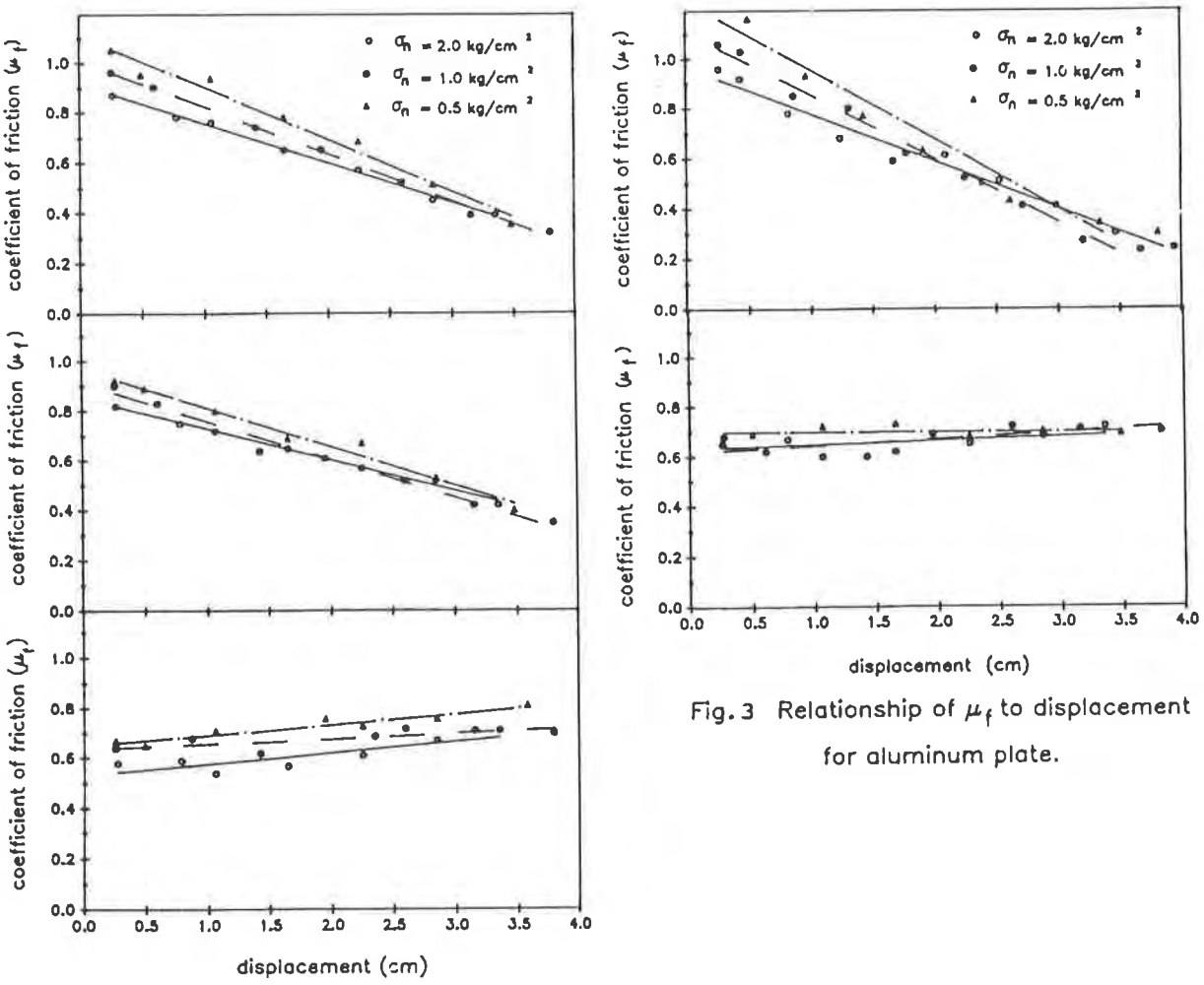

Fig. 3 Relationship of μ_f to displacement for aluminum plate.

Pullout behaviors. From pullout tests, coefficient of "μ" could be directly computed by Eq.4. For coefficient of "υ" , Eq.2 and Eq.6 were used for computation. Values for both coefficients are given in Table 3. By reviewing these data, both coefficients decrease with an increase of normal stress for soils S-1 and S-2. This may be due to the occurrence of dilation from these pure sand materials. For other soils, a contrary tendency was observed for changes of "μ" and no regularity was found with regard to changes of "υ". This finding is believed to be caused by the fines content engaged and more completely developed under high confining

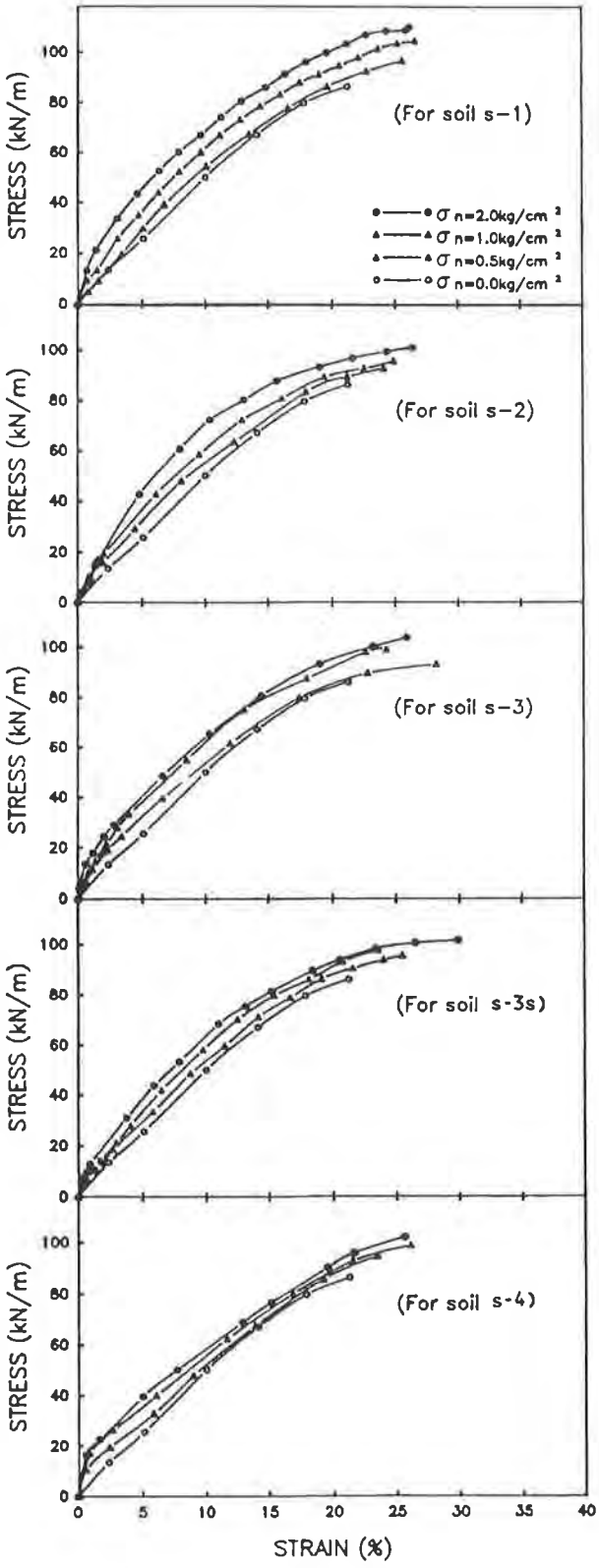

Fig.4 Tensile results for specimen A

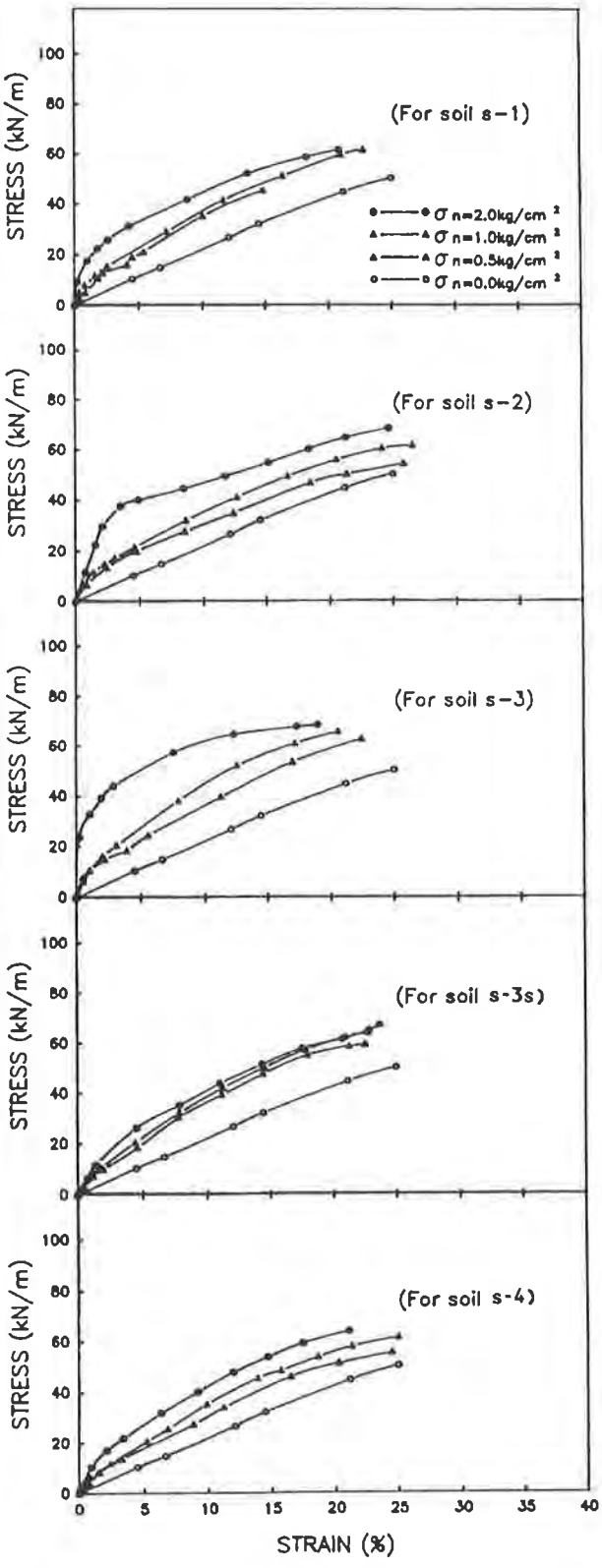

Fig.5 Tensile results for specimen B

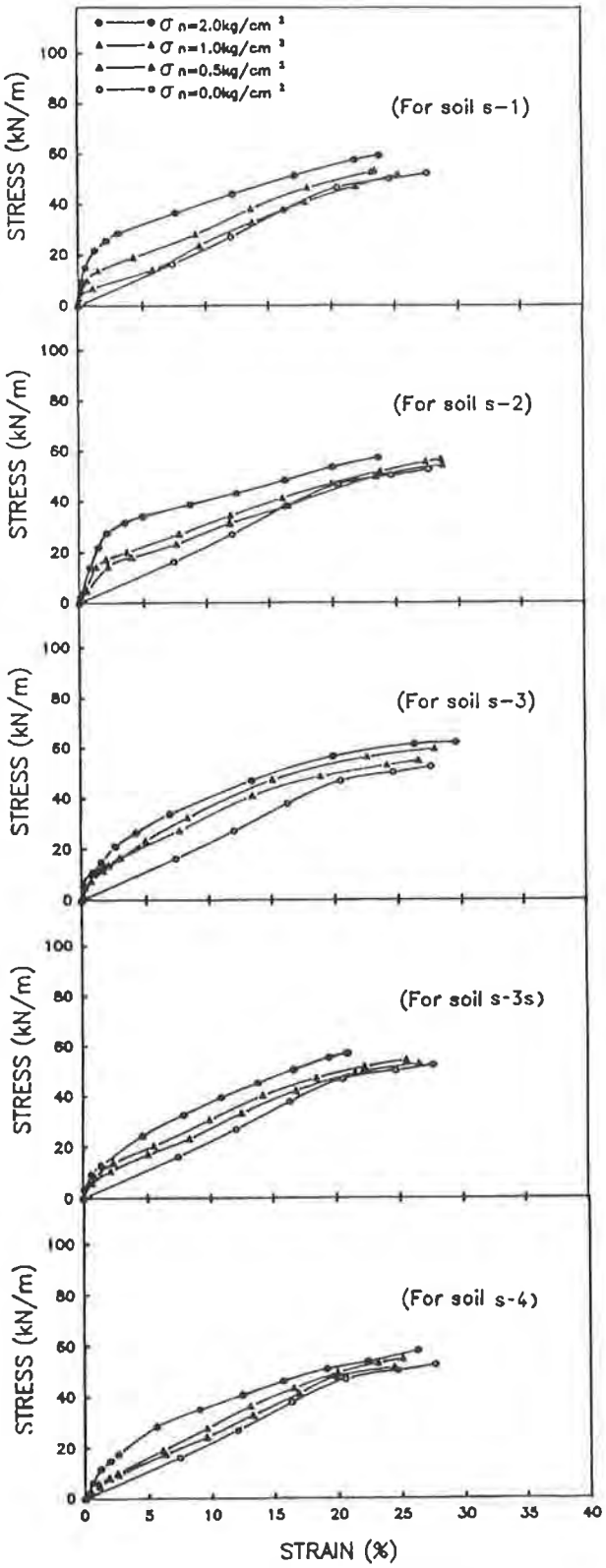

Fig.6 Tensile results for specimen C

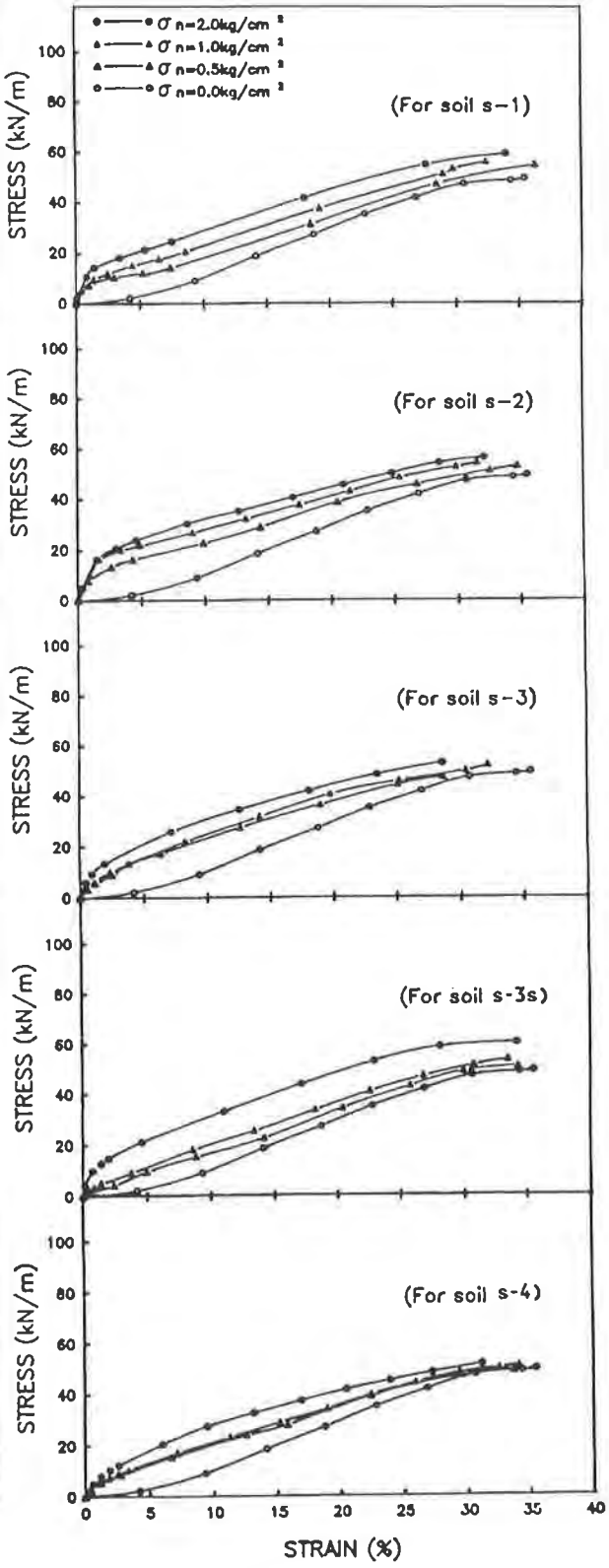

Fig.7 Tensile results for specimen D

pressure. But for the smaller relative movement of geotextile and soil in tensile testing, cohesion could not develop well. While comparing values of "μ" to "υ", it was observed that "μ" most likely presents the higher value. This is also due to the larger relative movement between geotextile and soil, leading the completion of frictional resistance. These differences for soils S-1 and S-2, are more significant. In explaining this phenomenon, interlock effect may be the best factor to discuss. It is known that for soils S-1 and S-2, grain size present as #20-#30 sieve and #40-#50 sieve, respectively. To the property of AOS (refer from Table 1), larger openings exhibits the more significant interlock effect, and resulted in a 30% to 40% difference (specimen B, C and D with S-1 soil).

Table 3 Produced results for coefficients of μ and υ

Materials soil	geotextile	σ_n= 0.5 kg/cm^2 μ	υ	σ_n= 1.0 kg/cm^2 μ	υ	σ_n= 2.0 kg/cm^2 μ	υ
S-1	A	1.34	0.52	1.32	0.63	1.19	0.57
	B	1.48	0.93	1.18	0.64	1.05	0.59
	C	1.34	0.23	0.86	0.54	0.80	0.60
	D	1.22	0.93	1.10	0.70	1.01	0.49
S-2	A	1.29	0.87	1.16	0.71	0.99	0.59
	B	1.23	1.13	1.16	0.68	0.77	0.91
	C	1.27	1.10	1.01	0.72	0.93	0.76
	D	1.22	1.19	0.91	0.86	0.82	0.67
S-3	A	1.24	0.79	1.26	0.78	1.25	0.48
	B	1.40	1.25	1.25	0.95	1.02	1.01
	C	1.19	1.17	1.24	0.76	1.03	0.55
	D	1.30	1.38	1.34	0.80	0.98	0.57
S-3s	A	0.77	0.46	0.81	0.58	0.91	0.56
	B	0.80	0.90	0.91	0.78	1.16	0.66
	C	0.68	0.44	0.77	0.39	0.98	0.63
	D	0.81	1.06	0.98	0.75	1.03	0.62
S-4	A	1.04	0.50	1.15	0.72	1.33	0.57
	B	0.96	0.70	1.05	0.58	1.36	0.63
	C	0.75	0.89	1.04	0.63	1.07	0.63
	D	0.89	0.82	0.79	0.59	1.10	0.76

Overall design consideration. Based on the discussion above, the stress-strain behavior of geotextiles used for design consideration may be summarized and sketched in non-scaled Fig.8. In this figure, the design range was followed by the suggestion from Christopher and Holtz (1985). $T_{5\%}$ is the load for design at 5% strain. In the design range, frictional resistance significantly increase the tensile stress while in confined state. On the other hand, design load using $T_{5\%}$ obtaining the unconfined wide-width tensile test, may be too conservative. During the design process, a pullout test should be performed to determine the anchorage length of geotextile behind the failure plane. While picking up the "μ" value from the result of the pullout test, "υ" could be quantitatively defined and Fig.8 can be obtained. In this study,

the summerized values for μ and υ with the specified materials are given in Table 4, for reference.

Table 4. Summary of μ and υ

Soil Types	$\sigma_n \leq 0.5$ kg/cm^2		$\sigma_n \geq 1.0$ kg/cm^2	
	μ	υ	μ	υ
Dry Sand	1.2	0.5-0.6	1.0	0.5-0.6
Wet Sand	0.7	0.4-0.5	0.9	0.5-0.6

Review the Boundary Conditions of Confining Box. In the testing progarm, the rigid loading plate was used to transfer the normal stress (confining pressure), this has made the stress to possibly concentrate along the wedge. In addition, the influence of box depth and the influence of rigid door may also reflect on the testing performance. Althought the findings of this study are significant, some boundary conditions need to be considered into this. Since this research was the initial progarm on the topic of tensile strength with soil confinement condition, the boundary conditions should be considered in the future progarm. Moreover, the flexible type of loading method by air bags and in coupling confinement condition will also be suggested in the following study.

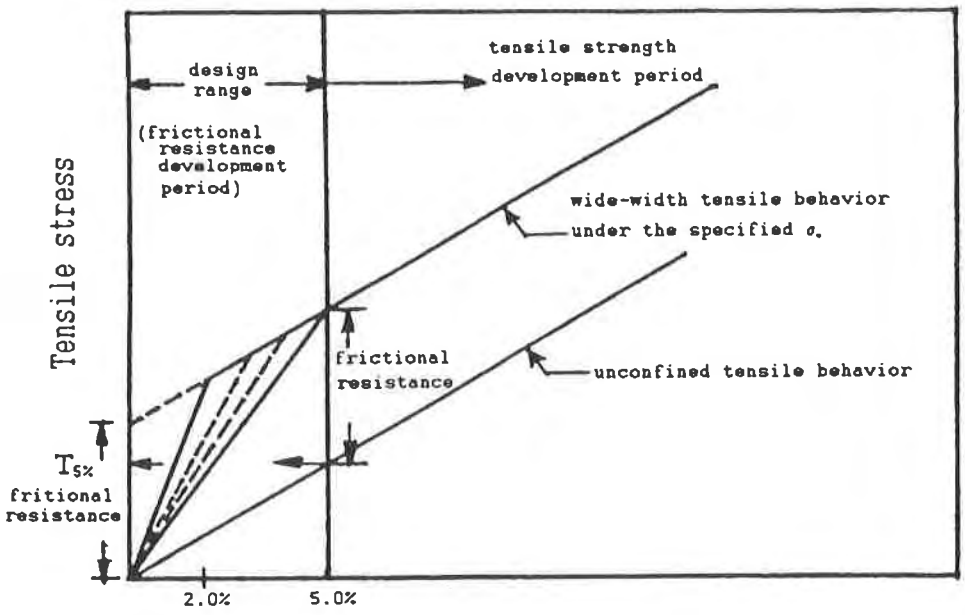

Fig.8 Design consideration

CONCLUSION

Through the analysis and discussion of results, some conclusions can be made.

1. The effect of soil confinement significantly increase the tensile strength for four woven geotextiles.

2. The stress-strain behaviors of geotextiles with soil confinement, can be divided into the friction development period and tensile strength development period.
3. The frictional resistance (F_c) was to be developed by the effects of surface friction and interlocking.
4. To properly select a load level for design, it is suggested that the additional component of frictional resistance (F_c) be included.

ACKNOWLEDGEMENTS

Authors extend the deepest thanks to the National Science Council, Taiwan, R.O.C., for Grant Number, NSC-79-0414-p033-18, which supported this study.

REFERENCE

American Society for Testing and Materials, (1991), Tensile Properties of Geotextiles by the Wide Width Strip Method, ASTM.

Chang, D.T.T., Chen, T.C. and Su, K.H. (1991) "Utilization of geotextile-reinforced retaining wall for stabilizing weathered mudstone slope", Geosynthetics '91 conference Proceeding, Vol.2, pp. 739-774.

Christopher, B.R., Berg, R.R., (1990) "Pullout evaluation of geosynthetics in cohesive soils", Proceedings of 4th International Conference on Geotextiles, Geomenbranes and Related Products, pp. 731-736.

Christopher, B.R. and Holtz, R.D. (1985) "Geotextile Engineering manual", Federal Highway administration National Highway Institute, Washington, D.C., U.S.A.

Christopher, B.R., Holtz, R.D., and Bell, W.D., (1986) "New tests for determining the in-soil stress-strain properties of geotextiles ", Proceeding of 3rd International Conference on Geotextiles, Geomembranes, and Related Products, Viennam Vol.3, pp. 683-688.

Kokkalis, A., and Papacharisis, N.,(1989) "A simple laboratory method to estimate the in-soil behavior of geotextiles", Journal of Geotextiles and Geomembranes, Vol.8, pp. 147-157.

McGown, A., Andrawes, K.Z. and Kabir, M.H., (1982) "Load-extension testing of geotextiles confined in-soil", Proceeding of 2nd International Conference on Geotextiles, Las Vegas, Nevada, Vol.3, pp. 793-798.

Wu, C.S. (1990) "Stress-elongation behavior of geotextile under the normal load (I)", Technical Report, Nation Science Council of Taiwan, R.O.C.

Yu, S.C. (1990) "Stress-elongation behavior of geotextile under soil confinement", Master Thesis of Tamkang University, Taiwan, R.O.C.

The Influence of Selected Testing Procedures on Soil/Geomembrane Shear Strength Measurements

S.M. Bemben
GZA GeoEnvironmental Inc., USA

D.A. Schulze
GZA GeoEnvironmental Inc., USA

ABSTRACT

Results of Direct Shear testing with a modified commercial direct shear box and various soil and geomembranes are presented. Modifications include the additions of a precise vertical loading control, a vertical deformation measurement device, and an increased range of accurate rates of horizontal shear movements. The use of a single set-up with multiple consolidation and shearing steps to obtain three or more points of a residual failure envelope is determined to be feasible and practical. The shear strength behavior for the wet soil/geomembrane combination tested is systematically related to the dilatency behavior of the soil during shearing and to the drainage states. The drainage states are related to the degree of saturation and to the rates of movement.

INTRODUCTION

The proposed ASTM "Standard Test Method for Determining the Coefficient of Soil and Geosynthetic or Geosynthetic and Geosynthetic Friction by the Direct Shear Method Draft Designation 01.81.07" (termed ASTM Guidelines hereinafter) is the sole guideline on the topic for the foreseeable future. It provides for user judgement regarding the rate of shearing to maintain a drained state during shearing. This judgement is in addition to the usual choices involving unit weights and water contents of the soil specimen at set-up.

The test method is intended to model field conditions. However, both designers and laboratory personnel currently have dilemmas. They involve two aspects; first, what are the critical design situations and, second, what laboratory testing procedures best simulate the critical design situations.

Critical design situations are typically addressed in EPA Design Manuals and texts but the shear stress - movement behavior at the soil/geomembrane interface is simply taken to be a fixed property; that is, variations in limiting stress under differing rates of movements, and with changes in the environmental setting (such as changes in water content) are not yet employed.

Takasumi, et. al. (1991), and others, have pointed out that for cohesive soils, the rates of movement during shear influence the developed shear stresses at failure and that "slow enough" rates are needed to develop drained state conditions.

The purpose of this research is fourfold. First, to give credibility to the equipment by showing that failure envelopes for Ottawa Sand/geomembranes match published values. Second, to evaluate the feasibility of a single set-up to determine failure envelopes. Third, to elaborate on the notion presented by Williams and Houlihan (1987) regarding the minimum amount of shear movements necessary to reach the onset of residual shear stress behavior. Fourth, to show that the range in the values for the shear stresses at failure for a wet, low permeability soil is very widespread but the variation is systematically related to the state of drainage.

DIRECT SHEAR BOX AND TESTING PROCEDURES

The shear box machine (Brainard-Kilman Model LG112) used in this study incorporates several features/modifications originated by the authors. These include a precise normal stress application system, a vertical movement measuring system, and a wide range of constant speed rates of shearing. The normal load is accurately controlled by an air cylinder system using precise air-bleed regulators. Vertical movements are monitored by an LVDT during consolidation and shearing steps. The rate of travel can be accurately controlled between 6.4 and 0.0025 mm/min (0.25 and 0.0001 in./min).

The design is similar to the fixed shear box design described by Takasumi et. al., (1991) except that, for the soil/geomembrane tests to be presented hereinafter, the bottom box has a solid block rather than soil filler. For soil/soil tests the bottom box is filled with soil. The leading edge of the lower box has a clamp into which the leading end of the membrane is inserted. The lower box, upon which the membrane rests, is 38 by 30 cm (15 by 12 in.) in plan. This allows for up to 7.6 cm (3 in.) travel without any change in the area of the interface being tested. A schematic of the shear box is shown as Figure 1.

The upper box, in which the soil specimens are fabricated, is 30 by 30 cm (12 by 12 in.) in plan. Specimens are fabricated with a height of 5.1 cm (2.0 in.). The desired exact weight of the wet (or dry) soil per layer is weighed in advance and compacted, by hand, until the exact desired height is achieved. Measurements of height are controlled by at least twenty measurements per layer using a caliper and crossbar system. The test specimen is covered with a 1.3 cm (0.5 in.) layer of Ottawa Sand upon which the loading plate bears.

The weight of the soil and loading plate as well as the small frictional resistance during shearing (which amounts to less than one percent of the normal load) are taken into account during calculations. Readings during testing may be made manually or automatically by a computerized data logging system.

Soil specimens may be tested at the water content at set-up or they may be tested

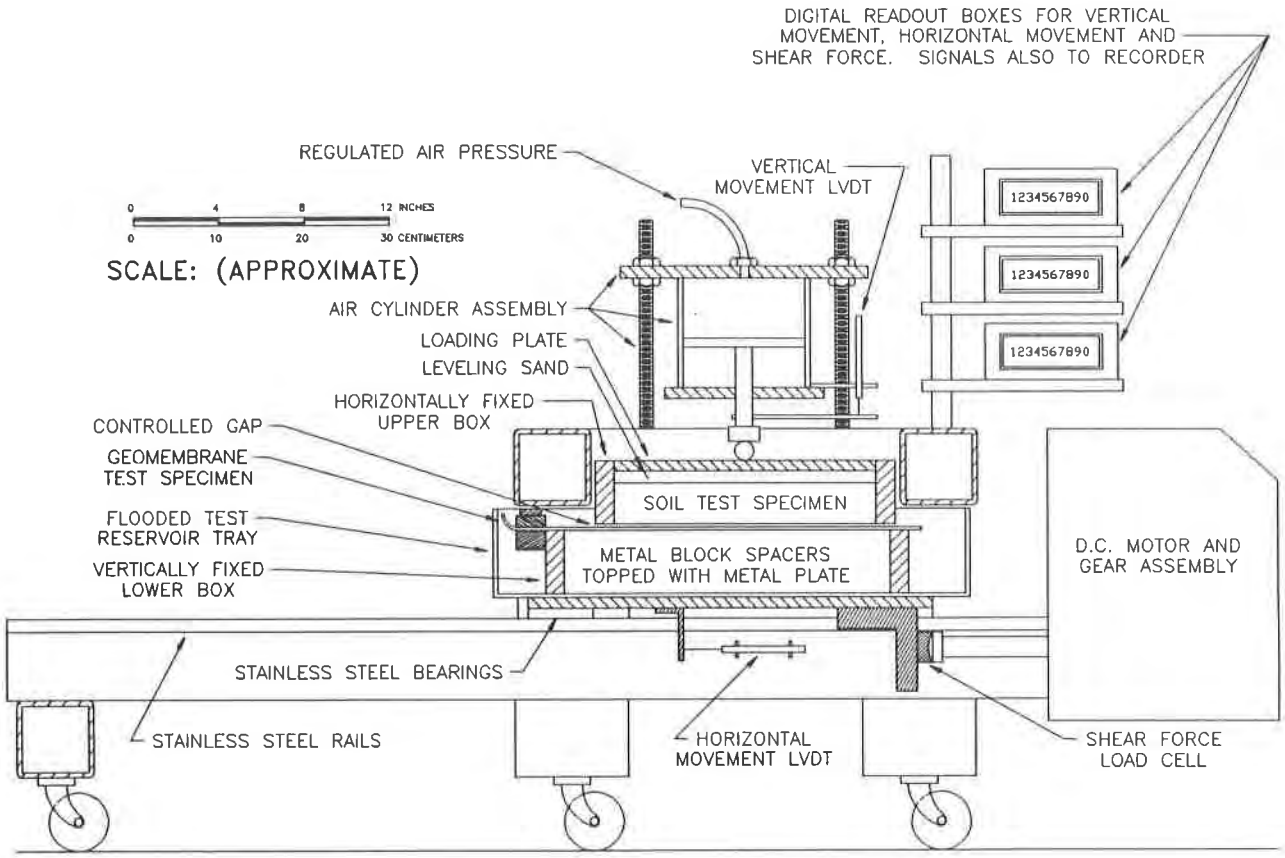

Figure 1. Schematic Section of Direct Shear Box During a Soil/Geomembrane Test

underwater by filling the bottom shear box with water. These test conditions are termed In-Air and Flooded, respectfully. A flooded specimen is always allowed to equilibrate for at least 18 hours prior to commencement of a shearing step.

SOIL AND GEOMEMBRANE MATERIALS

Two soils are involved, the first soil is Ottawa Sand. It is a uniform quartz sand composed of mostly subrounded particles. The sand was compacted air dry to a density of 17.7 $\pm$ 0.3 kN/m^3 (112.5 $\pm$ 2 pcf).

The second soil is remolded Connecticut River Valley glacial till. It was extensively deposited by glacial bulldozing. The till, in nature, contains particles from clay to boulder sizes; the soil employed in the testing contained only the minus 13 mm (0.5 in.) portion. It has very low plasticity. It was compacted to a dry density of 20.6$\pm$ 0.8 kN/m^3 (130.0 $\pm$ 2.5 pcf) at 8.0 $\pm$ 0.2% water content. These values correspond to about 95% Modified Proctor maximum dry density and about 2% higher than optimum water content, respectively.

Two commercial geomembranes are involved. They are Poly-Flex HDPE (smooth) and Gundline HDT (textured). Membrane specimens were usually 60 mil thick; a few were 40 mil and 80 mil.

EFFECTS OF SINGLE SET-UP TESTS ON FAILURE ENVELOPES

The tests involve the Ottawa Sand, Poly-Flex HDPE (smooth) membrane, and Gundline HDT (textured) membrane materials.

The ASTM Guidelines call for three point failure envelopes with each point being the result of a separate set-up which, in turn, is followed by a single consolidation step and a single shearing step. Figure 2 shows three such shear stress - total shear movement curves; these are designated 26-1, 27-1, and 28-1. With this labelling system to be used hereinafter, the first number refers to the soil specimen set-up number; the second number refers to the shearing step being experienced by the soil specimen. Each curve has a "peak portion" (including the peak shear stress point) plus a "residual portion". The label "total shear movement" refers to the amount of horizontal movement of the bottom shear box with respect to the top shear box. It therefore also means total movement of particles above the interface surface with respect to

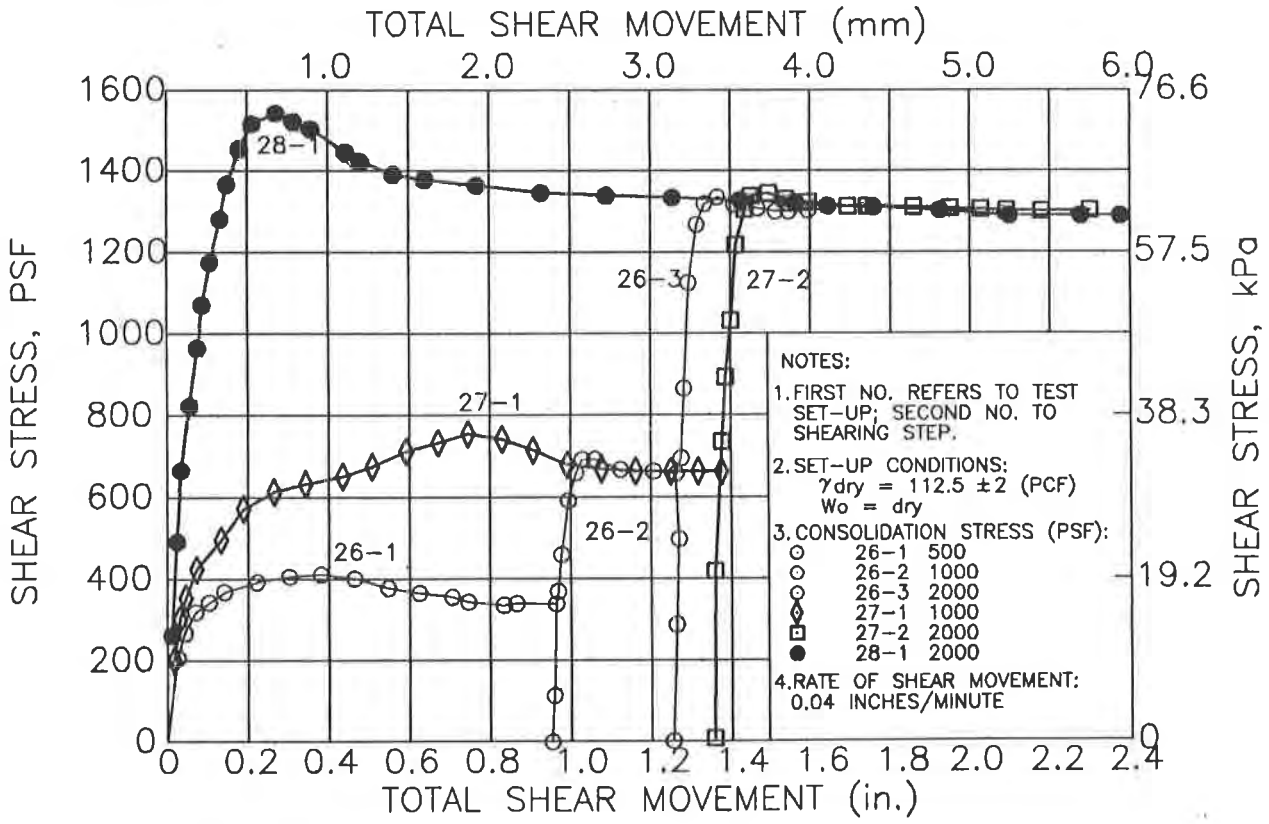

Figure 2. Ottawa Sand/Ottawa Sand. Effects of total movements on behavior of stress–movement curves.

particles below the interface surface. Total movement is referenced to the condition at set-up irrespective of the number of consolidation steps and shearing steps following set-up. Total movement is employed rather than the term "strain" because the amount of total movement experienced by soil elements is not related to the size of the soil specimen.

Figure 2 also introduces the notion of a single set-up followed by three consolidation steps and three shearing steps. Shearing step 26-1 at 23.9 kPa (500 psf) was followed by a consolidation step at 47.8 kPa (1,000 psf), which was followed by shearing step 26-2; this was followed by a consolidation step at 95.5 kPa (2,000 psf), which was followed by shearing step 26-3. Similarly, shearing step 27-1 at 47.8 kPa (1,000 psf) was followed by a consolidation step at 95.5 kPa (2,000 psf), which was followed by shearing step 27-2. In each case, the shearing stress-horizontal movement curve of a subsequent shear step join into and coincide with the corresponding initial (and sole) shear step curves of shearing steps 26-1, 27-1 and 28-1. (The reader should note that the summations of the "horizontal movements" of all the individual shearing steps following a set-up comprise the instantaneous "total horizontal movement"). This occurs irrespective of whether the joining is in either the peak portion or the residual portion of the initial shear step curve. That is, the shear stress-total shear movement curve following each initial consolidation step is unique. Figure 2 also shows that residual stress failure values can be interchangeable by either multiple set-up or single set-up testing; however, except for the initial consolidation step and initial shearing step, peak failure points cannot be obtained from single set-up testing.

The notion of a necessary minimum amount of total movement to the onset of residual stress noted by Williams and Houlihan (1987) is confirmed. Additionally, it is observed that the minimum amount increases with increasing values for normal stress.

First step consolidation and first step shearing curves for Ottawa Sand/Ottawa Sand, Ottawa Sand/smooth membrane and Ottawa Sand/textured membrane are shown by Figure 3. There is a wide difference in behavior among the curves. The principle of the unique curves depicted on Figure 2 for Ottawa Sand/Ottawa Sand also apply to the combinations of Ottawa Sand/smooth membrane, and Ottawa Sand/textured membrane

Figure 4 shows the residual stress failure envelopes for the three described combinations of materials. The benefit of a textured membrane in comparison to a smooth membrane is significant. In fact, nearly the entire shear stresses of Ottawa Sand/Ottawa Sand is mobilized by the textured membrane. The failure envelopes are in good agreement with the published values for the same materials by Martin, et. al. (1984) and Druschl and O'Rourke (1991).

EFFECTS OF RATES OF SHEAR MOVEMENTS ON SHEAR STRESSES

All tests involve the Connecticut River Valley glacial till and Gundline HDT (textured) materials.

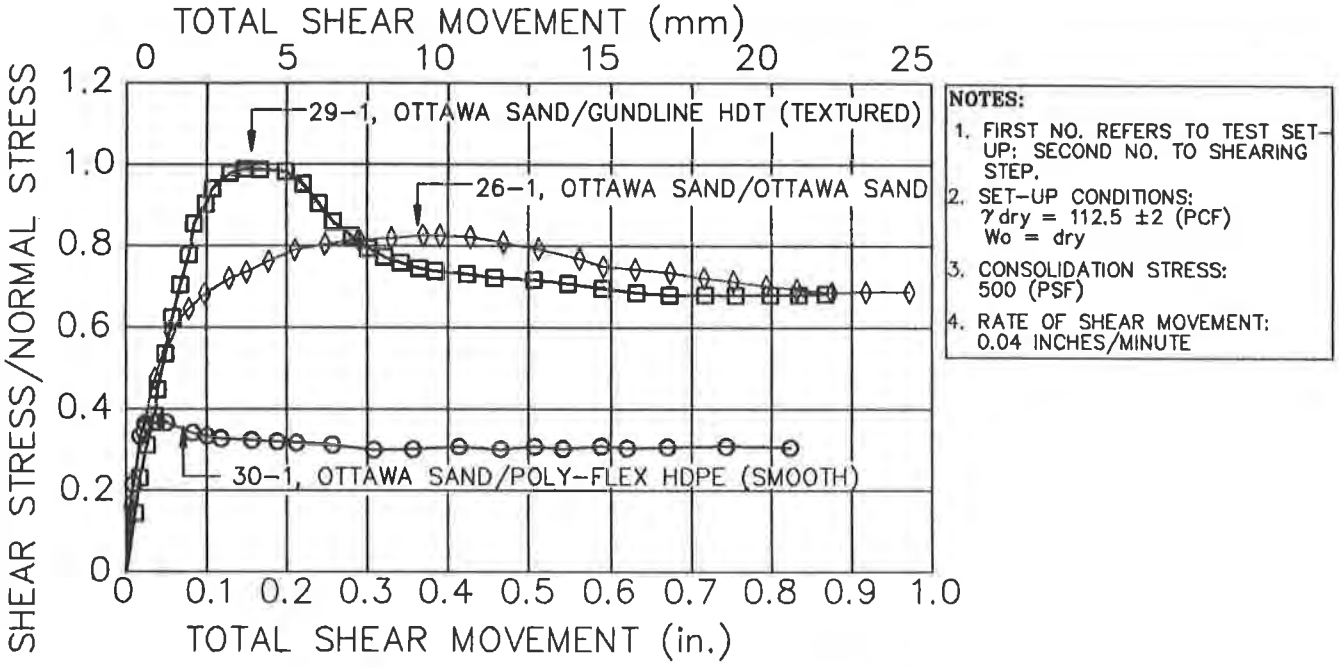

Figure 3. Shear stress – Shear movement curves for Ottawa Sand/Ottawa Sand, smooth geomembrane, and textured geomembrane interfaces.

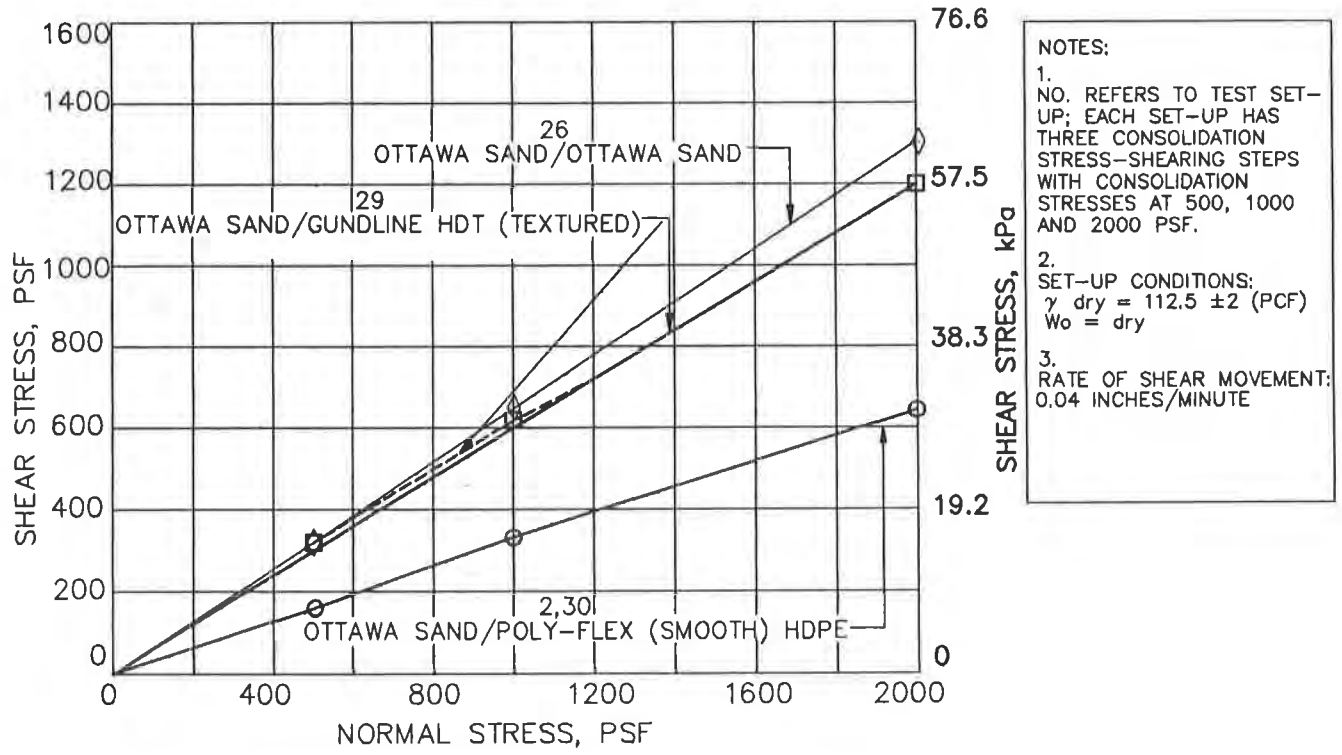

Figure 4. Residual stress failure enevelopes for Ottawa Sand/Ottawa Sand, smooth geomembrane, and textured geomembrane interfaces.

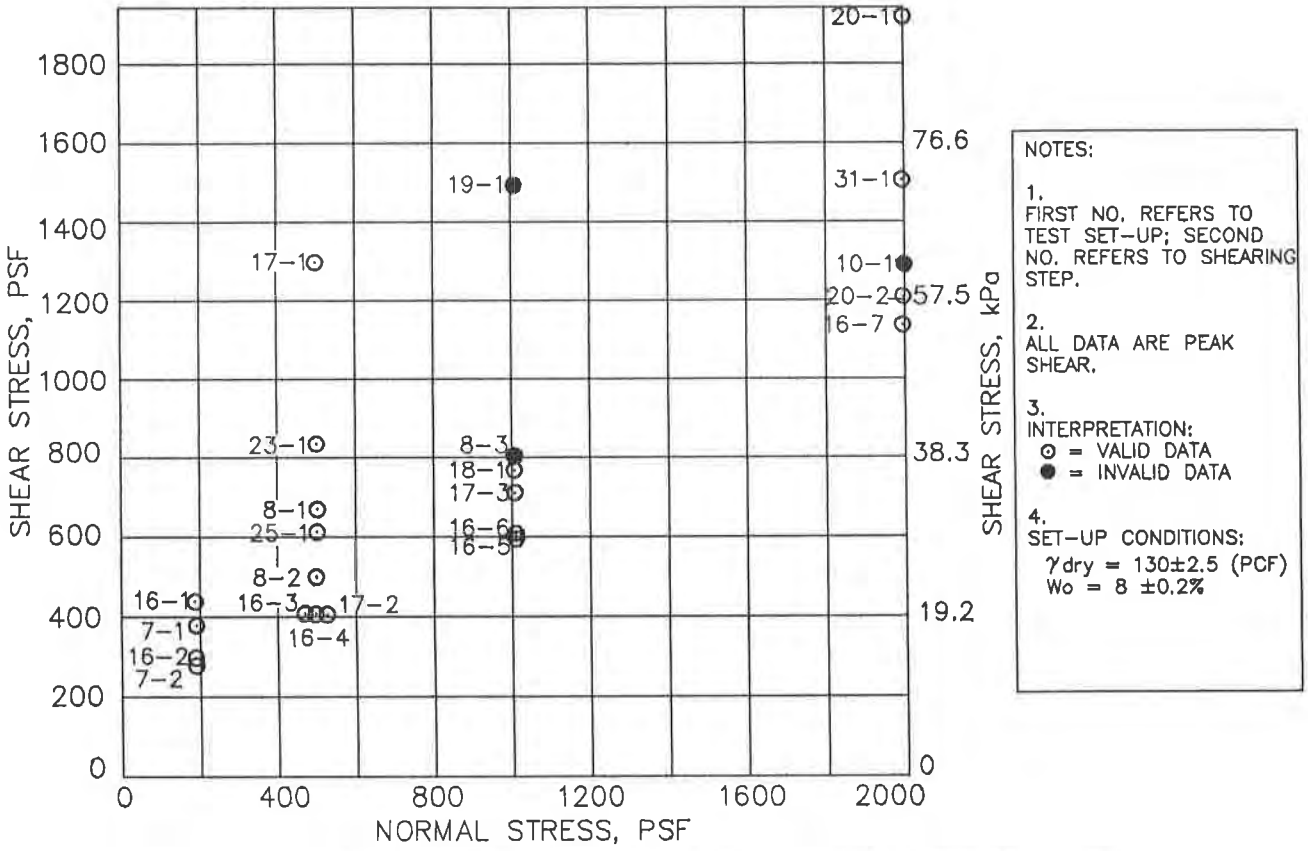

Figure 5. Connecticut River Valley Glacial Till/Gundline HDT (Textured). Locus of data for peak stress with varied rates of shear movements, varied total movements at peak stress, and states of saturation.

Peak shear stresses ensuing from eleven set-ups are presented by Figure 5. Many of the test set-ups were followed by multiple consolidation steps each of which, in turn, are sometimes followed by two steps of shearing (at two different rates) rather than the conventional one step. For example, test sixteen involves one set-up, four consolidation steps, and seven shearing steps. The principles previously described for single set-up test failure envelopes are again employed. At first glance, the data seems to represent a woefully imprecise state of measurements.

Three data points are noted to be invalid data. For these three shearing steps, the unusual shapes of the stress-horizontal movement curves are distinguishable to the trained eye. The curve of shearing step 10-1 contains fluctuations in the initial loading branch and a rapid drop in shear stress following the (apparent) peak load; this is a manifestation of sliding of the membrane out of the holding clamp. At teardown, the slippage of the membrane was visible. The shear stress-movement curves of steps 19-1 and 8-3 have shapes which indicate unusually stiff behavior and high peak stresses. This behavior is a manifestation of binding of a stone particle in the fixed gap between the steel boxes.

The shear stress - total shear movement curves for eight shearing steps, all following consolidation steps at 23.9 kPa (500 psf) are shown by Figure 6. Four aspects of behavior during shear are discerned. First, the unique shear stress-total shear movement curve for drained state behavior is characterized, successively, by the peaks of shearing steps 25-1, 8-2, 16-3, 16-4 and 17-2. The drained state peak stress and the onset of residual stress occur at about 5.1 mm (0.2 in.) and 25.4 mm (1.0 in.), respectively. Second, maximum shear stress occurs for the combination of high degree of saturation (flooded specimen) and high rate of shear movement. This comprises the maximum "undrained" shear strength. Third, curves which are above the unique drained state behavior curve (such as steps 17-1 and 23-1) eventually tend toward the unique drained state behavior curve but do not reach it because of the limitations of the total shear movement of the test equipment. Fourth, (as with the case with Ottawa Sand) peak drained shear stress can only be achieved by a shearing step immediately following set-up.

Similar behavior exists for each of the other consolidation stress steps at the four stress steps of 9.5, 23.9, 47.8 and 94.5 kPa (200, 500, 1,000 and 2,000 psf). The total horizontal movements to drained peak shear stress are approximately 2.5, 5.0, 10.2 and 12.7 mm (0.1, 0.2, 0.4 and 0.5 in.), respectively, and the minimum total horizontal movements required for the onset of drained state residual stress levels are approximately 19.1, 25.4, 38.1 and 50.8 mm (0.75, 1.0, 1.5 and 2.0 in.), respectively. Although not shown on Figure 6, a shear stress- total shear movement curve can also be maintained above the drained residual region; this will be discussed later.

Three failure envelopes are shown by Figure 7. Envelope A comprises the peak shear "undrained" points (such as 17-1 of Figure 6). Naturally, some small unknown amount of drainage had to occur during shearing, so the term "undrained" merely refers to essentially undrained. Envelope B comprises the peak shear, drained points (such as 25-1 of Figure 6).

Envelope C comprises the residual stress, drained points (such as 16-3, 16-4 and 17-2 of Figure 6). The initial woeful impression of Figure 4 is overcome.

The shape of the shear stress-total shear movement curves is reflective of the rearrangement of particles within the soil specimen during shearing. The particles are compacted and consolidated in a random state. As shearing occurs, they tend to align in the plane of shearing along the soil/membrane interface. The rearrangement typically causes volume changes to occur. For this soil, the tendency is to expand (dilate) during early shear movements as evidenced by the vertical dial movements (not shown). This tendency develops the peak shear, drained points. Completion of the rearrangement of particles by continued, total shear movements results in the onset of drained state residual behavior.

Whenever a shear stress-total shear movement curve for any shearing step does not quickly seek and join the unique drained state behavior curve, a pore pressure "problem" exists. The presence of water in the pores hinders the volume changes which the soil particle are seeking.

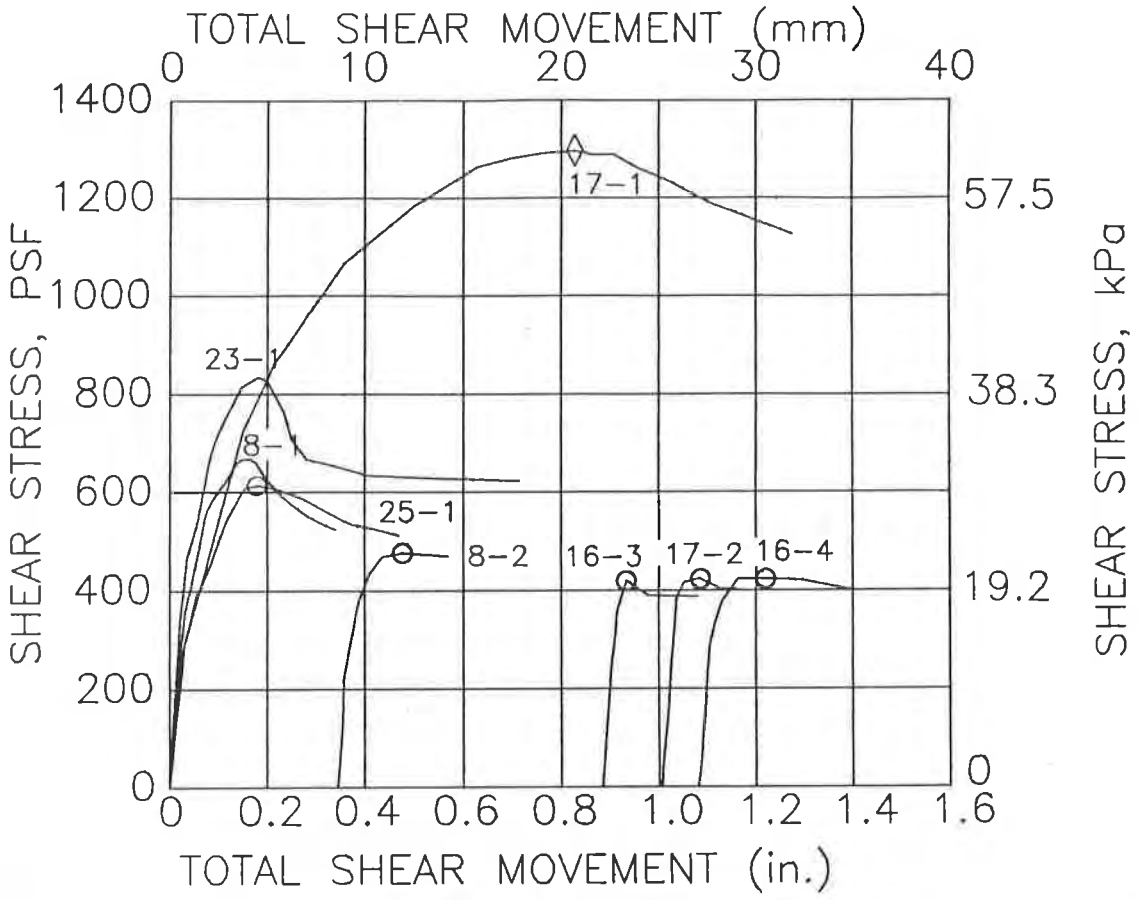

TEST, STEP	DEG. SAT. (%)	RATE OF MOVEMENT (IN./MIN.)	DISTINGUISHING FEATURES
25-1	±90	0.001	PEAK DRAINED STRENGTH
8-1	±75	0.04	INTER. "UNDRAINED" PEAK STRENGTH
23-1	±75	0.002	
8-2	±75	0.0002	INTER. DRAINED STRENGTH COMBINED WITH INTER. TOTAL SHEAR MOVEMENT
17-1	±90	0.04	MAX. "UNDRAINED STRENGTH"
16-3	±75	0.04	RESIDUAL DRAINED STRENGTH; MIN. STRENGTH COMBINED WITH "SUFFICIENT" TOTAL SHEAR MOVEMENT
16-4	±75	0.0002	
17-2	±90	0.0002	

NOTES:

1. FIRST NO. REFERS TO TEST SET-UP; SECOND NO. TO SHEARING STEP
2. SET-UP CONDITIONS:
   γ dry = 130.0± 2.5 (PCF)
   Wo = 8 ±0.2%
   CONSOLIDATION STRESS = 500 (PSF)

Figure 6. Connecticut River Valley Glacial Till/Gundline HDT (Textured). Effects of total movement, rates of movement, and states of saturation on behavior of stress–movement curves.

The "problem" is that the pore (water) pressure is at an unknown value other than zero; that is, a zero value constitutes the drained state. Soils that are essentially dry do not develop pore pressure problems. For this soil, pore pressure problems develop at rates of shearing faster than "critical" for both the 75% and 90% degrees of saturation; likewise, they do not develop at rates slower than "critical".

ASTM Guidelines offer a recommendation for selection of the "critical" rate of shearing movement to ensure essentially drained conditions during shearing. That is, the "critical" rate (or any slower rate) allows essentially complete diffusion of the pore pressures being generated during shear. The "critical" rate is estimated as the ratio of the horizontal movement for peak shear stress to the time required to reach that amount of movement. The procedure is actually a trial and error method. To illustrate the method, consider shearing step 25-1 of Figure 6. Assume that the total shear movement to peak shear stress will be 4.8 mm (0.19 in.). This, of course, is known in hindsight from the test data. In the ordinary case, the initial assumption may be little more than a guess. The time to reach 50% consolidation was determined from the vertical dial readings to be 6.25 minutes. The recommended time to reach peak stress is 50 times the time to reach 50% consolidation. In this case, the recommended time, accordingly, is 312 minutes. The "critical" rate is estimated to be (4.8 mm/312 min), or 0.0154 mm/min. (0.0006 in./min).

The actual rate of shear movement employed for the shearing step was 0.0305 mm/min. (0.001 in./min). The expectation is that some negative pore pressure (that is, incomplete diffusion) existed and that accordingly, the measured peak stress strength was slightly higher that the correct drained shear strength would have been. Referring to Figure 7, it appears that such is the likely situation.

Two significant applications of the critical rate of shear movement to commercial testing applications are as follows:

First, if only residual shear stress levels are desired and only one consolidation step is involved, one can travel to the minimum total shear movement to reach residual conditions at a high rate of movement (as, say, 1.0 mm/min) and then switch to a lower rate commensurate with drained state conditions. The shear stress will quickly equilibrate to the residual stress level. The process is shown by shear steps 17-1 and 17-2 of Figure 6.

Second, if only residual stress levels are desired and multiple consolidation and shearing steps are involved, one must travel at least to the minimum shear movements required for each successive residual condition. This aspect is shown by Figure 5. Here, shearing step 17-2 at 23.9 kPa (500 psf) experienced drained behavior; it was followed by consolidation step 47.8 kPa (1,000 psf), and followed afterward by shearing step 17-3 at 1.02 mm/min (0.04 in/min). The total shear movement at the onset of step 17-3 was 29.2 mm (1.15 in.); this is less movement than is required at this stress level for the onset of residual behavior. The specimen experienced some negative pore pressure and, accordingly, the measured shear stress was higher than that for

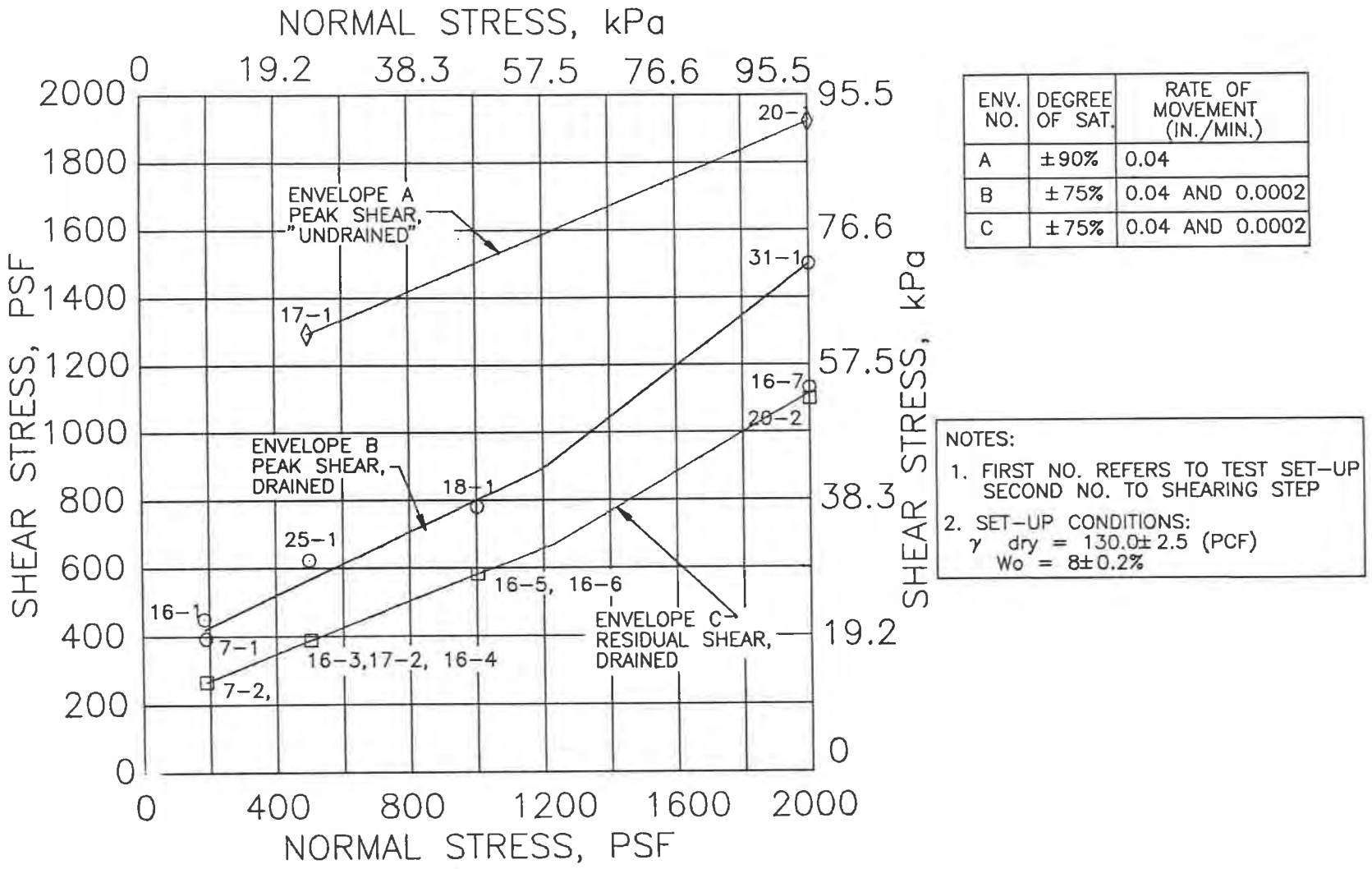

ENV. NO.	DEGREE OF SAT.	RATE OF MOVEMENT (IN./MIN.)
A	±90%	0.04
B	±75%	0.04 AND 0.0002
C	±75%	0.04 AND 0.0002

NOTES:

1. FIRST NO. REFERS TO TEST SET-UP SECOND NO. TO SHEARING STEP
2. SET-UP CONDITIONS:
   γ dry = 130.0± 2.5 (PCF)
   Wo = 8±0.2%

Figure 7. Connecticut River Valley Glacial Till/Gundline HDT (Textured). Shear strength envelopes.

the drained residual stress of step 16-5.

The effects of rates of movements on measured peak shear stresses at failure is shown by Figure 8. It is seen that the influence of rate of movement is dramatically significant. That is, high rates of movements together with the flooded condition produce dramatically large peak shear stresses. The data is too meager to allow comments on the effects of rates of movements on measured residual shear stresses.

The reader is also reminded that for many of the shearing steps (such as the cited step 25-1), the calculated critical rate of movement is between 0.025 mm/min (0.001 in./min) and 0.0051 mm/min (0.0002 in./min); hence, Figure 8 shows good correlation between the calculated critical rate of movement by the ASTM Guidelines and the observed critical rate of movement.

CONCLUSIONS

The following conclusions derive from the research described. The data is limited. The possible extension of the conclusions to other soils and geomembranes requires extensive further testing.

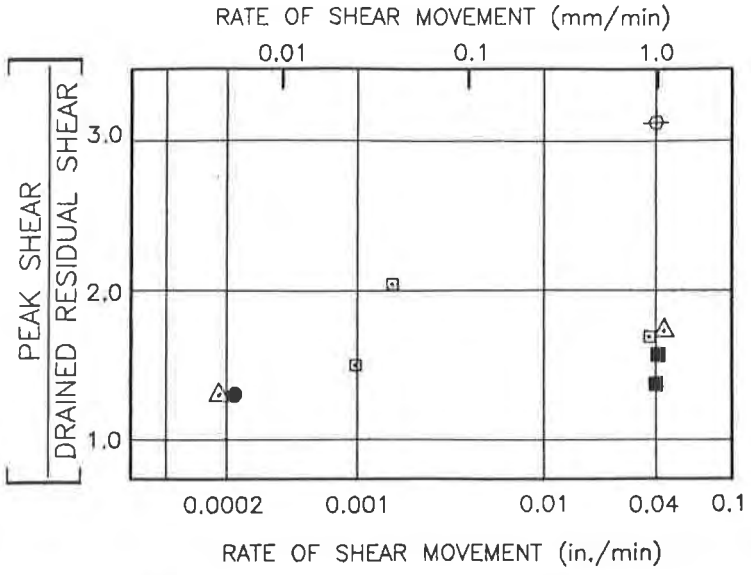

SYM.	NORMAL STRESS (PSF)	NORMAL STRESS (kPa)	DRAINAGE AT BOUNDARIES
■	200	9.6	IN–AIR
⊡	500	23.9	IN–AIR
⊕	500	23.9	FLOODED
●	1000	47.9	FLOODED
△	2000	95.8	FLOODED

NOTES:

1. PEAK SHEAR REFERS TO INITIAL SHEARING STEP FOLLOWING A SET–UP.
2. SET–UP CONDITIONS:

   γ_{dry} = 130.5 ± 2.5 (PCF)

   w_o = 8 ± 0.2%

Figure 8. Connecticut River Valley Glacial Till / Gundline HDT (Textured). Effect of rates of movements on peak shear stress at failure.

1. The use of a single set-up with multiple consolidation and shearing steps to obtain three or more points of a residual stress failure envelope is feasible and practical. The procedure is applicable to soil/soil, soil/smooth geomembrane, and soil/textured geomembrane combinations.
2. The advantages of a single set-up procedure are cost savings and exact duplication of test specimens.
3. The disadvantage of a single set-up procedure is that the correct peak shear stress can only be obtained for the initial shearing step for granular soils such as the Ottawa Sand and glacial till tested herein.
4. The ASTM Guideline method for selecting the critical rate of movement appears to be reasonable for use with the glacial till tested. It is not applicable to the Ottawa Sand soil because the uppermost allowed rate of shearing governs.
5. The shear strength behavior for the wet till soil/geomembrane combination tested is systematically related to the dilatency of soil during shearing and to the drainage tates.

ACKNOWLEDGEMENTS

This research was funded by GZA GeoEnvironmental, Inc. as an in-house research learning experience. The senior author originated the research notions. On behalf of GZA, the authors purchased, modified and calibrated the direct shear box; developed testing and data processing procedures; and, prepared this paper. The authors express their gratitude to Matt Trettel, the laboratory technician who performed all of the tests.

REFERENCES

Druschel, S.J., and O'Rourke, T.D. (1991) "Shear Strength of Sand-Geomembrane Interfaces for Cover System and Lining Design," Proc. Geosynthetics '91 Conference, Atlanta, USA, pp. 159-173.

Martin, J.P., Koerner, R.M. and Whittey, J.F., (1984) "Experimental Friction Evaluation of Slippage Between Geomembranes, Geotextiles and Soils," Proc. International Conference on Geomembranes, Denver, USA, pp. 191-196.

Takasumi, D.L.; Green, K.R. and Holtz, R.D. (1991) "Soil Geosynthetics Interface Strength Characteristics: A Review of State-of-the-Art Testing Procedures," Proc. Geosynthetics '91 Conference, Atlanta, USA, pp. 87-100.

Williams, N.D. and Houlihan, M.F. (1987) "Evaluation of Interface Friction Properties Between Geosynthetics and Soils," Proc. Geosynthetics '87 Conference, New Orleans, USA, pp. 616-627.

Large-Scale Pull-Out Test Results on Geosynthetics

R.J. Fannin
University of British Columbia, Canada

D.M. Raju
University of British Columbia, Canada

ABSTRACT

The design, control and data acquisition features of a large, 1.30 m x 0.64 m x 0.60 m, pullout test apparatus are described. Interpretation of load vs. displacement curves for a grid reinforcement, and the associated normalized pullout resistance, is used to distinguish between a pullout failure, an impending tensile failure, and other intermediate responses to pullout loading. Detailed examination of a pullout test on a geomembrane sheet illustrates the development of a progressive pullout failure.

INTRODUCTION

The development of adequate pullout resistance is essential to the performance of reinforced soil structures, such as walls and slopes. It is also pertinent to the requirements of an anchor trench on the side slopes of a waste containment facility. In design, the available pullout resistance should exceed the tensile force in the geosynthetic by a specified factor of safety.

Pullout resistance is governed by soil-geosynthetic interaction. It is evaluated in the laboratory by performing pullout tests under controlled conditions: a draft ASTM Standard Test Method is currently being developed for such a test. Factors that significantly influence the mobilisation of pullout resistance are summarised in Table 1. Some requirements for the dimensions of a pullout test apparatus, and therefore soil sample, have been investigated by Palmeira and Milligan (1989), who conclude that larger scale tests minimize the influence of the front wall boundary on pullout resistance. However, the influence of boundary conditions is not well-understood, Juran et al. (1988). This uncertainty relates mostly to the top boundary, which may be flexible or rigid, and the front wall boundary which typically is rigid, but may include a sleeve that protrudes into the soil sample, for example Bonczkiewicz et al. (1989).

Table 1. Factors affecting pullout resistance

Pullout Test Apparatus	Soil Sample	Geosynthetic Test Specimen
• Depth of sample	• Type	• Type
• Front wall boundary	• Density	• Length
• Top boundary		• Width
• Confining stress		
• Pullout rate		

This paper describes features of a large pullout test apparatus located at the University of British Columbia. Emphasis is placed on the arrangement of the pullout box, the control system used to mobilise pullout resistance, and the data acquisition system. Some factors influencing test preparation are described. The general response of test specimens subject to a pullout force is illustrated for different confining stresses. Implications for interpretation of test results are examined. One test result is then reported in detail to illustrate both the development of pullout resistance, and the behaviour of the soil sample in the pullout box. The influence of boundary conditions on the pullout response is discussed.

PULLOUT TEST APPARATUS

The apparatus comprises several components: a pullout box which contains the soil sample and geosynthetic test specimen; a hopper for controlled placement of soil in the box; an hydraulic system for application of pullout force ; a clamp assembly for gripping the test specimen; and a reaction frame. A schematic diagram is given in Fig. 1.

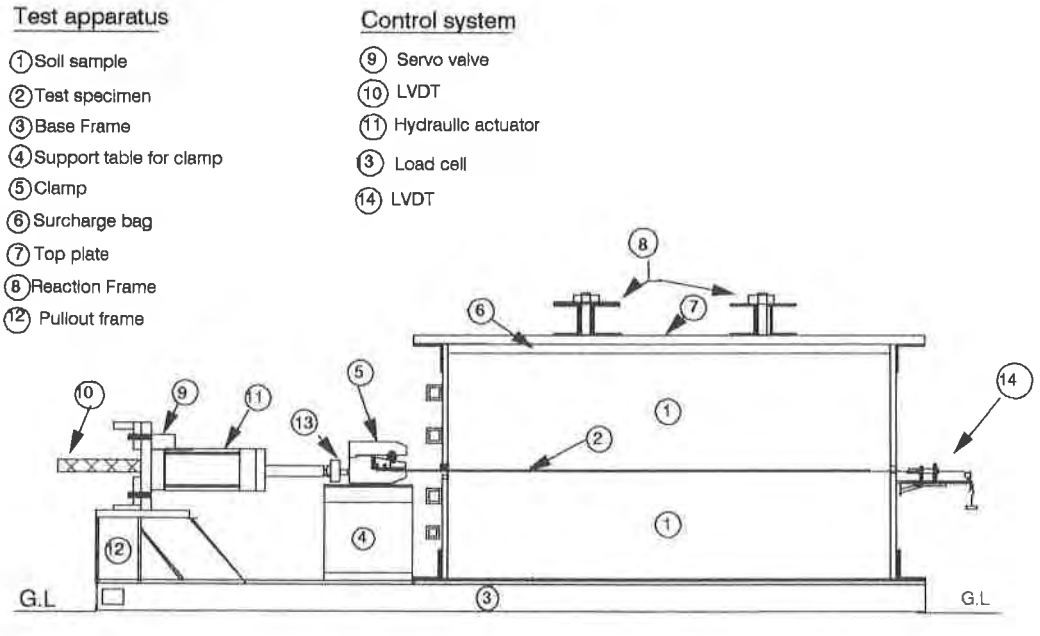

Figure 1 Schematic illustration of test apparatus

The pullout box is a rigid container which accommodates a soil sample 1.30 m long, 0.64 m wide and 0.60 m deep. The front wall, base, and back wall are made of aluminum. The side walls are made of glass sheet fixed to plexiglass. The rigid container imposes strain-controlled (zero displacement) boundaries on all sides of the sample except the top. The top is a flexible bag which is filled with water and pressurised to create a stress-controlled boundary. The surcharge bag reacts against a top plate that is tied to the base frame of the apparatus.

A hopper is used to prepare homogeneous (uniform) soil samples. The soil, a coarse-grained sand, is pluviated into the box. The hopper includes two perforated mild steel plates, each with 6.3 mm holes on a 12.5 mm spacing and diagonally offset, that are overlapped to create a regular pattern of holes. It is placed such that the plates are 0.8 m above the box, giving a maximum fall of 1.4 m (bottom layer) and a minimum of 0.8 m (top layer). Pluviation is initiated by releasing two trap doors beneath the steel plates.

The hydraulic system comprises a pump and several pressure and flow control valves that are used to govern delivery of oil to the double-acting actuator. Control of the actuator is achieved through a closed-loop electro-hydraulic system. A servo-valve mounted directly on the actuator is the interface between electric and hydraulic control. The actuator is fixed on the base frame of the apparatus, and connects to the test specimen through a load cell and clamp, see Fig. 1.

The clamp is made of aluminum and comprises three pieces: a lower jaw; an upper jaw; and a central insert. It connects to the actuator rod through a ball-swivel connection. The clamp is specially designed to grip either grid or sheet test specimens, by modification of the central insert. Details of the clamp assembly are reported by Raju (1991).

CONTROL SYSTEM

A closed-loop control system is used in testing. The principle of operation is illustrated in Fig. 2. For closed-loop control, the function to be controlled is continuously measured and used as feedback for comparison with the demand for that function. The difference between the feedback and demand signal, termed error, is then used to correct the system.

Pullout tests are typically performed under displacement control, for which the feedback signal is that from a displacement transducer monitoring the position of the actuator rod. However, tests may be performed under load control, in which case the feedback signal is that from a load cell recording tensile force on the test specimen. The closed-loop control options are illustrated schematically in Fig. 3.

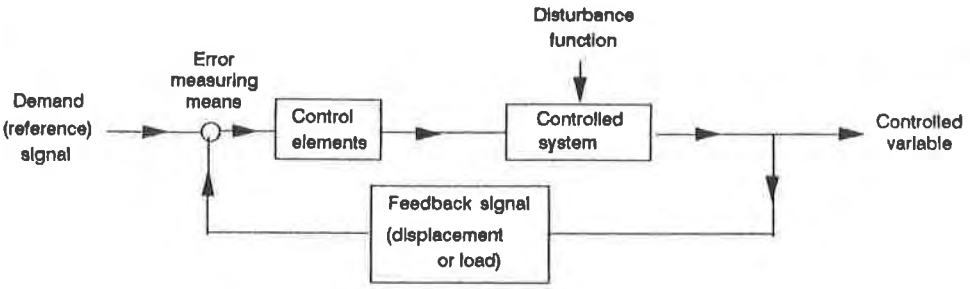

Figure 2 Principle of feedback control

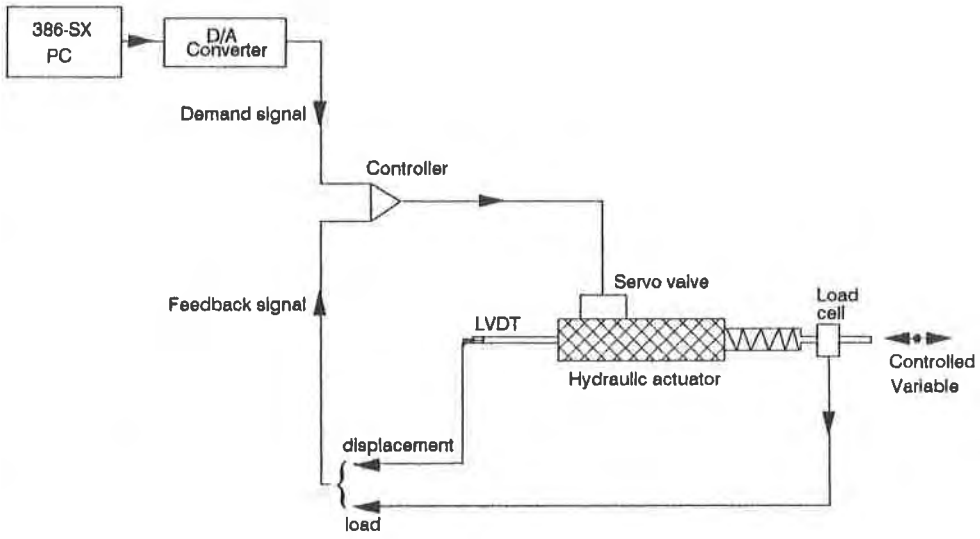

Figure 3 Feedback control system

An electro-hydraulic loading system is used in testing. The servo-valve controls either the rate of displacement of the actuator rod, or the load applied to the test specimen. It operates on an input signal which is the error signal from the controller. The controller compares the demand and feedback signals, and generates a compensating error signal. This error signal drives the servo-valve.

The demand signal for the closed-loop control system, in either position or load control, is generated from software on a 386-SX personal computer. Digital-to-analog conversion of the demand is made using a D/A board in the computer, and the signal is then output to the controller. If the requirement of testing is to apply a constant rate of displacement (CRD), or a constant rate of load, to the geosynthetic specimen, then the demand signal is a linearly (CRL) increasing voltage with time, termed a ramp function. If however, the requirement of testing is to study the influence of dynamic loading, then the demand signal is changed to a waveform.

INSTRUMENTATION

Instrumentation is used to measure pullout force, pullout displacement, strain in the test specimen, displacement of the embedded end of the test specimen, total pressure on the front face of the box, and applied surcharge pressure.

Pullout force is measured using a load cell mounted between the actuator rod and the clamp on the test specimen. Pullout displacement is measured from a displacement transducer located on each end of the clamp. Strain in the test specimen is determined from the output of electric wire resistance strain gauges bonded to the geosynthetic. Five gauges are mounted along the centreline of a test specimen at selected distances from the front wall, see Fig. 4. These gauges are selected for their versatility, and suitability for measuring dynamic strains in both geogrids and geomembranes. A full description of the gauges, and the procedure used to bond them, is reported by Raju (1991). Movement of the embedded end of the specimen is monitored by a tell-tale cable connected to a displacement transducer that is mounted outside the back wall of the box, see Fig. 3. An array of six total pressure transducers, see Fig. 5, is used to measure normal stress on the front face of the box during sample preparation and pullout testing. Surcharge pressure applied to the sample is measured using a water pressure transducer connected to the flexible bag.

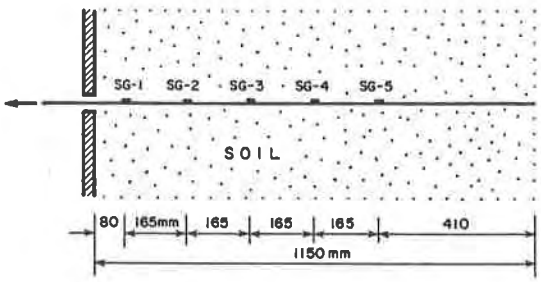

Figure 4 Strain gauge transducer locations

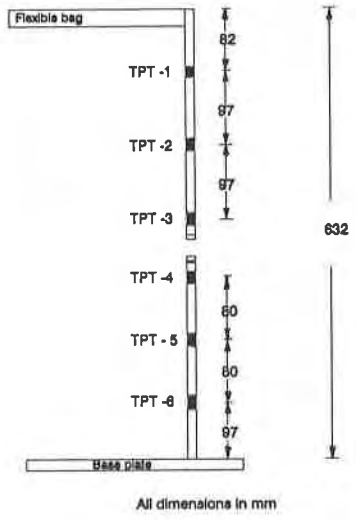

Figure 5 Total pressure locations

FACTORS INFLUENCING TEST PREPARATION

Preparation of the geosynthetic test specimen involves bonding the strain gauges. A cyanoacrylate adhesive is used because of the simple, quick curing procedure. Some excess wire is provided at each location to accommodate movement of the test specimen during pullout. The remaining wire for each gauge is sheathed in a protective tube and taken out through the back-face of the box. The tell-tale cable is then fixed

to the end of the specimen that will be embedded, and similarly taken out.

It is necessary to replicate many soil samples to allow a comparative evaluation of soil/geosynthetic interaction. Examination of terminal velocities has shown the density of a sand sample prepared by air pluviation is sensitive only to rate of pouring and drop height, Vaid and Negussey (1988). Consequently, there is a height of drop beyond which little significant change in void ratio, or increase in density, occurs with increase in drop height. Some experiments on pluviation were performed with the test sand to establish a relationship between density achieved and height of drop, for various pouring rates. A minimum value of 0.8 m was established. During sample preparation, sand is poured from the hopper in a series of eight layers, each 7.5 cm thick.

CHARACTERISTIC CRD PULLOUT RESPONSE

A series of tests was performed at different vertical effective stress on a grid reinforcement. The backfill was a uniformly graded coarse-grained angular sand, for which d_{85} = 0.9 mm. The uniaxial geogrid is made of high density polyethylene. Properties of the material are reported in Table 2. Long-term strength relates to 1 x 10^6 hours from extrapolation of rapid loading creep tests carried out to 1 x 10^4 hours. The test specimens were 1.15 m long and 0.63 m wide. It should be noted that all specimens tested are now prepared to a narrower width of 0.5 m, providing a 7 cm set-back from the sidewalls of the apparatus.

A constant rate of displacement of 0.5 mm/min was used in testing. A slow rate of testing has been considered appropriate for standardization of pullout testing, and is used to allow comparison with results of other established test programs.

Results of the test are summarized in Fig. 6. The curves describe a broad response to applied pullout force. Tests at small vertical effective stress tend to a constant force per unit width that represents a pullout type of failure. Tests at high vertical effective stress also tend to a constant force per unit width, but one that is in excess of the allowable tensile strength and indicative of impending tensile failure of the reinforcement.

This aspect of the response behaviour is further illustrated by the mobilised values of $F^*\alpha$, see Fig. 7, a parameter describing normalized pullout resistance. It is defined as:

$$F^*\alpha = \frac{P}{2\,LW\,\sigma_v'} \qquad (1)$$

where P/W = pullout force per unit width
L = embedment length
σ_v' = vertical effective stress on the specimen

Table 2 Description of the test specimens

Geogrid Property	Value	Geomembrane Property	Value
Apertures		Thickness	
• Machine direction (MD)	14.5 cm (nom)	• Sheet	60 mil
• Cross machine direction	1.7 cm (nom)	Strength	
• Open area	60% (nom)	• Break	27 MPa
		• Yield	14 MPa
Thickness		Elongation	
• Ribs	0.13 cm (nom)	• Break	700%
• Bearing member	0.43 cm (nom)	• Yield	10%
Strength			
• Long-term design load in MD	31 kN/m (min)		

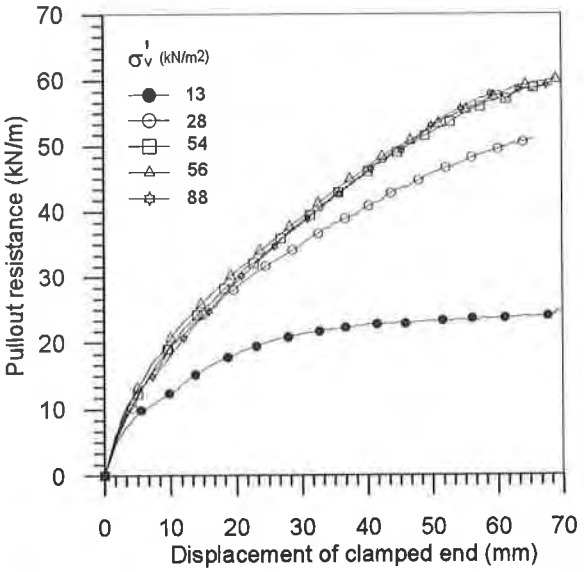

Figure 6 Force-displacement curves

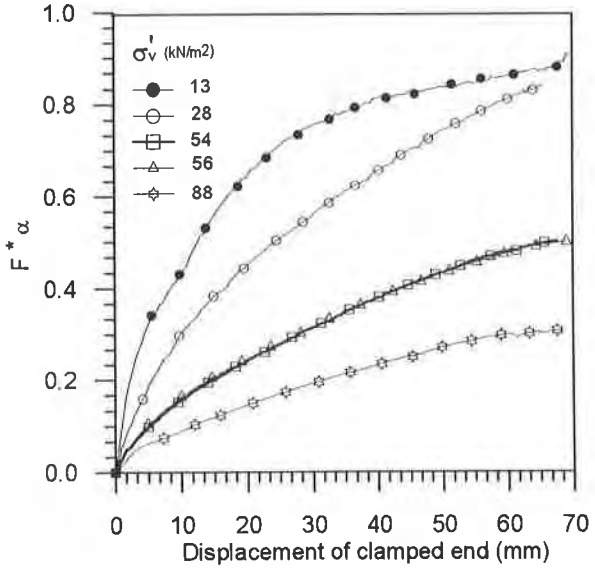

Figure 7 Normalized pullout resistance

Pullout failure is associated with a constant maximum value of $F^*\alpha$, for example the test at $\sigma_v' = 13$ kN/m^2. An impending tensile failure is associated with a constant value of $F^*\alpha$ that is significantly smaller: the test at $\sigma_v' = 88$ kN/m^2 is tending toward such a condition. Repeatability of the test results is confirmed by good agreement between the tests at $\sigma_v' = 54$ and 56 kN/m^2.

Implications of these general responses for interpretation of pullout tests are as follows. First, performing pullout tests at values of vertical effective stress that will mobilise a tensile force per unit width which is large in comparison to the ultimate tensile strength of the geosynthetic test specimen does not achieve a pullout failure. The shape of the load-displacement curve is similar in each case, see curves for σ_v' = 54, 56 and 88 kN/m^2 in Fig. 6, and dominated by in-air extension of the test specimen rather than pullout. Second, pullout failure is best established from examination of the trend of normalized pullout resistance $F^*\alpha$ with increasing displacement, and the maximum value that is achieved.

DEVELOPMENT OF PULLOUT RESISTANCE

Results of a pullout test performed on a smooth HDPE geomembrane are reported in detail in Figs 8 to 12. Properties of the material are reported in Table 2; strength and elongation properties are reported from ASTM D638. The test specimen was 1.0 m long and 0.5 m wide. The backfill soil was a uniformly graded coarse-grained rounded sand, for which d_{85} = 0.9 mm. Surcharge loading applied an effective vertical stress of 12 kN/m^2 on the geosynthetic test specimen. A constant rate of displacement of 0.5 mm/min was used in testing.

Measured rate of displacement of the clamped end of the test specimen increased rapidly at the start of the test, see Fig. 8, to achieve the designated value. The mobilisation of pullout resistance is illustrated in Fig. 9. The curve shows a marked peak value at a small displacement of approximately 4 mm, and a nearly constant value at large displacement. Peak pullout resistance ocurs when displacement of the embedded end is first observed, see Fig. 10. Thereafter the test is characterized by equal displacements of the clamped and embedded ends, and there is essentially no confined elongation of the specimen. The peak value is associated with an apparent mean interface friction angle of 11.9°, while the residual value is associated with an apparent mean interface friction angle of 7.9°. The angle of shearing resistance for this sand at large displacement was found to be 30° from a direct shearbox.

A progressive development of strain is observed along the geosynthetic test specimen, see Fig. 11. Some fluctuation of strain is observed at these small strain magnitudes, as the specimen is pulled through the soil. The rate of strain is greatest at the loaded end of the specimen, and least near the embedded end. Initially no strain is measured at location SG-5. At small displacement, corresponding with peak pullout resistance, largest strains are measured near the loaded end and strain magnitudes decrease at each location toward the embedded end. With increasing displacement the trend is one toward a uniform strain along the test specimen of approximately 0.2 to 0.3%. While the mean interface friction angle that is deduced at peak pullout resistance may have little significance because of progressive, non-uniform strain in the specimen, it is appropriate for a residual value.

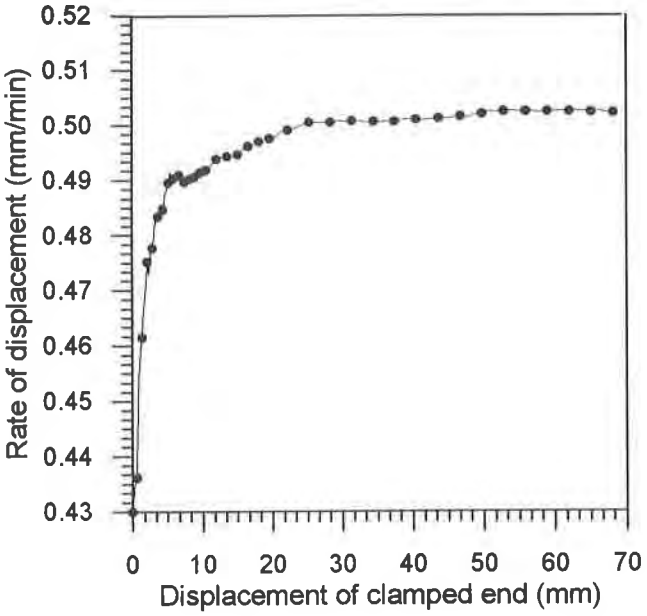

Figure 8 Rate of displacement

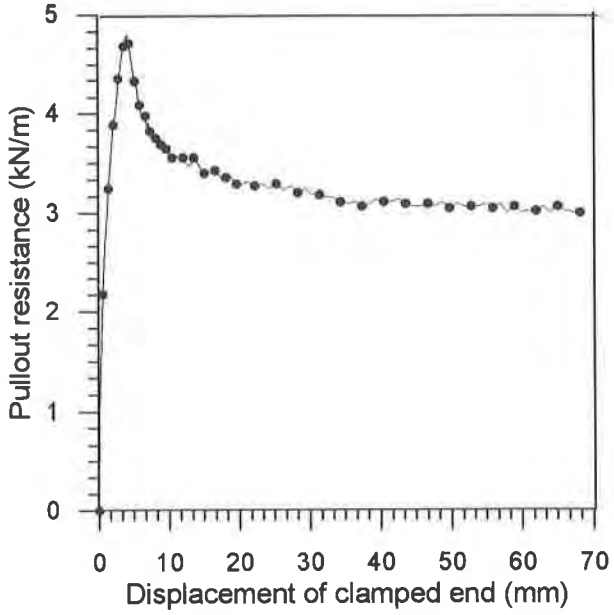

Figure 9 Development of pullout resistance

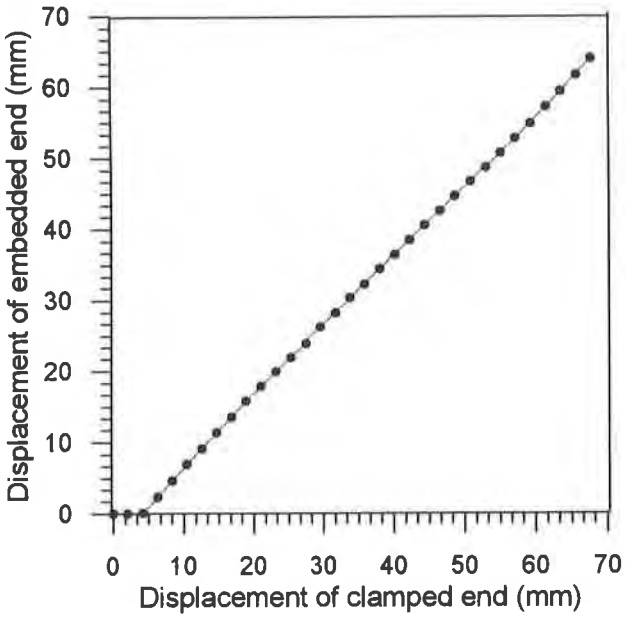

Figure 10 Onset of pullout failure

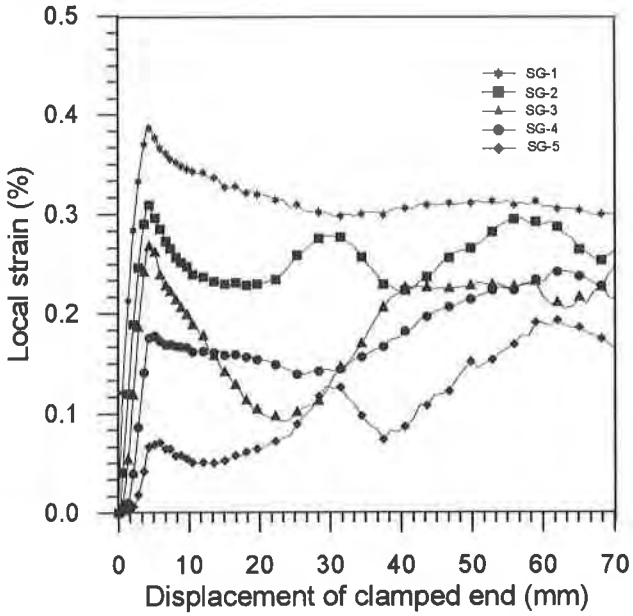

Figure 11 Development of strain

Horizontal stress acting on the front wall of the pullout box changes in response to loading. The response of the two transducers nearest to the test specimen, TPT3 and TPT4, shows greatest variation. Transducers TPT1, TPT5 and TPT6 show no significant change. The response of TPT2 shows a moderate increase. The increment of horizontal stress on the bottom face of the front wall is less than that on the top one: a similar response has been observed in all pullout tests.

The comprehensive acquisition of data shows clearly a progressive development of pullout resistance, up to a peak value, and a decrease thereafter to a constant residual value that is associated with a generally uniform strain in the test specimen.

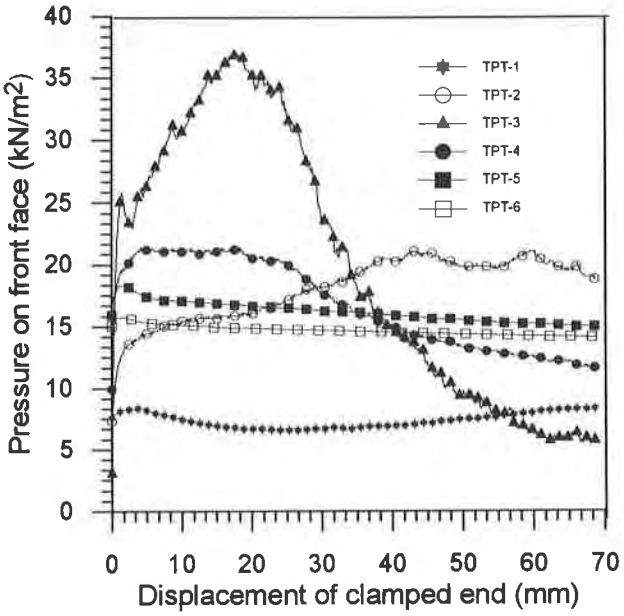

Figure 12 Pressure on the front wall

DISCUSSION

Currently, pullout testing of geosynthetics is not governed by a Standard Test Method. Results of a series of tests on geogrids have been compared, and measurements from one test on a smooth geomembrane reported in detail. Repeatibility of the pullout test apparatus is largely dependent on the sample preparation technique, and is shown to be very good. This is important for any comparative evaluation of soil/geosynthetic interaction. The influence of boundary conditions on pullout testing is not well-understood. An array of pressure cells on the front well defines the shape of the pressure bulb mobilized during pullout, which is not symmetrical about the elevation of the test specimen. Development of pullout resistance is shown from the measurements to be characterized by progressive strain.

CONCLUSIONS

The failure mechanism that is mobilized is essentially one of (a) pullout, (b) tensile failure or (c) some combination of these two responses. Results of pullout tests performed on the geogrid show:

1. For a given width of test specimen, tests performed at relatively low values of vertical effective stress that cause the pullout resistance to be small in comparison to the ultimate tensile strength will tend toward a pullout failure. Conversely, at relatively high vertical stress, tests will tend toward a failure in tensile extension.

2. Pullout force versus displacement curves are necessary, but not sufficient, to define the nature of the failure mechanism. Normalizing the curves with respect to the vertical effective stress helps establish the dominant mechanism.

ACKNOWLEDGEMENTS

This research is supported by grant OGP0046397 from the Natural Sciences and Engineering Research Council of Canada. The tests were performed by D.M. Raju.

REFERENCES

Bonckiewicz, C, Christopher, B.R. and Amatzidis, D.K. (1989) "Evaluation of soil-reinforcement interaction by large-scale pull-out tests," Transportation Research Record No.1188, Washington, D.C.

Juran, I., Knochenmus, G., Acar, Y.B. and Arman, A. (1988) "Pull-out response of geotextiles and geogrids (synthesis of available experimental data)," Proceedings of Symposium on Geotextiles for Soil Improvement, ASCE, Geotech. Special Publication 18, pp. 92-111.

Palmeira, E.M. and Milligan, G.W.E. (1989) "Scale and other factors affecting the results of pull-out tests of grids buried in sand," Geotechnique, Vol. 39, No. 3, pp. 511-524.

Raju, D.M. (1991) "Large scale pullout testing of geosynthetics," A thesis submitted in partial fulfilment of the M.A.Sc. degree at the University of British Columbia.

Vaid, Y.P. and Negussey, D. (1988) "Preparation of reconstituted sand specimens," Advanced Triaxial Testing of Soil and Rock, ASTM STP 977, ASTM, Philadelphia, pp. 405-417.

Diffusivities of Organic Contaminants in High Density Polyethylene Geomembranes

D.R. Ramsey
University of Texas/Los Alamos National Laboratory, USA

ABSTRACT

The solubility and diffusivity of organic containments in high density polyethylene (HDPE) geomembranes was investigated. Using HDPE geomembranes from four manufacturers, sorption and desorption experiments were conducted with benzene, toluene and chlorobenzene to determine equilibrium solubilities and four different diffusivities for each contaminant and geomembrane. Detailed statistical analyses were conducted and revealed that variation in solubility and diffusivity does exist between different geomembranes. In terms of the diffusivity, the variation was slight in most cases. A method for estimating a range of expected diffusivities for any plasticizing contaminant also was developed and presented along with supporting data for benzene, toluene and chlorobenzene.

INTRODUCTION

Polymer liners are employed extensively to protect the environment from the tremendous amount of wastes disposed of by our nation. Geomembranes (liners) are barriers used to separate chemicals in waste impoundments, landfills, ponds and underground storage tanks (USTs) from the surrounding environment. A variety of polymers are used to manufacture commercial liners. Polyethylene, especially high density polyethylene (HDPE), is the most common and represents 40-45% of the raw material used in the manufacture of geomembranes (Jagielski,1990). Polyethylene liners are used extensively in waste and petroleum storage facilities. About 490 million square feet of geomembranes were installed in 1990 with 70-80% of all geomembrane applications related to waste and liquid containment (Jagielski,1990). Clearly, the application of polyethylene, either alone or in conjunction with other barrier materials, in environmental protection is large.

Only four different studies (August and Tatsky, 1982; August and Tatsky, 1984; Haxo et al., 1984; Haxo, 1988; Britton et al., 1989) have been performed to investigate the characteristics of geomembranes in

deleterious chemical environments. Even though little research has been conducted using geomembranes, the transport behavior of many chemicals in polymeric barriers has been thoroughly investigated in other disciplines; namely, in the chemical engineering and industrial hygiene fields. One of the most significant results from these studies is that similar materials from different manufacturers can exhibit variation in permeation, sorption and diffusive phenomena. Thus, HDPE geomembranes from different manufacturers will likely exhibit different characteristics. Studies on HDPE geomembranes either have directly observed variation in permeation phenomena (August and Tatsky, 1982) or have eluded to the potential for its existence.

An effective method for estimating the chemical compatibility of a chemical penetrant/geomembrane system is to perform sorption/desorption tests to determine diffusion and sorption characteristics. These tests are simple and inexpensive. Other chemical compatibility tests, Method 9090 (USEPA, 1984) and permeation tests using permeation cells such as ASTM F739-85, are expensive and can be quite difficult to perform. Results from sorption/desorption tests can be used to determine the characteristics of a penetrant/polymer's diffusivity and solubility: unlike other compatibility tests.

The objective of this research was to investigate diffusivity and solubility differences between HDPE geomembranes from different manufacturers and to develope a procedure, using sorption and desorption tests, for estimating the diffusivities of organic contaminants in typical environmental managment situations.

PREVIOUS RESEARCH ON GEOMEMBRANES

Concerns about the performance of geomembranes in potentially deleterious chemical environments have been expressed by many researchers. Initial research on transport behavior focused on the determination of water vapor transmission rates (Haxo et al., 1984; Lawson and Ingles, 1984; Giroud, 1984; Giroud and Bonaparte, 1989) and gas permeation rates (Haxo et al., 1984) for different penetrant/geomembrane combinations. Geomembrane manufacturers have conducted limited research on the permeability to the contaminants which they were designed to contain. The bulk of experiments conducted on geomembranes have been dedicated to the determination of the chemical compatibility using the Method 9090 developed by the United States Environmental Protection Agency (USEPA).

The earliest research on transport phenomena in geomembranes was conducted by August and Tatsky in the early 1980s to determine the permeation behavior of five different polymer sheets, including polyethylene, challenged against concentrated and dilute aqueous organic solvents. Haxo et al.(1984) determined the gas transmission rates, solvent vapor transmission rates and the water vapor transmission rate for 13 different membranes. Haxo (1988) also conducted a series of experiments to ascertain the degree of partitioning between contaminants and HDPE geomembranes under different conditions. Britton et al. (1989) performed immersion and permeation experiments with different thicknesses of HDPE and eight organic solvents at two temperatures. A

general description of the experiments and results from these researchers is presented in Table 1.

CHARACTERISTICS OF DIFFUSION

The fundamental law of mass transport was derived by Adolf Fick in 1855 from an analogy to Fourier's law of conductive heat transfer. Fick proposed that the flux of a substance permeating a membrane is proportional to the concentration gradient across the membrane and a coefficient of mass transfer designated as the diffusion coefficient. It was originally expressed as

$$J = - D \frac{\partial C}{\partial x} \qquad (1)$$

where

J = mass flux of a substance diffusing across a unit area in unit time,
D = proportionality constant called the diffusion coefficient, and
$\frac{\partial C}{\partial x}$ = concentration gradient.

Diffusion is a complex summation of all polymer-polymer, penetrant-polymer and penetrant-penetrant interactions and each different penetrant-polymer combination has a unique diffusion coefficient describing the diffusive process.

The usual application of Equation 1 is in the diffusion of two different components and the measured diffusion coefficient is termed the integral diffusion coefficient, D. As diffusion proceeds and the concentration of a penetrant increases in a penetrant/polymer medium, the integral diffusivity usually approaches an upper limit which is related to the maximum penetrant concentration (the concentration at equilibrium sorption): the maximum concentration diffusion coefficient, $D_{C \rightarrow Co}$. Conversely, one can define an infinite dilution diffusion coefficient, $D_{C \rightarrow 0}$ as the diffusivity of one molecule of penetrant in a pure polymer medium. Similar to the concept of $D_{C \rightarrow Co}$, the infinite dilution diffusivity implies that as the concentration of a penetrant is reduced to zero, a point will occur where so little of the penetrant remains that each penetrant molecule "sees" only a pure polymer matrix.

In the original expression of Equation 1, known as Fick's first law, the diffusion coefficient was assumed to be independent of penetrant concentration. If this is the case, the three definitions of the diffusivity will have the same value. In fact, researchers conducting experiments using geomembranes have made this assumption. However, this conclusion is often incorrect. Diffusion phenomena of low sorbing gases and vapors may exhibit concentration invariance but vapors and liquids with a high activity may have diffusion coefficients which exhibit a strong concentration dependence. This results in different values for the diffusivities described above; sometimes many orders of magnitude.

For non-polar organic liquids, which are ubiquitous in environmental control situations, the diffusion coefficient usually increases with increasing penetrant concentration due to swelling of the amorphous polyethylene. As the polymer swells, additional penetrant molecules sorb into the ever-growing penetrant-polymer matrix instead of a pure polymer medium. Since each penetrant molecule must occupy a characteristic volume within the polymer, a new penetrant molecule will "see" the volumes created by the segmental motion of the polyethylene segments as well as the volumes occupied by diffusing penetrant molecules. Thus, as the penetrant concentration increases, the penetrant is able to diffuse more easily into the penetrant-polymer matrix resulting in a diffusion coefficient that increases with concentration. This type of concentration dependent diffusion is known as plastization and the diffusing species is termed a plasticizing penetrant.

Sorption/Desorption Tests. Fick's second law of diffusion describes diffusion under non-steady state conditions and can be derived for a one dimension case in an isotropic medium by applying Fick's first law to a volume element:

$$\frac{\partial C}{\partial t} = D \frac{\partial^2 C}{\partial x^2} \tag{2}$$

It can be shown that one solution to Equation 2 has the form of series relating the amount of mass diffusing into a plane sheet during time t, M_t, to the amount of mass diffusing after infinite time, M_∞ (Crank, 1976);

$$\frac{M_t}{M_\infty} = 1 - \frac{8}{\pi^2} \sum_{n=0}^{\infty} \frac{1}{(2n+1)^2} \exp\left(\frac{-D(2n+1)^2 \pi^2 t}{l^2}\right) \tag{3}$$

where

l = sheet thickness,
t = time after contact between diffusant and plane sheet,
x = distance within the region of the plane sheet, and

all other variables retain their previous meaning.

If $M_t/M_\infty=0.5$, Equation 3 can be approximated by

$$D = 0.049 \frac{l^2}{t_{1/2}} \tag{4}$$

where $t_{1/2}$ is the time at which $M_t/M_\infty=0.5$ with the error on the order of 0.001 percent.

Equations 3 and 4 are applicable to the diffusion of a penetrant into as well as out of a geomembrane. Noting the complexity of the

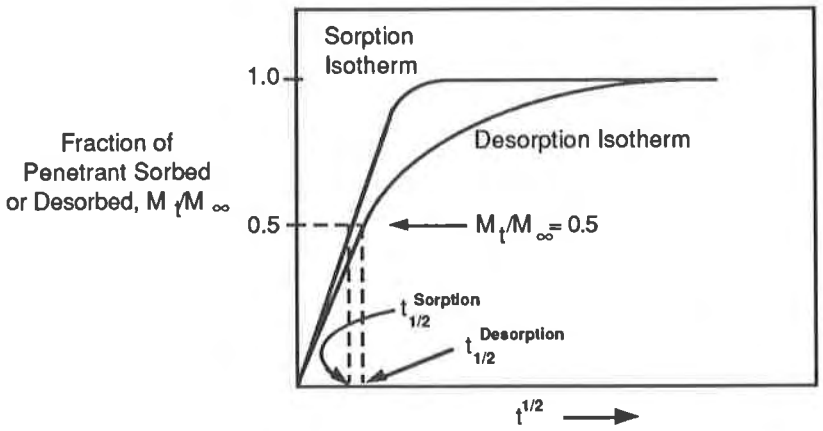

Figure 1. Functional form of sorption and desorption isotherms.

diffusion coefficient as described in the previous section, it is reasonable to expect differences between a diffusion coefficient measured during sorption and one measured during desorption; even if all other variables remain constant. As shown in Figure 1, this is the case if the diffusivity is a function of concentration. If transport plastization is occurring, the diffusion coefficient will increase as the penetrant concentration increases, thus the rate of mass uptake during sorption will be greater than the rate of mass loss during desorption. Therefore, two integral diffusivities, D_S and D_D, can be determined by applying Equation 4 to sorption/desorption data.

In the later stages of diffusion, only the first term in Equation 3 needs to be considered yielding an equation of the form

$$\ln\left(1 - \frac{M_t}{M_\infty}\right) = - \frac{Dt\pi^2}{l^2} \qquad (5)$$

Similar to the determination of D_S or D_D, a plot of $\ln[1-M_t/M_\infty]$ versus time will allow the determination of $D_{C\rightarrow Co}$ or $D_{C\rightarrow 0}$ from the slope of the sorption or desorption data, respectively. Thus from a single sorption/desorption experiment one can determine the concentration dependence of the diffusivity as well as the equilibrium solubility of the penetrant/polymer system.

In research conducted on geomembranes, sorption tests have been used to determine degree of weight and volume change for neat and aqueous solutions of organics (August and Tatsky, 1984); partitioning coefficients between geomembranes and absorbing organic constituents (Haxo,1988); and the solubility, diffusivity, and permeability of organic solutions in geomembranes (Britton et. al., 1989). However, desorption tests have not been performed and the possibility of a concentration dependent diffusivity has not been addressed.

METHODOLOGY AND MATERIALS

HDPE geomembranes in four thicknesses were procured from four liner manufacturers: Gundle Lining Systems Inc., National Seal Company, Poly-America Inc. and SLT North America Inc. To augment and confirm data supplied by the manufacturers, the geomembrane crystallinity content was determined for each manufacturer using a Polymer Laboratories Differential Scanning Calorimeter, PL-DSC. The density was determined using a simple immersion density technique (ASTM, 1986).

Sorption and desorption experiments were performed on 2.5 cm x 7.5 cm coupons sectioned from the 1.5 mm (60 mil) sheets donated by each manufacturer. Three penetrants were examined: benzene, toluene and chlorobenzene. The sorption experiments consisted of placing the coupons in the pure penetrant (contained in a vapor tight 300 ml glass jars with teflon-lined phenolic resin tops) and periodically weighing the coupons to determine the rate of penetrant uptake. After equilibrium sorption had been attained, the coupons were placed in 300 ml glass jars fitted with a butyl rubber stopper to facilitate the connection of a vacuum system (15-25 in. Hg). The coupons were weighed periodically to determine weight loss. For statistical accuracy, ten coupons were used in all sorption and desorption experiments except in sorption experiments to determine $D_{C \rightarrow Co}$ (three coupons). All experiments were conducted at 23±1°C.

RESULTS AND DISCUSSION

The geomembrane density and crystalline content determined during this research for each manufacturer is presented in Table 2. The results are similar to values contained in manufacturer data sheets as well as previous research (Cadwallader and Burkinshaw, 1991). Using the notation in Table 2, differences in densities between manufacturers A and D are not distinguishable whereas the densities of manufacturers A (or D), B and C are significantly different.

The equilibrium sorption results are shown in Table 3 and indicate that for each penetrant the lowest equilibrium sorption can be attributed to manufacturer A while manufacturer B retains the greatest value. Also, variation within data recorded for manufacturer D is almost an order of magnitude greater than variation noted for the other manufacturers in all cases (similar variation generally was not observed in diffusivity calculations). Since similar experimental techniques were employed for all manufacturers, this may imply greater variation in manufacturer D's product as compared to the other manufacturers. If a baseline variance is calculated by averaging the measurements recorded for manufacturers A, B and C it is found that, approximately, only 5% of manufacturer D's variation can be attributed to a general, industry-wide product variance while 95% is product specific. Solubility trends in Table 3 follow trends in the geomembrane density: manufacturer A always has the lowest solubility while manufacturer B the greatest.

The sorption/desorption isotherms for the toluene/manufacturer A system are presented in Figures 2 and 3. All penetrant/manufacturer

Table 2. Density and crystallinity content for four HDPE geomembranes[1].

Manufacturer	Density [g/cm^3]	Percent Crystallinity
A	0.9514**a**	57.1%**a**
B	0.9459**b**	57.3%**a**
C	0.9532**c**	57.0%**a**
D	0.9517**a**	59.9%**a**

[1] Analysis of variance was conducted using a Fischer test statistic with the following values: df_1=3, df_2=8, α=0.05 and F_c=4.07. Different bold letters within a column represent data significantly dissimilar using two standard deviations. For example, the density of manufacturer A's geomembrane is significantly different from the values determined for manufacturers B and C but not that calculated for manufacturer D.

Table 3. Equilibrium solubility [g penetrant/g geomembrane] and standard deviation for four HDPE geomembranes and three penetrants[1].

Manufacturer	Benzene		Toluene		Chlorobenzene	
A	0.0796**ad**	s=0.00030	0.0869**ad**	s=0.00028	0.1042**ad**	s=0.00044
B	0.0842**b**	s=0.00016	0.0920**b**	s=0.00022	0.1166**b**	s=0.00031
C	0.0823**cd**	s=0.00012	0.0882**cd**	s=0.00024	0.1061**cd**	s=0.00008
D	0.0814**d**	s=0.00089	0.0884**cd**	s=0.00132	0.1067**cd**	s=0.00155

[1] Analysis of variance was conducted using a Fischer test statistic with the following values: df_1=3, df_2=36, α=0.05 and F_c=2.87.

Table 4. Diffusion coefficients for four HDPE geomembranes and three penetrants[1].

Penetrant	[x 10^8 cm^2/s] D_S	D_D	$D_{C\rightarrow Co}$	$D_{C\rightarrow 0}$	Manufacturer
Benzene	2.19**a**	3.93**a**	9.88**a**	0.492**a**	A
	3.30**b**	4.49**bc**	11.51**b**	0.587**b**	B
	2.69**c**	4.33**c**	11.01**b**	0.540**c**	C
	2.77**c**	4.57**bc**	13.05**c**	0.581**b**	D
Toluene	2.65**a**	4.58**a**	11.23**a**	0.487**a**	A
	3.96**b**	5.01**bd**	9.61**b**	0.544**b**	B
	2.56**a**	4.85**cd**	11.80**a**	0.493**a**	C
	3.26**c**	5.10**bd**	11.83**a**	0.512**c**	D
Chlorobenzene	2.41**a**	3.66**a**	8.59**a**	0.484**a**	A
	3.19**b**	4.33**b**	11.39**bcd**	0.564**b**	B
	2.22**c**	3.78**c**	10.43**bc**	0.495**a**	C
	2.84**d**	3.98**d**	11.79**bd**	0.585**b**	D

[1] Analysis of variance was conducted using a Fischer test statistic with the following values: df_1=202-122, df_2=205-125, α=0.05 and F_c=1.77. Three replications were used for experiments to determine $D_{C\rightarrow Co}$ resulting in the following parameters: df_1=52, df_2=55, α=0.05 and F_c=2.73.

combinations exhibited similar curves differing only in the rate of approach to equilibrium. The curves in Figures 2 and 3 represent "anomalous" diffusion, non-Fickian, which is typical of penetrant/polymer systems of this type. These curves reveal that the initial rate of desorption is greater than the initial rate of sorption. As time progresses, the rate of desorption decreases and then finally levels off, falling well below that recorded for sorption.

The form of the curves in Figures 2 and 3 does not precluded a diffusion coefficient solely dependent on penetrant concentration (Crank, 1976), however, curves such as these usually indicate an additional time and/or spatial dependence. To test the possibility of time dependence, three consecutive sorption/desorption cycles were performed (in triplicate) using samples from manufacturer D. No change in the shape or relative location of the curves was observed upon plotting consecutive sorption/desorption cycles. The spatial dependence of the diffusion coefficient was investigated by performing additional sorption/desorption experiments on different thicknesses. Experiments were performed in triplicate using samples of 1 mm (40 mil), 1.25 mm (50 mil), 2 mm (80 mil) and 2.5 mm (100 mil) thickness from manufacturer D. No macroscopic variation in the sorption/desorption curves was observed indicating that spatial considerations (i.e., membrane thickness) do not play a significant role in determining the functional form of the diffusion coefficient. Since spatial and time coordinates are not a factor in the diffusivity, penetrant concentration and its effects must be primarily responsible for the type of sorption/desorption phenomena observed in these penetrant/manufacturer systems.

Carbon black, variable between each manufacturer, may play a role in the functional form of these isotherms. This assertion is supported by the variability in degree of anomalous behavior between penetrants: chlorobenzene (which has a greater affinity for carbon black that either benzene or toluene) isotherms showed greater deviation from Fickian diffusion than either benzene or toluene.

Examples of the graphs used to determine the four diffusion coefficients are presented in Figures 4 and 5. These plots represent either magnified perspectives of curves similar to the sorption/desorption isotherm shown in Figure 2 or magnified perspectives of graphs used to determine $D_{C \rightarrow Co}$ or $D_{C \rightarrow 0}$. Diffusion coefficients determined from these graphs as well as the remaining data are displayed in Table 4.

The data presented in Table 4 indicates that the integral sorption and desorption diffusion coefficients, D_S and D_D, are similar (even though each D_S/D_D pair, i.e. between columns, is different). Furthermore, even though statistical variation exist between manufacturers within a penetrant grouping as well as between penetrants in most cases, the diffusion coefficients are very similar. An average sorption and desorption diffusion coefficient, calculated from the integral sorption and desorption diffusion coefficients, can be calculated for each penetrant with little resulting error: usually less than 20 percent. Thus, an average integral diffusion coefficient can be assumed to adequately represent the four manufacturers. The same

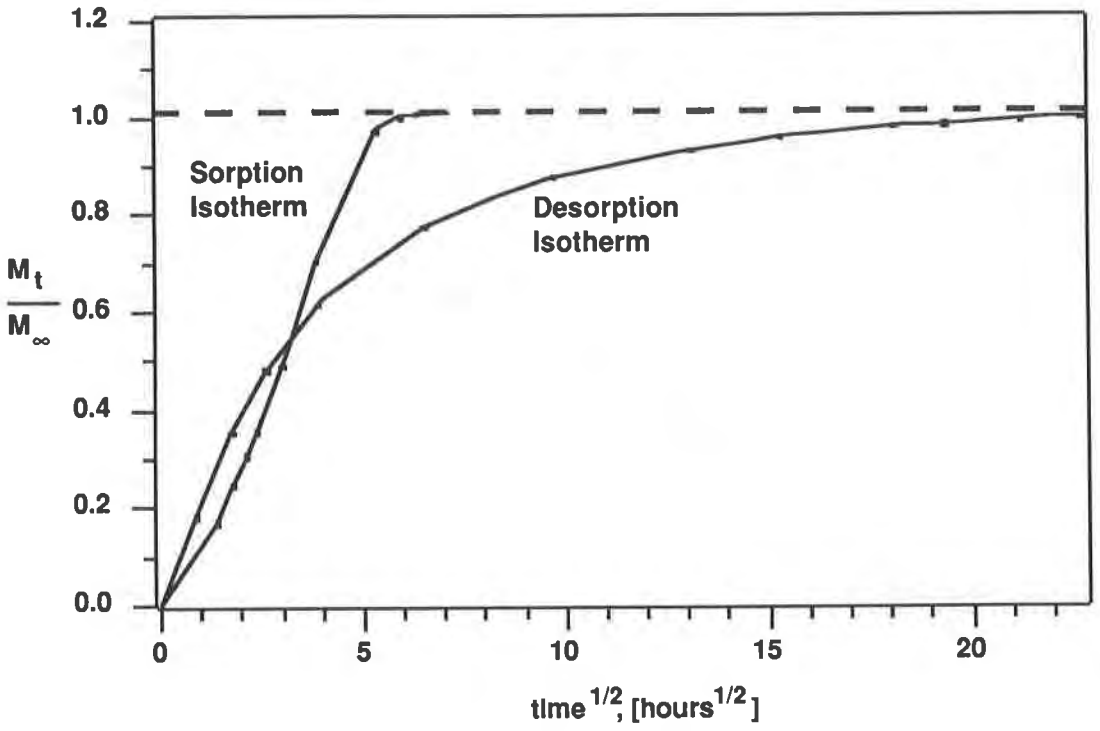

Figure 2. Sorption/desorption isotherm for toluene/manufacturer A.

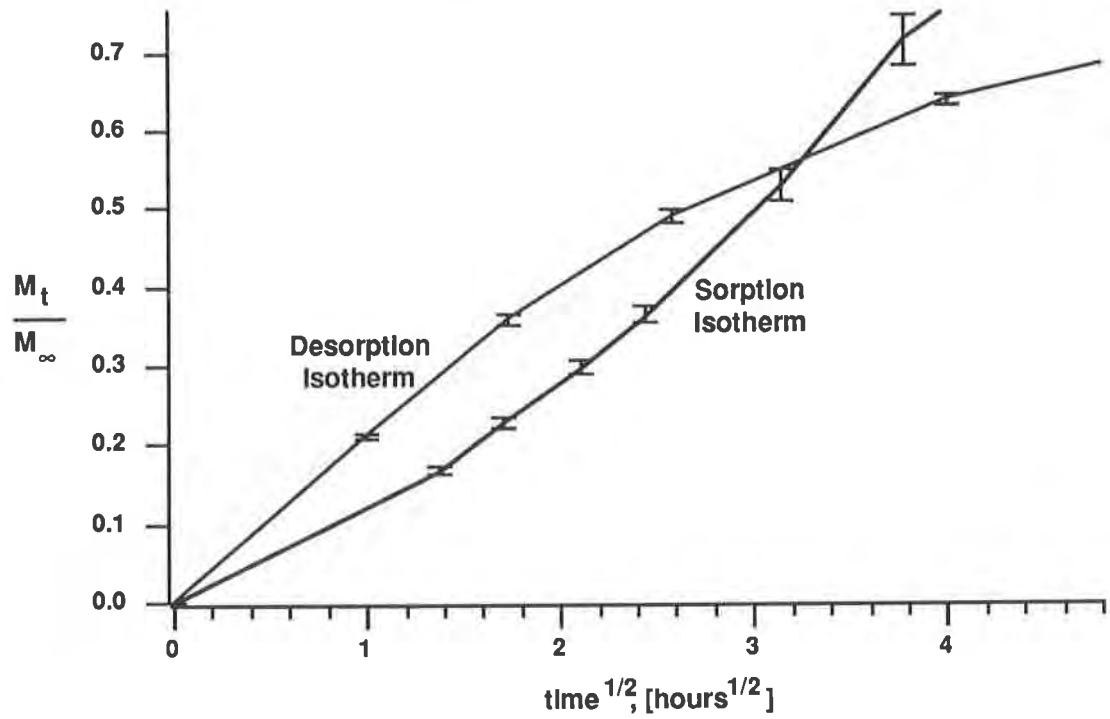

Figure 3. Expanded view of sorption/desorption isotherm for toluene/manufacturer A (error bars represent the range of data recorded).

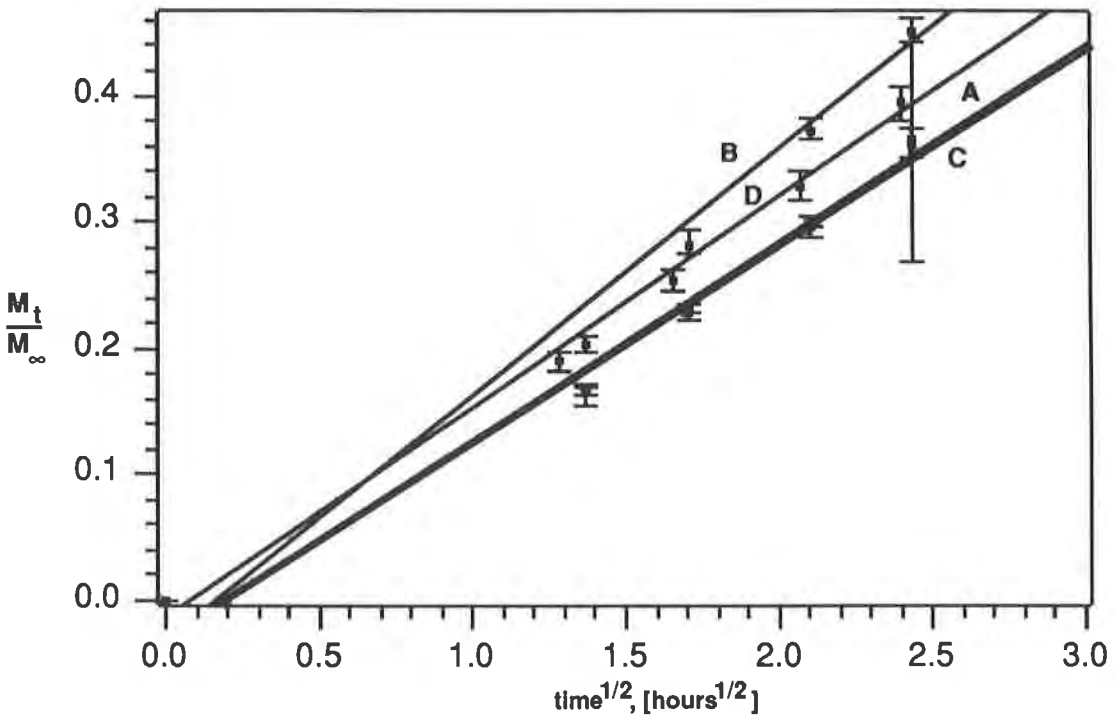

Figure 4. Plot of mass uptake (sorption) for four manufacturers with penetrant toluene.

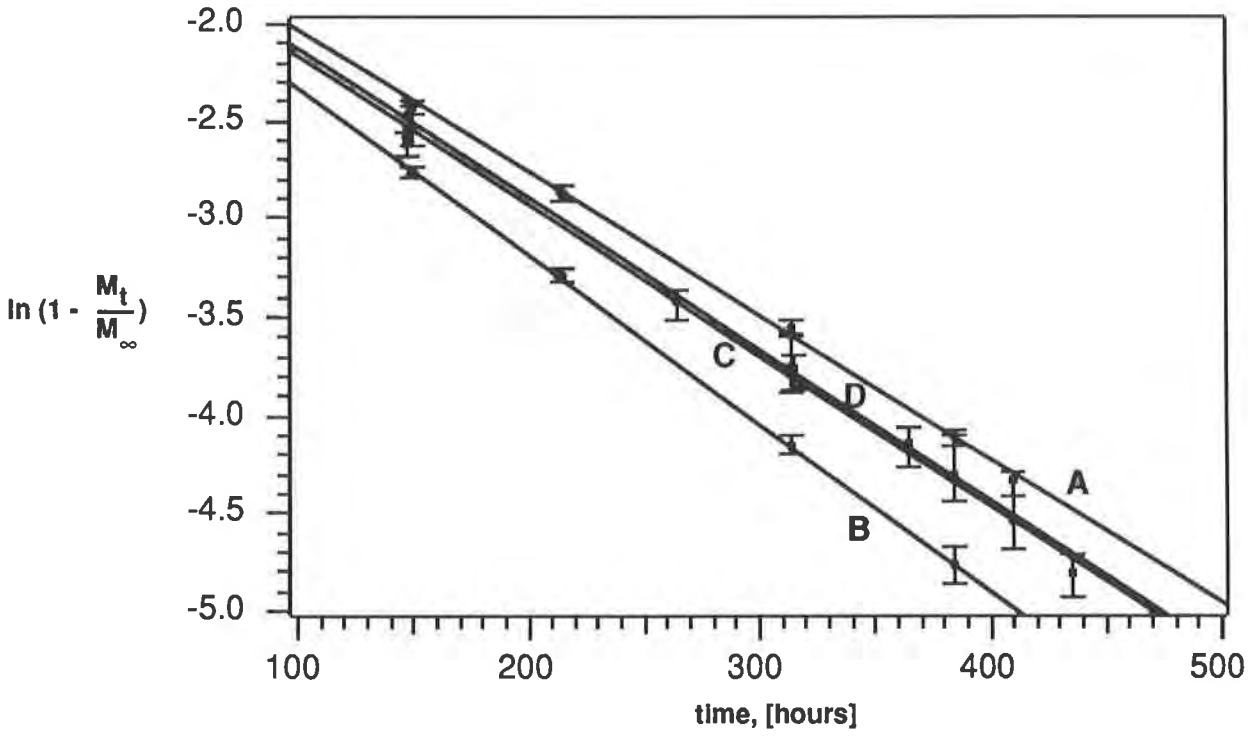

Figure 5. Plot of mass loss (desorption) for four manufacturers with penetrant chlorobenzene.

position can be argued for calculating a diffusion coefficient representing the average of each D_S/D_D pair.

Comparing data for $D_{C\rightarrow Co}$ and $D_{C\rightarrow 0}$ indicates that a significant range exists between these two diffusivities with D_S and D_D always falling somewhere within this range. This is to be expected given the sensitivity of the diffusivity to penetrant concentration. It can be argued that this range represents the range of diffusivities one would expect from any chemical environment containing plasticizing compounds. The infinite dilution coefficient, $D_{C\rightarrow 0}$, is independent of the original penetrant concentration since it symbolizes the diffusion of a single penetrant molecule in an infinite medium of HDPE and will always represent a lower limit for diffusivities. All diffusivities, irrespective of the chemical environment, will be greater than this limiting value; even for the case of organic compounds in dilute aqueous concentrations which is typical of landfill leachate.

Similarly, since the effects of plasticizing penetrants other than the diffusing penetrant (e.g., benzene in toluene) should be similar to that of the diffusing penetrant, $D_{C\rightarrow Co}$ can be interpreted as an upper limit of the diffusivity range. Again, this limit is assumed to be independent of the original chemical environment of the diffusing penetrant. One can devise a situation where greater plasticizing compounds exist such that the penetrant's diffusivity, $D_{C\rightarrow Co}$, is not a definitive upper limit. However, given the high solubility of most plasticizing hydrocarbons, this diffusivity should be at least within an order of magnitude and likely very similar.

As noted previously, the integral sorption and desorption diffusion coefficients fall between these two diffusivities in all cases. However, it is not possible to determine their exact location within this range because the diffusivities calculated using this method are a complex function of concentration and position. As the penetrant diffuses into the HDPE sheet, the concentration is not constant at each location within the sheet as was assumed for the calculation of $D_{C\rightarrow Co}$ and $D_{C\rightarrow 0}$, but rather a function position. Consequently, the integral diffusion coefficients are more sensitive to the characteristics of the chemical environment and, likely, not as reproducible.

Engineering Significance. The diffusivity range discussed above could be used to estimate the range for diffusion coefficients that would exist in waste management and petroleum storage situations. Since the determination of diffusivities for all conceivable applications involving geomembranes is impossible if not unreasonable, an upper and lower operational limit would enable the estimation of performance as well as guide the design of future waste management technologies and facilities. Moreover, the technique employed to determine the range, the sorption/desorption method, is very simple and inexpensive; especially when compared to other testing procedures often required for regulatory compliance. For these types of compounds, the variance introduced by this technique is within acceptable limits compared to the inherent variation of geomembranes. Finally, any significant deviation of a

diffusivity from this range would indicate an inferior or misinterpreted penetrant/geomembrane combination or structural problems (e.g., holes).

Regulatory Significance. USEPA has long recognized the potential for adverse environmental effects resulting from the application of HDPE geomembranes in waste containment applications. This diffusivity range could used to determine the performance and establish standards for the application of geomembranes in regulatory situations.

CONCLUSIONS

The solubility and diffusivity of penetrant/geomembrane pairs have been deduced and the form of the diffusion coefficient inferred for benzene, toluene and chlorobenzene in HDPE. Differences between manufacturers of HDPE geomembranes have been observed: however, in most cases the variation is minimal. It was shown that significant chemical compatibility data can be obtained by performing simple sorption and desorption tests. More importantly, it is possible to realize the range and form of the diffusion coefficient for any plasticizing chemical environment using this technique.

ACKNOWLEDGEMENTS

Support for the research was provided by Environmental and Water Resources Engineering (Department of Civil Engineering) at The University of Texas at Austin and the Research and Development Section of the Industrial Hygiene and Safety Group, Health and Safety Division at Los Alamos National Laboratory. Geomembranes were graciously donated by Gundle Lining Systems Inc., National Seal Company, Poly-America Inc. and SLT North America Inc. This research was conducted under the auspices of The University of Texas and Los Alamos National Laboratory independent of financial or technical support from geomembrane manufacturers. Reference or mention of a geomembrane does not constitute an endorsement of a manufacturer's product or service.

REFERENCES

American Society for Testing and Materials (1986), Specific Gravity (Relative Density) and Density of Plastics by Displacement, D792-86, Philadelphia, PA.

August,H. and R. Tatsky, (1982) "Permeation Behavior of Plastic Waterproof Sheeting to Seal Dump Bases Against Organic Solvents", Forschungshar. Bundesanst. Meterialpruef. (BAM),12(1), pp 9-14.

August,H. and R. Tatsky, (1984) "Permeabilities of Commercially Available Polymeric Liners for Hazardous Landfill Leachate Organic Constituents", Proceedings of the International Conference On Geomembranes, Vol. 1, Denver, CO, Industrial Fabrics Association International, St. Paul, MN, pp163-168.

Britton, L.N., R.B. Ashman, T.M. Aminabhavi, and P.E. Cassidy, (1989) "Permeation and Diffusion of Environmental Pollutants Through Flexible Membrane Polymers", J. App. Poly. Sci., Vol 38, pp 227-236.

Cadwallader, M.W. and J.R. Burkinshaw, (1991) "Molecular and Rheological Changes in Polyethylene Occurring From Heat Seaming HDPE Liners", In GeoSynthetics 1991 Conference Proceedings, Industrial Fabrics Association International, St. Paul, MN, pp 287-302.

Crank, J., (1975) The Mathematics of Diffusion, 2nd Edition, Oxford University Press.

Giroud, J.P., (1984) "Impermeability: The Myth and a Rational Approach", Proceedings of the International Conference On Geomembranes, Vol. 1, Denver, CO, Industrial Fabrics Association International, St. Paul, MN, pp157-162.

Giroud, J.P. and R. Bonaparte, (1989) "Leakage Through Liners Constructed with Geomembranes - Part I. Geomembrane Liners", Geotextiles and Geomembranes, 8, 27-67.

Haxo, H. E. Jr., J. A. Miedema, and N. A. Nelson, (1984) "Permeability of Polymeric Membrane Lining Materials", Proceedings of the International Conference On Geomembranes, Vol. 1, Denver, CO, Industrial Fabrics Association International, St. Paul, MN, pp151-156.

Haxo, H.E. Jr., (1988) "Transport of Dissolved Organics from Dilute Aqeuous Solutions through Flexible Membrane Liners", Presented at the 14th Annual Solid Waste Research Symposium on Land Disposal, Remedial Action, Incineration and Treatment of Hazardous Waste, Cincinnati, OH, May 9-11.

Jagielski, K., (1990) "Geomembrane Market Report: A Solution That Ensures Growth", Geotechnical Fabrics Report, Vol. 8, No. 8.

Lawson, C.R. and O.G. Ingles, (1984) "Water Repellency Requirements for Geomembranes", Proceedings of the International Conference On Geomembranes, Vol. 1, Denver, CO, Industrial Fabrics Association International, St. Paul, MN, pp169-173.

United States Environmental Protection Agency, (1984) EPA Method 9090 - Compatibility Test for Wastes and Membrane Liners, Office of Solid Waste and Emergency Response, Washington, D.C.

United States Environmental Protection Agency, (1985) Assessment of Synthetic Membrane Successes and Failures at Waste Storage and Disposal Facilities, Hazardous Waste Engineering Research Laboratory, Cincinnati, OH, EPA/600/2-85/100.

United States Environmental Protection Agency, (1987b) Technical Considerations for De Minimis Pollutant Transport Through Polymeric Liners, Hazardous Waste Engineering Research Laboratory, Cincinnati, OH, EPA/600/2-88/042.

Shaking Table Tests for Geosynthetic Interfaces

A.M. Lahlaf
GEI Consultants Inc., USA

M.K. Yegian
Northeastern University, USA

ABSTRACT

This paper presents the results of a research program undertaken to investigate the dynamic interface shear strength properties of geosynthetic systems using shaking table tests. Tests were performed on geomembrane-geotextile and geomembrane-geomembrane interfaces. The results indicate that during dynamic tests, there is a limited shear stress, hence a limited acceleration, that can be transmitted from one geosynthetic to another. Beyond this acceleration, relative displacement is initiated between the two geosynthetics. Also, for the geosynthetics used, there was no appreciable difference between the dynamic interface friction angles measured at the onset of sliding and those from static tests. Therefore, shaking table tests can be used to provide values for dynamic as well as static interface friction angles. The orientation of the geomembrane, the normal stress, and the frequency of motion were found to have no effect on the measured dynamic friction angles. Wetting of the geosynthetic interface was found to slightly reduce the dynamic friction angle.

INTRODUCTION

Significant progress was made in the field of geosynthetics during the last decade. Recent research efforts have been targeted mainly at investigating the behavior of geosynthetic-geosynthetic and geosynthetic-soil systems under static loads, while the dynamic behavior of such systems is not yet adequately addressed. The results of extensive static tests on the interface shear strength properties of geosynthetics have been reported in the literature. Investigations of the dynamic interface shear strength properties of geosynthetics have been limited.

This paper presents the results of a research program undertaken to investigate the dynamic interface shear strength properties of geosynthetic systems using shaking table tests. The shaking table tests consisted of subjecting a concrete or a steel block, the base of which was covered with a geosynthetic, to a periodic motion. The block was resting freely on another geosynthetic fixed to the table. The calculation of the angle of internal friction between the geosynthetics

was based on measurements of the accelerations of the block. Tests were performed on geomembrane-geotextile and geomembrane-geomembrane interfaces for both dry and wet conditions.

While the concept of using a sliding block to determine the dynamic interface shear properties is in essence a simple one, a thorough understanding of the nature of sliding friction in general, and the factors affecting it is an essential component toward developing a better understanding of the dynamic interface shear properties of geosynthetics. The subject of friction between moving bodies has received great attention from researchers for a long time. Deresiewicz (1986) reported that in 1699 Guillaume Amontons introduced the idea that the frictional force is proportional to the normal force. Also, one of the earliest comprehensive testing programs was undertaken by Charles Augustin Coulomb in 1785. He determined that factors that can affect sliding friction include: the nature of the materials in contact and their coating, the surface area, the normal force, the time of contact before motion begins, and the relative velocity. More recent research indicates that additional parameters such as temperature (West and senior, 1962), and sliding distance (Sung and Suh, 1979) can also affect sliding friction. In this research some of the factors listed above were investigated, and the results are reported.

Finally, in this paper the applicability and limitations of using a shaking table to measure dynamic friction properties of geosynthetics are discussed.

TEST APPARATUS

Figure 1 shows a schematic of the shaking table facility used to evaluate the dynamic interface properties between geosynthetics.

The shaking table apparatus consisted of a vibration exciter connected to a rigid aluminum table, which was mounted on frictionless linear bearing pillow blocks, and moving on two stainless steel guide rails. The vibration exciter has a capacity of 1.11 KN (250 lb), a stoke

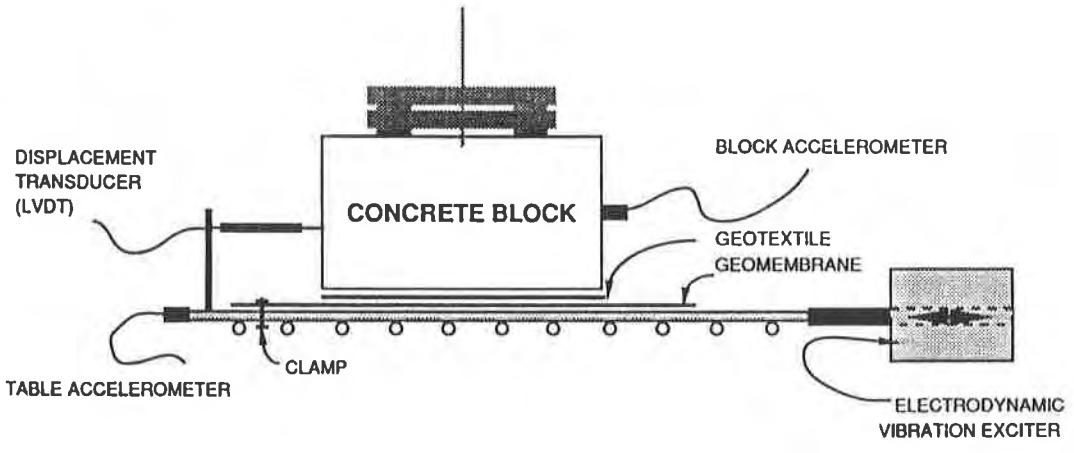

Figure 1. Shaking Table Apparatus

of 2.54 cm (1 in.), and a usable frequency range of 5000 Hz. The dimensions of the table are 91 cm (3 ft) in the direction of motion, and 81 cm (2.65 ft) in the transverse direction. The results presented herein correspond to a periodic excitation of the vibration exciter.

A concrete block with weights placed on top of it, rested on a segment of a geotextile which in turn rested on a large piece of geomembrane that was fixed to the shaking table. When a wet condition was required, the block-geosynthetic system was placed in a tub full of water and fixed to the shaking table.

The acceleration of the table and that of the block were measured simultaneously by piezometric accelerometers. The output signals from the accelerometers were amplified using charge amplifiers. The displacement of the block relative to the table was recorded using a linear variable displacement transducer (LVDT) attached to the shaking table.

For data acquisition, the outputs of the two accelerometers and that of the LVDT were fed into a personal computer via a screw terminal board as shown in Figure 2. Upon conversion of the signals from analog to digital, the data was retrieved and analyzed by commercially available software.

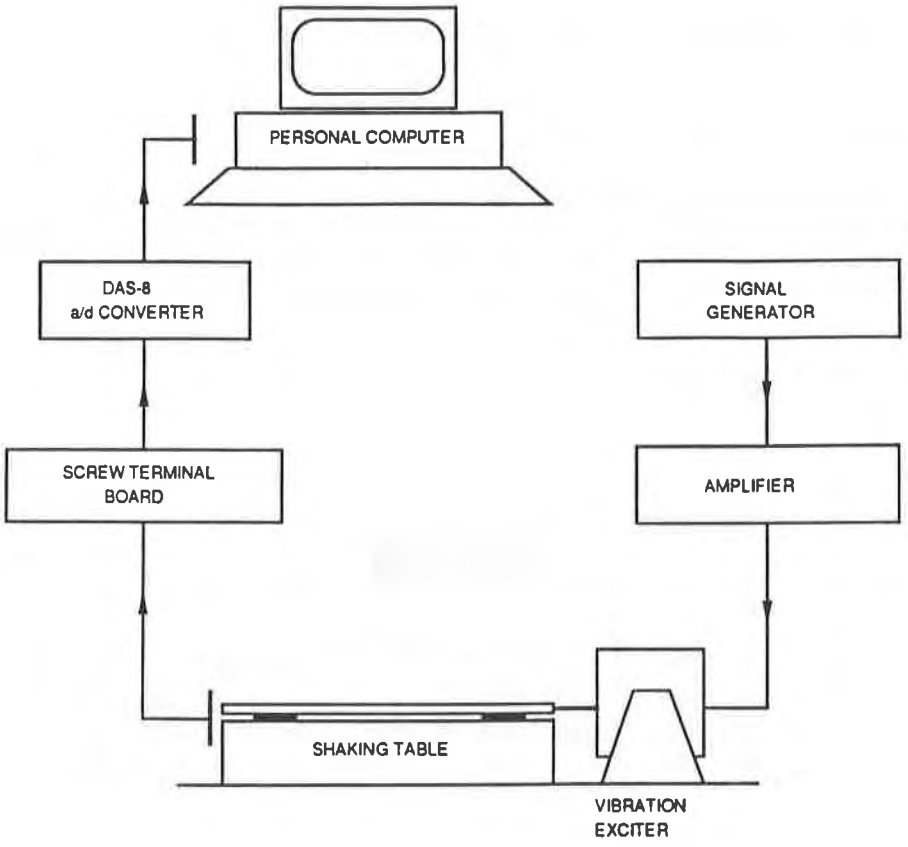

Figure 2. Schematic of Test Apparatus and Data Acquisition System

The geosynthetics used in this research consisted of a hard smooth high density polyethylene geomembrane (Gundle HD60), and a nonwoven geotextile (Polyfelt TS700).

TESTING PROCEDURE

After the desired geosynthetic interface was selected, the concrete block was placed atop it. The vibration frequency was set to 2 Hz, and the incoming current from the signal generator to the vibration exciter was set to cause the table to move with a certain acceleration. Measurements of the 3 channels were recorded immediately after the table started its motion. The measurements were made for a duration of 4 seconds. The sampling frequency for the 3 channels was 100 Hz, i.e., 100 samples per second.

After one test was finished, the data was stored for later analysis. The incoming current to the vibration exciter was increased so as to increase the acceleration of motion of the table, and another test was performed. This procedure was repeated for each test.

For the tests where the table acceleration was large enough to cause sliding of the block, the block was repositioned at the start of each test.

EVALUATION OF THE INTERFACE SHEAR STRENGTH

The calculation of the angle of friction between the geosynthetics tested is based on the measurement of the acceleration of the block.

Consider the block shown in Figure 3. Since the frictional resistance between the concrete block and the geotextile is significantly larger than that between the geomembrane and the geotextile, sliding always takes place between the geotextile and the

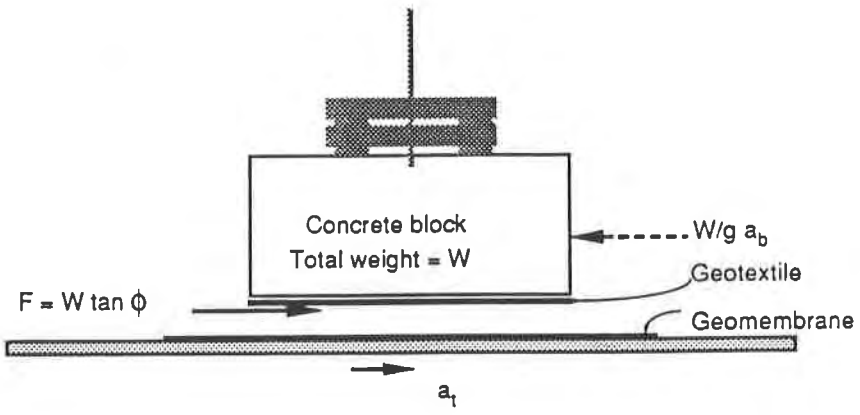

Figure 3. Forces Acting on the Block

geomembrane. Hence, as the table accelerates, it transmits a force F to the block. This frictional force cannot exceed the interface shear strength between the geosynthetics.

$$F = W \tan\phi \qquad (1)$$

where

W is the weight of the block and added weights
ϕ is the interface friction angle between the geosynthetics.

The force F causes the block to move with an acceleration given by

$$W \tan\phi = \frac{W}{g} a_b$$

or

$$a_b = \tan\phi \; g \qquad (2)$$

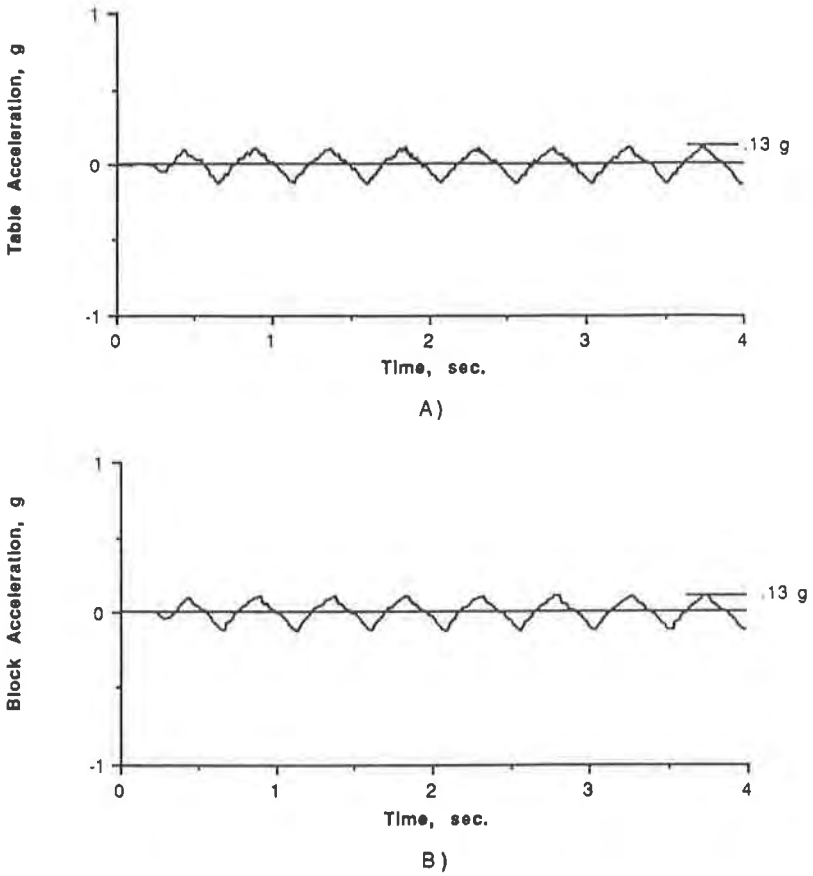

Figure 4. Shaking Table Test Results for Geomembrane-Geotextile Interface, Dry Condition, (No Sliding)
A) Table Acceleration Record with a Peak value of 0.13g
B) Block Acceleration Record with a Peak Value of 0.13g

Equation 2 implies that during tests where the table acceleration is smaller than the limiting block acceleration given by equation 2 the block and the table move together ,i.e., the table and the block accelerations are equal as shown in Figure 4. When the acceleration of the table exceeds the limiting block acceleration, however, relative displacement between the block and the table is induced as shown in Figure 5. Thus, measurement of the limiting acceleration of the block can provide the dynamic interface friction angle between the geosynthetics.

$$\phi = \arctan\left(\frac{a_b}{g}\right) \qquad (3)$$

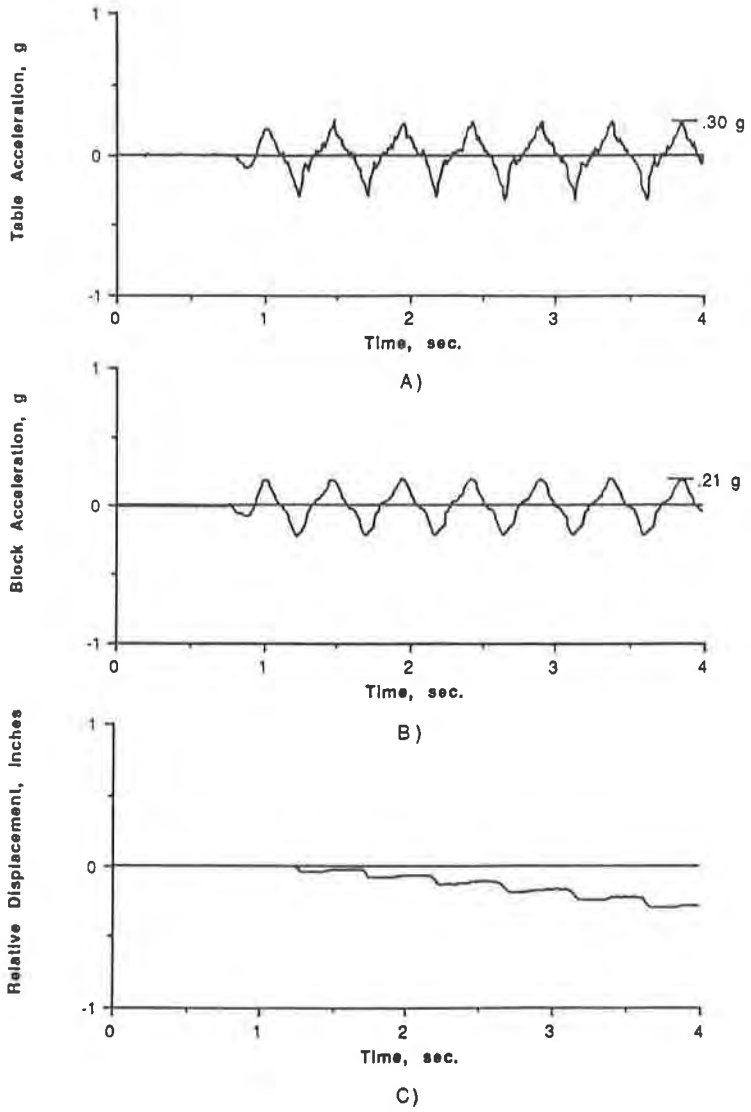

Figure 5. Shaking Table Test Results for Geomembrane-Geotextile Interface, Dry Condition,
A) Table Acceleration Record with a Peak Value of 0.30 g.
B) Block Acceleration Record with a Peak Value of 0.21 g.
C) Relative Displacement.

TEST RESULTS

Geomembrane-Geotextile Interface. Tests similar to those presented in Figures 4 and 5 were performed for values of peak table acceleration ranging from 0.10 g to 0.40 g. The tests were conducted for a dry geomembrane-geotextile interface condition with a normal stress of 8.5 KPa (1.2 psi), and a frequency of excitation of 2 Hz.

A plot of the peak block acceleration versus the peak table acceleration is shown in Figure 6. The solid lines shown in Figure 6 represent the least square fit of the data. A number of significant observations can be made from these and other similar results. The initial segment that has a slope angle of about 45° confirms that the block initially moves with the table (no sliding occurs between the geomembrane and the geotextile) up to a limiting table acceleration of about 0.20 g. This corresponds to a block acceleration, a_b = 0.20 g, or a friction angle of $\tan^{-1}$ (0.20) = 11.3°. Immediately after sliding of the block is initiated, the block acceleration invariably drops slightly. This reduction is attributed to the residual shear strength of the geomembrane-geotextile system (Mitchell et al. 1990, Yegian and Lahlaf, 1992). The block acceleration associated with the interface residual strength is about 0.19 g. This corresponds to a friction angle of $\tan^{-1}$ (0.19) = 10.7°. These numbers are very similar to those obtained for the same geosynthetic interface from static interface strength tests obtained by Yegian and Lahlaf (1992).

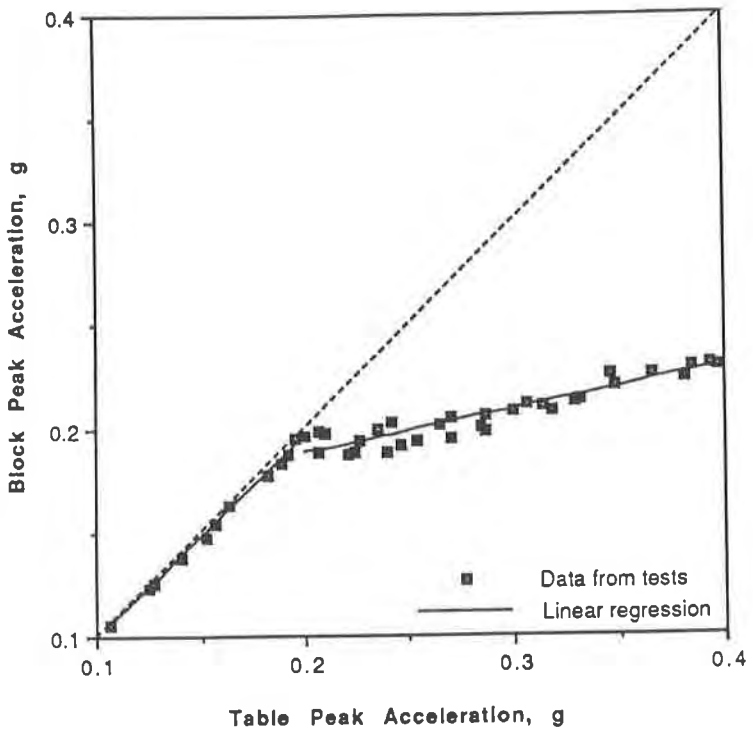

Figure 6. Shaking Table Test Results for Dry Geomembrane-Geotextile Interface, Normal Stress = 8.5 KPa (1.2 psi), Frequency of Excitation = 2 Hz.

The second segment of the regression line shown in Figure 6 represents the behavior of the block for table accelerations greater than 0.20 g. In this case, the block slides relative to the table; therefore, its acceleration is smaller than that of the table. The acceleration of the block, however, increases slightly with increasing table acceleration, meaning that the frictional force, F, transmitted to the block by the table is a function of the table acceleration. The residual friction angle, calculated using Equation 2, increases from 10.7° to 13° within the range of table acceleration of 0.20 g to 0.40 g. Similar observations were made by Lai (1979) and Jacobson (1980) during shaking table tests on model retaining walls sliding on sand.

Geomembrane-Geomembrane Interface. The results of dynamic tests on a geomembrane-geomembrane interface, conducted under a normal stress of 8.5 KPa (1.2 psi) and an excitation frequency of 2 Hz, are shown in Figure 7. The first segment in the graph indicates that, initially, the block moves with the table up to a limiting acceleration of about 0.14 g. This corresponds to a dynamic peak friction angle of $\tan^{-1}$ (0.14) = 8°. At the onset of sliding, the block acceleration drops to about 0.11 g, corresponding to a dynamic residual friction angle of $\tan^{-1}$ (0.11) = 6.3°. Note that the drop from peak to residual friction angle measured at the onset of sliding for a geomembrane-geomembrane interface is larger than that observed for a geomembrane-geotextile interface.

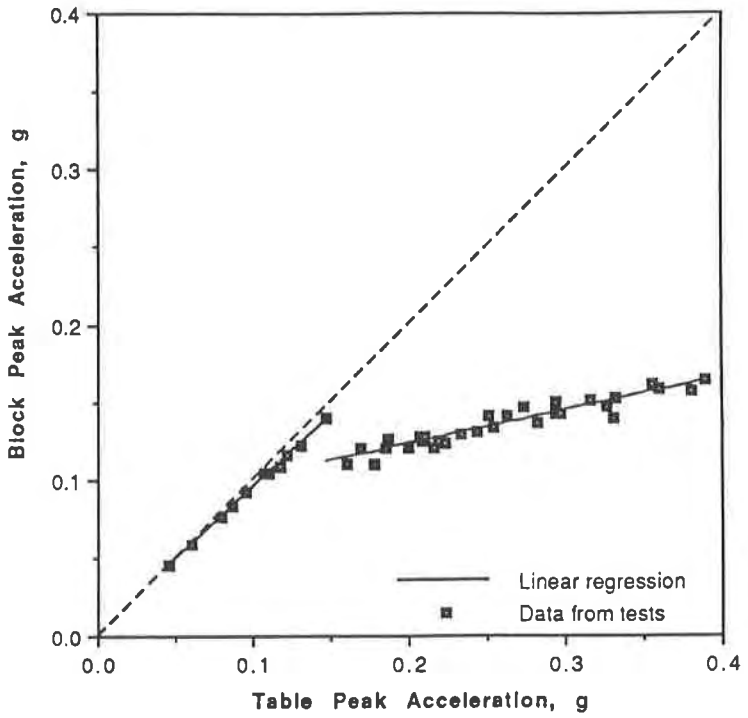

Figure 7. Shaking Table Test Results for Dry Geomembrane-Geomembrane Interface, Normal Stress = 8.5 KPa (1.2 psi), Frequency of Excitation = 2 Hz.

This is due to the stick-slip nature of sliding between two smooth geomembranes. In fact, stick-slip behavior was also observed for geomembrane-geomembrane interface in static tests during which the measured peak and residual friction angles were 8° and 5.7° (Lahlaf and Yegian, 1991), respectively.

Similar to the observation made for the geomembrane-geotextile interface, once sliding occurred along the geomembrane-geomembrane interface, the measured block acceleration increased with increasing table acceleration. When the table acceleration was 0.40 g, the measured block acceleration was about 0.16 g, corresponding to a friction angle of 9.1°.

The results are summarized in Table 1.

Table 1. Measured Dynamic Friction Angles for Dry Geomembrane-Geotextile and Geomembrane-Geomembrane Interfaces

Interface condition	Acceleration Transmitted to the Block at the First Observation of Sliding (Peak Dynamic Friction Angle)	Acceleration Transmitted to the Block After Sliding is Initiated (Residual Dynamic Friction Angle)
a. Geomembrane[1]/Geotextile[2] Dry	.20 g (11.3°)	.19g[3] - .23g[4] (10.7° - 13°)
b. Geomembrane[1]/Geomembrane[1] Dry	.14 g (8°)	.11g[3] - .16g[4] (6.3° - 9.1°)

[1] Gundle HD60: hard, smooth HDPE.
[2] Polyfelt TS700: Nonwoven, continuous filament, needlepunched geotextile.
[3] at first observation of sliding.
[4] at table acceleration of .4g

Factors Influencing the Dynamic Interface Friction Angle. To determine if the geomembrane orientation has an influence on the measured dynamic friction angles, tests were conducted on a geomembrane-geotextile interface where the direction of motion of the shaking table was perpendicular to the cross machine direction of the geomembrane. The normal stress was 8.5 KPa (1.2 psi) and the frequency of motion of the shaking table was 2 Hz. The results indicate that the peak and residual friction angles obtained from these tests, as well as the variation of the residual angle with the table acceleration, are similar to those obtained for the machine direction and shown in Figure 6. It is, therefore, concluded that the geomembrane orientation with respect to the direction of motion of the shaking table does not have any appreciable effect on the measured dynamic peak and residual friction angles of a geomembrane-geotextile interface.

Other tests were conducted to investigate the effect of geomembrane surface conditioning, wetting, normal stress, and effect of shaking table frequency. It was found that the geomembrane surface was very sensitive to surface conditioning. A mere touch of the geomembrane surface by hand would place enough perspiration on it and thus lower the measured dynamic interface angles. Wetting was found to slightly reduce the measured dynamic friction angles (about 1°), while the normal stress and the frequency had no effect on the measured results. Details about these tests can be found in Lahlaf and Yegian (1991), and Yegian and Lahlaf (1992).

CONCLUSION

Previous investigations of interface shear strength of geosynthetics have been focused mainly on the static behavior. In the research reported in this paper, dynamic interface shear strength properties of geosynthetics were investigated. For this purpose, shaking table tests were successfully utilized. Shaking table tests offer the advantage of using large representative samples of geosynthetics, especially if field samples need to be tested. It was shown that shaking table tests can provide both static and dynamic friction angles between geosynthetics. During such tests the influence of normal stress, and frequency of motion can be easily studied. In addition, tests can be performed using actual time histories, where not only the response of the system on top of the geosynthetic interface is obtained, but also any change in the frequency characteristics of the transmitted motion is detected.

There are, however, some limitations associated with shaking table tests. These include factors such as: difficulty of achieving a perfectly horizontal table; data acquisition problems and noise in the measured responses; difficulty in adapting the testing procedure for geosynthetic-soil systems because of problems such as densification of soil during testing; and difficulty of achieving very high normal stresses.

Current research is underway at Northeastern University to devise tests for geosynthetic-soil systems, and to improve the shaking table apparatus to allow tests at high normal stresses.

ACKNOWLEDGEMENT

The work described in this paper was partially funded by the Stone and Webster Corporation and the National Science Foundation. This support is greatly appreciated. The authors also extend their gratitude to Polyfelt, Inc., and Gundle Lining Systems, Inc. for contributing the geosynthetics used in this research.

REFERENCES

Deresiewicz, H. (1986), "Amontons and Coulomb, Friction's Founding Fathers", Proceedings of the Workshop on the Use of Surface Models to Predict Tribology Behavior, Columbia University, New York, pp. 56-60.

Jacobson, P. N. (1980), "Translational Behavior of Gravity Retaining Walls During Earthquakes", M. E. Report 80-9, University of Canterbury, New Zealand.

Lahlaf, A. M., and Yegian, M. K. (1991), "Dynamic Interface Shear Strength Properties Between Geomembranes and Geotextiles", Report No. CE-91/08, Civil Engineering Department, Northeastern University.

Lai, Cho sim (1979), "Behavior of Retaining Walls Under Seismic Loading", M. E. Report 79/9, University of Canterbury, New Zealand.

Mitchell, J. K., Seed, R. B., and Seed, B. H. (1990), "Kettleman Hills Waste Landfill Slope Failure. I: Liner-system Properties", Journal of Geotechnical Engineering, ASCE, Vol. 116, No. 4, pp. 647-668.

Sung, N-N., and Suh, N. P. (1979), "Effect of Fiber Orientation on Friction and Wear of Fiber Reinforced Polymeric Composites", Wear, Vol. 53, pp. 129-141.

West, G. H., and Senior, J. M. (1962), "Frictional Properties of Polyethylene", Wear, Vol. 19, pp. 37-52.

Yegian, M. K., and Lahlaf, A. M. (1992), "Dynamic Interface Shear Strength Properties of Geomembranes and Geotextiles", Journal of Geotechnical Engineering, ASCE, Vol. 118, No. 5, pp. 760-779.

Highlighting the Process Defects by Means of Mass Per Unit Area Analysis

D.C. Adolphe
École-National Superieure, France

J.Y. Drean
École-National Superieure, France

B. Burckle
École-National Superieure, France

T. N'Guyen
École-National Superieure, France

ABSTRACT

The control and the regulation of the non-woven textile manufacturing processes seem in fact to be more involved in the know-how and the empirical knowledge of the engineers than in the scientific analysis of the product and the output processes.

In this paper, a scientific approach of the control and the regulation of these processes will be presented.
By means of a specific device which closely performs the measurement of the mass per unit area [400 points/m(122 points/ft)]and with the help of statistic tools developed for the analysis of the textile lap and implemented on the computer device, we show that it is possible to highlight the presence of process defect, especially the periodic ones, and to control and optimize the regulation processes.

This work takes place into two frames works :

-first, the implementation of the statistical tools in a spirit of theoretical study;

-then, the optimization of the regulation processes in an industrial spirit carried out with a non-woven textile manufacturer.

INTRODUCTION

The control and the regulation of the non-woven textile manufacturing processes seem in fact to be more involved in the know-how and the empirical knowledge of the engineers than in the scientific analysis of the product and the output processes.

The target of this study is to prove that both control and regulation can be done by means of a control of the non-woven textile lap.

Using specific tools, measurement device and calculation algorithms, developed in our laboratory, we carried out two kinds of study, a theoretical one, and an industrial one.

The effected control was done on the distribution of the mass per unit area.

MEASUREMENT DEVICE

This device used a method based on the absoption of a laser beam by the non-woven textile lap [ADO90-1].

Presentation. The main component are as follows :

-a HeNe laser beam (5mW) equipped with crossed plates to control the output power of the beam;

-a photomultiplier equipped with an interferential plate centred on the wawelength of the laser beam emission so as to reduce the influence of the external light;

-a set of optical fibres to guide the beam on the testing point;

-a micro-computer which monitors all the measurement devices; performs all the data calculations and stores and displays the results.

-The scanning of the lap is done with the help of a travelling attachement combined with a lap motion device.

This device provides a very small scanning area close to $5mm^2$ so that the resolution of the device reaches 160,000 points/m^2 (14884 points/ft^2).

Figure 1 shows a general view of the measurement device previously described.

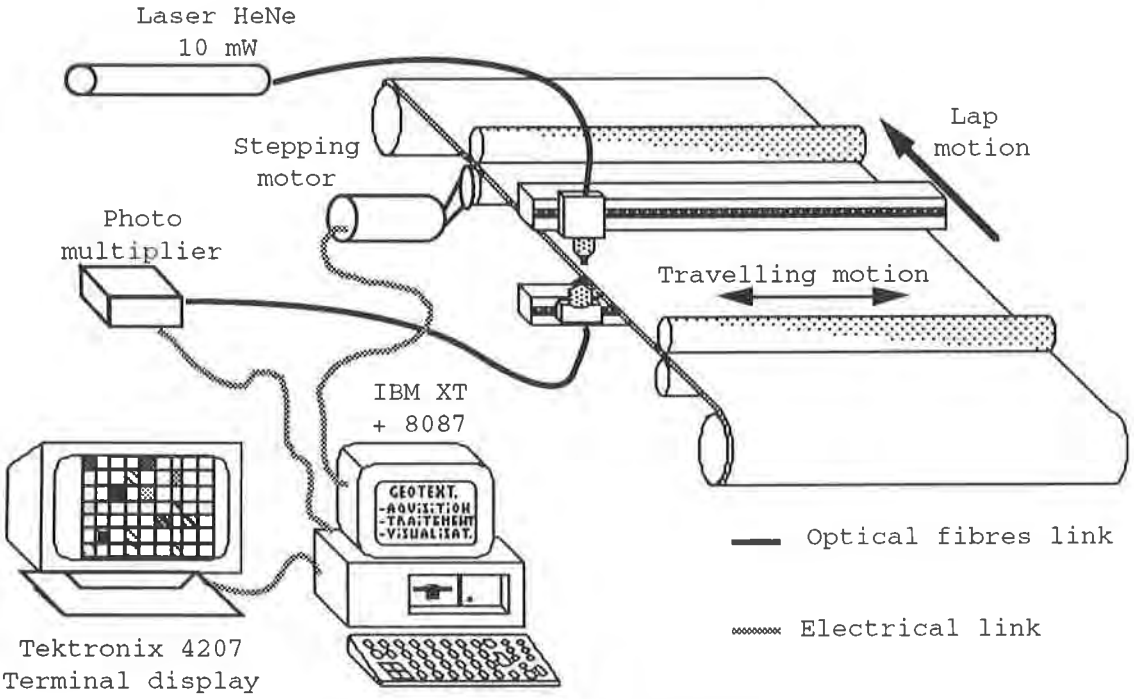

Figure 1 : Overview of the measurement device

Experimental procedure. A modelization of the laser beam absorption law in case of non-woven textile media, is given by the following formula [ADO 90-2]:

$$I = A + B\, e^{-Cm} \qquad (1)$$

where:

I = resulting intensity,

m = mass per unit area,
A,B,C = absorption coefficient; these coefficients depend on the kind of tested non-woven textiles.

Due to the method of measurement, a calibration procedure is implemented. This procedure allows the device to determine the A,B,C coefficients of the absorption law which is specific to each non-woven textile lap.

THE STATISTICAL ANALYSIS TOOLS

Surface variance. The classical statistical analysis such as variance analysis scans the sample unidirectionaly. The total unevenness of the sample is given by a longitudinal scanning and a transversal one.

Based on the theory and the methods developed to characterize the structural unevenness of the linear textiles (sliver, roving and yarns) [MAR 45], [BRE 57],[BRE 58], it is possible to conceive a new method of evaluation of the mass unevenness of textile surfaces. This method is based on a bidirectional scanning of the sample.
Let S_i be the mass per unit area of an element of the fibrous population P (textile lap). The distribution of the S_i random variable is described by means of the classical statistical parameters, such as: the mean

$$S = \frac{\sum s_i}{N} \qquad (2)$$

with N = Σ xi number of elements of the sample
and with the variance

$$\mathrm{Var.S} = \frac{\sum (s_i - S)^2}{N} \qquad (3)$$

with N >> 100

The mass unevenness of the lap can be characterized by studying the variance dispersion as a function of the size of the sample. The variance can be symbolically denoted as B(s,c) and named as "interclass surfacic variance" with s as the surface of the element, S as the surface of the given sample. The variance of the mother population is called "TOTAL VARIANCE" and corresponds to the limit case:
s -> O
N -> ∞ so S -> ∞
so the total variance explained with the help of Plamer's notations. will be as follows :

$$VT = B(0,\infty) \qquad (4)$$

But in fact, such a value is not measurable and can only be estimated by extrapolation. The variability of B(s,S) can be studied by choosing the s element size and the N = S/s number of measurements as a function of the statistical reliability to be obtained. With such an approach, interclass surfacic variance curves can be plotted.The previous formulae can be simplified by using the following notations:

$$B(0,\infty) = B(0) \qquad (5)$$

$$B(s,S) = B(s) \qquad (6)$$

The properties of the linear length variances [WRO 661],[WRO 662],

[MON 60] are transposable to the surfacic interclass functions especially in cases of pure random massic unevenness.

Between variances B(S) Let a S surface band (strip) [KIR 76-1] of x abcissa (versus an 0 arbitrary origin) of an L constant width and of an 1 length taken from an ideal lap (figure 2).

Let s be an elementary band of S (of t abcissa versus O) and M(t) be the punctual mass taken in cross section
The mass per unit area of the S surface band is denoted as M (x,S).The mathematical expression of B(S) has now to be determined.

B(S) is the variance related to the surfacic mass of the bands of S surface (M (x,S) variable).

The surfacic mass M(x,S) belonging to an s surface corresponds to the average value of M(t) in the interval [x, x = 1] = [x, x+S/L]

$$M(x,S) = \left(\frac{L}{S}\right).\int_{x}^{x+\frac{S}{L}} M(t)dt \qquad (7)$$

Let **M** be the expected value of the M(x,S) variable

$$\mathbf{M} = E(M(x,S)) \qquad (8)$$

$$B(S) = E(M(x,s)- \mathbf{M})^2 \qquad (9)$$

so

$$B(S) = E\left(\frac{L}{S}\int_{x}^{x+\frac{S}{L}} (M(t)dt - \mathbf{M})^2\right) \qquad (10)$$

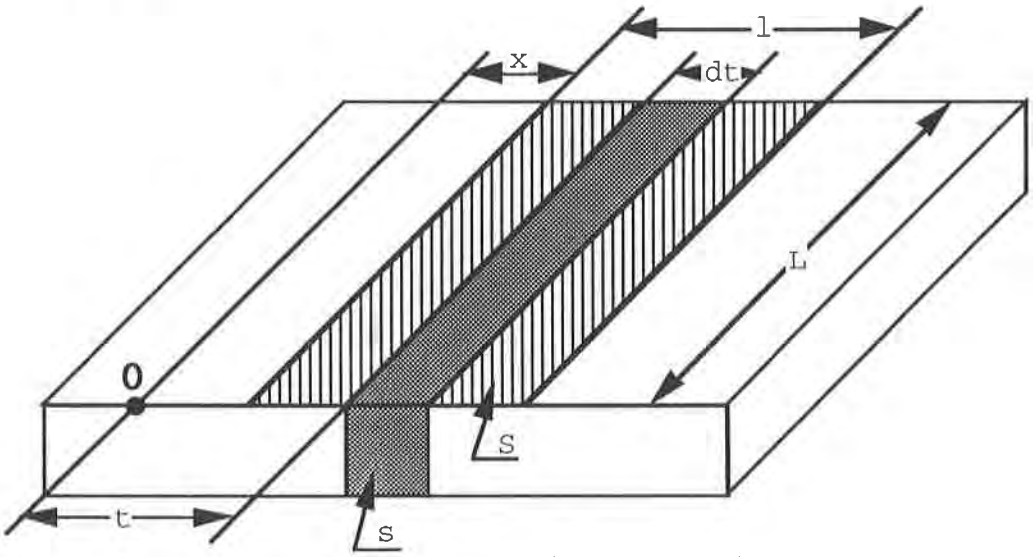

Figure 2 : Representation of an ideal lap

By using the properties of the E operator, expliciting the covariance and changing variables, the following expression of B(S) is to be obtained :

$$B(S) = 2\,\frac{L^2}{S^2}\int_{0}^{\frac{S}{L}} \Gamma(u)\left(\frac{S}{L} - u\right)^2 du \qquad (11)$$

with rS(u) autocorrelation surfacic function defined as follows:

$$r_S(u) = \Gamma(u)\ \Gamma(0) \quad (12)$$

The B(O) value is obtained from the following relationship:

$$B(S) = E(\ M(x,s) - \mathbf{M})^2 \quad (13)$$

When s -> O, S/L -> O, M(x,s) -> M(t) which designates the punctual surfacic mass. So, at the limit, the total variance of the lap can be obtained as follows :

$$B(O) = E(M(t) - \mathbf{M})^2\ Ss^2 \quad (14)$$

so,

$$B(S) = 2\ \frac{L^2}{S^2}\ B(0) \int_0^{\frac{S}{L}} \left(\frac{S}{L} - u\right) r_s(u)\ du \quad (15)$$

The plot of the interclass surfacic variance curve needs the knowledge of the fibres or filament yarns distribution function within the lap. As an example, figure 3 represents the theoretical interclass surfacic variance curve of a lap whose fibre distribution function is modelized by the combination of an isoprobable law and two sinusoidal laws.

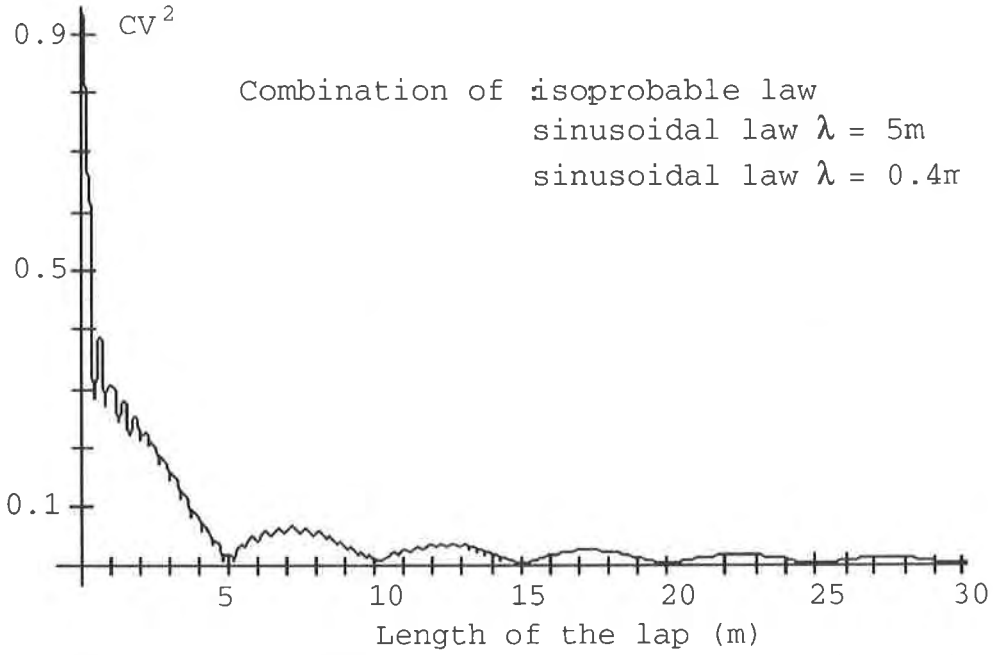

Figure 3 : Display of a theoretical interclass surfacic variance curve

NON-WOVEN TEXTILE TESTS

Experimental procedure. As previously shown, the use of statistical tools can allow some periodic defects to be highlighted, the main goal of this study being to validate this hypothesis in the case of non-woven textiles.

For the validation of the method, five samples have been tested. These samples came from different manufacturing and linking processes and were tested on 5, 10 and 15 meter length (16.4; 32.8;49.21feet) . This set of samples is composed of:

- -3 Heat-bonded
- -2 Needles

The avèrage of the mass per unit area ranges from 110 to 280 g/m^2

(0.36 to 0.91ounce/ft^2); the scanning steps set to 2.5mm (0.098 inch)(X axis), 5mm (0.19 inch)(Y axis) [80,000 points/m^2 (7432 points/ft^2)].

Each set of data, has been computed through the stastistical software tools, and the following table (table 1) was carried out.

Adjustment of an indutrial process. The purpose of this study is to use the specific measurement device to adjust industrial processes. This work takes place within the frame of a industrial/university collaboration. The two members were, on one hand Freudenberg SpunWeb S.A. for the industrial part, and on the other hand the Ecole Nationale des Industries textiles de Mulhouse through the Laboratoire de Physique et Mécanique Textile.

The device is used to display the non-uniformity of the fibre distribution while the lap is built up. In this kind of study, the main thing is not to know the exact mass per unit area of the lap but to obtain a qualitative information about the mass per unit area distribution.

Samples	Area density g/m^2	Max. value Vmax g/m^2	Min. value Vmin g/m^2	Average Vmoy g/m^2	Variance V(x)	Coeff. CV%	Standard deviation σ	β_1 Pearson	β_2 Pearson
A Heat bonded	110	272.0	66.3	114.4	611.3	21.6	24.7	0.31	3.71
B Heat bonded	180	320.1	94.2	164.4	313.5	10.5	17.2	0.42	3.82
C Heat bonded	180	301.6	83.5	175.8	435.2	11.8	20.8	0.25	3.71
AD350 needle punched	280	355.9	179.2	218.9	370.5	8.7	19.2	0.45	3.81
AD350.1 Needle punched	280	355.9	179.2	218.9	370.5	8.7	19.2	0.45	3.81

Table 1 : Statistical analysis of the sample

Based on these results, some specific calculations were developed; based on the tribology coefficient calculation the "skewness" [VIA-91]; to quantify the non-uniformity and the imbalance in the mass per unit area distribution.

Presentation of the "skewness coefficient";consider the curve in figure 4. To evaluate the skewness "S" criteria, the following formulae are used :

$$S = \frac{1}{N.\sigma^3} \sum_{i=1}^{N} g(X_i)^3 \qquad \text{with } g(X_i) = (X_i - \bar{X}) \tag{16}$$

Where :

σ = standard deviation;

σ^2 = variance.

$$\sigma = \sqrt{\frac{\sum g(X_i)^2}{N}} \qquad (17)$$

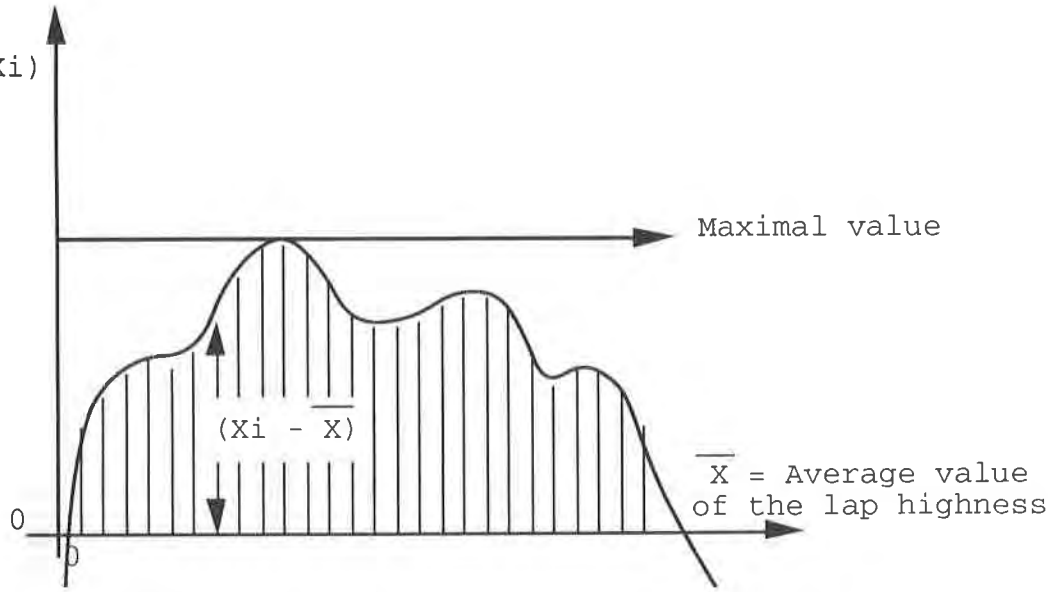

Figure 4 : Evaluation of the "S" criteria

Variation of the "S" criteria :
S >0 , more material over the average value line;
S >0 , more material under the average value line;
S = 0, total symetrical area

In fact; the S criteria expected is S >0 ; more material under the average value line then the distribition is more regular.

To carry out this study, the M.R.E. methods [PHA 83] were used to define the experience plan.

Experience plan setting. Thanks to specific MRE software used by our industrial partner we have obtained the following experience plan. It seems evident that for problems of industrial secret we won't give the name of the different components taken into account in this study, but we have defined them as P1, P2, etc…

The following experience matrix is obtained (figure 5):

	P4	P5	P6	P7		
	1	1	-1	1	I	
	-1	1	-1	1	II	
	1	-1	-1	1	III	
	-1	-1	-1	1	IV	
	1	1	1	1	V	Nf = 8
	-1	1	1	1	VI	
	1	-1	1	1	VII	
	-1	-1	1	1	VIII	
	$-\alpha$	0	0	0	IX	
	α	0	0	0	X	
	0	0	$-\alpha$	0	XI	
	0	0	α	0	XII	Na = 6 with α= 1.5 or 1
	0	0	0	$-\alpha$	XIII	
	0	0	0	α	XIV	
	0	0	0	0	No1	
	0	0	0	0	No2	No3 = 0
	0	0	0	0	No3	

P1	P2	P3		
1	1	1	I	
-1	1	1	II	
1	-1	1	III	
-1	-1	1	IV	
1	1	-1	V	Nf = 7
-1	1	-1	VI	
1	-1	-1	VII	
0	0	0	No1	
0	0	0	No2	No = 3
0	0	0	No3	

Figure 5 : The experience matrix

RESULTS ANALYSES

The different results obtained are shown taking the two parts of the study into account.

Highligting the periodic defects. For this analysis, we present two kinds of display, an iso-massic one for a overview of the lap, and the length variance curve for the analysis of the periodic defects.

Experimental control in the case of the length variance curve. Let us consider a L length lap part. Thanks to our measurmement device,80,000 points per m^2 are picked up; this collection can be schematized by figure 6

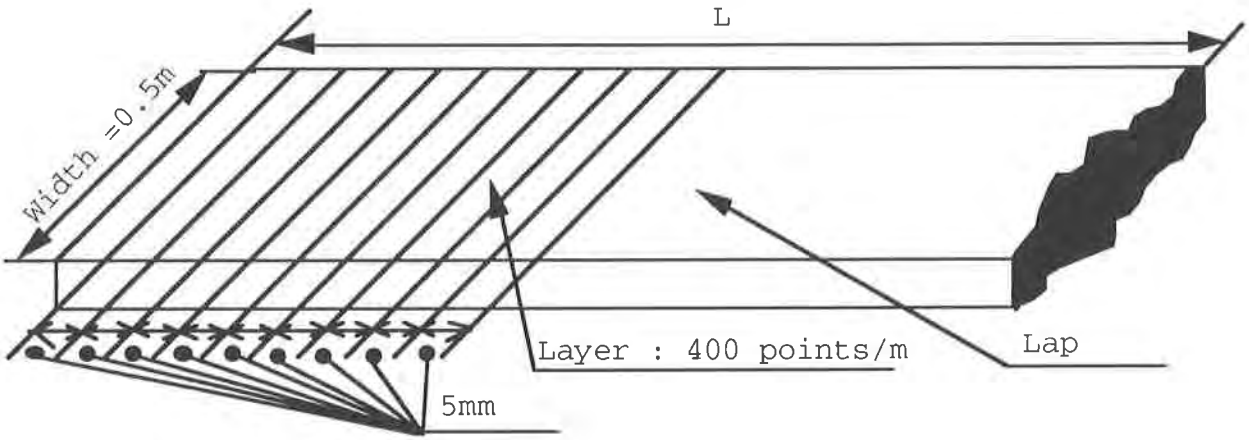

Figure 6 : Schematization of the calculation method

To obtain the curve B(l), the scanning length l will increase; first let's calculate the average value for each layer mi (individual

average), the lap will be displayed by a "vector" where each element is the mass par unit area average value of each 5mm mi layer.Then the total average can be calculated :

$$m_T = \sum_{i=1}^{N} \frac{m_i}{N} \qquad (18)$$

Where
N = Number of layer

Then, the measurement area will grow, associating the layer 2 by 2, 3 by 3, etc…

The obtained curves are presented in figure 7 to 10.

All the displays are not presented but only the most significant ones. Different non-woven textiles were analysed:

Figure 7 shows the obtained results for a needled non-woven textile, 280g/m^2 (0.91ounce/ft^2); carded; polypropylene; AD350; this analysis is done on a 5m length lap. The curve is first analysed. The curve is composed of a continous component and two major periodic components with respectively 0.24 (0.78ft)and 0.64m (2.09ft) wave-length; some other defects; with shorter wave-length can be carried out. These defects are very sharp and could derive from pulsatory defects (non-periodic ones). In a second stage these defects and the components of the manufacturing process tried to be linked. At this point of the study, only few hypotheses can be defined about the defect generation:

The short wave-length defects could be due to the needle frames and the needle action.

The medium and long wavelength defect could be generated by the card output roller or the flock transport.

Analysis of the iso-massic map. This sample being the heaviest one, it is impossible to clearly distiguish the low-zone and high-zone of mass per unit area. In fact only longitudinal stripes can be noticed due to the output rollers or the needles frame (hypothesis).

Figure 8 shows the obtained results for a heat-bonded non-woven textile, uncarded; needled; 180g/m^2 (0.589ounce/ft^2); polyesther; B; this analysis was performed on a 5m length lap. In this case, the defect [0.86m (2.82ft) wave-length] is difficult to highlight and may be due to the lack of card and could be due to the yarn-moving device or and the yarn generation device.

Analysis of the iso-massic map. Low and high mass area could be noticed; the mass per unit area distribution is unsymetrical; the right side presents a higher mass per unit area than the left side. A periodic defect clearly appears on this map; its wavelength is approximatly 0.80m (2.62ft) (highlight by the length variance curve). Due to the mass per unit area average; the difference between high and low mass per unit area is better than the previous display.

Figure 10 shows the obtained results for a heat-bonded non-woven textile, uncarded; needled; 180g/m^2 (0.589ounce/ft^2); polyesther; C; this analysis was performed on a 5m length lap. In this case the defect [0.92m (3.018ft) wavelength] that has been found seems to be a sinusoidal one, in fact the slopes are sharper than previous examples and the harmonic less visible. The defect could be due to a problem of yarn driving or an imbalance of the moving roller.

Analysis of the iso-massic map. The low mass per unit area zone appears as a net on the lap. The distribution of the mass per unit area

is still asymetrical; but the stastistic results (Table 1) give a quasi-normal mass per unit area distribution.

In the case of this sample, the length variance curve is drawn for 5, 10, 15m scanning length (figue 10, 11, 12). Some differences can be noticed between them; as expected, when the scanning length grows, the wavelength of the defect that can be detected, grows too. This is a well known aspect of the data treatment (Shannon law). Then the longer the lap, the longer the wavelength of the detected defect will be. In fact, a few more periodic defects could be highlighted thanks to the other curves (except for the harmonic point).

Figure 9 shows the obtained results for a heat-bonded non-woven textile, uncarded; needled; 110g/m^2 (0.36ounce/ft^2); polyesther; A; this analysis was done on a 5m length lap. Periodic defects with a greater wave-length than previously [0.72m (2.36ft)] are remarked and the width of the harmonics are lower than previously. This defect (0.72m) could (hypothesis) be due to a lack in the drawing and projecting yarn devices. The hypothesis for the short wave-length defect is still true.

Analysis of the iso-massic map. It is the lighter sample; the difference between high and low mass per unit area is very clear, the mass per unit area distribution on the width of this sample is totally unsymetrical; the right side seems to present a mass per unit area higher than the left side; this defect could be due to the yarn distribution device.

Adjustment of an industrial process. The plan of experience was followed and the main results obtained are the following: the presented displays are the most significant, in terms of mass per unit area distribution. In fact we pulled out one of the parameter as the essential one for the lapping process; and we present the evolution of the mass per unit area distribution in relation to the parameter evolution. Two kinds of display are used, one is the "well known" iso-massic display, the other presents the profile of the lap (in fact the average value of the mass per unit area for each measurement point). The skewness can be calculated thanks to the $g(x_i)$ curve. Figures 13 to 16 show the different displays and some conclusions can be carried out after the interpretation of these curves; in fact we can notice that the parameter P1 has a real influence on the mass per unit distribution. In a practical point of view, the use of our device allows the engineers to visualize and quantify the non-homogeneity of the mass per unit distribution and then to optimize the process driven by the experience plan.

CONCLUSION

Each of the different results that has been found and presented in these studies embodies the beginning of a new study.

For highlighting the periodic defects, a systematic analysis of the mass per unit area distribution due to the deviation of process parameters is started and we expect to get some new results soon. In this way we want to achieve a catalogue of defects and of the produced effects on the mass per unit area distribution and vice-versa to facilitate the adjustment of the process and the defect detection and correction alike; and later on an on-line regulation of the mass per

unit area distribution all over the lap.
For the adjustment of industial process this study was a punctual one but it meets again the first topic, some other behaviour studies being expected in relation to our industrial partner.

ACKNOWLEDGEMENTS

This study was made possible thanks to the firm Feudenberg SpunWeb S.A.

REFERENCES

ADOLPHE, D.C., DREAN, J.Y., SIGLI, D., (1990) "Laser beam used in mass per unit area measurement", Experimental Techniques, March/April 1990, pp.48-50.

ADOLPHE, D.C., (1990) "Contribution à l'étude de certaines propriétés physiques et hydrauliques de géotextiles", Thèse de Docteur en "Sciences pour l'Ingénieur", Université de Haute-Alsace, Mulhouse.

BRENY, H., (1957) "Elément d'une théorie statistique des faisceaux de fibres parrallèles", Annalles Scientifiques Textile Belges, Décembre 1957.

BRENY, H., (1958) "Elément d'une théorie statistique des faisceaux de fibres parrallèles", Annalles Scientifiques Textile Belges, Mars 1957.

MARTINDALE, J.G., (1945) "A new method of measuring the irregularity of yarn with some observations on the origin of irregularities", Journal of Textile Institute.

PHAN TAN, LUU, R.,FENEUILLE, D.,MATHIEU,D., (1983) "Methodologie de la recherche experimentale -Etude des surfaces de réponse -Introduction -Outils mathématiques", Laboratoire de prospective réactionnelle et d'analyse de l'information.

VIALLIER-REYNARD, P.,(1991) "Cours de tribologie de D.E.A.", Ecole Nationale Supérieure des Industries Textiles de Mulhouse, Université de Haute-Alsace, Mulhouse.

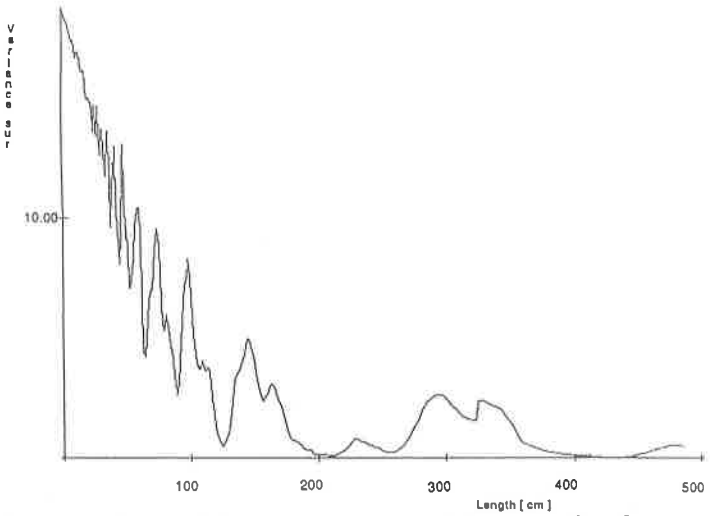

Figure 7 : Experimental B(l) curve; needlepunched non-woven textile - AD350 - 280g/m^2 PP

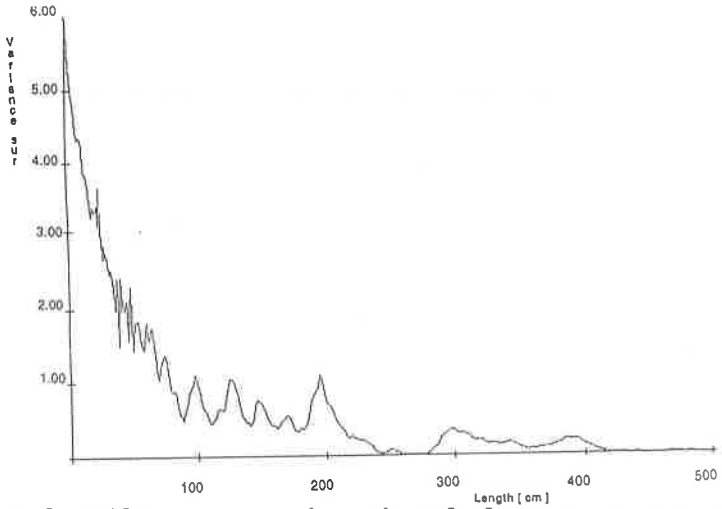

Figure 8 : Experimental B(l) curve; heatbonded non-woven textile - B - 180g/m^2 PETP

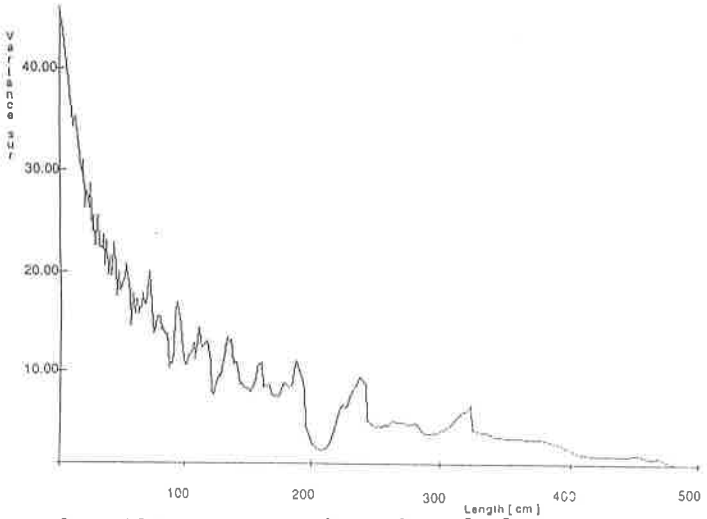

Figure 9 : Experimental B(l) curve; heatbonded non-woven textile - A - 110g/m^2 PETP

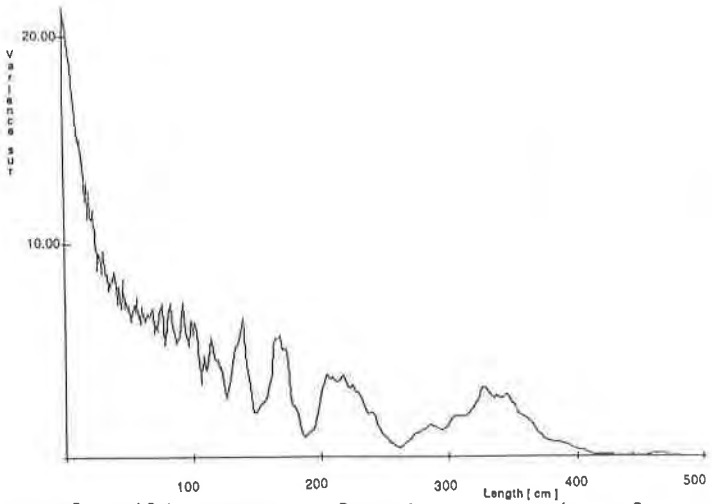

Figure 10 : Experimental B(l) curves for 5m scanning length; heatbonded geotextile - C - 180g/m^2 PETP.

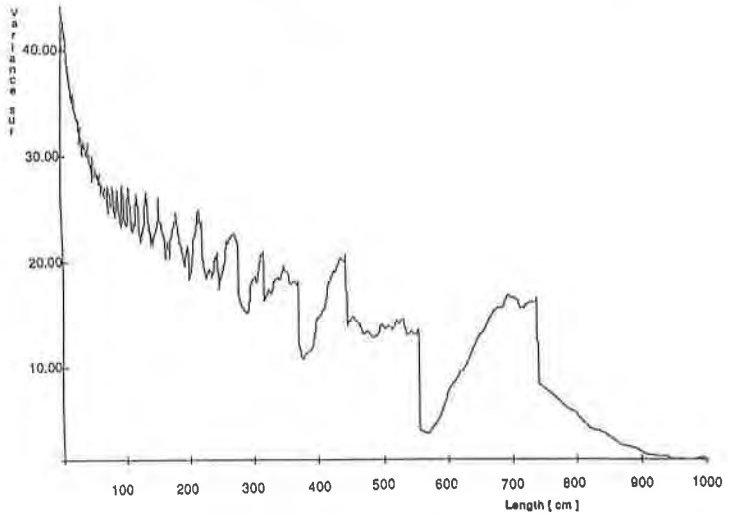

Figure 11 : Experimental B(l) curves for 10m scanning length; heatbonded geotextile - C - 180g/m^2 PETP.

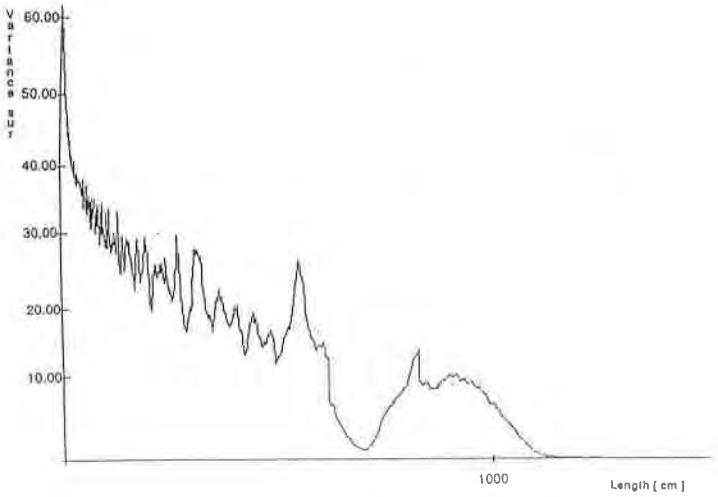

Figure 12 : Experimental B(l) curves for 15m scanning length; heatbonded geotextile - C - 180g/m^2 PETP.

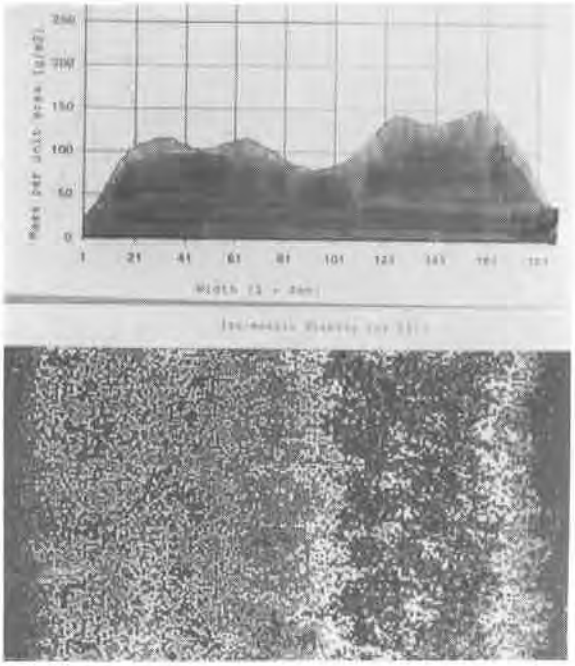

Figure 13 : Evolution of the mass per unit area distribution (Profile and iso-massic display)in relation to the parameter evolution P1 = P1.1

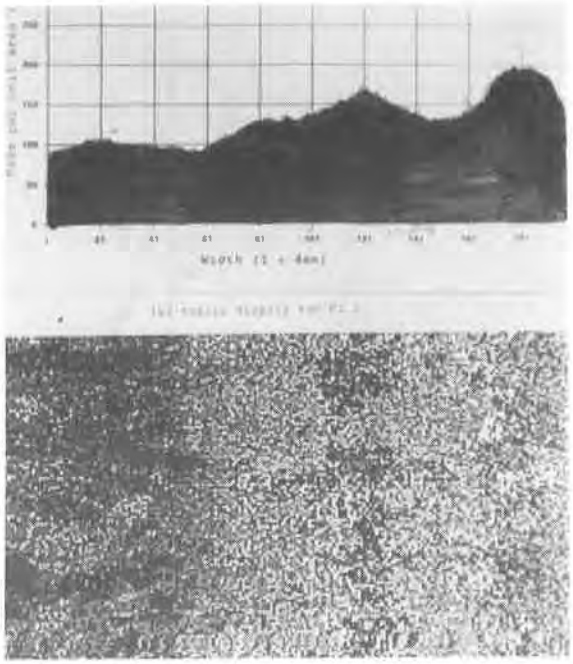

Figure 14 : Evolution of the mass per unit area distribution (Profile and iso-massic display)in relation to the parameter evolution P1 = P1.2

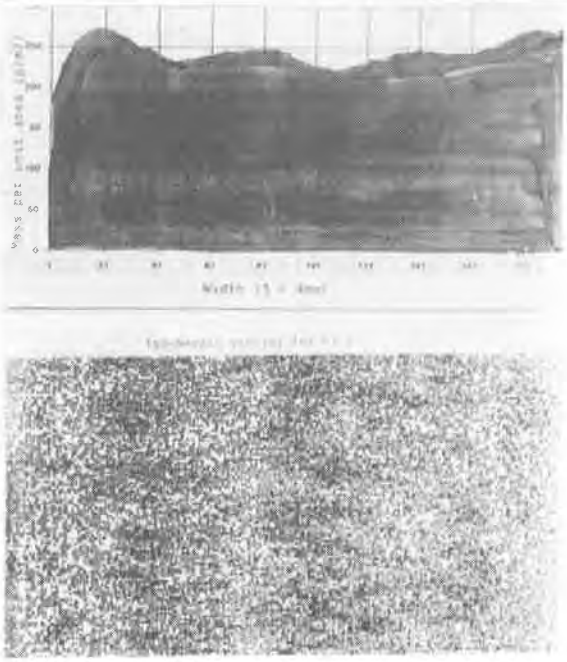

Figure 15 : Evolution of the mass per unit area distribution (Profile and iso-massic display)in relation to the parameter evolution P1 = P1.3

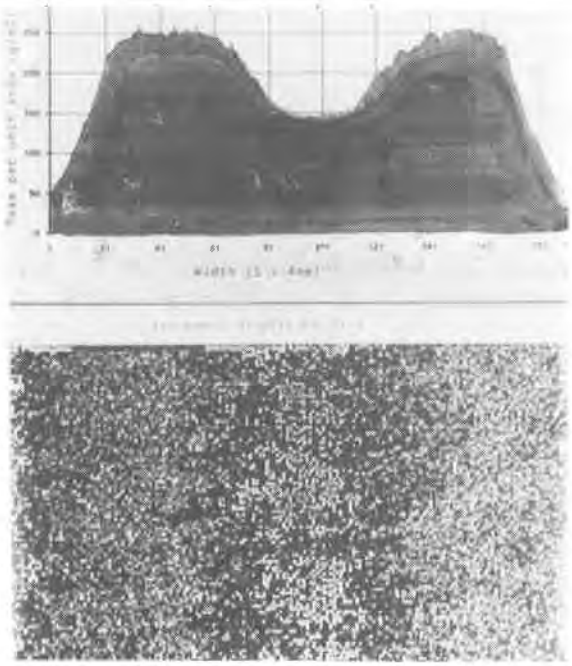

Figure 16 : Evolution of the mass per unit area distribution (Profile and iso-massic display)in relation to the parameter evolution P1 = P1.4

The Use of Multi-Axial Burst Test to Assess the Performance of Geomembranes

J. Nobert
Poly-America Inc., USA

ABSTRACT

Many of the tests used to specify geomembranes do not reflect field performance. One test that can be used by the design engineer to evaluate a liner's performance is the multi-axial burst test. In this test a force is applied perpendicular to the geomembrane liner. This subjects the liner to bi-axial stresses which can then be measured and converted to stress-strain diagrams.

To make the information from this test more realistic and useful, geomembrane liners were subjected to various conditions of temperature, strain rate, and chemical environments. Results show that the liner's performance in the multi-axial burst test may mimic responses of the standard index tensile tests. Also, evaluations were done on various geosynthetic systems. In these tests it was found that geotextiles can greatly improve the performance of the liner, whereas the addition of drainage nets had little effect.

INTRODUCTION

Many of the tests used to specify geomembranes fail to evaluate the true performance of the liner. These tests serve only as index tests and only evaluate the relative performance for a given class of liner. For example, when tensile testing HDPE geomembranes, the liners are required to pass 750% elongation before failure. Under real world conditions, failures have occurred with little or no elongation. Likewise, materials such as PVC, which are elastic and appear to be puncture resistant when tested at room temperature, can fail at relatively mild temperatures of 0°F. Although these index tests do not always evaluate the liner's true performance, they are not without value. As quality control guidelines, they assist in assuring that the product is uniform and is of high quality. These tests are not intended to be used for design criteria.

A better way to obtain more realistic data on geomembrane performance is to test the liners in a hydrostatic pressure vessel. This relatively large scale testing device is valuable in evaluating the performance of liners in contact with various subgrades. With this test, the subgrade of interest is spread across a 7.5 cm deep by 45 cm (or larger) diameter pan which is placed inside the test chamber. A geomembrane is then placed on top of the subgrade and held in place along the edges of the pressure vessel. As pressure is increased on the liner, the liner will attempt to conform to the subgrade. If the liner is not sufficiently durable, small holes develop. Pressure will then be lost and the liner fails the test. This method is particularly useful for evaluating liners intended for mining applications where sharp, angular rocks are found in the subgrade, or on top of the liner, as in the case of leach pads.

Another manner in which the hydrostatic pressure vessel can be used is the multi-axial burst test. This test attempts to simulate a subsidence (void) in the subgrade below the liner. Such voids are problematic in landfill caps, but may also occur in clay subgrades if the clay is dry and cracked. In this test the liner sample spans the diameter of the pressure vessel. There is no subgrade or other support beneath the liner. As pressure increases, the liner deforms. The amount of out-of-plane deflection vs pressure is recorded. This raw data is transformed into stress-strain curves through a series of geometric formulas as prescribed by Beyer (1987).

Results based on these tests are more realistic and therefore more valuable for design considerations, compared to the standard tensile tests (ASTM D 638) for the following reasons:

1. Force is applied perpendicular to the sheet simulating actual field conditions.
2. The sheet is responding to bi-axial stress instead of uni-axially.
3. Material defects and flaws are more likely to be found since 100 times more surface area is being tested compared to the typical tensile tests.

The study of geomembranes based on test equipment that recreates these real-world conditions gives the engineer great advantage when designing a geosynthetic lining system.

SCOPE

Over 140 tests were conducted to evaluate numerous variables. Although the information provided has been compiled from testing conducted under controlled conditions, variability in this data has not been fully studied or understood. The major objective of this study was to gain insight into some of the problems that may confront engineers when they design with geomembranes.

The variables examined with this data are as follows:

Testing Variation	Rate of Strain
Effect of Temperature	Textured vs Smooth HDPE
Effect of Thickness	Effect of Seams
Effect of Chemicals	Geosynthetic Systems
Comparison of Liners	Cyclic Stress

Although various types of liners were evaluated during this study, the majority of testing was conducted on HDPE since it was readily available, and most of all, it could be tested to failure in the apparatus.

PROCEDURE

A schematic of the hydrostatic tester is shown in Figure 1. The internal diameter is 48 cm across with a depth of 23 cm. The applied pressure in the top section is controlled by an air pressure regulator. Deflection is measured by a rod which protrudes up through the bottom half of the vessel and contacts the liner at the very center of the sample. Viewing ports around the top of the apparatus allow the sample to be observed during the test.

To run the test at other than ambient conditions, tempered water (or other liquids) are brought into direct contact with the liner. Pressure is still controlled by the air regulator on top of the hydrostatic tester (air over water).

The controlled pressure increase at increments of 6.9 KPa/min. (1 psi/min.) allows accurate measurements and will keep the duration of most tests to within 1/2 hour. A more rapid rate of pressure increase does not permit the liner to reach steady state, thus the deflection indicator is constantly moving and prevents accurate measurements from being made. When rupture occurs a loud noise is heard and air rushes through the hole in the liner.

CALCULATIONS

The pressure-deflection values yield information on the out-of-plane performance of the liner, but do not indicate the in-plane stress-strain relationships that are occurring. In calculating these relationships it is assumed that the tested geomembrane shall deform spherically to the point where the amount of deflection equals the radius of the pressure vessel. The apparatus used for this study is designed so that the maximum deflection cannot exceed the radius of the vessel.

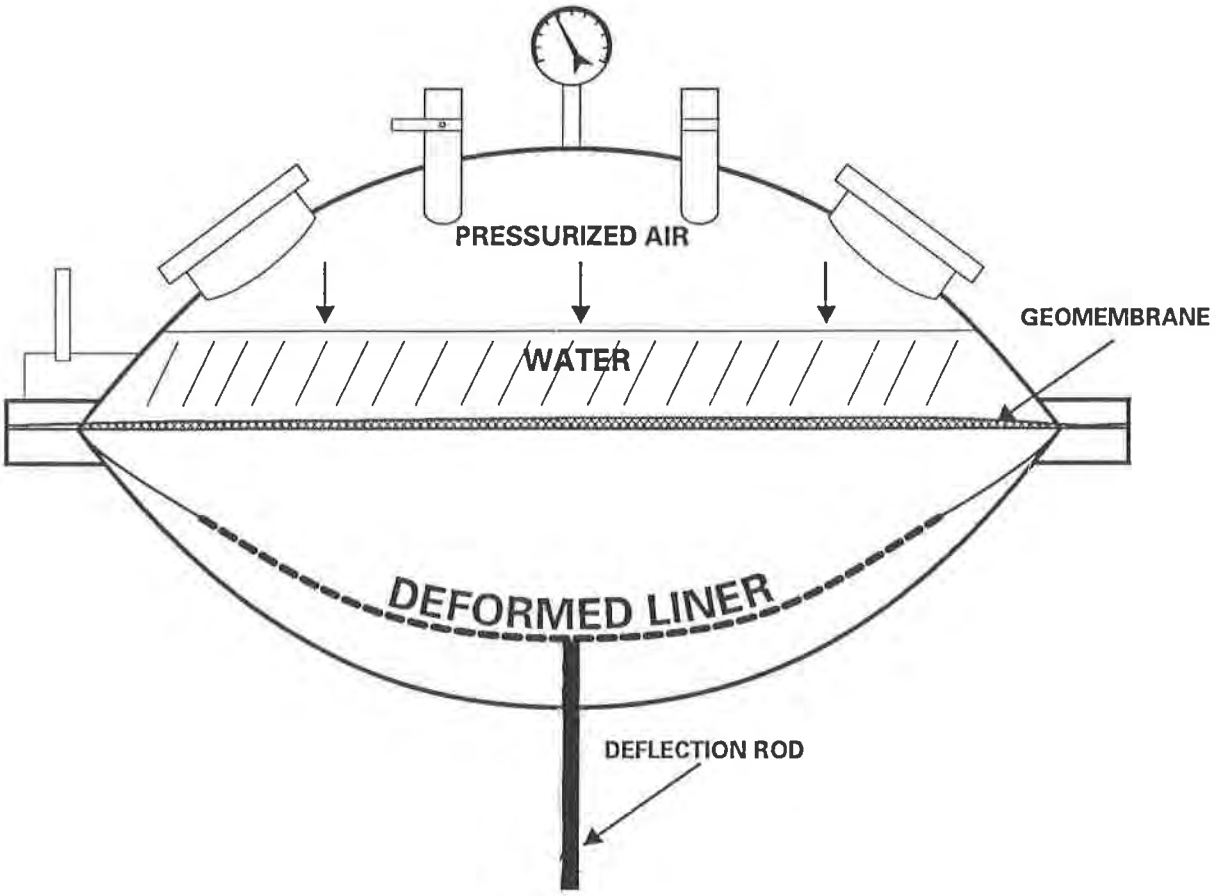

FIGURE 1
HYDROSTATIC PRESSURE TEST VESSEL

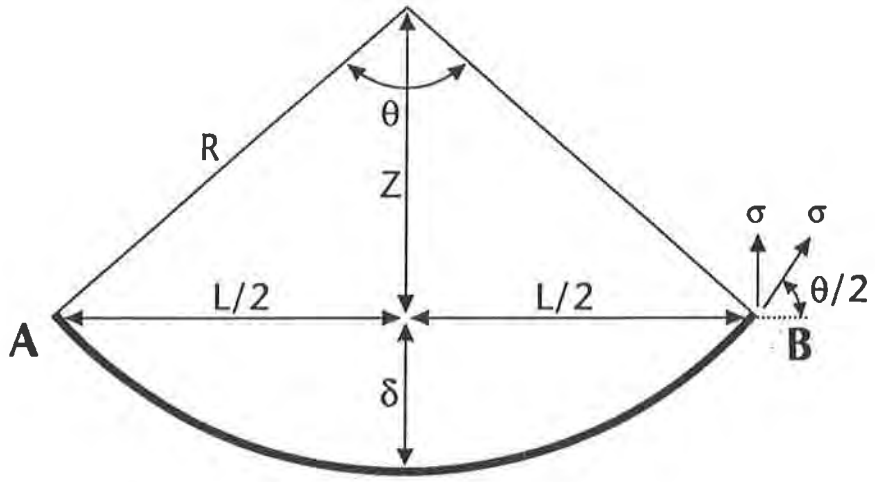

FIGURE 2

To calculate the stress-strain values, refer to Figure 2 and the following equations:

STRESS

$$\sigma = \frac{Lp}{4t*\sin(\phi/2)}$$

STRAIN

$$\epsilon = \frac{\text{arc AB}-L}{L} \cdot 100$$

A more detailed progression of these mathematical expressions can be found in GRI's GM 4 test method.

DISCUSSION

Test Variability (Figure 3). The first variable to be investigated is the ability to reproduce results. Figure 3 shows the results of five different tests on 1.5 mm (60 mil) HDPE sheet. These tests were conducted over a period of nine months. The results represent not only the variability of the test, but also reflect some product variation. Although some variation in results is indicated, all follow the same general curve.

Overlaid on this graph is a tensile curve per ASTM D 638. This curve, up to the yield point, is similar to the curve generated by the multi-axial burst test (this curve may also vary to a significant degree). In the tensile test, specimens continue to elongate past the yield point and become thinner (cold draw) across the entire test area. After this occurs, stress builds on the polymer chains (strain harden) until the specimen ruptures.

In the multi-axial burst test, after the yield point has been reached, a "fish eye" in the machine direction (MD) forms at the weakest point (usually the thinnest spot). With little or no pressure increase, this "fish eye" lengthens, but only in the machine direction due to the anisotropic nature of the sheet. Simultaneously, the material within the "fish eye" elongates and thins as in the tensile test. At some point, this thin section can no longer withstand the pressure exerted on it, and ruptures. It is likely that within this "fish eye" region the cold draw and strain hardening effect occurs in the same fashion as in the tensile test.

This test demonstrates that real-world performance of an HDPE liner will depend on a design criterion based on yield stress as opposed to break stress and ultimate elongation.

Figure 3. Multi—axial Burst

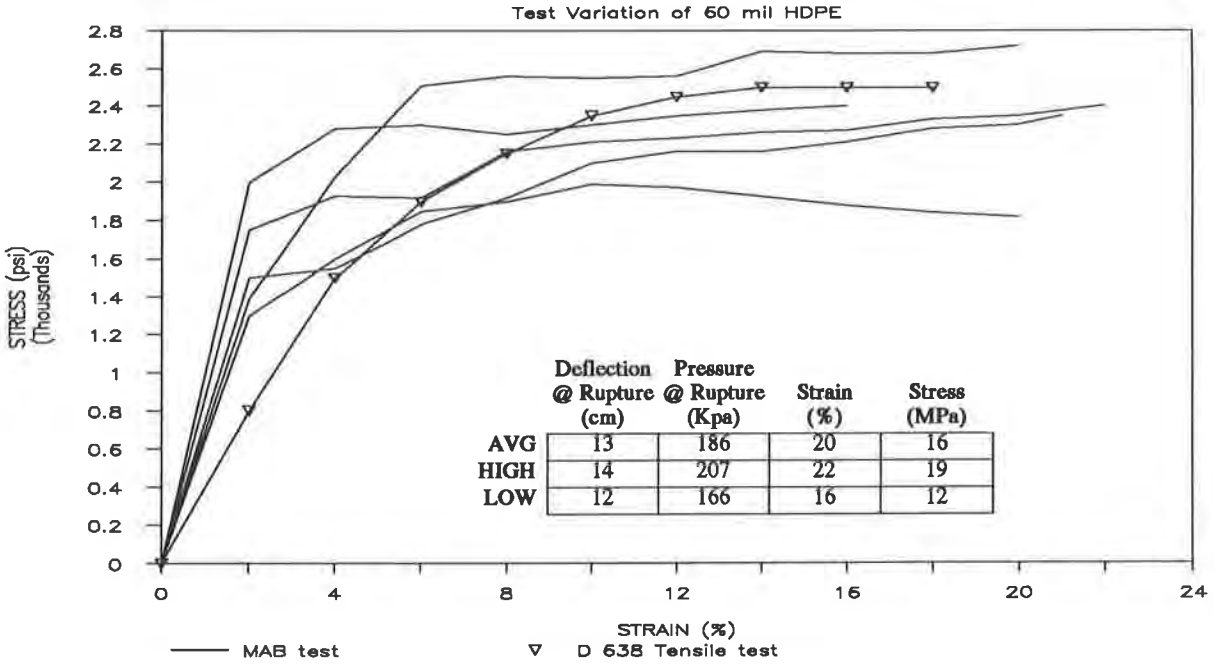

	Deflection @ Rupture (cm)	Pressure @ Rupture (Kpa)	Strain (%)	Stress (MPa)
AVG	13	186	20	16
HIGH	14	207	22	19
LOW	12	166	16	12

Figure 4. Multi—axial Burst

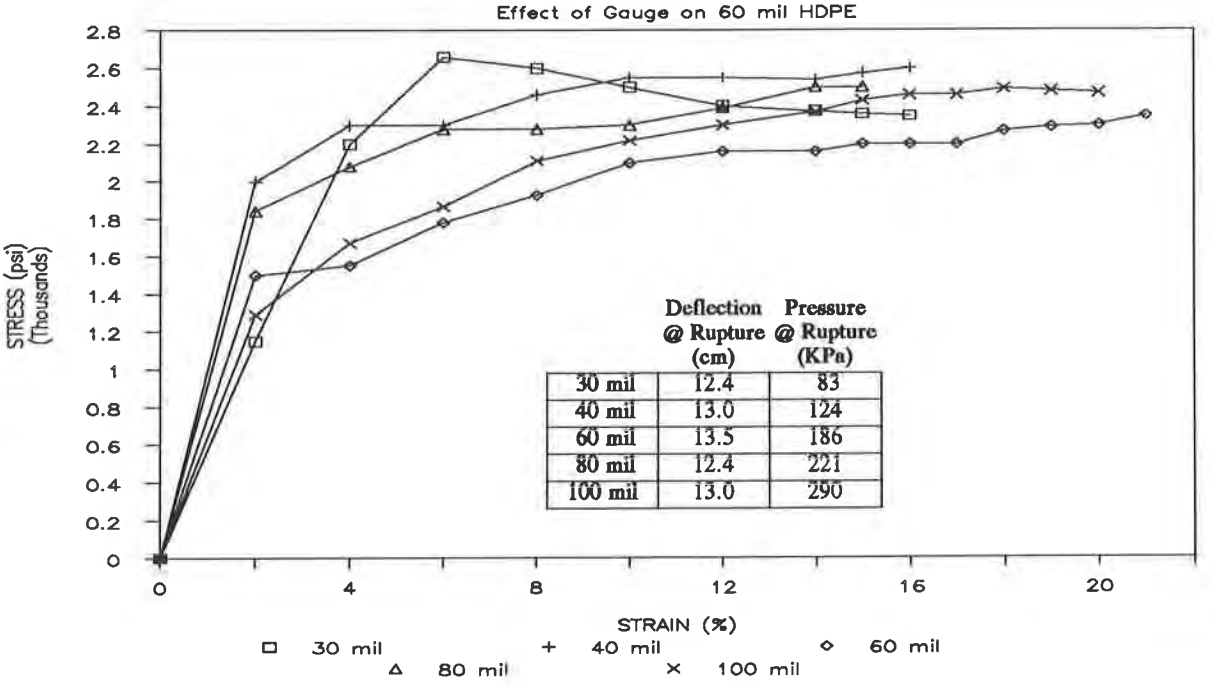

	Deflection @ Rupture (cm)	Pressure @ Rupture (KPa)
30 mil	12.4	83
40 mil	13.0	124
60 mil	13.5	186
80 mil	12.4	221
100 mil	13.0	290

1000 psi = 6.9 MPa

40 mil = 1 mm

Response to Changes in Gauge of HDPE (Figure 4). This Figure represents the effect of thickness (or gauge) on the performance of HDPE liners. No trend is indicated based on this data. This is what is expected based on results from ASTM D 638 tensile testing when values are normalized for gauge (psi).

Reviewing the pressure vs deflection values, the deflection values at rupture remain fairly constant with gauge, but increased air pressure is required to cause rupture as gauge increases.

Effect of Temperature on HDPE (Figure 5). Since liners are exposed to a range of temperatures and most data concerning liner performance comes from tests conducted at room temperature, it was appropriate to investigate liner response to a realistic set of temperature conditions. Tests were conducted between -25°C (-13°F) and 65°C (149°F). These are considered the "normal" extremes of temperature that a liner will be subjected to. This range also represents the limits of what can be achieved by the testing equipment.

Between 0°C and 50°C, elongation was found to remain fairly constant. Above 50°C, the liner appeared to undergo a change and started to behave as if it did not have a yield point. At 65°C, elongation doubled and the liner still did not rupture (DNR). Also at 65°C, it was expected that the stress value would drop significantly. The data does show some decrease but still remains much higher than anticipated. Other types of confirmation tests need to be conducted, but this data suggests HDPE may be capable of being used at higher temperatures than currently recommended!

Below room temperature, stress values for HDPE increased, and at temperatures below 0°C, strain values began to decrease. At -25°C, a rupture of 13% indicated that the polymer chains were becoming much less mobile and ductile. This also suggests that specifications based on ASTM D 746 low temperature impact may inadequately reflect minimum use temperature.

Effect of Temperature on VLDPE (Figure 6). The effect of temperature on VLDPE using this hydrostatic tester is not fully known because the unit is not deep enough to allow VLDPE to elongate beyond its rupture point (49% strain the liner bottoms out in the vessel). Even at -25°C, VLDPE still elongated 47%. Like HDPE as temperature decreases, break strength increases. Therefore, if chemical resistance is not critical, and when low temperature is expected, VLDPE may be the material of choice.

Effect of Temperature on PVC (Figure 7). PVC, like VLDPE, elongated beyond the capacity of the testing unit. Also like VLDPE, stress values increased considerably and strain values decreased slightly as temperature decreased to -20°C. This is where the comparison ends. With only slightly lower temperatures PVC quickly changed character. At -25°C, PVC ceased exhibiting its elastic properties and turned glassy and brittle. Elongation values at failure decreased from over 40% down to just 12% when the sample catastrophically failed, shattering like glass.

Figure 5. Multi–axial Burst

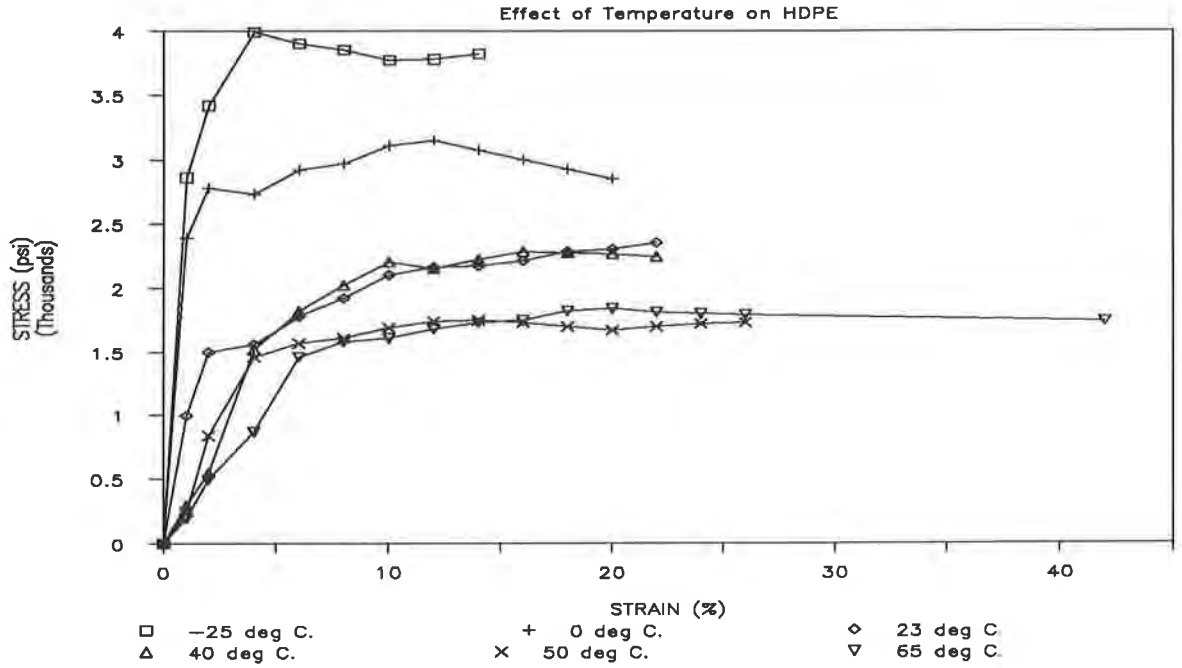

Figure 6. Multi–axial Burst

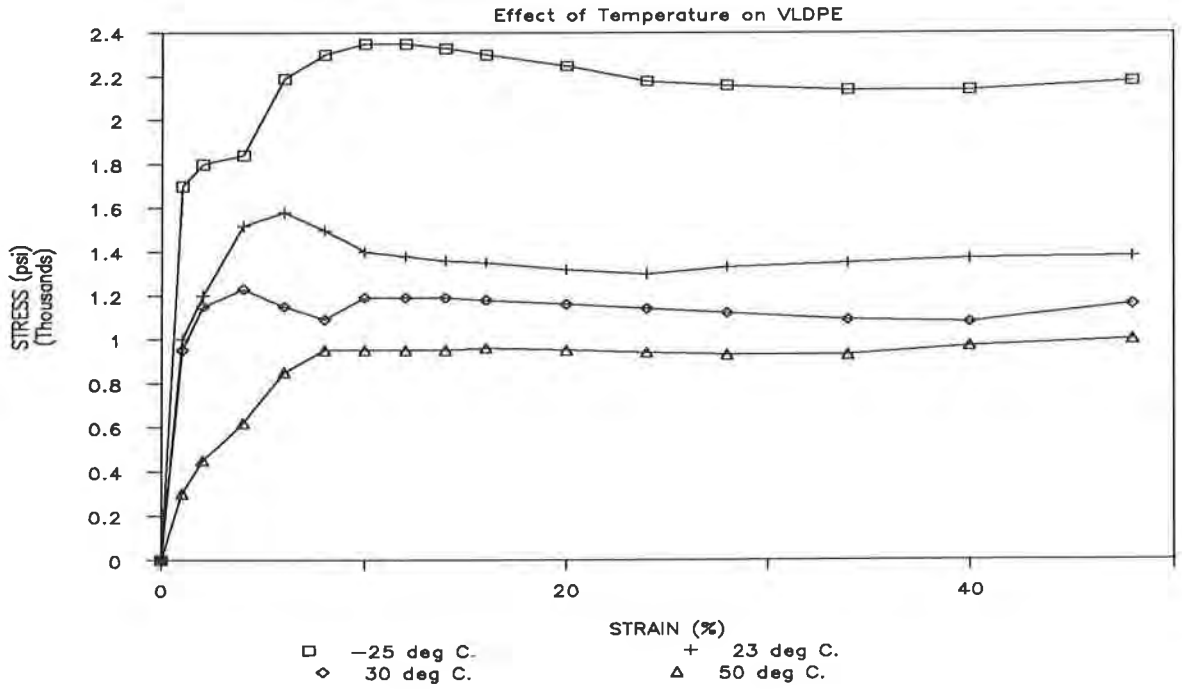

1000 psi = 6.9 MPa

Figure 7. Multi—axial Burst

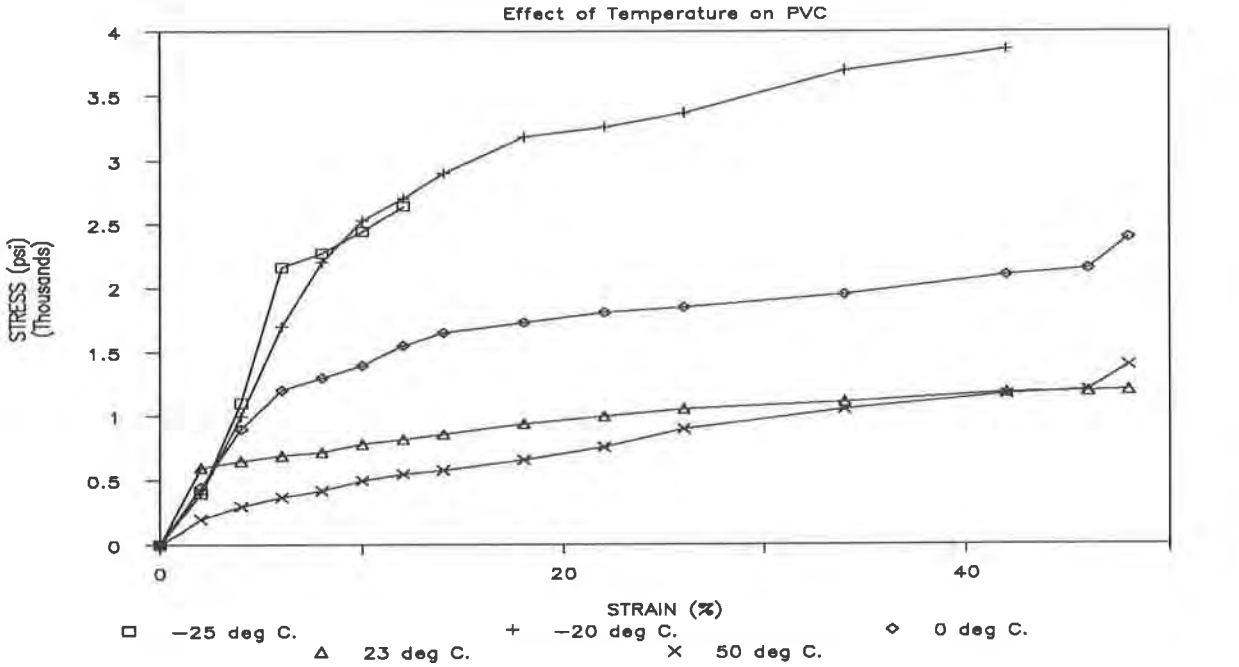

Figure 8. Multi—axial Burst

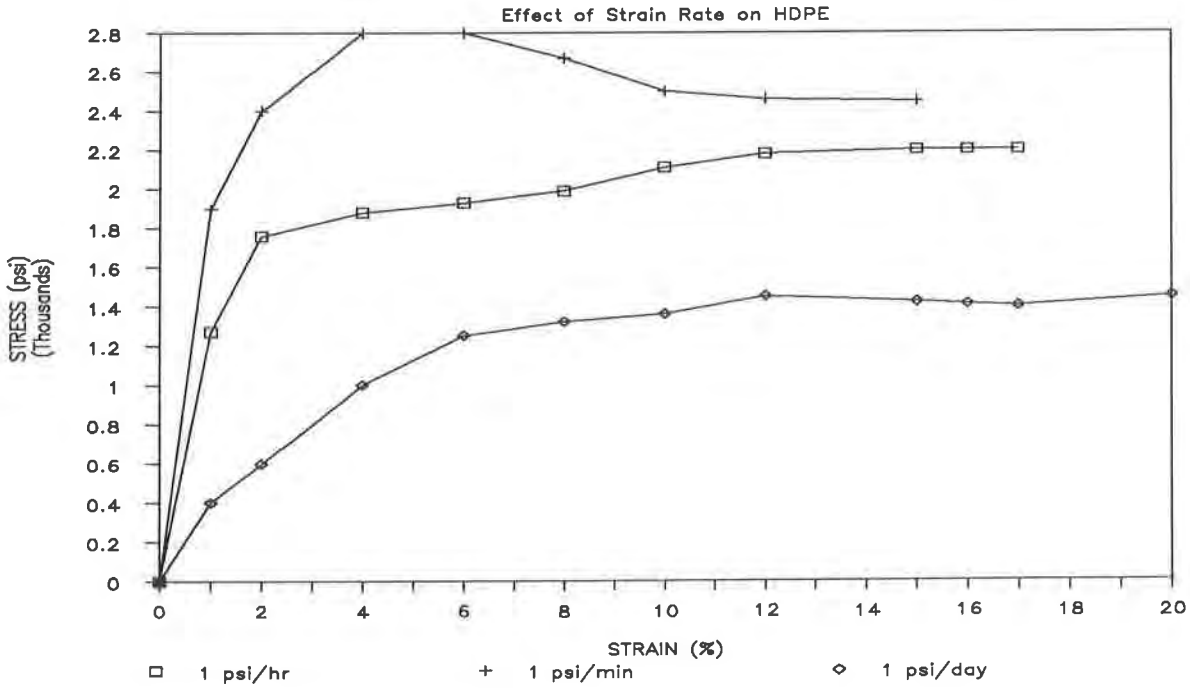

1000 psi = 6.9 MPa

Effect of Strain Rate (Figure 8). During most of this study 6.9 KPa/min. (1 psi/min.) increments were used because they enable brief and accurate testing. It was assumed that a slower rate would enhance results. To prove this, tests were conducted with pressure rates of 6.9 KPa/hr. (1 psi/hr) and 6.9 KPa/day (1 psi/day). The results in Figure 8 show the difference between these rates. At the slower rates the liner behaved more elastically, exhibiting lower moduli. However, it does not exhibit significantly increased elongation, as expected, from an elastic material. This may be due to the fact that the stress being applied has a longer time to act upon a flaw and cause failure, or it may be the stress forces, over a longer period of time. This caused the polymer chains to untangle, thereby resulting in decreased performance. In either case, this phenomenon needs to be explored and quantified further.

Comparison of Geomembrane Liners (Figure 9). Figure 9 shows how various types of liners perform in the multi-axial burst test. As previously stated, VLDPE and PVC cannot be tested to failure in a multi-axial burst test, therefore, comparisons with HDPE and CSPE are misleading. Also included is a new polyolefin copolymer which is being promoted for use as a flexible membrane liner. It too could not be tested to failure.

CSPE quite naturally gave the highest stress values due to the scrim reinforcement. Elongation was similar to HDPE. When rupture did occur, the liner tore in many pieces as opposed to HDPE where only a small hole would develop. Of the elastic materials, VLDPE was shown to have the highest resistance to deformation at any given pressure. For landfill caps it is desirable to combine properties of strength and elasticity so that the liner's integrity is not breached, even in the presence of large subsidences.

Textured vs Smooth HDPE Sheet (Figure 10). It can be misleading to evaluate a liner's performance by relying on results from index tests such as ASTM D 638. This is particularly true when comparing HDPE textured and smooth sheet.

In some processes, the textured layers and core layer are co-extruded and act as a single material. In other processes the textured surface is sprayed on.

Table 1. Tensile Properties (D 638) of HDPE Sheet

	SMOOTH	CO-EXTRUDED TEXTURED	SPRAYED TEXTURED
Yield MPa (psi)	17 (2500)	17 (2500)	17 (2500)
Elong. @ Yield (%)	18	18	18
Break MPa (psi)	31 (4500)	10 (1500)	21 (3000)
Elong. @ Break (%)	800	100	600

Figure 9. Multi—axial Burst

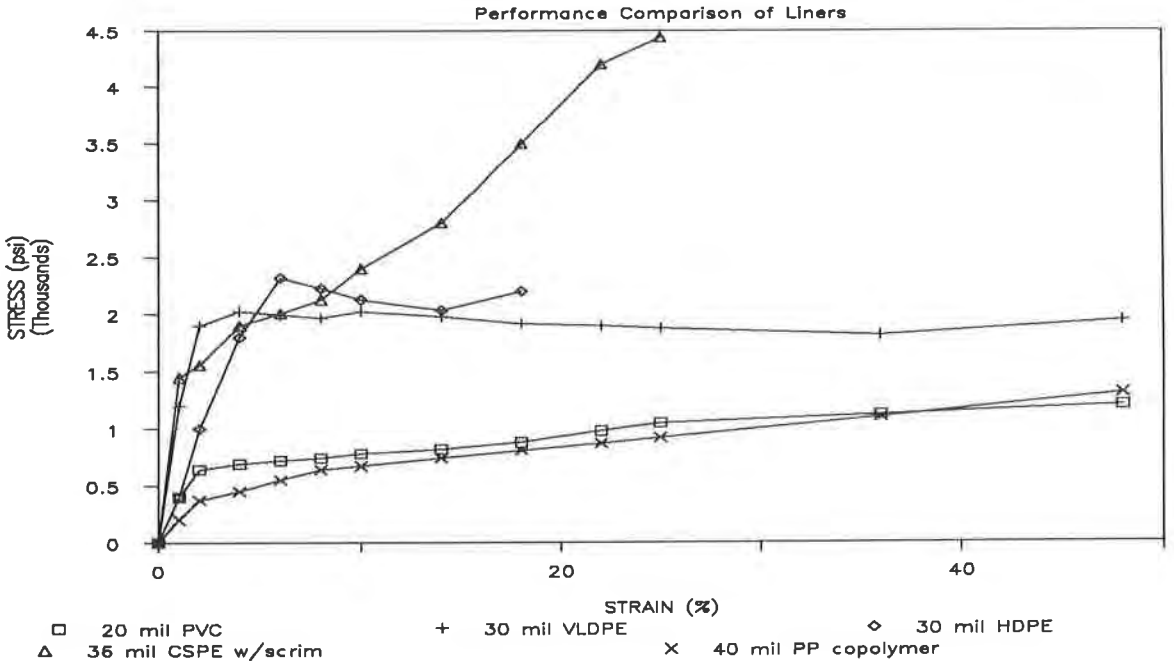

Figure 10. Multi—axial Burst

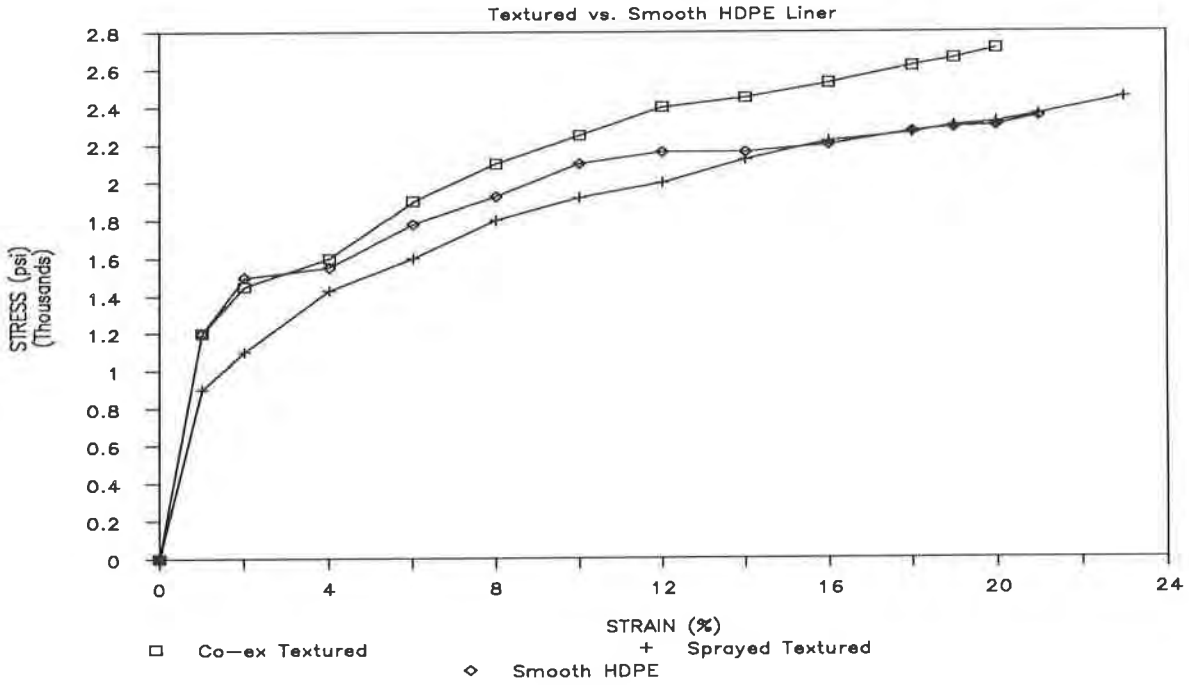

1000 psi = 6.9 MPa

40 mil = 1 mm

In the coextrusion process the textured layers and core layer act in unison as evidenced by the lower tensile elongation values in ASTM D 638 testing (see Table 1). These lower values are expected because of nonuniformity of the surface, which results in stress focal points being developed after the material is well beyond its yield point. With either process, the performance, as demonstrated by the multi-axial burst test (Figure 10), is the same and is also similar to the smooth sheet. Tensile break and elongation numbers are irrelevant for design. Note that because the true core thickness in textured sheet is hard to measure, the normalized stress values for these curves could vary slightly depending on the average gauge used for the thickness of the sample. Hence, the curves in Figure 10 may more closely resemble each other if an accurate means of gauging the entire textured sheet was found and used for these stress calculations.

Comparison of Seams (Figure 11). The possibility that the seam is the weak point in a liner is a commonly raised concern. Multi-axial burst testing reveals that a properly welded seam is not the weak point in a liner. It appears that the seam area, which is twice as thick as the rest of the liner, acts as a reinforcement bar and makes the sheet stronger. Failures in these tests occurred away from the welded area.

On the other hand, an improperly welded seam or a liner with excessive overgrinding in the seamed area can cause premature failure in the multi-axial burst test, when compared to the base material. This problem of premature failure has only been experienced in samples with extrusion welds. In Figure 11, the curve of the "poor extrusion weld" shows that the strain value is only 2/3 of the parent sheet, even though the stress values exceed the value of the sheet.

Although the sample size is too large for quality control testing, the multi-axial burst test demonstrates that it can be an effective tool in seam evaluations.

Reinforcement Effect of Drainage Net (Figure 12). Another problem confronting engineers is a means to evaluate geosynthetic systems. Figure 12 shows the effect of a drainage net under a 1.5 mm (60 mil) HDPE liner. Although the drainage net seemed to stiffen the liner initially, failure occurred at the same point as with the liner alone. Viewing the failed sample, it appeared that the net gave way first, thereby increasing the stress on the liner, which in turn failed immediately. However, this testing only represents one grade of net (foamed polyethylene with a juncture thickness of 0.5 cm) and results could vary with different nets.

Reinforcement Effect of Geotextiles (Figure 13). Geotextiles are designed for filtration or they act as a cushion when used in combination with geomembranes. Cushioning the liner against such items as sharp rocks is particularly important in the mining industry where liners serve as leach pads. They also act to reinforce the liner. To quantify this effect, testing was done with .23 kg and .45 kg (8 and 16 oz.) needlepunch polypropylene beneath 1 mm and 2 mm (40 and 80 mil) HDPE.

Figure 11. Multi—axial Burst

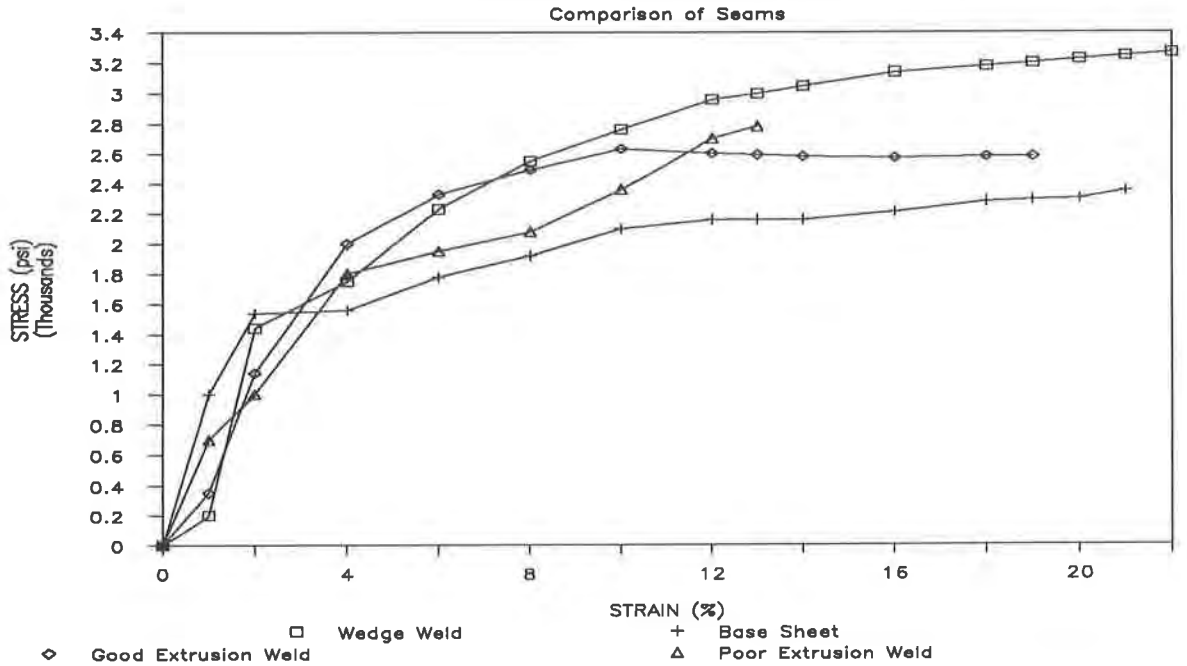

Figure 12. Multi—axial Burst

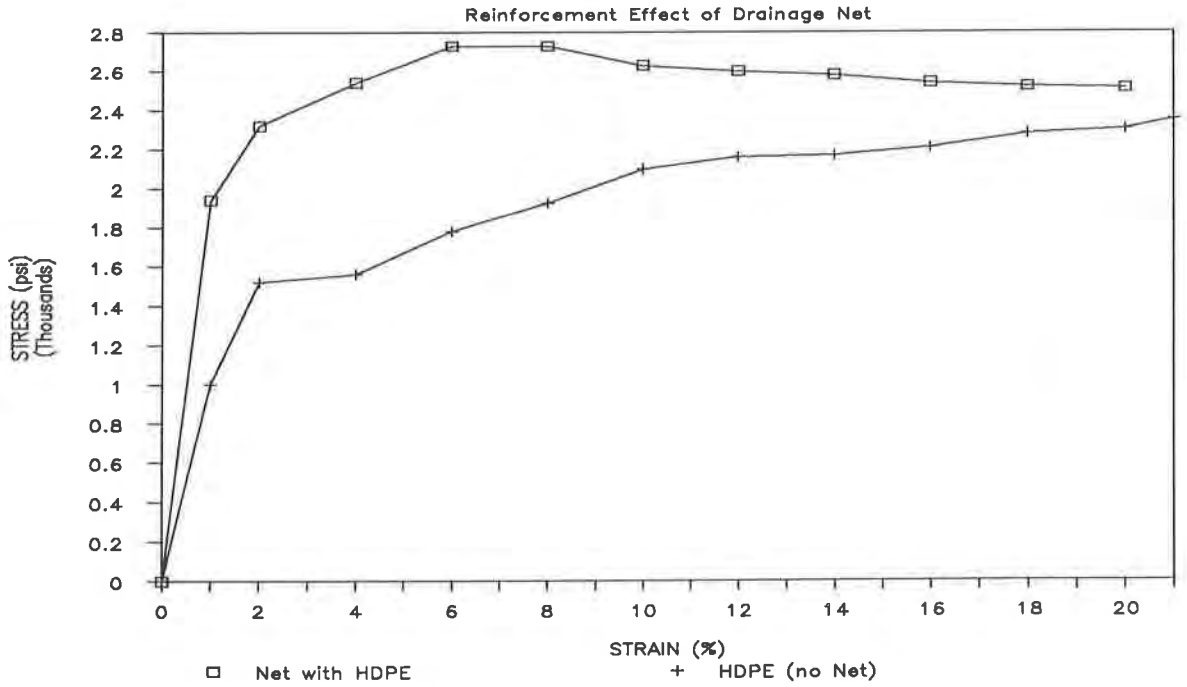

1000 psi = 6.9 MPa

Figure 13. Multi—axial Burst

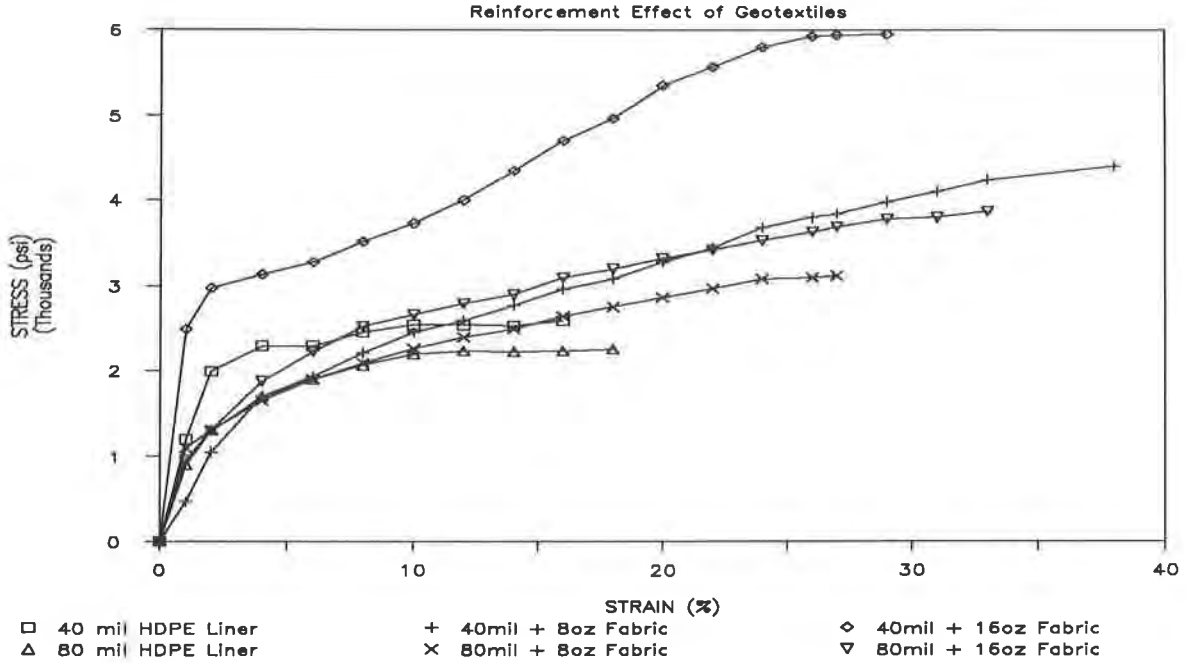

Figure 14. Multi—axial Burst

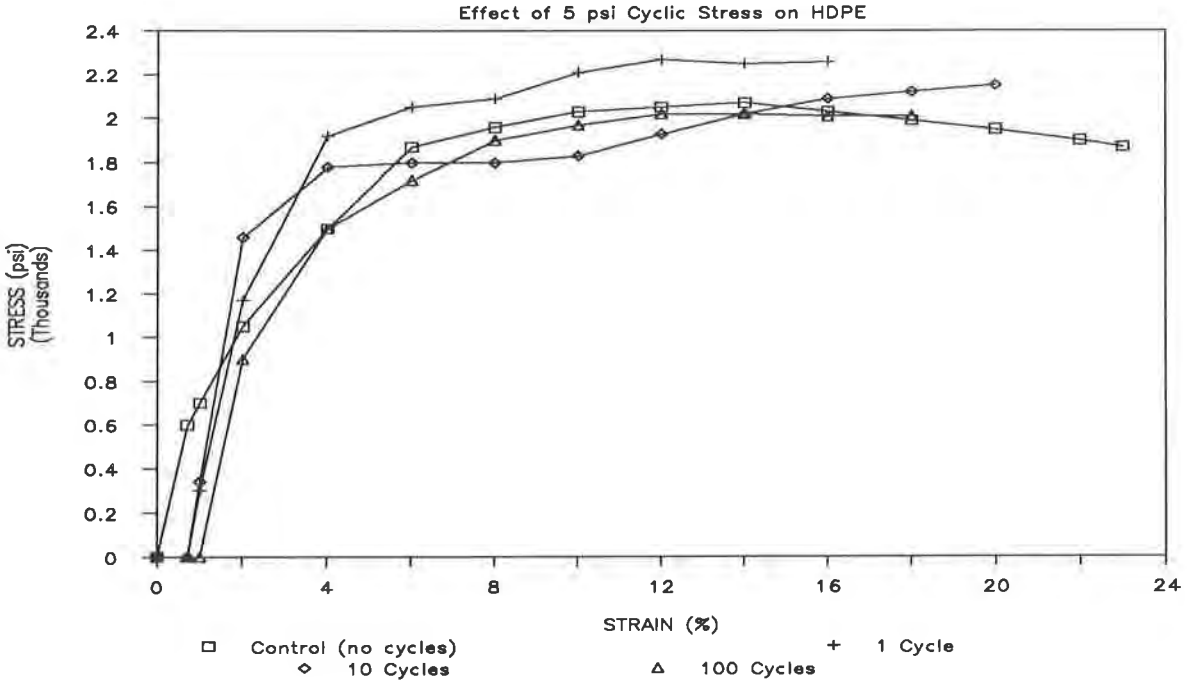

1000 psi = 6.9 MPa

40 mil = 1 mm

Results show that the textiles greatly increased the strength of the liner as expected. However quite unexpectedly, elongation at rupture values increased by over 50%. Similar to the drainage net testing, the traditional development of a "fish eye" in the liner prior to failure did not occur. Instead, it is suspected the textile tore first, causing the liner to tear and immediately fail.

Effect of Cyclic Stress (Figure 14 & 15). In real life, liners are subjected to cyclic stress due to loadings on the liner or temperature fluctuations. Normal index tests do not address the consequences of such action.

To simulate the above situation, the hydrostatic tester was used in a multi-axial burst test mode. Pressure was applied in a cyclic manner on the geomembrane sample. Pressure of 35 KPa (5 psi), which is one quarter the pressure at break, was applied, held for one minute and then released. The liner was then subjected to a multi-axial burst test with pressure being increased at 6.9 KPa/min. (1 psi/min) until rupture occurred. This entire procedure was run again, except the addition and release of the 35 KPa (5 psi) pressure was repeated 10 and 100 times. This cyclic effect was also evaluated with a pressure increment of 104 KPa (15 psi), which is three quarters of the normal break strength.

As can be seen in Figure 14, repeated cycles of 35 KPa did not have much effect. When the liner was cycled through 104 KPa of applied pressure (Figure 15), the ultimate performance went unaltered, but the initial portion of the stress-strain curve was shifted to the right. This indicates that some permanent deformation had occurred, even at one cycle of 104 KPa, to cause the liner to bag.

Chemical Compatibility of HDPE (Figure 16). The last variable to be studied was the effect of chemicals on the liner. Assessment of chemical compatibility has been a problem in the design of waste containment facilities. The most widely accepted test for determining chemical compatibility has been the EPA 9090 method. Although this test reveals much useful information, it is based on index properties and takes a minimum of four months to run.

To discover if the multi-axial burst test method could be used to determine chemical compatibility, a series of tests were run on HDPE liner in contact with various chemicals (leachate could also be used). The first chemical chosen was dichloroethane since it is known to be fairly detrimental to polyethylene and other materials. The sample was first immersed in dichloroethane for seven days. After this incubation time, the liner was removed from the chemical, immediately placed in the hydrostatic pressure device and tested.

The results in Figure 16 show that the liner had softened and lost about 1/3 of its strength and elongation. Also in Figure 16 are results from additional testing done with other chemicals. As will be noted, some chemicals demonstrated a larger detrimental affect on the liner than others.

Figure 15. Multi–axial Burst

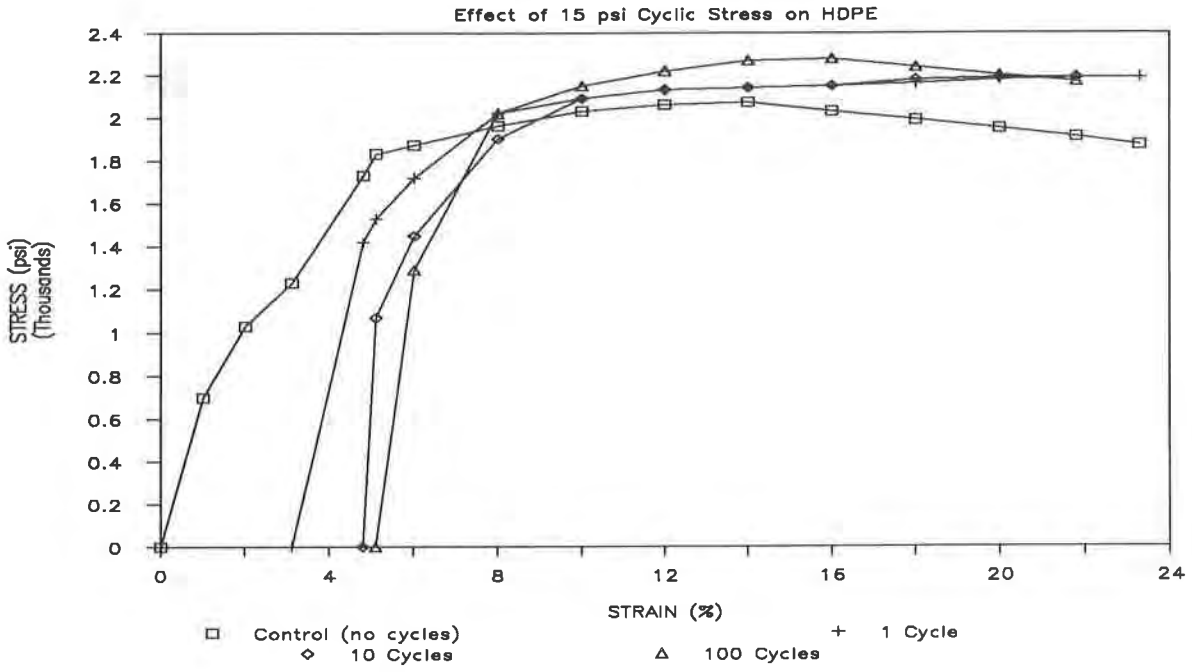

Figure 16. Multi–axial Burst

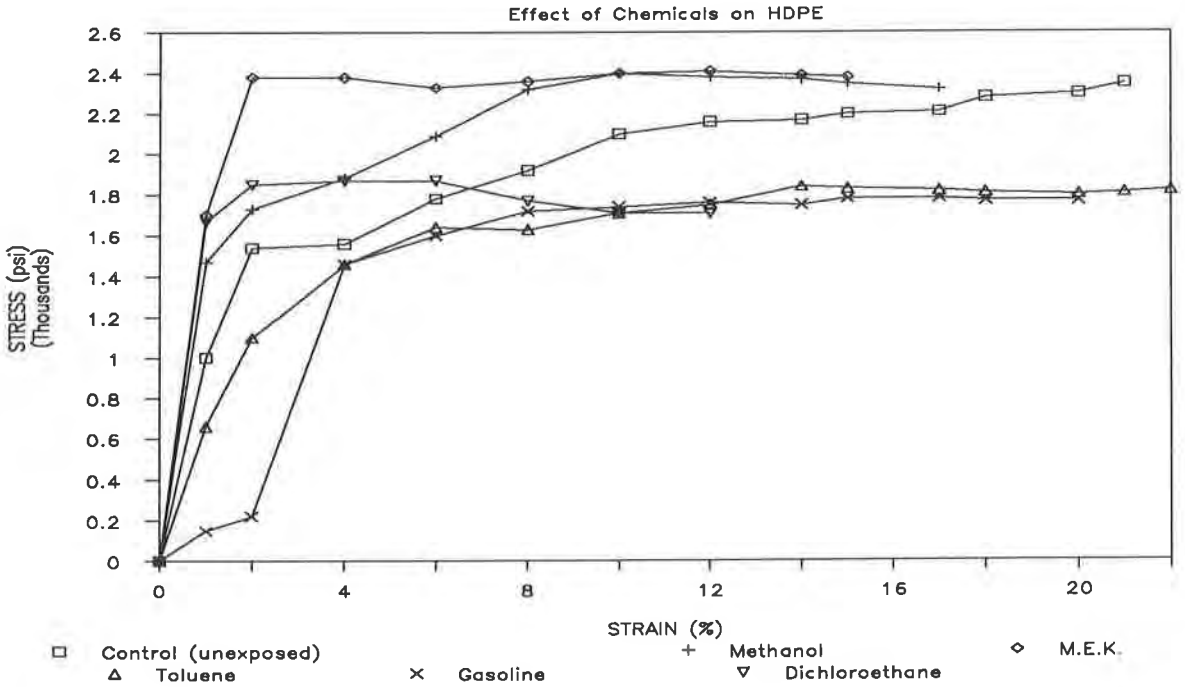

1000 psi = 6.9 MPa

Chemical Effect on Other Geomembranes (Figure 17). Figure 17 shows some additional testing done with other combinations of chemicals and liners. In the case of PVC in contact with dichloroethane, the liner had dissolved during the seven-day immersion period and could not be removed for testing. In the case of supported CSPE in contact with dichloroethane, the loss of strength is mainly due to the loss of strength of the scrim. As with the other variables studied, elastic materials were difficult to evaluate fully since they elongated beyond the capacity of our test unit.

SUMMARY

The hydrostatic pressure vessel has proven to be valuable in assessing geomembrane performance under real world conditions. The effects of temperature, strain rate, and chemicals have all been investigated.

In the case of HDPE, the multi-axial burst test produces results similar to the ASTM D 638 tensile test up to the yield point. This verifies that only the yield point needs to be specified for design purposes (this is especially true in textured sheet).

Changes in temperature affected different polymers to various degrees compared to their room temperature data. As expected, as temperature increased all liners tested became more elastic. As temperature decreased they became stiff and brittle. However, this occurred at temperatures far warmer than what some index tests would suggest.

Chemical compatibility is always a question of determining whether a liner's diminished physical properties are adequate for the application. The use of multi-axial burst test data can go beyond simple index testing to yield a realistic insight into the problem of liner-chemical interaction.

Quite surprisingly the change in strain rate or cyclic stresses did not have a major affect on HDPE in the ranges studied, other than possibly reducing the modulus of elasticity. This type of endurance testing is valuable in demonstrating long-term field survivability.

CONCLUSION

The data presented is meant only as an overview of the capabilities of the hydrostatic tester and the multi-axial burst test method. Extensive work still needs to be done to fully explore these variables along with others. However, this data should give some guidance as to how liners perform under real conditions.

REFERENCES

Beyer, W. H., "Standard Mathematical Tables", 28th Edition CRC Press, Inc.; Boca Raton, FL, 1987

GRI Test Method GM-4, "Three Dimensional Geomembrane Tension Test", Geosynthetic Research Institute, Philadelphia, PA, 1989

Figure 17. Multi—axial Burst

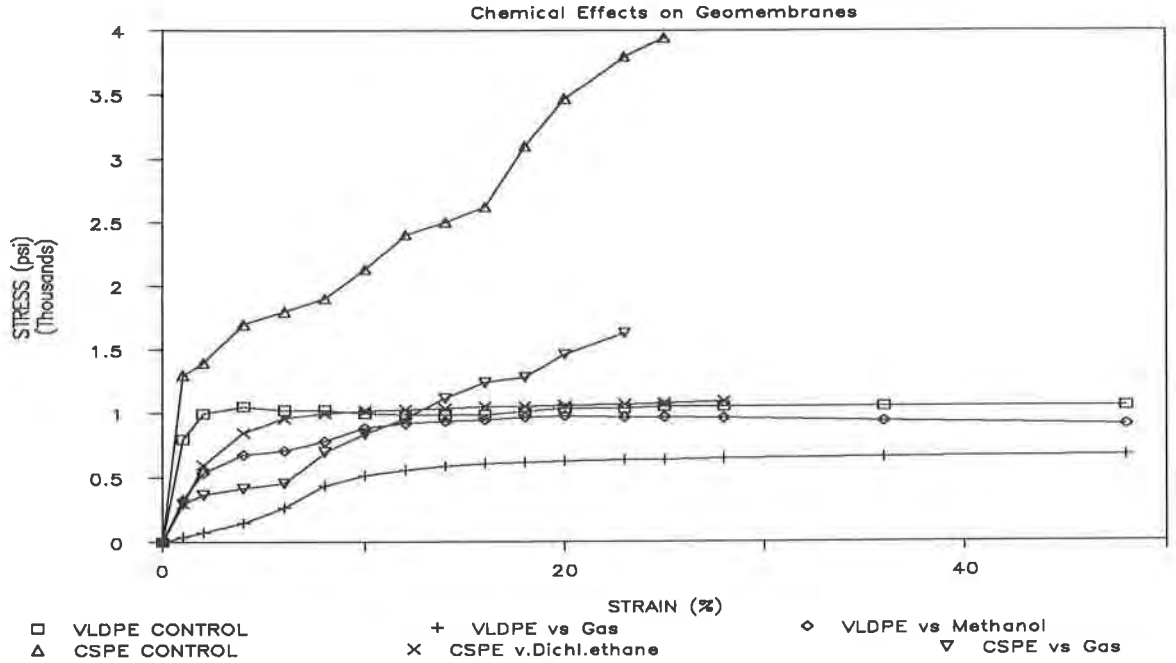

1000 psi = 6.9 MPa

Strain Compatibility Considerations and Tensioning Analysis for Geosynthetic Lining Systems

W.L. Deutsch Jr.
Roy F. Weston Inc., USA

ABSTRACT

This paper presents a quantitative procedure to assess whether internal slippage between components of a geosynthetic "sandwich" will occur from the tension force generated from the weight of an overlying soil cover. Governing equations for both an infinite slope and a slope with a toe buttressing effect are developed, and the effects of an applied extraneous force (e.g., equipment loading) are also considered. In addition, a quantitative procedure is presented that allows the developed tension force to be distributed among the geosynthetic "sandwich" components in the situation where internal slippage between these materials will not occur (i.e., where the geosynthetic "sandwich" behaves as a single block mass in which all components of the "sandwich" strain equally under the tension loading).

INTRODUCTION

When designing a geosynthetic lining system that is to be placed on a sloping surface and covered with soil, the designer must rely on the interface shear strength between the various components of the lining system to ensure internal stability of the geosynthetic "sandwich." This shear strength, consisting of both interface friction and adhesion, is necessary to prevent slippage between the various components of the lining system. This shear strength also determines the magnitude of the tension load that the geosynthetics within the lining system must support. In particular, the shear strength parameter that governs this behavior is the minimum interface friction angle of the lining system as determined by direct shear testing of the various geosynthetic/ geosynthetic and geosynthetic/soil interfaces within the lining system. Assuming that the adhesion resistance component of the shear strength is neglected, it will be shown in this paper that, under the developed tensile loading, the components of the lining system will strain as a "single block mass" (i.e., no slippage between the various components of the lining system will occur) if all of the individual interface

friction angles between these components exceed a minimum required value determined from a quantitative relationship between the slope angle and the minimum interface friction angle of the geosynthetic lining system.

It is the present practice in many designs to assume that the most rigid material within the geosynthetic "sandwich" carries the developed tensile load. However, if the individual geosynthetic components are acting as a single block mass, they must, under the developed tensile loading, strain the same amount as the most rigid material. From stress-strain relationships, it therefore must be concluded that, while the most rigid geosynthetic in the single block mass carries a high percentage of the tensile load, it does not carry the entire tensile load. The remainder of this loading is instead distributed among the remaining geosynthetics. A quantitative procedure will be presented in this paper that distributes this tensile loading among the various geosynthetics within the lining system based on the stress-strain relationships of these materials. A design example will also be presented that will illustrate these quantitative analysis procedures.

ASSUMPTIONS

Assumptions used in the derivations of the mathematical equations presented in this paper are as follows:

1. The soil cover atop the geosynthetic "sandwich" is free-draining and cohesionless; therefore, the shear strength of this material is derived solely from internal friction. In addition, no seepage forces are present within this material.

2. The shear strength between the soil to geosynthetic and geosynthetic to geosynthetic interfaces within the lining system is due solely to interface friction between these materials. Adhesional resistance, if present, is neglected in the analyses.

3. The entire geosynthetic "sandwich" is positioned atop a prepared subgrade or clay liner and beneath a cohesionless cover soil. There are no soil layers internal to the geosynthetic "sandwich."

4. The geosynthetic components of the lining system carry all of the developed tension loading. The underlying prepared subgrade or clay liner and overlying soil cover layer are assumed to carry none of this loading due to the minimal, if any, tensile strength of these materials.

SINGLE BLOCK MASS DERIVATION

To develop the quantitative expression that defines the single block mass condition, consider the free body diagram shown in Figure 1. For purposes of this analysis, the free body will be assumed to be of infinite slope in geometry, that is, the slope is assumed to be of great

length, and a buttressing force at the toe of slope, which develops when a cover soil thickness on a sloping surface frictionally interacts with cover soil on a flatter surface at the toe of the slope, does not exist. The impact of these assumptions on the developed quantitative relationship will be discussed in a subsequent section of this paper.

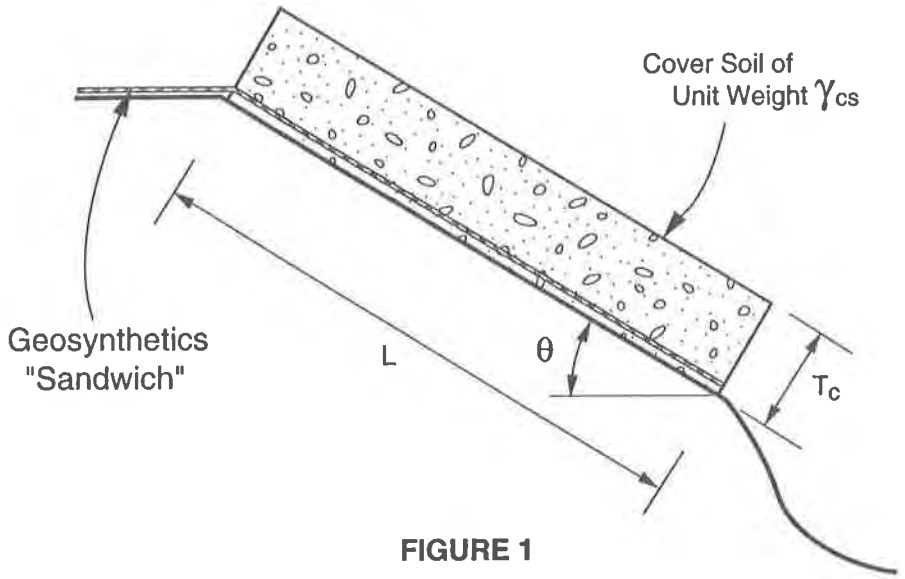

FIGURE 1

Under the infinite slope assumption, the tension force that develops in the underlying geosynthetic "sandwich" from the weight of the cover soil is calculated as follows on a pounds per foot width of lining system basis:

$$W = \text{Cover soil weight} = \gamma_{cs} L T_c \quad (1)$$

$$W_x = \text{Downslope component of weight of cover soil} = \gamma_{cs} L T_c \sin\theta \quad (2)$$

$$W_y = \text{Component of weight of cover soil normal to geosynthetic sandwich} = \gamma_{cs} L T_c \cos\theta \quad (3)$$

Also, it is evident from the definition of these forces that:

$$F_D = \text{Driving force} = W_X = \gamma_{cs} L T_c \sin\theta \quad (4)$$

$$F_R = \text{Resisting force} = W_Y \tan\delta_{min} = \gamma_{cs} L T_c \cos\theta \tan\delta_{min} \quad (5)$$

in which δ_{min} = Minimum value of the interface friction angle between adjacent geosynthetic to geosynthetic or soil to geosynthetic interfaces within the lining system.

The developed tension loading (T) is then:

$$T = F_D - F_R \tag{6}$$

or $$T = \gamma_{cs} L T_c (\sin \theta - \cos \theta \tan \delta_{min}) \tag{7}$$

For all components of the geosynthetic "sandwich" to move as a single block mass (i.e., strain equally) with no slippage between contacting materials under this developed tension loading, there must be sufficient frictional resistance between each interface which is numerically greater than the developed tension force. Based on the laws of physics, this will be true if:

$$F_{friction} (\text{at each respective interface}) \geq T \tag{8}$$

where $$F_{friction} = N_{\mu_s} \tag{9}$$

in which N = normal force to the potential slippage interface, and μ_s = coefficient of static friction = tan δ, in which δ is the interface friction angle for the particular interface being evaluated.

Also, from the free body diagram of Figure 1:

$$N = W \cos \theta = \gamma_{cs} L T_c \cos \theta \tag{10}$$

Therefore, substitution into Equation 8 yields:

$$\gamma_{cs} L T_c \cos \theta \tan \delta \geq \gamma_{cs} L T_c (\sin \theta - \cos \theta \tan \delta_{min}) \tag{11}$$

Dividing this expression by $\gamma_{cs} L T_c \cos \theta$ and designating δ as δ_{REQD} yields

$$\tan \delta_{REQD} \geq \tan \theta - \tan \delta_{min} \tag{12}$$

or $$\delta_{REQD} \geq \tan^{-1} (\tan \theta - \tan \delta_{min}) \tag{13}$$

Equation 13 quantifies the single block mass condition. From an inspection of this equation, it is evident that two cases are possible.

1.) Case I: All $\delta_i \geq \delta_{REQD}$

In this instance, all of the interface friction angles (soil to geosynthetic or geosynthetic to geosynthetic) within the lining system exceed δ_{REQD}. The entire geosynthetic "sandwich" should therefore strain equally without slippage under the developed tensile loading at any and all interfaces, that is, the entire "sandwich" should strain as a single block mass. Under this scenario, the developed tensile loading would be distributed among all of the various geosynthetics that comprise the "sandwich" according to the quantitative relationships developed subsequently in this paper.

2.) Case II: One or more $\delta_i < \delta_{REQD}$

In this instance, slippage will occur under the developed tension loading at the first interface, measured from the soil cover layer downward, at which $\delta < \delta_{REQD}$. Under this scenario, only those geosynthetics above the slippage interface will behave as a single block mass within which all will strain equally. In this case, the developed tensile loading would be distributed only among those geosynthetics above the slippage interface according to the quantitative relationships developed subsequently in this paper. It is important to note that the author does not recommend that geosynthetic lining system designs proceed under this scenario. If the single block mass analysis indicates that slippage will occur within the lining system, then the components of the geosynthetic "sandwich" should be altered to produce a higher δ_{min} until the single block mass equation is satisfied. For example, this may be achievable by changing a smooth HDPE geomembrane/ nonwoven needled geotextile interface to a textured HDPE geomembrane/ nonwoven needled geotextile interface to take advantage of the "Velcro" effect and resulting higher interface friction angle which develops between these latter two materials.

To check the validity of the derived quantitative relationship, consider the boundary condition when $\delta_{min} = \theta$. Under this assumption, Equation 13 shows that δ_{REQD} can be as low as 0^0 (i.e., a totally frictionless interface within the "sandwich" would not slip). This is consistent with the case of zero developed tension within the geosynthetic "sandwich" that will occur under the infinite slope assumption when $\delta_{min} \geq \theta$. (This can be shown by substituting $\delta_{min} = \theta$ into Equation 7, in which case $T = 0$ will result. It is obvious that, for any $\delta_{min} > \theta$, a zero tension condition will also result.) This boundary condition analysis therefore shows that, as anticipated, when no tension is developed within the geosynthetic "sandwich," no interface friction is necessary to prevent slippage at the interfaces within the "sandwich."

DISTRIBUTION OF TENSION LOADINGS

To develop this quantitative concept, consider the stress/strain diagram of Figure 2 (expressed in terms of tensile loading (T) versus

strain (ϵ)), in which four geosynthetics within a proposed lining system "sandwich" are assumed to have the straight line stress/strain behavior as shown in this figure. The most rigid of these materials is assumed to have a modulus of elasticity E_1 with the remaining three materials having modulus values of E_2, E_3, and E_4 in the order of decreasing rigidity.

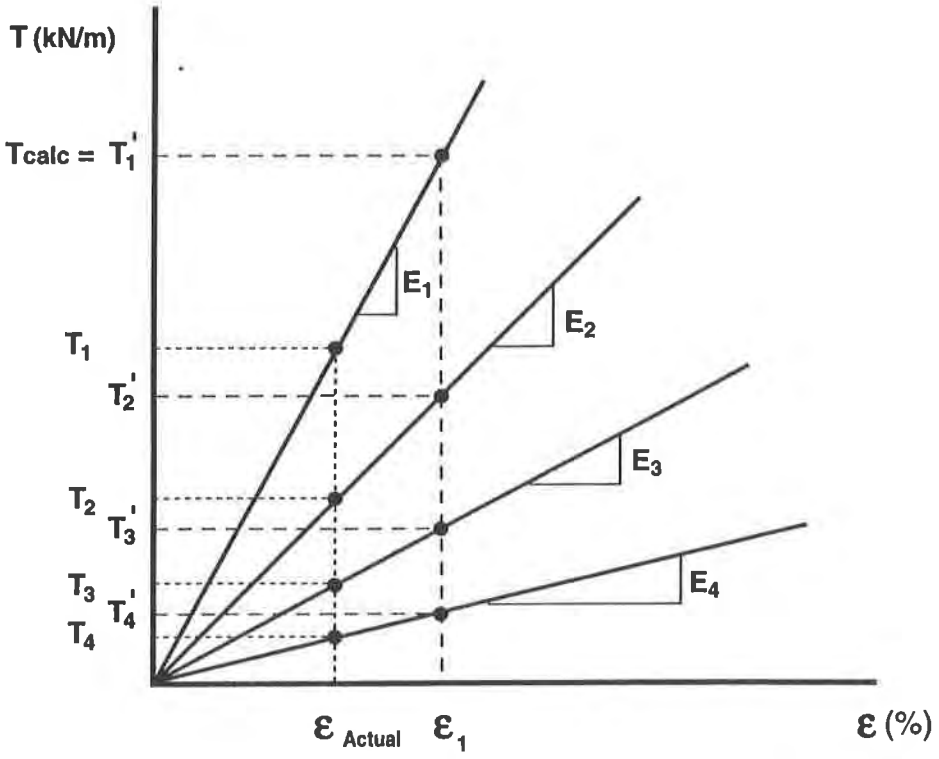

FIGURE 2

The magnitude of the tension loading (T_{calc}) generated within a sloping geosynthetic "sandwich" from the weight of the overlying cover soil is also necessary for this analysis. This value can be calculated from Equation 7 for the case of an infinite slope having the geometry shown in both Figure 1 and Figure 3A. This same parameter can be calculated for the case of a geosynthetic "sandwich" with a uniform thickness of cover soil and a buttressing effect at the toe of slope (see Figure 3B) using the following equation developed by Giroud and Beech (1):

$$T_{calc} = \frac{\gamma_{cs} T_c^2}{\sin 2\theta} \left[\left(\frac{2H \cos \theta}{T_c} - 1 \right) \frac{\sin (\theta - \delta_{min})}{\cos \delta_{min}} - \frac{\sin \phi}{\cos (\theta + \phi)} \right] \qquad (14)$$

An extension of the procedures of the Giroud and Beech paper to the case of a tapered cover soil thickness (see Figure 3C) in which a greater buttressing effect will develop, as well as the case of a uniform thickness of cover soil with an overlying equipment loading, was

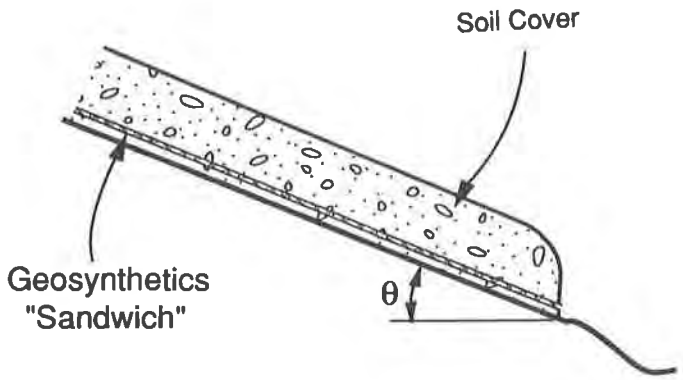

A). INFINITE SLOPE (NO TOE OF SLOPE BUTTRESSING EFFECT)

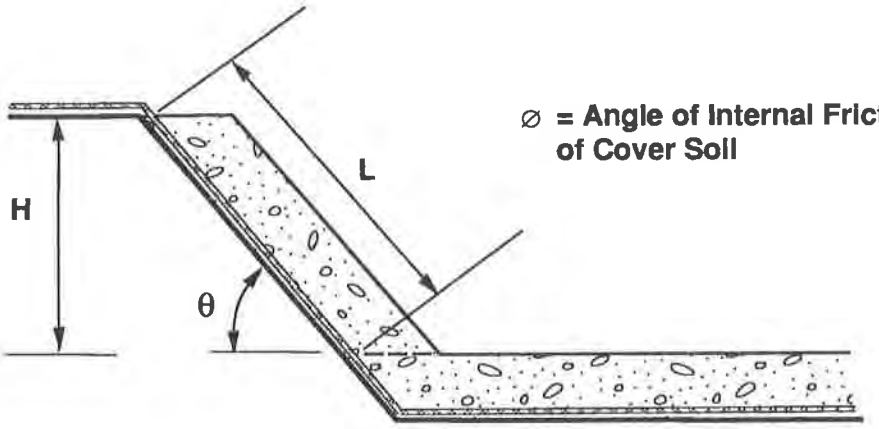

B). SLOPE WITH UNIFORM COVER SOIL THICKNESS AND TOE OF SLOPE BUTTRESSING EFFECT

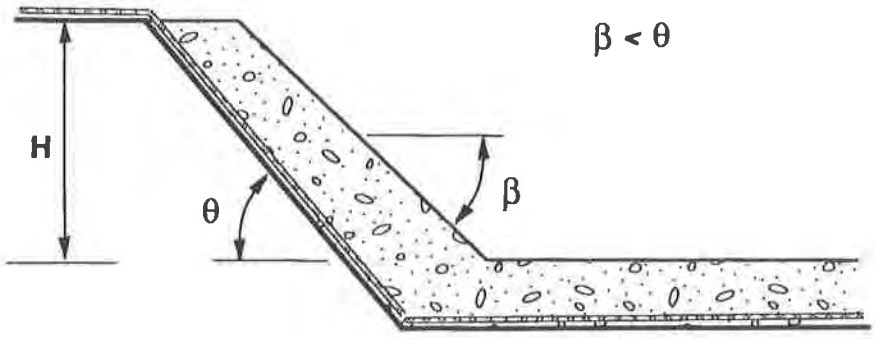

C). SLOPE WITH TAPERED COVER SOIL THICKNESS AND TOE OF SLOPE BUTTRESSING EFFECT

1251-459 12/4/92

FIGURE 3

presented by McKelvey and Deutsch (2). This paper allows direct computation of T_{calc} for these two cases.

If it is now assumed, for the sake of argument, that the most rigid geosynthetic (material 1) carries all of the calculated tension loading (i.e., $T_1' = T_{calc}$), it must, according to its stress/strain relationship, strain amount ϵ_1 in the process of carrying this load.

The value of ϵ_1 may be calculated as:

$$\epsilon_1 = \frac{T_1'}{E_1} \quad \text{where } T_1' = T_{calc} \tag{15}$$

However, if all of the remaining geosynthetics have strained equally as a single block mass under this loading, each of them must also have strained an amount ϵ_1. At this level of strain, their respective stress/strain diagrams indicate that they must also carry loadings of T_2', T_3' and T_4' in magnitude (see Figure 2). Based on this argument, it is therefore evident that $T_1' + T_2' + T_3' + T_4'$ must be greater than T_{calc} since T_1' was initially assumed to be equal to T_{calc}. But this cannot be true. Therefore, the assumption that the most rigid geosynthetic in the lining system "sandwich" carries <u>all</u> of the developed tension loading is inaccurate. (Only in the case of a perfectly rigid geosynthetic (i.e., a vertical stress/strain curve within the stress range of interest) will this assumption be true, and this behavior simply does not exist, even for the most rigid currently available geosynthetics.) Instead, there must be a distribution of this tension loading among all of the geosynthetics within the lining system "sandwich" with more rigid geosynthetics carrying a proportionately greater percentage of T_{calc} as demonstrated subsequently. In addition, the single block mass movement of these geosynthetics will strain equally to a value of ϵ_{actual} which must be less than the value of ϵ_1 noted above as also demonstrated subsequently.

The quantitative distribution of the calculated tension loading among the four geosynthetics assumed in this discussion may be easily determined by noting that:

$$T_1 + T_2 + T_3 + T_4 = T_{calc} \tag{16}$$

in which T_1 through T_4 are the initially unknown tension loadings carried by each of the four geosynthetics. Since, from the basic definition of modulus of elasticity for linear stress/strain behavior, $T = E\epsilon$, the above expression may be written as:

$$E_1 \epsilon_1 + E_2 \epsilon_2 + E_3 \epsilon_3 + E_4 \epsilon_4 = T_{calc} \tag{17}$$

If the entire geosynthetic "sandwich" is straining as a single block mass, then $\epsilon_1 = \epsilon_2 = \epsilon_3 = \epsilon_4 = \epsilon_{actual}$. Therefore, Equation 17 may be rewritten as:

$$\epsilon_{actual} (E_1 + E_2 + E_3 + E_4) = T_{calc} \tag{18}$$

or $$\epsilon_{actual} = \frac{T_{calc}}{E_1 + E_2 + E_3 + E_4} \tag{19}$$

This equation can be generalized to the case of "n" geosynthetics as follows:

$$\epsilon_{actual} = \frac{T_{calc}}{\sum_{i=1}^{n} E_i} \tag{20}$$

Following calculation of ϵ_{actual} from Equation 20, the tension force in each of the four geosynthetics within the "sandwich" initially assumed for this discussion can then be calculated as:

$$\begin{aligned} T_1 &= \epsilon_{actual} E_1 \\ T_2 &= \epsilon_{actual} E_2 \\ T_3 &= \epsilon_{actual} E_3 \\ T_4 &= \epsilon_{actual} E_4 \end{aligned} \tag{21}$$

This may also be generalized to the case of "n" geosynthetics as:

$$T_i = \epsilon_{actual} E_i \qquad \text{for } i = 1 \text{ to } n \tag{22}$$

Note from Figure 2 that the actual value of strain (ϵ_{actual}) which all of the geosynthetics will undergo, as well as the tension loadings (T_1 through T_4) which each of these materials will carry, are numerically less than the corresponding values of these parameters (i.e., ϵ_1 and T_1' through T_4') determined under the incorrect initial assumption that the most rigid of the geosynthetics in the "sandwich" carries <u>all</u> of the tension loading. In addition, through the very nature of the derivation, this solution must also satisfy the boundary condition that:

$$\sum_{i=1}^{n} T_i = T_{calc} \tag{23}$$

Following computation of ϵ_{actual} for the strained geosynthetics single block mass system from Equation 20, this value may be compared to an allowable strain for the lining system (e.g., 1%). If the calculated

strain is greater than that permitted by the design, the value of ϵ_{actual} may be reduced in one of two ways:

1. Alter the components of the lining system to increase the value of δ_{min} (e.g., change a smooth HDPE to needled geotextile interface to textured HDPE to this same needled geotextile to create a "Velcro" effect). This will have the direct effect of reducing the value of T_{calc} and therefore ϵ_{actual} as indicated in Equation 20.

2. Add a high modulus reinforcing geosynthetic (e.g., a geogrid) to the lining system. Assuming that this addition does not create a new interface which reduces δ_{min} (i.e., T_{calc} remains the same), this new material will significantly increase the value of the denominator of Equation 20, thereby decreasing ϵ_{actual}.

Following computation of T_1 through T_n from Equation 22, these values may be compared to allowable tensile strengths for these materials to define a Factor of Safety against tensile failure. If one or more of these Factor of Safety values is unacceptable, the following measures should be implemented:

1. Select a more competent member within the geosynthetics family that has exhibited an unacceptable Factor of Safety. For example, a 16 oz/yd^2 needlepunched geotextile has significantly greater tensile strength than an 8 oz/yd^2 needled geotextile.

2. Add a high modulus reinforcing geosynthetic (e.g., a geogrid) to the lining system. Assuming that this addition does not create a new interface which reduces δ_{min} (i.e., T_{calc} remains the same), the addition of this material means that T_{calc} is now distributed among "n+1" instead of "n" geosynthetics, thereby reducing the value of T_i carried by each of the original "n" geosynthetics in the "sandwich." In addition, since this geosynthetic addition is recommended to be of high modulus value, it will carry a much higher percentage of T_{calc} than the remaining geosynthetics, thereby proportionately reducing T_i for each of the remaining geosynthetics in the process.

It is recognized that most geosynthetic materials do not exhibit linear stress/strain behavior. However, it is suggested that the mathematical analysis procedures discussed above can also be adapted to this condition using the modified approach illustrated in Figure 4 and as outlined below for the case of an assumed 4-component geosynthetic "sandwich."

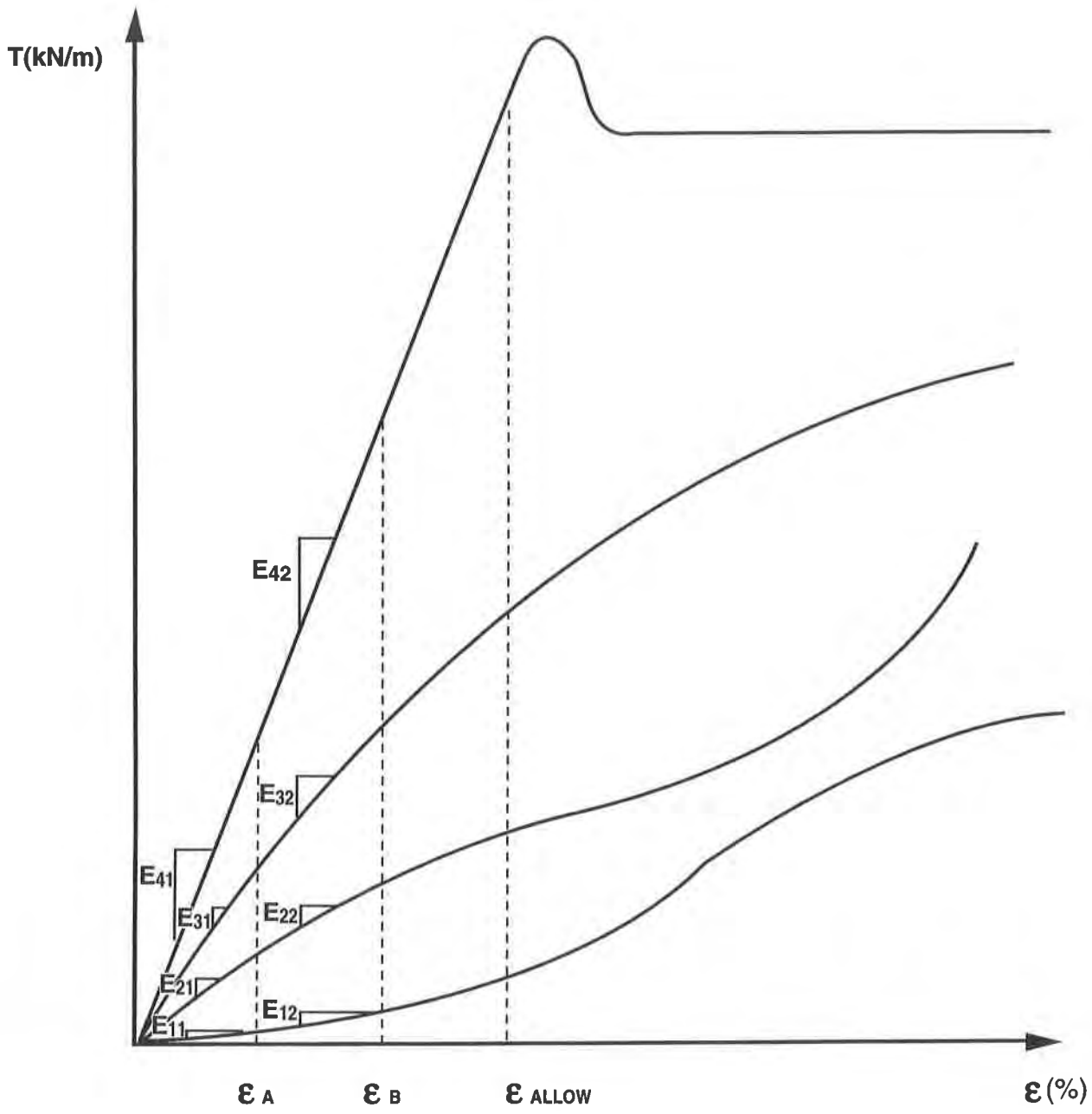

1251-461 12/4/92

FIGURE 4

1. Assume an initial range of strains from 0 to ϵ_A in which ϵ_A is less than the allowable strain (ϵ_{ALLOW}) of the lining system. In addition, the stress/strain curves should be approximately linear within the assumed strain range.

2. Using the modulus of elasticity values E_{11} through E_{41} as shown in Figure 4, calculate ϵ_{actual} from Equation 20.

3. If $\epsilon_{actual} \leq \epsilon_A$, the initial assumption in Step 1 is valid. In this instance, ϵ_{actual} represents the strain which the single block mass of straining geosynthetics should experience. Use Equation 22 to calculate the tensile load which each of the geosynthetics is carrying. Use modulus of elasticity values E_{11} through E_{41} in this computation.

4. If $\epsilon_{actual} > \epsilon_A$, the initial assumption in Step 1 is invalid. Therefore, assume a revised strain range from ϵ_A to ϵ_B in which ϵ_B is less than the allowable strain of the lining system. In addition, the stress/strain curves should be approximately linear within this newly-assumed strain range.

5. Using the modulus of elasticity values E_{12} through E_{42} as shown in Figure 4, calculate ϵ_{actual} from Equation 20.

6. If $\epsilon_A < \epsilon_{actual} \leq \epsilon_B$, the revised strain range assumption of Step 4 is valid and the tensile loads in each of the geosynthetics may be calculated from Equation 22 using the modulus values E_{12} through E_{42}.

7. If $\epsilon_{actual} > \epsilon_B$, repeat the process of Steps 4 through 6 with increasing strain ranges until the revised strain range assumption is valid. Note that the upper limit of the revised strain range may not exceed ϵ_{ALLOW}. If the computations indicate that this will occur, use one of the two procedures discussed previously to reduce ϵ_{actual}.

EFFECTS OF TOE OF SLOPE BUTTRESSING

As discussed previously in this paper, toe of slope buttressing develops when a cover soil thickness on a sloping surface frictionally interacts with cover soil on a flatter surface at the toe of slope. Toe of slope buttressing has the effect of reducing the tension load that develops within the geosynthetic "sandwich" on the sloping surface from the weight of overlying cover soil. This can be quantitatively expressed using Equation 6, which, when modified to include the toe of slope buttressing effect (F_B), becomes:

$$T = F_D - F_R - F_B \qquad (24)$$

Equation 8 can be used to assess the effect of toe of slope buttressing on the quantitative expression for δ_{REQD}. This relationship

will be derived below for the case of a uniform thickness of cover soil placed over the more steeply-sloping surface. In this instance, the theoretical value of tension developed within the geosynthetic "sandwich" is given by Equation 14 as developed by Giroud and Beech (1). In the following derivation, it is also assumed that Equation 10 is representative of the normal force to the various "sandwich" interfaces that results from the weight of the overlying soil cover. (There is a slight inaccuracy in this assumption because the geometry of the soil cover at the top of the slope as shown in Figure 1 is different than that assumed by Giroud and Beech. However, this inaccuracy is insignificant for typical landfill slope lengths.) Therefore, Equations 8, 9, 10 and a slight algebraic variation of Equation 14 may be used to define the following governing equation for single block mass movement:

$$\gamma_{cs}\, LT_c \cos\theta \tan\delta \geq \frac{\gamma_{cs}\, T_c^2}{\sin 2\theta}\left[\left(\frac{2H\cos\theta}{T_c}\right)\left(\frac{\sin(\theta-\delta_{min})}{\cos\delta_{min}}\right) - \frac{\sin(\theta-\delta_{min})}{\cos\delta_{min}} - \frac{\sin\phi}{\cos(\theta+\phi)}\right] \quad (25)$$

Expanding the right hand side of this equation and noting from Figure 3B that $H = L \sin\theta$, the following expression results:

$$\gamma_{cs}\, LT_c \cos\theta \tan\delta \geq \frac{2\,\gamma_{cs}\, T_c\, L \sin\theta\cos\theta}{\sin 2\theta}\left(\frac{\sin(\theta-\delta_{min})}{\cos\delta_{min}}\right) - \frac{\gamma_{cs}\, T_c^2}{\sin 2\theta}\left(\frac{\sin(\theta-\delta_{min})}{\cos\delta_{min}}\right) - \frac{\gamma_{cs}\, T_c^2}{\sin 2\theta}\,\frac{\sin\phi}{\cos(\theta+\phi)} \quad (26)$$

Dividing this expression by $\gamma_{cs}\, LT_c \cos\theta$ then yields the following:

$$\tan\delta \geq \frac{2\sin\theta}{\sin 2\theta}\,\frac{\sin(\theta-\delta_{min})}{\cos\delta_{min}} - \frac{T_c}{L\cos\theta}\,\frac{\sin(\theta-\delta_{min})}{\sin 2\theta\cos\delta_{min}} - \frac{T_c}{L\cos\theta}\,\frac{\sin\phi}{\sin 2\theta\cos(\theta+\phi)} \quad (27)$$

Designating δ as δ_{REQD}, the governing equation for single block mass movement of the geosynthetics "sandwich" for the case of a uniform thickness of cover soil with toe of slope buttressing then becomes:

$$\delta_{REQD} \geq \tan^{-1}\left\{\left[\frac{2\sin\theta}{\sin 2\theta}\,\frac{\sin(\theta-\delta_{min})}{\cos\delta_{min}}\right] - \frac{T_c}{L\cos\theta\sin 2\theta}\left[\frac{\sin(\theta-\delta_{min})}{\cos\delta_{min}} + \frac{\sin\phi}{\cos(\theta+\phi)}\right]\right\} \quad (28)$$

Note that, in addition to the variables θ and δ_{min} which define the single block mass relationship under the infinite slope assumption, the

variables T_c, L and ϕ also influence the single block mass relationship for a uniform cover soil thickness with toe of slope buttressing.

To check the validity of this equation, it is only necessary to determine if the expression reduces to Equation 13 for the conditions of an infinite slope. For the case of an infinite slope, L is very long (infinite in the limit) with its dimension being much greater than T_c. Therefore, the term T_c/L reduces to zero. Equation 28 then becomes:

$$\delta_{REQD} \geq \tan^{-1}\left(\frac{2 \sin\theta}{\sin 2\theta}\frac{\sin(\theta - \delta_{min})}{\cos\delta_{min}}\right) \quad (29)$$

Through trigonometric substitutions, it can be shown that this equation will reduce to Equation 13, thereby confirming the validity of Equation 28.

Note also that the toe of slope buttressing effect (i.e., the second term of the right hand side of Equation 28) is negative, indicating that this contribution will decrease the value of δ_{REQD} necessary to prevent slippage of one or more interfaces within the lining system, as anticipated. Also note that an initially apparent infinite slope case similar to Figure 3A can occur in which no toe of slope buttressing effect is present (i.e., $\phi = 0°$), but the slope face is of limited length (i.e., T_c/L is significant). In this case, the negative second term of the right hand side of Equation 28 can be significant, thereby resulting in a reduction of δ_{REQD} from that predicted by the more conservative Equation 13.

McKelvey and Deutsch (2) have shown that, for the case of an equipment loading W_A (expressed as lb/ft width of lining system) existing atop the cover soil, the Giroud and Beech tension equation for a uniform thickness of cover soil with toe of slope buttressing can be expressed as:

$$T_{calc} = \frac{\gamma_{cs} T_c^2}{\sin 2\theta}\left[\left(\frac{2H\cos\theta}{T_c} - 1 + \frac{W_A \sin 2\theta}{\gamma_{cs} T_c^2}\right)\frac{\sin(\theta - \delta_{min})}{\cos\delta_{min}} - \frac{\sin\phi}{\cos(\theta + \phi)}\right] \quad (30)$$

Using Equations 8, 9, 10, 30, and the derivation procedure noted above, the governing equation for single block mass movement of the geosynthetic "sandwich" for the case of a uniform cover soil thickness with both toe of slope buttressing effects and the presence of an equipment load becomes:

$$\delta_{REQD} \geq \tan^{-1} \left\{ \left[\frac{2 \sin \theta}{\sin 2\theta} \frac{\sin (\theta - \delta_{min})}{\cos \delta_{min}} \right] \right.$$

$$- \frac{T_c}{L \cos \theta \sin 2\theta} \left[\frac{\sin (\theta - \delta_{min})}{\cos \delta_{min}} + \frac{\sin \phi}{\cos (\theta + \phi)} \right]$$

$$\left. + \frac{W_A}{\gamma_{cs} L T_c \cos \theta} \frac{\sin (\theta - \delta_{min})}{\cos \delta_{min}} \right\} \qquad (31)$$

Note that the equipment loading term is positive, indicating that this loading will increase the value of δ_{REQD} necessary to prevent slippage at one or more interfaces within the lining system, as anticipated.

The extension of the single block mass derivation to the case of a tapered cover soil thickness is straightforward using the derivation procedures noted above and can be accomplished using the theoretical tension equation for this condition as developed by McKelvey and Deutsch (2).

DESIGN EXAMPLE

Consider a four component geosynthetic "sandwich" consisting of a needled geotextile underliner (GTX1), a smooth HDPE geomembrane (GM), a drainage net (DN) and a needled geotextile filter (GTX2). The sandwich rests on a prepared 2.5H:1V silty sand subgrade (S1) and is overlain by a 0.61 meter (i.e., 2 feet) thick free draining sandy cover soil (S2) having a unit weight of 18.6 kN/m^3 (i.e., 118.5 pcf) and a ϕ angle of 32°. The interface friction angles between these various components are as follows:

$\delta_{S1/GTX1} = 22°$ $\qquad$ $\delta_{DN/GTX2} = 19°$

$\delta_{GTX1/GM} = 10°$ $\qquad$ $\delta_{GTX2/S2} = 26°$

$\delta_{GM/DN} = 14°$

Assume that this lining system is used as a landfill cap in which no buttressing effect is present as in Figure 3A. From the above data, $\delta_{min} = 10°$ and $\theta = 21.8°$ for a 2.5H:1V slope inclination. Therefore, Equation 13 yields $\delta_{REQD} = 12.6°$. The friction angle of the GTX1/GM interface (10°) is less than δ_{REQD}. Therefore, slippage should occur at this interface under the developed tension loading. It is therefore necessary to improve the frictional resistance of this interface. Assume that this will be done by using a textured instead of a smooth HDPE geomembrane. Under this design modification, the two new interface friction values are assumed to be:

$\delta_{GTX1/GM(T)} = 15°$ $\qquad$ $\delta_{GM(T)/DN} = 18°$

For a revised δ_{min} = 15° and θ = 21.8°, Equation 13 yields δ_{REQD} = 7.5°. All δ values are now greater than δ_{REQD} and no slippage between the components of this modified lining system should occur on the 2.5H:1V slope, i.e., the geosynthetic lining system should behave as a single block mass.

Now assume that the revised lining system has a slope length (L) of 15.2 meters (i.e., 50 feet). Using Equation 7 in which all input parameters have now been defined, T = 21.1 kN/m^2 (i.e., 1,453 lb/ft). If the modulus of elasticity (E) values of the four geosynthetics are determined from their stress strain properties, Equation 20 can be used to calculate the strain which the revised geosynthetic sandwich, acting as a single block mass, will experience. Equation 22 can then be used to calculate the tension force in each of the four geosynthetics. These values, when summed, will total the calculated tension load. These tensile forces can then be compared with the tensile strengths of these same materials to define a Factor of Safety against tensile failure for each geosynthetic.

Now assume that the original geosynthetic "sandwich" (i.e., using the smooth HDPE geomembrane in which δ_{min} = 10°) is used as a bottom lining system within a landfill as shown in Figure 3B. Under this scenario, toe of slope buttressing will occur. For the same 2.5H:1V slope inclination, as well as the above referenced values of L, T_c and ϕ, Equation 28 yields δ_{REQD} = 8.8°. All of the individual interface friction angles are greater than this value. Therefore, the original geosynthetic "sandwich" should not experience internal slippage under this toe of slope buttressing scenario, and, therefore, can be used in this design. Equation 14 can then be used to determine the developed tension loading for this situation. The procedures discussed in the above paragraph can subsequently be used to distribute this tension loading among the four geosynthetics of this "sandwich," as well as to calculate the strain which the "sandwich," acting as a single block mass, will experience, and the Factors of Safety against tension failure for each geosynthetic.

REFERENCES

1. Giroud, J.P. and Beech, J.F., "Stability of Soil Layers on Geosynthetic Lining Systems." Conference Proceedings: Geosynthetics 1989, San Diego, CA, pp. 35-46.

2. McKelvey, J.A. and Deutsch, W.L., "The Effect of Equipment Loading and Tapered Cover Soil Layers on Geosynthetic Lined Landfill Slopes." Conference Proceedings: Fourteenth Annual Madison Waste Conference, University of Wisconsin-Madison, September 25-26, 1991.

The Use of Differential Scanning Calorimetry to Follow the Hydrolysis of Polyethylene Terephthalate

R.W. Thomas
National Seal Co., USA

S.R. Allen
TRI/Environmental Inc., USA

ABSTRACT

There has been great interest in the long term durability of woven and nonwoven polyesters in geosynthetic applications. Of major importance is the detection of hydrolysis, which is the principal life-limiting mode of environmental degradation for these materials. A common result of related studies is that there are few, if any, methods of tracking hydrolysis before catastrophic loss in strength is observed. Additionally, the methods that have been used successfully all involve the measurement of a change in molecular weight, and are generally time consuming and/or expensive. This paper will report on a new method for the detection of changes in poly(ethylene terephthalate) (PET) caused by hydrolysis with the use of a differential scanning calorimeter (DSC). This method appears to be a simple, fast, and relatively inexpensive way to monitor the effects of hydrolysis in polyesters.

Two hydrolysis experiments were performed. The first one involved aging a powdered, bottle-grade PET in boiling water for 54 days. The second one was performed in water at 80°C and involved a commercial, nonwoven fabric. The aged samples were analyzed with a DSC by heating the specimens to above the melting point and allowing them to cool naturally until recrystallization occurred.

The results showed that the temperature of crystallization, the heat of crystallization, and the maximum amount of heat evolved during crystallization all change as a function of aging time. Additionally, these changes can be related to changes in the molecular weight of the samples. This paper will discuss these results along with industry applications for material screening and long term life-time predictions.

INTRODUCTION

The hydrolysis of polyesters has been studied for over thirty years and still remains somewhat controversial (Schneider, 1987, Jailloux, 1990, and Risseeuw, 1990). One of the most detailed studies of this reaction was published by McMahon, et.al. in 1959. They used tensile properties, electrical properties, infrared spectroscopy, and dilute solution viscosity (DSV), to study films and sheets exposed to temperatures between 50 and 130°C and relative humidities from 20 to 100%. The results showed that a large change in molecular weight (MW) occurred before a change in tensile properties was detected. They also reported that the rate did not change at the glass transition temperature (Tg) and that the rate remained constant throughout a pH range of 2 to 7 at 130°C. The most controversial result concerned the mechanism of hydrolysis. Although the rate versus time plot showed an increasing rate, these authors believed that there were two regions with different slopes rather than a curve, which would be consistent with an autocatalytic reaction. They believed that the reaction proceeded in a linear manner up to a point at which rapid degradation would occur.

Other researchers have used a variety of techniques to study this reaction. The combinations of techniques used include end group analysis and DSV (Zimmerman, 1980), melt flow index (Kelleher, 1982), weight loss, DSV, breaking twist angle, and strength (Ellison, 1982), tensile properties, DSC, and scanning electron microscopy (Ansell, 1983), weight loss, tenacity and strength (Gawish, 1986), and finally, physical properties, DSC, thermal mechanical analysis (TMA) and dynamic mechanical analysis (DMA) (Thomas, 1990). The main results of all these studies were that the mechanism was either linear or autocatalytic and that only techniques sensitive to changes in MW were appropriate for tracking hydrolysis.

Although DSC was used in several of these studies, the focus was always on crystallinity changes seen in the melting of the polymer, which proved to be inappropriate for studying hydrolysis (Thomas, 1990). This study will demonstrate that much more information can be extracted from the recrystallization of PET from the melt in a DSC.

EXPERIMENTAL

DSC Method. A sample weighing 5-10mg was carefully pressed into a sample pan with an aluminum barrel and plunger designed to compress fibers or powders into the pan. The sample was placed in a DSC and a nitrogen flow of 50-75 ml/min was started. The sample was then heated at 10°C/min to 290°C, held at 290°C for 2 min and allowed to cool naturally through the recrystallization process to a lower temperature of around 160°C. The resulting crystallization exotherm was then analyzed for onset and peak temperatures, peak height, and heat of crystallization.

Gel Permeation Chromatography (GPC). The GPC results were generated by Jordi Associates, Inc., Billingham, Massachusetts. The samples were dissolved in hexafluoroisopropanol (HFIP) and 0.01M sodium trifluoroacetate and filtered. They were then run in the same solvent as a mobile phase at 0.6 ml/min using a Jordi Gel Mixed Bed column at room temperature. The injection volume was 100ul of a 0.25% (W/V) solution. The detectors used were a Waters 401 IR and a Waters 440 UV.

Hydrolysis Experiment Number 1. A typical bottle grade PET molding compound was converted from pellets to a powder by dissolution in m-cresol and precipitation in a large excess of methanol. After filtration and drying, about 20g of powder was placed in about 200ml of D.I. water and heated at reflux. Duplicate set-ups were assembled and samples were extracted periodically from both reaction vessels. The reactions proceeded at reflux for 54 days. Upon removal, the samples were simply washed with deionized water, dried in a vacuum desiccator, and stored in glass vials for DSC analysis.

Hydrolysis Experiment Number 2. This experiment included a commercial nonwoven fabric. The fabric was cut into squares about 5cm by 5cm. The specimens were placed in a 1L canning jar filled with D.I. water. The jar was placed in a forced flow oven at 80°C and samples extracted from the jar periodically. The water was replaced every week by removing the old water, rinsing all the samples three times with fresh water, and replacing the water. At this time, the samples for analysis were removed, rinsed with deionized water, and dried in a vacuum desiccator. Samples were exposed for 70 days.

RESULTS AND DISCUSSION

DSC Method. DSC is an analytical method that is sensitive to heat flow into and out of a specimen. Therefore, it is a sensitive way to detect changes in thermodynamic heat caused by transitions such as melting or boiling. Classically, a DSC melting profile experiment involves heating a specimen at a constant rate until the molecular transition is completed. The method used in this study was to monitor the spontaneous recrystallization behavior of a specimen after controlled melting. A thermal curve showing the behavior of PET to a heating and cooling cycle is shown in figure 1. In all the curves shown in this paper, peaks pointing up are exothermic and peaks pointing down are endothermic. The main difference between the heating and cooling cycles are that during the melt, heat has to be absorbed from the DSC and power must be added to the heaters to drive the transition. Alternatively, the recrystallization process occurs spontaneously and when it begins, the temperature is essentially isothermal,

since heat is evolved. Therefore, the specimen controls the crystallization temperature without any input from the calorimeter. This difference may seem trivial, but this study has shown that it is very important.

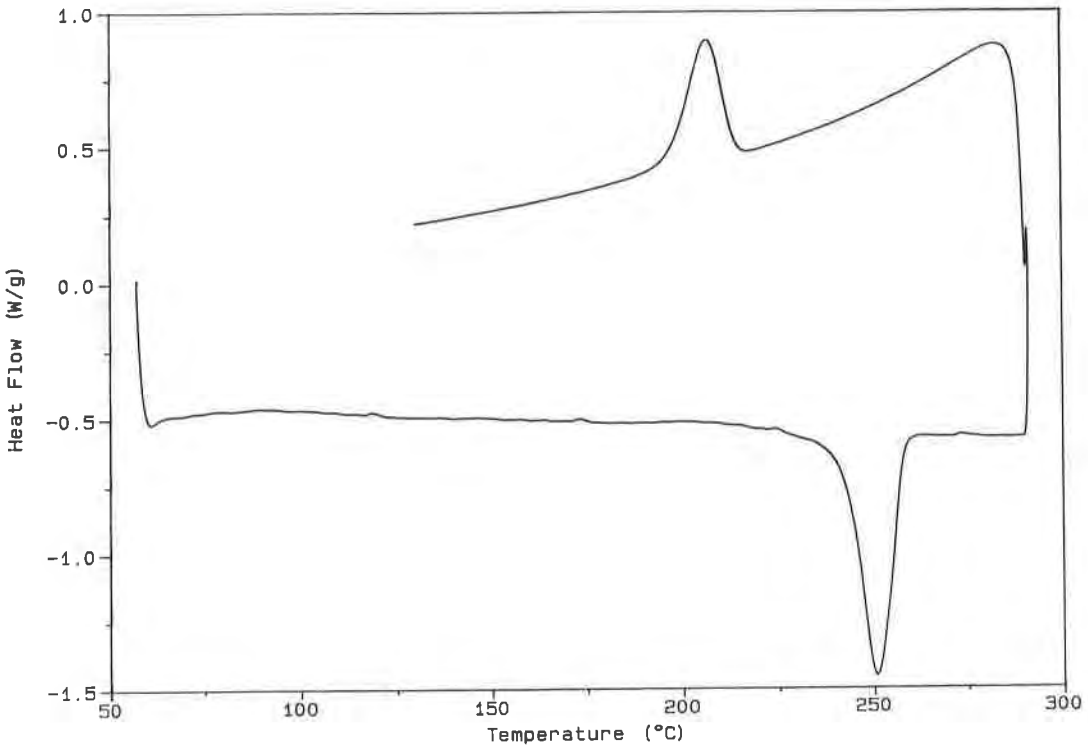

Figure 1. A Typical DSC Heating and Cooling Curve for a Nonwoven PET Fabric.

For example, figure 2 shows the effect of aging a PET nonwoven fabric for 70 days in water at 80°C. This figure magnifies the upper, cooling portion of the thermal curve. Notice that the crystallization peak moved to higher temperatures and became taller and more narrow after exposure. This is typical behavior for the changes observed throughout this study.

One of the first characteristics noticed about this technique was that the reproducibility of the crystallization measurements (onset and peak temperatures) was not as good as seen in the melting curves. Therefore, the cooling rate was programmed at 5°C/min. in an effort to improve the precision of the recrystallization. And, since the natural cooling rate was 7-9°C/min, the rate was actually controlled by adding heat. This controlled cooling resulted in the same samples seen in figure 2 becoming indistinguishable, just as they were during the melting cycle. It is believed that when the instrument was adding heat to the samples, the spontaneous recrystallization could not occur. Therefore, the samples appeared to be identical. The same logic helps explain why the effect of hydrolysis was not seen during the heating cycle. Apparently, this process only occurs when the DSC is not adding heat to the specimen.

Another interesting observation was made concerning the effect of purging the sample compartment. When there was no purge gas, the samples again became indistinguishable. This seems consistent since the temperature would not remain constant if the heat of crystallization is not removed by the flowing atmosphere. Therefore, the results showed that the sensitivity of a DSC to certain phenomena can be dramatically enhanced by allowing a sample to cool spontaneously from the melt, under a flowing gas blanket.

Hydrolysis Experiment Number 1. The first experiment was on a bottle grade PET injection molding compound of unknown origin. The pellets were converted to a powder

by solvent/nonsolvent precipitation and aged in boiling water for times up to 54 days. The changes seen in the resulting DSC cooling curves are shown in figure 3.

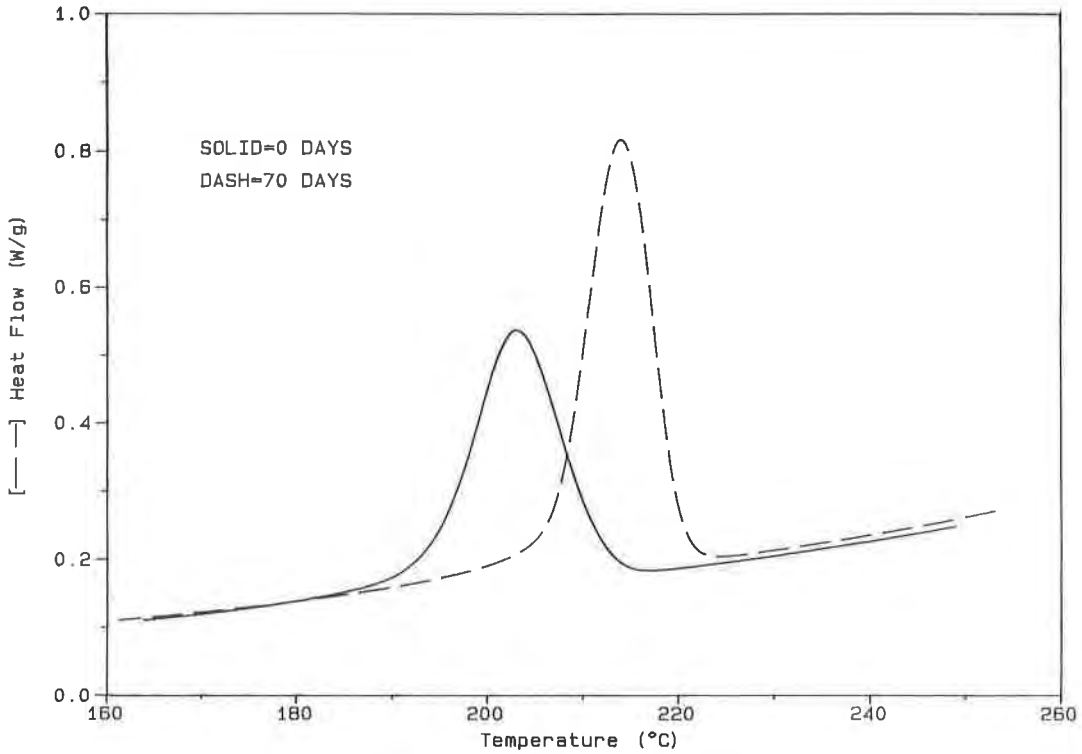

Figure 2. The Effect of 70 Days in Water at 80°C on the Crystallization of a Nonwoven PET Fabric

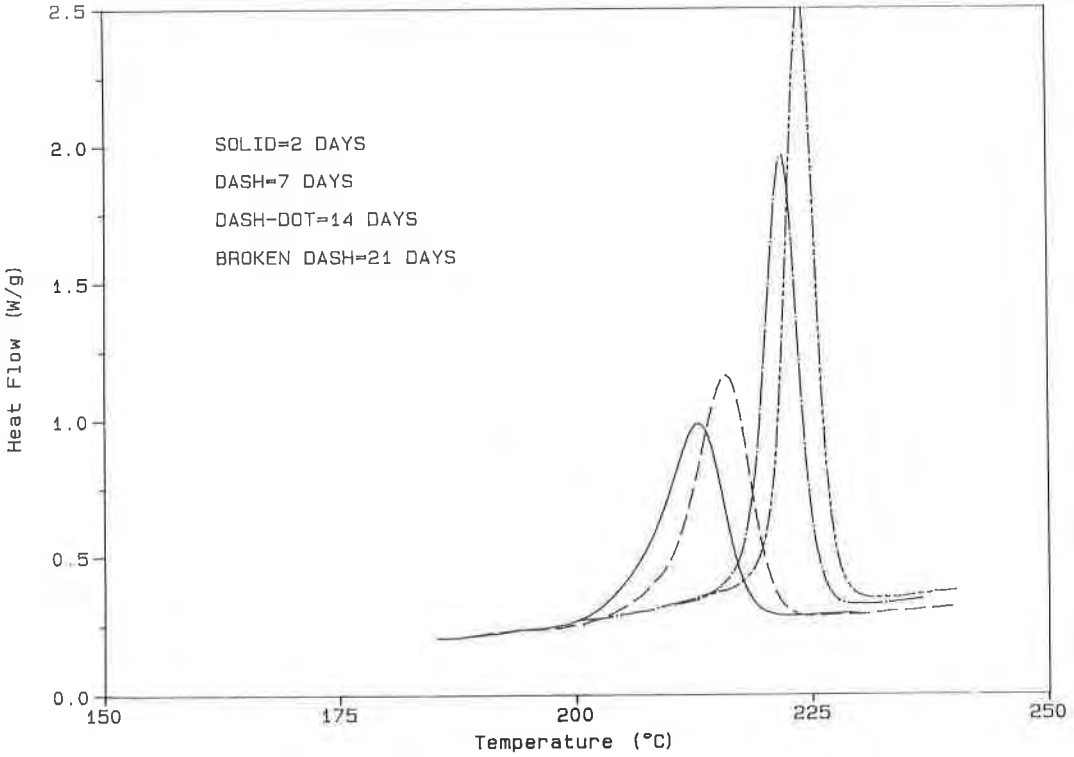

Figure 3. The Effect of Aging a Bottle Grade PET in Boiling Water

Notice that as hydrolysis proceeded, the crystallization peak became sharper, taller, and shifted to higher temperature. Table 1 shows the changes in crystallization temperatures (onset and peak), heat of fusion, and peak height as a function of aging time. Notice that at around 20 days, the temperatures reached a maximum and began to decrease. It is believed that this reflects an increase in the concentration of terephthalic acid, which was a hydrolysis product. The basis of this belief is that over 95% of the 54 day sample was found to be soluble in 10% sodium hydroxide and that upon acidification, the solution produced a compound identified as terephthalic acid by IR spectroscopy. Therefore, since we knew that total hydrolysis took place, it was assumed that terephthalic acid became a contaminant at some point. Nonetheless, hydrolysis appeared to proceed in a linear fashion for the first 20 days. Additionally, crystallization appeared to increase with aging time, which has been previously reported (McMahon,1959 and Ansell, 1983).

Table 1. The Effect of Boiling Water on the Crystallization Behavior of a Bottle Grade PET

Exposure Time(Days)	Onset Temp. (˚C)	Peak Temp. (˚C)	Peak Width (˚C)	Peak Height (W/g)	ΔH_f
0	217.3(5.3)*	208.2(3.6)	9.1(1.7)	0.35(0.04)	37.0(1.1)
2	218.0(1.1)	212.7(0.9)	5.3(0.4)	0.67(0.08)	40.4(1.0)
7	220.7(0.2)	216.0(0.3)	4.7(0.2)	0.93(0.13)	44.6(0.7)
14	225.0(0.2)	221.9(0.3)	3.1(0.2)	1.59(0.13)	47.9(3.4)
21	226.7(0.2)	224.0(0.2)	2.7(0.1)	2.10(0.07)	55.1(1.3)
28	226.8(0.0)	223.9(0.3)	2.9(0.3)	2.13(0.03)	56.1(0.7)
35	226.1(0.1)	222.8(0.1)	3.3(0.1)	1.86(0.05)	53.4(3.0)
54	222.8(0.1)	219.0(0.1)	3.8(0.2)	1.26(0.08)	47.4(3.0)

* Standard deviation in parentheses

Hydrolysis Experiment Number 2. The second aging experiment was performed on a nonwoven PET fabric used in geosynthetic applications and was done at 80˚C. The exposure was carried out for 70 days, and the results are presented in Table 2.

Notice that the same trend was seen in these results (Table 2) as with the ones in the previous section (Table 1). The crystallization peak became more narrow and moved toward increasing temperature. And, the change in the onset and peak temperatures was linear with exposure time. However, in this experiment, the peak height had a point that appeared out of place (see Table 2). Although the exact cause of this is not known, it is believed to be associated with an experimental variable that has yet to be discovered. The basis for this belief is that throughout the development of this method, more and more variables came to light that, at first, did not seem very important. In each case, there was a period when no meaningful results were generated, followed by the discovery of another variable. Therefore, it is expected that further study will yield another variable not yet known that may affect the peak height. Nonetheless, in general, the results for a nonwoven fabric were nearly identical to those observed in the bottle grade resin.

Table 2. The Effect of Exposure to Water at 80°C on the Crystallization Behavior of a Nonwoven PET Fabric

Exposure Time(Days)	Onset Temp. (°C)	Peak Temp. (°C)	Peak Width (°C)	Peak Height (W/g)	ΔH_f
0	212.3(0.7)	203.6(0.9)	8.7(0.3)	0.38(0.02)	37.8(1.9)
22	215.0(0.8)	207.0(0.8)	8.0(0.3)	0.47(0.02)	38.2(1.1)
49	217.5(0.7)	210.2(0.8)	7.3(0.4)	0.49(0.08)	39.1(2.6)
70	220.1(0.2)	213.9(0.7)	6.3(0.5)	0.61(0.06)	41.3(1.7)

The molecular weights of these samples were also measured by GPC and a linear relationship between MW and aging time was found. Therefore, the onset and peak crystallization temperatures were correlated with the MW values. The result is seen in figure 4. This is a plot of crystallization temperature vs. weight average molecular weight (M_w). The four data points are the values measured at the four exposure times from Table 2. Notice the excellent correlation for both the crystallization onset and peak temperatures. The correlation coefficients for the two lines are 0.9981 and 0.9959 for the onset and peak temperatures, respectively. These results support the conclusion that the changes detected by DSC correlate with the molecular weight of the samples. And, since smaller chains can more readily form crystals that are more stable, it follows that as MW decreases, the crystallization temperatures increase.

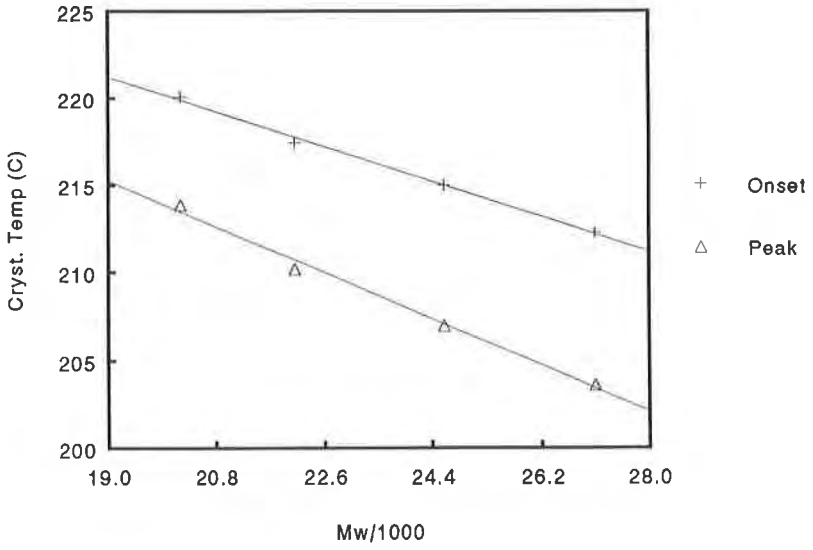

Figure 4. The Relationship Between Crystallization Temperature and Molecular Weight for a Nonwoven Fabric Aged in Water at 80°C

Miscellaneous Results. This technique has also been used on a number of different types of materials used in geotechnical applications so the purpose of this section is to briefly show the longer term possibilities of this method. First, figures 5 and 6 show the effect of water at 80°C on a different nonwoven fabric and a high tenacity fiber used for reinforcement applications. Both of these show similar results, although the magnitude of the changes are smaller than the material discussed in the

last section. These differences reinforce the belief that this method can be used to measure the rate of hydrolysis of different PET products in different environments.

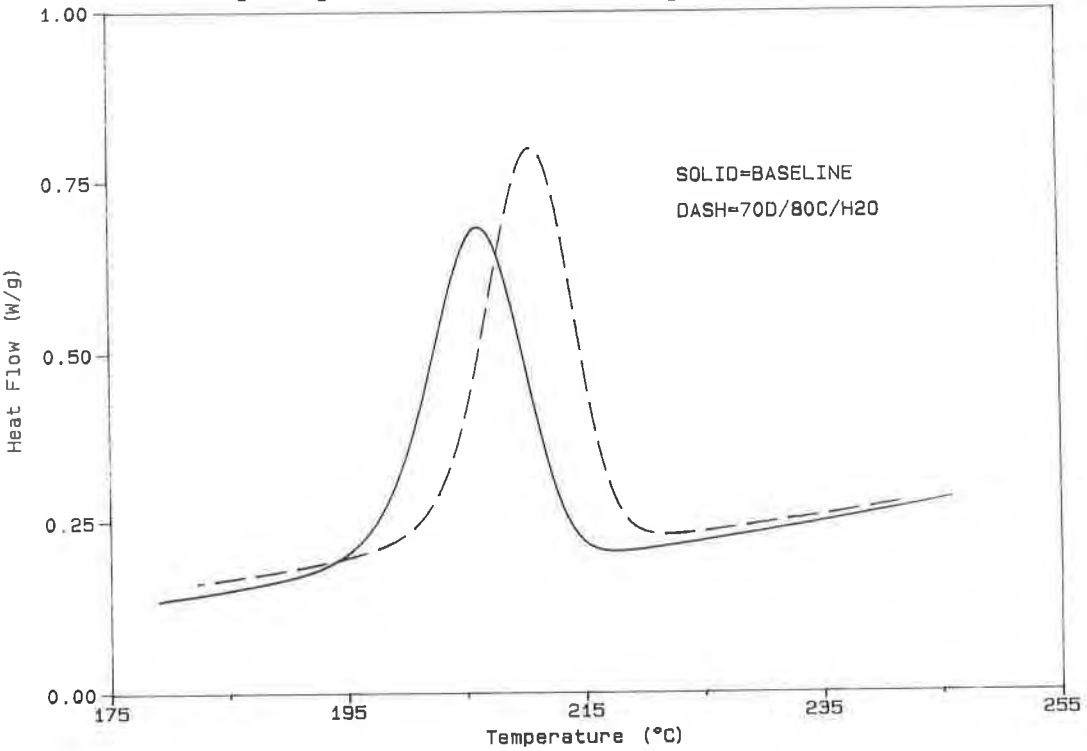

Figure 5. The Effect of Aging in Water at 80°C on the Crystallization of a Different Nonwoven PET Fabric

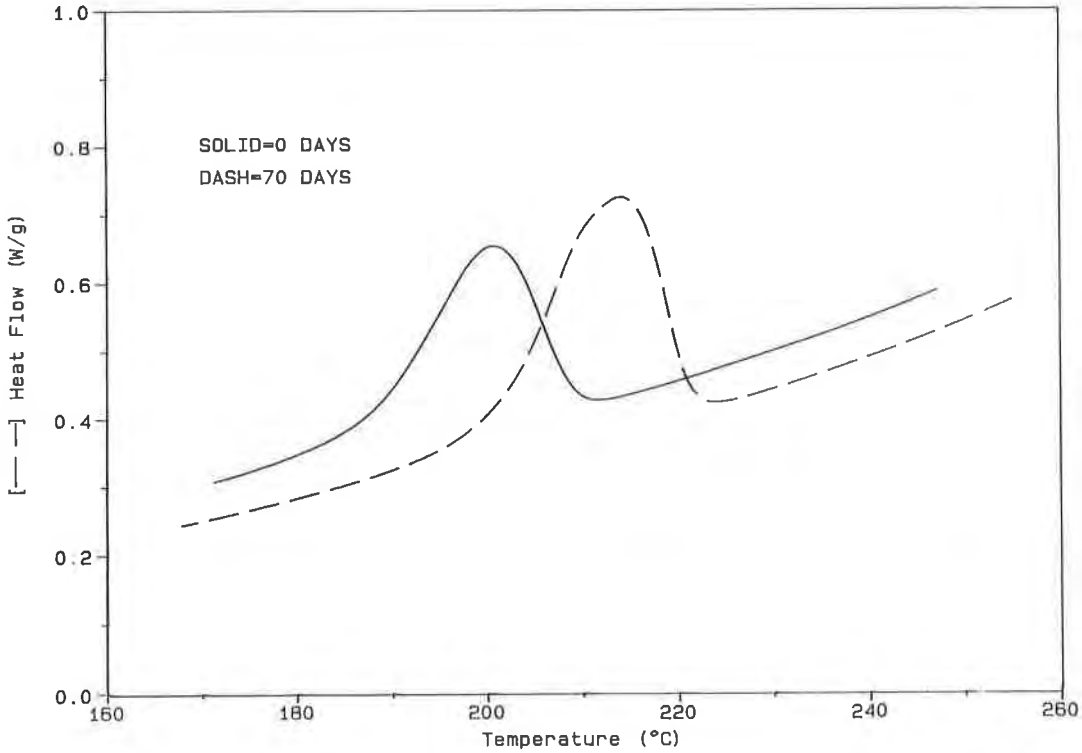

Figure 6. The Effect of Aging in Water at 80°C on the Crystallization of a High Tenacity PET Yarn

Figures 7 and 8 show, remarkably, that this technique may not be limited to polyester materials. Figure 7 shows the effect of 50 days of exposure to 1N sulfuric acid on a nonwoven polypropylene fabric. Notice for this polyolefin, the peak also moved toward increasing temperature, but became smaller and wider after exposure.

Finally, figure 8 shows the effect of U.V. exposure on the behavior of polyethylene. This sample was from a sheet made without carbon black for U.V. protection and was aged in a UVCon machine. For this sample, the peak moved towards lower temperature and became wider. It should be stated that this sample had become brittle around 400 hours of exposure, so the changes seen here had occurred after the sample had reached an advanced state of degradation. However, the DSC technique still shows promise as a general tool for monitoring changes in molecular weight for a variety of materials used in geotechnical applications.

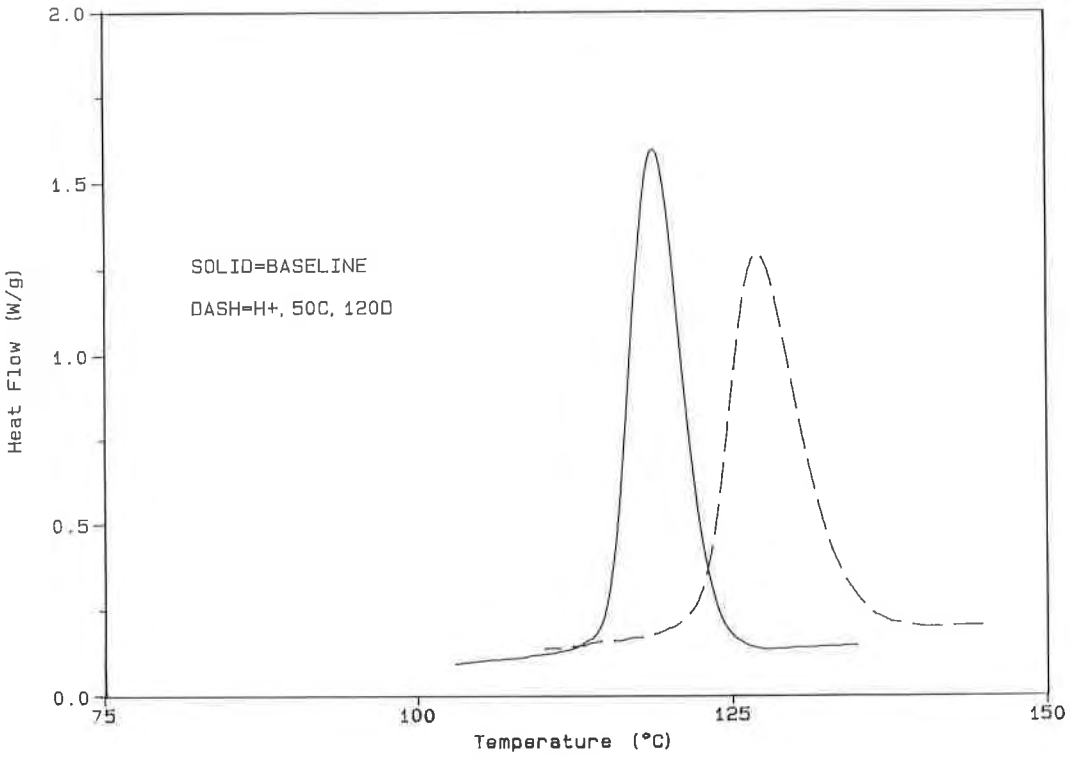

Figure 7. The Effect of 120 Days in 1N Sulfuric Acid at 50°C on a Polypropylene Geotextile

CONCLUSIONS

The research efforts described in this paper serve to validate differential scanning calorimetry as a viable and sensitive tool to detect the onset and monitor the rate of hydrolysis in polyester geotextiles. The major significance of this work may be in the potential of this test method to determine the relative performance of various geotextiles and other geosynthetic products exposed to severe environments. While molecular weight analyses performed using more traditional methods are well established, they are often time consuming and costly. The development of DSC for long term durability studies may provide a very cost efficient alternative for monitoring degradation.

The next phase of this research is in progress. Work is being performed that will compare mechanical properties of geotextiles at various states of hydrolysis-aging to DSC crystallization test results. This effort will seek to establish a relationship between DSC results, molecular weight loss, and material tensile properties. Ultimately, this DSC test procedure may serve to better define long term durability of geosynthetics.

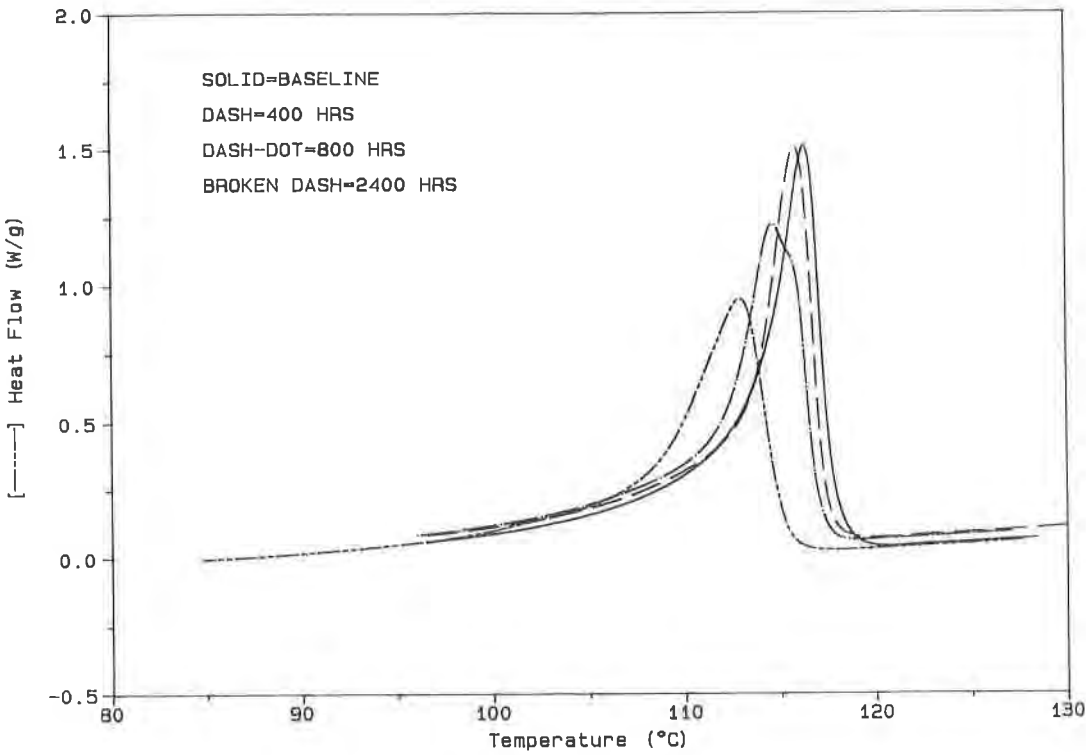

Figure 8. The Effect of U.V. at 50°C on a HDPE Sheet without Carbon Black

REFERENCES

Ansell, M.P.,(1983) "The Degradation of Polyester Fibres in a PVC-Coated Fabric Exposed to Boiling Water", J.Text.Inst., No. 5, pp. 263-271.

Ellison, M.S.,et.al.,(1982) "Physical Properties of Polyester Fibers Degraded by Aminolysis and by Alkaline Hydrolysis", J.Appl.Polym.Sci., Vol.27, pp. 247-257.

Gawish, S.M., and Ambroise, G.,(1986) "Alkaline Hydrolysis of Polyester Fabrics", American Dyestuff Reporter,Feb., pp. 30-32.

Jailloux, J.M., and Verdu, J.,(1990) "Kinetic Models for the Prediction in PET Hygrothermal Ageing: A Critical Survey", Proceed. of the 4th Int. Conf. on Geotextiles, Geomembranes, and Related Products, The Hague, Netherlands, p. 727.

Kelleher, P.G., Wentz, R.P., and Falcone, D.R.,(1982) "Hydrolysis of Poly(butylene terephthalate)",Polym.Eng.Sci.,Vol. 22, No. 4, pp. 260-264.

McMahon, W., et.al.,(1959) "Degradation Studies of Polyethylene Terephthalate", J.Chem.Eng.Data, Vol. 4, No. 1, pp. 57-79.

Risseeuw, P., and Schmidt, H.M.,(1990) "Hydrolysis of HT Polyester Yarns in Water at Moderate Temperatures", Proceed. of the 4th Int. Conf. on Geotextiles, Geomembranes, and Related Products, The Hague, Netherlands, pp. 691-696.

Schneider, H., and Groh, M.,(1987) "An Analysis of the Durability Problems of Geotextiles",Proceed. of the Geosyn. '87 Conf., New Orleans, Louisiana, pp. 434-441.

Thomas, R.W., and Verschoor, K.L.,(1990) "Thermal Analysis of Nonwoven Polyester Geotextiles", in "Geosynthetics: Microstructure and Performance", I.D.Peggs, Ed.,ASTM STP 1076, pp. 4-16.

Zimmerman, H., and Kim, N.T.,(1980) "Investigations on Thermal and Hydrolytic Degradation of Poly(Ethylene Terephthalate)", Polym.Eng.Sci., Vol.20, No.10, pp.680-683.

Construction Induced Reduction in Tensile Strength of Polymer Geogrids

T. Rainey
Tensar Earth Technologies Inc., USA

R. Barksdale
Georgia Institute of Technology, USA

ABSTRACT

A comprehensive full-scale field study to evaluate construction-induced reductions in the tensile strength of polymer geogrids is reported. The study included eleven polymer geogrid materials, three fill materials, two fill thicknesses, and two types of commercial compaction equipment. The tests were conducted in general accordance with procedures recommended by the Geosynthetic Research Institute. The basic sequence of study was as follows: (1) geogrid placement on prepared subgrade; (2) fill placement and compaction; (3) geogrid recovery; and (4) geogrid tensile testing. The tensile testing was performed using the wide-width test method (ASTM) to evaluate both damaged and undamaged geogrid specimens. For the range of materials and conditions studied, reductions of 0 to 50 percent in short-term geogrid tensile strength were found. The results of this study may be used to estimate partial factors of safety on geogrid design strength to account for construction-induced damage.

INTRODUCTION AND SCOPE

The increased use of polymer geogrids has led to the need to better understand their material properties and the potential for short and long-term property changes due to field installation and exposure. For example, polymer geogrids placed in compacted earthworks are susceptible to mechanical damage from fill placement and fill compaction during earthwork construction. Such construction induced damage may cause changes in geogrid properties such as short-term tensile load response, long-term tensile load response (creep), or resistance to chemical or biological degradation. The study reported in this paper focuses on the potential reduction in short-term tensile load response of polymer geogrids caused by construction-induced damage.

The effect of construction-induced damage on the short-term tensile load response is typically quantified by the ratio of the short-term tensile strength of undamaged (control) material to that of damaged material. This ratio is typically used in design as a partial factor of safety applied to the measured tensile strength of undamaged geogrid material. The Geosynthetic Research Institute (GRI) at Drexel University, USA has addressed the issue of construction-induced tensile strength reduction in geogrid materials in its publication GG4(a) (GRI 1990) and GG4(b) (GRI 1991). These standard of practice documents give guidelines for determining the partial factor of safety, FS_{CD}, described above.

The study reported in this paper was conducted using procedures that were generally consistent with GRI's guidelines, in order to determine representative partial factors of safety for construction-induced damage. The only deviations from GRI's guidelines was a 54 sq. ft. sample area was used instead of 100 sq. ft. and 10 specimens were taken for testing instead of 30. This study was comprehensive in that

it included full-scale outdoor testing using eleven polymer geogrid materials, three fill materials, two fill thicknesses, and two types of commercial compaction equipment. The eleven geogrids were commercial products manufactured using different base polymers and different production techniques. The three fill materials were crushed stone, sand, and silty sand. The fills were compacted using: (i) a light walk-behind compactor with approximately 15 cm (6 in.) of fill between the compactor and the geogrid; and (ii) a heavy motor-driven compactor with approximately 25cm (10 in.) of fill between the compactor and the geogrid.

The study progressed in the following general sequence:

- subgrade preparation;
- geogrid bedding layer placement;
- geogrid placement;
- fill placement;
- fill compaction;
- geogrid exhumation;
- geogrid specimen selection;
- specimen tensile testing (ASTM D4595); and
- tensile testing data reduction.

These steps are described in the following sections.

PREVIOUS STUDIES

Construction induced damage testing on polymer geogrids has been conducted by manufacturers, independent researchers, and government agencies. Publication has been limited since some programs were project specific or only qualitatively analyzed (Elias (1990), Allen (1991), Bush and Swan (1988), Watts & Brady (1990), and Wrigley (1987).

Several studies have suggested that the level of damage induced by construction to a polymer geogrid is a function of the following primary factors (Allen 1991, Bush & Swan 1988, Elias 1990):

- Geogrid Thickness
- Compactive effort and lift thickness
- Type and weight of construction equipment used for fill spreading
- Type and weight of compaction equipment
- Grain size distribution of backfill
- Angularity of backfill
- Polymer used in manufacturing the geogrid
- Geogrid manufacturing process

Some specific previous findings include [Allen 1991, Bush & Swan 1988, Elias 1990]:

- Compactive effort has relatively little effect on the loss of strength for sands and silts but for gravelly soils there is an effect.
- The loss of strength increases with decreasing geogrid thickness.
- Lift thickness has relatively little effect on the loss of strength for sands and silts but for gravelly soils there is an effect.
- The loss of strength increases with increasing backfill particle size.
- Partial factors of safety, FS_{CD}, have generally been found to vary between 2.0 and 1.0

The study reported in this paper augments the previously published information on reduction in tensile load capacity of polymer geogrids resulting from construction-induced damage by providing results from a comprehensive and systematic, full-scale testing program.

MATERIALS AND CONSTRUCTION EQUIPMENT

Geogrid Materials. Geogrids were selected for this study to represent common geogrid materials used in construction. The geogrids were obtained in full roll width dimensions. A description of each of the eleven geogrids is provided in Table 1.

Fill Materials. The fill materials were selected for this study to represent a wide range of grain sizes and particle irregularities. The classification (ASTM D2487) of each of the three fill materials was as follows: (i) crushed stone with maximum 5cm (2 in.) particle size - GP (poorly graded gravel), (ii) sand - SP (poorly graded sand) although it very nearly classified as SW (well graded sand), and (iii) residual soil - SC (clayey sand). Grain size distribution curves for these materials are given in Figure 1. The crushed stone and sand were produced by a crushing operation and therefore had angular grains; the angularity of the residual soil is unknown.

Construction Equipment. Commercial earthwork construction equipment was used for this study. A summary of the pieces of equipment used and their application is presented in Table 2.

FIELD TESTING PROCEDURE

The soil types both above and below the geogrids, as stated above, were a fine grained material (Silty Sand) and large grain material (51 mm (2 in.) minus crushed stone) along with an intermediate size material (Concrete Sand). The compaction energy used in placing the fill material above the geogrid was also chosen to represent extremes and will be discussed later.

Subgrade Preparation. The site chosen for the test was a vacant level lot already graded for the future location of an office building. The on-site silty sand was chosen as one of the fill materials. The test bay areas were surveyed and staked to the dimensions as shown in Figure 2. Before placement of a 10.2 cm (4 in.) fill, constructed with the respective material for each bay, all three bays were rolled with a large sheeps-foot vibrating roller (Bomag BW 213PD) five times to provide a sound and competent subgrade free from soft spots or pumping. Next, a large, smooth drum vibrating roller (Bomag BW 212D) was used to smooth out the subgrade to permit the actual measurement of the 10.2 cm (4 in.) fill to be placed over the subgrade. This process took approximately three passes of the roller to provide a firm subgrade and adequate support needed for the test areas.

Initial Four Inch Fill Placement. The initial 10.2 cm (4 in.) lift of crushed stone in bay number 1 and sand in bay number 2 was placed and spread by a small front end loader (New Holland L783) and motor grader (CAT 12G). The crushed stone and silty sand were first leveled and prepared for the compactor. The large smooth drum vibrating roller, used previously for the proof-rolling, traversed the crushed stone and sand bays with four passes back and forth. The crushed stone and silty sand showed no signs of movement, sinking, or heaving. The objective was to obtain 95% standard proctor compaction. The silty sand bay was already prepared from the proof-rolling noted above. Therefore, it was not traversed again since the on-site material is the fill required.

Placement Of Geogrids. The geogrids were placed on top of the 10.2cm(4 in.) of prepared fill previously described. The geogrids were obtained in full roll width dimensions from their manufacturer or distributor.

Care was taken during mobilization and cutting of the geogrids to not induce any damage. The geogrids were cut to their appropriate size for each bay with the across the roll direction as the 1.4 m (4.5 ft.) minimum dimension. The specimens were cut in the longitudinal direction if required to meet the 1.4m (4.5 ft.) dimension. The geogrids were cut with a gasoline powered rotary blade saw using a masonry blade. The control geogrid sections were cut also at this time and tagged for identification. Control geogrid sections were taken from the same roll as the sections to be buried. The geogrid specimens to be buried were also tagged to identify in which bay they were located. The geogrids were all made long enough to allow 3.7 m (12 ft.) for the 15.3

Table 1. Geogrid structure, polymer type, and properties

Geogrid	Structure Type	Polymer Type*	Mass/Unit Area* ASTM D3776-84 g/m^2 (oz/yd^2)	Aperture Size* mm (in) MD	Aperture Size* mm (in) XD	Thickness* ASTM D1777-64 mm (mils) At Rib	Thickness* ASTM D1777-64 mm (mils) At Junction
A	Uniaxial	PE	858(25.3)	241.3(9.50)	16.8(0.66)	2.03(80)	5.46(215)
B	Flexible	P-AL	203.4(6)	25.4(1.0)	20.3(0.8)	1.4(55)	1.52(60)
C	Uniaxial	PE	1065(31.4)	137.2(5.40)	16.8(0.66)	1.78(70)	5.84(230)
D	Flexible	P-AL	390(11.5)	22.5(0.9)	21.5(0.85)	2.2(85)	2.3(90)
E	Uniaxial	PE	824(24.3)	144.7(5.70)	16.8(0.66)	1.27(50)	4.32(170)
F	Flexible	P-PVC	475(14.0)	60.7(2.39)	25.6(1.01)	1.05(42)	1.30(51)
G	Uniaxial	PE	495(14.6)	144.7(5.70)	16.8(0.66)	0.76(30)	2.79(110)
H	Flexible	P-PVC	508(15.0)	22.8(.9)	22.8(.9)	2.54(100)	3.30(130)
I	Biaxial	PP	306(9.0)	25(1.0)	33(1.3)	1.27(50)	4.0(16.0)
J	Biaxial	PP	215(6.4)	25(1.0)	33(1.3)	0.75(30)	2.8(110)
K	Flexible	P-PVC	746(22.0)	81.3(3.2)	7.62(.3)	N/A	N/A

*Information taken from Geotechnical Fabrics Report, December 1991.

PP - Polypropylene
PE - Polyethylene
PET - Polyester
P-PVC - Polyester, PVC-Coated
P-AL - Polyester, Acrylic Latex Coated
MX - Machine Direction
XD - Cross Machine Direction

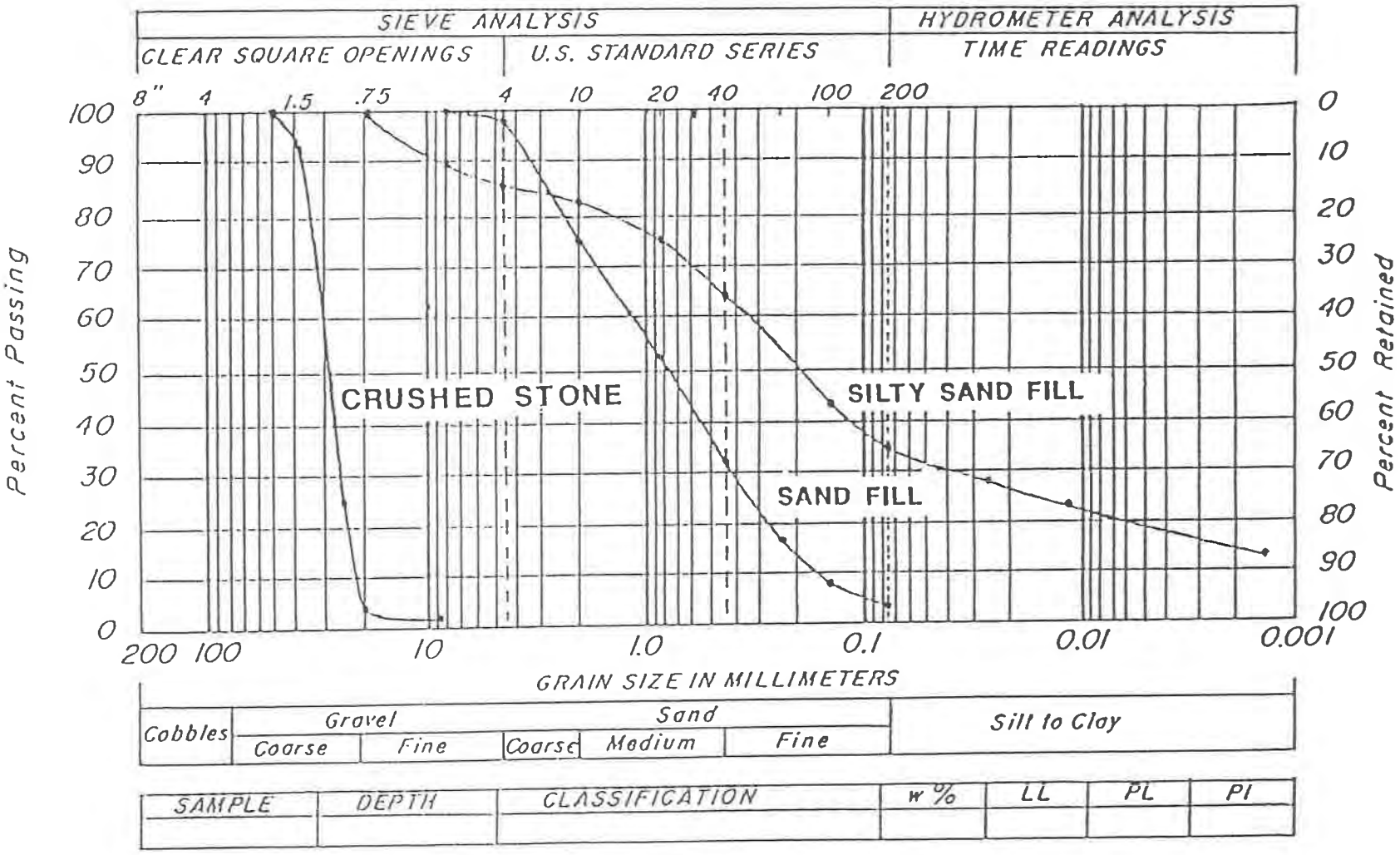

Figure 1. Gradation test results

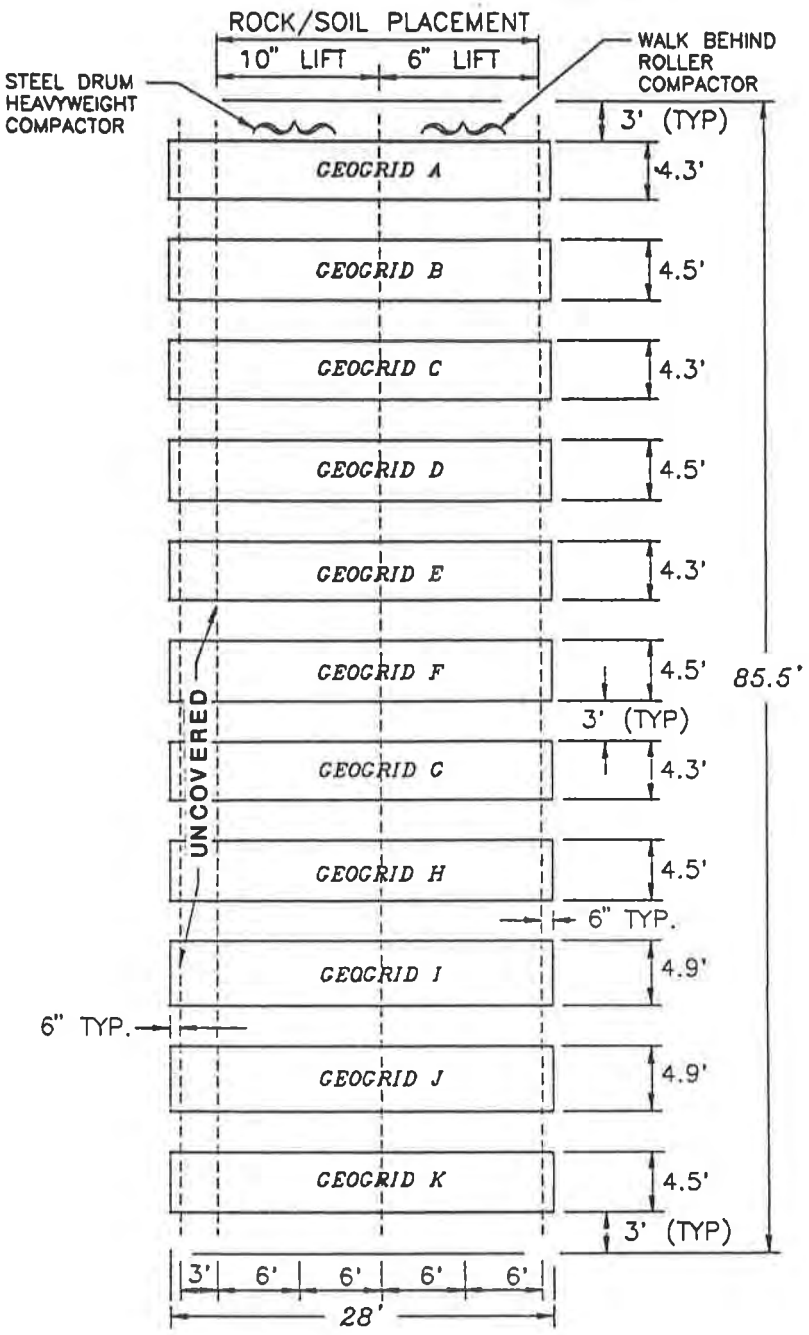

Figure 2. Bay layout for each fill material

Table 2. Summary of construction equipment used for study

Type	Manufacturer	Model	Use in Study
Front end loader	New Holland	L783	fill placement
Front end loader	Gehl	4615	fill placement
Motor grader	Caterpillar	12G	subgrade prep. geogrid traff.
Motor driven Vibratory drum compactor	Bomag	BW212D	crushed stone and sand compaction
Walk-behind vibrator drum compactor	Wacker	W55	crushed stone & sand compaction
Motor-driven sheeps-foot compactor	Bomag	BW212PD	residual soil compaction
Walk-behind sheeps-foot compactor	Thomas	SDT30	residual soil compaction

cm (6 in.) and 25.4 cm (10 in.) lift areas. All geogrids were laid parallel to each other and separated by 0.91 m (3 ft.) to allow walking room and permit the front end loader to strattle the geogrid while placing fill on top. Also, the loader did not have to traverse on top of one geogrid more than another using this approach. Placing the geogrids parallel in this manner allowed the compactor to pass perpendicular to all the geogrids with each pass giving each geogrid the same compactive effort.

Fill Placement. Fill was placed on top of the in place geogrids by a small front end loader always beginning on the 15.3 cm (6 in.) lift side and working toward the 25.4 cm(10 in.) side. Some of the geogrids were slightly wider than others. For this case, the loader operator when traversing over the fill material, already placed on the geogrid, kept the wheels on the outside edges of the geogrid. Therefore, specimens had to be taken from the center of the geogrid to avoid areas traversed more by the loader. Approximately 7 to 10 trips with the small loader were required to place all of the fill required to cover both the 15.3 cm (6 in.) and 25.4 cm (10 in.) thick lift areas for each geogrid. The material was placed working from the 15.3 cm (6 in.) lift side with a single lift. The fill height of each bay was monitored with a measuring tape keeping the lifts as close as possible to the required depth.

Fill Compaction. Compaction of the crushed stone bay began first using the large BoMag smooth drum vibratory roller. The compactor traversed the 25.4 cm (10 in.) thick lift area of the bay four times for each drum width until the entire area was covered. After the last pass over the lift, no movement, sinking, or heaving occurred indicating the crushed stone was well compacted.

The 15.3 cm (6 in.) thick lift area was compacted with the same number of passes on each drum path width until the entire area was covered. However, the compaction equipment used was a walk behind smooth drum vibratory roller (Wacker W55). The sand bay was compacted following exactly the same procedures as the crushed stone bay.

The silty sand bay was compacted with the same method as the crushed stone and sand except a sheeps-foot roller was used rather than a smooth drum roller. The 15.3 cm (6 in.) thick lift area was compacted with a walk-behind dual-drum Thomas SDT30 sheepsfoot vibratory roller. The 25.4 cm (10 in.) thick lift area was compacted with the large BoMag sheeps-foot vibrating roller.

Exhuming Geogrids. The geogrids buried in the crushed stone fill were exhumed first. Initially, the use of hand shovels was attempted to exhume the geogrids, but was found to be very difficult and time consuming. A front end loader was also tried, but caused shifting of the crushed stone directly on top of the geogrid, which could have resulted in additional damage. The area of geogrid where these exhuming procedures were carried out was on the edges which were not in the area specimens were taken. Therefore, a third method was employed which consisted of using water from a local fire hydrant to wash the crushed stone off of the geogrid. The water did create the movement of gravel on top of the geogrid once the overburden of gravel was removed. However, there was very little vertical normal force on the gravel moving on the geogrid since the water was sprayed from the side. Therefore, additional damage was minimized being no more than damage induced from placing the gravel on the geogrid. Also, any damage induced would be relatively even along all geogrids. This technique worked well and was used to remove all of the crushed stone from above the geogrids. This method was also employed for the sand bay.

The washing method was also attempted to remove the fill on top of the geogrids with the silty sand. Washing, however, only separated the few rocks in the silty sand which could have possibly further damaged the geogrids more than the fine materials. Therefore, all of the geogrids buried in the silty sand were exhumed by hand. During hand excavation, shovels damaged the geogrid periodically. Damaged geogrid areas were immediately painted so that specimens taken for later testing would not come from damaged areas.

Before removal, a white line was also painted on the top side of each geogrid at the uncovered end. Therefore, the orientation of the geogrid in the bay would be known in the testing laboratory. All geogrids were immediately rolled up and taken to the testing laboratory for safe storage.

TESTING

Eighty-five percent of the geogrid tests were run in the Quality Control laboratory at the Tensar Corporation under the direction of GeoSyntec Consultants who helped set up equipment and observe the initial wide width tests. The remaining geogrid tests were performed by GeoSyntec Consultants in their Boynton Beach, Florida laboratory.

Compaction tests and grain size distribution tests were performed on the fill material and wide-width tensile tests (ASTM D4595) were performed on the geogrids. This testing program and its results are briefly described below.

Fill Material. Before exhuming the geogrids, tests were performed on the fill materials to determine their lift height and density in place. The average height for the 15.3cm (6 in.) lift areas was 17.5cm (6.9 in.) and for the 25.4cm (10 in.) lift areas 23.0cm (9.4 in.). The average density of the compacted sand was 93.2% of standard proctor maximum dry density and 88.7% for the silty sand. The desired compaction was 95%. Moisture content of the silty sand was wet of optimum and probably prevented the desired result. The crushed stone was not tested for compaction.

Geogrid Laboratory Testing Procedures. Prior to cutting the exhumed samples for wide-width testing, they were washed down with water to remove any soil and debris approximately three days after exhumation. The geogrids were then rolled back up and stored in a warehouse storage area where temperatures varied from a minimum of 16^0C (60^0F) to a maximum of 32^0C (90^0F). The lighting was standard Halogen bulbs typically used in warehouse lighting. While in storage, the geogrids from each lift height were all photographed for documentation and for future viewing of construction induced damage.

A layout for cutting specimens from each geogrid was predetermined to obtain specimens as close to the centerline of the geogrid test strip and centered along each section within the test strip. The specimens were cut beginning at the center of the 15.3 cm (6 in.) and 25.4 cm (10 in.) lift areas. Also, the center line along the 8.5

m (28 ft.) dimension was located to avoid specimens along the edges. Because this testing was controlled, a random sampling location was not as important as being consistent from one geogrid to the next. Ten (10) samples were taken from the six (6) inch lift area as well as the ten (10) inch lift area. Forty (40) specimens were taken from each control for each geogrid. Again, ten (10) additional specimens were taken from the biaxial geogrids to account for the machine and cross machine directions.

The exhumed geogrids were then systematically tested to determine their ultimate tensile strength. In total, over 1000 wide width tensile tests were performed over a period of approximately 15 months.

Uniaxial and biaxial geogrids are typically tested with wedge-type clamps. The same clamps were used for this study. The flexible geogrids however, are typically tested with roller clamps. Therefore each of these three classes of geogrids involved different testing equipment and are discussed separately.

The uniaxial stiff geogrids were cut out and labeled before the tensile testing began. The desired test results were (1) Tension force at 2% strain; (2) Tension force at 5% strain; (3) Tension force at Ultimate; and (4) Strain at Ultimate.

The test used for all geogrids was ASTM D4595 - "Test Method for Tensile Properties of Geotextiles by the Wide-Width Strip Method". This test was chosen because as noted in Elias (1990): "Examination of the standard deviation of test results for exhumed samples in each test indicates that the wide-width tensile test results exhibit the smallest standard deviations of the index test performed and therefore should be used as the sole index for calculation of retained strength". The conditions under which the uniaxial geogrid tests were performed are typical of uniaxial stiff geogrid tests and are summarized in Table 3. Using established testing conditions will produce better control. For example, the clamps used for the uniaxial stiff geogrids produced failures throughout the specimen length being tested.

The conditions under which the flexible geogrid tests were performed are also typical for their specific structure and stiffness. The flexible geogrid testing conditions are summarized in Table 4. Similarly, the testing conditions for the biaxial stiff geogrids are found in Table 5.

LABORATORY TEST RESULTS

Construction induced damage factors of safety were determined by comparing wide-width tensile strengths on undamaged and damaged geogrid specimens as outlined in GG4 [GRI 1990, GRI 1991]. Comparisons can not be made from the observed tensile force at different strain values since correlations were not made to variables like specimen size and preload values. Therefore, an evaluation of the strains measured during the wide width tests was not made. Only the tensile force at ultimate is used in evaluating construction induced damage.

The partial factor of safety for construction induced damage (FS_{ID}) is computed as follows [GRI 1990, GRI 1991]:

$$FS_{ID} = T(\text{Original}) \,/\, T(\text{Exhumed}) \qquad (1)$$

Where:
T (Original) = Original ASTM D4595 tensile strength (Force/Unit Length)
T (Exhumed) = Exhumed ASTM D4595 tensile strength (Force/Unit Length)

The average geogrid tensile force per unit length at ultimate is given for each group of test specimens in Table 6. These wide-width tensile strength values were used in equation (1) to calculate the factors of safety for each geogrid and can be found in Table 7. The difference in geogrid types and fill material is readily apparent when comparing values in Table 7.

Upon removal of the geogrids from the fill material, more damage was visually observed on those geogrids found in the crushed stone areas than in any other. There were broken ribs, splits, bruises, and scuff marks. The geogrids buried in sand and silty sand showed less visual damage.

Table 3. Testing Conditions for uniaxial stiff geogrids

Preload - (Load applied before test to remove slack)	Geogrid G - 0.122 kN 27.5 lbs. Geogrid E - 0.194 kN 43.7 lbs. Geogrid C - 0.252 kN 56.7 lbs.
Gauge Length -	Geogrid G - Control 312.1mm (Avg.) Geogrid G - Exhumed 309.0mm (Avg.) Geogrid E - Control 346.1mm (Avg.) Geogrid E - Exhumed 347.6mm (Avg.) Geogrid C - Control 319.9mm (Avg.) Geogrid C - Exhumed 320.9mm (Avg.)
Clamps -	Wedge-type wide-width jaws with serrated faces. No LVDT used.
Machine Speed	Crosshead speed - 10% of gauge length +/- 3% per minute.
Specimen Width - (Note: Measurement for width are to include 8 ribs (outer rib to outer rib)).	10 ribs cut - but 8 ribs tested. Avg. specimen width - 15.6 cm (6.13 inches).

Table 4. Flexible geogrid testing conditions

Preload - 222 N (50 lbs.)
Gauge Length - 101.6mm (4 inches)
Clamps - Roller Grips with LVDT
Speed - 10mm (4 inches)/min.
Specimen Width - Approximately 20.3 cm (8 in.)
(depending on grid type-to the nearest rib).

Table 5. Testing conditions for stiff biaxial geogrids

Preload - 1.25% of ultimate Tensile strength

	MD	TD
Geogrid J	42N(10 lbs)	59N(13 lbs)
Geogrid I	59N(13 lbs)	90N(20 lbs)

Gauge Length - Biaxial Grids (mm)

Control	MD	TD
Geogrid J	114.0	118.1
Geogrid I	114.1	121.9

Crushed Stone	MD	TD		MD	TD
Geogrid J			Geogrid I		
25.4 cm (10 in.)	114.6	117.0	25.4 cm (10 in.)	116.1	121.9
15.3 cm (6 in.)	114.4	118.8	15.3 cm (6 in.)	113.8	114.5
Traffic	117.0	119.3	Traffic	112.3	114.3

Sand	MD	TD		MD	TD
Geogrid J			Geogrid I		
25.4 cm (10 in.)	113.2	118.3	25.4 cm (10 in.)	116.1	121.9
15.3 cm (6 in.)	114.7	118.8	15.3 cm (6 in.)	113.5	117.2
Traffic	117.7	121.0	Traffic	113.0	115.7

Silty Sand	MD	TD		MD	TD
Geogrid J			Geogrid I		
25.4 cm (10 in.)	112.3	118.1	25.4 cm (10 in.)	113.1	114.6
15.3 cm (6 in.)	113.9	118.0	15.3 cm (6 in.)	114.5	114.6
Traffic	116.0	119.0	Traffic	112.3	115.0

Clamps - Channel jaw-no LVDT used
Machine Crosshead Speed - 10% ± 3%/min of gauge length (11 or 12 mm/min)
Specimen Width - Approximately 20.3 cm (8 in.) to 24.1 cm (9.5 in.) (Depending on apertures to the nearest rib)
MD - Machine Direction
TD - Transverse or Cross machine direction

Table 6. Polymer Geogrids Tension at Ultimate (lbs/ft)
(Conversion to SI units: lbs/ft*14.5939 = M/m)

Geogrid	Control	Sand Fill 6" Lift	Sand Fill 10" Lift	Crushed Stone Fill 6" Lift	Crushed Stone Fill 10" Lift	Silty Sand 6" Lift	Silty Sand 10" Lift
A	8929.0	8378.1	8516.2	8305.2	7400.4	8654.1	8414.5
B	2181.6	1687.3	1898.9	1458.4		Lost/Sam.	2069.4
(Gravel 10" Lift)	2414.5				1196.4		
C	8240.9	8308.8	8295.0	7861.1	7282.9	7857.6	7860.7
D	7376.6	5388.2	5546.1	4976.4		6536.5	6423.0
(Gravel 10" Lift)	7005.1				3723.5		
E	6405.3	5736.4	5703.5	5607.8	4947.9	6223.4	6007.4
F	6355.8	5215.0	5482.0	5043.0	3852.7	5572.0	5571.0
G	3614.4	3466.2	3547.0	3374.4	2541.1	3614.8	3495.9
H	4583.1	4274.6	3824.8	3397.8	2471.3	4831.7	4474.9
I - TD	2329.3	2387.7	2326.0	2310.8	2051.3	2278.0	2100.9
I - MD	1369.7	1461.4	1443.1	1406.6	1166.9	1389.5	1373.5
J - TD	1500.0	1535.2	1517.9	1381.5	1031.9	1485.6	1359.7
J - MD	875.3	937.1	934.0	906.0	636.5	894.7	880.9
K	13217.2	10173.0	10850.0	8604.0	7321.0	12439.0	12104.0

Table 7. Computed Construction Damage Factors of Safety

Geogrid Type		Control	Sand Fill 6" Lift	Sand Fill 10" Lift	Crushed Stone Fill 6" Lift	Crushed Stone Fill 10" Lift	Silty Sand 6" Lift	Silty Sand 10" Lift
A		1.00	1.07	1.05	1.08	1.21	1.03	1.06
B		1.00	1.29	1.15	1.50		ERR	1.05
		1.00				2.02		
C		1.00	0.99	0.99	1.05	1.13	1.05	1.05
D		1.00	1.37	1.33	1.48		1.13	1.15
		1.00				1.88		
E		1.00	1.12	1.12	1.14	1.29	1.03	1.07
F		1.00	1.22	1.16	1.26	1.65	1.14	1.14
G		1.00	1.04	1.02	1.07	1.42	1.00	1.03
H		1.00	1.07	1.20	1.35	1.85	0.95	1.02
I	- TD	1.00	0.98	1.00	1.01	1.14	1.02	1.11
	- MD	1.00	0.94	0.95	0.97	1.17	0.99	1.00
J	- TD	1.00	0.98	0.99	1.09	1.45	1.01	1.10
	- MD	1.00	0.93	0.94	0.97	1.38	0.98	0.99
K	- TD	1.00	1.30	1.22	1.54	1.81	1.06	1.09

Of particular interest were the coatings which were on the polyester geogrids. Upon removal from the fill, some of the geogrids coatings were cracked. Refer to Figure 3.

CONCLUSIONS

The comprehensive and systematic full-scale field study produced important data on the use of polymer geogrids in three different fill materials. The biggest effect contributing to damage of polymer geogrids during construction was the fill material. As expected, the most construction induced damage to the geogrids occurred in the crushed stone fill. For all geogrids studied, the average construction induced safety factor for the 25.4 cm(10 in.) thick crushed stone fill was 1.46 compared to only 1.07 for the concrete sand fill and 1.06 for the naturally occurring silty sand. Also, construction induced damage varied from 1.00 to 2.02 for geogrids placed within the crushed stone fill (Table 7). This wide variation in construction induced damage was related to the type of geogrid used and clearly indicates that careful geogrid selection is important in insuring good structural performance. The crushed granite gniess used in the study was gap graded and had a 5.1mm (2 in.) top size and only about 4% passing the 0.75 in. sieve (Figure 2). In contrast, the concrete sand was well graded and subangular in shape with about 98% passing the No. 4 sieve and 4% passing the No. 200 sieve. The silty sand was also subangular and had about 100% passing the 0.75 in. sieve and 35% passing the No. 200 sieve. The particles greater than about the 3/8 in. sieve size tended to be subrounded. Aggregate size, gradation and perhaps even angularity affected the construction induced safety factor.

The contribution to construction induced damage from compaction equipment and lift height was almost negligible for the concrete sand and silty sand materials. The light weight equipment had comparable degrees of damage to specimens as did the heavy weight equipment. Therefore, agreement was found with references cited that compaction for sands and silts do not have a large impact on construction induced damage. Also in agreement with references was for the crushed stone fill, the 25.4 cm (10 in.) thick lift, subjected to the heavy compaction equipment, experienced an average reduction in wide width tensile strength 21 percent greater than the 15.3 cm (6 in.) thick lift compacted with lightweight equipment. However, using the light compaction equipment with the thin lift may be nearly equivalent to using the heavy compaction equipment with the thick lift. Therefore, a more comprehensive test could be made varying lift thickness with the same compaction equipment or vice versa to even better investigate the compaction and lift thickness contribution to induced damage.

Comparing the standard deviation for the control to each respective damaged specimen, the damaged specimens on average had a standard deviation of 3.5 times the control. The damage tends to create more deviation of tensile strength from specimen to specimen, which this illustrates. The average standard deviation for the control specimen tensile tests was 3.2% of ultimate tension compared to 11.7% of ultimate tensile strength for the damaged specimens. When comparing control and damaged specimen results, the modulus (slope of the stress strain curve) for all geogrids is in general the same or greater up to the ultimate tensile strength.

Coatings on some of the polymer geogrids when present cracked and came completely off when buried in fill material. The severity of cracking tends to increase with the particle size of the fill. Therefore, caution should be used when relying on the coating to provide protection of the geogrid strands or ribs particularly when large aggregate is used.

In conclusion, the factors of safety given in Table 7 can be used for general guidance for determining an approximate value to use in design. However, site specific testing should continue to be used in critical applications especially where a large, angular aggregate is used.

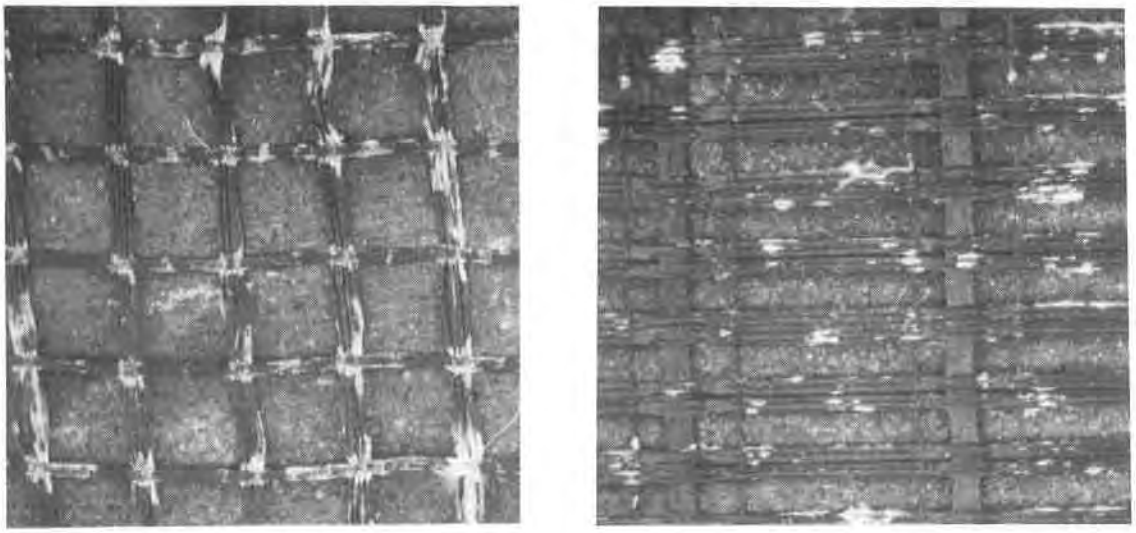

Figure 3. Cracking of coating in some of the exhumed polyester geogrids

References

Allen, Tony M. (1991) "Determination of Long-Term Tensile Strength of Geosynthetics: A State-of-the-Art Review". Geosynthetics '91 Conference, Atlanta, Georgia. pgs. 351-379.

Bush, D.I. and Swan, D.B.G. (1988) "An Assessment of the Resistance to Physical Damage During Construction of Tensar SR55, SR80, and SR110 Geogrids."

Bush, D.I. and Swan D.B.G. (1988) "An Assessment of the Resistance of Tensar SR2 to physical damage during the construction and testing of a reinforced soil wall."

Bush D.I. (1988) "Evaluation of the effects of construction activities on the physical properties of polymeric soil reinforcing elements." International Geotechnical Symposium on Theory and Practice of Earth Reinforcement, Fukuoka, Japan.

Elias, Victor, (1990) "Durability/Corrosion of Soil Reinforced Structures." Prepared for U.S. Department of Transportation Federal Highway Administration, FHWA-RD-89-186.

Geosynthetic Research Institute (1990). GRI Standard Practice GC4 (a), "Determination of the Long-Term Design Strength of Stiff Geogrids."

Geosynthetic Research Institute (1991). GRI Standard Practice GC4 (b), "Determination of the Long-Term Design Strength of Flexible Geogrids."

Geotechnical Fabrics Report (December 1991). 1992 Specifiers Guide, Published by the Industrial Fabrics Association International, Volume 9 Number 9.

Watts, G.R.A. and Brady, K.C., (1990) "Site Damage Trials on Geotextiles". Proceedings of the Fourth International Conference on Geotextiles, Geomembranes and Related Products, The Hagne, pp. 603-607.

Shelton, W.S. and Wrigley, Nigel E., (1987) "Long-Term Durability of Geosynthetics Soil Reinforcement," Conference Proceedings of Geosynthetics '87, New Orleans, LA.

Installation Damage Testing of Four Polyester Geogrids in Three Soil Types

D. Sandri
Mirafi, USA

J.S. Martin
Mirafi, USA

C.W. Vann
Perini International Corp., USA

M. Ferrer
Ingeneria Epacta, Venezuela

I. Zeppenfeldt
Oficina De Ingenieria, Venezuela

ABSTRACT

Utilization of geogrids for reinforcement of soil structures has become a common method of construction. However, determining appropriate reduction factors for calculating design strength requires field testing. One factor which is project specific and varies with each site is construction induced damage (FS_{ID}). Investigation of resistance to installation damage for four polyester geogrids with three different soil types was conducted. The work was conducted on one project under very controlled conditions.

Nineteen tests on four geogrid types installed in three soils were conducted for the study. Compaction equipment and fill lifts similar to those proposed for final construction were used to simulate field conditions. Removal of the geogrids samples was conducted by laborers using shovels, brooms, and picks.

Strength testing of the damaged and new geogrid samples was done in accordance with single rib tensile testing methods. Strength results indicate installation damage factor of safety ranging from 1.05 to 1.18.

INTRODUCTION

Proper determination of "working" strength (Long Term Allowable Design Load (LTADL)) of geogrids is critical to the successful design of geogrid reinforced soil structures. Current design philosophy in the determination of geogrid working strength is influenced by guidelines from the Federal Highway Administration (Christopher, 1990), Task Force 27 (1989), and Geosynthetics Research Institute (Koerner, 1990). Each of the respective organizations have selected a partial factor-of-safety approach to be applied against a laboratory determined ultimate geogrid strength. An example of the partial factor-of-safety calculation is provided below, see Koerner (1990):

$$T_{allow} = \frac{T_{ULT}}{FS_{ID} \times FS_{BD} \times FS_{CD} \times FS_{CR} \times FS_{JNT}}$$

where;

T_{allow} = allowable strength for design
T_{ULT} = ultimate strength determined from wide width or single rib tensile tests
FS_{CR} = partial factor-of-safety for creep deformation
FS_{ID} = partial factor-of-safety for installation damage
FS_{BD} = partial factor-of-safety for biological degradation
FS_{CD} = partial factor-of-safety for chemical degradation
FS_{JNT} = partial factor-of-safety for joints (seams or connections)

The partial factors-of-safety for creep, installation damage, chemical degradation and biological degradation are affected by the soil properties within which the geogrid is placed and desired service life. These partial factors-of-safety are selected based on polymer type, design service life, and site specific testing. The partial factor of safety for joints is applied only when seaming or joining of geogrid (strength direction) is employed.

This paper focuses on providing specific installation damage test results for flexible geogrids manufactured from high tenacity polyester fibers coated with acrylic latex. More specifically, this paper discusses the test sequence and results of actual installation damage testing of four polyester geogrids in up to three different soil types.

The term "installation damage" is considered to encompass only that loss in strength associated with installing the geogrid. This includes damage incurred by cutting the geogrid to size, placing the geogrid on the subgrade, and placing (compacting) soil over the geogrid. Christopher and Holtz (1984) refer to the strength loss during installation as "survivability" which they define as "resistance to damage during construction and initial operation".

Other terms included in Equation 1 which affect the allowable design strength are addressed by Sutton and Leclercq (1982), Wisse and Birkenfeld (1982), Brorsson and Eriksson (1986), Bonaparte and Berg (1987), Bonaparte, et al. (1988) Wrigley (1989), Voskamp and Risseeuw (1987). For more information on partial factors of safety (other than FS_{ID}) the above papers may be reviewed.

BACKGROUND

Installation damage testing discussed herein was completed in conjunction with construction of massive reinforced soil slopes and walls required for grading of the new U.S. Embassy compound in Caracas, Venezuela. As part of the geogrid (soil reinforcement) approval process, the U.S. State Department (project owner) required comprehensive submittal information substantiating each of the terms in equation 1. The purpose of this work was determination of geogrid FS_{ID}. The FS_{ID} information was required to support product submittals for slope and wall reinforcements.

MATERIALS

The specifications for reinforced structures included two types of soil material into which the geogrid would be placed. The two soil materials were referred to as "Rock Fill" and "Slope Drain Material".

Rock fill was required to construct the mass of reinforced soil structures. The "Rock Fill" was obtained from on-site and is composed of angular particles (ASTM D-2448) of weathered calcarious granitic schist with intrusions of quartz. The "Rock Fill" was excavated from the mountain side during the grading process. The original specification gradation requirements as well as sample gradation curves are noted in Figure 1.

The second soil type, "Slope Drain Material", was required to accommodate drainage within the structures. Slope Drain Material had to meet original specification gradation requirements as shown on Figure 2. Example gradation curves for two borrow sources (Araguita pit and Cantera Nacional) are also included on Figure 2. The material obtained from the Araguita pit consist of subangular particles (ASTM D-2488) while the materials obtained from the Cantera Nacional source were crushed and exhibit angular to highly angular (ASTM D-2488) characteristics. Figure 3 is a photo of Slope Drain material obtained from the Araguita Pit.

The project specifications for geogrid allowed a variety of geogrid types. However, the specifications were very clear that substantiating back-up information would be required to support technical claims. The minimum requirements for the geogrid are noted below:

Aperture Size	-	≥ 15.2 mm
Percent Open Area	-	≤ 60%
Sliding Coefficient	-	0.7
Coating	-	Internal (provide creep tests showing that coating and base material act as a unit.
Long Term Allowable Design Load	-	14.6 kN/m to be calculated per GRI GG-4
Maximum Allowable Total Strain	-	Not more than 5% at sustained LTADL of 14.6 kN/m after 15,000 hours.

Made in America clauses in the specification required that U.S. made materials be sourced whenever possible.

The geogrids selected for the project consist of bi-directional flexible geogrids manufactured from high tenacity polyester multifilament yarns. The geogrids are coated with an acrylic latex finish which enhance their resistance to UV, biological and chemical attack. The geogrid physical properties are listed in Table 1.

Scrutiny of FS_{ID} data supplied during the review/submittal process and questions relative to its applicability to aggressive, angular, granular soils anticipated on this project necessitated that on-site field testing be conducted.

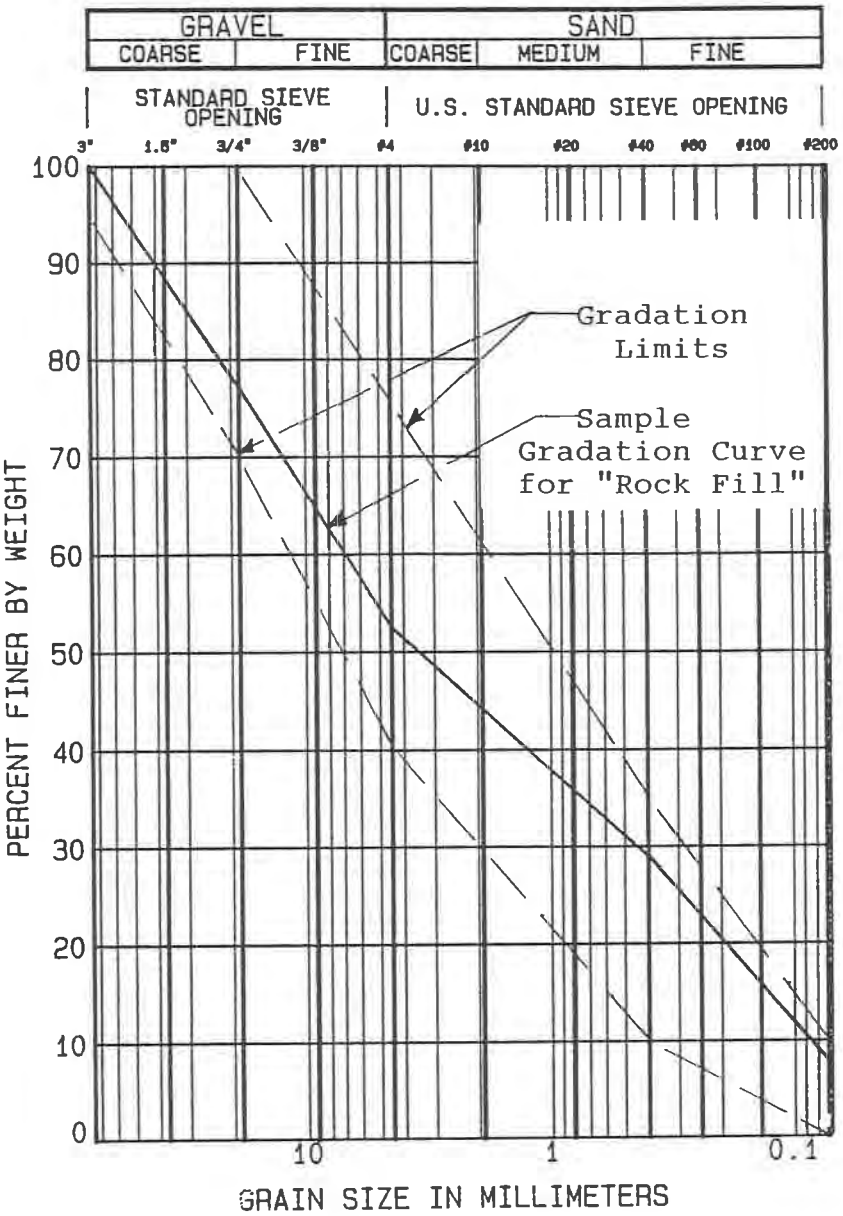

Figure 1. Soil Gradation Curve for Rock Fill Material

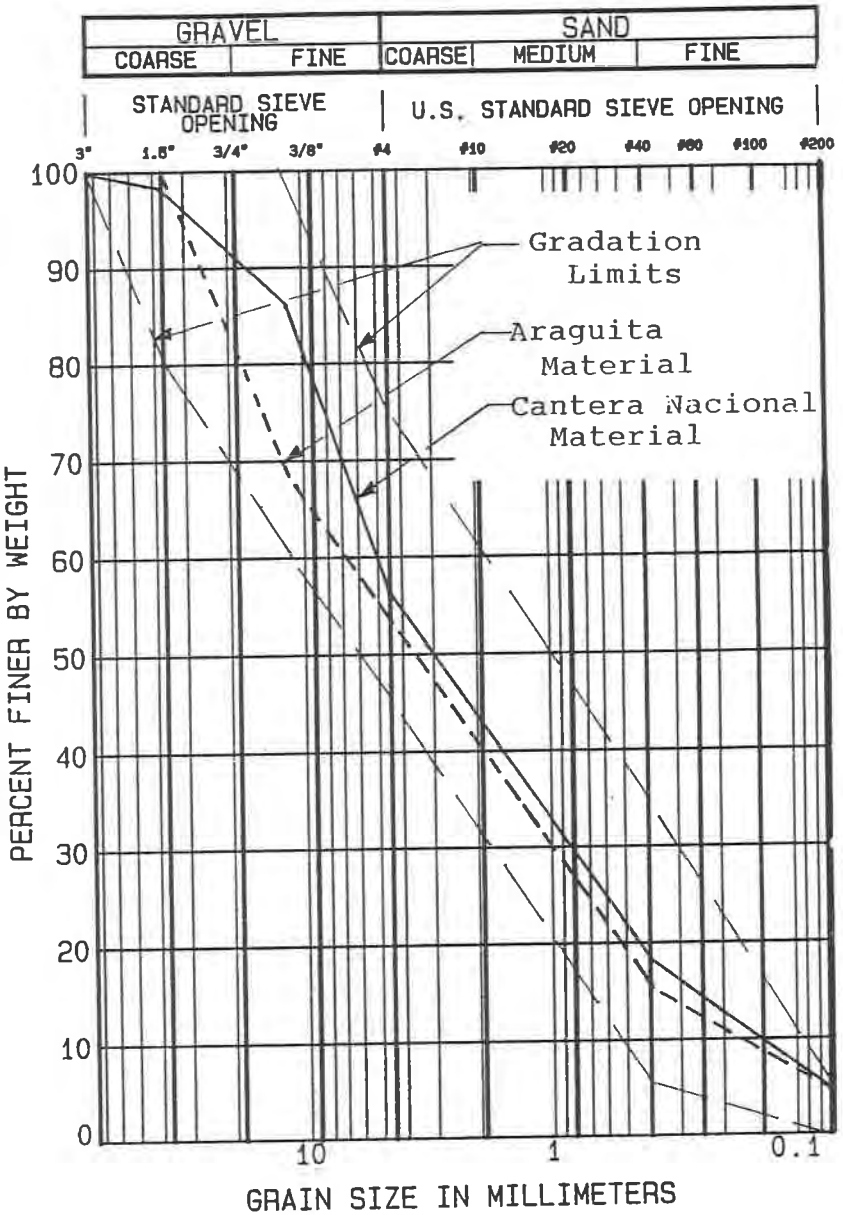

Figure 2. Soil Gradation Curve for Slope Drain Material

Figure 3. Stockpiled Araguita Pit Slope Drain Material

Figure 4. Placement of Slope Drain Material on Installation Damage Test Pad

TABLE 1 - Geogrid Properties

PROPERTY	UNIT	TEST METHOD	GEOGRID A		GEOGRID B		GEOGRID C		GEOGRID D	
			WARP	FILL	WARP	FILL	WARP	FILL	WARP	FILL
Rib Tensile Strength	kN/m	GG1/ASTM D-4632	31.37	24.80	54.70	43.80	109.40	43.80	138.60	43.80
Rib Tensile Elongation	%	GG1/ASTM D-4632	21.00	26.00	18.00	16.00	25.00	20.00	26.00	16.00
Wide Width Tensile Strength	kN/m	ASTM D-4595	29.18	22.62	52.50	40.90	93.40	40.90	124.00	40.90
Wide Width Elongation	%	ASTM D-4595	15.00	20.00	15.00	19.00	19.00	19.00	16.00	19.00
Open Area	%	COE Method	>55		>65		>55		>55	
Grid Aperture Size	cm	Measured	3.00	3.30	2.40	2.50	2.30	2.20	2.30	2.20
Thickness	cm	ASTM D-1777	- 0.20 -		- 0.14 -		- 0.25 -		- 0.38 -	
Weight	g/m²	ASTM D-3776	- 271 -		- 237 -		- 356 -		- 424 -	
Roll Length	m	Measured	45.75		45.75		45.75		45.75	
Roll Width	m	Measured	4.0		4.0		4.0		4.0	

FIELD TESTING PROCEDURES

Field testing to determine FS_{ID} was scrutinized for compliance with GRI GG-4 by representatives of the U.S. State Department (owner), Perini International (General Contractor), Haley and Aldrich (owners geotechnical consultant), Oficina De Ingeneria (independent on-site testing facility) and Mirafi (geogrid supplier). All involved parties were persistent in ensuring that the field testing be conducted exactly in accordance with the specifications. In meeting that goal, handling, installation and compaction of the geogrid during field testing was conducted to simulate actual procedures, equipment and techniques anticipated during construction.

The procedures and equipment used to conduct the field portion of the installation damage testing are summarized below.

1. Unused (new) samples of geogrid were cut from the production rolls prior to being shipped to the jobsite. The new samples were stored for future testing and establishment of "baseline" material strength properties.

2. Test pads were prepared to receive geogrid samples. Preparation of the test pads included placement and compaction of soil conforming to the appropriate specifications ("Rock Fill" or "Slope Drain Material"). Equipment used to Compact the test pad included a D-8 Caterpillar sheepsfoot roller or an Ingersol Rand SP 54, 10 ton static, smooth drum roller, depending on soil type and equipment availability. Prior to geogrid placement, density and soil gradations were conducted on test pads to ensure compliance with project specifications.

3. Geogrid specimens were cut to size and placed on the smooth rolled or sheepsfoot imprinted, compacted subgrade. Geogrid specimens of approximately 2.5m x 4m (2.5m x one roll width) were placed on the prepared pad. A minimum sample size of 9.5m² (100 square feet) was used for each test.

4. Fill conforming to the appropriate specification was subsequently placed on the geogrid samples. Fill was placed with Caterpillar

tracked end loaders. Soil was first spread with the loader bucket and then pushed into final position to form a 9" uniform lift thickness (Figure 4).

5. The fill layer was compacted with equipment referenced in number 2 above (Figure 5).

6. Density testing by both sand cone and nuclear methods was conducted on the newly placed and compacted fill to ensure compliance with the project specifications. A 95% (modified proctor) density was required.

7. Exhumation of the geogrid samples was conducted by hand. Hand shovels, brooms and pick axes were used to break up and excavate the compacted material (Figure 6). Care was exercised in using the hand tools to prevent damage to geogrid during the excavation process. Any geogrid damage inflicted during the excavation process was marked and noted. Final removal of the geogrid from the loosened soil was effected by carefully pulling and lifting (Figure 7).

8. The exhumed (damaged) and new samples were packaged for shipping and forwarded to Westinghouse Geosynthetics Laboratories for subsequent tensile strength analysis.

9. Thirty (30) single rib tensile strength tests were conducted on each specimen. Single rib test specimens were selected by random with marked areas (damaged during exhumation) excluded from testing. Testing of both undamaged (new) and exhumed (damaged) geogrid samples was conducted. Rib tensile strength testing was conducted in accordance with GRI GG1 and in conformance with GRI GG4 requirements.

Single rib tensile testing of the higher strength products (Geogrid Types C & D) encountered significant difficulty due to grip slippage. Due to a combination of short grip length, moderate geogrid profile, strong high tenacity tensile elements and broad, flat jaw configuration, some of the strength fibers were pulling out of the clamping jaw rather than failing in tension. When fiber pullout occurs, misleadingly low tensile strengths result. The grip slippage problem was corrected by wrapping the jaw embedded sample portions with asphalt impregnated open mesh tape. The tape appeared to have the effect of uniformly applying gripping pressure to a larger sample surface area and hence minimized slippage.

RESULTS OF TESTING

Visual examination of the exhumed samples showed only minor damage. Visual damage was mostly noted as nicked coating and distortion of the geogrid which was the direct and verifiable result of gouging with excavation tools. General distortion of the geogrid (from the near orthoganal position) appeared to be created by both the exhuming process (pulling and lifting of the geogrid to free it from the soil cover) and by conformance to subgrade surface irregularities such as sheepsfoot cleat marks, protruding stones, wheel ruts, etc. Figures 8 and 9 show

Figure 7. Lifting of Geogrid to Remove Loosened Soil from Partially Excavated Geogrid

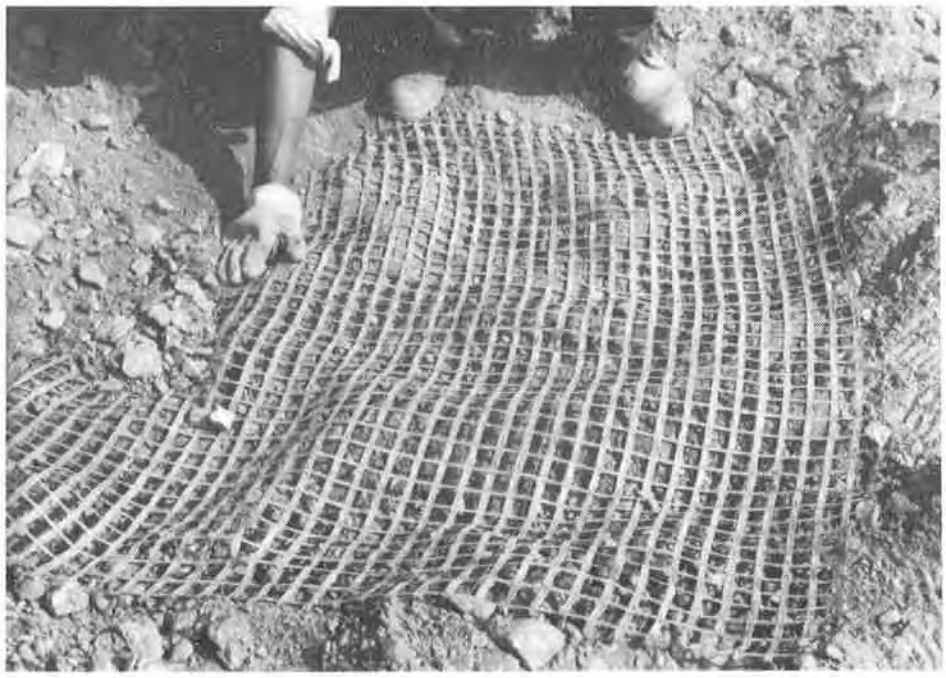

Figure 8. Partially Exhumed Geogrid Sample. Note Minor Distortion of Geogrid and Apparent Conformance to Underlying Sheepsfoot Cleat Marks in Subgrade.

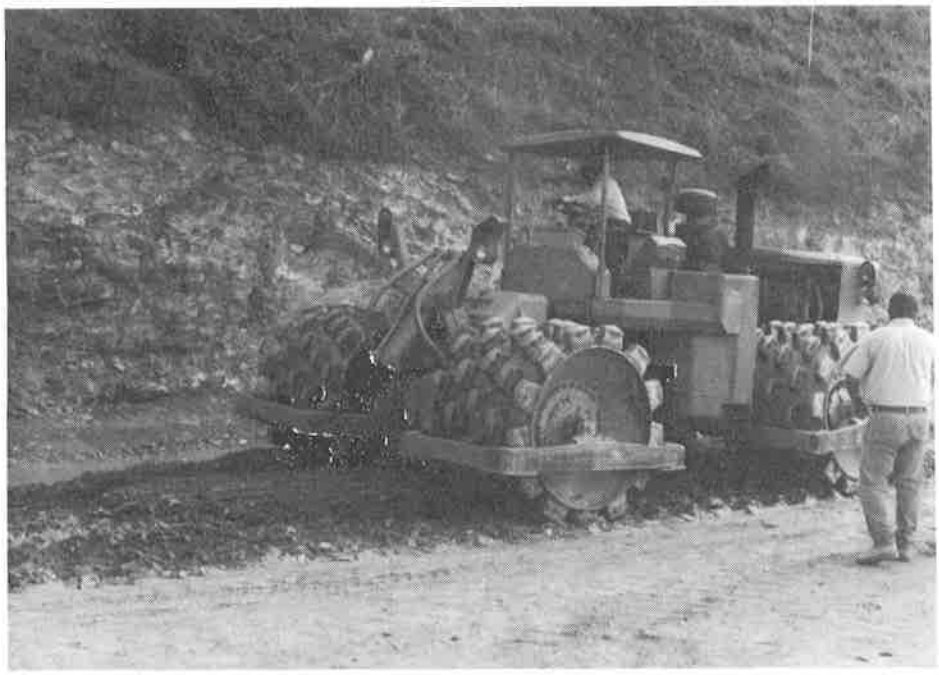

Figure 5. Compaction of Soil over Geogrid in Test Pad

Figure 6. Hand Excavation of Geogrid using Pick Axes and Shovels

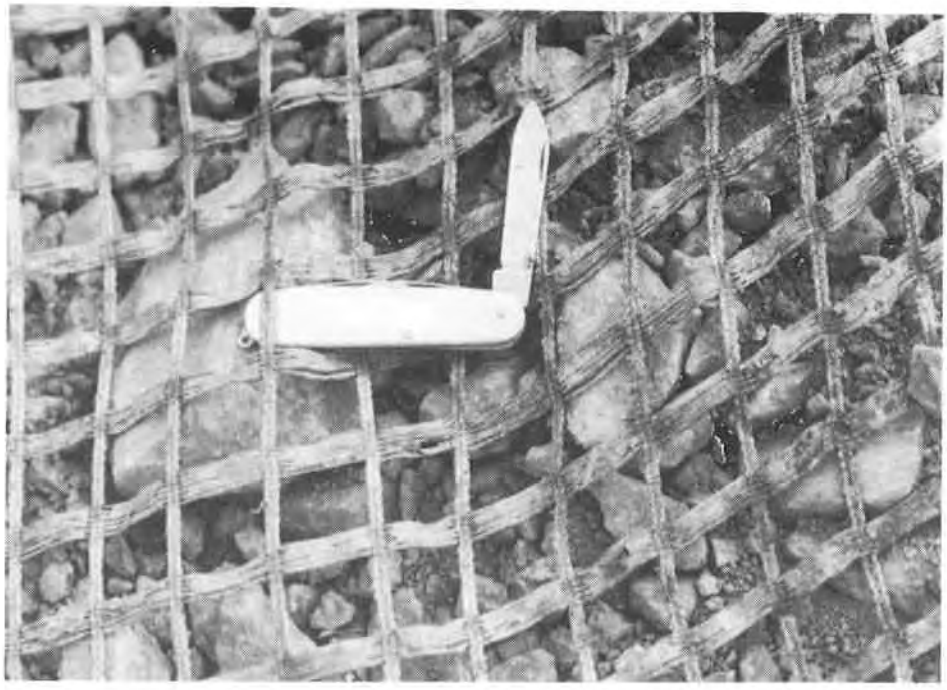

Figure 9. Close-up of View of Partially Exhumed Geogrid Sample. Note minor visual damage and distortion.

the exhumed geogrid and relative distortion noted above.

Three separate field tests were performed during the course of the project. The approximate dates on the field tests were May 1991, October 1991, and March 1992. Since different geogrid production runs and laboratory personnel were used for each test sequence, new base values were determined for each series of tests.

Tabular results of geogrid tensile strength testing are included in Table 2 and graphically represented in Figures 10 through 28. The dates noted in Table II and on Figures 10 through 28 correspond to the dates on which the samples were tested in the laboratory. The dates of laboratory testing were not the same as the dates of field testing. However, they are usually within about one month.

The bottom of Table 2 shows the FS_{ID} for each test series. Horizontal lines on Figures 10 through 28 labeled as "BV" and "Avg." provide the "Base Values" of new geogrid specimens and average strength values determined from testing of site damaged materials. The two values ("BV" and "Avg.") correspond to their respective tests and are also noted in Table 2. These values are again used to calculate FS (FS_{ID}) and are shown in the title of each figure. Calculation of FS_{ID} is shown in equation 2 below.

TABLE 2. Summary of Single Rib Tensile Test Results

PRODUCT	A	A	B	B	B	B	B	B	B	B	C	C	C	C	C	C	D	D	D
CONDITION	NEW	SD AR	NEW	SD RF	NEW	SD AR	SD CN	NEW	SD RF	SD AR	NEW	SD AR	SD CN	NEW	SD RF	SD AR	NEW	SD AR	SD CN
TEST DATE	11/27/91	12/02/91	7/15/91	7/15/91	11/25/91	12/02/91	12/02/91	3/23/92	3/23/92	3/20/92	11/25/91	12/02/91	12/02/91	3/20/92	3/20/92	3/20/92	11/25/91	12/05/91	12/04/91
SPECIMEN No.	Value (kN/rib)	Value (kN/rib)	Value (kN/rib)	Value (kN/rib)	Value (kN/rib)	Value (kN/rib)	Value (kN/rib)	Value (kN/rib)	Value (kN/rib)	Value (kN/rib)	Value (kN/rib)	Value (kN/rib)	Value (kN/rib)	Value (kN/rib)	Value (kN/rib)	Value (kN/rib)	Value (kN/rib)	Value (kN/rib)	Value (kN/rib)
1	1.00	0.85	1.68	1.56	1.89	1.39	1.77	1.83	1.67	1.69	3.34	3.13	3.17	2.84	3.24	3.02	4.44	3.58	4.03
2	0.96	0.78	1.57	1.54	1.90	1.51	1.64	1.83	1.68	1.68	3.51	3.23	3.15	3.20	3.24	2.88	4.25	3.41	3.73
3	0.97	0.85	1.69	1.60	1.88	1.55	1.69	1.89	1.65	1.73	3.46	3.24	3.09	3.19	3.28	2.96	4.47	3.76	3.79
4	0.98	0.77	1.67	1.60	1.88	1.66	1.71	1.86	1.48	1.61	3.46	3.12	2.90	3.53	3.24	3.03	4.45	3.43	3.95
5	0.95	0.85	1.70	1.63	1.83	1.69	1.68	1.91	1.62	1.69	3.33	3.28	2.70	3.57	3.23	3.17	4.40	4.01	3.91
6	0.95	0.87	1.71	1.55	1.86	1.50	1.71	1.84	1.62	1.63	3.35	3.31	3.13	3.37	3.11	3.06	4.37	3.96	3.79
7	0.93	0.86	1.72	1.58	1.88	1.64	1.70	1.84	1.49	1.75	3.29	3.29	2.96	3.62	3.09	2.96	4.36	3.90	3.82
8	0.99	0.73	1.72	1.51	1.87	1.67	1.65	1.77	1.64	1.69	3.45	3.13	3.12	3.45	3.29	3.13	4.22	3.94	4.01
9	0.99	0.90	1.69	1.29	1.91	1.68	1.73	1.85	1.58	1.49	3.32	3.13	2.76	3.46	3.28	3.12	4.28	3.92	3.81
10	0.95	0.82	1.67	1.63	1.90	1.62	1.73	1.74	1.64	1.75	3.38	3.18	3.01	3.52	3.29	2.47	4.45	4.01	3.85
11	0.97	0.83	1.68	1.51	1.87	1.80	1.74	1.92	1.49	1.57	3.37	3.33	2.98	3.43	3.28	2.95	4.08	3.79	3.93
12	0.95	0.71	1.68	1.43	1.89	1.77	1.74	1.81	1.62	1.38	3.34	3.18	3.05	3.46	3.32	3.24	4.26	3.95	3.98
13	0.98	0.85	1.66	1.60	1.89	1.73	1.68	1.85	1.62	1.54	3.40	3.28	3.03	3.34	3.28	3.14	4.35	3.91	3.87
14	0.96	0.88	1.64	1.60	1.84	1.73	1.78	1.79	1.60	1.77	3.32	3.11	2.88	3.46	3.22	3.36	4.28	3.88	3.98
15	0.82	0.70	1.57	1.53	1.84	1.71	1.70	1.91	1.27	1.78	3.47	3.24	3.23	3.50	3.24	3.18	4.48	3.68	3.73
16	0.97	0.77	1.43	1.56	1.88	1.72	1.70	1.81	1.57	1.69	3.41	3.08	3.17	3.00	3.15	3.17	4.33	3.45	3.89
17	0.97	0.90	1.69	1.57	1.82	1.63	1.66	1.89	1.57	1.72	3.45	3.07	2.85	3.14	3.25	3.17	4.17	3.52	3.92
18	0.93	0.82	1.66	1.57	1.84	1.66	1.76	1.78	0.89	1.45	3.48	2.95	3.00	3.29	3.18	2.82	4.30	4.06	3.67
19	0.99	0.89	1.64	1.64	1.86	1.66	1.77	1.92	1.61	1.73	3.49	3.17	3.10	3.45	3.28	3.17	4.37	3.47	3.98
20	1.00	0.89	1.73	1.57	1.83	1.72	1.72	1.87	1.58	1.53	3.53	3.30	2.71	3.63	3.26	3.17	4.38	3.99	3.79
21	1.00	0.84	1.67	1.42	1.87	1.60	1.66	1.91	1.66	1.73	3.47	3.36	3.12	3.52	3.25	3.22	4.60	3.48	3.87
22	0.98	0.78	1.72	1.54	1.89	1.68	1.68	1.85	1.67	1.61	3.55	2.95	3.05	3.43	3.19	3.23	4.42	3.80	3.78
23	0.86	0.85	1.77	1.59	1.87	1.65	1.59	1.73	1.56	1.71	3.43	3.05	3.10	3.49	3.10	3.06	4.47	4.10	3.78
24	0.99	0.91	1.73	1.21	1.87	1.63	1.63	1.92	1.62	1.55	3.46	3.13	3.31	3.45	3.22	3.12	4.41	4.05	3.62
25	0.97	0.82	1.68	1.66	1.84	1.61	1.68	1.90	1.55	1.68	3.51	3.10	2.94	3.45	3.43	3.06	4.44	3.81	3.95
26	0.95	0.73	1.73	1.65	1.89	1.64	1.58	1.86	1.60	1.68	3.49	3.24	3.19	3.35	3.18	2.92	4.37	3.78	4.04
27	1.05	0.82	1.78	1.73	1.85	1.68	1.53	1.86	1.67	1.71	3.50	3.20	3.12	3.17	3.17	3.11	4.42	3.85	3.70
28	0.97	0.82	1.76	1.65	1.83	1.85	1.67	1.83	1.60	1.69	3.56	3.36	3.07	3.38	3.12	3.24	4.43	3.68	3.64
29	0.97	0.79	1.77	1.63	1.86	1.73	1.61	1.86	1.66	1.70	3.35	3.13	2.96	3.46	3.17	2.59	4.15	3.81	4.04
30	0.98	0.83	1.81	1.67	1.88	1.62	1.73	1.91	1.60	1.72	3.40	3.27	3.05	3.43	2.83	2.99	4.27	3.99	3.94
Avg.	0.96	0.82	1.69	1.56	1.87	1.66	1.69	1.85	1.57	1.65	3.43	3.18	3.03	3.39	3.21	3.06	4.36	3.80	3.86
Std. Dev.	0.04	0.06	0.07	0.11	0.02	0.09	0.06	0.05	0.15	0.10	0.07	0.11	0.15	0.17	0.10	0.19	0.11	0.21	0.12
Base Value	0.96	0.96	1.69	1.69	1.87	1.87	1.87	1.85	1.85	1.85	3.43	3.43	3.43	3.39	3.39	3.39	4.36	4.36	4.36
FS_{ID}	1.00	1.17	1.00	1.08	1.00	1.13	1.11	1.00	1.18	1.12	1.00	1.08	1.13	1.00	1.05	1.11	1.00	1.15	1.13

KEY:
NEW = New, undamaged geogrid
SD RF = Site damage by "Rock Fill"
SD AR = Site damaged by "Slope Drain Material" from Araguita pit
SD CN = Site damaged by "Slope Drain Material" crusher rock from Cantera Nacional Pit

$$FS_{ID} = \frac{T_{BV}}{T_{SD}}$$

where;
T_{BV} = rib tensile strength of new, undamaged material per GRI GG1.
T_{SD} = rib tensile strength of exhumed, site damaged material GRI GG1.

The results of the testing indicates partial FS_{ID} ranging from a low of 1.05 to a maximum of 1.18 for the geogrids tested. Insufficient data is available to correlate the effects of geogrid weight, geogrid structural geometry, soil particle size or soil angularity. However, the above factors are believed to affect FS_{ID}.

The results presented above provide guidance for practicing engineers in selecting FS_{ID}'s for similar soil and material types. Soil media which may result in higher FS_{ID} may include fill which is comprised of larger particle sizes, same maximum size particles which are poorly or gap graded, and possibly smaller maximum sized particles which are more angular. Lower FS_{ID}'s are likely to be experienced in finer grained soils, soils which contain smaller maximum particle sizes and soils in which the particles are more rounded. Likewise, lighter weight equipment is also likely to result in less geogrid installation damage (ie. lower FS_{ID}'s).

ACKNOWLEDGEMENTS

The authors express sincere appreciation to Perini International for their time and equipment contributions toward field testing, and their support in the submittal process.

REFERENCES

Bonaparte, R., Ah-Line, C., Charron, R., and Tisinger, L., (1988), "Survivability and Durability of a Nonwoven Geotextile," Proc. Geosynthetics for Soil Improvement, R.D. Holtz, Ed., Geotech. Spec. Publ. 18, ASCE, pp. 68-91.

Brorsson, I., and Eriksson, L., (1986), "Long-Term Properties of Properties of Geotextiles and Their Function as a Separator in Road Construction," Third Int'l. Conf. on Geotextiles, Vienna, pp. 93-98.

Christopher, B.R., and Holtz, R.D., (1984), Geotextile Engineering Manual, FHWA DTFH 61-80-C0094, Washington, DC.

Christopher, B., Gill, S., Giroud, J., Junan, I., Mitchell, J., Schlosser, F., Dunnicliff, J., (1990), "Reinforced Soil Structures", Report No. FHWA-RD-89-043, Federal Highway Administration, Washington, D.C.

Koerner, R.M., (1990), Designing With Geosynthetics; Second Edition, Prentice-Hall Publishing Co., Englewood Cliffs, NJ.

Koerner, R.M., (1990), Determination of the Long-Term Design Strength of Flexible Geogrids", GRI Standard Practice GG4(b).

Sutton, M., and Leclercq, B., (1982), "Geotextiles and Aging Tests," Second Int'l. Conf. on Geotextiles, Las Vegas, pp 559-568.

Task Force No. 27 (1989), "Design Guidelines for Use of Extensible Reinforcements (Geosynthetic) for Mechanically Stabilized Earth Walls in Permanent Applications", Joint Committee of AASHTO-AGC-ARBTA on Materials.

Voskamp, W., and Risseeuw, P., (1987), "Method to Establish the Maximum Allowable Load Under Working Conditions of Polyester, Reinforcing Fabrics, Jour. Geotex. and Geomemb., Vol. 6, Nos., 1-3, pp. 173-184.

Wisse, J.D.M., and Birkenfeld, S., (1982), "The Long-Term Thermoxidative Stability of Polypropylene Geotextiles in the Oosterschelde Project," Second Int'l. Conf. on Geotextiles, Las Vegas, pp. 283-288.

Wrigley, N.E., (1989) "The Durability and Aging of Geogrids," Durability and Aging of Geosynthetics, R.M. Koerner, Ed., Elsevier Appl. Sci. Publ. London, pp. 110-134.

Analysis of an Exposed Polypropylene Geotextile

L.G. Tisinger
GeoSyntec Consultants, USA

B.S. Clark
GeoSyntec Consultants, USA

J.P. Giroud
GeoSyntec Consultants, USA

B.R. Christopher
Polyfelt Inc., USA

ABSTRACT

A continuous filament polypropylene nonwoven geotextile was exposed to sunlight in an empty landfill cell for approximately 7 months. Because some deterioration was expected, samples of the geotextile were periodically tested to check if the geotextile's properties would still meet project specifications. The rate of deterioration was low during the first five months and, then, accelerated. After 6.5 months of exposure, holes were observed in isolated areas of the geotextile, while the geotextile between the holes had retained more than 50% of its strength. Since the manufacturer recommended that the geotextile be exposed to sunlight for no longer than 500 hours, it was initially assumed that the geotextile deterioration was essentially due to ultraviolet radiation; however, similarities with previous work indicated that the deterioration could partially be attributed to the action of heat. The study confirmed that heat contributed to the geotextile's deterioration. This paper describes the steps taken to characterize the geotextile's deterioration, provides guidance for testing deteriorated geotextiles, and gives recommendations for minimizing deterioration of exposed geotextiles.

INTRODUCTION

A continuous filament polypropylene nonwoven geotextile with a mass per unit area of 540 g/m^2 (16 oz/yd^2) was exposed to sunlight for approximately 7 months (December 1990-June 1991) in a semi-tropical environment in the northern hemisphere. The geotextile was to function as a filter preventing clogging of the geonet leachate collection layer in a municipal solid waste landfill cell and was located on the bottom of the cell and on the slopes and crest of the perimeter berm. The geotextile was left uncovered until the project progressed to a stage at which a protective layer of sand could be placed. At the design stage, the exposure time was anticipated to be on the order of a couple of months; however, during construction, it became apparent that the exposure would be much longer, on the order of 6 months or more. The manufacturer's recommendation for the geotextile's maximum outdoor exposure time was 500 hours. It should be noted that the geotextile performed as expected during, and even beyond, the exposure period recommended by the manufacturer.

When the potential for deterioration of the geotextile was recognized, it was agreed that the exposed geotextile be tested periodically. Tests conducted after 4.5 months of exposure indicated that the mechanical properties of the geotextile had not significantly changed as compared to its properties measured before installation. Tests conducted after 6.5 months of exposure revealed that the geotextile had then suffered significant deterioration of its mechanical properties. After 6.7 months of exposure, a number of holes ranging in size from 2 cm to 20 cm (1 in. to 8 in.) were observed in the geotextile. Tests on samples taken at different locations after the holes were observed showed that the deterioration was not uniformly distributed.

The nature of the exposure led to initial speculation that the deterioration was due to ultraviolet (UV) radiation; however, previous field and laboratory work (Tisinger et al., 1990) suggested that the deterioration could also be attributed to heat. Microstructural analyses, helpful in the earlier studies, were employed to help determine the mechanisms of deterioration. For example, spectrometric and thermal analyses indicated that the geotextile filaments had experienced change consistent with previously documented effects of high temperatures. Moreover, the physical evidence of deterioration (alteration of mechanical properties and appearance of holes) was similar to that of a polypropylene geotextile analyzed in a previous study addressing the effect of high temperature on polypropylene geotextiles. It was concluded that heat was at least partially responsible for the observed deterioration of the geotextile.

Only one geotextile was involved in this study, and it was exposed to conditions unique to the site. Therefore, the results of this study apply only to the geotextile's behavior under the conditions at this site and should not be used to predict the geotextile's performance under other conditions or to predict the performance of other geotextiles under the same conditions.

Topics of the paper are discussed in the following order: (i) description of site conditions; (ii) properties of the geotextile; (iii) characterization of the mechanism of deterioration; (iv) recommendations for testing exposed geotextiles; and (v) recommendations to minimize geotextile deterioration.

DESCRIPTION OF SITE CONDITIONS

Description of the Application. The considered geotextile is part of a landfill double-liner system, which consists of the following, from top to bottom:

- protective sand layer (not constructed during the 6.7-month period discussed in the paper);
- geotextile filter with a 540-g/m^2 (16-oz/yd^2) mass per unit area;
- geonet drainage layer;
- 2.0-mm (80-mil) thick HDPE textured geomembrane;
- geocomposite drainage layer; and
- 2.0-mm (80-mil) thick HDPE textured geomembrane.

Exposure Conditions. The site is located in a semi-tropical environment in the northern hemisphere where the geotextile was exposed to high ambient temperatures up to 38°C (100°F), humidity, sun, wind, and rain. Figure 1 presents the site's average temperature versus the geotextile's duration of exposure. The prevailing winds were from the north (November, December), the north-northwest (January), the east-southeast (February, April, and May), and the southeast (March and June). Some runoff water carrying soil particles was occasionally in contact with the geotextile on the north side of the cell. Uplift of the geosynthetics due to gas buildup occurred on several occasions. In addition, there was a large population of seagulls at the site. The seagulls deposited on the geotextile droppings and various debris they had retrieved from the waste stored in another cell, such as pieces of glass and bones. The seagulls also picked at the geotextile with their claws and beaks.

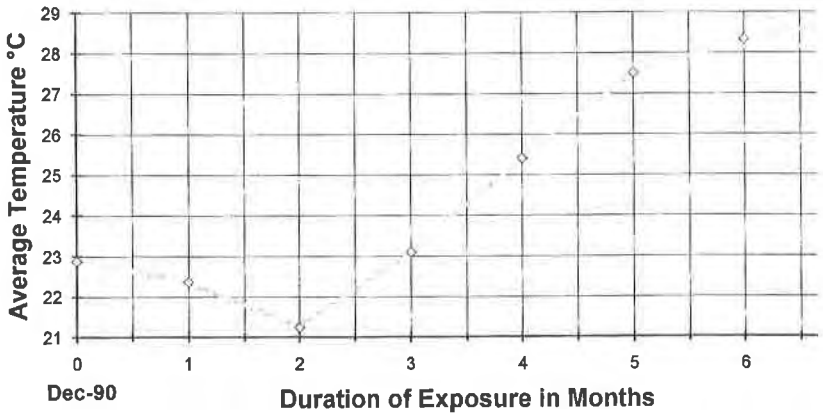

Figure 1. Monthly average ambient temperature versus duration of exposure.

PROPERTIES OF THE GEOTEXTILE

Description of Geotextile. The needlepunched nonwoven geotextile was made with polypropylene continuous filaments stabilized against ultraviolet (UV) radiation with hindered amine light stabilizers (a type of antioxidant). The geotextile did not contain carbon black.

Geotextile Selection. The project specifications included survivability requirements expressed by the following minimum geotextile mechanical properties:

Grab Strength	>	800 N	(180 lbs)
Tear Strength	>	220 N	(50 lbs)
Puncture Strength	>	355 N	(80 lbs)
Burst Strength	>	2000 kPa	(290 psi)

These requirements could be met by a geotextile with a mass per unit area of 270 g/m^2 (8 oz/yd^2). However, a geotextile with a mass per unit area of 540 g/m^2 (16 oz/yd^2) and with published properties (Table 1) that far exceed the project specifications was selected, anticipating that this geotextile would still retain enough strength after exposure to meet the project specifications.

Table 1. Pre-exposure physical and mechanical properties of the geotextile.

Property	Unit	Manufacturer's Published Values	Conformance Tests Average Values	Conformance Values vs. Published Values
Mass/area	g/m^2	540	586	109%
Grab Strength	N	1424	2358	166%
Tear Strength	N	534	811	152%
Puncture Strength	N	623	954	153%
Burst Strength	kPa	3100	4206	136%

Pre-Exposure Properties of Geotextile. Conformance testing was performed on samples taken at random from the geotextile rolls delivered to the site. Five samples were taken in accordance with the conformance testing frequency required by the project specifications. Each sample was taken from a different roll. On each sample: 10 specimens each were tested for mass per unit area, puncture, and burst strength; and 20 specimens each were tested for grab and tear strength, 10 in each direction. Conformance test average values given in Table 1 show that the properties of the geotextile delivered to the site exceeded all of the manufacturer's published values.

Properties of Exposed Geotextile. The geotextile was left exposed until protective sand placement began approximately 7 months after geotextile placement. At the construction stage, it was recognized that the geotextile would be exposed longer than originally anticipated. The site owner and the site designer, therefore, agreed to take samples of the geotextile before sand placement to verify whether the geotextile properties still met project specifications. Only mechanical properties were measured. The mass per unit area measurements were not relevant because the samples were dirty. On the other hand, cleaning the samples would have resulted in removal of a significant number of weakened filaments, a process that would bias the test results. Samples were taken at three different times as discussed below.

Four samples were taken from the bottom of the cell after approximately 4.5 months of exposure (from December 15 to April 30). On each sample: 10 specimens each were tested for puncture and burst strength; and 20 specimens each were tested for grab and tear strength, 10 in each direction. The average test results are reported in Table 2. Examination of the data in Table 2 reveals that the geotextile did not undergo significant change as the result of 4.5 months of exposure. The average burst and tear strength values after 4.5 months of exposure are even greater than the corresponding pre-exposure values. This increase is attributed to: (i) shrinking of the fibers by exposure, causing an increase in the test specimens' mass per unit area; and (ii) embrittlement of the fibers due to exposure, increasing slightly the fibers' strength.

Table 2. Properties after 4.5 and 6.5 months of exposure.

Property	Unit	Pre-exposure Value	4.5 Months Value	4.5 Months Change	6.5 Months Value	6.5 Months Change
Grab Strength	N	2358	2140	-9.2%	1818	-22.9%
Tear Strength	N	811	890	9.7%	535	-34.0%
Puncture Strength	N	954	867	-9.1%	724	-24.1%
Burst Strength	kPa	4206	4600	9.4%	4076	-3.0%

Four samples were again taken from the bottom of the cell after approximately 6.5 months of exposure (from December 15 to June 30). On each sample: 10 specimens each were tested for puncture and burst strength; and 20 specimens each were tested for grab and tear strength, 10 in each direction. The average test results are presented in Table 2. These results showed significant deterioration of the geotextile; however, the samples still met the specifications. As a result, approval was given for placement of the protective sand layer.

A few days later, before sand placement, a number of holes were observed in the geotextile. The holes ranged from approximately 2 cm (1 in.) to 20 cm (8 in.) in diameter. All the holes were in the same area: at the crest of the north slope near the northwest corner and, to a lesser degree, at the crest of the west slope near the northwest corner (the crest refers to the horizontal portion of the perimeter berm, next to the anchor trench; the berm is 1.2 m (4 ft) high and the slope is 2H:1V). No holes were found on the slopes or the bottom. Figures 2 and 3 show the condition of the geotextile at this stage, i.e., after 6.6 months of exposure (from December 15 to July 3), in the area where the holes developed.

Additional samples were taken after 6.7 months of exposure (from December 15 to July 7). The samples were taken from the following locations: the crest in the vicinity of the northwest corner; bottom of the cell, next to the toe of the slope; bottom of the cell, 8 m (25 ft) from toe of slope; and bottom of the cell, 25 to 50 m (80 to 175 ft) from the toe of the slope. Samples taken from the crest had holes occurring at a frequency of approximately 5 to 10 holes per m^2 (4 to 8 holes per yd^2). The average test results from testing these samples are presented in Table 3. These results are also presented in Figure 4 in terms of residual strength, defined as the percentage of strength retained using the conformance test results as a basis. As found from inspection of Table 3, the geotextile's mechanical property values are smaller at the crest than at the three other locations, which are at the bottom of the cell. In particular, the burst test value at the crest does not meet the project specifications. Figure 4 indicates that the various tests do not have the same sensitivity to deterioration and suggests that the sensitivity may depend on the degree of deterioration. Clearly, this is an area where more research is needed.

Figure 2. Typical holes in the deteriorated geotextile.

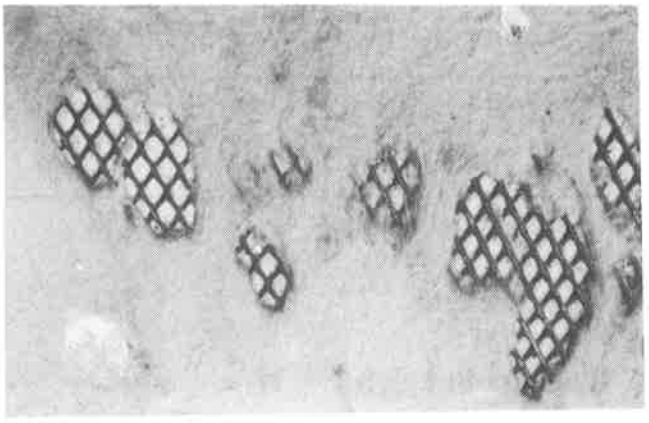

Figure 3. Typical holes in the deteriorated geotextile. (close-up view)

Rate of Deterioration. The residual strength of the geotextile at the bottom of the cell (25 to 50 m from the toe of the slope) as a function of time is given in Figures 5, 6, 7, 8, and 9. It appears in these figures that the rate of deterioration is not a linear function of time. The increase in the rate of deterioration in the last two months may be due to greater temperature and UV radiation in the late spring and summer (May and June), but may also be due to the accelerative nature of the deterioration. Similar results were reported in a study by Brand and Pang (1991) where the rate of deterioration of exposed geotextiles was found to increase with increasing intensity of UV radiation. The increase in the rate of deterioration may also be due to the synergistic effect of mechanical action and exposure, once the geotextile has reached a certain degree of deterioration.

Table 3. Properties after 6.7 months of exposure.

Location*	Number of Samples	Grab (N)	Tear (N)	Puncture (N)	Burst (kPa)
Crest	2	883	285	494	1793
Next to Toe of Slope	3	902	384	686	3697
8 m from Toe of Slope	2	915	368	737	3607
25 to 50 m from Toe of Slope**	3	1691	***	***	***

* All samples were horizontal; no samples were taken on the slopes; all samples were taken at the bottom of the cell, except two at the crest.

** Samples taken at bottom of the cell, 25 to 50 m from the toe of the slope, were located adjacent to samples taken after 6.5 months of exposure.

*** These samples were tested only for grab strength.

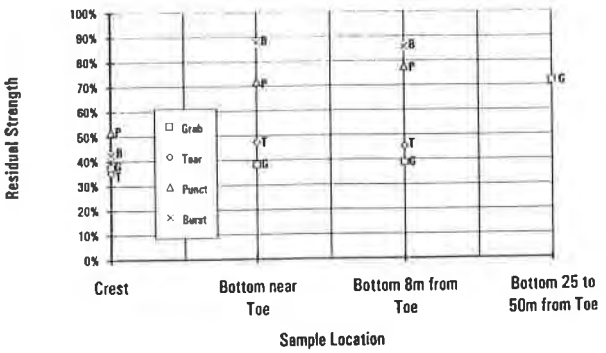

Figure 4. Geotextile residual strength after 6.7 months of exposure depending on location.

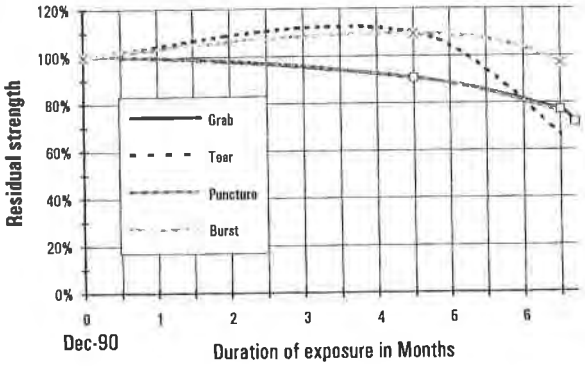

Figure 5. Geotextile residual strength at cell bottom (average curves only - see Figures 6 to 9 for ranges).

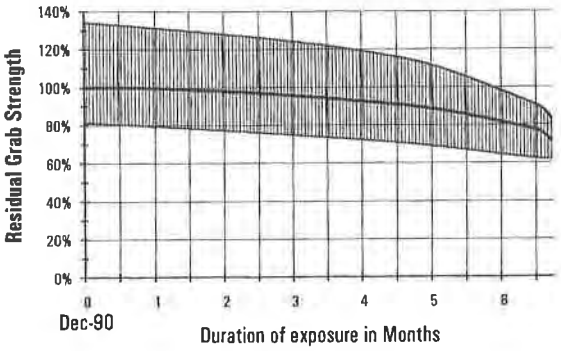

Figure 6. Geotextile residual grab tensile strength at cell bottom after exposure.

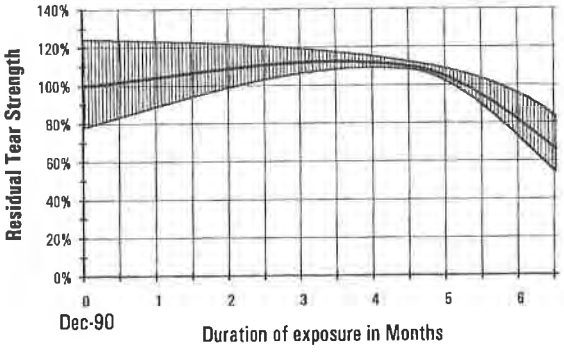

Figure 7. Geotextile residual trapezoid tearing strength at cell bottom after exposure.

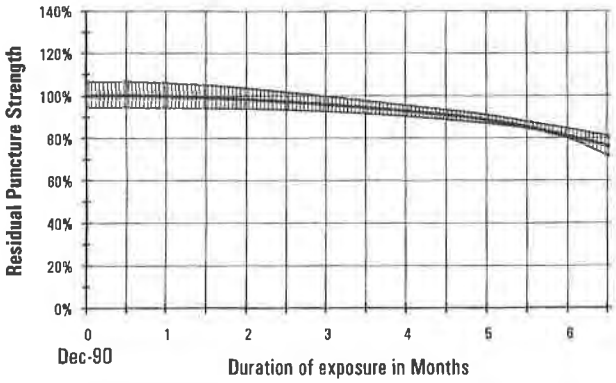

Figure 8. Geotextile residual puncture strength at cell bottom after exposure.

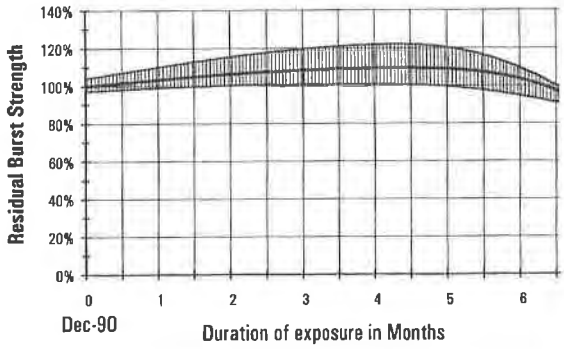

Figure 9. Geotextile residual burst strength at cell bottom after exposure.

Discussion of Test Results. At 4.5 months of exposure, the differences in the geotextile's properties could be attributed to material and experimental variability. At 6.5 months of exposure, property deterioration was clearly measured. The geotextile's grab, tear, and puncture strengths were reduced by approximately 23%, 34%, and 24% respectively, compared to

conformance test results, while the change in its burst strength was insignificant. At both the 4.5 and 6.5-month exposure times, the geotextile's properties met project specifications and the geotextile was apparently able to function as designed. However, shortly after the 6.5 month exposure time, many holes developed at the crest in the vicinity of the northwest corner of the cell. The tests, then conducted, showed that all of the mechanical properties were reduced significantly; however, with the exception of burst strength along the crest, the geotextile properties still met the project specifications, which seemed inconsistent with the presence of holes. Suspecting errors in testing, the test procedures were carefully reviewed: no errors were found. This led to a review of specimen selection procedures, revealing that, when samples had holes, specimens had been selected from areas between the holes. Accordingly, the measured property values did not reflect the extent of the geotextile's deterioration. Random selection of specimens from samples with holes would have provided some specimens with zero strength. As a result, the average values reported for the samples taken from the crest would have been much more representative of the worst conditions in the field, and the project specifications would not have been meet by the measured properties of the geotextile at the crest.

CHARACTERIZATION OF THE MECHANISM OF DETERIORATION

Microstructural Analytical Techniques. Changes at the molecular level in polymers are evaluated using microstructural analytical techniques that characterize molecular structure, crystallinity, and oxidative stability, as discussed below:

- Molecular structure is characterized using infrared spectrophotometry (IR), a technique that subjects a sample to infrared radiation scanning from high to low frequency. Molecules consist of individual components that each respond at different frequencies to infrared radiation: when the infrared frequency matches the vibrational frequency of a molecular component, the molecular component absorbs infrared radiation. An infrared spectrum of the sample is thus obtained. Every polymer has a unique infrared spectrum, making IR a useful technique for characterizing polymers. Structural changes, such as those imparted by deteriorative processes, are detected using IR.

- Crystallinity is determined using differential scanning calorimetry (DSC). In a DSC analysis, polymeric materials are heated at a controlled rate, while the amount of heat emitted or absorbed by the material is monitored. Since only crystalline areas melt, the crystallinity of a polymeric material can be calculated from the amount of heat required to melt it, which is measured in a DSC analysis in terms of energy per unit mass.

- Oxidative stability is also measured by DSC. The effectiveness of the antioxidants in the considered polymeric material is evaluated by the time, or the temperature, at which oxidation of a polymer occurs, as measured by DSC.

Previous Study. In a previous study, the deterioration of exposed polypropylene needlepunched nonwoven geotextiles was investigated (Tisinger et al., 1990). Two geotextiles were studied:

(i) a black geotextile containing carbon black; and (ii) a white geotextile not containing carbon black. Both contained antioxidants. After approximately 6 months of outdoor exposure in the upper mid-west United States, holes developed randomly in the geotextiles, the black geotextile appearing to be more deteriorated than the white geotextile. Because the geotextiles were exposed to sunlight, preliminary conclusions were that the observed deterioration had been induced by UV radiation. Accordingly, microstructural analyses were conducted to evaluate the molecular deterioration of the polypropylene fibers. In these analyses, the fibers' molecular structure, crystallinity, and oxidative stability were evaluated. The analyses indicated that:

- the polymer molecular structure had not undergone significant deterioration (a finding that, first, seemed inconsistent with the visual appearance of the geotextiles);
- the crystallinity had increased (approximately 10%); and
- the oxidative stability had not changed significantly.

In addition, the exposed fibers were examined using optical microscopy. From this examination, the fibers appeared to be wrinkled, as though they had shrunk. The deterioration, therefore, appeared to be related more to physical changes, such as changes in the fiber's crystallinity, than to deterioration of the polymer in the fibers. Since the molecular structure of the polypropylene molecules in the fibers had not changed, it seemed unlikely that the geotextile's deterioration was caused by heat induced or by UV induced oxidation (which is a chemical reaction that changes the molecular structure of polymer molecules). It was therefore apparent that another mechanism of deterioration was operating. Since the fibers had undergone a change in crystallinity, it was speculated that heat from the sun had an impact on the fibers (heat causes molecular motion, UV radiation does not).

To evaluate this speculation, two samples of unexposed black geotextile were placed in a forced-air laboratory oven at 100°C for 72 days. (Samples of the white geotextile were not available when the oven test was conducted.) One sample was restrained (pulled tight, biaxially) when oven-aged, because it was speculated that any mechanical stress imparted on the geotextile in the field may have pulled the geotextile's fibers apart, causing the holes to develop. The other sample was not restrained. Holes developed randomly in the unrestrained geotextile in the same way they had developed in the field-exposed sample. In addition, the unrestrained sample shrank. The restrained geotextile did not develop holes. As with the field-exposed fibers, the unrestrained sample's crystallinity also increased (up to 30%). Conversely, the restrained sample's crystallinity did not change.

These findings showed that heat alone as an energy source has a significant impact on polypropylene fibers, because the deterioration of the geotextile exposed to heat only (no UV radiation) in the laboratory was similar to that observed in the field, where both UV radiation and heat were energy sources. These findings also indicated that black fibers, because of their ability to absorb heat, may undergo more deterioration than white fibers. In addition, these findings indicated that restriction of the fibers' movement, such as by biaxial restraint, improves significantly a geotextile's ability to withstand the physical effect of heat.

Results of this Study. The geotextile discussed in this paper was subjected to the microstructural analyses described above. Results of the analyses performed on samples exposed for 6.7 months and taken next to holes observed at the crest of the north berm are presented in Table 4 for DSC analysis (crystallinity and oxidative stability), and in Figure 10 for IR analysis.

Table 4. Results of DSC analysis after 6.7 months of exposure.

Property	Unit	Unexposed	Exposed	% Change
Crystallinity (energy/mass)	J/g	96	105	9.4
Oxidative Induction Time	min	7.2	1.2	-83

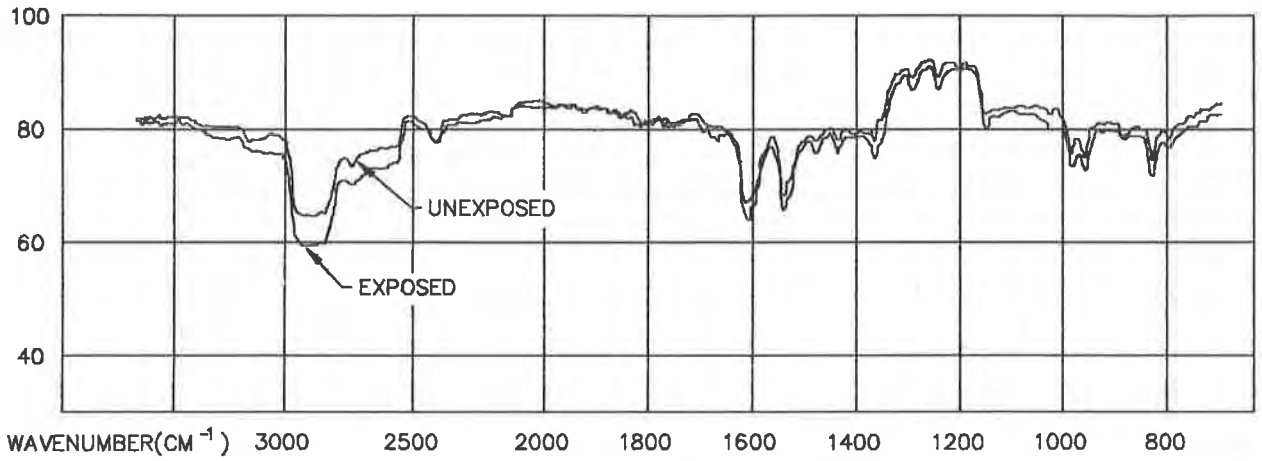

Figure 10. Results of IR analysis after 6.7 months of exposure.

As shown in Table 4, the crystallinity increased approximately 10% after 6.7 months of exposure, an increase consistent with heat aging of polypropylene (Schneider, 1988; Tisinger et al., 1990).

As shown in Table 4 and as expected, oxidative induction time decreased after exposure, indicating that antioxidants had been consumed by the action of heat or UV radiation from outdoor exposure and that some oxidation occurred.

IR analysis was conducted to determine the extent to which the polypropylene molecules had undergone structural change due to oxidation. Examination of Figure 10 indicates that the IR spectra for the unexposed and exposed samples are nearly the same. Had the exposed sample been severely oxidized, a significant difference between the two curves would have appeared at a band (i.e., a range of frequencies) at approximately 1750 cm^{-1} (oxidation by-product band) in the IR spectrum. Since such a band had not developed, it is likely that oxidation had not significantly affected the fibers.

Discussion of Mechanisms of Deterioration. UV radiation, heat, and other mechanisms are discussed below.

UV Radiation. UV radiation causes oxidation (referred to as UV-oxidation) of polypropylene fibers. Oxidation is evidenced by fiber embrittlement, by a reduction in oxidative induction time (OIT), and by appearance of a characteristic oxidation by-product band in polypropylene's IR spectrum (Carlsson and Wiles, 1976; Tisinger, 1989). The fibers of the exposed geotextile were slightly embrittled and had lowered OIT values (which can also occur from heat exposure), but their IR spectrum did not indicate the presence of the characteristic oxidation band. It therefore appears that the extent of the fibers' oxidation was not significant enough to be evident in the fibers' IR spectrum, probably because of the effectiveness of the fibers' UV-stabilizers (hindered amine light stabilizers).

Heat. As discussed previously, prolonged exposure to high temperatures can change the physical features of polypropylene fibers. The mechanism is as follows: when polypropylene fibers are extruded, their molecules are oriented and are in a stressed state, a condition that remains when the fibers cool ("residual stresses"); as the fibers are heated, increasing portions of the polypropylene molecules become mobile ("segmental chain motion"); as a result, the intermolecular forces linked to the residual stresses bring the molecules closer together ("shrinkage"), which relaxes the residual stresses and increases the molecular organization, hence the increase in crystallinity. As a result of increase in crystallinity, fibers become stiffer and more brittle. In addition, polypropylene fibers subjected to heat may also undergo oxidation (referred to as thermo-oxidation), which may cause the polypropylene fibers' embrittlement (Schneider, 1988). The effect of heat is confirmed by the fact that oven-aged samples showed similar physical and microstructural changes, i.e., development of holes and increase of crystallinity, to samples exposed to the outdoors, an environment with both UV radiation and heat. This study (which is consistent with a previous one discussed earlier in this paper) confirms that heat is a significant cause of deterioration of polypropylene geotextiles.

It was mentioned earlier in this paper that fibers exposed to heat, while maintained under tension, did not undergo increase in crystallinity and, therefore, did not become more brittle. In accordance with the above discussion, this observation can be explained as follows: tension prevents fiber shrinkage, i.e., restricts molecules from moving closer together as they become more mobile under the effect of heat; since molecules do not move closer, crystallinity does not increase and the fibers do not become more brittle.

The study also shows that exposure to high temperatures can cause significant changes in the performance of polypropylene fibers without causing severe molecular deterioration, such as by oxidation. These changes occurred without detectable change in the molecular structure of the polypropylene molecules, illustrated by the IR spectra of the exposed polypropylene geotextiles. The OIT values were reduced, indicating that some oxidation probably occurred; however, the effect of oxidation on the molecular structure of polypropylene was not detectable by IR.

Other Mechanisms. As an attempt to explain the presence of holes at the crest of the berm near the northwest corner, other mechanisms of deterioration may be considered:

- Foot traffic was possibly more intensive at the crest of the berm than anywhere else; therefore, abrasion due to foot traffic may have been a cause of the greater number of holes on the crest, but this does not explain the greater concentration of holes near the northwest corner.

- Birds, certainly weakened the geotextile by pulling at its fibers; however, this action is believed to have occurred randomly, which does not explain the presence of holes only in the crest area.

- The debris such as pieces of glass and bones brought by birds could conceivably cause abrasion of the geotextile. However, these debris were randomly scattered, which does not explain the presence of holes only in one area (crest of slope).

- The pieces of glass, by focusing sunlight, could accelerate heat action in small areas, but this cannot explain the fact that the holes were large and localized in one area.

- Improper storage of the geotextile rolls could have caused some deterioration of the first wrap prior to installation. This assumption is not relevant because the first two wraps of each roll were systematically discarded. Furthermore, the geotextile at the crest was not always from the beginning of a roll.

- Chemical deterioration by runoff water has been envisioned as a potential cause for development of holes at the crest; this assumption was dismissed because polypropylene has excellent resistance to any chemical likely to be in runoff water. Polypropylene has also an excellent chemical resistance to bird droppings; in addition, these droppings were randomly distributed, which cannot explain the presence of holes only at the crest.

- Uplift of the geosynthetics due to gas buildup occurred on several occasions, causing tension in the geotextile; however, this type of uplift took place on all berms and does not explain hole concentration near the northwest corner.

- Wind action seems the most likely cause of hole concentration near the northwest corner because, in June, when the geotextile was significantly deteriorated, the prevailing winds were blowing toward the northwest corner. It is known that maximum wind action occurs at the crest of slopes exposed to the wind. Therefore, the geotextile in the vicinity of the northwest corner was exposed to such deteriorative wind actions as fiber breakage, fiber removal, and abrasion by windblown particles. These actions were able to cause significant damage to the geotextile because by June the geotextile had been significantly weakened by exposure.

RECOMMENDATIONS FOR TESTING EXPOSED GEOTEXTILES

Testing exposed geotextiles should address bulk properties to evaluate the extent of deterioration, and microstructural properties to investigate the mechanism of deterioration.

Bulk Properties. Two aspects must be considered regarding the measurement of bulk properties: test selection and specimen selection.

Test Selection. The tests used to measure the geotextile bulk properties should be selected using the following criteria: (i) the tests should be related to the function (e.g., opening size) and survivability (e.g., puncture) of the geotextile in the considered application; and (ii) the tests should have the sensitivity to detect geotextile deterioration and be reproducible. Regarding the latter requirement, the best tests are those that use large specimens and where the relevant property is measured rather uniformly throughout the specimen area (which is the case of a wide-width tensile test, but not of a puncture test).

Specimen Selection. When samples include holes, there is a natural tendency to select specimens for testing from areas located between the holes, where the geotextile is in good condition. This provides a false indication of the geotextile's condition. It is recommended that selection of test specimens be done at random (for example, through the use of a preexisting template) to include in specimens holes and other distressed areas. Such a specimen selection process ensures that holes or thinning areas will not be avoided and that zero values will be reported for strength (or infinite values for opening size or permeability) for specimens that cannot be tested, because they were selected from a hole in the sample.

Microstructural Properties. Clues regarding mechanisms of deterioration can be provided by microstructural analyses. For this study, IR was used to identify molecular structure, and DSC was used for the measurement of crystallinity and oxidative stability. Other techniques may be used, such as gel permeation chromatography (GPC) (Carraher and Seymour, 1983) and scanning electron microscopy (Tisinger et al., 1990) to determine molecular weight and surface changes. Other microstructural analysis techniques are being studied.

RECOMMENDATIONS TO MINIMIZE GEOTEXTILE DETERIORATION

Geotextile Selection. If long-term outdoor exposure cannot be avoided, UV-stabilized geotextiles should be used. Also, light-colored geotextiles may be preferred to black geotextiles. Manufacturers should be consulted when geotextiles may be exposed to extreme conditions, since it is possible to modify UV and thermal stabilizers to extend the anticipated life of the geotextile. The manufacturer's recommendations regarding the useful lifetime of an exposed geotextile should be considered seriously. The geotextiles' properties should be monitored periodically, and the test results evaluated cautiously, since, as shown in this study, properties may display linear behavior as a function of exposure time, but later deteriorate drastically, once a critical exposure time is reached. In addition, the synergistic effect of mechanical actions and

deterioration due to exposure must be taken into account (i.e., light mechanical actions can cause large holes in a geotextile weakened by exposure). Selecting a geotextile that initially far exceeds project specifications and will still meet project specifications after deterioration can be considered. This strategy seems justified by the fact that mechanisms of deterioration, such as UV radiation and heat, stop as soon as the source of energy is cut off by the placement of a layer of soil on the geotextile. However, using an oversized geotextile may not be the best strategy because the partially deteriorated fibers have imperfections that make them sensitive to stress concentrations. As a result, a deteriorated geotextile may not resist stresses (such as those due to abrasion or construction damage) as well as a new geotextile (assuming that both have the same strength). Therefore, protecting the geotextile in the event of long-term outdoor exposure may be the best strategy.

Geotextile Protection. A geotextile can be protected using a layer of material that stops (and even partially reflects) sunlight and/or provides thermal insulation. Assuming, in the context of this paper, that the placement of a soil barrier is not an available option, possible materials include: a geotextile (of light color to minimize the amount of heat transmitted to the protected geotextile), a white geomembrane (potentially more effective than a geotextile, but more expensive), and panels of expanded polymeric foam. These protective materials must be properly secured against wind action and must be removed prior to placing soil as they could cause a slip surface and/or otherwise impair the function of the geotextile.

CONCLUSIONS

Conclusions regarding the mechanism of deterioration are:

- the rate of deterioration is not linear, it is slow for several months and, then increases;
- the deteriorative action of heat may be greater than that of UV radiation, consequently black geotextile may deteriorate more rapidly than light-colored geotextile; and
- when a geotextile has deteriorated to a certain degree due to UV radiation and heat, holes may result from mechanical actions (e.g., tensions and abrasion due to wind).

Conclusions regarding testing are:

- specimens for measuring geotextile bulk properties must be selected at random for a representative evaluation of deterioration; and
- microstructural analyses are necessary to identify mechanisms of deterioration.

Conclusions regarding design strategy are:

- manufacturers' recommendations regarding the useful lifetime of an exposed geotextile should be considered seriously;

- manufacturers should be consulted, when a geotextile is to be exposed to extreme conditions, to extend its lifetime by modifying the stabilizers; and

- a removable protective layer is preferable to a non-protected oversized geotextile.

REFERENCES

Brand, E.W. and Pang, P.L.R., (1991) "Durability of Geotextiles to Outdoor Exposure in Hong Kong", Journal of Geotechnical Engineering, ASCE, Vol. 117, No. 7, pp. 979-1000.

Carlsson, D.J. and Wiles, D.M., (1976) "Effects of UV Light on the Chemical and Mechanical Properties of Fiber Forming Polymers", Ultraviolet Light Induced Reactions in Polymers, ACS Symposium Series 25, Labana, S.S., Editor, American Chemical Society, Washington, D.C., pp. 321-339.

Schneider, H., (1988) "Long-Term Performance of Polypropylene Geosynthetics", Durability and Aging of Geosynthetics, Koerner, R.M., Editor, Elsevier, NY, pp. 95-109.

Seymour, R.B., and Carraher, C.E., (1981) "Polymer Chemistry: An Introduction", Dekker, New York, 564 p.

Tisinger, L.G., (1989) "Microstructural Analysis of The Durability of a Polypropylene Geotextile", Proceedings of Geosynthetics '89, San Diego, California, pp. 513-524.

Tisinger, L.G., Peggs, I.D., Dudzik, B.E., Winfree, J.P., and Carraher, C.E., (1990) "Microstructural Analysis of a Polypropylene Geotextile After Long-Term Outdoor Exposure", Geosynthetic Testing for Waste Containment Applications, ASTM STP 1081, Koerner, R.M., Editor, American Society for Testing and Materials, Philadelphia, pp. 335-351.

Creep and Accelerated Creep Testing for Geogrids

P. Rimoldi
Tenax SpA., Italy

F. Montanelli
RDB Plastotecnica SpA., Italy

ABSTRACT

The determination of the long-term design strength of a reinforcing geosynthetic is always a very challenging task. The creep test is quite simple: the elongation of a loaded specimen is measured by the time at constant external conditions. On the other hand there is the difficulty of defining the various aspects of the test procedure, such as the type of clamping, the loading time, the minimum length of the specimens, the required testing time, the extrapolation procedure and the level of accuracy of the prediction. All these aspects are discussed in the paper, and suggestions for the standardization of this test procedure are included. Different creep tests at 20°C (standard condition) and at 30°C and 40°C (accelerated testing) were performed on different geogrids for periods up to 10000 hours; isochronous load and tensile creep modulus curves, as a function of time and temperature, are analyzed to determine the time-temperature relationship between standard and accelerated testing.

INTRODUCTION

Early use of geogrids was limited to small walls and slope, but nowadays it is quite easy to find geogrid reinforced slopes and walls in excess of 20 m in height as in Rimoldi and Ricciuti (1992). The geogrid reinforced slopes and walls, sometimes impressive for size and criticality, are more and more used for permanent structures, having design lives between 50 and 120 years. Therefore geogrids will be subject to an almost constant load for a time of the order of 10^6 hours. Design engineers need to have reliable data concerning the long term behaviour of geogrids under constant loads at different temperatures. Hence there is the need of focusing the attention on tests aimed to quantify the long-term mechanical properties of the different available geogrids, which depend on the creep behaviour of the products. Creep is the result of the elastic-plastic-viscous response of a material under a sustained constant load. Creep of geogrids is known to depend on temperature, load, time,

loading conditions, polymer and structure of the product.

Extensive research programs are going on in different countries, trying to obtain creep data on all the available geogrids and to define the testing procedures. One of these testing programs is being conducted at the Tenax Geosynthetics Testing Laboratory in Italy. The Authors have been involved for many years in ASTM and CEN committees on Geosynthetics testing. This paper refers on the results of such tests, performed on different geogrids types.

Geogrids are classified as stiff or flexible in GRI-GG3-90 (1990) creep test method, based on their flexural stiffness. In this paper the geogrids available on the market are classified according to Tab. 1.

Table 1: Geogrid type

TYPE A) integral extruded, cold punched, uniaxially or biaxially drawn in PP or HDPE
TYPE B) integral extruded, hot formed, uniaxially or biaxially drawn, in PP or HDPE
TYPE C) woven PET yarns, arranged in bundles, covered with PVC or other types of sheating
TYPE D) PET strips sheated in LDPE, thermally bonded at the strips intersections

Only the first 3 geogrid types were tested in the research program here presented: type A) will be referred as "cold punched integral geogrids", type B) as "hot formed integral geogrids", while type C) as "woven geogrids" and type D) as "bonded geogrids".

SHORT AND LONG-TERM TENSILE BEHAVIOUR OF GEOGRIDS

The tensile strength, modulus and elongation behaviour of geogrids depend on the temperature; in general, strength and modulus will decrease and elongation will increase with increasing temperature. The creep of a geogrid largely depends on the basic polymer used to manufacture the product but also the creep of the geosynthetic structure is another important component of the total elongation: it is produced by the realignment of polymer fibers, necking, elimination of wrinkles, crimp; these phenomena give an unpredictable, unrecoverable immediate strain, usually significant in woven geogrids and geotextiles while it is totally negligible for integral geogrids. Therefore woven products, even if manufactured with the best available PET polymers, show a large elongation when tested.

Stress-strain-time data are usually presented as creep curves of strain versus log time. These same data may be presented in other ways to facilitate the selection of information for particular requirements. Sections may be taken through the creep

curves at constant times, yielding isochronous load versus strain curves, or at constant strain, giving isometric load versus log time curves. If the elongation of a geogrid subject to continuous loading is calculated using the modulus of elasticity obtained from short term tensile tests, E, the result is likely to be inaccurate since the effects of creep have not been considered. However, if the load level and the reference temperature are known and the creep curves are available at the reference temperature, an apparent or creep modulus, E_F, can be calculated using the creep curves as follows:

$$E_F = F / \epsilon(t) \qquad (1)$$

where: F = applied load;
$\epsilon(t)$ = total strain from the creep curve at time t, for a specific temperature, produced by the load F.

The data from the extrapolated curves of Creep Modulus can be used to extrapolate an Isochronous load diagram. It must be noted at this point that the loading time is a very important aspect of creep tests on plastic products: in general, the shorter the loading time the larger the instantaneous elongation. After a certain elapsed time, the total strain ϵ becomes almost the same, while the creep strain ϵ_c (total strain minus instantaneous strain) is very different. Therefore the Authors feel that it is totally incorrect to quote figures of the creep strain ϵ_c, instead of the total strain ϵ, without a precise reference to the loading time used for testing.

TENSILE CREEP TESTS

The creep tests research here presented was aimed at measuring the uniaxial unconfined creep behaviour at various constant temperature and for different sustained tensile loads. The testing program included more than 80 testing positions, with geogrids type A), B) and C), for a total of 8 different product grades, at 3 different temperatures (20°C, 30°C, 40°C). All the tests were performed in accordance with the GRI-GG3-90 test method for "The tension creep testing of geogrids" (GRI 1990), and in general accordance with the actual CEN and ISO draft proposals for creep testing of geosynthetics.

The geogrid specimens were cut as a narrow tensile strip having a width of approximately 100 mm and a length of about 1200 mm. In practice, the integral geogrids specimens were three ribs wide by eight bars long. The gauge length selected was 1000 mm in order to increase the accuracy without incurring in highly expensive measuring devices. Since geogrids are meshed products, the 1000 mm gage length was choosen to include several geogrid mesh units, thus giving more accurate and averaged results. The extruded and oriented geogrids which were tested did not suffer, when loaded, the effect of edge contraction (necking) typical of

geotextiles, since the thick and stiff transversal bars prevent this necking phenomena. In lieu of this consideration the width of three ribs was selected as the representative dimension for the integral geogrids to be tested. The gauge length was marked with white paint lines on the samples while they were layed flat between two smooth surfaces. No preloads were applied during the marking of the gauge length. In fact the authors were concerned with the significant magnitude and variability of the initial crimp of the fibers present in the wowen products. The total elongation was monitored by the means of a direct reading graduate ruler, mounted directly on the geogrid in such a way that the origin position was exactly at the top gauge line (see Fig. 1 and 2). The measurements were accurate up to 0.05 % of the original gauge length and accurate up to 1.0 % of the actual average total elongations measured. This accuracy is in accordance with the requirements of ASTM D2990 test standard for tensile, compressive and flexural creep rupture of plastics. The constant loads were applied by means of dead weights. These loads were applied in a one step process, loading in tension the specimens in a time of maximum 5 seconds. The dead weight procedure was selected over the knife-edges lever method for its accuracy over the full range of extension, for its simplicity and conveniency. The applied loads were, for all the products, equal to the 15%, 25%, 35% and 40% of the peak tensile strength when tested in accordance with the GRI-GG1 test method for geogrid rib tensile strength. The data shown in the creep modulus diagrams in this paper are those relative to the manufacturers' suggested Long Term Design Strength in term of percentage of the peak load or, in the case of the wowen geogrids, to the load corresponding to a 10% creep strain at 10^6 hours at 20°C. Woven geogrids were tested also at 60 % of peak tensile strength. The applied load range was selected to span across the 10 % long term strain, which is the strain limit as proposed by Mc Gown et Al. (1984) and Allen (1991) as a safe and conservative design criteria for reinforcing geosynthetics.

Great care was taken when selecting the appropriate type of clamping to hold the specimens. The clamps for the integral geogrids were designed to hold the specimens through the geogrid junctions, in order to transmit the stresses in the same way as they are transmitted to the geogrid when embedded in the soil. At the same time the clamps were designed to prevent slipping or damage to the specimen. Since polymeric geogrids are very sensible to high concentrate point load sustained for long period of time and at elevated temperature, the final clamping system consisted of precasting a bar of a cold-setting resin at the end of the geogrid in a rectangular shaped mould. The resin used was an industrial resin compound (Sikadur 31 produced by Sika) designed to attach concrete joints in civil engineering projects. The small resin blocks, finished after 24 hours of curing at ambient temperature, were then inserted in "C" shaped tubular clamps, as shown in Fig. 2. On one side of the clamp, a slit aperture allows the passage of the ribs of the geogrids, while on the other side of the clamp, a welded ring allows the connection to the weight through an universal joint to minimize any eccentric loading on the specimen. This system has proven effective and no failures in the clamps has been noted so far. Clamping

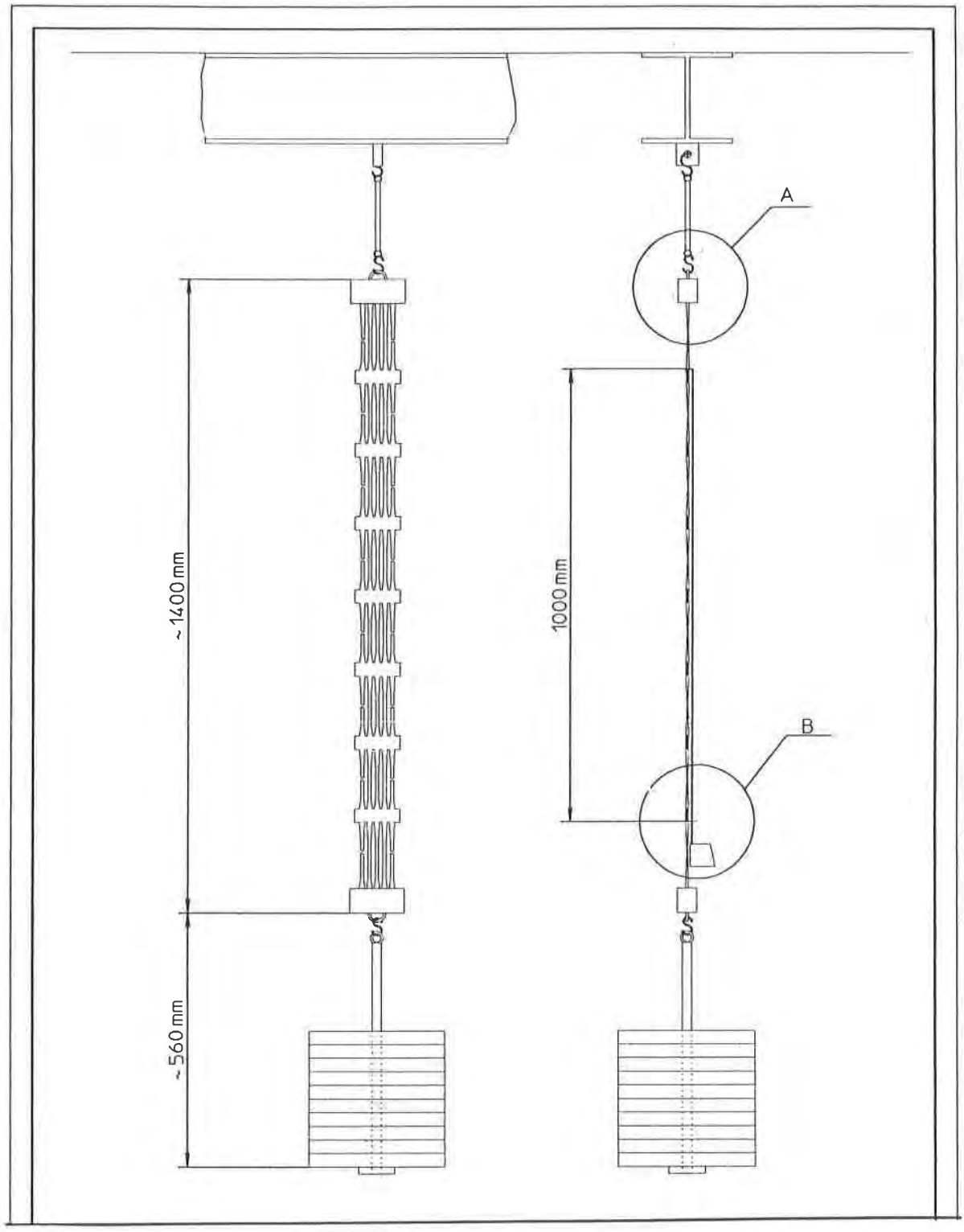

Fig. 1. Scheme of the tensile creep tests; details A and B are shown in Fig. 2.

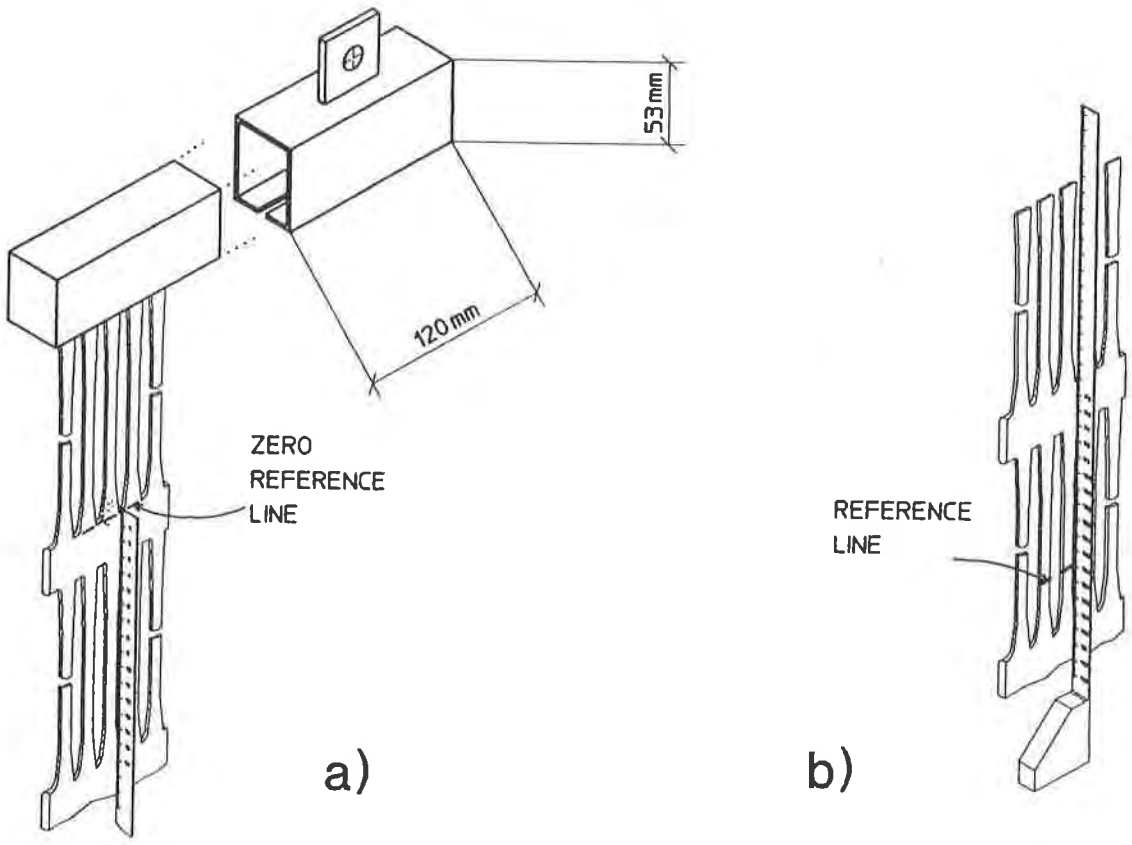

Fig. 2. Detail of the clamps for integral geogrids (A) and of the elongation measurement system (B).

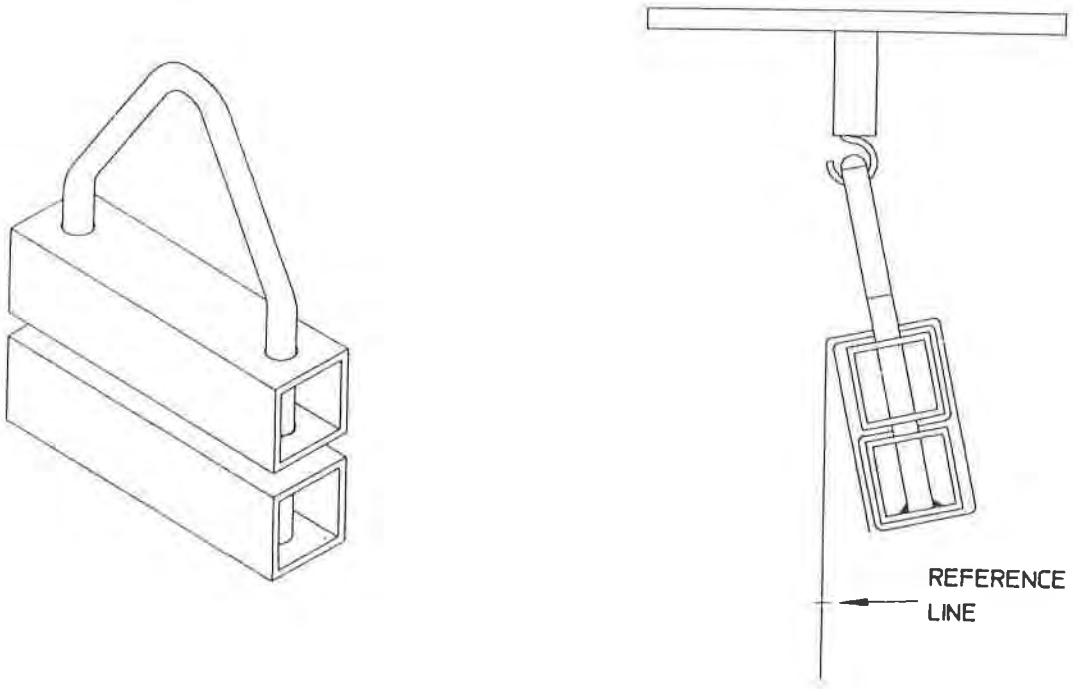

Fig. 3. The clamps used for woven geogrids.

through the junctions was not possible for the woven geogrids, because the junctions break in the clamps: therefore capstan type clamps, especially designed, were used for these geogrids (see Fig. 3). They are made with two pieces of commonly available "square" steel tubes, connected by a shaped steel bar (Φ 12 mm) which is welded at the base of the bottom steel tube; the top clamp can freely move up and down along the steel bar. When the woven geogrid is wrapped around the top and bottom steel tubes according to the pattern shown in Fig. 3, it become very firmly gripped when the load is applied and the top clamp is consequently pressed against the bottom clamp. No sliding was observed in the clamps at the application of the load and during the whole loading period. The specimens were still three ribs wide by 1200 mm long, and only a minor necking occurred: the specimen width, originally equal to 50 mm (3 ribs), became 49 mm after the application of the load. This type of clamps is suitable also for woven geotextiles. The authors noted that, when tested with the clamping-through-the-junctions method, only the PVC coating of the woven geogrids remained embedded in the clamps, while the PET fibers were pulled out by the loads. It shall be interesting to investigate if the same behaviour occurs when woven geogrids are placed in the soil.

The test temperatures were recorded and controlled in the ±2°C range, giving an average level during the time of testing of 20.2°C, 29.8°C and 39.8°C. The humidity level was monitored in the range of 55 % to 65 % for the three different temperature rooms.
Some tests were carried out to investigate the influence of the loading time: a hot formed integral geogrid and a woven geogrid were tested with loading times varying from instantaneous loading to 1 hour loading, always with a load equal to 40 % of the peak tensile strength, at 20°C.

TENSILE CREEP TESTS RESULTS

The results are presented for the products listed in table 2.

Table 2: Characteristics of the tested geogrids.

GEOGRID REF. n.	PRODUCT NAME	GEOGRID TYPE	MADE IN	POLYMER TYPE	PEAK TENSILE STRENGTH (kN/m)
1	TENAX TT401 SAMP	B	ITALY	HDPE	80.0
2	TENSAR SR2/UX 1500	A	U.S.A.	HDPE	80.0
3	AKZO FORTRAC 55/30-20	C	GERMANY	PET/PVC	55.0
4	TENAX TT201 SAMP	B	ITALY	HDPE	45.0
5	TENAX TT301 SAMP	B	ITALY	HDPE	65.0
6	TENAX TT601 SAMP	B	ITALY	HDPE	100.0
7	TENAX TT701 SAMP	B	ITALY	HDPE	110.0

Figure 4 shows the typical elongation - log time curves for geogrid type 1 at 20°C, 30°C, 40°C. At 10,000 hours, at 20°C and at 40 % of peak tensile strength, the total elongation measured was lower than the 10 % limit strain. Figure 5 shows the tensile creep modulus derived from the above test results, calculated applying eq. 1 to the creep curves at a load level of 35% as shown in Fig. 4. These curves show a linear viscoelasticity behaviour, that is successive creep modulus versus time curves for different loads superimpose upon each other. The superposition is performed in Figure 5, where the curves for 30° C and 40° C are time-shifted to continue the one at 20°C. This tecnique allows the confident prediction of the long term modulus for periods up to two orders of magnitude greater than the actual testing time range. It can be noted that the time shift between the curves at 20°C and 30° C is equal to 100 or $10^{2.0}$, while the time shift between 20°C and 40°C is equal to 2000 hours or $10^{3.301}$. This means, practically, that 1 hour of creep testing at 30°C produce the same elongation than 100 hours at 20°C, for the same testing condition; or 10^4 hours at 30°C correspond to 10^6 hours at 20°C. And similarly for the 40°C testing, with a 2000 factor.

Figure 6 shows the cartesian Isochronous Load - Elongation curves for the same geogrid. This diagram indicates loads plotted against strain for different time intervals. This is useful for the design engineers to select the appropriate design load and elongation for the given life of the structure. The isochronous curves at 20°C are directly obtained from the creep curves in Fig. 4 up to a design life of 10,000 hours, that is up to the testing duration. The Isochronous Load curves at 10^6 h at 20°C and 30°C were extrapolated from the Creep Modulus curve of Fig. 5 and from the other similar curves for different loads. In fact the Creep Modulus E_F obtained from Fig. 5, relative to a load F equal to 35 % of the peak tensile strength, at a given time t yields, through Eq. 1, the elongation $\epsilon(t)$ produced by the load F.
Fig. 7 shows the results of some of the tests with geogrid 2, Fig. 7a shows the failure of this type of geogrids at 40 % of the peak tensile strength at 40°C. Fig. 7b shows the Creep Modulus curves and the time-temperature superposition. The time shift between 20°C and 30°C results equal to 40, or $10^{1.602}$, while the one between 20°C and 40°C is equal to 700, or $10^{2.845}$. Data reported by Bush (1990) on a geogrid similar to geogrid 2 (produced in U.K.), showed a time shift coefficient of $10^{3.2}$ between 20°C and 40°C. Taking into account that the products tested by Bush (1991) and by the Authors are manufactured by different producers and they were tested at a slightly different load level, the obtained results seems to be fundamentally in the same range (i.e. 2.845 vs. 3.2).

Figure 8 shows the initial results (1000 hours) of the tests with geogrid 3. The 1000 hours time scale was selected to show the initial behavior of these geogrid. It is interesting to note that, even if the creep behaviour becomes early asymptotic, the total elongation corresponding to a load equal to 40 % of the peak tensile

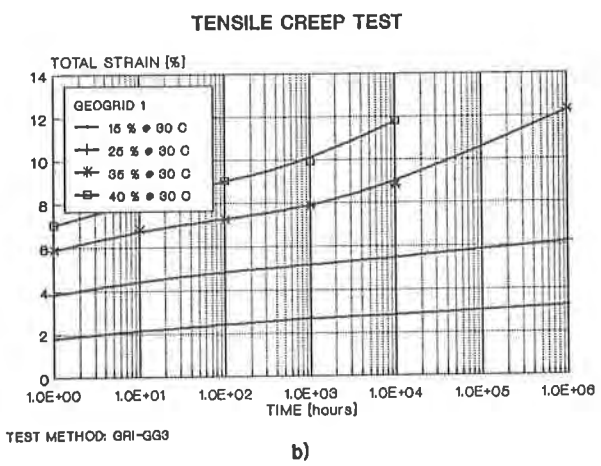

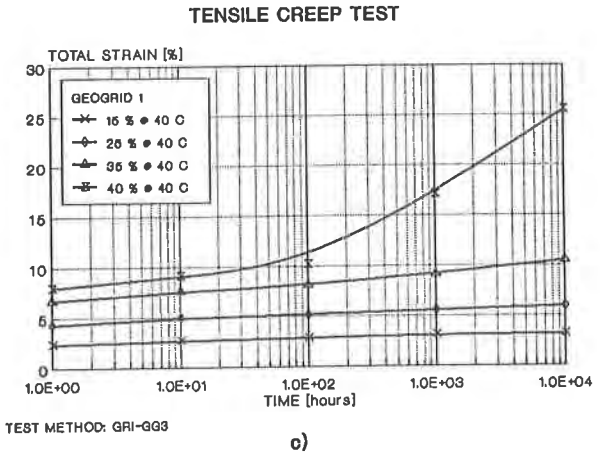

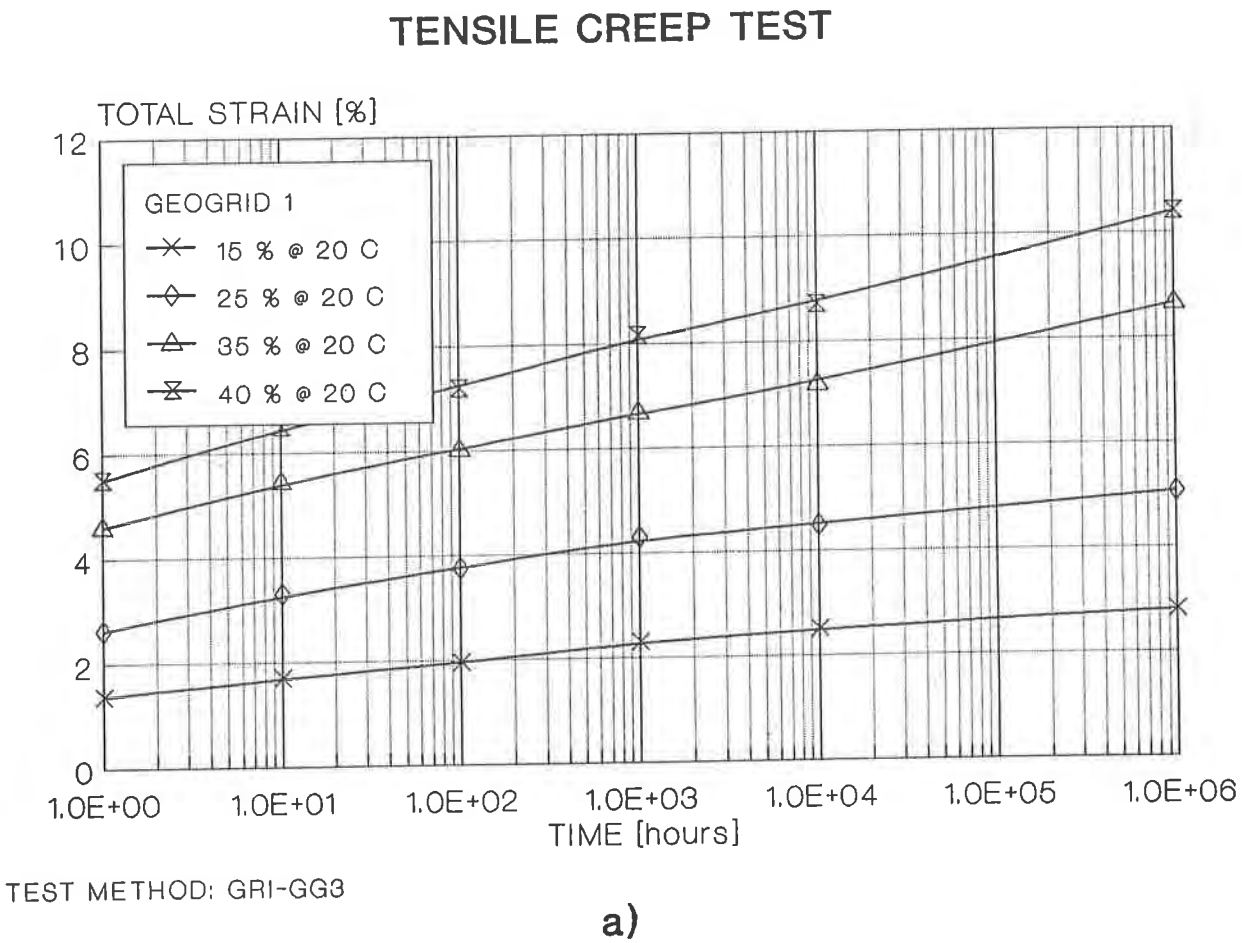

Fig. 4. Elongation - log time curves (creep diagram) for GEOGRID 1: a) at 20°C; b) at 30°C; c) at 40°C.

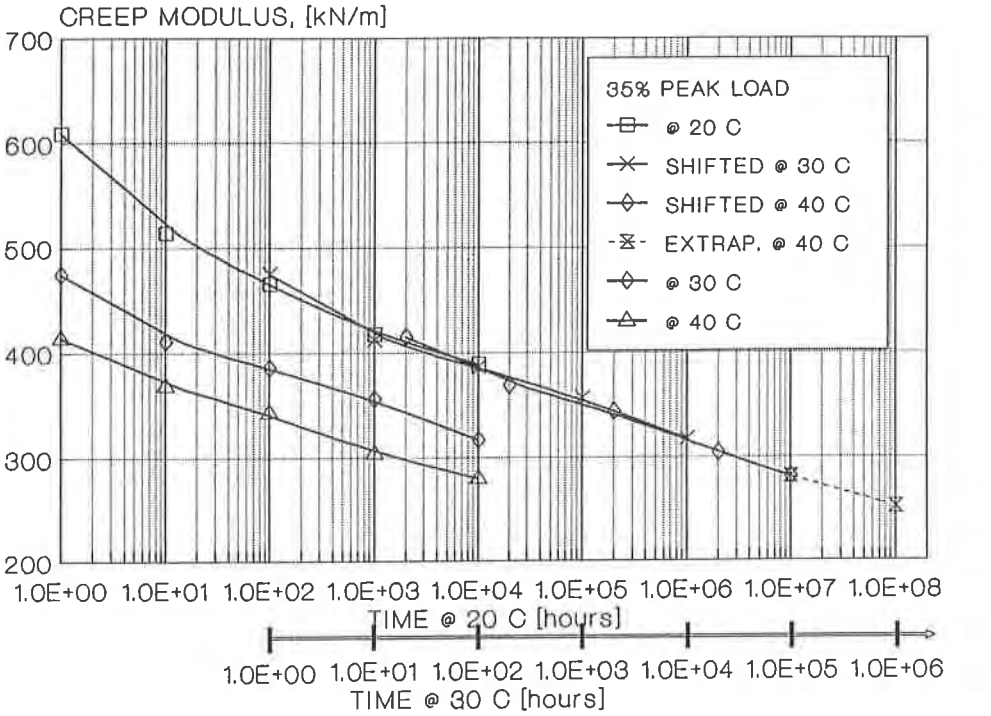

Fig. 5. Creep modulus versus time for GEOGRID 1 geogrids; curves at 20°C, 30°C, 40°C and time-temperature superposition curve.

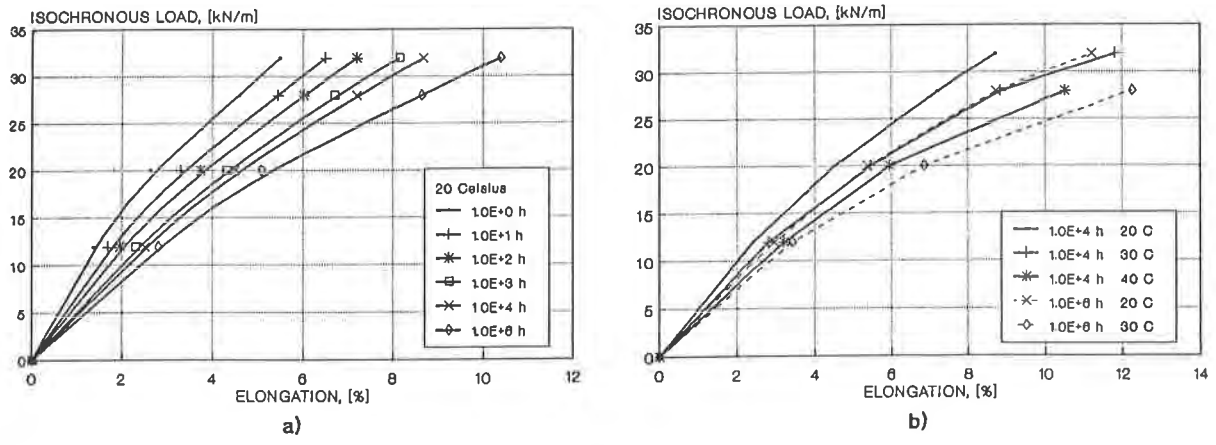

Fig. 6. Isochronous load - elongation diagrams for GEOGRID 1: a) at 20°C; b) extrapolation to 10^6 hours.

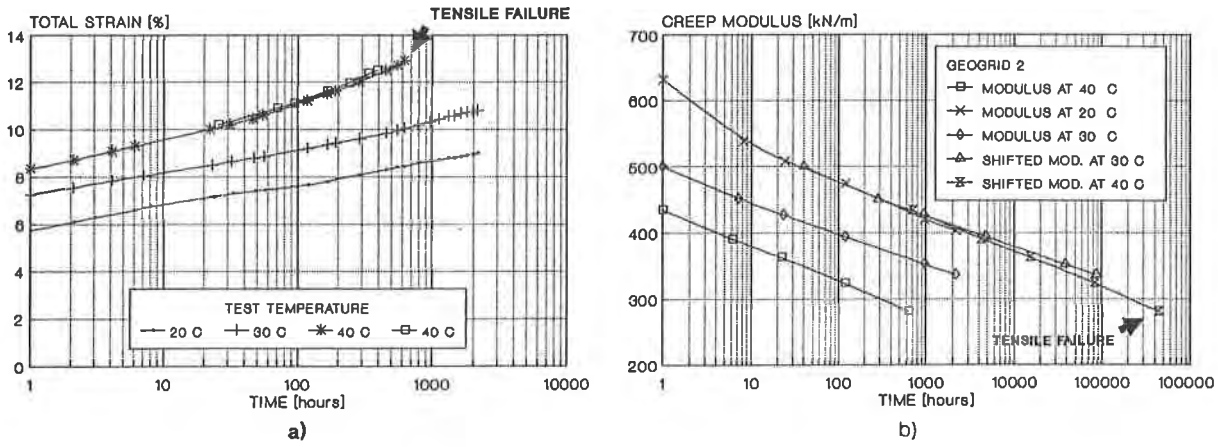

Fig. 7. Creep tests results for GEOGRID 2 at 40% load level: a) creep curves; b) creep modulus curves and time-temperature supurposition of the creep modulus curves.

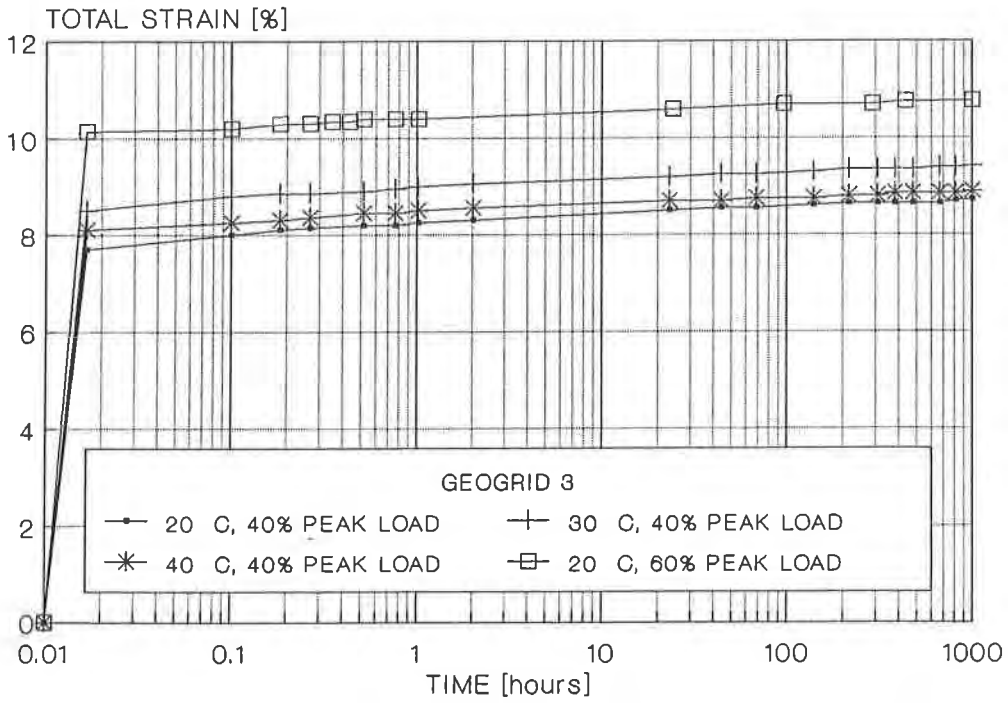

Fig. 8. Some creep tests results for GEOGRID 3.

strength is immediately in excess of 8 % and, considering the results obtained at 10000 hours, the creep strain tends to a 10 % value in the long term, while the total elongation at 60 % of the peak tensile strength is immediately in excess of 10 % and tends to a 12 % value in the long term. This is due to the elastic and plastic elongation of the threads and of the woven structure: when the load is applied, the strands, which are not straight in the junctions due to the weaving with the intersecting perpendicular strands, become initially straight (with a consequent, only partially recoverable, elongation) and then elongate elastically and plastically. These results are in substantial agreement with the findings of other researchers as Muller-Rochholz (1991). Therefore, in the Authors' opinion, the common belief that PET woven geogrids have around 2 % creep may be applicable only to the single strands, previously straightened, and not to the whole geogrid structure. Hence, as already reported by Greenwood (1991), the creep tests on single strands of woven geosynthetics is absolutely not representative of the behaviour of the products. The Authors feel that, for woven geogrids, the minimum width of the sample shall be 3 ribs or, even better, 5 ribs (for avoiding almost totally the necking effect). Fig. 9 shows the results of the tests performed with different loading time for geogrid 1 and 3. It can be noted that HDPE integral geogrids are more sensitive than PET woven geogrids to the loading time. However both types of geogrids show significant differences in the instantaneous elongation when the loading time just changes from instantaneous to 3 minutes. For the woven geogrids the influence of the loading time disappear after about 2 h, while for the integral geogrids after about 50 h.

Fig. 10 shows the variation of the long term design strength at 120 years with the average temperature (from 10°C to 40°C) for the different types and grades of the tested geogrids reported in Tab. 1. As made by Bush (1990), Fig. 10 was obtained from the data in Fig. 4 to Fig. 8 and from the equivalent diagrams for the other geogrids (not shown here for limited space). The LTDS in Fig. 10 is relative to a total elongation of 10 % when extrapolated to 10^6 hours (120 years). The LTDS at 20 °C results in the range from 35 % to 40 % of the peak tensile strength (the actual one, not the nominal one) for HDPE integral geogrids, while it is almost equal to 40 % of the actual peak tensile strength for PET woven geogrids. The LTDS for the woven geogrids was determined on the base of the following considerations: 1) the variation of the elongation with the temperature is almost negligible in the range of 20°C to 40°C, hence a limited time shifting extrapolation is obtainable; 2) the creep behavior at 10000 hours at 40 % load level is clearly asymptotic based on Sherby Dorn analysis made by the Authors. Therefore, even if the overall elongation was close to 10% and even without using superposition techniques, the Authors feel that, for the geogrids showing such a behavior, it is possible to define the Long Term Design Strength at 10^6 hours simply extrapolating the last two log cycles behavior.

Since, for practical reasons, it is impossible to perform testing at more than four temperatures (usually 10°C, 20°C, 30°C and 40°C), then the LTDS at 40°C for the

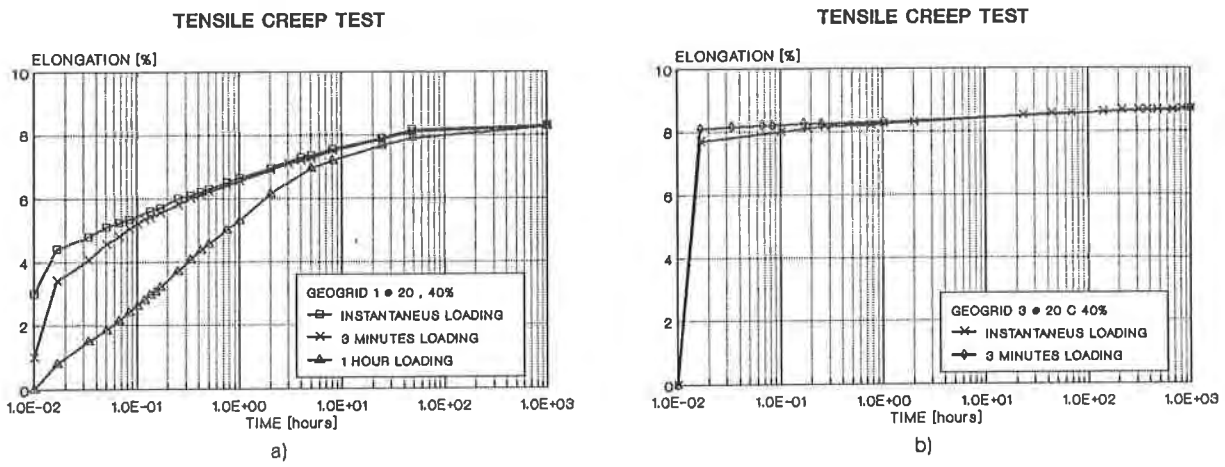

Fig. 9. Effect of the loading time on the creep curves: a) GEOGRID 1 hot formed integral geogrids; b) GEOGRID 3 woven geogrids.

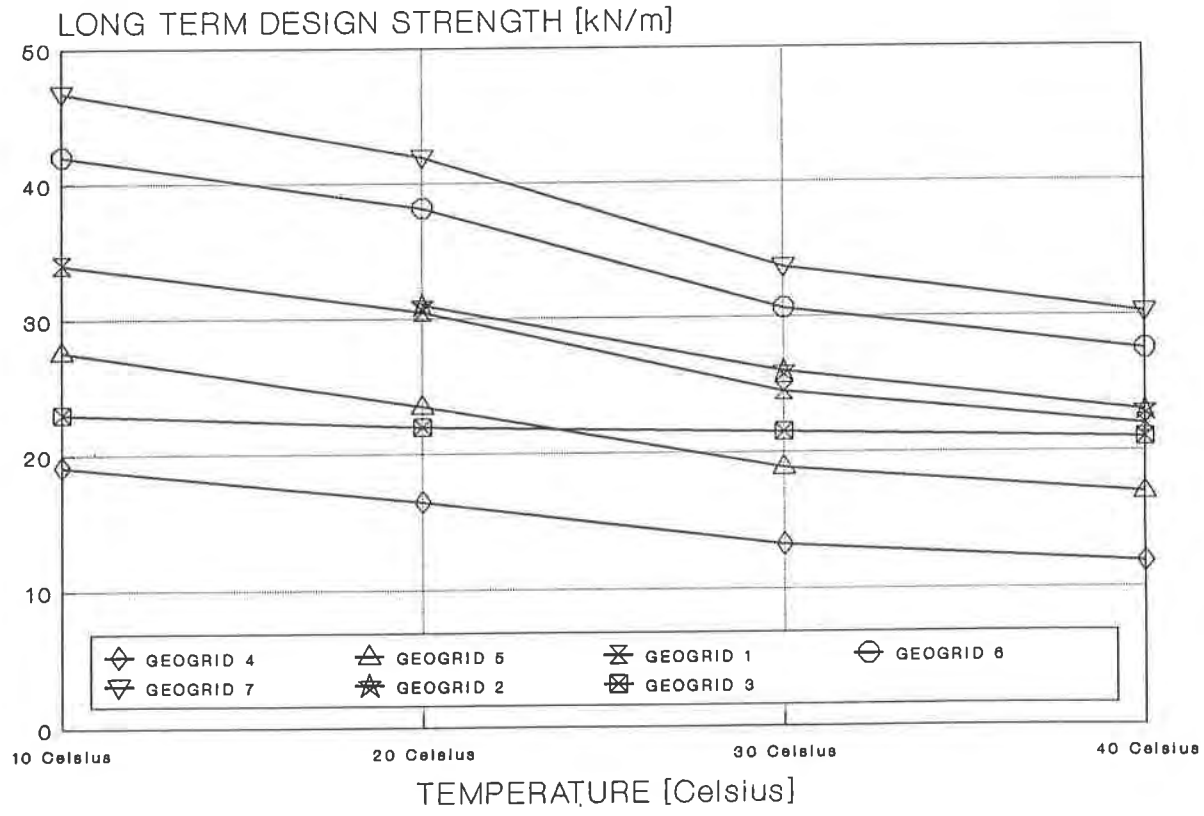

Fig. 10. Variation of the Long Term Design Strength at 120 years with the average temperature, for the tested geogrids.

geogrids tested (see Fig. 10) was determined by extrapolating the data at 10000 hours within the limits of two orders of magnitude, to a design life greater than 100 years, as indicated by the american standard GRI-GG3-87 (GRI, 1987)

CONCLUSIONS AND PROPOSALS FOR STANDARDIZATION

A laboratory research was performed to investigate the creep properties of different geogrid products. Some conclusions can be drawn from this research. The Authors suggest the following points as a proposal for the standardization of tensile creep tests on geogrids and woven geotextiles:

- the minimum width of the specimens, for both integral and woven geogrids, shall be minimum three ribs; for woven geotextiles the minimum width will be the one that produces a lower necking than 5% of the initial specimen width;
- the gauge length shall be equal to 1000 mm: this size allows a very simple yet very precise measurement of the elongation, with an accuracy of 0.05 % on the initial length and of 1.0 % on the average final elongation, using a common tape ruler: infact the ruler is in contact with the geogrid, therefore there are no parallax measurements errors; moreover being the test temperature constant even the ruler length is constant throughout the test;
- clamps shall be differentiated between integral and woven geogrids or geotextiles: integral geogrids can be clamped through the junctions, while woven geogrids break in this type of clamps and therefore capstan or roller type clamps are required;
- two very simple and inexpensive, yet very effective types of clamps have been proposed: the through-the-junctions clamps make use of a cold-setting resin, while the capstan type clamps are made with commonly available square steel tubes;
- the time-temperature superposition, using the creep modulus curves, has been used to extrapolate the behaviour of Type A and B integral geogrids to 10^6 hours. The method appear to be quite reliable and simple;
- the influence of the loading time has been investigated: it appears extremely important that all the tests shall be performed with the same loading time. Five seconds appears to be a reasonable option;
- loading by dead weight appears to be the most reliable, precise, cheap and fast method; it allows to change easily the loading time. In the Authors' opinion it is a preferable option than the knife-edged lever or other methods.

ACKNOWLEDGEMENT

The Authors wish to thank Mr Italo De Feo for his professional help in performing the tests and in developing the testing devices.

REFERENCES

Rimoldi, P., and Ricciuti, A, (1992) "The role of geogrid reinforced embankments in landslide stabilization: theory and practice in Italy.", Proc. VI Int. Symp. on

Landslides, Christchurch, New Zealand.

GRI, (1987) "GRI Test Method GG3: Creep behavior and long term design load of geogrids", Geosynthetics Research Institute, Philadelphia, PA, USA.

GRI, (1990) "GRI Test Method GG3: (a) Tension creep testing of stiff geogrids; (b) Tension creep testing of flexible geogrids.", Geosynthetics Research Institute, Philadelphia, PA, USA.

ASTM, (1990) ASTM D2990-90, "Standard test method for tensile, compressive and flexural creep and creep-rupture of plastics.", Annual book of ASTM Standards Vo. 08.02. ASTM, Philadelphia, PA, USA.

Mc Gown, A., Andrawes, K.Z., Yeo, K.C., DuBois, D., (1984) "The load - strain - time behaviour of Tensar geogrids.", Polymer grid reinforcement, Thomas Telford, London.

Allen, T.M., (1991) "Determination of long term tensile strength of geosynthetics: a state of the art review.", Proc. Geosynthetics '91 Conf., Atlanta, USA.

Bush, D.I., (1991) "Variation of long term design strength of geosynthetics in temperatures up to 40°C.", Proc. IV Int. Conf. on Geotextiles, Geomembranes and Related Products, The Hague, the Netherlands.

Muller-Rochholz, J, and Kirschner, R., (1991) "Creep of geotextiles at different temperatures.", Proc. IV Int. Conf. on Geotextiles, Geomembranes and Related Products, The Hague, the Netherlands.

Greenwood, J.H., (1991) "The creep of geotextiles.", Proc. IV Int. Conf. on Geotextiles, Geomembranes and Related Products, The Hague, the Netherlands.

Using the Arrhenius Equation and Rate Expressions to Predict the Long-Term Behavior of Geosynthetic Polymers

W.S. Shelton
The Tensar Corp., USA

D.G. Bright
The Tensar Corp., USA

ABSTRACT

Geosynthetic polymers used in critical structures have minimum performance requirements to be maintained over a service life from 1 to 100 years. Predicting the behavior of these polymers with time facilitates proper design of the structure and assures the polymer's adequate performance over a service life.

Over the past few years, there has been a proliferation in the use of rate expressions to represent a polymer's behavior with time within geotechnical environments. Elevated temperatures are used to accelerate a polymer's behavioral response, facilitate data acquisition, and evaluate rate parameters. The Arrhenius equation is commonly used to represent temperature dependency within a rate expression, and its activation energy (E) is suppose to remain constant over its temperature range of evaluation and extrapolation. Literature shows that E is frequently not a constant, and any small error in E causes a large error in the rate expression.

Caution should be exercised when using rate expressions and the Arrhenius equation to represent the behavioral response of polymers in geotechnical environments, especially when the rate expression has to change with time to represent polymeric behavior.

INTRODUCTION

Polymeric materials used in geosynthetics for reinforcement of earth structures and waste containment sites have minimum performance requirements to be maintained over a service life ranging from 1 to 100 years. The ability to predict the long-term behavior of these materials would assure their adequate performance over the structures design life. However, the mechanism and profile of a material's response to geotechnical environment must be known or be predictable.

The common modes that change the properties of geosynthetic polymers within a geotechnical environment are installation damage, mechanical deformation, weathering, chemical degradation, and biological deterioration. Prediction of long-term performance is usually accomplished by the extrapolation of relatively short-term data collected on a polymer's response to a particular mode. Typically, extrapolation is limited to one order of magnitude, e.g., one year of data is necessary to predict ten year behavior (ASCE 1985). Time frames exceeding ten years necessitate the utilization of time-temperature-superposition principles or a rate expression with which to extrapolate short-term data.

Over the past few years, there has been a proliferation in the use of rate expressions to represent a polymer's response with time to a specific geotechnical environment. Rate parameters are determined experimentally, usually at elevated temperatures so as to expedite collection of sufficient data within a reasonable time frame. These parameters are then extrapolated to temperatures common to a specific environment, and the subsequent integration of the rate expression predicts a material's behavior with time.

The objective is to review the problems and pitfalls in establishing a rate expression and its kinetic parameters to represent the response of a geosynthetic polymer to a geotechnical environment with time. Means of circumventing problems and pitfalls are suggested.

A GENERIC METHODOLOGY

In the development of a rate expression modeling a particular deteriorative mode with time, the first step is to determine which physical properties respond to that mode, which chemical structure(s)/group(s)/constituent(s) reflect changes in those physical properties, which agent(s) in the service environment are likely to attack these structure(s)/groups(s)/constituent(s), and in which physical state the polymer resides while in service when responding to a particular deteriorative mode (Flynn 1981 and 1988).

Assume a geosynthetic product is composed of polymer A. An agent B within the surrounding environment reacts with polymer A causing a change in a property, e.g., molecular weight. The overall or net change in a property may be the net result of several intermediate reactions, e.g., initiation, propagation, and eventually termination. Thus, an overall or net reaction scheme incorporating only the reactants (A and B) and products (A') can be:

$$A + B \rightarrow A' \qquad (1)$$

where A' is lower molecular weight A. If progression of the reaction is dependent upon the amount of A and B present and temperature, a representative kinetic rate expression can be (Boudart 1968, Levenspiel 1962, Smith 1970):

$$-r_A = -d[A]/dt = k*[A]^a*[B]^b \qquad (2)$$

where $-r_A$ is the rate of change of A; d/dt is the time derivative; [ ] represents the residual concentration (quantity) of the reactant constituents A and B; superscripts a and b are the rate order by constituent; k is the kinetic rate constant, and t is the time parameter.

The second step is to select a means of accelerating the reaction. Temperature accelerates exponentially nearly all reactions. If all other factors are held constant, then a single mathematical relation, the Arrhenius equation, can describe such temperature dependence (Flynn 1981, Levenspiel 1962, Smith 1970):

$$k = k_0 \, e^{-E/RT} \tag{3}$$

$$\ln k = \ln k_0 - E/R * 1/T \tag{4}$$

where:

k	=	kinetic rate constant,
k_0	=	pre-exponential kinetic rate constant,
E	=	apparent activation energy,
R	=	universal gas constant,
T	=	absolute temperature, and
ln	=	natural logarithm.

E is considered the apparent activation energy because it represents the overall or net reaction between reactants A and B. Assumptions associated with the Arrhenius equation are (Boudart 1968, Levenspiel 1962, Smith 1970, Flynn 1969 and 1980):

- k is only a function of temperature;
- k_0 does not affect the temperature sensitivity of the reaction; and
- E remains constant over the time and temperature range for evaluation, extrapolation, and prediction.

The third step is to determine the validity of the selected rate expression and constituent order, e.g., Equation 2, by recording the concentration of constituents with time at various elevated temperatures (T_i) for a particular deteriorative reaction. Plot concentration verses time for each T_i according to the integrated rate expression (e.g., Equation 2). If the correlations of concentration as a function of time per temperature (T_i) result in straight lines as shown in Figure 1, then the chosen rate expression represents the overall kinetic reaction (Levenspiel 1962, Smith 1970) between polymer A and deteriorative agent B. The rate constant k_i is the slope of each concentration-time correlation for T_i .

The fourth step is to determine if -E/R in Equation 3 is constant with changes in both temperature and constituent(s) conversion (Flynn

1966, 1969, 1977, 1980, 1988) for the rate expression established in step three. The Arrhenius' parameters (k, k_0, and E) are usually determined by either isothermal or isoconversion experiments. For isothermal experiments, ln k is plotted as a function of reciprocal temperature, 1/T, to determine k_0 and -E/R in Equation 4 as shown in Figure 2. If the ln k verses 1/T is a straight line, then k is solely a function of temperature, as it should be for applicability of the Arrhenius equation (Equation 3) in a rate expression (e.g., Equation 2) (Levenspiel 1962, Flynn 1966 & 1969).

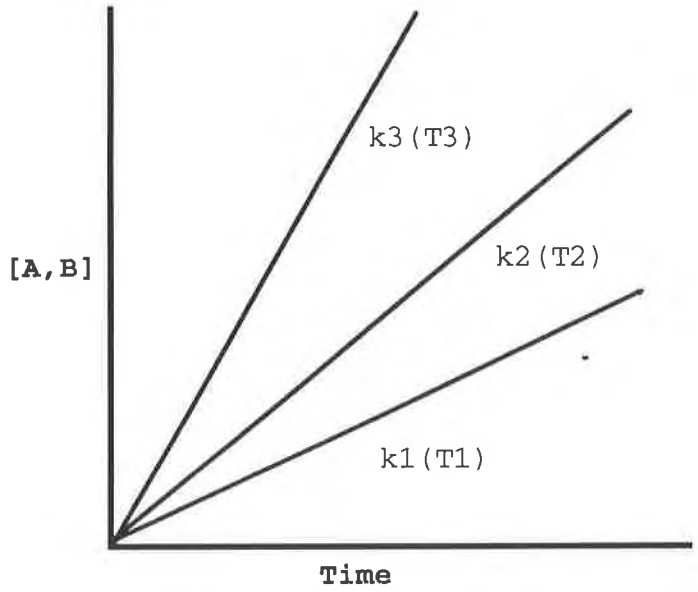

Figure 1. Concentration of Constituents with Time at Various Temperatures

The fifth step is to determine a rate constant k at temperature T of a specific environment from Figure 2. Now the rate expression (e.g., Equation 2) can be integrated to predict the state of polymeric material A with time t:

$$\int [A]^{-a} * [B]^{-b} * d[A] = - k \int dt \qquad (5)$$

To summarize, first a rate expression is selected by correlating constituent concentration and order with time. Second, a representative function for temperature dependency is assumed; this is usually the Arrhenius equation. Verification of the rate expression and validity in using the Arrhenius equation for temperature dependency are the third and fourth steps, respectively. The fifth step is the extrapolation of the Arrhenius' parameters to a service temperature and then integration of the rate expression for prediction of the state of a polymeric material after exposure to a particular of deteriorative reaction after a given time, t.

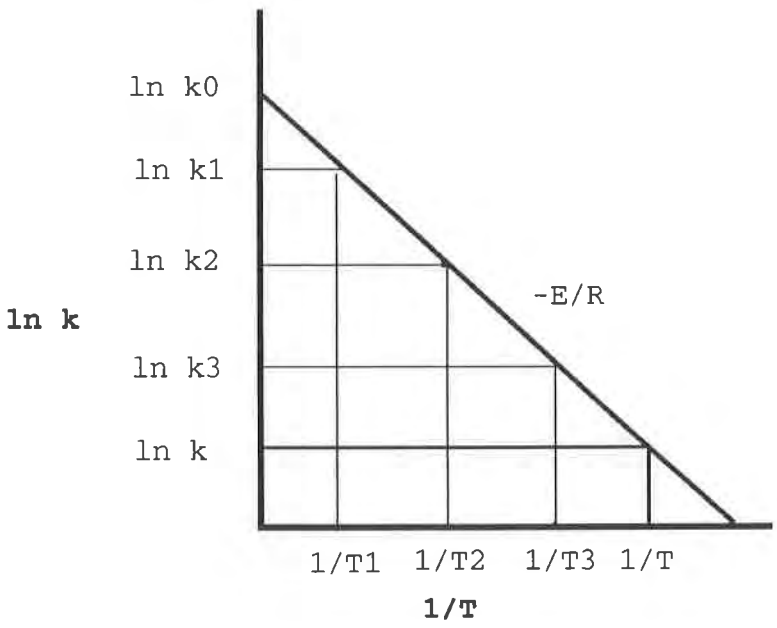

Figure 2. Rate Constant as a Function of Temperature

ESTABLISHING A REPRESENTATIVE RATE EXPRESSION

Physical State and Properties. Deteriorative processes are quite complex and usually take place within a heterogeneous environment (Flynn 1981 & 1988) such as a solid geosynthetic product attacked by agent(s) dispersed in the soil (e.g., pyritic, dolomitic, microbic) or fluid media (e.g., air, water). The reaction mechanisms within the physical state (e.g., glassy or viscoelastic) are affected by physical properties such as density and crystallinity. Thus, it is advantageous to minimize the elevation of temperature above service conditions so as to minimize changes in pertinent physical properties.

Elevated Temperature Range. As temperature is elevated to accelerate the reaction, physical properties vary with temperature changing the rate limiting step of the kinetics, thus changing the form of the rate expression. At the low end of the overall temperature range (i.e., ambient), diffusion mechanisms commonly control; whereas at the high end of the range, chemical reactions usually dominate. (Flynn 1988) The atmospheric degradation of poly(vinyl chloride) is a classic example of this phenomenon as discussed in a previous paper (Bright 1992). Thus, kinetic parameters development at elevated temperatures may have questionable usefulness in service life predictions at ambient temperatures (Flynn 1981). So, it is desirable to minimize the elevation of temperature above the service conditions.

If the elevated temperature range is sufficiently high to traverse a phase transition (e.g., glass transition, melt range), a sharp change in rheological, physical, thermal properties will occur (van Krevelen 1972). These changes will affect the kinetic mechanisms of the

deteriorative reaction necessitating a change in the representing rate expression. This phenomenon was discussed in a previous paper (Bright 1992) addressing the hydrolytic degradation of poly(ethylene terephthalate) below, within, and above its glass transition and the oxidative degradation of polyethylene below and above its melt range.

Validity of Arrhenius' parameters determined above and/or within a phase transition and then extrapolated to service temperatures where the polymer is in a different state is questionable. A very small error in E translates into a large error in $-r_A$ upon its extrapolation from elevated temperatures to service temperatures (Flynn 1981 and 1988). Typical thermal transitions of polymers used in geosynthetic are given in Table 1.

Table 1. Thermal Transitions of Polymers Used in Geosynthetics

Polymer	Glass Transition, C	Melt Range C
Low Density Polyethylene	-80	60-100
Medium Density Polyethylene	-80	80-120
High Density Polyethylene	-80	100-140
Polypropylene	-10	100-165
Poly(ethylene terephthalate)	~75	200-260
Poly(vinyl chloride)	80	-

Thus, the maximum range of temperature elevation should be limited to within the temperature range of the physical state in which the polymer resides at service conditions, and this range should be minimized.

Constituent Representation. In homogeneous, fluid phase reactions, constituent concentration is fairly straight forward such as the classical weight/volume for a fluid phase constituents, and partial and total pressure changes for purely gas phase constituents (Boudart 1968, Levenspiel 1962, Smith 1970). But in mixed state reactions (e.g., fluid/solid), constituent concentration can be in various units of measure: weight loss or dimensional reduction for a solid phase constituent and weight/volume for a fluid phase constituents. Thus, a single rate expression for a heterogeneous state reaction can have mixed units of measure for constituent concentration. Through constituent density and dimensional change, classical concentration units (i.e., weight/volume) could be calculated. Thus a reaction's progression may have to be defined as the change in material thickness or weight or residual chemical groups (e.g., end group concentration or count) for solid state polymer A with time (Gomes 1961, McMahon 1959).

Constituent Order. For many deteriorative reactions associated with polymers, the rate expression (e.g., Equation 2) is commonly assumed first-order by constituent. Thus, the superscripts a and b are both equal to one, and the rate expression becomes second-order overall (a+b) (Levenspiel 1962, Smith 1970):

$$-r_A = -d[A]/dt = k_1 * [A]^1 * [B]^1. \quad (6)$$

The integration of Equation 6 is (Levenspiel 1962, Smith 1970):

$$\ln\{[B]*[A_0]/[A]/[B_0]\} = -\{[A_0] - [B_0]\} * k_1 * t. \quad (7)$$

If the plot of concentration verses time (i.e., Equation 7) is a straight line correlation per temperature (T_i) as illustrated in Figure 3, then the chosen rate expression (i.e., Equation 6) represents the kinetic reaction (Levenspiel 1962, Smith 1970) of a particular mode of deterioration between A and B. If not, then superscripts a and b are usually adjusted first to achieve a straight line.

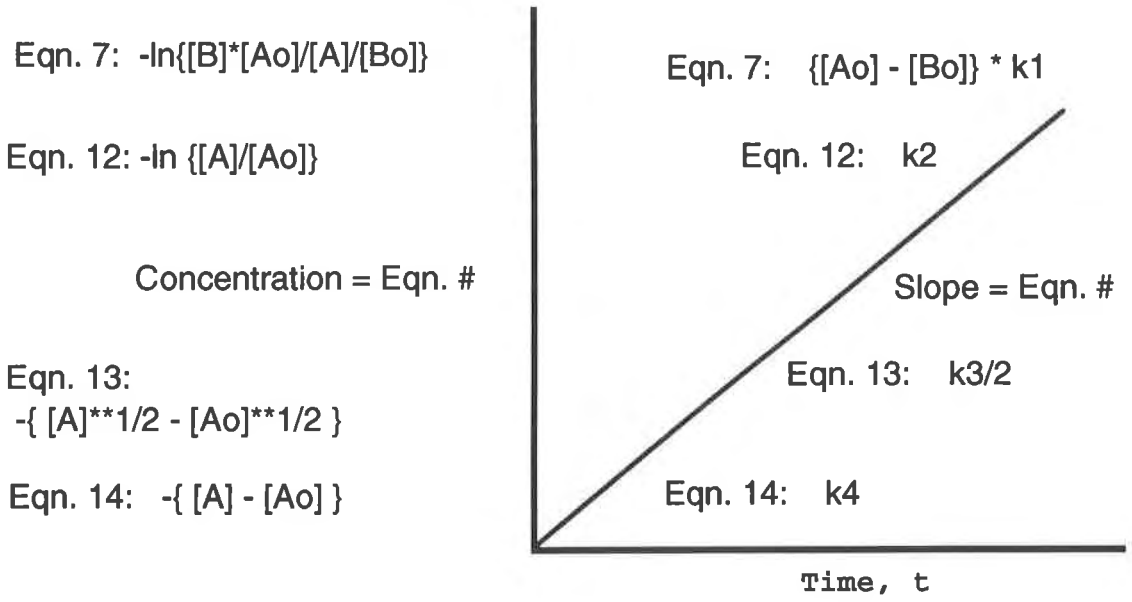

Figure 3. Correlation of Concentration by Rate Order with Time for a given Temperature, T_i

In typical geotechnical environments, the concentration of agent B is commonly in considerable excess relative the concentration of polymeric material A. Thus, progression of the reaction is dependent upon [A] and independent of [B]. The reaction is still first-order by A but now zero-order by B; thus superscripts a and b are one and zero, respectively. Now Equation 2 becomes an overall pseudo first-order rate expression and reduces to:

$$-r_A = -d[A]/dt = k_2 * [A]^1 \quad (8)$$

But, it is not uncommon for a rate expression representing a polymeric deterioration to be half-order by the polymeric constituent A (Ravens 1961 & 1964). Thus, superscript a becomes 1/2, and the rate expression (e.g., Equation 2) becomes half-order (Levenspiel 1962, Smith 1970):

$$-r_A = -d[A]/dt = k_3 * [A]^{1/2} . \quad (9)$$

Initially, some deteriorative reactions depend solely on temperature (Gomes 1961, Ravens 1960). Thus, the superscripts are zero, and the rate expression (e.g., Equation 2) becomes zero order (Levenspiel 1962, Smith 1970, Garn 1972):

$$-r_A = -d[A]/dt = k_4 . \quad (10)$$

The integration of Equations 8, 9, and 10 (Levenspiel 1962, Smith 1970) are respectively:

Pseudo First-Order $$\ln \{[A]/[A_0]\} = - k_2 * t \quad (12)$$

Half-Order $$[A]^{1/2} - [A_0]^{1/2} = - k_3/2 * t \quad (13)$$

Zero-Order $$[A] - [A_0] = - k_4 * t \quad (14)$$

These equations correlate concentration with time, as shown in Figure 3, to determine representation of the kinetic reaction by constituent and its order for a particular deteriorative reaction. It should now be apparent that constituency and their order within a rate expression have a significant impact on the correlation of kinetic data, and the prediction of polymeric behavior with time.

Some deteriorative reactions (e.g., oxidation and hydrolysis) become autocatalytic with time changing the form of the rate expression as the reaction progresses. By definition, an autocatalytic behavior means that the reaction accelerates with the increasing presence (concentration) of a particular product constituent (Boudart 1968, Levenspiel 1962, Smith 1970), for example constituent C:

$$A + B + C \rightarrow A' + C . \quad (15)$$

A kinetic rate expression representing autocatalytic behavior can be (Levenspiel 1962, Smith 1970):

$$-r_A = -d[A]/dt = k*[A]^a*[B]^b*[C]^c \quad (16)$$

where the integrated form is considerably more complex than Equation 7. The concentration of C must be incorporated into the initial rate expression (e.g., Equation 2) at some time after the reaction has begun, but when (i.e., time) and at what order (i.e., superscript c) ?

Prediction is complicated when a particular mode of deterioration exhibits a changing reaction order with time. Some deteriorative reactions (e.g., hydrolysis) initiate with a zero-order behavior (e.g., Equation 10) (Gomes 1961, Ravens 1960), progress to pseudo first-order (e.g., Equation 8) (Golike 1960, McMahon 1959) or second-order (e.g., Equation 6) (Golike 1960) behavior, and eventually become autocatalytic (e.g., Equation 16) (Marshall 1953, Risseeuw 1990). Thus, over the service life of a polymer, its representing rate expression can be changing thus compounding the ability to accurately predict its behavior with time. Multiple rate expressions could be employed, each over a specific time frame, but now the problem becomes one of the time interval for changing from one rate expression to another.

Initial Rate Data. The relevancy of initial rate data are clouded by such complicating factors as the release of absorbed gases, absorbents and/or solvents, plasticizers (e.g., water), and the effect on kinetic mechanisms by residual catalysts, antioxidant and stabilizer packages, and general impurities (Flynn 1977). Volatilization of these gases and liquids affect the kinetics of the initial rate process representing the condensed phase but are not directly measurable (Flynn 1980). Thus, rate parameters determined on initial kinetic data will not likely have the same value when determined after these factors have either dissipated or stabilized.

Isothermal Thermogravimetric Analysis (TGA) of the geosynthetic product at the elevated temperature (T_i) can determine the time (t) to a stable plateau in weight loss, after which the rate data should more accurately represent deteriorative kinetic reaction.

Degree of Conversion. At low conversions where $-r_A \sim 0$ for $t \sim 0$, a reaction may behave like zero order expression due to the dominance of the Arrhenius equation temperature term, -E/R/T (Flynn 1967). At low conversions, plot concentration data versus time according to a zero-order expression (e.g., Equation 14). At a time (t_0) when the data depart from the straight line correlation of the zero-order expression, switch to a higher order expression such as first-order or even second-order (e.g., Equation 12 or 7, respectively) as illustrated in Figure 4. If the reaction becomes autocatalytic, concentration data will correlate with time at t_1 according to an integrated form of a rate expression similar or analogous to Equation 16. Thus, it is necessary for the reaction to progress sufficiently with time so as to acquire meaningful data to determine parameters for a rate expression with progressing constituent order.

APPLICABILITY OF THE ARRHENIUS EQUATION

With liquid/solid state reactions initially being diffusion limited, the conventional concept of constituent concentration and their order have questionable significance. Thus, it may be difficult to determine whether the rate expression exhibits an exponential dependency with temperature (Garn 1972, Gomes 1961, Jost 1960) as would be described by the Arrhenius equation (i.e., Equation 3). Temperature

dependency as described by the Arrhenius equation should not be so readily assumed for solid/liquid state reactions (Gomes 1961, Jost 1960). Some other correlation describing temperature will be necessary.

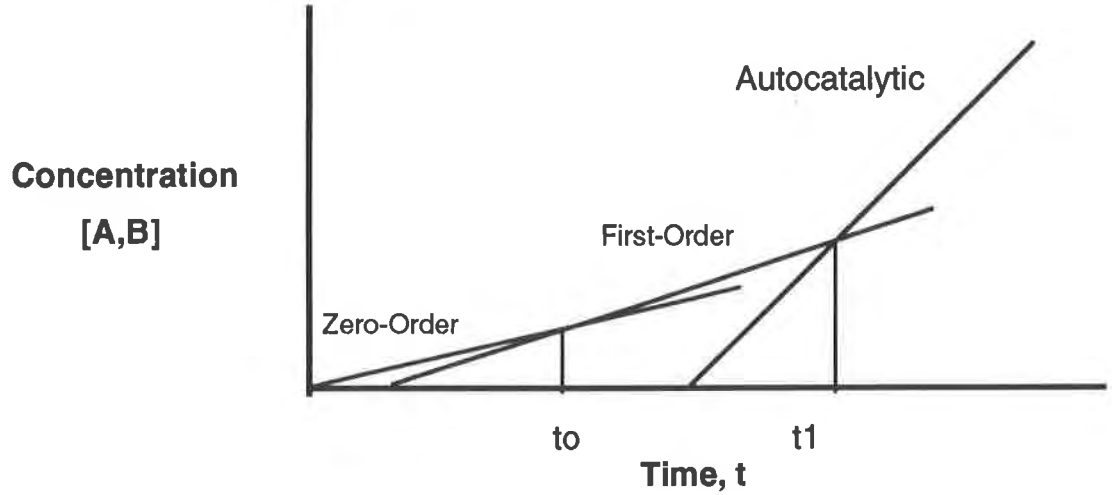

Figure 4. Multiple Order Rate Expressions Used to Correlate Data

DETERMINATION OF ARRHENIUS' PARAMETERS

Temperature Range. Rate parameters are determined experimentally at elevated temperatures so as to expedite collection of sufficient data within a reasonable time frame. Changes from traversing across and within physical states (e.g., glassy to viscoelastic, viscoelastic), in physical properties (e.g., density, crystallinity), and/or in activity/mobility of the deteriorative agent(s) maybe sufficient to alter reaction mechanisms (Flynn 1988) thus causing rate expressions representing the extreme ends of the temperature range to be different. This leads to different E values as well. Also, a material's thermal history can affect dramatically the kinetic parameters (Flynn 1981) through effects on physical properties such as density and crystallinity.

At the low end of temperature range (i.e., ambient), diffusion mechanisms commonly control leading to low activation energies (E); whereas at the high end temperatures, chemical reactions dominate leading to high E values (Flynn 1988). Thus, E values development at elevated temperatures have questionable usefulness in service life predictions at ambient temperatures (Flynn 1981). Thus, it is desirable to minimize the elevation of temperature above the service conditions so as to minimize changes in pertinent physical properties keeping the polymer in a physical state common to its conditions (Flynn 1988).

Activation Energy. The magnitude of E reflects the temperature dependency of the rate expression. Thus, it is important to determine E as precisely as possible to provide meaningful estimates in service

life with time after the extrapolation of the rate expression ($-r_A$) to service temperatures (Flynn 1979). Since a slight error in E translates into a large error in $-r_A$ upon its extrapolation to service conditions (Flynn 1981), the greater the temperature difference between service and elevated temperatures, the smaller the error in E must be for a given accuracy at service conditions (Flynn 1979). Thus, it is desirable to minimize the elevation of temperature above service conditions.

For example, a 1/2 kilo calorie/mole error in E will cause a 50% uncertainty at the 90% confidence level for an extrapolation of the $-r_A$ from 400 to 25 C (Flynn 1988). Or, an error in E of as small as 1.0 kilo calorie/mole will cause an error of +/- 100% at the 95% confidence level in extrapolation of $-r_A$ from 225 to 25 C (Flynn 1988). Unfortunately, values of E for the degradation of some well-investigated polymers commonly resemble a list of random numbers (Flynn 1981).

Any error in the rate expression ($-r_A$) is compounded again by its integration for prediction of polymeric behavior with time at 25 C in response to a particular deteriorative environment.

THE STEPS IN ESTABLISHING A PROTOCOL

1. Identify the primary constituent(s) involved in the deteriorative reaction.

2. Establish a rate expression incorporating all constituents and assume an order of one per constituent.

3. Assume applicability of the Arrhenius equation being cognizant that it may not actually be applicable.

4. Establish the maximum elevated temperature range by keeping the polymer within the same physical state as in the service environment.

5. Establish time for volatilization of absorbed gases, adsorbed liquids, plasticizers, additives, etc.

6. Record kinetic data being aware of the problems with initial data and low conversions.

7. Correlate data according to the integrated form of the initial expression adjusting the number of constituents and/or their order as necessary. The net order of the rate expression may very well change as the reaction progresses.

8. Determine the Arrhenius' parameters and their relative accuracy.

9. Extrapolate the rate parameters to service conditions and then integrate the rate expression to predict behavior after exposure to a mode of deterioration with time.

CONCLUSIONS

Thus, modeling the kinetics of polymer deterioration is difficult and complex, and compounded by the fact that a single rate expression developed in the short-term may not be representative or valid over the long-term service life.

REFERENCES

_____, (1985) "Structural Plastics Selection Manual", ASCE Manuals and Reports on Engineering Practice No. 66, American Society Civil Engineers: New York.

Boudart, M., (1968) Kinetics of Chemical Processes, Prentice-Hall: Englewood, New Jersey.

Bright, D. G., (1992) "Problems with Current Medhodology in using the Arrhenius Equation to Predict the Long-Term Behavior of Polymeric Materials in geotechnical Environments", Symposium on Advances in Fatigue Lifetime Predictive Techniques, 2nd Volume, STP #1211, American Society for Testing and Materials: Philadelphia.

Flynn, J. H. and Wall, L. A., (1966) "A Quick Direct Method for the Determination of Activation Energy from Thermogravimetric Data", J. Polymer Science, Polymer Letters, Vol. 4, No. 5, pp. 323-8.

Flynn, J. H. and Wall, L. A. (1967) "Initial Kinetic Parameters from Thermogravimetric Rate and Conversion Data", Journal Polymer Science, Polymers Letters, Vol. 5, No. 2, pp. 191-6.

Flynn, J. H., (1969) "The Historical Development of Applied Nonisothermal Kinetics", Thermal Analysis, Vol. 2, R. F. Schwenker and P. D. Garn editors, Academic Press: New York, pp. 1111-23.

Flynn, J. H., et al., (1977) "Initial Weight-Loss Kinetics for the Thermal Degradation of Polyurethanes", ACS Polymer Preprints, Vol. 18, No. 1, pp. 757-60.

Flynn, J. H. and Dickens, B., (1979) "Applications of New Kinetic Techniques to the Lifetime Prediction of Polymers from Weight-Loss Data", Durability of Macromolecular Materials, R. K. Eby editor, ACS Symposium Series 95: Washington, D. C., pp. 97-113.

Flynn, J. H., (1980) "Degradation Kinetics Applied to Lifetime Predictions of Polymers", Polymer Engineering and Science, Vol. 20, No. 10, pp. 675-7.

Flynn, J. H., (1981) "The Role of Thermal Analysis in The Lifetime Prediction of Polymers", Proceedings of the Second European Symposium on Thermal Analysis, D. Dollimore editor, Heyden: London, pp. 223-6.

Flynn, J. H., (1981) "Analysis of the Kinetics of Thermogravimetry: Overcoming Complications of Thermal History", Thermal Analysis in Polymer Characterization, E. A. Turi editor, Heyden: Philadelphia, pp. 43-59.

Flynn, J. ,(1988) "Lifetime Prediction for Polymeric Materials from Thermal Analytical Experiments-Problems, Pitfalls, and How to Deal with Some of Them", 46th Annual Technical Conference, Society Plastics Engineers: Atlanta, Georgia, pp. 930-2.

Flynn, J. H., (1988) "Thermal Analysis Kinetics-Problems, Pitfalls and How To Deal with Them", Journal Thermal Analysis, Vol. 34, No. 1, pp. 367-81.

Garn, P. D., (1972) "Kinetic Investigations by Techniques of Thermal Analysis", CRC Critical Reviews in Analytical Chemistry, Vol. 3, No. 1, pp. 66-111.

Golike, R. C. and Lasoski, S,. W., (1960) "Kinetics of Hydrolysis of Polyethylene Terephthalate Films", Journal Physical Chemistry, Vol. 64, No. 7, pp. 895-8.

Gomes, W., (1961) "Definition of Rate Constant and Activation Energy in Solid State Reactions", Nature, Vol. 192, No. 4805, pp. 865-6.

Jost, W., (1960 Diffusion in Solids, Liquids, Gases, Academic Press: New York, pp. 367-8.

Levenspiel, O., (1962) Chemical Reaction Engineering, Wiley: New York.

Marshall, I. and Todd, A., (1953) "The Thermal Degradation of Polyethylene Terephthalate", Transactions Faraday Society, Vol. 49, pp. 67-78.

McMahon, W., et al., (1959) "Physical Properties Evaluation of Compounds and Materials", Journal Chemical Engineering Data, Vol. 4, No. 1, pp. 57-79.

Ravens, D. A. S., (1960) "The Chemical Reactivity of Poly(ethylene terephthalate): Heterogeneous Hydrolysis by Hydrochloric Acid", Polymer, Vol. 1, pp. 375-83.

Ravens, D. A. S. and Ward, I. M., (1961) "Chemical Reactivity of Polyethylene Terephthalate", Transactions Faraday Society, Vol. 57, No. 1, pp. 150-9.

Ravens, D. A. S. and Sisley, J. E., (1964) "Cleavage Reactions", Chemical Reactions of Polymers, E. M. Fettes editor, Interscience: New York, pp. 551-64.

Risseeuw, P. and Schmidt, H. M., (1990) "Hydrolysis of HT Polyester Yarn in Water at Moderate Temperatures", 4th International Conference on Geotextiles, Geomembranes, and Related Products, G. den Hoedt editor, The Hague, Netherlands, pp. 691-6.

Smith, J. M., (1970) Chemical Engineering Kinetics, McGraw-Hill: New York.

van Krevelen, D. W., (1972) Properties of Polymers Correlation with Chemical Structure, Elsevier: Amsterdam.

Long-Term Heat Aging Stabilization Study of Polyethylene and Its Relationship With Oxidative Induction Time (OIT)

G. Yim
Novacor Chemicals Ltd., Canada

M. Godin
Novacor Chemicals Ltd., Canada

ABSTRACT

The long term heat aging property of polyethylene used for geomembranes has been a subject of intense discussion for a long time. Controversy arises from the tests used to evaluate the long term thermal stability performance of geosynthetic products in the field.

Currently, Oxidative Induction Time (OIT) is a test used to decide "go or no go" for polyethylene geomembranes in the industry. Unfortunately, high OIT is mistakenly considered by most people as meaning that the material will have good long term thermal stability. The results of our heat aging study show that there is no correlation between the long term thermal stability and OIT for polyethylene materials. Our study also indicates that the long term thermal stability in polyethylene can be optimized through the use of proper heat stabilization systems.

For a given formulation, OIT by itself is a good test for quality control to ensure that the right amounts of antioxidants or UV-stabilizers are added, but using it to judge the long term thermal stability of a material is certainly inappropriate, and it may lead to product failure in the field. Heat aging is a good test to compare polyethylene resins with different stabilization packages as well as predicting the service life of the product under various temperatures. However, the time required to complete the test is too long for it to be used for quality control. It is recommended that the industry should develop a heat aging test method and standards that would be used to qualify resins used for geomembrane.

INTRODUCTION

Although high density polyethylene resins have been used for geomembranes for many years, the question, "How long will the geomembranes last?", still has not been satisfactorily answered. Geomembranes may fail in the field due to many reasons, such as inadequate strength, poor resistance to chemicals, poor environmental stress cracking property, photodegradation, and thermal oxidative degradation etc. This paper will discuss the long term thermal stability of polyethylene geomembranes.

Thermal Oxidation Can Be Divided Into Two Kinds:

1) High temperature thermal degradation in the presence of oxygen. - This kind of oxidation typically occurs during processing where radicals are generated due to high temperature and excessive mechanical shear. Thermal degradation can lead to molecular chain scissions and/or crosslinking, depending on the type of polymers involved and the processing conditions. Secondary antioxidants such as phosphites or thioesters are often added not only to minimize the degradation during processing, but also helps to minimize the primary antioxidants from being consumed during the

processing. As a rule, processing temperatures should always be kept as low as possible to minimize degradation without causing other problems in the operation.

2) Low temperature thermal degradation. - Low temperature here means the temperature is well below the melting point of the polymer. For geomembranes, it is very seldom that the sheet are exposed to temperatures higher than 60°C for an extended period of time. At such low temperatures, the rate of degradation is extremely slow, and it requires a long time before significant degradation in the polymer can be detected. Nevertheless, the degradation does occur and continue, and it becomes a concern in the long run. To slow down this kind of degradation, primary antioxidants such as sterically hindered phenols are often added into the polymers. Recent research (Ciby - Geigy, 1988) reported that hindered amine light stabilizers (HALS) can also provide good long term thermal stability. Long term low temperature thermal stability is what we are interested in this study.

Thermal oxidation of polyethylene geomembranes, to a different degree, can happen under various conditions in the field. The conditions in the field, such as temperature, contact with solvents and leachates, presence of oxygen, and exposure to sunlight, etc., can greatly affect the rate of degradation.

The mechanism of thermal oxidation is similar to that of photo-oxidation. The mechanisms are outlined in the following steps (Hawkins, 1975):

Step 1 : Initiation heat
(polyolefin) RH ------>R. + H. (1)

Step 2 : Propagation
R. + O_2 ------>ROO. (2)
ROO. + RH ------>ROOH + R. (3)

Step 3 : Branching
ROOH ------>ROO. + RO. + HO. (4)
RO. (ROO.) + RH. ------>ROH (ROOH) + R. (5)

Step 4 : Termination
R. + R. ------> R-R (6)
ROO. + HA (primary A/O) ------> stable products (7)
ROOH + HA (secondary A/O) ------> stable products (8)

As almost all the commercial polyethylene resins cannot be one hundred percent pure, they always contains trace amounts of chromophores which absorb UV-radiation (sunlight), and impurities which accelerate the chemical radical reactions. Even in the absence of UV-radiation, radical initiation can still occur because of the presence of impurities such as catalyst metal residues and low concentration of carbonyls induced during processing. Once the radicals are formed, they will continue to propagate to form more radicals, unless heat stabilizers are present to slow down or terminate the harmful reactions.

Some attempts had been made to differentiate the thermal stability of various polyethylene materials (Thomas, 1988). These studies focused on the thermal stability of the material in its molten state. It had been reported that some heat stabilizers behave very differently in molten state versus solid state due to the differences in mobility, volatility, solubility, and most of all the reaction kinetics of these additives in the two states. Therefore, it is inappropriate to select a material simply based on some thermal stability data in the molten state, such as the differential scanning calorimetry (DSC) tests.

Presently, in the geomembrane industry, DSC OIT measured at 200°C in oxygen is widely used as a guide for material selection in terms of thermal stability. OIT by itself is a good quality control test to ensure the right amounts of particular heat stabilizers have been added to the polymers. However, OIT should neither be used to differentiate the thermal stability of various materials nor be used to predict the long term thermal stability performance in the fields.

There are two objectives in this study. One is to optimize the stabilization system for polyethylene geomembranes, and the other is to confirm if there is any relationship between long term heat aging property and OIT.

EXPERIMENTAL

The polyethylene base resin used in this study has a melt flow rate, (I_{21}) of 6.5 g/10 min. and a density of 0.946 g/cm^3. The resin was compounded in a 20 mm diameter screw Brabender extruder with a carbon black masterbatch and three different commercially available heat stabilizers according to the formulations listed in Table 1.

Table 1. Formulations for the Oven Aging Study at 110°C

Formulation	Base Resin (1)	Heat Stabilizer, HS-A, ppm (2)	Heat Stabilizer, HS-B, ppm (3)	Heat Stabilizer HS-C, ppm (4)	Carbon Black Master Batch, % (5)
1	balance	3000	0	0	6
2	balance	1500	1500	0	6
3	balance	0	3000	0	6
4	balance	0	1500	1500	6
5	balance	0	0	3000	6
6	balance	1500	0	1500	6
7	balance	1500	750	750	6
8	balance	750	750	1500	6
9	balance	750	1500	750	6
10 (control)	balance	0	0	0	6

(1) Base Resin melt flow rate 6.5, density 0.946
(2) HS-A is a hindered phenol
(3) HS-B is a hindered amine light stabilizer (HALS)
(4) HS-C is a phosphite
(5) Carbon black loading 35%

The masterbatch has 35% loading of carbon black which has particle size of 19 nm. The compounding conditions were basically maintained constant for all the runs to ensure that they were compounded under the same shear and heat environment. After the materials were compounded, each formulation was pressed into six 9"x9" plaques (1.9 mm thick). One plaque from each formulation was retained for the zero-month tests, while the rest were placed inside a forced air oven by hanging them with hooks to the frame of the oven. The temperature of aging was set at 110°C ± 2°C, and the temperature inside the oven were mapped with the samples in place. This made sure that the temperatures inside were uniform, and there was no hot spot within the oven. During the course of aging, the samples were moved around once a month to make sure the exposure environment among the samples was as even as possible.

One plaque of each formulation was taken out every two months for melt flow rate, tensile properties, embrittlement, and OIT tests. The melt flow rate and the tensile were tested according to ASTM D-1238 and D-638 respectively, while the OIT was measured according to ASTM D-3895 using aluminium pans. The embrittlement test was performed by bending ten specimens which had the same dimensions as those used for ASTM D-1693 ESCR test. The ten specimens were placed in the bending device used for the ESCR test, and were bent 180 degrees at a constant rate. The number of brittle failures was expressed in percentage.

As degradation occurs, there must be some changes in the molecular structure. In order to confirm such changes, Gel Permeation Chromatography (GPC) was performed on some of the samples. Samples of five formulations, both the zero-month and the 12th month, were selected for the GPC test. The test was performed on a GPC instrument manufactured by Waters, model 150CV, fitted with mStyragel columns.

RESULTS AND DISCUSSIONS

Table 1 lists the nine formulations studied, which are illustrated in a tertiary composition diagram in Figure 1.

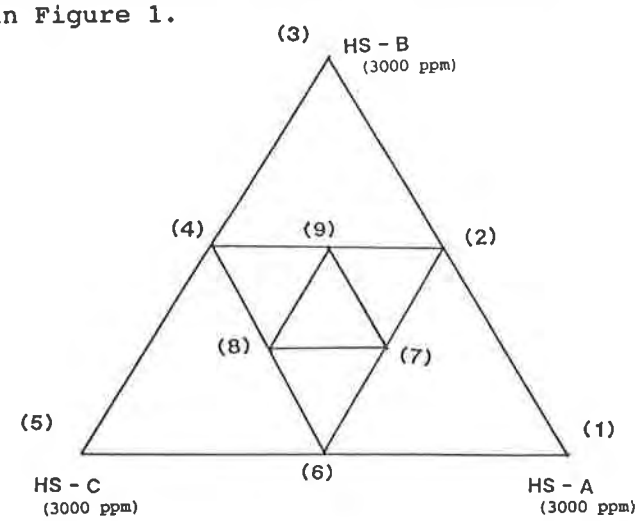

Figure 1. Nine Formulations Shown in the Tertiary Composition Diagram

We suggest the readers spend some time to familiarize themselves with this diagram because it is very useful in analyzing the data. It helps to follow the discussions as the diagram will be referred to frequently.

The physical and mechanical properties tested were melt flow rate, ultimate elongation, ultimate tensile, and embrittlement. Increases in melt flow rate generally indicate molecular chain scission, while decreases in melt flow rate means crosslinking between molecules has occurred. In heat aging, both chain scissions and crosslinking occur simultaneously, but to different extents, depending on the kinds of polyethylene.

As the polyethylene degrades, most of the mechanical properties will deteriorate. Tensile and embrittlement properties are very sensitive to polymer degradation.

Table 2 shows the aging results of the control formulation. After only three weeks of aging, significant degradation had already taken place, and it became so bad in the sixth week that the material was untestable. This demonstrates that heat stabilizers must be added in order to provide long term thermal stability to polyethylene.

Table 2. Oven Aging Results for Formulation #10 (Control) at 110°C

Weeks of Aging	0	3	6	9
Melt Flow rate (I21), g/10 min	7.40	3.60	1.05	no flows[1]
Ultimate elongation, %	800	244	N/A [2]	N/A [2]
Ultimate Tensile, MPa	33	16	N/A [2]	N/A [2]
Embrittlement failure, %	0	70	100	100
OIT, minutes	3	3	1	2

(1) The material was crosslinked and degraded; it was not able to be measured.

(2) The material was too brittle to be cut out for testing.

Overall Observation. The changes in melt flow rate, ultimate elongation, and ultimate tensile after twelve months of aging are shown in Tables 3, 4, and 5 respectively. The changes are also expressed as percentages of the original values, i.e., the zero-month properties, so that the formulations can be compared on an equal basis.

Table 3. Oven Aging at 110°C, Property Tested - Melt Flow Rate (I21)

Formulation	Month					
	0	2	4	6	8	12
1	6.70	5.79	5.60	5.20	5.20	0.10
% original	100	86	84	78	78	2
2	6.70	6.27	5.90	6.00	5.40	2.80
% original	100	94	88	90	81	42
3	7.80	7.41	8.00	6.90	6.90	5.70
% original	100	95	103	89	89	73
4	8.10	7.94	8.60	7.60	7.60	7.10
% original	100	98	106	94	94	88
5	7.90	8.07	8.50	9.10	0.10	0.10
% original	100	102	108	115	1	1
6	7.70	7.40	7.38	6.80	6.20	0.10
% original	100	96	96	88	81	1
7	7.87	7.19	7.35	7.20	6.60	3.70
% original	100	91	93	92	84	47
8	7.50	7.40	7.60	7.70	6.30	0.10
% original	100	99	101	103	84	1
9	7.20	7.19	7.40	7.50	7.00	6.00
% original	100	100	103	104	97	83

Note: Melt flow rate values of 0.10 are simply assigned values because the materials were badly crosslinked, and they were not able to be measured.

Table 4. Oven Aging at 110°C, Property Tested - Ult Elongation, %

Formulation	Month					
	0	2	4	6	8	12
1	770	800	688	755	829	5
% original	100	104	89	98	108	1
2	790	890	878	820	784	471
% original	100	113	111	104	99	60
3	700	670	711	610	624	756
% original	100	96	102	87	89	108
4	800	790	736	680	425	750
% original	100	99	92	85	53	94
5	820	784	749	780	5	5
% original	100	96	91	95	1	1
6	790	722	785	740	783	5
% original	100	91	99	94	99	1
7	830	752	826	750	662	460
% original	100	91	100	90	80	55
8	810	730	804	752	756	5
% original	100	90	99	93	93	1
9	810	770	849	940	784	827
% original	100	95	105	116	97	102

Note: Elongation values of 5% are simply assigned values because the materials were very brittle, and they broke during the sample preparation.

Table 5. Oven Aging at 110°C, Property Tested - Ultimate Tensile, MPa

Formulation	Month					
	0	2	4	6	8	12
1	31	29	25	27	34	10
% original	100	94	81	87	110	32
2	32	34	35	33	30	18
% original	100	106	109	103	94	56
3	25	22	21	23	20	24
% original	100	88	84	92	80	96
4	30	27	23	24	19	26
% original	100	90	77	80	63	87
5	34	30	24	29	28	10
% original	100	88	71	85	82	29
6	32	27	27	25	29	10
% original	100	84	84	78	91	31
7	36	25	30	26	21	19
% original	100	69	83	72	58	53
8	35	23	26	27	27	10
% original	100	66	74	77	77	29
9	34	26	29	26	30	31
% original	100	76	85	76	88	91

Note: Ultimate tensile values of 10 MPa are simply the assigned values because the materials were too brittle to be tested. However, generally the brittle materials can still have certain tensile stress strength.

The results are plotted in Figures 2, 3, and 4. Table 6 and Figure 5 show the embrittlement property.

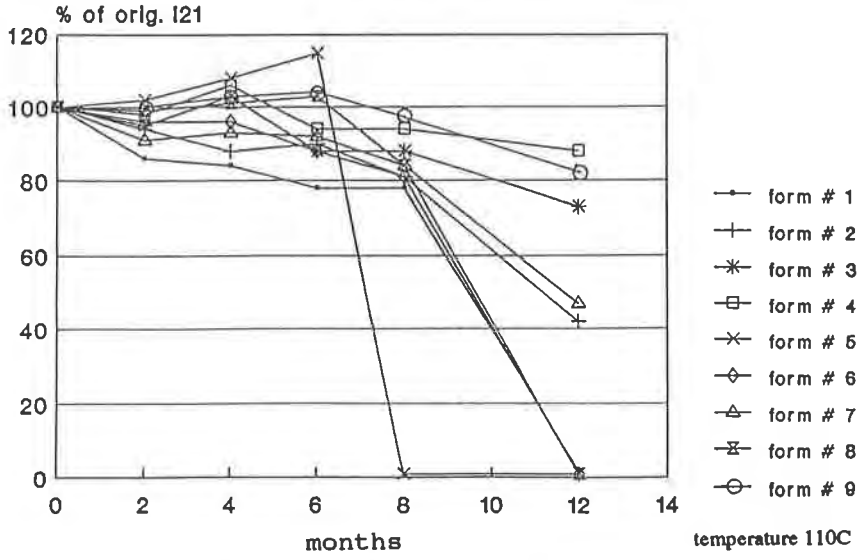

Figure 2. Oven Heat Aging Study
Change in Flowrate (I_{21})

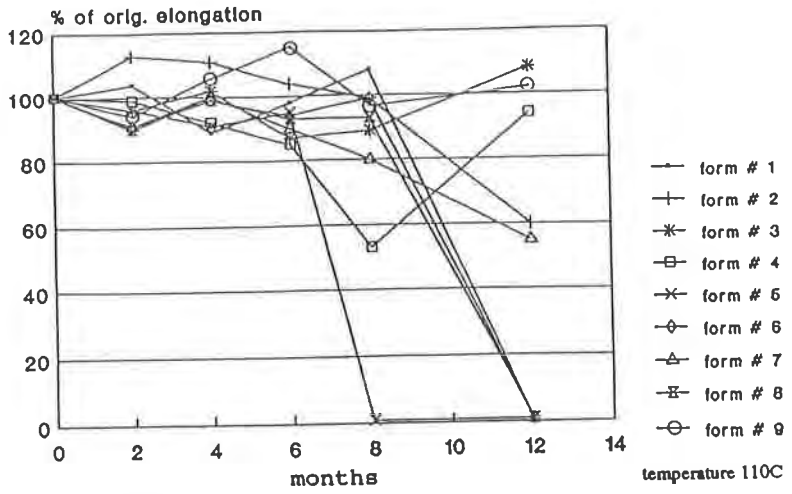

Figure 3. Oven Heat Aging Study
Change in Ultimate Elongation

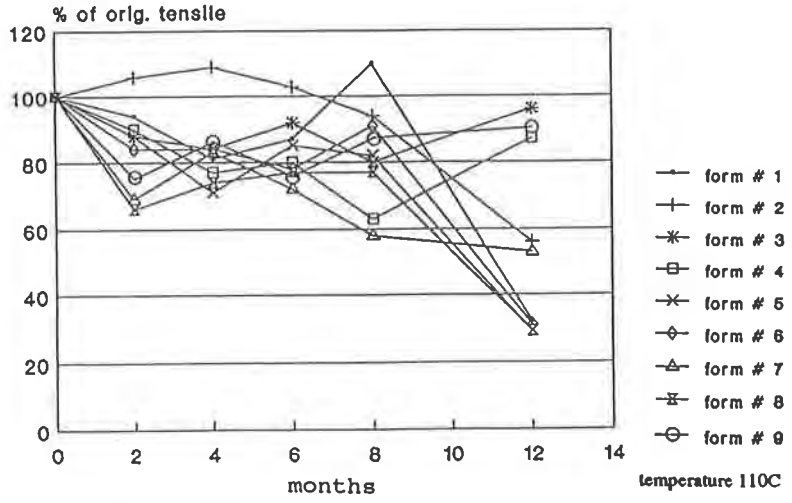

Figure 4. Oven Heat Aging Study
Change in Ultimate Tensile

Table 6. Property Tested - Embrittlement (Percent Failure)

Formulation	Month					
	0	2	4	6	8	12
1	0	0	0	0	0	100
2	0	0	0	0	0	20
3	0	0	0	0	0	10
4	0	0	0	0	10	10
5	0	0	0	10	100	100
6	0	0	0	0	0	100
7	0	0	0	0	0	0
8	0	0	0	0	0	100
9	0	0	0	0	0	0

Note: Percent Failure was calculated based on ten specimens tested.

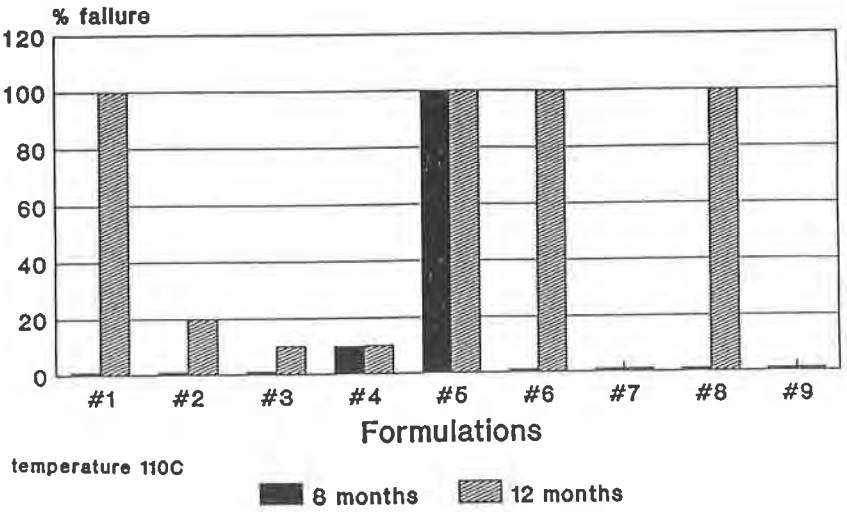

Figure 5. Oven Heat Aging Study
Embrittlement Failure in 8 & 12 Months

Figures 2, 3, and 4 show that the nine formulations have very different heat aging behaviour. In the first six months of aging, the changes in all the formulations were relatively similar and small, and the differences did not really show up until the eighth month. Formulation 5, which had the poorest retained flow rate and elongation, indicates that the material had badly degraded. The embrittlement results in Figure 5 undoubtedly confirmed the complete failure of the material.

For the other formulations, though some differences are observed after eight months of aging, the differences are not large enough to be conclusive at this stage. However, after twelve months, the differences amongst the formulations had become so obvious that one can differentiate the good ones from the bad ones without detailed data analyses.

Ranking The Thermal Stability Of The Formulations. At the beginning of the study, it was attempted to use 50% retained properties as failure criteria. After twelve months of aging, it was found that some of the samples still retained very good properties, above 50% of the original properties. One may suggest to extrapolate the data to obtain the failure time for 50% retained property. The data obtained in this study strongly suggests that the rates of degradation for these formulated materials are nonlinear, and the onset of degradation is different for each formulation. Therefore, extrapolating the data may lead to substantial errors in the analyses. In order to rank the thermal stability of these formulations, the following empirical scoring method is used.

A = flow rate score = 100 x percent of the 12th month retained property
B = elongation score = 100 x percent of the 12th month retained property
C = tensile score = 100 x percent of the 12th month retained property
D = embrittlement score = 200 if 0% failure,
= 100 if 10% failure,
= 50 if 20% failure,
= 0 if 30 % or more failure.

Total score = A+B+C+D

This scoring method emphasizes the importance of the embrittlement property. Embrittlement is a better test than flow rate and tensile tests for the polymers which have undergone chain scission and/or crosslinking during the course of degradation.

The scores for each formulation are shown in Table 7, in which the formulations 1, 5, 6, and 8 show significantly poorer heat aging property than the other five

formulations. According to the scores, the heat aging property of the formulations are ranked as 9, 3, 4, 7, 2, 1, 6, 5, and 8, with 5 and 8 being the poorest.

Table 7. Scores of the Formulations based on the 12th Month Aging Properties

Formulation	Score on I21	Score on Ult. Elongation	Score on Ult Tensile	Score on Embrittlement	Total Score
1	2	1	32	0	35
2	42	60	56	50	208
3	73	108	96	100	377
4	88	94	87	100	369
5	1	1	29	0	31
6	1	1	31	0	33
7	47	55	53	200	355
8	1	1	29	0	31
9	83	102	91	200	476

Gel Permeation Analysis. In order to study how the molecular structure had changed due to heat aging, GPC was performed on the zero and the 12th month samples of three high score formulations, 3, 7, 9, and two low score formulations, 5 and 6. The GPC results and the GPC curves are shown in Table 8, Figures 6 & 7 respectively. The GPC results show the large molecular weight differences between the zero-month and the 12th month for the formulations 5 and 6, confirming that severe degradation had definitely occurred.

Table 8. Results of Gel Permeation Chromatography (GPC) on Formulations # 3, #5, #6, #7 and #9

Formulation	0 Month Aged Sample				12th Month Aged Sample			
	$Mnx10^{-3}$	$Mwx10^{-3}$	M_zx10^{-3}	Dispersity(1)	$Mnx10^{-3}$	$Mwx10^{-3}$	M_zx10^{-3}	Dispersity(1)
3	16	144	490	8.9	15	145	500	9.9
5	16	139	470	8.8	9	29	90	3.1
6	16	166	600	10.1	10	43	170	4.3
7	16	163	590	10.5	16	159	570	10.1
9	18	195	780	10.6	16	158	570	9.9

(1) Dispersity is defined by Mw/Mn.

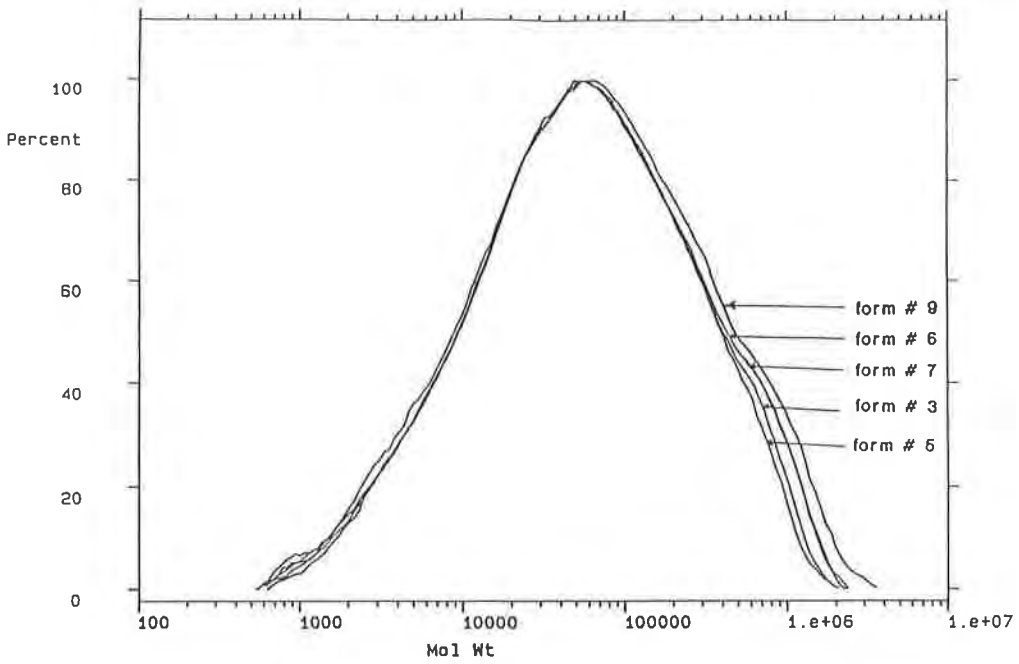

Figure 6. GPC Curves, 0 Month Aging Formulations #3, #5, #6, #7, and #9

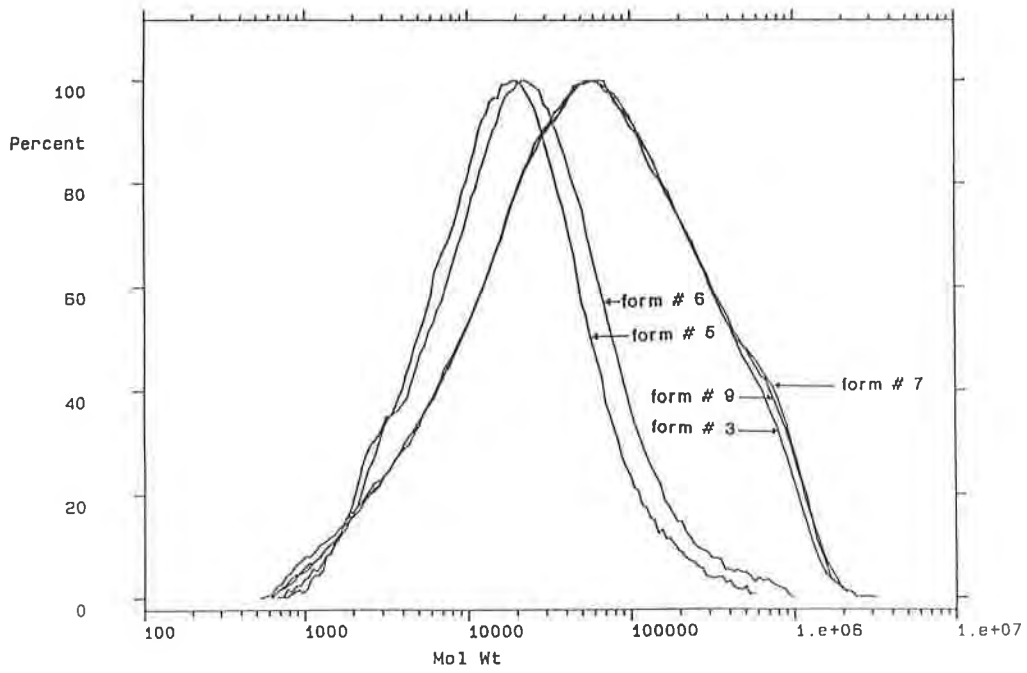

Figure 7. GPC Curves, 12 Months Aging Formulations #3, #5, #6, #7, & #9

The GPC values for the formulation 9 seems to be slightly deviated from the others. It is because this formulation was not tested side by side with the others due to equipment problems.

Relationship Between OIT and Heat Aging Property. The results, shown in Table 9, indicate that OIT had dropped significantly after two months for most of the formulations. So, does it mean that majority of the stabilizers had been consumed within two months? The answer is not. We can see that almost all of the samples after aged for four, six, and even up to eight months still retained good physical and mechanical properties. During these periods, the molecular structures of the heat stabilizers within the polymer had probably changed, but functionally they were still active, and protected the polymer from degradation. However, these structurally changed stabilizers could no longer provide good OIT. This is one piece of evidence showing that there is no relationship between OIT and heat aging property.

Table 10 shows the initial OIT and the total score for each formulation. The data are plotted in Figure 8, which clearly indicates there is no relationship between the initial OITs and heat aging property.

Table 9. Oven Aging at 110°C, Property Tested - OIT, min. (O2, 200°C)

Formulation	Month					
	0	2	4	6	8	12
1	139	91	75	41	18	2*
2	126	41	6	11	8	9
3	13	10	6	8	9	8
4	32	7	4	6	7	8
5	46	9	4	4	2	2*
6	125	46	21	11	6	2*
7	127	57	11	9	8	5
8	105	26	6	5	5	1
9	101	15	6	7	9	7

* Plaques won't press properly, indicating the material was badly crosslinked and degraded.

Table 10. Relationship Between OIT and Heat Aging Property

Formulations	Initial OIT, Minutes	Scores
1	139	35
2	126	208
3	13	377
4	32	369
5	46	31
6	125	33
7	127	355
8	105	31
9	101	476

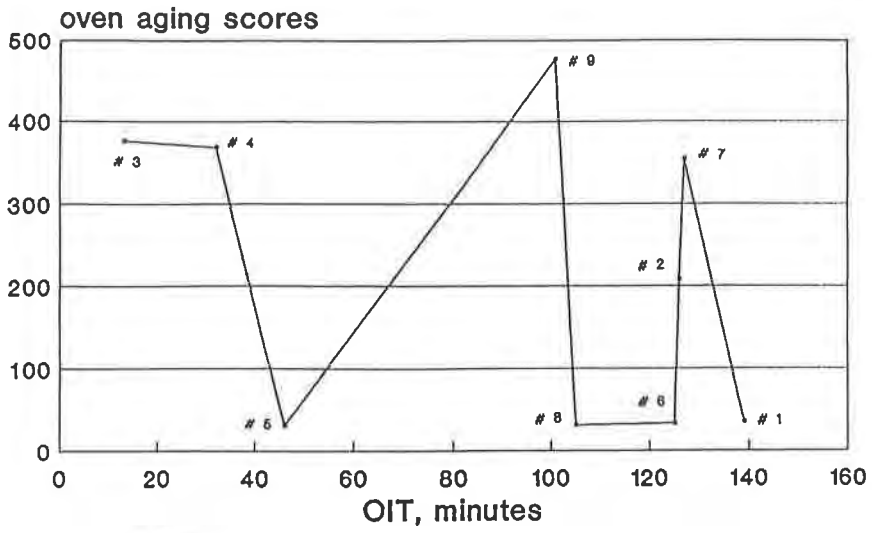

OIT (200C,oxygen @ 7 psi, 10 mil plaque)
Aging temperature 110C

Figure 8. Relationship Between Oven Aging and Oxidative Induction Time

Analysis Of The Effects Of The Heat Stabilizers

1) Effects of the Heat Stabilizer by Itself.

Figure 9 shows the scores in the tertiary composition diagram. The results are interesting, and it gives a lot of information about the heat stabilizers used in this study. The formulations in the diagram are designed in such a way that maximum information can be obtained in the data analysis, and the design itself can cross check the reliability and the consistency of the data.

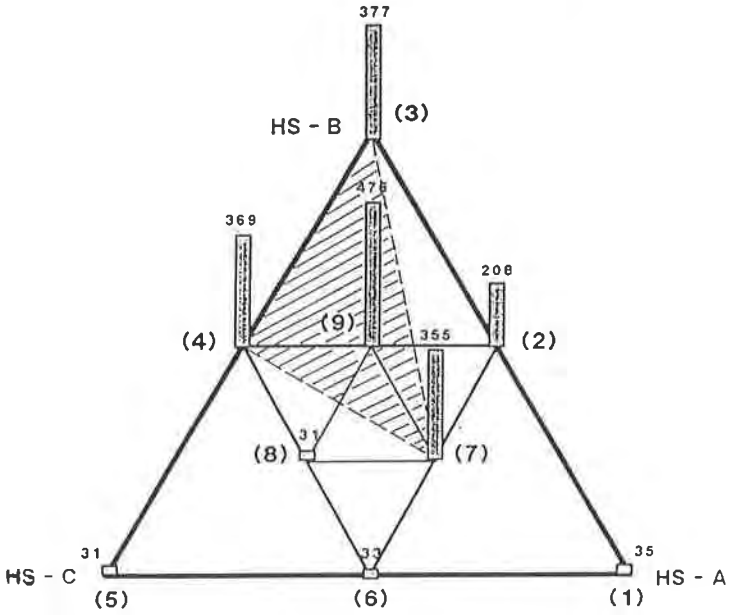

Figure 9. Oven Aging Scores

The results in Figure 9 indicates that amongst the three heat stabilizers by itself, i.e., the formulations 1, 3, and 5, HS-B has by far the best heat aging property. Moving from the formulations 3 to 1, or from 3 to 5, the heat aging property (the scores) decreases. This is further supported by the low score of formulation 6 which has equal concentrations of HS-A and HS-C, but no HS-B.

2) Synergistic Effects Amongst the Heat Stabilizers.

The study demonstrated strong synergistic effects amongst the three stabilizers studied. Each of these stabilizers has its own characteristics in terms of processing and long term thermal stabilization.

In Figure 9, as we move along the formulations 2, 9, and 4, the concentrations of HS-A and HS-C change simultaneously, while the concentration of HS-B remains constant. The heat aging property reaches the optimum at the formulation 9. Similarly, for the path of the formulations 2, 7, and 6, where the concentrations of HS-A remains constant, the optimal stability is reached at the formulation 7. On the path of the formulations 6, 8, and 4, where the concentration of HS-C remains constant, the formulation 4 has the best heat aging property. The results suggest that, the area bounded by the formulations 3, 4 and 7, would provide good long term thermal stability to the material.

CONCLUSIONS

In this oven heat aging study, the following conclusions are drawn:

1. There is no relationship between the initial OIT and the long term thermal stability in polyethylene.

2. Good optimal long term thermal stability can be achieved through appropriate combinations of heat stabilizers.

As mentioned earlier, the long term thermal stability of a material can be affected by other factors such as the abundance of oxygen, contact with solvents and chemicals, use of carbon black and its dispersion, etc., studies need to be done to ensure the products when subjected to these conditions will perform satisfactorily in the field for a long period of time. It is recommended that the industry should develop a heat aging test method and standards that would be used to qualify resins used for geomembranes.

ACKNOWLEDGEMENTS

We would like to thank the personnel at the Novacor Technical Centre and Nova Husky Research Centre, who carried out the work, and to Novacor Chemicals Ltd. for its permission to publish this paper.

Thanks are particularly due to Sandra Barber who coordinated the tests during the course of the study.

REFERENCES

Ciba - Geigy, 1988, "Processing and Long-Term Heat Stabilization of Polyolefins", Technical Brochure.

Hawkins, W.L., 1975, "The Thermal Oxidation of Polyolefins - Mechanisms of Degradation and Stabilization", "Degradation and Stabilization of Polymers", A Halsted Press Book.

Thomas, R.W., Bartz, A.K., Vershoor, K.L., 1988, "Evaluation of the Oxidative Stability of High Density Polyethylene Geomembranes by Isothermal and Dynamic Differential Scanning Calorimtry", in Durability and Aging of Geosynthetics, Elsevier Applied Science.

Creep and Stress Rupture Testing of a Polyethylene Geomembrane Under Equal Biaxial Tensile Stress

D.E. Duvall
L.J. Broutman & Associates Ltd., USA

ABSTRACT

Specimens of a medium density (approximately 0.94 g/cm^3) polyethylene geomembrane, approximately 1.5 mm thick, were subjected to equal biaxial tension stresses at room temperature and elevated temperatures. The loads were $\leq$ 60% of the product's ultimate load capability under the test conditions. Stress & strain data were obtained at room temperature and put into the form of an isochronous stress-strain curve for this material and loading condition. The elevated temperature data were used to estimate the ultimate stress-rupture performance of the geomembrane at room temperature. Results of the stress rupture testing and creep data from approximately 15,000 hours of room temperature testing are presented.

INTRODUCTION

So called "Commodity" thermoplastic polymers, e.g. polyethylene, polypropylene, or PVC, are being utilized in an increasing number of long term, load bearing applications. Examples of this are the utilization of medium- and high-density polyethylene resins for natural gas distribution pipe, and the use of PVC pipe for drinking water distribution pipe and sewer pipe. In order to intelligently design for such applications, it is necessary to know how the materials will respond to stresses and deformations which will be well below the nominal yield stress or strain of the material but which will be applied to the product for periods of years or decades.

In addition to the use of thermoplastic materials for piping, another application of this type is in "Geomembrane" products. A geomembrane is a sheet of polymeric material with a thickness which may range from less than one millimeter to nearly three millimeters and which is used as a liner for a waste pond or landfill. Such liners are placed on the bottom of an impoundment and are intended to inhibit the migration of undesirable chemicals contained within the landfill or waste pond into the surrounding environment. They must also be able to withstand, without rupture, stresses and strains which will be created by subsidence of the underlying ground. Civil engineers who design structures with geomembranes have identified several potential occurrences which could result in depressions developing beneath a portion of the geomembrane; see for example Giroud (1984) or Borea (1990). Once such a depression occurs, the weight of the material above this part of the liner would then force the geomembrane to stretch down into the depression. The result will be the creation of stresses which, over a long period of time, could result in failure of the liner and leakage of whatever was being contained.

In the present work, a method for evaluating the creep and stress rupture response of one specific medium density polyethylene liner under equal biaxial loading is presented. This type of loading is what is expected in a geomembrane which is exposed to the conditions cited in the previous paragraph. Specimens have been tested at 23°, 60° and 80°C. Both creep data and stress vs. failure time data have been obtained. The results of these experiments provide information on the time dependent, stress vs. strain properties for this geomembrane product along with strain-at-failure data for long-time exposures. This kind of information is needed by design engineers in order to determine limits on the stresses and strains to which the geomembrane can be exposed while in service.

EXPERIMENTAL PROCEDURES

The geomembrane used in this study is a commercially available product, manufactured from a medium density polyethylene (PE) resin. Certain PE material properties were measured and are presented in Table 1. Density values were determined at 23°C. The as received value was obtained on specimens cut from the membrane sample. The annealed density was measured on a strand of material from the melt index test which was annealed prior to testing for one hour in boiling water. The base resin density was calculated per ASTM D3350-84, Section 6.5.1.

Details of the apparatus developed for conducting these tests have been presented in a previous paper by Duvall and Edwards (1992); a summary only will be presented here. In order to subject the geomembrane specimens to an equal biaxial stress, sections of the sheet were cut from the roll and clamped to the face of a 2" IPS size polyethylene pipe flange adapter. Two metal back-up rings are used to pin the sheet specimen to the face of the flanged section of the adapter. A PE pipe end cap is butt heat fused to the other end of the flange adapter and tapped to permit internal pressurization of the assembly. The geomembrane specimen expands outward from the flange ring as the assembly is pressurized. The face of the adapter has ridges which grip the sheet sample and keep it from slipping during the test.

The thickness of the sheet was nominally 1.52 mm (0.060 inches). Thickness measurements were made on individual test specimens and actual thicknesses were found to range from 1.49 to 1.56 mm. Compressed gas (air or nitrogen) was used to pressurize the test cells. Gas pressure regulators maintained a constant pressure inside each manifold of three cells. The internal pressure in each set of test cells is given in Table 2. Tests were conducted at 23°, 60°, and 80°C.

Several authors have conducted a stress analysis of a thin membrane or sheet loaded in this geometry; Kirkland, et. al. (1970), Koerner, et. al. (1990), Williams (1980), and Giroud, et. al. (1990). Because of the geometry, the tensile stress in the plane of the sheet should be the same in any direction in that plane. If the sheet thickness is much smaller than the dimensions of the specimen in the plane of the sheet, then the stress through the thickness is small enough compared to those in the plane that it can be ignored. The stress analysis problem then becomes one of evaluating the plane stress state in the plane of the deformed sheet. The stress and strain in that plane can then be reasonably approximated by a calculation using the specimen dimensions, internal pressure in the test cell, and the outward deflection of the center point of the geomembrane.

Currently the geosynthetics industry utilizes the analysis of Giroud, et. al. (1990); therefore, that method will be used here also. The equation for calculating an average strain in a geomembrane deformed in this manner is:

Table 1. Properties of MDPE Geomembrane Resin

Melt Flow Rate	(ASTM D1238)	
190°C/2.16 kg		0.18 g/10 min.
190°C/5.0 kg		0.94 g/10 min.
Density - as received	(ASTM D1505)	0.950 g/cm^3
Density - annealed	(ASTM D1505)	0.947 g/cm^3
Carbon Black Content	(TGA Method)	2.48 %
Density - base resin	(ASTM D3350)	0.939 g/cm^3
Ash Content	(TGA Method)	0.02 %

Table 2. Test Conditions

Tests at 23° C

Internal Pressure (kPa)	Average Stress (MPa)
205	5.2
275	6.2
345	7.1
415	8.3
485	9.2
550	10.1
690	12.2
830	14.5

Tests at 60° C

Internal Pressure (kPa)	Average Stress (MPa)
550	9.5
620	10.8
690	12.4

Tests at 80°C

Internal Pressure (kPa)	Average Stress (MPa)
415	7.1
485	8.6
550	9.9

$$e_s = 2 * \Omega * \sin^{-1}[1/(2*\Omega)] - 1 \quad (\text{if } \delta/L < 1) \qquad (1)$$

where $\Omega = 0.25*[(2\delta/L) + (L/2\delta)]$. The symbol δ denotes the center point deflection of the geomembrane specimen, and L is the diameter of the test cell. These are illustrated in Figure 1.

In order to verify the calculated strain values, two experiments were carried out to compare calculated strains to strains measured directly. First, three liner specimens mounted in test cells were prepared with strain gages bonded to the outer surface at the center point. These cells were then pressurized step-wise and the strain measured with the gage as well as being calculated by Equation 1. Measurements had to be discontinued at around 2% strain because the gages debonded from the geomembrane specimen surfaces.

In a second set of experiments, a small square of known size was drawn on the center of three more specimens. The pressure was again increased stepwise and the increased size of the square at each step was measured among with the centerpoint deflection of the specimen. Strain was calculated from the increase in length of the sides of the square and from Equation 1. Figure 2 is a plot of the results of all of these tests, showing the strain measured by either the gages or dimensional changes of the drawn square versus the strain calculated by Equation 1. The agreement is seen to be quite good.

The calculation of an average stress in the specimen, requires, first, calculation of the tension created in the geomembrane:

$$\alpha = P * L * \Omega / 2 \qquad (2)$$

with α = the geosynthetic tension, P = the pressure behind the geomembrane, and L and Ω as before. The approximate average stress in the specimen can then be estimated by dividing this tension by the thickness of the liner. Because the specimen thins appreciably when deformed to these strain levels, the thickness of the stretched specimen was estimated in the following way. It can be reasonably assumed that the polyethylene material is incompressible; therefore, the product of the extension ratios in the three principal stress directions (extension ratio = engineering strain + 1) equals one. Two of these directions are in the plane of the deformed sheet (hoop and meridional); the third is through the thickness of the sheet. Thus, the strain in the thickness direction of the sheet, e_t, can be determined from:

$$(e_t + 1) = 1/(1 + e_s)^2 \qquad (3)$$

with e_s calculated by Equation 1. From e_t one can calculate the reduction in sheet thickness as it stretches and estimate an average true stress in the geomembrane.

The deflection at the center of the liner disks for all other tests was measured periodically in order to calculate the stress and strain in the specimen. A dial gage, mounted in a fixture, was used to measure the deflection. The gage has a resolution of 0.025 mm (0.001 inches). The deflection data, along with the geometric parameters were then used to calculate the stress and strain of the samples during the test. The 60^{o} and 80^{o}C tests were conducted in forced air ovens, which are stable to within +/-1 degree C. The deflection measurements are made quickly with the dial gage fixture to assure that any temperature drop is minimal as the measurements are taken. The temperature of the ovens is monitored using thermometers, which are checked against our standard calibrator probe. Stresses in the elevated temperature specimens were corrected for thickness changes due to thermal expansion using the method presented by Crissman (1991).

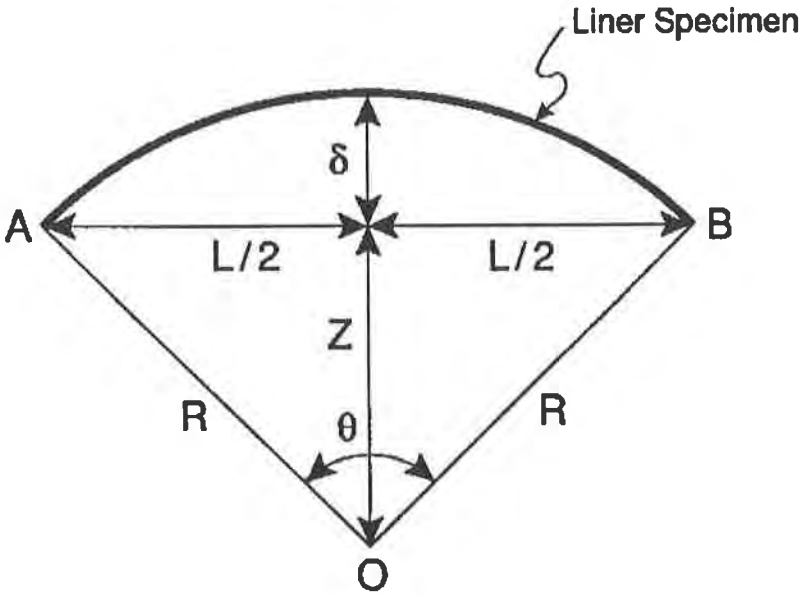

Figure 1. Schematic of Geomembrane Specimen on Test.

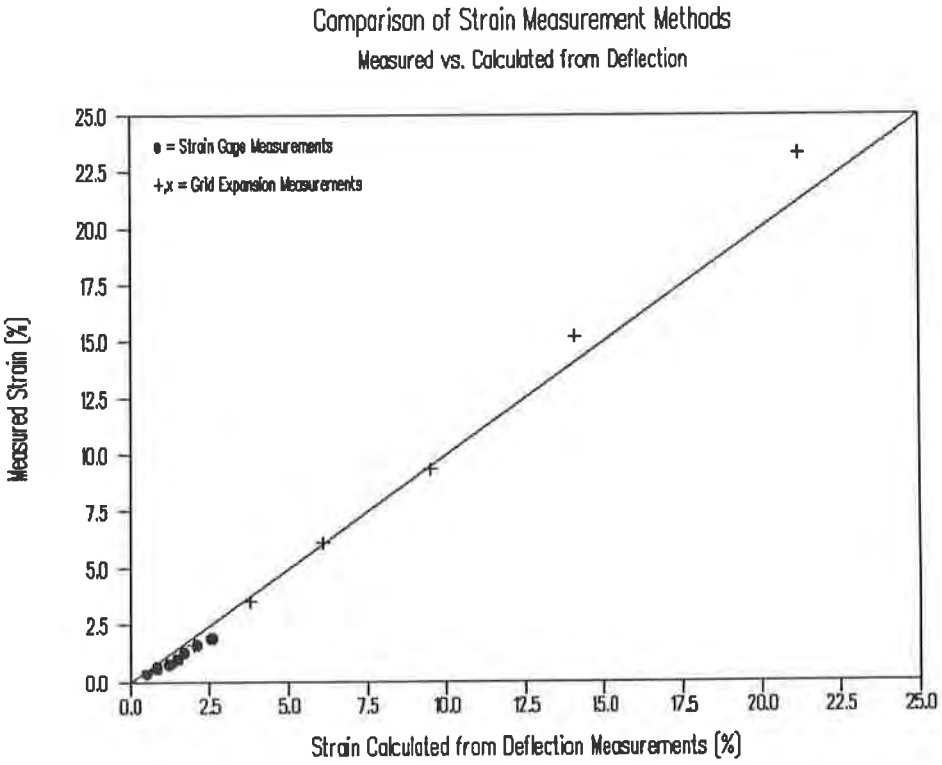

Figure 2. Comparison of Measured Strain and Strain Calculated from Equation 1.

RESULTS AND DISCUSSION

Three geomembrane specimens were tested under each of the conditions listed in Table 2. Figure 3, a plot of creep strain vs. time for the three specimens at room temperature and 415 kPa test pressure, is typical of the results obtained. The stress calculated in each geomembrane specimen from a set of three tested under the same temperature and pressure conditions varied by less than $\pm$ 2% from the average for the set. It is recognized that the stress in one of these test specimens is not truly constant with time, especially at the beginning of the experiment. However, after two or three days, the stress stabilizes and is essentially unchanged from that point on. Because of the long duration of these experiments, it is reasonable to treat the data as being from a true, constant stress creep test.

The room temperature creep strain data were utilized to construct isochronous stress-strain curves, as shown by Heger, et. al. (1979). For each time at which deflection measurements were made, the stress and strain at that time were calculated. A plot was constructed of stress vs. strain for all measurements made after 0.3 hours, 23 hours, 455 hours, etc. Each of these sets of constant time (isochronous) results was fitted by a least squares regression analysis to an equation of the form

$$S = A \times e^{b}. \tag{4}$$

The curve fitting products are presented in Figure 4 as a set of isochronous stress-strain curves for times ranging from 0.3 hours to 13,500 hours.

he creep data from each load were also fitted by a least squares method to an equation of the form

$$e = A \times t^{n}. \tag{5}$$

The line through the data points in Figure 3 is a result of this curve fitting procedure. The values of A and n determined can then be utilized to extrapolate an estimate of the strain in the liner at any time, for the values of stress in these tests. A 50 year isochronous curve was constructed by extrapolating the 50 year strain, for each stress level at room temperature, from the appropriate version of Equation 5. The 50 year isochronous curve is also contained in Figure 4.

Another observation on the room temperature creep data concerns the total strain in the most highly stressed test specimens. To date, after > 15,000 hours on test, these have reached strains of approximately 20% without yielding. In a normal ASTM D638 tensile test, run with a crosshead speed of 50 mm/minute, this type of polyethylene will yield and neck at around 12% strain. It appears then that under conditions of long time loading (i.e. low strain rates) the yield strain is substantially greater than that measured in a short time test. This was also observed in the results of uniaxial tensile creep tests conducted on a similar polyethylene resin by Crissman (1991), where strains at yield of 20% - 70% were observed at 24°C.

The elevated temperature testing was carried out for two primary purposes. The first was to assess whether or not the failure mechanism would change from the highly ductile yielding type of failure seen in short time testing of polyethylene to a non-ductile crack initiation and growth mechanism. That such a change in failure mechanism can occur for medium and high density polyethylenes is well documented; see, for example, the review by Lustiger (1986). Such a transition causes the "knee" observed in stress rupture curves obtained on many polyethylene materials. It has also been clearly shown that testing under creep loading at superambient temperatures will accelerate the molecular precesses and cause the transition to

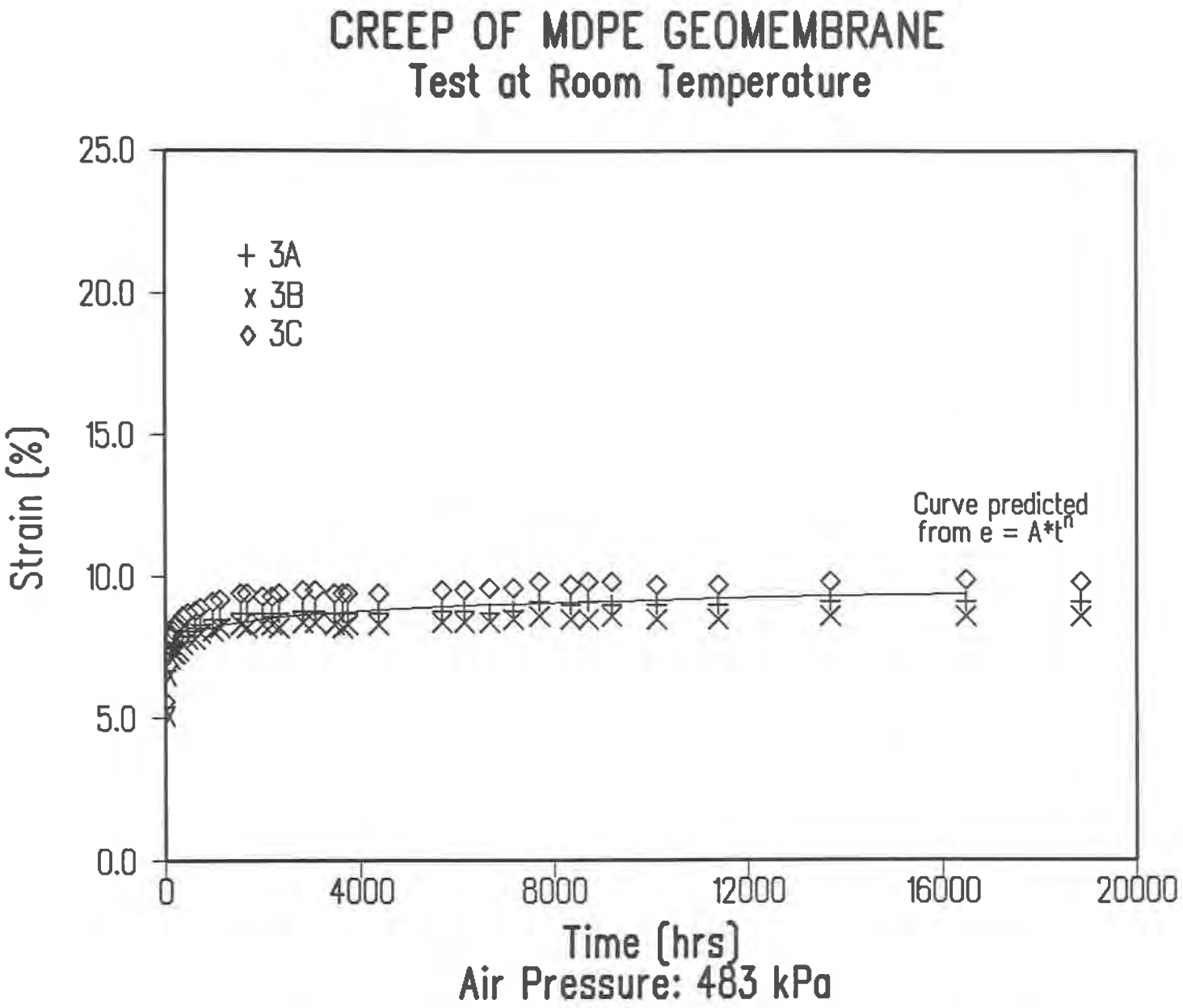

Figure 3. Typical Creep Data.

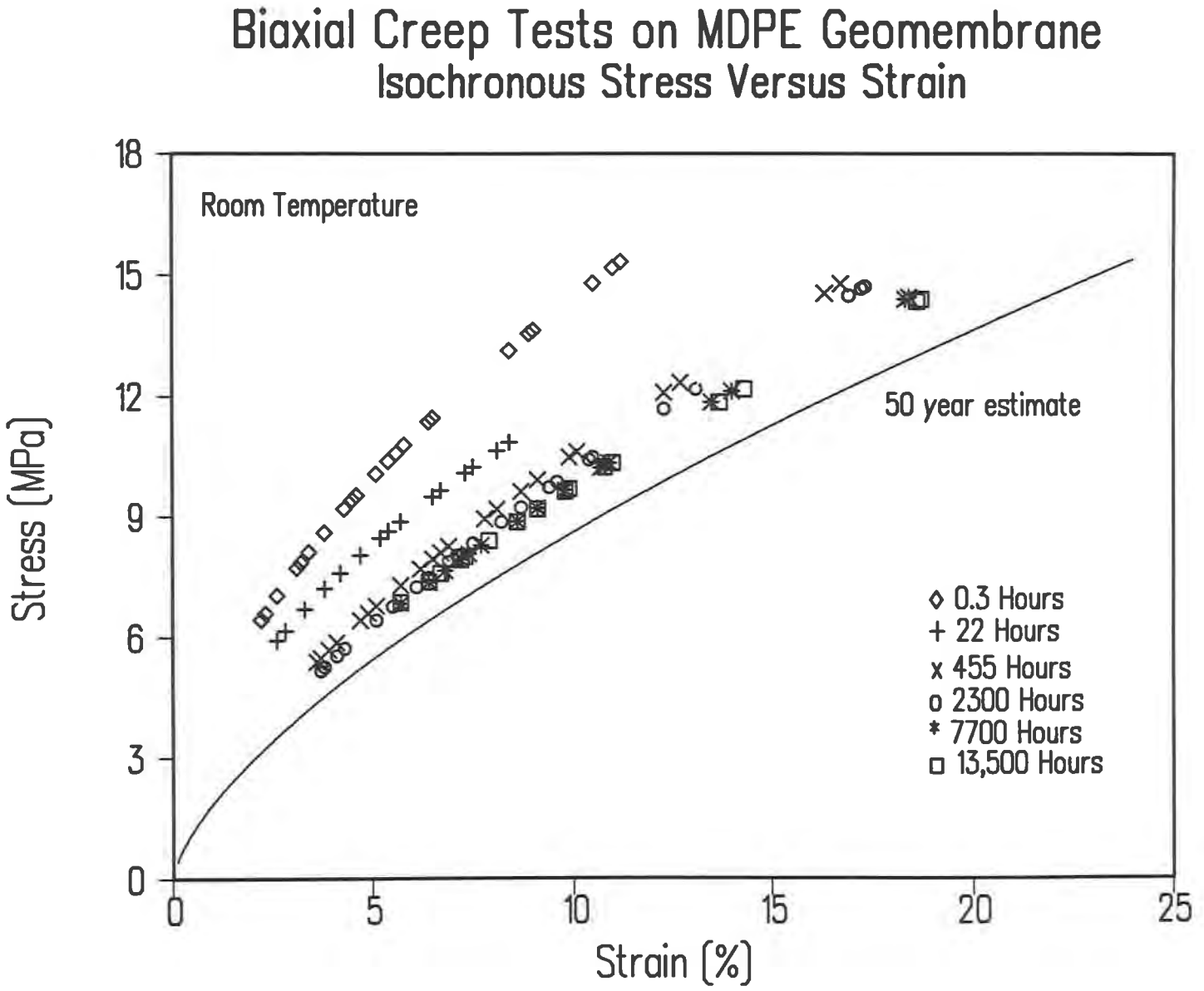

Figure 4. Isochronous Stress vs. Strain for Axisymmetric Creep.

occur at shorter times: see, for example, Richard, et. al. (1959), or Palermo and DeBlieu (1985).

The second reason for conducting the tests at 60° and 80°C is to utilize the elevated temperature data to estimate failure times at room temperature. This is a common practice in material performance characterization and many different mathematical relationships have been proposed to use for this extrapolation. Two will be considered here; the semi-logarithmic equation developed from work by Eyring (1941), Tobolsky and Eyring (1943) and others; and a double logarithmic equation used by the Plastics Pipe Institute and presented by Mruk (1985).

Elevated temperature tests were carried out under the conditions already listed in Table 2. To date, 16 of the 18 specimens have failed: two remain on test at 9.5 MPa stress and 60°C. Both ductile yielding and non-ductile, slow crack growth failures have occurred. Almost all of these failures occurred near the center of the specimen; however, two of the 60°C, 8.6 MPa samples developed slits at the edge near the clamping ring. These edge slit failures were atypical and may have been partly due to the clamping mechanism used. Due to space restrictions for these proceedings, they cannot be discussed further here.

Figure 5 is a plot of stress vs. failure time for these experiments. Figure 6 is a photograph of a ductile failure. The sheet specimen bursts near the center point and the material yields prior to failure. Specimens burst at room temperature in periods as short as 1-2 minutes have the same appearance. Strains in each ductile failure specimen obtained from the last measurement prior to failure are listed in Table 3. It is apparent that these geomembrane specimens can attain strains in excess of 30% before yielding. This also agrees with Crissman's (1991) uniaxial tension results.

Table 3 also has a listing of the strains measured in the non-ductile failure specimens prior to their leaking. Figure 7 is a photograph of one of these failures; note that there is no yielding as found in the ductile failure piece and the slit leak in this specimen is too small to be seen in this photo. The maximum strains attained by these are much lower than in the ductile yield failures. Also, the strain at failure is decreasing as the time to failure is increasing, consistent with polyethylene pipe hydrostatic pressure test results. The implication from this is that geomembrane specimens at lower stresses and consequently longer failure times, will fail at total strains even lower that the 19% - 20% seen thus far in these experiments. This fact is also recognized by the polyethylene pipe industry; for example, Janson (1981) recommends that long term strain in buried PE pipes be limited to 5%.

Regression analyses were performed on the ductile failure data. The results of fitting these data to a semilogarithmic and a double logarithmic equation are:

$$\log(\text{time}) = -35.0124 + (16{,}333/T) - (317.90/T)*S \quad (6)$$

$$\log(\text{time}) = -28.1735 + (17{,}506/T) - (6764/T)*\log(S) \quad (7)$$

where T is the test temperature in degrees Kelvin, S is the stress in MPa, and the time is in hours. The correlation coefficients for both equations are $r^2=0.760$.

An examination of Figure 5 shows that the non-ductile failures occur mostly at times well below what would be predicted by Equations 6 or 7. This is evidence that the "knee" which appears in uniaxial tension stress-rupture testing also appears in this axisymmetric, biaxial tension system. The non-ductile data can also be fitted to relationships like Equations 6 or 7; this has not yet been done here because these failures are all quite recent and two of the 60°C specimens which will be non-ductile failures are still on test.

Table 3: Strain at Failure for Elevated Temperature Tests

Ductile Failures

No. of Specimens	Avg. Stress (MPa)	Temp. (°C)	Failure Time Range (hrs.)	Strain before Yield (%)
3	9.8	80	121 - 341	> 35
1	8.6	80	634	> 35
3	12.4	60	86 - 270	28 - 33

Non-ductile (Slit) Failures

3	7.1	80	14,086-14,829	~21
2	10.8	60	4675 - 11,689	~24
1	9.5	60	16,005	~19.5

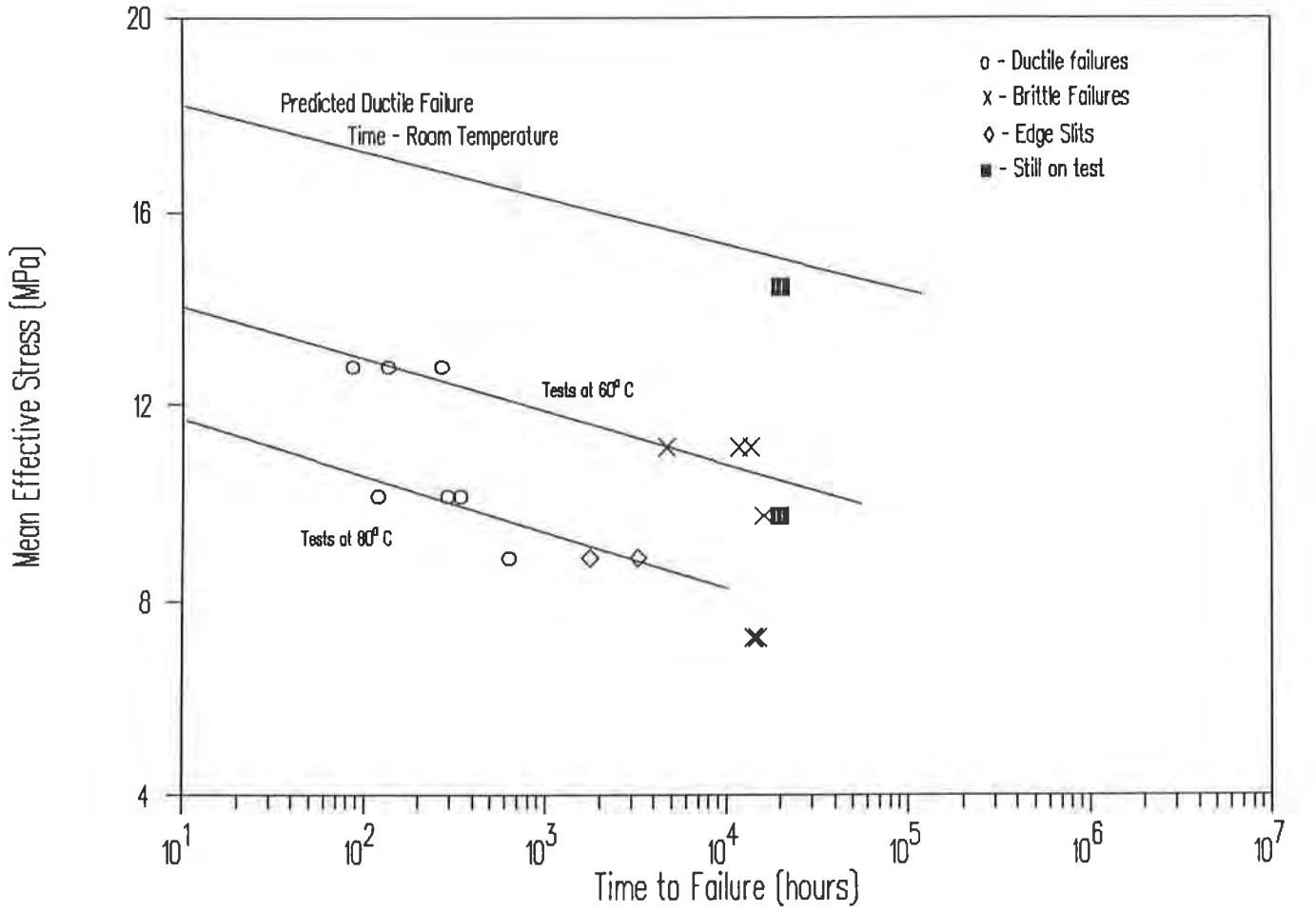

Figure 5. Semi-logarithmic Plot of Stress Rupture Data Obtained on MDPE Geomembrane. Ductile failure data have been shifted to 24°C.

Figure 6. Ductile Failure Specimen.

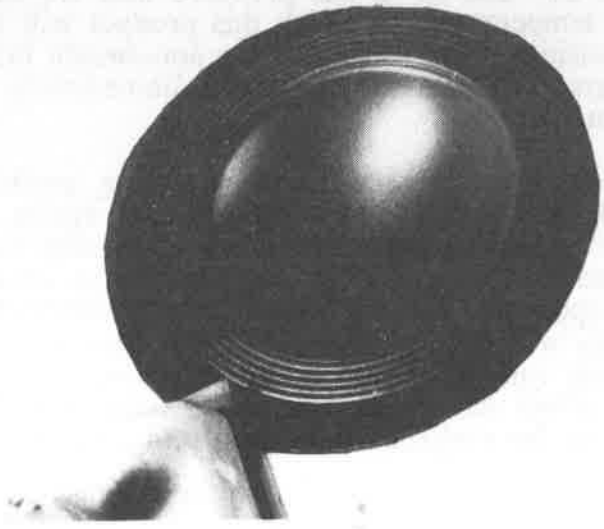

Figure 7. Brittle Failure Specimen.

Finally, an experiment was carried out to assess the effect of specimen size on the results of this project. A geomembrane sample was attached to the face of a 12" IPS polyethylene flange adapter, yielding a test specimen 340 mm in diameter. The apparatus was pressurized at 80°C and deflection measurements made as with the smaller samples. Due to problems in manipulating this large assembly in the constant temperature oven, the sheet burst (ductile failure) in less than a week. A second such assembly was made and tested; it too burst in a few days. It was observed that the pressure inside the test cell required to achieve a certain stress and strain level was much less for the large assembly than for the smaller ones. These two were run at 83 kPa pressure (12 psig) while a small cell would have to be run at around 450 kPa (65 psig) to get the same stress and strain.

Figure 8 shows the strain versus time data that was obtained on the two pieces, along with a prediction of the strain-time response made from the 80°C data obtained on the small test specimens. Even though there were difficulties in handling such a large specimen in the oven, the predicted creep curve matches the data reasonably well. It is concluded that the data obtained on the 63.5 mm diameter specimens are valid for evaluating the creep behavior of larger sized geomembrane samples. While it is believed that the elevated temperature stress rupture data obtained on 63.5 mm specimens is also valid for extrapolation to larger sized samples, an understanding of why the 340 mm specimens burst sooner than expected must be obtained before that belief is confirmed.

CONCLUSIONS

1) A test method has been developed by which the creep and stress rupture characteristics of polymeric sheet products can be studied with the specimens exposed to equal biaxial (axisymmetric) tension stresses.

2) Tests using this method have been conducted on one sample of a MDPE geomembrane liner. Creep data have been accumulated at 23°C and several stress levels for over 15,000 hours. These data have been presented in the form of a set of isochronous stress-strain curves.

3) Stress rupture testing at 60° and 80°C has provided data for estimation of time to failure under constant stress at temperatures to which this product will be exposed when in service. The existence of a transition from a ductile to a non-ductile failure mode has been demonstrated for this loading geometry. Also, the strains immediately prior to failure are decreasing as time to failure is increasing.

It should be noted that the results of the stress rupture testing, particularly the transition from ductile yielding failures to slow crack growth failures, are highly dependent upon the nature of the polyethylene resin. Other polyethylene materials having similar melt flow and density characteristics to the material evaluated here could behave quite differently in the stress rupture tests, depending upon each material's resistance to slow crack growth failure. Polyethylenes of different density will behave very differently than this material, both in the creep response and in the stress rupture performance. Crissman (1989) has shown that processing conditions can also affect the stress rupture behavior of polyethylene products. Each geomembrane product should be evaluated individually to asses its creep and long term stress rupture performance.

ACKNOWLEDGEMENTS

The author wishes to thank Mr. Dale Edwards and Mr. Joe Grzetic for their assistance in carrying out the testing. This material has been submitted by the author in partial fulfillment

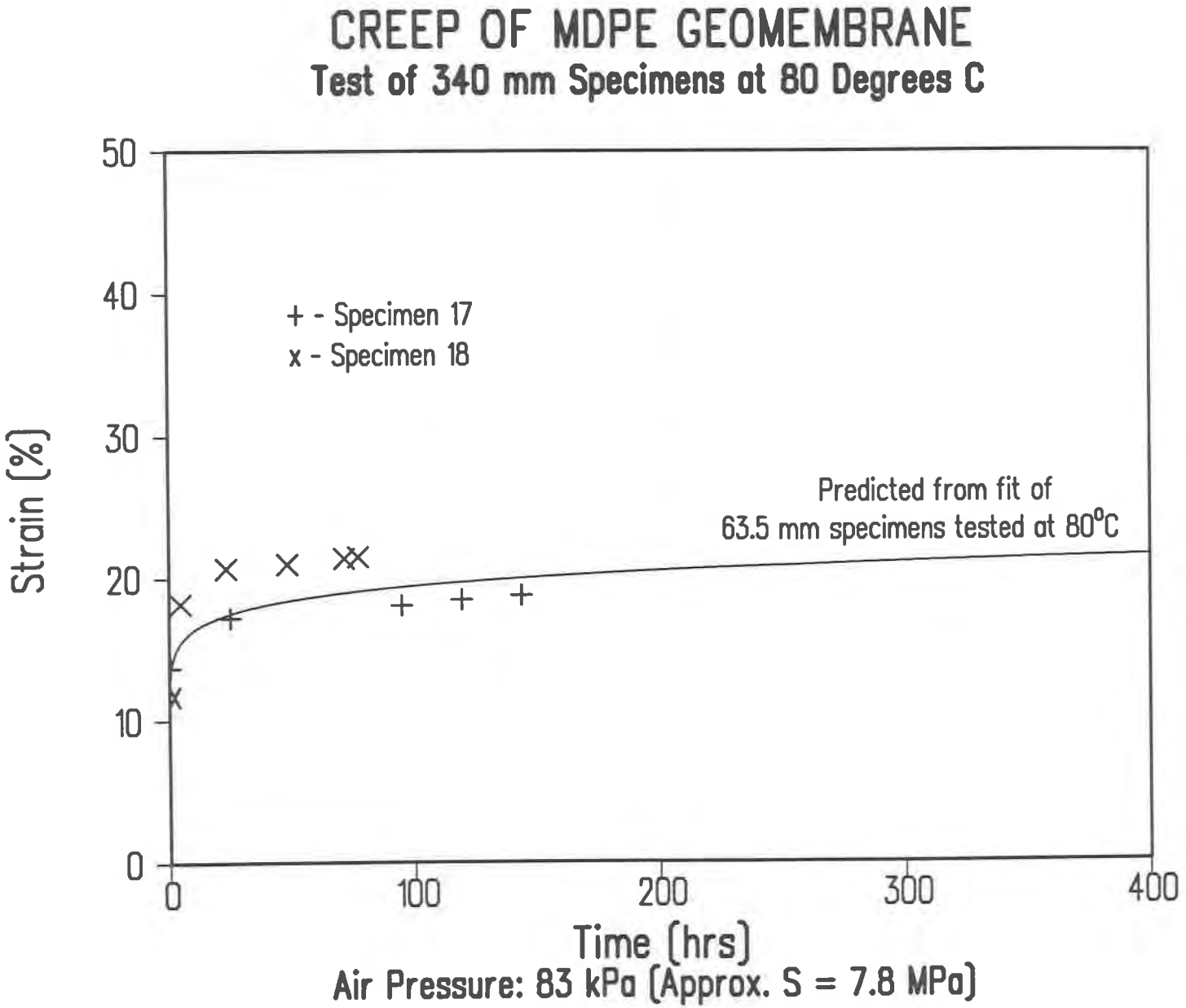

Figure 8. Strain vs. Time for 340 mm Diameter Test Specimens.

of the requirements for the Ph.D. degree in the Department of Metallurgical and Materials Engineering at Illinois Institute of Technology, Chicago, Illinois.

REFERENCES

S. J. Barton and B. W. Cherry, (1979) Polymer Eng. & Sci. **19** (8), 590.

A. Borea, (1990) Proceedings of the 4th International Conference on Geotextiles, Geomembranes, and Related Products, Volume 2, 524.

J. M. Crissman, (1989) Polym. Eng. & Sci. **29**(22), 1598.

J. M. Crissman, (1991) Polymer Eng. and Sci. **31**(8), 541.

D. E. Duvall and D. B. Edwards, (1992) Proceedings of the Society of Plastics Engineers 50th Annual Technical Conference, **38**, 128.

S. Glasstone, K. J. Laidler and H. Eyring (1941), The Theory of Rate Processes, McGraw Hill, New York.

J. P. Giroud, (1984) Proceedings of the International Conference on Geomembranes, Vol. II, (Denver, CO, June 1984), 481.

J. P. Giroud, R. Bonaparte, J. F. Beech, and B. A. Gross, (1990) Geotextiles and Geomembranes **9**, 11.

F. J. Heger, R. Chambers, and A. G. Dietz, (1979) Structural Plastics Design Manual, Phase 1, Chapters 1-4, Chapter 2, Section 2.3, FHWA-TS-79-203, U. S. Government Printing Office, Washington, DC.

L. E. Janson, (1981) Proceedings of the International Conference on Underground Plastic Pipe, New Orleans, LA, Mar. 30-Apr. 1, 1981, ASCE, New York.

J. T. Kirkland, J. L. Duncan, and R. N. Haward, (1970) Polymer **11**, 562.

R. M. Koerner, G. R. Koerner, and B.-L. Hwu, (1990) Geosynthetic Testing for Waste Containment Applications, ASTM STP 1081, 170, ASTM, Philadelphia, PA.

A. Lustiger, (1986) Failure of Plastics, ed. by R. D. Corneliussen and W. Brostow, Chapter 12, Hanser Publishers, New York.

S. A. Mruk, (1985) Proceedings of the 9th Plastic Fuel Gas Pipe Symposium (New Orleans), 202.

E. F. Palermo and I. K. DeBlieu, (1985) Proceedings of the 9th Plastic Fuel Gas Pipe Symposium (New Orleans), 215.

A. Tobolsky and H. Eyring (1943), J. Chem. Phys. **11**, 125.

K. Richard, E. Gaube, and G. Diedrich, (1959) Kunststoffe **49**(10), 516.

J. G. Williams, (1980) Stress Analysis of Polymers, 2nd Edition, Chapter 5, Ellis Horwood Ltd., West Sussex, England.

A Methodology for Forecasting the Lifetimes of Geomembranes that Fail by Slow Crack Growth

M.F. Kanninen
Southwest Research Institute, USA

I.D. Peggs
I-Corp International Inc., USA

C.H. Popelar
Ohio State University, USA

ABSTRACT

It is suggested that a fundamentally-based fracture mechanics approach, initiated and validated for polyethylene gas pipe materials, be extended to quantify the stress cracking processes responsible for the premature failure of numerous geomembranes used in uncovered liquid impoundment and solid waste lining systems. It is shown that slow crack growth measurements and time-temperature shifting can be used to develop a correlation of crack growth rate with the stress intensity factor. The resulting equation of motion of the crack tip could be used to predict the life expectancy of a geomembrane subjected to different applied stresses, operating temperatures, and defect sizes. The basis of the approach and a heuristic application to failure at a seam in a geomembrane are provided to illustrate this approach.

INTRODUCTION

There are an estimated one-quarter million uncovered liquid impoundment and solid waste lining systems in the United States and Canada. Stress cracking and environmental stress cracking have been responsible for premature failure in some of these systems [Peggs, et al, 1989; Peggs 1990]. So far, there have been no known failures in soil-covered liners. But, increases in leakage rate that may be related to slow crack growth (SCG) suggest that it may be only a matter of time before such failures do occur. Nonetheless, no analyses or material characterization procedures currently exist to assist the industry in preventing failures that are based on quantifying the SCG mechanisms that can erode geomembrane durability. Fortunately, as a similar set of concerns for polyethylene (PE) gas distribution pipes has already been addressed, a base exists to develop a corresponding methodology for forecasting the service performance of geomembrane liners. That methodology is based on bi-directional time-temperature shifting that is coupled with modern fracture mechanics technology [Kanninen, et al 1991; Kenner, et al 1992; Kuhlman, et al 1992; Popelar, et al, 1991(a); Popelar, et al, 1991(b)]. As a result, a procedure that requires only the convenient laboratory measurement of the crack growth rate at one temperature to forecast real time performance under service conditions is available for applications that will greatly improve geomembrane reliability and durability.

The preliminary study described in this paper strongly indicates that the technology, developed and validated for medium density and high density polyethylene (MDPE and HDPE) gas pipes, can be extended to geomembrane applications. Specifically, it is suggested that a correlation of SCG rates with the stress intensity factor can be developed from elevated temperature crack growth tests of laboratory specimens of HDPE geomembranes. The use of fracture mechanics techniques [Kanninen, 1985], which essentially provide the equation of motion of the crack tip, also ensures that the SCG data will be "transferable" from the test specimen to an actual application. It is further suggested that temperature-dependent shift functions can be established to account for the influence of differences in temperature from the accelerated laboratory testing of a geomembrane to its performance following installation in actual service.

BASIS OF THE LIFETIME PREDICTION METHODOLOGY

In contrast to the constant tensile load test and other similar tests used to rank material behavior, in this approach SCG data on gas pipe materials are obtained using laboratory test procedures that are in turn correlated with a linear elastic fracture mechanics (LEFM) approach. This quantitatively characterizes the ability of a PE material to resist SCG. The validity of the LEFM approach requires that the craze zone size at the onset of crack growth be significantly less than the wall thickness of the pipe from which the SCG specimen was machined. If this is the case, Category I type material behavior is said to exist and LEFM is valid. Otherwise the material is designated as one exhibiting Category II behavior for which LEFM is inappropriate. Note that this designation is based on the crack tip deformation state and not upon the flexibility of the material itself. The work described in this paper is strictly confined to Category I material behavior which, for heuristic purposes, is assumed to also apply to HDPE geomembranes. A common situation for SCG initiation in a geomembrane is shown in Figure 1.

Acquiring Accelerated SCG Test Data. In gas pipes SCG testing consists of applying a constant load to a test specimen that contains an initial crack. The displacement of the load point is monitored as a function of time. Viewing the displacement as the sum of the viscoelastic deformation of the uncracked specimen and the displacement due to crack growth allows the crack length to be determined without a direct measurement of the crack tip position. This is accomplished by equating the convolution integral for the load-point displacement to the measured displacement record with the crack length history then inferred from the resulting equation. The requisite viscoelastic material data needed in this procedure are obtained from the displacement time record prior to the time of the initiation of crack growth [Kanninen, et al., 1990].

In an LEFM approach the crack length (a) history as a function of time (t) is differentiated to give the crack growth rate as a function of the stress intensity factor (K) for the test specimen. Here, K represents the crack driving force which generally is a function of the crack length, applied stresses, and component geometry. It is usually found that an adequate representation of the SCG data for PE materials is given by the simple power relation

$$\frac{da}{dt} = AK^m \tag{1}$$

In Equation (1) the material constants A and m are determined from test data, and therefore empirically characterize the material resistance to SCG at the test temperature.

Note that the time that SCG initiates (t_i) can also be obtained from the test data as a function of K. Recent work on butt fusion joints [Popelar, et al., 1991(b)] indicates that

$$t_i = BK_o^{-m} \tag{2}$$

where B also is a material parameter and K_o is the stress intensity factor corresponding to the initial crack depth in the SCG test.

Analyzing SCG Under Service Conditions. Equation (1) can be integrated to arrive at the time required for an SCG process to fail a pipe or joint. In combination with Equation (2), this gives a lifetime relation that is the sum of two processes: the time to grow a crack, and the time to initiate crack growth. It is usually assumed that the crack front is very long in comparison to its depth into the pipe wall, and that the small difference between the critical crack depth and the wall thickness can be neglected. The lifetime (t_f) is then given by

$$t_f = \frac{1}{A}\int_{a_0}^{h} \frac{da}{K^m} + BK_o^{-m} \tag{3}$$

where a_o is the initial flaw depth, h is the pipe wall thickness, and, as above, A, B and m are material properties determined from standardized SCG testing. Note that, because the applied loads and crack sizes in service are usually smaller than those selected for test purposes, K and K_o are generally less in service than for the test specimen.

Bi-directional Time-Temperature Shift Functions. It is important to recognize that Equation (3) will apply only at the temperature for which the material constants were measured. Thus, a very powerful analysis tool for PE gas pipe materials are shift functions that allow test results at one temperature to be shifted to any other temperature. Because elevated temperature accelerates the SCG process in PE materials, tests can be performed relatively quickly at elevated temperature with the results readily converted to ascertain the equivalent material response at any other temperature. Not only does the bi-directional procedure correctly shift data; in so doing it preserves the regions of dominance of brittle and ductile PE behavior while showing no more scatter than did the original data. To date, all available tensile test, burst test, and SCG data collected on PE materials (45 sets) to which the shift functions could be applied have been analyzed with unfailing success [Kenner, et al 1991; Popelar, et al, 1991(a)].

To utilize the bi-directional shifting procedure, if T_l is the laboratory test temperature and T_s is the service temperature in °C, data are shifted horizontally by multiplying the time by a factor a_T that is given by

$$a_T = \exp[-0.109(T_s - T_l)] \tag{4}$$

while the dependent variable (e.g., failure stress in a sustained pressure test) is shifted vertically by dividing by a factor b_T given by

$$b_T = \exp[0.016(T_s - T_l)] \tag{5}$$

To illustrate the power of the shift functions, in Figure 2(a) are shown SCG data on a material designated only as an HDPE material [Kenner, et al, 1991]. Nonetheless, these data can be correlated with a scatter no greater than the original data. This is shown in Figure 2(b). With this outstanding agreement as a basis, note that crack growth data can be shifted such that

$$\left(\frac{da}{dt}\right)_{T=T_s} = \frac{1}{a_T}\left(\frac{da}{dt}\right)_{T=T_t} \tag{6}$$

While the stress intensity factor is shifted by

$$(K)_{T=T_s} = b_T\,(K)_{T=T_t} \tag{7}$$

Generalized Life Prediction Relation. By substituting Equations (6) and (7) into Equation (3), noting that K is a function of both the instantaneous crack length and the applied stress, the life prediction equation can be generalized to

$$(t_f)_{T=T_s} = \frac{a_T}{(b_T)^m}\left[\frac{1}{A}\int_{a_o}^{h}\frac{da}{K^m} + B\,K_o^{-m}\right] \tag{8}$$

which allows SCG data obtained at an arbitrary temperature T_t to predict time-to-failure t_f at a service temperature T_s initiating from a pre-existing surface defect. Here, A, B, and m are typically determined from SCG data obtained at a temperature of 80°C, with a_T and b_T then accounting for the difference between the test temperature and the service temperature of interest. This methodology has been shown to be capable of making life time predictions of PE pipe and butt-fused joints subjected to internal pressure, rock impingement, soil overburden, and residual stresses [Kanninen, et al, 1990; Kanninen, et al, 1991; Kuhlman, et al, 1992; Popelar, et al, 1991(b)].

A HEURISTIC PROCEDURE FOR GEOMEMBRANE LINERS

It has been found that in-service failures of geomembrane liners generally occur in or near a seam [Peggs, et al., 1990(a); Peggs, et al., 1990(b)]. In some cases, these are in the form of a leak; in others, rapid crack propagation (RCP) occurs to shatter very large areas. Figure 3 shows typical examples of the former situation. Figure 4 shows a simple plane strain (i.e., a very long but finite depth crack) approximation that can be used to demonstrate the use of the SCG fracture mechanics technology. Assuming that the liner and seam behave in a linear elastic manner, that residual stresses can be ignored, and that the loads are solely due to in-plane uniaxial tensile stresses that act in the direction normal to the crack line, the stress intensity factor can be taken as [Kanninen, et al, 1985]

$$K = 1.12C\sigma(\pi a)^{1/2} \tag{9}$$

where σ is the remote in-plane tensile stress, a is the crack depth, and C is a dimensionless geometric factor that simply combines a stress riser with the seam/membrane area difference. For the two cases illustrated in Figure 4, $C = 2.8$ (corner flaw) and $C = 0.5$ (center flaw).

From the results of an uninstrumented constant load SCG test on a face notched strip of a 0.060-inch thick HDPE liner material, making the assumption that the detailed behavior of PE liner material will be similar to the class of PE gas pipe materials that behave in accordance with linear elastic fracture mechanic principles, the SCG rate can be assumed to have the form of Equation (1). To a reasonable first approximation it was found that $A = 10^{-14}$ (English units) and $m = 2$. Just as for gas pipes, Equation (8) can be used to obtain a relation for the lifetime where h is the thickness of the liner (or the liner plus seam).

To illustrate how Equation (8) can be applied to forecast the long-term service performance of geomembranes, assume that the loads are due only to the thermal stresses arising from the difference between the installation and service temperatures. If no significant synergisms arise between the stress and temperature effects, then the applied stress can be taken as time-independent and given by

$$\sigma = \alpha E \Delta T \tag{10}$$

where α is the coefficient of thermal expansion of the geomembrane, E is its elastic modulus, and ΔT is the long-time average installation/service temperature differential during service. Substituting Equation (10) into Equation (9) and using the result in Equation (8) then gives a relation for t_f as a function of ΔT. Generally, a numerical procedure must be used to perform the integration. But, for the simple case where $m = 2$, the integration can be made in closed form. Ignoring t_i (a conservative assumption), the lifetime is

$$t_f = \frac{1}{(1.12)^2 \pi A (\alpha E C)^2} \quad \frac{\ln(h/a_o)}{(\Delta T)^2} \quad \frac{a_T}{b_T^2} \tag{11}$$

The results obtained using Equation (11) for the time-to-failure in the two conditions shown in Figure 4 are provided in Figures 5 and 6.

Figures 5 and 6 illuminate several interesting aspects of geomembrane durability that follow from the use of fracture mechanics methods to quantify SCG. First, there is clearly a difference in lifetime arising from the location of the initiating defect; i.e., defects located at the edge of a seam are much more detrimental than those in the center of seam. Second, because the SCG process tends to be dominated by the time spent in propagating very small cracks, there is a significant effect of the initial defect size. Third, a low service temperature produces tensile thermal stresses that can significantly diminish the lifetime that can be anticipated in service.

These observations notwithstanding, perhaps the most important element that is offered by results such as those in Figures 5 and 6 is that, for the first time, the potential for developing explicit relations among material variables and installation and service conditions for geomembranes has been demonstrated. Nonetheless, it must be recognized that this heuristic example, for the sake of providing an illustrative example of the current technology, ignored a number of complicating aspects that are involved in geomembrane durability. These are discussed in the following section of this paper.

DISCUSSION

As firmly established in work for the gas industry, SCG can be quantified by already established fracture mechanics methodologies. For geomembranes, use of this technology would allow an accelerated SCG test like that employed for PE gas distribution piping systems to determine the SCG properties in the form of crack growth rate (da/dt) and time for initiation of crack growth as functions of a fracture mechanics parameter like the stress intensity factor K. Lifetime estimates could then be made to account for applied loads (constant or cyclic), residual stresses, temperature changes (constant or cyclic), geomembrane and seam geometry, and, above all, defect size, orientation and location. In addition, it would become possible to quantify inspection targets for an installed geomembrane.

Further research to achieve the above benefits must include specific work on SCG for the initial growth through the thickness, and for the subsequent growth of a through-thickness crack. Work on the potential of the latter to become unstable and thereby produce rapid crack propagation (RCP) is needed to help define the limits of the SCG process. This expanded view of the problem is indicated schematically in Figure 7 which comprehensively depicts the manner in which a geomembrane service failure could occur.

As shown in Figure 7, the modeling and material characterization work for geomembrane durability can be categorized as follows:

- Stage 1 - SCG initiated at a small manufacturing or installation-induced surface defect that eventually punctures the geomembrane to produce a relatively small leak.
- Stage 2 - Through-geomembrane SCG initiated at a small Stage 1 leak that expands to produce a large leak.
- Stage 3 - Through-geomembrane catastrophic RCP that occurs after a transition from SCG when a Stage 2 crack reaches a critical size.

In addition to ignoring these fundamental aspects of geomembrane behavior, the heuristic result shown in Figure 5 made several expedient simplifications (e.g., plane strain conditions), and glossed over some major issues. Examples of measurement and analysis issues that must be addressed in further research certainly include the effect of the seaming process and the service temperature on the geomembrane SCG properties, the validity of the PE gas pipe bi-directional shift functions, and the legitimacy of the use of LEFM; i.e., whether or not geomembranes exhibit Category I behavior.

CONCLUSIONS

This paper described a heuristic study aimed at illustrating how existing gas pipe technology can be extended and transferred to geomembrane applications to predict the life expectancy (durability) of a defective geomembrane in service conditions. The goal of the further work is to provide assessments of geomembrane lifetimes that are dictated by the presence of surface scratches and defected seams. The establishment of this approach will benefit manufacturers, installers, regulators and, above all, owners of liquid and solid waste impoundment sites by enabling them to select appropriate HDPE materials, guide the installation procedures, and establish defect sizes for quality assurance inspection.

ACKNOWLEDGEMENT

Much of the PE gas pipe work reported in this paper was performed in a joint SwRI/OSU project that was supported by the Gas Research Institute under Contract No. 5088-271-1822. The GRI project manager was Dr. Michael M. Mamoun. Useful discussions on geomembrane uses and issues have been held with Dr. Mary McLearn of the Electric Power Research Institute.

REFERENCES

Kanninen, M.F. and Popelar, C.H., (1985) Advanced Fracture Mechanics, Oxford University Press, New York.

Kanninen, M.F., O'Donoghue, P.E., Popelar, C.H. and Kenner, V.H., (1990), "A Viscoelastic Fracture Mechanics Assessment of Slow Crack Growth in Polyethylene Gas Distribution Pipe Materials," Engineering Fracture Mechanics, Vol. 36, pp. 903-918.

Kanninen, M.F., Popelar, C.F., Tweedy, L.K. and Popelar, C.H., (1991) "Time-Temperature Accelerated Procedures for Forecasting Long-Term Service Performance of Polyethylene Gas Distribution Pipes," Twelfth Plastic Fuel Gas Pipe Symposium, American Gas Association, Arlington, VA, pp. 113-127.

Kenner, V.H., Popelar, C.H. and Wooster, J.P., (1991) "An Approach for Interpreting Accelerated Performance Data for PE Gas Pipe Materials," Twelfth Plastic Fuel Gas Pipe Symposium, Boston, MA, pp. 180-189.

Kuhlman, C.J., Kanninen, M.F. and Tweedy, L.K., (1992) "Forecasting the Long-Term Service Performance of Polyethylene Gas Distribution Pipes," Plastic Pipes VIII, Koningshof, The Netherlands.

Peggs, I.D. and Carlson, D. S., (1989) "Stress Cracking of Polyethylene Geomembranes: Field Experience," Durability and Aging of Geosynthetics, R.M. Koerner, Ed., Elsevier Applied Science, London, pp. 195-221.

Peggs, I.D., (1990) "Durability of Geosynthetics," Florida Society of Professional Engineers presentation, West Palm Beach, Florida.

Peggs, I.D. and Carlson, D.S., (1990)(a) "Brittle Fracture in Polyethylene Geomembranes," Geosynthetics Microstructure and Performance, ASTM STP 1081, pp. 57-77.

Peggs, I.D. and Carlson, D.S., (1990)(b) "The Effects of Seaming on the Durability of Adjacent Polyethylene Geomembranes," Geosynthetic Testing for Waste Containment Applications, ASTM STP 1076, R.M. Koerner, Ed., pp. 132-142.

Popelar, C.H., Kenner, V.H. and Wooster, J.P., (1991)(a) "An Accelerated Method for Establishing the Long-Term Performance of Polyethylene Gas Pipe Material," Polymer Engineering and Science, Vol. 31, pp. 1693-1700.

Popelar, C.H., Kenner, V.H., Popelar, S.H. and Pfeil, M.C., (1991)(b) Life Predictions of Butt Heat Fusion Joints in Polyethylene Gas Pipe Materials, Final Report to the Gas Research Institute on GRI Contract No. 5088-271-1739, The Ohio State University, Columbus, OH

(a) Craze has developed into crack at edge of seam

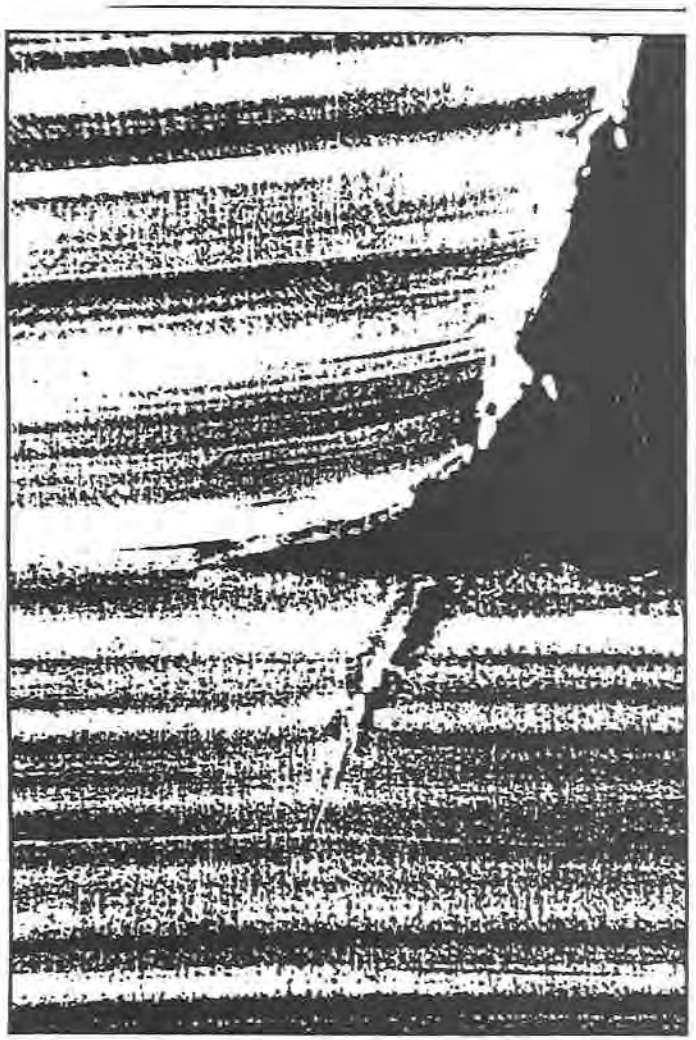

(b) Crazing at edge of seam under extrude lead

Figure 1 Slow crack growth in geomembrane seams

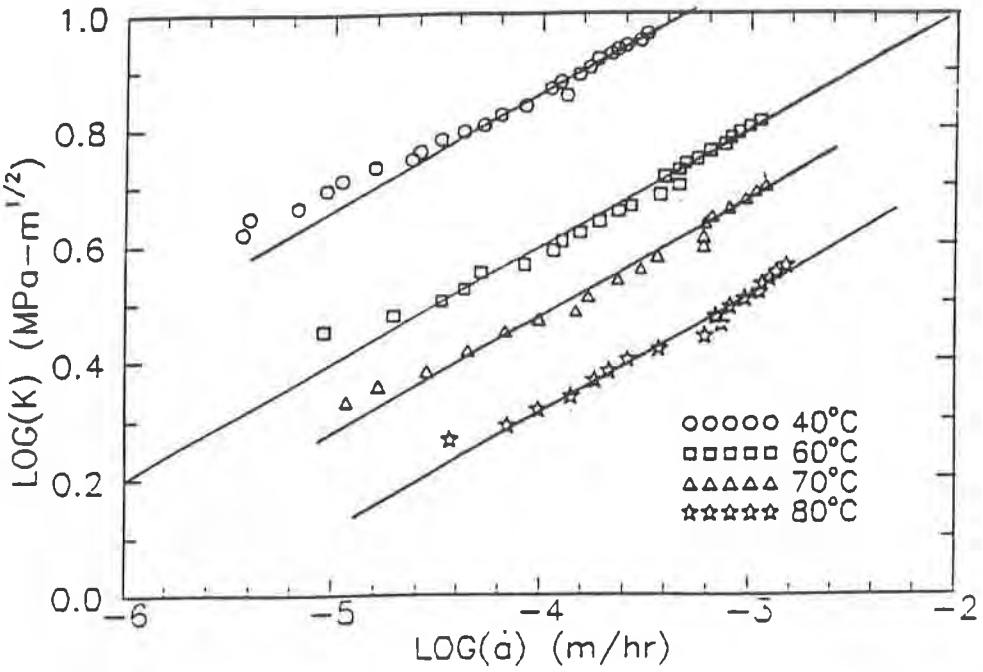

(a) SCG data at various temperatures

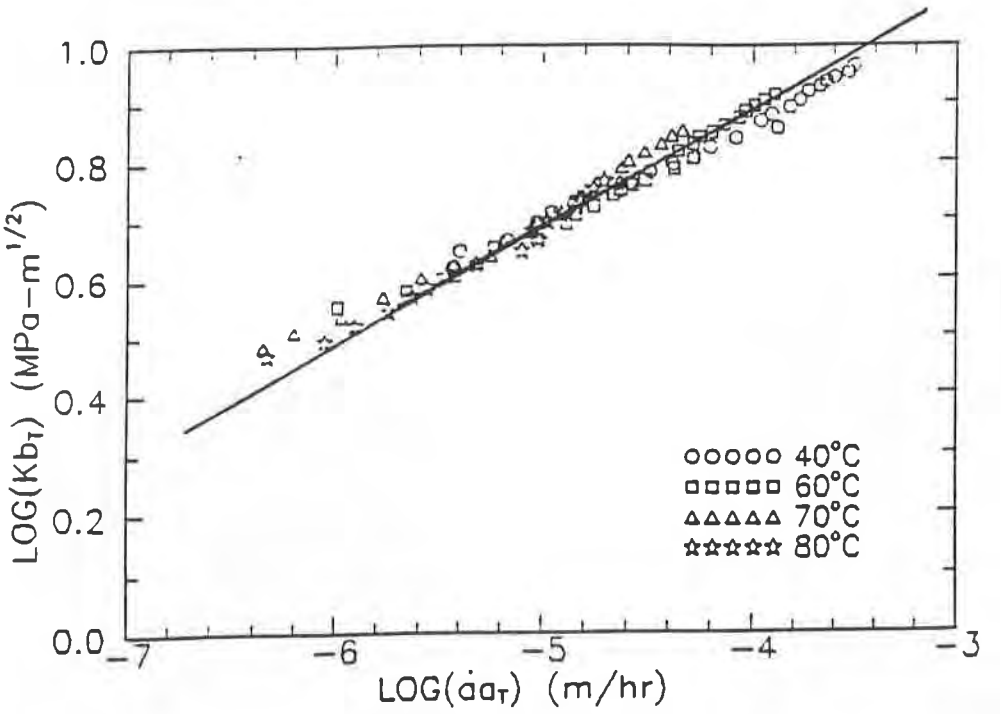

(b) Consolidation of data at reference temperature of 40°C

Figure 2 Use of the bi-directional shift functions to effectively consolidate SCG data on an HDPE gas pipe material [Peggs 1990]

(a) Short crack (arrowed) along edge of seam

(c) Crack along edge of hot wedge seam

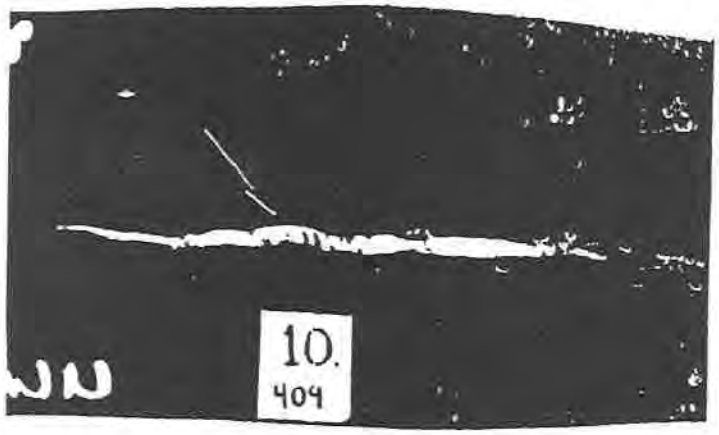

(b) Cracking within extruded seam

(d) Cracking within fused seam

Figure 3 Examples of field failures in seamed geomembranes

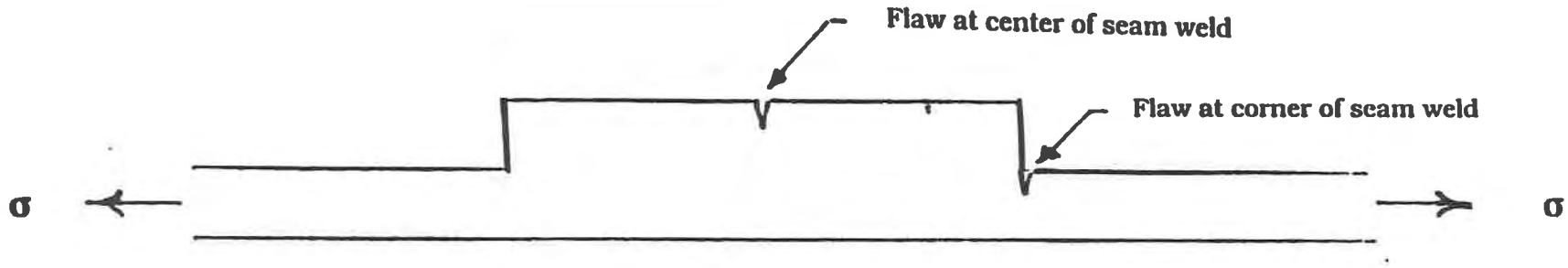

Figure 4 Basis of heuristic calculation for lifetime of polyethylene seam welded membrane

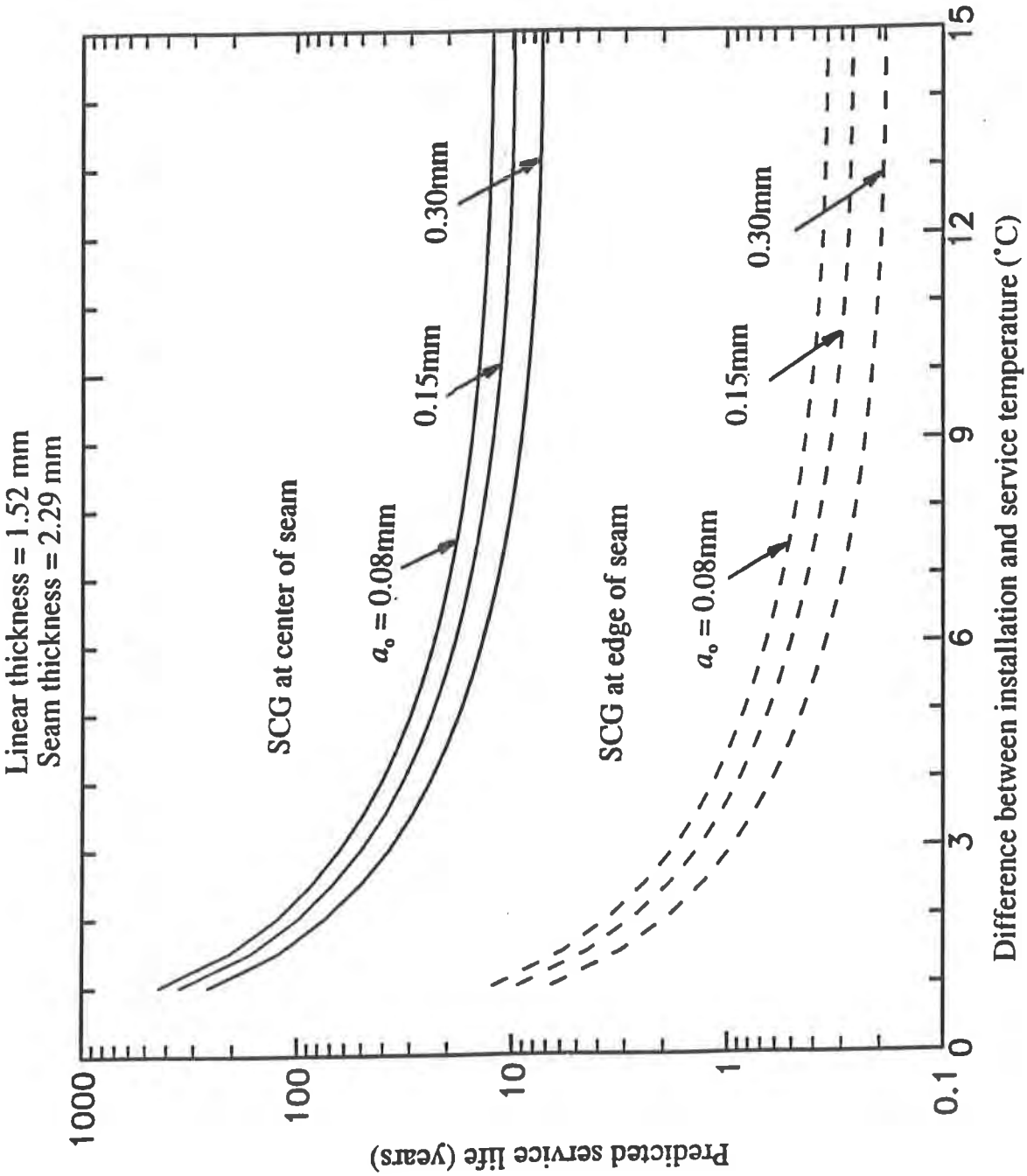

Figure 5 Predicted service life in a seamed geomembrane liner as a function of initial flaw size and thermal stresses

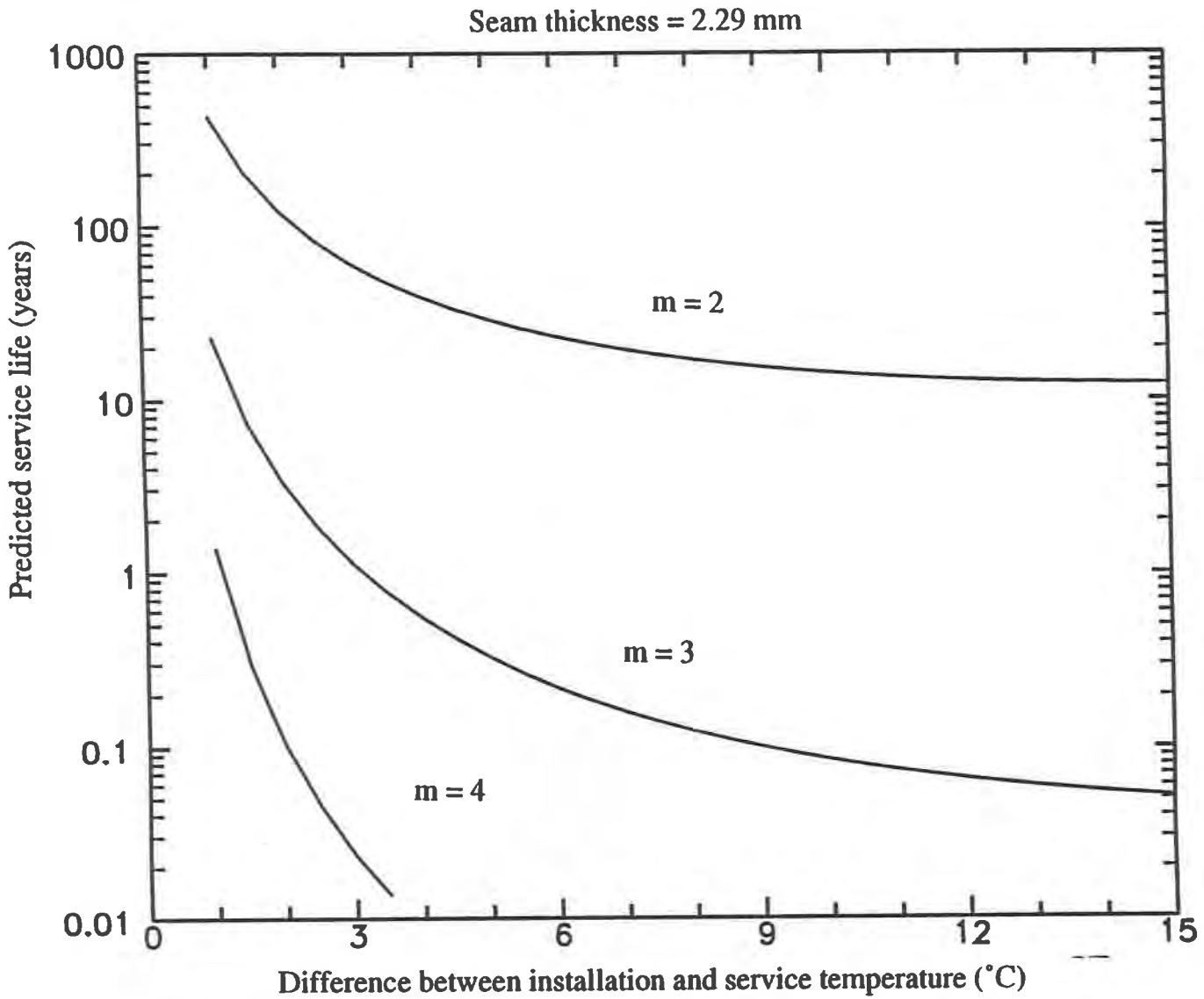

Figure 6 Predicted service life for an initial flaw of 0.08 mm at the center of a seamed geomembrane liner as a function of material and thermal stresses

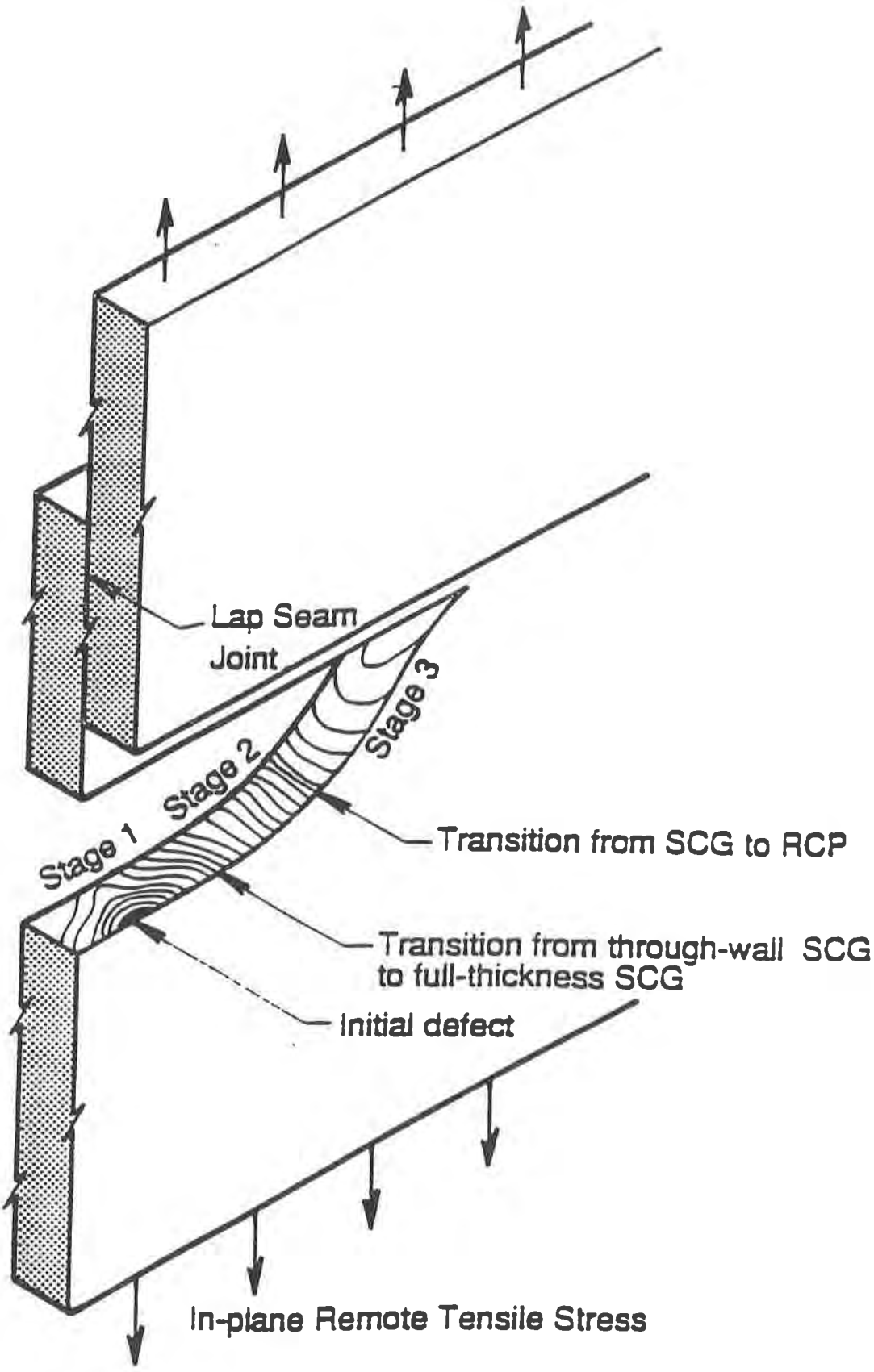

Figure 7 Schematic view of long-term failure process in a seamed geomembrane

Chemical Compatibility of Four Geosynthetics With Two MSW Incinerator Ash Leachates

H.E. Haxo Jr.
Matrecon, USA

P.D. Haxo
Matrecon, USA

ABSTRACT

EPA Method 9090 compatibility tests of four geosynthetics that may be used in the construction of landfills were performed with samples of two municipal solid waste (MSW) incinerator ash leachates. The geosynthetics that were tested included three geomembranes [a 60-mil high-density polyethylene (HDPE), a 36-mil fabric-reinforced, industrial-grade chlorosulfonated polyethylene (CSPE-I), and a 30-mil unreinforced polyvinyl chloride (PVC)], and one polyester nonwoven geotextile. The test results indicate that the HDPE geomembrane and the polyester geotextile are compatible with both MWC ash leachates. The PVC geomembrane appears to be compatible for short-term exposure with these leachates, but it tends to lose extractables (i.e., plasticizers), increase in volatiles, and soften. Extrapolation of these changes would result in adverse changes in physical properties. Though the polyester fabric reinforcement maintained its strength, the CSPE-I is of concern because of its high water absorption, loss of extractables, and apparent softening, all of which may affect seam strength.

INTRODUCTION

In spite of the effort to use incineration to reduce and, if possible, eliminate the volume of municipal solid waste (MSW) requiring disposal, there still remains solid waste residuals that can contain many trace metals. These residuals must still be disposed of on the ground in a landfill. The U.S. Environmental Protection Agency (EPA) initiated this study to investigate the effects of municipal waste combustion (MWC) ash monofill leachate on properties of geosynthetic materials used in the construction of the lining, drainage, detection, and collection systems for an MWC monofill and the ability of these materials to perform their design function for the life of the facility and post-closure period. The EPA desired this information to support future regulations for the design and construction of MWC ash disposal facilities.

Four geosynthetics commonly used in liner systems, including three geomembranes and one polyester nonwoven geotextile, were selected for test. Chemical compatibility testing was performed with samples of two MSW incinerator ash leachates in accordance with EPA Method 9090 (EPA, 1986) for geomembranes and the EPA's draft supplementary guidance (EPA, 1989) for testing other geosynthetics. Samples of each of the geosynthetics were exposed at 23° and 50°C for up to 120 days to the two leachates as required by the test procedure, removed from the exposure, and tested for changes in properties at the end of every 30 day increment to determine whether these materials were adversely affected by exposure to the leachates. Analytical testing was performed to characterize the geomembranes and the geotextile so that the results of these studies could be used to aid in assessing other geosynthetics that might be potential candidates for use in constructing lining systems for MWC ash monofills.

MATERIALS TESTED

The three geomembranes selected for test were:

- A 60-mil high-density polyethylene (HDPE).
- A 36-mil industrial-grade chlorosulfonated polyethylene (CSPE-I). The membrane was reinforced with a 10 x 10 ends per inch polyester scrim.
- A 30-mil unreinforced polyvinyl chloride (PVC).

The geotextile selected for testing was a nonwoven polyester fabric that had a nominal thickness of 125 mils and a nominal mass per unit area of 10 oz per square yard. This geotextile is intended for filtration and separation.

The MWC ash leachates used in the study were collected from two sources, one based on a current and the other based on an older technology. Leachate No. 1 came from a state-of-the-art MWC ash monofill leachate facility. This facility had a scrubber, and ash disposed of in the monofill contained bottom ash, fly ash, and scrubber residue. Leachate No. 2 came from an older MWC ash monofill facility that did not have a scrubber. Ash disposed of in the monofill contained bottom ash and fly ash. Analyses of the two leachates are summarized in Table 1. Even though analysis for pH, electrical conductivity (EC), and total dissolved solids (TDS) indicated that there were only insignificant differences between the drums in which the leachates were shipped, it was decided to mix equal aliquots from the contents of the different drums of a single leachate together before placing the blended leachate in the individual exposure cells.

COMPATIBILITY TEST PROCEDURE

Description of the Test Method. EPA Method 9090 was specifically designed to assess the chemical compatibility of geomembranes and waste liquids (EPA, 1986). This test method is basically divided into two parts; the first part deals with the exposure of the geosynthetic samples to a waste liquid, and the second part is concerned with the specific tests that are performed on geomembranes before and after exposure. In this test, slab samples are immersed for up to four months at 23° and 50°C in a representative sample of the waste liquid or leachate that would be contained by the geomembrane. Analytical and physical tests are performed on the unexposed geomembranes for baseline data and on samples exposed to the waste liquid for 30, 60, 90, and 120 days. Testing of all the exposed samples is performed at 23°C. Table 2 presents the procedures used in testing the geomembranes before and after exposure. The specific procedures used depend on the construction of the geomembrane (i.e., whether it is fabric-reinforced) and the type of polymer used in its manufacture.

A "significant" change in any of the measured properties resulting from exposure to a leachate or a trend showing continuing percent change in the positive or negative direction at the end of the fourth month probably indicates long-term incompatibility of the geosynthetic with that leachate. A "significant" change would be one that affects the performance of that geosynthetic in a field installation. Absolute quantification of significant changes for different geosynthetic applications has not been developed, and interpretation of exposure tests results still depends on judgment and guiding principles. It is recognized that there is an inherent variability in the tests used to monitor the changes in properties of geosynthetic materials (e.g., tensile strength and tear resistance), and that this variability can make interpretation of the data difficult. It is also recognized that all materials can be affected by immersion in a liquid medium and that some changes in properties are to be expected. Figure 1 presents schematically four general ways in which a geosynthetic property can change during exposure to a waste liquid. Curve A indicates an initial rapid change in a property value, and even though the rate of change slows down, the trend continues with exposure time. Curve B indicates that the change from the initial value goes through a maximum before beginning a continuous change in the opposite direction. For example, a plasticized composition may increase in weight as it absorbs constituents

Table 1. Analysis of MWC ash leachates

Species	Concentration	
	MWC-1	MWC-2
Chloride, mg/L	13,000	14,000
Electrical conductivity, mmho/cm	19	36
Sulfate, mg/L	120	5,500
Total dissolved solids, mg/L	20,000	30,000
Total suspended solids, mg/L	14	19
Nitrate, mg/L	0.27	0.02
Total organic carbon, mg/L	85	48
Aluminum, mg/L	0.093	0.84
Arsenic, mg/L	ND	ND
Cadmium, mg/L	0.019	ND
Calcium, mg/L	4,300	170
Chromium, mg/L	0.031	ND
Copper, mg/L	0.58	ND
Iron, mg/L	5.4	1.6
Lead, mg/L	ND	0.008
Magnesium, mg/L	7.2	4.0
Manganese, mg/L	3.7	0.40
Mercury, mg/L	ND	ND
Nickel, mg/L	0.064	ND
Selenium, mg/L	ND	ND
Silicon, mg/L	2.8	3.9
Silver, mg/L	0.034	ND
Zinc, mg/L	0.073	0.27

ND= Not detected.

Table 2. Methods used to test geomembranes before and after exposure in MWC ash leachate compatibility study

Property	Geomembrane type[a]		
	CSPE-I	HDPE	PVC
Analytical properties			
Volatiles	MTM-1	MTM-1	MTM-1
Extractables	MTM-2	MTM-2	MTM-2
Weight	---------Direct Measurement---------		
Dimensional properties			
Thickness	ASTM D374	ASTM D374	ASTM D374
Area	---------Direct Measurement---------		
Physical Properties			
Tensile properties	ASTM D751, Method B	ASTM D638	ASTM D638
Modulus of elasticity	...	ASTM D638	...
Tear resistance	...	ASTM D1004	ASTM D1004
Ply adhesion	ASTM D413, 90° peel	...	...
Puncture resistance	ASTM D4833	ASTM D4833	ASTM D4833
Hydrostatic resistance	ASTM D751	ASTM D751	ASTM D751
Hardness	...	ASTM D2240	ASTM D2240

[a]MTM=Matrecon test method as described in Matrecon (1988); ASTM = American Society for Testing and Materials.

of a waste liquid, and then lose weight once the waste liquid begins to leach plasticizer. Both Curves A and B indicate that the geosynthetic is probably not compatible with the immersion liquid. Curve C shows that the geosynthetic property value has reached a plateau after an initial, relatively large change. Depending on the property and the effect such a change could have on the field performance of the geosynthetic, the geosynthetic may or may not be compatible with the liquid to which it is exposed. Curve D, which shows that the geosynthetic property has reached a plateau after an initial, relatively small change, indicates that the geosynthetic is probably compatible with the immersion liquid. It should be noted that a polymeric composition has a combination or set of interrelated properties. A change in the value of one property of the material resulting from exposure to environmental conditions such as immersion in a liquid will be accompanied by changes in other properties. For example, the swelling of a material usually results in a loss of tensile strength, and the extraction of plasticizer usually results in shrinkage and an increase in tensile strength. Because a significant change in one property would be accompanied by significant changes in others, no one property of a geosynthetic exposed in a Method 9090 test should be analyzed separately for significance.

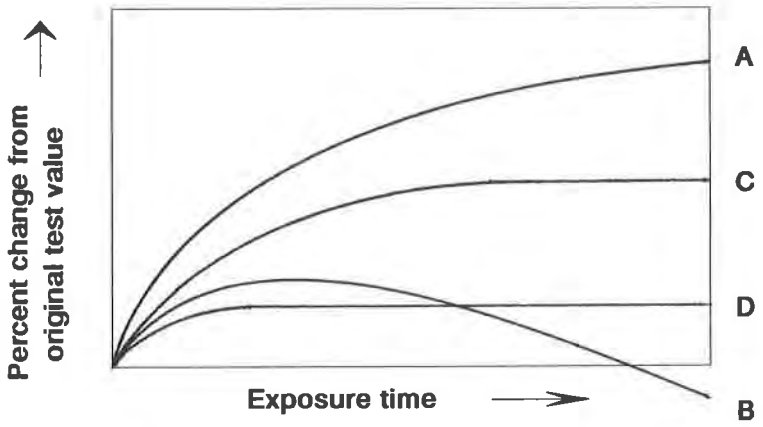

Figure 1. Four general trends by which the properties of a geosynthetic can change from initial values on exposure to a waste liquid.

Current EPA regulations require that all materials used in constructing a liner system for a RCRA hazardous waste management facility be tested for chemical compatibility with the waste to be contained. In recognition of this requirement, the EPA has proposed supplementary guidelines so that geosynthetics other than geomembranes can be tested in accordance with EPA Method 9090 (EPA, 1989). This guidance requires all geosynthetics to be exposed under the conditions described in Method 9090 and to be tested by appropriate test methods for changes in properties, and it lists specific methods for testing geotextiles, geonets, geogrids, and plastic pipes before and after exposure. Table 3 presents the tests used to determine the properties of the geotextile before and after exposure. Baseline properties were measured on wet specimens. The different geotextile test specimens were cut prior to exposure and exposed in specially designed metal holders that were placed in the exposure tanks.

Sampling of the Geosynthetics. The geomembrane samples tested for the exposure study were taken on a diagonal across the width of the received roll, excluding the outer foot on each side. Each sample was measured for thickness, width and length, and weighed. In addition, each sample was inspected for scratches or other damage that might have occurred during shipment or handling. Twenty samples of each geomembrane that were of essentially the same thickness were selected for the actual exposure test.

A similar procedure was used in sampling the geotextile to take into account the inherent variability in the mass per unit area of nonwoven fabrics. Individual 11 x 15-in. pieces were cut from the 15-ft wide geotextile roll. Specimens for the individual tests were cut from each of these pieces in accordance with a set pattern. Selection of individual test specimens for exposure was based on approximate equality

Table 3. Methods used to test polyester geotextile before and after exposure in MWC ash leachate compatibility study

Property	Test method
Thickness	ASTM D1777[a]
Mass per unit area	ASTM D3776[a]
Grab tensile	ASTM D4632
Trapezoidal tear resistance	ASTM D4533
Hydraulic burst strength	ASTM D3786
Index puncture resistance	ASTM D4833
Permittivity	ASTM D4491, constant head method

[a]Measured on specimens prior to exposure.

in weight of the specimens for a given test. The specimens were grouped so that the average weight of the specimens for a given test and directional orientation was essentially the same for all exposures. This procedure resulted in a specimen population that was significantly more uniform in its mass per unit area than a random selection, thus reducing the variations in test results that could be related to variations in the geotextile.

Exposure Cells. Exposure cells designed and fabricated to meet the demands of compatibility testing were used in conducting the exposure tests. The Matrecon cell, which is presented schematically in Figure 2, has the following features:

- The tanks, lids, stirrers, and specimen racks are constructed of 316 stainless steel.
- The volume of leachate held by a cell is 5.2 gallons.
- A Teflon gasket is installed between the tank lid and the flange around the top of the tank. The gasket is used to prevent loss of volatiles. Teflon was selected to minimize the absorption of leachate constituents by the gasket.
- The leachate is stirred continuously to prevent stratification within the waste liquid.
- The cell can be operated at 23° or 50°C by being placed in water baths controlled to these temperatures. Temperature in the individual cells is monitored by mercury thermometers.
- Two short standpipes are secured in the lid of each tank and used for filling the tank to its capacity, thus minimizing the possibility that volatiles will leave the leachate to enter a headspace.
- Each lid is equipped with a septum through which sampling or spiking of leachate can be performed.

Monitoring the Leachate Throughout the Exposure. Because the two leachates had very low total organic carbon contents, it was not necessary to change the leachate at the beginning of each 30-day exposure period. At the end of each 30-day exposure period, the leachates in the individual cells were sampled and tested for pH, EC, and TDS to determine whether the leachates had changed significantly. The results of analyzing the leachate samples indicate that the contents of the cells remained essentially constant throughout the exposures. A slight decrease in the pH of some of the cells containing MWC Ash Leachate No. 2 is probably related to the corrosion of the stainless steel tanks and wire frames.

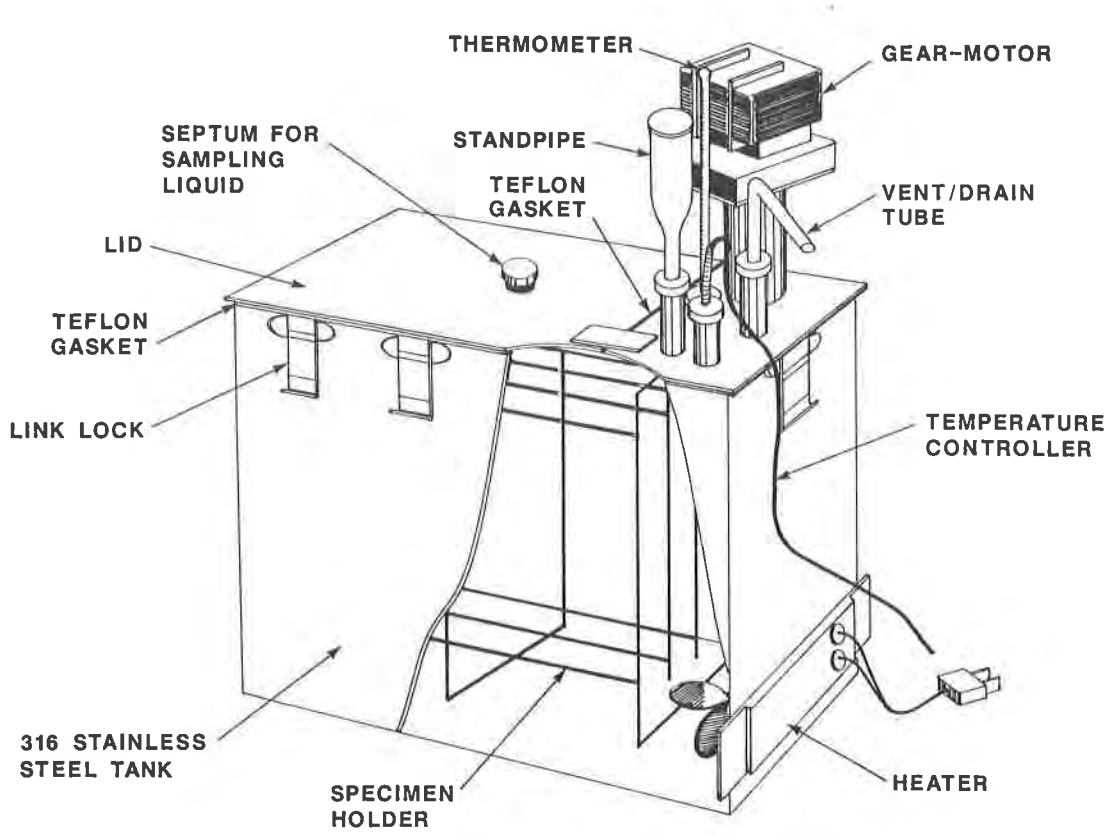

Figure 2. Schematic of the cell used in performed the exposure portion of the EPA Method 9090 compatibility studies.

RESULTS OF METHOD 9090 EXPOSURE TESTS

At the end of each exposure period, the appropriate slabs and specimens were removed from the cells and after cleaning (in the case of the geomembranes) or draining (in the case of the geotextile), they were sealed in individual polyethylene bags until they were tested (within 48 hours). During the exposure a relatively hard deposit formed on the surface of the geomembrane slabs. The variability in the effectiveness of removing the deposits without causing damage to the geomembrane surfaces resulted in some variation in the weight and thickness measurements. The brown color of the depositions indicated that they were probably iron oxide. The geotextile specimens also appeared rust-stained, but no effort was made to try to remove the deposits prior to testing. After the individual test specimens were labelled, they were allowed to hang in a hood until liquid no longer drained easily from them. After hanging for a short time, the specimens for each leachate-temperature combination were placed in separate polyethylene bags until they were tested.

Results of the Exposure Testing of the CSPE-I Geomembrane. The results of monitoring the volatiles and extractables of the CSPE-I on immersion in the two MWC ash leachates are illustrated in Figures 3 and 4, respectively. There were progressive small changes with immersion time in the values of the analytical properties of the exposed slabs. All of the slabs increased in weight with time. The maximum increase was 7.42% for the slabs immersed for 4 months in MWC Ash Leachate No. 1. The changes in weight were paralleled by increases in the volatiles contents, indicating that the increases in weight were primarily due to water absorption. The slabs exposed at 50°C absorbed somewhat more than did those exposed at 23°C. All of the slabs also showed a gradual decrease in extractables with those immersed at 50°C showing greater decreases than those immersed at 23°C. Overall, the effects of the immersion on the analytical properties were comparatively small, but they showed trends that indicate possible long-term effects on the CSPE-I coating.

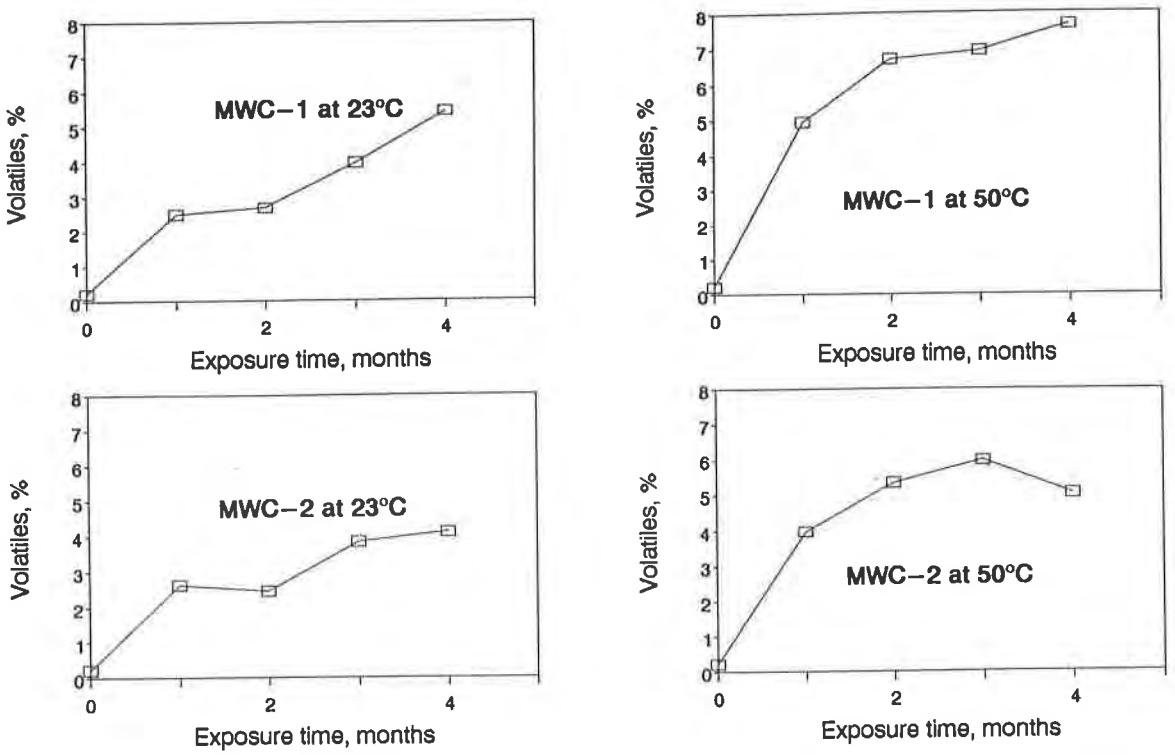

Figure 3. Volatiles of 36-mil CSPE-I geomembrane samples immersed in MWC ash leachates. Value for the unexposed membrane is 0.22%.

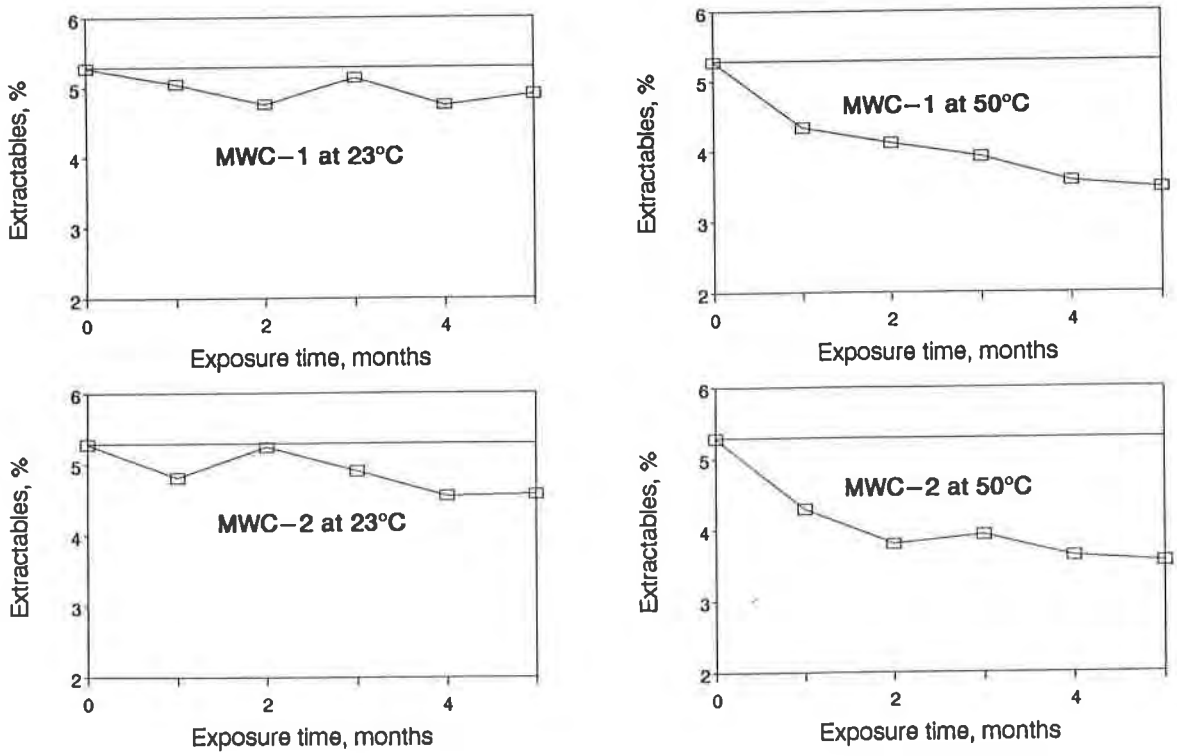

Figure 4. Extractables of 36-mil CSPE-I geomembrane samples immersed in MWC ash leachates. Value for the unexposed membrane is 5.28%.

The physical properties of the CSPE-I membrane were largely determined by the reinforcing fabric, which was a 10 x 10 polyester scrim. This open-weave fabric is designed to impart tear resistance, tensile strength, and dimensional stability to the geomembrane. This fabric is also designed to have a low adhesion to the CSPE-I coating so that under stress conditions, such as in tearing, the fabric threads will debond from the CSPE-I coating and take the stresses independently, thereby reinforcing the geomembrane.

Overall, the results indicate that the reinforcing fabric was not affected by immersion in either of the two leachates, nor were there any trends toward long-term changes in this polyester fabric. Nevertheless, there was some scatter in the values in some of the tests, because some of the threads had pulled out of the test specimens without breaking during testing, particularly in the case of the 1-in. strip tensile test specimens. Such behavior may reflect the high strength and looseness of the weave of the fabric coupled with its low adhesion to the CSPE-I matrix and the shortness of the confined length of the specimen threads in the test equipment grips. Such pullout would not occur in an in-service liner due to the extended length of the individual threads. As a result, it was decided to test a fifth slab that had been retained in immersion for an additional month, but there was the same scatter in the data. In the hydrostatic resistance test, all of the fabric threads broke, resulting in test values that remained essentially constant, as is shown in Figure 5 for the samples immersed at 50°C. These results indicated that the polyester fabric was chemically compatible with the two leachates.

The ply adhesion values gradually decreased during the immersion period, as is shown in Figure 5 for the samples immersed at 50°C. The unexposed geomembrane had a ply adhesion of 7.2 and 8.3 pounds per inch (ppi) for the machine and transverse directions, respectively, and after five months of immersion the values had decreased approximately 1-2 lbs with those immersed at 50°C showing greater decreases than those immersed at 23°C. This decrease may reflect a loss of adhesion of the CSPE-I to the fabric and a softening of the CSPE-I. Reflecting the results of the analytical testing, this result indicates that, even though the effects were small, there was a trend that could indicate adverse long-term effects on the CSPE-I coating.

Results of the Exposure Testing of the HDPE Geomembrane. The average percent retentions and changes in properties of the samples immersed in MWC Ash Leachate No. 1 at 23°C are summarized in Table 4, and the results of testing the samples immersed in MWC Ash Leachate No. 2 at 50°C are summarized in Figure 6.

The changes in the analytical properties of the HDPE geomembrane were small, with essentially no change in either the volatiles or the extractables. The immersed samples appeared to have a very slight weight loss.

Immersion in the two leachates also resulted in only small changes in the physical properties of the HDPE geomembrane. Averaging the data measured in the machine and transverse directions and correcting for thickness variations indicate that the tensile at yield, the stresses at 100 and 200% elongation, the modulus of elasticity, the tear strength, the hydrostatic resistance, and the hardness of the geomembrane appeared to have increased slightly. On the other hand, there were slight decreases in the tensile at break and elongation at break from the baseline data. The results of the exposure at 50°C were quite similar to those from the 23°C exposure. Overall, these results indicate that the HDPE hardened slightly during exposure.

It is concluded from these results that the HDPE geomembrane is compatible with both MWC ash leachates.

Results of the Exposure Testing of the PVC Geomembrane. The results of testing the samples immersed in MWC Ash Leachate No. 1 at 23°C are summarized in Figure 7.

The effects of the immersion on the analytical properties of the PVC slabs were slight on an absolute basis (i.e., <1%), but they showed trends which, on extrapolation, may indicate long-term incompatibility of the PVC with the MWC ash leachates. As shown in Figure 8, the volatiles increased from 0.18% to 0.5-0.97%. Concurrently, as shown in Figure 9, the extractables gradually decreased. These results are con-

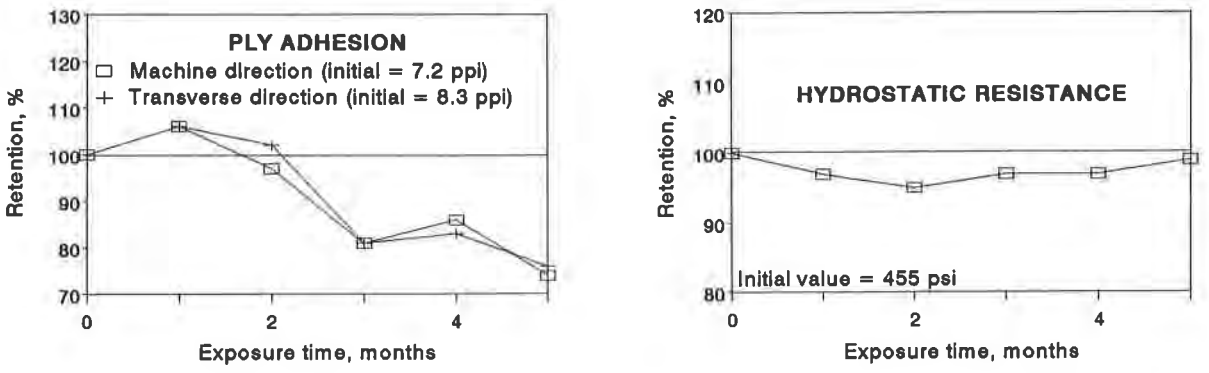

Effect of immersion in MWC Ash Leachate No. 1 at 50°C

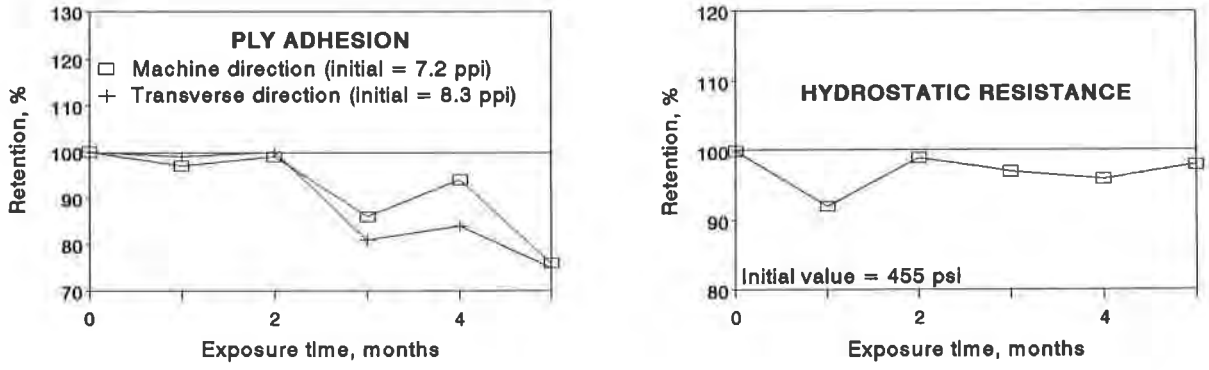

Effect of immersion in MWC Ash Leachate No. 2 at 50°C

Figure 5. Effects of exposure at 50°C in both MWC Ash Leachate No. 1 and No. 2 on the ply adhesion and hydrostatic resistance of the CSPE-I geomembrane.

firmed by the results of monitoring the weight of the immersed slabs. Both sets of slabs immersed in Leachate No. 2 initially increased in weight but began to lose weight after the initial gains. The slabs exposed at 50°C gradually decreased in weight to an overall loss of -0.37% of the original weight at four months of exposure after having increased +0.49% of the original weight at one month of exposure.

The effects of the immersion on the physical properties of the PVC slabs were only slight; however, there were trends which basically confirmed the analytical data and, when extrapolated, indicate possible long-term effects. Averaging the data for the machine and transverse direction and plotting against exposure time indicated that the tensile strength at break tended to decrease and the elongation at break tended to rise. This is generally consistent with the softening of a PVC compound. This softening is also indicated with the downward trends with exposure time for the stresses at 100 and 200% elongations and the hardness values. In all cases, there was a trend for the tear resistance to increase a few percent and then to decrease with exposure time. In those tests that do not result in separate values for machine and transverse directions, i.e., hydrostatic resistance and puncture resistance, the test values initially tended to decrease, but by the end of four months of exposure they appeared to be increasing.

The results of the four-month exposure indicate that, for short-term exposure, the PVC geomembrane is compatible with the two MWC ash leachates, but the apparent changes in analytical properties of the test slabs, particularly the decrease in extractables probably due to a loss of plasticizer, indicate that for long-term applications the PVC may not be compatible with the MWC ash leachates. To determine whether these trends continue on longer exposure, a fifth PVC slab is continuing in immersion.

Table 4. EPA Method 9090 compatibility test of 60-mil HDPE geomembrane[a] in MWC Ash Leachate No. 1 at 23°C

Property	Direction of test	Initial value	Exposure time, months			
			1	2	3	4
Analytical properties			Test values			
Volatiles, %		0.28	0.22	0.19	0.17	0.21
Extractables[b], %		1.06	1.09	1.07	0.82	0.91
Dimensional properties			Change, %			
Weight		...	-0.04	-0.09	-0.17	-0.18
Thickness		...	0.16	1.15	-1.25	1.80
Area		...	-0.19	0.10	-0.48	-0.19
Physical properties						
Tensile properties:			Retention, %			
Tensile at yield	Machine	2560 psi	104	98	103	108
	Transverse	2810 psi	101	94	95	104
Elongation at yield	Machine	15%	100	100	100	100
	Transverse	15%	100	100	100	100
Tensile at break	Machine	5195 psi	95	88	101	90
	Transverse	5250 psi	102	102	96	93
Elongation at break	Machine	855%	98	94	102	95
	Transverse	845%	104	104	101	98
Stress at 100% elongation	Machine	1970 psi	101	98	103	105
	Transverse	1930 psi	97	97	95	101
Stress at 200% elongation	Machine	1995 psi	101	101	102	103
	Transverse	1950 psi	99	98	96	102
Modulus of elasticity	Machine	96,600 psi	108	101	98	105
	Transverse	98,800 psi	114	113	110	110
Tear resistance	Machine	815 ppi	102	99	99	106
	Transverse	775 ppi	103	100	100	104
Hardness, Shore D:			Change in points			
Instant reading		57	5	5	3	3
5-second reading		54	4	4	2	2
Hydrostatic resistance:			Retention, %			
Thickness		60.5 mil	104	101	101	105
Value		485 psi	106	103	110	109
Puncture resistance:						
Thickness		60.8 mil	101	104	102	102
Force at puncture		132 lb	104	105	104	104
Probe travel at puncture		0.60 in.	108	100	97	97

[a]Matrecon Identification No. P793.
[b]The solvent used in determining the extractables was methyl ethyl ketone.

Results of the Exposure Testing of the Nonwoven Polyester Geotextile. There were only slight changes in the properties of the geotextile during the course of the exposure, although there tended to be slight increases in breaking load and index puncture resistance, and slight decreases in apparent elongation at breaking load. There also appeared to be a slight increase in permittivity, but the increase is within experimental error. These results indicate that the nonwoven polyester geotextile is compatible

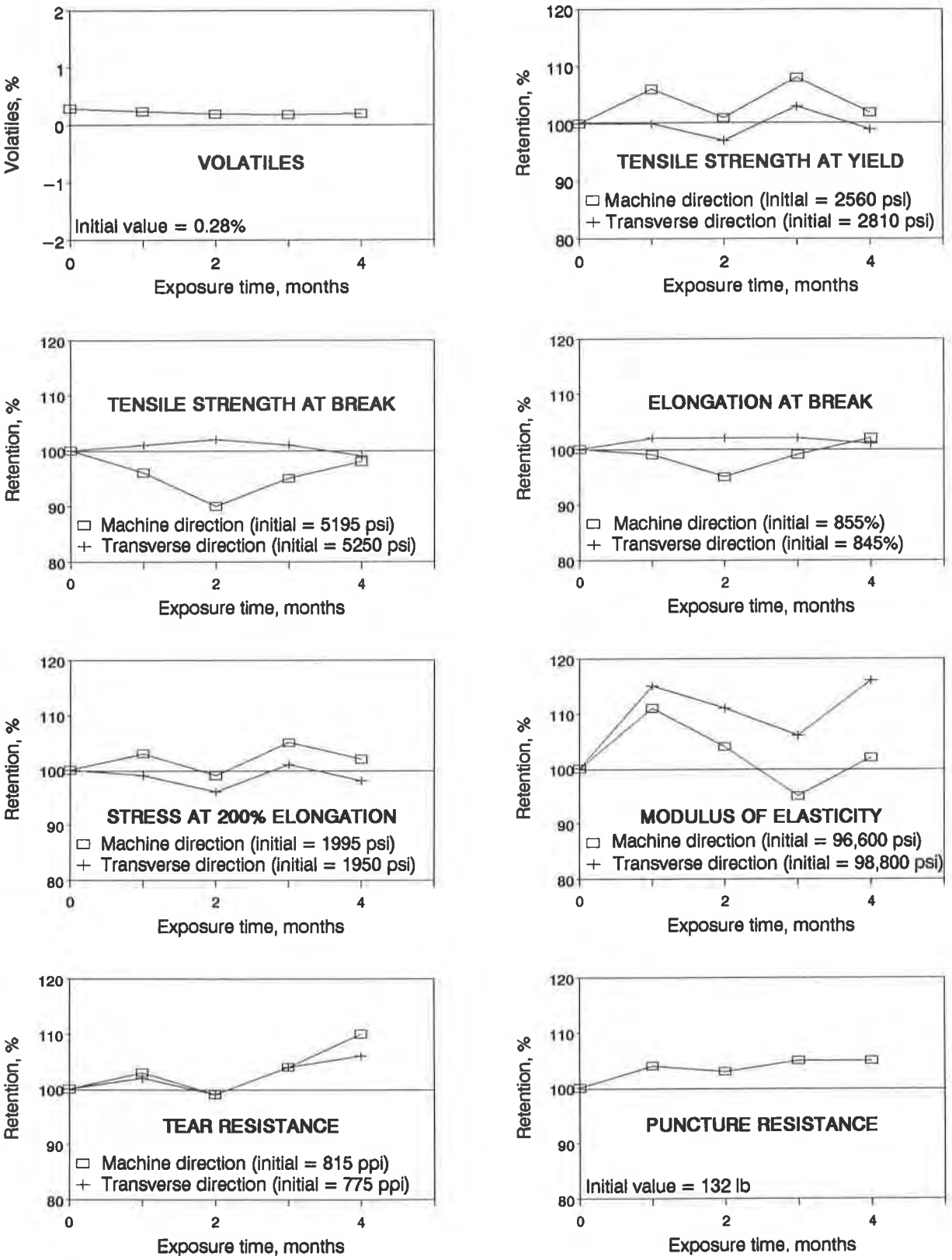

Figure 6. Change in selected properties of a 60-mil HDPE geomembrane after immersion in MWC Ash Leachate No. 2 at 50°C.

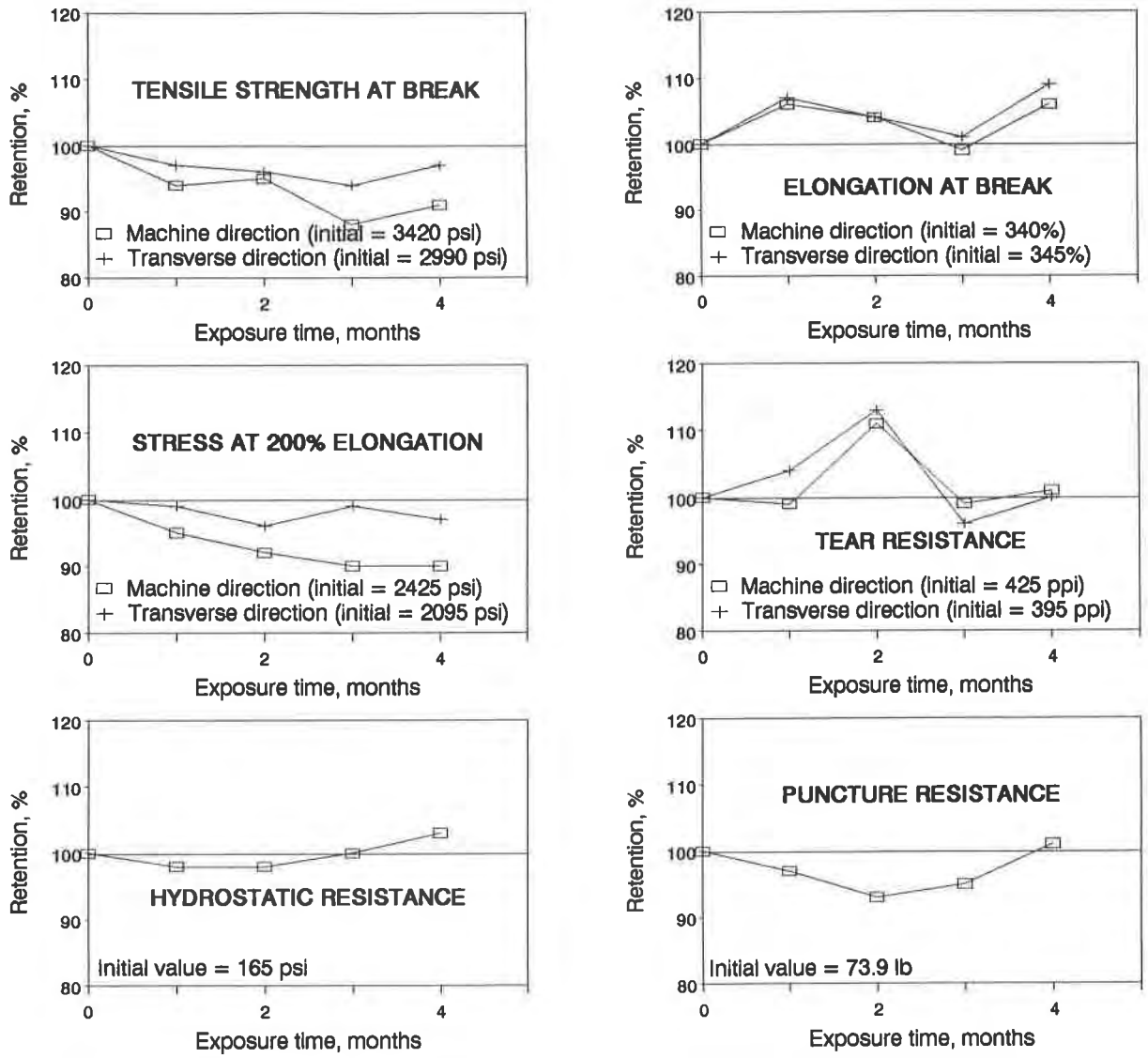

Figure 7. Change in selected properties of a 40-mil PVC geomembrane after immersion in MWC Ash Leachate No. 1 at 23°C.

with the two MWC ash leachates, which have pHs of 7.0 to 8.0. The results of testing the samples immersed in MWC Ash Leachate No. 2 at 50°C are summarized in Figure 10.

CONCLUSIONS

The results of the EPA Method 9090 compatibility tests indicate that, within the four months of exposure required by the method, exposure to the two MWC ash leachates caused only comparatively small changes in the analytical and physical properties of all four materials. These results also indicate that the four-month exposure period may not be long enough to establish long-term compatibility. Both the HDPE geomembrane and the polyester geotextile were not significantly affected by the immersion and thus are compatible with the two MWC ash leachates to which they were exposed. The CSPE-I geomembrane showed essentially no change in strength characteristics; however, the analytical properties which relate to the CSPE coating showed slight increases in volatiles and weight and a decrease in extractables. The values for all three of these properties were continuing to change at the end of the four months of exposure. Also, there was a slight trend downwards in ply adhesion between the top and bottom layers

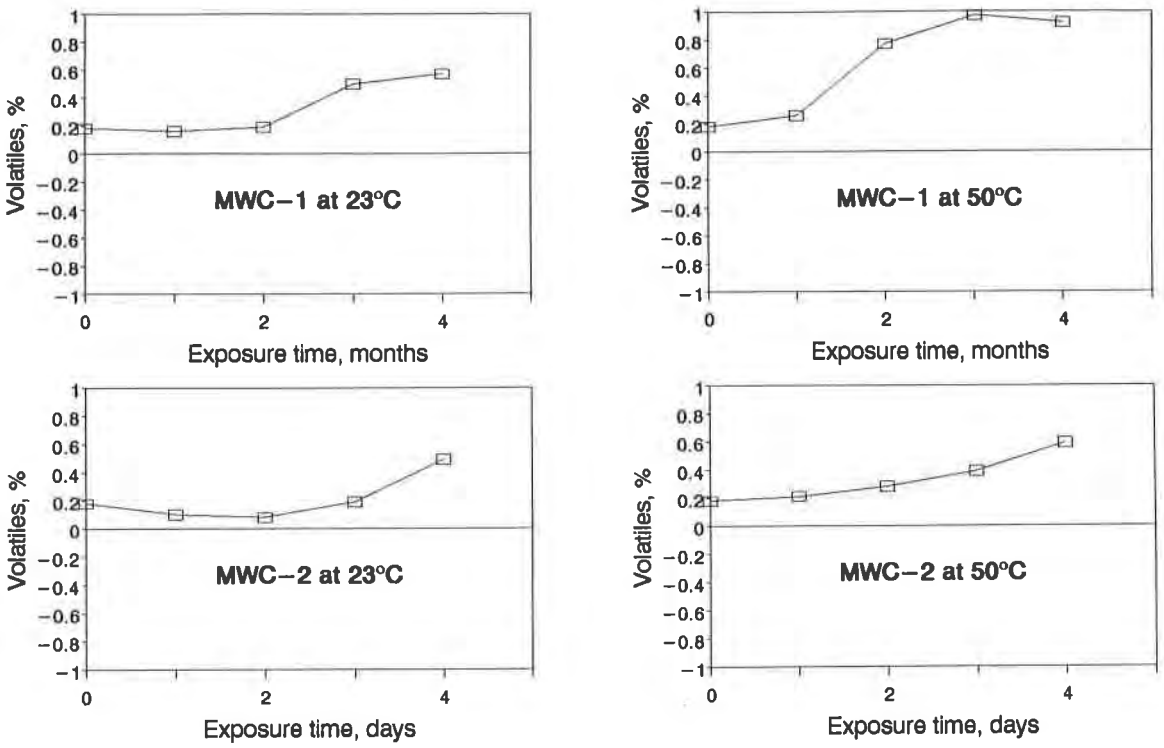

Figure 8. Volatiles of 40-mil PVC geomembrane samples immersed in MWC ash leachates. Value for the unexposed membrane is 0.18%.

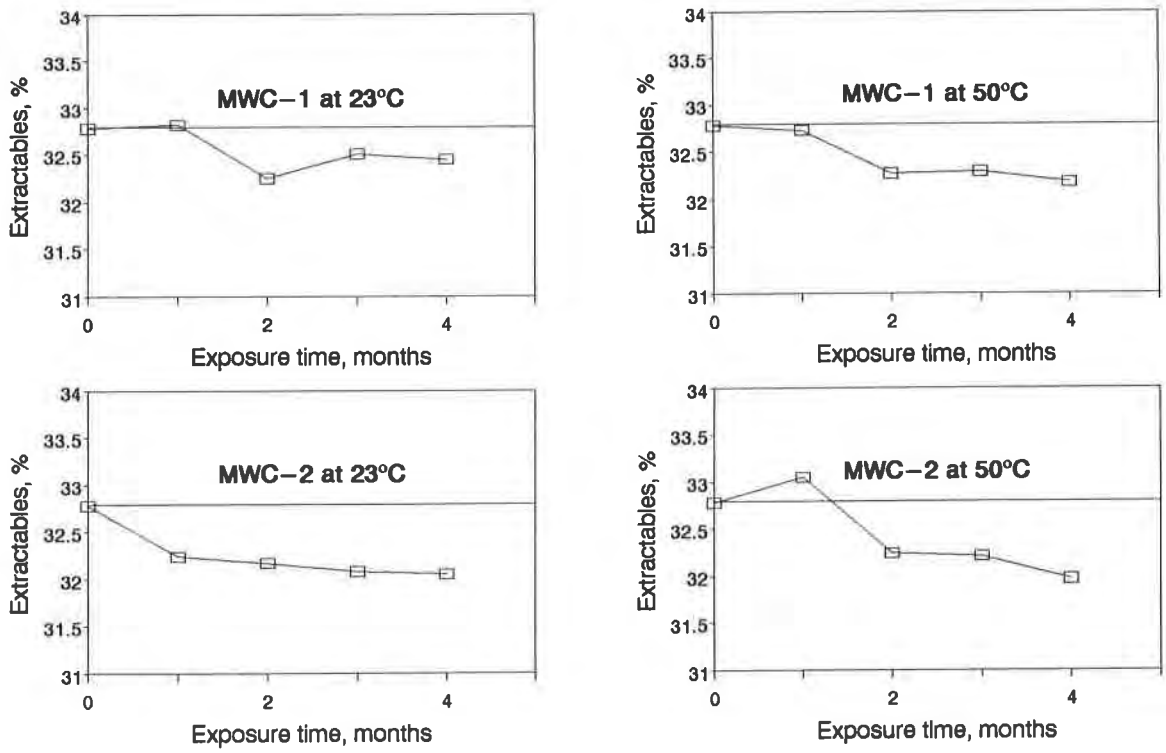

Figure 9. Extractables of 40-mil PVC geomembrane samples immersed in MWC ash leachates. Value for the unexposed membrane is 32.78%.

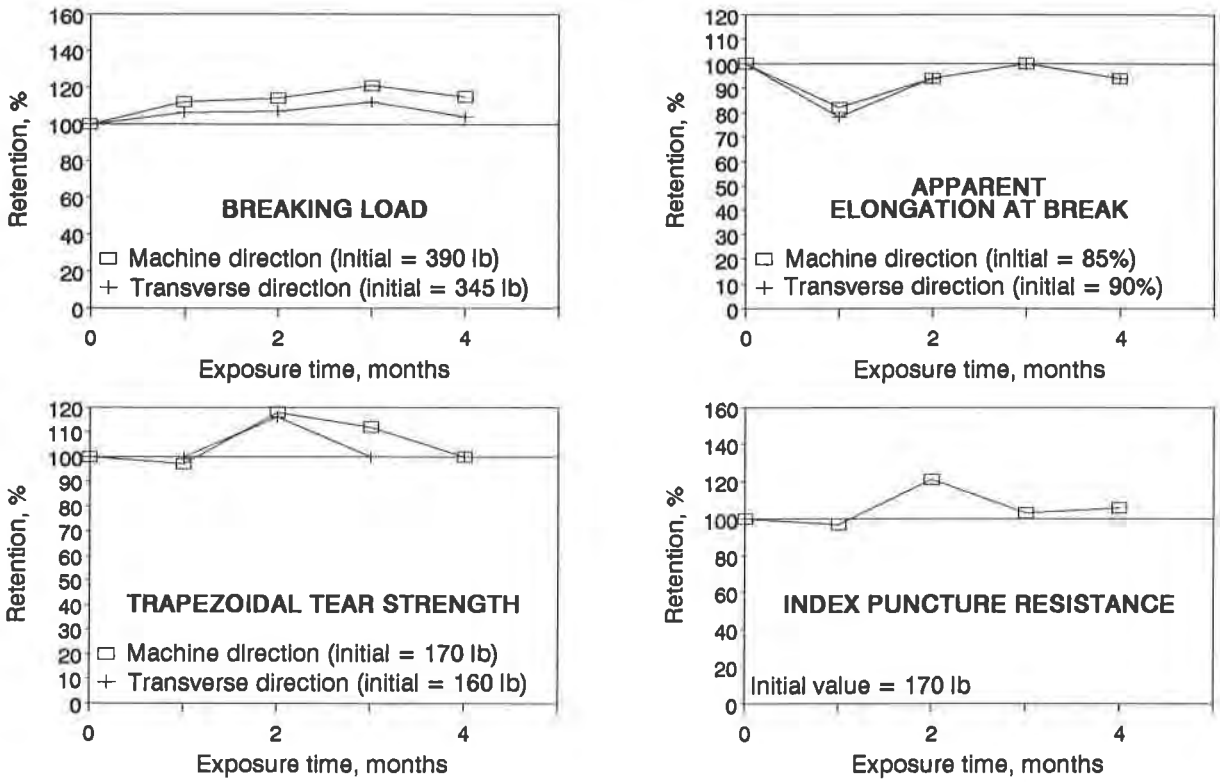

Figure 10. Change in selected properties of a nonwoven polyester geotextile after immersion in MWC Ash Leachate No. 2 at 50°C.

of CSPE. This decrease may reflect loss of adhesion to the fabric or some swelling and softening of the CSPE-I coating layer, which may affect seam strength. The four months of exposure resulted in little change in the analytical and physical properties of the PVC geomembrane, indicating short-term compatibility. However, the volatiles tended to increase with exposure time and the extractables tended to decrease, and during the last two months of exposure the PVC showed some trends towards stiffening which could indicate long-term incompatibility. To determine whether the trends would continue on prolonged exposure, a fifth PVC slab sample is continuing in immersion in the two leachates and will be tested at a later date after more than two years of immersion.

ACKNOWLEDGMENTS

The work presented in this paper was performed under a subcontract to International Technology, Subcontract No. 1044-91 to EPA Contract No. 68-C9-0036. The authors would like to gratefully acknowledge the support of the Project Manager for International Technology, Thomas A. Janszen, and the Project Officer for the EPA, David Carson.

REFERENCES

EPA, (1986) "Method 9090: Compatibility Test for Wastes and Membrane Liners", Test Methods for Evaluating Solid Waste, Vol. 1A: Laboratory Manual, Physical/Chemical Methods, 3rd ed., SW-846, U.S. Environmental Protection Agency, Washington, D.C.

EPA, (1989) "Supplementary Guidance in Geosynthetic/Leachate Chemical Resistance Testing", an internal memo to the Hazardous Waste Management Division Directors, Regions I-X, dated September 21, 1989.

Durability and Aging Study of Two Chlorosulfonated Scrim Reinforced Geomembranes

Y.G. Hsuan
Geosynthetic Research Institute, Drexel University, USA

R.M. Koerner
Geosynthetic Research Institute, Drexel University, USA

T.Y. Soong
Geosynthetic Research Institute, Drexel University, USA

ABSTRACT

The geomembranes evaluated in this study were field retrieved from two different sites. Both sites are lined surface impoundments approximately 10 years old. Geomembrane "A" was covered by soil and water while Geomembrane "B" was exposed and partially contained paper mill sludge. Seven test coupons of Geomembrane "A" were retrieved at periods of 1, 2, 3, 4, 5, 7, and 10 years. In addition, a sample of the original geomembrane was archived and served as a reference material. For Geomembrane "B", test samples were exhumed from various exposure environments; including soil covered, sunlight exposure, and liquid covered, however the original geomembrane was not available.

The properties of the samples were evaluated using a number of mechanical, physical and chemical analyses. The results indicate that a greater degree of curing has occurred in the sunlight exposed geomembrane samples than those covered by soil and/or liquid. In addition, a slight softening effect has been observed in the liquid covered samples after 10 years. For the PET scrim yarns, hydrolytic reaction has been detected in the sunlight exposure samples. In spite of these subtile changes, both geomembranes continue to serve their intended barrier functions.

INTRODUCTION

The focus of this study is to evaluate the durability and aging behavior of two scrim reinforced chlorosulfonated polyethylene (CSPE-R) geomembranes. While the geomembranes are somehow similar to one another and both had 10 years of service life when sampled (both are still in service), there are some quite meaningful differences, in particular their exposure environments. Table 1 lists and counterpoints the differences between the two geomembranes which are designated as Geomembranes "A" and "B".

The retrieved samples were evaluated by a large array of mechanical, physical, and chemical test methods. The purposes of the study are to track the aging process for Geomembrane "A" and the effects of exposure conditions in Geomembrane "B".

Table 1. General characteristics of the two geomembranes evaluated in this study

Characteristics	Geomembrane "A"	Geomembrane "B"
Resin Type	CSPE and CPE blend	CSPE
Scrim Type	PET	PET
Installed	1980	1982
Sampling Time	1990	1991
Purpose	reservoir	surface impoundment
Liquid Contained	water	paper mill sludge
Covering	0.3 m (12 inch) soil	none (exposed)
Reference Material	archived sample	anchor trench sample
Samples for Evaluation	retrieved at various times: 1,2,3,4,5,7, and 10 years	retrieved at 10 years of service life but at 4 different locations

CROSS LINKING MECHANISMS IN CSPE POLYMER

The function of the two geomembranes under investigation is as a liquid barrier. The integrity of the geomembrane sheet is the primary concern with regard to the durability of the material. The functions of the scrim are to provid additional strength, reduce thermal effects, and improve the tear and puncture resistance of the geomembrane. With respect to the geomembrane sheet material, it is important to recognize the aging process of CSPE polymer; in particular the cross-linking mechanism.

As-produced CSPE geomembrane sheet is a rubbery thermoplastic material called an elastomer. It is a multicomponent compound consisting of polymer resin, filler, carbon black and stabilizers. The CSPE polymer resin is made from chlorinating branched (or linear) polyethylene with SO_2, as shown in Equation 1, (Rodriguez, 1989). The chlorine and sulfur content vary with the type of product. The typical range for sulfur is 1 to 1.5% and chlorine is from 25 to 35%, (Schoenbeck, 1988).

$$-CH_2- + Cl_2 + SO_2 \rightarrow -\underset{\displaystyle \underset{\displaystyle Cl}{|}SO_2}{\overset{|}{CH}}- + HCl \qquad (1)$$

The resulting chlorosulfonyl (SO_2Cl) groups in the polymer act as preferred cross-linking sites and there is about one site for 100-200 carbon atoms in the polymer chain. The cross-linking process, commonly called "curing", refers to the chemical reactions between chlorosulfonyl groups and metal oxide in the presence of moisture, as expressed in Equations (2) to (4), (Maynard and Johnson, 1963).

$$2\ RSO_2Cl + 2H_2O \rightarrow 2RSO_3H + 2HCl \qquad (2)$$

$$2\ HCl + MO \rightarrow MCl_2 + H_2O \qquad (3)$$

$$2\ RSO_3H + MO \rightarrow (RSO_3)_2M + H_2O \qquad (4)$$

In addition to the above described sulfur bearing vulcanization, cross-linking can occur in the branch points of the polymer (i.e. chlorine atoms at tertiary carbon atoms), as described by Smith, 1966. The metal oxides play a dual role in the curing of chlorosulfonated polyethylene since they act both as acid acceptors [Equation (3)], and as crosslinking agents [Equation (4)]. The most widely used metal oxides in CSPE geomembrane are either lead oxide for industrial grade sheet or magnesium oxide for potable water grade sheet. The amount of water present in commercial polymers and fillers is sufficient to start the cycle of curing reactions, since water is also produced by the reaction shown in Equation (3).

Over time, curing takes place and the polymer gradually changes from a thermoplastic into a thermoset material. Subsequently, the chemical resistance of the material increases as well as its stiffness. Other properties change in a related manner.

LOCATIONS AND AGES OF FIELD RETRIEVED SAMPLES

Geomembrane "A". This geomembrane is currently being used as a water reservoir liner by the U.S. Bureau of Reclamation. The site is situated in Colorado and it was constructed in 1980. Test coupons were placed on the bottom of the reservoir during construction. The geomembrane was covered with approximately 30 cm (12 inch) of soil, thus the samples are exposed to water but not the atmosphere, per se. Test coupons were retrieved after 1, 2, 3, 4, 5, 7, and 10 years. As a result of excellent foresight, a sample of the original geomembrane was archived as a reference material.

Geomembrane "B". This geomembrane is currently being used as a surface impoundment liner and was installed approximately 10 years ago. The site is situated in the north central part of the United States. The facility stores liquid waste generated from manufacturing paper. Test samples were taken from four different locations on the northerly exposure side slope. Sample S-1, which was located in the anchor trench, was never exposed to either sunlight or liquid during the entire service period. Hence the properties of Sample S-1 will be considered as the base reference liner in comparison with the others. While it did not have direct exposure, it did have burial aging over the 10 years, hence it probably has some modified properties from the original material but to an unknown degree. Sample S-2 was located at the upper portion of the side slope and was constantly exposed to the surrounding ambient environment, but never to the liquid waste. Sample S-3 was located within the liquid fluctuating zone which was exposed to the waste liquid periodically. When not covered by the liquid, it was exposed to the same environment as Sample S-2. Finally, Sample S-4 was located at the toe of the slope which was always covered by the waste liquid.

TEST MATERIALS

Both Geomembranes "A" and "B" are scrim reinforcement geomembranes which are a 3-ply material consisting of two 0.38 mm (15 mil) thick geomembrane sheets on the top and bottom surfaces, with a woven fabric scrim between them. The total thickness of the composite geomembranes are each 0.90 mm (36 mil). For the geomembrane sheet materials, the polymer resin in Geomembrane "A" was made from blending approximately 51% chlorinated polyethylene (CPE) with 49% CSPE resins. Hence it contains less sulfur cross-linking sites than the pure CSPE polymer. The predominant curing mechanisms would be the branch points cross-linking. However,

for simplification, the geomembrane will still be referred as CSPE in the paper. The polymer resin in Geomembrane "B" was made from 100% CSPE. The scrim of both of the laminated composite geomembranes was made from polyethylene terephthalate (PET) yarns.

For the purpose of the analysis, it was sometimes necessary to separate the geomembrane sheets from one another and from the fabric scrim. This results in three groups of materials for each geomembrane sample: upper and lower geomembrane sheets and the woven scrim. In the case of Geomembrane "B", it is very important to identify the upper and lower geomembranes since the upper geomembrane was the layer always facing either sunlight or liquid, and the lower geomembrane was the layer always facing the subgrade soil.

MECHANICAL TEST PROCEDURES AND RESULTS

The changes in the macroscopic behavior of the various materials were evaluated using conventional tensile tests. Tests were performed on three groups of materials: complete scrim reinforced chlorosulfonated polyethylene CSPE-R composite geomembranes, separated CSPE geomembrane sheets, and removed PET yarns.

Test Procedures. The CSPE-R composite geomembranes were tested using 25 mm (1") wide by 100 mm (4") long strip specimens. The gage length was 50 mm (2") and strain rate was 8 mm/sec (20 inch/min.). The evaluation of CSPE sheets were using 6 mm (0.25") wide and 100 mm (4") long test specimens. The gage length was 4 mm (1.5") and strain rate was at 6 mm/sec (15 inch/min.). For the reinforcing scrim yarns, only warp direction yarns were tested. The tensile tests were performed using a gage length of 50 mm (2") and a strain rate of 0.8 mm/sec (2 inch/min).

Test Results. The results of the mechanical tests are summarized in two groups based on the type of geomembranes. Three tests were performed in each sample and the average values reported.

1. Geomembrane "A". - The original(0 year), 3 year, 7 year, and 10 year old samples were tested. The average test result values and coefficient of variation are shown in Table 2. A typical load/elongation curve of the composite geomembrane can be seen in Figure 1. The first peak at high load and low elongation corresponds to the breakage of the PET scrim yarns. After that the geomembrane sheets carry the load until failure.
   The CSPE-R composite geomembrane samples show no noticeable changes in the properties until 10 years at which time a slight increase in elongation is observed in the 1st peak and at breakage.

   For the geomembrane sheet materials, the elongation also increases in the 10 year old sample, consistent with the CSPE-R results. The breaking load has not changed, but the load at 200% elongation decreases noticeably.

   Regarding the PET reinforcing scrim yarns, the elongation increases in the 10 year old sample as did the composite material. This suggests that there may be some shrinkage occurring in the PET yarns. On the other hand, the strength of the PET yarns remain constant throughout the 10 years of service. This is not consistent with the results obtained by Morrison and Gray (1991) who found a 20% drop in grab breaking strength and burst resistance.

Table 2. Tensile test results of Geomembrane "A"

Age (years)	CSPE-R Geomembrane				CSPE Sheet			PET Yarn		
	1st peak load (KN)	1st peak elong. (%)	break load (KN)	break elong. (%)	break load ($KN \times 10^{-2}$)	break elong. (%)	load @ 200% elong. ($KN \times 10^{-3}$)	break load ($KN \times 10^{-2}$)	break elong. (%)	load @ 5% elong. ($KN \times 10^{-2}$)
0	0.80	28	0.22	600	2.7	773	9.3	7.6	26	1.1
	(6%)	(4%)	(1%)	(4%)	(1%)	(7%)	(7%)	(5%)	(8%)	(8%)
3	0.80	26	0.22	591	3.6	733	9.8	8.0	24	1.7
	(4%)	(7%)	(2%)	(7%)	(4%)	(1%)	(2%)	(4%)	(8%)	(4%)
7	0.83	29	0.22	571	3.6	737	10.2	7.6	26	1.7
	(6%)	(7%)	(2%)	(6%)	(2%)	(2%)	(0%)	(8%)	(7%)	(5%)
10	0.89	32	0.21	665	3.1	947	6.7	8.5	34	1.2
	(8%)	(8%)	(2%)	(4%)	(1%)	(2%)	(4%)	(3%)	(3%)	(4%)

Note : The percentage value within the parentheses is the coefficient of variation value of three tests

Table 3. Tensile test results of Geomembrane "B"

Sample	CSPE-R Geomembrane				CSPE Sheet						PET Yarn		
	1 peak load (KN)	1 peak elong. (%)	break load (KN)	break elong. (%)	break load ($KN \times 10^{-2}$)		break elong. (%)		load at 100% elong. ($KN \times 10^{-2}$)		break load ($KN \times 10^{-2}$)	break elong. (%)	load @ 5% elong. ($KN \times 10^{-3}$)
S-1	0.22	45	0.32	235	4.0		293		1.8		2.7	28	9.8
	(5%)	(0%)	(2%)	(4%)	(10%)		(10%)		(6%)		(2%)	(10%)	(3%)
S-2	0.24	42	0.36	180	4.9(U)	4.0(L)	204(U)	207(L)	2.5(U)	2.2(L)	2.7	27	4.0
	(2%)	(7%)	(2%)	(6%)	(8%)	(2%)	(13%)	(3%)	(1%)	(1%)	(1%)	(4%)	(6%)
S-3	0.21	38	0.37	220	5.3(U)	4.0(L)	284(U)	229(L)	2.0(U)	1.8(L)	2.7	28	4.9
	(2%)	(7%)	(1%)	(6%)	(3%)	(2%)	(3%)	(2%)	(3%)	(2%)	(1%)	(10%)	(0%)
S-4	0.18	40	0.29	210	3.6(U)	3.6(L)	256(U)	229(L)	1.6(U)	1.5(L)	2.2	35	7.6
	(5%)	(%%)	(2%)	(3%)	(5%)	(3%)	(6%)	(1%)	(2%)	(4%)	(1%)	(0%)	(0%)

Note: (U) = Upper geomembrane sheet, (L) = Lower geomembrane sheet
The percentage value within the parentheses is the coefficient of variation value of three tests

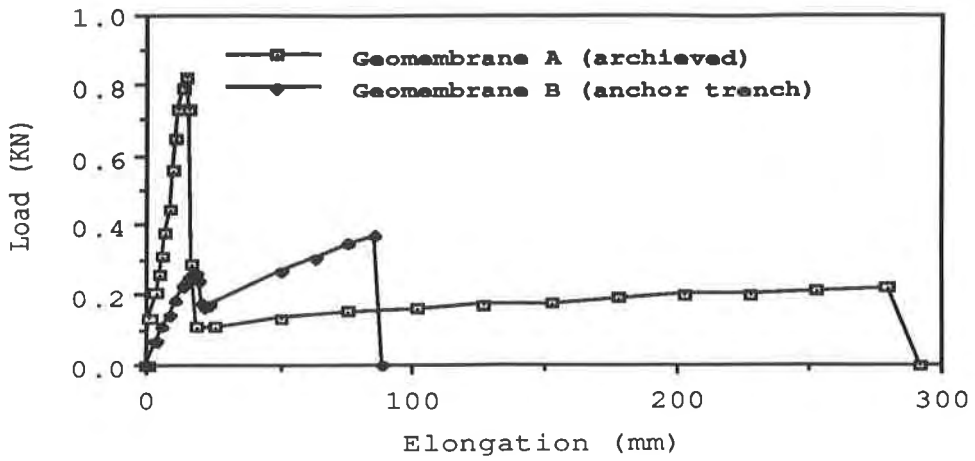

Figure 1. Typical load versus elongation curves of CSPE-R geomembrane composite materials

2. Geomembrane "B". - The average test result values and coefficient of variation are listed in Table 3. A typical load/elongation curve of CSPE-R composite geomembrane is displayed in Figure 1 so as to compare with that of Geomembrane "A". There is a noticeable difference between the two tensile curves. The breaking load of Geomembrane "B" is much higher then the load at first peak. This is opposite to the behavior of Geomembrane "A", and indicates that the scrim strength is less than the combined effect of the geomembrane sheets.

In the CSPE-R composite geomembranes, there is a slight increase in the breaking load of Samples S-2 and S-3. However, only Sample S-2 shows a drop in the breaking elongation. For Sample S-4, a small reduction in breaking load was measured.

For the properties of geomembrane sheets, the breaking strength of Samples S-2 and S-3 show an increase, consistent with the results of CSPE-R, but only Sample S-2 exhibits a drop in elongation. The gain in strength seems to be mainly contributed by the upper layer of geomembrane sheets, since the strength of lower geomembrane sheets show no change. Also the load at 100% elongation increases in both Samples S-2 and S-3. This appears to signify that cross linking probably has taken place in Samples S-2 and S-3, in particular in the upper geomembrane sheets. In Sample S-4, a slight reduction in strength is indicated.

Regarding the PET scrim yarns, there is no significant variation in the breaking strength and elongation of Samples S-2 and S-3 using Samples S-1 as the comparison. However, the loads at 5% elongation exhibit a large reduction. This may suggest some transition taking place in the PET yarns during the 10 years exposure. For Sample S-4, which covered by the waste liquid, the strength of the yarns decrease modestly as the elongation increases. This may indicate some shrinkage in the yarns.

ANALYTICAL TEST PROCEDURES AND RESULTS

The changes in the microscopic properties of the materials were evaluated using

a variety of analytical tests. The applicability of each test depends on the material. Some of the tests only can be applied to one type of material due to sample configuration, resolution of the results, or composition of the material.

CSPE Geomembrane Sheet. The evaluation of CSPE geomembrane sheet materials included density, mass per unit area, thermogravimetry (TG) and dynamic mechanical analysis (DMA). Three tests were repeated in each type of analyses for each sample and the average values are reported.

1. Density and Mass per Unit Area.- The density of geomembrane sheet material were evaluated using ASTM D 792 test method. The liquid used in this test was heptane, having a density of 0.684 g/cc. In addition, the weight of specimen in air was recorded for calculating the mass per unit area.

   Geomembrane "A". - All seven field exhumed samples together with the original archived sample were evaluated and the results are listed in Table 4. The mass per unit area of the geomembrane sheet gradually increases until the fifth year and then it declines slightly. The most noticeable change in density occurred during the first year. After that there is very little change as the material approached equilibrium.

   Geomembrane "B". - The mass per unit area and density of the geomembrane sheets were measured and their results are listed in Table 4. There is some reduction in the mass per unit area of upper geomembrane in Sample S-4. This may be part of reason for the reduction in its breaking load (see Table 3). On the other hand, density of upper and lower geomembrane sheets maintains almost the same.

Table 4. Average density and mass per unit area values of geomembrane sheets

Age (Years)	mass/unit area (g/m^2)	density (g/cc)	Samples	mass/unit area (g/m^2) Upper	mass/unit area (g/m^2) Lower	density (g/cc) Upper	density (g/cc) Lower
Geomembrane A			Geomembrane B				
0	280	1.48	S-1	570	-	1.30	-
1	320	1.50	S-2	570	510	1.31	1.33
2	340	1.50	S-3	600	520	1.30	1.31
3	340	1.50	S-4	460	550	1.29	1.29
4	350	1.50					
5	310	1.51					
7	330	1.50					
10	310	1.50					

2. Thermogravimetry (TG).- In order to assess the amount of different components in the material and their corresponding decomposition temperatures, the geomembrane sheets were analyzed by TG. Any reactions that induce a change of the mass can be detected and quantified. The test specimens were heated from 30°C to 650°C at a heating rate of 10 °C/min under a nitrogen atmosphere. Air was then introduced to oxidize the residue for determining the ash content.

   Geomembrane "A". - All eight samples were evaluated. The thermal curve of a typical CSPE sheet material is depicted in Figure 2. The graph is presented

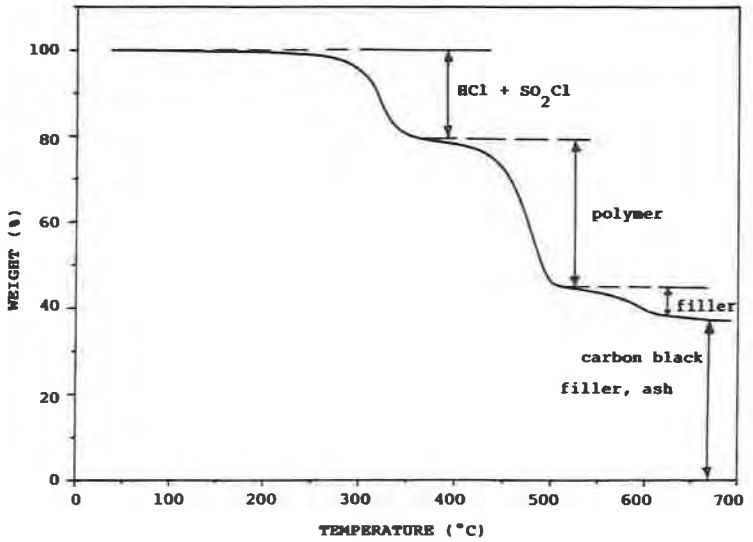

Fig. 2. TGA thermograph of Geomembrane "A" sheet material

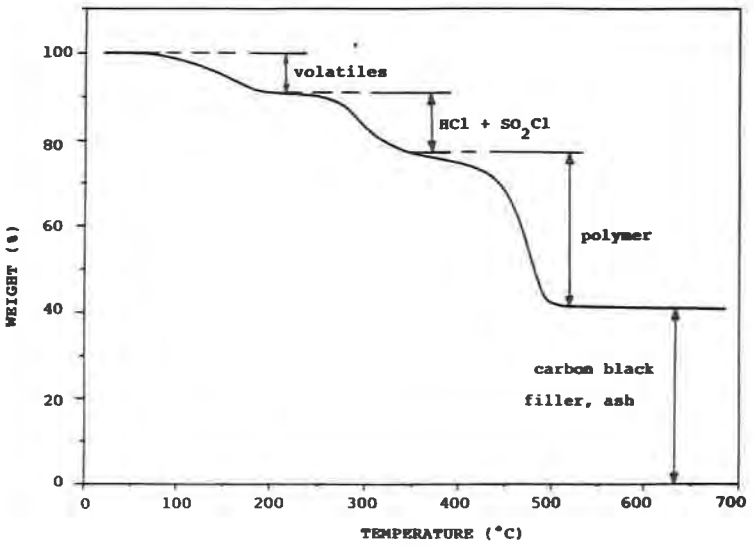

Fig. 3. TGA thermograph of Geomembrane "B" sheet material

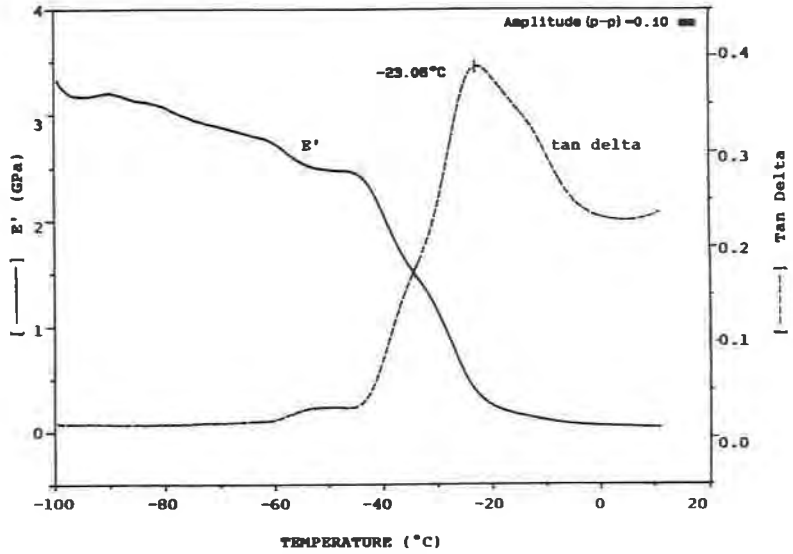

Fig. 4. DMA thermograph showing storage modulus (E') curve
tan delta curve

in weight percent plotted against temperature. There are four distinguishable groups of components. The components which decompose at the lowest temperature are predominantly HCl with small amount of SO_2Cl. The second component represents the polymer carbon chains, followed by a small amount of inorganic matter. Finally, carbon black and filler are obtained. Ash content is obtained after oxidation and is not shown on this thermal curve. The analysis results are tabulated in Table 5. There is no change either in decomposition temperatures and amount of each component during the 10 years of service. The amount of HCl in the polymer remains the same suggesting that curing probably has not yet taking place. In addition, there is no moisture detected in any of the samples. Thus the absorbed water probably was chemically bonded with one of the components. Calcium carbonate is a common type of filler and it reacts with water to form calcium hydroxide which has a dehydration temperature around 550°C, inducing a weight loss by losing water.

Table 5. TG results of geomembrane sheet in Geomembrane "A"

Age (years)	HCl + SO2Cl T(°C)	%	polymer T(°C)	%	filler T(°C)	%	C.B. + filler %	ash %
0	285	21	449	34	548	7	7	31
1	284	22	449	32	550	9	6	31
2	288	22	452	32	549	9	6	31
3	283	22	446	34	550	7	6	31
4	286	21	446	34	550	7	7	31
5	288	21	449	34	547	8	6	31
7	286	21	449	35	549	7	7	31
10	288	21	450	33	549	7	7	32

Note : C.B. = carbon black + carbonaceous polymer residue

Geomembrane "B".- The thermal curve of CSPE geomembrane sheet basically is similar to that of Geomembrane "A", but with an additional distinguishing groups of components. As shown in Figure 3, the additional component in the geomembrane is volatile matter which has a low decomposition temperature range from 60 to 90 °C. The analysis results are tabulated in Table 6. Sample S-1 has a higher volatile decomposition temperature and content than the others which were exposed to atmosphere or the waste liquid. This is expected since

Table 6. TG results of geomembrane sheet in Geomembrane "B"

Samples	volatiles T(°C)	%	HCl + SO2Cl T(°C)	%	polymer T(°C)	%	C.B. + filler %	ash %
S-1	91	8	268	15	448	37	37	4
S-2(U)	68	3	262	17	447	37	39	4
S-2(L)	63	2	265	16	449	39	39	3
S-3(U)	79	3	261	18	448	37	39	3
S-3(L)	73	3	255	17	447	37	39	3
S-4(U)	72	3	262	17	450	37	40	3
S-4(L)	67	3	255	17	447	37	37	3

Note : C.B. = carbon black + carbonaceous polymer residue, (U) = upper, (L) = lower

the volatiles could be either evaporated by heat or extracted by the liquid. Other than that, the data are fairly similar to one another regardless of the sampling locations.

3. Dynamic Mechanical Analysis (DMA).- CSPE is a highly amorphous material. Hence the glass transition temperature (T_g) can be detected without further sample treatment. T_g is a property which is sensitive to the degree of cross-linking. If cross-linking has taken place, the T_g value should increase, (Struik, 1978). The DMA apparatus used in this study is TA Instrument Model 983. The tests were performed at 1 Hz fixed frequency using 0.1 mm amplitude. The specimens were heated from -100 to 50°C at a heating rate of 4 °C/min. A typical DMA curve is shown in Figure 4 where "tan delta" and storage modulus (E') are plotted against temperature. The peak temperature of the tan delta curve corresponds to T_g of the specimen. As the tan delta increases, the storage modulus decreases due to transition of the material from glassy to rubbery.

Geomembrane "A". - Only the 0, 3, 5, 7, and 10 year old samples were tested. The resulted T_g values from the DMA curve are listed in Table 7. The T_g values are fairly consistent throughout the first seven years. Then it increases 6 degrees with the 10 year old sample. This is rather unexpected, since no sign of stiffening was indicated by the mechanical properties of the CSPE sheet materials. In contrast, the opposite behavior was observed as signified by the gain in elongation. It seems that the change in T_g is more likely due to variation of blending between CPE and CSPE rather than aging in material.

Geomembrane "B". - The T_g values of all four samples are also shown in Table 7. The values are almost identical for all samples, implying that cross-linking has not occurred in the polymer. This is contradicting the mechanical test results which indicate that some amount of cross linking has occurred in the upper sheet of Samples S-2 and S-3. Another explanation may be that the amount of cross linking present in those two samples is not sufficient to influence the overall T_g values of the geomembrane sheets.

Table 7. Glass transition temperature (T_g) determined by DMA

Age (years)	Tg (°C)	Sample	Tg (°C)	
Geomembrane A		Geomembrane B	(Upper)	(Lower)
0	-14	S-1	-25(2)*	-
3	-14	S-2	-24	-24
5	-13	S-3	-24	-24
7	-14	S-4	-25	-25
10	-8(1)*			

* Standard deviation of triplicate analyses

PET Scrim Yarns. The analytical techniques used to evaluate the properties of the removed PET yarns include mass per unit length, density, TGA, differential scanning calorimetry (DSC), and Fourier transform infrared (FTIR) spectrometry. Three

repeated tests were performed in each analytical technique for each sample and the average values are reported.

1. Density and Mass per Unit Length. - For these tests the procedures and conditions are same as those used for testing CSPE sheet materials.

Geomembrane "A". - All eight samples were evaluated with the average results shown in Table 8. The mass per length decreases after two years, but then it remains constant, except for the 5 year old sample. Also the density shows a noticeable increase after first year. It then remains constant.

Table 8. Average density and mass per unit length values of PET yarns

Age (years)	mass/unit length (g/m) x10^{-2}	density (g/cc)	samples	mass/unit length (g/m) x10^{-2}	density (g/cc)
Geomembrane A			Geomembrane B		
0	11.8	1.30	S-1	3.7	1.30
1	11.6	1.40	S-2	2.8	1.17
2	11.0	1.36	S-3	2.8	1.24
3	11.0	1.39	S-4	3.8	1.27
4	11.0	1.38			
5	11.4	1.37			
7	11.0	1.37			
10	11.1	1.37			

Geomembrane "B". - The average resulting values for the PET yarns can be seen in Table 8. There is large reduction in the unit weight of two exposed samples, Samples S-2 and S-3. Reduction of density can also be observed in the PET yarns of Samples S-2 and S-3, especially in Sample S-2.

2. Thermogravimetry (TG).- The test conditions for these tests are same as that used for investigating CSPE geomembrane sheets.

Geomembrane A. The typical thermal curve can be seen in Figure 5. The graph is presented in weight percent plotted against temperature. There are three different components in the material. The substances at the lowest temperature probably corresponds to some type of coating material on the yarn surfaces to improve the bonding between the yarns and geomembrane sheets. The subsequent decomposed material is PET polymer followed

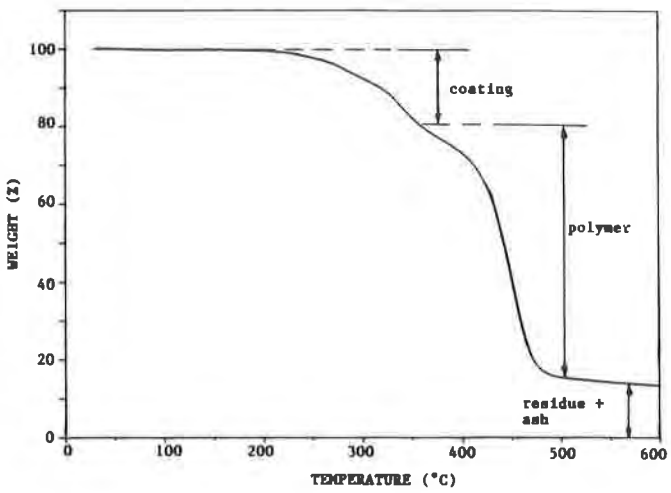

Fig. 5. TGA thermograph of PET yarns in Geomembrane "A"

by the carbonaceous polymer residue. Ash is obtain after oxidation and is not shown on the thermal curve. The average resulting data is listed in Table 9. The only meaningful change occurs in the coating material. The amount of the coating decreases approximately 40% after 2 years of service. After that, it stays essentially constant, except for the 5 year sample which has values similar to those of the one year sample. This is consistent to the mass per unit length measurements, and seems to suggest that part of the coating material has been dissolved away after two years of service. However, this assumes that the amount of coating is the same throughout all samples.

Table 9. TG results of PET yarns in Geomembrane "A"

Age	coating		polymer		residue	ash
(years)	T (°C)	%	T (°C)	%	%	%
0	284	23	427	62	14	1
1	281	20	428	64	15	2
2	292	13	428	70	15	1
3	299	13	428	71	15	2
4	301	13	429	70	15	1
5	285	19	428	65	15	1
7	295	14	429	69	16	1
10	292	14	429	70	16	1

Geomembrane "B". The large variation in the TG thermal curves of Geomembrane "B" depends on the location of the sample. Table 10 lists the analytical results of the tests. The covered samples, Samples S-1 and S-4 exhibit a thermal curve essentially the same as that of Geomembrane "A". In contrast, the exposed samples (Samples S-2 and S-3) result in a very different thermal curve, as seen in Figure 6. They contain small amounts of volatile matter. In addition, the polymer now consists of two components, Component "1" and "2", with different decomposition temperatures. This indicates that the PET yarns in Samples S-1 and S-3 have somewhat chemically reacted yielding two new components with decomposition temperatures different than the reference sample.

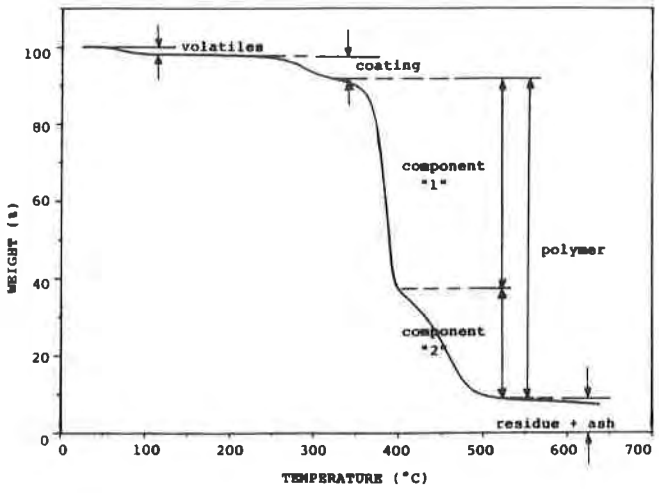

Fig. 6. TGA thermograph of PET yarns in Geomembrane "B"

Table 10. TG results of PET yarns in Geomembrane "B"

Samples	volatiles		coating		polymer component-1		polymer component-2		residue	ash
	T(°C)	%	T(°C)	%	T(°C)	%	T(°C)	%	%	%
S-1	-	-	309	15	418	68	-	-	16	1
S-2	41	3	266	4	383	58	434	28	5	1
S-3	39	6	263	6	372	52	434	29	7	3
S-4	-	-	307	30	417	53	-	-	16	1

3. Differential Scanning Calorimetry (DSC). - DSC was used to assess the melting, crystallization, and T_g of the PET polymers. The test specimens were heated from 20°C to 275°C at a heating rate of 20 °C/min under nitrogen atmosphere (i.e. first heating cycle) to obtain the melting temperature(T_m). After the specimens reached equilibrium at the upper temperature, they were quenched in liquid nitrogen to obtain as much amorphous phase as possible. Then the test was repeated on the quenched specimen, (i.e. the second heating cycle) in order to obtain T_g, crystallization temperature(T_c), and corresponding melting temperature.

Geomembrane "A". - All eight samples were evaluated and the results are shown in Table 11. There is no changes in any of the thermal properties through out the 10 years. This seems that the structure of the yarns remained the same.

Table 11. DSC results of PET scrim yarns in Geomembrane "A"

Age (years)	T_m - 1st cycle(°C)	T_g(°C)	T_c(°C)	T_m - 2nd cycle(°C)
0	241	61	126	237
1	241	68	132	236
2	243	64	126	236
3	240	65	128	235
4	243	69	132	238
5	244	63	126	235
7	241	66	129	237
10	242	64	125	236

Geomembrane "B". - In the first heating cycle, there is no substantial variation in the melting point values of all four samples, as shown in Table 12. However, the datum of the thermal curves in Samples S-2, S-3, and S-4 are no longer straight lines but now exhibit a broad endothermal peak. A more interesting finding occurs in the 2nd heating cycle. Sample S-1 shows similar properties as those in Geomembrane "A", i.e. a classic PET material. In contrast, the sunlight exposed samples, Samples S-2 and S-3 show very different thermal property values than S-1. The T_g , T_c and T_m all shift to lower values. Also the crystallization and melting peaks consist of a shoulder. These changes are somehow consistent with those observed in the TG results. The double melting peaks probably correspond to the new components, component "1" and "2", detected by the TG analysis. For Sample S-4, its

thermal curve is unexpectedly different compared to the Sample S-1, in spite of the similarity in their TG response. A sharp exothermal peak is observed at about 60°C followed by a extremely broad melting peak with onset temperature at around 150°C. One possible hypothesis may be that chemical reactions occurred during the first heating cycle.

Table 12. DSC results of PET scrim yarns in Geomembrane "B"

Sample	T_m - 1st cycle (°C)	T_g (°C)	T_c (°C)	T_m - 2nd cycle (°C)
S-1	250	65	128	242
S-2	251	-	72	212
S-3	250	-	84	184
S-4	247	-	57	153

4. Fourier Transform Infrared Spectrometer (FTIR). Both TG and DSC results indicate that the PET yarns in Samples S-2 and S-3 consist of two new components. FTIR was performed in order to analysis the chemical components of the PET yarns. Tests were performed using a Perkin-Elmer Model 1610 FTIR device. The diffuse reflectance technique was utilized so that the scrim samples could be examined directly. The number of scans was 264. Data was collected at wavenumbers ranging from 400 cm^{-1} to 4000 cm^{-1}. As an illustration of the type of data which is generated in a FTIR test, Figure 7(a) shows a FTIR spectrum of a PET yarn. It can be seen that the spectrum is very complicated, containing more than 10 peaks. However, the focus of the test was not on the identification of each of the peaks but to note any differences from one sample to another.

Geomembrane A.- All eight samples were scanned and their spectra show no changes.

Geomembrane B. - For Samples S-1 and S-4, their spectra are very similar and are the same as those obtained from Geomembrane A, a typical PET yarn. This signifies that no degradation has taken place in the yarns of either sample. For Samples S-2 and S-3, they produced very different spectra, as shown in Figure 7(b). The broad absorption region at 1100-1700 cm^{-1} and the aborption peak at 3325 cm^{-1} suggests that these two samples contain a high concentration of acidic group (—COOH) and hydroxide (—OH) end groups. This probably resulted from a reaction between PET and water (or moisture) yielding products with either —COOH or —OH end group. This reaction is called hydrolysis of PET and is expressed in Equation (5), (Risseeuw and Schmidt, 1990).

$$-[OC-C_6H_6-COOCH_2CH_2O-] + H_2O \rightarrow -OC-C_6H_6-COOH + HOCH_2CH_2O- \quad (5)$$

(PET) (water) (acid compound) (hydroxide compound)

The moisture came from the diffusion of surface water, creating a 100% relative humidity atmosphere around the PET scrim. Under sunlight exposure, the temperature of the black liner could reach 70°C which accelerated the rate of the hydrolysis, as observed by Mohammadian et al, 1991. Based on this analysis, the two new components in Samples S-2 and S-3 detected by TG and DSC may be the products of hydrolysis, acid and hydroxide compounds.

Temperature is one of the key acceleration factors for the hydrolytic reaction. At ambient temperature the rate of reaction is very slow. This is perhaps why hydrolysis was not observed in Sample S-4. The waste liquid maintained the temperature at ambient levels.

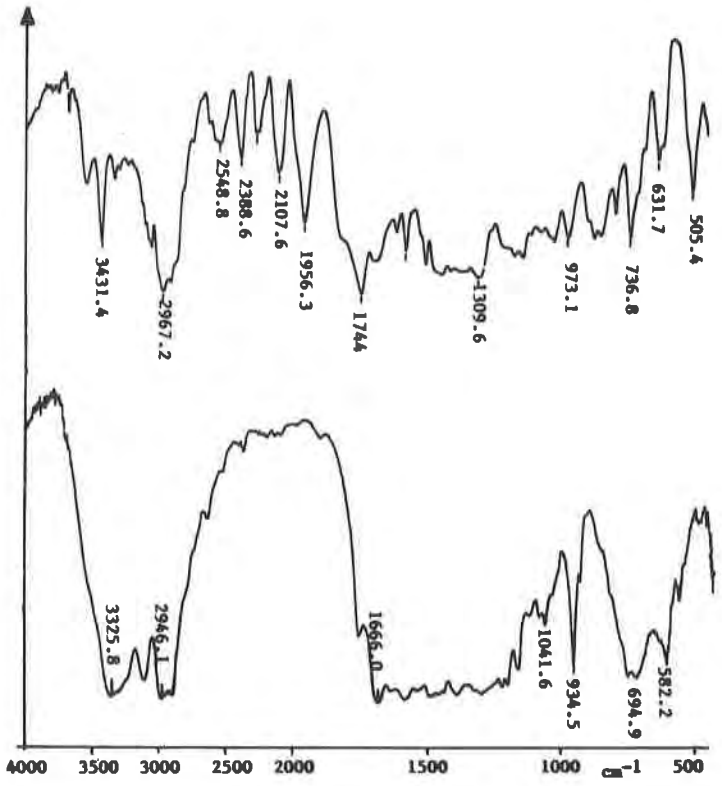

Fig. 7. FTIR spectra of PET yarns.
(a) original PET yarns
(b) Sample S-2

SUMMARY AND CONCLUSIONS

The property changes in two field retrieved CSPE reinforced geomembranes were monitored by mechanical, physical, and chemical analyses. The large amount of data resulting from the analysis presented in the paper is summarized in Table 13.

Regarding the properties of CSPE geomembrane sheets, there is no substantial change in the tensile properties of Geomembrane "A" after 10 years of service. This suggests that cross-linking probably has not yet begun or is proceeded very slowly during the 10 years period. On the other hand, for the sunlight exposed samples of Geomembrane "B", the breaking load and load at 100% elongation have slightly increased together with some decrease in elongation. This may signify that more cross-linking has taken place in the sunlight exposed materials (Sample S-2 and S-3) than the soil covered material (Sample S-1) but to a very slight amount. The overall glass transition temperature of the materials was not affected.

Thus it can be concluded that there are no significant changes in the sheet materials of either Geomembrane "A" or Geomembrane "B", other than the slight amount of stiffening being detected in the sunlight exposed surface layer.

Table 13. The summary of entire test results

Test Methods	Geomembrane "A"	Geomembrane "B"
Tensile Test		
• CSPE-R	slight increase elongation in 10 year old sample	increase breakage load in S-2, S-3 decrease break elongation in S-2
• CSPE	increase breaking elongation & decrease load at 200% elongation in 10 year old sample	increase load in upper sheet of S-2,S-3 decrease elongation in S-2 slight decrease load in S-4
• PET	increase breaking elongation in 10 year old sample	increase breaking elongation in S-4 decrease load at 5% elongation in S-2, S-3
Physical Properties		
• CSPE	increase in mass/unit area density increase after 1 year	Upper S-4 decrease in mass/unit area no change in density
• PET	mass/unit length decrease after 2 years density increase after 1 year	decrease mass/unit length in S-2, S-3 decrease density in S-2 and S-3
Chemical Analysis		
TG		
• CSPE	no change	no change
• PET	decrease coating after 2 years	S-2, S-3 contain volatiles and reveal two new components
DMA		
•CSPE	T_g decrease in 10 year old sample	no change
DSC		
• PET	no change	S-2,S-3 contain double melting peaks
FTIR		
• PET	no change	—COOH and —OH end groups formed in S-2,S-3

For the PET scrim yarns, there is no change in Geomembrane "A" throughout the 10 years of service. In Geomembrane "B", the covered Samples S-1 and S-4, maintained their tensile and chemical properties after 10 years service. However, noticeable change has occurred in the atmosphere exposed Samples S-2 and S-3. The thermal analyses, TG and DSC, clearly indentified the existence of two new components. The analysis of FTIR suggests that they are acidic and hydroxide compounds which are products of PET hydrolysis. In contrast, the only change in tensile properties is the load at 5% elongation. It seems that thermal and chemical analyses may be more sensitive to monitor the changes of PET due to hydrolysis.

The above noted changes in the PET scrim yarns should not have a large impact on the performance of "Geomembrane B". This is because the design function of the geomembrane is containing liquid and would not be challenged directly by the changes of the scrim after its installation.

ACKNOWLEDGEMENTS

The funding for this study was provided by the Geosynthetic Research Institute consortium of member organizations. Our sincere appreciation is extended.

REFERENCES

Maynard, J.T., and Johnson, P.R., (1963) "Crosslinking Chlorosulfonated Polyethylenes", Rubber Chem. Technol., No. 36, PP. 963-974.

Mohammadian, M., Allen, N.S., and Edge, M., (1991), "Environmental Degradation of Poly(ethylene Terephthalate)", Textile Res. J., 61 (11), pp. 690-696.

Morrison. W.R., and Gray, E.W., Jr., (1991), "Performance of Mount Elbert Forebay Reservoir Flexible Membrane Lining after 10 Years of Service", Geosynthetics'91 Conference, Altanta, USA.

Risseeuw, P., and Schmidt, H.M., (1990) "Hydrolysis of HT Polyester Yarns in Water at Moderate Temperatures", Proceedings of the 4th International Conference on Geotextiles, Geomembranes, and Related Products, The Hague, pp. 691-696.

Rodriguez, F., (1989), Principles of Polymer Systems, 3rd Edition, Hemisphere Publishing Co., New York.

Schoenbeck, M., (1988), "Performance of Chlorosulfonated Polyethylene Geomembranes after Long Term Weathering Exposure", 2nd. GRI Seminar on Durability and Aging of Geosynthetics, Ed. by Koerner, R.M., Elsevier Scientific Publishing Co., New York, pp 136-151.

Smith, D.A., (1966), "Characterization of the Thermal Decompositon of Chlorosulfonated Polyethylenes by Thermal Analysis", Polymer Letters, Vol. 4, PP 215-221.

Struik, L.C.E., (1978), Physical Aging in Amorphous Polymers and Other Materials, Elsevier Scientific Publishing Co., New York.

Oil-Resistant PVC Geomembrane Chemical Compatibility for Residual Waste

F.X. Taylor
Palco Linings Inc., USA

J.C. Hutwelker
American Resource Consultants Inc., USA

ABSTRACT

This paper documents an extensive geomembrane chemical compatibility program developed to evaluate an oil-resistant grade of PVC geomembrane for use in a Pennsylvania landfill accepting both municipal and residual industrial wastes.

Testing was performed in accordance with United States Environmental Protection Agency (US EPA) Method 9090 procedures. A unique feature of the test was the creation of a "spiked" leachate to be used in the immersion test. The spiked leachate was the product of an extensive evaluation by the landfill engineer of historical and potential future leachate constituents and was developed to provide a "worst case" simulation for the test. The landfill engineer worked with the Pennsylvania Department of Environmental Resources (PA DER) in developing the leachate for the test. Results from the tests would then be used to aid in the evaluation of future residual wastestreams proposed for acceptance at the landfill.

BACKGROUND

Grand Central Sanitary Landfill, Inc. (GCSL) is a municipal landfill that operates under Pennsylvania Department of Environmental Resources (PA DER) regulations which include specific requirements for geomembranes. The landfill is located in Plainfield Township in northeastern Pennsylvania. GCSL was one of the first landfills in the Commonwealth of Pennsylvania to use a geomembrane. A total of seven lined areas have been built at GCSL since the first geomembrane was installed in 1984.

GCSL accepts a wastestream that is comprised of approximately 65% municipal or household waste and 35% residual industrial waste that is classified as nonhazardous. The landfill liner system is of double geomembrane design and includes a primary and secondary leachate collection system above each layer of geomembrane. The PA DER regulations require that the geomembrane be compatible with the waste and leachate that is to be contained. Compatibility is usually determined by performing a Method 9090 immersion test with leachate from the site. Individual residual wastestreams must be examined and approved by the PA DER on a case by case basis to determine compatibility through a permitting process known as a Module One permit. The timely review and approval of these applications is important to the landfill owner and to the generator of the residual waste.

The compatibility evaluation is normally based on laboratory test data detailing the chemical make-up and leaching characteristics of a particular waste. This evaluation is performed by the landfill engineer, geomembrane manufacturer and PA DER and may be somewhat subjective based on the availability of specific compatibility data and the difficulty in predicting the effect a single waste may have on the overall leachate generated by a facility. Consequently, getting all parties involved to eventually agree on a waste may be a lengthy process. Thus, the landfill engineer worked with the local PA DER office to develop a more objective approach to evaluating liner-leachate chemical compatibility and hopefully streamline the review and approval of future applications.

Although GCSL had successfully used a standard Polyvinyl Chloride (PVC) geomembrane in constructing the first four lined areas at the landfill, an oil-resistent PVC (OR-PVC) geomembrane was specified for the newly approved Northern Expansion facility. The reason for the change in geomembrane type was to take advantage of the greater range of chemical resistance afforded by the OR-PVC that would allow for the approval of residual waste applications for the acceptance of wastes containing hydrocarbons or other VOC's not considered compatible with standard grade PVC.

The PA DER had rejected applications on the basis of geomembrane chemical incompatibility in cases where the geomembrane manufacturer and other PA DER offices had deemed similar concentrations to be acceptable for standard PVC. The disparity that existed was based on fundamental differences in the evaluation of chemical compatibility. The PA DER office now responsible for reviewing waste at GCSL based their evaluation on general compatibility charts and the potential effect of any individual waste, or its leachate, on the geomembrane. The previous office and geomembrane manufacturer had taken the more realistic approach of looking first at the effect any individual waste may have had on the leachate as a whole, then at the resulting leachate's potential effect on the geomembrane. This latter method was supported by results from analytical testing performed on a waste and its leachate that would be submitted with the applications and on historical analytical data from leachate not being generated at the facility.

Proof of the dilution effect that the total landfill leachate has on any one wastestream was demonstrated by several 9090 immersion studies performed on PVC geomembranes with leachate taken directly from the leachate collection system at GCSL (Precision Laboratories, 1988). The leachate used in those studies contained numerous constituents that were considered by most published literature to be incompatible with PVC geomembranes, specifically aromatic and halogenated solvents. The PVC geomembrane performed successfully in the tests even though the leachate contained these potentially harmful constituents.

Despite the satisfactory results from the early 9090 tests and the demonstrated performance of the PVC liner system in both their older disposal areas as well as at other facilities (Taylor, 1991), GCSL opted to change to the OR-PVC geomembrane to expedite the review and approval of new residual wastes. Delays in the approval of an application by the PA DER or the outright rejection of an application meant lost revenue to GCSL and also created a disposal problem for the generator of the waste. The chemical resistance of the OR-PVC encompasses a wider range than that of the standard grade PVC. The OR-PVC manufacturer provided a chemical compatibility table to be used in evaluating new wastes (see Table 1). Accordingly, based on this change in liner materials, an application for disposal of petroleum contaminated soil, for instance, could theoretically be approved without delay by the PA DER.

Although the broader range of OR-PVC chemical resistance helped speed the review of some applications, it did not provide a sure method for the approval of all. Consequently, the landfill engineer and the PA DER decided that a more consistent method of determining Module acceptance could be provided by developing a list of selected chemical compounds and concentrations to be added to the existing GCSL leachate that would be used in the immersion tests. The spiking would encompass a range of constituents and concentrations that were in some cases beyond the allowable range given in the OR-PVC literature. Future Module applications could then be compared to this range of leachate constituents for approval based upon the successful performance of the geomembrane in the spiked 9090 test. The list of compounds in the leachate would provide greater detail than the more general list supplied by the geomembrane manufacturer (see Table 1.).

Table 1. Chemical Resistance of OR-PVC Geomembrane
(Adapted from Occidental Chemical Corp., 1990)

Maximum Solid Waste Values	
pH range	3-12
Cyanide	< 5000 mg/kg
Sulfides	< 5000 mg/kg
Oil and Grease (Freon Extractable)	10%
Total Petroleum Hydrocarbons	10%
Volatile Organic Compounds	< 2000 mg/kg
Total Solids Content	Waste shall be non-flowable and not pass through a paint filter.
Maximum Leachate Values	
pH range	4-10
Arsenic	1000.0 mg/l
Barium	5000.0 mg/l
Cadmium	5000.0 mg/l
Chromium (total)	5000.0 mg/l
Cyanide	500.0 mg/l
Lead	500.0 mg/l
Mercury	500.0 mg/l
Selenium	500.0 mg/l
Silver	5000.0 mg/l
Nickel	< 25000.0 mg/l
Copper	< 25000.0 mg/l
Zinc	< 25000.0 mg/l
Fluoride	< 5000.0 mg/l
Ammonia	< 5000.0 mg/l
Phosphates	< 30000.0 mg/l
Chlorides	< 30000.0 mg/l
Sulfates	< 30000.0 mg/l
Phenolic Compounds	< 5000.0 mg/l
Oil and Grease (Freon Extractable)	< 20000.0 mg/l
Total Petroleum Hydrocarbons	< 20000.0 mg/l
Volatile Organic Compounds	< 2000.0 mg/l
Endrin	100.0 mg/l
Lindane	100.0 mg/l
Methoxychlor	100.0 mg/l
Toxaphene	100.0 mg/l
2,4 D	100.0 mg/l
2,4,5 - TP (Silvax)	100.0 mg/l

DEVELOPING THE SPIKE

The landfill engineer examined records of the facility's leachate analytical data for the period including July 1985 through July 1991. A compilation of the most frequently occurring organic compounds and their detected concentrations was then developed from this research. Various inorganic compounds contained in the leachate were not considered during this review since those compounds are known to have little or no adverse effect on the PVC geomembrane. For purposes of developing the worst case leachate, and to allow for possible increases in leachate strength at the facility over time, the maximum observed concentrations of the organic compounds were increased by a factor of at least ten and in some cases one hundred. This increase in the concentrations of compounds that were common to wastes frequently proposed for acceptance at the landfill would provide assurance that future requests for waste approvals could be approved.

Additional compounds that historically had not been detected in leachate from the facility were added to the list to allow for other wastes under consideration and also increases in the volumes of wastestreams currently being accepted at the facility. One source used to help identify these other potential compounds was the PA DER technical guidance document for National Pollutant Discharge Elimination System (NPDES) permitting of landfill leachate treatment plants. This document was developed by the PA DER Bureau of Water Quality and provides a list of constituents and concentrations to be used as a design basis for treatment plants being proposed at new landfills or facilities where site specific leachate data is not available.

Along with the list of constituents from the historical data, the NPDES additions produced a comprehensive list of worst case compounds that could potentially be found in the GCSL leachate. This list of compounds would then be "spiked" at the appropriate dosage into raw leachate taken from a leachate collection manhole at the landfill. In theory, this spiked leachate would contain VOC concentrations well in excess of those commonly found in a MSW leachate (Ham et. al. 1979). Considering current restrictions on waste acceptance at Pennsylvania municipal landfills, this would provide a comfortable factor of safety in the performance of compatibility testing for the facility. PA DER agreed (after much discussion) that this simulated leachate would be acceptable for assessing the chemical compatibility of wastes with the OR-PVC geomembrane. The final list of spiked and existing constituents would then be the basis for the evaluation of future Module applications.

TEST PROCEDURES

Immersion testing was performed by an independent laboratory. Samples of 0.762 mm (30 mil) OR-PVC and 1.27 mm (50 mil) OR-PVC were sent to the laboratory by the manufacturer. Samples were identified by roll number and lot number.

Raw leachate was collected from an existing GCSL leachate collection manhole and sealed in 208 liter (55 gallon) drums. A total of 18 drums was shipped to the laboratory for the testing. The raw leachate was analyzed for the analytes and properties listed in Table 2.

Table 2. Leachate Analysis

TEST METHOD	TEST DESCRIPTIONS/ANALYTES	RESULTS	DETECTION LIMITS	UNITS OF MEASURE
EPA 418.1	Total Petroleum Hydrocarbons	3.1	2	mg/L
EPA 150.1	pH	7.3	-	Std. Units
EPA 160.1	Total Dissolved Solids	6,600	-	mg/L
EPA 160.2	Total Suspended Solids	22	-	mg/L
EPA 413.2	Oil & Grease	9.0	2	mg/L
EPA 405.1	Biochemical Oxygen Demand	339	10	mg/L
EPA 410.4	Chemical Oxygen Demand	1090	10	mg/L
SM 407 A	Chloride	2070	1	mg/L
EPA 340.2	Fluoride	0.6	0.1	mg/L
EPA 350.2	Ammonium	634	0.1	mg/L
EPA 374.4	Sulfate	13	1	mg/L
	Total Organic Carbon	720	10	mg/L
EPA 120.1	Specific Conductance	11,400	10	µmhos/cm
206.2	Arsenic	0.01009	0.0005	mg/L
208.1	Barium	0.56	0.02	mg/L
213.1	Cadmium	0.016	0.008	mg/L
219.1	Cobalt	0.071	0.003	mg/L
236.1	Iron	4.01	0.03	mg/L
245.1	Mercury	0.0023	0.0003	mg/L
242.1	Magnesium	369	0.001	mg/L
200.7	Manganese	1.22	0.1	mg/L
270.3	Nickel	0.21	0.02	mg/L
200.7	Potassium	369	29	mg/L
272.1	Silver	0.016	0.005	mg/L
289.1	Zinc	0.079	0.005	mg/L
624	Volatile Organic Compounds, Various	24.00	3.0	µg/L

Exposure to the leachate was conducted in glass tanks. The leachate was constantly agitated by the use of an epoxy coated submersible pump. The OR-PVC samples were placed in the tank and suspended from quartz glass frames using polyethylene monofilament. Stainless steel weights were attached to the bottom of the geomembrane sheets to prevent their movement. The leachate was added to the tank along with the spiked compounds (see Table 3.). To prevent volatilization, headspace was minimized, allowing for expansion only. Glass lids were applied to the tanks with a silicone sealant to prevent the loss of volatile materials. The tanks were stored in rooms maintained at 23° C. and 50° C. with the leachate changed after each thirty day test period.

After each thirty day immersion period, the geomembrane sheets to be tested were removed from the leachate. The 50° C. sheets were allowed to cool to room temperature while covered with leachate. The sheets were then lightly rinsed with tap water and the excess water was then gently wiped from the surface using paper towels. The weights and dimensions were taken, then the test specimens cut. The sheets and test specimens were wrapped with aluminum foil in sealed plastic bags whenever not in use to minimize volatile and / or moisture loss.

Testing of physical properties was performed on unexposed samples of the geomembrane to provide a baseline for comparison of the immersed sample test results.

Table 3. 9090 Spiked Leachate Organic Compounds

Compound	Concentration, µg/l				
	Target Min.	30 day	60 day	90 day	120 day
Acetone	22,216	74,000	20,300	75,300	82,000
Methylene Chloride	14,000	23,600	21,400	35,800	45,800
Methyl Ethyl Ketone	200,000	720,000	352,000	308,000	302,000
Carbon Disulfide	2,500	5,000	*	*	*
Phenol (Total)	5,000	*	*	*	*
Toluene	1,800	2,100	400	2,000	4,500
Ethyl Benzene	1,760	*	*	1,250	2,000
1,1,1-Trichloroethane	1,500	31,500	400	*	3,750
Xylenes	840	1,650	*	1,000	2,750
Benzene	500	520	*	500	750
Carbon Tetrachloride	500	700	*	1,750	1,500
Chloroform	6,000	69,500	2,400	9,250	13,500
Chlorobenzene	100,000	69,600	26,500	103,000	168,000
1,2-Dichloroethane	500	650	*	*	*
Tetrachloroethylene	700	600	*	1,250	3,250
Trichloroethylene	500	420	*	388	750
Vinyl Chloride	200	*	*	*	*
Total	358,516	999,840	423,400	539,488	630,550

* Compound not detected or difficult to maintain detectable concentration.

Tensile properties were determined in accordance with ASTM D638 using Type IV dumbbell specimens and a strain rate of twenty inches per minute. Tear resistance was conducted in accordance with ASTM D1004, DIE C. Hardness was measured in accordance with ASTM D2240 using a Type A shore durometer. Puncture resistance was tested according to FTMS 101C, Method 2065. Hydrostatic resistance was tested in accordance with ASTM D751, Procedure 1. Volatile and extractable contents were determined in accordance with EPA 600 / 2-88 / 092, Appendices G and E respectively. Weight and dimension changes were determined in accordance with EPA Method 9090. Specific gravity was determined in accordance with ASTM D792, Method A.

Summaries of the immersion test results are presented in Tables 4 and 5.

Table 4. Material Property Summary, 0.762 mm (30 mil) PVC/OR Grade Liner

EXPOSURE TIME (DAYS)		0	30	60	90	120	% CHANGE 0 vs 120
		23 degrees C.					
Stress at 100%	MD	11.42	12.66	13.69	12.82	12.00	5.0
Elongation (MPa)	TD	10.51	11.20	11.64	11.44	10.92	3.0
Stress at Break (MPa)	MD	20.21	20.00	20.20	19.90	19.12	-5.4
	TD	22.00	20.00	21.70	21.27	21.00	-4.6
Strain at Break (percent)	MD	336	329	271	300	315	-6.2
	TD	506	451	481	474	493	-2.6
Tear Resistance (kN/m)	MD	70.35	59.15	72.28	67.55	58.28	-17.1
	TD	60.73	67.20	56.88	61.43	51.28	-15.5
Puncture Resistance Load (N)		249	209	200	214	200	-19.6
Hydrostatic Resistance (kPa)		923	930	958	909	882	-4.5
Hardness (Type A)		94	92	92	91	93	-1.1
		50 degrees C.					
Stress at 100%	MD	11.42	11.02	10.78	10.86	10.62	-7.0
Elongation (MPa)	TD	10.51	9.38	10.48	9.36	9.49	-9.8
Stress at Break (MPa)	MD	20.21	18.59	17.91	18.27	17.82	-11.82
	TD	21.97	19.14	20.33	19.33	19.81	-9.8
Strain at Break (percent)	MD	336	334	316	324	330	-1.8
	TD	506	455	471	480	501	-1.0
Tear Resistance (kN/m)	MD	70.35	59.15	61.78	47.60	53.38	-24.1
	TD	60.73	52.33	49.18	51.28	45.68	-24.8
Puncture Resistance Load (N)		249	227	196	227	254	1.8
Hydrostatic Resistance (kPa)		923	903	868	848	882	-4.5
Hardness (Type A)		94	92	92	92	92	-2.2

Table 5. Material Property Summary, 1.27 mm (50 mil) PVC/OR Grade Liner

EXPOSURE TIME (DAYS)		0	30	60	90	120	% CHANGE 0 vs 120
		23 degrees C.					
Stress at 100%	MD	11.07	11.34	12.44	11.86	11.91	7.6
Elongation (MPa)	TD	10.58	10.97	11.71	11.09	10.76	1.8
Stress at Break (MPa)	MD	21.97	20.23	22.25	21.66	21.11	-3.9
	TD	20.77	18.94	20.99	20.33	20.42	-5.0
Strain at Break (percent)	MD	507	437	460	468	461	-9.0
	TD	531	452	513	515	502	-5.5
Tear Resistance (kN/m)	MD	66.33	64.93	64.75	65.63	60.90	-8.2
	TD	61.08	59.85	57.40	61.95	55.83	-8.6
Puncture Resistance Load (N)		356	329	289	396	312	-12.5
Hydrostatic Resistance (kPa)		1530	1612	1578	1626	1654	8.1
Hardness (Type A)		94	93	91	91	93	-1.1

Table 5. Continued

EXPOSURE TIME (DAYS)		0	30	60	90	120	% CHANGE 0 vs 120
		50 degrees C.					
Stress at 100%	MD	11.07	10.47	11.11	10.22	10.29	-7.12
Elongation (MPa)	TD	10.58	9.96	10.75	10.03	9.93	-6.1
Stress at Break (MPa)	MD	21.97	19.80	21.73	20.02	20.58	-6.3
	TD	20.77	18.33	19.96	18.72	19.95	-3.9
Strain at Break (percent)	MD	507	454	499	462	494	-2.6
	TD	531	460	503	462	526	-0.9
Tear Resistance (kN/m)	MD	66.33	62.83	60.20	55.83	55.83	-15.8
	TD	61.08	57.40	54.93	51.80	53.20	-12.9
Puncture Resistance Load (N)		356	365	316	365	369	3.8
Hydrostatic Resistance (kPa)		1530	1502	1440	1481	1461	-4.5
Hardness (Type A)		94	93	91	90	91	-3.9

CONCLUSIONS / RECOMMENDATIONS

The OR-PVC liner performed well in the test. Values remained relatively unchanged over the 120 day test period for tensile strength at break, elongation at break, modulus at 100% and 200% elongation, hydrostatic resistance and hardness. The lack of change or absence of any significant trend in these values between the 30 day immersion periods indicates that the geomembrane was not affected by or was chemically resistant to the leachate. Although there was evidence of weight gain in some of the samples this may be considered typical of a polymerically plasticized PVC membrane immersed in an aqueous solution at elevated temperatures and is not necessarily evidence of a chemical reaction with the leachate. The apparent changes in tear resistance were attributed to anomalies in the testing since trends or changes in tear resistance should correlate directly with changes in modulus and tensile properties. As indicated by the test results, this was not the case. Changes in the membrane tensile properties were of a lesser magnitude and did not trend the same as the changes in tear resistance.

Throughout the development of this testing program and it's concomitant "worst case" leachate it was apparent that the difficulties in evaluating the suitability of a geomembrane for use in a Municipal / Residual Waste Landfill center not only on accurate chemical compatibility data but also on predicting the composition of the leachate to be generated over the life of a particular facility.

Although considerable work has been performed in the area of predicting MSW leachate quantity it remains difficult to predict its quality. This is due primarily to the variability of MSW and is especially true for landfills that accept a high percentage of residual wastes. For the moment, characterization of a leachate to be generated at a new facility is best accomplished by thoroughly evaluating historical data from similar facilities that are operating and accepting similar wastes. Unfortunately, reliable data is not easy to come by and due to the dynamic nature of landfilling regulations and techniques even recent data may become outdated quickly.

Considering the wide variation in published qualitative leachate data that was reviewed during the course of this project, it is no wonder that opinions differ when predicting leachate strength and constituents. One can hardly fault the

regulators for taking a conservative approach when evaluating the effects of individual wastestreams on a geomembrane. However, the authors feel that the development of a spiked leachate, with compounds and concentrations developed both from historical site-specific data and predicted future wastestream characteristics is a viable approach to obtaining a representative leachate to be used in compatibility testing of a membrane. As an ongoing check, future analytical data for a facility leachate should be compared with the leachate used in the test to determine whether further testing is necessary.

The successful performance of the OR-PVC membrane in a leachate containing compounds generally considered to be incompatible with PVC membranes demonstrates the need for additional research in the area of geomembrane chemical compatibility. Engineers and regulatory agencies continue to rely on outdated, generalized charts and tables developed over the years by the plastics industry. In most cases these charts were not even developed for geomembrane applications and may have been compiled from testing of resins or polymers bearing little resemblance to those used in the production of modern geomembranes. Due to the continuing evolution of polymers and advances in polymer chemistry they should be considered only as a starting point for assessing compatibility and be supplemented with up-to-date compatibility data or testing.

ACKNOWLEDGEMENTS

The authors would like to acknowledge Mr. Nolan Perin, of Grand Central Sanitary Landfill, Mr. Dave Lauwers of Occidental Chemical, Inc., and Mr. Larry Kamp of Palco Linings, Inc., for their support and assistance in the preparation of this paper.

REFERENCES

Ham, Robert, et al, University of Wisconsin Engineering Department. U.S.E.P.A. Report No. 600/2-79-109, "Background Study on the Development of a Standard Leaching Test", U.S.E.P.A., Cincinnati, Ohio, May 1979.

Landreich, R.E., "Flex - An Expert System to Assess Flexible Membrane Liner Materials", U.S.E.P.A., Geosynthetics '89 Conference Proceedings, San Diego, California, February, 1989.

Little, A.D. Inc., "Resistance of Flexible Membrane Liners to Chemicals and Wastes", U.S.E.P.A. Report PB86-119955, October, 1985.

Occidental Chemical Corp., "Chemical Resistance of Oxyflex OR Geomembrane", Oxychem, Pottstown, Pennsylvania, October, 1990.

Taylor, F.X., "Lycoming County Landfill Protected with Geomembrane", Geotechnical Fabrics Report, July, 1991.

U.S.E.P.A. Method 9090 Immersion Tests, October, 1988, May, 1989 and October, 1989, Precision Laboratories, Inc., Orange, California.

Geomembrane Protection by Nonwoven Geotextiles

E.S. Motan
SEC Donohue Inc., USA

L.S. Reed
National Seal Co., USA

C.M. Lundell
SEC Donahue Inc., USA

ABSTRACT

A testing program was initiated to develop a methodology to quantify the physical damage, from a subgrade of very angular particles, to unprotected and geotextile-protected HDPE geomembrane specimens. Both polypropylene and polyester non-woven geotextiles were used. Testing consisted of, 1. Pressurizing geotextile-protected and unprotected 60-mil smooth geomembrane specimens against a subgrade of AASHTO #57 gravel inside a pressure chamber and, 2. Subsequent multi-axial stress-strain testing of the same geomembrane specimens within a multi-axial pressure chamber. The test results suggested that during the first stage of testing, the permanent tensile strains induced in the geomembrane specimens affect the outcome of testing in the second stage.

INTRODUCTION

Current landfill liner system designs frequently require the use of geomembranes placed on a prepared subgrade or below a drainage or a protection soil layer. The grain-size distribution and the grain-shape characteristics of such layers may produce adverse conditions for the integrity of the geomembrane under certain circumstances. Where the potential for physical damage to the geomembrane exists from the adjacent layers of soil, a widely used practice to reduce this potential is to provide a cushion layer of non-woven geotextile between the geomembrane and the soil. Manufacturer's literature and rules of thumb are often used to establish the type and thickness of geotextile required for geomembrane protection.

As landfill design heights are increased in attempts to maximize the air space, the base liner systems are being placed under correspondingly larger normal pressures. Such pressures can be on the order of 15,000 to 20,000 lb/ft^2. The role of geosynthetics in the protection of geomembranes under such large pressures needs to be evaluated for a range of soil materials that typically comprise subgrade or drainage layers.

The purpose of this study was to assess the extent of physical damage in a geotextile-protected geomembrane subjected to typical landfill base-grade pressures. Under such pressures, even though geomembrane puncture is not necessarily induced, partial physical degradation of the geomembrane material may take place as a result of particle indentations and localized excessive deformations.

Previously, attempts have been made to evaluate HDPE geomembrane damage by modeling anticipated field conditions in a pressurized chamber, and monitoring for punctures. If puncturing did not occur, the geomembrane sample was visually observed for signs of damage. In some cases, uniaxial testing across dimples or other imperfections was attempted in an effort to quantify the damage. In this study, geomembrane samples that were pressurized against a bed of granular subgrade were later tested in a multiaxial stress test in an effort to quantify damage to the samples. It was anticipated that structural weakness in the geomembrane samples resulting during pressurizing against the subgrade would be more easily detected using this procedure.

This paper examines the effectiveness of three types of non-woven geotextiles in protecting a smooth 60-mil thick HDPE geomembrane. The geotextiles were placed between the geomembrane and a subgrade bed consisting of granular gravel size material with angular particles. The granular subgrade of gravel size particles was intentionally selected to subject the geotextile-geomembrane system to rather severe point-loading conditions without considerably deviating from the reality.

STANDARD METHODOLOGY TO EVALUATE GEOMEMBRANE PROTECTION

The ASTM Standard Test Methods D3786 (Mullen Burst Test) and D4833 (Index Puncture Resistance Test) have been utilized to establish an index of geotextile strength. When applied to geotextile-geomembrane combinations, the Index Puncture Resistance Test results could be used as an indicator of the protective capacity of the geotextile against puncture by small objects. Mullen Burst Test, on the other hand, could be useful in assessing the extent of geomembrane protection provided by geotextiles in the presence of loading distributed over a larger area.

The three-point puncture test (Frobel, et al., 1987; Hullings, 1990) used in evaluating the puncture resistance of geomembranes is a move toward establishing geomembrane performance criteria based on a more realistic modeling of soil-to-geomembrane contact irregularities. The height of truncated cones used to establish the geomembrane puncture resistance during the test can be varied by adjusting the thickness of the bed of subgrade soil around the cones. The three-point puncture test does provide a methodology for comparative evaluation of protection offered by different geotextiles. However, because of its standardized nature, it fails to provide a base of comparison in situations that can be site-specific with regard to the characteristics of the subgrade material.

MATERIAL CHARACTERISTICS

Geotextiles. Non-woven geotextiles of four different weights (8, 10, 12, and 16 oz/yd^2 nominal) of three different brands were utilized in the testing program. The generic descriptions of these geotextiles are presented below:

Type A Geotextile: Continuous-filament, polyester, non-woven needle-punched.

Type B Geotextile: Continuous-filament, polypropylene, non-woven, needle-punched.

Type C Geotextile: Staple, polypropylene, non-woven, needle-punched.

Geotextile weights and thicknesses reported in Table 1 are the average values determined by actual measurements on a minimum of three and a maximum of six samples of each geotextile type and weight used. Table 1 also presents the typical strength characteristics of these geotextiles on the product data sheets.

Subgrade Material. The subgrade utilized during the tests consisted of a layer of AASHTO #57 aggregate. Predominant particle size in the subgrade material ranges from 1/2" to 1". Crushed stone aggregate was used instead of rounded river bed material in order to present a more severe condition. Aggregate was mounted to a 1/4"-thick plywood base with epoxy resin so that no mobilization of the particles occurred between tests. This ensured that the subgrade conditions did not vary from one sample to another during the testing program.

TESTING PROCEDURE

The geomembrane protection test program was conducted at the National Seal Company Technical Center using a modified point-stress test device and a multi-axial pressure chamber (National Seal Company, 1992).

Laboratory program consisted of determining the multi-axial stress -strain characteristics of geomembrane specimens for the conditions listed below:

1. Virgin specimens not subjected to initial pressurizing against the subgrade (base-line tests),
2. Specimens subjected to pressurizing without geotextile protection, and
3. Specimens protected by geotextiles during initial pressurization.

Testing was performed in two stages as detailed below. For the virgin specimens Stage 1 was omitted.

Stage 1 - Application of hydrostatic pressure on the geomembrane. Subgrade was placed in the point stress device such that the plane of the base was even with the rim of the apparatus. A layer of geotextile

TABLE 1. GEOTEXTILE CHARACTERISTICS

	Measured Thickness (mils)	Measured Mass Per Unit Area (oz/yd^2)	Grab Tensile Strength (*) ASTM D4632 (lb)	Puncture Resistance ASTM D4833 (lb)	Mullen Burst Strength ASTM D3786 (psi)	Trapeziodal Tear (*) ASTM D4533 (lb)
Type A						
8 oz	105.6	6.9	300	115	390	105
10 oz	140.2	9.6	420	155	560	140
12 oz	176.9	13.4	540	185	700	180
16 oz	177.4	15.9	650	225	855	225
Type B						
8 oz	98.5	7.2	240	115	350	100
10 oz	120.7	9.7	300	140	425	120
12 oz	130.1	11.4	350	150	450	150
16 oz	165.1	15.7	480	180	550	200
Type C						
8 oz	85.3	7.9	275	130	575	140
10 oz	123.1	11.3	315	165	650	160
12 oz	144.6	14.6	410	185	825	185
16 oz	164.5	15.1	510	220	920	220

(*) MACHINE DIRECTION

was placed on the subgrade. The geomembrane was, in turn, placed over the geotextile (Figure 1). The diameter of the geomembrane was identical to the outer diameter of the rim to achieve a positive anchorage of the geomembrane perimeter and prevent any slippage during the tests. The upper chamber was then bolted in place and compressed air was introduced into the chamber at a rate of 1 psi/minute. Pressure was held at 5000 lb/ft^2 for one hour after which the specimen was removed and visually inspected.

Subsequent geomembrane samples were tested under 10,000 lb/ft^2, 15,000 lb/ft^2, and 17,000 lb/ft^2. A puncture developing in the geomembrane samples was made evident by a rapid drop in the chamber pressure. The initially planned test series at 20,000 lb/ft^2 pressure could not be performed because of the limitations in the air pressure that could be supplied to the equipment.

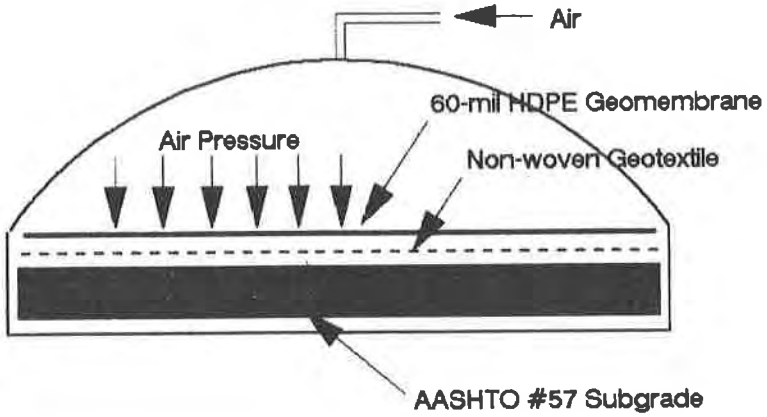

Figure 1. Geomembrane, Geotextile and Subgrade Configuration during Stage 1 Testing

Stage 2 - Multiaxial Tensile Testing. The geomembrane specimens removed from the point stress device were subsequently taken to a hydrostatic pressure chamber for multi-axial tensile testing. Only those membranes that did not exhibit puncture were tested in this stage. Testing was conducted according to GRI test standard GM-4. Air pressure was gradually increased during the test and the center deflection of the inflated geomembrane was recorded by means of a sonic range finder. The pressure and geomembrane deflection were continuously recorded by a strip-chart device for visual inspection of the curves after each test. Following rupture, a photograph of each tested geomembrane specimen was taken for a visual record of the pattern of failure.

All testing was performed at 23±2 C temperature and 50±5% relative humidity.

At least three tests were performed at each pressure to confirm the repeatability of the results.

TEST RESULTS

As described above, the multi-axial tensile stress-strain curves for a set of 60-mil HDPE virgin geomembrane specimens were obtained prior to the start of the protection testing program with each geotextile. The average values of stress and strain at break were 2321 lb/in^2 and 24.9 percent, respectively. The average values, as well as the associated standard deviations are illustrated in Figure 2.

Break Stress. Figure 3 presents the multi-axial break stress values obtained with unprotected and geotextile-protected specimens. Prior to the start of testing with each geotextile, a set of three geomembrane specimens were tested with no protection. The solid squares represent the data points obtained with the unprotected geomembrane specimens. The average baseline stress value for the virgin geomembrane is also shown for reference. In Figure 3, as well as Figure 4, each subgrade stress pressure was repeated three times to show the results of three tests performed with each geotextile.

There is a certain amount of scatter in both Figures 2 and 3 that can not be readily explained. It is suspected that the considerable scatter observed in Figure 2 for the baseline values is a major cause of the scatter in Figure 3. Several aspects of the geomembrane behavior with and without protection, however, can be observed in Figure 3:

- Unprotected membranes pressured beyond 10,000 lb/ft^2 failed during Stage 1 pressurization against the subgrade material.
- A large portion of the test points lie below the baseline average of the virgin specimens.
- For a given weight non-woven geotextile, there is no clearly defined trend in the break pressure as the subgrade test pressure varies between 5000 and 17,000 lb/ft^2.
- So long as the unprotected geomembrane remains intact -i.e, does not develop punctures- during Stage 1 pressurization, it will withstand multi-axial pressures comparable to those protected by geotextiles.
- There is no clear indication that one type of geotextile is superior to the others for the protection it provides.

Stress-Strain Behavior of Geomembrane Specimens. Figure 4 presents the multi-axial strain at break for the unprotected and geotextile-protected geomembrane specimens. Most of the observations made above for the break stress appear to also apply to multi-axial strain at break.

However, The standard deviation of the strain at break (Figure 2) is considerably less than the break strain range in Figure 4. Therefore, the scatter shown in Figure 4 leads to more significant observations than those listed above for the break stress:

- The multi-axial strain at break for unprotected specimens is smaller than the average break strain obtained from the baseline tests.
- For a given weight non-woven geotextile, the multi-axial strain

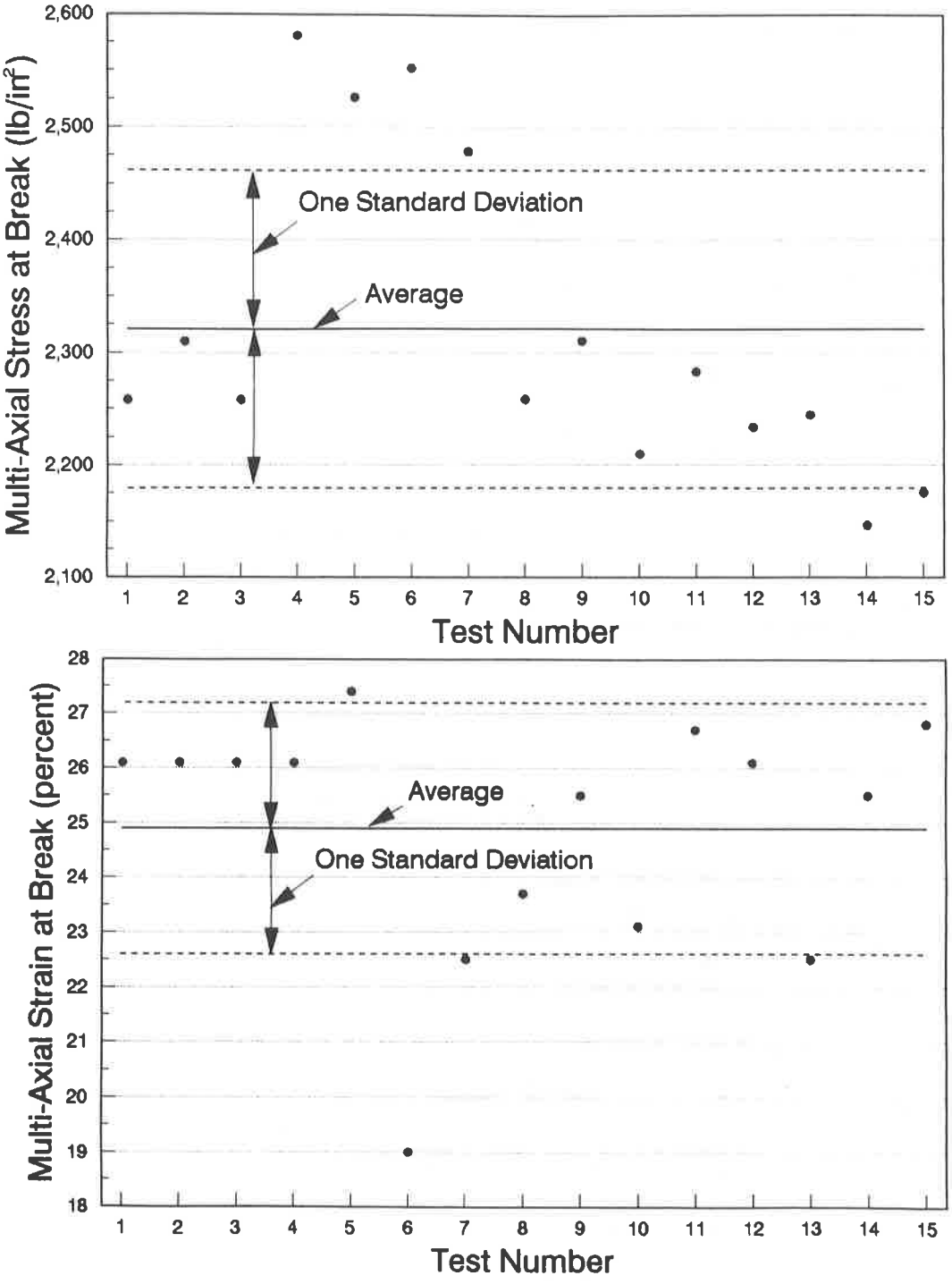

Figure 2. Break stress and break strain values obtained during baseline testing

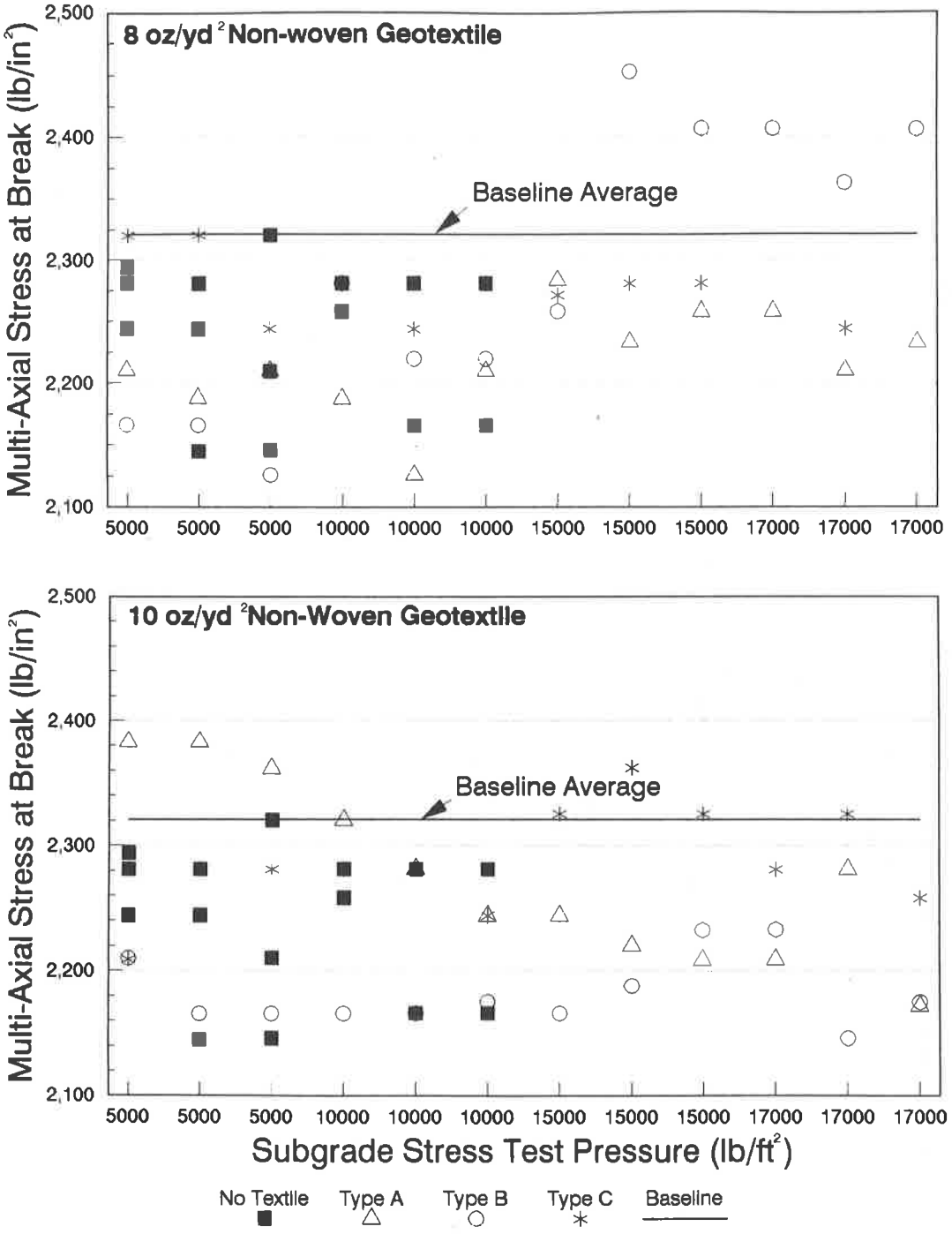

Figure 3. Break stress values obtained during Stage 2 testing

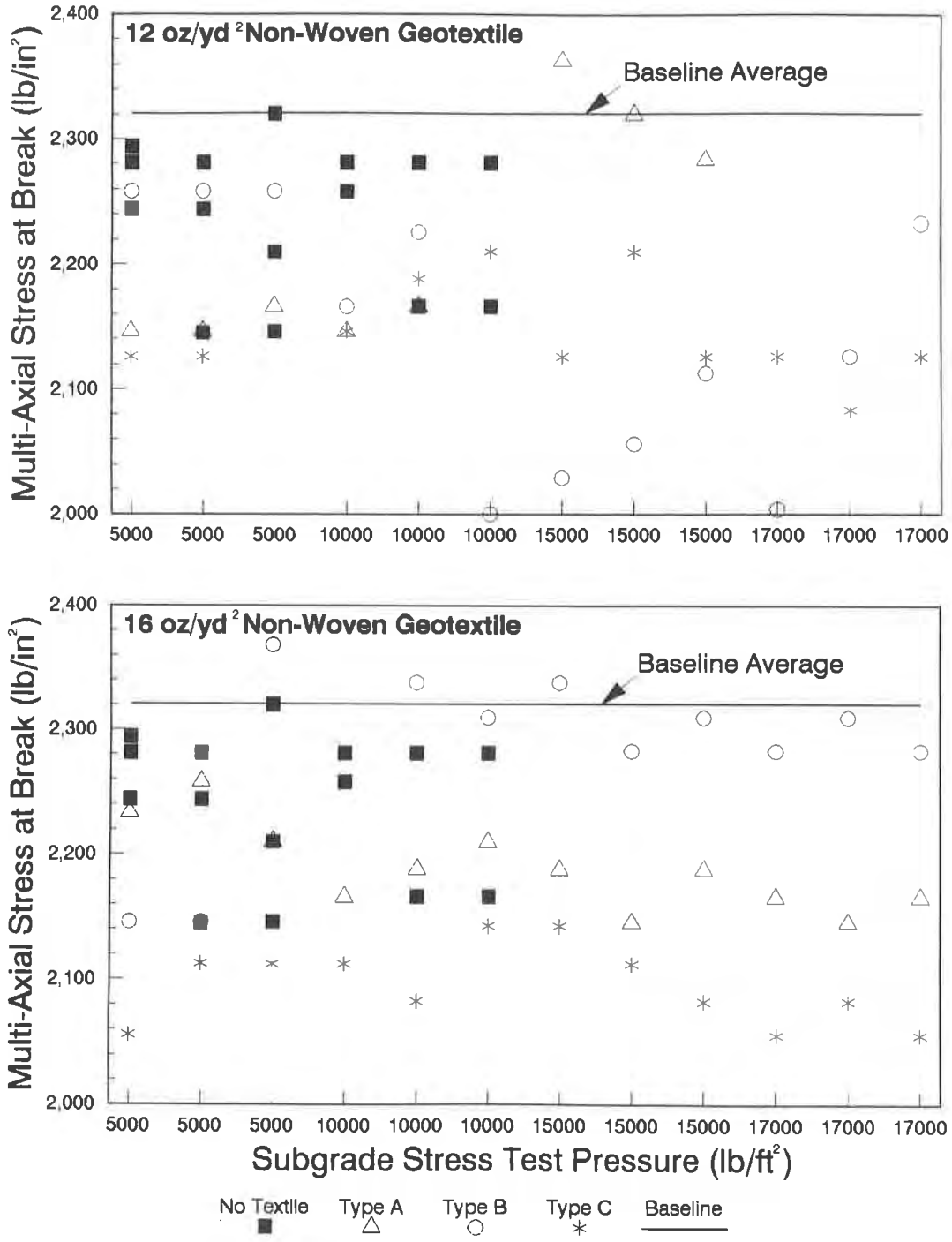

Figure 3. Break stress values obtained during Stage 2 testing

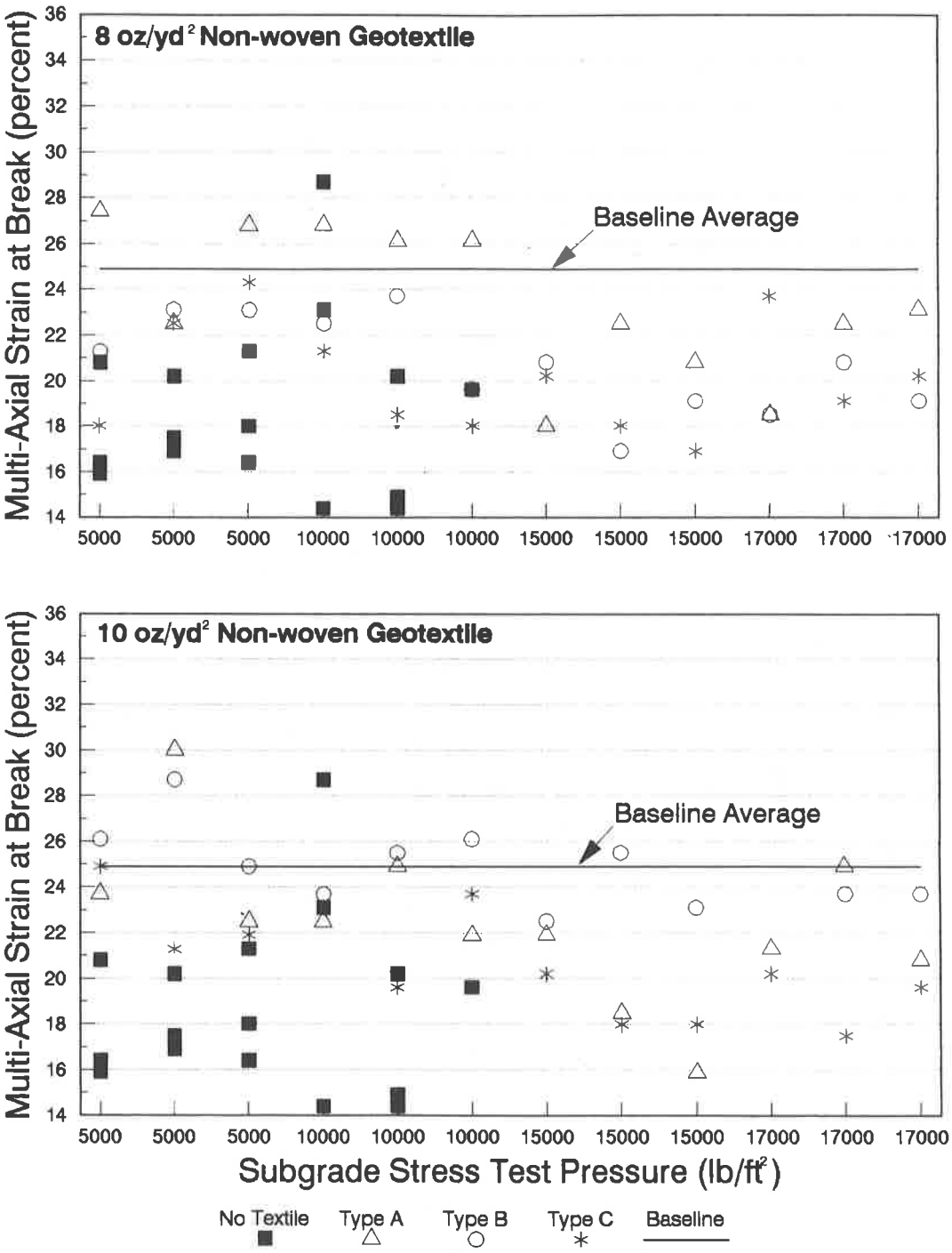

Figure 4. Break strain values obtained during Stage 2 testing

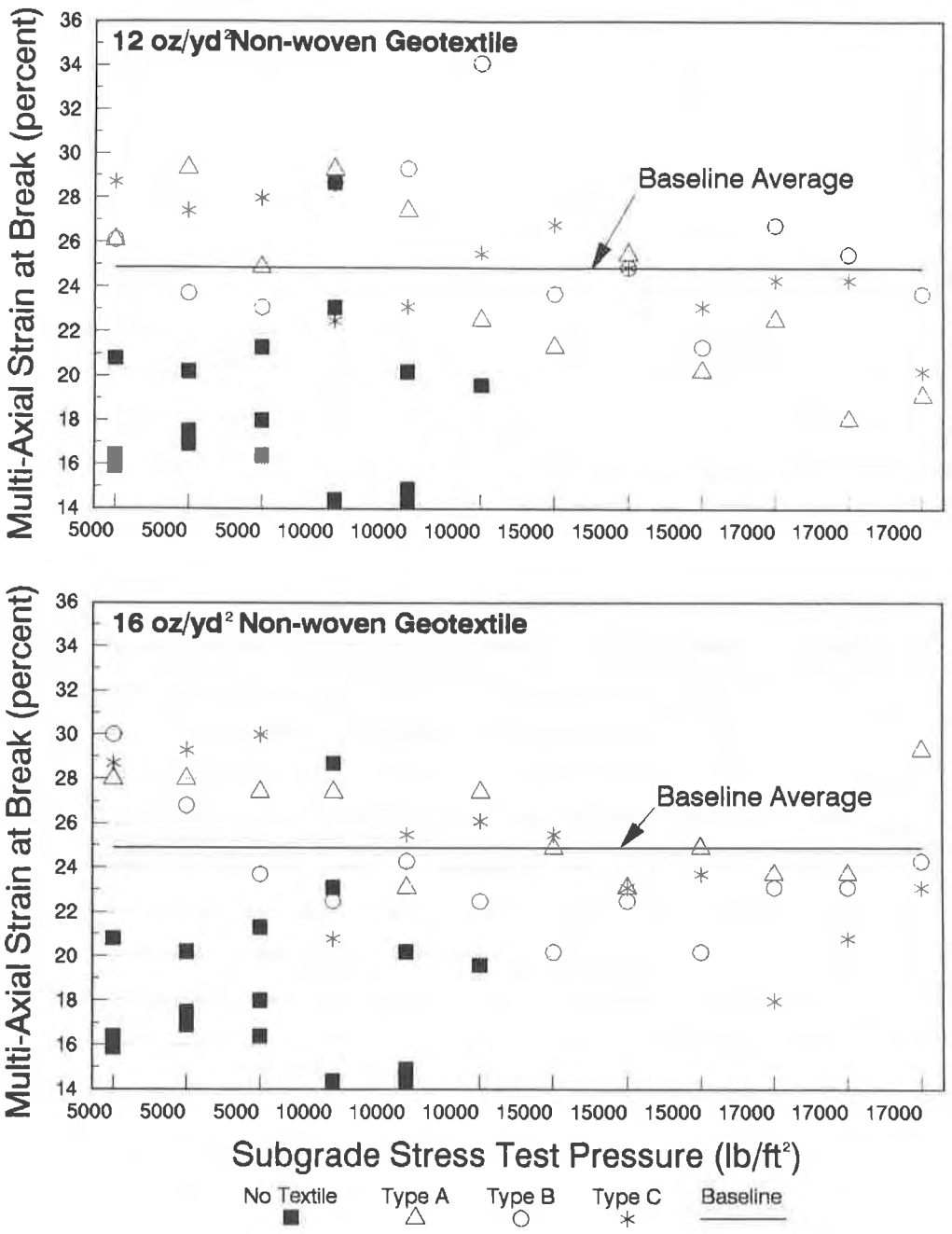

Figure 4. Break strain values obtained during Stage 2 testing

at break appears to decrease with an increase in the subgrade test pressure. This situation is more evident when the data points for all three geotextiles are observed as a group.
- The break strain appears to shift slightly toward larger values with increasing weight of the protective geotextile.
- A significant number of data points lie above the baseline. This appears to be particularly the case at subgrade test pressures below 15,000 lb/ft^2.
- There is no clear indication that one type of geotextile is superior to the others.

DISCUSSION

The results of this study generally point toward a need for a larger-scale test program in which statistically significant numbers of data points under different conditions can be collected and compared. This is particularly evident in the case of break stress. The variations in the multi-axial stress behavior of different specimens of HDPE geomembranes from the same manufacturer appear to interfere with any conclusions that may be drawn regarding the effectiveness of protection by a certain type of geotextile.

The test results appear to indicate that, generally, the effects of damage caused by a coarse-grained subgrade can be quantitatively identified by means of the two-stage testing methodology described above. This can be accomplished either in the form of measuring multi-axial stress, or strain, at break. As initially expected, the mechanical damage in the geomembrane specimens exhibited itself in the form of lower multi-axial stress, as well as lower strain, at break.

Modes of membrane breakage obtained during multi-axial testing also varied. Types of observed failure ranged from loss of pressure through pinholes to large-scale split, or tear, of the geomembrane. Geomembranes subjected to subgrade pressure test with no geotextile protection generally failed after developing pinholes. A large number of the geotextile-protected geomembrane specimens failed as a result of holes that developed at the points of localized strain after some material yield. Therefore, there was no uniform description of the state of failure during the tests.

It is conceivable that, in some of the tests in Stage 2, the pressure at which some of the indentations developed into very small punctures may have not been accurately recorded by the recording device. This situation can potentially occur because the volume of air beneath the expanded membrane and the constant supply of pressurized air can make it difficult to detect small pressure changes that result from leakage of air through pinhole-size holes within the geomembrane.

Fine-tuning of the methodology will be needed in order to minimize the scatter. This may be achieved in the form of increased precision in the measuring systems, very strict control on the testing methodology, precise definition of the state of failure, and possibly a change in the sampling methods of the geomembrane and geotextile specimens.

It should be realized that the methodology presented herein is not the only way to quantify geomembrane damage. Actual measurements of the depth of indentation taken at a number of points on the damaged geomembrane can also be used for this purpose. These measurements, however, can not easily be translated into a numerical value pertaining to physical performance of the damaged geomembrane.

It is recognized that the relative stiffness of the materials facing the geomembrane on both of its sides is a significant factor that may modify this type of behavior considerably. In this study, the membranes were pressured against a bed of stiff granular material using air pressure. Had a much stiffer medium such as a metal plate been used to force the geomembranes against the granular bed, geomembrane puncture may have taken place to a larger extent. In practice, the stiffness of the subgrade material is likely to be intermediate between these two extremes. This study covered only one of the extremes.

The effects of long-term loading were not considered in this study, and need to be addressed in future studies to better understand the effectiveness of geomembrane protection by geotextiles.

CONCLUSIONS

This study was undertaken as an attempt to quantify the damage to HDPE geomembrane that can result from adjacent materials. In particular, the testing program evaluated the damage caused by AASHTO #57 stone and protection provided by various geotextiles. It is the authors' concern that past studies have not been able to evaluate damage except at puncture, and that mechanical properties of geomembranes may be significantly changed by exposure to adjacent materials under certain conditions even if puncture does not occur.

The results indicate that material properties measured during testing, specifically stress and strain at break, can be modified by adjacent materials. Geotextile protection appears to be useful in minimizing such effects, depending upon the overburden pressure applied. Since only one type of granular material was used in this program, it is not possible to conclude how significant a factor the particle size may be, although it seems logical that it can be important.

Further testing is necessary to determine if important design trends or data can be obtained from this type of approach.

ACKNOWLEDGMENTS

Financial support for this project was provided by the Waste Management of North America, Inc. The National Seal Company made their laboratory facilities and personnel available for testing. This support by both companies is gratefully acknowledged.

REFERENCES

National Seal Company (1992) Research Report on Geomembrane Protection by Selected Non-Woven Geotextiles, A report to Waste Management of North America, Inc.

Frobel,R., Youngblood, W. and Vandervoort, J. (1987) "The Composite Advantage in the Mechanical Protection of Polyethylene Geomembranes", Geosynthetics '87 Conference, New Orleans, USA, pp. 565-576.

Hullings, D.E. (1990) "Puncture Behavior and Protection of Geomembranes Using Large Scale Hydrostatic Testing", Master of Science Thesis submitted to the Faculty of Drexel University.

HDPE & VLDPE Geomembrane Survivability

C.L.Y. Wong
Golder Associates Ltd., Canada

D. Wijewickreme
Golder Associates Ltd., Canada

ABSTRACT

The survivability of 40 mil HDPE and 30 mil VLDPE geomembranes to the puncture stresses caused by construction vehicles trafficking over a crushed gravel cover was assessed in a field test. The main issues addressed were confirmation of the thickness of cover material and geotextile blanket to protect the geomembranes, the type of bedding material suitable for this application, and the acceptability of shallow disturbance of sand bedding. The results of the field test indicated that 40 mil HDPE has superior survivability compared to 30 mil VLDPE and that braking/acceleration of vehicular traffic is the most critical loading condition which should be evaluated. A simplified model to simulate the survivability of the HDPE geomembrane was developed and appeared to be successful in reflecting the survivability performance of the HDPE geomembrane observed in the field tests for the given performance criteria.

INTRODUCTION

The survivability of a geomembrane during and after installation is a common concern. Survivability as defined herein is the ability of a geomembrane to withstand the puncturing stresses caused by the placement of soil cover and subsequent vehicular traffic on the soil cover.

Where possible, the survivability of a geomembrane can be addressed by selecting bedding and cover materials of a suitable gradation and by specifying a suitably thick surface on which all vehicular traffic must travel. However, it is not always possible to satisfy these conditions and the issue of survivability becomes a significant concern. This paper discusses the results of field testing and computer modelling of a geomembrane cap system to assess the survivability of 40 mil high density polyethylene (HDPE) and 30 mil very low density polyethylene (VLDPE) geomembranes to the puncture stresses caused by vehicular traffic over a gravel soil cover.

DESIGN CRITERIA

The Pacific Place residential/commercial project covers an area of about 82 hectares in downtown Vancouver, British Columbia, Canada. The Parcel 9 area will be a park. The soils underlying Parcel 9 are contaminated with coal tars, PCBs and chlorophenols. The remedial plan for the park site includes a containment barrier around the site and groundwater control and treatment of the contained leachate. To reduce precipitation and irrigation recharge to the groundwater, thereby reducing the amount of leachate generated and requiring treatment, and to provide a physical marker to indicate the zone of potentially contaminated soils, an impermeable cover over the Parcel 9 area was specified.

The criteria for selecting an impermeable cover were as follows:

a) The cover should significantly reduce the infiltration of water into the underlying contaminated soils. However, a perfectly impermeable barrier is not an absolute necessity because any leakage through the impermeable cover will be collected by the groundwater control and treatment system.
b) The cover material should be readily identifiable as a physical marker.
c) The cover should provide a "thin" cross-section thereby minimizing the volume of excavation of contaminated soils to achieve the specified grades.
d) The cover should be cost-effective.
e) In the playfield area of the park, the impermeable cover should be able to support a 300 mm thick clear crushed gravel cover overlain by an additional 300 mm of granular material, with potentially heavy vehicular traffic on top of the granular cover material. This criterion was specified by others to meet landscaping and park use requirements.

Geomembranes were considered to be the most appropriate class of materials meeting the above criteria. The performance criteria selected for the geomembranes specified that very shallow, local deformations of the geomembrane material, due to gravel imprints, would be acceptable provided they do not appear to compromise the integrity of the liner. Deformations which result in puncture or significant straining of the geomembrane material would be unacceptable. It should be noted that for applications such as hazardous waste landfill liners, where the consequences of leakage through a liner are severe, even such imperfections of the geomembrane material may not be acceptable.

MATERIALS

The proposed cap design for the playfield area is shown on Figure 1. Details of each component of the cap system are discussed below.

Bedding. The thin cross-section of the geomembrane resulted in fill being required in most of the playfield area to achieve the playfield surface drainage requirements specified by others. A medium to fine sand was selected as the fill and geomembrane bedding material. However, there was a concern that the sand bedding could be easily disturbed during installation and therefore consideration was also given to the use of a 20 mm crushed sand and gravel road base material for bedding.

Geomembrane. Based on the design criteria, both 40 mil high density polyethylene (HDPE) and 30 mil very low density polyethylene (VLDPE) geomembranes were considered to be

potentially acceptable impermeable cover materials. The manufacturer's minimum average roll value for puncture resistance (FTMS 101, 2065) of 40 mil HDPE and 30 mil VLDPE is 0.23 kN and 0.19 kN, respectively.

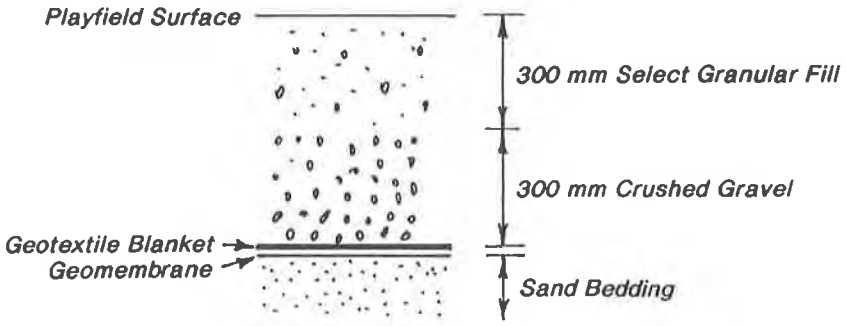

SCHEMATIC ONLY
Not to Scale

Figure 1. Proposed Cap Design

Geotextile Blanket. A thick non-woven needle-punched geotextile blanket was considered to be a requirement to protect the geomembrane from the angular gravel cover material. A 400 grams/m² (minimum average roll value) polypropylene material was selected because of its local availability. The manufacturer's minimum average roll specifications for tensile strength (ASTM D-4632), Mullen burst (ASTM D-3786), and ball burst resistance (ASTM D-3787) were 1.33 kN, 4,490 kPa, and 0.82 kN, respectively.

Cover. The 300 mm thick crushed gravel cover material was specified by others to be 12 mm to 38 mm sieve size. A 300 mm thickness of granular material is to be placed above the crushed gravel, upon which a permeable synthetic turf is to be installed.

To address the design concern of the survivability of the geomembrane during and after construction, field simulation testing was carried out. The survivability issues which were to be addressed by the test program included confirmation of:

a) The thickness of soil cover above the geomembrane to protect it from heavy vehicular traffic. It was decided to evaluate 300 mm of soil cover, rather than 600 mm of soil cover, to assess whether heavy truck traffic could be permitted to drive over the 300 mm thickness crushed gravel surface during construction.
b) The requirement for a non-woven needle-punched geotextile blanket to protect the geomembrane from the angular gravel.
c) The acceptability of shallow disturbance and loosening of the sand bedding due to foot traffic by construction personnel during geomembrane installation.
d) The acceptability of 20 mm crushed sand and gravel as a bedding material.

FIELD TESTING - PROCEDURE

The field test program was carried out using the test arrangement shown on Figure 2. The bedding under two-thirds of the test section was a medium to fine sand (see Figure 3). Half of the sand section was compacted smooth with a 100 kN vibratory roller. The other half of the

sand section was loosened to a depth of about 50 mm by foot traffic imprints. The bedding under the other one-third of the test section was 20 mm minus crushed sand and gravel (see Figure 3) compacted smooth with a roller.

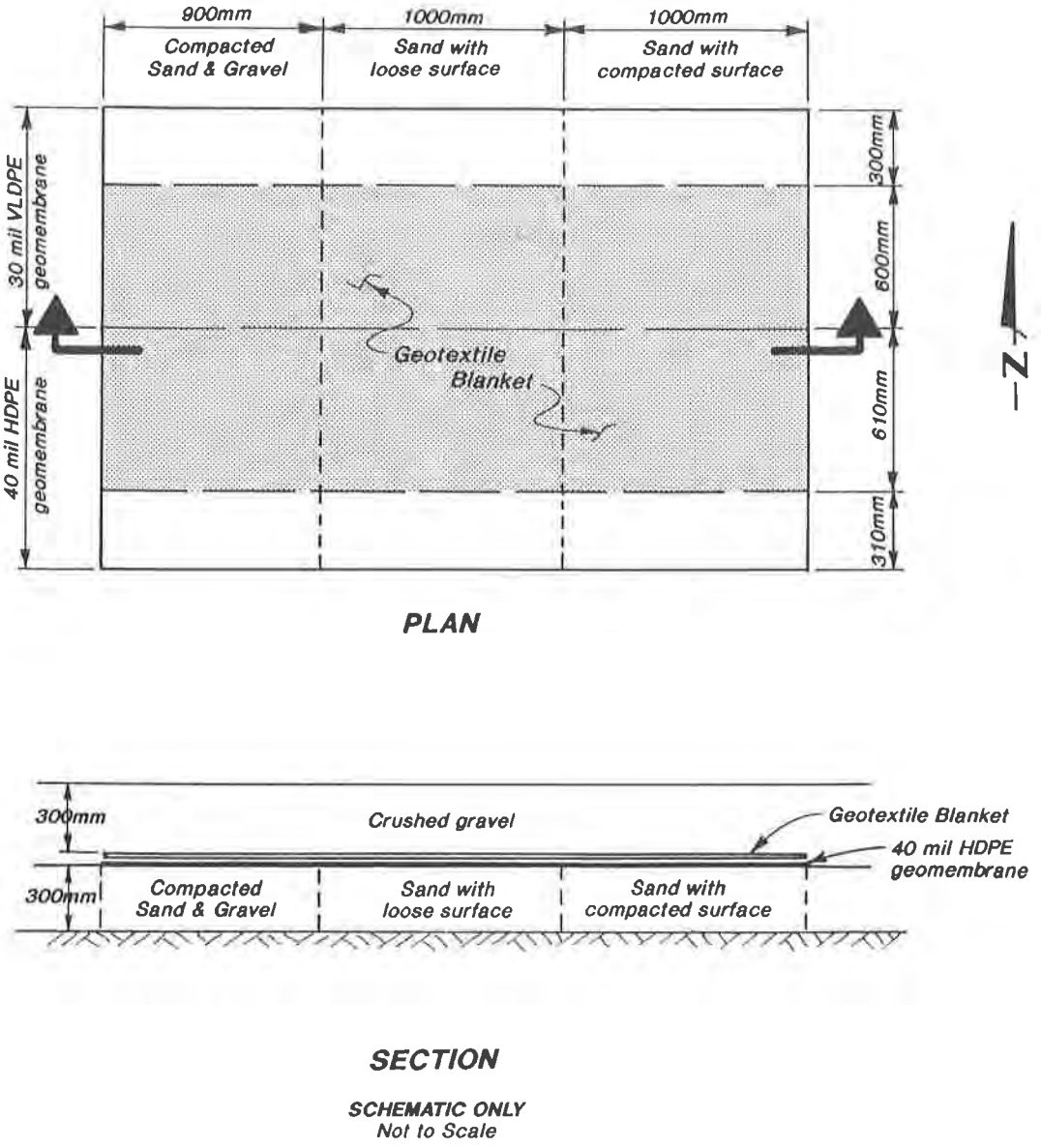

Figure 2. Field Test Arrangement

Both geomembranes had smooth surfaces and none of the geomembrane or geotextile specimens had seams or welds. The geotextile blanket covered only about two-thirds of each of the HDPE and VLDPE geomembranes to allow an assessment of the effect of the lack of the blanket on the performance of the geomembranes. The cover over the geotextile/geomembranes was initially 300 mm thickness of 12 mm to 38 mm clear crushed angular gravel (see Figure 3).

After placement of all materials, the gravel surface over all areas was compacted in a north-south direction by 10 passes of a 100 kN vibratory roller having a 2.13 m wide drum. A fully loaded tandem truck, having a 229 kN (51,477 lbs) gross vehicle weight and 620 kPa

(90 psi) tire pressure, then made 8 passes at 5 kph along the same north-south alignment (during each pass) over the test section. After these 8 passes, 2 passes were made by braking the truck at the test section and then reaccelerating from the stopped position. The purpose of the stop/start passes was to more closely simulate construction conditions. The stop/start condition exposes the cap system to the highest stresses since the cap is subjected to not only the vertical weight of the truck but also to the shearing stresses associated with decceleration/acceleration of the truck.

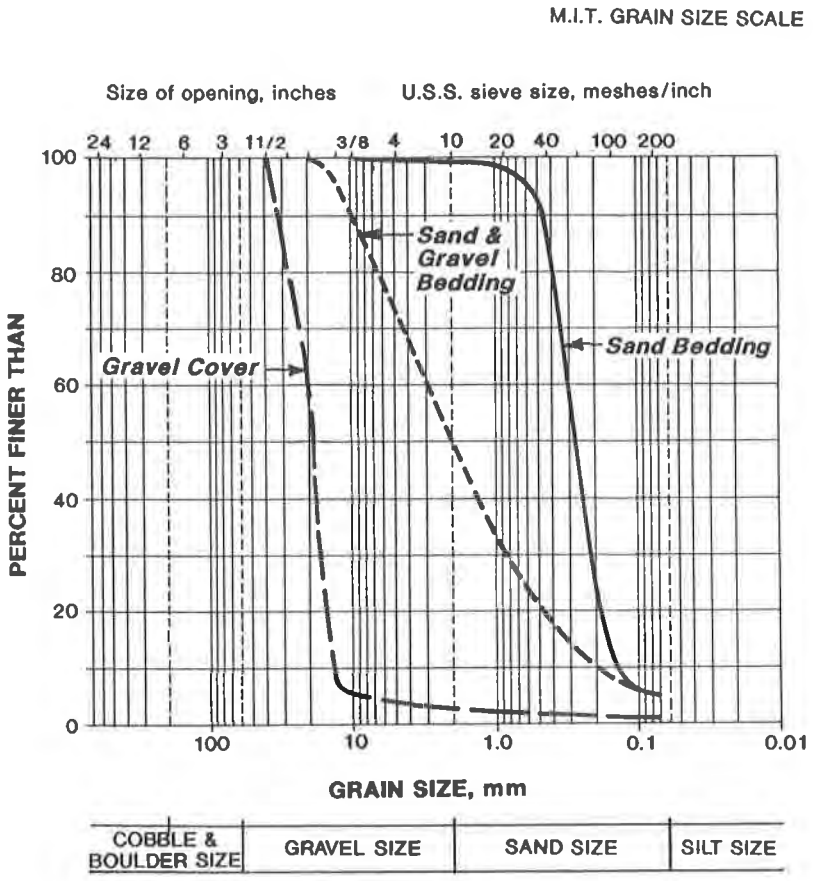

Figure 3. Grain Size Distribution Curves

After these 10 passes, the truck was realigned to make a similar 8 plus 2 passes in a north-south direction such that all areas received reasonably equal traffic coverage. Ruts in the gravel were formed by the truck tires along all alignments, which reduced the thickness of gravel over the geotextile/geomembrane to an estimated average of about 250 mm. The truck became stuck during one of the stop/start passes due to rutting in the HDPE / Compacted Sand area. It is estimated that the truck tires in this rut were about 160 mm above the geomembrane.

Upon completion of the truck passes, the geomembrane was carefully exhumed by hand labour and inspected. The in situ density of the upper 100 mm of the sand and gravel bedding material was determined, using a nuclear densometer, to average 97% of standard Proctor maximum dry density. Both the loosened surface and compacted sand areas averaged 100% of standard Proctor maximum dry density in the upper 100 mm of the bedding material. It should be noted that although the Proctor compaction test is not intended for sand, it is generally accepted locally as a suitable method for compaction control.

FIELD TESTING - RESULTS

The number of "holes" and "pressure points" within each test area is shown on Figure 4. "Holes" denotes punctures through the geomembrane determined by using a bright light and probing with a sharp pencil. "Pressure Points" were determined qualitatively by judgement and denote permanent deformations of the geomembrane which are not holes through the geomembrane but which are significant deformations and indicate unacceptable performance. It should be noted that all areas of the geomembranes experienced very shallow indentations, caused by gravel imprints. These minor indentations, which were considered to be acceptable performance, were more discernable by the variations in the reflection of sunlight off the geomembrane surface than by close-up inspection or feel.

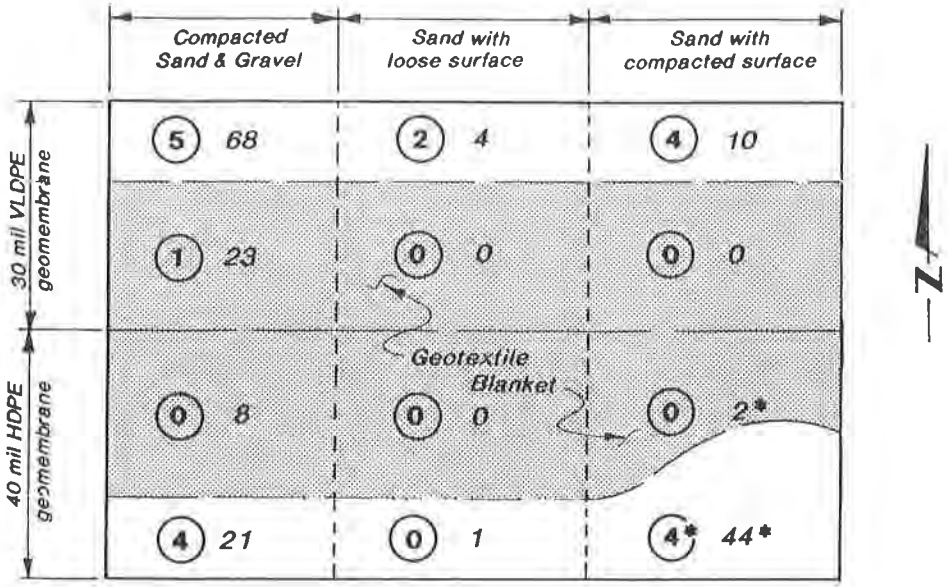

PLAN

SCHEMATIC ONLY
Not to Scale

LEGEND :

(5)	*Number of Holes*
8	*Number of Pressure Points*
*	*Due to Rutting*

Figure 4. Field Test Results

Despite efforts to achieve reasonably uniform coverage with the truck tires, rutting of the gravel had a pronounced effect on the field test results, since the ruts allowed the truck tires to be closer to the geomembrane surface, thus increasing the gravel contact stress on the geotextile blanket and geomembrane. The most significant rutting was caused during the stop/start passes of the truck and was most severe in the 40 mil HDPE / Compacted Sand section, where the truck tires even caused the geotextile blanket to locally shift and reduce the area of the HDPE covered by the geotextile blanket. Holes and pressure points thought to be due to rutting are identified in Figure 4.

The following discusses the field test results for each area of the test section.

Sand Bedding and Geotextile Blanket. With the exception of the Compacted Sand / HDPE area, no holes or pressure points were identified in the sand bedding areas covered by a geotextile. The two pressure points identified in the Compacted Sand / HDPE area were associated with rutting which resulted in the truck tires being within about 160 mm above the geomembrane. The test results demonstrated that both the 40 mil HDPE and the 30 mil VLDPE are capable of surviving heavy vehicular traffic provided the bedding is sand, there is a non-woven needle punched geotextile blanket having a weight of at least 400 grams/m^2, and the gravel cover is at least 250 mm thickness.

The test results also indicated that disturbance of the sand bedding due to foot traffic is not noticeably detrimental to the survivability of the geomembrane. Intuitively, one would expect that the area where the sand bedding was compacted would perform better than the area where it was loose. One possible explanation for this apparent discrepancy is that during preparation of the bedding prior to placement of the geomembrane, the vibratory roller did not compact the top few centimetres of sand and therefore it did not make a difference whether the surface was loosened or rolled. This explanation is supported by D'Appolonia, et al. (1969) who showed that a vibratory roller does not compact the upper 50 mm to 100 mm of sand.

A second possible explanation is that the initial compaction of the gravel with the 100 kN vibratory roller also caused compaction of the underlying sand bedding in this area and therefore the initial state of compaction of the sand did not matter. It is notable that compaction testing of the upper 100 mm of the sand (using a nuclear densometer) after exhuming the geomembranes indicated that the sand in both the area where the sand was compacted and the area where the surface of the sand was loosened had identical average in situ densities of 100 percent of standard Proctor maximum dry density. Thus, whether due to the vibratory roller or the truck traffic, the loosened sand eventually becomes compacted.

Sand & Gravel Bedding and Geotextile Blanket. One hole in the VLDPE area, and 8 and 23 pressure points in the respective HDPE and VLDPE areas were identified. The test results suggest that, for the given test conditions, 20 mm minus crushed sand and gravel is an unsuitable bedding material for the geomembranes. The results of similar field testing on PVC, CPE and elasticized polyolefin geomembrane materials by Gunkel (1981) support this observation. Although the sand and gravel surface was smooth and undisturbed, the holes and pressure points of the geomembranes appeared to be due more to the gravel particles in the bedding material than due to the gravel cover. It appears that the gravel acts as a "hard point" while the sand matrix compresses with respect to the gravel piece, thereby exposing the geomembrane to the gravel. It is likely that, if the sand and gravel bedding surface had been disturbed, the indentations would have been even deeper.

Sand Bedding Without Geotextile Blanket. The HDPE and VLDPE portions in the loose sand area which were not covered by a geotextile blanket experienced 1 and 4 pressure points and 0 and 2 holes, respectively, compared to no damage observed in areas with a geotextile blanket. In the compacted sand bedding area, it appeared that all the damage to the HDPE sheet was likely due to the rutting. The VLDPE sheet in the compacted sand bedding areas experienced about twice the number of holes and 2.5 times the number of pressure points compared to the loose sand bedding area. However, all the holes and pressure points were along the north-south alignment of the rut in the gravel and may be associated with higher gravel contact stresses due to a gravel cover of between 160 and 250 mm thickness. The top surface of both geomembranes

was scored, compared to the generally smooth surface of the geomembranes protected by the geotextile blanket. This scoring was considered to be unacceptable performance because the scratches increase the potential for stress cracking.

Sand & Gravel Bedding Without Geotextile Blanket. Both the HDPE and the VLDPE portions which were not covered by a geotextile blanket experienced significantly more pressure points and punctures than the areas which were provided with a geotextile blanket. The performance of the area having a sand and gravel bedding and no geotextile blanket was clearly unacceptable.

40 mil HDPE Versus 30 mil VLDPE. The 40 mil HDPE and the 30 mil VLDPE appeared to perform similarly well when protected by a geotextile and when underlain by sand bedding. However, this does not necessarily indicate equal survivability characteristics since it was not possible to determine from the field data the available factor of safety with respect to yield or puncture of each material. When the bedding material is crushed sand and gravel or when the geomembranes are not provided with a geotextile cover in the loose sand bedding area, the 30 mil VLDPE sustained more holes and pressure points than the 40 mil HDPE. In general, it appeared that the thinner 30 mil VLDPE was more susceptible to damage than the thicker 40 mil HDPE.

COMPUTER MODELLING

From a designer's perspective, it would be advantageous to have a model which could predict the potential survivability of a geomembrane. To date, very few attempts have been made to model the survivability of geomembranes.

In an effort to address this deficiency, a simple computer model simulation of the cap system under a vertical load was carried out. It was not intended that this be an accurate model of the field conditions, since the "real world" situation is highly complex. Rather, it was intended that an empirical model having a theoretical basis be developed with the object of matching the model results to field observations using common material parameters. In particular, it was anticipated that the puncture stresses acting on a geomembrane by a piece of gravel could be determined from the computer model. These stresses could then be compared to a criterion, such as the yield stress, to determine if the material has acceptable survivability. The field test results described above would be used to select the appropriate criterion to calibrate the model.

Model Definition. The computer program FLAC (Fast Lagrangian Analysis of Continua) Version 2.2 (1989) was used to model the cap. FLAC uses a finite difference solution scheme to model two dimensional elastic or plastic continua. This program was selected because it is relatively easy to use and can accommodate relatively large deformations through mesh regeneration. For simplicity, linear elastic material properties were used for the geomembrane, geotextile and gravel. Elastic, perfectly-plastic properties were assumed for the sand bedding.

The cap system was modelled as a single "typical" piece of gravel, having a vertical stress acting on it, pressing down on the geotextile (or geomembrane if there is no geotextile blanket), with a sand bedding underlying the geomembrane. The vertical stress experienced by the gravel resting on the geotextile (or geomembrane) was determined by computing the contact area of the dual tires of one side of the rear axles of a fully loaded tandem truck, applying the tire pressure

of 620 kPa to this contact area and determining by "1 horizontal to 2 vertical" stress distribution the force acting on the piece of gravel bearing on the geotextile (or geomembrane). The piece of gravel was assumed to have a plan area the same as the 50 percent passing sieve opening (19 mm by 19 mm), with the stress acting on the gravel at a height of 10 mm above the geotextile (or geomembrane) surface. The force on the gravel piece was distributed over a hemispherical point having a 3 mm radius, to represent the point of the piece of gravel. The hemispherical 3 mm radius point was selected to approximately match the point of the puncture tool used in FTMS 101C Method 2065. Figure 5 summarizes how the stress acting on the 3 mm radius point was computed.

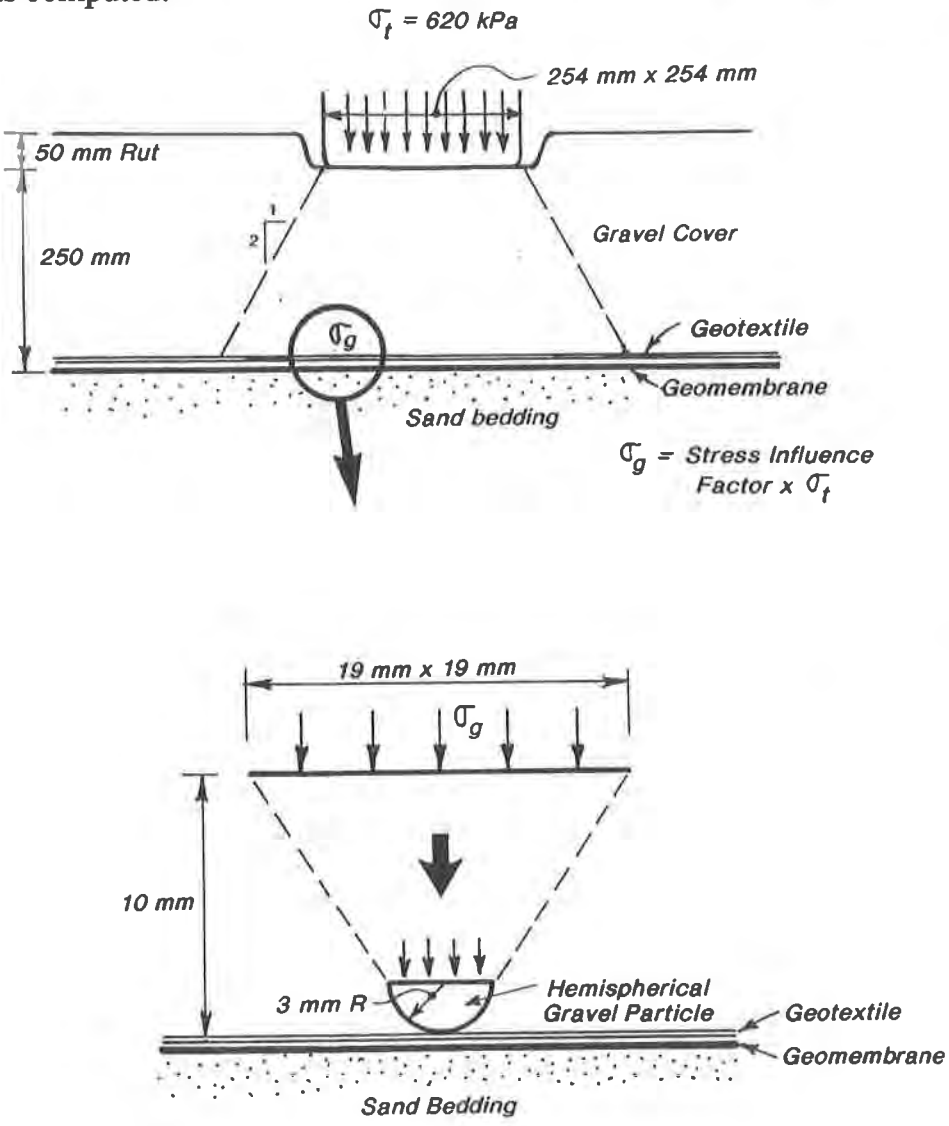

Figure 5. Stress Acting on Gravel Particle

Three vertical stress levels acting on the 3 mm radius point were selected for analysis. A stress of 3,200 kPa corresponds to the stress induced when only 160 mm of gravel cover overlies the geomembrane, as occurred in the deep rut during the field test. A 2,100 kPa stress corresponds to the stress with 250 mm of gravel cover, which was the average cover thickness over most of the field test section during the truck passes (the actual gravel cover thickness ranged from 300 mm to 210 mm, depending on the particular pass). A 700 kPa stress corresponds to 600 mm of gravel cover, which is the ultimate design cover thickness.

Figure 6 shows the mesh used for the axisymmetric computer analysis of the above conditions. Table 1 summarizes the elastic parameters assumed for each material. Under the hemispherical point, the thickness of the geotextile was assumed to be 1 mm to reflect the compressed state of the geotextile under load. The geotextile properties in Table 1 are for a compressed state.

Table 1. Material Properties.

Material	Young's Modulus (MPa)	Poisson's ratio
Gravel Particle	200,000	0.35
Geotextile	10	0.10
HDPE Geomembrane	550	0.40
Sand Bedding	30	0.35

A Mohr-Coulomb yield criterion of no cohesion and an effective angle of internal friction of 33° was assumed for the sand bedding.

Only 40 mil HDPE geomembrane was selected for the computer modelling because the nonlinear, strain-hardening plastic properties of VLDPE cannot be easily modelled using linear elastic analyses. HDPE, on the other hand, has a definable yield stress which can be used as a failure criterion. The HDPE geomembrane was modelled for the two cases of with and without a geotextile blanket.

Results. Figure 7 shows plots of "two times the maximum shear stress" with distance from the axis of symmetry for the cases of with and without a geotextile blanket. The stresses presented are those acting on the element located second from the bottom of the HDPE geomembrane portion of the mesh. Stresses were not calculated at the axis of symmetry because the stresses are computed only at the center of an element.

It is proposed that a three dimensional axisymmetric tensile yield stress of 11 MPa, as shown on Figure 7, be used as a survivability criterion for the model. This value was selected by multiplying the typical uniaxial tensile yield stress (ASTM D-638) for HDPE of 15.2 MPa by a factor of 0.72, which is a scaling factor, derived from Koerner's (1990) data, for converting the uniaxial yield stress to a value appropriate for three dimensional axisymmetric conditions.

The computer model results indicate that when the maximum predicted geomembrane stress significantly exceeds the 11 MPa criterion, such as the case of 160 mm gravel cover (due to rutting) without a geotextile blanket, some holes and numerous pressure points in the HDPE sheet were experienced in the field test. For the case of 160 mm of gravel cover and a geotextile blanket, the predicted geomembrane stress is slightly above the 11 MPa criterion and corresponds to the field test results which identified only 2 pressure points within a limited area. In both these cases, the damage sustained by the HDPE sheet was also roughly comparable to the radius where the model stresses exceeded the 11 MPa criterion.

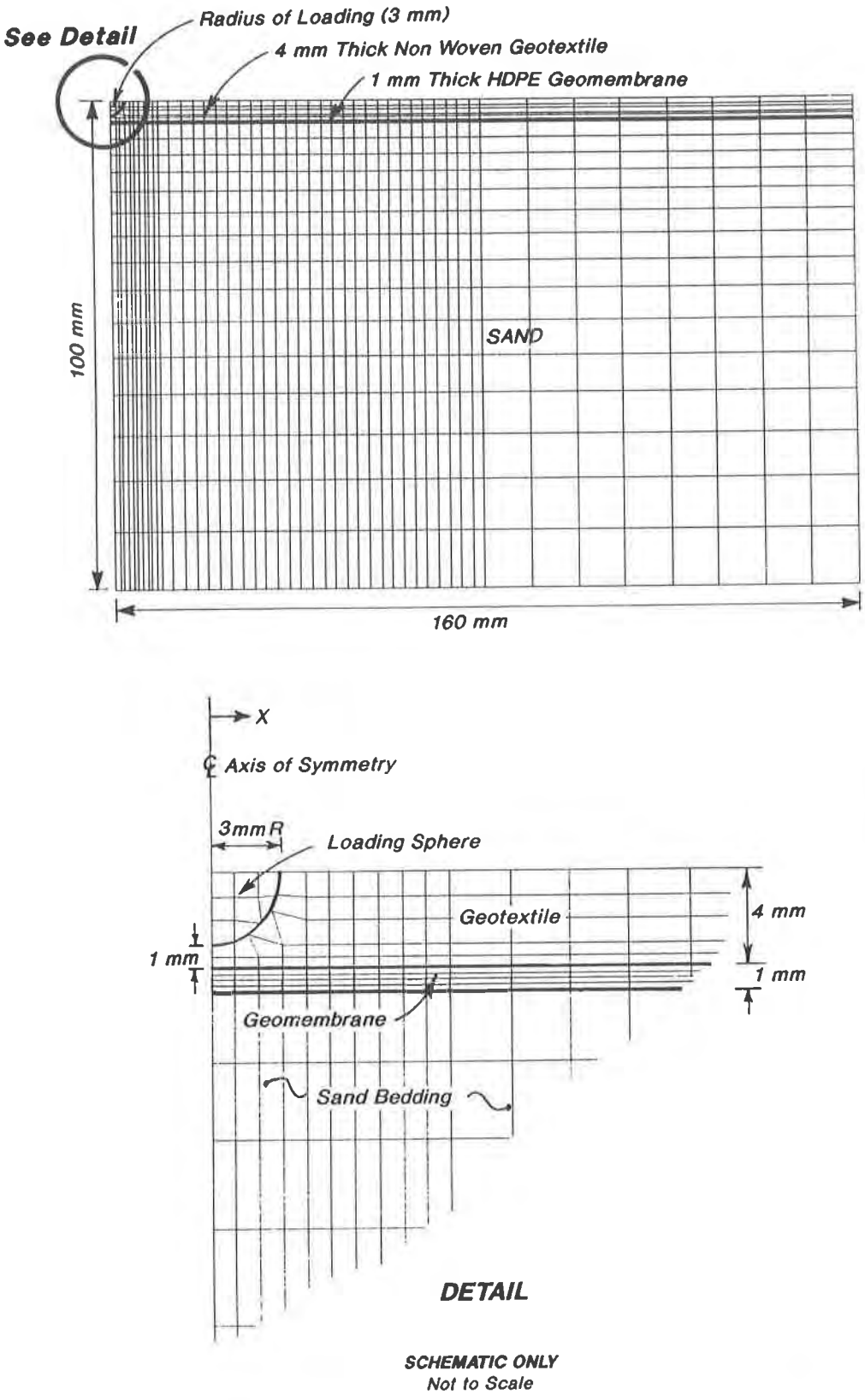

Figure 6. FLAC Model Mesh

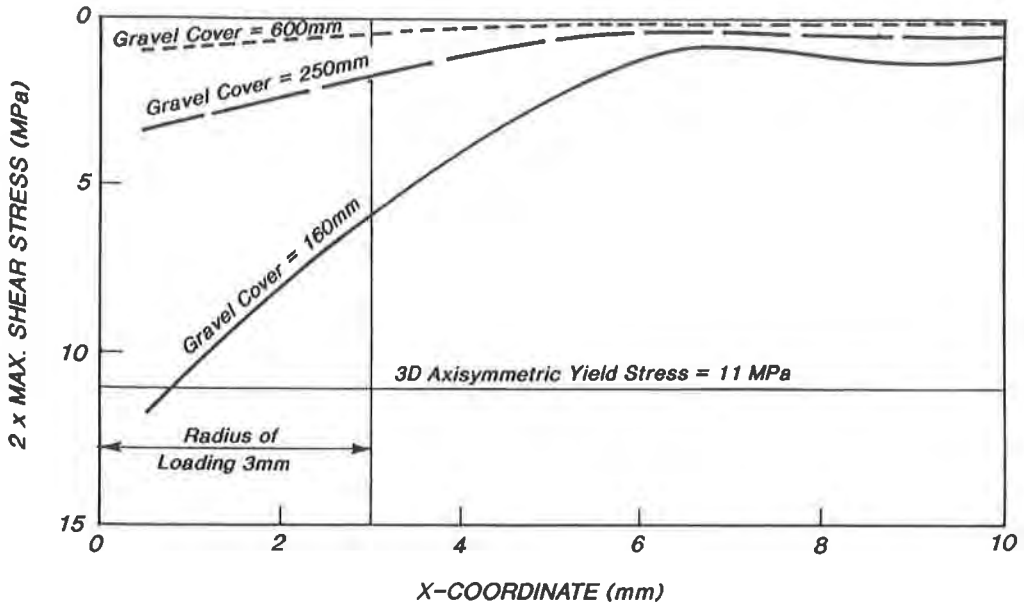

a) WITH GEOTEXTILE

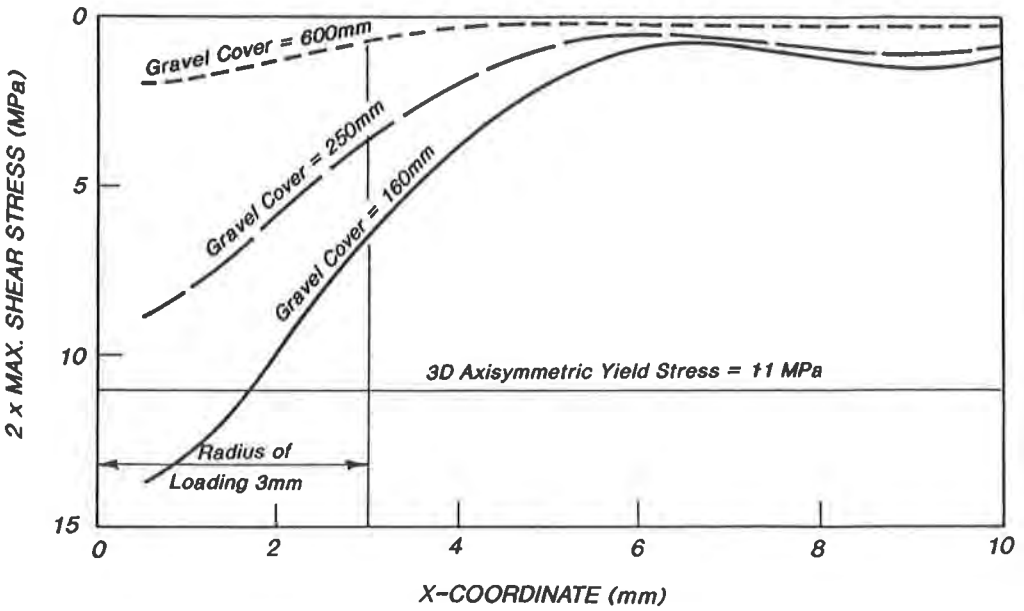

b) WITHOUT GEOTEXTILE

Figure 7. FLAC Model Results

When the maximum geomembrane stress predicted by the model is near the 11 MPa criterion, such as the case of 250 mm cover and no geotextile blanket, only one pressure point was identified in the field test, indicating a marginal condition. When the maximum stress predicted by the model is significantly less than 11 MPa, such as the case of 250 mm cover and a geotextile blanket, no punctures or pressure points were experienced in the field tests, indicating acceptable performance.

The above results indicate that the model appears to provide a satisfactory correlation with field performance, when the three dimensional axisymmetric tensile yield stress is used as a failure criterion, and validates the model for the given conditions. The model demonstrates that the effect of the geotextile blanket is to reduce the stresses on the geomembrane. The model further indicates that 600 mm of soil cover will substantially reduce the stresses on the geomembrane and will provide a significant margin of safety with respect to survivability of the geomembrane.

In summary, it appears that the survivability of a geomembrane can be empirically modelled by simplifying the loading conditions to that of a single piece of gravel having a 3 mm hemispherical radius acting on the geotextile or geomembrane. However, it is important to remember that the model was calibrated to the type of performance considered to be acceptable (i.e. very shallow indentations of the geomembrane were considered to be acceptable) and that these performance criteria may not be acceptable for other applications.

CONCLUSIONS

The results of the field testing indicated that a cap system consisting of sand bedding, 40 mil HDPE or 30 mil VLDPE, a 400 grams/m^2 non-woven needle-punched geotextile blanket, and a minimum 250 mm thickness of 12 to 38 mm clear crushed gravel soil cover would be capable of surviving heavy truck traffic.

The stop/start action of vehicular traffic imposed the highest stresses on the cap system and is considered to be the most critical loading condition, especially on the geotextile protective blanket. While the start/stop action may not directly affect the geomembrane if it is covered with a geotextile blanket, the resulting rutting decreased the thickness of granular material overlying the geomembrane, thus increasing the contact stress of the gravel on the geomembrane. To ensure that the geomembrane is not damaged, the thickness of soil cover should be increased such that, if rutting occurs, 250 mm of soil cover would still remain between the truck tires and the geomembrane.

The field testing indicated that a geotextile blanket over the geomembrane was required to minimize damage due to a gravel soil cover. The testing with a gravel soil cover also indicated that a 40 mil HDPE geomembrane had superior survivability compared with a 30 mil VLDPE geomembrane.

It appeared that loosening of the surface of the sand bedding due to foot traffic did not make a difference on the survivability of the geomembrane. Use of crushed sand and gravel as a bedding layer significantly decreased the survivability of geomembranes.

For the sand bedding and cap conditions described in this paper, it appeared that the survivability of the cap system could be modelled with the computer program FLAC using linear elastic parameters for the geomembrane and geotextile. The computer model results, when correlated against the three dimensional axisymmetric tensile yield stress, appeared to reflect the type of behavior and performance observed in the field test for the given performance criteria.

ACKNOWLEDGEMENTS

The permission of B.C. Environment to publish the results of the field testing is appreciated. The authors also wish to thank the following organizations for contributing geosynthetic materials for this study: Columbia Geosystems Ltd., National Seal Company, and Nilex Geotechnical Products.

REFERENCES

D'Appolonia, D.J., Whitman, R.V., and D'Appolonia, E.D. (1969), "Sand Compaction with Vibratory Rollers", Journal of the Soil Mechanics and Foundations Division, ASCE, Vol.95, SM1, pp. 263-284.

FLAC Version 2.2 (1989), Itasca Consulting Group, Inc. Minneapolis, Minnesota, U.S.A.

Gunkel (1981), "Membrane Liner Systems for Hazardous Waste Landfills", Proceedings of the 7th Annual Research Symposium, U.S. EPA-600/9.81-002b, pp. 131-139.

Koerner, R.M., Designing with Geosynthetics, Prentice Hall, New Jersey, 1990.

The Effect of Temperature, Pressure and Oven Aging on the High-Pressure Oxidative Induction Time of Different Types of Stabilizers

R.W. Thomas
National Seal Co., USA

C.R. Ancelet
National Seal Co., USA

ABSTRACT

There has recently been a great deal of discussion concerning the usefulness of the oxidative induction time (OIT) of polyolefins as determined by differential scanning calorimetry. The current belief is that when the test is performed at 200°C, as required by ASTM D3895, the results have no relationship to real-life aging and may or may not relate to the concentration of stabilizer. Also, the same test performed at lower temperatures and under a high oxygen pressure has been proposed as a more realistic test, but no definitive data have yet been generated.

This study was designed to deepen the understanding of the test and the effects of temperature and pressure. Samples of HDPE geomembranes were prepared that contained different types and amounts of stabilizers. Twelve experimental formulations were prepared from six different additives that included three hindered phenols, two hindered amines and one phosphite. The samples were evaluated by the OIT test at different temperatures and pressures, and the effect of oven aging at 115°C was also studied.

The results showed that for the additives tested, the high pressure OIT showed Arrhenius behavior for temperature and was inversely dependent on pressure at temperatures between 140 and 160°C and at pressures between 1.38MPa(200psi) and 5.52MPa(800psi). Results of oven aging showed that for volatile additives, the high pressure OIT test does not simulate oven aging and therefore may be inappropriate as a durability tool when used by itself. However, the combination of oven exposure followed by high pressure OIT appears to be a promising new technique for following the effects of oven aging on stabilized geomembranes.

INTRODUCTION

One of the most popular ways to evaluate the thermooxidative stability of polyolefins is to determine the OIT of a sample in a differential scanning calorimeter (DSC). The method most often used (ASTM D3895) was designed to measure the stability of plastic insulation on copper wires. In recent years the test has been used to evaluate a variety of materials including oils, greases, waxes, and different types of polyolefins. Basically, the method involves heating a sample at a predetermined temperature in an oxidizing atmosphere (air or oxygen) and waiting until spontaneous decomposition of the polymer occurs. The time from the addition of oxidizer to decomposition is the OIT and is the time in which the protective additives have reacted with oxygen, evaporated, or decomposed. Once most of the additives are consumed, the rate of polymer decomposition auto-accelerates and can be detected by a large evolution of heat. The test has been harshly criticized for the lack of correlation between it and oven aging tests performed at much lower temperatures (Gugumus,1987, Thomas,1989, Gray,1990). However, it is well documented that a better correlation exists if the

temperature at which the OIT is determined is similar to the oven aging temperature (Gugumus,1987, Kramer,1986). Therefore, the main reason for the lack of correlation has been that the OIT test is generally run at temperatures that induce chemical reactions and physical phenomena that do not occur at lower temperatures.

Besides increasing temperature, another way to accelerate thermooxidation is by increasing the concentration of oxygen (Faulkner, 1982,1985). This method involved placing samples in pressurized vessels and performing oven aging under high oxygen pressure. The method was reported to accelerate the rate of thermooxidation from 3.6 times (Faulkner,1982) to 70 times (Faulkner,1985) depending on sample geometry. Additionally, similar energies of activation were determined with and without high pressure, which suggests that the appropriate reactions are accelerated without introducing new ones or changing the mechanism of degradation.

The acceleration due to high oxygen pressure has also been demonstrated in a pressurized DSC (Dugan,1984, Cadwallader,1987,1990, Rhee,1990, Thomas,1992). The test requires a high pressure DSC and involves performing an OIT experiment at pressures as high as 5.52MPa(800psi). The test can generally produce data at much lower temperatures than conventional OIT. In fact, temperatures as low as 130°C have been reported (Cadwallader,1987,1990). This should be a more appropriate test than an OIT measured at 200°C, but the effect of high oxygen pressure has not been addressed, especially for volatile stabilizers. Also, the lowest temperature at which the decomposition can be detected is still above the melting point of HDPE (128°C). Therefore, this study was designed to look at the effect of high pressure on a series of additives and determine if the results of the high pressure OIT test can be correlated to oven aging at temperatures below the melting point of HDPE.

EXPERIMENTAL

Experimental Additive Packages. A total of 14 different samples were investigated during this study. There were 12 experimental additive packages compounded into a "barefoot" resin and converted to either 2.03mm (80mil, samples A-1 through A-6) or 1.52mm (60mil, samples B-11 through B-16) sheet on a one foot wide flat sheet extruder with a 6.35cm (2.5in) screw. Additionally, two commercially available, proprietary formulations were investigated. The formulations of the 12 experimental packages are given in Table 1. The hindered phenols used were Irganox 1010, Irganox 1076 and Santowhite Crystals, the HALS were Tinuvin 622 and Chimassorb 944, and the phosphite was Irgaphos 168. All additives were supplied by the Ciba-Geigy Corp., except Santowhite Crystals (Monsanto Company).

OIT Analysis. All of the DSC experiments were performed in a TA Instruments Model 910 DSC. Both high and low pressure cells were used in the analysis of different stabilizer packages. The baseline samples from packages A-1 through A-6 were cryogenically ground before testing. All other samples were shaven from the test coupons. To avoid the exposed edges of the coupons, the shavings were taken from a freshly cut interior edge.

The low pressure experiments closely followed the procedure outlined in the ASTM Method D3895. Five to ten milligrams of the sample shavings were placed in a tared aluminum sample pan. The sample was then weighed and placed in the DSC cell. An empty aluminum pan was placed on the reference platform. Next, the cell was covered and purged with an inert gas (nitrogen) at a rate of 50 ml/min for five minutes to assure displacement of oxygen from the cell. While still under purge, the sample was heated at a rate of 20°C/min to 200°C. The instrument was programmed to hold the sample at this temperature using the "isotrack" mode. The sample was then allowed to equilibrate at the test temperature for five minutes prior to the introduction of oxygen. The time from the introduction of oxygen to the onset of an oxidative exotherm was taken as the oxidative induction time or OIT.

Table 1. Experimental Additive Formulations

SAMPLE NUMBER	IRGANOX 1010(PPM)	IRGANOX 1076(PPM)	SANTOWHITE CRYS.(PPM)	TINUVIN 622(PPM)	CHIMASSORB 944(PPM)	IRGAPHOS 168(PPM)
A-1	1500					750
A-2*	1500					750
A-3	3000					750
A-4	750			1000		750
A-5*	750			1000		750
A-6	750			2000		750
B-11	1000					
B-12		1000				
B-13			1000			
B-14				1000		
B-15					1000	
B-16						1000

* All experimental formulations except A-2 and A-5 contained 2.5% carbon black

The high pressure cell was configured for constant volume operation according to the operator's manual. The procedure for the high pressure OIT test consisted of three basic steps: 1) Loading the cell; 2) Purging and pressurizing the cell; and 3) Performing the experiment. Typically, the cell was loaded in the same manner as a normal DSC cell. All gas valves were closed and the tank regulator was set at the desired pressure. The cell was then purged with oxygen by opening the outlet and inlet valves to the cell a few turns. The cell was purged for several minutes to assure complete displacement of the air in the cell. The outlet valve on the cell was then closed off and the cell pressure allowed to equilibrate. The inlet valve was then closed and the experiment started. A typical temperature program for these experiments included a 20°C/min ramp to the test temperature and an isotrack segment long enough to observe the oxidative exotherm. The time varied with the type of stabilizer. The OIT was taken as the time from the start of the test (heating) to the onset of the oxidative exotherm.

Air-Oven Aging. The air-oven aging experiments were performed in a Baxter Model DN-83 Mechanical Convection Oven. The air flow through the oven was adjusted by opening the air intake about 50%. The samples were placed in the oven two different ways. The first set, A-1 through A-6, were about 22cm X 28cm and were hung on cubical, stainless steel racks by their four corners with stainless steel wire. The samples were placed in a way to maintain at least 1cm of space between the samples. The second set, B-11 through B-16, were about 14cm X 22cm and were hung on stainless steel or glass rods through a hole punched in the top center. Spacers made from Tygon tubing, 1cm wide, were placed on the rods between the samples to prevent close contact. The rods were then suspended under the oven's racks.

RESULTS AND DISCUSSION

The types of samples investigated during this project were divided into three groups. The first group (A-1 through A-6) were made to study the effects of concentration, carbon black, and the addition of a hindered amine light stabilizer (HALS) on a basic stabilizer formulation. The basic package consisted of a hindered phenol and a phosphite (sample A-1, Table 1). Sample A-2 was the same formulation without carbon black and sample A-3 had twice as much phenol. The next three, A-4 through A-6, had a HALS at two concentrations and samples with and without carbon

black. The second group of experimental rolls (B-11 through B-16) were prepared with single components at a constant level of loading (1000 ppm by weight) and the third group tested were two commercially available packages (M-1 and M-2).

The high pressure OIT test has not yet been standardized and involves many more variables than the low pressure method. The pressure cell from TA instruments can be configured so that the purge gas flows across the sample compartment from top to bottom or bottom to top, or the flow can be around the sample compartment to pressurize the high pressure canister. Also, the cell can be run static or with a high pressure flow of oxygen. Another variable is the actual pressure inside the sample compartment. There is a pressure gauge mounted in the cell, but it seems too imprecise for this type of work. Therefore, the actual pressure of the experiment was questionable. In this study, the cell was pressurized at room temperature to the target pressure, then the experiment started with a temperature ramp to the target temperature. The resulting increase in temperature created a corresponding change in the pressure that was estimated to be about a 10% increase. It was not possible to calculate the pressure increase because only a small portion of the gas volume was heated. It is recognized that this is probably not the most favorable way to perform this experiment, but an attempt was made to quickly find a way that would provide reasonable precision. The method chosen involved a constant volume of gas at pressure, the pressure was set at room temperature, and the experiment started under pressure at room temperature.

Table 2 shows a comparison between low and high pressure OIT for eight different rolls. The values with standard deviations next to them were those samples run in triplicate; all others were in duplicate.

Table 2. Comparison Between Low and High Pressure OIT For Different Additive Packages

SAMPLE	LPOIT(min) 200°C,0.10MPa (14psi)	HPOIT(min) 150°C,5.52MPa (800psi)
A-1	87(2)*	132
A-2**	69(3)	208
A-3	125(2)	174
A-4	73(2)	476(24)
A-5**	48	1018
A-6	81(4)	863
M-1	95	141
M-2	90	206

* Standard deviation of triplicate analyses
** No Carbon Black

Several interesting results are found in this table. First, the effect of adding carbon black on OIT can be seen by comparing samples A-1 with A-2 and A-4 with A-5. Notice that under low pressure and high temperature, the addition of carbon black increases the OIT. Conversely, under high pressure at lower temperature, the addition of carbon black significantly decreases the OIT. It has been suggested that carbon black adsorbs the additives (Gray,1990). Assuming this is true, it is possible that at 200°C, the additives have been desorbed and are available to do whatever it is that they do during the OIT experiment. Nonetheless, this difference is one piece of information suggesting that different phenomena occur at the two different conditions of temperature and pressure.

Another interesting result is seen in the behavior of the HALS under the different conditions. Notice that HALS are nearly invisible at 200°C (samples 4,5 and 6) but become active at the lower temperature, which has also been previously reported (Gray,1990). Again, this is strong evidence that these two conditions are dramatically different. Since it has been shown that oxygen pressure does not change the reaction mechanisms at 90°C (Faulkner,1982), it was assumed that the differences seen in Table 2 are mostly due to differences in temperature.

Other information found in this table include the effect of concentration and a dramatic display of the fact that the high pressure conditions seem to readily distinguish different additive packages. And finally, it appears as if the two commercial packages are different in some way, based on the high pressure results. More evidence concerning the differences between the two conditions of temperature and pressure is shown in Table 3, which shows the high and low pressure OIT values for the individual component samples (Thomas, 1992).

Table 3. Comparison Between Low and High Pressure OIT For Individual Stabilizers

SAMPLE	LPOIT(min) 200°C,0.10MPa (14psi)	HPOIT(min) 150°C,3.45MPa (500psi)
B-11(Irganox 1010)	56	152
B-12(Irganox 1076)	23	103
B-13(Santowhite Cry.)	23	291
B-14(Tinuvin 622)	5	245
B-15(Chimassorb 944)	3	473
B-16(Irgaphos 168)	6	129

Notice that the high pressure experiments were performed at 3.45MPa(500psi), while the Table 2 results were done at 5.52MPa(800psi). Also notice that the ranking does not hold between the two conditions and that the HALS are again, invisible at 200°C and very active at 150°C. Of additional interest is the fact that the Santowhite Crystals gave the highest HPOIT value of the three hindered phenols (B-11,B-12,B-13), and that the HALS (B-14,B-15) produced the highest values of all.

The effect of temperature was determined at three temperatures from 140°C to 160°C on 5 samples. The results are shown in Table 4 and the corresponding Arrhenius plots are found in figure 1.

Table 4. The Effect of Temperature on the HPOIT at 3.45MPa(500PSI)

SAMPLE	OIT(min) 140°C	OIT(min) 150°C	OIT(min) 160°C
A-1	353	186(9)	102
A-3	478	246	134
A-4	1290	606(18)	271
M-1	408	214	112(2)
M-2	655	295	138

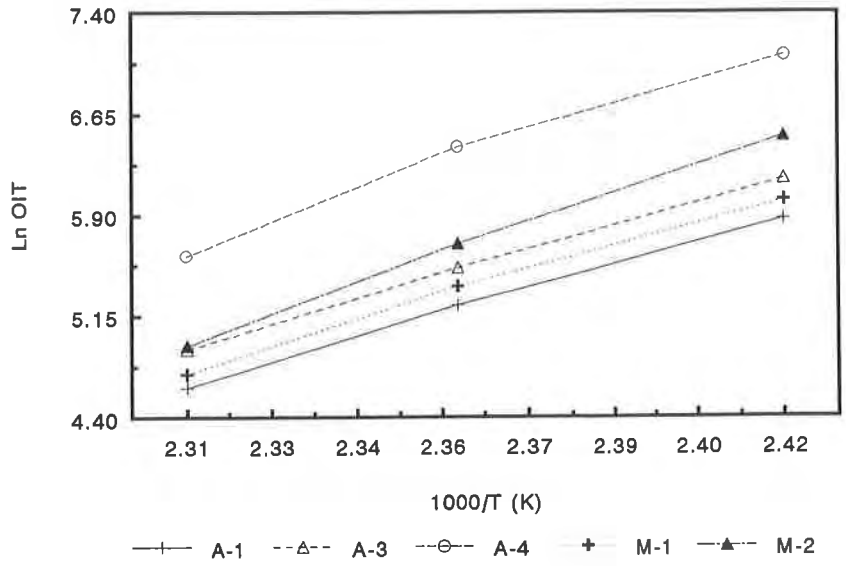

Figure 1. The Effect of Temperature on the HPOIT at 3.45MPa(500PSI)

The slopes of the lines, which give the relative energies of activation seem to fall into two groups. Samples A-1, A-3 and M-1 all have slopes about 20% lower that samples A-4 and M-2. This indicates that samples A-4 and M-2 are more stable to the condition of high pressure at these temperatures.

The effect of pressure was also evaluated on the same samples from 1.38MPa(200psi) to 5.52MPa(800 psi). The results are shown in Table 5 and a plot of HPOIT versus inverse pressure is given in figure 2. These results are essentially the same as those previously reported (Dugan,1984).

Table 5. The Effect of Pressure on the HPOIT at 150°C

SAMPLE	OIT(min) 1.38MPa (200psi)	OIT(min) 3.45MPa (500psi)	OIT(min) 5.52MPa (800psi)
A-1	356	186(9)	132
A-3	495	246	174
A-4	960	606(18)	476(24)
M-1	397	214	141
M-2	550	295	206

Figure 2 shows that the samples fall into two groups, with sample A-4 being significantly different than the others. Since we know that A-4 is a HALS and A-1 and A-3 contain a phenol and a phosphite, this difference might be due to the type of stabilizer. Or, it could be related to vapor pressure. Either way, the pressure dependence of sample A-4 is different than the others. This fact suggests that pressure does play a role in this test, and that the mechanism of degradation (chemical or physical) may be changed by high oxygen pressure.

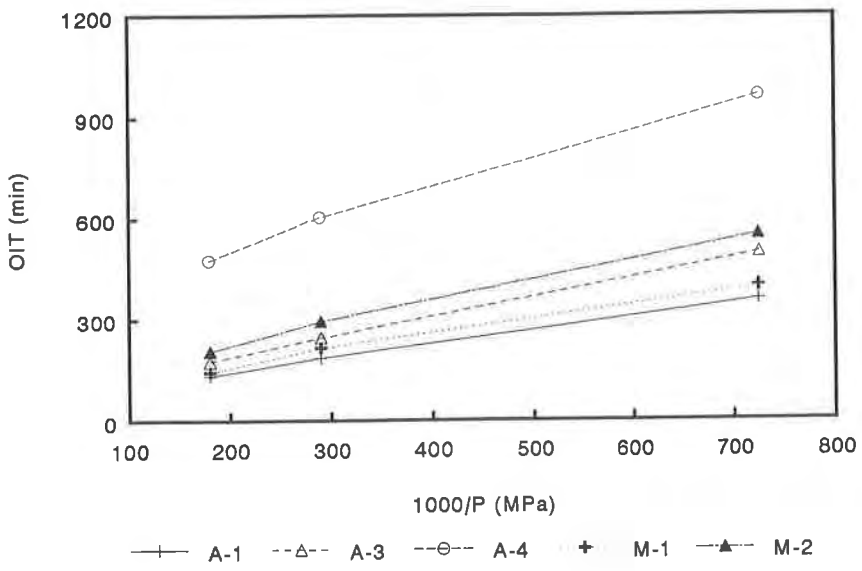

Figure 2. The Effect of Pressure on the HPOIT at 150C

Another way to evaluate the effects of pressure and temperature is to attempt to correlate the HPOIT results to oven aging. Since the time to failure by embrittlement is months or years, the change in HPOIT as a function of oven exposure time was measured. This way, the HPOIT was used as a measure of the materials lifetime and the loss of lifetime by air oven aging was monitored. If the mechanisms are the same, one would expect that the change in HPOIT with aging would be smallest for the sample with the highest initial value. The results of the aging experiments are shown in Table 6.

Table 6. The Effect of Oven Aging at 115°C on HPOIT [150°C,3.45MPa(500 psi)]

SAMPLE	OIT(min) 0 DAYS	OIT(min) 21 DAYS	OIT(min) 50 DAYS
A-1	186(9)	134	95(5)
A-3	246	199	158(4)
A-4	606(18)	484	447(17)
A-6	1175	817(23)	694
B-11	152	120	80
B-12	102	85	56
B-13	291	85(15)*	58
B-14	245	199	189
B-15	473	420	372
B-16	129	75	31
M-1	214	154	127
M-2	295	278(9)	268

* 5 Replicates

These results suggest that, by itself, the HPOIT is not a measure of the products durability. Compare the behavior of samples B-12, B-13, and M-2. B-13 has an initial value equal to M-2 and three times larger than B-12. However, after only 21 days of exposure, its value becomes comparable to B-12 and much lower than M-2. The difference in behavior between the components in samples B-12 and B-13 might be explained by comparing their chemical structures. Irganox 1076 (B-12) is a monofuntional phenol with a molecular weight of about 530. Santowhite Crystals (B-13) is a difuntional phenol with a molecular weight of about 358. This means that Santowhite Crystals is both more active at constant loading (lower equivalent weight) and more volatile (lower molecular weight) than Irganox 1076. Therefore, it is essentially an OIT booster, since the oven aging results show that it readily diffuses out of the plastic. Notice that the precision for B-13 at 21 days was very poor. The cause of this has not been determined but the poor precision appears to be restricted to this sample. The overall performance of the 12 formulations in Table 6 is shown graphically in figure 3 and figure 4 (Thomas, 1992).

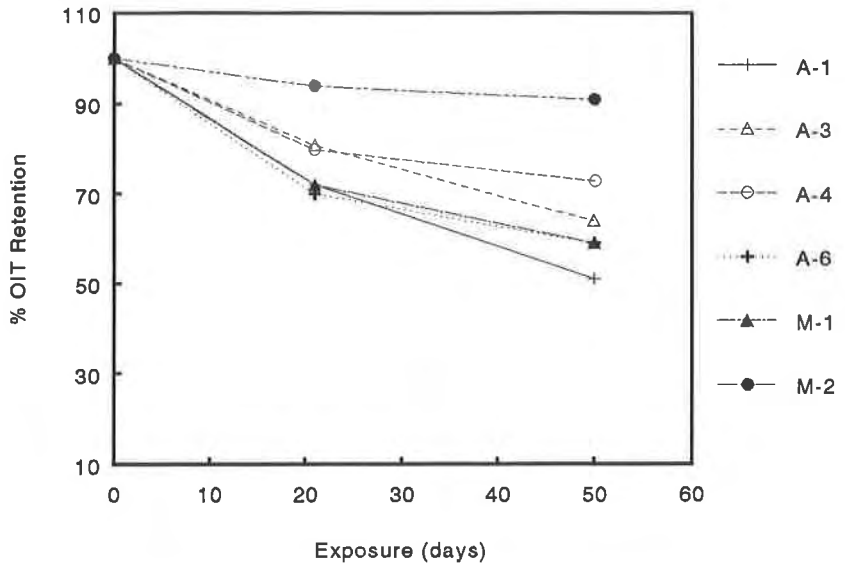

Figure 3. The Effect of Oven Aging at 115C on HPOIT [150C,3.45MPa(500psi)]

Two types of behavior seem typical. Either the loss of HPOIT is linear or shows up as a curve. It is possible that the curves relate to diffusion controlled changes. This is suggested because the two most volatile components are Irgaphos 168 (B-16) and Santowhite Crystals (B-13), and loss of volatiles would be diffusion controlled. The other curves are found in samples containing HALS. In this case, the curves show up at higher concentrations, so the samples may be supersaturated. Therefore, the excess additive may be lost through a diffusion controlled process, producing a curve. Nonetheless, it is clear from these results that the processes are complex and involve all the components in a formulation. And, since some formulations may contain up to six components, the type of analysis presented here must be done cautiously. However, it does appear that the combination of oven aging and HPOIT shows promise for extracting durability information in a short period of time.

For example, recall that samples M-2 and A-4 both displayed higher energies of activation in the Arrhenius plots. Figure 3 shows that these two formulations lose their HPOIT values slowly. It is also clear that formulations with volatile components will change very rapidly during the initial stages of oven aging. But, once the volatiles are gone, it is possible that the changes may be slower. Therefore, it may be possible to follow the effects of oven aging until a linear state is reached, which might be indicative of the true rate of degradation.

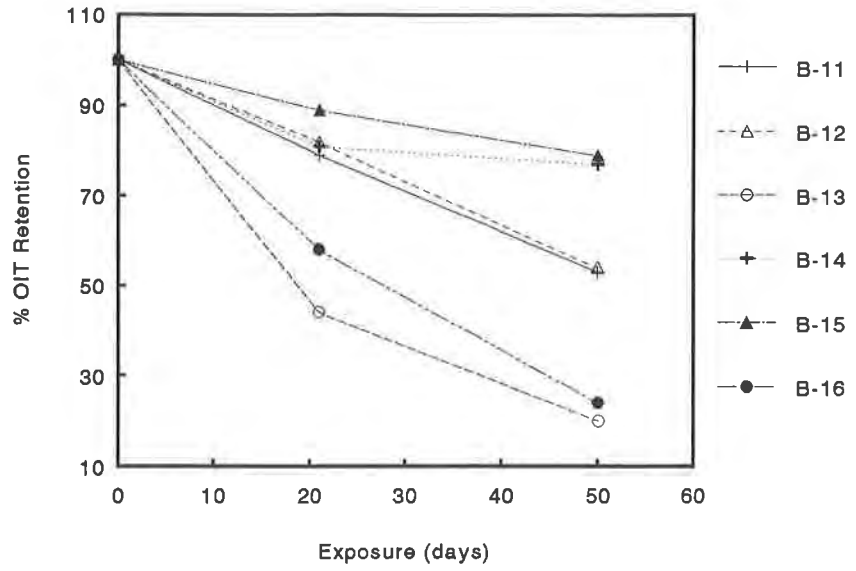

Figure 4. The Effect of Oven Aging at 115C on HPOIT [150C,3.45MPa(500psi)]

CONCLUSIONS AND RECOMMENDATIONS

The results of this study showed that although the high pressure OIT test accelerates the degradative processes and can produce results at lower temperatures, the effects of the high pressure cannot be ignored. These effects are most evident in volatile additives. It was also demonstrated that each component of a formulation contributes to the HPOIT and a complex situation is found when trying to follow changes in HPOIT during oven aging. However, the combination of HPOIT with oven aging shows promise as a method for evaluating the effects of oven aging without waiting for brittle failure. If this is true, then it would be possible to evaluate the thermooxidative resistance of geomembranes in months rather than years.

To accomplish this goal, much more research is needed. First, the current samples need to be aged for longer periods to evaluate the longer range effects. Next, the effects of pressure on volatile additives should be investigated. Other combinations of additives in different concentrations should be evaluated to determine if the loss of HPOIT is related to a decrease in concentration of a particular additive. And finally, some samples must be aged to failure to absolutely determine if the technique is viable. If some of these goals can be reached, then perhaps long term information can really be found in the results of short term tests. This, of course, is a major goal for everyone involved in durability and accelerated life testing.

REFERENCES

Cadwallader, M.W. and Metzger, P., (1987) "Accelerated Ageing of High Density Polyethylene Geomembranes: A Novel Approach", Proceedings of the 42nd Purdue Industrial Waste Conference, West Lafayette, Indiana.

Cadwallader, M.W., (1990) "The Relation of High Pressure OIT to Oven Ageing for HDPE Liners", Proceedings of the 4th International Conference on Geotextiles, Geomembranes, and Related Products, The Hague, Netherlands, p. 593.

Dugan, G. and McCarty, J.D., (1984) "An Improved Differential Scanning Calorimetry Method for Studying the Oxidative Stability of Polymers and Resins", Proceedings of the 13th North American Thermal Analysis Society Conference, Philadelphia, Pennsylvania.

Faulkner, D.L., (1982) "Effects of High Oxygen Pressure and Temperature on the Aging of Polypropylene", Polym.Eng.Sci., Vol.22, No.8, pp. 466-471.

Faulkner, D.L., (1985) "Aging of Polypropylene Using High Oxygen Pressure", Proceedings of the 189th American Chemical Society Meeting, Miami, Florida, pp. 515-519.

Gray, R.L., (1990) "Accelerated Testing Methods for Evaluating Polyolefin Stability",in "Geosynthetic Testing for Waste Containment Applications", R.M.Koerner, Ed., ASTM STP 1081, pp. 57-71.

Gugumus, F., (1987) "The Use of Accelerated Tests in the Evaluation of Antioxidants and Light Stabilizers", in "Developments in Polymer Stabilisation", Vol.8, G.Scott, Ed., Elsevier Applied Science Pubs., New York, New York, pp. 239-287.

Kramer, E., and Koppelmann, J., (1986) "Measurement of Oxidation Stability of Polyolefins by Thermal Analysis", Polym.Deg.Stab., Vol.16, pp. 261-275.

Rhee, I., (1990) "Development of a New Oxidation Stability Test Method for Greases Using a Pressure Differential Scanning Calorimeter (PDSC)", Proceedings of the 57th Annual Meeting of the National Lubricating Grease Institute, Denver, Colorado.

Thomas, R.W., Bartz, A.K., and Verschoor, K.L., (1989), "Evaluation of the Oxidative Stability of High Density Polyethylene Geomembranes by Isothermal and Dynamic Differential Scanning Calorimetry", in "Durability and Ageing of Geosynthetics", R.M. Koerner, Ed., Elsevier Applied Science Pubs., New York, New York, pp. 230-243.

Thomas, R.W., and Ancelet, C.R., (1992), "High Pressure OIT for Geomembranes", Geotechnical Fabrics Report, Vol.10, No.5, pp.12-13.

The Environmental Stess Cracking of Polymers Used in Geosynthetic Products

D.G. Bright
The Tensar Corp., USA

ABSTRACT

Geosynthetic polymers used in critical earth structures and hazardous waste containment sites have a minimum performance requirement to be maintained over a service life ranging from 1 to 100 years. During service, these polymers experience stress and contact with environmental agents. Sufficiently high stresses can cause crazes and cracks which, when exposed to agents, can propagate leading to the deterioration of the mechanical properties of the polymer. This is environmental stress cracking (ESC).

A polymer may be ductile when stressed in air, and may resist a particular stress cracking agent when exposed in an unstressed state. But, if the polymer is exposed to a particular agent while under stress, it may fail in a brittle manner at low strains in the short-term. The general perception is that ESC is a phenomenon associated only with polyethylenes. However, other polymers used in geosynthetics are subject to ESC as well. The objective is to address the ESC phenomenon, mechanism, test conditions and limitations, and performance of polymers used in geosynthetic products.

INTRODUCTION

Critical applications of polymeric products in the ground include natural gas pipe, geomembranes in municipal and hazardous landfills, and geogrids in soil reinforcement. These products are designed for a service life ranging from 1 - 100 years. Over their service life, these products experience stress and contact with environmental agents. Typically, these conditions do not present a problem for these products to perform at design conditions. Only where conditions of high stress are concentrated at a particular point causing crazing and cracking aggravated by exposure to an agent(s) is there a concern for a product not maintaining a minimum level of performance. This is the phenomenon of environmental stress cracking (ESC).

Historically, this phenomenon is commonly associated with polyethylenes (PE) because of its strict testing for use in so many critical applications, e.g., natural gas pipe, telephone cable coating, and chemical reagent containers. However, the ESC phenomenon applies to other polymers as well (Gomez 1975, Howard 1964, Jabarin 1992, Wolters 1987). The ESC failure of PE is merely a particular mechanism of stress failure exclusive to polyethylenes (PEs) (Gomez 1975, Howard 1959).

Resin selection, product development, methods of fabrication, and design procedures are all intended to push the time table for possible brittle failure significantly beyond the service life expectancy of the product.

ENVIRONMENTAL STRESS CRACKING

A polymer may exhibit failure in ductile or brittle manner, depending upon stress level and time duration. See Figure 1. The same polymer will likely resist attack of any stress cracking agent when exposed in an unstressed state at ambient conditions (Brown 1980, Powell 1983) for a very long time. But, when subjected to stress levels, normally inducing a ductile failure, and exposure to an agent(s), the polymer may experience premature failure in a brittle manner (Brown 1980, Powell 1983). See Figure 2. Applied stresses can cause crazes to develop. These regions are porous and prone to adsorb fluids (Powell 1983), particularly chemical agent(s) exhibiting a surfactant behavior. These agents accelerate the relaxation of the polymer's yield point at the tip of the craze (Ward 1991). This initiates additional crazes and propagates existing crazes into cracks. Eventually, crack propagation and growth becomes sufficiently rapid and extensive that brittle fracture can occur (Powell 1983). Elevated temperatures accelerate the process of stress cracking thus further reducing the time to stress rupture as shown in Figure 3. The combination of stress, sufficiently elevated temperatures, and exposure to a particular agent(s) can accelerate stress cracking promoting brittle rupture within the very short-term, e.g., hours (Ward 1990). Thus, the time to a forced, premature brittle failure has little correlation to the time-to-failure in an ambient environment. The time frame for rupture also depends on several pertinent polymeric properties: such as molecular weight and distribution, copolymer branching and frequency, density and crystallinity, molecular orientation (Howard 1964), and physical state.

THE VARIOUS MECHANISMS OF ESC

Polymeric Morphology. A semicrystalline polymer is comprised of crystalline and amorphous regions. Within the crystalline regions, the long molecular chains orient themselves in a folding manner parallel to one another forming lamella. Multiple lamella (lamellae) emanate outward from a common nuclei forming a spherulitic geometry. These spherulites are predominately crystalline. There are regions of amorphous polymer between lamellae within a spherulite (intra-regions).

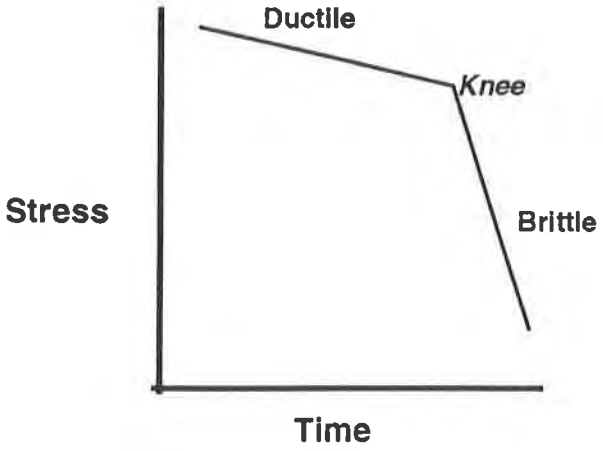

Figure 1. ESC Behavior in Air

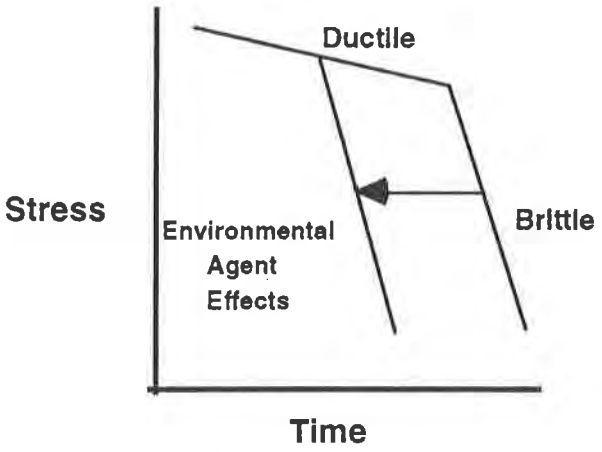

Figure 2. Effect of Environmental Agents

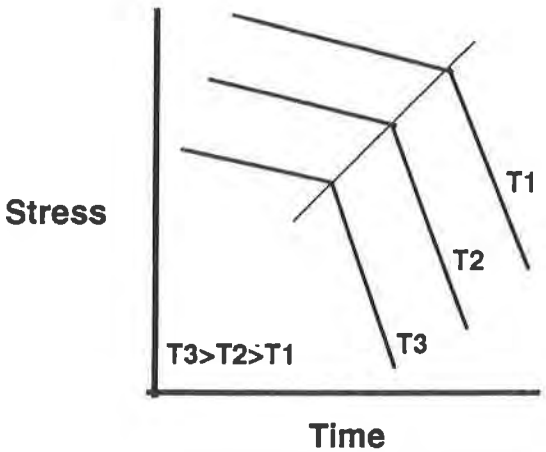

Figure 3. Effect of Temperature on ESC

Molecular chains bridging between spherulites (inter-regions), called tie molecules, achieve no specific orientation and thus makeup the principal amorphous regions within the polymer matrix.

An amorphous polymer has no specific arrangement or alignment of molecular chains and thus possesses essentially no crystallinity.

Polymeric States. A polymer in its viscoelastic state responds to stress as if it were a combination of an elastic solid and a viscous fluid. In this state, a polymer exhibits the solid characteristics of elasticity and strength, and the liquid characteristics of viscosity. The glass transition of the polymer is the reversible change that occurs when it is heated or cooled through a thermal transition where its traverses from a hard, glassy state to a viscoelastic state, and vice versa respectively. (Whittington 1978) Below its glass transition, a polymer responds to stress according to the limits of its modulus of elasticity, beyond which its experiences permanent deformation.

Viscoelastic State. Some semicrystalline polymers are in their viscoelastic state at common geotechnical temperatures (20 °C), such as polyethylenes (PE), causing behavior to be time dependent (Popelar 1991). A polymer's behavior can lead to a failure given sufficient time. Failure is ductile or brittle depending upon the stress level. When failure occurs in a ductile manner, stress levels are sufficiently high to cause plastic flow of the molecular structure in the short-term. Tie molecules stretch out, and some lamellae separate and start unfolding, causing spherulites to fracture (Lustiger 1983, Peggs 1989). The fracture interface exhibits a coarse, fibrillar character (Peggs 1989). Applied stresses cause crazes to form in the intra- and inter-spherulitic regions of the molecular matrix where stress cracking agents can be adsorbed and accelerate fracture.

When failure occurs in a brittle manner, stress levels are usually lower permitting sufficient time for the tie molecules to slowly disentangle themselves from adjacent spherulites. Failure occurs predominately in the amorphous regions between the spherulites producing a smoother fracture interface. (Lustiger 1983, Peggs 1989) Applied stresses cause crazes to form principally in the inter-spherulitic regions of the molecular matrix where stress cracking agents can be adsorbed and accelerate fracture.

Stress cracking agents accelerate relaxation of the polymer's yield point at the craze tip sufficiently to initiate crack formation followed by slow crack growth (Ward 1991). In PEs, the time for slow crack growth to cause failure is about 90% of the total time to failure (Wolters 1987, Broutman 1990).

Glassy State. Some semicrystalline polymers are in their glassy state at 20 °C, such as poly(ethylene terephthalate) (PET). The physical and mechanical aging of such polymers occurs with time when below their

glass transition. (Struik 1987) The glass transition temperature of high tenacity PET fiber is about 75 °C. At ambient temperatures (20 °C), PET changes from a tough or ductile to a brittle fracture mode with time (Aref-Azaf 1983, Jabarin 1992, Mininni 1973). Thus, PET, like other polymers, is also subject to ESC brought about by the impact of stress and the environment (Jabarin 1992).

Due to its chemistry, PET adsorbs some moisture (Davis 1988), primarily in the amorphous regions. Water sorption produces stress at the amorphous/crystalline interface, causing the formation of microcavities (Bastioli 1990) or voids. These voids permit adsorption of additional water, if available, facilitating more plasticization and microcavitation or void volume generation. These voids are frequently associated the formation of crazes (Mininni 1973). The presence of environmental agents while under stress could initiate ESC of PET.

Some polymers are amorphous and in their glassy state at 20 °C, such as unplasticized poly(vinyl chloride) (uPVC). Although the grades of PE and uPVC used in gas, water, and sewer pipe, show little variation in ductile long-term strength, they differ considerably in long-term brittle-like failure behavior. The transition from ductile to brittle fractures is gradual for uPVC. Brittle failure in uPVC is caused by a process of craze initiation, growth, and breakdown. Breakdown is the transition of crazes into cracks followed by almost immediate fracture. Thus, the time for crack initiation is about 90% of total time to failure. The time to failure is strongly affected by the quality of the entanglement network within the craze (material quality), surrounding medium environmental agent(s), temperature, and applied stress. (Wolters 1987)

Plasticized Vinyl Polymers. Some vinyl polymers are plasticized prior to fabrication into geosynthetic products. A plasticizer is added to a rigid polymer (e.g., uPVC) to lower its glass transition temperature (T_g) to below 20 °C so that the plasticized polymer blend (e.g., plasticized PVC) exhibits a viscoelastic behavior permitting flexibility. For economic reasons, no more plasticizer is added than necessary.

Any loss of plasticizer(s) with time due to leaching (Ansell 1985, Seaman 1976), and/or microbiological attack (Bessems 1979, Bright 1992, Cadmus 1977, Tirpak 1970) results in the plasticized PVC becoming progressively brittle and crack prone (Ansell 1985) as its T_g rises above 20 °C towards the T_g of uPVC (~80 °C). Then, the less plasticized PVC could start to mimic the ESC behavior of uPVC.

LIMITING CONDITIONS FOR TESTING OF ESC

The gas industry has used PE plastic pipe for distribution of natural gas since the early 1950s. The ASTM D 2837 test standard is commonly used to qualify a new resin and quality control pipe product for slow crack growth, but this test generally takes more than a 10,000 hours. The gas industry desires a much shorter term test.

Ward, Lu, and Brown (1990) have established the test conditions for greatly accelerating crack growth in MDPE sufficiently to force premature brittle failure in the very short-term, e.g., << 1000 hours. A notched test specimen of a specific geometry loaded to 2.4 MPa exposed to a 10% IGEPAL® CO-630 solution at 80 °C can experience brittle fracture in < 2 weeks (280 hours), the same mode of fracture that occurs in MDPE gas pipe after long-term field service, e.g., 50+ years. However, they warn that 80 °C is the upper temperature limit to prevent introduction of morphological changes in MDPE, and 2.4 MPa (350 psi) is the upper stress limit at 80 °C producing the same mode of brittle fracture in MDPE that occurs at ambient temperatures for the long-term. Thus, there is apparently an upper limit combination of stress, temperature, and agent type and concentration for a polymer in a particular specimen geometry with notch configuration that will induce brittle fracture in the very short-term that is characteristic of the long-term.

IGEPAL® CO-630 is the most common chemical agent used to accelerate stress crazing and cracking of polyethylenes promoting premature failure. It is a nonionic surfactant having a cloud point range of 52-56 °C (PHÔNE-POULENC 1990). By definition, the cloud point is the temperature at which turbidity first appears caused by separation or egress of water from the solution (PHÔNE-POULENC 1990, Whittington 1978). This phenomenon results in concentrating the original solution, and this solution concentration can increase with temperature. A change in surfactant concentration will change its wetting angle relative to a commmon material. This will affect the relaxation rate of the polymer's yield point at the craze tip, in turn, affecting the time to to premature failure. Thus, the evaluation of ESC of polyethylenes, or other polymers, at temperatures above and below the cloud point of IGEPAL® CO-630, or other stress cracking agent, would reflect differing ESC behaviors rendering correlation of such data of suspect.

REPRESENTATIVE TESTING OF ESC

Howard (1964) with Bell Laboratories warns that there cannot be just one universal test for stress crack evaluation. The test should mimic the end-use application. Pressured gas pipe will be under a constant internal loading, thus a constant load test is indicated. An end-use application experiencing repetitive flexure warrants the bent-strip test for realistic results. Test results will be as different as the modes of loading. Strips of a common PE resin tested under the bent mode will experience shorter times to the ductile-brittle transition knee than under the constant load test. (Howard 1964)

ESC PERFORMANCE BY POLYMER AND TEST METHOD

Polyethylenes. Data in Table 1 show how the time to a brittle failure, if it occurs, varies with test method. Comparison of data by Lustiger and Markham (1983) to data by Reinhart (1966) clearly shows the impact

that specimen notching, exposure to a stress cracking agent, and elevated stress has on the earliest time to a brittle failure (ductile-brittle transition: the knee). These test conditions are intended to force premature failure. With a hydrostatic design basis (HDB) of 1250 psi for thermoplastic pipe of PE 2406 (PPI 1990), the higher stress levels coupled with the impact of notching and exposure to an agent in the Lustiger and Markham data (1983) yield results having questionable correlation to long-term field performance. However, data taken at various temperatures and stress levels, in the absence of stressing cracking agents, result in correlations more meaningful to long-term performance as shown in data by Popelar (1991) and Wolters (1987) in Table 1. Bidirectional shifting of stress verses time data at 80, 60 and 40 °C to coincide with 20 °C data by Popelar (1991) enables the selection of a stress level ensuring ductile behavior of PE for very long times, 100+ years, with confidence.

Table 1. The ESC behavior of polyethylenes by test method.

Author	Specimen	Test Method	Performance Data
Reinhart 1966	MDPE Pipe	ASTM D 1598	MDPE, Conditions with NO Knee Water @ 23 °C: 50 years & 1220 psi
	HDPE Pipe		HDPE, Conditions with NO Knee Water @ 23 °C: 50 years & 1250 psi
Lustiger, Markham 1983	MDPE Pipe	Constant Tensile Load Axially notched	MDPE, Conditions at Knee Igepal @ 23 °C: 100 hours & 2000 psi air @ 23 °C: 150 hours & 2250 psi
	HDPE Pipe	1% Igepal & Air	HDPE, Conditions with NO Knee Igepal @ 23 °C: 1,000 hours & 1800 psi air @ 23 °C: 1,000 hours & 2300 psi
Popelar, Kenner, Wooster 1991	MDPE Pipe	ASTM D 2837	Conditions at Knee @ 80 °C: ~160 hours & 6.0 MPa (870 psi) @ 60 °C: ~1,260 hours & 7.4 MPa (1037 psi) @ 40 °C: ~6,300 hours & 9.5 MPa (1378 psi) Conditions at No Knee @ 20 °C: ~80,000 hours & 11.7 MPa (1697 psi)
Wolters 1987	HDPE Pipe	Hoop Stress	Conditions at Knee @ 80 °C: ~15 hours & ~5.7 MPa (826 psi) @ 60 °C: ~400 hours & ~6.4 MPa (924 psi) @ 40 °C: ~7,000 hours & ~7.2 MPa (1044 psi) @ 20 °C:~300,000 hours & ~8.2 MPa (1189 psi)

CONCLUSIONS

1. The mechanisms of environmental stress cracking depend upon the polymer and its morphology, formulation, and physical state.

2. There is apparently an upper limit combination of stress, temperature, and agent concentration for each polymer that will induce a brittle fracture in the short-term.

3. Specimen notching and agent(s) used to accelerate premature brittle failure do not generate data with which to predict long-term performance.

4. ESC test methods should mimic the end-use application of the geosynthetic to be definitive.

5. Polymers used in fabrication of geosynthetics, such as PE, PET, unplasticized PVC, and plasticized PVC, are subject to environmental stress cracking.

REFERENCES

Ansell, M. P., (1985) "The degradative effect of boiling water on polyester fibres in a PVC-coated fabric", Journal Coated Fabrics, Vol. 14, pp. 242-255.

Aref-Aref, A., et al., (1983) "The effect of physical ageing on the properties of poly(ethylene terephthalate)", Polymer, Vol. 24, No. 10, pp. 1245-1251.

Bastioli, C. et al., (1990) "Effects of water sorption on the physical properties of PET, PBT, and their long fibers composites", Polymer Composites, Vol. 11, No. 1, pp. 1-9.

Bessems, E., (1979) "Some microbiological problems of fabrics coated with plasticized PVC", Journal Coated Fabrics, Vol. 9, pp. 26-37.

Bright, D. G., (1992) "Biological stability of geosynthetics in critical earth structures", International Conference on Implication of Ground Chemistry/ Microbiology for Construction, IGCC'92: Bristol, England.

Broutman, L. J. et al., (1990) "Application of crack initiation and growth data to plastic pipe failure analysis", Annual Technical Conference '90, Society Plastic Engineers: Dallas, Texas, pp. 1495-1496.

Brown, R. P., (1980) "Testing Plastics for Resistance to Environmental Stress Cracking", Polymer Testing, Vol. 1, No. 4, pp. 267-282.

Cadmus, E. L., 1977 "The biological stability of polymers", Journal Coated Fabrics, Vol. 7, No. 7, pp. 33-42.

Davis, G. W., (1988) "Aging and durability of polyester geotextiles", Durability and Aging of Geosynthetics, Geosynthetic Research Institute: Philadelphia.

Gomez, I. L., (1975) "Testing Rigid PVC Products--analysis of Test Results", Encyclopedia of PVC, Vol. 3, L. I. Nass editor, Marcel Dekker: New York, pp. 1675-80.

Howard, J. B., (1959) "A review of stress-cracking of polyethylene", SPE Transactions, Vol. 15, No. 5, pp. 397-412.

Howard, J. B., (1964) "Why do plastics stress-crack?", SPE Transactions, Vol. 4, No. 3, pp. 217-223.

Jabarin, S. A. and Lofgren, E. A., (1992) "Environmental aging and stress-cracking of poly(ethylene terephthalate)", Polymer Engineering Science, Vol. 32, No. 2, pp. 146-158.

Lustiger, A., (1983) "The molecular mechanism of slow crack growth in polyethylene", Proceedings, Eight Plastic Fuel Gas pipe Symposium, American Gas Association: Arlington, Virginia, pp. 54-56.

Lustiger, A. and Markham, R. L., (1983) "Importance of tie molecules in preventing polyethylene fracture under long-term loading conditions", Polymer, Vol. 24, No. 12, pp. 1647-1654.

Mininni, R. M. et al., (1973) "The effect of excess volume on molecular mobility and on the mode of failure of glassy poly(ethylene terephthalate)", Journal Macromolcular Science, Vol. B8, No. 1-2, pp. 343-359.

Peggs, I. D. and Carlson, D. S., (1989) "Brittle fracture of polyethylene geomembranes", Geosynthetics: Microstructure and Performance, I. D. Peggs editor, ASTM STP 1076: Philadelphia, pp. 57-77.

PHÔNE-POULENC, (1990) Surfactants & Specialties Catalogue.

Plastics Pipe Institute, (1990) Recommended Hydrostatic Strength and Design Stresses for Thermoplastic Pipe and Fittings Compounds, TR-4/90, Society of Plastics Industry: New Jersey.

Popelar, C. H. et at., (1991) "An accelerated method for establishing the long term performance of polyethylene gas pipe materials", Polymer Engineering Science, Vol. 31, No. 24, pp. 1693-1700.

Powell, P. C., (1983) Engineering with Polymers, Chapman & Hall: New York, pp. 128-132.

Reinhart, F. W., (1966) "Long-term hydrostatic strength characteristics of thermoplastics pipe", Polymer Engineering Science, Vol. 6, No. 4, pp. 285-295.

Seaman, R. N. and B. Venkataraman, (1976) "Utilization of vinyl coated synthetic fabrics in industrial applications", Journal Coated Fabrics, Vol. 5, No. 4, pp. 225-247.

Struik, L. C. E., (1987) "The Mechanical and physical ageing of semicrystalline polymers: 1", Polymer, Vol. 28, No. 9, pp. 1521-1533.

Tirpak, G., 1970 "Microbial degradation of plasticized PVC", SPE Journal, Vol. 26, No. 7, pp. 26-30.

Whittington, L. R., (1978) Whittington's Dictionary of Plastics, Technomic: Westport, CT.

Ward, A. L. et al., (1990) "Accelerated test for evaluating slow crack growth of polyethylene copolymers in Igepal® and air", Polymer Engineering Science, Vol. 30, No. 18, pp. 1175-1179.

Ward, A. L. et al., (1991) "The mechanism of slow crack growth in polyethylene by an environmental stress cracking agent", Polymer, Vol. 32, No. 12, pp. 2162-2168.

Wolters, M., (1987) "Prediction of long-term strength of plastics pipe systems", Tenth Plastic Fuel Gas Pipe Symposium, New Orleans: American Gas Association, pp. 164-174.

Soil Reinforcement with Strips of Reclaimed HDPE

C.H. Benson
University of Wisconsin-Madison, USA

M.V. Khire
University of Wisconsin-Madison, USA

ABSTRACT

The feasibility of reinforcing soil with strips of reclaimed HDPE was investigated in this study. Strips of HDPE were mixed with Portage sand and tested to determine CBR, secant subgrade modulus, resilient modulus, and shear strength. Tests were conducted on mixtures containing plain, punched, and kinked strips. The tests showed that reinforcing sand with HDPE strips enhances its resistance to deformation and increases its strength. The tests showed that addition of strips increased the CBR and the secant modulus, with the CBR increasing by as much as a factor of 5. The resilient modulus also increased with addition of strips with the greatest increases (35% increase) occurring for strip contents of 3%. Direct shear tests also showed that addition of HDPE strips increased the shear strength of the sand, with increases in friction angle of 18^{o} measured at normal stresses below the critical confining stress.

INTRODUCTION

In recent years, plastic jugs made of high density polyethylene (HDPE) have been used with increasing frequency for storage and marketing of various liquids such as milk, motor oil, and laundry detergents. Generally, the jugs have a short life span and are discarded when empty. As a result, landfills have been continually filled with a valuable resource that has been used for only a short time. In many communities, however, HDPE is now being collected for recycling or reuse.

Unfortunately, secondary markets for reclaimed HDPE have not developed as quickly as recycling programs. The number of buyers for reclaimed HDPE remains small and the quantity of HDPE that is reused is only a fraction of the total volume that is collected. Reclaimed HDPE is also difficult to incorporate in feedstock for many new products. Because of the relatively low temperatures at which it is melted, the U.S. Food and Drug Administration does not permit addition of reclaimed HDPE in feedstocks that are used to produce containers for food, drugs, or cosmetics. Furthermore, many processors of HDPE currently produce plastic for use by a variety of industries (i.e., food and non-food products) and hence are reluctant or unable to incorporate reclaimed HDPE in their feedstock.

The small secondary market and restrictions on re-melting often make recycling of HDPE uneconomical. For example, in 1990, the average price for used HDPE milk jugs was 7 cents/lb and ranged between 0 and 13 cents/lb. When the cost of shipping is considered (about 3 cents/lb), the resulting profit is, on average, about 4 cents/lb. At this small profit margin, recyclers are reluctant to deal in reclaimed HDPE. Hence, to promote recycling and reuse of HDPE, new ways to reuse it need to be identified. In this paper, the feasibility of using small strips of HDPE to reinforce soils is investigated. In particular, highway applications for soil reinforcement are considered because millions of cubic meters of earth are used in highway projects each year.

BACKGROUND

Reinforcement of soil using strips or pieces of plastic, fabric, or metal embedded in the soil has been studied by many investigators. In most cases, reinforcement has increased the strength and stiffness of the soil and hence have improved its mechanical properties. Nevertheless, most studies have focused on reinforcing soil with virgin materials and few studies have considered the use of HDPE.

Fletcher and Humphries (1991) conducted CBR tests on fine sandy silt reinforced with polypropylene fibers. Fibers of two different lengths and diameters were used and the fiber content was varied between 0.09 to 1.5% by weight. Fletcher and Humphries found a maximum increase in CBR of 133% which occurred at a fiber content of 1%. They also found that higher CBR values were obtained with longer fibers.

Dynamic tests have been conducted by Noorany and Uzadavines (1989) and Maher and Woods (1990). Noorany and Uzadavines conducted undrained cyclic triaxial tests on saturated sand reinforced with randomly distributed hair-like polypropylene fibers having a length of 20 mm. They found the reinforcement increased the resistance to liquefaction. Lower pore water pressures developed during testing which was attributed to the tensile resistance provided by the fibers which increases the elasticity of the composite material.

Maher and Woods (1990) conducted resonant column and torsional shear tests on fiber reinforced Muskegon dune sand. They found that fibers increased the rigidity of the sand. They also found that the increase in rigidity decreases as the confining pressure increased.

Gray and Ohashi (1983) conducted direct shear tests on sand reinforced with natural and synthetic fibers. Their study showed that fibers improve the shear strength and stress-deformation characteristics of sand. They found that reinforcement increased the peak strength of the sand and reduced or eliminated the post-peak loss in strength. Gray and Ohashi also found that improvements in strength and deformation characteristics of the sand increased with as the percentage of strips increased. Similar results have been obtained by Lawton, et al. (1992).

Large-scale direct shear tests were conducted on dry uniformly graded sand by Shewbridge and Sitar (1989). The sand was reinforced with six different materials. They found that reinforcement increased the residual strength of the soil, but concluded the increase in strength was not linearly proportional to the quantity of reinforcement. They also found that the width and shape of the shear zone in reinforced soil is altered by the quantity of the

reinforcement, stiffness of reinforcement, and bond between the reinforcement and surrounding soil.

MATERIALS

Soil

Portage sand was selected for use in this study. It is a uniformly graded medium sand composed of rounded quartz particles. It has been used in numerous studies at the University of Wisconsin-Madison and hence has been thoroughly characterized. Figure 1 is a particle size distribution curve for Portage sand; it has a coefficient of uniformity of 1, coefficient of curvature of 1, and is classified as SP in the Unified Soil Classification System.

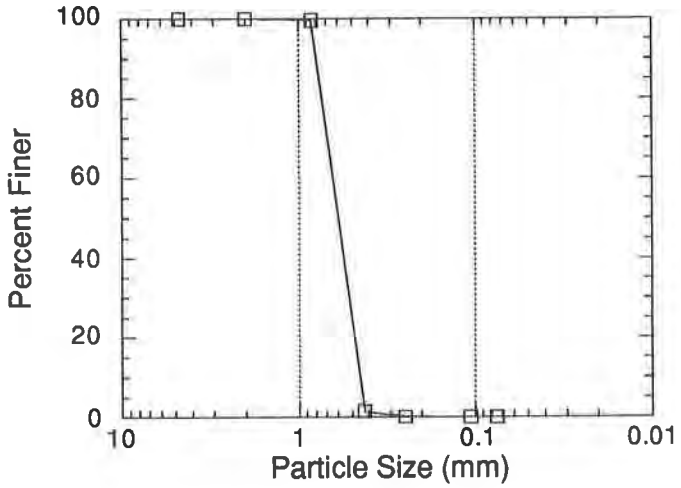

Figure 1. Particle Size Distribution for Portage Sand.

A relative density test was performed on the sand using procedures described in ASTM 4254. The maximum dry unit weight was found to be 17.8 kN/m^3 whereas the minimum dry unit weight was 15.2 kN/m^3.

HDPE Strips

Translucent HDPE milk jugs were selected as stock for producing reinforcing strips. Milk jugs were selected because they can be cleaned easily and are stockpiled in abundance at recycling centers in the Madison area. Strips were cut from milk jugs using a sharp knife mounted on a table. No particular concern was placed on selecting portions of the jugs to be used for the strips with the exception of necks and handles, which were omitted. Some strips were naturally bent by the contours in the jugs. Other strips had rough portions because of the dimpled section present on some jugs. It was decided not the eliminate these potentially confounding factors because they would likely exist if HDPE strips were used commercially.

The strips were cut to a length of 5 cm and a width of 0.6 cm resulting in an aspect ratio of 8. These dimensions were selected so the strips would be smaller than the dimensions of

specimens ordinarily used in geotechnical testing (7 to 10 cm). It was also believed that strips of this size could be easily handled and mixed into soils.

Three types of strips were evaluated as shown in Fig. 2. The first type is made by cutting strips 5 cm long by 0.6 cm wide; these strips are herein referred to as "plain" strips. The second type of strip is cut to the same dimensions as plain strips, but are punched with 2 holes equally spaced along the center of the strip. Herein, these strips are referred to as "punched" strips. For the third type, strips were cut to the same dimensions as plain strips, but were kinked using a pliers. Hence, they are referred to as "kinked" strips. The latter two types of strips were evaluated to determine if adding holes for interlocking or folds for entanglement would enhance the reinforcing characteristics of the strips.

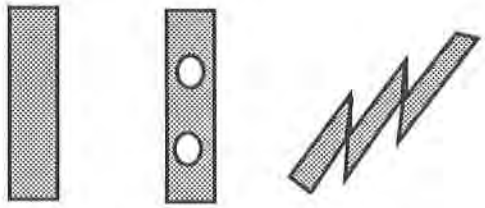

Figure 2. Schematic of (a) Plain Strips, (b) Punched Strips, and (c) Kinked Strips.

TESTING APPARATUS AND PROCEDURES

To evaluate the reinforcing characteristics of HDPE strips, California Bearing Ratio (CBR), resilient modulus, and direct shear tests were conducted. These tests were selected because they are commonly used to determine parameters for use in the design of rigid and flexible pavements, shallow foundations, and small retaining structures and slopes.

California Bearing Ratio (CBR)

CBR tests were performed to determine the CBR value, a measure of the bearing strength of soil that is used in the design of rigid and flexible pavements. The secant subgrade modulus was also determined from the CBR tests. Procedures in ASTM D1883 were used to conduct the tests.

Specimens were molded in a steel CBR mold with a 15.2 cm inside diameter. Sand and strips were pre-mixed by hand and then a pre-determined weight of the mixture was placed in the mold. This procedure produced a sand/strip mixture having randomly oriented strips. The mixture was vibrated on a shaking table until soil in the mold settled to a volume yielding a density of the sand fraction equal to 17.8 kN/m^3, which corresponded to a relative density of 1. Three lifts of the sand/strip mix were used to prepare each specimen. Undoubtedly, some segregation occurred during vibration. Nevertheless, when specimens were dissected after testing, the strips still appeared to be randomly oriented and uniformly distributed throughout the sand.

A surcharge plate yielding a pressure of 2.44 kPa was placed on the specimen prior to testing. Then, the specimen was placed in a load frame and dial gauges were mounted to measure deformation of the specimen and the penetration of the loading piston (Fig. 3). The tests were conducted at a penetration rate of 0.002 cm/sec and were continued until a penetration exceeding 2.5 cm was achieved.

Figure 3. Specimen in Load Frame for CBR Test.

Resilient Modulus

The resilient modulus is an elastic modulus of soil determined in a test using dynamic loading. It characterizes the recoverable deformation of sub-base materials under repeated loading and is used in elastic analyses of flexible pavements. Testing methods described in SHRP Protocol P46 were used to conduct the tests (see SHRP, 1989).

The resilient modulus tests were conducted in a large triaxial cell (specimen has diameter of 15 cm and height of 30 cm) and an MTS system was used for dynamic loading (Fig. 4). The specimens were formed in the triaxial cell by mixing sand and strips and placing a pre-determined weight of the mixture in the membrane. This procedure resulted in randomly oriented strips. The sand was vibrated using a shaking table until a sand density of 17.8 kN/m^3 (relative density = 1) was achieved. Six lifts were used to mold each specimen. After the

specimen was molded, a top cap was placed on the soil and sealed to the membrane using two O-rings. Then, a 70 kPa vacuum was applied to further consolidate the specimen.

A special membrane was required that would not be punctured by sharp edges of the strips. The membrane was constructed from a piece of 20 mil PVC geomembrane and was welded at the seam with solvent. This membrane was also used by Edil, et al. (1991) to measure the resilient modulus of soil/tire chip mixtures and was found to have little effect on the test results even though it is somewhat stiffer than the more commonly used latex membranes.

The following sequence was used to test each specimen. First, the specimen is conditioned by applying a confining pressure of 105 kPa and subjecting it to 200 cycles of a deviator stress of 105 kPa. Then, the specimen is subjected to a series of cyclic loadings beginning at a confining pressure of 21 kPa and ending at a confining pressure of 140 kPa. At each confining pressure, a sequence of increasing deviator stresses is applied. Each deviator stress is applied 100 times and the average recovered strain is determined from the last five cycles. The resilient modulus is defined as the deviator stress divided by the recovered strain. Additional details regarding the testing procedure can be found in SHRP (1989).

Figure 4. Triaxial Cell Mounted in MTS Load Frame for Resilient Modulus Test.

Direct Shear

Direct shear tests were performed to determine how reinforcement with HDPE strips affects the shear strength of the sand. Tests were performed in accord with ASTM Standard D3080. To measure full-scale effects of the strips and to avoid boundary problems, a large-scale direct shear device was constructed (Fig. 5). It consists of a direct shear ring 28 cm in diameter and 25 cm deep. Shear and normal stresses were applied with pneumatic and hydraulic actuators driven by an MTS system. Loads were measured with load cells and deformations were monitored using LVDTs.

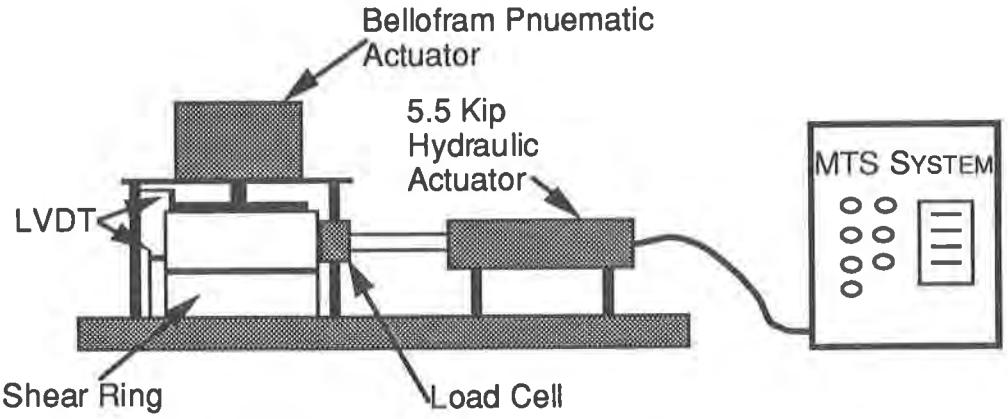

Figure 5. Schematic of Large-Scale Direct Shear Machine.

Specimens were molded directly in the shear ring. A loose mixture of sand and randomly oriented strips was placed in the ring and tamped with a rod until a sand density of 17.8 kN/m^3 was attained. Typically, 5 lifts of the sand/strip mixture were used to form a specimen. Normal stresses were applied to the soil and the specimen was then sheared by applying a horizontal force at a rate of 0.004 cm/sec. Normal stresses of 11.5, 20.7, 36.2, 69, and 159.8 kPa were applied. The tests were conducted until the shear ring was displaced 2.5 cm and a peak was observed in the load-displacement curve.

To ensure the large-scale direct shear machine was operating properly, tests were also conducted on unreinforced sand in a standard Wykeham-Farrance direct shear machine (Model No 25301) having a square shear box 6.4 cm wide. The specimens were prepared using vibration to obtain a dry unit weight of 17.8 kN/m^3 (relative density of 1). Mohr-Coulomb failure envelopes (corresponding to peak shear stress) that were obtained with both machines are shown in Fig. 6; it shows the large and small-scale direct shear machines yield essentially the same friction angle (36^o).

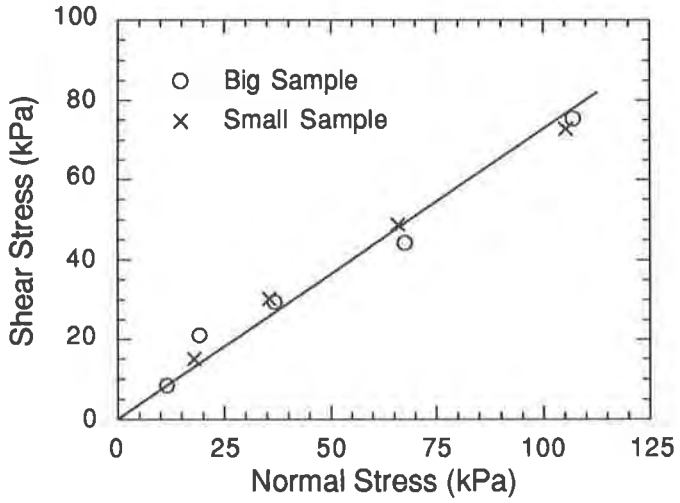

Fig. 6. Mohr-Coulomb Diagram for Unreinforced Portage Sand.

RESULTS

Each test was conducted with strip contents, defined as strip weight/sand weight, of 0, 1, 2, 3, and 4%. For the CBR and resilient modulus tests, at least one replicate measurement was conducted for each testing condition. No replicates were conducted for the direct shear tests because of the time and quantity of soil/strip mixture that was required. Results presented in this section are averages if replicates were performed.

CBR and Secant Subgrade Modulus

Results of the CBR tests are shown in Figs. 7. The CBR value was computed by dividing the piston stress by 6900 kPa at a displacement of 2.5 mm and multiplying by 100. A seating correction was applied when the load-displacement curves had a visible offset. The secant subgrade modulus was computed by dividing the piston stress at a penetration of 2.5 mm by 2.5 mm.

For each strip type, increases in CBR were generally observed as the strip content was increased, except in one case where CBR initially decreased (kinked, 1%) and then increased when the strip content was raised higher. The decrease in CBR was small, however, and was most likely the result of sample variability. The most significant increases in CBR occurred for specimens containing plain and kinked strips. At strip contents of 3 to 4%, the CBR value increased by a factor of 4 to 5 in comparison to the CBR of unreinforced sand. A smaller increase in CBR was observed for specimens reinforced with punched strips (factor of 2 increase).

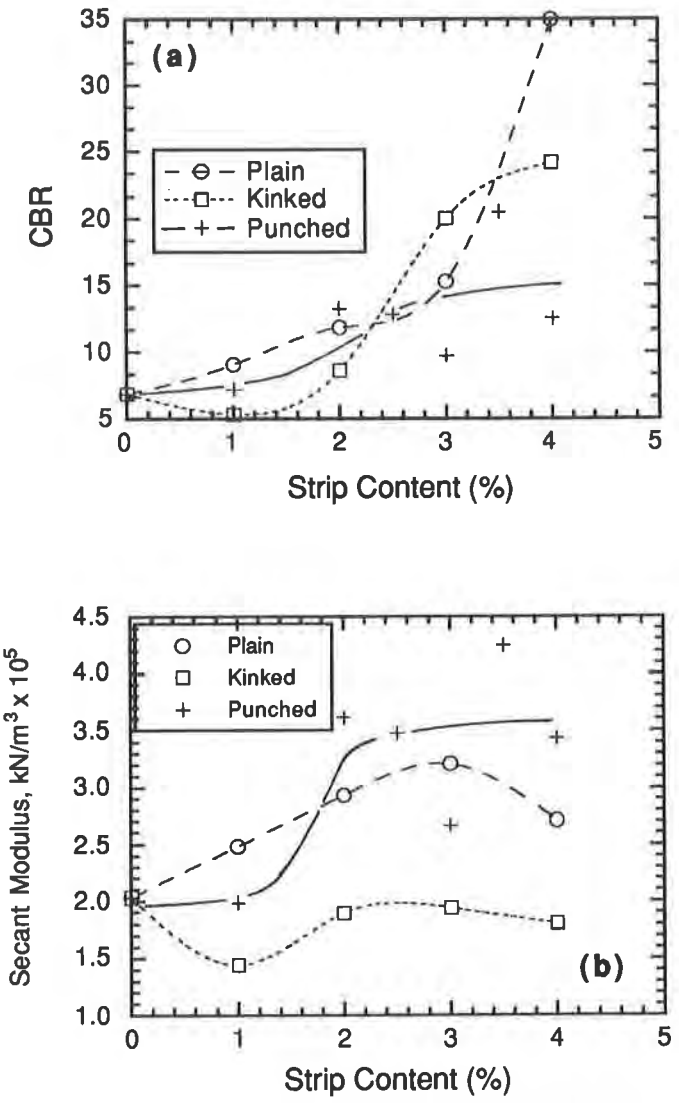

Figure 7. CBR (a) and Secant Subgrade Modulus (b) vs. Strip Content.

The secant subgrade modulus also increased when strips were added to the sand (Fig. 7b). However, the secant modulus increased for specimens reinforced with plain and punched strips, but did not increase for specimens reinforced with kinked strips. The increase in secant modulus was similar for the plain and punched strips, but the modulus was larger for the punched strips at a lower strip content.

When the tests were completed, the specimens were dissected and the strips were examined. Many of the strips showed elongation and thinning and clear impressions of sand particles in the plastic. Apparently, as the soil sheared during penetration, strips fixed in the sand by friction elongated as the soil tried to deform. The resistance to deformation provided by the strips was the likely cause of the increase in CBR that was measured. It was also

observed that punched strips exhibited most of their deformation in the thin sections of plastic surrounding the holes. Apparently, the thinner sections around the holes provided less resistance to deformation and hence a smaller increase in CBR occurred.

Resilient Modulus

The CBR tests suggested that no benefit was gained by punching or kinking the strips; similar CBR values were obtained for plain and kinked strips whereas similar secant moduli were obtained for plain and folded strips. Based on the results of these tests, it was decided that only plain strips would be used in the resilient modulus and direct shear tests.

Results of the resilient modulus tests are presented in Fig. 8 as normalized modulus vs. strip content. Normalized modulus was defined as the resilient modulus (M_r) for a given strip content and bulk stress divided by the resilient modulus of an unreinforced specimen (M_{ro}). Bulk stress was defined as the sum of the three principal stresses. Values for M_{ro} were 85.4, 118.7, and 140.6 MPa at bulk stresses of 138, 345, and 552 kPa.

Figure 8 shows that the resilient modulus increases as the strip content is increased. Increases were observed, however, only when the strip content was increased to at least 2% and a maximum resilient modulus was observed for a strip content of 3%. Beyond 3%, however, the modulus decreased. Figure 8 also shows that the increase in resilient modulus caused by addition of strips depends on the bulk stress; greater resilient modulus was measured with increasing bulk stress provided the strip content exceeded 2%.

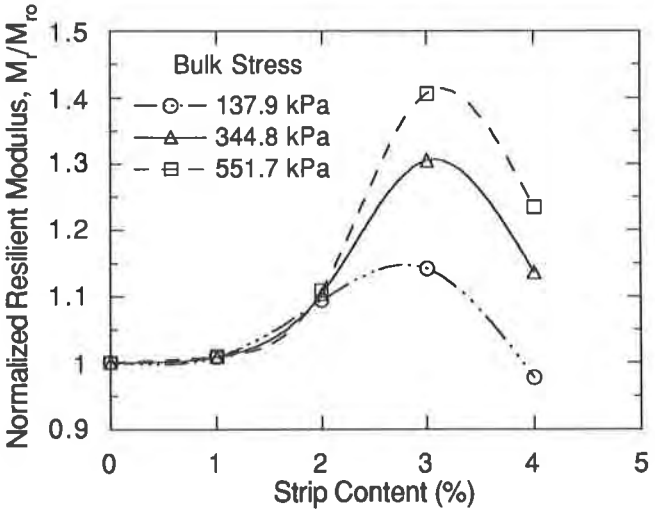

Figure 8. Normalized Resilient Modulus vs. Strip Content.

Examination of the strips after the tests showed little deformation or marking by the sand particles. This result is not surprising, however, even though it contrasts observations made for the CBR tests. In the resilient modulus test, the specimen undergoes numerous small shear displacements whereas in a CBR test the soil is sheared significantly in a single penetration of the piston. Hence, less deformation of the strips is expected during a resilient modulus test.

Shear Strength

Mohr-Coulomb envelopes for the direct shear tests are shown in Figure 9. The envelopes show that the friction angle (ϕ) increases when strips are added provided the normal stress is low. For unreinforced sand, the friction angle was 36°, whereas friction angles as large as 54° were measured for sand reinforced with strips. Hence, at low stresses, the friction angle increased as much as 18°.

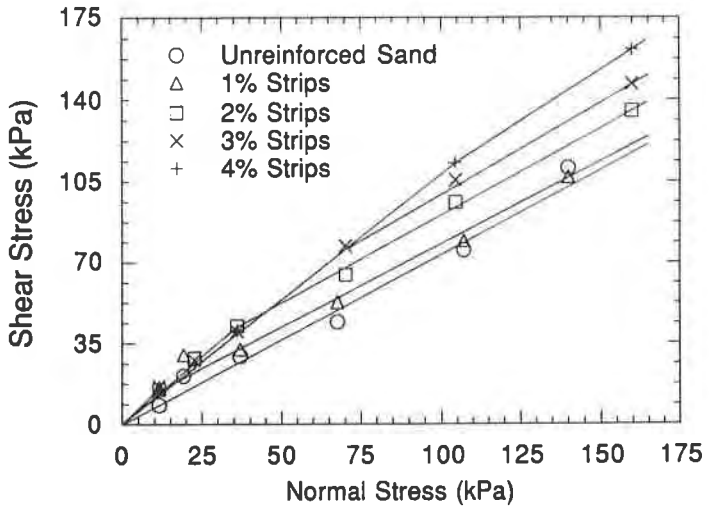

Figure 9. Mohr-Coulomb Envelopes for Various Strip Contents.

The increase in friction angle can also be interpreted in terms of efficiency (ε), defined as:

$$\varepsilon = \frac{\tan\phi_r}{\tan\phi_o} \times 100 \qquad (1)$$

where ϕ_r is the friction angle for reinforced sand and ϕ_o is for unreinforced sand. Essentially, the efficiency is the ratio of the coefficient of friction for reinforced sand to the coefficient of friction for unreinforced sand. Table 1 summarizes the increase in efficiency obtained by reinforcement. The greatest efficiency (191) was realized for a strip content of 1%, but was limited to low normal stresses (see Fig. 10). Efficiencies of 150 were more typical and correspond to a increase in coefficient of friction by a factor of 1.5.

Table 1. Summary of Efficiencies and Critical Confining Stresses for Various Strip Contents.

Strip Content (%)	f	σ_{crit}' (kPa)	ε(%)
0	36	-	100
1	54	11.5	194
2	50	36	166
3	48	70	156
4	47	104	152

Increases in friction angle, however, were only observed at lower stresses. Once the normal stress reached a particular level, the slope of the failure envelope decreased and became parallel to the failure envelope obtained for unreinforced sand. Nevertheless, the reinforced soil still had greater shear strength, only the additional strength caused by the frictional component appears as an apparent cohesion at high stresses.

Similar break points in the failure envelope for reinforced soil have been observed by Gray and Ohashi (1983). They coined the term "critical confining stress" (σ_{crit}') to describe the normal stress at which the break point in the failure envelope occurs. In these tests, σ_{crit}' increased with increasing strip content. Table 1 summarizes the σ_{crit}' measured at various strip contents.

Examination of the strips after the test revealed that only a few strips were significantly deformed during shearing. Apparently, the load applied to the strips was sufficiently small such that little to no deformation occurred. Similar results were observed by Gray and Ohashi (1983). They found that the fibers did not break during shear but instead were either pulled out or stretched. Apparently, the HDPE strips tested in this study pulled out during shear and hence did not undergo significant deformation. Also, when the soil was removed from the rings, the strips did not exhibit a preferential orientation. The strips appeared to remain randomly oriented and embedded in the sand.

SUMMARY AND CONCLUSIONS

The feasibility of reinforcing soil with strips of reclaimed HDPE was investigated in this study. Strips of HDPE were mixed with Portage sand and tested to determine CBR, secant subgrade modulus, resilient modulus, and shear strength. Tests were conducted on mixtures containing plain, punched, and kinked strips. The tests showed that reinforcing sand with HDPE strips enhances its resistance to deformation and strength. Based on the test results, the following conclusions are drawn:

1. Addition of HDPE strips to Portage sand increased its CBR by a factor of 5 with the largest increases occurring for strip contents of 3 to 4%. The secant subgrade modulus also increased substantially. It was found, however, that punching or kinking the strips did not provide a any improvement over plain strips. Examination of the strips after the tests showed they had deformed during shearing of the sand.

2. Sand reinforced with HDPE strips had higher resilient modulus than unreinforced sand. The greatest increase in modulus occurred at a strip content of 3%; however, for strip contents greater than 3%, the resilient modulus decreased. Larger resilient modulus also occurred as

the bulk stress was increased when the strip content was at least 3%. For lower strip contents, the normalized resilient modulus was independent of bulk stress.

3. Shear strength was measured in a large scale direct shear machine to avoid boundary and scale effects. Preliminary tests on unreinforced sand showed that the large-scale direct shear machine gave results similar to a standard small-scale machine. Tests conducted with the large-scale machine showed that addition of HDPE strips increases the shear strength of the sand. Mixtures of sand and strips resulted in increases of friction angle ranging between 11 to 18° in comparison to unreinforced sand provided the normal stress was below the critical confining stress.

4. Break points in the Mohr-Coulomb envelopes were observed at which the friction angle of the sand/strip mixture became essentially the same as friction angles for unreinforced sand. This break point is called the critical confining stress (Gray and Ohashi, 1983) and ranged between 11 to 104 kPa. Nevertheless, at high normal stress, the shear strength of the reinforced sand was still greater than the strength of unreinforced sand. It was also found that the critical confining stress increased as the strip content increased.

The results of this study suggest that strips cut from reclaimed HDPE may prove useful as soil reinforcement in highway and light-duty geotechnical applications. Further study is needed, however, to optimize the size and shape of the strips to obtain maximum increases in properties of soil/strip mixtures. Further study is also needed to evaluate the durability and aging of the strips and the economic benefits that can be accrued through their use.

ACKNOWLEDGMENT

Financial support for the study described in this paper was provided by the State of Wisconsin's Solid Waste Research Council (SWRC). This support is greatly appreciated. However, the results and opinions presented in this paper are those solely of the authors and do not necessarily represent the policies or opinions of SWRC. This paper has not been reviewed by SWRC.

REFERENCES

Edil, T.B., P.J. Bosscher, and N. Eldin (1991), "Executive Summary: Development of Engineering Criteria for Shredded or Whole Tires in Highway Applications," Interim Report to the Wisconsin Department of Transportation, May 1991.

Fletcher, C.S., and Humphries, W.K. (1991), "California Bearing Ratio Improvement of Remolded Soils by the Addition of Polypropylene Fiber Reinforcement.," presented at the 70th Annual Meeting of the Transportation Research Board, Washington, D.C., January.

Gray D.H., and Ohashi, H. (1983), "Mechanics of Fiber Reinforcement in Sand," Journal of Geotechnical Engineering, ASCE, Vol. 109, No. 3, pp. 335-353.

Jewell, R.A. & Wroth, C.P. (1987), "Direct Shear Tests on Reinforced Sand," Geotechnique, 37, No. 1, pp. 53-68

Lawton E.C., M.V. Khire, and N.S. Fox (1992), "Reinforcement of Soils By Multi-Oriented Geosynthetic Inclusions," Journal of Geotechnical Engineering, ASCE, in press.

Maher, M.H., and Woods, R.D. (1990), "Dynamic Response of Sand Reinforced with Randomly Distributed Fibers," Journal of Geotechnical Engineering, ASCE, Vol. 116, No. 7, pp. 1116-1131.

Noorany, I., and Uzdavines, M. (1989)," Dynamic Behavior of Saturated Sand Reinforced with Geosynthetic Fibers," Proceedings of Geosynthetics '89, San Diego, Vol. 2, pp. 385-396.

Shewbridge S.E. and Sitar N. (1989), "Deformation Characteristics of Reinforced Sand in Direct Shear," Journal of Geotechnical Engineering, ASCE, Vol. 115, No. 8, pp. 1134-1147.

SHRP (1989), "Sharp Protocol P46 - Resilient Modulus of Unbound Granular Base/Subbase Materials and Subgrade Soils," SHRP-LTPP Laboratory Material Testing Guide, Version 1.0, August 1989, pp. P46-1, 34

Polyethylene Sheathing for Downdrag Mitigation in Piles

K.S. Tawfiq
FAMU/FSU College of Engineering, USA

J.A. Caliendo
Utah State University, USA

ABSTRACT

To overcome problems associated with bitumen coating in reducing downdrag forces in piles, an alternative method is suggested herein to sheathe piles with polyethylene sheets. The effectiveness of this method was investigated in the laboratory along with the conventional bitumen coating method. Concrete blocks were prepared and coated with polyethylene sheets and bituminous material and tested under different temperature and loading conditions using direct shear apparatus. The results showed that the changes in temperature or rate of loading did not influence the shearing characteristics of the concrete-polyethylene-soil samples, whereas, in bitumen coated samples, these two parameters complicated the viscous behavior of the bitumen-soil matrix. Based on the findings of this study, it is believed that polyethylene sheathing with two 6 mil lubricated sheets can provide better performance over bitumen coating in mitigating downdrag forces in piles.

INTRODUCTION

Proprietary Mechanically Stabilized Earth (MSE) walls are typically constructed at bridge abutments on Florida Department of Transportation (FDOT) projects. Prior to wall construction, end bent concrete piles are driven behind the proposed wall. Subsequently, as the wall is constructed, fill is placed and compacted adjacent to the piles. This process induces a relative settlement between the pile and the adjacent soil causing the friction resistance along the pile shaft to decrease and, eventually, to reverse its direction (Figure 1). The amount of settlement that causes this reversal is about 1% of the shaft diameter. This negative skin friction gives rise to downdrag forces on the pile shaft and represents one of the major causes of pile settlement or pile failure (Johannessen and Bjerrum, 1965).

The magnitude of the downdrag force developed in piles depends mainly on the friction characteristics of the pile-soil contact surface. This friction, in turn, depends on the pile type, soil type, and the rate of relative settlement.

Several methods have been suggested to determine the negative skin friction on piles (Bjerrum, et al. 1969; Vesic, 1972; Zeevaert, 1972; Baligh, et al. 1975, and 1981). Some of these methods are empirical, and others are based on the principles of Mohr-Coulomb yield criterion. Vesic (1972) expressed the negative skin friction of cohesionless and cohesive soils as:

$$NF = N_o \, \sigma_o \, A \qquad (1)$$

where:
NF = Negative skin friction;
N_o = Dimensionless factor and varies from 0.01 to 0.8;
σ_o = The mean normal effective stress;
A = The area of the shaft in the zone of settling soil.

This expression can also be used to estimate the positive skin friction of piles. For different soil layers, the negative skin friction is the sum of the contribution of each soil layer that settles with respect to the pile.

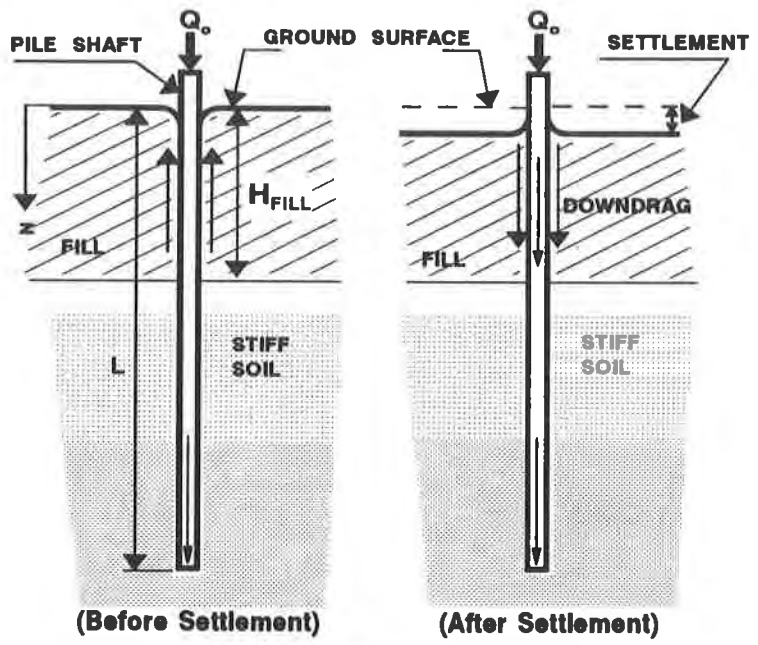

Figure 1 Downdrag in Piles

METHODS FOR DOWNDRAG REDUCTION

On vertical and end bearing piles, small downdrag forces can be resisted by increasing the pile capacity, by providing additional piles, or by reducing the spacing between piles in a group. However, when large downdrag forces are expected, other methods are used to reduce these forces including:
1- preloading;
2- electro-osmosis to increase the pore water pressure around the cathode pile;
3- casing to prevent direct contact between the pile and the soil;
4- Coating the pile with a friction reducer such as bitumen or bentonite admixtures.

Today, coating piles with bitumen represents the most common method for downdrag reduction. Federal and State highway agencies have set certain requirements for furnishing and applying bituminous coating and primer to concrete pile surfaces. According to these requirements, pile coating requires asphalt type bitumen conforming to ASTM D946, with minimum penetration grade (pen. 25°C) equal to 50 at the time of pile driving. The primer should conform to the requirements of ASTM D41. Also, bitumen coating should be applied uniformly at a temperature of not less than 149°C (300°F), nor more than 176°C (350°F). The bitumen coating should be applied to a minimum dry thickness of 3.2 mm (1/8 in). But in no case should the quantity of application be less than 8.6 gallons/10 m^2.

The performance of bitumen coated piles subjected to downdrag loading depends on the characteristics of the pile, the soil, and the bitumen coating. Other unpredictable factors that are related to the nature of the bituminous materials can

adversely impact the effectiveness of the coating in mitigating downdrag. Among these factors are: storage distortions, dripping off of unprotected coating during installation, temperature/strain rate susceptibility of the bitumen material, and soil penetration into bitumen coating.

Experimental studies (Baligh, et al., 1975) have shown that after soil particle penetration, the negative skin friction, f_s, on bitumen coated piles could reach 50% to 100% of the skin friction on an uncoated pile. Also, negative skin friction of bitumen coated piles in coarse grained soils reaches a maximum value in less than a month. At this stage, the bitumen coating behaves as a visco-frictional material with very complex properties. Moreover, it has been found that 0.6 mm reduction in the coating thickness could double the downdrag force in clayey soils, and that 5°C change in the ground temperature could change the downdrag force by a factor of 4 (Baligh, et al., 1981).

POLYETHYLENE SHEATHING METHOD

Considering the above mentioned uncertainties, it becomes necessary to search for an alternative method for downdrag reduction in piles. A friction reducer performs as a pile coating to prevent direct contact between the soil and the pile surface and to reduce the friction resistance.

With the successful use of the geosynthetics in civil engineering applications, it was decided to investigate the use of polyethylene sheathing as a friction reducer. The surface characteristics of the polyethylene sheets would accommodate the relative settlement between the pile surface and the surrounding soils with little or possibly no friction.

Polyethylene sheets, with their improved physical and mechanical properties, have been used in numerous engineering practices. They are continuous polymeric sheet geomembranes, and their primary function is always as a barrier. Martin, et al. (1984) showed that angles of friction of soil-to-geomembrane are always less than those of soil-to-soil. The magnitudes of the friction angle depend on the type of soil and geomembrane. It is believed, however, that when a pile is sheathed with more than one layer of polyethylene, the shearing forces along the pile would transfer to another surface of contact which could ease the effect of the relative settlement on negative skin friction (Tawfiq and Ping, 1992).

LABORATORY INVESTIGATION

The effectiveness of the polyethylene sheathing method in reducing negative skin friction has been investigated in the laboratory using sets of concrete samples covered with different configurations of polyethylene sheets and tested under direct shear conditions. To draw a meaningful comparison between this method and the conventional bitumen coating method, other sets of concrete samples covered with bituminous materials were prepared and tested under the same conditions.

MATERIAL CHARACTERIZATION

Soil properties. Two types of soils were used to shear the polyethylene and the bitumen coated samples. The first type was reddish brown sandy soil with some fines, and the natural water content, w_c, of this soil was 4%. The second type was light tan coarse-grained crushed limestone. The sieve analysis results indicated that the first soil contains 2% fines, and the second one comprises gravel with less than 2% fines. According to the Unified Soil Classification System (USCS) the first soil is well graded sand with some fines (SW), and the second one is well graded gravel (GW) (Figure 2). These two types of soils conform to those typically used by the FDOT in the construction of MSE wall systems.

Polyethylene Sheets. From the wide range of polyethylene sheets available in the market today, two types of sheets were selected for this investigation. The first type was 6 mil clear polyethylene sheets, and the second type was the 40 mil HDPE, which is a High Density Polyethylene containing approximately 97.5% polymer and 2.5% of carbon, anti- oxidants and heat stabilizers. The purpose for this selection was to investigate

the effect of layer thickness on the friction characteristics of polyethylene sheathed concrete samples.

Bitumen Properties. Bitumen samples for this investigation were prepared from a material known commercially as AC-30 bitumen. This type of bitumen has a minimum penetration of 50 at 25° C, viscosity of 3000 to 3600 poises at 60° C, and a ductility of 40 at 25°C. The penetration grade for this bitumen conforms to the FHWA requirements for pile coating.

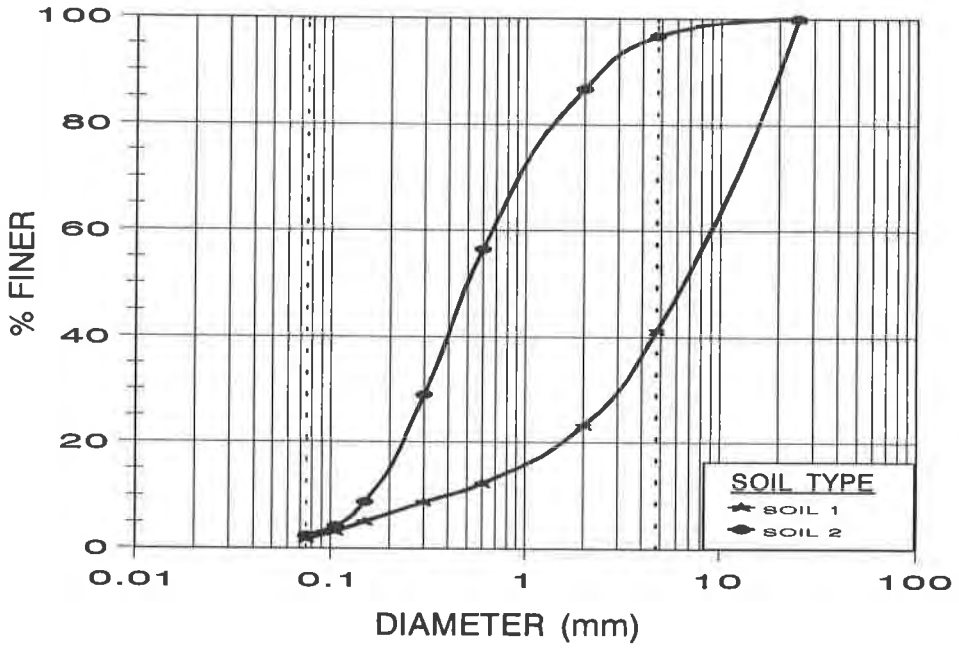

Figure 2 Grain Size Distribution

TESTING PROCEDURE

The required samples for the testing program were divided into two sets. The first set consisted of concrete blocks covered with polyethylene sheets, and the second one included concrete blocks coated with AC-30 bitumen The dimensions of the concrete blocks were 13 cm x 13 cm x 1.3 cm. This size was chosen to suit the slight modification that was introduced to fit the concrete blocks into the direct shear box (Figure 3).

For the 40 mil polyethylene sheets, preparation of a typical concrete-polyethylene sample was started by wrapping a concrete block with one polyethylene sheet and fastening the sheet to the block using duct tape. Other samples were prepared with one 40 mil sheets set unfastened on the blocks. The same setup was followed in the case of the 6 mil polyethylene sheathed samples. For some of the samples, concrete blocks were covered with two unfastened sheets. Also, some of these sheets were lubricated with oil and others were left without any lubrication. The purpose of these arrangements was mainly to separate the soil particles from the concrete surface and to transfer the shearing stresses to the polyethylene sheets. In addition, lubricating the polyethylene sheets in some samples was another way to facilitate the relative displacement between the sheets with little or no friction resistance. All these combinations of boundary conditions were investigated in order to come up with the most effective arrangement of the polyethylene sheathing.

Bitumen samples were prepared by pouring the preheated AC-30 bitumen in lubricated metal molds placed on the top of the concrete blocks. After the curing period, each concrete-bitumen sample was transferred to the direct shear apparatus for testing. Bitumen material is very susceptible to temperature changes; therefore, extra

care was exercised to avoid any distortion during sample preparation, and testing.

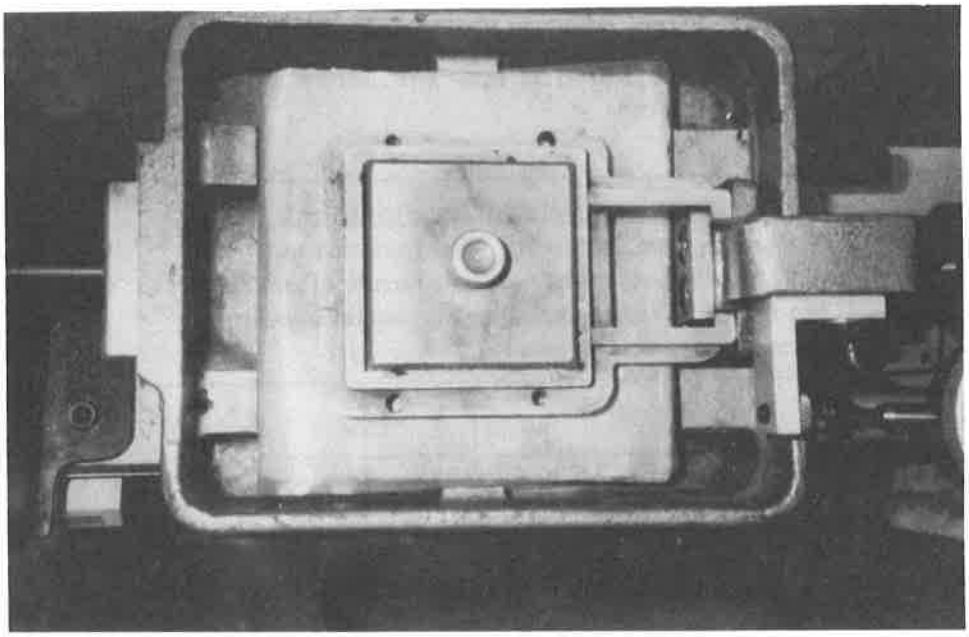

Figure 3 Direct Shear Test Apparatus

To compare the results from the polyethylene and the bitumen coated samples with the shear resistance of concrete and soil without any friction reducer, some concrete blocks were prepared and tested using both types of soils. Results from these samples were taken as control data for comparison with the other results.

The testing procedures for the concrete-polyethylene samples and the concrete-bitumen samples using the direct shear test were the same in both cases. After placing the samples in the direct shear apparatus, the upper half of the shear box was positioned on the top of the coating, and then the soil was poured in layers and tamped to the desired density. The loading frame, the loading bar, and the dial gauges were then attached to the head and set for testing.

Three normal stress increments (18.85 KPa, 27.02 KPa, and 40.65 KPa) were applied on the polyethylene and the bitumen coated samples. Also the samples were tested at different temperatures (5°C, 25°C, and 56°C) and subjected to the control strain type of loading with rates of loading equal to 0.0025 mm/min, 0.25 mm/min, and 1.0 mm/min. For each sample, measurements of the horizontal displacement, vertical displacement, and shearing stresses were recorded for further analysis. The stress-displacement relationships exhibited similar trends in all the samples. The upper limit of each relationship was considered when the shearing stress attained constant value while the shearing displacement continued to increase. The tests were terminated at about 2 mm to 3 mm total shearing displacement. After the completion of each test the polyethylene and the bitumen coated samples were visually examined to determine the amount of damage that could have occurred during shear testing.

ANALYSIS OF RESULTS

The scope of this study was to investigate the effectiveness of polyethylene sheathing as compared to the bitumen coating in mitigating downdrag in piles. Several parameters that are considered to impact the shearing behavior of the polyethylene sheathing and the bitumen coating have been selected and investigated in this study. These parameters include: soil type, normal stress, temperature, and rate of loading. The effect of boundary conditions on the shearing resistance of the polyethylene sheathing was added to these parameters.

Test results showed that when polyethylene sheathing method was employed, the friction coefficient of the concrete-polyethylene-soil samples reduced by 62% for the 40 mil single sheets. This ratio was related to the friction coefficient of the concrete-soil samples without any friction reducer. A single 6 mil polyethylene sheet reduced the friction coefficient by approximately 67%. When two loose layers of polyethylene were added, the reduction progressed to 78% (Figure 4). The effect of temperature and the rate of loading did not influence the shearing behavior of the concrete-polyethylene-soil samples.

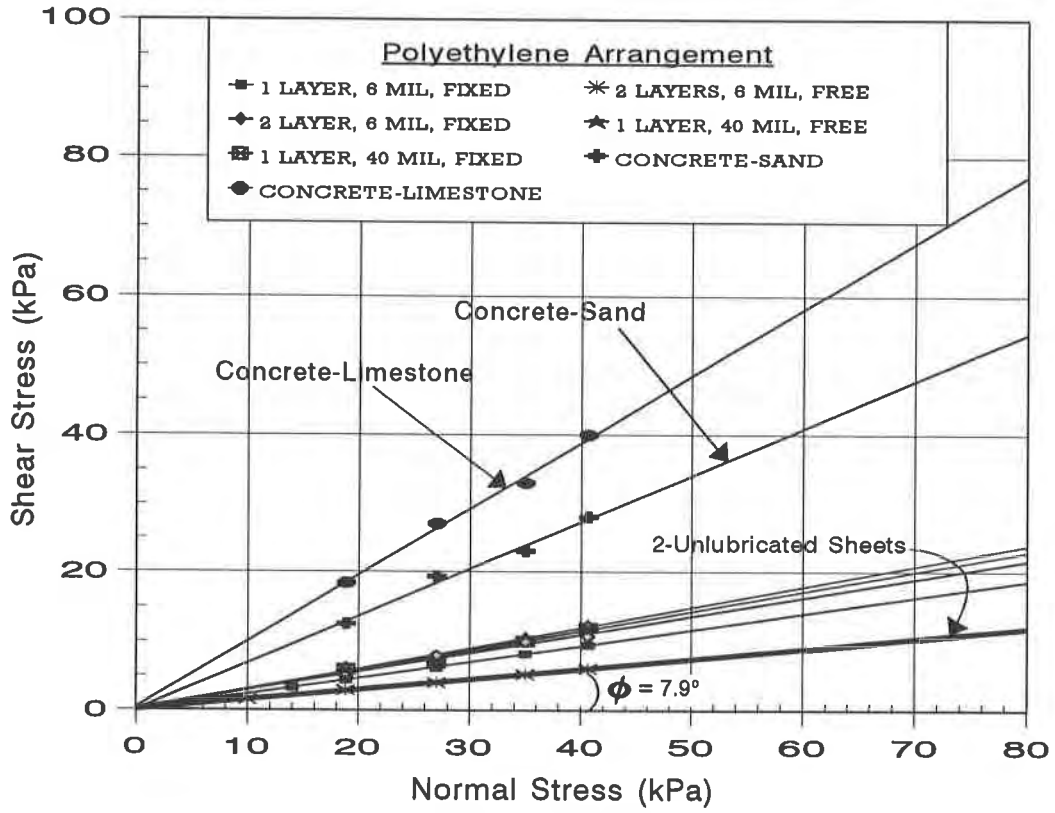

Figure 4 Shearing Characteristics of Polyethylene Sheathed Samples.

The least shearing resistance of the concrete-polyethylene-soil samples resulted when two 6 mil sheets were lightly lubricated with oil. This arrangement reduced the coefficient of friction for the two soils by 95% at 0.0025 mm/min rate of loading and 25°C temperature. For the lubricated sheets the shearing resistance was slightly higher at a shearing rate 1.0 mm/min than at 0.0025 mm/min.

Test results on the bitumen coated samples showed that bitumen was more effective than polyethylene sheathing in reducing the friction resistance between the soil and the concrete surface at 56°C temperature. However, it was also found that increasing the normal stress on the concrete-bitumen-soil samples caused a drastic increase in the shearing resistance. The effect of the temperature, the rate of loading, and the soil type on the shearing behavior of the bitumen-soil matrix was very pronounced. Conventionally, the shearing behavior of bitumen is always presented in terms of shear stress versus strain rate. This is because the shearing characteristic of bitumen is strain rate dependent. However, for the purpose of this study the shearing behavior of the bitumen coated samples was expressed in terms of Mohr-Coulomb yield criterion, and compared with the shearing behavior of the polyethylene sheathed samples. Figures 5 and 6 show the effect of different parameters on the shearing resistance of the concrete-bitumen-soil samples as compared with the concrete-polyethylene-soil with two lubricated layers.

Unexpectedly the 40 mil sheets exhibited higher shear resistance than the 6 mils sheets. This behavior may be related to the surface texture of the 40 mil sheets used in the study. However, this type of polyethylene sheet showed no signs of damage

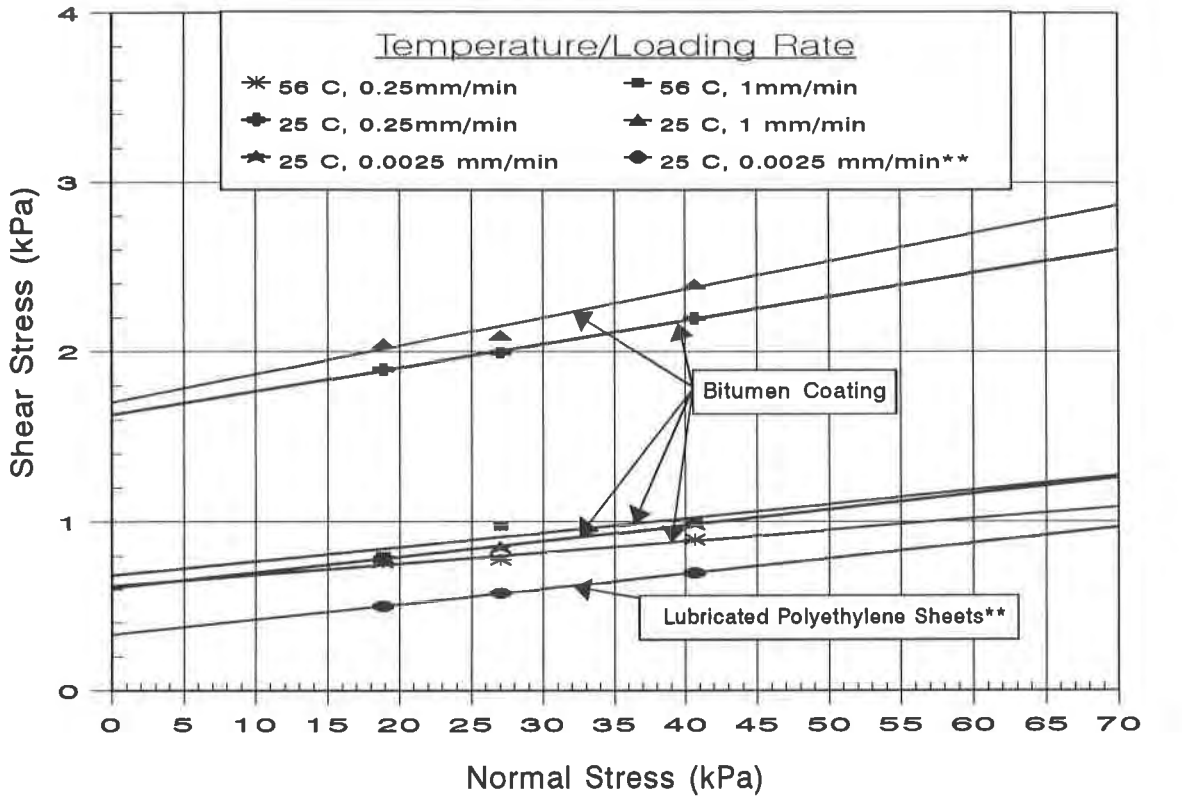

Figure 5 Shearing Behavior of Bitumen and Lubricated Polyethylene Coated Samples; Sandy Soil.

except for some scattered scratches from the coarse particles. For the 6 mil sheets, some marks and depressions were noticed on the fixed single sheets, but no damage had occurred during shear testing. The disturbance due to the soil particle penetration was very noticeable on the bitumen coated samples. For the coarse soil samples, the particles fully penetrated the bitumen layer (3.2 mm) and came to a full contact with the concrete surface at normal stresses of 35 KPa and 40.65 KPa. This contact caused an increase in the friction resistance of the samples.

As the test results show, the two lubricated polyethylene sheets exhibited the lowest shearing resistance at normal stress of 40.65 KPa as compared with the bitumen coating at the same temperature and normal stress. For the unlubricated sheets, the shearing resistance was found to be comparable to the bitumen coating for the coarse soil at 25°C.

CONCLUSION

The aim of this study was to evaluate the effectiveness of polyethylene sheeting as compared with the bitumen coating in reducing downdrag in piles. It is evident from the laboratory results that using polyethylene sheathing method can significantly reduce the shearing resistance between the soil and the concrete surface. The two 6 mil polyethylene sheets reduced the shear resistance by an amount that was comparable to the bitumen coating in coarse soils. Lubricating these sheets would further reduce the shear resistance, and with this arrangement the polyethylene sheathing became more effective than the bitumen coating under all the tested conditions, except at high

temperatures (T > 56°C), at which bitumen coating exhibited the least friction. These temperatures, however, may not be attainable in the actual field conditions.

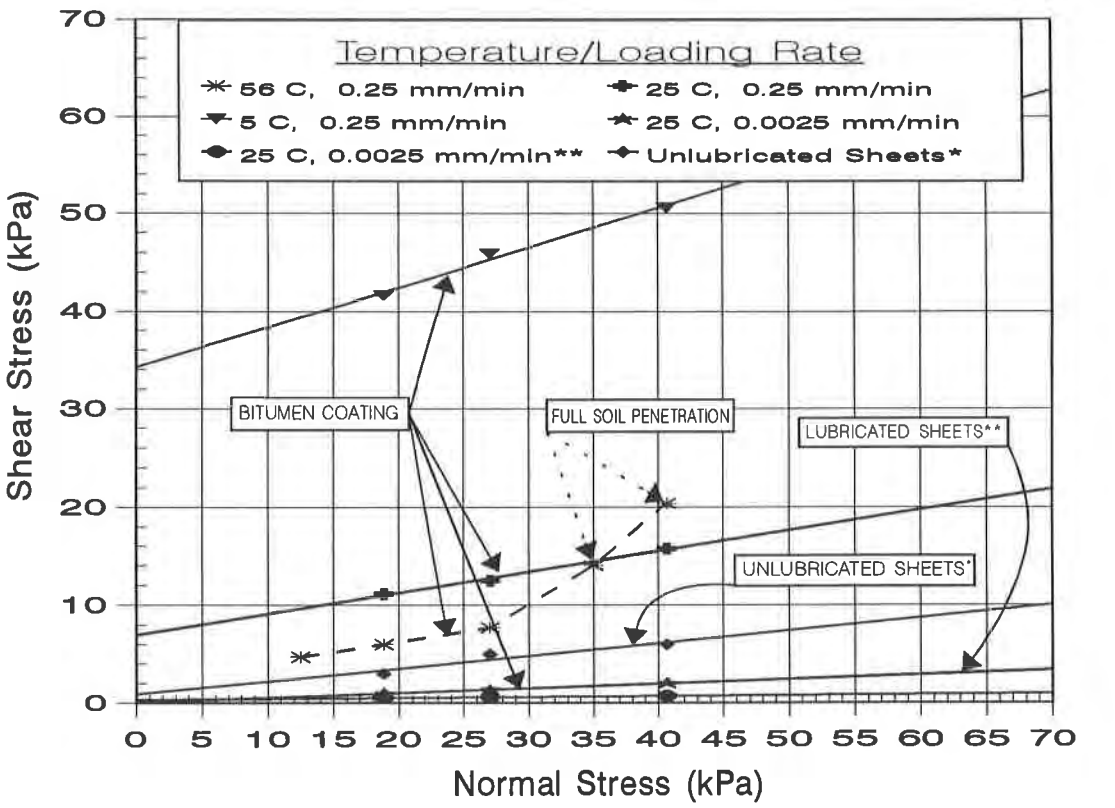

Figure 6 Shearing Behavior of Bitumen and Lubricated Polyethylene Coated Samples; Coarse Soil.

Disturbance of the bitumen coating due to soil particles penetration was significant, and this occurrence can not be avoided, especially in cases of soft bitumens and coarse soils. Full penetration occurred at stresses corresponding to fill height on the order of 4.5 meters. On the contrary, the polyethylene sheets showed no signs of damage during shear testing. Moreover, the installation process does not require extra precautions as in the case of bitumen coating. Whereas in bitumen coating, dripping off of unprotected bitumen coating represents one of the major problems in hot climates.

The selectivity of the type of polyethylene sheets depends upon the requirements of the engineering design. For the purpose of mitigating downdrag forces, it is believed that polyethylene sheets with high strength, smooth surface texture, and appropriate workability could satisfy the requirements of an acceptable friction reducer in piles.

ACKNOWLEDGMENTS

Financial support was provided by the Florida Department of Transportation and the Department of Civil Engineering at FAMU/FSU College of Engineering. This support is gratefully acknowledged. Also, the authors would like to express their gratitude to Dr. Jean Louis Briaud from Texas A & M University for his valuable suggestions on this project.

REFERENCES

Baligh, M. M., and Vivatrat, V., (1975 A) "A Manual on Prediction of Pile Downdrag On End Bearing Piles", Research Report R75-38, CFD-518, Department of Civil Engineering, Massachusetts Institute of Technology, Cambridge, Mass., 22 p.

Baligh, M. M., Figi, H., Vivatrat, V., (1975 B) "Design of Bitumen Coating to Reduce Downdrag on Piles", Research Report R78-5, CFD-596, Department of Civil Engineering, Massachusetts Institute of Technology, Cambridge, Mass.

Baligh, M. M., Figi, H., Vivatrat, V., and Azzouz, A. S., (1981) "Design of Bitumen Coating to Reduce Downdrag on Piles", Research Report R80-42, Department of Civil Engineering, Massachusetts Institute of Technology, Cambridge, Mass.

Bjerrum, L., Johnessen, I. J., and Eide, O., (1969) "Reduction of Negative Skin Friction on Steel Piles to Rock", Proceedings, the Seventh International Conference on Soil Mechanics and Foundation Engineering, Mexico City, Mexico, Vol. 2, pp. 27-34.

Johannessen, I. J. and Bjerrum, L., (1965) "Measurements of the Compression of a Steel Pile to Rock due to Settlement of Surrounding Clay", Proceedings, the Sixth International Conference on Soil Mechanics and Foundation Engineering, Vol. II, Canada, pp. 261-264.

Martin, J. P., Korner, R. M. and Whitty, J. E., (1984) "Experimental Friction Evaluation of Slippage Between Geomembranes, Geotextiles and Soils," Proceedings, International Conference on Geomembranes, IFAI, Denver, Colorado, pp. 191-196.

Tawfiq, K. S., and Ping W. V., (1992) "Effectiveness of Polyethylene versus Bitumen Coating on Downdrag Forces", Final Report Submitted to the Florida Department of Transportation.

Vesic, A. S., (1972) "Design of Pile Foundations", Report No. 42, Transportation Research Board, National Research Council, Washington D.C.

Zeevaert, L., (1972) "Foundation Engineering For Difficult Subsoil Conditions", Van Nostrand Reinhold Company, New York.

Full Scale Geotextile Rock Barrier Wall Testing, Analysis and Prediction

D.K. Burroughs
Parsons De Leuw Inc., USA

H.H. Henson
Parsons De Leuw Inc., USA

S.-S. Jiang
King County (Washington) Public Works, USA

ABSTRACT

Rockfalls are a constant danger to motorists and to highway facilities in mountainous terrain. An experimental full size rock barrier wall measuring 27.4 m (90 ft.) in length, 3.05 m (10 ft.) in height, and 1.82 m (6 ft.) thick with layers of geotextile fabric placed horizontally between layers of soil was built and tested in August, 1991, at Rifle, Colorado, USA. Various sized rocks from 0.6 m (2 ft.) to 1.8 m (6 ft.) in diameter and weighing up to 4000 N (18,000 lbs.) were rolled down a 180 m (600 ft.) high incline into the barrier. A sophisticated monitoring system was designed to measure the maximum static and dynamic deformations along the vertical faces of the wall during each rock impact.

A three dimensional solid element model using finite element analysis was then used to model the wall. Static loads were applied to the model at the approximate point of impact of the rock. Energy verses deformation curves were then plotted for certain material properties. These curves were then compared to the test results to determine the appropriate material properties for the model. Material properties were based on the composite strength of the soil and fabric. Using the selected material properties, other wall sizes have been modeled and energy deformation curves have been created to predict the maximum rock energy which can be absorbed by the wall.

INTRODUCTION

Rockfalls are a constant danger to motorists where vehicles moving at a high rate of speed may collide with rocks on the roadway. There is also danger of rockfalls at highway facilities such as rest areas. The construction of 21 km (13 miles) of I-70 through a narrow river canyon near Glenwood Springs, Colorado has led to new research and methods for mitigating this problem. This canyon has walls of rock reaching at least 600 m (2000 ft.) above the roadway.

One structure which has been considered for use to control rockfalls is a reinforced geotextile fabric and soil wall which provides an impact barrier to rolling rocks as shown in Figure 1. These structures ranging in width from 1.5 m (5 ft.) to 2.5 m (8 ft.) and ranging in height from 2.5 m (8 ft.) to 3 m (10 ft.) are a space-efficient and cost-effective solution to absorb the massive energies in a rockfall. In certain situations, rocks 1.8 m (6 ft.) in diameter and traveling at over 18 m/s (60 ft/s) with over 1,400,000 J (1,000,000 ft.-lbs.) of energy must be stopped within a narrow 2.5 m (8 ft.) space.

Figure 1. Photograph of Test Wall Showing Front Face

Previous tests of rock barrier walls undertaken by the Colorado Department of Transportation (CDOT) have shown that they can absorb massive amounts of energy. This particular test was undertaken to accurately measure and record the wall deformations during impact and to find a way to estimate the required rock barrier wall size for certain rockfall energy levels.

At the present time, there is not an established method to estimate the required wall size to stop rockfalls. An approximate design method is needed to predict required wall sizes for various rock energy levels.

An exact or even an approximate design method may be difficult to develop for the following reasons:

(1) Impact problems by their nature are difficult to solve since the impact of the rock on the rock barrier wall occurs in a very short time period with very high dynamic forces.

(2) The motion of the rolling rock is unpredictable. It's motion consists of a horizontal component, a vertical component, and a rotational component of velocity. It is also bounding down the incline which has an uneven surface.

(3) The shape of the rock is seldom spherical but can be oblong in shape with rough projections.

(4) The barrier wall behaves as a three dimensional solid. Analysis should consider the three dimensional behavior of the wall.

(5) The barrier wall is built from a composite material which consists of geotextile fabric and soil. Although uniform in construction, this wall type is difficult to model as a composite material.

(6) The forces imposed on the barrier wall are very high and may result in non-linear stress-strain behavior. Large deformations and in-elastic behavior will occur near the point of impact.

(7) The contact area at the point of impact varies in size during the duration of the impact.

(8) Computer software is available for the analysis of both static and dynamic three dimensional problems. The cost and time to implement a more sophisticated solution which includes the non-linear material properties and dynamic modeling is time consuming and not cost-effective as a production design technique.

Presented with these factors, it was decided to use a simplified method of analysis that could be implemented efficiently and in a cost-effective manner. Design figures for rock barrier walls of various sizes for different rockfall energy levels will be developed. Although the results will be approximate in nature, they are adequate for the design of these types of structures.

SITE CONDITIONS

The wall test site was at Rifle, approximately 275 km (170 miles) west of Denver, Colorado, USA. The wall was built at the base of a slope of approximately 460 m (1500 ft.) in length with a drop of elevation of 180 m (600 ft.). The top of the slope has a natural slope of about 45 degrees and the bottom of the slope near the wall has been graded to about a 30 degree incline. A channel has been removed about 18 m (60 ft.) in width to guide the rolling rocks into the center of the wall. The soil on the surface of the slope consisted of exposed rocks, boulders, and mixed silty sand and clay.

The test wall was constructed directly on a graded level natural soil foundation. The undisturbed material beneath the wall varies from boulders to fine granular soil and is considered to be a firm and sound foundation for the wall.

TEST WALL

An experimental full size rock barrier wall measuring 27.4 m (90 ft.) in length, 3.05 m (10 ft.) in height, and 1.82 m (6 ft.) thick was built. The test wall layout is shown on Figure 2. The wall was reinforced with horizontal layers of geotextile fabric at 30 cm (1 ft.) spacing as shown in Figure 3. The fabric used was Poly-felt TS-700 non-woven geotextile. A 15 cm (6 in.) by 15 cm (6 in.) nominal timber facing was used on both sides of the wall. The timber facing was used to provide dimensional control for construction of the wall. The horizontal members were discontinuous to minimize the effect of adding additional strength to the wall. The purpose of the test was to evaluate the reinforced earth mass. The soil fill was roadbase material. It consisted of mixed gravel, sand, and silt and was slightly compacted in 30 cm (1 ft.) layers.

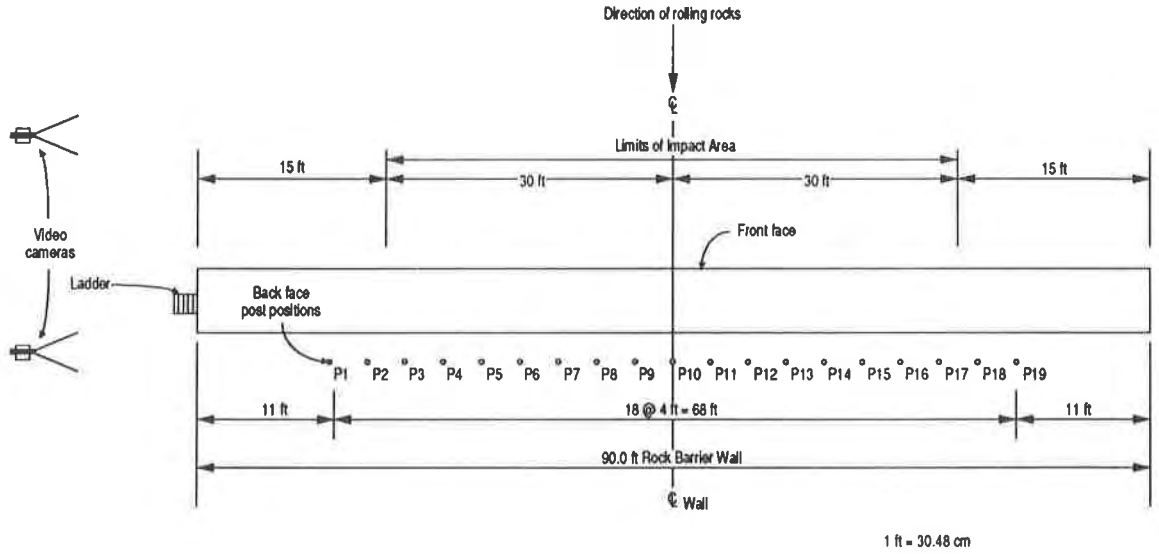

Figure 2. Test Wall Layout

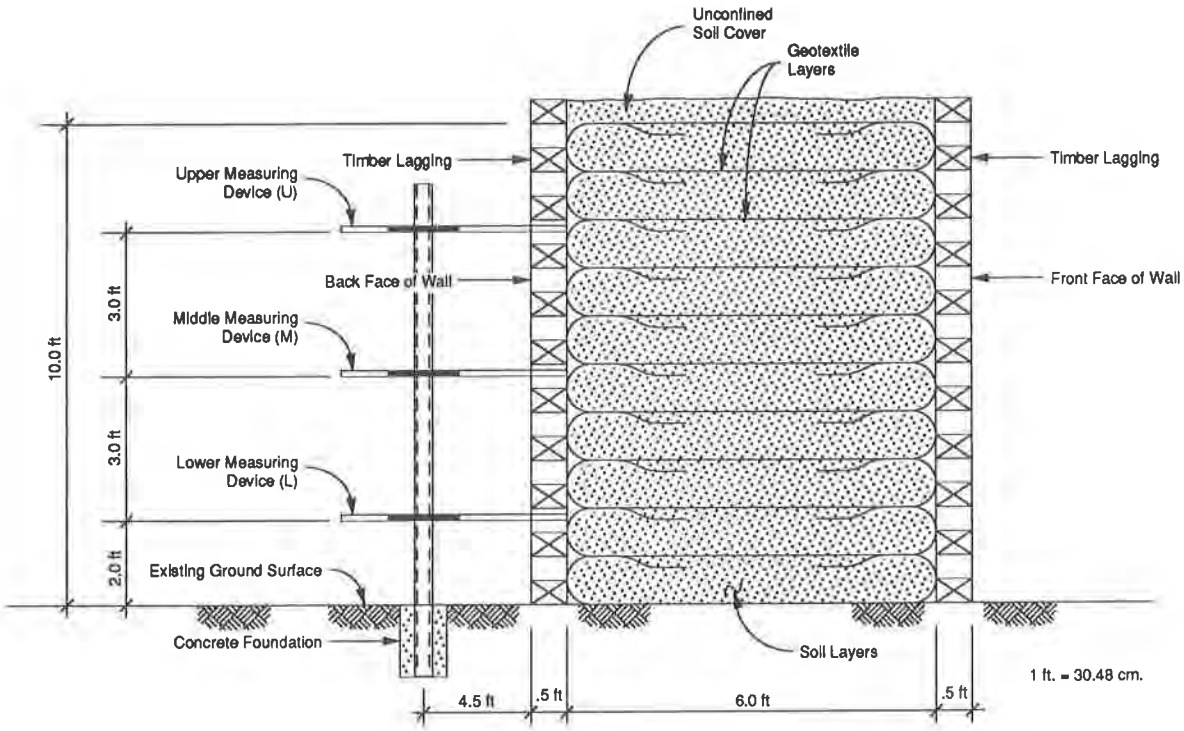

Figure 3. Cross-Section of Test Wall

MONITORING PROCEDURE

All testing was monitored with video cameras which were recording at 30 frames per second or 0.033 seconds per frame. White lines were placed parallel to the wall at 3.05 m (10 ft.) increments up the incline to assist in recording the velocity of the rocks. Rock velocities can be determined by counting the number of video frames recorded between successive lines as the rock rolls down the incline. Video cameras also recorded the behavior of the front face and back face of the wall during impact.

Both the front and back faces of the wall were instrumented to record the deformation during and after each impact. The front face had a steel cable which was raised and lowered to serve as a reference line to measure the permanent deformation of the front of the wall. This system could not measure the maximum deformation which occurred during impact. Video tape of the impact was reviewed to estimate the amount of deformation at the front face. On the back face, steel posts were spaced at 1.21 m (4 ft.) intervals with mechanical measuring devices which could record both the permanent deformation of the wall due to a succession of rock impacts and the maximum deformation during each impact.

TEST PROCEDURE

A total of 18 rocks were used in the test. Each rock was measured and numbered during the preparation for the test. The rocks varied in diameter from 50 cm (1.7 ft.) to 1.8 m (5.8 ft.). The weights varied from 100 N (500 lbs.) to 4,100 N (18,000 lbs). The weights were computed from the average diameter of the rocks and the estimated density. The different sizes of rocks were selected to provide different levels of rock energy at the point of impact with the barrier wall. The rocks were released at the same point at the top of the incline beginning with the smaller rocks to slowly increase the impact energy on the wall. After each rock impact, the rock was removed to clear the test area. Damage to the barrier wall was not repaired during the test.

Data was recorded for the permanent deformation at the front face of the wall and the permanent deformation and the maximum deformation at the back face after each rock impact.

TEST RESULTS

Test results, shown on Table 1, include the test number, rock diameter, estimated rock weight, velocity, computed energy, estimated contact duration measured from the video tape, front face deformation at the point of impact, back face deformation at the mid-height of the wall, and the height of the point of impact from the ground surface. Note that certain rocks did not impact the wall or that other rocks impacted with no significant deformation. These tests were not investigated further. The significant tests were Test Nos. 6, 7, 12, 13, 15, and 18.

Successive rock impacts created greater and greater deformation of the rock barrier wall. The data was adjusted to provide the net deformation for each rock impact. Table 2 shows the net back face deformation for each test. The data is presented at each post location which are at 1.2 m (4 ft.) spacing. It is also shown at the upper, middle, and lower measuring locations. From the data, it is useful to note the relative locations of each rock impact along the wall and the deformation in the proximity of the point of impact.

Figure 4 shows the front face of the test wall after the impact of Test No. 18. This was the last test rock and it shows the large amount of damage to the wall at the point of impact.

Figure 4. Test Wall After Rock Impact of Test No. 18

METHOD OF ANALYSIS

The energy method of analysis can be used to simplify the analysis and design procedure. The energy concept relates the kinetic energy of the rolling rock to the energy absorbed through deformation of the rock barrier wall. The kinetic energy of the rock consists of vertical, horizontal, and rotational components. For this analysis, the horizontal component of velocity and its energy will be used. The vertical and rotational components do not create large horizontal deformations of the wall. The energy absorbed by the rock barrier wall includes the strain energy of the wall as it is deformed.

FINITE ELEMENT MODEL

A three dimensional solid element model using the finite element program SAP90 was used to model the wall. Figure 5 is a picture of the finite element model. It consists of 440 elements and has a wider base section to model the undisturbed material under the base of the wall. Point loads were applied to the model at the location shown. The length of the model was greater than the influence length as determined from the test results.

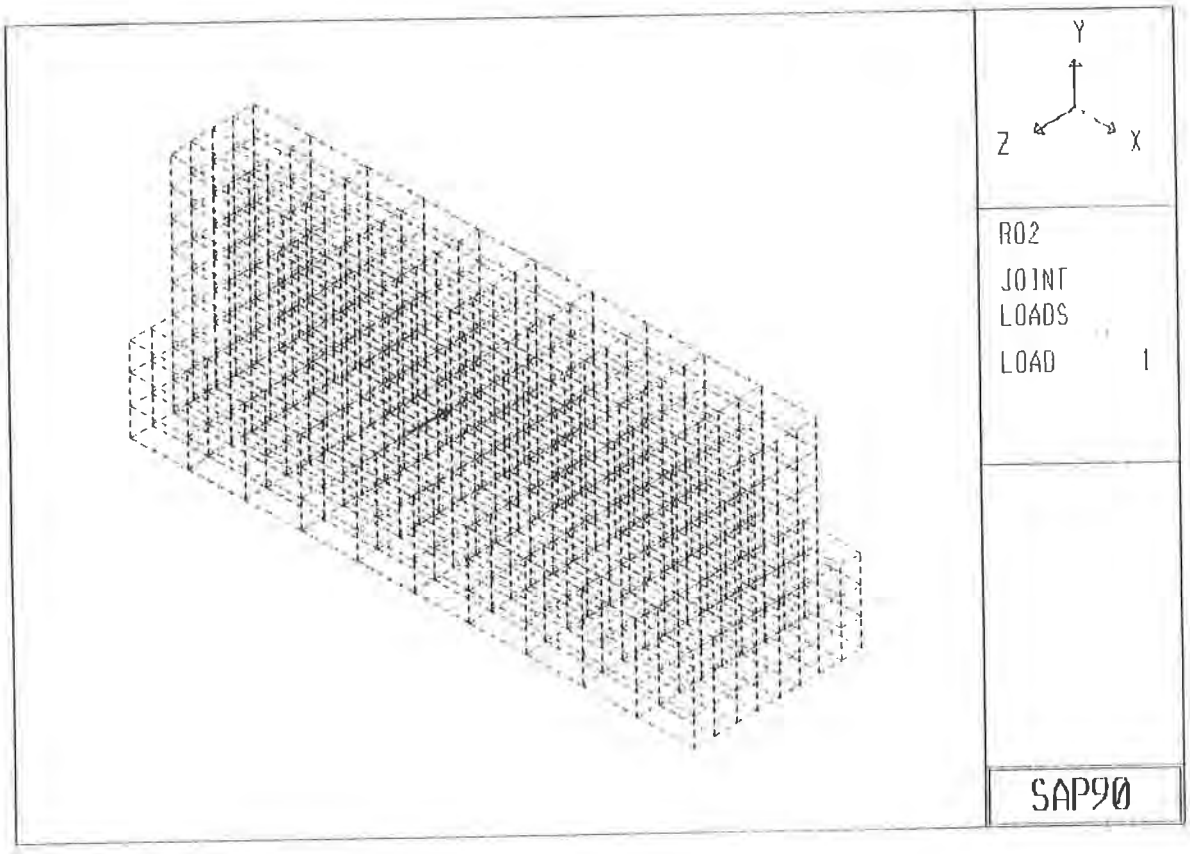

Figure 5. SAP90 Rock Barrier Wall Model

MATERIAL PROPERTIES

The material properties of the model were considered to be isotropic, linear, elastic, and composite with the soil and fabric. The model material properties were determined as follows. From the test data, it is known what the maximum deformations of both the front and back wall were during the rock impact. The energy level of the rock was also determined from the computed velocity from the video data. The value of Young's Modulus, E, is varied in the wall and in the base material of the model with the base material being a higher value. The value of the shear modulus was equal G=0.3*E in all cases. The amount of deformation at a certain energy level is matched at the point of impact and at the back face.

To simplify the solution, the point of impact was considered to be at 0.4 times the wall height. The amount of deformation of the wall at the point of impact and at the back face at mid-height for a constant energy level is not appreciably different for different heights of impact up to approximately 0.6H. The back face deformation used is at the mid-height of the wall and is at the same level as the middle measuring device shown on Figure No. 3.

Figure 6 shows the wall deformations of the finite element model due to a point load at 0.40*H on the front face. The rock has been shown graphically at the point of impact.

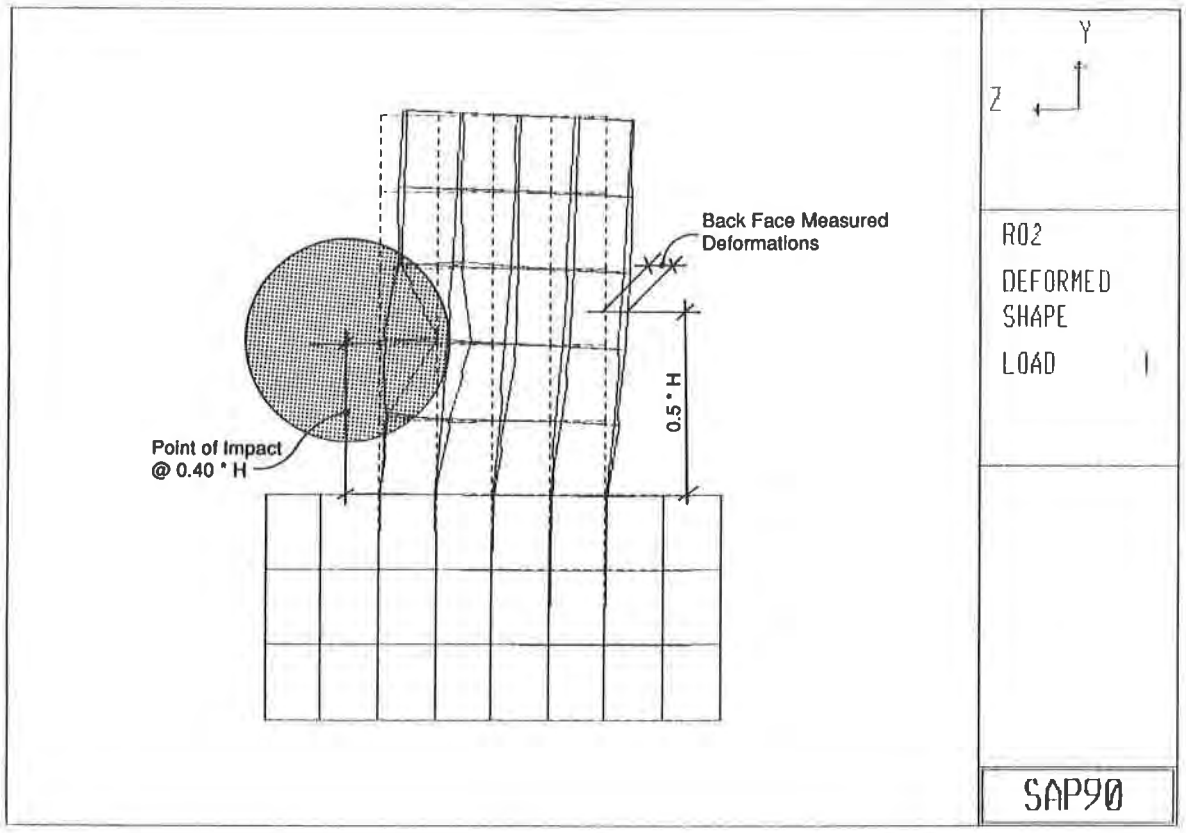

Figure 6. Model Deformation

Figure 7 shows the front face and back face measured deformations from the wall test at the various rock energy levels. The value of E in the model for the base material and the wall has been adjusted so that the model deformations match the test deformations at the point of impact and at the back face for the rock energy of Test No. 15. The value of E determined in this model was 13,800,000 Pa (2000 psi) for the wall material and 62,000,000 Pa (9000 psi) for the undisturbed base material. Figure 8 represents the back face deformations at mid-height along the back face and the deformations of the finite element model with the adjusted E values for Test No. 15. It can be seen that the transverse distribution of deformation closely matches the model.

DESIGN CURVES

The theoretical curves shown in Figure 7 represents the energy absorbed by the wall to cause certain deformations at the front face at 0.40*height and at the back face at mid-height. It can be seen that the test data correlates closely to the theoretical curve due to the adjustment of the material properties of the wall. The curve is a second order equation from the origin to the test data at Test No. 15. The backwall deformation at Test No. 15 was about 20 cm (8 in.) At Test No. 18 the deformation was over 70 cm (29 in.). It was decided to connect these two points with a straight line to represent the dramatic increase in deformations with a small amount of increase in energy.

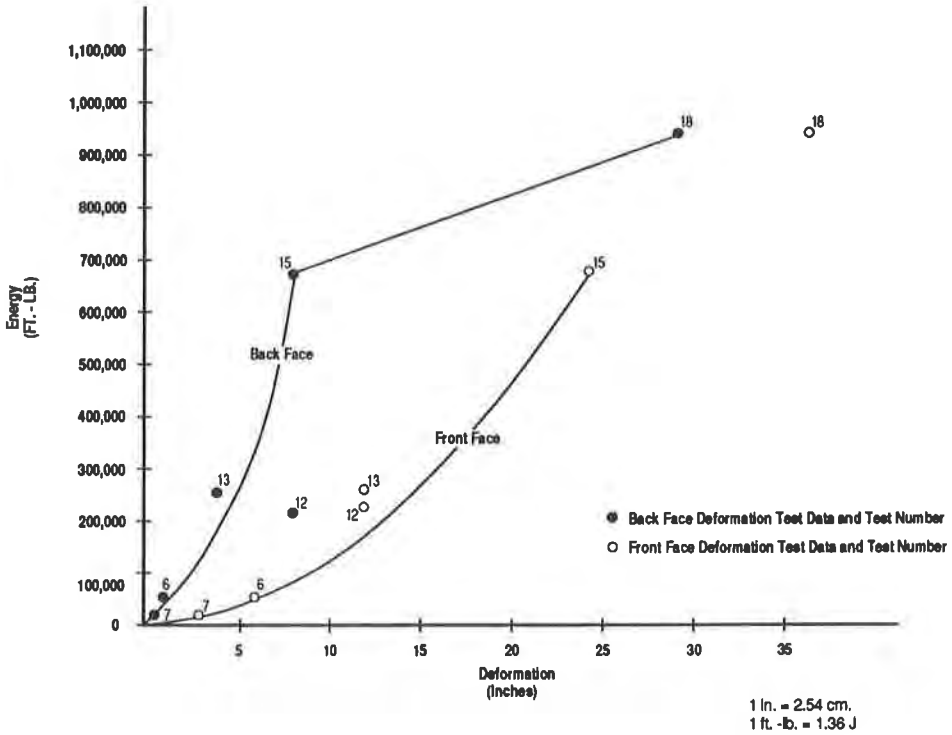

Figure 7. Test Data and Theoretical Curves

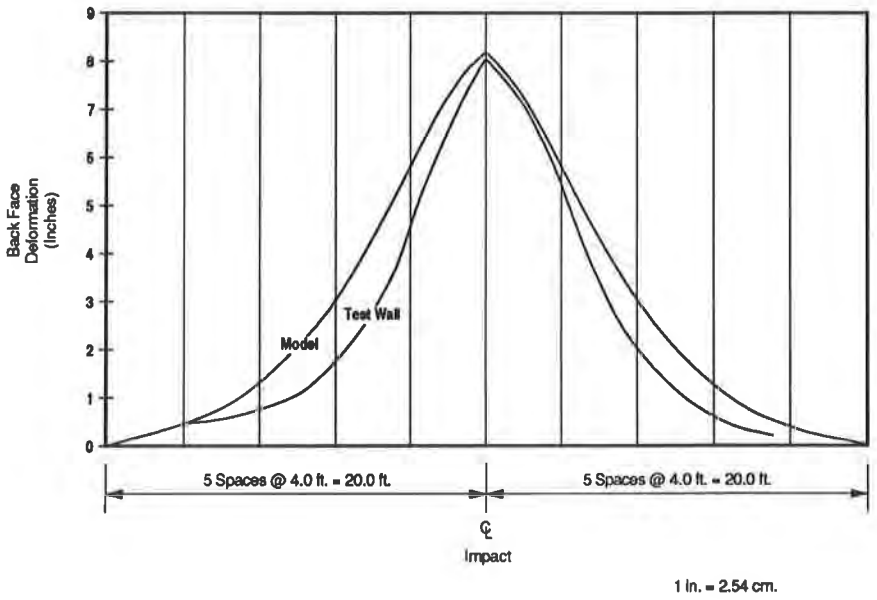

Figure 8. Comparison of Back Face Transverse Wall Deformation for Test No. 15 Between the Test Wall and the Finite Element Model

PREDICTION

Using the selected material properties, other wall sizes have been modeled and energy deformation curves have been developed to predict the maximum rock energy which can be absorbed by the wall. Figure 9 shows the energy deformation curves for the 1.8 m (6 ft.) by 3.05 m (10 ft.) wall, a 1.5 m (5 ft.) by 2.43 m (8 ft.) wall, and a 2.13 m (7 ft.) by 3.35 m (11 ft.) wall. The curves were discontinued at 30 cm (12 in) of back face mid-height deformation. The end of the second order curve has been uniformly discontinued at 20 cm (8 in.).

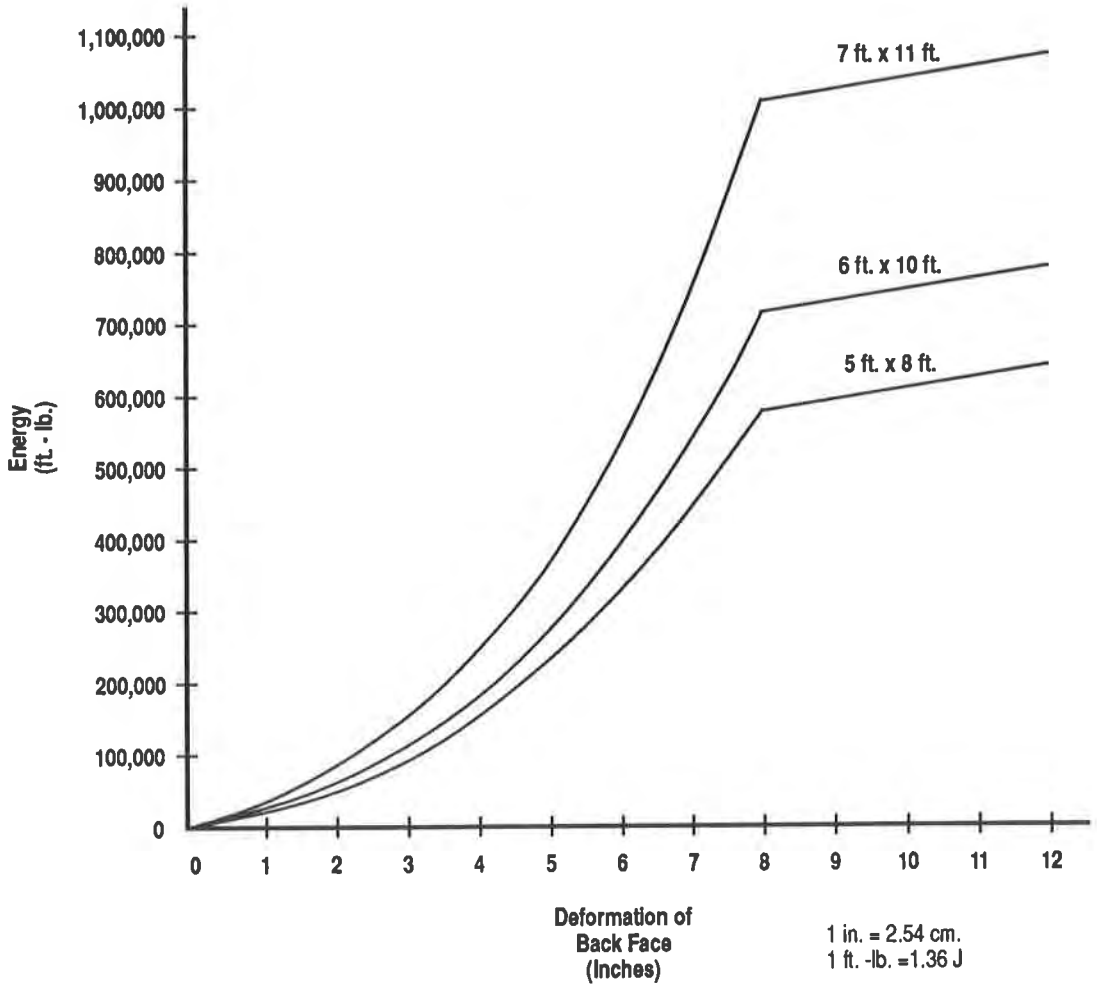

Figure 9. Rock Barrier Wall Energy Deformation Curves

CONCLUSIONS AND RECOMMENDATIONS

(1) Full scale testing has demonstrated that geotextile reinforced earth rock barrier walls are an economical and practical structure to absorb the energy of falling rocks. The desired results for wall performance were achieved and the performance of the geotextile fabric met all expectations.

(2) The rock barrier test wall absorbed over 1,300,000 J (1,000,000 ft-lbs) of energy from a rolling rock.

(3) An energy method for the prediction of rock barrier wall sizes for certain rock energy levels has been presented. Although this approach is a simplified method of analysis, it can be implemented efficiently and in a cost-effective manner. The results are approximate in nature, but they are reasonable for the design of this type of structure.

(4) The information presented in Figure 9 is directly related to the wall size tested. For walls of largely varying sizes and shapes, results should be verified with further testing. Rock impacts should be below 0.6H of the wall height. This energy method of analysis was limited to isotropic, linear, and elastic material properties. At the point of rock impact with the barrier wall, plastic behavior will occur.

(5) The timber facing was used as an aid in the construction of the wall and had little effect on the strength of the wall. In the future, facing materials should be considered that would provide protection against adverse environmental conditions and the abrasive action of rock impacts.

(6) The ultimate failure of the wall is the point at which a rock just continues movement through the wall and out the back face. Failure of the wall occurs when a rock seriously damages the wall and in fact may be stopped within the wall. Extensive repair measures are required. No test rocks had enough energy to subject the wall to ultimate failure. Test rocks 15 and 18 did fail the wall to the extent that repairs to the wall would be necessary.

(7) In the future, other barrier walls of varying sizes and different geotextile fabric reinforcing patterns and properties should be built and tested to provide additional test data and to confirm the material presented.

ACKNOWLEDGEMENTS

The test wall was built and monitored by the Colorado Department of Transportation as part of their on-going rockfall studies research program.

The authors wish to express their appreciation to the Colorado Department of Transportation and in particular to Bob Barrett who has promoted the use and testing of geotextile reinforced earth structures as energy absorbing rock barriers.

Protective Shelter Construction With Reinforced Earth

C.Y. Tuan
Applied Research Associates Inc., USA

D.H. Merkle
Applied Research Associates Inc., USA

ABSTRACT

Protective shelters for military applications are traditionally constructed with reinforced concrete. However, the use of prefabricated wall panels anchored to a soil backfill reinforced with geosynthetics for hardened shelter construction could reduce cost by at least thirty percent, as opposed to the use of reinforced concrete. These shelter components can be prepositioned in theater and rapidly erected by unskilled labor as the need arises. Furthermore, damage to the shelter from airblast and ground shock would be localized due to the modular wall construction. Thus, expedient repair methods can be applied to these prefabricated reinforced soil shelter facilities with little difficulty. The objective of this research is to develop a simple analytical model that characterizes shock wave propagation through reinforced soil and the dynamic interaction with modular wall panel sections. Centrifuge model test data have been used to validate the model. It is expected that this innovative construction will increase the survivability of protective shelters, while at the same time reducing construction and maintenance costs.

INTRODUCTION

Conventional protective shelters are generally constructed with cast-in-place reinforced concrete requiring skilled labor, materials and equipment, which may not be available on site. These constructions usually take a long time and cost millions of dollars.

The use of reinforced soil in the construction of retaining walls has received much attention during the past decade. Barrett (1992) reported that retaining wall systems with synthetic soil reinforcement frequently save fifty percent or more than concrete systems. Recent field explosive tests on a reinforced earth shelter conducted in Israel(Raudanski 1990) have shown that such shelters can be constructed rapidly and can provide good protection from blast loading. Prefabricated wall panels attached to horizontal metal strips in a backfill were utilized in that shelter construction. These suggest that geosynthetics may find applications in the

construction of protective shelters.

This study focuses on the dynamic response of a reinforced earth protective shelter under ground shock wave loading. A one-dimensional mathematical model was first developed to describe the characteristics of shock wave propagation through reinforced soil and to determine the dynamic interaction between the wall and reinforced soil. The results were then compared with centrifuge test using replica models.

ONE-DIMENSIONAL MODEL

As shown in Figure 1, a typical wall can be constructed with interlocking modular panels or blocks connected to the soil reinforcement. The soil reinforcement is assumed to be layers of geogrids running parallel to the direction of wave propagation. Figure 2 shows a wall panel with a layer of reinforced soil attached to it. It is implied in this model that any tension developed in the soil will be taken by the geogrid, and that the soil and wall panel stay bonded at the interface. Furthermore, the shear and bending resistance from connections between the panels has been left out to simplify the analysis.

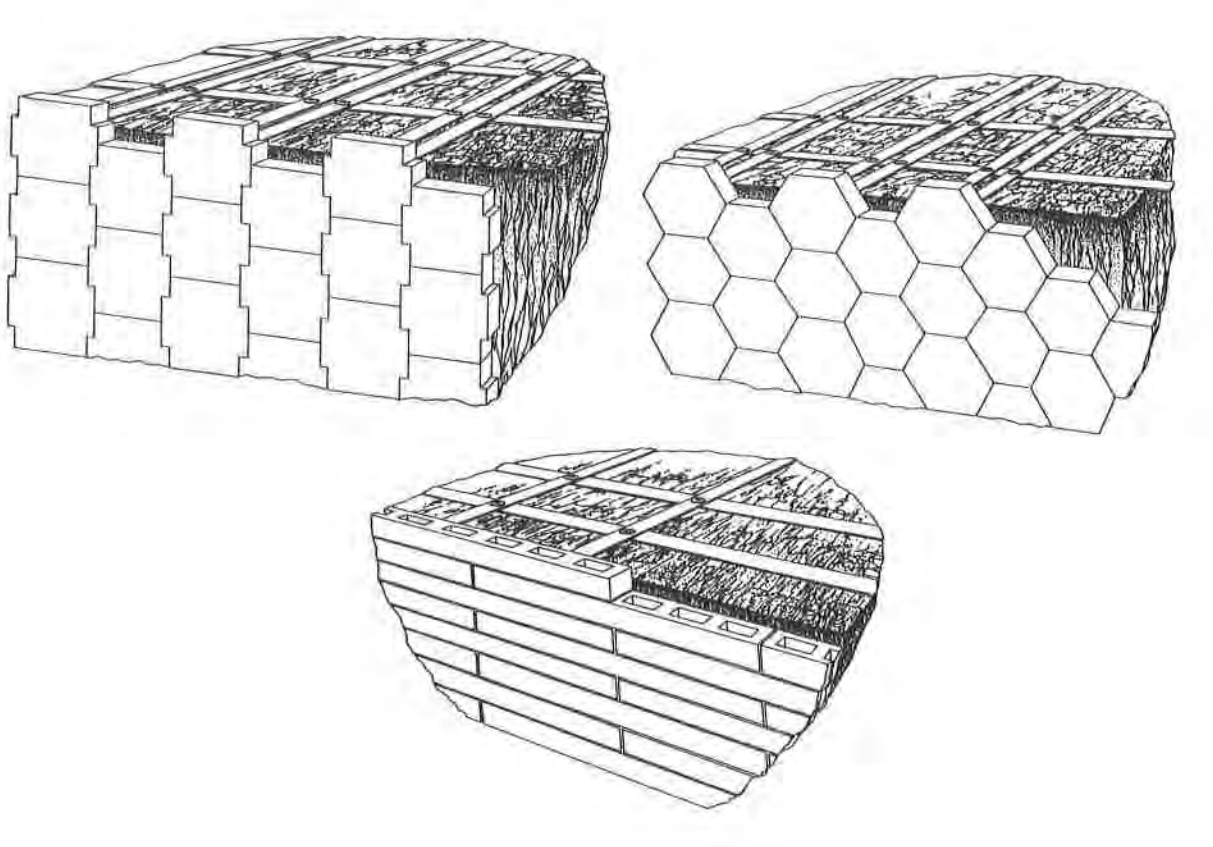

Figure 1 Modular Wall Panels with Soil Reinforcement

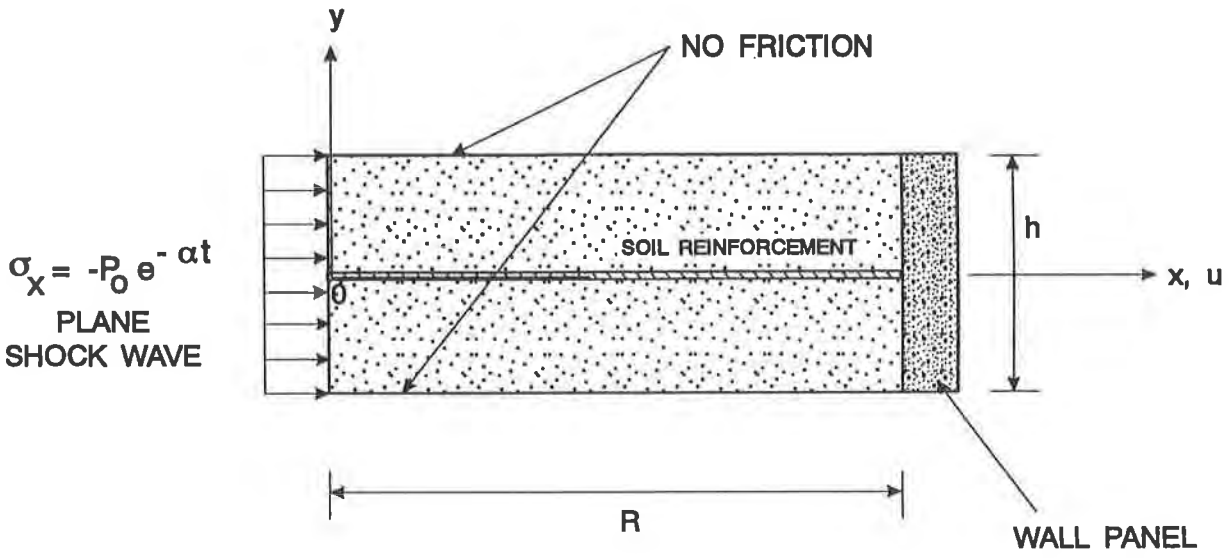

Figure 2 One-dimensional Model of Wall Panel and Soil Reinforcement Connection System

The elastic behavior of sheet-reinforced soil can be modeled as that of a composite material. Jones(1975) showed that the "macromechanical" behavior of a composite material can be described in terms of the mechanical properties of its constituents and their volume ratios in the composite construction. Harrison and Gerrard (1972) treated reinforced soil as a cross-anisotropic (or transversely isotropic) material consisting of layers of stiff and soft isotropic materials with a vertical axis of symmetry. Assuming strain compatibility, the constrained modulus of the reinforced soil in the apparent stress-strain relation in the x-direction, $\sigma_X = K_X \varepsilon_X$, can be expressed as

$$K_x = \frac{E_s(1-\nu_s)}{(1+\nu_s)(1-2\nu_s)}(1-V_g) + \frac{E_g(1-\nu_g)}{(1+\nu_g)(1-2\nu_g)}(V_g)$$

$$-V_g(1-V_g)\frac{\left[\dfrac{E_s\nu_s}{(1+\nu_s)(1-2\nu_s)} - \dfrac{E_g\nu_g}{(1+\nu_g)(1-2\nu_g)}\right]^2}{\dfrac{E_s(1-\nu_s)}{(1+\nu_s)(1-2\nu_s)}(V_g) + \dfrac{E_g(1-\nu_g)}{(1+\nu_g)(1-2\nu_g)}(1-V_g)} \qquad (1)$$

where E_s and E_g, and ν_s and ν_g are, respectively, the Young's moduli and Poisson's ratios of the soil and reinforcement. The volume ratio of the reinforcement in a reinforced soil medium is denoted by V_g.

Governing Equation. The 1D wave equation for the particle displacement, $u(x,t)$, in a homogeneous medium is

$$\frac{\partial^2 u}{\partial t^2} = c^2 \frac{\partial^2 u}{\partial x^2} \tag{2}$$

where c, the wave propagation velocity of reinforced soil, is given by

$$c = \sqrt{\frac{K_x}{\rho_o}} \tag{3}$$

and ρ_o is the mass density of the reinforced soil.

Boundary Conditions. At x = 0, the shock wave front, having an initial particle velocity, v_o, arrives at time t = 0 and decays exponentially, so that

$$\frac{\partial u}{\partial t}(0,t) = v_o \exp(-\alpha t) \qquad (t > 0) \tag{4}$$

where α is the decay rate. The shock front pressure, P_o, is the product of soil's impedance ρc and the initial particle velocity v_o.

At x = R, the equation of motion of the wall panel is

$$M \frac{\partial^2 u}{\partial t^2} = -\sigma_x hb - T_g \tag{5}$$

where M is the mass of the wall panel, h is the panel height, b is the panel width, and T_g is the geogrid tension at the wall-soil interface. Casting this geogrid tension in terms of the interface displacement, Eq.(5) becomes

$$\mu \frac{\partial^2 u}{\partial t^2} + \frac{\partial u}{\partial x} = 0 \tag{6}$$

where

$$\mu = \frac{M}{K_x hb + E_g A_g} \tag{7}$$

and E_g and A_g are the Young's modulus and cross-sectional area of the geogrid, respectively.

Initial conditions. The wall panel and reinforced soil system is at rest before the shock front arrives, and thus the initial conditions are:

$$u(x,0)=0 \qquad (0\le x\le R) \tag{8}$$

$$\frac{\partial u}{\partial t}(x,0)=0 \qquad (0\le x\le R) \tag{9}$$

Solution. Eq.(2), together with boundary and initial conditions, was solved by the Laplace transform method. Taking the Laplace transform of Eqs.(2), (4), and (6) yields the transformed wave equation

$$\frac{\partial^2 U(x,s)}{\partial x^2}-\frac{s^2}{c^2}U(x,s)=0 \tag{10}$$

and the transformed boundary conditions

$$U(0,s)=\frac{v_o}{s(s+\alpha)} \tag{11}$$

$$\frac{\partial U(R,s)}{\partial x}=-\mu s^2 U(R,s) \tag{12}$$

where s is a complex variable in the Laplace domain, and x is held fixed throughout the transformation. The solution of Eqs.(10)-(12) is

$$U(x,s)=\frac{v_o}{s(s+\alpha)}\left[\cosh\theta-\left(\frac{\sinh\beta+\mu sc\times\cosh\beta}{\cosh\beta+\mu sc\times\sinh\beta}\right)\sinh\theta\right] \tag{13}$$

where

$$\beta=\frac{sR}{c} \tag{14}$$

and

$$\theta=\frac{sx}{c} \tag{15}$$

The particle displacement, u(x,t), was obtained by taking the inverse transform of Eq.(13), for which purpose Eq.(13) is rewritten in the form of

$$U(x,s)=\frac{v_o}{s(s+\alpha)}\left(e^{\theta}-\frac{e^{\theta}-e^{-\theta}}{1+\eta}\right) \tag{16}$$

where

$$\eta=\left(\frac{1-\mu sc}{1+\mu sc}\right)e^{-2\beta} \tag{17}$$

Because $\eta < 1$,

$$\frac{1}{1+\eta}=\sum_{j=0}^{\infty}(-1)^j\,\eta^j \tag{18}$$

and

$$U(x,s)=\frac{v_o}{s(s+\alpha)}\left[e^{\theta}-\left(e^{\theta}-e^{-\theta}\right)\sum_{j=0}^{\infty}(-1)^j\,\eta^j\right] \tag{19}$$

Keeping only the first three terms of the infinite series along with using Laplace transform pairs yields solution for u(x,t) in the form

$$u(x,t)=\sum_{1}^{5}u_i \tag{20}$$

where, using the variables,

$$t1=t-\frac{x}{c} \tag{21}$$

$$t2=\left(t+\frac{x}{c}\right)-2T \tag{22}$$

$$t3=\left(t-\frac{x}{c}\right)-2T \tag{23}$$

$$t4 = \left(t + \frac{x}{c} \right) - 4T \tag{24}$$

$$t5 = \left(t - \frac{x}{c} \right) - 4T \tag{25}$$

$$T = \frac{R}{c} \tag{26}$$

$$m = \mu\alpha c \tag{27}$$

$$p = m + 1 \tag{28}$$

$$q = m - 1 \tag{29}$$

$$\gamma = \frac{1}{\mu c} \tag{30}$$

the terms on the right hand side of Eq.(20) take the form

$u1 = 0 \qquad (t1 < 0)$

$$= \frac{v_o}{\alpha}\left(1 - e^{-\alpha \cdot t1}\right) \qquad (t1 > 0) \tag{31}$$

$u2 = 0 \qquad (t2 < 0)$

$$= -\frac{v_o}{\alpha q}\left[p\left(1 - e^{-\alpha \cdot t2}\right) - 2m\left(1 - e^{-\gamma \cdot t2}\right) \right] \qquad (t2 > 0) \tag{32}$$

$u3 = 0 \qquad (t3 < 0)$

$$= \frac{v_o}{\alpha q}\left[p\left(1 - e^{-\alpha \cdot t3}\right) - 2m\left(1 - e^{-\gamma \cdot t3}\right) \right] \qquad (t3 > 0) \tag{33}$$

$u4 = 0 \qquad (t4 < 0)$

$$= -\frac{v_o}{\alpha q^2}\left\{ p^2\left(1 - e^{-\alpha \cdot t4}\right) - 4m^2\left(1 - e^{-\gamma \cdot t4}\right) + 4mq\left[1 - (1 + \gamma \cdot t4)e^{-\gamma \cdot t4}\right] \right\} \quad (t4 > 0) \tag{34}$$

$u5 = 0 \qquad (t5 < 0)$

$$= \frac{v_o}{\alpha q^2}\left\{p^2\left(1-e^{-\alpha \cdot t5}\right)-4m^2\left(1-e^{-\gamma \cdot t5}\right)+4mq\left[1-(1+\gamma \cdot t5)e^{-\gamma \cdot t5}\right]\right\} \quad (t5>0) \quad (35)$$

The expressions for the longitudinal normal stress, particle velocity, particle acceleration of the soil medium can be readily derived from Eqs.(20) and (31)-(35). Although higher order terms could be added to the solution, the transient response of the reinforced soil system due to shock loading will have been damped out before they become effective.

CENTRIFUGE MODELING

A series of model tests was conducted to provide data for the validation of the one-dimensional analysis.

Setup. Based on standard static design procedures, 1:30 scale model walls were constructed with soil reinforcement in a 457 mm (18 in.) square centrifuge bucket. As shown in Fig. 3 , a 100 mm (4 in.) sand base was prepared to simulate foundation soil. A 150 mm (6 in.) high, 457 mm (18 in.) long model wall constructed with 51 mm (2 in.) square gypsum panels was built on this base. There were six layers of reinforcement attached to the panels. The reinforcement extended 150 mm (6 in.) from the panels. Horizontal movement along the perimeter of the wall was restrained. A clean sand with a unit weight of 1685 Kg/m^3 (105 pcf) was used for backfill. An explosive charge of 3 g RDX was detonated at 178 mm (7 in.) from the center of the wall while the centrifuge was operated at 30 g .

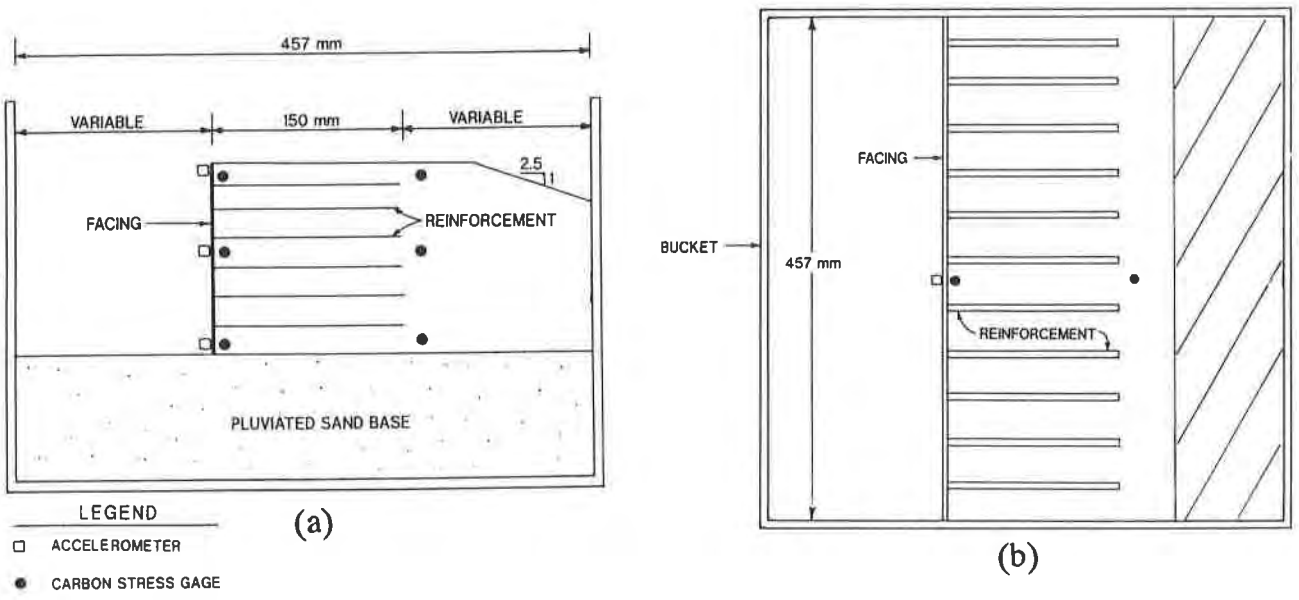

Figure 3 Model Wall Centrifuge Test
(a)Side View (b) Plan View

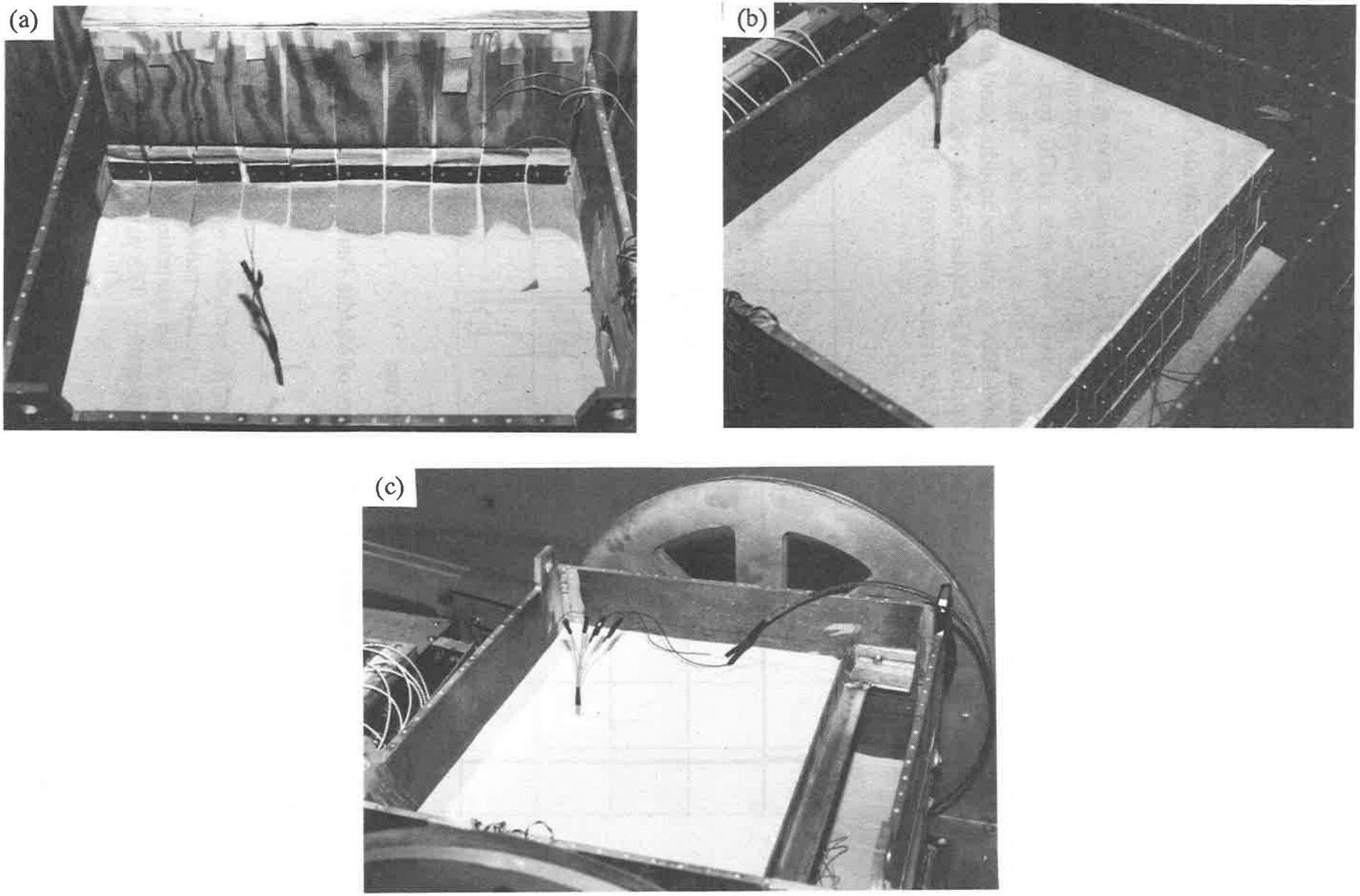

Figure 4 Instrumentation in the Centrifuge Tests
(a) Model Wall Construction (b) Accelerometer Locations (c) Constraint at Top of Wall

Instrumentation. Three accelerometers were placed on the exterior of the wall at the top, middle, and bottom along the centerline. Six carbon resistance pressure gages were used for each test. Three were placed immediately behind the panels at the top, middle, and bottom along the centerline of the wall. The other three were placed at the same elevations and just behind the reinforced soil zone. Fig. 4 shows the model wall and geogrid as well as the locations of the transducers. Three blasting caps were bundled together to provide the necessary energy release in the soil.

Results. The carbon gages provided the times of arrival of the shock wave at different locations. From the time of arrival and the standoff from the explosive, the wave propagation velocity of the reinforced sand was computed to be about 494 m/s (1620 fps). The accelerometers provided the time-histories of acceleration of the wall panels. The top and bottom panels had peak accelerations in the range of 4000-5000 g, and the middle panel had a peak acceleration of about 1500 g. The top and bottom panels had higher values because of the boundary constraints. All accelerograms basically had the same waveform. Fig. 5 shows a typical acceleration time-history of the middle panel.

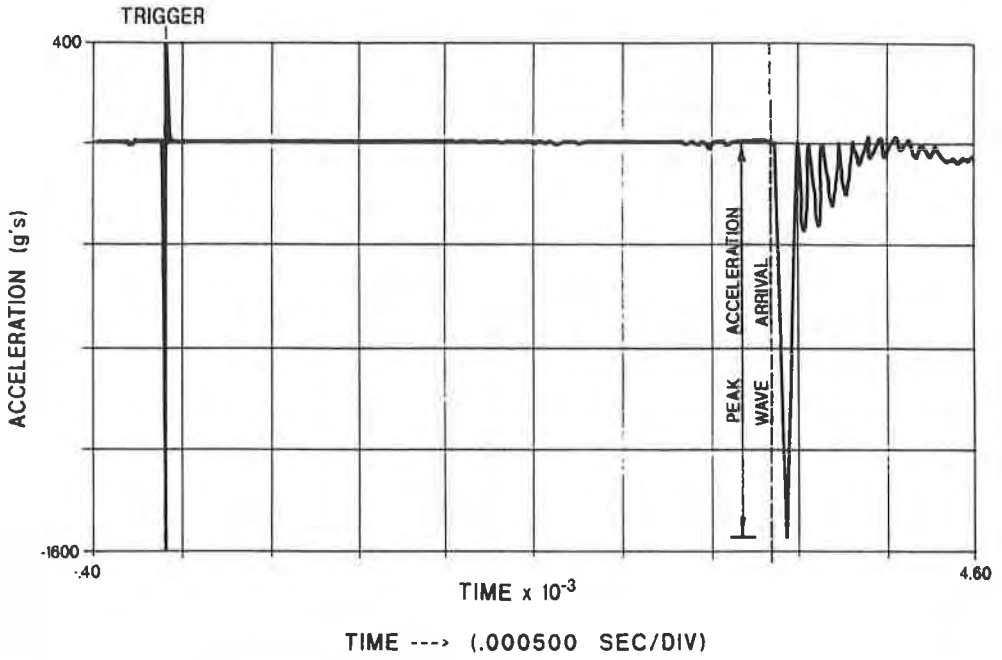

Figure 5 Acceleration Time-history of Middle Panel

VALIDATION OF THE 1D MODEL

The full-scale protective shelter simulated with the centrifuge models was analyzed using the 1D mathematic model. The scaling laws for using replica models in ground shock studies(Baker et al. 1991) were strictly observed. Therefore, all quantities with dimensions of pressure and velocity are the same in both prototype and model. The parameters used in this analysis are given in Table 1.

Table 1 Model Parameters for the 1D Analysis

Young's Modulus of Soil	255 MPa (37,000 psi)
Poisson's Ratio of Soil	0.35
Dry Unit Weight of Soil	1685 kg/m^3 (105 pcf)
Geogrid Modulus	66 MPa (9,600 ksi)
Poisson's Ratio of Geogrid	0.30
Volume Ratio of Geogrid	0.05%
Pressure at Shock Front	2 MPa (290 psi)
Ground Shock Decay Rate	300 Sec^{-1}
Standoff Distance	5.33 m (210 in.)

The free-field particle velocity due to the given detonation was obatined using a one-dimensional, spherically symmetric, large strain, explicit finite element hydrodynamic code - SABER(Zimmerman et al. 1991). Common explosives and many pre-defined soil models are available for use in a ground shock calculation. A JWL type of equation of state is used to predict the shock front pressure and volume expansion of the explosive. The free-field particle velocity was then used as a boundary condition in the 1D analysis. The time-histories of the response parameters of the wall panel as well as the soil-panel interface stress are shown in Fig. 6. For theoretical interest, higher-order terms in Eq.(20) were also included in the analysis. However, only the first two terms have physical significance.

The time of arrival of shock wave was about 0.01 sec., which is equal to that observed in the centrifuge tests multiplied by the scale factor of 30. The first peak in the acceleration time-history is about 1250 g, which compares well only with the peak acceleration of the middle panel in the centrifuge tests. This is because the 1D model does not take boundary constraints of the panel into account.

CONCLUSION

The 1D mathematical model proposed in this study provides a simple method for predicting the dynamic interaction between reinforced soil and wall panels under ground shock loading. The analytical results compared well with the centrifuge test data, for a short duration after time of arrival of the shock wave. The model treats reinforced soil as a linearly elastic and homogeneous medium, and as such cannot model the hysteretic compaction or other plastic behavior of soil under stress wave propagation.

ACKNOWLEDGMENTS

This research was conducted under Scientific and Engineering Technical Assistance (SETA) contract F08635-88-C-0067 with the Air Force Civil Engineering Support Agency, Engineering

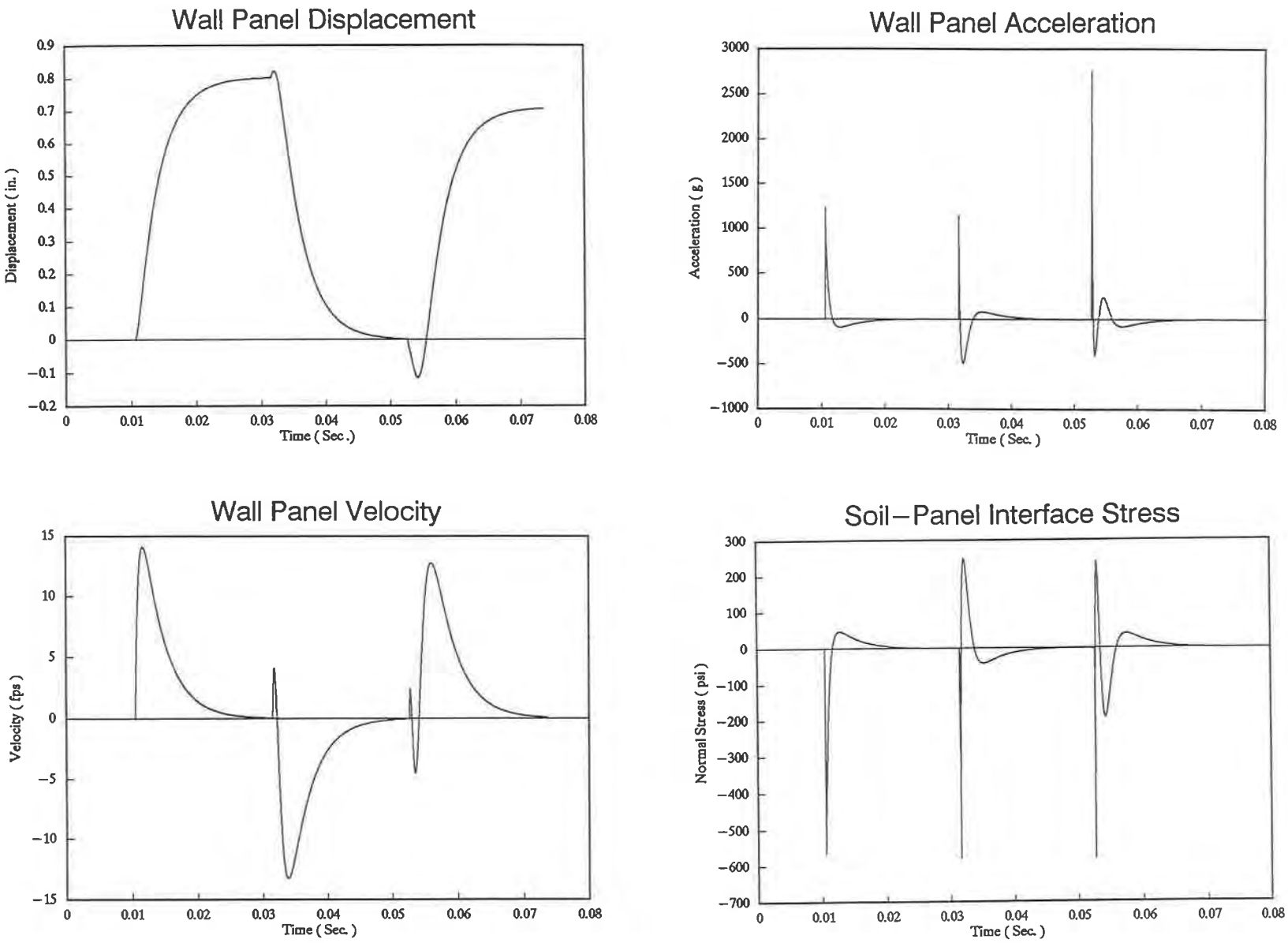

Figure 6 Time-histories of Reponse Parameters of Wall Panel
(a) Wall Displacement (b) Wall Acceleration (c) Wall Velocity (d) Interface Stress

Research Division (AFCESA/RAC), as part of SETA Subtask 2.14, "Advanced Panel and Connection System for an Airbase Protective Shelter Employing Reinforced Earth."

The authors wish to thank Mr. Michael R. Purcell of Applied Research Associates, Inc., for preparing the shelter wall models and conducting the centrifuge tests.

REFERENCES

Baker, W.E., et al.(1991), Similarity Methods and Applications in Engineering Dynamics, 2nd Ed., Elsevier Book Company.

Barrett, R.K., (1992), "Can you build a retaining wall for less cost?," Geotechnical Fabrics Report, pp.14-17.

Harrison, W.J., and Gerrard, C.M.(1972), "Elastic Theory Applied to Reinforced Earth," J. of the Soil and Foundation Division, ASCE, Vol.98, No.SM12, pp.1325-1345.

Jones, R.M.(1975), Mechanics of Composite Materials, McGraw-Hill Book Company, New York, N.Y., pp.31-84.

Raudanski, E., Eytan, R., and Sweiry, G.(1990), "Reinforced Soil Ammunition Magazine, Full-scale Tests-1990, Testing Program," Headquarters Israeli Air Force Civil Engineering Division, Engineering and Products Branch.

Zimmerman, H.D., et al.(1991), Users Guide for SABER-PC/CWE, Structures Laboratory, US Army Engineers Waterways Experiment Station, Vicksburg, Mississippi.

New Materials for Ancient Worlds: The Application of Geosynthetics to the Conservation of Cultural Sites

M. Demas
Getty Conservation Institute, USA

P.-M. Lin
Getty Conservation Institute, USA

N. Agnew
Getty Conservation Institute, USA

M. Taylor
National Park Service, USA

ABSTRACT

The growing recognition of the world's cultural sites as finite resources that are rapidly vanishing has created a demand for effective measures to preserve them for future generations. Technology transfer is one of the approaches being investigated. The new engineering technologies and materials represented by the geosynthetics industry offer considerable potential for transfer and adaptation to the conservation of cultural sites. This paper examines the limitations imposed on technology transfer by the special requirements of cultural conservation and presents some of the testing being carried out in applying geosynthetic technology to the conservation and implementation of cultural sites in the U.S. and in China.

INTRODUCTION

The loss of so much of the world's cultural heritage to modern development and natural deterioration has created a demand for effective and appropriate measures to protect and conserve what remains. Among the solutions being sought is the transfer of existing technologies and materials from other fields to the conservation of cultural sites. Technology transfer--if it is to be truly successful--requires establishing a common ground between the needs of the one field and the technologies of the other.

One of the aims of this paper is to begin to establish this common ground between the field of geotechnical engineering and cultural conservation. This means foremost making clear the goals and needs of cultural conservation to the audience whose technology we are seeking to use. The paper, therefore, begins with a review of the field of cultural conservation. Another aim of the paper is to stimulate the interest of the geosynthetic community in the problems of cultural conservation. We trust that our 'clientele'--the cultural sites of the world--will be sufficient stimulus in itself. Finally, we hope to lay the groundwork for a dialogue between the two fields by presenting actual and potential applications of geosynthetics to the conservation of cultural sites.

CULTURAL CONSERVATION: A REVIEW OF AIMS AND NEEDS

Cultural sites are the buildings, sites, and landscapes that constitute the physical manifestations of the past and that continue to have meaning and value for society today. These places are as diverse, culturally and chronologically, as the peoples and circumstances that created them. They are prehistoric cave sites, ancient monuments and archaeological sites (Fig. 1), historic buildings and historic city centers, and battlefields and sacred landscapes.

Cultural 'resources' is a term commonly applied to these sites. It is an apt description because it recognizes the manifold values they hold for society: they are of cultural value as places with historic or scientific interest, religious association, or aesthetic and artistic significance; they are of educational value as places that inform society about the past; they are of social value as places that provide a communal focus and a community spirit; and they are of economic value as places that generate tourist income.

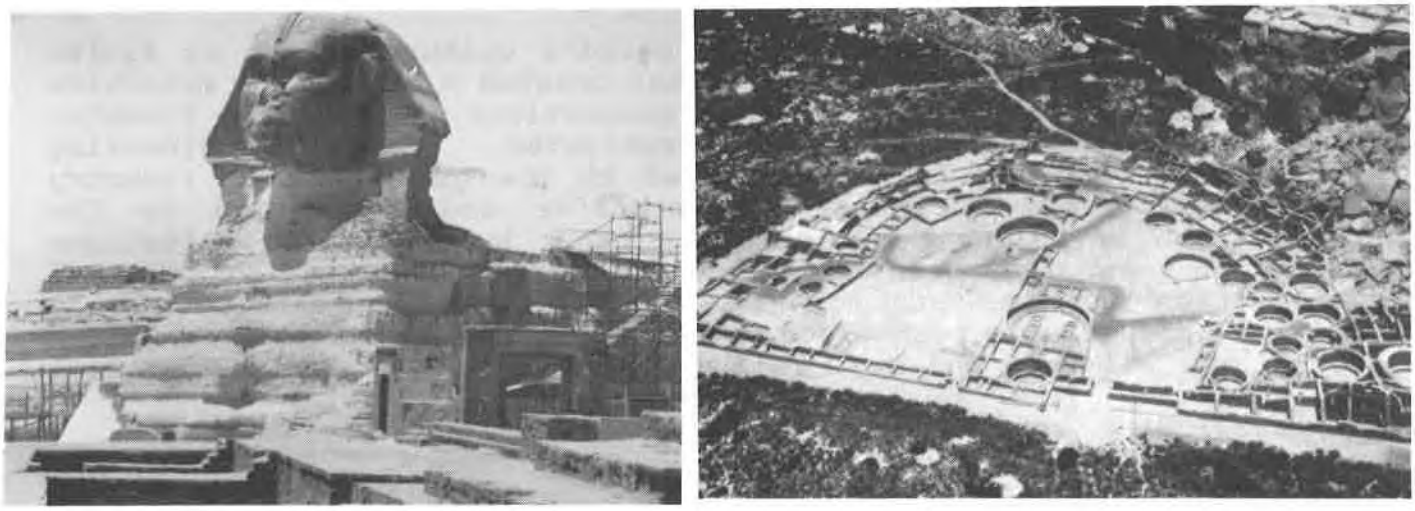

Fig. 1. Ancient monuments such as the Great Sphinx (left) and archaeological sites, such as Pueblo Bonito (right), are among the world's most fragile cultural resources.

Like many of our natural resources, cultural resources are finite and nonrenewable, and they are rapidly vanishing. As the world's cultural resources have shrunk, the movement to conserve them has grown. The central aim of conservation is to ensure their physical survival and cultural integrity--that is, to ensure the survival of the resource as a physical entity, but to do this in such a way that its significance and value to society are not impaired or destroyed. Over the last few decades, the conservation profession has made significant strides in protecting cultural sites through legislation and planning policies.

Saving a site from the bulldozer or designating it as a national park or landmark is, however, only half the battle of ensuring its survival. Cultural resources need also to be protected from the processes of natural deterioration. Unlike objects in a controlled museum environment, sites are exposed to the effects of the rain, snow,

sun, and wind, to periodic flooding or a high water table, to temperature and humidity fluctuations, and to many other agents of decay.

The greatest challenge for conservation is to find acceptable methods of intervention to prolong the life of cultural sites without sacrificing original materials and aesthetic values. Technical solutions have long been sought in the allied fields of architecture and engineering, and from the building and construction industries. Too often, however, the use of modern technologies or materials has resulted in the loss of original materials and aesthetic values. The example of cement will suffice to illustrate the problem.

Throughout the 20th century, cement has been extensively used on cultural sites as the favored material for structural stabilization work--for grouting, re-pointing, rebuilding, and capping or facing of walls. Its hardness, strength, and durability--the very qualities that make it such a desirable construction material--are, however, a disadvantage when used in conjunction with the softer and porous sedimentary stones or earthen materials (adobe) of which many ancient monuments are constructed. Differential weathering properties of cement and traditional building materials have resulted in loss of original material. Cement has the further disadvantage of introducing soluble salts to a structure and being visually intrusive.

The use of cement illustrates the desire for permanent solutions and the belief that modern technology and materials can solve all our problems. Mistakes of the past have resulted in significant loss of cultural material, but they have also had two beneficial consequences for conservation: they have spurred the development of professional standards and guidelines, and they have led to re-newed interest in the use of traditional materials and techniques.

The return to traditional techniques has represented a healthy and necessary swing of the research pendulum for the profession. However, it is equally necessary that the profession continue to explore the applicability of new technologies and materials to the conservation of sites. The needs of conservation are too great for the field to stagnate.

CURRENT APPLICATIONS OF GEOSYNTHETICS TO CULTURAL SITE CONSERVATION

Research and testing of new materials and technologies for use in cultural conservation is one of the activities of The Getty Conservation Institute (GCI), which was established in 1985 to further scientific knowledge and professional practice in cultural conservation. Through its scientific research, training courses, and field work, the GCI seeks to develop, apply, and make available appropriate solutions to conservation problems. Since 1989 it has been investigating the potential application of geosynthetic materials to the conservation of cultural sites.

There are many reasons for selecting geosynthetics for investigation. Their functions--especially drainage and erosion

control--correspond to the conservation needs of many cultural sites. The variety of products, the range of grades available, and the potential for creating composites make geosynthetics versatile and adaptable. Most important for cultural sites, geosynthetics often require less intervention in sub-grade applications and less maintenance over the long-term than traditional applications.

In collaboration with other cultural resource agencies in the U.S. and abroad, the GCI is currently testing and using geosynthetics in two of its field projects--both concerned with the conservation of ancient monuments.

Chaco Project. This project is a collaborative effort of the GCI with the National Park Service to test strategies for protecting archaeological sites with standing architectural remains. The venue for the testing is Chaco Culture National Historical Park (Chaco) in New Mexico, administered by the Southwest Regional Office of the National Park Service.

The 34,000 acres of Chaco park contain hundreds of sites of the Anasazi culture, which flourished in the southwestern U.S. between the 9th and 13th centuries A.D. Many of these sites display monumental architecture. The largest is Pueblo Bonito (Fig. 1) with 650 rooms, which include dwellings, storage spaces, round ceremonial structures (kivas), communal plazas, and masonry walls up to four stories in height. Chaco was designated a World Heritage Site in 1984.

Chaco exemplifies many of the problems that are common to archaeological sites worldwide. Its monumental, ruined buildings are fully exposed to the weather and to the structural instability of roofless structures. There are two major problems being addressed by the current tests: drainage related problems, and erosion of the bases and tops of masonry walls.

A. Drainage. Drainage problems at archaeological sites may be caused by any number of conditions: poorly graded surfaces, impermeable sub-soils, seasonal high water table, or periodic flooding. Equally problematic, but unique to archaeological sites, are the unequal fills that characterize most excavated sites. The reasons are threefold. Archaeological sites commonly exhibit multiple, successive building phases that may span decades, centuries, or even millenia. They are rarely excavated completely. And, once excavated, they may subsequently be partly reburied to protect portions of a structure from deterioration. The result is frequently a complex intra-site topography, such as that which characterizes the sites at Chaco (Fig. 2).

Unequal fills within architectural complexes result in hydrostatic pressure on walls and lateral migration of water through walls, leading to crystallization of salts on the exposed face of the wall and erosion of mortar and stone. Equitable distribution of fills in adjacent rooms alleviates the problems arising from differential fills, but since this is not always possible or desirable, a means of reducing pressure and preventing lateral migration of water is required.

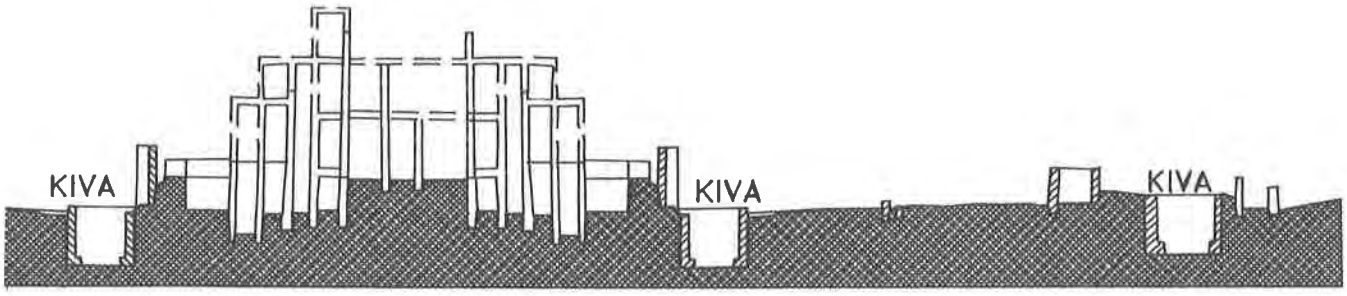

Fig. 2. Composite cross-section through an archaeological site illustrating differences in fill levels.

Previous methods that have been used at Chaco and other archaeological sites to address the problems caused by differential fills have been the construction of concrete curtain walls; attempting to seal the face of walls with impervious materials, such as bitumen; sub-surface drainage using gravel fills; and experimentation with various moisture-resistant mortars.

These methods have often impacted severely the original fabric of structures and have not always addressed the underlying problem. The use of geodrains was proposed as an alternative method that would be less intrusive and would respond to the need to drain excess water from fills. Two tests employing vertical and horizontal geodrains were designed and installed at the site of Pueblo Bonito in November 1991.

The use of vertical geodrains on archaeological sites is appropriate only in circumstances where trenching for installation will not disturb cultural deposits--this means rooms that have already been excavated. Two adjacent rooms--one (Room 128) completely backfilled, the other (Room 340) with only a shallow backfill--were selected for the test. The geodrain was installed against the vertical face of the filled side of the wall separating the two rooms (Fig. 3). A one meter

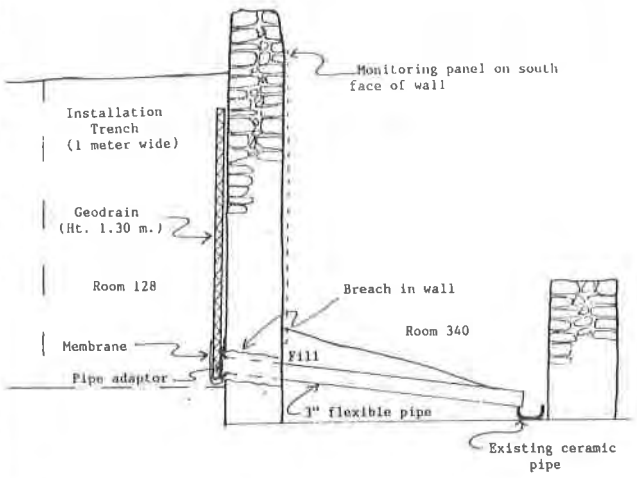

Fig. 3. Vertical Geodrain: Backfilled room during installation of geodrain (left) and cross-section through test room (right).

wide trench was dug in the existing backfill to install the geodrain. A geodrain with a core of webbed nylon filaments was selected as providing maximum flexibility to conform to the uneven wall surface.

The discharge system necessitated breaching the wall and connecting the out-flow pipe to a pre-existing drainage system. This constituted the only physical intrusion to the wall. While unsatisfactory, a discharge system is an inevitable consequence of any drainage system and the disturbance of a minimal amount of wall fabric must be weighed against the overall benefits of drainage.

An horizontal geodrain can be utilized in rooms or areas that retain their original archaeological deposit and where trenching is therefore not possible. The test room (Room 368), with its original fill, is an island surrounded by excavated rooms. The horizontal geodrain is intended to drain surface water from rain and snow melt, thus preventing seepage into the fill and thereby reducing erosion of the vertical exposed wall faces. The geodrain was placed on top of a geomembrane and covered with a layer of gravel, rather than soil, in order to reduce weed growth (Fig. 4). The discharge pipe leads directly into drums installed for the purpose of monitoring water collection efficiency.

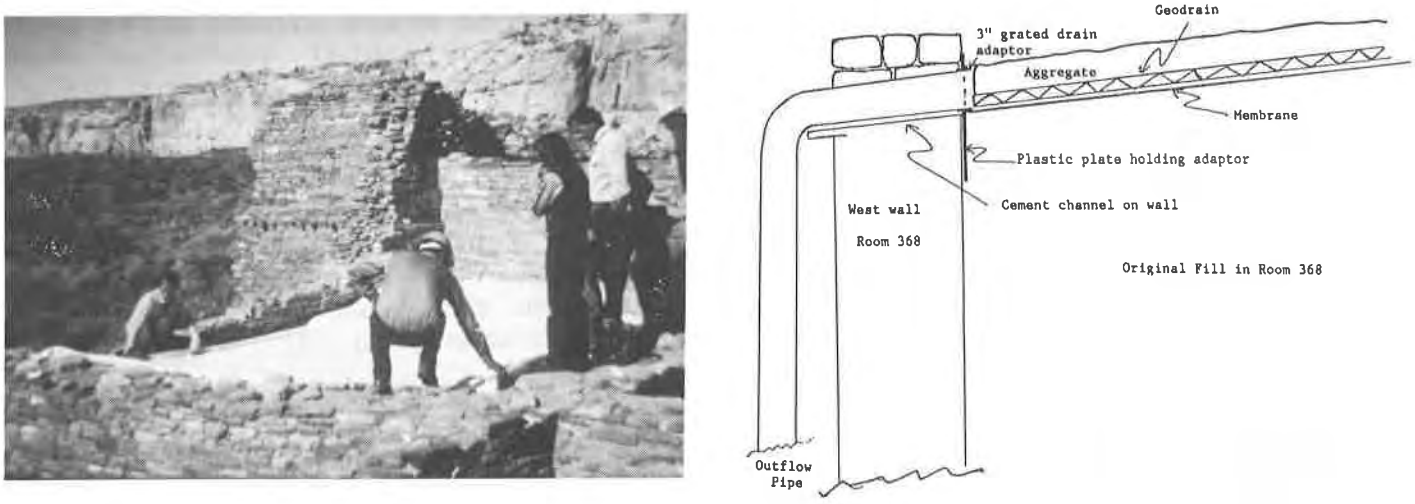

Fig. 4. Horizontal Geodrain: Geodrain being positioned in test room (left) and cross-section through test room (right).

B. Erosion of the base and tops of walls. The oft quoted adage "all you need is a good hat and good boots to protect your walls" sums up the problems inherent to exposed archaeological structures. Most walls in an archaeological setting are not afforded the protection of roofs, which have long since deteriorated. The wall tops are thereby exposed to the weather in a manner that was never intended originally. The bases of walls are frequently in contact with archaeological fill, which provides a conduit for moisture and cannot be removed or re-graded because it is a cultural deposit.

At Chaco, deterioration of the wall bases from ground moisture is a serious problem, due mainly to the accumulation of snow over extended

periods of time (Fig. 5). Because of great diurnal fluctuations in temperature, freeze-thaw cycles allow seepage of moisture into the substrate and capillary rise of moisture in the walls. The result is destruction of mortar and stone and, if unchecked, the potential for structural failure.

A standard method of controlling moisture at the base of a wall is to create a positive slope away from it. This is effective for shedding rain water, but not for eliminating moisture that results from the slow melting of snow. A method currently being practiced at Chaco, is to manually remove snow from the base of the walls. This is effective, but with some eight miles of exposed wall surface to maintain, ultimately impractical. To address the problem of basal erosion, two tests were designed using geosynthetics and were implemented in November 1991 at the site of Pueblo Bonito.

For one test, a 0.66 meter wide geodrain was laid lengthwise along the base of the wall and above an impermeable geomembrane (Fig. 5); the second test employs only the geomembrane. Both geodrain and membrane are covered with a layer of soil. The rationale is simply to prevent saturation of the soil from snow melt adjacent to the wall. This method is appropriate for archaeological sites because it does not involve trenching or disturbance to the cultural deposit.

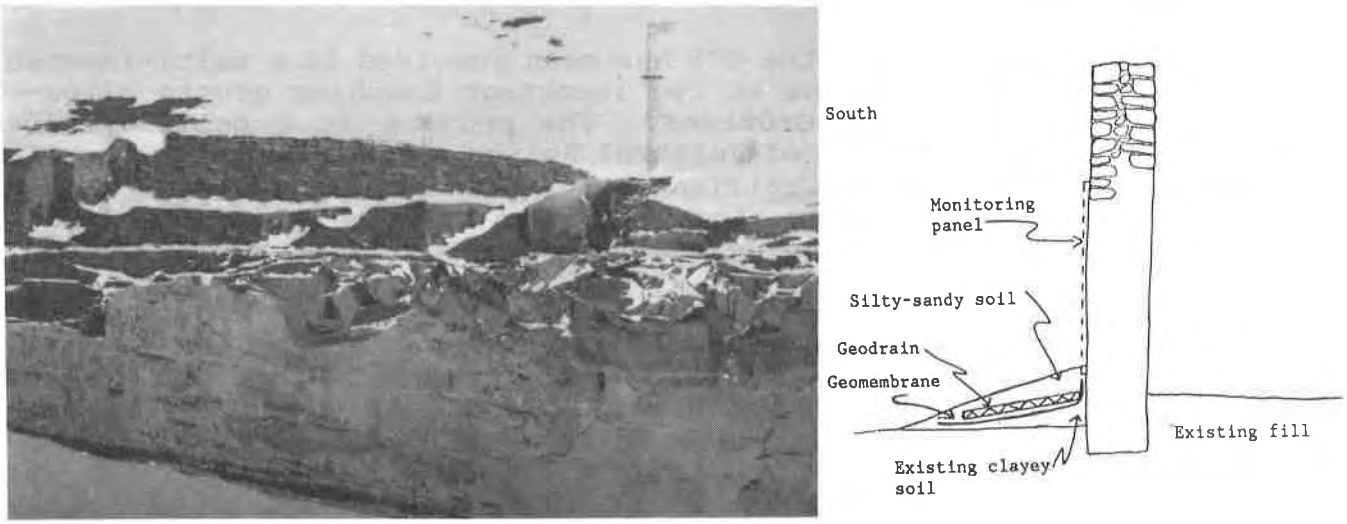

Fig. 5. Basal Protection: Snow accumulation at the bases and tops of walls during winter months (left); the cross-section (right) shows installation of geodrain to protect the base of walls.

Problems affecting the tops of roofless walls are also due to moisture penetration from snow melt. During the winter and spring, the exposed walls at Chaco are subject to snow accumulation and melt (Fig. 5). Water penetrating into the wall freezes and causes buckling of the exterior facing stones. Evaporation of moisture on the wall surface brings with it soluble salts, whose efflorescence creates a distinct and destructive tide mark along the top of the wall face.

The present practice is to remove snow from the tops of the walls using a snow blower. To eliminate this labor-intensive task and protect

the wall from infiltration of water, an impermeable membrane cap was designed for temporary (seasonal) protection. The wall capping test employs two different geomembranes draped over four meter segments of a wall top. One membrane is of polyester material with a slick urethane coating; the other is a composite membrane with a polyester geotextile bonded to one side. Selection criteria for the membranes were resistance to ultraviolet degradation, flexibility, resistance to tear and puncture from protruding stones and tethering attachments, and aesthetics (color).

The membrane is intended primarily to protect the horizontal surface of the wall top; it overlaps the vertical face of the wall c. 15-20 cm. The caps are tethered to anchor stones at the base of the wall. Although these caps do constitute a visual intrusion to the site, they are intended for use only during the winter season.

All four tests will be monitored for a period of four years. The protocol includes monitoring rates of mortar erosion on re-pointed wall segments; moisture readings of soil fills using a carbide meter and dielectric probes; and measuring water flow in a collection system for the horizontal geodrain. Monitoring data are insufficient at present to evaluate the tests, but the membrane caps have already proven effective in eliminating salt efflorescence.

China Project. Since 1988, the GCI has been involved in a multi-faceted conservation project in China at two important Buddhist grotto sites--the Yungang and the Mogao Grottoes. The project is a collaborative effort with the State Bureau of Cultural Relics of the People's Republic of China. Drainage, sand stabilization, and reinforcement of weakened roofs of the rock carved grottoes are the three problems for which geosynthetic solutions are being designed and tested at these sites.

The Mogao Grottoes are near Dunhuang, Gansu Province, in northwestern China, some 1,100 miles from Beijing. Mogao is an oasis site on the edge of the Gobi Desert, along the great trade and caravan route--the Silk Road--that once linked China with the Mediterranean world and carried goods and ideas between east and west. Some 500 grottoes were carved in the mile-long cliff face between the 4th and 14th centuries AD. The Buddhist art of the grottoes is among the masterpieces of Chinese art. It consists of some 2,000 figures sculpted in clay and painted and 45,000 sq. meters of wall paintings. The Mogao Grottoes were designated a World Heritage Site in 1986.

Mogao is a desert site surrounded by sand and it is only by continuous, active maintenance that the sand is kept at bay and prevented from engulfing the site. The sand dunes on the plateau of the cliff are especially problematic. Prevailing seasonal winds drive the sand in the direction of the cliff face, depositing it along the cliff edge and at the cliff base below (Fig. 6). In a typical year, 2,000 cubic meters of sand are swept up from the base of the cliff.

To control the movement of sand on the plateau and reduce its deposition at the base of the cliff, a windbreak fence of knitted

Fig. 6. Mogao Grottoes: Sand on the plateau erodes cliff face (left) and cascades down to the base of the cliff below (right).

polyethylene fabric was installed. The A-shaped windbreak is 3,600 meters in length (1.8 m. high), protecting the full length of the grottoes below (Fig. 7). Each of its broadly angled arms corresponds with the prevailing NW and SW wind directions. The prevailing winds thus form a large intersect angle with their respective arms, depositing wind-blown sand along their base. Since its installation in 1990, the fence has reduced by 62% the amount of sand at the base of the cliff. A 'live' windbreak fence of drought resistant plants is being designed to eventually supplant the fabric fence.

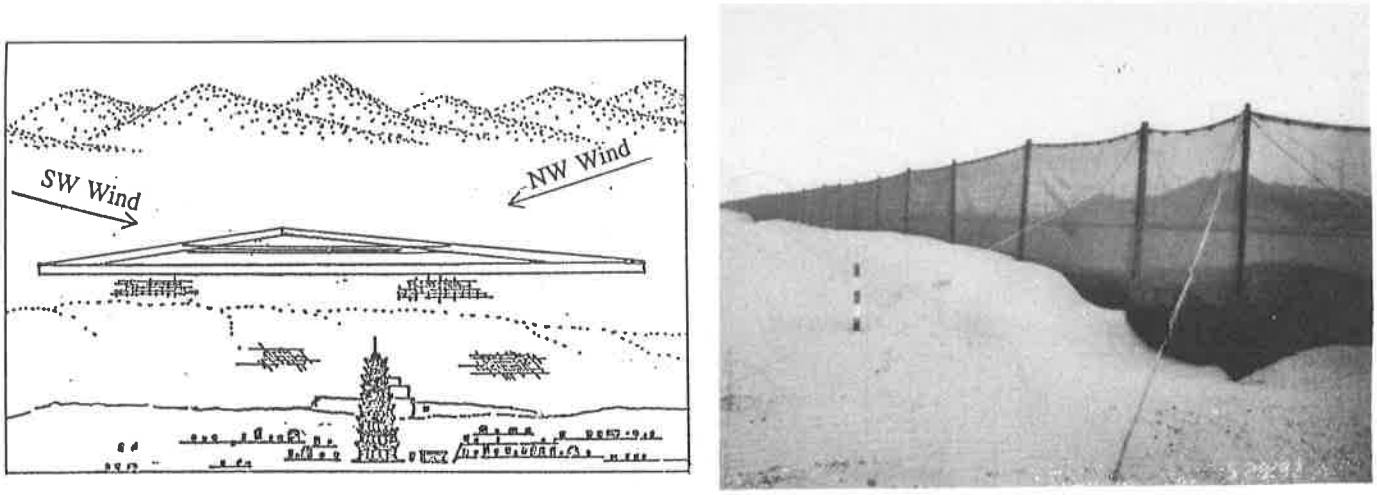

Fig. 7. Relationship of wind break fence to grottoes and wind directions (left) and build-up of sand along fence (right).

Centuries of sand abrasion have eroded the conglomerate out of which the grottoes are carved. Along the edge of the plateau this erosion has created a bevelled edge, causing the roofs of the upper tier of caves to become thin and structurally weak; in some cases these have worn through completely, creating holes and allowing ingress of sand and occasional rain. The thin-roofed caves require protection against

further erosion. The application of geosynthetics is one of the solutions being investigated for these roofs. The requirements of the design are that it utilize light-weight materials, that it seal openings, that it be flexible enough to withstand earthquake vibrations, that it be visually non-intrusive, and that it be reversible. The steep slope of the eroded cliff edge is the backdrop against which these requirements must be set (see Fig. 6).

A geosynthetic composite has been designed to meet these requirements and testing of the design off-site is being conducted. The geocomposite uses an impermeable geomembrane and a geomatrix of webbed construction; it is designed to be laid over the thin roofs as a protective capping. The function of the membrane is to prevent the infiltration of sand or water where the roofs have worn through. A webbed geomatrix, in conjunction with the underlying membrane, was selected to provide a structure to retain a layer of chemically consolidated sand that will camouflage the materials and provide a natural appearance over the rock face. The sand is chemically consolidated with potassium silicate. If the consolidated sand layer is subjected to earthquake vibrations, it may break, but it will be held by the geomatrix and prevented from falling to the cliff base below. Testing has shown that the potassium silicate performs well in consolidating the sand and bonding it to the geomatrix.

Where the geocomposite must cover a hole in the roof (the largest is approximately 2 by 5 meters), additional support will be provided by an underlying layer of expandable metal mesh (Fig. 8). The metal mesh will also act as the lath to retain a mud plaster facing on the interior

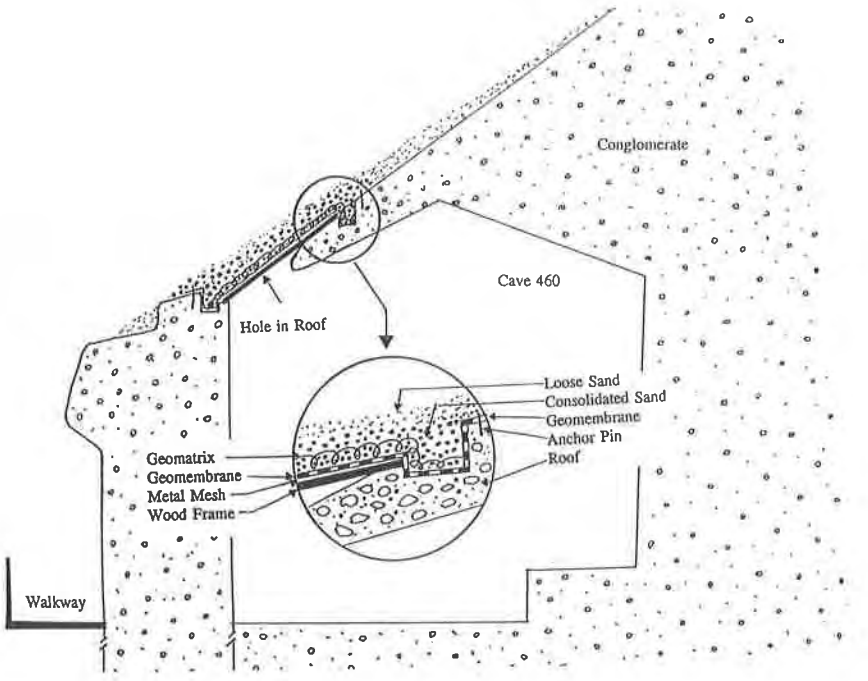

Fig. 8. Cross-section through thin-roofed grotto showing geocomposite cap over hole and detail of construction and installation.

of the cave. A simulated cave has been constructed near the site to evaluate the resistance of the geocomposite cap and mesh to sagging. The cave consists of a ground pit (2 m. diameter; 1.9 m. deep) covered with the geocomposite and the mesh, and supported on a wooden frame. Pre-fabricated geocomposite panels are being considered to reduce sagging and simplify installation on the steep slope of the cliff edge.

The Yungang Grottoes are located near the city of Datong, 200 miles west of Beijing, in Shanxi Province. The 52 caves carved into the sandstone cliffs contain an exceptional array of rock-carved reliefs and sculptures, the largest of which is a 17 m. high seated Buddha (Fig. 9). The grottoes date mainly to the Northern Wei Dynasty (460-524 AD). During the Ming Dynasty (1368-1644 A.D.), many of the deteriorated rock-carved sculptures were restored with mud-plastered coating and painted in brilliant polychrome.

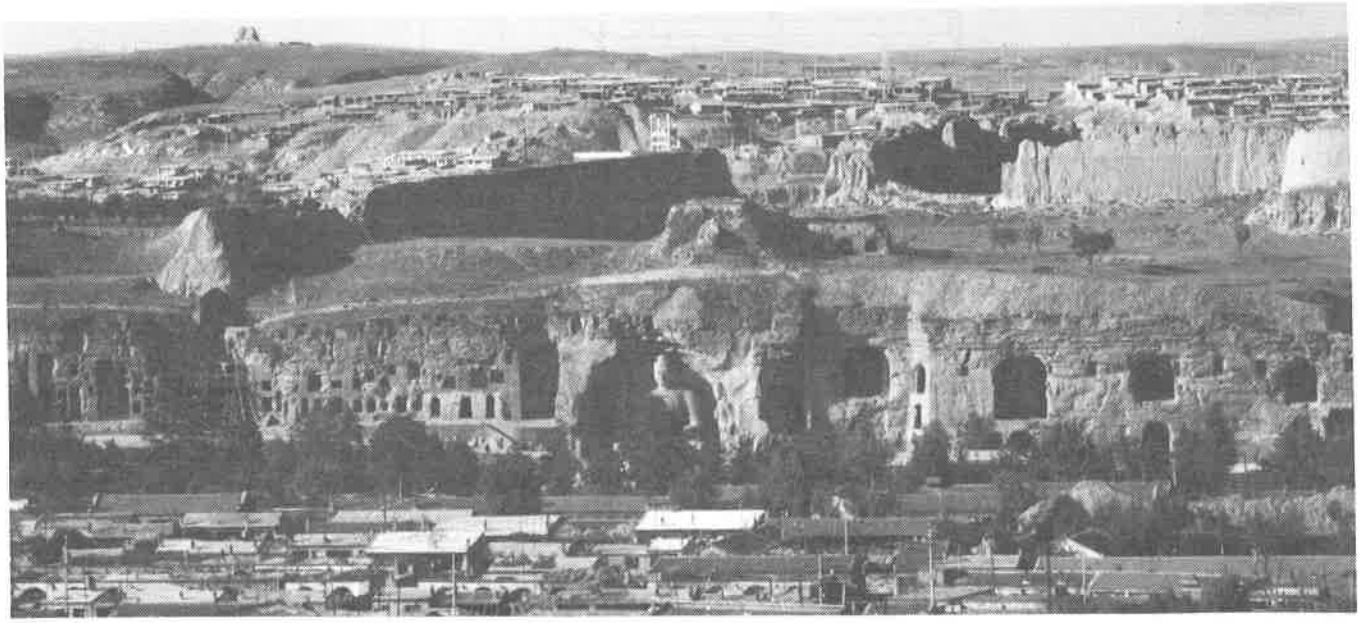

Fig. 9. The Yungang Grottoes carved in the sandstone cliff face and the Ming Dynasty fort on the plateau above.

The accumulation of water on the cliff plateau has been a major cause of deterioration of the sandstone. The water infiltrates through the rock matrix into the grottoes. A Ming Dynasty adobe fort on the plateau of the cliff top (Fig. 9) exacerbates the problem by trapping water and thereby functioning as a catchbasin. Water percolating through the rock and shale lenses in the sandstone enters the grottoes, carrying with it soluble salts that crystallize on the surface and corrode the sculpture. Control of ground water on the plateau is therefore a key element in stabilizing the site and reducing decay. The area of the plateau requiring drainage is approximately 50,000 sq. m.

Two tests utilizing geosynthetics were implemented in the Fall of 1992 (Fig. 10). The test sites (each approximately 2,500 sq. m.) are located along the edge of the cliff. One test is a straightforward application of geodrains. Using stripdrains, a system of parallel lateral drains (25 m. in length) feed into a central collector line (50

m. long). The other test employs only a geomembrane laid over the resurfaced test area and covered with a layer of soil. Its purpose is simply to eliminate water infiltration to the underlying rock strata.

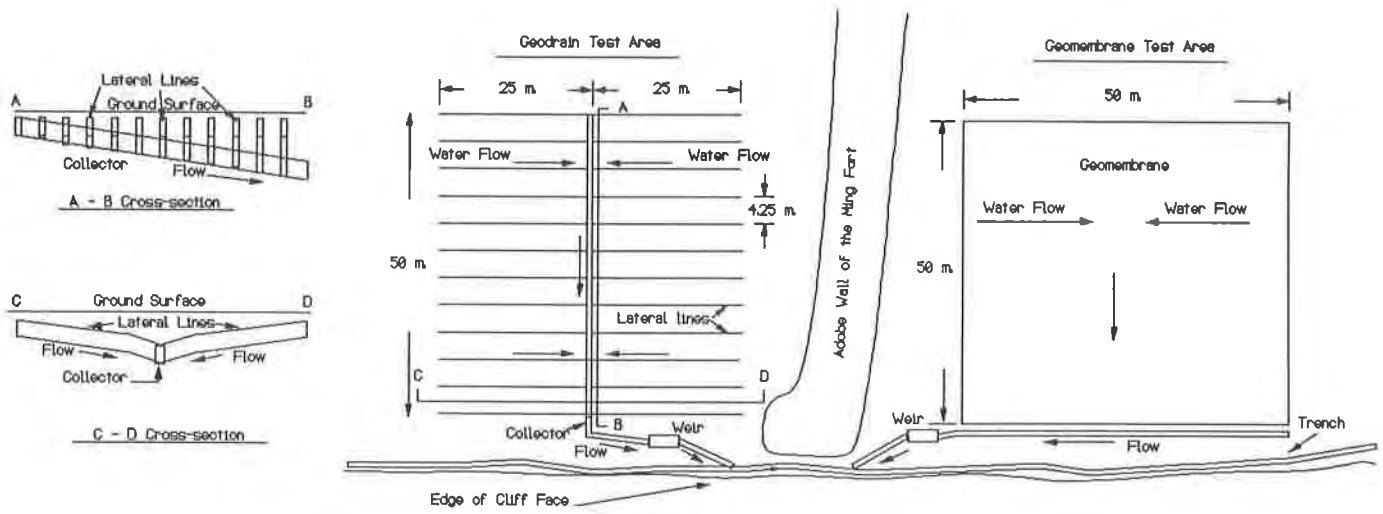

Fig 10. Design schematic of the geodrain and geomembrane tests.

The tests are the prelude to a more comprehensive drainage design for the plateau. They will determine the effectiveness of the two systems in draining water and preventing infiltration to the rock strata. Dielectric probes are being used to measure the water content of soil and rock strata inside bore holes. A water collection weir equipped with ultra sonic depth gauge will monitor the amount of water collected by each system. The tests will be equally important for evaluating any adverse effects on the cultural resource and for gauging the degree and type of disturbance to the archaeological area resulting from the installation process.

Other applications. Two other applications of geosynthetics are already finding some acceptance in archaeological contexts. One is a traditional application--erosion control--the other an adaptation of traditional functions--separation and filtration. The separation and filtration functions of geotextiles are useful in re-burial or capping of archaeological sites. Reburial refers to the practice of filling an exposed site with soil to protect it from deterioration. Capping is the burial of an unexcavated site with soil, sand, or aggregate fill to protect it from road or building construction, grazing, and other adverse surface impacts.

These types of operations are frequently long-term, although short-term reburial is also a common practice. In either case, there is the potential or certainty that the site will be re-excavated or uncovered at a future date. It is therefore essential to provide a separator material to distinguish the unexcavated matrix or feature from the fill. The properties required of a separator material are precisely the properties of filtration, permeability, resistance to biological degradation, flexibility and strength that characterize geotextiles.

Geotextiles have already begun to be used on a limited scale in this capacity (Fig. 11). The excavated remains of the Elizabethan Rose Theatre in London--the venue of the first performance of many of Shakespeare's plays--were provided with a temporary protective fill, which incorportaed a geotextile as the horizon marker (Ashurst et al. 1989). In a reburial experiment at the historic adobe site of Fort Selden in New Mexico, adobe test walls have been sheathed with geotextile fabric and reburied (Fig. 11). Since 1988, the fabric-wrapped wall and a control wall without fabric have been exposed to accelerated weathering using a water spray system (Agnew 1990). The fabric-wrapped wall has shown considerably less weathering than the control wall.

Geotextiles may not be appropriate in all circumstances. The weight or pressure of fills may press the fabric into a wet, clayey matrix or plaster surface, causing damage when removed. Further research and testing is clearly required to determine the conditions under which geotextiles can be used in an archaeological context.

Fig. 11. The use of geotextiles in a reburial operation (left) and to protect adobe test walls at Fort Selden (right).

The second application of geosynthetics is for erosion control, which remains one of the principal causes of the destruction of archaeological sites. The transfer of geosynthetic technology and materials is fairly straightforward--whether it be the use of geotextiles below gabions or riprap; revegetation mats or geomatrices to control erosion; or woven or knitted fabrics to control wind erosion. All of these solutions have potential application to archaeological contexts and many have already been implemented (Engineers 1988, III-1; Thorne 1985, 40ff.). However, the presence of cultural material requires consideration of potential impacts of soil compaction from the use of riprap or heavy equipment and the impact of land re-formation by grading on sub-surface archaeological remains.

FUTURE DIRECTIONS

Applications of geosynthetics described in this paper only begin to address the potential that exist for adapting geosynthetic technologies

and materials to the conservation of cultural sites. In order to realize the full potential and ensure a successful technology transfer, efforts toward achieving the following goals are critical:

Testing. One of the appeals of technology transfer is that product testing and development has already been undertaken. The danger lies is in assuming that this testing will have taken into consideration contexts for which the products were not originally designed. Testing of geosynthetics in specific archaeological contexts is essential for building a repertoire of effective applications and for evaluating adverse impacts.

Publication. In the case of technology transfer, a little knowledge can truly be a dangerous thing. There is a great deal of oversimplified or mis-information circulating informally among conservation professionals about geosynthetics. The dissemination of information about the properties, uses, limitations, and durability of geosynthetics to the conservation community is, therefore, critical.

Collaboration. Collaboration between the geosynthetic engineering and conservation fields will provide the combined expertise that is needed to ensure a successful transfer of technology. We hope this paper will elicit an interest in such collaboration from the geosynthetic community.

ACKNOWLEDGEMENTS

All photographs and drawings used in this paper are courtesy of The Getty Conservation Institute and the Southwest Regional Office of the National Park Service. The geotechnical design engineer for the projects was Dr. Po-Ming Lin. Mr. Lynn E. Ward, Product Manager at Akzo Industrial Systems, provided advice at Yungang.

REFERENCES

Agnew 1990: Neville Agnew, *The Getty research project at Fort Selden I: experimental design*. In **Sixth International Conference on the Conservation of Earthen Architecture. Adobe 90 Preprints** (Las Cruces, New Mexico, October 14-19, 1990), 243-249. Los Angeles, CA: The Getty Conservation Institute.

Ashurst et al. 1989: John Ashurst, Nick Balaam, and Kate Foley. *The Rose Theatre*. **Conservation Bulletin**, no. 9, 9-10.

Engineers 1988: U.S. Army Corps of Engineers. **The Archaeological Site Protection and Preservation Notebook** (Environmental Impact Research Program). Vicksburg, MS: U.S. Army Engineer Waterways Experimental Station.

Thorne 1985: Robert M. Thorne. **Preservation is a Use: Archaeological Site Stabilization, An Experimental Program in the Tennessee River Valley**. Archaeological papers of the Center for Archaeological Research, no. 5, University of Mississippi; Tennessee Valley Authority Publications in Anthropology no. 40.

Geotextile Composites Comprised of Mineral Layers for Special Applications

K.P. von Maubeuge
Naue-Fasertechnik, Germany

G. Heerten
Naue-Fasertechnik, Germany

C. Mills
Terrafix Geosynthetics Inc., Canada

Summary

The development of new geotextile composites has intensified to penetrate into applications, where common geotextile structures such as nonwovens and wovens cannot be used due to insufficient mechanical or physical properties. Combinations of geosynthetics and minerals, like bentonite powder, sand and fine gravel, have shown to be able to fulfill the missing properties in protection, filtration, erosion control, sealing and drainage applications.

Geosynthetic clay liners (bentonite mats) are not only used in applications such as water reservoirs, groundwater protection for petro-chemical tank farms, but also also as gas barrier, sealing systems in landfills and as a very effective protective layer for geomembranes. Sand mats show very good filter characteristics with soil types finer than sand and allow placement in water depths greater than 26 feet (8 meters) even under turbulent conditions. Geotextile/gravel composites allow an easy installation and longterm permeability even at high loads. Furthermore they can be installed on slopes as erosion control mats.

This paper will show how synthetic products can be combined with minerals using needle-punching or heat-bonding techniques to manufacture products for many applications where common geotextiles cannot be used. The latest test results, field trials and case histories will be presented for new and unique products.

1. Introduction

For more than 25 years geotextiles have been used in soil mechanics. In many applications, nonwovens, wovens, geogrids, geonets and geomembranes are installed as a current practice to contain harmful contaminents, to achieve a stable soil condition or prevent ecological damage, by using inexpensive geosynthetic solutions and saving natural resources.

The professional groups most strongly influenced (by advances in geosynthetics) are geotechnical engineering, heavy construction, building construction, hydrogeology, and environmental engineering, although all soil- , rock- and groundwater-related activities fall within the general scope of the various applications [1].

For approx. 10 years, the market of geocomposites - various combinations of geotextiles, geogrids, geonets, geomembranes and/or other materials - has been rapidly increasing (see Fig. 1) due to their variety in geosynthetic applications. Geocomposites are able to be constructed in such a way that the new product can fit properties of nearly any kind of application. With the integration of soil particles such as gravel, sand, silt and/or clay within the composite system, the amount of synthetic raw materials could be reduced using the positive soil attributes to achieve properties which a geosynthetic alone does not have, such as [2]:

- improved filter properties
- higher protection efficiency
- larger drainage capacity at high loadings
- better creep behaviour.

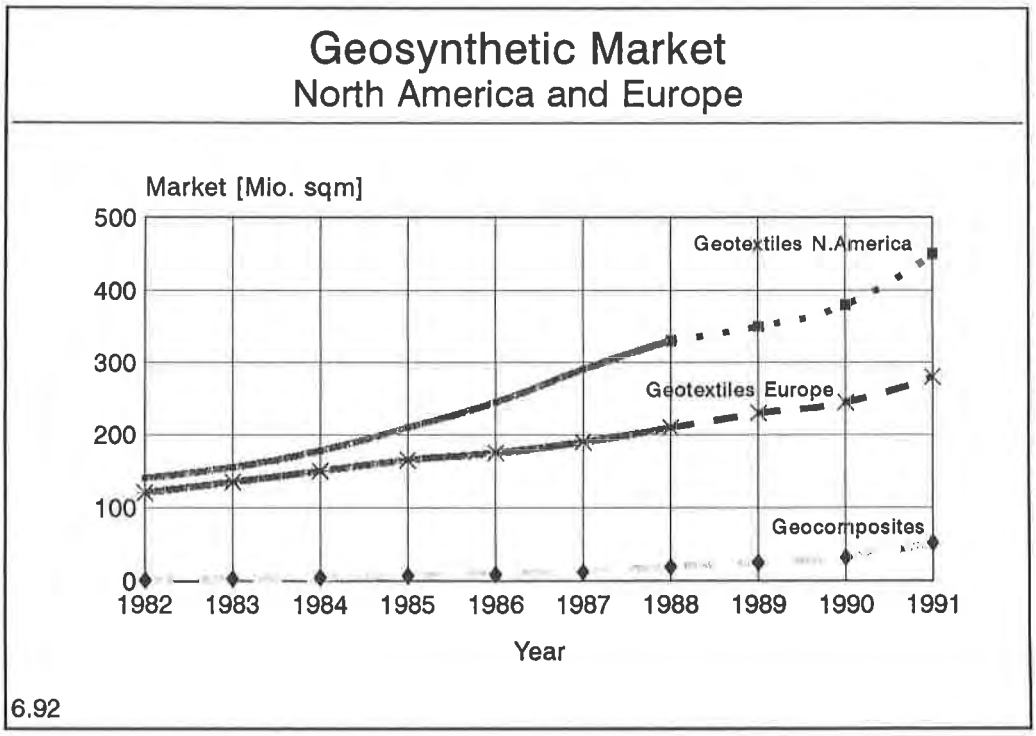

Fig. 1: Approximate geosynthetic market for geocomposites [1, 6] dotted lines are estimations

For these new geotextile/mineral composite products for earth construction and hydraulic engineering, the suitability of various soil types had to be examined. In the case of gravels and sands it was the properties to resist very high pressures without considerable deformations. The colloids on the other hand in clayey minerals have the advantage that they can absorb high amounts of water and swell so that a high sealing effect is achieved. Thus, all of the three grain types (Fig. 2) show certain properties which cannot be fulfilled by a geotextile alone.

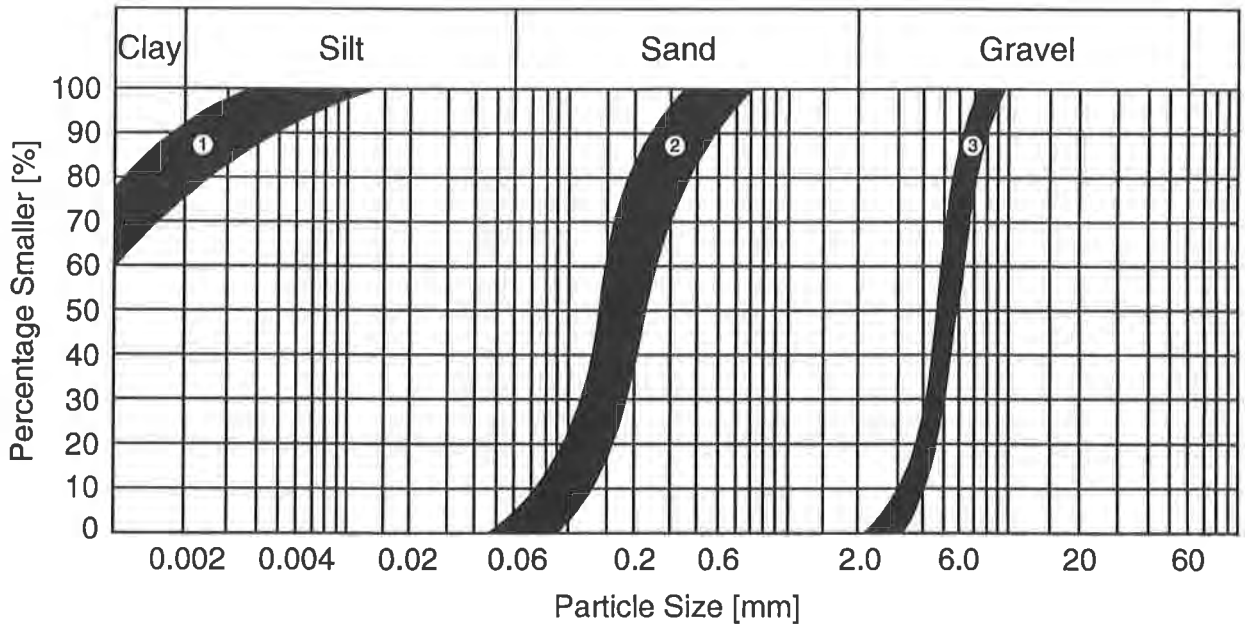

Fig. 2: Grain size distribution curves of the used mineral materials
1 = bentonite; 2 = quartz sand; 3 = gravel 3/8 mm

2. Geocomposites of clay and geotextiles

The examination of the clay minerals showed that the surface activity of the montmorillonites of the bentonites is the highest compared to the illites and kaolinites, so that the bentonite can deposit far more water molecules directly into the voids of its crystal lattice and achieves a lower permeability. This leads to a higher swelling capacity. Due to this property the bentonite can be considered as the suitable construction material for applications where high sealing effects are required. In 1988, this resulted in the development of the needle-punched geosynthetic clay liner (GCL) Bentofix (Fig. 3) as a new sealing and protection element consisting of two geotextile layers with an intermediate layer of encapsulated bentonite powder. Both geotextiles are needle-punched together through the bentonite layer, thus forming a compact mat. This GCL is a fibre-reinforced sealing system in which the bentonite powder is encapsulated over the whole surface in a way that it cannot erode. In hydrated condition this compound guarantees a hydraulic conductivity coefficient of typically 1 x 10^{-9} cm/s [11, 12], even under conditions such as:

- elongation (< 35%) [13]
- loadings [11, 12]
- high hydro-static head pressures (for example 2-10 m (6 - 33 ft)) [14].

It is important to note that permeability varies according to confining stress, hydration time, consolidation pressure, permeant water composition and to a lesser extent head pressure. For this reason a comparison of test data is not always possible [18].

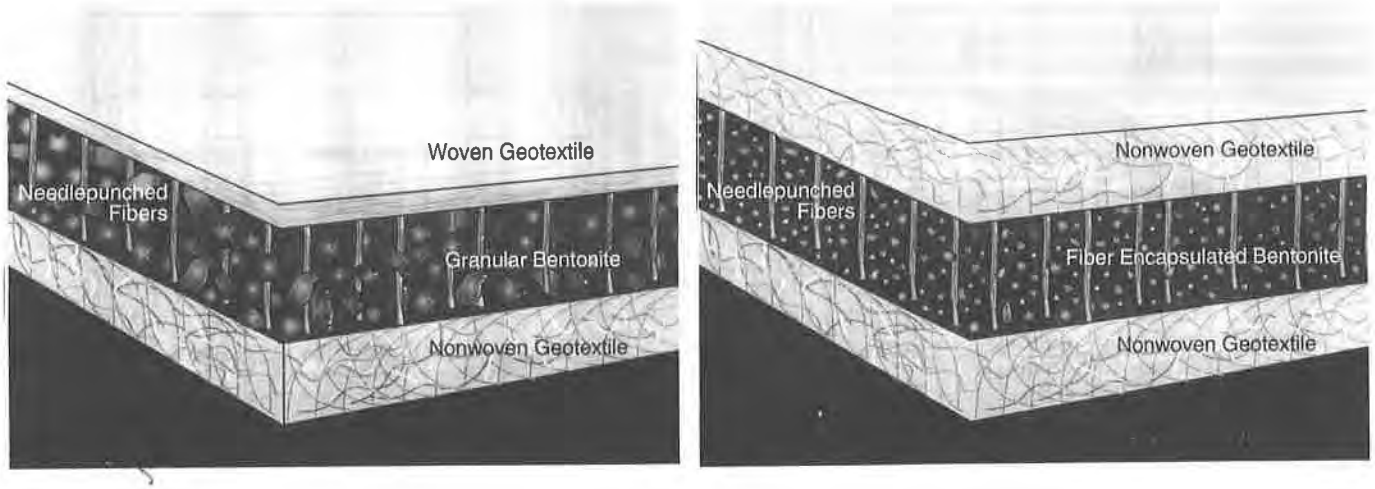

Fig. 3: Needle-punched GCL compsite product (encapsulated erosion stable) and at least one mechanically bonded nonwoven

The friction angle is an important value for the installation of the needle-punched geosynthetic clay liner (GCL) in slopes. Tests in the shear box resulted in - depending on soil type - interface friction angles of 28° to 34° of the hydrated and unhydrated needle-punched GCL [15, 16].

A new field of application for GCL´s is the use as a gas barrier (Fig. 4). Several European regions have for example a high portion of radon containing minerals (radon is a gaseous decay product of radium with a radioactive period of 3.8 days). In the case of incorporation due to releasing radionuclides the release of the radon can cause damage to health. For this reason the radon permeability of Bentofix was tested. Results from various institutes ("Institut für angewandte Isotopen-, Gas- und Umweltuntersuchungen" Wörthsee/München and "Universitätsklinik Homburg") show that a hydrated Bentofix can be considered as a radon barrier [17]. Furthermore it is presently being tested to determine how effective a partly saturated needle-punched GCL is at maintaining permissible limiting values. In order to increase the absorption capacity of ß-radiation some technical production changes are necessary, about which will be report in time.

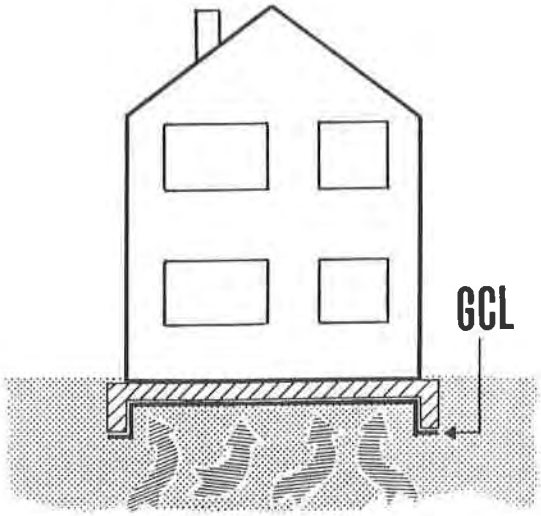

Fig. 4: Needle-punched GCL as radon barrier

Furthermore, needle-punched geosynthetic clay liners have entered with an increasing market share applications in landfill design. Geomembrane systems are continuously subjected to loads during the lifetime of the landfill, so that damage can occur due to [3]:

- loads imposed during installation (dynamic loads)
- loads resulting from waste weight (static loads).

To protect the geomembrane against penetration and puncturing from coarse drainage aggregate, a protection layer must be installed between the geomembrane and the drain material to ensure that local deformations in the geomembrane remain below a permissible limit [10]. Test trials carried out by Prof. Dr. Biedermann in Germany [4] have shown that up to now only a needle-punched geosynthetic clay liner will provide sufficient protection against a coarse drainage material such as 16/32 mm (0.6 to 1.25 in) as used in German base seals. Biedermann's aim is to avoid any puncturing or deformation of the geomembrane. The protection layer should be able to absorb all puncture loadings and not be affected by creep under load. Needle-punched geosynthetic clay liners currently provide the most effective protection because the reinforced sandwiched bentonite absorbs these loadings and additionally withstands creep forces. Scrim (minimum 220 g/m² (24 0z/yd²) HDPE wovens) reinforced mechanically bonded HDPE nonwovens are also sufficient protection layers as needle-punched nonwoven layers if they fulfill the minimum value (test field experience according to [4]) of:

$$t_{geo} > t_{gr}$$

(t_{geo} = thickness geotextile [mm], but min. 600 g/m² (17.6 oz/yd²) ; t_{gr} = smallest particle size)

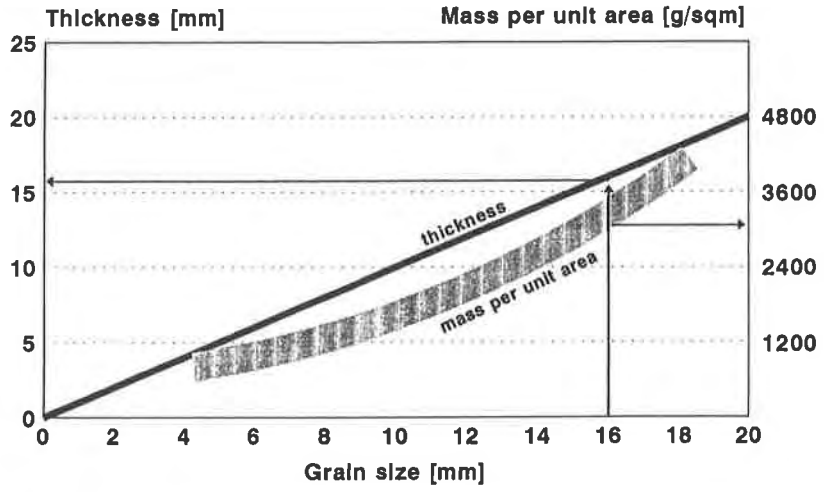

Fig. 5: A granular material 16/32 mm (0.6/1.25 in) would require a nonwoven protection with a thickness of >16 mm (0.6 in) and a mass per unit area of 3200 g/m² (94 oz/yd²)

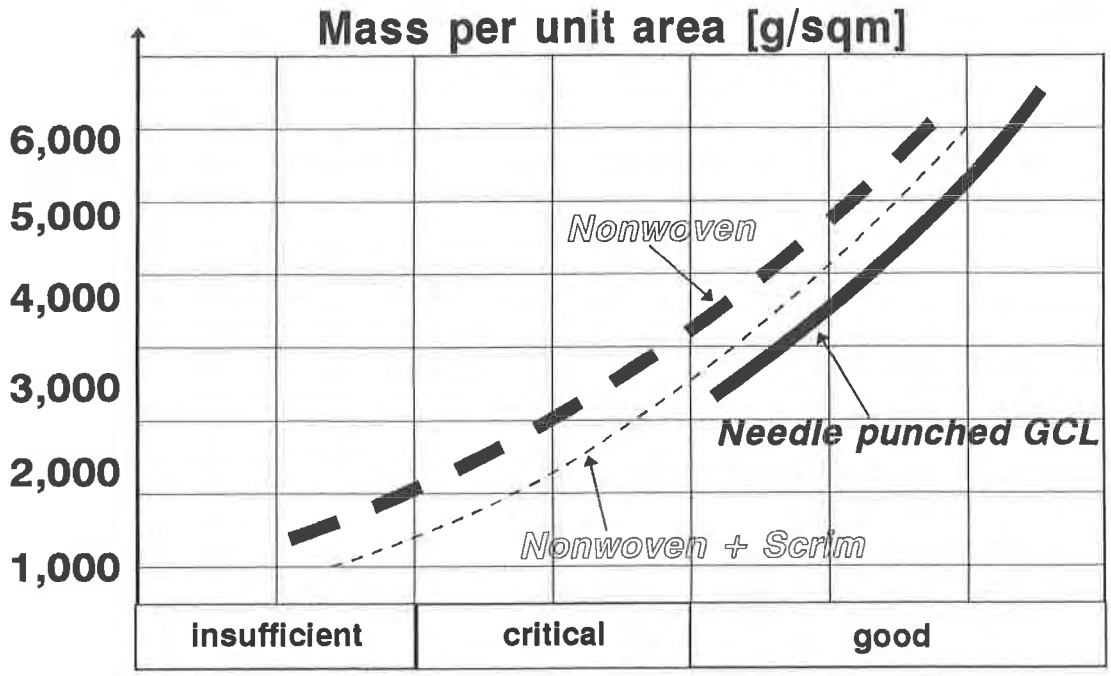

Efficiency of protection layers on geosynthetic liners by using 16/32mm drainage gravel

Fig. 6: Efficiency of protection layers on lining systems to protect against 16/32 mm [3]

To prove the protection efficiency of protection layers in landfill designs German recommendations rely on two test methods:

- the modified load bearing test for static loads (lining elongation less than 0.25% after the test)
- field trials for dynamic loads (no reasonable damage at all).

The German approach is that the dynamic installation conditions can best be addressed by carrying out full scale site trials with the specific materials which are intended to be installed whereas the long-term static load condition can be best tested by the laboratory 1000-hour plate-bearing tests and prove the best protection efficiency for a base seal design. The chemical resistance should be at least as high as the one expected from the geomembrane (HDPE) allowing the protection layer to last one day longer than the expected lifetime of the geomembrane.

Above mentioned tests have shown over all that a needle-punched HDPE geosynthetic clay liner cannot only withstand static and dynamic stresses but can also protect the geomembrane against a chemical attack and acts as an additional seal for the landfill system.

David E. Daniel and Robert M. Koerner favour as an additional barrier underneath the primary geomembrane layer a geosynthetic clay liner instead of a compacted clay liner because of several advantages:

- installation with light-weight equipment minimizing the risk of damage to underlaying components
- avoiding consolidation water flowing into the underlying drainage layer where it could be misinterpretated as liner leakage
- self-sealing effectiveness of bentonite and therefore minimizing or even stopping leakage flowing through the damaged geomembrane. [5]

To prove the intimate contact between the geomembrane and the GCL, several tests with different kinds of GCL products underlying a geomembrane leak were carried out to test whether the in-plane transmissivity of geotextiles could impair the effective composite action.

The tests were carried out by using a round-shaped sample of different GCL products with 18.5 cm in diameter. On top of the GCL a geomembrane sample (HDPE 2.5 mm (100 mil) thick) was placed. A plexiglass pipe of approx. 1 m (3 ft) height and a diameter of 1 cm (0.4 in) was connected to a hole in the middle of the geomembrane sample. The GCL/geomembrane composite was loaded with steel rings giving a relatively low vertical loading of approx. 7.5 kN/m² (1.2 psi) to the system. By filling up the pipe with 70 cm (2.3 ft) dyed water (in 10% Neocarmin W-solution) a hydraulic head of 0.90 m (2.9 ft) was applied. Over a period of 7 days the waterhead was controlled and held on a constant level by refilling the necessary quantity of water. The test results are shown in Fig. 7.

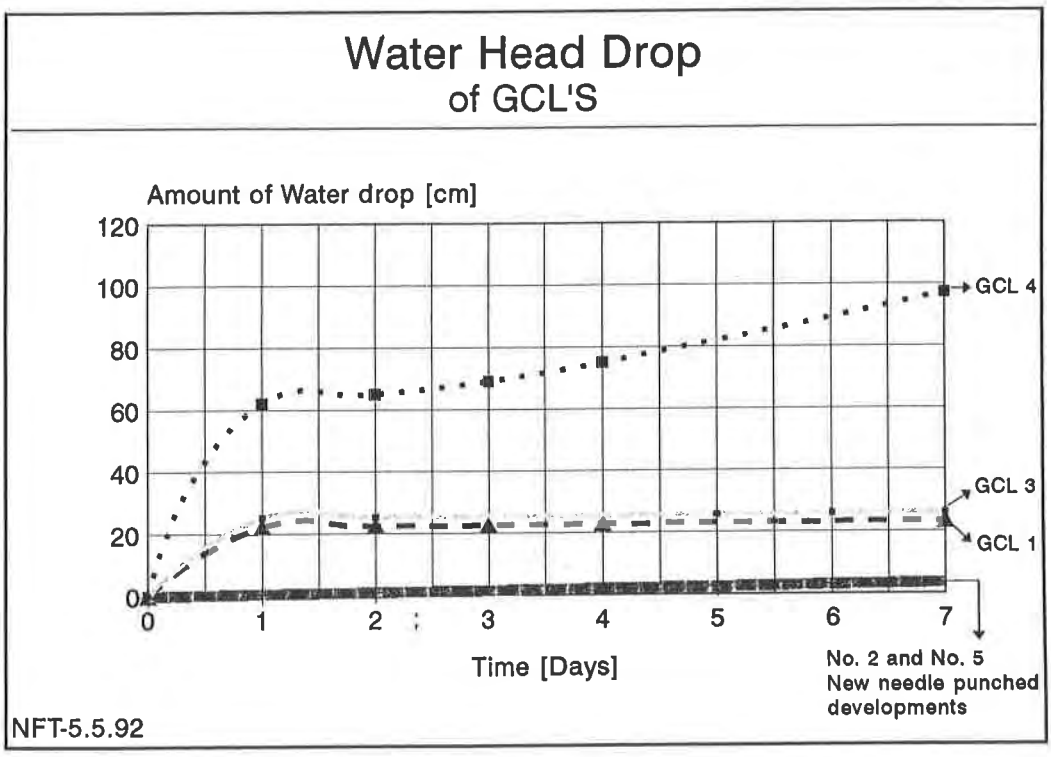

Fig. 7: Waterhead drop - 7 day period; (Sample 1,3 and 4: not needlepunched GCL´s; Sample 2: needlepunched GCL and topside filled with bentonite powder; Sample 5: needlepunched GCL and topside layer woven).

Fig. 7 shows clearly that the new Bentofix types No. 2 and No. 5 (needle-punched GCL with top layered nonwoven filled and fixed with bentonite powder and needle-punched GCL with one woven layer) which were developed for this special application performed best in this test. The aim was to reduce the transmissivity in-plane to an absolute minimum value at the critical low loads. Even the special selected woven in sample 5 reduced the transmissivity in-plane. The other developed sample No. 2 was designed in such a way that the geomembrane faced side was filled and fixed (not glued) with loose powder bentonite so that a small amount of water would immediately cause a swelling of the bentonite and therefore perform as an excellent intermediate contact between GCL and geomembrane. The new developments performed all in the range of No. 2 (Fig. 7).

3. Compound product of sand and nonwovens

Similar to a needle-punched GCL, the sandmat development Terrafix 1004 RB consists of two mechanically bonded nonwovens between which 4000 g/m² (118 oz/yd²) quartz sand is being needle-punched as ballast and as additional filter layer. A nonwoven used in hydraulic engineering with a thickness of 6.0 mm (0.25 in) and a mass per unit area of 800 g/m² (23 oz/yd²) (filter stable for soil types 1 to 4 according to BAW recommendations [7], Fig. 8) is used as carrier layer. The sand layer on top of this is covered with a 300 g/m² (8.9 oz/yd²) nonwoven. All three layers are needle-punched together over the whole surface (Fig. 9).

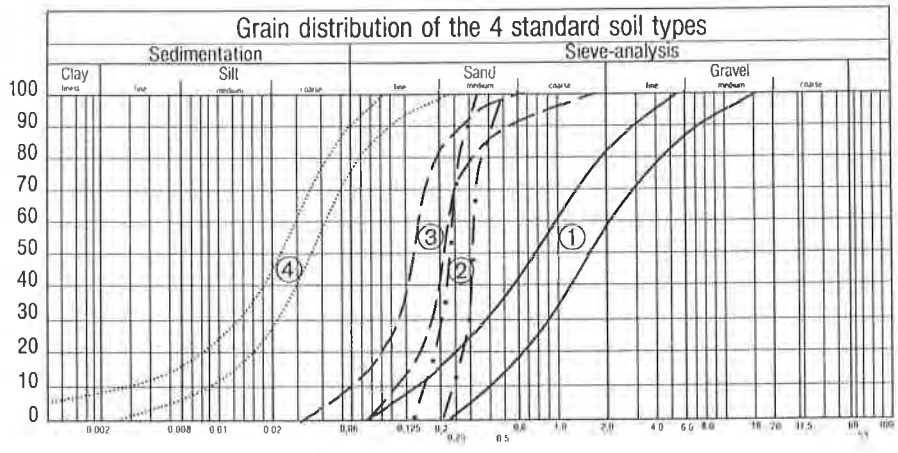

Mean coefficients of water permeability:

Soil type ① k-value = 4 x 10⁻⁴ m/s
Soil type ② k-value = 3 x 10⁻⁴ m/s
Soil type ③ k-value = 6 x 10⁻⁵ m/s
Soil type ④ k-value = 1 x 10⁻⁹ m/s

Fig. 8: BAW soil types 1 to 4

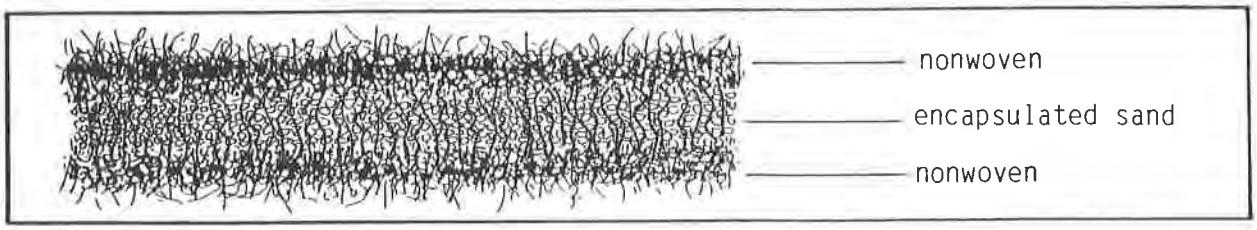

Fig. 9: Needle-punched compound product of sand and two mechanically bonded nonwovens [2]

The mass per unit area with approx. 6000 g/m² (177 oz/yd²) allows an easy handling and exact installation, even in considerable water depths. First underwater installations were done at the Bremer Weser Weir in 1991 (approx. 1,500 m² (15,000 ft²) in water depths of up to 12 m (40 ft)) and at the hydro-electric power station Pielweichs on the river Isar in March 1992 (approx. 40,000 m² (400,000 ft²) in a water depth of up to 4 m (13 ft)). In both cases the sandmat was installed on site contrary to usual installation methods and without considerable technical efforts. Even in unloaded condition the sandmat has proven to be remarkably stable when it is installed. This high stability was additionally proven in current overflow tests at the Leichtweiß-Institute of the TU Braunschweig.

According to BAW suitability tests, the mechanical filter efficiency of the sandmat particularly towards soil type 4, has been improved considerably due to the sand layer. The total soil passage reduces from nearly 300 g (10 oz) (permissible total soil passage for soil type 4 according to MAG, 1987) for a usual nonwoven filter to less than 50 g (1.8 oz) for the sandmat Terrafix 1004 RB (Fig. 10).

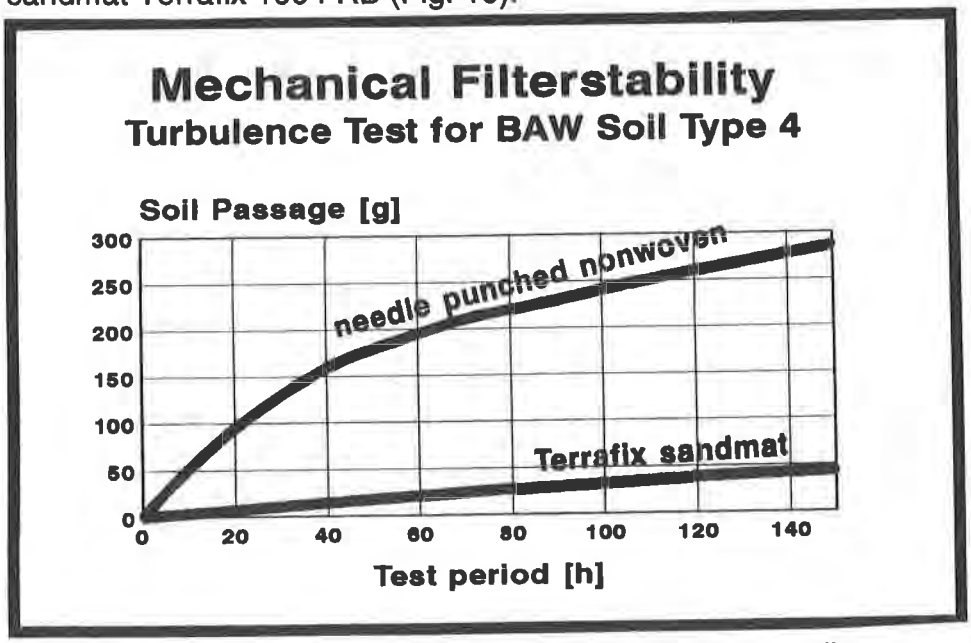

Fig. 10: Soil passage of soil type 4 through geotextiles

For the first time a geotextile with an effective opening size in the range $O_{90,w} < 0.055$ mm (smaller than US sieve 200) was manufactured due to the special production method and the sand encapsulation. This guarantees the filter capacity towards fine-grained soils (for example fine silt or generally for soils with a grain size distribution curve on the left side of BAW soil type 4) (compare DVWK, 1992 [8]).

4. Geocomposites with gravel material

To resist compressive loads and still maintain the drain capacity, gravel was chosen for a new compound product. The developed product - a combination of needlepunched nonwovens, a three-dimensional drainage mat and a joint-rigid Tensar geogrid, filled with quartz gravel 3/8 mm (Fig. 11) - was designed to be used in several applications:

- as a base and cap drainage in waste landfills
- as protection layer
- in steep slopes
- as erosion control and
- as sink mattress.

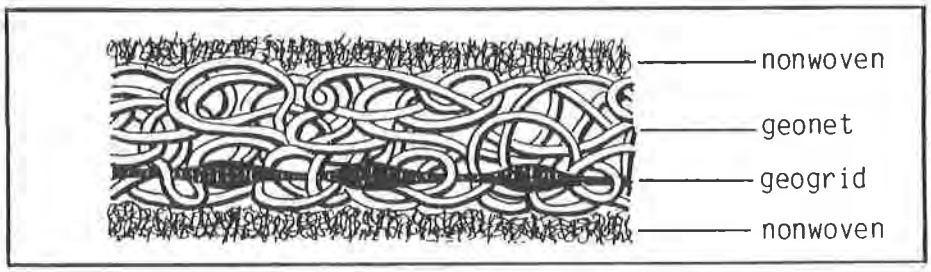

Fig. 11: Compound product of drainage mat reinforced with Tensar (here without gravel embedding) and two mechanically bonded nonwovens [9]

Whereas a new joining technique - the partial melting before the nonwoven is attached - makes it possible to physically connect even thick non-wovens heavier than 2000 g/m² (59 oz/yd²) to the intermediate layers, the filled drain structure can take over the diversion of liquids and the geogrid takes over the force transmission.

In cases of high loads - such as in base lining systems of landfills - the compactability of the drainage mat considerably influences the water permeability. For this reason, the

"Prüfamt für Grundbau, Bodenmechanik und Felsmechanik der TU München" carried out compression tests with this gravel drainage mat.

Whereas the thickness of mechanically bonded nonwovens can be reduced by approx. 50% under high loads, the gravel drainage mat filled with 3/8 mm gravel only reduces by less than 16%. The horizontal water permeability is only slightly affected, as can be seen in Fig. 12. The water permeability shows a relatively low reduction of the k_h-value from 3.2×10^{-2} m/s down to 2.3×10^{-2} m/s under a normal stress from 2 to 800 kPa (0.3 to 116 psi). Thus, the suitability of the gravel drainage mat as drainage layer has been proven for high normal stresses. Comparison tests showed that the permeability coefficients of unfilled synthetic drainage structures reduced by 1 to 2 orders of magnitude when the normal stress is increased from 2 to only 200 kPa (0.3 to 29 psi) (in the short-time test without consideration of the long-term durability).

Shear tests (with the slope angle apparatus) showed that the decisive shearing surface does not occur in the composite but always between the adjoining soil and the composite product. Here, slope angles of up to 1.5 : 1 (approx. 33°) were achieved.

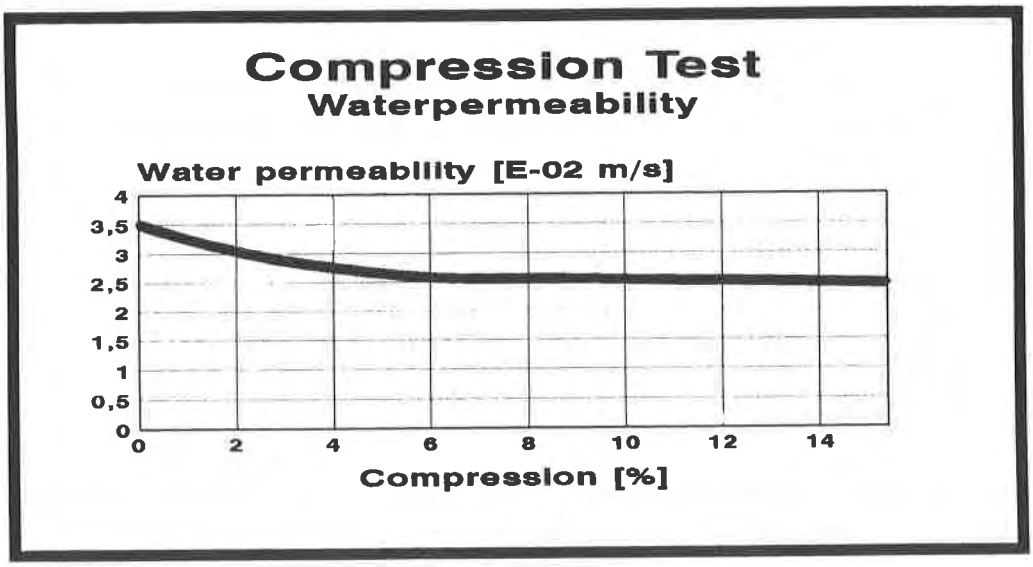

Fig. 12: Water permeability coefficients of the gravel drainage mat depending on the compression

5. Final Remarks

Since the early days of geotextile applications experience has shown that the installation of geosynthetics is justified because the durability of the construction is increased this way and in most cases less mineral substances are needed [6]. From the ecological point of view, this fact shows that using geotextiles can save raw materials and decrease construction costs.

The products which were available up to now could not always fulfill the requirements for long-term drainage performance under high loads, high protection efficiency of the geomembrane in a base seal and guaranteed groundwater protection or erosion control and filter stability in case of fine-grain soils. In the meantime, the geotextile technology has reached a state where the additional use of mineral materials does not only achieve the above mentioned properties but also prevents long-term ecological damage, since:

- ground water is protected,
- less mineral materials are required for maintenance works and therefore costs can be reduced for long periods,
- the environment is not impaired by intensive construction works because the new mineral compound materials, a higher lifetime and easier installation result in a shorter construction period and reduced transport capacities.

If all these marginal effects were included in an economical calculation, nothing would prevent the use of compound products made of mineral materials and textiles.

Literature

[1] Robert M. Koerner "Designing with geosynthetics", ISBN 0-13-202300-8, New Jersey/USA, 1990

[2] K. von Maubeuge/J. Witte "Geotextile Verbundstoffe aus Mineralstoffen und Textilstrukturen (Geotextile composites made of mineral materials and textile structures)", 2. Kongreß "Kunststoffe in der Geotechnik" K-Geo 92, Luzern, 1992

[3] K. von Maubeuge/J. Dixon "Geomembrane protection layers for landfills. A summary of German experience", WASTEMAN, Birmingham, 1992

[4] Prof. Dr. Biedermann "Das Zusammenwirken von mineralischer Basisabdichtung, Schutzvlies und Filterschicht am Beispiel der Reststoffdeponie Hopferstadt (The combination of mineral base sealing, protective nonwoven and filter layer such as in the combinated sealing for the residue landfill Hopferstadt)", SKZ, Würzburg, 1989

[5] Daniel/Koerner "Landfill liners from top to bottom", Civil Engineering, Dec. 1991

[6] K. von Maubeuge "Anwendung von geotextilen Asphalteinlagen (Use of geotextile asphalt layers)", Baugewerbe Heft 8/91

[7] BAW Recommendation "Anwendung von geotextilen Filtern an Wasser-straßen (Use of geotextiles in waterways)", Karlsruhe 1987

[8] DVWK 221/1992 "Anwendung von Geotextilien im Wasserbau (Use of geotextiles in water constructions)", Hamburg 1992

[9] Heerten/Saathoff/v. Maubeuge "Neue Verbundstoffe aus Mineralstoffen und Vliesstoffen für den Erd- und Wasserbau (New composites made of mineral materials and nonwovens for earth construction and hydraulic engineering)", 4. Internationales Techtextil Symposium für technische Textilien und textilarmierte Werkstoffe, Frankfurt, Juni 1992

[10] Saathoff/Scheu "Zum Einsatz von Geotextilien im Deponiebau (The use of geotextiles in landfills)", Abfallwirtschaftsjournal 4, 1992

[11] Naue Fasertechnik and Albarrie Naue, "Quality Control Data", since 1988

[12] University of Texas, "Results of Permeability Tests on Bentofix", Austin, Oct 1992

[13] University of Hanover, IGBE, "Results of Laboratory Tests of Naue Bentofix Sealing Matting", Munich, March 1990

[14] Institute for Foundation Enrineering, Soil and Rock Mechanicsat the University of Munich, "Permeability in Relationship to Hydraulic Gradient", Munich, Oct 1992

[15] University of Hanover, Franzius Institute, "Tests of Shear Behaviour", April 1988

[16] Kohlhase/Saathoff, Franzius Institute, "Selected Investigations of Sealing Systems Bentonite Matting", Hanover, July 1989

[17] Keller, University Saarland, "Behaviour of Bentofix against Radon", Homburg, Mai 1991

[18] Heerten/ von Maubeuge/ Simpson/ Mills, "Manufacturing Quality Control of Geosynthetic Clay Liners - A Manufacturers Perspective", GRI Seminar " MQC/MQA and CQC/CQA of GCL´s", Philadelphia PA, Dec. 1992

The Durability and Development of Optimum Seaming Parameters for an FCEA Geomembrane

I.D. Peggs
I-Corp International Inc., USA

R.D. Bowen
Akzo Industrial Systems Co., USA

S.E. Hoekstra
Akzo Industrial Systems BV, Netherlands

J.M. Rigo
University de Liège, Belgium

L. Courard
University de Liège, Belgium

ABSTRACT

A new polymeric material proposed for geomembrane applications must be carefully evaluated. The material must have adequate chemical resistance to the liquids and leachates it is intended to contain. Likewise, it must have adequate mechanical durability, and be easily installed under a wide range of ambient conditions so that seam integrity can be assured at the time of installation and throughout the liner's service life.

Tuff-Ply is a fully cross-linked elastomeric alloy that has been proposed for, and used in, geomembrane applications. An international testing program is described that confirms the suitability of using this thermoplastic elastomer as a geomembrane.

INTRODUCTION

As the geomembrane market grows rapidly and as our technological understanding of existing geomembranes increases, the demand for new geomembrane materials also increases. New materials must provide advantages over conventional materials. They must be easier to handle in the field, they must be more durable, have significant improvements in some properties without displaying reductions in others, be easier to seam, suffer less installation damage, or simply provide the same performance at a significantly reduced installed cost.

High density polyethylene (HDPE) made such an impact on the geomembrane market several years ago because of its excellent chemical resistance, low cost, weathering resistance, and ability to be essentially homogeneously seamed among other properties. But, like all materials, it has undesirable properties, which, with time, have been identified. Not surprisingly, since technological advancements never cease, there is now a window of opportunity for new materials to meet the challenges that HDPE cannot. Such a material may be Tuff-Ply (TP), a fully cross-linked elastomeric alloy (ASTM D5046-90, "Standard Specification for Fully Cross-linked Elastomeric Alloys (FCEAs)") of polypropylene (PP) and ethylene propylene diene monomer (EPDM). However, before any claim can be made that a new material is a candidate for geomembrane applications, a significant amount of testing must be done. Such a program of testing is described.

In addition to the basic mechanical and physical property requirements that all construction materials must meet, there are three predominant characteristics required by geomembranes: they must be chemically resistant to the chemicals and leachates they will contain, they must have adequate mechanical durability, and their seaming characteristics must be known and understood.

This paper reviews the testing program performed to assess the performance of TP in these three critical areas, with most emphasis being placed on the development of optimum seaming parameters and the definition of seam specifications. The testing

program was devised in light of 1991/1992 geomembrane technology and concerns expressed at that time about the performance of conventional geomembranes such as PVC, VLDPE, and HDPE.

The emphasis was placed on seams because they are frequently the weak link of field installation and long-term performance. In practical terms, it is therefore essential that seaming performance be understood in order to provide adequate guidelines to field seaming crews dealing with new materials for the first time, and thus to assure the integrity and durability of field seams; the latter is often completely ignored during installation.

SCOPE OF WORK

The testing program discussed in the paper covers the following items:

- A comparison of the stress cracking rates between a typical HDPE and TP.
- The chemical resistance of TP to a municipal solid waste leachate and to a pulp mill black liquor; the latter is an environment in which HDPE does not perform well.
- Seams fabricated by hot wedge and hot air equipment over a range of machine temperatures and speed settings and over a range of ambient temperatures (-9 to 40°C).

MATERIAL EVALUATION - DURABILITY

Stress Cracking Resistance. Since it has been determined that medium and high density polyethylenes (PE) are subject to stress cracking (SC), significant advances have been made in developing PE resins that have a high resistance to stress cracking. Stress cracking is a brittle fracture phenomenon that occurs at a constant applied stress below the yield stress. It occurs in many materials, even in some stainless steels. Since it can be accelerated, for instance by chemical environments (environmental stress cracking), overheated seams, notch geometries (seams and scratches), and high service stresses (low temperature contraction), it will remain one of the less desirable properties of HDPE. New materials will have to be assessed for stress cracking resistance (SCR) in comparison to HDPE, since SC is the Achilles heel of HDPE and since most engineers use HDPE performance as the reference against which new materials are judged. Shortly there will be a method to relate laboratory stress cracking characteristics to mechanical durability in the field (Kanninen et al).

In this project, the stress crack growth rate of TP was compared to that of a frequently used HDPE with higher than average SCR. The work was performed at GeoSyntec Consultants' Materials Testing Laboratory according to the basic procedure of GRI standard GM5.

Dogbone specimens of 1.5 mm TP and PE were notched and placed in water at 50°C at a constant load providing an initial stress equivalent to 25% of each material's room temperature yield stress (TP at 11.5 MPa, PE at 17.7 MPa). Igepal, normally used to accelerate the stress cracking process in PE, would not necessarily accelerate the process in TP. It was, therefore, decided to expose both materials in water. Since the SC process would not be accelerated, except by temperature, times to failure would be long. Crack growth rates were, therefore, monitored by removing specimens from the test rig after various exposure times, preparing thin slice microsections, and measuring the extension of the notch initially placed in the specimen. The crack growth rates are summarized in Table 1 which shows that after 736 hours there was no crack growth in TP. In fact, the notch in TP was clearly blunted. TP is clearly not susceptible to stress cracking in its as-manufactured state.

Table 1. Results of Notched Constant Tensile Load Testing in Water
GRI Standard GM-5

HDPE @ 25% Yield Strength		TUFF-PLY @ 25% Yield Strength	
Time (hr)	Craze Length (μm)	Time (hr)	Craze Length (μm)
4	37	5	0
12	52	26	0
98	58	121	0
548	58	170	0
750	64	406	0
835	65	736	0

While geomembranes such as PVC and VLDPE may become susceptible to stress cracking as they age (by loss of additives or oxidation), it is expected that the elastomeric component of TP and its non-phthalate, non-volatile additive content will minimize the aging-induced initiation of SC.

It is encouraging to note that TP is not susceptible to stress cracking; it does not, therefore, require measurement of seam elongation in the shear test and seam separation in the peel test as does HDPE.

Chemical Resistance. The polymer from which TP is extruded consists of cross-linked EPDM suspended in a PP matrix during a dynamic vulcanization process. The two polymer systems interact synergistically, giving rise to properties and performance above and beyond what would rationally be expected from a physical blend of the systems. For many years this polymer had been used in high temperature applications for gaskets and seals in automobiles. It has also been used on a regional basis in the United States as an extruded membrane in roofing applications.

Some of the same characteristics that made it an ideal product for high temperature and for roofing applications naturally make it a logical candidate for geomembrane applications. It became necessary to demonstrate that TP was compatible with municipal solid waste leachate (MSW) before any designer would even consider it as a candidate geomembrane for waste containment.

In an independent EPA Method 9090 laboratory study (conducted by GeoSyntec Consultants), TP was immersed for 120 days at 23°C and 50°C in a MSW leachate that had some aggressive organic traces. The results showed that increases in mass were generally less than 1.5%, indicating that the TP geomembrane did not significantly absorb constituents from the leachate. According to the laboratory, lower variability in mechanical property values of the TP was observed than were typically measured in other families of geomembranes immersed in leachate of a similar composition.

These initial data suggest that TP may be a viable alternative to HDPE as a material for spent sulfite (low pH) and black liquor (high pH) pond liners (in the pulp and paper industry), since it appears not to suffer from stress cracking, and has been shown to be chemically resistant to the liquors, even at their elevated operating and inlet temperatures. For example, in a two-year test in spent sulfite liquor (pH 1.3-2.4), TP showed little interaction and retained over 92% of its original mechanical property values, as shown in Table 2 (Akzo).

In a parallel immersion test (Akzo) at an elevated temperature of 70°C, TP showed no significant degradation of mechanical properties over 90 days (Table 3). A three-week test during which TP, VLDPE, HDPE, XR-5, and Hypalon were exposed to black liquor at 70°C (Peggs et al), then examined by structural and thermal analytical methods, showed TP to offer excellent resistance to the high pH, high temperature black liquor.

In a 60-day immersion test in NaOH at 100°C, TP showed no appreciable change in physical or mechanical properties (Table 4).

Table 2. Resistance of Tuff-Ply to Spent Sulfite Liquors (pH 1.3-2.4) at 23° for 24 months

Property	Procedure	1 Month	6 Months	12 Months	24 Months
Hardness, Shore D (Units Change)	ASTM D2240	-1	-1	-2	-2
Ultimate Tensile Strength (% Retention)	ASTM D412	102	103	101	92
Ultimate Elongation (% Retention)	ASTM D412	99	103	101	93
Modulus @100% Strain (% Retention)	ASTM D412	98	99	99	98
Volume Swell (%)	ASTM D471	1.09	3.6	5.5	7.7

Table 3. Resistance of Tuff-Ply to Spent Sulfite Liquors (pH 1.3-2.4) at 70°C for 90 days

Property	Procedure	6 Days	24 Days	90 Days
Hardness, Shore D (Units Change)	ASTM D2240	-1	-1	-2
Ultimate Tensile Strength (% Retention)	ASTM D412	102	102	99
Ultimate Elongation (% Retention)	ASTM D412	97	100	99
Modulus @100% Strain (% Retention)	ASTM D412	99	100	97
Volume Swell (%)	ASTM D471	2.8	3.4	5.3

Table 4. Resistance of Tuff-Ply to -50% NaOH at 100°C for 1440 hours

Property	Procedure	168 Hours	360 Hours	720 Hours	1440 Hours
Hardness, Shore D (Units Change)	ASTM D2240	-2	-2	-4	-5
Ultimate Tensile Strength (% Retention)	ASTM D412	106	102	102	111
Ultimate Elongation (% Retention)	ASTM D412	98	96	93	100
Modulus @100% Strain (% Retention)	ASTM D412	101	101	105	100
Weight Change (%)	ASTM D471	0.02	0.20	0.45	2.10

SEAMING

Uniaxial Tensile Properties. Since seam acceptance criteria are generally related to the uniaxial yield stress of the material, it is necessary to establish the index uniaxial tensile properties of the material. Typical uniaxial stress/strain curves for TP and HDPE are shown in Figure 1.

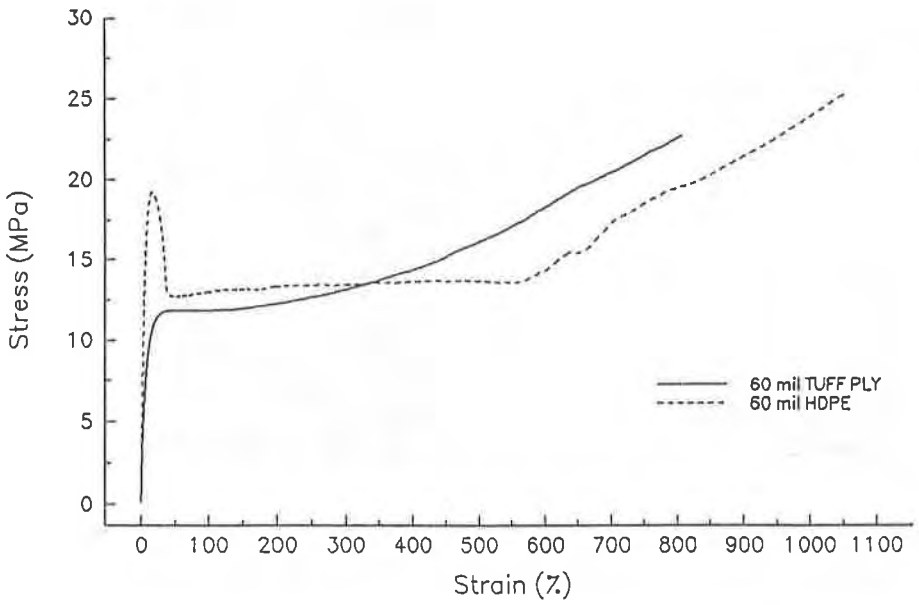

Figure 1. Uniaxial Stress-Strain Curves of Tuff-Ply and HDPE geomembranes.

The yield and break parameters (stress, elongation) are 11.8 MPa and 34%, and 23.1 MPa and 810%, respectively. The yield point of HDPE occurs at a higher stress (17.7 MPa), but at a lower elongation (13%). This pronounced yield point is a point of instability and is a restrictive feature for designers to accommodate. The higher the strain at which the yield point occurs, and the smoother the curve (provided it does not become horizontal), the better. TP's other mechanical properties are in line with those required for geomembranes in National Sanitation Foundation International Standard 54.

It is evident that TP, with its identifiable yield point that provides a basic material reference point, has satisfactory uniaxial tensile mechanical properties for use as a geomembrane.

Hot Air Seaming. Hot air seaming methods are not often used. Hot air seaming is probably felt not to be as controllable as the similar hot wedge technique due to the perceived difficulty of maintaining a constant geomembrane heating/cooling profile in windy conditions. It is also somewhat slower than hot wedge techniques for seaming HDPE. However, one of its advantages may be that the temperature profile of the heat-affected zone in the parent geomembrane (at the edge of the melted and solidified material) is less sharp than in hot wedge seams, and, therefore, capable of providing an "easier" transition of service stresses from geomembrane to seam. FCEA materials similar to TP have a long history of successful hot air seaming, so it was felt appropriate to take advantage of this proven technology in this study.

In order to be able to seam at sub-zero temperatures, the seam fabrication program was performed by Matériaux Techniques Côté in Montreal, Canada. A Leister X-10 machine was used to make the seams. The hot air temperature was measured by placing the thermocouple supplied by the manufacturer through the slots at the nozzle exit back into the supplied air stream (Figure 2). The speed of the machine was determined on each sample by measuring the distance traveled in a known time. When temperatures were reset, the hot air was allowed to reach an equilibrium temperature before seaming was initiated. At specific machine temperatures, the speed was adjusted to different

settings, approximately each meter of seam. The peel and shear specimens were always cut from the last 65 cm of each 1 m test length. In both cases, double track seams were made over a range of machine temperature settings from 200 to 500°C and speed settings from 0.5 to 2.5 m/min. Seaming was performed in the plant at a temperature of 20°C and outside at -9°C.

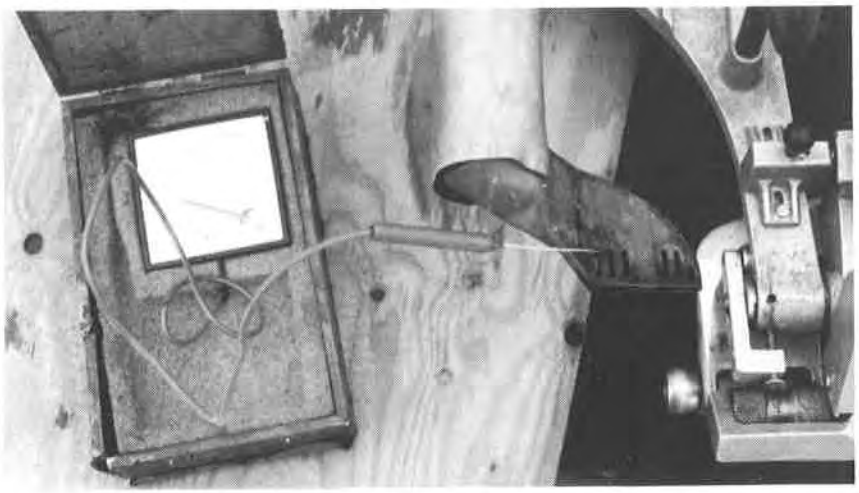

Figure 2. Measuring hot air temperature.

When seaming at the low temperature it was snowing and windy, the wind blowing directly into the gap between the two sheets being joined. Unsuccessful attempts were made to clean the snow from the areas to be joined. Subsequently, the hot air was allowed to melt the snow and blow the water away from the surfaces to be seamed.

All samples were peel-tested on an instrumented field tensiometer at a cross head displacement rate of 50 mm/min. Only the inside track of the double track seam was tested. A number of specimens were also tested on a calibrated tensile machine in a temperature and humidity-controlled, independent testing laboratory (GeoSyntec Consultants MTL). Seam samples made in U.S. were sent to Belgium for confirmatory testing.

A few seamed and tested specimens were cut on a microtome to produce thin-slice microsections for viewing by light transmission microscopy, in order to assess the homogeneity and quality of the seam and to define the characteristics of peel test breaks.

It appeared, quite early in the testing program, that the seams were either good or bad: there appeared to be very little grey area in which their quality was uncertain. Peel strength would be very low or very high: optimally within 90% of the measured yield strength. At high peel strengths, there were two characteristic breaks: break would occur at an angle of approximately 45° (Figure 3) from the root of the squeeze-out bead through the geomembrane, or the seam would appear to peel completely (Figure 4). However, this latter figure and a microsection (Figure 5) do show that separation does not occur along the joined interface but, in fact, occurs along the edge of the heat-affected zone (HAZ) in the parent geomembrane. Break is, therefore, occurring in solid material, hence the high strength. The results of testing are summarized in Figure 6.

Figures 6 b, d, f, and h show that at any hot air temperature, between 200°C and 500°C, there is an optimum speed range over which there is a minimum "apparent peel separation". (We will use the term "apparent" since the seam interface itself is not separating). At higher and lower speeds, the peel strength is still high but the apparent peel separation increases to 100%. Only at very low speeds would the peel tension fall sharply to zero. Although it is clear that there will be a high speed at which a weld will not be effected, it is higher than the maximum speed of 2.5 m/min. used in this study. At a constant seaming machine speed, there is also an optimum temperature range that produces a sweet spot seam with minimum apparent peel separation (Figure 6).

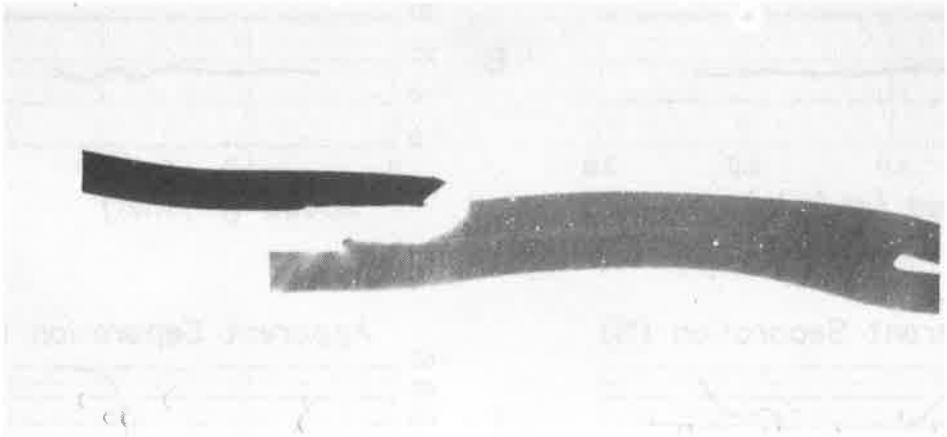

Figure 3. Peel test break at 45° at edge of seam. (x3.5)

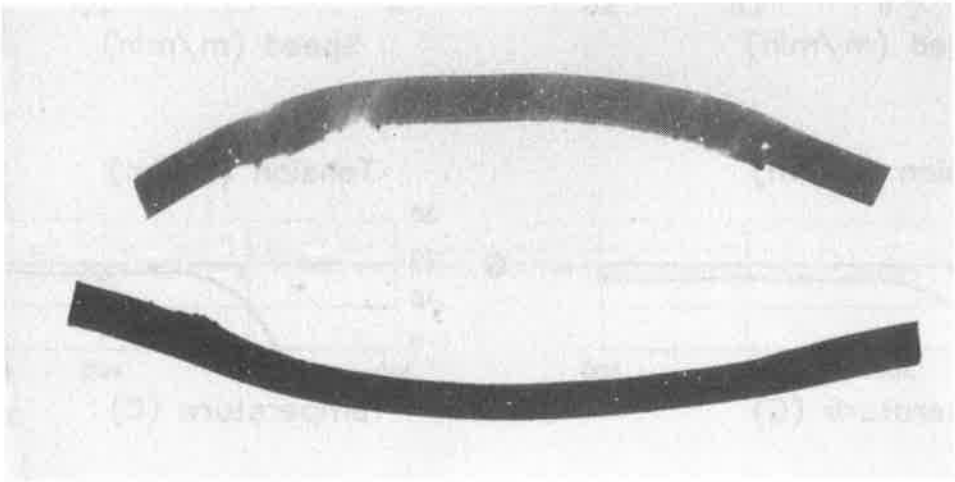

Figure 4. Peel test apparent separation. Top part is thinner than lower part. (x3.5)

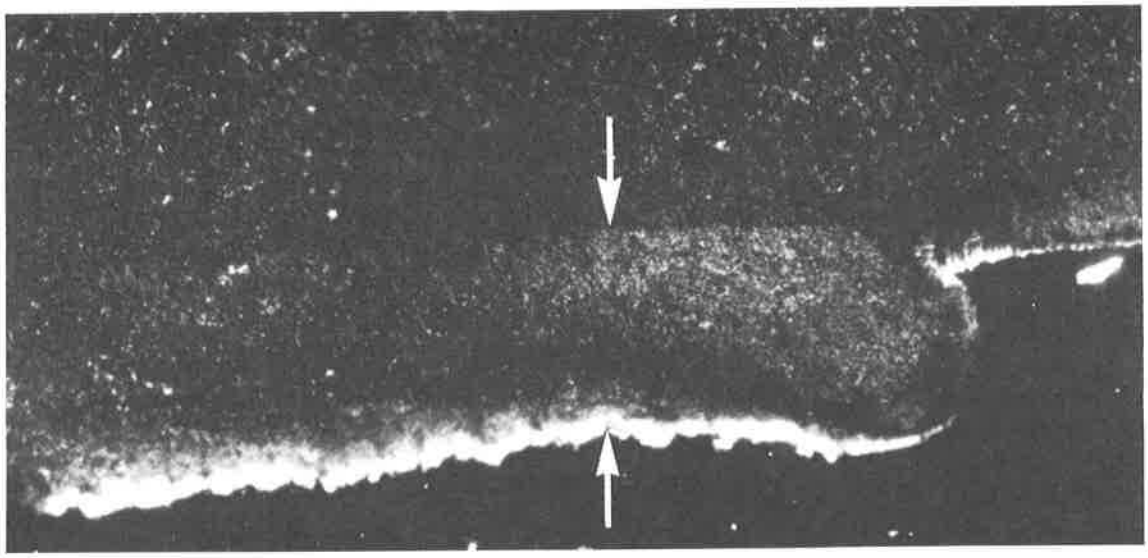

Figure 5. Apparent separation along edge of HAZ. Weld zone is between arrows. (x65 polarized)

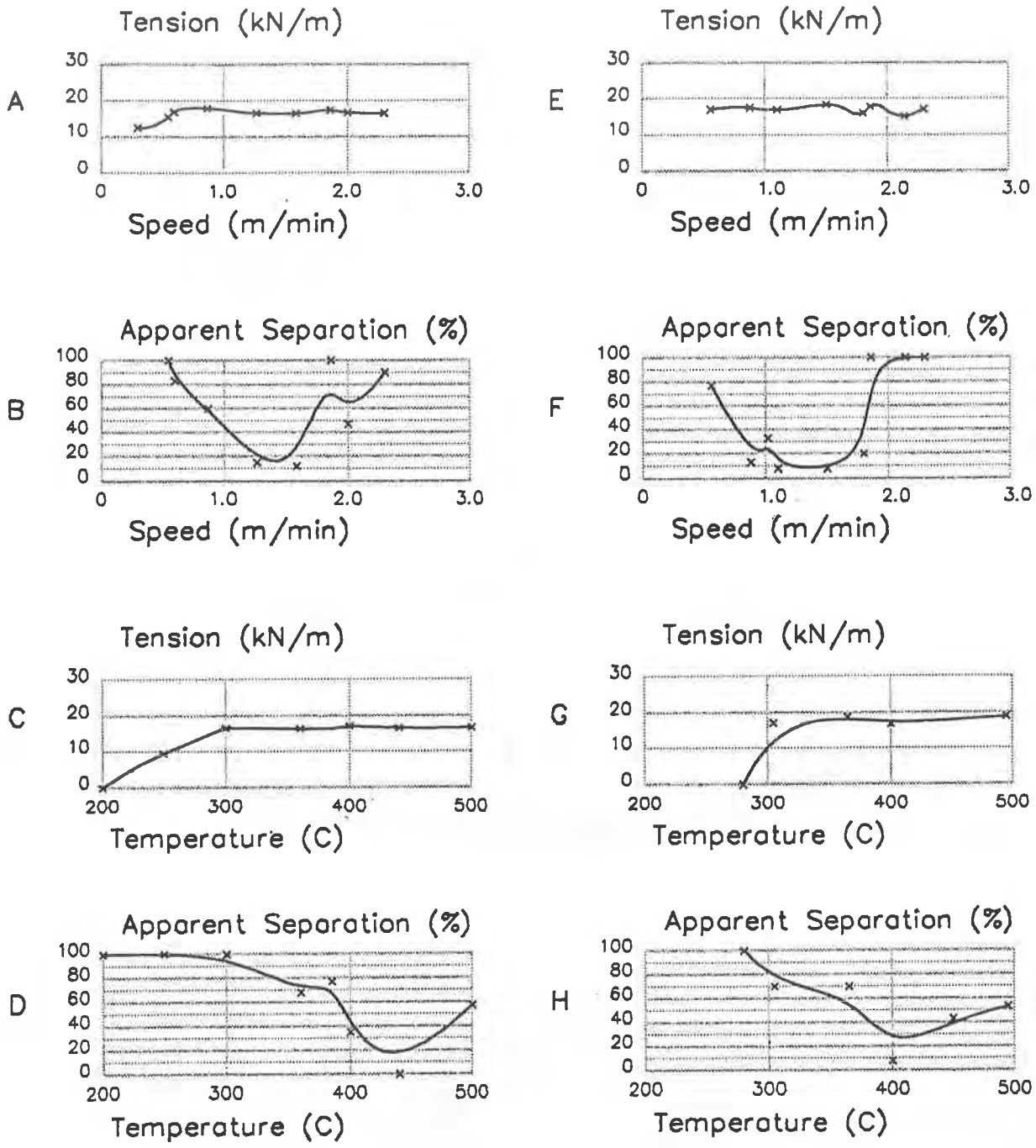

Figure 6. Seam Peel Tensions and Apparent Peel Separations at:

a,b) 410°C hot air, 20°C ambient
c,d) 1.56 m/min machine speed, 20°C ambient
e,f) 405°C hot air, -9°C ambient
g,h) 1.1 m/min machine speed, -9°C ambient

The minimum in curves b, d, f, and h is the sweet spot, or optimum seaming condition.

From Figure 6, it can be seen that there is very little difference between the tests performed at ambient temperatures of 20°C and -9°C, except that the optimum machine speeds are approximately 1.5 m/min. and 1.3 m/min., respectively. This would be expected since, at lower ambient temperatures, the machine speed would need to be a little slower in order to provide the required thermal energy input for effective seaming.

From the test results, appropriate conditions for producing good seams (that still provide room for error) in 1.5 mm thick TP geomembrane over a geomembrane temperature range from -10°C to 20°C are summarized in Table 5.

Table 5. Hot Air Seaming Parameters for 1.5 mm Tuff-Ply

LINER TEMP (°C)	HOT AIR TEMP (°C)	SPEED (m/min)
20	400	0.8 to 2.5
20	300 - 500	1.6
-9	400	0.5 to 2.5
-9	350 - 500	1.1

With additional testing it should be possible to generate, from a statistically treated set of data, a family of curves that relate optimum temperature and speed ranges. For thicknesses of 1.5 mm and above, these ranges will probably be approximately 1.5 to 2.0 m/min. and 400 to 450°C.

Apparent Peel Separation. When apparent peel separation occurs, it is clear from the full microsection, Figure 4, that separation does not occur along the original interface of the two geomembranes, but instead occurs along the edge of the heat affected zone (HAZ). The edge of the HAZ is not necessarily the edge of the molten pool, but is the boundary to which the parent geomembrane microstructure is modified by the input of thermal energy during seaming. One part of the separated seam is significantly thicker than the other. Separation along the edge of the HAZ is more clearly shown at higher magnification in Figure 5.

The microsections examined in this project revealed that the only apparent difference between those specimens that break in the geomembrane at the edge of the seam and those that apparently peel, is the sharpness of the boundary of the heat-affected zone. The specimens that fail at the edge of the seam have an almost undefinable transition (Figure 7), while those that appear to peel have a relatively distinct transition between the weld and the parent geomembrane (Figure 8).

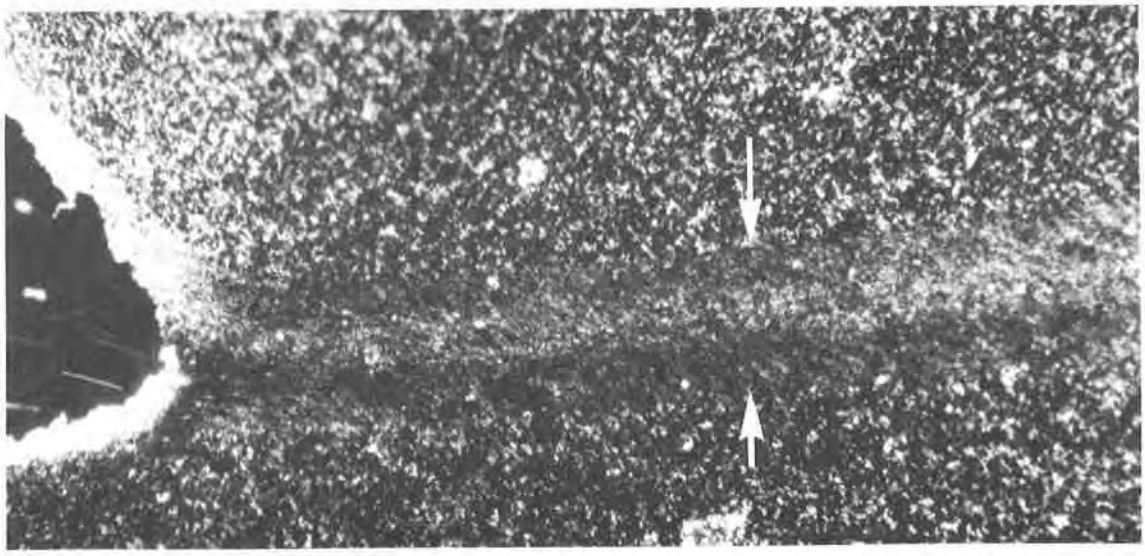

Figure 7. HAZ (arrowed) blends in to parent geomembrane. (x65 polarized)

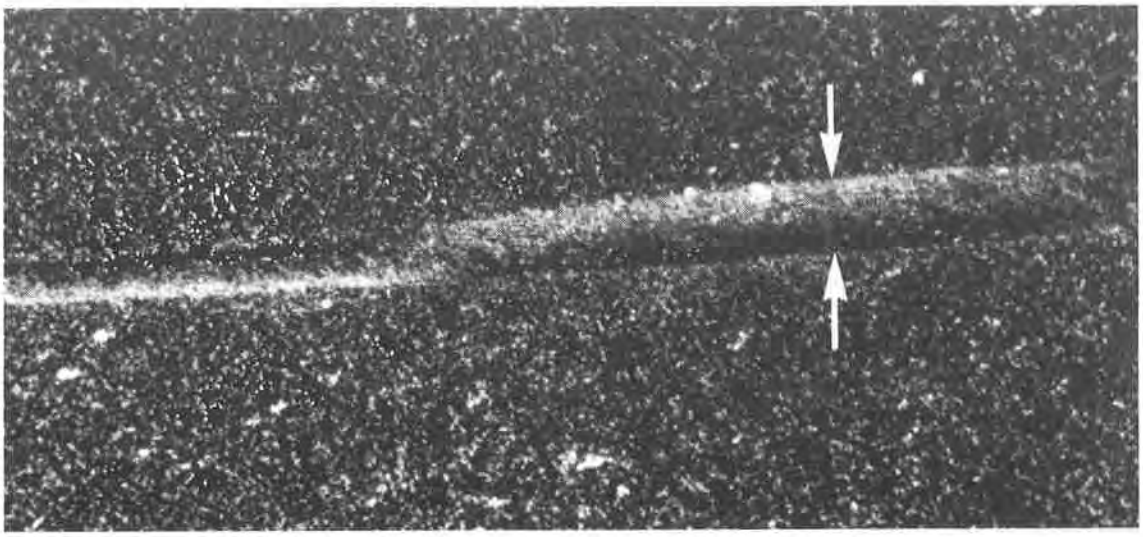

Figure 8. HAZ (arrowed) has distinct edges. (x65 polarized)

In comparison, the specimens that clearly separate in the conventional peeling mode along the original interface between the two geomembranes show a distinct interface line, clearly a lack of bonding across the interface. Seams that are extremely badly made contain very apparent defects (Figure 9).

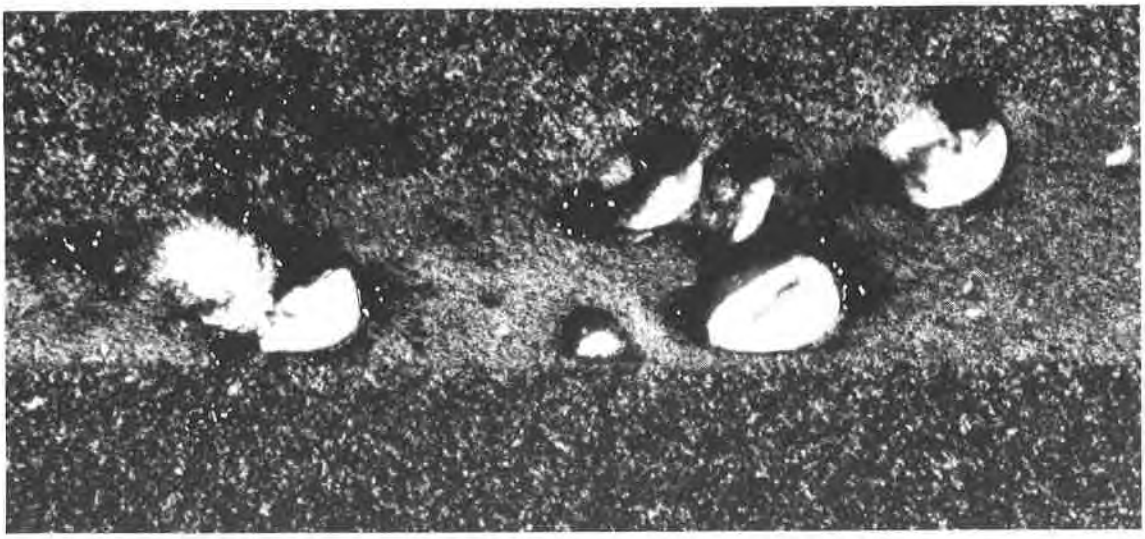

Figure 9. Voids in weld zone (across middle of photograph). (x65 partial polarization)

Hot Air Welding with a Hand Tool. Seam shear test data generated by GeoSyntec Consultants on seams in 0.75 mm, 1.0 mm, and 1.5 mm thick geomembrane made using a Leister Triac hand held hot air tool set at 600°C are shown in Table 6. The normal pressure was applied by a nylon roller. In all cases, the residual peel strengths were very high, exceeding 90%.

At patches, appurtenances, and wherever detailed seaming is required, hot air seaming using a hand-held tool could, apparently, produce seams of the same quality as the long-run seams.

Hot Wedge Seaming. Dual track hot wedge seams were constructed on 1.5 mm TP both in the USA and in Belgium at the University of Liege. A Pfaff type 8365/002 computerized hot wedge seaming machine was used in Belgium to run three series of seaming experiments.

Table 6. Hot Wedge Seam Test Results

Sample No.	No. Spcms	Thick. (mm)	Ambient Temp(°C)	Wedge Temp(°C)	Machine Speed(m/min)	Shear (kN/m)	Peel (kN/m)	Residual Yld Strength (%) Shear	Residual Yld Strength (%) Peel	Sheet Yld Tension (kN/m)	Equip Mfg.	Welded/ Tested
1	13	1.0	20	260	3.7	12.43	10.51	103	87	12.08	Columbine	USA/USA
2	4	1.0	20	260	4.0	---	11.21	--	93	12.08	Columbine	USA/USA
3	8	1.0	19	260	3.0	---	11.38	--	94	12.08	Columbine	USA/USA
4	8	1.0	19	260	3.7	---	11.21	--	93	12.08	Columbine	USA/USA
5	8	1.0	19	260	4.0	---	10.51	--	87	12.08	Columbine	USA/USA
6	8	1.0	19	260	4.6	16.25	11.03	135	91	12.08	Columbine	USA/USA
7	4	1.0	19	260	3.7	13.13	11.25	105	90	12.50	Columbine	USA/USA
8	4	1.0	23	260	2.8	12.96	10.36	96	76	13.50	Pfaff	Bel/Bel
9	4	1.0	23	260	1.9	15.80	9.59	117	71	13.50	Pfaff	Bel/Bel
10	4	1.0	23	360	3.0	Material Melted		--	--	13.50	Pfaff	Bel/Bel
11	4	1.0	23	183	1.9	18.43	13.30	97	70	19.00	Pfaff	Bel/Bel
12	4	1.5	20	300	3.7	20.88	14.58	106	74	19.7	Columbine	USA/Bel
13	4	1.5	20	260	3.7	19.70	13.40	100	68	19.7	Columbine	USA/Bel
14	4	1.5	20	300	4.6	20.88	13.59	106	69	19.7	Columbine	USA/Bel
15	4	1.5	23	300	1.5	19.95	13.68	105	72	19.0	Pfaff	Bel/Bel
16	4	1.5	23	260	1.5	20.33	14.06	107	74	19.0	Pfaff	Bel/Bel
17	4	1.5	23	260	2.5	19.38	14.63	102	77	19.0	Pfaff	Bel/Bel
18	4	1.5	23	292	2.4	22.61	14.75	119	75	19.0	Pfaff	Bel/Bel
19	4	1.5	23	200	2.3	19.00	14.82	100	78	19.0	Pfaff	Bel/Bel
20	4	1.5	23	200	1.5	22.99	14.25	125	75	19.0	Pfaff	Bel/Bel
21	4	1.5	-10	300	1.5	17.88	13.63	101	77	17.7	Pfaff	Bel/Bel
22	4	1.5	-10	260	1.5	17.88	14.16	101	80	17.7	Pfaff	Bel/Bel
23	4	1.5	-10	200	1.5	18.76	14.16	106	80	17.7	Pfaff	Bel/Bel
24	4	1.5	-10	200	2.5	18.76	12.21	106	69	17.7	Pfaff	Bel/Bel
25	4	1.5	23*	200	2.5	19.29	13.63	109	77	17.7	Pfaff	Bel/Bel
26	4	1.5	40	300	1.5	19.82	12.39	112	70	17.7	Pfaff	Bel/Bel
27	4	1.5	40	260	1.5	18.41	13.10	104	74	17.7	Pfaff	Bel/Bel
28	4	1.5	40	200	1.5	19.12	13.98	108	79	17.7	Pfaff	Bel/Bel
29	4	1.5	40	200	2.5	18.76	13.10	106	74	17.7	Pfaff	Bel/Bel
30	10	1.5	20	300	4.6	18.48	11.38	104	64	17.78	Columbine	USA/USA
31	10	1.5	20	260	3.7	17.58	10.31	99	58	17.78	Columbine	USA/USA
32	10	1.5	20	300	3.7	18.55	13.15	104	74	17.78	Columbine	USA/USA
33	10	1.5	20	365	1.5	---	15.24	--	90	16.87	Resicon	USA/USA
34	10	1.5	20	365	1.5	---	15.57	--	86	18.18	Resicon	USA/USA

*Sheet cooled at -10°C; seamed at +23°C with condensate from the air.

In the first series of tests, the seaming was done at room temperature (23 ± 2°C) with seaming speeds varied between 1.5 and 2.5 m/min. and hot wedge temperatures ranging from 200°C to 300°C.

The second series was executed on TP samples that had been previously conditioned at -10°C for three hours in a cold chamber. The seaming was done in the cold chamber at the same speeds and hot wedge temperatures as used in the first run. The third series was made in another chamber set a +40°C with the same parameters as the second series.

A seam was also constructed on 1 mm TP at 23°C with the wedge temperature varied between 183°C and 300°C and speeds adjusted to 1.9, 2.8, and 3.0 m/min.

Specimens for peel and shear testing were then cut from the last-seamed sections of the 1 m long double track test seams and tested according to ASTM D4545. Samples cut from test seams made at an ambient temperature of 23°C with a hot wedge temperature of 300°C and seaming speeds of 1.3 and 2.5 m/min were sent to the USA for cross-examination.

The results of all peel and shear testing conducted on dual track hot wedge welded seams are shown in Table 7, including the data from the seams effected in the USA. In order to account for any differences in tensile yield strength, the authors felt it important to also identify the peel strength as a residual percentage of the parent geomembrane tensile yield strength.

Table 7. Hot Air (Hand Gun) Seam Test Results

	SAMPLE/THICKNESS (mm)		
PARAMETERS	1.5	1.0	0.75
Ambient Temperature (°C)	20	20	20
Nozzle Temperature (°C)	600	600	600
Shear (kN/m)	16.08	12.47	9.74
Peel (kN/m)	18.09	12.00	9.53
Residual Shear Strength (%)	106	103	105
Residual Peel Strength (%)	90	99	102
Sheet Yield Strength (kN/m)	17.08	12.08	9.30

The hot-wedge seams made in the U.S.A. (except for samples 34 and 35) were constructed with Columbine International's Wedge-It, an automated hot wedge welder. All the peel and shear tests done in Belgium were conducted in a controlled atmosphere laboratory, whereas in the USA they were done on a portable field tensiometer at a strain rate of 50 mm/min. Samples 34 and 35 were done at an independent laboratory.

The seams constructed on the 1 mm geomembrane, consistently showed residual peel strengths between 87% and 94% at a constant wedge temperature of 260°C at speeds between 3.0 and 4.6 m/min. at room temperatures.

The seaming of the 1.5 mm TP identified some interesting trends. For example, at an ambient temperature of -10°C and seaming speed of 1.5 m/min., the peel strength values varied only slightly with wedge temperatures of 200, 260, and 300°C. The residual peel strengths of these three test seams were 80% at 200 and 260°C and 77% at the 300°C wedge temperatures.

Similarly, the seams produced at 23°C and wedge temperatures ranging from 200 to 292°C and seaming speeds between 1.5 and 2.5 m/min. consistently showed residual peel strengths greater than 75%. Thus, ambient temperature fluctuations that might be experienced during a working day in a high desert climate, may not necessitate the adjustment of the equipment settings for satisfactorily welding TP.

The tests conducted on material welded at an ambient temperature of 40°C (which is quite common in the southwestern part of the United States), provide very comparable data to those obtained at 23°C over a similar range of wedge temperatures and speeds.

Test seams 34 and 35 were made on material welded at an ambient temperature of

20°C by professional installers at a machine speed setting of 1.5 m/min. and a wedge temperature of 365°C. The material was seamed in both the roll and cross roll directions and showed excellent consistency in the peel strength values. The residual peel strength was 90% in the roll direction and 86% in the cross roll direction.

Although most of the results from the 23°C tests indicated satisfactory seams, the higher peel strength values obtained from samples 34 and 35 seem to indicate that the wedge temperature has not yet been optimized at a seaming speed of 1.5 m/min.

It should be noted that in all cases (except three) the seam shear values were equal to, or greater than, the yield strength of the parent geomembrane. Although a compilation was not made during the testing program, it qualitatively appeared that there were many more "apparent" separations during peel testing of hot wedge seams than there were in hot air seams.

Comparative Seam Tests. Table 8 summarizes the data generated when the uniaxial tensile yield properties and the seam peel and shear properties of TP geomembrane were measured on the different pieces of test equipment.

Table 8. Interlaboratory Test Results

SPECIMEN	TEST LOCATION/DETAILS	Yield Tension (kN/m)	Yield Elong. (%)
1.5 mm TP gmb	Montreal, Tensiometer, Strip	21.7	--
1.5 mm TP gmb	Belgium, Laboratory	17.7	20.4
1.5 mm TP gmb	GeoSyntec, Laboratory	17.6	24.6
1.5 mm TP gmb	Akzo, Laboratory	16.1	30.0
1.5 mm TP gmb	Brochure specification	17.5	31.0
		Average Peel Tension (kN/m)	
Montreal Seam	Montreal, Tensiometer	15.1	
Montreal Seam	GeoSyntec, Laboratory	14.9	
Belgian Seam	Belgium, Laboratory	13.8	
Belgian Seam	GeoSyntec, Laboratory	14.4	
Belgian Seam	Akzo, Laboratory	14.4	

The data in Table 8 show that when the geomembrane tensile properties are measured using the same (dogbone) type of specimens, the yield strength values are within 1% of each other. However, there can be a difference of about 25% between yield strength values measured on dogbone specimens and strip specimens. A large (>20%) variation in yield elongation measurements can occur, even when using the same specimen geometry. The seam peel strengths are surprisingly consistent: within approximately 5% of each other. If all parent geomembrane tests are performed using the same dogbone specimen geometry and all seam tests are done using strip specimens, the test data will be uniformly consistent.

DISCUSSION

The three most significant features of this seaming study are: a) the wide window of environmental conditions over which satisfactory seams can be made; b) the effectiveness of hot air seaming methods, even under adverse ambient conditions; and c) the apparent peel separation characteristic of the seams.

Unlike HDPE seams, which essentially break in a peel test through the geomembrane or by interface separation, TP breaks in an additional mode: by separation along the edge of the HAZ. It has been shown that this "apparent" peel behavior occurs through solid material and, therefore, occurs at a stress very close to the yield stress of the parent material. Such a breaking mode should be considered acceptable. For comparison, National Sanitation Foundation International Standard 54 specifies that a peel separation in PVC geomembrane is acceptable at 10% of the tensions measured in this study.

Within the range of seaming conditions that produce adequate peel strength

values, and bounded by "apparent" separation characteristics, is a zone where peel break occurs through the geomembrane at the edge of the seam, without any apparent peel separation. This is the "sweet spot" (as in a tennis racquet) or the zone of optimum seam strength. It appears that in this region the weld zone has optimum homogeneity and blends smoothly into the parent geomembrane structure. As the seaming parameters move away from the sweet spot, apparent separation begins to occur as the boundary between the HAZ and the parent geomembrane becomes more distinct, i.e., the microstructural changes between one region and the next are less smooth. The orientation of the crystalline/amorphous microstructure apparently provides a plane of preferred failure, not necessarily a significantly weaker plane but one on which fracture can initiate and propagate more easily than elsewhere.

On a qualitative basis, there appeared to be more hot wedge specimens that failed by apparent peel separation than hot air specimens. This may simply be because the sweet spot for hot wedge seams was not identified, because the sweet spot is not as broad, or does not occur. If the latter is the case, this must be because the hot wedge, with its definite "footprint" produces a sharper transition between HAZ and parent geomembrane. The hot air seams, on the other hand, may have a more diffuse extremity that encourages the smooth transition from weld zone to parent geomembrane. Such a hypothesis requires further investigation. However, if it is found to be true, some geomembrane materials (depending on their microstructure) such as TP, may provide more durable seams by hot air seaming. Even though this seaming process may be a little slower than hot wedge seaming, the actual seam strength and durability may be better.

CONCLUSIONS

Preliminary fundamental stress cracking studies and chemical resistance studies performed on Tuff-Ply, a fully cross-linked elastomeric PP/EPDM alloy, in spent sulfite liquors and a municipal solid waste leachate indicate that the material may perform very well as a geomembrane for the containment of solid and liquid wastes. It has good resistance to high and low pH liquors at elevated temperatures.

A comprehensive series of hot air and hot wedge seaming tests over a wide range of machine parameters and seaming conditions show that the material is easy to seam in the field:

- It can be successfully seamed at -10°C in blowing snow.
- It can be successfully seamed over a wide range of machine speed and temperature settings.
- Hot air seaming techniques will probably produce the most durable seams.
- Seam test specimens may appear to peel apart, but if the peel stress is close to the yield stress, such seams are acceptable.

REFERENCES

Kanninen, Melvin F., Peggs, I.D., and Popelar, C. (1993). "A Methodology for Predicting the Lifetimes of HDPE Geomembranes". Geosynthetics '93. IFAI, St. Paul, Minnesota.

AKZO Industrial Systems, Inc. Unpublished work.

Peggs, I.D., Dewijn, T., and Lewis, D. R. (1993). "Geomembranes for the Containment of Pulp Mill Hot Black Liquors: Problems and Remediation". Geosynthetics '93. IFAI, St. Paul, Minnesota.

Using a Spray-on Liner for Secondary Containment at an Oil Tank Field

S.J. Druschel
CH2M Hill Inc., USA

R.A. Callaghan
Exxon Co., USA

L.W. Well
CH2M Hill Inc., USA

ABSTRACT

This paper describes the design and construction of a spray-on lining system for secondary containment used at a petroleum products terminal in the northeastern United States. The primary purpose of the containment system is to capture any product release before it contacts soil, groundwater, or surface water. Spray-on liners offer many advantages over conventional, prefabricated sheet-lining systems. Two types of spray-on liner were evaluated: polyurethane sprayed onto needlepunched, polypropylene geotextile, and polysulfide sprayed onto lightweight, spunbound polyester geotextile. The final installation uses a polysulfide liner system, although both systems met design requirements. This paper concludes with a summary of the observations made and the lessons learned during the construction process.

SITE HISTORY AND PURPOSE OF SECONDARY CONTAINMENT

This facility has been in operation for more than 100 years. Begun as a refinery, the facility ceased refining operations in the early 1970s and is now a terminal for petroleum products. There, a secondary containment system was constructed to keep oil and other products out of the groundwater, underlying soil, and nearby surface water. The containment system was designed to capture releases such as those caused during the connection or disconnection of transfer hoses or by slow leaks from valves, piping connections or pump seals. The proximity of tanks and piping made designing a secondary containment system for the terminal particularly challenging. Piping, often only 0.3 meters (m) above the ground, occupied the limited space between tanks. The liner had to accommodate many penetrations, including numerous pipe supports, stair supports, and cups for collecting steam condensate.

DESIGN PARAMETERS OF SECONDARY CONTAINMENT

Specific design parameters at the terminal were the state regulatory requirements, reliability, and cost. State regulations require that new secondary containment systems be constructed of materials that have a permeability, at the maximum anticipated hydrostatic pressure, of no more than 1×10^{-9} meters per second (m/sec) for the product being contained. The need for reliability requires the system to be chemically compatible with the products stored at the terminal and physically durable enough to withstand stresses caused by foot traffic, dropped tools, and maintenance vehicles. A cost effective system was important (with costs based on both construction and maintenance) to meet annual budgetary requirements.

Another design consideration was that no stone or soil could cover the containment system because they are absorbent and make leak detection difficult. Soil and stone materials must be removed and disposed of after a leak, which would increase the cost and effort of using them. Therefore, without the protection of a soil or stone cover, materials had to be weather resistant.

EVALUATION OF ALTERNATIVES

Alternatives were evaluated on the basis of four criteria: performance, constructability, ease of maintenance and repair, and safety. Could the system contain site products and resist degradation from chemical contact and from exposure to weather and facility maintenance traffic? What would the system cost to construct and maintain given the narrow passageways, tanks, pipes, pipe-rack supports, and numerous other penetrations around which the cover had to be sealed? How well would the system retard fire and how safe a footing did exposed parts of the system provide workers?

Traditionally, high-density polyethylene (HDPE) geomembranes or geosynthetic clay liner (GCL) have been used for secondary containment in petroleum tank fields. HDPE offers superior chemical resistance, but is relatively difficult to seal around many odd-shaped penetrations. GCL swells snugly around any shape. However, both HDPE and GCL systems require soil cover to ensure the best performance. HDPE wrinkles when exposed to light, and ambient temperature changes. GCL is unstable and becomes irregular without soil cover pressure. Because a soil cover would have been incompatible with performance requirements at the facility, these two alternatives ranked poorly in the selection criteria.

Similarly, when conventional asphalt and concrete surfaces were evaluated, they too ranked poorly in the selection criteria. Conventional asphalt requires costly overcoats and reapplication of sealants to mitigate oxidation and other effects of exposure. Concrete is relatively expensive for this type of installation, and requires continual maintenance to ensure impermeability. Both surfaces are difficult to seal around penetrations and difficult to install in the narrow pipe alleyways.

However, the durability and a lower initial cost of asphalt paving could not be ignored. A petroleum-resistant asphalt pavement was selected for use in all maintenance accessways. The pavement was designed to provide sufficient support for all maintenance and fire protection equipment. In the areas where installation of the asphalt pavement would have been difficult and durability was unimportant (e.g., under piping runs), a second system, spray-on liners, was selected.

DESCRIPTION OF SPRAY-ON LINERS

Spray-on liners are elastomeric membrane systems consisting of fabric substrates and spray-on coating. Typically, the substrate is a non-woven polypropylene or polyester textile chosen for its structure, strength, and uniformity. The coating is a plural component elastomer with low permeability and high chemical resistance. The two products bond to form a flexible, durable, and easily installed waterproof barrier. The roofing and corrosion-protection industries have used similar coating products for more than twenty years.

Spray-on liners offer three major advantages. First, installation is relatively easy because the liner is practically cast in place. The fabric substrate is spread out and cut to size. Then the coating is sprayed on for a custom-made fit. Second, the coating's resistance to ultraviolet light degradation without any soil cover ensures its longevity. Because the coating encapsulates the fabric substrate, the substrate also is protected. Third, spray-on liners are a easily maintained because preparation and patching can be done quickly by "painting on" the coating.

There are several disadvantage to the use of spray-on liners. Performance levels are practically undocumented. Existing test results in many cases were the product of test standards different from those usually applied to geomembrane testing. Because there are few installations, liners have not been tested under a wide range of conditions. Quality control for spray-on liners is based primarily on the requirements for painting and corrosion resistance, not environmental protection requirements. Many painting contractors familiar with plural component spray coatings are unfamiliar with spray-on liners. Because of the limited number of installations, reliable cost data do not exist.

TESTING PROGRAM

A laboratory testing program was conducted to evaluate the physical characteristics and strength of the spray-on liners considered for use at the petroleum products terminal. Two spray-on liner systems were selected for consideration on the basis of the chemical compatibility of the liners and the experience of the respective manufacturers. In the first system, a polyurethane coating was applied to a 200 gram-per-square-meter (g/m^2) needlepunched polypropylene substrate. In the second system, a polysulfide coating was applied to a 140 g/m^2 spunbound polyester substrate. Figure 1 shows each material considered for use at the terminal. Representative samples of completed liner, 3 m^2 in size and at least 1.27 mm thick, were supplied by each vendor. Testing was done in accordance with published standards whenever possible. Table 1 lists the applicable test standards and the minimum and average results of each test.

DESIGN ASPECTS

There were several aspects involved with the evaluation and design of the spray-on liner for this site:

- Liner strength

Table 1. Test Results: Physical Characteristics of Spray-on Liners

Test	Test Method	Polyurethane Liner		Polysulfide Liner[2]	
		Minimum	Average	Minimum	Average
Unit Weight	ASTM D-3776	1,638 g/m^2	1,767 g/m^2	2,244 g/m^2	2,697 g/m^2
Thickness	ASTM D-1777	2.36 mm	2.42 mm	1.49 mm	1.95 mm
Effective Coating Thickness	See text	1.27 mm	1.38 mm	1.36 mm	1.66 mm
Trapezoidal Tear (machine direction)[1]	ASTM D-4533	180.2 N	194.0 N	55.2 N	62.3 N
Trapezoidal Tear (cross direction)[1]	ASTM D-4533	135.3 N	164.7 N	50.3 N	55.6 N
Wide-width Tensile (machine direction)[1]	ASTM D-4595	22.7 kN/m	23.5 kN/m	6.89 kN/m	7.78 kN/m
Wide-width Tensile (cross direction)[1]	ASTM D-4595	18.66 kN/m	18.82 kN/m	5.33 kN/m	5.71 kN/m
Puncture (liner side up)	ASTM D-4833	586.5 N	655.5 N	186.0 N	190.5 N
Puncture (textile side up)	ASTM D-4833	698.7 N	743.2 N	185.6 N	197.6 N

N = newtons
kN = kilonewtons
[1]Machine direction and cross direction refer to the orientation of the substrate fabric within the test specimen.
[2]Polysulfide liner incorporated a 140-g/m^2 spunbound polyester substrate. Substrate was later changed to strengthen the installed product.

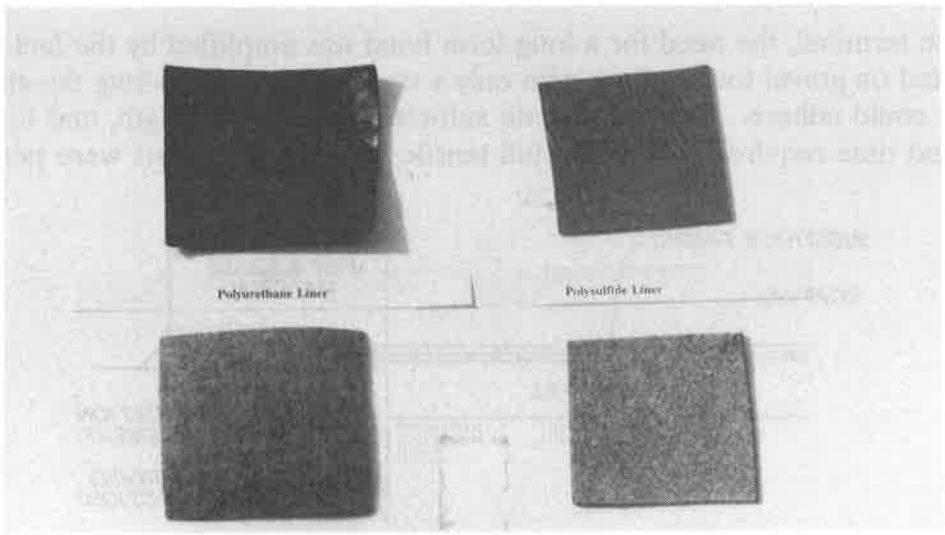

Figure 1. Illustration of Spray-On Liners

- Connections of tanks and other penetrations
- Puncture resistance
- Measurement of liner thickness
- Gas venting
- Skid resistance

Liner Strength. The spray-on liner needed to survive the maximum probable tensile forces caused by wind loading. High winds create suction, especially around the tanks, containment berms, and other structures. Suction creates an uplift loading on the unballasted spray-on liner, which can sever connections and tear open the liner. Wind forces were calculated using the Factory Mutual System (Factory Mutual Engineering Corporation, 1983). A 5.83-pascal (Pa) uplift loading was computed at ground surface of the terminal on the basis of the Factory Mutual System design event. The design event is a theoretical annual extreme wind speed with a 100-year recurrence, 145 kilometers per hour (km/hr), for the location and the site topography. For the largest open area of the spray-on liner, about 25 meters by 25 meters, a maximum tensile force of about 4.4 kilonewtons per meter (kN/m) could be generated at the perimeter. According to the Factory Mutual System, some areas near edges or corners of the liner could sustain higher uplift pressures.

Tests showed that both vendors' liners could resist large-area wind loading, but that the polysulfide liner would fail under higher, localized loadings. Because the polysulfide liner could not withstand probable maximum tensile forces, it was not initially considered. When the vendor replaced the original polysulfide liner with one whose strengths was similar to that of the polyurethane liner, both liner systems were retained for the bid selection process.

Connections to Tanks and Other Penetrations. Although most flexible membrane liners (e.g., HDPE) must be attached mechanically to a penetration, spray-on liners adhere to prepared concrete, asphalt, and steel when used with a primer (Figure 2). However, the adhesion must be adequate to ensure a long-term bond that can withstand the probable maximum tensile

forces. At the terminal, the need for a long-term bond was amplified by the fact that many of the tanks rested on gravel foundations, with only a small surface area along the annular ring to which a liner could adhere. To demonstrate sufficient adhesive strength, and to evaluate the minimum bond time required to develop full tensile strength, field tests were performed.

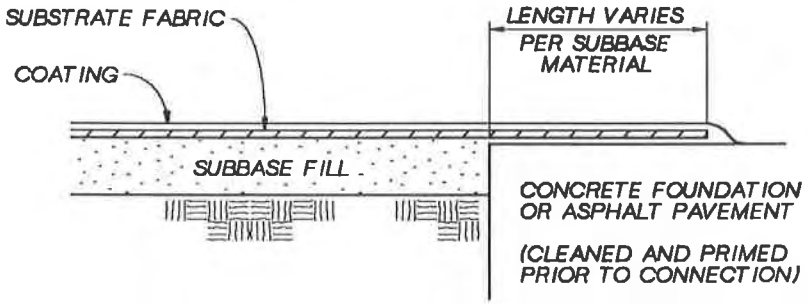

Figure 2. Adhesive Connection Detail

During the initial phase of the liner installation, typical samples of spray-on liner material were attached to asphalt and concrete tank foundation surfaces using installer's recommended methods and materials. After a 7-day curing period, 25 mm wide specimens of liner were cut perpendicular to the connection. 200 mm of length was bonded to the asphalt or concrete. 100 mm of free length was used to apply tension. A tension load cell, with an integral gauge automatically recorded the peak measurement (Figure 3). When the liner was stretched all tests pulled the liner parallel to the connection surface, simulating the most probable loading condition for these connections. Table 2 lists the results of these tests.

The strength of all connections exceeded the specification requirement of 8.74 kN/m. Although asphalt connections had an average strength of 13.36 kN/m, typically the liner membrane failed before the connection did. The membrane-failure load levels were less than the tensile strength required for the liner membrane. The testing methods used in this study are different than those used for the membrane alone, and therefore the results do not directly reflect the strengths of the membrane. During an asphalt-connection test, strain occurred within the bonded section of the membrane as far as 125 mm from the asphalt edge. Post-test inspection showed that the asphalt subbase frequently failed 50 to 75 mm from the edge, leaving a 5-mm layer of asphalt attached to the specimen.

Concrete connections had an average strength of 14.40 kN/m, and typically failed the gauge clamp rather than the liner membrane or the concrete subbase. During a concrete-connection test, strain occurred within the bonded section as far back as 25 mm from the concrete edge.

Table 2 Results of Adhesive Connection Test					
Test	**Type of Connection**	**Width (mm)**	**Load (N)**	**Strength (kN/m)**	**Comments**
1-A	Asphalt	24.6	321	13.05	Liner failed
2-A	Asphalt	24.6	325	13.88	Liner failed
3-A	Asphalt	23.4	317	12.89	Liner failed
4-A	Asphalt	24.4	347	14.22	Liner failed
5-A	Asphalt	25.1	233	not used	Too much up-angle on pull
6-A	Asphalt	24.4	311	12.74	Liner failed
1-C	Concrete	25.7	377	14.67	Clamp failed
2-C	Concrete	25.7	337	13.11	Clamp failed
3-C	Concrete	25.4	308	12.14	Clamp failed
4-C	Concrete	24.6	>489	>19.86	Gauge limit exceeded
5-C	Concrete	25.4	311	12.24	Clamp failed

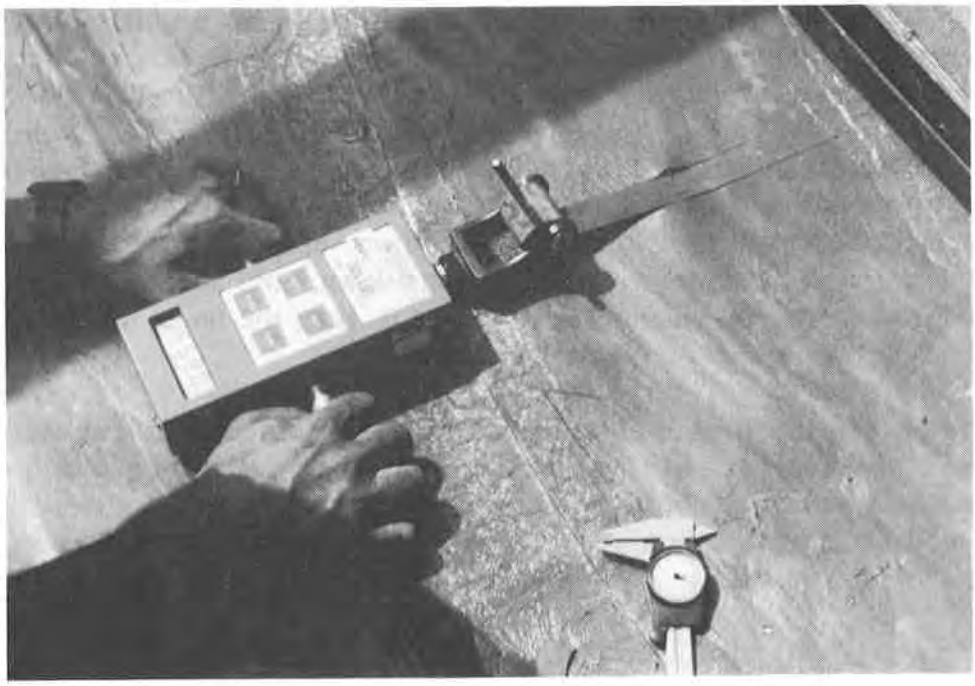

Figure 3. Adhesive Connection Testing

These tests showed that adhesive connections to asphalt and concrete were acceptable for this project. Testing also revealed that long connection bonds enhanced bond strength. Therefore, it was imperative to use minimum connection bond lengths of 150 and 50 mm for asphalt and concrete, respectively. To ensure bond strength, typical bond lengths were twice the minimum length, or 300 and 100 mm for asphalt and concrete, respectively. Typical bond lengths were used for the majority of connections, but the minimum bond lengths were used for special conditions. During installation, adhesive connections were inspected to verify both the length of the bond and the surface preparation met manufacturer specifications. Applications of coating without fabric or beyond the primed surface were not considered part of the bond length.

Where there was insufficient space to install adhesive connections, or substrate fabric could not accommodate penetration shape, special connection details were used to develop both adequate strength and a definitive contact between the liner material and the penetration. Two general types of connections were used, one used a rope or band clamp to physically hold the substrate fabric against the penetration, the other used an anchorage trench (see Figures 4 and 5). Both connections were sized according to penetration diameter to resist maximum large-area wind force. The larger the penetration, the greater the required strength, which is based on the hoop tensile forces required to resist a pull perpendicular to the connection.

Puncture Resistance. The puncture resistance necessary for long-term integrity is difficult to determine because punctures have many causes, each difficult to quantify. The secondary containment liner could be punctured by the impact of a dropped tool, by the pressure of a stone in the sole of a worker's boot, or by the weight of the liner resetting on the point of a frost-heaved stone. Although low puncture strength may not be as serious a problem as low tensile strength, the liner is routinely exposed to puncture-causing forces.

To test liner resistance to damage caused by dropped tools, a 0.9-kilogram wood-splitting wedge was dropped onto samples of liner resting on a concrete floor. The liner materials were affected similarly. When the wedge was dropped from a height of about 1 meter with the sharpened point or a corner pointing down, both liners were split. However, when the wedge was dropped butt end down or on its side, the liners usually retained their form, despite slight bruises and occasional pin-holes.

The results of the puncture tests attest to the durability of the spray-on liners. Puncture resistance (determined by ASTM D-4833) averaged about 670 N for the polyurethane-based liner and about 190 N for the laboratory tested configuration of the polysulfide-based liner. Although a worker's weight on a small stone could produce a point load of about 190 N, unless the stone were nearly rod shaped, the liner would flex around the stone.

On the basis of these results, a 50-mm-thick layer of medium-sized sand was specified for the subbase fill and leveling course beneath the liner. Although sand may not prevent all punctures, medium-sized sand was selected for its uniformity and ability to cushion point loads.

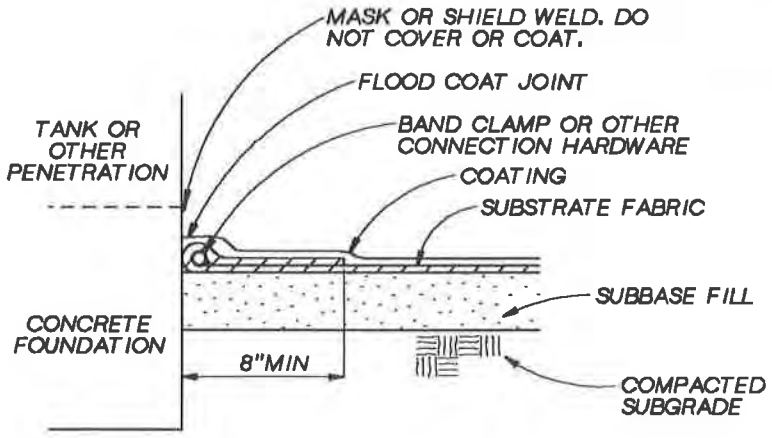

Figure 4. Band Clamp Connection Detail

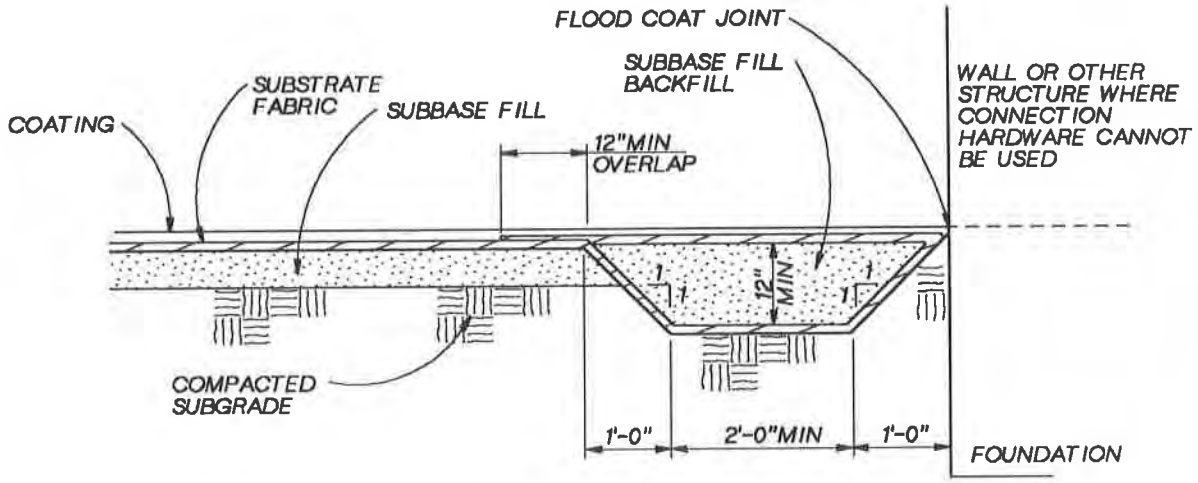

Figure 5. Perimeter Anchorage Detail

Because of their geometry and shape, almost all membrane liners are susceptible to punctures. The placement of cushioning geotextiles or sand blankets over the liner would distribute the effects of a point load and increase puncture resistance. These additions increase the effort and cost of liner installation. If substantially increased puncture resistance is needed, then perhaps another lining system such as polymer- modified asphalt or concrete should be used. The decision to use spray-on liners must be viewed as a choice between level of service and cost.

Measurement of Liner Thickness. Because liner strength and puncture resistance depend on liner thickness, thickness was measured during installation. Samples for thickness measurement were cut every 90 m^2 from the installed liner. The thickness of the spray-on liner was initially measured using a micrometer at a standard contact pressure, according to ASTM D-1777. However, this test method inflates results because the coating does not fully penetrate the substrate fabric. The extra uncoated substrate fabric beneath the coated composite material contributes to the thickness, not to the barrier. A more accurate indicator of barrier thickness was developed by determining the liner's mass per unit area. Subtracting

the substrate fabric's mass per unit area from the spray-on liner's mass per unit area gives the mass per unit area of the coating alone. Dividing the coating mass per unit area by the coating unit weight gives the average or effective coating thickness. Examples of the difference between the micrometer measurement and the effective coating measurement are shown in Table 1.

Gas Venting. Soils naturally give off small amounts of gas. The lack of ballast on the liner, the relative high permeability of the subbase fill sand, and the transmissivity of any substrate fabric that is not saturated by the coating during installation (typically, the lower portion of the substrate fabric) all help move gas to high points. If not vented, these gases can collect under the liner and create a bubble that lifts the liner off the contact surface. Such a bubble could become large enough to impede operations. At the terminal, gas vents were installed using 0.1-m-diameter slotted riser pipes and crushed stone, both of which are 0.9 m below grade to prevent frost heave. The gas vents were located primarily at the grading ridge lines because gas generally collects at high points. Intervals of 15 m were selected for the vents, a distance judged sufficient to prevent gas buildup. No gas has collected since the liner was installed.

Skid Resistance. A skid-resistant surface was necessary where liner access would be required. On the basis of discussions with vendors, a method was developed for applying grit to the surface of a previously installed liner. The grit was composed of 20-30 sieve sand (sand that passes through a 0.85-mm opening [No. 20 sieve] but does not pass through a 0.60-mm opening [No. 30 sieve]) that has an average diameter of about 0.7 mm. An extra 0.25-mm-thick coating was applied to the installed liner, and the grit was spread onto the uncured coating at a rate of 0.50 to 0.75 kilogram per 10 square meters. Grit of this size was large enough to protrude above the 0.25-mm coating without penetrating the liner.

CONSTRUCTION OBSERVATIONS

Two contractors built the secondary containment system at the petroleum products terminal. A general civil contractor did earthwork and paving. An industrial painting contractor, experienced with plural-component coatings installed the liner. Coordination between the two contractors was sometimes challenging because of their closely related responsibilities. For example, the general civil contractor prepared the subgrade and subbase fill for immediate liner installation, but weather delayed liner installation. Such delays increased the general civil contractor's costs because of increased subbase exposure and maintenance time. One way to mitigate this problem could be to subcontract the liner installer to the general civil contractor.

The liner was not installed in the usual way. Instead of spreading out the substrate fabric and coating in-place, sheets of spray-on liner were prepared in a nearby warehouse. By coating uncut substrate fabric the liner was protected from most of the effects of weather. After the sheets cured, they were cut into panels, transported to the project site, and put in place. Final trims and connections followed. Painters coated the liner and roofers deployed panels and made the connections. Joints between adjacent panels were made by using a paint brush to apply a glue-like layer of coating between the two over-lapping layers. A hand roller, 100-mm wide, was used to force the two layers together, then more coating was applied.

Installation started at a rate of about 30 m^2 per day, and reached about 60 m^2 per day. Penetrations and site constrictions, not methods, slowed installation. Advantages to this method of installation are: provides a uniform and consistent product; reduces vulnerability to effects of weather on the coating process; eliminates time required to move raw material stockpiles and mixing equipment as the working locations change; and reduce the amount of masking and other overspray precautions that must be taken. Also, sliding a panel underneath a pipe rack that has a 0.3-m clearance is easier than spraying in the same space.

Disadvantages to warehouse liner preparation were: moving heavy, completed panels; increasing health and safety precautions to mitigate the effects of fumes produced during the liner coating and curing processes; and preventing damage to sufficiently cured panels. A xylene rinse can be used, if necessary, to clean panels used for a joint or connection.

The vendor's limited experience with substrate fabric for spray-on liners resulted in a couple of construction problems. Liner substrate fabric must have a light pre-applied coating to seal the fabric to a specified level. One shipment was insufficiently precoated. In another shipment, an improper precoating mixture prevented curing. Another time, the wrong substrate fabric was sent. Each of these shipments was rejected. To the vendor's credit, coating batches were satisfactory and the vendor facilitated component measuring by providing premeasured, matched bulk containers of each component. Overall, the installation went smoothly, and, in the limited time since installation, the spray-on liner is performing well.

SUMMARY

Spray-on liners provide a unique and cost-effective method of secondary containment, and they have many advantages over other containment systems. However, this technology is new, and few other projects similar in size and complexity to the petroleum products terminal have been completed. Therefore, the use of spray-on liners must be considered carefully. Special attention to installation details may be required for exposed-liner secondary containment to provide uniform and long-lasting performance. Field quality assurance also is critical to a successful installation. With proper design and construction, spray-on liners can provide high-quality secondary containment at a reasonable price even at complex sites.

REFERENCES

"Soil and Rock; Dimension Stone; Geosynthetics," *Annual Book of ASTM Standards*. American Society for Testing and Materials. Philadelphia, PA. 1991. Vol. 04.08.

"Wind Forces on Buildings and Other Structures," *Loss Prevention Data 1-7*. Factory Mutual Engineering Corporation. Norwood, MA. 1983.

Standard Method of Fire Tests for Flame-Resistant Textiles and Films, National Fire Protection Association, Inc. Quincy, MA. 1989.

WDCM87/038.51

Design and Installation of a High-Wind Load Floating Diversion Baffle Constructed of Reinforced Geomembranes

F.R. Wilson
Seaman Corp., USA

W.L. Watkins III
Therma Fab Inc., USA

ABSTRACT

Operational theory and construction details for Floating Diversion Baffles constructed of reinforced geomembranes are presented. Forces on baffles, along with typical required geomembrane stress-strain characteristics are presented. Differential hydraulic forces are discussed to provide a basis for determining strength requirements of the geomembrane portion of the baffle system. A case history is presented detailing a typical Floating Diversion Baffle, which was replaced after failure due to several failure possibilities.

INTRODUCTION

Beginning with the Clean Water Act in 1972, the United States launched a massive program to provide secondary treatment for all collected wastewater through Federal funding. In the 1980's, the Federal funding was largely changed to State Revolving Funds (SRF's), which are a type of loan offered to municipalities. Treatment plants that are hydraulically or organically overloaded, or which employ pond-based treatment systems that have solids build-up, face major costs for continued compliance with secondary treatment standards. Floating Diversion Baffles (FDB), constructed of reinforced geomembranes are rapidly gaining popularity as a method of extending hydraulic retention time, and thus upgrading and increasing treatment plant capacity. Figure 1 illustrates a treatment impoundment subject to short circuiting, and with short circuiting eliminated with the use of Floating Diversion Baffles. In a typical application, an impoundment can loose 50% of its hydraulic retention time because of short circuiting. FDB's are used in both new construction and in retrofit situations. Installation does not interrupt treatment facility operation.

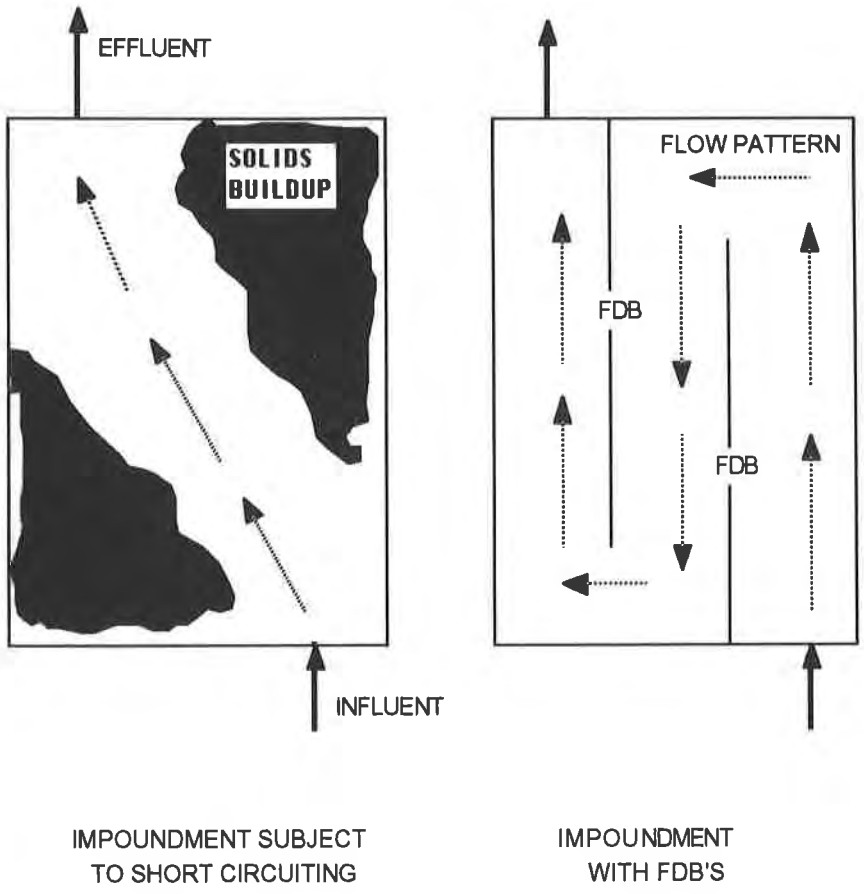

Figure 1. Impoundment Upgrading using Floating Diversion Baffles

FDB CONSTRUCTION

The principal and core component of a FDB system is a highly reinforced geomembrane. The Baffle acts as a curtain which causes flow to occur parallel or around the barrier. The geomembrane must have a concentrated reinforcing in order to resist hydrostatic pressure, have minimal elongation and creep, and possess sufficient yield tensile strength to carry some of the longitudinal loading transmitted to the load bearing units. Fabric reinforced geomembranes with fabric density exceeding 18 x 18 are used in order to achieve the high Yield tensile strength and low elongation illustrated in Figure 2.

Figure 3 illustrates the construction of a typical FDB. A description of each component follows.

Float. A unicellular foam log, of varying diameter (typically 10 to

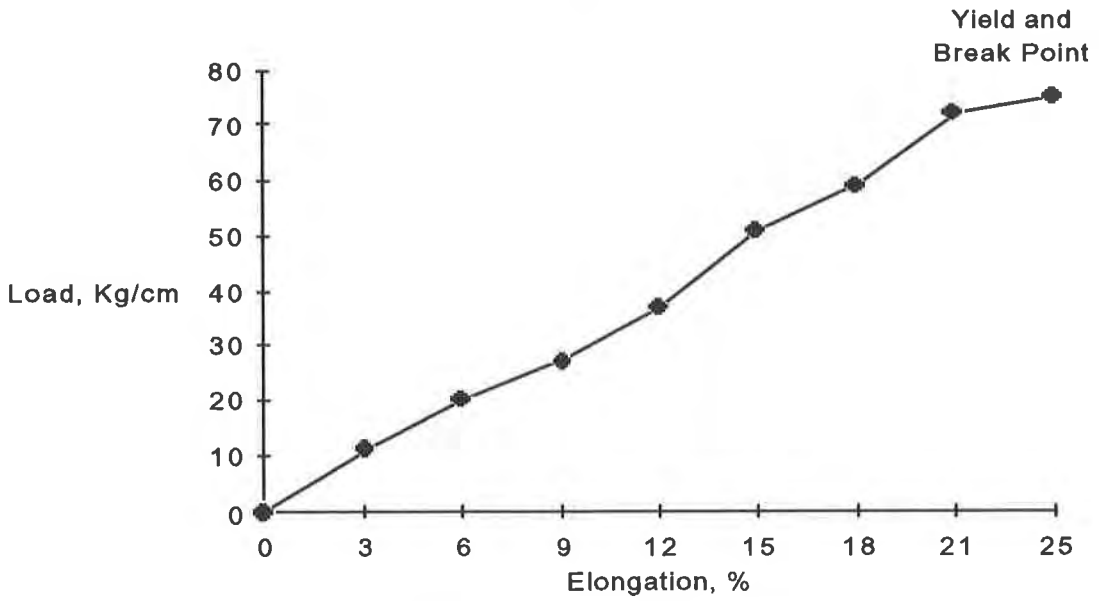

Figure 2. Stress vs. Strain for a Coated Fabric Geomembrane (XR-5),Test Method FTMS 191
(Reprinted by Permission of Seaman Corporation)

30 cm) is wrapped with a reinforced geomembrane. The float, of course provides stability for the baffle and must be of sufficient diameter to hold the submerged curtain somewhat vertical, although below water wrinkling is not unusual or detrimental. The geomembrane encasing the float must provide mechanical and environmental resistance.

Curtain. As discussed above, the geomembrane itself is the core of the baffle. All other components function merely to ensure the geomembrane remains in place and functional for hydraulic routing.

Top Load Bearing Member. In most FDB applications, a cable is provided near the top of the baffle to carry most of the tensile load transmitted to the baffle. The cable can be of varying size and type and can be either exposed, or encapsulated by the geomembrane. In Figure 3, the cable is encapsulated by the geomembrane and is contained immediately below the float mechanism.

Bottom Weight Member. Typically, a highly flexible weight such as a steel chain is attached to the bottom of the FDB in order to minimize the amount of "ballooning" by the baffle, and to keep it vertical. This bottom weight member can also act as an added Load Bearing Member in some situations.

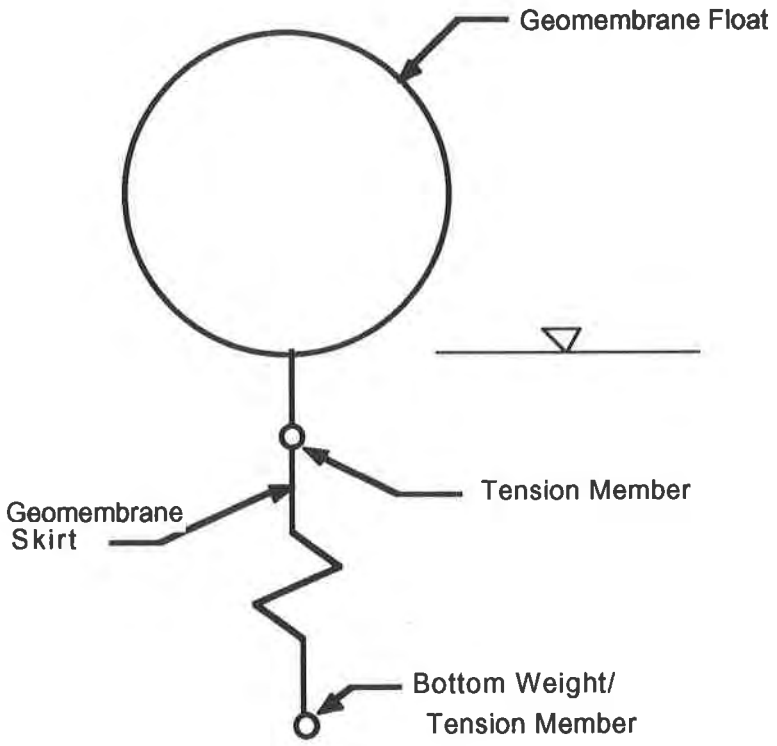

Figure 3. Construction of a Typical FDB
(Reprinted by Permission of Therma Fab Inc.)

FORCES AND DEGRADATION MECHANISMS ON FLOATING DIVERSION BAFFLES

A Floating Diversion Baffle is subjected to a variety of forces and degradation mechanisms which are induced from hydraulic and environmental surroundings. Figure 4 illustrates the major forces acting upon the FDB system. A discussion of these forces follows.

Tensile Forces (1). Loads acting in a perpendicular manner translate into tensile loads upon the baffle. Tensile forces are derived from hydraulic and/or wind forces. Load bearing members at the top and bottom of the baffle are designed to carry this load, but actual hydraulic conditions often cause loads to be placed on the geomembrane curtain itself. Figure 5 shows a pond/FDB system installed for a paper mill wastewater treatment facility, which is also illustrated graphically in Figure 6. Here, the aerators impede the free flow of wastewater through the system and an actual head differential exists from influent to effluent. Figure 7 shows the hydrostatic loading on the baffle float as a result of differential water levels.

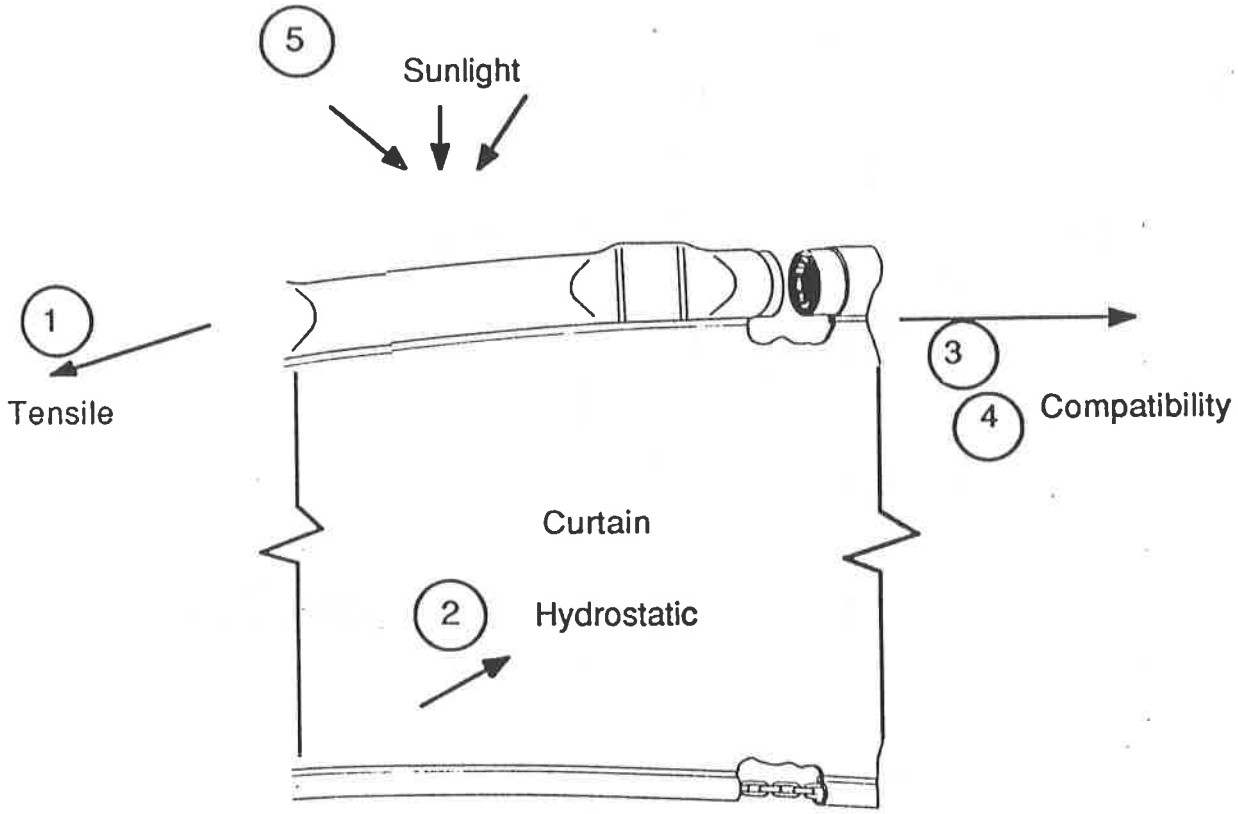

Figure 4. Major Forces and Degradation Mechanisms Acting on FDB System

Figure 5. FDB System at Paper Mill Wastewater Treatment System

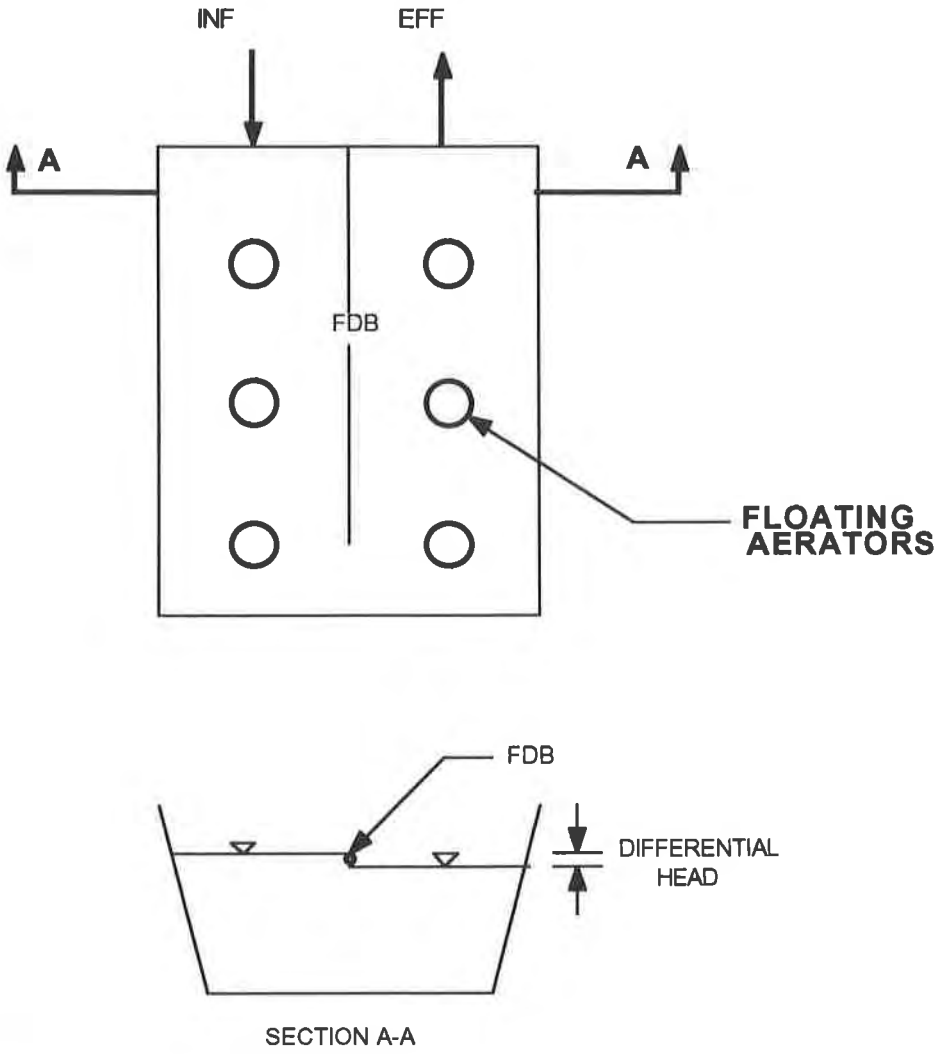

Figure 6. Schematic of Treatment System Subject to Head Differential

Assuming a float diameter of 15 cm and worst case conditions where the hydraulic differential is the diameter of the float, the force can be calculated:

Hydrostatic Force on Float = (1/2) (b) (h) (1)

where w = weight of water = 1004 kg/cu m

b = load at float bottom = (1004 kg/cu m) (0.15 m)

h = height of float = 0.15 m

Hydrostatic Force on Float = (0.5) (150.6) (0.15)

= 11.3 kg/m

For a 30 m long FDB, this force would total almost 350 kg acting on the FDB and translating into a tensile force. Ideally, this force is transmitted in an incremental manner to the tension member, but Point A as shown in Figure 7 would be subject to tensile stress. For instance, the point stress at the bottom of the Float area would be equivalent to 150 kg/m of baffle or 150 kg/ sq m of area. Because it is a point load, less area is affected and thus the total loading is less. However, the geomembrane must have high strength to carry this loading, but yet be flexible to allow movement as necessary to effectively transmit all tensile loading to the tension member.

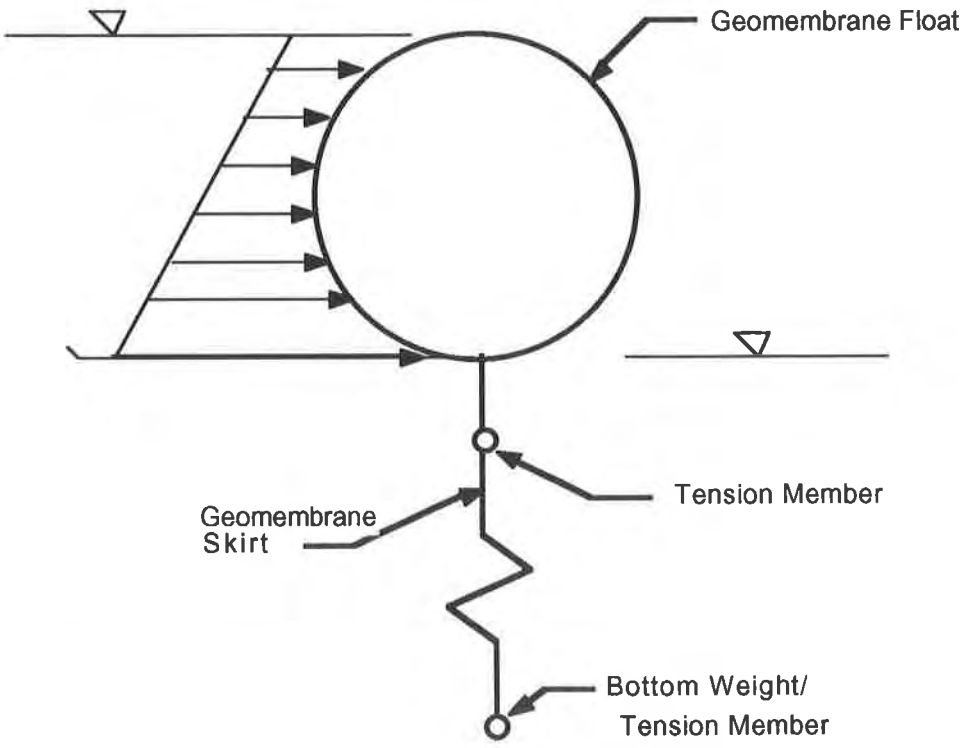

Figure 7. Differential Hydraulic loading on FDB

Hydrostatic Force on Curtain (2). Wastewater is balanced on each side of the curtain except in differential head situations as described previously. Because water seeks a lower energy position (lower hydraulic head or position), the geomembrane receives constant pressure in the form of hydrostatic loading. The flexibility of the reinforced membrane allows movement in both normal load directions. Overall, hydrostatic loads translate into tensile load, but throughout the baffle, the membrane is loaded hydrostatically.

Chemical Compatibility (3,4). Typically, a wastewater can have several chemical components, depending on the wastewater composition and the energy level of the basin. The geomembrane portion of the FDB must be compatible with the diverted wastewater below the water level and also at the water surface. The latter is significant in many impoundments, including both municipal and industrial, where free oils accumulate and concentrate at the water surface. If the geomembrane is not long term compatible with hydrocarbons, a relatively short service life will result. This situation can occur in an opposite manner when non water soluble organics with specific gravities greater than 1.0 are present and chemical attack can occur at the impoundment bottom. Such a phenomenon can occur in treatment systems with industrial contributions. The geomembrane portion of the baffle must have a broad range of chemical resistance.

Sunlight Resistance (5). The float portion of the geomembrane is exposed to sunlight. It therefore is subject to UV exposure and thermal heating and cooling cycles. It must therefore have good UV resistance and low thermal expansion-contraction properties.

Mechanical Properties-Float Section (6). Abrasion, ice, mechanical damage, and freeze-thaw are all degradation mechanisms which act upon the float section. The physical properties of a geomembrane which a designer evaluates for a lining application are also important for a FDB. Puncture resistance and the ability to prefabricate the majority of the baffle are considerations.

MUNICIPAL TREATMENT SYSTEM

A large impoundment complex adjacent to the Arkansas River forms the basis of the municipal wastewater treatment system for the City of Pine Bluff Arkansas. A series of aerated and facultative ponds are used in series at the plant. The subject treatment facility receives 20% hydraulic contribution from industrial sources including such industries as poultry processing. The overall average influent flow is over 0.9 cu m/sec (20 MGD).

In 1986, the effluent limits on organics, as measured by BOD5 were being exceeded. After a series of studies, it was concluded hydraulic short circuiting in the facultative ponds was occurring with resulting reduction in organic removals. A system of Floating Diversion Baffles were proposed for all ponds, including the aerated ponds. The selected FDB system was designed, manufactured and installed by Therma Fab Inc., Lexington, South Carolina. The geomembrane component was specified to be a 0.75 kg/sq m (22 oz/sq yd) reinforced PVC. Therma Fab manufactured the FDB system using 8422 PVC manufactured by Seaman Corporation, Wooster, Ohio.

FDB layout for a typical pond (Pond No. 2) at the subject

facility is shown in Figure 8, along with the assumed flow routing. The large ponds mean a large open area that is subject to high winds. Initially, this baffle system was constructed of nylon-reinforced PVC, with one side anchored at wooden piles spaced on 30 m centers. The float mechanism consisted of a 15 cm diameter flotation device wrapped with reinforced PVC and a 0.6 cm diameter galvinized load bearing cable was provided to give a 2700 Kg Yield Tensile Strength. All portions of the baffle system were constructed in this manner. Figures 9 and 10 illustrate the FDB system which consisted of over 4000 m of baffle with relatively shallow depths ranging from 1.4 m to 1.7 m. With such a large surface area to depth ratio, the impoundments relied primarily on aerobic processes for wastewater treatment.

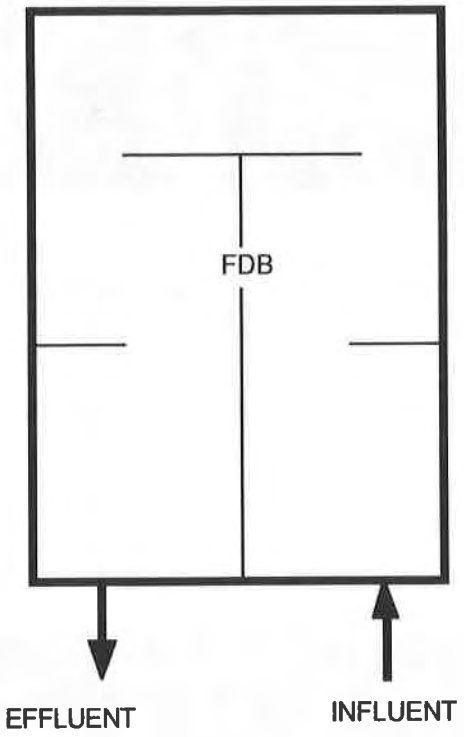

Figure 8. FDB Layout in Typical Impoundment

After six months of operation, the baffle system was exhibiting failure in the form of tearing and separation throughout its length.

ANALYSIS AND CORRECTED DESIGN

Several conditions were believed to have contributed to the failure of the geomembrane portion of the design. A discussion and summary of each follows.

Figure 9. FDB in Municipal Wastewater Treatment Impoundment

Figure 10. FDB in Municipal Wastewater Treatment Impoundment

Chemical Compatibility. A 30-day test immersion using a 0.75 Kg/sq m (22 ounce per square yard) reinforced PVC and a reinforced Ethylene Co-Polymer Alloy (XR-5) geomembrane was conducted. Laboratory testing of control and immersed samples showed no significant loss of tear or tensile properties, but an increased amount of softness was noted in the reinforced PVC samples. Therefore, it was concluded that some degree of incompatibility existed and likely had caused decreased tensile properties. This apparent degradation at the end of 30 days of constant immersion would have been more pronounced with longer immersion time. The XR-5 geomembrane was unaffected during the immersion period and was utilized in the replacement baffle.

Tensile Loading. The subject site was open and subject to very windy conditions. Table 1 illustrates statistical return period extreme wind data. Additional data showed that typical wind speed of approximately 32 Km/hour (20 mph) occurred.

Table 1. Wind Speed Extremes, Little Rock, AR Airport

Return Period ,Years	Wind Speed, Km/hr (MPH)
2	72 (45)
5	87 (54)
10	97 (60)
20	106 (66)
50	119 (74)
100	129 (80)

Using standard wave generation data techniques,a marine engineering consultant determined the critical point to be Point 1 as shown on Figure 11. The Fetch, or open wind distance was greatest at that point. Predicted wave heights were 0.15 m under typical condition and 0.4 m under extreme conditions. Wave forces were calculated assuming:

-15 cm diameter float (sail area)

-Wind as shown above

-Water force pushing against geomembrane float to overtopping conditions

Based on this analysis, extreme loading on the FDB was calculated to be 112 to 134 kg/m along the length of the baffle. The solution to this loading was solved by a two-fold approach. First and most obvious was to increase the strength of the primary

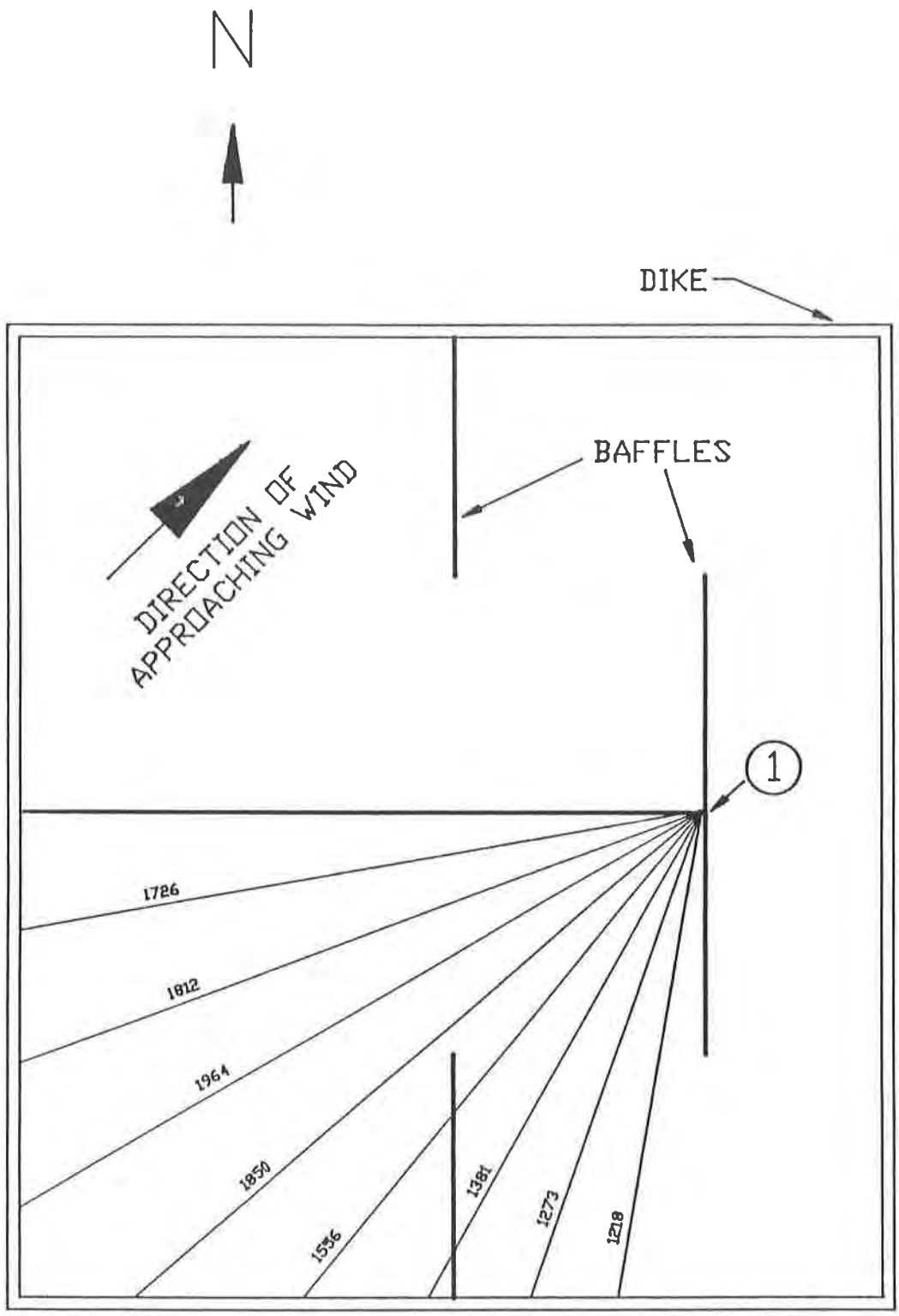

Figure 11. Fetch Diagram (Jones, 1991)
Note: Distances shown are in feet (1 ft = 0.305m)

tension member. A 0.95 cm diameter cable instead of the original 0.6 cm diameter was used which increased the load bearing capacity to 5400 Kg. Second, the sail area of the FDB was reduced. The diameter of the float portion of the baffle was reduced from 15 cm diameter to 10 cm diameter. As discussed previously, and shown in Figure 7, a smaller float will allow less hydrostatic force to accumulate. This is magnified when the sail area for wind loading is calculated. Under these conditions, some overtopping of the baffle will occur, but it should be remembered the FDB purpose is to divert wastewater, not provide absolute containment.

Intermediate Anchoring. Originally, the FDB was anchored on one side to driven piles spaced at 60 m intervals. These were also the point where 60 m sections of FDB were mechanically attached. The corrected design employed two piles on 60 m centers and the baffle was positioned between the piles. This arrangement allowed tensile strength to be transferred to the posts on an intermediate basis while not subjecting the geomembrane to any tear or peel forces as had been present in the first design. Figure 12 is a photograph of the baffle replacement and shows the intermediate anchoring.

Figure 12. FDB Replacement in Municipal Wastewater Impoundment

CONCLUSIONS

Through a combination of design modifications, a high tensile load diversion baffle was provided for a municipal wastewater impoundment application. The FDB was composed of a reinforced Ethylene Co-Polymer Alloy Geomembrane (XR-5) with a 0.22 Kg/sq m (6.5 ounce per square yard) polyester base fabric which provided Yield Tensile Strengths of approximately 90 Kg/cm (500 lb/in) and hydrostatic resistance of over 35 Kg/sq cm (500 psi), with virtually no elongation. Primary reinforcing and intermediate load bearing connections were provided. While the exact mechanisms and mechanics of the original failure are not known, the factors discussed herein were, at a minimum, contributors.

REFERENCES

Bio Separator Diversion Baffle Specifications, Therma Fab Inc., Lexington, SC, 1992.

Jones, C. P., "Report to Kyzer Associates, Wave Analysis for Pine Bluff, AR Wastewater Treatment Plant", Charleston, SC, September 1991.

Technical Data and Specifications, XR-5 Geomembrane, Seaman Corporation, Wooster, OH, 1992.

Evaluation of a Friction/Drainage Structured Geomembrane

I.D. Peggs
I-Corp International Inc., USA

S. Lewis
A/A Manufacturing Inc., USA

P. Riegl
Agru, Austria

ABSTRACT

The components of a structured, high density polyethylene (HDPE) geomembrane consisting of: 1) spikes on the bottom surface that provide frictional resistance; 2) stubs on the top surface that provide drainage; and 3) geotextile bonded to the stubs to provide filtration, are evaluated. Friction angles are compared to a conventional textured geomembrane, and transmissivity values are compared to a conventional geonet.

Transmissivity shows little effect of confining pressure between steel plates at pressures up to 2.40 MPa. A performance test with soil over the geotextile demonstrates the advantages of using a woven monofilament rather than a nonwoven geotextile for filtration purposes.

The shear strength between the structured geomembrane and a clay is significantly higher than that for a conventional textured geomembrane due to a very high apparent adhesion value, despite the former's lower friction angle.

INTRODUCTION

It is economically advantageous to the owners of landfills to increase the steepness of landfill cell side slopes in order to increase available airspace. Various methods of roughening the surfaces of high density polyethylene geomembranes to increase their friction angles with adjacent geosynthetics and soils have been developed in order to stabilize the geomembrane on steeper slopes.

In one method, nitrogen gas is blown onto the surface of the geomembrane just before it exits the extruder die. Another method involves spraying fine HDPE fibers on to the surface of the geomembrane after extrusion. A third method, used to generate structured geomembrane, is to form bottom surface spikes by a profiled calender roll immediately after flat cast extrusion. By using two profiled rolls, different (friction and drainage) structures can be generated on opposite surfaces of the flat cast geomembrane. The flat cast technique allows basic geomembrane thickness to be controlled to ± 1% if required.

A double structured geomembrane with spikes on the underside and a raised, squared grid pattern on the top side, both to provide increased friction, was tested at the Institute for Foundation Engineering and Soil Mechanics (IGB) in Braunschweig, Germany in 1984. The geomembrane was developed for, and successfully used on, 30° slopes at an industrial waste disposal facility in Hamburg, Georgswerder.

Early in 1992, the profile of the top surface structure was changed to a pattern of stubs, to provide a synthetic drainage structure - the equivalent of a built-in geonet.

With this structuring approach, the filtration geotextile may be thermally-bonded to the drainage structure to provide a single geocomposite that has all the required characteristics of a single geosynthetic lining system: high shear strength with subgrade soil, and filtration and drainage of leachate or leakage liquids. Such a geocomposite lining system can be deployed in one action as opposed to the three deployment activities required for geomembrane, geonet, and geotextile, or the two activities if a geonet/geotextile composite is used.

In mid-1992, a double-structured, filtration/drainage geomembrane was in the development stages, but was not then available for testing. However, geomembrane containing the two structures separately was available and is the subject of this testing program.

SCOPE OF WORK

The results of a testing program to assess the effects of the structures on the friction angle, transmissivity, and uniaxial tensile strength of the geomembrane are described. The performance of this new geomembrane is compared to the performance of conventional textured geomembrane and geonet.

STRUCTURED GEOMEMBRANE

The profile of the initial European structured friction geomembrane is shown in Figure 1. The spikes are cone-shaped with a height of 6 mm, a base diameter of 5 mm, and a square spacing (parallel to roll and cross-roll directions) of 25 mm.

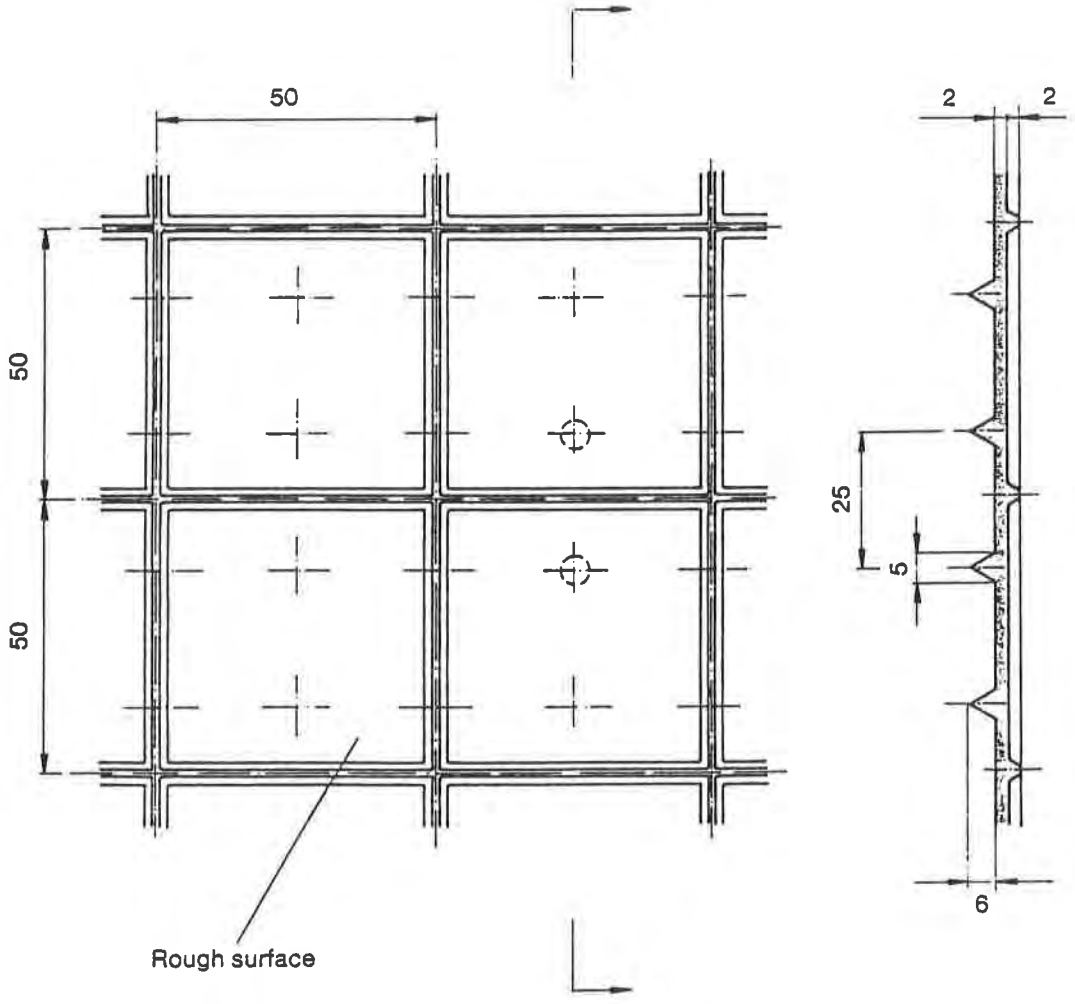

Figure 1. Profile of European friction/friction structured geomembrane.

This material has been successfully installed on 30° slopes in Laakirchen, Austria and on 42° slopes at the Vereinigten Ville project in Germany.

In 1991 and 1992, the friction structure profile was modified, as shown in Figure 2, to place the spikes at an angle of 18° to the roll direction, thereby preventing each spike from following in the furrow of the preceding one should slippage occur.

The drainage structure shown in Figure 3 was added to the geomembrane after two prototype structures were investigated. Figure 4 shows a prototype drainage geomembrane with a nonwoven geotextile bonded to it.

TEST PROCEDURES

Uniaxial tensile strength and elongation. Tests on geomembranes incorporating the spike and stub structures separately were performed according to ASTM methods D638 and D882, using dogbone and strip specimens respectively. Type 4 dogbone specimens were used to determine the tensile parameters of the basic geomembrane without spikes or stubs. Type 1 dogbone specimens were used to assess the effects of a single row of spikes or stubs. Strip specimens were used to assess the effects of two rows of drainage stubs, and, for comparative purposes, to assess a single row of friction spikes.

Transmissivity. The tests were performed according to the procedure of the American Society of Testing and Materials (ASTM) Method D4716, "Test for Constant Head Hydraulic Transmissivity (In-Plane Flow) of Geotextiles and Geotextile Related Products", using 2 mm thick geomembrane.

Index tests were performed as follows:

- Drainage geomembrane between steel plates at pressures between 0.96 and 2.40 MPa.
- Poly-Net PN-3000 geonet between steel plates at pressures between 0.24 and 2.40 MPa.

In order to assess the extent of intrusion of the geotextile filter between the drainage profile stubs, performance tests were done on the following model lining systems:

- Drainage geomembrane covered by nonwoven geotextile (Trevira 1125) and sand at pressures between 0.24 and 2.40 MPa. The geotextile was not bonded to the geomembrane.
- Poly-Net PN-3000 geonet covered by nonwoven geotextile (Trevira 1125) and sand at pressures between 0.24 and 2.40 MPa. The geotextile was not bonded to the geonet in order to provide conditions comparable to those above.
- Drainage geomembrane covered by woven monofilament geotextile (Synthetic Industries' Erosion 1) and sand at pressures between 0.24 and 2.40 MPa. The geotextile was not bonded to the geomembrane.

The woven Erosion 1 geotextile was selected since it had an apparent opening size similar to that of the nonwoven material. It also had relatively high grab tensile and puncture strengths and low grab tensile elongation at break, all of which would contribute to minimizing intrusion.

At each confining pressure, the transmissivity was measured at hydraulic gradients of 0.25, 0.50, and 1.00.

In order to prevent sand being washed into the inlet side of the 30 cm x 30 cm specimens, the sand was contained in a flexible polyethylene bag. Due allowance was made in the pressure and hydraulic head calculations for the reduction in effective length of the specimen caused by the rounding effect at the ends of the bag.

Direct Shear. Friction angle tests were performed according to the procedure of ASTM draft standard test method D35.01.81.07, "Determination of the Coefficient of Soil and

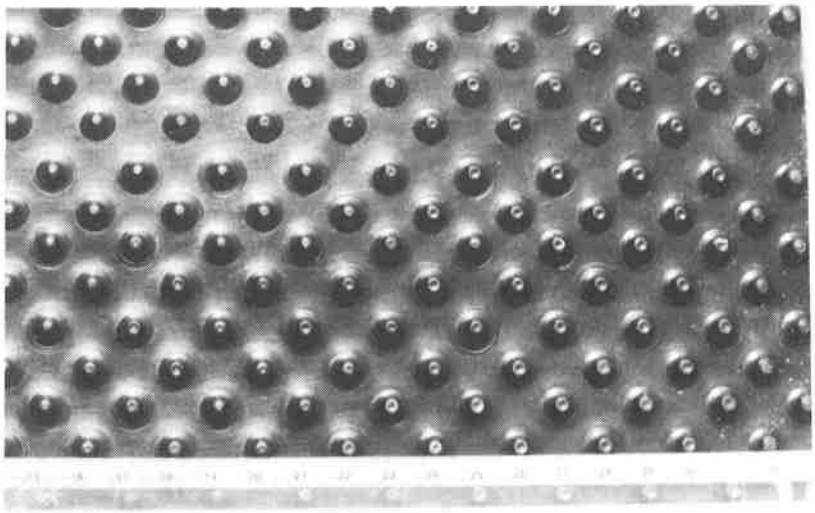

Figure 2. Friction structured (spikes) geomembrane used in test program.

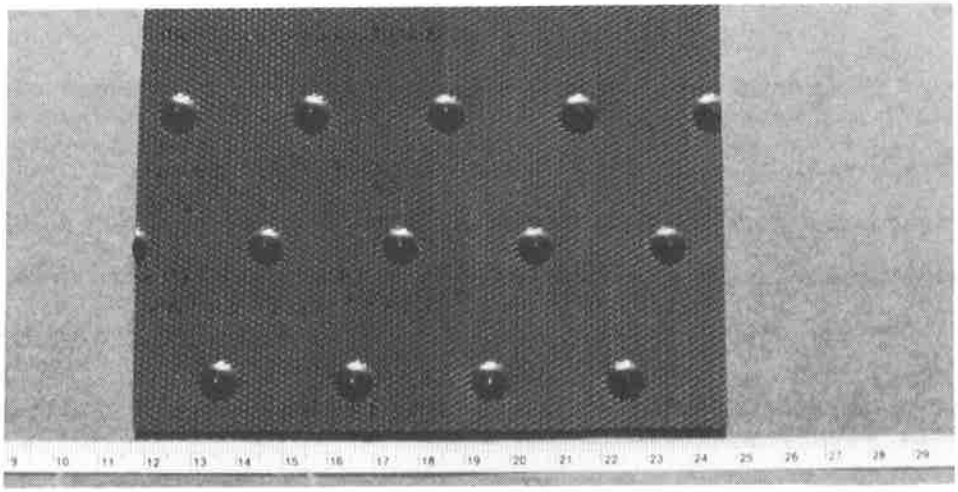

Figure 3. Drainage structured (stubs) geomembrane used in test program.

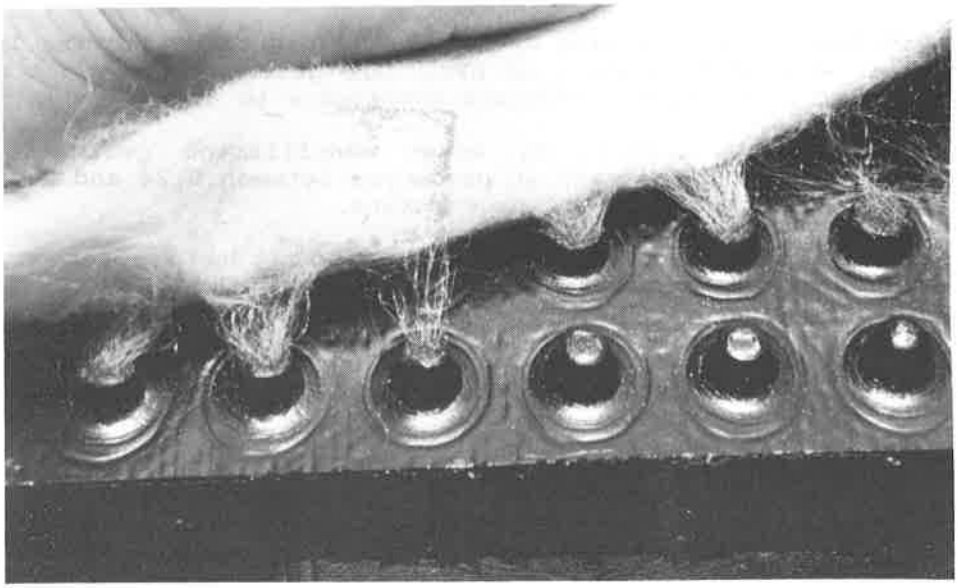

Figure 4. Geotextile filter bonded to drainage geomembrane. Prototype sample.

Geosynthetic or Geosynthetic and Geosynthetic Friction by the Direct Shear Method", on the following interfaces:

- Friction geomembrane (spikes) against Ottawa sand, a glacial till, and a lean Gulf clay.
- Drainage geomembrane (stubs) against the same three soils (included for general interest only).
- HDPE textured geomembrane (Gundle HDT, 2 mm thick) against the same three soils.

Tests were performed in a 30 cm x 30 cm shear box at confining pressures of 0.24, 0.48 and 0.72 MPa.

The geomembrane was placed (structure upward) with the smooth surface on a bed of compacted concrete sand. The test soils were placed on top of the geomembrane structure to a depth of approximately 75 mm and were compacted to 95% of maximum dry unit weight, at a moisture content 2 percentage points wet of optimum, as determined by ASTM D698. The top section of the shear box containing the soil was moved on top of the restrained geomembrane.

TEST RESULTS

Uniaxial Tensile Tests. The values of yield stress, break stress, and break elongation are summarized in Table 1. There is no consistent reduction in uniaxial tensile strength or elongation properties at yield or break due to the presence of the spikes or the stubs.

Table 1. Uniaxial Tensile Test Results

SAMPLE	SPECIMEN	YIELD Stress (MPa)	BREAK Stress (MPa)	BREAK Elongation (%)
Drainage sheet	D638 Type 4	18.0	16.6	452
Drainage sheet 1 row stubs	D638 Type 1	17.8	21.3	813
Drainage sheet 2 rows stubs	D882	18.6	16.2	221
Friction sheet	D638 Type 4	18.9	15.8	436
Friction sheet 1 row spikes	D638 Type 1	16.9	14.7	348
Friction sheet 1 row spikes	D882	20.5	22.6	520

Similar results (Taprogge) were also generated on the original friction/friction structured geomembrane at the IGB. They also performed multiaxial burst testing on 1 m diameter specimens of both unseamed and seamed specimens. Both types of specimens failed at strains exceeding 19% without significant stress concentrations being caused by the structures. Conventional textured HDPE geomembrane ruptures at strains of approximately 20% in the same test.

Transmissivity. The index (between steel plates) transmissivity test results generated during this test program and during a previous test program on a slightly different structure profile are shown in Figure 5. The previous tests showed no significant differences in transmissivity at confining pressures up to 0.96 MPa. There is good consistency between the two sets of tests and very little effect of confining pressure up to 2.40 MPa on the transmissivity of the structured geomembrane.

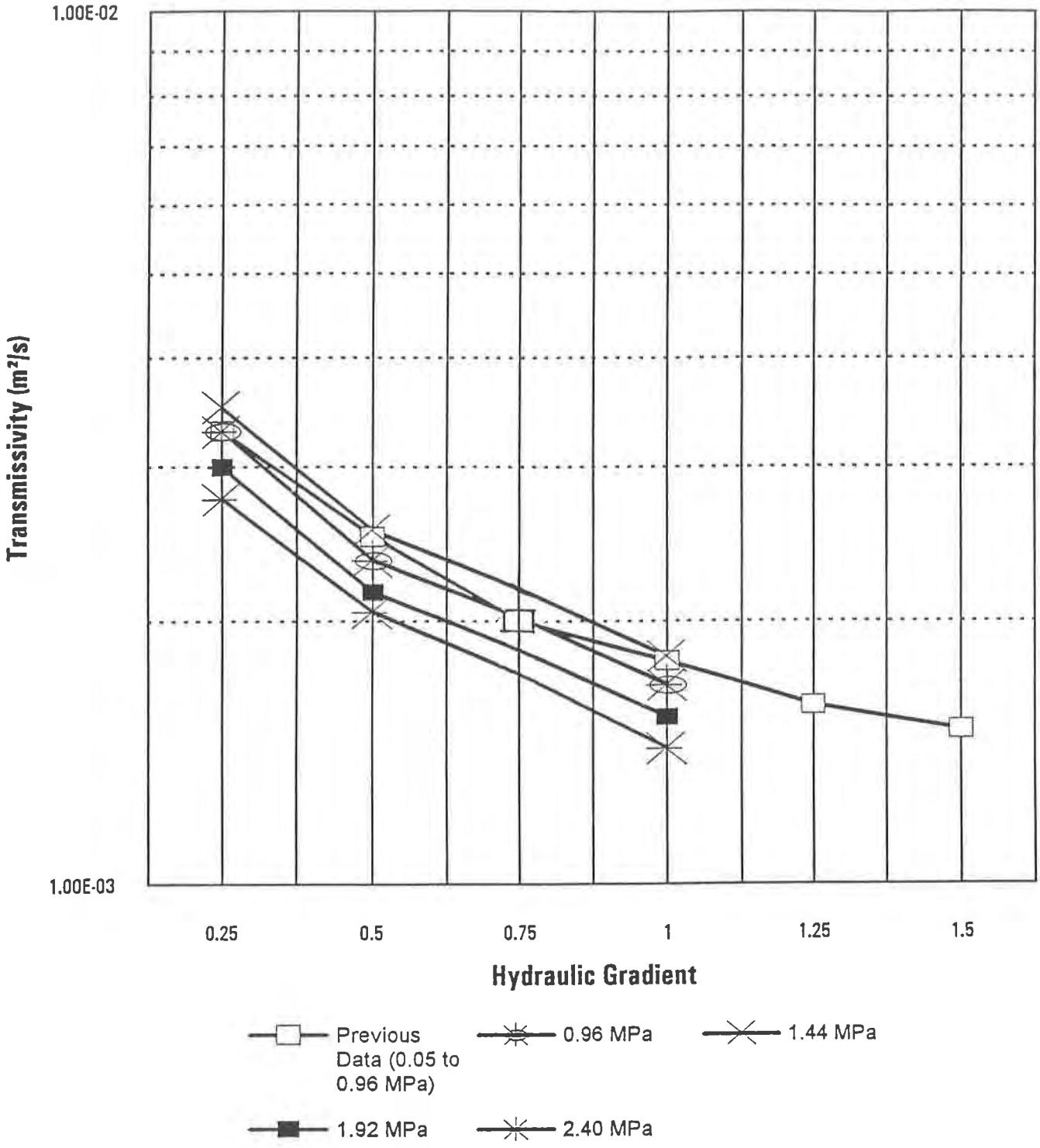

Figure 5. Index transmissivity test results on drainage geomembrane.

Figure 6 shows a comparison between the drainage geomembrane and the conventional geonet. The drainage geomembrane is a more rigid structure at higher confining pressures, having a transmissivity that is a factor of 3 higher than the geonet at 2.40 MPa. At lower pressures, up to 0.96 MPa, the two products have essentially the same transmissivity values.

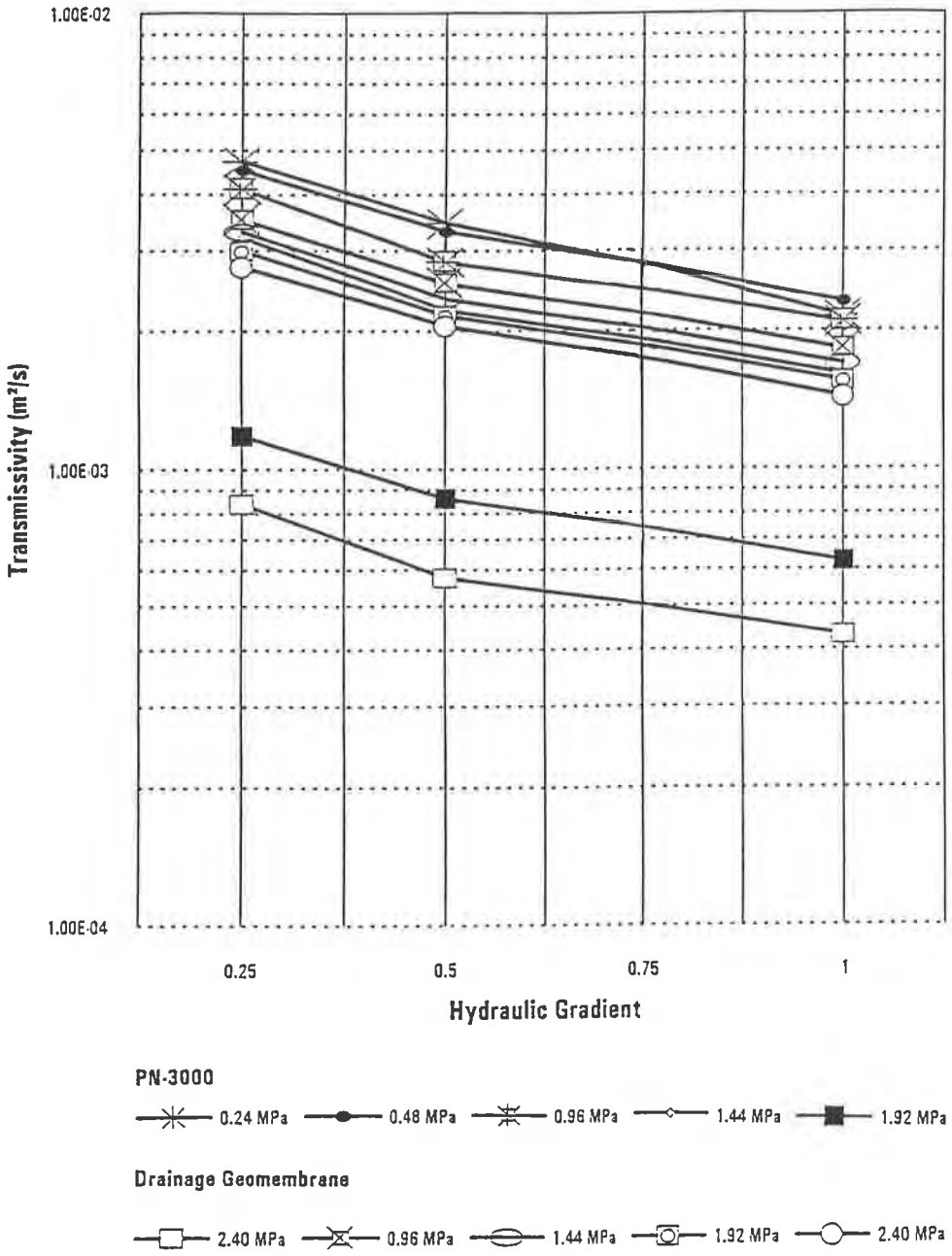

Figure 6. Index transmissivity of drainage geomembrane and PN3000 geonet.

The performance test results, summarized in Figure 7, show that significant geotextile intrusion occurs in both products at pressures considerably higher than 0.50 MPa. There is more intrusion into the drainage geomembrane. This is not surprising since intrusion can proceed without hindrance down to the surface of the geomembrane. In the geonet, when intrusion reaches halfway to the geomembrane surface, there are transverse geonet strands that inhibit further intrusion.

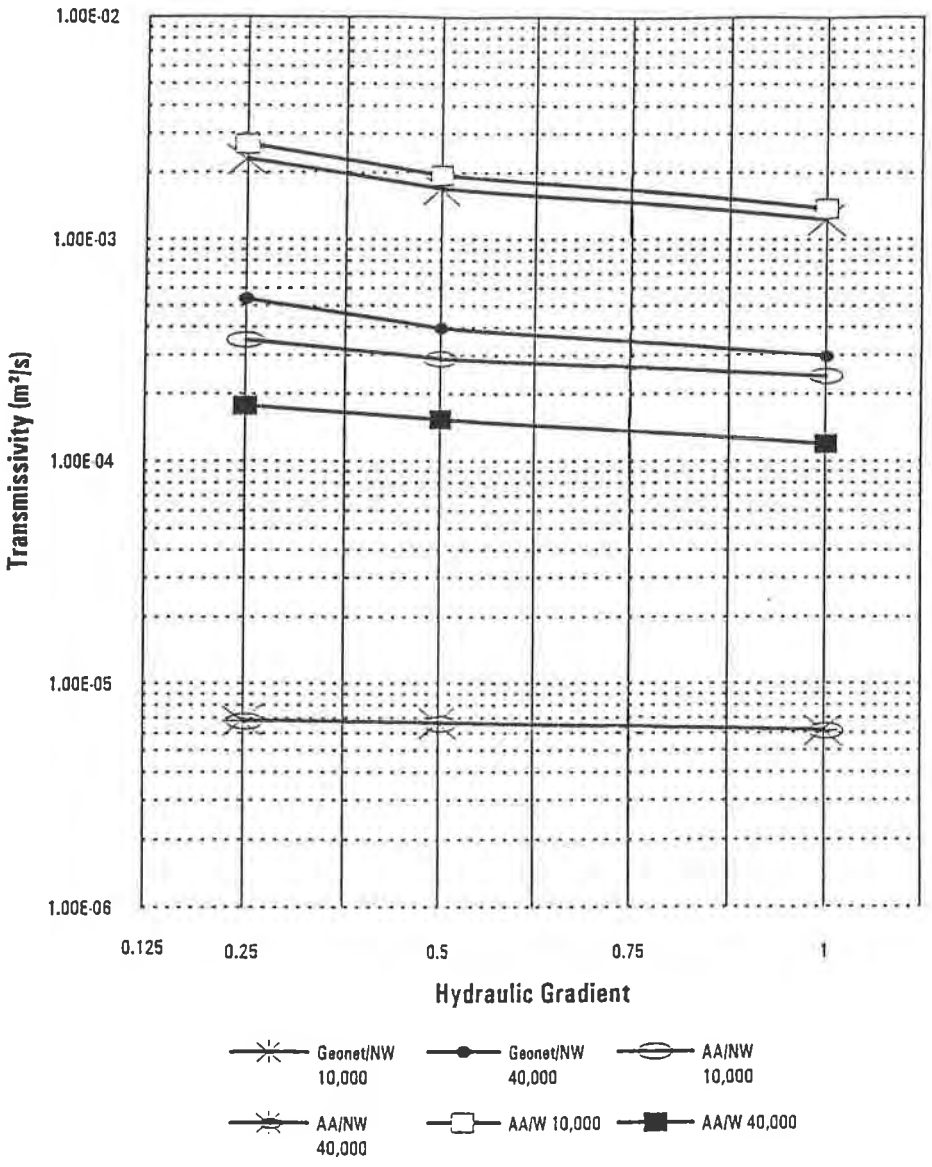

Figure 7. Performance test results.
AA - drainage geomembrane
W - woven geotextile
NW - nonwoven geotextile

As expected, the woven geotextile does not intrude into the drainage geomembrane as much as the nonwoven. Nevertheless, at a confining pressure of just over 1.92 MPa, there is essentially no flow through the drainage geomembrane with either geotextile.

Direct Shear. Table 2 summarizes the peak and residual friction angles and the peak and residual adhesion values for all combinations of the three materials against the three soils.

Table 2. Summary of Direct Shear Results on Friction, Drainage, and Textured Geomembranes [Friction Angle (°)/Adhesion (kPa)]

SOIL	FRICTION GEOMEMBRANE	DRAINAGE GEOMEMBRANE	TEXTURED GEOMEMBRANE
Ottawa Sand			
- Peak	26/16.3	26/ 7.9	31/0
- Residual	25/19.9	24/17.5	29/10.8
Glacial Till			
- Peak	25/10.8	26/ 8.2	31/17.0
- Residual	20/33.8	21/24.5	31/17.0
Clay			
- Peak	5/90.2	4/85.0	11/ 7.2
- Residual	4/74.6	4/56.9	8/ 5.3

The friction angles of the two structured geomembranes against the Ottawa sand and the glacial till (approximately 26°) are essentially the same as the values typically recorded for smooth geomembrane against the same soils. In comparison, the textured geomembrane against the same soils shows friction angles (31°) essentially the same as those for the soils themselves, confirming that the surface texture has transferred the shear plane from the geomembrane/soil interface into the soil itself.

Similarly, the friction angles of the two structured geomembranes against the lean clay is lower than that for the textured geomembrane against the clay. However, with the high value of adhesion the shear stresses required to mobilize the interfaces of the structured geomembranes are significantly higher than those for the textured geomembrane at all confining pressures below 0.81 MPa. It is, therefore, apparent that despite the lower friction angle, the structured geomembranes will adhere to steeper slopes, or will be more stable on the same slopes, when compared to the textured geomembrane. Such behavior raises the possibility of defining an "apparent" friction angle.

Figure 8 shows the extrapolated failure envelopes of the friction (spiked) and textured geomembranes against lean clay. The slope of a line between the origin and any point on the failure envelopes will be the apparent friction angle of that interface at the point's confining pressure. For instance, at a normal pressure of 0.20 MPa, the apparent friction angle for the friction geomembrane is 26°, while for textured geomembrane it is 12°. Table 3 lists additional calculated values of the apparent friction angle. The apparent friction angles of the friction geomembrane are considerably higher than those for the textured geomembrane, the difference decreasing as the confining pressure increases to 0.81 MPa.

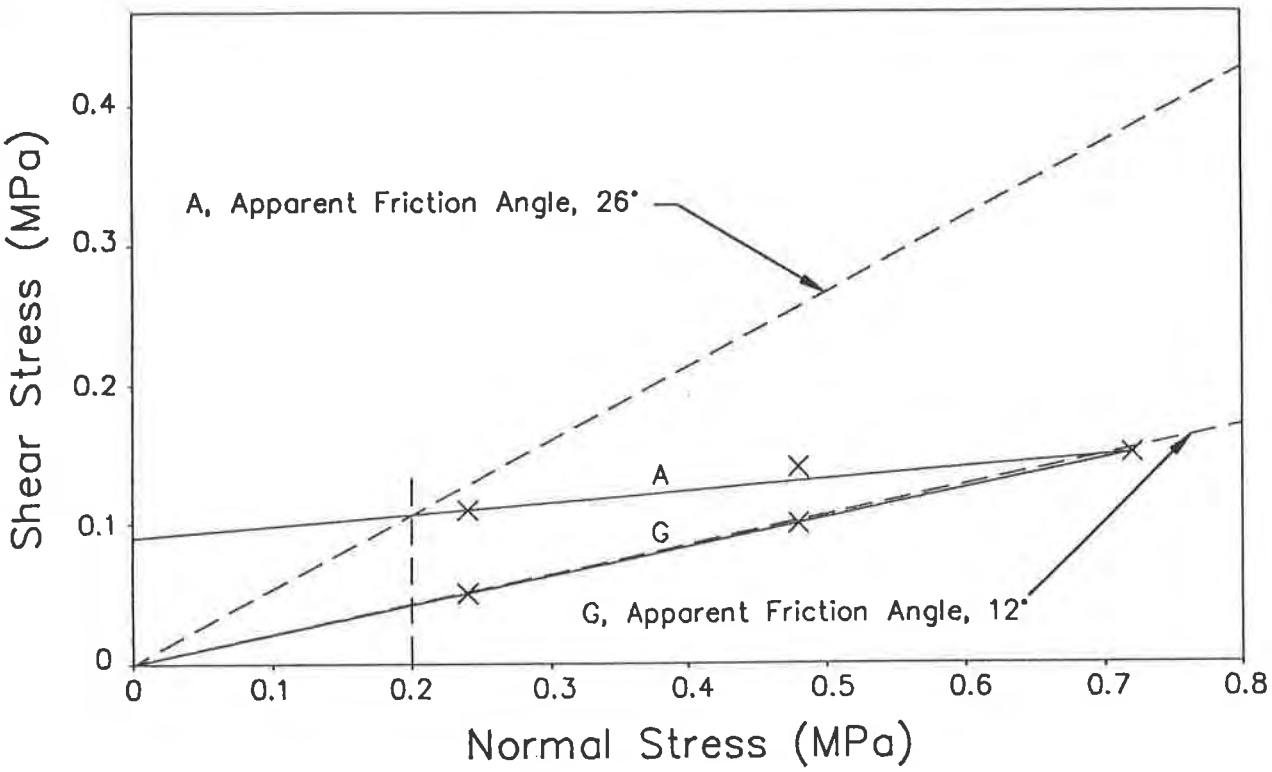

Figure 8. Shear failure envelopes for friction geomembrane (A) and textured geomembrane (G) against lean clay. "Apparent" friction angles shown at 0.20 MPa.

Table 3. "Apparent" Friction Angles (Degrees)

CONFINING PRESSURE (MPa)	FRICTION GEOMEMBRANE	TEXTURED GEOMEMBRANE
0.20	26	12
0.40	16	11
0.60	13	10
0.80	10	10

DISCUSSION

Uniaxial Tensile Properties. The uniaxial tensile test data show that there is very little detrimental effect of the structural elements (spikes and stubs) on the short-term mechanical properties of the geomembrane. It would, therefore, be expected that the biaxial tensile properties (those used in design) should also not be affected by the structural profiles, as shown in other studies (Taprogge).

To assure the long-term mechanical durability of the structured geomembranes, it will be necessary to perform stress rupture tests on the basic geomembrane and to determine if there are any residual stresses or extreme geometrical notch profiles at the roots of the structural elements. A preliminary microscopy study showed there was no extreme residual stress present at the roots of the spikes. In Europe, the structured geomembrane is made with Hoechst's Hostalen GM5040 T12 HDPE resin, known to have high stress cracking resistance. The structures were specifically designed with no sharp notches that might act as stress concentrators.

Transmissivity. The transmissivity data indicate that while there is some intrusion of geotextile into the drainage geomembrane at lower confining pressure, significant geotextile intrusion does not start to occur until high confining pressures of about 1.92 MPa (equivalent to about 160 m of waste), the minimum transmissivity (3×10^{-5} m^2/s) allowable within EPA's Final Rule for Liners and Leak Detection Systems (1992) is not reached until the same confining pressures (2.0 MPa) are reached.

EPA's minimum requirement for transmissivity for liquid impoundment synthetic drainage media is 3×10^{-4} m^2/s, but a geotextile filter would not be required in such an application, thus avoiding the concerns about intrusion. If a thick, rigid primary geomembrane were placed directly on top of the secondary drainage structured geomembrane, the performance of the drainage layer under normal pressure would be closer to that shown in Figure 5. It would, however, be desirable, in addition, to generate data to confirm the creep component of geotextile intrusion and the related performance of a liquid impoundment primary geomembrane. The woven geotextile will provide better creep performance than the nonwoven geotextile.

Direct Shear. The direct shear testing provided the most interesting results. There are two basic reasons why the friction geomembrane does not quite have the friction angle that the textured geomembrane has. The first is that there are considerable surface areas of geomembrane that are not roughened and, consequently, behave essentially as smooth geomembrane. Even the file-finished surface on the friction geomembrane effectively behaves as smooth material in the sand and glacial till soils. If this file-finished profile were made somewhat coarser, there might be an improvement in friction angle. Secondly, some confining pressure on the geomembrane surface is lost at the base of the spikes and stubs (on the drainage geomembrane) due to the inability to properly compact the soils in these localized regions.

There are some differences in adhesion between the textured and structured geomembranes in the sand and glacial till, the structured geomembranes being slightly higher, but additional data are needed to assess the significance of differences between the two structured profiles. However, the higher adhesion and apparent friction angles of the structured products in the clay are quite significant.

The increased adhesion is probably a function of both the vertical component of the surface area of the spike and stub profiles and the fact that the shear plane is displaced further away from the surface of the soil than for the textured geomembrane; the shear stress within the body of the soil is somewhat higher than it is near the surface. With further refinement of the height, shape, and distribution of the structures, it is possible that the adhesion and apparent friction angles could be further increased. The shear plane of the present friction geomembrane is shown schematically in Figure 9a as the accumulation of many shear zones initiated by the tip of each spike. If the spike heights and distribution can be varied in a controlled way, it may be possible to initiate overlapping shear zones (just prior to peak shear failure) with a total shear area larger than the geomembrane/soil interface shear area, as shown in Figure 9b. This possibility, of increasing the apparent friction angle, will be investigated further.

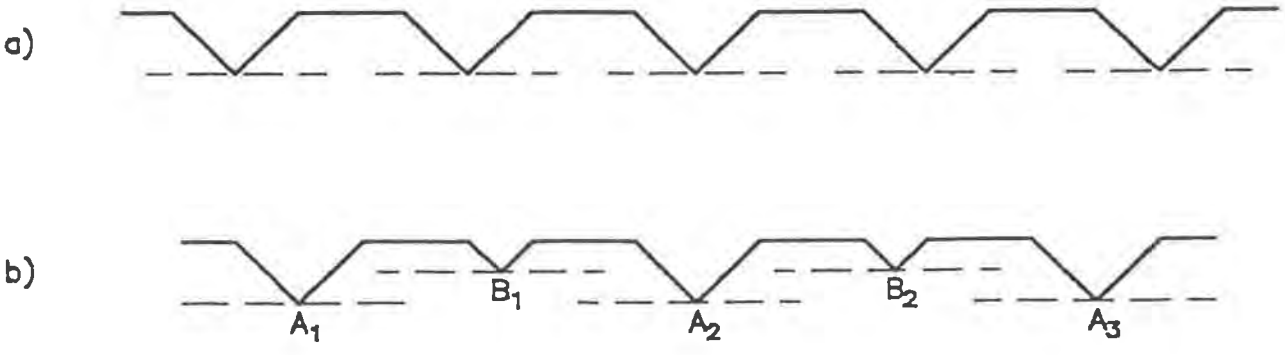

Figure 9. a) Shear plane aligned with tips of single set of spikes.
b) Overlapping, shear planes with two sets of spikes.

It is important that designers and engineers remain mindful of the term "apparent", since it is not yet clear that adhesion at zero normal stress actually exists. Whether the friction angle curve continues in a straight line to intercept the shear stress axis at a finite value of adhesion, or whether the slope of the curve gradually increases at lower normal stresses to pass through the origin, has not yet been experimentally confirmed and published. With appropriate test equipment, there are indications that adhesion does exist in some systems. If there is significant mechanical interlocking of the geomembrane in the clay, it would seem logical to expect some adhesion.

CONCLUSIONS

A double-structured HDPE geomembrane consisting of spikes to provide friction resistance and stubs to provide drainage has the following characteristics:

- Potential for rapid deployment in the field.
- Excellent transmissivity between rigid planar components at high normal pressures.
- High apparent friction angles with clay and, probably, other cohesive soils.
- Higher transmissivity with a woven geotextile filter than with a nonwoven geotextile at higher normal pressures.

When used as a drainage medium under low cohesion soils, due allowance should be made for intrusion of the filtration geotextile at the higher normal pressures, as it should with all synthetic drainage components.

Further optimization of the friction and drainage performance of these types of geocomposites should be possible.

REFERENCES

Taprogge, R., "AGRU Waterproof Sheeting Structure Made of Polyethylene". Expert opinion, Hamburg, Germany. (From AGRU, Bad-Hall, Austria).

U.S. Environmental Protection Agency (USEPA)(Jan/1992). "Final Rule for Liners and Leak Detection Systems for Hazardous Waste Landfill Disposal Units". Federal Register. p.3468.

White-Surfaced HDPE Geomembranes: Assessing Their Significance to Liner Design and Installation

M. Cadwallader
Gundle Lining Systems Inc., USA

M. Cranston
Chemical Waste Management, USA

I.D. Peggs
I-Corp International Inc., USA

ABSTRACT

A significant temperature reduction under typical weather conditions was found to occur for a white-surfaced HDPE geomembrane compared to a standard black-surfaced geomembrane. Under clear skies at an ambient air temperature of approximately 30°C, geomembrane temperature was reduced as much as 24°C compared with black sheet. Effects of temperature reduction in terms of expansion/contraction of geomembranes, subgrade soil desiccation, and long term aging are reviewed and discussed. Identical installation damage in both white-surfaced and black geomembrane was observed and photographed in order to assess relative inspection visibility.

INTRODUCTION

White-surfaced geomembranes have been used over the last few years in a number of different applications. Because of the two-color scheme, these materials have become attractive to geotechnical and geosynthetics engineers for the ease of detecting damage during installation, as well as for subgrade desiccation protection and wrinkle reduction due to reduced geomembrane temperatures resulting from the light colored surface. With their increasing application in the liner industry has come a need to clearly and scientifically document their performance and behavior.

SOLAR ENERGY ABSORPTION STUDY

The degree of solar thermal energy absorption is one distinct difference between standard black geomembranes and white-surfaced geomembranes, a white surface being more reflective than a black surface. In order to measure the degree of solar thermal energy absorption, temperature sensors were embedded in black geomembrane and in white-surfaced geomembrane. Textured black geomembrane was also compared with smooth black geomembrane in this thermal energy absorption study.

Specimens and Instrumentation Each specimen was cut about 60 cm (2 ft) or 30 cm (1 ft) square. Uninsulated Type K (chromel/alumel) thermocouples manufactured from 25 μm (1 mil) diameter wire were attached to top and bottom surfaces of each specimen. The beads on the thermocouples were approximately 3 μm diameter and, are, therefore, capable of measuring the true temperature of the surface layer without significantly affecting the surface temperature. Conventional surface-contact thermocouple probes would affect the temperature being measured and could not respond quickly to changes in surface temperature.

Prior to assembly, all the thermocouples were placed in iced water for calibration. They all read to within 0.5°C of one another.

Each thermocouple bead was fixed in place by heating it, and the adjacent geomembrane surface, with the 1 mm diameter spherical tip of a pointed soldering iron. A very light pressure and quick contact were made to ensure that the thermocouple bead was not buried in the geomembrane, but remained in the surface layer. On the textured geomembrane, the thermocouple bead was placed on a raised part of the surface. The final assembly was very delicate and needed extremely careful handling to prevent the thermocouples from breaking. The specimens were placed on a 50 mm thick layer of sand and exposed to sunlight. The edges of the specimens were weighted to prevent convection of air between the specimen and the sand. The temperature of the sand under one specimen was also measured.

Results An abbreviated summary of measured reference and geomembrane temperatures under a clear sky follows. Two specimens of different degrees of "whiteness" were tested:

Equilibrium Conditions (°C)

Air	32.0	33.0	32.6	32.0	30.3	30.6	32.0
Sand	34.2	34.8	35.7	36.2	32.6	36.0	38.0
Black smooth, top	65.4	68.0	66.6	67.7	57.8	64.6	67.0
Black textured, top	62.4	65.6	64.2	66.4	55.1	60.6	61.8
White/grey smooth, top	48.1	48.7	48.9	49.7	42.6	47.1	50.0
White smooth, top	43.4	43.3	44.3	44.0	39.4	41.8	43.8

The bottom surface temperatures were consistently about 2°C lower than the top surface temperatures.

In summary, at an ambient temperature of approximately 30°C, the geomembrane temperatures were as follows:

Smooth black geomembrane, top	67°C	
Textured black geomembrane, top	64°C	(-3°C)
White/grey geomembrane, top	49°C	(-18°C)
White geomembrane, top	43°C	(-24°C)

The black textured geomembrane had a surface temperature that was lower than the smooth black geomembrane surface temperature, by about 3°C. This lends credence to the many comments from field installation

crews and CQA monitors that textured HDPE geomembrane is cooler than smooth geomembrane and does not wrinkle as much.

Depending on the degree of "whiteness", the non-black smooth geomembrane surface temperatures were up to 24°C (43°F) lower than smooth black geomembrane surface temperatures.

Temperature differences due to varying degrees of solar thermal absorption have a number of significant, geotechnical benefits and geosynthetic durability consequences as discussed below.

GEOMEMBRANE EXPANSION/CONTRACTION CONSIDERATIONS

In northern desert environments, where black geomembrane temperatures can be near 80°C (170°F) in the summer and -30°C (-22°F) in the winter, there can obviously be a change in geomembrane temperature of 100°C (180°F) or more. In more temperate climates, the change can easily be 50 to 75°C (90-135°F). White-surfaced geomembrane will reduce these temperature swings by 25 to 50%.

Thermal expansion/contraction makes it necessary to consider the amount of waviness (compensation) that must be built into, or kept out of, geomembrane liners when they are installed. This is necessary to prevent excessive contraction stresses at low temperatures, and to prevent excessive wrinkling when a soil cover has to be placed on the liner at a higher temperature than at installation. Temperature reduction through reflection of solar energy can result in easier more effective geomembrane installation, with a final seamed geomembrane less prone to expansion/contraction stresses, and, therefore, less prone to potential failures due to stress cracking.

Using the temperatures obtained in the above study and a low temperature of -18°C (0°F), the calculated contraction of a white-surfaced geomembrane will be 39% less than the contraction of a black geomembrane.

GEOMEMBRANE AGING PHENOMENA

Advantages of maintaining a lower geomembrane temperature are also evident in long term aging tests. Exposing any material to a high temperature is one of the most effective ways of promoting general degradation.

Increasing temperature accelerates both stress crack phenomena and oxidative degradation. Chan and Williams (1983) have indicated that stress crack growth rates in HDPE increase 40% for every degree (Celsius) rise in temperature. Klemchuck and Horng (1985) have found measurable rates of oxidation at only 40°C (72°F). Thermal stresses in geomembranes have been surveyed and oxidative degradation measured by Cadwallader and Metzger (1987), revealing considerably shortened oxidative stability in polyethylene with increasing temperature. In consideration of improved long term aging, Halse et al (1990) surveyed various methods of geomembrane temperature reduction under solar

exposure including soil covers, geotextile covers, and white painted surfaces.

The HDPE gas pipe industry presently uses a lifetime prediction technique based on the stress rupture performance. The prediction method, ISO TC 138/WG5, involves measuring the stress rupture performance of the pipe material at two elevated temperatures and then projecting such curves to 20°C. Figure 1 is a family of such curves for polyethylene pipe. The projected 20°C regression line is based on the Rate Process Method (RPM) mathematical model introduced by Bragaw, (1980):

$$\log t = A + B/T + C \log p \qquad (1)$$

where t = time to failure
p = applied stress
T = temperature
A, B, and C are constants

The RPM incorporates three variables (time, temperature, and stress) into a mathematical model that describes the stress rupture curves. With stress rupture data obtained at three elevated temperatures, the three unknown constants, A, B, and C, can be determined. Subsequently, the complete stress rupture curve at 20% can be plotted, with the exception that the actual transition time and stress are not accurately known.

The experimental technique used to generate stress rupture curves in pipes has been extended to geomembranes. A procedure described in the Geosynthetic Research Institute standard GRI.GM5 (1992) uses a single face notched specimen in a constant tensile load test to determine the stress rupture behavior of geomembranes and seams in geomembranes. These tests are presently done at elevated temperatures but in a surface-active agent used to promote stress cracking which makes actual field lifetime predictions impossible to make. However, Kanninen et al (1993) (this conference) have reported initial work using fracture mechanics theory coupled with time/temperature shifting methods (developed in pipe studies) that should enable geomembrane lifetime predictions to be made after crack growth testing at only one elevated temperature.

It is illuminating to note in Figure 1 that under a sustained stress of 2400 kPa (350 psi) at 40°C, the polyethylene pipe lasts fifty years. If the temperature is increased to 60°C, the lifetime is reduced to 30,000 hours or 3.4 years. As seen previously, when an exposed black geomembrane is 60°C, a white-surfaced geomembrane will only be 40°C.

The temperatures of exposed liners can be very high due to absorption of solar energy. Temperatures of 80°C (170°F) have been noted for black synthetic liners. It follows, therefore, that surface temperature moderation will promote lengthened lifetimes of exposed stressed geomembranes.

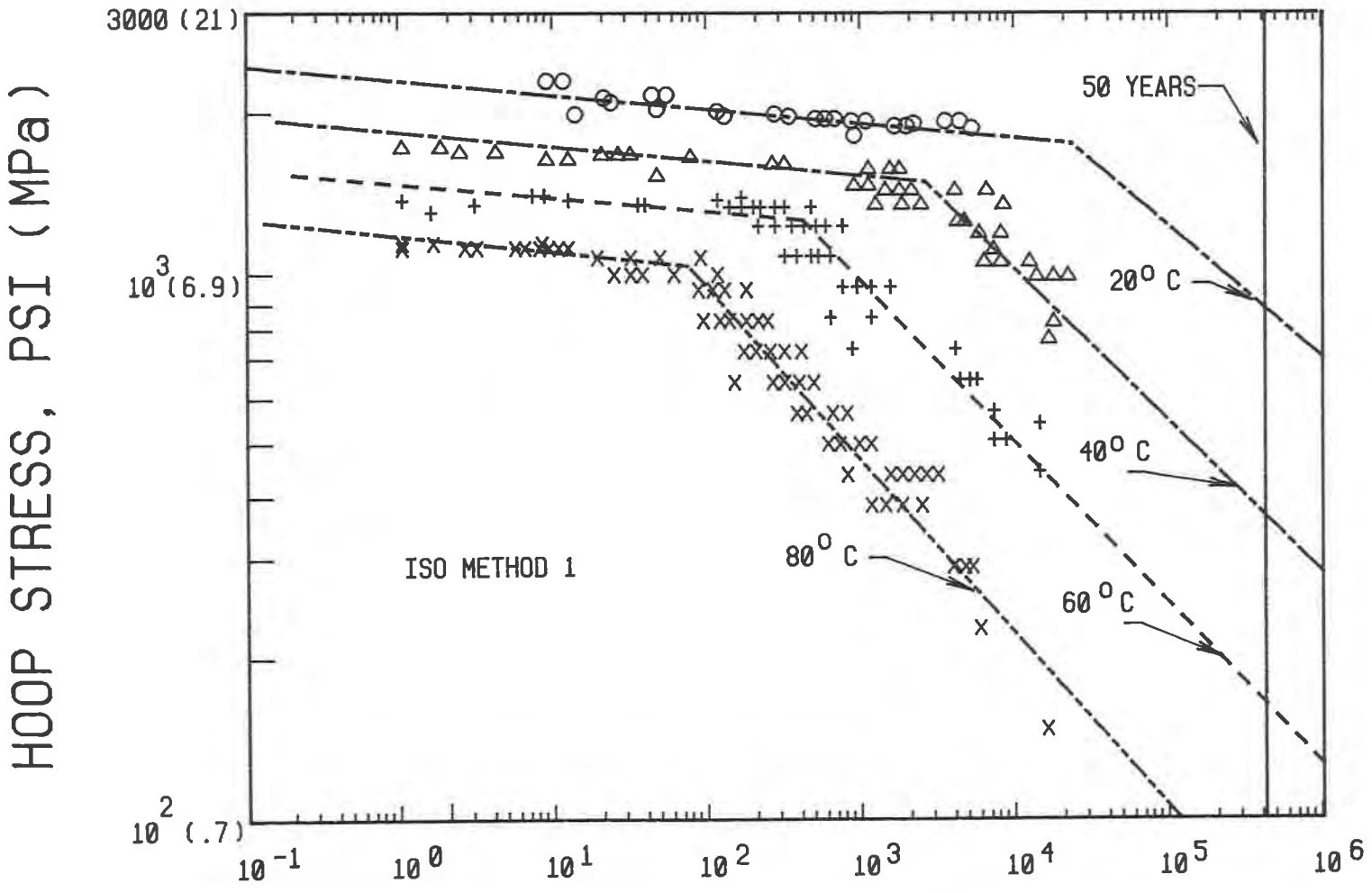

PE PIPE STRESS RUPTURE CURVES

FIGURE 1

FEB - 84

It should be noted that carbon black (used in black geomembranes) is still regarded as the best ultraviolet (UV) radiation stabilizer, with a long history of experience under solar exposure. Hindered amine light stabilizers (HALS) for nonblack applications are also proving to be excellent UV stabilizers for polyolefins, though perhaps not quite as effective as carbon black. The pertinent consideration for aging of geomembranes under sunlight is thus a comparison of the effectiveness of UV protection by carbon black or HALS, and the reduction in geomembrane temperature generated by switching from carbon black to HALS in a reflective surface. The answer varies depending on incident amounts of ultraviolet light and solar thermal energy, and on quality of UV stabilization. A white surface reflects incident UV as well as heat, therefore necessitating less UV stabilization. With good UV stabilization, temperature (especially in conjunction with contraction stresses) becomes the life-determining variable for most exposed geomembrane applications.

SUBGRADE DESICCATION

Geomembranes which reflect heat and maintain a lower surface temperature should retard subgrade desiccation.

Basnett & Brungard (1992) have reported severe desiccation of a clay subgrade under a geomembrane-lined landfill slope. Clay along the cell bottom was found to be adequately moist while clay on the side slopes was heavily desiccated with cracks averaging 10 to 25 mm (.5-1 in.) wide and extending the full depth of the clay layer, i.e., 30 cm (1 ft.). Figure 2 shows subgrade desiccation under the geomembrane.

Because the desiccation extended at least 30-50m (100-165 ft.) back from the edge of the HDPE geomembrane cover, contact with air is assumed not to be necessary in order to effect subgrade desiccation. The following mechanism of desiccation under the geomembrane was therefore proposed. It was reported that liquid pooling under the liner at the toe of the landfill slopes had been observed. Daily summertime surface temperatures of 66°C (150°F) or greater caused the geomembrane to wrinkle and, therefore, to form air pockets between the HDPE and subgrade clay surface. The hot air in the pocket would, therefore, become humid due to moisture leaving the clay under the temperature gradient. When the liner cooled at night, the relative humidity of the trapped air would increase to 100%, condensation would form on the underside of the geomembrane and surface of the clay, and drain downslope to the toe. Further heating and cooling cycles would cause desiccation of the clay from the top of the slope to the bottom of the slope. This proposed mechanism can be expected to occur whenever there are above freezing temperature variations, and the geomembrane has not been pressed into intimate contact with the subgrade clay.

Basnet and Brungard's hypothesis fits data reported by Corser and Cranston (1991) and by Corser, et al (1992). These engineers studied subgrade desiccation under typical liner and cover sections and

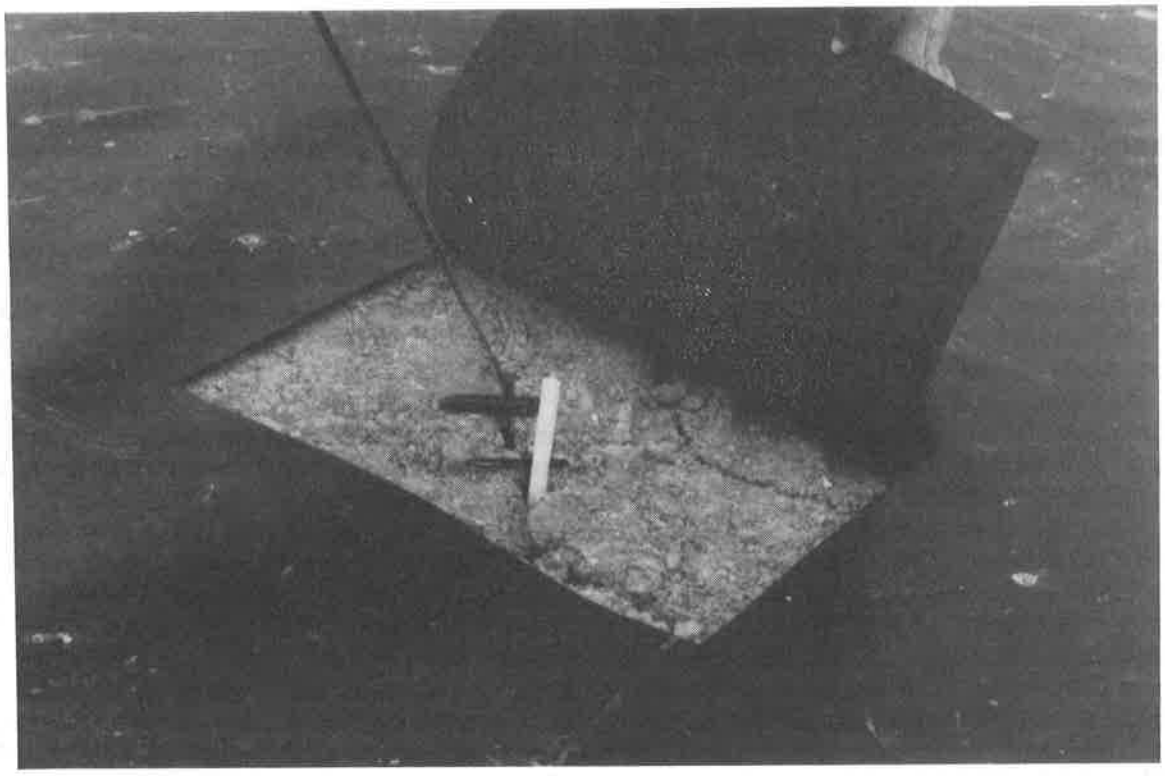

Figure 2. Subgrade Desiccation Under Exposed Geomembrane. Note Condensation On Underside of Membrane (Courtesy of CH2M Hill)

tracked the relationship between the amount of soil desiccation and the soil temperatures and tensions.

CALIFORNIA CLAY DESICCATION STUDY

To investigate the moisture-loss/clay desiccation mechanism, a test fill pad was constructed for the Corser and Cranston study with three feet of compacted clay and included a lower portion with a two percent slope and an upper portion with a slope of 3H:1V. The test fill was subdivided into three sections consisting of: 1) 0.5m (1.5 ft) of vegetative soil cover, 2) 1.5 mm (60 mil) HDPE, and 3) 1.5 mm (60 mil) HDPE with 0.6 m (2 ft) of vegetative soil cover. Instruments installed in the test fill include the following:

- Thermistors - to measure soil temperature fluctuations
- Tensiometers - to measure relative soil suctions

The instruments were installed at various depths throughout the day and vegetative soil cover components of the composite liner/cover systems in both the floor and slope portions of each of the three test sections. Double-ring infiltrometer tests were conducted on two of the test sections to confirm that minimum clay field permeabilities were achieved.

The test fill was constructed in April 1990 at the Chemical Waste Management, Inc. (CWM), Kettleman Hills Facility in Kettleman City, California. The clay material was obtained from a local borrow source and consisted of a high plasticity clay. The instruments were monitored by CWM on a daily basis initially and since on a weekly basis with regular periods of daily monitoring.

In October 1990, May 1991, and December 1992, site inspections of the clay test fill were conducted. In each of the three test sections, one excavation was made on the floor and one on the slope. The materials overlying the clay were removed exposing approximately .5 m x 1.5 m (5 ft x 5 ft) test sections, sketches and photographs taken of the exposed areas and test pits dug for the collection of moisture content samples and pocket penetrometer readings. The field data collected during each inspection was used for correlation with the instrumentation field data collected by CWM.

Desiccation was observed through monitoring the tensiometer probes and confirmed via periodic inspection and laboratory soil moisture content determinations. Tensiometers measure soil suction pressure which decreases as the soils dry out.

Based upon the monitoring and testing conducted in this study, it can be concluded that compacted cover/liner systems can lose moisture content, and desiccation cracks may form even after limited exposure to arid climates.

The moisture loss is suspected to be a result of moisture evaporation caused by hot surface temperatures. In the case of the liner section with only the HDPE over the compacted clay, the moisture is suspected to have collected in air pockets in the areas where the HDPE was not in contact with clay, then either passing through the HDPE as a vapor or running down to lower areas where the HDPE remains in contact with the clay. Soil suction profiles indicated increased soil tension both in the tensiometers near the surface and near the bottom of the clay in the section. Temperature profiles for this section indicated the clay surface undergoes large temperature fluctuations and soil temperatures could be significantly higher than the air temperatures, as much as 11°C (20°F). Surface temperatures in the clay were as high as 46°C (115°F) while air temperatures were approximately 35°C (95°F).

The cover section with only vegetative soil cover over the compacted clay did not perform well during the summer months. Increased soil suctions recorded by the tensiometers near the surface of the clay have indicated drying of the clay. Erratic readings of the vegetative soil cover tensiometers appear to confirm this clay surface moisture loss. Moisture leaving the clay material and passing through the vegetative cover results in drops in the tensiometer readings as the moisture passes by the tensiometer tips and then returns as drier conditions are re-established.

The test section with the best test performance was the section with both an HDPE cover and a vegetative soil cover. The vegetative

soil cover not only acted to insulate the clay from major daily temperature fluctuations but also weighted down the HDPE cover to maintain direct contact with the clay, thereby eliminating air pockets where drying occurs. In addition, the HDPE cover acts as a vapor barrier to reduce the moisture loss migration from the clay component. This section exhibited fairly consistent readings indicating very little change in moisture content both at the top and bottom of the clay layer.

During the visual site inspections, it was determined the cover section with the HDPE cover and vegetative soil cover exhibited the best performance. Only minor hairline cracks were noted in the surface of the clay. The section with the vegetative soil cover over the compacted clay exhibited extensive cracking. In October 1990, the crack widths varied from 25-100 mm (0.1-0.4 in) and depths varied between 25-100 mm (1-4 in). In May 1991, crack depths and widths had not significantly changed, however, by December 1992, the cracking had increased to widths of nearly 25 mm (1 in) and depths over .3 m (1 ft).

The section with an HDPE liner over the compacted clay simulates a typical landfill liner system. Depending on the construction phasing and the rate of fill placement, portions of landfill liner systems could be exposed to direct sunlight and weather conditions similar to this test section. In areas where the HDPE liner remained in contact with the clay, the moisture content of the clay appeared to have increased and in areas where no contact occurred, the clay had dried and cracked. Observed cracks had widths up to 6 mm (0.25 in) and depths up to 76 mm (3 in) when observed in May 1991. With this information and other observations noted during landfill construction and post-construction observations, it may be surmised that this type of liner section, when exposed to arid weather conditions could dry out in some areas and the drying depth may be substantial.

Clay Subgrade Under White-Surfaced Sheet

In February, 1992, a white HDPE liner was installed over the top of the exposed black HDPE liner on the test pad. This material was placed to reflect sunlight and thereby reduce clay surface temperatures and daily temperature fluctuations. Tables 1 and 2 present a representative comparison of some of the thermistor and tensiometer data respectively collected in Section 1 where the HDPE liner was placed over the compacted clay without any vegetative soil cover. The temperature recorded by thermistors and the soil suction pressures recorded by the tensiometers, both set at various depths are shown for similar dates in 1990 before the placement of the white reflective HDPE liner and compared to 1992 dates after the white HDPE liner had been installed.

The preliminary data indicates the temperatures of the compacted clay have been reduced by an average of 7°C (12°F) at all depths in the clay. Temperature decreases of 8-11°C (15°-20°F) were not uncommon near the surface of the clay during the peak of the hot summer period and substantial decreases in daily temperature

CHEMICAL WASTE MANAGEMENT, INC.
KETTLEMAN HILLS FACILITY
CLAY TEST PAD THERMISTOR DATA

BLACK LINER							WHITE REFLECTIVE LINER						
			THERMISTOR DEPTH AND TEMPERATURE (°F)							THERMISTOR DEPTH AND TEMPERATURE (°F)			
DATE	TIME	AMB. AIR TEMP(°F)	3 in.	9 in.	15 in.	27 in.	DATE	TIME	AMB. AIR TEMP(°F)	3 in.	9 in.	16 in.	27 in.
10-Apr-90	16:15	86	64.4	64.4	66.2	68.0							
19-Jun-90	08:13	78	81.9	83.3	85.1	87.4	18-Mar-92	11:41	62	58.1	57.9	57.6	55.8
28-Jun-90	08:15	75	85.5	87.1	89.4	92.1	28-Jun-92	08:20	72	75.4	76.1	77.0	77.2
2-Jul-90	08:17	80	86.5	88.2	90.3	92.8	2-Jul-92	07:40	78	75.0	75.6	76.1	76.1
10-Jul-90	09:20	87	87.6	89.2	91.0	94.1	8-Jul-92	10:17	85	75.0	75.6	75.9	77.0
13-Jul-90	09:19	90	88.7	89.8	91.9	96.1	15-Jul-92	14:05	100	76.1	76.6	77.5	79.7
20-Jul-90	13:45	95	91.2	92.8	95.0	97.9	22-Jul-92	15:07	93	77.5	78.4	79.3	80.6
27-Jul-90	09:35	87	91.9	93.6	95.7	95.5	29-Jul-92	15:28	106	76.6	78.6	78.4	82.9
6-Aug-90	09:40	90	93.0	94.3	95.9	97.3	5-Aug-92	15:06	99	78.6	79.2	80.6	81.5
10-Aug-90	12:39	96	93.7	95.2	97.2	99.5	12-Aug-92	16:01	105	79.9	80.6	81.7	84.9
20-Aug-90	11:15	83	92.8	93.2	93.2	90.5	20-Aug-92	15:50	107	81.3	81.7	83.7	86.2
27-Aug-90	13:38	84	90.9	91.2	91.6	91.2	28-Aug-92	15:10	100	80.6	81.7	81.1	81.7
7-Sep-90	13:45	94	90.9	91.2	91.9	92.3	4-Sep-92	15:27	83	79.5	79.3	79.3	77.2
14-Sep-90	09:58	78	90.7	91.2	91.6	90.3	11-Sep-92	15:36	91	78.1	78.4	78.4	78.3
17-Sep-90	09:07	90	90.1	90.3	90.5	88.3	15-Sep-92	12:50	88	78.1	77.9	77.0	76.6
21-Sep-90	11:11	79	89.4	89.6	89.6	88.2	23-Sep-92	11:29	89	77.9	78.1	78.4	78.4
24-Sep-90	09:30	72	88.7	88.5	88.2	84.7	29-Sep-92	15:49	102	77.2	77.7	77.9	80.2
26-Sep-90	10:57	76	88.0	87.8	87.6	84.7	5-Oct-92	14:36	89	76.5	75.6	75.9	75.7
1-Oct-90	09:19	98	87.3	87.1	87.3	86.5	13-Oct-92	15:08	95	76.1	75.9	75.7	77.9
15-Oct-90	11:25	85	84.9	84.6	84.0	81.1	19-Oct-92	09:26	74	75.0	71.4	73.8	72.9
18-Oct-90	14:28	92	89.4	89.4	89.4	88.3	23-Oct-92	15:25	81	73.9	73.2	72.3	66.0
31-Oct-90	12:26	67	82.2	80.8	78.6	71.4	5-Nov-92	15:00	76	70.9	69.8	68.5	68.2
10-Nov-90	13:15	62	76.4	76.0	74.9	70.2	11-Nov-92	15:28	62	70.2	68.5	67.6	63.1
							16-Nov-92	14:29	74	67.6	66.0	63.7	62.4

TABLE 1 - STATION 1A THERMISTOR DATA (Section 1 Floor Data)

CHEMICAL WASTE MANAGEMENT, INC.
KETTLEMAN HILLS FACILITY
CLAY TEST PAD TENSIOMETER DATA

BLACK LINER							WHITE REFLECTIVE LINER						
			TENSIOMETER READINGS (Centibars)							TENSIOMETER READINGS (Centibars)			
DATE	TIME	ATM PRESSURE	3 in.	9 in.	15 in.	27 in.	DATE	TIME	ATM PRESSURE	3 in.	9 in.	15 in.	27 in.
10-Apr-90	16:15	29.45	38	24	42	14							
19-Jun-90	08:13	29.30	4	12	33	7	18-Mar-92	11:15	29.23	10	8	5	49
28-Jun-90	08:15	29.37	6	16	34	7	28-Jun-92	08:10	29.15	10	8	12	28
2-Jul-90	08:17	29.22	6	20	34	6	2-Jul-92	07:40	29.20	11	7	12	26
10-Jul-90	08:23	29.27	6	24	32	4	8-Jul-92	10:14	29.28	11	5	6	22
13-Jul-90	09:19	29.29	10	26	30	4	15-Jul-92	14:02	29.14	11	8	4	20
20-Jul-90	13:45	29.17	8	22	33	1	22-Jul-92	14:55	29.12	10	8	6	20
27-Jul-90	09:35	29.25	6	28	38	4	29-Jul-92	15:25	29.09	10	9	6	20
6-Aug-90	09:40	29.20	8	35	33	4	5-Aug-92	15:04	29.11	12	9	6	17
10-Aug-90	12:35	29.20	25	37	39	4	12-Aug-92	15:41	29.04	12	10	6	16
20-Aug-90	11:15	29.20	17	42	45	6	20-Aug-92	15:45	29.07	12	8	7	16
27-Aug-90	11:20	29.40	14	48	48	11	28-Aug-92	15:09	29.19	14	10	10	22
7-Sep-90	13:45	29.34	17	51	50	10	4-Sep-92	15:30	29.24	12	12	12	26
14-Sep-90	09:55	29.30	7	56	58	19	11-Sep-92	15:32	29.19	12	8	9	28
17-Sep-90	09:05	29.11	16	63	56	18	15-Sep-92	12:46	29.08	12	8	10	28
21-Sep-90	11:09	29.17	2	67	66	22	22-Sep-92	14:37	29.10	12	8	8	24
24-Sep-90	08:59	29.33	6	58	60	23	25-Sep-92	15:10	29.10	10	9	12	28
26-Sep-90	10:56	29.33	17	68	62	22	29-Sep-92	15:48	29.09	11	11	10	26
1-Oct-90	09:17	29.22	10	66	62	21	5-Oct-92	14:36	29.19	10	8	11	30
15-Oct-90	11:23	29.21	12	68	64	26	13-Oct-92	15:05	28.99	10	6	10	29
18-Oct-90	14:18	29.35	70	48	26	17	19-Oct-92	09:38	29.30	9	8	16	38
31-Oct-90	12:18	29.42	34	44	32	23	5-Nov-92	14:16	29.26	9	8	13	40
10-Nov-90	13:15	29.40	45	48	34	26	10-Nov-92	15:18	29.39	9	9	18	44
							16-Nov-92	14:26	29.20	11	10	18	44

TABLE 2 - STATION 1A TENSIOMETER DATA (Section 1 Floor Data)

fluctuations were recorded. Additionally, clay temperatures never exceeded the ambient air temperature after installation of the white HDPE liner.

The temperatures of the clay beneath the exposed white HDPE liner were even lower than the adjacent soil covered HDPE/clay composite test pad, by typically 1-2°C (2°-3°F). Desiccation cracks observed during the December 1992 inspection revealed only minor cracking had occurred. Typical cracks were 2.5 mm (0.1 in) in width and 25-38 mm (1-1.5 in) deep, indicating some healing of the previously existing cracks underneath the black HDPE had taken place.

The preliminary tensiometer data indicates an overall decrease in soil suction pressures in 1992 because moisture content of the clay had dried in the two year period since the placement of the clay. Soil suction pressures appear much more stable in 1992, after the installation of the white-surfaced HDPE liner, showing a decrease in the fluctuation of soil pressures throughout the recording period. Tensiometer data collected in 1991, before installation of the white HDPE liner, indicates a pattern of fluctuating soil suction pressures similar to the 1990 data and continuance of the overall decrease of moisture content in the clay.

Detailed evaluations of all the instrumentation test data and complete results of the December 1992 site inspection are forthcoming. Final results, observations, and recommendations will be presented in a later summary report.

INSTALLATION CONSIDERATIONS

Installation of white-surfaced polyethylene geomembranes is conducted in exactly the same way as for standard polyethylene liner installations, with the same heat seaming methods and quality control procedures. In addition to the benefits of reduced expansion/contraction due to lower temperatures, such materials enable engineers and inspectors to detect installation damage more easily. The white surface layer, when impacted by routinely used installation equipment, reveals slits, scratches, abrasion marks, and holes with much better contrast than standard all-black geomembranes. The damage becomes visible because the black underlayer is revealed against a white background.

Detection of leaks is, of course, an important part of standard quality control efforts during an installation. The present emphasis on the use of soil/synthetic composite liners, barrier layers, and leak detection systems has occurred because agencies and regulators realize that it is extremely difficult to install a perfectly leak-free geomembrane. Darilek, et al (1989) published electrical resistance leak location data indicating an average of 26 leaks per 10,000 m^2 of geomembrane (ten leaks per acre). Although most of these leaks were pinhole leaks in seams, 26% of the reported leaks were panel tears and other such damage made during installation. These results indicate that there is room yet for improved inspection methods for geomembrane installations.

To assess whether the white-surfaced geomembranes make such inspections easier and more effective, identical scratches, slits and abrasion marks were made in adjacent samples of white-surfaced geomembrane and standard black sheet.

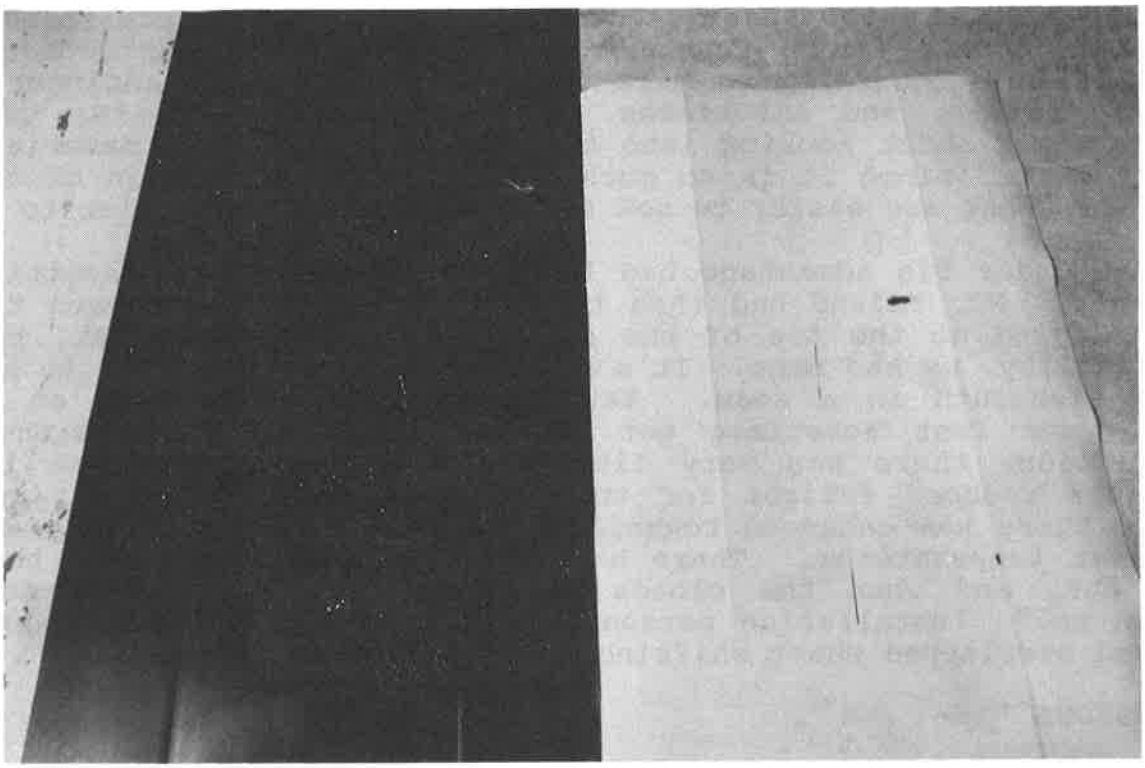

Figure 3. Visibility Comparison of Identical Damage In Standard Black and White-Surfaced HDPE

The white-surfaced geomembrane was 1.5 mm (60 mil) thick with a 0.125 mm (5 mil) coextruded white HDPE surface layer. Abrasion marks were made with a table saw blade elevated 0.375 mm (15 mils) from the tabletop. Punctures almost penetrating the geomembranes were made in each 1.5 mm sheet from the top surface down as well as from the bottom up. All types of damage were more visible in the case of the white-surfaced geomembrane. Figure 3 shows two of the samples in this installation damage comparison.

Discussions with project supervisors and quality assurance engineers verify the improvement of visual inspection for installation damage at white-surfaced geomembrane installations.

WHITE-SURFACED HDPE LINER DURING LANDFILL INSTALLATION

Envirite Corporation runs the Livingston Landfill in Livingston County, Illinois accepting metropolitan sanitary waste as well as nonhazardous waste. They constructed a double composite system consisting of 60 mil thick white-surfaced HDPE in combination with

three feet of clay, single-sided geotextile/geonet composite, and a secondary liner consisting of 60 mil white-surfaced HDPE and a single foot of recompacted clay. Conversations with the third party inspection engineer revealed that the white-surfaced sheet was much preferred over standard black sheet for various reasons.

One problem which had presented itself to third party inspectors was the uncertainty accompanying visual inspection of the geomembrane installation. According to Mike Friend, certification engineer with Vegrzyn, Sarver, and Associates of Pontiac, Illinois, "We usually inspect black sheet looking into the sun, but with this material, it doesn't matter since it is so much easier to see things in or on the sheet. Patches are easier to see and damage marks are easier to see."

The other big advantage had to do with temperature reduction in the liner. Mr. Friend had this to say: "It's very uncommon to not have bridging at the toe of the slopes on a site in August, but at this facility, we had none. It's also unusual in August not to have a single fishmouth in a seam. Yet we had none. Standing on black sheet, your feet sometimes get so hot they burn, but with this installation, there was very little heat radiation off the liner. There was reduced fatigue for the installation technicians, and we believe there was enhanced technician productivity and quality due to the lower temperatures. There have been less wrinkles when the sun comes out, and when the clouds block the sun, the sheet doesn't tighten up." Installation personnel did not have to worry about the deployed overlapped sheet shifting before it could be seamed.

CONCLUSIONS

Under solar exposure, white-surfaced geomembranes are cooler than black geomembranes. Lower temperatures provide several physical benefits such as lower expansion/contraction, greater resistance to long-term degradation, and increased protection of soil subgrades from desiccation. In addition, installation damage is usually more easily detected. Other aspects of installation and inspection appear to be made simpler as well.

REFERENCES

Basnett, C. and Brungard, M., (1992) "The Clay Desiccation of a Landfill Composite Lining System", Geotechnical Fabrics Report, January/February, pp. 38-41.

Bragaw, C. G., (1980) Proceedings of the Seventh Plastic Pipe Symposium, Vol. 20.

Cadwallader, M. W. and Metzger, P., (1987) "Accelerated Aging of High Density Polyethylene Geomembranes: A Novel Approach", 42nd Annual Purdue Industrial Waste Conference Proceedings.

Chan, M. K. V. and Williams, J. G., (1983) "Slow Stable Crack Growth in High Density Polyethylenes", Polymer, Vol. 24.

Corser, P., and Cranston, M., (1991) "Observations on Long-Term Performance of Composite Clay Liners and Covers", Proceedings of Geosynthetics Design and Performance Conference, Vancouver, British Columbia Geotechnical Society, May.

Corser, P., Pellicer, J., and Cranston, M., (1992) "Observations on Longterm Performance of Composite Clay Liners and Covers", Geotechnical Fabrics Report, November, pp 6-16.

Darilek, G. T., Laine, D. L., and Parra, J. O. (1989) "The Electrical Leak Location Method for Geomembrane Liners: Development and Applications", Geosynthetics '89 Conference Proceedings, Vol. 2, pp. 456-466.

GRI (1992) Test Method GM5, Geosynthetic Research Institute, Drexel University, Philadelphia, PA, April.

Halse, Y. H., Hullings, D. E., Koerner, R. M., and Lord, A. E., (1990) "Methods to Evaluate the Stress Crack Resistance of High Density Polyethylene FML Sheets and Seams", 16th Annual Research Symposium of the U. S. EPA, April.

Kanninen, M. F., Popelar, C. H., and Peggs, I. D. (1993). "A Methodology for Predicting the Lifetimes of HDPE Geomembranes", Proceedings of Geosynthetics '93. IFAI, St. Paul, MN.

Klemchuk, P. and Horng, P., (1985) "Longterm Aging Study of Antioxidants in Polyolefins", Plastics Compounding, Sept/Oct.

Polypropylene Geomembranes—The Alternative Containment Solution

A. Shah
Himont USA Inc., USA

R.K. Frobel
R.K. Frobel & Associates, USA

ABSTRACT

Polypropylene based olefinic polymers are not new to the geosynthetic community as they have been used for many years as fibers in the manufacture of geotextiles. In response to the growing need for an alterantive geomembrane system that is low in crystallinity, resistant to chemicals and ultra-violet (UV) light, flexible and easily seamed, polypropylene based olefinic polymers were developed. These polymers can be converted into high quality sheet by: air quenched blown sheet and slot die extrusion processes, and the calendering sheet production technology. Sheet thickness can range from 0.5 mm (0.02 in.) to 5.0 mm (0.2 in.). It has been demonstrated that the sheet made from these polyolefins can be factory seamed into large pre-fabricated panels that can be accordion folded and shipped to the site for installation. This paper highlights some of the physical/performance properties of polypropylene based geomembranes that will justify their utilization for a variety of containment applications. In addition, photographs of a representative installation and field seaming details are included.

INTRODUCTION

For many years, geomembrane systems have been used as a liquid and/or gas barrier primarily due to their low permeability, ability to be fabricated into large panels, ease of installation, and generally good environmental and chemical resistance. More specifically, the following additional performance characteristics are desired in a geomembrane system:

* Tensile Properties: Stress strain/characteristics that can be related to the overall design requirements.

* Toughness: High resistance to installation stresses where the material must be flexible and have excellent puncture resistance.

* Deformability/Conformability: Resistance to deformation under load and the ability to conform to various subgrade conditions while having

the potential for a reasonable amount of movement during service without rupture.

* Chemical Resistance: Little or no loss of performance properties when exposed to a variety of chemically aggressive environments.

* Durability: High resistance to a variety of environmental stresses, including constant long term exposure to UV, ozone, large changes in exposure temperatures and biological attack.

* Factory and Field Seaming: A material that can be seamed by a variety of thermal processes to produce a homogeneous bond over a wide range of seaming equipment temperatures.

* Repairability: Easily repaired after years of installation, preferably by the site owner.

* Lowest possible coefficient of linear thermal expansion.

* High surface coefficient of friction against a variety of construction materials.

A polypropylene based olefinic polymer was developed that satisfies the above listed specific requirements. The polymer that will be discussed in this paper is designated as KS-056P. The focus of this paper will be on the performance characteristics of the sheet made from this polymer, along with a brief discussion of the methods of sheet production and liner installation.

POLYMER DEVELOPMENT

The invention of the Ziegler Natta type catalyst was the origin for the polymerization of high density polethylene (HDPE) and isotactic polypropylene (PP). Both the HDPE and the PP first polymerized were very stiff materials having flexural moduli of about 1050 MPa (150,000 psi) and 1750 MPa (250,000 psi), respectively. Since then, both polymers have traversed parallel development paths towards softness, flexibility and higher impact resistance.

In the case of polyethylene (PE), the flexibility was achieved by the incorporation of alpha olefins as comonomers, e.g., butene, hexene, octene, etc. The incorporation of a comonomer lowered the polymer crystallinity, which resulted in a higher degree of flexibility and softness. By copolymerization, the flexural modulus of polyethylene can be reduced from 1050 MPa (150,000 psi) in the case of HDPE to about 70 MPa (10,000 psi) for very low density polyethylene (VLDPE).

Initially, copolymerization was utilized to make PP resins more impact resistant, but the copolymers of PP still had high flexural moduli, about 1135 MPa (165,000 psi). For further reduction in stiffness/flexural modulus, rubber compounds such as ethylene propylene diene monomer (EPDM), ethylene propylene rubber (EPR), etc. were added to PP resins. These compounds are commonly known as thermoplastic polyolefins (TPO's). The isotactic polypropylene and its copolymers had

very sharp melting points, which made them very difficult to seam thermally. Basically, the high stiffness and the difficulty in heat seaming did not allow the use of earlier polypropylenes as geomembranes.

New technology has been developed to produce propylene based polyolefins in a reactor that have flexural moduli less than 135 MPa (20,000 psi). In addition to the significantly higher degree of flexibility, these polymers have a broad melting transition, which allows them to be thermally seamed over a wide range of seaming equipment temperature set points. These flexible PP based olefins maintain the inherent characteristics of polypropylene, which include:

* The thermodynamic melting point is 20° (68°F) higher than polyethylene.

* Resistance to chemicals - no chemically reactive species in the polymer molecule.

* Very high environmental stress crack resistance (ESCR) to chemical/thermal environments that can include stress cracking in polyolefins.

* Very high resistance to other forms of detrimental environmental agents, i.e., ultra violet (UV) light, ozone, etc.

* Very low coefficient of thermal expansion (less than half that for HDPE).

GEOMEMBRANE SHEET MANUFACTURING PROCESSES

The KS-056P polymer was desiged for processing on all available processes used for the manufacture of sheet in the geomembrane industry. Being a polyolefin, this material can be converted into a high quality sheet using both the extrusion processes, i.e., slot die and air quenched blown as well as calendering manufacturing methods.

Prior to the development of KS-056P polymer, the calendering sheet manufacturing process was limited to non-polyolefin type polymers, i.e., polyvinyl chloride (PVC), chlorosufonated polyethylene (CSPE or Hypalon) and various rubbers. The morphology and thermal stability of the KS-056P polymer allows it to be converted into a high quality sheet using PVC or Hypalon calendering lines. The sheet can be easily scrim reinforced for applications that require higher modulus, higher ultimate strength and even more dimensional stability compared to the nonreinforced PP.

SHEET PROPERTIES OF THE KS-056P POLYMER

Stress-Strain Characteristics. Table 1 illustrates the index mechanical properties of 1.0 mm (0.040 in.) thick nonreinforced KS-056P sheet. Although this material is in the flexibilty range of plasticized PVC, it does show a distinct yield point in a tensile test at approximately 25% strain. The tensile strength of this material increases as a function of strain to values over 20 MPa (3000 psi). It should be noted that the

uniaxial elongation to break for this material is in excess of 800% of the original length.

Table 1 Mechanical Properties of 1 mm (.040 in.) KS-056P Geomembrane

Property	ASTM Test Method	Direction of Test	Value
Tensile Properties:			
Yield Strength, MPa	D638	Machine	6.2
		Transverse	5.3
Yield Elongation, %	D638	Machine	30.0
		Transverse	25.0
Breaking Strength, MPa	D638	Machine	22.0
		Transverse	21.5
Break Elongation, %	D638	Machine	805.0
		Transverse	850.0
Stress @ 100% Elongation, MPa	D638	Machine	6.0
		Transverse	5.2
Stress @ 200% Elongation, MPa	D638	Machine	8.0
		Transverse	5.5
Modulus of Elasticity, MPa	D882	Machine	112.0
		Transverse	81.3
Tear Resistance, Kg	D1004	Machine	157.0
		Transverse	159.0
Hardness, Shore D	D2240		
Instant Reading			37.0
5-Second Reading			32.0
Puncture Resistance	D4833		
Force, Kg			21.0
Probe Travel, cm			2.3

The multiaxial stress strain behavior of the KS-056P sheet was compared to other materials commonly used for geomembranes using Geosynthetics Research Institute (GRI) test procedure GRI/GM4 (GRI, 1991). The 1.0 mm (0.040 in.) sheet sample of KS-056P demonstrated very high deformability. This sample finally failed at over 150% elongation which is the maximum allowable strain limit of the test device. The failure was truly multidirectional and was not affected by the sheet manufacturing process. This property shows that the KS-056P sheet has exceptional capacity to deform under axisymetic loading and resist failure. Figure 1 illustrates the Multiaxial Stress-strain characteristics as compared to other geomembranes.

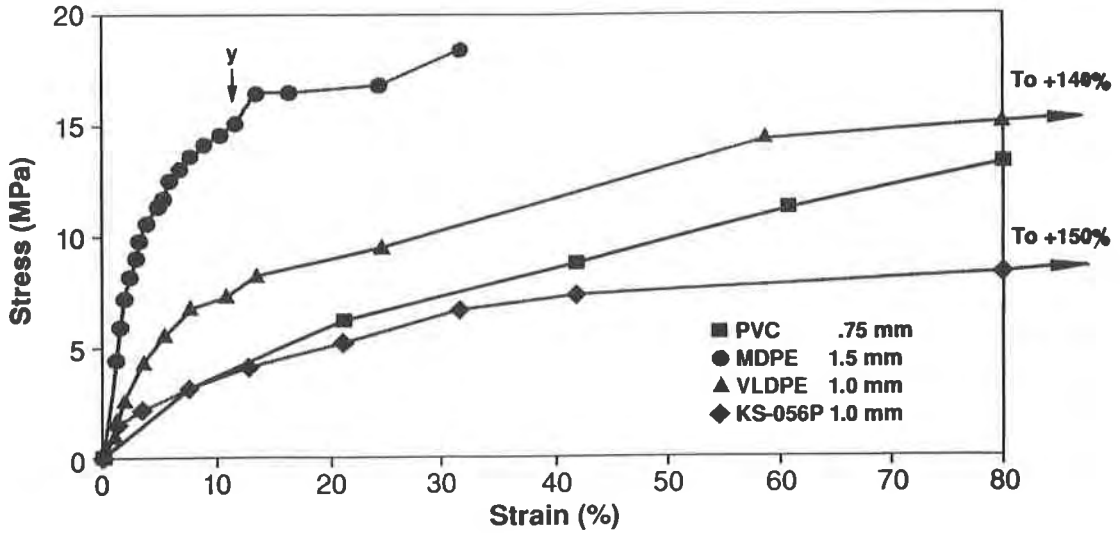

Figure 1 Comparative Multiaxial Stress/Strain Properties of Various Geomembranes.

In a point stress test, the KS-056P sheet sample was tested over truncated cones as specified in the GRI/GM3 (GRI, 1991) test procedure. The pressure loading rate was 6.9 kPa/min. (1.0 psi/min). The 1.0 mm (0.040 in.) non reinforced KS-056P sheet did not fail up to 820 kPa (120 psi) pressure over 10 cm. (4.0 in) cone heights. From this test, the critical cone height for KS-056P sheet was determined to be 10.0 cm (4.0 in.) as compared to 8.9 cm. (3.5 in.) for 1.0 mm (0.040 in.) VLDPE. This test again shows that the KS-056P sheet has superior elongation/ conformance properties when subjected to loading over rough substrates. A scrim reinforced KS-056P sheet sample was also tested and the critical cone height was found to be higher than either Hypalon or HDPE. The comparative data is shown in Table 2.

Table 2: Critical Cone Heights of Various Geomembranes

Geomembrane	Thickness (mm)	CCH (cm)
MDPE	1.5	1.0
CSPE-R	0.9	1.8
PVC	0.5	7.0
VLDPE	1.0	8.9
Polpropylene	1.0	10.0
Polypropylene-R	1.14	4.0

CCH=Critical Cone Height
R=Reinforced with Scrim

Dimensional Stability. Inherently, PP has a lower thermal coefficient of expansion as compared to polyethylene (Rodriguez, 1970). The lower coefficient of linear thermal expansion results in a higher degree of dimensional stability of the sheet when exposed to large temperature

changes, which is a common occurrence when black geomembranes are exposed to daily temperature extremes and direct sun light.

This property of KS-056P also inhibits excessive expansion of the sheet in the areas exposed to high temperatures during the seaming process. Excessive expansion in areas of the sheet that are exposed to high temperatures while seaming can result in residual stresses, which in turn can cause premature liner failure along the seamed areas. In addition, contraction of the sheet due to excessive low ambient temperatures can cause stresses that will result in premature failure of the seams.

Seaming and Thermal Behavior. The KS-056P has a very wide melt transition temperature range as compared to the polyethylenes and in particular medium density polyethylene (MDPE) as measured by differential scanning calorimetry (DSC). The advantage of the wider melting transition observed in the case of KS-056P as compared to the MDPE is clearly demonstrated by the thermal seaming characteristics of these two materials.

Figure 2 shows the peel strength values for thermally bonded sheet samples of KS-056P when seamed over a wide range of seam equipment temperatures at a low ambient temperature of 7°C (45°F). The average peel strength of 256 KN/m (45 lbs/in) for KS-056P was obtained over a wide thermal seaming equipment temperature range of over 200°C (392°F) which was substantially wider than either HDPE or VLDPE. In all cases, specimens failed at the seam edge in the Film Tear Bond (FTB) mode of failure with no indications of bonded seam area failures. The relative ease of thermal seaming over a wide range of seaming equipment temperatures is in itself a great advantage to the liner installer.

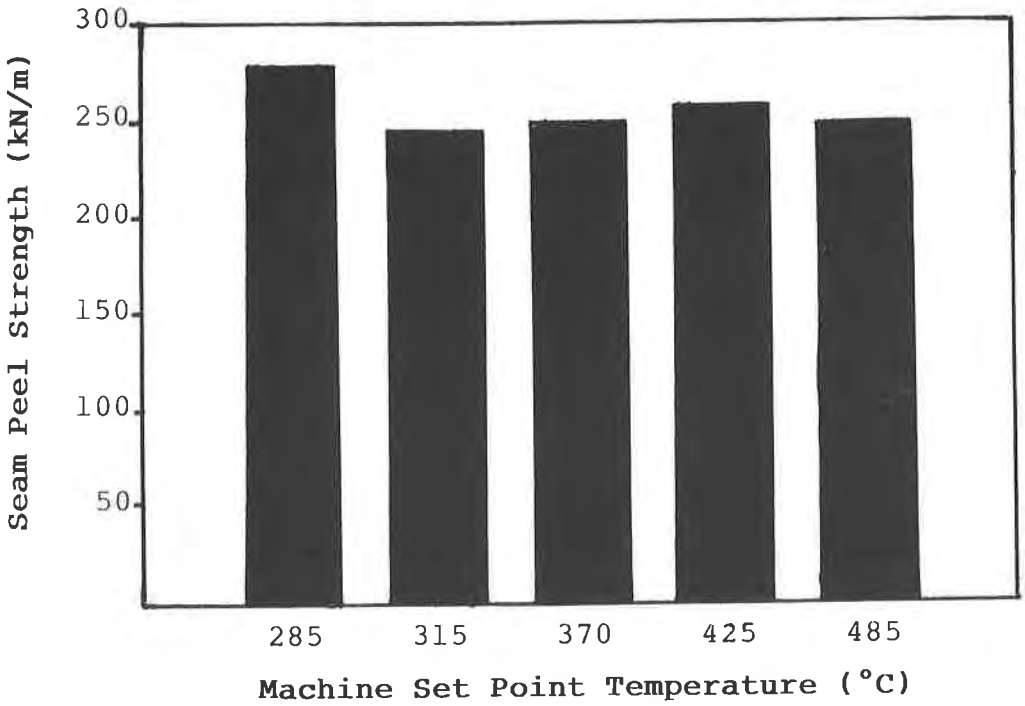

Figure 2. Seam Peel Strength vs. Machine Temperature (KS-056P)

Figures 3 and 4 show typical thin cross sections of the thermally seamed KS-056P sheet at 50X magnification. The photos clearly demonstrate that the seamed interface is completely invisible over a 170°C (300°F) seam temperature range due to the perfect fusion of the two sheets and thus a true homogeneous bond.

Environmental Stress Crack (ESC) Behavior. Using the ASTM Method D-1693 (ASTM, 1991) ESCR under constant strain, the KS-056P sheet was tested in 10% Igepal/acqueous solutions at three temperatures, 23°C, 50°C and 95°C (73°F, 122°F, 203°F) with no failures or surface cracking observed. One set of specimens was exposed to Igepal for 3000 hours to 50°C (122°F) and these specimens were found to be completely resistant to stress crack failure.

The samples of KS-056P sheet material were also tested using the GRI/GM5 (GRI, 1991) test method, also known as the constant load environmental stress crack resistance test. In this test, a black liquor effluent from a paper processing facility was used. The test was conducted for 525 hours with no failures, surface cracking or notch propagation under 60X magnification.

Chemical Resistance. The chemical resistance of KS-056P sheet samples was tested against saturated solutions of a variety of organic solvents. Upon reaching equilibrium, (i.e. no further organic absorption in the polymer), the sheet samples were tested for physical properties changes. The results are shown in Table 3. The data indicates no significant detrimental effect on the 1.0 mm (0.040 in.) thick KS-056P sheet samples after exposure to a variety of organics.

In an EPA 9090 membrane immersion test, no discernable loss of physical properties of KS-056P sheet was noted when exposed to a municipal solid waste leachate. The leachate was obtained from Delaware Solid Waste landfill in Sandtown, Delaware. The test was conducted at two temperatures, 23°C (73°F) and 50°C (122°F). In this test, various critical properties were monitored over four months of sheet sample immersion in the leachate with little or no change in physical/mechanical properties.

Table 3. Resistance of KS-056P to Saturated Aqueous-Organic Solutions

Solution	Concentration (ppm)	Weight Gain, %	Tensile Yield,MPa	Tensile Break,MPa	Ultimate Elongation
Control			8	23.5	840
Distilled Water		0.1	8.7	22.3	800
2% NaCl		0.1	7.8	22	815
MEK	1000	0.18	8.7	21.4	775
TCE	475	2	8	25	835
O-Xylene	150	1.1	7.8	22.6	840
Tolulene	475	2.25	7.2	20	775
Tolulene +2% NaCl	475	2.5	7.6	20	765

Figure 3. Thin cross section of KS-056P thermal seam made at 315°C (600°F) 50X magnification. (Arrow indicates seam area)

Figure 4. Thin cross section of KS-056P thermal seam made at 480°C (900°F) - 50X magnification. (Arrow indicates seam area)

PREFABRICATED PANEL INSTALLATION

As previously mentioned, the KS-056P polymer can be manufactured into geomembrane sheet by a variety of processes. If the sheet is calendered or extruded into relatively narrow roll widths of 1.8 to 3m (6 to 10 ft.), these rolls can then be factory fabricated into very large individual panels. Due to the high degree of flexibility and low crystallinity of the KS-056P sheet, these panels can be accordion folded and packaged for protective shipment to the site. Once at the site, individual panels are easily moved into position by fork lift or front end loader, unpackaged and unfolded into the specific panel location as shown in figures 5 and 6. Once the specified overlaps for the panels are set, the seams are thermally welded by hot air or hot wedge methods as shown in figure 7. Custom boots are easily fabricated out of KS-056P sheet stock or factory extruded. Boots and patches are completed by using a hand held hot air gun and hand roller as shown in figure 8. The KS-056P material can be readily repaired even after aging by using a commercially available hot air gun and hand roller with no special surface preparation.

SUMMARY

Utilizing the latest olefinic polymerization technology, a new polymer for the manufacture of geomembrane sheet materials was successfully developed. It has been shown that this polymer can be converted into high quality sheet of varying thicknesses using the air quenched blown and slot die extrusion manufacturing processes as well as calendering sheet production methods. The sheet manufactured from this polymer has been shown to exhibit the following outstanding characteristics:

* In a tensile test, KS-056P sheet shows a distinct yield point, over 800% ultimate elongation and ultimate tensile strength over 20 MPa (3000 psi).

* In a large diameter multiaxial rupture test the material exhibits high extensibility and deformation under axisymetic loading.

* The KS-056P sheet shows excellent puncture resistance in standard index puncture and large scale point stress testing, which means that the material has excellent subgrade conformance and puncture resistance.

* Laboratory and field testing has shown that the sheet from these polymers can be thermally bonded over a wide range of seaming equipment set points. In addition, analytical work has shown that the seam is a true homogeneous bond between two sheets.

* The sheet manufactured from this polymer did not fail when exposed to very aggressive ESCR liquid mediums and thus is not subject to environmental stress cracking.

* These materials being true polyolefins show outstanding resistance to a wide variety of chemicals and landfill leachates.

* Recent installations have demonstrated the ease of all aspects of liner installation in the case of KS-056P sheet, e.g. fabrication into large panels, transportation of these panels to the field, deployment of the fabricated panels and thermal sealing.

* Factory and field thermal seaming has been successfully accomplished using three seaming processes, i.e. hot air, hot wedge and extrudate, without any surface preparation.

REFERENCES

Geosynthetics Research Institute, GRI (1991) "Three Dimensional Geomembrane Tension Test, GRI/GM4," GRI Test Methods & Standards, GRI, Drexel University, Philadelphia.

Rodriquez, F. (1970), Principles of Polymer Science, McGraw-Hill, New York, pp. 524.

American Society for Testing and Materials, ASTM (1991), "Test Method for Environmental Stress-Cracking of Ethylene Plastics," D1693, Volume 8.02, ASTM, Philadelphia.

Geosynthetics Research Institute, GRI (1991) "Notched Constant Load Environmental Stress Crack Resistance Test for Polyolefins - GRI GM/5," GRI Test Methods & Standards, GRI, Drexel University, 1991.

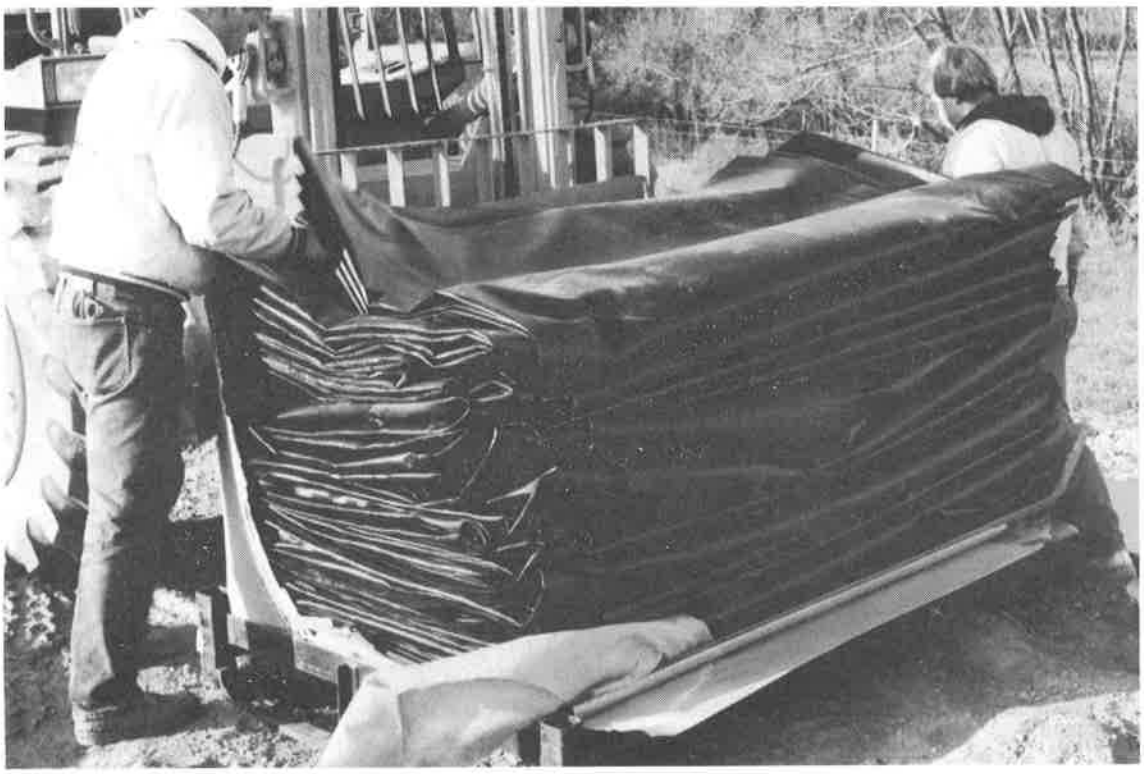

Figure 5. Prefabricated 1100m² (11,700 ft²) Accordion folded panels as delivered to the site.

Figure 6. Panel Deployment.

Figure 7. Hot Air Thermal Seaming of Panel Field Seams.

Figure 8. Field fabrication of boots and thermal seaming around penetration by hot air methods.

The European Standardization on Design and Testing of Geosynthetics

J.M. Rigo
University de Liège, Belgium

P. Delmas
Bidim Geosynthetics, France

ABSTRACT

The European Committee for Standardization has set up a Technical Committee devoted to Geotextiles, Geomembranes and related-products (CEN Technical committee 189). This technical committee has been requested to prepare :
- testing standards on products and systems;
- design methods, requirements and criteria for products and structures including geosynthetics.

Geosynthetic applications have been classified in load transfer, hydraulic and lining applications.

This paper describes the approach that is envisaged to deal with these matters.

INTRODUCTION

The European Unification and the recent political changes in Central Europe will create the biggest unified market in the world. For the 12 E.E.C. countries and the seven E.F.T.A. countries, this will be a reality after 1992/12/31. This means free circulation of goods and persons.

With regards to construction materials (including geosynthetics), this will also mean the unification of basic requirements, design and testing methods.

The CEN (European Committee for Standardization) was officially appointed to achieve the standardization work. CEN is basically composed of the Standard Institutes of the 12 Member States (Belgium, Denmark, France, Germany, Greece, Ireland, Italy, Luxemburg, The Netherlands, Portugal, Spain and United Kingdom). The seven countries grouped in the EFTA (European Free Trade Association) are also associated with the CEN work : Austria, Finland, Iceland,

Liechtenstein, Norway, Sweden and Switzerland.
Presently, Poland, Czechoslovakia, Hungary, Turkey and Cyprus have received the status of observer. Other countries are expected to join soon.

In addition, an ISO Technical committee 38 SC 21 (Geotextiles) delegation is an observer. Non-European delegates were invited to take part in this ISO delegation.

As a first step a CEN Technical Committee on geotextiles and geotextile-related products have been created : CEN Technical committee 189. It is a Belgian initiative. J.M. RIGO is the Chairman and I.B.N. (Belgian Standards Institute) together with CENTEXBEL (Belgian Textile Research Centre) are the secretary.

Later a CEN Technical committee on Flexible Sheeting for waterproofing was also created, covering roof, linings, bridge decking, ... : CEN Technical committee 254. This Technical committee is mostly "Materials" oriented. These two Technical committee's decided to create a joint working group to work on geomembranes : Technical committee 254 working on materials aspects and Technical committee 189 working on performance and end uses aspects for geomembranes. M. SOMMERFELD (Germany) is the Convenor of this Joint Working group.

The European regulations gave the standards produced by such a committee a mandatorily level. As soon as a CEN Technical committee starts harmonization work, a standstill procedure is applied by which all the engaged standards institutes are not allowed to produce anymore new standards in the investigated field. On the other hand, once the Eurostandards are published, the corresponding national standards are mandatorly replaced by the Europeans. This explains the reasons why most of the CEN National Standards Institutes actually give the priority to the development of standardization in Europe.
The standards produced by such a Technical committee will replace the national standards and have to be revised after a period of 5 years maximum.

The rapid development of geotextiles in Europe has brought about wide variations in testing methods and in the acceptance criteria for different geotextile applications between countries. RIGO (1990) on behalf of the I.G.S., recently published an "Inventory of current geotextile test methods and standards" where about 300 test methods were pointed out. A wide majority of these were published by European Standards Institutes or Associations. ROLLIN and RIGO (1991) also published a review of the test methods available for geomembranes.

The CEN Technical committee 189 organization. For efficiency reasons, the CEN Technical committee 189 has been divided in 5 working groups with the following objectives (figure 1) :
- Working group 1 : general and specific requirements, performance criteria and review of design methods (Chairman : Ph. DELMAS, France);

- Working group 2 : terminology, identification, sampling and classification (Chairman : B. THAMM, Germany);
- Working group 3 : mechanical testing (Chairman : D. CAZZUFFI, Italy);
- Working group 4 : hydraulic testing (Chairman : B. B. MYLES, United Kingdom);
- Working group 5 : durability (Chairman : J. GREENWOOD, United Kingdom).

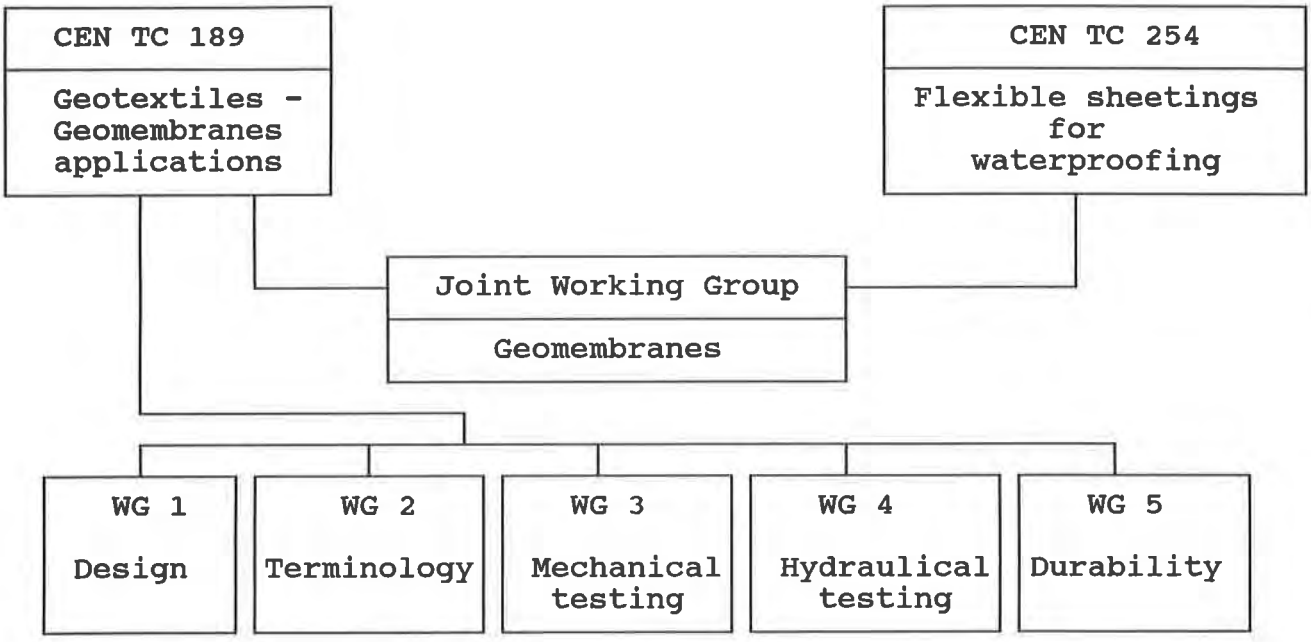

Figure 1 : the CEN TC 189 organization

Design and testing standardization. CEN standardization on geosynthetics is not restricted to the harmonization of testing methods. Indeed, requirements, performance and design are of prime importance. The Working group 1 is requested :

1) to review the existing functional design procedures for various applications (separation, filtration, drainage, reinforcement, protection and lining). These procedures include functional requirements of geosynthetics and possible design methods in general terms or ways of arriving at specifications for relevant properties. Design methods will be studied as far as they concern the process of specifying a geosynthetic in a specific structure;
2) to develop general requirements of structures incorporating geosynthetics : embankments, retaining walls, paved and unpaved roads and railways, erosion control, drainage trenches, lining systems...;
3) to develop specific requirements to be met by geosynthetics used within the above mentioned structures and applications;
4) to define the performance tests to relate index tests to the in-situ applications. Corresponding developments will be made by the other Working groups.

In fact, Working group 1 is in charge of the technical direction of the Technical committee work. The other working groups are referring to Working group 1 for the development of the testing procedures.

Table 1 below gives a list of the work items for the 5 working groups and the expected date of publication of the standards under development. This table will be updated soon by the Technical Committee in order to cover new items related to geomembrane applications.

Once the technical work of the Technical committee is achieved, the normal enquiry procedure request approximately one year between the achievement of the Technical committee work and the final vote and publication. All the dates mentioned in the previous table refer to the second step of the procedure.

The geotextiles and geotextile-related products classification. Presently, work is starting in CEN on the classification of geotextiles and geotextile-related products.
Various alternatives are possible :

- classification of products through each characteristic as it has been developed in France. The whole range of values for a given characteristic is subdivided into classes with upper and lower limits (CFGG - 1984);
- classification of products through a set of characteristics as it has been proposed by RATHMAYER (1982) in Finland. A group of characteristics (weight, weight variation, strength, elongation, friction, cone penetration test,...) is used to evaluate a classification index directing the product to families of applications. This method is applicable for non-woven products in roads construction;
- classification of products for a given application through an important characteristic to be played as it has been proposed in Germany (CEN Technical committee 189 doc. 39 - 1990). For example, for road construction, the German experts set up a classification system of the products on the basis of the puncture test (C.B.R. test) with 4 classes. This method is applicable to non-woven products.

On the other hand, discussions are now held to study the possibility of classifying products through functions and characteristics. This should take into account the tendency of design by function. Important characteristics for a given function should be grouped to evaluate the ability of a given product to act as drainage layer, filter, separator, protective layer, reinforcement. The classification should than be characterized by two indexes : a function and a level of performance for this function (for instance R 4 means class 4 for reinforcement). This work has just started. The above information is an indication of possible solutions.

Table 1. Actual CEN Technical committee 189 work items

WG	WORK ITEMS AND EXPECTED PUBLICATION DATE FOR ENQUIRY (month / year)
WG 1	- Review of design procedures - General requirements (12/1993) - Specific requirements (7/1994) - Performance criteria
WG 2	- Vocabulary (10/92) - Identification (10/92) - Sampling (6/1992) - Thickness (4/1992) - Mass per unit area (10/1992) - Classification (3/1993)
WG 3	- Tensile (4/1993) - Tensile on seams (4/1993) - Strength of structural joints (12/1994) - Static puncture (10/1992) - Dynamic perforation (3/1994) - Damage during installation (6/1994) - Tear propagation (3/1995) - Impact (12/1994) - Abrasion (12/1993) - Friction (10/1994) - Anchorage (10/1994) - Tensile creep (6/1994) - Compressive creep (6/1994)
WG 4	- Permeability normal to the plane without load (3/1993) - Permeability normal to the plane under load (1/1994) - Opening size (6/1994) - Flow capacity in the plane (1/1994) - Water penetration resistance (1/1994)
WG 5	- Thermal oxidation (6/1994) - Weathering (6/1993) - Chemical degradation (1/1994) - Microbiological degradation (6/1994) - Hydrolysis (6/1994) - Tests for evaluation of durability (6/1993)

Geosynthetics applications classes. Geosynthetics applications have been grouped in three different classes on the basis of the main function to be achieved :

- load transfer applications of geotextiles and related-products where reinforcement and/or separation are important. For example :
  . road and railways;
  . foundation;
  . retaining structures and walls; ...

- hydraulic application of geotextiles and related-products where drainage and/or filtration are important. For example :
  . drainage systems;
  . erosion control;
- lining applications where geotextiles, geomembranes and related-products are used in fluid (liquid and/or gas) barriers, leachate, leakage detection systems. For example :
  . waste disposal lining and capping systems;
  . canals;
  . dams;
  . tunnels; ...

These classifications permit a harmonized approach of the geosynthetics design and characterization.

Geosynthetics characterization. Currently, each application has been analysed on the basis of the functional design procedures. This work allows clarification of the knowledge of the real behavior of the geosynthetics in specific conditions.

Tables 2, 3 and 4 give the actual analysis for one example of Load transfer, Hydraulic and Lining application classes respectively. These tables show the tests to be referenced in the specifications of the different types of work. Either the usual index tests or the performance tests are related to the functions needed in the structures. Then the requirements will be analyzed on the basis of the performance criteria of the structures using geosynthetics.

The previous functional analysis will help to clarify the discussions and to establish guidelines to define the specifications on the geosynthetics.

This work has started and will take at least 3 years to complete.

CONCLUSIONS

The publication of Euro-standards on geotextiles, geomembranes and related-products will surely have very positive impacts on the market.

CEN standards not only cover test methods but also requirements, criterion and design aspects which are not commonly developed in other standardization bodies. One could say that we actually know enough and sometimes too much about test methods. The basic requests are now centered on design aspects. Some countries have no recommendations at all.

The production of European unified codes of design, practice... will certainly clarify these situations. On the other hand, the free circulation of goods together with unified codes will increase the competition between the producers. Adaptations of the products characteristics will be necessary in order to fulfil the next requirements and new products will be proposed.

Table 2. Geosynthetics characterization for a load transfer application earthwork foundations

Type of test	Filtration	Separation	Reinforcement
Specifications	Traffic loads mainly during installation	Traffic loads mainly during installation	Traffic loads mainly during installation
Performance tests	Filter stability (A) Durability : chemical (A)	Durability : chemical (A)	Friction (eg pull out) (A) in soil creep test (A) in soil tensile test (A)
Index tests	Opening size (N) Permittivity (N) Thickness (N)	Opening size (N)	Tensile test (strain stress) (N) Creep test (A) Friction test (N) Tensile of joints (A) Tensile of connections (A) Transmissivity (A)
Installation tests	Tensile test (strain-stress) (N) Damage during installation (N) Static puncture test (N) Durability UV (A) Identification of roll (N) Mass per unit area (A) Thickness (A)	Tensile test (strain-stress) (N) Damage during installation (N) Static puncture test (N) Durability UV (A) Identification of roll (N) Mass per unit area (A) Thickness (A)	Tensile test (strain-stress) (N) Damage during installation (N) Static puncture test (N) Durability UV (A) Identification of roll (N) Mass per unit area (A) Thickness (A)

(N) necessary
(A) when applicable

Table 3. Geosynthetics characterization for an hydraulic application : erosion control

Type of test	Separation	Filtration
Specifications	Advise installation joints	Advise installation joints
Performance tests	Abrasion test (A)	Filter stability (A) Surface erosion control (A) Durability : biological, chemical, UV (A) Long term permittivity in soil (A)
Index tests	Opening size hydro sieving (N) Static puncture test (N) Tensile test (strain-stress) (N) Burst test (A)	Opening size hydro sieving (N) Permittivity (N) Thickness (N) Static puncture test (N) Tensile test (strain-stress) (N)
Installation tests	Tensile test (strain-stress) (N) Damage during installation (N) Durability (UV) (A) Identification of roll (N) Mass per unit area (A) Thickness (A)	Tensile test (strain-stress) (N) Damage during installation (N) Dynamic puncturing test (N) Durability (UV) (A) Identification of roll (N) Mass per unit area (A) Thickness (A)

(N) necessary
(A) when applicable

Table 4.a. Geotextiles characterization for lining systems application

Type of test	Filtration	Reinforcement
Specifications		
Performance tests	Filter stability (A) Puncture resistance (A) Durability : chemical, biological (A)	Friction properties (e.g. pull out, slope shear)(A) In soil creep test (A) In soil tensile test (A) Durability : chemical, air, weathering, UV (A) Temperature (A)
Index tests	Opening size (N) Permittivity (N) Chemical resistance (A) Thickness (N)	Tensile test (strain stress) (N) Friction test (direct shear) (N) Tensile of joints (A) In isolation creep test (A)
Installation tests	Tensile test (N) Damage during installation (N) Durability (UV) (A) Deformability on site (A) Temperature (junction of gmb) (A) Joints strength (A) Dynamic puncture test (A) Identification of roll (N) Mass per unit area (A) Thickness (A)	Tensile test (strain stress) (N) Damage during installation (N) Dynamic puncturing test(N) Durability UV (A) Identification of of roll (N) Mass per unit area (A) Thickness (A)

(N) necessary
(A) when applicable

Table 4.a. (continued) : Geotextiles characterization for lining systems applications

Type of test	Drainage	Protection	Protection of environment
Specifications			
Performance	Long term transmissivity and corresponding compression (A) Durability : biological, chemical, temperature (A) Long term draining capacity (biological, clogging) (A)	Long term puncture test (A) (1,2) Durability : chemical (A) Multi-axial tensions (A)	
Index tests	Transmissivity (N) Water penetration resistance	Pyramidal puncture test (N) (1,2)	
Installation tests	Tensile test (N) Damage during installation (N) Deformability on site (A) Identification of roll (A) Mass per unit area (A) Thickness (A)	Tensile test (N) Damage during installation (N)(2) Durability (UV)(A) Dynamic puncture test (A)(2) Identification of roll (N) Mass per unit area (A) Thickness (A)	Inflammability(A) Smoke (A) Toxicity (A) Development drip behavior (A) Electrostatical properties (A)

(1) Gmb integrity after long term puncturing
(2) Tested in association with geomembranes
(N) Necessary
(A) When applicable

Table 4.b. Geomembranes in lining systems (continued)

Type of test	Fluid barrier (1)
Specifications	
Performance tests	Gas permeation (A) (2) Long term liquid "permeability" (N) Durability (2) Friction properties (anchorage, slope,...) (N) (5) Tensile performance (A) (4) Tensile performance on joints (N) Puncturing (5) : hydraulic stability performance (A) mechanical stability performance (A) Creep / relaxation (A) Bursting (A) (5) Durability : chemical, biological, UV, Oz, water, roots tested on gmb and joints (A)
Index tests (3)	Water vapor transmission (A) Thickness (N) Stress crack (A) Carbon black (content, dispersion) (A) Tensile test (strain stress) (N)
Installation tests	Tensile test (strain stress) (N) Impact test : gmb, joints (A) (5) Damage during installation (N) (5) Straightness, flatness (A) (3) Low T° folding (N) (3) High T° stability (N) (3) Coefficient of linear expansion (A) (3) Identification of roll (N) (3) Mass per unit area (A) (3) Thickness (A) (3) Joints (3) : peel test (A) and tensile shear test (A), vacuum box (N), spark test (A) and dual seams test (A), air lance test (A)

(1) fluid means liquids and gases
(2) weathering, chemical, biological, permanent elongation
(3) to be completed in coordination with Technical committee 254
(4) strain stress behavior; static and cyclic
(5) tested on the system geotextiles and geomembranes
(N) necessary
(A) when applicable

ACKNOWLEDGEMENTS

The authors would like to express their thanks to all the European experts working actively to the development of the CEN standards.

REFERENCES

CEN Technical committee 189 document n° 39 (1990). European Committee on Geotextiles and related-products, 44 pages

CEN Technical committee 189 Working group 1 document n° 32 (1992). European Committee on Geotextiles and related-products, 10 pages.

C.F.G.G. (Comité Français des Géotextiles et Géomembranes). "Recommandations générales pour la réception et la mise en oeuvre des géotextiles". Normes françaises d'essai CFGG - 1984.

Rathmayer (1992) "Experiences with "VTT-GEO" classified non-woven geotextiles for finnish road construction". Second International Conference on Geotextiles. Las Vegas, pp. 307-312.

Rigo, J.M., Mathieu Y., Smolders K. and Alexandre E. (1990). "I.G.S. Inventory of current test methods on geotextiles". The International Geotextiles Society, 154 pages.

Rollin A. and Rigo J.M. "Geomembranes. Identification and Performance testing". R.I.L.E.M. report 4. Chapman and Hall, London. 335 pages.

Geosynthetics '93
Conference Proceedings

Volume 1
Opening Session
Roads and Pavements
Walls, Slopes, Embankments and Foundations
Geotextile Filtration Design and Testing

Volume 2
Geosynthetics Testing
Durability and Long-Term Performance of Geosynthetics
Technical Advances, Innovations, Challenges

Volume 3
Waste Containment Case Histories
Landfill Design, Performance and CQA

Organized by
The North American Geosynthetics Society
(NAGS)
The Industrial Fabrics Association International
(IFAI)
under the auspices of
The International Geotextile Society
(IGS)

GEOSYNTHETICS '93
CONFERENCE
VANCOUVER, BRITISH COLUMBIA

March 30-April 1, 1993

Vancouver Trade & Convention Centre

Waterfront Centre Hotel

Vancouver,
British Columbia,
Canada

GEO'93

CONFERENCE PROCEEDINGS

VOLUME 3

SPONSORED BY

SOLMAX

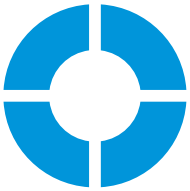

agru

The Plastics Experts.

Geosynthetics '93
Conference Proceedings

Volume 3

Waste Containment Case Histories
Landfill Design, Performance and CQA

This volume consists of papers presented at the
Geosynthetics '93 Conference held
March 30 - April 1, 1993 in Vancouver, BC, Canada

Sponsored By:

North American Geosynthetics Society
Industrial Fabrics Association International
under the auspices of the International Geotextile Society

Geosynthetics '93 Organizing Committee

Barry R. Christopher, Co-Chairman
Robert Denis, Co-Chairman
Joseph A. Dieltz, Secretary General
Richard J. Bathurst, Technical Committee Chairman
Robert G. Carroll
Jonathan Fannin
Mark L. Marienfeld
Frank Taylor
John F. Beech, Advisor

Publisher

Industrial Fabrics Association International
345 Cedar Street, Suite 800, St. Paul, MN 55101, USA
612-222-2508, fax 612-222-8215

Notice and Disclaimer

Forward

The 120 papers and invited lecture contained in these volumes represent the Proceedings of Geosynthetics '93 held in Vancouver, British Columbia, Canada, March 30 - April 1, 1993. The conference was co-sponsored by the North American Geosynthetics Society and Industrial Fabrics Association International and held under the auspices of the International Geotextile Society.

The papers in these volumes began with 307 abstracts that were received by the Organizing Committee of Geosynthetics '93 in answer to an international call for papers issued in 1991. A Technical Committee comprising seven knowledgeable persons employed with universities, manufacturers, distributors, consultants, testing laboratories and government agencies reviewed all abstracts. Based on this initial selection process, 179 authors were invited to submit full papers. Each paper was carefully reviewed by at least two qualified referees and the result of this peer-review is the collection of valuable papers gathered here. These 120 papers were presented in 24 technical sessions and a poster session at Geosynthetics '93 and represent the largest number of papers ever presented at a North American Conference devoted to geosynthetics.

A great number of individuals gave their valuable time to review papers and to offer constructive advice to the authors. The efforts of the Technical Committee of Geosynthetics '93 and the session leaders who organized the paper reviews are also gratefully acknowledged. Without their help, Geosynthetics '93 and these Proceedings would not have been possible. In addition, acknowledgements would be incomplete without thanking Mr. Joseph A. Dieltz, Timothy J. Arens and the IFAI staff who smoothly executed the formidable logistics required to organize Geosynthetics '93 and to produce these Proceedings.

This collection of technical papers is not only a valuable record of the state-of-the-art for geosynthetics in North America and worldwide, but also a testament to the co-operative spirit of the geosynthetics community in Canada and the United States.

Richard J. Bathurst
Chairman, Technical Committee
Geosynthetics '93

Table of Contents

Volume 1

Opening Session

Roads and Pavements

Walls, Slopes, Embankments and Foundations

Geotextile Filtration Design and Testing

Volume 2

Geosynthetics Testing

Durability and Long-Term Performance of Geosynthetics

Technical Advances, Innovations, Challenges

Volume 3

Waste Containment Case Histories

Landfill Design, Performance and CQA

WASTE CONTAINMENT CASE HISTORIES

GEOSYNTHETICS '93 CONFERENCE
VANCOUVER, BRITISH COLUMBIA

Geosynthetic Floating Silt Curtain in Environmental Protection Control: A Laboratory Study

M.M.K. Kan
Hong Kong Polytechnic, Hong Kong

K.H. Chang
Hong Kong Polytechnic, Hong Kong

K.W. Chau
Hong Kong Polytechnic, Hong Kong

ABSTRACT

Large scale dredging and reclamation in coastal waters will create a tremendous amount of mud and silt dispersion which will endanger the maritime ecological system as well as the environment. This paper reports the results of a laboratory study on the effectiveness of geosynthetic floating silt curtains in an open channel. Different types of floating silt curtains were set up across the channel and then tested under different water flow rates and water depths. Mud slurry, comprising a mixture of the fine particles of marine clay and water, was released upstream of the silt curtain. Water samples were then collected at various selected locations and depths, both upstream and downstream, of the silt curtain. Water samples were simultaneously drawn via a suction device at normalized time intervals. Suspended solids analysis of the water samples was then conducted. The percentages of suspended solids were used as an index value to demonstrate the effectiveness of the floating silt curtain.

INTRODUCTION

In the last four decades, Hong Kong has always faced the problem of land shortage. Reclamation has been practiced to increase the supply of useable land. Hong Kong's Port and Airport Development Strategy (PADS) and Metroplan are in the process of being implemented, therefore extensive measures for reclamation, in excess of 2,500 hectares of land, will be carried out in Hong Kong's foreshore and seabed in the next few years. Before filling material is deposited on the seabed of a coastal area, the low-bearing capacity material is either stabilized, or removed by dredging. Dredging is a process by which sediments are removed from the bottom of streams, rivers, lakes or coastal waters. The desired bed configuration of the filling material can also be achieved by dredging.

Dredging will inevitably cause some impact on the environment. The impact of dredging on the environment may be either short- or long-term, and can be classified into three categories: 1) physical, 2) chemical, and 3) biological. During the dredging process, a large quantity of sediment, which may be highly contaminated, mobile, and with a high risk of impact on the environment, will be disturbed and stirred up. Dredged sludge generally constitutes a large amount of fine matter, which is typically more than 60% by dry weight. The sediment is usually contaminated by bio-chemicals from industrial and domestic wastes. A large quantity of suspended solids in the water will cause turbidity, which is the most obvious effect of dredging on the water quality. Increased turbidity is likely to have an adverse effect on the environment. It also reduces the amount of sunlight penetration into the water, thus affecting the photosynthesis of plants. Turbidity can be reduced by

increasing the settling rate of sediments or confining the affected area (Baillard et al, 1984). The settling rate is related to the terminal velocity of a grain, and is dependent on the size of the grain. Hong Kong's marine mud contains a large quantity of fine particles by weight, which favors the spreading of suspended solids and also turbidity.

The objective of this study is to investigate the effectiveness of floating silt curtains to control the area of turbidity. Such a curtain physically prevents the suspended solids from spreading over the sea and limits the level of damage to the natural environment.The main component of silt curtains comprises geosynthetics, which involve woven or nonwoven geotextiles or a combination of the two. To allow water movement through the fabric of the silt curtain, it should provide sufficient permeability for water flow. At the same time, the silt curtain should serve the purpose of retaining soil particles and floating substances. Various types of geosynthetics will serve the purpose of the silt curtain, and their effectiveness can be tested in an open channel, as the flow rate and water depth may be varied to determine the effect on the efficiency. The geosynthetics tested in this study included three types of geotextiles - used by themselves, or in combinations to form composites, and one type of geogrid. Comparison of percentages of suspended solids both upstream and downstream of the curtain were used to demonstrate the effectiveness of silt curtain. Synthetic polymers are relatively insensitive to the action of different chemicals and to environmental effects. In many cases this is an advantage over traditional materials. Nonetheless each polymer has a lot of weaknesses which must be taken into consideration in the design of the curtain. The result is that mechanical properties such as strength, elasticity and strain absorption capacity deteriorate and the materials eventually become brittle and cracked. Since the silt curtain will be submerged in sea water and exposed under sunlight for a long time, the materials should be able to resist the combined effect of sunlight and sea water. For these reasons, the durability of the materials was also studied.

GENERATION OF TURBIDITY

The grab dredger is the most common form of mechanical dredger, and it is constructed in a variety of forms. All designs incorporate a grabbing system characterized by a slewing crane which lowers and hoists the grab into and out of the water. Wires from the crane system operate the grab mechanism. Suspended solid concentrations generated by a typical grab dredging operation can be traced to four major sources (Bray, 1979):-

(a) The grab is lowered to impact the seabed which generates the sediment suspension.
(b) Subsequently the grab is closed and removed from the bottom.
(c) Sediment erosion from the open top and mud covered grab surface as the grab is hauled upward through the water column.
(d) Barge loading and draining.

A typical grab dredging operation, such as that shown in **Figure 1**, will produce a turbidity plume several hundred meters downstream with average water column concentrations generally less than 100mg/l (Hayes, 1984), while the suspended solids concentration would be higher at the bottom of the channel.

To simulate the turbidity plume caused by the dredging operation in an open channel, marine mud slurry was released upstream via the mud slurry release device. Initially the sediment dispersed in all directions, then steadily spread along the direction of flow, and finally settled at the bottom of the channel. The distance

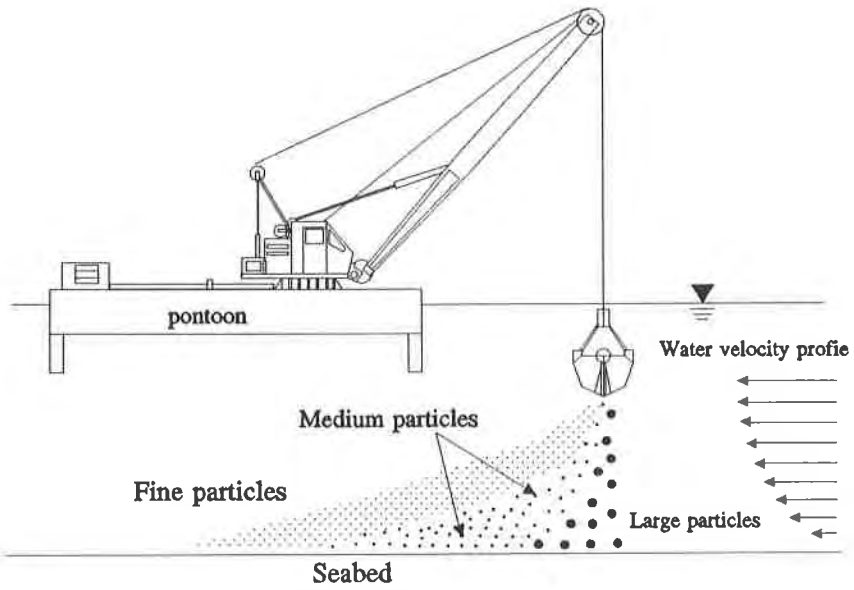

Figure 1. A Schematic Drawing showing the Dredging Operation

travelled by the particles depended on the particle size and the flow rate (Uchrin et al, 1980). A high proportion of fines in marine mud slurry would provide an excellent picture of the general mechanism of turbidity generation in the vicinity of dredging (Johnson, 1980).

Fine silt particles tend to create turbidity. The degree of turbidity is dependent upon the percentage of fine particles in the marine deposit. The chemical and physical properties of marine sediments may vary from place to place, according to the geological origin of the source. In this study, mixtures of a specified quantity of oven-dried fine particles of marine clays, less than 63μm in size, and water were used. The marine clays were pretreated by removing the sandy fractions and marine shells, since turbidity is mainly caused by fine particles and their removal also served to prevent blockage of the mud slurry release device. The marine mud were obtained from two reclamation areas in Hong Kong - West Kowloon and Junk Bay. Both of the marine clays contained a high percentage of silt and clay particles, i.e., approximately 94%. Their particle size distribution are as shown in **Figure 2**. The sample from West Kowloon contained more fine particles than the corresponding one from Junk Bay. Dredging marine mud which contains a large proportion of fine particles will cause serious turbidity in the water (Huggett et al, 1980).

DESCRIPTION OF SILT CURTAIN

The geosynthetics used in this project consisted of a tape-on-tape woven; a heat-bonded nonwoven; a needle-punched nonwoven; composites combining woven with heat-bonded, and woven with needle-punched geotextiles, which were sewn together; and a geogrid. Their individual properties are tabulated in Table 1 (Koerner, 1985). The function of the silt curtain is to prevent polluted water from spreading by screening the water, therefore the depth of silt curtain should be the same as the water depth. Since water pressure acts on the silt curtain, a reinforcing and supporting system was necessary to provide the structural stability. The following were the basic components of silt curtain:

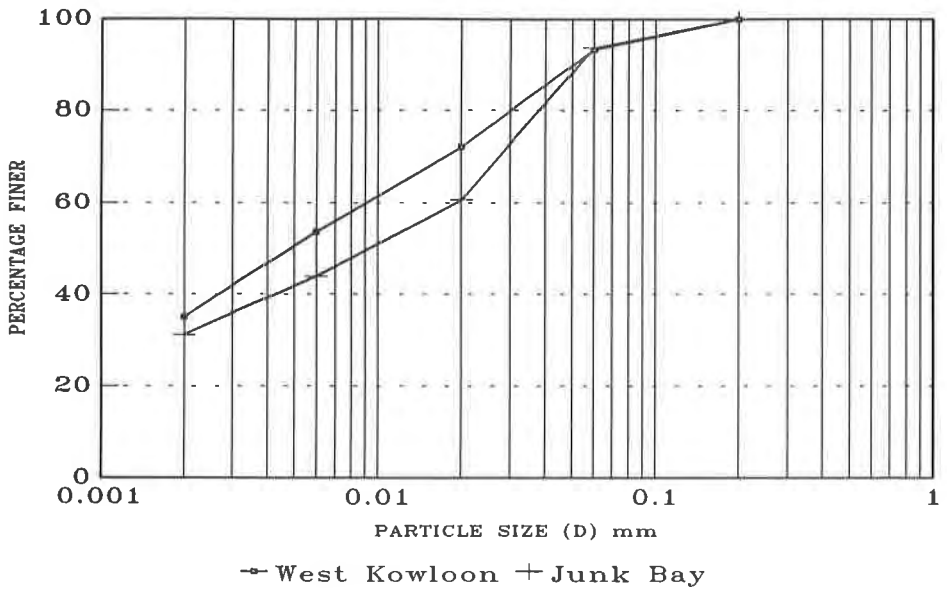

Figure 2. Particle Size Distribution of Marine Deposits.

(1) Floats - These are the main supports of the silt curtain in water, they provide uplift thrust to erect the silt curtain in water. In practice, anchorage should be provided at reasonable span length along the silt curtain, usually at 10m (32.8ft) intervals; so that the silt curtain can be properly secured at its designated location. The anchorage system consists of ties which are fastened to the floats at their designated positions, and then connected to either deadmen or anchors, which are secured at the bottom of the seabed. Since the silt curtain was supported by the two side walls of the open channel in this laboratory study, floats were not necessary.

(2) Reinforcing system - this was required because the silt curtain would be subjected to water pressure. As the flow rate increases, the pressure also increases. The hydrostatic pressure exerted on the curtain would create tensile stresses on the geotextile silt curtain, and eventually would rupture and damage the curtain. In order to provide sufficient resistance against tensile failure, stiff and high strength reinforcement should be introduced to strengthen the geotextile silt curtain in both longitudinal and transverse directions. In this project, two layers of geogrids were employed to form a pocket-like structure. The geotextile silt curtain was inserted and sandwiched between the geogrids as shown in Figure 3. The rigid structure of the geogrids provided additional stiffness to the overall system to withstand the high water pressure and to maintain the curtain in the upright position as far as possible. In practice, this system would facilitate the replacement of a damaged or clogged geotextile silt curtain. The geogrids can be reused many times. By using higher strength geogrids, serviceability can be guaranteed. Anti-fouling can be coated on the surfaces of geogrids to reduce the possibility of attack by marine life.

(3) Weight chain - The water pressure would cause the silt curtain to deflect. Thus sufficient weight should be provided to ensure that the silt curtain remains vertical across the channel.

Table 1 Properties of geosynthetics (Manufacturer Data)

Geosynthetics Type	Woven	Heat bonded	Needle punched	Geogrid
Type of Fibres	tape-on-tape	continuous filament	continuous filament	composite
Polymer Type	PP	PP/PE	PP	PE(casing)/PET(bands)
Mass per unit area (g/m^2)	155	140	165	530
Thickness (mm)	0.4	0.7	1.6	4.0
Permeability ($l/sec/m^2$)	2.7	50.0	54.5	---
AOS (μm)	0.6 to 0.2	100	150	---
Tensile Strength (kN/m) MD/XD	18.8/18.8	8.0/8.0	14.2/14.2	50/50
% at break MD/XD	10/6	30/30	50/50	11/11

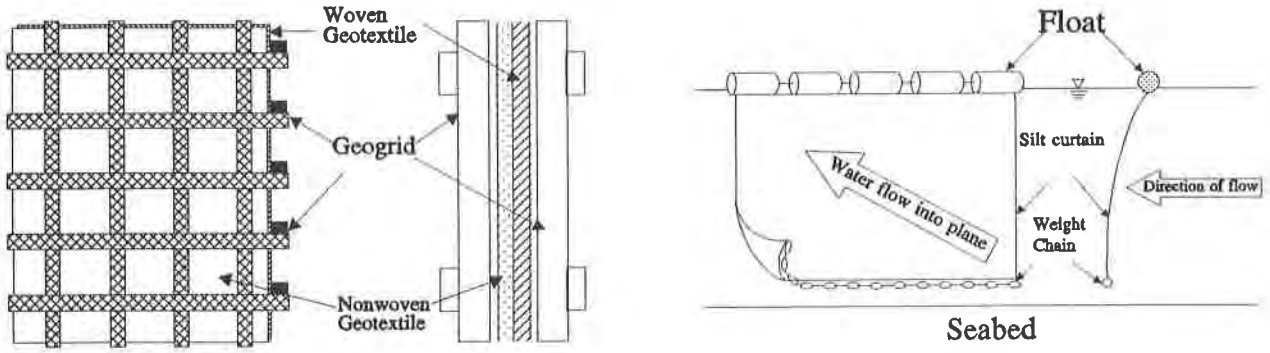

Figure 3. A Schematic Drawing showing Details of Silt Curtain.

MECHANISM OF SILT CURTAIN IN TURBIDITY CONTROL

Using the silt curtain, the pollution caused by dredging or reclamation operations can be closely confined. The mechanisms of the silt curtain in turbidity control are two fold and they are as follows:-

(1) Effect on surface water velocities - Generally the velocity profile of the water flow in the steady state is parabolic in form. The speed of water is higher in the upper layers than in the lower layers (Featherstone et al, 1982). In this study, the marine mud mixture was released at the surface of the water. Fine soil particles were spread across the surface and the upper layers of flow to the downstream regions of the source almost instantly by the fast moving water. This process most closely resembled the effluent discharge, rather than the dredging operation method. Nevertheless, the process served the purpose for the study of the effectiveness of the silt curtains. With the installation of the floating silt curtain obstructing the flow, the water flow near the curtain became slightly turbulent and behaved in a rather random, disorderly manner due to the rebounding and deflected water waves. Thus the

velocities of flow at the surface and the upper layer were retarded. But the water flow speeds at the lower layers were increased due to the convective effect of the water current. These increased velocities of water flow carrying the suspended solids would tend to get through the silt curtain via the underside of the silt curtain. The suspended solids which passed through the underside of the silt curtain would settle in a very short period of time, because of the limited settling depth, and thus turbidity would not occur. These phenomena are shown in **Figure 4**. Nevertheless, at very high levels of turbulece, the particles may not settle. The loosely settled particles, at further downstream, may be disturbed and recurrence of turbidity is possible.

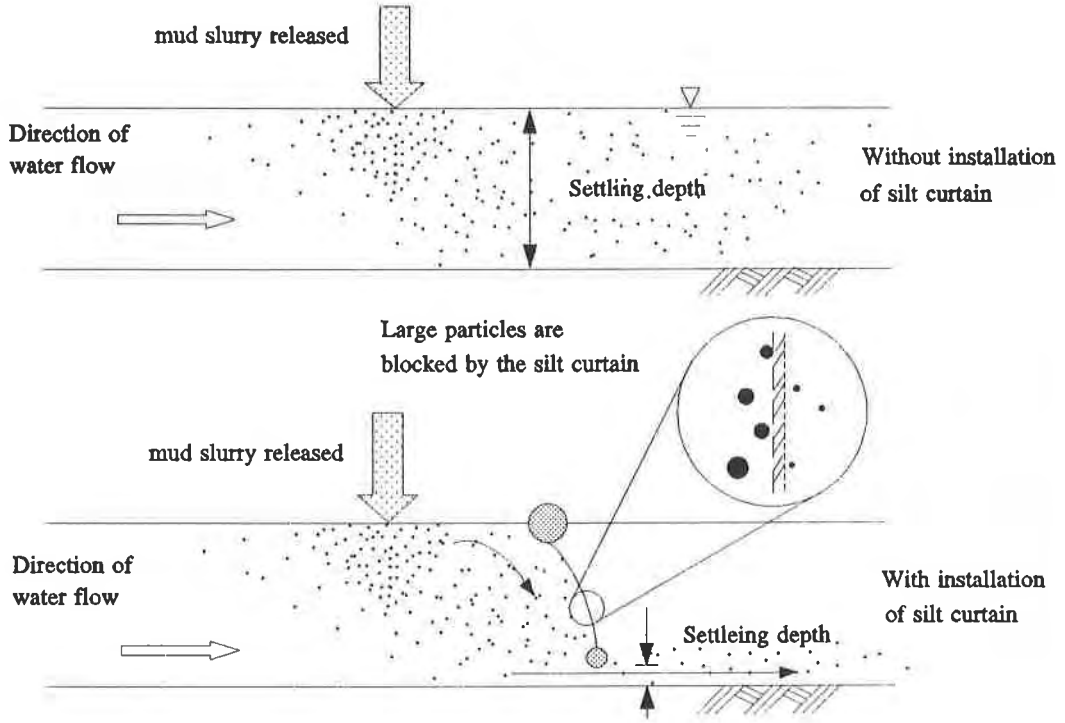

Figure 4. A Schematic Drawing showing the Mechanism of Blocking Effect.

(2) Blocking effect - The vertical velocity component of the water flow is much smaller than that of the horizontal. Therefore, the small suspended solids raised from the seabed during dredging or reclamation work move more quickly in the horizontal direction than in the vertical direction. Thus, turbidity dispersion to the vicinity occurs almost immediately when the engineering work has begun. The rate of expansion of boundary of the turbidity spread depends on the water velocity. The main function of the silt curtain is to block the spreading of suspended solids, while allowing water to flow through. In the experiment, the silt curtain was set across the direction of flow in the channel. When the turbidity cloud moved forward to the silt curtain, the spreading of turbidity was blocked. Only very fine soil particles of sizes less than the pore size of silt curtain could pass through the silt curtain and finally reach the downstream regions. Nevertheless, larger soil particles might be transported to the downstream regions by the water flow through the gaps between the curtain and the side walls of the channel. Similarly, particles could pass under the silt curtain, as the curtain would be raised up by the water uplift. In practice, the effectiveness of the silt curtain depends on the joining details. In the case of insufficient overlapping of

such panels, the pressure generated by the water flow would force the joints to open, allowing large quantities of effluent to pass through at the joints. Therefore the panels must be properly fastened and sufficient overlapping has to be ensured in order to achieve the utmost effectiveness. Due to the blocking effect, the suspended solids would be confined in the upstream region of the curtain for a longer period of time, and thus the particles settled in the upstream region of the curtain.

DESCRIPTION OF APPARATUS

This laboratory study to determine the effectiveness of geosynthetic floating silt curtains was performed in an open channel, which was designed to simulate the coastal water environment. Flowing water was generated by a pumping system. The water depths inside the open channel were varied to simulate the effect of tides. The components were as follows: (i) open channel, and (ii) sampling device.

Open channel - The open channel used in this investigation was 3m (9.8ft) in length by 0.6m (2.0ft) in width. The silt curtain was set at one third length of the channel from the inlet end. Mud slurry, comprising a mixture of the fine particles of marine clay and water, was released upstream of the silt curtain. A schematic drawing of the open channel is as shown in Figure 5. The individual components and accessories were as follows:

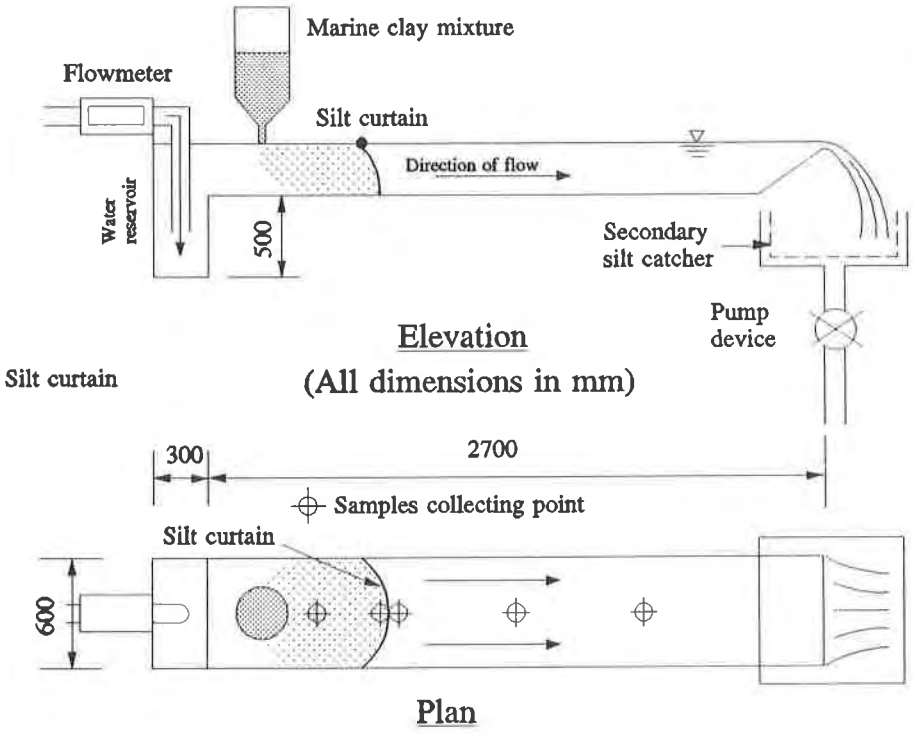

Figure 5. A Schematic Drawing showing Layout of Open Channel.

(1) Inclined plane - A flat smooth plane was installed at the end of open channel, and the inclination of the plane could be adjusted to vary the water depth.
(2) Water pump - A centrifugal pump was used to generate a steady water flow to the open channel. In this study, three water flow rates of 2.523 (0.667), 3.785 (1.000), 5.047 (1.333) l/sec (gal/sec) respectively were generated.
(3) Flow meter - The water flow rate was measured by a flow meter which was connected to the water inlet pipe.

(4) Secondary silt catcher - At the end of the open channel, a secondary silt catcher was installed and its purpose was to ensure that no soil would enter the centrifugal pump, since the water flow out from the channel was recycled by means of the pumping device.

(5) Water reservoir - It extended to a greater depth than the channel at the inlet and its purpose was to act as an energy dissipator. This was to prevent the increase of turbulent suspectibility of the flow caused by the pounding of inlet water flow.

Water sampling device - The water and suspended solids samples were collected by a vacuum pump system as shown in **Figure 6**. The system included an electric vacuum pump, which was connected to 15 sampling bottles, each bottle being connected to a plastic intake tube. Totally 15 plastic tubes were then immersed into water along the open channel in 5 different locations at 3 different depths, which could be taken simultaneously.

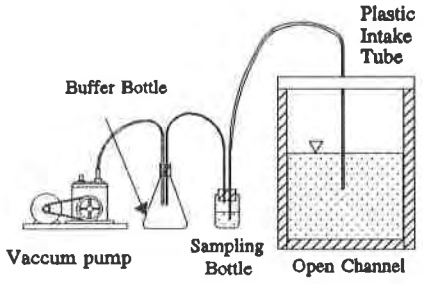

Figure 6. Schematic Drawing showing Details of Sampling System.

TESTING METHODOLOGY

A designated water flow was released into the open channel, and once the water flow was steady, the rate and water depth were recorded. A silt curtain with known mass was then mounted across the open channel so that it was perpendicular to the flow. The vacuum pump system was connected to the sample taking system, and sample-taking tubes were fixed at selected locations. It was very important to ensure that the sample-taking system was well connected without leakage.

Marine mud slurry was released upstream of the curtain, and timing of the experiment began from this moment. The time of release of the slurry was recorded to calculate the mean rate of pollutants added. When all the slurry had been released, the vacuum pump was activated to take up water samples. A brand new silt curtain was used for each variation of flow rate or flow depth. Before commencement of each test, the sediment remaining in the channel was removed. In order to determine the amount of soil retained on the silt curtain after each test, the curtain was dried and reweighed.

Total suspended solids tests, designed to comply with the relevant standard (Standard Methods for the examination of water and waste water :1985), were conducted on the collected water samples at various selected locations. The percentages of the suspended solids were used as the comparison indexes.

Durability test - The geosynthetics used in this study were immersed in sea water and placed under sunlight in a transparent tank with cover. The salinity and pH value of the sea water were maintained within a range of 27 - 33 ppt and 7.8 - 8.0 respectively. Tensile tests were then carried out on samples at regular time intervals in order to obtain the percentage loss in strength as compared to the controlled samples. For each testing batch, 10 samples of each type of geosynthetic were tested; except for the geogrids, for which only 2 samples were tested each time.

PERFORMANCES OF SILT CURTAINS

The performances of different kinds of silt curtains under different water velocities and at different sampling depths are as shown in **Figures 7(i) to (iii)** respectively. All of them indicate that there was a sudden drop in the percentages of suspended solids at distances beyond the silt curtain. These drops implied that the silt curtains functioned effectively. The four kinds of silt curtains used in this testing programme showed good performance in turbidity control. Generally they reduced the percentages of suspended solids to less than 20% of their initial values, and confined the concentration of the turbidity just upstream of the silt curtain. This effect was much more pronounced at high water velocity and as indicated in Figure 7(iii). Beyond the silt curtain, the suspended solids concentrated at lower layers. This indicated that the silt particles were settling very quickly. Thus it was demonstrated that the installation of silt curtain was a very effective means in reducing turbidity and promoted settling of sediments.

At low water speed, 14mm/sec (0.05ft/sec) as shown in Figure 7(i), the drop of percentages of suspended solids was less obvious. The reason was that the majority of the particles had already settled before they arrived at the silt curtain as the flow was much more steady and laminar. However, there was still improvement as compared to the case without a silt curtain, since fine particles require a long time to settle. The results indicated that the silt curtain was effective in retaining fine particles.

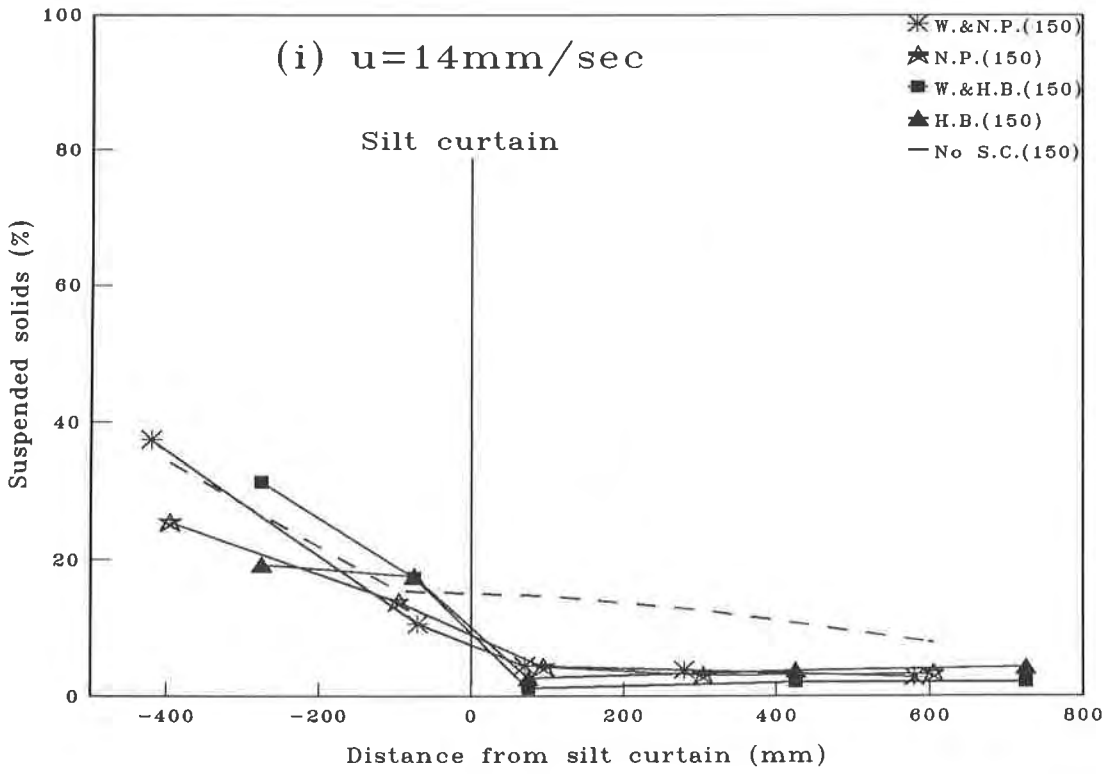

W.=Woven; H.B.=Heat Bonded; N.P.=Needle Punched; No S.C.=No Silt Curtain
The number inside ( ) is sampling depth. u= mean water velocity.

Figure 7. The Performances of different kinds of Silt Curtain under different Water Velocities.

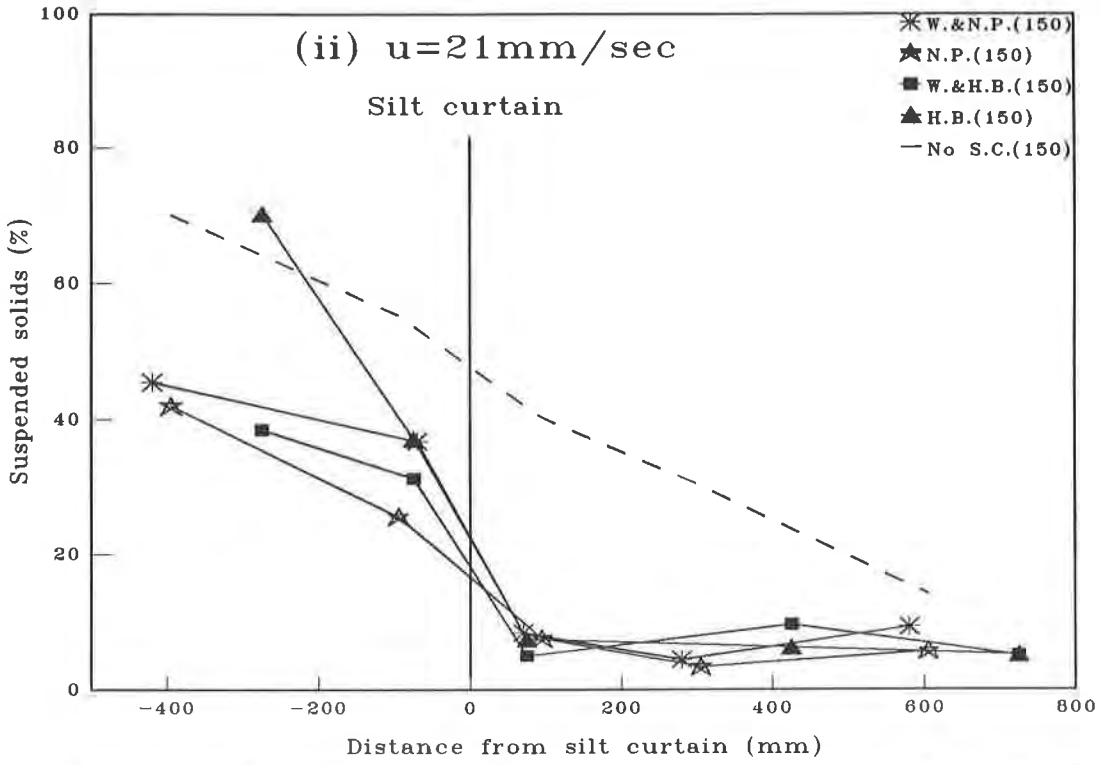

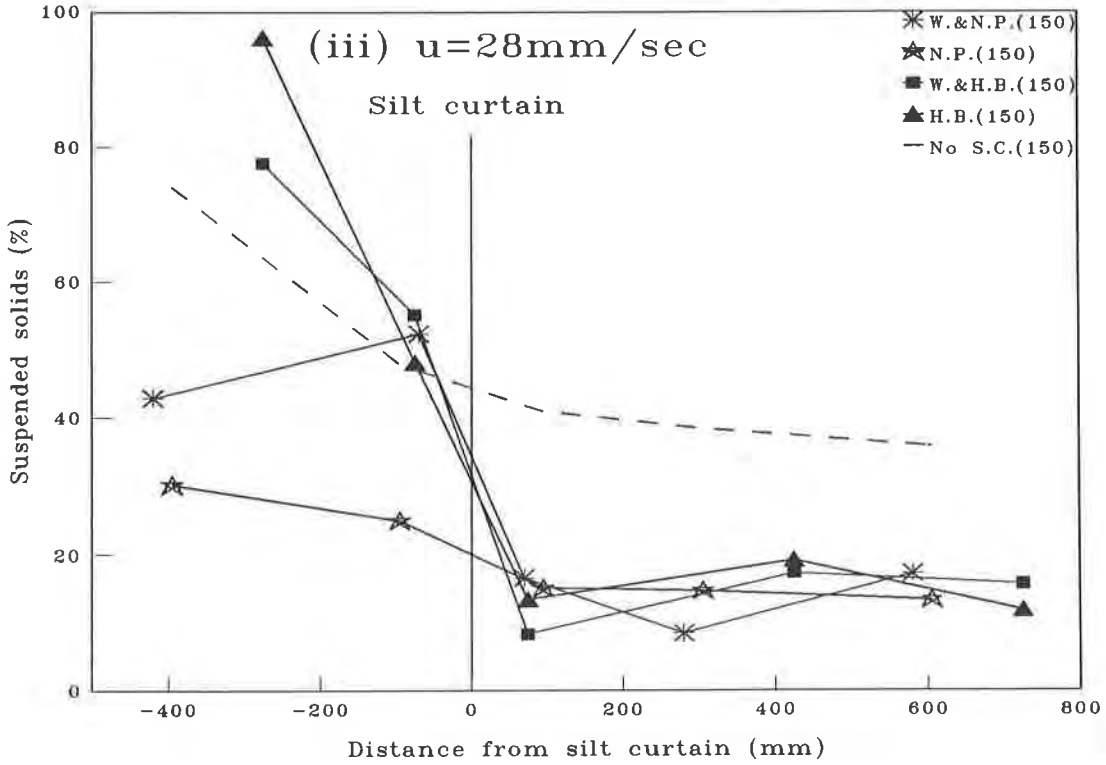

W.=Woven; H.B.=Heat Bonded; N.P.=Needle Punched; No S.C.=No Silt Curtain

The number inside ( ) is sampling depth. u= mean water velocity.

Figure 7. The Performances of different kinds of Silt Curtain under different Water Velocities.

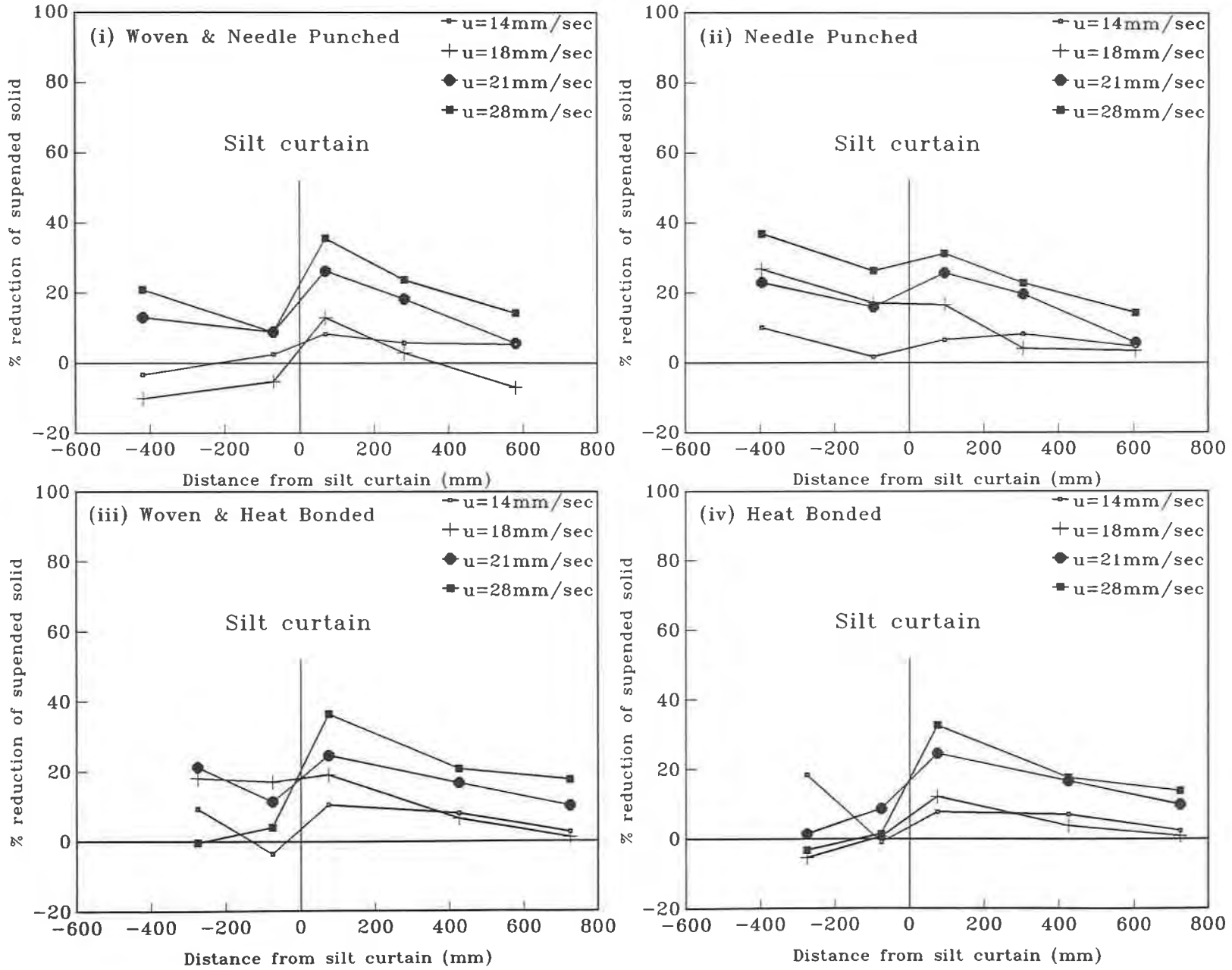

Fig.8 Percentage reduction of suspended solid compared with those without silt curtain

The results also showed a slight increase in percentages of suspended solids downstream of the channel which was due to turbulence and reflective waves caused by the inclined plane at the end of the channel. Water flow which pounded on the inclined plane and then reflected backward caused the resuspension of sediment.

Effect of water speed on the performance - **Figure 8(i) to (iv)** showed the mean percentage reduction of suspended solids against distances from the silt curtain at various water speeds. The mean value represented the average concentration of suspended solids at different sampling depths for the same location. The performance levels for silt curtains were different under different water speeds. Generally, at high velocity flow, the settling time for fine particles increased. Therefore, fine soil particles would be suspended longer in the water, and carried by the swift water flow to the downstream regions. With the installation of silt curtain, high concentration of suspended solids gathered behind the barrier, and an increasing amount of the suspended solids carried by the flow would pass through the under-side of the silt curtain and along its sides rather than directly passing through the curtain. Wakes and turbulence, generated by water flow through the silt curtain would also promoted these kinds of passage. The high water speed also caused resuspension of sediments which had already settled both upstream and downstream of the curtain. Turbulence was also increased at the inclined plane near the end of the channel. The occurrence of resuspension of particles was demonstrated very distinctively in those results of high water velocities. Higher water speed also implied higher pressure acting on the silt curtain. This thrust generated tensile stresses on the geotextile and tended to increase the opening size of the geotextile, such that more particles would pass through the silt curtain. The high velocity flow also tended to force the fine soil particles to penetrate into the silt curtain. From the results of the tests on the needle-punched geotextile, the amount of soil retained on the silt curtain became lessened as the speed of water was increased. These effects were obvious in the needle-punched geotextile, because of its rather loose and flexible structure. On the other hand, the combined structure sewn with the woven geotextile could provide higher tensile strength and thus increase the structure's stiffness. They were clearly indicated in **Figures 8(i) to (iv)**. Also, as indicated in **Figures 7(i) to (iii)**, the percentages at lower depth were usually greater than those at the upper layers irrespective of water speeds. These results have further verified the efficiency of the installation of silt curtain in turbidity control.

Environmental effect - Since the silt curtain was submerged in sea water, the resistance of geosynthetics to chemical, sunlight and water stability were also of interest in terms of the design. In this study, we have examined the strength loss in geosynthetics subjected to the combined effects of attack. **Figure 9** shows the percentage strength retention of geosynthetics under the combined effects of sea water and sunlight. The results showed that, after 8 weeks exposure to sunlight and water, the percentage loss in strength of the woven geotextiles was reduced by only 4.1% while the percentage loss in strengths for the needle-punched and heat-bonded geotextile were 36.5% and 55.5% respectively. The loss in strength for the needle-punched and heat-bonded geotextiles was significant. Polypropylene is usually subjected to thermal oxidation and photo-oxidation when exposed to ultraviolet radiation, which promotes deterioration of fibre mechanical properties. All the geotextiles used in this study were made of polypropylene polymer, but each one showed different results in the stability tests. The differences were mainly due to the manufacturing process. The geogrids had lost 35% of their strength in 8 week's exposure, it is believed that, hydrolysis of the ester group in the polyester fibres had occurred. It is because the rate of hydrolysis depends on the temperature, and the ambient temperature inside the covered transparent samples container was very high, approximately 60°C or above.

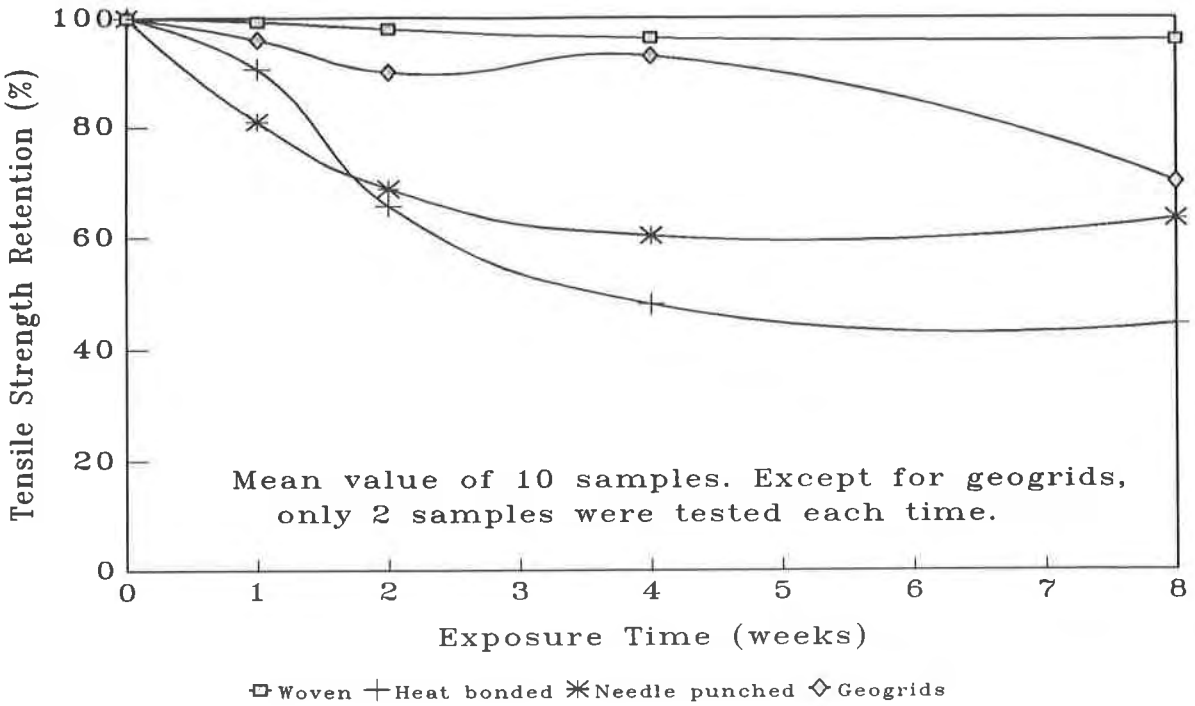

Figure 9. Percentage tensile Strength Retention of Geosynthetics after exposed to UV light and Seawater.

CONCLUSIONS AND RECOMMENDATION

A silt curtain proved to be effective to prevent widespread silt dispersions in the laboratory simulation study. The percentage contents of suspended solids downstream of the silt curtain were quite different under different water speeds. Although at higher water speed, the percentage of suspended solids was increased both upstream and downstream of the silt curtain, the results indicated obvious improvement in water quality. Utilization of a longer channel in the laboratory study can avoid the increasing amount of resuspensed sediment downstream of the curtain, which is the result of the reflected waves caused by the pounding water on the flow depth controlling device. Furthermore, the heat-bonded geotextile and the woven/heat-bonded geotextile composite showed better results than the needle-punched geotextile at high water speed. This is because of the rigid, tough and compact fabric structure of the heat-bonded geotextile. This implies that the stiffness of materials is an important factor and should be taken into consideration in the design of silt curtains.

From the results of the durability tests, it was found that the woven geotextiles provide better resistance to sunlight and sea water attack than the two nonwovens. In comparing the results of the two nonwovens, the needle-punched geotextiles exhibited slightly better results over the heat-bonded geotextiles. The main reason for this is their thick, bulky structures and only the fibres at the top surfaces of fabrics were attacked. Whereas for the thin but rigid heat-bonded geotextile, the penetration of UV light and the chemicals from the sea water were tremendous. They lost 50% of their original strength over a period of eight weeks. Therefore, constant replacement or the use of heavier fabrics with UV stabilizer is required for long-term service. It is believed that, by changing the polymer type to polyester (Van Zenten, 1986), the structure's stability against sea water and UV light attack could be improved. Nevertheless, we should bear in mind that the

polyester fibres can be slowly plasticized by water which enters the amorphous regions of the polymer and enhances molecular mobility. This would lead to a reduction in modulus and strength, but the effect is completely reversible when the water is removed (Davis, 1989). Geocomposites with woven geotextiles were proved effective in use as silt curtain because of the high moduli and stregths and low permeabilities; and thus, promoted the blocking effect; especially under high water speeds.

Since a floating silt curtain remains to be installed in water for a long time, maritime life will grow all over its surface, thereby altering the mechanical and hydraulic properties, and reducing the efficiency. In order to prevent this problem, a preferable solution would be to input antifouling agents into the polymer resins during the manufacturing process of geosynthetics. Such antifouling treatments should be stable to the silt curtain and non-polluting to the environment. Besides, the design of the silt curtain should incorporate ease of installation and maintenance. Based on the above reasons, geotextiles are highly suitable for silt curtain applications.

REFERENCE

Baillard,J.A., & Jenkins,S.A., (1984) "Systems for Reducing Sedimentation in Berthing Facilities ", Proceeding of the Conference Dredging'84, Vol. 1, pp. 311-320.

Bray,R.N., (1979) "Dredging: A Handbook for Engineers", Edward Arnold.

Davis,G.W., (1989) "Aging and Durability of Polyester Geotextiles", Durability and Aging of Geosynthetics, Edited by Koerner,R.M., Elsevier Applied Science, pp. 65-81.

Featherstone,R.E., & Nalluri,C., (1982) "Civil Engineering Hydraulics", Collins.

Hayes,D.F., & Raymond,G.L., (1984) "Sediment Resuspension from Dredging Activities", Proceeding of the Conference Dredging'84, Vol. 1, pp. 72-82.

Huggett,R.J., Nichols,M.M. & Bender,M.E., (1980) "Kepone Contamination of the James River Estuary", Contaminants and Sediments, Vol. 1, pp. 33-52.

Johnson,B.H., (1980) "Discussion of Mathematical Models for Computing the Physical Fate of Solids Released in Open Water During Dredging or Dredged Material Disposal", Contaminants and Sediments, Vol. 1, pp. 331-348.

Koerner,R.M., (1985) "Designing with Geosynthetics", Prentice-Hall.

Standard Methods for the Examination of Water and Wastewater, (1985), APHA, AWWA, WPCF.

Uchrin,C.G. & Weber,W.J., (1980) "Modeling of transport Processes for Suspended Solid and Pollutants In River - Harbor - Lake System", Contaminants and Sediments, Vol. 1, pp. 407-425.

Van Zanten,R.V. (Ed.), (1986) "Geotextiles and Geomembranes in Civil Engineering", John Wiley & Sons, New York.

Guidance for Design of Watertight Geomembrane Attachments to Concrete Surfaces

L.W. Well
CH2M Hill Inc., USA

ABSTRACT

The failure of thin rubber gaskets that allowed leakage in waste treatment lagoons and the need for a gasket designed to function under a 60-foot head in a water storage reservoir prompted the evaluation of gasket seals for geomembrane attachments to concrete structures. Mechanical watertight seals of geomembranes to structures require careful design and selection of materials. This paper presents general design methods to limit the compression of neoprene rubber gasket material so that the range of elasticity for the rubber is not exceeded. Without proper design, gaskets may be too thin, may be overtightened, and may distort the compression strip, which in turn subjects the gasket to uneven compression and results in leakage. Adhesive anchors (rather than mechanical anchors) are recommended for attaching the gasket system to concrete for improved reliability of the clamping method.

INTRODUCTION

This paper presents an approach to designing seals of geomembranes to concrete structures. It is based on an analysis of systems that have been developed and used to seal geomembranes to structures.

To achieve an essentially watertight, leak-proof seal against a concrete structure, several key elements must be considered by the designer. These elements are briefly described as follows:

- The condition of the geomembrane at the location of the attachment to the structure is important. The smoothness of the lap joints, the absence of wrinkles or defects, and the control of stresses on the geomembrane must be considered and specified in the design.

- The clamping pressure for the sealing system is provided by the anchor bolt and nut acting on the rigid, continuous batten strip. The hardness and type of elastomeric materials must be considered by the designer in order to distribute the clamping pressure evenly. Controlled stress ensures that the gasket seal is not tightened beyond the material's elastic limit and maintains the sealing pressure on the interface of the

geomembrane and structure contact. Many cases have been observed in which very thin gasket strips were overtightened until the rubber failed because its elasticity was exceeded. In those cases, the rubber no longer functioned as a compression seal to hold the materials in close contact with each other. The special factors that will be considered are related to thickness, shape, durometer hardness, and elastic properties. References and design graphs are included for the designer.

- The finish and strength of the concrete to which the geomembrane will be sealed must be known or specified. In particular, the smoothness of the surface and the age and strength of concrete inlet/outlet structures, walls, headworks, and pipe collars must be evaluated. The condition of the concrete may affect the choice of systems to be considered and the speed with which the work is completed. New concrete work will need time to cure and develop sufficient strength to resist pullout of the anchor bolts. Existing concrete that is deteriorating or of low strength may require some form of remediation or replacement before anchoring systems will work.

- The fastening or anchorage system that holds the gasket system to the structure is an important construction and performance factor. The advantages and disadvantages of wedge anchors, adhesive anchors, and cast-in-place anchor bolt systems are presented.

- The selection of the batten strip or clamping bar to be used for applying pressure to the sealing system and the spacing of the anchor bolts are critical elements to making the sealing system work. The factors that guide their selection will be described.

The mechanical compression seal of a geomembrane, as described in this paper, also reduces stress concentrations in the geomembrane along the attachment that may come under tension or compression stress. This compression sealing system may lessen the possibility of the geomembrane tearing at the anchor bolt if the geomembrane comes under severe stress.

DESIGN CONCEPTS

Condition of the Geomembrane. The purpose of the seal is to provide a watertight attachment. It must hold the geomembrane to the wall, outlet box, or whatever it is attached to and not allow leakage of gas or liquid through the attachment. In order to do this, the geomembrane under the sealing and clamping system should be free of folds, ridges, tears, holes, thick lap joints, and other features that will make it difficult to achieve a seal. A thick, extrusion-welded seam on a material such as high-density polyethylene may need to be ground smooth mechanically in the location of the gasket to achieve an effective seal. Thinner lap joints, such as those made by solvent welding PVC and Hypalon, wedge welding, and extrusion fusion welding, may be accommodated by the elastic properties of the rubber gasket material. In some cases, a stiff caulking material such as butyl rubber tape may be placed on the joint to make a smooth transition over the ridge caused by the lap joint.

The geomembrane must be free of defects under the gasket sealing system. The design drawings and specifications should note this requirement regarding the condition of the geomembrane at the seal.

Rubber Gasket Properties. Thin gaskets that attach geomembranes to structures are often overtightened. Discussions with some installers revealed that nuts on the anchor bolts are sometimes tightened again after initial installation. Often, this tightening is done because the workers think the nuts on the anchor bolts are not as tight as they could be, so they tighten them again. The reason the anchor bolt nuts seem loose to them is that the compression stress on the rubber is great enough to exceed the elastic limit and cause the rubber to "cold flow" and lose its resiliency. The rubber gasket is seen to be actually squeezed out from under the clamping strip and anchor bolt.

Rubber Hardness. When some rubber materials are compressed beyond their elastic limit, they become reformed or remolded and are no longer effective seals. The compression of the rubber in a gasket system should be kept within the elastic limit for the rubber so the rubber retains its resiliency. Tables presented in the Goodyear Handbook of Molded and Extruded Rubber (1959) provide a range of hardness values. The tables show the relationship between compression stress and percent compression deflection for intermittent and continuous loading conditions.

The compression-deflection relationship is to the hardness of the rubber and the shape factor for the gasket configuration, as shown in Figure 1. Graphs are presented for each rubber hardness and the various shape factors. Limits are shown on the plots for occasional loading (e.g., for a shock absorber) and for continuous or frequent loading (e.g., for a sealing gasket).

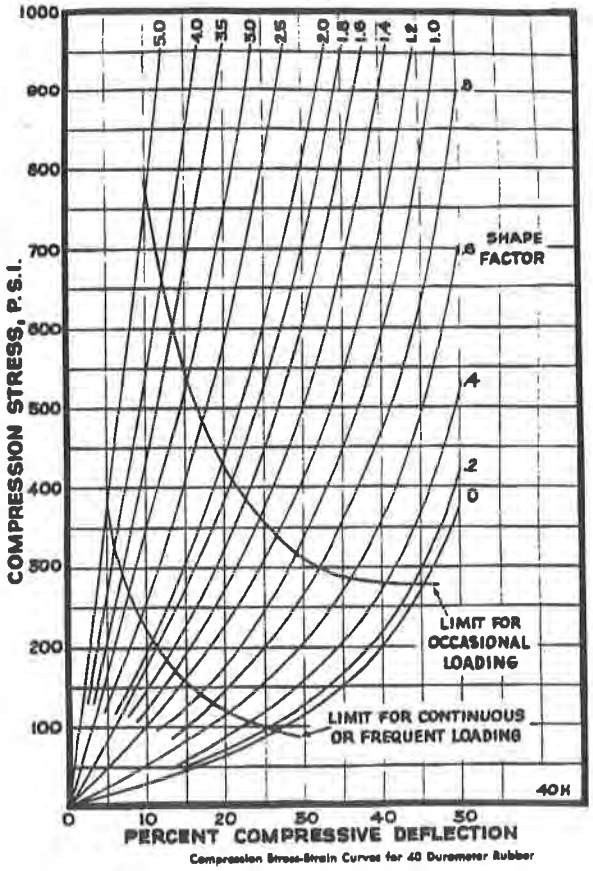

Figure 1. Relation of Rubber Compression to Deflection
(Reprinted by permission of The Goodyear Tire & Rubber Company, 1959)

Hardness is broadly defined in two ways. One way is the relative ability of one material to scratch another, and the other way is the relative resistance to surface indentation. The first method is not applicable to rubber. The second method, surface indentation, is based on measuring the penetration of a rigid ball into the rubber specimen under specified conditions. This is described in ASTM D 1415-83, Test Method for Rubber Property—International Rubber Hardness. Readings in International Rubber Hardness degrees are approximately the same as those given by the durometer in ASTM D 2240-84, Test Method for Rubber Property—Durometer Hardness.

A practical tolerance on durometer requirements is plus or minus 5 points. The recommended hardness value for geomembrane gasket materials is 40 durometer. The 40-durometer material is recommended based on evaluation of the compressive stress required to provide a watertight seal and a reasonable and measurable amount of deflection of the gasket to develop that force. Experience with this recommendation has shown it to be effective. The 40-durometer value provides a balance between resistance to lateral pressures on deeply submerged gaskets and the ability to measure and control the tightening of threaded anchoring systems. That property should be specified with the plus or minus 5-point tolerance because specimens and quantities that are exactly 40 durometer are rarely found. For those not familiar with the durometer hardness scale for rubber, the following table gives the hardness of some common rubber articles. A reading of 100 is obtained on a polished steel or glass plane surface.

Table 1. Examples of the Durometer Scale of Hardness

Article	Durometer
Rubber band	35 - 40
Inner tube	35 - 50
Heel on shoe	40 - 50
Tire tread	60 - 70
"Hard" rubber	95 - 99

Rubber in Compression. To function as a gasket, the rubber must be placed in compression. When rubber is compressed between two surfaces, there is a tendency for the rubber to move out from the center of the contact area. The modulus of elasticity or stiffness of rubber under compression is determined by three interrelated components.

- The inherent stiffness of the rubber
- Stiffness added by surface restraint or lack of freedom in planes normal to the line of external force
- Stiffness added by the shape of the piece

The effect of apparent stiffness varies depending on surface conditions and the amount of lateral restraint the surface offers to the rubber. The effects of various surface conditions are shown in Figure 2. Bonded or rough surfaces develop more restraint and higher compression stress per unit of deflection than do lubricated or very smooth surfaces.

Figure 2 indicates the importance of providing a clean, dry contact surface for the gasket. Lubrication of the surface of rubber contact greatly reduces the apparent stiffness. The apparent stiffness of a single piece of rubber is altered on the order of 6 to 1 by extremes in surface condition.

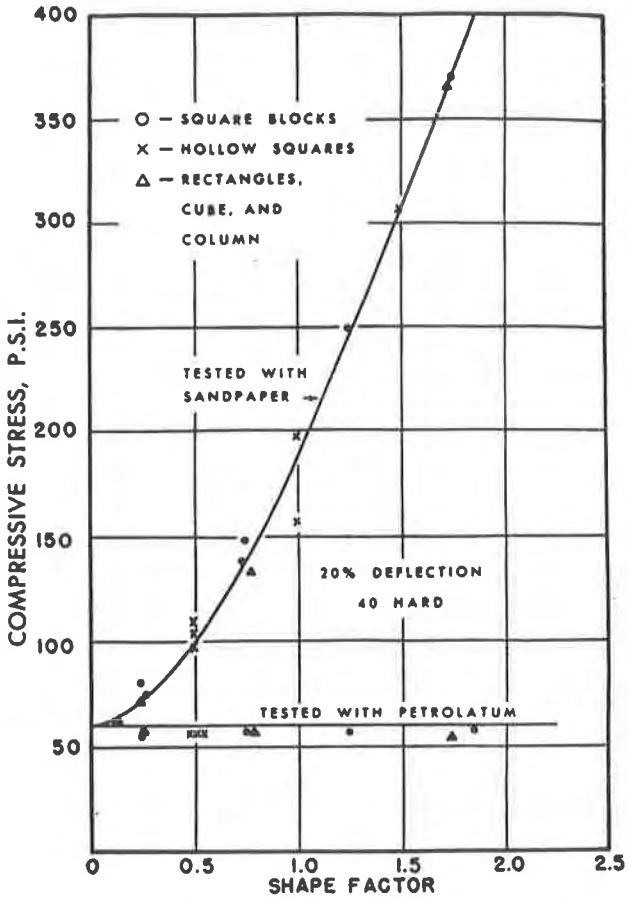

Figure 2. Compression Test Results
(Reprinted by permission of The Goodyear Tire & Rubber Company, 1959)

Another factor to consider is compression creep. Creep may be defined in simple fashion as the additional deformation of a body under stress over time. Creep is in addition to immediate elastic deformation. In rubber, creep is present in some degree at any stress level and at any temperature. Comparisons by Goodyear researchers of shear, tensile, and compression creep of a large number of samples over a three-year period showed that, on the average, compression creep is about 20 percent less than shear creep; tension creep is about 30 percent less than shear creep. The data developed during this testing were "scattered"; however, it can be stated reliably that a series of samples with significant differences in creep value will be shown to be in the same relative order with respect to creep regardless of whether the samples are loaded in tension, shear, or compression. The lowest creep values result from 35- to 40-durometer hardness, high-quality, well-vulcanized natural rubber or neoprene. These materials may have a creep value in shear of 15 percent of the original deformation in 60 days and 25 percent in 3 years. Goodyear also found that, as hardness increased, creep values tended to be higher. High temperatures increase the creep rate of rubber materials of all kinds. Where

dimensional stability is important, it may be generally said that operating temperatures must be kept substantially below vulcanizing temperatures, and usually below 65°C.

The designer considering installations of these materials at temperatures significantly higher than ambient temperatures is advised to make a special evaluation of the effects of the higher temperatures on rubber materials. That kind of special high temperature evaluation is beyond the scope of this paper.

The effects of compression creep and the influences of temperature on creep are important reasons to limit the compression of the rubber gasket to the range of 10 to 15 percent of the total thickness. According to Goodyear studies (1959), creep occurs at a relatively high rate in the initial stages and then proceeds at a progressively reducing rate. If the period is very long or if the stress is very high, the material may enter a failure phase where the rate of creep increases rapidly until actual fracture of the rubber results. Keeping the compressive stress low by limiting the deflection lessens the effects of creep on the gasket. Goodyear researchers also found that high temperature increases the creep rate of rubber materials of all kinds. Where stability of dimension is important, they recommend keeping operating temperatures substantially below vulcanizing temperatures, and usually below 65°C.

Shape Factor. The unit compressive stiffness is significantly affected by the shape of a rubber piece in compression. The shape factor for a rubber gasket, presented in the Goodyear Handbook, must be determined to identify the appropriate shape factor curve from Figure 1 to be used in design. For pieces that have parallel loading faces and sides normal to these faces, a convenient empirical "shape factor" is defined as the ratio of the area of one load face to the area of those surfaces free to expand laterally.

$$\text{Shape factor} = \frac{\text{One load area}}{\text{Total free area}}$$

The shape factor for pieces having parallel loading faces and sides normal to these faces is the total area of the loaded surface divided by the total area of both edges 2t (a+b), as shown in Figure 3. The thicker the gasket, the lower the shape factor will be. Low shape factors are the most desirable.

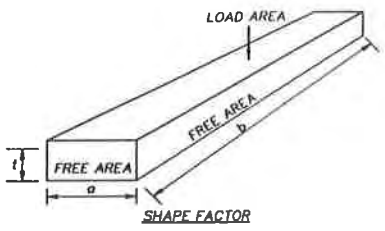

Figure 3. Shape Factor

Gaskets for geomembranes are ordinarily rectangular prisms:

$$s = \frac{ab}{2t(a + b)} \qquad (1)$$

where:
a and b = lateral dimensions
t = thickness
s = shape factor

For example, the shape factor of a cube is 0.25. A more typical shape for a geomembrane seal may be a 12.7-mm (0.5 inch) thick material that is 63.5 mm (2.5 inches) wide and 3.05 m (10 feet) long. The shape factor for this example is 2.45. To achieve the same compressive stress as the example, high value of shape factors, like 4 or 5, will limit the allowable compressive deflection to about 3 to 4 percent, which is undesirable. It is difficult to limit the compression of the gasket to 3 percent when the tightening mechanism is commonly a threaded anchor bolt. Lower shape factors allow greater and more controllable deflection dimensions for the same compression stress under a continuous load.

As indicated by Figure 1 and the limit for continuous loading, the deflection of the gasket by tightening should be limited to about 10 percent. The total thickness of the gasket is the key element to providing the clamping pressure needed to obtain a watertight seal. Because the thickness factor is in the denominator of the equation, reducing the thickness in half would double the shape factor. Again, it is not desirable to have high shape factors.

Just what does all this mean? To tighten a 12.7-mm (0.5-inch) thick gasket by 10 percent, the actual compression of the gasket is 1.27 mm (0.05 inch or less than 1/16 of an inch). Threaded anchor bolts of the size normally used, 9.5 mm to 12.7 mm (3/8 to 1/2 inch), have 16 to 13 threads per inch. Using a 16-thread-per-inch bolt would allow less than one complete turn of the nut to achieve the 10-percent compressive deflection limit. This limited amount of tightening would not be practical to rely on for construction. A more practical approach is to use gaskets thick enough to allow the 10 percent tightening to be done in one and one-half to two turns of the nut on the anchor bolt. The tightening will have to be measured after the assembly of the geomembrane, rubber gasket strip, clamping bar or batten, washers, and nuts is snug and finger-tight.

Concrete Surface and Condition. The most common substrate that geomembranes are fastened to is concrete. In some applications, geomembranes are installed in steel or glass fiber tanks. The principles of the gasket thickness, size, shape, and clamping pressure would be the same. Geomembrane attachment to steel and glass fiber structures is not covered in this paper, but similar design considerations would be required for successful attachments. Those attachments may be more straightforward than when dealing with the vagarious nature of concrete structures.

The concrete that the geomembranes will be sealed to may be old and cured, fresh and "green", nonreinforced or reinforced with steel bars, smooth finish or rough surface, with horizontal or vertical faces. All of these factors will control the approach to designing the watertight gasket system.

Aged and cured concrete will ordinarily have the strength required to withstand the pullout forces of the anchor bolts. The concrete must be competent and free of structural cracks, voids, rock pockets, and other features that would limit the development of pullout resistance. Existing concrete may have reinforcing steel in locations that will make it difficult to drill anchor bolt holes. The section of concrete for installing the gasket system has to be wide enough so the alignment of the anchor bolts may be placed away from the edge. In this way, the cone of influence from the pullout forces of the anchor bolts will not fail the concrete.

Fresh, green concrete presents another set of conditions. It may take 28 days or more for the concrete to develop the strength needed to resist the pullout forces. To try to clamp the geomembrane sealing system before adequate curing has taken place will undoubtedly lead to failure. In addition, there may be damage to the concrete that will make restoration of the concrete surface and reattachment of the gasket a challenge. Another approach is to embed anchor bolts by attaching them to reinforcing steel. A bar drilled to receive the anchor bolts may also be placed and secured in the form work. When the concrete is poured, a sufficient length of protected, threaded anchor bolt must be left exposed for the geomembrane gasket attachment.

The surface of the concrete that will receive the gasket system should be smooth and free of voids, ribs, cracks, tie-holes, and other defects that can interfere with the sealing of the gasket. Old concrete will need to be ground smooth or grouted to correct surface defects. Grouting, using special nonshrink grout products, would be useful in filling voids, large cracks, rock pockets, tie-holes and similar features. The surface that will receive the gasket should also be relatively flat and in true alignment for the clamping system to develop uniform clamping pressure.

Attaching a geomembrane to a horizontal surface offers advantages in many cases. There is less stress on a geomembrane that does not make the transition from a horizontal position to a vertical surface. The anchor holes are easier to drill, and the finish on a horizontal surface can be made better than a vertical form will typically allow. New concrete work, such as pipe support collars, inlet/outlet structures and spillways, may have horizontal sections designed to conform to the finish elevation to accommodate the geomembrane attachment. Sealing the geomembrane at the corners of structures is somewhat easier on a horizontal surface using the gasket attachment system.

Attachments to vertical surfaces are common, especially on existing structures being retrofitted for a geomembrane. It is best to bring the edge of the geomembrane above the maximum liquid level. When this cannot be done, great care must be taken in the design and construction of the gasket system to achieve the watertight seal.

Anchor Bolts. Anchor bolts for attaching geomembranes to concrete structures are usually specified to be stainless steel. There are many stainless steel alloys from which to select. The American Iron and Steel Institute (AISI) 300 series of corrosion-resistant austenitic stainless steels are used for a myriad of commercial and industrial uses, usually providing complete satisfaction and a lifetime of trouble-free service. The most common alloys specified for this application are AISI Type 304 and Type 316. It is important to understand that no structural metal or alloy is resistant to all corrosive environments. A qualified corrosion engineer should be involved in recommending the alloy for anchor bolts and clamping bars, with respect to the solutions or chemicals with which the material may be in contact.

The pitch of the threads of anchor bolts is an important factor in controlling the compressive deflection to about 10 percent when tightening. Special order bolts in the 12.7-mm (0.5-inch) diameter size with 24 threads per inch are available. This high thread-pitch count offers obvious advantages in controlling the clamping pressure.

The anchor bolts must be long enough to allow enough embedment in the concrete to develop the full pullout resistance. The forces that will be developed by the stress on the bolt at 10 percent compressive deflection are indicated in Figure 1. The spacing and embedment depth of anchor bolts requires close evaluation and design to ensure that uniform clamping pressure is applied to the gasket system (i.e., the rubber compression strip, geomembrane, batten strip, washers, and nut) and that the stresses on the concrete do not exceed the tensile strength of the concrete. The anchor bolt also needs to be long enough for the thickness of the gasket. It is important to have three threads exposed after the nut is tightened to allow for "locking" of the nut with marking paint. This will prevent subsequent changes of the rubber compression strip by additional tightening or will allow observation of overtightening if it occurs.

Anchor bolts come in a variety of anchorage systems. Drilled anchor systems use expansion anchors, wedge anchors, undercut anchors, and chemical (epoxy or adhesive) anchors.

Expansion anchors provide frictional resistance by side hole contact applied from the expanding action of shields or wedges.

Wedge anchors, like expansion anchors, rely on side hole frictional resistance. Wedge anchors have soft metal sleeves of zinc, lead, or a combination of both, that expand on tightening to conform to drill hole irregularities. They usually have lower load capacity than expansion anchors do.

Undercut anchors do not rely on friction to transfer the applied load to the concrete. Instead, the anchor bears directly against an undercut (inverted ledge) made by a separate drilling device, thereby transferring the load by compression.

Chemical anchors transfer the forces from the anchor into the surrounding concrete by the chemical bond. A chemical reaction between a liquid resin and a catalyst provides a high-strength bond.

Chemical anchors have proved to be more reliable than mechanical anchors in achieving anchorage for gasket systems. This is partly because a poorly drilled hole for a mechanical anchor may not allow the anchor to grip the hole and develop full strength without pulling some distance out from the bottom of the hole. This reduces the embedment length and development of full pullout resistance against the concrete. Anchor bolts are usually placed from 152 to 305 mm (6 to 12 inches) on center along the battening strip into the concrete. An anchor bolt that does not properly grip the hole made for it defeats the possibility for uniform compression along the gasket. To correct the situation when mechanical anchors do not work entails removing the whole gasket system in that area and drilling replacement holes on either side of the failed anchor bolt hole. This solution is difficult, expensive, and usually ineffective.

Chemical anchors that are installed according to the manufacturer's recommendations stay anchored and can still develop the necessary bond even in a poorly drilled hole.

Batten Strips. Batten strips (name derived from "battening down the hatches") can be bar, channel, and angle shapes. The rigidity of a flat bar of the typical 6.35-mm (1/4-inch) thickness may not be sufficient to develop the uniform clamping pressure across the gasket. The size, type of material, and thickness of the batten strip should have a flexural modulus sufficient to withstand bending at the anchor points resulting from compression forces. The compression of the batten strip should be uniform so that equal pressure is applied along all points of the gasket. The use of thicker bar stock material to provide the rigidity requires costly materials and fabrication when working with stainless steel alloys.

Channel and angle sections should be evaluated during the design to find which ones are acceptable. The spacing requirements for the anchor bolts and the pullout resistance of the concrete must be considered. Predrilled sections of batten strips are often used to locate the anchor bolts. When anchor bolts are cast in place in new concrete work, the predrilled sections are used as templates to hold the bolts in alignment while the concrete sets up. A typical section of the gasket system is shown in Figure 4.

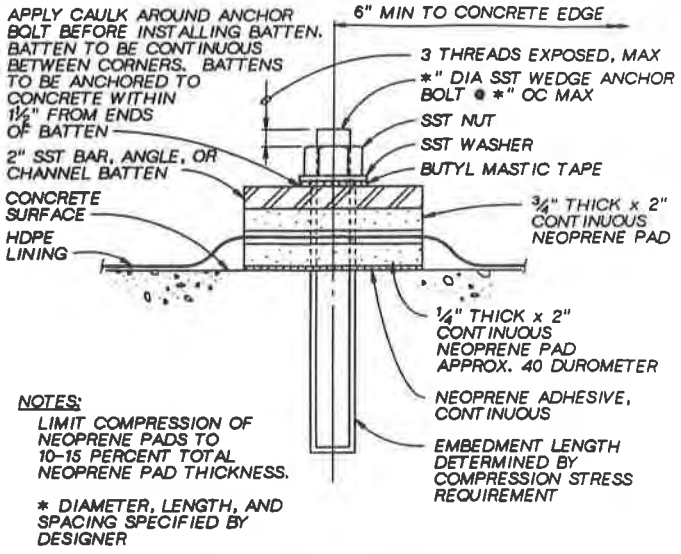

Figure 4. Gasket System

Tightening Method. The design is complete when it takes into account the shape factor, the durometer hardness of the rubber, the rigidity of the batten strip, the integrity of the anchor bolts, and the tightening procedure. These are the key elements for this gasket system to provide a watertight seal. The degree of compressive deflection (about 10 percent) and the total thickness of the rubber compression material dictate the amount of tightening required. The threads per inch of the anchor bolt will allow the degree of tightening to be judged without actual deflection measurements.

The tightening sequence should follow this sequence:

- Install a thin portion (e.g., 6.35 mm [1/4 inch]) of the total rubber compression strip over the anchor bolts and bond to the prepared concrete surface with manufacturer's recommended adhesive.

- Install the geomembrane over the anchor bolts so that it is smooth and free of wrinkles.

- Place the thicker portion (e.g., 19.05 mm [3/4 inch]) of the rubber compression strip over the geomembrane and through snug fitting holes in the strip for the anchor bolts.

- Install the predrilled batten strip over the anchor bolts onto the sandwich of rubber and geomembrane.

- Install the machine washer, lock washer, and nut on the anchor bolt and press the system together firmly to eliminate any gaps and bring all layers into contact while tightening the nut by hand or using light pressure on a wrench.

- When all the slack is out of the system, tighten the nut to the designed compressive deflection.

For example, when the compressive deflection is 10 percent, the total gasket thickness is 25.4 mm (1 inch) and the desired deflection is 2.54 mm (0.1 inch). Using an anchor bolt with 16 threads per inch, or 15.9 mm (0.62 inch) per turn, it will take a little over one and one-half turns to tighten the gasket the prescribed amount.

CONCLUSION

Watertight attachments of geomembranes to concrete structures can be achieved following the guidelines presented in this article. The properties of rubber limit the amount of compression it can undergo before it fails and loses its resiliency. To perform as a gasket, the rubber compression must be limited to about 10 percent of the total thickness. This is done by making gaskets thicker and controlling the tightening of the anchor bolt nuts.

REFERENCES

American Society for Testing and Materials, (September 1988) Standard Test Method for Rubber Property—International Hardness D1415-88, Vol 09.01, pp. 223 to 226.

American Society for Testing and Materials, (May 1986) Standard Test Method for Rubber Property—Durometer Hardness D2240-86, Vol. 09.01, pp. 227 to 230.

The Goodyear Tire & Rubber Company, (1959) Handbook of Molded and Extruded Rubber, 2nd edition.

Geosynthetic Landfill Cover Design Methodology and Construction Experience in the Pacific Northwest

R.S. Thiel
EMCON, USA

M.G. Stewart
EMCON, USA

ABSTRACT

The use of geosynthetics in landfill covers has increased in recent years and are likely to be required for most municipal solid waste (MSW) landfills in the U.S. by the new Environmental Protection Agency (EPA) subtitle D regulations. Critical cover-design concerns are stability and drainage. An infinite slope analysis that uses the properties of site-specific materials is considered appropriate for evaluating stability. Estimating the amount of seepage into the drainage layer above a geomembrane cover on steep slopes is critical for designing proper spacing of the layer's drainage outlets. The design should be based on interface shear strength and permeability testing with site-specific materials.

Well-prepared specifications and a construction quality assurance program are crucial to successful geosynthetic cover installations. This paper reflects experience gained from designing and constructing landfill covers with geomembranes on 11 projects totaling over 200 acres in Oregon and Washington. Lessons learned from these projects will lead to improvements in future designs.

INTRODUCTION

Geomembranes are increasingly used in landfill cover designs because they

- Are often preferred in regulations
- Reduce long-term leachate generation better than soil-only covers, especially in wet climates
- May reduce long-term liability by limiting future leachate generation and controlling gas
- Often cost less than low-permeability soil

Recent EPA regulations (Federal Register, 1991) will likely require composite covers (geomembrane over soil) on most new MSW landfills that have bottom geomembrane liners. Koerner and Daniel (1992) discuss the trends, benefits, and issues related to using geomembranes in landfill covers. Special design issues for landfill covers with geomembranes include

- Cover slope stability
- Settlement (total and differential)
- Landfill gas control
- Side slope seeps
- Construction methods and materials

Other more standard civil design items such as access roads, erosion, surface drainage structures, and vegetation must account for the special issues listed above.

All elements of the completed design must be considered when budgeting for long-term maintenance and planning for future site end use.

This paper describes a typical landfill cover design using a geomembrane barrier layer. The design discussion focuses on slope stability, taking into account partial saturation and seepage forces in the cover. Construction issues and production rates relating to the layered elements of the cover design are described at the end of the paper.

TYPICAL COVER DESIGN ELEMENTS AND MATERIALS

The following are the elements, from bottom to top, of a typical landfill cover with a geomembrane barrier layer (see Figure 1).

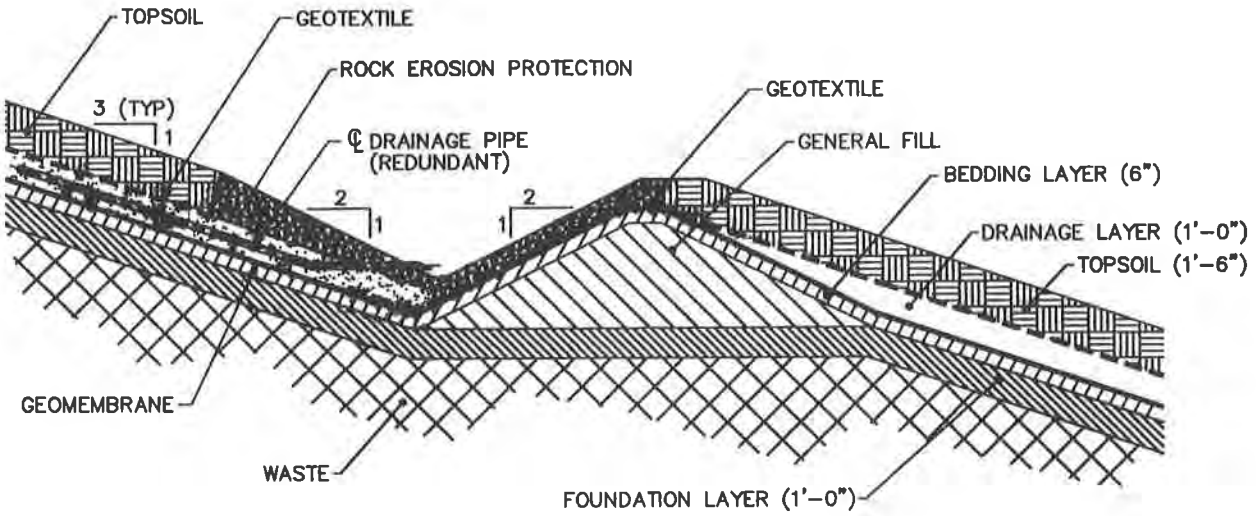

FIGURE 1. TYPICAL LANDFILL COVER SECTION WITH GEOMEMBRANE BARRIER LAYER AND INTERMEDIATE BENCH DITCH

Foundation Soil Overlying the Waste. This layer provides a firm foundation for subsequent cover construction. It is usually installed during landfill operations, or during cover construction when regrading is required. Typically at least 1 foot (30 cm) thick, it consists of general soil material that can be compacted. Some types of waste, such as ash, can even be used. Compaction requirements are not stringent (approximately 90 percent of standard Proctor maximum dry density) because the layer is not expected to support footings for structures. Structures can be constructed on the final cover but require considerations beyond the scope of this paper.

Geomembrane Bedding Layer. This layer typically consists of 6 inches (15 cm) of sand because sand particles have good frictional characteristics, are easy to grade, are of appropriate size for intimate contact with the geomembrane, can convey side slope seeps, and can transmit gas from shallow horizontal collection trenches. Cover design under Subtitle D (EPA, 1992a) will generally require this layer to be part of a composite cover to act as a hydraulic barrier and consist of 18 inches (46 cm) of soil with a hydraulic conductivity no greater than 2×10^{-5} feet/minute (1×10^{-5} cm/sec) for most MSW landfills that have bottom geomembrane liners.

Geomembrane. This is the barrier layer that replaces the conventional soil barrier. Key design concerns relating to the geomembrane include interface shear strength with adjacent materials and ability to handle differential settlement. EMCON has found only textured polyethylene products provide the required interface shear strength for steep (3:1) slopes at a reasonable cost. These products, especially the lower density variety, also have three-dimensional strain capabilities that would generally not be exceeded by differential settlements expected on landfill covers.

Drainage Layer. This is typically 1 foot (30 cm) of sand or gravel. Geosynthetic drainage elements, such as a geonet-geotextile composite, are generally not cost competitive with natural drainage materials in the Northwest. Most natural drainage material can be obtained and installed for about $10 per cubic yard (0.76 m^3) or about $0.37 per square foot (0.09 m^3) for a 1-foot (30 cm) thick layer. The cost of geocomposite drainage layers is usually significantly more than this, depending on the materials selected. No compaction requirements are specified for this layer.

Geotextile Filter. A filter is generally required between the topsoil and the drainage layer. Sometimes the relative gradations of the drainage and topsoil layers act as a natural filter, precluding the need for an additional filter. In either case the potential for clogging and piping should be checked either by strict filter design criteria, such as those developed by the Corps of Engineers (Cedergren, 1989), or by geotextile filter design methods with site-specific soils, as published in literature (GRI, 1991). If it is not known at the design stage what soil materials will be used, the specifications should require a method for selecting the proper geotextile.

Topsoil. The thickness of this layer depends on the type of vegetation to be established. The layer can be divided into two sublayers: a lower, rooting layer with less organic content and an upper, organic-rich layer. Most designs specify a rooting layer at least 1-foot (30 cm) thick overlain by 6 inches (15 cm) of organic soil. The topsoil layer should be at least as thick as the rooting depth of the proposed vegetation. Although compaction is generally not specified, to avoid overly loose placement the material should be subjected to at least two passes of construction equipment. If permeability is a concern, a minimum compaction can be specified for the rooting layer.

The elements described above are typical of the cover designs used in the Northwest. The following discussions on cover stability and construction reference these elements, but would be applicable to any layered cover section.

LABORATORY TESTING FOR THE COVER DESIGN

Topsoil. Tests required for topsoil include saturated unit weight, gradation, and permeability. Gradation is used to evaluate the filter design between the topsoil and the drainage layer. Looser (more permeable) soil produces more conservative permeability test results. Laboratory sample preparation should replicate as closely as possible the expected field placement condition.

Drainage Layer. This material also requires saturated unit weight, gradation, and permeability testing. Gradation test results should be checked for maximum allowable fines content, gap gradation, and filter compatibility with the topsoil. A dense sample would produce a more conservative permeability test result than a loose sample.

Geotextile. The main criteria for selecting a geotextile, if one is needed, are construction survivability and filtration between the topsoil and drainage layer. The GRI (1991) or Christopher and Holtz (1985) references are recommended as good sources that discuss the appropriate testing and material selection criteria for geotextile filters. The requirement for interface shear strength with adjacent soils is discussed below.

Geomembrane. Geomembrane cover material selection criteria (other than those required by state regulations) include construction survivability, ability to maintain integrity under total and differential landfill settlement conditions, cover slope stability, and cost. Secondary considerations, which could be primary considerations for certain projects, include ease of installation; construction quality assurance requirements; susceptibility and resistance to animal and plant penetration; ability to install in climatic extremes of hot and cold; aging durability; and, if the liner needs solvents for welding, health, safety, and environmental considerations. The testing and specifications required for the project will depend on the project's design considerations. Once a product type is selected, product specifications will generally require a cover geomembrane to meet minimum physical requirements for strength and elongation and provide minimum required interface friction with the adjacent soils (discussed below).

Geosynthetic-Soil Interfaces. Shear strength should be evaluated for the following interfaces:

- Topsoil-geotextile
- Geotextile-drainage material
- Drainage material-geomembrane
- Geomembrane-bedding soil

Typically the critical interface is where the drainage material meets the geomembrane, which should be the only interface where pore pressures may build up. With proper materials selection, the other interfaces should be able to provide adequate stability for slopes up to 33 percent.

The American Society for Testing and Materials is currently preparing a standard for interface direct-shear testing. It would be prudent to perform the testing with a minimum 1-foot (0.09 m^2) square shear box; under saturated conditions; to sandwich the geosynthetic between the actual materials it will experience in the design; and to use the range of normal loads anticipated in the final cover (e.g., 150 to 400 pounds per square foot [7.2 to 19.1 kPa]). An experienced laboratory with proper testing equipment sensitive at these low, normal loads should be used.

STABILITY ANALYSIS

The following procedure is for a potential cover failure sliding parallel to the slope, with the drainage layer-geomembrane interface the primary plane of weakness.

Description of the Problem. The stability analysis theory for a cover on a slope is well documented (Koerner, 1990; Lambe and Whitman, 1969; Giroud and Beech, 1989). It can consist of calculating the force vectors for the entire slope, including toe resistance, or it can be simplified somewhat for a uniform cover section by performing an infinite slope analysis. The method used will depend on the degree of conservatism wanted, its impact on design decisions, and the relative magnitude of the toe resistance compared to overall slope resistance. In many cases with long cover slopes toe resistance accounts for less than 5 percent of slope resistance. If an infinite slope analysis yields a factor of safety (FS) less than desired then the results can be checked by including toe resistance and re-evaluating the FS.

The method discussed in this paper is the infinite slope analysis. The most important parameters to consider in such an analysis are the slope angle, the shear strength of the potential failure plane parallel to the slope, and the amount of water above the potential failure plane (i.e., pore pressures acting on that plane). The unit weights of the materials above the potential failure plane have a small influence on the analysis. The most difficult of the parameters to estimate are the pore pressures acting on the potential failure plane. The potential failure plane of a geomembrane cover is assumed to be the drainage layer-geomembrane interface.

The problem is relevant to slopes steeper than about 15 percent (6.7H:1V), depending on the interface shear strength. Figure 2 depicts the variation in FS with slope angle (β) for a fully saturated infinite slope (worst case condition) assuming an interface friction parameter (ϕ) of 28 degrees (a typical low-end value between textured polyethylene and granular drainage materials). In this case imminent failure (FS=1.0) would occur at a slope of about 22 percent (4.5:1) and FS equal to 1.5 is obtained at a slope of about 15 percent (6.7:1). Landfills in Oregon and Washington are commonly constructed with slopes as steep as 33 percent.

Pore Pressures Acting on the Drainage Layer-Geomembrane Interface. Estimating the amount of head that builds up over the geomembrane requires consideration of the spacing and orientation of underdrain collectors, which collect water from within the drainage layer and discharge it outside the cover section. At a minimum the drainage layer will discharge at the slope toe. The need for additional intermediate discharge locations from the drainage layer is determined by the amount of water it collects and the minimum FS required for stability.

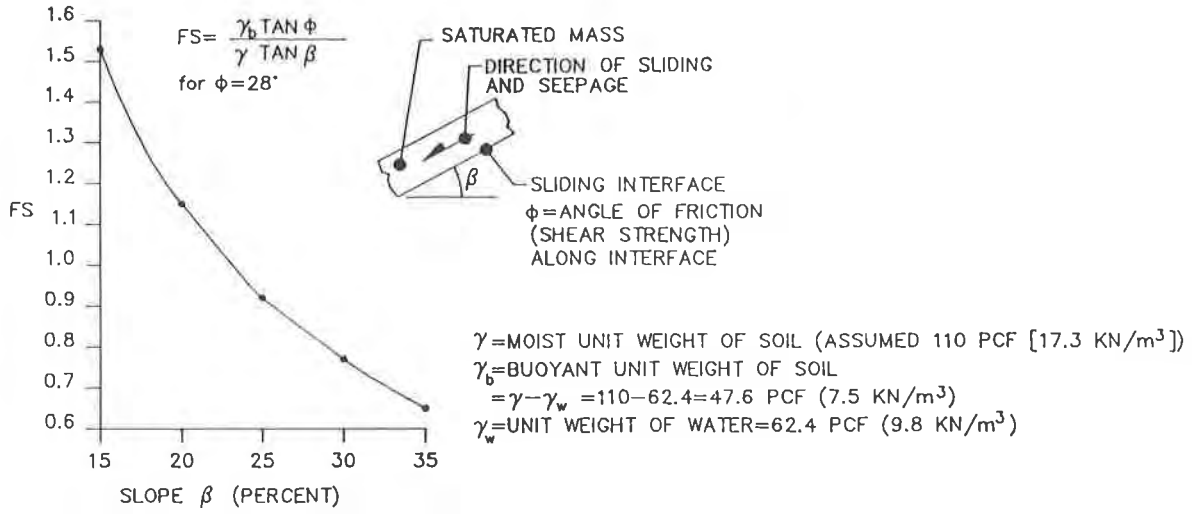

FIGURE 2. SLOPE ANGLE VS. FACTOR OF SAFETY FOR SATURATED INFINITE SLOPE

At least two methods can be used to provide intermediate discharge from the drainage layer: pipes (or collection ditches) running up and down the slope, and pipes (or collection ditches) running subparallel to the slope contours. The latter method seems to be more efficient and has been preferred in Oregon and Washington. The methods of analysis discussed here use this method. Figure 1 shows an example of an intermediate bench ditch that allows discharge from the drainage layer and that controls surface water runoff. The required spacing between drainage outlets is obtained by estimating the head buildup over the geomembrane and performing an infinite slope stability analysis. Head buildup can be estimated as follows (see Figure 3):

1. Assume that the topsoil is saturated during heavy rain, sheet flow is occurring over the surface, and water is percolating through the topsoil at a rate governed by its hydraulic conductivity (k_1). Using a hydraulic gradient (i_1) of 1 over an area (A_1) of unit width and length (L), the percolation into the drainage layer (Q_{in}) from the topsoil is based on Darcy's law as

$$Q_{in} = (k_1)\ (i_1)\ (A_1) = (k_1)\ (1)\ (1)\ (L) = (k_1)\ (L) \qquad (1)$$

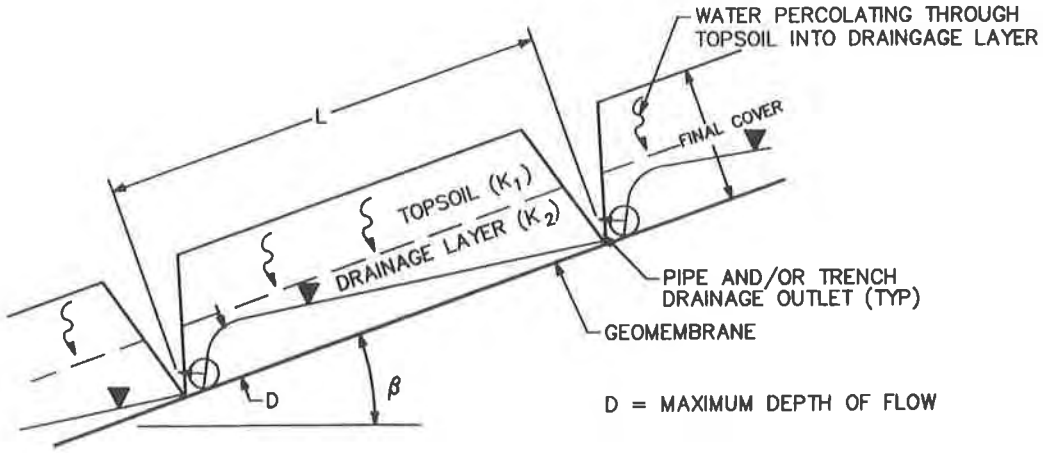

FIGURE 3. SCHEMATIC OF HEAD BUILDUP IN DRAINAGE LAYER

2. Apply the equation of continuity: $Q_{(in)} = Q_{(out)}$. $Q_{(out)}$ is the discharge flow rate in the drainage layer (assumed to flow parallel to the slope) at the downstream (discharge) end of a slope length (L). $Q_{(out)}$ is governed by the hydraulic conductivity of the drainage material (k_2); the gradient (i_2), which is the sine of the slope angle (β); and the area (A_2) normal to the flow equal to a unit width times the flow depth (D).

$$Q_{(out)} = (k_2)\ (i_2)\ (A_2) = (k_2)\sin(\beta)(1)(D) \qquad (2)$$

3. Keep the maximum flow depth (D) less than the drainage layer thickness in this model because it is assumed that the topsoil is fully saturated. If the flow in the drainage layer rises to touch the bottom of the topsoil layer, according to this model there will be an incremental jump in pore pressures exerted on the geomembrane from the depth of the drainage layer to the full depth of the cover section. Therefore, by setting (D) equal to the drainage layer thickness, an equation can be written to solve for (L), which immediately shows the importance of estimating the relative permeabilities of the topsoil and drainage layers.

$$L = (k_2)\sin(\beta)(D)/(k_1) \qquad (3)$$

This method of estimating head buildup is conservative, though may not be unrealistic, because it does not account for evapotranspiration reducing the amount of water percolating through the topsoil. Some engineers promote the use of HELP (Schroeder, 1989) or other water balance models to estimate percolation into the drainage layer. The conservative model discussed here, however, is preferable for Northwest conditions. During the critical winter months soils are saturated by substantial antecedent rainfall, and plants are not only subject to long periods of total saturation during this time but are either dormant or relatively inactive. It is not difficult to imagine that such percolation conditions modeled above occurred in the Northwest several times during the winters of 1989-90 and 1990-91, both of which had up to 100-year storm events. Only a few minutes of these conditions can initiate a slope failure. It may not be prudent for a water balance model to include evapotranspiration for a condition during several minutes of an intense rainstorm after weeks of antecedent rainfall.

The following results were calculated for a site near Portland, Oregon, to illustrate the discrepancy between the results of the model described above and those of the HELP model to predict the maximum anticipated flow into the drainage layer. A hydraulic conductivity of 2×10^{-5} ft/min (1×10^{-5} cm/sec) was used for the topsoil in both methods.

Water Percolating into Drainage Layer through Topsoil:
- HELP Model: 0.007 inch per hour
- Method described in this paper: 0.14 inch per hour
- Difference: Factor of 20
- Influence on selecting spacing of discharge points: Factor of 20

Although on average the HELP model may produce a good, and even conservative, estimate of the amount of liquid that would percolate annually through the topsoil, it may not estimate the peak amount that would control the stability analysis in an extreme, yet reasonable, situation. Estimating the maximum reasonable amount of water percolation through a topsoil layer is an area for potential future study and refinement.

Infinite Slope Analysis. The general geometry of a partially-saturated slope with seepage parallel to the surface is shown in Figure 4(a). The free-body diagram and force polygon for a vertical slice of the cover soils above the geomembrane are shown in Figure 4(b). Note that the pore pressure uplift force is based on the partial flow net shown in Figure 4(a).

a) INFINITE SLOPE GEOMETRY AND MATERIAL PARAMETERS

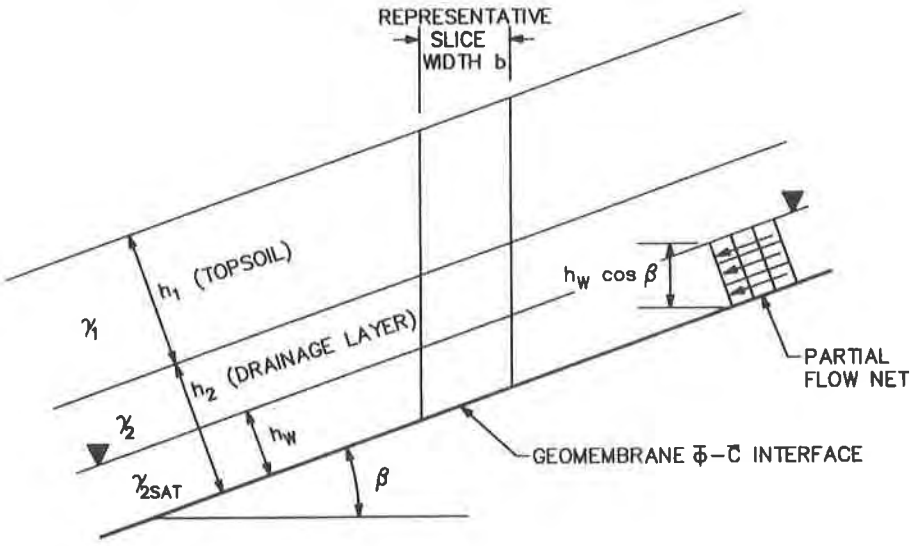

b) FORCES

$W = [h_1 \gamma_1+(h_2-h_w)\gamma_2+h_w \gamma_{2SAT}]\, b/\cos\beta$

$u = \gamma_w h_w \cos\beta$

$U = ub/\cos\beta = \gamma_w h_w b$

$N = W\cos\beta$

$T = W\sin\beta$

$\bar{N} = N-U$

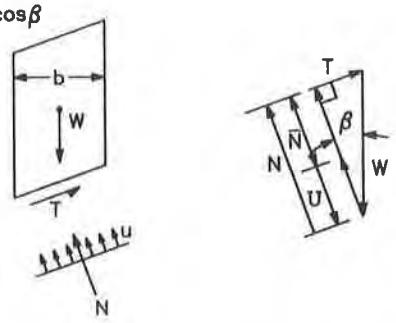

FREE BODY DIAGRAM FORCE POLYGON

Geometric Parameters: β = slope angle; h_1 = thickness of topsoil; h_2 = thickness of drainage layer; h_w = average height of water in drainage layer normal to slope; b = width of representative slice.

Material Parameters: γ_1 = saturated unit weight of topsoil; γ_2 = moist unit weight of drainage layer; γ_{2SAT} = saturated unit weight of drainage layer; γ_w = unit weight of water; $\bar{\phi}$ = effective friction parameter for shear strength at base of drainage layer; $\bar{c}$ = effective cohesion parameter for shear strength at base of drainage layer.

Forces: u = pore pressure on base of drainage layer; U = uplifting water force; W = total weight of slice; N = total force normal to slope exerted by weight; T = tangential force to slope exerted by weight; $\bar{N}$ = effective normal force.

FIGURE 4. INFINITE SLOPE STABILITY WITH SEEPAGE PARALLEL TO SLOPE
(MODIFIED AFTER DUNN ET AL, 1980, p.241)

The effective stress normal to base of the slice, $\bar{\sigma}$, is

$$\bar{\sigma} = \frac{\bar{N}}{b/\cos\beta} = [h_1\gamma_1 + (h_2 - h_w)\gamma_2 + h_w\gamma_{2\,SAT} - h_w\gamma_w]\cos\beta \qquad (4)$$

The shear stress exerted tangential to the slice base, τ, is

$$\tau = \frac{T}{b/\cos\beta} = [h_1\gamma_1 + (h_2 - h_w)\gamma_2 + h_w\gamma_{2SAT}]\sin\beta \qquad (5)$$

The shear strength at base of the slice, S, is

$$S = \bar{c} + \bar{\sigma}\tan\bar{\phi} \qquad (6)$$

The factor of safety, defined as the ratio of the resisting shear strength divided by the driving shear stress, is

$$FS = \frac{S}{\tau} = \frac{\bar{c} + [h_1\gamma_1 + (h_2 - h_w)\gamma_2 + h_w\gamma_{2SAT} - h_w\gamma_w]\tan\bar{\phi}}{[h_1\gamma_1 + (h_2 - h_w)\gamma_2 + h_w\gamma_{2SAT}]\tan\beta} \qquad (7)$$

Because the depth of saturation in the drainage layer varies, the FS would vary also. A common procedure is to compute the average FS by using the average water depth in the drainage layer, assumed to be half the maximum water depth (D) used in Equation (2). The method therefore computes an average factor of safety for the slope length between drainage discharge points. Locations upgradient of the average flow depth will have a slightly higher FS, and downgradient locations, a slightly lower FS.

The design methodology would be to compute the FS for a given cover geometry and materials properties using Equation (7), and using one half the maximum water depth (D) used in Equations (2) and (3). If the FS is acceptable, use the maximum drainage discharge spacing (L) computed in Equation (3). If the FS is unacceptably low, reduce the distance (L), recompute the average flow depth (D/2) in the drainage layer, and recompute the FS. Iterate until the FS is acceptable.

Design Example. Given: thickness (h_1) of 1.5 feet (45 cm) of topsoil with a saturated unit weight (γ_1) of 115 pcf (18 KN/m^3) and hydraulic conductivity (k_1) of 2×10^{-4} ft/min (1×10^{-4} cm/sec); thickness (h_2) of 1 foot (30 cm) of drainage layer with moist unit weight (γ_2) of 100 pcf (15.7KN/m^3), saturated unit weight (γ_{2SAT}) of 105 pcf (16.5 KN/m^3) and hydraulic conductivity (k_2) of 0.2 ft/min (0.1 cm/sec); slope angle (β) of 3:1 (18.4 degrees); and interface friction parameter (ϕ) of 30 degrees. Unit weight of water (γ_w) = 62.4 pcf (9.8 KN/m^3).

Find: Maximum allowable spacing (L_{max}) between drainage outlets designed subparallel to slope contours such that the maximum depth (D) of accumulated water in the drainage layer is one foot (30 cm), and a minimum average FS of 1.5 is maintained.

Solution:

$$L_{(max)} = (k_2)\sin(\beta)(D)/(k_1) = 0.2\sin(18.4)(1)/0.0002 = 316\,ft\,(96\,m)$$

$$FS = \frac{[(h_1)(\gamma_1) + (h_2 - D/2)(\gamma_2) + (D/2)(\gamma_{2SAT}) - (D/2)(\gamma_w)]\tan(\phi)}{[(h_1)(\gamma_1) + (h_2 - D/2)(\gamma_2) + (D/2)(\gamma_{2SAT})]\tan(\beta)} \qquad (8)$$

$$= \frac{[(1.5)(115) + (1 - .5)(100) + (.5)(105) - (.5)(62.4)]\tan(30)}{[(1.5)(115) + (1 - .5)(100) + (.5)(105)]\tan(18.43)} = 1.5\ (ok)$$

Factor of Safety. Geotechnical engineers often feel comfortable with a minimum FS of 1.5 for long-term static slope stability conditions. This value originated from dam

designs and may or may not be applicable to landfill slope stability in general, or cover stability in particular. The EPA (1992b) suggests that a FS between 1.25 and 1.5 might be acceptable depending on the level of certainty in the shear strength parameters. The following factors should be considered when selecting a minimum FS for a landfill cover: experience with geosynthetics has a relatively short history; level of confidence in assumed material properties; factors of safety may already be included in the estimated material properties; and the situation being analyzed is considered a worst case that will occur a small percentage of the time. A minimum FS of 1.5 has been used without failures attributable to underdesign of the drainage layer in the Northwest.

Seismic Considerations. New Subtitle D regulations require checking all elements of landfill design for stability due to seismic loading. A Newmark-type analysis (Newmark, 1965) is recommended for the cover. Consideration should be given to how much saturation should be allowed for in the drainage layer for the analysis (using the maximum amount computed for static stability would probably be overly conservative), and what amount of deformation would be acceptable. Because cover deformation is not life-threatening, and because it could be inspected and repaired after the event, the acceptable amount should be somewhat higher than the amount for a bottom liner. Acceptable deformations for bottom liners have been cited as 6 to 12 inches (15 to 30 cm) for a conservatively selected design earthquake (Seed and Bonaparte, 1992). One approach is to use these same criteria for covers modeled in a dry condition because the chance of an earthquake occurring at the same time as the maximum conservative saturation condition discussed in this paper is much more remote than the earthquake alone. Another approach is to recognize that the cover system does not directly affect the ability of a lined landfill to contain waste, and that it can be inspected and repaired. Therefore, the cover could be allowed to sustain a higher level of deformation, say on the order of one to three feet (30 to 90 cm). Often a design that is satisfactory for the worst case static condition with a reasonable FS is acceptable for a seismic condition.

CONSTRUCTION ISSUES AND PRODUCTION

The following paragraphs describe construction issues related to major elements of a final cover section, surface water ditches, and geomembrane penetrations. Anticipated production rates for constructing major elements of a cover are also provided for planning and scheduling purposes.

Settlement Considerations. Design changes on landfill closures are nearly unavoidable, mainly because landfills settle. Landfill owners and operators, however, expect the designer to achieve the lowest possible construction costs by preparing such complete bid packages that contractor claims and change orders during construction are minimized. Nevertheless, design changes to account for settlement must be expected, planned for, and executed during the construction phase of the project.

Design elements particularly susceptible to settlement are the horizontal and vertical control for roads, ditches and pipelines. For example, the design of both the

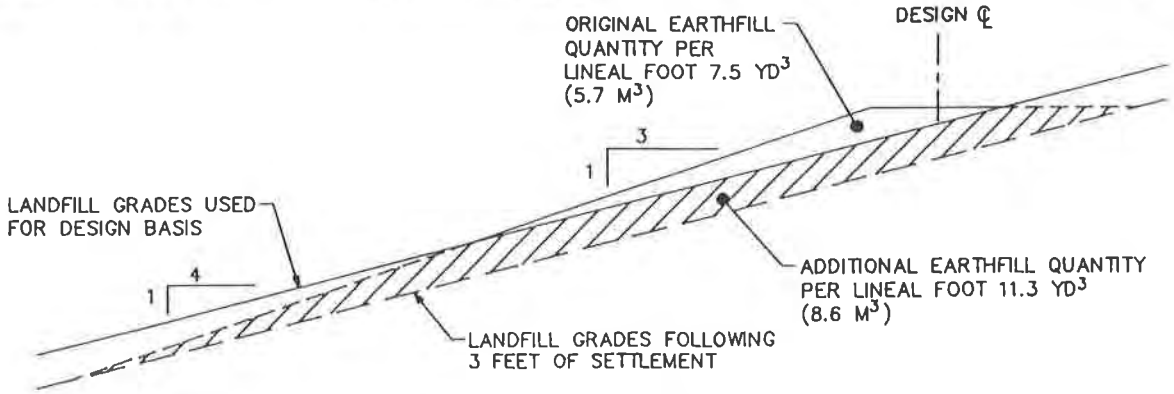

FIGURE 5. EFFECT OF SETTLEMENT ON ROAD DESIGN WITH SET HORIZONTAL AND VERTICAL CONTROL

horizontal and vertical alignment of a road for the side hill of a landfill was based on topographic mapping prepared 12 months before construction. Figure 5 shows the effect of 3 feet of settlement on an actual road section designed on a 4:1 side slope. Accommodating this settlement required either increasing the material to construct the road to design grades and alignments or rapidly redesigning the horizontal and vertical alignment during construction. The increased quantity of soil required to build the road to design grades was 11.3 cubic yards ($8.6m^3$) per lineal foot (0.3m) at a potential additional cost to the client of $158 per lineal foot. This would have added approximately $450,000 to the total project cost. Redesigning the road was the less expensive option, even if the contractor had put in a claim for delay.

Such design problems can be avoided. Instead of specifying set horizontal and vertical control in the bid documents, it would be better to design a typical road cross section relative to the final cover, set a general horizontal alignment, and require minimum cross slopes and longitudinal grades. Although more field engineering is involved, settlement makes this extra work inevitable. Final alignment of items that can be affected by settlement should not be fixed until the construction phase of the project.

Foundation Soil. A critical element in planning foundation layer construction is estimating the quantity of soil required to meet the design intent. Often landfill surfaces are poorly graded, have refuse exposed in areas, and have areas requiring significant earthfills to meet minimum final slope requirements. Assuming an average depth of foundation soil based on a typical cover cross section usually results in underestimating the quantity required to complete the work.

Experience has shown that for poorly graded landfills, where the refuse was recently placed and where daily cover is minimal, the quantity of soil required to provide a uniform grade and a 1-foot (30 cm) minimum depth of soil cover is 2 to 3 cubic feet (0.06 to $0.08m^3$) of soil per square foot ($0.09m^2$) of landfill area.

Production rates for placing foundation layer soil depend on the source of the material, available equipment, and site access. If soil is available on-site near the construction area daily quantities of 5,000 to 10,000 cubic yards (3,800 to $7,650m^3$) per day can be achieved. If the soil source is from off-site, a large trucking fleet will be required and production of more than 6,000 cubic yards ($4,600m^3$) per day is difficult to achieve.

Bedding Soil. The critical element in placing bedding layer soil is preparing a well graded subgrade (top of foundation soil). A well graded subgrade will minimize the quantity of bedding soil required to meet minimum thickness requirements. A rough graded subgrade with holes or ridges will require higher quantities of bedding soil, raise costs, and slow the schedule. Closely spaced grade control is also a key to constructing a quality uniform-depth bedding layer. Spacing grade control on a 50-foot (15m) grid is common.

Bedding soil, particularly where it is used to transmit gas or leachate, is typically a processed and imported soil. Production rates of 1,500 to 2,000 cubic yards (1,150 to $1,500m^3$) per day can be achieved which result in 2 to 3 acres (0.8 to 1.2 hectares) of completed bedding layer per day.

Geomembrane. Critical elements for geomembrane installation are maintenance of the bedding layer grades during deployment, quality seaming, and protection of the geomembrane during placement of the drainage layer.

Equipment and foot traffic can rut and put holes in a sandy bedding layer. Repair of this disrupted grade is required for a quality geomembrane installation. A smooth foundation for geomembrane installation is also critical to seaming operations and for avoiding undue stress on the geomembrane materials.

A large amount of information has been written concerning obtaining quality geomembrane seams. It is not the intent of this paper to describe geomembrane seam

construction in detail (see, for example, EPA, 1989). However, in summary, the following should be considered:

- Qualified personnel should perform the work.
- Welding equipment should be well maintained and checked frequently to assure proper operation. This is particularly important for the heating elements of welding machines.
- The installer should have a well planned quality control plan and the Owner should provide on-site representation to assure compliance with the plan and provide quality assurance testing.
- Test equipment should be well maintained, properly calibrated, and meet the requirements of the test procedures.

Production rates for geomembrane installation vary significantly based on complexity of projects, project size and schedule. Installations of 100,000 square feet (9,300m^2) per day for polyethylene are not uncommon. For planning purposes, however, production rates of 30,000 to 40,000 square feet (2,800 to 3,700m^2) per day are reasonable.

Drainage Layer. The drainage layer component of a final cover, particularly for steep slopes, is the most difficult to construct and the most important for the design. Many things can go wrong and planning to prevent problems is essential to success.

The drainage material must meet gradation and permeability requirements. Discovering that a product does not meet these requirements following its placement on the geomembrane can be costly. Removing material from the top of geomembrane is much more difficult than placing it.

A good quality control plan can avoid this problem by verifying material compliance with specifications before the material is placed. This may include source sampling and testing before approval of the material is granted. Monitoring delivery of material to the site is also important. Providing on-site testing capabilities can speed up the quality assurance monitoring of the material.

Drainage material placement should be monitored closely to assure no damage is done to the geomembrane, wrinkles are controlled, and proper thickness is achieved. Low ground pressure dozers work well to place this material but often require long pushes from the point where the material is delivered.

Drainage material placement is often the critical path in scheduling a cover project. The time required to produce the material, available trucking for delivery, and equipment necessary to handle the material on-site all need to be considered. Production rates of 3,000 to 4,500 cubic yards (2,300 to 3,400m^3) per day can be achieved, but logistical plans for this production rate must take into account that this means about 250 truck loads of material will be delivered per day.

Geotextile. Installation of geotextile is straight forward. Items to consider are protection from ultraviolet degradation and seaming of the product in the field. Production rates to meet schedules are usually not a problem.

Topsoil. Topsoil is placed at the end of a project, and the key to its success is constructing it in time to seed it, get vegetation to germinate, and protecting top soil from erosion. Simple methods of erosion protection that have proven effective are track walking a slope so that dozer tracks are deep and perpendicular to the line of slope, and covering the completed soil layer with 2 to 4 inches (5 to 10 cm) of straw. In colder climates this helps insulate seed and provides additional erosion protection. More sophisticated erosion control methods are available if needed. Production rates are usually between those for foundation soil and drainage layer.

Ditches. The most common construction error for surface water ditches is not paying attention to the cross sectional details of the ditch. The ditch in Figure 1 is a good example. In this ditch the design water depth is the highest elevation of geomembrane. If during construction the geomembrane is not brought up on the downstream side of the ditch and the contractor decides to maintain the overall depth of ditch with soil, then the soil above the geomembrane on the downstream side of the ditch must contain the water. If this soil is permeable or erodible the ditch can fail at high water levels, and damage the downslope cover. Protection against this problem is a good design, quality ditch installation, good quality control, and detailed construction staking and construction techniques.

Geomembrane Penetration. Two common problems occur with penetrations through geomembrane covers: (1) stresses are put on the geomembrane boot during drainage layer construction that result in boot failures or failures of the pipe penetrating the geomembrane, and (2) landfill gas escapes.

Figure 6 shows a detail that has been constructed successfully on cover projects that prevents these problems. The key to this detail is not the detail itself, but the timing of installation. The geomembrane boot should not be welded to the geomembrane cover until the major portion of drainage layer is placed. Geomembrane covers move during drainage layer placement, particularly on slopes. If the boot is installed prior to drainage layer placement then movement of the geomembrane transfers stresses to the area of the rigid pipe penetration. Landfill gas losses through the boot are prevented by the hydrated bentonite shown on the detail.

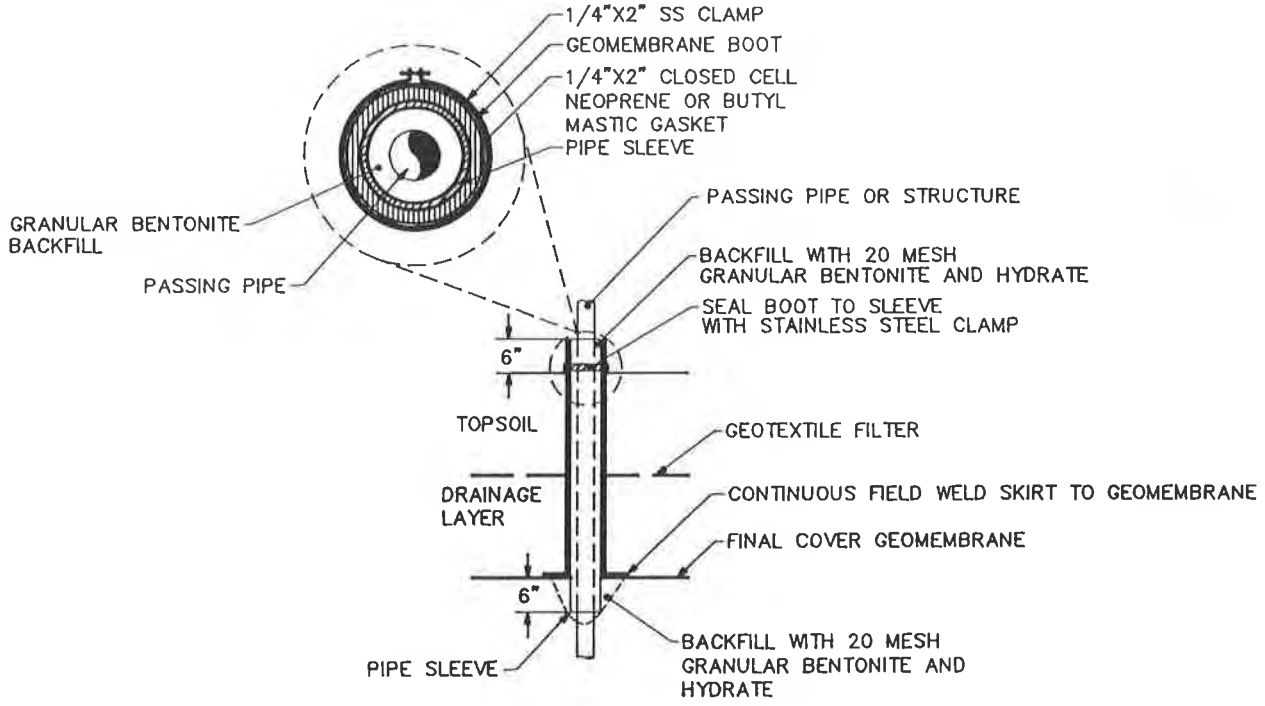

FIGURE 6. GEOMEMBRANE BOOT PENETRATION

Overall Production Rate. Overall construction time for a typical 25-acre (10-hectare) project is on the order of 3 to 4 months, although projects up to twice this size have been constructed in the same amount of time. Key factors affecting the schedule are the amount of equipment and manpower used by the contractor, efficient scheduling and construction management, well prepared drawings and specifications, and cooperation between the owner, engineer, and contractor.

SUMMARY AND DISCUSSION

1. Using geomembranes for landfill covers has increased in recent years because they perform better and are often more cost-effective than soil-only covers. The new Subtitle D regulations will likely require geomembrane final covers on most new landfills that have bottom geomembrane liners. Engineers need to develop an understanding and methodology for designing such landfill covers.

2. Two important considerations in designing geomembrane covers are the interrelated issues of slope stability and drainage. The infinite slope method is appropriate for modeling cover slope stability. Applying Darcy's law to an assumed saturated topsoil condition is a conservative yet rational method for estimating maximum head buildup in the drainage layer above the geomembrane for use in the infinite slope analysis.

3. The actual materials that will be used for each project should be tested to obtain design parameters. In cases where material selection is left to the contractor, provisions should be made in the specifications to address minimum or maximum allowable material properties and conformance testing so that the design intent is met.

4. Construction project planning should include provisions for field engineering modifications to allow for landfill settlement.

5. Construction quality control and quality assurance monitoring is important for

- Soil material conformance testing
- Geosynthetic material conformance testing and installation observation
- Grade tolerances and layer thickness control
- Construction details such as ditch cross sections and pipe boot installation

6. Construction planning and sequencing can improve efficiency and allow realistic scheduling.

REFERENCES

Cedergren, H.R., (1989) "Seepage, Drainage, and Flow Nets", 3rd Ed., John Wiley and Sons, New York.

Christopher, B.R. and Holtz, R.D. (1985) "Geotextile Engineering Manual", Federal Highway Administration, FHWA Contract No. DTFH61-83-C-00150.

Dunn, I.S., Anderson, L.R., and Kiefer, F.W., (1980) "Fundamentals of Geotechnical Analysis", John Wiley and Sons, New York.

EPA, (1989), "Technical Guidance Document: The Fabrication of Polyethylene FML Field Seams", EPA/530/SW-89/069, September 1989.

EPA, (1992a) "Final Cover Requirements for Municipal Solid Waste Landfills", Environmental Fact Sheet, EPA/530/SW-91084, March 1992.

EPA, (1992b) "Draft Technical Manual for Solid Waste Disposal Facility Criteria - 40 CFR Part 258", April 1992.

Federal Register, (1991) "Solid Waste Disposal Facility Criteria; Final Rule", 40 CFR257 and 258, Part II Environmental Protection Agency, Vol. 56, No. 196, Wednesday October 9, 1991 Rules and Regulations, U.S. Department of Commerce, Washington, D.C.

Giroud, J.P. and Beech, J.F., (1989) "Stability of Soil Layers on Geosynthetic Lining Systems", Geosynthetics '89 Conference Proceedings, Vol. 1, pp. 35-46.

GRI, (1991) "Proceedings of the 5th GRI Seminar on Geosynthetics in Filtration, Drainage, and Erosion Control", Geosynthetics Research Institute, Drexel University, Philadelphia, December 12 and 13, 1991.

Koerner, R.M., (1990) "Designing With Geosynthetics", Prentice Hall, New Jersey.

Koerner, R.M., and Daniel, D.E., (1992) "Better Cover-Ups", Civil Engineering, May, 1992, pp. 55-57.

Lambe, W.T. and Whitman, R.V., (1969) "Soil Mechanics", John Wiley and Sons, New York.

Newmark, N.M, (1965) "Effects of Earthquakes on Dams and Embankments", Geotechnique, Vol. 5, No. 2, London, England, June, 1965.

Seed, R.B. and Bonaparte, R., (1992), "Seismic Analysis and Design of Lined Waste Fills: Current Practice", Stability and Performance of Slopes and Embankments - II, ASCE Geotechnical Special Publication No. 31, New York, NY.

Schroeder, P.R. (1989), "The Hydrologic Evaluation of Landfill Performance (HELP) Model" U.S. EPA, Cincinnati, Ohio.

In-Situ Soda Ash Treatment for Contaminated Geosynthetic Clay Liners

T.N. Dobras
James Clem Corp., USA

J.M. Elzea
McCrone Associates Inc., USA

ABSTRACT

In 1986, approximately 195 m^2 (2100 square feet) of geosynthetic clay liner (GCL) was installed at a fuel storage tank site in the eastern United States. The site provided secondary containment of No. 2 fuels for a utility company. After several years of successful operation, the site began to experience an increase in its hydraulic conductivity.

After an extensive laboratory investigation and analysis, it was concluded that the bentonite had become contaminated by the intrusion of positively charged, soluble ions which had been present in the cover material. The investigation concluded that the cover contained a significant proportion of dolomitic limestone. The contamination had the effect of depleting the sodium content while increasing the concentration of calcium and magnesium ions. The result was a flocculation of the clay platelets, decrease in pH, reduction of water absorption capabilities of the bentonite and an increase in permeability.

After further testing, it was determined that the contaminated liner could be effectively treated, in-situ, with the addition of soda ash (sodium carbonate) spread over the existing liner. Laboratory investigations provided evidence that bentonite properties, which have been detrimentally affected by external contaminants, can be reversed by replenishing the depleted sodium ions. The permeability, water absorption, pH properties and platelet orientation all were restored to pre-alteration levels.

As a result of this investigation, the site was restored to its original condition by spreading a uniform layer of powered soda ash over the existing liner. The existing soil cover was replaced with a clean, freely draining aggregate, relatively free of adverse exchangeable cations. The bentonite was re-activated by hydrating the liner with fresh water and allowing the head of water to remain for a period of 48 hours. To date, no noticeable leakage has occurred.

INTRODUCTION

For over a century bentonite has been used for the containment of fluids in a variety of applications including ponds, oil well seals and, more recently, landfills, reservoir caps, heap leach pads and tank farms. With the introduction of easy to install bentonite-based geosynthetic clay liners (GCL's) in the early 1980's, this use of bentonite has grown considerably. Over the past decade more than 20 million square feet of GCL has been used in secondary containment applications.

GCL's are manufactured by combining bentonite with various geotextile materials. Installation is relatively rapid and requires less heavy equipment. They are self-repairing if punctured, can effectively seal against structures and penetrations and have manufacturing-controlled uniform properties. Although GCL's have been in use in waste management, secondary containment and waterproofing applications for more than ten years, there is little data and information available addressing long term performance under the various physical and chemical environments. This investigation is a first step in gaining that understanding.

A GCL, manufactured by the James Clem Corporation, was installed in 1987 at a site in the eastern United States. The GCL was made by sandwiching approximately 5mm of high-swelling Wyoming bentonite between two geotextiles. The GCL was initially performing satisfactorily for a few years. A change in performance was observed in 1989 where the liner lost its ability to effectively contain water. The change was noticed when storm water, which previously had been retained, appeared to be permeating through the liner at higher than normal rates. In order to understand why this increase in permeability occurred, a laboratory and field investigation was undertaken. The results of the investigation and the subsequent remediation measures performed on the affected liner at the site are the topic of this paper.

Site Description. The site is small, consisting of a 510m^3 (135,000 gallon) fuel storage tank, having a 6m (20 feet) diameter. The tank is surrounded by a concrete ring wall which is 4.2m (14 feet) away from the tank. The total lined area of the basin is 195m^2 (2100 sf). The GCL was placed on a compacted sand subgrade and under a 20cm cover soil which consisted primarily of dolomitic limestone. **Figure 1** shows the tank and perimeter wall at the site.

Figure 1. Overview of Site

PROBLEM IDENTIFICATION

Based on visual inspection of the liner, it was speculated that the chemistry of the bentonite had been altered such that the water retention and sealing properties were affected. In order to determine the cause of liner failure, the chemical and physical properties of bentonite removed from samples of failed and unused liner were tested. The objective of the laboratory portion of this investigation was to: 1) characterize and document the amount and type of chemical alteration, if any, which had occurred, 2) determine the reason for the surface alteration, and 3) make a preliminary proposal for reactivating the liner and removing the source of the problem. In order to meet the goals of this investigation, several different components of the liner system were examined. The samples of bentonite separated from the liner were examined by a number of analytical techniques (see below). In addition, samples of the cover material, unused GCL and raw Wyoming bentonite were examined. A rainwater sample was also analyzed for composition.

X-Ray Diffraction. Clay mineralogy of the new GCL, the existing liner and the cover soils were determined by x-ray diffraction. All samples were prepared and analyzed following standard procedures. The actual analysis was performed with a fully automated Siemens X-Ray Diffractometer using CuK_{α} radiation. This procedure was performed to identify the mineralogy of the various soil and clay samples. It also was used to examine the structure of the clay. Every crystalline substance scatters x-rays to produce an unique diffraction that may be considered a "fingerprint" of its atomic and molecular structure.

Electron Microscopy. Some of the samples were examined under a JEOL 840 electron microscope and a JEOL 8600 superprobe. This was done to obtain detailed chemical information as well as to examine microtextures.

Inductively Coupled Plasma Spectrometry (ICP). The exchangeable cation and major element chemistry of the bentonite was determined using a Perkin Elmer Model 6500 ICP-AES. The concentrations of exchangeable cations were measured by exchanging the bentonite with a 1N ammonium acetate solution adjusted to a pH of 7. The chemistry of the water sample was also determined by ICP.

RESULTS

Three samples of unused GCL, one sample of raw bentonite from the mine and two samples of the failed GCL from the site, were examined for exchangeable cation chemistry, major element chemistry, pH and mineralogy. Both the raw bentonite and unused GCL were analyzed.

The samples of failed GCL exhibited a severe depletion in exchangeable sodium and a significant increase in exchangeable calcium and magnesium relative to the unused clay (**Tables 1 and 2**). Another change in the chemistry of the clay was pH. The pH of the clay as mined is normally between 8.5 and 10.5. Bentonite removed from the failed liner exhibited a pH of approximately 7.

The major element chemistry of the clay was examined in order to determine whether or not the sodium was totally removed from the bentonite through cation exchange or had migrated from the clay surface to other parts of the structure. Results of this analysis suggest that the sodium was completely removed from the clay. Other changes noted in bentonite removed from the failed liner were a change in color, from blue-gray to brown-yellow, and a reduction in the ability to hydrate.

The mineralogy of the samples of cover material was determined by optical microscopy and x-ray diffraction. The cover was found to contain quartz, dolomite, feldspar (albite), mica and chlorite. Minor constituents include magnetite, montmorillonite, kaolinite, and illite/smectite. The amounts of each of the major mineral components was semi-quantitatively estimated on a relative basis, using a computer routine based on x-ray diffraction peaks. Results of this analysis are summarized in **Table 3**. Dolomite (nearly 90%) has a predominance of calcium and magnesium ions.

The last component of the system that was characterized was a sample of rainwater. The rainwater was determined to have a typical chemistry relative to other rainwater samples from the northeastern United States and has a pH of 6.2. The rainwater indicated normal concentration of the various constituents and was not considered further as a possible contaminant source.

TABLE 1

WT % Oxides

SAMPLE	Na_2O	MgO	K_2O	CaO	Fe_2O_3
Typical GCL	2.8	2.1	0.2	0.5	2.1
Commercial Bed Blue Bentonite	3.8	3.2	0.2	0.8	2.7
Site Sample #1	0.1	3.4	0.3	1.2	2.9
Site Sample #2	0.6	3.1	0.3	1.3	3.1

TABLE 2

Exchangeable Cations (%)

SAMPLE	Na	Ca	Mg	K	D (001) SPACING	pH
Typical GCL	84.1	8.9	4.0	3.1	10.2	10.2
Commercial Bed Blue Bentonite	77.6	14.5	4.0	4.0	N/A	10.0
Typical Values as Reported in Literature	75.0	18	6.0	1	11.0	9.5
Site Sample #1	0.4	59	40	0.4	11.4	7.3
Site Sample #2	17.3	65	16	2	11.6	7.3

TABLE 3

Mineralogy (%) of the East Hampton Cover Soil

Quartz	Dolomite	Feldspar	Mica	Chlorite
9	88.6	1.6	0.6	0.1

DISCUSSION OF RESULTS

Alteration of the GCL. Bentonite samples separated from failed GCL removed from this site were chemically and structurally altered relative to unused GCL and raw bentonite from the mine. Since the time of emplacement the bentonite has lost most of its exchangeable sodium which has been apparently replaced with calcium and magnesium. This loss of sodium has altered the chemistry of the clay, which has resulted in a change in the behavior of the clay. Other observed changes include a decrease in pH and the probable oxidation of octahedral iron. The degree of oxidation of iron has not been quantitatively determined but, based on the yellow color of the clay, it is reasonable to conclude that most of the iron is in the ferric state.

It has been experimentally demonstrated that bentonite with sodium as the major exchangeable cation yields the lowest permeabilities (Grim, 1962). This is because the presence of sodium effectively reduces particle size by enhancing dispersion. In addition, the hydration properties of sodium compared to other exchangeable cations, such as calcium, allow more water to be absorbed between clay particles. This increased water absorption impedes fluid flow by reducing inter-particle pore diameters and by physical interference. In addition, calcium predominant bentonites typically exhibit a lower pH than sodium predominant bentonite, explaining the lower pH values observed in the failed liner. It has been theorized that the presence of calcium ions, combined with a lower pH, promote flocculation of the particles (Lagaly, 1989). Flocculation results in the opening of small channels through which fluids flow, thereby increasing the permeability. As permeability increases, more water is able to pass through, creating additional opportunities for the exchange reaction to take place.

SUMMARY OF CONCLUSIONS

The exchange of calcium for sodium in the bentonite apparently has occurred after the liner was installed. The mechanism and timing of the exchange reaction, however, cannot be determined from the available data. Two conclusions can be drawn: a) The dolomitic cover soil appeared to be a logical source for both the calcium and magnesium ions; and b) Based on the analytical tests performed, the rainwater did not appear to contain these cations in sufficient concentrations to be considered as a likely contaminant source. Because the rate of dissolution of dolomite is a slow reaction, it is likely that several factors may have combined at the site to enhance dolomite dissolution, increase the concentration of calcium and magnesium in solution and promote the exchange of calcium for sodium on the clay surface. These factors are described below:

- Dolomitic limestone cover creating a source of calcium and magnesium ions which exchanged with the sodium of the bentonite;
- Excessive quantity of soil fines and silty clays in the cover soil, leading to poor site drainage. This potentially increased the extent of dissolution because of prolonged contact with the standing head of water. In addition, the time of exposure between the dissolved contaminants and the bentonite also became a factor;
- A slightly acidic rain water, possibly also increasing the solubility of the dolomite cover;
- Once the calcium and magnesium had a chance to react with the bentonite to the point where the water absorbing and low permeability properties were affected, the water was better able to pass through the bentonite, thereby further promoting the exchange reactions.

SODA ASH TREATMENT

Introduction. One of the unique features of sodium bentonite is its chemical reactivity. Because of this property, most reactions that alter the bentonite structure and behavior can be reversed, such that those affected properties can usually be restored to their original levels.

It has long been known by the bentonite suppliers that the addition of soda ash can reactivate sodium depleted bentonite and improve its swelling and absorption properties. In fact, suppliers of calcium bentonite routinely add soda ash to their product to enhance the sodium concentration. Before this treatment could be carried out in the field, several questions had to be answered, which included: a) will the sodium treatment be effective in re- exchanging with the calcium and magnesium?; b) even if the sodium is able to be successfully exchanged, how will this process affect the other properties, such as permeability, swelling and self-healing?; c) what effect would it have on the pH of the bentonite and orientation of the platelets?; d) how would the soda ash be applied in the field?; e) how long will the reaction take?; and f) at what rate should the soda ash be applied and in what form, solid or liquid?

A laboratory investigation was undertaken to determine if the soda ash treatment could effectively restore the bentonite to its original condition. Based on this investigation, as described below, we decided to use soda ash to reactivate the liner.

Swell Tests on Sodium Treated Bentonite. The first test was a simple swell test on two, 25cm^2 samples of affected liner obtained from the site. One sample was sprinkled with one gram of powdered soda ash (400g/m^2) and the other was left untreated. Both samples were hydrated with fresh water. Within a matter of a few hours, the treated sample swelled to three times its original height, while the untreated sample showed no visible signs of swelling or change in volume to any significant degree.

Tests on Bentonite Properties of Treated Bentonite. The next step was to perform the same quality control testing on a treated sample that the Clem Corporation follows when testing bentonite as it is delivered to the manufacturing plant. The application rate was again 400g/m^2. As before, the results were positive and are summarized in **Table 4** below:

Table 4

SAMPLE	TREATED (T) or UNTREATED (U)	FLUID LOSS (ml) per API-13A	SWELL INDEX (ml) per USPF XVII	PLATE WATER ABSORPTION (%) per ASTM E946
JCC QC Criteria	----------	12 (max)	27 (min)	700 (min)
Sample #1	U T	32 13	10 22	295 1150
Sample #2	U T	16 14	12 28	280 865
Sample #3	U T	16 14	18 28	370 905

As indicated, the bentonite properties were significantly improved in virtually every category.

Permeability Tests on Treated Bentonite. Next, we were able to determine that the permeability was reduced with the addition of soda ash. It was decided to use the same parameters and test methods used in the permeability test during routine quality control testing in the Clem manufacturing process. Those parameters included a five day test duration, 20N/cm^2 (30 psi) effective stress over the liner, and 10cm flexible wall permeameters. The results are presented in **Table 5** on the next page.

Table 5

PERMEABILITY TEST RESULTS OF SODA ASH TREATED BENTONITE LINER

SAMPLE	TREATED (T) or UNTREATED (U)	PERMEABILITY COEFFICIENT (cm/sec) per ASTM D5084 modified	DAY NUMBER
Baseline Acceptance Criteria	----------	4 x 10E-10 (maximum)	1 - 5
Sample #1	U	1.0 x 10E-9 1.4 x 10E-7 6.0 x 10E-10	1 2 3 - 5
Sample #2	T	4.0 x 10E-10 3.0 x 10E-10	1 2 - 5

Although not quite as pronounced, the results were once again quite positive. The most obvious conclusion is that we have successfully lowered the overall permeability to an acceptable level after the addition of soda ash. The treated sample behaved similarly to newly manufactured GCL with the low permeability achieved immediately and remaining unchanged over the course of the test.

It is not completely clear why the permeability of the untreated sample started out at 10E-9, increased to 10E-7 in day two and finally achieved its equilibrium valued of 6 x 10E-10 (approximately double that of the treated sample) by day three. It is possible that the high effective stress of 20N/cm^2 (30 psi) enabled the clay to orient itself into an overlapping configuration of the platelets, creating a shingle effect, and close any desiccation cracks which may have formed. In retrospect, the test should have been conducted at a lower, more representative pressure. The decision was made to perform the test under these conditions because of time constraints and due to the considerable amount of previous data available at the higher pressure, which would serve as a comparison.

Cation Exchange Capacity and pH Tests on Treated Bentonite. The last test that was performed on the treated bentonite liner was a pH measurement and a determination of the exchangeable cation capacity. These analyses were performed to determine if the exchangeable cation concentrations have truly been restored to the original levels. The results are shown below in **Table 6:**

Table 6

SAMPLE	TREATED (T) or UNTREATED (T)	EXCHANGEABLE CATIONS (%) Na	Ca	Mg	K	pH	D-SPACING (A)
Normal, New GCL	----------	84	9	4	3	9-11	10
Sample #1	U	3	60	24	14	7.5	13.7
Sample #2	T	80	13	7	0.2	10.2	10.4

All values of exchangeable cations, pH and d-spacing have been converted to levels typically found in unaltered bentonite, verifying the conclusion that the contaminated bentonite has been effectively treated with the addition of soda ash.

OPTIONS FOR REMEDIATION

Replacement of Dolomitic Cover Material. Based on the evidence provided by the laboratory testing to date, it was decided that in order to restore the liner and

ensure long term service, the dolomite cover should be removed. A new cover consisting of a clean, freely draining quartz aggregate was selected to minimize contamination by deleterious cations and to maximize drainage. A representative sample of the selected new cover was analytically tested to determine compatibility between the aggregate material and the bentonite. Relative concentrations of the various contaminants in the soil were determined. We specifically analyzed the soil for multi valent cations such as calcium, magnesium, potassium and iron.

Restoration or Replacement of the Existing GCL. The next decision was whether the existing GCL at the site should be restored to its original condition with an in-situ soda ash treatment, or if the GCL should be completely removed and replaced. The former alternative, with an estimated cost of $22,000 including the removal and replacement of the cover soil, was determined to be the most cost effective and timely alternative over the replacement option which was estimated at nearly $35,000. The cost differential would likely be more significant on larger sites.

As indicated previously, laboratory investigations on the affected liner suggested that the soda ash would rejuvenate the bentonite. Although the laboratory analysis was very positive, many questions remained regarding the feasibility of an in-situ treatment process on a relatively large scale. Questions, such as field application rate of soda ash method of application, and whether or not the dolomitic cover soil could be effectively removed without damaging the liner, remained. It was decided to proceed with the soda ash treatment at this site on an experimental basis. The small size of the area minimized the cost of the experiment. Additionally, it was felt that, because of the severely degraded liner, this site would be a good indicator of the general feasibility of the process.

SITE RESTORATION

Construction Problems. One of the biggest difficulties in the site restoration was its limited size and accessibility. The existing 20cm (8") layer of dolomitic cover had to be removed manually, using hand shovels and brooms, to ensure the GCL would not be damaged and to enable a visual inspection of the GCL. The four meter wide working area between the tank and the steel wall was the only access in which the contractor had to work. Numerous pipes and penetrations through the liner further impeded the progress (**Figure 2**). After two working days, using a five man team, the contractor completed the cover soil removal operation.

Inspection of Existing Liner. Following the removal of the cover soil, the existing liner was visually inspected. The surface of the liner was relatively firm with localized pockets of swelled, soft bentonite.

In general, the condition of the existing liner was poor (**Figure 3**). Although somewhat soft and gelatinous, it was very thin (approximately 5mm). A hydrated GCL, with an initial unhydrated thickness of 5mm, should swell to a thickness of 15-20mm under a confining load of 5KPa (0.7 psi) upon hydration. The liner appeared to be partially desiccated and cracked. Samples of the liner were hydrated over a period of 24 hours. The sample did not undergo any visual sign of swelling and hydration after the 24 hour period in an unconfined state. Additional samples were cut for further laboratory and field testing, as described below.

The original seams were butt-joined together with a cap strip over the top of the butt joint, rather than the recommended practice, which is a minimum 15cm (six inch) overlap of one panel over another. After inspection of the butt-joined seams, it was decided to replace the cap strips with new GCL. In addition, all seals around the tank, perimeter well and pipes were completely restored using a combination of granular bentonite, bentonite mastic and new GCL skirts and strips (**Figures 4 and 5**).

Soda Ash Treatment. The laboratory investigation utilized a soda ash application rate of approximately 400g of soda ash per square meter of liner (0.08 lbs/ft^2). To ensure the effectiveness of the treatment, it was decided to increase the application rate in the field by a factor of 5 to 2000g/m^2 (0.40 lbs/ft^2). For the site area of 195m^2, a total of 390 kilograms (860 lbs) of soda ash would be required.

Each bag of soda ash contained 23 kilograms (50 lbs) and, therefore, 17 bags were used. An area of the liner equal to 11.5 square meters (124 ft^2) was marked on the liner. Using a standard drop-type fertilizer spreader, each bag was evenly distributed over the marked area (**Figure 6**). Areas where new GCL was installed were not treated with soda ash.

Cover Soil Placement. Finally, with the entire area uniformly spread with soda ash, the cover operation began. The cover soil (consisting of 20mm nominal diameter gravel) was installed. A crane loader was used to dump the gravel onto the liner, which was first protected with plywood boards. Because of the limited accessibility, a small tractor had to be crane lifted in to the site (**Figure 7**). The material was spread using both the tractor, operating on plywood boards to prevent damage to the liner, and manually with shovels (**Figure 8**). **Figure 9** illustrates the completed site prior to the flood test. An inspection port consisting of an outer plastic ring to hold the cover soil in place, and bucket which could be lifted to gain access to the liner, was installed to enable a quick inspection of the liner to determine the hydration condition (**Figures 10 and 11**). The ring and bucket had holes drilled in the side to allow the flow of water through the bucket.

The lined area was slowly flooded from the sump area outward (in order to minimize the possibility of washing away the soda ash before it had a chance to react with the bentonite) to a height 25mm below the top of concrete ring wall (**Figure 12**).

The water level in the basin was measured using two graduated cylinders placed vertically on the liner (**Figure 13**). The first cylinder had holes drilled in the side and, therefore, always read the same level as the water in the basin. The second cylinder was closed on all sides, except on the top, which was open. This cylinder was used to measure the approximate effects from evaporation and precipitation. Both cylinders initially contained the same water level.

The cylinders were taped together to facilitate water level measurements and comparative readings between the two. Measurements were made on day two (to allow the bentonite hydration to take place during the first 48 hours) and again on day 10, using an engineer's scale and measuring from the top of the cylinder down to the water surface.

FIELD AND LABORATORY INVESTIGATIONS

To confirm the effectiveness of the soda ash treatment, a series of on-site and laboratory investigations were undertaken. A total of six samples were collected from the original, untreated liner. Three samples were treated with soda ash at the same rates as used in the site. The other three were left untreated. Each set of treated and untreated samples were used in each phase of the field investigation as described below:

Phase I - On-Site Permeability Testing. Two 20cm samples of liner were collected and placed in the bottom of two buckets, which had holes drilled in the bottom (**Figure 14**). To prevent sidewall leakage, a bentonite mastic was used around the sample sides. Soda ash was applied to one of the samples at the same rate that was applied in the field. A 20cm layer of the new cover soil was placed over each liner in the buckets and 25cm of water was poured in. Periodically, over the course of 30 hours, the water level in each bucket was accurately measured. After the 30 hour period, the water level in the bucket with the untreated sample dropped 24mm, while the treated sample dropped only 3mm, most of which occurred during the first few hours and can, therefore, be attributed to water absorption during hydration.

Phase II - On-Site Flood Test Results. The best indicators of the effectiveness of the soda ash treatment are the flood testing and the independent laboratory permeability testing, phases II and III of the investigation, respectively.

A new GCL under a confining stress of 5KPa (0.7 psi or 30cm of soil) should exhibit a permeability on the order of $1x10^{-9}$cm/sec. Under a head of 23cm (9 inches) of water and assuming a hydrated thickness of 1cm, the total expected loss through the liner should be no more than 0.2cm (0.08 inches) over a 10 day period. This, then,

should be our performance measuring gauge on the soda ash treated liner.

Between days two and 10 of the hydration/flood test program, the water level in the open cylinder rose 16mm, while the cylinder which only monitored precipitation and evaporation rose 13mm, indicating precipitation had occurred. Certainly, it can be concluded that there was no measurable drop in elevation in the basin after 10 days, and the slightly higher reading in the open cylinder might be attributed to slight differences in either precipitation capture or evaporation loss between the two cylinders. The permeability of the treated liner appears, on the basis of this test, to be on the order of the expected value of 10^{-8}cm/sec. After two weeks, with still no noticeable drop, the water was pumped out.

Phase III - Independent Laboratory Permeability Testing. Adjacent samples of both treated and untreated GCL from the site were carefully packaged and shipped to an independent testing laboratory. Flexible wall permeability testing of both samples were conducted in accordance with ASTM D5084.

The tests were conducted under an effective confining stress of 5KPa (0.7psi), which was approximately equivalent to the depth of soil cover used at the site. The test ran for six days, or until the in-flow change over time consistently equalled the out-flow change.

The reported permeabilities on the untreated and treated samples were 4.2×10^{-5} and 1.2×10^{-8}cm/sec respectively, which represents an improvement of nearly three orders of magnitude. The latter result is also consistent with reported laboratory permeability values on new GCLs under similar effective confining stresses.

CONCLUSION

It is apparent from both the on-site and laboratory investigations that the soda ash treatment on a severely contaminated bentonite liner is capable of restoring the bentonite to its original condition. On certain projects where similar contamination has occurred, the soda ash treatment can be a very cost effective alternative to replacing the liner system.

Additional testing still needs to be conducted to determine the feasibility of applying the soda ash in liquid form without removing the cover soil. If it has been determined that the cover soil is the contaminant source, additional testing should be conducted to determine how frequently the treatment would be required if the soil is not removed. Even a bi-annual treatment might prove to be more cost effective than replacing entire cover soil, as was done for this site.

REFERENCES

Grim, 1962 Applied Clay Mineralogy, McGraw Hill Books, Inc., pp. 242

Lagaly, G., 1989 "Principles of Flow of Kaolin and Bentonite Dispersions," Applied Clay Science, pp 105-123.

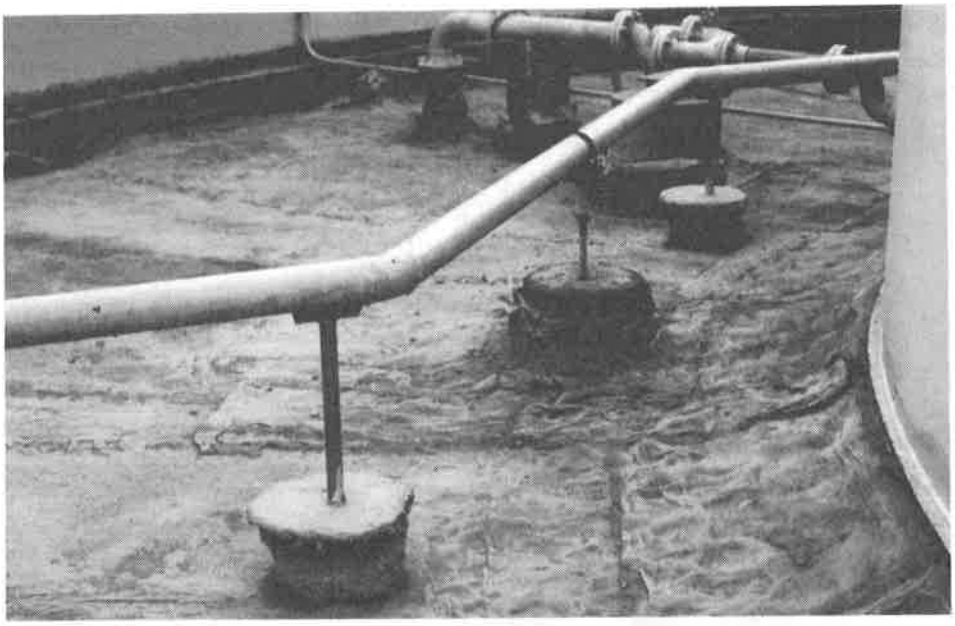

Figure 2. Numerous Pipes and Penetrations

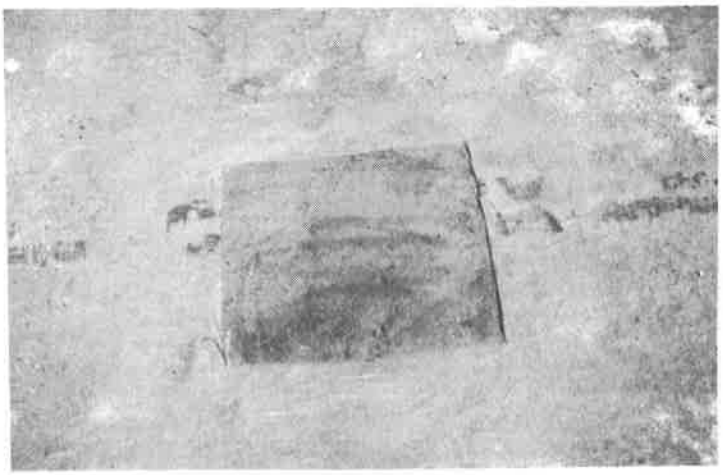

Figure 3. Condition of Existing Liner

Figure 4. Repair of seal around perimeter wall

Figure 5. Repair of seal around tank wall

Figure 6. Soda Ash application using standard drop spreader

Figure 7. Crane lifting tractor into site

Figure 8. Soil cover placement. A minimum protection layer of 8" of soil or plywood boards were used.

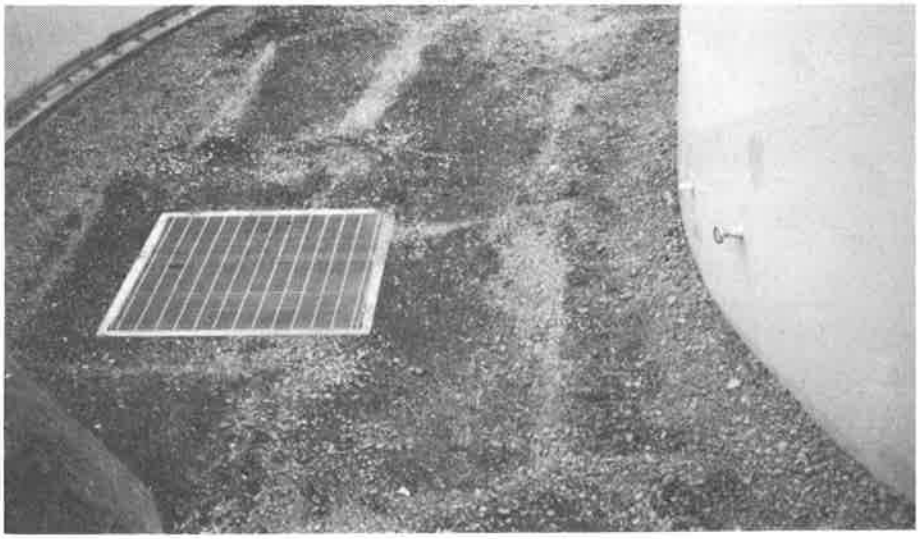

Figure 9. Completed site restoration

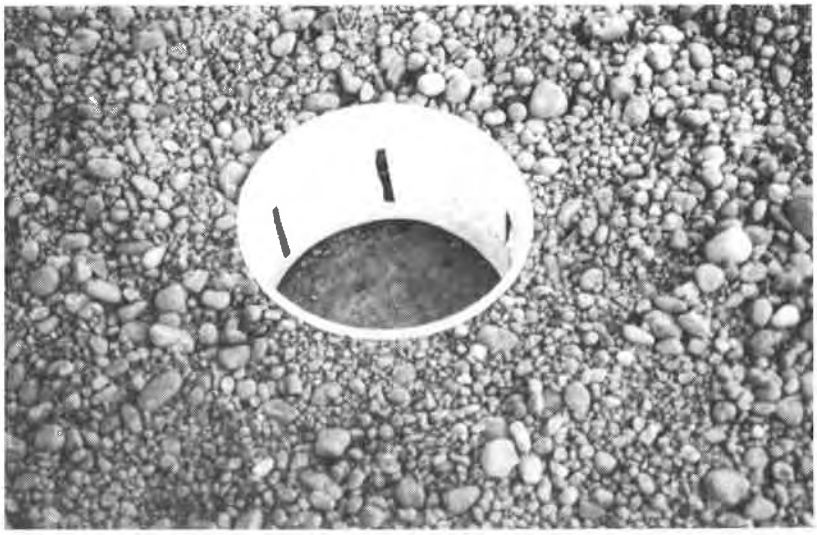

Figure 10. Outer ring for liner inspection port

Figure 11. Inspection Port

Figure 12. Flood test of restored site

Figure 13. Graduated cylinders for water level measurement

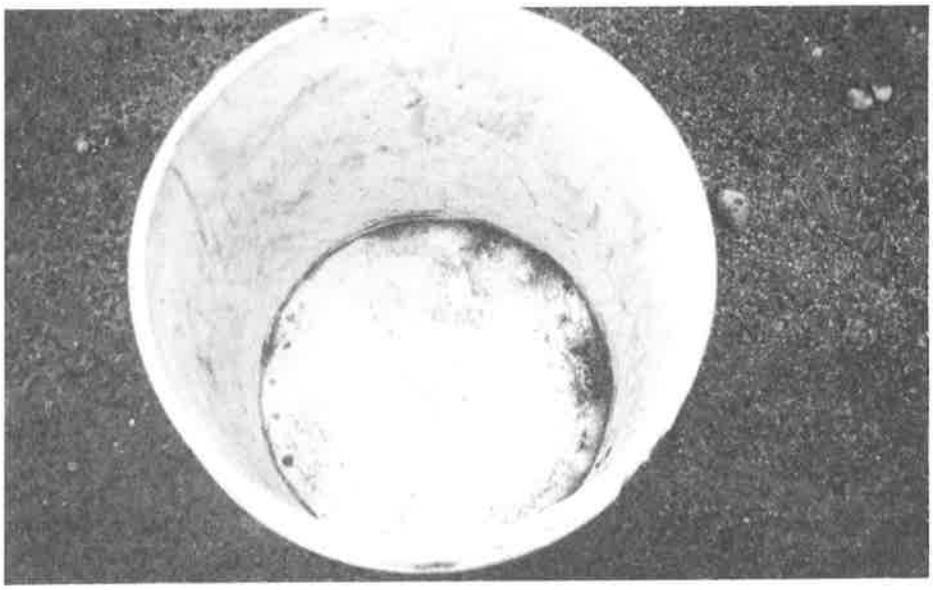

Figure 14. Soda Ash treated sample for on-site permeability test

Geomembrane Floating Covers: Technology for the Nineties

R.T. Taylor
JPS Elastomerics Corp., USA

L.R. Schader
JPS Elastomerics Corp., USA

ABSTRACT

Today, hundreds of properly designed floating covers have been installed worldwide. Dependable, yet continuously evolving technology, installation techniques and quality material can be credited with helping to grow this market. This paper will provide a look at these key elements as well as highlight and evaluate some of the critical factors in geomembrane installation.

In addition, the paper will offer comparative information on: how early, less effective floating cover designs compare to cutting edge technology (i.e., untensioned peripheral sump, bi-axially tensioned defined sump and post-tensioned cover systems and anaerobic digester covers); and how several floating cover membrane types stack up against one another (High Density Polyethylene, Hypalon, Polypropylene and XR-5).

INTRODUCTION

Since their introduction 30 years ago, the flexible geomembrane floating cover has evolved into a proven technology for protecting finished water resources from evaporation, contamination and algae growth. Custom designed floating covers not only provide reliable performance over the life of the installation, but are also environmentally sound alternatives for bio-gas collection and an economical solution for the coverage of industrial applications, including finished product storage and hazardous waste ponds.

As the geomembrane industry has evolved, so too has the selection of available flexible materials and the variety of installation designs. Installations have ranged from the earliest design of placing a blanket of membrane material directly onto liquid, to sophisticated tensioned, pre-determined sump location and ballasted cover configurations. However, there is no single floating cover design or material that is best suited for all applications. A thorough analysis of the specific site, and performance-related requirements of the proposed material is necessary prior to specifying a material and appropriate cover design.

SELECTION CRITERIA

While every geomembrane liner used as a protective barrier is designed to provide long term secure containment in a static environment, such as a reservoir or landfill, engineers must use special criteria in selecting a floating cover material to survive in a dynamic environment. This criteria includes:

1) Proven history
2) Weatherability
3) Strength
4) Seamability
5) Flexibility (fatigue resistance)
6) Potable water compatibility
7) Chemical compatibility
8) Repairability
9) Floatability

Engineers who neglect these factors when selecting a floating cover design and geomembrane, often learn difficult lessons from their omissions. For example, an engineer who selected an anaerobic digester cover at a chicken processing plant was so impressed by the widespread use of a certain geomembrane that he failed to consider the membrane's chemical incompatibility with chicken fats. As a result, the material failed. Another failure involved the use of a certain membrane in a Northern climate, without considering the material's inability to withstand continuous stress that would be exerted on the seam area in a subzero environment. When the outside temperature dropped to minus 25°F the membrane contracted and seam areas experienced severe stress due to the high co-efficient of contraction and expansion. This eventually led to stress cracking and the design failed. In both of these installations failures resulted from the selection of improper materials for the installation.

STATE OF THE ART MATERIALS

The first floating cover installations utilized Neoprene, Butyl or EPDM geomembranes. These materials -- all types of vulcanized rubbers -- proved incapable of handling the low levels of stress on the seams and anchorage locations caused by a reservoir's often changing liquid level. Seam integrity was virtually impossible to achieve and maintain in a dynamic water environment, and as a result, these materials literally came apart at their seams. These failures spawned the development of a new generation of high performance materials.

Hypalon. In the late 1950's, DuPont developed a polymer known as Chlorosulphonated Polyethylene (CSPE), now called Hypalon®. After nearly 20 years of outstanding performance in exposed applications such as cable jacketing, commercial roofing, and special coatings, DuPont encourage the introduction of Hypalon to the geomembrane floating cover market. Hypalon, which was approved by the FDA for use in potable water applications in the early 1970s, has been particularly successful in the exposed applications because of its proven weatherability and outstanding ultraviolet (UV) resistance. In addition, a geomembrane based on Hypalon, is highly flexible, easily contours to the installation site and is simple to install with chemical fusion or a hot air or wedge welder. A scrim reinforced Hypalon geomembrane provides a high level of puncture and tear resistance and superior dimensional stability. Once installed, the seams increase in strength with time and exposure. The first Hypalon floating covers were installed in Alcoa, Tennessee in 1973 and are still in operation. Since that time, Hypalon has dominated the market as the material of choice in potable water floating cover applications. Finally, while Hypalon is highly chemical resistant (resisting 95% of the chemicals normally found in containment applications), it does not typically perform well in the presence of fats and/or oils and may be somewhat difficult to repair after longterm exposure.

The key to the success of Hypalon over Neoprene, Butyl and EPDM was its seaming technology. The early membranes used a contact adhesive to bond both the factory and field seams. Although these seams exhibited very high shear values, they exhibited poor peel adhesion, often less than five pounds. This low value in combination with the breakdown in properties that occurred with many of the contact adhesives, resulted in seam failures with most of the early floating covers.

Hypalon seaming technology is based on the use of bodied chemical fusion technology. When a Hypalon bodied chemical fusion agent is applied to the seam, it actually causes the surface on the top and bottom sheets to fuse together, forming a homogeneous bond which increases in strength as the geomembrane ages. Therefore, with the improved Hypalon seaming technology, seam failure was substantially reduced.

XR-5. In the late 1970's, a new market developed for anaerobic digester floating covers. The first membrane successful in these applications was XR-5 (ethylene interpolymer alloy). This product exhibits superior chemical resistance which enabled it to be used where Hypalon could not. It was designed with a reinforcing fabric which gave it the strength to survive without yielding flexibility. XR-5's seaming technology, utilized a fusion method, which produced seams that were strong enough to survive in the dynamic floating cover environment. XR-5 is usually only warranted for 10 years for weathering exposure (compared to Hypalon's 20-year warranty), is not approved for potable water storage, and can be very difficult to repair once it has been installed in a chemical environment.

HDPE. High Density Polyethylene was first used as a floating cover on an anaerobic digester in the early 1980's. Its principle desired characteristic over XR-5 and Hypalon was its lower cost, floatability, and the available 20-year weathering warranty for this application. Despite the inherent very high stiffness of the membrane, HDPE is well-suited to this application because flexural stress is limited by design: ie: the fluid level of these cover applications rarely varies more than a few feet placing little stress on the cover.

Due to its low specific gravity, HDPE has an inherent ability to float. This gave designers the freedom to avoid the use of floats or counter weights that some designers felt were necessary to keep the material buoyant should the material develop a crack or tear. However, HDPE's excellent floatability is still not the ideal floating cover material because of its inherent high coefficient of thermal expansion and contraction. When expanded, large air pockets can develop and cause gas transmission problems beneath the cover and rainwater collection problems above the cover. Floats beneath the cover are often used with HDPE to provide gas transmission pathways. Its stiffness also makes fatigue failure a major concern especially in potable water applications, where it is common for reservoir levels to change 10 - 20 feet per day, subjecting the membrane to constant bending.

PP. Polypropylene is a proven material with more than 15 years successful exposure history and was introduced into the geomembrane market in 1991. It has many performance advantages over traditional flexible geomembranes. All the geomembranes described thus far have performance advantages and disadvantages. There is a tendency for materials with high flexibility to lack chemical resistance and materials with a high degree of chemical resistance to degrade with long-term exposure to UV, or suffer from a lack of flexibility and be difficult to repair.

Polypropylene is a high strength, scrim reinforced product with a low coefficient of expansion and contraction. PP's flexibility allows it to easily contour to all existing floating cover designs. It also has a wide temperature tolerance and can operate successfully in environments where ambient temperatures can range from -40°F to 120°F. It offers excellent chemical resistance to animal fats and greases common in anaerobic digester applications. In addition, PP is easy to repair using a hot air welder, even after long-term exposure to weathering.

The first polypropylene geomembrane installations were completed in 1991. The first polypropylene floating covers were installed in 1992 on an anaerobic digester in a wastewater treatment application and as covers on cyanide ponds in the gold mining industry. Polypropylene has all of the performance strengths required for a successful floating cover operation yet has few of the seam quality problems and other performance drawbacks associated with traditional floating cover materials.

FLOATING COVER DESIGNS

History. The earliest floating covers were plagued with design and installation problems, including surface-water collection and removal, entrapped air and gas, wind uplift, perimeter anchoring and seam reliability, as well as operational maintenance and safety issues.

The first commercial geomembrane reservoir cover, made from a high-strength reinforced Neoprene®-coated fabric, was installed in 1959 in California. The design consisted of a low-rise, air-inflated cover supported by cables and it rested on a

cushion of air pumped beneath the cover. Several covers with this design were installed, but performance problems plagued each one. For instance, once the material was installed, the seams, which were made with a gum tape system, could not withstand the low stress imposed by the air inflation and seam failure would occur.

The first commercial geomembrane floating cover design to actually be in direct contact with water was installed in 1964 by Globe Linings, Inc. in California. It is credited with being the predecessor of modern floating cover technology. A pattern of floats were attached to the underside of the cover membrane in the central portion of the reservoir. When the reservoir was filled, the excess slack (or slope allowance) was gathered into a rainwater collection trough around the periphery of the cover. Because of the absence of weights, this cover was known as the first "stress-free" peripheral sump cover. At this point, interest in floating covers was so strong that this stress-free cover was patented in 1967 as the ROOFLOAT® Cover System.

FLOAT DESIGNS

Floats are constructed from semi-rigid closed cell polyethylene and are attached on either the underside or topside of the cover membrane.

For most designs the term float is a misnomer. Despite the fact that floats do provide some buoyancy they will not insure cover survival in the event of a membrane or design failure. No matter how many floats are used, if the cover has not been designed to prevent stresses from exceeding 15 percent of the yield factor of the membrane, the life of the cover will be shortened. The ultimate failure will be due to either the stress causing the membrane to yield, or eventual membrane failure due to creep. The main purpose of the floats on a cover that is not used for bio-gas collection is to define the location of either the tensioned or the untensioned peripheral sump.

While the float patterns will vary depending on the reservoir configuration, the most common is a parallel arrangement in the center of the cover or two rows parallel to the sump (one on each side).

The original Globe Roofloat® design called for a parallel arrangement of floats centrally located on the cover and defined by the bottom plan dimensions of the reservoir with termination points of the floats at the inside boundary of the rainwater collection sump. The outer boundary is at the top anchor system resulting in a floating central plate and a peripheral rainwater collection sump.

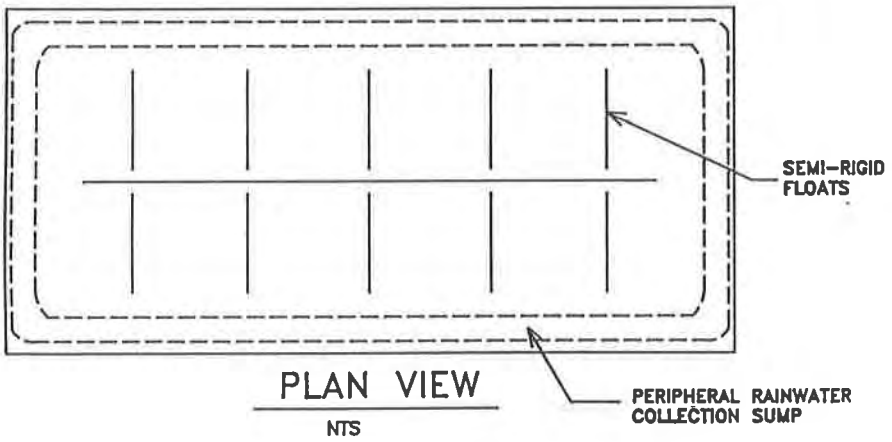

Figure 1. Untensioned Cover

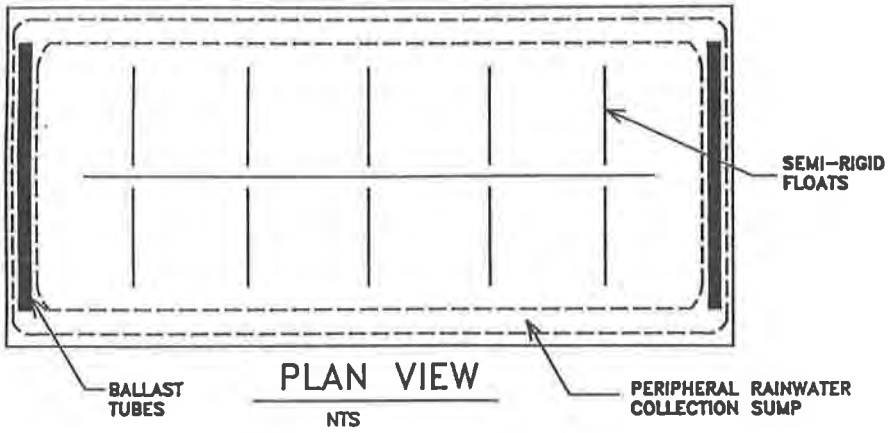

Figure 2. Uniaxial Tensioned Cover

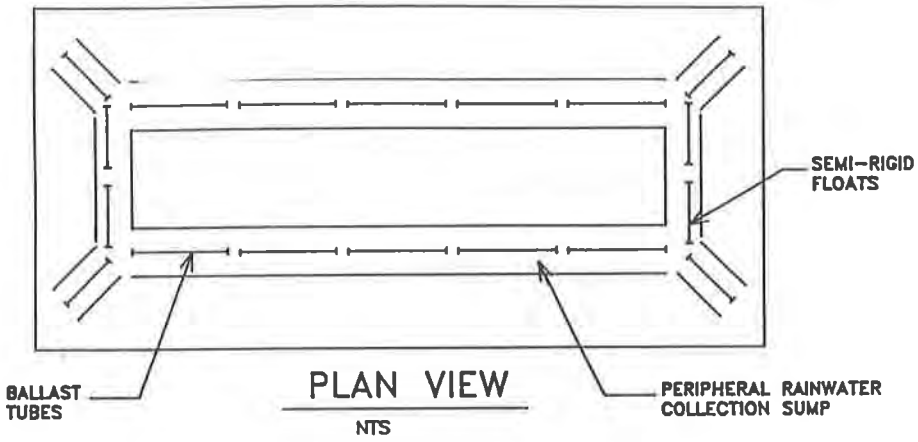

Figure 3. Biaxial Tensioned Cover

While the original Globe design did not call for any tension in the sump areas, current designs are modified to use tension at least parallel to the floats. Tension enhanced the cover's ability to drain surface water into the collection sumps. The tensioned plate system was developed as an answer for applications that require continuous access to the cover. This design incorporates a pattern of paired semi-rigid floats and segmented sand-filled tubes, attached to the topside of the cover, in a parallel arrangement (see figure 3). The location of the sand tube weights is dictated by the reservoir design. The array of floats and weights creates a slight biaxial tension in the cover which flattens it and allows for the drainage of surface water into the collection sumps. In addition, the weight design precisely locates the collection sumps regardless of weather or operating conditions. This design makes it easier for workers to walk on the cover when making repairs or performing water quality testing.

It is imperative that during design, the precise location of the sumps be determined and the distance between the paired floats be uniform and exact, otherwise the sumps will be improperly located and formed, resulting in poor surface water collection and drainage.

ASSESSMENT OF COVER TECHNOLOGY

Assessing floating cover technology can be a challenge for the consultant, engineer, designer and the owner/operator because of the variety of designs and materials available. There are several basic floating cover designs that are used currently and have more than a decade of successful installations

PERIPHERAL SUMP SYSTEM

The peripheral sump system is the most common and considered the simplest system to design and construct. This system creates a rainwater collection trough on the cover referred to as a sump that is located just inside of the toe of the slope or inside the base of a vertical wall. This sump maintains the same horizontal distance from the edge of the reservoir regardless of the depth of the water and has two purposes: to create a collection area for rain or surface water; and to form an area where slack membrane could gather as the water level changes.

There are two peripheral sump designs -- untensioned and tensioned plate design.

Untensioned Plate Design. The first untensioned plate design, developed by Globe, used no weights, cables or columns to hold the cover in place. It was considered a revolutionary design because it was free from stress caused by seismic loadings. This feature was particularly important in California where there is a great concern over seismic loadings that could result from an earthquake. Rigid covers have no natural immunity to seismic loadings and must rely upon proper reinforcement to perform without failure (see figures 4 and 5).

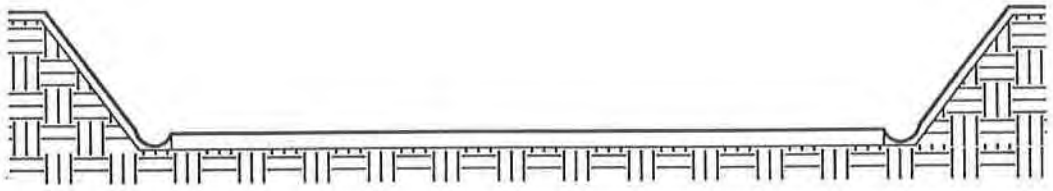

SYSTEM EMPTY

NTS

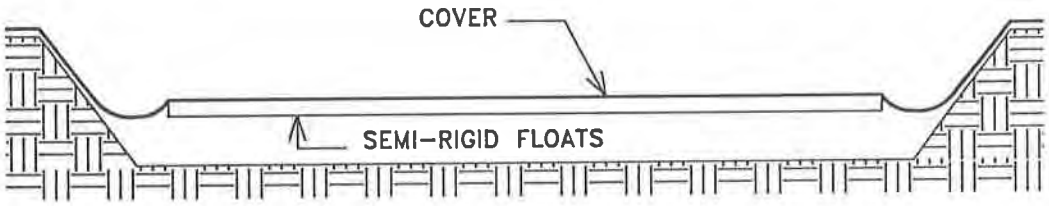

SYSTEM FULL

NTS

Figures 4 and 5. Untensioned Plate Cover System

The major drawback to the untensioned peripheral sump floating cover system is maintenance. It is difficult for workers to walk on the cover's free-standing central floating plate design because they must pass over the peripheral rainwater trench onto the plate, a potentially dangerous situation. A gang plank made of the semi-rigid float material is usually used to provide access.

Another problem with this system occurs when the owner fails to remove all of the rainwater from the sump area. Rainwater then accumulates in random stresses on the membrane which could lead to premature failure of the cover system.

Despite these drawbacks, a successful modification to the Globe Roofloat® design was installed recently at the Rocky Mountain Arsenal in Denver, Colorado. This cover was installed to prevent evaporation on a hazardous waste lagoon. Though the design parameters for this installation presented some dilemmas (parameters included: cover had to allow for high wind conditions, and no removal of surface water or maintenance), a solution was developed. That solution was a six-inch uniform ballast of water on the cover surface. The lack of any tension in the trenches coupled with the even distribution of water on the surface allowed the cover to remain in a virtually stress and maintenance-free environment. Unlike the Rocky Mountain Arsenal, however, most current peripheral sump floating cover system designs allow for maintenance and surface water removal.

Tensioned Plate Design. The tensioned plate floating cover design was developed to enhance surface water removal, make the cover safer and easier to maintain and repair, and to extend the life of the cover by predefining cover stress. This design uses sand-filled and segmented ballast tubes or pipes located within the peripheral rainwater collection sump which place minimal uniform tension on the cover surface, and help to form the peripheral sump. In addition, this design defines a uniform, weighted low area in the collection sumps where rain and/or surface water will flow. Surface water can be easily removed from collection troughs with a siphon or discharge pump. The weights also stabilize the central floating plate under windy conditions.

The earliest tensioned plate cover design was a simple modification of the untensioned design. Sand-filled weights were installed on the cover parallel to the floats (see figures 6 and 7). These weights provided cover tension in one direction across the float. This uniaxial tension made the cover easier to maintain and repair. Workers could walk on the cover safely. The tensioned design also prevented rainwater from pooling on the surface, reducing random stress. In addition, in the event of a tear developing in a cover, provided the installed cover material has a density greater than water, the entire surface will not sink. Only if the damaged portion of the cover is located between the floats is the cover at risk of sinking. The balance of the cover should remain afloat, enabling workers to install a patch while the reservoir remains in service. Such an incident happened several years ago in Pennsylvania. An automobile fell off of an embankment onto a floating cover. After the car was removed, workers installed a 50' by 80' patch onto the damaged area of the cover.

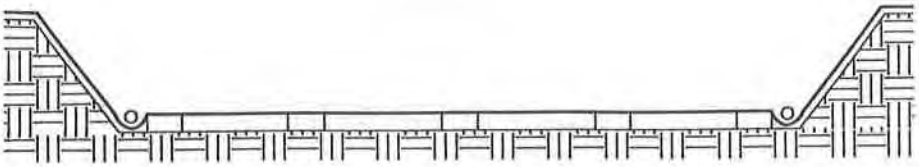

SYSTEM EMPTY

NTS

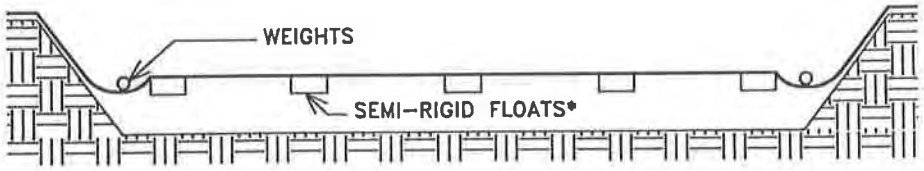

SYSTEM FULL

NTS

*NOTE: FLOATS CAN BE ATTACHED ABOVE OR BELOW COVER.

Figures 6 and 7. Uniaxial Tensioned Plate Cover System

The second tensioned plate design incorporates the use of pairs of floats around the periphery of the cover, placing uniform stress on all sides of the central floating plate (see figures 8 and 9). Thus the cover provides a much firmer surface for completing repairs or maintenance. In addition, the rainwater collection trough is usually narrower than five feet, providing easy access to the cover even during rainy weather. Another advantage to this design is the number of floats is less than the uniaxially-tensioned floating cover, lowering the overall installation cost. Some experts say that because this biaxially-tensioned design contains less floats than the uniaxially-tensioned design, the cover may sink should a tear develop in the material. To date, no proof exists to substantiate this concern. There are currently over 50 covers in operation with this design.

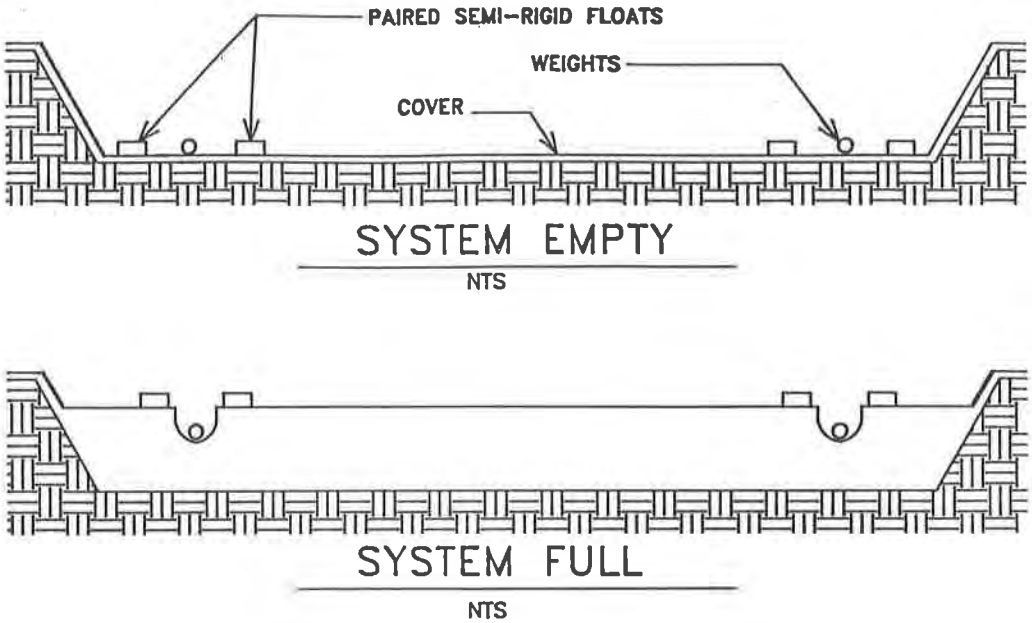

Figures 8 and 9. Biaxial Tensioned Plate Cover System

History has shown that subjecting a flexible membrane to continuous non-uniform tension can result in decreased service-life and/or premature failure due to creep or outright yielding of the geomembrane. However, experience with tensioned floating cover designs has shown that when a stress level of less than 15% of the yield of the material is designed into the system, the chance of premature failure of the system is minimal.

MECHANICALLY TENSIONED COVER SYSTEM

The mechanically tensioned cover system is a proprietary design that requires specific consultation with the designer to establish the proper size, number and location of the mechanical tensioning devices such as posts, cables, clamps, weights and hardware. When the mechanically tensioned cover is in service on a filled reservoir, the excess surface material is gathered around the top perimeter of the reservoir, forming a collection sump. These sumps form in a predominantly closed fold and substantially limit the collection of debris and require minimal cleaning. Surface drains on the cover collect rainwater and allow for drainage by pump or gravity through subsurface discharge piping. Because the cover is tensioned by exterior cables, surface floats are not necessary to predefine rainwater collection troughs and the cover rests directly on the water's surface, maintaining a low profile, and minimizing potential stress on the cover material at the mechanical attachments. The sump design also confines snow and ice build-up to the top surfaces of the cover and diminishes the potential for damage to the cover during winter months. Since the sump is almost closed and located at the perimeter of the reservoir, the system also allows easy access for workers to safely walk on, clean or repair the cover without taking the system out of service (see figures 10 and 11).

Mechanically tensioned cover systems are currently the most expensive floating covers available (and typically cost between 15% to 30% more than their tensioned plate system counterparts) due to the hardware necessary for the system to operate accurately. Additionally, this cover design has certain limitations relative to reservoir size, configuration and maximum potential depth on which it can be utilized.

BIO-GAS COLLECTION COVERS

In addition to traditional waste and fresh water floating cover applications, floating cover designs are also useful in bio-gas collection.

Flexible floating covers are an excellent low-cost alternative to expensive concrete digesters for the collection of gasses from anaerobic digester and other gas generating applications, especially in the processing of slaughter house waste, vegetable processing waste and municipal sewage sludge facilities.

In high-volume gas-generating applications, the cover design must be equipped with special gas mining hardware and adequate gas collecting and venting channels beneath the cover. In order to provide these channels, the floats are always installed on the underside of the bio-gas covers on such installations. The covers also have additional gas collection manifolds or piping either in the center, where there is a peripheral sump, or on the edge of the reservoir, where there are centrally located sumps.

If the cover is improperly designed, and inadequate provisions are made for the collecting and venting of gas, then the cover may inflate or balloon. Ballooning or inflation of a bio-gas cover should be avoided. Although ballooning may not affect the integrity of the cover material itself, it can cause stress at the perimeter anchor areas and access hatches. The affects of wind on the cover surface should also be taken into consideration when designing a cover.

THE IMPORTANCE OF PRE-DESIGN EVALUATION

Since different covers suit different types of reservoirs, it is important to conduct a complete evaluation and diagnosis of the critical factors for all geomembrane installations and the operational requirements specific to floating covers. It is therefore highly recommended that a competent and experienced flexible geomembrane manufacturer be consulted to review the design and application before any final design, contract award or construction begins.

For example, a recent potable water application in Tennessee called for concrete-filled ballast pipes in the rainwater collection troughs. The excessive stress caused from this weight would have lead to premature failure of the cover system. An alternative design was recommended by the geomembrane manufacturer, one that would provide sand-filled flexible tubes to give the cover uniform tension without excessive stress.

In the past 30 years, floating cover technology has radically evolved from designs and membranes that would only survive a few years to current sophisticated designs with expected lifespans of 15-20 years. When carefully selected, flexible geomembrane floating covers are a cost-effective, proven design alternative to concrete tanks and other rigid structures for finished water protection, and an environmentally sound approach to bio-gas collection. As a result, hundreds of floating covers in more than 30 countries have been installed on drinking water reservoirs and tanks, wastewater treatment ponds, product storage ponds as a solution to odor control and for methane gas collection on waste pits or anaerobic digesters.

Figure 10. Mechanically Tensioned Cover System

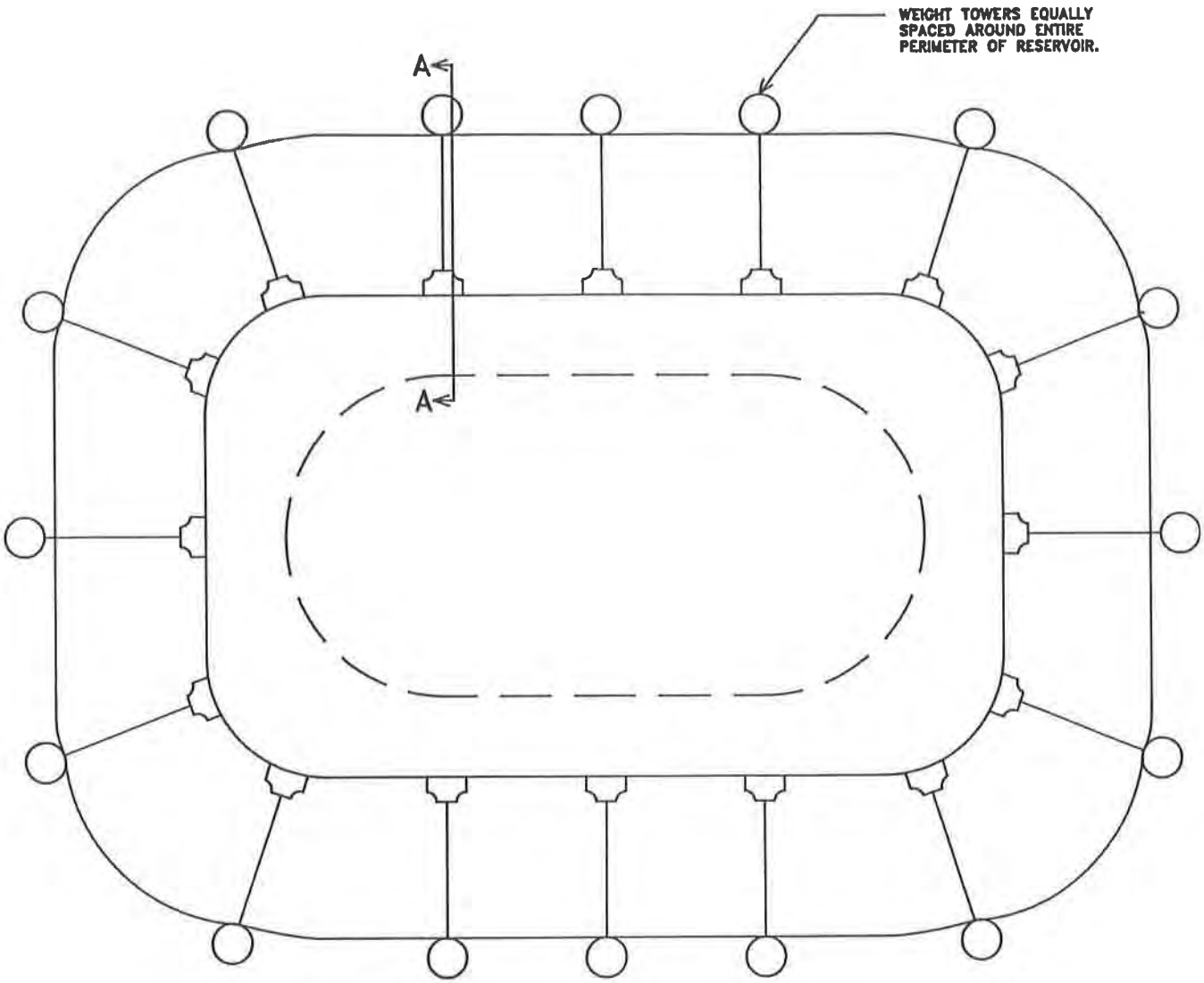

Figure 11. Section A - A System Empty

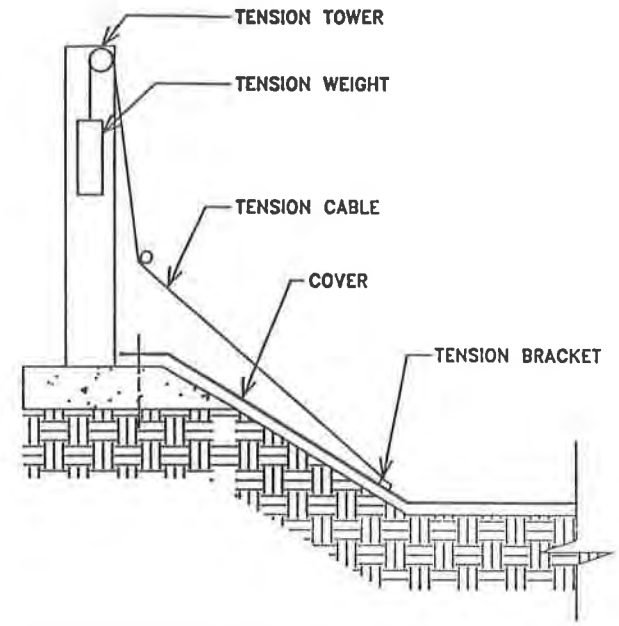

Section A - A System Full

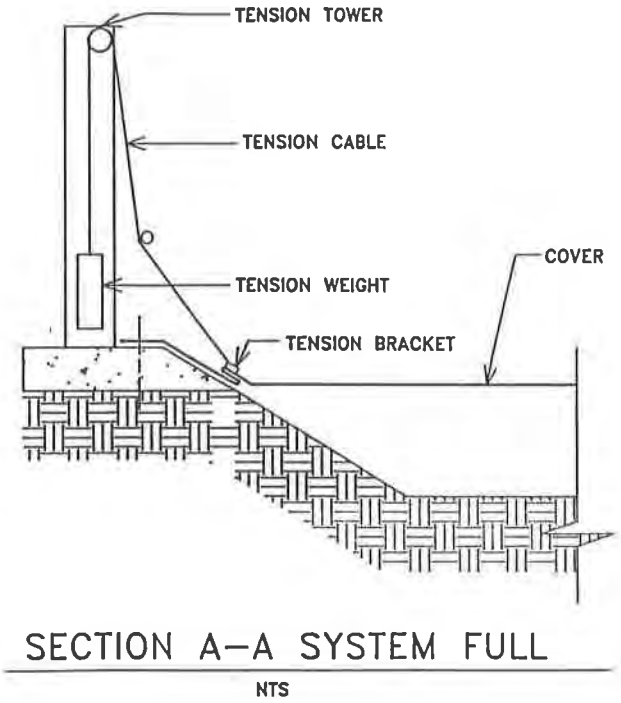

REFERENCES

Evans, Mark L, and Meade, John B., (1984) "Floating Cover Systems for Waste Lagoons: Potential Application at Old Inger Site, Louisiana", JRB Associates, McLean, VA and Anthony N. Tafuri, U.S. EPA, Oil and Hazardous Materials Spills Branch Edison, NJ, Alternative Technology.

Gerber, Dennis H., (1987) "Floating Reservoir Cover Designs", Burke Industries, International Conference on Geomembranes, Denver, CO.

Kays, William B., (1986) "Construction of Linings for Reservoirs, Tanks and Pollution Control Facilities", John Wiley & Sons, Second Edition.

Kittredge, David, (1987) "Performance of Flexible Membrane Floating Covers", Manchester Water Works, International Conference on Geomembranes, Denver, CO.

Taylor, Richard, (1989) "Installing Floating Covers on Intricately Shaped Reservoirs", JPS Elastomerics Corp, Northampton, MA.

"Floating Covers, A Comprehensive Technical Discussion", AWWA Convention Philadelphia, PA, June 23-27, 1991. Watersaver Company, Denver, CO.

"Flexible Membrane Covers and Linings for Potable Water Reservoirs", (1987) American Water Works Association, M25, First Edition.

"Flexible Membrane Lining and Floating Cover Materials for Potable Water Storage", (May 28, 1987) American Water Works Association, ANSI/AWWA D130-87, First Edition.

"Palco Floating Cover Manual", (September 1, 1991) Palco Linings, Inc., Stanton, CA.

Soweto's Unique 125 Megaliter (33 Million U.S. Gallons) Floating Cover Reservoir

H.I. Hollander
Soweto City, South Africa

T.P. Neilsen
Du Toit, Lombard & Malan Inc., South Africa

SYNOPSIS

This paper discusses the unique features of a combination earth embankment/reinforced concrete wall, floating cover, flexible membrane lined reservoir with particular reference to the various geosynthetics used in the alternate design submitted to the Soweto City Council in lieu of a conventional reinforced concrete design and the cost saving arising from their use. The alternate design of the 125 Megaliter (Ml) (33 Mil U.S. Gallons) reservoir, which finally cost R7,04m (US $2,44m) resulted in a saving of 36% (R3,96m = US $1,37m) on the original reinforced concrete design estimated cost of R11,0m (US $3,81m). This saving is directly ascribed to the use of the various geosynthetics which had a total value in excess of R2m (US $0,7m) or 28,5% of the total final cost of the reservoir.

1. INTRODUCTION

This 125Ml Floating Cover Reservoir was constructed for the City of Soweto, which, with a population in excess of 1,5 million, is one of the largest cities in South Africa. (Soweto lies adjacent to the south western boundary of Johannesburg.) The application of geosynthetics in a Third World environment raised considerable criticism from a number of parties involved during the decision-making process. Objections raised ranged from adaptability to a restricted site, weatherability under the extreme South African climatic conditions, to the security of the completed product, all compared with a reinforced concrete structure. The innovative floating cover alternate design and proposal, however, took care of most of these objections, as will be discussed later in this paper.

This design is indeed unique firstly because of its L-shape necessitated because of a very restricted site and secondly because of the application of the combinations of geosynthetics used. Geosynthetics were used in the following areas:

(1) Underfloor drainage
(2) Embankment and floor protection
(3) Embankment and subsurface drainage
(4) Geomembrane lining
(5) Floating cover

2. GEOSYNTHETICS

The use of various geosynthetics in the design and construction of this reservoir was paramount to the lowering of the overall cost and the efficiency of the whole concept. A 2,5m (+-8 ft) high reinforced concrete retaining wall atop an earth embankment, all lined with a flexible membrane liner (FML) and completed with a flexible floating cover has, as far as can be ascertained, never before been used in the southern hemisphere, certainly not on the African continent.

A number of challenging issues were dealt with as far as the geosynthetics were concerned each of which is discussed separately, namely:

2.1 The design of the civil works & geometric configuration of the reservoir.
2.2 Surface finish required.
2.3 Choice of a geotextile.
2.4 Leak detection/underfloor drainage system.
2.5 Choice of liner material and thickness thereof.
2.6 Transition of geomembrane from the sloping earth embankment to the vertical reinforced concrete wall.
2.7 Choice of the floating cover construction materials combination with special reference to the vertical wall.
2.8 Rainwater removal in view of the requirement that no pumps were allowed for reasons of maintenance and theft prevention.

Each of the above points is now discussed in more detail.

2.1 Design of the civil works. Because of an extremely confined site, use was made of the natural slope of the site to be able to achieve the required storage capacity. The site is entirely underlain by solid sandstone and it was thus decided that it would be uneconomical to excavate to any great extent to obtain a level floor. The floor thus has a natural slope of approximately 1 in 26 which was used to great effect in designing the underfloor drainage system.

Further, because of existing site restrictions, an L-shape had to be utilized in order to occupy the available space to the maximum. (See sketch no. 1) This presented its own complication in the cover design (discussed later in this paper).

Sketch no. 2 shows clearly how the reinforced concrete retaining wall is positioned atop the engineered earth embankment. Twenty-five percent (25%) of the total reservoir capacity is contained within this zone. This 2,5m high retaining wall also acts as a barrier to vandals which is an important consideration as this reservoir is located in the middle of a residential area. Because of the use of a geosynthetic lining, use was made of non-water-retaining concrete, thereby effecting a considerable cost saving. Expansion joints were positioned every 6,3m (+-21 ft) in this vertical wall which will limit the effect of differential movement in the wall in the unlikely event of a localized subsidence beneath a section of the wall footing. Strict compaction control of embankment fill, especially the final three layers, was imperative in order to prevent differential settlement.

The incorporation of an adequate overflow structure into the reservoir was a relatively simple matter due to the vertical concrete wall. The overflow structure was designed and constructed as a water retaining concrete structure since its complicated design and construction excluded the application of a geomembrane for water tightness.

2.2 Surface finish required. Due to the fact that the geomembrane would, for its life, be covered by the floating cover and the difficulty this presents should a leak develop in the lining system, the preparation of the earth surface finish was of the utmost importance. Any irregularities that existed in the surface were smoothed out sothat the geomembrane would be in an entirely unstressed condition for the rest of its operational life. Due to the nature of the borrow pit material used in the construction of the embankment, it became necessary to stabilize the entire embankment surface in order to obtain the smooth and regular surface required to accept the geotextile and the lining.

The borrow pit material used was a weathered dolerite with a high Plasticity Index (>14). Stabilization was effected by mixing in 3% lime, whereafter a compaction of 88 - 90% MOD AASHTO density was achieved prior to laying the geotextile.

2.3 Choice of geotextile. A relatively thin geotextile of 270g/sq.m (0,055 lb/sq.ft) underneath the geomembrane was chosen to perform the function of directing any water flow to the nearest drain, as well as providing the required protection to the 1,5mm (+-60 mils) thick HDPE geomembrane over the stabilized surface.

The maximum pressure exerted on the geofabric at full supply level is 1,1 bar (15.4 psi) and under these conditions the fabric has a porosity in excess of 11 liters per hour per meter width of fabric which is sufficient to accommodate flow from leaks through small holes in the lining should these occur.

2.4 Leak detection/underfloor drainage system. Due to the size of the reservoir, its embankments, its unique shape and the requirement that each 2000 sq.m of lining area should be serviced by a separate dedicated leakage detection drain, it was decided that flownet strips would be placed in a herringbone system against the sloped embankment over the geotextile. The purpose of this was that should a leak develop, the nearest flownet drain would intercept its flow and be carried away to the nearest perforated pipe drain which was installed along the perimeter of the floor of the reservoir. These drains exit into a leak detection sump where leaks can be monitored and traced to a particular area inside the reservoir.

The flownet used was an LDPE Type DN1 with a flow rate in excess of 70 liters/min/m width at a pressure of 1 bar (14 psi) consisting of 1.0m wide strips of 6mm (0,25 ins) thick flownet laid at an angle down the embankment slope. The flownet is also placed in a herringbone pattern of 1,0m wide strips over the entire floor area. This did away with the necessity of blasting trenches into solid rock.

2.5 Choice of geomembrane liner material and thickness. After having considered the surface finish required, the contractor offered a 1,0mm (45 mils) thick liner. However, the client's consulting engineers with the agreement of the client, insisted on a 1,5mm (60 mils) HDPE lining, because they were concerned with the possibility of puncture damage. The liner used has excellent elongation and puncture resistance properties, comes in 6,86m (22,5 ft) seamless wide sheets of up to 100m in length, is odourless, has exceptional chemical resistance as far as sterilisation of the reservoir is concerned and can be reliably seamed by means of extrusion welding. Furthermore High-Density Polyethylene is extremely cost effective and carries the South African Bureau of Standard Mark SABS 1526.

2.6 Transition of geomembrane from sloped earth wall to vertical reinforced concrete wall.

As previously mentioned, an interesting feature of the reservoir is its unique shape and combination of sloped earth embankment and non-water-retaining vertical reinforced concrete wall. The reinforced concrete wall was founded on top of the earth wall. This presented challenges to the designer of the Civil Works as well as to the Lining Contractor to ensure that the lining would, at all times, be stress-free and watertight. In order to achieve this, the liner was anchored both against the vertical and the horizontal faces at the toe of the concrete wall and watertightness was ensured by installing an HDPE skirt from the bottom of the vertical reinforced concrete wall to the top of the sloped embankment, covering the two anchors. Also contained in this toe arrangement was a triangular shaped no-fines drain which would direct any leakage through the vertical wall liner to the outside of the reservoir by means of a built in drainpipe. (See Sketch no. 3)

2.7 Choice of the floating cover construction materials combination, with special reference to the vertical wall.

In order to provide the most cost effective design of the floating cover, the lining contractor, Aquatan cc, proposed a combination of a 1,0mm (45 mils) thick High-Density Polyethylene (HDPE) co-polymer and a Chlorosulphanated polyethylene (CSPE) to construct the floating cover. As HDPE is not meant to flex continuously, the CSPE was installed in the areas of the floating cover where flexing was designed to take place, i.e. in the valleys, the centre-fold and vertical side walls. A 45 mil 5-ply scrim-reinforced CSPE was chosen to fulfil this requirement. This material was chosen because of the better lamination that can be achieved through the reinforcing scrim due to the thinner CSPE laminate layers which reduce the risk of delamination in the future. Furthermore, the CSPE used has proven itself over many years under the very harsh climatic conditions and high ultra-violet exposure experienced in South Africa. The CSPE is also approved for use in potable water applications, is easy to repair and due to it maintaining its flexible characteristics over time, can handle the continuous rise and fall of the water level in the reservoir during its lifetime. It further exhibits no evidence of stresscracking after extended periods of use.

The HDPE co-polymer used in the flat areas of the cover where major flexing is considered unlikely, is a proprietary compound of High-Density Polyethylene and EPDM (a synthetic elastomer based on ethylene, propylene and diene). Although this material has good flexibility, this property was not really required in this application where it would normally be in a flat unflexed and unstressed condition during its operational life. However, slight wave forming during windy conditions and folding on the sloped embankments do result in a limited amount of flexing in these areas. Hench the choice of this particular HDPE co-polymer. In addition to its flexibility, this HDPE copolymer has a very good track record in Southern Africa despite the regions extreme UV problems and exhibits all the excellent elongation and puncture resistance properties required to meet the demands of this application. It is also designed to resist the impact of hail better than most available materials in South Africa. This was considered important since the Witwatersrand area of the Transvaal Highveld is sometimes subjected to violent hailstorms. These two incompatible materials, used in the cover, CSPE and HDPE, were joined using a specially-designed flexible mechanical fixing. (See sketch no. 4)

Floats in the cover were arranged in such a pattern that they complement the stress-free configuration of the cover and ensure the formation of the flexible CSPE trough in the correct position. They further assist in ensuring that rainwater is removed from the cover in a controlled manner and provide some

rigidity in the cover, thus counteracting wind disturbance. The L-shape of the reservoir presented an unusual challenge to the floating cover designer in that an outside corner had to be dealt with such that where this corner intersected the central trough, stresses would be avoided. The effect of the wind on the vertical wall of the floating cover was largely eliminated by the use of automatic air extraction ventilators placed strategically around the perimeter of the reservoir, in the cover, which create a suction under the cover when the wind blows.

2.8 Rainwater removal system. It was an express requirement of the Client that maintenance should be limited to the absolute minimum and in the Third World environment where the reservoir was constructed, theft is a reality. For this reason, the conventional submersible pump arrangement for rainwater removal was not acceptable. In order to cater for this and because the reservoir was designed to be operated within the top 25% of its capacity, it was possible to install a gravity rainwater removal system. The system was so designed to carry rainwater from the bottom of the CSPE trough when the reservoir is full via a flexible pipe through the vertical concrete wall to discharge into the stormwater system on the outside of the reservoir.

3. QUALITY CONTROL

Geomembrane: The South African Bureau of Standards developed a standard for polyolefin sheeting used as geomembranes. The HDPE geomembrane used on this contact carries the SABS Mark. This means that it conforms in all respects to the requirements of this Standard. As there is no manufacturer of a flexible enough reinforced membrane which conforms to the behaviour characteristic required for the floating cover application in South Africa, Aquatan imported a 45 mil 5-ply scrim-reinforced CSPE from the USA.

Geotextile: The geotextile chosen for the contract had to comply with certain requirements and was chosen on the basis of complying with certain SABS and ASTM Standards, particularly considering its limited requirement for transverse permeability under the 1,3 Bar (18 psi) head and its ability to improve the puncture resistance of the geomembrane.

Flownet: The transverse permeability of the flownet as well as its compressibility under 1,3 Bar (18 psi) head was considered in its choice.

Site Quality Control: The success or failure of any geomembrane lining installation depends on the application or not of a detailed quality assurance programme. Aquatan has therefore introduced, in accordance with the South African Bureau of Standards, the Code of Practice for Quality Systems Part 11 (SABS ISO 9002) which describes a model for quality assurance in production and installation and which is the South African equivalent to ISO 9002-1987. This Code of Practice is for use when conformance with specified requirements is to be assured by the supplier, during production and installation. Aquatan, in order to implement its quality assurance programme, appointed a full-time Quality Control Inspector on site, who was responsible for the implementation, controlling and documentation of the site quality assurance procedures as required by the South African Bureau of Standards.

In accordance with the project quality plan, every facet of the project was properly controlled and documented. Amongst various issues controlled and documented were:

(1) the receipt of all geosynthetic materials on site:

(2) the maintenance of geomembrane-related equipment:
(3) the handing over of surfaces for lining:
(4) the handling of material on site
(5) the laying and seaming of the geosynthetic materials to specification drawings:
(6) the testing of seams, both destructive and non-destructive:

As previously mentioned, aspects that received considerable attention during the installation of the lining system were the preparation of the final surface of the earthworks that would receive the liner. In this case, due to the nature of the material, the surface had to be cement-stabilized as previously discussed. The seaming of the adjacent HDPE sheets was done by extrusion welding which were 100% vacuum-tested on completion. Completed areas were barricaded off to avoid unauthorised human traffic. Where the two incompatible materials were joined, special attention had to be paid to ensure a continuous and strong seam. (See Sketch 4)

4. MAINTENANCE

Information gathered from many reservoir owners and operators in various countries would suggest that maintenance costs on these types of reservoirs are very low. Certainly the owners of reservoirs built in Southern Africa seem to agree with this view.

Because of very limited funds and the cost effectiveness of the alternate design offered, the Soweto City Council opted for this type of reservoir and one of the factors that prompted a decision for a floating cover type reservoir was the low maintenance cost.

Cleaning of the roof only needs to be done for aesthetic reasons and because of its size will probably only be done once every 3-4 years. Based on South African experience it should not be necessary to clean the inside of the reservoir more than once in ten years, while rainwater removal pipes which could become clogged with debris will only need infrequent cleaning. Other than the above regular general inspections of the reservoir, it is also envisaged that monitoring of other aspects like the functioning of the liner/cover, anchor mechanisms and the operation of the overflow clap valves will take place on a regular basis.

5. CONCLUSION

Had the original reinforced concrete design for this reservoir been used, an additional R4,0m (US $1,4m) would have been required to finance the project. The abundant, yet judicious use of geosynthetics allowed a very cost effective design to be submitted and accepted by the client (despite much opposition from various quarters) which released additional funds for other much needed projects in the depressed community which this reservoir now serves.

The conclusion, then, from the experience gained on this project, is that the use of geosynthetics proved extremely cost effective and without a doubt justified the decision to depart from tradition and accept the innovative alternate design.

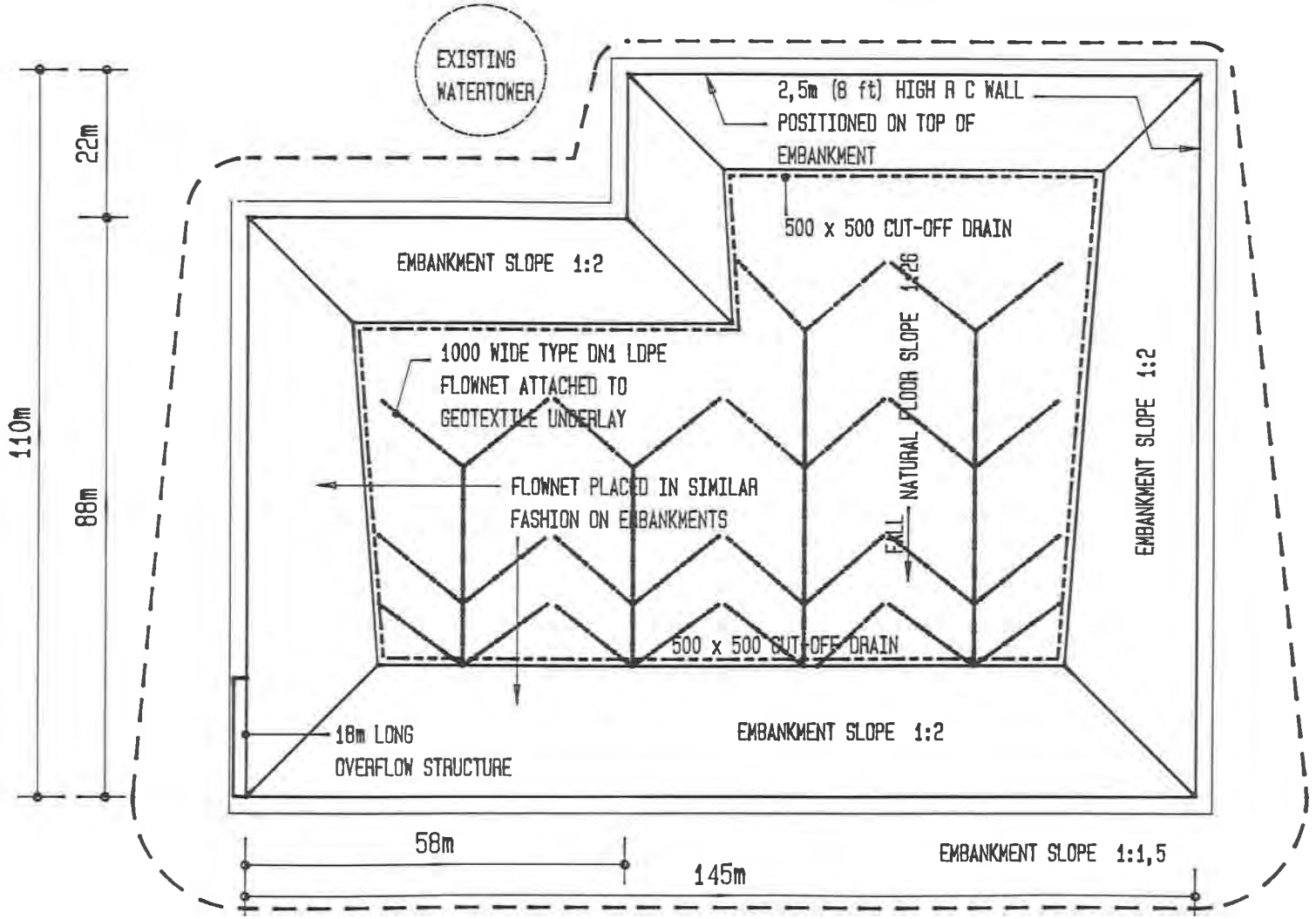

SKETCH No 1 : RESERVOIR LAYOUT

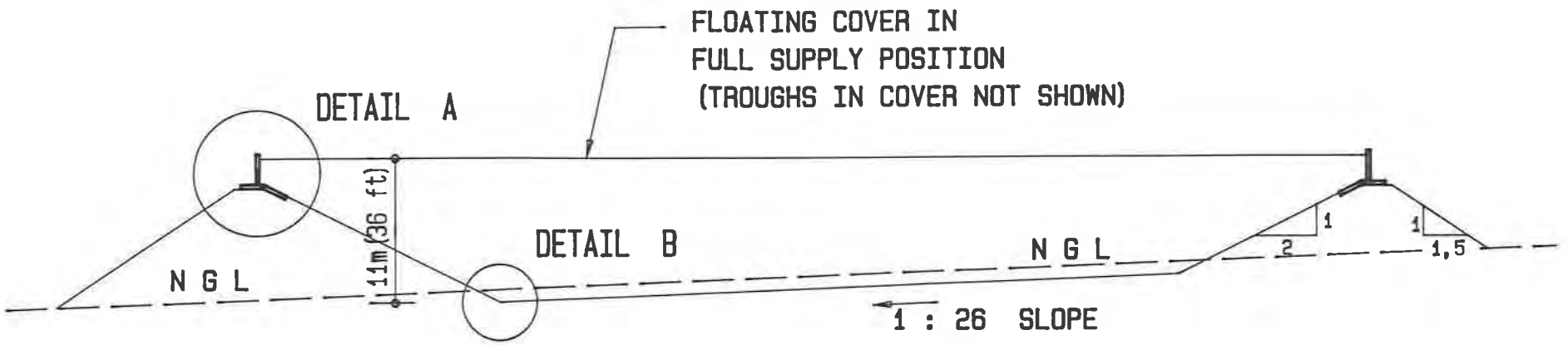

TYPICAL CROSS-SECTION THROUGH RESERVOIR

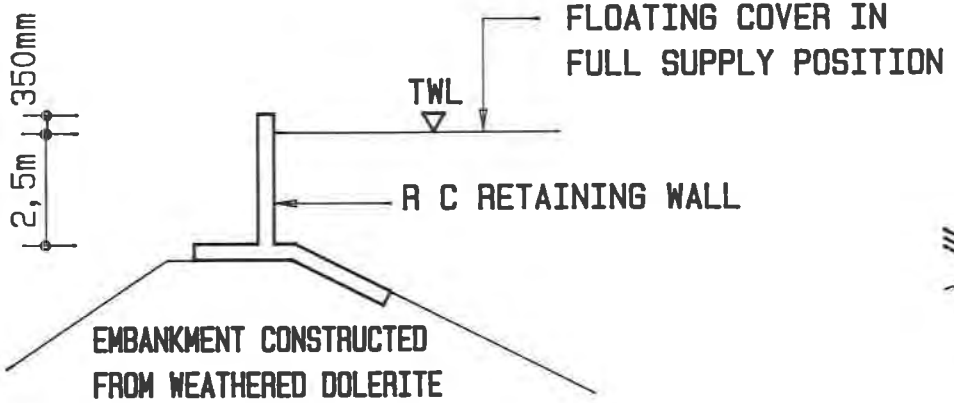

DETAIL A

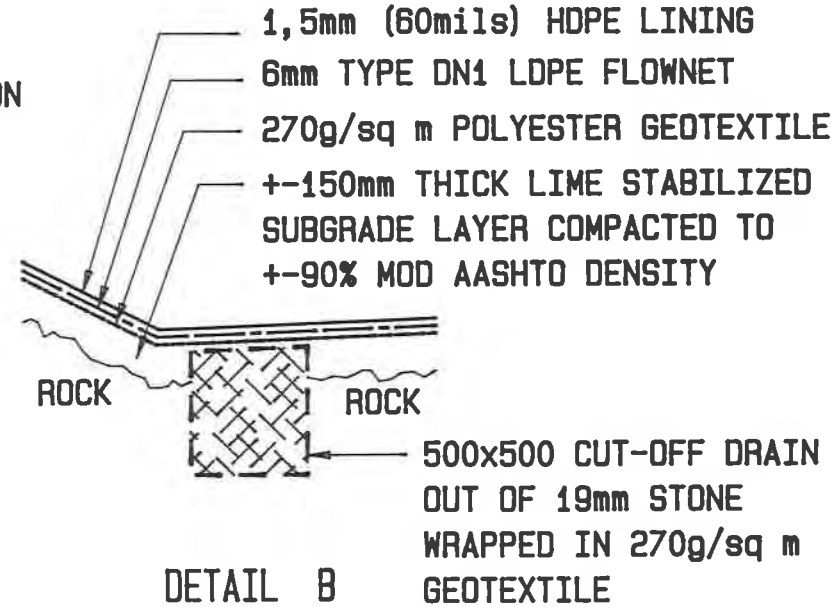

DETAIL B

SKETCH No 2 CROSS-SECTION THROUGH RESERVOIR AND DETAILS

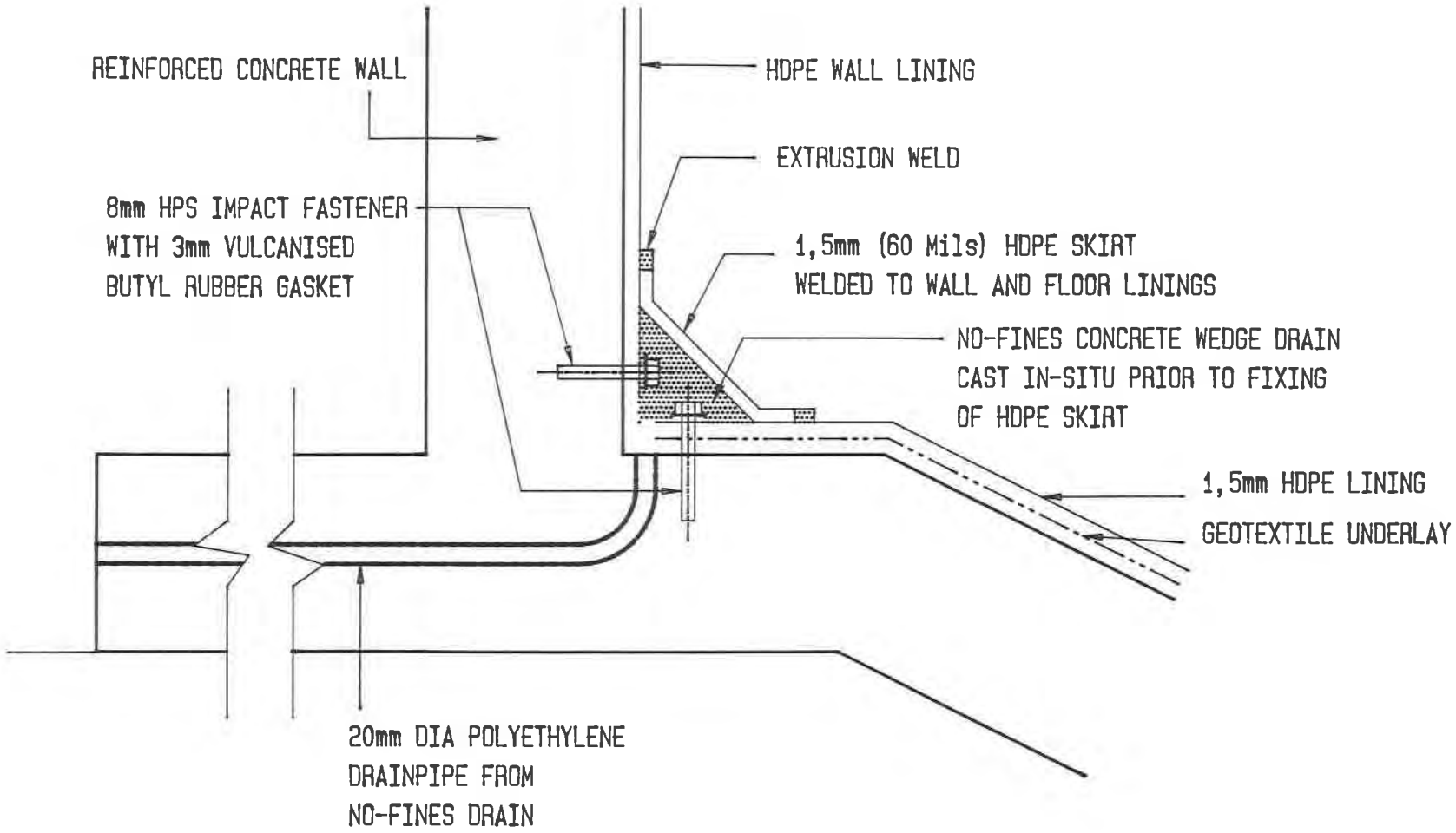

SKETCH No 3 DETAIL: LINING FASTENING AT INTERSCETION OF WALL AND FLOOR

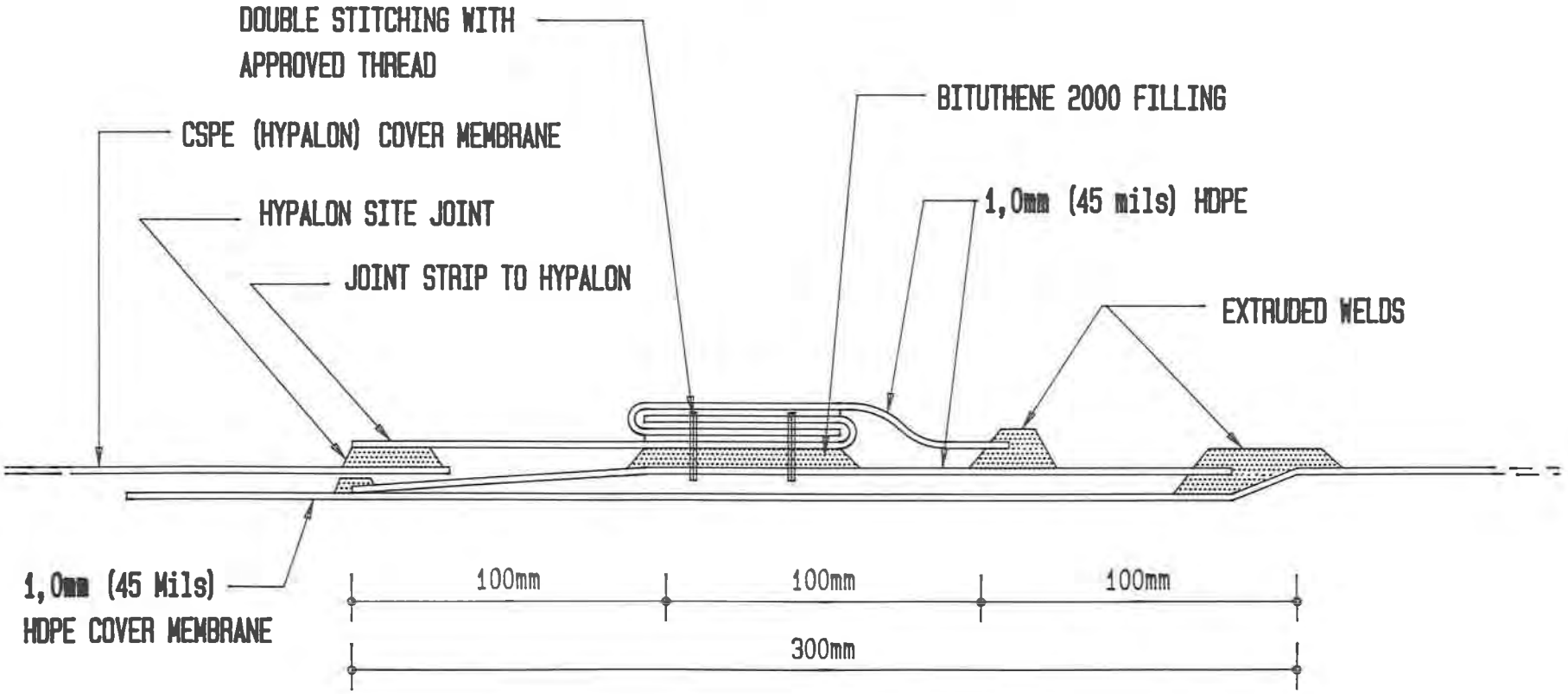

SKETCH No 4 TYPICAL CROSS-SECTION THROUGH STITCH JOINT BETWEEN HDPE AND CSPE IN FLOATING COVER

Custom Geocomposite for Superfund Closure Cap—A Case Study

J. Boschuk Jr.
J & L Engineering Inc., USA

W. Goeckler
General Electric Company, USA

M. Simpson
James Clem Corp., USA

S.D. Walker
Polyfelt Inc., USA

ABSTRACT

Four (4) sites encompassing 20.6± hectares (51 ±) acres along the Hudson River near Fort Edward, New York were mandated by the USEPA to be covered to secure PCB contaminated soils. Methane gas also had to be collected and vented. Due to very soft subgrade conditions consisting of silts, organics and wood debris, the compacted clay component of the cap required by the USEPA Record of Decision could not be placed. The Record of Decision was reviewed by the Owner and Engineer and the design was changed to replace the clay cap element with a custom made geobentonite fabric composite. The composite was designed to serve as an impervious barrier, gas collection system as well as soil reinforcing layer during placement of the overlying soil cover and topsoil components. A modified generic bentonite geomat (Geosynthetic Clay Layer [GCL]) was married with a generic polypropylene continuous filament needle punched nonwoven geotextile to create the liner system. Through an extensive testing program and demonstrations to both the USEPA and local citizens, this custom made geocomposite was approved for use on the project. This customized fabric reduced construction time by one (1) year and the cost of the project by several million dollars. This paper presents how this system was selected, developed, tested and installed.

INTRODUCTION

Remediation of contaminated sites often involves construction of a relatively impervious cover or capping containment system over the contaminated materials to prevent further migration of the contaminates within the soil and groundwater or exposure to the environment, namely air and surface water. One such site is located along the Hudson River, near Fort Edward, New York, approximately 88 kilometers (55 miles) upstream of Troy, New York. See Figure 1.

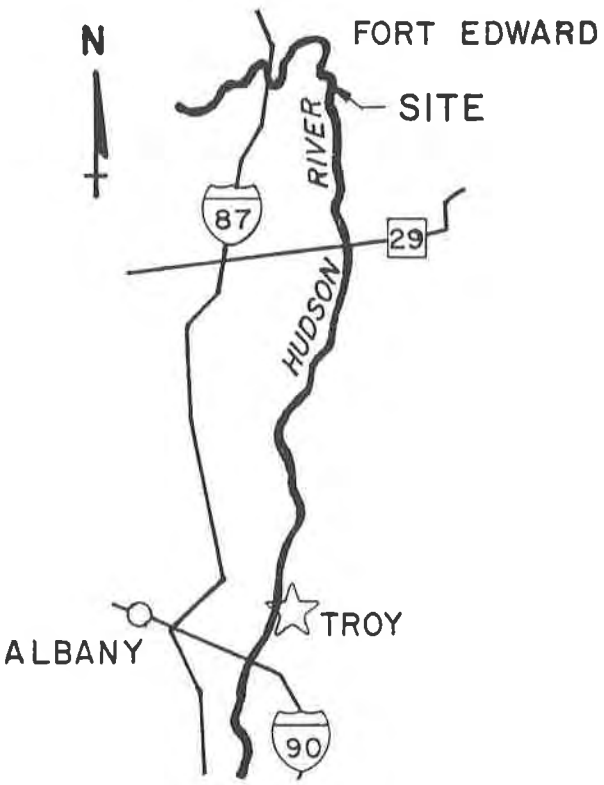

FIGURE 1 LOCATION PLAN

At one time, a dam existed across the Hudson River adjacent to a paper processing facility, immediately downstream of this site. See Figure 2. Upstream of the dam, a transformer manufacturing facility operated for many years and PCB contaminated liquids were disposed in the river under local and state permits. Over the years, the dam was no longer required for paper processing and was eventually razed, lowering the impoundment and discharging the water and sediment downstream. As a result of dam removal, PCB levels downstream were elevated causing an investigation of the impoundment area by the USEPA, Region II and the New York Department of Environmental Conservation (NYDEC). With the razing of the dam and removal of the impoundment area, remnant contaminated sediments or deposits were exposed which contained elevated levels of PCB's.

SITE CONDITIONS

Consistent with the USEPA and NYDEC's responsibilities to protect the environment, a Remedial Investigation and Feasibility Study (RI/FS) was initiated. Their findings delineated five (5) areas of elevated PCB levels noted as Remnant Deposit Sites 1, 2, 3, 4 and 5, as shown on Figure 2. Remnant Site 1 was a small island in the river which eventually eroded and ceased to exist as a designated site. Over the years of investigations and studies, these areas became overgrown with vegetation and trees. Due to the local topography, these relatively flat areas located at the base of the bluffs on both sides of the river, received seepage from the bluff creating constantly wet conditions. Site 4 even developed wetland vegetation and was eventually designated a wetland area by the state.

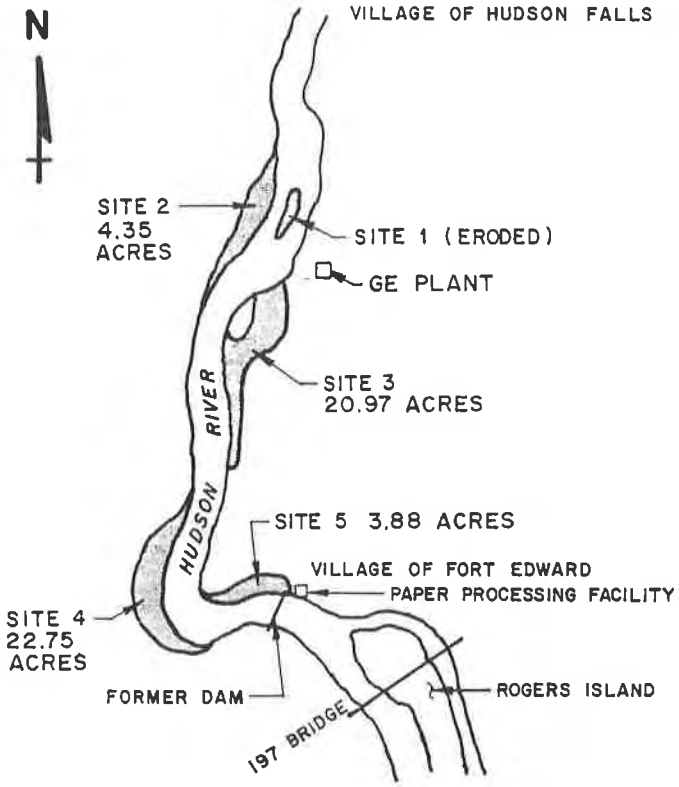

FIGURE 2 SITE PLAN

Sampling of the areas were performed by consultants under contract with the regulatory authorities. Their studies determined that levels of PCB's in excess of 5 ppm would serve as the criteria to delineate the site boundaries. Test borings performed by these consultants in the area showed the sediment deposits contained soft organic materials with remnants of logs and timber debris associated with the paper processing plant located near the dam site. A typical stratigraphic cross section is presented in Figure 3 together with a typical boring log.

INTERVAL DEPTH, FEET	SAMPLES: SAMPLE	BLOWS/ 6 in.	SAMPLE NUMBER	SAMPLE TYPE	REC/ATT	SOIL PROFILE: DESCRIPTION
0						
		4		SS		Brown fine medium SAND some silt, roots, with wood debris
		4		SS		
5		2		SS		
		1		SS		Dark brown organic SILT and fine sand, brown firm sand and silt, wet
		WORH		SS		Brown fine medium organic SAND, some silt, wet
10		4		SS		
		16		SS		
		12		SS		Gray to brown fine coarse SAND and silt, shale fragments, wet
15		100/.2		SS		
						Refusal at 17.2 feet
20						

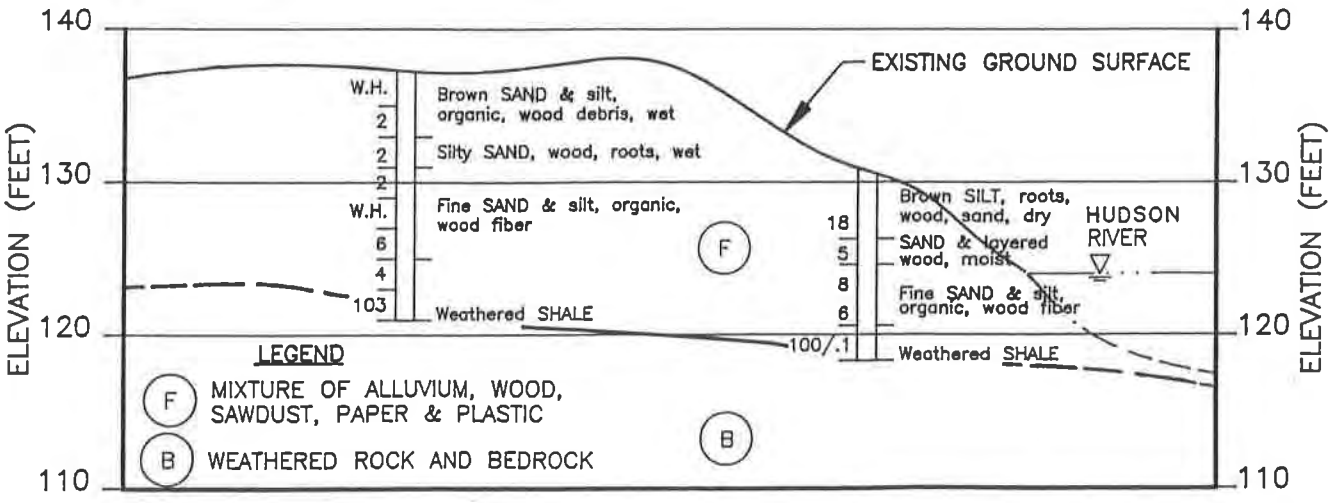

TYPICAL BORING LOG AND STRATIGRAPHIC CROSS SECTION

FIGURE 3

The data clearly shows the sediments to be wet, soft organic deposits having Standard Penetration Resistance values typically less than 5 and more typically 2 to 4 near the surface. Although a number of remediation options were considered, the final Record of Decision (ROD) issued by the USEPA recommended construction of a relatively impervious clay cover over these areas. This design is considered a temporary containment solution until cost effective technology is developed to eliminate these areas of PCB contaminates.

REGULATORY DESIGN

Using conventional cover design components, the regulatory agency's consultant prepared a cap design consisting of a sand leveling course over the contaminated soils, compacted clay (K $\leq 1 \times 10^{-7}$ cm/sec) impervious barrier, sand cover and top soil layer. A typical cross section of the ROD design is shown on Figure 4.

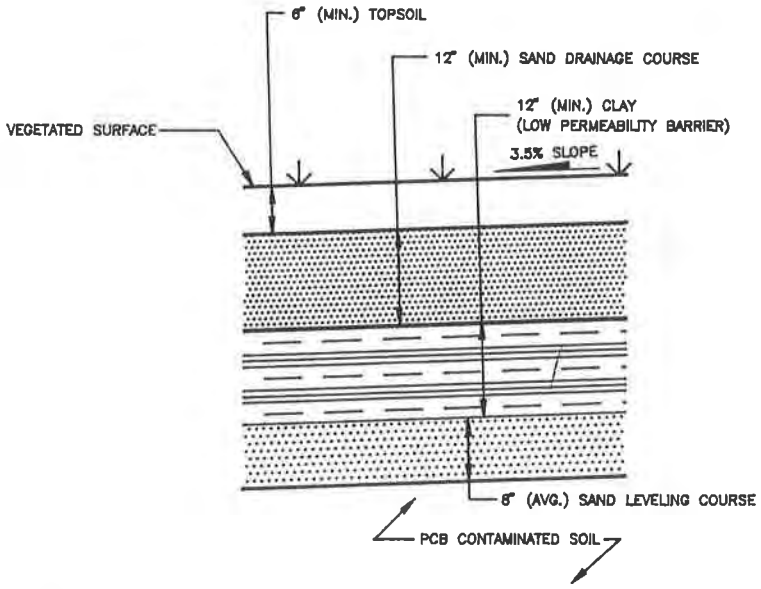

FIGURE 4 PROPOSED COVER DETAIL
PER RECORD OF DECISION

Consistent with this conceptual design, surface vegetation would be removed, the area rough graded to drain at a 3.5% slope to the river and then capped. At this point of the design process, the firm (General Electric Company) which accepted financial responsibility to remediate the sites also accepted the responsibility to perform the remedial repairs. As part of this agreement with the regulators, the firm had the option to explore other means of satisfying the ROD.

ASSESSMENT OF PROBLEMS

General Electric engaged an independent remedial design consultant to review USEPA's design concepts and to search for more economical solutions for this remediation without changing the basic design concept of the ROD. Upon completion of a site evaluation program, assessment of the RI/FS report, the USEPA's engineer's conceptual design, and detailed review of the ROD, a number of problems were delineated. Those directly associated with this cap system are:

1. The nature of the remnant deposits were too soft to traverse with conventional construction equipment.

2. The recommended compacted clay layer could not be constructed over the soft subgrade and compacted to meet the project specifications.

3. Clay was not readily available from areas local to the sites and the routes of travel were very restricted, due to bridge weight limits and the width of streets leading to the remediation areas.

4. Haul truck traffic volume limitations through the towns would limit daily remediation construction activities and extend the work through a period of in excess of two (2) years. Over 22,000 truck loads of imported impervious materials would be required to cap the sites.

5. The design did not consider decomposition of the organic deposits and the production of methane gas.

Considering only these design problems, an alternate cap had to be developed to accommodate these technical and construction problems, reduce the projected 2-1/2 year construction time and overall cost of the project. However, the basic concept of a cap configuration could not be changed appreciably from the concept presented in the ROD to preclude significant regulatory delays.

REMEDIAL ACTIONS

Considering the cross sectional configuration requirements of the ROD, the final design dictated the following basic components of the cover system:

From Top to Bottom:

Top Soil Layer;
Drainage Layer;
Low Permeability Layer;
Cosmetic Leveling Layer; and,
Contaminated Soil.

To eliminate problems with hauling, depositing and compacting a clay layer, it was decided

to consider a standard geosynthetic clay layer (GCL) as the low permeability material. See Figure 5. If impervious borrow soils were used, over 22,000 truck loads of clay would have to be hauled on site through narrow streets and across weight restricted bridges. If a GCL were used, only nineteen (19) tractor trailer loads of geosynthetic clay materials would be required. Furthermore, this material can be unrolled at an average rate of 0.5 hectares (1 acre) per day, greatly reducing construction time and cost. Furthermore, no compaction is required, material consistency is much greater with a manufactured product and the permeability of bentonite composites is approximately 1.5 to 2 orders of magnitude less than compacted clay available in the area.

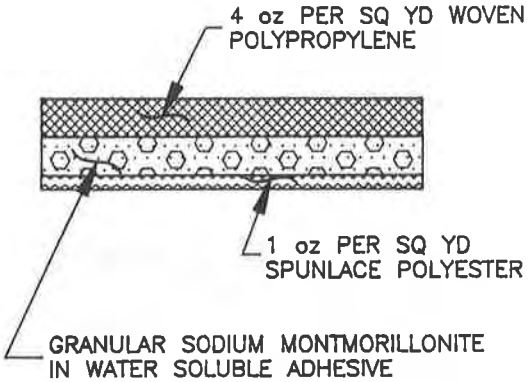

FIGURE 5 STANDARD GEOSYNTHETIC CLAY LINER

However, the soft subgrade would need a reinforcing larger layer of geotextile to support construction equipment for placement of the impervious materials and overlying granular fill and topsoil. In addition, the ROD did not consider methane gas generation. Venting of this gas would have to be addressed in the final design.

Consequently, various geotextile manufacturers were researched to determine which geotextile would serve the job requirements as a reinforcing layer and what products or design adjustments would be required to function as a gas collection system. Subsequent to this research, it was determined that a 340 grams per square meter (10 oz. per square yard) geotextile would satisfy reinforcing requirements and it could also serve as a pervious blanket to collect gas and feed the methane to gravel trenches and vent pipes. At this point, the engineer explored the possibility of using this 340 grams per square meter geotextile as part of the geosynthetic clay layer. The engineer visited the manufacturers of the GCL products, explored the possibilities of using alternate geotextiles in their manufacturing process and selected the most appropriate manufacturer and components of the proposed GCL. Confident the design section could be manufactured, arrangements were made to deliver the geotextile from the selected geotextile manufacturer to the GCL manufacturer and a prototype was fabricated. See Figure 6. The proposed corresponding cap design then consisted of the configuration shown on Figure 7.

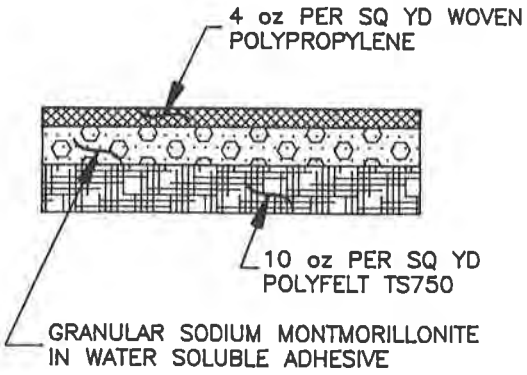

FIGURE 6 CUSTOM GEOSYNTHETIC CLAY LINER

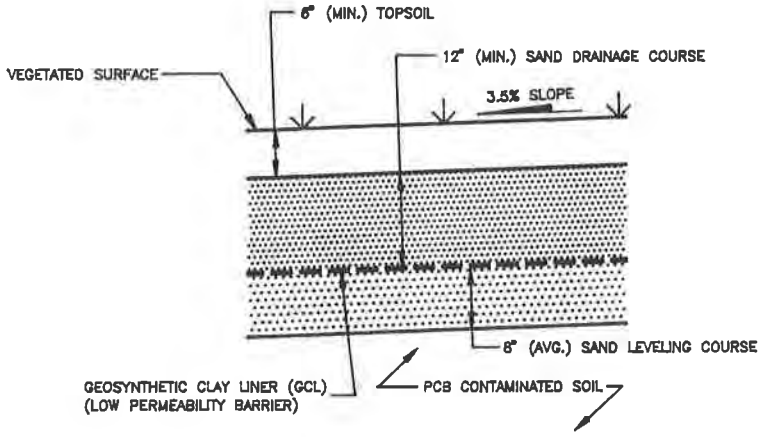

FIGURE 7 REVISED COVER DETAIL

This custom-made product was tested in the engineer's laboratory and found to have permeability on the order of 5×10^{-9} cm/sec, far less than the ROD requirement of $K \leq 1 \times 10^{-7}$ cm/sec. Additional standard laboratory tests were performed which verified the geotextile material bonded to the bentonite layer and had the strength to serve as a reinforcing layer. Wide width tensile and biaxial stress tests were performed to make these basic engineering assessments. Furthermore, hydraulic conductivity tests performed on biaxial stressed samples confirmed that permeability was maintained in the stressed samples. The last task was to determine if the lower geotextile reinforcing layer had the capability of collecting and transmitting gas under confined and biaxial stress conditions without upward flow of gas through the bentonite layer. A description of the basic testing programs are described as follows.

TESTING AND APPROACH

Once the custom manufactured GCL was produced and preliminary tests indicated an acceptable product, the regulatory authorities were approached to seek general approval of the concept. The engineer and project sponsor met with the agency representatives and presented the product and attributes of its uses on the site. In general, the agencies were told and presented data and a preliminary evaluation which addressed the following issues.

1. The initial laboratory tests demonstrated the GCL met the requirement of hydraulic conductivity ($K \leq 1 \times 10^{-7}$ cm/sec).

2. Calculations and basic laboratory tests were presented which demonstrated the ability of this custom manufactured product to serve as reinforcing layer for placement of the overlying soils without detrimental effects on hydraulic conductivity.

3. Calculations were presented to demonstrate the geotextile base layer of the GCL could serve as a viable gas collection blanket.

The concept was given general approval, pending a formalized testing program. The idea of reducing construction time by over one (1) year had a significant impact on the general acceptance of the product. Following this meeting a formal testing program commenced.

PERMEABILITY AND STRESS TESTING

A series of hydraulic conductivity tests were performed on the GCL using both flexible wall and rigid wall permeability equipment. A schematic of each test apparatus is presented on Figures 8 and 9. In addition, the product was subjected to biaxial stress tests to simulate stresses of settlement and loads applied by construction equipment under both dry and saturated conditions. See Figure 10. Permeability tests were performed on the product in the biaxial chamber during the stress tests while the material was in a deformed state. The results demonstrated the ability of the product to maintain its hydraulic conductivity properties during and after stress tests.

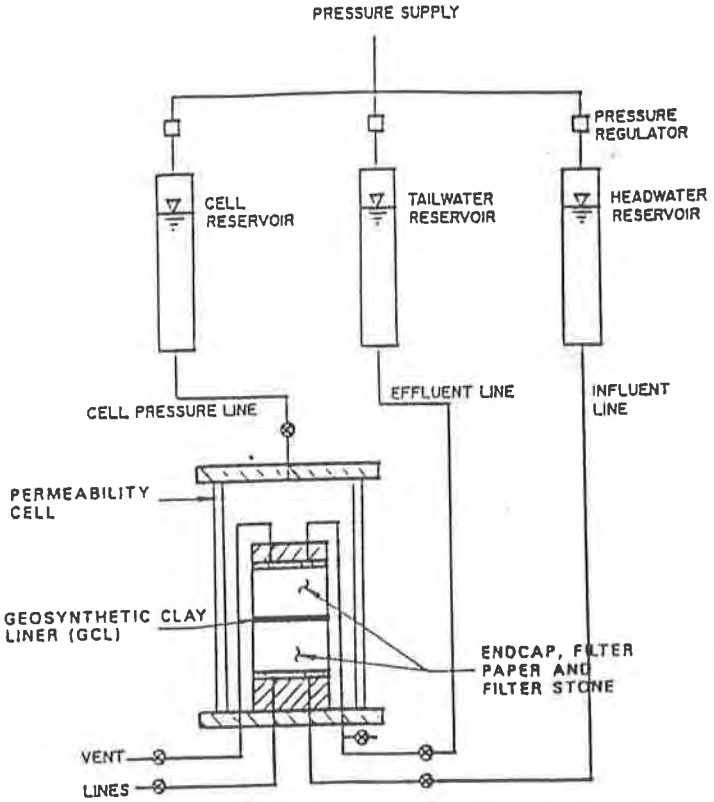

FIGURE 8 FLEXIBLE WALL PERMEABILITY APPARATUS

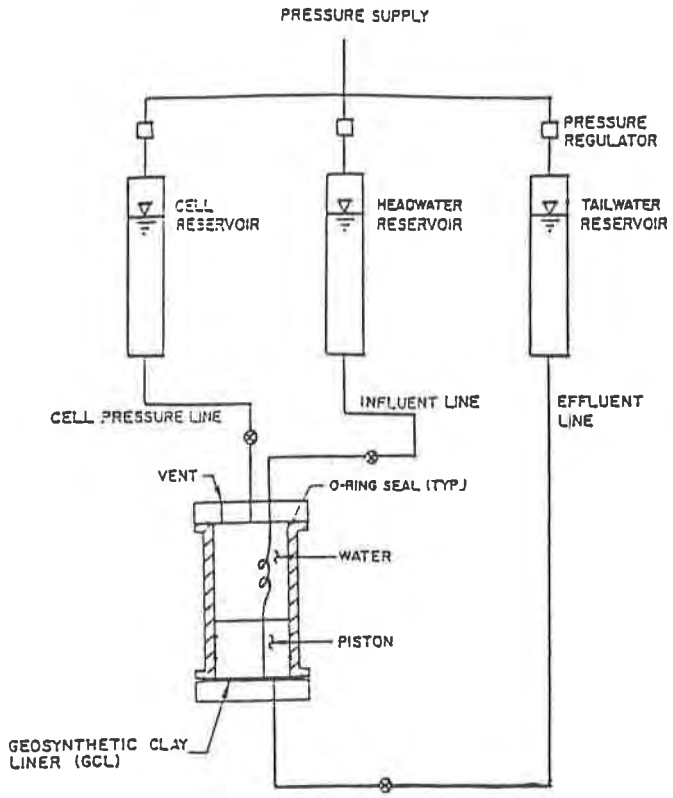

FIGURE 9 (25 mm) DIAMETER
RIGID WALL PERMEAMETER APPARATUS

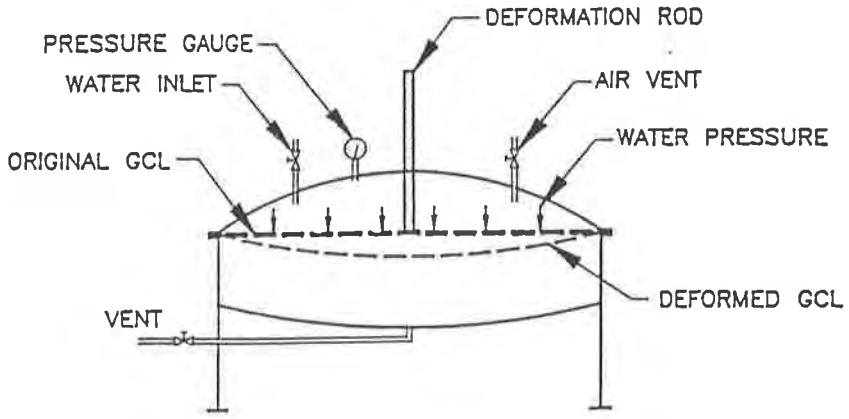

FIGURE 10 SCHEMATIC OF BIAXIAL TEST APPARATUS

GAS TRANSFER TESTING

Since standard test procedures for evaluating gas flow characteristics of a geotextile in a confined state affixed in a GCL product configuration have not been established, an apparatus was constructed to perform these tests. A schematic of this apparatus is presented on Figure 11.

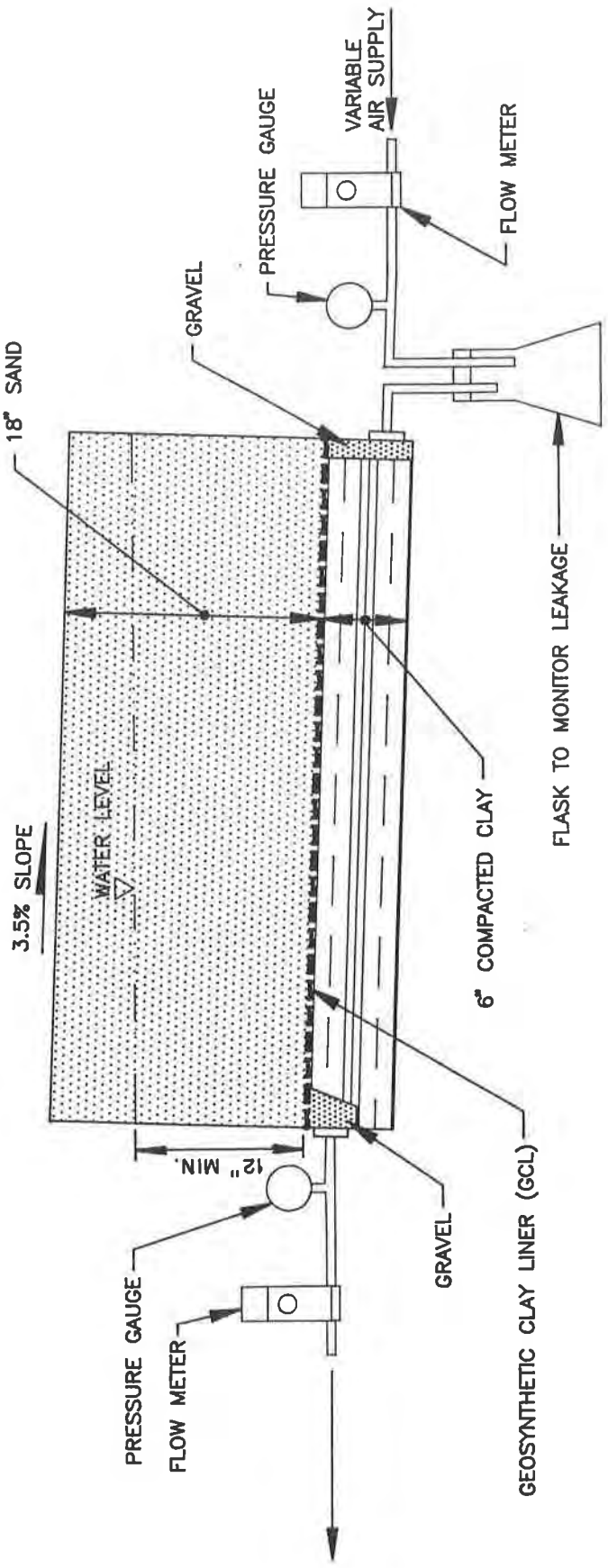

FIGURE 11 GAS FLOW EVALUATION APPARATUS

Subsequent to fabrication of the test configuration, the cover layer was saturated with water and the GCL was given time to fully hydrate. It is important to note that during this saturation process no water exited through the GCL. Once saturated, air was pumped into the system under the GCL and passed laterally through the geotextile. Pressure differentials and flow volumes at the points of entry and exit were measured. Using available technology, rough estimates of the amount of potential methane generation were computed. The goal of this program was to have the geotextile capable of transmitting at least 100 times this computed methane quantity. The tests performed demonstrated the 340 grams per square meter product met and exceeded this design criteria under simulated field conditions.

Once all tests were completed, the regulatory agencies were presented the data and the design was accepted. Furthermore, a public meeting was conducted and the data was presented to the local citizens. The gas model test was also demonstrated at this public hearing and the client received public acceptance of the modified design.

IMPLEMENTATION

Immediately after acceptance of the design, the regulatory agencies issued a modification to the Record of Decision which specified this custom made product. Bid documents and technical specifications were written and a contractor was selected to implement the remediation program. To improve stability of the subgrade (contaminated soils), vegetation was cut, shredded and disposed directly on the site. This eliminated the need to dispose of potentially PCB contaminated materials at off-site sources and created somewhat of a reinforcing layer to allow for placement of the sand leveling course using low ground pressure equipment. With the leveling sand layer in place, the GCL was unrolled, deployed and seamed by overlapping the sheets. It was immediately covered with the drainage sand in sections often exceeding 4700 square meters per day.

Although adverse weather often caused deployment/construction delays, the granular drainage cover soil over the GCL provided sufficient vertical load to allow the GCL to hydrate per the manufacturer's and engineer's requirements. At the edge of the GCL layer where the granular cover was terminated at the end of the work day and only nominal loads applied to the GCL, these areas were generally covered with plastic to provide sufficient protection from load free hydration during rainfall events. If these edge areas did hydrate without load, the sand was removed until suitable GCL was located and the area overlapped with another layer of GCL and work resumed with the placement of the cover drainage sand.

This work phase progressed without any major problems and was completed on schedule and within the budget estimate for this project. During the manufacture of the GCL product, one (1) foot wide strips, the width of the roll, were cut from every 10,000 square meters of product and tested for permeability, material adhesion, density of bentonite ($\geq$ 4800 grams per square meter) and quality of the geotextiles.

SUMMARY AND CONCLUSIONS

To our knowledge, this project represents the first use of a "custom-designed and fabricated" multiple layer geosynthetic used for a remediation project. Furthermore, it also represents the first

use of a GCL product as the main impervious barrier for a cover system on an USEPA project.

This proposed design alternative was reviewed and accepted by the USEPA, NYDEC and the U.S. Army Corps of Engineers. Acceptance was based on a successful laboratory test program, excellent cooperation between all parties involved in the project and constant open communications between the design engineer and regulatory agencies. As a result of this cooperative effort, a new concept in custom-designed and manufactured geosynthetics for remediation of hazardous waste sites has been achieved for our industry. The time from initial construction through the closure phase was reduced by over one (1) full construction season with a savings of several millions of dollars to the funding party. The impact on the local community was also minimized by eliminating thousands of trucks from hauling soils through their community.

POST SCRIPT

Since completion of this project in the Fall of 1990, we have had the opportunity to excavate areas at one (1) site and inspect performance of the GCL. We found the GCL to be functioning as designed meeting all of the requirements for low permeability, reinforcing and gas transfer.

ACKNOWLEDGEMENTS

The authors wish to express their sincere gratitude to Mr. Douglas Tomchuk, USEPA, Region II, Project Coordinator for his efforts and cooperation. The James Clem Corporation manufactured the product with the principal geotextile being supplied by Polyfelt. General Electric Company sponsored the project and J&L Engineering, Inc. and J&L Testing Co., Inc. performed the design, testing and construction engineering services.

(RHR.01)

Venezuelan Experience in Geosynthetics

A. Vidovic
Geosinteticos Trical C.A., Venezuela

R. Denis
Materiaux Techniques Coté Inc., Canada

M. Ardin
Techoconsult, Venzuela

ABSTRACT

An historical overview and current state of practice of the use and applications of geosynthetics in Venezuela is presented along with a documented case history. Highlighted is the case history of the first Venezuelan maximum security landfill for mercury contaminated sludges. Located at the heart of the petrochemical industry, this 53.000 m^2 double-lined cell was designed using high density polyethylene geomembranes and geonets (Figures 1. and 2.). Also described are the actions and methodology of the Venezuelan Government, consulting engineers and private industry that have enabled Venezuela to be considered one of the leading South American countries in environmental control using geosynthetics technology.

INTRODUCTION

Geosynthetics have been part of Venezuelan engineered projects since the early 1970's. Their path of development in this South American country has been guided by specific engineering challenges along with the availability of nationally produced materials. Venezuela has been very perceptive towards world-wide industry developments. Especially in environmental applications, whereby national regulations now allude to the use of geosynthetic containment systems, double-lined structures and leachate management for hazardous and toxic wastes.

THE EARLY BEGINNINGS

The birth of geosynthetics in Venezuela seems to be associated with the early 1970's where nationally produced polymeric geogrids were already being used for both subgrade and retaining wall reinforcement especially in the north-central part of the country, characterized by a geologically recent orogenesis (end of Miocene) of foliated metamorphic deposits (schists) and erodible soils. Domestic design methods had been developed by both academics and private consultants. Imported non-woven geotextiles were also being used, mainly for applications such as drainage and separation in roadwork and wall structures.

Figure 1. Primary Liner Deployment

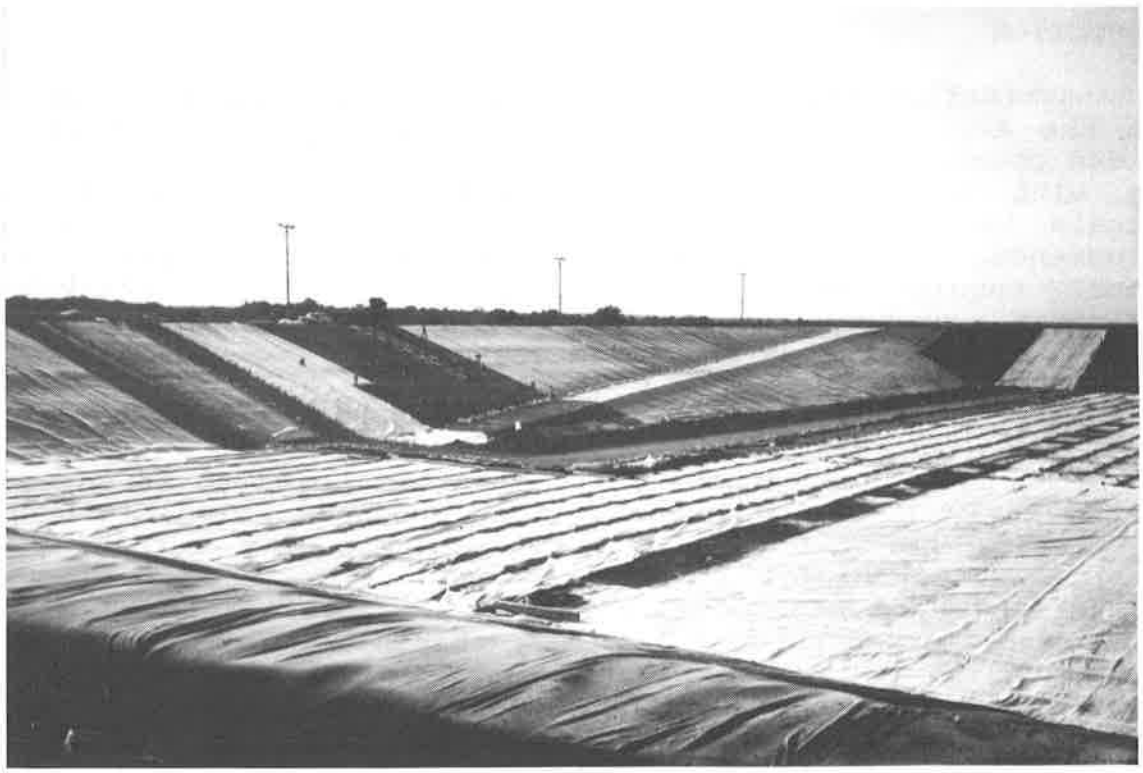

Figure 2. Access Ramp

THE 1980's

The 1980's witnessed the introduction of nationally produced non-woven staple-fibers geotextiles. Bonding was achieved through either needle-punching, stitching or surface heating. Roll widths of up to 3,6 m were then readily available locally with mass varying between 140 and 180 g/m^2. Parallel developments were also being achieved locally for the production of low density polyethylene geomembranes of up to 0,5 mm thickness and 2,1 m width, eventually leading to the production of high density geomembranes (HDPE). Double-sided adhesive tape and manual hot air welders were the only seaming methods available then. Main applications included single-lined containment systems for petroleum exploration sludges, fresh water and secondary containment of underground service station fuel tanks. By the end of the decade, Venezuela's geosynthetic industry was offering non-woven geotextiles of up to 650 g/m^2, 1,0 mm HDPE geomembranes and world-class reinforcement geogrids and geopipes.

THE CURRENT SITUATION

On account of Venezuela's growing concern for the conservation of its environment, government agencies and engineering consultants began searching for proven waste management technologies. Venezuela is a most industrialized nation characterized by its major petrochemical activity. The country was thus being confronted with characteristic industrial waste disposal challenges. Environmental restoration projects such as Lake Maracaibo's have most likely triggered deep interests for double-lined geosynthetic landfills. In spite of locally unavailable thick HDPE geomembranes (i.e. > 1,0 mm), Venezuela has nevertheless opted for state-of-the-art containment designs which involves, for the time being, import of both materials and skilled manpower. A direct outcome of Venezuela's recent geosynthetic endorsement has already prompted the national production of HDPE geonets.

FIRST VENEZUELAN MAXIMUM SECURITY LANDFILL

General Information. A Venezuelan petrochemical enterprise, a subsidiary of PDVSA (Petroleo De Venezuela Sociedad Anonima) produces a wide range of chemical compounds. Among other products, one of its plants has been producing chlorine and caustic soda for an extended number of years from brine electrolysis using mercury electrodes. As part of a process modernization program towards a more environmentally friendly technology, the enterprise was first confronted with the disposal of both mercury contaminated construction debris and stabilized sludges from its previous activities. In view of Venezuela's new environmental regulations and requirements on hazardous wastes management (1,2,3), this petrochemical plant opted for a state-of-practice geosynthetic double-lined landfill, with a composite secondary hydraulic barrier and a geosynthetic primary barrier.

Siting. For logistical purposes, location of the landfill site was chosen on the plant's premises adjoining a natural incline, the subgrade mainly being characterized by a 13 m deep cenozoic fine clayey-sand deposit ($k=10^{-4}$ cm/s) intertwined with four distinct 500 mm thick clay lenses. The water table at this emplacement was reported to be approximately 20 m below existing grade. The bottom elevation of the cell basically corresponded to the existing grade and necessitated up to 6 m of excavation (east portion) and fill (west portion) for its preparation. A one percent slope was purveyed to the bottom of the cell towards its south-west corner and a five percent grade interior access ramp was also provided by the design.

Secondary System. A 300 mm layer of drainage sand ($k=10^{-3}$ cm/sec) was first placed in the bottom of the cell (Figure 3.) along with a rectangular matrix of perforated high density polyethylene (HDPE) geopipes (50 mm dia.) equally spaced at every 40 m approximately. The geopipes had been pre-wrapped in a non-woven geotextile held against a thin geomesh. A one meter thick layer of clay was then placed in 200 mm lifts all over the cell's area (53.000 m^2); bottom, slopes and access ramp. The 3H:1V slopes extended 12 m above the cell's bottom. This clay layer was compacted at 95% Modified Proctor for its required $k=10^{-7}$ cm/s. This first composite segment was then followed by the installation of a 2,0 mm thick HDPE geomembrane, a 5 mm thick HDPE geonet (1.17×10^{-3} m^2/s, under a unity gradient, at 718 kPa), and a 180 g/m^2 stitched non-woven geotextile. A rectangular matrix of HDPE geopipes (50 mm dia.) was then installed and connected to a 100 mm dia. HDPE collector pipe, followed by a 300 mm layer of compacted sand (65% Modified Proctor) in the bottom only, thus completing the secondary system. This collector pipe extended 80 m across the west slope, leading to a 16 m^3 concrete retention basin located outside the cell, 4 m below the bottom of the cell. The secondary collection system was thus designed using a most efficient gravity flow.

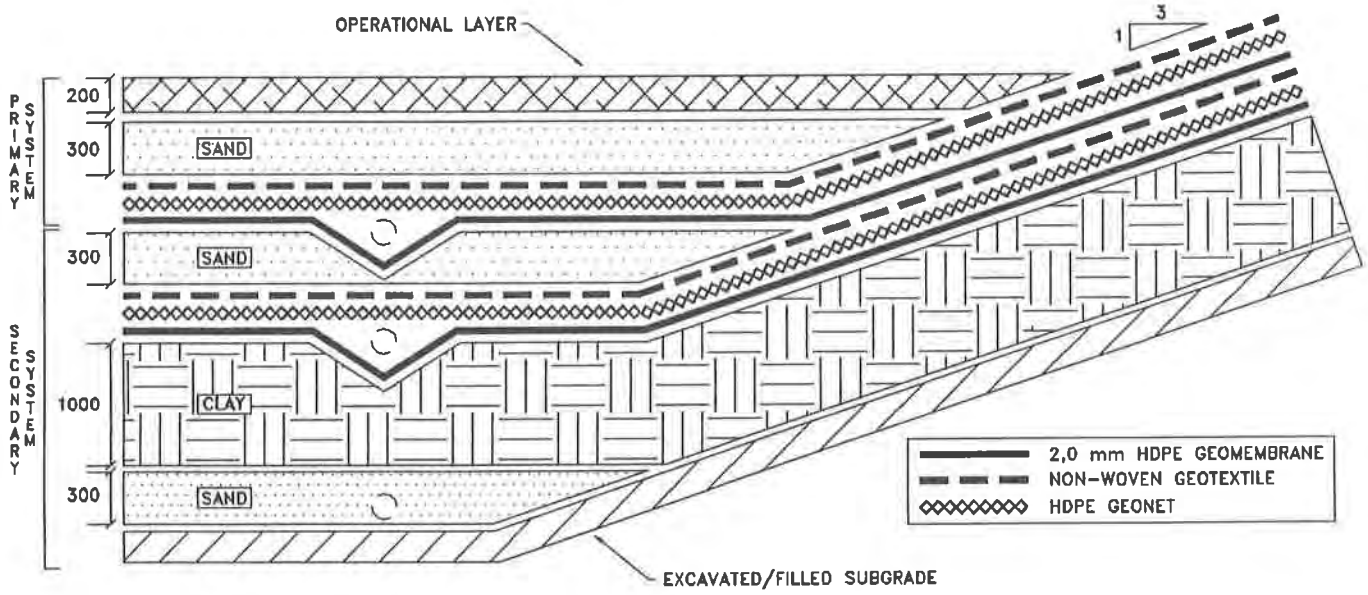

FIGURE 3. TYPICAL CROSS-SECTION
N.T.S.

Primary System. The primary system was then installed using a similar cross-section as the secondary system (Figure 1.) i.e a 2,0 mm HDPE geomembrane, a 5 mm HDPE geonet, a 180 g/m^2 stitched non-woven geotextile (its seams oriented downslope), a matrix of HDPE perforated geopipes and a 300 mm layer of compacted sand. Only this time the access ramp was also back-filled with the sand layer. The primary collection system was designed using gravity flow as well. A 200 mm clayey-sand operational layer was finally placed all over the cell's bottom and access ramp.

Construction and Quality Controls. All in all, 16 weeks of earthwork were required to complete the preparation of the cell for its geosynthetic components, which in turn required 9 weeks to install. Automated double hot wedge welders were used for all geomembrane structural seaming (approximately 20 km) while both automated hot air and manual extrusion were used for detail and patch work. A total of 218 trial and destructive tests were performed yielding an average peel value of 12.7 MPa, i.e. over 75% of the parent material's stress at yield (4). All structural seams were non-destructively tested with 200 kPa air pressurization, while details and patch work required 35 kPa vacuum boxing. In summary, all material and installation quality controls specified and performed for this project were as stringent and exhaustive as any comparable hazardous waste landfill requirements in the geosynthetic industry. Standard test methods, methodologies and frequencies, along with proper and sound documentation, revision and approbation procedures were closely abided upon throughout the whole project.

Problems Encountered. On account of the region's typical wide temperature spread between nocturnal and diurnal conditions, tremendous geomembrane trampoline effects were at first encountered at the toe of slopes (up to 2 m high). Induced stresses from thermal contraction were thereafter prevented by slightly postponing the back-filling of the anchor trenches, allowing each deployed panel a few days to find its comfortable position. Exceptionally strong north-easterly winds (80 km/h) also proved problematic at first, and a design modification was requested to circumvent the situation. Partial back-filling of the anchor trenches following the deployment of the secondary system was thus eventually permitted as opposed to the original design which had called for complete back-filling following the placement of all geosynthetics only. Nonetheless, high winds had still to be handled with during deployment itself and unorthodox placement procedures had to be adopted. Panels were pulled off the spreader bars as usual, but their wind-exposed edges had to be dragged under the adjoining panel's overlap in order to prevent uplift. As a result of this procedure, leading portions (approximately 10 m length) of secondary geomembrane panels obviously developed deep and clay-contaminated scratches from the rather abrasive underlying subgrade and welding proved problematic at first. Extensive cleaning and quality controls were thus specially implemented for those areas and some liner portions even had to be discarded altogether. Placement of the primary liner did not prove as problematic, the

underlying subgrade being sand.

CONCLUSION

The cell was completed in May 1992 and is scheduled to remain active for the disposal of stabilized sludges and mercury contaminated construction debris in accordance with stringent operational procedures until June 1993. Closure is planned thereafter with the utilization of composite liners, bio-barriers, drainage layers, gas collection, re-vegetation and prolonged monitoring. This very first project of its kind in Venezuela will have required the participation of Venezuelan, Canadian and American enterprises.

On account of its environmental regulations and recently acquired experience, Venezuela may undoubtedly be considered a leading nation in geosynthetic hazardous waste containment systems. State-of-the-art double-lined designs, adequate materials and stringent manufacturing and installation quality controls constitute regulating agencies expectations.

ACKNOWLEDGEMENTS

The authors are grateful to the Instituto para el Control y la Conservacion de la Cuenca del Lago de Maracaibo (ICLAM), under the leadership of Alicia Soto de Leon, for their valuable contribution.

REFERENCES

1- (1987) "Decreto 1800", Ministerio de Sanidad y Asistencia Social y del Ambiente y de los Recursos Naturales Renovables, Gobierno de la Republica de Venezuela, October 21 (in spanish).

2- (1988) "Instructivo Sobre Criterios Tecnicos y Procedimientos Para el Control de la Generacion y Manejo de Desechos Toxicos o Peligrosos no Radioactivos", Ministerio de Sanidad y Asistencia Social y del Ambiente y de los Recursos Naturales Renovables, Gobierno de la Republica de Venezuela, August 11 (in spanish).

3- (1992) "Normas para el Control de la Generacion y Manejo de Desechos Peligrosos", Decreto 2.211, Gaceta Oficial, Gobierno de la Republica de Venezuela, April 23 (in spanish).

4- (1992) "Report on Quality Control Procedures Conducted on Site by Construction Technique Jacques Cote Inc.", PEQUIVEN El Tablazo, Celda a Maxima Seguridad Para Lodos Mercuriales, Maracaibo, Venezuela, Internal Report prepared for TRICAL Geosinteticos C.A., June.

The Gilt Edge Asphalt Leach Pad: A Case History

M.E. Smith
Vector Engineering Inc., USA

ABSTRACT

The Gilt Edge is a gold mine using cyanide heap leaching on a reusable asphaltic and geomembrane lined leach pad. Ore is processed on reusable pads by stacking and leaching the ore on the liner, then unloading. The liner must be capable of maintaining containment integrity after many cycles of loading with heavy equipment. The selected primary liner was asphaltic concrete with an internal asphalt-saturated-geotextile membrane.

The primary liner leaked at rates exceeding the permit limitations. The leakage occurred through the joints in the pavement and defects in the geotextile membrane.

The liner was repaired with spray-applied liquid asphalt followed by a cover liner system consisting of a sand bedding layer, VLDPE, and a protective gravel cover. The cover liner system has been in service since 1989 and is continuing to perform within the permit limitations.

PROJECT DESCRIPTION

The Gilt Edge mine is located at an elevation of 1,700 meters (5,600 feet), about 3 miles (5 km) south of the historic town of Deadwood in the Black Hills of South Dakota. Gilt Edge is an open pit gold mine using cyanide heap leaching for gold recovery. Construction began in 1987 and the facility was commissioned in September 1988.

In the heap leach process, ore is crushed and stacked on a lined area, then a weak cyanide solution is irrigated over the heap. As the solution percolates down through the heap the cyanide reacts with the gold to form an aqueous gold-cyanide complex. The gold bearing solution is collected on the liner, drained to a collection pond (commonly referred to as the pregnant pond)

and then pumped to the recovery plant. The gold is removed from the solution and the now barren liquor is pH adjusted and more cyanide is added, then recirculated to the heap.

The unique aspect about Gilt Edge is the leach pad. Conventional heap leaching uses "permanent heaps" where the ore is placed on the pad, leached, detoxified and reclaimed on the pad. The leach pad is both a process element and the containment for final disposal. The height of the ore is controlled by geotechnical and metallurgical factors, and is typically limited to between 30 and 60 meters (100 and 200 feet). But this approach requires vast expanses of relatively level land. In the mountainous region surrounding Gilt Edge level land is scarce.

The alternative, which has been employed at about four other mines in North America, is an "on-off" pad. In this approach the ore is stacked on the pad, leached, then detoxified and removed to a disposal area. Since metallurgical control and uniform percolation of the leach solutions are not an issue in the waste disposal area, the waste dumps can be of virtually unlimited heights and dumped in any manner. Additionally, the waste is now essentially inert and only minimal containment criteria applies.

Photo 1 presents a view of the asphalt pad and the toe of the ore heaps. The piping shown is the pregnant and barren distribution piping. The slope is lined with HDPE.

THE ORIGINAL LEACH PAD DESIGN

The challenge with permanent pads is balancing permeability and structural requirements. The ore is stacked by end-dumping from Catapillar (Cat) 773B 50t trucks and pushed up with Cat D-9 dozers. Spent ore is removed with a Cat 992C front-end loader and 50t trucks. The design load is the loader, which has a gross weight of 87,000 kg (191,000 pounds) and a maximum wheel load of 52,000 kg (115,000 pounds). The accepted approach for the primary liner, and the one used for Gilt Edge, is to employ a structural asphalt section combined with a hydraulic barrier. According to South Dakota regulations, the containment was also required to include a composite secondary liner and an intervening leak detection, collection and recovery system (LDCRS).

The approach for the primary liner settled on by the owner and the design team was and asphalt pad constructed in two lifts. Between the bottom and top lifts was a membrane liner constructed by spraying hot liquid paving-grade asphalt (AC-10) over the bottom lift, then deploying a highway-grade, 0.014 grams per square centimeter (g/cm^2) (4 ounces per square yard (oz/sy)) non-woven geotextile while the AC-10 was still hot. The AC-10 was applied at the rate of 0.6 to 0.9 liters per square meter (l/m^2) (0.20 to 0.30 gallons per square yard). The result was an asphalt-saturated-geotextile membrane. Figure 2 presents a schematic of the leach pad liner system as originally designed and constructed.

The containment design also included a provision for storage of the probable maximum precipitation. The leach pad perimeter consisted of a level berm on all four sides, ranging in

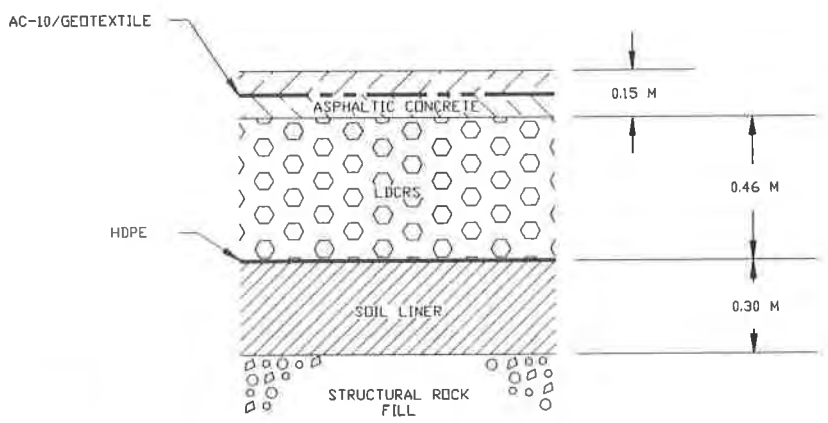

FIGURE 1
Original Leach Pad Liner System

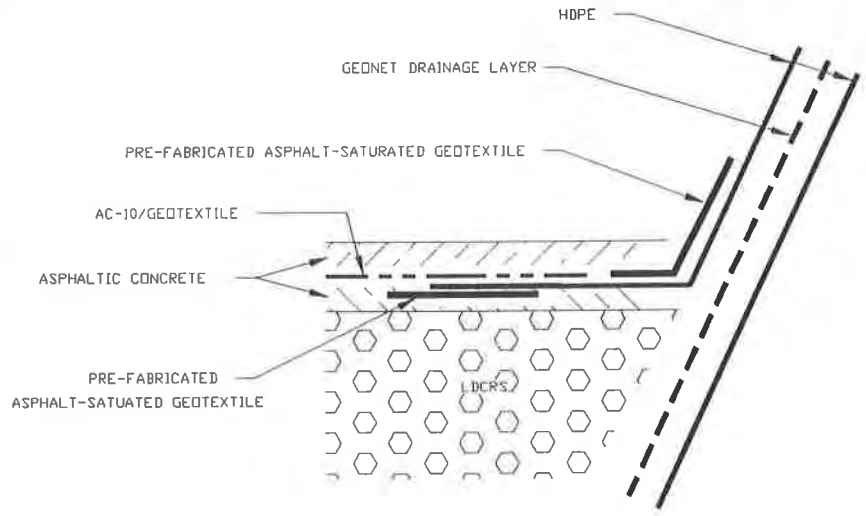

FIGURE 2
Slope Connection Detail

height from 2 to 5 meters (7 to 16 feet), as shown in photo 1. During extreme storm events excess solution would be stored on the leach pad. The interior slopes of the berms also required a double liner system to allow for storm water storage. It was impractical to construct the berm slopes at an low enough angle to allow for extension of the asphalt liner system up the slopes, and the design included HDPE geomembranes along the slopes. The connection of the HDPE slope liner and the asphalt pad liner is presented in Figure 2.

The leach pad was divided into seven cells, each nominally 8,000 square meters (2 acres) in plan dimension. The liner system is continuous, and a small berm over the asphalt provides hydraulic separation of the process liquors. The purpose of this division is to allow adjacent cells to be stacked, leached, rinsed and off-loaded independently.

Construction of the primary liner included specifications and construction quality control typical of highway pavement projects. The asphalt mix design focused on structural integrity. Quality control included measuring quantities of asphalt used, testing the asphalt pavement for AC content and density, and observing placement operations.

LINER SYSTEM PERFORMANCE

The permit issued by the State of South Dakota included an action leakage rate schedule for the leach pad, which is presented in Table 1. Within a few days of commissioning the first cell, seepage was detected in the LDCRS collection sump. The flow rate in the LDCRS slowly increased over the next month until the rates exceeded the allowable limits set in the action leakage rate (ALR) schedule. At this time several cells were on-line, and the leakage rate varied substantially from one cell to the next. Table 2 presents the stabilized leakage rates for each of the cells. It was determined that some cross-connection between the LDCRS beneath adjacent cells was occurring, and the data required substantial manipulation to allocate the total seepage to the appropriate cells. Cell 5 was repaired before it was commissioned, and cells 3 and 4 were only leached briefly before stopping irrigation, and the reported rates for these two cells are not stabilized rates.

At this point the author was engaged to trouble-shoot the leach pad and recommend a strategy to reduce the leakage through the primary liner. Since the ore was routinely cycled on and off of the leach pad on roughly a bi-monthly schedule, the approached used was to investigate and repair one cell at a time during the regularly scheduled off-load period. This afforded the minimum disruption to gold production. Leakage rates where held to acceptable levels by strict control of the irrigation rates and by reducing the total active area.

Table 1. Action Leakage Rate Schedule

Leakage Band liters/1000m^2/day (Ltd) or (gallons/acre/day)	Response Action Required
0 to 20	No response required.
20 to 100	Initiate response action, additional monitoring and reporting required, and areas of leakage located.
100 to 300	Change pad loading/spraying sequence to reduce leakage.
300 to 500	Repair leaks.
>500	Shutdown of sections contributing to leakage, replace primary liner as necessary.

Table 2. Stabilized Leakage Rates

Cell Number	Stabilized Leakage Rate liters/1000m^2/day (gallons/acre/day)
1	1,000
2	3,600
3	700
4	400
5	none
6	600
7	1,600

INVESTIGATION OF LEACH PAD

The leach pad was investigated in several ways to isolate the leakage mechanism. Monitoring wells were installed in one of the heaps, using drive-point well screens common in construction dewatering operations, to determine the hydraulic head in an active heap. This resulted in maximum water levels of less than 0.6 meters (2 feet), lower than predicted in the design and too low to be responsible for the elevated leakage rates.

Cracks along the contact between the HDPE slope liner and the asphalt leach pad were common all around the leach pad. Major cracks ran perpendicular to the edge of the pad from the edge in about 1.5 meters (5 feet), or to about the edge of the HDPE. These were located every 1.5 to 6 meters (5 to 20 feet) around the perimeter and were open at the surface as much as 2 to 5 cm (1 to 2 inches). Discontinuous, smaller open cracks were also present parallel to the edge of the pavement. Both types of cracks were determined to have been caused by the differential thermal expansion between asphaltic concrete and HDPE, and the relatively low tensile strength of asphalt.

Cores were taken of the asphalt through some of these cracks, and it was observed that in every case the cracks did not penetrate the AC-saturated geotextile. This was substantiated in the field by probing the cracks and by filling some with water, which did not seep away. Also, attempts to isolate the leach solution away from these cracks had no measurable affect on the measured flow rates in the LDCRS sumps.

Cores were also obtained to investigate the permeability of the asphalt/geotextile system. The cores were visually observed for macro-structure which might serve as a conduit for seepage, and they were tested in the laboratory for permeability. In each case test results on both the entire core including the geotextile layer, and a single lift of asphalt without the geotextile, indicted permeabilities lower than could be measured in the lab ($1x10^{-8}$ cm/sec), which is consistent with testing done during the design phase. Air voids where visually identified in the core, primarily near the bottom of each lift, indicating that the lift thickness of 8 to 10 cm (3 to 4 inches) may have been excessive for the compactive effort applied. While these air voids would allow the asphaltic concrete to pass water, the AC-saturated geotextile layer effectively acted as an hydraulic barrier in the cores tested.

During the investigation, leaching and neutralization of individual heaps continued and the first cell had been completely off-loaded and cleaned of mud. While this cell was air drying we noticed that the paver joints would still be visibly wet when the balance of the area was dry. The paver joints were spaced every 3 meters (11 feet) and the partially dried cell was zebra-stripped with thin wet lines. One transverse joint was also present in the first cell off-loaded, representing the end of a day's paving operation, and this joint was wet also. We also observed that solution from the adjacent active cell was crossing under the berm in some of the paver joints.

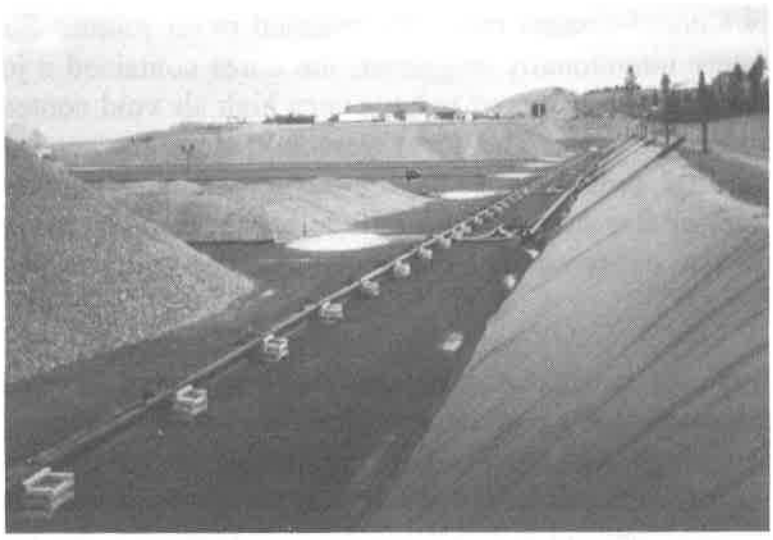

Photo 1

View of Leach Pad and Heap

Photo 2

Asphalt Cores from Cell No. 5

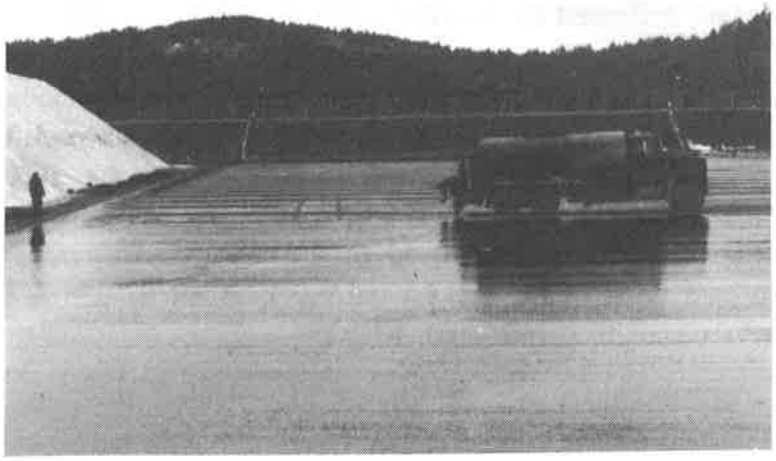

Photo 3

Repair of Cell No. 5

To investigate this phenomena we cored several randomly selected paver joints. Since the joints in the upper and lower lifts were intentionally staggered, the cores contained a joint in the upper lift only. The asphaltic concrete was observed to have very high air void contents; in fact, one could literally blow air through the core. The cores were split along the geotextile layer and laboratory tests of the top lifts (with the geotextile layer removed) indicated permeabilities greater than $1x10^{-3}$ cm/sec, or five orders of magnitude higher than the material away from the joints. In one core it was observed that the geotextile was not completely saturated with asphalt, a significant finding.

To follow-up on this core testing, the construction records were reviewed in greater detail, including the photo logs, and the contractor's and owner's staff were interviewed. The interviews, and to a lesser extent the photo logs, indicated that the application rate of the spray-applied asphalt was quite variable across the leach pad, and that "dry" spots (that is, areas where the geotextile was not fully saturated) were present but not extensive. However, by back-calculation we determined that it was only necessary for each cell to have one or two such dry spots, occurring directly beneath a paver joint, to achieve the measured leakage rates.

From this investigation we concluded that the mechanism of the leakage was as follows. The paver joints would be saturated, and at a few locations randomly spaced dry spots in the geotextile would be present beneath a paver joint. This would allow solution to flow horizontally along the geotextile/asphaltic pavement contact until a paver joint in the bottom lift allow the solution to penetrate into the LDCRS layer. While there was no practical way to prove this hypothesis, it was the only scenario which was consistent with the physical evidence.

REPAIR OF THE ASPHALTIC CONCRETE

A repair program was developed, which called for spraying the cell with a prime coat of a medium-cure cut-back liquid asphalt (with heaviest application on the paver joints), followed by a heavy chip seal over the entire cell using asphalt cement. Cut-back asphalts are a mixture a asphalt and light oil and are commonly used for prime- and tack-coats in road construction. A cut-back asphalt was selected because of the low viscosity and ability to penetrate into the voids. Chip-seals consist of a spray applied liquid asphalt cement followed by the immediate application of fine gravel, and in this plan, followed by another coat of asphalt cement.

The first cell to be repaired was Cell 5, and this was scheduled for the winter. Because of the extremely low temperatures at the mine site, certain precautions were taken. The cell was dried and pre-heated with flame-throwers immediately before application of the surface treatment. MC-250 was selected for the prime coat. The MC-250 was applied at an average rate of 0.9 l/m^2 (0.30 gal/s.y.) over the paver joints, and 0.45 l/m^2 (0.15 gal/s.y.) over the entire cell, for an average application rate of 0.76 l/m^2 (0.24 gal/s.y.). Cell 6, which was repaired in colder weather, used a lower viscosity prime coat, MC-70.

The chip seal used AC-5, which has a low viscosity relative to other paving grade asphalts. A high viscosity asphalt cement, AC-10, was used for cells constructed in warmer weather.

Cell 5 was repaired with ambient temperatures in the range of 5 to 12° C (42 to 54 degrees F), well below the recommended operating range for asphalts. However, the only significant problem was application of the gravel for the chip seal. The AC-5 cooled almost instantly upon distribution, and even with the gravel spreader close behind the distributor truck the AC-5 would set before the chips could be applied. Therefore, application of the chips was terminated and the total planned AC-5 volume was applied in one application of 1.7 l/m^2 (0.54 gal/s.y.), which was the maximum rate without puddling or run-off.

After repair Cell 5 was stacked with ore and brought into production. The leakage rate through the asphaltic liner system was nominally 200 l/1000m^2/d (200 gpad). Although this cell had not been activated prior to being repaired and we therefore had no datum to compare with, the repair was considered a success because the leakage rate was an order of magnitude below the other cells.

This repair procedure was repeated on 3 of the other cells with similar results. Cell 6 had the highest post-repair leakage rate which is explained by the fact that it was constructed in the coldest weather, with construction temperatures between -7 to -1° C (20 to 30° F). On the other hand, Cell 1, which was repaired in the spring, reported only 20 Ltd (20 gpad). The average leakage rate of all four cells was 180 Ltd (180 gpad).

THE COVER LINER CONCEPT

The repair work was performed under a temporary variance by the State of South Dakota on the permit's ALR. This agreement set a threshold leakage rate of 300 Ltd (300 gpad); leakage rates greater than this required termination of operation. While the average leakage rate of 180 Ltd (180 gpad) complied with the State's criteria, it provided a very small factor of safety. Because the consequential costs of interrupting operations were very high, the decision was made to re-line the leach pad to ensure that the ALR could be complied with on a continuing basis.

The concept developed was to provide a geomembrane cover liner over the asphalt leach pad. The LDCRS layer beneath the asphalt would remain as the point of compliance and the cover liner would provide both containment and hydraulic head control over the asphalt. The cover liner was to be installed in the same manner as the asphalt repair: one cell at a time as the leach cycles were completed. The cover liner needed to meet the following design criteria:

- Withstand the loading imposed by the stacking and off-loading equipment;
- Resistant to solvents contained in the asphalt products;
- Resistant to ultra violet light exposure and extreme cold weather;

- Resistant to sodium cyanide solution at Ph 11;
- Conform to the very tight geometry of the existing pad;
- Suitable for cold weather installation.

The materials considered included polyvinyl chloride (PVC), high density polyethylene (HDPE), very low density polyethylene (VLDPE), and chlorosulfonated polyethylene (CSPE). PVC was ruled out due to the extended exposure to sun light, and the problems associated with seaming PVC at low temperatures. CSPE was ruled out due to cost and cold weather seaming problems. The final comparison was between HDPE and VLDPE. In 1989 VLDPE was still a relatively new product and the cold weather performance was somewhat speculative; but we were reluctant to use HDPE because of the difficulty of having it conform to the tight geometry. The final material selection was 2.0 mm (80 mil) VLDPE as manufactured by Gundle Lining Systems of Houston, Texas.

The cover liner system consisted of: surface treatment of the existing asphaltic liner (for only those cells not previously treated), a sand bedding and leachate collection system, the VLDPE liner and a protective cover system. The cover liner system design is presented in Figure 3.

The surface treatment of the asphaltic liner was an abbreviated version of the program implemented on four of the cells. Only a tack coat of MC-70 was used, and the asphalt cement was omitted.

The sand bedding layer was not designed as a conventional LDCRS layer because the geometry of the pregnant solution collection system would only allow a very thin layer. Therefore, emphasis was placed on protection against puncture and abrasion rather than drainage. A pervious sand was used and drainage was also provided.

The protective cover layer needed to protect the liner against mechanical attack from the heavy mining equipment. The protective

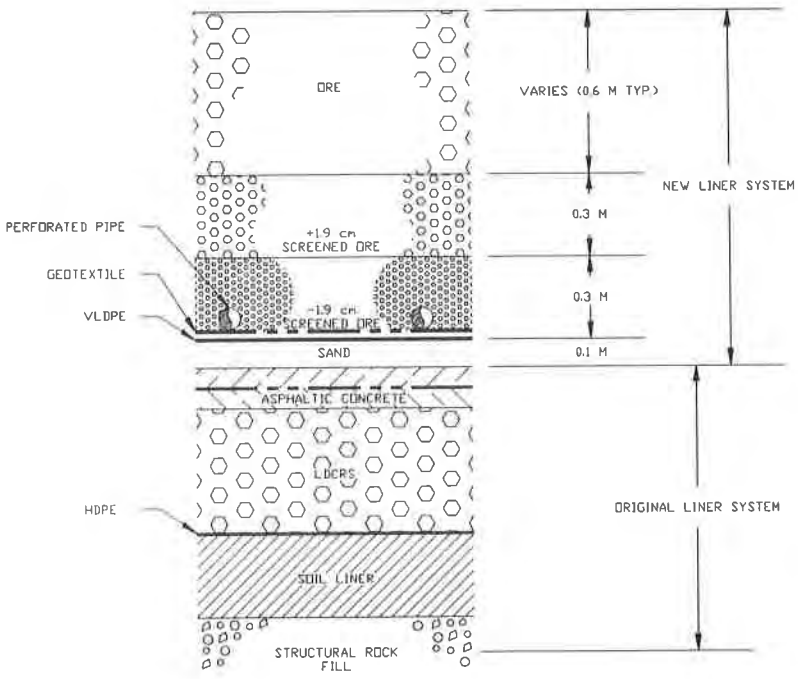

FIGURE 3
Final leach Pad Liner System

cover design was based upon field-scale testing performed for prior projects (Smith, et al 1987) and laboratory testing performed for this project using a test method similar to that used in research for the EPA (Laine, et al, 1988). The system consisted of a non-woven geotextile followed by a layer of fine ore and perforated drainage pipe. Over this layer coarse, clean ore was placed to enhance drainage, followed by a layer of random ore to isolate the engineered materials from the loading equipment.

COVER LINER PERFORMANCE

The cover liner was expected to perform well initially, but the unknown was its endurance under the loading conditions. At start-up (January 1990) no leakage was detected from the secondary leachate collection system. During the period between January 1990 and June 1992 the leakage reached a stabilized rate of a few liters per day per cell. At this low rate into the secondary collection system the primary LDCRS, which is the point of compliance, is reporting negligible leakage rates.

CONCLUSIONS

Two conclusions were drawn from this project. Structural asphalt liners can be constructed to provide reasonable containment, but cannot be made to perform equal to geomembrane liners. Secondly, geomembrane liners can be designed to withstand very large cyclic loads.

Design and construction of an asphaltic liner system must incorporate multiple redundancies to ensure proper performance. Relying only on the asphalt-saturated geotextile for containment made the system very susceptible to construction defects. Multiple redundancies, including designing the asphaltic concrete for low permeability by using a finer aggregate and higher oil content, constructing the paver joints more carefully (including saw-cutting and tack coating), and providing a seal coat may have allowed the original liner system to comply with the permit conditions.

To the author's knowledge this is the only double-lined project which has used a geomembrane under these conditions. The geomembrane has continued to perform within acceptable limits. This technology is now being applied at a larger facility in Chile.

ACKNOWLEDGEMENTS

The author wishes to acknowledge the contributions of the management and staff of Brohm Mining Company both in investigating and implementing the repair, and in assisting with the preparation of this paper. Also, the State of South Dakota Division of Water and Natural Resources cooperative approach to this project is greatly appreciated.

REFERENCES

Laine, D.L., M.P. Miklas, Jr. and C.H. Parr, (1988) "Loading Point Puncturability Analysis of Geosynthetic Liner Materials:, EPA contract No. 68-03-3231, pp. 14-20.

Smith, M.E., M. Henderson and B. McIntosh, (1987) " Puncturing of Geomembranes", Heap and Dump Leaching, Vol.4, No. 3, pp 3-9.

Use of Increased Frictional Resistance in Landfill Liner System Design and Construction

E.D. Chiado
Almes & Associates Inc., USA

S.D. Walker
Polyfelt Inc., USA

ABSTRACT

This paper provides a case history of the design, testing, and installation of a liner system that incorporated laminated continuous filament needlepunched polypropylene drainage geocomposites and textured high density polyethylene (HDPE) geomembranes. This liner system was installed in 1991 at a 4.5 hectare (11-acre) municipal solid waste landfill. Because of the relative newness of these products at that time, several unique laboratory tests were conducted to evaluate the shear strength of the laminated interface, the effect of lamination and normal stress on interface friction, and the adequacy of the texturing process applied to the geomembrane. These tests included two modifications of wide-width tensile strength to evaluate the shear strength of the bond between the nonwoven geotextile and HDPE geonet and unbonded versus bonded direct shear tests. In addition, simple field conformance tests were developed to provide minimal acceptance criteria for the adequacy of lamination and texturing. These conformance test procedures are provided and their suitability discussed. Finally, problems encountered during installation of bonded geocomposites in contact with textured geomembranes are presented, and solutions for overcoming the problems are suggested.

INTRODUCTION

Sideslopes of 3 horizontal to 1 vertical (3H:1V), or even steeper, are common in most modern landfills. Until recently, the liner system applied to these slopes usually contained one or more interfaces with low frictional resistance, such as geonet to smooth geomembrane, geonet to geonet, or unlaminated geotextile to smooth geomembrane. Steep sideslopes combined with low interface frictional resistance can result in the development of significant tensile stress. To maintain stability, tensile stress can be resisted through the incorporation of geosynthetic reinforcing, which is usually located directly above the other liner system components. Traditionally, this reinforcing has consisted of geogrids or woven geotextiles, which provide high strength at low strain. Figure 1 provides a cross section of a typical geosynthetic reinforced liner system. Based on the authors involvement with several landfill

projects, geosynthetic reinforcing has been used to successfully stabilize long, steep slopes that incorporated liner systems with low frictional resistance. However, geosynthetic reinforcing requires the use of an additional liner material, it usually increases the complexity of construction, and perhaps most importantly, it can result in a significant cost increase.

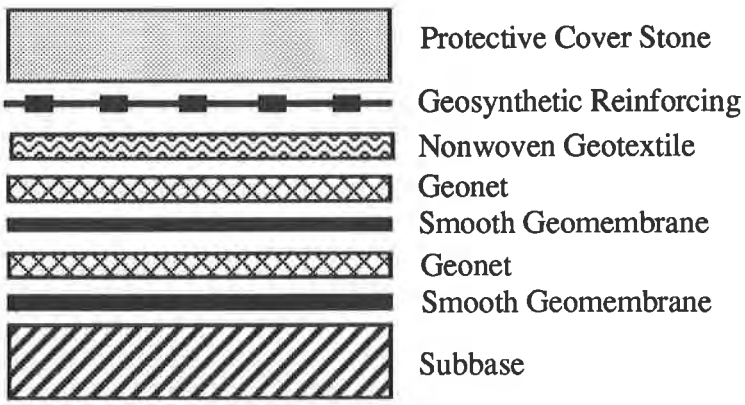

Figure 1. Typical Reinforced Liner System

The recent development and significant production of laminated drainage geocomposites (nonwoven geotextile(s) bonded to geonet) and textured geomembranes has permitted an alternative method to be developed to insure adequate liner stability. (Please note that the words laminated and bonded are used interchangeably throughout this paper.) When used in combination, the textured geomembrane and bonded drainage geocomposite provide a significant increase in frictional resistance, relative to a typical "smooth" geosynthetic liner system. This increased frictional resistance can eliminate or greatly reduce tensile stress, and is therefore, often sufficient to reduce or eliminate the need for additional geosynthetic reinforcement.

CASE HISTORY BACKGROUND

Chrin Brothers Sanitary Landfill (Chrin) is located in southeastern Pennsylvania, approximately 65 kilometers (40 miles) north of Philadelphia. Figure 2 provides a plan view of the permitted landfill area. The site was originally permitted for disposal of municipal solid waste on 4.5 double-lined hectares (11 acres). By the spring of 1991, about 2.8 of the 4.5 hectares (7 of 11 acres) had been lined and were receiving waste. At this time, the owner decided to expand the landfill onto adjacent property. The liner system for the expansion area was designed to contain a double liner system with high density polyethylene (HDPE) geomembranes. This was different from the geomembrane configuration used in the existing landfill area. Rather than have a different type of liner system for each area, which would eliminate the ability to fill over the interface between the existing and expansion areas, it was decided that the 1.7 remaining hectares in the existing area would be lined with the same liner system as that proposed for the expansion area. The 2.8 hectares that were already lined and overlain by waste would be excavated and retrofitted with a new HDPE liner system at a later time.

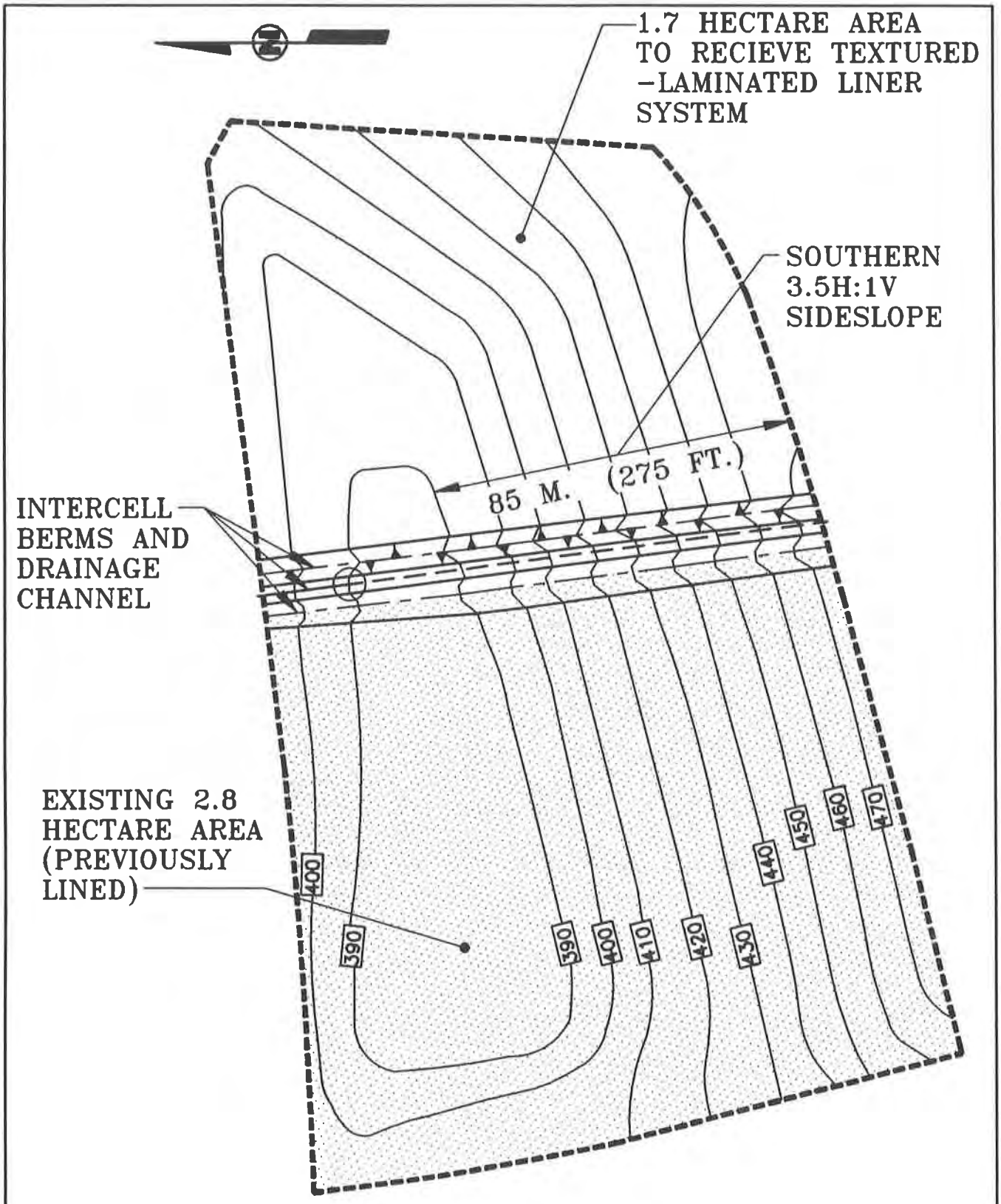

FIGURE 2
PLAN VIEW OF SUBJECT AREA

NOT TO SCALE

Landfill slopes within the remaining 1.7 hectares were designed to range from 2 percent to 28.5 percent (3.5H:1V), with the majority of the cell area located on the later. Average lengths of sideslope along the southern edge of the cell were about 85 meters (275 feet). Benches were not incorporated along this southern sideslope, since this would have necessitated pushing the limit of the landfill further south, which was not possible due to space restrictions. During the subsequent liner analysis and design, this southern sideslope provided the main area of focus, since the other sideslopes within the 1.7 hectare area were either short in length or minimal in slope.

Initially, it was decided that a smooth HDPE geomembrane would be used for the primary and secondary liner. These geomembranes would be coupled with one or more layers of HDPE geonet that would form the primary and secondary leachate collection zones. Direct shear tests of these interfaces indicated that low interface friction would probably exist along several of the interfaces. Subsequent analyses using these direct shear test results indicated that substantial tensile stress would theoretically be developed on the long southern 3.5H:1V sideslopes. As such, a liner system that incorporated geosynthetic reinforcing was anticipated along the remaining 1.7 hectare area.

During the initial analysis, several liner manufacturers were beginning to introduce textured HDPE geomembranes. In addition, drainage geocomposites, wherein either continuous filament needlepunched polypropylene or polyester nonwoven geotextiles are bonded to HDPE geonet, were also introduced. Limited independent laboratory testing suggested that large increases in interface friction were possible between the interface of textured geomembrane and bonded drainage geocomposite. Further analyses of liner stability with the limited direct shear test results indicated that if the reported frictional properties could be achieved, the need for geosynthetic reinforcing could be eliminated from the liner system proposed for the 1.7 hectare area. These initial favorable results provided the impetus to develop a "textured/laminated" liner system for the remaining 1.7 hectare area. Figure 3 provides a cross section of the textured/laminated liner system proposed for the 1.7 hectare area. During the subsequent design it was determined that insufficient data existed for several key design features concerning the bonded geocomposite and the textured geomembranes. As such, a series of unique laboratory tests were undertaken to attempt to address these issues.

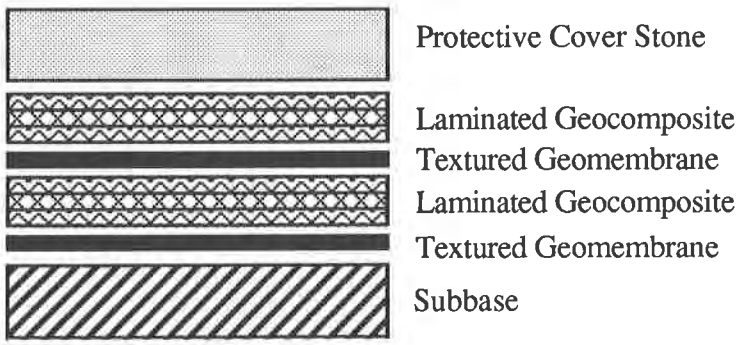

Figure 3. Textured/Laminated Liner System Proposed for 1.7 Hectare Area

TESTING

As stated above, the relative newness of the textured/laminated liner system, coupled with the lack of substantial laboratory data, necessitated the development of a laboratory testing program to address several design issues. After a review of existing data, the following issues were determined to be those that needed additional testing or consideration:

1. Peel tests (ASTM D413), which had previously been used as an index test to determine the strength of the bond, did not produce a shear-type failure, which would be the anticipated mode of failure in the field. As such, this test method was entirely inadequate for design purposes. A new test needed to be developed to better model and evaluate the shear strength of the bond between the nonwoven geotextile and geonet, so as to produce meaningful information that could be used in design;

2. The effect, if any, of lamination on interface friction between the nonwoven geotextile and the textured HDPE geomembrane needed to be evaluated, since the majority of testing to date had been performed on unlaminated nonwoven geotextiles in contact with textured geomembrane;

3. The influence of large normal loads on interface friction was relatively unknown, which was of concern since large overburden stress from overlying waste was anticipated; and

4. The effect, if any, of long-term loading on the ability of the textured geomembrane and bonded geocomposite to maintain enhanced frictional resistance was relatively unknown.

These issues needed to be addressed because the textured/laminated liner system derives its stability almost exclusively through increased frictional resistance. This system acts in a much more composite manner, relative to a geosynthetic reinforced liner system. Therefore, it was vital that knowledge of the interaction of bonded geocomposite and textured geomembrane, their strengths and weaknesses, be understood and accounted for in the design.

Shear Strength of Bond Between Nonwoven Geotextile and Geonet: The shear strength of the bond between the HDPE geonet and nonwoven geotextile was one of the most important physical properties of the proposed textured/laminated liner system. Since ASTM D413 (Ply Adhesion) does not produce a shear mode of failure, a new method for shear strength evaluation of the bond was needed.

In order to develop more field and design orientated data, two new laboratory tests were evaluated. These two methods were essentially variations of ASTM D4595 (Wide Width Tensile Strength). Although this test method also has several shortcomings, it was felt that a modification of the wide width tensile test represented a step in the right direction for determining the strength of a bond. The tests were conducted on 10 ounce per square yard (oz/sy) continuous filament needlepunched polypropylene and polyester nonwoven geotextiles that were bonded to HDPE geonet.

The two test setups are shown in Figure 4. Test Configuration 1 consisted of clamping the HDPE geonet in one clamp head and a nonwoven geotextile in the other clamp head. The bonded interface was located midway between the two clamp heads, and was then pulled apart in shear, similar to shear testing for geomembrane welds. This first test was felt to provide a "worst case" scenario, since the bond was the only component providing resistance to the load. Furthermore, this test should have provided the minimum strength that can be expected from the bond between the geonet and nonwoven geotextile. Test Configuration 2 consisted of clamping both the HDPE geonet and 10 oz/sy nonwoven geotextile in one clamp head and just the 10 oz/sy nonwoven geotextile in the other clamp head. This second test configuration was developed to simulate anchoring of the components and may provide a better simulation of how failure would occur in the field.

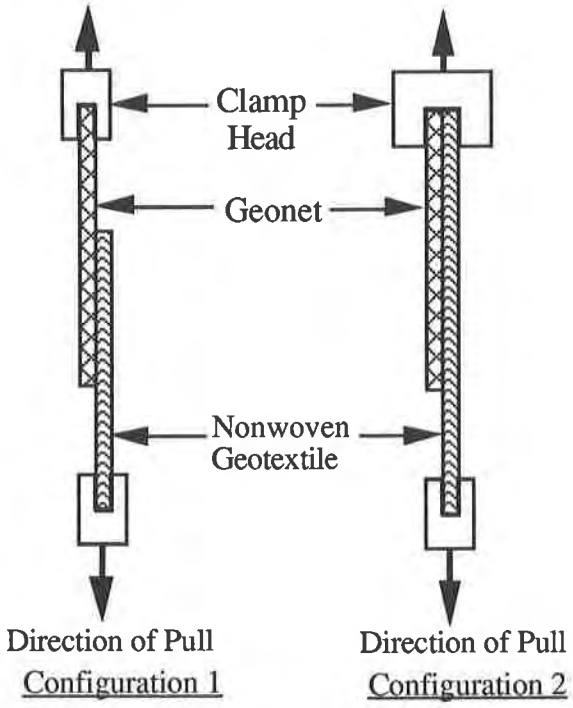

Figure 4. Modified Wide Width Tensile Test for Bond Shear Strength

Typical test results from Test Configuration 1 are provided in Figure 5. Some general conclusions from Test Configuration 1 are that both the polypropylene and polyester bonded geocomposites failed in similar manners. Only the magnitude of peak shear strength was different. The polypropylene bonded geocomposites generally achieved a peak shear stress of about 95 Newtons per meter (N/m) (130 pounds per foot) at 15 percent strain, whereas the polyester bonded geocomposites achieved a peak shear stress of approximately 210 N/m (285 pounds per foot) at 30 percent strain. All Test Configuration 1 results demonstrated a fairly well defined peak shear stress, with a linear stress-strain curve to peak. After peak shear stress was achieved, a rapid decrease in strength resulted until residual shear strengths of about 18 N/m (25 pounds per foot) were realized. Residual shear strength was maintained over a

strain range from 30 to 70 percent, with complete breaking of the bond generally occurring around 70 percent strain. Residual shear strengths were similar for both polypropylene and polyester bonded geocomposites.

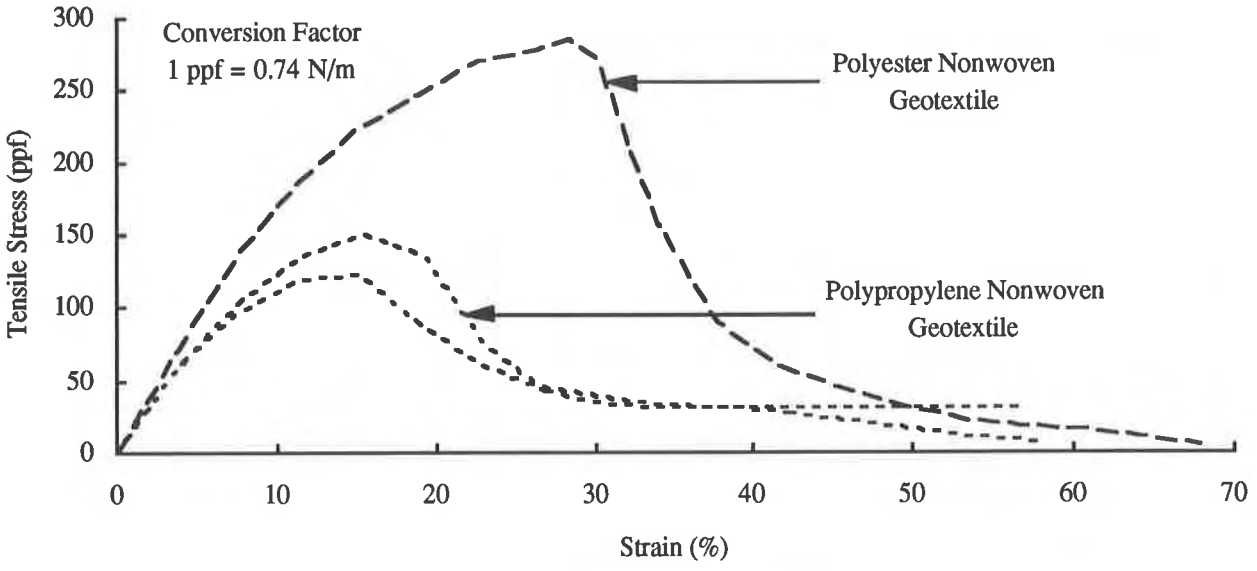

Figure 5. Modified Wide Width Tensile (Test Configuration 1)

Typical results from Test Configuration 2 are provided in Figure 6. Again, the stress-strain curves for the polypropylene and polyester bonded geocomposites are similar up to a point. However, the mode of failure and the magnitude of stress and strain at failure was very different for the two materials. The polypropylene bonded geocomposite specimens demonstrated a linear increase in stress with strain to a peak shear stress of about 625 N/m (850 pounds per foot) at 45 percent strain. Peak shear stress was followed by a rapid drop to residual shear strength. All of the bonded polypropylene geocomposite samples failed by rupture of the nonwoven geotextile and not by failure of the bond between the geonet and nonwoven geotextile. The polyester bonded geocomposite specimens demonstrated two distinct peak shear stresses. These specimens demonstrated a linear increase in stress-strain to an initial peak shear stress of approximately 465 N/m (630 pounds per foot) at 30 percent strain. At this initial peak stress the bond began to fail (delaminate). Beyond this initial peak, the shear stress began to increase as the nonwoven geotextile accepted the load. A second peak shear stress of approximately 625 N/m (850 pounds per foot) was achieved at an average strain of 70 percent, followed quickly by rupture of the polyester nonwoven geotextile.

In general, the results from both test configurations showed that the polypropylene and polyester bonded geocomposites behaved similarly over the range of strain needed to maintain stability (i.e., no more than about 10 percent strain). Within this limited strain range, the shear stress varied linearly with strain, and shear strengths of the bond were similar between the two different types of bonded geocomposites. Based on this testing program, Test Configuration 1 was felt to provide a good index test to determine the minimum shear strength of a bonded geocomposite. However, results from Test Configuration 2 were used in the liner

system design, since it was felt that this test better represented field conditions. Shear strengths determined at acceptable strains were used in the liner system analysis to provide the design shear strength of the liner system, which is different from a typical analysis of a "smooth" liner system where the tensile strength of the geomembrane(s) or geosynthetic reinforcing controls. In this manner, the design of the liner system was such that shear stresses would not exceed the bond strength of the drainage geocomposite.

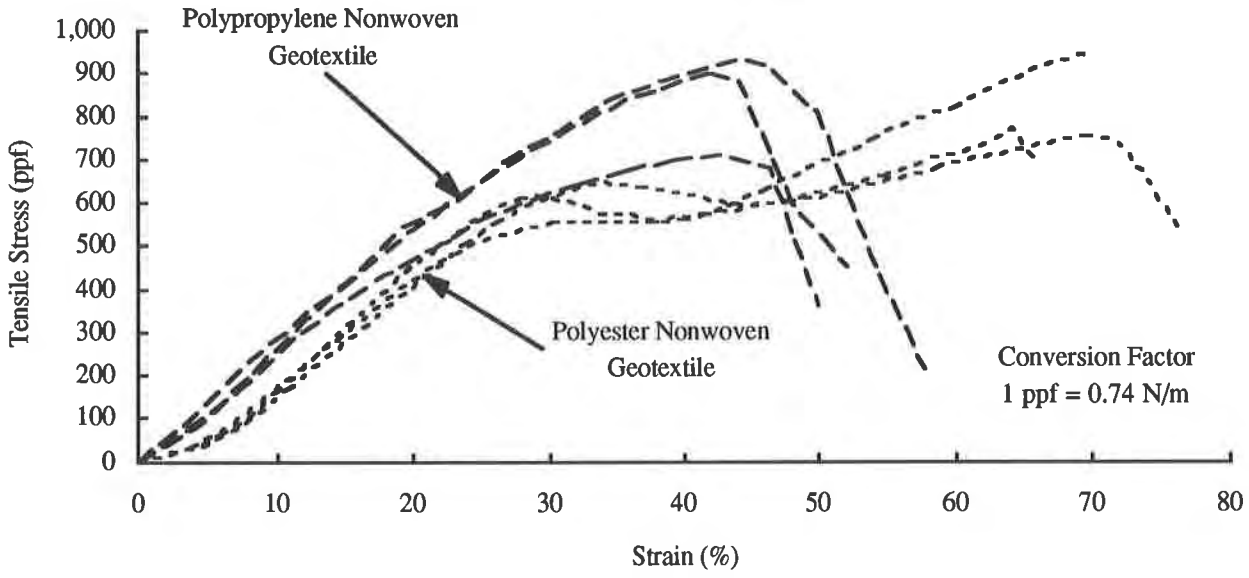

Figure 6. Modified Wide Width Tensile (Test Configuration 2)

Effect of Bonding on Interface Friction: During the manufacture of a thermally bonded geocomposite, the surface of the HDPE geonet is heated until it is molten. The nonwoven geotextile is then placed on top of the molten surface, and the two components are calendered so that fibers within the nonwoven geotextile melt into the HDPE geonet. Although heat-bonding only occurs on one side of the nonwoven geotextile, it is conceivable that the other side, which will eventually be in contact with the textured geomembrane, may be effected by the heat-bonding process.

Current geonet to nonwoven geotextile lamination processes are designed with three lamination bond strength determinants, which are:

1. Temperature of geonet upon contact with the nonwoven geotextile;

2. Method of heat transfer; and

3. Off-line or on-line lamination, which determines line speed and thus, time of heat exposure.

Sufficient heat must be applied to the geonet during lamination in order to assure an adequate bond strength as determined by the designer for site conditions. At the same time,

due to differences between softening points of the various polymers used for the production of the various nonwoven geotextiles, it is appropriate to adjust the heat applied to the geonet so as not to damage the lower softening point of nonwoven geotextile materials.

Some of the more common methods of heat transfer are flame, hot air, and heated calendar. These methods will require a specific line speed and distance from the heat source to the geonet in order to obtain an appropriate geonet temperature for a sufficient bond to be made with a given nonwoven geotextile.

When geonet to nonwoven geotextile lamination is performed in a separate step after the geonet is produced in an earlier, separate step, the lamination speed is usually faster than those processes which combine the two steps. Thus, higher temperatures or increased exposure time must be applied to the geonet to provide an adequate bond.

In order to evaluate whether heat-bonding had an effect on interface friction, direct shear testing was conducted on the two interfaces shown in Figure 7. One interface contained an unlaminated (not bonded) nonwoven geotextile in contact with a textured geomembrane. The second interface consisted of a bonded geocomposite in contact with a textured geomembrane. The nonwoven geotextiles used in this testing program were all 10 oz/sy and were either continuous filament needlepunched polypropylene or polyester. The textured HDPE geomembrane was 60 mils thick.

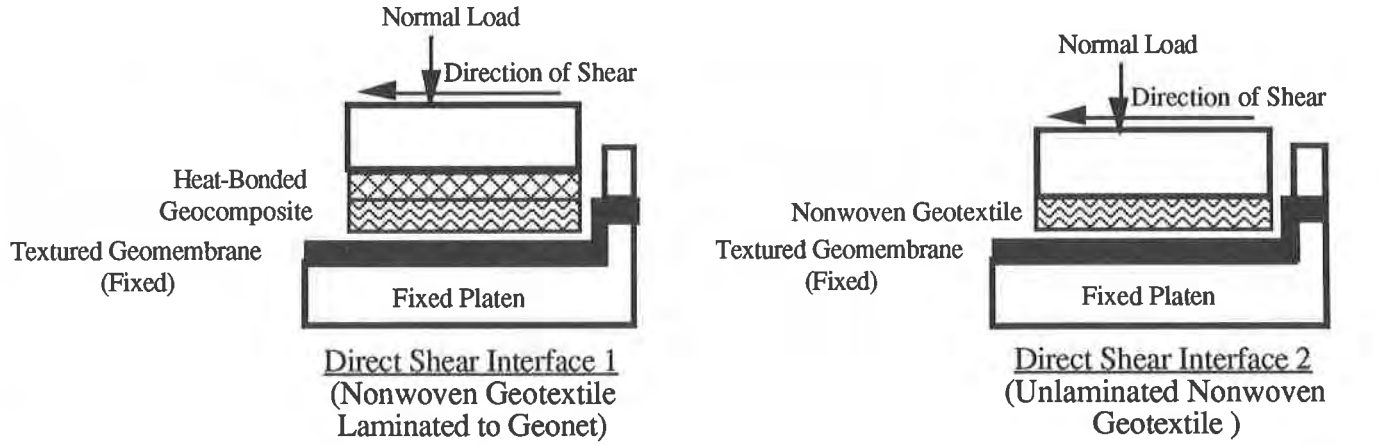

Figure 7. Direct Shear Test Setups

Typical results from both direct shear tests are provided in Figure 8. Referring to these results, it can be seen that for the materials tested, bonding did not appear to effect interface friction, since these interface friction angles are very similar to friction angles obtained on unlaminated nonwoven geotextiles in contact with textured geomembrane. It was believed that the 10 oz/sy nonwoven geotextile was sufficiently thick to prevent heat from the bonding process to affect the side of the nonwoven geotextile that was in contact with the textured geomembrane. Generally, nonwoven geotextiles become more sensitive to heat

treatments and other lamination processes as thickness of the nonwoven geotextile decreases. Therefore, all nonwoven geotextile used in the production of bonded geocomposites was specified to be at least 10 oz/sy for this project.

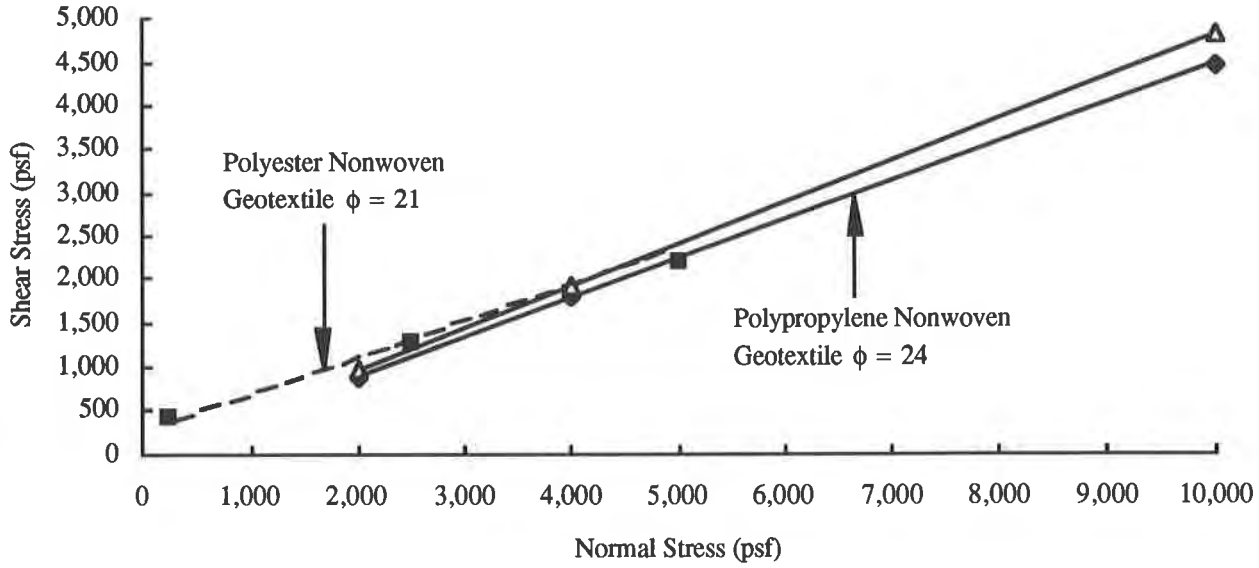

Figure 8. Results of Direct Shear Tests

Effect of Large Loads on Interface Friction: The maximum overburden stresses from overlying waste in the 1.7 hectare area was anticipated to be about 480 kiloPascals (kPa) [10,000 pounds per square foot (psf)]. Prior to this design, direct shear testing on a bonded geocomposite/textured geomembrane interface was typically performed at much lower normal stresses. For this design it was important to evaluate what effect, if any, large normal stresses would have on interface friction. As such, direct shear testing was conducted at 10, 95, 190, 240, and 480 kPa (250, 2,000, 4,000, 5,000, and 10,000 psf) on both continuous filament needlepunched polypropylene and polyester bonded geocomposites.

Test results from this direct shear testing program are provided in Figure 8. Referring to this figure, it is seen that at the higher normal stresses there was essentially no decrease in the slope of the intercept line. This result suggested that the interface friction angle was relatively constant at higher normal stresses, compared to lower normal stresses. This result was somewhat unexpected, since it was assumed that the higher normal stresses would contribute to elastic deformation of the textured surface, with corresponding decrease in interface friction. However, this assumption was not supported by the limited laboratory direct shear test data shown in Figure 8. Even if the results had shown slight differences in interface friction as a function of normal stress, attempting to account for these small differences in the analysis would have been difficult for a 1.7 hectare landfill area, let alone a much larger landfill area.

Effect of Long-Term Loading on Interface Friction: Intuitively, the textured surface on the geomembrane should become slightly smoother with time. This assumption is based on the

knowledge that the texturing will experience elastic and creep deformation under load. Furthermore, creep of the overlying liner components, specifically the bonded geocomposite, may tend to striate and possibly align the textured surface or nonwoven geotextile fibers along preferential paths, with the passage of time. Unfortunately, time constraints on the design of the 1.7 hectare area did not permit for a determination of how long-term loading effects interface friction.

The active design life of the 1.7 hectare area was anticipated to be about 2 years. Therefore, long-term loading effects were of concern, since it was likely that elastic and creep deformation would occur within this time frame. Because long-term loading effect data was not available, it was decided to apply a partial factor of safety to the design interface friction angle. This partial factor of safety was based in part on work by others for creep of plastic geomembranes and was felt to be satisfactory, in the absence of better data.

CONSTRUCTION QUALITY ASSURANCE

In addition to the usual conformance testing conducted during a typical construction quality assurance program, it was decided to add two additional conformance tests, during installation of the liner system in the 1.7 hectare landfill area. These tests were designed to measure the adequacy of texturing applied to the surface of the geomembrane and to evaluate the adequacy of the bond between the nonwoven geotextile and HDPE geonet. Specifications for the 1.7 hectare area were written to permit the use of either polypropylene or polyester bonded drainage geocomposites, based on the satisfactory results obtained for both of these materials in this testing program. The actual bonded drainage geocomposite selected for installation in the 1.7 hectare landfill area consisted of a 10 oz/sy continuous filament needlepunched polypropylene nonwoven geotextile bonded to an HDPE geonet. The actual primary and secondary geomembranes consisted of textured 60-mil material.

The first additional conformance test required that direct shear tests be conducted for every 9,300 square meters (100,000 square feet) of textured geomembrane and bonded geocomposite installed. In order to maintain consistency between the individual conformance tests, the material in contact with the textured geomembrane was the actual bonded geocomposite installed in the liner system. Initially, a 3-point direct shear test was conducted on the first conformance sample. Normal stresses applied during the 3-point test were 48, 240, and 360 kPa (1,000, 5,000 and 7,500 psf). These results were then combined with the existing direct shear data (conducted during the design phase) to develop a "master baseline " direct shear curve. This master baseline direct shear curve is shown in Figure 9. All subsequent direct shear conformance tests were 1-point, conducted at a normal stress of 360 kPa (7,500 psf). As each 1-point direct shear result was made available it was plotted on the master baseline direct shear curve. Direct shear conformance tests were acceptable when the 1-point datum point lay within or above the range of data exhibited in the master baseline curve. In this manner, it was not necessary to define a passing interface friction angle, since the master baseline curve had been used in the design phase, and all passing conformance tests would provide either the same or higher interface friction, relative to that used in the design. This procedure also permitted the use of 1-point direct shear tests, resulting in substantial savings, compared to a 3-point direct shear test for every conformance sample.

The second additional conformance test was a simple field peel, wherein the CQA Consultant would remove a sample of the bonded geocomposite every 9,300 square meters (100,000 square feet) and physically peel the nonwoven geotextile off of the HDPE geonet. The CQA Consultant would then determine the percentage of area of the sample where bonding was complete, relative to the entire area of the sample. A lower limit was then placed on the percentage of adequately bonded area to total area. Passing conformance tests had to achieve at least this minimum percentage. In retrospect, this second conformance test was not entirely appropriate or adequate for a couple of reasons. First, it was very difficult for the CQA Consultant to actually physically separate the bonded interface, leading to many frustrating and failed attempts at conducting the test. This did however, promote confidence in the adequacy of the bond between the nonwoven geotextile and geonet. More importantly though, this test did not place any qualitative measure on the shear strength of the bond, which was all important for this application. In essence, the unique laboratory testing that was performed during the design phase was of little value if we could not be sure that the actual installed material did not possess a minimum shear strength sufficient to meet the intent of the design. As such, subsequent installations at other landfills in which the authors have been involved, required wide width tensile testing of the bonded geocomposite, to correspond with the design information.

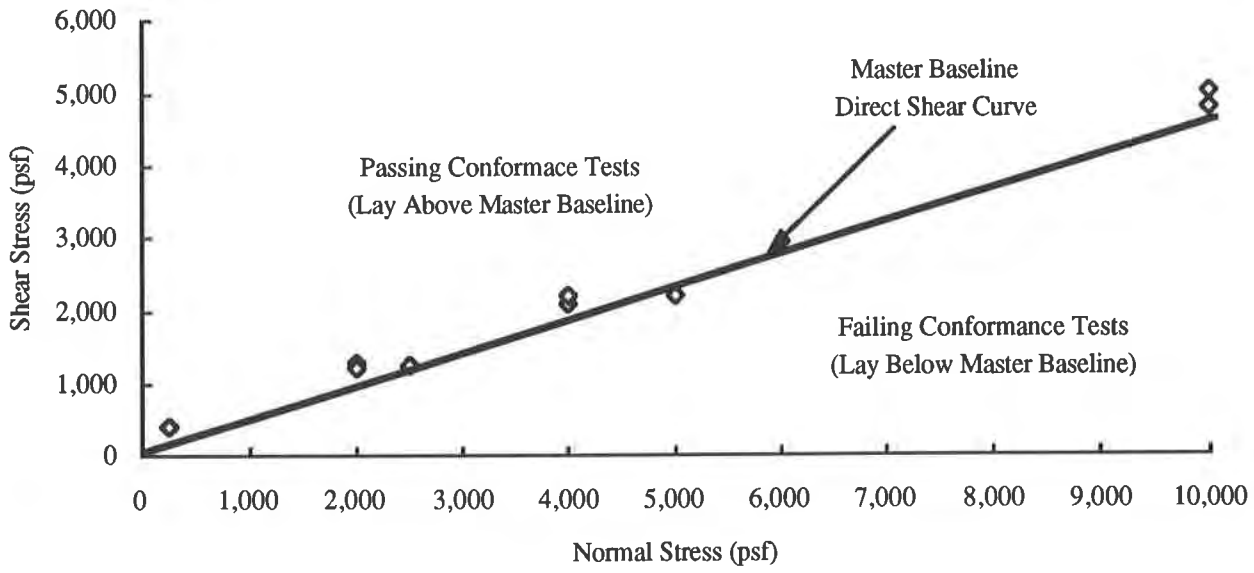

Figure 9. Master Baseline Direct Shear Curve for Conformance Testing Evaluation

INSTALLATION

Problems Encountered During Installation and Suggested Solutions: A primary difficulty experienced during installation of the bonded geocomposite had been the inability to make minor adjustments to the orientation of the panels once they are placed on the textured geomembrane. Once placed, the textured surface "grabs" hold of the nonwoven geotextile fibers, and it is virtually impossible to move the panels into final position. This problem was avoided in the 1.7 hectare area by allowing the liner installer to use scrap sheets of either

smooth geomembrane or loose HDPE geonet. These scrap pieces were placed on top of the textured geomembrane prior to placement of the bonded geocomposite. As the geocomposite was placed and positioned, the scrap pieces of material where withdrawn. As added protection, installation specifications clearly stated that dragging of the bonded geocomposite over the textured surface was forbidden. The CQA Consultant constantly monitored installation to ensure that this condition was achieved. This precaution should not be underestimated, since dragging of the geocomposite will result in stretching and possibly tearing of the individual geotextile fibers, resulting in residual shear strength being developed before the first load of waste is even placed.

One other difficulty that was identified during installation was due primary to the manner in which the installation specifications were written. Originally, it was required that each adjacent panel of bonded geocomposite would have 10 to 15 centimeters (4 to 6 inches) of its nonwoven geotextile pulled back so that the geonets between adjacent panels would be in intimate contact with each other, ensuring a continuous flow zone. In reality, this proved to be very difficult and time consuming. After a review of the situation it was decided that intimate contact between adjacent geonets was not required to maintain a continuous flow zone, since the geotextiles could also convey flow. As such, the installation specifications were modified to allow a simple overlap of adjacent panels with plastic ties pushed through all of the geotextiles and geonet in the overlap area.

Advantages Encountered During Installation: There were several advantages realized during installation of the textured/laminated liner system, relative to a typical "smooth" liner system. The usual requirement for temporary anchoring of liner components with either sandbags or partial backfill of the anchor trench was not needed. The enhanced frictional resistance was sufficient to prevent each individual component from sliding down the slope during installation. However, during high winds, sandbags were still used. Additionally, the good "grip" between the textured geomembrane and bonded geocomposite essentially eliminated geomembrane wrinkles, even on the longest slopes. This in turn, resulted in easier seaming, and a decrease in the number of "fishmouths." A final advantage was that there was savings in construction time, relative to a more typical liner system where each component of the drainage systems (geonet and filter geotextiles are installed individually.

CONCLUSIONS

The 1.7 hectare area was successfully lined with liner system that incorporated 60-mil textured geomembranes and 10 oz/sy continuous filament needlepunched polypropylene bonded geocomposite drainage systems. This area has reached final grade and was projected to be closed by the end of 1992. To date, the liner system has performed as expected and has shown no sign of instability or excessive stress. The confidence with which the liner system was developed and deployed would not have been possible without a realistic estimate of the shear strength of the bond between the nonwoven geotextile and geonet and knowledge of the functioning of the bonded geocomposite when in contact with the textured geomembrane. Through testing conducted as part of the design, it was possible to design an unreinforced liner

system for a relatively steep and long sideslope. Additional conformance testing, which was above and beyond that typically encountered, assured the designers that the enhanced frictional resistance that was being counted upon in the design was, in fact, developed in the actual liner.

The testing program highlighted several issues that need further research. Perhaps most importantly, there is little information available on the long-term ability of the textured geomembranes to continue to provide a sufficiently roughened surface and therefore, enhanced frictional resistance. Intuitively, one would expect the textured surface to become less rough with time, due to elastic and creep deformation coupled with ordinary shear stress along the face of the geomembrane. Additionally, little is known about the effect of high normal stresses on interface friction between textured geomembranes and bonded geocomposites. Although testing did not show any effect, intuitively again, it would be expected that interface friction at large normal stress might be slightly smaller than that at lower normal stress.

Finally, it should be realized that a limited amount of testing on select materials was conducted for this design. Only two 60-mil HDPE geomembranes, one 10 oz/sy continuous filament needlepunched polypropylene heat-bonded geocomposite, and one 10 oz/sy continuous filament needlepunched polyester nonwoven geotextile were included in the testing program. Differences in manufacturing by each producer may result in widely varying results from that presented. Specifically, there are several methods for applying textured surfaces to geomembranes, and nonwoven geotextiles can be needled in number of ways, or not even needled at all. Therefore, the results and conclusions from this testing program may not be applicable to other materials and should be reviewed and used with caution.

ACKNOWLEDGMENTS

The authors would like to acknowledge the assistance and guidance of Mr. Greg Chrin in preparing this paper. The authors would also like to acknowledge the assistance of Polyfelt, Incorporated, Hoechst-Celanese Corporation, Gundle Lining Systems, Inc., and National Seal Company for providing the materials used in this testing program.

REFERENCES

American Society for Testing and Materials "ASTM D413 Standard Test Method for Rubber Property - Adhesion to Flexible Substrate."

American Society for Testing and Materials "ASTM D4594 Test Method for Tensile Properties of Geotextiles by the Wide-Width Strip Method."

Geogrid Provides Design Solutions at Midway Landill

G. Fox
Parametrix Inc., USA

ABSTRACT

Midway Landfill closed in 1990. The typical final cover system consists of (bottom to top) interim cover/subgrade, geomembrane, drainage net, geotextile, and cover soil.

Three unique physical features of the landfill required individual design solutions. The first was a small section of 2:1 slope. The safety factor for the typical cover system was not acceptable and was increased by adding a geogrid below the cover soil and above the geomembrane.

The second feature was a sink hole which continually developed in the interim cover despite refilling. The third feature was a 180 meter (600 foot) long reoccurring crack in the interim cover. The crack was located above an interface of refuse against a vertical rock wall remaining from past gravel pit operations. The cover system was supported in these areas by adding a geogrid over the subgrade and below the geomembrane.

To date, no indications of slope instability or subgrade failure have been observed.

SITE HISTORY

The Midway Landfill is located in southern King County, Washington, within the City of Kent. The site is approximately 24 kilometers (15 miles) south of the City of Seattle and about 1.6 kilometers (one mile) east of the Puget Sound. The site was operated as a gravel pit from 1945 through 1966.

In 1966, the City of Seattle Solid Waste Utility leased the 22 hectare (55-acre) site from the pit operators for use as a landfill for non-putrescible wastes. The landfill was primarily used for disposal of demolition debris and municipal non-household wastes. After 1980, some

industrial wastes were also disposed of in the landfill. The landfill covers approximately 20 hectares (50 acres) with an average depth of 30 meters (100 feet) and was closed in 1983 (Figure 1).

Figure 1. Midway Landfill

In 1985, combustible landfill gas was detected in the basements of homes near the Midway Landfill. The City of Seattle installed a gas control system which drew the landfill gases back to the landfill and now prevents further off-site migration.

In 1986, the EPA added the Midway Landfill to the National Priorities List of hazardous waste sites. Remedial Investigation/Feasibility Study documents indicated that the landfill was having no significant impact on ground water, surface water, or air quality.

SCOPE OF PROJECT

The purpose of this project was to design and construct a final cover over the landfill which would protect human health and the environment by minimizing surface water infiltration. It must continue to perform this function, even in areas of differential settlement.

The criteria used in evaluating the various options for the cover design were:

1) availability of materials
2) ease of construction
3) susceptibility to weather conditions
4) implementation schedule
5) compatibility with future land uses
6) ease of maintenance and repair.

The project design began in February 1989.

Generally, the site can be described as having gentle slopes of between 4 and 6 percent grade, covering 18 hectares (45 acres), and steeper slopes of 25 percent (4H:1V), covering 4 hectares (10 acres). The typical cover system chosen consisted of (from bottom to top) a firm interim cover/subgrade foundation, geomembrane, geonet, geotextile, soil layer and vegetative layer (Figure 2).

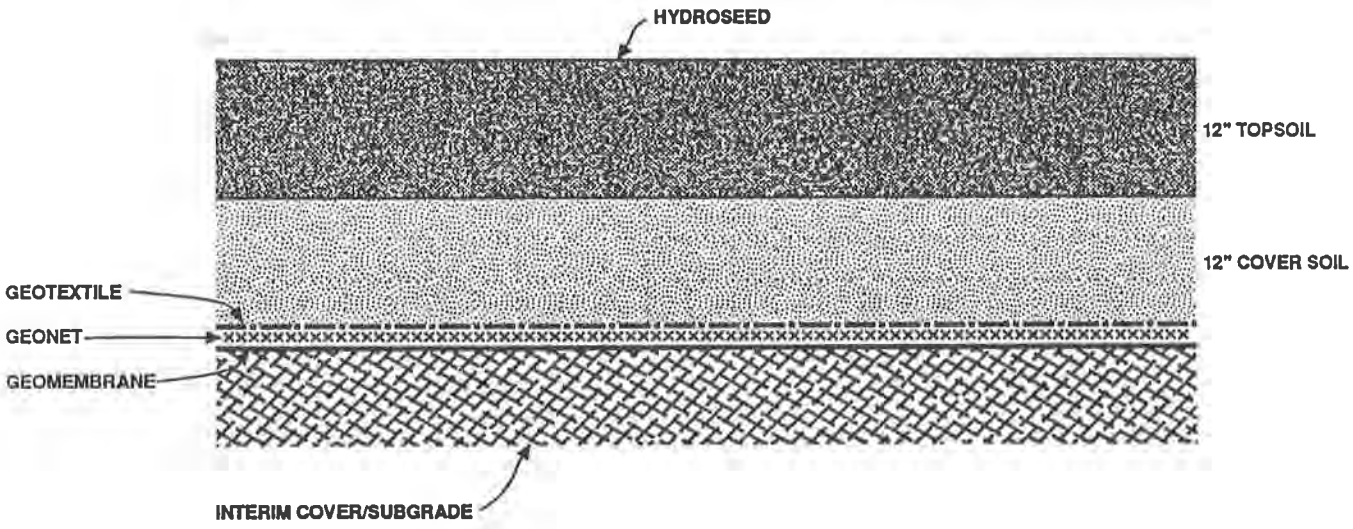

Figure 2. Typical Final Cover System

A geonet drainage layer was chosen because of its increased capacity over available aggregate drainage materials. With the majority of the cover on fairly flat slopes, the geonet allowed the subsurface collection lines to be spaced at 150 meter (500 foot) intervals. Use of available aggregate drainage material would have required spacing subsurface collection lines at 30 meter (100 foot) intervals, which would have increased the overall construction difficulty.

A geomembrane was chosen for the barrier layer because of its availability, cost and reduced susceptibility to weather compared to clay barrier layers.

Construction began in late summer 1989. After most of the excavation and embankment work was completed, to bring the site to subgrade, the project was shut down for the winter. The work began again in the spring of 1990 and was completed in early 1991.

DESIGN PROBLEMS

The design of the cover system was typical in many ways. Roads were designed to provide access around the site. Surface water and subsurface water collection facilities where provided. Liner penetration details for the numerous gas wells were developed, which allowed slippage to occur as the cover system settled, without losing a watertight seal. Interface friction tests were performed on all geosynthetic/geosynthetic and soil/geosynthetic interfaces being considered to assure adequate factors of safety on the 4H:1V side slopes. As a result of the interface testing, the typical cover section was modified for the side slope areas to increase stability by using textured geomembrane and drainage sand in place of smooth geomembrane and geonet. Due to the increased slope and short distance, the deletion of the geonet was not a problem.

Three individual physical features at the Midway Landfill required additional consideration. In these areas the typical cover system chosen for the landfill would not provide the performance desired throughout the post-closure period. The areas of concern were:

1) a small section of steeper side slope with a 2H:1V grade,
2) a 180 meter (600 foot) long crack in the interim cover of the landfill which reoccurred despite continued attempts to fill, and
3) a sink hole which developed in the interim cover despite continued attempts to fill it.

Slope Stability. A small section of the landfill side slope located adjacent to the sedimentation pond was too steep (2H:1V) for even the modified cover section with textured geomembrane. The factor of safety against sliding, calculated using graphic statics as described by Koerner (1986), was 0.8. The slope was 10 meter (35 foot) long by 45 meter (150 foot) wide.

Placement of additional embankment material was considered to flatten the slope angle. However, this was dismissed because the toe of the slope would have unacceptably encroached on the sedimentation pond.

Excavation of the slope to reduce the angle was not an acceptable option because the excavated material would have been predominately refuse. Removal of refuse from the site, to other landfills in the community, was not allowed due to Midway's statutes on the National Priorities List of hazardous waste sites. Also, excavation into refuse opens all sorts of possible scenarios for project delay due to possible uncovering of unknown materials.

Modification of the cover section was required to provide additional stability for this slope.

Subgrade Cracking. Large differential settlement of the subgrade was expected along the south end of the landfill. During earlier quarry operations, the original ground was cut almost vertical, leaving a rock wall approximately 6 meters (20 feet) high. During waste disposal operations, the waste was piled up against the wall. Since the landfill was closed and interim cover was placed in 1983, a surface crack approximately 180 meter (600 feet) long had developed above this area annually. The City's maintenance crew filled the voids with soil and bentonite in attempts to plug the crack as it reoccurred.

Modification of the cover section was required to assure continued integrity of the cover system in this area throughout this post-closure period.

Sink Hole. Another area where large differential settlement was anticipated was in a localized area at mid slope along the east side of the site. Since the interim cover was placed in 1983, a sink hole had continued to develop in the same location. The City's crew filled the hole approximately every two years, after it developed to approximately 1.8 meter (6 foot) deep and 1.5 meter (5 foot) across. The hole was approximately 1 meter (3 foot) deep in early 1989 when design for this project began.

Modification of the cover section was required in this area to assure the continued integrity of the cover system throughout the post-closure period.

DESIGN SOLUTIONS

Slope Stability. To increase the stability of the cover section on the 2H:1V slope, an HDPE geogrid was used to reinforce the soil placed on top of the textured geomembrane. The use of textured geomembrane and sand drainage layer resulted in an increase in the interface friction angle and hence an increase in the restraining force. However, as previously discussed, this force is not sufficient to assure stability. The geogrid, anchored at the top of the slope, provides the additional resisting force needed to minimize the potential for sliding of the soil cover layers.

The geogrid was designed based on the manufacturer's recommended design procedures (TTN:WM2, Tensar 1988). For a factor of safety of 1.5 a geogrid with a long-term allowable design strength of 32 KN/m (2,200 lb/ft) was used. The specified tensile modulus of 1,500 KN/m (100,000 lb/ft) (min.) allowed high tensile stress to develop at low strain levels.

Stress is transferred between the geogrid and the reinforced soil by mechanical interlocking of the soil particles with the geogrid. This stress transfer is greatest when the soil is placed on both sides of the geogrid. However, on this project the geogrid was placed directly on the geomembrane and the sand drainage material was then placed over the geogrid (Figure 3). This promoted quick installation of the geogrid and sand drainage material. Also, placing

a thin layer of soil over the geomembrane prior to placing the geogrid would be difficult to do without damaging the geomembrane, especially on the steep slope.

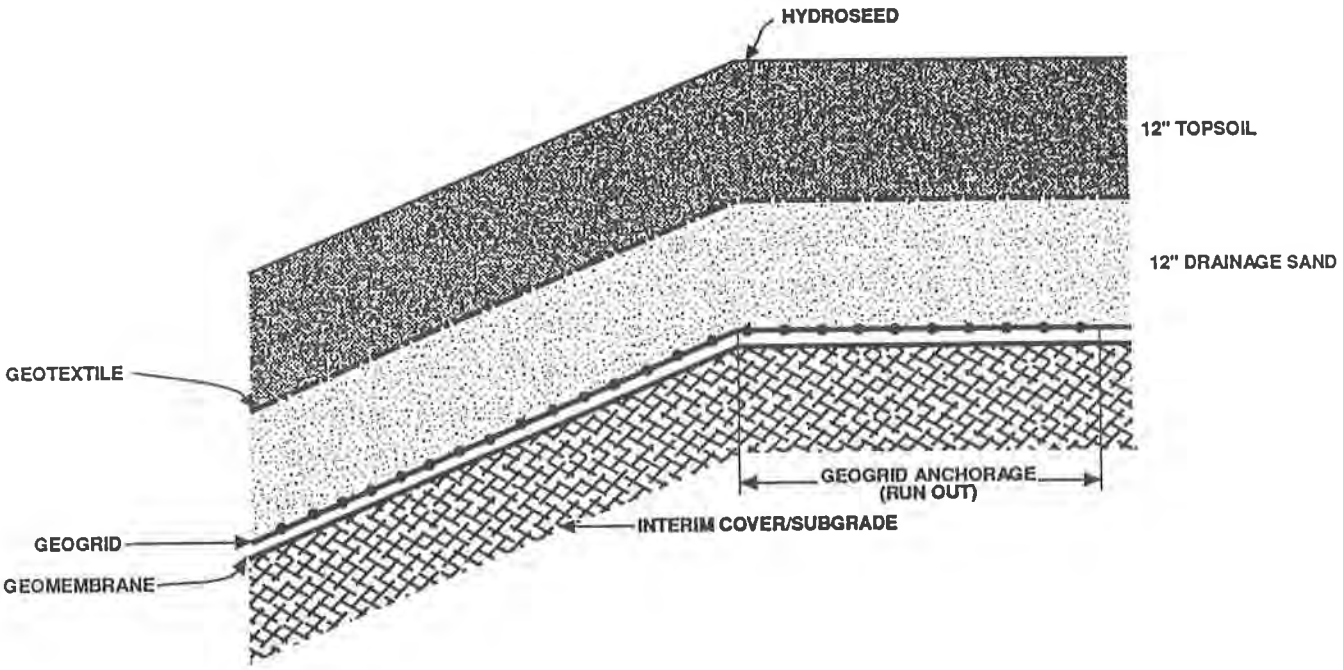

Figure 3. Geogrid Reinforced Slope

The geogrid was anchored at the top of the slope by embedding it a calculated distance beyond the crest. Because the geogrid was placed directly on the geomembrane and was in contact with the soil on only the top side, the runout length of 6 meters (20 feet) was approximately twice as long as would have been necessary if soil was placed on both sides. The cost for the extra geogrid used in the runout was estimated to be less than the savings from the decreased installation cost associated with the quicker and simpler construction required and the reduced potential for damaging the geomembrane. See Figures 4 through 7.

Subgrade Cracking. Differential settlement above the interface of refuse against the vertical rock wall, left from the quarry operations, is expected to continue for many years. City personnel estimated that the largest cracks seen, since closure in 1983, were approximately 15 centimeters (6 inches) wide. The crack was filled before it grew any larger.

Since no refuse has been placed since 1983, it is estimated that much of the total settlement has occurred. However, to be conservative it was assumed that the maximum crack that would develop under the cover system would be 60 centimeters (2 feet) wide. The cover system along the south end of the site must be able to span this assumed crack without failing.

Figure 4. Subgrade Preparation

Figure 5. Geomembrane Was Placed First

Figure 6. Geogrid Placed Over Geomembrane

Figure 7. Drainage Sand Being Placed Over Geogrid

Some consideration was given to placing a layer of bentonite under the geomembrane in the vicinity of the cracking to fill future cracks and to seal any areas of the geomembrane which may fail due to loss of the cover system foundation by cracking. Since the cracking was only slightly evident at the time of the design, the exact location where it would develop next could not be well defined, and as demonstrated in past years the bentonite may be swallowed up by the crack, this option was not considered further.

A geogrid was employed to provide support for the cover system over future cracks in the subgrade. The geogrid was placed under the geomembrane directly on top of the prepared subgrade (Figures 8 and 9). It was designed based on the manufacturer's recommended design procedures (TTN:WM3, Tensar 1989). The specified long-term allowable design strength to span the assumed 60 centimeter (2 foot) wide crack, using a factor of safety, was 15 KN/m (1,000 lb/ft). The specified tensile modulus of 730 KN/m (50,000 lb/ft) (min.) allowed high tensile stress to develop at low strain levels.

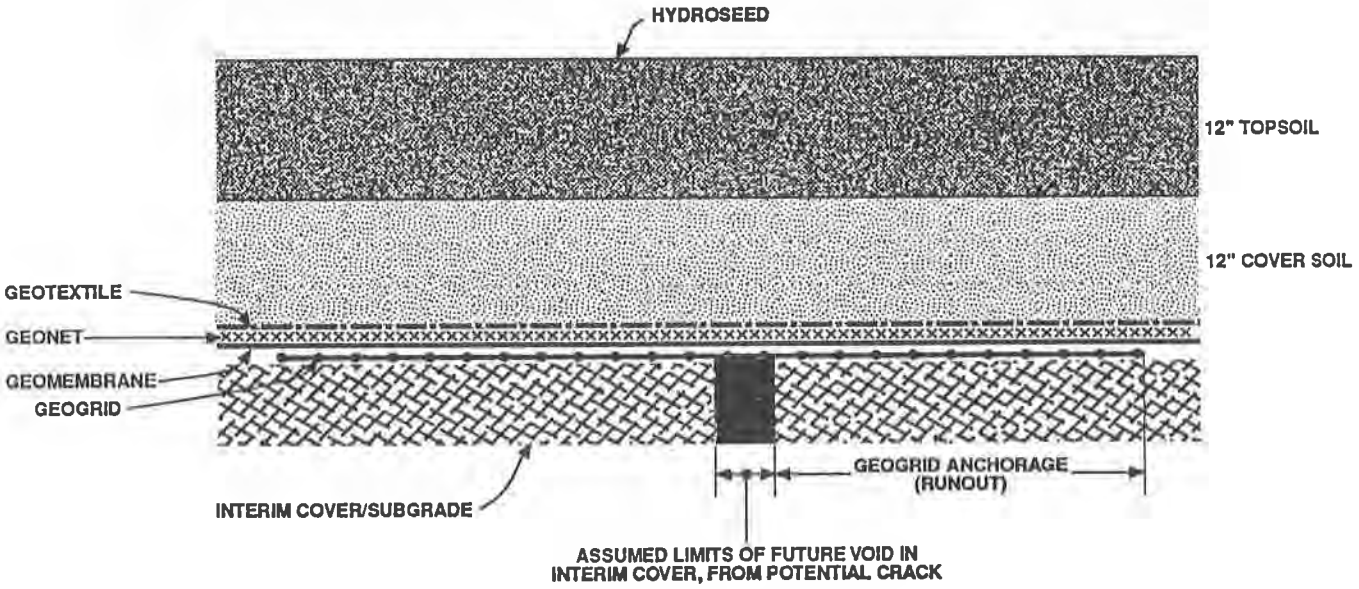

Figure 8. Geogrid Reinforced Foundation Over Potential Crack

The probable limits of where the crack may develop in the future were identified and the geogrid was anchored beyond those limits by running out an additional 1.8 meters (6 feet) or more. The runout distance required to anchor the geonet was approximately twice the length which would have been required if a layer of subgrade soil had been placed over the geogrid. Placing a layer of soil above the geogrid would have been simpler in this application, compared to the slope situation mentioned above, because the geomembrane would not be installed until

afterwards. However, it was estimated that the material savings would not be significant and would not offset the increased costs associated with the greater construction difficulty.

Figure 9. Geomembrane Being Placed Over Geogrid

Sink Hole. Due to the continued development of the sinkhole over the last few years, despite repeated filling, it is anticipated that differential settlement in this area will continue for many years. Based on City personnel's estimates, the maximum size of future development of the sink hole was assumed to be 3 meters (10 feet) in diameter. The cover system must be able to span this assumed sink hole in the foundation without failing.

Excavation in the vicinity of the sink hole was considered in order to investigate the cause and possibly fill in or plug the subsurface void causing the situation. However, because of the unknown depth and width of excavation that may be required, the unknown types of refuse that may be encountered, the regulatory requirement stating that no refuse shall be removed from site, and the lack of an area on site for disposal of relocated refuse this option was rejected.

Again, a geogrid was employed to provide support for the cover system over the potential future sink hole that may develop in the subgrade. The geogrid was placed under the geomembrane directly on top of the prepared subgrade (Figures 10 and 11). It was designed based on the manufacturer's recommended design procedures (TTN:WM3, Tensar 1989). The specified long-term allowable design strength to span the assumed 3 meters (10 foot) diameter

sink hole, using a factor of safety, was 44 KN/m (3,000 lb/ft). The specified tensile modulus of 1,900 KN/m (130,000 lb/ft) allowed high tensile stress to develop at low strain levels.

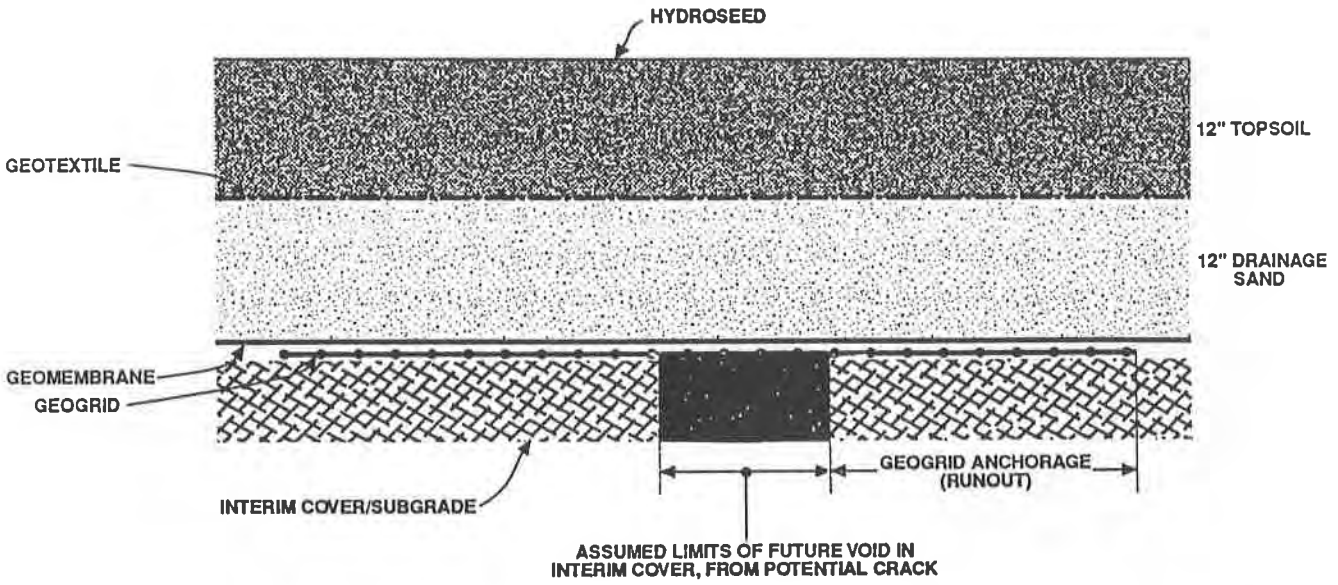

Figure 10. Geogrid Reinforced Foundation Over Potential Sink Hole

Figure 11. Geogrid Placed on Subgrade

Use of biaxial geogrid or two layers of uniaxial geogrid placed 90 degrees to each other were considered for this application. However, the sink hole was located adjacent to an access road with a surface water ditch. The location and geometry of the ditch did not allow sufficient room to anchor the geogrid over a continuous surface. Therefore, a single layer of uniaxial geogrid was placed running parallel with the access road. (Figure 12.)

Figure 12. Geogrid Placed Parallel to Access Road Centerline

The runout distance required to anchor the geogrid was 4.5 meters (15 feet) if soil was placed on both sides of the geogrid and 9 meters (30 feet) if placed on one side only. For the same reasons as previously noted, the geogrid was placed on the subgrade with the geomembrane placed directly over it and a 9 meters (30 foot) runout was used.

POST CONSTRUCTION SERVICE

Since construction of the landfill was completed in early 1991, routine inspection has been performed. As of October 1992, no sign of slope instability or foundation failure has been identified. The cover system has performed as designed on the 2:1 slope and in the areas of subgrade cracking and the sink hole.

SUMMARY

Use of geogrid provided design options at the Midway Landfill which

- allowed cover to be placed on the existing steep side slopes, which saved construction time and money by eliminating the need to reduce the slope by importing embankment material to build out the slope or excavating into the refuse fill.

- allowed reinforcement of the existing subgrade, thereby eliminating the need to repair the subgrade by excavating into the underlying refuse fill with all the associated problems and delays which may result from such an operation.

- provided confidence that the cover system would continue to perform throughout the post-closure period without the need for major repair in these areas where significant subgrade deficiencies have been identified.

The use of geogrid saved time and money during construction and reduced construction uncertainties. It is anticipated that post-closure maintenance will be significantly reduced by the use of geogrid to reinforce the subgrade versus the other options for subgrade repair which were considered.

REFERENCES

TTN:WM2, (1988) "Tensar Geogrid Reinforcement of Landfill Soil Veneer Covers," Tensar Technical Note (Draft).

TTN:WM3, (1989) "Design of Tensar Geogrid Reinforcement to Support Landfill Lining and Cover Systems," Tensar Technical Note.

Koerner, Robert M., (1986) "Designing with Geosynthetics."

Design, Construction and Performance of a Test Embankment on Hydraulically Placed Ash

D.W. Armour Jr.
Fuller, Mossbarger, Scott and May, Engineers Inc., USA

C.M. Avery
Fuller, Mossbarger, Scott and May, Engineers Inc., USA

ABSTRACT

Expansion of disposal facilities for a coal fired electric generating station in central Kentucky required construction of a 609.6 meter (2,000 feet) long, 12.2 meter (40 feet) high dike on hydraulically placed ash consisting primarily of fly ash. Construction of the dike on the loose, saturated ash foundation by conventional methods required either in-situ densification or removal and replacement of the ash. As an alternate, geosynthetic materials were designed to temporarily bridge the soft foundation; reduce construction pore pressures and speed consolidation; reinforce the embankment in the short-term; and reduce long-term seepage through the pervious foundation.

Because of the importance of the disposal facilities to plant operation, repercussions of a dike failure, and industry inexperience with reinforced embankments on saturated ash, an instrumented test embankment was constructed to (1) verify design assumptions, (2) evaluate and refine construction practices, and (3) monitor embankment, foundation and geosynthetic performance with time. Instrumentation within the embankment consisted of slope inclinometers and settlement transducers. Foundation instrumentation included slope inclinometers and pneumatic piezometers. In addition, reinforcing geosynthetic materials were monitored via strain gages.

This paper presents a case history study of design, construction, and performance monitoring of the test embankment. In addition, benefits of using the geosynthetic materials over conventional techniques will be discussed.

INTRODUCTION

Background. Kentucky Utilities Company (KU) owns and operates the E.W. Brown Generating Station in Burgin, Mercer County, Kentucky. A vicinity map indicating the location of the E. W Brown Station is presented in Figure 1. The station consists of three coal fired generating units and has a maximum output of 666,000 kilowatts. By products of coal fired electric power generating

include bottom ash, a coarse grained residue and fly ash, a fine grained material consisting of silt-sized rounded silica particles. The bottom and fly ash is disposed of by sluicing with water to an impoundment located on Curds Creek, a tributary to Herrington Lake.

The original 12.2 meter (40 feet) high impoundment was constructed approximately 30 years ago to a crest elevation of 243.8 meters (800 feet) (MSL). Between 1964 and 1973 the main embankment was raised to elevation 265.2 meters (870 feet) in two 10.7 meter (35 feet) increments. In 1989 KU decided to raise the embankment to elevation 274.3 meters (900 feet), the maximum elevation of the watershed. Due to existing topography, the presence of an access road, and railroad siding immediately north of the impoundment, a 12.2 meter (40 feet) dike around the northern perimeter was required. Figure 2 presents a general site layout and the configuration of the dike and main embankment.

Figure 1. Vicinity Map

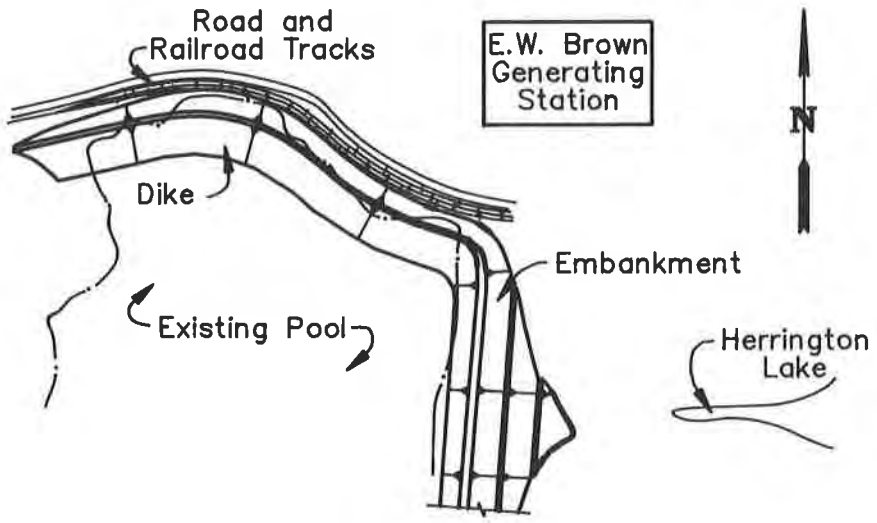

Figure 2. General Site Layout

Initial geotechnical exploration of the dike foundation soils revealed loose saturated fly ash deposits up to 6 meters (20 feet) thick underlain by approximately 1.5 meters (5 feet) of firm natural residual soil. In some areas the fly ash was covered with bottom ash. Based on observations of existing bottom ash deposits and conversations with plant personnel, between 1.5 and 3.7 meters (5 and 12 feet) of bottom ash was required to bridge over the saturated fly ash. Standard penetration testing and Shelby tube sampling of the fly ash during the initial exploration was largely unsuccessful due to the extremely loose and wet nature of the deposits. Subsequently, mechanical Dutch cone penetration tests were conducted to obtain additional information regarding thickness of fly ash and natural soils, and short term strength properties. Typical cone penetration test results are presented as Figure 3. Table 1 presents classification data for each of the three main foundation soils and Table 2 presents short and long term strength parameters used in design.

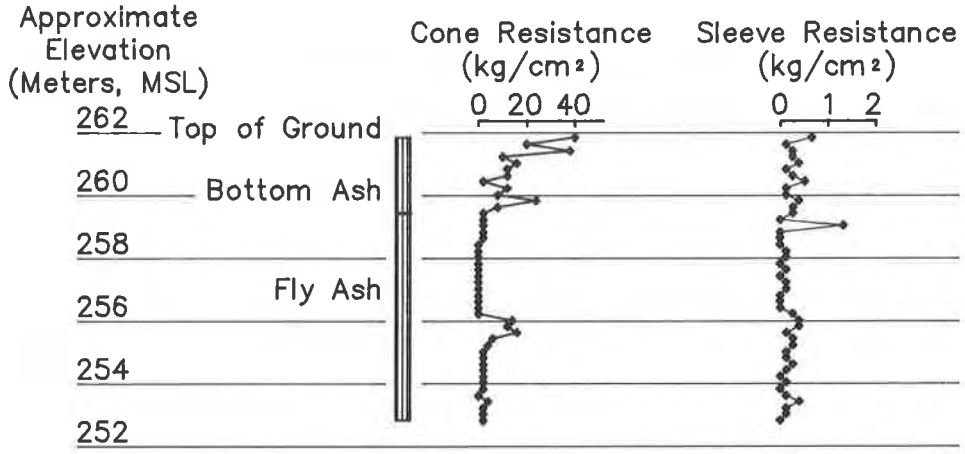

Figure 3. Typical Cone Penetration Test Data

Table 1. Engineering Classification Data

	Bottom Ash	Fly Ash	Natural Soil
% Gravel (-76mm to +No. 4)	35	4	3
% Sand (-No. 4 to +No. 200)	47	37	25
% Silt (-No. 200 to +.005mm)	14	46	28
% Clay (-.005mm)	4	13	44
Liquid Limit	NP	NP	53
Plastic Limit	NP	NP	22
Plasticity Index	NP	NP	31
Unified Classification	SM	ML	CH
AASHTO Classification	A-1-6(0)	A-4(0)	A-7-6(22)

Table 2. Design Strength Parameters

	Total Stress			Effective Stress		
	ϕ (degrees)	c kg/m^2*	γ kg/m^3**	ϕ' (degrees)	c' kg/m^2	γ kg/m^3
Embankment Soil	0	7320	1890	32	0	1890
Foundation Soil	0	5858	2003	32	0	2003
Working Platform	35	0	1842	35	0	1842
Fly Ash	10	0	1602	32	0	1602
Bottom Ash	32	0	1842	32	0	1842

* Tabulation based on kg/m^2. Multiply by 0.2048 to obtain lbf/ft^2.

** Tabulation based on kg/m^3. Multiply by 0.0624 to obtain lbf/ft^3.

Design Alternates. In addition to topographic and transportation constraints, the existing ash disposal facility had to remain in service during raising of the main embankment and construction of the new dike. Also, project construction had to be completed prior to November 1, 1990, resulting in a limited construction time. To accommodate these constraints and provide an environmentally safe long term facility, the design alternates listed below were considered.

- Excavate the saturated fly ash foundation and replace with compacted fill.
- Improve the foundation using stone columns.
- Chemically stabilize the foundation in-situ.
- Mechanically stabilize the foundation in-situ.
- Improve the foundation and mechanically stabilize the embankment using geosynthetic materials.

Each of the alternates was evaluated for construction feasibility, quality control, and cost. Excavating of the saturated fly ash and replacing with compacted fill provided good quality assurance, quality control and relatively low cost. However, excavating the saturated fly ash while maintaining pond operations was impractical. Stone column foundation improvement, while constructible and controllable was not cost effective. Chemical stabilization of the fly ash using lime injection and mixing in-situ was considered practical, however, quality assurance and quality control was questionable and this option had a relatively high cost. Mechanically stabilizing the fly ash by mixing with shot rock was also considered impractical from a quality assurance and quality control standpoint. The final selected alternate included improving the foundation using strip drains, mechanically stabilizing the embankment using geogrids and providing seepage control with a geomembrane. This alternate was (a) constructible, as demonstrated in the literature[1]; (b) assurable, since quality of materials could be documented through certifications and generally accepted test techniques; (c) controllable, since all construction operations were easily verified and

documented; and (d) cost effective, saving KU over one million dollars based on preliminary cost estimates. Table 3 presents a summary of the design alternate selection process and Figure 4 shows a typical section of the selected alternate.

Table 3. Design Alternate Summary

Alternate Number	Feasibility of Construction	Quality Assurance/ Quality Control	Preliminary Cost
1	Low	High	$ 4,800,000
2	High	High	$ 7,000,000
3	High	Low	$ 7,000,000
4	Low	Low	$ 5,000,000
5	High	High	$ 3,300,000

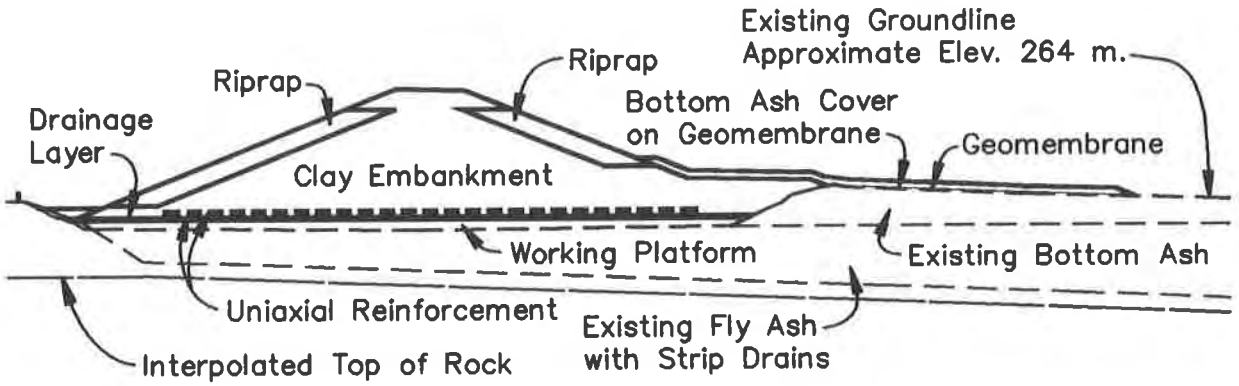

Figure 4. Typical Section

Because of the importance of the disposal facilities to plant operation, repercussions of a dike failure, and industry inexperience with reinforced embankments on saturated ash, an instrumented test embankment was designed, constructed and monitored to verify design assumptions, evaluate and refine construction practices, and monitor embankment, foundation and geosynthetic performance with time. Figure 5 shows a profile of the instrumented test embankment.

DESIGN

Four main portions of the embankment required evaluation and design; the working platform, foundation improvements, embankment reinforcing and seepage control. The design of each of the portions is discussed in subsequent paragraphs.

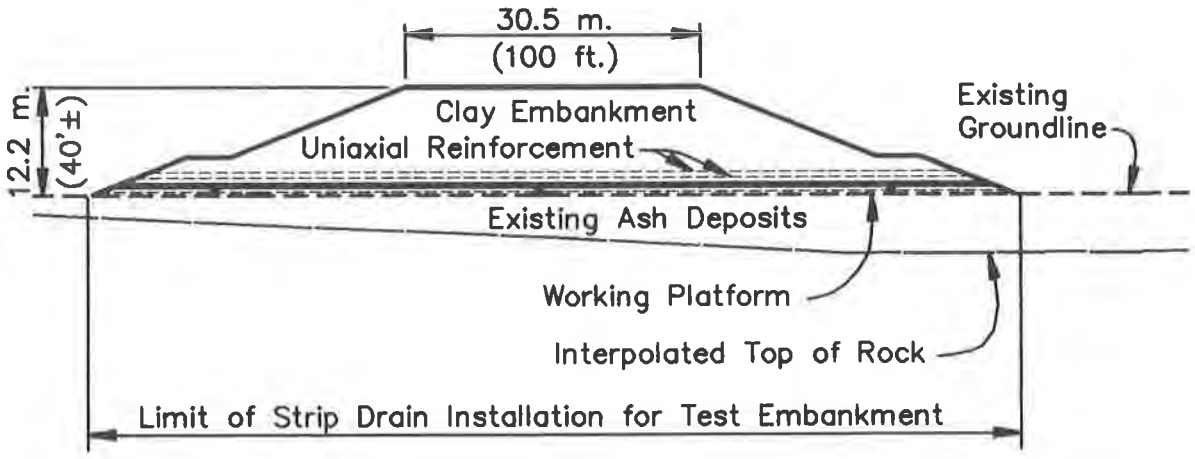

Figure 5. Profile - Instrumented Test Embankment

Working Platform. The geotechnical exploration, site observations, and site history revealed the fly ash deposits exhibited a thin crust due to desiccation that was underlain by saturated deposits which were very soft and thixotropic. KU reported that on at least two occasions small dozers broke through the crust and became trapped. A FMSM employee also broke through the crust while surveying and sank to his waist. Therefore, it was deemed necessary to design a working platform from which future construction operations could take place.

Geogrid manufacturers' experience indicates that typically a layer of biaxial geogrid overlain by 0.6 to 0.9 meters (2 to 3 feet) of free draining material, usually a well graded sand, provides a suitable platform for most earth moving and foundation improvement equipment. However, because the nearest acceptable sand source that could provide the quantity needed was near Cincinnati, Ohio; and considering the laboratory classification test results on bottom ash obtained as part of the geotechnical exploration, it was decided to incorporate bottom ash into the working platform in lieu of sand. The applicability of using bottom ash in the working platform was also verified in a small scale field trial. Based on geogrid manufacturer's experience, and the small scale field trial the working platform shown on Figure 6 was selected.

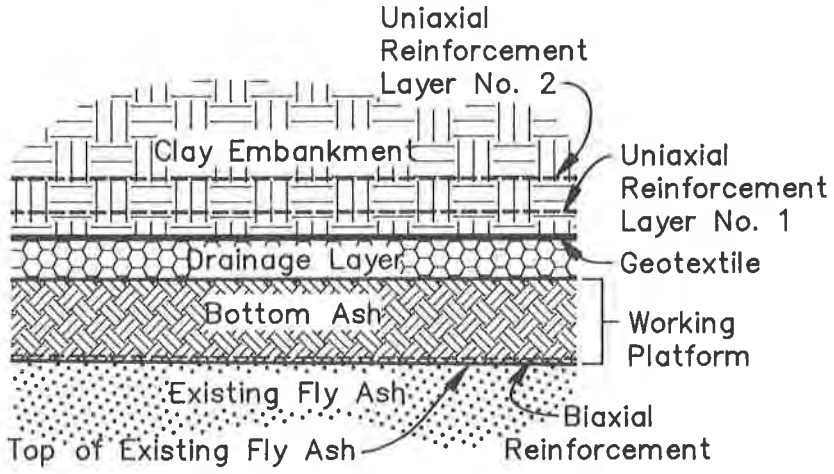

Figure 6. Typical Section of Working Platform and Embankment Reinforcement

Embankment Reinforcement and Foundation Improvement. The next element in the design process was configuration of an embankment which would remain stable during all operating and loading conditions. Initial stability analyses were conducted to evaluate short and long term embankment stability without embankment reinforcing or foundation improvement. The results of initial stability analyses indicated unacceptable short and long term factors of safety based on a desired factor of safety of 1.5. Therefore, embankment reinforcing consisting of uniaxial geogrids were added to reinforce the embankment. Strip drains were also designed to control excess pore pressures during construction, and increase the rate of consolidation.

Design of embankment reinforcement first required selection of an allowable geogrid stress (working stress). The working stress of a particular geogrid is dependent on its long term creep strength, allowable design strain, chemical and biological degradation of the geogrid over the design life of the structure and construction induced damage.[1] Because of the uniqueness of this application, and the importance of the structure, allowable strain was selected at five percent and a combined factor of safety against long term degradation and construction damage of 1.5 was chosen. This combination of allowable design strain and factor of safety against degradation and damage resulted in a reduction in ultimate geogrid strength of 60 percent.

Subsequent to selection of geogrid working stress a trial and error procedure was used to optimize the type, number, orientation and spacing of uniaxial geogrids. Circular and wedge slope stability analyses were conducted using the UTEXAS2[2] slope stability program. In addition to standard geometric and soil parameter input, the horizontal and vertical orientation of geogrid layers and the calculated working stress are entered. After determining the critical failure surface, the user must then verify that a sufficient length of geogrid extends beyond the failure surface to prevent pullout of the geogrid. Typical results of slope stability analyses showing the final geogrid configuration are presented in Figure 7.

Evaluating the strip drain performance required determination of consolidation properties of the fly ash, estimating the time of construction and selecting a time desired for primary consolidation to be completed. Laboratory consolidation testing of the fly ash and review of the literature indicated a coefficient of consolidation for sluiced fly ash of 929 square centimeters per day (1 ft^2/day)[3]. Because of time constraints and expected high rate of construction, the decision was made to require at least 90 percent consolidation by the end of construction. This high percentage of consolidation resulted in two benefits; (1) excess pore pressure within the fly ash would remain low, thereby increasing short term stability and (2) settlement would be essentially complete at the end of construction allowing for a shorter monitoring time, thereby decreasing the overall construction period.

Evaluation of different strip drain spacings was conducted using previously published and currently accepted methods.[4] Results of the analyses are presented as Figure 8 and show the effect of strip drains on 1.8 meter (6 feet) centers as compared to no strip drains. In addition to design of strip drain spacing, a drainage blanket was installed to provide a pathway for excess water flowing from the strip drains. The drainage blanket was designed to provide sufficient permeability to prevent pore pressure buildup in the blanket and to satisfy filter criteria based on the bottom ash working platform material.

Summary of Stability Anaylses		
Loading Condition	Circle	Factor of Safety
Short Term, Upstream, Piezometric Level at Existing Top of Ash	A	1.8
Short Term, Downstream, Piezometric Level at Existing Top of Ash	B	1.6
Long Term, Upstream, Piezometric Level at Existing Top of Ash (Deep Failure)	C	2.9
Long Term, Downstream, Piezometric Level and Fly Ash at Maximum Pool	D	1.5
Long Term, Upstream, Piezometric Level and Fly Ash at Existing Pool (Dynamic)(Shallow Failure)	E	1.4

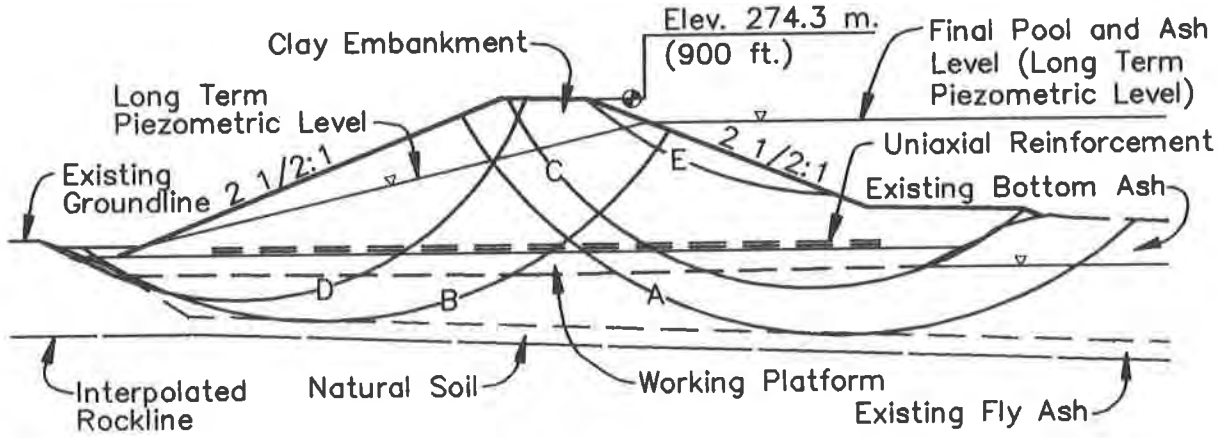

Figure 7. Final Slope Stability Analyses

Seepage Control. During construction of the test embankment, and the remainder of the dike and dam, the existing impoundment surface elevation was controlled, and remained near Elevation 262.1 meters (860 feet) (MSL). Therefore, control of seepage through the foundation during construction and monitoring of the test embankment was not required. However, the control of seepage through these media is extremely important for the long term integrity of the dike, therefore the methods designed to control seepage will be briefly discussed.

Several methods are available to provide seepage control through pervious foundations including slurry and sheet pile cut off walls, deep cut off trenches and upstream impervious blankets. Slurry walls and sheet pile cutoff walls were relatively expensive at this site when compared to other alternatives. Construction of a deep cutoff trench was impractical due to the nature of foundation soils and using a clay "impervious" blanket was impractical due to borrow quantity limitations, and constructibility. Therefore, it was decided to place a 40 mil HDPE geomembrane to a distance of 30.5 meters (100 feet) upstream of the dike to provide an "impervious" blanket. Flow nets were then constructed and analyzed to verify that a 30.5 meter (100 feet) impervious blanket was appropriate.

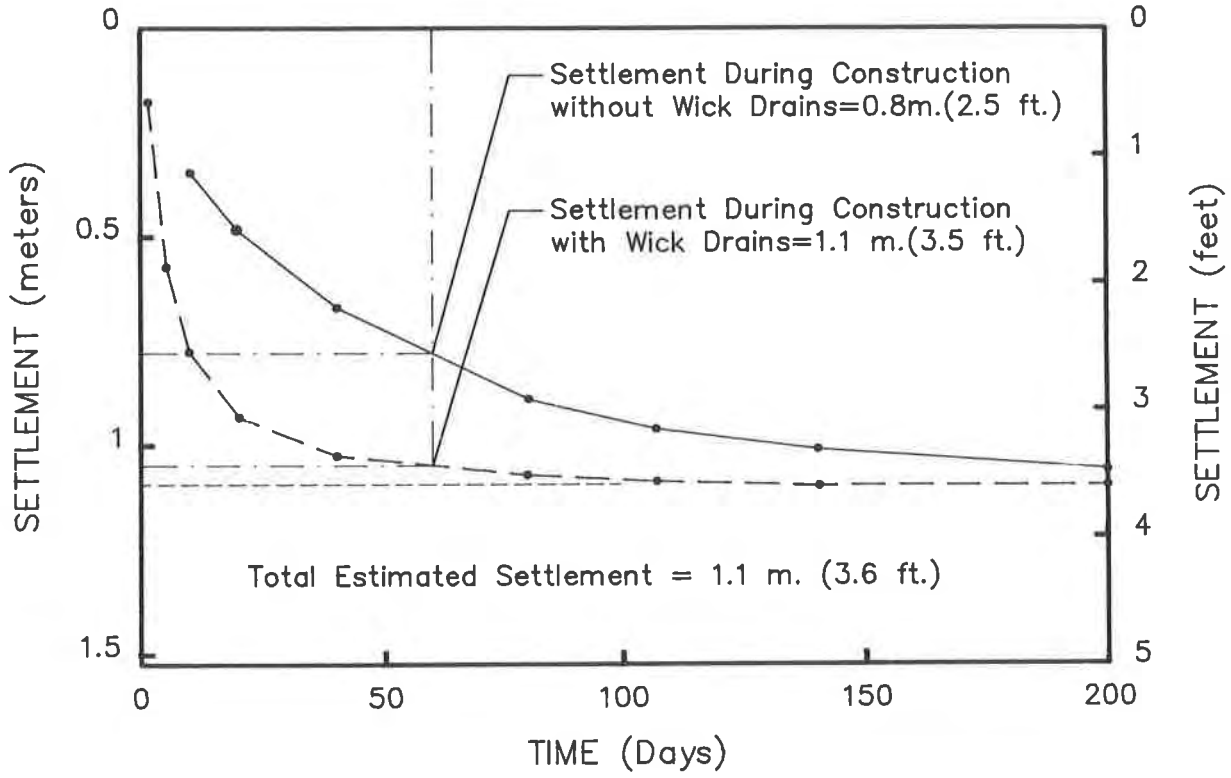

Figure 8. Calculated Time Rate of Settlement

CONSTRUCTION

Construction Sequence. Test embankment construction began November 13, 1989, and was completed January 11, 1990. A summary of construction activities and dates is presented as Figure 8. Initial work consisted of removing cattails from the area and diverting plant discharge lines away from the test embankment area. Biaxial geogrid was then placed in strips perpendicular to the test dike centerline directly over the cattail stubble allowing personnel to walk freely over covered areas. As the geogrid was placed, a Caterpillar D3C dozer pushed bottom ash across the geogrid parallel with individual strips to form the working platform. Because the bottom ash material proved to contain more fine-grained particles than samples tested during design, an additional layer of geotextile was added between the working platform and the crushed stone drainage layer. Initial crushed stone placement was accomplished by pushing the stone over the top of the working platform from the sides using the Caterpillar D3C dozer. This was very successful and allowed loaded 32,000 kilogram (35-ton) dump trucks to travel across the top of the crushed stone. After the crushed stone portion of the embankment was completed, strip drains were installed through the drainage layer, working platform and hydraulically placed ash to mandril refusal. In addition, pneumatic piezometers and settlement transducers were installed between the strip drains. Installation of strip drains through the one-foot thick crushed stone layer allowed this layer to act as a drainage medium relieving excess pore pressure buildup in the foundation and speeding consolidation.

Table 4. Summary of Construction Dates

Construction Activity	Time Period
Biaxial Geogrid	Nov. 13, 1989 - Nov. 17, 1989
Bottom Ash	Nov. 17, 1989 - Nov. 20, 1989
Drainage Layer	Nov. 20, 1989 - Nov. 21, 1989
Wick Drains	Nov. 27, 1989 - Dec. 1, 1989
Embankment	Dec. 1, 1989 - Jan. 11, 1990

After this foundation treatment system was in place, construction of the dike began. Since the crushed stone material beneath the clay embankment material did not meet design filter requirements, a layer of geotextile meeting design filter requirements was placed between these two materials. Next, a 15 centimeters (6-inches) layer of clay material was placed over the geotextile by placing approximately 25 centimeters (10 inches) of clay and scraping the excess off using a grader. At this point, one layer of uniaxial geogrid was placed followed by 30 centimeters (12 inches) of clay and then another layer of uniaxial geogrid. One strip on each layer of geogrid was instrumented with strain gauges. Installation of the last geogrid layer was completed December 14, 1989. Due to extremely bad weather conditions, work essentially ceased until January 5, 1990. The remaining clay portion of the test embankment was completed January 11, 1990.

Construction Difficulties. Three primary construction difficulties had to be conquered as the test embankment was constructed. The first and most serious was the bottom ash material that was used for constructing the working platform. This material contained higher than expected fine-grained (fly ash) particles that did not allow pore pressures to dissipate as the working platform was constructed. Because this material was not free draining as assumed during design, boils of fly ash developed on the surface of the working platform. These boils were created by excess pore pressures that developed as the dozer pushed layers of bottom ash across to the far sides of the working platform. The more the dozer traversed the site, the more pronounced surface deflection became until finally, a boil would occur allowing the excessive pore pressures to dissipate. Generally, after a few days with no dozer traffic the working platform stabilized and no additional boils occurred.

A second minor problem was installation of the strip drains. Due to concerns of equipment weights in the initial phase of construction, the contractor selected a moderately sized strip drain mandril that could not adequately push through the geotextile. The equipment was replaced with a larger wick installation system that could adequately install the wicks with no adverse deflection of the working platform. Subsequently, installation of the strip drains was completed without difficulty.

The third construction difficulty was Mother Nature. Almost from the beginning, the contractor suffered from sub-freezing weather conditions coupled with snow and rain. This made it impossible to meet the moisture requirement for the clay portion of the embankment.

Subsequently, the moisture requirement for construction of the test embankment was waived. The contractor removed and replaced the clay soil the following summer during the construction of the main dike embankment.

PERFORMANCE

Working Platform. Monitoring of working platform performance during construction was accomplished by visually observing the construction procedures and effects on the surface of the working platform. As presented previously, some difficulties were encountered during construction due to the unexpected presence of fine-grained material in the bottom ash. The fines prevented excess pore pressure from dissipating, causing boils at several locations. Figure 9 presents a photograph of a typical boil encountered. After dissipation of the initial excess pore pressure, further boils were not encountered and the working platform performed beyond expectations.

Reinforcement. The performance of uniaxial reinforcement was monitored directly by strain gages mounted on two individual grids, one on the bottom layer, and one on the top layer. A total of 26 strain gage pairs were mounted on the two geogrids, 13 on each grid. Eleven of these gages were destroyed during installation and/or fill compaction, leaving 15 gages available for monitoring of grid performance. Figures 10 and 11 present long term performance data for several of the reinforcing geogrids. As expected, the strain in the geogrids increased during construction, then remained relatively constant after construction.

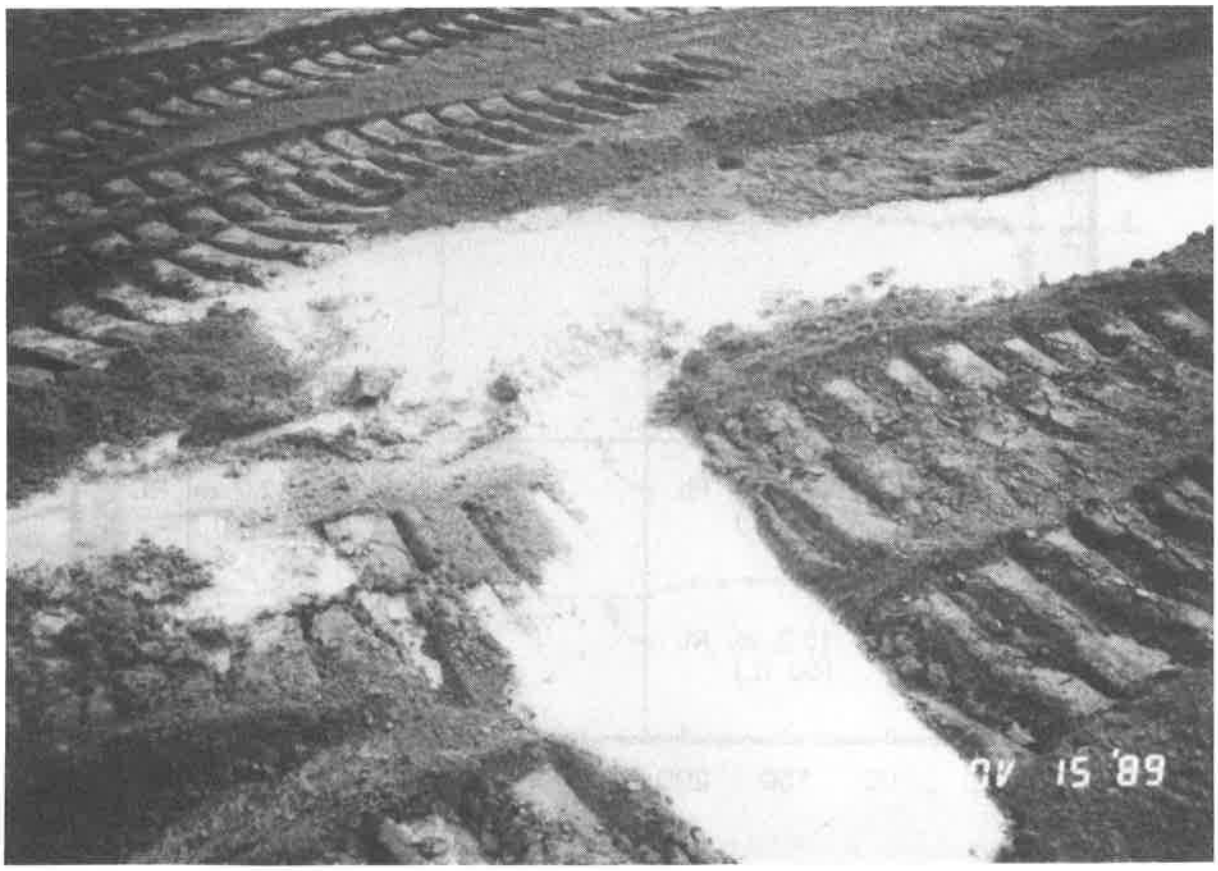

Figure 9. Typical Fly Ash Boil

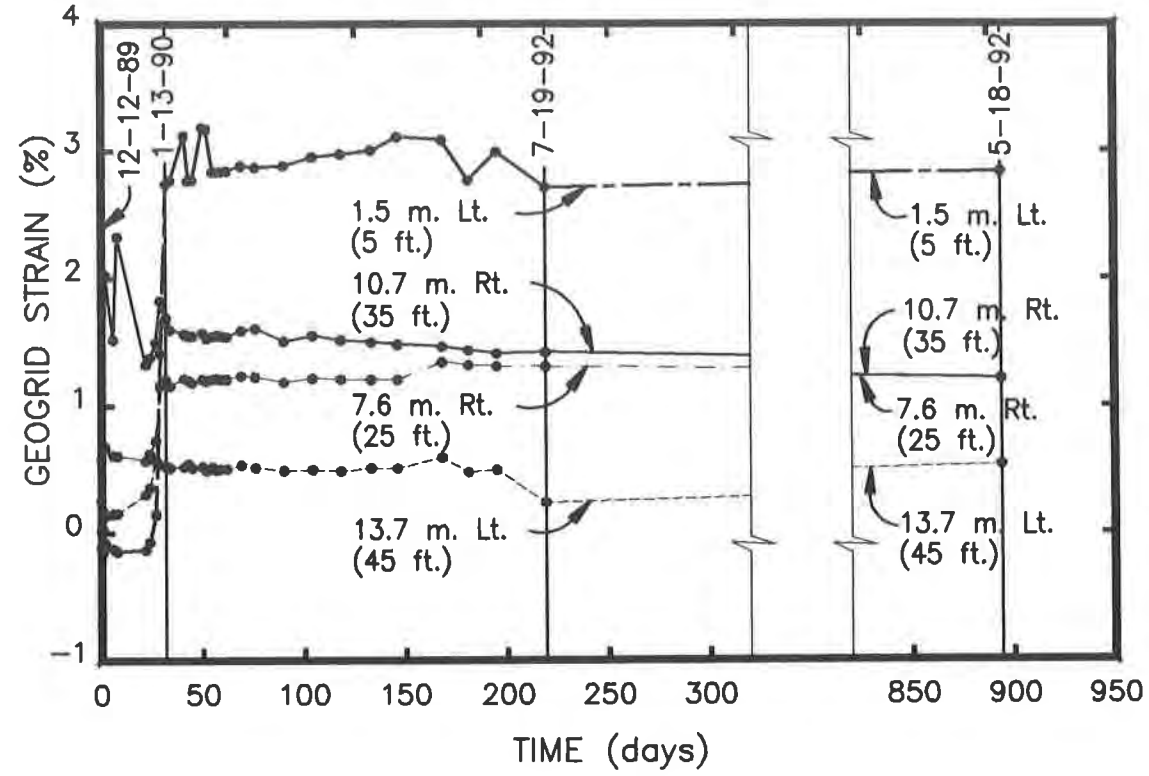

Figure 10. Geogrid Strain - Reinforcement Layer No. 1

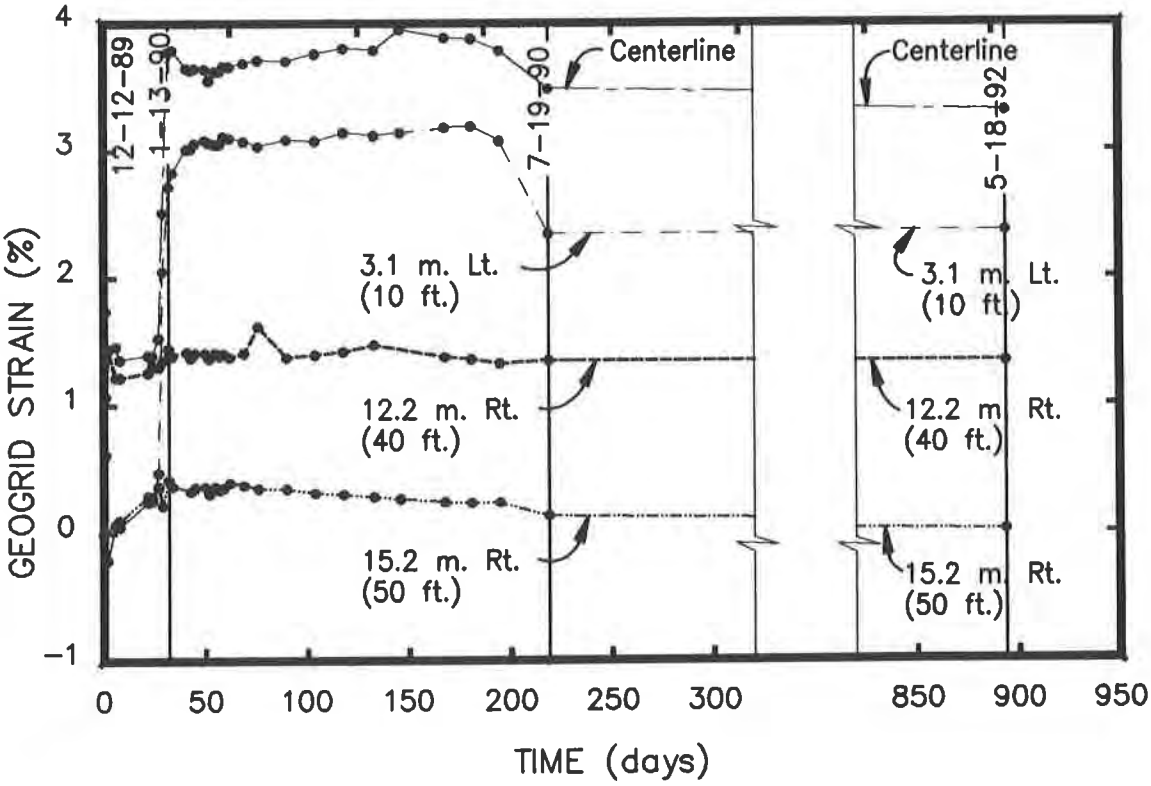

Figure 11. Geogrid Strain - Reinforcement Layer No. 2

In addition to direct monitoring of strain gage performance, slope inclinometers were installed to measure embankment and foundation lateral movement, providing an indirect measurement of geogrid performance. Five inclinometers were installed along the cross-section and centerline of the test embankment, and were monitored during and after construction. All but one of the inclinometer casings remained in service until late May, 1990. Typical results of inclinometer monitoring are presented in Figure 12. The relatively large deflections indicated at the top of the casing are attributed to the effects of construction equipment. This plot indicates lateral displacement of the working platform occurring during a five day period of maximum construction rate. After the embankment was completed (January 12, 1990), virtually no lateral displacement was indicated. It is hypothesized that this lateral displacement is due to the required strain to mobilize the strength of the working platform. This hypothesis is derived from the relatively little compactive effort exerted on the working platform, and the lack of continued lateral displacement after construction was completed. Finite element analysis would have to be undertaken to verify this hypothesis.

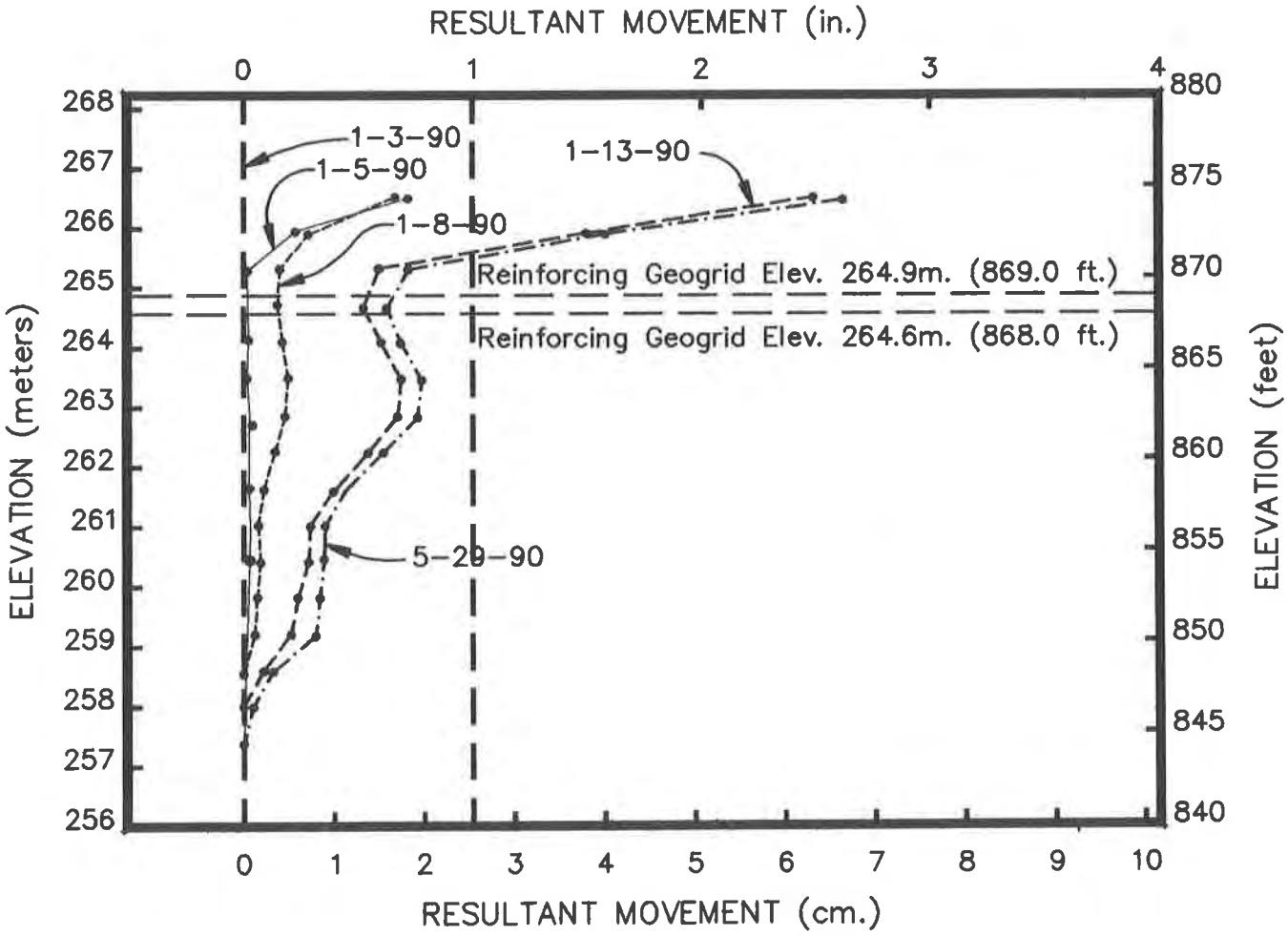

Figure 12. Typical Slope Inclinometer Results

Foundation Improvements. Strip drain foundation improvement performance was monitored by measuring foundation pore pressure and settlement during and after construction. Fourteen pneumatic piezometers and five pneumatic settlement transducers were installed to measure pore pressure and settlement, respectively. Results of long term pore pressure measurements versus time for several of the installed piezometers are presented in Figure 13. As expected, these plots indicate relatively minor excess pore pressure development during construction, then a gradual decline. Also as would be expected, greater excess pore pressures were found near the center of the embankment.

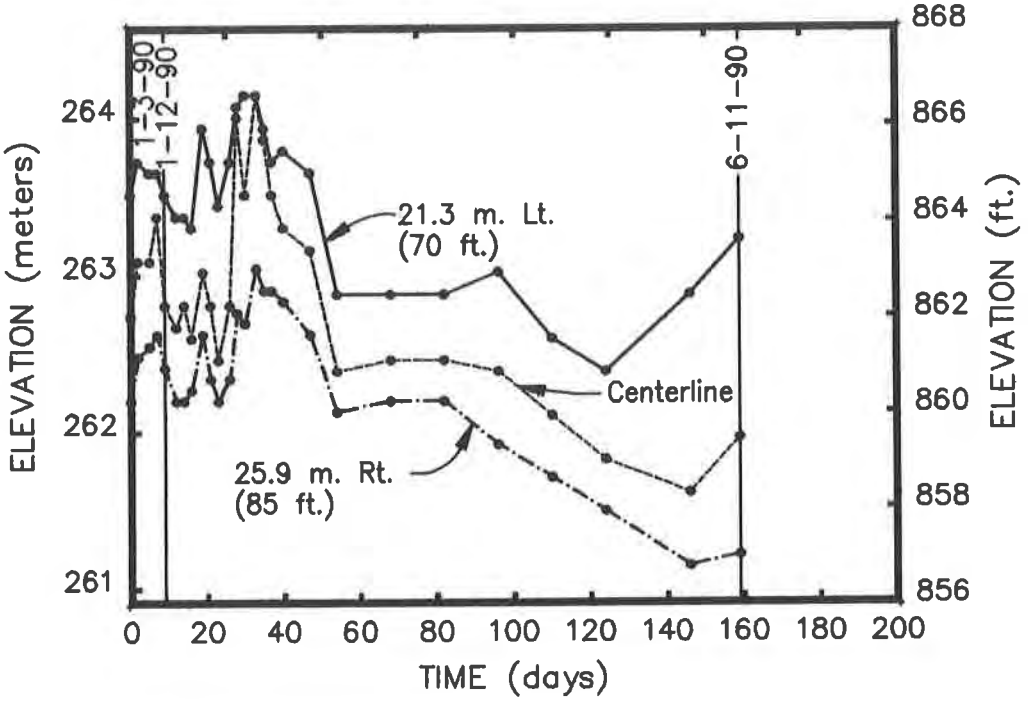

Figure 13. Typical Pore Pressure Response

Typical results of settlement transducers monitoring are included as Figure 14. The data is very erratic and it is difficult to draw any conclusions.

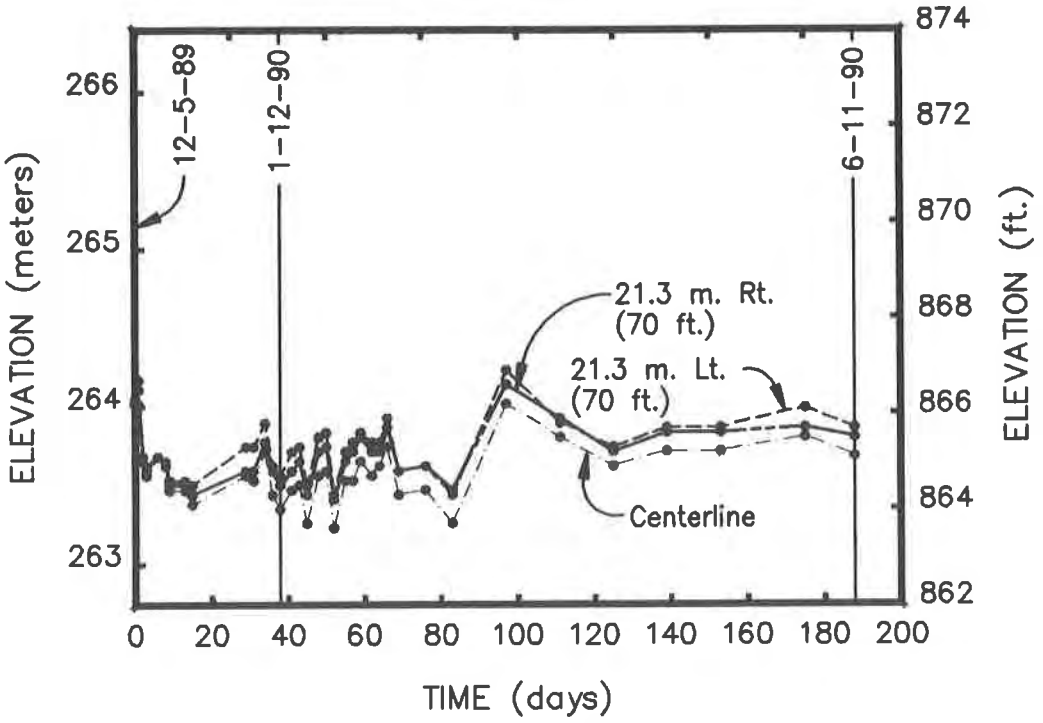

Figure 14. Typical Settlement Transducer Results

SUMMARY

This paper has presented a case history of the design, construction and performance of an embankment on sluiced fly ash. The design included constructing a working platform to temporarily bridge soft foundation soils, installing strip drains to speed consolidation and control excess pore pressure, reinforcing the embankment with geogrids and controlling seepage using a geomembrane. Construction proceeded relatively smoothly with only minor problems encountered due to unexpected fine grained material in the working platform. All phases of the design performed as expected. After several months of monitoring the test embankment, the remaining portion of the dike was constructed with little difficulties . The new ash pond is currently in service and performing well. The method of foundation improvement and mechanical stabilization for this project permitted a compressed construction schedule and saved the owner over one million dollars.

Successful completion of the ash pond modification at KU's E. W. Brown Generating Station has illustrated the following:

- Geosynthetic materials can safely and effectively be used to bridge over and construct upon hydraulically placed fly ash.

- Significant cost savings can be realized by use of by-products by using bottom ash in-lieu of sand. Although some construction difficulties were encountered, the effective use of strip drains eliminated long term construction and performance problems.

- Using geosynthetic materials and good engineering practice, the electric utility industry, and potentially many other industries, can vertically expand, or construct new facilities, on top of existing ash ponds. Expanding existing facilities can lead to significant cost savings, and reduce potential permitting difficulties and public opposition.

ACKNOWLEDGEMENTS

The writers gratefully acknowledge the engineering staff and management of KU for being cooperative, flexible and innovative. Tensar provided engineering assistance on geogrid design. Bizzack Construction Company successfully constructed this complex project in a tight construction schedule. Finally, we are appreciative of the FMSM staff who worked many hours including a lot of overtime to deliver a quality design project.

FMSM and KU received a National Honor Award from the American Consulting Engineers Council for the innovative design of the dike.

REFERENCES

1. Seawell H., Mattox, R.M. "An Economical Solution to Increasing the Capacity of an Industrial Waste Facility with a Geogrid Reinforced Dike," Proceedings of Geosynthetic '87, New Orleans, February 1987a pp 341 - 352.

2. Bonaparte, R. and Berg, R.R. "Long-Term Allowable Tensile Load for Geosynthetic Reinforcement," Proceedings of Geosynthetic '87, New Orleans, February, 1987a, pp 181-192.

3. Edris, E.V., Jr., and Wright, S.G., "Users Guide: UTEXAS2 Slope - Stability Package" Department of the Army, August, 1987, p. 171.

4. Hansbo S., "Consolidation of Fine-Grained Soils by Prefabricated Drains", Proceedings Tenth International Conference on Soil Mechanics and Foundation Engineering, Vol. 3 1981, Paper 12/22.

Geosynthetics Interface Friction: A Challenge for Generic Design and Specification

R.F. Lopes
Golder Associates Ltd., Canada

P.A. Smolkin
Golder Associates Ltd., Canada

P.J. Lefebvre
Regional Municipality of Ottawa - Carleton, Canada

ABSTRACT

This paper presents a case history of design, specification and performance of geosynthetic barrier systems from an interface friction perspective. The experiences reported involve various stages of design and construction of final capping and bottom liner systems for a municipal landfill near Ottawa, Ontario, over the period of 1987 to 1991.

The paper focuses on the difficulty of developing "generic" specifications for geosynthetics, while satisfying interface friction requirements of the design and requirements for competitive tenders for the supply of the materials. The adopted approach began with an assessment of the critical interfaces and the interface friction requirements of an initial design configuration. A final design and specification-basis testing program was then undertaken by the designer. The final design was confirmed on the basis of the results obtained and, where appropriate, minimum required interface friction and compliance laboratory testing were specified as part of the construction contractor's responsibilities. In addition, in some cases field scale testing was performed to further evaluate the stability of the constructed works. This generic design and specification approach allowed the owner to select the most economical system, while satisfying slope stability and other design concerns.

INTRODUCTION

The "design by function" principle for civil engineering application of geosynthetics (Koerner, 1990) has received broad acceptance and is followed by many design professionals. However, there is still a widespread practice of specifying geosynthetic products by brand name or past experience.

Consideration of the interests of all stakeholders in the geosynthetics industry, ranging from material manufacturers, through design practitioners and project owners, leads to the conclusion that specifying geosynthetics by brand-name or on the basis of past "similar" projects is inappropriate (Giroud, 1991).

The generic specification approach (ie. specifying properties rather than brand-name products) is not, however, the easiest route for the design professional to take, in light of the complexity of some of the design issues involved, particularly where a very broad range of test results can be obtained within the same class of product. This problem is particularly acute when specifying interface friction properties of geosynthetic products. The designer is then faced with the challenge of having to prepare a safe and economic design using frictional parameters which can be expected to be achievable by a sufficient number of products on the market, in order to allow for competitive bids for the supply of materials for the project. However, time and economic constraints seldom afford the luxury of performing beforehand a comprehensive interface friction testing program using all the available brand name products which meet the other design requirements. An example of this challenge and the specific solutions adopted are described in this paper, which is based on the Trail Road Landfill project, near Ottawa, Ontario (Figure 1).

Figure 1. Location Plan

OVERVIEW OF INTERFACE FRICTION ISSUE

General The issue of interface friction between geosynthetic components and along soil to geosynthetic contacts is a focus of major interest, research and testing. Published values of interface friction are available from numerous sources, however because these values are based on a wide variety of materials, test conditions, and test methods, they cannot and should not be used for design of a specific project, without at least careful critical review. Use of such published data in design is generally considered to be inappropriate (Giroud, 1991), because either they are potentially over conservative and lead to uneconomical designs or they unnecessarily introduce a potential risk of unacceptable performance/failure of the system. Published data demonstrate clearly that a significantly wide range of interface friction values can be obtained, even in controlled interlaboratory test programs.

Factors Affecting Interface Friction Selection of a representative design value for the interface friction between various geosynthetics requires the performance of representative tests. Currently there is no official/accepted test method for interface friction between geosynthetics. Various authors have addressed the issue of influence of test apparatus and methods on the measured values. Lydick and Zagorski (1991) listed the factors affecting geomembrane/geonet interface results, which include the following:

- **Profile** (Testing one interface at a time or testing the full set of interfaces at once);
- **Type of Geosynthetic** (Polymer type, Thickness, Surface Texture, etc.);
- **Testing Device** (Tilt Table or Direct Shear Box);
- **Geosynthetic Attachment** (Fixed, Partially Fixed and Free);
- **Normal Load** (Low for cap applications; high for bottom liner applications);
- **Condition of Sample** (Clean, Scratched, Folded, etc.);
- **Strain Rate** (Generally 5 mm/min. or less);
- **Moisture Condition** (Wet or dry interfaces); and
- **Preloading** (Relevant for cap applications; irrelevant for bottom liner applications).

The above factors can contribute to variations in interface friction test results not only between generically-specified products (ie. when only required properties are listed) but also between brand-name-specified products (ie. Gundline 80 mil HD, interfacing with Gundnet XL-14). Some of these factors are mentioned below, however for more detailed discussions the reader should refer to Lydick and Zagorski (1991).

Variety of Products and Interfaces Published data (Geotechnical Fabrics Report, 1991) shows that in 1992 geosynthetics supply in North America was classified into five (5) product categories, totalling well over fifteen hundred (1500) individual brand-name products, supplied by approximately 30 manufacturers.

Typically, the design-by-function approach and consideration of all design requirements except for interface friction, would narrow the choice of each individual geosynthetic component of a design to:

- 3 to 7 manufacturers of the required geomembrane
- 3 to 15 manufacturers of the required geotextile
- 2 to 7 manufacturers of the required drainage media (geonet or geodrain)

A project-specific design-basis interface shear testing program should therefore consider the appropriate normal stress and geosynthetic/soil profile as well as a minimum combination of the above candidate products. The number of tests to be performed would be a function of the degree of confidence required in the interface friction properties of the geosynthetic/soil profile. For example, where stability analyses of the critical slope configuration show that the required interface friction is well below the expected range of values from a careful review of available information, the number of design-basis tests can be significantly reduced, whereas if the expected range of values straddles the required interface friction value a more comprehensive testing program (or a design change) would be warranted.

In this context, it is generally recognized that there are three typical problem interfaces in landfill design and construction:

- Geomembrane/geonet interfaces in capping side slopes.
- Geomembrane/geotextile interfaces in bottom liner systems.
- Geomembrane/compacted clay liner interfaces in composite bottom liner systems.

Laboratory Results Versus Field Performance There is generally a lack of published information relating performance predictions based on laboratory test results and actual performance of completed facilities. Information of particular value would be that obtained from controlled field-scale tests carried out to failure. Laboratory-scale testing does not properly account for the effect of field-scale profile irregularity (depressions, bumps, patches, seams, etc.) of the geosynthetics/soil interfaces.

Waste Age (1991) reported the results of full scale tests involving geomembrane/geonet interfaces on 3 horizontal:1 vertical slopes. Artificial rainfall (equivalent to a storm having a 100 year return period for the site) was induced to evaluate the interface friction performance of two alternate geomembrane products (textured and smooth faced) with a geonet drainage medium. Neither full scale test section failed, and the minimum interface friction value of the interfaces from back-analysis was not reported. However, this experience suggests a field interface friction angle at the upper bound of the range of published geomembrane/geonet laboratory test results (ie. >18 degrees).

Paŕuvakat et.al.(1990) reported the results of large scale (3.65 m x 1.52 m x 0.91 m) tilting table tests that also suggest better interface frictional performance of geomembrane/sand interfaces at large scale, than at the scale of conventional laboratory shear box testing (ie. typically 0.30 m x 0.30 m box size).

Geomembrane/clay interface friction is a particularly difficult topic, and the subject of ongoing research by various investigators (eg. Seed and Boulanger, 1991). The Kettleman Hills Landfill failure (Mitchell et.al. 1990) is a good example of the "problem interfaces" (geomembrane/geonet, geomembrane/clay, and geomembrane/ geotextile) in landfill design. It is also a good illustration of the need for controlled field-scale tests carried out to failure. The back analysis of an uncontrolled unanticipated failure is significantly more complex and subject to interpretation.

While controlled field scale testing is the ideal approach, the authors' recognize that in the majority of projects the design and specification decisions will continue to be based on laboratory test results, tempered with the judgement/experience of the designer.

TRAIL ROAD LANDFILL PROJECT: GENERAL DESCRIPTION

The Trail Road landfill, owned and operated by the Regional Municipality of Ottawa-Carleton, is contained within a total land area of about 205 hectares (507 acres). The licensed landfill area occupies some 70 hectares (175 acres) which, between 1980 and 2000, is currently licensed to accept a total of some 8.8 million cubic metres (11.5 million cubic yards) of solid non-hazardous waste and domestic sewage sludge (J.L. Richards & Associates Limited, 1985 and 1990). Development of the landfill is in four stages as shown on Figure 2, each of which is designed to contain waste to a height of some 20 metres (66 feet). Disposal in Stage 1 took place between 1980 and 1986 and in Stage 2 from 1986 to 1991; landfilling operations are presently in Stage 3.

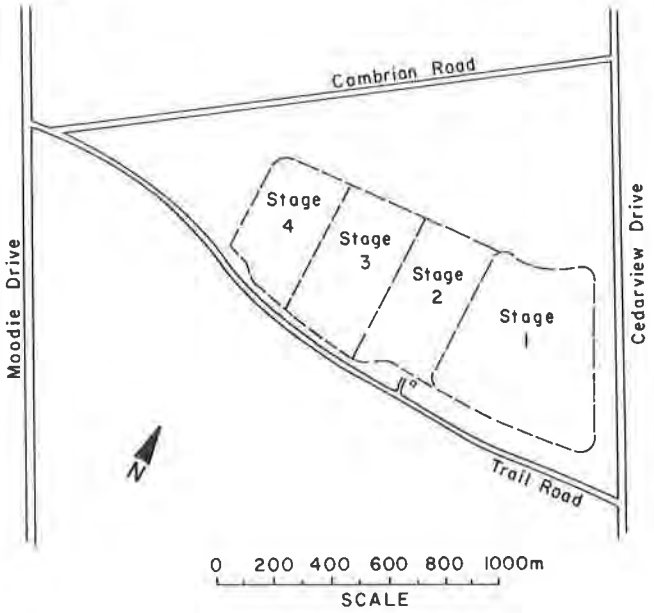

Figure 2. Trail Road Landfill

The landfill site was initially designed to function as a natural attenuation facility; that is one in which natural attenuation (dilution and chemical adsorption) within the hydrogeologic setting would primarily be responsible for reducing the impact from the landfill on groundwater quality to acceptable levels at the site property boundaries. The acceptable levels are defined by the Ontario Ministry of Environment's Reasonable Use Policy (MOE, 1986).

In order to meet these groundwater quality objectives, hydrogeological analyses indicated that the long term infiltration through the final cover on the landfill cells would have to be limited to 100 millimetres (4 inches) or less. To achieve this design objective a final closure cover system which incorporates a geomembrane as the hydraulic barrier component was selected. Stages 1 and 2 were developed without an engineered bottom liner system, and with a geomembrane final closure cap.

In 1989/90 various alternatives for development of the Stage 3 and 4 cells were assessed in terms of operations, long term leachate management and implementation of contingency plans. From this assessment, it was decided to construct an engineered low permeability bottom liner and leachate collection system prior to placement of waste in Stages 3 and 4, and to utilize geomembrane cover systems as described above for their closure.

From 1986 to 1991, the various construction stages have incorporated some 550,000 m^2 (6 million $ft.^2$) of geomembrane; 675,000 m^2 (7.3 million $ft.^2$) of non-woven geotextiles, and; 115,000 m^2 (1.2 million $ft.^2$) of geonet drain. This landfill is the largest user of geomembrane hydraulic barrier systems in Canada.

The Regional Municipality of Ottawa-Carleton has required from the outset that all geosynthetics for the project be specified on a generic (non brand-name) basis.

STAGE 1 COVER (1987 - 1988)

General Concept and Critical Interfaces The closure cover design concept developed in 1987 for the Stage 1 Capping Program consisted of a single geomembrane barrier system, with appropriate drainage systems to achieve the objective of minimum hydraulic head acting on the geomembrane. The initial design concept also included the use of a fine pea-gravel layer as drainage medium on 80 mil HDPE smooth geomembrane on the landfill side slopes (Figure 3).

Stability analyses performed on the critical slope configuration established a minimum required interface friction angle of 19 degrees between the geosynthetics/soil interfaces shown on Figure 3. Based on a critical review of published interface friction values available in 1987 (Martin, et.al, 1984) (Williams et.al., 1987) it was concluded that the geomembrane/pea gravel interface would be the critical interface.

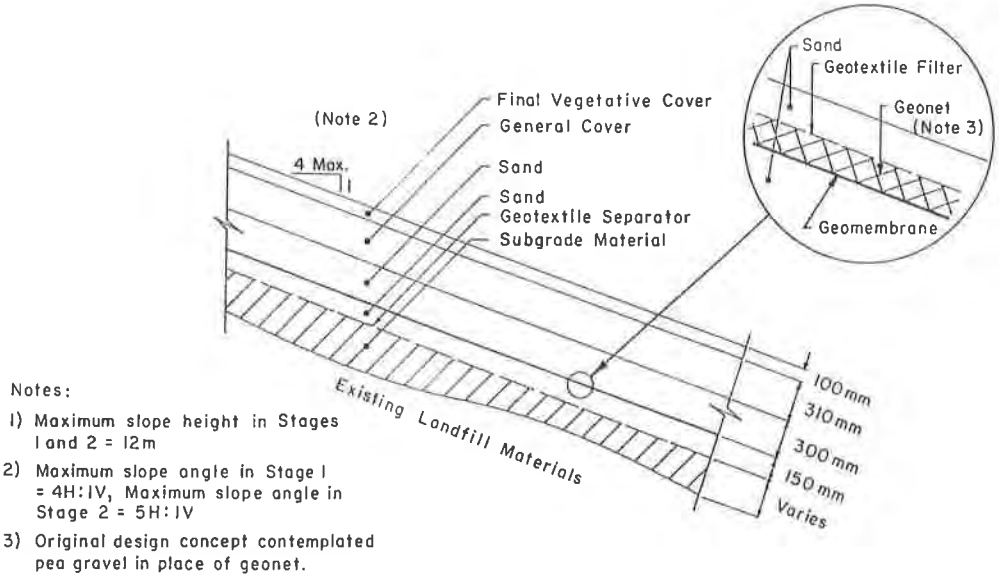

Figure 3. Stages 1 & 2 - Side Slope Cover Schematic

Interface Friction Specification The available information on a geomembrane/gravel interface was limited at the time, however published test results for geomembrane/soil indicated interface friction angles of greater than 19 degrees, which provided a good degree of confidence in the design. Due to time constraints tenders were issued without the benefit of project specific testing to verify the design; in addition it was generally not the practice at the time (1988) to specify interface friction properties of geosynthetics.

The successful tenderer proposed an alternate drainage design for the slopes (Figure 3) which entailed the use of Tensar NS-1400 geonet on 40 mil HD Gundline smooth geomembrane. Given the paucity of published data on geomembrane/geonet interfaces at the time, the design team retained the Geosynthetics Research Institute (GRI) to conduct a specification-basis testing program.

The specification basis testing program was performed on a 450 mm x 450 mm shear box at a strain rate of 4 mm per minute. Ten tests were performed on separate samples at

a normal stress of 15 kPa, after one hour of pre-loading at 60 kPa. All geosynthetics were free to move and failure (sliding) occurred at the geomembrane/geonet interface in all cases. The friction angle results obtained were in the range of 17 to 20 degrees, as graphically summarized on Figure 4 below.

On the basis of these test results a minimum interface friction angle of 19 degrees was specified for the proposed geomembrane-geonet materials, as condition of acceptance of the contractor's alternative.

In addition, recognizing the possibility of product quality fluctuations and in view of a general lack of experience with this combination of materials, a compliance testing program was specified which obliged the Contractor to provide a similar set of test results on random samples of the materials delivered to the project.

Compliance Laboratory Test Results The Contractor's compliance testing was performed by Geosyntec Inc. using test method ASTM 3080 and ASTM Draft Standard Test Method D35.01.87.07 modified such that the assembled test samples were preloaded at 60 kPa for one hour, then unloaded and sheared at a rate of 5 mm per minute at a single normal stress of either 15 or 23 kPa. The shear box size was 305 mm x 305 mm and all geosynthetics were free to move, as in the GRI Testing program. Ten tests were performed, with the failure occurring again at the geomembrane/geonet interface. The friction angle results obtained were in the range of 19 to 22.6 degrees, as summarized also on Figure 4 below.

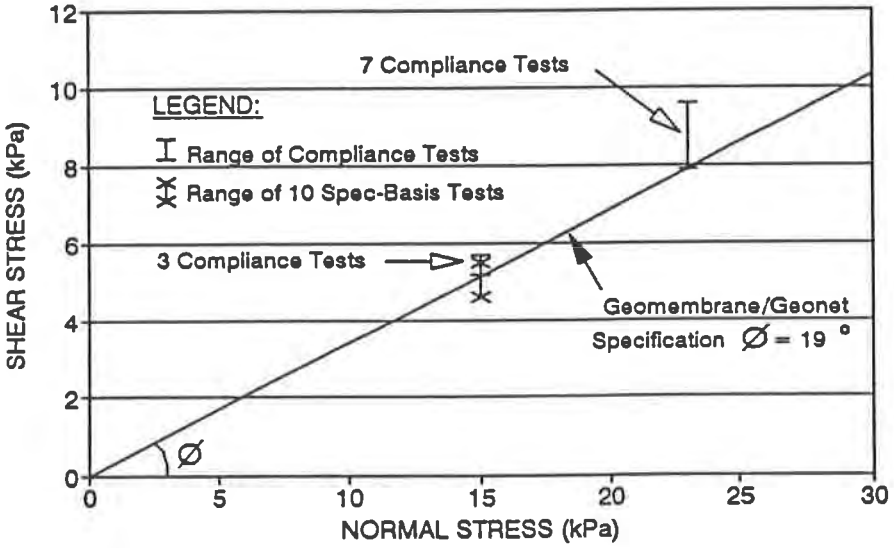

Figure 4. Summary of Laboratory Test Results - Stage 1 Cover

Field Scale Testing In order to provide additional supporting evidence for acceptability of the frictional resistance along the geonet/geomembrane interface, the Contractor was required to construct a 30 metre (100 ft wide) by 20 metre (60 foot) long test section of the complete cover cross-section on the 4H:1V side slope. Both the up slope and down slope ends of the section were left uncovered to avoid restraining any potential movements. A grid of monitoring stakes was established and monitored for movement over a two week period, during which three natural rainfall events occurred and a 25 year return period storm event was simulated by artificial methods. No significant observable movement of the test cover cross-section occurred during the monitoring period. Although the test section was not loaded to failure to determine the actual effective interface friction angle and factor of safety, it did provide an additional degree of confidence in the expected stability at a time when laboratory test methods and test results were much debated.

STAGE 3A BOTTOM LINER (1989 - 1990)

General Concept and Critical Interfaces The bottom liner concept developed for Stage 3A is a single composite liner, consisting of 0.6 metres (2 feet) of compacted silty clay soil with a design permeability objective of 1 x 10^{-7} cm/sec. overlain by an 80 mil HDPE geomembrane. On the bottom portion of the liner system the geomembrane is overlain by a thick non-woven geotextile as a protection layer for the overlying 0.65 metres (26 inches) of 19 millimetre (3/4 inch) angular clear crushed stone drainage blanket.

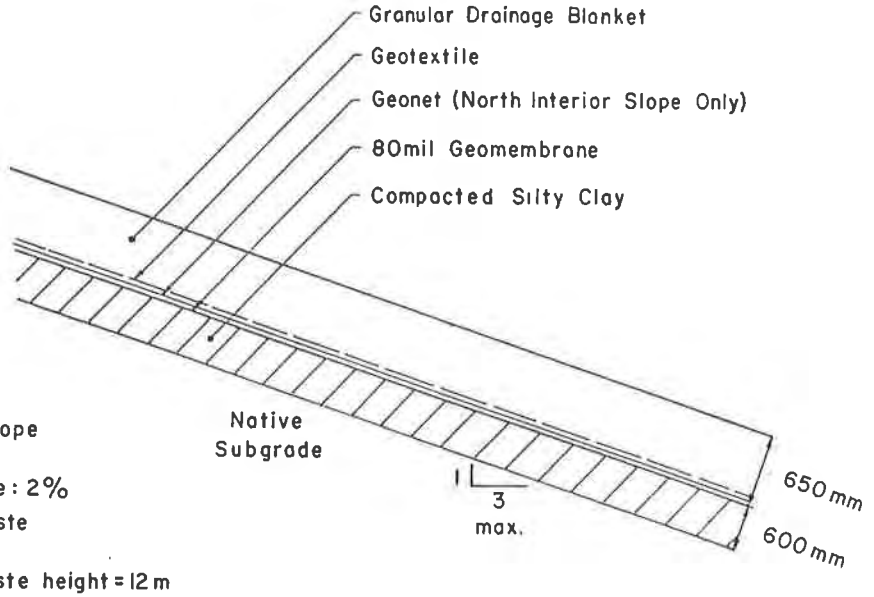

Notes:

1) Maximum interior side slope height: 25m
2) Maximum base slope grade: 2%
3) Maximum final exterior waste slope angle = 5H:1V
4) Maximum final exterior waste height = 12m

Figure 5. Stage 3 - Bottom Liner System

The time frame available for design and tendering of this phase of the project did not allow for a design and specification basis testing program to be carried out. Interface friction values based on published and other available information was used in stability evaluations of a design profile proposed by the project owner.

Since the design cross section involved geomembrane/clay and geomembrane/geotextile interfaces it was considered that the geomembrane/geotextile interface would clearly not meet the north interior side slope interface friction requirement based on published data. Therefore a geonet element was added between the geomembrane and the geotextile on the slope section to eliminate the perceived critical geomembrane/geotextile interface (see Figure 5).

The redesigned north interior side slope geosynthetics profile was not considered to merit design basis specific testing since alternate solutions to maintain stability of the drainage blanket were available, such as construction of the slope portion of the blanket in short vertical segments, or stages, as waste placement proceeds. Nonetheless, based on the successful experience with the 19 degree specification in the Stage 1 cover construction, it was decided that the same value and compliance testing would be required and this was written into the specification for the geonet material.

Various solutions were also available to maintain stability of temporary and final waste slopes (ie. filling sequence and maximum temporary waste slopes) therefore, it was decided that no interface friction requirements would be specified in the tenders for the geomembrane/geotextile and geomembrane/clay interfaces. However, given the known sensitivity of geomembrane/clay interface friction to density and water content of the compacted clay, stringent specifications were prepared in this regard.

In addition, after contract award an interface friction testing program was undertaken for the specific soil and geosynthetics materials proposed for use on the Stage 3A construction.

Design Verification Test Results The geosynthetic products initially proposed by the contractor for the design profile (Figure 5) were:

- PC Geomembrane Inc.'s Plastaliner 80 mil smooth HDPE geomembrane
- Tenax CE301 Geonet
- Terrafix 400R Geotextile

The proposed geomembrane was later replaced with PolyAmerica (Polyflex) Inc.'s 80 mil smooth HDPE. The testing was performed at Golder Associates' laboratory in Calgary, in a 430 mm x 300 mm size shear box. Both base liner and side slope liner geosynthetic/soil profiles were tested, at strain rates of 1 mm per min. The clay component of the profiles was placed at various density and water content values to represent normal and upper bound field conditions and all geosynthetic components were free to move in all tests. The base liner profiles were tested at normal stress values of 10 kPa, 75 kPa and 150 kPa and the side slope liner profiles were tested at a normal stress level of 10 kPa in all cases.

The base liner profile test results are summarized on Figure 6 below and the side slope profile test results are summarized on Figure 7. For the bottom liner profile the failure interface was along the geomembrane/geotextile contact, with a friction angle of about 12.5 degrees. From tests on the side slope liner profile the geomembrane/geonet was the critical interface, with a measured friction angle of about 15.5 to 16.5 degrees from 5 tests on Polyflex "blown film" HDPE geomembrane; of interest is that the measured friction angle was about 22 degrees from 3 tests between the same geonet and the "extruded" HDPE geomembrane manufactured by PC Geomembrane Inc. (Figure 7).

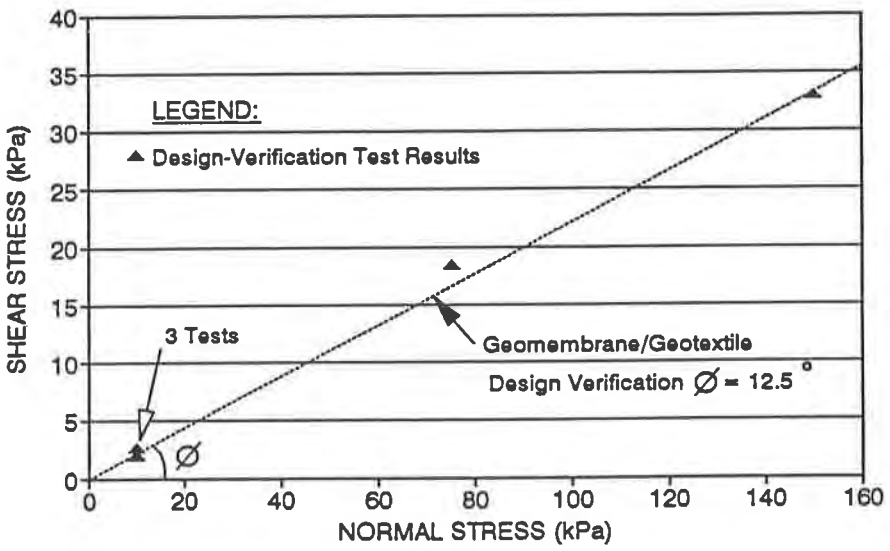

Figure 6. Summary of Laboratory Tests Results - Stage 3A Bottom Liner, Base Profile

Compliance Laboratory Test Results The contractors compliance testing was performed by Geoservices Inc. (now Geosyntec Inc.). The materials assembled in the shear box apparatus consisted of drainage blanket stone, Terrafix 400 g/m^2 (12 oz/yd^2) non-woven geotextile, Tenax CE-9 geonet, Polyflex 80 mil (minimum) HDPE geomembrane, and compacted silty clay. Initial direct shear tests carried out by Geoservices at their Boynton Beach laboratory at a shearing rate of 5 mm/min, and at normal stresses of 11,

21 and 42 kPa failed along the geonet/geomembrane interface and gave an angle of frictional resistance of 12.1 degrees with an "apparent interface adhesion" of 7.9 kPa; GeoServices then elected to verify these results by replicate tests at their Norcross laboratory and obtained an interface friction angle of 12.6 degrees with apparent adhesion of 2.3 kPa. The fact that the same operator, shear box size, test procedures and materials were used suggests that shear test results can be equipment specific.

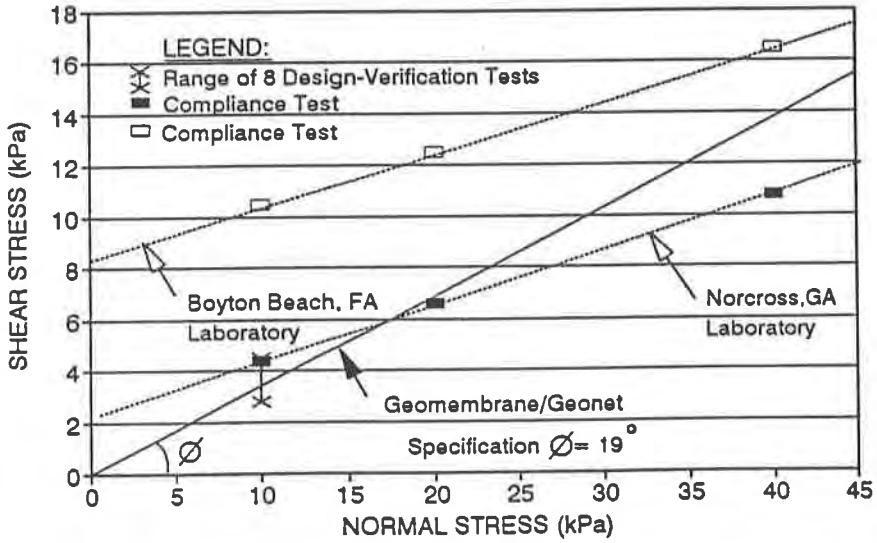

Figure 7. Summary of Laboratory Test Results - Stage 3A Bottom Liner - Side Slope Profile

Field Scale Testing As a result of the uncertainty posed by the wide range of compliance and verification laboratory test results for the 80 mil HDPE geomembrane/ geonet interface friction it was decided that a field test should be performed on the north side slope.

A 15 metre (50 foot) long trial slope section was constructed to the configuration shown on Figure 8 below, which included a surcharge of granular drainage stone on the upper part of the slope. The geosynthetics were anchored such that the geonet was free to slide on the anchored geomembrane. The position of the geonet was monitored for slippage relative to the geomembrane by survey control over a two week period, and no measurable movements were recorded; the configuration appeared stable and the remainder of the north side slopes was constructed as designed.

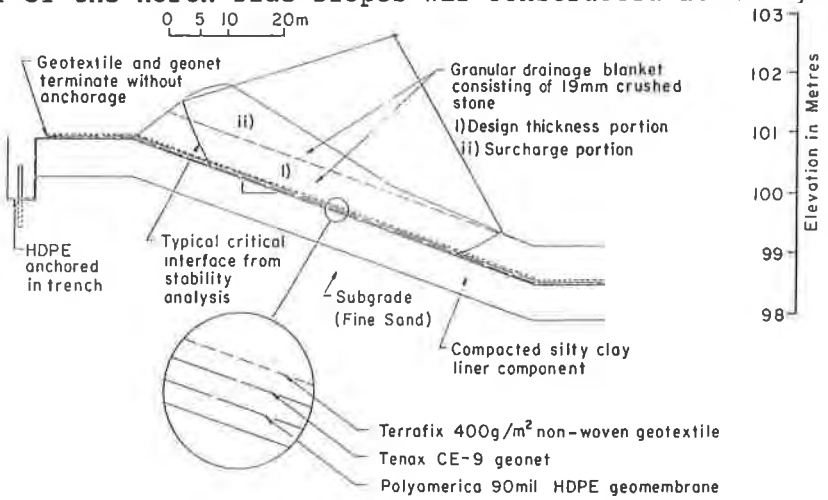

Figure 8. Geonet Test Section, Stage 3A Bottom Liner

To further investigate the observed successful behaviour of this side slope, a direct shear test was carried out on the granular drainage stone in Golder Associates 300 mm (12 inch) shear box. A shear strength envelope was determined, and it was considered that the range in internal friction angle could be from 45 to 55 degrees (ie. much higher than the conservative 30 degrees assumed in the initial stability analyses which established the required angle of friction). The results of Morgenstern-Price stability analyses using a 45 degree friction angle are shown on Figure 8 below, and indicate that even at geosynthetic interface friction angles less than 12 degrees the surcharged trial slope configuration should be expected to be stable. Analyses using the method of Giroud and Beech (1989) indicated that an overall factor of safety against instability for the actual slope of 1.3 can be achieved with geonet/geomembrane friction as low as 10 degrees. The sensitivity of the factor of safety and computed geonet/geomembrane friction to the assumed drainage stone friction angle is also shown on Figure 9 below.

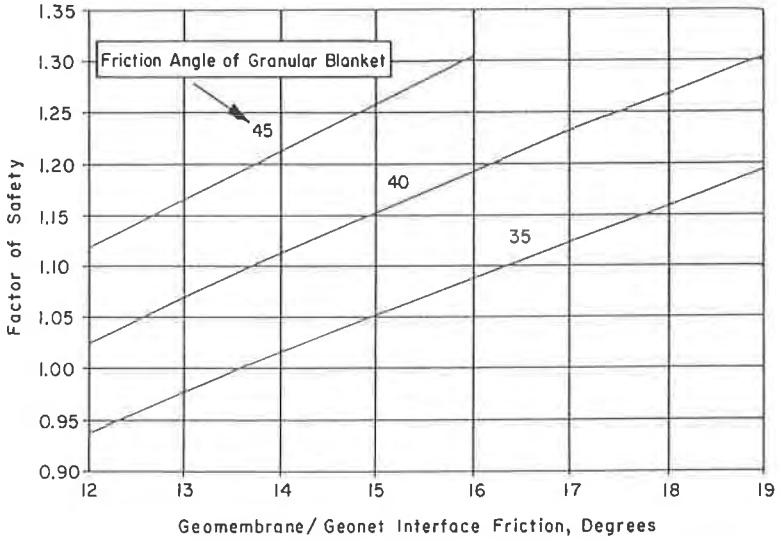

Figure 9. Stage 3 Bottom Liner, Parametric Stability Analysis

STAGE 2 COVER AND 3B BOTTOM LINER (1990 - 1991)

General Concept and Critical Interfaces The design for the Stage 2 Capping Program was initiated in 1990. The adopted design concept was similar to the as-constructed Stage 1 cover, ie. single geomembrane barrier system with geonet drainage medium on the side slopes. (see Figure 3).

The existing waste slopes were generally 5 horizontal to 1 vertical in Stage 2, whereas the Stage 1 waste slopes were 4 horizontal to 1 vertical. Therefore, stability analyses for the same general cap profile on 5 horizontal to 1 vertical slopes indicated a minimum required interface friction angle of only 15 degrees for the interfaces shown on Figure 3. However, based on the inconsistency of compliance and verification test results obtained in the 1989 - 1990 Stage 3A construction campaign, as well as the need to specify the geonet and 40 mil geomembrane generically for the Stage 2 cover (geomembrane/geonet evaluations, were still brand-name specific for Stage 1 cover and Stage 3A bottom liner), it was decided that a final design and specification - basis testing program was necessary.

The Stage 3B Bottom Liner design is essentially a duplication of the design used in the 1989-1990 Stage 3A construction, when laboratory interface shear testing indicated the geonet/80 mil geomembrane interface was critical and gave angle of friction values in the range of 12 to 16.5 degrees. However, the Stage 3A field testing indicated that the geonet/geomembrane interface friction angle can be as low as 10 degrees for a factor of safety of 1.3 against sliding, depending on the angle of friction of the gravel drain material (ie. 45 to 55 degrees).

Interface Friction Specifications VLDPE geomembranes came into use since the design and construction of the Stage 1 cover, therefore it was decided that the specification-basis testing program should evaluate 40 mil VLDPE as well as 40 mil HDPE geomembranes. The materials used in the specification-basis testing program were as follows:

Geomembranes	Geonets
National Seal 40 mil VLDPE	Tensar NS 1400
Gundle Hyperlastic 40 mil VLDPE	Gundnet XL-4
PolyAmerica Duraflex 40 mil VLDPE	Tenax CE-3
Gundle 40 mil HDPE	
National Seal 40 mil HDPE	

The testing was performed in Golder Associates' laboratory using the same shear box apparatus and procedures as in the Stage 3A design verification testing program. Twenty tests were performed on various combinations of the geosyn-thetic materials listed above, assembled as per design profile given on Figure 3. The test results are shown graphically on Figure 10 and can be summarized as follows:

- In all cases the plane of sliding was the geomembrane/geonet interface.
- VLDPE/Geonet interfaces gave friction angle results of 15 to 16.5
- HDPE/Geonet interfaces gave friction angle results of 19 to 21 degrees

On the basis of these results and consideration of the better puncture and elongation properties of VLDPE, it was decided to specify VLDPE geomembrane and a minimum friction angle of 15 degrees for the geonet/VLDPE interface for the Stage 2 cover.

In addition, both pre-qualification and compliance testing were specified for the Stage 2 cover contract. The pre-qualification requirements were a minimum of three satisfactory historic tests on samples of the proposed materials from general roll stock. The compliance program required seven (7) tests performed on samples from the rolls of materials produced for the project, prior to their use in the construction.

For the Stage 3B contract, the 80 mil HDPE/geonet interface friction angle was specified as equal to or greater than 13 degrees, on the basis of the 1990 Stage 3A laboratory testing and the field scale testing results. A compliance testing program was also specified for the geomembrane/geonet combination, similar to the Stage 2 cover requirements, but requiring only 3 tests on materials produced for the project.

These compliance testing programs by the contractors were considered essential in view of the minimum range of products tested in the specification-basis program and the possibility of product quality fluctuations due to manufacture.

In Plant Monitoring As part of the QA/QC program specified for geosynthetic materials and installation on the Trail Road Landfill projects in 1990/92 (Stage 2 cover and Stage 3B bottom liner), Golder Associates carried out in plant monitoring during geomembrane production for these contracts. Rather than the approach adopted in the Stage 1 cover (1988) where the manufacturing documentation and random physical property test results were received and reviewed by the QA/QC team and compared to the project specifications, in plant production monitoring was incorporated into the QA/QC program to observe the manufacturing of the geomembrane, verify the raw materials being used, check the physical property conformance test procedures and results and to participate in and review the production documentation and occurrence/resolution of any production difficulties. In plant monitoring for HDPE was carried out at the facilities of PolyAmerica Inc. in Grand Prairie, Texas and at Columbia Geosystems Ltd. in Calgary, Alberta, and for VLDPE at Gundle Lining Systems in Houston, Texas. As a result, only rolls of geomembrane which met the project specifications were allowed to be delivered to the job site, the on site review of production documentation was eliminated except for inventory control, and the uniformity of the materials provided to the project was verified.

Compliance Laboratory Test Results The contractor's compliance testing for the Stage 2 cover contract was performed by Geosyntec Inc. The testing apparatus was the same as in the Stage 1 cover contract, however the shearing rate used was 1 mm/minute and normal stress applied was 15 kPa, as used by Golder Associates in the specification basis testing. The 40 mil geomembrane material used was Gundle Hyperlastic VLDPE and the geonet was Tensar DN4. The 7 tests performed all produced failure along the geonet/geomembrane interface, with resulting friction angle results of 17 to 21 degrees.

The results are summarized on Figure 10 below and show compliance with the specification, and generally higher values than the 16 degrees obtained by Golder Associates in specification-basis testing of the same materials.

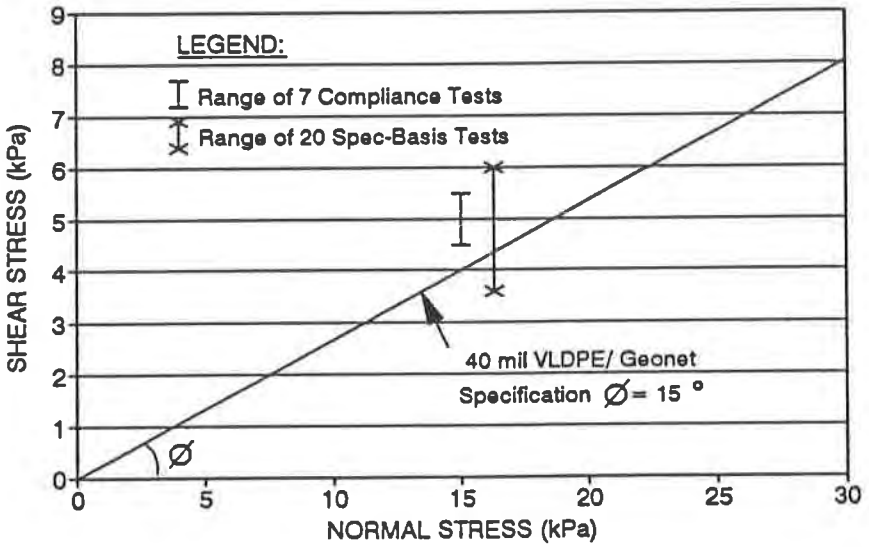

Figure 10. Summary of Laboratory Test Results - Stage 2 Cover

The contractor's compliance testing for the Stage 3B bottom liner contract was performed by the University of Alberta. The laboratory direct shear testing was carried out using the methods described for Stage 3A at a normal stress of 15 kPa on an assembly consisting of drainage stone, 400 gm/m^2 Matador non-woven geotextile, National Seal PN-3000 geonet, Columbia Geosystems 80 mil HDPE geomembrane and clay. Testing by the University of Alberta for the contractor reported peak geonet/geomembrane friction values ranging from 21.1 to 25.7 degrees, averaging 23.5 degrees; interpretation by Golder Associates of the shear stress plots gave residual friction values of 14 to 15 degrees. A verification test on the same materials by Golder Associates (Calgary) large direct shear apparatus gave a peak geonet/geomembrane friction of 19.3 degrees and a residual friction of 14 degrees. Because the peak value only occurs at very low strains, it was considered appropriate to use the residual friction value which met the specified project requirements. However, the peak shear stress results are shown on Figure 11, below.

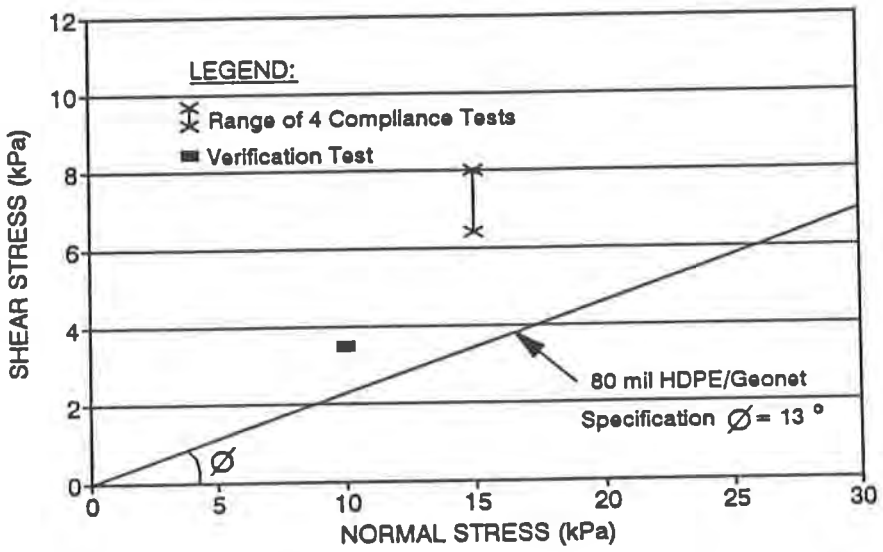

Figure 11. Summary of Laboratory Test Results - Stage 3B Bottom Liner, Side Slope Profile

CONCLUSIONS

The laboratory direct shear testing carried out as part of the Trail Road Landfill projects on a wide variety of geosynthetic products under low normal stresses which are typical of top cover designs or unloaded bottom liner systems highlights the following technical issues:

- interface friction values obtained from laboratory shear tests are very sensitive to the test apparatus (mode of application of normal loads, alignment of shear boxes, equipment friction, etc.) and on the physical characteristics (relative rigidity and surface texture) of the specific materials being tested. Good agreement was not always obtained between different testing laboratories even when using the same type of equipment, procedures and materials.

- field scale surface irregularities (bumps, depressions, liner seams, etc.) probably have a significant positive effect on stability which cannot be accounted for in laboratory scale testing.

- field scale tests taken to failure are needed in order to evaluate effective frictional properties compared to the laboratory results, and thereby further optimize geosynthetic designs.

The approach to generic design and generic specifications developed and utilized at the Trail Road Landfill has been successfully used in the public tender process to provide a technically sound, safe and cost effective means of successfully constructing containment facilities which incorporate geosynthetic products. This approach highlights the following practical considerations:

- lead time is required for the designer to carry out design and specification-basis testing as appropriate for the specific project requirements.

- at the time of tendering the contractors/suppliers need to have confidence in interface friction properties of various combinations of materials under a range of normal stresses, in order that their bid price is realistic and that unfavourable surprises are not encountered when their project specific materials are tested.

All final cover and bottom liner projects constructed to date at the Trail Road Landfill have been observed to perform acceptably, and have been constructed cost effectively utilizing the approach described in this paper.

ACKNOWLEDGEMENTS

The authors wish to acknowledge the Regional Municipality of Ottawa-Carleton, in particular the Environmental Services Department, for their progressive and active participation in advancing the technology in the expanding and evolving geosynthetics industry.

REFERENCES

Giroud, J.P. and Beech, J.F., "*Stability of Soil Layers on Geosynthetic Lining Systems, Proceedings of Geosynthetic*" 89 Conference, San Diego, 1989, pp. 35 to 46.

Giroud, J.P., "*Tips on Specifying Geosynthetics*", Geotechnical Fabrics Report, 1992 Specifications Guide, December 1991.

J.L. Richards & Associates Limited, "*Trail Road Landfill Development Plan*", report prepared for the Regional Municipality of Ottawa-Carleton, April 1985.

J.L. Richards & Associates Limited, "*Trail Road Landfill Development and Operations Plan*", report prepared for the Regional Municipality of Ottawa-Carleton, February 1990.

Lydick, L.D. and Zagorski, G.A., "*Interface Friction of Geonets: A Literature Survey*", Geotextiles and Geomembranes, No. 10, 1991.

Martin, J.P., Koerner, R.M. and Whitly, J.E., "*Experimental Friction Evaluation of Slippage Between Geomembranes Geotextiles and Soils*" International Conference on Geomembrane, Denver, 1984.

Mitchell, J.R., Seed, R.B. and Seed, H.B., "*Kettleman Hills Waste Landfill Slope Failure: Liner System Properties and Stability Analyses*" ASCE Journal of Geotechnical Engineering, Vol. 116, No. 4, April 1990.

Ontario Ministry of the Environment, "*The Incorporation of the Reasonable Use Concept into the Groundwater Management Activities of the Ministry of the Environment*", April 1986.

Paruvakat, N., Sevick, G.W., Boschuk Jr., J. and Kollodge, S., "*Design and Testing of a Landfill Final Cover with Geomembrane*" ASTM, Special Technical Publication, No. 1081, 1991.

Seed, R.B. and Boulanger, R.W., "*Smooth HDPE - Clay Liner Interface Shear Strengths: Compaction Effects*" ASCE Journal of Geotechnical Engineering,Vol. 117, No. 4, April 1991.

Waste Age, "*Protect the Geomembrane Cap!*", March 1990

Williams, N.D. and Houlihan, M.F., "*Evaluation of Interface Friction Properties Between Geosynthetics and Soils*", Proceedings, Geosynthetics '87, New Orleans, February 1987.

Design and Installation of a Lined Mill-Effluent Containment Facility

M.J. Brodie
Steffen Robertson and Kirsten (Canada) Inc., Canada

P.M. Healey
Steffen Robertson and Kirsten (Canada) Inc., Canada

ABSTRACT

A lined effluent containment pond was constructed in 1991 at Placer Dome Inc.'s Campbell Mine in western Ontario. The pond was designed to contain approximately three years of mill effluent from a pressure autoclave system that was recently installed at the mine.

The sideslopes and pond bottom are lined with 80 and 60 mil high density polyethylene (HDPE) respectively. The 80 mil liner was used on the sideslopes to provide additional protection against erosion and tearing by ice in the winter.

An underdrain system consisting of a 100 mm diameter HDPE perforated pipes was installed beneath the liner to assist in controlling groundwater and runoff during construction, and to act as a leak detection system.

During construction of the pond, poor weather threatened to delay the completion date of the project. Several measures were taken which allowed the project to be completed only 6 days late of the original completion date. This paper highlights the key aspects of the design and discusses the measures which were taken to address the problems which arose during construction.

INTRODUCTION

The growing trend in North America is towards lining surface impoundment facilities with geomembranes. A recent example is a project in Western Ontario which involved the construction of a lined effluent containment pond using a high density polyethylene (HDPE) geomembrane. The facility was constructed to contain effluent from a pressure autoclave which was recently installed at Placer Dome Inc.'s, Campbell Mine, located in Balmertown, Ontario. The pressure autoclave was installed to recover gold from arsenite bearing, ore concentrate. The mine processes about 1220 tonnes (1200 tons) of ore per day, yielding 270 tonnes per day (265

tpd) of the effluent. Design and construction supervision of the facility was conducted by Steffen Robertson and Kirsten (Canada) Inc. (SRK) of Vancouver, British Columbia. The supply and installation of the liner was provided by Columbia Geosystems Ltd. (Columbia) of Calgary, Alberta.

This paper highlights some of the key aspects of the design and discusses the measures which were taken to address the construction problems. Portions of the paper was originally published in the April, 1992 issue of the Geotechnical Fabrics Report.

DESIGN

The facility has a capacity of 290,000 cubic metres (10.2 million ft^3) which is sufficient to store 3 to 3.5 years production, based on a settled dry density of 1280 kg/m^3 (80 pcf) and a production rate of 270 tonnes/d (265 tpd). The general layout of the pond is shown on Figure 1. The pond was lined with the HDPE geomembrane as a measure to reduce contaminant migration from the stored effluent to the environment. The pond has an area of about 46,500 m^2 (500,000 ft^2), contained by five embankments, ranging in height from 4 to 12.2 m (13 to 40 ft). The embankments have 4.5 m (15 ft) wide crests and internal slopes of 2.5:1 (H to V). The external slopes vary from 2.0 to 3.8:1 (H to V). The embankments were constructed of compacted silty clay and the foundation soil at the base of the pond consisted of a silty sand.

Two liner options were considered during the design of the facility. The first option involved the use of the locally available silty clay which has a hydraulic conductivity ranging from 10^{-6} cm/sec to 10^{-7} cm/sec. The second option was the use of a geomembrane, such as HDPE. It was felt that although the geomembrane would not be completely impermeable, it would be less permeable than the clay liner. Consequently, as minimizing the risk of leachate loss from the facility was a key design requirement, the geomembrane option was selected. HDPE was the selected geomembrane material because of its superior resistance to degradation by chemical attack and ultra-violet radiation.

The liner thickness was the next design consideration. Although a 60 mil liner would sufficiently limit leachate migration from the pond, the action of ice, which would form on the pond during the winter months and possibly cause damage to the liner, prompted the use of 80 mil HDPE on the upstream face of the embankment. The selection of 80 mil HDPE, as opposed to any other thickness, was based on a subjective assessment of the experience of several geomembrane manufacturers. To protect the liner, the pond was designed to operate with a water level within 3 to 4 feet of the embankment crest. A soil cover over the liner would have required flatter slopes and would have added to the overall cost of the project. Furthermore, maintaining a maximum water level in the pond allowed the use of a thinner, 60 mil geomembrane on the base. The junction between the 80 and 60 mil material was located about 2 m (6 ft) beyond the toe of the embankment slope so that any trampolining stress which occurs at the tow of slope would not be concentrated on a welded seam.

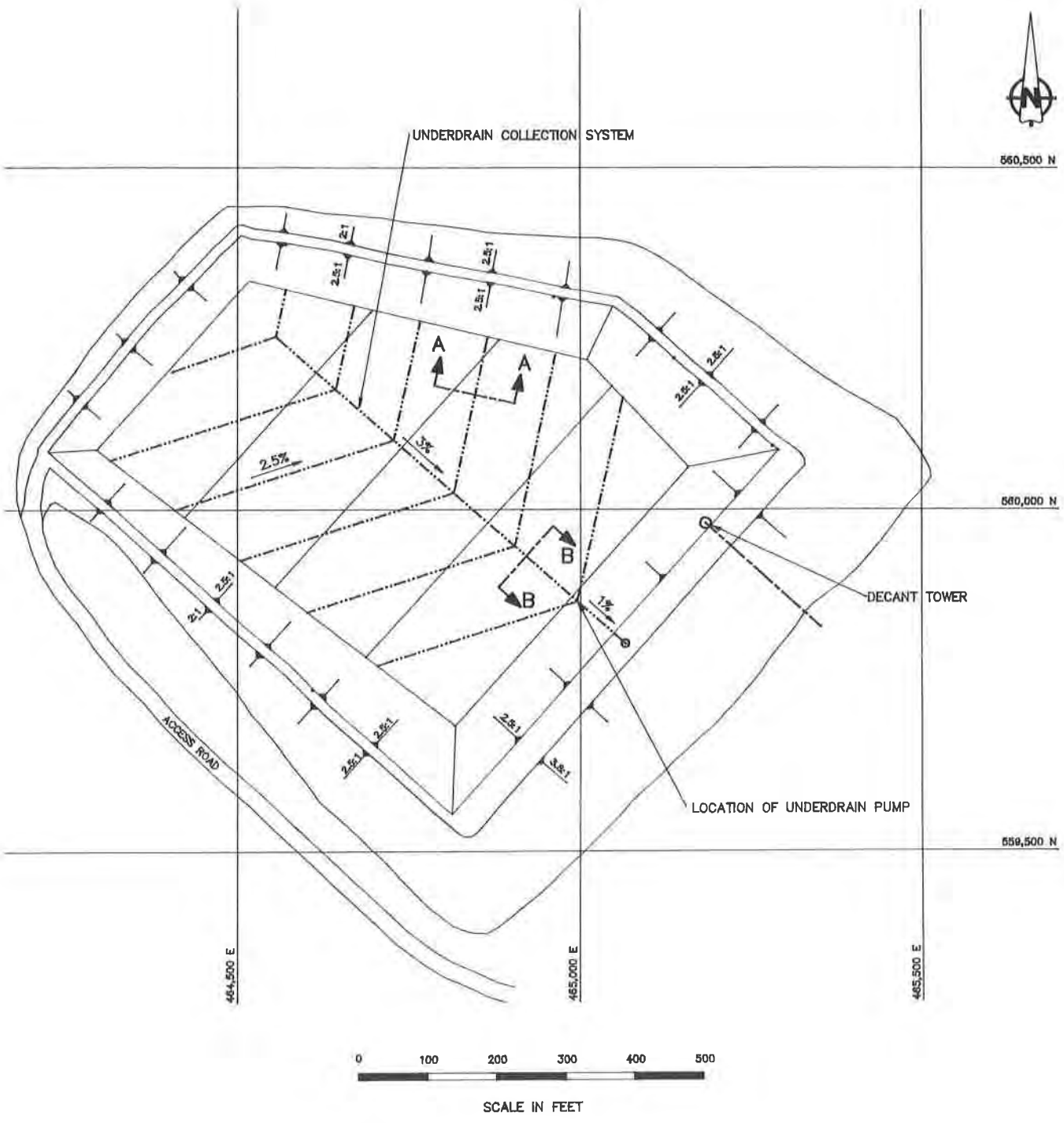

Figure 1. General Layout

An underdrain system consisting of a series of pipes was installed beneath the liner as shown on Figure 1. The lateral drains consisted of 10 cm (4-inch) diameter perforated PVC pipes (standard dimension ratio = 17) laid in trenches backfilled with drain rock. The drains were connected to a 20 cm (8-inch) collector pipe located down the center of the pond which discharged to a sump at the upstream toe of the southeast embankment. Water that collected in the sump would be pumped to the surface when required. A typical cross section of the lateral drains and collector pipe is shown on Figure 2. The underdrain system was primarily intended to control groundwater during construction. During operation of the pond, quality of water collected in the sump would also provide early detection of leakage from the pond. Monitoring wells were installed downgradient of the facility to monitor for any groundwater contamination.

CONSTRUCTION

The contract for construction of the embankment and installation of the liner was awarded in late April, 1991. Deployment of the liner began on June 22, 1991, and it took 30 days to complete the installation.

During construction, an unusually wet spring resulted in delays totalling 38 days in a planned construction period of 69 days. Modifications to the design, to make up for this lost time, included placement of geotextile filter fabric on the embankment slopes, sequencing deployment of the liner to allow early discharge into the lower end of the pond, and co-ordinating subgrade preparation to minimize lost effort due to precipitation. A second, 4-man liner installation crew complete with welding equipment was mobilized to the site to increase production during periods of good weather.

On several occasions, heavy rain caused extensive erosion of the prepared subgrade. The erosion produced rills and gullies of up to six inches deep on the embankment faces and pond bottom. At one time, about 20 percent of the pond bottom was flooded to a depth of one metre and was pumped out before subgrade preparation could resume (see Figure 3).

During subgrade preparation for the geomembrane, the silty clay fill on the embankment slopes would dry into irregular lumps, up to 15 cm (6 inches) in diameter during warm dry periods. Removal of these lumps of hardened clay, left unacceptable voids and backfilling with sand was found to be very slow because of the difficulty of moving machinery on the 2.5:1 slopes.

In order to resolve these problems, it was decided to place an 8-ounce nonwoven polypropylene geotextile filter fabric over the internal slopes of each embankment. The geotextile fabric protected the geomembrane from the sharp edges of the clay lumps and allowed subgrade preparation to proceed more rapidly. Between 5 to 8 days were trimmed off the construction period by using the geotextile.

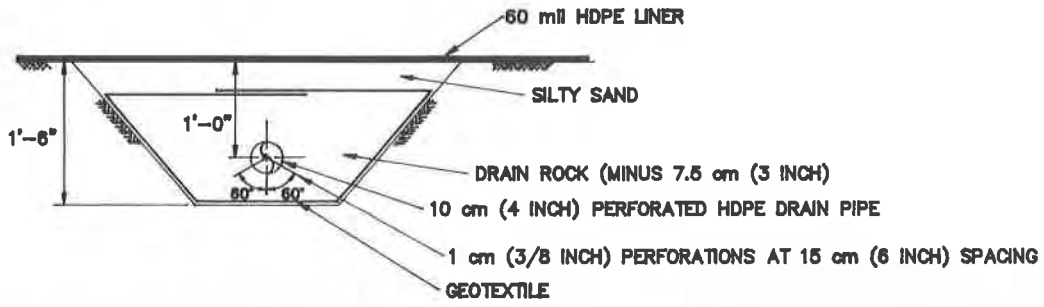

SECTION A–A
LATERAL PIPE DETAIL

SCALE IN FEET

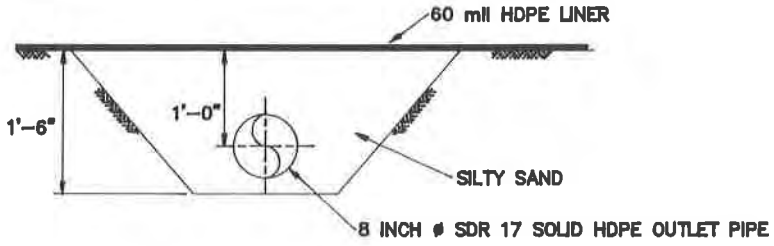

SECTION B–B
OUTLET PIPE
BENEATH POND DETAIL

SCALE IN FEET

Figure 2. Underdrain Details

Figure 3 Water ponded at the lower end of the impoundment. Liner deployment had commenced on the northern embankment.

An alternative solution to the clay lump problem was considered but was not adopted because of the level of uncertainty. It was thought possible that after placement of the geomembrane liner, the clay lumps would be softened by moisture drawn to the surface by capillary action. As the pond filled the weight of the material deposited into the pond would remould the softened clay lumps, eliminating the potential for the liner to puncture.

The subgrade at the pond bottom consisted of a sandy material, which required minimal preparation effort and geotextile filter fabric was therefore not required in this area.

Because of the threat of disturbance to the prepared subgrade by precipitation, it was necessary to keep subgrade preparation just ahead of geomembrane deployment. The procedure involved preparing an area of subgrade, ahead of the geotextile placement, equivalent to about three 8 x 30 m (25 x 100 ft) liner panels. Similarly, geotextile was laid, the equivalent of about three liner panels ahead of the geomembrane deployment.

As the pond bottom was sloped, it was possible to continue liner deployment at the shallow end of the pond while discharging into the completed area at the deep end. The risk, however, was that heavy runoff could wash sand and debris under the exposed, upstream edge of the geomembrane. In this event, the geomembrane would have to be removed to repair the subgrade.

To prevent this, a contingency plan was developed which would involve "tucking" a section of the upstream edge of the liner into the subgrade and excavating a ditch about 15 m (6 inches) deep upstream of the remainder of the "untucked" liner edge as shown in Figure 4. This would route runoff onto the liner via the "tucked" section. In the final 10 days of the project, however, there was no rainfall and the contingency measures were never implemented.

All seams, including the tie-in seams along the floor were welded using the dual (split) hot wedge method. A fillet extrusion weld was used for repairs and for welding the tie-in seams at T-junctions. During the installation of both the 80 mil geomembrane on the slopes and the 60 mil geomembrane on the pond floor, all the required non-destructive testing was performed by the site QA/QC personnel. Most of the field seams were pressure tested at 80 pounds per square inch (psi) for a period of 5 minutes. A pressure drop of up to 6 psi over the 5 minute period was acceptable. All 80 mil to 60 mil tie-in extension seams along the toe of the pond were vacuum box tested, as were any repaired areas and cross seams. Any seam failures that occurred during pressure testing were removed by cutting out the failed section and the panels were welded using the hot wedge fusion method. No field seams were capped. Construction quality control was also performed by the installer's personnel by pressure testing each of the hot wedge, welded seams.

The destructive testing of the liner was combined with the pre-weld qualification to avoid geomembrane destructive test specimens from being obtained within the geomembrane containment area. In order to satisfy the specified destructive testing requirements, test samples were taken from inside the anchor trenches and overlapping field seams on the floor. All destructive and pre-weld qualification tests exceeded the specified values, as recommended by the National Sanitation Foundation Standard No. 54, of 18.9 KN/m (108 pounds per inch (ppi)) shear strength for both 60 and 80 mil, and 14.7 and 17.2 KN/m (84 and 98 ppi) peel adhesion for the 60 and 80 mil, respectively.

The pond was designed to operate with a continuous decant system. The supernatant is decanted through a vertical 1.22 m (4-foot) diameter, corrugated metal tower, which penetrates the liner. The 80 mil geomembrane is attached to the tower using an HDPE anchorage strip which was set into a concrete base constructed around the tower. A fillet extrusion weld was used to connect the geomembrane to the anchor strip. The tie-in was non-destructively tested using the vacuum box method. A layer of asphaltic sealant was placed over any exposed concrete between the edge of the HDPE and the tower. A seepage barrier was also embedded into the concrete collar. Details of the tower penetration through the liner are shown on Figure 5.

Discharge from the underdrain installed beneath the pond is pumped from a sump at the toe of the southeast embankment to the adjacent tailing pond. A 20 cm (8 inch diameter HDPE pipe buried into the internal slope of the embankment, houses a dedicated submersible pump of 55 lpm (12 igpm) capacity as shown on Figure 6. The underdrain is pumped out about once per month and has produced about 7260 litres (1600 imp. gallons) over the last 11 months, which is believed to be groundwater as described below.

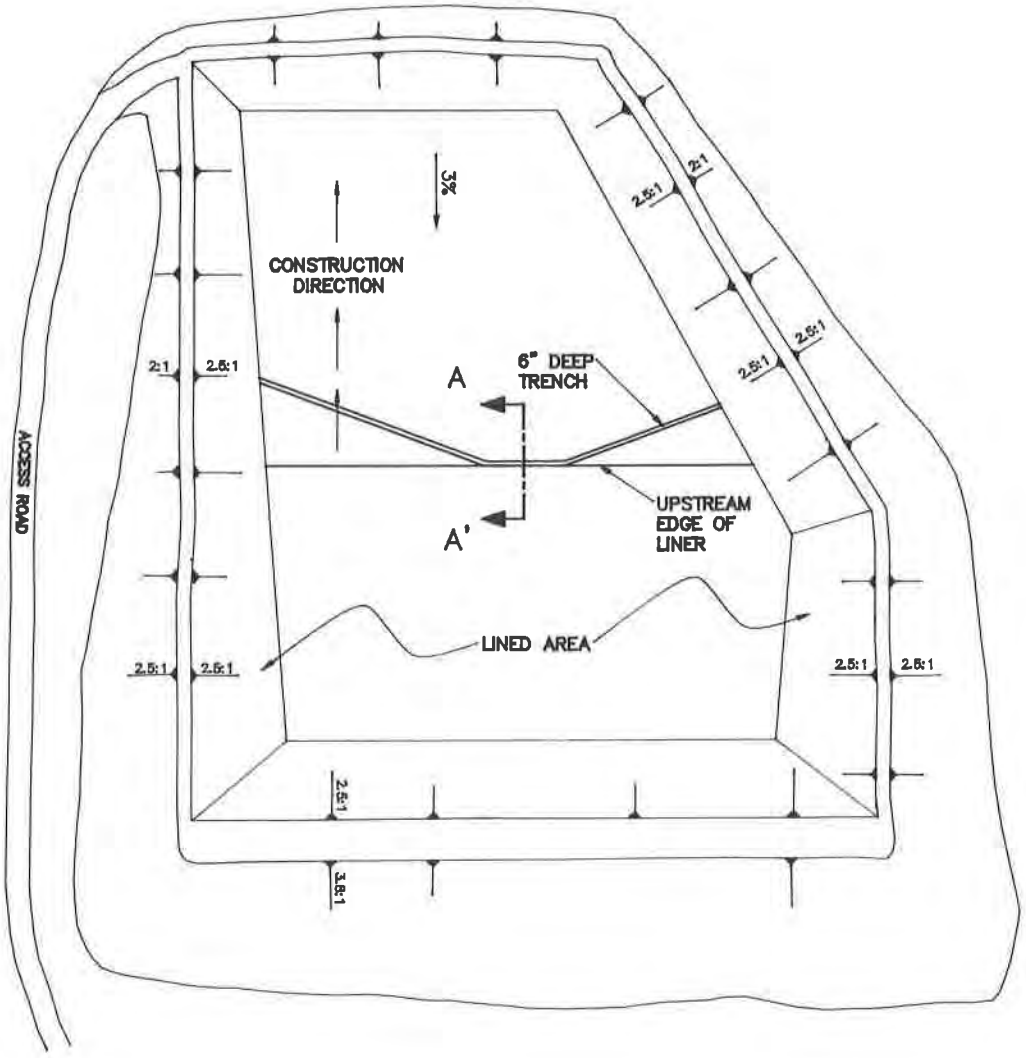

PLAN

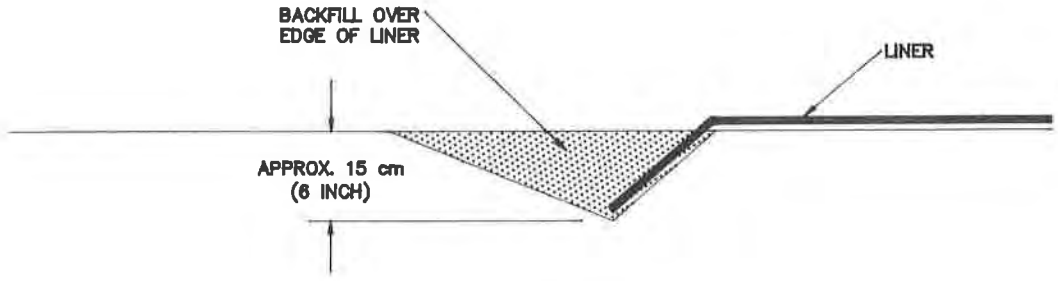

SECTION A–A'

Figure 4. Geomembrane "Tuck in"

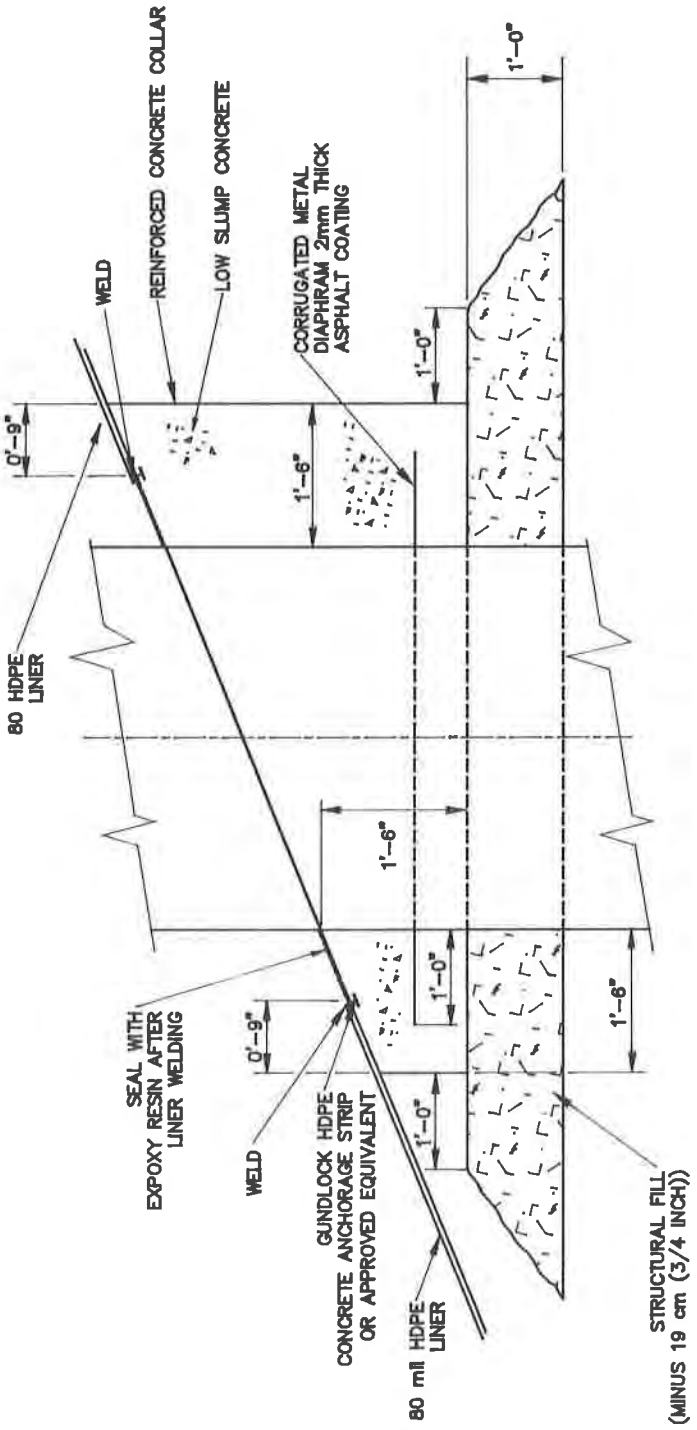

Figure 5. Schematic of Seal Around Decant Tower

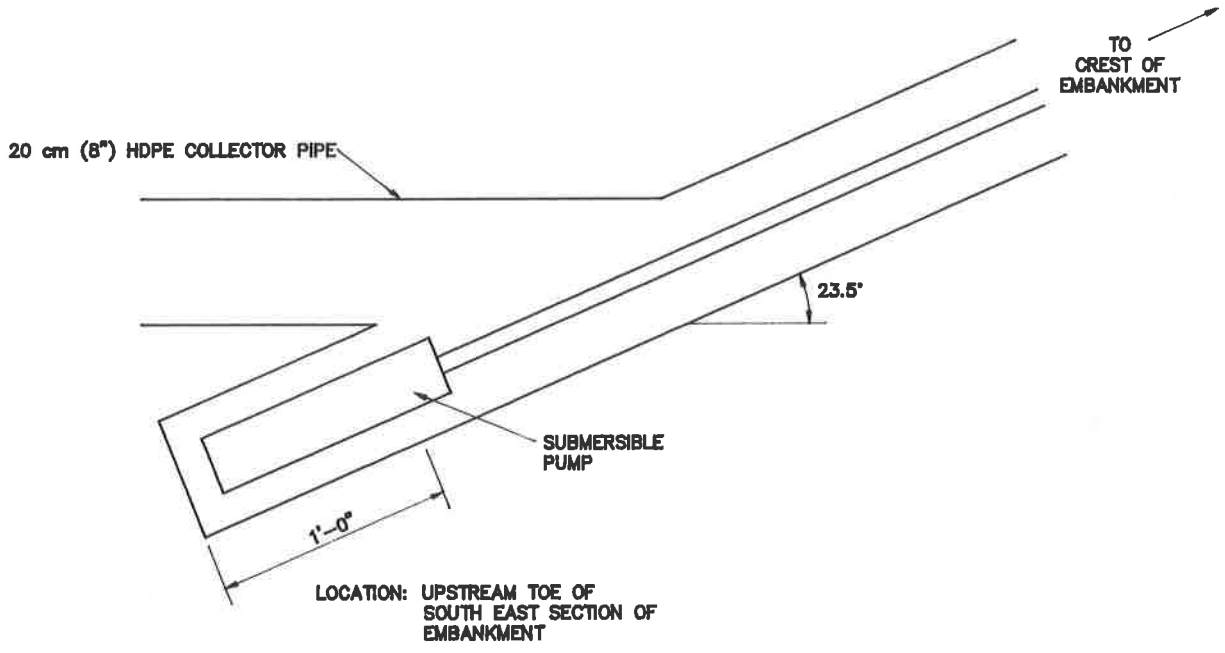

Figure 6. Underdrain Connection

Water quality samples obtained from the underdrain between August 1991 to May 1992 were analyzed for total and dissolved metals. Results of the analyses are presented in Table 1 and indicate levels of iron, arsenic and zinc that are typical of the background water quality based on previous sampling as the site. The monitoring of the water quality in the groundwater wells downgradient of the pond also show background levels.

Table 1
Summary of Underdrain Discharge Water Quality

DATE	Aug. 9/91	May 12/92
IRON,mg/l	1.62	2.41
ARSENIC, mg/l	-	<0.05
ZINC, mg/l	.03	<0.03

An anchor trench was excavated along each embankment crest to prevent downslope movement of the liner. A factor of safety of about nine was calculated for the pullout resistance. This high factor of safety was due to the minimum practical trench geometry which could be constructed with conventional equipment. A smaller trench could have been constructed but was not considered cost effective. A typical section through the trench is shown on Figure 7.

Excavation of the anchor trench revealed an unexpected problem. Because of the cohesive nature of silty clay used in the embankment, the edge of anchor trench developed sharp irregularities up to 20 cm (8 inches) deep. This raised concerns about stresses developing in the liner along the edge and prompted the contractor to use a ditch excavator to cut a 10 cm (4 inch) wide slot along the liner-side of the trench. The backhoe was then able to construct a clean edge along the trench using the precut slot.

The anchor trenches remained open during liner deployment to allow geomembrane expansion and contraction to occur and avoid material stress (trampolining) along the toe of the pond and in the corners. Upon completion of the geomembrane installation, the anchor trenches were backfilled during the cooler hours of the morning to avoid material stress.

The embankment was originally designed with a 4.6 metre (15 foot) wide crest, which would normally be sufficient for earthmoving equipment to raise the embankment to its full height. However, with the anchor trench being 1 m (3 ft) wide (which was the narrowest backhoe bucket on site) and set back 60 cm (2 ft) from the crest, the available working area for liner deployment was reduced to less than 3 m (10 ft). This made deployment of the 8 m (26 ft) wide rolls of HDPE difficult. The problem was solved by placing the material from the excavated anchor trench onto the downstream face of the embankment to temporarily widen the

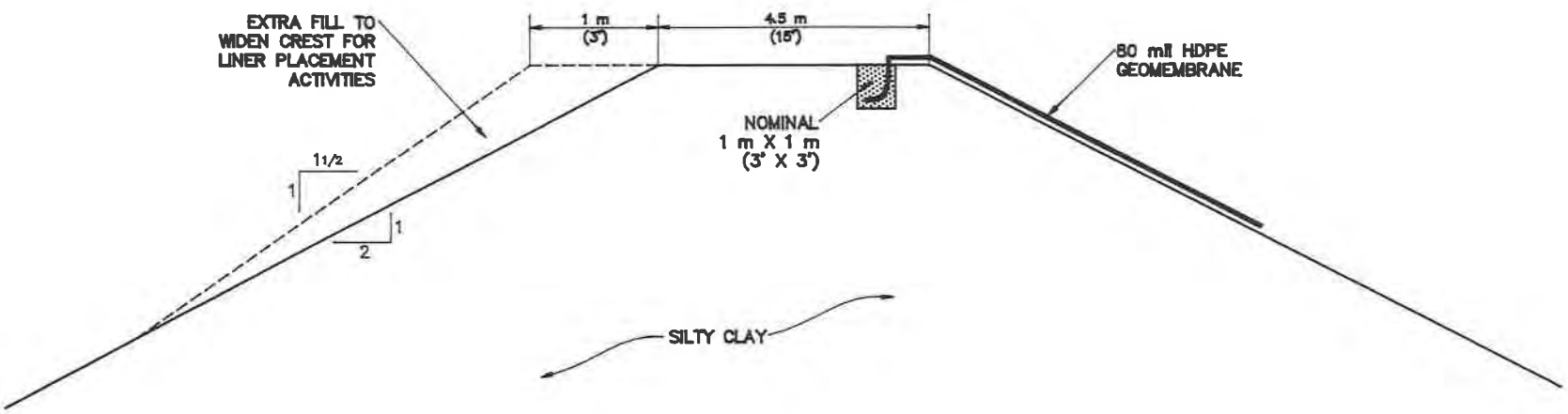

Figure 7. Anchor Trench Detail and Crest Width Modification

crest by about 1 m (3 ft), as shown in Figure 7. On completion of geomembrane installation, the material placed on the slope was removed and used to backfill the anchor trench.

CONCLUSION

The containment facility has now been in full operation for over 12 months and recent monitoring of both the underdrain and the groundwater wells has indicated that the liner is performing satisfactorily with respect to the design objective of minimizing loss of leachate.

REFERENCES

Brodie, M.J. and Healey, P.M., 1992. The Design and Installation of an Effluent Containment Facility. Geotechnical Fabrics Report, Volume 10, Number 3, April 1992.

Multiple Geotextile Layers Used for Geomembrane Support in a Landfill: The Marion County (Florida) Landfill Project

J.N. Paulson
Exxon Chemical Co., USA

L.W. Parker
Jones, Edmunds & Associates Inc., USA

ABSTRACT

The Baseline Landfill in Marion County, Florida, is located in highly irregular Karst geology. The initial geotechnical evaluation of a proposed landfill expansion indicated potential foundation support inadequacies. Geologic conditions were then rigorously evaluated based on data from standard penetration test borings, cone penetrometer tests, flat plate dilatometer tests, ground penetrating radar, and temporary groundwater piezometers. To improve existing foundation conditions a three element foundation design was implemented:

An impermeable geomembrane liner system to provide foundation condition protection by eliminating stormwater flow into the underlying strata,

Two layers of geosynthetic reinforcement designed to safely span subsidences up to 1.5m in diameter, thereby supporting the landfill, and

Deep compaction grouting to provide the third level of foundation improvement by densifying potentially raveling sands, thus reducing sinkhole potential and overall landfill foundation settlement.

The final design results in a safe and cost effective system. This presentation describes the site investigation, and development and implementation of the compaction grouting and geotextile reinforcement program.

INTRODUCTION

Baseline Landfill in Marion County, Florida, consists of three municipal solid waste (MSW) landfill cells covering a total area of about 60 acres, as shown on Figure 1. Landfilling began in 1978 in the unlined 33-acre Urban Cell until 1988. In 1988 the addition of the composite (clay-supported) synthetic-lined 12-acre Cell III-A was completed. As the first two cells approached maximum permitted capacity, construction began in September 1990 on an additional 15-acre cell, identified as Cell III-B. This cell incorporates a composite double synthetic bottom liner.

This Landfill is located in Karst topography generally characterized by the presence of sinkholes and ground surface depressions. During the 1988 construction of Cell III-A, limestone was present at or near ground surface throughout most of the proposed bottom liner area. Investigation and evaluation of these limestone

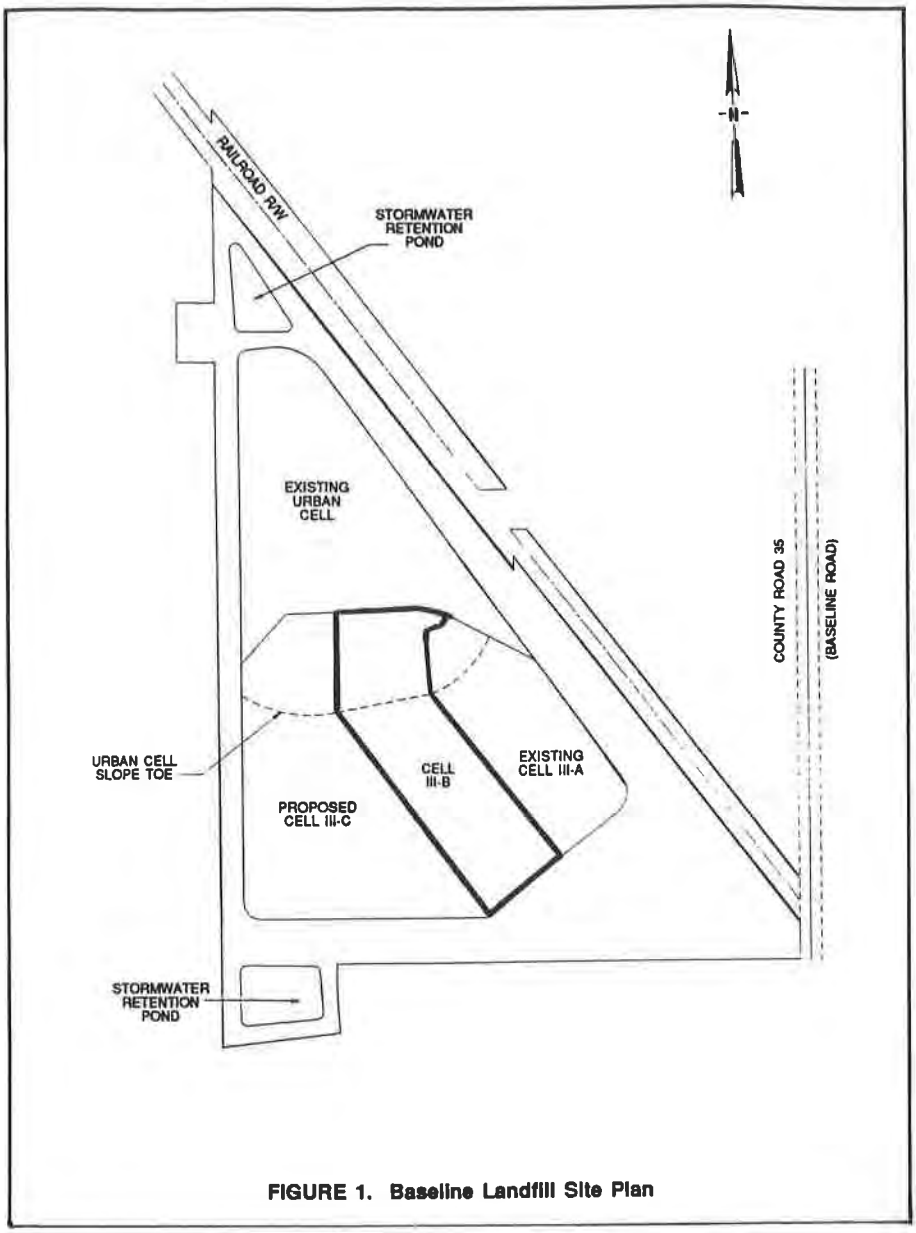

FIGURE 1. Baseline Landfill Site Plan

subsurface conditions revealed that subgrade improvement measures were needed to ensure stability and integrity of the landfill containment system. A three stage construction program was developed.

The first stage consisted of deep compaction grouting to stabilize foundation conditions. The second stage consisted of the installation of a two-layer geotextile reinforcement system. Finally, the impermeable geomembrane liner, and accompanying drainage systems were installed. The following describes the geotechnical investigation, development of the compaction grouting plan and compaction grouting construction, and the design and subsequent installation of the reinforcement geotextiles for Cell III-B of the Baseline Landfill.

GEOTECHNICAL INVESTIGATION CHRONOLOGY

PHASE I

As indicated previously, during the 1988 construction of Cell III-A, limestone was present at or near ground surface over most of the proposed bottom liner area. Similar conditions were anticipated to exist in the adjacent Cell III-B area.

The initial geotechnical field investigation for cell III-B consisted of an electrical resistivity survey and 14 Standard Penetration Test (SPT) borings. The investigation was proposed to confirm that limestone existed at shallow depths and would provide support in the III-B area, similar to those found at the previously constructed Cell III-A. However, conditions encountered during the initial investigation differed greatly from original expectations. Consequently the investigation expanded and was later termed Phase I.

The Phase I investigation included a geological literature review, 14 SPT borings (12 to 32 m deep), 2 electrical resistivity surveys, and 6 cone penetrometer test (CPT) soundings (18 to 33m deep). Analyses of the initial and phase I data revealed Cell III-B to be underlain by discontinuous clay and sand strata, limestone pinnacles, highly weathered limerock, and soft, soil-filled remnants of ancient cavities and sinkholes. Figure 2 shows a typical stratigraphic cross-section of these conditions.

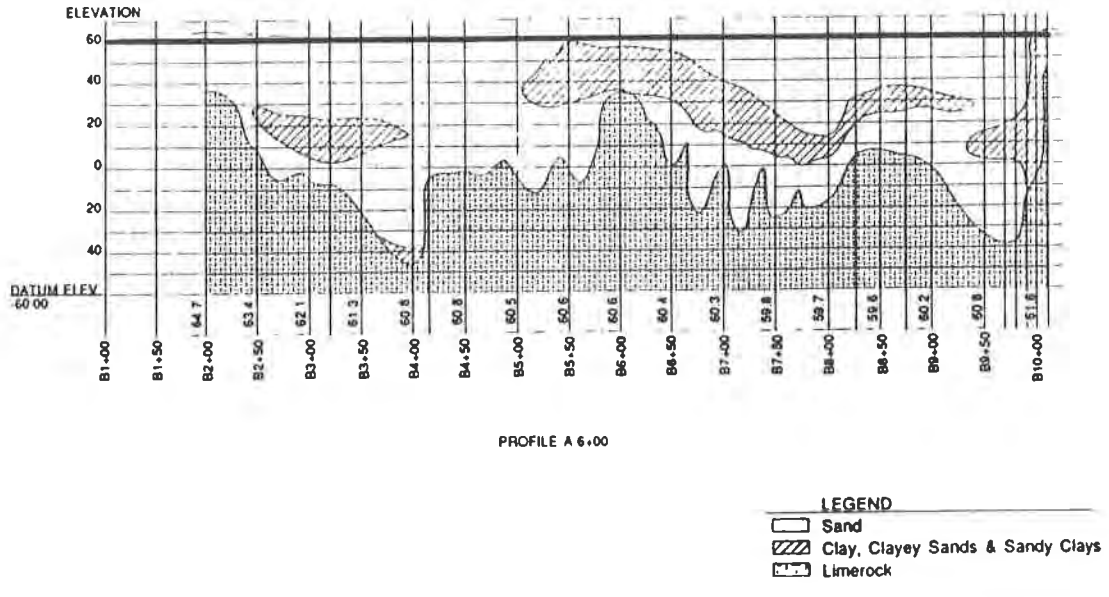

FIGURE 2. Typical Stratigraphic Cross-Section

The past sinkhole action and apparent sinkhole potential for the cell III-B area was much greater than for the existing Phase III-A cell. Because of these concerns, John H. Schmertmann, Ph.D., P.E. of Schmertmann & Crapps, Inc. was consulted for advice on developing the design for a sinkhole/subsidence protection system.

Dr. Schmertmann reviewed the available data and concluded that there was little likelihood for the formation of sinkholes, especially large sinkholes. This was based on the following considerations: The very irregular nature of the limerock surface, both in depth and degree of weathering; the lack of any evidence of major activities; a groundwater surface elevation about 4.5m below the liner and controlled by the piezometric level in the rock without perching; and the virtually complete cutoff of downward water seepage by the geomembrane liner underlying the landfill.

To provide protection against potential sinkholes under the bottom geomembrane liner, however, a blanket type protection system was designed using two layers of woven reinforcement geotextile. This was intended to safely span a cylindrical cavity of 4.5m in diameter or a slot cavity 3m wide. Figures 3 and 4 show the schematic geometry developed for the reinforcement analysis.

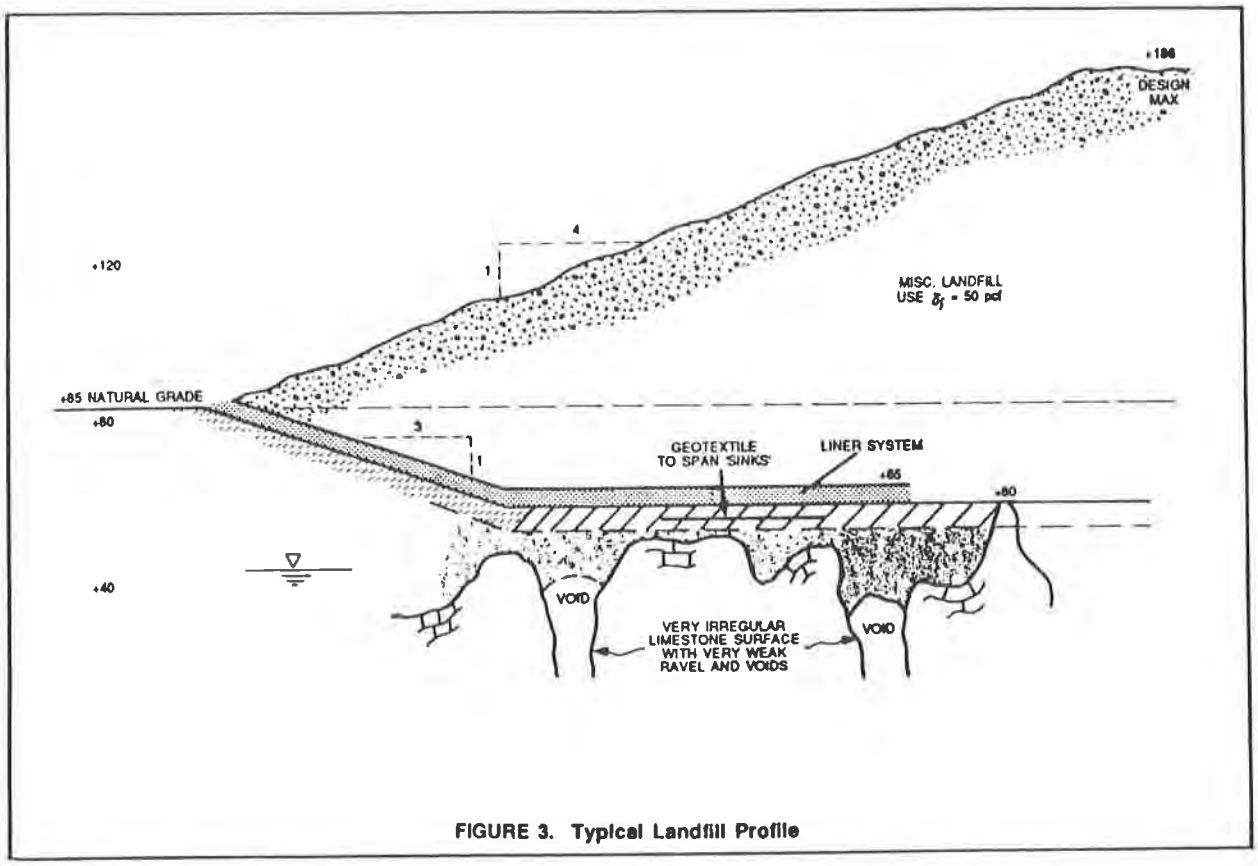

FIGURE 3. Typical Landfill Profile

During design review, the Florida Department of Environmental Regulation (FDER) expressed concern about the possibility of cavities larger than 4.5m and asked for more data supporting this proposed design. Additionally, design requirements were

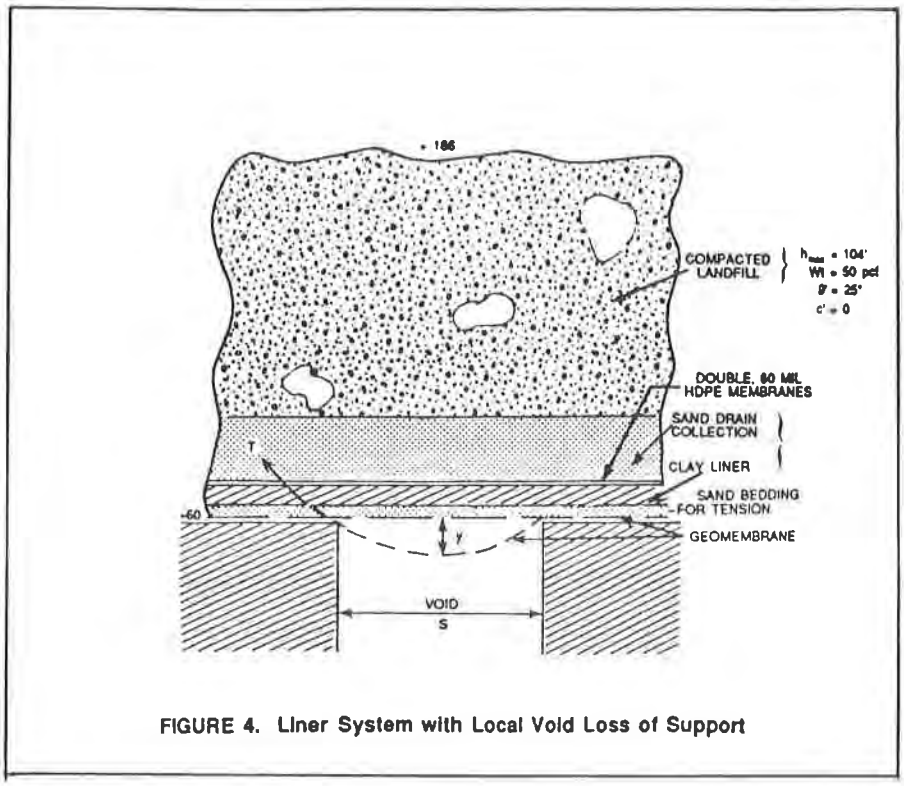

FIGURE 4. Liner System with Local Void Loss of Support

introduced requiring that no more than 30 cm of leachate head could develop above the liner. The reinforcement design depends on liner deformation to develop tensile strength for spanning cavities. The potential deflection of 0.85m resulting from the 4.5m diameter void assumption exceeded the 0.3m allowable maximum leachate head.

Design water balance calculations showed that the leachate head would be no greater than .15m under normal conditions (i.e., no subsidences). As such, the allowable design sag or settlement was therefore reduced to .15m, and a foundation stabilization technique was then required which would limit potential overall liner deformation to this height. Additionally, the stabilization technique would also be required to reduce the potential for any size sinkholes in order to satisfy FDER concerns for permitting.

As a result of the requirements imposed by FDER, additional investigations were begun, herein termed Phase II through IV to better define geological conditions for Cell III-B, and to determine an appropriate foundation stabilization technique to reduce the risk of sinkhole subsidence.

PHASE II

A site inspection was conducted in March 1990, when most of the site had been excavated to at or near the approximate +60 planned elevation of the liner bottom. A soils transect map of the +60 surface was prepared at FDER's request with the intent of defining potentially raveling sand areas that might require improvement. Potentially raveling sand was defined as gap-graded sand with very few (less than 5%) fine particles passing the US Sieve Size No. 200. Site inspection of surficial materials indicated that approximately half of the Cell III-B bottom liner area (5 of 10 acres) exhibited potentially raveling sand at elevation +60.

Trenching work was then performed with a backhoe to better define the depth profiles in these sands. This, in turn, led to additional concerns about the horizontal extent of raveled sands under the areas which showed clay at the +60 surface. It was thus decided to perform a major extension of the investigation, designated Phase III.

PHASE III

This investigation phase consisted of 36 additional mechanical CPT soundings and ground penetrating radar (GPR). This work was intended to be the precursor to a more extensive investigation, the scope of which would depend on the phase III investigative findings. (GPR) profiles were performed on 30m centers two ways across the site. The CPT and GPR results were used to guide the final phase of the exploration program, Phase IV.

PHASE IV

Based on the available data from the phases I,II,and III investigations, an additional 60 CPT sounding locations were selected. These were completed during April 1990. Seven additional SPT borings were performed adjacent to previous CPT soundings to provide specific comparisons between CPT data and SPT soil data in order to confirm CPT soil descriptions. Lastly, five Dilatometer (DMT) soundings were performed around the site to better establish the compressibility characteristics of the various types of soil existing under the liner. The DMT soundings were also performed in April 1990.

To supplement available groundwater data, 6 to 7.5m lengths of PVC pipe (2.5cm O.D. with slotted lower sections) were installed in 38 completed CPT holes to provide for water level determination and monitoring. Five 6m long, 5cm O.D. PVC pipes with 1.5m screened intervals were augered in place to verify the groundwater readings obtained from the 2.5cm O.D. piezometers in selected locations.

REVIEW OF GROUNDWATER CONDITIONS

The information from the Phase I investigation gave equilibrium water levels in the boreholes at about elevation +45. This was considered the approximate piezometric level in the underlying Ocala limestone, thus indicating little or no perched water table or artesian conditions.

The groundwater flow conditions within the overburden above the limerock surface appear to be the simple case of rainwater percolating to a groundwater level controlled by deeper piezometric levels. Such vertical flow is conducive to the vertically downward erosion of overburden sands into underlying rock cavities. The future presence of the III-B landfill and liner would essentially cut off this vertical flow and produce conditions unfavorable for sinkhole formation. However, concern still existed about possible lateral and vertical flow due to cycles in the piezometric level in the underlying limestone.

The long-term piezometric elevation fluctuations in the rock at this site are not fully known. However, groundwater levels are not expected to fluctuate the 4.5m required to reach the bottom of the cell liner.

ALL PHASES SUMMARY

The total field investigation included 21 SPT borings to a maximum depth of 35m, 102 CPT soundings to a maximum depth of 35m, 5 DMT soundings to a maximum depth of 18m, 43 water level monitoring locations, a GPR survey along 30m grid lines in perpendicular directions, 2 resistivity surveys, and a +60 surface soil transect survey. These results were used to design a supplemental compaction grouting program to reduce sinkhole and subsidence potential and reduce potential overall landfill foundation settlements.

THE REMEDIAL GROUTING PROGRAM

Based on the previously described foundation stabilization requirements, a deep compaction grouting program was developed intended to reduce overall settlement to .15m, and reduce the potential for future sinkholes to occur. The grouting plan was developed based on the results of the intensive geotechnical/geological investigation and guidance provided by a specialty contractor.

The main purpose of the grouting program was to provide protection against sinkhole formation by stabilizing those areas that have a higher risk for sinkhole formation, based on the extensive exploration work previously described. It was not expected that sinkholes would form without the grouting, but rather that grouting would further reduce the possibility that sinkhole subsidence could develop under the liner system.

It was felt that the completed grouting would have only a minor, negligible effect on groundwater conditions within the overburden. Based on Dr. Schmertmann's experience, it was estimated that no more than 20% of the contact area between limestone and overburden would be covered by grout. The remaining 80% should provide ample seepage paths to allow the low-gradient groundwater flow movements described previously.

COMPACTION GROUTING

Compaction grouting, was used to stabilize the Cell III-B foundation. Compaction grouting typically consists of a volumetric mixture of 10% cement and 90% sand, with possible additives to control setting time, pumpability, and slump. Compaction grout is mixed in a continuous-run grout plant and pumped at a very low slump, typically 5 to 10cm. Compaction grout does not flow away from the point where it is injected but instead forms a pressure bulb of grout which expands in diameter as the pressure increases. Injection pressures can become quite large, typically 700 to 2000kPa, typically much higher than with slurry grouting.

The result of the displacement is a compaction of the surrounding soils displaced by the grout. The high stresses tend to also result in beneficial higher residual stresses in the ground after compaction completion. Figure 5 shows the compaction grouting design concept used for this project. The grout columns are founded on limerock for good foundation support, while allowing for the arching action stress transfer to the columns by the enhanced shear action produced by the compaction grouting.

Several references describe the compaction grouting methods for preventing sinkholes or for doing remedial work after sinkholes have formed (see Henry

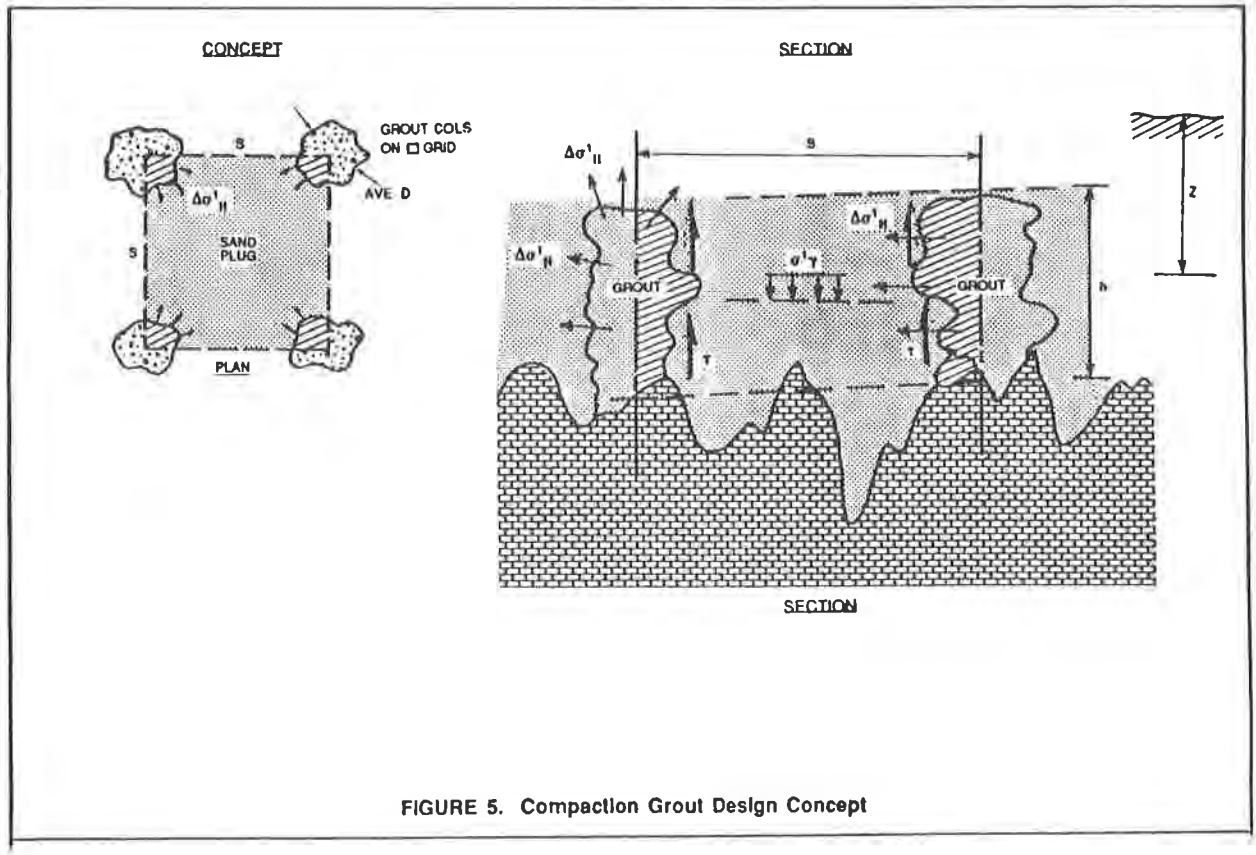

FIGURE 5. Compaction Grout Design Concept

Several references describe the compaction grouting methods for preventing sinkholes or for doing remedial work after sinkholes have formed (see Henry (1986,1989)). Wilson and Beck (1987) also describe a sinkhole-threatened landfill liner support problem where compaction grouting was used to correct the problem. It presumably took thousands of years for the geological processes to form the raveled soils present on site. If these soils can be densified by compaction grouting, it will presumably again take thousands of years for the raveling process to again threaten to form sinkholes. This is in addition to the stabilizing effect of eliminating vertical groundwater flow because of the capture of all the rainwater by the liner system.

THE PROPOSED GROUTING PLAN

Cell III-B site conditions are variable and not clearly definable; however, the extensive investigation described herein defined areas where significant raveling has or may have occurred. Those areas were treated with compaction grouting.

After review of the available data, three classifications of areas were created where, as a first approximation, it appeared that; 1) grouting would clearly be of benefit, 2) would clearly not be necessary, and 3) where there was some uncertainty. These preliminary classifications were then reviewed for patterns to define nine areas which should receive primary coverage with compaction grouting. Depending on actual grout take and grout pressures during primary grout construction, those areas which did not meet specified grouting objectives would be further stabilized with additional grout points located between the primary point.

In addition, if the primary coverage showed that the originally planned pattern should be extended outward, it could be so extended.

In this way, the grouting program itself would form the final, Phase V process of site investigation. Based on judgement, literature information, and experience, a 20 foot grid pattern was selected for the primary coverage.

The grout design objective was to reduce sinkhole potential by constructing an 11 foot thick zone of compaction grout, including the compacted and horizontally densified sand, covering those areas of limerock surface most likely to provide points for sand ravel inflow and subsequent sinkholes.

GROUT CONSTRUCTION

Grout construction was performed by a specialty contractor in accordance with specifications prepared by consultants, and approved by FDER. The low-slump compaction grout column was intended to compact any raveling soils between the grout columns to form a mat-type arching zone, supporting the landfill overburden. Initial grouting layout results were supplemented with additional grout points to maximize the stabilization benefits. More detailed information on this extensive grouting program can be obtained in Parker, (1991).

POST GROUTING SPT BORING CHECKS

In accordance with FDER requirements, Standard Penetration test borings were performed after completion of the grouting program (SPT, ASTM D1586) to check the effectiveness of the compaction grouting. It was agreed with FDER to use a minimum of 1 SPT check boring per 10 primary grout points. With a total of 311 primary grout points having been performed, a minimum of 32 SPT check borings were required. This minimum was met and exceeded by performing a total of 38 borings. All borings were located in-between actual grout locations so as to test grout-compacted soils instead of grout. The check borings were distributed approximately randomly over the nine grouted areas and in approximate accord with the number of primary points in each area.

The preset minimum acceptable SPT N-values were: depth divided by 10 for clean sands (SP or SW) and depth divided by 20 for silty sands (SM). Clayey soils were exempt from minimum N-value requirements since these soils would not readily ravel. All the SPT check borings showed after-grouting N-values that met or exceeded the preset minimum N-value requirements throughout the depth of the grout-mat zone in soil possibly susceptible to ravelling.

GROUTING SUMMARY

One method for assessing the overall reasonableness of the compaction grouting achieved for this project is to compare what was actually done vs. what was originally expected. Originally, 206 primary points were planned for this site with the assumption that field data would require approximately 188 more grout points. The total number of locations actually grouted totaled 400 (13 locations encountered limerock less than 3m deep and did not require pressure grouting). Actually, 1.5% more points were used, 10% more grout hole length was performed, and the total grout volume was 13% greater than expected; all in the conservative direction. Figure 6 outlines the grouting and SPT boring locations.

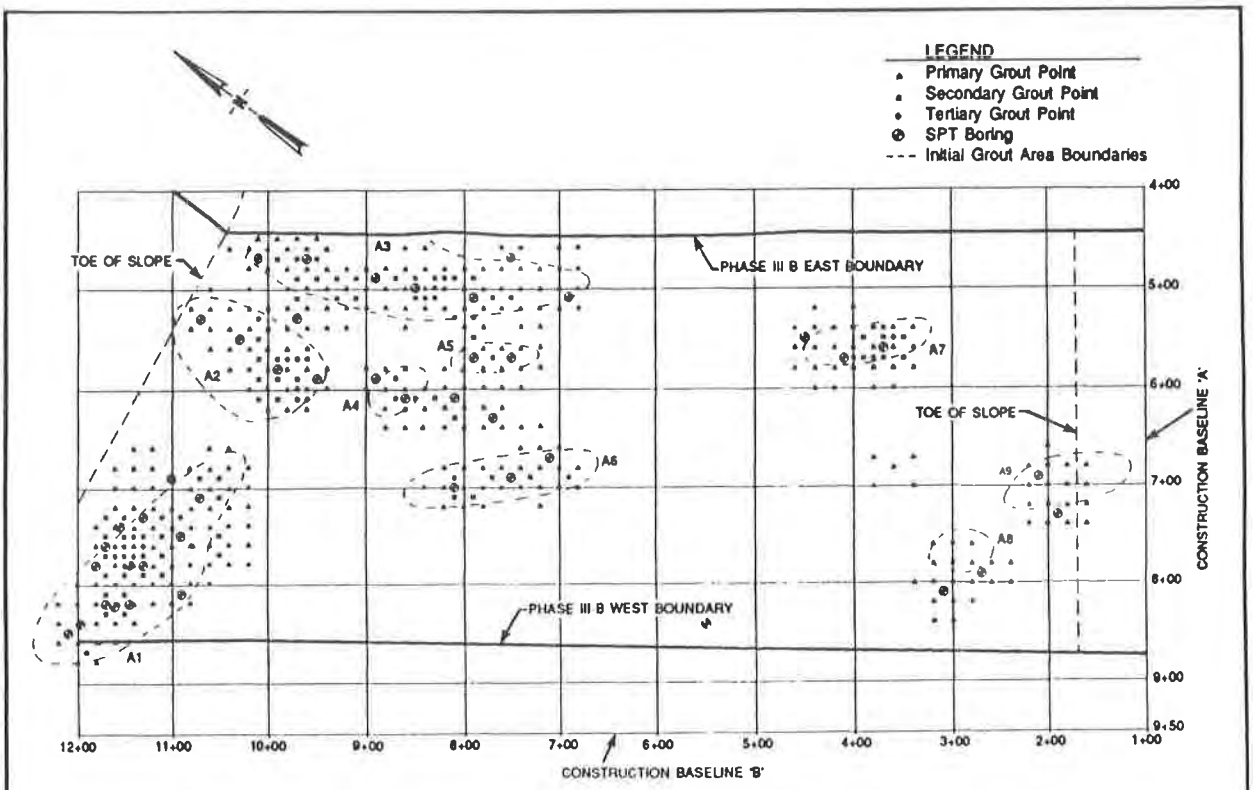

FIGURE 6. Final Grout Point and Check Boring Locations

The purpose of the compaction grouting was to reduce sinkhole potential and potential large differential settlements under the landfill liner system. The presence of the liner prevents vertical downward water flow, which greatly reduces sinkhole potential. The double geotextile layer reinforcement at the bottom of the liner system protects against subsidence should subsurface cavities form and eventually migrate upward to the liner. The arching in the landfill itself, and in the compacted geomembrane liner, and in the proofrolled 3M of soil below the liner also help protect against differential settlements.

In view of the supplemental nature of the compaction grouting and its implementation, as described herein, in good accord with the plans and expectations and specifications of the engineers involved. The FDER authorized the beginning of geotextile reinforcement installation in the fall, followed by liner construction in December 1990.

GEOTEXTILE REINFORCEMENT

As described, the second form of protection consisted of two layers of geotextile reinforcement. This reinforcement was designed to enhance landfill liner integrity by providing support in the event that a sinkhole developed. This section describes the design concepts, the material requirements and finally, the installation of the reinforcement.

DESIGN CONCEPT

The liner support concept has been presented previously (Giroud,et al,1987 Koerner, 1991) wherein a void or depression is assumed to develop under the geomembrane, which threatens the liner integrity. Geotextile reinforcement provides support for the liner over this assumed area, reducing deformations or strain in the liner system.

The strength required in design is determined by several factors, including the size of the assumed void, its shape, (i.e., circular, or strip-like) and the amount of overburden. Additionally, the strength and deformation characteristics of the reinforcement material is required as input, as well as whether the reinforcement will provide one directional or bi-directional strength. Figure 7 illustrates schematically the depressed shape of a geotextile supporting a geomembrane over a void area of radius 'R'.

Conditions assumed for design at the Baseline Marion County Landfill Cell III-B were a void in the overburden soils small sinkholes up to 1.5m in diameter, with only .15m local deflection.

The geotextile was to be installed in two layers, one at 90 degrees from the other. Seam strengths were assumed to develop only 50% of the geotextile tensile's strength. As a result no seams were allowed across the machine direction in either layer. This allowed the full material strength without reductions because of sewn seams to be utilized in design. The biaxial strength was determined to be the intact machine direction strength added to the seam strength for each direction.

GEOTEXTILE MATERIAL REQUIREMENTS

Geotextile specification requirements called for a woven high strength polyester material which achieved a minimum average roll (MARV) ultimate wide width strip tensile strength of 77 kN/m in the machine and x-machine direction at 10% strain, determined using ASTM D4595 test procedures.

Additionally, each layer required sewing of the individual rolls into one complete panel. This required that the two geotextile layers would be field fabricated to completely cover the site area. Seams were stitched, J type, with two parallel rows of stitchlines.

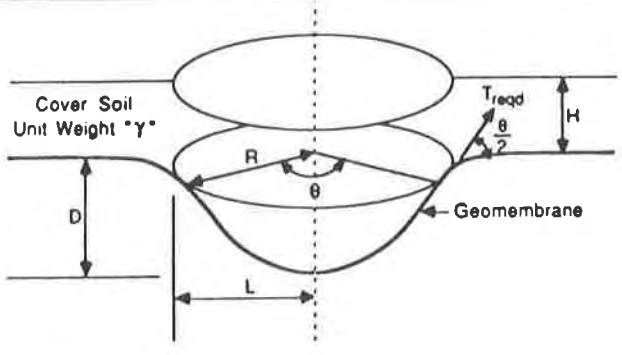

Fig. 7. Tensile stresses in a geomembrane mobilized by cover soil and caused by subsidence. (after Koerner)

Minimum and average seam efficiencies were specified to be 40 and 50 percent of the unseamed strength, respectively, based on ASTM D4595 testing on cut-piece field samples taken from every 228m of seam. Both pre-installation, and onsite sampled conformance testing of material was required as part of the contractors obligation. Numerous seam tests were performed during installation.

High tenacity polyester yarns exhibit excellent creep resistance, allowing very small long term creep strains and relatively high tensile strengths to be developed.

Manufacturing Requirements

The long dimension of the cell mandated an intact geotextile roll to be produced with unseamed lengths of more than 375m. Because of this, manufacturing required special care and attention. Each roll length was to be slightly different because the area to be covered by reinforcement Geotextile was not rectangular, but rather trapezoidal in shape. This was due to the angle the reinforcement layout pattern assumed when it came into contact with the previous cell surface on the existing northern slope (Figure 8).

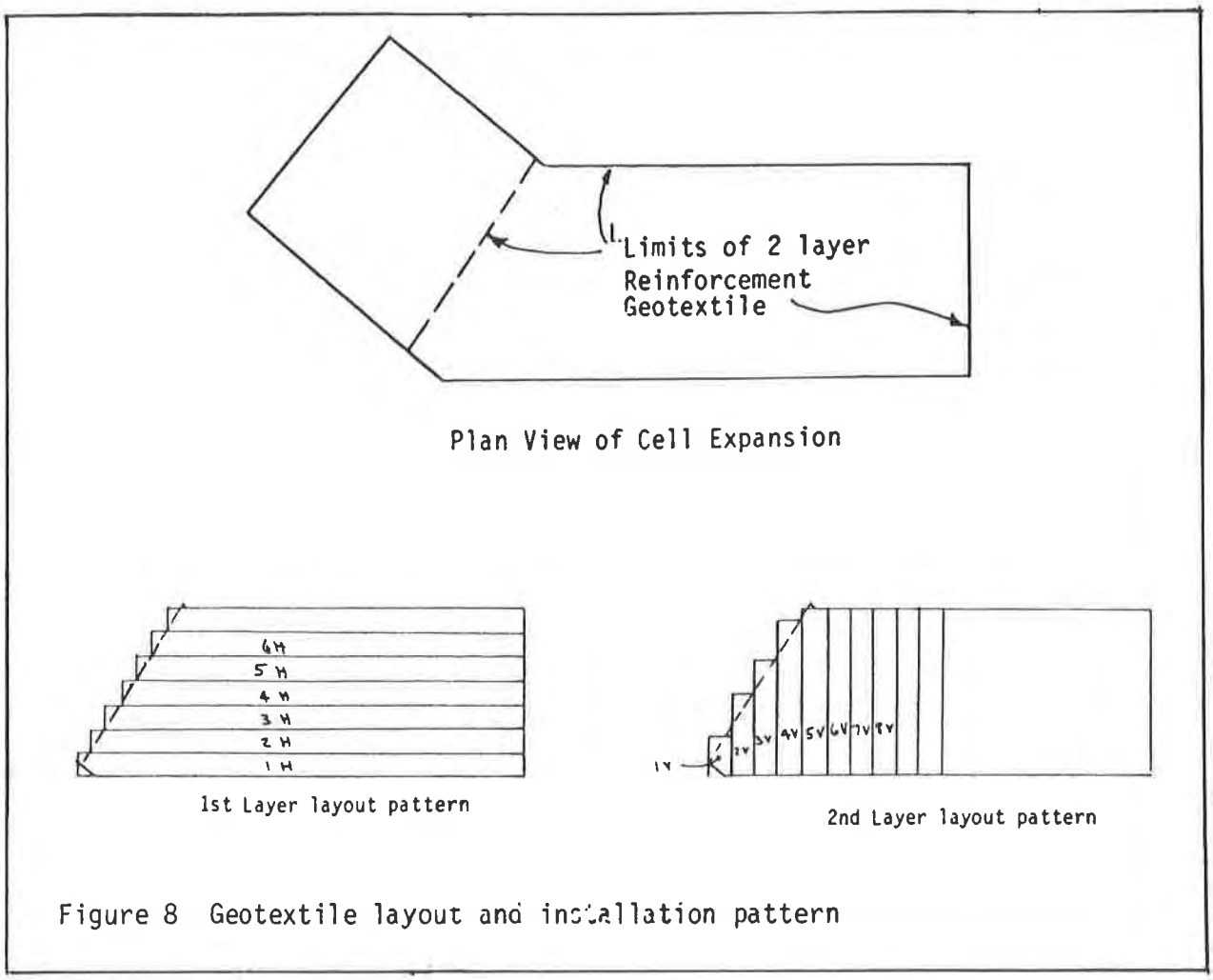

Figure 8 Geotextile layout and installation pattern

The geotextile supplied was woven into 3.75m width rolls approximately 450m long. This length meant roll lengths in the long direction could be cut from the roll, with the remaining piece used for the 90^{o} direction second layer. Roll weights of almost 680 kg required the use of steel cores to facilitate handling.

Geotextile Installation

The sequence of construction was to begin with the site grading, shaping the bottom of the new cell to facilitate drainage. A series of swales running across the cell bottom parallel to each other provided the drainage gradients across the site.

Once subgrade preparation was complete, and the site contoured to the leak detection system lines and grades, the geotextile installation began. The long dimension layer was placed first, with each roll unrolled, cut to the appropriate length. The remainder of that roll was retagged and stored for later installation in the 90^{o} direction. Each roll was laid out, cut to the proper length, then sewn to the previously installed roll. Seams were all sewn in the 'up' position, for visual inspection.

These long roll lengths, and the accompanying weight required that steel cores be used in the roll manufacturing process. This allowed field equipment to attach to the end of the rolls, then unroll the roll of material. This equipment was rubber tired, with low contact pressures. Care was taken by the installation contractor to not turn sharply or stop abruptly when running over the geotextile. The two layer design required that equipment be allowed on top of the Geotextile to sew the upper layer.

All seams were sewn using a machine which sews a two parallel stitchlines and a lock-type stitch. The weight of the machine required it to be vehicle mounted. The sewing machine was hung from a boom attached to the back of a small, four-wheel rubber tired one person vehicle. A portable generator was mounted on the front of the vehicle for balance, and to provide power to the machine. High strength polyester sewing thread was used to sew the seams. Once a new roll was sewn onto the panel, it was pulled smooth and tight, then prepared for the next roll to be unrolled and sewn.

Field sewing took approximately two weeks, from start to finish. A four man crew was utilized for the sewing and positioning of the geotextile. Seam samples were selected by the field engineer for outside testing at pre-selected locations over the site. All exceeded the specified requirements.

CONCLUSIONS

The unique subsurface conditions of this site mandated that a three component prevention and protection approach be used to design the foundation support system for the III-B Cell in Marion County, Florida. A compaction grouting program was developed and executed to minimize or eliminate the potential for sinkhole development.

This was followed by a two-layer geotextile reinforcement design and installation to provide liner support and maintain liner integrity. This reinforcement was designed to support the landfill overburden in the remote event that subsidence developed at a later date. The two layers were positioned at 90^{o} to each other and field sewn.

The geomembrane liner provided the isolation medium that would contain leachate and eliminate the potential for water flow into the underlying soils, potentially initiating sinkhole development. This was the third component in the three component design.

Both the grouting programs and geosynthetic installation were essentially completed in late 1990, and the landfill is operational today.

ACKNOWLEDGMENTS

Sincere thanks go to Dr. J. H. Schmertmann for his assistance throughout this project. The successful review of this innovative project design by FDER was significantly due to his efforts.

The geotextile field sewing and installation was performed by Geosynthetic Systems of Pembroke, GA, as a subcontractor to Phoenix Construction Services, Inc., general contractors for Cell III-B Construction.

Exxon Chemical GTF-550T was selected for this application. This is a high strength reinforcement geotextile, one of a series from the Custom Engineered Fabrics family of products.

Hayward Baker Inc. Contributed significantly to the design of and field construction for the grouting program.

REFERENCES

J.F. Henry (1986), "Low Slump Compaction Grouting for Correction of Central Florida Sinkholes," presented at a conference titled "environmental Problems in Karst Terrain and Their Solutions," Bowling Green, KY, Oct. 28-30, 6 pp. (Reprints available from GKN-Hayward Baker, (813) 844-3441).

J.F. Henry (1989), "Ground Modification Techniques Applied to Sinkhole Remediation," Proceedings, Third Multi-Disciplinary Conf. on Sinkholes, Florida Sinkhole Institute, pp. 327-332.

W.L. Wilson and B.F. Beck (1987), "Investigation of Karst-Related Subsidence Near The Southwest Landfill, Alachua County, FL, Using Ground Penetrating Radar," Florida Sinkhole Research Institute Report No. 87-88-1.

J.P. Giroud, et al (1987) "Load Carrying Capacity of a Soil Layer Supported by a Geosynthetic Located on a Void," proceedings of the International Geotechnical Symposium Theory and Practice of Soil Reinforcement. Kyushu, Japan, Balkema, Rotterdam pp. 185-90.

R.M. Koerner, and Bao-Lin HWU (1991) "Stability and Tension Considerations Regarding Cover Soils on Geomembrane Lined Slopes," Geotextiles and Geomembranes Vol. 10 No. 4, Elsevier Publications, pp. 335-355.

L.W. Parker, (1991) "Compaction Grouting Stabilizes Landfill Foundation" Project Report 9095-000-00, Jones, Edmunds and Associates, Inc Gainesville, Fl

Installation of Geosynthetic Materials for Seepage Control at the Black Mountain (Arizona) Operating Reservoir

A.I. Comer
U.S. Bureau of Reclamation, USA

R.E. Straubinger
U.S. Bureau of Reclamation, USA

ABSTRACT

In the summer of 1990, approximately 9.3 hectares (23 acres) of 1.14-mm (45 mils) PVC geomembrane were used to line the Black Mountain Operating Reservoir, located about 14.5 kilometers (9 miles) southwest of Tucson, Arizona. This water-regulating/storage reservoir was designed by the Bureau of Reclamation, and constructed as part of the Central Arizona Project. The geomembrane was anchored at the top of the side slopes in a "V"-shaped soil trench and at concrete structures by a solvent weld to an embedded PVC anchor strip. On the 3H:1V side slopes, a geotextile was used to provide protection for the geomembrane during placement of the riprap on the side slopes. To protect the PVC during cleaning operations, the bottom of the reservoir was covered with a 150-mm (6 inch) thick layer of unreinforced concrete. While on a site visit, we noted a condition where non-yielding point contacts, between the small, sharp rocks under the geomembrane and the reservoir concrete lining above the geomembrane, might puncture the liner following an application of a vertical load to the concrete. This concern, led to a laboratory investigation which would evaluate the effect of point loading on the geomembrane. This paper summarizes the construction activities associated with the installation of the geosynthetic materials in the Black Mountain Operating Reservoir, the design details associated with the attachment of the geomembrane to concrete structures, and the possible effect of small aggregate point loads on the geomembrane as revealed by the subsequent laboratory investigation.

INTRODUCTION

The Black Mountain Operating Reservoir (BMOR), located approximately 14.5 kilometers (9 miles) southwest of Tucson, Arizona, (Figure 1), was constructed, in 1990, to minimize on-peak pumping at the Black Mountain pumping plant (BMPP) by providing adequate storage for the worst case mismatch conditions of water demand and delivery schedules. This storage provides sufficient water to reduce the number of pump starts and stops as water is delivered from this part of the system. The delivered water will be used by the San Xavier Indians for land irrigation.

Reclamation's typical water level drawdown rate is 150 mm (6 inches) in the first hour or a uniform rate of 300 mm (1 foot) per day. In order to permit a faster than typical drawdown rate of 6.1 m/day (20 foot/day), a watertight lining design was selected. A conventional reinforced concrete lining system would require the use of an underdrain system, and when combined with site constraints was deemed too expensive. Therefore, a geomembrane liner system was selected as the primary means of water retention in the reservoir.

DESIGN CONSIDERATIONS

Geomembrane

The decision to use a geomembrane liner as the primary means of water retention in the reservoir made it possible to choose from a wide range of geomembrane lining system possibilities. Each lining system had several advantages and disadvantages depending on the material selected and if the geomembrane would be left exposed to sunlight. Initially three geomembrane materials (all 1.02-mm (40 mils) thick) were proposed: polyvinyl chloride (PVC), high density polyethylene (HDPE), and very low density polyethylene (VLDPE). The latter two liners were considered both as covered and exposed liners because they were considered ultra-violet-resistant. The remoteness of the site, with its attraction to wildlife and vandalism precluded the use of an exposed geomembrane lining system because of the geomembrane damage potential. The VLDPE liner was dropped from consideration because it was a fairly new material at the time and Reclamation did not have enough long-term experience to warrant using this material in this critical application.

Protective Cover Material

With the selection of a covered geomembrane lining system, the designer began considering different types of cover materials. Reclamation has over 20 years of experience using locally excavated soils as the cover material for PVC-lined canals.[1] These soils are generally easy to place and inexpensive. When a soil thickness of 250 mm (10 inches) plus an additional 25.4 mm (1 inch) for each 300 mm (1 foot) of water depth is used, the soil can protect the geomembrane from the elements, animal traffic, vandalism, and mechanical damage during canal cleaning operations. An initial thickness of 460 mm (18 inches) of clayey or silty sands was specified for placement on the reservoir invert. However, further evaluation of design criteria showed that this soil depth or cover would not satisfy the design requirements. A 910-mm (36 inches) thick soil layer would have to be used wherever construction haul roads were located. This additional material in excess of 460 mm (18 inches) design thickness would have to be removed prior to job completion.

A large shallow reservoir with a soil bottom could easily support plant growth, thus leading to an ongoing O&M problem. Draining the reservoir and cleaning the reservoir bottom would be a problem due to the amount of time it would take for clayey sand to dry out enough to support equipment loads, and there would be an increased risk of damaging the geomembrane if too much soil cover is removed. Due to problems with a soil cover, consideration was given to using either soil-cement, or reinforced or unreinforced concrete. Soil-cement was not specified because the local soils were not

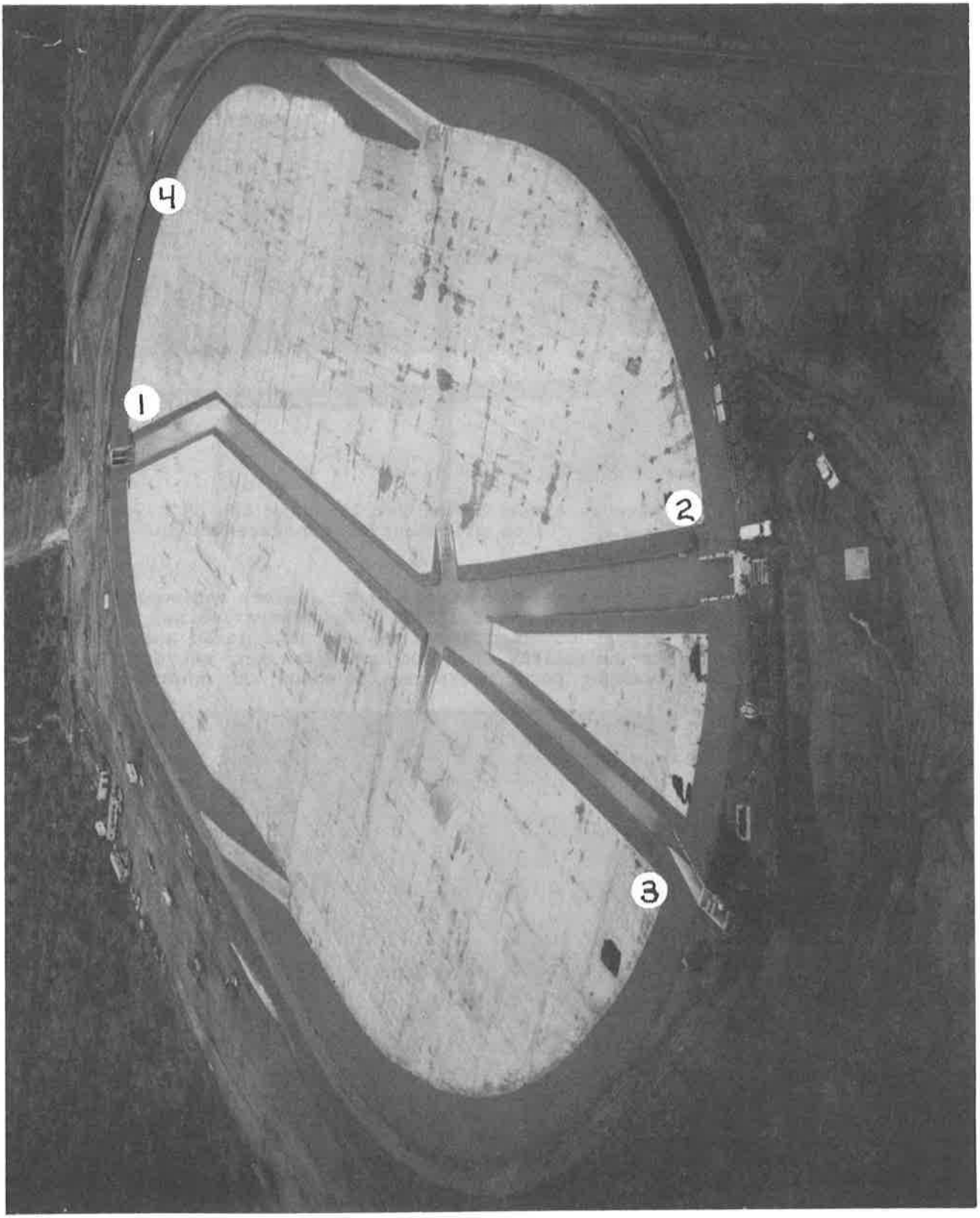

Figure 1: An October 2, 1990, aerial view of the Black Mountain Operating Reservoir during its construction. Looking south. 1) Reach Six Inlet Structure. 2) The San Xavier Turnout. 3) Black Mountain Outlet Structure. 4) Emergency Spillway.

conducive to use in soil-cement and because all construction traffic would be prohibited for a minimum of 7 days to permit sufficient strength development. These restrictions, when combined with the site geometry, led to the selection of a 150-mm (6 inches) thick unreinforced concrete cover for the geomembrane-lined reservoir invert. Figure 2 shows the lining system during construction.

Figure 2: A section of PVC liner in the BMOR invert prior to placement of concrete cover.

Design considerations for the cover material on the 3H:1V side slopes were different from those used on the reservoir invert. The cover material must be stable during normal reservoir operations and not break down under temperature extremes. The native soils are sensitive to excess pore pressure and would be unstable when subjected to the proposed operating conditions. Consideration was then given to using either a concrete or riprap cover. Shotcrete was considered and was rejected because of concerns about its durability when subjected to many wet/dry or hot/cold cycles and concerns that excess pore pressures between the shotcrete and the geomembrane could displace the shotcrete during rapid drawdown operations. If a smooth lining was utilized instead of a rough riprap type surface, the freeboard requirements would be increased by 40 percent.[2] Since riprap was free draining, durable, and stable on a 3:1 side slope (Figure 3), it was selected for use on the side slopes.

Figure 3: Placement of riprap protection on the 3:1 side slope.

Installation of the riprap over the geomembrane required special construction considerations in order to protect the geomembrane from damage. The use of a geotextile between the riprap and the geomembrane provides the necessary

geomembrane protection, but it also introduces some stability problems. Where riprap would be stable if placed over either a geotextile or a geomembrane on a soil foundation, it might not remain in place if a geotextile was sandwiched between the riprap and the geomembrane. The side slope stability of the various materials depends on the shear friction characteristics between the materials, rather than the tensile capacity of either material. The failure slip surface or the minimum friction angle between material interfaces occurs at the geomembrane-to-geotextile interface. The interface friction angle has to exceed the tangent of the embankment slope, or 18.43 degrees in this design, in order to be stable. For a HDPE to geotextile interface, the friction angle was 9 degrees, as compared to the PVC-to-geotextile friction angle of 23 degrees.[3] Thus, only the PVC geomembrane was selected for use. The initial proposed liner thickness of 1.02 mm (40 mils) was increased to 1.14 mm (45 mils) when rigid concrete was selected as the cover material for the reservoir invert.

Attachment to Concrete Structures

There are four main structures on the BMOR, the Black Mountain Outlet Structure, the San Xavier Turnout, the Reach Six Inlet Structure, and the Emergency Spillway. These structures have to tie into the geomembrane lining system in order for the whole system to be watertight. Since three structures were placed adjacent to a depressed channel in the reservoir, the interface point between the liner and the structures was more complicated than a simple pipe penetration through the geomembrane.

There are two basic ways of attaching the geomembrane to concrete structures. A watertight connection can be obtained either by using batten strips to attach the geomembrane to the concrete or by embedding a geosynthetic anchor strip in the concrete and field seaming the geomembrane to the anchor strip. The batten strip method has typically been used for this type of work, but was not used for this job because of some inherent problems.

The batten strip method is a mechanical type connection that obtains its seal by sandwiching either a full-bodied adhesive/mastic or neoprene closed cell foam between the concrete and the geomembrane. Then pressure is applied to the system via the

Figure 4: A geosynthetic anchor strip, compound bend at left side of inlet structure.

Figure 5: A geosynthetic anchor strip, compound bend at right side of inlet structure.

batten strips. Typically the batten strip is held tightly against the concrete structure by expansion anchor bolts threaded into expansion anchor inserts in the concrete, usually located on 150- to 300-mm (6- to 12-inch) centers. The batten strip can be constructed of either wood or metal, but is usually a 6.5- by 100-mm (1/4- by 4-inch) wide stainless steel strip because it is more durable. Water leakage past the joint is very much dependent on the long-term integrity of the batten strip, the anchor bolts, and the mastic/foam sealer. There are few mastic/adhesives that can bond to both concrete and PVC. Thus, a seal is obtained through the application of a constant mechanically-induced pressure. This pressure can easily be lost through the corrosion of the metal batten strips or the anchor bolts, slippage of the expansion anchor, deterioration of the foam, mastic, or adhesive utilized in the joint, or simply because a reasonably sized expansion anchor cannot provide a large enough normal force to the batten strip.

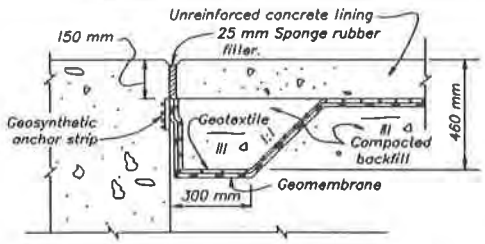

FIGURE 6A TYPICAL SECTION WHERE UNREINFORCED CONCRETE LINING JOINS STRUCTURE

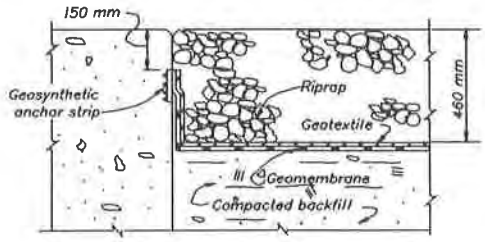

FIGURE 6B. TYPICAL SECTION WHERE RIPRAP JOINS STRUCTURE (NORMAL TO SLOPE)

FIGURE 6. GEOMEMBRANE ATTACHMENT TO CONCRETE STRUCTURES

The embedded geosynthetic anchor strip does not have these problems. The geosynthetic anchor strip's embedment in the concrete forms the watertight seal between the dissimilar concrete and PVC materials. The PVC geomembrane can be field-seamed to the anchor strip. This joint is not expected to deteriorate with time. The solvent-welded field seam is very easy to inspect and test for watertightness. But this type of joint is hard to repair if the geosynthetic anchor strip is dislodged from its concrete embedment or is not installed during the initial concrete placements. Careful installation of the geosynthetic anchor strip is necessary as it is either bent or transitioned around corners of the concrete structures. Butt welds or splices in the geosynthetic anchor strip are relatively easy to make in the field, while field construction of compound bends (combined bends in two different planes occurring at the same point) in the field is much more difficult, as illustrated by Figures 4 and 5. Factory joints can greatly improve the quality of the joints, and eliminate some of the joint discontinuities that can occur if the proper deflection angle of the anchor strip joint is made.

The geomembrane-to-structure attachment details, as shown in Figures 6 and 7, show how the geomembrane is transitioned from its basically horizontal position on the reservoir invert to the vertical face of the structure. The geomembrane was transitioned in this way to limit the amount of load or stress being transferred from the geomembrane into the geosynthetic anchor strip and then into the concrete structure. These details utilize the geosynthetic material's best characteristics while limiting the adverse impacts.

The embedded geosynthetic anchor strip can handle shearing load transfers much better than normally applied tensile loads. Similarly, an overlapped seam loaded in shear is 3 times stronger than an overlapped seam loaded by a normal

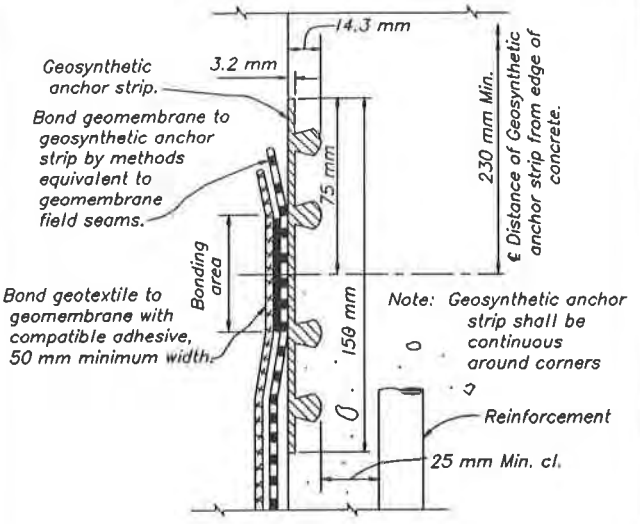

FIGURE 7. GEOSYNTHETIC ANCHOR STRIP DETAIL
(150 mm PVC Base Seal Shown)

tensile load that would tend to peel the seam apart.[3] The 300-mm (1 foot) vertical rise in the geomembrane before its attachment to the anchor strip allows for load distribution from the probable point of load application to the point of load resistance. The PVC geomembrane elongation characteristics can be fully utilized by these design details. The continuous solvent seam weld of the geomembrane to the anchor strip will be subjected to considerably less stress concentration when compared with the typical batten strip method of geomembrane attachment. By design the geomembrane is supposed to be installed in a slack condition, thus further limiting the amount of load that has to be carried by the geomembrane attachment to the structures.

Figure 8: Geomembrane over one of the small, sharp rocks.

CONSTRUCTION

The geomembrane was installed in accordance with the specifications [4], however, in retrospect, there were some details pertinent to the geomembrane subgrade preparation and the liner attachment to structures that we believe should be improved to enhance the long-term serviceability of the liner.

During construction a large number of unavoidable, small, sharp rocks were observed beneath the geomembrane. Figure 8 shows the geomembrane over one of these rocks. The rolled subgrade was so firm that the small rocks could not be forced into the subgrade just by a man standing on them. The nonyielding point contact between the small sharp rocks under the geomembrane and the reservoir concrete lining above the geomembrane might puncture the liner when a load is applied to the concrete. Additionally the effect of elevated temperatures on the puncture resistance of the geomembrane was a concern. The sharp, smaller than 19-mm (3/4 inch) size aggregate could affect the geomembrane when the liner softened during hot temperatures and then stiffened with cool temperatures. These effects had not previously been studied in the laboratory. As a result, a laboratory investigation was initiated to study point loading of a geomembrane following its exposure to elevated temperatures.

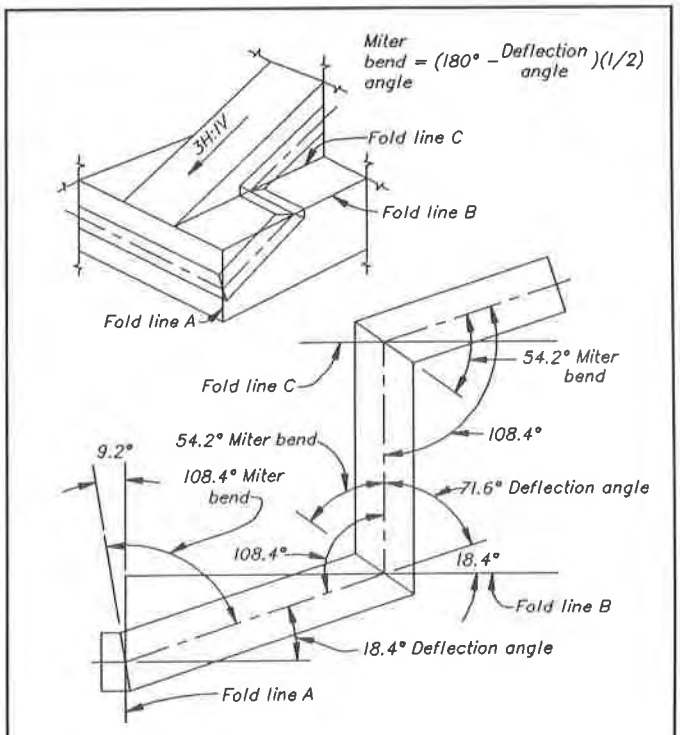

Figure 9: Miter bend details. Shows how the anchor strip bends or folds around corners.

Another area for consideration included our observations of a new method of attaching the geomembrane to structures. The use of an embedded PVC anchor strip has much promise, but some portions of the anchor strip installation highlights the need for detailed drawings whenever the anchor strip makes a bi-directional or compound bend. Figure 9 illustrates the

proper construction and alignment of a miter bend angle in relationship to a bi-directional, bi-plane bend. Figures 4 and 5 illustrate what might be assembled if the contractor tries to align the miter bend parallel to only one of the bend's axes, without regard to the bi-directional, bi-plane nature of a compound bend. Any compound bend can be described in terms of a single in-plane deflection angle, which in turn can be used to determine the proper miter bend angle. Typically a simple in-plane miter bend, or butt joint, can be made in the field, especially when the length of the joint is less than 1.5 times the anchor strip's width. But when the miter bend is an odd angle, is greater than 1.5 times the width, or is between two different planes a special jig is needed to aid in the joint construction. Fold lines B or C in Figure 9 illustrate just such a joint. Due to the long joint lengths, the flexible anchor strips should be supported and assembled on either a large flat surface or a corner jig where appropriate. The use of factory constructed corner joints or multiple joint intersections can greatly increase the quality of the overall product.

Figure 10: Geomembrane attachment to emergency spillway. An area where the installation did not have enough slack thus the geomembrane was tented.

The authors did observe one contractor-related problem. When the geomembrane is attached to structures, it has to be placed loosely against the structure and the foundation soils. However, at the site, the liner was attached to the structure in a stretched condition, as if the liner was cut too short but made to fit anyway. Figure 10 shows this condition. The resulting tenting action of the geomembrane next to the structure could result in liner damage when the cover material is placed or when the reservoir is filled. The thermal expansion and contraction properties of the geomembrane have to be accommodated when attaching the geomembrane to structures. In general, the installation should occur either during the cooler portion of the day or with the appropriate amount of slack.

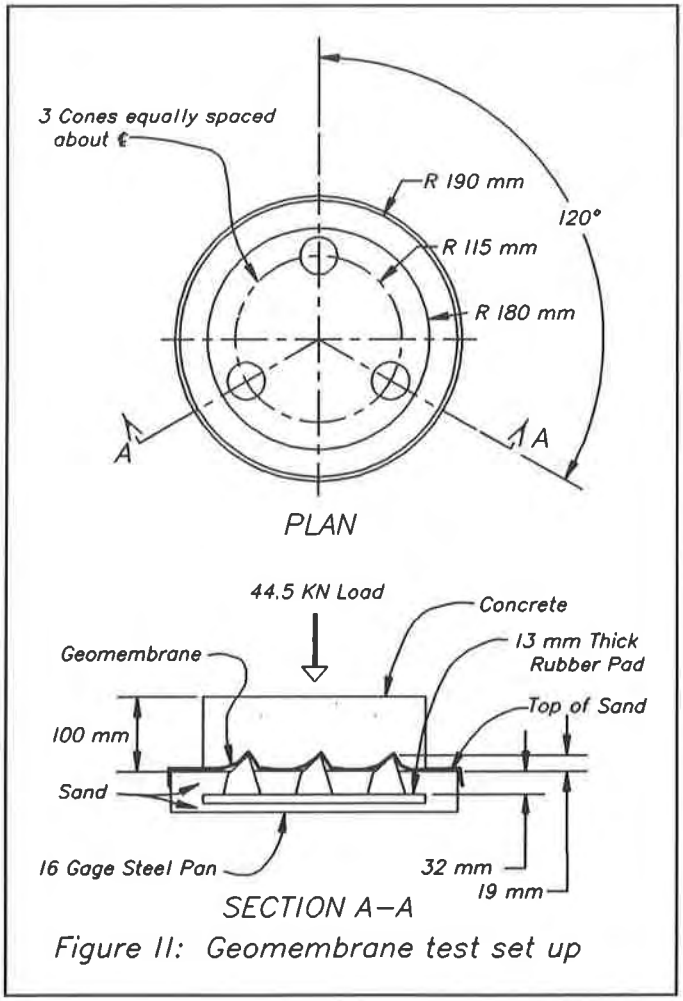

Figure 11: Geomembrane test set up

LABORATORY TESTING

Test Procedures

The laboratory test program developed to study the point loading of a geomembra-

ne, consisted of a series of 10 PVC geomembrane samples having the configuration shown in Figure 11. These samples were tempered in a calorimeter room maintained at 37.7 °C (100°F). This higher temperature was used to simulate actual conditions in Arizona. The samples were loaded with a vertical nearly instantaneous compressive force of 44.5 kN (10,000 lbf) after curing periods of 7, 28, and 90 days. The 44.5-kN load was intended to simulate an approximate loading of the concrete cover by a medium-sized front end loader that might be used to clean sediment out of the bottom of the reservoir. The load application rate was 11.1 kN/sec (2,500 lbf/sec).

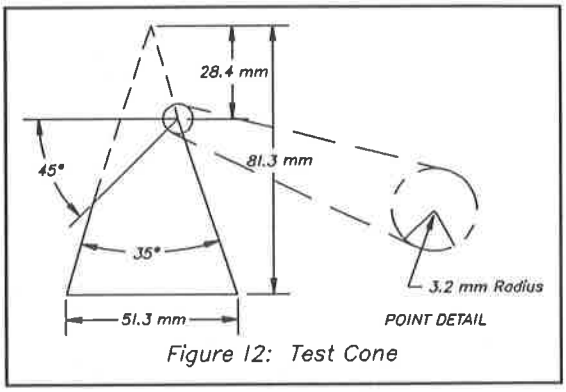

Figure 12: Test Cone

The subgrade for the concrete cover and geomembrane, consists of a rubber bearing pad, with three cones, partially covered by sand. The exposed cones will model the presence of small aggregate resting on a firm subgrade. The three cones are scaled down versions of the cone configuration in Geosynthetics Reaserch Institute (GRI) GM 3, test procedure, "Large Scale Hydrostatic Puncture Test." The test cones were machined of cast clear-acrylic rod to the dimensions shown in Figure 12 and bonded with rubber cement to a rubber bearing pad. The rubber bearing pad, with type A Durometer reading of 67, was intended to simulate the limited subgrade deformation which could take place beneath small aggregate particles. Sand was then placed over this system until approximately 19-mm (3/4 inch) of the cones protruded above the sand.

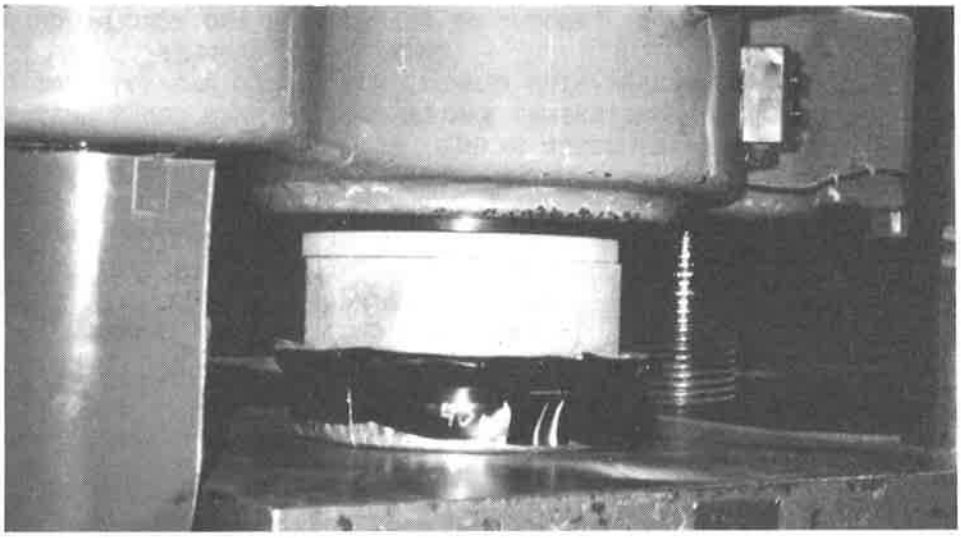
Figure 13: Test specimen ready to be loaded.

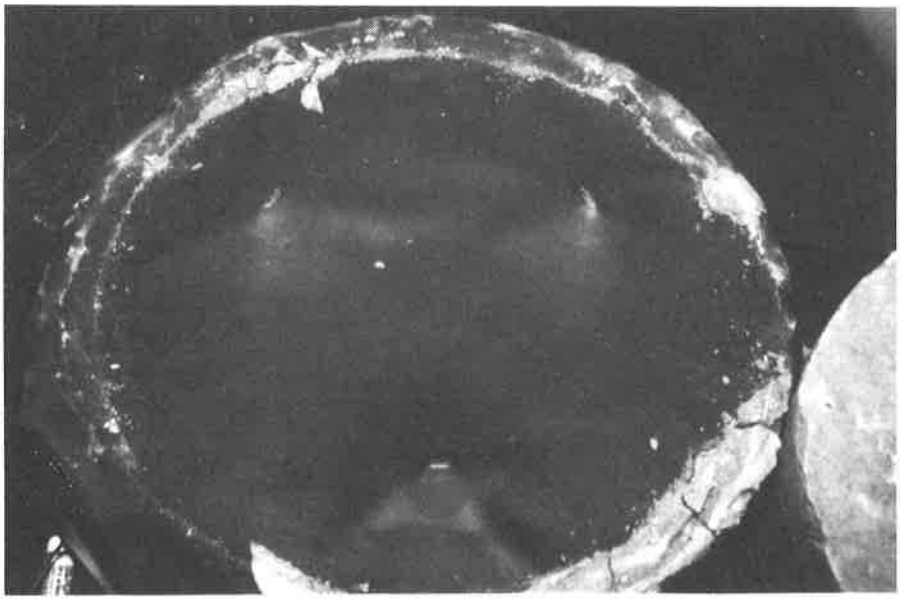
Figure 14: Test specimen after application of the test load and removal of the concrete cover.

The geomembrane was placed over the cones and anchored to the sides of the test pan, by a pipe clamp, to simulate actual field conditions limiting lateral movement of the geomembrane. Next,

a lift of fresh concrete was placed on top of the geomembrane. This concrete was allowed to cure at room temperature for approximately 4 hours before the entire test system was placed in a calorimeter room maintained at 37.7 °C (100°F). Samples were removed from this room just prior to vertical loading of the specimen with approximately 44.5-kN (10,000 lbf). Figure 13 shows a test specimen prior to loading. Figures 14 and 15 show a sample with the concrete cover removed after loading.

Test Results

The entire laboratory program took place over a 3-month period. Results are found in Tables I and II. Geomembrane samples were tested for plasticizer loss using ethyl ether (ASTM D-3421) and retained bi-axial strength by the Mullen Hydrostatic Burst strength (ASTM D-751, procedure A). For comparisons, each test period was preceded by a test of scrap parent material, followed by testing of unstressed and point-stressed test specimens both of which were heat tempered.

TABLE I - AMOUNT OF PLASTICIZER AND PERCENT CHANGE IN PVC GEOMEMBRANE SAMPLES

OS = BASE LINE SAMPLE, NOT LOADED AND NOT HEAT CURED
US = UNSTRESSED SAMPLE FROM BETWEEN CONES HEAT CURED
PS = STRESSED SAMPLE, HEAT CURED

SAMPLE NUMBER	GEOMEMBRANE THICKNESS mm (mils)	DAYS IN 37.7 °C CURING ROOM	LOAD TYPE	PERCENT OF PLASTICIZER IN SAMPLE	%DECREASE IN PLASTICIZER FROM OS
1	1.02 (40)	7	OS	32.4	0.0
			US	31.0	4.4
			PS	31.2	3.9
2	1.02 (40)	7	OS	32.4	0.0
			US	31.7	2.4
			PS	31.8	1.9
3	1.14 (45)	28	OS	29.7	0.0
			US	28.4	4.5
			PS	26.9	9.4
4	1.02 (40)	28	OS	32.8	0.0
			US	28.8	12.2
			PS	29.0	11.5
5	0.76 (30)	90	OS	28.9	0.0
			US	23.6	18.3
			PS	23.5	18.7
6	0.50 (20)	90	OS	30.8	0.0
			US	22.2	27.9
			PS	25.4	17.5
7	1.14 (45)	90	OS	30.4	0.0
			US	25.4	16.4
			PS	26.3	13.5
8	1.02 (40)	90	OS	32.9	0.0
			US	26.1	20.7
			PS	28.2	14.3
9	0.76 (30)	90	OS	28.9	0.0
			US	23.2	19.7
			PS	22.7	21.5
10	0.50 (20)	90	OS	30.9	0.0
			US	24.1	22.0
			PS	25.2	18.4

TABLE II - MULLEN BURST TEST RESULTS AND PERCENT CHANGE FOR THE VARIOUS PVC GEOMEMBRANE SAMPLES

OS = BASE LINE SAMPLE, NOT LOADED AND NOT HEAT CURED
US = UNSTRESSED SAMPLE FROM BETWEEN CONES HEAT CURED
PS = STRESSED SAMPLE FROM THE AREA DIRECTLY OVER THE CONES, HEAT CURED
KPa = psi x 6.89475

SAMPLE NUMBER	GEOMEMBRANE THICKNESS mm (MILS)	DAYS IN 37.7 °C CURING ROOM	LOAD TYPE	MULLEN BURST TEST IN KPa						
				SPECIMEN A	SPECIMEN B	SPECIMEN C	SPECIMEN D	SPECIMEN E	AVERAGE SPECIMEN VALUE	%CHANGE IN AVG VALUE TO AVG OS
1	1.02 (40)	7	OS	896	896	862	862	896	883	0.0
			US	862	862	896			873	1.0
			PS	793	827				810	8.2
2	1.02 (40)	7	OS		See	Sample	1		883	0.0
			US	896	931	896			908	-2.9
			PS	758	793				776	12.1
3	1.14 (45)	28	OS	1207	1207	1207	1207	1207	1207	0.0
			US	1241	1207	1276			1241	-2.9
			PS	1172	1207				1189	1.4
4	1.02 (40)	28	OS		See	Sample	1		883	0.0
			US	1034	1034	1034			1034	-17.2
			PS	931	896				914	-3.5
5	0.76 (30)	90	OS	758	793	793	793	827	793	0.0
			US	1103	1103	1000			1069	-34.8
			PS	1207	1172				1189	-50.0
6	0.50 (20)	90	OS	448	414	448	448	414	434	0.0
			US	448	724	621			598	-37.6
			PS	345	379				362	16.7
7	1.14 (45)	90	OS		See	Sample	3		1207	0.0
			US	1310	1586	1551			1482	-22.9
			PS	1276	1379				1327	-10.0
8	1.02 (40)	90	OS		See	Sample	1		883	0.0
			US	1207	1172	1241			1207	-36.7
			PS	965	1103				1034	-17.2
9	0.76 (30)	90	OS		See	Sample	5		793	0.0
			US	1069	1103	931			1034	-30.4
			PS	862	1482				1172	-47.8
10	0.50 (20)	90	OS		See	Sample	6		434	0.0
			US	621	621	689			644	-48.1
			PS	414	448				431	0.8

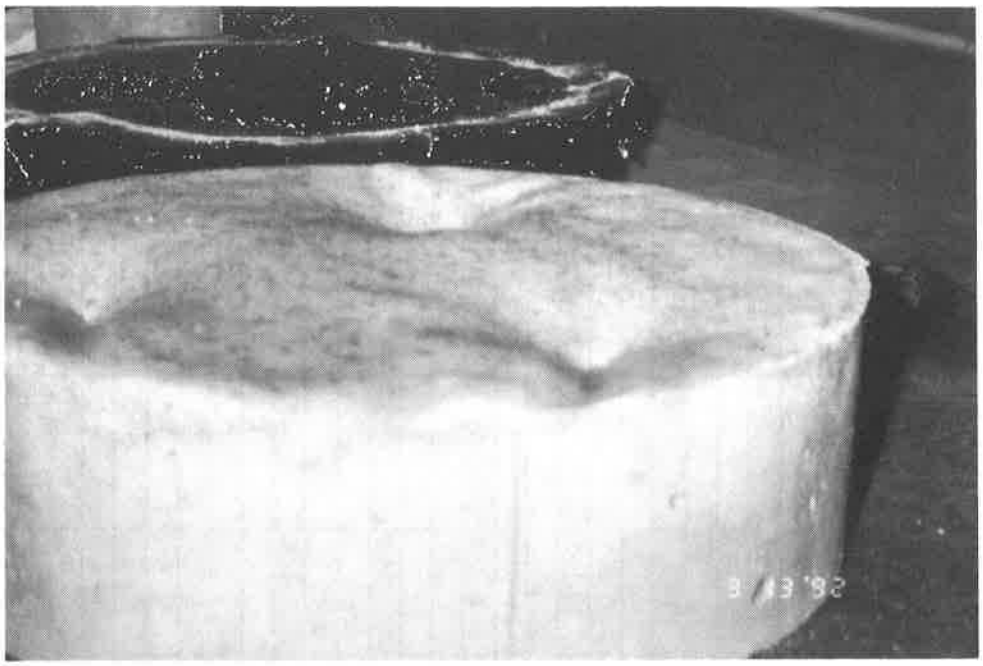

Figure 15: Concrete cover displaying signs of how the geomembrane was draped over the cones.

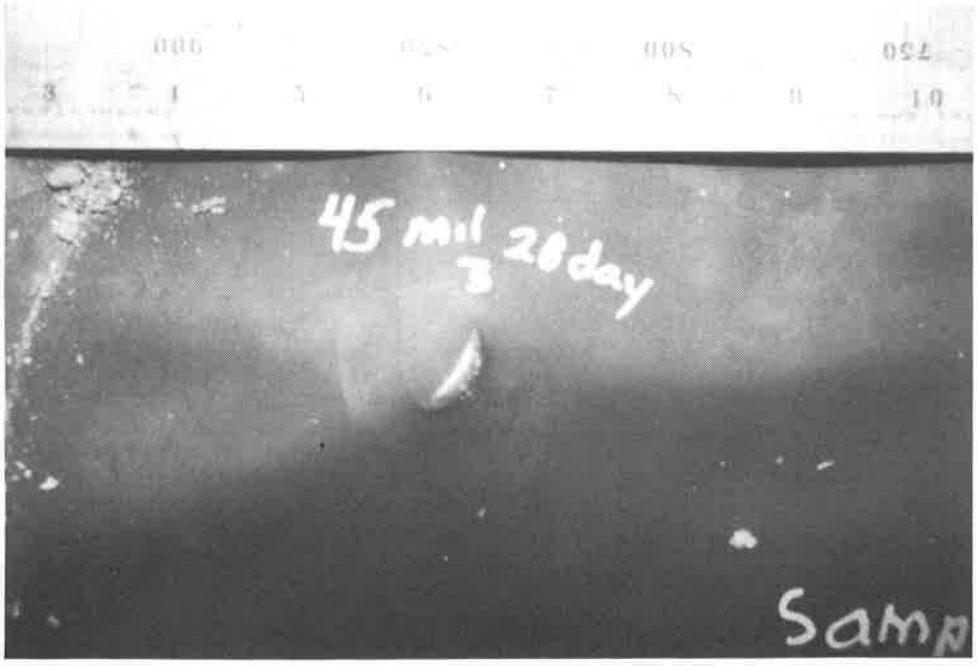

Figure 16: A 1.14 mm PVC geomembrane shows evidence of stretching at the cone point following the application of a 44.5 kN load to a sample tempered for 28 days.

As expected, the plasticizer loss increased with time in the elevated temperature exposure. When the geomembrane samples were loaded after being exposed to elevated temperatures, the cone-stressed portions of the samples had slightly less plasticizer than the unstressed-but-loaded samples. Slight change in geomembrane color around the point of the cones is an indication of this change (Figure 16). However, the measured differences may not be significant when considering the normal precision of the plasticizer measurement test and the limited number of specimens tested. In the case of the heat cured and stressed sample only one specimen per set was tested for plasticizer loss, while two specimens were tested for hydrostatic burst strength.

When the results from the Mullen Burst Hydrostatic test were studied, there was a greater loss in burst strength for the stressed and heat cured samples then there was with the samples that were only heat cured. The only exception to this observation was the 0.76 mm (30 mil) thick samples. The 28 and 90 day heat cured samples had burst strengths that were greater than the base line samples which were neither stressed nor heat cured. For the base line samples we were able to run 5 specimens or replicates per sample type and the standard deviation ranged from 18 to 24 kpa. For the heat cured but unstressed samples we were able to run 3 replicates per sample type. For the heat cured and stressed samples we were able to run 2 replicates per sample type. The latter two data sets may indicate trends but do not contain enough replicates to allow for significant statistical analysis.

CONCLUSIONS

The use of an embedded geosynthetic anchor strip is a viable method for attaching PVC geomembranes to structures. Where compound bends occur, a factory joint should be assembled, leaving only simple butt joints to be installed in the field.

Results from the laboratory investigations indicate that elevated temperatures will cause plasticizer loss in the PVC geomembrane. However, even with the plasticizer loss the application of a vertical load through a rigid concrete cover does not result in a puncture failure of the PVC geomembrane. The typical lack of intimate contact between the 19 mm (3/4 inch) high angular protrusions in the subgrade and the geomembrane causes a reduction in the foundation bearing area for the concrete cover. This reduction however, did not cause the PVC geomembrane to fail. Both of these results can amount to significant savings in future construction costs. The amount of subgrade preparation can be reduced by not requiring the removal of 19 mm (3/4 inch) high or less angular protrusions. Also, a geotextile is not required either over the protrusion or between the geomembrane and the concrete cover.

From our experience, the above conclusions also show that a load application through a rigid cover is different from either a hydrostatic load application or a load application through a flexible cover material such as soil. The ability of the cover material to span and redistribute the load is a big factor when considering how big a void the geomembrane can span. The ability of the geomembrane to span voids is also limited by its flexibility. Our limited Mullen Burst tests data show that some plasticizer loss results in test specimens with somewhat higher Mullen Burst strengths. Thus, we recognize that although the BMOR PVC geomembrane testing program was successful, future study will be needed to determine at what point, if any, the plasticizer loss will have an adverse impact on the geomembrane's ability to handle single or repetitive loads.

ACKNOWLEDGEMENTS

William R. Morrison for his assistance in reviewing the paper.

Cheryl A. Kramer for drawings and test assembly.

William F. Kepler for concrete mix design.

Cheryl Kramer, Steve Reo, and Kurt Mitchell for laboratory testing.

Louis DiMattia for chemical analysis data.

REFERENCES

[1] Morrison, W. and Starbuck, J. (1984) "Performance of Plastic Canal Linings" Bureau of Reclamation REC-ERC-84-1 report.

[2] Saville, T. Jr. (1962) "Journal of the WATERWAYS AND HARBORS DIVISION Proceedings of the American Society of Civil Engineers".

[3] Koerner, R. (1990) Designing with Geosynthetics, 2nd ed., Englewood Cliffs, N.J., Prentice Hall, Inc.

[4] USBR Solicitation Specification 9-CC-32-00760/DC-7786, "Tucson Aqueduct-Black Mountain Operating Reservoir", Tucson Division, Central Arizona Project, Arizona.

Geomembranes for the Containment of Sulphur: A Case History

J.A. Mills
Layfield Plastics (1978) Ltd., Canada

ABSTRACT

This paper presents a case history which examines the feasibility of several lining materials for the application of sulfur storage. The Shell Caroline Gas Development produces 4,100 metric tons of sulfur daily. A number of site linings at the project's sulfur handling facility were proposed, this case history deals with the liners proposed for the sulfur storage blocks.

Sulfur block liners may be exposed to 125°C molten sulfur. A material selection testing program explored the suitability of four geomembrane materials. Measurements were taken before and after sulfur exposure to measure material shrinkage and tensile properties. A second large scale test was carried out at the construction site where 3 m x 3 m samples were exposed to a 50 mm thick layer of molten sulfur. The large scale test samples were evaluated for tensile properties and shrinkage. A material recommendation was made based on the test results.

INTRODUCTION

The Shell Caroline Gas Development is the most significant sour gas development in the last twenty years. The development of the estimated 56 billion cubic meters of raw gas in this field is being undertaken by Shell Canada Limited along with their partners. The estimated production from this field is to be 2,550,000 cubic meters of natural gas (methane) per day, along with 4,100 metric tons of liquid sulfur and 7,200 cubic meters of natural gas liquids and condensates. In order to handle the sulfur produced by this development, the Shantz sulfur handling facility was built near Harmattan, about 80 kilometers north west of Calgary, Alberta. Molten sulfur is extracted from natural gas at the Shell gas plant in Caroline and then transferred by pipeline 41 kilometers to the Shantz sulfur facility. At the Shantz site molten sulfur is formed into pellets and transferred to rail cars for shipment.

In the event of a malfunction of the pellet manufacturing equipment, or in the event of an overabundance of sulfur on the world market, the sulfur produced by the Caroline gas field may need to be stored. A common storage technique used in Alberta is to pour liquid molten sulfur into an aluminum form and allow it to solidify into a block. Additional layers are placed on top of the previous layers by repositioning the forms. The yellow blocks of solid sulfur that are formed can reach twenty meters in height and are typically the size of a football field. Most Alberta sulfur blocks have been remelted and sold in recent years due to a strong demand for sulfur.

Decommissioning of sulfur blocks in the province of Alberta has revealed costly contamination problems. During sulfur re-melt, the sulfur melting equipment can recover all but the last 100 mm of sulfur from a well prepared block base. The remaining sulfur is chipped out which leaves a large quantity of sulfur contaminated with soil. Efforts to separate the soil from the sulfur have not yet proven successful. This results in quantities of contaminated sulfur which are not saleable and substantial quantities of contaminated soil that must be treated as hazardous waste. The ground below the sulfur block can also contain low pH contamination and remediation of between 150 mm to 300 mm beneath the base is common.

Alberta Environment, a department of the provincial Government of Alberta, required from Shell Canada a plan to prevent the migration of contaminants from the site. It was clearly stated that the long range goal was to restore the Shantz site to farm land at the completion of the life cycle of the facility. The Shell plan included a series of monitors around the site to detect the presence of H_2S gas, sulfur dust, the accumulation of sulfates in the surrounding area, and groundwater contaminants. All site run-off water was to be collected in a double lined retention pond, neutralized, and recycled. This water would be utilized in the cooling towers which would effectively eliminate the release of liquid run-off water from the site. In an effort to prevent soil contamination beneath the sulfur block base it was proposed that a geomembrane liner be placed at the interface of the soil and sulfur which would also result in reduced decommissioning clean-up cost. This paper describes the research that led to the construction of a geomembrane liner beneath the sulfur block facilities at the Shantz site.

SCOPE OF PROJECT

The sulfur block storage area is designed to store five months of production from the Shantz sulfur plant. Two sulfur block pads are built on weathered clay. Each of the two sulfur blocks is designed to be 35 meters wide and 324 meters long with a height of 15 meters. Alberta Environment proposed that a geomembrane liner be used under each sulfur block to prevent contamination of underlying soils.

The principle requirement of the sulfur storage block lining material is that it must withstand the molten sulfur pouring temperature of approximately 125°C. Each pour of sulfur is about 100 mm deep and takes about sixteen hours to cool sufficiently before the next pour is placed. It was felt that the insulating properties of the sulfur would protect the liner after the first 150 to 200 mm of solid sulfur was in place. The proposed liner might also have to remain exposed to the

elements for many years before use as pouring a sulfur block at the Shantz site was considered a remote possibility under the current market conditions.

Since operating temperatures of 125°C are well beyond the temperature range of common geomembrane plastics (Modern Plastics Encyclopedia' 92) it was suggested that specific material selection testing be done.

There are a number of factors that come into play in the application of a containment liner. Material selection is a function of chemical resistance, heat resistance, weathering resistance (for an exposed liner), and mechanical properties. There were other factors that needed to be considered as well including: cost, installation requirements, cold temperature performance, and conformability to subgrade. A two part testing program was proposed that would attempt to determine a suitable lining material for the containment of molten sulfur. This two part testing program consisted of a small scale test to determine basic suitability of a number of materials, and a large scale test that would confirm the results of the small scale test under actual field conditions.

SMALL SCALE TESTING

The first step was to make a preliminary selection of a lining material that would meet the basic performance requirements of this project. The scope of this first phase was to canvass suppliers for likely materials and then perform some initial selection tests. The initial problems expected were difficulties with the heat of the sulfur and the possibility of chemical reactions with the lining materials and molten sulfur at elevated temperatures. Initial material selections were based on material cost and availability. A secondary selection was made from materials that had proven high temperature applications. Table 1 lists the materials selected for the small scale test.

Table 1. Materials for Small Scale Test.

1. High density polyethylene (HDPE) 80 mil, blown film.
2. Polyvinyl chloride (PVC) 20 mil, regular containment grade.
3. Ethylene interpolymer alloy material (EIA) "Solar" grade.
4. Silicone Coated Fibreglass (SCF) cloth.

The HDPE and PVC materials are standard containment materials that are widely available and low in cost. The EIA (Solar) material is a high temperature version of the standard ethylene interpolymer alloy style material. A 540 g/m^2 (16 oz/yd^2) silicone coated fibreglass cloth with a service temperature in excess of 260°C was selected to test the high end of the temperature spectrum.

The small scale test was a simple contact test between the molten sulfur and the lining material in question. After exposure, the material was tested for property changes and evaluated as to performance. Peak temperatures were measured under the liner to ensure that the liner was not damaged by sulfur pouring temperatures. Liner samples exposed to the molten sulfur were cut into rectangles approximately 216 mm by 260 mm. Reference marks were placed at equal distances along the side of each sample, three along the length and two along the width. Measurements were taken between opposite marks, before and after exposure to the molten sulfur to determine shrinkage. A suitably sized metal tray was filled with sand and a thermistor was placed in the center of the tray on top of the sand. The sample was centered over the thermistor. A metal container approximately 150mm x 150mm x 150mm was centered over the sample. Sand was placed around the outside of the metal container to prevent the sulfur from leaking out between the metal container and the sample.

Sulfur chips were heated to 150°C in a laboratory sulfur melting pot. The molten sulfur was then ladled into the metal container. The molten sulfur level was brought to approximately the top of the metal container. After substantial cooling of the sulfur, the samples were removed and examined for shrinkage/elongation, discoloration, warping, and bonding to the sulfur. Two tensile test samples were cut from where the material was in contact with the molten sulfur, and two control samples were cut from material outside the contact area. Samples from the control and exposed area were tensile tested according to ASTM D882. The tensile properties of the control samples were compared to the tensile properties of the sample that had been in contact with the molten sulfur.

Small Scale Test: Results Visual observations were made of each material after contact with the molten sulfur. The observations are summarized in Table 2.

Small Scale Test: Discussion. The purpose of the small scale testing was to determine if it was physically possible to utilize a geomembrane in contact with molten sulfur. Original expectations were that the EIA (Solar) and the silicone would show better performance than the HDPE and the PVC. The tensile strength trends in Table 3 show that the PVC and the HDPE exhibited performance equal to, or better than the EIA (Solar). The results from the silicone coated fibreglass cloth showed that strength lost after exposure was much higher than was expected in a high temperature fabric.

After these initial test results a cost estimate was prepared which clearly favoured the HDPE and the PVC. This cost comparison assisted us in limiting our initial material selection to HDPE and PVC. Table 4 shows the cost estimates.

Table 2. Small Scale Test
Visual Observations.

Material	Observations
HDPE	Showed warping during placement of the sulfur. In the initial test the warping of the HDPE lifted the metal form away from the sample and allowed the sulfur to spill out from the test area. A second test was performed with a substantial weight on the metal form to prevent lifting. The warping observed was permanent. The HDPE showed a slight surface discoloration; the contact area was lighter in color after the test and the color could not be removed. No significant shrinkage was observed.
PVC	Showed some warpage from the heat. An outline of the metal form was clearly set into the PVC sample after the test. The sample showed discoloration in the contact area but did not show measurable shrinkage. The PVC sample showed some bonding to the solid sulfur.
EIA (S)	Showed some warping from the heat. No discoloration or shrinkage was apparent in this sample. Some bonding of the sulfur to the sample was present.
SCF	Showed no warping, no discoloration, or shrinkage. Some bonding to the sulfur was present but the sample separated cleanly.

Table 3. Small Scale Test.
Tensile Strength Trends.

Material Type	Average Peak Tensile Strength	Average Peak Strain
HDPE	9% increase	no change
PVC	8% decrease	3% increase
EIA (Solar)	10% decrease	9% decrease
SCF	21% decrease	23% decrease

Table 4. Cost Estimates

Material Type	Installed Cost (Taxes Extra)
HDPE	CDN $ 206,000
PVC	CDN $ 114,000
EIA (Solar)	CDN $ 440,000
SCF	CDN $ 439,000

Using cost as a selection criteria limited the next considerations to HDPE and PVC. It was apparent from the testing that both the PVC and the HDPE did exhibit some physical changes, but it appeared that these changes were not of significant magnitude to affect the performance of the liner system.

A temperature of 125°C is above what may be considered the melting point of HDPE and PVC lining materials. Although processing temperatures for both these materials are normally in the range of 250°C or higher, a sustained temperature in the 125°C range could be expected to cause some significant changes. The small scale testing showed, however, that the temperature below the liner was much lower than the pouring temperature (approximately 80°C). Both the PVC and the HDPE appeared to be performing as insulators. Initial sulfur contact with the cool liner may have been providing an initial layer of solid sulfur that helped to mitigate the effects of temperature. The slow placement of sulfur in the small scale test may have contributed to a crust of sulfur forming.

HDPE Discussion. The HDPE initially warped so as to lift the sulfur mold off the material surface, spilling molten sulfur and requiring a repeat test. This warping was permanent as the sample remained warped after cooling. It was expected that the HDPE warpage was due to stress relaxation. No significant shrinkage was found. It was felt that the warpage observed in the HDPE could cause problems. Large scale warpage could cause mobilization of sections of the liner system or the raising of voids under large wrinkles in the liner.

The visual observations of the surface of the HDPE (Table 2) indicated that after contact with the molten sulfur the HDPE had taken on a lighter color. An attempt was made to wash off this color but it was a permanent change. HDPE has an extremely high chemical resistance and is normally not affected by inorganic compounds. At the elevated temperatures of the test, however, a chemical reaction on the surface of the material may have occurred. The physical strength trends (Table 3) showed a tendency toward higher tensile strengths after exposure.

One factor that must always be taken into consideration with a new HDPE application is environmental stress cracking resistance (ESCR). Evidence pointed to a physical change, albeit small, in the HDPE. Since ESCR is a surface phenomenon of polyethylene, and evidence was observed of possible chemical changes to the surface of the HDPE sample, it was possible that the risk of ESCR had changed. It was not possible, given this simple test, of knowing whether the observed changes would have improved or deteriorated the ESCR performance of the material. Additional testing would have needed to be done to determine if the ESCR of the HDPE material had changed. Determining any effects on the HDPE's ESCR performance was beyond the scope of this material selection testing. The recommendation for continuing investigation of HDPE as a lining material was that an ESCR test be performed to determine if the HDPE liner performance had changed.

PVC Discussion. Original expectations of the PVC's performance were that the high temperatures would produce an unacceptable softening of the material. In fact, the temperature plots on the PVC sample showed that the maximum temperature reached, as measured under the

liner, was only 80°C, well below the softening point of PVC. Observations in Table 2 indicated that the PVC sample did show some permanent deformation; the outline of the metal sulfur mold made an impression in the PVC that did not relax after the test. The PVC did not appear damaged by this deformation and showed no signs of distress. It was felt that the mould served as a heat sink for the sulfur, directing the heat in a concentrated line on the PVC material. The small amount of deformation present, and the absence of shrinkage, indicated that the PVC would not exhibit any unexpected large scale deformations in contact with molten sulfur. The visual observations of the surface of the PVC (Table 2) indicated that after contact with the sulfur the PVC had taken on a lighter color. An attempt was made to wash off this color but it was a permanent change. As with the HDPE, this color change may have indicated a chemical change to the surface of the geomembrane. Flexible PVC is not however, susceptible to environmental stress cracking.

Flexible PVC geomembrane materials are mixtures of (rigid) PVC resin with a number of additives; the most important being the plasticizer. The plasticizer gives the material its flexibility. When plasticizers are extracted from PVC the material shows a characteristic increase in tensile strength and decrease in tensile elongation. If sufficient plasticizer is extracted then brittleness may occur. What was shown by the physical test data for the PVC testing is opposite to what would be expected from the scenario where plasticizer is extracted. The physical data showed a tendency for the PVC to decrease tensile strength and to increase strain at break. It is possible that the additional heat continued the dispersion of the plasticizer into the PVC matrix. In this case it appeared that the heat of the sulfur had acted to further plasticize the material and to make it more flexible.

Small Scale Test: Recommendations. At the conclusion of the small scale test two materials appeared largely suitable for the containment of molten sulfur. Both the PVC and the HDPE had stood up well to the heat of contact, and the observed changes were reasonable for the expected use of the liner. Before a final selection could be made however, a larger scale test would be required.

LARGE SCALE TEST

Large Scale Test: Material Selection. Given the results from the small scale testing it was possible to narrow the field of possible materials to two. HDPE and PVC appeared to withstand the molten sulfur and were within budgeted cost estimates. South-central Alberta, where the proposed sulfur block liners were to be installed has a temperature range of +30 to -35°C. In order to allow for thermal effects on an exposed liner, it must be installed with sufficient slack to allow for contraction at cold temperatures without inducing stress. Three problem areas arose with the HDPE liner as a result of the required compensation slack. The sulfur block areas had a grade of only 0.7 meters vertical to 100 meters horizontal. HDPE compensation wrinkles typically stand up between 100 and 200 mm and may have impeded drainage on this very flat pad. Pouring molten sulfur onto standing water was possible, but drainage was a concern. The second area of concern was with the possibility of void spaces under HDPE wrinkles as the sulfur block was poured. The small scale test had shown warpage in the HDPE after exposure

to molten sulfur. It was possible that this warpage could exacerbate the compensation wrinkles already in place in the liner, or cause wrinkles to run together to form large additive wrinkles. The sulfur is poured in lifts of 100 mm at a time and impediments to the flow of the sulfur in the initial pours can make it difficult to set up a solid base. Since it is impossible to access the lined area once molten sulfur has started to flow, the possibility of forming void spaces of 300 to 400 mm high and of considerable length was a concern. It was felt that void spaces could induce unacceptable cracks in the block as it grew in size. The final area of concern was the construction schedule. The proposed time for the installation of the sulfur block was very late in the season. HDPE liners had been successfully installed in weather as cold as -20°C but maintaining a quality installation at these temperatures is very difficult.

The PVC material offered to solve a number of the problems that the HDPE had shown. Compensation wrinkles in PVC lie flat and do not normally impede drainage. PVC wrinkles also compress under low pressure, and are not expected to create void spaces. The warpage seen in the PVC during the small scale testing was of a different nature than the warpage of the HDPE. The PVC warpage was one of conformance to the base, while the HDPE warpage forced the mold up and out of position. The PVC was expected to lie flat and not interfere with sulfur pouring. PVC could also be installed much more quickly than HDPE allowing installation within the tight construction schedule. Two problem areas did exist for PVC: UV exposure and cold temperature flexibility. It is not common in Alberta for regular PVC lining materials to be exposed over the winter months. Although experience has shown that the UV stability of regular PVC is approximately 5 to 7 years at Alberta latitude, the cold temperature resistance of regular grades of PVC are marginal for an exposed liner. An exposed life expectancy of 7 years was acceptable to the client. Liner replacement or repair was possible after this time if sulfur had not been poured.

A PVC-style flexible liner would have a number of advantages over the stiffer HDPE liner. The UV resistance of a regular PVC liner was sufficient for the client's purpose, and the speed of construction and repairability was an advantage for this application. The limitation of the regular PVC material was that the cold temperatures expected at the site could possibly contribute to damage to the liner if the liner were impacted at cold temperatures. Since regular PVC materials have a typical cold temperature resistance of -26°C, available blends of PVC that might perform better were investigated.

The final selection for the large scale test were two styles of PVC material. The first, a regular PVC material blended for improved cold temperature resistance had a cold temperature resistance (ASTM D1760) of -29°C. The second material was an alloy of PVC and a modified rubber compound (PVC Alloy). This alloy material has a cold temperature resistance of -30°C and had the additional advantage of being a UV stabilized grade. Experience with this PVC Alloy grade had shown that installations as low as -35°C were possible. After reviewing our report on the small scale testing, the client accepted the proposal for a large scale test utilizing the improved cold temperature regular PVC and the PVC Alloy material.

Large Scale Test: Method. Would the sustained heat of a large quantity of sulfur create different reactions or physical changes in the PVC materials ? If a crust of solid sulfur had formed directly on the cool liner surface during the small scale test (as we suspected) would a larger amount of sulfur re-melt this crust and adversely affect the liner ? The large scale test was designed to answer these questions.

The large scale test exposed the two liner samples to molten sulfur at conditions expected during service at the site. Two samples were prepared to represent the materials. One sample each of regular PVC and PVC Alloy were prepared in panels approximately 3 meters square. These sample panels were marked for later shrinkage measurements. Each sample contained a fusion welded factory seam and a solvent seam placed approximately 600 mm apart and running across the full width of the sample. A 2.7 meter square wooden frame was prepared on the Shantz site for each sample. Thermistors were placed to measure temperatures; two below the lining samples and one suspended in the sulfur above the liner to measure actual pouring temperature. A 50 mm thickness of molten sulfur was placed on each sample and allowed to cool.

A basic comparison between an unexposed sample and the exposed liner sample was made. Tests of seams determined if exposure reduced seam properties to values below acceptable values. The tensile strength of the factory and solvent welded seams were compared to the exposed material strength. Destructive tests were performed to ASTM D882 (5 samples from each location tested).

Large Scale Test: Results. Observation of the samples removed from the large scale test showed that the sulfur had bonded to the PVC materials but was relatively easy to chip away from the liner (see Figure 1). The discoloration evident in the small scale test was present in this large scale test. The PVC materials had conformed to the subgrade during the application of the molten sulfur which "set" in a position that mirrored the irregularities of the subgrade.

The temperature under the lining samples reached a maximum of 103°C under the PVC liner and 116°C under the PVC Alloy. These maximum temperatures were reached about three and a half minutes after the start of the pour. The maximum observed temperature of the molten sulfur during pouring was approximately 125°C. The sulfur was allowed to cool for about two hours before stripping the liner samples for testing. Both samples were marked and measured for shrinkage. Both the PVC and the PVC Alloy showed negligible shrinkage (less than 1%).

Large Scale Test: Discussion. The results of the large scale test showed that additional heating of the regular PVC material continued the reaction shown during the small scale test. The 19% strength reduction of the PVC material (Table 5) indicated that additional heating from a large amount of molten sulfur created additional changes.

The seam shear results in Table 6 however, showed that the seam shear strengths after exposure were still within 10% of the initial material strength. Seam shear strengths were compared to the strength of unexposed, unseamed sheet samples.

Table 5. Large Scale Test.
Unseamed Sheet Tensile Test Results

Material Type	Average Tensile Strength (MPa)	% Change
PVC Unexposed	9.5	
PVC Exposed	7.7	19 % decrease
PVC Alloy Unexposed	4.9	
PVC Alloy Exposed	5.0	2 % increase

Table 6. Large Scale Test.
Seam Shear Tensile Test Results
Exposed Samples

Material Type	Average Tensile Strength (MPa)	% of Initial Material Strength
PVC Factory Seam	9.0	9.0 vs 9.5 95%
PVC Field Seam	8.7	8.7 vs 9.5 92%
PVC Alloy Fact.	4.9	4.9 vs 4.9 100%
PVC Alloy Field	5.0	5.0 vs 4.9 102%

All seam samples exhibited film tear bond failures for all shear tests.

Table 7. Large Scale Test.
Seam Peel Tensile Test Results
Exposed Samples

Material Type	Average Peak Load (N/mm)	% of Unexposed Material Peak Load (N/mm vs N/mm)
PVC Factory Seam	5.72	5.72 vs 7.35 78%
PVC Field Seam	5.04	5.04 vs 7.35 69%
PVC Alloy Fact.	4.29	4.29 vs 4.03 106%
PVC Alloy Field	3.25	3.25 vs 4.03 81%

All peel test samples showed a film tear bond in peel except the PVC Alloy field seam. One of the PVC Alloy field seams showed a film tear bond, the rest showed a failure in peel.

The PVC Alloy material showed negligible change in material tensile strength after exposure to the molten sulfur (Table 5). The PVC Alloy material also showed seam shear tensile strengths (Table 6) that were substantially equal to the unexposed material strength. The seam peel test

results in Table 7 showed that the factory seam exposed to molten sulfur was equal in strength to the unexposed material strength. The PVC Alloy solvent weld peel strength after exposure of 81% of initial material strength (Table 7) was considered to be an excellent peel strength result for a solvent weld. A solvent weld peel strength of over 70% of initial material strength is considered a very good result.

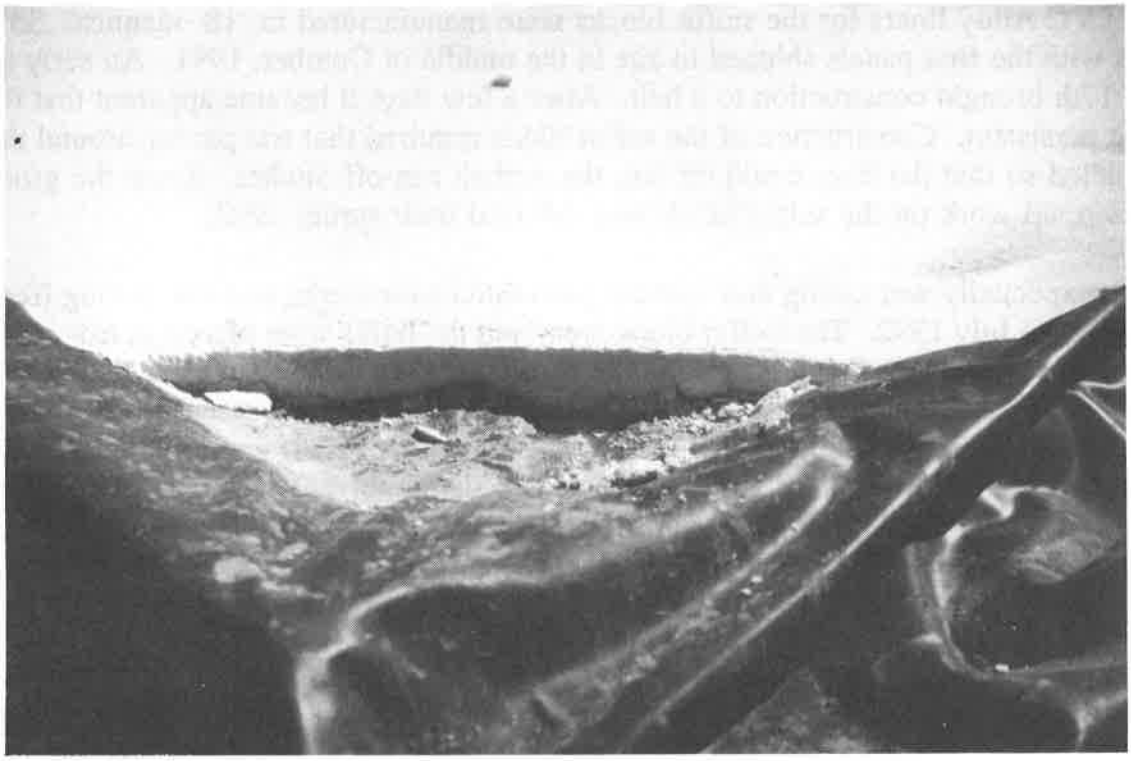

Figure 1. Solidified sulfur is removed from the sample at the completion of the large scale test.

The PVC Alloy material showed an overall excellent response to the large scale molten sulfur test. As a result of this large scale test the PVC Alloy material was selected. A cost comparison was prepared and the PVC Alloy material was estimated at CDN $ 149,000, which compared favourably to the PVC and HDPE material cost estimates prepared earlier. A report based on the test results was forwarded to the client recommending that the PVC Alloy would meet the project requirements.

Large Scale Test: Conclusion. On August 1st, 1991, Shell Canada Limited requested that a representative from Layfield Plastics attend a meeting with Alberta Environment. The environmental protection plan that Shell Canada Limited had proposed was reviewed at this meeting. A substantial part of the discussion pertained to the requirements of the sulfur block linings. The test results were discussed and a number of questions were answered. At the conclusion of this meeting Shell Canada Limited was informed that their permit for the Shantz site was approved.

The testing program had shown that a geomembrane liner of reasonable cost could meet the requirements of ground protection for a sulfur block. The geomembrane would allow for the complete removal of sulfur from the site without creating contaminated sulfur or soil.

CONSTRUCTION

The PVC Alloy liners for the sulfur blocks were manufactured in 18 identical 33 m x 36 m pieces with the first panels shipped to site in the middle of October, 1991. An early snow on October 17th brought construction to a halt. After a few days it became apparent that the snow would be persistent. Construction of the sulfur block required that site paving around the block be completed so that the liner could tie into the asphalt run-off ditches. Since the ground was now frozen, all work on the sulfur block was deferred until spring 1992.

An unexpectedly wet spring and summer prevented earthworks and site paving from being completed until July 1992. The Sulfur block areas and the liners were placed in August of 1992. A 400 mm high berm was prepared around the perimeter of each block to mark the liner location and to allow the aluminum sulfur forms to be placed. A strip of lining material was placed under each of these small berms during construction. The main liner panels were welded to these strips using solvent bonding. Repairs were accomplished using solvent welding techniques. Field welding was carried out in accordance with established Quality Control practices which included frequent qualification welds. All field welds and repairs were tested using the air lance test.

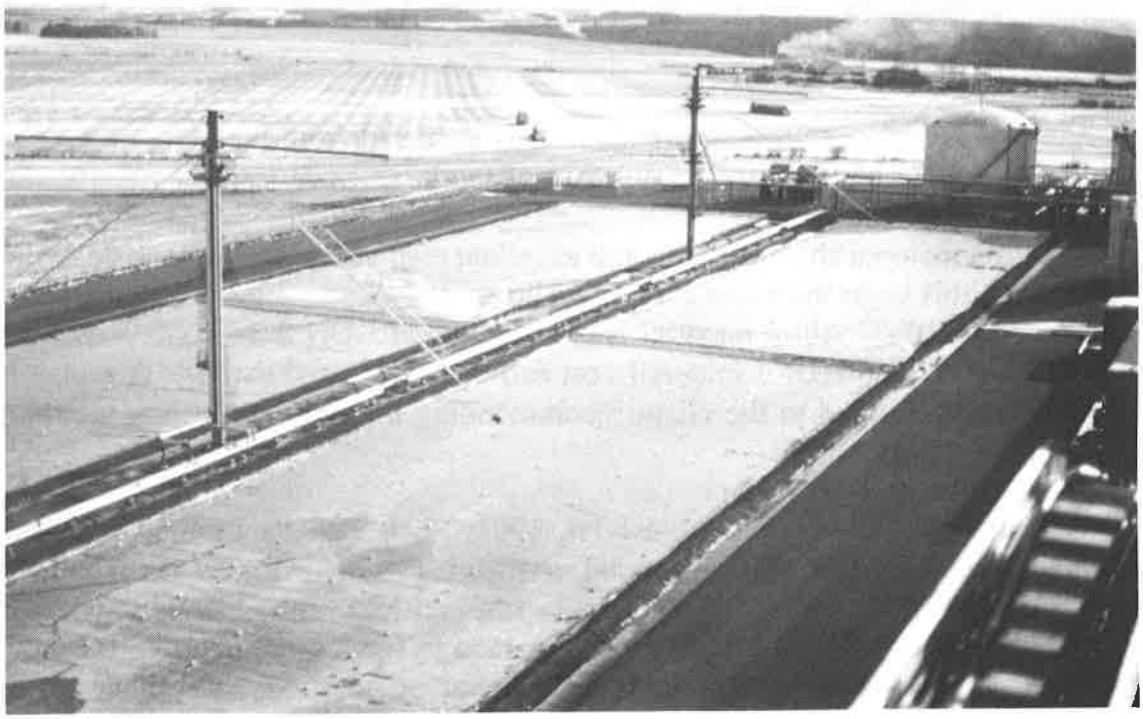

Figure 2. Sulfur Block Construction.
Four of the six cells are shown.

The sulfur block liners were permanently ballasted against wind uplift by using concrete weights. These concrete weights were actually concrete test cylinders collected from local engineering laboratories. The cylinders occasionally had small pieces of solid sulfur left over from compression testing. These ballast weights were available at low cost, and the attached traces of sulfur were not a concern on this particular project.

CONCLUSION

The Shantz sulfur facility is an example of the successful selection of a suitable geomembrane material in an application that had not been attempted previously. No one geomembrane meets all the lining needs of every application. The high temperatures expected in this project, as well as some unique site conditions required a logical approach to the determination of a suitable liner. This program of testing, that modelled site conditions, allowed the establishment of a high level of confidence in the material selected. This confidence allowed Shell Canada to receive construction permits for a previously untried application.

ACKNOWLEDGEMENTS

Layfield Plastics would like to thank Tom Moffat of Shell Canada Limited for his support. We would also like to thank Mike Kaut of Petrotech Lavalin and Tim Murphy of EBA Engineering for their assistance.

REFERENCES

Greene,R., (1991) "Engineering Data Bank", Modern Plastics Encyclopedia '92, 1992 Edition, pp. 378-428.

Clay Desiccation of a Single-Composite Liner System

C.R. Basnett
CH2M Hill Inc., USA

R.J. Bruner
CH2M Hill Inc., USA

ABSTRACT

During construction of a single-composite liner system in a north-central Florida municipal solid waste landfill, severe desiccation cracking occurred in the clay liner along the exposed slopes. In addition, water accumulated between the high-density polyethylene (HDPE) geomembrane and the clay liner along the toe of the slope. The suspected cause was moisture in the clay that was condensing on the geomembrane and migrating to the slope toe. To confirm this, clay samples were collected throughout the landfill and analyzed for moisture content.

The analytical results indicate that the lowest moisture content occurred near the clay surface and that, generally, the clay became drier as distance from the toe increased. Severe desiccation cracking had occurred within 2 months after the liner had been placed on the slopes, indicating rapid development of cracking and water accumulation. Significant changes in the design of exposed composite liners could reduce these tendencies in the clay materials.

INTRODUCTION

The construction of two sections of a Class 1 municipal solid waste landfill in north-central Florida demonstrates the need for changes in the design of exposed composite liners. Section 1 of the landfill involved construction of a 5.3-hectare (13-acre) disposal area equipped with a single-composite liner system. Construction of Section 2, an expansion of Section 1, involved the addition of 6.1 hectares (15 acres) of lined disposal area.

BACKGROUND

Landfill Sections 1 and 2 are now the active Class 1 disposal areas, serving two counties and approximately 200,000 people. Figure 1 is the overall site plan showing the locations of

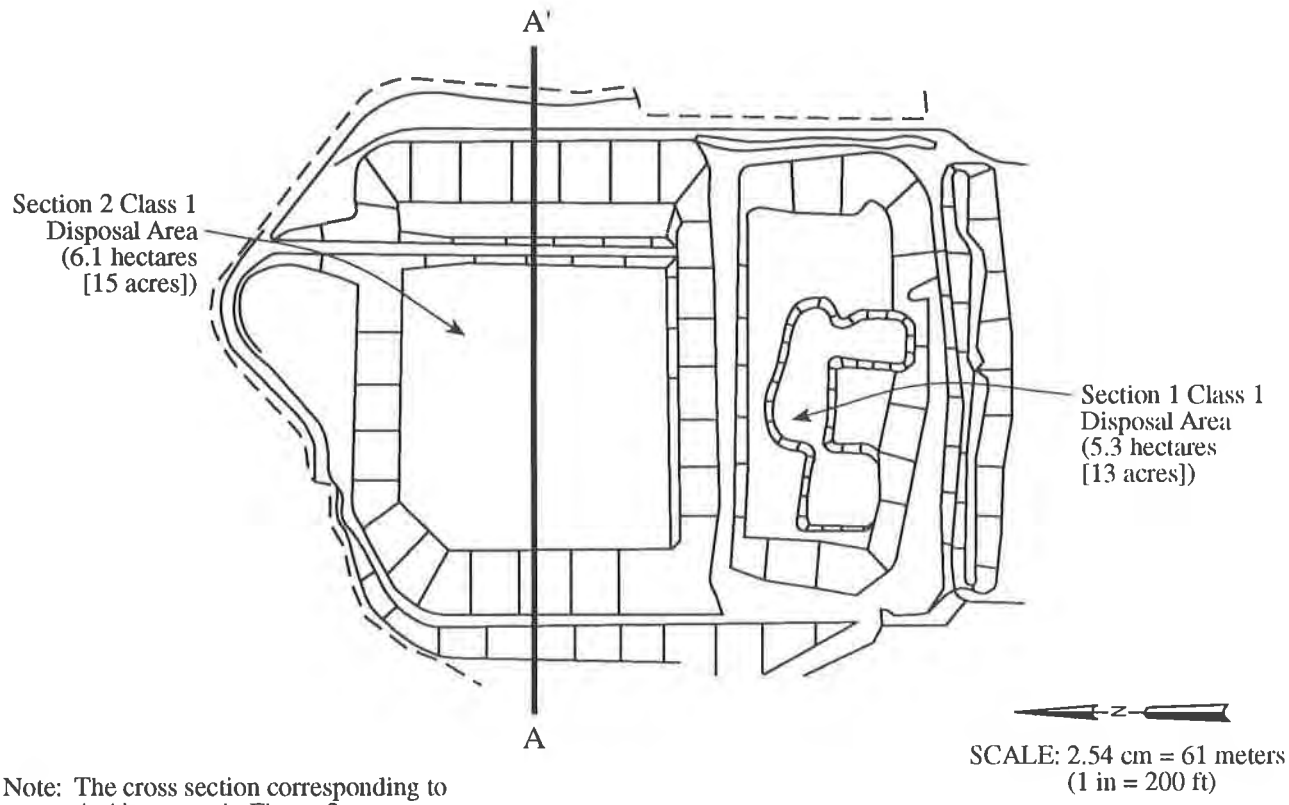

Figure 1. Overall Site Plan

Sections 1 and 2. Section 1 was constructed from late 1987 through mid-1988; Section 2 was constructed in 1991.

Design. The single-composite liner system consists of subgrade reinforcing geotextile, 30.5 centimeters (cm) (12 inches) of compacted natural clay, and a 1.5-millimeter (mm) (60-mil) HDPE geomembrane. Along the bottom of the disposal area, the geomembrane is covered by at least 61 cm (24 inches) of drainage sand. Because of the relatively steep (3:1) side slopes of the landfill berm, low friction between the geomembrane and sand, and locally intense rainfalls, the composite liner remains exposed along the slopes to where landfilling begins. The specifications required the compacted natural clay liner to provide a minimum coefficient of permeability of 10^{-7} centimeters per second (cm/sec).

Figure 2 is a typical cross section of the liner system. As shown, the disposal area bottom is below natural grade, with side slope embankments partially above natural grade. The ground water surface elevation is approximately 8 meters (m) (26 feet) below the bottom of the disposal area.

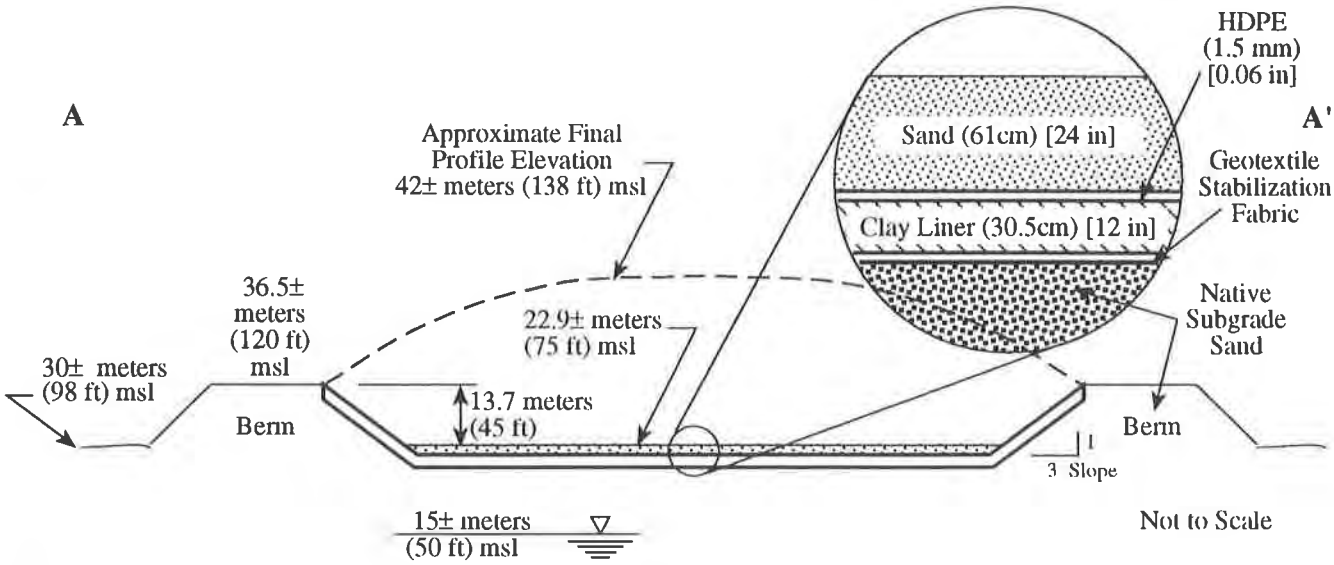

Note: See Figure 1 for the location of the cross section.

Figure 2. Typical Liner System Cross Section

Construction. Liner system construction included compacting and grouting the subgrade, placing the clay liner in two lifts, and installing the HDPE geomembrane and subsequent drainage sand cover. The natural clay for the liner consists of a clayey sand mixture, with an average of 38 percent passing the No. 200 sieve. The average plasticity index for this clay is about 33 percent. (Although the liner material exhibits excellent clay properties [low permeability and moderate to high plasticity], it is a clayey sand rather than a clay according to the United Soil Classification System [USCS]. To differentiate between this layer and the subgrade sand, however, the clayey sand layer is hereafter called *clay* in this paper).

The clay for the Section 1 disposal area was compacted to at least 95 percent of the maximum dry density determined by American Society for Testing and Materials (ASTM) D-698. The average moisture content of the clay after placement, compaction, and acceptance by the engineer was about 21.8 percent.

The clay for Section 2 was compacted to at least 95 percent of the maximum dry density determined by ASTM D-1557. After the clay had been placed, compacted, and accepted by the engineer, the moisture content of the clay averaged about 16.9 percent. The topography of the landfill site is characterized by karst formations. Because small chimney sinkhole formations are characteristic of the subgrade sand, compaction grouting of the subgrade sand and increased compaction of the clay liner were required.

In general, during placement and compaction, the clay moisture content in both sections was at or within 5 percent above the optimum moisture content.

After the clay was in place and before it was covered with the HDPE geomembrane, desiccation cracking was controlled by applying water from a wagon equipped with spray bars and nozzles. In most instances, the clay was covered with the geomembrane within 24 hours after the engineer had accepted the clay placement.

Landfill Operation. Typically, no drainage sand or protective covering is placed on the side slope geomembrane during construction. This covering is usually added during landfill operations. As refuse is placed up the slope, the drainage sand layer is placed ahead of the refuse. The length of time the side slopes remain exposed is a function of the landfilling rate. Consequently, sections of the side slopes can be exposed for up to 3 to 5 years.

OBSERVATIONS

Section 1. During construction of the Section 1 liner system, the resident engineer observed that a significant amount of water was trapped between the newly placed geomembrane and the clay at the toe of the landfill slopes. The drainage sand covering the geomembrane provided sufficient confining pressure to trap the water. At that time, the water was thought to be the result of storm water from intense rainfall that had flowed under the newly placed panels of geomembrane. Because Section 1 contained the first clay-lined disposal area at the landfill, the long-term effects of exposed slopes on the condition of the clay liner were unknown.

Section 2. When Section 2 construction began, Section 1 was active and filled approximately 70 percent with refuse. When existing panels of the Section 1 geomembrane were rolled back to prepare for attachment of the Section 2 panels, severe clay cracking was observed (see Figure 3). The cracks were about 2.5 cm (1 inch) wide and penetrated the full depth of the clay liner.

Figure 3. Cracking under the Existing Geomembrane Panels

To determine if this cracking was an isolated occurrence, an inspection port measuring 0.6-meter (2-foot) square was cut into the geomembrane approximately 30 meters (100 feet) south of the initial discovery area and about 2 meters (6 feet) down from the crest of the slope. Under the inspection port, the clay was also found to be severely desiccated throughout the full clay thickness. Figure 4 shows the inspection port in the geomembrane and the underlying desiccated clay. Moisture beading on the underside of the geomembrane is visible in Figure 4.

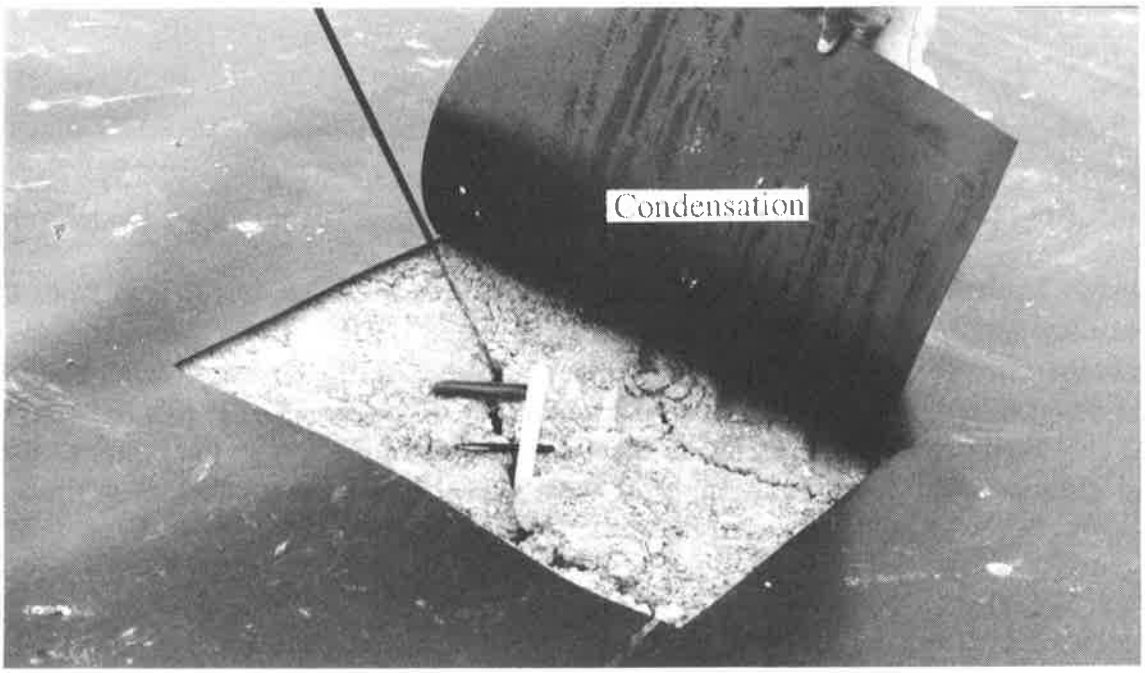

Figure 4. Section 2 Geomembrane Inspection Port Showing Underlying Liner System Conditions

As in construction of the Section 1 liner system, large quantities of water (estimated to be hundreds of liters) were observed trapped between the geomembrane and the clay on the side slope. This water mounding occurred about 6 weeks after geomembrane liner placement. In some areas, it was so significant that small water-pressure relief holes were cut into the geomembrane. These holes were patched after the excess water had drained. Figure 5 shows a typical area of trapped water. Leachate cleanout piping is visible in the background of the mounding area.

Figure 5. Area of Water Retention between the Geomembrane Liner and the Underlying Clay

Hypothesis. These observations led to the hypothesis that moisture was driven from the clay when the clay was heated during the day and condensed on the HDPE geomembrane as the geomembrane cooled at night. After condensing on the HDPE geomembrane, the moisture migrated down to the slope toe where water mounding was observed. If this hypothesis were true, the clay liner would be expected to lose moisture from the top to the bottom. Exposure time and distance away from the berm crest were also suspected to be factors in the moisture loss.

INVESTIGATION

To test the proposed hypothesis, clay samples were obtained from the Section 1 and Section 2 slopes at various distances from the berm crest and analyzed for moisture content.

Section 1. Six clay sample locations were established at the following distances down from the berm crest (see Figure 6):

Section 1 Sample Location	Distance (meters)	Distance (feet)
A	12.2	40
B	21.3	70
C	25.9	85
D	30.5	100
E	35	115
G	39.5	130

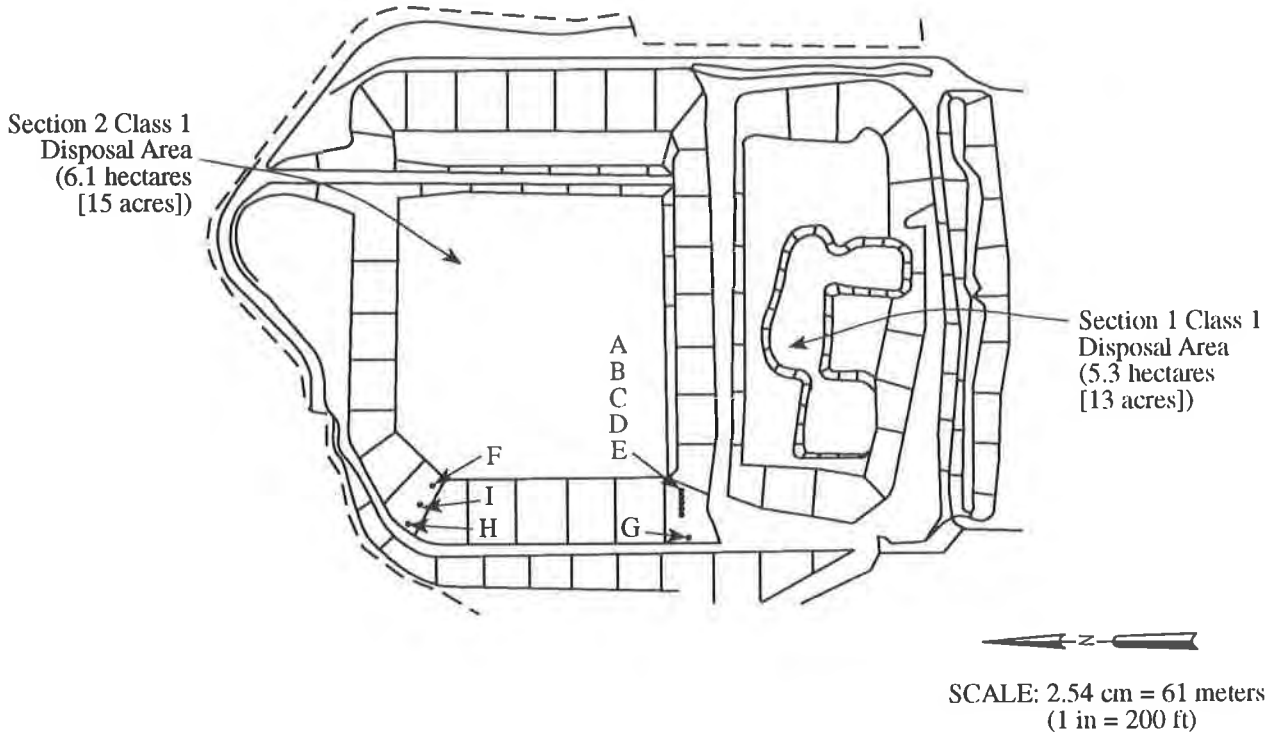

Figure 6. Clay Sample Locations

Samples were collected from these locations at depths of 5 cm (2 inches), 15 cm (6 inches), and 20 cm (8 inches) with a 2.5-cm-diameter (1-inch-diameter) hand auger. A subgrade sand sample was also obtained approximately 6 cm (2.5 inches) below the clay liner. Construction records for clay placement in this area indicate that the average moisture content during placement was approximately 22 percent. The clay samples analyzed were collected about 3.5 years after placement.

Results of the current clay moisture content analysis indicate a significant loss of moisture for shallow samples close to the berm crest. For example, Sample G showed about a 70 percent reduction in moisture between placement and sampling, with an average moisture content of 6.7 percent. Surface samples collected at a depth interval of 5 cm (2 inches) averaged about 10 percent moisture content. Figure 7 illustrates the overall moisture-content trend along the sampling strip. As shown, the clay loses moisture from the surface downward and as a function of the distance from the crest.

Although no records of as-constructed moisture content of the subgrade sand are available, the subgrade sand samples exhibited extremely low moisture contents, averaging about 2 percent, and a dust-like consistency. These characteristics indicate that significant moisture reduction may be occurring, even in the clay subgrade materials.

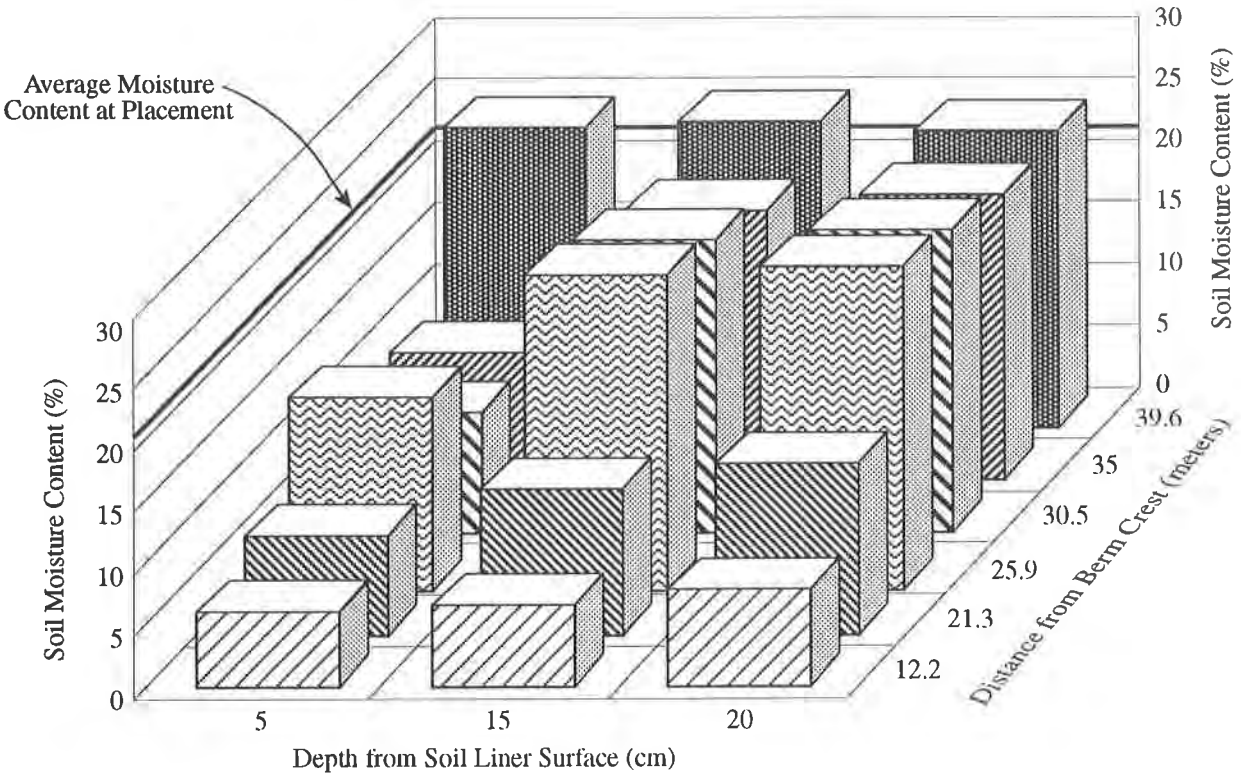

Figure 7. Relationship of Moisture Content and Soil Depth for Section 1

Section 2. Three clay sample locations were established at the following distances down from the berm crest (see Figure 6):

Section 2 Sample Location	Distance (meters)	Distance (feet)
F	6.4	21
H	16.9	55.5
I	27.4	90

Samples were collected from these locations at depths of 5 cm (2 inches), 15 cm (6 inches), and 20 cm (8 inches) with a 2.5-cm-diameter (1-inch-diameter) hand auger. A subgrade sand sample was also obtained approximately 6 cm (2.4 inches) below the clay liner. Construction records for clay placement in this area indicate that moisture content during clay placement averaged about 18 percent. The clay samples were obtained approximately 2 months after the clay was placed, compacted, and covered with geomembrane.

Results of the Section 2 sample analyses revealed that severe clay desiccation had already begun (see Figure 8). Figure 8A shows the clay condition at 6.4 meters (21 feet) down from the crest, and Figure 8B shows the clay condition at 27.5 meters (90 feet) down from the crest. The clay cracks measured about 1.3 cm (0.5 inch) wide and extended to a depth of about 20 cm (8 inches).

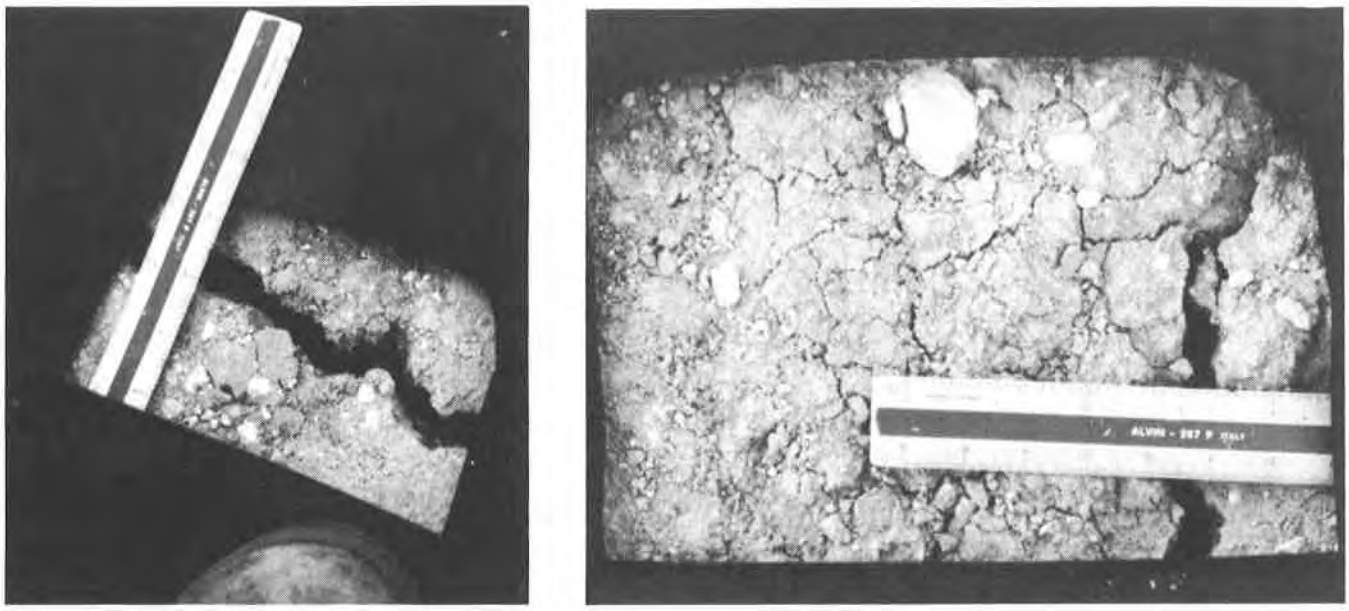

A. Conditions at 6.4 Meters from the Berm Crest

B. Conditions at 27.5 Meters from the Berm Crest

Figure 8. Severe Desiccation in the Section 2 Clay Layer

The moisture contents obtained reflect the visual condition of the clay. The average moisture content at locations H and I at 5 cm (2 inches) below the surface was about 8 percent, which is less than half of the original placement moisture content. Location F exhibited no loss of moisture throughout the depth range of the clay. As shown in Figure 9, moisture loss occurs from the clay surface downward and possibly as a function of distance from the berm crest. However, evidence of this condition in Section 2 is not as strong as it is for Section 1 (see Figure 7).

Causes. These observations and analyses provide considerable support for the hypothesis. Coarser and Cranston (1991) reported that on slopes [clay] "moisture either passes through the HDPE as a vapor or condenses on the backside of the liner and runs to low spots where it will collect and potentially absorb into the clay liner." Seed and Bonaparte (1992) state the following:

> Thermal effects associated with cyclic heating and cooling of geomembranes placed over compacted liner clays (due to exposure to sunshine during daytime, until the

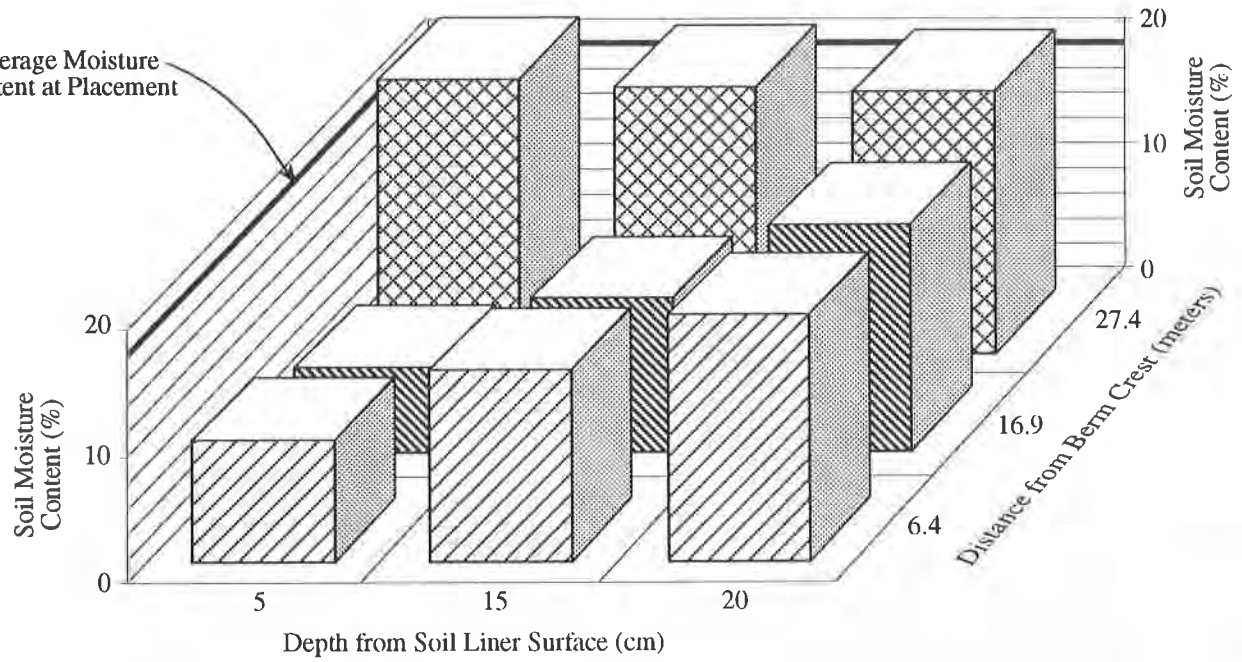

Figure 9. Relationship of Moisture Content and Soil Depth for Section 2

geomembrane is subsequently covered with soil) will draw water from the clay and cause this water to condense on the underside of the geomembrane. In some circumstances, this will result in wetting of the interface.

These statements, along with the evidence produced in this investigation, suggest that a combination of thermal effects and low recharge of subgrade soil pore water were major factors in the severe desiccation cracking.

Thermal Effects. Throughout Section 2 construction, the HDPE geomembrane surface temperatures were monitored during peak ambient air temperature periods. With average peak ambient air temperatures of about 35 degrees Celsius (°C) (95 degrees Fahrenheit [°F]), the HDPE geomembrane surface temperature exceeded 65°C (150°F). Low average HDPE geomembrane temperatures were estimated to be about 24°C (75°F). These conditions indicated about a 40°C (75°F) temperature fluctuation in the HDPE liner. As a result, HDPE liner wrinkles due to thermal expansion are significant. In addition, during hot afternoons, aerodynamic effects tend to lift portions of the side slope liner by as much as 0.5 meter (18 inches) above the clay liner.

Because large areas of HDPE geomembrane were not in direct contact with the clay liner, moisture that condensed along the underside of the HDPE would migrate down the slope until the liner recontacted the clay or until the water reached the lowest possible collection level, which would be the toe of the slope.

Low Subgrade Recharge. Because a significant portion of the side slope subgrade is above natural grade, low pore-water recharge of the subgrade from permeation of surface storm water can occur. Most rainfall in this region is intense and of short duration; therefore, water that would otherwise permeate a natural grade may not do so here. Instead, most storm water would simply run off the 3:1 outside slopes of the berm. The top of berm does not provide adequate area to collect significant amounts of water to rehydrate the clay. Consequently, the clay would receive little, if any, subgrade pore water to replace the loss.

CONCLUSION

The results of this investigation and the findings of other researchers suggest that exposed side-slope composite liners are likely to cause the clay liner to desiccate, sometimes severely and within a relatively short time. Coarser and Cranston's (1991) research was "intended to provide a qualitative large scale field assessment of whether this was an isolated occurrence or a mechanism that could apply to all landfills in arid areas" (p. 4). The findings of this investigation provide evidence that the same process is occurring and may be more severe than previously suspected, even in a semitropical area such as north-central Florida where average annual rainfall may exceed 140 cm (55 inches).

ALTERNATIVE DESIGN APPROACH

One design change that could mitigate the clay desiccation problems would be eliminating exposed liner. If eliminating exposed liner is impossible (because of side slopes), however, the side-slope grade should be below the surrounding natural grade to help rehydrate the clay materials.

The alternative designs listed below are intended to reduce or prevent clay desiccation on exposed side slopes in future landfill facilities. However, because they have not been applied and proven in practice, further research is recommended. Most of the following recommendations would have a significant effect on the design and, consequently, would lead to increased construction cost.

- Place a geosynthetic reinforcement for drainage material on the slope. This action would help prevent the drainage material from sloughing and eroding and would reduce slope stability difficulties along this plane. It would also maintain continuous contact between the clay and HDPE geomembrane along the side slope and help stabilize temperature fluctuations.

- Install an intermediate geotextile barrier in the clay layer. As a horizontal sheet within the clay layer, this feature would potentially impede the loss of clay moisture.

- Provide a rough, uncompacted clay surface to break capillary water movement.

- Install a reflective solar surface over the slope lining to reduce the temperature of the HDPE geomembrane.

- Add hydrophilic calcium chloride to the clay to retain water.

- Use a polyurethane spray foam insulation or solar barrier on the HDPE liner to reduce liner temperature.

- Cover the HDPE liner with a fabric-form containing a weak cementatious grout to reduce liner temperature and maintain contact between the geomembrane and the clay.

- Provide a system to recirculate the mounding water at the toe of the slope to continually rehydrate the clay until the slope is covered. This recirculation would also reduce stress on the geomembrane liner from mounding water at the slope toe.

ACKNOWLEDGEMENTS

The authors thank J.H. Water Systems, Inc., for providing assistance during this investigation. In addition, appreciation is extended to Larry Well and Martin Brungard of CH2M HILL for providing encouragement and information to produce this paper, and to Carla Bare for editing the text.

REFERENCES

Well, Larry, (February 1991) "Internal CH2M HILL Memorandum," Portland, Oregon.

Coarser, P., and Cranston, M., (1991) "Observations on Long-Term Performance of Composite Clay Liners and Covers," Presented at Geosynthetics Design and Performance, Vancouver Geotechnical Engineering Society, Vancouver, B.C., May 24, 1991, pp. 2, 4.

Seed, R.B., and Bonaparte, R., (1992) "Seismic Analysis and Design of Lined Waste Fills: Current Practice," Presented at Stability and Performance of Slopes and Embankments-II, University of California at Berkeley, June 30, 1992, ASCE Geotechnical Special Publication No. 31, pp. 1540-1541.

Design of Lining and Cover System Sideslopes

S.J. Druschel
CH2M Hill Inc., USA

E.R. Underwood
CH2M Hill Inc., USA

ABSTRACT

In this paper, a design methodology is presented for evaluating the stability of various lining and cover sideslope configurations. Traditional sliding-block analysis is the basis of the methodology, but it has been expanded to include seepage forces, equipment loads, geosynthetic anchorage, and factors of safety. As an aid to "real world" application of the methodology, equations are included in this paper to simplify the working analysis of stability and to allow the optimization of factors such as slope geometry, strength, and applied loads. In addition, figures are included that show the maximum slope height attainable for a range of slope angles, interface frictions, soil strengths, soil layer thicknesses, seepage depths, equipment loads, and geosynthetic anchorages. Use of this methodology is demonstrated in a project example in which slope angles are balanced against bench heights, soil characteristics, geosynthetic anchorage, and economics.

GLOSSARY OF SYMBOLS

The symbols used in the text, figures, and equations that appear in this paper are explained in the following list.

H	=	sideslope height
T_c	=	cover soil thickness
β	=	sideslope angle
γ_w	=	unit weight of water (62.4 lbs/ft^3)
γ_c	=	unit weight of cover soil
δ	=	interface friction angle
δ_m	=	interface friction angle (mobilized)
ϕ	=	soil shear strength angle
ϕ_m	=	soil shear strength angle (mobilized)
W_2	=	weight of sideslope soil
W_1	=	weight of toe buttress soil
W_e	=	weight of equipment on the sideslope
F_b	=	equipment braking force

T_w	=	thickness of seepage
W_{w1}	=	weight of seepage water in toe buttress
W_{w2}	=	weight of seepage water in sideslope soil
F_s	=	seepage force
F_a	=	geosynthetic anchorage force
F_1	=	toe buttress reaction force
F_2	=	sideslope reaction force
P	=	sideslope-toe buttress reaction force

INTRODUCTION

The capacity of a waste-containment facility such as a landfill is determined by the facility's area, height, and sideslope angles. Although the area and height are usually determined by property limits and regulations, the sideslope angle is based on engineering judgment and operational performance. Steeper sideslopes provide greater capacity, and greater capacity provides higher profits, so the sideslope angle should be as steep as possible. However, when the sideslope angle is too steep, the protective soil cover can become unstable and slide down slope. At best, such movement increases maintenance costs. At its worst, such movement can destroy a containment facility and cause its premature closure. Designs must balance the need for capacity against the risk of failure.

STABILITY ANALYSIS

Typical modern liner and cover systems consist of both soil and geosynthetic materials in a layered arrangement. When a liner or cover system becomes unstable, stronger overlying layers will tend to remain somewhat intact and slide over the weaker layers. Because the slope length is much greater than the liner or cover system thickness, the system can be modeled by a block sliding on an inclined plane. Figure 1 shows a sideslope with forces that typically act on it.

The sliding-block analysis is a traditional geotechnical technique in which all the forces acting on the sliding block are summed and the resultant must equal zero for the block to be stable. Sliding-block analysis is similar to the infinite slope analysis, another traditional geotechnical technique, but includes the contribution of the slope change at the bottom of the sideslope, described below as the toe buttress force. Factors of safety for sliding block analysis are developed by evaluating the shear strengths required to balance the forces and achieve stability. A full discussion of sliding-block analysis may be found in Lambe & Whitman (1969) or U.S. Navy (1986). Each of the forces that affects sideslope stability is briefly discussed below.

Interface Shear Strength. In any liner or cover system, the weakest interface governs stability. From the many studies of interface friction (for example, Martin, et al. [1984], Saxena and Wong [1984], Williams and Houlihan [1986], Negussey, et al. [1989], O'Rourke, et al. [1990], Mitchell, et al. [1990], and Yegian and Lahlaf [1992]), two classes of commonly encountered interface strengths have emerged: low-strength interfaces and high-strength interfaces.

Low-Strength Interfaces

Geotextile-geomembrane Geonet-geomembrane Geotextile-geonet (unless heat-bonded) Geomembrane- clay(saturated)	δ = 6 to 9 degrees

High-Strength Interfaces

Sand-geomembrane Sand-geotextile Clay-geotextile	δ = 15 to 18 degrees

Factors of Safety. Factors of safety are calculated on the basis of the ratio of the actual shear strength to the mobilized shear strength (that is, the shear strength required for stability):

$$\text{Factor of safety} = \frac{\tan \phi}{\tan \phi_m} \text{ or } \frac{\tan \delta}{\tan \delta_m} \qquad \text{(Equation 1)}$$

Alternatively, a factor of safety can be set and maximum values of ϕ_m and δ_m calculated. This value may be used in the sliding block model to determine the maximum conditions (that is, H or β) that can be tolerated while still maintaining the factor of safety.

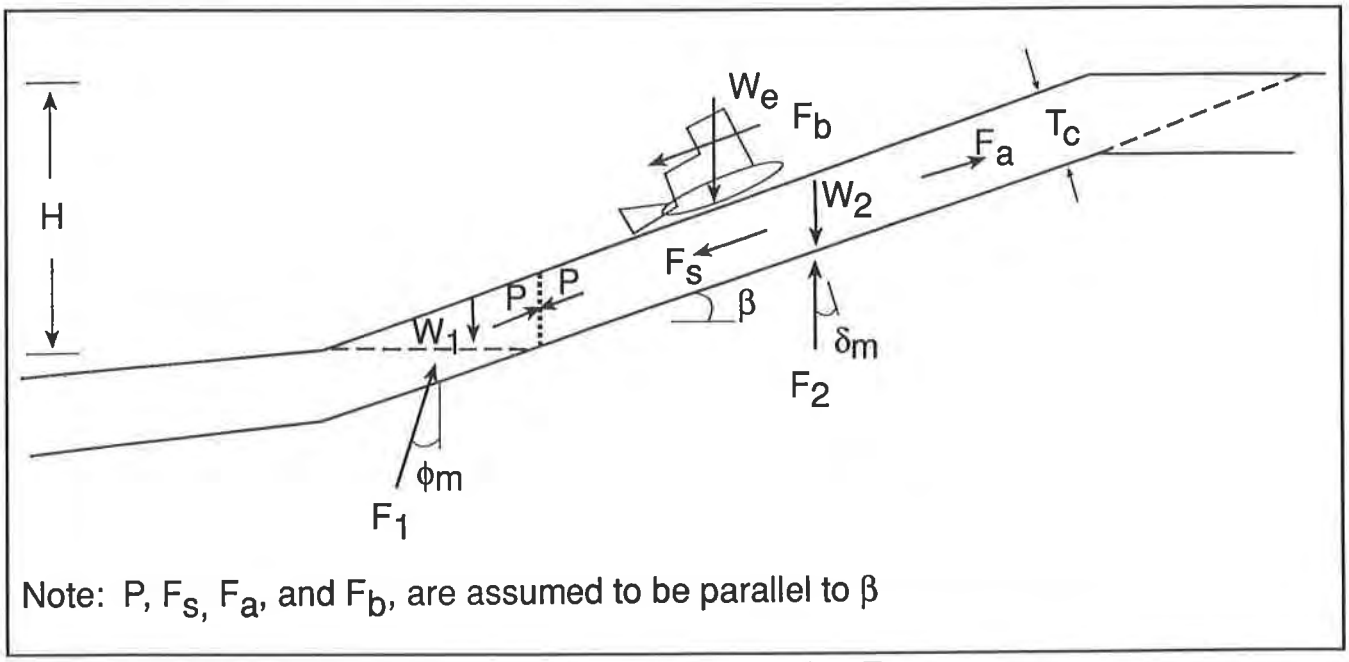

Figure 1. Sideslope with Typical Forces

One important point about shear strength values used for evaluation of cover and liner systems: because each material used in the system has a different shear stress-displacement response, peak or ultimate strengths may occur at different strain levels, or not at all. For this reason, residual shear strengths instead of peak strengths are strongly recommended for use in all slope evaluations.

Toe Buttress. Multilayered geosynthetic or composite liners and covers that have low-strength interfaces (δ values in the range of 6 to 9 degrees) are especially prone to stability problems. What allows liner and cover systems with low-strength interfaces to be stable when $\beta > \delta$? The answer lies with the soil cover at the bottom of the slope, through which any failure surface must propagate. This wedge of soil acts as a toe buttress, holding back the soil cover and increasing its stability. The strength of an effective toe buttress is provided by the friction developed along the failure surface. This friction is a function of ϕ and a combination of W_1 and P (the force of the soil cover acting on the wedge as it tries to slide). While the reaction force is determined graphically, W_1 is given by the following equation:

$$W_1 = \frac{\gamma_c T_c^2}{2 \sin \beta \cos \beta} \qquad \text{(Equation 2)}$$

More detail on the effect of the toe buttress on stability may be found in Beech and Giroud (1989).

Soil Cover. W_2 can be calculated using the following equation:

$$W_2 = \frac{\gamma_c T_c}{\sin \beta} \left(H - \frac{T_c}{2 \cos \beta} \right) \qquad \text{(Equation 3)}$$

This equation addresses soil covers of uniform thickness. It should be noted that this equation also reflects a simplifying assumption in that the upper end of the failure plane passes through the cover soil, but this length is treated as if it has the same strength as the interface. This is a conservative assumption because the actual strength is generally higher.

Equipment Load. Equipment that operates on the sideslope has a static weight, W_e, that acts in the same manner as W_2. However, additional forces are generated by acceleration and braking of the equipment as it moves on the sideslope. Koerner and Richardson (1987) suggest that these forces be treated as a separate braking force, F_b, equal to 30 percent of the equipment's weight and acting downslope, parallel to the interface. While a gross simplification, this approximation is sufficient to allow for the effects of equipment of different sizes. Intuitively, we know there must be a difference in the effects of a D-4 and a D-7 bulldozer, since there is a threefold increase in weight but only a moderately larger footprint.

W_e is calculated using the equipment weight divided by the contact width. The contact width is simply the width over which the load is distributed to the interface of interest. Because soil arching typically will mobilize the zone of soil between the tracks, the contact width may be based on the full width of the equipment.

Seepage Force. F_s is treated as a negative static load on the basis of the buoyancy applied to the cover soil. Simply put, the buoyancy normally reduces frictional shear stress because of the reduction in effective stress normally applied to the sliding plane. Instead of applying the reduction to the strength parameters as is done in most areas of soil mechanics, Lambe and Whitman (1969) suggest using a negative resisting force. A major assumption of this approach is that the seepage is parallel to the slope and of uniform thickness. The seepage force may then be calculated in the same way as the soil loads, changing only T_w.

$$W_{W1} = \frac{\gamma_W T_W^2}{2 \sin\beta \cos\beta} \qquad \text{(Equation 4)}$$

$$W_{W2} = \frac{\gamma_W T_W}{\sin\beta}\left(H - \frac{T_w}{2 \cos\beta}\right) \qquad \text{(Equation 5)}$$

$$F_S = W_{W1} \tan\phi_m + W_{W2} \cos\beta \tan\delta_m \qquad \text{(Equation 6)}$$

It should be noted that no interwedge force exists with seepage because water can sustain no shear stress.

Geosynthetic Anchorage. F_a represents the force provided by geogrids or by high-strength geotextiles anchored at the top of the slope. Strengths typically are taken from the 2 percent strain level of the geosynthetics, a level that generally can be accommodated by the other components of a liner or cover system. The direction of F_a is parallel to the slope and upward. Anchorage trenches or other means of attachment must be sufficiently strong to keep the geogrid or geotextile from pulling out. Geomembranes, geonets, and general-use geotextiles should not be considered for F_a because useful levels of strength would require unacceptable levels of strain.

Earthquake Force. While beyond the scope of this paper, pseudo-static earthquake forces can be applied easily, parallel to the slope. The earthquake force, which is equal to the soil weight multiplied by the acceleration factor (percentage of gravity), is entered into the model as a negative geosynthetic anchorage force. Soil and interface shear strengths should reflect appropriate factors of safety.

Reaction Forces. Reaction forces include P, F_1, and F_2 and are a function of the static equilibrium. These variables drop out of the calculations through some physical and mathematical relationships.

STABILITY CALCULATION

All forces are plotted on a force vector diagram, as shown in Figure 2. The magnitudes of the reaction forces are unknown, but their directions are set by the problem geometry. We can eliminate F_1 and F_2 by using Newton's first law, which states that the sum of the forces in any direction must equal zero for stability to exist. Therefore, the forces perpendicular to F_1 in Polygon 1 and perpendicular to F_2 in Polygon 2 are each summed and set equal to zero. Solving the remaining terms for P sets up the next step.

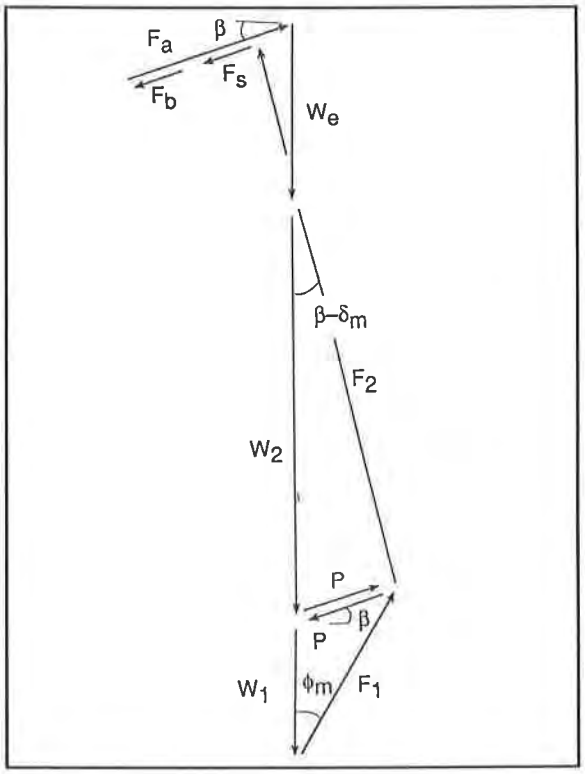

Figure 2. Force Vector Diagram

Polygon 1: $$P = \frac{W_1 \sin\phi_m}{\cos(\beta + \phi_m)}$$ (Equation 7)

Polygon 2: $$P = \frac{(W_e + W_2)\sin(\beta - \delta_m)}{\cos\delta_m} + F_b + F_s - F_a$$ (Equation 8)

Equations 7 and 8 are now equated, and P drops out:

$$\frac{W_1 \sin\phi_m}{\cos(\beta + \phi_m)} = \frac{(W_e + W_2)\sin(\beta - \delta_m)}{\cos\delta_m} + F_b + F_s - F_a \quad \text{Equation 9)}$$

Equation 9 can be rearranged to solve for F_a:

$$F_a = F_b + F_s + \frac{(W_e + W_2)\sin(\beta - \delta_m)}{\cos\delta_m} - \frac{W_1 \sin\phi_m}{\cos(\beta + \phi_m)} \qquad \text{(Equation 10)}$$

Equation 10 provides the basis for the overall method. Simply stated, if anchorage forces are positive in value, the slope is not stable without them. Solving for F_a to equal zero will give the maximum stable height for a particular set of slope conditions.

To make the calculation, insert the actual values for F_b, F_s, W_1, and W_2:

$$F_a = [\,0.3W_e\,] + \left[\frac{\gamma_w T_w^2 \tan\phi_m}{2\sin\beta\cos\beta} + \frac{\gamma_w T_w \cos\beta \tan\delta_m}{\sin\beta}\left(H - \frac{T_w}{2\cos\beta}\right)\right]$$
$$+ \left[\frac{W_e \sin(\beta-\delta_m)}{\cos\delta_m}\right] + \left[\frac{\gamma_c T_c \sin(\beta-\delta_m)}{\sin\beta\cos\delta_m}\left(H - \frac{T_c}{2\cos\beta}\right)\right] \qquad \text{(Equation 11)}$$
$$- \left[\frac{\gamma_c T_c^2 \sin\phi_m}{2\sin\beta\cos\beta\cos(\beta+\phi_m)}\right]$$

Equation 11 may be expanded as follows:

$$F_a = W_e\left[0.3 + \frac{\sin(\beta-\delta_m)}{\cos\delta_m}\right] + \left[\frac{\gamma_w T_w^2 \tan\phi_m}{2\sin\beta\cos\beta} + \frac{\gamma_w T_w H \cos\beta \tan\delta_m}{\sin\beta} - \frac{\gamma_w T_w^2 \cos\beta \tan\delta_m}{2\sin\beta\cos\beta}\right]$$
$$- \left[\frac{\gamma_c T_c^2 \sin\phi_m}{2\sin\beta\cos\beta\cos(\beta+\phi_m)} + \frac{\gamma_c T_c^2 \sin(\beta-\delta_m)}{2\sin\beta\cos\delta_m\cos\beta} - \frac{\gamma_c T_c H \sin(\beta-\delta_m)}{\sin\beta\cos\delta_m}\right]$$

(Equation 12)

Rearrange and combine in terms of the sideslope geometry:

$$F_a = \frac{\gamma_w T_w^2}{2\tan\beta}\left(\frac{\tan\phi_m}{\cos^2\beta} + \frac{2H\tan\delta_m}{\cos\beta} - \frac{\tan\delta_m}{\cos\beta}\right) + W_e\left(0.3 + \frac{\sin(\beta-\delta_m)}{\cos\delta_m}\right) - \frac{\gamma_c T_c^2 \sin(\beta-\delta_m)}{2\sin\beta\cos\beta\cos\delta_m}\left(\frac{\sin\phi_m\cos\delta_m}{\cos(\beta+\phi_m)\sin(\beta-\delta_m)} + 1 - \frac{2H\cos\beta}{T_c}\right) \quad \text{(Equation 13)}$$

PARAMETRIC EVALUATION

This methodology can be used to evaluate stability of a single landfill configuration. Another use—possibly more instructive—would be to test the impact of a single variable, keeping all other variables unchanged. In this way, a designer would gain an understanding of how sensitive stability is to changes in certain variables such as interface friction or slope angle. Given a particular set of conditions, a designer can determine the interface friction value and slope angle required for stability. This methodology enables the designer to tailor the slope design to existing conditions, thereby enhancing performance of the facility.

An understanding of the effect of each variable on stability may be gained by placing Equation 13 in a spreadsheet and changing certain values. Figure 3 shows the maximum stable height for a range of δ_m. The trend of the data is clear. For each value of δ_m, a high slope (slopes with a height greater than 30), T_c can be obtained at a β equal to or less than δ_m. At greater angles, the maximum stable height is quickly reduced to values between 2 T_c and 5 T_c. The rapidity with which this change occurs shows that both β and δ_m are major factors in determining the maximum slope height. These data are useful to set β or bench height of a particular lining or cover system or to select the components for a particular slope geometry.

The influence of the cover soil characteristics is demonstrated in Figures 4 and 5. Thicker cover soils allow stability to be maintained despite higher slopes, by approximately a proportional amount, but changes in γ_c make no appreciable difference. Increasing ϕ_m also increases the maximum stable slope height. These trends suggest that the characteristics of a cover soil may be manipulated to develop a stable slope of a given height and configuration.

Seepage and equipment loadings are evaluated in Figures 6 and 7, respectively. T_w has a relatively moderate effect on maximum stable slope heights. W_e has a substantial effect, especially when β is greater than δ_m.

For slopes that require geosynthetic anchorage to be stable, the magnitude of F_a required for stability is the key question of design. Figures 8 and 9 are examples of this analysis, showing F_a required for particular slope heights and angles, with δ_m of 12 and 9 degrees, respectively. The trend of the data is linear, with higher slopes requiring proportionally greater F_a. Increasing β or decreasing δ_m will significantly increase the magnitude of F_a required. A cost-benefit analysis may be performed by using the stability model in this way, in which the height or angle between benches and the associated value of space may be optimized against the cost of the required anchorage.

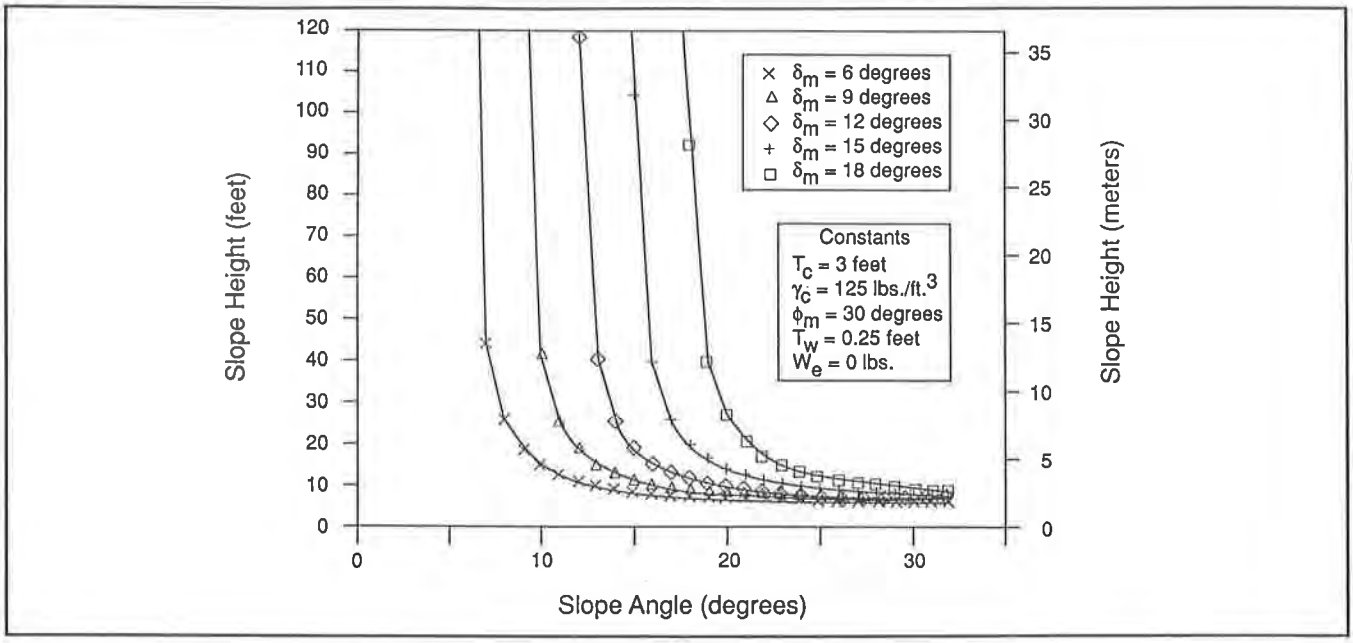

Figure 3. Height as a Function of δ_m and β

PROJECT EXAMPLE

Use of this design methodology is demonstrated in the following example, which simulates design of a typical landfill.

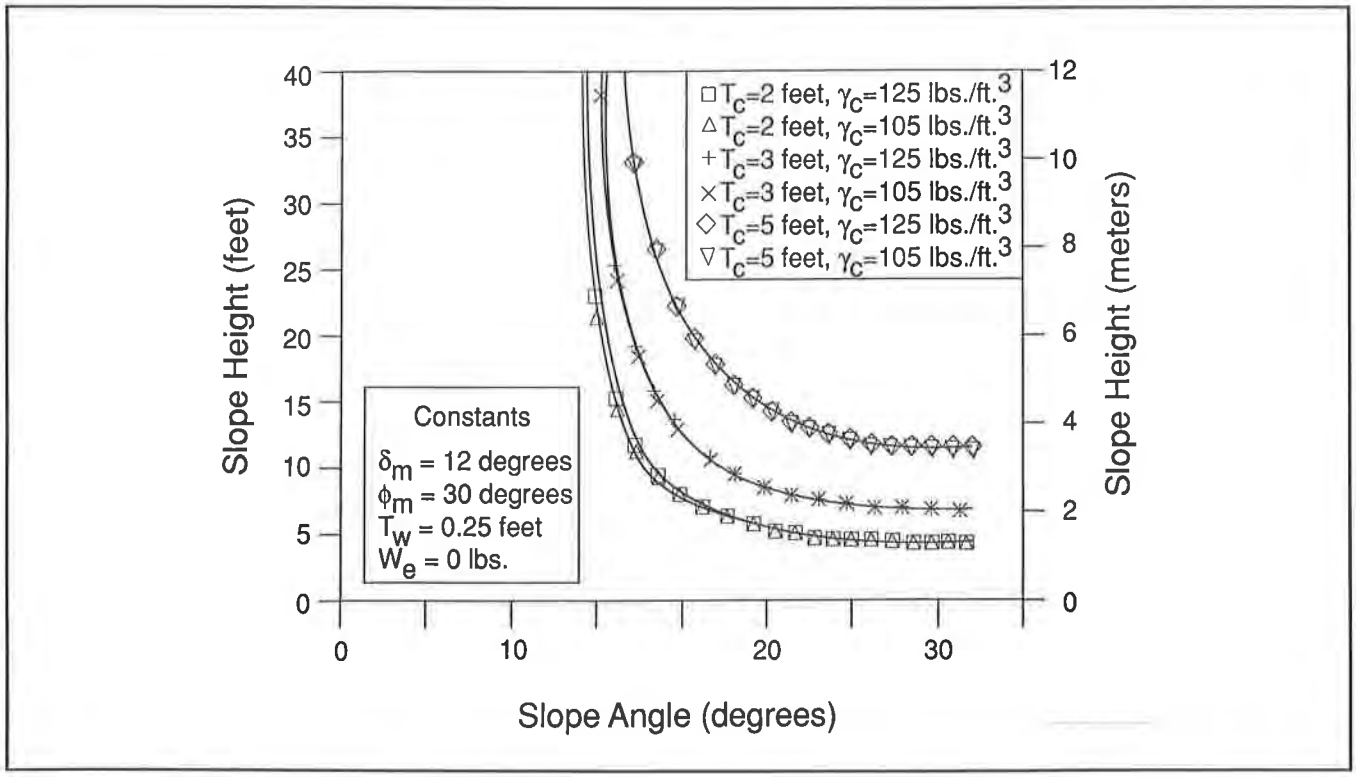

Figure 4. Height as a Function of Soil Cover Characteristics

For a slope 6 meters (20 feet) high, two configurations are considered. The first configuration is a 4:1 (β = 14.0 degrees) straight slope. The second configuration has two 3:1 slopes (β = 18.3 degrees), each 3 meters (10 feet) high, separated by a bench 6 meters (20 feet) wide. Constants for this example are:

- ϕ = 35 degrees (maximum residual value)
- δ = 12 degrees (maximum residual value)
- T_w = 76 mm (0.25 feet)
- γ_c = 19.6 kN/m^3 (125 lbs/ft^3)
- W_e = 0

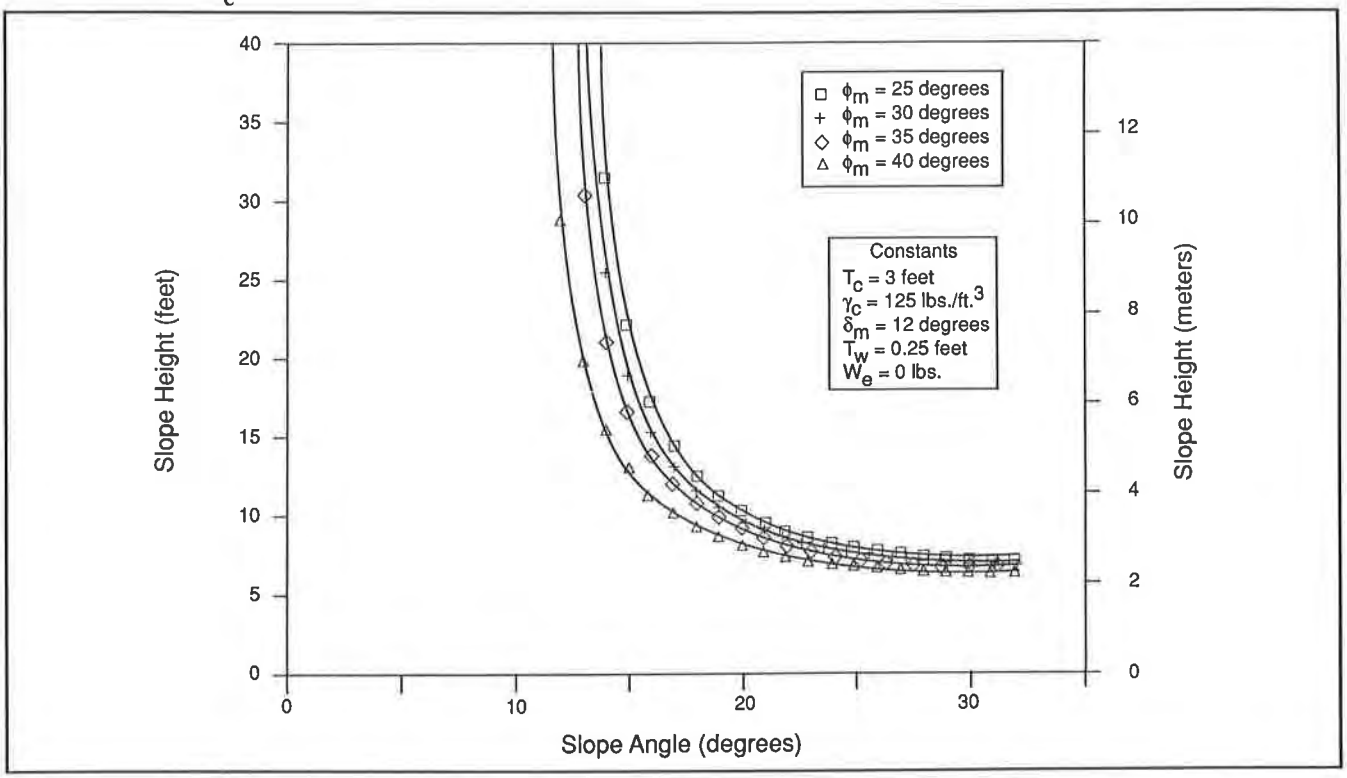

Figure 5. Height as a Function of ϕ_m

In the example, several combinations of T_c and F_a are evaluated to find a design that minimizes costs and maximizes performance while providing a minimum safety factor (FS) of 1.25. The safety factor is determined by finding the highest mobilized strength levels for which F_a equals zero or less. Different combinations of ϕ_m and δ_m, calculated using the same factor of safety for each combination, are inserted into the equation until F_a equals zero.

Table 1 shows the results of the evaluation. Factors of safety for slopes with no geosynthetic anchorage are given, as well as the value of F_a, which is required to provide a factor of safety of at least 1.25 for each of the thinner soil covers. The thinnest T_c to provide a factor of safety of 1.25 without any geosynthetic anchorage is 1.30 meters (4.25 feet) for the 4:1 slope and 1.07 meters (3.5 feet) for the 3:1 slopes with the intermediate bench. These results may be used

in evaluating the relative cost benefit of geosynthetic anchorage and various thicknesses of soil cover in order to optimize the design.

Table 1. Evaluation Results (Example)

Cover Soil Thickness (T_c)	4:1 Slope, H = 6 Meters (20 Feet)		3:1 Slope, H = 3 Meters (10 Feet)	
	FS for $F_a = 0$	F_a Required for FS = 1.25	FS for $F_a = 0$	F_a Required for FS = 1.25
0.61 m (2 ft.)	<1.00	14.83 kN/m (1,009 lbs/ft)	<1.00	7.73 kN/m (526 lbs/ft)
0.91 m (3 ft.)	1.11	11.89 kN/m (809 lbs/ft)	1.16	3.68 kN/m (250 lbs/ft)
1.22 m (4 ft.)	1.22	3.07 kN/m (209 lbs/ft)	1.37	0
1.52 m (5 ft.)	1.34	0	1.60	0

F_a = Geosynthetic anchorage force; FS = Factor of safety;
kN/m = KiloNewtons/meter

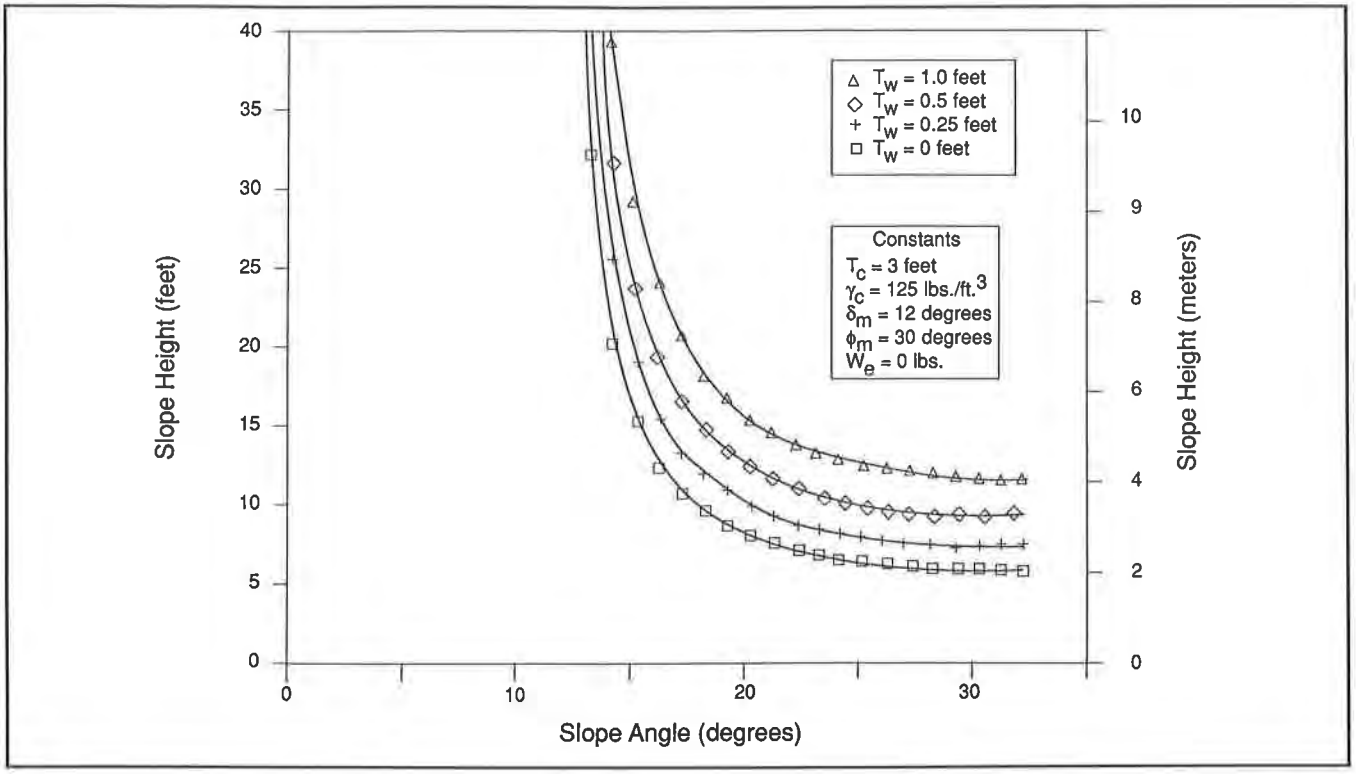

Figure 6. Height as a Function of T_w

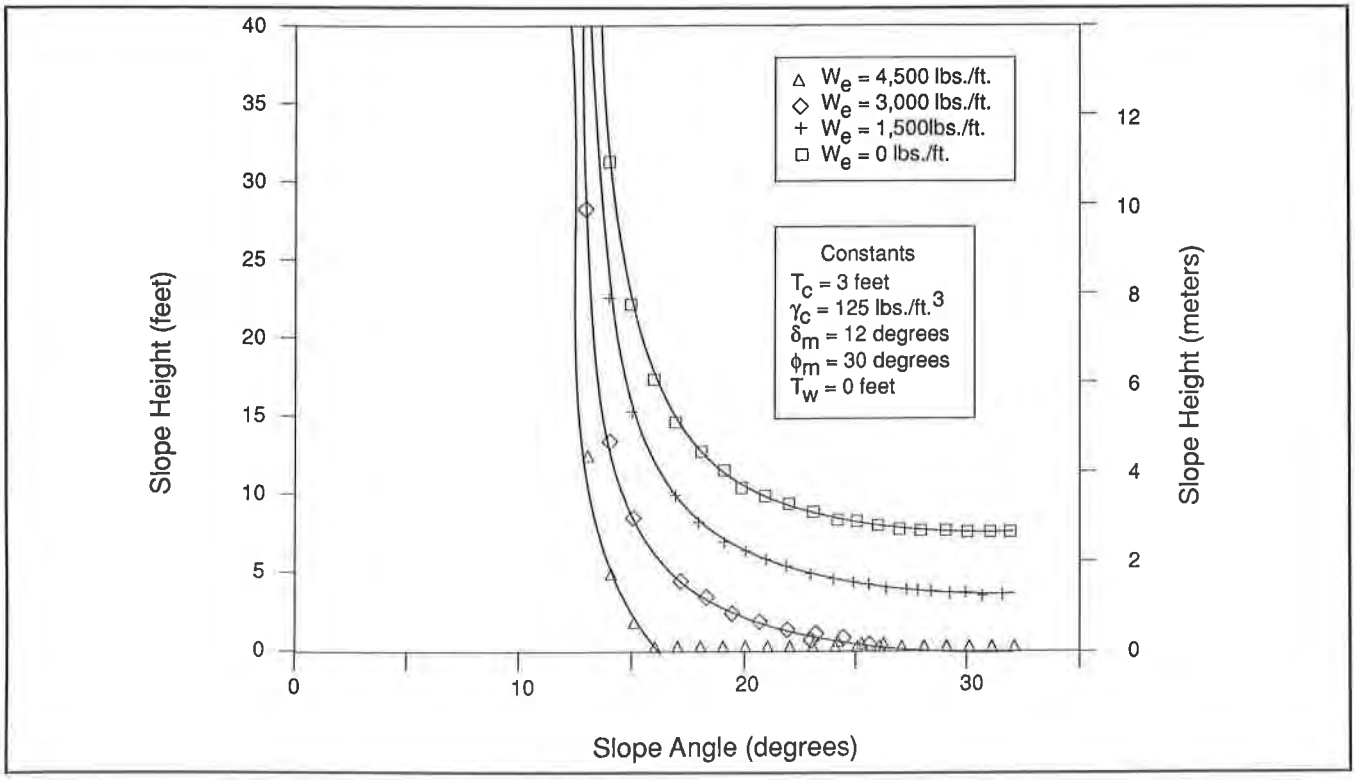

Figure 7. Height as a Function of W_e

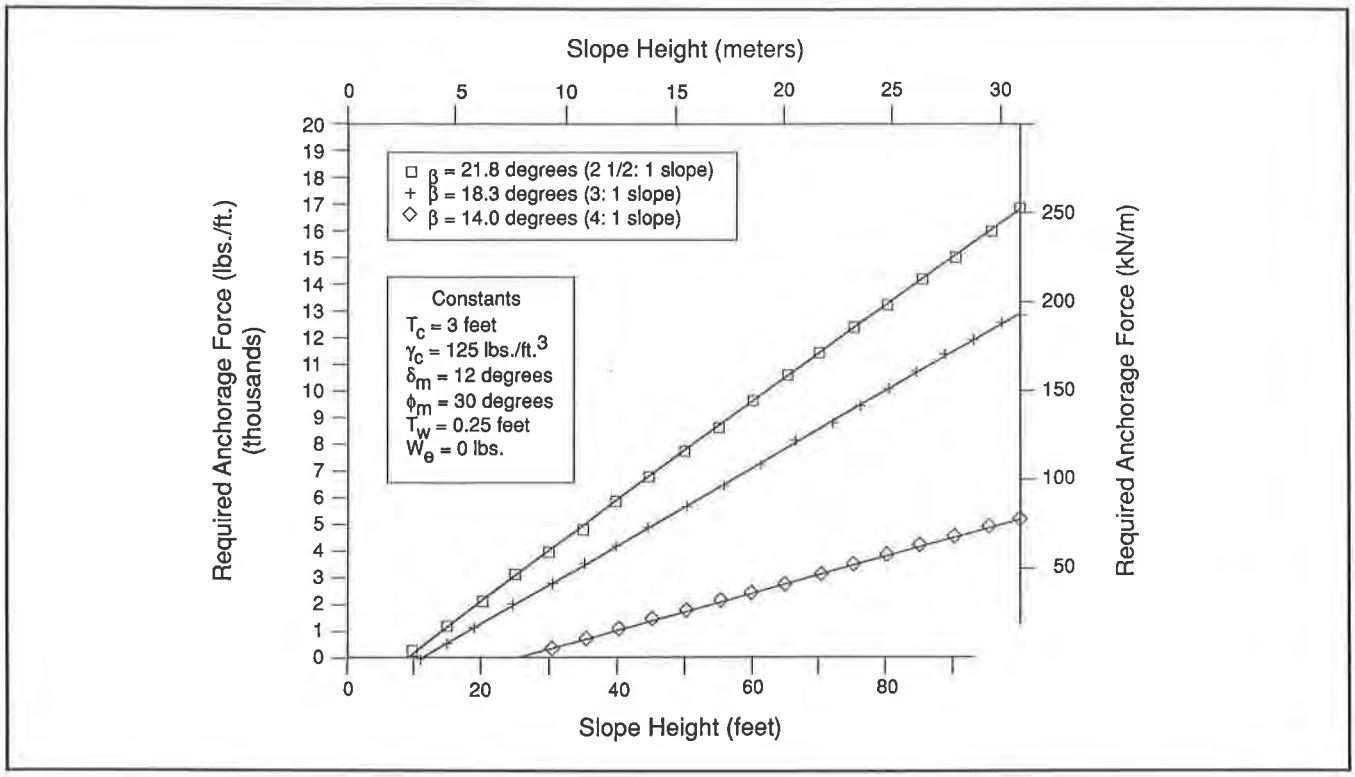

Figure 8. Anchorage Required for Slopes where δ_m = 12 Degrees

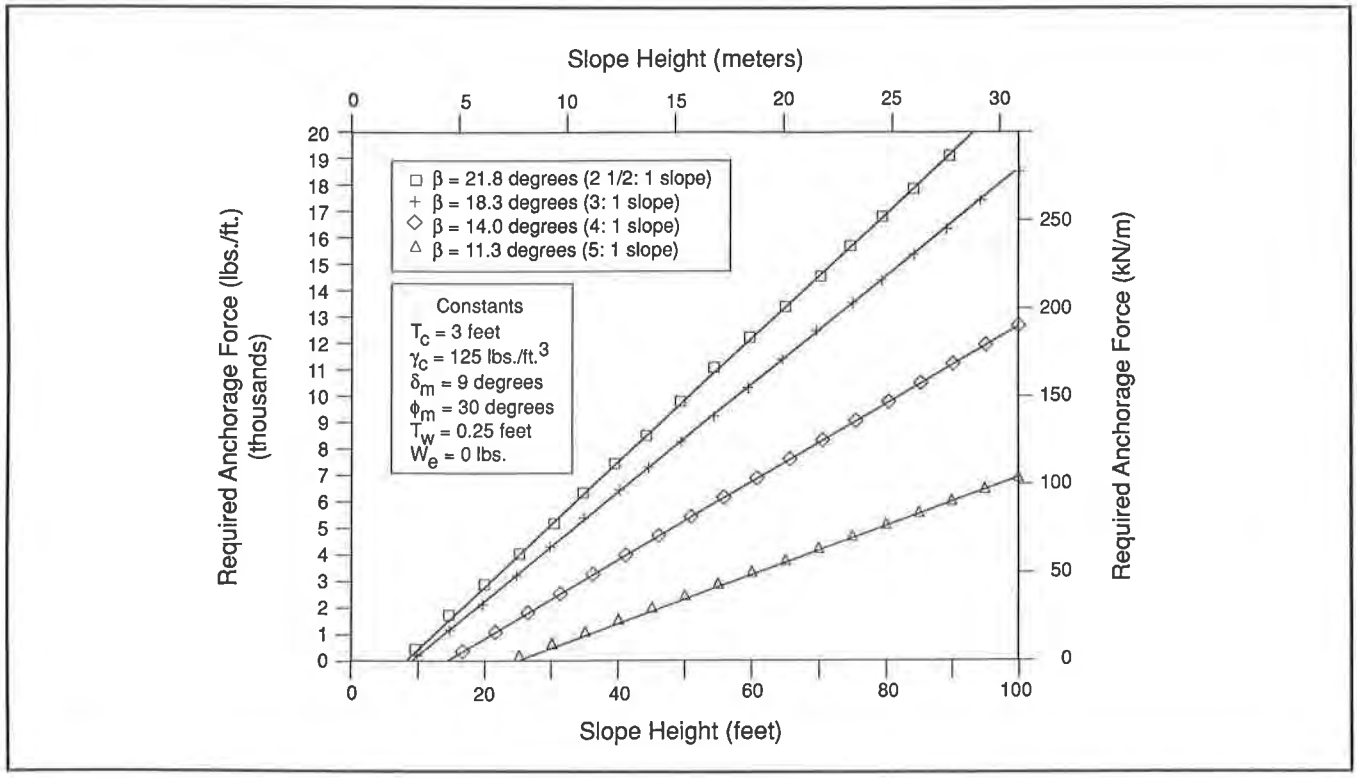

Figure 9. Anchorage Required for Slopes where δ_m = 9 Degrees

SUMMARY

The stability of lining and cover system sideslopes can be evaluated using a design methodology that is described in this paper. This methodology is based on the traditional sliding-block analysis, but has been expanded to include seepage forces, equipment loads, geosynthetic anchorage, and factors of safety. Equations are included in this paper to simplify application of the methodology to "real world" situations and to allow the optimization of factors such as slope geometry, strength, and applied loads.

Figures are presented to show the maximum stable slope height attainable at given slope angles for a range of slope characteristics and external loads. Geosynthetic anchorage can be used to achieve a stable slope, and figures are presented to show the relationship between slope height and required anchorage force (F_a) for various slopes. A project example is included to demonstrate how a landfill sideslope can be designed for best performance.

REFERENCES

Giroud, J.P., and Beech, J.F. (1989) "Stability of soil layers on geosynthetic lining systems," Proceedings, Geosynthetics '89 Conference, IFAI, San Diego, California, pp. 35-46.

Lambe, T.W., and Whitman R.V. (1969) Soil Mechanics, John Wiley and Sons, Inc., New York.

Martin, J.P., Koerner, R.M., and Whitty, J.E. (1984) "Experimental friction evaluation of slippage between geomembranes, geotextiles, and soils," Proc. Int. Conf. on Geomembranes, Industrial Fabrics Association International, Denver, Colorado, pp. 191-196.

Mitchell, J.K., Seed, R.B., and Seed, H.B. (1990) "Kettleman Hills waste landfill slope failure. I: liner-system properties," J. Geotech. Engrg., ASCE 116(4), pp. 647-668.

Negussey, D., Wijewickreme, W.K.D., and Vaid, Y.P. (1989) "Geomembrane interface friction," Canadian Geotech. J., 26 (Feb.), pp. 165-169.

O'Rourke, T.D., Druschel, S.J., and Netravali, A.N. (1990) "Shear strength characteristics of sand-polymer interfaces," J. Geotech. Engrg., ASCE, 116(3), pp. 451-469.

Richardson, G.N., and Koerner, R.M. (1987) Geosynthetic Design Guidance for Hazardous Waste Landfill Cells and Surface Impoundments, Geosynthetic Research Institute, Drexel University, Philadelphia, Pennsylvania.

Saxena, S.K., and Wong, Y.T. (1984) "Frictional characteristics of a geomembrane," Proc. Int. Conf. on Geomembranes, Denver, Colorado, pp. 187-190.

U.S. Navy (1986) "Design manual—soil mechanics, foundations and earth structures," NAVFAC DM-7, Department of the Navy, Washington, D.C.

Williams, N.D., and Houlihan, M. (1986) "Evaluation of friction coefficients between geomembranes, geotextiles, and related products," Proc., 3rd Int. Conf. on Geotextiles, Vienna, Austria, pp. 891-896.

Yegian, M.K., and Lahlaf, A.M. (1992) "Dynamic interface shear strength properties of geomembranes and geotextiles," Journal of Geotechnical Engineering, ASCE, Vol. 118, No. 5, May, pp. 760-779.

WDCP295/003.51

Geomembranes for the Containment of Pulp Mill Hot Black Liquors: Problems and Remediation

I.D. Peggs
I-Corp International Inc., USA

T. Dewijn
Northwood Pulp and Timber Ltd., Canada

D.R. Lewis
Stothert Engineering Ltd., Canada

ABSTRACT

High density polyethylene (HDPE) geomembrane has been used in a number of pulp mills to contain hot black liquor (pH>12) at inlet temperatures of approximately 80°C in uncovered surface impoundments. Several of these installations have failed after being in service for no more than 12 months. One of these failures, at Northwood Pulp & Timber Ltd. in Prince George, B.C. was thoroughly investigated. Failure was found to be due to environmental stress cracking at folded compensation wrinkles caused by a soap solution associated with the black liquor. The black liquor itself also promoted environmental stress cracking. The field investigation and laboratory testing programs are described.

Preliminary chemical resistance testing was performed on a number of candidate geomembranes that might safely contain black liquor. Geomembranes based on polypropylene (PP) appear to be excellent candidates. Very low density polyethylene (PE) may be a candidate if it is provided with a soil cover.

INTRODUCTION

An inexpensive goemembrane-lined impoundment that will contain hot black liquor during service period outages can provide significant economic advantages to pulp mills. Over the past ten years, a number of geomembrane materials such as butyl rubber, polyvinyl chloride (PVC), chlorosulfonated polyethylene (CSPE, Hypalon), and high density polyethylene (HDPE) have been used to contain black liquor which has a pH exceeding 12 and is discharged to the pond at approximately 80°C.

Although there have been a number of delamination failures, the material that appears to have provided the best uncovered service is Hypalon. However, until recently, none of the installations have incorporated adequate leakage monitoring systems to confirm that the Hypalon lining systems are working satisfactorily.

In the early 1980s, two HDPE geomembranes were installed at mills in Georgia. In the mid-1980s, both liners are reported (private communications, 1990) to have failed by cracking along the top of wrinkles. One pond was taken out of service and replaced by tanks; the other was frequently repaired and appeared to slowly stop leaking, perhaps as the cracks and holes were clogged by cool viscous black liquor. This latter installation is presently being reassessed to see if it can be refurbished with another geomembrane. HDPE was not used again until 1986, when it was installed in one facility, but with a cover of gunite and clay to insulate/separate the geomembrane from the liquor.

In the late 1980s four additional HDPE liners were installed in black liquor ponds. One was installed at the Prince George, B.C. mill of Northwood Pulp & Timber, Ltd. (Northwood) in 1988. The liner failed in 1989. The nature of the failure, the

investigation performed, and suggestions for remediation are the topics of this paper. The initial investigation and testing programs were performed while the principal author was President of GeoSyntec, Inc.

BACKGROUND

The lining system installation was completed on a fast-track basis in the Fall of 1988. The lining system consisted of a 1 mm thick secondary HDPE geomembrane placed on a prepared sand subgrade. A geonet separated the secondary geomembrane from a 1.5 mm thick primary HDPE geomembrane. In order to complete the project within the required time frame, the primary HDPE geomembrane was supplied by a different manufacturer than the one that supplied the secondary geomembrane. The primary geomembrane was made on indexing drum equipment and, therefore, contained transverse flow marks approximately every 35 cm. At these flow marks, the geomembrane is considerably thicker than its nominal thickness. Neither the primary nor secondary geomembranes were installed by their manufacturers.

The primary geomembrane was seamed using double hot wedge equipment. In order to best accommodate the variations in thickness of the primary geomembrane, alternate panels were laid upside down so the smooth surfaces were placed together for seaming. When the finished seams were found to contain many small leaks, not surprisingly at the flow marks, repairs were attempted by extrusion seaming the edges of the original seams and covering the seams with epoxy paint. These problems and inadequate procedures were not identified during installation because there was no independent Construction Quality Assurance (CQA) monitoring performed during construction.

The initial intent of the installation was to provide black liquor containment for 20 days during a major renovation to the plant's recovery boiler. However, when the benefits of the installation were realized, Northwood was hoping for a 10-year service life.

In July of 1989, the first cracks were observed on wrinkles, particularly on those that had obviously folded over under the hydrostatic head of black liquor. The liquor level had been varied from zero up to approximately 3.5 m. Not surprisingly, liquor was being collected in the leakage collection system.

Attempts to repair the cracks were made, but the leaks could not be prevented as other cracks became active. Further cracking occurred at the edges of extruded beads placed to repair original cracks.

SCOPE OF WORK

This paper describes the field investigation performed on the primary and secondary geomembrane liners, the laboratory tests performed to confirm the cause of failure, tests performed on possible alternative materials of construction, and recommendations for CQA and operational procedures.

BLACK LIQUOR

The black liquor at the Northwood mill enters the pond as a 52% solution (pH≥12) containing several sodium salts: sulfates, sulfides, sulfites, carbonate, and hydroxide. It is delivered to the pond at a temperature of 82°C. Through dilution with water, it is stored as a 12% solution in the pond.

SITE INVESTIGATION

The installation is approximately 107 x 103 m with 3:1 side slopes. At one end, a concrete ramp is used to allow the hot liquor to cool as it cascades down the ramp towards a concrete sump. There is a floating pump in the sump which is used to remove the black liquor from the pond. Northwood records showed that although the liquor exited the pipe on to the top of the ramp at 82°C, the temperature in the pond had never exceeded 62°C. At the first filling, and whenever the pond had been empty, water was pumped into the pond before any black liquor was added to ensure that the liner was

not excessively heated. Northwood had been informed that the liner could not operate safely for extended time periods at temperatures in excess of 73°C. This is unusual since no concern is expressed about exposed HDPE geomembrane in hot sunny environments that can easily achieve temperatures of 75 or 80°C.

The installation was first visited and examined by the authors in August, 1990. At a time when the primary geomembrane was not very hot, the first impression gained was that there was an unusually large number of wrinkles in the liner (Figure 1). The same impression was gained when the secondary geomembrane (Figure 2) was examined in September, 1990. Figure 2 also shows that there were areas of significant ponding on the secondary liner.

An examination of the primary geomembrane seams showed, as expected, that the epoxy paint had not adhered to the HDPE and was peeling off (Figure 3). At some locations, where an extruded bead had been laid on top of the seam, the bead could easily be pulled off by hand and, in some locations, could make a hole in the geomembrane as shown in Figure 4: the geomembrane failed by a brittle cracking mechanism and not by ductile tearing.

It was apparent that there had been excessive compensation built into the primary geomembrane as evidenced by folded and creased wrinkles (Figure 5). However, all folded and creased wrinkles were not cracked. Even some small wrinkles that could not have been folded were cracked (Figure 6). As shown in Figures 7 to 9, the cracks were short jagged relatively parallel cracks, long clean cracks occurring on the tops of wrinkles, and long cracks initiated at surface scratches.

At various locations, in areas that had been underneath the maximum liquid level, soft deposits were observed on the liner. These are "soap" deposits from the layer that floats on top of the black liquor. Similar deposits were found within the geonet (Figure 10), confirming that significant amounts of liquor had leaked through the primary liner. These deposits show how a leak may eventually be clogged and sealed.

When the primary geomembrane and the geonet had been completely removed, the same characteristics of folded wrinkles and cracking were observed in the secondary geomembrane. The cracking was not quite as extensive in the secondary geomembrane as it had been in the primary geomembrane. Stains in the subgrade sand clearly indicated that liquor had been leaking through the secondary geomembrane liner.

In a number of areas, there was evidence of patches having been placed on patches and multiple reseaming (Figure 11) of obviously leaking seam intersections. From stains on the sand, it was apparent the such repairs had not been successful or had so badly degraded the geomembrane, that failure occurred after a short time in service.

Adjacent to the sump was an area where there were large (3 cm) stones in the subgrade protruding into the secondary geomembrane (Figure 12), eventually puncturing the geomembrane. Several samples were cut out of this and other areas of the geomembranes and taken to the laboratory for further examination.

LABORATORY INVESTIGATION

Conformance Testing. In the laboratory, conformance tests were performed on visually undamaged samples of the primary geomembrane to determine whether or not it met the manufacturer's specifications. The results are shown in Table 1.

Considering the installation damage that the material might have suffered and the two years' exposure it had experienced, most of the parameters could be projected to have met specifications at the time of installation. Even the break stress and elongation, the two parameters that show most influence of installation and service damage, met specifications. The puncture strength was a little low (514 N, compared to the specified 534 N), but this is of little significance with respect to the cracking mode of failure. Tear resistance was adequate, as was low temperature impact resistance at -70°C. The latter parameter was not tested at the manufacturer's specified temperature (-100°C), but its value (<-70°C) is adequate for the service conditions.

Table 1. Conformance test and manufacturer specification data.

PROPERTY		UNIT	MEAN	SPECIFICATION
Specific Gravity	ASTM D792		0.952	> 0.942
Density	ASTM D792	g/cc	0.950	> 0.940
Thickness	ASTM D394	mm	1.88	> 2.0
Yield Stress	ASTM D638	MPa		
RD			18.0	> 17.3
XD			19.3	> 17.3
Yield Elongation	ASTM D638	%		
RD			13.9	> 15
XD			14.0	> 15
Break Stress	ASTM D638	MPa		
RD			34.0	> 31.1
XD			30.1	> 31.1
Break Elongation	ASTM D638	%		
RD			1395	> 800
XD			1216	> 800
Tear Resistance	ASTM D1004(c)	N		
RD			36.3	> 33.4
XD			36.7	> 33.4
Puncture Strength	FTMS101C (2065)	N	514	> 534
Carbon Black Content	ASTM D1603	%	2.35	1.5-3.0
Carbon Black Dispersion	ASTM D2663(B)		A-3	A-1,A-2,B-1
Melt Flow Index	ASTM D1238 (190/2.16)	g/10min	0.52	> 0.45
Low Temperature Brittleness	ASTM D746B	°C		
RD			<-70	< -100
XD			<-70	< -100

RD - roll direction XD - cross direction

The carbon black dispersion was poor, at a rating of A-3, but this also was not a prime factor in the failure since all cracking had occurred under the maximum level of liquid in the pond. There appeared to be no cracking on the upper levels of the side slopes where the primary geomembrane had only been exposed to UV radiation. It is, however, possible that some carbon agglomerates may have been responsible for the initiation of some stress cracks, as has previously been reported (Rollin et al, and Peggs and Carlson) although the extent of the present investigation was not sufficient to confirm this.

Seam Testing. Two seam samples from the primary geomembrane were tested. One sample was from an original double track seam, and the other was from a section that had been repaired with an extruded bead over the edge of the seam. Both tracks of the first sample peeled apart completely, and the inner track of the second sample also peeled completely. The outer track of the repaired sample did not peel.

Seam tests were also performed on samples removed from the secondary geomembrane. All of these samples showed satisfactory peel characteristics as well as satisfactory shear strengths, but two of the eight samples displayed low elongation values, shown later to be due to the presence of non-penetrating stress cracks along the edge of the seam.

Analytical Testing. Differential scanning calorimetry (DSC), thermalgravimetric analysis (TGA), and infrared spectophotometry (IR) tests were performed on the primary geomembrane in the region of cracks to determine if the geomembrane had been degraded by heat in these areas (as was proposed by the manufacturer and installer). As shown in Table 2, none of the parameters measured by DSC (crystallinity, oxidative induction temperature, temperature at maximum energy absorbtion, and temperature at onset of endotherm) and TGA (temperature at onset of decomposition) showed significant deviations from data typically generated on the same material when new. The IR spectra showed no evidence of oxidation.

Table 2. DSC and TGA test results.

PARAMETER	UNIT	FIELD SAMPLE	NEW SAMPLE
Crystallinity	%	44	48
Temperature at maximum energy absorption	°C	127.11	125.20
Oxidative induction temperature	°C	264.18	264.70
Onset of endotherm (DSC)	°C	118.54	117.57
Onset of decomposition (TGA)	°C	438.43	428.85

According to all these tests, the geomembrane met conventional materials property specifications at the time of installation and showed no evidence of microstructural degradation while in service. Only two low elongation values in seam shear tests (a parameter that is not normally measured) indicated the potential cause of failure.

Stress Crack Testing. Stress cracking tests were then performed on unused archive material manufactured in 1988 by the primary geomembrane manufacturer. The only apparent difference from the field material was that the test material was 2 mm in thickness. Specimens were tested according to the procedure of Geosynthetic Research Institute (GRI) standard GM5 "Notched Constant Load Test for High Density Polyethylene Geomembranes", at a liquid temperature of 50°C and at a stress of 5.9 MPa, approximately 30% of the room temperature yield stress of the geomembrane. Batches of specimens were tested in the following liquids:

- water
- 1% Igepal
- 52% black liquor from the Northwood pulp mill
- 5% solution of soap from the Northwood pulp mill. (An arbitrary solution of 5% was selected to be midway between the 1% and 10% solutions of Igepal normally used.)

After various exposure times, specimens were removed from the liquid, thin slice (15μm) microsections were prepared from across the artificial notch placed in the specimen, and the microsection examined under a light transmission microscope to determine the extension of the notch caused by the constant load. From these data, a crack growth rate curve was developed as shown in Figure 13.

Igepal is the solution usually used in the laboratory to accelerate the stress cracking behavior of HDPE. Figure 13 clearly shows that the stress crack growth rate in Igepal is far higher than in water. However, the crack growth rate in the 5% soap solution is even higher than it is in Igepal. The black liquor itself also has an accelerating effect but not as significant as Igepal or the soap. It is quite evident that the black liquor, and particularly the soap solution, cause serious environmental stress cracking in the tested HDPE. Environmental stress cracking is the fundamental stress cracking that is accelerated in the presence of a chemical environment.

Microsections were prepared across the cracks in the samples removed from the field. Figure 14 shows a number of straight, parallel cracks without any ductile deformation in the geomembrane, that are typical of (environmental) stress cracks. For every major penetrating crack, there are many more partially penetrating cracks and crazes. The secondary geomembrane shows the same features, although, in Figure 15, there appear to be many more fine cracks. All of the evidence indicates that the liner has cracked by a process of environmental stress cracking at the stress points caused predominantly, but not completely, by folding of excessive wrinkles in the geomembrane.

Puncture Hole Analysis. The secondary geomembrane samples containing holes made by the subgrade stones were examined. All of them have failed simply by mechanical puncturing and tearing, as shown by the typical sample in Figure 16. The break edges all show the thinning feature of the yield process and subsequent ductile tearing leaving fibrils on the fracture edges. HDPE cannot conform to a rough profile as well as other geomembrane materials. If failure had not occurred at these points by yielding, it would have occurred eventually by stress cracking.

Replacement Geomembrane Chemical Resistance Testing. Laboratory testing then moved toward making a preliminary assessment of geomembrane materials that could be used to safely contain hot black liquor. Five materials: very low density Polyethylene (VLDPE), Tuff-Ply (TP - a polypropylene/EPDM alloy), Hypalon, HDPE, and XR-5 (a PVC alloy) were exposed to the 52% hot black liquor at 70°C for up to 3 weeks. After 7, 14, and 21 days, the samples were subjected to a series of physical, mechanical, and microstructural analyses. Subsequently to this program, KS-056P (a Himont polypropylene geomembrane) was also subjected to a similar series of mechanical, physical, structural, and stress cracking tests. The chemical resistance tests were carried out for 21 days.

Both the Hypalon and XR-5 show much larger changes in uniaxial tensile properties than do the other materials. They also show much larger changes in mass and dimensions.

None of the KS-056P specimens in the stress cracking tests (Figure 17) failed in a brittle manner in the 5% soap solutions within the 525 hr test period. All the specimens simply elongated until they reached the 40% (approximately) strain limit of the equipment. The initial notch did not extend; it was simply blunted. This KS-056P PP geomembrane is, therefore, not susceptible to stress cracking in the soap solution.

Separate studies on Tuff-Ply© (Peggs et al 1993) reported at this conference, and by Akzo show that it does not display fundamental stress cracking characteristics. When tested in hot water, alongside HDPE, it would deform and cause notch blunting, while HDPE showed notch/craze growth.

The mechanical and physical test data are shown in Tables 3 and 4; the microstructural data in Table 5. From a purely chemical resistance standpoint, Hypalon and XR-5 are not as appropriate as the other materials for the containment of black liquor. HDPE, VLDPE, TP and KS-056P show good resistance. Since it has been shown that TP (Peggs et al 1993) and KS-056P are not susceptible to stress cracking in black liquor, and are probably not susceptible to stress cracking at all (for all practical purposes), they are the preferred candidate materials. Although VLDPE appears to be a candidate the principal author has seen a VLDPE sample that has suffered from stress cracking after only a few months exposed service. Further investigation of VLDPE's aging characteristics is required.

DISCUSSION

When geomembranes are installed for uncovered service in areas where the temperature in the winter can be very low, it is necessary that, due to the high coefficient of linear thermal expansion, they be installed with sufficient slackness so that they do not develop high tensile stresses when their contraction is restrained. This is particularly important in the case of semi-crystalline materials, such as HDPE, that may be susceptible to stress cracking. The expansion coefficient of HDPE can be as high as $2 \times 10^{-4}/°C$ at elevated installation temperatures (Giroud

Table 3. Effect of exposure to black liquor on tensile properties.

MATERIAL/PROPERTY	UNITS	CONTROL	7 DAYS	14 DAYS	21 DAYS
HYPALON (ASTM 751)					
Scrim break tension	N/m	17.7	12.3	12.5	12.4
Scrim break elongation	%	43	25	27	29
Ultimate break tension	N/m	16.0	7.35	8.02	10.17
Ultimate break elongation	%	45	299	315	35
XR-5 (ASTM D751)					
Scrim break tension	N/m	40.1	23.6	23.3	21.1
Scrim break elongation	%	26	22	26	23
Ultimate break tension	N/m	40.1	10.5	12.7	14.1
Ultimate break elongation	%	26	43	40	33
HDPE (ASTM D638)					
Yield stress	MPa	16.9	19.7	19.6	19.5
Yield elongation	%	18	17	17	16
Break stress	MPa	30.3	31.5	31.1	32.0
Break elongation	%	1325	1231	1201	1238
VLDPE (ASTM D638)					
Break stress	MPa	10.6	7.49	11.6	15.2
Break elongation	%	967	882	1006	1070
Yield stress* (Z-slope)	MPa	6.76	7.80	8.03	8.19
Yield elongation* (Z-slope)	%	46	81	68	82
TUFF-PLY (ASTM D638)					
Break stress	MPa	14.4	12.7	14.0	13.6
Break elongation	%	711	431	550	567
Yield stress* (Z-slope)	MPa	11.3	11.0	11.0	11.2
Yield elongation* (Z-slope)	%	43	47	47	54
KS-056P (ASTM D638)					
Yield stress	MPa	6.58	--	--	6.62
Break stress	MPa	16.6	--	--	16.8
Break elongation	%	1152	--	--	1084

* Material did not generate a detectable yieldpoint. Calculation of this property was performed at the point on the stress-strain curve where the slope of a computer-generated tangent line was zero.

Table 4. Change in physical properties (%).

	MASS	DIMENSIONS RD	XD	THICKNESS
7 Days				
HDPE	0.03	0.68	-1.00	1.00
TUFF-PLY	0.30	0.00	0.00	-0.70
HYPALON	2.50	0.21	-0.44	-0.20
XR-5	-2.06	0.00	0.00	-3.80
VLDPE	0.00	0.00	0.00	-1.20
KS-056P	---	---	---	---
14 Days				
HDPE	0.03	-0.03	0.22	0.25
TUFF-PLY	0.34	0.00	0.00	-1.24
HYPALON	1.76	0.23	-0.03	-0.71
XR-5	-6.80	0.10	0.40	-5.13
VLDPE	0.20	0.00	0.00	-1.23
KS-056P	---	---	---	---
21 Days				
HDPE	0.03	-0.03	0.22	-0.50
TUFF-PLY	0.35	0.00	0.00	-1.00
HYPALON	1.76	0.30	-0.04	-0.71
XR-5	-6.80	0.17	-0.70	-5.44
VLDPE	0.24	0.00	0.00	-1.72
KS-056P	0.02	0.28	0.75	1.00

Table 5. Effects of exposure to black liquor on parameters measured by DSC and TGA.

PROPERTIES OF HDPE/VLDPE	UNIT	CONTROL	7 DAY EXPOSURE	14 DAY EXPOSURE
Crystallinity	%	39.5/ 12.0	39.1/ 10.5	41.0/ 12.5
Temperature at maximum energy absorption	°C	125.4/120.9	125.2/120.3	124.2/120.6
Oxidative induction temperature	°C	263.6/269.7	261.8/259.0	259.1/259.1
Temperature at onset of endotherm	°C	117.6/110.3	117.1/109.9	115.6/110.4
Temperature at onset of decomposition	°C	405.9/402.9	399.2/390.7	437.4/448.8

PROPERTIES OF TUFF-PLY/KS-056P	UNIT	CONTROL	7 DAY EXPOSURE	14 DAY EXPOSURE	21 DAY EXPOSURE
Heat of fusion	cal/gm	8.6/ 4.43	7.8/--	9.6/--	--/ 6.78
Temperature at maximum energy absorption	°C	157.8/141.0	157.1/--	157.1/--	--/139.4
Oxidative induction temperature	°C	251.8/245.0	244.7/--	246.1/--	--/243.4
Temperature at onset of endotherm	°C	145.4/119.3	144.8/--	143.4/--	--/ 85.1
Temp. at onset of decomposition	°C	207.3/291.8	277.1/--	275.2/--	--/289.6

and Peggs). Stress cracking is a phenomenon that occurs in many materials. It is a brittle fracture failure that occurs under a constant tensile stress lower than the yield stress of the material.

Naturally, it is important that too much compensation not be built in so that, at service temperatures, the wrinkles do not fold over and crease. If they do fold over, there will be significant bend stresses at the folds. Whether or not the geomembrane will crack under these conditions depends on its fundamental stress cracking resistance (which can be qualitatively measured) and the degree of acceleration of stress cracking provided by the contained liquid. It is clear that the two different types of HDPE geomembranes used in the Northwood facility are very susceptible to environmental stress cracking in black liquor and its associated soaps. It is also evident that the wrinkles do not have to fold over to be a problem. From the descriptions of the mid 1980s failures in Georgia, those failures appear to have been identical to the Northwood failure. Of the three other installations recently made, one has failed, a second has a few cracks, and there is no information on the third. From the evidence generated in this report it is the principal author's opinion that all will eventually fail.

While in service, the Northwood pond was emptied and filled frequently. Each time the liquid level was lowered, deposits of soap from the layer on top of the liquor would be deposited on the side slopes and on the geomembrane that was newly-exposed. At the liquid level, not only would the geomembrane be exposed to the soap and some stress, but it would also be at an elevated temperature from the sun. The potential for cracking would be very high in these regions. The deposited soap could also enter scratches and seam overlap flaps to facilitate further cracking when the liquid re-covered the liner.

If adequate independent CQA had been in place during construction of the lining system, it is possible that the excessive amount of compensation may have been defined and prevented. It is almost certain that the inadequate seaming problem, which is not the major cause of failure of this particular lining sytem, would have been detected during destructive and/or nondestructive seam testing.

For any HDPE-lined black liquor ponds still in service, in order to minimize the potential for stress cracking in the liner it would be desirable: a) to skim the soaps from the liquor before it enters the pond (the soap is a more agressive stress cracking agent than the black liquor itself); b) to keep the liquid temperature as low as possible consistent with the ability to pump it out of the pond; and c) to keep the liquid at a constant level and as low as possible in the impoundment. If the liner does not have excess compensation, the liquid level should be maintained as high as possible during winter months to minimize the amount of liner subjected to possible contraction stresses. A program of visual monitoring should be instituted to look for small cracks on the peaks of wrinkles, at crimps in wrinkles, and on the edge of extruded fillet seams on the lower sections of the geomembrane.

Remediation. In the principal author's opinion and experience it is impossible to satisfactorily repair an HDPE geomembrane that has suffered environmental stress cracking due to the action of black liquor and related soaps. The only solution is to re-line the facility with another material.

Preliminary tests indicate that there are two lining materials, both based on polypropylene, that should, uncovered, satisfactorily contain black liquor. It may also be possible to use VLDPE, provided it is covered to protect it from UV radiation and oxidation. Before using these materials in any installation, a series of confirmatory chemical resistance tests should be performed on samples of geomembrane and seams, both under stress, using the specific black liquor and soap solutions to be contained.

When an appropriate geomembrane has been identified, the lining system should be designed by a designer experienced in geosynthetic lining systems, or, at the very least, the design should be reviewed by an experienced geosynthetics designer. The necessary specifications will be developed and a CQA plan should be prepared by the designer or, preferably, an independent CQA expert who knows geomembrane performance.

The next important phase is to ensure that an installer is selected who thoroughly understands and acknowledges the project specifications and can meet the requirements of the CQA plan. During liner installation, the CQA team must pay special attention to trial seam and production seam testing results, since the peel test characterstics of at least the TP geomembrane seams can be different to those usually encountered with HDPE geomembranes: seams that are well-made can appear to separate during a peel test (Peggs et al). All seams should be 100% nondestructively tested.

While it is not necessary to be as concerned about liner contraction stress if TP or KS-056P geomembranes are used (since they do not stress crack), it is still good practice to build a geomembrane that will not be too highly stressed under any service condition. Therefore, adequate compensation should still be built-in, but using an expansion coefficient that is appropriate for the material being used. If the material is based on PP, the expansion coefficient will be considerably less than the expansion coefficient used for HDPE. The CQA consultant should ensure that an excessive amount of compensation is not provided.

Prior to placing any black liquor in the impoundment, the impoundment should first partially be filled with water, preferably starting in the evening when the temperature is low and there are few wrinkles in the liner. An electrical leak survey could then be performed to determine if there are leaks in the complete liner, not just at the seams. When this final stage of CQA has been completed, the liquor can be placed in the pond. The pond should then be operated so that it is never completely empty - to prevent uplift of the liner in winds, and to prevent more wrinkles forming on the bottom. During cold periods, the pond should be operated as full as possible so that most of the liner is not subjected to contraction stresses.

CONCLUSIONS

Despite a number of HDPE geomembrane liner failures that occurred in the mid and late 1980s in pulp mill hot black liquor ponds the authors are confident that geomembrane materials exist that can provide safe, durable service in such applications.

HDPE geomembrane failures in pulp mill hot black liquor ponds have occurred because HDPE is susceptible to environmental stress cracking by black liquor and, particularly, the soap solution associated with black liquor.

Geomembranes based on Polypropylene (PP) appear to offer a viable alternative for the safe, durable containment of black liquor. Very low density polyethylene (VLDPE) may also be a candidate material, provided it is used under a soil cover to protect it from excessive oxidation.

ACKNOWLEDGEMENTS

The authors are grateful to: a) Northwood Pulp and Timber for having the courage and confidence to provide this information and, thereby, to help prevent similar failures in the future; b) GeoSyntec Consultants for the provision of archive information; and c) Akzo Industrial Systems and Himont for permission to incorporate test data.

REFERENCES

Akzo Industrial Systems, "Notched Constant Tensile Load Testing of Seamed Tuff-Ply© and High Density Polyethylene Geomembranes in Water". GeoSyntec Consultants Report. May, 1991.

Geosynthetic Research Institute (1990), Ductile/Brittle Transition Time for Notched Polyethylene Specimens Under Constant Stress, GRI Test Method GM5.

Giroud, J.P. and Peggs, I.D., (1990) "Geomembrane Construction Quality Assurance", Waste Containment Systems: Construction, Regulation and Performance, Geotechnical Special Publication No. 26, ASCE, pp. 190-225.

Peggs, I.D., Carlson, D.S., (1990) "Brittle Fracture in Polyethylene Geomembranes". Geosynthetics: Microstructure & Performance. ASTM STP 1076. pp. 57-77.

Peggs, I.D., et al. (1993) "Development of Optimum Seaming Parameters for an FCEA Geomembrane". Proceedings of Geosynthetics '93, IFAI, St. Paul, Minnesota.

Rollin, A.L., et al. (1991) "Evaluation of Field Seam Quality by the Impact Test Procedure". Geotechnical Fabrics Report. July/Aug. pp. 6-21.

Figure 1. General view of primary liner. Note wrinkles.

Figure 2. General view of secondary liner; note wrinkles and ponding.

Figure 3. Epoxy paint peeling off a seam. Note flow marks (arrowed) on left panel; smooth surface on right panel.

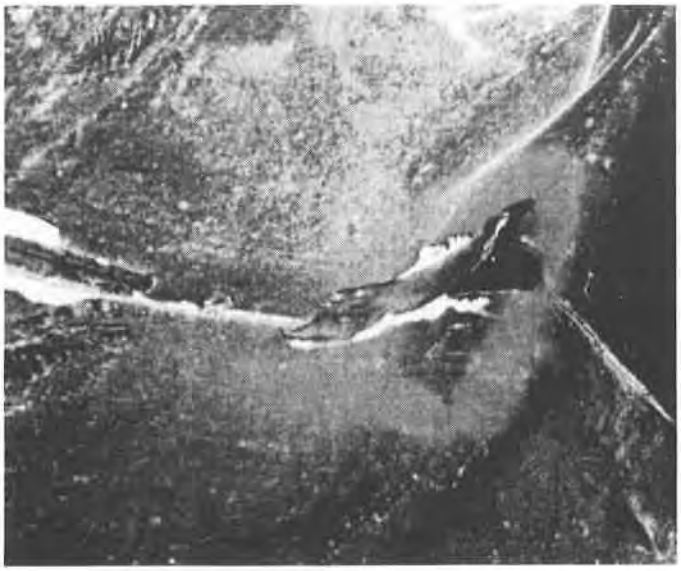

Figure 4. Repair bead pulled off seam. Note hole.

Figure 5. Wrinkle that has folded over.

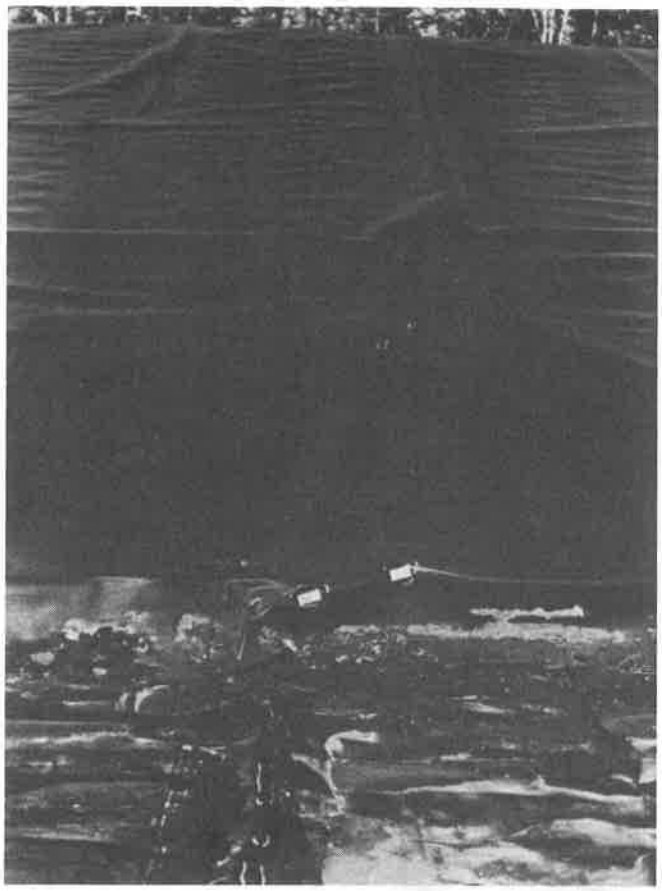

Figure 6. Cracks in folded wrinkles (at white labels) and on bottom unfolded wrinkle (outlined by white pen).

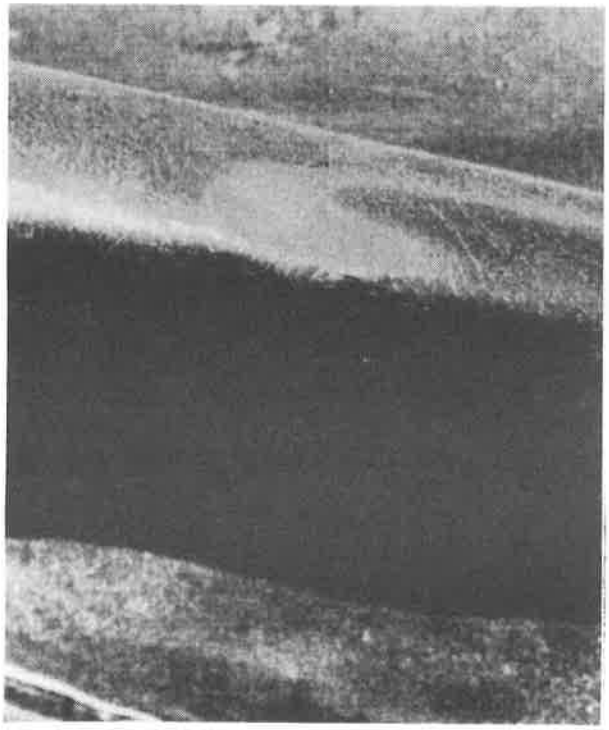

Figure 7. Short, jagged stress cracks basically parallel to one another on peak of wrinkle.

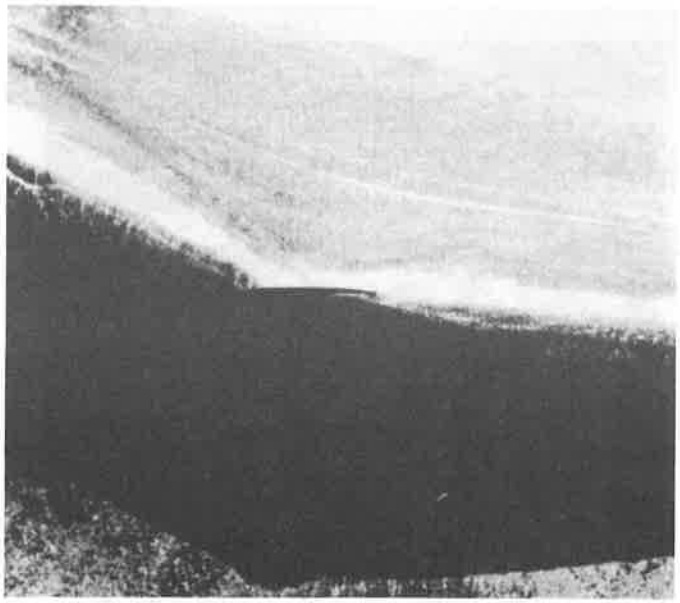

Figure 8. Long, clean crack on peak of wrinkle.

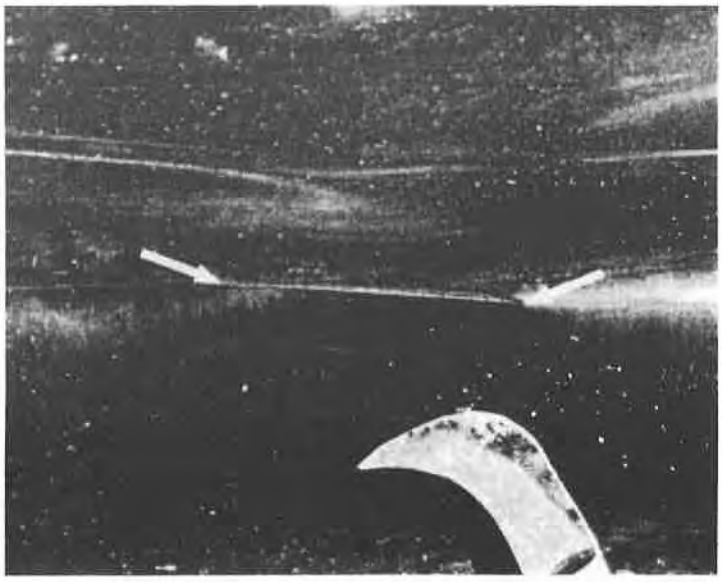

Figure 9. Long crack initiated by scratch along peak of wrinkle.

Figure 11. Multiple repair beads at seam intersection.

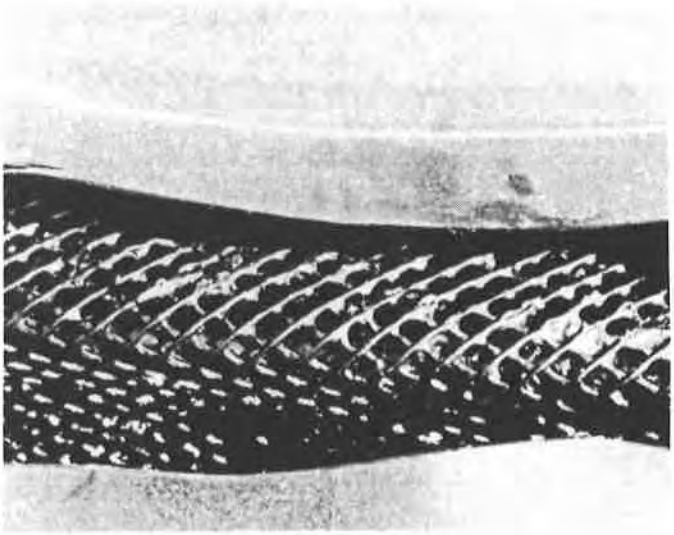

Figure 10. Soap deposit within geonet.

Figure 12. Stones protruding against underside of secondary liner.

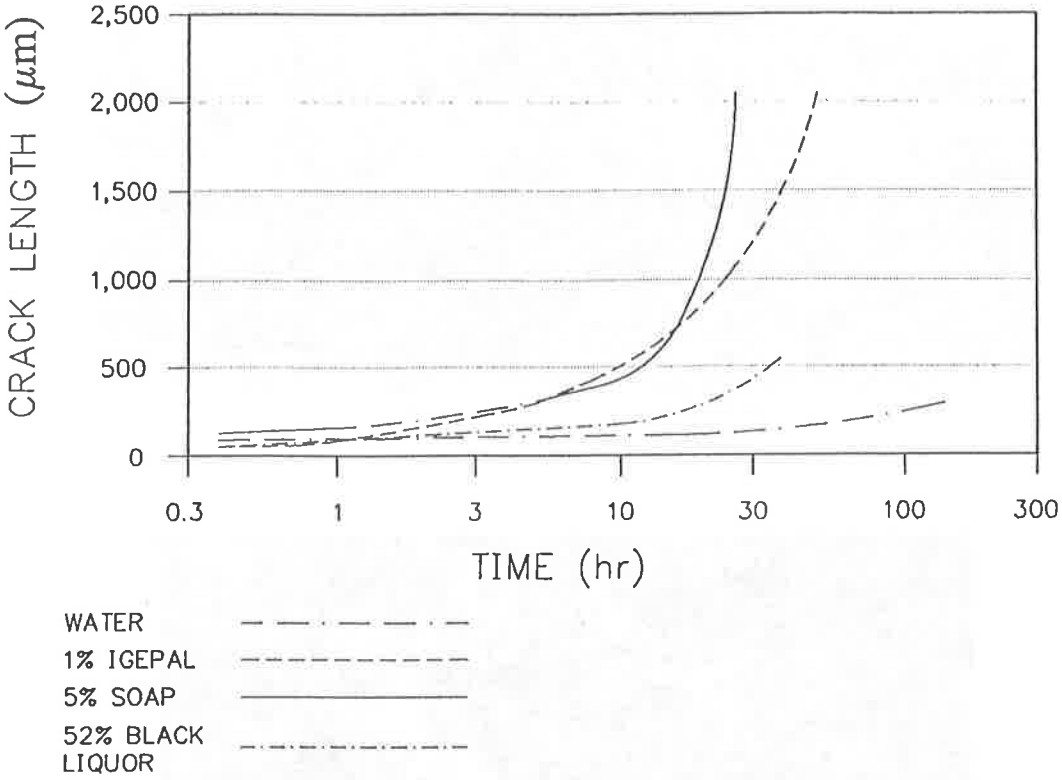

Figure 13. Stress crack growth rates.

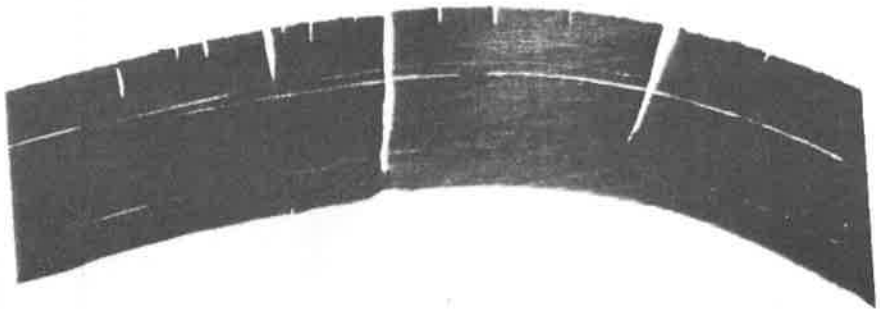

Figure 14. Cross section through primary liner showing stress cracks (x 12).

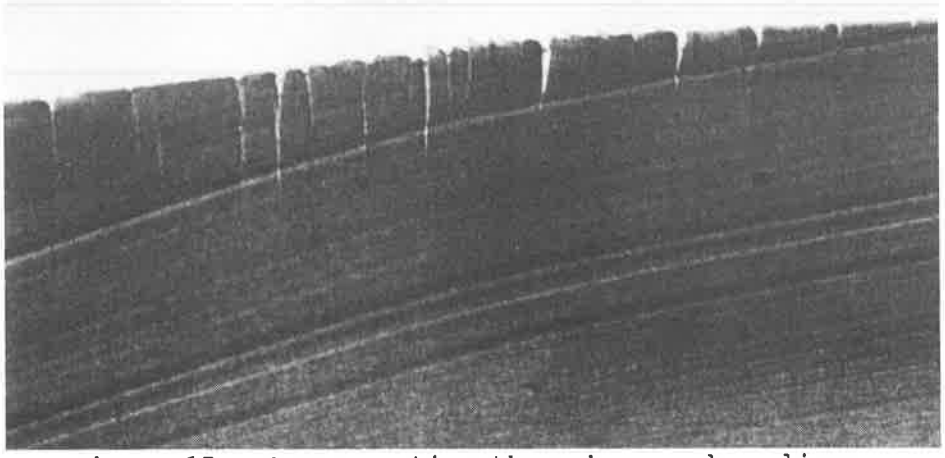

Figure 15. Cross section through secondary liner showing stress cracks (x 65).

Figure 16. Stone puncture hole in secondary liner.

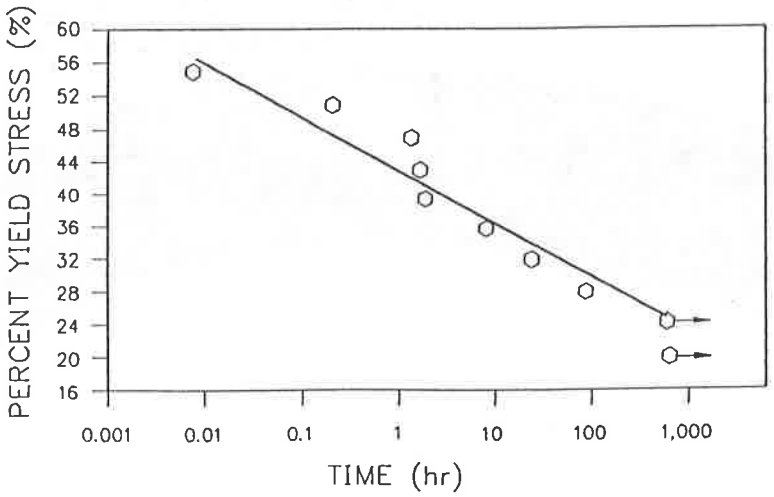

Figure 17. KS-056P stress cracking results. Curve shows time to approximately 40% elongation.

Field Performance of Double-Liner Systems in Landfills

M.T. Feeney
Jordon, Jones & Goulding Inc., USA

A.E. Maxson
Chemical Waste Management Inc., USA

ABSTRACT

The performance of liner systems in landfills is critical in protecting the environment. Analytical methods and models are available to predict the performance of lining systems and some test liners have been constructed and tested. Little data is available, however, on the field performance of actual geosynthetic lining systems in landfills.

This paper presents data on the field performance of double liner systems in 49 landfill units, including 8 damaged units, at eight facilities. All liner systems consist of at least two geomembranes, and all but two landfill units have a composite geomembrane/compacted clay liner on the landfill base. These two remaining landfill units have a primary liner consisting of a geomembrane underlain by a bentonite clay mat. Strict construction quality assurance programs were employed during the construction of each of the landfill cells studied. Data on observed primary and secondary leachate flow rates is presented and evaluated. For some of the landfill units, the influence of clay liner consolidation on observed flow rates will be presented. The effect of facility closure on flow rate will be also be evaluated.

INTRODUCTION

The performance of liner systems in landfills is critical in protecting the environment. Analytical methods and models are available to predict the performance of lining systems and some test liners have been constructed and tested. Little data is available, however, on the field performance of actual geosynthetic lining systems in landfills. This paper presents data on the field performance of double liner systems in 49 landfill units at eight facilities.

In preparing this paper, the authors wish to present real data on the field performance of double liner systems in landfills and to examine the variation in flow rates observed in landfills. The effect of the time period over which flow rates are averaged is also examined. An evaluation is also presented of the effect on flow rates from consolidation of the clay component of composite liners and closure of landfill units.

The 49 landfill units (including 8 damaged units discussed separately) for which data is presented in this paper were constructed between 1985 and 1990 and, except as described below, have similar lining systems. All of the units were constructed to exceed the U.S. Environmental Protection Agency's Minimum Technology Guidance for RCRA Subtitle C Solid Waste Landfill units. The base liner system for all units, except two, consists of a double composite liner. The waste is underlain by a primary leachate collection and removal system, which is then underlain by a composite liner of both geomembrane and compacted clay. The primary composite liner is underlain by a secondary leachate collection and removal system followed by another composite liner of geomembrane and compacted clay. The geomembrane component of both liners consists

of 1.5 millimeters (60 mils) of high density polyethylene. The compacted clay component is nominally 0.46 meters (1.5 feet) thick in the primary liner and at least .91 meters (3 feet) thick in the secondary system. The compacted clay component of the liner system is constructed to have a coefficient of permeability which does not exceed 1 x 10^{-7} centimeters per second. The side slope lining system of each landfill unit is very similar to the base liner, except that the compacted clay component of the primary liner and the granular portion of the leachate collection systems are not present on the side slope of any of the units. Figure 1 illustrates the base and side slope lining systems described above. The only units which have lining systems different from that described above are units 42 and 43, for which a bentonite mat has been used as the clay component of the primary composite liner, and in which the bentonite mat also covers the landfill side slopes. The average depth of waste in the landfill units varies from about 15 meters (50 feet) to about 45 meters (150 feet), and is typically 24 meters (80 feet) to 30 meters (100 feet).

Strict construction quality assurance programs were employed during the construction of each of the landfill units. Construction quality assurance personnel were present throughout construction of the landfill units. Comprehensive quality assurance reports documenting the construction of each unit were prepared and typically have been reviewed by state and/or federal regulatory agencies. The landfill units reviewed are considered to be in excellent condition and to be performing well. However, eight units did require repair subsequent to the initial construction. These units will be described later in the paper.

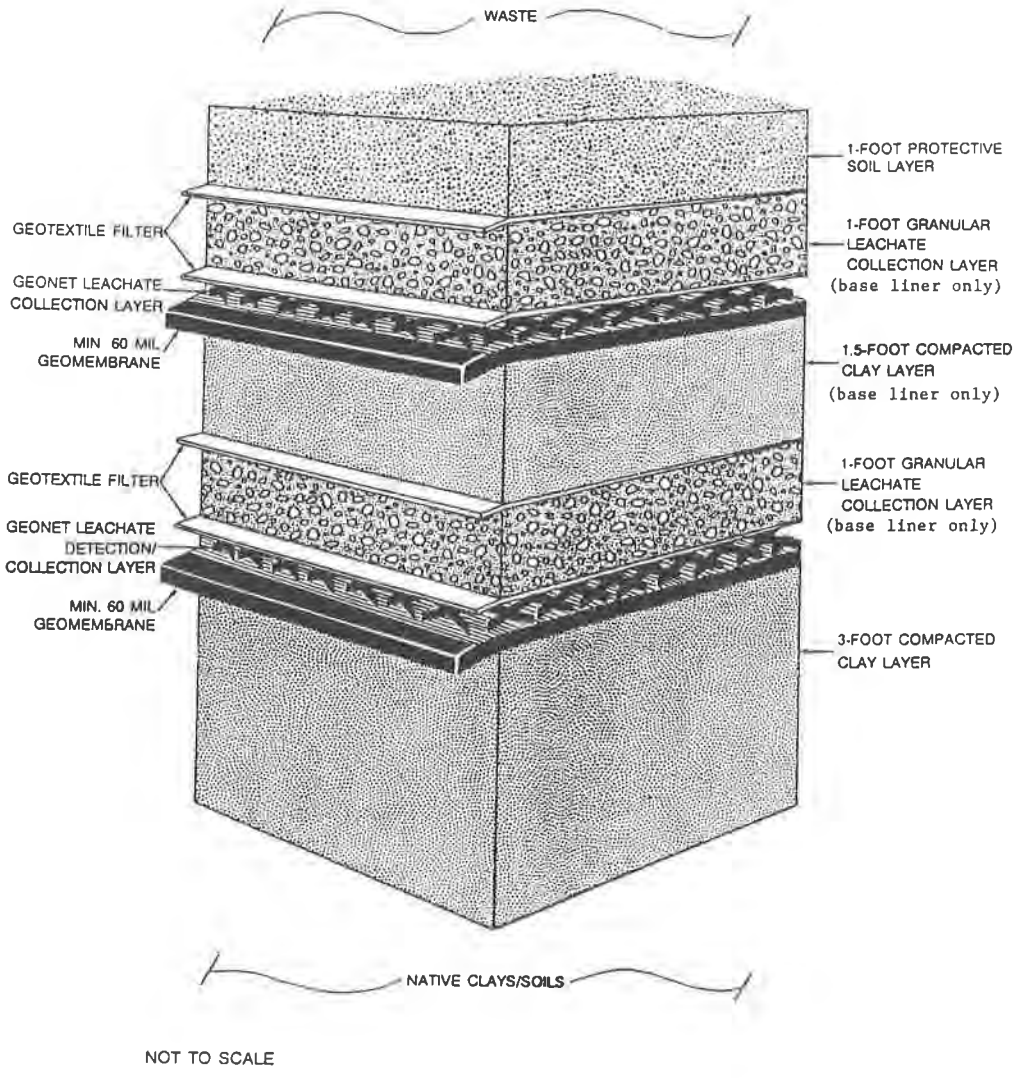

Figure 1. Typical Double Liner System

FLOW RATE DATA

The information presented in this paper consists of flow rates observed in primary and secondary leachate collection and removal systems. As described in the preceding section of this paper, the primary leachate collection system is in direct communication with the landfilled waste and is subject to the direct, or nearly direct, influence of precipitation. The secondary leachate collection system lies beneath the primary lining system and, because of its location, is termed a "leak detection system" by some practitioners. In the authors' experience, the secondary leachate collection system is almost never completely dry, although the presence of liquid in this system does not necessarily indicate a failure of the primary lining system. The U.S. Environmental Protection Agency also recognizes, most recently in regulations promulgated on January 29, 1992, that the presence of liquid in the secondary leachate collection system of a double-lined solid waste landfill unit is to be expected. One of the authors' primary purposes in preparing this paper is to present information on flow rates observed in the secondary leachate collection systems of well constructed landfills for future use by landfill designers, operators, and permit writers.

The data presented in this paper has been collected by personnel employed on a full time basis at each of the landfill facilities. The length of the study period presented in this paper varies according to the landfill unit, with the shortest period studied being four months and the longest being 60 months. A considerable amount of data has been reviewed. One measure of the amount of data presented is the "unit month". One unit month represents the collection of data from one landfill unit for one month. The collection of data from two units for two months each would result in four unit months of data. Similarly, this paper will also make reference to comparably defined unit weeks of data. The data presented in this paper represents 1,485 unit months of flow rate observations. The data collection periods studied cover a wide range of operational conditions, from newly constructed landfill units to closed units.

The flow rates presented have been normalized as flow rate per unit area of liner, or cubic meters per hectare per day (m3/ha/d). The United States unit of measure is gallons per acre per day (gpad), with one acre equalling 43,560 square feet. The original data was collected in United States units and has been converted to S.I. units for presentation in this paper. The flow rates available for study had previously been collected by landfill site personnel, usually on a daily or weekly basis, and then averaged over one week (7 day) or one month time periods. For some landfill units, flow rates averaged for both weekly and monthly intervals are presented in this paper. This weekly and monthly average data is presented to examine the significance of the time period over which the flow data is averaged. When data on a single landfill unit is available for both weekly and monthly intervals, the same calendar period may not be represented by the different groups of data. Table 1 indicates the type of data presented for each landfill unit, and the amount of data available for both the weekly and monthly intervals. Primary and secondary leachate collection systems continue to be operated at each of the landfill units studied.

OBSERVED FLOW RATES IN PRIMARY LEACHATE COLLECTION SYSTEMS

Primary flow rates vary considerably with time, as would be expected due to the variation of precipitation over time, the continued placement of waste in the landfill, and the eventual closure of the landfill. The authors have not attempted to evaluate all of these factors for each of the landfill units, though the effect of closure on one unit is presented later in this paper. Also, previous unpublished work by the authors has convinced them that primary leachate collection system flow is correlated with precipitation. Consequently, the summary values and average flow rates for the primary leachate collection system should be read with a great deal of caution. The data presented in this paper does not include the volume of water removed from the surface of the landfill unit during operations. The authors' purpose in summarizing the primary flow rates is to provide an indication of the real primary flow rates observed in landfills.

Flow rate data from primary leachate collection systems is available from 41 landfill units. For 19 of the units, flow rates which have been averaged on a weekly basis (weekly flows) are available for a total monitoring period of 3,688 unit weeks. Flow rates which have been averaged on a monthly basis (monthly flows)are available for all 41 units over a total monitoring period of 1,477 unit months. The observed weekly and monthly primary flows are presented in the following paragraphs. In this paper, the term "average flow" will be often used. However, because the base data which has been reviewed has already been averaged, for a weekly or monthly interval, the term "average flow" actually refers to the average of weekly or monthly average flows.

For the 19 units for which primary weekly average data is available, the average primary weekly flow rate was 5.88 m3/ha/d (629 gpad). The average minimum primary weekly flow rate was 0.07 m3/ha/d (7 gpad), while the average maximum primary weekly flow rate was 83.31 m3/ha/d (8,910 gpad). The observed primary weekly average, maximum, and minimum flow rate values for individual units are summarized in Table 2 (S.I. units) and Table 2A (U.S. units) for all landfill units.

The average primary monthly flow rate for all 41 landfill units was 6.17 m3/ha/d (660 gpad). The average minimum primary monthly flow rate was 0.45 m3/ha/d (48 gpad) while the average maximum primary monthly flow rate was 27.87 m3/ha/d (2981 gpad). The observed primary monthly average, maximum, and minimum flow rate values for individual units are summarized in Table 2 (S.I. units) and Table 2A (U.S. units) for all landfill units.

The primary flow rates reported vary widely, reflecting the various geographic locations of the landfill units, changes in the operational condition of the units, and seasonal precipitation. The data collected on a weekly basis exhibits a greater range of fluctuation than the monthly data. The increased fluctuation reflects the effect of intense, short-term, rainfall events, and fluctuation is greatest at units subject to the most intense rainstorms. At facilities subject to intense rainstorms, average monthly primary flow rates tend to be higher than average weekly primary flow rates. The use of weekly averaging periods for primary flow rate data seems to be reasonable, although it must be understood that the use of weekly averaging may result in some very high individual weekly values. Such high individual values do not necessarily indicate the presence of problems within the landfill. Finally, while additional study of the primary flow rates presented may lead to useful conclusions, the authors have not further examined this data in the preparation of this paper.

OBSERVED FLOW RATES IN SECONDARY LEACHATE COLLECTION SYSTEMS

For the 30 units for which secondary weekly average data is available, the average secondary weekly flow rate is 0.12 m3/ha/d (13 gpad). The average minimum secondary weekly flow rate was 0.004 m3/ha/d (0.4 gpad), while the average maximum secondary weekly flow rate was 0.98 m3/ha/d (105 gpad). The average secondary weekly flow rate is lower than the observed primary weekly flow rate by a factor of about 77, for the 18 units for which comparable data is available. The observed secondary weekly average, maximum, and minimum flow rate values for individual units are summarized in Table 2 (S.I. units) and Table 2A (U.S. units) for all landfill units.

The average secondary monthly flow rate for 41 landfill units is 0.10 m3/ha/d (11 gpad). The average minimum secondary monthly flow rate was about 0.02 m3/ha/d (2 gpad), while the average maximum secondary monthly flow rate was 0.60 m3/ha/d (64 gpad). The average secondary monthly flow rate is lower than the observed primary monthly flow rate by a factor of about 137, for the 39 units for which comparable data is available. The observed secondary monthly average, maximum, and minimum flow rate values for individual units are summarized in Table 2 (S.I. units) and Table 2A (U.S. units) for all landfill units.

As a comparison to the flow rate data previously presented, the authors have reviewed data collected from eight landfill units where the liner is known to have been damaged. In these eight landfill units, strict construction quality assurance programs were employed during construction and the units were initially completed with the same level of quality and integrity as those units previously discussed. However, during operation of these eight units the primary liner system was damaged, usually by heavy

equipment operating within the landfill. While repairs have been made to these landfill units and the observed flow rates have decreased, the data collected while the liners were in the damaged condition is illustrative. The average primary weekly flow rate observed in the eight damaged landfill units was 10.39 m3/ha/d (1,111 gpad), a value comparable with the primary flows in other landfills. The average secondary weekly flow rate was 1.08 m3/ha/d (116 gpad), considerably greater than the average secondary weekly flow rate observed in other units. The average maximum secondary weekly flow rate was 6.56 m3/ha/d (701 gpad), while individual weekly maximums observed varied from 3.10 m3/ha/d (332 gpad) to 17.48 m3/ha/d (1,870 gpad). The authors note that the individual maximum secondary weekly flow rates observed in the eight damaged units are not significantly different than some of the individual weekly secondary flow rates observed in intact units. This indicates that individual high flow rates may not result from a damaged liner, and that continued observation of elevated flow rates is important in detecting liner damage. Summary flow rate data from the eight damaged landfill units is presented in Table 3 (S.I. units) and Table 3A (U.S. units).

EFFECT OF SPECIAL CONDITIONS

Fluid from Consolidation of the Primary Clay Liner. The majority of the landfill cells studied contained primary composite liner systems along the base of the landfill. While the clay portion of the primary liner system was designed to prevent large amounts of leakage through defects in the primary HDPE geomembrane, it has been anticipated that fluids would be expelled into the secondary leachate collection system from the clay liner itself when landfill loadings were applied. Therefore, the secondary leachate collection system data from several landfill cells were studied to determine the volumes of fluid which could be expected from consolidation of the clay components of the primary liner system.

To enable the operator to predict the flow rates expected in the secondary leachate collection system from the consolidation of the primary clay liner, a model was developed by Chemical Waste Management, Inc. This model is designed to calculate the volume of fluids which would be expelled by the primary clay liner under simulated waste loading conditions. The model uses the clay liner properties determined by a one-dimensional consolidation test and applies a linearly increasing load to the specified maximum waste height to simulate the effects of waste placement in the cell. The volumes of flow resulting from permeation of fluids through the primary liner and the infiltration of groundwater can also be simulated with the model where necessary. The typical output results of the model are shown in Figure 2.

The secondary flow rate data collected from landfill cells were examined to determine if the fluid generation versus time compared with what would be expected from the consolidation model. In general, the observed secondary flow rates in units studied reached peak values within one year of the date of opening, and exhibited slowly decreasing flows thereafter. One plot of actual flow rate data compared with predicted results is shown in Figure 3. The pattern of increased initial secondary flow rates slowly decreasing over time predicted by the consolidation model was observed in most of the landfill cells studied.

Landfill units 31, 32, 33, and 34 were examined for the presence of fluids introduced from the consolidation of the primary compacted clay liner. These landfill cells are particularly well suited to examination for consolidation water in the secondary system because of the cells' location in an arid region of the U.S. There are few sources of fluids in the secondary system other than consolidation water because of the deep ground water conditions at the facility and the low volumes of primary leachate generated because of low rainfall. Therefore, the majority of fluids present in the secondary leachate collection system is expected to be from expulsion of water from the primary clay liner during consolidation.

The primary compacted clay liner for these cells is constructed of a silty clay/bentonite admixture which had significant amounts of water added during processing to facilitate compaction of the clay liner. Testing conducted during construction indicated that liner was approximately 95% saturated when it was placed.

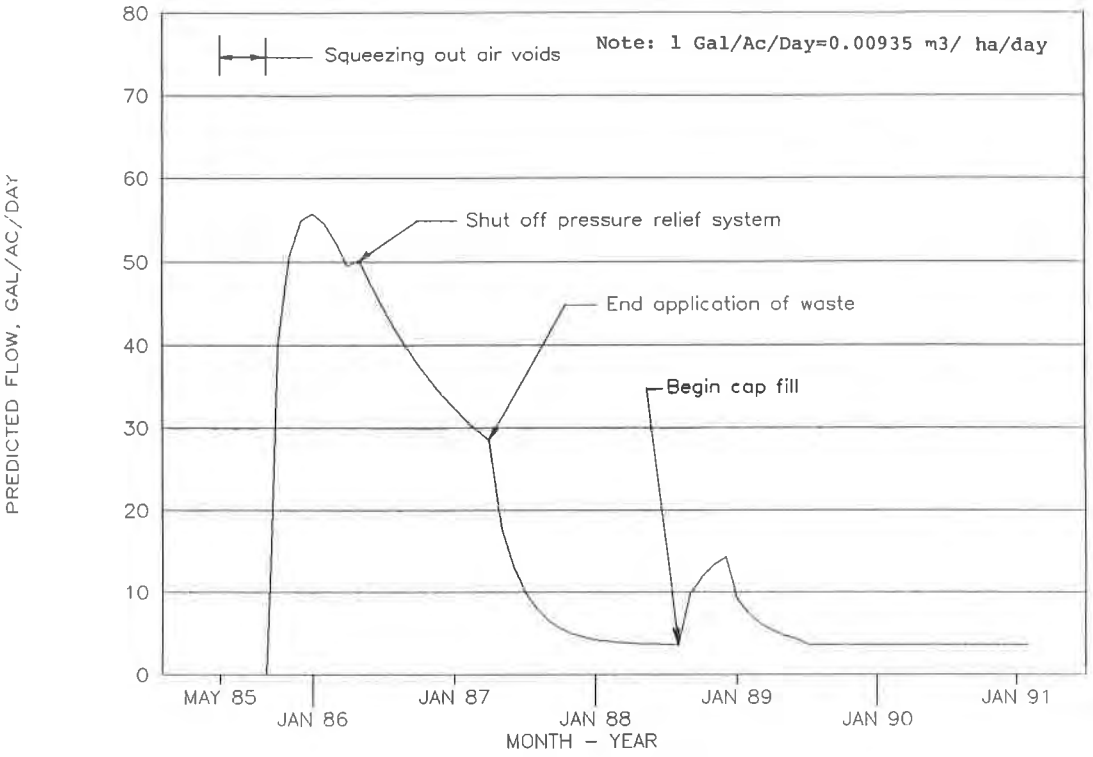

Figure 2. Typical Output Results of Secondary Collection System Flow Model (After K. A. Anderson, Chemical Waste Management, Inc.)

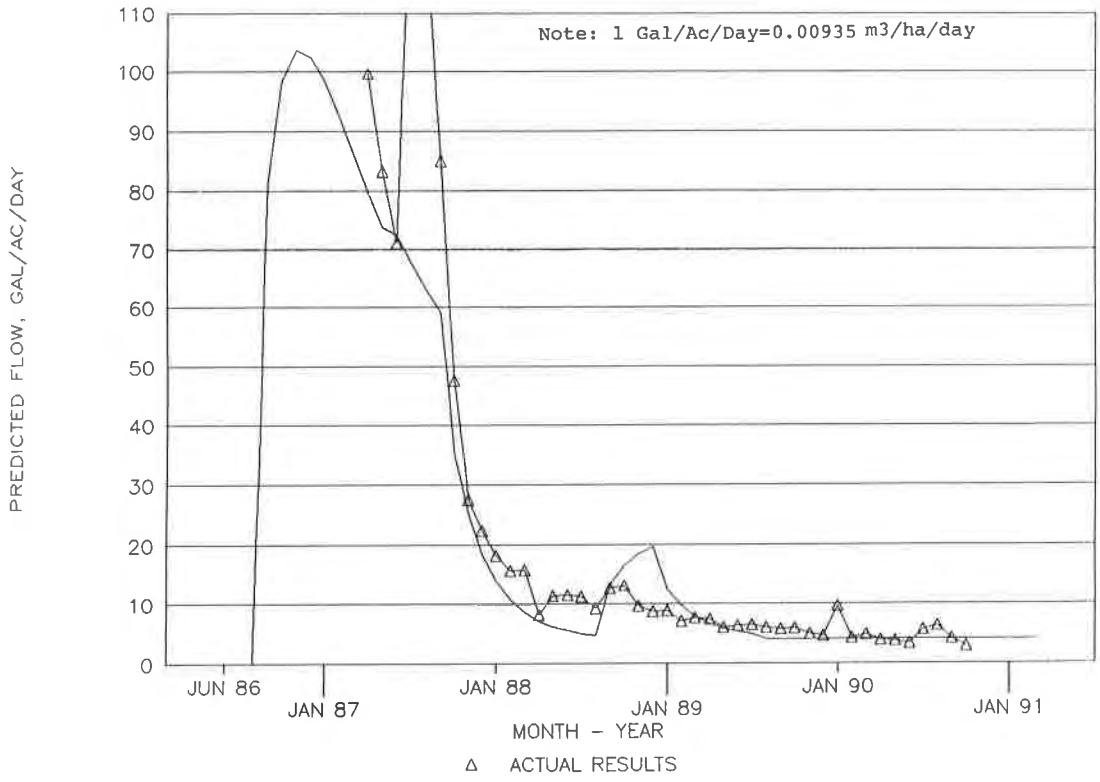

Figure 3. Model Output Results versus Actual Results for Landfill Unit 31 (After K. A. Anderson, Chemical Waste Management, Inc.)

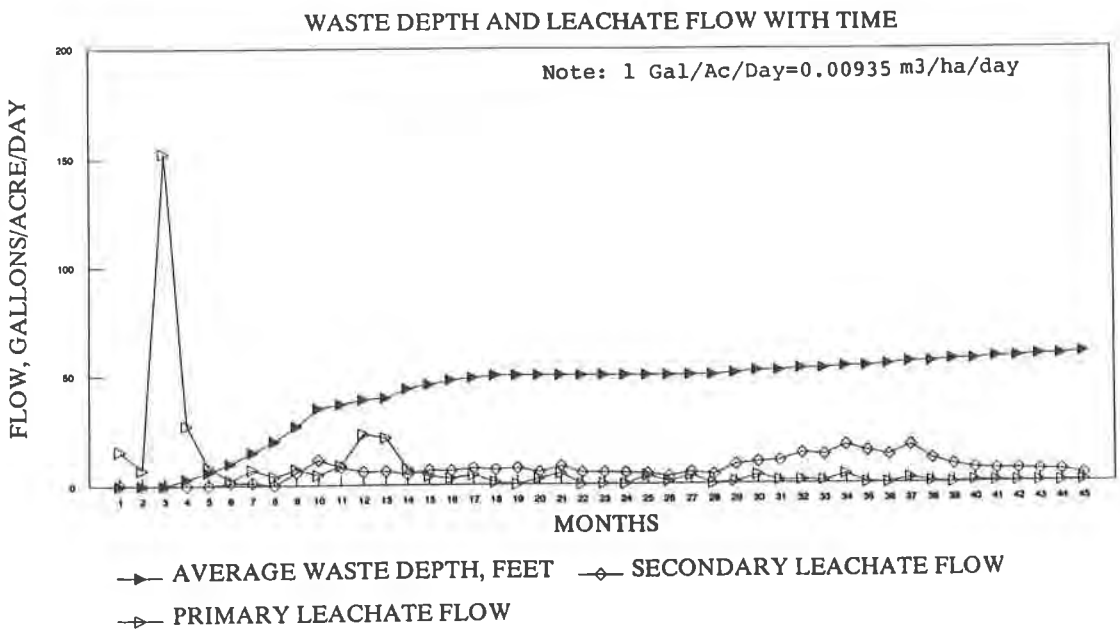

Figure 4. Monthly Average Leachate Collection System Flow Volumes and Average Waste Depth Versus Time for Landfill Unit 32

A plot of the primary and secondary leachate flow rates as compared with average waste depth for landfill unit 32 is presented in Figure 4. This unit was initially filled with waste to a average depth of 15 meters (50 feet) within a span of 13 months. Substantial amounts of fluid were not generated in the secondary system of the unit until approximately six months after waste filling began. At this point in time, the average waste depth over the compacted clay layer was approximately 7.6 meters (25 feet), corresponding to an overburden stress on the liner of approximately 120 kiloNewtons per square meter (2,500 pounds per square foot). Secondary flow rate initially peaked during the ninth month of filling with a monthly average of 0.11 m3/ha/d (12 gpad). No waste filling took place in the cell during the fourteenth to the twenty-sixth months after opening. During this period, primary fluid collection volumes were very low, averaging 0.02 m3/ha/d (2 gpad) monthly, while secondary fluid collection volumes were larger, averaging about 0.05 m3/ha/d (5 gpad) monthly. Filling in the cell was again initiated at 27 months after the cell was opened. Although waste depths only increased about 3 meters (10 feet) during the next 14 months, the secondary volumes once again peaked at a monthly average of 0.17 m3/ha/d (18 gpad) 30 months after the cell was opened.

The performance of the secondary leachate collection system in landfill unit 32 can be accounted for in general terms by the consolidation of the clay liner. The appearance of fluids in the secondary system in significant amounts during the sixth month of filling probably indicates the point at which the air voids had been squeezed out of the clay liner and further consolidation expelled water from the voids of the clay into the secondary system. Once the waste overburden pressure had initially stabilized at the depth of 15 meters (50 feet), normal consolidation of the clay liner proceeded until the rate of settlement and fluid generation rate were gradually reduced. Once further waste was placed in the landfill cell, the clay liner was reloaded and the rate of settlement and fluid generation increased, stabilized, and finally decreased.

Effect of Landfill Closure. Approximately 18 of the 49 landfill units studied by the authors received final caps during the time leachate flow data was collected for this paper. All of the final closure caps in this study consisted of a 0.6 meter (2 feet) layer of compacted clay soil overlain by a 1.0 millimeter (40 mil) HDPE geomembrane and a geonet/geotextile drain and varying amounts of protective soil cover/vegetative cover. The typical final cap is illustrated in Figure 5.

Landfill units 26 through 31 of this study were closed during a single operation in August through November of 1988. These units were subdivisions of one larger landfill that had a plan area of approximately 7.7 hectares (19 acres). The effects of final closure on primary and secondary flow levels was monitored by examining data gathered between January of 1987 and August of 1991. A graph of these flow rates is presented in Figure 6. Volumes decreased substantially over time, dropping significantly in the primary leachate collection system after cap placement. Flow rates in the secondary leachate collection system dropped substantially, even prior to capping, probably due to decreased fluids being expelled from consolidation of the primary clay liner and decreased amounts of primary fluid permeating to the secondary collection system.

When the cells were in operation, the generation of primary leachate varied considerably due to the rainfall and thickness of waste placed within the cell, and depended on the amount of rainfall removed directly from the module before it reached the primary collection system. During the operating period of units later closed, average monthly primary flow values ranged from 1.87 m3/ha/d (200 gpad) to 14.96 m3/ha/d (1600 gpad). Average monthly flows after closure initially decreased from 1.40 m3/ha/d (150 gpad) to 0.47 m3/ha/d (50 gpad) within six months. Over the next two years flows have slowly dropped to the current typical values of 0.09 m3/ha/d (10 gpad). The mean values of primary fluid flows were 3.74 m3/ha/d (400 gpad) prior to cap placement. The mean value after cap placement has been reduced to approximately 0.37 m3/ha/d (40 gpad).

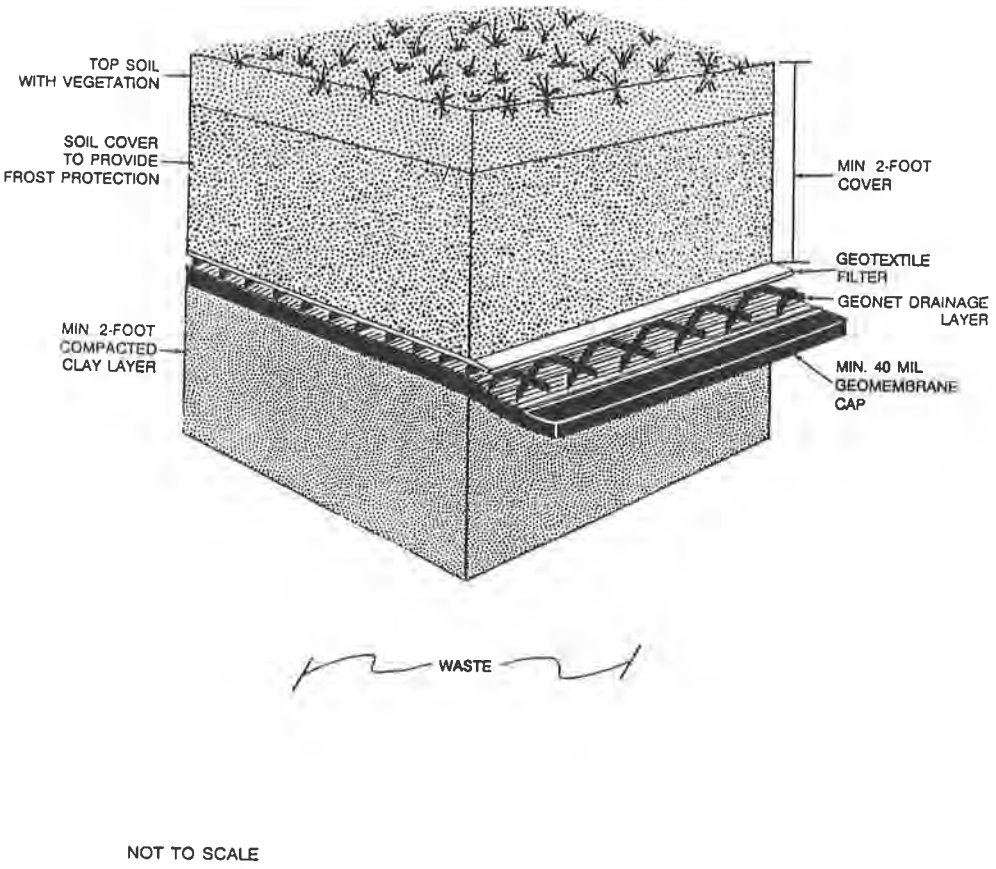

Figure 5. Typical Final Cap

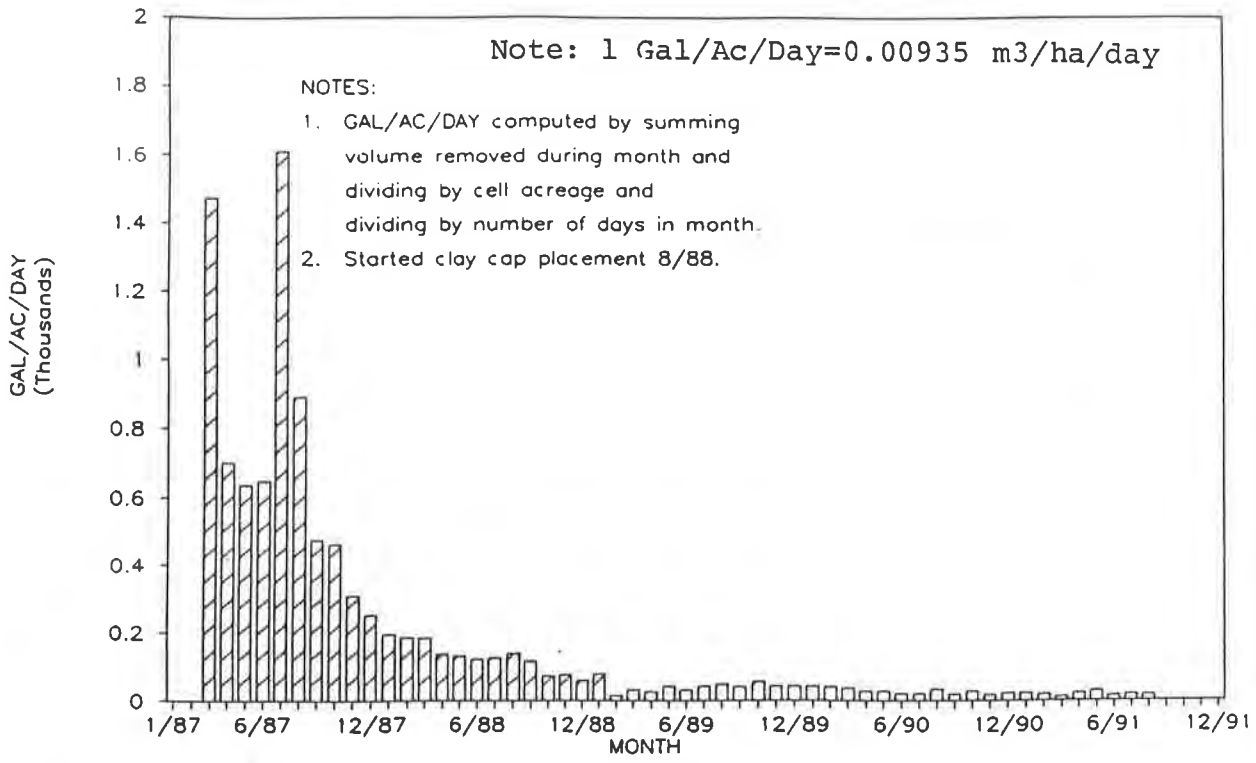

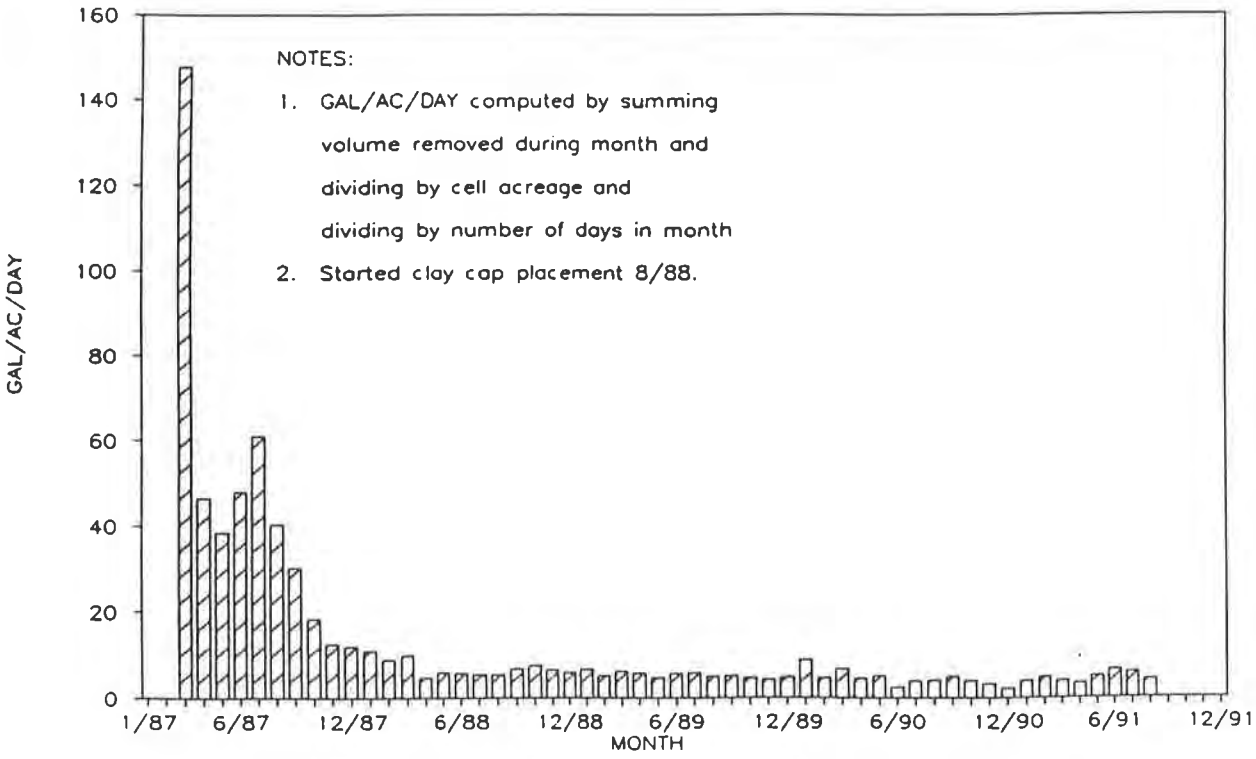

Figure 6. Flow Volumes for Landfill Units 26 through 31 versus Time. (After K. A. Anderson, Chemical Waste Management, Inc.)

SUMMARY AND CONCLUSIONS

This paper has presented actual data regarding flow rates observed in primary and secondary leachate collection systems of double lined landfills. In reviewing the data presented, the authors have reached several conclusions:

1. The double-lined landfill units studied appear to be functioning reliably and as designed. Approximately 98 percent of the leachate removed from the landfills studied is removed from the primary leachate collection system.

2. The data clearly indicate that liquids and flow will be present in the secondary collection systems of well constructed and operated landfills. Liner systems of the type studied, when constructed to a high standard, have exhibited weekly average secondary flow rates less than 0.56 m3/ha/d (60 gpad).

3. The use of weekly averaging periods for computing flow rates appears reasonable. It must be recognized, however, that the use of weekly averaging periods will probably result in the occasional computation of very high flow rates, 10 to 50 times greater that the accumulated average flow rate. Such occasional high flow rates do not necessarily indicate liner damage or failure. Response action levels developed for secondary collection systems should be higher if they are based on weekly average, rather than monthly average, computations.

4. The flow rate observed in secondary collection systems of intact units is not correlated to flow in the primary system, indicating the integrity of the primary lining system and the effectiveness of pumping in the primary system to reduce the head on the primary liner and the resultant flow to the secondary system.

5. The average flow rate observed in secondary collection systems of intact units is approximately two orders of magnitude lower than average primary flow rate. However, much larger reductions in flow have been noted at facilities subject to intense rainfall. On average, approximately 98 percent of the liquid removed from landfill units studied was removed from the primary leachate collection system.

6. The data presented shows that the consolidation of the clay component of a primary liner system can contribute significant quantities of liquid to the flow measured in the secondary collection system. During the early stages of landfill operation, the contribution due to consolidation may even dominate the observed flow rate.

7. Previous calculations (Giroud and Bonaparte, 1989) based on theory, which predict the flow rates to be anticipated from good, fair, and poor quality liners, predict somewhat lower secondary flow rates than those presented in this paper. The reason for this difference has not been established. Previous presentations of actual leachate flow data (Bonaparte and Gross, 1990), are consistent with the data presented in this paper.

ACKNOWLEDGMENTS

The authors would like to express their appreciation to Chemical Waste Management, Inc. for their support and for the use of the flow rate data presented. We would also like to thank our families for their patience and understanding during the preparation of this paper. The authors would specifically like to thank Mr. Bob Gilbert for his assistance in the preparation of the data summaries, and Mr. Ken Anderson of Chemical Waste Management, Inc. for his contributions regarding the impact of clay consolidation and landfill closure on the secondary leachate collection system flow rate. The assistance of our colleagues and support staff in the preparation and review of this paper is also gratefully acknowledged.

REFERENCES

1. United States Environmental Protection Agency, Federal Register, Volume 57, No 19, January 29, 1992, page 3462-3497.

2. Anderson, Kenneth A., unpublished Chemical Waste Management, Inc. company correspondence.

3. Giroud, J.P. and Bonaparte, R., "Leakage through Liners Constructed with Geomembranes-Part II. Composite Liners", Geotextiles and Geomembranes, 1989.

4. Bonaparte, R. and Gross, B.A., "Field Behavior of Double Liner Systems", Waste Containment Systems: Construction, Regulation, and Performance, ASCE Geotechnical Special Publication No. 26, 1990.

TABLE 1
FLOW MONITORING DATA

UNIT	MONITORING PERIOD	
	MONTHLY DATA PERIOD	WEEKLY DATA PERIOD
1	1/87-12/91	5/89-6/91
2	1/87-12/91	5/89-6/91
3	1/87-12/91	5/89-6/91
4	1/87-12/91	5/89-6/91
5	1/89-5/91	1/89-5/91
6	1/89-5/91	1/89-5/91
7	1/89-5/91	1/89-5/91
8	1/89-5/91	1/89-5/91
9	1/89-5/91	1/89-5/91
10	1/89-5/91	1/89-5/91
11	1/89-5/91	1/89-5/91
12	1/89-5/91	1/89-5/91
13	1/89-5/91	1/89-8/91
14	1/89-5/91	1/89-8/91
15	10/90-3/91	9/90-3/91
16	10/91-3/91	9/90-3/91
17	11/87-7/91	3/90-7/91
18	6/88-7/91	3/90-7/91
19	12/88-7/91	3/90-7/91
20	12/88-7/91	3/90-7/91
21	9/89-7/91	3/90-7/91
22	9/89-7/91	3/90-7/91
23	11/90-7/91	11/90-7/91
24	11/90-7/91	11/90-7/91
25	1/87-7/91	3/90-7/91
26	1/87-7/91	3/90-7/91
27	1/87-7/91	3/90-7/91
28	1/87-7/91	3/90-7/91
29	1/87-7/91	3/90-7/91
30	1/87-7/91	3/90-7/91
31	4/87-6/91	NOT AVAIL
32	11/87-6/91	NOT AVAIL
33	6/89-6/91	NOT AVAIL
34	7/89-6/91	NOT AVAIL
35	2/90-5/90	2/90-5/90
36	2/90-5/90	2/90-5/90
37	1/90-8/90	NOT AVAIL
38	1/90-8/90	NOT AVAIL
39	1/90-8/90	NOT AVAIL
40	1/90-8/90	NOT AVAIL
41	1/90-8/90	NOT AVAIL
42	1/90-8/90	NOT AVAIL
43	6/88-4/90	NOT AVAIL
44	NOT AVAIL	4/90-1/91
45	NOT AVAIL	4/90-1/91
46	NOT AVAIL	4/90-1/91
47	NOT AVAIL	4/90-1/91
48	NOT AVAIL	4/90-1/91
49	NOT AVAIL	4/90-1/91

TABLE 2
LEACHATE FLOW IN DOUBLE LINED LANDFILLS
(S I. UNITS)

	PRIMARY LEACHATE COLLECTION SYSTEM FLOW						SECONDARY LEACHATE COLLECTION SYSTEM FLOW						
UNIT	RANGE OF MONTHLY AVG. (M3/HA/D)		MONTHLY AVG. (M3/HA/D)	RANGE OF WEEKLY AVG. (M3/HA/D)		WEEKLY AVG. (M3/HA/D)	RANGE OF MONTHLY AVG. (M3/HA/D)		MONTHLY AVG. (M3/HA/D)	RANGE OF WEEKLY AVG. (M3/HA/D)		WEEKLY AVG. (M3/HA/D)	
	max	min	avg	max	min	avg	max	min	avg	max	min	avg	REMARKS
1	1.68	0.00	0.29	1.22	0.00	0.29	0.55	0.00	0.09	0.24	0.00	0.08	NOTE 1
2	8.04	0.00	1.60	3.93	0.19	1.50	0.05	0.00	0.03	0.08	0.00	0.03	NOTE 1
3	28.05	0.00	6.92	29.92	0.00	7.57	3.37	0.00	0.31	3.53	0.00	0.50	NOTE 1
4	24.31	0.73	4.76	46.75	0.00	5.14	0.49	0.00	0.14	0.57	0.00	0.16	NOTE 1
5	11.22	0.46	3.65	NA	NA	NA	0.48	0.07	0.17	0.53	0.00	0.17	
6	7.20	0.19	1.87	NA	NA	NA	0.32	0.07	0.18	0.50	0.00	0.18	
7	14.96	0.32	2.34	NA	NA	NA	0.59	0.09	0.23	1.40	0.00	0.24	
8	5.33	0.37	1.59	NA	NA	NA	0.30	0.06	0.18	0.73	0.00	0.18	
9	38.34	1.22	12.16	NA	NA	NA	2.99	0.02	0.25	8.51	0.00	0.26	
10	34.60	0.06	5.61	NA	NA	NA	0.50	0.04	0.22	1.22	0.00	0.22	
11	11.22	0.06	2.34	NA	NA	NA	0.50	0.03	0.09	0.75	0.00	0.09	
12	82.28	0.94	19.64	NA	NA	NA	0.39	0.03	0.09	0.75	0.00	0.10	
13	28.05	0.31	3.83	NA	NA	NA	0.25	0.00	0.06	1.03	0.00	0.06	
14	44.88	0.33	15.90	NA	NA	NA	0.62	0.01	0.06	0.94	0.00	0.05	
15	39.27	4.11	16.83	NA	NA	NA	0.03	0.01	0.01	0.20	0.00	0.03	NOTE 1
16	39.27	4.11	16.83	NA	NA	NA	0.06	0.00	0.02	0.17	0.00	0.03	NOTE 1
17	53.30	0.50	6.73	2.90	0.34	1.50	1.12	0.01	0.08	1.68	0.00	0.07	NOTE 1
18	39.27	0.00	7.95	5.98	0.00	1.96	1.12	0.03	0.19	1.31	0.01	0.15	NOTE 1
19	43.01	0.57	8.18	8.42	0.07	2.71	0.41	0.01	0.10	0.34	0.01	0.05	NOTE 1
20	51.43	0.00	11.22	30.86	0.00	4.02	0.43	0.05	0.16	0.45	0.04	0.11	NOTE 1
21	20.57	0.94	5.24	6.17	0.59	3.09	1.22	0.04	0.31	2.15	0.02	0.30	NOTE 1
22	112.20	0.88	25.25	486.20	0.04	20.57	0.36	0.02	0.11	0.60	0.03	0.15	NOTE 1
23	187.00	0.02	32.73	635.80	0.00	32.73	0.36	0.01	0.06	0.75	0.00	0.09	
24	86.02	2.15	25.25	233.75	0.00	23.38	0.11	0.02	0.04	0.07	0.00	0.04	
25	0.75	0.00	0.11	0.18	0.00	0.00	0.61	0.00	0.05	0.19	0.00	0.04	NOTE 1
26	3.27	0.00	0.64	0.94	0.00	0.16	1.50	0.00	0.07	0.11	0.00	0.02	NOTE 1
27	28.99	0.00	4.02	2.62	0.00	0.50	0.67	0.00	0.10	0.11	0.00	0.05	NOTE 1
28	4.39	0.00	0.35	1.12	0.01	0.10	1.50	0.00	0.09	0.09	0.00	0.04	NOTE 1
29	78.54	0.22	7.01	2.34	0.02	0.56	1.40	0.00	0.15	0.26	0.00	0.08	NOTE 1
30	0.20	0.00	0.03	0.46	0.00	0.07	1.31	0.00	0.20	0.08	0.01	0.04	NOTE 1
31	0.39	0.00	0.07	NA	NA	NA	0.21	0.00	0.06	NA	NA	NA	ARID REGION
32	1.43	0.00	0.07	NA	NA	NA	0.13	0.00	0.05	NA	NA	NA	ARID REGION
33	0.04	0.00	0.01	NA	NA	NA	0.16	0.00	0.07	NA	NA	NA	ARID REGION
34	0.07	0.00	0.01	NA	NA	NA	0.16	0.00	0.04	NA	NA	NA	ARID REGION
35	0.02	0.00	0.00	NA	NA	NA	0.15	0.00	0.02	NA	NA	NA	
36	0.05	0.00	0.01	NA	NA	NA	0.00	0.00	0.00	NA	NA	NA	
37	0.72	0.00	0.14	NA	NA	NA	0.01	0.00	0.00	NA	NA	NA	
38	0.09	0.00	0.03	NA	NA	NA	0.02	0.00	0.01	NA	NA	NA	
39	5.28	0.00	1.05	NA	NA	NA	0.05	0.00	0.01	NA	NA	NA	
40	0.11	0.00	0.04	NA	NA	NA	0.04	0.00	0.01	NA	NA	NA	
41	6.81	0.00	0.84	NA	NA	NA	0.01	0.00	0.00	NA	NA	NA	SEMI-ARID
AVG.	27.87	0.45	6.17	83.31	0.07	5.88	0.60	0.01	0.10	0.98	0.0037	0.12	

NOTE 1: CALENDAR PERIOD FOR WEEKLY AND MONTHLY AVERAGES DO NOT COINCIDE.
NOTE 2: (M3/HA/D) REPRESENTS UNITS OF CUBIC METERS/HECTARE/DAY.

TABLE 2A
LEACHATE FLOW IN DOUBLE LINED LANDFILLS
(U.S. UNITS)

UNIT	PRIMARY LEACHATE COLLECTION SYSTEM FLOW						SECONDARY LEACHATE COLLECTION SYSTEM FLOW						REMARKS
	RANGE OF MONTHLY AVG. (GPAD)		MONTHLY AVG. (GPAD)	RANGE OF WEEKLY AVG. (GPAD)		WEEKLY AVG. (GPAD)	RANGE OF MONTHLY AVG. (GPAD)		MONTHLY AVG. (GPAD)	RANGE OF WEEKLY AVG. (GPAD)		WEEKLY AVG. (GPAD)	
	max	min	avg	max	min	avg	max	min	avg	max	min	avg	
1	180	0	31	130	0	31	59	0	10	26	0	9	NOTE 1
2	860	0	171	420	20	160	5	0	3	9	0	3	NOTE 1
3	3000	0	740	3200	0	810	380	0	33	378	0	54	NOTE 1
4	2600	78	509	5000	0	550	52	0	15	61	0	17	NOTE 1
5	1200	49	390	NA	NA	NA	51	8	18	57	0	18	
6	770	20	200	NA	NA	NA	34	7	19	54	0	19	
7	1600	34	250	NA	NA	NA	63	10	25	150	0	26	
8	570	40	170	NA	NA	NA	32	6	19	78	0	19	
9	4100	130	1300	NA	NA	NA	320	2	27	910	0	28	
10	3700	6	600	NA	NA	NA	54	4	23	130	0	24	
11	1200	6	250	NA	NA	NA	54	3	10	80	0	10	
12	8800	100	2100	NA	NA	NA	42	3	10	80	0	11	
13	3000	33	410	NA	NA	NA	27	0	6	110	0	6	
14	4800	35	1700	NA	NA	NA	66	1	6	100	0	5	
15	4200	440	1800	NA	NA	NA	3	1	1	21	0	3	NOTE 1
16	4200	440	1800	NA	NA	NA	6	0	2	18	0	3	NOTE 1
17	5700	53	720	310	36	160	120	1	9	180	0	8	NOTE 1
18	4200	0	650	640	0	210	120	3	20	140	1	16	NOTE 1
19	4600	61	875	900	8	290	44	1	11	36	1	5	NOTE 1
20	5500	0	1200	3300	0	430	46	5	19	48	4	12	NOTE 1
21	2200	100	560	660	63	330	130	4	33	230	2	32	NOTE 1
22	12000	94	2700	52000	4	2200	39	2	12	64	3	16	NOTE 1
23	20000	2	3500	68000	0	3500	39	1	9	80	0	10	
24	9200	230	2700	25000	0	2500	12	2	4	7	0	4	
25	80	0	12	19	0	0	65	0	5	20	0	4	NOTE 1
26	350	0	68	100	0	17	160	0	7	12	0	2	NOTE 1
27	3100	0	430	260	0	54	72	0	11	12	0	5	NOTE 1
28	470	0	37	120	1	11	160	0	10	10	0	4	NOTE 1
29	8400	24	750	250	2	60	150	0	16	28	0	9	NOTE 1
30	21	0	3	49	0	7	140	0	21	9	1	4	NOTE 1
31	42	0	8	NA	NA	NA	22	0	6	NA	NA	NA	ARID REGION
32	153	0	8	NA	NA	NA	14	0	5	NA	NA	NA	ARID REGION
33	4	0	1	NA	NA	NA	17	0	8	NA	NA	NA	ARID REGION
34	8	0	1	NA	NA	NA	17	0	4	NA	NA	NA	ARID REGION
35	2	0	0	NA	NA	NA	16	0	2	NA	NA	NA	
36	5	0	1	NA	NA	NA	0	0	0	NA	NA	NA	
37	77	0	15	NA	NA	NA	1	0	0	NA	NA	NA	
38	10	0	3	NA	NA	NA	2	0	1	NA	NA	NA	
39	565	0	112	NA	NA	NA	5	0	1	NA	NA	NA	
40	12	0	4	NA	NA	NA	4	0	1	NA	NA	NA	
41	728	0	90	NA	NA	NA	1	0	0	NA	NA	NA	SEMI-ARID
AVG	2981	48	660	8910	7	629	64	2	11	105	0.4	13	

NOTE 1: CALENDAR PERIOD FOR WEEKLY AND MONTHLY AVERAGES DO NOT COINCIDE

TABLE 3
LEACHATE FLOW THROUGH DAMAGED PRIMARY LINERS
(S I. UNITS)

UNIT	PRIMARY LEACHATE COLLECTION SYSTEM FLOW						SECONDARY LEACHATE COLLECTION SYSTEM FLOW						REMARKS
	RANGE OF MONTHLY AVG. (M3/HA/D)		MONTHLY AVG. (M3/HA/D)	RANGE OF WEEKLY AVG. (M3/HA/D)		WEEKLY AVG. (M3/HA/D)	RANGE OF MONTHLY AVG. (M3/HA/D)		MONTHLY AVG. (M3/HA/D)	RANGE OF WEEKLY AVG. (M3/HA/D)		WEEKLY AVG. (M3/HA/D)	
	max	min	avg	max	min	avg	max	min	avg	max	min	avg	
42	NA	NA	NA	NA	NA	NA	4.53	0.10	1.41	17.48	0.00	1.61	LINER DAMAGED
43	NA	NA	NA	NA	NA	NA	4.39	0.00	1.20	5.50	0.00	0.56	LINER DAMAGED
44	NA	NA	NA	66.67	0.00	9.12	NA	NA	NA	3.48	0.00	0.43	LINER DAMAGED
45	NA	NA	NA	3.91	0.00	0.49	NA	NA	NA	4.70	0.00	0.48	LINER DAMAGED
46	NA	NA	NA	7.38	0.00	1.97	NA	NA	NA	3.10	0.00	0.31	LINER DAMAGED
47	NA	NA	NA	23.04	0.00	2.66	NA	NA	NA	5.21	0.00	0.77	LINER DAMAGED
48	NA	NA	NA	75.58	0.00	13.56	NA	NA	NA	6.10	0.00	0.81	LINER DAMAGED
49	NA	NA	NA	104.54	0.00	34.54	NA	NA	NA	6.88	0.00	0.86	LINER DAMAGED

NOTE 1: (M3/HA/D) REPRESENTS UNITS OF CUBIC METERS/HECTARE/DAY.

TABLE 3A
LEACHATE FLOW THROUGH DAMAGED PRIMARY LINERS
(U.S. UNITS)

UNIT	PRIMARY LEACHATE COLLECTION SYSTEM FLOW						SECONDARY LEACHATE COLLECTION SYSTEM FLOW						REMARKS
	RANGE OF MONTHLY AVG. (GPAD)		MONTHLY AVG. (GPAD)	RANGE OF WEEKLY AVG. (GPAD)		WEEKLY AVG. (GPAD)	RANGE OF MONTHLY AVG. (GPAD)		MONTHLY AVG. (GPAD)	RANGE OF WEEKLY AVG. (GPAD)		WEEKLY AVG. (GPAD)	
	max	min	avg	max	min	avg	max	min	avg	max	min	avg	
42	NA	NA	NA	NA	NA	NA	484	11	151	1870	0	172	LINER DAMAGED
43	NA	NA	NA	NA	NA	NA	470	0	128	588	0	60	LINER DAMAGED
44	NA	NA	NA	7130	0	975	NA	NA	NA	372	0	46	LINER DAMAGED
45	NA	NA	NA	418	0	52	NA	NA	NA	503	0	51	LINER DAMAGED
46	NA	NA	NA	789	0	211	NA	NA	NA	332	0	33	LINER DAMAGED
47	NA	NA	NA	2464	0	284	NA	NA	NA	557	0	82	LINER DAMAGED
48	NA	NA	NA	8083	0	1450	NA	NA	NA	652	0	87	LINER DAMAGED
49	NA	NA	NA	11181	0	3694	NA	NA	NA	736	0	92	LINER DAMAGED

Structural Integrity of Composite Geosynthetic Lining and Cover Systems

R.B. Gilbert
University of Illinois, USA

J.H. Long
University of Illinois, USA

J.J. Daly
University of Illinois, USA

ABSTRACT

Composite lining and cover systems containing geosynthetic and soil components are used extensively in waste containment facilities. The structural integrity of these systems must be maintained throughout the lifetime of the facility in order to provide for adequate performance. The state of practice for predicting the stresses generated within composite systems considers only limit state equilibrium. A finite difference method which considers both force equilibrium and load-displacement compatibility for predicting these stresses is presented and compared with the state of practice.

INTRODUCTION

Composite lining and cover systems containing geosynthetic and soil components are used extensively in waste containment facilities. These systems serve as barriers to control the migration of contaminants to the environment. Stresses are generated within lining and cover systems during construction, waste placement and waste settlement. Rupture of any of the geosynthetic components within a composite system due to high stresses may compromise its ability to serve as an effective barrier. In addition, the expected loads carried by geosynthetic components are needed to design geosynthetic anchorage systems (e.g. anchor trenches at slope crests) properly. Finally, the long term performance of a geosynthetic (e.g. creep, stress cracking, etc.) is a function of the stress level in the geosynthetic. Therefore, accurate predictions of stresses within the geosynthetic components of lining and cover systems under different loading conditions can be of considerable importance.

The current state of practice for evaluating stresses within lining and cover systems is to consider limit state equilibrium (e.g. Mitchell, et. al. 1990; Koerner, 1990; and Giroud and Beech, 1989). The tensile force in each geosynthetic layer required to maintain equilibrium within the system is calculated by assuming that the maximum shear stress is mobilized at each interface within the system. There are two major limitations to this approach. First, the mobilized interface shear resistance is a function of relative displacement between adjacent layers. For relative displacements less than that required to mobilize peak interface strength, interface

shear resistance is roughly proportional to displacement. As the relative displacement increases beyond that required to mobilize peak strength, the shear resistance decreases from peak to a residual or large displacement strength. Therefore, a range of mobilized shear resistances is available for each interface, and selection of a single resistance value for use in the limit analysis is unclear. Second, limit state equilibrium methods ignore the axial stress-strain relationship within each layer. The initial axial stiffness may be significantly different among various geosynthetic and soil materials. As a lining or cover system is loaded, the stiffer components within the system tend to support more load than the less stiff components. Therefore, consideration of axial load behavior in addition to interface behavior is necessary to predict stresses accurately.

To account for the limit equilibrium limitations discussed above, Wilson-Fahmy and Koerner (1993) adopted a two-dimensional finite element approach. The finite element method provides a powerful computational tool for investigating two-dimensional effects while considering both shear resistance-displacement compatibility at interfaces and axial stress-strain compatibility within components. However, finite element tools typically require a level of effort in discretizing the geometry and performing numerical calculations that is more suitable for checking a final design configuration. Finite element methods generally are too cumbersome for analyzing multiple configurations required for design optimization and extensive parametric studies.

A finite difference method is presented herein to analyze composite lining and cover systems. This approach offers the advantage of simplicity in formulating the problem and in performing the numerical calculations while considering shear resistance-displacement and axial stress-strain compatibility. An example using a typical cover system is presented to compare results of the approach proposed with the currently accepted limit state approach and to evaluate factors which influence the distribution of stresses in composite systems.

PROPOSED APPROACH

The approach proposed for evaluating stresses within lining and cover systems uses inelastic, non-linear springs to model the shear resistance-displacement behavior at each interface and to model the axial load-displacement behavior within each component. Let m represent the number of components or layers within the system and let L represent the total length of the system. Each layer within the system is modeled one-dimensionally, and it is divided into a series of n nodes along the layer as shown on Fig. 1. Nodes are numbered successively down a column starting in the upper left corner of the system (Fig. 1), yielding N total nodes where N is equal to the number of nodes per layer (n) multiplied by the number of layers (m). Shear springs with stiffness k_s are located between nodes of adjacent components (layers). k_s is related to the interfacial shear modulus by the following relationship

$$k_s = \frac{\tau (L/n+1) W}{\Delta} \qquad (1)$$

where τ represents the shear stress, Δ represents the relative displacement at the interface, L/(n+1) represents the distance between adjacent nodes in a layer, and W represents width. In this analysis, a unit width is assumed. In addition, axial springs with stiffness k_a are located between adjacent nodes within a given layer.

k_a is related to the axial modulus of the material by the following relationship

$$k_a = \frac{E_a A}{L/(n+1)} \tag{2}$$

where E_a represents the secant modulus, A represents the cross-sectional area for a unit width, and L/(n+1) again represents the distance between adjacent nodes. The boundaries at the perimeter of the system are assumed to be fixed.

The tensile load in each geosynthetic layer is evaluated by satisfying both system equilibrium and load-displacement compatibility. Consider an individual node as shown on Fig. 1 where i represents the node of interest. By evaluating force equilibrium in the x direction, the following equation is obtained

$$\sum F_x = S_i - k_{a(i,i-m)}(\delta_i - \delta_{i-m}) + k_{a(i+m,i)}(\delta_{i+m} - \delta_i) - k_{s(i+1,i)}(\delta_i - \delta_{i+1}) + k_{s(i,i-1)}(\delta_{i-1} - \delta_i) = 0 \tag{3}$$

where δ represents displacement and S_i represents the external shear force per unit width that is applied to node i.

In considering force equilibrium for each node within the system, a system of N equations with N unknowns (i.e. each δ_i) is obtained. This system of equations is represented by the following in matrix form

$$[C] \cdot [\delta] = [S] \tag{4}$$

where [C] represents a NxN matrix of coefficients, $[\delta]$ is a 1xN matrix of displacements for each node, and [S] represents a 1xN matrix of external shear forces for each node. For a given row i in [C], the non-zero coefficients are given by the following

$$C_{i,i-m} = -k_{a(i,i-m)} \tag{5}$$

$$C_{i,i-1} = -k_{s(i,i-1)} \tag{6}$$

$$C_{i,i} = k_{a(i,i-m)} + k_{s(i,i-1)} + k_{a(i+m,i)} + k_{s(i+1,i)} \tag{7}$$

$$C_{i,i+1} = -k_{s(i+1,i)} \tag{8}$$

$$C_{i,i+m} = -k_{a(i+m,i)} \tag{9}$$

The system of N equations can be solved using standard algorithms to obtain the

displacement matrix for a given set of coefficients.

Since relationships between axial load and displacement and between shear load and displacement are nonlinear for most geosynthetic and soil components, an iterative approach is used to solve for displacements. The first iteration assumes initial values for each k_a and k_s and an initial set of displacements is obtained. The next iteration is based on displacements of the previous analysis. Values of k_a and k_s are re-evaluated, the analysis is performed, and a second set of displacements is obtained. The analysis is repeated until convergence in the displacements is achieved. A graphical representation of the iterative approach is shown on Fig. 2. An interactive computer program, GEOSTRES, has been developed to perform these calculations.

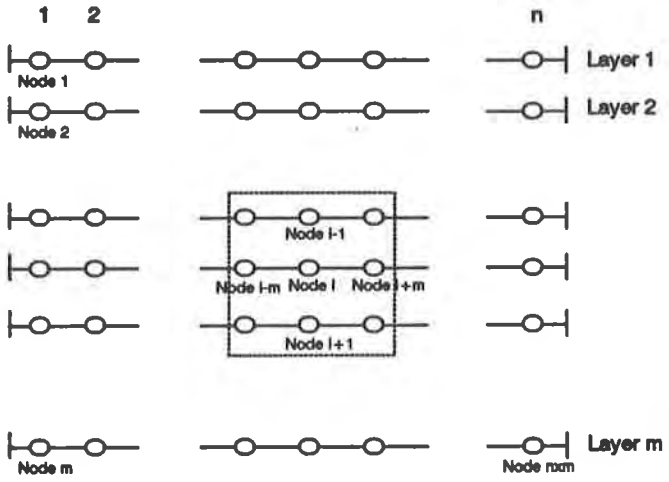

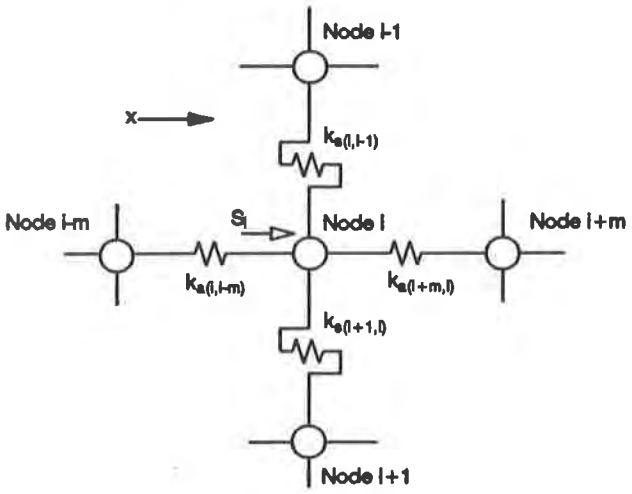

Figure 1. Model of lining or cover system.

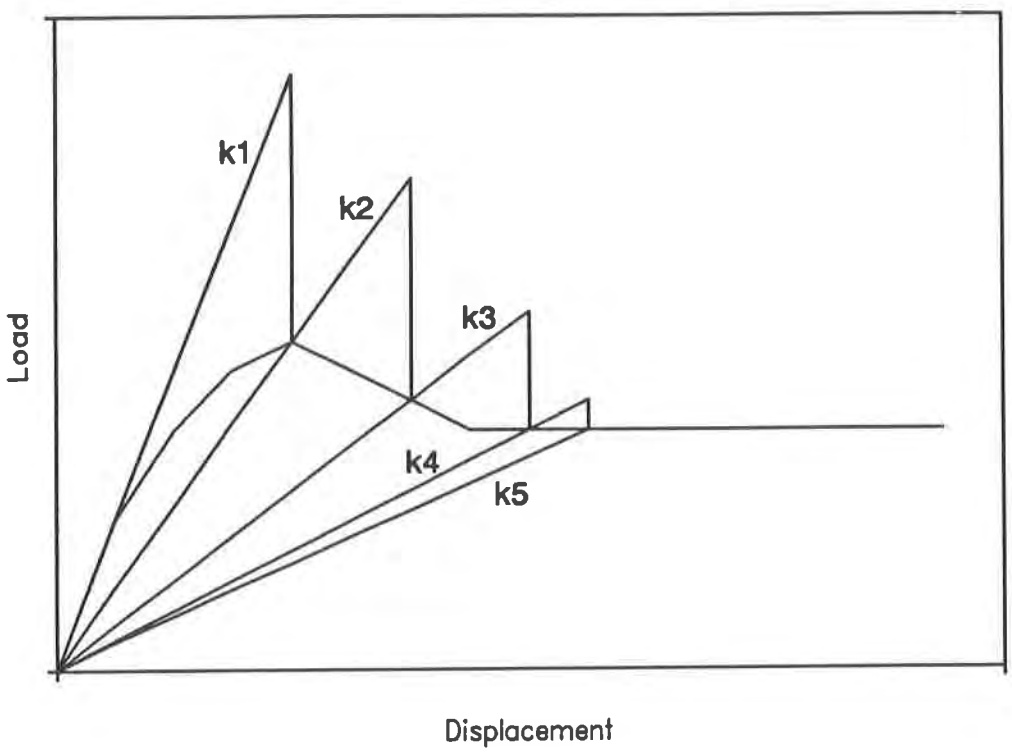

Figure 2. Graphical representation of iterative approach to obtain load-displacement compatibility.

ILLUSTRATIVE EXAMPLE

An example problem is presented to demonstrate the approach proposed for evaluating stresses in lining and cover systems. A typical composite cover system as shown on Fig. 3 is used for this purpose. A constant slope height of 8 m will be assumed in all calculations, while the grade of the slope will be varied. The soil cover is 0.92 m thick with a unit weight of 18.7 kN/m^3. The shear resistance parameters are presented in Table 1 for the various interfaces, and the load-displacement relationships used as input to GEOSTRES are shown on Fig. 4 for a given normal stress of 16.7 kN/m^2 (i.e. the normal stress at the bottom of 0.93 m of cover soil at 25 percent grade). The shear resistance versus displacement relationships are based on both a review of published data and unpublished large scale direct shear testing results. The sample sizes for these large scale tests are typically on the order of 300 mm by 300 mm. The axial load versus strain relationships for the various components are shown on Fig. 5. These relationships are typical of results from tensile tests on wide width specimens (Koerner, 1990), and represent short-term strengths (i.e. creep is not considered). As shown on Figs. 4 and 5, point-wise linear load-deformation relationships have been assumed for simplicity; however, the finite difference approach is general and non-linear relationships can readily be accommodated.

Limit Equilibrium Approaches Stresses within the cover system are predicted using the limit equilibrium approach proposed by Giroud and Beech (1989). Two slight

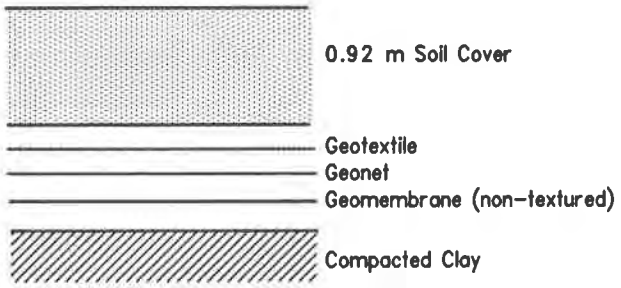

Figure 3. Composite system configuration for example problem.

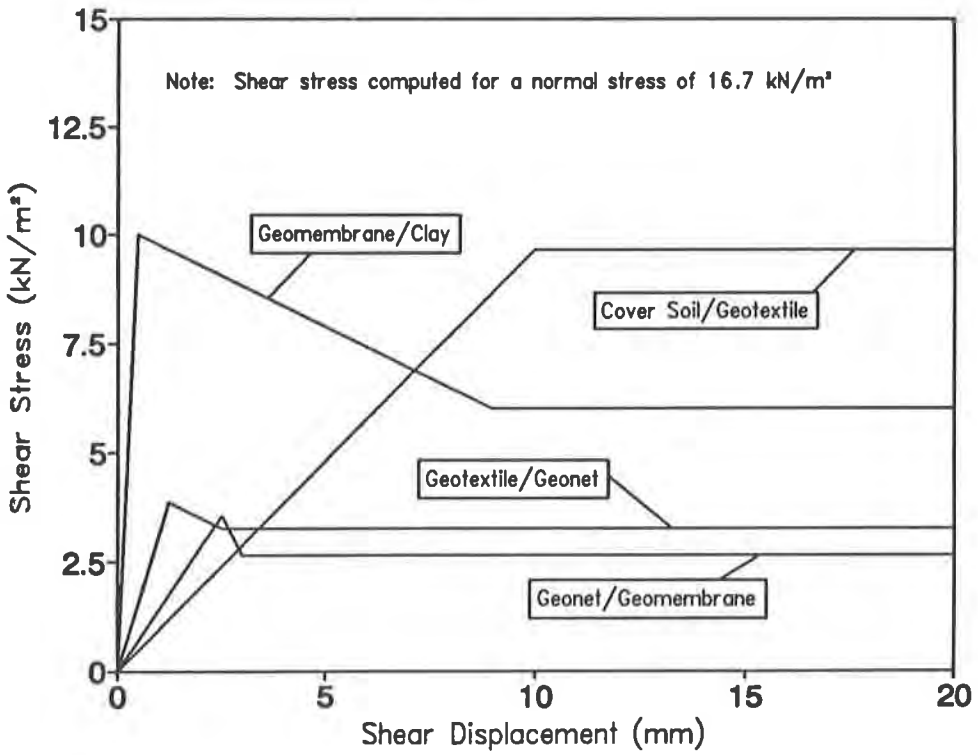

Figure 4. Shear resistance versus displacement for interfaces in example problem.

Table 1. Interface shear resistance versus displacement relationships for example problem.

	Peak			Large Displacement		
Interface	Friction Angle (°)	Intercept (kN/m)	Displace-ment (mm)	Friction Angle (°)	Intercept (kN/m)	Displace-ment (mm)
Cover Soil/ Geotextile	30	0	10	30	0	10
Geotextile/ Geonet	13	0	1.25	11	0	2.5
Geonet/ Geomembrane	12	0	2.5	9	0	3
Geomembrane/ Clay	0	10	0.5	0	6	9

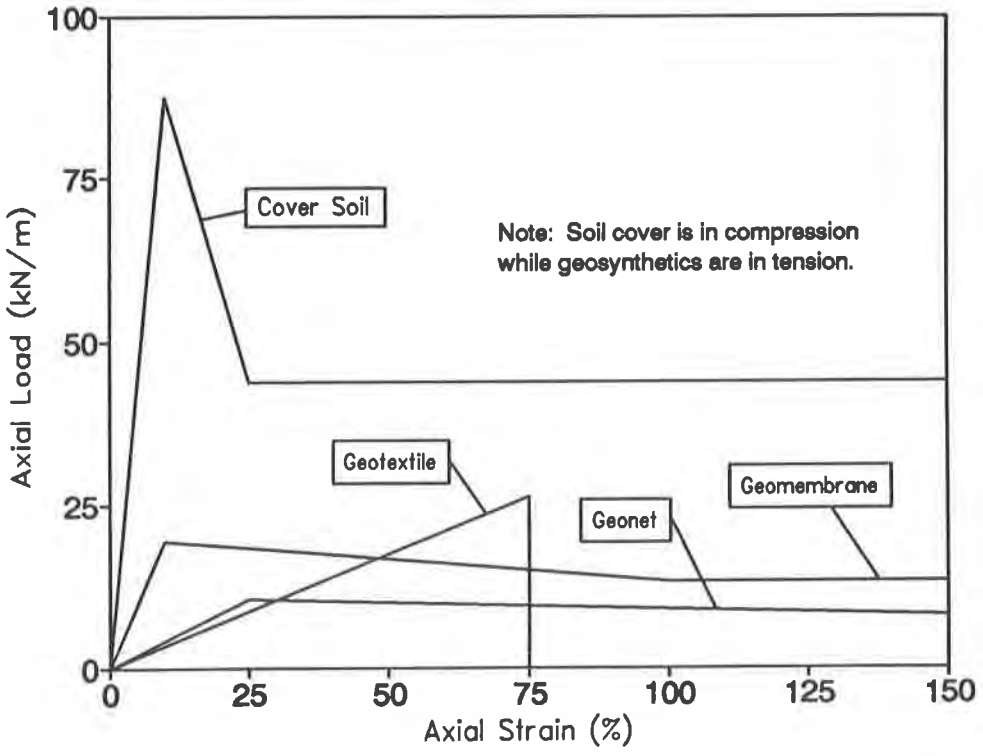

Figure 5. Axial load versus stress for components in example problem.

variations of the Giroud and Beech method are also used to illustrate the effect of buttress load on axial loads in the components. The limit equilibrium approach assumes a mobilized soil resistance at the toe (buttress) and a mobilized interface strength along the slope of the potential sliding surface. Any unbalanced forces are carried by tensile loads in the components above the potential failure surface. Results from three limit equilibrium methods are compared. Each of the methods are distinguished by assumptions that affect mobilization of the buttress load.

The first limit approach is consistent with the Giroud and Beech (1989) method. The method requires that all driving forces be resisted first by interface shear and compressive load in the soil. Tensile loads are carried by the geosynthetics only after driving forces exceed resisting forces provided by shear and the soil compressive load. The approach follows a rationale that the soil cover is the stiffest element (Fig. 5) in the cover system; therefore, a significant portion of the total driving force should be resisted by compressive loads in the soil. For limit analysis, the total driving force less the axial capacity of the soil is mobilized at the soil/geotextile interface while the large displacement resistance is mobilized at the other interfaces. The total tensile load that must be carried by the geosynthetic components (i.e. the summation of the individual geosynthetic loads) to satisfy equilibrium is plotted as a function of slope grade in Fig. 6 as the curve labeled "Maximum Soil Buttress." Since the geonet/geomembrane interface provides the minimum shear resistance (Table 1), the system will slip along this interface and the total tensile load in the geosynthetics is carried by only the geotextile and the geonet. The geosynthetics carry no tensile load until the soil reaches its axial capacity at a slope grade of approximately 44 percent (23.7°). This approach provides a lower bound estimate of the tensile stresses in the geosynthetics.

A conservative approach would assume the buttress carries no axial load; therefore, the driving forces are resisted only by a combination of tensile load in the geosynthetics and shear between the underlying geosynthetics. Analysis is conducted by applying the total driving force along the soil/geotextile interface and using the large displacement strengths at all other interfaces. Results are plotted on the curve labeled "No Soil Buttress" in Fig. 6. For slope grades less than 16 percent (9.0°), the geosynthetics carry no load since the interface friction angle for the geonet/geomembrane is 9°. The tensile load indicated by the "No Soil Buttress" curve in Fig. 6 exceeds the combined tensile strength of the geotextile and geonet for slope grades greater than about 20 percent (11.3°). This approach yields very high values for loads in the geosynthetics and is considered to provide an upper-bound estimate for geosynthetic load. Therefore, the results of limit analyses using the "No Soil Buttress" and the "Maximum Soil Buttress" approach provide upper bound and lower bound estimates of load expected in the geosynthetic components, respectively.

A limit approach that yields results between the two extremes assumes that the axial load in the soil and the shear resistance at the soil/geotextile interface are both at the same proportion of their limits. Therefore, at a slope grade just prior to failure of the soil cover, the axial load and the shear resistance at the soil/geotextile interface will both be at their respective limits. Large displacement resistances are assumed for all of the interfaces below the soil/geotextile interface. The curve labeled "Proportioned Soil Buttress" in Fig. 6 represents the results obtained for this case. The magnitude of the geosynthetic tensile load is between the extreme cases of "No Soil Buttress" and "Maximum Soil buttress." Axial loads for each component are shown in Fig. 7 as a percentage of their maximum strength. The axial load in the soil cover increases gradually as the slope angle increases. The geonet carries load for a slope grade exceeding 18 percent (10°). This identifies where

sliding initiates along the geonet/geomembrane interface. Similarly, the geotextile begins to carry load when the slope grade exceeds 22 percent (12.4°). Once slippage occurs along the geotextile/geonet interface, the geotextile load increases significantly with increasing slope. The combined tensile load of the geonet and geotextile is equal to the geosynthetic load shown in Fig. 6 as "Proportioned Soil Buttress." The geomembrane carries no tensile load.

Proposed Method - GEOSTRES Results from limit analyses (Figs. 6 and 7) demonstrate that a wide range of loads in the soil and geosynthetic components can be predicted. Unfortunately, the limit methods provide no guidance to assess which assumptions result in reasonable predictions for load. To evaluate the consequence of these assumptions, a consideration of shear resistance-displacement and axial stress-strain compatibility is necessary. The example problem has been analyzed using GEOSTRES by dividing each layer into 100 nodes. Results are shown on Figs. 6 and 8. The total load carried by the geosynthetics (Fig. 6) falls between the limit state assumptions of "Proportioned Soil Buttress" and "Maximum Soil Buttress," indicating that to rely on the soil to provide the full resistance is unconservative, and to assume no buttressing at the toe of the soil cover is overly conservative. For slope grades less than about 21 percent (i.e. a slope angle of 12° which is the minimum peak friction angle at any interface), the geosynthetics carry small loads; however, for slope grades greater than 21 percent, the load carried by the geosynthetics increases rapidly over a small increase in the slope grade. The sharp jump in the axial load carried by the geosynthetics results from the post peak behavior of the interface resistance between the geonet and the geomembrane (Fig. 4). Once peak resistance is mobilized, additional deformation in the system causes the shear resistance to decrease to its large displacement value and the load in the geosynthetic components correspondingly increases. After the initial jump, the tensile load increases gradually as the slope grade steepens.

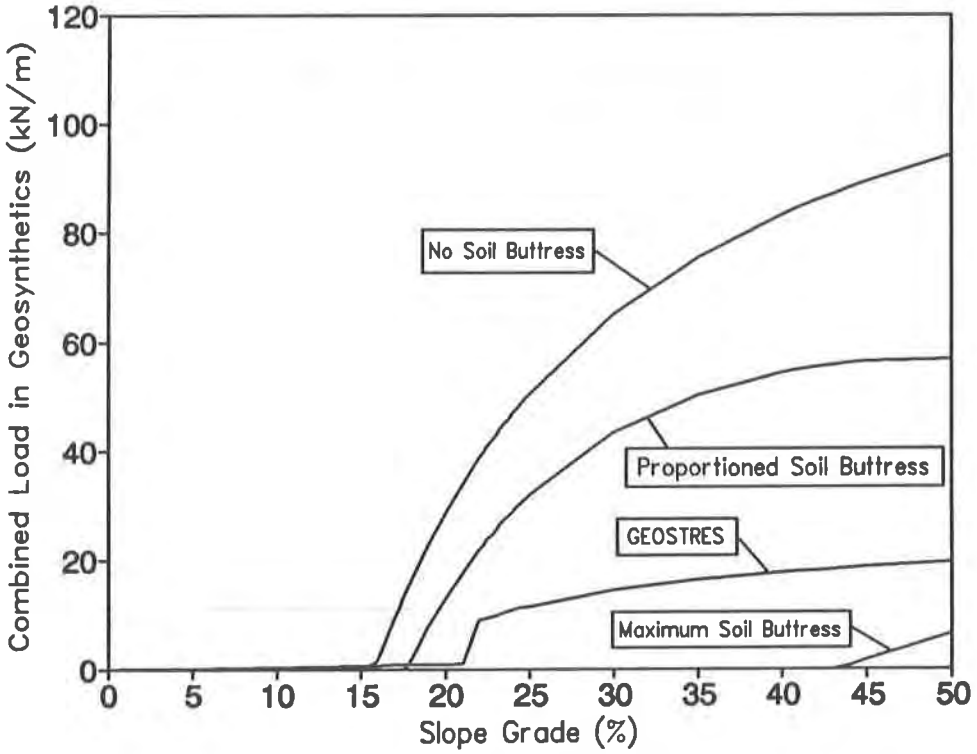

Figure 6. Geosynthetic load versus slope grade for example problem.

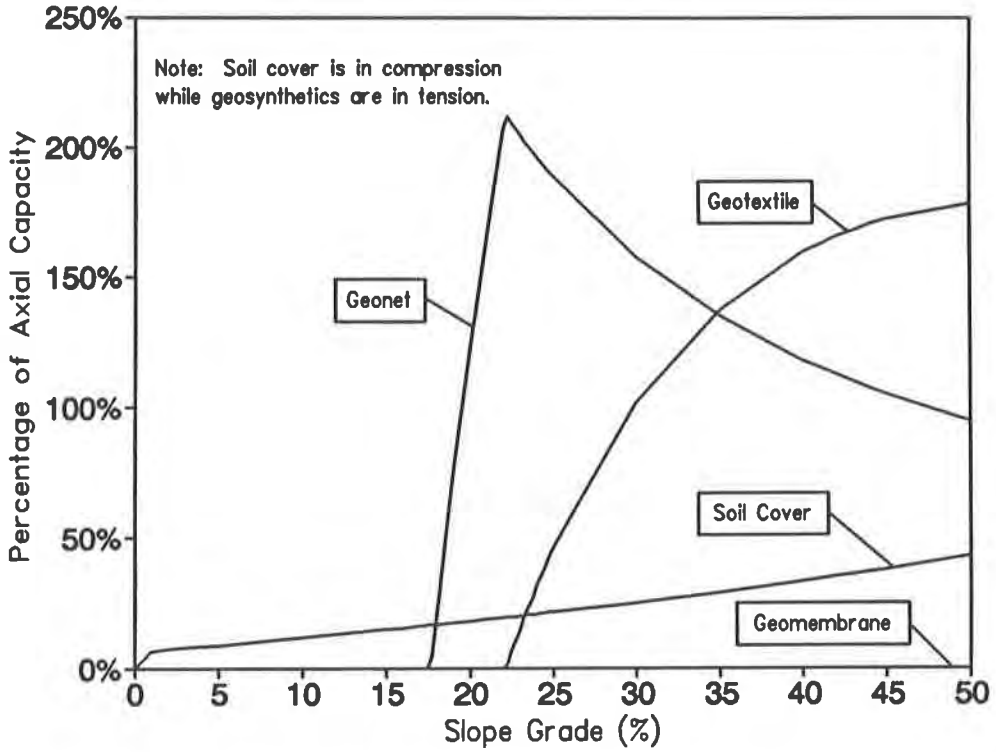

Figure 7. Predicted axial loads example problem using limit state analysis with proportioned soil buttress.

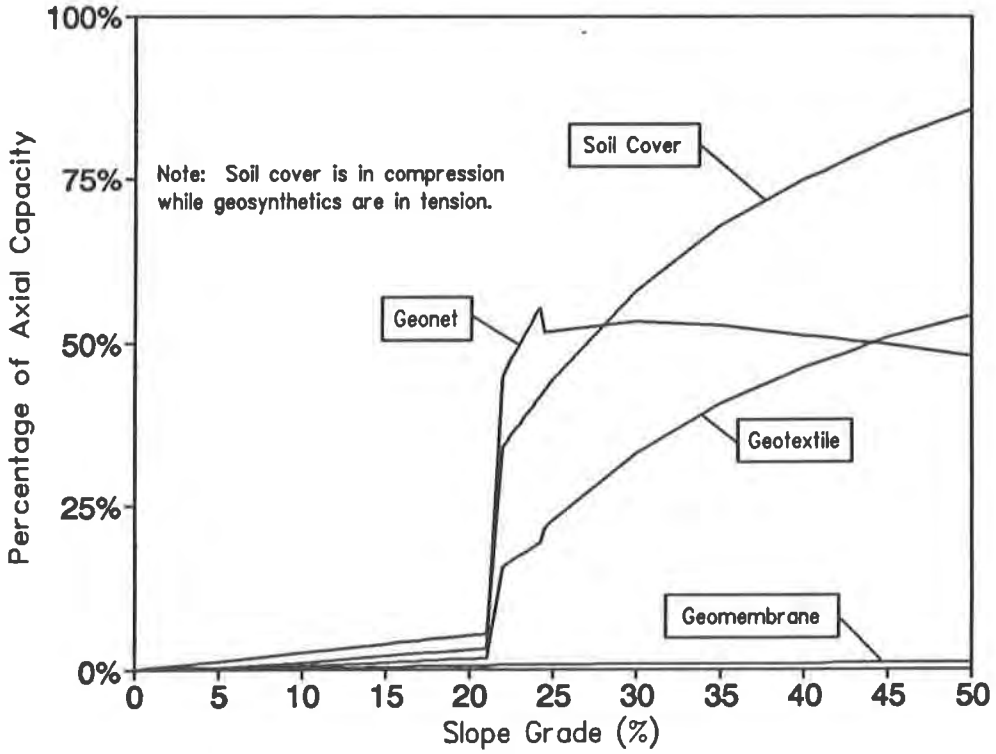

Figure 8. Predicted axial loads for example problem using GEOSTRES.

Predictions for loads in the cover system components using GEOSTRES are shown on Fig. 8. A comparison with Fig. 7 demonstrates that very different loads result from methods that consider equilibrium only. The loads in the geonet and the geotextile predicted by GEOSTRES are generally much smaller than those predicted using the limit approach due to greater resistance provided by the cover soil. Additionally, insight into the complex behavior of the system due to interactions between components can be obtained from Figure 8. For example, the tensile load in the geonet climbs sharply after initial slippage along its lower interface with the geomembrane [i.e. at a slope grade of 21 percent or 12° which is the peak friction angle of the geonet/geomembrane interface (Fig. 4)] and peaks at approximately 25 percent where slippage initiates along its upper interface with the geotextile. Here, the resistance at the geotextile/geonet interface decreases rapidly to its large displacement strength and less load can be transferred to the underlying geonet; thus, the load in the geonet decreases. Also, the load in the geotextile increases in response to the decrease in interface resistance at its base. As the slope grade increases further, the axial loads in the soil cover and geotextile continue to increase to resist the larger driving forces while the axial load in the geonet decreases slightly. Finally, it is interesting to note that some loads are predicted in the components even at slope angles less than 12° (i.e. the peak friction angle for the interface providing the minimum resistance). A limit approach would predict no loads at slope angles lower than 12°; however, the finite difference method predicts mobilization of axial loads due to deformations within the system to accommodate even small driving forces. This example demonstrates that it is important to have a complete understanding of how components interact within the system to design the system effectively, especially considering that the most complex behavior occurs at slope grades commonly used in practice (i.e. 10 to 50 percent).

The influence of strength and deformation parameters on component stress levels is demonstrated using results from a limited sensitivity study for the illustrative example. GEOSTRES was used to conduct the study. The following parameters were considered: the initial axial stiffness of the cover soil, the peak shear displacement at the geomembrane/clay interface, and the available shear resistance at the geomembrane/clay interface. A slope grade of 25 percent was selected for the study, and the results are presented in Table 2.

Since the cover soil carries a significant portion of the total resistance as a compressive load, the axial stiffness of the soil may have a significant influence on the results. The initial soil stiffness was increased and decreased by a factor of 2, and the results are presented as Cases 1 and 2, respectively, in Table 2. Increasing the soil stiffness by a factor of 2 results in greater load carried by the soil and less carried by the geosynthetic components, while the opposite result occurs when the soil stiffness decreases by a factor of 2. However, the magnitude of load change is less than a factor of 2. For example, increasing soil stiffness by 2 results in approximately 25 percent less load in both the geotextile and geonet. Decreasing the soil stiffness results in 29 percent greater load in both components. Therefore, the axial stiffness of a single component within the system can substantially influence the loads developed within that component as well as within other components in the system.

Importance of the interface shear-displacement behavior is illustrated below. The shear resistance versus displacement relationships for interfaces with geosynthetic components are typically obtained in the laboratory; however, these relationships are sensitive to test conditions, test methods, and scale of the test. The peak shear displacement for the non-textured geomembrane/clay interface was increased by a factor of 10 (i.e. the shear displacement at peak was increased from 0.5 mm to 5.0 mm) and is

noted as Case 3 in Table 2. The axial load in the geomembrane increases from 0.13 kN/m to 0.73 kN/m due to the increase in the peak displacement while the axial loads in the other components are essentially unaffected. Since larger displacement is required to mobilize peak shear resistance at the base of the geomembrane, the geomembrane carries more load axially as axial strains are developed. However, the increase in axial load within the geomembrane is insignificant.

Table 2. Sensitivity study results for example problem with 25 percent slope grade.

	Cover Soil		Geotextile		Geonet		Geomembrane	
	Axial Load (kN/m)	Ratio with Base	Axial Load (kN/m)	Ratio with Base	Axial Load (kN/m)	Ratio with Base	Axial Load (kN/m)	Ratio with Base
Base Case	-39	1.00	6.0	1.00	5.4	1.00	0.13	1.00
Case 1	-42	1.09	4.5	0.75	4.1	0.76	0.13	1.00
Case 2	-36	0.92	7.8	1.29	7.0	1.29	0.13	1.00
Case 3	-39	1.00	6.0	1.00	5.4	1.00	0.73	5.5
Case 4	-42	1.08	6.1	1.01	5.5	1.01	6.7	51

Notes:

Case 1 - Increase axial stiffness of cover soil by 2.
Case 2 - Decrease axial stiffness of cover soil by 2.
Case 3 - Increase peak shear displacement at geomembrane/clay interface by 10.
Case 4 - Replace compacted clay with bentonite panels.
Tension is indicated by positive values.
Compression is indicated by negative values.

Replacement of the compacted clay with bentonite panels is considered as Case 4. A typical shear resistance versus displacement relationship for the bentonite panel interface with a non-textured geomembrane is given as follows: a peak friction angle of 9° mobilized at 5 mm and a residual friction angle of 8° mobilized at 13 mm. The resulting geosynthetic loads for the 25 percent slope grade with the bentonite panels are presented as Case 4 in Table 2. The axial load in the geomembrane increases to 6.7 kN/m due to the smaller available shear resistance at the base of the geomembrane, while the axial loads in the other components remain essentially unchanged. Therefore, the available shear resistance at the interfaces has a significant influence on the axial loads developed within the geosynthetics.

CONCLUSIONS

A finite difference method for evaluating stresses in soil and geosynthetic components of lining and cover systems is developed in this paper. The approach satisfies force equilibrium and load-deformation compatibility at interfaces and within components. A typical cover system is analyzed to compare the results of the proposed approach with results of the currently accepted limit state approach. While limit state methods can identify upper and lower bounds for component loads, the difference between the two bounds is too great to assess a realistic load in the geosynthetics. Compared to the approach proposed, the limit state approach can significantly over-

predict, or under-predict loads in components. Furthermore, the limit state approach predicts tensile load in a geosynthetic layer only when slippage occurs on its lower interface. The proposed approach also shows that a geosynthetic can develop tensile load from slippage on its lower interface, but in addition, can develop load when slippage occurs along other underlying interfaces.

The importance of strength and deformation parameters are illustrated with results of a limited sensitivity study. The results demonstrate that changes in strength and deformation parameters of individual components can be significant, or insignificant, depending on the type of parameter varied, and how the other components in the system interact. Methods that consider only limit state equilibrium predict no effect of deformation parameters.

Results from analyses of an example cover system and a sensitivity study demonstrate that stresses within lining and cover systems are affected significantly by both stiffness and strength of the soil and geosynthetic layers. Therefore, both shear resistance-displacement and axial stress-strain compatibility must be satisfied to evaluate stresses accurately within geosynthetic components of lining or cover systems.

ACKNOWLEDGMENTS

Support for this research effort was provided by the Illinois Office of Solid Waste Research, the Institute for Environmental Studies, and the University of Illinois at Urbana-Champaign under contract OSWR-06-005. Their support is gratefully acknowledged.

Results of unpublished laboratory tests, such as large-scale direct shear tests, on soil/geosynthetic and geosynthetic/geosynthetic interfaces, and on bentonite panels, were provided by Golder Associates Inc. Their contribution and cooperation is greatly appreciated.

REFERENCES

Giroud, J. P. and Beech, J. F. (1989), "Stability of Soil Layers on Geosynthetic Lining Systems," Proceedings, Geosynthetics '89 Conference, San Diego, CA, pp. 35-47.

Koerner, R. M. (1990), Designing with Geosynthetics, Prentice-Hall, Englewood Cliffs, NJ.

Mitchell, D. H., McLean, M. A. and Gates, T. E. (1990), "Stability of Lined Slopes at Landfills and Surface Impoundments," EPA/600/2-89/057, Office of Research and Development, USEPA, Cincinnati, OH.

Wilson-Fahmy, R. F. and Koerner, R. M. (1993), "Finite Element Analysis of Stability of Cover Soil on Geomembrane Lined Slopes," Proceedings, Geosynthetics '93 Conference, Vancouver, B. C.

Locating Leaks in Geomembrane Liners of Landfills Covered With a Protective Soil

D.L. Laine
Leak Location Services Inc., USA

G.T. Darilek
Leak Location Services Inc., USA

ABSTRACT

The electrical leak location method was used to locate leaks in the geomembrane liners of single-lined and double-lined landfills covered with a protective soil cover. The landfills ranged in size from 0.40 hectare (one-acre) to 3.2 hectares (eight-acre). Water in the leak detection system under the primary liner indicated the primary liners were leaking.

The principal of the electrical leak location method is to place a voltage across the geomembrane liner and then to detect areas where electrical current flows through leaks in the liner. The electrical leak location method proved to be a practical and efficient method to locate leaks under a protective soil cover. This method was very successful in locating leaks to solve the leak problems at the landfills.

INTRODUCTION

Geomembrane liners are covered often with sand or soil to protect the liner from mechanical damage and damage from solar ultraviolet radiation. Geomembrane liners covered with soil materials are also used to cap landfills. Because the geomembrane liner may be damaged while emplacing the protective soil, an electrical leak location survey of the soil-covered geomembrane is a highly effective method for ensuring that leaks will be located in the liner. The method is particularly valid because the liner is tested under load, and after the liner has been exposed to possible damage.

The development of the electrical leak location method began in 1980 and commercial surveys have been available for the past seven years. Electrical leak location surveys with soil cover have been conducted commercially for the past five years. The commercial surveys have been overwhelmingly successful in that many leaks were efficiently and accurately located in installations that had been previously tested with other methods.

Description of Method. The electrical leak location method has been described previously by the authors in several papers. The basic method is to connect an electrical power supply to electrodes above and below the liner and then detect areas of localized electrical current flow through leaks in the otherwise insulating liner. When no leaks are present, the voltage impressed across the liner produces a very low current flow and a relatively uniform voltage distribution in the material above the liner. If the liner has a leak, electrical current flows through the leak causing a localized anomaly in the potential gradient. Leaks are located by measuring potential gradients in the material above the liner to search for these localized areas of relatively high electrical potential gradients. The electrical leak location method is used in liquid impoundments, and for pre-service inspection of solid waste landfills with soil cover.

With the proper implementation of equipment and survey procedures the electrical leak location method is a very sensitive and accurate method. The measured amplitude of the leak signal is proportional to the amount of electrical current flowing through the leak. Therefore, leak location surveys should be conducted with the maximum practical safe impressed voltage. To increase the leak detection reliability the detector electronics must be optimized for maximum sensitivity. In addition, extraneous electrical conductors such as metal pipes and pump wiring that provide an electrical conduction path through or around the geomembrane liner should be eliminated or insulated.

SURVEYS OF WATER-FILLED LINERS

Surveys of water-filled liners are conducted while wading in the liquid or standing on the side slope using electrical search probes and associated instrumentation. This system is for inspection of non-hazardous liquid-filled impoundments and for pre-service inspection of water-filled impoundments and landfills. Figure 1 shows the operation of the equipment.

FIGURE 1. LEAK LOCATION SURVEY WITH WATER COVERING THE LINER

The authors have previously reported an average density of located leaks at 2.6 per 1,000 m^2 (2.4 per 10,000 sq. ft.) Darilek, et al (1989) and 3.4 leaks per 1,000 m^2 (3.1 per 10,000 sq. ft.) Laine and Miklas (1989) with several liners having more than 12.5 leaks per 1,000 m^2 (11.6 per 10,000 sq. ft.). To date the authors have surveyed over 850 thousand square meters (9 million sq. ft.) of liner material. The results of the most recent surveys are presented in Figure 2 and Table 1.

ELECTRICAL LEAK LOCATION METHOD WITH SOIL COVER

Systematic Surveys. The electrical leak location method for surveying surface impoundments was adapted to make surface soil potential measurements for locating leaks in geomembranes covered a protective or cap soil layer. The soil is dampened with water for electrical contact and to allow the water to percolate through leaks in the geomembrane liner. Water may be sprayed on the soil using a water truck or sprinkler hoses. In some cases, the natural moisture and rain may be sufficient for the survey. Surface potential measurements are made on the dampened soil in a systematic manner using specialized measurement electrodes and a portable digital data acquisition system.

Figure 3 shows the data collection operation for a leak location survey with soil cover. Surveys are conducted by making point-by-point potential measurements along predetermined survey lines with a fixed measurement electrode separation. The data in the portable digital data

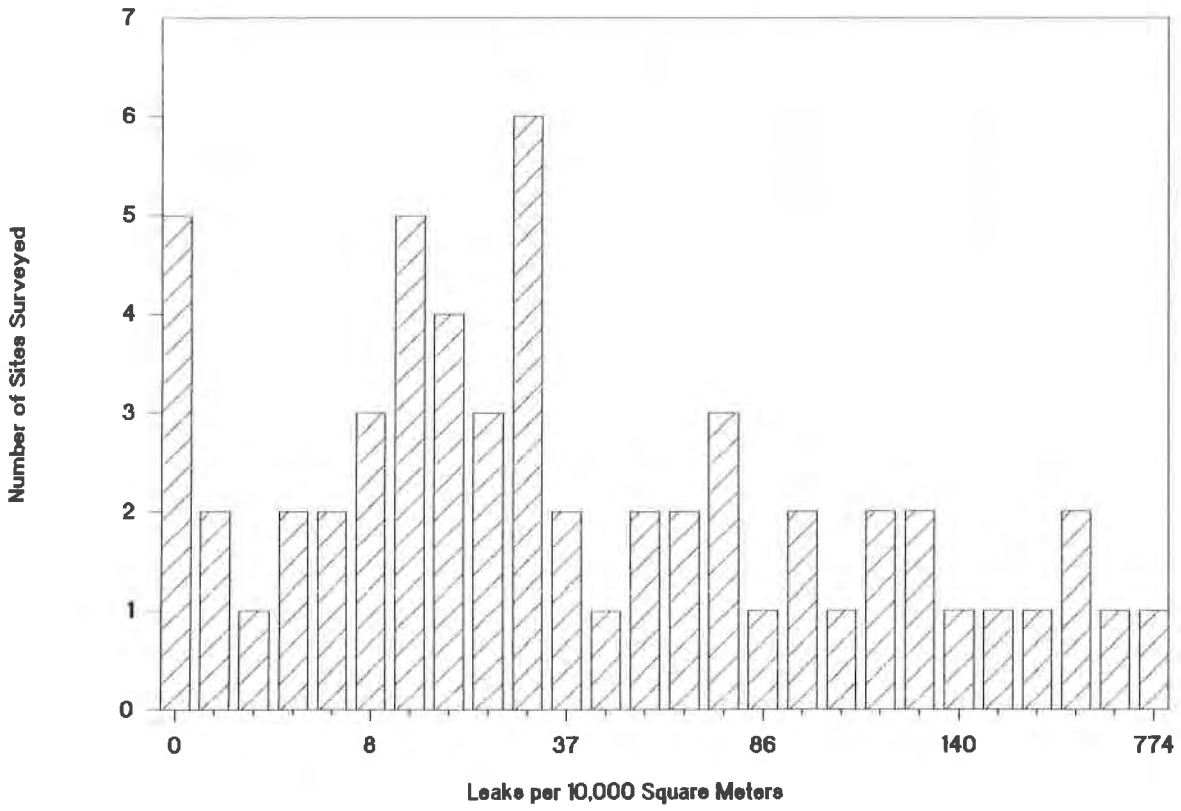

FIGURE 2. NUMBER OF SITES vs NUMBER OF LEAKS PER 10,000 M^2

TABLE 1. LEAK LOCATION SURVEY DATA FOR WATER-FILLED SURVEYS

SURVEY NO.	SIZE SQ. METERS	TOTAL LEAKS	LEAKS LOCATED SEAM	LEAKS LOCATED SHEET	10,000 SQ. METERS
1	195	0			0.0
2	223	6	2	4	269.1
3	232	2	1	1	86.1
4	281	0			0.0
5	290	1	1		34.4
6	302	7	6	1	231.8
7	302	2	1	1	66.2
8	330	4	3	1	121.3
9	358	0			0.0
10	372	1	1		26.9
11	393	9	9		229.3
12	393	1	1		25.5
13	393	1	1		25.5
14	530	8	8		151.1
15	530	4	2	2	75.5
16	530	41	41		774.2
17	530	1		1	18.9
18	530	4	4		75.5
19	697	4	2	2	57.4
20	798	15	10	5	188.0
21	1,347	3	3		22.3
22	1,457	18	18		123.6
23	1,457	0			0.0
24	1,457	11	7	4	75.5
25	1,457	14	12	2	96.1
26	1,906	4	4		21.0
27	1,906	22	22		115.4
28	2,007	24	24		119.6
29	2,007	4	4		19.9
30	3,066	43	43		140.3
31	3,066	9	9		29.4
32	3,530	34	29	5	96.3
33	4,047	3	1	2	7.4
34	4,181	19	19		45.4
35	4,645	18	18		38.8
36	4,645	3	3		6.5
37	4,645	31	30	1	66.7
38	6,000	10	10		16.7
39	6,039	65	62	3	107.6
40	6,039	32	29	3	53.0
41	6,039	7	5	2	11.6
42	6,039	5	3	2	8.3
43	6,070	2	2		3.3
44	6,070	0			0.0
45	7,432	6	4	2	8.1
46	7,479	13	6	7	17.4
47	8,094	6		6	7.4
48	8,919	19	17	2	21.3
49	8,919	25	25		28.0
50	8,919	12	9	3	13.5
51	12,141	4	3	1	3.3
52	14,864	6	5	1	4.0
53	22,297	61	61		27.4
54	28,328	37	37		13.1
55	28,328	40	40		14.1
56	28,328	34	34		12.0
57	33,751	21	12	9	6.2
58	48,562	41	31	10	8.4
TOTALS	363,684	817	734	83	22.5

FIGURE 3. LEAK LOCATION SURVEY WITH SOIL COVER

acquisition system is downloaded to a portable computer for storage, analysis, and plotting. The data is then analyzed in the field to identify leak signatures. When a suspect area is located, manual measurements are made to further isolate the leak.

Sensitivity and Accuracy. The sensitivity of electrical leak location method increases as the thickness of the soil decreases. Typically, leaks with a diameter greater than 0.30-centimeters (0.12-in.) can be located in a geomembrane covered with up to 60 centimeters (2 ft.) of soil. Typically surveys are conducted on the sand filtration layer or on the soil placed above the filtration layer. Surveys can be successfully conducted with geotextile separating the soil layers. To optimize leak detection sensitivity, testing for leaks with only a portion of the soil cover in place is recommended if the thickness of the soil cover will be greater than approximately 30 centimeters. Damage to the liner will most likely occur during the placement of this first layer of soil.

The leak location accuracy for surveys conducted with soil cover also depends upon the closeness of the spacing of the point-by-point measurements and the homogeneity of the soil cover. A practical accuracy guideline for leak location surveys with soil cover is approximately one-half of the soil thickness. When a leak signal is detected the soil is removed or the thickness of the soil decreased and follow-up measurements are made to exactly locate the leak.

The design of the surveys must be based on the physics of the electrical leak location method. The survey parameters must be designed for proper coverage and leak detection sensitivity. These include survey line spacing, spacing of measurements, and spacing of measurement electrodes.

LEAK LOCATION SURVEYS WITH SOIL COVER - CASE STUDIES

Isolated Leaks Under 60 Centimeters of Soil Cover. An electrical leak location survey was conducted on the floor area of a doubled-lined two-acre landfill. The primary liner and secondary liners were 1.5 millimeter (60-mil) high-density polyethylene material separated by a synthetic drainage net. The primary liner was covered with a sequence of approximately 30 centimeters (1 ft.) of gravel, a geotextile, and 30 centimeters (1 ft.) of sand. Water leakage after rainfalls indicated that the primary liner was leaking at a rate of approximately 1,150 liters (300 gal.) per day. Therefore, a small leak was suspected in the primary liner. Figure 4 shows a view of the survey site.

The floor area of the 8,100 square meter (87,000 sq. ft.) landfill was surveyed on a 60 centimeter (2 ft.) survey grid with the electrodes spaced 60 centimeters (2 ft.) apart. Three small leaks were located in the primary liner. Figure 5 shows a raster plot of the data collected near one of the leaks. The leak signature is clearly detectable on survey lines that are located 3 meters (10 ft.) from the leak. The detected leak was a 0.25-centimeter (0.1-in.) diameter hole through the liner.

FIGURE 4. VIEW OF DOUBLE-LINED LANDFILL CELL SURVEYED

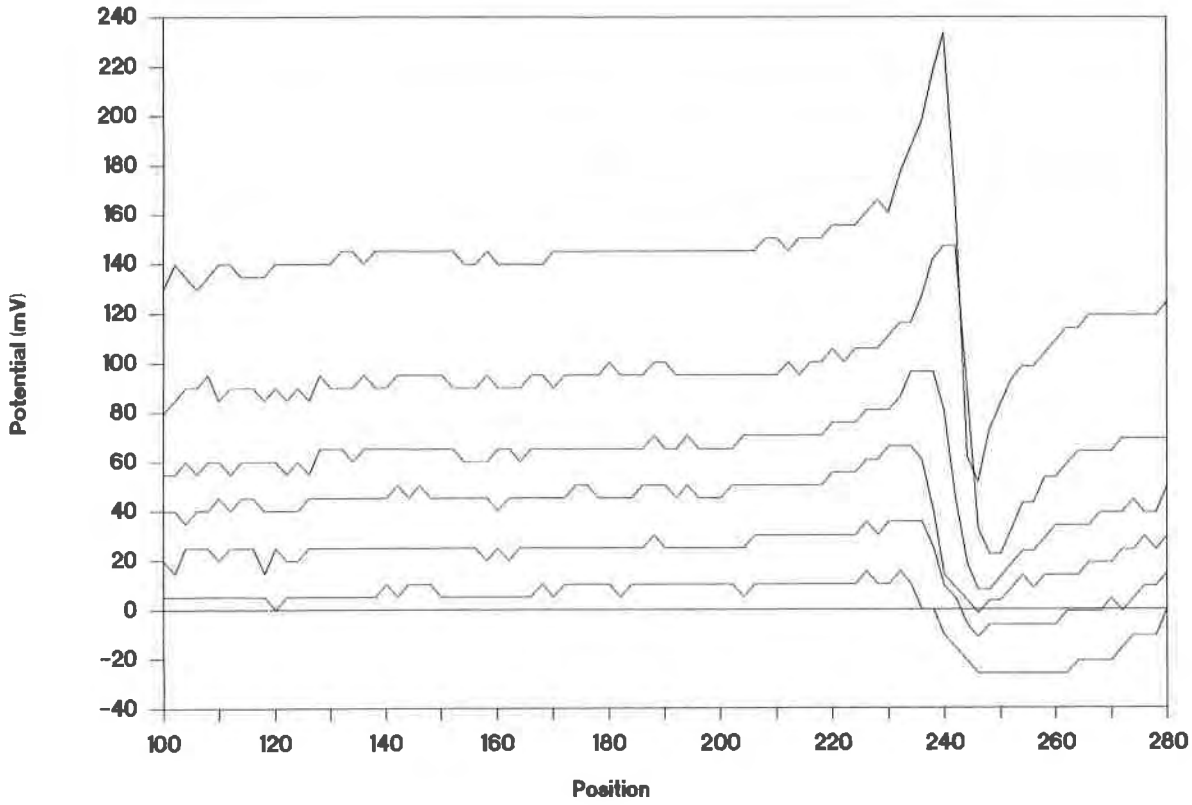

FIGURE 5. SURVEY DATA FOR 0.25 CENTIMETER DIAMETER LEAK LOCATED UNDER 60 CENTIMETERS OF SOIL COVER

Multiple Leaks. Isolating multiple closely-spaced leaks under soil cover requires a thorough, in-depth understanding of the physics of the electrical leak location method and extensive practical field experience. The superposition of the leak signatures results in a complex leak signature. The presence of multiple leaks must be recognized and subsequent measurements and excavations must be performed to isolate the leaks. Figure 6 shows a raster plot of some of the data taken on a single scrim-reinforced chlorosulfonated polyethylene (CSPER) liner with multiple leaks. The data is characterized by many leak signal excursions. The signals from several single leaks are evident on adjacent lines.

The liner was protected with large rock rip-rap placed on a 15-centimeter (6-in.) to 30-centimeter (12 in.) soil bed. The rock rip-rap was removed prior to the survey. The leak area shown between positions 60 and 190 on the survey lines was investigated further to isolate approximately 50 leaks. Figure 7 shows a 5-centimeter (2-in.) puncture leak that provided one of the larger leak signals previously shown in Figure 6. Figure 8 shows a 0.5-centimeter (0.2-in.) long puncture/abrasion.

Reconnaissance Surveys. A reconnaissance survey methodology for geomembranes with soil cover can be successful, particularly when an electrical leak location survey was previously conducted before the liner was covered with soil. Rather than performing a systematic survey on closely spaced survey lines to locate smaller leaks, the reconnaissance measurements are intended

to isolate a few large leaks. The reconnaissance methodology assumes that no smaller leaks are present in the geomembrane liner. The measurement sequence is to make measurements in the suspect areas to locate a leak, expose the leak, insulate the leak, and then measure the power supply output current. This sequence is repeated until the output current level is decreased to a level indicating that all of the major leaks have been found. Figure 9 shows a reconnaissance survey being performed on a 0.40-hectare (one-acre) landfill cell. The area in the lower left of Figure 9 was uncovered to expose a located leak.

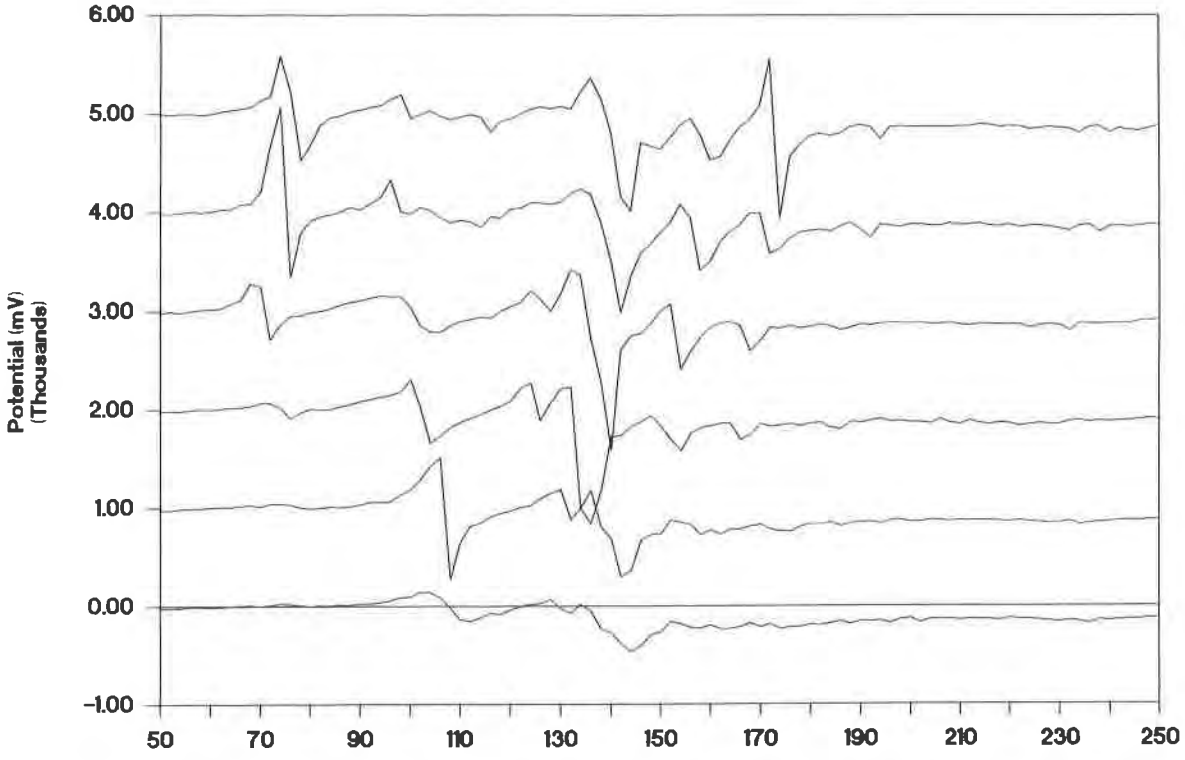

FIGURE 6. SURVEY DATA SHOWING MULTIPLE LEAK SIGNALS

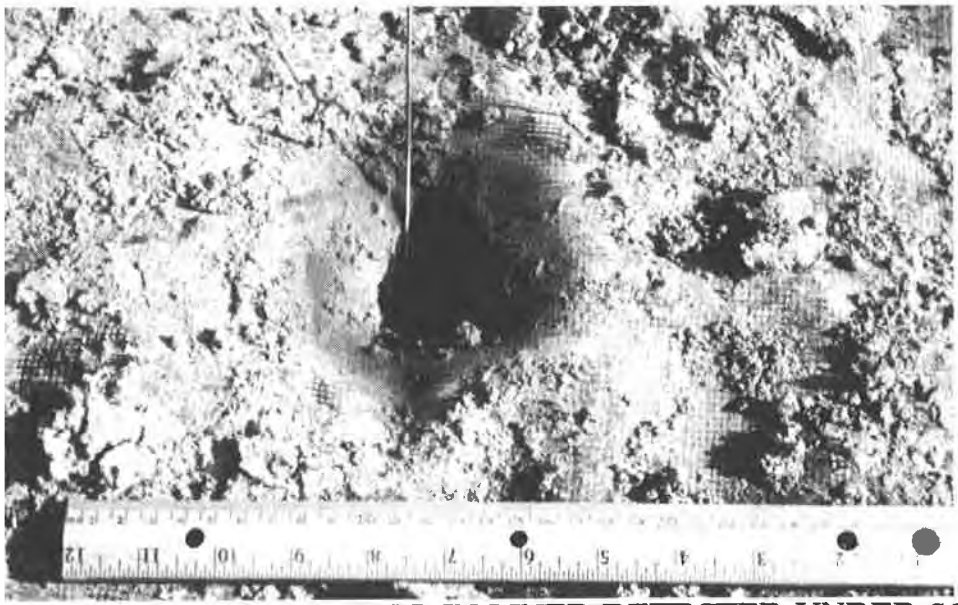

FIGURE 7. FIVE CENTIMETER HOLE IN LINER DETECTED UNDER SOIL COVER

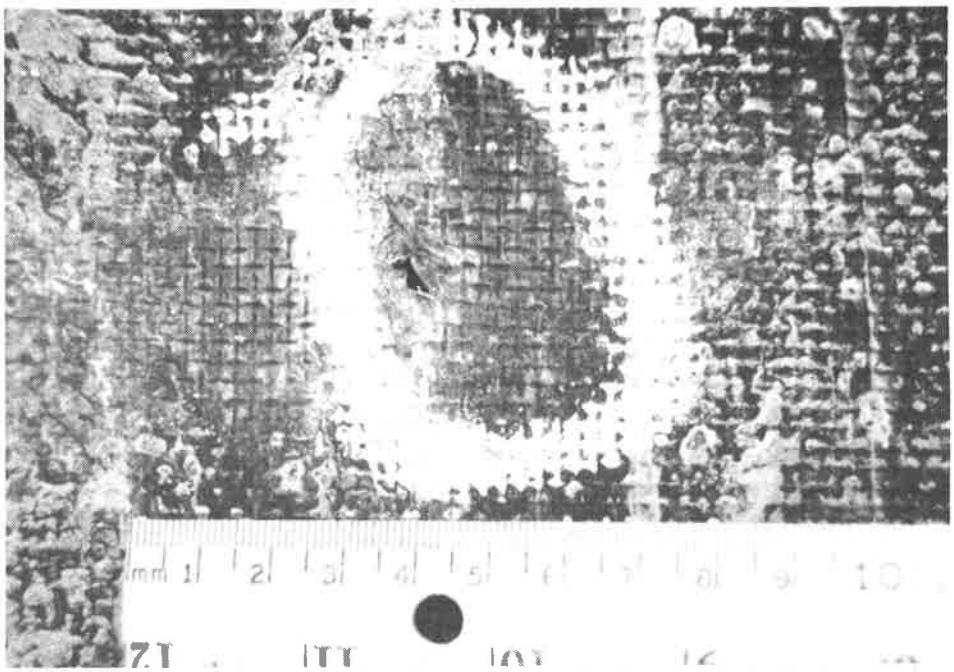

FIGURE 8. 0.5 CENTIMETER HOLE IN LINER DETECTED UNDER SOIL COVER

FIGURE 9. VIEW OF LANDFILL CELL WITH AN ELECTRICAL LEAK LOCATION RECONNAISSANCE SURVEY IN PROGRESS

CONCLUSIONS

An electrical method for locating leaks in geomembrane liners of waste impoundments and landfills has been developed and demonstrated successfully in a wide variety of applications. The validity and usefulness of the electrical leak location method has been demonstrated for testing the integrity of the geomembrane for single and double-liners with and without protective soil cover systems. The method will not damage the liner.

The technique is used for construction quality assurance and in-service performance monitoring. The electrical leak location method can be used in liquid impoundments, as a pre-service inspection of solid waste landfills, and to locate leaks in the final cover for landfills or impoundments. In addition, if leaks are suspected in the primary liner covered with up to two-feet of protective material, then they can be effectively located in a systematic manner using this method without removing the material covering the liner.

REFERENCES

1. Darilek, G.T., Laine, D.L., Parra, J.O., The Electrical Leak Location Method for Geomembrane Liners-Development and Applications, Industrial Fabrics Association International Geosynthetics '89 Conference, San Diego, CA, February 21-23, 1989.

2. Laine, Daren L., and Miklas, Michael P., Detection and Location of Leaks in Geomembrane Liners Using an Electrical Method: Case Histories, Superfund '89, 10th National Conference, Washington, DC, Nov. 27-29, 1989.

LANDFILL DESIGN, PERFORMANCE AND CQA

GEOSYNTHETICS '93 CONFERENCE
VANCOUVER, BRITISH COLUMBIA

Deflection Analysis of Polyethylene Leachate Collection Pipes

N. Paruvakat
Foth & Van Dyke, USA

ABSTRACT

This paper examines the use of Marston's formula with Iowa formula for evaluating vertical deflection of leachate collection pipes under high landfills. For these cases, one needs to account for soil-structure interaction between the buried flexible pipe and its backfill to obtain realistic pipe deflections and loads on the pipes. The approach is examined by employing the procedure to predict the vertical deflection of and load on a corrugated polyethylene pipe placed under a 30.48 m (100 feet) high embankment. Test results for this case history are taken from published data. Agreement between the predicted and observed results is good. Due to the similarity of the geometries of this case and that of leachate collection pipes under high landfills, the results of the comparison indicate that this approach may also be applicable to deflection analysis of leachate collection pipes under high landfills.

INTRODUCTION

With the passage of Resource Conservation and Recovery Act (RCRA) Subtitle D, new solid waste landfills will, to a great extent, be designed with at least one composite liner. The Subtitle D rules also require an efficient leachate collection system to be placed above the liner. The leachate collection systems of existing landfills typically consist of granular drainage layers sloping towards ditches containing leachate collection pipes embedded in pipe-zone backfill (PZB) of clean gravel or stone. Figure 1 shows a typical configuration. This paper addresses the design of polyethylene pipes for leachate collection in situations similar to the one shown in Figure 1.

Buried plastic pipes to convey fluids have been designed and constructed for a long time. For plastic pipes with stress relaxation properties and typically used in civil engineering construction, Goddard (1983) has demonstrated that the design need only

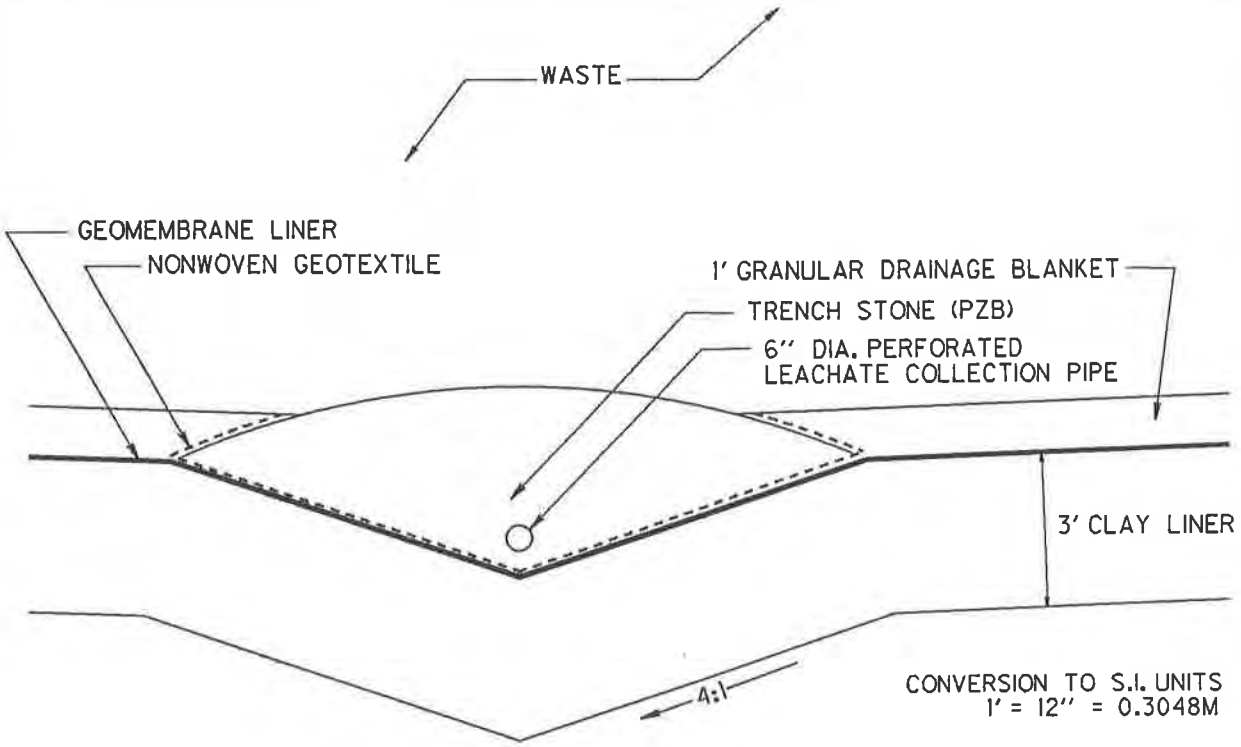

FIGURE 1: TYPICAL V-SHAPED TRENCH
FOR LANDFILLS WITH COMPOSITE LINERS

/dl/users/jow/prgetren.dgn

address the deflection (shortening of the vertical axis) under the imposed loads. The strain in the pipe wall and the buckling stress are extremely small when the pipe deflection under the imposed load reaches the limiting value. However, for pipe designers it is prudent to check the factors of safety against wall crushing and buckling failure. For this paper only deflection was considered.

The Iowa Deflection Formula or any of its variations is generally used to predict the vertical deflection of a buried flexible plastic pipe. In this deflection formula the pipe deflection is equal to the load on the pipe divided by the sum of the pipe stiffness and the soil stiffness (Goddard, 1983). The effect of soil stiffness is much more pronounced compared to the pipe stiffness.

The Iowa formula for pipe deflection is:

$$\Delta x = \frac{(DL)\ (k)\ (W_c)}{\frac{EI}{r^3} + 0.061\ E'} \qquad (1)$$

where:

Δx = horizontal deflection (which is also equal to the vertical deflection);
DL = deflection lag factor;
k = bedding factor;
W_c = load per unit length of pipe;
E = Young's Modulus for the pipe material (short term);
I = moment of inertia of pipe wall;
E' = modulus of soil reaction;
r = pipe radius.

This formula has served well under normal burial conditions and has found its way into design manuals. But for deflection analysis of pipes under deep burial such as under high landfills, the use of this formula needs to be critically examined.

Traditionally, landfills have been designed and constructed such that the refuse depths are in the 30-metre range. But stricter and stricter regulations with regard to locational criteria have led to fewer landfills being designed today. Since the quantity of waste going to the landfills has not declined, the new landfills tend to be larger and taller. The increased waste depths and the resulting increase in the overburden pressure at the pipe elevation have raised questions as to the validity of currently used procedures for analyzing plastic pipes, the preferred material for leachate collection pipes in view of their desirable chemical resistance properties.

Tests at Utah State University (Watkins, 1990) and field tests and analytical studies of a buried high-density polyethylene pipe (Hashash and Selig, 1990, Goddard, 1991) showed that the Iowa formula or its variations did not correctly predict pipe

deflection when buried under large depths. The deflections were highly over-predicted when the formula was used in the conventional manner.

Hashash and Selig (1990) have described the results of an excellent field test on a corrugated polyethylene pipe under a 30.48 m (100′) high embankment of Interstate 279 near Pittsburgh, Pennsylvania, U.S.A. They compared the results observed with those predicted using two finite element codes SOILCON (SOIL CONduit analysis) and CANDE (Culvert ANalysis and DEsign). Both codes are powerful tools for analyzing soil-structure interaction where soil properties as a function of soil types and percent compaction can be input as one option. Hashash and Selig concluded that both codes gave similar predictions which were in reasonable agreement with the measured values.

Watkins (1990) proposed a method of computing the pipe deflections which will correspond to incipient failure under high landfills. He concluded that for pipes enveloped in select PZB, incipient failure condition will not occur up to ring deflection of 18 percent (assuming PZB has an angle of internal friction (ϕ) of 0.524 rad (30 degrees) and 21 percent for ϕ = 0.611 rad (35°) for different cases analyzed, irrespective of the height of the landfill. His results also showed that for ϕ greater than 0.262 rad (15°) and initial ring deflections less than 20 percent, a factor of safety of 2 with respect to deflection in the design of the pipe will result in a factor of safety greater than two with respect to loads applied to the pipe.

Thus, a review of pertinent literature shows that the designer of leachate collection pipes for high landfills is in need of a simple and relatively inexpensive design procedure to predict pipe deflections under imposed loads.

PROPOSED DEFLECTION ANALYSIS

Typical leachate collection systems in a modern landfill consist of perforated or slotted pipes (generally 0.1524 m (6") in diameter to facilitate cleaning operations) embedded in PZB. The PZB typically will be placed above the pipe for heights of 0.3 to 0.6 m or more. When waste is placed over the backfill of a leachate collection pipe, the weight of the fill will cause the pipe to deflect. This deflection will result in a redistribution of stresses within the PZB in the vicinity of the pipe. For the purpose of this paper, the redistribution of stresses are assumed not to extend beyond the PZB. The behavior of the pipe under this condition can be considered to be similar to that of a positive projecting conduit within an embankment.

The compacted clay liner in this case will be analogous to the natural ground and the PZB to the embankment, if one were to use existing theories such as Marston's formula for load on positive projecting conduit, to obtain loads acting on the leachate collection pipe.

Use of Marston's Formula. When a positive projecting conduit deforms under the embankment load, shearing stresses are induced in the embankment soils. Marston's Formula is derived on the assumption that relative movements take place along imaginary vertical planes extending upwards from the sides of the conduit. For the case of a flexible plastic pipe backfilled with a stone or clean gravel PZB, the case is illustrated in Figure 2. For this condition, Marston's Formula for the load on the conduit is given by: (Spangler and Handy, 1982)

$$W_c = \gamma\ (C_c)\ (B_c)^2 \tag{2}$$

$$C_c = \frac{e^{\pm 2k\mu(He/B_c)} - 1}{\pm 2k\mu} + \left(\frac{H}{B_c} - \frac{H_e}{B_c}\right) e^{\pm 2k\mu(He/B_c)} \tag{3}$$

where:

W_c = load per unit length of conduit;
γ = unit weight of soil above the conduit;
B_c = outside width of conduit = 2r;
H = height of fill above conduit;
H_e = height of plane of equal settlement above the critical plane;
k = lateral pressure ratio (earth pressure coefficient);
μ = tan ϕ; where ϕ = angle of internal friction of PZB material;
e = base of natural logarithm.

Figure 3 illustrates the deformation of the positive projecting conduit in an embankment where the relative stiffness of the conduit is smaller than the surrounding soil and therefore shortening of the vertical height of the conduit is more than the deformation of the adjacent columns of soil. This condition therefore is an incomplete ditch condition provided the plane of equal settlement is within the PZB. Figure 3 also illustrates the plane of equal settlement and the critical plane as well as the terms required to define the settlement ratio in equation (4). The height of plane of equal settlement above the critical plane (H_e) can be evaluated from the equation (4).

$$\left[\frac{1}{2k\mu} \pm \left(\frac{H}{B_c} - \frac{H_e}{B_c}\right) \pm \frac{r_{sd}\ p}{3}\right] \frac{e^{\pm 2k\mu(He/B_c)} - 1}{\pm 2k\mu} \pm \frac{1}{2}\left(\frac{H_e}{B_c}\right)^2$$
$$\pm \frac{r_{sd}\ p}{3}\left(\frac{H}{B_c} - \frac{H_e}{B_c}\right) e^{\pm 2k\mu(H_e/B_c)} - \frac{1}{2k\mu}\left(\frac{H_e}{B_c}\right) \mp \left(\frac{H}{B_c}\right)\left(\frac{H_e}{B_c}\right) = \pm r_{sd}\ (p)\left(\frac{H}{B_c}\right) \tag{4}$$

where:

r_{sd} = settlement ratio;
p = ratio of the conduit projection above the natural ground surface to the diameter of the conduit.

The settlement ratio can be found using equation (5)

$$r_{sd} = \frac{(Sm + Sg) - (Sf + dc)}{Sm} \tag{5}$$

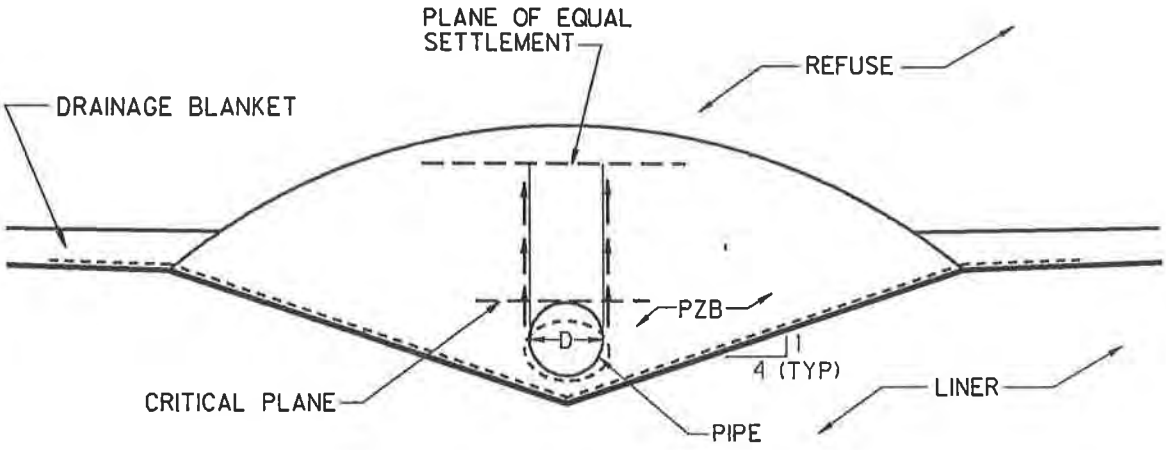

FIGURE 2: SETTLEMENT OF LEACHATE PIPE INDUCING SHEAR STRESSES IN PZB

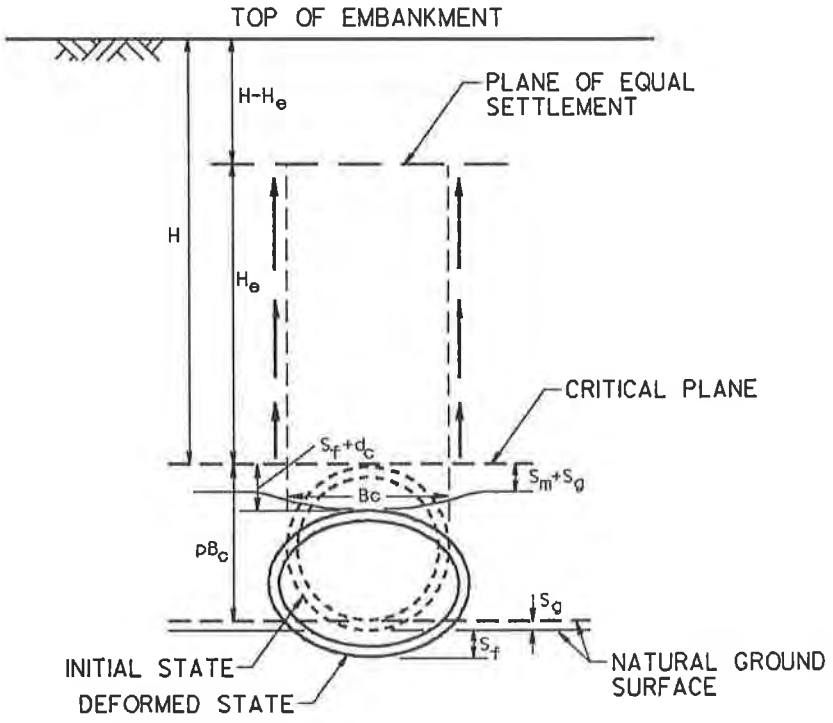

FIGURE 3: CASE OF AN INCOMPLETE DITCH CONDITION FOR A POSITIVE PROJECTING CONDUIT

/dl/users/jow/prgetren.dgn

where:

Sm	=	compression deformation of soil column adjacent to the conduit of height p B_c;
Sg	=	settlement of the natural ground surface adjacent to the conduit;
Sf	=	settlement of the conduit into its foundation;
dc	=	shortening of the vertical height of the conduit.

In equations 3 and 4, wherever + and - signs are used together, the upper signs are used for cases where r_{sd} is positive and the lower signs are used where r_{sd} is negative. For the case of a polyethylene leachate collection pipe where *Sg* and *Sf* are the same, the settlement ratio will reduce to

$$r_{sd} = \frac{Sm - dc}{Sm} \tag{6}$$

Since the PZB material is stiffer than the pipe, *dc* is invariably larger than *Sm* and so r_{sd} is negative thereby indicating an incomplete ditch condition in Marston's analysis cases.

An equilibrium condition will be indicated when Equations 3, 4 and 6 are simultaneously satisfied. Equations 3 and 4 correlate C_c, r_{sd} and H_e while r_{sd} and *dc* are correlated in equation 6. The Iowa formula can be used to determine *dc* for a given value of W_c which is a function of C_c. The resulting values of *dc* and W_c are of interest to the designer of the leachate collection pipes.

STEP BY STEP PROCEDURE

As mentioned previously, the load on the pipe as well as pipe deflection can be obtained through simultaneous solution of equations 3, 4, and 6. Equation 4 contains the term r_{sd} which is a function of *dc*, the pipe deflection. Evidently, the deflection of the pipe depends on the load on the pipe which can be obtained by the use of equations 2 and 3. It must be noted that both equations 3 and 4 contain the term H_e, the height of the plane of equal settlement. Therefore, it is possible to initiate a trial and error solution by assuming a value of H_e. It is also possible to initiate the process by assuming a value of r_{sd}. The latter method was proposed here because recommended design values of the settlement ratio r_{sd} have been used in the past (Spangler and Handy,1982). A step by step procedure is enumerated below.

Step 1
Assume a value of settlement ratio r_{sd}

Step 2
Calculate the value of *Sm* based on the estimated vertical stress at the level of the pipe and the deformation modulus E of the PZB. (*Sm* may be estimated in a number of

ways, but a simplified procedure is illustrated in Step 2 of the Analysis of the Case Study which follows.)

Step 3
Using the assumed value of r_{sd} and the calculated value of *Sm*, enter equation 6 and determine pipe shortening *dc*.

Step 4
Substitute the calculated values of *dc* for Δx in Equation 1 and calculate W_c using equation 1. Since Iowa formula is widely used, appropriate parameters for this equation can readily be determined (for example, Goddard, 1983). It is suggested that for the present, the soil modulus values be obtained from available literature on pipes under shallow burials. Future research may dictate changes in this value.

Step 5
Using equation 2 and W_c, calculate C_c

Step 6
Using equation 3 and C_c, calculate $\frac{H_e}{B_c}$

Step 7
Verify whether equation 4 is satisfied by using the calculated value of $\frac{H_e}{B_c}$ and assumed value of r_{sd}. If not, assume another value of r_{sd} and repeat steps 1 through 7. When Equation 4 is satisfied, both the pipe deflection and load on the pipe are available.

Step 8

Verify that the PZB extends to a minimum height of H_e above the crest of the pipe. This condition is required based on the assumptions of this approach.

Step 9

Once the load on the pipe is known, the compressive stresses in the pipe wall and factor of safety against crushing can be calculated. Also the pipe deflections can be compared against the allowable design values.

ANALYSIS OF CASE STUDY

Use of the proposed deflection analysis for the case of pipes under large depth of burial, is demonstrated here by analyzing the field test conducted in Pittsburgh for which the observations are reported by Hashash and Selig (1989, 1990) and Goddard (1991).

This test data was used for demonstration because, as far as is known, this is the only test data on an instrumented plastic pipe placed at a large depth.

A 0.61 m (24-inch) diameter corrugated polyethylene pipe was installed in a trench 1.52 m (5 feet) deep and 1.52 to 1.83 m (5 to 6 feet) wide at the base of a 30.48 m (100 feet) high embankment.

The backfill consisted of 1.07 m (3.5 feet) of structural fill (granular soil with a maximum of 5 percent passing U.S. sieve No. 100 and maximum grain size of 38 mm, i.e., 1.5 in.) and the rest CL material which was the material the embankment was made of. The pipe and the surrounding zone was well instrumented to monitor horizontal and vertical soil pressure on the pipe, free-field soil strain, pipe strain, pipe wall strain at various locations, pipe wall circumferential compression and change in pipe diameter.

From a design standpoint, the most important observation was that at a geostatic stress of 661 kPa (96 psi) due to 30.48 m (100 feet) soil at a unit weight of 21.7 kN/m^3 (138 pcf), the shortening of the vertical axis of the pipe was about 4.3 percent of the pipe diameter. The load on the pipe was measured as 151 kPa (22 psi). Following is an example analysis of pipe deflection for the above described case study using the approach proposed in this paper. In order to perform an analysis of the test data, certain assumptions have to be made. These are identified when they are used for the first time in the example.

Step 1
Assume settlement ratio r_{sd} = - 1.73

Step 2
Calculate *Sm*
Vertical stress = 661 kPa = 96 psi (test data)
Deformation modulus E_s = 47.88 MPa = 1 x 10^6 psf (conservatively assumed based on E_s = 732.6 MPa = 15.3 x 10^6 psf at low strains for PZB and 23.9 to 38.3 MPa ((0.5×10^6 to 0.8×10^6 psf) for embankment material from published data).

Mean pipe diameter = 0.654 m (25.75 in.)

$$Sm = \frac{(vertical\ stress)(mean\ pipe\ diameter)}{E_s}$$
$$= 9.04\ mm\ (0.356\ in.)$$

Step 3
Calculate *dc*

$$dc = Sm\ (1 - r_{sd})$$
$$= 0.356\ (1 + 1.73) = 24.68\ mm\ (0.972\ in.)$$

Step 4

Use Iowa formula to calculate W_c

$$W_c = \frac{d_e}{(DL)\,k}\left(\frac{EI}{r^3} + 0.061\,E'\right)$$

Use

DL = 1.5 (assumed)
k = 0.1 (assumed)
E = 75.8 MPa (11,000 psi)(manufacturer's data)
I = 1901 mm^4/mm (0.116 in^4/in)(manufacturer's data)
E' = 13.8 MPa (2,000 psi)(assumed)
r = .328 m (12.9 in)

W_c = 138.5 kN/m (791 pounds/in)

It may be noted that all assumed values are conservative values, i.e., those likely to produce larger calculated pipe deformation.

Step 5

Calculate C_c

$$C_c = \frac{W_c}{\gamma\,B_c^{\,2}}$$

γ = 21.7 *kN/m*^{3} (138 *pcf*) (*test data*)
B_c = 0.654 *m* (25.75 *in.*)
$\therefore C_c$ = 14.94

Step 6

$$C_c = \frac{e^{-2k\mu\left(\frac{H_e}{B_c}\right)}-1}{-2k\mu} + \left(\frac{H}{B_c} - \frac{H_e}{B_c}\right) e^{-2k\mu\left(\frac{H_e}{B_c}\right)}$$

Assume kμ = 0.13 (Spangler and Handy, 1982)

$$\frac{H}{B_c} = \frac{100(12)}{25.75} = 46.6$$

By trial and error $\frac{H_e}{B_c}$ = 4.74

Step 7

Substitute $\frac{H_e}{B_c}$ in equation 4, use p = 1

Left Hand Side of equation (LHS) = 95.2
Right Hand Side of equation (RHS) = 80.618

Since RHS ≠ LHS, assumed value of r_{sd} = -1.73 needs to be changed. For the second trial, assume r_{sd} = -1.9.

By following Steps 1 through 7, it is found that Equation 4 is satisfied i.e., r_{sd} is equal to -1.9. For this case:

W_c is calculated as 147 kN/m (840.2 lb/in) or 231 kPa (32.63 psi)

Observed load on the pipe = 151.7 kPa (22 psi)

$\frac{H_e}{B_c}$ is calculated as 4.46 and *dc* or pipe deflection is calculated as 26 mm (1.03 in.) or 4 percent (observed = 4.8 percent)

Thus, it is seen that the load on the pipe is over-predicted and the pipe deflection is under-predicted, but both are within acceptable limits.

Step 8

The example above showed $\frac{H_e}{B_c}$ to be 4.46 or in other words, the stress transfer from the pipe to the soil on the sides took place due to shear resistance developed for a length of (4.46)(0.654) = 2.92 m (115 inches). The plane of equal settlement is within the embankment, thus obtaining incomplete ditch conditions assumed in the approach proposed in this paper.

CONCLUSIONS

A method which is simple is described for design of flexible pipes under high landfills. Analysis of a field test has been carried out to demonstrate the deflection analysis capabilities of the method for deep burials. Designers of landfills, who are required to demonstrate the adequacy of their leachate collection pipe design can use the approach to justify the use of plastic pipes under tall landfills. Additional research in terms of field measurements and/or comparison with more sophisticated but expensive numerical techniques to analyze differing field conditions are necessary to evaluate this approach more fully.

REFERENCES

Goddard, J.B. (1983) "Structural Design of Plastic Pipes" Support Document presented to AASHTO Flexible Pipe Committee, March.

Goddard, J.B. (1991) "The Structural Performance of Polyethylene Pipe" Geotechnical Fabrics Report, September.

Hashash, N. and Selig, E.T. (1989) "Results of Field Measurements on Polyethylene Pipe Taken in July 1989" Department of Civil Engineering, University of Massachusetts, November.

Hashash, N. and Selig, E.T. (1990) "Analysis of the Performance of a Buried High Density Polyethylene Pipe" Proceedings Conference on Flexible Pipes Columbus, Ohio, October.

Spangler, M.G. and Handy, R.L. (1982) "Soil Engineering, Fourth Edition," Harper & Row, New York.

Watkins, R.K. (1990) "Plastic Pipes Under High Landfills" Buried Plastic Pipe Technology, ASTM STP 1093. Buczala, G.S. and Cassady, M.J. Ed. American Society of Testing and Materials, Philadelphia.

Finite Element Analysis of Stability of Cover Soil on Geomembrane-Lined Slopes

R.F. Wilson-Fahmy
Geosynthetic Research Institute, Drexel University, USA

R.M. Koerner
Geosynthetic Research Institute, Drexel University, USA

ABSTRACT

This paper is focused on the development of a plane strain finite element analysis for the purpose of studying the stability of nonreinforced and reinforced cover soils on geomembrane lined slopes. Various types of elements are used in the analysis including continuum elements, line elements and interface elements to represent soil, geosynthetics and interface friction respectively. In the analysis, the cover soil can be applied in an incremental manner and in various configurations in order to simulate the actual construction sequence. Nonlinear stress-strain relationships of the various system components are simulated using hyperbolic and polynomial formulations. Results obtained using the finite element procedure are compared with those computed using limit equilibrium techniques. They indicate that failure heights predicted using both methods are in reasonable agreement. The finite element method, however, provides significant insight to deformation behavior throughout the loading process. The presence of a geosynthetic reinforcement layer on top of the liner is shown to improve the stability of the cover soil. The degree of improvement is a function of the reinforcement load-extension modulus and is quantified via the program for a given example problem.

INTRODUCTION

Soil covering on geomembrane lined slopes has undergone slumping and stability failure in a number of instances (Boschuk, 1991). This is often due to the relatively low interface friction between the covering soil and the underlying geomembrane. Where stability is questionable, a layer of geogrid or geotextile reinforcement is often placed on top of the liner system which by virtue of its high-modulus provides an additional stabilizing component. Two landfill liner configurations, which are also used in landfill caps, are illustrated in Figure 1. It should be noted, however, that this same situation can also occur in a number of geotechnical and transportation engineering applications, e.g., in geomembrane lined earth dams and highway slopes.

Current design methods which consider the stability of the cover soil are based on

simplified limit equilibrium wedge type of analyses. Tension is assumed to develop in the geosynthetic elements based on static equilibrium and the available frictional resistance at the interfaces between the layers. Because strain compatibility is overlooked in these types of analyses, they may or may not lead to conservative design. Clearly, they cannot predict any behavior up to the time of incipient failure. This is not the case, however, with the finite element method which allows for strain compatibility between the various system components. This, in addition to the ability to model construction sequence and nonlinear material properties, make the finite element method appealing in dealing with the stability of multiliner geosynthetic systems.

The finite element method is used in this paper to study the stability of cover soils on geomembrane lined slopes. After development of the model, two examples are presented to demonstrate the method's capability. The first shows how the finite element results compare to limit equilibrium predictions. The second example investigates the effect of geosynthetic reinforcement on the system stability.

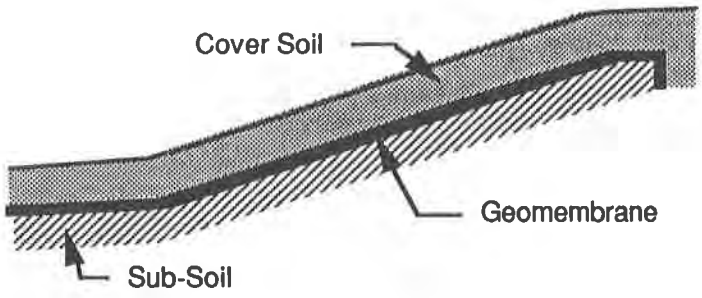

(a) Liner with Soil above Geomembrane

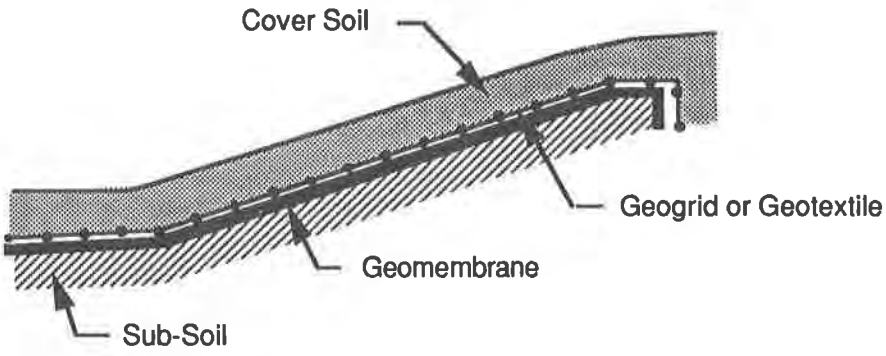

(b) Liner with Geosynthetic Reinforcement above Geomembrane

Fig. 1 Geomembrane Liner With and Without Geosynthetic Reinforcement

FINITE ELEMENT ANALYSIS

The literature is replete with cases in which the finite element method has been used to study soil - geosynthetic interaction in various applications. It was suggested for use on this problem by Boschuk (1991). Details of the different finite element modeling techniques can be found in many publications (e.g., Andrawes et al, 1982, Rowe et al, 1984 and Mylleville and Rowe, 1991). Only a brief description of the method used herein is given below. This particular finite element program has been developed using a 386 IBM compatible computer.

Finite Element Configuration

Figure 2 shows the discretization scheme used in the finite element analysis. As can be seen, various types of elements are used. The cover soil is represented by quadrilateral elements with each element consisting of four constant strain triangular elements. The sub-soil is considered stationary in the finite element formulation. However, shearing of the soil can be accounted for in the shear stress-displacement behavior of the interface elements connecting the bottom geosynthetic to the soil.

The geomembrane liner is represented by line elements which only provide in-plane tensile resistance (i.e. no bending stiffness). Geogrid or geotextile reinforcement, if any, is treated in the same manner. Spring elements are used to simulate soil / geomembrane interfaces by allowing relative displacement parallel to the side slope while preventing relative movement in the perpendicular direction. In order to avoid numerical errors arising from the inclination of the spring elements, the axes of the finite element mesh are rotated such the side slope becomes the horizontal axis (x-axis) before carrying out the finite element analysis.

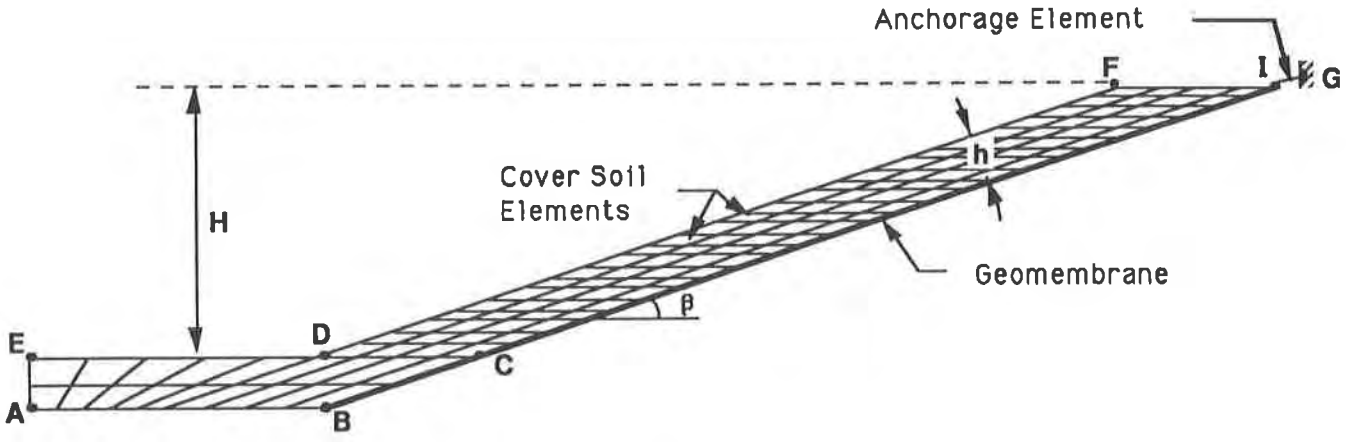

Fig. 2 Finite Element Configuration

Anchorage of the geomembrane at the top of the slope is simulated by a line element parallel to the side slope and connected to a fixed point (point G in Figure 2) above the slope. This assumption does not contradict the fact that in actuality the geomembrane is laid horizontal from the top of the slope to the anchor trench where it bends to become vertical. In determining the anchorage capacity of geomembranes, it is customary to assume the presence of imaginary frictionless pulleys at each change in the geomembrane direction, thus implying no effect of the geomembrane inclination on the mobilized force.

Material Properties

(i) Cover Soil

The finite element program allows for nonlinear stress-strain behavior of the cover soil using the hyperbolic formulation of Duncan and Chang (1970). Elastic-plastic stress-strain curves can also be modeled using the appropriate constants in the hyperbolic formulation. It should be cautioned, however, that the stress-strain properties may be difficult to obtain at the low stress levels involved in cover soil. Furthermore, the failure criterion in the hyperbolic formulation is based on triaxial test results which, for the stress-strain conditions of the cover soil, may not be appropriate. It may be noted that in treating infinite slopes, failure is assumed to occur when the shear stress on a plane parallel to the slope is equal to or greater than the shearing resistance along this plane. It appears that this failure criterion is more adequate for the cover soil than one that considers the critical state of stresses in all directions as implied by the hyperbolic formulation.

This paper concludes with two examples to demonstrate the capability of this particular finite element procedure. In the analysis, the failure criterion is taken as described above for infinite slopes except at the bottom of the slope where failure is also governed by shearing on any plane in the soil element which satisfies the Mohr-Coulomb failure criteria.

(ii) Geosynthetics

Load-extension curves of geosynthetics are represented in the finite element program in a polynomial form, thus allowing for nonlinear behavior. Since the plane strain condition is representative of most cases of cover soil stability, it is logical to determine these load-extension properties using wide width tests. Because the stress-strain behavior of some geosynthetics is likely to be affected by confinement, it further seems appropriate to use confined wide width test data in the finite element analysis for these materials. Various geosynthetics used in liner systems are currently being tested at the Geosynthetic Research Institute, Drexel University, to investigate their behavior in-isolation and under confinement.

It should be mentioned that standardized wide width tension tests differ depending on the type of geosynthetic. For example, ASTM D4595 test method specifies that geotextiles be tested at a rate of strain of approximately 10% per minute. There is no specific test method focused on geogrids, however, a modified form of the geotextile test method is generally used. On the other hand, the testing rate of geomembranes is about 1% per minute according to the ASTM D4885 test method. This method, however, allows for faster rates to simulate fast loading conditions in

the field. It seems logical to use the same rate of strain for all geosynthetics involved in a particular multiliner system. The choice of a representative rate of strain should be based on whether short-term or long-term conditions are investigated. Furthermore, where long-term stability is considered, creep and stress relaxation data may be required to characterize the material behavior. Thus, rather than following the ASTM protocol blindly, the designer should attempt to simulate site specific conditions as closely as possible.

In addition to the above data, pullout test data will be required to determine the anchorage behavior of the geosynthetic layers. Pullout tests representative of the actual field conditions can be carried out for this purpose. In the finite element idealization, the length of an anchorage element is taken equal to 0.30 m (1 ft). As shown in Figure 2, the anchorage element is treated as a line element with its top end prevented from movement. By assuming that the pullout load-displacement curve results from the extension of a 0.3 m length of the material, a fictitious load-extension curve can be established which would yield the same response to load as the actual anchored geosynthetic.

(iii) Interface Friction

The hyperbolic formulation was also used to model the relationship between shear stress and relative displacement at the interface between two geosynthetics or between soil and geosynthetic. The method is described by Clough and Duncan (1971).

It should be recognized that interface friction is a major factor in the stability of the liner system and, hence, great care should be excercised in measuring it. Interface angles of friction published in the literature should not be used unless verified by accurate testing. It is recommended that large shear box tests (300 mm x 300 mm) be used for this purpose.

All interfaces should be evaluated in their anticipated moisture states and conditions and under appropriate normal stresses. Again the rate of testing should be chosen based on expected field conditions and whether short-term or long-term conditions are to be evaluated.

LOADS

Cover soil is placed on the side slope by spreading and compacting the soil from bottom to top. In the finite element analysis, construction is simulated by activating the self weight of the newly placed cover soil layer. For example, in Figure 2, there are 25 soil layers above the horizontal cover soil. If each layer represents a soil lift, the program considers the effect of the self weight of each layer one at a time starting from the bottom layer upwards. All soil elements above the specific applied soil lift are not included in the finite element analysis. A soil lift may consist of two or more finite element layers depending on the height of the soil element and the thickness of the soil lift. For improved accuracy, the self weight of each soil lift is applied in four equal increments. The moduli of the soil, geosynthetic and interface elements are updated after each increment in order to accurately follow their stress-strain response. Thus, for the finite element mesh given in Figure 2, the program will run 100 times if the soil is placed in 25 soil lifts. Variations to this construction sequence can be also modeled depending on the actual field conditions.

Construction equipment moving on the slope are represented in the finite element analysis by nodal loads acting on the face of the cover soil. Because the finite element program deals only with plane strain conditions, the three-dimensional loading due to the weights of such equipment must be approximated in an appropriate manner.

TYPICAL FINITE ELEMENT RESULTS

Two hypothetical examples using this finite element program are presented below. The first considers the stability of cover soil above a geomembrane for different interface friction angles while the second investigates the beneficial effect of a geogrid or geotextile reinforcement over the geomembrane liner. The assumptions used in these examples have been arbitrarily chosen to highlight the effect of one or more of the parameters involved in the stability of cover soil on geomembrane lined slopes. Therefore, the results should be viewed in association with these assumptions.

Example 1

Consider the case shown in Figure 3 where cover soil is placed directly on a geomembrane at a slope angle of 18.4^{o} (i.e., 3 to 1 slope) with a maximum height of 12 m. It is required to determine the stability of the cover soil as it progresses up the slope for different interface angles of friction. The data used in the finite element analysis are given in Figure 3.

The cover soil is assumed to be cohesionless with an angle of shearing resistance equal to 32^{o}. For simplicity, the stress-strain curve of the soil is assumed to follow an idealized elastic-plastic behavior and to have a Poisson's ratio of 0.3. The modulus E_s is assumed to be independent of the minor principal stress σ_3 as indicated in Figure 3. The material constants are chosen to give adequate levels of deformation. In order to limit the variables involved, the soil elements in the zone below line CDE (see Figure 3) have been assigned high angles of shearing resistance to force failure to occur in the cover soil on or above this line. Also, this allows comparison with limit equilibrium techniques which are based on similar assumptions.

For smooth behavior at the interfaces, the shear stress - relative displacement relationships are assumed to be hyperbolic and dependent on the magnitude of the normal stresses. In all cases considered, the top and bottom interface friction angles are taken equal in magnitude.

The load-extension curve of the geomembrane is assumed to follow an elastic-plastic response. The load-extension modulus used in the analysis is of the same order of magnitude of that of HDPE geomembranes. Other geomembranes can readily be simulated by other modulus values.

Construction is assumed to be carried out in lifts with each lift represented by a row of finite elements. This procedure is advantageous in that the failure height can be detected from the

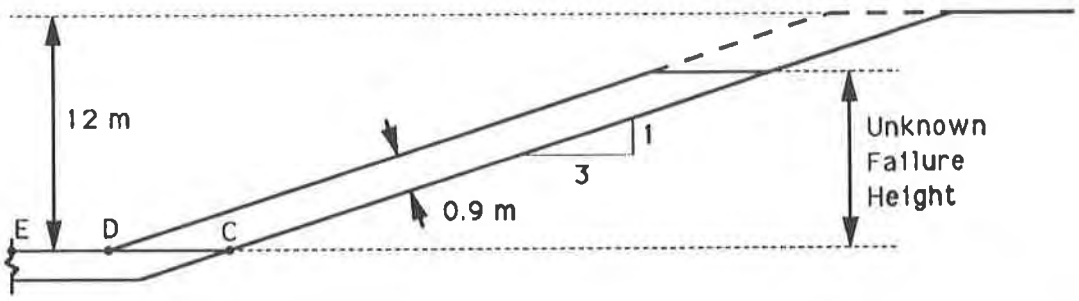

(a) Geometry

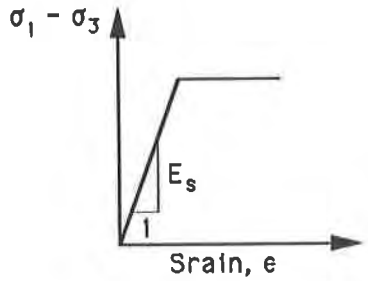

$E_s = K P_a (\sigma_3/P_a)^n$
P_a = atmospheric pressure
= 101.3 kN/m^2
K = 45
n = 0

(i) Soil

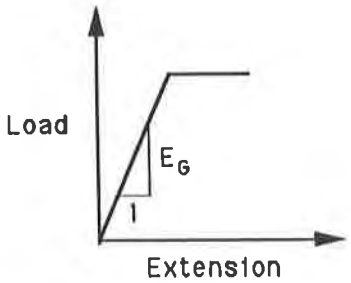

E_G = 350 kN/m

(ii) Geomembrane

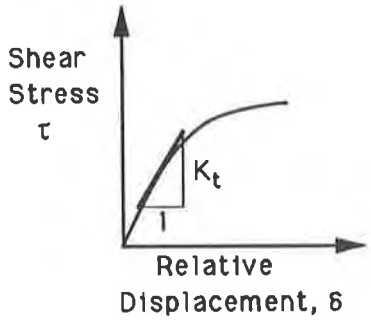

$K_t = [1 - (R_f \tau)/(\sigma_n \tan\delta)]^2 K_1 P_a (\sigma_n/P_a)^m$
σ_n = normal stress
R_f = 0.9
K_1 = 1300
m = 1

(iii) Interface Friction

(b) Material Properties

Fig. 3 Data for Example 1

output data after the addition of each layer. It should be recognized, however, that this is an idealized simulation of the construction sequence. In the field, the process of placing soil on the side slope starting from the bottom upwards may initially involve an irregularly tapered soil condition.

Utilizing the finite element program for a sequential series of deformations gives a single curve such as that represented by a "δ" value of 10°. Using a series of different "δ" values gives the series of curves shown in Figure 4. The relationship between the construction height and the maximum displacement experienced by the cover soil is in a direction parallel to the side slope. In general, the maximum displacement occurs at or close to the interface with the liner at a height ranging between 40% to 50% of the cover soil height. It can be seen that in all cases, except for the cases of the interface angles of friction of 20° and 24°, the displacement increases gradually up to a certain soil height where instability starts to increase dramatically. This soil height corresponds approximately to the development of failure of the cover soil as depicted from the finite element stress results.

Failure always initiates at the bottom row of elements above line CD (see Figures 2 and 3). It is characterized by failure of one element followed by another until all the elements in the row reach their ultimate strengths. Complete failure will be assumed to occur at this point. This failure mode substantiates the mechanism postulated in limit equilibrium techniques which involves sliding of the cover soil over the horizontal interface at the bottom of the slope (line CD in Figure 3). The height corresponding to the first sign of failure and that corresponding to failure of all the elements in the bottom row are plotted against the interface angle of friction in Figure 5. The failure heights predicted using the limit equilibrium method of Koerner and Hwu (1991) for a factor of safety of 1.0 and adapted to account for a level soil at the top of the slope are also shown in Figures 4 and 5. Similar values are predicted by the method of Giroud and Beech (1989). Both Figures 4 and 5 indicate good agreement between the finite element model at failure and limit equilibrium methods.

The finite element results show that stability can be greatly enhanced by using high friction liner materials such as textured geomembranes (see curves at 20° and 24° in Figure 4). However, these results are for equal interface friction angles above and below the liner. If the bottom interface is weaker than the top interface and the geomembrane has a low load-extension modulus, it can be readily assumed that stability will be governed by the lowest interface friction. On the other hand, a high-modulus geomembrane will provide an additional restraining effect, thereby improving overall stability but at the risk of tension failure of the geomembrane. Alternatively, a stabilizing effect can also be provided by placing a high-modulus geosynthetic reinforcement over the geomembrane as discussed in the example below.

Example 2

Using the same cover soil in Example 1, we now determine the effect on stability of a geosynthetic reinforcement placed above the geomembrane. Consider two reinforcement materials, one with a load-extension modulus of 1000 kN/m and the other with a higher modulus of 2000 kN/m. In all cases, assume that the interface angle of friction is 16° above and below the

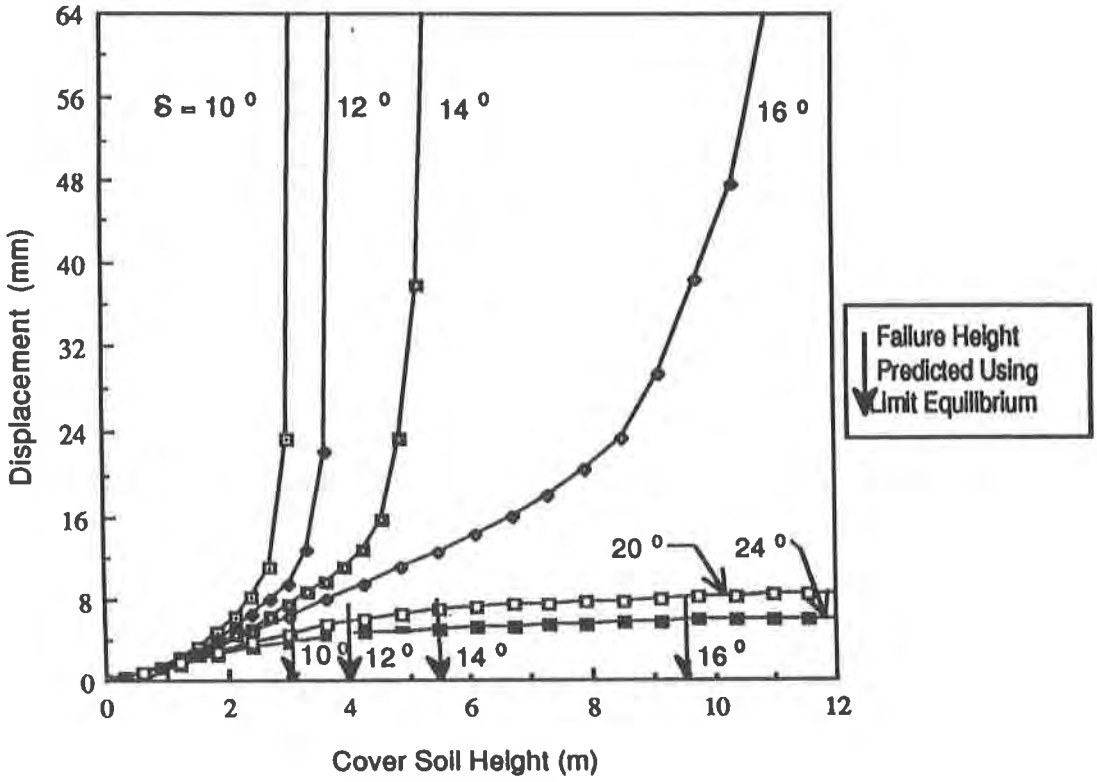

Fig. 4 Relationship between Cover Soil Height and Maximum Displacement (shown as curves) and Correlation to Limit Equilibrium (shown as arrows) (Note that the soil slope is at 18.4)

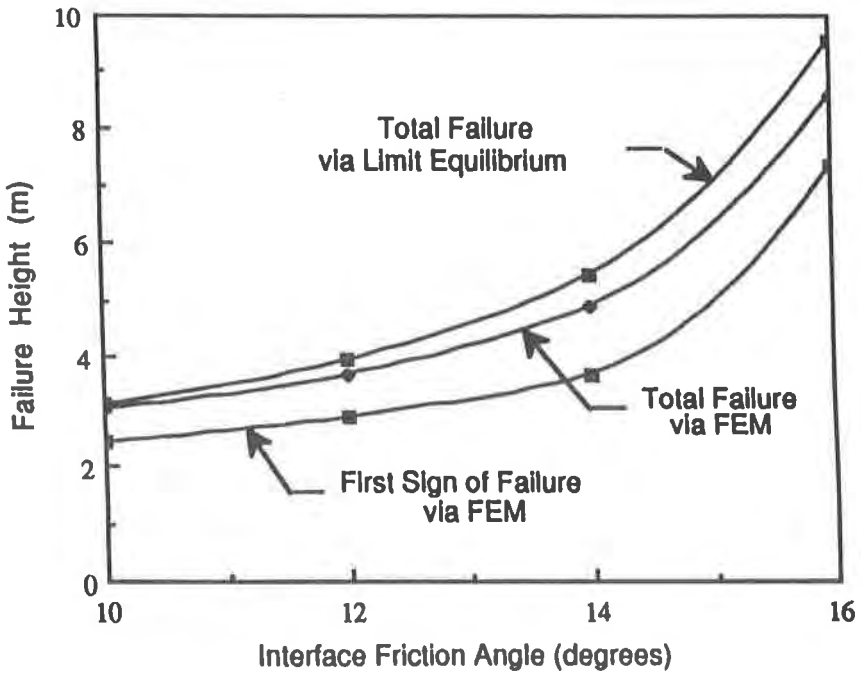

Fig. 5 Prediction of Failure Heights by Various Methods

liner. Hence, comparison can be made with the case already investigated in Example 1 of a geomembrane with an interface angle of friction equal to 16° which was seen to fail at a height of 8.5 m (recall Figure 5). For the interface between the reinforcement and the cover soil, assume an angle of 32° which is equal to the angle of shearing resistance of the soil.

Figure 6 shows the predicted relationship between the soil height and the maximum displacement experienced by the cover soil with and without reinforcement. The geomembrane alone shows a subtle change in slope at a certain point on the curve. As already mentioned, this point is indicative of instability. On the other hand, the displacement is shown to increase in a more gradual manner up to the maximum cover height when reinforcement is used. The fact that, over part of the curve, the weaker reinforcement shows a slightly greater displacement compared to that in the case of the geomembrane alone is due to the presence of three interfaces in the former case compared to two in the latter case. Relative displacement mobilized at the additional interface provides an extra displacement component. The less extensible the reinforcement is, the more restraint will be imposed on overall displacement.

A better illustration of the effect of reinforcement is given in Figure 7 which displays the height of cover soil corresponding to the first local failure and to complete failure for both the reinforced and unreinforced cover soils. Both reinforcement materials are shown to delay local and total failure. However, in general, the stronger reinforcement has a greater stabilizing effect than the weaker reinforcement. As seen in Figure 6, no complete failure is detected for the stronger reinforcement up to the maximum cover soil height of 12 m. This suggests that the load-extension modulus of the reinforcement is an important consideration in checking the stability of the cover soil. Note that modulus is not accounted for in limit equilibrium techniques. Its importance, however, was emphasized by Giroud and Beech (1989) who arbitrarily imposed a limit on the amount of strain in the reinforcement material.

The maximum tension force developing in the geosynthetic sheets during construction of the cover soil and up to failure is plotted against soil height in Figure 8 for the cases with and without reinforcement. It can be seen that the presence of the reinforcement reduces the tension transmitted to the geomembrane liner. However, in general, the tension in the geomembrane is much smaller compared to that taken by the reinforcement. Note that the tension in the reinforcement increases with the cover soil height in a highly nonlinear manner. For example, at half the maximum height the tension force is equal to about 15% of that at full height.

Although not shown, the finite element predictions indicate that at maximum height of the cover soil, only the top half length of the reinforcement is subjected to tension while the other bottom half is not carrying any load. This suggests that a shorter length of the reinforcement may achieve the same effect as a reinforcement extending over the full length of the side slope.

It should be recognized that the degree of improvement provided by reinforcement is dependent on various factors including thickness, height and properties of the cover soil, frictional behavior of the interfaces involved and load-extension properties of the geosynthetics in the liner system including its reinforcement. Therefore, the results given in Figures 6, 7 and 8 should be viewed only in terms of the geometry and material properties assumed in the example.

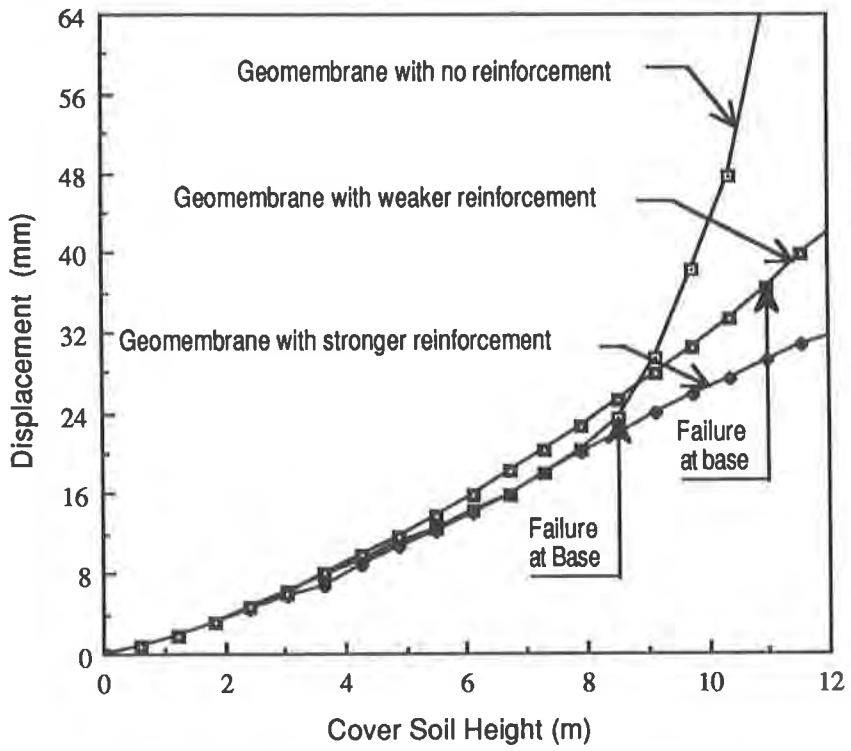

Fig. 6 Relationship between Maximum Displacement and Height of Cover Soil with and without Reinforcement

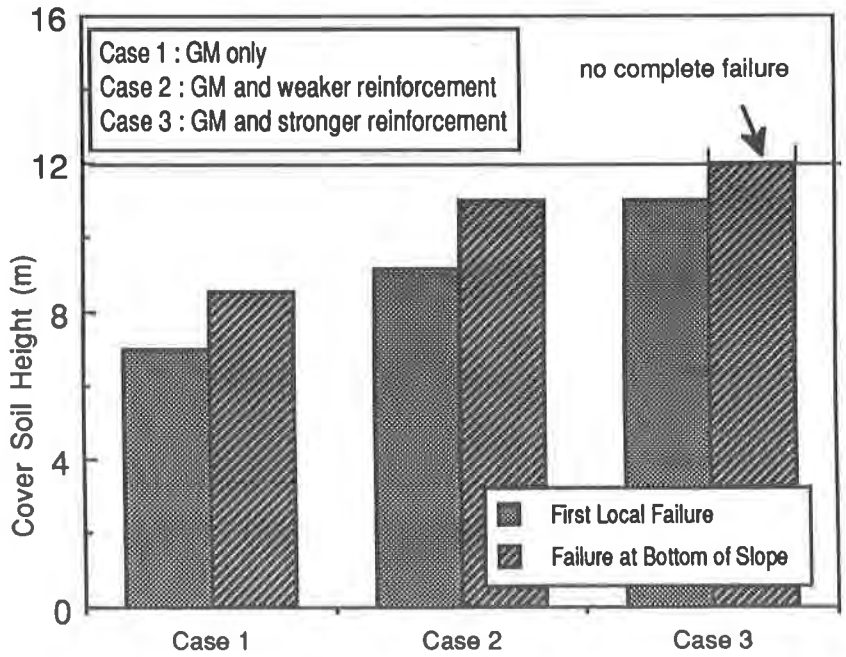

Fig. 7 Effect of Geosynthetic Reinforcement on Failure Height

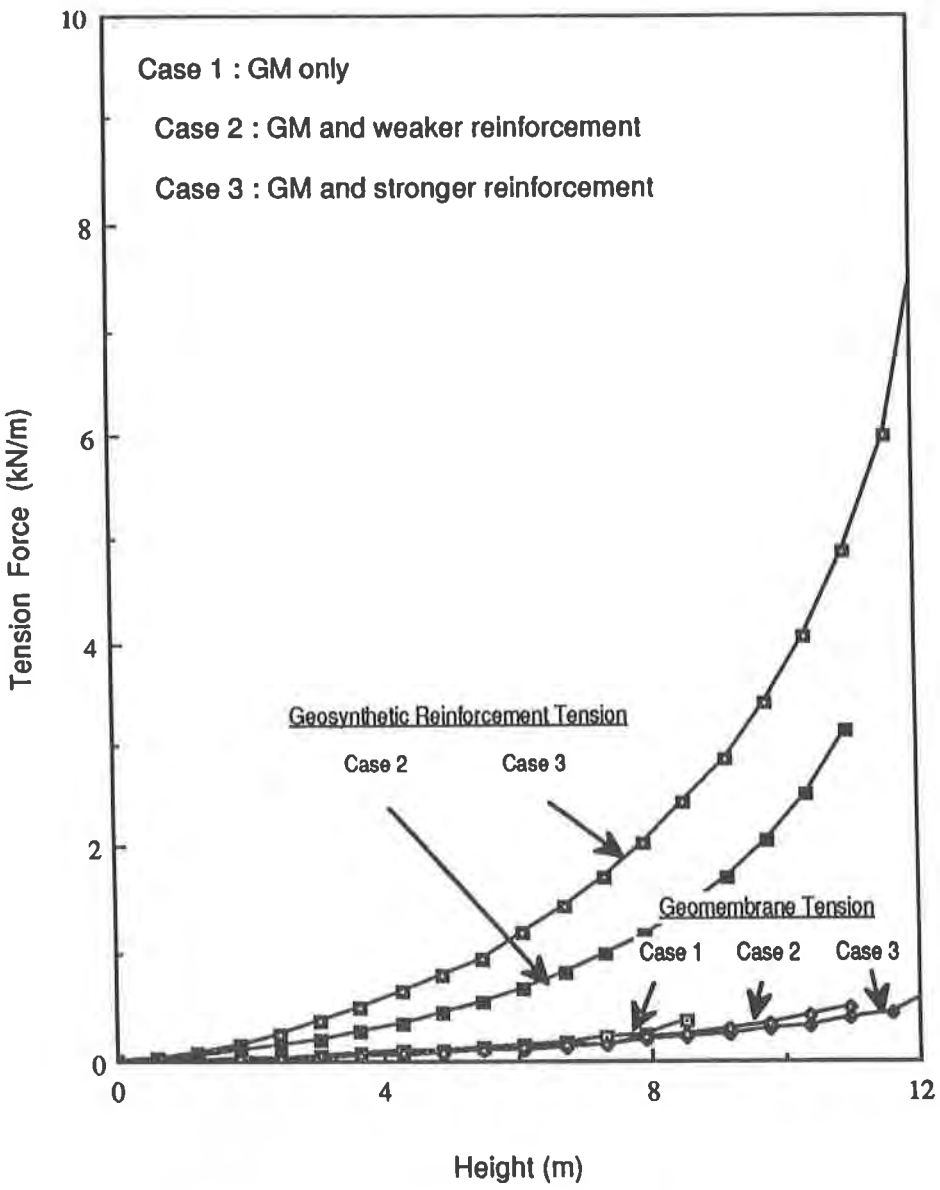

Fig. 8 Variation of Tension Force in both the Reinforcement and the Geomembrane with Cover Soil Height

CONCLUSIONS

A finite element procedure is presented for the analysis of the stability of cover soil on gemembrane lined slopes. The method allows for nonlinear material properties and incremental construction loading. Two examples are presented which illustrate the use of the technique. The first example demonstrates the effectiveness of the method in predicting the height of the cover soil at incipient failure. Results show that failure heights determined with the aid of limit equilibrium methods agree reasonably well with those predicted using finite element analyses. The second example shows that geosynthetic reinforcement, geogrids or geotextiles, can be effective in delaying local failure and in increasing the stable height of the cover soil.

ACKNOWLEDGEMENTS

This study is part of the overall research and development efforts undertaken by the Geosynthetic Research Institute of Drexel University. Funding is by the 50 member organizations who form the consortium and to whom the authors express sincere appreciation.

REFERENCES

Andrawes, K.Z., McGown, A., Wilson-Fahmy, R.F. and Mashhour, M.M. (1982) "The finite element method of analysis applied to soil-geotextile systems", Proc. 2nd Int. Conf. on Geotextiles, Vol. 3, pp. 695 - 700.

Boschuk, J. (1991) "Landfill covers - an egineering perspective", Geotechnical Fabrics Report, Vol. 9, No. 2, pp. 23-34.

Clough, R.W. and Duncan, J.M. (1971) "Finite element analysis of retaining wall behavior", Jl. of Soil Mechanics and Foundation Engineering Div., ASCE, Vol. 97, SM12, pp. 1657-1673.

Duncan, J.M. and Chang, C.Y. (1970) "Non-linear analysis of stress and strain in soils", Jl. of Soil Mechanics and Foundation Engineering Div., ASCE, Vol. 96, SM5, pp 1629-1653.

Giroud, J.P. and Beech, J.F. (1989) "Stability of soil layers on geosynthetic lining systems", Proc.of Geosynthetics' 89, pp. 35-46.

Koerner, R.M. and Hwu, B.L. (1991) "Stability and tension considerations regarding cover soils on geomembrane lined slopes", Geotextiles and Geomembranes, Vol. 10, pp. 335-355.

Mylleville, B.L.J. and Rowe, R.K. (1991) "On the design of Reinforced Embankments on Soft Brittle Clays", Proc. of Geosynthetics' 91, Vol. 22, pp. 395-408.

Rowe, R.K., MacLean, M.D. and Soderman, K.L. (1984) "Analysis of a geotextile-reinforced embankment constructed on peat", Canadian Geotechnical Journal, Vol. 21, No. 3, pp. 563-576.

Design of Landfill Liners Over Yielding Foundations

R.R. Berg
Ryan R. Berg & Associates Inc., USA

J.G. Collin
Tensar Environmental Systems Inc., USA

ABSTRACT

A methodology which is currently used for the design of landfill liner systems over a potentially yielding foundation is reviewed. This methodology assumes axisymmetric deflection, a fixed geometry, strain limits based upon quick testing of the geomembrane, and use of geosynthetic reinforcement material to carry the entire tensile load. Limitations of this current design methodology are discussed, and a new design approach is presented. The proposed procedure is based upon definition of a long-term allowable tensile stress, and corresponding strain, in the geomembrane material. The proposed procedure is specifically applicable to low strain conditions where the geomembrane, and reinforcement as applicable, remain in their linear viscoelastic response range. Polyethylene geomembranes are specifically examined. Use of a geosynthetic reinforcing element is optional, though load carrying capacity may be significantly increased with a combination of geomembrane and reinforcement materials. Example calculations for design of liners over yielding foundations with the current methodology and with the proposed procedure are presented. Both liner systems with and without geosynthetic reinforcement are considered for the proposed procedure. The paper is directed toward practitioners and regulatory authorities.

INTRODUCTION

Landfills are normally designed to eliminate, or minimize, mobilization of tensile stresses in the liner components. However, tensile loadings may not be eliminated for applications where landfill liners are constructed over yielding foundations. Examples of yielding foundations include landfill construction over areas prone to sinkhole formation, mine subsidence, and earth fissures; lateral and vertical expansions of existing landfills; and settlement of landfill caps. Much of the work to date on development of design methodologies for these applications has focused on definition of geometric configuration and boundary loading

conditions. Viscoelastic material response of the geosynthetic liner system components under long-term loading are examined within this paper.

CURRENT DESIGN PRACTICE

Components. A typical cross section of a landfill liner system that may be constructed over a yielding foundation is shown in Figure 1. The primary function and performance of the geosynthetics relative to a deformed foundation are discussed below.

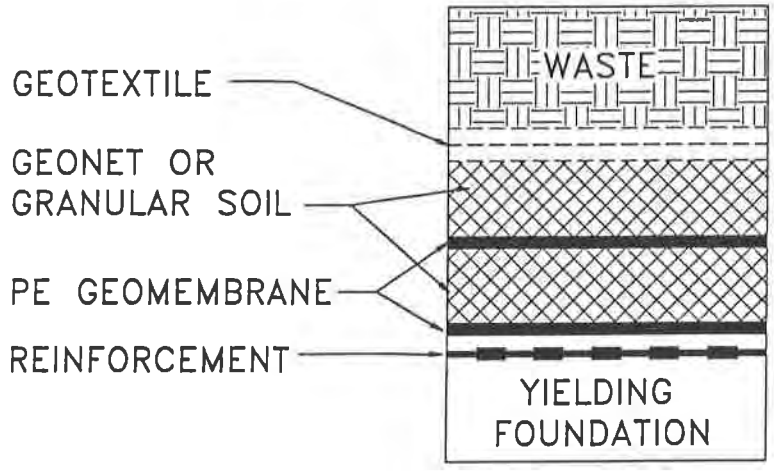

Figure 1. Typical Landfill Liner

The geotextile used for filtration is typically a light weight (eg., 200 g/m^2), nonwoven material. The geotextile is installed with adjacent rolls overlapped. It should be capable of conforming to deformations created by foundation settlements without impairing its function. Geonets used in landfills are typically 5 to 6 mm thick and manufactured of polyethylene. Geonets are usually installed with sides of adjacent rolls butted together and held in place with plastic ties. The geonets also should be capable of conforming to deformations without impairing their overall function of drainage, though localized drainage could be impaired if deformations occur directly beneath a butted seam and edges of adjacent rolls are separated.

Two polyethylene (PE) geomembranes, 1.5 to 2.5 mm (60 to 100 mil) thick, are typically used in the bottom of landfills. Adjacent panels of geomembranes are overlapped and joined by welding. In current design practice, it is assumed that deformations will not affect their function if strain in the geomembrane is below a *safe* limit. Geogrids (Tieman et al., 1990; Curtis and Butchko, 1991; Stephens and Bodner, 1991) and geotextiles (Parker and Paulson, 1993) have been added to landfill liner systems to support geomembranes where construction is over yielding or potentially yielding foundations soils. Roll ends of geogrids may be overlapped or mechanically joined. Edges of geogrid rolls may be butted or overlapped. Geotextile ends and edges may be joined by sewing or be overlapped. Grids and textiles are designed to maintain their reinforcement function over a deforming foundation.

Structural Properties. The current state-of-practice of designing lining systems over yielding foundations is documented by project examples (Tieman et al., 1990; Curtis and Butchko, 1991; Stephens and Bodner, 1991; Parker and Paulson, 1993). It is assumed that tensile load in the filtration textile and drainage net are negligible in addressing foundation settlements. This assumption implies that the textile and net strain, to the degree set by the membrane and/or reinforcement limitation, without substantial stress.

Membrane and reinforcement geosynthetics are then of specific concern in addressing performance over yielding foundations. Geomembranes are typically designed to a *safe* level of strain, and another geosynthetic component (reinforcement) is designed to carry the tensile load. Based upon the work of Giroud (1984), the present state of practice in the U.S. for design with PE geomembranes is to limit the allowable tensile strain to the short-term yield strain divided by a factor of safety. The yield strain is typically defined with use of American Society for Testing and Materials D 638, *"Standard Test Method for Tensile Properties of Plastics"* (ASTM, 1991). The safety factor applied to the yield strain is typically taken as 1.5 to 2. Thus with a range of yield strains of 10% to 15%, a *safe* strain level of 5% to 10% has been used in the projects cited above. This *safe* strain level is taken as the allowable long-term (i.e., design life) strain on the PE geomembrane.

The structural geosynthetic reinforcement component is designed at a tensile capacity defined at the *safe* strain value of the membrane. The structural capacity of the reinforcement may be defined with a partial factor of safety approach (e.g., Bonaparte and Berg, 1987a; Jewell and Greenwood, 1988; GRI, 1990, 1991, 1992; Koerner, 1990; Allen, 1991; Berg, 1992). Creep, installation damage, degradation, seams, and an overall safety factor for uncertainties are addressed in these procedures. A stress-strain relationship (i.e., isochronous curve) at a given time or design life is defined with these procedures. The limit state strain is then set equal to the *safe* geomembrane strain for lateral and vertical expansions.

Deformation Models. The state-of-practice, as defined by case histories (Tieman et al., 1990; Curtis and Butchko, 1991; Stephens and Bodner, 1991), is to utilize an axisymmetric deflection model. Diameters of 1.8 m and 2.4 m have been used for applications of lateral and vertical expansions of landfills. The basis for this diameter is not clearly documented.

Design. A common approach to design for lateral and vertical expansion applications is to use tension membrane theory, illustrated in Figure 2, and soil arching theory, illustrated in Figure 3, in conjunction with an axisymmetric deflection. It is assumed that the depression is a void, thereby suspending the geosynthetics between the depression edges. The geomembrane components of the lining system define the *safe* strain, but it is assumed that they carry zero tensile load. The reinforcement component of the lining system is then selected to carry the entire membrane tensile load at a strain compatible with the allowable *safe* strain of the geomembrane and at a time equal to the design life of the facility. Application of this design method for a landfill expansion application, with the deformation model and material properties noted above, is presented in Example Calculation # 1.

Use of tension membrane and arching theories has been documented by Giroud et al. (1990) and Bonaparte and Berg (1987b). Application of these theories to design of lateral and vertical expansion of landfills has been documented by Tieman et al. (1990) and Curtis and Butchko (1991).

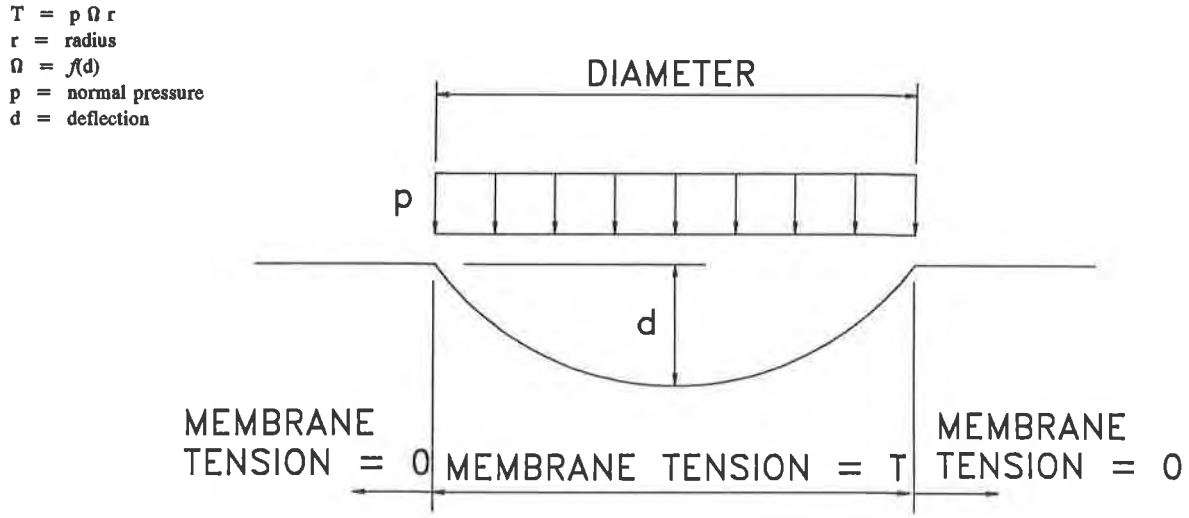

Figure 2. Tension Membrane

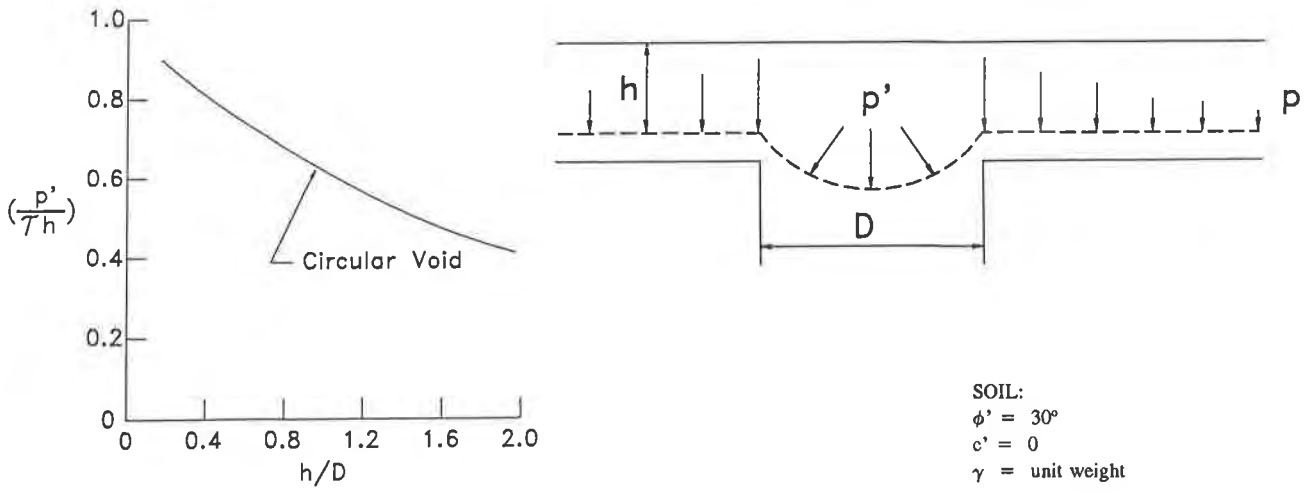

Figure 3. Soil Arching
(from Bonaparte and Berg, 1987b)

Example Calculation # 1. An example calculation for a lining system to be constructed over an existing landfill is presented below. The liner system consists of two 1.5 mm PE geomembranes, two geonets, one filtration geotextile, and a layer of geosynthetic reinforcement. Soil arching and tension membrane theories are used in computing the required reinforcement tension.

Assumptions:

- a 1.8 m diameter depression, or void, models possible foundation deformations
- liner system does not touch bottom of depression
- geomembranes are subject to a load-controlled boundary condition
- 30 m of waste will be placed above the lining system
- waste unit weight equals 10 kN/m^3
- yield strain of the PE geomembranes is 10 % (per ASTM D 638)
- a safety factor on yield strain of 2 is desired/required
- long-term tensile load in the geomembranes $\approx$ 0
- long-term tensile load in the geonets $\approx$ 0
- long-term tensile load in the filtration geotextile $\approx$ 0

Pressure, p, on the liner system computed with arching theory (equation from Giroud et al., 1990) is

$$p = 2 \gamma r (1 - e^{-0.5 H / r})$$

$$p = 2 \times 10\ kN/m^3 \times 0.9\ m \times (1 - e^{-15\ m\ /\ 0.9\ m})$$

$$p = 18\ kN/m^2$$

The safe design strain limit is

$$\epsilon_d = \frac{\epsilon_y}{2} = 5\ \%$$

Membrane tension, α, on the liner system (equation and Ω from Giroud et al., 1990) is

$$\alpha \approx p\ r\ \Omega$$

$$\Omega = 0.97 \quad for \quad \epsilon_d = 5\ \%$$

$$\alpha \approx 18\ kN/m^2 \times 0.9\ m \times 0.97$$

$$\alpha \approx 15.7\ kN/m$$

Therefore, a reinforcement geosynthetic with an isotropic long-term allowable strength of 15.7 kN/m at a strain of 5% is required.

Limitations. The primary function of these two types of geosynthetic materials, membranes and reinforcement, has led to dissimilar procedures for evaluating long-term

structural performance. The state-of-practice for establishing allowable stress (i.e., by definition of a *safe* strain) for PE geomembranes neglects to account for several important factors including time, temperature, exposure environment, presence of seams, and boundary loading or deformation conditions, as discussed by Berg and Bonaparte (1993).

Ideally, the procedure for establishing the allowable stress in geomembranes should account for all these factors and synergism between factors, particularly whether boundary conditions are load- or deformation-controlled. The procedure for geomembranes should be consistent with that used for the geosynthetic reinforcement component of the liner system. Long-term geomembrane tensile test requirements and a procedure for reduction of data to design parameters have recently been presented by Berg and Bonaparte (1993) for PE geomembranes subject to load-controlled boundary conditions.

PROPOSED DESIGN APPROACH

Procedures for design of liner systems are presented within. These procedures are applicable to any deformation model or geometry, and to any analytical technique. The procedures incorporate the mobilized tensile strength of the geomembrane and address systems without and with geosynthetic reinforcing elements. Two example calculations are presented for the landfill expansion examined in example calculation # 1.

Assumptions on which geosynthetic(s) contribute to structural support, deflection model, analytical procedure, and waste properties must be made by the designer. Long-term tensile properties of the membrane and reinforcement (if applicable) materials need to be defined with laboratory testing. Long-term allowable stress in the geomembrane may be quantified with the method presented by Berg and Bonaparte (1993), for PE geomembranes under load-controlled boundary conditions. This method should be modified for materials other than polyethylene and to model actual loading conditions. The long-term tensile strength of reinforcement should be quantified with one of several similar methods presented in the literature (e.g., Bonaparte and Berg, 1987a; Jewell and Greenwood, 1988; GRI, 1990, 1991, 1992; Koerner, 1990; Allen, 1991; Berg, 1992). Alternatively, the geosynthetic composite liner system, or those components significantly contributing to support, could be tested under assumed geometric and boundary loading conditions.

An assumption on the relationship of strain magnitudes of the geosynthetic components, which contribute to support, also must be made. Equal strains in the geosynthetic components carrying tensile load may be applicable if components are closely spaced, or if a large size deflection (eg., sinkholes) is assumed. Unequal strains may be applicable for geosynthetic components subject to a small size deflection (eg., 1.8 m diameter) that are separated by soil layers 0.3 m to 0.6 m thick. Strain magnitude in the geosynthetic components, for the case of unequal strains, may be estimated by scaling the assumed deflection model to the liner system geometry.

A factor of safety against rupture of the liner system must be defined by the designer. This factor should reflect judgement used in other assumptions, reliability of material properties, and consequences of rupture of the liner system.

Liner systems with geosynthetic reinforcement differ from the example without reinforcement in how the factor of safety against rupture is defined. The factor of safety against rupture for a system with only geomembranes carrying loads is dependent upon the rupture stress and safety factor against rupture of the geomembrane. The factor of safety against rupture of a liner system with reinforcement is dependent upon rupture stress of the geomembrane, the mobilized stress in the reinforcement at the rupture strain of the geomembrane, and the mobilized stress in the reinforcement at the working strain (i.e., at the allowable stress) of the geomembrane.

For example, the overall factor of safety against rupture of a PE geomembrane, subject to load-controlled boundary conditions, from Berg and Bonaparte (1993) is equal to:

$$FS = \frac{\sigma_r \; x \; FC \; x \; FW \; x \; FI}{\sigma_a} \qquad \textbf{Eq. (1)}$$

where

FS = overall factor of safety against rupture of the geomembrane (dimensionless);

σ_r = geomembrane rupture stress at the design life/temperature as illustrated in Figure 4 (N/mm^2);

FC = reduction factor to account for chemical (or radiation) degradation over the design life (dimensionless);

FW = reduction factor (i.e., weld factor) to account for long-term seam strength (dimensionless); and

FI = reduction factor to account for installation damage (dimensionless);

σ_a = geomembrane allowable long-term tensile stress at the design life/temperature as illustrated in Figure 4 (N/mm^2).

An overall factor of safety of 2 to 3 for PE geomembranes appears reasonable, as discussed by Berg and Bonaparte (1993). The factor of safety against liner system rupture is equal to the factor of safety against rupture of the geomembrane(s) when a geosynthetic reinforcement component is not included.

The overall factor of safety against rupture of a liner system which incorporates reinforcement elements may be defined as:

$$FS_{ls} = \frac{(\sigma_f \; x \; t_m \; x \; N) + T_{reinf}}{(\sigma_a \; x \; t_m \; x \; N)} \qquad \textbf{Eq. (2)}$$

where

N	=	number of geomembranes of equal thickness t_m (dimensionless);
FS_{ls}	=	factor of safety against rupture of the liner system (dimensionless);
σ_f	=	failure stress of the geomembrane at the design life and temperature (i.e., $\sigma_f = \sigma_r$ x FC x FW x FI, as illustrated in Figure 4) (N/mm^2);
t_m	=	minimum thickness of geomembrane(s) (mm); and
T_{reinf}	=	mobilized tension (σ_R x t_R) in the reinforcement element(s) at a strain compatible with σ_f (σ_R illustrated in Figure 5) (kN/m).

Assuming equal strain in geomembrane and reinforcement elements, the allowable tensile load, T_{ls}, in liner systems with and without reinforcement is:

(a) without reinforcement

$$T_{ls} = \sigma_a \; x \; t_m \; x \; N \qquad \textbf{Eq. (3)}$$

and

(b) with reinforcement

$$T_{ls} = (\sigma_a \; x \; t_m \; x \; N) + T_a \qquad \textbf{Eq. (4)}$$

where T_a equals mobilized tension in the reinforcement element(s) at a strain compatible with the mobilized tension in the geomembrane(s) (σ_{a2} or σ_{a3}), illustrated as ϵ_{a2} and ϵ_{a3} in Figure 5. In incorporating reinforcement and assuming strain compatibility at a time equal to the design life, it is inherently assumed that both the geomembrane(s) and reinforcement(s) remain within their linear viscoelastic limit. This assumption is justified by the low levels of initial and final strains anticipated.

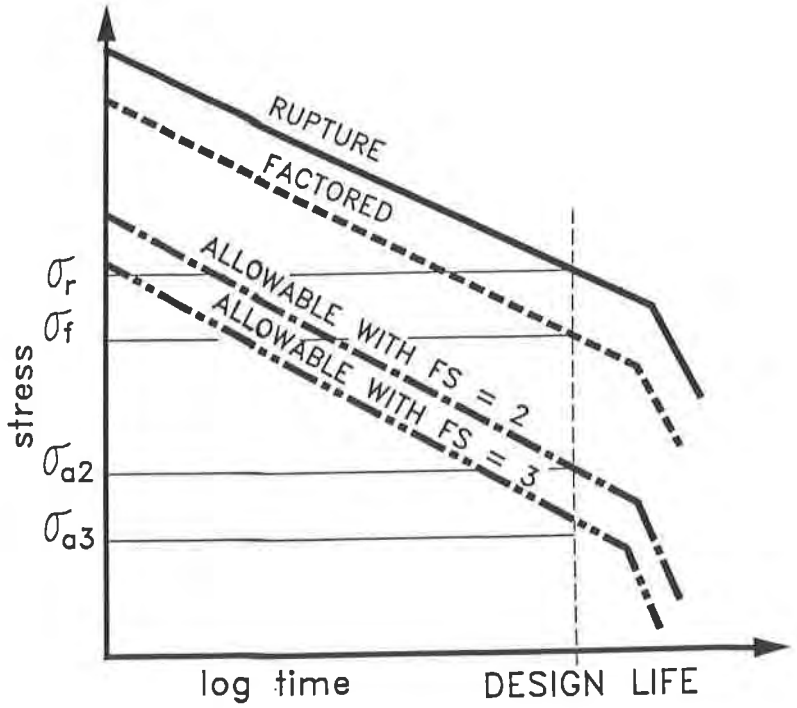

Figure 4. Geomembrane Rupture Lines

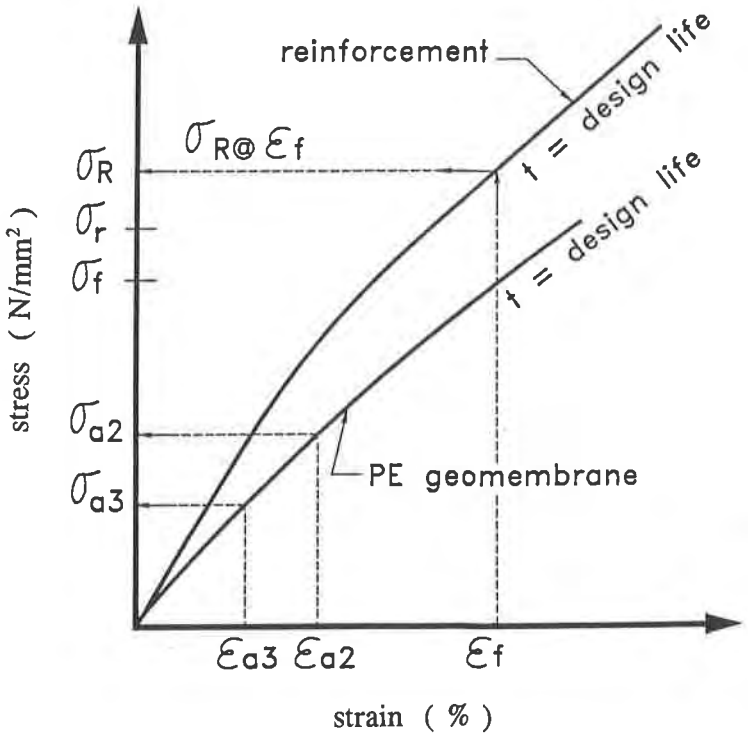

Figure 5. Isochronous Curves

The following example calculations are presented as an illustration, comparing the tensile load capacity of two liner systems, one without (example #2) and one with a reinforcement element (example #3). The relative performance difference between the two systems is quantified by using the same normal load, deflection model, and geomembrane partial safety factor assumptions in the two sets of calculations. The assumptions on deflection model and normal pressure are also similar to those used in example calculation #1, to enable a comparison to current design practice.

Example Calculation # 2. The liner system consists of two 1.5 mm PE geomembranes, two geonets, and one filtration geotextile.

Assumptions:

- a circular depression, or void, models possible foundation deformations
- liner system does not touch bottom of depression
- geomembranes are subject to a load-controlled boundary condition
- 30 m of waste will be placed above the lining system
- the stress rupture-time relationship of the geomembrane is defined by Figure 6
- waste unit weight equals 10 kN/m^3
- long-term tensile load in the geonets $\approx$ 0
- long-term tensile load in the filtration geotextile $\approx$ 0

Example Calculation # 2. (*continued*)

Pressure,p, on the liner system from Example Calculation # 1 is

$$p = 18\ kN/m^2$$

Computation of the allowable stress on the PE geomembrane (from Berg and Bonaparte, 1993) is

STEP 1: Establish in-service environment and design life
Assumption - service temperature is 23°C
Assumption - design life equals 50 years

STEP 2: Establish stress-strain and rupture characteristics
From Figure 6, $\sigma_r = 7.2$ N/mm^2

STEP 3: Quantify a chemical degradation factor
Assumption - degradation factor, FC = 1.0

STEP 4: Quantify a seam factor
No data available, assume that the long-term seam factor, FW = 0.8

STEP 5: Quantify an installation damage factor
Assumption - installation damage factor, FI = 1.0

STEP 6: Select an overall factor of safety for the PE geomembranes
Select an overall factor of safety against rupture of 3.0

STEP 7: Compute long-term allowable tensile stress

$$\sigma_a = \frac{\sigma_r \ x\ FC \ x\ FW \ x\ FI}{FS}$$

$$\sigma_a = \frac{7.2\ N/mm^2\ x\ 1.0\ x\ 0.8\ x\ 1.0}{3.0} = 1.9\ N/mm^2$$

Thus, allowable long-term tensile stress in this (Figure 6) polyethylene geomembrane is $\sigma_a = 1.9$ N/mm^2. The strain at this long-term stress level, from extrapolated 50-year isochronous line on Figure 7, is approximately 1.0%.
The tensile load capacity of the liner system, at the allowable stress level of the geomembranes is

$$T_a = \sigma_a \ x\ 2\ x\ t_m$$

$$T_a = 1.9\ N/mm^2\ x\ 2\ x\ 1.5\ mm = 5.7\ kN/m$$

The design strain limit is $\epsilon_d \approx 1.0$ %, therefore $\Omega = 2.07$ (from Giroud et al., 1990)

Example Calculation # 2. (*continued*)

Membrane tension, α, on the liner system (equations from Giroud et al., 1990) is

$$\alpha \approx p\, r\, \Omega$$

$$\alpha \approx 5.7\ kN/m \approx 18\ kN/m^2 \times r \times 2.07$$

$$r \approx 0.15\ m$$

Therefore, this liner system is capable of carrying an allowable isotropic tensile load, under load-controlled boundary conditions, of 5.7 kN/m and can span a circular deflection or void of 0.3 m in diameter.

Example Calculation # 3. This liner system consists of two 1.5 mm PE geomembranes, two geonets, one filtration geotextile, and a geosynthetic reinforcement element.

Assumptions:

- a circular depression, or void, models possible foundation deformations
- liner system does not touch bottom of depression
- geomembranes are subject to a load-controlled boundary condition
- 30 m of waste will be placed above the lining system
- the stress rupture-time relationship of the geomembrane is defined by Figure 6
- waste unit weight equals 10 kN/m^3
- long-term tensile load in the geonets $\approx$ 0
- long-term tensile load in the filtration geotextile $\approx$ 0

Pressure,p, on the liner system from Example Calculation # 1 is

$$p = 18\ kN/m^2$$

Computation of the allowable stress on the PE geomembrane (from Berg and Bonaparte, 1993) is

STEPs 1 through 5: same as example calculation # 2

STEP 6: Select an overall factor of safety for the PE geomembranes
Select an overall factor of safety against rupture of the geomembranes of 2.0, provided the inclusion of the geosynthetic reinforcement raises the overall factor of safety against rupture of the liner system to 3.0 or larger.

STEP 7: Compute long-term allowable tensile stress

$$\sigma_a = \frac{\sigma_r \times FC \times FW \times FI}{FS}$$

$$\sigma_a = \frac{7.2\ N/mm^2 \times 1.0 \times 0.8 \times 1.0}{2.0} = 2.9\ N/mm^2$$

Example Calculation #3. (*continued*)

Thus, allowable long-term tensile stress in this (Figure 6) polyethylene geomembrane is
$\sigma_a = 2.9$ N/mm^2.

The strain at this stress level, from extrapolated 50-year isochronous line on Figure 7, is $\approx$ 1.8%.

Check factor of safety against liner rupture and determine minimum requirements of geosynthetic reinforcement. Factor of safety against rupture of the geomembranes is applied to the rupture stress, σ_r. The factor of safety against rupture of the liner system may be computed as the ratio of tensile stress, or load, at rupture to the allowable stress, or load, in the geomembrane(s). The factor of safety is equal to

$$FS_{ls} = \frac{\sigma_f (t_m \; x \; N) + T_{reinf}}{\sigma_a (t_m \; x \; N)} \geq 3.0$$

where T_{reinf} is at ϵ_f of the geomembrane

$$\sigma_f = \sigma_r \; x \; FC \; x \; FW \; x \; FI$$

$$\sigma_f = 7.2 \; N/mm^2 \; x \; 1.0 \; x \; 0.8 \; x \; 1.0 = 5.76 \; N/mm^2$$

$$\frac{5.76 \; N/mm^2 \; x \; (\; 1.5 \; mm \; x \; 2 \;) + T_{reinf}}{2.9 \; N/mm^2 \; x \; (\; 1.5 \; mm \; x \; 2 \;)} \geq 3.0$$

$$T_{reinf} = 8.8 \; kN/m$$

where

T_{reinf} = minimum isotropic tensile strength of the reinforcement at the geomembrane failure strain of 5% as determined form Figure 7, at the design temperature and life (kN/m)

Assume the reinforcement, with an isotropic tensile strength of 8.8 kN/m at a 5% strain, has an isotropic tensile strength of 3.3 kN/m at a strain of 1.8%. Therefore tensile strength, T_a, equals 3.3 kN/m.

The tensile load capacity of the liner system, at the allowable stress level of the geomembranes is

$$T_{system} = (\sigma_a \; x \; t_m \; x \; N) + T_a$$

$$T_{system} = (2.9 \; N/mm^2 \; x \; 1.5 \; mm \; x \; 2) + 3.3 \; kN/m$$

$$T_{system} = 8.7 + 3.3 = 12 \; kN/m$$

The design strain limit is $\epsilon_d = 1.8$ %, therefore $\Omega = 1.52$ (from Giroud et al., 1990)

Example Calculation #3. (*continued*)

Membrane tension, α, on the liner system (equations from Giroud et al., 1990) is

$$\alpha \approx p\, r\, \Omega$$

$$\alpha = 12\ kN/m \approx 18\ kN/m^2 \times r \times 1.52$$

$$r \approx 0.44\ m$$

Therefore, this liner system is capable of carrying an allowable axisymmetric tensile load of 12 kN/m and can span a circular deflection or void of 0.9 m in diameter.

STEP 8: Check that both the geomembrane and reinforcement remain in their linear viscoelastic limits under initial and final strains.

DISCUSSION

Procedures for design of liner systems over potentially yielding foundations were proposed. These procedures vary from past practice by incorporating the geomembranes as a tensile carrying element in the design. Definition of a long-term allowable stress of the geomembrane(s) is required with the proposed procedure, which requires long-term laboratory testing.

Example calculations illustrate design for a specific case of an assumed axisymmetric deflection analyzed with application of tension membrane and soil arching theories. The geomembrane strength model used was based on actual load-controlled testing. The tested geomembrane is predicted to undergo a transition from ductile to brittle failure within the assumed design life. Equal strains in the geomembranes and reinforcement was also assumed, which inherently assumes both materials remain within their linear viscoelastic limits. Although the examples were limited to specific case, the proposed procedure is applicable to other deflection models, loading conditions, and analytical techniques for yielding foundations. The proposed procedure for margin of safety against rupture of the liner system also may be applied to cases where unequal strains are assumed in the tensile load carrying geosynthetic elements.

Liner systems may be designed with geomembranes providing the entire tensile force, or with inclusion of geosynthetic reinforcing elements with the proposed procedure. A designer or regulatory agency may use a lower factor of safety against rupture of the geomembranes if a reinforcement geosynthetic is used, provided that the overall margin of safety against rupture of the liner system meets designer and regulatory agency requirements.

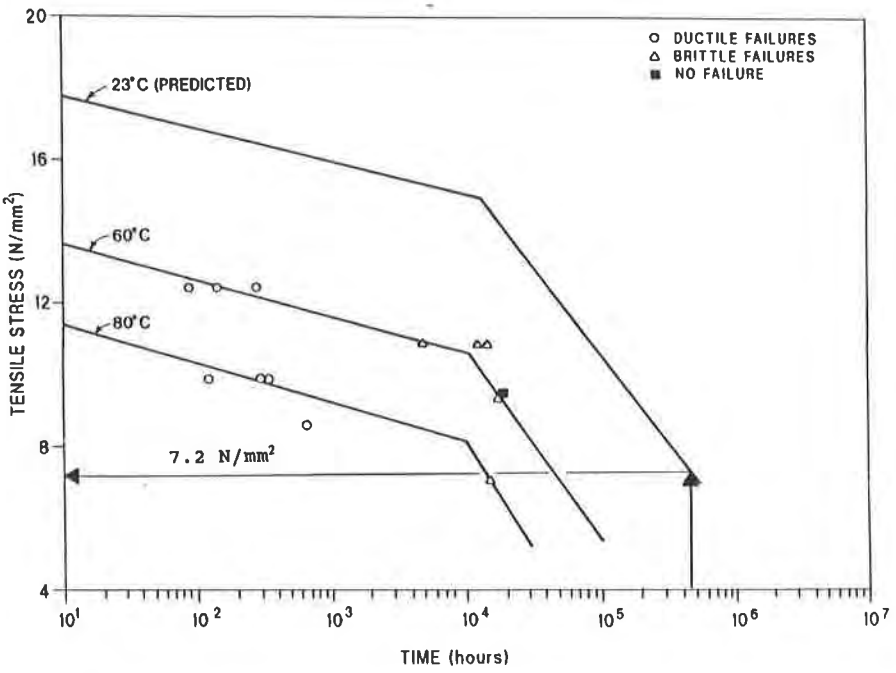

Figure 6. Stress Rupture Line for Axisymmetric Loading of a PE Geomembrane, at 23°C, Derived with Elevated Temperature Testing (after Berg and Bonaparte, 1993)

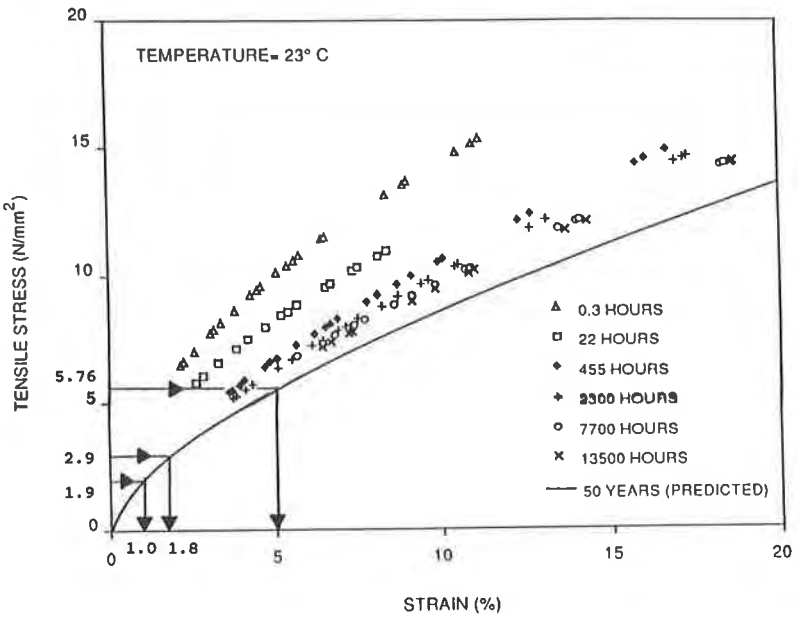

Figure 7. 50-Year Isochronous Curve for Axisymmetric Loading of a PE Geomembrane, Derived with Elevated Temperature Testing (after Berg and Bonaparte, 1993)

REFERENCES

Allen, T.M. (1991). Determination of long-term tensile strength of geosynthetics: a state-of-the-art review. In *Proceedings of the Geosynthetics '91 Conference*, Vol. 1. Atlanta, pp. 351-380.

ASTM (1991). Standard Test Method for Tensile Properties of Plastics, D 638, American Society for Testing and Materials, Philadelphia.

Berg, R.R. and Bonaparte, R. (publication pending (1993)). Long-term allowable stresses in PE geomembranes. *Geotextiles and Geomembranes*, Elsevier Applied Science, England.

Berg, R.R. (1992). *Guidelines for Design, Specification, & Contracting of Geosynthetic Mechanically Stabilized Earth Slopes on Firm Foundations*, U.S. Department of Transportation, Federal Highway Administration, Washington, D.C., 87 p.

Bonaparte, R. and Berg R.R. (1987a). Long-term allowable design loads for geosynthetic soil reinforcement. In *Proceedings of the Geosynthetics '87 Conference*, Vol. 1. New Orleans, pp. 181-192.

Bonaparte, R. and Berg, R.R. (1987b). The use of geosynthetics to support roadways over sinkhole prone areas. In *Proceedings of the Second Multidisciplinary Conference on Sinkholes and the Environmental Impact of Karst*. Orlando, pp.437-445.

Curtis, V.E. and Butchko, S.T. (1991). Innovative use of structural geogrids in waste containment applications. In *Proceedings of Third International Landfill Symposium*. Sardina, Italy, pp.547-561.

Giroud, J.P. (1984). Analysis of stresses and elongations in geomembranes. In *Proceedings of the International Conference on Geomembranes*, Vol. 2. Denver, pp. 481-486.

Giroud, J.P., Bonaparte, R., Beech, J.F. and Gross, B.A. (1990). Design of soil layer-geosynthetic systems overlying voids. *Geotextiles and Geomembranes*, Vol. 9, No. 1. Elsevier Applied Science, England, pp.11-50.

Jewell, R.A. and Greenwood, J.H. (1988). Long term strength and safety in steep soil slopes reinforced by polymer materials. *Geotextiles and Geomembranes*, Vol. 7, Nos. 1 & 2. Elsevier Applied Science, England, pp.81-118.

Koerner, R.M. (1990). Designing With Geosynthetics. 2nd Edition, Prentice-Hall, Englewood, New Jersey, 652 p.

Parker, L.E. and Paulson, J.N. (1993). Multiple geotextile layers used for geomembrane support in a landfill: the Marion County, Florida, landfill project. In *Proceedings of the Geosynthetics '93 Conference*, Vancouver, B.C.

Stephens, A. and Bodner, R. (1991). Geogrid liner support at Empire sanitary landfill. In *Proceedings of the Geosynthetics '91 Conference*. Atlanta, pp. 15-22.

Tieman, G.E., Druback, G.W., Davis, K.A., and Weidner, C.H. (1990). Stability of vertical piggyback landfill expansions. *Geotechnics of Waste Fills - Theory and Practice, ASTM STP 1070*, Arvid Landa, G. David Knowles, eds. American Society for Testing and Materials, Philadelphia, pp.285-302.

GRI (1992). *Determination of Long-Term Design Strength of Geotextiles*, GRI Test Method GT7. Geosynthetic Research Institute, Drexel University, Philadelphia, 13 p.

GRI (1991). *Determination of Long-Term Design Strength of Flexible Geogrids*, GRI Test Method GG4(b). Geosynthetic Research Institute, Drexel University, Philadelphia, 13p.

GRI (1990). *Determination of Long-Term Design Strength of Stiff Geogrids*, GRI Test Method GG4(a). Geosynthetic Research Institute, Drexel University, Philadelphia, 16p.

Mechanical Design of Geomembrane Applications

J.P. Giroud
GeoSyntec Consultants, USA

K.L. Soderman
GeoSyntec Consultants, USA

M. Monroe
GeoSyntec Consultants, USA

ABSTRACT

This paper provides quantitative data intended to increase the safety of geomembrane applications compared to the present design practice. The first part of the paper summarizes the results of a testing program that included 500 tensile tests on high density polyethylene (HDPE) geomembranes at temperatures ranging from -20°C to 70°C. An equation is introduced to model the non-linear stress-strain behavior of HDPE geomembranes and this equation proves to be an effective design tool. The second part describes methods to quantify strain concentrations induced in geomembranes by scratches and seams. The third part presents a methodology that combines data from the preceding two parts to evaluate the factor of safety of geomembrane applications. A design example shows that geomembrane failures observed in service can be quantitatively explained and that HDPE and other geomembranes can be safely used if non-linear mechanical behavior and strain concentrations are integrated into the design.

INTRODUCTION

A comprehensive study was undertaken to better understand the conditions that lead to mechanical failure of geomembranes. The study involved systematic laboratory testing of 900 geomembrane specimens (including 500 specimens of HDPE geomembrane) and analytical evaluations of strains that govern geomembrane failures observed in the field. A thesis and eight technical papers present the study in detail. The main results of the study are presented in this paper where, for the sake of clarity, most data and examples are related to HDPE geomembranes.

The first part of the paper is devoted to tensile properties of HDPE geomembranes. Comprehensive data on the stress and strain at the yield peak in uniaxial tension are provided and an equation is proposed to describe the non-linear stress-strain curve of HDPE geomembranes. The equation is shown to model the observed stress-strain behavior with a high degree of accuracy. Also, relationships between strains in uniaxial and biaxial states of stress

are proposed to account for biaxial conditions in the field. Special attention is paid to strains rather than stresses because geomembranes in service are not normally required to support loads, however, they are required to strain without exhibiting failure; therefore, strains govern their performance.

The second part of the paper is devoted to strain concentrations that occur in geomembranes in service. Simple, yet rigorous, methods are presented to quantitatively evaluate strain concentrations in geomembranes caused by the presence of seams and surface scratches. The equation of the HDPE geomembrane stress-strain curve plays an important role in the development of the methods.

The third and final part of the paper presents a methodology to evaluate the factor of safety of geomembranes against mechanical failure based on the experimental data and strain concentration evaluations provided in the first two parts of the paper. A design example illustrates the methodology and shows that geomembrane failures observed in the field can be explained quantitatively. The design example also shows that the methodology can be used easily by engineers for designing geomembrane applications.

1. TENSILE PROPERTIES OF HDPE GEOMEMBRANES

1.1 Tensile Properties from Uniaxial Tests. More than 500 tensile tests were conducted on HDPE geomembrane specimens from five U.S. manufacturers at temperatures ranging from -20°C to 70°C (Monroe, 1993; Monroe et al., 1993). Geomembrane thicknesses ranged from 0.5 to 3 mm (20 to 120 mils). The tests were conducted on dumbbell specimens according to ASTM standard test method D 638 (ASTM, 1990), at a speed of 50 mm/minute with geomembrane elongations measured using an extensometer.

The following test data and discussion focus on the portion of the stress-strain curve up to the yield peak, since this is the portion of the HDPE stress-strain curve pertinent to design. Strains beyond the yield peak in a tensile test should not be considered in design because they are greatly influenced by the test procedure. Furthermore, they do not correspond to strains at failure in many field situations. As shown in Section 2.1, under certain field conditions, HDPE geomembranes may fail at strains significantly smaller than the strains at break measured in laboratory tests. In addition, it is shown in Section 2.1 that the failure mechanism is initiated at the yield peak, confirming the importance of the yield peak in design.

The tests did not show large differences between the stress-strain curves for HDPE geomembranes from different manufacturers. Figure 1 presents the average stress-strain curves obtained for HDPE geomembranes at each testing temperature, i.e., each stress-strain curve in Figure 1 was obtained by averaging stress-strain curves from all tests conducted at that temperature on all HDPE specimens included in the testing program, regardless of manufacturer. Only the portions of the stress-strain curves between the origin and the yield peaks are shown in Figure 1. The yield stress, σ_Y, and the yield strain ε_Y, are defined as the stress and strain, respectively, at the yield peak. Average values of σ_Y and ε_Y obtained at various temperatures

are given in Figures 2 and 3, respectively. (Values beyond the -20°C to 70°C range were extrapolated.) Inspection of Figure 2 indicates that the relationship between σ_Y and temperature is virtually linear. Also, extrapolation of the straight line in Figure 2 at temperatures greater than 70°C gives $\sigma_Y = 0$ at the temperature of fusion of HDPE (140°C), which is logical. Figure 3 shows that the relationship between ε_Y and temperature can be considered approximately linear between -40°C and 80°C.

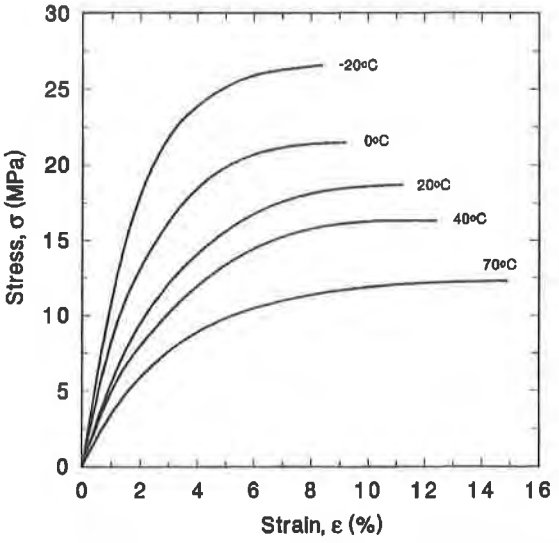

Figure 1. Average HDPE stress-strain curves from origin to yield peak (each curve is the average of 100 tests).

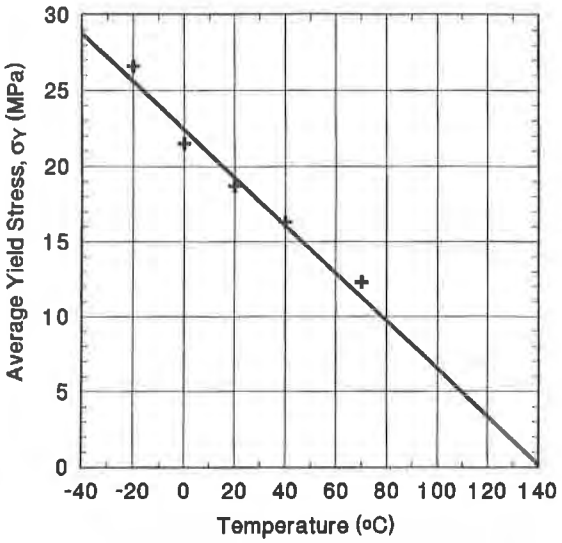

Figure 2. Average HDPE yield stress, σ_Y, as a function of temperature (from 100 tests at each of five different temperatures).

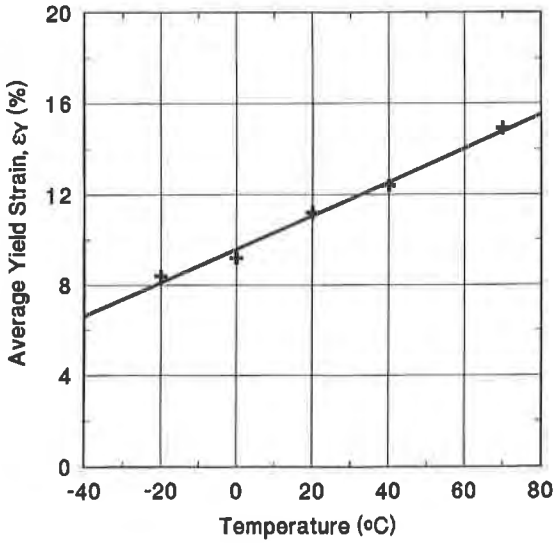

Figure 3. Average HDPE yield strain, ε_Y, as a function of temperature (from 100 tests at each of five different temperatures).

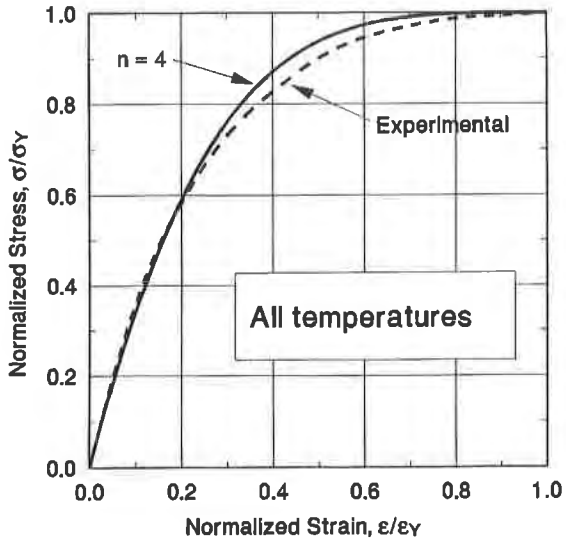

Figure 4. HDPE geomembrane normalized stress-strain curves. The experimental curve is the average of the curves in Figure 1.

A remarkable result was obtained from the testing program: the average stress-strain curves for HDPE geomembranes at different temperatures become nearly identical when presented in normalized axes, σ/σ_Y and $\varepsilon/\varepsilon_Y$. (It is possible that this result stems from a fundamental rheological trait of HDPE, but this was not investigated.) Furthermore, it has been shown that the normalized average stress-strain curve (i.e., the unique normalized stress-strain curve that represents with a good approximation all tested HDPE geomembranes regardless of temperature) can be represented by an n-order parabola (Giroud, 1993), the equation of which is:

$$\sigma/\sigma_Y = 1 - \left(1 - \varepsilon/\varepsilon_Y \right)^n \quad (1)$$

An excellent approximation of the normalized average stress-strain curve from the testing is obtained with Equation 1 when $n = 4$ (Figure 4). Knowing only the stress and strain at the yield peak for a given temperature, Equation 1, with $n = 4$, gives the stress-strain curve of an HDPE geomembrane between the origin and the yield peak at that temperature. If the stress and strain at the yield peak are not known, they can be obtained from Figures 2 and 3. Therefore, with the n-order parabola (Equation 1), it is possible to describe in a quantitative manner the portion of the stress-strain curve that is relevant to the design of HDPE geomembrane applications. This has major design consequences, as illustrated in the remainder of this paper.

The above results are related to smooth HDPE geomembranes. Systematic tests conducted with geomembranes textured using various processes gave results close to the above results for the portion of the stress-strain curves between the origin and the yield peak. With some textured geomembranes, tensile properties beyond the yield peak, in particular the stress and strain at break, were significantly different from the corresponding tensile properties for smooth geomembranes. However, the difference has no impact on design since the portion of the stress-strain curve that is relevant to design is the portion before the yield peak.

All the results presented above were obtained from tests where the strains were calculated from elongations measured using an extensometer attached to the central portion of the dumbbell specimen. When dumbbell specimens are used, extensometer measurements are essential to obtain accurate strain values. Extensometer measurements are indeed specified in the ASTM standard test method D 638 (ASTM, 1990). However, the use of an extensometer is cumbersome, and the current practice in the United States consists of following the NSF 54 Standard on Flexible Membrane Liners (NSF, 1991). The 1991 version of the NSF Standard indicates that "the test does not require the use of extensometers" and specifies that the yield strain should be calculated by dividing the change in grip separation by a gauge length equal to 33 mm (i.e., the length of the central, narrow portion of the dumbbell specimen).

Giroud et al. (1993b) have analyzed the strain distribution in a dumbbell specimen and conducted tests to compare the strain obtained as specified in the NSF Standard to the strain obtained from extensometer measurements. They concluded that strains determined according to the NSF Standard can be as much as 50 percent higher than the strains more accurately determined using an extensometer. For example, a yield strain calculated as 16% according to the NSF Standard is actually significantly less and may be as low as 11%. Also, the NSF

Standard specifies that the minimum yield strain of HDPE geomembranes should be 12% at 21°C. U.S. manufacturers typically publish yield strain values of 13% to 15%, which is reasonable since they typically use the NSF Standard method. However, it should be recognized that the minimum standard value of 12% and the published values of 13% to 15% are greater than actual values (indeed, Figure 3 for 20°C gives $\varepsilon_Y = 11\%$). These exaggerated yield strain values give the design engineers an illusion of safety, which is not conducive to safe design.

1.2 Relationships Between Uniaxial and Biaxial States of Stress. In the field, geomembranes are often subjected to planar biaxial tensile states of stress. In the laboratory, any given planar biaxial tensile state of stress can be modeled by subjecting a cross-shaped geomembrane specimen to controlled tensile stresses and/or strains in the two perpendicular directions. Such tests require sophisticated equipment only available in some research centers at the present time. Research and development in this area must be intensified to develop a simple laboratory test method that simulates field conditions.

Another laboratory test intended to simulate a planar biaxial tensile state of stress is the "hydrostatic test" or "large-diameter burst test", where a circular geomembrane specimen, clamped along its perimeter, is subjected to a uniform pressure on one of its faces. The deflection of the geomembrane increases as the pressure increases until the geomembrane fails. This test is easy to perform, but it has an inherent flaw: the state of stress varies from the center to the perimeter of the geomembrane specimen. Consequently, the interpretation of this test requires certain arbitrary assumptions; therefore, the hydrostatic test results are, at best, questionable.

A practical approach consists of using data from uniaxial tensile tests, which are easy to conduct, and adapting these data to biaxial situations using relationships between uniaxial and biaxial states of stress based on the theory of elasticity. Soderman and Giroud (1993) proposed to use the following relationship for an isotropic biaxial state of stress:

$$\varepsilon_{Yb} / \varepsilon_{Yu} = 1 - \nu \tag{2}$$

and the following relationship for a plane-strain biaxial state of stress:

$$\varepsilon_{Yb} / \varepsilon_{Yu} = (1 - \nu^2) / \sqrt{\nu^2 - \nu + 1} \tag{3}$$

where:

ε_{Yb} = yield strain in a biaxial state of stress;
ε_{Yu} = yield strain in a uniaxial state of stress; and
ν = geomembrane Poisson's ratio.

For incompressible materials such as HDPE geomembranes, $\nu = 0.5$, hence:

$$1 - \nu = 0.5 \quad \text{and} \quad (1 - \nu^2) / \sqrt{\nu^2 - \nu + 1} = 0.87 \ .$$

Using these values, a uniaxial yield strain of 11% becomes 5.5% for an isotropic biaxial state of stress, and 9.6% for a plane-strain biaxial state of stress.

2. STRAIN CONCENTRATIONS IN GEOMEMBRANES

2.1 Effect of Scratches on Geomembrane Stresses and Strains. A study published almost ten years ago (Giroud, 1984a) showed that geomembranes that have a stress-strain curve with a yield peak, such as HDPE geomembranes, can fail at strains close to the yield strain if their surface has long, continuous scratches that are approximately perpendicular to the direction of the applied tensile stress. That earlier study established that the relevant strain for the design of HDPE geomembrane applications is the yield strain, not the strain at break. The original study considered a geomembrane with a linear stress-strain curve between the origin and the yield peak, which led to the following relationship between the yield strain of a scratched geomembrane, ε_{Ys}, and the yield strain, ε_Y, of an intact geomembrane:

$$\varepsilon_{Ys} / \varepsilon_Y = 1 - d_s / t_g \tag{4}$$

where:
d_s = depth of scratch; and
t_g = thickness of geomembrane (Figure 5).

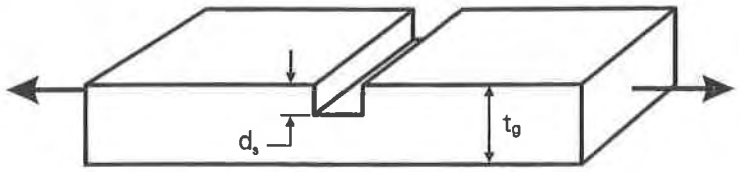

Figure 5. Geomembrane specimen with a scratch.

To more accurately model HDPE geomembranes, the study has been extended to the case where the geomembrane stress-strain curve is represented by the n-order parabola defined by Equation 1 (Giroud et al., 1993a). In this case, the relationship between ε_{Ys} and ε_Y becomes:

$$\varepsilon_{Ys} / \varepsilon_Y = 1 - (d_s / t_g)^{1/n} \tag{5}$$

where:
n = exponent in the equation of the n-order parabola (usually, n = 4).

HDPE geomembrane thicknesses are generally greater than 0.75 mm (30 mils). Scratches with depths between 0.1 and 0.4 mm (4 to 16 mils) have been observed. Therefore, d_s / t_g ratios of up to 0.5 can be considered. Values calculated using Equation 5 with n = 4 are given in Figure 6; they show that the strain, ε_{Ys}, at which a scratched HDPE geomembrane yields can be significantly less than the yield strain, ε_Y, of an intact geomembrane. For example, with a scratch depth equal to 10% of the geomembrane thickness, an HDPE geomembrane yields at a strain that is only 44% of the yield strain of the intact geomembrane. In addition, Figure 6

shows that assuming a linear stress-strain curve underestimates the effect of scratches on the behavior of HDPE geomembranes.

The strain at which a scratched HDPE geomembrane yields can be obtained as a function of temperature from data in Figures 3 and 6. For example, if the yield strain of an intact HDPE geomembrane is 7% (a typical value at -35°C, according to Figure 3), the same geomembrane, with a scratch depth equal to 10% of its thickness, has a yield strain of 3%. This small yield strain quantitatively explains why HDPE geomembranes exposed to very cold temperatures sometimes fail even though they are only subjected to a few percent strain.

Since the governing parameter in Equation 5 is the ratio between the scratch depth and the geomembrane thickness, it is clear that a thicker geomembrane will be less sensitive to given scratches than a thinner geomembrane. However, because of the shape of the curve in Figure 6, the benefit resulting from the use of a thicker geomembrane is not proportional to geomembrane thickness.

In the above discussions, the effect of a scratch on geomembrane behavior has been accounted for as a decrease in yield strain, because this is physically the clearest way. However, to be consistent with the way other causes of strain concentration are accounted for in factor of safety calculations, it is preferable to use a strain concentration factor. Such an approach is usually complex because the strain concentration factor for a given scratch depends on the strain level. However, if the factor of safety is based on yield strain (as recommended in Section 3.2), the strain concentration factor, λ, has the following simple expression which is directly derived from Equation 5:

$$\lambda = \frac{1}{1 - (d_s / t_g)^{1/n}} \tag{6}$$

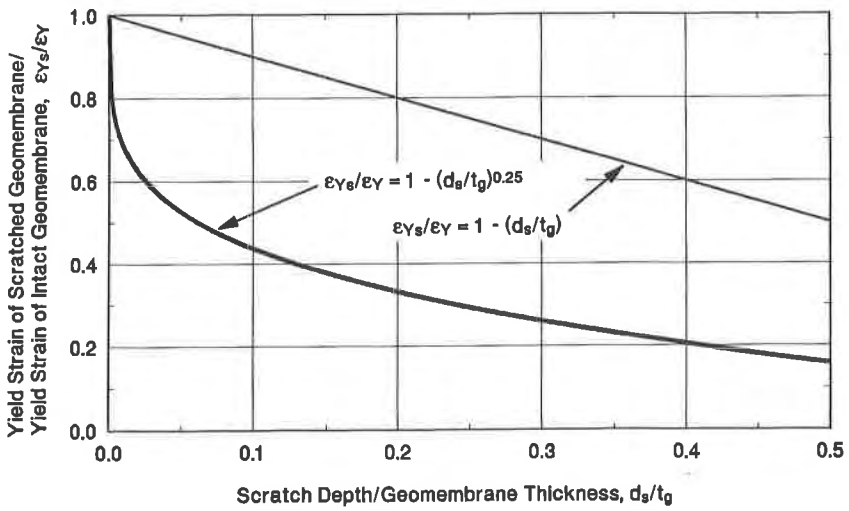

Figure 6. Ratio of scratched HDPE geomembrane yield strain/intact geomembrane yield strain.

Finally, it is important to note that scratches have a maximum effect when they are perpendicular to the direction of the applied tensile stresses (as assumed in the development of Equation 5 and Figure 6) and when they are long and continuous, which precludes stresses in the geomembrane from becoming redistributed around or between scratches. A random distribution of short scratches will probably have a limited effect on the tensile behavior of an HDPE geomembrane, whereas one long continuous scratch, perpendicular to the direction of maximum stresses, has a maximum effect. This is particularly true for scratches located along seams (possibly due to grinding), because their effect is amplified by the strain concentrations due to seams.

2.2 Strain Concentration due to Seams. As shown by Giroud [1984a, 1984b], seams rotate when a geomembrane is in tension because the equilibrium of the tensile forces applied on the geomembrane requires the portion of geomembrane on one side of a seam to be in the same plane as the portion of geomembrane on the other side of the seam. As a result, the geomembrane bends on each side of the seam (Figure 7). A detailed analysis of the bending of the geomembrane has been performed by Giroud et al. (1993c). The analysis shows that the maximum tensile strain due to bending occurs at the connection between the lower geomembrane and the seam. The analysis provides equations to determine the maximum tensile strain due to bending as a function of the following parameters: geomembrane thickness, geomembrane modulus, seam type (Figure 8), seam thickness (in the case of extrusion seams), seam width, and the average tensile strain in the geomembrane that causes bending next to the seam. The equations are too numerous and complex to be reproduced here. However, in Figure 9, the maximum tensile strain due to bending is given in graphs for two geomembrane thicknesses and for several different types of seams.

It is clear from the graphs that the tensile strain due to bending is less for fusion seams than for extrusion seams. However, even for fusion seams, the tensile strain due to bending is significant: it is equal to approximately 80% of the average tensile strain in the geomembrane. In other words, the total tensile strain next to a fusion seam (i.e., the sum of the average tensile strain and the maximum tensile strain due to bending) is equal to 1.8 times the average tensile strain in the geomembrane. It has also been shown by Giroud et al. (1993c) that seams narrower than those considered in Figure 9 would generally give greater strain concentrations. It should be noted that significant bending strains occur even though the seam rotation angle is small (typically only a few degrees).

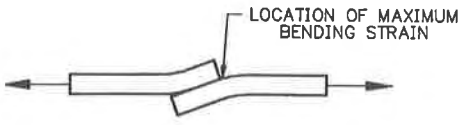

Figure 7. Geomembrane bending

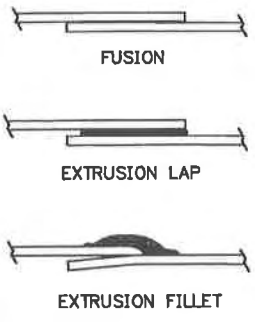

Figure 8. Types of seams

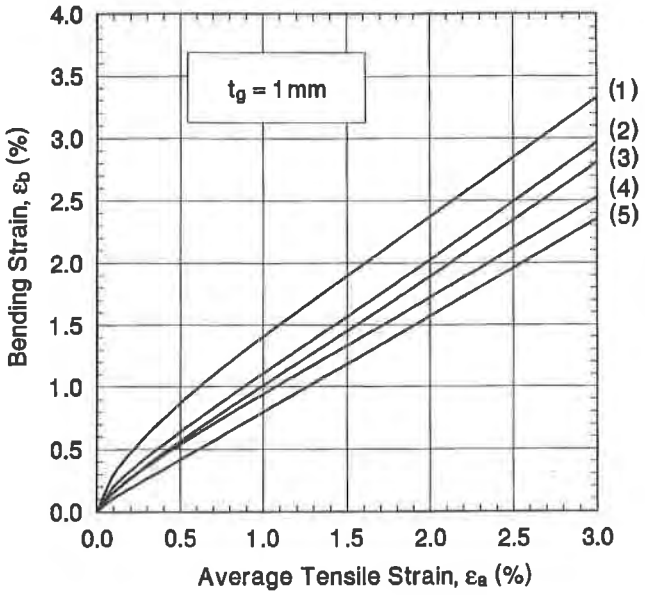

(1) Extrusion Lap [4 mm](*)
(2) Extrusion Lap [3 mm] (*)
(3) Extrusion Fillet [4 mm] (*)
(4) Extrusion Fillet [5 mm] (*)
(5) Fusion [2 mm] (*)

Geomembrane Thickness:
1 mm (40 mils)
Seam Width:
38 mm (1.5 in.)

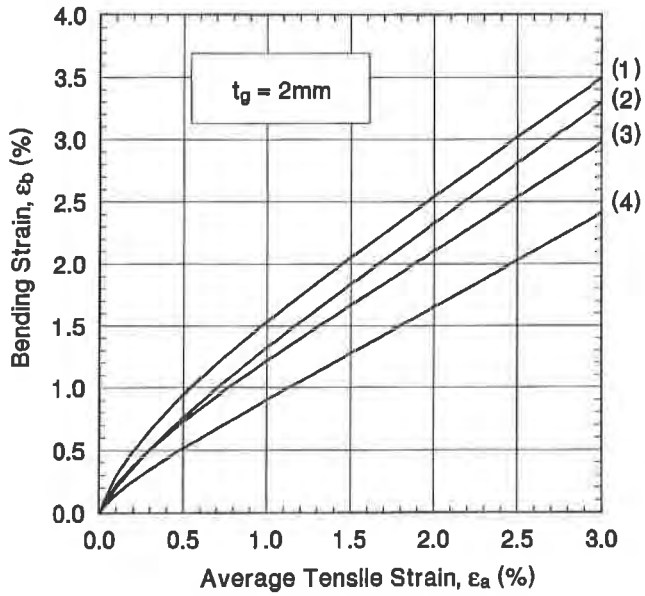

(1) Extrusion Lap [6 mm] (*)
(2) Extrusion Fillet [6-7 mm] (*)
(3) Extrusion Lap [5 mm] (*)
(4) Fusion [4 mm] (*)

Geomembrane Thickness:
2 mm (80 mils)
Seam Width:
38 mm (1.5 in.)

Figure 9. Tensile strain due to geomembrane bending next to a seam, ε_b, as a function of the average tensile strain, ε_a, in the geomembrane. The charts are applicable to seams that are free to rotate; in the case of seams that are subjected to normal stresses that limit their ability to rotate, the bending strains should be less than indicated on the charts. (*) Note: The value indicated in square brackets is the total seam thickness, i.e., thickness of extrudate, if any, plus thickness of two geomembrane layers.

3. DESIGN OF GEOMEMBRANE APPLICATIONS

3.1 Methodology. Geomembranes do not normally play a structural role and it is more appropriate to express mechanical design criteria for geomembranes in terms of strains than in terms of stresses. Therefore, the proposed methodology consists of calculating a factor of safety on the basis of strains. The three steps of the methodology are described below, followed by a design example and comments.

3.2 Selection of the Maximum Allowable Strain. The first step consists of selecting the maximum allowable strain, ε_{maxall}, which is the strain that triggers the mechanism that leads to geomembrane failure. This strain depends on the type of geomembrane. For example, the maximum allowable strain is the break strain for a geomembrane that does not exhibit a yield peak or plateau, and it is the break strain of the scrim for a scrim-reinforced geomembrane. In the case of HDPE geomembranes, discussions in the preceding sections show that the maximum allowable strain is the yield strain.

Ideally, the maximum allowable strain should be obtained from a biaxial test that simulates field conditions, including temperature and strain rate. If such a test is not available, the strains measured in a uniaxial tensile test conducted at room temperature can be used with appropriate corrections. For example, in the case of HDPE geomembranes, the effect of temperature can be accounted for using Figure 3, and the yield strain for a biaxial situation can be derived from the yield strain obtained in a uniaxial tensile test as shown in Section 1.2. The influence of strain rate was not evaluated in this study. However, it should be noted that for cases where the factor of safety is calculated on the basis of strains, such as the cases discussed in this paper, the data obtained from the relatively high speed testing conducted for this study should be considered conservative.

To calculate the factor of safety, it is essential that the maximum allowable strain be accurate. Therefore, strains must be obtained from tensile tests using an extensometer (see Section 1.1). Strains derived from grip separation, which is often the case with strains reported in the literature, may be significantly inaccurate. However, they can be corrected as shown by Giroud et al. (1993b).

3.3 Determination of the Effective Strain. The second step consists of evaluating the effective strain, which is equal to the average strain modified to account for strain concentrations. The average strain results from the mechanisms that deform the geomembrane, such as: thermal contraction, differential settlements, lack of support beneath the geomembrane, etc. A description of the methods used to determine the average strain is beyond the scope of this paper. Methods to evaluate average strains in geomembranes are, however, readily available: methods have been published, for example, by Giroud (1982, 1984b), Giroud and Stone (1984), Giroud et al. (1990), and Koerner (1990), and new design methods have been developed as part of this study (Giroud et al., 1993d,e). The strain-generating mechanism considered in the design example in Section 3.5 is thermal contraction because, in this case, strain calculation is relatively simple.

The average strain, ε_a, must then be modified for strain concentrations to obtain the effective strain, ε_e. In the case of HDPE geomembranes, the factor λ defined by Equation 6 with n = 4 can be used to account for strain concentration due to scratches, as follows:

$$\varepsilon_e = \frac{\varepsilon_a}{1 - (d_s / t_g)^{0.25}} \tag{7}$$

Regardless of the type of the geomembrane, strain concentrations due to the presence of seams that are free to rotate can be accounted for according to Section 2.2, as follows:

$$\varepsilon_e = \varepsilon_a + \varepsilon_b \tag{8}$$

where:
ε_b = bending strain given in Figure 9.

For HDPE geomembranes, the following equation, obtained by combining Equations 7 and 8, can be used in the case of scratches next to seams:

$$\varepsilon_e = \frac{\varepsilon_a + \varepsilon_b}{1 - (d_s / t_g)^{0.25}} \tag{9}$$

3.4 Calculation of a Factor of Safety. In the last step, the maximum allowable strain and the effective strain are used to calculate a factor of safety that is defined as follows:

$$FS = \frac{\text{Maximum Allowable Strain}}{\text{Effective Strain}} = \frac{\varepsilon_{maxall}}{\varepsilon_e} \tag{10}$$

The factor of safety thus calculated must be greater than an allowable factor of safety selected by the design engineer. The allowable factor of safety must be greater than 1.0 and it depends on the structure (critical nature, design life), the level of confidence in the design method and design parameters, and applicable regulations, if any.

3.5 Design Example. A 2 mm (80 mil) thick geomembrane is installed without wrinkles or compensation at a temperature of 20°C. Extrusion fillet seams are used. The geomembrane is not covered with a protective layer, and is expected to be exposed in the winter to a temperature of –30°C. The geomembrane coefficient of thermal expansion-contraction is 1.5 x 10^{-4} $°C^{-1}$. What is the factor of safety assuming that there might be 0.1 mm (4 mil) deep scratches on the surface of the geomembrane next to seams due to grinding prior to seaming?

According to Figure 3, the yield strain measured in a uniaxial test at -30°C is 7.3%. The state of stress due to thermal contraction is close to isotropic biaxial and a factor of 0.5 should be used according to Section 1.2, hence a maximum allowable strain:

$$\varepsilon_{maxall} = 7.3\% \times 0.5 = 3.65\%$$

The average tensile strain due to thermal contraction is:

$$\varepsilon_a = 1.5 \times 10^{-4} (20 + 30) = 0.0075 = 0.75\%$$

Then, strain concentration due to the combined effect of a seam and a scratch next to the seam can be evaluated using Equation 9 with $d_s = 0.1$ mm (4 mils), $t_g = 2$ mm (80 mils), $\varepsilon_a = 0.75\%$, and $\varepsilon_b = 1.05\%$ (obtained from Figure 9 for $t_g = 2$ mm, $\varepsilon_a = 0.75\%$, and an extrusion fillet seam). The resulting effective strain is:

$$\varepsilon_e = \frac{0.75 + 1.05}{1 - (0.1 / 2)^{0.25}} = 3.41\%$$

The factor of safety is then given by Equation 10 as follows:

FS = 3.65/3.41 = 1.07

Using the same method as above, it can be determined that the factor of safety would be: 0.84 if the geomembrane temperature during installation had been 35°C; 0.89 if the considered scratch depth had been 0.2 mm (8 mil); 0.98 if the thickness of the geomembrane had been 1.0 mm (40 mil); and 0.58 with all of the above. In addition, the factor of safety is about 5 for locations that are not next to a seam and are not scratched. This factor of safety is much higher than factors of safety for locations affected by seams and scratches.

The above example shows quantitatively that HDPE geomembranes subjected to very low temperatures can have a small factor of safety. However, it should not be concluded from the above example that the factor of safety of HDPE geomembrane applications is always low. In fact, it can be high, even for an HDPE geomembrane exposed to a very low temperature, if adequate precautions are taken at the design and construction stages. For example, if fusion seams (which cause less strain concentration and do not require grinding) are used, the factor of safety for a 2 mm (80 mil) thick geomembrane becomes 1.5 (assuming a scratch depth of only 0.05 mm (2 mils)). The factor of safety is even greater if the geomembrane is installed with wrinkles and/or compensation panels, which alleviate tension due to thermal contraction. Furthermore, if the geomembrane were covered with soil, thermal contraction would be much less and strain concentration due to the presence of seams would decrease as seam rotation would not be free.

3.6 Comments on the Methodology. Every method has its limitations. The proposed methodology results from theoretical developments based on data from uniaxial tensile tests. A more direct approach, but involving a considerable testing effort, would consist of conducting systematic biaxial tests, at various temperatures, on large specimens of geomembranes with seams, scratches, and possibly other features likely to cause strain concentrations; these tests should be conducted at various strain rates to investigate time-dependent effects. It will take years before results of such an ambitious program are available. In the meantime, the methodology proposed in this paper should be useful.

CONCLUSION

A systematic testing program has provided quantitative data on the tensile properties of various types of geomembranes over a wide range of temperatures. For the sake of simplicity, only data on HDPE geomembranes were presented in this paper. An n-order parabola has been proposed to represent the non-linear mechanical behavior of HDPE geomembranes. The n-order parabola was used to evaluate the strain concentrations due to scratches at the geomembrane surface (whereas a linear stress-strain curve does not allow an accurate evaluation of this major effect). Strain concentrations due to the presence of seams were also evaluated.

Using the above data, a rigorous methodology to evaluate the factor of safety of geomembranes against mechanical failures has been proposed and it has been illustrated using a design example. The factors of safety obtained in the design example explain quantitatively why a geomembrane may fail under some circumstances, and why, at a given site, a geomembrane fails at some locations (e.g., in the vicinity of seams) and not elsewhere. The design example also shows that a satisfactory factor of safety can be achieved if appropriate precautions are taken at the design and construction stages.

This paper shows that it is essential to know the geomembrane stress-strain curve with great accuracy to safely design geomembrane applications. In particular, with HDPE geomembranes, it is necessary to know in detail the portion of the stress-strain curve between the origin and the yield peak, whereas the current design practice consists of giving only the yield stress and strain and the stress and strain at break, virtually ignoring the only portion of the stress strain curve that is relevant to design. Therefore, changes in the current design practice are required for all types of geomembranes. The results and the methodology presented in this paper, although they were mostly illustrated with examples pertaining to HDPE geomembranes, are intended to promote the safe use of all types of geomembranes.

ACKNOWLEDGEMENTS

The authors are indebted to J.F. Beech, R. Bonaparte, R.M. Charron, and J.E. Fluet, Jr. for valuable comments. (Note: M. Monroe is now at ATEC Associates.)

REFERENCES

American Society for Testing and Materials (ASTM), (1990) "Standard Test Method for Tensile Properties of Plastics", D 638, 12 p.

Giroud, J.P., (1982) "Design of Geotextiles Associated with Geomembranes", Proceedings of the Second International Conference on Geotextiles, Vol. 1, Las Vegas, Aug 1982, pp. 37-42.

Giroud, J.P., (1984a) "Analysis of Stresses and Elongations in Geomembranes", Proceedings of the International Conference on Geomembranes, Vol. 2, Denver, CO, pp. 481-486.

Giroud, J.P., (1984b) "Geotextiles and Geomembranes. Definitions, Properties and Design", IFAI Publishers, 325 p.

Giroud, J.P., Bonaparte, R., Beech, J.F., and Gross, B.A., (1990) "Design of Soil Layer-Geosynthetic Systems Overlying Voids", Geotextiles and Geomembranes, Vol. 9, No. 1, pp. 11-50.

Giroud, J.P., and Stone, J.L., (1984) "Design of Geomembrane Liner for the Proton Decay Experiment", Proceedings of the International Conference on Geomembranes, Vol. 2, Denver, CO, pp. 469-474.

Giroud, J.P., (1993) "Mathematical Model for Geomembrane Stress-Strain Curve with a Yield Peak", submitted to Geotextiles and Geomembranes.

Giroud, J.P., Beech, J.F., and Soderman, K.L., (1993a) "Yield of Scratched Geomembranes", submitted to Geotextiles and Geomembranes.

Giroud, J.P., Monroe, M., and Charron, R.M., (1993b) "Measurement of Geomembrane Strain in Tensile Test", submitted to Geotechnical Testing Journal, ASTM.

Giroud, J.P., Tisseau, B., Soderman, K.L., and Beech, J.F., (1993c) "Analysis of Strain Concentrations Next to Geomembrane Seams", submitted to Geotextiles and Geomembranes.

Giroud, J.P., Soderman, K.L., and Beech, J.F., (1993d) "Design Method to Prevent Geomembrane Failures in Tank Corners", submitted to Geotextiles and Geomembranes.

Giroud, J.P., Beech, J.F., and Soderman, K.L., (1993e) "Effects of Differential Settlements on Geomembranes", submitted to Geotextiles and Geomembranes.

Koerner, R.M., (1990) "Designing with Geosynthetics", Prentice Hall, Englewood Cliffs, 652 p.

Monroe, M., (1993) "Effect of Temperature on the Tensile Characteristics of Geomembranes", M.S. Thesis submitted at Florida Atlantic University.

Monroe, M., Fluet, J.E., and Giroud, J.P., (1993) "Geomembrane Tensile Characteristics as a Function of Temperature", submitted to Geotextiles and Geomembranes.

National Sanitation Foundation (NSF), (1991) "Flexible Membrane Liners", NSF Standard 54, 29 p. plus appendices.

Soderman, K.L. and Giroud, J.P., (1993) "Relationships Between Uniaxial and Biaxial Stresses and Strains in Geomembranes", submitted to Geotextiles and Geomembranes.

Direct Shear Testing for HDPE/Amended Soil Composites

H.D. Sharma
CH2M Hill Inc., USA

D.E. Hullings
EMCON Associates, USA

ABSTRACT

As landfill excavation and refuse slopes become steeper and most regulations mandate composite liners, slope stability becomes an even more important consideration. Composite liners (a low permeability soil layer underlying a geomembrane) often contain the weakest plane within the lining and leachate collection systems. Although the low permeability soil is usually clay, more sites are being located where clay is not readily available and therefore amended soils (on-site soil admixed with bentonite or other clay material) are being used. For such sites, the interface strength between amended soils and high density polyethylene (HDPE) geomembrane must be determined to evaluate slope stability.

The most commonly used method for evaluating this strength is a direct shear test. Although many direct shear tests have been performed by various laboratories, the current lack of an ASTM standard results in great variations in the procedures and widely varying results. In order to provide a basis for interface friction values between amended soils and HDPE, the authors have conducted tests generally consistent with the Geosynthetic Research Institute (GRI) standard GS6 and ASTM draft standard D35-01.87.07. This paper presents the residual and peak interface friction angle (δ) values for various amended low permeablity soil/HDPE interfaces obtained from a large (12-inch by 12-inch) direct shear device and the case for developing standard test methods that would simulate field conditions for landfills.

INTRODUCTION

As solid waste landfills have grown from local dumps to state-of-the-art engineered facilities, more attention has been placed on the geotechnical aspects of "landfill engineering." One task now required for all new landfills is a complete slope stability analysis. This is particularly important given recent slope failures such as Kettleman Hills (Mitchell, et al., 1990 and Seed, et al., 1990). As is true for any analysis, the accuracy of the slope stability analysis depends, in part, on material parameters such as strength. One of the most critical parameters, and the focus of this paper, is the interface shear strength between the flexible membrane liner (FML) and the compacted amended soil layer in a composite liner.

Almost all new landfills now require, at a minimum, a composite liner consisting of an FML over a compacted soil layer (EPA Subtitle D). Although the composite liner is more effective than either component alone, the shear strength between the two components is often low, resulting in the most critical plane in the stability analysis. Another composite liner requirement is low permeability soil (hydraulic conductivity no greater than 1×10^{-7} centimeters per second [cm/sec]). For projects where the appropriate low permeability material is not available on site, amended soils (on-site soil mixed with off-site bentonite or other low permeability soil) have been used to obtain the desired permeability.

This paper discusses the direct shear test procedures used by the authors and presents interface shear strength values for various composites. After reviewing existing test methods, a large-scale direct shear method was used for the investigation. No standard exists, however, so variables were chosen to represent field conditions while keeping the test method practical. The data are also interpreted and compared to available information.

DIRECT SHEAR TESTING

The first direct shear apparatus, built about 150 years ago, was stress controlled (Collin, 1846). Its main disadvantage was that the soil behavior beyond peak shearing resistance could not be measured. The evolution of the constant rate of displacement test allowed the stress beyond peak to be measured, but the cross sectional area of the sample changed during displacement, which led to problems with determining stress distribution within the specimen. The development of the Ring Shear Test and Simple Shear Test during the 1930's solved the area problem, but as with any direct shear test, other problems remained. The direct shear test causes the samples to fail along a predetermined plane and drainage conditions are difficult to control. A different method, the triaxial test, was developed during the 1930's to measure the shear strength of soil samples and mitigate the above problems. The direct shear test is still appropriate, however, when the material's behavior along a certain interface must be evaluated (Mathews, 1988). With the increased use of geosynthetics, more attention has been given to the direct shear test.

The interface between the low permeability soil layer and a geomembrane in a composite liner is particularly suited for evaluation by a direct shear apparatus. During the last 10 years, many investigators have performed such interface shear tests in direct shear machines (Seed and Boulanger, 1991; Takasumi, et al., 1991; Koursourais, et al., 1990; Williams and Houlihan, 1986 and 1987; Eigenbrod and Locker, 1987; Richards and Scott, 1985). These tests have been performed in box sizes from 5 centimeters (cm) by 5 cm to 30.5 cm by 30.5 cm, and larger. Besides size, conditions such as displacement rates and sample anchorage also vary. Although there is no unanimity on type or size of the test apparatus, there is a need to follow a consistent testing procedure in a standardized apparatus. Takasumi, et al. (1991) suggests

that a 12-inch by 12-inch box be used and further recommends that the test be performed in accordance with American Society for Testing and Materials (ASTM) draft D35-01.81.07.

APPLICATIONS

Interface friction values from direct shear testing are used as input into the stability analysis. The stability analysis begins with identifying potential problem areas whether they be cut (excavation) or fill (refuse) slopes. Potentially weak planes, usually associated with material interfaces, should also be identified (see Figure 1). The correct analytical technique is then chosen to evaluate the stability.

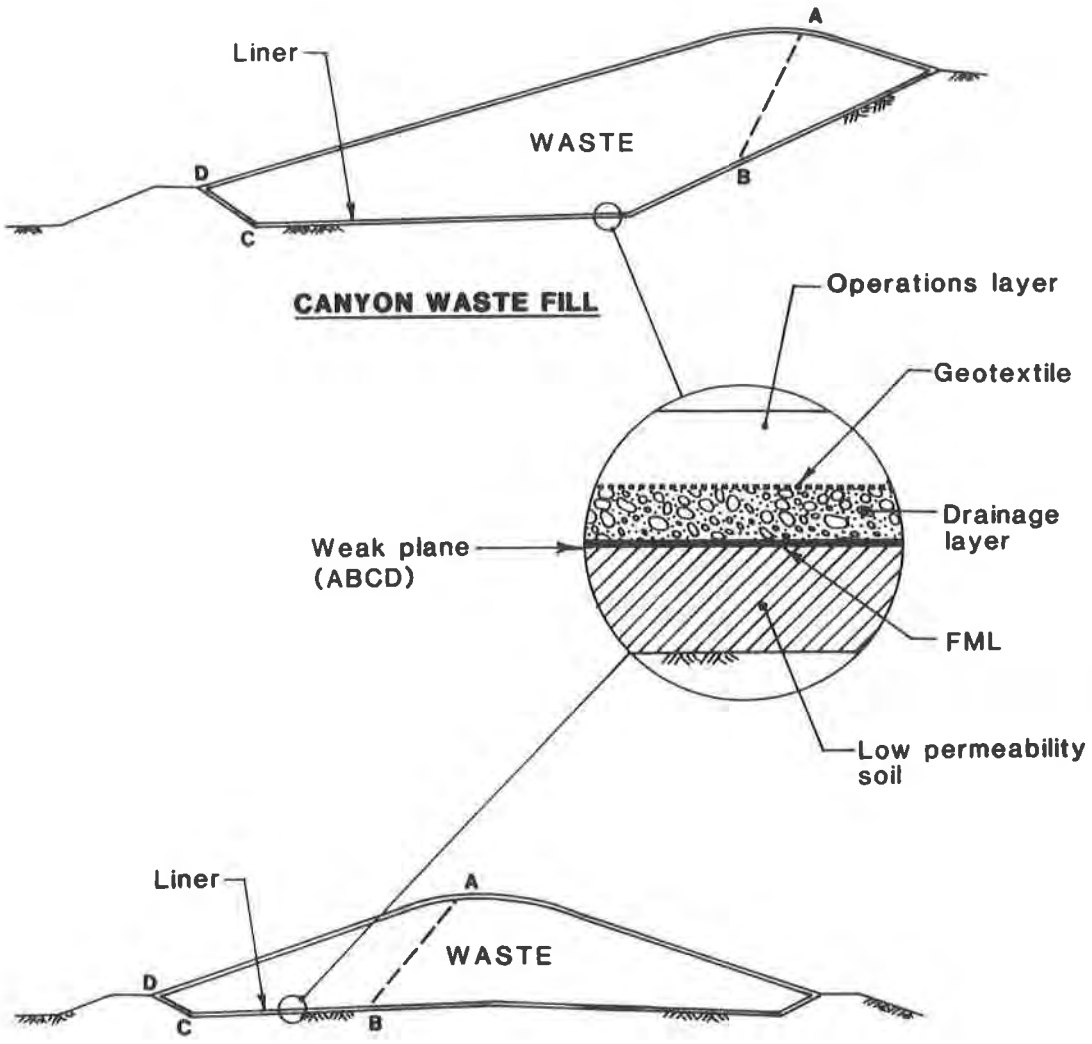

Figure 1 Potential Weak Plane

Such an analysis typically computes a factor of safety by dividing the resisting forces or moments by the driving forces or moments and is based on established geotechnical procedures such as the modified Bishop's or Janbu's approach. Circular failure surfaces are still analyzed, but because of weak planes associated with liner components, block failure analyses are usually more critical. A wide variety of computer programs are available to "crunch the numbers," but engineering judgement and experience are still required to determine potential failure surfaces. Even the most sophisticated program run by the most experienced engineer still requires the selection of suitable material parameters for an accurate analysis.

Materials usually associated with landfills or waste fills include soil, refuse, and synthetics. Testing for soils is well established, with soil strengths measured in friction angle and cohesion. Refuse properties vary widely, but at this time (1992) soil-like properties have been applied to refuse to describe its shear strength (Converse, 1975; Singh and Murphy, 1990). Because the use of synthetics in landfills is relatively new, strength testing is not as advanced as it is for soil. Direct shear testing apparently will be used, however, to measure the shear strength of synthetic interfaces although the testing parameters have not been completely standardized

The importance of identifying potentially weak interfaces and accurately testing shear strengths cannot be underestimated. Often a half dozen or more synthetic-to-synthetic or synthetic-to-soil interfaces exist in a landfill, any one of which may be the weakest plane. Each interface should be tested using state-of-the-art testing under simulated field conditions. If the engineer decides to forego testing and uses unrealistically conservative values, valuable landfill airspace may be lost. Conversely, if higher than actual values are used in the analysis, a catastrophic failure could result. The time and expense to accurately measure shear strengths are negligible when faced with the possible alternatives of inaccurate testing and evaluation.

TESTING APPARATUS AND PROCEDURE

Test Apparatus. The shear strengths of the geosynthetic/soil interfaces were determined by direct shear testing in general accordance with Geosynthetic Research Institute (GRI) Test Method GS6 and ASTM draft method D 35.01.81.07. Tests were performed in a large square box with inside length and width dimensions of 30.5 centimeters (12 inches) and a total height of 20.3 centimeters (8 inches). The box has two components: a fixed lower half and an upper half capable of moving at a controlled rate. Pneumatic loading devices are used to apply a controlled normal pressure over the interface being tested and to move the upper half in a shearing action. The device is instrumented to measure normal load (accurate to about 10 kPa), shear force (accurate to about 1 kPa), and horizontal and vertical displacements (accurate to about 0.25 mm).

Sample Preparation. A 30.5-centimeter by 30.5-centimeter square geomembrane sample is cut and affixed to wooden blocks to achieve full fixation and then placed in the lower box. Full fixation allows no

extension in the material and leads to lower bound friction values, according to GS6. The upper box is then aligned with the lower box and the soil is compacted to the specified density and moisture content in the upper box above the geomembrane. Steel plates are then placed in the upper box to evenly distribute the normal load. A "frictionless" plate, consisting of ball bearings held in a metal frame, is placed between the upper steel plate and the loading device to reduce "internal" friction in the apparatus.

Procedure. The direct shear box lies within a larger box, which is flooded with water. The normal load is applied in two different ways to represent two conditions. A normal load consistent with anticipated loads on the liner is applied overnight to represent partially consolidated undrained (PCU) conditions. To model uncondolidated undrained (UU) conditions, a 500 psf load is applied overnight to counteract swelling and the full load is applied just before shearing. The terms "consolidated" and "unconsolidated" are used for discussion and do not necessary reflect the true condition of the soil. After the normal load is applied, the alignment pins are used to separate the upper and lower boxes by 6.4 millimeters (0.25 inch) and then the pins are removed. The horizontal displacement gauge is set to zero and the shearing force is applied. The upper box moves at a constant displacement rate of 0.762 mm (0.03 inch) per minute and both displacement and shearing force are measured. Shearing continues until a maximum displacement of 30.48 mm (1.2 inches) is achieved. The geosynthetic types, normal load, horizontal displacements, and shearing force are recorded on the data sheets.

The data for each geosynthetic combination at each overburden pressure is plotted as displacement versus shear stress. These plots are used to obtain both the peak and residual shear stresses. Both values are used to create normal stress versus shear stress plots. The best fit straight line is then drawn through the data points. The slope of this line determines the friction angle (δ) and the y-intercept value is the adhesion (a).

MATERIAL PROPERTIES

Testing was performed for eight different soil sources collected from five landfill sites. Several properties of the soils are presented in Tables 1 and 2.

Table 1 Low Permeability Material Properties

Site	1	2	3	4
Percent passing #200 sieve	94	51	43	>50
Liquid Limit (LL)	46	38	27	
Plasticity Index (PI)	25	22	5	
Maximum dry density[1](pcf).	107	129	114	102
Optimum Moisture[1] (%)	18.2	9.6	13.5	12.0
Permeability (cm/sec)	$4x10^{-8}$	$5x10^{-8}$	$2x10^{-7}$	$1x10^{-8}$

[1] In accordance with ASTM D1557

Site 1 is an on-site clay obtained from a landfill in southern California. The results are presented here for comparison to admixed soils. Site 2 is a mixture of sand, found on site at another southern California landfill, with 10 percent bentonite (by weight). A mixture of on-site sandy silt and 5 percent bentonite was used for the soil liner at Site 3. Site 4 is a mixture of high plasticity clay that was mixed with on site soil in an attempt to increase its interface strength. Site 5 is a northern California site that may use one of four admixes of on site soil with high plasticity clay (mix D also contains 2 percent sodium bentonite). All admixes met the applicable requirements for a soil liner at the time of construction.

Table 2 Site 5 Low Permeability Material Properties

Site Mixture	5A 70% Alluvium/ 30% Clay	5B 70% DG[2]/ 30% Clay	5C 60% DG/ 40% Clay	5D 78% DG/ 20% Clay
Percent passing #200 sieve	43	52	59	47
Liquid Limit (LL)	38	41		
Plasticity Index (PI)	20	21		
Maximum dry density[1](pcf).	117	113	112	114
Optimum Moisture[1] (%)	12.7	15.8	16.0	15.0
Permeability (cm/sec)	$3x10^{-7}$	$8x10^{-8}$	$1x10^{-8}$	$1x10^{-8}$

[1] In accordance with ASTM D1557 [2] decomposed granite

INTERFACE STRENGTHS

The soils were tested in the direct shear apparatus with the FML that was to be used for the particular project. Shear stress/displacement curves are presented for sites 1 and 5 as examples and shear stress/normal load curves are presented for these and other combinations. The resulting interface friction strengths are summarized in Table 3. The Site 1 clay was compacted to 90 percent relative compaction at 5 percent wet of OMC and tested with textured Gundle high density polyethylene (HDPE) geomembrane. The site 2 amended soil was compacted to 90 percent relative compaction at 4 percent over OMC and tested with both smooth and textured Gundle HDPE. The site 3 amended soil was also compacted to 90 percent compaction at 3 percent OMC and the interface strength was tested with SLT textured HDPE geomembrane. Site 4 soil was compacted to 90 percent compaction at 3 percent OMC and was tested with Gundle textured sheet. Site 5 soils were compacted to 95 percent relative compaction and placed at 3 percent wet of OMC. Textured SLT and Gundle HDPE geomembranes were used in combination with these soils.

"Peak" and "residual" are used to describe interface strengths at different displacements. The peak value is based on the highest shear stresses recorded during testing and usually occurs at low displacements. The residual strengths are based on shear stresses recorded at displacements of 30.5 cm (10 percent of the original

length). Where residual strengths are determined is a judgement call; this is discussed in a later section.

Table 3 - Interface Friction Strength

Site	Peak a (kPa)	Peak δ	Residual a (kPa)	Residual δ	Test Condition	Soil/FML
1	0	20	0	12	PCU	Clay/Gundle textured
2	0	19	29	7	PCU	Bentonite-sand/Gundle smooth
3	14	25	12	25	PCU	Bentonite-SM/SLT textured
5A	24	19	17	19	PCU	Clay-Alluvium/SLT textured
5B	9.6	21	9.6	17	PCU	Clay-Granite/SLT textured
5C	19	10.5	19	8.5	PCU	Clay-Granite/Gundle textured
5D	18	11.5	18	11.5	PCU	Clay-Granite/Gundle textured
4	12	12	12	9	UU	Clay-SM/Gundle textured
5B	24	10	24	9.5	UU	Clay-Granite/Gundle textured
5C	20	9	17	7	UU	Clay-Granite/Gundle textured
5D	16	11	16	10	UU	Clay-Granite/Gundle textured

PCU - partially consolidated undrained
UU - unconsolidated undrained

At Site 1 the peak δ is a relatively high 20 degrees, but the residual strength is 12 degrees. This is consistent with what the authors have seen for interface testing involving clays. At Site 2 the peak is again relatively high (19 degrees), but the residual strength is much lower. In this case the high peak value may be attributable to the coarse nature of the amended soil. Although the drop from peak to residual is substantial, it is not surprising. Results involving amended soils and textured sheet are somewhat different. The peak values are consistantly high and do not differ much from Sites 1 and 2. The residual values for amended soils are not, however, much lower than peak values. Some amount of adhesion is also apparent. The difference in behavior can be seen in the typical displacement versus shear stress curve in Figures 2 and 3 (Sites 1 and 5A). Normal versus shear stress curves for selected sites are presented in Figures 4 through 7.

DISCUSSION

Test Results. The results of this limited study indicate that there are differences between the shear strength behavior of the clay/HDPE geomembrane interface and the amended soil/textured HDPE geomembrane interface. There is apparently no substantial difference between peak and residual values for amended soil/HDPE geomembrane interfaces, as is found for interfaces with clay. The residual δ for Site 1, which involved clay, is about half the peak value. The authors' experience has been that for tests involving clay interfaces, the residual value is typically 30 to 70 percent of the peak values. If amended soils and textured sheet are used, the residual strength is 80 to 100 percent of the peak. This is a substantial difference when one considers that it is the residual values that should be used in any design.

The differences between peak and residual values are probably attributable to the creation of a smooth plane along the interface during shearing. For textured sheet against typical clays, the residual interface strengths are close to the residual clay strengths. The failure surface may pass through the clay instead of along the interface. At site 1 the residual interface strength is 11 degrees and tests show that the residual soil strength is 12 degrees, indicating that the interface strength may indeed reflect the clay strength. The higher residual strengths for tests involving amended soils may be the result of higher soil strengths.

Test Parameters. Comparing the data presented here with other published data would be valuable but may not be reasonable because the investigators do not all use similar test procedures. A few factors that need to be considered in developing standard test procedures and methods of interpretation are as follows:

- During the flooding stage before shear testing, the sample may be placed under the full test normal load or just enough normal load to counteract swelling. Data provided in Table 3 indicate that the two loads result in different interface strengths. For example the friction angle for material 5C against textured HDPE decreased from 8.5 degrees under PCU conditions to 7 degrees under UU conditions.

- The gap size between the upper and lower box influences the failure surface. Limited testing indicates that different failure surfaces resulted when the gap was reduced from 6.4 mm to 2.5 mm.

- The displacement rate of 0.762 mm per minute does not allow the sample to drain, but undrained conditions cannot be assured. The strain rate and soil condition need to be determined.

- The type of geomembrane used in addition to the type of soil affects the results.

Other factors affecting the test results are discussed by Takusumi et al. (1991).

Interpretation. All the tests performed in this study were stopped at the 30.5 mm displacement. The strength at 30.5 mm displacement was lower than peak strengths. There are no guidelines regarding the displacement levels that will be providing residual strengths. This is an important factor because refuse strengths are generally argued to be fully mobilized at large displacements and therefore residual interface strengths should be used in the stability analyses.

Simulation of Field Conditions. After installation of the FML on top of the low permeability layer, the interface may get wet due to a combination of rain, leachate migration, migration of water caused by the consolidation of soil, and water vapor collecting under the FML from thermal effects that would draw moisture from the underlying soil (Seed and Boulanger, 1991).The field conditions that exist at a composite

liner interface during and after construction should be assumed to be saturated and may consist of one of two scenarios:

- Unconsolidated undrained conditions representing the construction or refuse placement phases.
- Partially consolidated undrained conditions representing long-term final slope configurations where the refuse has been in place for some time.

CONCLUSIONS AND RECOMMENDATIONS

Based on the test results and discussions presented in this study, the following conclusions and recommendations are made:

- A database for interface shear strength parameters between textured HDPE and amended soil has been started. Residual interface friction values range from 7 to 25 degrees. These data are being compiled so they can be used for feasibility design when the site-specific amended soil has not yet been tested. Site-specific soil must, however, be tested for the final design.
- The interface strength parameters between HDPE and amended soil indicate slightly lower residual values when compared to peak values. These residual values are recorded at a displacement of 30.5 mm.
- Various factors that may affect the interface strength parameters are normal load during flooding, level of consolidation, gap between the two boxes, and the definition of residual strength.
- In the authors' opinion, an industry-wide standard test procedure and interpretation methods should be developed so that the results can be uniformly applied in the design of waste fills.

REFERENCES

Collin, A., (1846) "Recherches Experimentales Sur Les Glissements Spontanes Des Terrains Argilleux," Carilian-Goewig et Dalmont, Paris.

Converse Davis Dixon Associates, (1975) "Slope Stability Investigation, Proposed Final Slope Adjacent to the Pomona Freeway," Operating Industries Disposal Site.

Eigenbrod, K.D., and Locker, J.G., (1987) "Determination of Friction Values for the Design of Side Slope Lined or Protected with Geosynthetics," Canadian Geotechnical Journal, No. 24, pp 509-519.

Koutsourais, M.M., et.al., (1990) "Interfacial Friction Study of Cap and Liner Components for Landfill Design," Proceedings of the Fourth GRI Seminar- Landfill Closures: Geosynthetics, Interface Friction, and New Developments, R. Koerner, ed., Elsevier Publishers Ltd., England, pp 149-166.

Mathews, M.C., (1988) "The Engineering Application of Direct and Simple Shear Testing," Ground Engineering, March, pp 15-20.

Mitchell, J.K., et.al., (1990) "The Kettleman Hills Waste Landfill Slope Failure - I: Liner Interface Properties," Geotechnical Engineering, ASCE, Vol 116, No 4, pp 647-668.

Richards, E.A., and Scott, J.D., (1985) "Soil Geotextile Frictional Properties," Proceedings of the Second Canadian Symposium on Geotextiles and Geomembranes, Edmonton, Alberta, pp 13-24.

Seed, R.B., and Bonaparte, R., (1992) "Seismic Analysis and Design of Lined Waste Fills: Current Practice," Stability and Performance of Slopes and Embankments - II, Geotechnical Engineering Division, ASCE.

Seed, R.B., and Boulanger, R.W., (1991) "Smooth HDPE-Clay Liner Interface Shear Strengths: Compaction Effects," Geotechnical Engineering, ASCE, Vol 117, No 4, pp 686-693.

Seed, R.B., et al., (1990) "The Kettleman Hills Waste Landfill Slope Failure - II: Stability Analysis," Geotechnical Engineering, ASCE, Vol 116, No 4, pp 669-690.

Singh, S., and Murphy, B.J., (1990) "Evaluation of the Stability of Sanitary Landfills," Geotechnics of Waste Fills: Theory and Practice, STP 1070, pp 240-258.

Takasumi, D.L., et. al., (1991) "Soil-Geosynthetics Interface Strength Characteristics: A Review of State-of-the-Art Testing Procedure," Proceedings of Geosynthetics '91 Conference, Atlanta, pp 87-100.

Williams, N.D., and Houlihan, M., (1986) "Evaluation of Friction Coefficients Between Geomembranes, Geotextiles and Related Products," Proceedings of Third International Conference on Geotextiles, Vienna, Austria, pp 891-896.

Williams, N.D., and Houlihan, M.F., (1987) "Evaluatin of Interface Friction Properties Between Geosynthetics and Soils," Proceedings of Geosynthetics '87 Conference, New Orleans, pp 616-627.

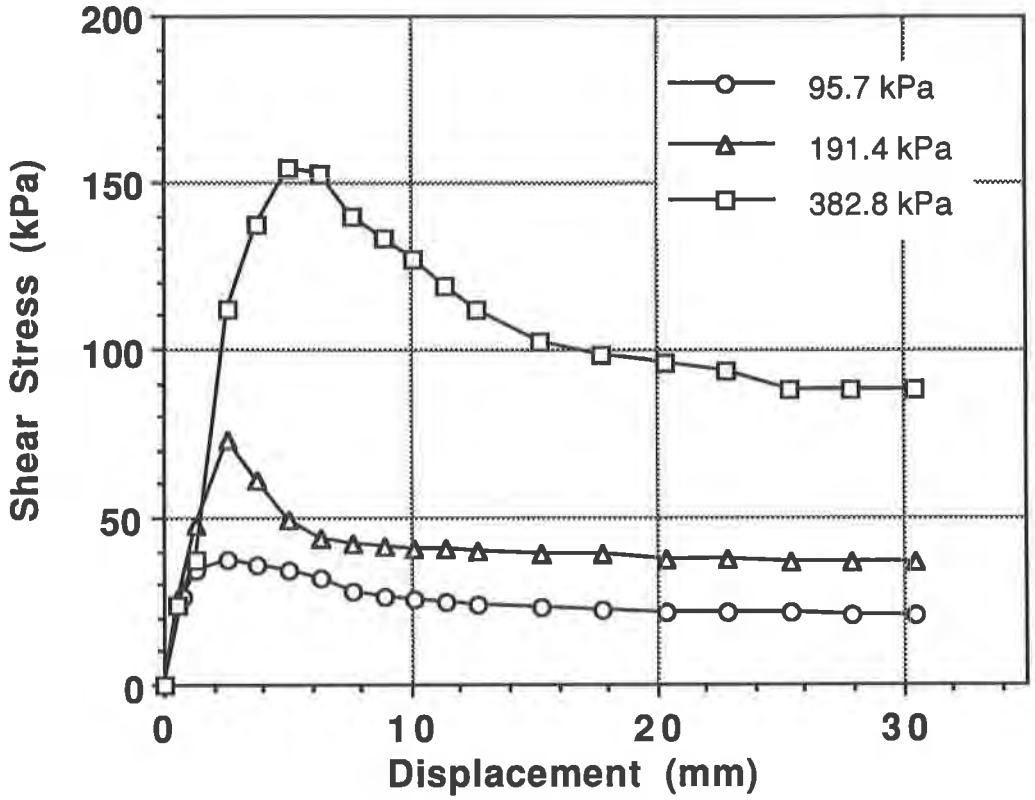

Figure 2. Site 1 - Typical Clay Interface

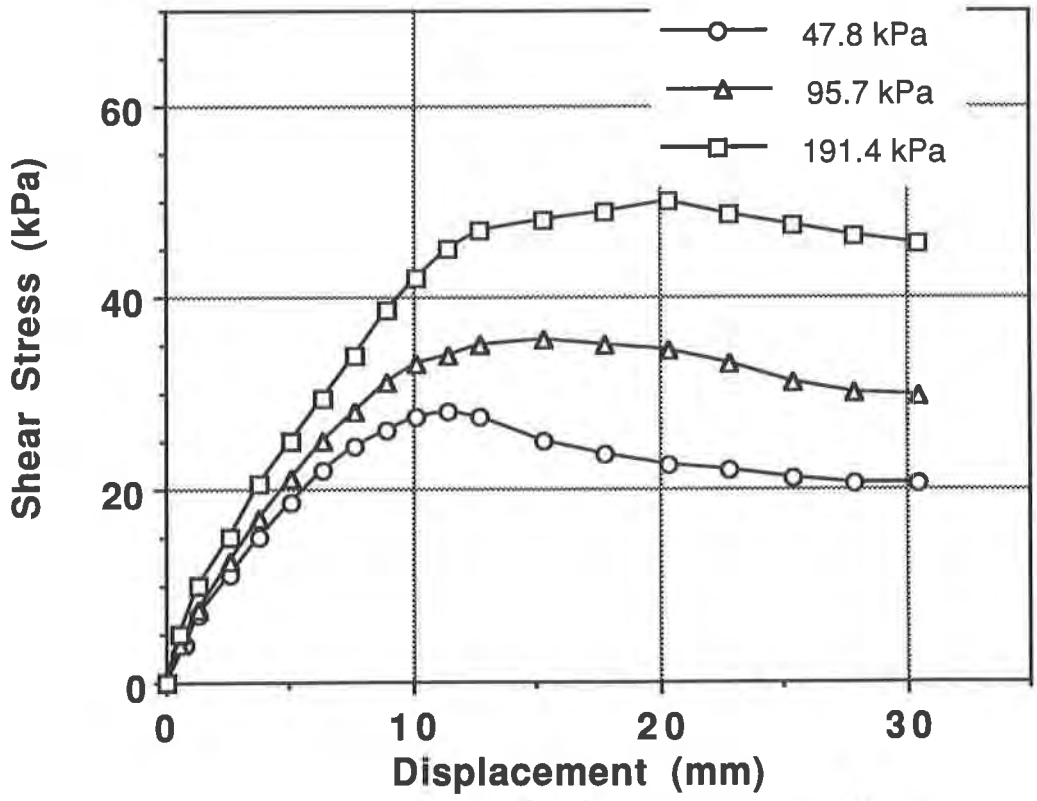

Figure 3. Site 5C - Typical Amended Soil Interface

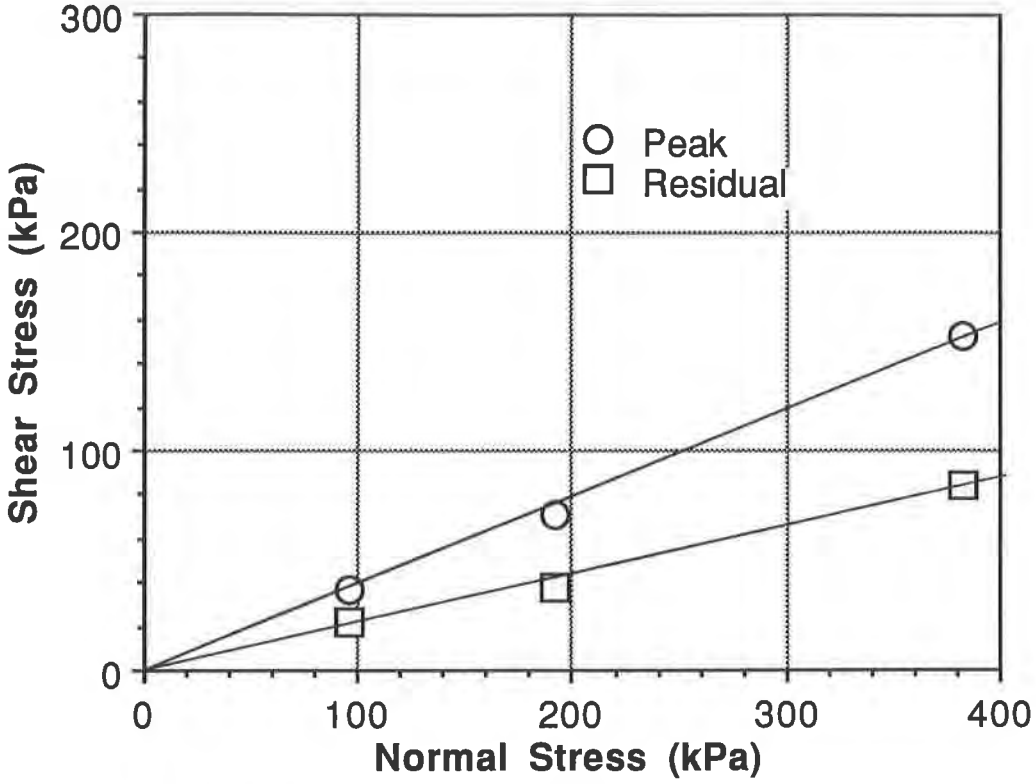

Figure 4 - Site 1 Clay/Textured HDPE Interface

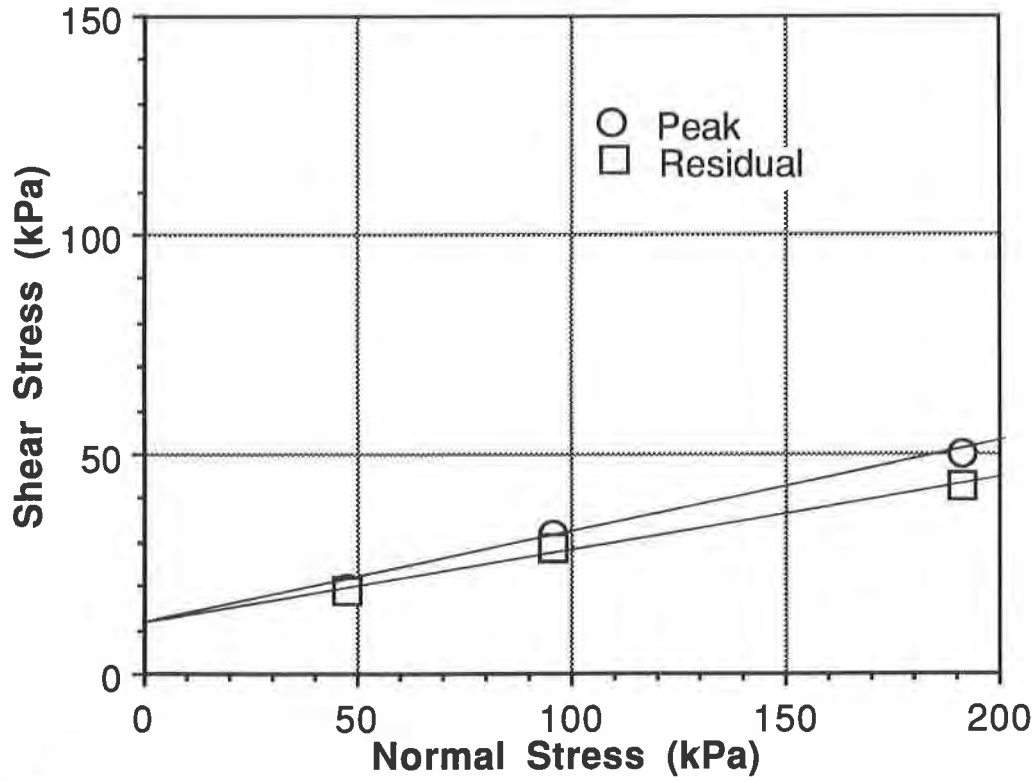

Figure 5 - Site 4 Amended Soil/Textured HDPE Interface

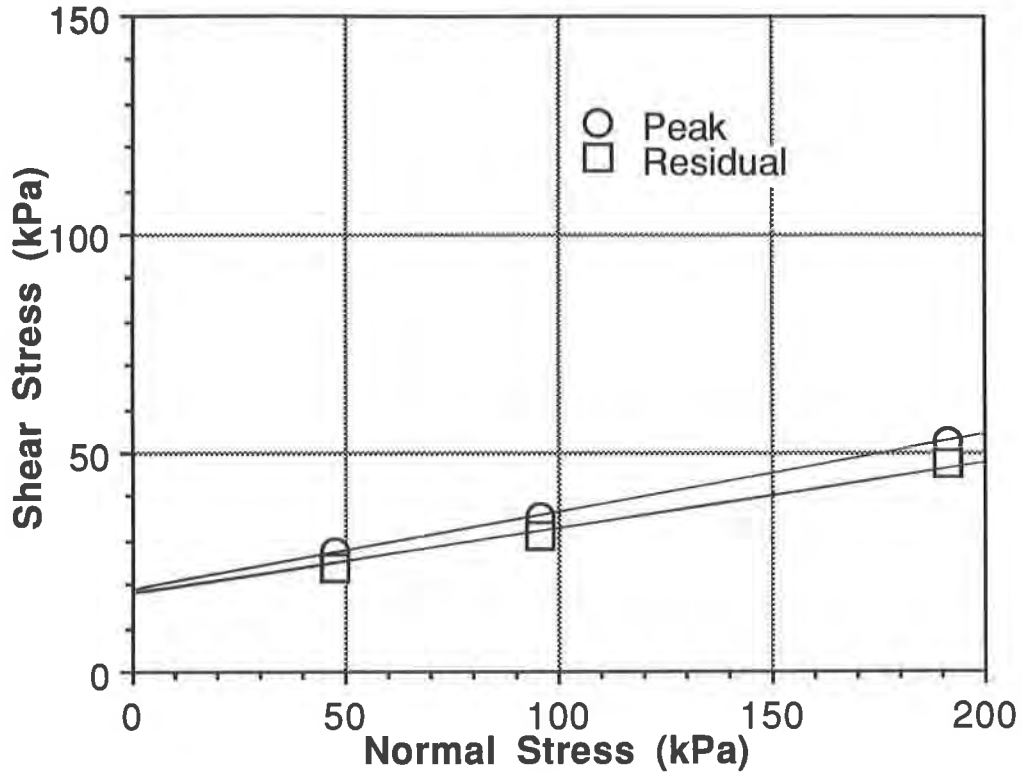

Figure 6 - Site 5C Amended Soil/Textured HDPE Interface (PCU)

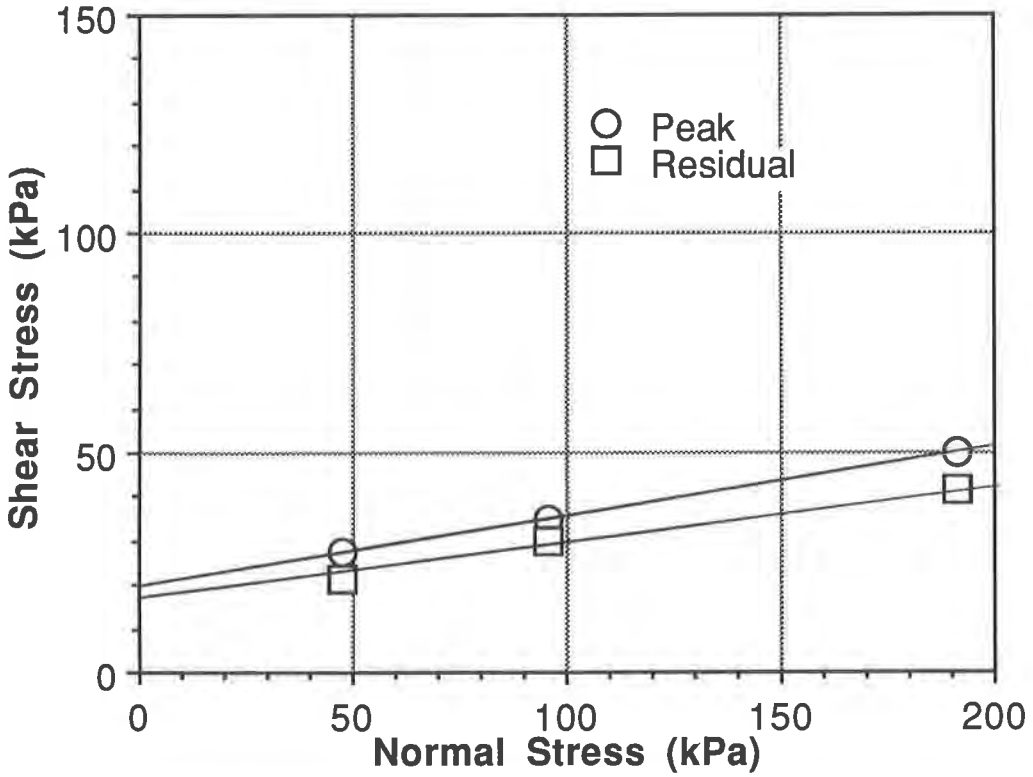

Figure 7 - Site 5C Amended Soil/Textured HDPE Interface (UU)

Effects of Partial Wetting on the Performance of the Bentonite Component of a Geosynthetic Clay Liner

D.E. Daniel
University of Texas, USA

H.-Y. Shan
University of Texas, USA

J.D. Anderson
Gundle Lining Systems Inc., USA

ABSTRACT

The bentonite component of samples of a geosynthetic clay liner (GCL) was moistened under controlled conditions. Three separate items were investigated: soil suction or soil water potential, permeability to hydrocarbons, and shear strength. The first two interrelate to the ability of the GCL to act as a barrier to hydrocarbons while the shear strength is a more general issue. The water content of the bentonite stabilized in 1 to 3 weeks at 50% when the soil suction was 15 bars and 100% for a soil suction of 1 bar. The long-term shear strength of the bentonite was insensitive to water content for water contents ≥ 50%. When the water content was ≤ 50%, the bentonite was very permeable to hydrocarbons (permeability ≈ 10^{-7} m/s), but when the water content was ≥ 100%, the permeability was very low (< 10^{-11} m/s).

INTRODUCTION

Geosynthetic clay liners (GCL's) consist of a layer of clay (typically sodium bentonite) sandwiched between two geotextiles or attached with an adhesive to a geomembrane. The bentonite in the manufactured GCL's is essentially dry (water content ≈ 15 to 20%). Dry bentonite is strong, but bentonite saturated with water has very low shear strength. For example, Shan and Daniel (1991) report that the angle of internal friction (ϕ) for dry, unreinforced bentonite in a GCL is about 30°, but for water-saturated bentonite ϕ drops to approximately 10°. Shan and Daniel (1991) also demonstrated that dry bentonite in a GCL does not hydrate and achieve low permeability when the dry GCL is permeated directly with a concentrated organic liquid. However, Shan and Daniel showed that bentonite hydrated with water can maintain a low permeability to organic liquids for at least several months.

Gundseal® (Figure 1) consists of a 3.5-mm-thick layer of sodium bentonite mixed with an adhesive and attached to a geomembrane (typically high density polyethylene, or HDPE). The GCL may be installed with the bentonite facing downward as shown in Figure 1 or upward. If the bentonite faces downward and the GCL is placed on soil, the bentonite will normally absorb moisture from the soil but will not become fully saturated. The properties of the partly wetted bentonite are expected to be intermediate to those of dry and water-saturated bentonite, but no quantitative data were available at the beginning of this study.

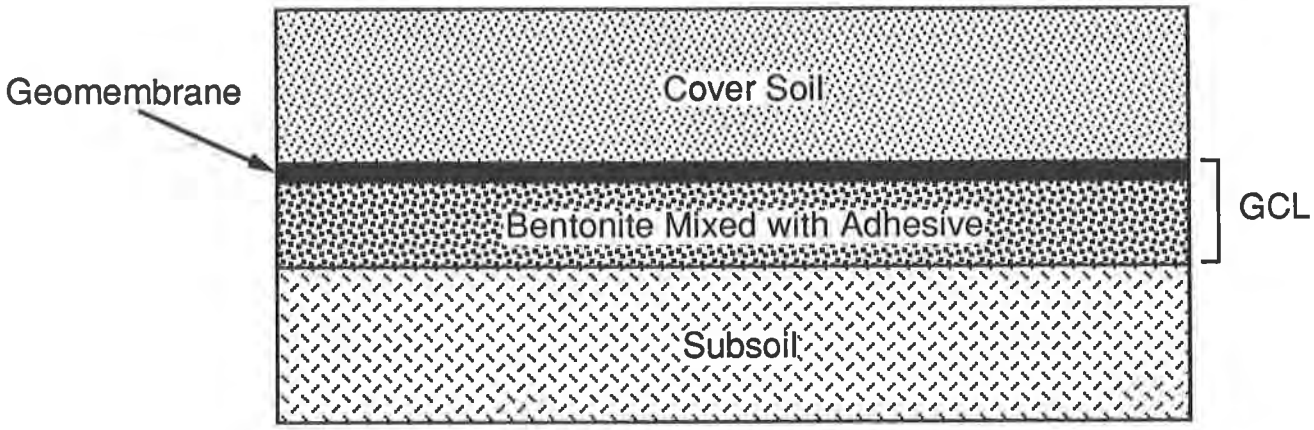

Figure 1. Geosynthetic Clay Liner (GCL) Installed with Bentonite Component Facing Downward.

The purpose of this investigation was to determine the effects of partial wetting of the bentonite component of a GCL on: (1) the shear strength of the bentonite, and (2) the permeability of the bentonite to hydrocarbons and common organic solvents. The shear strength is relevant to final cover systems for waste containment units (Koerner and Daniel, 1992) and other situations in which the GCL is placed on a permanent slope. Permeability to hydrocarbons is relevant primarily to linings for secondary containment structures for petroleum hydrocarbon and chemical storage tanks but in some situations may be relevant to landfill or impoundment liners (Daniel and Koerner, 1991).

APPROACH TO ASSESSMENT OF WATER CONTENT

If the bentonite in a GCL is placed against soil, the bentonite will either absorb water from the soil or yield water to the soil, depending on the relative energy of water in the soil and in the bentonite. Water always flows down a gradient in energy, i.e., from higher hydraulic head to lower hydraulic head. The hydraulic heads in unsaturated soils are negative relative to atmospheric pressure and are usually given names such as "soil water potential," "capillary pressure," "suction," and others. The term "suction" (defined as the negative of the soil water potential and expressed in units of pressure) is used in this paper. The unit of measure is bar (1 bar $\approx$ 1 atm $\approx$ -10 m of water head).

Dry bentonite has an extremely negative water potential. If the bentonite component of a GCL is placed against soil, water will almost always tend to flow from the soil to the bentonite. If the bentonite in a GCL is placed in contact with a soil having a known suction, the bentonite will eventually equilibrate at approximately the same suction as the soil (assuming the volume of soil is much larger than that of the bentonite). Once the relationship between water content and suction is defined for the bentonite in a GCL, the water content of the bentonite placed against soil can be predicted from the measured or estimated suction of the soil. The approach taken in this investigation was to measure the relationship between water content and suction in the bentonite component of a GCL with two independent methods. Engineers can determine the equilibrium water content of the bentonite from knowledge of the suction in the soil (measured or estimated) and the water content-suction relationship for the GCL.

MATERIALS AND METHODS

Geosynthetic Clay Liner. The GCL used in this investigation was Gundseal®. Standard material with a 0.5 mm (20 ml) thick high density polyethylene (HDPE) geomembrane and 42 g/m^2 of bentonite was tested. All tests except permeability tests were performed on the HDPE/bentonite composite. Permeability tests were performed on the bentonite alone; the bentonite layer was carefully separated from the HDPE sheet with a knife for the permeability tests.

Water Content Measurements. All water content measurements were performed by drying specimens overnight at 110°C in accordance with procedures outlined in ASTM D-2216. All water contents reported herein are gravimetric values, i.e., mass of water lost upon drying divided by the oven-dry mass of solids and expressed as a percentage.

Soil Suction Measurements. Soil suctions were measured with two techniques. With the first technique, a piece of GCL that measured about 175 by 25 mm was slowly wetted by spraying a known mass of water onto the surface of the bentonite. The moistened GCL was placed in a large test tube with the bentonite facing inward. A thermocouple psychrometer was positioned in the center of the test tube, and the test tube was sealed with a rubber stopper (Figure 2). The psychrometers were supplied by Wescor, Inc., and were read with a Keithley microvoltmeter. The test tubes were stored in a heavily insulated container and were read for 2 weeks, at which point equilibrium had been reached. The GCL specimen was then removed and oven dried to determine water content.

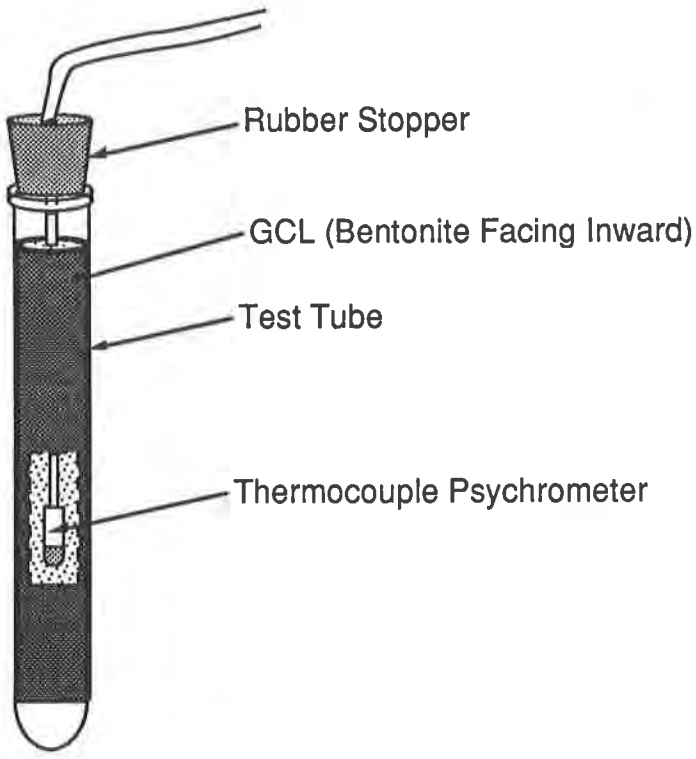

Figure 2. Suction Measurement with Thermocouple Psychrometer.

The second method of measurement involved placing 25 mm square pieces of GCL samples in sealed vessels that contained salt solutions with known vapor pressures. Test specimens were periodically removed and oven dried to determine water content. The salt solutions that were used and the corresponding equilibrium suction values were as follows:

Salt Solution	Equilibrium Suction (bars)
0.0218 M NaCl	1
0.110 M NaCl	5
0.357 M NaCl	16
1.13 M NaCl	52

The water contents reported herein were measured on specimens that had been exposed to the controlled vapor pressures for 66 days.

Rate of Wetting. To evaluate rate of wetting, 6 pieces of GCL, each measuring 100 by 25 mm, were placed directly in contact with sand in 20 L buckets. The sand in each bucket was wetted to a different water content. The GCL specimens were buried below about 75 mm of sand, and every several days a specimen was removed to determine the water content of both the bentonite and the sand beneath the bentonite. The last (sixth) sample was removed 42 to 44 days after each test had begun.

A grain-size distribution curve for the sand, developed with procedures described in ASTM D-422, is shown in Figure 3.

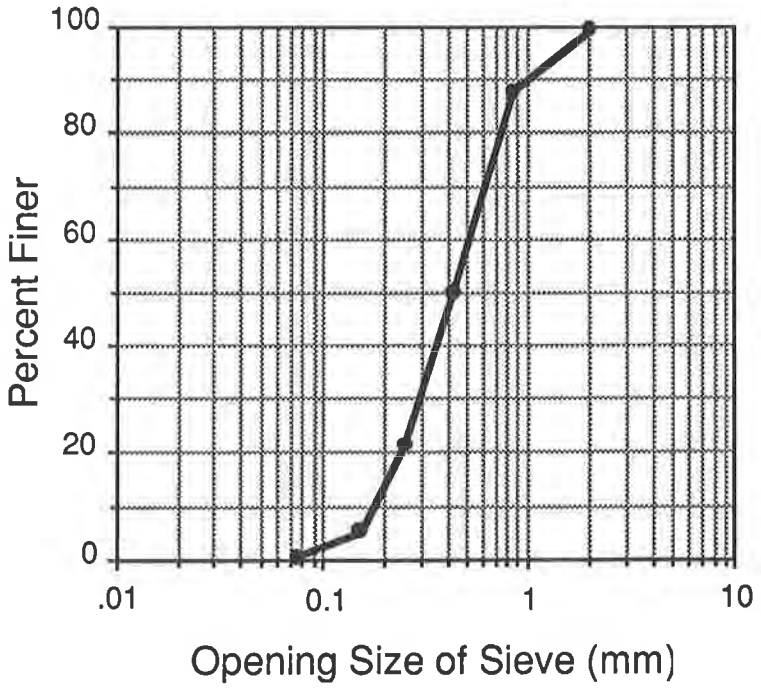

Figure 3. Grain Size Distribution Curve for Sand.

Direct Shear Tests. Direct shear tests on 60 mm diameter specimens were performed per ASTM D-3080. Samples that were sheared in a dry condition were placed in the shear box, subjected to a normal load, and then sheared. To shear saturated samples, samples of dry GCL were first placed in the direct shear box, subjected to the desired normal load, soaked with water until swelling ceased (≈ 2 weeks), and then sheared. Partially wetted samples of GCL were moistened to water contents of approximately 50% or 100% outside of the shear box, then placed in a shear box, consolidated to the desired normal stress, and sheared. Two rates of shear were used: 0.26 mm/min (16 mm/hr) and 0.0003 mm/min (0.02 mm/hr). The slow rate was selected to ensure full dissipation of excess pore water pressure generated during shear. (Consolidation rates were determined on separate specimens.) The fast shear rate is more typical of shearing rates used for geosynthetics interfacial shear tests (≈1 mm/min is common). Failure was forced through the bentonite as close to the center of the bentonite as possible. After shear, the water content of the bentonite was determined.

Permeability. Permeability tests were performed on 100 mm diameter specimens of GCL without the HDPE. Specimens were slowly wetted to a nominal water content of 50%, 100% or 125% and then placed in permeability cells. Tests on dry and water-saturated materials were also performed. The permeameters were equipped with stainless steel and Teflon® components. Teflon® sheeting separated the test specimens from the surrounding latex membranes. After the cells were assembled, the chambers were filled with water and the specimens were consolidated to a stress of 14 kPa. Then the organic liquid of interest was introduced. However, for tests on water-saturated samples, the bentonite was first permeated with tap water and then with the organic liquid. The head of liquid was approximately 300 to 600 mm, and the resulting hydraulic gradient was 80 to 120. The thicknesses of the specimens used for calculating permeability were 3.5, 4.0, 5.5, 6.0, and 6.5 mm for initial water contents of 17, 50, 100, 125, and 145%, respectively. The tests were performed per ASTM D-5084, except that the samples were not back pressured. Testing duration was typically 2 months.

The organic liquids used in the investigation were benzene, gasoline, methanol, tert-butylethylether (MTBE), and trichloroethylene. Some of the properties of the liquids used in this study (obtained from the literature) are summarized in Table 1.

Table 1. Typical Properties of Permeant Liquids

Liquid	Dielectric Constant	Density (g/cc)	Viscosity (cp)
Benzene	2.284	0.8765	0.652
Gasoline	-	0.68	0.43
Methanol	32.63	0.7914	0.597
MTBE	-	-	-
TCE	3.4	1.4996	0.55
Water	81	1	1.002

RESULTS

Water Content - Suction Relationship. Table 2 summarizes the water content and suction data that were obtained with the thermocouple psychrometer and vapor equilibrium methods. The relationship between water content and suction is plotted in Figure 4. The measured water contents ranged from 17% (dry bentonite) to 145% (bentonite soaked in water at a compressive stress of 14 kPa). The suctions ranged from 0 to about 50 bars.

Table 2. Water Content - Suction Results

Water Content (%)	Suction (bars)	Method of Measurement
17	---	(Water Content of GCL as Received)
17	43	Thermocouple Psychrometer
18	44	Thermocouple Psychrometer
24	49	Thermocouple Psychrometer
28	43	Thermocouple Psychrometer
29	52	Vapor Equilibrium
31	25	Thermocouple Psychrometer
46	14	Thermocouple Psychrometer
54	16	Vapor Equilibrium
56	8	Thermocouple Psychrometer
66	7	Thermocouple Psychrometer
79	6	Thermocouple Psychrometer
89	5	Vapor Equilibrium
96	4	Thermocouple Psychrometer
101	1	Vapor Equilibrium
145	0	Direct Soaking with 14 kPa Compressive Stress

Many people are unaccustomed to dealing with suction values. One or two points of reference may be helpful. One useful reference is 15 bars of suction, which is approximately equal to the wilting point of many plants. Plants can suck water out of unsaturated soils that have suctions as large as approximately 15 bars. Plants will wilt and die if the soil suction exceeds about 15 bars. If the bentonite in the GCL studied is placed against soil at the wilting point (15 bars of suction), the water content of the bentonite is expected to equilibrate at about 50%. In all but very arid climates, it is reasonable to assume that the water content of the bentonite will be at least 50% if the bentonite is placed against the soil.

Moist soils that support lush vegetation are likely to have suctions in the range of 0 to 1 bar. The equilibrium water content of the bentonite in the GCL placed upon such soils would be at least 100% and probably closer to 140% if the suction approaches 0.

The following table summarizes the practical implications of the test results:

Soil on Which the GCL is Placed	Approximate Water Content (%) of Bentonite in GCL
Extremely Dry Soil that Will Not Support Plant Growth (Soil Suction > 15 bars)	< 50%
Damp Soil that Will Support Sparse Growth of Plants (1 bar ≤ Soil Suction ≤ 15 bars)	50% - 100%
Moist Soil that Will Support Growth of Lush Vegetation (0 bars ≤ Soil Suction ≤ 1 bar)	100% - 140%
Wet (Practically Saturated) Soil (Soil Suction ≈ 0)	> 140%

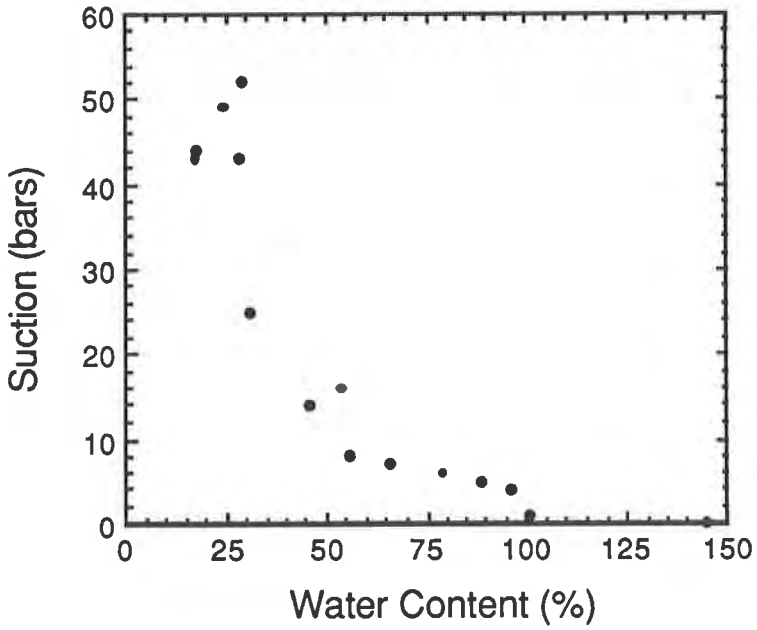

Figure 4. Relationship between Water Content and Suction for Bentonite in the GCL.

Rate of Water Content Change. The water content of the GCL samples placed in contact with sands having various water contents is plotted versus time in Figure 5. The equilibrium water content ranged from 50% for the driest sand to 190% for the wettest sand. Most of the change in water content occurred in less than 1 week for the wettest sand and less than 2 to 3 weeks for the driest sand. From a practical standpoint, the equilibration time for bentonite placed in contact with soil was 1 to 3 weeks.

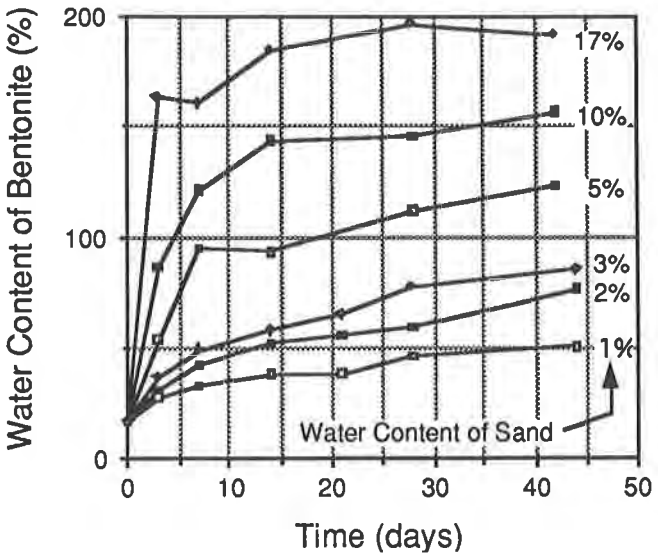

Figure 5. Water Content Versus Time for Samples of GCL Placed in Contact with Sand at Various Water Contents.

Shear Strength. The results of the direct shear tests are plotted in Figure 6. The shear and normal stresses at failure, and water contents, are tabulated in Table 3. Linear failure envelopes shown were computed by regression analysis. Cohesion and friction angles associated with the failure envelopes plotted in Figure 6 are summarized in Table 4.

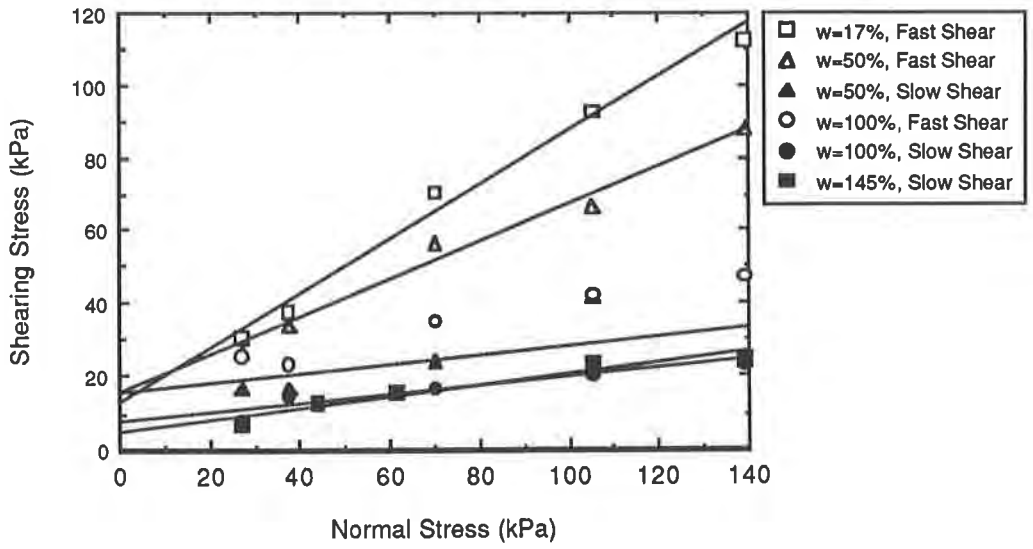

Figure 6. Mohr-Coulomb Diagrams for GCL Sheared at Various Water Contents.

Table 3. Results of Direct Shear Tests.

Water Content (%)		Shearing	Conditions at Failure	
			Normal	Shearing
Nominal	After Failure	Rate	Stress (kPa)	Stress (kPa)
17	17	Fast	26.8	30.9
17	17	Fast	37.3	37.7
17	17	Fast	70.1	70.2
17	17	Fast	105	92.8
17	17	Fast	139	112
17	17	Slow	27.1	19.1
17	17	Slow	35.9	26.5
17	17	Slow	71.0	36.3
17	17	Slow	106.2	52.9
50	58	Fast	26.8	27.0
50	57	Fast	37.3	33.8
50	58	Fast	70.1	56.2
50	57	Fast	105	66.3
50	56	Fast	139	87.4
50	38	Slow	26.8	16.8
50	46	Slow	37.3	17.0
50	51	Slow	70.1	24.5
50	46	Slow	105	41.8
50	81.7	Slow	139	23.9
100	82	Fast	26.8	25.9
100	111	Fast	37.3	23.2
100	92	Fast	70.1	35.0
100	94	Fast	105	42.4
100	79	Fast	139	47.2
100	128	Slow	26.8	8.4
100	101	Slow	37.3	14.7
100	96	Slow	70.1	17.0
100	66	Slow	105	20.9
100	83.01	Slow	139	23.6
145	---	Slow	26.8	7.4
145	---	Slow	44.1	13.0
145	---	Slow	61.5	15.5
145	---	Slow	105	23.2
145	---	Slow	139	25.2

Notes:
1. Samples were wetted to the approximate desired water content, placed in direct shear box, consolidated under specified normal load, and then sheared.
2. Shearing speeds were 0.26 mm/min (fast shear) and 0.0003 mm/min (slow shear).

Table 4. Results of Least Square Linear Regression Analysis.

Nominal Water Content (%)	Shearing Speed	Cohesion (kPa)	Friction Angle (Degrees)
17	Fast	13	36
17	Slow	10	22
50	Fast	15	27
50	Slow	15	7
100	Fast	19	12
100	Slow	8	7
145	Slow	5	9

The rate of shear had an important impact on the test results. For dry material, the angle of internal friction dropped from 36° to 22° when the rate of shear was decreased from 0.26 mm/min to 0.0003 mm/min. However, the most significant conclusion from this work is that for samples sheared slowly, even a slight wetting of the soil causes a significant reduction in the angle of internal friction of the bentonite. For example, the friction angle for bentonite with a nominal water content of 50% was 7°, which, within the limits of experimental accuracy, is virtually identical to the value for saturated bentonite (9°).

Permeability to Hydrocarbons. Results of the permeability tests are summarized in Table 5. The permeability of the bentonite component of the GCL to hydrocarbons was relatively high (on the order of 10^{-7} m/s, which corresponds to 10^{-5} cm/s) when the initial water content (w_o) was 17% or 50%. However, when the water content was increased to 100% or greater, the permeability was 10^{-11}m/s or less. For samples marked "no flow" the permeability decreased to a value that was too small to measure (< 10^{-12} m/s). These results are consistent with those published by Shan and Daniel (1991) and demonstrate that the beneficial effects of hydration of the bentonite occur when the bentonite is less than fully saturated with water.

Table 5. Summary of Results of Permeability Tests.

	Permeability (m/s)				
Permeating Liquid	w_o = 17%	w_o = 50%	w_o = 100%	w_o = 125%	w_o = 145%
Benzene	3×10^{-7}	2×10^{-7}	5×10^{-11}	No Flow	No Flow
Gasoline	4×10^{-7}	4×10^{-7}	4×10^{-11}	No Flow	No Flow
Methanol	3×10^{-7}	3×10^{-7}	3×10^{-11}	No Flow	No Flow
MTBE	2×10^{-7}	3×10^{-7}	$<1 \times 10^{-11}$	No Flow	No Flow
TCE	4×10^{-5}	4×10^{-7}	3×10^{-10}	No Flow	No Flow
Water	$1\text{-}2 \times 10^{-11}$	----	----	----	----

Plots of permeability versus pore volumes of flow are presented in Figures 7 - 12.

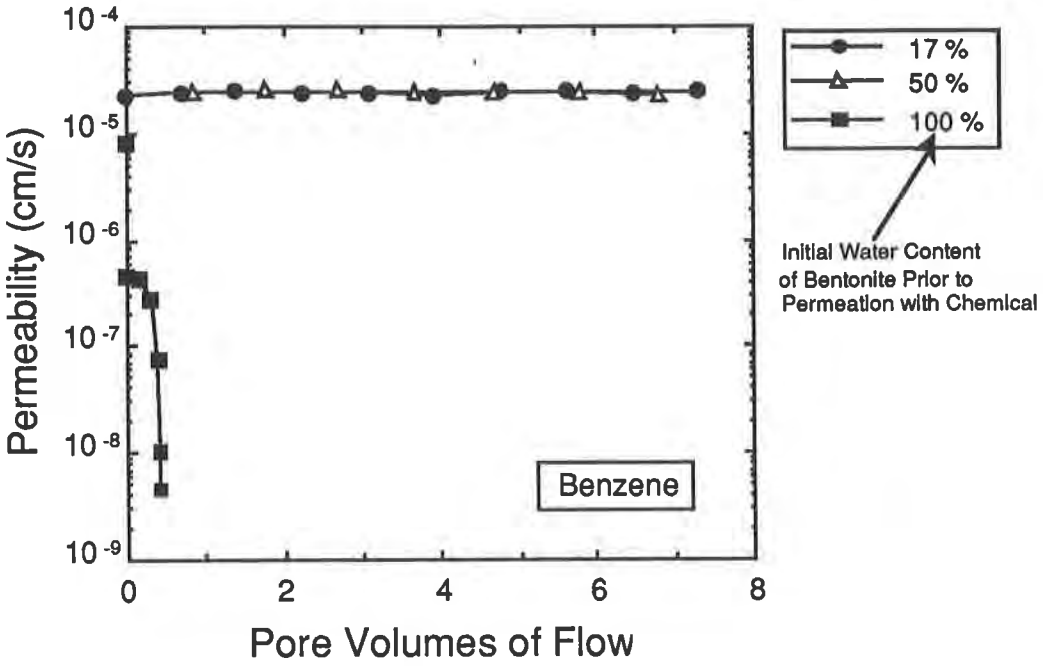

Figure 7. Coefficient of Permeability Versus Pore Volumes of Flow for Samples of the Bentonite Component of a GCL Permeated with Benzene.

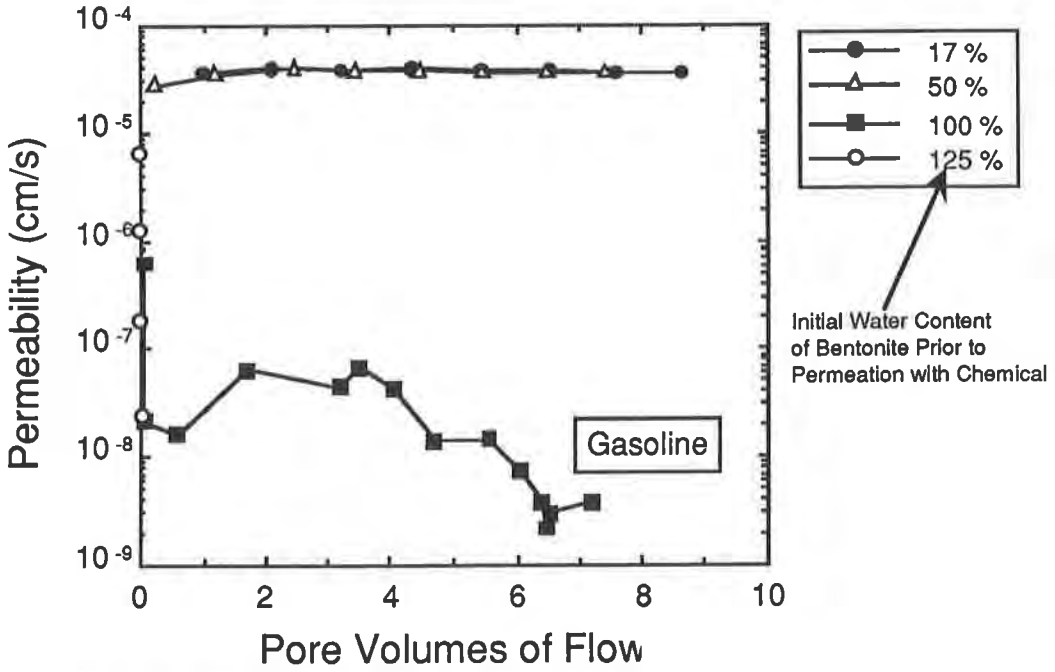

Figure 8. Coefficient of Permeability Versus Pore Volumes of Flow for Samples of the Bentonite Component of a GCL Permeated with Gasoline.

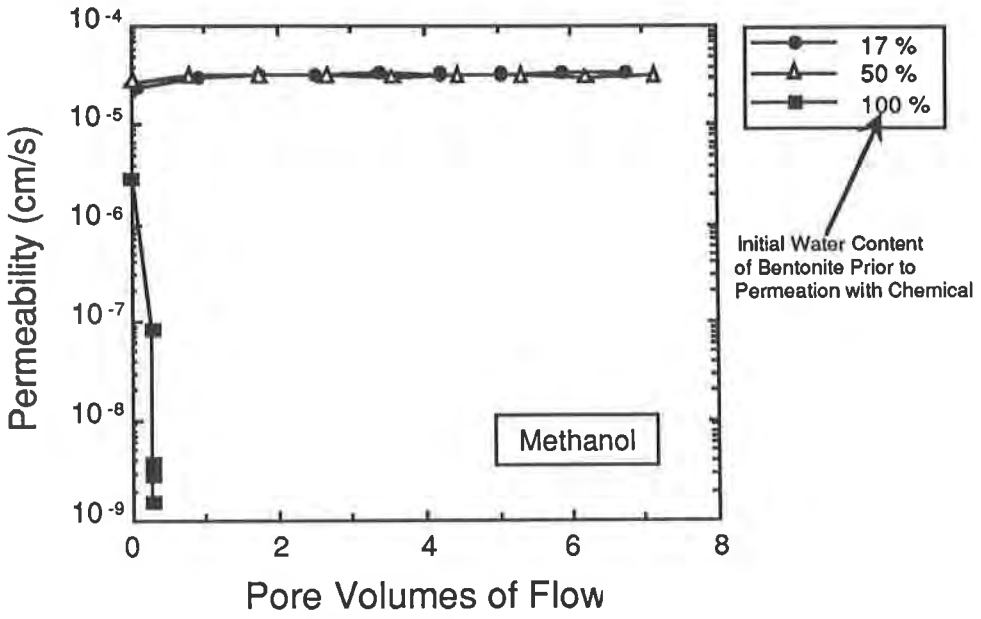

Figure 9. Coefficient of Permeability Versus Pore Volumes of Flow for Samples of the Bentonite Component of a GCL Permeated with Methanol.

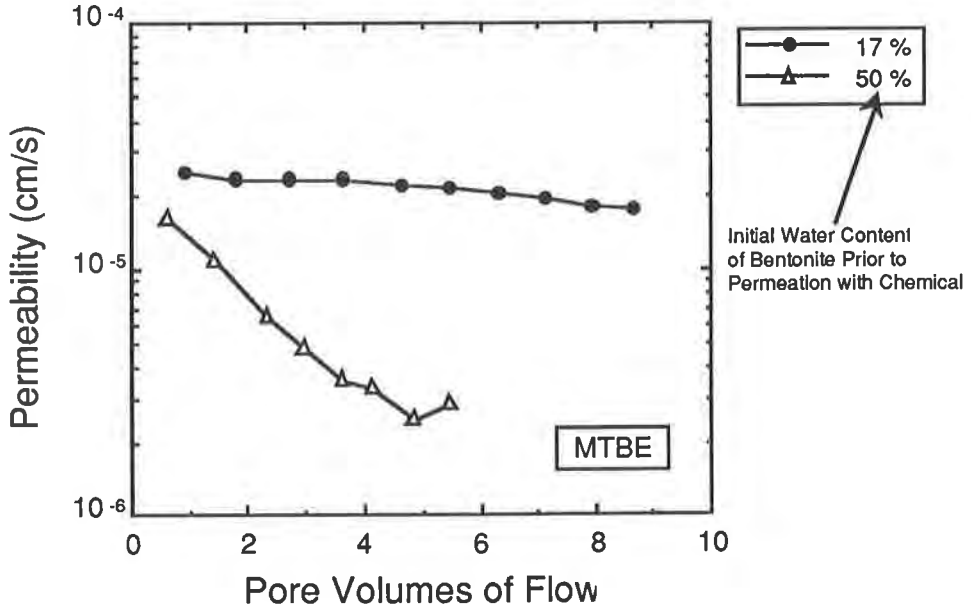

Figure 10. Coefficient of Permeability Versus Pore Volumes of Flow for Samples of the Bentonite Component of a GCL Permeated with MTBE.

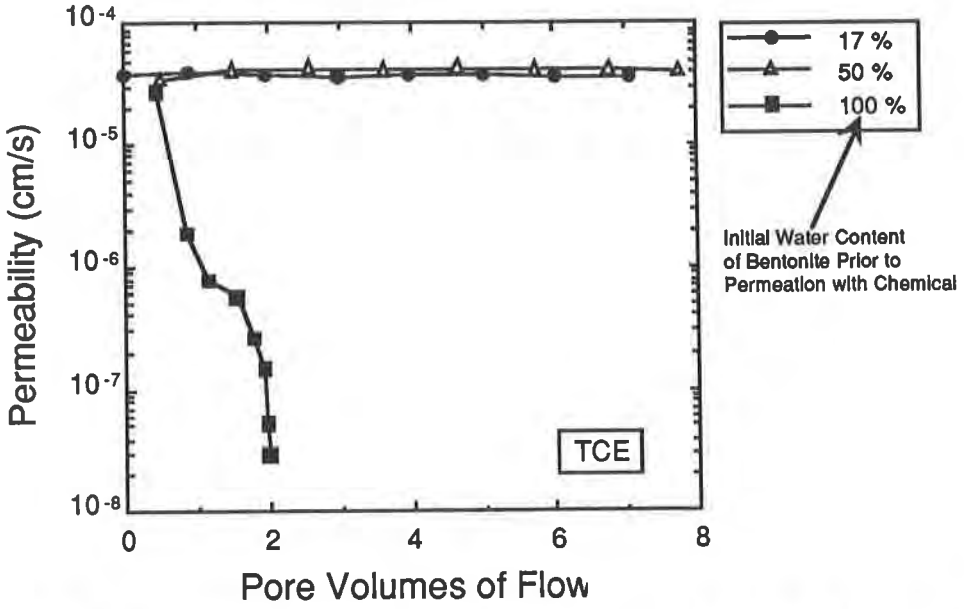

Figure 11. Coefficient of Permeability Versus Pore Volumes of Flow for Samples of the Bentonite Component of a GCL Permeated with Trichloroethylene.

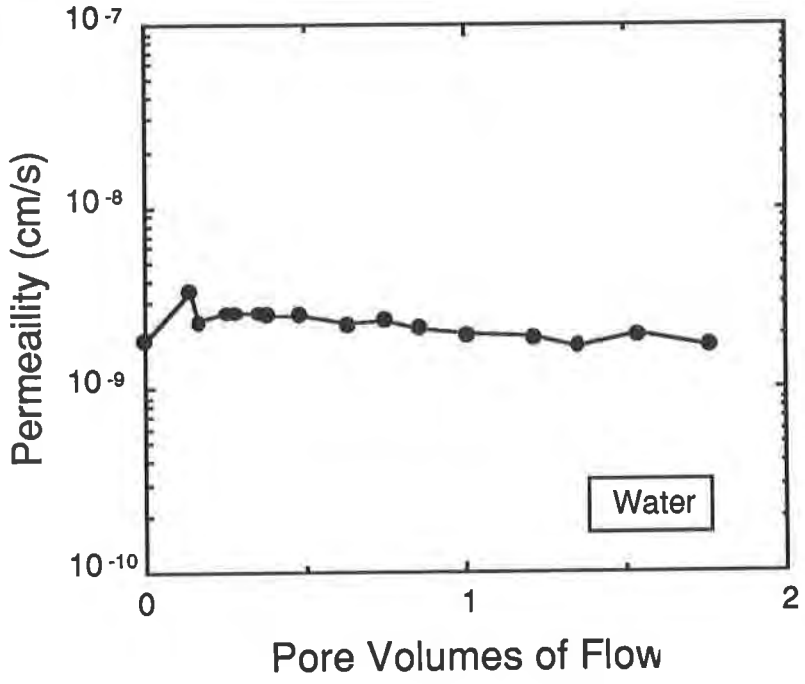

Figure 12. Coefficient of Permeability Versus Pore Volumes of Flow for Samples of the Bentonite Component of a GCL Permeated with Water.

CONCLUSIONS

The following conclusions are drawn from the results of tests described in this paper.

1. A relationship exists between the equilibrium water content of the bentonite component of the GCL that was investigated and the soil water potential (soil suction). Dry bentonite in the GCL has a water content of approximately 17%. If the bentonite side of the GCL is placed against soil that has a suction of 15 bars (the wilting point of typical plants) and the GCL is buried beneath cover soil, the bentonite will absorb moisture from the soil and equilibrate at a water content of approximately 50%. If the bentonite side of the GCL is placed against moist soil with a suction < 1 bar, the water content of the bentonite is likely to rise to 100% or more. The time required for the bentonite to absorb water and reach equilibrium is approximately 1 to 3 weeks.

2. The shear strength of the bentonite component of the GCL that was investigated was found to be sensitive to the water content of the bentonite and the rate of shear. For rapid shear of dry bentonite, a friction angle of 36° was measured. For slow shear on bentonite with a water content ≥ 50%, friction angles on the order of 10° were measured.

3. The permeability of the bentonite component of the GCL to hydrocarbons and organic solvents was found to be sensitive to the water content of the bentonite at the time that the organic liquid was introduced into the test specimens. For dry bentonite and bentonite moistened to a water content of 50%, the permeability to hydrocarbons was relatively high (on the order of 10^{-7} m/s or 10^{-5} cm/s). When the bentonite was at a water content of 100% or greater, the permeability remained low (on the order of 10^{-11} m/s or less) for the duration of the tests, which was approximately 2 months. It was not necessary for the bentonite to be completely saturated with water for it to have a low permeability to hydrocarbons and solvents.

ACKNOWLEDGMENTS

This research was sponsored by Gundle Lining Systems, Inc., Houston, Texas. The authors thank Mark Cadwallader and Fred Struve of Gundle for their continued support and for their suggestions and insights into issues concerning GCL and related products.

REFERENCES

Daniel, D.E., and R.M. Koerner (1991), "Landfill Liners from Top to Bottom," *Civil Engrg.*, 61(2), 46-49.

Koerner, R.M., and Daniel, D.E. (1992), "Better Cover Ups," *Civil Engrg.*, 62(5), 55-57.

Shan, H. Y., and D. E. Daniel (1991), "Results of Laboratory Tests on a Geotextile/Bentonite Liner Material," *Geosynthetics 91*, Industrial Fabrics Association International, St. Paul, MN, Vol. 2, pp. 517-535.

Design of Liner Systems Under Vertical Expansions: An Alternative to Geogrids

D.-J. Jang
Golder Associates Inc., USA

C. Montero
Golder Associates Inc., USA

ABSTRACT

Acquiring and permitting new landfill sites is often a difficult task. An attractive alternative to present landfill owners is to permit expansions to existing landfills. This option often involves the design and permitting of vertical expansions over old landfill areas that were constructed before liners and leachate collection systems were required. At present, the literature on vertical expansions suggests that liners and collection systems overlaying old landfill areas require some type of reinforcement. The purpose of the reinforcement is to minimize the tensile strains in overlaying liner and leachate collection systems assuming a void, created by progressive degradation and sudden collapse of large objects buried in the old landfill areas, occurs.

This paper presents the results of a model study aimed to analyze and define the expression of a void occurring at depth, on the surface of a liner and leachate collection system. The purpose of the model is to define the shape of the deformed surface, and to predict the actual tensile strains on the liner surface. The model in this paper suggests that given a finite void size, excessive tensile strains will not occur; unless the object collapsing and creating a void is assumed to be in very close proximity to the liner. The model presented in this paper shows that if large objects likely to decay and create a void, are not present within 1.8 to 3 m (6 to 10 feet) (depending on the void size and the material properties used in the analysis) underneath the liner system, excessive tensile strains are not created and reinforcement of the liner is not necessary.

Four analytical models, which may be used to evaluate void-induced settlement, are briefly discussed in this paper. This paper illustrates how one of these models, which is based on an elastic solution, may be applied to the evaluation and design of a liner and leachate collection system over an existing landfill that is proposed to be expanded vertically.

INTRODUCTION

Leachate containment and removal systems are presently being constructed on existing landfills, which were developed before low-permeability liners and leachate collection systems became a regulatory and industry standard of practice. These systems are being constructed below proposed vertical expansions to reduce the infiltration of leachate generated within the newly placed waste, into the underlying old landfills.

A liner and leachate collection system constructed on an existing landfill is potentially subject to large differential settlements. The long-term performance of these systems is thus a major design consideration. Large differential settlements within existing refuse may occur due to the collapse or degradation of large objects, which have been disposed of in the old landfill. These settlements could result in tensile strains at the surface of a liner system. If the tensile strains within the liner exceed the tensile capacity of the material, whether it is a soil or a geomembrane, tension cracks or tensile failure will develop. Under extreme conditions, tension cracks will reduce the effectiveness of the liner as a hydraulic barrier by providing a direct flow path through the liner system.

Differential settlements occurring below a liner and leachate collection system could also affect the slope at which the liner and leachate collection systems have been constructed. Again, under extreme conditions, this could result in the reversal of leachate flow grades. If grade reversal takes place at the surface of a liner and leachate collection system, leachate will pond on the liner, and the potential for infiltration of the leachate into the old landfill will increase.

This paper presents an approach to analyze the differential settlement at the surface of a liner system caused by the collapse of a void within an existing landfill. On the basis of this analysis, a new design method is presented and described. This paper summarizes methods currently available to estimate "void-induced" differential settlements. One of these methods is further discussed and an example using this design method is provided. Conclusions and recommendations based on the proposed analysis and results are also presented.

Current Design Practice. Presently, two methods are being used to minimize the potential damage of a liner and leachate collection system constructed between an existing landfill and a vertical expansion. These methods consist of either reinforcing the liner system with synthetic geogrids or improving the subgrade by stabilizing the in-situ refuse before constructing a liner and leachate collection system above it.

Geogrid reinforcement is one of the techniques most frequently applied in these cases. The design of the reinforcement is based on the assumption that a void is located immediately underneath the liner. The liner is then treated as a plate bridging over the void and carrying the loading from the overlying waste. Structural geogrids are placed to support and protect the integrity of the liner system (12, 13). The design methodology used in geogrid reinforcement is based on the tensioned membrane theory. When differential settlement takes place, the

geogrid deflects into the depression as tensile stresses develop in the geogrid.

The other method, stabilizing existing refuse areas, includes surcharging, deep dynamic compaction, and lime/fly ash slurry injection, among others (2). Time and/or field constraints often render these methods impractical for the development of vertical expansions.

All the methods currently in use are based on the assumption that "void-induced" settlement will impair the liner. Since none of these methods require the calculation of the settlement, it is unknown whether "void-induced" settlement is a real or perceived problem. And, whether other alternatives such as providing a thick buffer, or a strain-transition zone offers as effective a solution as those methods currently in use. The calculation of "void-induced" settlement, and the evaluation of an alternative design methodology are the subjects of this paper.

REVIEW OF METHODS FOR ESTIMATING DIFFERENTIAL SETTLEMENT

To date, the authors are not aware of a specific methodology used to quantify the settlement resulting from the presence of a void within a landfill. However, similar situations are often encountered in mining and classical geotechnical fields. Several methods to analyze "void-induced" settlement have been developed and are documented in mining and geotechnical journals and conference proceedings. The following four methods of analysis are briefly discussed in this paper:

- Mining Subsidence Empirical Methods (3,4), which include influence and profile functions;
- Numerical Methods (5,18), which include finite element (FE) and finite difference (FD) methods;
- Displacement Method (11);
- Two-dimensional and Three-dimensional Elastic Solutions (15, 16).

Mining Subsidence Empirical Methods. A mechanism similar to the collapse of a large object within an existing landfill and the resulting differential settlement at the surface of a liner system exists in mining (3,4). Mining subsidence occurs in a bowl-shaped pattern. Empirical methods have been developed to analyze the subsidence of "long-wall" mines, an underground mining technique mainly used in rock formations. The method applied in a specific geographical region is unique, based on the geological characteristics of the region. Because there is no generic solution available for all geographical regions, this method is not suitable for the analysis of differential settlements for a landfill vertical expansion configuration.

Numerical Methods. Finite element analyses of a void within a soil layer have been conducted in several research fields other than landfill engineering. Wang, M. C., et. al. used a finite element analysis and a physical model to analyze the bearing capacity of a shallow footing above a void embedded in clay (18). The results of Wang's finite element analysis and the results of

the model tests appear to confirm one another.

Drumm, E. C., et. al. also used finite element analysis to evaluate the deformation of highly plastic soils in contact with cavitose bedrock. The calculated settlements were presented as a function of cavity size in a paper titled "Analysis of Plastic Soil in Contact with Cavitose Bedrock" (5).

Displacement Method. "Closed-form" solutions for the strain field in an initially isotropic and homogeneous incompressible soil due to near-surface ground loss were presented by Sagaseta, C. (11). The differential settlement of a point on a plane is calculated in this method, as a function of the displacement of other points. The applications of the closed form solutions to some typical problems indicate that the calculated movements agree quite well with experimental observations and compare favorably with other commonly used numerical methods.

Elastic Solution. In the Conference of Engineering Geology of Underground Movements, in September 1987, an analytical elastic method to evaluate settlements caused by voids at depth was presented by Y. Tsur-Lavie, et. al. The method can be used to calculate the surface settlement as a function of the dimension of the void, thickness of medium (soil/rock) over the void, and Poisson's ratios. The method presented is based on a solution developed by Golecki (7,8) for stresses and displacements in an infinite homogeneous elastic half space, with discontinuous step-like uniform boundary displacement representing the collapsing of a void. The displacement in the surrounding medium and the resulting differential settlement at the medium surface is then calculated by the elastic method.

The results obtained from the analytical elastic method were compared with British National Coal Board (NCB) mining subsidence field measurement data by Tsur-Lavie, et. al., and are in close agreement with one another.

Summary. Several analytical and numerical methods are presented in the previous sections. All the methods discussed are capable of calculating differential settlements resulting from the existence of a void at depth.

The numerical methods discussed, i.e., the finite element and the finite difference methods, are suitable for the analysis of problems with nonhomogeneous, anisotropical materials. However, the displacement method and the elastic solution method discussed above, require little or no material properties for the analysis, and therefore can be readily applied to a vertical expansion design. Of these two methods, the elastic solution has the advantage that it has been calibrated by field measurements and it allows the performance of sensitivity analyses based on different soil or waste characteristics. The elastic solution method is easier to apply than the finite element analysis, and since it neglects arching in the waste, it also provides conservative results.

The following section discusses how Tsur-Lavie, et. al's Elastic Solution Method was

used to analyze the effect of "void-induced" differential settlement on a liner system constructed underneath the proposed vertical of an existing landfill.

ELASTIC SOLUTION MODEL APPLIED TO A VERTICAL EXPANSION LINER SYSTEM DESIGN

Differential Settlement Mechanism. Differential settlement in a vertical expansion liner system takes place when the surrounding waste in the existing landfill moves toward and, in the extreme case, fills in the void created by the degradation of a large object such as a large household appliance. A model was developed to analyze this mechanism, as shown on Figure 1. In this model, soil and waste are represented by a half space medium. Surface differential settlements in the model are influenced by the following factors:

- Engineering properties of the medium;
- The thickness of the medium over the void (T);
- The containment liner system grade (α); and
- The void size (length L_x x width L_y x depth D).

To quantify the influence of these factors on surface deformation, an influence function is first developed. The differential settlement can then be calculated and evaluated with the influence function.

The following sections describe the approach, assumptions and procedures used in the application of the elastic solution model, to the design of a liner constructed for the vertical expansion of an existing landfill.

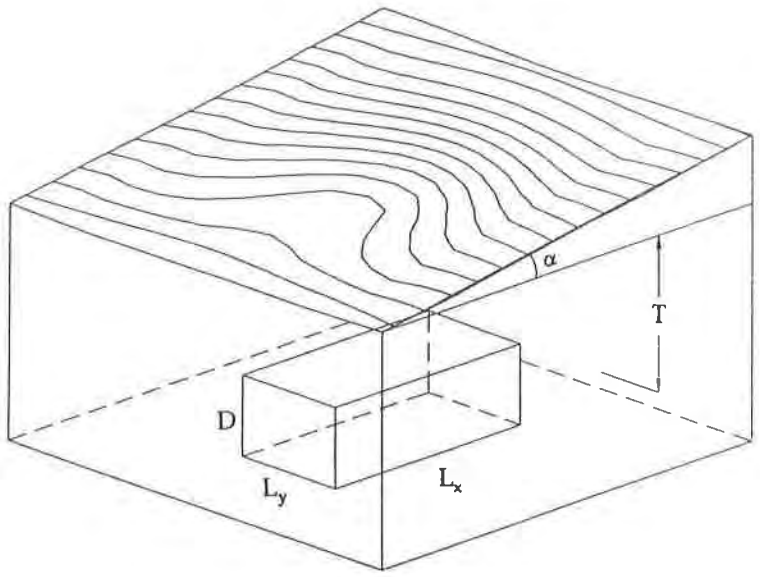

Figure 1 Differential settlement model - three dimensional Elastic Solution Model

Approach. A computer program was developed to solve the three-dimensional equations presented in Tsur-Lavie, et al's analytical elasticity solution. This computer program is capable of evaluating the differential settlement caused by voids at depth. The input variables in the program consist of the following:

- The void size (defined by L_x x L_y x D);
- The soil thickness over the void (T); and,
- Poisson's ratio of the subsiding material.

The computer program was verified by comparing its output with the characteristic curves presented in Tsur-Lavie, et. al's paper.

Assumptions. Three basic assumptions were made to model the deformation of a surface due to the presence of a void at depth. These assumptions are as follows:

- The liner surface is stress free;
- Differential settlement on a horizontal plane is projected to a graded surface; and
- A constant Poisson's ratio.

Each of the assumptions listed above is further discussed in the following sections.

Stress Free Surface. A stress free surface is one of the assumptions made in the solution of the Elastic Model. This is a conservative assumption because the strains at the liner surface are reduced by the arching effect of the material, i.e., waste, overlaying it. Mathematically, incorporating the waste above the liner could reduce the magnitude of the settlement by approximately half.

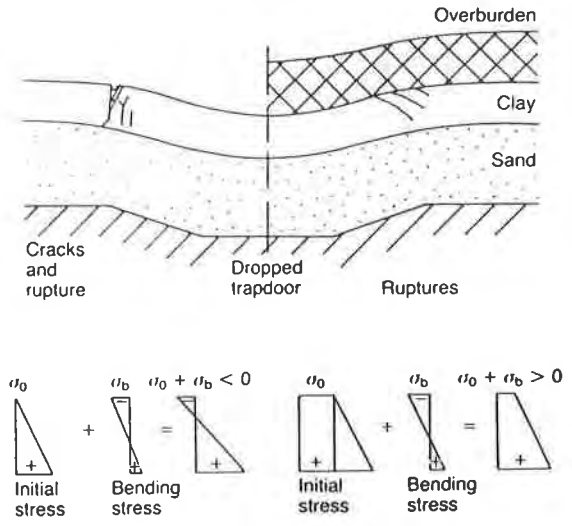

Figure 2 Influence of overburden on lateral stress level (After Jessberger and Stone, 1991)

A study on the response of clay layers subjected to differential deformations by centrifuge model tests was presented by Jessberger, et. al. (9). In this study, the effects of overburden and choice of clay liner material on the response of a model liner subjected to deformations were investigated. The test results show no tension cracks at the surface. Jessberger, et al. suggested that the suppression of tension cracking can be explained, in part, by a simple elastic interpretation of the material response, as illustrated in Figure 2. The increased initial lateral stresses generated within the liner as a result of the overburden allowed greater differential settlement of the clay liner to occur before tensile stresses could be generated. However, before reaching such stress levels, localized dislocation would take place to form multiple shear ruptures in the areas of greatest liner deformation. Consequently, tensile stresses did not arise and no tension cracks were created once rupturing occurred. It was observed from the test that the presence of shear ruptures did not affect the performance of the liner as an effective hydraulic barrier.

Differential Settlement Approximation On a Sloped Surface. To evaluate the impact of differential settlement on the liner grade, it is necessary to define the configuration of the deformed liner surface on a sloped plane. However, the Elastic Method was developed for horizontal surfaces. The model does not evaluate differential settlements on sloped surfaces.

To evaluate the surface deformation of a sloped liner surface, an approximation was made by projecting the differential settlements calculated on a horizontal surface to a sloped surface. This results in a conservative approximation because the distances between the points along the sloping surface and the void are always greater than or equal to those in the horizontal case. Therefore, the differential settlements so calculated in the sloped surface will be slightly higher than those in the horizontal case.

Poisson's Ratio. Tsur-Lavie, et. al. (15) compared the maximum differential settlement calculated with the analytical elastic model with field measurements for mining subsidence. With a Poisson's ratio of 0.5, the results of the analysis were close to the field results obtained with a void found at shallow depths. Tsur-Lavie, et. al. thus concluded that the differential settlement resulting from shallow voids was associated with a state of failure extending into the medium surface. This resulted in an increase in volume (dilatancy) and, therefore, was best represented by a model with a large Poisson's ratio. Following Tsur-Lavie, et. al's recommendations, a Poisson's ratio of 0.5 was used in the design example presented in this paper.

Calculation Procedures. An example of the application of the elastic model to design a liner system for an actual case where the vertical expansion of an existing landfill is being planned, is presented below.

EXAMPLE CALCULATION FOR THE DESIGN OF A SLOPED LINER SYSTEM

Design Problem. A void 0.9 m (3 feet) long by 0.9 m (3 feet) wide by 1.8 m (6 feet) deep is

used in the analysis. These dimensions represent a typical household refrigerator, what may be the largest object to be disposed of at a sanitary landfill.

The analysis of a liner system sloping at a 7 percent grade is presented as an example. The 7 percent sloping surface, and soil/waste thicknesses of 1.8, 2.25, 2.7, and 3.6 m (6 7.5, 9, and 12 feet), were analyzed over an area 6.4 m (21 feet) long by 6.4 m (21 feet) wide. The void is assumed to be located in the center of this area.

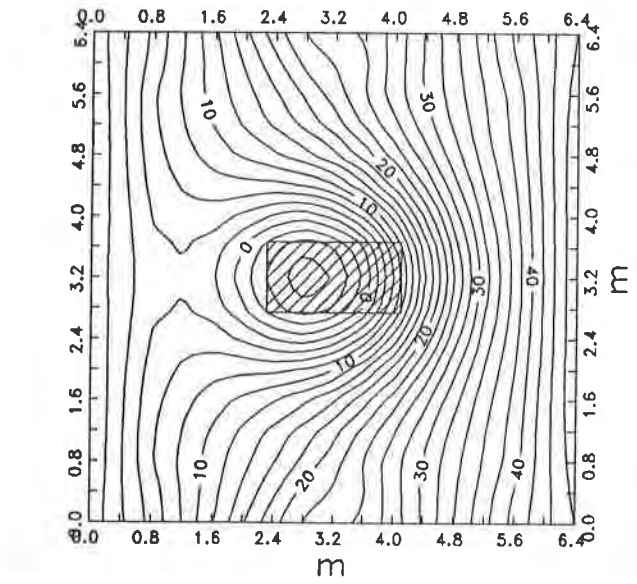

Surface Contours (cm) on 7% Slope
over 1.8 m (6 ft.) Controlled (Soil/Waste) Fill

Figure EX_1

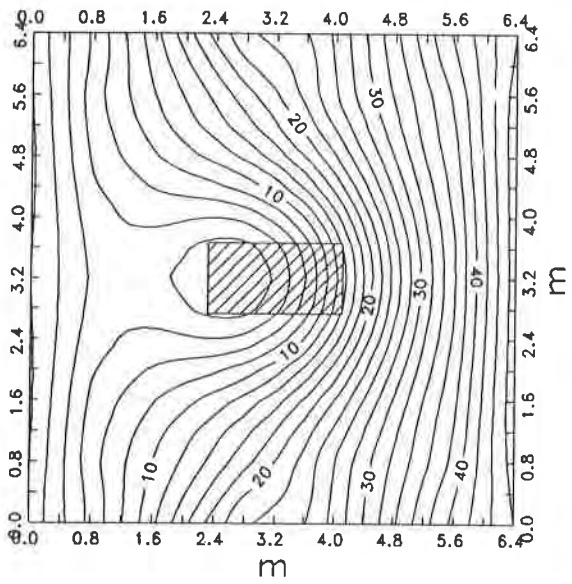

Surface Contours (cm) on 7% Slope
over 2.25 m (7.5 ft.) Controlled (Soil/Waste) Fill

Figure EX_2

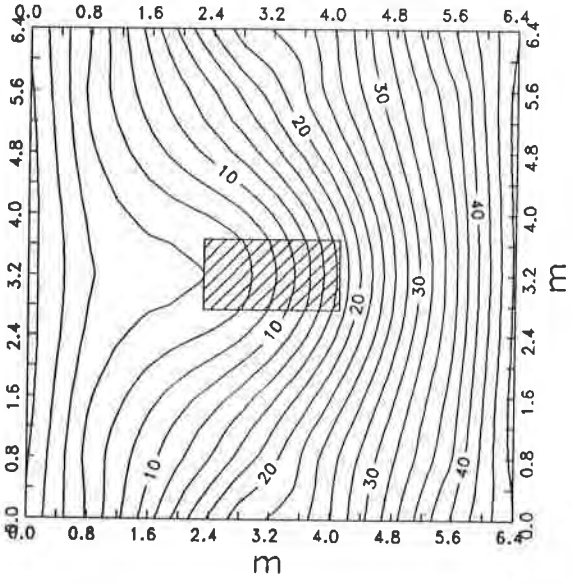

Surface Contours (cm) on 7% Slope
over 2.7 m (9 ft.) Controlled (Soil/Waste) Fill

Figure EX_3

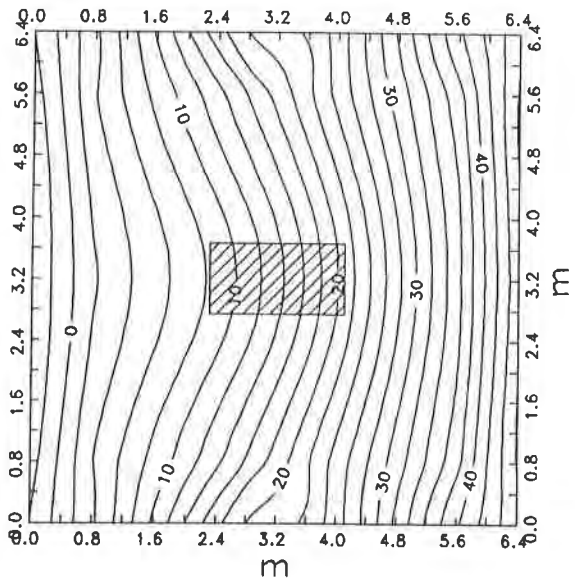

Surface Contours (cm) on 7% Slope
over 3.6 m (12 ft.) Controlled (Soil/Waste) Fill

Figure EX_4

Presentation and Discussion of Results. In a contour plot, a contour line represents the same elevation along a line. A closed contour therefore indicates either a depression or a mound. The presence of closed contours representing a deep depression is an unacceptable condition in the design of a liner system.

The deformed surface elevations in each grid point are calculated by the computer program. The deformed surface contours on the 7 percent sloping surface are then plotted for each case, as shown on Figures EX_1 - EX_4.

Where the thickness of the soil/waste layer is 1.8 m (6 feet), as shown on Figure EX_1, the presence of the void will create a depression 9 cm (0.3 feet) deep. This depression could trap and accumulate liquids, hindering the free flow of leachate towards a collection point.

When the thickness of the soil/waste layer above the void is increased to 2.25 m (7.5 feet), the depression is reduced to less than 3 cm (0.1 foot), as shown on Figure EX_2. With a 2.7 m (9 foot) thick soil/waste layer over the void, the depression disappears. The disturbance in the liner surface decreases as the depth to the void increases, as seen when the thickness of the soil/waste layer is increased to 3.6 m (12 feet) (Figure EX_3 and EX_4).

To evaluate the potential for grade reversal, a characteristic curve of required soil/waste thicknesses (T) over a 0.9 m (3 feet) wide by 0.9 m (3 feet) deep by 1.8 m (6 feet) long void versus liner surface grades (α) is illustrated on Figure 3.

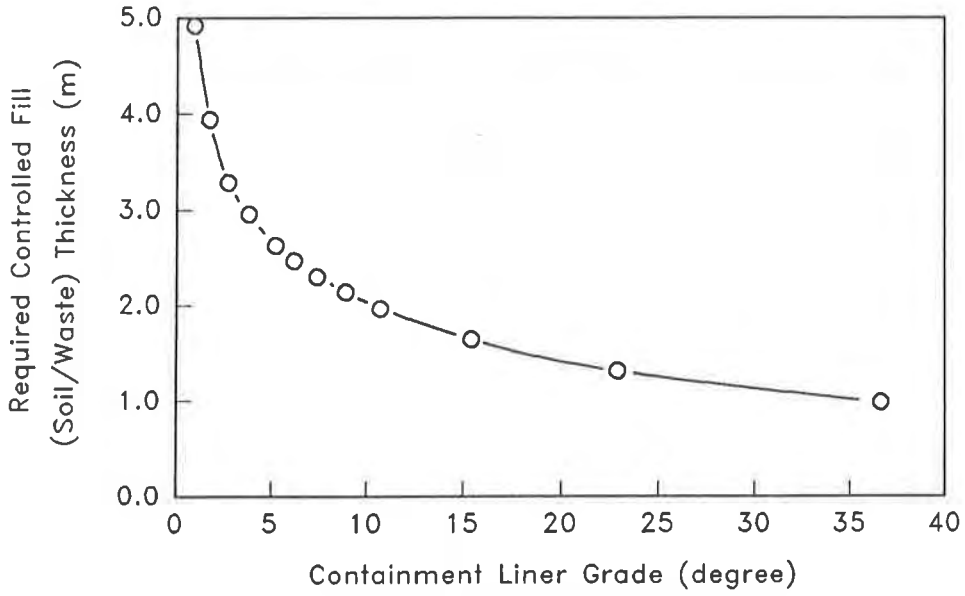

Figure 3 Required controlled fill thickness to prevent grade reversal (T) versus containment liner grade (α) on 0.9m x 0.9m x 1.8m (3'x3'x6') void

For each analysis, the tensile strains were calculated from the deformed spacing between adjacent grid points in the surface against the initial grid spacing. A characteristic curve of the maximum tensile strains versus ratio of void width (L_y) to controlled fill thickness (T) was developed from the analyses' results. This curve is presented in Figure 4.

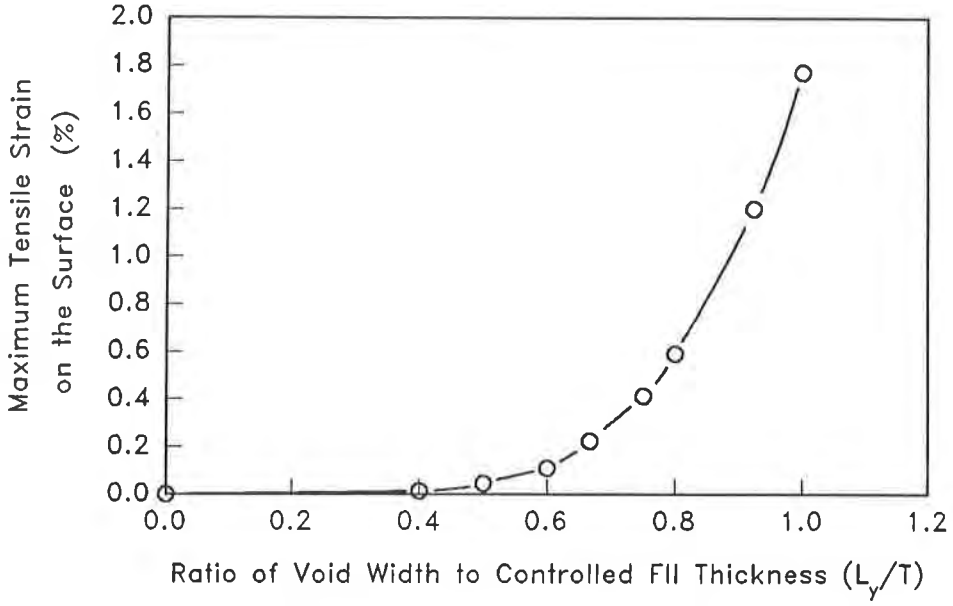

Figure 4 Maximum tensile strain versus ratio of void width/controlled fill thickness on 0.9m x 0.9m x 1.8m (3'x3'x6') void

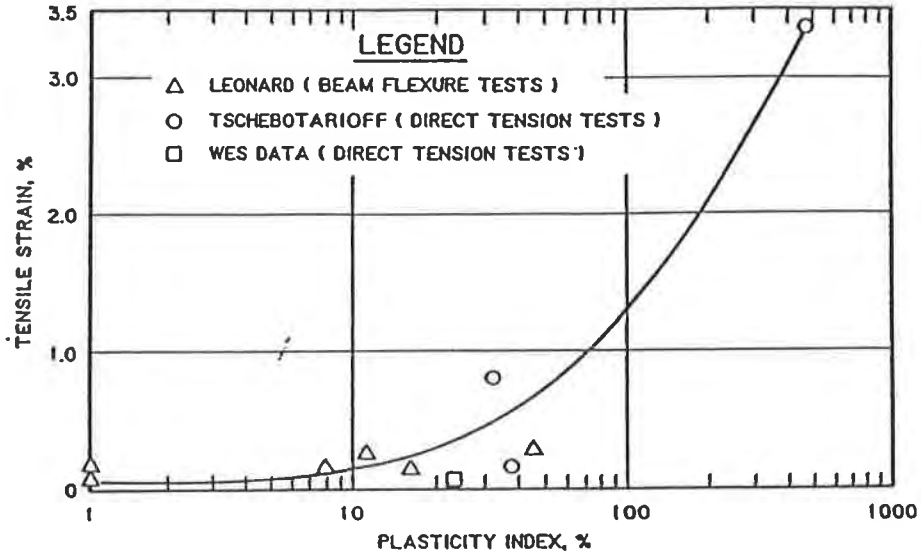

Figure 5 Tensile strain versus plasticity index (After Gilbert and Murphy, 1987)

The maximum tensile strain generated by the differential settlements was examined to evaluate the integrity of a composite liner, which included a geomembrane and a clay layer. The geomembrane can sustain tensile strains higher than those that the clay component of the composite liner can sustain before tensile failure or tension cracks develop within the clay component. Therefore, the tensile strain limit of the clay component can be used as an acceptable design criterion to evaluate the integrity of composite liners.

From the maximum tensile strains versus soil/waste thickness (T) characteristic curve, a soil layer thickness (T) equals to 2.7 m (9 feet), the maximum tensile strain caused by the 0.9 m (3 foot) wide by 0.9 m (3 foot) deep by 1.8 m (6 foot) long void is 0.2 percent. This strain is within acceptable limits for a clay layer as illustrated on Figure 5 from Gilbert and Murphy (6).

On the basis of the above example analysis, a 2.7 m (9 foot) thick soil/waste layer can serve as a strain transition zone to prevent grade reversal, excessive tensile strains and stresses developed in a liner system. Therefore, a 2.7 m (9 foot) thick layer of soil or "select" waste can be placed, in this example, before constructing the vertical landfill containment liner.

Summary. For slope angles other than the 7 percent used in the example analysis, the tensile strains and potential for grade reversal on a liner surface can be evaluated according to the thickness versus maximum tensile strain and thickness versus liner grade characteristic curves, settlement contours and containment liner design criteria. From this evaluation, the required backfill thicknesses in different liner grades and liner systems can be determined and designed to prevent grade reversal and excessive tensile strains on a vertical expansion liner and leachate collection system.

CONCLUSIONS

The Elastic Method provides a conservative and efficient method to evaluate the potential differential settlement caused by a void within an existing landfill when a vertical expansion of the landfill is planned. The results from this method closely agree with the results from British NCB's field mining subsidence surveys. The method provides a conservative estimate of the potential differential settlement, and therefore can be used to design a vertical expansion liner system.

Characteristic curves of thickness over the void (T) versus maximum tensile strain, and of thickness (T) versus maximum differential settlement slope can be developed for specific void size, as shown in the example presented in this paper. These characteristic curves can then be used for the design of containment liner systems in a landfill vertical expansion.

As shown in the characteristic curves provided, the differential settlement diminishes as the soil/waste thickness over the void increases. Thus, it is possible to increase the distance between the potential void and the surface of the liner, to reduce the differential settlement to

harmless levels.

The example analysis presented in this paper demonstrates that placing controlled fill (soil or waste) above an existing landfill is a viable and economical method to protect a non-reinforced liner system from the impact of potential excessive differential settlement. This is of particular importance because vertical expansions are often in the design phase while the existing landfill is still operating. This provides the opportunity to select the waste placed in the upper zone of the existing landfill, such that large objects are not placed in the zone immediately below the base grades of the vertical expansion liner system.

ACKNOWLEDGEMENTS

The authors would like to thank the staff of Waste Management of North America, Inc. for providing the opportunity and the means to perform this study. Also, the authors would like to thank Kuantsai Lee and Leo Overmann of Golder Associates for their support and for the time they provided to review this paper.

REFERENCES

1. Al-Hussaini, M., "Tensile Properties of compacted Soils," Laboratory Shear Strength of Soil, ASTM STP 740, 1981, pp. 207-225.

2. Blacklock, James R., "Landfill Stabilization for Structural Purposes," Proceedings of Geotechnical Practice for Waste Disposal '87, June 1987, pp. 275-293.

3. Brauner, Gerhard, "Subsidence Due to Underground Mining," (in two parts), 1973, U.S. Department of the Interior, Bureau of Mines, Denver Mining Research Center, Denver, Colorado.

4. British National Coal Board, Mining Department, Subsidence Engineers' Handbook, 1975, London, U.K.

5. Drumm, E. C., Kettelle, R. H., Manrod, W. E., "Analysis of Plastic Soil in Contact with Cavitose Bedrock," Proceedings of Geotechnical Practice for Waste Disposal '87, June 1987, pp. 418-431.

6. Gilbert, Paul A. and Murphy, William L., "Prediction/Mitigation of Subsidence Damage to Hazardous Waste Landfill Covers," Report No. EPA/600/2-87/025, U.S. EPA, March 1987, Cincinnati, Ohio.

7. Golecki, J. J., "Boussinesq-Trefftz Solution and Related Representations in Compressible and Incompressible Elastostatics," Solid Mechanics Archives, Vol. 3, Issue 2, May 1978, pp. 109-129.

8. Golecki, J. J., "Displacement Potentials and Corresponding Stress Functions in Two-Dimensional Problems of Elasticity," Solid Mechanics Archives, Vol. 4, Issue 3, August 1979, pp. 183-205.

9. Jessberger, H. L. and Stone, K. J. L., "Subsidence Effects on Clay Barriers," Geotechnique 41, No. 2, June 1991, pp. 185-194.

10. Leonards, G. A. and Narain, J., "Flexibility of Clay Cracking of Earth Dams," Journal of Soil Mechanics and Foundations Division, ASCE, Vol. 89, No. SM2, March, 1963, pp. 47-98.

11 Sagaseta, C., "Analysis of Undrained Soil Deformation Due to Ground Loss," Geotechnique 37, No. 3, September 1987, pp. 301-320.

REFERENCES
(CONT'D)

12. Stephens, A. and Bodner, R., "Geogrid Liner Support at Empire Sanitary Landfill," Conference Proceedings Geosynthetics '91, February 1991, pp. 15-22, Atlanta, Georgia.

13. Tieman, G. E., Druback, G. W., Davis, K. A. and Weidner, C. H., "Stability Consideration of Vertical Landfill Expansions," Geotechnics of Waste Fills - Theory and Practice, ASTM, STP 1070, 1990, pp. 285-302.

14. Tschebotarioff, Gregory P., Ward, Edward R. and DePhilippe, Alexander A., "The Tensile Strength of Disturbed and Recompacted Soils," Proceedings of the 3rd International Conference on Soil Mechanics and Foundations Engineering, 1953, Vol. 1, pp. 207-210, Zurich, Switzerland.

15. Tsur-Lavie, Y. and Denekamp, S., "A Boundary Element Method for the Analysis of Subsidence Associated with Longwall Mining," Proceedings of 2nd International Conference on Ground Movements and Structures, April 1980, pp. 65-74, Cardiff, UK.

16. Tsur-Lavie, Y., Denekamp, S. A. and Fainstein, G., "Surface Subsidence Associated with Longwall Mining: Two and Three Dimensional Boundary Element Model," Engineering Geology of Underground Movements, 1988, pp. 225-231.

17. U. S. EPA, "Design and Construction of RCRA/CERCLA Final Covers," Report No. EPA/625/4-91/025, May 1991, Cincinnati, Ohio.

18. Wang, M. C. and Badie, A., "Effect of Underground Void on Foundation Stability," Journal of Geotechnical Engineering, Vol. 111, No. 8, August, 1985, pp. 1008-1019.

Stability of Soil-Covered Geosynthetic-Lined Slopes: A Parametric Study

P.L. Bourdeau
Purdue University, USA

S.J. Ludlow
Purdue University, USA

B.E. Simpson
Purdue University, USA

ABSTRACT

In recent years, the use of geosynthetics has become increasingly popular, particularly in the environmental field, for the containment of solid waste. However, reported failures have resulted in a concern of the stability of soil-covered, geosynthetic-lined slopes. A parametric study was undertaken to evaluate the relative influence of the governing factors on the stability of soil-covered, geomembrane-lined slopes and on tensile forces developed in the geomembrane. The analysis was based on a modified version of the model of the static equilibrium at the interface between a cover soil layer and a geomembrane-lined slope recently proposed by Koerner and Hwu (1991). This modified formulation enables to account for the effect of the mobilized resistance to shearing at the cover soil-geomembrane interface on the tensile force developed in the geomembrane.

INTRODUCTION

Geosynthetics are commonly used for the containment of solid waste. Various liner configurations involving natural cover soils and geosynthetics are employed for such designs and are illustrated in Figure 1. Optimum design of a geosynthetic-lined system is expected to minimize the risk of subsurface (soil and groundwater) contamination by collecting leachate and maximize the volume available for the waste fill by steepening the side slopes. However, recently reported failures [e.g. Mitchell et.al. (1990)] have resulted in a concern of the stability of soil-covered, geosynthetic-lined slopes. Investigations of these failures have shown that sliding may occur at the interfaces between the components of the liner system. It is also generally agreed that significant tensions can develop in the geosynthetic layers when they are subjected to unbalanced interface friction forces. The stability of the liner system is controlled by such factors as:

- the geometry (e.g. slope length and angle);
- the shear resistance developed along the interfaces between the cover soil, geosynthetic, and sub-soil;
- the tension developed in the geosynthetic, and it's tensile strength as well as anchorage resistance;
- the passive soil resistance available at the toe of the slope; and
- the pore pressure that may develop beneath impervious flexible membranes.

Thus to prevent such failures, methods of analyses have been proposed to assess the stability of an overlying soil layer as well as the tensile stresses induced in the geomembrane [e.g. Martin and Koerner (1985), Giroud and Beech (1989) and Koerner and

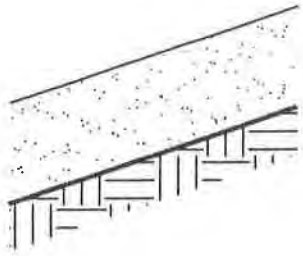

(a) single geomembrane with granular cover soil layer.

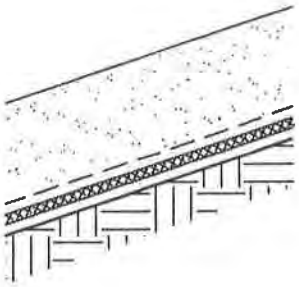

(b) single geomembrane with geotextile filter and geonet drainage layer.

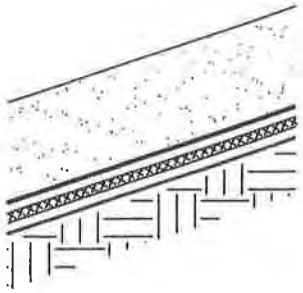

(c) double geomembrane with geonet drainage layer between.

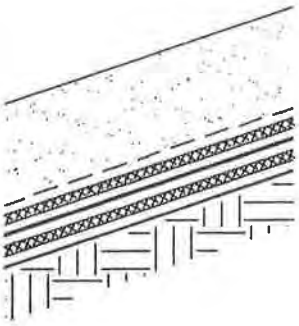

(d) double geomembrane with double geonet darainage layers.

FIGURE 1 – Various Liner Systems

Hwu (1991)]. These methods provide useful information and lead generally to conservative designs. However, they cannot account in their present form for the interaction between the mobilized shear strength of the cover soil and the tensile force development in the geomembrane because they use uncoupled equations to analyze these mechanisms.

The purpose of this paper is two fold: 1) propose a modification to the Koerner and Hwu (1991) method in order to account for the interaction between shear strength mobilization in the cover soil and the tensile force developed in the geomembrane; and 2) evaluate by a parametric study the relative influence of the governing parameters on the stability of the cover soil and on the tensile forces developed in the geomembrane. To evaluate the relative influence of the controlling parameters, a single geomembrane located between a cover and sub-soil as shown in Figure 1 (a) is considered. Although this is a simplified situation in comparison to multiple liner systems, it does help in understanding the mechanisms of the stability of a liner system.

METHOD OF ANALYSIS

Background. The basis for the method of analysis used in the present study is the analysis originally proposed by Koerner and Hwu (1991) for the static equilibrium at the interface between a cover soil layer and a geomembrane-lined slope. Their method utilizes a two wedge model represented in Figure 2. Sliding of the active wedge is resisted by the resistance to shearing along the interface with the geomembrane and by the passive soil wedge at the toe of the slope. The critical sliding surface is assumed horizontal beneath the passive wedge. Another simplification for this limit equilibrium analysis is that the interwedge forces, E_A and E_P, are assumed to act parallel to the sliding surface of the active wedge, i.e. parallel to the geomembrane. The cover soil is of uniform thickness and constant unit weight. The factor of safety, FS, with respect to sliding of the two wedge system is a solution of the quadratic equation:

$$a(FS)^2 + b(FS) + c = 0 \qquad (1)$$

where:

$$a = 0.5\gamma LH\sin^2(2\omega)$$

$$b = -[\gamma LH\cos^2\omega\tan\delta_U\sin(2\omega) + C_U L\cos\omega\sin(2\omega) + \gamma LH\sin^2\omega\tan\phi\sin(2\omega) + 2CH\cos\omega + H^2\tan\phi]$$

$$c = (\gamma LH\cos\omega\tan\delta_U + C_U)(\tan\phi\sin\omega\sin(2\omega))$$

and where:
γ, unit weight (kN/m^3)
L, slope length (m)
H, thickness of cover soil (m)
ω, slope angle (deg.)
C, cohesion of cover soil (kPa)
ϕ, angle of internal friction - cover soil (deg.)
C_U, adhesion at upper interface (kPa)
δ_U, interface friction angle (deg.) at upper interface

Readers interested in the detailed formulation of this stability equation are referred to the original paper by Koerner and Hwu (1991). It is noted that according to this methodology, the safety factor has the same value at every point along the sliding surface defined by the two wedge mechanism. In particular, the safety factor is the same with respect to the shearing resistance at the active wedge-geomembrane interface as that with respect to the shearing resistance of the cover soil beneath the passive wedge. This result, although consistent with limit equilibrium theories, is questionable from a physical standpoint. Its implication on the geomembrane liner design will be shown in the parametric study.

Another model is proposed by Koerner and Hwu (1991) to assess the tension in the geomembrane due to unbalanced interface shear forces as shown in Figure 3. Due to the downward-acting shear stresses applied by the cover soil to the geomembrane, shear stresses are developed by the underlying soil in the opposite direction at the lower

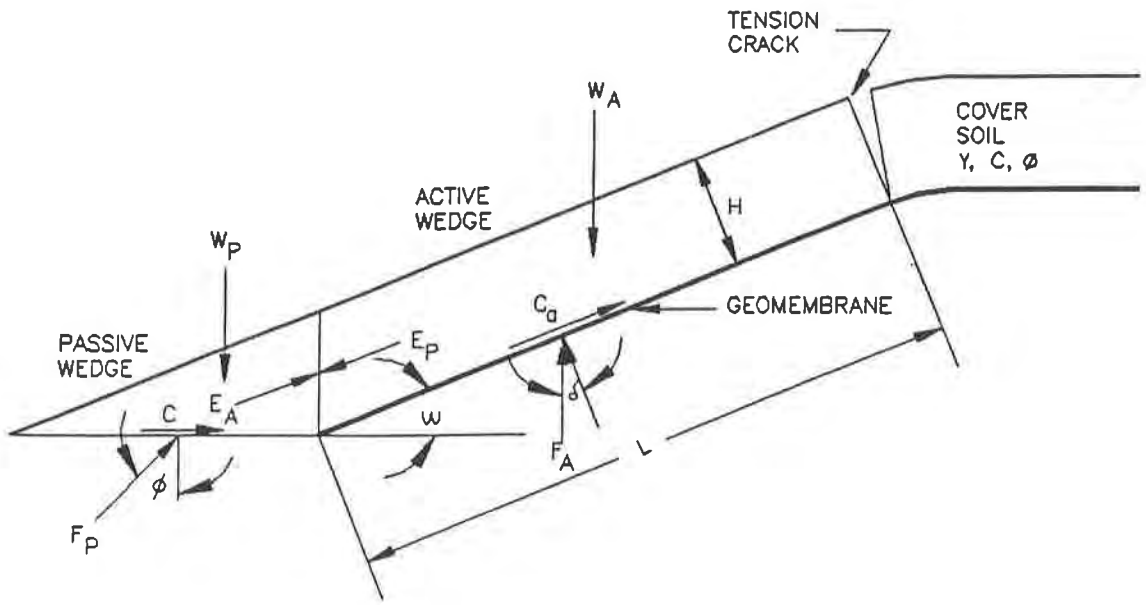

FIGURE 2 - Stability Model of Cover Soil Over Geomembrane
(Modified From Koerner and Hwu, 1991)

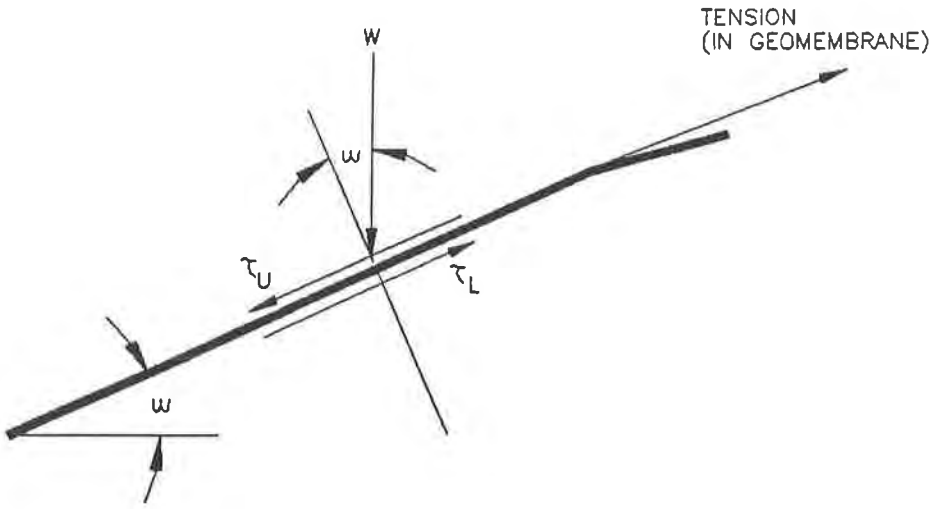

FIGURE 3 – Shear Stress Interaction on the Tensile Force in the Geomembrane
(Modified From Koerner and Hwu, 1991)

interface. According to Koerner and Hwu (1991), three cases have to be considered:

1. If the resistance to shearing at the upper interface, τ_U, is equal to the resistance at the lower interface, τ_L, the geomembrane goes into a state of pure shear where no tension exists in the geomembrane.

2. If $\tau_U < \tau_L$, the geomembrane goes into a state of pure shear up to a magnitude of τ_U and the balance of $\tau_L - \tau_U$ is not mobilized. Hence, no tension exists in the geomembrane.

3. If $\tau_U > \tau_L$, the geomembrane goes into a state of pure shear up to a magnitude of τ_L and the balance of $\tau_U - \tau_L$ is carried by the geomembrane in tension.

Assuming uniform mobilization of the interface resistances along the geomembrane the expression for the developed tensile force per unit width of slope is given by:

$$T = [(C_U - C_L) + \gamma H \cos\omega(\tan\delta_U - \tan\delta_L)]L \qquad (2)$$

where:
C_L, adhesion at lower interface (kPa)
δ_L, interface friction angle (deg.) at lower interface

Proposed Modification. Equation (2) expresses the unbalance between the maximum shear force that can act at the geomembrane upper interface and the maximum shear force at the lower interface. In concept, the shear force at the upper interface is a demand to the geomembrane free body system and the lower interface force is a capacity of reaction. When the demand is lower than the capacity (i.e. $T < 0$), the geomembrane is in equilibrium under the effect of interface forces. However, when the demand is greater than the lower interface capacity (i.e. $T > 0$), equilibrium must be ensured by a tensile force in the geomembrane equal to T. A shortcoming of this model is that the tensile force, T, computed using Equation (2) is independent of the level of shear stress effectively mobilized at the upper interface. In effect, the demand term in the expression of the force T should only represent the mobilized portion of the interface shear strength instead of the full (ultimate) resistance. In order to modify the Koerner and Hwu (1991) model in this sense, it is necessary to introduce coupling between equations (1) and (2). This can be done by replacing in equation (2) the terms

$C_U + \gamma H \cos\omega \tan\delta_U$

by:
$1/FS(C_U + \gamma H \cos\omega \tan\delta_U)$

The new expression for the tensile force in the geomembrane is then:

$$T = [(C_U/FS - C_L) + \gamma H \cos\omega(\tan\delta_U/FS - \tan\delta_L)]L \qquad (3)$$

By incorporating the two proposed models into a single model, a direct assessment of the stability of the liner system and required tension in the geomembrane can then be made which considers the mobilized shear strength at the upper interface. While, the original model assumed full mobilization.

PARAMETRIC STUDY

The modified model [equations (1) and (3)] was programmed in a spreadsheet software environment. For a given slope geometry, cover soil shear strength and a modest variation of interface properties, an evaluation of the stability of a soil-covered, geomembrane-lined slope and tensile forces developed in the geomembrane was performed. Again, a system as shown in Figure 1 (a), with parametric conditions as indicated below in Table 1 was assumed for this study. Four parametric cases were analyzed. For each case, two parameters were varied. These cases, including the parameters that were varied, consisted of: $\delta_U\delta_L$; C_UC_L; $C_U\delta_U$; and $C_L\delta_L$. In addition, a study was performed where the mechanical parameters were kept constant but the slope

angle was varied with constant slope height, D.

Table 1. Summary of Parameters

PARAMETER	VALUE
γ, unit weight (kN/m^3)	19(1)
L, slope length (m)	100(1)
D, slope height (m)	33(1)
H, thickness of cover soil (m)	0.9(1)
ω, slope angle (deg.)	18.4(2)/10 to 30(3)
C, cohesion of cover soil (kPa)	15(1)
ϕ, angle of internal friction - cover soil (deg.)	32(1)
C_U, adhesion at upper interface (kPa)	2(2)/0 to 20(3)
δ_U, interface friction angle (deg.) at upper interface	15(2)/5 to 20(3)
C_L, adhesion at lower interface (kPa)	2(2)/0 to 10(3)
δ_L, interface friction angle (deg.) at lower interface	5(2)/5 to 20(3)

Notes: (1) Typical for all cases.
(2) Constant case.
(3) Range of interest for parametric case.

DISCUSSION OF RESULTS

Mechanical Parameters. Figure 4 illustrates the relative influence of the variation of the upper (δ_U) and lower (δ_L) interface friction angles on the tension required in the geomembrane. Observations indicate the tension required in the geomembrane decreases as τ_U decreases until the shear stress state at the upper interface is equal to or less than τ_L at the lower interface. At this point, there is no tension in the geomembrane and the plot is discontinuous as shown on the left side of Figure 4. Further observation of Figure 4 confirms that if $\tau_U > \tau_L$, the geomembrane goes into a state of pure shear up to a magnitude of τ_L and the balance of $\tau_U - \tau_L$ is carried by the geomembrane in tension.

A second aspect of the computation results which also requires particular attention is the stability of the cover soil over the geomembrane (Figure 5). Although the computed tension in the geomembrane may be less than the available strength, the stability with respect to sliding of the cover soil over the geomembrane may not be adequate. Reinforcement techniques have been proposed to handle this type of situation (e.g. Giroud and Beech, 1989), however these are not analyzed herein. Observations of Figure 5 indicate the stability of the cover soil is increasing proportional to δ_U but is independent of δ_L. On the other hand, although the upper interface may have an adequate δ_U, the tension in the geomembrane may be considerably high and exceed the available strength if δ_L is low.

Figures 6 and 7 illustrate the relative influence of the variation of the upper (C_U) and lower (C_L) adhesion on the tension required in the geomembrane and the stability of the cover soil over the geomembrane. Similar observations for the interaction mechanisms of the cover soil, geomembrane and sub-soil can also be made here as in the previous case for the interface friction for δ_U and δ_L.

Figure 8 illustrates the relative influence of the variation of the upper interface strength properties (δ_U, C_U). Although C_U may provide a significant contribution to the strength along the upper interface, as indicated in Figure 8, it is often neglected in design. As the upper interface strength increases, the required tension in the geomembrane increases. The tension required in the geomembrane reaches a maximum value which is controlled by the geometry.

Figure 9 illustrates the relative influence of the variation of the lower interface strength properties (δ_L, C_L). As the lower interface shear strength is decreased, the tension required in the geomembrane increases. When τ_U is less than or equal to τ_L, tension is not developed in the geomembrane. Hence, the geomembrane is

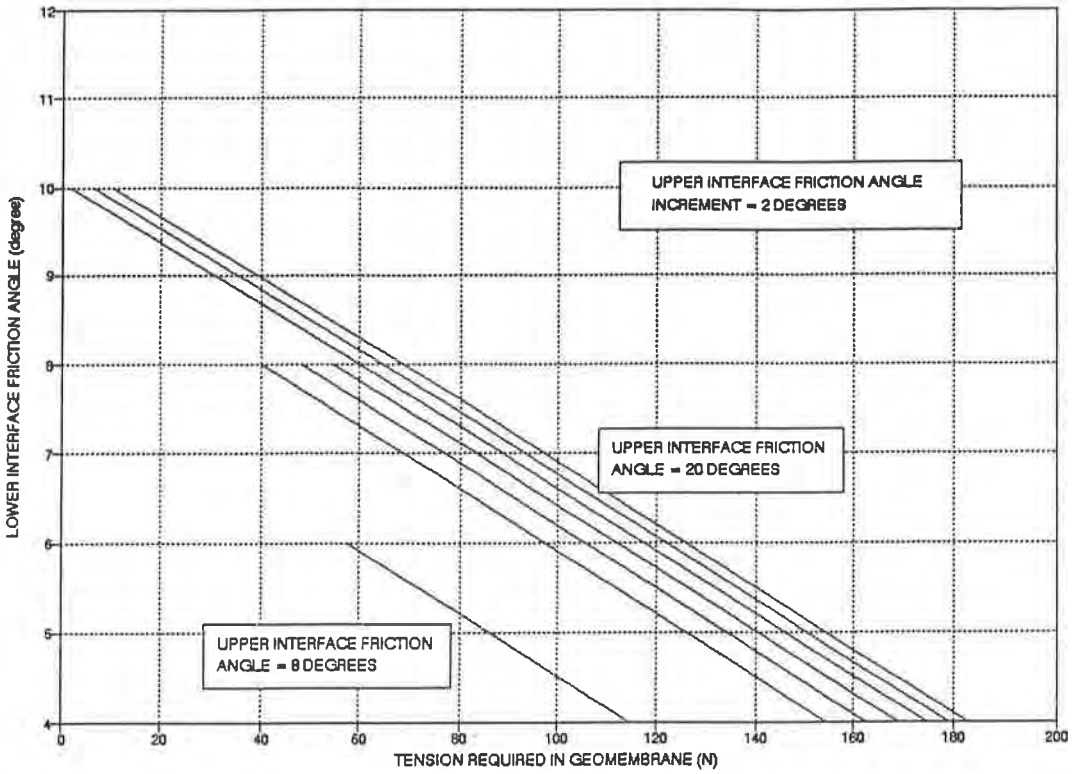

FIGURE 4 - Upper - Lower Friction Angle Variations

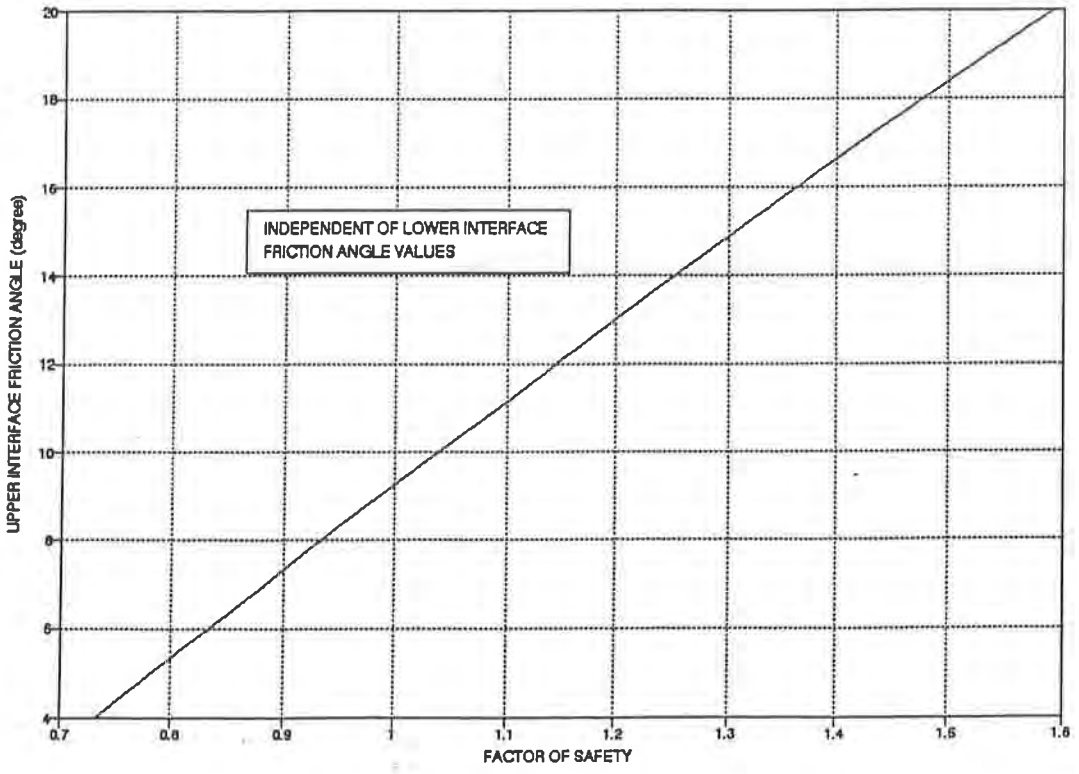

FIGURE 5 - Factor of Safety V. Upper Interface Friction Angle

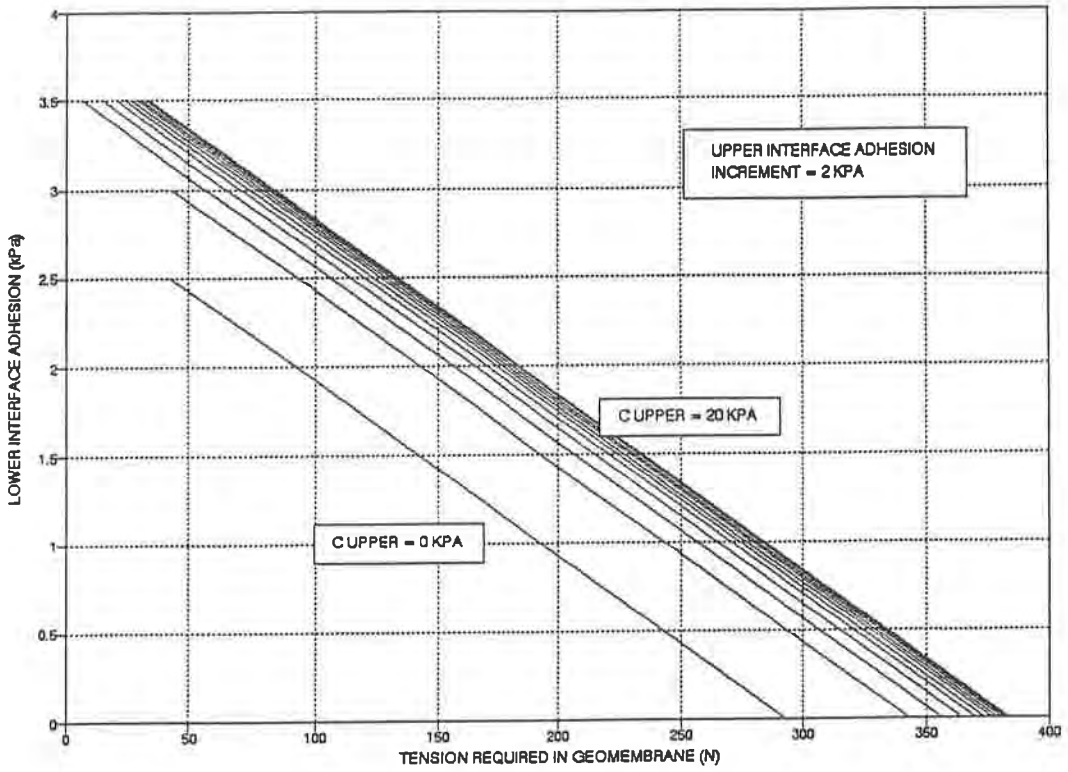

FIGURE 6 - Upper - Lower Adhesion Variations

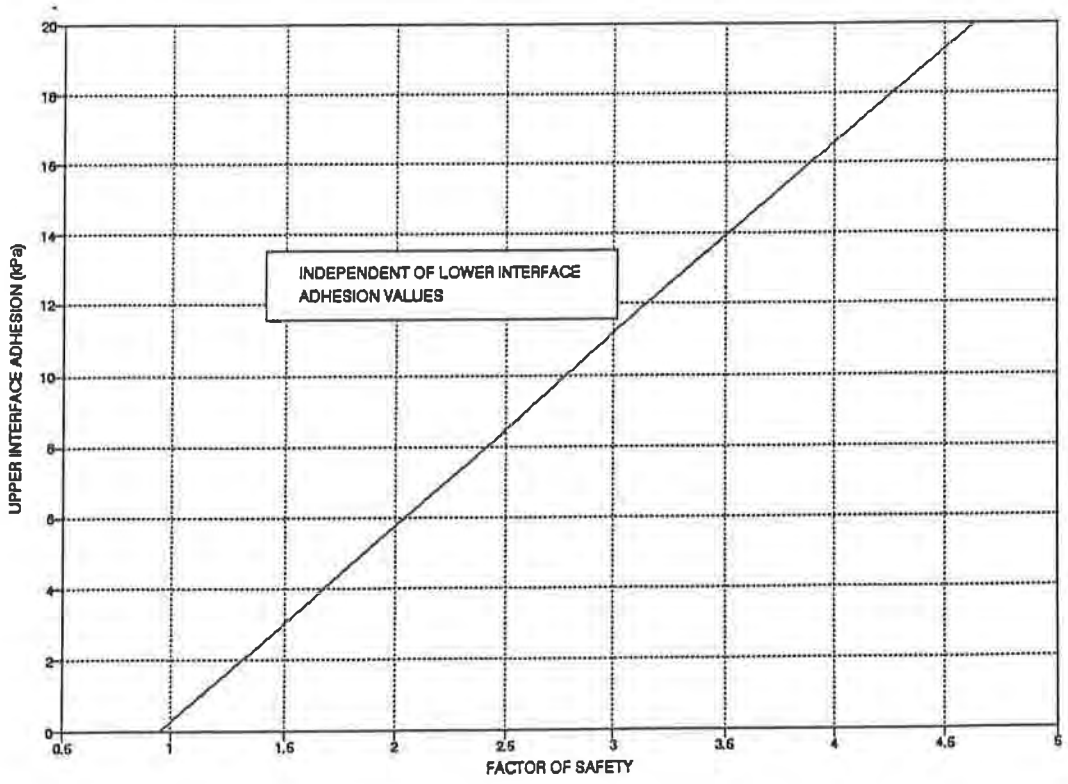

FIGURE 7 - Factor of Safety V. Upper Interface Adhesion

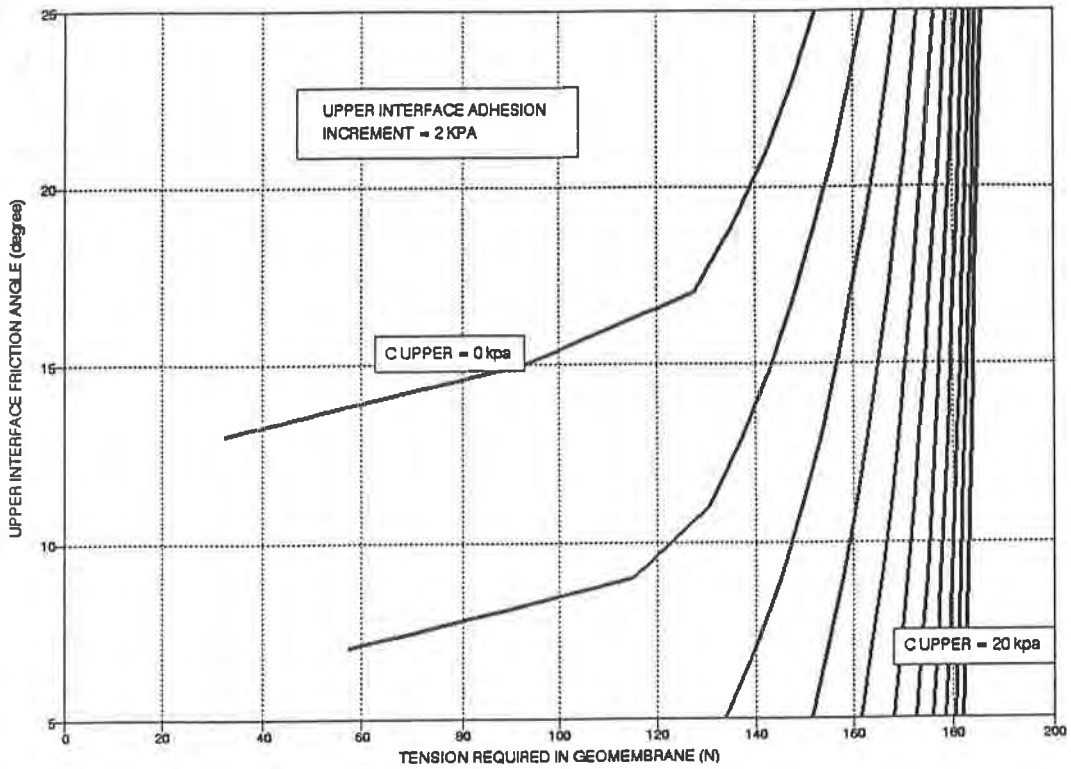

FIGURE 8 - Upper Interface Strength Variations

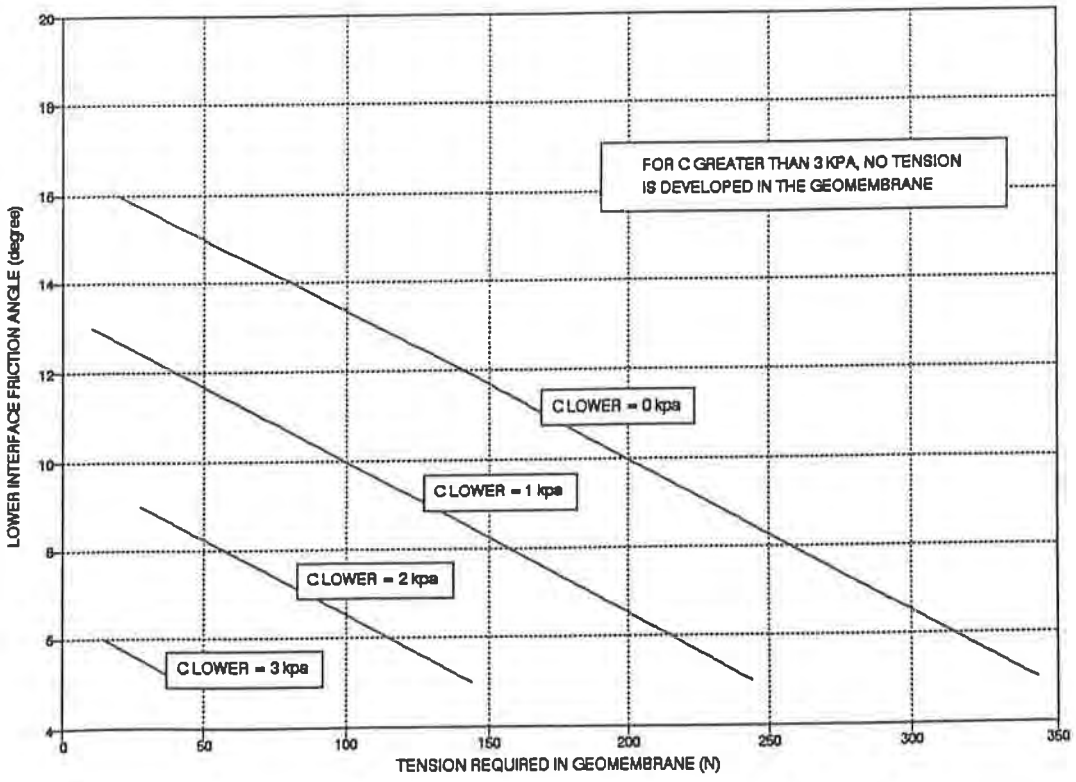

FIGURE 9 - Lower Interface Strength Variations

in a state of pure shear.

Slope Angle. The influence of the slope angle on the stability of the cover soil and the tension developed in the geomembrane is illustrated in Figure 10. Computations were performed for a constant value of slope height, D = 33 m, and strength parameters indicated in Table 1. When the slope angle is varied from 10 to 30 degrees, the safety factor with respect to sliding decreases from 2.4 to 0.83. It is equal to 1 for an angle of 24.3 degrees. In the range of angles for which the slope is theoretically stable (i.e. FS > 1, ω < 24.3 degrees), no tension is mobilized in the geomembrane up to approximately ω = 13 degrees. At values of slope angle greater than 13 degrees, greater tension is mobilized with increasingly mobilized shear stress at the upper interface. The tension in the geomembrane reaches a peak for ω = 24.3 degrees and FS =1. When the slope angle is further increased, the tension in the geomembrane indicated by the model decreases because the upper interface shear strength is mobilized at its maximum (constant) value and, simultaneously, the slope length decreases. It is noted that in this range of slope angles, the stability of the cover soil is not ensured and reinforcement would be required.

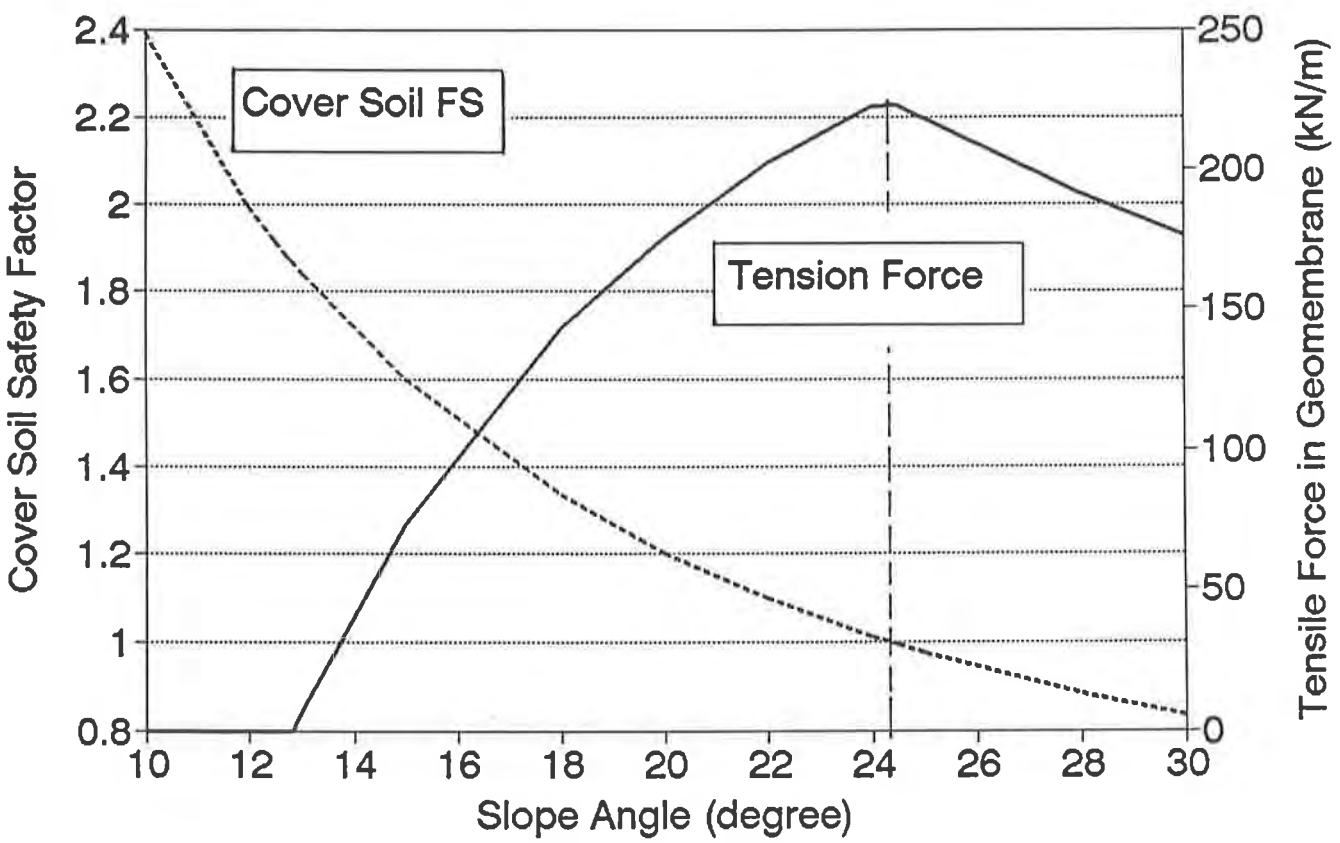

Figure 10. Influence of the slope angle on the stability of the cover soil and the tension in the geomembrane (Note: height of slope, 33m, is constant.)

CONCLUSIONS

A modification to the Koerner and Hwu (1991) method of analysis for the stability of geosynthetic-lined slopes is proposed. This modification allows to account for the amount of resistance to shearing mobilized at the interface between a cover soil and geomembrane in the computation of the tensile force due to unbalanced friction developed in the geomembrane. The modified model consists of coupling the stability and tensile force equations.

A parametric study was performed using this model to study the relative influence of mechanical and geometric parameters on the sloped liner response. The dominant factors are shown to be the ratio between upper and lower interface strengths as well as the slope angle. It is emphasized by this study that the stability of a sloped-liner system including geosynthetic components is critical even at moderate slope angles and is controlled by interface strength that are usually low and difficult to assess. Hence, better understanding of the complex interaction between the liner components is needed in order to develop improved methods of analysis and optimum use of available experimental databases.

ACKNOWLEDGEMENTS

Contribution of Mr. Brian Simpson to this study was supported by a fellowship grant from Golder Associates. Additional support for the preparation of this paper was provided by the School of Civil Engineering of Purdue University. The computations were performed at the Bechtel Geotechnical Research Laboratory of Purdue University.

REFERENCES

Giroud, J.P., and Beech, J.F., (1989) "Stability of soil layers on geosynthetic lining systems", Geosynthetics '89 Conference Proceedings, IFAI, San Diego, CA, pp. 35-46.

Koerner, R.M., and Hwu, B.L., (1991) "Stability and tension considerations regarding cover soils on geomembrane lined slopes", Geotextiles and Geomembranes, Vol. 10, pp. 335-355.

Martin, J.E., and Koerner, R.M., (1985) "Design methods for slippage of lined waste embankments and reservoirs", International Journal of Geotextiles and Geomembranes, Vol. , pp.

Mitchell, J.K., Seed, R.B., and Seed, H.B., (1990) "Kettleman Hills waste landfill slope failure. I-liner-system properties", Journal of Geotechnical Engineering, Vol. 116, No. 4, pp. 647-660.

Practical Geoelectric Leak Surveys With Hand-Held, Remote and Water Lance Probes

I.D. Peggs
I-Corp International Inc., USA

ABSTRACT

Geoelectric leak surveys using handheld and remote drag probes in a waste water treatment plant concrete basin retroactively fitted with a 2.5 mm thick HDPE geomembrane are described. Despite the presence of steel inlet and outlet pipes penetrating the geomembrane, and metal agitator paddles being immersed in the water, a successful leak survey was performed.

A new "water lance" probe was used for the first time to examine the uncovered side slope geomembrane liner of a surface water run-off pond, and the side slopes of a geotextile-covered liner in an industrial waste cell, the latter during rain showers. The water lance probe was found to be extremely sensitive in finding leaks, but requires specific types of liner subgrades to be successfully applied. Contrary to popular opinion, the presence of wetness on the surface of the geomembrane, provided it is not running water, need not necessarily prevent a geoelectric leak survey from being performed.

INTRODUCTION

The electric, or geoelectric, method of locating leaks in geomembrane liners was developed almost simultaneously by the Foote Mineral Company (patent now assigned to Leak Sensors, Inc., 1985) and the Southwest Research Institute. In both cases, the technique was developed to locate leaks in liquid impoundments. It has recently been extended to soil covered liners and exposed liners.

The principle behind the technique has been described by Peggs and Darilek et al. In summary, the assumption is made that the geomembrane is essentially an insulator. An electrical potential is applied across the geomembrane between the liquid contained by the liner and the subgrade or the leakage detection system. A probe is then traversed through the liquid measuring potential gradients, thereby identifying the steep gradients and the high currents that occur in the region of a hole. Under favorable conditions, the hole can be exactly located.

SCOPE OF WORK

This paper describes the procedures used to search for leaks in two unusual installations: a lined concrete basin containing small and very large steel inlet and outlet pipes respectively, and an industrial waste cell covered with a thick nonwoven geotextile. It also describes the first application of the "water lance" technique to examine the uncovered and geotextile-covered side slopes of two geomembrane liners. The Leak Sensors equipment was used for these surveys.

TEST PROCEDURES - CONCRETE BASIN

A large concrete basin, approximately 36 x 28 x 10 m, was part of a large industrial wastewater treatment plant. The low pH of the incoming waste water was damaging the concrete, so the basin was lined with 3.0 mm thick high density polyethylene (HDPE) geomembrane. The basin contained 24 pillars supporting a roof structure, a 30 cm diameter stainless steel drain valve in the center of the floor, and a 1.3 m diameter steel outlet pipe (closed with a blind flange) in one of the walls (Figure 1). A geonet had been installed between the geomembrane liner and the concrete with a small leakage collection drain pipe at the side of the floor drain. The geomembrane was suspended from, and sealed to, the top of the walls by a stainless steel batten strip. All geomembrane seams were extruded fillet seams.

Previous History. Since completion of the lining system 9 months previously, the liner had been leaking. The owners had performed careful visual inspections of the liner, they had monitored leakage rate with reference to water level, and had used dyes, in a series of attempts to locate the leak(s). The leaks remained undetected. Meanwhile, a second lined basin had been performing satisfactorily even when filled with water. Finally, a geoelectric leak survey was commissioned.

Leak Survey Procedure. Before any leak surveying was done, the empty basin and liner were examined to determine the approach that would be taken. This was considered essential because of the steel inlet and outlet pipes. In addition, there were four metal paddles suspended from the ceiling providing agitation in the water, and there was a metal-edged overflow weir controlling maximum water level.

It was decided to survey the floor of the basin first to cover the most likely areas of leakage: the corners between the walls and the floor and the pillars and the floor. The stainless steel floor drain valve was approximately 30 cm in diameter and would have to be insulated from the water in the basin to prevent it appearing as a large leak, conducting most of the current through the liner and seriously reducing the sensitivity of the method to locate small leaks elsewhere in the liner. The owners decided to weld a 75 cm high HDPE standpipe to the floor liner around the valve, thereby keeping water required for the floor survey from contacting the valve. The floor of the basin was flooded with water to a depth of approximately 60 cm.

A calibration cell containing a cap with a 1 mm diameter hole (Figure 2) was filled with basin water and placed on the liner. The cell was connected into the electrical circuit as shown diagrammatically in Figure 3. The sensitivity and gain controls on the meter were adjusted until the potential gradient disruption in the basin water caused by the hole in the calibration cell could be clearly defined from a distance of approximately 1.25 m. The current flowing through the 1 mm hole between the injector electrode in the basin water and the negative (ground) electrode in the cell was measured with a multimeter to be 0.21mA. The cap with the 1 mm hole was replaced with a cap containing a 6 mm diameter hole, and the current was found to be 0.50mA.

The calibration cell was removed from the negative electrode of the 12 VDC battery power supply. A separate wire was then used to connect the negative electrode of the battery to the water stream from the leakage collection drain pipe under the basin. The 12 VDC potential was, therefore, applied directly from the water in the basin to the leaking water only through holes in the liner. The current measured through the geomembrane (and any leaks) was found to be 0.42mA. The magnitude of this current clearly indicated that there was a leak in the liner.

When the floor of the basin was flooded, it was observed that a small amount of water was leaking, at two locations, underneath the standpipe and draining to the stainless steel drain valve. Therefore, it was impossible to say whether there was a leak in the liner or whether the current was due to the leak through the standpipe/liner weld. When the hand-held search probe was traversed within 2.5 m of the standpipe, there was a distinct change in signal confirming the presence of the leak through the standpipe. It was found, as observed, that there were two spots in the weld between pipe and liner that were leaking.

The Leak Sensor signal is presented in analog fashion on a dial gage and as an audible signal. The latter is far more sensitive to small leaks. In regions where

there is no hole in the liner, there is a steady background signal. Near a leak, as one traverses the probe steadily in the water over the liner, there is a step increase or decrease in the audio signal, depending on the orientation of the probe electrodes. When one electrode of the probe is placed directly on the hole, the audio signal is very high; with the other electrode, it is very low.

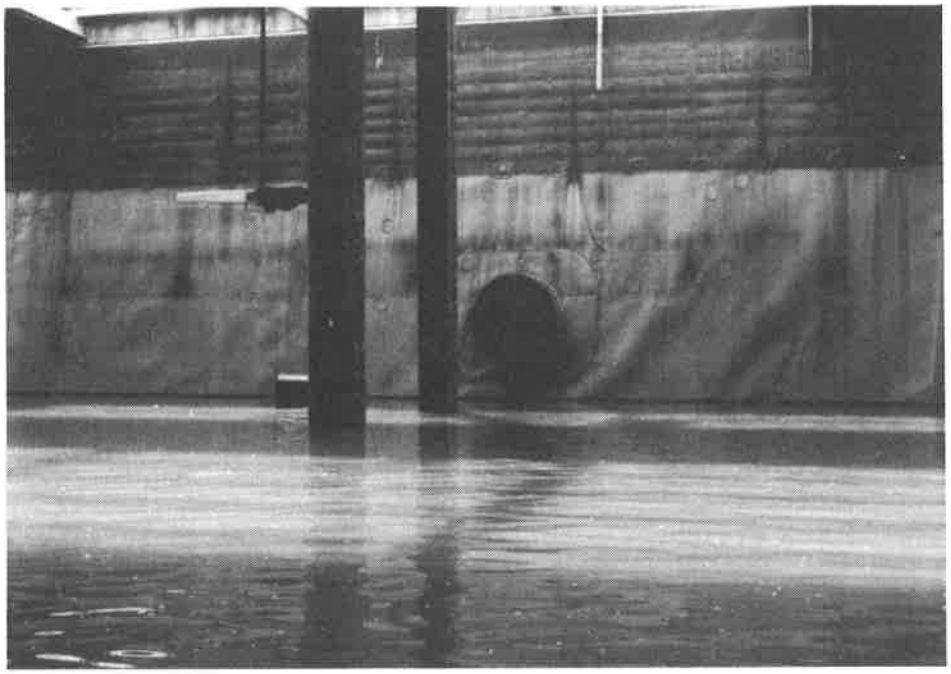

Figure 1. Geomembrane-lined basin. Agitator paddle, 2 columns, and large diameter outlet pipe are shown.

Figure 2. Calibration cell. White cap contains 1 mm hole. The "ground" electrode is inside the cell.

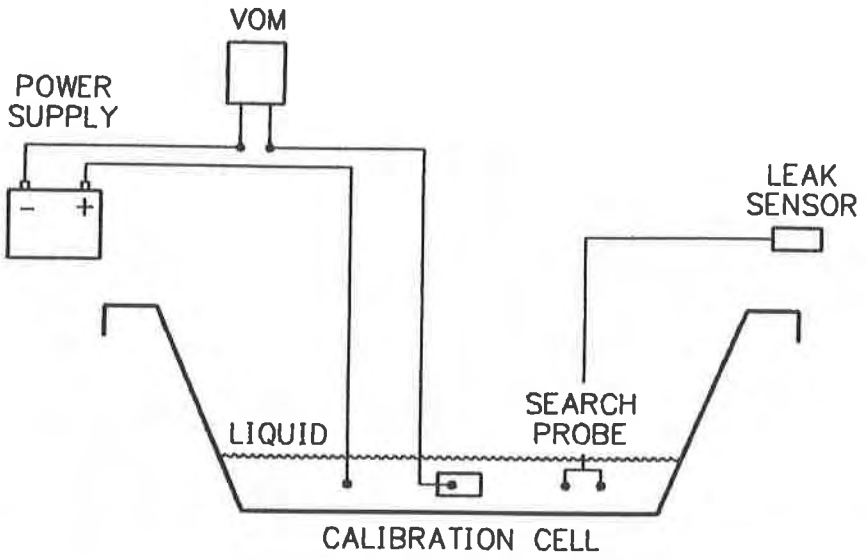

Figure 3. Electrical circuit

After checking the standpipe, the liner surface covered by water was surveyed on a 1 m grid spacing, paying special attention to the corners at the bases of the columns and walls. The change in geometry at these locations did cause changes in signals requiring detailed searching in these areas to distinguish between such signals and leak signals.

Four hours later, three leaks had been found. Two were on the floor in the middle of a geomembrane panel, and one was in a vertical seam in the corner between the wall and floor of the basin. The seam leak could not be identified visually. One of the leaks on the floor was a 1 cm long cut made by dropped equipment. The second leak on the floor consisted of two similar parallel cuts.

The water was pumped from the basin, the leaks patched, and the basin refilled to a depth of 60 cm. The bottom of the liner no longer leaked.

The rest of the basin was completely filled and promptly started leaking. Over the next two months, the owners again varied water levels, monitored leakage rates, and used dyes but could not locate the remaining leaks, except that they appeared when the water level was close to the top of the 1.3 m diameter outlet pipe. Another geoelectric survey was commissioned.

Prior to this second survey, it was requested that the floor valve and all exposed metal associated with the large outlet pipe (pipe, blind flange, bolts, circular batten strip fastening pipe boot to the wall) be painted with a coal tar epoxy paint to electrically insulate the steel from the water in the basin. The integrity of the paint was examined with a holiday detector (spark discharge method) and the few holes that were detected were repaired. The basin was filled to the top of the outlet valve, and the paint coating checked one more time, this time with the leak detector's hand-held probe, to define remaining holidays in the paint that would appear as leaks. While the paint coating performed a significant insulating function, insulation was not complete, and it was found necessary to reduce the gain setting on the meter to its minimum level to obviate the signal due to the current conducted through the pipe, in order to detect the holidays.

The liner on the walls of the basin away from the outlet pipe was surveyed first, using a remote probe that was lowered from a boat down the liner walls at intervals of 2 m. Each vertical seam was carefully examined. Subsequently, each column was carefully surveyed. No leaks were found. It therefore remained to examine the outlet pipe and batten strip, the only possible source of the leak.

Due to the high signals obtained in the region of the pipe, it was thought that a survey in this area would be an impossible task. Nevertheless, the hand-held probe was manipulated from the boat stabilized above the pipe. The sensitivity switch used to account for the conductivity of the liquid was turned to its most insensitive position (normally used for high-conductivity liquids), and the gain was turned to zero. The bolts on the flange and the flange/pipe joint were examined. The only abnormal signal was provided by the holidays in the paint coating. Next, the batten strip clamping the pipe boot to the wall was examined, and two distinct signals were found over distances of 1 cm and 3 cm near the top of the strip. They were marked as suspected leaks.

The basin was further filled to a level just below that at which four agitator paddles suspended from the roof would contact the water. The walls and columns were again surveyed with the remote probe; no leaks were found.

As the basin was then filled to its maximum level, the current flow through the geomembrane was monitored. An expected increase in current was observed when the paddles were contacted and again when the steel edge of the overflow weir was contacted. A final survey of the walls and columns was performed without finding any leaks. A changing signal was noted when columns in the vicinity of the agitator paddles were examined, but this could easily be confirmed as being associated with the paddles. Except for the time spent waiting for the water to rise, the survey was completed in a matter of hours.

Subsequently, when the batten strip was removed, the two leaks were quite evident. These leaks occurred despite many assurances from the owners that the batten strip had been very carefully placed and torqued down. Repairs were made, the basin filled, and only an acceptable slow dripping leak occurred. Despite the electrically conducting penetrations through the geomembrane, the leak survey had been successful.

Nevertheless, it will not be surprising, due to the difficulty of retrofitting thick geomembrane in concrete basins, if new leaks periodically occur in this installation, particularly in seams in 90 degree corners where the liner cannot be totally supported by the concrete.

TEST PROCEDURES - SOLID WASTE CELL AND RUN-OFF POND

Solid Waste Cell. An industrial solid waste cell, approximately 52 x 25 x 8 m with 1:1.5 side slopes had been lined with a 2 mm HDPE geomembrane liner covered by a thick nonwoven geotextile leachate drainage and cushioning layer. The cell had partially filled with rain water prior to being placed in service. It was suspected of leaking.

Due to the depth of water, a hand-held probe wading survey could not be performed. Instead, a remote drag probe survey was performed from side to side of the cell. The equipment was calibrated only to the 6 mm diameter hole in the calibration cell due to the expected large size of the leak and the low conductivity of the rain water in the cell. The cell was surveyed on a 1 m grid spacing using the stitched geotextile seams as guides.

At one corner of the cell, close to the toe of the slope, a leak indication was found. Being close to the toe of the slope, it was possible that the signal could have been generated by the change in slope at that area. (Changes in signal also occur: a) as the probe is moved up a side slope and approaches the surface of the water; b) at large wrinkles; and c) around the sides of whales.) The signal was found to be consistent along the toe of the slope for about 3 m and then did not occur along the remainder of the toe of the slope. The indication was, therefore, believed to be a leak. Subsequently, the geotextile was removed from this area to reveal an unsatisfactory repair bead about 30 cm long.

Surface Water Run-Off Pond. The surface water run-off pond was on the same site as the waste cell. It was a square pond with two basins separated by a low dike, each basin containing two geomembrane-penetrating concrete inlet and outlet pipes. The water level was just above the top of the dividing dike.

A conventional remote, drag probe survey was performed parallel to the dividing dike, and a number of leak indications were found, particularly in the region of the concrete pipes.

Although the signal at the pipe openings was very high (water in the pipe acted as a large leak), there were a few discrete peaks in signals on top of the basic high signal that were construed to be leaks. As yet, this pond has not been emptied to confirm the leak survey indications.

In addition to the pipe problems, two additional problems that frequently occur were experienced in this survey: false signals from heavy metal and oily sludge deposits. A uniform soil cover up to 1 m thick does not prevent a survey being performed, but due to the distance between the probe and the geomembrane, the grid spacing is required to be much smaller than usual. However, a variable thickness layer, particularly if it contains metallic deposits, can be a significant problem if the metallics contact and stick on the probe electrodes. If such signals are suspected, the probe must be lifted to the water surface and dunked several times to clean off the sludge, and several passes in both directions must be made over the suspect area to determine whether the signal is due to a leak or to the nature, or profile, of the sludge deposits.

Similar influences on the signal occur when the probe passes through an oily sludge, evidenced by a bloom appearing on the surface of the water as the sludge is disturbed. Such an occurrence makes it extremely difficult to survey small run-off ponds around, for example, the railroad loop at a coal-fired generating station. If the pond is large and the oily deposits less frequent, a good background signal can be obtained that helps distinguish between leak and oil signals.

Water Lance Technique. After the underwater areas of the waste cell and run-off pond had been surveyed, the owners requested that the above-water sections of the side slopes be examined using the new water lance technique. The water lance technique (Leak Sensors (1988)) is outlined schematically in Figure 4. A positively-charged source of water is directed in a solid jet (not a discontinuous spray) on the surface of the liner being examined, through the hand-held water lance (Figure 5). The lance incorporates two electrodes connected to the leak sensor meter. When the water jet falls onto, and penetrates a hole, thereby contacting the negatively charged subgrade, a current flows through the circuit and is recorded (analog and audio) on the meter.

During the calibration procedure, a large signal was produced when the water jet fell on the 1 mm diameter hole of the calibration cell. In fact, the technique was so sensitive that additional leaks were found through two sealing fittings in the calibration cell. These latter leaks were then effectively sealed. In the run-off pond, a gasoline powered portable immersion pump was used to pump the positively charged water from the pond, via garden hoses, through the water lance. The ground electrode remained in a manhole monitoring leaking water under the pond.

Since this was the first commercial use of the water lance, 1 mm and 5 mm diameter holes were placed in the geomembrane at the top of the slope. When the water jet fell on the holes, a large signal was generated. The level of the signal was different for the two holes and was also different depending on whether the full jet of water was falling on the hole (Figure 6) or whether peripheral water was over the hole (Figure 7). If water and air were allowed to mix on top of the 1 mm hole it was quite evident, from the brief loss of signal, when an air bubble was preventing water from flowing down the hole. The method is very sensitive.

It was also apparent that even though a signal could be generated if a thin film of static water on the surface of the geomembrane was connecting the jet of water to the hole, a larger signal occurred when the jet fell directly on the hole. It is, therefore, not necessary that the liner be completely dry in order to perform such a survey.

The water lance survey was performed over the complete side slope area above the water level, but no leaks were found. Considerable time was provided for the water jet to penetrate any leaks that might exist in the extrusion seams. The seams were

examined from the water level towards the top of the slope. When the water jet contacted the grade soil at the top of the slope, a signal, as expected, was produced.

The steep side slopes of the waste cell were next examined. The water jet was directed through the geotextile to where the geomembrane seam was felt to be. The jet was directed between the outer flap and the bottom geomembrane. Part way through the survey, it started to rain. The survey could be satisfactorily performed until the rain saturated the geomembrane and water started running down the geomembrane. When the rain stopped, and water stopped running down the geomembrane, the survey was restarted. The residual wetness in the geotextile only became a problem when the water jet came within about 1.5 m of the grade soil at the top of the side slopes. At this point, too much current was being drawn up the wet geotextile to the soil (the soil was in electrical contact with the leaking water). No leaks were identified in the cell liner above water level.

More time was provided for the water jet to saturate the double track fusion seams in the waste cell liner than for the extrusion seams in the run-off pond liner. It must be recognized that a leak will only be detected in double track seams if there is a hole through both tracks, and if the hole through the inner track is below the hole in the outer track.

DISCUSSION

Although no "natural" holes through the liner were found using the water lance technique, this new methodology was found, through an intentionally-made 1 mm diameter hole in the liner, and through inadequate seals in the calibration cell, to be very sensitive. It must, however, be recognized that the tortuosity of any hole through a seam will influence the time required for the hole to be detected by this method. This situation is even more complicated in a double track seam. In fact, a double track seam will behave in the same way as a double lining system: the pressure of the water jet will drive the water through a hole in the outer track, but only gravity will act on water flowing over a hole in the inner track (unless the channel is blocked lower down the slope and water backs-up in the channel).

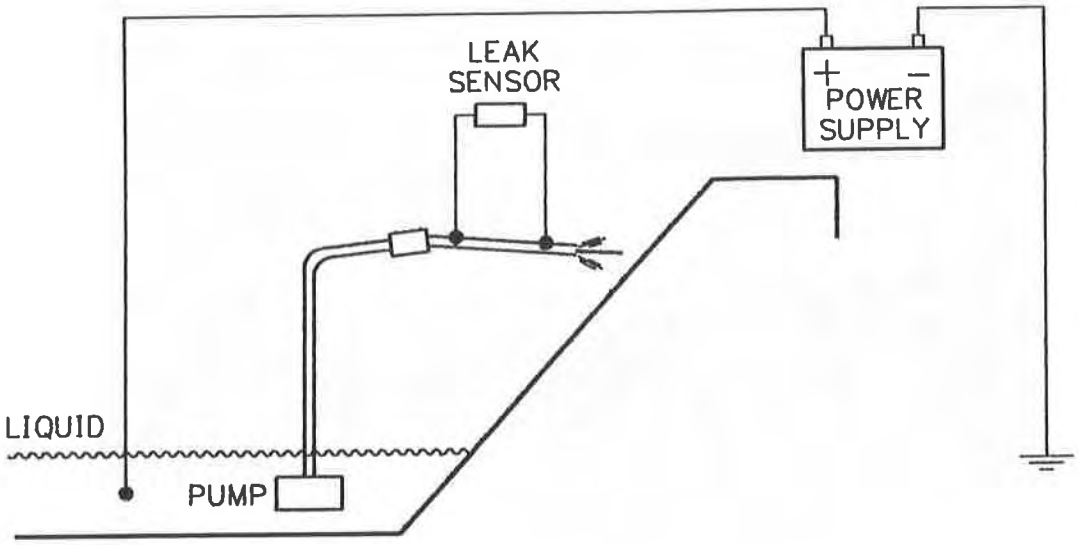

Figure 4. Schematic view of the water lance technique.

Figure 5. Searching for leaks with the water lance.

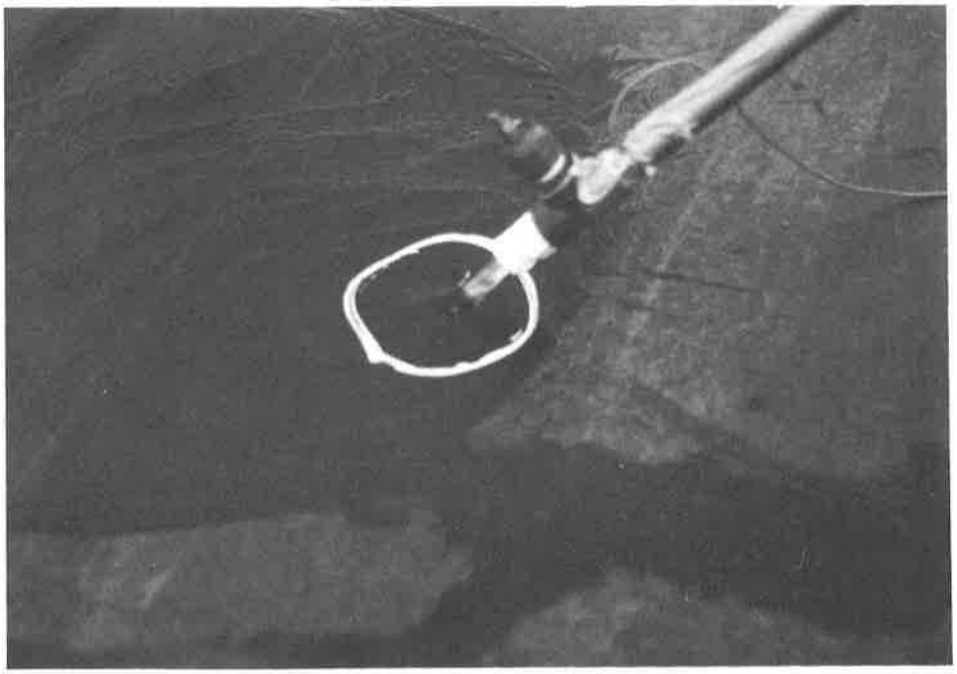

Figure 6. Jet from water lance falling directly on hole (center of white circle) in liner.

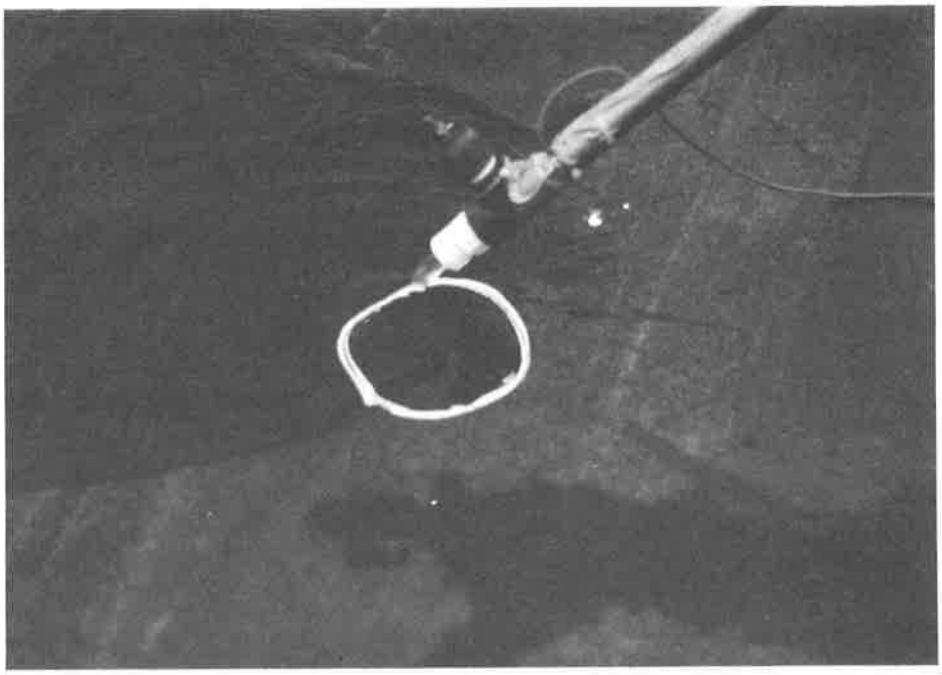

Figure 7. Periphery of jet from water lance just covers the hole.

When leaking water has penetrated the liner, for the water lance technique to be effective, the leaking water must come into immediate contact with an electrically conducting medium to which the ground electrode of the power supply can be connected. Wet soil, or a leakage drainage system that can be back-filled with water, would be appropriate. Since a newly-installed liner would not have been completely covered by water, there will not be a continuous leak path to a sump that can be accessed by an electrode from the periphery of the liner. It would, therefore, not be practical to perform a water lance leak survey on the slopes of a newly installed geomembrane-geonet-geomembrane lining system. It would be most appropriate to do it on a single geomembrane placed directly on soil, such as the secondary and primary geomembranes of a double composite lining system during construction.

The observations that water lance surveys can be successfully done even when the liner is wet (but not with running water), and that the conventional survey using hand-held probes can be performed in installations with sizeable metal (pipe and valve) penetrations through the liner, indicate that it is not necessary to go to great lengths to insulate the contained water from the ground. Certainly one must recognize the resultant restrictions that are imposed on the technique, and the reductions in sensitivity that may occur (close to anchor trenches, around penetrations) but useful information on a practical scale can be generated, without, for instance, digging an isolating trench in the soil cover around the periphery of the covered liner. As an example, the author was recently able to locate a tear in a liner under 1.5 m of sand only 5 m from a soil covered side slope.

With the addition of the water lance to other leak survey probes, the geoelectric method of locating leaks in geomembranes can be performed on liners covered by water, liners covered by a soil layer with free-standing water over the soil, liners covered only by soil, and liners that contain no cover and are dry. The American Society for Testing and Materials Committee D35 on Geosynthetics is now drafting a standard method of test using the electrical technique, an indication that it has become accepted by the industry. At present, it is the only available method that can rapidly evaluate leak defects in 100% of a geomembrane liner. Experience indicates that it can do so at the rate of about 9,000 to 13,000 m^2 per day.

CONCLUSIONS

The conventional geoelectric method for locating leaks in geomembrane-lined installations can successfully be applied to installations containing metal penetrations through the geomembrane.

The novel water lance technique can successfully be applied to dry geomembranes, provided leaking water has direct access to an electrically conductive medium to which the ground electrode of the power supply can be connected.

A light rainfall or static wetness on the geomembrane above the water level does not preclude the ability to perform a leak survey.

ACKNOWLEDGEMENTS

The author wishes to acknowledge the support of Mr. Robert H. Hurwit of Leak Sensors, Inc., by providing the prototype "water lance" for this survey and for reviewing this paper.

REFERENCES

Darilek, G.T., Laine, D., and Parra, J.O., (1989) "The Electrical Leak Location Method for Geomembrane Liners: Development and Applications". Proceedings of Geosynthetics '89. Industrial Fabrics Report International, St. Paul, Minnesota, pp. 456-462.

Leak Sensors, Inc. US Patent #4,543,525. "Method for Determining a Leak in a Pond Liner of Electrically Insulating Sheet Material". 1985.

Leak Sensors, Inc. US Patent #4,771,246. "Method for Determining the Location of a Leak in a Pond Liner Formed of Electrically Insulating Material". 1988.

Peggs, I.D., (1990) "Detection and Investigation of Leaks in Geomembrane Liners". Geosynthetics World, Vol.1, Issue 2, pp. 7-14.

Ultrasonic Field Seaming of PVC Geomembranes

L.J. Stearns
OHM Remidiation Services Corp., USA

R.S. Lacey
Geotechnics, USA

J.E. Magnoli
New England Liner Systems Inc., USA

ABSTRACT

Ultrasonic field seaming of thermoplastic geomembranes is an emerging application of established technologies. For pollution remediation sites, ultrasonic field seaming can offer an effective alternative to traditional solvent seaming of polyvinyl chloride (PVC) geomembranes. This paper presents relative advantages and limitations of ultrasonic field seaming based on a case history plus laboratory testing of various seam samples. Key advantages of ultrasonic field seaming include quality cold temperature seams, dual-bond seam geometry capability, rapid field seaming rates, immediately available full seam strength, reduced operator dependence for uniform quality seams, and reduced seaming costs. Current limitations include equipment availability, lack of experienced operators, relatively high capital investment, and restrictions in performing detail work.

A case history is presented where 0.76-mm (30-mil) PVC geomembrane was ultrasonically field seamed during cold weather conditions (below 4°C) to cap a hazardous waste landfill. Average destructive test results were 4.9-kN/m (28 ppi) with a film tear bond for peel and 10.8-kN/m (62 ppi) for shear strength. In addition to the case history data, laboratory destructive testing results are presented for dual-bond sample seams that were ultrasonically welded at 10°C in 0.50-, 0.76-, and 1.0-mm (20-, 30-, and 40-mil) PVC, 0.91-mm (36-mil) chlorosulfonated polyethylene (CSPE-R), and 0.76-mm (30-mil reinforced ethylene interpolymer alloy (EIA-R) geomembranes.

INTRODUCTION

Ultrasonic dual-bond (UDB) field seaming of geomembranes at pollution remediation sites is a recent technology transfer of polymer seaming techniques that are well established in the manufacturing and packaging industries (Lord, et al., 1989; Bove and Smith, 1989; USEPA, 1988). With rapid, uniform seam rates and full strength being immediately available, UDB field seaming can offer an effective alternative to the traditional solvent seaming of PVC geomembranes.

In the past, dual-bond seam geometry has not been practical for PVC geomembranes due to the limitations of solvent style bonding techniques (Koerner, 1990; Morrison and Swihart, 1989; USEPA, 1991). Ultrasonic welding offers an alternative to this limited seam geometry plus several associated advantages based on our field experience:

- Immediately available, full seam strength
- Quality cold weather seams
- Rapid nondestructive field seam testing
- Rapid seam installation rates
- Uniform seam quality
- Reduced dependence on operator skill
- Cost reduction and schedule improvement.

In comparison to solvent seaming, ultrasonic welding produces a bond with immediately available and greater strength while eliminating the need and inconvenience of a seam curing period (Johnson and Rivette, 1989; Bove and Smith, 1989). The ultrasonic welding device is a piezoelectric- or magnetostrictive-driven horn that produces a frictional thermal melting in contacted thermoplastic materials. The ultrasonic horn vibrates longitudinally at about 40-kHz with an amplitude of 0.038-mm (0.0015 inch). A molten surface layer forms on the two geomembrane sheets to be bonded which are then pressure rolled together forming the seam. The dual-bond geometry is shaped during the post-molten rolling. Welding speed is rapid involving only a few seconds depending upon weather conditions and certain material characteristics such as thickness and friction coefficient (Obeda, 1986; Lord, et al., 1989).

Ultrasonic welding appears to be far less susceptible to detrimental moisture and temperature effects than solvent welding. It is not unusual for project specifications to restrict solvent welding to ambient temperatures above 10°C, yet as the case history will show, acceptable ultrasonically welded field seams can be produced from -8 to 4°C. The ultrasonic machine atomizes both surface and molecular adsorbed moisture then blows it off the sheet with heated air just prior to welding. This can reduce "dry sheet" requirements in specifications. Because the ultrasonic welding equipment is automated and can be preadjusted to field conditions, it tends to produce seams of more uniform quality than solvent welding which requires constant attention to the quantity of solvent applied, solvent coverage, setup time prior to sheet contact, and proper pressure and duration of rolling (USEPA, 1991; Koerner, 1990). In addition, there is no risk of spilt or extraneous solvent dissolving unseamed areas of the geomembrane. Ultrasonic seaming is clearly faster than solvent seaming and can be performed at sustained field rates of 1.8 to 2.1 meters per minute (6 to 7 feet per minute) with an experienced two-man crew.

A key advantage of ultrasonic welding is the capability to produce a dual-bond seam in materials such as PVC. Each bonded area is between 13 and 19-mm (0.5 and 0.75 inches) wide and individually will typically exhibit a film tear bond (FTB) in peel. The redundancy of a primary and secondary bonded area is also a significant advantage of this seam geometry. However, a second benefit of this seam geometry is that the included air channel can be pressurized in the field to evaluate the integrity of the two bonded areas along the entire length of the seam (USEPA, 1991; Koerner, 1990; Haxo and Kamp, 1989). This nondestructive quality control test is relatively quick to perform compared to the vacuum box or air lance tests necessary for solvent welded

seams. The pressurized air channel test provides a semi-quantitative indication of seam strength while also testing the interior edges of the two bonded areas which are otherwise not readily accessible for continuous evaluation.

CASE HISTORY

Introduction. During the winter of 1989-1990, a 6,225-square-meter (67,000-square-foot) cap was installed over a hazardous waste landfill near the coast of Connecticut, United States. From top to bottom, the cap consisted of: 152-mm (6 inches) of unvegetated, gravelly coarse sand; 542-gram-per-square-meter (16-ounce-per-square-yard) nonwoven, needle-punched geotextile; 0.76-mm (30-mil) PVC geomembrane; 271-gram-per-square meter (8-ounce-per-square-yard) nonwoven, needle-punched geotextile; and regraded, smooth-rolled waste. The approved project specifications required either thermal or solvent geomembrane welding techniques and allowed seaming only when ambient temperatures were above 10°C. Field seam acceptance criteria were FTB and/or 1.75-kN/m (10 ppi) in peel, and 80-percent of sheet tensile strength in shear.

Construction startup was delayed until late Fall 1989 yet the project had an absolute, regulatory deadline for completion with significant liquidated damages. To make matters more difficult, unusual and extraordinary cold weather conditions delayed the geomembrane installation. This eventually resulted in the willingness of all parties to consider alternative geomembrane seaming techniques.

Demonstration. Ultrasonic dual-bond seaming was successfully demonstrated on the 0.76-mm (30-mil) PVC geomembrane with the destructive peel and shear tests giving more than acceptable results. The test seam was welded at an ambient temperature of -8°C on a clear, sunny day. Following the demonstration, UDB seaming was approved for the geomembrane installation although more frequent than previously specified destruction seam testing was recommended. In addition, the ambient temperature restriction was lifted and the specified definition of a FTB, taken from the NSF (1985) Standard No. 54, was redefined to be a failure of one of the bonded sheets by tearing or breaking prior to the complete separation of the bonded area being tested. This redefinition of FTB was believed to be necessary because the demonstration seams typically did not "snap" cleanly in a 180-degree tee peel test.

Installation. The geomembrane installation and field seaming occurred during the first week of February 1990 when ambient temperatures ranged between -1 and 4°C. Weather conditions otherwise were clear and sunny, but at times quite windy. Six field seams were installed including a total of 130-meters (425 linear feet) of UDB seam. All seams were tested both destructively and nondestructively. Field seam length varied from 15-m (50 feet) to 38-m (125 feet). Quality assurance was provided by an independent, third-party consulting firm. Twice each day, test seams were visually inspected and destructively tested for peel and shear to calibrate and monitor the performance of the ultrasonic welding equipment.

Three UDB field seam samples were destructively tested for shear and 180-degree tee peel at a measured cross-head speed of 53-mm per minute (2.1 inches per minute). Ten uniform test coupons, each 25-mm wide by 200-mm long (1 inch wide by 8 inches long), were carefully cut for testing from each seam sample with a razor knife and steel template. Five coupons from each

sample were then tested for peel and five for shear with the results average to represent the reported strength. Both shear and peel tests were performed on portable tensiometers which were firmly set on a countertop inside an on-site trailer heated to 18°C during all testing. The tensiometers used digital displays of the tensile force values and the maximum value displayed became the peak load test result for that coupon.

During on-site confirmatory material testing, ten coupons of the 0.76-mm (30-mil) PVC geomembrane material to be installed were tested for tensile sheet strength and averaged 14-kN/m (81 ppi) with a 0.7-kN/m (4 ppi) standard deviation. Elongation was 342-percent with a 19-percent standard deviation.

Nondestructive testing was performed on all UDB seams by pressurizing the air channel to a minimum of 138-kPa (20 pounds-per-square-inch) gauge pressure, allowing a 2-minute relaxation period, then taking gauge pressure readings at 1-minute intervals over a 5-minute test duration. The acceptance criteria was not more than a 28-kPa (4-psig) pressure loss at the end of the 5-minute test. To confirm an acceptable test, the sealed end of the air channel was slit open. If an audible release of air pressure was obvious, then the seam's air channel was considered to be continuous for the tested section of seam.

Results. None of the six UDB seams failed the nondestructive pressurized air channel test criteria. One seam did show a gauge pressure loss of 14-kPa (2 psig), however, this seam appeared to be leaking at the entry point of the needle into the air channel.

Shear strength test results are given in Table 1. Individual coupon values ranged from 9.8 to 12.4-kN/m (56 to 71 ppi) with an overall average of 10.8-kN/m (62 ppi) and a 0.6-kN/m (3.5 ppi)

Table 1. Case History Shear Strength Results for 30-mil PVC (ppi)*

Test Replicate	Peak Load (ppi) and Break Classification					
	Sample 1		Sample 2		Sample 3	
1	61	FTB	64	FTB	62	FTB
2	58	FTB	62	NF	61	FTB
3	57	FTB	66	NF	66	FTB
4	56	NF	67	FTB	71	FTB
5	62	FTB	59	NF	59	FTB
MEAN	59 ppi		64 ppi		64 ppi	
STD	2.6 ppi		3.3 ppi		4.8 ppi	

*FTB - Film Tear Bond 1 kN/m = 5.714 ppi 1 mil = 0.0254 mm
NF - No failure at limit of tensiometer crosshead travel

standard deviation. All of the shear test coupons that failed (12 of 15 coupons) produced a FTB. The remaining three coupons elongated to the maximum cross-head distance of the tensiometer prior to failure. These three coupons had peak recorded shear strengths from 9.8 to 11.6-kN/m (56 to 66 ppi) and were included in the above overall strength value. Using the measured tensile sheet strength of 14-kN/m (81 ppi), the individual shear coupons ranged from 69 to 88-percent of the tensile strength with a 76-percent average.

Peel test results are presented in Table 2. Individual test coupons ranged from 4.4 to 5.8-kN/m (25 to 33 ppi) with an overall average of 5.2-kN/m (29.5 ppi) and 0.35-kN/m (2.0 ppi) standard deviation for the 22 tests. All coupons produced an FTB.

Table 2. Case History Peel Strength Results for 30-mil PVC (ppi)*

Test Replicate	Peak Load (ppi) and Break Classification					
	Sample 1		Sample 2		Sample 3	
1	28	FTB	31	FTB	29	FTB
2	25	FTB	31	FTB	29	FTB
3	27	FTB	31	FTB	28	FTB
4	28	FTB	32	FTB	29	FTB
5	27	FTB	30	FTB	29	FTB
6	27	FTB	30	FTB		
7	30	FTB	33	FTB		
8			32	FTB		
9			31	FTB		
10			32	FTB		
MEAN	27 ppi		31 ppi		29 ppi	
STD	1.5 ppi		0.9 ppi		0.5 ppi	

*FTB - Film Tear Bond 1 kN/m = 5.714 ppi 1 mil = 0.0254 mm
NF - No failure at limit of tensiometer crosshead travel

The overall peel test results indicated an average of 36-percent of the measured tensile sheet strength was achieved with a 31 to 41-percent range for the individual coupons.

LABORATORY TESTING

Introduction. No data known to the authors has been previously published on the strength of ultrasonically welded dual-bond seams in PVC, EIA-R, or CSPE-R. To address this data gap, the following laboratory test study was performed.

Method. Ultrasonically dual-bond seam samples were prepared under shop conditions at an ambient temperature of 10°C for laboratory destructive testing. Seams were made in 0.5-, 0.76-, and 1.0-mm (20-, 30-, and 40-mil) PVC, 0.91-mm (36-mil) CSPE-R, and 0.76-mm (30-mil) EIA-R geomembranes. Twenty 25-mm wide by 150-mm long (1-inch by 6-inch) specimens were die cut from each sample seam, ten specimens for testing each in peel and shear.

The tests were performed on a screw-driven, universal test machine equipped with pneumatic grips in accordance with ASTM-D4437-84 as modified by Appendix A of NSF (1991). Crosshead displacement rates were 50.8-mm per minute (2 inches per minute) for the peel testing and 508-mm per minute (20 inches per minute) for the shear testing in PVC materials, and 50.8-mm per minute (2 inches per minute) for all reinforced material testing in peel. Locus of break codes were determined in accordance with NSF (1991).

Results. The destructive testing results in PVC materials for shear and peel are presented in Tables 3 and 4, respectively. All of the PVC test specimens achieved film-tearing bond in both peel and shear. The predominant break mode in peel was a tensile break at the outer edge of the welds with less than 10-percent peel incursion. The shear specimens failed in sheet tension at the outer edge of the welds. Table 5 presents the results of peel adhesion testing in the reinforced geomembranes. The peel specimens delaminated in the plane of the scrim reinforcement producing a FTB.

Discussion. From a laboratory testing standpoint, the ultrasonic seams exhibit two notable characteristics which contrast them with solvent-welded seams. The most significant of these is the consistent FTB failure mode for all of the geomembrane specimens tested in peel. For seams in the PVC geomembranes, this failure mode also produced significantly higher peak loads than is typically required in solvent-welded seams (NSF, 1991).

The second characteristic is the absence of uncertainty and delays associated with the curing of solvent-welded seam samples prior to laboratory testing. From an engineering point of view, the accelerated oven curing of solvent-seam samples prior to laboratory testing gives, in our opinion, a distorted representation of realtime field seam strength conditions. This is not a concern with the ultrasonically-welded specimens.

Table 3. Laboratory Peak Shear Strength Results (ppi) for PVC Geomembranes*

Test Replicate	20-mil PVC		30-mil PVC		40-mil PVC	
1	43.8	FTB	58.7	FTB	95.3	FTB
2	46.8	FTB	58.6	FTB	101.1	FTB
3	38.6	FTB	66.2	FTB	97.4	FTB
4	47.3	FTB	64.8	FTB	100.8	FTB
5	41.8	FTB	61.5	FTB	100.6	FTB
6	42.3	FTB	62.5	FTB	102.1	FTB
7	40.4	FTB	67.4	FTB	96.9	FTB
8	47.8	FTB	60.9	FTB	93.5	FTB
9	43.5	FTB	62.1	FTB	89.8	FTB
10	45.9	FTB	62.6	FTB	100.1	FTB
MEAN	43.8 ppi		62.5 ppi		97.8 ppi	
STD	3.1 ppi		2.9 ppi		3.9 ppi	

Table 4. Laboratory Peak Peel Adhesion Results (ppi) for PVC Geomembranes*

Test Replicate	20-mil PVC		30-mil PVC		40-mil PVC	
1	22.6	FTB	36.7	FTB	44.4	FTB
2	23.5	FTB	33.9	FTB	48.8	FTB
3	25.7	FTB	31.5	FTB	46.7	FTB
4	24.8	FTB	34.0	FTB	43.5	FTB
5	25.4	FTB	35.3	FTB	44.3	FTB
6	24.6	FTB	33.6	FTB	44.8	FTB
7	23.3	FTB	34.2	FTB	42.4	FTB
8	25.5	FTB	32.2	FTB	47.5	FTB
9	25.3	FTB	33.2	FTB	43.3	FTB
10	27.0	FTB	31.2	FTB	44.4	FTB
MEAN	24.8 ppi		33.6 ppi		45.0 ppi	
STD	1.3 ppi		1.7 ppi		2.0 ppi	

*FTB - Film Tear Bond 1 kN/m = 5.714 ppi 1 mil = 0.0254 mm

Table 5. Laboratory Peak Peel Adhesion Strength Results (ppi) for Reinforced Three-Ply Geomembranes*

Test Replicate	20-mil EIA-R		30-mil CSPE	
1	49.9	FTB/DEL	22.3	FTB/DEL
2	48.2	FTB/DEL	25.3	FTB/DEL
3	48.1	FTB/DEL	24.9	FTB/DEL
4	45.8	FTB/DEL	25.1	FTB/DEL
5	43.0	FTB/DEL	23.3	FTB/DEL
6	44.2	FTB/DEL	28.8	FTB/DEL
7	47.0	FTB/DEL	28.8	FTB/DEL
8	41.1	FTB/DEL	24.3	FTB/DEL
9	45.0	FTB/DEL	29.4	FTB/DEL
10	46.2	FTB/DEL	22.8	FTB/DEL
MEAN	45.8 ppi		25.5 ppi	
STD	3.5 ppi		2.6 ppi	

*FTB - Film Tear Bond DEL - Delamination 1kN/m = 5.714 ppi 1 mil = 0.0254 mm

CONCLUSIONS

Ultrasonic field seaming of PVC geomembranes is an effective alternative to solvent welding that offers several practical advantages including immediate full-seam strength, dual-bond seam geometry, and quality cold weather seaming without excessive adjustments to installation technique. Nondestructive seam testing is greatly simplified in the field with the dual-bond geometry and can reduce geomembrane installation cost and schedule. Seam strength in peel and shear is excellent and a FTB failure mode is normally observed.

However, the ultrasonic geomembrane seaming technique has some limitations worth consideration. The seaming machine is patented and is currently available from only one vendor on a made-to-order basis. Since the machine has a relatively high capital cost, roughly twice that of a conventional hot-wedge seaming machine, there is usually only one ultrasonic welding machine available at the construction site. This could lead to problems if the machine breaks down and cannot be field repaired in a reasonable time.

Operator training and experience is crucial to proper ultrasonic geomembrane seaming in non-ideal field conditions. Although it was not a problem in the case history discussed here, machine parts do wear out or experience fatigue (particularly the horn) and not always on a predictable basis (Smith and Magnoli, 1992). Careful inspection is important to maintain the machine in proper operational condition. Handheld ultrasonic seaming units are not currently available and solvent welding is still necessary for detail and patching work. The machine is awkward to handle through steep, shallow depressions. Although burn-through is very unlikely, it can be difficult to maintain overlap and straight seam runs in these areas. For thin geomembranes, such as 0.5-mm (20-mil) PVC, the high mounting of the ultrasonic horn on the machine frame can also present difficulties with maintaining overlap (Smith and Magnoli, 1992).

Additional research is needed to fully define the capabilities and optimal performance specifications for ultrasonic field seaming. The ultrasonic seaming machine welds the two sheets from the interface outward, and the depth of influence of the resulting bond can vary. Further research of the seam strength and bonding depth versus the adjustable operational parameters should be considered. The ergonomics of the machine itself could be improved to better accommodate the demands of field seaming.

ACKNOWLEDGEMENTS

The authors are grateful to William L. Smith of Staff Industries, Inc., for his review comments during the preparation of this paper.

REFERENCES

American Society for Testing and Materials (ASTM). Annual Book of ASTM Standards; Philadelphia, Pennsylvania.

Bove, J.A., and Smith, W.L. (1989) "Ultrasonic Seams," in Proc. 3rd GRI Seminar on the Seaming of Geosynthetics; Geosynthetics Research Institute, Drexel University, Philadelphia, Pennsylvania; December 14-15, 1989; pp. 43 to 51.

Haxo, H.E., and Kamp, L.C. (1989) "Destructive Testing of Geomembrane Seams - I: Testing of Seam Strength;" Proc. 3rd GRI Seminar on the Seaming of Geosynthetics; Geosynthetics Research Institute, Drexel University, Philadelphia, Pennsylvania; December 14-15, 1989; pp. 91-115.

Johnson, G.W., and Rivette, C.A. (1989) "Concerns Regarding Polyethylene Geomembrane Seams: One Owner's Perspective;" Proc. 3rd GRI Seminar on the Seaming of Geosynthetics; Geosynthetics Research Institute, Drexel University, Philadelphia, Pennsylvania; December 14-15, 1989; pp. 169-177.

Koerner, R.M. (1990) Designing with Geosynthetics; 2nd edition, Prentice-Hall Publishers; pp. 493-497.

Lord, A.E., Halse, Y.H., and Koerner, R.M. (1989) "Emerging Methods for Geomembrane Seaming;" Proc. 3rd GRI Seminar on the Seaming of Geosynthetics; Geosynthetics Research Institute, Drexel University, Philadelphia, Pennsylvania; December 14-15, 1989; pp. 80-90.

Morrison, W.R., and Swihart, J.J. (1989) "Bureau of Reclamation Experiences with PVC Seams;" Proc. 3rd GRI Seminar on the Seaming of Geosynthetics; Geosynthetics Research Institute, Drexel University, Philadelphia, Pennsylvania; December 14-15, 1989; pp. 67-79.

National Sanitation Foundation (1991) Standard Number 54 - Flexible Membrane Liners; Ann Arbor, Michigan, revised May 1991.

National Sanitation Foundation (1985) Standard Number 54 - Flexible Membrane Liners; Ann Arbor, Michigan.

Obeda, E.G. (1986) "Apparatus and Method for Ultrasonically Joining Sheets of Thermoplastic Materials;" U.S. Patent 4,713,131; U.S. Patent Office Official Gazette; December 15, 1987.

Smith, W.L. and Magnoli, J.E. (1992) personal communication.

USEPA (1988) "Lining of Waste Containment and Other Impoundment Facilities;" EPA-600/2-88/052; U.S. Department of Commerce-NTIS, Springfield, Virginia; September 1988; p. 4-39.

USEPA (1991) "Inspection Techniques for the Fabrication of Geomembrane Field Seams;" Technical Guidance Document EPA/530/SW-91/051; U.S. Department of Commerce-NTIS, Springfield, Virginia; May 1991.

Laboratory Evaluation of HDPE Geomembrane Seams

D.S. Carlson
GeoSyntec Consultants, USA

R.M. Charron
GeoSyntec Consultants, USA

J.P. Winfree
GeoSyntec Consultants, USA

J.P. Giroud
GeoSyntec Consultants, USA

M.E. McLearn
Electric Power Research Institute Inc., USA

ABSTRACT

This paper presents a study intended to develop laboratory test measures to help improve the performance of seams of exposed high density polyethylene (HDPE) geomembranes. The first part of the paper presents a discussion of relationships between seam performance and parameters measured in seam testing such as peel separation and shear test elongation. The second part presents results from 74,643 HDPE geomembrane seam specimens tested from 1986 to 1991; various types of seams are ranked based on the degree of peel separation and the elongation exhibited during the shear test. The third part presents results from notched stress rupture testing of over 300 HDPE geomembrane specimens with and without seams; these results support the use of the notched stress rupture test in the selection process of HDPE geomembranes for exposed applications. In conclusion, enhanced quality assurance procedures are proposed for exposed HDPE geomembranes.

INTRODUCTION

In the past decade, geomembranes have become reliable construction materials, due largely to quality assurance methods developed for the installation of geomembrane liners in landfills. However, failures are still observed, particularly in exposed geomembranes, i.e., geomembranes that are not covered with a layer of material that protects them. Geomembranes in liquid impoundments are partially exposed, whereas in landfills geomembranes are generally covered with soil and waste shortly after their installation.

Failures of exposed HDPE geomembranes have been observed at seams or next to seams which are produced by the same seaming techniques under the same quality assurance procedures as are presently specified for landfills. In this paper it is proposed that seaming quality assurance for exposed geomembranes follow stricter seaming procedures and acceptance criteria than those used for landfills. The stricter specifications would take into account the fact that exposed geomembranes are subjected to more stresses than covered geomembranes. In particular, tensile stresses due to thermal contraction and shrinkage in exposed HDPE

geomembranes have contributed to stress cracking failures.

A study was undertaken to address the concerns of owners, designers, and constructors of facilities where geomembranes are exposed. This study included: (i) a review of the state of practice regarding seam testing that is done for quality assurance purposes; (ii) an analysis of a data base including the results of 74,643 quality assurance seam tests; and (iii) a testing program to investigate the influence of seams on geomembrane stress crack resistance. The study was restricted to HDPE geomembranes and with only minor exception addresses four types of seams: extrusion fillet; extrusion lap; hot wedge fusion, single track; and hot wedge fusion, double track (Figure 1). This paper describes the study, summarizes the results, and provides recommendations regarding seam type selection, seam testing, and geomembrane selection.

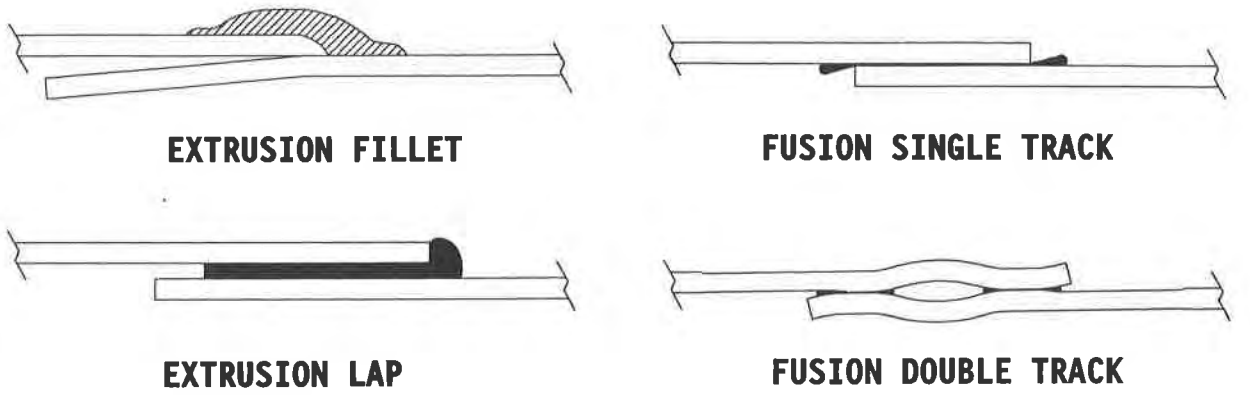

Figure 1. Seam configurations.

1. REVIEW OF HDPE GEOMEMBRANE SEAM TESTING STATE OF PRACTICE

1.1 Seam Testing Methodology. Seams are generally tested using peel and shear tests according to ASTM standard method D 4437. This standard method presents procedures for specimen preparation, laboratory testing instrumentation, and test conditions; however, seam acceptance criteria are not addressed in ASTM D 4437. Typically one measurement is made in each test: the maximum peel force per unit width in the peel test, and the maximum shear force per unit width in the shear test. However, in this study, two additional parameters were systematically recorded: the amount of separation, if any, which occurs during the peel test; and the amount of elongation that occurs during the shear test. The amount of peel separation is the percentage of the initially bonded area that becomes separated during the peel test and is determined by an informed observational judgement. The amount of elongation is calculated by dividing the change in grip separation during the shear test by a gauge length of 50 mm (2 in.), which is equal to the initial grip separation minus the width of the seam.

1.2 Significance of Peel Separation. Microscopic examination of surfaces separated during a peel test shows that small crazes, which are precursors to cracks, or cracks themselves, often appear on these surfaces (Peggs and Charron, 1989). Such crazes and cracks have been found to propagate through liners, along or through seams, in a direction normal to the applied tensile stress and normal to the plane of the geomembrane. Propagation accelerates on a very small,

localized scale during combined exposures to wetting agents (such as surfactants) and oxidizing agents (such as oxidizing acids), infra-red or ultraviolet radiation, and tensile loading. (These mechanisms will be discussed further in Section 3.2.)

As a result of tensile loading, seams tend to rotate slightly, causing bending of the geomembrane, with maximum bending next to the seam (Giroud, 1984a, 1984b; Giroud et al., 1993b). As a result of seam rotation, the forces exerted by one geomembrane on the other through the bonded area act partially in shear and partially in peel. When seam separation occurs, the location of maximum bending moves with the separation to abut the area that remains bonded. Consequently, maximum bending occurs in a previously bonded area that has just separated. This previously bonded portion of geomembrane may be susceptible to crazing due to surface imperfections resulting from the separation process. Consequently, geomembrane failure may ultimately result in such an area in the seam.

A maximum allowable seam separation of 10% was proposed by Peggs (1987) to eliminate, at the quality assurance stage, seams that tend to peel excessively and, therefore, are susceptible to crazing as discussed above. In order to investigate the validity of this criterion, a microscopic investigation of 10 partially or totally separated specimens including each seam type was undertaken. Examples of photomicrographs are shown in Figure 2. The results of the microscopic investigation are as follows:

- crazing may not always occur, but was found in every instance investigated during this study;
- all seam types exhibited crazing on both sides of the separated interfaces; and
- when crazing occurs, it may occur at very small peel separation (i.e., less than 10%) irrespective of seaming method.

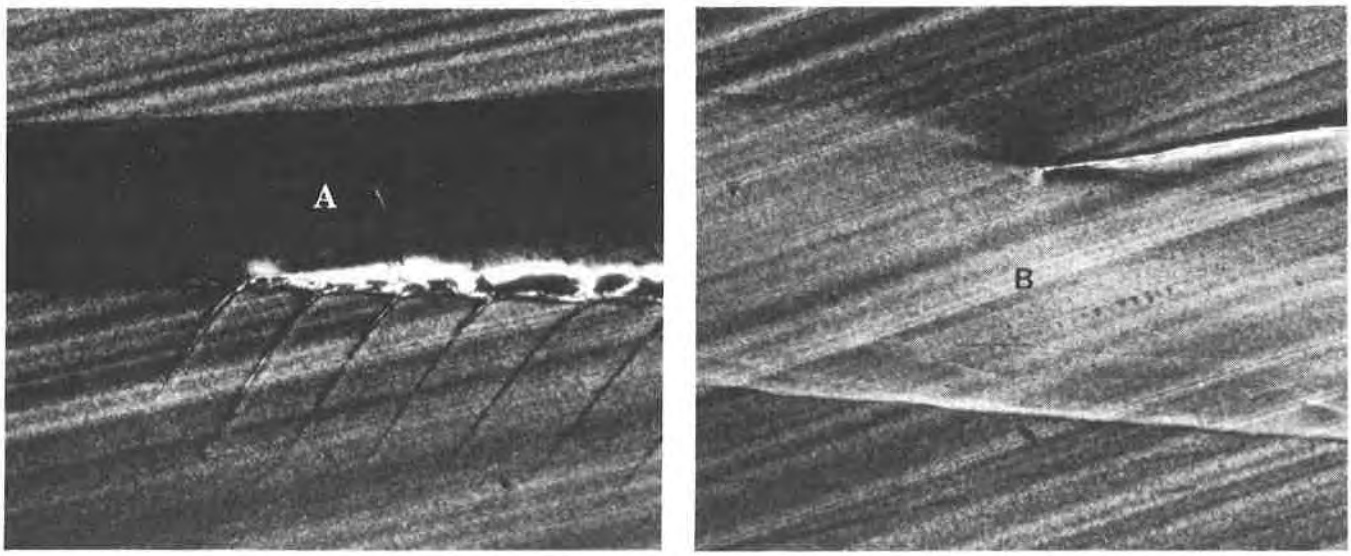

Figure 2. Evidence that peel separation influences initiation of crazing: (a) separated interface with crazing; and (b) specimen prior to peel testing with no crazing.

It is important to note that the 10 specimens subjected to microscopic investigation after peel testing were also subjected to microscopic investigation prior to peel testing and no crazing was observed at that stage (Figure 2b).

It should be noted that the peel conditions imposed by testing in the laboratory are much more severe than those experienced in the field (where the peel forces are only a fraction of the shear forces). On the other hand, a 10% peel separation under actual peel forces in the field would be unacceptable in light of the above discussion. Therefore, an ideal criterion would require no peel separation at all in a laboratory peel test conducted with the same peel forces as those likely to be exerted in the field. Clearly, more research is needed to evaluate these forces and define testing procedures that properly model field conditions.

1.3 Significance of Shear Elongation. Causes of low elongation during a shear test include geomembrane embrittlement in the seam area (which may be due to excessive temperature during seaming) and localized decrease (potentially due to the seaming process) in geomembrane thickness adjacent to the seam, as shown by Giroud (1984a, 1984b) and quantified by Giroud et al. (1993a). Both geomembrane embrittlement and lack of thickness may result in inadequate performance of the geomembrane next to a seam, even though the seam itself may remain watertight. Because both factors cause low elongation, measuring elongation in a shear test is an effective means of detecting seam areas of inferior performance potential.

1.4 Seam Acceptance Criteria. Based on the experience summarized above, acceptance criteria have been proposed (Giroud and Peggs, 1990) for seams, such as those in exposed locations, where a high level of quality assurance is required. Two categories of acceptance criteria are included: specimen acceptance criteria and sample acceptance criteria. The applicability and importance of the proposed criteria will be discussed in the context of the data base analysis which follows.

Specimen Acceptance Criteria. A peel test must be conducted until rupture of the geomembrane or complete (100%) peel separation occurs, and a specimen peel test result is considered acceptable if it meets the following two requirements:

- strength of at least 60% of the parent geomembrane yield strength; and
- less than 10% separation at the end of the test.

A specimen shear test result is considered acceptable if it meets the following two requirements:

- strength of at least 90% of the parent geomembrane yield strength; and
- more than 50% elongation.

Sample Acceptance Criteria. On each sample five peel specimens and five shear specimens are tested. The seam sample acceptance criteria are as follows: four of the five peel specimens tested must pass the criteria for peel specimens and four of the five shear specimens tested must pass the criteria for shear specimens.

2. DATA BASE ANALYSIS

2.1 Overview. A data base was assembled from results of laboratory seam testing conducted from 1986 through 1991 for HDPE geomembrane quality assurance related to the construction of a number of landfills and other facilities in the USA. The purpose of this data base assembly and analysis was to: (i) evaluate the proposed seam testing criteria and their parameters; and (ii) compare the various seaming techniques using these criteria.

Results from 47,896 specimens tested in peel and 26,747 specimens tested in shear are included in the data base. All results in the data base are for individual specimens only, without regard to their parent sample. Consequently, sample acceptance criteria mentioned in Section 1.4 are not considered in the study; only the specimen acceptance criteria mentioned in Section 1.4 are considered. Extrusion seam failures in the fillet are not included for lack of relevancy to the analysis.

Peel and shear data presented in the following sections are related to specimens from "initial samples" and specimens from "secondary samples". Initial samples are those taken with an average frequency that is in accordance with the site-specific quality assurance plan, e.g., one sample per 150 m (500 ft). These samples are typically selected by the on-site quality assurance manager either at random or because the quality assurance manager has a particular reason to take a sample at a specific location (e.g., changing weather conditions, seaming done by a new crew member). Secondary samples are typically taken approximately 3 m (10 feet) on each side of initial samples that do not meet site specific acceptance criteria. The importance of this practice is supported in Section 2.2.

The numbers of specimens for each type of test and seam are indicated in the legends of Figures 3, 4, 5, and 6. The number of specimens was much larger for two types of seams, the fusion double track and the extrusion fillet, than for the others. Therefore, the conclusions drawn for these two types of seams are more valid than for the others.

2.2 Analysis of Peel Separation Data. Information pertaining to seam failure in the peel test for specimens from initial and secondary samples is contained in Figures 3 and 4, respectively, according to three categories: 11-50%, 51-99%, and 100% seam peel separation. In cases other than 100% seam peel separation, the test ended with geomembrane rupture outside the seam.

The seam failure rates (Figure 3) for extrusion lap seam specimens (16.1%) and single-track fusion seam specimens (23.5%) are large compared to the failure rates for extrusion fillet seam specimens (9.0%) and double-track fusion seam specimens (4.1% for the outside track and 3.5% for the inside track). However, because of the small amount of data for single track fusion seams and extrusion lap seams no conclusive statements can be made concerning these seams.

A comparison of Figures 3 and 4 shows that peel separation occurred in significantly more specimens from secondary samples than from initial samples (e.g., 33.3% for extrusion fillet seam specimens; 7.9% for the outside track of double-track fusion seam specimens; and 6.8% for the inside track of double-track fusion seam specimens). This statistical result is believed to

be the first quantitative data supporting the quality assurance practice of taking secondary samples when primary samples fail the tests (see Section 2.1).

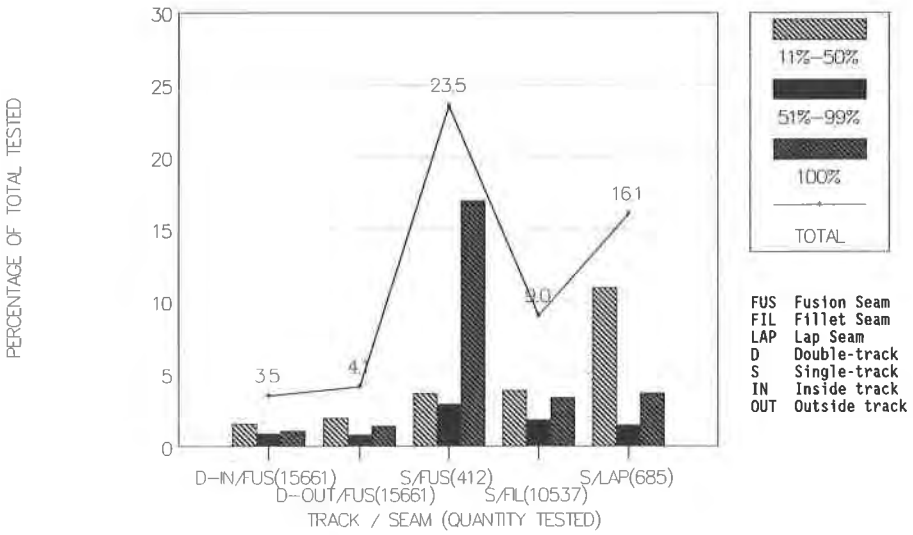

Figure 3. Peel separation data for specimens from initial samples.

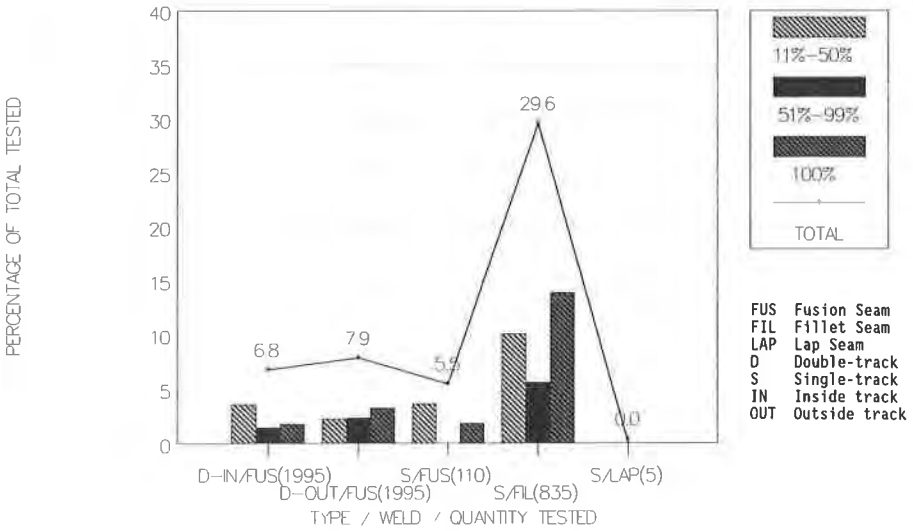

Figure 4. Peel separation data for specimens from secondary samples.

Figures 3 and 4 show that the 51-99% peel separation category contains the smallest number of specimens; i.e., most seams exhibit either a relatively small seam separation percentage (i.e., less than 50%) or peel completely.

Figure 5 was obtained by combining results from Figures 3 and 4 and reorganizing the categories as follows: the category "> 10%" in Figure 5 includes all the peel separation categories of Figures 3 and 4, namely "11-50%", "51-99%", and "100%". Figure 5 shows that if the "< 10%" peel acceptance criterion were adopted, instead of the "< 100%" peel acceptance criterion (i.e., film tearing bond (FTB)), the number of specimens of fusion double-

track seams and extrusion fillet seams rejected for peel separation would increase by a factor of approximately 2.5. However, since the distribution of failed specimens with respect to samples is unknown, it is possible that the sample failure rates will increase by a factor less than 2.5 because some samples produce two or more specimen failures.

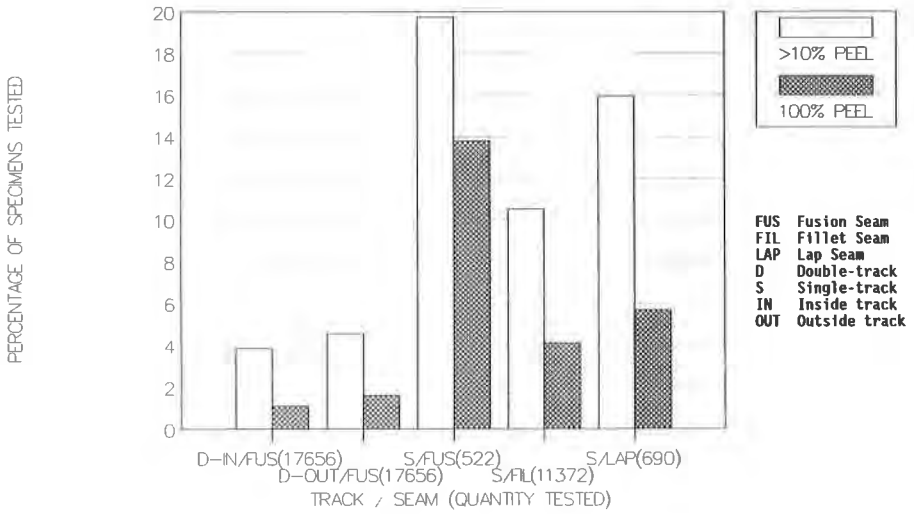

Figure 5. Separation comparison for specimens from initial and secondary samples.

2.3 Shear Data Analysis. Geomembrane seam specimens rarely fail a shear test using a criterion based solely on strength. The shear test, however, provides the opportunity to measure the elongation in and adjacent to the seam. Elongation of magnitudes close to that of geomembrane provides some assurance that the material in or near the seam has not been altered drastically during the seaming process. Reduced elongation values indicate that the seam area has been altered, as discussed in Section 1.3. Figure 6 shows the percentage of specimens that fail to meet the criterion requiring elongation greater than 50% in the shear test. This figure shows seam failure rates of 3.0% for extrusion fillet seam specimens and 1.0% for double-track fusion seam specimens. These data show that double-track fusion seams perform better than other seam types analyzed in this study, which was also concluded from the peel test data.

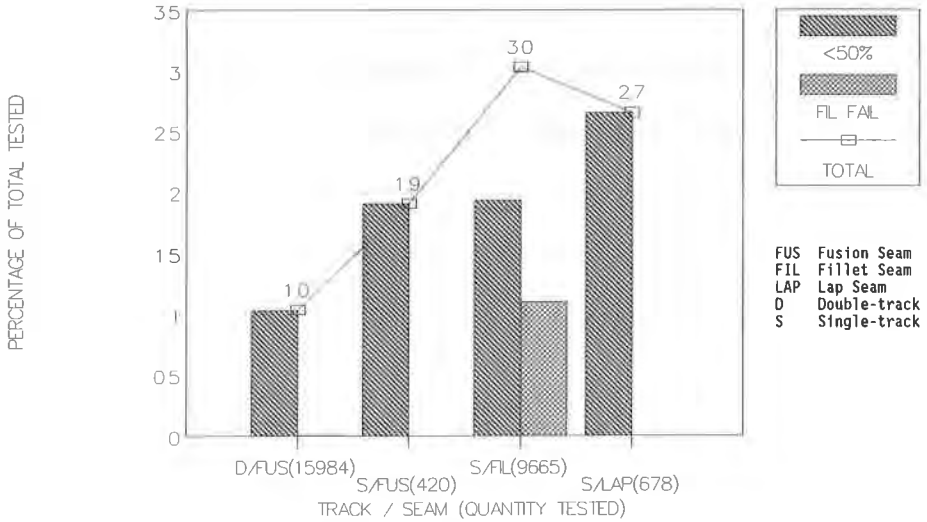

Figure 6. Shear elongation data for specimens from initial samples.

3. INFLUENCE OF SEAMS ON STRESS CRACKING RESISTANCE

3.1 Purpose of the Investigation. A significant proportion of the HDPE liner system failures which the authors have investigated have evidenced incipient stress cracking in and along seams. It was hypothesized, therefore, that seaming processes or the presence of a seam decreases geomembrane stress crack resistance. To evaluate this hypothesis, notched stress rupture tests were performed on HDPE geomembrane with and without seams and the results were compared.

3.2 Relationship Between Microstructure and Stress Cracking of HDPE. A semicrystalline material, HDPE consists of two phases: (i) crystalline; and (ii) amorphous. In the crystalline phase, polyethylene molecules are packed into highly organized plates also called lamellae. Adjacent lamellae are held together by the amorphous phase, consisting of tie molecules, which include: (i) polyethylene molecules that extend from one lamella to another; and (ii) physically entangled molecules that extend out of adjacent lamellae but that do not extend from one lamella to another. Stress cracking occurs primarily between, but not across, adjacent lamellae. Accordingly, any process (such as chemical reaction or swelling) that causes tie molecules either to break or to become disentangled should accelerate stress cracking in HDPE.

Infrared, ultraviolet, and high energy radiation create chemically reactive sites on amorphous polyethylene molecules since these molecules are not tightly packed. These reactive sites react with chemicals such as oxygen and nitric acid, breaking the tie molecules that connect adjacent lamellae. Stress cracking in HDPE may be further accelerated by chemical agents which reduce the cohesive forces between molecules, a process that occurs more readily in the amorphous phase since its molecules are disorganized and are not tightly packed together. These chemical agents cause HDPE to swell, causing the polyethylene molecules in the amorphous phase to disentangle, eventually leading to disconnection of adjacent lamellae.

3.3 Overview of the Notched Stress Rupture Test. The notched stress rupture test is a laboratory test intended to evaluate a material's stress crack resistance (it is usually conducted on specimens without a seam). The notched stress rupture test employs a constant tensile load and a uniform stress concentrator (notch). This test has been referred to as (i) Constant Tensile Load (CTL) Test and (ii) Single Edge Notched (SEN-CTL) Test. These are differences only in name and not in procedures. This test method is currently in the draft stage at ASTM. An earlier ASTM test was conducted for similar purposes on un-notched specimens.

The notched stress rupture test provides data about the stress crack resistances of different polymeric materials by either: (i) performing tests at given stress levels and comparing times to rupture; or (ii) performing tests at one stress level and comparing craze growth at that stress level. The first approach was selected.

The mode of failure of HDPE geomembrane in the notched stress rupture test can be described as ductile, transitional, or quasi brittle depending on the fracture face (Figure 7). The type of fracture face morphology is normally determined by informed observational judgement. Ductile failure is a type of fracture producing noticeable cold drawing (where cold drawing is the plastic deformation of fracture face material, occurring parallel to the applied load.) Quasi

brittle failure is a type of fracture producing cold drawing on a micro-level (i.e., not readily noticeable). A transitional mode of failure is a type of fracture evidencing roughly equal degrees of both ductile and quasi brittle fracture characteristics. For example, when subjected to a sustained stress less than approximately 40% of its room temperature yield strength, HDPE will, in a conducive environment, display a quasi brittle mode of failure known as stress cracking. (Truly brittle cracking occurs in HDPE at high propagation rates under low temperatures.)

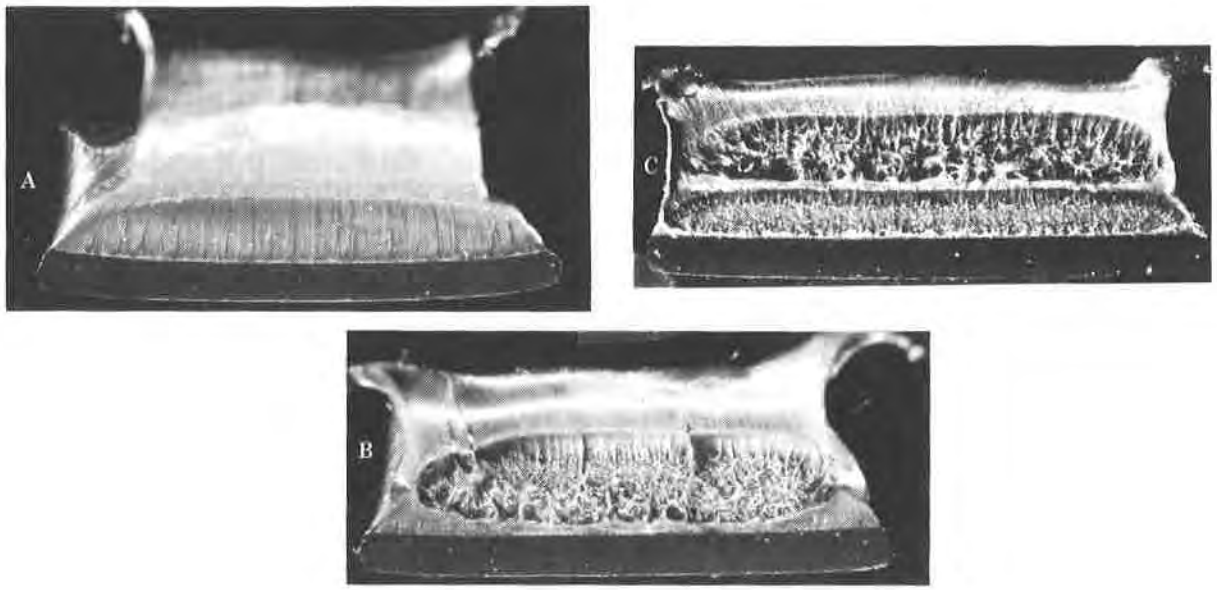

Figure 7. Notched stress rupture specimen fracture faces illustrating (a) ductile failure, (b) transitional failure, and (c) quasi brittle failure.

3.4 Geomembrane Material Used in Testing Program. Notched stress rupture testing was employed to compare the stress rupture behaviors of nine samples of seamed HDPE geomembrane materials supplied by five different manufacturers. These samples were large enough so specimens with seams and without seams could be excised. Table 1 summarizes the materials tested.

Table 1. Summary of the nine HDPE samples subjected to notched stress rupture tests.

MANUFACTURER LETTER CODE	SAMPLE CODE	NOMINAL THICKONESS OF SHEET (mm)	TYPE OF SEAM
A	A-1	1.5	Double-Track Extrusion
	A-2	2.0	Extrusion Lap
B	B	1.5	Single-Track Fusion
C	C-1	2.0	Extrusion Fillet
	C-2	2.0	Double-Track Fusion
D	D-1	2.0	Extrusion Fillet
	D-2	2.0	Double-Track Fusion
E	E-1	2.0	Extrusion Fillet
	E-2	2.0	Double-Track Fusion

3.5 Test Procedures. For all tests, dumbbell ASTM D 638 Type IV specimens were used. To ensure proper comparison between tests with and without seams, specimens without seams were taken (a) from the same samples as the specimens with seams and (b) parallel with the specimens with seams. More than 300 HDPE specimens were tested. Specimens with seams were excised so that the outer seam edge (notch location) was positioned at the center of the dumbbell specimens.

All notches were cut to a controlled depth equal to 20% of the geomembrane's thickness at that location. Notching was done by very slowly pressing a fresh razor blade into the top surface of the geomembrane sheet. The specimens with seams were notched in the top surface of the bottom sheet of geomembrane immediately adjacent to the root of the squeeze-out bead at the seam edge. The specimens were notched in this location because it has been found to be the predominant location of field stress cracking, as shown by Peggs and Carlson (1990). Seam edge notching of fusion seams required the removal of some extraneous material before notching, as illustrated in Figure 8. Whether the specimen included a seam or not, the notch was located approximately equidistant between the grips.

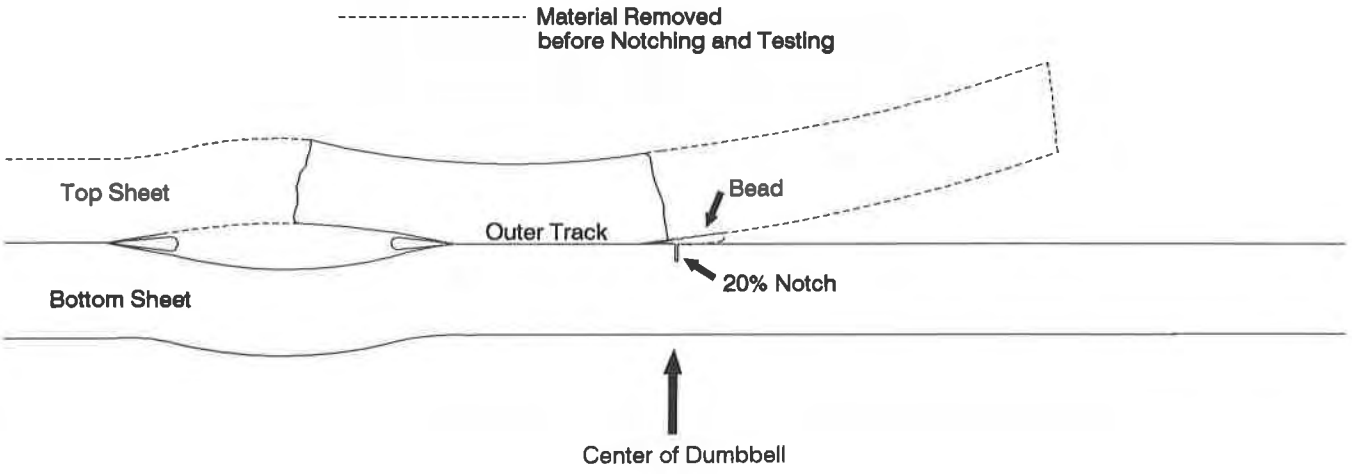

Figure 8. Cross section of notched stress rupture specimen from a double track fusion seam showing a side-view of the notch location.

The stress applied to each specimen was calculated based on the applied load and the initial cross-sectional area of the geomembrane at the test notch (i.e., excluding the area of the notch itself). Steady loads were applied to induce the following stress levels in the tests: 5500, 6200, 6900, 7600, and 8300 kPa (800, 900, 1000, 1100, and 1200 psi). The yield stress of the tested geomembranes at 50°C was on the order of 13,000-15,000 kPa (1900-2200 psi).

The 1% Igepal CO-630 surfactant bath, maintained at 50°C, provided for a standard accelerated test environment. Igepal CO-630 is 100% nonylphenoxy poly(ethylene-oxy) ethanol, manufactured by General Analine Film (GAF) Corporation.

3.6 Test Results. The notched stress rupture test results (Figure 9) show small and inconsistent differences, measured in stress rupture lives, between specimens with and without seams from a given sample provided by a given manufacturer. The test did not show a consistent difference between specimens with and without seams either because there was no difference or because the test was unable to show a difference.

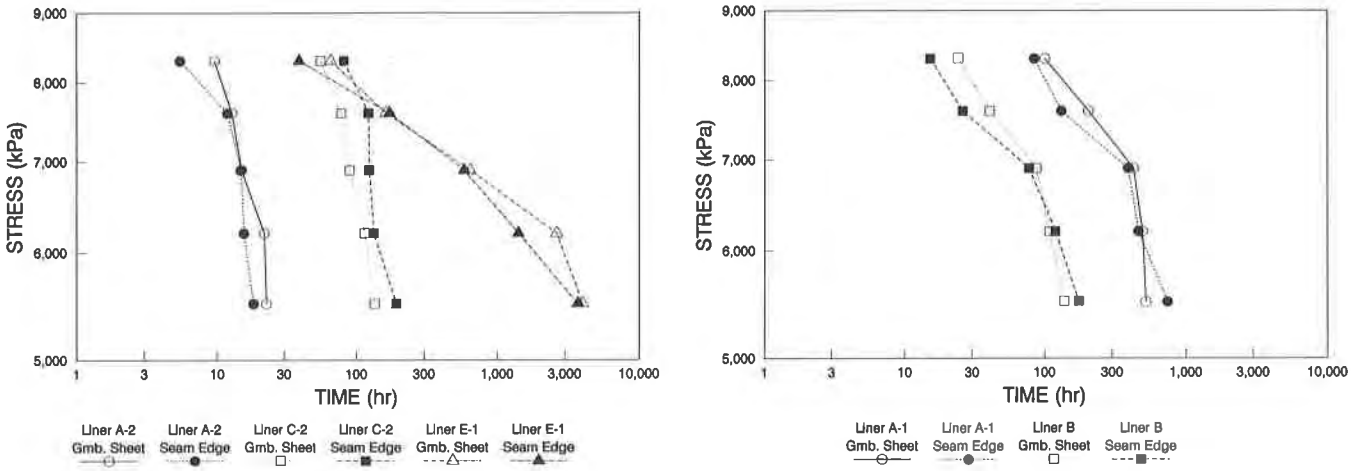

Figure 9. Notched stress rupture test results illustrating relatively small differences in rupture lives between specimens with and without seams from a given sample of material from a given manufacturer.

The absence of a "seaming effect" may reflect the care which was exercised in seaming the samples supplied by the geomembrane manufacturers for this study. If the results are attributable to optimized seaming, the following observations may be made:

- under well controlled conditions, it is possible to seam HDPE geomembranes without reducing their stress cracking resistance;
- seamed material which shows reduced resistance to stress cracking has been sensitized by something done improperly during seaming; and
- seaming practices which may sensitize geomembrane should be monitored by testing.

Test results did show, however, that rates of crack growth through HDPE geomembrane can vary by as much as two orders of magnitude depending on the geomembrane sample. This is readily evidenced from Figure 10 which presents most of the same data as Figure 9 in a different form. This variability between geomembranes (which may be due to differences in resins and/or manufacturing processes) suggests that notched stress rupture testing can be used as a tool when selecting geomembranes for exposed applications.

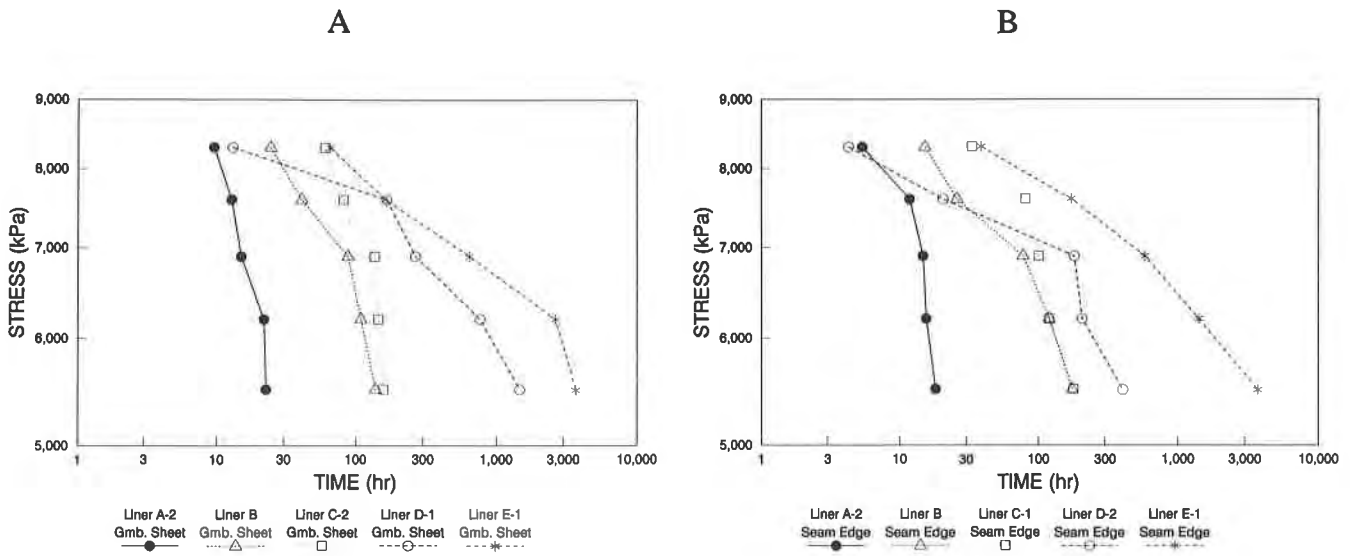

Figure 10. Stress rupture properties of HDPE geomembrane supplied by five manufacturers (a) without seam, and (b) with seam.

3.7 Selection of Stress Level for Geomembrane Comparison. A geomembrane that has a greater time to rupture than another geomembrane at all stress levels is likely to have a greater stress crack resistance in the field. However, as shown in Figure 10, a given geomembrane compared to another one may have a greater time to rupture at one stress level and a smaller time to rupture at another. Therefore, to use notched stress rupture testing as a tool for comparing different HDPE geomembranes, both a stress level and a time to rupture should be specified. The specified stress level should be low enough to induce quasi brittle stress cracking, but should not be so low that it takes months to complete a test. The 7600 kPa (1100 psi) and 8300 kPa (1200 psi) stress levels are therefore ruled out for HDPE because specimen failures occurred in a ductile mode. The 6900 kPa (1000 psi) stress level is ruled out because many specimen failures exhibited ductile to quasi brittle transitional behaviors. The 6200 kPa (900 psi) stress level is selected because quasi brittle stress cracking was induced in all specimens, and because times to rupture were shorter than those at 5500 kPa (800 psi), a stress level at which quasi brittle stress cracking was also induced in all specimens.

3.8 Selection of Minimum Pass Criterion. Selecting a "minimum pass criterion" time to rupture at the selected stress level is difficult and arbitrary because the relationship between specimen rupture times to real life expectancy is not known. Guidance may be provided by the frequency distribution of rupture times for all HDPE specimens tested at 6200 kPa (900 psi) presented in Figure 11. This distribution shows that 57 % of the specimens ruptured after 200 hours, and that 11 % of the specimens ruptured after 1000 hours. Guidance may also be provided by the ranking of the nine HDPE geomembranes according to their times to rupture at 6200 kPa (900 psi) in the accelerated test (Table 2). It appears that a minimum pass criterion of 200 to 500 hours could be considered. A new study drawing correlations between field failures of exposed material and times to rupture (at 6200 kPa) of identical, but unexposed, material should provide

further data supporting the selection of a "minimum pass criterion" time to rupture. The authors have not yet begun this new study.

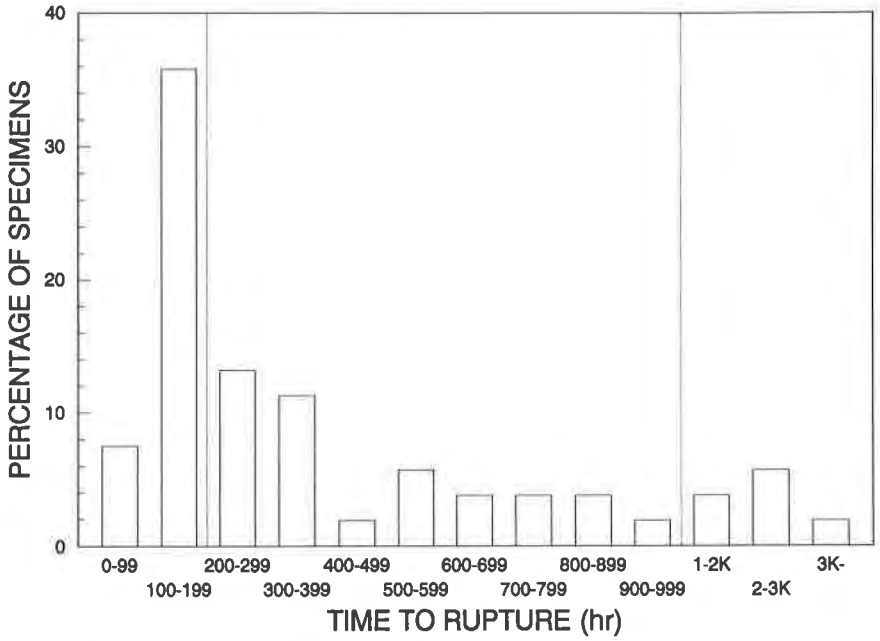

Figure 11. Frequency distribution of rupture times for over 50 HDPE specimens (with and without seams) tested at 6200 kPa (900 psi).

Table 2. Ranking of nine HDPE geomembranes according to notched stress rupture lifetimes at 6200 kPa. (Tests conducted on geomembrane specimens without seams.)

Ranking (Longest to Shortest)	1	2	3	4	5	6	7	8	9
Sample Code	E-1	E-2	D-1	A-1	D-2	C-1	C-2	B	A-2
Average Time to Rupture (Hours)	2630	805	762	431	168	161	130	108	22

CONCLUSIONS

A review of the seam peel and shear testing state of practice has shown that:

- The seam peel and shear failure criteria considered are closely related to failure mechanisms that affect exposed geomembranes.

- Both seam peel and seam shear test acceptance criteria are necessary and complementary because: (i) both peel and shear stresses are present in the field; (ii) the peel test is currently the only way to evaluate the uniformity of adhesion between geomembranes; and (iii) the shear test provides important information on low elongation failure, which may result from damage to the geomembrane caused by the seaming procedure and affects the performance of the seam.

- The need for a peel separation criterion is confirmed by microtome analyses, showing that seam separation causes crazing of the geomembrane which may lead to inadequate seam performance in service.

- The formulations of the seam acceptance criteria could be improved. For example, research could be undertaken to develop test procedures that would allow the "less than 10% peel criterion at failure in the peel test" to be replaced by a "0% peel criterion at working stresses".

Data from peel and shear testing of 74,643 HDPE geomembrane seam specimens were systematically assembled and analyzed by the authors. The main results from the data base analysis are the following:

- Although the extent of the data base may not be sufficient to draw firm conclusions for single-track extrusion lap seams, it appears that these seams exhibit a relatively large number of specimen failures as determined by the criteria considered.

- According to the two seam criteria investigated, a much lower specimen failure rate occurred with double-track fusion seams than with single track fusion and extrusion fillet seams.

The main results of the notched stress rupture tests are:

- Using the notched stress rupture test, the authors were unable to demonstrate in this study that seaming processes or the presence of a seam consistently decreases the stress crack resistance of HDPE geomembrane. At this stage, it is not possible to conclude whether the presence of the seam has no effect on geomembrane performance, or the type of test used is unable to evaluate the influence of the seam.

- The stress crack resistance of HDPE geomembrane materials produced from different sources can vary by as much as two orders of magnitude as measured by time to rupture in accelerated notched stress rupture testing.

- The notched stress rupture test is recommended for consideration as a tool for geomembrane selection for applications where the geomembrane is to be exposed.

- The 6200 kPa (900 psi) stress level is recommended to compare HDPE geomembranes subjected to notched stress rupture testing under standard accelerated conditions (Igepal solution at 50°C).

ACKNOWLEDGEMENTS

The financial support of Electric Power Research Institute for this work, and in preparing this paper, is gratefully acknowledged.

The technical assistance of Mr. Louis G. Tisinger in describing material and environmental interactions and the data base assembly by Mr. Robert Heyen are appreciated.

REFERENCES

Giroud, J.P., (1984a) "Analysis of Stresses and Elongations in Geomembranes", Proceedings of the International Conference on Geomembranes, Vol. II, pp. 481-486.

Giroud, J.P., (1984b) "Geotextiles and Geomembranes. Definitions, Properties and Design", IFAI Publishers, 325 p.

Giroud, J.P. and Peggs, I.D., (1990) "Geomembrane Construction Quality Assurance", Waste Containment Systems: Construction, Regulation, and Performance, Geotechnical Special Publication No. 26, ASCE, R. Bonaparte, Editor, pp. 190-225.

Giroud, J.P., Beech, J.F., and Soderman, K.L., (1993a) "Yield of Scratched Geomembranes", submitted to Geotextiles and Geomembranes.

Giroud, J.P., Tisseau, B., Soderman, K.L., and Beech, J.F., (1993b) "Analysis of Strain Concentrations Next to Geomembrane Seams", submitted to Geotextiles and Geomembranes.

Peggs, I.D., (1987) "Evaluating Polyethylene Geomembrane Seams", Proceedings of Geosynthetics 87, Vol. II, pp 505-518.

Peggs, I.D. and Charron R.M., (1989) "Microtome Sections for Examining Polyethylene Geosynthetic Microstructure and Carbon Black Dispersion", Proceedings of Geosynthetics 89, Vol. II, pp 421-432.

Peggs, I.D., and Carlson, D.S., (1990) "The Effects of Seaming on the Durability of Adjacent Polyethylene Geomembranes", Geosynthetic Testing for Waste Containment Applications, ASTM STP 1081.

The Use of Impact Test Procedure to Assess Seams' Brittleness

A.L. Rollin
École Polytechnique, Canada

M. Marcotte
Solmers Internationale, Canada

J. Lafleur
École Polytechnique, Canada

J. Mlynarek
École Polytechnique, Canada

ABSTRACT

This paper presents the behavior of more than 700 HDPE seam's samples that were analyzed under the impact test procedure. This procedure was developed to detect seams brittleness since none of the commonly used testing procedures permit its evaluation within the bonded strip. This testing procedure, modified from an existing ASTM standard for HDPE pipe, has been developed to determine the energy level required to fail specimens upon impact. The required energy level is evaluated using a drop-weight apparatus and depends mainly upon the sheet's tickness and on the quality of the seam itself.

The tests were performed on both hot air seams and hot wedge seams. Sheet thickness, welding speed, roller pressure, ambient and welding temperature were varied to evaluate their relative importance as determining factor. In each case, the impact test has been sensitive enough to detect brittle specimens. In order to implement the impact test in a quality assurance program, consideration is given on the base of the results presented in the paper. It is pointed out that this testing procedure can easily be performed on site since the conditions of testing, the size of the apparatus and the cost of the necessary equipment are minimal.

INTRODUCTION

It is well known that the service life of lined facilities is influenced by the ageing of the polymer and by any other aggressive parameters such as very low or high ambient temperature, localized impact, chemical attack, UV attack and excessive welding conditions. However, seam brittleness has recently been identified as a predominant factor in the long term behavior of HDPE lined facilities (Peggs 1988, Rollin 1989)

Rupture of degraded HDPE sheets usually happened at stresses lower than expected because of propagation of micro-cracks within its molecular structure. The micro-stress cracking phenomenon is a result of local residual stresses as well as degradation of the molecular structure from overheating, excessive pressure, chemical and weathering attacks. This degradation within the molecular structure of the polymer may be related to the mechanical behavior of the geomembrane itself. Actually, under that kind of degradation, the stress-strain curve of the material will exhibit stiffer modulus along with a more brittle behavior. Since the manufacturing process affects obviously the molecular structure, it is also well known that the welding process will greatly affect the long term behavior of the molecular structure.

Still, none of the commonly used testing procedures implemented by construction Quality-Assurance/Quality-control (QAQC) programs of these lined facilities permit the identification of a brittle behavior within the bonded strip. The shear test and the peel test are both used to measure seam strength. More and more attention is drawn to the stress-strain relationship but it appears that the measured parameters are not sensitive enough to be related to the brittleness level of a HDPE sheet.

A dynamic test has been developed to determine the energy level required to fail specimens upon impact. It has been shown by Rollin et al (1991) that the impact test is sensitive enough to detect brittle seams. In this paper, the mechanical behavior of more than 700 seam samples are analyzed under impact test procedure. This behavior is also compared to the parent material in the vicinity of the seams along with the results of peel and shear tests. Finally, microscopic analyses were also performed on cross sections of ruptured seams to characterized the rupture mechanism.

THE SEAMING EFFECT

HDPE is a semi-crystalline polymer composed of both amorphous and crystalline areas. The crystalline portion is responsible for many of the characteristics of polyethylene, including strength and rigidity. The more crystalline the HDPE, the higher the tensile strength and elastic modulus. Since modulus is the ratio of stress to strain, several types of modulus values are used to define the tensile behavior of HDPE. The two most common for HDPE geomembranes are modulus of elasticity and secant modulus (figure 1). Experience has demonstrated that seaming of HDPE geomembrane is as critical as the manufacturing process is. Specifically, to demonstrate the effect of seaming on the parent material located along the bonded strip, two series of seams were tested in shear: one series of normal seams ECD80-A and one series of brittle seams ECD80-B. Eight sets of four sheet specimens were collected at different distances from the seam axis randomly along both seams as shown in Figure-2. The secant shear modulus at yield (E1) and the secant shear modulus at break (E2) are presented in Figure-3.

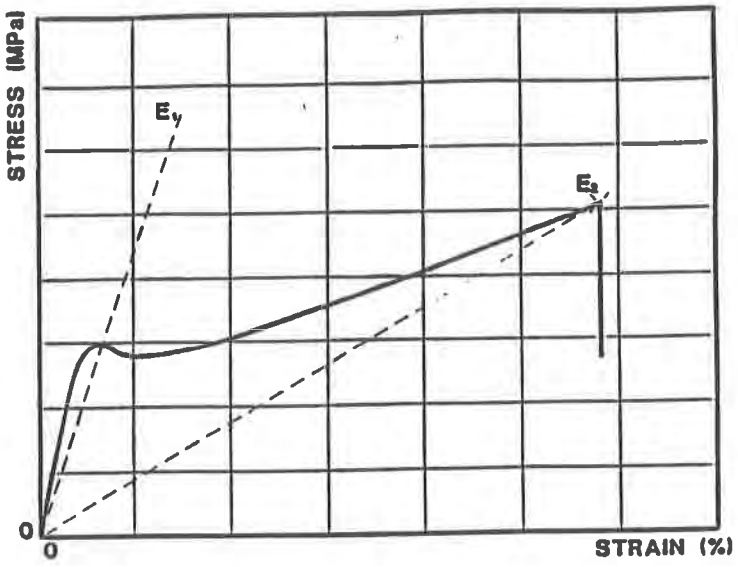

Figure 1 - HDPE parent material stress-strain curve

It can be observed that the values of both secant modulus increased toward the seam axis indicating an increasing rigidity of the parent material near the edge of the seam. However, the results does not permit to identify the brittle seam (ECD80-B). These results support the fact that the test is not sensitive enough to identify brittle seams. Finally, it should be pointed out that "rigid" is used in this paper as opposite to "deformable" and "brittle" is opposed to "ductile".

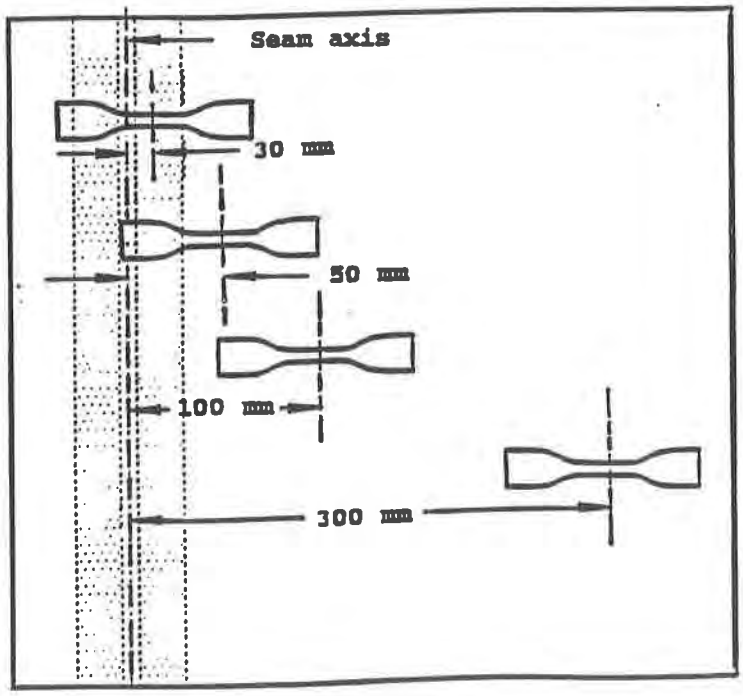

Figure 2 - HDPE sheet specimen locations from seam axis

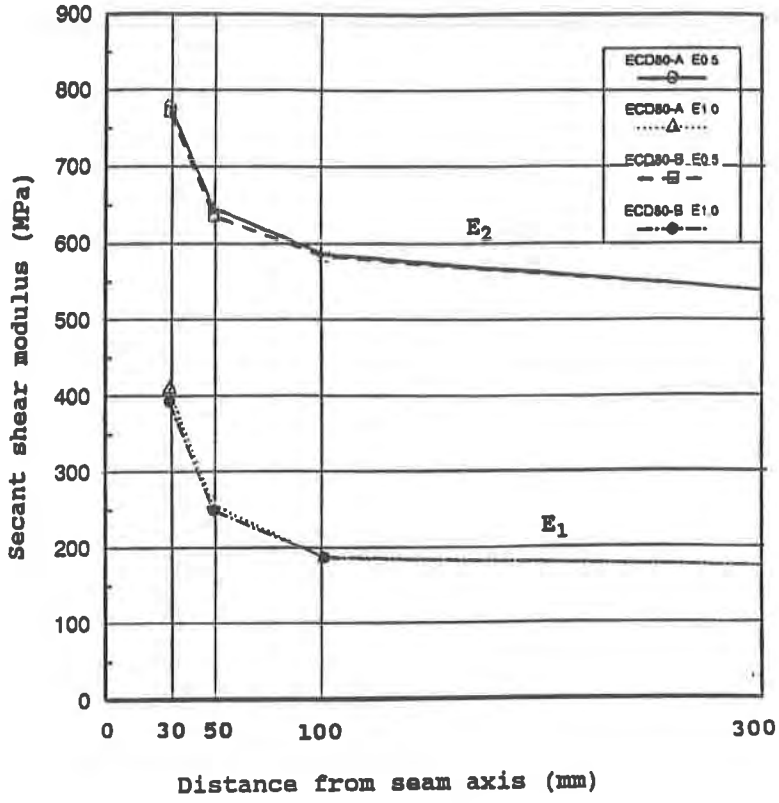

Figure 3 - Secant shear modulus of welded HDPE sheets

PROCEDURE AND TESTING

Drop-weight apparatus The drop-weight apparatus is a modified version of the equipment used to measure the impact resistance of corrugated plastic drainage pipe (ASTM-D-3029 (1984)). The main components are a vertical steel pipe installed on a support, a metallic mass and a seam specimen holder as shown in Figure-4. A release mechanism is installed at different locations along the tube to set the falling distance. The impact on the seam specimen is produced by the falling mass releases from a predefined height (the distance between the specimen surface and the position of the release rod). The 400 mm width and 266 mm long specimen is installed between grips of the holder such as to obtain a convex surface at the impact location. On impact, a flexion is imposed on the edge of the seam and a brittle or ductile rupture could happen as shown in Figure-5. The fracture is located at the top sheet and the crack propagated along the edge of the seam as shown in Figure-6. As exposed by Rollin et al. (1991) in a previous paper, the resistance of an HDPE sheet to an impact force can be expressed by the average energy, W_{50}, defined as the energy necessary to fail 50% of the tested specimens. Two different experimental approaches can be used: the Probit method or the Bruceton Straircase method.

The Probit method consists in grouping an equal number of specimens (20 to 40 according to Pergelhof et al.(1985) selected at random from a seam into many sets and to test the specimens belonging to a set at a selected energy level, the energy used for each set being different.

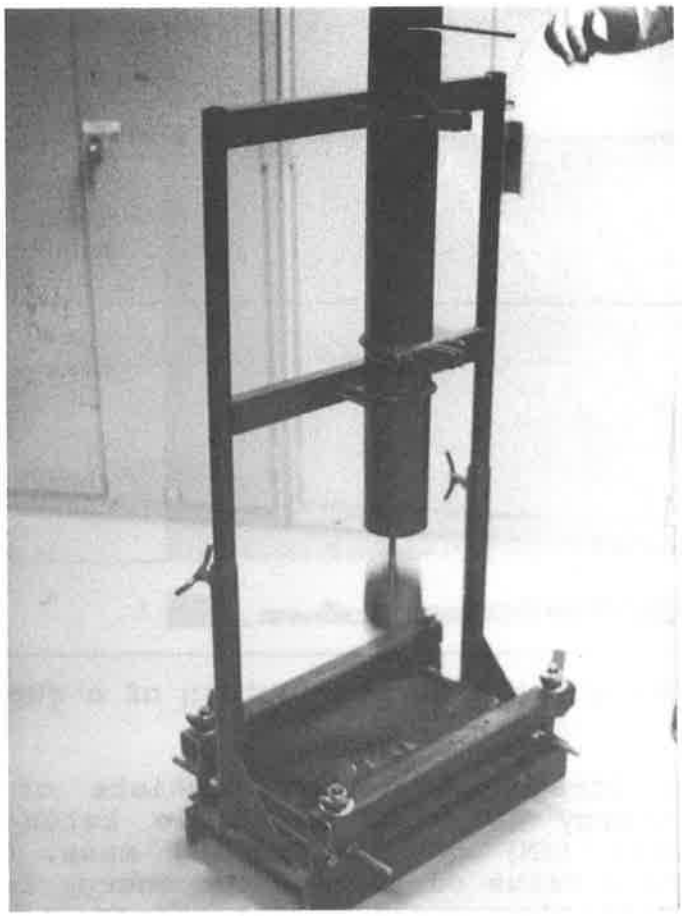

Figure 4 - Photograph of the impact apparatus

Figure 5 - Photograph of a ruptured seam

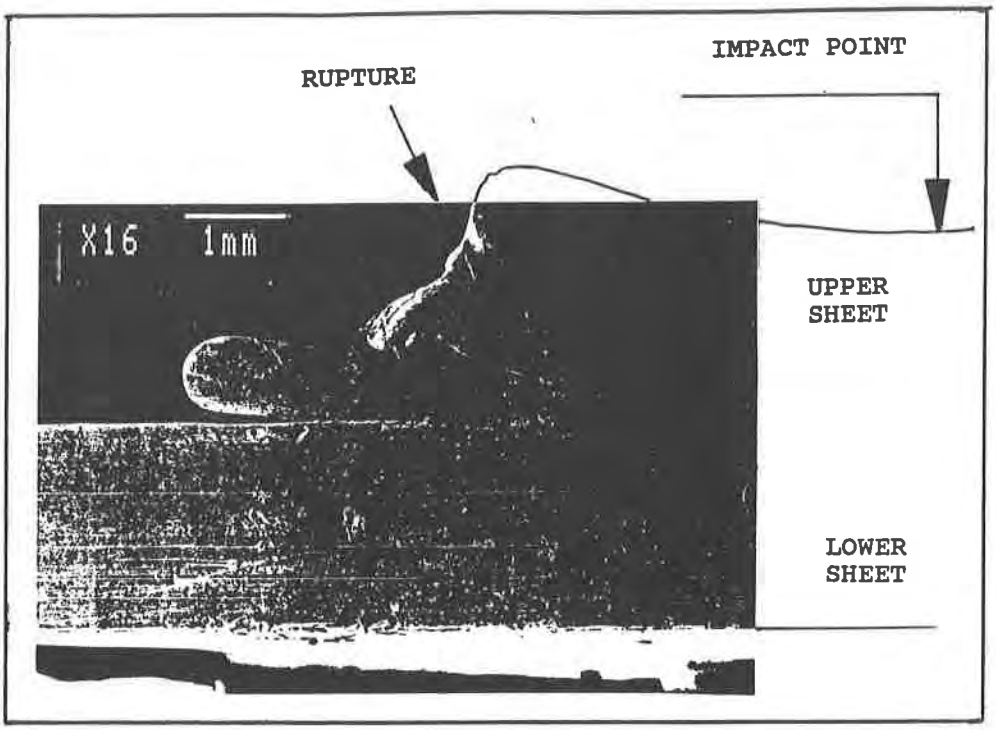

Figure 6 - Photograph of cross-section of a ruptured seam

The Bruceton Straircase method consists of determining the average rupture energy (W_{50}) of a single batch of specimens by incremental increase (dM) of the falling mass. Following trial tests, an approximate value of the average energy is determined and a specimen is tested at this energy level. If failure is observed, an additional test is performed with a lighter mass. On the other hand, if no failure is observed, the next test is performed with an increased mass. As recommended by Weaver (1986), this technique is used to determine the average value but should not be used to evaluate the minimum and maximum energy values since only few specimens are tested at these limits. The main advantage of this method lies in the low number of specimens to be tested as compared to other methods (Progelhof (1895). The Bruceton Staircase method is presented in the ASTM-D-3029 standard.

The energy increment was obtained by increasing or decreasing the falling mass's weight by 230g (0.5 pound) while the height of drop was kept constant at a value of 1130 mm. This procedure was retained to minimize the effect of impact velocity that could otherwise affect results. (ASTM-D-3029).

MICROSCOPIC ANALYSIS

Cross sections of seams were observed under electronic scanning microscope to observe facies along ruptured HDPE specimens. Prior to the microscopic analysis, each cross section of the specimen must be coated with gold-palladium mixture to obtain the necessary electrical conduction. Two well defined facies patterns are usually observed and can either be related to a brittle or a ductile failure as explained by Lefebvre (1991). Photographs of both types of cross-section facies are presented in Figures 7 and 8.

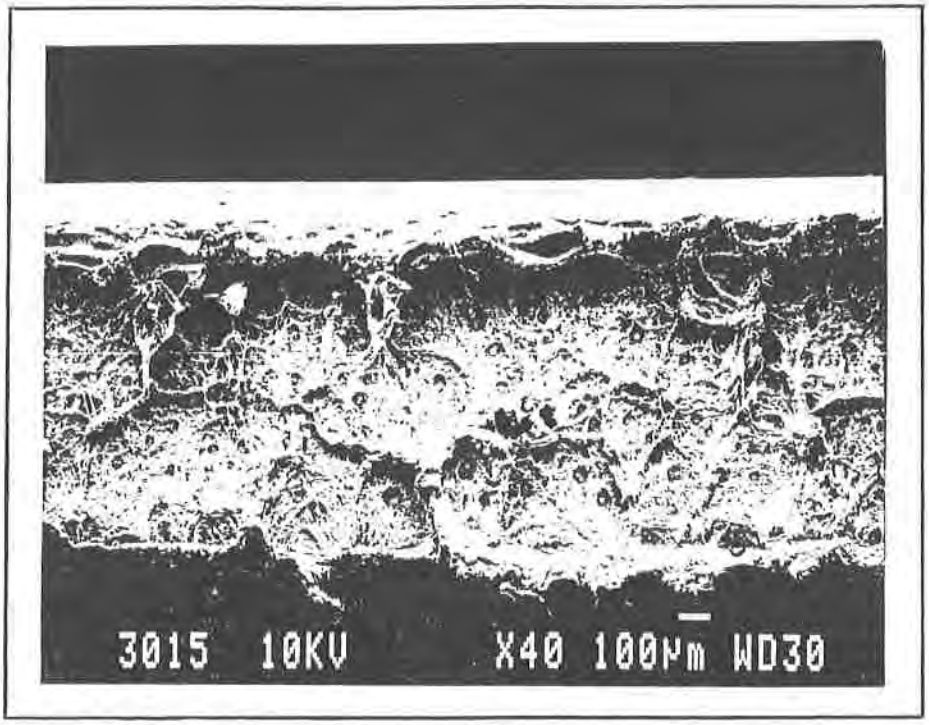

Figure 7 - Photograph of a brittle facies

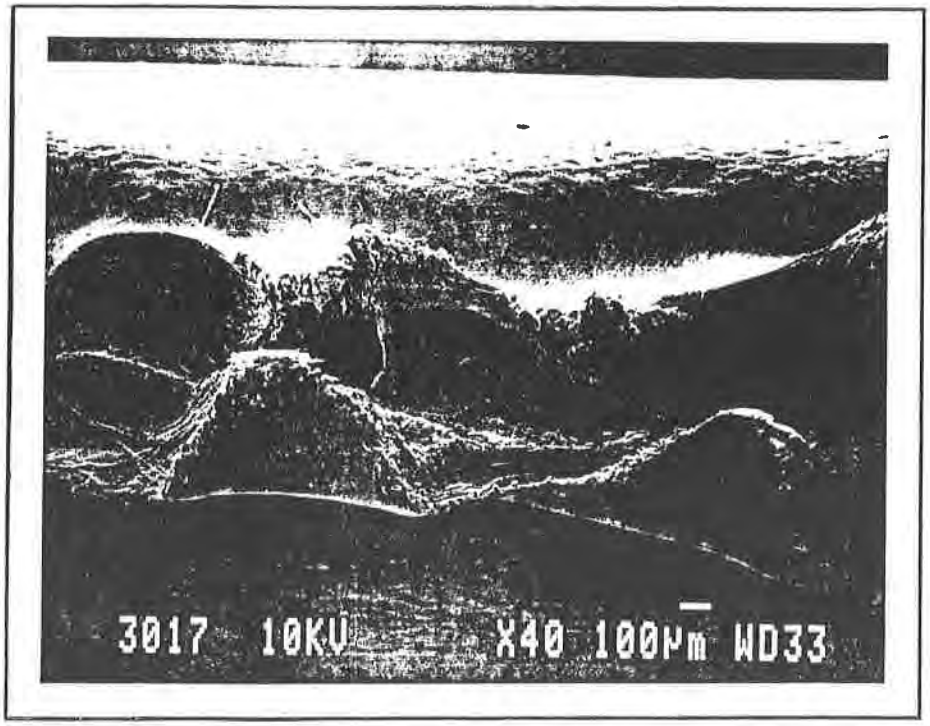

Figure 8 - Photograph of a ductile facies

SEAMS PREPARATION

HDPE sheets of two different thicknesses were used to produce the following:

- hot air single seam on 1.5mm thick sheet (ACS60 series)
- hot air double seam on 1.5mm thick sheet (ACD60 series)
- Wedge double seam on 2.0 mm thick sheet (ECD80 series).

HDPE sheets were welded inside a warehouse building. The welding parameters were selected to obtain different brittleness levels and are presented in Table-1.

Table 1 - Welding parameters and series identification

Series	Speed m/min	Pressure	Temperature (^{o}C) sheet	air	wedge
ACD60	0.5	normal	23.0	400	-
ACS60-A	0.5	normal	23.0	400	-
ACS60-B	0.55-0.58	normal	23.0	400	-
ACS60-D	0.5	normal	23.0	430	-
ACS60-F	0.5	high	23.0	430	-
ECD80-A	1.25	normal	23.2	-	400
ECD80-B	0.80	normal	23.2	-	400
ECD80-C	1.25	high	23.2	-	400
ECD80-D	1.05	normal	23.2	-	400

The sheet temperature was kept approximately constant at a value of 23^{o}C while the hot wedge and hot air temperatures were set at 400^{o}C except series ACS60-D and ACS60-F where the air temperature was increased to 430^{o}C. The welding speed for the 1.5 mm thick sheet was set at 0.5 m/min while it was set at some different values for the 2.0 mm thick sheet (ranging from 0.8 to 1.25 m/min).

During the calibration of the welding equipment, the pressure was set as to obtain acceptable peel strength, identified as normal, and to obtain brittle seams, identified as high, for seams of series ACS60-F and ECD80-C.

RESULTS

The results are presented in regard to the welding procedure and sheet's thickness. Differences in welding parameters are underlined along with the observed consequences.

Impact energy associated with ruptured seams - ECD80 series; Hundred of samples of double hot wedge seams (ECD80) were tested with the impact test. The samples were grouped into four series (ECD80-A, ECD80-B, ECD80-C and ECD80-D) and were tested using 8 to 9 different impact energy levels (an increment of 3 to 6 Joules between tests). The results are presented in Figure-9.

The range of the impact energy was between 50 to 120 Joules. It can be observed that for specimens from series ECD80-B, ECD80-C and ECD80-D the percent of specimens that rupture ranges from 10 to 90 while specimens from series ECD80-A the percent ranges from 10 to 55.

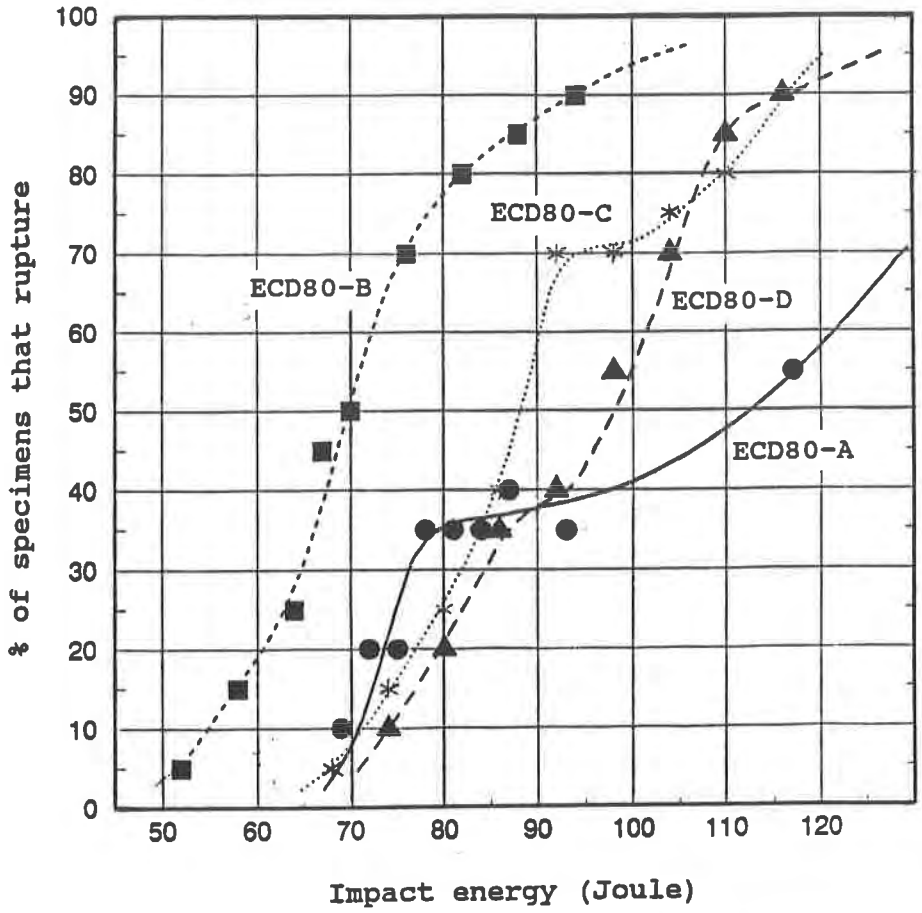

Figure 9 - Results for ECD80 samples

Failures were obtained at lower impact energy for ECD80-B specimens while greater impact energy was needed to rupture specimens from other series. This result was expected since the seams of series ECD80-B were produced at lower welding speed to favour overheating of the seams. Seams of series ECD80-A, ECD80-C and ECD80-D were produced at approximately the same welding speed and the observed energy curves are shifted to the right and very similar. This was not expected for seams of series ECD80-C because higher welding pressure was used to obtain a brittle condition.

These data were transformed into logarithmic scale and the PROBIT model was used to calculate the minimum, median and maximum impact energy level. They represent the energy levels at which respectively 10% (W10), 50% (W50) and 90% (W90) of the samples will rupture (at 95% confidence level). The calculated energies are presented in Table-2.

Table 2 - Impact energies for seams of series ECD80			
Series	IMPACT ENERGY (Joules) W10	W50	W90
ECD80-A	71	113	140
ECD80-B	55	71	91
ECD80-C	71	90	114
ECD80-D	75	98	117

Impact energy associated to welding speed - ECD80 series; The energy necessary to rupture seams of series ECD80-A, ECD80-B and ECD80-D are presented in Figure 10. As presented in Table 1, the welding speed used to produce seams of these series ranges from 0.8 to 1.25 m/min. As expected, the impact energies needed to rupture the seams produced at the lower speed (ECD80-B) are lower than the energies needed to rupture ECD80-D and ECD80-A seams because of the induced brittleness.

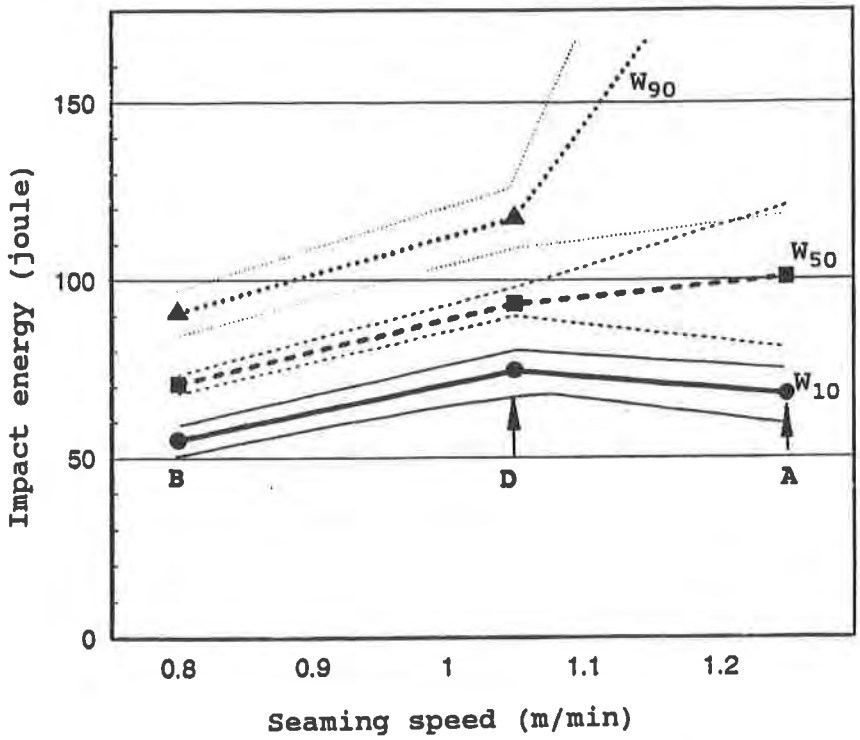

Figure 10 - Results versus ECD80 welding speed

Impact energy associated to welding pressure - ECD80 series; The energy necessary to rupture seams of ECD80-A and ECD80-C series are presented in Figure-11. Seams from both series were produced with identical welding speed but the welding pressure used to produce seams of series ECD80-C was higher than the pressure used to produce ECD80-A series.

The impact energies needed to rupture seams of series ECD80-C are lower than the energies needed to rupture seams of series ECD80-A. These results are supporting that brittle seams can be produced by applying too high pressures during welding process as already pointed out by Rollin et al (1989, 1991).

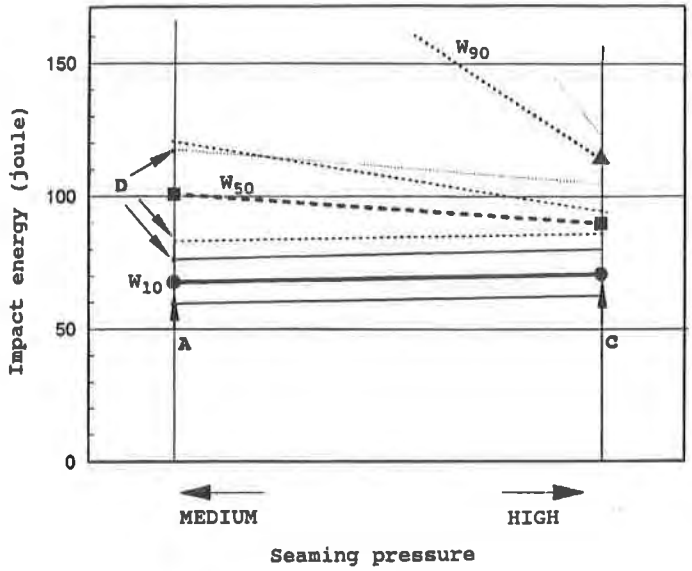

Figure 11 - Results versus ECD80 welding pressure

Rupture analysis - ECD80 series; Rupture of seams were visually observed and electron scanning microscopic analysis of their cross sections was performed to identify the fracture mechanism. On impact, a flexion is imposed on the edge of seams and a brittle or ductile rupture happened. From observation, rupture is always initiated in the top HDPE sheet along the edge of the seam as shown in Figures 7 and 8. More frequently the crack is uniform with its center at the impact point. The length of the cracks ranges from few millimeters to 80 millimeters with a width of 1 to 2 millimeters.

Brittle or ductile fractures could easily be identified using the electron scanning microscope. A systematic study of the facies of ruptured seams permitted to determine the number of specimens with a brittle rupture. The results are presented in Table-3.

Table 3 - Brittle fractures of ECD80 seams

Series	brittle type	brittle facies
ECD80-A	61%	58%
ECD80-B	93%	79%
ECD80-C	35%	35%
ECD80-D	53%	13%

The percentage reported are the average for all rupture specimens at all level of impact energy. As expected the percentage of brittle fractures is higher for ECD80-B seams while the percentages are lower for ECD80-C and ECD80-D seams. On the other hand, the results indicate higher values than expected for ECD80-A seams because most of the rupture seams were obtained at low energy level (as indicated in Figure 9). The percentage of brittle failure was observed to be very high at low energy level indicating that as the brittleness of a seam is greater, the impact energy necessary to rupture it is lower.

ACD60 series: Double seams produced using a hot air technique were tested to obtain a correlation between the specimen temperature and the impact energy needed to rupture it. This phase of the project was performed to obtain results that could support the use of the impact test at field temperatures. The impact energies measured for seam specimens tested at temperatures of -10, -5, 0, 5, 15 and 21 °C are presented in Figure 12 and the median impact energies (W50) calculated using the Bruceton Staircase model are presented in Table-4.

Table 4 - Median impact energy for ACD60 seams

Temperature °C	Impact energy (Joules) W50	variance
- 10	30	0.33
- 5	36	0.81
0	39	0.61
5	44	0.43
15	47	0.84
21	45	0.64

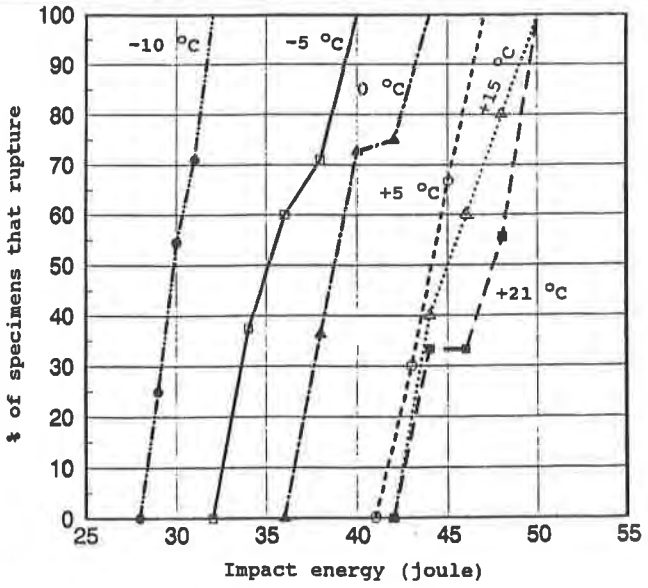

Figure 12 - Impact test results for ACD60 seams

The median impact energies are presented in Figure 13. It can be observed that the lower the temperature of the specimen, the less impact energy necessary to rupture the brittle seams. On the other hand, for temperatures higher than 10°C, the required impact energy to rupture brittle seams is more or less constant. From these results one can conclude that results obtained at ambient temperature are not affected by a slight variation in temperature. This would support the use of the impact test on site at ambient temperature.

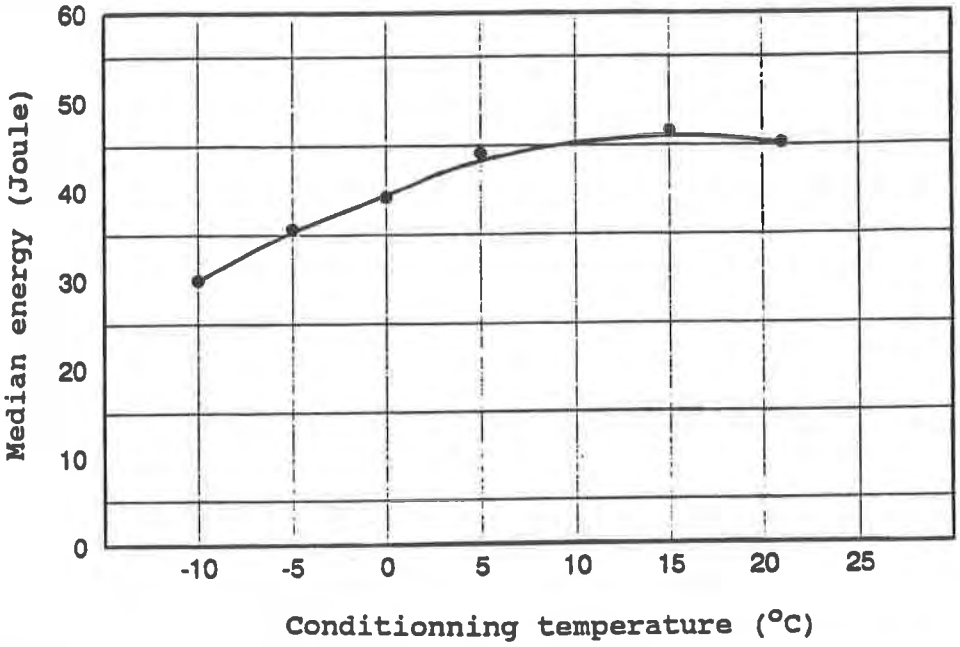

Figure 13 - Impact energy level versus specimen temperatures

Impact energies of ACS, ACD and ECD seams; Table 5 presents all the series tested and the results obtained.

Table 5 - Welding parameters vs W50

Series	Speed m/min	Pressure	Temperature (oC) sheet	air	wedge	W50 (Joules)
ACD60	0.50	normal	23.0	400	-	45
ACS60-A	0.50	normal	23.0	400	-	51
ACS60-B	0.55-0.58	normal	23.0	400	-	49
ACS60-D	0.50	normal	23.0	430	-	41
ACS60-F	0.50	high	23.0	430	-	42
ECD80-A	1.25	normal	23.2	-	400	101
ECD80-B	0.80	normal	23.2	-	400	71
ECD80-C	1.25	high	23.2	-	400	90
ECD80-D	1.05	normal	23.2	-	400	94

While high temperature and high pressure (ACS60-D and ACS60-F) are combined to positively affect the seam, the result gathered from a average of 20 test samples for each series clearly indicate the effect of badly calibrated equipment. ECD80 series were conducted on more than 700 samples. Not only from a statistical point of view but also from numeric consideration, the results obtained under that condition showed a clearly defined trend: ECD80-B is definitely apart from the other series.

The average energy level required for 80 mils thick samples is approximately twice as high as the energy required for 60 mils thick samples; 95 joules against 47. It should also be observed that the required energy are pratically the same for series ACS60 and ACD60 indicating that the same impact energy level is needed to rupture either a single or a dual seam.

Finally, one may observed that the energy level required to rupture a brittle seam is 20% and 25% lower than the energy level obtain on a normal seam normal, respectively for the 60 and 80 mils series.

CONCLUSION

The growing use of High Density Polyethylene (HDPE) geomembranes as liners in hydraulic barriers relies on a proper evaluation of their long term performance. It is actually well known that long term performance can be reduced by production problems, carbon black dispersion or low quality carbon black, weathering, chemical and bacteriological attacks and more likely by inappropriate or excessive welding conditions such as too high roller pressure, overheating of the sheets and thermal shock in the vicinity of the bonded strip (Rollin et al (1990)).

This question of long term performance addresses the structural stability of the polymer as well as the quality of the sheet's installation. Brittle failures of the seams originate from crazes or micro-stress cracks existing within the base material and it has been shown that equipment calibration like welding speed, temperature and roller pressure can affect the polymer structure which in turn will modified the stress-strain behavior of the material. Since proper equipment performance requires appropriate calibrations, quality control testing programs must then be implemented to include a test procedure that can easily be performed on-site, to efficiently assess the brittleness of the bonded strip. It has been demonstrated from the behavior of more than 700 HDPE seam's samples that this impact test procedure can easily and rapidly be performed at normal ambient temperature, to assess seam's brittleness. The presented results also support the fact that impact energy is basically a function of the sheet's thickness.

Finally, it is proposed that the impact test procedure should be used to analyse ageing of HDPE geomembrane seams from samples extracted from existing landfills.

ACKNOWLEDGEMENT

The work presented in this paper was conducted by Mr. Marc Lefebvre in the course of a master's degree program. Partial funding of this work is due to NAGS. The seams were constructed by Matériaux Techniques Côté Inc. with HDPE geomembrane liners furnished by PLASTALENE CORPORATION.

REFERENCE

Lefebvre, M. (1991), "Développement d'un essai d'impact pour la mesure de la fragilité des joints de géomembranes en polyéthylène", Master thesis, Ecole Polytechnique of Montreal, Quebec, Canada

Rollin A.L., Lefebvre M., Lafleur J. and Marcotte M., (1991),"Evaluation of field seams quality with the impact test procedure", Geosynthetics '91 Conference Proceedings, Atlanta, Ga.

Rollin, A. L., Fayoux, D., Benneton, I . P . et Emond, G. (1990), "Non-Destructive and Destructive seam Testing" , Rilem Technical Publication "Geomembranes: Identification and Performance testing" Editor: Chapman and al., Chap. 4,

Rollin, A.L., Vidovic, A., Denis, R. and Marcotte, M.,(1989), "Evaluation of HDPE Geomembrane Field Welding Techniques ; Need to Improve Reliability of Quality Seams", Proceedings of the Geosynthetics'89 Conference, San Diego, USA pp 443-455.

Halse, Y., Koerner, R. and Lord, A. E., (1989) "Laboratory Evaluation of Stress Cracking in HDPE Geomembrane seams", Proceeding GRI-2, Durability and Aging of Geosynthetics, Journal Geotextiles and Geomembranes, Elsevier, May 1989

Peggs, I.D. (1987), "Evaluating Polyethylene Geomembrane Seams", Proceedings of the Geosynthetics'87 Conference, New Orleans, USA, pp 505-518

Ami, S. R. (1987), "Drainage Pipe Testing Manual" , Canadian International Development Agency technical report, Hull, Canada.

Peggs, I.D. and Rose, S., (1985), "Practical aspect of polyethylene geomembrane seam welding", Geotechnical Fabric Report, Feb, pp. 12-16

Weaver, O.R. (1986), "Using Attributes to Measure a Continuous Variable in Impact Testing Plastic Bottles", Material Research and Standards, vol. 6, no. 6, June pp 285-292

Progelhof, R.C., Throne, J.L. and Patel, U. (1985), "Drop Weight Testing: What it Tells Designers", Modern Plastics Encyclopedia,

ASTM-D-3029 (1984), "Standard Test Methods for Impact Resistance of Rigid Plastic Sheeting or Parts by Means of Tip (falling weight) ".

Assessment of Hot-Air Fusion Welding for HDPE Geomembranes

M. Marcotte
Solmers Internationale, Canada

A.L. Rollin
École Polytechnique, Canada

S. Lagace
Solmers Internationale, Canada

R. Denis
Solmax Geosynthetics Inc., Canada

ABSTRACT

An in-depth analysis of more than a thousand HDPE fields seam specimens demonstrates that automated hot air fusion welding is unquestionably a bona fide geomembrane fusion welding method, using convection as its heat transfer mechanism. The method yields reliable and consistent fusion welds which, from experience and analysis, compare well with automated hot wedge fusion in all aspects of the seams' mechanical properties. Inherent pre-heating, cleaning and drying of surfaces resulting from the use of this method should also be pointed out as major advantages.

In order to compare the mechanical performance of the two methods, over 1200 test results from actual job site destructive specimens were examined. The mean peel strength value obtained through both methods is similar, as is standard deviation on that property.

The results presented in this paper confirm that automated hot air fusion compares well as a permanent welding method with the more widely used hot wedge fusion method. Moreover, it is suggested that specification documents should not restrain its use in that respect.

INTRODUCTION

High Density Polyethylene (HDPE) is a thermoplastic polymer composed of very long hydrocarbon chains. About half of its mass is crystalline, having a fixed melting point, and the other half is amorphous, without any definite melting or freezing point; it is thus called a semi-crystalline polymer. The crystalline portion is responsible for many of the useful characteristics of polyethylene, including strength and rigidity. Polyethylenes with greater crystalline portions are usually more rigid, denser, and have higher tensile strengths, while their "weldability" is usually reduced.

Because they exhibit high chemical stability, and thus resist well solvents and glues, HDPE geomembranes can only successfully assembled through polymer fusion. In these processes, a set quantity of calorific energy (heat) is supplied at the sheets' interface in order to blend the two melted surfaces and to create a continuous seam. As such, the welding equipment merit close attention as do the methods available to evaluate the quality of the joining system. Means to evaluate the mechanical strengths of seams are easily available but very few references compare the actual performance of the different welding techniques commonly used to assemble HDPE geomembranes.

FUSION WELDING TECHNIQUES

Fusion or melt bonding methods are used on thermoplastics, where the base polymer is sensitive to heat and readily melts upon supply of energy. In practical applications, the surfaces of the two sheets to be joined are first heated, melted and then immediately pressed together to form a bonded strip that extends into the thickness of the sheet. The melt depth is mainly a function of the quantity of heat supplied, pressure and sheet temperature.

Hot-Wedge Fusion. As one of the most commonly used methods, the hot wedge method employs heated elements to convey the required heat. This method relies on a combination of radiation and conduction heat transfer mechanism. The basis of the system consists of an electrically heated V-shaped resistance element that passes between the two sheets to be sealed, thus melting the surfaces. Pressure is then applied by nip rollers to form a homogeneous seal between the two sheets (figure 1). Typical welding speeds for HDPE geomembrane range from 1 to 4 m/min (3 to 12ft/min) while wedge temperature is around 375 to 400 C (700 to 750 F). Because of the comparatively high welding speeds obtained, most installers find an economical interest in relying heavily on this method.

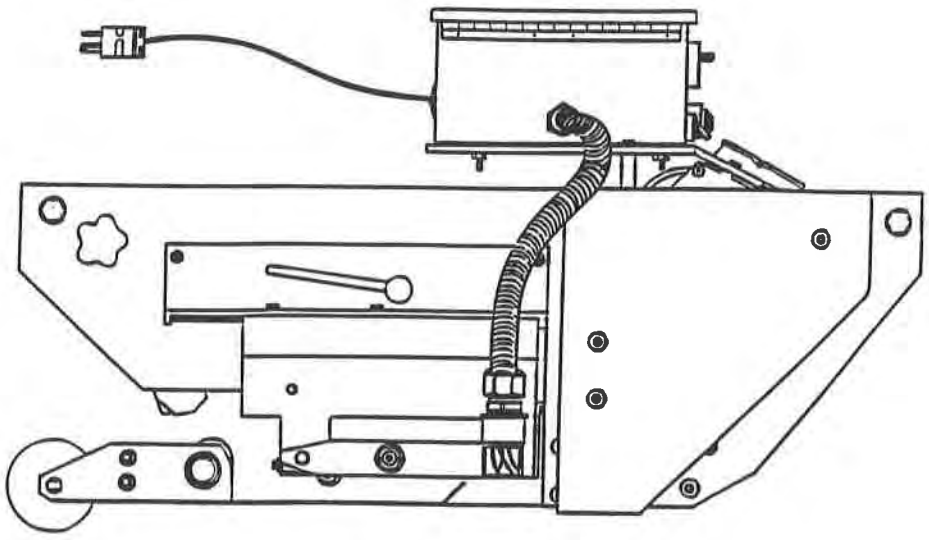

Figure 1 - Typical Hot-Wedge Welding Apparatus

Hot-Air Fusion. Using convection as its heat transfer mechanism, hot air can also be used on most thermoplastics. For HDPE geomembrane seaming, heated air is supplied at temperatures usually ranging from 400 to 450°C (750 to 850°F). In a process similar to the one described above for hot-wedge fusion, the hot air jet is blown between the sheets to join; these are then pressed together by nip roller. On most automated hot air seaming machines (figure 2), temperature, pressure and speed can be adjusted by the operator. Typical welding speeds for HDPE geomembrane range from 0.3 to 2m/min (1 ft/min. to 6 ft/min). The principle of hot-air welding is simple, the technology is well-known and the equipment is easily available.

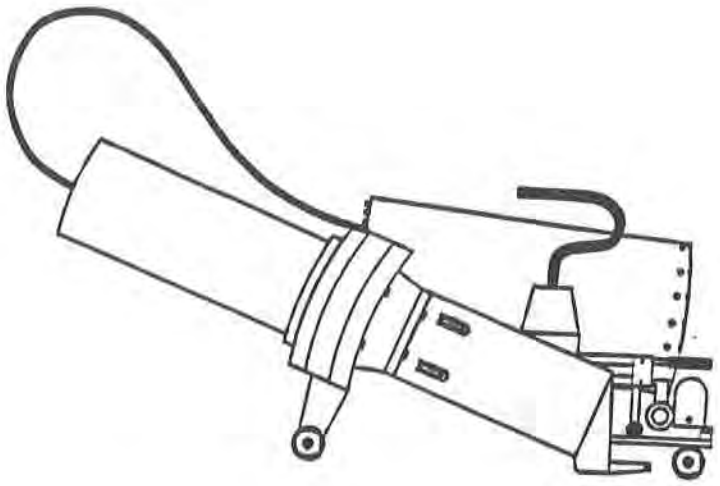

Figure 2 - Typical Hot Air Welding Apparatus

For both methods, too much melting or too much pressure usually weakens the geomembrane by inducing brittleness. On the other hand, too little melting will result in low seam strengths due to poor adhesion (cold weld). Proper calibration of welding parameters is essential to achieve acceptable and consistent assemblies for both methods.

STRENGTH TESTING METHODS

Tensile stress is defined by ASTM as "the tensile load per unit area of minimum original cross-section, within the gage boundaries, carried by the test specimen at any given moment". It is expressed in force per unit area, usually in megapascal (MPa) or pounds force per square inch (psi). Stress units of MPa (psi) are preferred for HDPE since the sheet is homogeneous and the tensile stress defines a property of the manufactured polyethylene which is essentially independent of thickness over the range of most HDPE geomembranes. Tests are generally conducted under ASTM D638.

Two mechanical test methods are widely used in testing the bond strength of geomembrane seams. Those methods are commonly known as shear and peel testing.

In Shear testing (ASTM D3083/mod.NSF54), a load is applied at the constant rate along the assembly, subjecting the bond's interface to a shearing force (figure 3). Results are recorded in Newtons per meter (pounds force per inch) of nominal seam width. Shear testing is generally considered to be a performance test, indicative of the seam's behavior in service.

Figure 3- Shear Test

Peel testing (ASTM D413/mod.NSF54) is accomplished by applying a load such that the bonded interface is subjected to a peeling force attempting to separate the bonding system from the geomembrane sheet (figure (4). Results are also recorded in Newtons per meter (pounds force per inch) of seam width. Pell testing is usually considered as an index test, indicative of the general quality of bonding obtained between the joined elements.

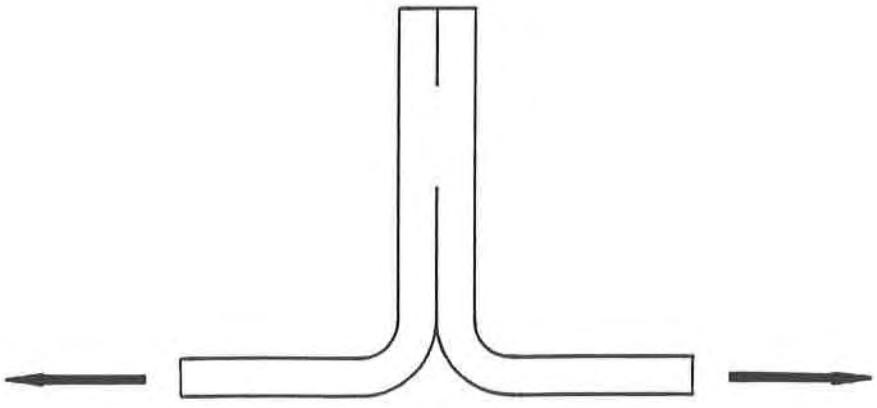

Figure 4 - Peel Test

DATA COLLECTION

In order to compare the mechanical performance of automated hot air seams to that of automated hot wedge seams, peel and shear test results were collected from the field installation of more that 2,000,000 square meters (21 million square feet) of HDPE geomembrane liners.

Over 1200 test results were included in a database and analyzed. Calibration tests as well as destructive tests on seam samples were included in the database for purposes of comparison. In order to compare the results of different thickness, the values of the seams' strength shown in the following tables are presented as stresses in MPa (psi), where the maximum force recorded is divided by the width of the tested sample (25.4mm, or 1") an d by the sheet's nominal thickness.

Data was gathered over five years from more than thirty different projects, four different manufacturers, four sheet thickness, two types of automated hot wedge welders as well as two types of automated hot air welders. The peel tests were conducted both in the field with calibrated portable tensile testers as well as in a certified laboratory, while all shear tests were conducted in a certified laboratory. For purposes of discussion, the results were compared to current National Sanitation Foundation's Standard 54 specifications (NSF 54).

DATA ANALYSIS

All materials, all phenomenon present a certain amount of intrinsic variation. If a parameter is systematically measured on a large sample, and the results observed are plotted against their frequency of appearance, we obtain a distribution curve of the characteristic surveyed.

The normal distribution being extremely widespread, and applying to a large number of phenomenon, the database discussed in this paper was treated as a normal (gaussian) distribution. This assumption seems reasonable in view of the histograms obtained from the treated data.

A few simple statistical notions were employed in the analysis of the database. These included the following basic definitions.

A normal, or Gaussian, distribution has a symmetrical, bell-shaped curve (figure 5); it is completely defined by its mean and its standard deviation (or its mean and its variance). In such a distribution, the mean, the median and the mode coincide. The mean is obtained from the sum of all results multiplied by their respective weight. The median is a second measure of central tendency. It is the point at which the distribution is divided in two equal halves, 50% of the results being situated below the median value and 50% above it. The mode is another measure of central tendency and is defined as the value that appears the most frequently in the sample.

The variance is a measure of distribution, defined as the sum of all differences between each observation. The standard deviation is another measure of distribution. It is defined as the positive square root of the variance. In a normal distribution, about 67% of all observations are comprised within one standard deviation on each side of the mean (x+/-s), and about 95% are comprised within two standard deviations (x+/-2s).

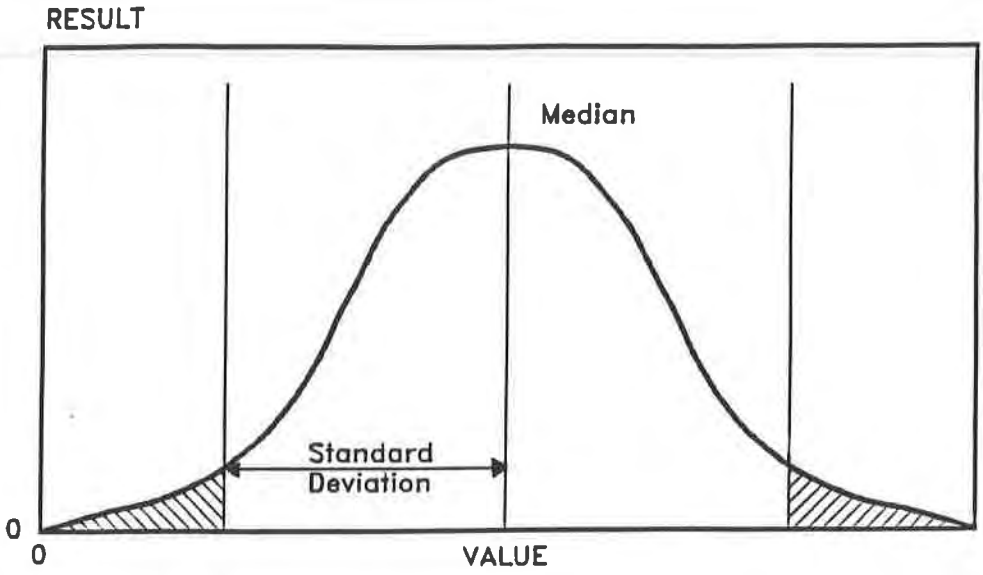

Figure 5 - Normal (Gaussian) Distribution Curve

RESULTS

Peel Test Results. 873 peel test results are summarized in Table 1, including some results on fillet extrusion given only for information purposes. Mean values for hot air and hot wedge are 14.3 and 14.1 MPa respectively and may be considered equivalent, while standard deviations, although comparable, prove slightly lower for hot wedge welding.

Table 1 - Peel Test Results

MPa (psi)	HOT WEDGE	FILLET EXTRUSION	HOT AIR
Nb of tests	48	46	343
Minimum	6.5 (928)	8.4 (1218)	3.0 (428)
Mean	14.1 (2016)	12.9 (1871)	14.3 (2046)
Maximum	22.3 (3196)	18.8 (2727)	21.9 (3137)
Std dev.	2.1 (300)	2.4 (348)	2.7 (388)

Figures 6 and 7 show the distribution of the results presented in Table 1.

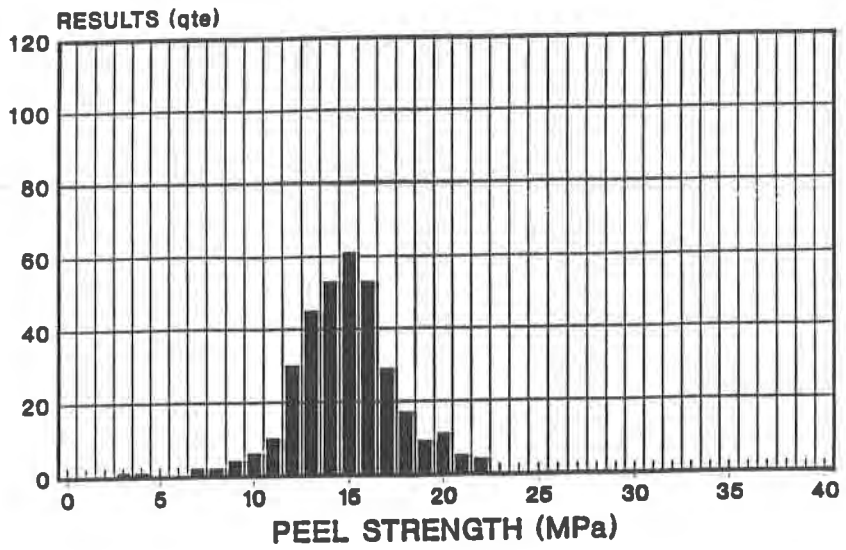

Figure 6- Peel Test Results for Hot-Air

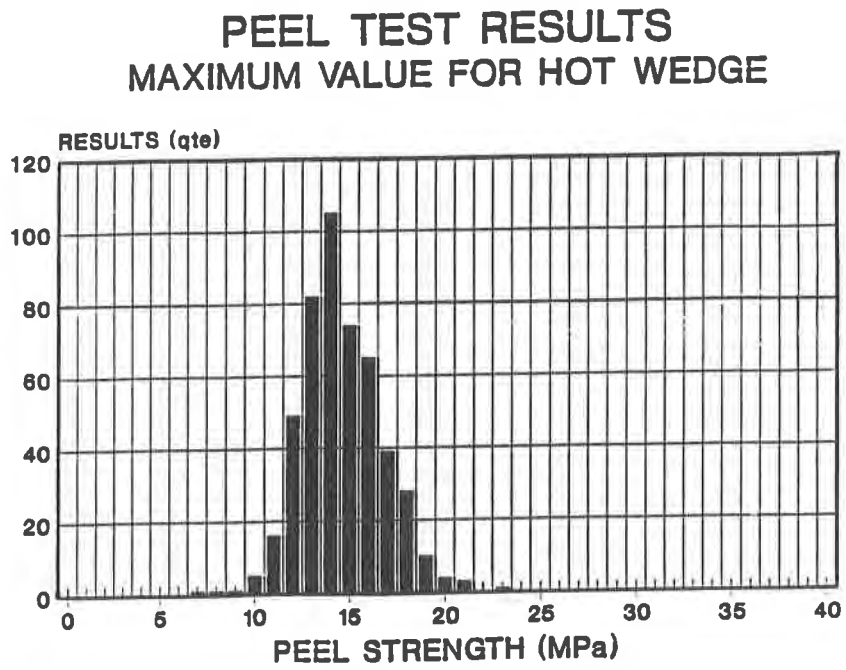

Figure 7 - Peel Test Results for Hot-Wedge

Shear Test Results. Table 2 shows values of stresses at yield for 347 shear test results. Mean value is slightly higher for hot air at 24.9 MPa versus 21.2 MPa; its corresponding standard deviation is lower than that of hot wedge welding, 2.2 versus 5.8 MPa. Again, the two methods yield similar results, albeit on a limited sampling population.

Table 2 - Shear Test Results			
MPa (psi)	HOT WEDGE	FILLET EXTRUSION	HOT AIR
Nb of tests	305	25	42
Minimum	1.6 (231)	17.3 (2509)	19.0 (2715)
Mean	21.2 (3031)	23.3 (3380)	24.9 (3561)
Maximum	32.5 (4653)	27.9 (4047)	30.2 (4331)
Std dev.	5.8 (833	2.6 (377)	2.2 (308)

Parent Material Tensile Test Results. Since it is reasonable to believe that the mechanical behavior of the bonded strip is related to the behavior of the sheet itself, parent material conformance test results were also compared with reported manufacturing quality control test results (Table 3).

Table 3 - Parent Material Tensile Tests Results		
CONFORMANCE TESTING	STRESS AT YIELD	STRESS AT BREAK
Number of tests	140	140
Minimum: MPa (psi)	16.8 (2437)	6.5 (943)
Average: MPa (psi)	21.1 (3061)	24.2 (3510)
Maximum: MPa (psi)	25.0 (3626)	36.8 (5338)
Standard deviation	2.3 (334)	6.9 (1001)
MANUFACTURING QC PROGRAM-STRESS AT YIELD		STRESS AT BREAK
Number of tests	119	119
Minimum: MPa (psi)	16.1 (2330)	26.3 (3810)
Average: MPa (psi)	17.9 (2590)	31.2 (4527)
Maximum: Mpa (psi)	19.7 (2840)	35.8 (5200)
Standard deviation	2.4 (347)	5.9 (862)

Conformance and manufacturing quality control testing show similar standard deviations for stress at yield (2.3 and 2.4 MPa), while stress at break gives slightly higher standard deviations on peel and shear strength values shown in Tables 1 and 2, ranging from 2.1 MPa to 5.8 Mpa. Thus, it seems that fusion welding procedures, whether they use the hot air or the hot wedge method, do not induce significantly greater variations in the observed tensile behavior; rather, it looks as if they simply make the mean value of that parameter slide.

Test Results as Compared to Specifications. Table 4 shows data from the point of view of specification documents. In NSF 54 specifications, the bonded seam strength (shear strength) is set to a certain value according to the thickness of the sheets. If NSF 54 had been the sole acceptance criterion, almost 95% of all tests included in the database would have been found acceptable.

Most peel test results from both methods would also have been found acceptable if NSF54's value (67% of the nominal tensile stress at yield) had been used as an acceptance value for peel and shear.

Table 4 - NSF 54 specification as acceptance criterion			
SHEAR STRENGTH	HOT WEDGE	FILLET EXTRUSION	HOT AIR
Nb of Tests	305	25	42
Average (MPa)	21.2	23.5	24.9
Std Deviation	5.8	2.6	2.2
95% Lower Limit	9.6	18.1	20.5
NSF 54 Criterion	9.4	9.4	9.4
95% Lower Limit	8.9	8.1	9.9
Std Deviation	2.7	2.4	2.1
Average (MPa)	14.3	12.9	14.1
Nb of Tests	343	46	484
PEEL RESULTS	HOT AIR	FILLET EXTRUSION	HOT WEDGE

A CASE HISTORY

Information concerning trial seaming peel test results was gathered from one specific project (70,000 square meters) for three welding methods: automated hot wedge fusion, manual fillet extrusion and automated hot air fusion. Out of 440 trial seam tests, hot air fusion welding shows the best performance on a first trial basis(qualitative pass/fail criterion), indicating the ease with which operators were able to calibrate their equipment. Table 6 resumes the results obtained while evaluating the reliability of different welder types.

Table 5 - Summary of Trial Seaming Data			
PASS/FAIL	HOT WEDGE	FILLET EXTRUSION	HOT AIR
Nb of Tests	202	174	64
Passes	131	109	63
Failures	71	65	1
Percentage	35%	37%	<2%

To give a frame of reference, trial fusion test results were extracted from the database presented before and are shown in table 6.

Table 6 - Results from Trial Peel Tests			
	HOT WEDGE	FILLET EXTRUSION	HOT AIR
Nb of tests	215	46	176
Minimum (MPa)	10.3	8.4	10.5
Average	14.2	12.9	15.5
Maximum (Mpa)	20.9	18.8	21.9
Std deviation (Mpa)	1.8	2.4	2.3

As the table shows, the mean values for trial peel test are slightly higher than the database mean values and the standard deviation values lower. Since these values are recorded as QAQC documentation before starting a new weld, it is likely that the destructive test results would show higher variability and lower average value. In other words, at the start of the shift, welding equipments are adjusted to give an excellent seam, but the actual seam quality will be influenced locally by variations in ambient temperature, sheet thickness, sheet tensile strength, and by residual dirt and other site conditions, yielding slightly lower overall results.

DISCUSSION OF RESULTS

Shear and peel strengths from both automated hot-air and hot wedge seaming methods show mean and standard deviation values that are in the same order of magnitude. Both methods yield bonded seam strengths significantly higher than NSF 54 specifications.

From the study of lab manufacturing QC programs on tensile stress in parent material, the standard deviation observed for both stress at yield and stress at break vary between 2.4 and 6.9 MPa, which is in the same order of magnitude that the standard variation observed for the whole database of peel and shear tests presented herein (between 2.1 and 5.8 Mpa). In that respect, the seaming method in itself may not be a s important a factor as the parent material variability.

Finally, the authors surmise that the slightly higher standard deviation value observed for automated hot-air fusion may be related in some way to the equipment's lighter weight. As a matter of fact, the speed of the hot-air automated welder is controlled by the pressure rollers, while for the generally heavier hot wedge welder, traction is independent of the pressure rollers. When the sheet's temperature varies, the actual speed of the hot air welder may be affected by a slight change in the parent material stiffness, while this may not be true for the heavier wedge welder. In that respect, the experience of the operator may well have greater influence on seam quality for hot-air fusion that for hot wedge fusion.

There is currently no reason to dismiss automated hot air fusion as a "true" fusion seaming method, as has sometimes been the case. With the assessment tools currently available, no significant difference can be highlighted between automated hot air fusion and hot wedge fusion in terms of mechanical performance (peel and shear strength). Automated hot air seaming is simple, practical, and dependable. Very useful in areas where maneuvering space is limited, it is especially well suited for detail and patch work. Because of its proven reliability and automation, it may even be preferred over alternate manual fillet extrusion methods. Although its typical slow seaming rates (compared to hot wedge welding) may be an installation drawback, its inherent sheet pre-heating, cleaning and drying abilities should be recognized as important advantages.

REFERENCES

Frobel R. K., (1984), "Methods of Constructing and Evaluating Geomembrane Seams", International Conference on Geomembranes, Denver, USA

Koerner, G.R., and Bove, J.A., (1989) Inspection of HDPE Geomembrane Installation, Geosynthetics'89 Conference Proceedings, San Diego, CA, USA, pp. 70-83

Marcotte M. and Lagacé S., Technical note on hot air seaming of HDPE geomembranes, Geotextiles and Geomembranes, vol. 9, nos. 4-6, Elsevier Applied Science, 1990

Peggs, I.D. (1987), "Evaluating Polyethylene Geomembrane Seams", Geosynthetics'87 Conference proceedings, New Orleans, USA, pp 505-518

Peggs, I.D. and Rose, S., (1985), "Practical aspect of polyethylene geomembrane seam welding", Geotechnical Fabric Report, February 1985, pp 12-16

Peggs, I.D., (1988), "Failure and Repair of Geomembrane Lining Systems", Geotechnical Fabrics Report, 13-16, November 1988

Rollin A.L., Lefebvre M., Lafleur J. and Marcotte M., (1991), "Evaluation of field seams quality with the impact test procedure", Geosynthetics'91 Conference Proceedings, Atlanta, Georgia, USA

Rollin A.L., Vidovic, A., Denis R. et Marcotte M., (1989), "Microscopic Evaluation of HDPE Geomembrane Field Welding Techniques", Microstructure and Performance of Geosynthetics Conference Proceedings, Orlando, Florida, USA

Rollin, A.L., Vidovic, A., Denis, R. and Marcotte, M., (1989), "Evaluation of HDPE Geomembrane Field Welding Techniques; need to Improve Reliability of Quality Seams", Geosynthetics'89 Conference Proceeedings, San Diego, USA pp 443-455

SOLMERS INTERNATIONALE, Internal reports, 1986-1991

Chemical Fingerprinting of Geosynthetics, Is There Still a Need?

R.E. Landreth
U.S. Environmental Protection Agency, USA

ABSTRACT

The U.S. Environmental Protection Agency (EPA 1986) has developed EPA Method 9090 for evaluating the chemical resistance of geosynthetics in hazardous waste land disposal facilities since the implementation of RCRA. This evaluation has been required for each unit within each facility. Many facilities are expanding their waste disposal capacity and using the same geosynthetics. If the owner/operator could demonstrate that the incoming waste stream characteristics had not changed and that the geosynthetic materials were essentially the same, the EPA generally did not require a duplication of the Method 9090 test. To demonstrate this a "fingerprint" was required. The Agency developed a series of recommended tests for fingerprinting each type of geosynthetic material. To discuss the most efficient way of obtaining accurate information, the EPA held a workshop to discuss chemical fingerprinting. Results of that workshop suggested there was no clear agreement as to the objective of fingerprinting nor was there agreement on tests and protocols for such testing. These conclusions present a real dilemma for users of geosynthetics and regulators. Since the test protocols for fingerprinting are unclear, should the Agency reconsider the need for fingerprinting?

This paper will present a discussion on the status and future of chemical resistance testing and U.S. EPA Test Method 9090, and the relationship between fingerprinting and chemical resistance testing.

INTRODUCTION

The U.S. EPA currently requires that any geosynthetic material to be installed in a waste management facility be essentially similar to the material that was evaluated during the design and permitting phases. This requirement was based on information obtained during the Agency's early research with geomembranes (EPA 1982, EPA 1985) which indicated that generic names such as polyvinyl chloride (PVC), chlorinated polyethylene (CPE) and chlorosulfonated polyethylene (CSPE) were insufficient to describe a specific material. Later studies (EPA 1988c) also found differences in the polyethylene products such as high density (HDPE), low density (LDPE), linear low (LLDPE) and very low (VLDPE).

Within each generic group the performance of the class of geomembrane could be traced, in part, to material formulation. At that time physical properties were unable to definitively identify the individual products. Additional analytical techniques such as thermogravimetric analysis, differential scanning calorimetry, etc. could improve the ability to distinguish individual materials. After these tests were run, the data was sufficiently clear that individual materials, within each generic group, could be identified. The purpose for the fingerprint, as defined by the Agency, was to "ensure that the geosynthetic material evaluated in chemical resistance testing was essentially the same as that material installed in the permitted facility."(EPA 1988a)

IDENTIFICATION OF NEED

The need for fingerprinting came about for two primary reasons (1) chemical resistance and (2) construction lagging design phases. The basic EPA research program determined that within a given generic class of geomembranes there could be noticeable differences in material performance. Physical properties of the geomembranes were similar. Further evaluation of the material indicated differences in basic resin and polymer material due to compounding. The purpose of the fingerprint was not to identify all of the components in the compound, but to characterize the material in terms of: the polymer type and amount; the amount of extractables; and the carbon black and ash contents. The investigation into the make-up of the material was difficult and began raising questions such as "what influence does a processing aid have on the performance of a geomembrane and what if the manufacturer changed the type of processing aid?" These questions were not easily answered by the EPA or by those manufacturers willing to discuss these issues.

In addition to the basic questions of how changes in the manufacturing process impact performance, the Agency was continually asked to give a "blanket" approval of generic materials used in waste management facilities. One of the prime reasons for asking for the approval was the Agency's requirement that a chemical resistance test, i.e. Method 9090, was required to approve geosynthetic materials for each facility. Owner/operators agreed to perform these tests for each new facility. However, the Agency continued to receive comments on high costs of the test procedure, the extended (4-5 months) time required to perform the tests and questions on how to interpret the test data.

When owner/operators became more involved with expansion activities, utilizing the same materials as those in the original disposal unit became a popular economic decision. Automatic approval of these materials for use in the expanded unit was sought. Owner/operators argued that time and money could be saved if Method 9090 did not have to be used. The Agency concurred with this approach providing the type and amount of waste received at the facility was essentially the same and that no problems had been encountered with the performance of the geosynthetics in the original facility. The Agency also required the geosynthetic material be the same type as that used in the original disposal unit.

This requirement created some concern since the resin suppliers and manufacturers were reevaluating their materials to improve their performance. These improvements included new resins, new performance additive packages and new manufacturing processes. In total, the improvements resulted in superior geosynthetic products. The question remained about qualifying two materials as the same.

Added to this problem was the fact that more types e.g. nets, grids, geotextiles, etc. of geosynthetics were being used as design engineers became more familiar with

their uses. To complicate the issue new resin types were being used in different products, and as the manufacturing industry became more aware of the durability and long-term performance issues facing the designer, different and improved additives were utilized to minimize polymer degradation during the manufacturing and installation process and to improve long-term performance either in an exposed or unexposed design.

WORKSHOP ON FINGERPRINTING

Clearly there is confusion in the industry, including the regulators, who are required to approve the use of the geosynthetic materials. The need to hold a workshop to clarify these issues became clear to EPA. The EPA agreed to host such a workshop in July 1991. The objectives of the workshop were very broad:

- to review analytical procedures that will prove that the material tested for chemical resistance is the same as that that will be installed in accordance with the design
- to review procedures to determine the amount of reprocessed product (regrind) in the finished product and the potential impact on performance and durability
- to review the impact on performance and durability when additives are changed (origin, amount, or type.)
- to review procedures as a means of rapidly detecting the onset of degradation and as a means of determining chemical resistance
- to provide information of a forensic nature that can be used to analyze geosynthetics retrieved from field installations and provide feedback for improved resins, additives and compounding agents.

In retrospect, the objectives were too broad for the short meeting time. Each objective could have been the subject of a separate meeting and perhaps then some consensus could have been obtained. This is not to say the meeting did not produce meaningful results. In fact, the meeting was indeed a success if for no other reason it clearly pointed out the need to continue the education process involving the resin supplier, manufacturer, designer, regulator and facility owner/operator. Perhaps now more specific questions can be asked.

The term "fingerprint" is used to identify cause and effect changes, and while there are similarities between each of the objectives, the Agency is still faced with the dilemma of which tests to use for each material type that will verify that the geosynthetic material tested and used in the original construction is essentially the same as the material to be used in the expanded unit.

From the Agency's perspective, fingerprinting when used as a substitute for the chemical resistance test (Method 9090) should provide information such as polymer type and amount, carbon black, additive packages and amount, processing aids, volatiles and ash content. There may be other constituents that require identification. New materials, new resins, new additive packages, etc. will dictate these requirements.

Obtaining the required information, noted above, should not take on the proportions of a research project. Standard procedures with known accuracy and bias should be used. These procedures should be reliable and reproducible, be able to be

performed by a majority of testing laboratories, identify changes when changes are made and perhaps most importantly result in data understood by the designer, regulator and owner/operator.

In addition, the design engineer needs to become more familiar with the analytical tests and interpretation of test results. Engineering designers and polymer scientists need to expand their dialogue. The geosynthetic industry has made tremendous strides in the last few years to improve the performance and durability of these materials. Continued improvement and increased use will depend on whether the engineering designer and polymer scientist can communicate their respective needs to each other.

FUTURE NEEDS AND DIRECTION

The Agency strongly supports the use of geosynthetics in waste management facilities as mandated by RCRA Part 264, 257 and 258 (CFR 1987, EPA 1991). Design engineers are increasing their use of geosynthetic materials as demonstrated by the continued growth in the industry and with new applications.

The Agency still requires, for Subtitle C hazardous waste management facilities, the evaluation of geosynthetic chemical resistance via EPA test Method 9090. In some site specific situations, the Agency may accept "fingerprinting data if the owner can verify that the material to be used in the new or expanded facility is essentially the same as the material used in the original unit".

An alternative immersion procedure is being developed by the American Society for Testing and Materials (ASTM) Committee D-35 on Geosynthetics. This ASTM procedure closely follows the immersion procedure of EPA Method 9090 but adds details regarding test conditions and the immersion vessel. This procedure is under review by the EPA for potential acceptance in lieu of portions of Method 9090.

As a part of the Method 9090 test, procedures are described for evaluating the physical properties of geomembranes, but other types of geosynthetics are being used in waste management facilities and a consistent set of physical property evaluation tests were needed. Therefore, the Agency in consultation with several research and testing firms developed initial recommendations for evaluating the chemical resistance of geosynthetics. These recommendations are compiled in (Landreth 1990) and identify ASTM standard tests for geotextiles, geonets, geogrids and plastic pipe. Geomembrane test procedures can be found in the current version of Method 9090. Other tests may be required by the design engineer depending on site specific requirements.

Fingerprinting will continue to be used to verify that the material tested is essentially the same as used in the final construction process. Tests to be used depend on polymer type. Thermogravimetric analysis, differential scanning calorimetry, infrared spectrometry and gas chromatography should be used to determine composition, melting point, glass transition temperatures, crystallinity, oxidation induction time, plasticizers and additives.

In addition, government/industry partnerships need to be established to develop data bases on relationships between analytical, mechanical and physical properties of the various geosynthetics and long-term performance for different applications. Procedures have already been established to protect propriety information. The end result of this process will be beneficial for everyone. The environment and public health will be protected through superior waste disposal unit design, the use of

geosynthetics for all types of applications will be accepted by the general public and the costs of the materials will be reasonable.

SUMMARY

Fingerprinting is commonly used in the geosynthetic industry to differentiate between materials. An Agency sponsored workshop, originally intended to clarify procedures, raised many more issues without direct answers. The workshop demonstrated what is known and what is still in the research arena. The requirement for fingerprinting, depending on the specific function e.g. qualify material, identify on set of degradation, identify regrind, etc. can be performed if single clearly thought objectives are defined.

The Agency requires geosynthetic chemical resistance evaluation either through Method 9090 type of testing, for new units, or by fingerprinting, for expansion units. The Agency will also continue to evaluate the development of thermo analytical and mechanical procedures. In addition, the Agency should undertake the development of partnerships with industry to develop data bases on test results with long-term performance.

The geosynthetic industry is growing at a rapid rate. Continued advancements in basic polymers and additives, coupled with improved analytical techniques, will provide improved geosynthetic performance in waste containment. It is essential that the design engineers and polymer scientists increase their dialogue if the industry is to continue with these advances.

REFERENCES

Landreth, R.E., (1990) "Chemical Resistance Evaluation of Geosynthetics Used in Waste Management Applications," Geosynthetic Testing for Waste Containment Applications," ASTM STP 1081, Robert M. Koerner, editor, American Society for Testing and Materials, Philadelphia.

CFR, (1987) Title 40, Part 264.

U.S. EPA, (1982) "Liner Materials Exposed to Municipal Solid Waste," Report No. EPA/600/2-82/097, Office of Research and Development, U.S. Environmental Protection Agency, Cincinnati, Ohio. NTIS PB-83-147801.

U.S. EPA, (1985) "Liner Materials Exposed to Hazardous and Toxic Wastes," Report No. EPA/600/2-84/169, Office of Research and Development, , U.S. Environmental Protection Agency, Cincinnati, Ohio. NTIS PB-85-121333.

U.S. EPA, (1986) "Test Methods for Evaluating Solid Waste, 3rd Edition," Report No. EPA/SW-846, Office of Solid Waste and Emergency Response, Washington, D.C.

U.S. EPA, (1988a) "Guide to Technical Resources for the Design of Land Disposal Facilities," Report No. EPA/625/6-88/018, Office of Research and Development, U.S. Environmental Protection Agency, Cincinnati, Ohio.

U.S. EPA, (1988b) Land Disposal Restrictions for First Third Scheduled Wastes, Final Rule, 53 FR 31138.

U.S. EPA, (1988c) "Lining of Waste Containment and Other Impoundment Facilities," Technical Resource Document, Report No. EPA 600/2-88-052. NTIS PB-129670.

U.S. EPA (1991) Solid Waste Disposal Facility Criteria, Final Rule, 56 FR 196.

Construction Management in the Landfill Industry

S.W. Taylor
Golder Construction Services Inc., USA

R.A. Gould
Golder Construction Services Inc., USA

A.T. Stockman
Waste Management of Ohio, USA

ABSTRACT

The regulatory environment in which landfills are constructed requires a clear understanding of the relationships among the parties involved. In particular, Construction Managers must curb their "can do" attitude in order to work in harmony with Quality Assurance (QA) and Quality Control (QC) personnel. Definitions of construction management (CM), QA, and QC are provided and working relationships are illustrated through the authors' experiences on two projects in Ohio.

While the goals of CM, QA, and QC are similar there is a substantial difference in emphasis. It is, therefore, important to establish protocols for the resolution of conflicts and to maintain a non-adversarial relationship among the various parties. A decision was made early in the projects discussed that the requirements of QA would take precedence over those of CM; at the same time QA personnel were not insensitive to the objectives of CM, particularly with respect to schedule.

The paper addresses relationships with other parties which the Construction Manager must establish and develop towards a goal of optimum and efficient project execution. These other parties include the Contractor, the Designer, the Regulator and public agencies. It is concluded that the responsibility of the CM must extend far beyond the traditional realm of time and money.

INTRODUCTION

Government regulations pertaining to landfills (including Environmental Protection Agency (EPA) Subtitle D) are designed to protect human health and the environment, and to increase public confidence in and decrease opposition to municipal solid waste landfills. However, landfills conforming to the best designs and regulations will only achieve their objectives if they are properly constructed. Implementation of an independent construction management program can assist the Owner in achieving those objectives.

Experience in providing construction management (CM) services in conjunction with quality assurance (QA) and quality control (QC) for environmental projects has identified the need to better define the unique relationship among regulators, designers, facility owners, CM personnel, QA personnel, and QC personnel. Construction Managers, by education and temperament, are prone to think in terms of getting the job done and tend to act accordingly. While this "can do" attitude works well on more conventional civil heavy construction projects it can have negative effects on landfill construction projects in a regulatory environment where the dictates of QA and QC need to prevail.

Construction Managers engaged in the construction or the closure of landfills must balance the constraints of weather, schedule, budget, airspace, QA, QC and, on many sites, an active environmental lobby. Under such conditions Construction Managers will find it necessary to modify, if not curb, their inclination to provide immediate solutions to field problems; rather they must rethink their objectives in harmony with QA and QC priorities in order to meet the demands of the mandated permit requirements.

This paper addresses particulars of this dilemma focusing on experience gained at numerous landfills for which the authors represented Owner, CM, and/or QA/QC. The authors draw especially from experiences at Countywide Regional Disposal Facility (CWRDF) in East Sparta, Ohio where CM and QA/QC were provided by the same entity under separate contracts during construction of a new solid waste cell; and from Statewide Regional Disposal Facility (SRDF) in Canton, Ohio, where CM and QA were provided by a single entity under one contract and QC was provided by the contractor. Both of these sites are owned by Waste Management of Ohio, their perspective of the sometimes conflicting demands of CM, QA, and QC is reflected in this paper.

The authors recognize that this paper does not conform to the more traditional *"technical paper"*, in that it offers little in the way of startling new discoveries. It does however, offer the reader insight into the application of construction management techniques to the landfill construction industry.

DEFINITIONS

Before any discussion of Construction Management, Quality Assurance or Quality Control can be undertaken it is first necessary to have a clear understanding of these terms. For the purpose of this paper the authors have adopted the following:

Construction Management. Construction Management was defined by Heery (1974) as: "... that group of management activities related to a construction program, carried out during the pre-design, design, and construction phases, that contributes to the control of time and cost in the construction of a new facility."

Construction Quality Assurance. A document prepared by the United States Environmental Protection Agency (USEPA 1986) provides a clear and concise definition of quality assurance as: "a planned system of activities that provide assurance that the facility was constructed as specified in the design". The document further states that "CQA is performed independently of CQC" and that it "includes inspections, verifications, audits, and evaluations of materials and workmanship necessary to determine and document the quality of the constructed facility."

Construction Quality Control. The same document (USEPA 1986) defines quality control as: "a planned system of inspections that are used to directly monitor and control the quality of a construction project". The document states that "CQC is performed by the construction contractor(s) and consists of inspections necessary to control the quality of the constructed or installed component". Finally, this document states that "These activities are completely independent of the CQA activities."

Landfill lining system. A landfill lining system may be described as a combination of liners (soil and geomembrane) and liquid collection layers. The purpose of the lining system is to contain and direct leachate flow within the landfill for systematic removal and treatment outside the landfill area.

The above definitions for CQA and CQC are about to be expanded and refined in a new EPA Technical Guidance Document being prepared by Professors David E. Daniel and Robert M. Koerner.

Another minor point that should be clarified is the difference between QA and CQA and QC and CQC. The "C" refers to construction as distinct from manufacturing. To this end, QA and QC tend to be used in a general context referring to the manufacture of products and the construction using those products.

GOAL IDENTIFICATION

Providing successful construction management services in today's quality intensive and often highly regulated field of landfill construction or landfill closure requires that CM personnel understand the need for and the benefit of both QC and QA. The Construction Manager must systematically define and develop his role towards achieving the project goals while adhering to the strict CQA demanded by environmental concerns. Identifying the project goals and establishing non-adversarial relationships with the Owner, Contractor, QA and QC personnel which is based on trust and confidence

is fundamental to the ultimate success of the project and the services the Construction Manager hopes to provide.

Properly identifying the project goals requires some research on the part of CM personnel. Meeting with the Owner at the start of the project to review and understand the events leading to actual construction makes the Construction Manager aware of elements which may be both important and unique to the project. Concurrent research regarding the history of site activity will help the Construction Manager gain an understanding of site perception by parties other than the Owner. In addition, a familiarization with all levels of regulation governing operations at the site is essential. With this information at hand, the project goals will start to emerge.

For the Countywide RDF new cell construction the project goal was readily identified as completing construction and certification of cell 2 to have it ready to receive waste by mid May 1992 while at the same time satisfying the concerns of the citizens group, Club 3000. This latter constraint was particularly significant since Club 3000 and the Owner had some differences of opinion relating to construction of cell 1 during the previous construction season. Cost was also a factor to be considered but the Owner was the Contractor and the Construction Manager's role with regards to construction cost was therefore to advise the Owner of means of limiting costs while still achieving project milestones.

An entirely different set of goals emerged for the closure of the Statewide RDF. Following meetings with the Owner it was learned that as a result of delays caused by winter weather, the 60 acre landfill was in violation of Ohio Environmental Protection Agency (OEPA) time constraints for closure. In addition, since the landfill was acquired and operated by the current owner only for the last quarter of its active life information on the characteristics and limits of refuse was incomplete. Due to the close proximity of densely populated residential neighborhoods, the landfill had been the source of ongoing tension between the current owner and the town. This information, combined with a thorough review of OEPA Solid Waste Regulations, made this project's goal quite clear: implement the most cost effective, Best Available Technology (BAT) closure design in the shortest time frame possible, keeping quality in strict accordance with OEPA and county health department regulations. Due to the degree of scrutiny on the part of regulatory agencies and local residents, community awareness and sensitivity was identified as being an essential and guiding factor to the successful completion of this project.

PROJECT EXECUTION

Once the project goals have been established, its successful completion is largely dependent upon the relationships established between CM personnel and all participants involved in the project. These participants include the Owner, Quality Assurance and Quality Control personnel, Contractor, Designer, regulatory personnel, and various other affected groups such as community officials, residents, etc.

During this stage of the project CM personnel attempt to provide the Owner with options to field problems which offer the best available solutions with respect to cost, project goals and the requirements of QA. The Owner should be presented with alternatives to any aspect of construction determined to be unsuitable or questionable by CM personnel. Properly researched, the identification of sound construction alternatives by the Construction Manager and their ultimate use can prove invaluable to the Project.

The Construction Manager established an office on the Countywide RDF project site and began the process of coordinating the construction efforts of the Contractor (Owner) by developing a time scaled logic diagram schedule for use as a management tool. While the Construction Manager and the QA Certifying Engineer were both from the same company they had distinctly different responsibilities so they promptly established the protocol by which conflicts between the two interests would be resolved. One manifestation of that protocol was the decision that the requirements of QA would take precedence over those of schedule. Examples of cooperation between CM and QA were common as described below.

Early in the Countywide RDF project it became apparent that the soils QA monitor had a very difficult task of maintaining an accurate record of test elevations because a survey crew was not always available to determine each test location and elevation. At the Construction Manager's initiative a rotating laser was brought to site by the surveyor and the QA Monitor was able to determine test elevations independent of the survey crew. This approach to solving a problem impacting the cost and responsiveness of QA proved valuable in that the cost of survey was reduced by minimizing the on-site survey crew involvement in support of the QA effort. An additional benefit to the project was that the construction superintendent was able to use the rotating laser as a means of controlling lift thickness of the material placed. This reduced the construction superintendent's dependence on the survey crew for grade checks and accelerated the progress of the work.

An example of CM and QA cooperation occurred early in the Statewide RDF closure project, when CM personnel realized that verifying cover layer thickness would present unique difficulties due to differential settlement of the landfill cap. Conventional survey techniques would prove ineffective in maintaining cover layer thickness documentation which was necessary to the certification of the cover. CM personnel presented the Owner with the idea of using a series of specially fabricated settlement plates and poles to perform the function. At little cost to the Owner, the system was implemented and proved beneficial both for construction and QA documentation.

Another situation developed at the Statewide RDF closure project where the Owner was confronted with disposal of contaminated soil encountered during excavation of a 70 foot section of trench for installation of a leachate collection system toe drain. The contaminated soil had to be removed, placed in roll-off boxes and transported to a hazardous waste facility for treatment at substantial cost to the Owner. The cost of disposing of the contaminated soil was directly proportional to the volume of contaminated soil removed from the trench so steep slopes were desirable in order to minimize the volume. The risk of the excavation failing was a concern to CM personnel so several excavation options (comparing cost and risk) were researched and presented to the Owner. The Owner selected an option which entailed removing ten feet of overburden above the area delineated as contaminated, and providing full support of the remainder of the excavation utilizing 40 linear feet of trenchbox (Figure 1). The process was implemented and the minimal volume of contaminated soil was excavated at a predetermined cost to the Owner.

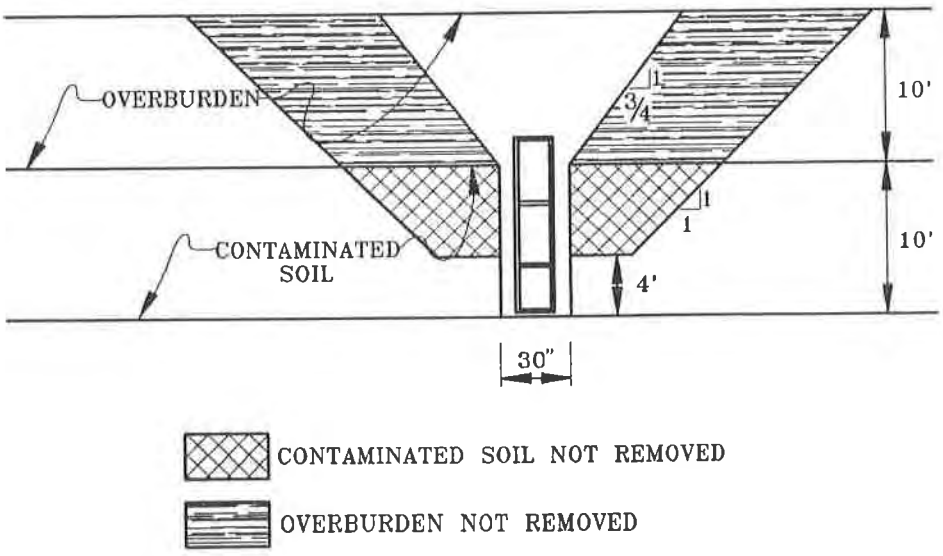

FIGURE 1

TRENCH BOX DETAIL

PROJECT RELATIONSHIPS

QA and QC. While the earlier noted definitions of QA and QC are quite clear there appears to be confusion and ambiguity in practice. Many individuals and groups use the terms *"quality assurance"* and *"quality control"* together and often interchangeably. Others suggest that QA and QC are completely separate and must be done by different organizations. The authors are of the opinion that neither position is correct! While QA should be performed by an independent (or third party) organization, QC does not require such independence. Furthermore, while the purposes of QA and QC are different, the mechanics of implementation may be essentially the same. Finally, our experience suggests that projects having separate firms for each activity are often the most difficult and the most costly without any attendant improvement in project quality.

CM, QA, and QC. Perhaps the most essential relationship in successfully achieving the project goals is that between CM, QA, and QC personnel. It is important that the Construction Manager demonstrate to QA and QC personnel that their goals are similar; CM, QA, and QC are all dedicated to quality although there may be a difference in emphasis. While the sole concern of QA is in complying with project specifications and permit conditions, that is only one of many concerns that the Construction Manager must consider in discharging his responsibility on behalf of the Owner. It is here that both parties must recognize the concerns of the other. The Construction Manager must see QA and QC as mandatory components often dictating the time requirement of the project. At the same time, QA and QC personnel must have an understanding of the concerns of CM and must be willing to work with the Construction Manager in identifying the most effective means of achieving the project goals while maintaining adherence to permit conditions and ensuring that quality is not compromised. If caution is not exercised from the start, adversarial relationships can develop in which QA and/or QC personnel refuse to contribute towards identifying the most efficient means of attaining a quality product. The relationship in which each party consistently questions the role and actions of the other can prove detrimental to the project goal.

For the Countywide RDF project the owner operated as contractor and entered first into a contract for QA/QC and then into a separate contract for CM. This latter contract was initiated when it became apparent that the Owner did not have the resources available from his own fully committed staff to adequately manage the work at hand. Both QA/QC and CM were performed by the same corporate entity but under different contracts. The roles of both were kept distinct and two different project managers (PM), one for CM and one for QA/QC, were involved with the project (Figure 2). This arrangement required close coordination between the two PMs but allowed each PM to concentrate his efforts on the area for which he was responsible. Consequently there were times when the interest of CM were in apparent conflict with those of QA/QC and a resolution involving both parties had to be reached. Because the potential for such conflicts was recognized early, protocols were established whereby the Construction Manager deferred any question involving quality of the project to the QA Certifying Engineer and the Certifying Engineer rendered the final decision in such matters. With this protocol established, decisions impacting quality of construction were rendered by the person responsible for QA and decisions not relating to quality, such as scheduling, were rendered by the Construction Manager.

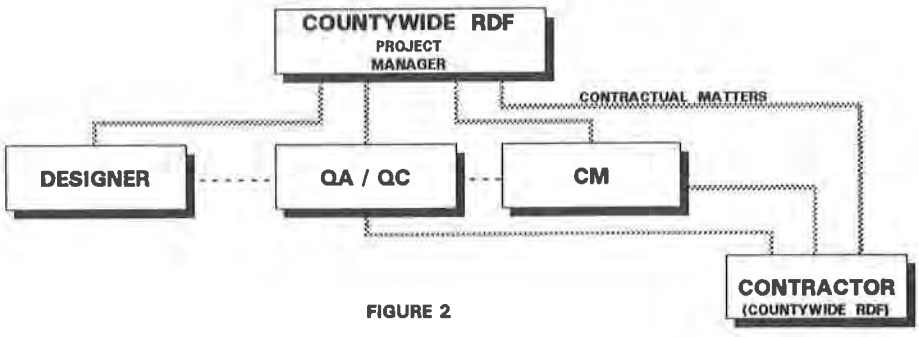

FIGURE 2

PROJECT RELATIONSHIPS - COUNTYWIDE RECYCLING AND DISPOSAL FACILITY

In the case of the Statewide RDF closure project, both CM and QA services were provided by one entity under the same contract and QC was provided for by the Contractor as part of his construction contract (Figure 3). This arrangement facilitated communication and proved to be effective. As illustrated by the following examples, CM personnel understood and yielded to the often time consuming remedial work necessitated by QA requirements. In one instance, subgrade material placed, tested and certified as a base for the placement of clay cap material was removed at the recommendation of QA personnel because, during winter frost conditions, the surface (top 4 to 6 inches) of the subgrade material had frozen. The Construction Manager, concerned about schedule, discussed the situation with several geotechnical specialists who agreed with the QA personnel. Their recommendation was to replace the frozen material with fresh subgrade prior to the placement of clay cap material. While the remedial action delayed the project schedule, CM personnel understood its purpose in achieving the project goal and, in that light, were able to satisfactorily explain the delay to the Owner.

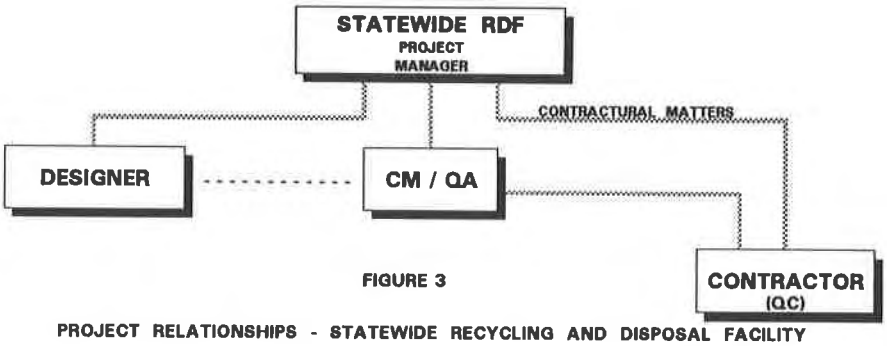

FIGURE 3

PROJECT RELATIONSHIPS - STATEWIDE RECYCLING AND DISPOSAL FACILITY

Another reason for the success experienced at the Statewide RDF was the willingness of QA personnel to provide the Construction Manager and the Contractor with a series of options when problems developed. In one instance it became apparent that clay, which had been placed and compacted as part of the cover, had absorbed excess moisture during a period of above normal precipitation and no longer provided the level of impermeability required. Instead of mandating that the material be removed and replaced, as is often the case, QA personnel discussed the problem with the Construction Manager. Both parties agreed to offer the Contractor the option of either removing and wasting the clay, or opening it (by disc or harrow) in order to promote air drying in the sun while placement continued in other areas. The Contractor chose the latter and, after the material was processed and the moisture content checked by QA personnel, the material was re-compacted and met the permit conditions with respect to permeability.

Finally, in addition to a good relationship between CM and QA personnel, a close affiliation with key laboratory personnel facilitated the process of incorporating preconstruction and construction testing into the project schedule. On several occasions, the Construction Manager advised QA personnel of the impact which the turnaround time of each sample would have on the project schedule. Careful planning and coordination was initiated in order to optimize the use of laboratory facilities with respect to attaching appropriate priority to those tests most impacting schedule. During critical stages of the project when the capacity of one laboratory to perform permeability tests was reached and a decision was made to involve other laboratories across the country in order that construction not be interrupted or delayed.

CM and Contractor. It is essential that the Contractor understand the Construction Manager's commitment to the project goal. A smooth running project requires an understanding and mutual respect between the Construction Manager and the Contractor. This understanding and respect needs to be recognized, developed and nurtured for without these essential ingredients projects may experience conflict, delay, claims and/or deterioration of quality. While the Contractor must recognize the Construction

Manager's desire for and knowledge of what is required to achieve a high quality product, the Construction Manager must recognize and accede to the Contractor's familiarity with his equipment and personnel capabilities. The easiest way to deteriorate this relationship is to dictate construction methods to the Contractor.

The Contractor must be recognized as a critical resource influencing the successful achievement of project goals. His knowledge and suggestions should always be carefully considered by the Construction Manager. In the case of the Statewide RDF project, the Contractor often suggested alternative procedures and options. It was then the responsibility of the Construction Manager to research the alternatives with respect to the project constraints and goals and recommend the most effective alternative. This included presenting alternatives to the Designer for comment on functional integrity and to QA personnel for possible effects on quality.

It is also important to recognize the Contractor's desire to approach the Construction Manager for ruling in cases where QA personnel have deemed remedial work necessary and the Contractor disagrees. This is an excellent example of when a good relationship between the Construction Manager, QA personnel and Contractor is beneficial. A basic confidence in the knowledge and understanding of QA personnel will encourage the Construction Manager to let QA dictate the progress of the work. Respect for the fairness and objectivity of the Construction Manager will encourage the Contractor to accept the decision.

CM and Designer. Another relationship essential in successfully achieving project goals is that between CM personnel and the Designer. In the form of drawings and written specifications, the Designer committed to paper the desired final product. It is the responsibility of CM personnel to aid in making the transition from paper to field as smooth as possible. In doing that, it is the duty of the on-site Construction Manager to make known any field conditions which may have effects on the proper implementation of the design. Often times this will include the timely coordination of data gathering to aid in developing solutions.

During construction of the Statewide RDF project, effective communications between CM personnel and the Designer helped in alleviating several potential construction delays and associated costs. In one instance, the designed alignment of the leachate collection toe drain called for the removal of several hundred feet of site fence as well as a group of pine trees providing a buffer between the landfill and an adjacent neighborhood. After bringing the situation to the attention of the Designer, the alignment of the collection drain was slightly altered away from the fenceline without hampering its functional integrity. That portion of the collection drain was successfully installed without the time consuming daily removal and replacement of the site fence and, at the same time, the trees buffering the adjacent houses were left untouched.

CM and Regulator. The Construction Manager for landfill projects should meet with representatives of regulatory agencies on a regular and frequent basis. It is important that the Construction Manager be in a position to provide assurance to these representatives that quality work is being performed. It is here that a Construction Manager's thorough understanding of all levels of regulation governing the project as well as a firm grasp on QA and QC procedures proves beneficial. When a regulator can discuss quality aspects of the project with someone whose abilities extend beyond the traditional concerns of schedule and budget he is sure to have confidence that the project requirements are being met.

While communication with the OEPA during construction of the Statewide RDF project was for the most part limited to the Owner, the Construction Manager met with county health inspectors on a regular basis. The Construction Manager made it a point to keep the health department apprised of all activity on the site. Setting aside time for immediate responses to concerns raised by the health department created a sense of confidence on the part of the health inspectors and was the basis for the non-adversarial relationship enjoyed by the Construction Manager and the county health department.

CM and Public Relationships. Public relations are vital to the success of a project. Community groups, lobbyists, town officials, etc. can make carrying out a landfill construction or closure project very difficult. It is important to maintain an up front, open and honest approach to all project activity. Furthermore, addressing the concerns of the people on an individual basis can result in positive, if not enthusiastic, support for the project.

At the start of the Statewide RDF project a full set of plans and specifications was forwarded to the township office for public access. In addition, CM personnel, accompanied by a representative of the Owner, conducted a door to door awareness campaign on two separate occasions. Residents were given a brief explanation of intended construction activity, construction schedules and a contact to call with any questions they may have.

During Statewide RDF construction the Construction Manager attended regular site meetings with township trustees to be available to answer questions. In addition, the township office was issued a copy of periodic construction progress reports for public access. On two occasions, CM personnel coordinated evaluations and written responses to surface water drainage concerns raised by land owners adjacent to the site. In all of these instances, keeping the community informed proved beneficial to the successful completion of the project and achievement of the project goals.

CONCLUSIONS

The authors' experience, as described in this paper, has shown that providing successful CM services to the landfill industry entails the traditional responsibility to look after the interests of the Owner; however, in the case of landfill projects, an Owner's interests, and a Construction Manager's responsibilities, go far beyond the traditional realm of schedule and budget. Because quality assurance has overriding consideration its importance must be recognized early in the construction phase of the project. As seen at both Countywide and Statewide RDFs, identifying the project goals and establishing vital working relationships with contractors and QA personnel were the keys to successful CM and, in turn, successful projects.

ACKNOWLEDGEMENTS

The authors wish to thank Waste Management of Ohio for permission to publish this paper and Mr. D.F. Fletcher for his assistance during its preparation.

REFERENCES

Heery, George T., (March-April 1974) "Construction Management Defined", The Military Engineer, No. 430, p.85.

United States Environmental Protection Agency (USEPA) Office of Solid Waste and Emergency Response, (October 1986) "Technical Guidance Document: Construction Quality Assurance for Hazardous Waste Land Disposal Facilities", EPA 530.SW.86.031, OSWER Policy Directive No 0472003, Section 1.4.1.

Authors Index

Subject Index

The pages listed indicate the first page of the paper in which the reference is found.

Know More.

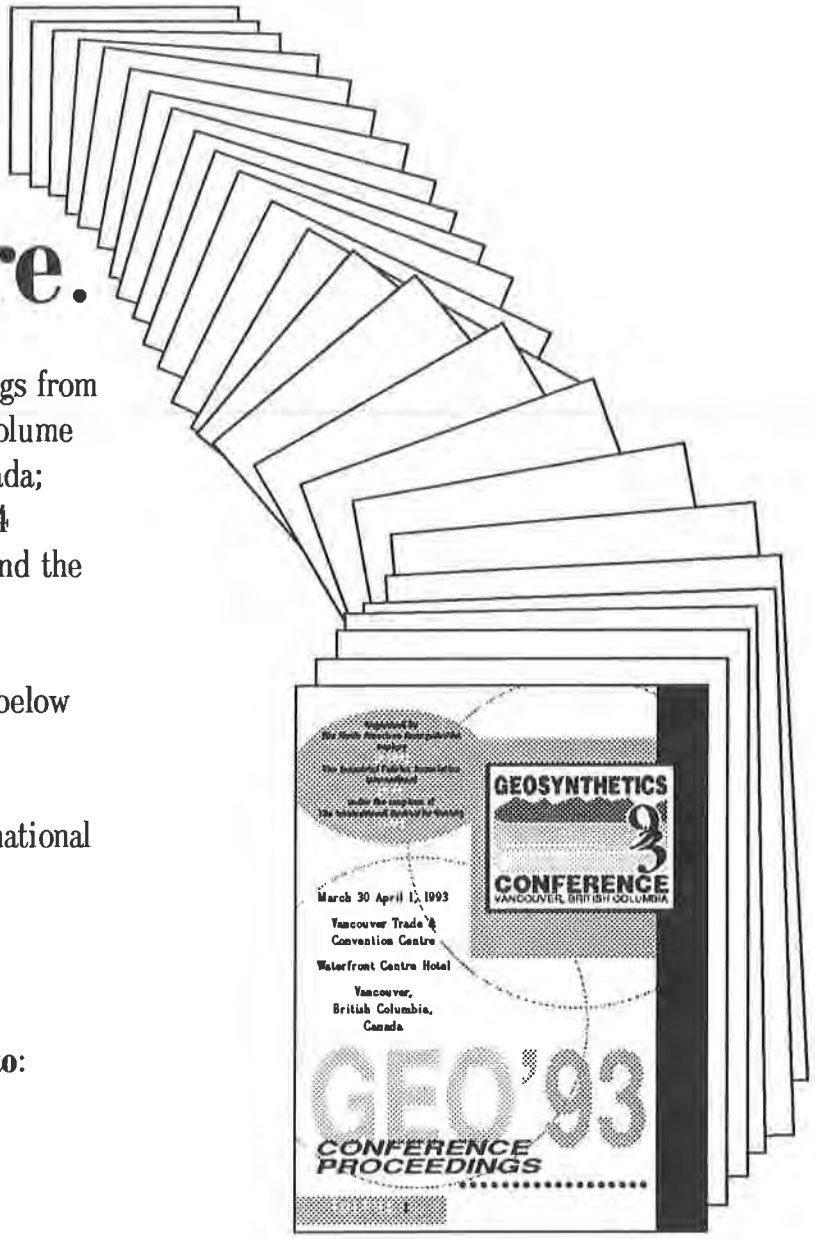

Order extra copies of the proceedings from Geosynthetics '93. Just $85 per 3-volume set, plus postage ($6 U.S.; $19 Canada; $58 South America and Europe; $34 Central America; $70 Asia, Africa and the Middle East).

To order, simply complete the form below and return with payment to:

Industrial Fabrics Association International
345 Cedar St., Suite 800
St. Paul, MN 55101
USA

For faster service, fax your order to:
612/222-8215

GEO'93

Please send _____ copies of Geosynthetics '93 Conference Proceedings @ $85 per set, plus postage

☐ Check enclosed ☐ Please bill my ☐ Visa ☐ Master Card Expiration date _____

Credit Card # _____

SIGNATURE (X) _____

Subtotal _____
Postage _____
TOTAL _____

NAME _____

COMPANY _____

ADDRESS _____

CITY _____ STATE/PROVINCE _____ ZIP/POSTAL CODE _____

COUNTRY _____

PHONE _____ FAX _____

Return to: Industrial Fabrics Association International
345 Cedar St., Suite 800, St. Paul, MN 55101 USA
612/222-2508 • fax 612/222-8215

Geosynthetics '93
Conference Proceedings

Volume 1
Opening Session
Roads and Pavements
Walls, Slopes, Embankments and Foundations
Geotextile Filtration Design and Testing

Volume 2
Geosynthetics Testing
Durability and Long-Term Performance of Geosynthetics
Technical Advances, Innovations, Challenges

Volume 3
Waste Containment Case Histories
Landfill Design, Performance and CQA